Electromagnetic Fields

SECOND EDITION

Jean Van Bladel

The IEEE Press Series on Electromagnetic Wave Theory
Donald G. Dudley, *Series Editor*

Electromagnetic Fields

Second Edition

Jean G. Van Bladel

IEEE Antennas and Propagation Society, Sponsor

IEEE Press Series on Electromagnetic Wave Theory
Donald G. Dudley, Series Editor

IEEE PRESS

WILEY-INTERSCIENCE
A JOHN WILEY & SONS, INC., PUBLICATION

Electromagnetic Fields

IEEE PRESS SERIES ON ELECTROMAGNETIC WAVE THEORY

The IEEE Press Series on Electromagnetic Wave Theory consists of new titles as well as reissues and revisions of recognized classics in electromagnetic waves and applications which maintain long-term archival significance.

BOOKS IN THE IEEE PRESS SERIES ON ELECTROMAGNETIC WAVE THEORY

Chew, W. C., *Waves and Fields in Inhomogeneous Media*
Christopoulos, C., *The Transmission-Line Modeling Methods: TLM*
Clemmow, P. C., *The Plane Wave Spectrum Representation of Electromagnetic Fields*
Collin, R. E., *Field Theory for Guided Waves, Second Edition*
Collin, R. E., *Foundations for Microwave Engineering, Second Edition*
Dudley, D. G., *Mathematical Foundations for Electromagnetic Theory*
Elliott, R. S., *Antenna Theory and Design, Revised Edition*
Elliott, R. S., *Electromagnetics: History, Theory, and Applications*
Felsen, L. B., and Marcuvitz, N., *Radiation and Scattering of Waves*
Harrington, R. F., *Field Computation by Moment Methods*
Harrington, R. F., *Time Harmonic Electromagnetic Fields*
Hansen, T. B., and Yaghjian, A. D., *Plane-Wave Theory of Time-Domain Fields*
Ishimaru, A., *Wave Propagation and Scattering in Random Media*
Jones, D. S., *Methods in Electromagnetic Wave Propagation, Second Edition*
Josefsson, L., and Persson, P., *Conformal Array Antenna Theory and Design*
Lindell, I. V., *Methods for Electromagnetic Field Analysis*
Lindell, I. V., *Differential Forms in Electromagnetics*
Stratton, J. A., *Electromagnetic Theory, A Classic Reissue*
Tai, C. T., *Generalized Vector and Dyadic Analysis, Second Edition*
Van Bladel, J. G., *Electromagnetic Fields, Second Edition*
Van Bladel, J. G., *Singular Electromagnetic Fields and Sources*
Volakis, et al., *Finite Element Method for Electromagnetics*
Zhu, Y., and Cangellaris, A., *Multigrid Finite Element Methods for Electromagnetic Field Modeling*

Electromagnetic Fields

Second Edition

Jean G. Van Bladel

IEEE Antennas and Propagation Society, Sponsor

IEEE Press Series on Electromagnetic Wave Theory
Donald G. Dudley, Series Editor

IEEE PRESS

WILEY-INTERSCIENCE
A JOHN WILEY & SONS, INC., PUBLICATION

IEEE Press
445 Hoes Lane
Piscataway, NJ 08854

Library of Congress Cataloging-in-Publication Data is available.

ISBN 978-0-471-26388-3

Printed in the United States of America

10 9 8 7 6 5 4 3 2 1

To Hjördis and Sigrid

Contents

Preface

When the first edition of *Electromagnetic Fields* was published in 1964, the digital revolution was still in its infancy and professional computers had been available at universities for only a decade or so. Since these early days, massive computing power has been deployed over time to solve ever more complex field problems. This happened in the traditional disciplines of telecommunications and power, but also in a number of industrial and medical areas of research, for example tumor detection, nondestructive testing, and remote monitoring of forests and vegetation. The new, updated edition was conceived to take these developments into account.

Its main focus remains the theory of the electromagnetic field. Numerical analysis receives only limited attention, and fine points such as the stability and robustness of algorithms or the manipulation of matrices to achieve computer economy are only cursorily mentioned. These topics are amply addressed in a number of outstanding treatises, many of which are listed in the general bibliography. The dividing line between theory and numerical analysis is fuzzy, however. Field theory, for example, remains a most important guide for the numerical analyst. It helps refine and simplify brute force numerical procedures. It also provides benchmarks for the validation of numerical codes, and predicts the singular behavior of potentials, fields and sources at sharp discontinuities, in particular at edges and tips of cones. Theoretical analysis also produced a series of useful numerical methods, some of which are described in the text, albeit in very concise form.

The number of topics in the general area of electromagnetism is exceedingly vast, even after subjects of a more computational nature are excluded. A drastic selection became unavoidable. The author based it on a broad survey of the literature of the last few decades and the frequency with which topics appeared in some leading periodicals. Within each topic, in addition, only papers which *directly* contribute to the flow of the theoretical development have been quoted. This procedure is subjective, of course, and leaves unmentioned many important articles, in general because of the complexity of their mathematical structure. It should be noted, in that respect, that *Electromagnetic Fields* is written for engineers and applied physicists. Potential applications of a theoretical result, for example, are mentioned whenever possible. More importantly, the mathematics remain practical, almost utilitarian, and it is only occasionally that a modicum of rigor is introduced. The main example is found in potential theory, more specifically in the analysis of the singularities of static potentials and fields. A fundamental understanding of these singularities is essential for derivations of integral equations such as the EFIE and the MFIE. The text has been made mathematically self-contained by including a number of specialized appendices. These were well received in the first edition, and are reproduced in the present one, in slightly expanded form.

Notwithstanding the book's 1100 pages, space limitations played a major role. They did not allow, for example, inclusion of some important subjects, and forced a fairly broad-brush treatment of others. In contrast, much space has been allotted to some aspects of the theory which are seldom gathered under a single cover:

- the already mentioned singularities of fields and sources;
- the low-frequency approximations;

– the electrodynamics of moving bodies; and
– the resonances which affect fields scattered by targets.

Space limitations have also precluded long analytical developments, particularly extended complex integrations, and have sometimes led to the omission of intermediate steps in a theoretical derivation (in which case suitable references are given). The abundant figures hopefully compensate for some omissions by clarifying, on their own, the underlying features of a phenomenon, for example the frequency-dependence of the scattering cross section of a target. The present text is the product of these various choices and compromises. It is a survey, a vade-mecum, which should be useful to graduate students, entry-level researchers, and even experienced engineers and physicists who wish to take on a novel subject of research. Power engineers involved in the design of electrical machines may find pertinent information in the chapters that cover "60 Hz approximations" and the evaluation of motion-induced eddy currents.

The task of integrating and accurately representing the contributions of so many researchers into a coherent whole has been arduous. Fortunately, more than ninety authors quoted in the text kindly reviewed the pages on which their work was cited. Their suggestions and corrections have decisively enhanced the accuracy of portions of the text. These scientists are too numerous to be thanked individually, but an exception must be made for A.T. de Hoop, D. De Zutter, E. Heyman, I.V. Lindell, J.R. Mautz, P.H. Pathak, F. Olyslager, H. Rogier, F. Tesche, and A.D. Yaghjian, who devoted so much time in offering their comments and criticisms. The manuscript as a whole has greatly benefited from the guiding hand of the late D.G. Dudley, the editor of the Series on Electromagnetic Wave Theory, and from the expert advice of five distinguished reviewers: R.E. Collin, E. Heyman, A. Ishimaru, D.S. Jones and, most particularly, C.M. Butler. These well-known authors pinpointed several passages which were in need of clarification, and they suggested changes in both the general structure and the tenor of the text. Many errors have undoubtedly remained undetected, for which the author begs the reader's forgiveness. Typographical errors, in particular, are inevitable in a text comprising some 5,000 equations and 300,000 words.

The elaboration of a manuscript as extensive as the present one required considerable administrative effort. In this regard, the author had the good fortune of enjoying the full support of his friend and colleague, Paul Lagasse, chairman of the Department of Information Technology at Ghent University. Ms. Isabelle Van der Elstraeten flawlessly typed every word and equation of the two versions of the manuscript, and, in doing so, exhibited rare professionalism, expertise, and dependability, so crucial in bringing this project to fruition. To her the author extends his special gratitude. Closer to home, he called upon his daughter Sigrid to read large parts of the text; her corrections greatly improved the style and form of those pages. The decisive support, however, came from his patient wife, Hjördis, who graciously accepted the role of "book widow" for close to nine years. Her warm encouragement and relentless support helped the author overcome frequent moments of writer's fatigue.

JEAN G. VAN BLADEL

Ghent, Belgium
April 2007

Chapter 1

Linear Analysis

The linear equations of mathematical physics can be solved by methods that have found applications in many disciplines (e.g., electrostatics, hydrodynamics, acoustics, and quantum mechanics). It is instructive, therefore, to describe these methods in very general and abstract terms. Such an approach avoids tedious repetition of steps that are essentially the same for each new equation that is encountered. A really rigorous discussion of the relevant methodology requires great precision of language. Such an approach is beyond the pale of the current chapter, whose sole ambition is to give a broad survey — only the bare essentials — of some of the most important topics. The reader is directed to more specialized texts for additional (and more rigorous) information [147, 150, 160, 168, 174, 186, 193].

To illustrate the basic abstract concepts of linear analysis, we will consider two particularly simple physical systems. The first one is the *flexible string*. When the string is subjected to a uniform longitudinal tension T and a vertical force density $g(x)$, its small static displacement $y(x)$ satisfies the differential equation

$$\frac{d^2y}{dx^2} = -\frac{g(x)}{T}. \tag{1.1}$$

Two different types of boundary conditions are pertinent. They correspond with (Fig. 1.1)

1. The *clamped* string, where the displacement $y(x)$ vanishes at both ends, $x = 0$ and $x = l$.
2. The *sliding* string, which is free to slide vertically at both ends but is constrained to keep zero slope there.

A second useful example is afforded by the *transmission line* (Fig. 1.2). The voltage and current on the line satisfy the system of equations

$$\begin{aligned} \frac{\partial v}{\partial x} &= -Ri - L\frac{\partial i}{\partial t} + \frac{\partial v_a}{\partial x} \\ \frac{\partial i}{\partial x} &= -Gv - C\frac{\partial v}{\partial t} + \frac{\partial i_a}{\partial x}. \end{aligned} \tag{1.2}$$

Electromagnetic Fields, Second Edition, By Jean G. Van Bladel

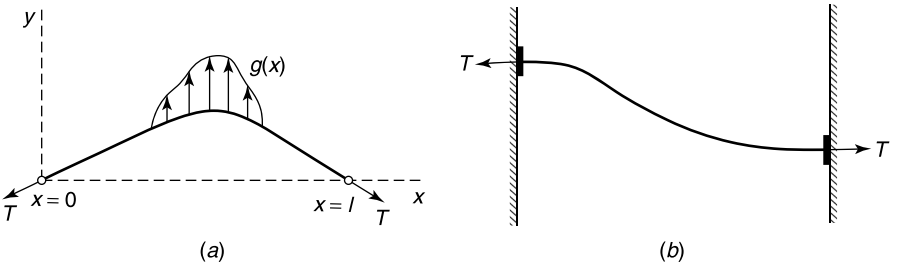

Figure 1.1 (*a*) Clamped string; (*b*) sliding string.

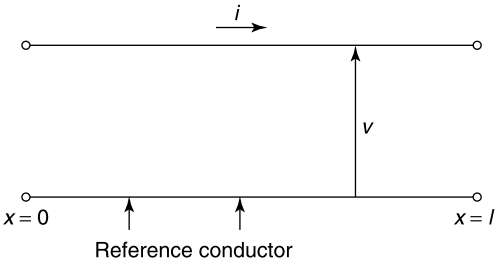

Figure 1.2 Open transmission line.

Here R, L, G, and C denote the linear resistance, inductance, conductance, and capacitance of the line, respectively, per unit length. The symbols $v_a(x,t)$ and $i_a(x,t)$ refer to externally applied voltages and currents. Function v_a, for example, could be the voltage $(-\partial\phi^i/\partial t)$ induced by a linear magnetic flux ϕ^i (in Wb m^{-1}) originating from exterior sources.

When phenomena are harmonic in time, $v(x,t)$ and $i(x,t)$ can be obtained from a knowledge of the phasors $V(x)$ and $I(x)$. Typically,

$$v(x,t) = \mathrm{Re}[V(x)\mathrm{e}^{j\omega t}].$$

The phasor voltage on a lossless line satisfies, with $I_a = 0$, the equation

$$\frac{d^2V}{dx^2} + \omega^2 LCV = \frac{d^2V_a}{dx^2}, \tag{1.3}$$

which must be supplemented by the conditions $I = 0$ and $dV/dx = 0$ at the end points $x = 0$ and $x = l$ (for an open line) and $dI/dx = 0$ and $V = 0$ at the end points (for a short-circuited line).

1.1 LINEAR SPACES

The field quantities that appear in a linear problem possess mathematical properties dictated by the physical nature of the phenomenon under investigation. The displacement of a string, for example, must be a continuous function of x. The electric field near a metallic edge must be square-integrable. In general, the nature of the problem requires the field quantities to belong to a linear space $\mathcal{S}$; that is, to a collection of elements f for which addition and multiplication by a scalar have been defined in such a manner that

1. Addition and multiplication are commutative and associative.

2. These operations create an element that is in $\mathcal{S}$.

3. The product of f and the scalar 1 reproduces f.

4. The space contains a unique null or zero element 0 such that $f + 0 = f$ and $f \cdot 0 = 0$.

5. To each f there corresponds a unique element $(-f)$ such that $f + (-f) = 0$.

The space of three-dimensional Euclidean vectors is obviously a linear space. Another example is the space of complex-valued functions that are Lebesgue-measurable and square-integrable in a given domain. This space is denoted by the symbol $\mathcal{L}_2$.

If $f_1, f_2, \ldots, f_N$ belong to $\mathcal{S}$, the set of elements $a_1 f_1 + a_2 f_2 + \cdots + a_N f_N$, where the a_i are complex numbers, constitutes the space spanned by the f_i. The f_i are *linearly independent* if $\sum_{i=1}^{N} a_i f_i = 0$ implies that all a_i coefficients are zero. If every element of $\mathcal{S}$ can be expressed uniquely as a linear combination of the f_i, the latter are said to form a *basis* for $\mathcal{S}$, and the value of N is the *dimension* of the space (which can be finite or infinite). To give an example, the space of vectors (v_1, v_2) is two-dimensional, and the elements $(1, 0)$ and $(0, 1)$ form a possible basis for that space.

The importance of the previous considerations will become clear when we discuss, in later sections and chapters, the representation of a function f by its *expansion*

$$f \approx a_1 f_1 + a_2 f_2 + \cdots + a_N f_N. \tag{1.4}$$

Here the f_i are given, and the a_i are unknown coefficients. The symbol $\approx$ indicates a *representation*, which will hopefully turn into a good approximation as N increases. The meaning of these various terms will be further clarified in the current section and in Section 1.7. The concept of *normed space* plays an important role in that respect. By definition, a linear space is *normed* if each element f is assigned a real number $\| f \|$ such that the following rules apply:

1. $\| f \| \geq 0$, with equality if, and only if, $f = 0$.

2. $\| af \| = |a| \ \| f \|$, where a is a real or complex number.

3. $\| f_1 + f_2 \| \leq \| f_1 \| + \| f_2 \|$ (triangle inequality).

For an N-dimensional vector $\mathbf{x}$ with components $x_1 \ldots x_N$, one often uses the following norms [198]:

1. The *unit* norm, sum of the absolute values of the components

$$\|\mathbf{x}\|_1 = \sum_{i=1}^{N} |x_i|. \tag{1.5}$$

2. The *Euclidean* norm

$$\|\mathbf{x}\|_2 = \sqrt{\left(\sum_{i=1}^{N} |x_i|^2 \right)}. \tag{1.6}$$

This norm corresponds with the Euclidean concept of length.

3. The *infinite* norm

$$\|\mathbf{x}\|_\infty = \max |x_i|. \tag{1.7}$$

A normed linear space provides a measure of the closeness of two elements f_1 and f_2. From rule 1 above, we note that $\| f_1 - f_2 \| = 0$ occurs only for $f_1 = f_2$. Therefore $\| f_1 - f_2 \|$, the *distance* between the elements, is a measure of their closeness. This remark leads directly to the concept of *convergence*, according to which a sequence of elements f_n converges to f if, for any given ϵ, there exists a number N such that

$$\| f - f_n \| < \epsilon, \qquad \text{whenever } n > N. \tag{1.8}$$

As a basis for some important numerical methods, we must go a step further and introduce the *inner product space*; that is, a space that is endowed with an inner (or scalar) product $\langle f_1, f_2 \rangle$. A *symmetric* scalar product satisfies the rules

1. $\langle f_1, f_2 \rangle_S = \langle f_2, f_1 \rangle_S$
2. $\langle a_1 f_1 + a_2 f_2, f_3 \rangle_S = a_1 \langle f_1, f_3 \rangle_S + a_2 \langle f_2, f_3 \rangle_S,$ (1.9)

where the various f are elements of S. Such a product is relevant for the concepts of reaction and reciprocity, which play an important role in later chapters. To illustrate by an example, the scalar product

$$\langle y_1, y_2 \rangle_S = \int_0^\ell y_1(x) y_2(x)\, dx$$

is suitable for the study of the real displacements of a string. However, there are other possibilities, such as

$$\langle f_1, f_2 \rangle = \int_0^\ell [\operatorname{grad} f_1 \cdot \operatorname{grad} f_2 + l^{-2} f_1 f_2]\, dx.$$

A most important scalar product is the *Hilbert* product, which is defined by the rules

1. $\langle f_1, f_2 \rangle_{\mathrm{H}} = \langle f_2, f_1 \rangle_{\mathrm{H}}^*,$ where the star denotes complex conjugation.
2. $\langle a_1 f_1 + a_2 f_2, f_3 \rangle_{\mathrm{H}} = a_1 \langle f_1, f_3 \rangle_{\mathrm{H}} + a_2 \langle f_2, f_3 \rangle_{\mathrm{H}}$
$\langle f_3, a_1 f_1 + a_2 f_2 \rangle_{\mathrm{H}} = a_1^* \langle f_3, f_1 \rangle_{\mathrm{H}} + a_2^* \langle f_3, f_2 \rangle_{\mathrm{H}}.$
3. $\langle f, f \rangle_{\mathrm{H}} \geq 0,$ where the equality sign holds only for $f = 0.$ (1.10)

Such a product is associated with the concept "power," as illustrated by its application to a transmission line in the sinusoidal regime. The relevant product is here

$$\langle V, I \rangle_{\mathrm{H}} = \frac{1}{l} \int_0^l V I^*\, dx. \tag{1.11}$$

The right-hand term of Equation (1.11) is clearly the average value of the complex power VI^* along the line. Property 3 above makes the Hilbert product particularly suitable for the introduction of the norm

$$\| f \| = \sqrt{\langle f, f \rangle_{\mathrm{H}}}, \tag{1.12}$$

and therefore for the study of convergence as measured by the magnitude of the error. With a Hilbert type of scalar product,

$$|\langle f, g \rangle_{\mathrm{H}}| \leq \| f \| \, \|g\| = \sqrt{\langle f, f \rangle_{\mathrm{H}}} \, \sqrt{\langle g, g \rangle_{\mathrm{H}}}. \tag{1.13}$$

This important relationship is the *Schwarz' inequality*.

Criterion (1.8) leads to *strong* convergence. The existence of a scalar product allows one to introduce *weak* convergence, according to which f_n converges to an element f of S if

$$\lim_{n\to\infty} \langle f_n, h\rangle_{\mathrm{H}} = \langle f, h\rangle_{\mathrm{H}}, \tag{1.14}$$

where h is any element of S. Convergence of functions has now been replaced by convergence of numbers, a property that has advantages from a numerical point of view. If the h are the testing functions of distribution theory defined in Appendix 8 (functions that are infinitely differentiable on a compact support), the convergence is said to hold in the *distributional* sense.

The concept of a scalar product is obviously inspired by classical vector analysis. Pursuing the analogy further, we will say that elements f_m and f_n are *orthogonal* if $\langle f_m, f_n\rangle = 0$. We will often use, in the sequel, *orthonormal* sets, defined by the property

$$\langle f_m, f_n\rangle = \delta_{mn}, \tag{1.15}$$

where δ_{mn} is the Kronecker delta, equal to one for $m = n$ and zero for $m \neq n$.

Consider now the problem of approximating an element f by a series such as (1.4), where the f_n form an orthonormal set. We write

$$f = \underbrace{\sum_{n=1}^{N} a_n f_n}_{f_N} + e_N. \tag{1.16}$$

The a_n are arbitrary coefficients, and e_N is the corresponding error. The norm $\|e_N\|$ of the error is given by

$$\begin{aligned}(\|e_N\|)^2 &= \langle f - f_N, f - f_N\rangle_{\mathrm{H}} \\ &= \langle f, f\rangle_{\mathrm{H}} - \sum_{n=1}^{N} \left(a_n\langle f_n, f\rangle_{\mathrm{H}} + a_n^*\langle f, f_n\rangle_{\mathrm{H}} - a_n a_n^*\right).\end{aligned}$$

If we choose $a_n = \langle f, f_n\rangle_{\mathrm{H}}$, that is, if we expand f as

$$f = \sum_{n=1}^{N} \langle f, f_n\rangle_{\mathrm{H}} f_n, \tag{1.17}$$

the norm $\|e_N\|$ vanishes, which means that an optimal approximation has been obtained.

1.2 LINEAR TRANSFORMATIONS

The basic problem for the clamped string is to determine the displacement $y(x)$ due to a given forcing function $g(x)$. We shall assume that $g(x)$ is piecewise continuous. The string problem is a particular case of a more general one, namely

$$\mathcal{L}f = g, \tag{1.18}$$

where $\mathcal{L}$ is an operator mapping the space $\mathcal{D}$ of elements f (the *domain*) into the space $\mathcal{R}$ of elements $\mathcal{L}f$ (the *range*). This mapping is a *transformation*. In the clamped string problem, the domain consists of functions that are continuous in $(0, l)$, vanish at $x = 0$ and $x = l$, and have piecewise continuous second derivatives in $(0, l)$. A transformation is *linear* when it is additive and homogeneous; that is, when $\mathcal{L}(f_1 + f_2) = \mathcal{L}f_1 + \mathcal{L}f_2$ and $\mathcal{L}(af) = a\mathcal{L}f$. These properties imply, first, that the operator is linear and, second, that the domain contains all linear combinations of any two of its elements. Such a domain is a *linear manifold*. The transformation associated with the clamped string problem is obviously linear. The transformation associated with the inhomogeneous boundary conditions $y = 1$ at $x = 0$ and $y = 3$ at $x = l$ is not. The reason is clear: The sum of two possible displacements takes the values $y = 2$ at $x = 0$ and $y = 6$ at $x = l$, and these values violate the boundary conditions.

An element f is said to satisfy Equation (1.18) in a *weak sense* if the left and right terms of Equation (1.18) have equal projections on any function w belonging to a space that includes $\mathcal{R}$. We write

$$\langle w, \mathcal{L}f \rangle = \langle w, g \rangle. \tag{1.19}$$

Weak solutions will often be encountered in future chapters. They are frequently easier to construct than direct (strong) solutions of the initial Equation (1.18). The solution of the latter is greatly facilitated when a linear operator $\mathcal{L}^a$, a scalar product $\langle f, g \rangle$, and a domain $\mathcal{D}^a$ can be found such that

$$\langle \mathcal{L}f, h \rangle = \langle f, \mathcal{L}^a h \rangle \tag{1.20}$$

whenever h belongs to D^a. The linear transformation defined by operator $\mathcal{L}^a$ and domain $\mathcal{D}^a$ is the *adjoint* of the original one. It allows transferring the operator $\mathcal{L}$, acting on f, to an operator $\mathcal{L}^a$ acting on h. In the case of the clamped string, the left-hand term of Equation (1.20) can be transformed by integrating by parts. One obtains

$$\langle \mathcal{L}f, h \rangle = \int_0^l \frac{d^2 f}{dx^2} h \, dx = \int_0^l f \frac{d^2 h}{dx^2} \, dx + \left[h \frac{df}{dx} - f \frac{dh}{dx} \right]_0^l. \tag{1.21}$$

It is seen that Equation (1.20) is satisfied if one chooses $\mathcal{L}^a$ to be the differential operator d^2/dx^2, and the domain $\mathcal{D}^a$ to consist of functions that are zero at $x = 0$ and $x = l$ [whereby the bracketed term in (1.21) vanishes] and possess piecewise-continuous second derivatives. Clearly, the adjoint of the clamped string transformation is the transformation itself, which is therefore termed *self-adjoint*.

The pattern suggested by Equation (1.21) is frequently encountered in mathematical physics. In general, the scalar product is an n-dimensional integral. The equivalent of Equation (1.21) is then obtained by using a suitable Green's theorem in n-dimensional space, in which the bracketed term is replaced by an $(n - 1)$-dimensional integral, linear in f and h, which is termed the *bilinear concomitant* $J(f, h)$. The domain $\mathcal{D}^a$ of h is determined by enforcing the condition $J(f, h) = 0$.

Self-adjoint transformations occur very frequently in mathematical physics, but they are by no means the rule in electromagnetism, in particular in the area of *scattering*, where

nonself-adjoint transformations are often encountered. Two simple examples of nonself-adjoint transformations will clarify the concept [146, 193]:

EXAMPLE 1.1

The operator is $\mathcal{L} = d/dx$ and $\mathcal{D}$ consists of real differentiable functions on the interval (a, b), which vanish at $x = a$. From

$$\int_a^b \frac{df}{dx} h \, dx = -\int_a^b f \frac{dh}{dx} \, dx + [f\,h]_a^b,$$

we conclude that $\mathcal{L}^a = -d/dx$, and that $\mathcal{D}^a$ consists of differentiable functions that vanish at $x = b$.

EXAMPLE 1.2

The operator is $\mathcal{L} = \text{curl}$, and the elements f are real differentiable vectors in a volume V, which, in addition, are perpendicular to the boundary S. From (A1.32):

$$\int_V \mathbf{h} \cdot \text{curl}\, \mathbf{f} \, dV = \int_V \text{curl}\, \mathbf{h} \cdot \mathbf{f} \, dV + \int_S (\mathbf{u}_n \times \mathbf{f}) \cdot \mathbf{h} \, dS,$$

where $\mathbf{u}_n$ is the unit vector along the outer normal to S. This relationship shows that the adjoint operator is the curl, and that $\mathcal{D}^a$ consists of differentiable vectors $\mathbf{h}$ (without any conditions imposed on their behavior on S).

The scalar product $\langle \mathcal{L}f, f \rangle$ is a quadratic form in f. This can easily be checked for the clamped string, where

$$\langle \mathcal{L}f, f \rangle = \int_0^l \frac{d^2 f}{dx^2} f \, dx = \left[f \frac{df}{dx} \right]_0^l - \int_0^l \left(\frac{df}{dx} \right)^2 dx = -\int_0^l \left(\frac{df}{dx} \right)^2 dx. \tag{1.22}$$

In this case, the quadratic form is real. This property holds for all self-adjoint transformations in a Hilbert space. We note, indeed, that the properties of the Hilbert scalar product imply that

$$\langle \mathcal{L}f, f \rangle_H = \langle f, \mathcal{L}f \rangle_H^*.$$

On the other hand,

$$\langle f, \mathcal{L}f \rangle_H^* = \langle \mathcal{L}f, f \rangle_H^*$$

because of the self-adjoint character of the transformation. Comparison of these two equations shows that the quadratic form is equal to its conjugate, hence that it is real. The quadratic form of the clamped string has the additional property, evident from Equation (1.22), that it is negative or zero. The same is true for the quadratic form of the sliding string. The corresponding transformations are termed *nonpositive*. In the case of the string, the vanishing of the quadratic form $\langle \mathcal{L}f, f \rangle$ implies that $df/dx = 0$ at all points of the interval $(0, 1)$. This, in turn, requires $f(x)$ to be a constant. For the clamped string, this constant must be zero because of the end conditions. The corresponding transformation is termed *negative-definite*, which means that it is a nonpositive transformation whose $\langle \mathcal{L}f, f \rangle$ is

always negative for nonzero elements f and vanishes for, and only for, the zero element. The transformation associated with the sliding string is *not* definite, because $\langle \mathcal{L}f, f\rangle = 0$ is satisfied by $f = \text{const.}$, a nonzero function that belongs to the domain of the transformation. Similar considerations hold for *nonnegative* and *positive-definite* transformations. To summarize, a transformation is

1. Nonnegative if $\langle \mathcal{L}f, f\rangle$ is real, and either positive or zero;
2. Positive-definite if, in addition, $\langle \mathcal{L}f, f\rangle = 0$ implies $f = 0$.

For the positive-definite transformation, it is useful to introduce an energy inner product[1]

$$\langle f_1, f_2\rangle_{\mathrm{E}} = \langle \mathcal{L}f_1, f_2\rangle_{\mathrm{H}} \tag{1.23}$$

and an associated energy norm

$$\|f\|_{\mathrm{E}} = \sqrt{\langle \mathcal{L}f, f\rangle_{\mathrm{H}}}, \tag{1.24}$$

which leads to the concept of *convergence in energy*. Note that this concept can be extended to nonpositive and negative-definite transformations by simply replacing $\mathcal{L}$ by $-\mathcal{L}$.

The notion *norm* can be applied to a linear transformation when the latter is *bounded*. Boundedness means that there exists a real number M such that

$$\|\mathcal{L}f\| \leq M\|f\|. \tag{1.25}$$

For such a case the norm $\|\mathcal{L}\|$ is the smallest value of M for which this holds, and we write

$$\|\mathcal{L}\| = \sup \frac{\|\mathcal{L}f\|}{\| f \|} \tag{1.26}$$

from which it follows that

$$\|\mathcal{L}f\| \leq \|\mathcal{L}\|\|f\|. \tag{1.27}$$

Differential operators are always unbounded [150].

1.3 THE INVERSION PROBLEM

A very fundamental problem consists in inverting a linear transformation; that is, finding an element f of the domain such that $\mathcal{L}f = g$, g being given in $\mathcal{R}$. This inverse transformation can be represented symbolically by $f = \mathcal{L}^{-1}g$. Three questions immediately arise:

1. Is there an inverse?
2. Is that inverse unique?
3. Is the solution stable?

The question of uniqueness can be answered quite simply. Assume that there are two distinct solutions, f_1 and f_2. These solutions satisfy the equations

$$\mathcal{L}f_1 = g \quad \text{and} \quad \mathcal{L}f_2 = g.$$

Subtraction of corresponding members shows that the difference $f_0 = f_1 - f_2$ must be a solution of the homogeneous problem

$$\mathcal{L}f_0 = 0. \tag{1.28}$$

If this problem does not possess a nonzero solution, f_1 and f_2 must be equal, and the solution of the original inhomogeneous problem is unique. If, on the contrary, the homogeneous problem has linearly independent solutions $f_{01}, f_{02}, \ldots, f_{0n}$, the solution of $\mathcal{L}f = g$ is determined to within an arbitrary linear combination of the f_{0i} terms. It is clear that uniqueness obtains for a positive-definite transformation, as $\langle \mathcal{L}f_0, f_0 \rangle = 0$ implies $f_0 = 0$ for such a case.

The concept *well-posed* is most important for practical numerical computations. It implies that

- The solution is unique;
- A solution exists for any g; and
- The solution is stable; that is, a small variation in the conditions of the problem (in $\mathcal{L}$ or g) produces only a small variation in the solution f.

These points are belabored further in Section 1.13, which is devoted to the solution of matrix problems. Note that instability can be remedied by methods such as *regularization* [175].

Turning now to the clamped string, we note, from direct integration of Equation (1.1), that the homogeneous problem only has the solution $f_0 = 0$. This result can be obtained in an indirect manner, frequently used for nonpositive or nonnegative transformations. The method consists in evaluating $\langle \mathcal{L}f_0, f_0 \rangle$. For the clamped string,

$$\langle \mathcal{L}f_0, f_0 \rangle = \int_0^l \frac{d^2 y_0}{dx^2} y_0 \, dx = \left[y_0 \frac{dy_0}{dx} \right]_0^l - \int_0^l \left(\frac{dy_0}{dx} \right)^2 dx = -\int_0^l \left(\frac{dy_0}{dx} \right)^2 dx.$$

Clearly, $\mathcal{L}f_0 = 0$ implies that $\langle \mathcal{L}f_0, f_0 \rangle = 0$, which in turn requires the first derivative dy_0/dx to vanish. For a clamped string, this means that y_0 is zero. The physical interpretation is obvious: The clamped string without forcing function remains stretched along the x-axis. For the sliding string, on the contrary, the homogeneous problem has the nonzero solution $y_0 = \text{const.}$, which means that the average height of the string is not defined or, equivalently, that any equilibrium configuration of the string can be displaced vertically by a given amount and yet remain an equilibrium configuration. A very important remark should be made in this connection. For the clamped string an equilibrium position can be obtained for any force distribution $g(x)$. For the sliding string, on the contrary, a stable displacement is possible only if the net vertical force vanishes, that is, if

$$\int_0^l g(x) \, dx = 0.$$

This obvious physical limitation is a particular form of a general mathematical requirement, which may be formulated by considering the homogeneous adjoint problem of (1.18), viz.

$$\mathcal{L}^a h_0 = 0 \qquad (h_0 \text{ in } \mathcal{D}^a). \tag{1.29}$$

Let this problem have a nonzero solution. Under these conditions, the original problem has no solution unless the forcing function g is orthogonal to h_0, that is, unless

$$\langle g, h_0 \rangle = 0. \tag{1.30}$$

The proof is straightforward: Equation (1.18) implies that $\langle g, h_0 \rangle = \langle \mathcal{L}f, h_0 \rangle$. However, the definition of the adjoint of a transformation allows us to write $\langle \mathcal{L}f, h_0 \rangle = \langle f, \mathcal{L}^a h_0 \rangle$, and this is zero because of Equation (1.29). In the case of the sliding string, h_0 is the function $y_0(x) = \text{const.}$, and the orthogonality condition reduces to the form $\int_0^l g(x)\,dx = 0$, that is, to the condition given above.

As f is defined to within a multiple of f_0, interest centers on the part that is not "contaminated" by f_0; that is, which has zero projection on f_0. Assuming that f_0 is normalized (so that $\langle f_0, f_0 \rangle = 1$), this *core solution* is given by

$$f_c = f - \langle f, f_0 \rangle f_0. \tag{1.31}$$

For the sliding string, the core solution is the displacement of the string about its average height. Clearly, $\langle f_c, f_0 \rangle = 0$. The original problem (1.18) may now be replaced by

$$\mathcal{L}f_c = g - \langle g, h_0 \rangle h_0. \tag{1.32}$$

The second term, where h_0 is again assumed normalized, obviously satisfies the requirement (1.30). It is the *core* part of g with respect to h_0. Note that (1.30) is a *necessary* condition for the existence of a solution but by no means a sufficient one. General statements can be made regarding the *existence* of a solution to Equation (1.18) for certain classes of transformations, but this subject is not pursued here [50, 160, 168, 174]. Note also that, if the homogeneous system (1.29) has N linearly independent solutions f_{0i}, requirement (1.30) must be satisfied for each of them. For such a case, Equation (1.28) also has multiple solutions, and the core solution for f is obtained by subtracting the projection of f on the linear manifold formed by the f_{0i} terms. Thus,

$$f_c = f - \sum_{i=1}^{N} \langle f, f_{0i} \rangle f_{0i}. \tag{1.33}$$

We have assumed that the linearly independent f_{0i} are normalized and orthogonal. If orthogonality does not originally hold, it can be obtained by means of the *Schmidt orthogonalization process*, by which a nonorthogonal set f_1, f_2, f_3 is replaced by

$$\begin{aligned}
f_1' &= f_1 \\
f_2' &= f_2 - \frac{\langle f_1', f_2 \rangle}{\langle f_1', f_1' \rangle} f_1' \\
f_3' &= f_3 - \frac{\langle f_1', f_3 \rangle}{\langle f_1', f_1' \rangle} f_1' - \frac{\langle f_2', f_3 \rangle}{\langle f_2', f_2' \rangle} f_2'.
\end{aligned}$$

More generally,

$$f_n' = f_n - \sum_{i=1}^{n-1} \frac{\langle f_i', f_n \rangle}{\langle f_i', f_i' \rangle} f_i'. \tag{1.34}$$

1.4 GREEN'S FUNCTIONS

We introduce the classic concept of a *Green's function* by considering the displacement of a beam under a distributed force $p(x)$. Let $y_G(x|x')$ be the vertical displacement at x due to a concentrated unit force at x'; that is, to a force acting on an infinitesimal interval $\Delta x'$ centered on x' and of amplitude $(1/\Delta x')$ (Fig. 1.3). The displacement under $p(x)$ can be expressed as

$$y(x) = \lim_{\Delta x' \to 0} \sum y_G(x|x')p(x')\,\Delta x' = \int_0^l y_G(x|x')p(x')\,dx'. \tag{1.35}$$

The function $y_G(x|x')$ is the *Green's function* (sometimes called the *influence function*). Once it is known, the response to an arbitrary load distribution can be obtained by means of a trivial integration.

Let us determine the Green's function for the clamped string (Fig. 1.4). Except at x' there is no force; hence, from Equation (1.1), y_G varies linearly and we write

$$y_G = \begin{cases} a(x')x & \text{for } x \le x' \\ b(x')(l-x) & \text{for } x \ge x'. \end{cases}$$

The deflection is continuous at $x = x'$, so that

$$a(x')x' = b(x')(l - x').$$

A second relationship between $a(x')$ and $b(x')$ can be obtained by evaluating the slope discontinuity of the function $y_G(x|x')$ at $x = x'$. Integrating Equation (1.1) over a small interval $(x' - \epsilon, x' + \epsilon)$ gives

$$\int_{x'-\epsilon}^{x'+\epsilon} \frac{d^2 y_G}{dx^2}\,dx = \left(\frac{dy_G}{dx}\right)_{x'+\epsilon} - \left(\frac{dy_G}{dx}\right)_{x'-\epsilon} = -\frac{1}{T}\int_{x'-\epsilon}^{x'+\epsilon} g(x)\,dx = -\frac{1}{T}. \tag{1.36}$$

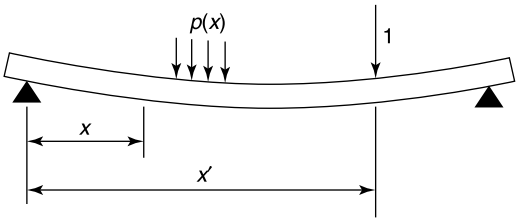

Figure 1.3 Loaded beam with unit force.

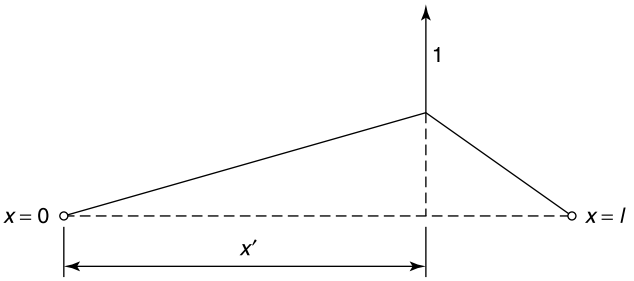

Figure 1.4 Clamped string with unit force.

The end result is the Green's function

$$G(x|x') = y_G(x|x') = \begin{cases} \dfrac{(l-x')x}{lT} & \text{for } x \le x' \\ \dfrac{(l-x)x'}{lT} & \text{for } x \ge x'. \end{cases} \tag{1.37}$$

Two important remarks should be made here:

1. The Green's function for the clamped string is symmetric; that is, the displacement at x due to a unit force at x' is equal to the displacement at x' due to a unit force at x. This reciprocity property is characteristic of self-adjoint problems but is also valid, in modified form, for nonself-adjoint problems (see Equation 1.54). Reciprocity properties, pioneered by H. A. Lorentz, play a fundamental role in electromagnetic theory.
2. The discontinuity in the first derivative defines the basic singularity of $y(x)$ at the point of impact of the unit force. It was obtained by analyzing the behavior of y_G in the immediate neighborhood of that point. Such an approach is used systematically in similar situations, for example, in Chapter 3. Distribution theory, however, allows one to represent the previously derived singularity in very concise form, using the techniques of Appendix 8. For the clamped string, for example, we would write

$$\frac{d^2G}{dx^2} = -\frac{1}{T}\delta(x-x'). \tag{1.38}$$

The reader is referred to Appendix 8 for a detailed discussion of the Dirac distribution and its generating function $\delta(x)$. From a practical point of view, the operational significance of $\delta(x)$ lies in the sifting property

$$\int_{-\infty}^{\infty} f(x)\delta(x-x_0)\,dx = f(x_0), \tag{1.39}$$

where $f(x)$ is continuous at x_0. Thus, $\delta(x-x_0)$ may be treated as a usual function, but whenever the integral in Equation (1.39) is encountered, it should be replaced by the right-hand term of the equation, that is, by $f(x_0)$. Setting $f(x) = 1$ gives

$$\int_{-\infty}^{\infty} \delta(x-x_0)\,dx = 1. \tag{1.40}$$

This relationship shows that a force density $p(x) = \delta(x)$ may be interpreted as a unit force concentrated at $x = 0$. If we now integrate Equation (1.38) over the small interval $(x'-\epsilon, x'+\epsilon)$ we obtain the basic discontinuity of G directly. Thus,

$$\int_{x'-\epsilon}^{x'+\epsilon} \frac{d^2G}{dx^2}\,dx = \left(\frac{dG}{dx}\right)_{x'+\epsilon} - \left(\frac{dG}{dx}\right)_{x'-\epsilon} = -\frac{1}{T}\int_{x'-\epsilon}^{x'+\epsilon} \delta(x-x')\,dx = -\frac{1}{T}.$$

The notion of Green's function is fundamental for the solution of the *general* linear differential problem of (1.18). We write this solution in the form

$$f(\mathbf{r}) = \mathcal{L}^{-1}g(\mathbf{r}) = \int_V G(\mathbf{r}|\mathbf{r}')g(\mathbf{r}')\,dV'. \tag{1.41}$$

This relationship should be valid for all points $\mathbf{r}$ of the volume V in which the differential equation is satisfied. In our search for $G(\mathbf{r}|\mathbf{r}')$, let us assume that the adjoint of the original transformation has been determined. This determination rests on the possibility of deriving a "Green's theorem"

$$\langle \mathcal{L}f, h\rangle_H = \int_V (\mathcal{L}f)h^*\, dV = \int_V f(\mathcal{L}^a h)^*\, dV + \int_S J(f,h)\, dS, \tag{1.42}$$

where one assumes that $f, h, \mathcal{L}f, \mathcal{L}^a h$ satisfy the necessary continuity conditions in V. Note that V is an n-dimensional volume (space and time coordinates can be included) and that S is its $(n-1)$-dimensional boundary (often written as ∂V). Equation (1.42) suggests that the operator of the adjoint transformation should be $\mathcal{L}^a$. The domain $\mathcal{D}^a$ of the transformation is defined by requiring the bilinear concomitant (which in this case is the surface integral) to vanish when f belongs to the domain of the original transformation and h belongs to $\mathcal{D}^a$. A glance at the particular case of the flexible string will readily clarify these rather abstract statements.

Consider now a function H that satisfies the boundary conditions associated with $\mathcal{D}^a$, and also

$$\mathcal{L}^a H = 0$$

everywhere except at $\mathbf{r} = \mathbf{r}_0$, where $\mathcal{L}^a H$ is discontinuous (Fig. 1.5). The nature of the discontinuity will be determined presently. If $\mathbf{r}_0$ is excluded by a small volume V_0, Equation (1.42) can be applied, because $\mathcal{L}^a H$ is continuous in $V - V_0$. Thus,

$$\int_{V-V_0} (\mathcal{L}f)H^*\, dV = \int_{V-V_0} f(\mathcal{L}^a H)^*\, dV + \int_S J(f,H)\, dS + \int_{S_0} J(f,H)\, dS_0.$$

The volume integral in the right-hand term vanishes because $\mathcal{L}^a H$ is zero in $V - V_0$. The surface integral over S vanishes because of the boundary conditions satisfied by $H(\mathbf{r})$. Replacing $\mathcal{L}f$ by g then yields

$$\lim_{V_0\to 0} \int_{V-V_0} g(\mathbf{r})H^*(\mathbf{r}|\mathbf{r}_0)\, dV = \lim_{V_0\to 0} \int_{S_0} J(f,H)\, dS_0. \tag{1.43}$$

The left-hand term is precisely the kind of volume integral that appears in the inversion Equation (1.41). To complete the identification, the right-hand term should generate $f(\mathbf{r}_0)$. This

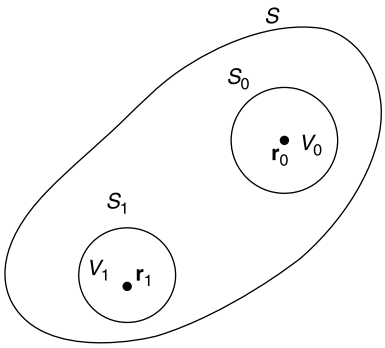

Figure 1.5 Finite volume, from which points $\mathbf{r}_0$ and $\mathbf{r}_1$ have been excluded.

requirement determines the nature of the discontinuity of $H(\mathbf{r})$ at $\mathbf{r} = \mathbf{r}_0$. More precisely, the condition takes the form

$$\lim_{V_0 \to 0} \int_{S_0} J(f, H)\, dS_0 = f(\mathbf{r}_0) \qquad \text{for all } f. \tag{1.44}$$

The practical meaning of this condition is clarified in later chapters through application to several examples (see Section 3.2 for an example). If (1.44) is satisfied, we may combine (1.43) and (1.44) to express the solution of (1.18) in the form

$$f(\mathbf{r}_0) = \lim_{V_0 \to 0} \int_{V - V_0} H^*(\mathbf{r}|\mathbf{r}_0) g(\mathbf{r})\, dV. \tag{1.45}$$

Comparing with (1.41) shows that $H^*(\mathbf{r}|\mathbf{r}_0)$ is an appropriate Green's function. We therefore write

$$G'(\mathbf{r}_0|\mathbf{r}) = H^*(\mathbf{r}|\mathbf{r}_0). \tag{1.46}$$

The differential equation satisfied by $H(\mathbf{r}|\mathbf{r}_0)$ can be found by first evaluating the scalar product

$$\langle \mathcal{L}f, H \rangle_H = \int_V g(\mathbf{r}) H^*(\mathbf{r}|\mathbf{r}_0)\, dV. \tag{1.47}$$

Equation (1.45) implies that this scalar product is equal to $f(\mathbf{r}_0)$. From the definition of the adjoint transformation, the scalar product (1.47) is also equal to

$$\langle f, \mathcal{L}^a H \rangle_H = \int_V f(\mathbf{r}) \left[\mathcal{L}^a H(\mathbf{r}|\mathbf{r}_0) \right]^*\, dV.$$

In δ-function terms, one may therefore write, using the three-dimensional form of (1.40),

$$\mathcal{L}^a H(\mathbf{r}|\mathbf{r}_0) = \delta^*(\mathbf{r} - \mathbf{r}_0) = \delta(\mathbf{r} - \mathbf{r}_0). \tag{1.48}$$

1.5 RECIPROCITY

The developments of the previous section can be repeated for the solution of the adjoint problem

$$\mathcal{L}^a h = s. \tag{1.49}$$

Let us introduce a function $G(\mathbf{r})$, which for the moment does not coincide with the Green's function G' in (1.46) but satisfies the boundary conditions on S associated with $\mathcal{D}$. It must also satisfy $\mathcal{L}G = 0$ everywhere except at $\mathbf{r}_1$, where G is expected to be singular. The nature of the singularity follows from an application of (1.42) to the volume V, from which a small volume V_1 containing $\mathbf{r}_1$ has been excised (Fig. 1.5). Thus,

$$\int_{V - V_1} (\mathcal{L}G)^* h\, dV = \int_{V - V_1} G^*(\mathcal{L}^a h)\, dV + \int_{S + S_1} J^*(G, h)\, dS.$$

The integral over S vanishes, $\mathcal{L}^a h = s$, and $\mathcal{L}G = 0$. Hence,

$$\lim_{V_1 \to 0} \int_{V - V_1} s(\mathbf{r}) G^*(\mathbf{r})\, dV = - \lim_{V_1 \to 0} \int_{S_1} J^*(G, h)\, dS_1.$$

The singularity of G (and derivatives) must be such that

$$- \lim_{V_1 \to 0} \int_{S_1} J^*(G, h)\, dS_1 = h(\mathbf{r}_1) \qquad \text{for all } h. \tag{1.50}$$

For such a case, we may write

$$h(\mathbf{r}_1) = \lim_{V_1 \to 0} \int_{V - V_1} s(\mathbf{r}) G^*(\mathbf{r}|\mathbf{r}_1)\, dV, \tag{1.51}$$

and $G^*(\mathbf{r}|\mathbf{r}_1)$ turns out to be a suitable Green's function $G^a(\mathbf{r}_1|\mathbf{r})$ for the adjoint problem. On the basis of $\langle h, \mathcal{L}G \rangle = \langle \mathcal{L}^a h, G \rangle$, we arrive at the relationship

$$h(\mathbf{r}_1) = \int_V s(\mathbf{r}) G^*(\mathbf{r}|\mathbf{r}_1)\, dV = \int_V h(\mathbf{r}) [\mathcal{L}G(\mathbf{r}|\mathbf{r}_1)]^*\, dV, \tag{1.52}$$

from which it may be concluded that

$$\mathcal{L}G(\mathbf{r}|\mathbf{r}_1) = \delta(\mathbf{r} - \mathbf{r}_1). \tag{1.53}$$

The reciprocity property can now be derived by invoking adjointness. Thus,

$$\int_V H(\mathbf{r}|\mathbf{r}_0) [\mathcal{L}G(\mathbf{r}|\mathbf{r}_1)]^*\, dV = \int_V \mathcal{L}^a H(\mathbf{r}_1|\mathbf{r}_0) G^*(\mathbf{r}|\mathbf{r}_1)\, dV.$$

On the basis of (1.48) and (1.53), one obtains

$$H(\mathbf{r}_1|\mathbf{r}_0) = G^*(\mathbf{r}_0|\mathbf{r}_1).$$

Taking (1.46) into account gives the sequence

$$G^{\mathrm{a}}(\mathbf{r}_1|\mathbf{r}_0) = G^*(\mathbf{r}_0|\mathbf{r}_1) = H(\mathbf{r}_1|\mathbf{r}_0) = [G'(\mathbf{r}_0|\mathbf{r}_1)]^*.$$

These equalities show that $G(\mathbf{r}|\mathbf{r}_0)$ and $G'(\mathbf{r}|\mathbf{r}_0)$ are equal, and also that

$$G(\mathbf{r}_0|\mathbf{r}_1) = [G^a(\mathbf{r}_1|\mathbf{r}_0)]^*. \tag{1.54}$$

This important result, arrived at by δ-function techniques, can also be obtained by a more rigorous method based on (1.42). The steps are left to the reader.

The actual singularity of the Green's function (and derivatives) can take various forms. In fact, the Green's function itself could be a symbolic function. Consider, for example, the wave equation

$$\nabla^2 p - \frac{1}{c_0^2} \frac{\partial^2 p}{\partial t^2} = g(\mathbf{r}, t), \tag{1.55}$$

where $g(\mathbf{r}, t)$ is different from zero in a finite time interval $(0, T)$ only. The *outgoing-wave* solution of (1.55) is [165]

$$p(\mathbf{r}, t) = -\frac{1}{4\pi} \int_{\text{all space}} \frac{g(\mathbf{r}', t - |\mathbf{r}' - \mathbf{r}|/c_0)}{|\mathbf{r}' - \mathbf{r}|} \, dV'. \tag{1.56}$$

There is no "usual" function G that allows representation of this relationship in the form

$$p(\mathbf{r}, t) = \int_{-\infty}^{+\infty} dt' \int_{\text{all space}} G(\mathbf{r}, t|\mathbf{r}', t') g(\mathbf{r}', t') \, dV',$$

but the desired result may be obtained by setting

$$G(\mathbf{r}, t|\mathbf{r}', t') = -\frac{1}{4\pi |\mathbf{r} - \mathbf{r}'|} \delta \left(\frac{|\mathbf{r} - \mathbf{r}'|}{c_0} + t' - t \right). \tag{1.57}$$

It is to be noted that G is not symmetric, for the exchange of t and t' does not leave G invariant but yields instead the Green's function for the *incoming-wave* solution of (1.55). More rigorous treatments of the Green's function for the wave equation involve a Laplace transformation of both terms. The point is further belabored in Chapter 7 (see also [151]).

When (1.28) has a nonzero solution, the original problem (1.18), coupled to condition (1.30), has no unique solution. The *core* solution, however, is unique and can be obtained with the help of a Green's function in the extended sense by the operation

$$f_c(\mathbf{r}) = \int_V G_e(\mathbf{r}|\mathbf{r}') g(\mathbf{r}') \, dV'. \tag{1.58}$$

This solution is valid only if $g(\mathbf{r})$ is orthogonal to the solution of (1.29). Instead of (1.52), the new Green's function must satisfy

$$\mathcal{L} G_e(\mathbf{r}|\mathbf{r}_0) = \delta(\mathbf{r} - \mathbf{r}_0) - h_0(\mathbf{r}) h_0^*(\mathbf{r}_0). \tag{1.59}$$

Similarly,

$$\mathcal{L}^a G_e^a(\mathbf{r}|\mathbf{r}_0) = \delta(\mathbf{r} - \mathbf{r}_0) - f_0(\mathbf{r}) f_0^*(\mathbf{r}_0). \tag{1.60}$$

As $f_c(\mathbf{r})$ in (1.58) must be orthogonal to f_0, in the sense that

$$\int_V f_c(\mathbf{r}) f_0^*(\mathbf{r}) \, dV = 0,$$

it is clear that the following condition must hold:

$$\int_V f_0^*(\mathbf{r}) G_e(\mathbf{r}|\mathbf{r}_0) \, dV = 0. \tag{1.61}$$

On the basis of this equation, it is easy to retrace the steps leading to (1.54) and to prove that the reciprocity property (1.54) holds for $G_e(\mathbf{r}|\mathbf{r}_0)$ (Problem 1.15).

1.6 GREEN'S DYADICS

The Green's function technique can be adapted to the solution of the linear vector problem

$$\mathcal{L}\mathbf{f} = \mathbf{g} \qquad (\mathbf{f} \text{ in } \mathcal{D}). \tag{1.62}$$

We first note that the solution cannot generally be expressed in terms of a single scalar Green's function, for example, as

$$\mathbf{f}(\mathbf{r}_0) = \int_V G(\mathbf{r}_0|\mathbf{r})\mathbf{g}(\mathbf{r})\, dV.$$

Such a relationship would imply that sources $\mathbf{g}$ everywhere parallel to the x-axis generate a field $\mathbf{f}$ parallel to the same axis. This is not usually true. It is therefore necessary to use nine scalar Green's functions to express the three components of $\mathbf{f}(\mathbf{r}_0)$ in terms of the three components of the forcing function. Thus,

$$\begin{aligned}
f_x(\mathbf{r}_0) &= \int_V [G_x^x(\mathbf{r}_0|\mathbf{r})g_x(\mathbf{r}) + G_y^x(\mathbf{r}_0|\mathbf{r})g_y(\mathbf{r}) + G_z^x(\mathbf{r}_0|\mathbf{r})g_z(\mathbf{r})]\, dV \\
f_y(\mathbf{r}_0) &= \int_V [G_x^y(\mathbf{r}_0|\mathbf{r})g_x(\mathbf{r}) + G_y^y(\mathbf{r}_0|\mathbf{r})g_y(\mathbf{r}) + G_z^y(\mathbf{r}_0|\mathbf{r})g_z(\mathbf{r})]\, dV \\
f_z(\mathbf{r}_0) &= \int_V [G_x^z(\mathbf{r}_0|\mathbf{r})g_x(\mathbf{r}) + G_y^z(\mathbf{r}_0|\mathbf{r})g_y(\mathbf{r}) + G_z^z(\mathbf{r}_0|\mathbf{r})g_z(\mathbf{r})]\, dV.
\end{aligned} \tag{1.63}$$

A function such as $G_x^y(\mathbf{r}_0|\mathbf{r})$ measures the contribution of an x-oriented source, acting at $\mathbf{r}$, to the y-component of the field at $\mathbf{r}_0$. The equation for $\mathbf{f}(\mathbf{r}_0)$ can be rewritten much more concisely as

$$\mathbf{f}(\mathbf{r}_0) = \int_V [g_x(\mathbf{r})\mathbf{G}_x(\mathbf{r}_0|\mathbf{r}) + g_y(\mathbf{r})\mathbf{G}_y(\mathbf{r}_0|\mathbf{r}) + g_z(\mathbf{r})\mathbf{G}_z(\mathbf{r}_0|\mathbf{r})]\, dV \tag{1.64}$$

where the $\mathbf{G}$ terms are the column vectors of the Green's dyadic $\overline{\overline{G}}(\mathbf{r}_0|\mathbf{r})$. Still more concisely, using dyadic notation,

$$\mathbf{f}(\mathbf{r}_0) = \int_V (\mathbf{G}_x\mathbf{u}_x\cdot\mathbf{g} + \mathbf{G}_y\mathbf{u}_y\cdot\mathbf{g} + \mathbf{G}_z\mathbf{u}_z\cdot\mathbf{g})\, dV = \int_V \overline{\overline{G}}(\mathbf{r}_0|\mathbf{r})\cdot\mathbf{g}(\mathbf{r})\, dV. \tag{1.65}$$

The point of departure for the calculation of the Green's dyadic is a relationship of the type

$$\int_V (\mathcal{L}\mathbf{f})\cdot\mathbf{h}^*\, dV = \int_V \mathbf{f}\cdot(\mathcal{L}^a\mathbf{h})^*\, dV + \int_S J(\mathbf{f},\mathbf{h})\, dS, \tag{1.66}$$

where it is assumed that the various functions satisfy the conditions of validity of the equation. Relationship (1.66) determines the adjoint of the transformation whose operator is $\mathcal{L}^a$ and whose domain $\mathcal{D}^a$ is such that the surface integral vanishes when $\mathbf{f}$ is in $\mathcal{D}$ and $\mathbf{h}$ is in $\mathcal{D}^a$. Let a vector $\mathbf{H}_x(\mathbf{r}|\mathbf{r}_0)$ satisfy the boundary conditions associated with $\mathcal{D}^a$, and in addition

$$\mathcal{L}^a\mathbf{H}_x = 0$$

everywhere except at $\mathbf{r}_0$, where $\mathcal{L}^a\mathbf{H}_x$ is singular. If $\mathbf{r}_0$ is excluded by a small volume V_0 (as in Fig. 1.5), the use of (1.66) yields

$$\lim_{V_0\to 0}\int_V \mathbf{g}(\mathbf{r})\cdot\mathbf{H}_x^*(\mathbf{r}|\mathbf{r}_0)\,dV = \int_{S_0} J(\mathbf{f},\mathbf{H}_x)\,dS. \tag{1.67}$$

The singularity of $\mathbf{H}_x$ is determined by requiring the right-hand term to be equal to $f_x(\mathbf{r}_0)$. Vectors $\mathbf{H}_y$ and $\mathbf{H}_z$ can be found in a similar fashion, and the three vectors together allow representation of $\mathbf{f}(\mathbf{r}_0)$ as

$$\mathbf{f}(\mathbf{r}_0) = \int_V \mathbf{g}(\mathbf{r})\cdot[\mathbf{H}_x^*(\mathbf{r}|\mathbf{r}_0)\mathbf{u}_x + \mathbf{H}_y^*(\mathbf{r}|\mathbf{r}_0)\mathbf{u}_y + \mathbf{H}_z^*(\mathbf{r}|\mathbf{r}_0)\mathbf{u}_z]\,dV. \tag{1.68}$$

Precisely as in the previous section, we now consider the adjoint problem and introduce a vector $\mathbf{G}_x$ whose singularity should produce h_x through the requirement

$$-\lim_{V_1\to 0}\int_{S_1} J^*(\mathbf{G}_x,\mathbf{h})\,dS = h_x(\mathbf{r}_1). \tag{1.69}$$

In distributional notation:

$$\mathcal{L}\mathbf{G}_x(\mathbf{r}|\mathbf{r}_0) = \delta(\mathbf{r}-\mathbf{r}_0)\mathbf{u}_x. \tag{1.70}$$

Similar requirements serve to define $\mathbf{G}_y$ and $\mathbf{G}_z$. These vectors must furthermore satisfy the required boundary conditions; that is, belong to $\mathcal{D}$. The basic reciprocity property is now

$$\mathbf{u}_i\cdot\mathbf{G}_k(\mathbf{r}_0|\mathbf{r}_1) = \mathbf{u}_k\cdot\mathbf{H}_i^*(\mathbf{r}_1|\mathbf{r}_0). \tag{1.71}$$

The x-component of (1.68) can be rewritten as

$$\begin{aligned} f_x(\mathbf{r}_0) &= \int_V \left[g_x(\mathbf{r})\mathbf{u}_x\cdot\mathbf{H}_x^*(\mathbf{r}|\mathbf{r}_0) + g_y(\mathbf{r})\mathbf{u}_y\cdot\mathbf{H}_x^*(\mathbf{r}|\mathbf{r}_0) + g_z(\mathbf{r})\mathbf{u}_z\cdot\mathbf{H}_x^*(\mathbf{r}|\mathbf{r}_0)\right]dV \\ &= \int_V \left[g_x(\mathbf{r})\mathbf{u}_x\cdot\mathbf{G}_x(\mathbf{r}_0|\mathbf{r}) + g_y(\mathbf{r})\mathbf{u}_x\cdot\mathbf{G}_y(\mathbf{r}_0|\mathbf{r}) + g_z(\mathbf{r})\mathbf{u}_x\cdot\mathbf{G}_z(\mathbf{r}_0|\mathbf{r})\right]dV \\ &= \mathbf{u}_x\cdot\int_V \left[g_x(\mathbf{r})\mathbf{G}_x(\mathbf{r}_0|\mathbf{r}) + g_y(\mathbf{r})\mathbf{G}_y(\mathbf{r}_0|\mathbf{r}) + g_z(\mathbf{r})\mathbf{G}_z(\mathbf{r}_0|\mathbf{r})\right]dV. \end{aligned}$$

Clearly, the integral in the right-hand term above stands for $\mathbf{f}(\mathbf{r}_0)$; hence, the vectors $\mathbf{G}_x$, $\mathbf{G}_y$, $\mathbf{G}_z$ are precisely those needed to construct the Green's dyadic. We therefore write, from (1.65),

$$\overline{\overline{G}}(\mathbf{r}_0|\mathbf{r}) = \mathbf{G}_x(\mathbf{r}_0|\mathbf{r})\mathbf{u}_x + \mathbf{G}_y(\mathbf{r}_0|\mathbf{r})\mathbf{u}_y + \mathbf{G}_z(\mathbf{r}_0|\mathbf{r})\,\mathbf{u}_z. \tag{1.72}$$

The fundamental singularity of $\overline{\overline{G}}$ is expressed by

$$\mathcal{L}\overline{\overline{G}}(\mathbf{r}|\mathbf{r}_0) = \delta(\mathbf{r}-\mathbf{r}_0)\,\overline{\overline{I}}. \tag{1.73}$$

The interpretation of $\mathbf{H}_x$, $\mathbf{H}_y$, and $\mathbf{H}_z$ in terms of building blocks for the Green's dyadic $\overline{\overline{G}}^a$ of the adjoint problem proceeds as in the previous section.

1.7 CONVERGENCE OF A SERIES

Convergence of a series, strong or weak, is defined in Section 1.1. To further discuss the topic, consider the representation shown in (1.4) and the convergence criterion

$$\lim_{N\to\infty} \left\| f - \sum_{n=1}^{N} a_n f_n \right\| = 0. \tag{1.74}$$

If the norm is defined by a Lebesgue integral $(\int_V f^* f \, dV)^{1/2}$, convergence in the mean does not imply point convergence. The situation is well exemplified by the Fourier series $\sum_{n=1}^{\infty} (\sin nx)/n$ of $(\pi - x)/2$ in the interval $0 \le x \le \pi$. The series converges to $(\pi - x)/2$ everywhere except at the origin, where its sum is equal to zero. The sum of the first N terms of the series oscillates about the function in the manner shown in Figure 1.6. These oscillations can be telescoped into smaller and smaller intervals as N grows larger, but their amplitude never approaches zero. In other words, it is not possible to find a number of terms large enough for the series to be within ϵ of the function at each point of the interval. This type of convergence, which is termed *nonuniform*, is frequently encountered in subsequent chapters, particularly in the study of resonant cavities. The lack of uniform convergence demands great care in performing operations such as the exchange of limiting and integration processes or term-by-term differentiation of the series. The function $f(x) = x$, for example, has the Fourier expansion

$$f(x) = x = 2\left(\sin x - \tfrac{1}{2}\sin 2x + \tfrac{1}{3}\sin 3x + \cdots\right), \qquad -\pi \le x \le \pi,$$

but its derivative $f'(x) = +1$ is *not* represented by the sum of derivatives of the terms, namely $2(\cos x - \cos 2x + \cos 3x + \cdots)$. The difficulty lies in the lack of uniform convergence resulting from the behavior of the series at the end points $x = \pm\pi$, where the sum of the series is equal to zero. More generally, the exact coefficients of the Fourier expansion of the derivative of $f(x) = \alpha_0 + \sum_{n=1}^{\infty} (\alpha_n \cos nx + \beta_n \sin nx)$ must be found by expanding $f'(x)$ separately as

$$f'(x) = a_0 + \sum_{n=1}^{\infty} (a_n \cos nx + b_n \sin nx). \tag{1.75}$$

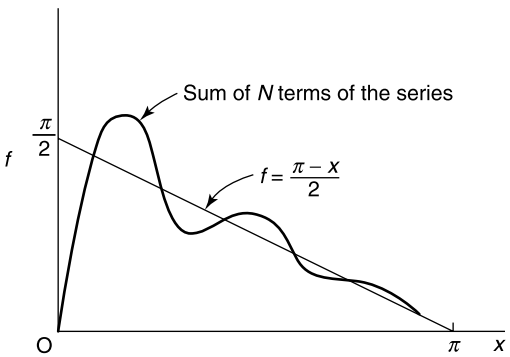

Figure 1.6 Nonuniform convergence.

The coefficients a_n and b_n can be obtained by integrating by parts. Thus,

$$a_n = \frac{1}{\pi}\int_{-\pi}^{\pi} f'(x)\cos nx\,dx = \frac{1}{\pi}[f(x)\cos nx]_{-\pi}^{\pi} + \frac{n}{\pi}\int_{-\pi}^{\pi} f(x)\sin nx\,dx$$
$$= n\beta_n + \frac{\cos n\pi}{\pi}[f(\pi) - f(-\pi)]. \tag{1.76}$$

Similarly, one finds that $a_0 = (1/2\pi)[f(\pi) - f(-\pi)]$ and $b_n = -n\alpha_n$. Clearly, term-by-term differentiation is allowed only if $f(\pi) = f(-\pi)$. This method of determining the expansion coefficients of the derivative is very basic and is used repeatedly in later chapters, where it will be called the *derivative of a sum* technique.

The set f_n appearing in (1.74) is said to be *complete* with respect to a class of elements f when each element of the class can be approximated in the mean by a series of the form $\sum_n a_n f_n$. Many complete sets encountered in practice are orthogonal and can be normalized according to (1.15). For example, the functions

$$\frac{1}{(2\pi)^{1/2}}, \frac{1}{\pi^{1/2}}\cos x, \ldots, \frac{1}{\pi^{1/2}}\sin x, \ldots, \frac{1}{\pi^{1/2}}\sin nx, \ldots$$

form a complete orthonormal set in the interval $(-\pi, \pi)$ with respect to the scalar product $\int_{-\pi}^{\pi} fg^*\,dx$ and $\mathcal{L}_2$ functions (i.e., functions for which $\int_V |f|^2\,dV$ exists). Similarly, the Bessel functions of the first kind $J_n(\lambda_{nk}r)$, where the λ_{nk} terms are the zeros of $J_n(x)$, form an orthogonal (but not normalized) set in the interval (0, 1) with respect to $\mathcal{L}_2$ functions and the scalar product $\langle f, g\rangle = \int_0^1 fg^* r\,dr$.

For a few simple domains in multiple dimensions, sets of functions that are complete in several variables can be formed from complete sets in one variable. For example, let $\phi_m(x)$ be complete in the interval $a \le x \le b$, and $\psi_n(y)$ in the interval $c \le y \le d$. The doubly infinite set $\theta_{mn}(x, y) = \phi_m(x)\,\psi_n(y)$ is then complete in the rectangle $a \le x \le b, c \le y \le d$. Illustratively, the set $(2/\sqrt{ab})\sin(m\pi x/a)\sin(n\pi y/b)$ is complete and orthonormal in the rectangle $0 \le x \le a$, $0 \le y \le b$.

In addition to the least-squared norm of convergence, which is suitable for functions belonging to $\mathcal{L}_2$, one could also apply the infinite norm (1.7) and base convergence on the criterion $\sup \|f - \sum a_n f_n\|$. This *maximum* norm is particularly useful when one wishes to achieve an assigned accuracy at every point of a volume.

The approximation by a series is often sought, in a one-dimensional situation, by means of a polynomial of degree N, N being required to increase until a given degree of accuracy is obtained. When N becomes unduly high, it often becomes preferable to approximate the series by the *ratio* of two polynomials, a_M and b_N, of respective degrees M and N. The point is further discussed in Section 12.4, where the *Padé approximation* is introduced.

1.8 EIGENFUNCTIONS

The notion of eigenfunction can be illustrated by considering the example of the short-circuited lossless transmission line. Equation (1.3) for the voltage has a unique solution unless the homogeneous problem, defined by

$$\frac{d^2V}{dx^2} + \omega^2 LCV = 0 \qquad V = 0 \text{ at } x = 0 \text{ and } x = l, \tag{1.77}$$

has a nonzero solution. Such a solution exists only if

$$\omega = (LC)^{-1/2}\frac{n\pi}{l}, \qquad n = 1, 2, 3, \ldots.$$

For the corresponding values (the resonant frequencies), (1.77) has the nonzero solution

$$V_n = A \sin \frac{n\pi x}{l},$$

where A is an arbitrary constant. The meaning of V_n is clear: It is a voltage that can exist along the transmission line in the absence of any external source. Such a voltage is a resonant mode of the line. If the line is excited at one of the resonant frequencies by a forcing function dV_a/dx, (1.3) has no finite inverse unless the forcing function is orthogonal to V_n; that is, unless

$$\int_0^l \frac{d^2V_a}{dx^2} \sin \frac{n\pi x}{l}\, dx = 0.$$

In other words, the forcing function must not couple to the resonant mode; otherwise, the voltage would increase without limit. These considerations can be extended to the general problem

$$(\mathcal{L} - \lambda)f = g \qquad (f \text{ in } \mathcal{D}), \tag{1.78}$$

where λ is a complex parameter. The problem has an inverse unless

$$(\mathcal{L} - \lambda_n)f_n = 0 \qquad (f_n \text{ in } \mathcal{D}) \tag{1.79}$$

has a nonzero solution. The corresponding values of λ are termed the *eigenvalues* of $\mathcal{L}$, and they form the point spectrum (or discrete spectrum) of $\mathcal{L}$. The functions f_n are the *eigenfunctions* of the problem. Similarly, the transformation $\mathcal{L}^a$ has eigenfunctions and eigenvalues defined by

$$(\mathcal{L}^a - \mu_k)h_k = 0 \qquad (h \text{ in } \mathcal{D}^a). \tag{1.80}$$

Under a wide range of conditions, the eigenvalues of $\mathcal{L}^a$ are the complex conjugates of the eigenvalues of $\mathcal{L}$ (more rigorous statements of this property can be found in texts on functional analysis, such as [168] or [174]). This theorem finds an interesting application in Equation (1.28), which can be interpreted as defining an eigenfunction f_0 with eigenvalue zero; the equation implies that (1.29) has a nonzero solution, too, a property that was implicitly assumed in Section 1.3.

The eigenfunctions of the transmission line form an orthogonal set. This property, which results from the well-known integral

$$\int_0^l \sin \frac{m\pi x}{l} \sin \frac{n\pi x}{l}\, dx = 0 \qquad \text{for } m \neq n,$$

is a particular case of a more general theorem that states that the eigenfunctions f_n and h_k are orthogonal when $\lambda_n \neq \mu_k^*$. The proof runs as follows. The definition of the adjoint of a transformation implies that

$$\langle \mathcal{L}f_n, h_k \rangle_H = \langle f_n, \mathcal{L}^a h_k \rangle_H.$$

Equations (1.79) and (1.80) and the general properties of the scalar product lead to

$$\langle \mathcal{L} f_n, h_k \rangle_H = \langle \lambda_n f_n, h_k \rangle_H = \lambda_n \langle f_n, h_k \rangle_H$$

and

$$\langle f_n, \mathcal{L}^a h_k \rangle_H = \langle f_n, \mu_k h_k \rangle_H = \mu_k^* \langle f_n, h_k \rangle_H.$$

Equating these expressions gives $(\lambda_n - \mu_k^*)\langle f_n, h_k \rangle = 0$; hence, the desired result

$$\langle f_n, h_k \rangle_H = 0, \qquad \text{when } \lambda_n \neq \mu_k^*. \tag{1.81}$$

In words, the eigenfunctions of the adjoint transformation form a *biorthogonal set* with those of the original transformation. For a self-adjoint transformation, the eigenfunctions form an *orthogonal set*, and the corresponding eigenvalues are real. This property can be established by writing

$$\langle \mathcal{L} f_n, f_n \rangle_H = \langle \lambda_n f_n, f_n \rangle_H = \lambda_n \langle f_n, f_n \rangle_H.$$

The left-hand term is real for a self-adjoint transformation, as shown in Section 1.2, and $\langle f_n, f_n \rangle$ is always positive. It follows that λ_n must be real. Moreover, λ_n is given by

$$\lambda_n = \frac{\langle \mathcal{L} f_n, f_n \rangle_H}{\langle f_n, f_n \rangle_H}. \tag{1.82}$$

This relationship implies that the eigenvalues of a positive (or negative) definite transformation are all positive (or negative). The point can easily be verified for the transformation of the clamped string, which is negative-definite, and whose eigenvalues $-(n\pi/l)^2$ are indeed negative.

It often happens that several linearly independent eigenfunctions correspond with the same eigenvalue. In general, these *degenerate eigenfunctions* are not orthogonal to each other. The *Schmidt orthogonalization process* described in Section 1.3 makes it possible to construct linear combinations that are mutually orthogonal. The generalization to higher order degeneracies and to biorthogonal sets is immediate.

The eigenfunction Equation (1.79) can be rewritten as

$$\mathcal{L} f_n = \lambda_n f_n \qquad (f_n \text{ in } \mathcal{D}).$$

If a Green's function exists for the problem embodied in (1.18), f_n can be expressed in terms of the second term $\lambda_n f_n$ to give

$$\int_V G(\mathbf{r}|\mathbf{r}') f_n(\mathbf{r}')\, dV' - \frac{1}{\lambda_n} f_n(\mathbf{r}) = 0. \tag{1.83}$$

Clearly, the eigenfunctions f_n of the differential problem are also eigenfunctions of the integral operator $\int_V dV' G(\mathbf{r}|\mathbf{r}')$. The converse is also true, as can be formally established by operating with $\mathcal{L}$ on both sides of Equation (1.83). We note that the eigenvalues of the integral operator are $1/\lambda_n$. For problems in which a Green's function in the extended sense must be used (see Section 1.5), a slight modification of our statements is necessary. In that case, all eigenfunctions except f_0 are eigenfunctions of the operator $\int_V dV' G_e(\mathbf{r}|\mathbf{r}')$.

1.9 INTEGRAL OPERATORS

Integral equations are frequently encountered in electromagnetism, both in their first and second forms. In the *first kind*, the unknown appears solely behind the integral sign. Thus,

$$\int_V K(\mathbf{r}|\mathbf{r}')f(\mathbf{r}')\,dV' = g(\mathbf{r}), \tag{1.84}$$

where the kernel $K(\mathbf{r}|\mathbf{r}')$ is often a Green's function. We immediately notice that this equation does not automatically have a solution. Such is obviously the case for the (degenerate) kernel $K = A(\mathbf{r})B(\mathbf{r}')$, for which (1.84) has no solution unless $g(\mathbf{r})$ is proportional to $A(\mathbf{r})$. Equation (1.84) may be interpreted as the search for a function $f(\mathbf{r})$ whose "K-transform" is known. The Fourier transform discussed in Appendix 7 is an obvious example of such an integral equation. In many cases $g(\mathbf{r})$ is obtained experimentally, and the solution of (1.84) may suffer from instabilities of the kind discussed in Section 1.13, which cause small errors in the data to generate much larger errors in $f(\mathbf{r})$. The reader is referred to the abundant literature that exists on the subject and in particular to discussions of the existence of a solution to (1.84) [147, 148, 159, 164, 167, 168, 176].

The integral equation of the *second kind* is of the general form

$$f(\mathbf{r}) - \lambda \int_V K(\mathbf{r}|\mathbf{r}')f(\mathbf{r}')\,dV' = g(\mathbf{r}), \tag{1.85}$$

where λ is a parameter. Its homogeneous version

$$f_n(\mathbf{r}) - \lambda_n \int_V K(\mathbf{r}|\mathbf{r}')f_n(\mathbf{r}')\,dV' = 0 \tag{1.86}$$

defines the eigenfunctions of an integral operator with kernel $K(\mathbf{r}|\mathbf{r}')$. The properties of the eigenfunctions depend strongly on the nature of the kernel. Two important types are

1. The *Fredholm* kernels, for which

$$\int_V \int_V |K(\mathbf{r}|\mathbf{r}')|^2\,dV\,dV'$$

has a finite value. The integral operator is *bounded* under these circumstances.

2. The *weakly singular* kernels

$$K(\mathbf{r}|\mathbf{r}') = \frac{H(\mathbf{r}|\mathbf{r}')}{|\mathbf{r} - \mathbf{r}'|^{\alpha}}, \tag{1.87}$$

where $H(\mathbf{r}|\mathbf{r}')$ is bounded, and α is a constant satisfying the inequality $0 < \alpha < n$ (where n is the number of dimensions of the space).

In 1902, *Fredholm* developed the general theory of equations such as (1.85), initially assuming that V was a finite region and the kernel nonsingular. Basically, his approach was to interpret (1.85) as the limit of a finite system of linear equations with a finite number of unknowns, a philosophy that allowed him to establish a link with matrix theory. His well-known *alternative*, to be enunciated presently, has been extended, under certain conditions

[158], to weakly singular, possibly complex kernels. It requires consideration of the adjoint integral equation

$$h(\mathbf{r}) - \mu \int_V K^*(\mathbf{r}'|\mathbf{r}) h(\mathbf{r}')\, dV' = s(\mathbf{r}). \tag{1.88}$$

The alternative — in fact a particular case of the general theory presented in Section 1.3 — can be formulated as follows:

1. Either (1.85) has a unique solution or (1.86) has at least one nontrivial solution. This occurs only when λ is an eigenvalue.
2. The same holds for the adjoint equation, where the nontrivial solutions are eigenfunctions satisfying

$$h_n(\mathbf{r}) - \mu_n \int_V K^*(\mathbf{r}'|\mathbf{r}) h_n(\mathbf{r}')\, dV' = 0. \tag{1.89}$$

   Both homogeneous equations, (1.86) and (1.89), have the same (finite) number of solutions. Further, $\mu_n = \lambda_n^*$, and biorthogonality takes the well-known form

$$\int_V f_m(\mathbf{r}) h_n^*(\mathbf{r})\, dV = 0 \qquad (m \neq n). \tag{1.90}$$

3. When λ (or μ) is an eigenvalue, (1.85) and (1.88) do not have solutions unless

$$\int_V g(\mathbf{r}) h_n^*(\mathbf{r})\, dV = 0$$
$$\int_V s(\mathbf{r}) f_n^*(\mathbf{r})\, dV = 0. \tag{1.91}$$

The usual properties of self-adjoint transformations hold when the kernel is Hermitian, that is, when $K(\mathbf{r}|\mathbf{r}') = K^*(\mathbf{r}'|\mathbf{r})$. More specifically [168],

1. The eigenvalues are discrete, and their only possible point of accumulation is at infinity.
2. The eigenvalues are real.
3. The eigenfunctions form an orthogonal set.
4. Each square-integrable function $g(\mathbf{r})$ can be approximated in the mean as

$$g(\mathbf{r}) = \sum_n f_n(\mathbf{r}) \int_V f_n^*(\mathbf{r}') g(\mathbf{r}')\, dV' + h(\mathbf{r}), \tag{1.92}$$

   where the f_n functions are normalized, and $h(\mathbf{r})$ is a solution of the homogeneous integral equation

$$\int_V K(\mathbf{r}|\mathbf{r}') h(\mathbf{r}')\, dV' = 0. \tag{1.93}$$

   If the only solution of (1.93) is $h(\mathbf{r}) = 0$, the set formed by the f_n terms is automatically complete. If there is a nonzero solution h_0, it should be added to complete the

set. Such a situation arises when the kernel is a Green's function of the extended type, a type discussed in Section 1.5. In the case of the sliding string, for example, the f_n are the $\cos(n\pi x/l)$ functions ($n = 1, 2, \ldots$) and h_0 is a constant.

The previous considerations can be extended to vector problems and their associated dyadic kernels $\overline{\overline{K}}(\mathbf{r}|\mathbf{r}')$. The adjoint kernel is now $[\overline{\overline{K}}^t(\mathbf{r}'|\mathbf{r})]^* = \overline{\overline{K}}^\dagger(\mathbf{r}'|\mathbf{r})$ (where t means transpose and $\dagger$ denotes Hermitian conjugate). The eigenvector equation becomes

$$\mathbf{f}_n(\mathbf{r}) - \lambda_n \int_V \overline{\overline{K}}(\mathbf{r}|\mathbf{r}') \cdot \mathbf{f}_n(\mathbf{r}')\, dV' = 0. \tag{1.94}$$

Here the nine components $K_i^j(\mathbf{r}|\mathbf{r}')$ of the kernel are individually Fredholm kernels or weakly singular kernels. Further, let $K_m^n(\mathbf{r}|\mathbf{r}') = [K_n^m(\mathbf{r}'|\mathbf{r})]^*$. For such conjugate-symmetric (or Hermitian) kernels, the following properties hold[2]:

1. Eigenvectors corresponding with different eigenvalues are orthogonal.
2. Any square-integrable vector $\mathbf{g}(\mathbf{r})$ can be approximated in the mean as

$$\mathbf{g}(\mathbf{r}) = \sum_n \mathbf{f}_n(\mathbf{r}) \int_V \mathbf{f}_n^*(\mathbf{r}') \cdot \mathbf{g}(\mathbf{r}')\, dV' + \mathbf{h}(\mathbf{r}). \tag{1.95}$$

Here the eigenvectors $\mathbf{f}_n$ are assumed normalized, and the rest term $\mathbf{h}(\mathbf{r})$ is a solution of the homogeneous integral equation

$$\int_V \overline{\overline{K}}(\mathbf{r}|\mathbf{r}') \cdot \mathbf{h}(\mathbf{r}')\, dV' = 0. \tag{1.96}$$

When this equation does not have a nonzero solution, the set of eigenvectors is complete.

A few additional comments should be made to conclude this overview:

1. A logarithmic kernel, of the type encountered in two-dimensional potential and scattering problems, is *weakly* singular. In fact, $|\mathbf{r} - \mathbf{r}'|^\alpha \log_e|\mathbf{r} - \mathbf{r}'|$ remains bounded for all positive α, however small α might be.
2. In Equation (1.87), the kernel becomes *strongly singular* when $\alpha = n$. Fredholm's theory now breaks down; new methods are needed [167]. The Hilbert transform mentioned in Appendix 7 is a typical example of such a case.
3. When V is unbounded, Fredholm's theory breaks down, too, and a continuous spectrum may appear. This is true, in particular, for the Picard equation

$$f(x) = \lambda \int_{-\infty}^{\infty} e^{-|x-x'|} f(x')\, dx',$$

which has solutions of the form [164, 167]

$$f(x) = c_1\, e^{\sqrt{1-2\lambda}\, x} + c_2\, e^{\sqrt{1-2\lambda}\, x}$$

for $0 < \lambda < \infty$. The spectrum is seen to be continuous. On the other hand,

$$f(x) = \lambda \sqrt{\frac{2}{\pi}} \int_0^{\infty} \cos(xx') f(x')\, dx'$$

has only *two* eigenvalues, $\lambda = \pm 1$, each of which has an infinite number of eigenfunctions

$$f_{\pm 1}(x) = \sqrt{\frac{\pi}{2}}\, e^{-ax} \pm \frac{a}{a^2 + x^2}, \qquad (x > 0),$$

where a is an arbitrary positive number.

1.10 EIGENFUNCTION EXPANSIONS

Expandibility in terms of eigenfunctions has just been discussed for the case of an integral operator. As a further example, let us use eigenfunctions to determine the voltage along a lossless transmission line when the forcing function $d^2V_a/dx^2 = H(x)$ in (1.3) is given, and the end voltages $V(0)$ and $V(l)$ are imposed (Fig. 1.2). Clearly, the line is subjected to a *volume* excitation and a *boundary* excitation. The problem can be solved with the help of the eigenfunctions of the clamped string, which are known to form a complete set. We write

$$V(x) = \sum_{n=1}^{\infty} V_n \sin \frac{n\pi x}{l}$$

$$H(x) = \sum_{n=1}^{\infty} H_n \sin \frac{n\pi x}{l}.$$

The expansion coefficients H_n are known because H is given, but the V_n must be solved for. To achieve this goal, both Fourier expansions are introduced in (1.3), after which the coefficients of $\sin(n\pi x/l)$ on opposite sides of the equation are equated. The trouble, however, is that the expansion of d^2V/dx^2 is not known. We have already emphasized in Section 1.7 that it may *not* be permissible to differentiate a Fourier series term by term. Rather, one should expand d^2V/dx^2 separately as

$$\frac{d^2V}{dx^2} = \sum_{n=1}^{\infty} A_n \sin \frac{n\pi x}{l}.$$

The connection between the coefficients A_n and V_n can now be established by the following calculation involving an integration by parts:

$$\begin{aligned} A_n &= \frac{2}{l}\int_0^l \frac{d^2V}{dx^2} \sin \frac{n\pi x}{l}\, dx \\ &= \frac{2}{l}\int_0^l V \frac{d^2}{dx^2}\left(\sin \frac{n\pi x}{l}\right) dx + \frac{2}{l}\left[\sin \frac{n\pi x}{l}\frac{dV}{dx} - V\frac{d}{dx}\left(\sin \frac{n\pi x}{l}\right)\right]_0^l \\ &= -\left(\frac{n\pi}{l}\right)^2 V_n + \frac{2}{l}\frac{n\pi}{l}[V(0) - \cos(n\pi)V(l)]. \end{aligned}$$

It is seen that termwise differentiation would give $-(n\pi/l)^2 V_n$ only and would not include the contribution from the end voltages. Insertion of the series expansions in (1.3) immediately yields $A_n + \omega^2 LCV_n = H_n$, from which V_n can be calculated directly. One obtains,

finally,

$$V(x) = \sum_n \sin\left(\frac{n\pi x}{l}\right) \frac{2}{l} \frac{1}{\omega^2 LC - (n\pi/l)^2} \times \left[\int_0^l H(x) \sin \frac{n\pi x}{l}\, dx - \frac{n\pi}{l}\, V(0) + \frac{n\pi}{l} \cos n\pi\, V(l) \right]. \tag{1.97}$$

The phenomenon of resonance is well demonstrated by this equation, in that the voltage becomes infinite when the frequency approaches one of its resonant values $\omega_n = (LC)^{-\frac{1}{2}} n\pi/l$. The phenomenon does not occur when the total excitation of the mode (as represented by the bracketed term) vanishes.

The generalization to the solution of the more abstract problem

$$\mathcal{L}f - \lambda f = g \tag{1.98}$$

is immediate. The method consists in expanding both members of the equation in terms of the normalized eigenfunctions of the transformation, which are assumed to form a complete set. Thus,

$$g = \sum_n a_n f_n \qquad f = \sum_n b_n f_n \qquad \mathcal{L}f = \sum_n c_n f_n.$$

To find a relationship between a_n and b_n, we make use of the biorthogonality relationship (1.81) to eliminate c_n by writing

$$c_n \langle f_n, h_n \rangle_H = \langle \mathcal{L}f, h_n \rangle_H .$$

Let us assume that the eigenfunctions are normalized, in the sense that

$$\langle f_n, h_n \rangle_H = 1.$$

We now invoke the fundamental relationship (1.42) to obtain

$$\begin{aligned} \langle \mathcal{L}f, h_n \rangle_H &= \left\langle f, \mathcal{L}^a h_n \right\rangle_H + \int_S J(f, h_n)\, dS \\ &= \lambda_n \langle f, h_n \rangle_H + \int_S J(f, h_n)\, dS \\ &= \lambda_n b_n + \int_S J(f, h_n)\, dS. \end{aligned}$$

Finally,

$$f = \sum_n f_n \frac{1}{(\lambda_n - \lambda)} \left[\langle g, h_n \rangle_H - \int_S J(f, h_n)\, dS \right]. \tag{1.99}$$

The term between square brackets represents the excitation of the corresponding eigenmode. It consists of a volume excitation, expressed by $\langle g, h_n \rangle_H$, and a boundary excitation,

represented by the surface integral. Specialization to a self-adjoint problem is immediate. For such a case, the λ_n are known to be real.

In the absence of boundary excitation, that is, when f belongs to $\mathcal{D}$,

$$f(\mathbf{r}) = \sum_n f_n(\mathbf{r}) \frac{1}{\lambda_n - \lambda} \int_V g(\mathbf{r}') h_n^*(\mathbf{r}')\, dV'$$

$$= \int_V g(\mathbf{r}') \left[\sum_n \frac{f_n(\mathbf{r}) h_n^*(\mathbf{r}')}{\lambda_n - \lambda} \right] dV'.$$

The Green's function of the problem can therefore be written in the form

$$G(\mathbf{r}|\mathbf{r}'|\lambda) = \sum_n \frac{f_n(\mathbf{r}) h_n^*(\mathbf{r}')}{\lambda_n - \lambda}. \tag{1.100}$$

Similarly,

$$G^a(\mathbf{r}|\mathbf{r}'|\lambda) = \sum_n \frac{h_n(\mathbf{r}) f_n^*(\mathbf{r}')}{\mu_n - \mu}. \tag{1.101}$$

These relationships are also valid for the Green's functions in the extended sense, provided the eigenfunctions f_0 and h_0 are not included in the summation.

The expansion in (1.100) can be obtained directly by a procedure that is often used in the sequel. The Green's function satisfies

$$\mathcal{L}G(\mathbf{r}|\mathbf{r}_1|\lambda) - \lambda\, G(\mathbf{r}|\mathbf{r}_1|\lambda) = \delta(\mathbf{r} - \mathbf{r}_1), \tag{1.102}$$

which is an immediate extension of (1.53). Proceeding in a similar way as for the solution of (1.98), and because G as a function of $\mathbf{r}$ belongs to $\mathcal{D}$, we write

$$\int_V \mathcal{L}G(\mathbf{r}|\mathbf{r}_1|\lambda) h_n^*(\mathbf{r})\, dV = \int_V G(\mathbf{r}|\mathbf{r}_1|\lambda) \mathcal{L}^a h_n^*(\mathbf{r})\, dV$$

$$= \lambda_n \int_V G(\mathbf{r}|\mathbf{r}_1|\lambda) h_n^*(\mathbf{r})\, dV.$$

On the other hand, an expansion of the Dirac function in terms of the biorthonormal set (f_n, h_n) yields

$$\delta(\mathbf{r} - \mathbf{r}_1) = \sum_n f_n(\mathbf{r}) h_n^*(\mathbf{r}_1), \tag{1.103}$$

where the equality sign must be interpreted in terms of the theory of distributions. Inserting this expansion in (1.102) leads directly to the sought form (1.100).

It is clear that the Green's function (1.100), considered as a function of the complex variable λ, has *pole* singularities located at $\lambda = \lambda_n$. Let C be a large circle of infinite radius (Fig. 1.7*a*). The integral along C is equal to the sum of the residues of the enclosed poles. Performing this simple operation yields the sought eigenfunction expansion. More precisely,

$$-\frac{1}{2\pi j} \int_C G(\mathbf{r}|\mathbf{r}'|\lambda)\, d\lambda = \sum_n f_n(\mathbf{r}) h_n^*(\mathbf{r}'). \tag{1.104}$$

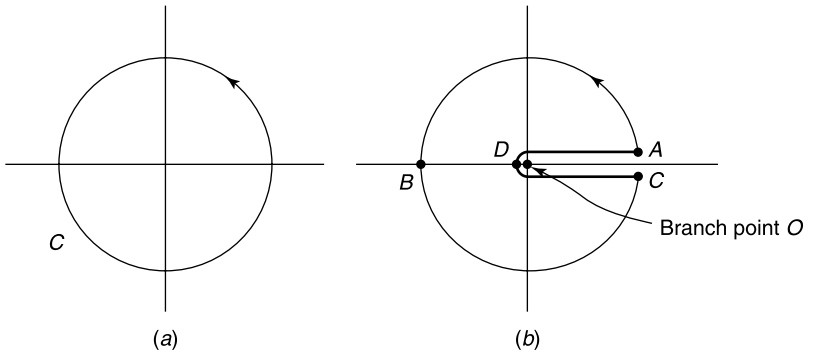

Figure 1.7 Contour of integration for a Green's function (*a*) without branch point and (*b*) with a branch point.

From (1.103), this can be rewritten as

$$-\frac{1}{2\pi j}\int_C G(\mathbf{r}|\mathbf{r}'|\lambda)\,d\lambda = \delta(\mathbf{r}-\mathbf{r}'), \tag{1.105}$$

a relationship that is of general validity [47, 150, 186] and is particularly interesting when the Green's function can be determined directly. Under these circumstances, the singularities of $G(\mathbf{r}|\mathbf{r}'|\lambda)$ will reveal whether there are only poles (in which case the discrete spectrum will lead to an expansion in terms of a complete set) or whether branch points are involved (in which case a continuous spectrum will appear). An example will clarify the matter. The Green's function for a short-circuited transmission line is readily found to be

$$G(x|x'|\lambda) = \begin{cases} \dfrac{\sin\sqrt{-\lambda}x\,\sin\sqrt{-\lambda}(x'-l)}{(-\lambda)^{1/2}\sin(-\lambda)^{1/2}\,l}, & \text{for } x \le x' \\ \dfrac{\sin\sqrt{-\lambda}x'\,\sin\sqrt{-\lambda}(x-l)}{\sqrt{-\lambda}\,\sin\sqrt{-\lambda}\,l}, & \text{for } x \ge x' \end{cases}$$

where $\lambda = -\omega^2 LC$. The rules given in Appendix 6 indicate that this function does not have any branch points; its only singularities are poles occurring at the zeros of $\sin(\sqrt{-\lambda}\,l)$, that is, at $\lambda = -(n\pi/l)^2$, where n is an integer. However, from (1.104), a function $u(\mathbf{r})$ admits the representation

$$u(\mathbf{r}) = -\frac{1}{2\pi j}\int_C d\lambda \int_V G(\mathbf{r}|\mathbf{r}'|\lambda)u(\mathbf{r}')\,dV'. \tag{1.106}$$

The sum of the residues now gives

$$u(\mathbf{r}) = \sum_{n=1}^{\infty}\frac{2}{l}\sin\frac{n\pi x}{l}\int_0^l u(x')\sin\frac{n\pi x'}{l}\,dx',$$

which is precisely the Fourier expansion of $u(x)$, confirming that the set formed by the $\sin(n\pi x/l)$ is complete. When the Green's function has a branch point, the integration contour for (1.105) becomes *ABCDA* (see Fig. 1.7*b*), and the value of $u(\mathbf{r})$ consists of the sum of the residues supplemented by the branch-cut integral *ADC*. In this case, the

eigenfunctions do not form a complete set, and the contribution of the discrete spectrum (the eigenvalues) must be supplemented by the contribution of the continuous spectrum (Problem 1.24).

1.11 DISCRETIZATION

Consider the very general problem

$$\mathcal{L}f(\mathbf{r}) = g(\mathbf{r}) \qquad (f \in \mathcal{D}), \tag{1.107}$$

where $\mathcal{L}$ is a linear operator (integral or differential), g a known forcing function, and f — the unknown of the problem — a function that must belong to a given domain $\mathcal{D}$ (e.g., the family of functions that are continuous in a volume V). Following Section 1.1, we shall seek an approximate solution of the problem in the form

$$f(\mathbf{r}) \approx \sum_{n=1}^{N} a_n f_n(\mathbf{r}). \tag{1.108}$$

The f_n are the *basis functions*, and the a_n are the unknown coefficients. The basis functions must be chosen so that the summation belongs to $\mathcal{D}$. Let us apply the operator $\mathcal{L}$ to both sides of (1.108). As N remains finite (although it is often very large in order to obtain the desired accuracy), $\mathcal{L}$ may be brought behind the summation sign, and we write

$$\sum_{n=1}^{N} a_n \mathcal{L} f_n(\mathbf{r}) \approx g(\mathbf{r}). \tag{1.109}$$

A simple-minded method to determine the a_n is to satisfy (1.109) at N points in the region of interest. This *collocation* (or *point-matching*) method reduces the problem to the solution of N linear equations with N unknowns, a discretized form that is eminently suitable for programming on a digital computer. Such steps had a revolutionary impact on the number of problems that could be solved numerically — in all fields of engineering and physics — when efficient computers became generally available in the 1950s. But how good is the approximation? An answer can be given on the basis of the *error*, or *residue*, defined as

$$e = g - \sum_{n=1}^{N} a_n \mathcal{L} f_n. \tag{1.110}$$

In the method of least squares, the a_n are chosen to minimize the norm of the error, viz. (Problem 1.26)

$$\begin{aligned} \| e \|^2 &= \left\| g - \sum_{n=1}^{N} a_n \mathcal{L} f_n \right\|^2 \\ &= \left\langle g - \sum_{n=1}^{N} a_n \mathcal{L} f_n, g - \sum_{k=1}^{N} a_k \mathcal{L} f_k \right\rangle_H . \end{aligned} \tag{1.111}$$

In the more general approach based on (1.109), it is clear that point-matching will yield values of a_n, and therefore of the error, that definitely depend on the choice of the matching points $\mathbf{r}_i$; that is, on the values of $g(\mathbf{r})$ at these points. It would certainly be advantageous to use better sampling and to involve the whole *range* of values of $g(\mathbf{r})$. This can be done[3] by taking the scalar products of (1.109) with N suitable *testing* (or *weighting*) functions w_i. The method generates N equations of the type [154]

$$\sum_{n=1}^{N} a_n \langle \mathcal{L} f_n, w_i \rangle = \langle g, w_i \rangle \qquad (i = 1, 2, \ldots, N). \tag{1.112}$$

In matrix form:

$$\begin{bmatrix} \langle \mathcal{L}f_1, w_1 \rangle & \langle \mathcal{L}f_2, w_1 \rangle & \cdots & \langle \mathcal{L}f_N, w_1 \rangle \\ \langle \mathcal{L}f_1, w_2 \rangle & \langle \mathcal{L}f_2, w_2 \rangle & \cdots & \langle \mathcal{L}f_N, w_2 \rangle \\ \vdots & \vdots & \ddots & \vdots \\ \langle \mathcal{L}f_1, w_N \rangle & \langle \mathcal{L}f_2, w_N \rangle & \cdots & \langle \mathcal{L}f_N, w_N \rangle \end{bmatrix} \cdot \begin{bmatrix} a_1 \\ a_2 \\ \vdots \\ a_N \end{bmatrix} = \begin{bmatrix} \langle g, w_1 \rangle \\ \langle g, w_2 \rangle \\ \vdots \\ \langle g, w_N \rangle \end{bmatrix} \tag{1.113}$$

or

$$\overline{\overline{L}} \cdot \mathbf{a} = \mathbf{g}. \tag{1.114}$$

It is seen that collocation corresponds with the choice $w_i = \delta(\mathbf{r} - \mathbf{r}_i)$. The matrix elements L_{mn} are typically space integrals, which bear some resemblance to moment integrals of the type $\int x^n f(x)\, dx$. This connection prompted Harrington to call the process described above (and apparently first used by Kantorovitch and Akilov) the *method of moments*.[4] The set of equations (1.112) can be interpreted to imply the requirement

$$\langle e, w_i \rangle_H = 0. \tag{1.115}$$

The equations therefore ensure that the error e is orthogonal to the subspace formed by the w_i or, expressed in a slightly different way, that e is constrained to be the zero element in that subspace. We notice, from (1.115), that e converges to zero in a *weak* sense.

By solving (1.112), we have replaced the original problem (1.107) by a different one, with evident questions concerning the validity and convergence of the solution as N increases.[1] A few answers can be given when the original transformation is positive, but most electromagnetic problems unfortunately yield transformations that are neither positive nor positive-definite [186]. The choice of basis and testing functions plays an important role in the matter, as it determines[5]

- The accuracy of the solution, and the numerical convergence of the process;
- The ease with which the matrix elements can be evaluated; and
- The character of the matrix, and the resulting influence on stability, a point that is further discussed in Section 1.12.

It is therefore appropriate to discuss the nature of the basis functions that have been used in practice. They sometimes have a support that covers the whole domain V of variation of $\mathbf{r}$, in which case they are termed *entire domain functions*. In a one-dimensional space, obvious examples are $\sin nx$ and $\cos nx$ in the interval $(0, 2\pi)$ or Legendre polynomials in the interval $(-1, +1)$. It is often advantageous, however, to choose *subdomain* functions;

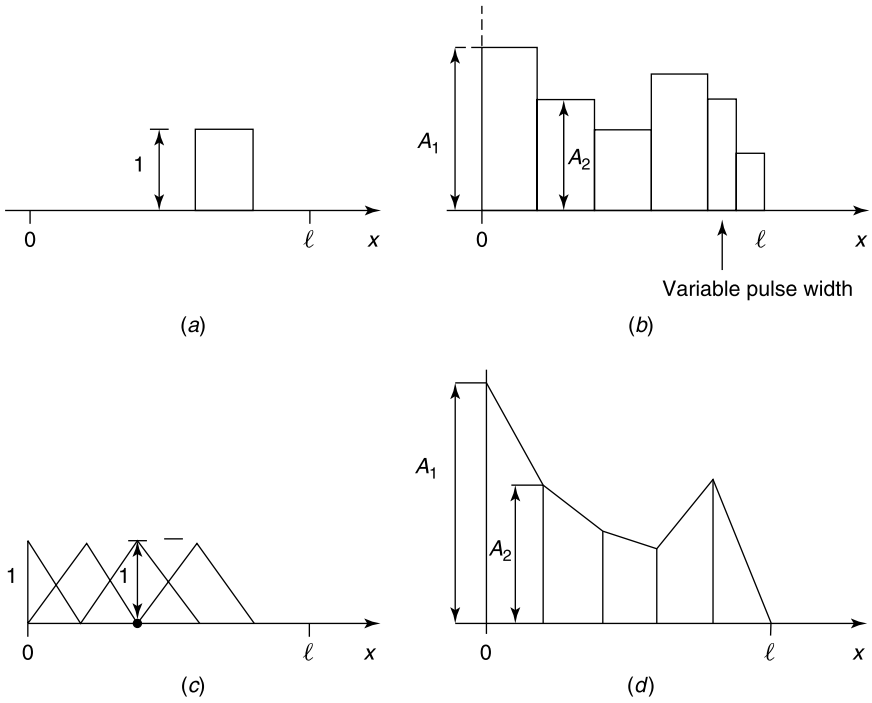

Figure 1.8 Typical subdomain basis functions.

that is, functions with a support V^* that covers only part of V. These functions are identically zero in $V - V^*$. Two frequently used one-dimensional subdomain functions are

1. The rectangular pulse (Fig. 1.8*a*, *b*): The function is approximated by a succession of horizontal plateaus. The width of the pulses may be chosen at will. It is advantageous, for example, to introduce a high density of pulses in those regions where $f(\mathbf{r})$ varies rapidly.
2. The triangle and the half-triangle (Fig. 1.8*c*, *d*): The function is now represented by a succession of linear segments.

There are many other possibilities, such as the half-sinusoid or the spline [145, 203]. *Spline functions* are defined on subintervals and join smoothly — in some given sense — at the connecting points. The straight segments in Figure 1.8*d* are actually first-degree splines, which join smoothly, but with discontinuous first derivatives. The often-used cubic splines are third-order polynomials, so chosen that the first and second derivatives remain continuous in the interval $(0, b)$. Cubic splines are particularly appropriate for differential operators of the second order, as a representation by line segments, such as in Figure 1.8*d*, introduces delta functions at the junction points, hence a representation that would not be in $\mathcal{D}$. The difficulty can sometimes be circumvented by switching to a weak type of solution, where a derivative is transferred to the testing functions, which now take over part of the smoothness requirement. It is shown in Section 2.2 how the order of the highest derivative present in the problem can be reduced.

In two and three dimensions, it is seldom possible to find *entire domain* basis functions in analytical form, except in simple space domains such as the rectangle or the cube. *Subdomain*

functions, of the kind discussed in Section 2.7, under the heading *finite elements*, are used extensively, in particular because of their flexibility in fitting domains of arbitrary shape.

Testing functions may be chosen among those discussed above or in the form of delta functions, as in the point-matching method. In the *Galerkin method*, they *coincide* with the basis functions. For such a choice, the typical matrix element is

$$L_{mn} = \langle \mathcal{L} f_m, f_n \rangle = \left\langle f_m, \mathcal{L}^a f_n \right\rangle. \tag{1.116}$$

When $\mathcal{L}$ is self-adjoint with respect to a Hilbert inner product,

$$\begin{aligned} L_{mn} &= \langle \mathcal{L} f_m, f_n \rangle_H = \langle f_m, \mathcal{L} f_n \rangle_H \\ L_{nm} &= \langle \mathcal{L} f_n, f_m \rangle_H = \langle f_m, \mathcal{L} f_n \rangle_H^* = L_{mn}^*. \end{aligned} \tag{1.117}$$

The property $L_{nm} = L_{mn}^*$ defines a *Hermitian matrix*. The $\overline{\overline{L}}$ matrix would be *symmetric* if we had adopted a symmetric inner product. Another possible choice for w_i is $\mathcal{L} f_i$, for which (1.112) becomes

$$\sum_{n=1}^{N} a_n \langle \mathcal{L} f_n, \mathcal{L} f_i \rangle = \langle g, \mathcal{L} f_i \rangle . \tag{1.118}$$

If $\mathcal{L} f_n$ and g are in the domain of $\mathcal{L}^a$, we may write

$$\sum_{n=1}^{N} a_n \langle \mathcal{L}^a \mathcal{L} f_n, f_i \rangle = \left\langle \mathcal{L}^a g, f_i \right\rangle, \tag{1.119}$$

which is the Galerkin discretization of

$$\mathcal{L}^a \mathcal{L} f = \mathcal{L}^a g. \tag{1.120}$$

In that case, we solve (1.120) instead of the original equation (1.107). It is advantageous that $\mathcal{L}^a \mathcal{L}$ is positive-definite (see Problem 1.10). Less advantageous is that $\mathcal{L}^a \mathcal{L}$ generates higher-order derivatives when $\mathcal{L}$ is a differential operator.

1.12 MATRICES

A matrix is a rectangular array of elements, denoted by L_{mn}. The literature on this important operator is very abundant, and the reader will find additional information in well-known texts such as [152, 157, 177]. A few essential notions will suffice for our purpose. They concern only $N \times N$ square matrices, where N is the *rank* of the matrix, and are direct applications of the theory of transformations discussed in Sections 1.2 and 1.3.

Let us first define two possible inner products relative to vectors $\mathbf{x}$ and $\mathbf{y}$ of dimension N, viz.

$$\langle \mathbf{x}, \mathbf{y} \rangle_{\mathrm{S}} = \sum_{i=1}^{N} x_i y_i \tag{1.121}$$

$$\langle \mathbf{x}, \mathbf{y} \rangle_{\mathrm{H}} = \sum_{i=1}^{N} x_i y_i^*. \tag{1.122}$$

The typical operator equation, corresponding with (1.18), is now

$$\overline{\overline{L}}\cdot\mathbf{f}=\mathbf{g}, \tag{1.123}$$

which stands for

$$\sum_{j=1}^{N} L_{ij}f_j = g_i. \tag{1.124}$$

The nature of the adjoint matrix depends on the choice of the inner product. In the *symmetric* case, for example, $\overline{\overline{L}}^a$ follows from the relationship

$$\left\langle \overline{\overline{L}}\cdot\mathbf{x},\mathbf{y}\right\rangle_{\mathrm{S}} = \left\langle \mathbf{x},\overline{\overline{L}}^t\cdot\mathbf{y}\right\rangle_{\mathrm{S}}. \tag{1.125}$$

Clearly, the *adjoint* is the *transpose* of $\overline{\overline{L}}$, with elements

$$L^t_{ik} = L_{ki}. \tag{1.126}$$

The matrix is self-adjoint when it is symmetric. Similarly, as

$$\left\langle \overline{\overline{L}}\cdot\mathbf{x},\mathbf{y}\right\rangle_{\mathrm{H}} = \left\langle \mathbf{x},\overline{\overline{L}}^\dagger\cdot\mathbf{y}\right\rangle_{\mathrm{H}}, \tag{1.127}$$

the adjoint with respect to a Hilbert scalar product is the *Hermitian transpose* $\overline{\overline{L}}^\dagger$, with elements

$$L^\dagger_{ik} = L^*_{ki}. \tag{1.128}$$

A matrix is now self-adjoint when it is Hermitian.

Following again the general theory, we introduce the eigenvector problem

$$\overline{\overline{L}}\cdot\mathbf{f}_n = \lambda_n\mathbf{f}_n. \tag{1.129}$$

Relationship (1.129) shows that, when $\overline{\overline{L}}$ operates on one of its eigenvectors, it produces the eigenvector itself, dilated by a factor λ_n. Such a property often has interesting physical implications, for example in elasticity. It is easy to see that the eigenvalues are the solutions of the determinantal *secular equation*

$$\det\begin{bmatrix} L_{11}-\lambda & L_{12} & \cdots & L_{1N} \\ L_{21} & L_{22}-\lambda & \cdots & L_{2N} \\ \vdots & \vdots & \ddots & \vdots \\ L_{N1} & L_{N2} & \cdots & L_{NN}-\lambda \end{bmatrix} = 0. \tag{1.130}$$

If the determinant of the L_{mn} vanishes, the matrix is singular, and $\lambda = 0$ is an eigenvalue. Such a situation arises when the original N linear equations leading to (1.123) are not linearly independent. As a consequence, there is now a nonzero solution to*

$$\overline{\overline{L}}\cdot\mathbf{x}_0 = 0. \tag{1.131}$$

*The extension to several linearly independent solutions proceeds as in Section 1.3.

Let us assume that a Hilbert inner product has been chosen. For such a case, the adjoint matrix $\overline{\overline{L}}^{\dagger}$ has eigenvalues μ_n that are the complex conjugates of λ_n and eigenvectors that form a biorthogonal set with the $\mathbf{x}_n$. It follows that zero is also an eigenvalue of $\overline{\overline{L}}^{\dagger}$, hence that there is a nonzero solution for

$$\overline{\overline{L}}^{\dagger} \cdot \mathbf{y}_0 = 0. \tag{1.132}$$

To conclude this brief overview, let us define a few terms that appear regularly in the literature:

1. The *product* of two matrices $\overline{\overline{a}}$ and $\overline{\overline{b}}$ of rank N is a matrix $\overline{\overline{c}}$ with elements

$$c_{mn} = \sum_{i=1}^{N} a_{mi} b_{in}. \tag{1.133}$$

2. The *inverse* of a matrix is a matrix $\overline{\overline{L}}^{-1}$ defined by

$$\overline{\overline{L}} \cdot \overline{\overline{L}}^{-1} = \overline{\overline{I}}, \tag{1.134}$$

where $\overline{\overline{I}}$ is the unit matrix.

3. The *trace* of a matrix is the sum of the diagonal terms. It is also the sum of the eigenvalues.

4. The *spectral radius* of a matrix is defined by

$$\rho\left(\overline{\overline{L}}\right) = \max|\lambda_i| \qquad (1 \le i \le N). \tag{1.135}$$

5. A matrix is of the *Toeplitz* type when its elements depend on the difference $|i - j|$ rather than on i and j independently. The form of the matrix, as given by Toeplitz,[6] is

$$\overline{\overline{a}} = \begin{bmatrix} \cdot & \cdot & \cdot & \cdot & \cdot & \cdot & \cdot \\ \cdot & a_0 & a_1 & a_2 & a_3 & a_4 & \cdot \\ \cdot & a_1 & a_0 & a_1 & a_2 & a_3 & \cdot \\ \cdot & a_2 & a_1 & \boxed{a_0} & a_1 & a_2 & \cdot \\ \cdot & a_3 & a_2 & a_1 & a_0 & a_1 & \cdot \\ \cdot & a_4 & a_3 & a_2 & a_1 & a_0 & \cdot \\ \cdot & \cdot & \cdot & \cdot & \cdot & \cdot & \cdot \end{bmatrix}. \tag{1.136}$$

Toeplitz called the associated quadratic form an L-form. There are numerical advantages in formulating a problem (when and if it is possible) in terms of such matrices: they contain only N unique elements, and rapid inversion algorithms are available.[7,8]

6. A matrix is *fully populated* if all of its elements are nonzero and is *sparse* if only a small proportion of its elements are nonzero.

7. A matrix is *diagonal* if nonzero elements only occur on the leading diagonal; that is, if $a_{mn} = 0$ for $m \neq n$.

8. A *band* matrix is characterized by elements that are clustered in a narrow band containing the main diagonal.

9. A *lower triangular* matrix is a square matrix having zero elements above the leading diagonal. Similarly, an *upper triangular* matrix has zero elements below the leading diagonal.

1.13 SOLUTION OF MATRIX EQUATIONS: STABILITY

When solving an equation such as (1.123), it is important first to investigate the existence and uniqueness of the solution. The homogeneous equation (1.132) plays a decisive role here. From (1.30) and (1.132), there is *no* solution to (1.123) unless[†]

$$\langle \mathbf{g}, \mathbf{y}_0 \rangle = 0. \tag{1.137}$$

When this is satisfied, $\mathbf{f}$ is defined to within a multiple of $\mathbf{x}_0$ (the solution of 1.131), but a *core* solution may be introduced to ensure uniqueness. Clearly, the existence of a zero eigenvalue should be a reason to proceed prudently. Even when the lowest eigenvalue is not zero, but very small, care should be the rule, as shown by the following simple example, in which the system to solve is

$$\begin{aligned} 4.1f_1 + 2f_2 &= 100 \\ 2f_1 + 1.1f_2 &= 50. \end{aligned} \tag{1.138}$$

The solution is simple: $f_1 = 19.608$ and $f_2 = 9.804$. Let us now slightly modify the second term of the system, and make it (101, 48). The new solution is $f_1 = 29.608$ and $f_2 = -10.196$. There obviously is instability. The difficulty is caused by the spread of the eigenvalues, which are $\lambda_1 = 0.1$ (quite close to zero) and $\lambda_2 = 5.1$. To support this statement, assume, to simplify matters, that $\overline{\overline{L}}$ is Hermitian, and that the eigenvectors $\mathbf{x}_n$ form an orthonormal set. Expanding $\mathbf{f}$ and $\mathbf{g}$ in the $\mathbf{x}_n$, and inserting into (1.123), yields

$$\mathbf{f} = \frac{\langle \mathbf{g}, \mathbf{x}_1 \rangle}{\lambda_1}\mathbf{x}_1 + \frac{\langle \mathbf{g}, \mathbf{x}_2 \rangle}{\lambda_2} + \cdots. \tag{1.139}$$

Assume now that the data $\mathbf{g}$ are shifted by a (small) amount $\Delta\mathbf{g}$. The resulting shift in $\mathbf{f}$ satisfies[‡]

$$\overline{\overline{L}} \cdot \Delta\mathbf{f} = \Delta\mathbf{g}.$$

An expansion in the $\mathbf{x}_n$ now gives

$$\Delta\mathbf{f} = \frac{\langle \Delta\mathbf{g}, \mathbf{x}_1 \rangle}{\lambda_1}\mathbf{x}_1 + \frac{\langle \Delta\mathbf{g}, \mathbf{x}_2 \rangle}{\lambda_2}\mathbf{x}_2 + \cdots. \tag{1.140}$$

[†]When (1.132) has several linearly independent solutions, the condition must be valid for each one of them.

[‡]If there exists a constant M such that, for any $\Delta\mathbf{g}$,

$$\| \Delta\mathbf{f} \| \leq M \| \Delta\mathbf{g} \|,$$

the computation is said to depend *Lipschitz continuously* on the data.

The product $\langle \Delta \mathbf{g}, \mathbf{x}_1 \rangle$ is small, but if it is divided by a very small λ_1, it may give rise to a very sizeable contribution. The same simplistic approach can be applied to

$$(\overline{\overline{L}} - \lambda) \cdot \mathbf{f} = \mathbf{g} \tag{1.141}$$

to yield

$$\Delta \mathbf{f} = \frac{\langle \Delta \mathbf{g}, \mathbf{x}_1 \rangle}{\lambda_1 - \lambda} \mathbf{x}_1 + \frac{\langle \Delta \mathbf{g}, \mathbf{x}_2 \rangle}{\lambda_2 - \lambda} \mathbf{x}_2 + \cdots. \tag{1.142}$$

Ill-posedness now becomes a danger when λ approaches an eigenvalue. Enhancing the influence of $\Delta \mathbf{g}$, combined with round-off errors during the solution process, can lead to unacceptably large errors.

To cast these rather loose considerations into a more rigorous mold,[9] let us use the concept of the *norm of a matrix* [198, 209]. From (1.26), the norm of $\overline{\overline{L}}$ is

$$\| \overline{\overline{L}} \| = \sup \frac{\| \overline{\overline{L}} \cdot \mathbf{f} \|}{\| \mathbf{f} \|}. \tag{1.143}$$

This important quantity can be of several types, as discussed in Section 1.1. It could be the *infinite norm*, for example, which for a matrix is the maximum value of $\sum_{i=1}^{N} |a_{ij}|$ for all rows. Whatever the choice, we define the *condition number* as[§]

$$\operatorname{cond} \overline{\overline{\mathrm{L}}} = \| \overline{\overline{\mathrm{L}}} \| \cdot \| \overline{\overline{\mathrm{L}}}^{-1} \|. \tag{1.144}$$

From (1.140), the shift $\Delta \mathbf{f}$ resulting from an error $\Delta \mathbf{g}$ is given by

$$\Delta \mathbf{f} = \overline{\overline{L}}^{-1} \cdot \Delta \mathbf{g}. \tag{1.145}$$

From the definition of the norm of a matrix, it follows that

$$\| \Delta \mathbf{f} \| \leq \| \overline{\overline{L}}^{-1} \| \, \| \Delta \mathbf{g} \|$$

$$\| \mathbf{g} \| \leq \| \overline{\overline{L}} \| \, \| \mathbf{f} \|.$$

Multiplying these two inequalities together, and dividing by $\| \mathbf{f} \| \, \| \mathbf{g} \|$, yields

$$\frac{\| \Delta \mathbf{f} \|}{\| \mathbf{f} \|} \leq \operatorname{cond} \overline{\overline{\mathrm{L}}} \frac{\| \Delta \mathbf{g} \|}{\| \mathbf{g} \|}. \tag{1.146}$$

By similar methods, one can show that the shift in $\mathbf{f}$ produced by a small perturbation $(\Delta \overline{\overline{L}})$ of the *matrix* itself satisfies [193]

$$\frac{\| \Delta \mathbf{f} \|}{\| \mathbf{f} \|} \leq \operatorname{cond} \overline{\overline{\mathrm{L}}} \frac{\| \Delta \overline{\overline{\mathrm{L}}} \|}{\| \overline{\overline{\mathrm{L}}} \|}. \tag{1.147}$$

[§]Other measures of condition have been proposed, such as Turing's M-number, or the value of the determinant of the normalized matrix [176].

Clearly, a small condition number favorably limits the relative error in $\mathbf{f}$ resulting from a shift in $\mathbf{g}$ or $\overline{\overline{L}}$. For the often-used Euclidean norm, the condition number is given by

$$\mathrm{cond}_2\,\overline{\overline{\mathrm{L}}} = \sqrt{\frac{|\nu_{\max}|}{|\nu_{\min}|}}, \tag{1.148}$$

where the $|\nu|$ are the extreme absolute values of the eigenvalues of $\overline{\overline{L}}^{\dagger}\cdot\overline{\overline{L}}$. When the matrix is real and symmetric, $\nu_n = \lambda_n^2$, whence

$$\mathrm{cond}_2\,\overline{\overline{\mathrm{L}}} = \frac{|\lambda_{\max}|}{|\lambda_{\min}|}. \tag{1.149}$$

We conclude that a large spread in the absolute values of the eigenvalues of $\overline{\overline{L}}$ leaves the door open to instabilities. For the simple example discussed under (1.138) the condition number is 51, and as $\| \Delta\mathbf{f} \| = 10\sqrt{5}$, $\| \mathbf{f} \| = 9.804\sqrt{5}$, $\| \Delta\mathbf{g} \| = \sqrt{5}$, and $\| \mathbf{g} \| = 50\sqrt{5}$, condition (1.146) is seen to be satisfied (fortuitously with the equality sign).

The stability problem, far from being a theoretical exercise, plays a fundamental role in numerical procedures and in particular in the solution of scattering problems of the kind discussed in later chapters.

1.14 FINITE DIFFERENCES

Discretization of differential operators has a long tradition of service in numerical analysis. Consider first the application of the method to the first derivative of $\phi(x)$. We start from the Taylor expansion around a central point O, viz. (Fig. 1.9)

$$\begin{aligned}\phi_2 &= \phi_0 + h\left(\frac{d\phi}{dx}\right)_0 + \frac{1}{2}h^2\left(\frac{d^2\phi}{dx^2}\right)_0 + \cdots \\ \phi_1 &= \phi_0 - h\left(\frac{d\phi}{dx}\right)_0 + \frac{1}{2}h^2\left(\frac{d^2\phi}{dx^2}\right)_0 + \cdots.\end{aligned} \tag{1.150}$$

From these expressions follow the *central difference* formulas[¶]

$$\left(\frac{d\phi}{dx}\right)_0 = \frac{1}{2h}(\phi_2 - \phi_1) + O(h^2). \tag{1.151}$$

$$= \frac{1}{12h}(-\phi_4 + 8\phi_2 - 8\phi_1 + \phi_3) + O(h^4). \tag{1.152}$$

The approximation consists in dropping the correction terms in h^2 or h^4 and keeping only the truncated version. This procedure improves in accuracy as the mesh size h decreases,

[¶]A function $f(x)$ is $O(x)$ when $\lim_{x\to 0} xf(x)$ is finite and nonzero, and $o(x)$ when the same limit is zero.

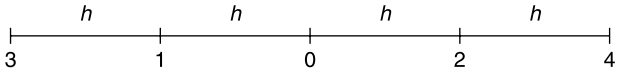

Figure 1.9 Equidistant points on an interval.

and particularly so in the case of (1.152). One may also use the *forward difference* forms

$$\left(\frac{d\phi}{dx}\right)_0 = \frac{1}{h}(\phi_2 - \phi_0) + O(h) \tag{1.153}$$

$$= \frac{1}{2h}(-\phi_4 + 4\phi_2 - 3\phi_0) + O(h^2) \tag{1.154}$$

or the *backward difference* forms

$$\left(\frac{d\phi}{dx}\right)_0 = \frac{1}{h}(\phi_0 - \phi_1) + O(h) \tag{1.155}$$

$$= \frac{1}{h}(3\phi_0 - 4\phi_1 + \phi_3) + O(h^2). \tag{1.156}$$

The last two approximations, in their truncated form, are less accurate than their central difference counterparts. When these various formulas are used in an array, the indices 0 to 4 are systematically replaced by $i-2$, $i-1$, i, $i+1$, $i+2$.

Turning now to the second derivative, adding a few truncated values of ϕ gives the *central difference* forms

$$\left(\frac{d^2\phi}{dx^2}\right)_0 = \frac{1}{h^2}(\phi_2 - 2\phi_0 + \phi_1) + O(h^2) \tag{1.157}$$

$$= \frac{1}{12h^2}(-\phi_4 + 16\phi_2 + 16\phi_1 - \phi_3) + O(h^4). \tag{1.158}$$

Relationship (1.158) can be written in the interesting form

$$\left(\frac{d^2\phi}{dx^2}\right)_0 = \frac{2}{h^2}(\phi_{\text{ave}} - \phi_0) + O(h^2), \tag{1.159}$$

where ϕ_{ave} is the average between ϕ_1 and ϕ_2. The partial second derivatives follow analogously, and give, for a uniform mesh size h in the x and y directions,

$$\nabla^2_{xy}\phi = \frac{4}{h^2}(\phi_{\text{ave}} - \phi_0) + O(h^2). \tag{1.160}$$

Analogously,

$$\nabla^2_{x,y,z}\,\phi = \frac{6}{h^2}(\phi_{\text{ave}} - \phi_0) + O(h^2). \tag{1.161}$$

In (1.161), ϕ_{ave} is the average of the values at the points of a six-rayed star. However, the formula is also valid[10] when the average is taken over the volume of a cube of

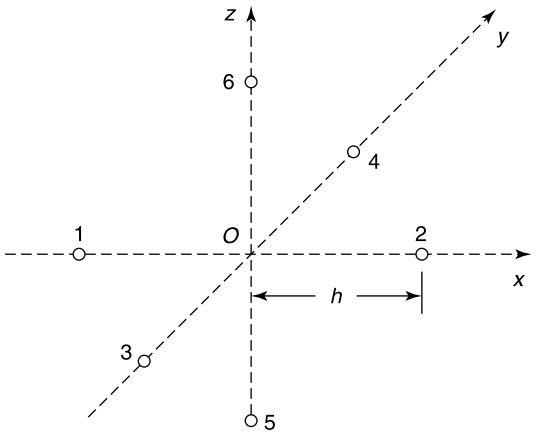

Figure 1.10 Six-rayed star pertinent to the evaluation of the Laplacian.

side $2h$ centered at 0 or over the surface, the edges, or the vertices of the cube. In particular, the value of a function ϕ satisfying $\nabla^2\phi = 0$ (a *harmonic function*) is equal to each one of these averages and to the average taken over a spherical surface of radius h (Fig. 1.10).

A short example will show how a truncated operator can be put to use in a numerical procedure. We seek the solution to the eigenvalue problem

$$\frac{d^2y}{dx^2} = \lambda y, \tag{1.162}$$

where y vanishes at the end points $x = 0$ and $x = l$. Application of (1.157) at the three intermediate points yields, with $h = \frac{1}{4}l$ (Fig. 1.9),

$$\begin{aligned} y_1\left(-\lambda\frac{l^2}{16} - 2\right) + y_0 &= 0 \\ y_1 + y_0\left(-\lambda\frac{l^2}{16} - 2\right) + y_2 &= 0 \\ y_0 + y_2\left(-\lambda\frac{l^2}{16} - 2\right) &= 0. \end{aligned}$$

In matrix notation,

$$\begin{pmatrix} -2 & 1 & 0 \\ 1 & -2 & 1 \\ 0 & 1 & -2 \end{pmatrix} \begin{pmatrix} y_1 \\ y_0 \\ y_2 \end{pmatrix} - \frac{\lambda l^2}{16} \begin{pmatrix} y_1 \\ y_0 \\ y_2 \end{pmatrix} = 0.$$

The 3×3 matrix has the eigenvalues and eigenvectors

$$\frac{\lambda l^2}{16} = -(2 - \sqrt{2}) \qquad y_1 = \frac{1}{2} \qquad y_0 = \frac{1}{\sqrt{2}} \qquad y_2 = \frac{1}{2}$$

$$\frac{\lambda l^2}{16} = -2 \qquad y_1 = \frac{1}{\sqrt{2}} \qquad y_0 = 0 \qquad y_2 = -\frac{1}{\sqrt{2}}$$

$$\frac{\lambda l^2}{16} = -(2 + \sqrt{2}) \qquad y_1 = -\frac{1}{2} \qquad y_0 = \frac{1}{\sqrt{2}} \qquad y_2 = -\frac{1}{2}.$$

The three λ terms are fairly good approximations to the three lowest eigenvalues $-9.87/l^2, -39.4/l^2$, and $-89/l^2$ of the clamped string. The agreement becomes much better as the number of division points increases. Increasing N would also reveal an interesting phenomenon, namely that the matrix has a *band structure*, fundamentally because formulas such as (1.157) and (1.158) connect the value of y at a given point to the y's of only *a few* neighboring points.

The truncated forms expressed in terms of ϕ_{ave} have the great advantage of leading to a semiintuitive, semiquantitative understanding of the behavior of functions satisfying differential equations involving ∇^2. For example,

1. A function that is harmonic in a volume cannot have a maximum or a minimum there, as $\nabla^2\phi = 0$ implies $\phi_0 = \phi_{\text{ave}}$. Extrema therefore only occur at the boundary.
2. Solutions of the source-free diffusion equation

$$\nabla^2 T = \frac{1}{a^2}\frac{\partial T}{\partial t} \tag{1.163}$$

have a tendency to converge to an equilibrium state. To justify this assertion, we investigate the equalization of temperature that follows an initial disturbance (Fig. 1.11*a*). At $t = 0$, the Laplacian is positive as $T_{\text{ave}} > T_0$. As a result, $\partial T/\partial t$ is positive, T grows, and the gap between T and T_{ave} narrows down. In the limit, the two curves will ultimately converge to a common asymptotic value, which will persist until a new perturbation occurs.

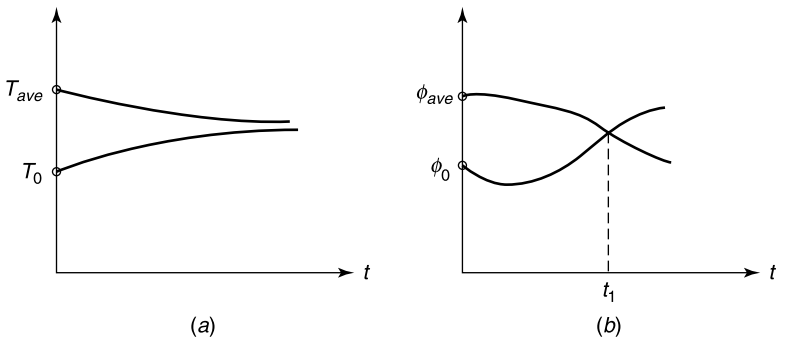

Figure 1.11 (*a*) The evolution of a temperature disturbance. (*b*) The birth of an oscillation.

3. A very different behavior is evidenced by the solution of the sourceless wave equation

$$\nabla^2\phi = \frac{1}{c^2}\frac{\partial^2\phi}{\partial t^2}. \tag{1.164}$$

This solution is fundamentally oscillatory, as shown by the following simple argument. At $t = 0$ (Fig. 1.11*b*), we start with a positive $\nabla^2\phi$, which implies a positive $\partial^2\phi/\partial t^2$, and therefore an *upward* curvature. The situation remains so until the curves cross each other at t_1, upon which the curvature turns *downward*. The oscillatory tendency is evident.

4. The last example concerns the Helmholtz equation in a source-free region, viz.

$$\nabla^2\phi + k^2\phi = 0 \qquad \left(k = \frac{2\pi}{\lambda}\right). \tag{1.165}$$

According to (1.161), this can be rewritten as

$$\frac{6}{h^2}\left[\phi_{\text{ave}} - \phi_0 + \frac{k^2h^2}{6}\phi_0 + O(h^4)\right] = 0. \tag{1.166}$$

Equation (1.166) shows that the solution behaves locally as a harmonic function, provided the distance h between net points remains much smaller than λ.

Finite difference methods are used extensively in the solution of differential equations such as the wave equation (1.164) [169, 199, 205, 209]. To follow the time evolution of the solution of that equation, let us start in one dimension, with a net of the kind shown in Figure 1.12. The value of ϕ at a net point is denoted by $\phi(i, j)$, where i and j refer to the coordinates $i\Delta x$ and $jc\Delta t$. The wave equation, discretized according to (1.157), now generates the *time-marching* equation

$$\phi(i, j+1) = 2(1-r)\phi(i, j) + r[\phi(i+1, j) + \phi(i-1, j)] - \phi(i, j-1), \tag{1.167}$$

where r is the aspect ratio

$$r = \left(\frac{c\Delta t}{\Delta x}\right)^2. \tag{1.168}$$

The influence of the choice of intervals on the stability of the algorithm is an important topic, which is within the pale of numerical analysis, and will not be pursued here [205, 209]. In one

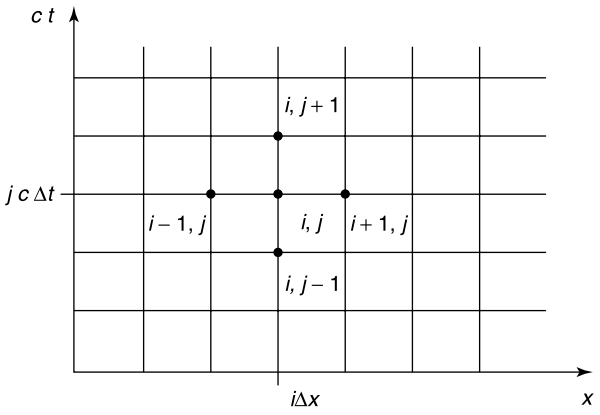

Figure 1.12 A mesh for the variables x and t.

dimension, for example, stability requires r to satisfy $r \leq 1$. With $r = 1$, Equation (1.167) becomes

$$\phi(i, j+1) = \phi(i+1, j) + \phi(i-1, j) - \phi(i, j-1). \tag{1.169}$$

A simple application of formulas of that type can be found in Section 12.8.

1.15 PERTURBATIONS

The essential features of the perturbation method can be revealed by solving the simple operator equation

$$(\mathcal{L} + \epsilon\mathcal{M})f = g, \tag{1.170}$$

where ϵ is a small parameter, and $\mathcal{L}$ and $\mathcal{M}$ are self-adjoint operators. Let f_0 be the solution of the undisturbed problem

$$\mathcal{L}f_0 = g.$$

The new solution is $f = f_0(1 + \alpha)$, where α approaches zero with ϵ. Keeping only terms of the first order leaves

$$\alpha\mathcal{L}f_0 + \epsilon\mathcal{M}f_0 = 0.$$

Taking the scalar product of both members with f_0 leads to the sought solution, viz.

$$f = f_0 - \epsilon\frac{\langle\mathcal{M}f_0, f_0\rangle}{\langle g, f_0\rangle}. \tag{1.171}$$

These ideas can now be applied to the eigenfunction equation

$$(\mathcal{L} + \epsilon\mathcal{M})\phi_n - \mu_n\phi_n = 0 \qquad (\phi \text{ in } \mathcal{D}). \tag{1.172}$$

In this example, the perturbation is again in the operator, but the method could equally well be applied to perturbations in the boundary conditions, or even in the boundary shape. Let λ_n and f_n be the nonperturbed eigenvalues and eigenfunctions of $\mathcal{L}$, and assume that the eigenfunctions are not degenerate and form an orthonormal set. We expand ϕ_n — the perturbed version of f_n — in a series

$$\phi_n = \sum_i A_{ni} f_i = A_{nn} f_n + \sum_{i \neq n} A_{ni} f_i.$$

Coefficient A_{nn} is close to one, and the other A_{ni} approach zero with ϵ. We next insert the expansion in (1.172). Keeping only terms of order ϵ leaves

$$\sum_i A_{ni}\lambda_i f_i + \epsilon\mathcal{M}A_{nn}f_n - \mu_n\sum_i A_{ni}f_i = \sum_i A_{ni}(\lambda_i - \mu_n)f_i + \epsilon A_{nn}\mathcal{M}f_n = 0.$$

Because of the orthonormality property of the f_n's, taking the inner product with respect to f_m cancels all terms but those in A_{nm}. Thus,

$$A_{nm}(\lambda_m - \mu_n) + \epsilon A_{nn}\langle\mathcal{M}f_n, f_m\rangle = 0.$$

Setting first $m = n$ gives

$$\mu_n = \lambda_n + \epsilon \langle \mathcal{M} f_n, f_n \rangle. \tag{1.173}$$

For $m \neq n$, one obtains

$$A_{nm} = \epsilon A_{nn} \frac{\langle \mathcal{M} f_n, f_m \rangle}{\mu_n - \lambda_m}$$

or, exploiting (1.173),

$$A_{nm} = \epsilon A_{nn} \frac{\langle \mathcal{M} f_n, f_m \rangle}{(\lambda_n - \lambda_m) + \epsilon \langle \mathcal{M} f_n, f_n \rangle}. \tag{1.174}$$

As the eigenfunction f_n is defined to within a multiplicative constant, we may set $A_{nn} = 1$. This gives immediately the final formula

$$\phi_n = f_n + \epsilon \sum_{m \neq n} \frac{\langle \mathcal{M} f_n, f_m \rangle}{\lambda_n - \lambda_m} f_m + \cdots. \tag{1.175}$$

By similar methods, one could obtain correction terms in ϵ^2 and higher, but at the cost of often unacceptable complexity.

A slight modification of the perturbation procedure is necessary when the *eigenvalue* λ_n is *degenerate*. Assume, for simplicity, that two degenerate *orthonormal* eigenfunctions f_{n1} and f_{n2} exist for $\lambda = \lambda_n$. The steps of the general theory can be retraced up to (1.172), but here a new element appears: The two perturbed eigenfunctions ϕ_{n1} and ϕ_{n2} do not normally converge to f_{n1} and f_{n2} as ϵ approaches zero. Instead, they converge to linear combinations $c_1 f_{n1} + c_2 f_{n2}$, where

$$c_1 = \epsilon \frac{\langle \mathcal{M} \phi_n, f_{n1} \rangle}{\mu_n - \lambda_n} = \epsilon \frac{\langle c_1 \mathcal{M} f_{n1} + c_2 \mathcal{M} f_{n2} \rangle}{\mu_n - \lambda_n} + \text{higher terms}, \tag{1.176}$$

and c_2 is given by a similar formula. These two homogeneous equations, in c_1 and c_2, will have nonzero solutions if, and only if, the determinant of the coefficients vanishes. Setting $\mu_n = \lambda_n + \epsilon \alpha_n$, this condition becomes

$$\det \begin{bmatrix} -\alpha_n + \langle \mathcal{M} f_{n1}, f_{n1} \rangle & \langle \mathcal{M} f_{n2}, f_{n1} \rangle \\ \langle \mathcal{M} f_{n1}, f_{n2} \rangle & -\alpha_n + \langle \mathcal{M} f_{n2}, f_{n2} \rangle \end{bmatrix} = 0, \tag{1.177}$$

from which two different values for the correction term α_n can be found. The corresponding eigenvalues are $\mu_n = \lambda_n + \epsilon \alpha_{n1}$ and $\mu_m = \lambda_n + \epsilon \alpha_{n2}$. Clearly, the perturbation has separated the eigenvalues, and the degeneracy has been removed. This effect is well-known in physics, where it is encountered, for example, in the splitting of spectral lines under a slight external disturbance. An electromagnetic example is discussed in Section 10.3.

The procedure outlined above is, of course, in need of a firmer theoretical basis, as important questions of validity of the power expansions in ϵ and of the magnitude of the relevant radii of convergence have been left unanswered. Great care should be exercised, for example, when ϵ is the coefficient of the highest derivative in a differential equation. The reader is referred to the specialized literature for additional information[11] [118, 149, 165, 166].

PROBLEMS

1.1 Show that orthogonal elements are always linearly independent.

1.2 The two sets $x_1, x_2, \ldots, x_i, \ldots$ and $y_1, y_2, \ldots, y_i, \ldots$ are said to be biorthogonal if $\langle x_i, y_k \rangle = \delta_{ik}$. Assuming that the x_i form a complete set for a class of functions $f(x)$, find the expansion coefficients of $f(x)$. Show that the two sets are composed of linearly independent elements.

1.3 Draw the locus of the tips of the unit vectors (vectors with unit norm) corresponding with the (1.5), (1.6), and (1.7) norms. Work in the (x_1, x_2) plane.

1.4 A sequence f_i converges in the *Cauchy sense* if, given an $\epsilon > 0$, there exists a number N such that $\| f_m - f_n \| < \epsilon$ as soon as m and n are larger than N. This means, more simply, that the distance between any of the elements of the sequence approaches zero as one penetrates deeper and deeper into the region of higher indices. Show that convergence, as defined in (1.8), implies Cauchy convergence.

1.5 Consider a *given* element f, and find its best approximation by a sum of the form $S_n = \sum_{n=1}^{N} a_n f_n$. As a criterion, require the error $(f - S_n)$ to have zero projection on the basis formed by the (possibly not orthogonal) linearly independent f_n. Show that the solution involves the conjugate transpose of the *Gram* matrix $\overline{\overline{G}}$ of the f_m (the elements of the *Gram matrix* are $G_{ik} = \langle f_i, f_k \rangle$).

1.6 Show that if a bounded transformation $\mathcal{L}^a$ is the adjoint of $\mathcal{L}$, then conversely $\mathcal{L}$ is the adjoint of $\mathcal{L}^a$.

1.7 Consider the transformation defined by the operator d^2/dx^2 and the boundary conditions $y(0) = 0$ and $y'(0) = y(1)$.

(**a**) Show that the transformation is not self-adjoint.

(**b**) Find the eigenvalues and eigenfunctions. Check that the former are complex.

(**c**) Find the adjoint transformation and the latter's eigenvalues and eigenfunctions.

(**d**) Check the biorthogonality property.

1.8 Show that, if the transformation $\mathcal{L}$ is positive-definite, the problem $\mathcal{L}f = g$ cannot have more than one solution.

1.9 Consider the transformation

$$\left(\frac{d^2}{dx^2} + \lambda\right) f = g$$

$$f'(0) = \alpha f(0)$$

$$f(1) = 0$$

where λ is real but α is complex. Show, with respect to the product

$$\langle u, v \rangle = \int_0^1 u v^* \, dx,$$

that the transformation is self-adjoint when α is real but not if α is an arbitrary complex number.

1.10 If the transformation $\mathcal{L}$ is not positive-definite, show, with respect to a Hermitian inner product, that a positive-definite transformation can be synthesized by forming $\mathcal{L}^a\mathcal{L}$. This is only valid if $\mathcal{L}f_0 = 0$ has only the zero element as a solution. The range of $\mathcal{L}$ must obviously be in the domain of $\mathcal{L}^a$ for $\mathcal{L}^a\mathcal{L}$ to have a meaning.

1.11 Investigate the transformation $(\nabla^2 + \lambda)f$ in a volume V when f is constrained to vanish at the boundary S. Is the transformation self-adjoint for complex, nonreal values of λ? Symmetric and Hilbert inner products should be considered separately.

1.12 Let $\mathcal{L}f = g$ and $\mathcal{L}^a h = s$ be two adjoint problems. Show that

$$\langle g, h\rangle = \langle f, s\rangle.$$

When the inner product is symmetric, the common value is termed the *reaction*. The left-hand term connects the *source* g in the original problem to the *effect* in the adjoint problem. Conversely, the right-hand term connects the source in the adjoint problem to the effect in the original problem. In a perhaps simpler notation, we would write $\langle g_1, f_2\rangle = \langle f_1, g_2\rangle$ or even $\langle 1, 2\rangle = \langle 2, 1\rangle$. The concept *reaction* is used extensively in later chapters.

1.13 Find the solution of $d^2y/dx^2 = -g(x)/T$ where $g(x)$ denotes the rectangular pulse defined by $g(x) = 0$ for $0 < x < x' - \epsilon$ and $x' + \epsilon < x < 1$, and $g(x) = \frac{1}{2}\epsilon$ for $x' - \epsilon \le x \le x' + \epsilon$. Confirm that the solution approaches the Green's function (1.37) as ϵ approaches zero.

1.14 Prove that the conditions (1.44) and (1.50) are equivalent when $\mathcal{L}$ is a self-adjoint transformation.

1.15 Derive the expression for the (extended) Green's function of the sliding string. Use it to derive the solution of (1.1), and check that the obtained expression

(**a**) Satisfies (1.1) if, and only if, $\int_0^l g(x)\,dx = 0$;

(**b**) Has zero slope at both ends;

(**c**) Has zero average value, which makes it acceptable as a "core" solution;

(**d**) Satisfies reciprocity; that is, the condition $G_e(x|x_0) = G_e(x_0|x)$.

1.16 Consider the differential problem

$$\frac{d}{dx}\left[(1-x^2)\frac{dy}{dx}\right] + \lambda y = 0, \qquad -1 \le x \le 1,$$

where y has continuous second derivatives and remains finite at both ends of the interval.

(**a**) Find the Green's function relative to $\lambda = 0$.

(**b**) Find the eigenvalues and eigenfunctions.

1.17 Consider the problem

$$\frac{d^2\phi}{dx^2} + \lambda\phi = f \qquad (\lambda \text{ real positive})$$

$$\phi + j\frac{d\phi}{dx} = 0 \qquad (\text{at } x = 0 \text{ and } x = 1).$$

(**a**) Show that this transformation is self-adjoint with respect to a symmetric inner product.

(**b**) Show that self-adjointness does not hold with respect to a Hilbert inner product, and determine the adjoint transformation for that type of product.

(**c**) Find the eigenfunctions in both cases.

(**d**) Verify the orthogonality properties.

1.18 Check by explicit calculation that the eigenfunctions $\sin(n\pi x/l)$ of the clamped string satisfy (1.83). (Use the expression for $G(x|x')$ given in Equation 1.37.)

1.19 Given the integral equation

$$y(x) + \lambda\int_0^l (x + x')y(x')\,dx' = 0$$

(**a**) Find the two eigenvalues and the two normalized eigenfunctions y_1 and y_2. Check that y_1 and y_2 are orthogonal.

(**b**) Show that the kernel is

$$-\left[\frac{y_1(x)y_1(x')}{\lambda_1}+\frac{y_2(x)y_2(x')}{\lambda_2}\right].$$

(**c**) Show that any function that can be expressed as $\int_0^l (x+x_0)f(x_0)\,dx_0$ is equal to $c_1y_1+c_2y_2$, where c_1 and c_2 are suitable expansion coefficients.

(**d**) Check that any function is equal to its expansion in terms of y_1 and y_2 plus a solution of the homogeneous equation $\int_0^l (x+x_0)f(x_0)\,dx_0 = 0$.

1.20 A heavy circular cylinder (of linear mass ρ kg m^{-1}) rotates with angular velocity Ω (Fig. P1.1). The end points $x = 0$ and $x = l$ remain fixed. In the absence of rotation, the displacement under a unit force in x' is $G(x|x')$, a known function. Derive an integral equation for the displacement from the axis under rotation by equating elastic and centrifugal forces. Show that a (possibly catastrophic) displacement will occur at *discrete* (critical) values of Ω.

1.21 Solve the integral equation

$$f(x) - 2\int_0^1 xf(y)\,dy = x, \qquad 0 \le x \le 1.$$

Show also that there is no solution to the integral equation

$$\int_0^1 (3x^2t + xt^2 + t^3)f(t)\,dt = \sin x, \qquad 0 \le x \le 1.$$

1.22 Consider the integral equation with degenerate kernel

$$f(x) - \lambda\int_0^1 x(x')^2 f(x')\,dx' = \alpha x + \beta. \tag{P1.1}$$

(**a**) Determine the eigenvalues λ_n and eigenfunctions f_n of the operator.

(**b**) Perform the same task for the adjoint kernel, and obtain the h_n eigenfunctions.

(**c**) With $\lambda = \lambda_n$, determine the values of α and β for which (P1.1) has a solution (which is known to be determined to within a multiple of f_n).

(**d**) Assume that the second member is $(4x - 3)$. Determine the core solution of (P1.1) for such a case.

1.23 Determine the eigenvalues and eigenfunctions of the kernel $x^2(3x - 2)$. (Answer: there are none.)

1.24 Consider the differential equation [186]

$$\left(\frac{d^2}{dx^2} - \lambda\right)f = g, \qquad \mathrm{Im}\sqrt{\lambda} < 0$$

over the interval $(-\infty, +\infty)$. The solution f is required to vanish at the (limit) end points $(-\infty)$ and $(+\infty)$.

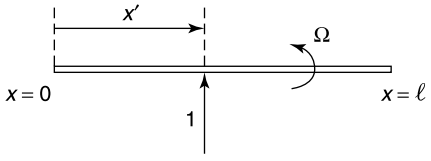

Figure P1.1

(**a**) Show that the Green's function is

$$G(x|x'|\lambda) = -\frac{1}{2j\sqrt{\lambda}}e^{-j\sqrt{\lambda}(x-x')}, \qquad \text{for } x > x'$$
$$= -\frac{1}{2j\sqrt{\lambda}}e^{-j\sqrt{\lambda}(x'-x)}, \qquad \text{for } x < x'.$$

(**b**) Investigate the singularities of $G(x|x'|\lambda)$.

(**c**) Perform the integration (1.105) around $ABCDA$, as in Figure 1.7*b*, and show that the result is

$$\delta(x - x') = \frac{1}{2\pi}\int_{-\infty}^{\infty} e^{jk(x-x')}\, dk,$$

which is the well-known Fourier spectral representation of the δ-distribution.

1.25 Show that the values of a_n that minimize $\| e \|^2$ in (1.111) are the solutions of the system

$$\sum_{n=1}^{N} a_n \langle \mathcal{L}f_n, \mathcal{L}f_i \rangle_H = \langle g, \mathcal{L}f_i \rangle_H.$$

Compare this result with (1.118).

1.26 According to (1.115) the error, which automatically belongs to the range $\mathcal{R}$, is constrained to be the zero element in the subspace of the weighting functions w_i. As $N \to \infty$, the latter must therefore be able to represent any excitation g, which means that the w_i should be in $\mathcal{R}$ for good convergence. If $\mathcal{R}$ is a subspace of $\mathcal{D}$, Galerkin can be used because f_n belongs to $\mathcal{D}$, hence automatically to $\mathcal{R}$. To illustrate the point, consider the problem

$$\frac{df}{dx} = 1, \qquad 0 \le x \le 1$$
$$f = 0, \qquad \text{for } x = 0.$$

(**a**) Determine the adjoint transformation; that is, the operator $\mathcal{L}^a$ and its domain $\mathcal{D}^a$.

(**b**) Choose basis functions $f_n = \sin(n\pi x/2)$ (n odd).

(**c**) First choose $w_m = \cos(m\pi x/2)$ (m odd) as testing functions, and determine the expansion coefficients. Show that this results in a least-squares solution.

(**d**) Apply thereafter the Galerkin method, with $f_n = w_n$, and again determine the expansion coefficients.

(**e**) Plot a few terms in each case, and compare convergence rates. Justify by applying the property that if w_m is not in $\mathcal{D}^a$, it cannot be in $\mathcal{R}$.

(Courtesy of T.P. Sarkar, *IEEE Trans.* **AP-33**, 436–441, 1985.)

1.27 Prove the statements in Section 1.12 concerning eigenvectors and eigenvalues when the inner product is of the Hilbert type. What do these statements become when the inner product is symmetric?

1.28 What is the condition number of the unit matrix $\bar{\bar{I}}$?

1.29 The following problem will give an idea of the sensitivity of solutions to shifts in the value of the matrix elements. The original system is

$$\begin{bmatrix} 1.012671 & 1.446949 \\ 1.446949 & 2.068528 \end{bmatrix} \begin{bmatrix} x_1 \\ x_2 \end{bmatrix} = \begin{bmatrix} 0.006324242 \\ 0.002755853 \end{bmatrix}.$$

Its solution is $(8.4448, -5.9059)$. Where only five significant figures are kept, the problem becomes

$$\begin{bmatrix} 1.0127 & 1.4469 \\ 1.4469 & 2.0685 \end{bmatrix} \begin{bmatrix} x_1 \\ x_2 \end{bmatrix} = \begin{bmatrix} 0.0063242 \\ 0.0027559 \end{bmatrix}.$$

Find the new solution (it is off by some 20%) [157].

1.30 Starting from an initial choice $\mathbf{x}_0$ in (1.129), form successively $\mathbf{y}_0 = \overline{\overline{L}} \cdot \mathbf{x}_0, \mathbf{y}_1 = \overline{\overline{L}} \cdot \mathbf{y}_0$, and so on. Show that, as one proceeds, $\mathbf{y}_n$ becomes proportional to $\mathbf{y}_{n+1}$, and find the proportionality factor [190].

1.31 Verify the various statements in Section 1.13 by considering the simple matrix

$$\overline{\overline{a}}_1 = \begin{pmatrix} 3 & j \\ 2+j & 1 \end{pmatrix}.$$

More specifically, find the eigenvalues and eigenvectors of $\overline{\overline{a}}_1$. Repeat for the adjoint $\overline{\overline{a}}_1^{\dagger}$, and for the Hermitian matrix

$$\overline{\overline{a}}_2 = \begin{pmatrix} 3 & j \\ -j & 1 \end{pmatrix}.$$

1.32 Investigate the properties of eigenvalues and eigenvectors of an antisymmetric matrix, such as

$$\begin{pmatrix} 0 & 1 \\ -1 & 0 \end{pmatrix}.$$

Show that the eigenvalues are imaginary.

1.33 Work out the steps (1.139) and (1.140) for the specific example of the matrix problem (1.138).

NOTES

1. D. G. Dudley, Error minimization and convergence in numerical methods, *Electromagn.* **5**, 89–97 (1985).
2. C. E. Weatherburn, Vector integral equations and Gibbs' dyadics, *Trans Cambridge Phil. Soc.* **22**(8), 133–158 (1916).
3. R. F. Harrington, Matrix methods for field problems, *Proc. IEEE* **55**, 136–149 (1967).
4. R. F. Harrington, Origin and development of the method of moments for field computation; in [208], and also in *IEEE Antennas Prop. Mag.* 31–35 (June 1990).
5. T. Sarkar, A. R. Djordjevic and E. Arvas, On the choice of expansions and weighting functions with numerical solution of operator equations, *IEEE Trans.* **AP-33**, 988–996 (1985).
6. O. Toeplitz, Zur Theorie der quadratischen Formen von unendlichvielen Veränderlichen, *Nachrichten K. Ges. d. Wiss. Göttingen*, *Klasse Math-phys.* **5**, 489–506 (1910).
7. D. H. Preis, The Toeplitz matrix: Its occurrence in antenna problems and a rapid inversion algorithm, *IEEE Trans.* **AP-20**, 204–206 (1972).
8. G. A. Watson, An algorithm for the inversion of block matrices of Toeplitz form, *J. Assoc. Comput. Mach.* **20**, 409–415 (1973).
9. C. Klein and R. Mittra, Stability of matrix equations arising in electromagnetics, *IEEE Trans.* **AP-21**, 902–905 (1973).
10. R. M. Redheffer and R. Steinberg, The Laplacian and mean values, *Quart. Appl. Math.* **9**, 315–317 (1951).
11. F. Rellich, Störungstheorie der Spektralzerlegung, *Math. Ann.* **113**, 600–619 (1936).

Chapter 2

Variational Techniques

The essence of the variational method may be understood by considering a *functional* $J(f)$; that is, an expression that takes a well-defined value for each f belonging to a given family of *admissible* functions. The functional is *stationary* about f_0 when a small variation δf_0 results in a (smaller) variation δJ, of the order $\| \delta f_0 \|^2$ or higher. In a crude quantitative way: An error in f_0 of the order ϵ (say 10%) results, when f_0 is inserted in $J(f)$, in an error on $J(f)$ of the order ϵ^2 (say 1%). Furthermore, stationarity is obtained when f_0 is the solution of $\mathcal{L}f_0 = g$, an equation that is termed *Euler's equation*. Function f_0 is correspondingly called the *Euler function* of $J(f)$.

This very superficial description of the method can nevertheless serve to illustrate the following points:

1. A good approximation for $J(f_0)$ can be obtained by inserting a less accurate approximation for f_0 into $J(f)$. This is important when $J(f_0)$ is a quantity of physical interest, say a scattering cross section. For such a case, $J(f_0)$ is often the main unknown of the problem. An example can be found in Section 5.9.
2. When $J(f)$ reaches a local minimum (or maximum) about f_0, an upper (or lower) bound for $J(f_0)$ results from inserting a trial function "close to f_0" into $J(f)$. It is sometimes even possible to derive complementary variational principles,[1] which together provide both upper and lower bounds for the desired value $F(f_0)$. An example is given in Section 4.2. Such methods were particularly useful before massive computing power became available.
3. In many applications, the goal is to solve $\mathcal{L}(f_0) = g$. The problem can be solved variationally if a functional can be found for which $\mathcal{L}(f_0) = g$ is the Euler equation. The solution then proceeds by inserting a parameter-laden trial f into $J(f)$ and subsequently enforcing the stationary character of $F(f)$. Numerous examples of this procedure are discussed in later chapters.

Electromagnetic Fields, Second Edition, By Jean G. Van Bladel

2.1 STATIONARY FUNCTIONALS

We shall first discuss the stationary properties of a *function* $f(x, y)$. They follow from a consideration of the power expansion of $f(x, y)$ in the vicinity of (x_0, y_0). Thus,

$$f(x,y) = f(x_0,y_0) + (x-x_0)\left(\frac{\partial f}{\partial x}\right)_0 + (y-y_0)\left(\frac{\partial f}{\partial y}\right)_0 + \frac{1}{2}\left[(x-x_0)^2\left(\frac{\partial^2 f}{\partial x^2}\right)_0 + 2(x-x_0)(y-y_0)\left(\frac{\partial^2 f}{\partial x \partial y}\right)_0 + (y-y_0)^2\left(\frac{\partial^2 f}{\partial y^2}\right)_0\right] + \cdots.$$

This function is stationary at (x_0, y_0) when its first-order derivatives vanish at that point. Under these conditions, small changes in the independent variables about the point $x = x_0, y = y_0$ result in small changes of a higher order in the function itself. If these changes are always positive (or negative), the stationary point corresponds with a local minimum (or maximum) of the function. If these changes are of undetermined sign, the stationary point is a saddle point of the function. Distinction among the three cases requires consideration of the second derivatives. Thus, a minimum exists at (x_0, y_0) if the three expressions $\partial^2 f/\partial x^2$, $\partial^2 f/\partial y^2$, and $(\partial^2 f/\partial x^2)\cdot(\partial^2 f/\partial y^2) - (\partial^2 f/\partial x \partial y)^2$ are positive there. The condition for stationarity is more difficult to determine when an auxiliary condition of the form $g(x, y) = 0$ is to be satisfied. In some cases, this condition allows explicit expression of y in terms of x, whereupon $f(x, y)$ becomes a known function of x, whose stationary points can be determined by setting the first derivative with respect to x equal to zero. In other cases, the method of *Lagrange multipliers* must be used. This method consists in evaluating dy/dx in two different ways. First, from $g(x, y) = 0$,

$$\frac{dg}{dx} = \frac{\partial g}{\partial x} + \frac{\partial g}{\partial y}\frac{dy}{dx} = 0.$$

Second, from the condition for the stationarity of $f[x, y(x)]$,

$$\frac{df}{dx} = \frac{\partial f}{\partial x} + \frac{\partial f}{\partial y}\frac{dy}{dx} = 0.$$

By elimination:

$$\frac{\partial f/\partial x}{\partial g/\partial x} = \frac{\partial f/\partial y}{\partial g/\partial y}.$$

This relationship implies the existence of a number λ such that

$$\frac{\partial f}{\partial x} + \lambda\frac{\partial g}{\partial x} = 0 \qquad \frac{\partial f}{\partial y} + \lambda\frac{\partial g}{\partial y} = 0.$$

These are precisely the conditions that the function of three independent variables $f(x, y) + \lambda g(x, y)$ must satisfy to be stationary.

The concept of stationarity can be extended to *functionals* $J(f)$. For instance, a functional has a local *minimum* at f_0 when δJ is positive for all possible variations δf. It should be emphasized that the existence or nonexistence of a minimum (or maximum) depends on the choice of the class of admissible functions. It is known, for example, that none of the

curves with continuous slope that connect A and B and are perpendicular to **AB** at both ends has minimum length, although all lengths have the lower bound $|\mathbf{AB}|$. If the perpendicularity condition is suppressed, a minimum becomes possible and is actually attained for the straight line connecting A to B.

The variation δf must be so chosen that $f_0 + \delta f_0$ remains an admissible function. The form of δf could be the *strong* variation $\delta f = f(\mathbf{r}, \epsilon) - f_0(\mathbf{r})$, where $f(\mathbf{r}, \epsilon)$ is an arbitrary parametric family satisfying the condition $\lim_{\epsilon \to 0}[f(\mathbf{r}, \epsilon)] = f_0(\mathbf{r})$ [22]. Following many authors, we shall only consider the more pragmatic version

$$f(\mathbf{r}) = f_0(\mathbf{r}) + \epsilon \eta(\mathbf{r}) \tag{2.1}$$

where ϵ is a small real parameter, and the η's are admissible functions; that is, functions that belong to the basket admitted for comparison. When the $f(\mathbf{r})$'s are inserted in $J(f)$, the resulting δJ must be of the order ϵ^2 or higher. This *stationarity* condition is not satisfied unless f_0 satisfies an equation of the type $\mathcal{L} f_0 = g$, where $\mathcal{L}$ is an operator that depends on the nature of the functional. The equation $\mathcal{L} f_0 = g$ is the *Euler equation* of the functional. In frequent cases, the Euler equation is insufficient to ensure stationarity, and f_0 is required to satisfy, in addition, some boundary conditions, which are then termed *natural*.

With the type of weak variation used in (2.1), the stationary character of $J(\phi)$ is expressed by the condition

$$\left(\frac{dJ}{d\epsilon}\right)_{\epsilon=0} = 0. \tag{2.2}$$

This condition leads to the relevant Euler equation and the natural boundary conditions.

Euler's equations are *necessary* conditions for the existence of an extremizing function, but it is not evident that they are *sufficient*. In fact, well-known counter examples attest to the contrary. These cases are exceptions, however, and the equivalence of an Euler equation and the variational problem can be assumed in most practical cases.

2.2 A SUITABLE FUNCTIONAL FOR THE STRING PROBLEM

To investigate in more detail the mechanics of the variational method, let us determine the Euler equation of the functional

$$J(y) = \int_0^l \left[\frac{T}{2}\left(\frac{dy}{dx}\right)^2 - g(x)y\right] dx, \tag{2.3}$$

where $g(x)$ is piecewise continuous, and the admissible functions are required to have piecewise continuous second derivatives. Inserting (2.1) into (2.3) gives

$$J(y) = \int_0^l \left[\frac{T}{2}\left(\frac{dy_0}{dx}\right)^2 - g(x)y_0\right] dx + \epsilon \int_0^l \left[T\frac{dy_0}{dx}\frac{d\eta}{dx} - g(x)\eta\right] dx + \epsilon^2 \int_0^l \frac{T}{2}\left(\frac{d\eta}{dx}\right)^2 dx.$$

The coefficient of ϵ should be set equal to zero. Because of the continuity properties of the admissible functions, this coefficient can be transformed as follows:

$$\left[T\eta\frac{dy_0}{dx}\right]_0^l - \int_0^l \eta\left[\frac{d}{dx}\left(T\frac{dy_0}{dx}\right) + g(x)\right]dx = 0. \tag{2.4}$$

If the behavior of $y(x)$ at the end points is left unspecified, stationarity will only be obtained for a y_0 satisfying

$$\frac{dy_0}{dx} = 0 \quad \text{at } x = 0, x = l. \tag{2.5}$$

Such a boundary condition is termed *natural*. Because the integral in (2.4) must vanish for all η's, the term between square brackets should vanish, otherwise one could always find an η for which the integral differs from zero. A *fundamental lemma* should really be invoked to support this simple argument, but for all practical purposes we have found the pertinent Euler equation in the form

$$\frac{d}{dx}\left[T\frac{dy_0}{dx}\right] = -g(x). \tag{2.6}$$

The search for $y_0(x)$ now reduces to the solution of the sliding string problem of Chapter 1, and both the stationarity condition and the condition for solvability of the differential equation require the average value of $g(x)$ to be zero. No Euler function exists if this condition is not satisfied.

It is important to note that not all problems generate natural boundary conditions. If the admissible functions for functional (2.3) are chosen to vanish at $x = 0$ and $x = l$, so that $\eta(x)$ vanishes there, too, all preceding steps can be retraced, but the condition at the end points disappears because the first square bracket in the left-hand term of (2.4) is automatically zero. In this case, the Euler function is the displacement of the clamped string, and an extremum exists for all piecewise continuous $g(x)$.

It is also important to know whether a functional $J(f)$ has a local extremum around f_0 or whether the equivalent of a saddle point exists. The answer is obtained by examining the expansion of $J(\epsilon)$ in powers of ϵ:

$$J(\epsilon) = J(0) + \frac{\epsilon^2}{2!}J''(0) + \ldots,$$

where the term in ϵ is absent because of the stationarity condition. It is clear that a minimum, for example, exists when $J''(0)$ is positive, a condition that is clearly satisfied in the case of the string.

The functions that were admitted for insertion in (2.3) had piecewise continuous second derivatives. It should be noted, however, that the second derivative does *not* appear in the functional, and that the latter has a perfectly well-defined value for functions with a piecewise continuous *first* derivative, such as the piecewise linear approximations 1 and 2 shown in Figure 2.1. These functions are suitable trial functions for the clamped string functional (2.3), in which we set $g(x) = T = 1$, to obtain

$$J(y) = \int_0^1 \left[\frac{1}{2}\left(\frac{dy}{dx}\right)^2 - y\right]dx. \tag{2.7}$$

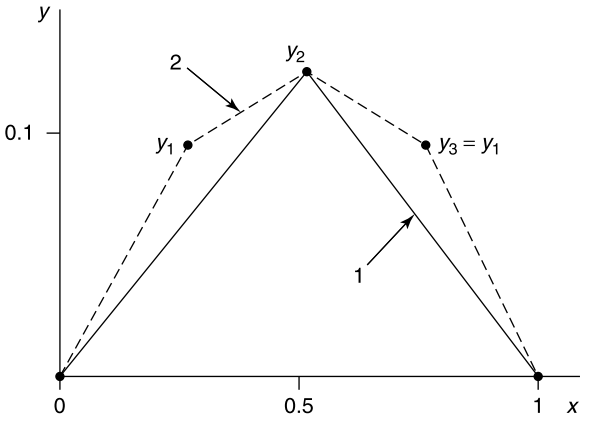

Figure 2.1 Linear approximations.

The sought Euler solution is $y_0 = \frac{1}{2}x(1-x)$. Inserting approximation 1 into (2.7) gives $J(y) = 2y_2^2 - \frac{1}{2}y_2$, and the stationarity condition $(\partial J/\partial y_2) = 0$ yields $y_2 = \frac{1}{8}$, the correct value. Repeating with approximation 2 produces values of y_1 and y_2, which again happen to be the correct ones. It will be noted that both trial functions have infinite second derivatives at the junction points. By considering them for insertion in (2.3), we have vastly broadened the supply of trial functions, a definite advantage from a numerical point of view. The danger, however, is that stationarity might be found for functions that are *not* admissible (i.e., which do not have a continuous *second* derivative). A more thorough theory, however, shows that the broader class of admissible functions nevertheless leads to stationarity for, and only for, a function of the narrower class (i.e., one having a piecewise *second* derivative). This statement, proved by Du Bois-Reymond, implies that the string problem may be solved by means of (2.3), a functional in which only first derivatives appear. It is clear that a considerable gain in numerical flexibility has been achieved. It should be remarked that the policy of eliminating higher derivatives is common to several numerical methods, a point that is clarified in later chapters.

2.3 FUNCTIONALS FOR THE GENERAL $\mathcal{L}$ TRANSFORMATION

Assume first that the transformation is self-adjoint with respect to a *symmetric* inner product. For such a case, a relevant functional is

$$J_1(f) = 2\langle f, g\rangle_S - \langle f, \mathcal{L}f\rangle_S . \tag{2.8}$$

We go once more through the steps outlined in the previous sections and set $f = f_0 + \epsilon\eta$. This gives

$$J_1(f) = 2\langle f_0, g\rangle_S - \langle f_0, \mathcal{L}f_0\rangle_S + \epsilon\left[2\langle \eta, g\rangle_S - \langle f_0, \mathcal{L}\eta\rangle_S - \langle \eta, \mathcal{L}f_0\rangle_S\right] - \epsilon^2\langle \eta, \mathcal{L}\eta\rangle_S . \tag{2.9}$$

Setting the term in ϵ equal to zero yields

$$2\langle \eta, g\rangle_S - \langle \mathcal{L}f_0, \eta\rangle_S - \langle \eta, \mathcal{L}f_0\rangle_S = 2\left[\langle \eta, (g - \mathcal{L}f_0)\rangle_S\right] = 0.$$

For this to hold for all η's belonging to $\mathcal{D}$ implies $\mathcal{L}f_0 = g$, the sought Euler equation. If, in addition, the transformation is positive-definite, the term in ϵ^2 in (2.9) is negative, and the stationary value $J_1(f_0) = \langle f_0, g\rangle$ corresponds with a maximum.

Applied to the transformation of the clamped string, (2.8) yields the already obtained functional

$$J_1(y) = 2\int_0^l y\left(-\frac{g}{T}\right)dx - \int_0^l y\frac{d^2y}{dx^2}dx = \frac{2}{T}\int_0^l \left[\frac{T}{2}\left(\frac{dy}{dx}\right)^2 - gy\right]dx.$$

Another functional that is made stationary by f is

$$J_2(f) = \frac{\langle \mathcal{L}f, f\rangle_S}{\langle f, g\rangle_S^2}. \tag{2.10}$$

Here, Euler's equation is actually $\mathcal{L}f = \lambda g$, where λ is an arbitrary constant. The form of this equation implies that the Euler function is determined to within a multiplicative constant. The value of J_2, however, is independent of that factor, and the accuracy of J_2 for a given trial function is therefore independent of the scale of the function f. The property is of importance for problems in which the stationary value of J_2 is a quantity of physical interest.

Let us next assume that self-adjointness holds with respect to a *Hilbert* inner product. The relevant functional is now

$$J_3(f) = \langle f,\, g\rangle_H + \langle g, f\rangle_H - \langle \mathcal{L}f, f\rangle_H. \tag{2.11}$$

The usual procedure leads to

$$\langle \eta, (g - \mathcal{L}f_0)\rangle_H + \langle (g - \mathcal{L}f_0), \eta\rangle_H = 2Re\,\langle \eta, (g - \mathcal{L}f_0)\rangle_H = 0,$$

and the condition for this to hold for all admissible η's is $\mathcal{L}f_0 = g$.

When the transformation is not self-adjoint (a situation that occurs, for example, when odd-order derivatives are present in $\mathcal{L}$, such as in dissipative systems), the pertinent functional becomes [183]

$$J_4(f, h) = \langle f, s\rangle + \langle g, h\rangle - \langle \mathcal{L}f, h\rangle. \tag{2.12}$$

In this expression, the nature of the scalar product is left unspecified (the choice will only influence the form of the adjoint transformation). The variable functions are f and h, and we determine the Euler equations by setting

$$\begin{aligned} f &= f_0 + \epsilon_1\eta_1 + \epsilon_1^2\mu_1 + \ldots \\ h &= h_0 + \epsilon_2\eta_2 + \epsilon_2^2\mu_2 + \ldots, \end{aligned}$$

where ϵ_1 and ϵ_2 are independent, small real parameters. Inserting in (2.12) gives

$$\begin{aligned} J_4(f, h) = \langle f_0, s\rangle + \langle g, h_0\rangle - \langle \mathcal{L}f_0, h_0\rangle + \epsilon_1\left\langle \eta_1, (s - \mathcal{L}^a h_0)\right\rangle \\ + \epsilon_2\,\langle (g - \mathcal{L}f_0), \eta_2\rangle - \epsilon_1\epsilon_2\,\langle \mathcal{L}\eta_1, \eta_2\rangle - \epsilon_1^2\,\langle \mathcal{L}\mu_1, h_0\rangle - \epsilon_2^2\,\langle \mathcal{L}f_0, \mu_2\rangle. \end{aligned}$$

Setting the coefficients of ϵ_1 and ϵ_2 equal to zero produces the Euler equations

$$\begin{aligned} \mathcal{L}f_0 &= g \\ \mathcal{L}^a h_0 &= s. \end{aligned} \tag{2.13}$$

Stationarity is achieved when f and h are close to f_0 and h_0. In that vicinity,

$$J_4(f,h) = \langle f_0, s\rangle - \epsilon_1\epsilon_2 \langle \mathcal{L}\eta_1, \eta_2\rangle - \epsilon_1^2 \langle \mathcal{L}\mu_1, h_0\rangle - \epsilon_2^2 \langle g, \mu_2\rangle + \ldots.$$

No general conclusions can be drawn concerning the existence of a maximum, a minimum, or a saddle point. Corresponding with (2.10) we now find

$$J_5(f,h) = \frac{\langle \mathcal{L}f, h\rangle}{\langle f, s\rangle \langle g, h\rangle}. \tag{2.14}$$

The condition $y = 0$ at the end points makes the transformation of the clamped string self-adjoint. The same would hold for other homogeneous conditions such as $y' = 0$ or, more generally, $y' + \lambda y = 0$. But self-adjointness disappears when an inhomogeneous condition such as $y = 1$ at $x = 0$ is imposed, which implies that (2.8), for example, loses its relevance. An obvious way out is to find a function u that satisfies the inhomogeneous condition and replace f by $(f - u)$, an element that now belongs to $\mathcal{D}$ and may validly be inserted in a functional such as (2.10). To find a suitable u is easy enough in one dimension (see Problem 2.5). But in a higher-dimensional space, the boundaries may be too irregular to allow a simple analytic continuation of f from boundary to main volume. An alternative method is to switch to a functional in which the boundary conditions are automatically incorporated. In two dimensions this could be, for example (Fig. 2.2),

$$J(\phi) = \int_S \left[\frac{1}{2}|\text{grad } \phi|^2 - \phi\right] dS + \frac{1}{2}\lambda \int_C (\phi - g)^2 dc. \tag{2.15}$$

Inserting $\phi = \phi_0 + \epsilon\eta$ in (2.15) and setting the coefficient of ϵ equal to zero gives

$$\int_S \eta(-\nabla^2\phi_0 - 1)\, dS + \int_C \eta\left[\frac{\partial\phi_0}{\partial n} + \lambda(\phi_0 - g)\right] dc = 0$$

from which we obtain

$$\nabla^2\phi_0 = -1$$

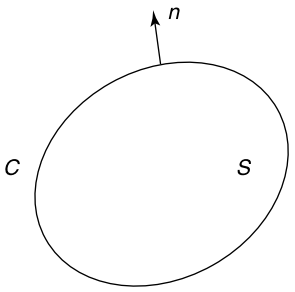

Figure 2.2 A bounded domain in the plane.

together with the natural boundary condition

$$\lambda\phi_0 + \frac{\partial\phi_0}{\partial n} = \lambda g.$$

2.4 EULER'S EQUATIONS OF SOME IMPORTANT FUNCTIONALS

2.4.1 Functionals for the Eigenvalue Problem

We shall only discuss the simple example of a self-adjoint transformation with respect to a symmetric inner product. A relevant functional is

$$J(f) = \frac{\langle \mathcal{L}f, f\rangle_S}{\langle f, f\rangle_S}. \tag{2.16}$$

$J(f)$ is easily shown to be stationary about the eigenfunctions of $\mathcal{L}$, and the stationary values are the corresponding eigenvalues. More can be said when the (normalized) eigenfunctions f_n form a complete set. For such a case, consider an arbitrary trial function f, whose expansion in terms of the f_n's is $f = \sum a_n f_n$. If this function is in the domain of $\mathcal{L}$, the rules given in Section 1.7 imply that $\mathcal{L}f = \sum a_n \mathcal{L}f_n$, whence it follows that

$$J(f) = \frac{\lambda_1 a_1^2 + \lambda_2 a_2^2 + \dots}{a_1^2 + a_2^2 + \dots}. \tag{2.17}$$

In most problems of interest in this book, the λ_n's approach $+\infty$ or $-\infty$ as $n \to \infty$. It is always possible to choose the sign of $\mathcal{L}$ to ensure an approach to $+\infty$, in which case only a finite number of eigenvalues are negative. For a positive-definite transformation, in particular, all λ_n's are positive. Under these conditions, (2.17) shows that $J(f)$ reaches an absolute minimum, equal to the lowest eigenvalue λ_1, when f is a multiple of the lowest eigenfunction f_1. Equivalently, an upper bound for λ_1 is obtained when an arbitrary admissible function is inserted in $J(f)$.

To apply these considerations to the clamped string, we must change the sign of the operator, using $-d^2/dx^2$ instead of d^2/dx^2. The transformation is now positive-definite, and functional (2.16) takes the form

$$J(y) = -\frac{\displaystyle\int_0^l y(d^2y/dx^2)\,dx}{\displaystyle\int_0^l y^2 dx} = \frac{\displaystyle\int_0^l (dy/dx)^2\,dx}{\displaystyle\int_0^l y^2 dx}. \tag{2.18}$$

To obtain an upper bound for λ_1, we use the trial function $x(l-x)$, which is an admissible function because it vanishes at both ends of the interval $(0, l)$ and has a piecewise-continuous second derivative. The corresponding value of $J(y)$ is $10/l^2$. This is only slightly higher than the exact value $\pi^2/l^2 = 9.869/l^2$. This excellent agreement is due to the fortunate choice of the trial function, which is almost proportional to the lowest normalized eigenfunction $(2/l)^{\frac{1}{2}} \sin(\pi x/l)$.

The usefulness of functional (2.17) is not limited to the calculation of the *lowest* eigenvalue. If admissible functions orthogonal to f_1 can be found, the coefficient a_1 vanishes, and

the minimum of J for these functions becomes equal to λ_2, the second-lowest eigenfunction. More generally, admissible functions orthogonal to the $(n-1)$ lowest eigenfunctions yield upper bounds for the nth eigenvalue λ_n. Actual use of the method hinges on a knowledge of these eigenfunctions. This requirement can often be bypassed when special symmetry properties exist. The lowest eigenfunction of the clamped string, for example, is symmetric with respect to $x = l/2$; hence all antisymmetric functions are automatically orthogonal to it and can be used to obtain an upper limit for λ_2.

2.4.2 Integral Equations as Euler's Equations

Consider the functional

$$J(\phi) = \int_V \phi(\mathbf{r})\, dV \int_V K(\mathbf{r}|\mathbf{r}_0)\phi(\mathbf{r}_0)\, dV_0 + \int_V \phi^2(\mathbf{r})\, dV - 2\int_V \phi(\mathbf{r}) f(\mathbf{r})\, dV \tag{2.19}$$

where $K(\mathbf{r}|\mathbf{r}_0)$ is a summable *symmetric* kernel. The first variation is obtained by setting $\phi = \phi_0 + \epsilon\eta$. Thus,

$$\begin{aligned}\delta J = \epsilon \Bigg[&\int_V \eta(\mathbf{r})\, dV \int_V K(\mathbf{r}|\mathbf{r}_0)\phi_0(\mathbf{r}_0)\, dV_0 \\ &+ \int_V \phi_0(\mathbf{r})\, dV \int_V \eta(\mathbf{r}_0)K(\mathbf{r}|\mathbf{r}_0)\, dV_0 + 2\int_V \phi_0(\mathbf{r})\eta(\mathbf{r})\, dV - 2\int_V \eta(\mathbf{r}) f(\mathbf{r})\, dV \Bigg] \\ &+ \epsilon^2 \left[\int_V \eta(\mathbf{r})\, dV \int_V \eta(\mathbf{r}_0)K(\mathbf{r}|\mathbf{r}_0)\, dV_0 + \int_V \eta^2(\mathbf{r})\, dV \right] + \ldots .\end{aligned}$$

Interchanging the order of integrations leads to the Euler equation

$$\phi_0(\mathbf{r}) + \int_V K(\mathbf{r}|\mathbf{r}_0)\phi_0(\mathbf{r}_0)\, dV_0 = f(\mathbf{r})$$

which is an integral equation of the second kind. We note that a local minimum is obtained when

$$\int_V \phi(\mathbf{r})\, dV \int_V K(\mathbf{r}|\mathbf{r}_0)\phi(\mathbf{r}_0)\, dV_0$$

is positive for all ϕ's. A *kernel* for which this is true is termed *positive-definite*.

By similar methods, it is easy to show that the integral equation of the first kind

$$\int_V \phi(\mathbf{r}_0)K(\mathbf{r}|\mathbf{r}_0)\, dV = f(\mathbf{r}),$$

is the Euler equation of the functionals

$$J_1(\phi) = \int_V \phi(\mathbf{r})\, dV \int_V \phi(\mathbf{r}_0)K(\mathbf{r}|\mathbf{r}_0)\, dV_0 - 2\int_V f(\mathbf{r})\phi(\mathbf{r})\, dV \tag{2.20}$$

and

$$J_2(\phi) = \int_V \phi(\mathbf{r})\, dV \int_V K(\mathbf{r}|\mathbf{r}_0)\phi(\mathbf{r}_0)\, dV_0, \tag{2.21}$$

where $\phi(\mathbf{r})$ in (2.21) is required to satisfy the auxiliary condition

$$A(\phi) = \int_V \phi(\mathbf{r}) f(\mathbf{r})\, dV = 1.$$

Such a variational principle is termed *constrained*, a concept already discussed in Section 2.1 for a *function* [178]. To determine its Euler equation, we set $\phi = \phi_0 + \epsilon\eta$ in the functional and the auxiliary condition. The condition $(dJ_2/d\epsilon)_{\epsilon=0} = 0$ gives

$$\int_V \eta(\mathbf{r})\, dV \int_V \phi_0(\mathbf{r}_0) K(\mathbf{r}|\mathbf{r}_0)\, dV_0 = \int_V \eta(\mathbf{r}) g(\mathbf{r})\, dV = 0. \tag{2.22}$$

This relationship must be satisfied for all $\eta(\mathbf{r})$ subject to the auxiliary condition

$$\int_V \eta(\mathbf{r}) f(\mathbf{r})\, dV = 0. \tag{2.23}$$

Let us show that $g(\mathbf{r})$ is proportional to $f(\mathbf{r})$ under those circumstances. As a possible $\eta(\mathbf{r})$ we select $g(\mathbf{r}) - \alpha f(\mathbf{r})$, an acceptable choice if we require α to satisfy

$$\int_V [g(\mathbf{r}) - \alpha f(\mathbf{r})] f(\mathbf{r})\, dV = 0.$$

This condition determines α uniquely. Combining now (2.22) with (2.23) leads to the requirement

$$\int_V \eta(\mathbf{r})[g(\mathbf{r}) - \alpha f(\mathbf{r})]\, dV = 0,$$

which must be satisfied by all admissible functions. Substituting $\eta(\mathbf{r}) = g(\mathbf{r}) - \alpha f(\mathbf{r})$ in that equation yields

$$\int_V [g(\mathbf{r}) - \alpha f(\mathbf{r})]^2\, dV = 0,$$

which implies that the bracketed term is zero; that is, that $g(\mathbf{r})$ and $f(\mathbf{r})$ are proportional to each other. Euler's equation is finally obtained in the form

$$g(\mathbf{r}) = \int_V K(\mathbf{r}_0|\mathbf{r}) \phi_0(\mathbf{r}_0)\, dV_0 = \alpha f(\mathbf{r}), \tag{2.24}$$

where α is a constant to be determined by the condition $A(\phi_0) = 1$.

The preceding developments are based on symmetric inner products and kernels. They can be extended to Hilbert inner products and Hermitian kernels, using general functionals such as (2.11).

2.5 DISCRETIZATION OF THE TRIAL FUNCTIONS

The stationary values of a functional can be determined, in principle at least, by inserting an infinite number of admissible functions into $J(f)$ and observing the behavior of the functional in the vicinity of each trial function. Ideally, the total supply of admissible

functions should be exhausted in the process. The *Rayleigh-Ritz method* achieves this goal by using a complete set of admissible functions f_n, termed *coordinate functions*, and expanding the trial function in terms of the f_n as

$$f = a_1 f_1 + a_2 f_2 + \ldots + a_n f_n + \ldots. \tag{2.25}$$

The stationarity problem for $J(\phi)$ with respect to weak variations $\epsilon\eta(\mathbf{r})$ can now be replaced by an analogous problem for $J(a_1 f_1 + \ldots + a_n f_n + \ldots)$ with respect to small variations in the values of the a's. The pertinent values of a_i are the solutions of the equations $\partial J/\partial a_i = 0$. In practice, the infinite sum is replaced by the first N terms of the expansion, and it is assumed that the function formed with the *best* coefficients a_i will ultimately converge to f_0 as N increases. Presumably, a good approximation to f_0 is obtained when a sufficiently large number of terms is used. It is to be noted in that respect that there is a limit to the additional accuracy that can be obtained by increasing N. It is found, indeed, that an increase in N also increases the round-off errors introduced by the algorithm, to the effect that accuracy is lost beyond a certain value of N. Note also that the speed of convergence to the actual Euler function depends on a good choice of the coordinate functions (power series, Fourier series, etc.). Many delicate points are involved in the evaluation of the errors caused by keeping N finite.

As an illustration, consider determination of the stationary value of the already discussed functional

$$J(y) = \int_0^1 \left[\frac{1}{2}\left(\frac{dy}{dx}\right)^2 - y \right] dx, \tag{2.26}$$

where $y(x)$ is restricted to vanish at $x = 0$ and $x = 1$. The Fourier series $\sin n\pi x$ forms a suitable set of coordinate functions. Using a single term $a_1 \sin \pi x$ we obtain, from the condition $\partial J/\partial a_1 = 0$, the value $a_1 = 4/\pi^3$ as the "best" value of a_1. With two terms, $a_1 \sin \pi x + a_2 \sin 2\pi x$, the conditions $\partial J/\partial a_1 = 0$ and $\partial J/\partial a_2 = 0$ give $a_1 = 4/\pi^3$ and $a_2 = 0$. With three terms, the best function turns out to be $(4/\pi^3) \sin \pi x + (4/27\pi^3) \sin 3\pi x$. A direct evaluation of the quality of the approximation is possible in this case because the Euler equation $d^2y/dx^2 = -1$ can be solved explicitly. The solution is $y(x) = x(1-x)/2$, and the best function $(4/\pi^3) \sin \pi x + (4/27\pi^3) \sin 3\pi x$ turns out to represent the first two terms of the Fourier expansion of the solution.

The method that consists in optimizing a trial function by loading it with undetermined parameters is very general and is not tied to the knowledge of a set of coordinate functions. The parameters can even appear in nonlinear fashion, as in $\cos x - \sin ax$. The best values are again determined by the conditions $\partial J/\partial a_i = 0$.

Let us apply the Rayleigh-Ritz method to functional (2.8), the Euler equation of which is $\mathcal{L}f = g$. Insertion of series (2.25) into (2.8) gives

$$J(f) = 2\sum_{n=1}^{N} a_n \langle f_n, g\rangle_S - \left\langle \sum_{n=1}^{N} a_n \mathcal{L} f_n, \sum_{m=1}^{N} a_m f_m \right\rangle_S.$$

The a_n coefficients are obtained through relationships of the kind

$$\frac{\partial J}{\partial a_n} = 2\langle f_n, g\rangle_S - 2\sum_{m=1}^{N} a_m \langle \mathcal{L} f_n, f_m\rangle = 0. \tag{2.27}$$

A look at (1.112) shows that the variational procedure has produced *exactly the same equations as the method of moments* in its Galerkin version, a point that caught earlier users of these methods by surprise.[2] An important advantage of the variational process, however, is that it delivers a stationary value for the functional (and often an upper or a lower bound for the latter). But an even more important feature, already mentioned in Section 2.2, is that functionals can be found that involve lower-order derivatives than the original $\mathcal{L}$ operator and therefore allow a greater choice of admissible functions. The example embodied in Figure 2.1 illustrates the point.

The argumentation presented above for a self-adjoint transformation can be extended to the more general case, for which the functionals (2.11) or (2.12) are appropriate. Two trial functions are now required, and we expand them as

$$f = \sum_{n=1}^{N} a_n f_n$$
$$h = \sum_{n=1}^{N} c_n h_n. \tag{2.28}$$

Assume a symmetric inner product, for example, and let $\mathcal{L}^a$ be the adjoint transformation. Inserting the series into (2.12) gives

$$J_4(f,h) = \sum_{n=1}^{N} a_n \langle f_n, s\rangle_S + \sum_{n=1}^{N} c_n \langle g, h_n\rangle_S - \sum_{n,m=1}^{N} a_n c_m \langle \mathcal{L}f_n, h_m\rangle_S.$$

Setting the partial derivatives with respect to a_n and c_n equal to zero yields

$$\sum_{m=1}^{N} c_m \langle \mathcal{L}f_n, h_m\rangle_S = \sum_{m=1}^{N} c_m \left\langle f_n, \mathcal{L}^a h_m\right\rangle_S = \langle f_n, s\rangle_S \quad (n = 1,\ldots,N)$$
$$\sum_{m=1}^{N} a_m \langle \mathcal{L}f_m, h_n\rangle_S = \sum_{m=1}^{N} a_m \left\langle f_m, \mathcal{L}^a h_n\right\rangle_S = \langle g, h_n\rangle_S. \tag{2.29}$$

These equations are precisely those generated by the method of moments when applied to $\mathcal{L}f = g$ (with h_n as testing function) and $\mathcal{L}^a h = s$ (with f_n as testing function).

2.6 SIMPLE FINITE ELEMENTS FOR PLANAR PROBLEMS

Trial functions that are defined over the complete simulation domain are difficult to express in closed analytical form when the area under consideration is of a complex shape. In exceptional cases, for example in a rectangle with sides parallel to the x and y axes, entire domain functions can be found in the form of double Fourier series, or series involving Bessel functions, Legendre polynomials, or Hermite polynomials [163]. But much greater suppleness is afforded by the subdivision of the surface* of interest into *small elements*,

*The extension of the finite element concept to three dimensions and vector fields is discussed in the next section and in Chapters 6 and 10.

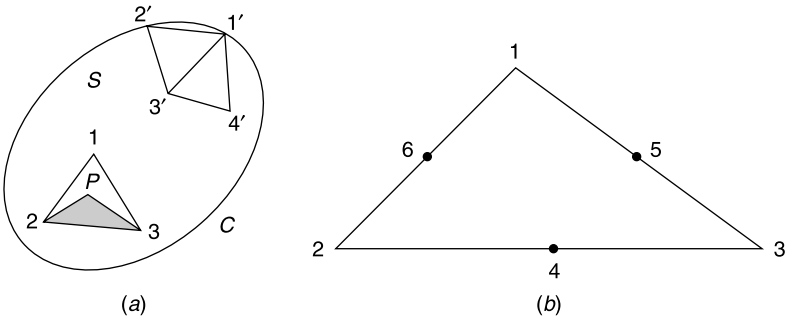

Figure 2.3 (*a*) Triangular elements. (*b*) Nodal points for a quadratic basis function.

a method first proposed in the early 1940s,[3] and which soon became popular in structural mechanics, particularly in aircraft design.

Fundamentally, a given area S is divided into a collection of simple subdomains, connected together at a number of *nodal points*. A typical element is the triangle 1–2–3 shown in Figure 2.3*a*. Irregular boundaries can easily be followed with such elements. In each element, a simple basis function is chosen, for example a linear function of the (x, y) coordinates. Thus, in triangle 1–2–3,

$$\phi = \phi_1 L_1(x, y) + \phi_2 L_2(x, y) + \phi_3 L_3(x, y). \tag{2.30}$$

In this expression $L_i(x, y)$ is a linear *shape function*, equal to one at node i and to zero at the other two nodes. It is clear that ϕ, as expressed by (2.30), varies linearly alongside 1–2. We may therefore conclude that the ϕ's are *continuous* across triangle boundaries, whereas their normal derivatives are not automatically so.

To express the (linear) shape functions analytically, we write

$$L_i(x, y) = a_i + b_i x + c_i y. \tag{2.31}$$

With indices that cycle between 1, 2, and 3:

$$\begin{aligned} a_i &= \frac{x_{i+1}y_{i+2} - x_{i+2}y_{i+1}}{2\Delta} \\ b_i &= \frac{y_{i+1} - y_{i+2}}{2\Delta} \\ c_i &= \frac{x_{i+2} - x_{i+1}}{2\Delta}. \end{aligned} \tag{2.32}$$

Δ is the area of the triangle 1–2–3, given by

$$\Delta = \frac{1}{2}\left[(x_1y_2 - x_2y_1) + (x_3y_1 - x_1y_3) + (x_2y_3 - x_3y_2)\right]. \tag{2.33}$$

It is clear that L_1, at p is the ratio of the area of the shaded triangle in Figure 2.3*a* to the total area Δ of the triangle.

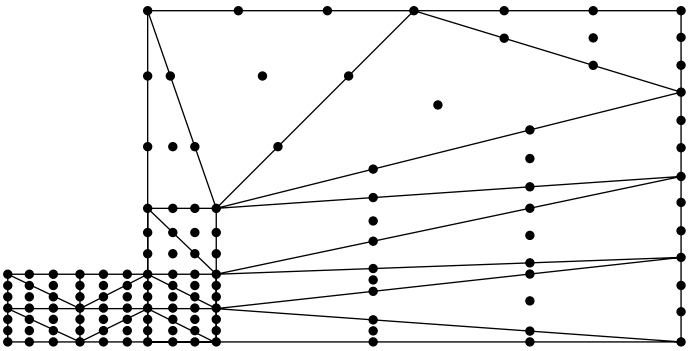

Figure 2.4 Subdivision of an area into triangular elements.

If we were to plot the surface $z = \phi(x, y)$ in three-dimensional space, basis functions of type (2.30) would generate an ensemble of joining triangles, which constitute an approximation to the exact surface generated by the correct function ϕ. A better match would result from the use of higher-order shape functions, such as the quadratic form

$$\phi = L_1(2L_1 - 1)\phi_1 + L_2(2L_2 - 1)\phi_2 + L_3(2L_3 - 1)\phi_3 + 4L_1L_2\phi_4 + 4L_2L_3\phi_5 + 4L_3L_1\phi_6. \tag{2.34}$$

Here, the 4, 5, 6 nodes are the midpoints of their respective sides (Fig. 2.3*b*). The improved accuracy obtained in the triangle itself makes it possible to either reduce the total number of triangles for a given *total* accuracy or to keep the number of triangles and increase accuracy. Higher-order elements have their advantages, but they also generate denser matrices, with in general a higher condition number. These elements also lead to more complex interaction integrals. The choice, which is a matter of compromise,[†] should also take into account the added programming complexity associated with higher-order functions [181, 183, 199, 206, 211].

Figure 2.4 shows a net based on cubic shape functions (with nine reference points per triangle). The net covers one quarter of the cross-section of a ridge waveguide. We notice that it is particularly dense in the region where the unknown is expected to vary rapidly.

A representation such as (2.30) is often used, as a trial function, in conjunction with a variational principle. The nodal values ϕ_i become the variable parameters, which must subsequently be optimized by the condition $\partial J/\partial\phi_i = 0$. The method has already been applied in Section 2.2, where the ϕ_i's in functional (2.7) are the coordinates y_1, y_2, y_3 shown in Figure 2.1, and the linear segments between vertices represent the *one-dimensional* equivalent of (2.30). We now extend our analysis to a *two-dimensional* example, centered on the functional

$$J(f) = \int_S \left\{ \frac{1}{2}\left[\left(\frac{\partial f}{\partial x}\right)^2 + \left(\frac{\partial f}{\partial y}\right)^2 \right] + fg \right\} dS, \tag{2.35}$$

where f is required to vanish on C (Fig. 2.3*a*). The Euler equation is Poisson's equation

$$\nabla^2 f = g.$$

[†]These topics, which are of great importance in numerical analysis, are beyond the pale of this book. The choice between elements remains a subject of lively interest in the current literature.

Let us insert trial functions of type (2.30) into the functional. The partial triangle 1–2–3 contributes

$$J_{123}(f) = \int_{123} \left[\frac{1}{2} (\phi_1 \text{ grad } L_1 + \phi_2 \text{ grad } L_2 + \phi_3 \text{ grad } L_3)^2 + (\phi_1 L_1 + \phi_2 L_2 + \phi_3 L_3) g \right] dS.$$

Enforcing the condition $\partial J / \partial \phi_1 = 0$ in that particular triangle gives

$$\begin{aligned} \frac{\partial J}{\partial \phi_1} &= \phi_1 \int_S (\text{grad } L_1)^2 dS + \phi_2 \int_S \text{grad } L_1 \cdot \text{grad } L_2 \, dS \\ &\quad + \phi_3 \int_S \text{grad } L_1 \cdot \text{grad } L_3 \, dS + \int g L_1 \, dS \\ &= \phi_1 C_{11} + \phi_2 C_{12} + \phi_3 C_{13} - g_1 = 0. \end{aligned} \tag{2.36}$$

Similar relationships may be written for ϕ_2 and ϕ_3. Together they define the *partial stiffness matrix* C_{mn} of the triangle, whose elements may be obtained by performing a few simple integrations. In a final step, all the partial contributions are added together, and a *global stiffness matrix* emerges. In evaluating the contribution from the outer triangles, one should remember that the nodes located at the boundary (e.g., $1'$ and $2'$ in Fig. 2.3*a*), are not free, but fixed, as the boundary condition leads to the requirement $\phi_{1'} = \phi_{2'} = 0$.

It is important to note that the global stiffness matrix C is *sparse*, as a node with value ϕ_i is part of only a small number of triangles and is therefore connected to only a small number of other nodes. It follows that only a few C_{in} differ from zero. In addition, the $\overline{\overline{C}}$ matrix can also be put in *banded* form. Random numbering of nodes will not achieve this goal, hence renumbering will be necessary, for which a number of specific methods exist [44, 205]. Ultimately, most nonzero elements will be concentrated in as narrow a band as possible, symmetrically distributed with respect to the main diagonal [189, 205]. We are finally confronted with the solution of a matrix problem of the form

$$\overline{\overline{C}} \cdot \boldsymbol{\phi} = \mathbf{g}, \tag{2.37}$$

which can be solved by the methods described in Sections 2.8 and 2.9 [192]. The solution gives only discrete values of the unknown function ϕ, namely those at the nodes. Some additional programming will be necessary to interpolate between these values (e.g., with the help of splines).

2.7 MORE FINITE ELEMENTS

The triangle is not the only shape suitable for the subdivision of an area into elements: the rectangle and the quadrilateral, with appropriate basis functions, are other possibilities. An often used basis function for the rectangle in Figure 2.5 is [182, 192]

$$\phi = \phi_1 \left(1 - \frac{x}{a}\right)\left(1 - \frac{y}{b}\right) + \phi_2 \frac{x}{a}\left(1 - \frac{y}{b}\right) + \phi_3 \frac{x}{a}\frac{y}{b} + \phi_4 \left(1 - \frac{x}{a}\right)\frac{y}{b}. \tag{2.38}$$

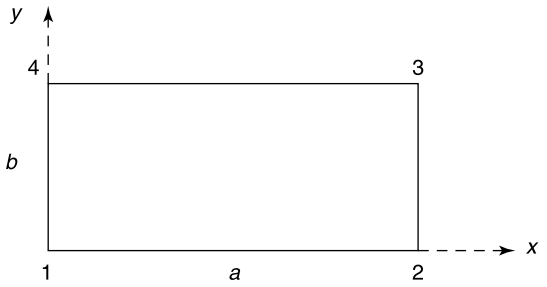

Figure 2.5 Rectangular element.

Rectangular and triangular elements can be used not only within the area of interest but also in contact with a boundary such as C in Figure 2.3*a*. Because straight segments (say $1'$ $2'$) may be too rough an approximation in following the curve, *curved* elements are often preferred. These can be synthesized by means of coordinate transformations based on *local coordinates* (u, v), which in Figure 2.6*a* range from (-1) to $(+1)$ [163, 182, 193, 203, 207]. The *global coordinates* (x, y) are expressed in terms of the (u, v) by relationships of the form

$$x = \sum_{i=1}^{8} x_i \alpha_i(u, v)$$

$$y = \sum_{i=1}^{8} y_i \alpha_i(u, v), \tag{2.39}$$

where the (x_i, y_i) are the arbitrarily chosen coordinates of the nodes. It is clear that α_i must be equal to one at node i and to zero at the other nodes. A possible choice is

$$\alpha_1(u, v) = \frac{1}{4}(u + 1)(v + 1)(u + v - 1) \tag{2.40}$$

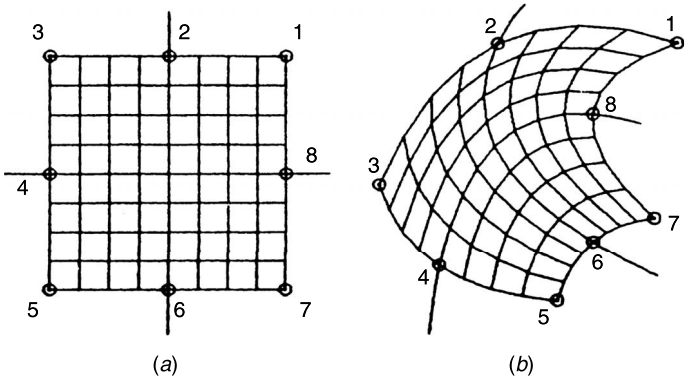

Figure 2.6 A coordinate transformation: (*a*) reference square and (*b*) (x, y) plane (from P. P. Silvester and R. L. Ferrari, *Finite elements for electrical engineers*, 2nd edition, 1990, with permission of Cambridge University Press).

for a corner node such as 1, and

$$\alpha_2(u, v) = \frac{1}{2}(u + 1)(v + 1)(-u + 1) \tag{2.41}$$

for a central node such as 2. The six remaining α_i can be obtained by simple coordinate rotations and reflections. Ultimately, the curved element will have a shape of the kind shown in Figure 2.6*b*. The *shape function* is chosen *isoparametrically*, when it is expressed in terms of the same α_i functions as the coordinates themselves. We write

$$\phi = \sum_i \phi_i \alpha_i(u, v). \tag{2.42}$$

It should be noted that simple elements such as triangles and rectangles lead to interaction integrals that can be evaluated analytically. This advantage is lost with general quadrilaterals or curved elements.

The structures encountered in *three-dimensional* problems are often greatly complex, inhomogeneous in their material properties, and endowed with points and lines where the fields become singular. Large alternators, or volumes of biological material such as the human body, are cases in point. The application of finite elements to such structures is discussed in later chapters. For *scalar* problems, the extension to three dimensions is evident, and Figure 2.7 displays two often used elements: the *tetrahedron* and the *brick*. Basis and shape functions can be synthesized just as in two dimensions. For the tetrahedron of Figure 2.7*a*, for example, the linear variation

$$\phi = \phi_1 L_1(\mathbf{r}) + \phi_2 L_2(\mathbf{r}) + \phi_3 L_3(\mathbf{r}) + \phi_4 L_4(\mathbf{r}) \tag{2.43}$$

is often selected, where $L_1(\mathbf{r})$ is given by [207]

$$L_1(\mathbf{r}) = \frac{1}{6V} \begin{bmatrix} 1 & x & y & z \\ 1 & x_2 & y_2 & z_2 \\ 1 & x_3 & y_3 & z_3 \\ 1 & x_4 & y_4 & z_4 \end{bmatrix}. \tag{2.44}$$

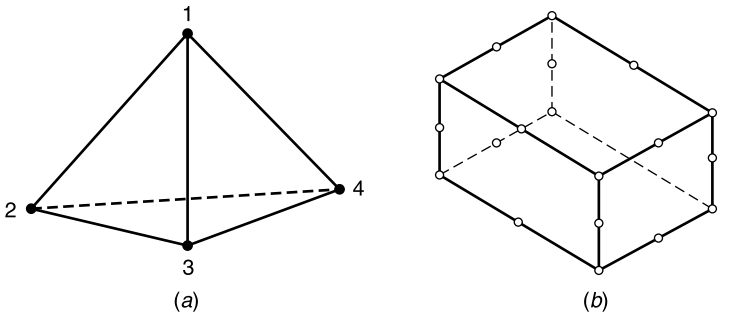

Figure 2.7 (*a*) Four-node tetrahedron (volume V); (*b*) 20-node rectangular prism (a brick).

In (2.44), V is the volume of the tetrahedron, equal to

$$V = \frac{1}{6}\begin{bmatrix} 1 & x_1 & y_1 & z_1 \\ 1 & x_2 & y_2 & z_2 \\ 1 & x_3 & y_3 & z_3 \\ 1 & x_4 & y_4 & z_4 \end{bmatrix}. \tag{2.45}$$

Similar expressions can be written for the other L_i.

The next extension is to *vector* unknowns, a category that is obviously of prime importance for electromagnetic applications. The elements of interest here belong to either the nodal or the edge families [189, 207]. *Nodal* elements follow the pattern shown in (2.43) and lead to basis functions of the form (2.44) for each scalar component of the field vector. Thus,

$$\boldsymbol{\phi}(\mathbf{r}) = \sum_i \boldsymbol{\phi_i} L_i(\mathbf{r}). \tag{2.46}$$

In the *edge element* approach, on the other hand, the basis vector function is expressed as

$$\boldsymbol{\phi} = \sum_i a_i \boldsymbol{\tau_i}(\mathbf{r}), \tag{2.47}$$

where the nature of the $\boldsymbol{\tau_i}(\mathbf{r})$ is discussed in Chapters 6 and 10.

Numerical codes of remarkable sophistication (e.g., HP-HFSS and Anscon-HFSS) are available commercially, for example for the automatic generation of meshes (e.g., by "Delaunay tessalation") but also for mesh refinement in regions where more detail is required. This can be done by the user (i.e., by direct human intervention) but also by *adaptive refinement*, based on an a posteriori error analysis followed by automatic correction [188, 190, 195]. Mesh refinement may proceed by several methods,[4,5,6] including the use of higher-order basis functions (termed p-refinement) in regions where more precision is needed or the progressive increase of the number of elements in the mesh (termed h-refinement), as illustrated in Figure 2.8.

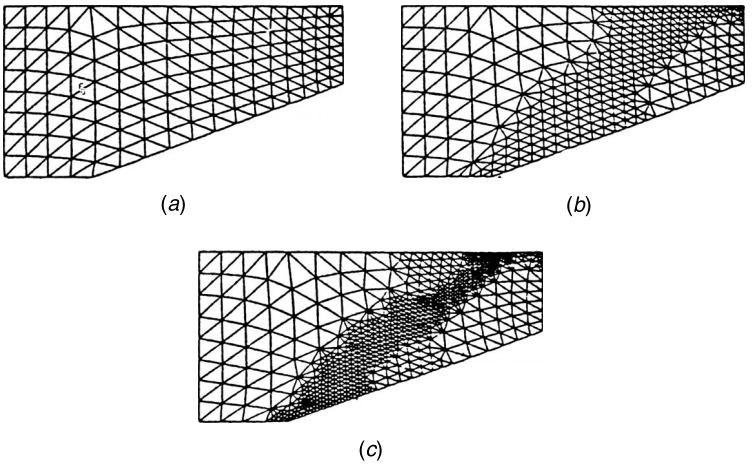

Figure 2.8 Mesh enrichment: (*a*) initial mesh, (*b*) after 101 steps, (*c*) after 201 steps (from D. C. Zienkiewicz and R. L. Taylor, *The finite element method in structural and continuous mechanics*, 4th edition, 1994, copyright 1967, 1994, with permission of the McGraw-Hill Companies).

2.8 DIRECT NUMERICAL SOLUTION OF MATRIX PROBLEMS

Discretization of problems, a technique routinely applied in numerous fields of physics, has generated an intense interest in the numerical solution of matrix problems. An extensive literature exists on the subject [156, 176, 188, 192, 193, 203, 207]. We shall limit ourselves to an outline of the main methods, which are either *direct* or *iterative*.

A direct method of continuing popularity is that of *Gaussian elimination*. The starting equation is

$$\overline{\overline{A}} \cdot \mathbf{x} = \mathbf{y}. \tag{2.48}$$

The original matrix $\overline{\overline{A}}$ is decomposed into a product $\overline{\overline{L}} \cdot \overline{\overline{U}}$, where $\overline{\overline{L}}$ is lower triangular and $\overline{\overline{U}}$ upper triangular. The solution proceeds by successively solving

$$\overline{\overline{L}} \cdot \mathbf{z} = \mathbf{y} \tag{2.49}$$

and

$$\overline{\overline{U}} \cdot \mathbf{x} = \mathbf{z}. \tag{2.50}$$

Such a factorization is possible, for example, when the principal minors of $\overline{\overline{A}}$ are nonsingular, a property that is automatically satisfied by positive-definite matrices. Methods for determining $\overline{\overline{L}}$ and $\overline{\overline{U}}$ can be found in standard texts. The application to the following simple matrix equation shows the mechanics of the process. We start with

$$\begin{aligned} 3x_1 + 2x_2 &= 8 \\ 6x_1 + 6x_2 &= 18. \end{aligned}$$

A possible decomposition of the matrix is

$$\begin{pmatrix} 3 & 2 \\ 6 & 6 \end{pmatrix} = \begin{pmatrix} 1 & 0 \\ 2 & 2 \end{pmatrix} \cdot \begin{pmatrix} 3 & 2 \\ 0 & 1 \end{pmatrix} = \overline{\overline{L}} \cdot \overline{\overline{U}}.$$

The first partial problem, that is, (2.49), takes the form

$$\begin{aligned} z_1 &= 8 \\ 2z_1 + 2z_2 &= 18. \end{aligned}$$

Its solution is $z_1 = 8$ and $z_2 = 1$. The second problem is now

$$\begin{aligned} 3x_1 + 2x_2 &= 8 \\ x_2 &= 1. \end{aligned}$$

Its solution yields the correct answer, viz. $x_1 = 2$ and $x_2 = 1$.

Well-tailored methods, adapted to symmetric matrices and matrices with special characteristics, have been developed to reduce computer time, memory requirements, and number of operations. A diagonal matrix a_{ii} can immediately be inverted in the form $(1/a_{ii})$.

It is therefore to be expected that *band* matrices, with elements centered on the main diagonal, should be advantageous from a numerical point of view. Sparse matrices are also advantageous, and their properties can also be systematically exploited [157].

Finally, the determination of eigenvalues and eigenvectors may be achieved by a number of specialized methods, such as those of Jacobi, Givens, and (for a real, symmetric matrix) Householder [177, 188, 193].

2.9 ITERATIVE NUMERICAL SOLUTION OF MATRIX PROBLEMS

Iterative methods converge to the solution after a series of steps, whose number depends on the required accuracy. There are many such methods, of which Jacobi and successive overrelaxation (discussed in Chapter 5) are well-known examples. Each method must be tested on its convergence properties and its performance when applied to an ill-conditioned matrix [176]. Fundamentally, iteration proceeds from an approximate solution $\mathbf{x}_n$ to a new one, of hopefully higher accuracy, through the general process

$$\mathbf{x}_{n+1} = \mathbf{x}_n + \Delta\mathbf{x}_n. \tag{2.51}$$

The method starts from an initial trial vector $\mathbf{x}_0$, which produces an error

$$\mathbf{e}_0 = \mathbf{y} - \overline{\overline{A}}\cdot\mathbf{x}_0. \tag{2.52}$$

It subsequently endeavors progressively to reduce the error. A functional is involved in this process, which, when $\overline{\overline{A}}$ is symmetric and positive-definite, is typically

$$F(\mathbf{x}) = 2\langle\mathbf{x},\mathbf{y}\rangle_S - \left\langle\overline{\overline{A}}\cdot\mathbf{x},\mathbf{x}\right\rangle_S. \tag{2.53}$$

From (2.8), the Euler equation of $F(\mathbf{x})$ is (2.48), and F reaches a maximum for the correct solution $\mathbf{x}$. Starting from $\mathbf{x}_0$, let us introduce a (small) correction $\Delta\mathbf{x}_0$, and insert it in $F(\mathbf{x})$. This yields

$$\begin{aligned} F(\mathbf{x}_1) &= F(\mathbf{x}_0) + 2\langle\Delta\mathbf{x}_0,\mathbf{y}\rangle_S - 2\left\langle\Delta\mathbf{x}_0,\overline{\overline{A}}\cdot\mathbf{x}_0\right\rangle_S - \left\langle\overline{\overline{A}}\cdot\Delta\mathbf{x}_0,\Delta\mathbf{x}_0\right\rangle_S \\ &= F(\mathbf{x}_0) + 2\langle\Delta\mathbf{x}_0,\mathbf{e_0}\rangle_S - \left\langle\overline{\overline{A}}\cdot\Delta\mathbf{x}_0,\Delta\mathbf{x}_0\right\rangle_S. \end{aligned} \tag{2.54}$$

In the *steepest descent method*, $\Delta\mathbf{x}_0$ is chosen in the direction of $\mathbf{e_0}$, in order to obtain a strong variation in F and potentially a faster convergence. Thus,

$$\mathbf{x}_1 = \mathbf{x}_0 + \alpha_0\mathbf{e_0}. \tag{2.55}$$

Inserting (2.55) into (2.54), and setting $\partial F/\partial\alpha_0 = 0$, gives the "best" value

$$\alpha_0 = \frac{\langle\mathbf{e_0},\mathbf{e_0}\rangle_S}{\left\langle\overline{\overline{A}}\cdot\mathbf{e_0},\mathbf{e_0}\right\rangle_S}. \tag{2.56}$$

These steps are repeated to obtain $\mathbf{x}_2$, starting from $\mathbf{x}_1$, and more generally $\mathbf{x}_n$ from $\mathbf{x}_{n-1}$. It turns out that better convergence can be obtained by applying the method of *conjugate*

gradients. We describe one of the several forms that this method can take [200, 203, 212]. Fundamentally, $\Delta\mathbf{x}_0$ is not chosen in the direction of $\mathbf{e_0}$ anymore, but according to the prescription[7]

$$\mathbf{x}_1 = \mathbf{x}_0 + t_0\mathbf{p}_0. \tag{2.57}$$

The various methods differ by the choice of both t_0 and the direction of the search vector $\mathbf{p}_0$. We choose [192]

$$\mathbf{p}_0 = \frac{\overline{\overline{A}}^t \cdot \mathbf{e}_0}{\| \overline{\overline{A}}^t \cdot \mathbf{e}_0 \|^2} \tag{2.58}$$

and

$$t_0 = \frac{1}{\| \overline{\overline{A}} \cdot \mathbf{p}_0 \|^2}. \tag{2.59}$$

The subsequent steps are obtained by iteration according to the scheme

$$\begin{aligned}
\mathbf{x}_{n+1} &= \mathbf{x}_n + t_n\mathbf{p}_n \\
\mathbf{p}_{n+1} &= \mathbf{p}_n + q_n\overline{\overline{A}}^t \cdot \mathbf{e}_{n+1} \\
t_n &= \frac{1}{\| \overline{\overline{A}} \cdot \mathbf{p}_n \|^2} \\
q_n &= \frac{1}{\| \overline{\overline{A}}^t \cdot \mathbf{e}_{n+1} \|^2} \\
\mathbf{e}_{n+1} &= \mathbf{e}_n - t_n\overline{\overline{A}} \cdot \mathbf{p}_n.
\end{aligned} \tag{2.60}$$

A simple numerical problem reveals the mechanics of the method. We start with the equation

$$\begin{pmatrix} 1 & 2 \\ 4 & 3 \end{pmatrix} \cdot \begin{pmatrix} x_1 \\ x_2 \end{pmatrix} = \begin{pmatrix} 3 \\ 2 \end{pmatrix}. \tag{2.61}$$

The solution is clearly $x_1 = -1, x_2 = 2$. To obtain this solution by iteration, we choose a trial vector $\mathbf{x}_0 = (0, 1)$ (Fig. 2.9). Following (2.56) to (2.60), we obtain successively (Problem 2.15)

$$\begin{aligned}
\mathbf{e}_0 &= (1, -1) \quad \text{(from the data)} \\
\mathbf{p}_0 &= (-0.3, -0.1) \\
t_0 &= 0.4 \\
\mathbf{x}_1 &= (-0.12, 0.96).
\end{aligned}$$

The next round gives

$$\begin{aligned}
q_0 &= 0.625 \\
\mathbf{p}_1 &= (-0.55, 0.65) \\
t_1 &= 1.6 \\
\mathbf{x}_2 &= (-1, 2).
\end{aligned}$$

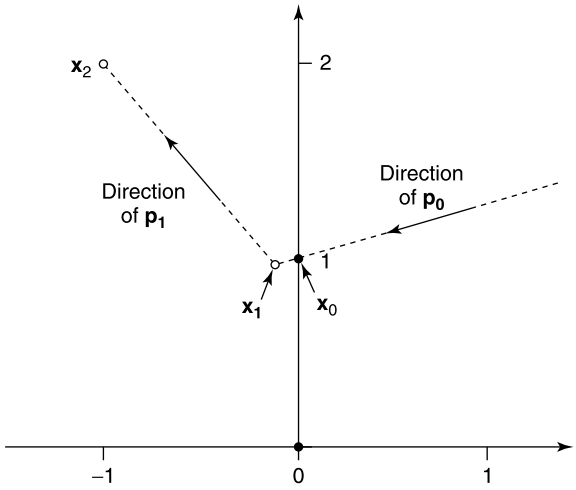

Figure 2.9 Application of the conjugate gradient method.

This is the correct value, obtained with only two steps. More generally, at most N steps are needed to arrive at the solution when the matrix is of the $N \times N$ type. Round-off errors, however, may require additional steps to achieve the desired accuracy.

The values obtained in our numerical experiment allow us to verify an important general orthogonality property, viz.

$$\left\langle \overline{\overline{A}} \cdot \mathbf{p}_1, \overline{\overline{A}} \cdot \mathbf{p}_0 \right\rangle = \left\langle \mathbf{p}_1, \overline{\overline{A}}^t \cdot \overline{\overline{A}} \cdot \mathbf{p}_0 \right\rangle = 0. \tag{2.62}$$

It is on the basis of this property that the directions of $\mathbf{p}_0$ and $\mathbf{p}_1$ are termed *conjugate*.[8] We note that orthogonality holds with respect to the — automatically positive-definite — operator $\overline{\overline{A}}^t \cdot \overline{\overline{A}}$ [155, 203].

When confronted with the choice of a method, the numerical analyst should take several criteria into account. Some of these are [176]:

1. Accuracy obtained; stability with respect to round-off.
2. Time required; convergence rate for iterative methods.
3. Applicability; type of matrix to which the method applies.
4. Each step of the process should be an improvement in the approximation.
5. As many of the original data as possible should be used.
6. Storage requirements.
7. Ease of coding.
8. Performance on ill-conditioned systems.

Direct methods are often preferred when the typical matrix problem (2.48) must be solved for many excitations $\mathbf{y}$, because these methods implicitly generate the inverse matrix. Iterative methods, on the other hand, are generally preferred for the solution of problems involving a single large, sparse matrix. The conjugate-gradient method has a distinct advantage compared with direct methods: the rounding errors do not build up from one iteration step to the next, which makes the method better suited to the solution of poorly conditioned systems.

PROBLEMS

2.1 Find a variational principle for the eigenvalues of a real $N \times N$ symmetric matrix. Use this principle to determine the lowest eigenvalue of the matrix in (1.138). Compare it with the exact value (which is given in the text). Determine the same quantities for the matrix

$$\bar{\bar{a}} = \begin{pmatrix} -2 & 1 & 0 \\ 1 & -2 & 1 \\ 0 & 1 & -2 \end{pmatrix}.$$

2.2 A transmission line with given linear impedance $Z(x)$ and given linear admittance $Y(x)$ is loaded with an impedance Z_L. A time-harmonic input voltage is applied to the line.

(**a**) Show that the Euler equations of the functional

$$J_1(V, I) = \frac{V(0)}{I(0)} + \frac{1}{I^2(0)} \int_0^l \left[I \left(\frac{dV}{dx} + ZI \right) - V \left(\frac{dI}{dx} + YV \right) \right] dx$$

are the transmission line equations. Verify that the stationary value of J is the input impedance of the line.

(**b**) Show that the input impedance is also the stationary value of the functionals

$$J_2(I) = \frac{1}{I^2(0)} \left\{ \int_0^l \left[\frac{1}{Y} \left(\frac{dI}{dx} \right)^2 + ZI^2 \right] dx + Z_0 I^2(l) \right\}$$

and

$$J_3(V) = \frac{V^2(0)}{\displaystyle\int_0^l [(1/Z)(dV/dx)^2 + YV^2]\, dx + (1/Z_0)V^2(l)}.$$

Verify that the extremizing functions are the line current and the line voltage.
(M. Namiki and H. Takahaschi, *J. Appl. Phys.*, **23**, 1056, 1952.)

2.3 Consider the problem

$$\frac{d^2y}{dx^2} = -6x \qquad (y = 0 \text{ at } x = 0 \text{ and } x = 1).$$

The exact solution is $x(1 - x^2)$. To effect the variational solution:

(**a**) Write down a suitable functional for the problem [use the form shown in (2.3)].

(**b**) Insert, as a first trial function, the triangular function shown in Figure 2.1, taking the maximum value y_2 as a parameter.

(**c**) Insert, as a second trial function, the function shown in Figure P2.1, and optimize with respect to y_1 and y_2.

(**d**) As a third trial function, choose $y = 4Cx(1 - x)$, and optimize with respect to C, which is the maximum value of the function obtained for $x = 0.5$.

(**e**) With the same trial function, determine C by way of the least squares method, in which C is required to minimize

$$\int_0^1 \left(\frac{d^2y}{dx^2} + Cx \right)^2 dx.$$

(**f**) For each case, compare the approximate values at $1/3$, $1/2$, and $2/3$ with the exact ones.

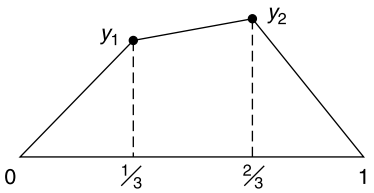

Figure P2.1

2.4 Find the Euler equation of

$$J(f,h) = \langle \mathcal{L}f, h\rangle - \langle g, h\rangle$$

when $\mathcal{L}$ is not self-adjoint, and f and h are the admissible functions.

2.5 Find the solution of the problem

$$\frac{d^2y}{dx^2} = -x \qquad \text{(with } y = 0 \text{ at } x = 0 \text{ and } y = 1 \text{ at } x = 1\text{)}$$

(**a**) Directly;

(**b**) By setting $y^* = y - x$, and using the clamped string functional (2.3) for y^*. Use the piecewise linear approximation shown in Figure P2.1, and determine y_1^* and y_2^* from stationarity. Compare the resulting values for y_1 and y_2 with the exact ones.

2.6 Find the Euler equation of the functional

$$J(\phi) = \int_0^\pi \left[p\left(\frac{d\phi}{dx}\right)^2 + q\phi^2 \right] dx \; + \; h_1 p(0)\phi^2(0) \; + \; h_2 p(\pi)\phi^2(\pi) \quad (p(x) > 0)$$

where the admissible functions satisfy the boundary conditions $\phi'(0) - h_1\phi(0) = 0$ and $\phi'(\pi) + h_2\phi(\pi) = 0$.

2.7 Find the Euler equation and natural boundary conditions of the functional (Fig. P2.2)

$$F(\phi) = \iint_S \left[|\text{grad } \phi|^2 - 2\phi\rho(x,y) \right] dS \; - \int_{c_1} 2\phi h(c)dc - 2\int_{c_2} \left[\phi - g(c)\right] \frac{\partial\phi}{\partial n} dc.$$

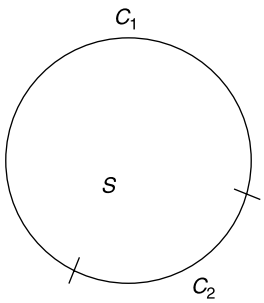

Figure P2.2

2.8 The adjoint problem is often found with the help of a Green's theorem of the form

$$\langle \mathcal{L}f, h\rangle_V - \left\langle f, \mathcal{L}^a h\right\rangle_V = \langle Bf, Ch\rangle_S - \left\langle C^a f, B^a h\right\rangle_S .$$

The scalar products are integrals over either the volume V or the boundary surface S. The direct problem is $\mathcal{L}f = g$ in V, $Bf = q$ on S, the adjoint problem $\mathcal{L}^a h = s$ in V, $B^a h = q^a$ on S. Show that the pertinent functional is

$$J = \langle \mathcal{L}f, h\rangle_V - \langle f, s\rangle_V - \langle g, h\rangle_V - \langle Bf, Ch\rangle_S + \left\langle C^a f, q^a\right\rangle_S + \langle q, Ch\rangle_S .$$

(Y. J. Xie and C. H. Liang, *Microwave Opt. Tech. Letts.*, **17**, 255–259, 1998.)

2.9 Consider the first s eigenvalues of

$$\mathcal{L}u - \lambda \mathcal{M}u = 0 \quad (u \in \mathcal{D}),$$

where $\mathcal{L}$ and $\mathcal{M}$ are self-adjoint positive-definite transformations:

(**a**) Generalize functional (2.16), which corresponds with $\mathcal{M} = 1$, to include the present case.

(**b**) Express a typical eigenfunction as a sum of S admissible functions, and insert into (**a**).

(**c**) Show that the (approximate) eigenvalues are the roots of the determinantal equation

$$\det \begin{pmatrix} L_{11} - \Lambda_k M_{11} & L_{12} - \Lambda_k M_{12} & \dots & L_{1S} - \Lambda_k M_{iS} \\ \dots & \dots & \ddots & \dots \\ L_{S1} - \Lambda_k M_{S1} & L_{S2} - \Lambda_k M_{S2} & \dots & L_{SS} - \Lambda_k M_{SS} \end{pmatrix} = 0,$$

where the matrix elements L_{ik} and M_{ik} are defined by the relationships

$$\begin{array}{llll} L_{ik} & = \langle u_i, \mathcal{L}u_k\rangle & = \langle \mathcal{L}u_i, u_k\rangle & = L_{ki} \\ M_{ik} & = \langle u_i, \mathcal{M}u_k\rangle & = \langle \mathcal{M}u_i, u_k\rangle & = M_{ki}. \end{array}$$

2.10 Find the Euler equation and the natural boundary conditions relative to the functional

$$J(\phi) = \int_{\mathcal{D}} F\left(\phi, \frac{\partial \phi}{\partial x}, \frac{\partial \phi}{\partial y}, \frac{\partial \phi}{\partial z}, x, y, z\right) dV + \int_S P(\phi, \dots)\, dS.$$

2.11 The equation for the *damped* vibration of a string is of the form

$$\frac{\partial^2 y}{\partial t^2} + 2k\frac{\partial y}{\partial t} - c^2 \frac{\partial^2 y}{\partial x^2} = 0.$$

Show that the proper Lagrangian is

$$L = \frac{\partial z}{\partial t}\frac{\partial y}{\partial t} + k\left(y\frac{\partial z}{\partial t} - \frac{\partial y}{\partial t}\right) - c^2 \frac{\partial z}{\partial x}\frac{\partial y}{\partial x}$$

and determine the equation satisfied by z.

2.12 Put the symmetric matrix

$$\begin{pmatrix} 0 & 1 \\ 1 & 0 \end{pmatrix}$$

in the $\overline{\overline{L}} \cdot \overline{\overline{U}}$ form. Is the matrix positive-definite?

2.13 Solve the matrix equation

$$\begin{pmatrix} 2 & 3 \\ 5 & 4 \end{pmatrix} \cdot \begin{pmatrix} x_1 \\ x_2 \end{pmatrix} = \begin{pmatrix} 4 \\ 3 \end{pmatrix}$$

by Gaussian elimination (i.e., by means of a decomposition $\overline{\overline{L}} \cdot \overline{\overline{U}}$). Notice that the decomposition is not unique, and that two degrees of freedom are available in choosing the matrix elements (N degrees of freedom when the matrix is $N \times N$).

2.14 Solve (2.61) by the method of steepest descent.

2.15 Solve (2.61) starting from the initial trial vector $\mathbf{x}_0 = (1, 0)$, and compare the convergence rate with that obtained from the $\mathbf{x}_0$ trial vector used in the text.

2.16 In the equation

$$\begin{pmatrix} 1 & j \\ j & 0 \end{pmatrix} \cdot \begin{pmatrix} x_1 \\ x_2 \end{pmatrix} = \begin{pmatrix} 0 \\ j \end{pmatrix}$$

the matrix is clearly non-Hermitian:

(**a**) Find the eigenvalues and eigenvectors of the matrix;

(**b**) Solve the equation by the method of conjugate gradients.

NOTES

1. P. D. Robinson and A. M. Arthurs, Some variational principles for integral equations, *J. Math. Phys.* **9**, 1364–1368 (1968).
2. See Ref. 4 in Chapter 1.
3. R. Coccioli, T. Itoh, G. Pelosi, and P. Silvester, Finite-element methods in microwaves: a selected bibliography, *IEEE Antennas Prop. Mag.* **38**, 34–47 (1996).
4. Z. J. Csendes and D. N. Shenton, Adaptive mesh refinement in the finite element computation of magnetic fields, *IEEE Trans.* **MAG-21**, 1811–1816 (1985).
5. D. N. Shenton and Z. J. Csendes, MAX — an expert system for automatic adaptive magnetic modeling, *IEEE Trans.* **MAG-22**, 805–807 (1986).
6. R. Hertel and H. Kronmuller, Adaptive finite element mesh refinement techniques in three-dimensional micromagnetic modeling, *IEEE Trans.* **MAG-34**, 3922–3930 (1998).
7. T. K. Sarkar, X. Yang, and E. Arvas, A limited survey of various conjugate gradient methods for solving complex matrix equations arising in electromagnetic wave interactions, *Wave Motion* **10**, 527–546 (1988).
8. M. R. Hestenes and E. Stiefel, Methods of conjugate gradients for solving linear systems, *J. Res. Nat. Bur. Standards* **49**, 409–436 (1952).

Chapter 3

Electrostatic Fields in the Presence of Dielectrics

The current chapter focuses on the theory of the Newtonian potential, a centuries-old discipline with applications in many branches of physics. The theory investigates integrals of the type $\int_V |\mathbf{r} - \mathbf{r}'|^{-\alpha} f(\mathbf{r}')\, dV'$ and shows that, if $0 < \alpha < 3$, these integrals can be given a meaning, although the integrand becomes infinite for $\mathbf{r} \to \mathbf{r}'$. The theory is further concerned with the properties of the derivatives of the integrals and also with those of the surface integrals $\int_S |\mathbf{r} - \mathbf{r}'|^{-\beta} g(\mathbf{r}')\, dS'$, where $0 < \beta < 2$. Such developments are clearly essential for a study of static fields, but they are equally important for the theory of time-harmonic fields. For such fields, the main kernel is $|\mathbf{r} - \mathbf{r}'|^{-1} \exp(-jk_0|\mathbf{r} - \mathbf{r}'|)$ instead of $|\mathbf{r} - \mathbf{r}'|^{-1}$, but the two kernels coincide in the limit $\mathbf{r} \to \mathbf{r}'$; that is, for $|\mathbf{r} - \mathbf{r}'|$ much smaller than $k_0^{-1} = (\lambda_0/2\pi)$. This simple remark is the key to the derivation of a number of integral equations and provides a basis for the study of low-frequency fields. Numerous examples in the text illustrate the importance of these aspects.

The investigation of potential — and derivatives — requires great precision of language and considerable mathematical rigor. We shall not endeavor to achieve such excellence, for which first-rate references are given, but follow the more pragmatic approach of quoting, without extensive discussions, the main results of the theory.

3.1 VOLUME CHARGES IN VACUUM

The fundamental equations for the electric field stemming from a volume charge distribution of density $\rho(\mathbf{r})$ are

$$\text{curl } \mathbf{e} = 0 \tag{3.1}$$

$$\text{div } \mathbf{e} = \frac{\rho}{\epsilon_0}. \tag{3.2}$$

We shall assume that all charges are at a finite distance and hence that $\rho(\mathbf{r})$ vanishes outside a sufficiently large sphere. The significance of the operators curl and div is discussed in

Electromagnetic Fields, Second Edition, By Jean G. Van Bladel

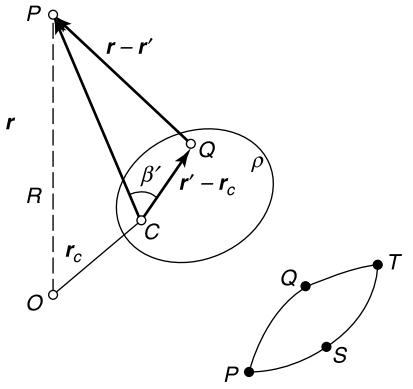

Figure 3.1 Charged volume with charge center C.

Appendices 1 and 8. The irrotational character of **e** implies that the field can be derived from a scalar potential. This can be seen by considering a contour $PQTS$ in a region in which **e** is continuous* (Fig. 3.1). By Stokes' theorem (A1.42), the integral of **e** around the contour is zero, hence

$$\int_{PQT} \mathbf{e}\cdot d\mathbf{l} = \int_{PST} \mathbf{e}\cdot d\mathbf{l}.$$

This relationship shows that the line integral of **e** from P to T is independent of the path and depends only on the end points P and T. In consequence, there exists a single-valued function ϕ, determined to within an additive constant, such that this line integral is equal to $\phi(P) - \phi(T)$. Therefore,

$$\mathbf{e} = -\text{grad}\ \phi \tag{3.3}$$

and (3.2) gives rise to *Poisson's equation*,

$$\nabla^2\phi = -\frac{\rho}{\epsilon_0}. \tag{3.4}$$

The differential equation (3.4) is not sufficient to determine ϕ uniquely. It is necessary, in addition, to specify the behavior of ϕ at large distances by means of the condition of *regularity at infinity*. This condition, which is dictated by experimental evidence, requires $R\phi$ and $R^2\partial\phi/\partial x_i$ to remain bounded in absolute value for all sufficiently large R, where R is the distance from an arbitrarily fixed point O. Uniqueness of the solution under these circumstances can be checked by verifying that the homogeneous problem

$$\nabla^2\phi_0 = 0 \qquad (\phi_0 \text{ regular at infinity}) \tag{3.5}$$

has no nonzero solution. The proof proceeds by applying Green's theorem (A1.30) to the volume bounded by a large spherical surface S_∞ centered at O. Thus,

$$\int_V [\phi_0\nabla^2\phi_0 + (\text{grad}\ \phi_0)^2]\, dV = \int_{S_\infty} \phi_0 \frac{\partial\phi_0}{\partial n}\, dS. \tag{3.6}$$

*The extension to square-integrable irrotational vectors can be found in Note 1.

The surface integral vanishes as R approaches infinity because, although dS_∞ is proportional to R^2, $\phi_0\ \partial\phi_0/\partial n$ is proportional to R^{-3} by virtue of the assumed regularity condition. It follows, in the light of (3.5), that grad $\phi_0 = 0$ throughout space or, equivalently, that ϕ_0 is a constant. But this constant is zero because of the regularity condition. We conclude that $\phi_0 = 0$.

The potential problem discussed above gives rise to a transformation characterized by an operator ∇^2 and a domain consisting of functions regular at infinity and endowed with the necessary second derivatives. This transformation is self-adjoint with respect to a real symmetric scalar product,[†] as can be verified by applying Green's theorem (A1.31) to a volume bounded by S_∞. Thus,

$$\langle \mathcal{L}u, v\rangle = \int_V (\nabla^2 u)v\, dV = \int_V u(\nabla^2 v)\, dV + \int_{S_\infty} \left(v\frac{\partial u}{\partial n} - u\frac{\partial v}{\partial n}\right) dS. \tag{3.7}$$

If v, together with u, is regular at infinity, the surface integral vanishes, hence $\langle \mathcal{L}u, v\rangle = \langle u, \mathcal{L}v\rangle$, which is the expression of self-adjointness. The transformation is, in addition, negative-definite because, from (A1.30),

$$\langle \mathcal{L}u, u\rangle = \int_V u\nabla^2 u\, dV = -\int_V |\text{grad } u|^2\, dV + \int_{S_\infty} u\frac{\partial u}{\partial n}\, dS. \tag{3.8}$$

The surface integral vanishes because of the regularity condition at infinity. As a consequence, $\langle \mathcal{L}u, u\rangle = 0$ implies $|\text{grad } u| = 0$ (i.e., $u = 0$ because of the same regularity condition).

It is useful to remark that Poisson's equation is the Euler equation of the functional

$$J(\phi) = \int_V \left[\rho\phi - \frac{1}{2}\epsilon_0 |\text{grad } \phi|^2\right] dV. \tag{3.9}$$

The admissible ϕ's belong to the domain mentioned above. The functional $J(\phi)$ reaches a local minimum when ϕ approaches the solution of (3.4). These properties are easily verified by means of the methods discussed in Chapter 2. The minimum is clearly equal to the electrostatic energy present in the system.[2]

An interesting reciprocity theorem can easily be derived for the solutions of the potential problem. Let ϕ_1 and ϕ_2 be the potentials generated by respective charge densities ρ_1 and ρ_2. From (A1.31), and because both ϕ's are regular at infinity,

$$\langle \phi_1, \rho_2\rangle = \int_V \phi_1(-\epsilon_0\nabla^2\phi_2)\, dV = \int_V \phi_2(-\epsilon_0\nabla^2\phi_1)\, dV = \langle \phi_2, \rho_1\rangle. \tag{3.10}$$

Reciprocity theorems of this kind are very useful in practice and are frequently encountered in subsequent chapters. As an example, let ρ_2 be a unit point-source in $\mathbf{r}_2$. The corresponding charge density is $\rho_2 = q\delta(\mathbf{r} - \mathbf{r}_2)$. With $q = 1$, (3.10) now yields

$$\int_V \phi_1\delta(\mathbf{r} - \mathbf{r}_2)\, dV = \phi_1(\mathbf{r}_2) = \int_V \rho_1(\mathbf{r})\phi_2(\mathbf{r}|\mathbf{r}_2)\, dV. \tag{3.11}$$

This relationship gives ϕ_1 in terms of its sources ρ_1 and shows that ϕ_2 has the nature of a Green's function. We shall derive the explicit form of this function in the next section.

[†]Because the current chapter is only concerned with real quantities, symmetric and Hermitian scalar products coincide, and no subscript (S or H) will be attached to $\langle a, b\rangle$.

3.2 GREEN'S FUNCTION FOR INFINITE SPACE

The derivation of the relevant $G(\mathbf{r}|\mathbf{r}_1)$ rests on (3.7), which corresponds with the general relationship (1.42). The bilinear concomitant is in the current case

$$\int_S J(u, v)\, dS = \int_S \left(v\frac{\partial u}{\partial n} - u\frac{\partial v}{\partial n} \right) dS, \tag{3.12}$$

where n is the outward-pointing normal direction. The sought Green's function $G(\mathbf{r}|\mathbf{r}_1)$

1. Must satisfy $\nabla^2 G = 0$ for $\mathbf{r} \neq \mathbf{r}_1$
2. Must be regular at infinity
3. Must have the right kind of singularity when $\mathbf{r}$ approaches $\mathbf{r}_1$.

The search for G is facilitated by the fact that this function should depend on $|\mathbf{r} - \mathbf{r}_1|$ only, because of the spherical symmetry of the field surrounding the unit source. The function that satisfies all these requirements is[‡]

$$G(\mathbf{r}|\mathbf{r}_1) = -\frac{1}{4\pi}\frac{1}{|\mathbf{r} - \mathbf{r}_1|} = G(\mathbf{r}_1|\mathbf{r}). \tag{3.13}$$

To verify this assertion, let us apply (3.7) to all space, from which a small volume V_1 around $\mathbf{r}_1$ has been excised (Fig. 3.2*a*). The boundary surface consists of a large sphere at infinity (for which the surface integral vanishes) and S_1. We are left with

$$\int_{S_1} \left[\phi(\mathbf{r})\frac{\partial G(\mathbf{r}|\mathbf{r}_1)}{\partial n} - G(\mathbf{r}|\mathbf{r}_1)\frac{\partial \phi(\mathbf{r})}{\partial n} \right] dS = \int_{\text{space}-V_1} G(\mathbf{r}|\mathbf{r}_1) \left[-\frac{\rho(\mathbf{r})}{\epsilon_0} \right] dV.$$

Let us check that the left-hand term generates $\phi(\mathbf{r}_1)$. The small area dS (Fig. 3.2*b*) is related to the elementary solid angle $d\Omega$ by

$$dS = \frac{d\Omega}{\cos\theta} R^2.$$

Let R approach zero, while the *relative* geometry (including the shape of V_1) remains invariant. Surface S_1 now shrinks toward $\mathbf{r}_1$. In the left-hand term G is proportional to $(1/R)$, but dS to R^2, hence the only contribution that survives as V_1 shrinks must come from $(\partial G/\partial n)$. Because

$$\text{grad } G = \text{grad}\left(-\frac{1}{4\pi R} \right) = \frac{1}{4\pi R^2}\mathbf{u}_R \tag{3.14}$$

it follows that

$$\frac{\partial G}{\partial n} = \frac{1}{4\pi R^2}(\mathbf{u}_R \cdot \mathbf{u}_n) = \frac{\cos\theta}{4\pi R^2}.$$

[‡]The perhaps unfamiliar minus sign in (3.13) is due to the choice of ∇^2 as the operator in (3.4). If we had written $-\nabla^2\phi = \delta(\mathbf{r} - \mathbf{r}')$, the Green's function would have been $(4\pi|\mathbf{r} - \mathbf{r}_1|)^{-1}$, a form that is more often encountered in the literature.

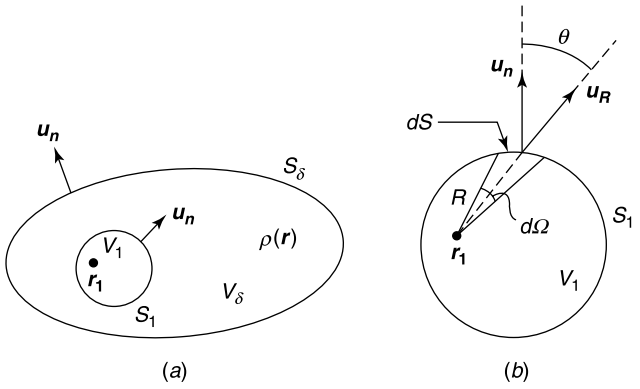

Figure 3.2 (*a*) Charged volume with interior point $\mathbf{r}_1$. (*b*) Geometry around the interior point.

Combining these various results gives rise to a left-hand term

$$\lim_{R\to 0}\int_{S_1}\phi(\mathbf{r})\frac{\partial G(\mathbf{r}|\mathbf{r}_1)}{\partial n}\,dS_1 = \phi(\mathbf{r}_1)\int_{S_1}\left(\frac{\cos\theta}{4\pi R^2}\right)\frac{d\Omega}{\cos\theta}R^2$$
$$= \phi(\mathbf{r}_1)\frac{1}{4\pi}\int_{S_1} d\Omega = \phi(\mathbf{r}_1). \tag{3.15}$$

Finally,

$$\phi(\mathbf{r}_1) = \frac{1}{4\pi\epsilon_0}\lim_{V_1\to 0}\int_{\text{space}-V_1}\frac{\rho(\mathbf{r})}{|\mathbf{r}_1-\mathbf{r}|}\,dV. \tag{3.16}$$

The integral in (3.15) is a *volume potential integral*, of the general type

$$I_1(\mathbf{r}) = \int_V f(\mathbf{r}')\frac{1}{|\mathbf{r}-\mathbf{r}'|}\,dV' = \int_V g(\mathbf{r},\mathbf{r}')\,dV', \tag{3.17}$$

where $\mathbf{r}$ is a point inside V. Integral $I_1(\mathbf{r})$ has been investigated extensively. It converges provided the limit

$$I_2(\mathbf{r}) = \lim_{\delta\to 0}\int_{V-V_\delta} g(\mathbf{r},\mathbf{r}')\,dV'$$

exists. In this equation, the symbol V_δ denotes a volume that contains $\mathbf{r}$ and whose longest chord does not exceed δ. A rigorous proof of the convergence property, for piecewise continuous $f(\mathbf{r})$, can be found in texts on potential theory [5, 153, 158, 162, 172]. Basic to the argument is the property that

$$I_3 = \int_{V_\delta}\frac{dV'}{|\mathbf{r}-\mathbf{r}'|^\alpha} \tag{3.18}$$

converges for $0 < \alpha < 3$ [158]. The proof is typical for potential theory. It consists in showing that the contribution from V_δ to I_3 approaches zero with δ. This is done in two

steps (Fig. 3.2*a*):

- First prove that the contribution from a small sphere V_1 of radius a vanishes. This is easily shown in *spherical coordinates*, as

$$I_3 = \int_0^a \frac{\pi R^2 dR}{R^\alpha} = \frac{\pi}{3-\alpha} a^{3-\alpha}.$$

  This integral approaches zero with a, provided $\alpha < 3$.
- Subsequently note that the contribution from $V_\delta - V_1$ also approaches zero, as the integrand remains finite in that region.

Derivatives of the Volume Potential

To investigate the derivatives of $I_1(\mathbf{r})$, consider the integral

$$\mathbf{I}_4(\mathbf{r}) = \int_V \frac{\mathbf{r}-\mathbf{r}'}{|\mathbf{r}-\mathbf{r}'|^3} f(\mathbf{r}')\, dV' \tag{3.19}$$

where $f(\mathbf{r})$ is integrable and bounded. Vector $\mathbf{I_4}$ is fundamental from a *physical* point of view because it represents a mathematical statement of Coulomb's law as applied to a volume charge. The electric field generated by a point charge q at the origin is, indeed,

$$\mathbf{e}(\mathbf{r}) = \frac{q}{4\pi\epsilon_0}\frac{\mathbf{u}_R}{R^2} = \frac{q}{4\pi\epsilon_0}\frac{\mathbf{r}}{R^3}.$$

If $f(\mathbf{r})$ is bounded and integrable in V, $I_1(\mathbf{r})$ can be shown to be differentiable, with partial derivatives that are Hölder continuous everywhere in space [153]. Note that a function $g(\mathbf{r})$ is *Hölder continuous* if there are three positive constants, c, A, α, such that

$$|g(\mathbf{r}) - g(\mathbf{r}')| \le A|\mathbf{r}-\mathbf{r}'|^\alpha \tag{3.20}$$

holds for all points up to a distance $|\mathbf{r}-\mathbf{r}'| \le c$. It can be further proved that

$$\mathbf{I}_4(\mathbf{r}) = -\text{grad}\, I_1(\mathbf{r}).$$

This important result shows that the derivatives of $I_1(\mathbf{r})$ may be obtained by *differentiating behind the sign of integration*. Applied to the electric field, this remark leads to the relationships

$$\begin{aligned}\mathbf{e}(\mathbf{r}) = -\text{grad}\,\phi(\mathbf{r}) &= -\frac{1}{4\pi\epsilon_0}\int_{\text{all space}} \rho(\mathbf{r}')\,\text{grad}\,\frac{1}{|\mathbf{r}-\mathbf{r}'|}dV' \\ &= \frac{1}{4\pi\epsilon_0}\int_{\text{all space}} \frac{\rho(\mathbf{r}')}{|\mathbf{r}-\mathbf{r}'|^2}\,\text{grad}\,|\mathbf{r}-\mathbf{r}'|\,dV'.\end{aligned} \tag{3.21}$$

Here, grad $|\mathbf{r}-\mathbf{r}'|$ is the unit vector in the direction from $\mathbf{r}'$ to $\mathbf{r}$, which we will denote by $\mathbf{u}_D$.

We note that convergence of $I_1(\mathbf{r})$ implies that the limit is independent of the *shape* of the small volume V_δ containing $\mathbf{r}_1$ or, equivalently, that the contribution from V_δ vanishes as

V_δ approaches zero in all its dimensions. The independence of the shape of the volume is most important for computations, for it allows the use of any convenient system of coordinates and the removal of volumes conveniently described in terms of these coordinates.

The *second* derivatives of $I_1(\mathbf{r})$ pose a more delicate problem, because the mere continuity of $f(\mathbf{r})$ does not ensure their existence. They will exist, however, when $f(\mathbf{r})$ satisfies a Hölder condition at each point inside the charged volume, in which case

$$\nabla^2 I_1(\mathbf{r}) = -4\pi f(\mathbf{r}). \tag{3.22}$$

The second derivatives are very sensitive to small errors in the numerical evaluation of potential I_1. It might be preferable, consequently, to let the derivatives operate on analytically known functions. This can be achieved, formally at least, by bringing ∇^2 behind the integral sign, where it finds the $\mathbf{r}$-dependent function $1/|\mathbf{r}-\mathbf{r}'|$ on which to operate. Great care must be exercised, however, when $\mathbf{r}$ is an *interior* point of the charge-carrying volume. For such a case, the second derivative produces a $|\mathbf{r}-\mathbf{r}'|^{-3}$ type of singularity, too strong for convergence to hold. A remedy to that difficulty is discussed in Section 3.9.

When Equation (3.22) is applied to the potential of a point charge (the Green's function), the following distributional equation is obtained

$$\nabla^2\left(-\frac{1}{4\pi|\mathbf{r}-\mathbf{r}'|}\right) = \delta(\mathbf{r}-\mathbf{r}').$$

3.3 MULTIPOLE EXPANSION

Attention is frequently focused on the calculation of the potential at large distances from a charge distribution. This problem is of particular importance in atomic physics, in particular in the evaluation of the fields produced by a nucleus and surrounding electrons. Restriction to large distances allows considerable simplification in the evaluation of the right-hand term of (3.16). The basis for an analysis of the far-field potential is the integral

$$I = \int_V \rho(\mathbf{r})\phi(\mathbf{r})\, dV. \tag{3.23}$$

In this expression, $\phi(\mathbf{r})$ (which is not necessarily a potential) is assumed to be continuous — with continuous derivatives — and to vary little over V. Under these conditions, it becomes appropriate to represent ϕ by its power series expansion

$$\begin{aligned}\phi(\mathbf{r}) &= \phi_0 + \sum_{i=1}^{3}\left(\frac{\partial\phi}{\partial x_i}\right)_0 x_i + \frac{1}{2}\sum_{i,j=1}^{3}\left(\frac{\partial^2\phi}{\partial x_i\partial x_j}\right)_0 x_i x_j + \cdots \\ &= \phi_0 + \mathbf{r}\cdot\operatorname{grad}_0\phi + \frac{1}{2}\mathbf{r}\cdot(\operatorname{grad}\operatorname{grad})_0\,\phi\cdot\mathbf{r} + \cdots .\end{aligned} \tag{3.24}$$

The subscript 0 refers to the value of ϕ (and derivatives) at an arbitrarily chosen origin O in V (Fig. 3.3). From the definition of the gradient of a vector given in (A4.48), the dyadic in the right-hand term is given by

$$\operatorname{grad}\operatorname{grad}\phi = \sum_{i,j=1}^{3}\frac{\partial^2\phi}{\partial x_i\partial x_j}\mathbf{u}_i\mathbf{u}_j. \tag{3.25}$$

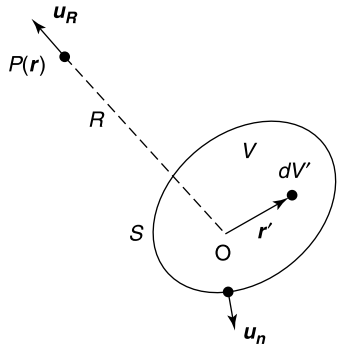

Figure 3.3 A volume containing sources.

Inserting expansion (3.24) into (3.23) yields

$$I = q\phi_0 + \mathbf{p}_e \cdot \text{grad}_0\, \phi + \frac{1}{2}\overline{\overline{q}}_e : (\text{grad grad})_0\, \phi + \cdots \tag{3.26}$$

The *colon double product* is defined in (A4.18). The various moments of ρ are given by

$$q = \int_V \rho\, dV, \qquad \mathbf{p}_e = \int_V \rho \mathbf{r}\, dV, \qquad \overline{\overline{\mathbf{q}}}_e = \int_V \rho \mathbf{r}\mathbf{r}\, dV. \tag{3.27}$$

These considerations may be applied to the potential at a distant point P. Because $|\mathbf{r} - \mathbf{r}'|$ in (3.16) varies little over V, its inverse $|\mathbf{r} - \mathbf{r}'|^{-1}$ is a suitable function for the application of (3.24), which then yields (Fig. 3.3):

$$\begin{aligned} \phi_0 &= \frac{1}{4\pi\epsilon_0 R} \\ \text{grad}_0\, \phi &= \frac{\mathbf{u}_R}{4\pi\epsilon_0 R^2} \\ (\text{grad grad})_0\, \phi &= \frac{1}{4\pi\epsilon_0 R^3}\,(3\mathbf{u}_R\mathbf{u}_R - \overline{\overline{I}}), \end{aligned} \tag{3.28}$$

where $\overline{\overline{I}}$ is the identity dyadic. The last equation is obtained from (A4.86) applied to a vector of radial component $a_R = 1/(4\pi\epsilon_0 R^2)$. Insertion of (3.28) into (3.24) yields, for the potential in P,

$$\phi(\mathbf{r}) = \frac{q}{4\pi\epsilon_0 R} + \frac{\mathbf{p}_e \cdot \mathbf{u}_R}{4\pi\epsilon_0 R^2} + \frac{1}{8\pi\epsilon_0 R^3}\mathbf{u}_R \cdot (3\overline{\overline{q}}_e - \overline{\overline{\mathbf{I}}}\, tr\, \overline{\overline{q}}_e) \cdot \mathbf{u}_R + \cdots . \tag{3.29}$$

The symbol *tr*, which denotes the *trace*, is defined in (A4.7). In (3.29), q is the total charge, $\mathbf{p}_e$ the *electric dipole moment*, and $\overline{\overline{q}}_e$ the *electric quadrupole moment*. The next term, in R^{-4}, is the octupole moment, a term that is not given further consideration in the current text.

The multipole expansion can be obtained directly from the distributional form of the charge density,[§] which is [133]

$$\rho(\mathbf{r}) = q\delta(\mathbf{r}) - \mathbf{p}_e \cdot \text{grad}\ \delta(\mathbf{r}) + \frac{1}{2}\overline{\overline{q}}_e : \text{grad grad}\ \delta(\mathbf{r}) + \cdots . \tag{3.30}$$

The meaning of the various operators is discussed in Appendix 8, for example in (A8.74). In distributional parlance, grad grad δ is defined by applying the general equation (A8.60) to $\delta(\mathbf{r})$, which yields

$$\langle \mathcal{L}\delta(\mathbf{r}), \phi \rangle \stackrel{\text{def}}{=} \left\langle \delta(\mathbf{r}), \mathcal{L}^a \phi \right\rangle = (\mathcal{L}^a \phi)_{\mathbf{r}=0}. \tag{3.31}$$

In such an equation, ϕ is a testing function, and $\mathcal{L}^a$ is the adjoint operator of $\mathcal{L}$. In (3.26), $\mathcal{L}$ is grad grad, and $\mathcal{L}^a$ is equal to $\mathcal{L}$, hence

$$\langle \text{grad grad}\ \delta, \phi \rangle \stackrel{\text{def}}{=} (\text{grad grad})_0\, \phi = \int \phi\ \text{grad grad}\, \delta\, dV. \tag{3.32}$$

This relationship means that, whenever the integral in (3.32) is encountered, it may be replaced by the dyadic $(\text{grad grad})_0\, \phi$. Application of that definition to $|\mathbf{r} - \mathbf{r}'|^{-1}$ reproduces the term in $\overline{\overline{q}}_e$ in (3.29).

The classic multipole expansion (3.29) clearly shows the hierarchy of the various terms of the series. At large distances R, the term in q dominates. If the total charge is zero, it is the dipole term in $\mathbf{p}_e$ that predominates. More generally, the first nonzero term determines the law according to which the potential decreases. These considerations are of major importance in physical chemistry, where the clouds of charge are formed by atoms and molecules [37, 69]. It is therefore useful to look at the various terms of the multipole expansion in some detail.

The first term in (3.29) gives rise to the radial field of a point charge.

The second term (the dipole term) becomes dominant when the particle is neutral, and the + and − charges tend to accumulate in two separate parts of the charged volume (Fig. 3.4*a*). In the simple example of Figure 3.4*b* $\mathbf{p}_e = qd\mathbf{u}$ and the field generated by the

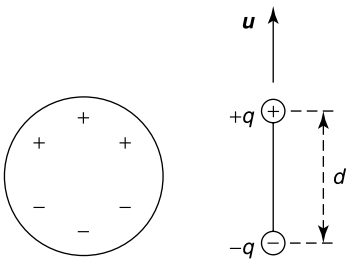

Figure 3.4 (*a*) General dipole source. (*b*) Typical example.

[§]When the charge cloud is concentrated around $\mathbf{r}_0$ instead of the origin, $\delta(\mathbf{r})$ should be replaced by $\delta(\mathbf{r} - \mathbf{r}_0)$ in (3.30).

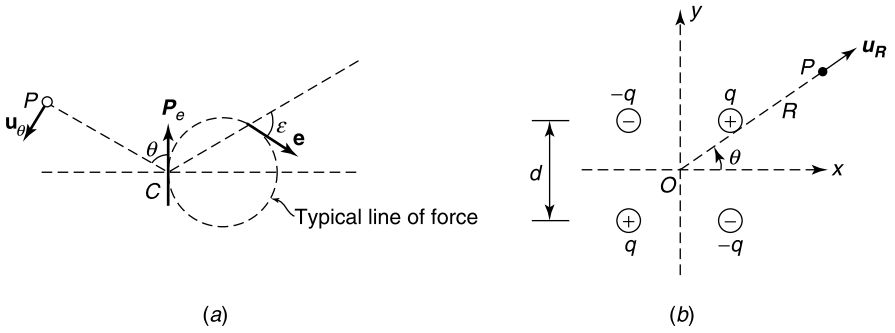

Figure 3.5 (*a*) Electric dipole and its field. (*b*) Point charges forming a square pattern.

dipole is given by (Fig. 3.5*a*)

$$\mathbf{e} = -\text{grad}\left(\frac{p_e \cos\theta}{4\pi\epsilon_0 R^2}\right) = \frac{1}{2\pi\epsilon_0}\frac{p_e\cos\theta}{R^3}\mathbf{u}_R + \frac{1}{4\pi\epsilon_0}\frac{p_e\sin\theta}{R^3}\mathbf{u}_\theta$$
$$= \frac{1}{4\pi\epsilon_0 R^3}\left[3(\mathbf{p}_e\cdot\mathbf{u}_R)\mathbf{u}_R - \mathbf{p}_e\right] = \frac{1}{4\pi\epsilon_0 R^3}\mathbf{p}_e\cdot\left[3\mathbf{u}_R\mathbf{u}_R - \bar{\bar{I}}\right]. \tag{3.33}$$

We notice that **e** decreases like $(1/R^3)$.

The third term gives rise to a quadrupole contribution. A simple quadrupole is shown in Figure 3.5*b*. It consists of two antiparallel dipoles in a square pattern, and the relevant dyadic is here

$$\bar{\bar{q}}_e = qd^2(\mathbf{u}_x\mathbf{u}_y + \mathbf{u}_y\mathbf{u}_x). \tag{3.34}$$

In the (xy) plane, the generated potential is of the form

$$\phi = \frac{3qd^2}{8\pi\epsilon_0 R^3}\sin 2\theta. \tag{3.35}$$

The corresponding field is proportional to $(1/R^4)$. We notice that, as we go down the multipole expansion [23, 29], the successive terms decrease like $(1/R), (1/R^2), (1/R^3)\ldots$. Clearly, the range of the potential goes down as the order of the multipole term increases. This property is germane for a proper understanding of the interactions between particles.

3.4 POTENTIAL GENERATED BY A SINGLE LAYER OF CHARGE

A single layer of charge density $\rho_S(\text{C m}^{-2})$ can be represented by a volume density

$$\rho(\mathbf{r}) = \rho_S(\mathbf{r})\delta_S \qquad (\mathbf{r} \text{ on } S). \tag{3.36}$$

The meaning of the distribution δ_S is defined in A8.24. Thus,

$$\int_{\text{all space}} \delta_S\phi(\mathbf{r})\,dV \overset{\text{def}}{=} \int_S \phi(\mathbf{r})\,dS. \tag{3.37}$$

Applied to the volume integral (3.16), this definition gives

$$\phi(\mathbf{r}) = \lim_{\delta \to 0} \frac{1}{4\pi\epsilon_0} \int_{S-S_\delta} \frac{\rho_S(\mathbf{r}')}{|\mathbf{r} - \mathbf{r}'|}\, dS' \tag{3.38}$$

where S_δ is a small area of arbitrary shape containing P and of maximum chord δ. The integral (3.38) implies that the contribution from S_δ can be ignored in a numerical process, as it is compressed "into oblivion" as δ approaches zero. In practice, however, S is divided into small elements S_i, one of which is taken to be S_δ. This element is *not* infinitely small, hence its contribution to the integral may not be negligible. Fortunately, this contribution (the "self-patch") is known for a few simple shapes of S_δ associated with simple laws of variation of ρ_S. Some of these are given at the end of the current section.

In potential theory, one discusses the general integral

$$I_5(\mathbf{r}) = \int_S \frac{f(\mathbf{r}')}{|\mathbf{r} - \mathbf{r}'|}\, dS' \qquad (\mathbf{r}' \text{ on } S). \tag{3.39}$$

The theory first proves that

$$I_6(\mathbf{r}) = \int_S \frac{dS'}{|\mathbf{r} - \mathbf{r}'|^\beta} \tag{3.40}$$

is convergent when $0 < \beta < 2$. In addition, if $f(\mathbf{r}')$ is bounded and integrable, $I_5(\mathbf{r})$ converges and is Hölder continuous in all space [153]. The surface S should be sufficiently regular for these properties to hold[¶] (the most important examples of irregularities are edges and vertices, which are discussed in detail in Chapter 5). Given the nature of the charge distribution (strongly concentrated in the normal direction), it is not surprising that the continuity of $f(\mathbf{r})$ may not suffice to ensure the existence of the *electric field integral* [158]

$$\mathbf{I}_7(\mathbf{r}) = \int_S f(\mathbf{r}') \frac{\mathbf{r} - \mathbf{r}'}{|\mathbf{r} - \mathbf{r}'|^3}\, dS'. \tag{3.41}$$

Examples are known for which $\mathbf{I}_7(\mathbf{r})$ is unbounded [153, 158]. On the other hand, if $f(\mathbf{r})$ is Hölder continuous on S,

$$\mathbf{I}_7(\mathbf{r}) = -\text{grad}\, I_5(\mathbf{r}),$$

and $\mathbf{I}_7(\mathbf{r})$ is Hölder continuous at points outside S. The theory also proves that the tangential components of $\mathbf{I}_7(\mathbf{r})$ approach a well-defined limit as $\mathbf{r}$ approaches a point P or S along the normal. The proof is delicate because the integrand in $\mathbf{I}_7(\mathbf{r})$ is affected by a $|\mathbf{r} - \mathbf{r}'|^{-2}$ type of singularity; that is, by an exponent $\beta = 2$ in (3.40). The first step consists in splitting S into two parts: a small *circle* S_δ of radius a, centered in $\mathbf{r}$, and the remaining part of S, viz. $(S - S_\delta)$ [158]. Because of the circular symmetry of S_δ, the *self-patch* contribution from S_δ

[¶]The *surface S* should be of the *Lyapunov* type; that is, it should have the following properties [153]:

- Have a well-defined tangent at each point.
- If β is the angle between the normals at points P and Q, and d is the distance between these points, β should satisfy the condition $\beta < Ad^\alpha$, where A and α are constants, and $0 < \alpha \leq 1$.
- For all points P of the surface, there exists a fixed length l such that the portion of S inside a sphere of radius l about P intersects lines parallel to the normal at P in at most one point.

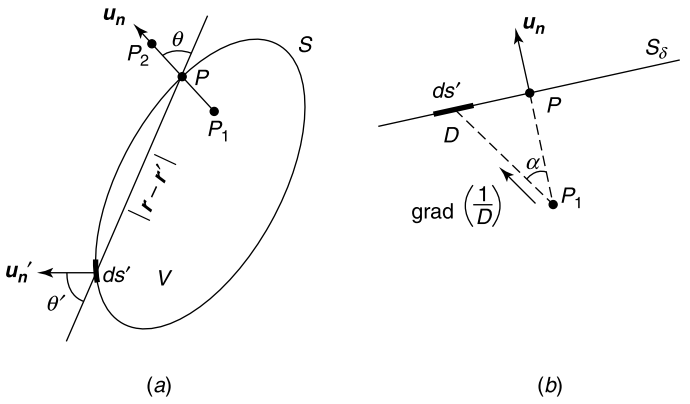

Figure 3.6 (*a*) Relevant for the properties of surface layers. (*b*) Evaluation of the self-patch contribution.

approaches zero with a (see also Section 12.1while the contribution from $(S - S_\delta)$ remains bounded. We shall therefore define $\mathbf{I}_7$ as the limit

$$\mathbf{I}_7(\mathbf{r}) = \lim_{\delta\to 0} \int_{S-S_\delta} f(\mathbf{r}') \frac{\mathbf{r}-\mathbf{r}'}{|\mathbf{r}-\mathbf{r}'|^3}\, dS' \tag{3.42}$$

where S_δ is a small circle centered on $\mathbf{r}$.

The study of the normal derivatives is simpler. If $f(\mathbf{r})$ is continuous at P, $\partial I_5/\partial n$ approaches limits as P_1 and P_2 approach P along the normal (Fig. 3.6*a*). To evaluate these limits, we shall again excise a *small* S_δ of *arbitrary shape* from S. For the approach $P_1 \to P$, we may write [assuming $f(\mathbf{r})$ to be practically constant on S_δ]

$$\begin{aligned}\frac{\partial}{\partial n}\int_{S_\delta} \frac{\mathbf{f}(\mathbf{r}')}{|\mathbf{r}-\mathbf{r}'|}\, dS' &= f(\mathbf{r}_P)\int_{S_\delta}\left(\mathbf{u}_n \cdot \operatorname{grad}\frac{1}{|\mathbf{r}-\mathbf{r}'|}\right) dS' \\ &= f(\mathbf{r}_P)\int_{S_\delta}\frac{1}{D^2}\cos\alpha \cdot dS' = f(\mathbf{r}_P)\int_{S_\delta} d\Omega',\end{aligned}$$

where $D = |\mathbf{r} - \mathbf{r}'|$, and $d\Omega'$ is the solid angle subtended by dS' (Fig. 3.6*b*). As P_1 gets closer to P, the integral $\displaystyle\int_{S_\delta} d\Omega'$ approaches 2π. A similar argument for P_2 gives (-2π). The final formulas are therefore[‖]

$$\lim_{P_1\to P}\frac{\partial I_5}{\partial n} = 2\pi f(\mathbf{r}_P) + \lim_{\delta\to 0}\int_{S-S_\delta} f(\mathbf{r}')\frac{\partial}{\partial n}\left(\frac{1}{|\mathbf{r}-\mathbf{r}_P|}\right) dS' \tag{3.43}$$

$$\lim_{P_2\to P}\frac{\partial I_5}{\partial n} = -2\pi f(\mathbf{r}_P) + \lim_{\delta\to 0}\int_{S-S_\delta} f(\mathbf{r}')\frac{\partial}{\partial n}\left(\frac{1}{|\mathbf{r}-\mathbf{r}_P|}\right) dS'. \tag{3.44}$$

[‖]For the sake of compactness, one often replaces the limits

$$\lim_{\delta\to 0}\int_{V-V_\delta} g(\mathbf{r},\mathbf{r}')\, dV'; \qquad \lim_{\delta\to 0}\int_{S-S_\delta} g(\mathbf{r},\mathbf{r}')\, dS'$$

by the symbols $\displaystyle\int_V g(\mathbf{r},\mathbf{r}')\, dV'$ or $\displaystyle\int_S g(\mathbf{r},\mathbf{r}')\, dS'$.

In electrostatics, $f(\mathbf{r})$ is $(\rho_S(\mathbf{r})/4\pi\epsilon_0)$, hence,

$$\lim_{P_1 \to P} \frac{\partial \phi(\mathbf{r})}{\partial n} = \frac{\rho_S(P)}{2\epsilon_0} + \frac{1}{4\pi\epsilon_0} \lim_{\delta \to 0} \int_{S-S_\delta} \rho_S(\mathbf{r}') \frac{\partial}{\partial n} \left(\frac{1}{|\mathbf{r}' - \mathbf{r}_P|} \right) dS' \tag{3.45}$$

$$\lim_{P_2 \to P} \frac{\partial \phi(\mathbf{r})}{\partial n} = -\frac{\rho_S(P)}{2\epsilon_0} + \frac{1}{4\pi\epsilon_0} \lim_{\delta \to 0} \int_{S-S_\delta} \rho_S(\mathbf{r}') \frac{\partial}{\partial n} \left(\frac{1}{|\mathbf{r} - \mathbf{r}'_P|} \right) dS'. \tag{3.46}$$

These equations show that $(\partial\phi/\partial n)$ *decreases* by (ρ_S/c_0) when the observer crosses S from P_1 to P_2. Because $\mathbf{e} = -\text{grad}\ \phi$, the normal component e_n *increases* by the same amount as the observer proceeds from P_1 to P_2.

Some Self-Patch Contributions

For a rectangle and a uniform ρ_S, [54, part 1] (Fig. 3.7*a*),

$$\phi(0) = \frac{\rho_S}{2\pi\epsilon_0} \left(a \log_e \frac{b + \sqrt{(a^2 + b^2)}}{a} + b \log_e \frac{a + \sqrt{(a^2 + b^2)}}{b} \right) \tag{3.47}$$

$$\phi(Q) = \frac{\rho_S}{4\pi\epsilon_0} \left(2a \log_e \frac{b + \sqrt{(4a^2 + b^2)}}{2a} + b \log_e \frac{2a + \sqrt{(4a^2 + b^2)}}{b} \right). \tag{3.48}$$

Formulas for the potential outside the rectangle can be found in [54, volume 1] and [188]. For a square, for which $a = b$,

$$\begin{aligned} \phi(0) &= (\rho_S a/\pi\epsilon_0) \log_e(1 + \sqrt{2}) = 0.2805\ \rho_S a/\epsilon_0 \\ \phi(Q) &= (\rho_S a/4\pi\epsilon_0) \log_e \left(\frac{11 + 5\sqrt{5}}{2} \right) = 0.1915\ \rho_S a/\epsilon_0. \end{aligned} \tag{3.49}$$

On a circular disk carrying a uniform charge density (Fig. 3.7*b*)

$$\phi(r) = (\rho_S a/\pi\epsilon_0) E(r/a), \tag{3.50}$$

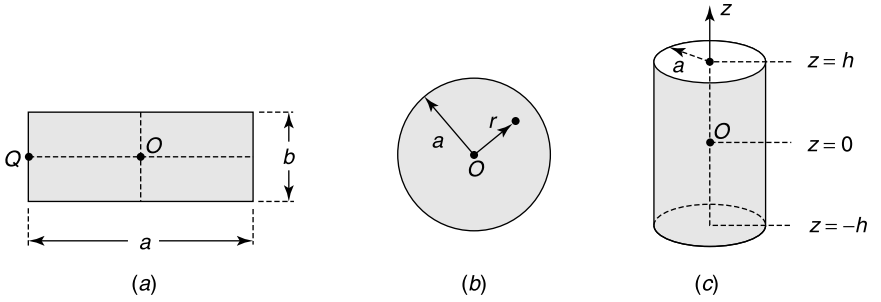

Figure 3.7 Uniformly charged surfaces: (*a*) rectangular plate, (*b*) circular disk, (*c*) hollow metallic circular cylinder.

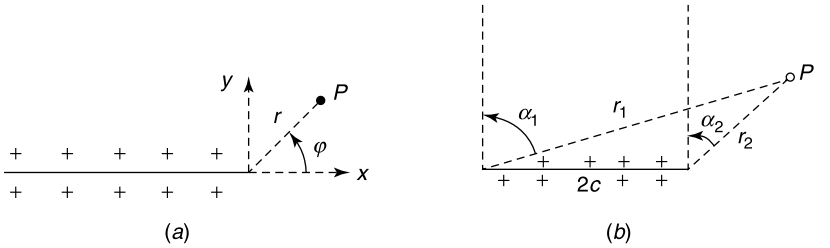

Figure 3.8 Surface charge distributions: (*a*) half plane carrying ρ_S, (*b*) band carrying ρ_S.

where E is the elliptic integral of the second kind [144]

$$E(x) = \int_0^{\frac{\pi}{2}} \sqrt{(1 - x^2 \sin^2 \varphi)} d\varphi. \tag{3.51}$$

At the center of the disk,

$$\phi(0) = \rho_S a / 2\epsilon_0. \tag{3.52}$$

At the central axial point 0 of a uniformly charged thin-walled cylinder (Fig. 3.7*c*)

$$\phi(0) = (\rho_s a/\epsilon_0) \log_e \left\{ h/a + \sqrt{[1 + (h/a)^2]} \right\}. \tag{3.53}$$

It is useful, for numerical purposes, to know how potential and electric field behave near the *edge* of an open surface (which could be a circular disk or a rectangular plate). To that effect, we consider the edge of a *half-plane* carrying a *uniform* charge density ρ_S (Fig. 3.8*a*). There [54, volume 1]

$$\begin{aligned} \phi &= \frac{\rho_S}{2\pi\epsilon_0} \left[x \log_e \frac{r}{L} - y\varphi - x \right] + \text{const.} \\ e_x &= \frac{\rho_S}{2\pi\epsilon_0} \log_e \frac{L}{r} \\ e_y &= \frac{\rho_S}{2\pi\epsilon_0} \varphi \end{aligned} \tag{3.54}$$

where L is a reference length. For a *band*** of width $2c$ (Fig. 3.8*b*):

$$\begin{aligned} \phi &= \frac{\rho_S}{2\pi\epsilon_0} \left[(c + x) \log_e \frac{L}{r_1} + (c - x) \log_e \frac{L}{r_2} + 2c - y(\alpha_1 - \alpha_2) \right] \\ e_x &= \frac{\rho_S}{2\pi\epsilon_0} \log_e \frac{r_1}{r_2} \\ e_y &= \frac{\rho_S}{2\pi\epsilon_0} (\alpha_1 - \alpha_2). \end{aligned} \tag{3.55}$$

These formulas hold for *curved* edges, provided r remains small with respect to the radius of curvature of the edge.

**Formula for ϕ courtesy of Dr. R. De Smedt.

3.5 POTENTIAL GENERATED BY A DOUBLE LAYER OF CHARGE

The layer consists of dipoles perpendicular to S and of density $\tau(\mathbf{r})$ (in C m^{-1}). The distributional form of the corresponding volume density is

$$\rho(\mathbf{r}) = -\tau(\mathbf{r})\frac{\partial \delta_S}{\partial n}. \tag{3.56}$$

The meaning of $(\partial\delta_S/\partial n)$ is defined in (A8.67). Thus,

$$\int_{\text{all space}} f(\mathbf{r})\frac{\partial \delta_S}{\partial n}\,\phi(\mathbf{r})\,dV \overset{\text{def}}{=} -\int_S f(\mathbf{r})\,\frac{\partial \phi}{\partial n}\,dS. \tag{3.57}$$

From (3.29), the potential in P due to the double layer takes the form (Fig. 3.9)

$$\phi(\mathbf{r}) = \frac{1}{4\pi\epsilon_0}\int_S \frac{\tau(\mathbf{r}')\cos\theta'}{|\mathbf{r}-\mathbf{r}'|^2}\,dS' = \frac{1}{4\pi\epsilon_0}\int_S \tau(\mathbf{r}')\frac{\partial}{\partial n'}\left(\frac{1}{|\mathbf{r}-\mathbf{r}'|}\right)dS'. \tag{3.58}$$

The dipole layer is assumed ideal, which implies that the distance d in Figure 3.9 is *infinitesimal*. If, on the contrary, the double layer is formed by a single layer of positive density ρ_{S1} on a surface S_1, separated by a *nonzero* (but small) distance d from a negative single layer $-\rho_S$ on S, charge neutrality requires that

$$\rho_{S_1} = \rho_S\frac{dS}{dS_1} = \rho_S\frac{1}{1-Jd} \approx \rho_S(1+Jd), \tag{3.59}$$

where J is the first curvature defined in (A3.5), viz.

$$J = \frac{1}{R_1} + \frac{1}{R_2}, \tag{3.60}$$

and R_1, R_2 are the principal radii of curvature, positive when the vector connecting P to the center of curvature is in the direction of $\mathbf{u}_n$ (both R_1 and R_2 are therefore negative for the convex surface shown in Fig. 3.9). If S_1 carries a charge ρ_S, instead of the value (3.59), the layer will consist of a genuine dipole layer supplemented by a single layer of density $-\rho_S Jd = -J\tau$ (Problem 3.8).

In potential theory, the attention is focused on the integral (Fig. 3.9)

$$I_8(\mathbf{r}) = \int_S f(\mathbf{r}')\frac{\partial}{\partial n'}\left(\frac{1}{|\mathbf{r}-\mathbf{r}'|}\right)dS' = \int_S f(\mathbf{r}')\frac{\cos\theta'}{|\mathbf{r}-\mathbf{r}'|^2}\,dS'. \tag{3.61}$$

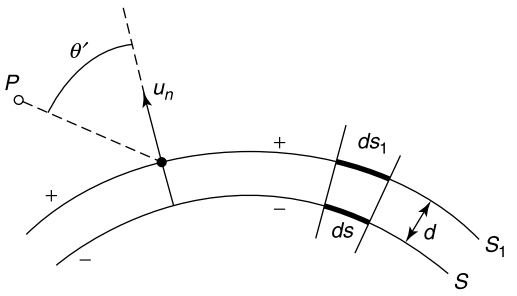

Figure 3.9 Details of a double layer.

Assume that $f(\mathbf{r})$ is piecewise continuous. We first note that $I_8(\mathbf{r})$ has a meaning when P is *on* the surface, in which case the integral converges to [158]

$$I_8(\mathbf{r}_P) = \lim_{\delta \to 0} \int_{S - S_\delta} f(\mathbf{r}') \frac{\partial}{\partial n'} \left(\frac{1}{|\mathbf{r} - \mathbf{r}'|} \right) dS'. \tag{3.62}$$

This integral is Hölder continuous at $\mathbf{r}_P$ when $f(\mathbf{r})$ is bounded and integrable [153]. Let now P_1 and P_2 approach P along the normal (Fig. 3.6*a*). To the value (3.62) we must now add the contribution ΔI_8 from the small excised area S_δ. This can be done by writing ΔI_8 in the form

$$\Delta I_8(\mathbf{r}) = \int_{S_\delta} \frac{f(\mathbf{r}') \cos \theta'}{|\mathbf{r} - \mathbf{r}'|^2} \, dS = \int_S f(\mathbf{r}') \, d\Omega' \tag{3.63}$$

where $d\Omega'$ is the elementary solid angle subtended by dS' (Fig. 3.10*a*). This angle is positive when P is on the positive side of the dipoles and negative in the opposite case. In the approach $P_2 \to P$, the solid angle subtended by S_δ approaches 2π, whereas for $P_1 \to P$ it approaches -2π. The (3.63) integrals then yield $2\pi f$ and $(-2\pi f)$, respectively, and this independently of the shape of S_δ. We may therefore write

$$\lim_{P_1 \to P} I_8(\mathbf{r}) = -2\pi f(\mathbf{r}_P) + I_8(\mathbf{r}_P) \tag{3.64}$$

$$\lim_{P_2 \to P} I_8(\mathbf{r}) = 2\pi f(\mathbf{r}_P) + I_8(\mathbf{r}_P). \tag{3.65}$$

Applied to the potential (3.58), these formulas give

$$\lim_{P_1 \to P} \phi(\mathbf{r}) = -\frac{\tau(\mathbf{r}_P)}{2\epsilon_0} + \frac{1}{4\pi\epsilon_0} \lim_{\delta \to 0} \int_{S - S_\delta} \tau(\mathbf{r}') \frac{\partial}{\partial n'} \left(\frac{1}{|\mathbf{r} - \mathbf{r}'|} \right) dS' \tag{3.66}$$

$$\lim_{P_2 \to P} \phi(\mathbf{r}) = \frac{\tau(\mathbf{r}_P)}{2\epsilon_0} + \frac{1}{4\pi\epsilon_0} \lim_{\delta \to 0} \int_{S - S_\delta} \tau(\mathbf{r}') \frac{\partial}{\partial n'} \left(\frac{1}{|\mathbf{r} - \mathbf{r}'|} \right) dS'. \tag{3.67}$$

It is clear that $\phi(\mathbf{r})$ suffers a jump τ/ϵ_0 when passing through the layer from the negative to the positive side. This property is in harmony with the common conception of a double-layer as representing a charged "battery."

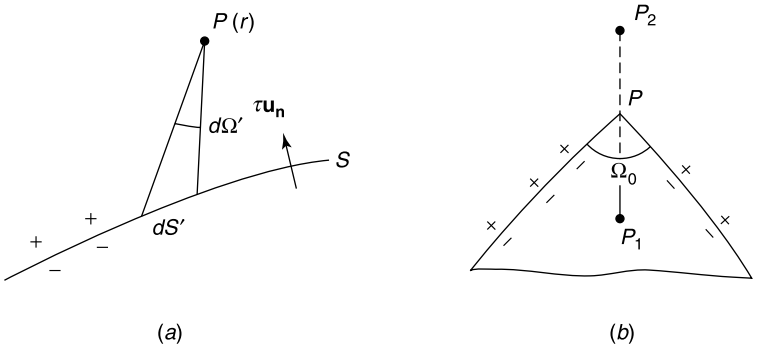

Figure 3.10 (*a*) Double layer and elementary solid angle. (*b*) A surface with a conical point P_0.

In the derivation of both (3.45, 3.46) and (3.66, 3.67), the evaluation of the contribution from a small S_δ was central. It is useful to recapitulate the main results of that analysis, namely

$$\lim_{P_1 \to P} \int_{S_\delta} \frac{\partial}{\partial n} \left(\frac{1}{|\mathbf{r} - \mathbf{r}'|} \right) dS' = - \lim_{P_1 \to P} \int_{S_\delta} \frac{\partial}{\partial n'} \left(\frac{1}{|\mathbf{r} - \mathbf{r}'|} \right) dS' = 2\pi \tag{3.68}$$

$$\lim_{P_2 \to P} \int_{S_\delta} \frac{\partial}{\partial n} \left(\frac{1}{|\mathbf{r} - \mathbf{r}'|} \right) dS' = - \lim_{P_2 \to P} \int_{S_\delta} \frac{\partial}{\partial n'} \left(\frac{1}{|\mathbf{r} - \mathbf{r}'|} \right) dS' = -2\pi. \tag{3.69}$$

Such equations will prove to be essential for the formulation of problems in terms of integral equations. Note that they can be modified to accommodate a point P at the apex of a *cone* of opening solid angle Ω_0 (Fig. 3.10*b*). The limit solid angles are now $(4\pi - \Omega_0)$ for P_2, and $(-\Omega_0)$ for P_1. The first terms on the right-hand sides of (3.66) and (3.67) must now be written as

$$\begin{aligned} -\frac{\Omega_0}{4\pi} \frac{\tau(P)}{\epsilon_0} \quad &\text{for } P_1 \\ \left(1 - \frac{\Omega_0}{4\pi}\right) \frac{\tau(P)}{\epsilon_0} \quad &\text{for } P_2. \end{aligned} \tag{3.70}$$

The potential jump remains equal to (τ/ϵ_0).

The previous analysis shows that, when a closed surface is covered with a uniform density of dipoles oriented along the outward-drawn normal, the external potential is zero, the internal potential is $(-\tau/\epsilon_0)$, and the potential at a point in the dipole layer is $-\tau/2\epsilon_0$.

Although ϕ suffers a step discontinuity across a double layer, the *normal derivatives* approach identical limits as P_1 and P_2 approach P, provided τ has continuous first and second derivatives at P. If τ is simply continuous, a weaker property holds, namely, that $(\partial\phi/\partial n)_{P_1} - (\partial\phi/\partial n)_{P_2}$ approaches zero when P_1 and P_2 approach P while remaining equidistant from that point. The *tangential derivatives* in any direction s satisfy

$$\left(\frac{\partial \phi}{\partial s}\right)_{P_2} - \left(\frac{\partial \phi}{\partial s}\right)_{P_1} = \frac{1}{\epsilon_0} \left(\frac{\partial \tau}{\partial s}\right)_P. \tag{3.71}$$

This relationship is a direct consequence of the discontinuity (τ/ϵ_0) suffered by ϕ across S. In terms of the electric field:

$$\mathbf{e}_{\tan}(P_2) - \mathbf{e}_{\tan}(P_1) = -\frac{1}{\epsilon_0} \mathrm{grad}_S\, \tau. \tag{3.72}$$

When τ is not distributed uniformly over S, continuity of the tangential component of $\mathbf{e}$ — often presented as a general property — does *not* hold (see Problem 3.9). A discontinuity in $\mathbf{e}_{\tan}$ arises, for example, when contact potentials vary from point to point under the influence of factors such as temperature gradients.

Near the edge of a *double layer* of uniform density τ, potential and field behave according to (Fig. 3.11)

$$\begin{aligned} \phi(P) &= \frac{\tau}{2\pi\epsilon_0}\, \varphi + \text{const.} \\ \mathbf{e}(P) &= -\frac{\tau}{2\pi\epsilon_0 r}\, \mathbf{u}_\varphi. \end{aligned} \tag{3.73}$$

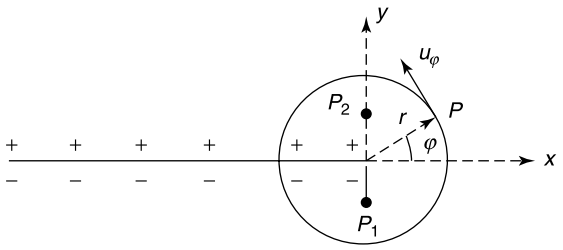

Figure 3.11 Half plane carrying a dipole density τ.

The equipotentials are radial and the lines of force circular. This edge behavior occurs, for example, at the end of a metallic junction, where τ represents a contact potential. A sudden interruption of the layer gives rise to a term $\text{grad}_S\, \tau = -\tau\delta(x)\mathbf{u}_x$ in (3.72). The resulting discontinuity in e_x may be verified by plotting $e_x(x)$ along horizontal lines through P_1 and P_2, at a very small distance y from the central plane (Problem 3.10).

3.6 POTENTIAL GENERATED BY A LINEAR CHARGE

The volume charge density of a linear charge of density ρ_l (in C m^{-1}) may be written as (Fig. 3.12*a*)

$$\rho = \rho_l \delta_l. \tag{3.74}$$

The operational definition of δ_l can be found in (A8.29). Thus,

$$\int_{\text{all space}} \rho_l \delta_l \, \phi(\mathbf{r})\, dV = \int_C \rho_l \, \phi(\mathbf{r})\, dc. \tag{3.75}$$

Such a linear charge generates a potential

$$\phi(\mathbf{r}) = \frac{1}{4\pi\epsilon_0} \int_C \frac{\rho_l(\mathbf{r}')\, dc'}{|\mathbf{r} - \mathbf{r}'|}. \tag{3.76}$$

This potential approaches infinity as the charge is approached, but in such a manner that

$$\lim_{Q \to P} D \frac{\partial \phi}{\partial D} = -\frac{\rho_l}{2\pi\epsilon_0}. \tag{3.77}$$

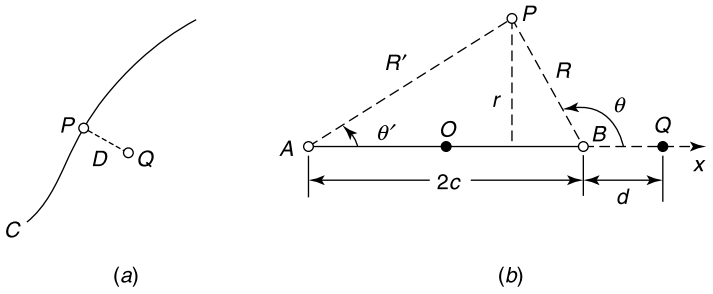

Figure 3.12 (*a*) Linear charge on an arc. (*b*) Straight segment carrying a uniform charge density.

Consider, in particular, a straight segment with uniform linear density ρ_l (Fig. 3.12*b*). Outside this segment the generated potential is

$$\phi(P) = \frac{\rho_l}{4\pi\epsilon_0}\int_{-c}^{+c}\frac{dx}{[(x-x_P)^2+r^2]^{\frac{1}{2}}} = \frac{\rho_l}{4\pi\epsilon_0}\log_e\frac{x_P+c+R'}{x_P-c+R}. \tag{3.78}$$

Let us see what happens when P is *on* the line. Setting $r = 0$ in (3.72) gives

$$\begin{aligned}\lim_{\epsilon\to 0}\phi &= \frac{\rho_l}{4\pi\epsilon_0}\left[\int_{-c}^{x-\epsilon}\frac{dx'}{x-x'}+\int_{x+\epsilon}^{c}\frac{dx'}{x'-x}\right]\\ &= \frac{\rho_l}{4\pi\epsilon_0}\left[\log_e(c^2-x^2)-2\log_e\epsilon\right].\end{aligned} \tag{3.79}$$

This integral does *not* converge [54, volume 1]. It becomes convergent, however, for a point on the axis *outside* the charges, say mean Q in Figure 3.12*b*. For such a point:

$$\begin{aligned}\phi(Q) &= \frac{\rho_l}{4\pi\epsilon_0}\log_e\frac{|x|+c}{|x|-c}\\ |e_x(Q)| &= \frac{\rho_l}{2\pi\epsilon_0}\frac{c}{x^2-c^2}.\end{aligned} \tag{3.80}$$

On the charged segment itself, the field is axial and equal to

$$|\mathbf{e}| = |e_x| = \frac{\rho_l}{2\pi\epsilon_0}\frac{|x|}{c^2-x^2}.$$

The equipotentials are prolate spheroids with foci at the end points, and the lines of force are hyperboles with the same foci. For P outside the charges:

$$\begin{aligned}\phi(P) &= \frac{\rho_l}{4\pi\epsilon_0}\log_e\frac{R+R'+2c}{R+R'-2c}\\ &= \frac{\rho_l}{4\pi\epsilon_0}\log_e\frac{\tan\left(\frac{\theta}{2}\right)}{\tan\left(\frac{\theta'}{2}\right)}.\end{aligned} \tag{3.81}$$

Also (Problem 3.11):

$$\begin{aligned}e_x &= \frac{\rho_l}{4\pi\epsilon_0}\left(\frac{1}{R}-\frac{1}{R'}\right)\\ e_r &= \frac{\rho_l}{4\pi\epsilon_0}\left[\frac{1}{R'}\tan\left(\frac{\theta'}{2}\right)-\frac{1}{R}\tan\left(\frac{\theta}{2}\right)\right].\end{aligned} \tag{3.82}$$

For an observer approaching a point on the segment, R and R' become

$$\begin{aligned}R' &\approx (c+x)+\frac{1}{2}\frac{r^2}{(c+x)}\\ R &\approx (c-x)+\frac{1}{2}\frac{r^2}{(c-x)}.\end{aligned}$$

These approximations yield a potential

$$\lim_{r\to 0}\phi(P) \approx \frac{\rho_l}{2\pi\epsilon_0}\log_e\frac{2\sqrt{c^2-x^2}}{r}. \tag{3.83}$$

The corresponding e_r is proportional to $\dfrac{1}{r}$ and dominates the e_x component. The electric field is therefore perpendicular to the segment.

It is important to determine how potential and field vary near the *tip* of the charged segment, say near B (Fig. 3.12*b*). In terms of R and θ one finds

$$\begin{aligned}\phi &\approx \frac{\rho_l}{4\pi\epsilon_0}\log_e\frac{2l}{R(1+\cos\theta)}\\ \mathbf{e} &\approx \frac{\rho_l}{4\pi\epsilon_0}\left[\frac{1}{R}\mathbf{u}_R - \frac{1}{R}\tan\frac{\theta}{2}\mathbf{u}_\theta\right].\end{aligned} \tag{3.84}$$

At point Q, on the axis:

$$|\mathbf{e}| \approx \frac{\rho_l}{4\pi\epsilon_0}\frac{1}{d}. \tag{3.85}$$

Formulas such as (3.84) are helpful in selecting trial functions for ϕ (or $(\mathbf{e})$ in the vicinity of A (or B). *Imposing* the behavior (3.84) on these functions can improve the convergence of the numerical algorithm. Furthermore, the validity of analytical solutions can be checked by observing whether the obtained results for ϕ and $\mathbf{e}$ behave according to (3.84). These remarks explain why so much attention is devoted to singularities in this book.

3.6.1 A Distributional Approach

Section 1.4 shows how a distributional equation such as (1.38) may serve to predict the singularity of a Green's function. It is instructive to investigate whether a similar approach can lead to the correct discontinuities of the potential across single and double layers of charge. To that effect, let a function $f(\mathbf{r})$ be continuous in space (together with its derivatives), except on a surface S, where f itself suffers a discontinuity $(f_1 - f_2)$ and its normal derivative a discontinuity $\left(\dfrac{\partial f}{\partial n}\right)_1 - \left(\dfrac{\partial f}{\partial n}\right)_2$ (Fig. 3.13). Under these circumstances, the distributional form of the Laplacian becomes, from (A8.96),

$$\nabla^2 f = \left\{\nabla^2 f\right\} + \left[\left(\frac{\partial f}{\partial n}\right)_1 - \left(\frac{\partial f}{\partial n}\right)_2\right]\delta_S + (f_1 - f_2)\frac{\partial \delta_S}{\partial n}. \tag{3.86}$$

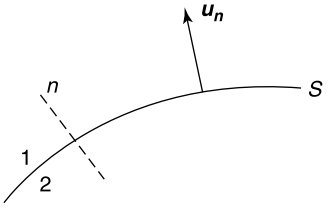

Figure 3.13 A surface of discontinuity.

The term between curly brackets is the value of the Laplacian everywhere but on S. On the other hand, from (3.36) and (3.56), Poisson's equation for single and double layers may be written as

$$\nabla^2\phi = -\frac{1}{\epsilon_0}\rho_S\delta_S + \frac{1}{\epsilon_0}\tau\frac{\partial\delta_S}{\partial n}. \tag{3.87}$$

Comparing (3.86) and (3.87) shows immediately that

$$\epsilon_0 e_{n1} - \epsilon_0 e_{n2} = \rho_S$$
$$\phi_1 - \phi_2 = \frac{\tau}{\epsilon_0}.$$

These are precisely the classic boundary conditions.

Consider now a vector $\mathbf{f}$, continuous everywhere outside S together with its derivatives. The tangential derivatives are assumed to suffer a discontinuity $(\mathbf{u}_n \times \mathbf{f})_1 - (\mathbf{u}_n \times \mathbf{f})_2$ across S. In addition, $\mathbf{f}$ becomes infinite in the (infinitely narrow) transition zone between 2 and 1, with the restriction that $\int_2^1 \mathbf{f}\cdot\mathbf{u}_n\, dn = U$. Then, from (A8.98),

$$\text{curl}\,\mathbf{f} = \{\text{curl}\,\mathbf{f}\} + \left[\mathbf{u}_n \times (\mathbf{f}_1 - \mathbf{f}_2) - \mathbf{u}_n \times \text{grad}_S\, U\right]\delta_S. \tag{3.88}$$

Let us apply this equation to the electric field $\mathbf{e} = -\text{grad}\,\phi$. Maxwell's equations require curl $\mathbf{e}$ to vanish throughout space. As a consequence, U becomes minus the potential increase $(\phi_2 - \phi_1)$. From (3.66) and (3.67), this increase is also (τ/ϵ_0). It follows that

$$(\mathbf{e}_{\text{tan}})_1 - (\mathbf{e}_{\text{tan}})_2 = -\text{grad}_S\frac{\tau}{\epsilon_0},$$

which is precisely (3.72).

We now turn to the divergence equation (A8.97), viz.

$$\text{div}\,\mathbf{f} = \{\text{div}\,\mathbf{f}\} + \mathbf{u}_n\cdot(\mathbf{f}_1 - \mathbf{f}_2)\delta_S + U\frac{\partial\delta_S}{\partial n}. \tag{3.89}$$

Comparison with

$$\epsilon_0\,\text{div}\,\mathbf{e} = \rho_S\delta_S - \tau\frac{\partial\delta_S}{\partial n}$$

now yields the classic boundary conditions

$$\epsilon_0(e_{n1} - e_{n2}) = \rho_S$$
$$U = -\frac{\tau}{\epsilon_0}.$$

3.6.2 An Equivalence Theorem

Let V be a volume in which no sources are present (Fig. 3.14). The potential in V satisfies

$$\nabla^2\phi = 0$$

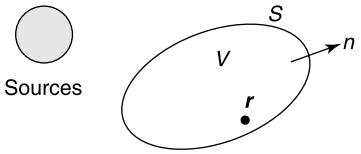

Figure 3.14 Relevant for the equivalence theorem.

while

$$\nabla^2\left(\frac{1}{|\mathbf{r}-\mathbf{r}'|}\right) = -4\pi\,\delta(\mathbf{r}-\mathbf{r}').$$

An application of Green's theorem (A1.31)[††] to these function gives, for $\mathbf{r}$ in V,

$$\phi(\mathbf{r}) = \frac{1}{4\pi}\int_S \left[\frac{1}{|\mathbf{r}-\mathbf{r}'|}\frac{\partial\phi}{\partial n'} - \phi\frac{\partial}{\partial n'}\left(\frac{1}{|\mathbf{r}-\mathbf{r}'|}\right)\right] dS'. \tag{3.90}$$

Potential ϕ is generated by the exterior sources, but to an observer in V who does not know of the existence of these sources, ϕ can be felt as produced by a surface charge density $\rho_S = \epsilon_0\dfrac{\partial\phi}{\partial n'}$ together with a dipole layer of density $\tau = -\epsilon_0\phi$. Note that $\dfrac{\partial\phi}{\partial n'}$ is the value of the normal derivative just inside S. We also note that the surface integral in (3.90) vanishes when $\mathbf{r}$ lies outside V.

The same kind of argument can be applied to the volume exterior to S, where $\nabla^2\phi = -(\rho/\epsilon_0)$. Green's theorem now yields

$$\phi(\mathbf{r}) = \underbrace{\frac{1}{4\pi\epsilon_0}\int_{\text{sources}}\frac{\rho(\mathbf{r}')}{|\mathbf{r}-\mathbf{r}'|}\,dV'}_{\phi^i(\mathbf{r})} + \int_S\left[\phi\frac{\partial}{\partial n'}\left(\frac{1}{|\mathbf{r}-\mathbf{r}'|}\right) - \frac{1}{|\mathbf{r}-\mathbf{r}'|}\frac{\partial\phi}{\partial n'}\right] dS. \tag{3.91}$$

The normal derivatives are taken just outside S.

3.7 SPHERICAL HARMONICS

In principle, finding $\phi(\mathbf{r})$ by performing the integration in (3.16) should be a simple matter. In reality, however, computation may be quite laborious, and it may become advantageous to solve Poisson's equation directly. This is possible when the surface bounding the charges is a coordinate surface in a coordinate system in which Laplace's equation is separable. As an illustration, consider the example embodied in Figure 3.15, where a spherical surface S is covered with a surface charge of known density $\rho_S(\theta)$. Given the rotational symmetry of the

[††]The conditions for applicability of Green's theorem, enunciated in Appendix 1, are not respected, given the singularity of $|\mathbf{r}-\mathbf{r}'|^{-1}$ as $\mathbf{r}'$ approaches $\mathbf{r}$. A rigorous method would require the excision of a small volume containing $\mathbf{r}$ from V. But Dirac decided to ignore these fine points and to represent the singularity by suitable δ-functions and derivatives. Professional mathematicians were not amused, but the physicists refused to let their δ-function go. The justification for their insistence is discussed in Appendix 8.

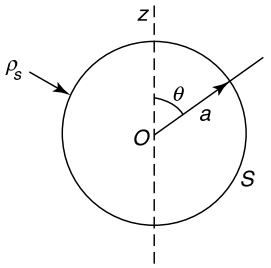

Figure 3.15 Charged spherical surface.

configuration, all derivatives with respect to φ vanish, and the potential satisfies Laplace's equation

$$\nabla^2\phi = \frac{1}{R^2}\frac{\partial}{\partial R}\left(R^2\frac{\partial\phi}{\partial R}\right) + \frac{1}{R^2\sin\theta}\frac{\partial}{\partial\theta}\left(\sin\theta\frac{\partial\phi}{\partial\theta}\right) = 0 \tag{3.92}$$

everywhere except on the charged surface S. To determine ϕ, we consider particular solutions of (3.92) in the form of a product $f(R)g(\theta)$. Introducing $f(R)g(\theta)$ in the equation gives

$$g(\theta)\frac{1}{R^2}\frac{d}{dR}\left(R^2\frac{df}{dR}\right) + \frac{1}{R^2\sin\theta}f(R)\frac{d}{d\theta}\left(\sin\theta\frac{dg}{d\theta}\right) = 0$$

or, after division by $f(R)g(\theta)$,

$$\frac{1}{f}\frac{d}{dR}\left(R^2\frac{df}{dR}\right) = -\frac{1}{\sin\theta g(\theta)}\frac{d}{d\theta}\left(\sin\theta\frac{dg}{d\theta}\right).$$

We notice that the left-hand term is a function of R alone, and the right-hand term is a function of θ alone. Thus, each must equal a common constant μ. This implies that $f(R)$ and $g(\theta)$ satisfy the equations

$$\frac{d}{dR}\left(R^2\frac{df}{dR}\right) = \mu f \tag{3.93}$$

$$\frac{1}{\sin\theta}\frac{d}{d\theta}\left(\sin\theta\frac{dg}{d\theta}\right) + \mu g = 0. \tag{3.94}$$

We shall now build up a solution of (3.92) in the form of a sum of product terms $f_n(R)g_n(\theta)$. To keep the solution general, and to ensure that the potential can be represented validly, we must select functions $g_n(\theta)$ that constitute a *complete* set. This is most important. To give an example, the functions $\cos nx$ (with $n = 0, 1, 2, \ldots$) form a complete set in $(-\pi, \pi)$ for *even* functions but are useless for the expansion of *odd* functions (for which the functions $\sin nx$ are appropriate). If we leave out the term $n = 0$ in the $\cos nx$ series (a constant), the truncated series can serve to expand functions with *zero* average value over $(-\pi, \pi)$ but would miss any "D.C. component" (to use a well-known engineering term). Keeping this in mind we note, from (A5.108) and (A5.139), that (3.94) is a Legendre equation, whose solutions $g(\theta)$ form a complete set when they are subjected to the condition "$g(\theta)$ finite" for $\theta = 0$ and $\theta = \pi$. Under these circumstances, (3.94) has solutions if, and only if,

$$\mu = n(n+1) \qquad n = 0, 1, 2, \ldots.$$

The corresponding normalized eigenfunctions are, from (A5.133),

$$\left(\frac{2n+1}{2}\right)^{\frac{1}{2}} P_n(\cos\theta).$$

The functions $P_n(\cos\theta)$ are known to form a complete set in the interval $-1 \leq \cos\theta \leq 1$. Inserting the value of μ given above in (3.93) leads to the tentative solution

$$\phi(R,\theta) = \sum_{n=0}^{\infty} P_n(\cos\theta)(A_n R^n + B_n R^{-(n+1)}). \tag{3.95}$$

In the configuration of Figure 3.15, separate expansions must be used for points inside and outside the sphere. In the exterior region, the condition of regularity at infinity excludes the possibility of including terms of the form $A_n R^n$, whence

$$\phi_e(R,\theta) = \sum_{n=0}^{\infty} C_n R^{-(n+1)} P_n(\cos\theta).$$

In the interior region, the potential must remain finite at $R = 0$, which prompts us to set

$$\phi_i(R,\theta) = \sum_{n=0}^{\infty} D_n R^n P_n(\cos\theta).$$

The coefficients C_n and D_n can be determined by utilizing the boundary conditions at $R = a$, which are

$$\phi_e = \phi_i$$

$$\frac{\partial\phi_e}{\partial R} - \frac{\partial\phi_i}{\partial R} = -\frac{\rho_S}{\epsilon_0} = \sum_{n=0}^{\infty} F_n P_n(\cos\theta).$$

Coefficient F_n can be expressed in terms of the known ρ_S by invoking (A5.133). Thus,

$$-\frac{1}{\epsilon_0}\int_{-1}^{1} \rho_S(\theta) P_n(\cos\theta)\, d(\cos\theta) = F_n \underbrace{\int_{-1}^{1} P_n^2(\cos\theta)\, d(\cos\theta)}_{(2/2n+1)}.$$

The two conditions at $R = a$ yield C_n and D_n, from which we obtain the following expressions for the potentials:

$$\phi_e(R,\theta) = -\sum_n P_n(\cos\theta)\frac{a^{n+2}}{2n+1}\frac{F_n}{R^{n+1}}$$

$$\phi_i(R,\theta) = -\sum_n P_n(\cos\theta)\frac{R^n}{2n+1}\frac{F_n}{a^{n-1}}. \tag{3.96}$$

The steps that have been outlined embody the essence of the technique of *separation of variables*. This technique can be extended to more complicated charge distributions; for example, to surface charges of the form $\rho_S(\theta, \varphi)$ [which require the use of spherical harmonics $P_n^m(\cos\theta)e^{jm\varphi}$ instead of Legendre polynomials] and to other coordinate systems in which ∇^2 is separable [20, 79, 165]. In the case of the (θ, φ) dependence, separation of variables yields the following expansion for a *harmonic function* (i.e., for a solution of Laplace's equation):

$$\phi(R,\theta,\varphi) = \sum_{n=0}^{\infty}\sum_{m=0}^{n}\Bigg[(C_{mn}\cos m\varphi + D_{mn}\sin m\varphi)P_n^m(\cos\theta)R^n + (F_{mn}\cos m\varphi + G_{mn}\sin m\varphi)P_n^m(\cos\theta)\frac{1}{R^{n+1}}\Bigg]. \tag{3.97}$$

The electric field associated with the term in C_{mn} is

$$\mathbf{e} = -R^{n-1}C_{mn}\Bigg[n\cos m\varphi P_n^m(\cos\theta)\mathbf{u}_R + \cos m\varphi\frac{d}{d\theta}P_n^m(\cos\theta)\mathbf{u}_\theta - m\sin m\varphi\frac{P_n^m(\cos\theta)}{\sin\theta}\mathbf{u}_\varphi\Bigg]. \tag{3.98}$$

Similar expressions hold for the other terms, the terms in $(1/R^{n+1})$ in (3.97) giving rise to fields proportional to $(1/R^{n+2})$. Clearly, at large distances, only the terms in $R^{-(n+1)}$ in (3.97) give rise to regular potentials. The various terms of that family can easily be identified with corresponding multipoles. Thus,

1. $1/R$ generates an omnidirectional potential, independent of θ and φ. It is the potential of a point charge (a monopole).
2. $1/R^2$ gives rise to three terms:

$$\frac{1}{R^2}P_1^0(\cos\theta) = \frac{1}{R^2}\cos\theta$$
$$\frac{1}{R^2}P_1^1(\cos\theta)\cos\varphi = \frac{1}{R^2}\sin\theta\cos\varphi$$
$$\frac{1}{R^2}P_1^1(\cos\theta)\sin\varphi = \frac{1}{R^2}\sin\theta\sin\varphi.$$

   From (3.29), these are the potentials of dipoles with moments oriented respectively along the z, x, and y axes.

The identification of the higher-order terms with quadrupoles, octupoles, and so forth, proceeds in a similar fashion.

If we require the electric field at large distances to remain *bounded* (a weaker condition than regularity), we are allowed to keep the terms in R in (3.97) in addition to the regular terms. There are three such terms, viz. $R\cos\theta = z$, $R\sin\theta\cos\varphi = x$, and $R\sin\theta\sin\varphi = y$. The corresponding electric fields are uniform and parallel to respectively the z, x, and y axes. We conclude that an electrostatic field that remains bounded at infinity (without vanishing there) must be uniform at large distances (i.e., for $R \to \infty$).

The multipole expansion in terms of spherical harmonics can be obtained directly from the potential expression (3.16) by means of the expansion of $1/|\mathbf{r}-\mathbf{r}'|$ in spherical harmonics, namely

$$\frac{1}{|\mathbf{r}-\mathbf{r}'|}=\sum_{n=0}^{\infty}\sum_{m=0}^{n}\epsilon_m\frac{(n-m)!}{(n+m)!}P_n^m(\cos\theta')P_n^m(\cos\theta)\cos m(\varphi-\varphi')A_n \tag{3.99}$$

with

$$A_n=\begin{cases}\dfrac{R^n}{(R')^{n+1}} & \text{for } R'>R\\[2ex] \dfrac{(R')^n}{R^{n+1}} & \text{for } R'<R.\end{cases}$$

Here ϵ_m is Neumann's factor, equal to 1 for $m=0$ and to 2 for $m=1,2,3,\ldots$. When (3.99) is inserted into (3.16), the following expression is obtained for the potential outside a sphere of radius a centered at C and containing all the charges:

$$\phi(R,\theta,\varphi)=\sum_{n=0}^{\infty}\sum_{m=0}^{n}[C_{mn}\cos m\varphi P_n^m(\cos\theta)+S_{mn}\sin m\varphi P_n^m(\cos\theta)]\frac{1}{R^{n+1}}. \tag{3.100}$$

The coefficients C_{mn} and S_{mn} can be found by applying the normalization integral (A5.162), which gives

$$\left.\begin{matrix}C_{mn}\\ S_{mn}\end{matrix}\right\}=\epsilon_m\frac{(n-m)!}{(n+m)!}\int_0^{2\pi}\left\{\begin{matrix}\cos m\varphi'\\ \sin m\varphi'\end{matrix}\right\}d\varphi'\int_0^{\pi}P_n^m(\cos\theta')\sin\theta'd\theta'$$
$$\times\int_0^a\rho(R',\theta',\varphi')(R')^{n+2}dR'.$$

At large distances, the terms corresponding with the lowest value of n will predominate, and it suffices to keep only these terms, possibly augmented with the next ones as a useful correction. As one gets closer to the sources, more and more terms will be needed, and the complexity of the potential pattern increases.

3.8 DIELECTRIC MATERIALS

The density $\rho(\mathbf{r})$ in (3.2) is a macroscopic concept. Essentially, using ρ implies that the charge in a small volume ΔV is $\rho\Delta V$. The volume must contain many charged particles for the concept to be statistically meaningful; the typical dimensions of the volume must therefore be large with respect to the classic particle dimensions, which are of the order 10^{-15} m. However, they must be small with respect to the dimensions of the electromagnetic system, which in optoelectronic applications, for example, might be as small as 10^{-6} m. It is clear that dN fluctuates constantly, by quantum steps, as particles enter and leave ΔV. Averages, both in time and in space, must therefore be introduced to move from the microscopic to the macroscopic; the techniques of quantum theory and statistical mechanics are the appropriate tools for the purpose. By means of averages, the charge is smeared out into a continuum, and the operations of the differential calculus may be performed without significant errors.

The medium discussed in the current section is a nonconducting dielectric, assumed to consist of *molecules* of zero net charge. The particles contain bound negative and positive charges, held in place by atomic and molecular forces. In certain materials, termed *polar*, the particles have a permanent dipole moment. Sometimes these dipoles are oriented at random, giving a zero net effect for the volume as a whole. *Electrets*, on the other hand, exhibit a spontaneous net polarization, each small volume having a net dipole moment, even in the absence of any external field. Barium titanate is an example of such a medium. *Nonpolar* materials consist of particles that have *no* permanent dipole moment. In the presence of an external field, however, negative and positive charges are pulled in different directions, and the centers of charge are shifted, albeit by very small distances. Something similar occurs when a conducting sphere of radius a is immersed in a uniform incident field $\mathbf{e}^i$ (Fig. 3.16*a*), in which case a dipole moment $\mathbf{p}_e = \epsilon_0 4\pi a^3 \mathbf{e}^i$ is induced, as shown in Section 4.6. In the presence of a local (microscopic) field $\mathbf{e}_0$, and for sufficiently moderate values of the latter, three mechanisms can generate a dipole density [37, 134]:

- A shift of electrons with respect to the positive charges. This is the electronic polarization.
- A relative displacement of atoms in an ionic band. This is the atomic polarization.
- A general orientation of the permanent dipoles. This effect is opposed by thermal agitation and is strongly temperature dependent.

The resulting dipole will be of the general form

$$p_{ei} = p_{0i} + \epsilon_0 \sum_{k=1}^{3} \alpha_{ik} e_{0k} + \epsilon_0 \sum_{j,k=1}^{3} \beta_{ijk} e_{0j} e_{0k} + \cdots . \qquad (\mathrm{C\,m}).$$

It is found experimentally that the terms of higher than first order are negligible at normal temperatures, and that saturation effects are unimportant except for very high external fields. Under these conditions

$$\mathbf{p}_e = \mathbf{p}_0 + \epsilon_0 \overline{\overline{\alpha}}_e \cdot \mathbf{e}_0 \qquad (\mathrm{C\,m}), \tag{3.101}$$

where $\overline{\overline{\alpha}}_e$ is the dyadic

$$\overline{\overline{\alpha}}_e = \sum_{i,k=1}^{3} \alpha_{ik} \mathbf{u}_i \mathbf{u}_k \qquad (\mathrm{m}^3).$$

The theoretical determination of $\mathbf{p_0}$ and $\overline{\overline{\alpha}}_e$ is a problem in atomic physics. The molecule may also acquire a quadrupole dyadic $\overline{\overline{q_e}}$, but this is often neglected because the resulting

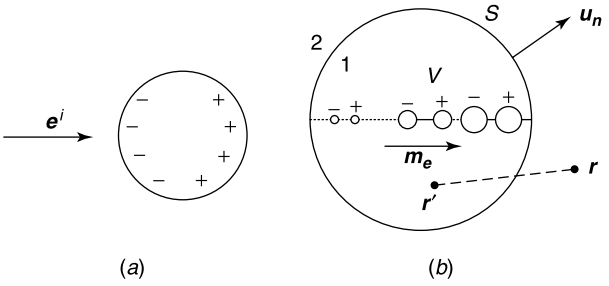

Figure 3.16 (*a*) Conducting sphere in an incident field. (*b*) Elementary polarization dipoles.

e-field decreases like $1/R^4$ at large distances R (i.e., at a faster rate than the competing dipole field). It can be shown, on the basis of energy considerations, that the molecular *electric polarizability tensor* $\overline{\overline{\alpha}}_e$ is symmetric, hence that $(\alpha_e)_{ik} = (\alpha_e)_{ki}$ [11].

The electric field ($\mathbf{e}_0$ mentioned above is the local microscopic field, which varies strongly in time and space. The transition to a macroscopic description involves suitable averaging procedures in space and time, which even out these rapid fluctuations [6, 37]. In the course of such averages a polarization per unit volume very naturally appears. This *electric dipole density* is given by

$$\mathbf{m}_{e_0} = n \langle \mathbf{p}_e \rangle_{\text{ave}} \qquad (\text{C m}^{-2}), \tag{3.102}$$

where n is the number of molecules per unit volume (the *number density*). For many substances, $\mathbf{m}_e$ is related to the macroscopic field by the simple law

$$\mathbf{m}_{e_0} = \mathbf{m}_0 + \epsilon_0 \overline{\overline{\chi_e}} \cdot \mathbf{e}_{\text{mac}} \tag{3.103}$$

where $\mathbf{m}_0$ is the permanent polarization (which must be included in the case of an electret) and $\overline{\overline{\chi_e}}$ is the (dimensionless) *electric susceptibility* of the dielectric. The macroscopic field $\mathbf{e}_{\text{mac}}$ is the field that appears in Maxwell's equations. This field has been shown by Lorentz to be the volume average of the microscopic fields. In the macroscopic vision, therefore, the dielectric reacts like the sum of elementary dipoles $\mathbf{m}_e\, dV$, which, according to (3.29), generate a potential (Fig. 3.16*b*)

$$\begin{aligned} \phi(\mathbf{r}) &= \frac{1}{4\pi\epsilon_0} \int_{\text{diel}} \frac{\mathbf{m}_e(\mathbf{r}') \cdot (\mathbf{r} - \mathbf{r}')}{|\mathbf{r} - \mathbf{r}'|^3}\, dV' = \frac{1}{4\pi\epsilon_0} \int_{\text{diel}} \mathbf{m}_e(\mathbf{r}') \cdot \text{grad}' \left(\frac{1}{|\mathbf{r} - \mathbf{r}'|} \right) dV' \\ &= \frac{1}{4\pi\epsilon_0} \int_V \frac{-\text{div}'\, \mathbf{m}_e(\mathbf{r}')}{|\mathbf{r} - \mathbf{r}'|}\, dV' + \frac{1}{4\pi\epsilon_0} \int_S \frac{\mathbf{u}_n \cdot \mathbf{m}_e(\mathbf{r}')}{|\mathbf{r} - \mathbf{r}'|}\, dS'. \end{aligned} \tag{3.104}$$

Clearly, the reaction of the dielectric may be accounted for by effective volume and surface charge densities, given by

$$\begin{aligned} \rho' &= -\text{div}\, \mathbf{m}_e \qquad (\text{in } V) \\ \rho'_S &= \mathbf{u}_n \cdot \mathbf{m}_e \qquad (\text{on } S). \end{aligned} \tag{3.105}$$

Figure 3.16*b* shows, in a simplistic way, how the tips of the dipoles produce a surface charge, and how the positive divergence of $\mathbf{m}_e$ (implied in the figure) tends to create a net negative ρ'. From a free space point of view, the total charge would then consist of unbound free charges and polarization charges, of respective densities ρ and ρ'. In consequence, in the absence of electrets, (3.2) becomes

$$\epsilon_0\, \text{div}\, \mathbf{e} = \rho - \text{div}\, \mathbf{m}_e = \rho - \text{div}(\epsilon_0 \overline{\overline{\chi}}_e \cdot \mathbf{e})$$

or, introducing the relative *dielectric constant* dyadic $\overline{\overline{\epsilon}}_r = \overline{\overline{I}} + \overline{\overline{\chi}}_e$,

$$\begin{aligned} \text{div}(\epsilon_0 \mathbf{e} + \mathbf{m}_e) &= \text{div}\, [\epsilon_0 (\mathbf{e} + \overline{\overline{\chi}}_e \cdot \mathbf{e})] \\ &= \text{div}\, (\epsilon_0 \overline{\overline{\epsilon}}_r \cdot \mathbf{e}) \;=\; \text{div}(\overline{\overline{\epsilon}} \cdot \mathbf{e}) = \rho. \end{aligned} \tag{3.106}$$

If we set

$$\mathbf{d} = \bar{\bar{\epsilon}} \cdot \mathbf{e} \qquad (\mathrm{C\,m^{-2}}) \tag{3.107}$$

we obtain Maxwell's equation

$$\operatorname{div} \mathbf{d} = \rho. \tag{3.108}$$

The vector $\mathbf{d}$ is the *electric displacement* (or *electric flux density*). Poisson's equation in a dielectric takes the form

$$\operatorname{div} (\bar{\bar{\epsilon}}_r \cdot \operatorname{grad} \phi) = -\frac{\rho}{\epsilon_0}. \tag{3.109}$$

At the boundary between two media (Fig. 3.16*b*):

$$\mathbf{u}_n \cdot (\mathbf{d}_2 - \mathbf{d}_1) = \rho_S. \tag{3.110}$$

3.9 CAVITY FIELDS

In the nineteenth century, physicists attempted to understand the mechanism of polarization by excising (in a *mental experiment*) a small volume from the dielectric and assigning the origin of polarization to the resulting cavity fields. The validity of the concept has been discussed at length (and critically) in an almost forgotten document published by the American Association of Physics Teachers (Coulomb Law Committee, 1950).[3] The problem is now mainly of historical interest [13, 42]. It remains mathematically relevant, however, for example, for the evaluation of the electric field in the interior of a current-carrying region, a topic further discussed in Section 7.9.

Figure 3.17 shows a linear dielectric from which a volume V has been excised. Let $\mathbf{e}$ be the original macroscopic field at P. The local field is now $(\mathbf{e} - \mathbf{e}_s)$, where $\mathbf{e}_s$ is the field contributed by the original dielectric material in V. The self field $\mathbf{e}_s$ may be evaluated by various methods, for example by means of difference equations. This way of obtaining the self-patch contribution is useful when, in a numerical process, a dielectric body is split into a net of cells, which are not necessarily small. From a theoretical point of view, however, it is instructive to consider very small volumes V, small enough for $\mathbf{m}_e$ to be practically uniform over these volumes. We shall denote such V's by V_δ. Potential (3.104) now takes the form

$$\phi(\mathbf{r}) = \frac{1}{4\pi\epsilon_0} \mathbf{m}_e(\mathbf{r}) \cdot \int_{V_\delta} \operatorname{grad}' \left(\frac{1}{|\mathbf{r} - \mathbf{r}'|} \right) dV' \;=\; \frac{1}{4\pi\epsilon_0} \mathbf{m}_e(\mathbf{r}) \cdot \mathbf{I}(\mathbf{r}).$$

Integral $\mathbf{I}(\mathbf{r})$ is of the type defined in (3.19) and is known to be convergent. The derivatives, however, which must be evaluated to obtain $\mathbf{e}_s$, introduce singularities of the order $|\mathbf{r} - \mathbf{r}'|^{-3}$. To take care of that difficulty, we shall use an approach often used in potential theory: remove from V_δ a small sphere V_0 that contains the field point $P(\mathbf{r})$ (Fig. 3.17). This artifice is resorted to because the contribution from V_0 , when it carries a uniform $\mathbf{m}_e$, can be determined analytically. From (3.105) this field, denoted by $\mathbf{e}_d$, is created by the surface charge (3.105), and by applying the techniques of Section 3.10 is easily found to be

$$\mathbf{e}_d = -\frac{1}{3\epsilon_0} \mathbf{m}_e.$$

Note that this value is uniform, in that it is independent of the position of P. The next step is to evaluate the contribution from the rest volume $(V_\delta - V_0)$. In that volume $|\mathbf{r} - \mathbf{r}'|^{-1}$ and derivatives are continuous, and we may apply Gauss' theorem (A1.29) to the evaluation of $\mathbf{I}(\mathbf{r})$. This yields

$$\mathbf{I}(\mathbf{r}) = \int_{S_\delta} \frac{\mathbf{u}_n(\mathbf{r})}{|\mathbf{r} - \mathbf{r}'|}\, dS' - \int_{S_0} \frac{\mathbf{u}_n(\mathbf{r}')}{|\mathbf{r} - \mathbf{r}'|}\, dS'.$$

The field $\mathbf{e}_1$ generated by $(V_0 - V_\delta)$ may therefore be written as

$$\begin{aligned}\mathbf{e}_1(\mathbf{r}) &= -\frac{1}{4\pi\epsilon_0}\,\text{grad}\left[\mathbf{m}_e \cdot \int_{S_\delta} \frac{\mathbf{u}_n(\mathbf{r}')}{|\mathbf{r} - \mathbf{r}'|}\, dS' - \mathbf{m}_e \cdot \int_{S_0} \frac{\mathbf{u}_n(\mathbf{r}')}{|\mathbf{r} - \mathbf{r}'|}\, dS'\right] \\ &= -\frac{1}{4\pi\epsilon_0}\,\mathbf{m}_e \cdot \left[\text{grad} \int_{S_\delta} \frac{\mathbf{u}_n(\mathbf{r}')}{|\mathbf{r} - \mathbf{r}'|}\, dS' - \text{grad} \int_{S_0} \frac{\mathbf{u}_n(\mathbf{r}')}{|\mathbf{r} - \mathbf{r}'|}\, dS'\right].\end{aligned}$$

In this equation, we have introduced the concept of *gradient of a vector*, a dyadic defined in (A4.48). Further manipulation gives

$$\begin{aligned}\text{grad} \int_{S_\delta} \frac{\mathbf{u}_n(\mathbf{r})}{|\mathbf{r} - \mathbf{r}'|}\, dS' &= \int_{S_\delta} \mathbf{u}_n(\mathbf{r}') \cdot \text{grad}\left(\frac{1}{|\mathbf{r} - \mathbf{r}'|}\right) dS' \\ &= \int_{S_\delta} \mathbf{u}_n(\mathbf{r}') \frac{\mathbf{u}_R(\mathbf{r}')}{|\mathbf{r} - \mathbf{r}'|^2}\, dS' \;=\; 4\pi \overline{\overline{L}}_{V_\delta}(\mathbf{r})\end{aligned}$$

where $\mathbf{u}_R = \dfrac{\mathbf{r} - \mathbf{r}'}{|\mathbf{r} - \mathbf{r}'|}$. The integral over S_0 similarly yields $\overline{\overline{L}}_{V_0}(\mathbf{r}')$. Collecting these results leads to

$$\mathbf{e}_1(\mathbf{r}) = -\frac{1}{\epsilon_0}\,\overline{\overline{L}}_{V_\delta} \cdot \mathbf{m}_e + \frac{1}{\epsilon_0}\,\overline{\overline{L}}_{V_0} \cdot \mathbf{m}_e.$$

A detailed evaluation of $\overline{\overline{L}}_{V_0}$ shows that this dyadic is independent of the position of $\mathbf{r}$ and is equal to $\dfrac{1}{3}\,\overline{\overline{I}}$. Combining this result with the value of $\mathbf{e}_d$ yields

$$\mathbf{e}_S(\mathbf{r}) = \mathbf{e}_d + \mathbf{e}_1 = -\frac{1}{\epsilon_0}\,\overline{\overline{L}}_{V_\delta}(\mathbf{r}) \cdot \mathbf{m}_e \tag{3.111}$$

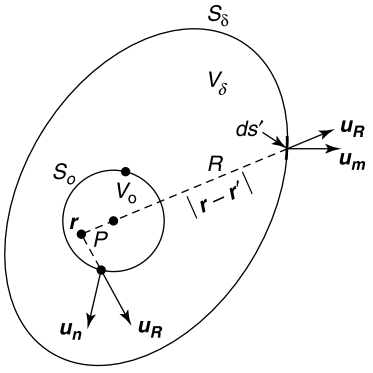

Figure 3.17 Cavity in a dielectric.

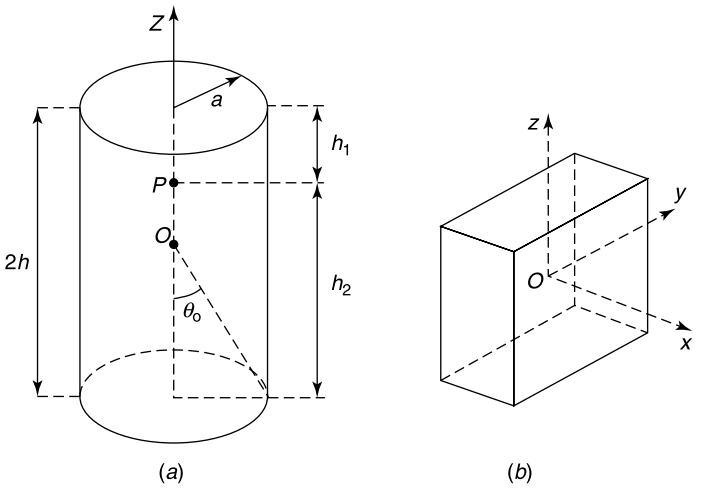

Figure 3.18 Typical volumes V: (a) circular cylinder, (b) rectangular box.

where $\overline{\overline{L}}_V$ is the dimensionless *depolarization dyadic*

$$\overline{\overline{L}}_V(\mathbf{r}) = \frac{1}{4\pi}\int_S \frac{\mathbf{u}_n(\mathbf{r}')\,\mathbf{u}_R(\mathbf{r}')}{|\mathbf{r}-\mathbf{r}'|^2}\,dS'. \tag{3.112}$$

This dyadic is real, symmetric, and its trace is unity.[4] $\overline{\overline{L}}$ varies generally with the position of P within the volume but is otherwise a function of the *shape* of V and not of the *scale* of V. More precisely, $\overline{\overline{L}}$ remains constant when V is magnified (or reduced) through a similarity transformation centered in $\mathbf{r}$. The specific value of $\overline{\overline{L}}$ is available for a few classic shapes:

1. At every point of a sphere, and at the center of a cube,[‡‡]

$$\overline{\overline{L}} = \frac{1}{3}\overline{\overline{I}}. \tag{3.113}$$

2. On the axis of a circular cylinder[§§] (Fig. 3.18a):

$$\overline{\overline{L}} = \left(1 - \frac{1}{2}\frac{h_1}{\sqrt{a^2+h_1^2}} - \frac{1}{2}\frac{h_2}{\sqrt{a^2+h_2^2}}\right)\mathbf{u}_z\mathbf{u}_z + \frac{1}{4}\left[\frac{h_1}{\sqrt{a^2+h_1^2}} + \frac{h_2}{\sqrt{a^2+h_2^2}}\right](\mathbf{u}_x\mathbf{u}_x + \mathbf{u}_y\mathbf{u}_y). \tag{3.114}$$

[‡‡]For the value of $\overline{\overline{L}}$ at an arbitrary point of the cube, see Note 5.

[§§]Formulas courtesy of Dr. R. De Smedt.

At the center, in particular,[4]

$$\overline{\overline{L}} = (1 - \cos\theta_0)\,\mathbf{u}_z\mathbf{u}_z + \frac{1}{2}\cos\theta_0(\mathbf{u}_x\mathbf{u}_x + \mathbf{u}_y\mathbf{u}_y). \tag{3.115}$$

For a needle-like cylinder, except close to the ends,

$$\overline{\overline{L}} = \frac{1}{4}\left(\frac{a^2}{h_1^2} + \frac{a^2}{h_2^2}\right)\mathbf{u}_z\mathbf{u}_z + \frac{1}{2}\left(1 - \frac{1}{4}\frac{a^2}{h_1^2} - \frac{1}{4}\frac{a^2}{h_2^2}\right)(\mathbf{u}_x\mathbf{u}_x + \mathbf{u}_y\mathbf{u}_y). \tag{3.116}$$

For a flat cylinder (a pillbox) of total height h:

$$\overline{\overline{L}} = \left(1 - \frac{h}{2a}\right)\mathbf{u}_z\mathbf{u}_z + \frac{h}{4a}(\mathbf{u}_x\mathbf{u}_x + \mathbf{u}_y\mathbf{u}_y). \tag{3.117}$$

In the limit $h \to 0$, $\overline{\overline{L}}$ becomes $\mathbf{u}_z\mathbf{u}_z$.

3. For a rectangular box, at the center (Fig. 3.18*b*),

$$\overline{\overline{L}} = \frac{1}{4\pi}(\Omega_x\mathbf{u}_x\mathbf{u}_x + \Omega_y\mathbf{u}_y\mathbf{u}_y + \Omega_z\mathbf{u}_z\mathbf{u}_z), \tag{3.118}$$

where Ω_x, Ω_y, and Ω_z are twice the solid angle subtended at $\mathbf{r}$ by a side perpendicular to the x, y, and z directions, respectively.

4. For an ellipsoid, (assuming that the principal axes are chosen as x, y, z axes)

$$\overline{\overline{L}} = L_1\mathbf{u}_x\mathbf{u}_x + L_2\mathbf{u}_y\mathbf{u}_y + L_3\mathbf{u}_z\mathbf{u}_z, \tag{3.119}$$

where the L_i are the depolarizing factors, discussed in more detail in [20].

Equations (3.116) and (3.117) lead directly to results of some historical importance.[¶¶] For a very long cylinder parallel to $\mathbf{m}_e$, $\overline{\overline{L}}\cdot\mathbf{m}_e$ is equal to zero, hence $\mathbf{e}_s = 0$, and the cavity field is equal to $\mathbf{e}$. For a flat box perpendicular to $\mathbf{m}_e$ (in which case $\mathbf{m}_e$ is z-oriented), $\overline{\overline{L}} = \mathbf{u}_z\mathbf{u}_z$, hence $\mathbf{e}_s = -\dfrac{1}{\epsilon_0}\mathbf{m}_e$. The cavity field is now

$$\mathbf{e} - \mathbf{e}_s = \mathbf{e} + \frac{1}{\epsilon_0}\mathbf{m}_e = \frac{1}{\epsilon_0}\mathbf{d} = \epsilon_r\mathbf{e}. \tag{3.120}$$

It is proportional to $\mathbf{d}$.

3.10 DIELECTRIC SPHERE IN AN EXTERNAL FIELD

Our aim, in this section, is to determine the fields in and around a homogeneous dielectric sphere of radius a, exposed to an incident[‖‖] potential ϕ^i. Such problems can be solved by

[¶¶] The authors of the report in Note 3 mention that these Kelvin cavity definitions of $\mathbf{e}$ and $\mathbf{d}$ have only a semblance of reality because they are never converted into concrete physical experiments.

[‖‖] We use the qualification *incident* for the preexisting potential, although such a choice is normally reserved for an incoming *wave*, which is pictured as "falling" on a target.

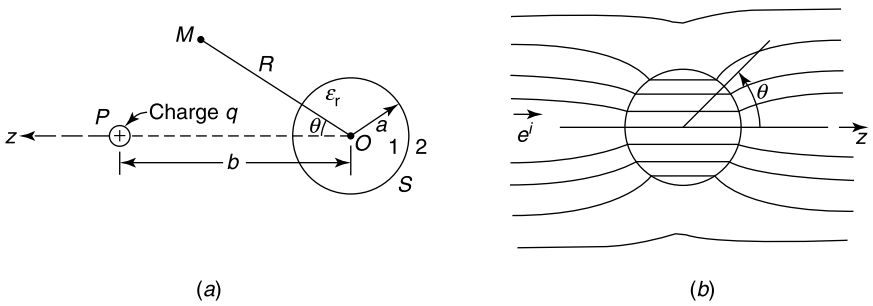

Figure 3.19 (*a*) Dielectric sphere in the field of a point charge. (*b*) Dielectric sphere in a uniform incident field.

separation of variables in a few cases, for example when the source is a point charge in P, and the obstacle a sphere (Fig. 3.19*a*). The potential generated by the point charge is actually the Green's function of the problem. Because the sphere is axisymmetric with respect to the z-axis, the potential depends only on R and z. Inside the sphere ϕ is harmonic. Hence, from (3.95),

$$\phi_1(\mathbf{r}) = \sum_{n=0}^{\infty} a_n R^n P_n(\cos\theta) \qquad R \le a.$$

The potential outside the sphere is the sum of the potential produced by the point charge and the potential $\varphi(\mathbf{r})$ stemming from the presence of the dielectric. At M, for example,

$$\phi_2(\mathbf{r}_M) = \frac{q}{4\pi\epsilon_0 PM} + \phi_d(\mathbf{r}_M)$$

where PM is the distance between P and M. The additional (or disturbance) potential may be written as

$$\phi_d = \sum_{n=0}^{\infty} \frac{b_n}{R^{n+1}} P_n(\cos\theta) \qquad R \ge a.$$

From (3.99), in which we now set $m = 0$,

$$\begin{aligned} \frac{1}{PM} &= \frac{1}{b}\sum_{n=0}^{\infty}\left(\frac{R}{b}\right)^n P_n(\cos\theta) \qquad R < b \\ &= \frac{1}{R}\sum_{n=0}^{\infty}\left(\frac{b}{R}\right)^n P_n(\cos\theta) \qquad R > b. \end{aligned} \tag{3.121}$$

It is now a simple matter to find the expansion coefficients a_n and b_n by applying the necessary boundary conditions. For $R < b$, for example,

$$\begin{aligned} \phi_1 &= \frac{q}{4\pi\epsilon_0}\sum_{n=0}^{\infty}\frac{2n+1}{\epsilon_r n + n + 1}\frac{R^n}{b^{n+1}}P_n(\cos\theta) \\ \phi_2 &= \frac{q}{4\pi\epsilon_0 PM} - \frac{q(\epsilon_r - 1)}{4\pi\epsilon_0}\sum_{n=0}^{\infty}\frac{n}{\epsilon_r n + n + 1}\frac{a^{2n+1}}{b^{n+1}}\frac{P_n(\cos\theta)}{R^{n+1}}. \end{aligned} \tag{3.122}$$

When P recedes to infinity, the incident field becomes homogeneous in the region occupied by the sphere. The incident potential takes the form $-e^i z = -e^i R\cos\theta$, and the method of separation of variables, applied as above, gives (Fig. 3.19*b*)

$$\phi_1 = -\frac{3}{\epsilon_r + 2} e^i R\cos\theta$$
$$\phi_2 = -e^i R\cos\theta + \frac{\epsilon_r - 1}{\epsilon_r + 2} e^i a^3 \frac{\cos\theta}{R^2}. \tag{3.123}$$

Clearly, the interior field is

$$\mathbf{e}_1 = \frac{3}{\epsilon_r + 2}\mathbf{e}^i.$$

The dipole moment induced by a uniform incident $\mathbf{e}^i$ is given by

$$\mathbf{p}_e = \int_V \mathbf{m}_e\, dV = (\epsilon_r - 1)\epsilon_0 \int_V \mathbf{e}\, dV = -(\epsilon_r - 1)\epsilon_0 \int_V \operatorname{grad}\phi\, dV$$
$$= -(\epsilon_r - 1)\epsilon_0 \int_S \phi\, \mathbf{u}_n\, dS. \tag{3.124}$$

This expression holds for a homogeneous isotropic dielectric body of arbitrary shape. For the sphere, it yields the value

$$\mathbf{p}_e = 4\pi\epsilon_0 a^3 \frac{\epsilon_r - 1}{\epsilon_r + 2}\mathbf{e}^i = \epsilon_0 \bar{\bar{\alpha}}_e \cdot \mathbf{e}^i \tag{3.125}$$

which shows that the *electric polarizability dyadic of the sphere* is

$$\bar{\bar{\alpha}}_e = 4\pi \frac{\epsilon_r - 1}{\epsilon_r + 2} a^3 \bar{\bar{I}}. \tag{3.126}$$

Computing ϕ_2 from (3.122) for a charge close to the sphere may require a large number of terms because of poor convergence. This difficulty can be avoided by the method of images, which in the current case shows that the contribution of the dielectric outside the sphere is that of an image source in B, viz.[6]

$$q_i = -\frac{\epsilon_r - 1}{\epsilon_r + 1}\frac{a}{d} q \tag{3.127}$$

augmented by a linear charge density stretched between O and B (Fig. 3.20*a*). Inside the dielectric, the total potential is that of a point charge in A, of value

$$q_i = \frac{2\epsilon_r}{\epsilon_r + 1} q \tag{3.128}$$

augmented by a linear charge stretched between A and infinity. With respect to a half-infinite medium (i.e., in the limit $a \to \infty$), the total potential in vacuum is generated by (Fig. 3.20*b*)

$$q \qquad (\text{in } A)$$

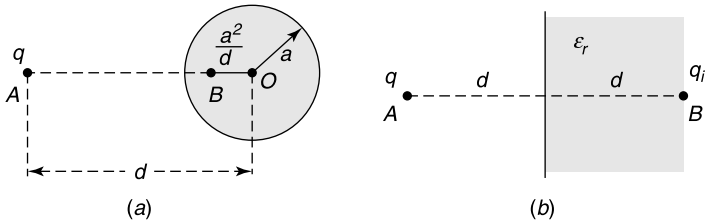

Figure 3.20 Image sources: (*a*) for a dielectric sphere, (*b*) for a dielectric half-space.

$$q_i = -\frac{\epsilon_r - 1}{\epsilon_r + 1}\, q \qquad (\text{in } B). \tag{3.129}$$

In the dielectric it stems from a source

$$q_i = \frac{2\epsilon_r}{\epsilon_r + 1}\, q \qquad (\text{in } A). \tag{3.130}$$

When the half-infinite space is *anisotropic* (a typical situation in geoelectromagnetic applications) images can be found when $\overline{\overline{\epsilon_r}}$ is real, positive-definite, and symmetric. With respect to the vacuum region, these images consist of a point charge in B plus a continuous surface distribution on an angular sector with apex located at the image point.[7]

3.11 DIELECTRIC SPHEROID IN AN INCIDENT FIELD

Separation of variables, already applied to a dielectric sphere in Section 3.10, can also provide a solution for a spheroid immersed in a uniform incident field $\mathbf{e}^i$ (Fig. 3.21). We shall start with a *prolate* spheroid. The problem is technically important, in particular in its magnetic version, which is relevant for the study of ferrite antennas. The solution proceeds by separating variables in prolate spheroidal coordinates (see A2.112 to A2.117). Cylindrical

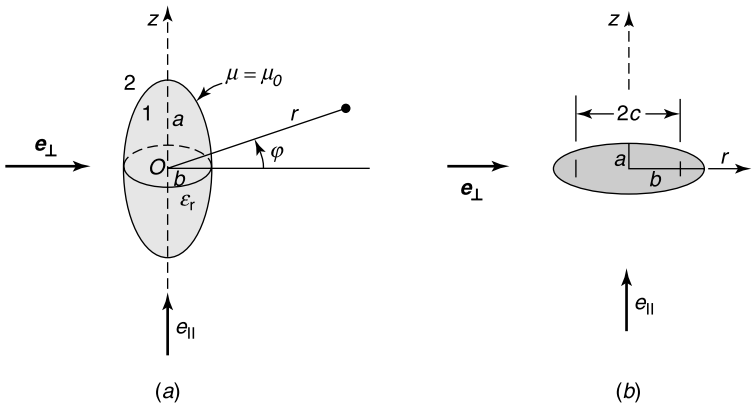

Figure 3.21 (*a*) Prolate dielectric spheroid in a uniform incident field. (*b*) Oblate dielectric spheroid in a uniform incident field.

and prolate coordinates are related by (Fig. 3.22)

$$x = c\sqrt{\mu^2 - 1}\sqrt{1 - \nu^2}\cos\varphi; \quad y = c\sqrt{\mu^2 - 1}\sqrt{1 - \nu^2}\sin\varphi; \quad z = c\mu\nu$$
$$r = c\sqrt{\mu^2 - 1}\sqrt{1 - \nu^2}. \tag{3.131}$$

The surfaces of constant μ are confocal ellipsoids of revolution defined by the equation

$$\frac{z^2}{\mu^2} + \frac{r^2}{\mu^2 - 1} = 1 \qquad \mu > 1. \tag{3.132}$$

The semi-axes are related to the half-focal distance by $c = \sqrt{a^2 - b^2}$. The surfaces of constant ν are hyperboloids of revolution defined by the equation

$$\frac{z^2}{\nu^2} - \frac{r^2}{1 - \nu^2} = 1 \qquad \nu < 1. \tag{3.133}$$

For $\mu = 1$, the spheroid degenerates into a segment of the z axis bounded by the points $z = c$ and $z = -c$. For μ slightly larger than 1, the ellipsoid is in the shape of a thin rod. For $\nu = 1$, the hyperboloids degenerate into two infinite segments of the z axis, extending, respectively, from $z = c$ to $z = +\infty$, and from $z = -c$ to $z = -\infty$. For ν slightly less than 1, the surface consists of two coaxial rods with rounded ends, and its geometry resembles that of a common type of spark gap. From (A2.117), Laplace's equation in prolate spheroidal coordinates takes the form

$$\frac{\partial}{\partial\mu}\left[(\mu^2 - 1)\frac{\partial f}{\partial\mu}\right] + \frac{\partial}{\partial\nu}\left[(1 - \nu^2)\frac{\partial f}{\partial\nu}\right] + \frac{1}{(\mu^2 - 1)(1 - \nu^2)}\frac{\partial^2 f}{\partial\varphi^2} = 0. \tag{3.134}$$

Following the method already used in the case of spherical harmonics, we try products of functions of respectively μ, ν, and φ as possible solutions. The equations in μ and ν are of

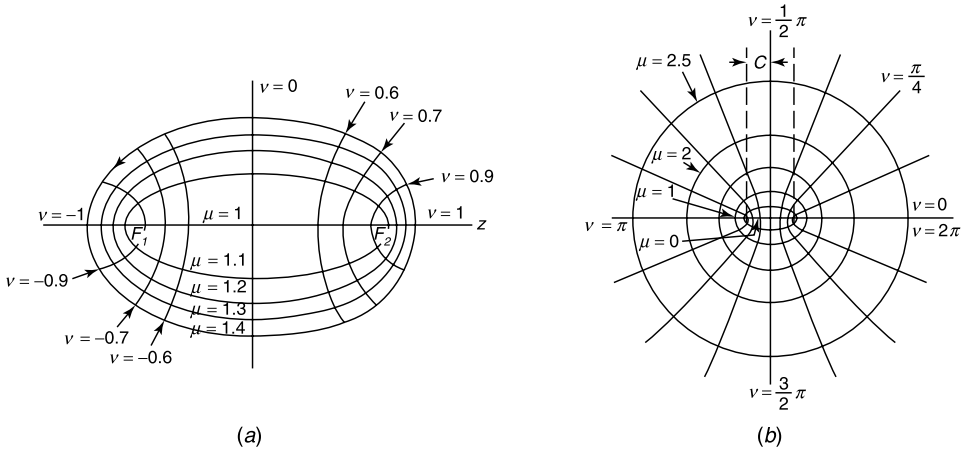

Figure 3.22 (*a*) Prolate spheroidal coordinates. (*b*) A series of confocal ellipses.

the Legendre type (see A5.138). They yield the double sum

$$\phi(\mu,\nu,\varphi)=\sum_{n=0}^{\infty}\sum_{m=0}^{n}[A_{mn}P_n^m(\mu)+B_{mn}Q_n^m(\mu)]$$
$$[C_{mn}P_n^m(\nu)+D_{mn}Q_n^m(\nu)](E_{mn}\sin m\varphi+F_{mn}\cos m\varphi). \tag{3.135}$$

The various coefficients must be detemined by means of the boundary conditions. Let us assume that the incident field in Figure 3.21*a* is uniform and *directed along the z-axis*. The sought potential is now independent of φ, and a possible solution is therefore

$$\phi(\mu,\nu)=\sum_{n=0}^{\infty}[A_nP_n(\mu)+B_nQ_n(\mu)][C_nP_n(\nu)+D_nQ_n(\nu)]\,. \tag{3.136}$$

The incident potential can be expressed as $-e_\parallel z=-e_\parallel c\mu\nu=-e_\parallel P_1(\mu)P_1(\nu)$. Clearly, satisfaction of the boundary conditions can be ensured by keeping only the terms in $n=1$ in the expansion. On these grounds, and because of the form of the incident potential, we set

$$\phi_1=A\mu\nu$$

in the dielectric, and

$$\phi_2=-e_\parallel c\mu\nu+\phi_d$$

outside the dielectric. The term ϕ_d represents the potential stemming from the presence of the dielectric. This potential must vanish at least as fast as $(1/R)$ at large distances (i.e., for μ approaching infinity). For infinite μ, $P_1(\mu)$ is infinite and must consequently be excluded from the solution. This suggests setting

$$\phi_2=-e_\parallel c\mu\nu+B\nu\,Q_1(\mu)$$

because $Q_1(\infty)=0$, from (A5.112). The constants A and B follow from the conditions at the boundary surface μ_0, which require ϕ and $\epsilon_r\dfrac{\partial\phi}{\partial\mu}$ to be continuous. A few simple steps now yield

$$A=-e_\parallel c\,\frac{1}{(\epsilon_r-1)g_\parallel+1}=-e_\parallel cD_\parallel \tag{3.137}$$

where

$$g_\parallel=(\mu_0^2-1)\left(\frac{1}{2}\mu_0\log_e\frac{\mu_0+1}{\mu_0-1}-1\right). \tag{3.138}$$

Clearly, the electric field inside the spheroid is uniform and parallel to the incident field $\mathbf{e}_\parallel$. More precisely,

$$\mathbf{e}_1=\frac{1}{(\epsilon_r-1)g_\parallel+1}\mathbf{e}_\parallel=D_\parallel\,\mathbf{e}_\parallel. \tag{3.139}$$

The quantity $g_\parallel$ is independent of the dielectric constant, but it depends on the *shape* of the spheroid. This can be seen by noting that $g_\parallel$ is a function of μ_0 alone and that μ_0 determines the shape of the spheroid through the ratio of the semiaxes

$$\frac{a}{b} = \frac{\mu_0}{(\mu_0^2 - 1)^{\frac{1}{2}}} \tag{3.140}$$

and the *eccentricity*

$$e = \frac{\text{distance between foci}}{\text{length of major axis}} = \frac{2c}{2a} = \frac{1}{\mu_0} = \sqrt{1 - \frac{b^2}{a^2}}. \tag{3.141}$$

A plot of $g_\parallel$ as a function of the eccentricity is given in Figure 3.23. For zero eccentricity, the spheroid reduces to a sphere, and $g_\parallel$ is equal to $\frac{1}{3}$. This result is in harmony with the field value derived from (3.123). For larger eccentricities, the spheroid becomes more and more prolate, $g_\parallel$ and $D_\parallel$ approach, respectively, the values 0 and 1, and the field in the dielectric approaches the undisturbed value $\mathbf{e}_\parallel$. Finally, the induced dipole moment is easily found to be proportional to $\mathbf{e}_\parallel$, with polarizability

$$\begin{aligned}(\alpha_e)_\parallel &= \frac{\mathbf{p_e}}{\epsilon_0 \mathbf{e}_\parallel} = \frac{4}{3}\frac{\epsilon_r - 1}{(\epsilon_r - 1)g_\parallel + 1}\pi a b^2 = \frac{\epsilon_r - 1}{(\epsilon_r - 1)g_\parallel + 1} V \\ &= \frac{4\pi}{3}\frac{\epsilon_r - 1}{(\epsilon_r - 1)g_\parallel + 1}\mu_0(\mu_0^2 - 1)\, c^3 \end{aligned} \tag{3.142}$$

where V is the volume of the spheroid, equal to $(4\pi a b^2/3)$.

When the incident field is *perpendicular* to the axis, the potential is proportional to $\cos\varphi$, and only terms in $\cos\varphi$ should be kept in general expression (3.135). Detailed developments show [104, 134] that the interior field is again proportional to the incident one.

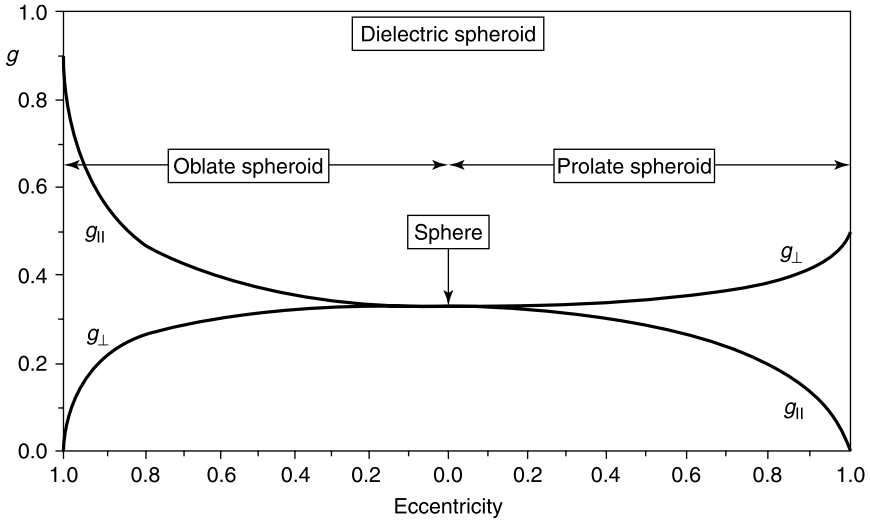

Figure 3.23 Shape factors $g_\parallel$ and $g_\perp$ for a dielectric spheroid. (Courtesy of Dr. R. De Smedt.)

More precisely,

$$\mathbf{e}_1 = \frac{1}{(\epsilon_r - 1)g_\perp + 1}\mathbf{e}_\perp \tag{3.143}$$

where

$$g_\perp = \frac{\mu_0(\mu_0^2 - 1)}{2}\left[\frac{\mu_0}{\mu_0^2 - 1} - \frac{1}{2}\log_e\frac{\mu_0 + 1}{\mu_0 - 1}\right]. \tag{3.144}$$

A plot of $g_\perp$ is given in Figure 3.23. For zero eccentricity (i.e., for a spherical body), $g_\perp$ and $g_\parallel$ must obviously be equal; this is confirmed by the figure. For large eccentricities (i.e., for a very thin spheroid), the figure shows that the internal field is given by

$$\frac{1}{(\epsilon_r - 1)\frac{1}{2} + 1}\mathbf{e}_\perp = \frac{2}{\epsilon_r + 1}\mathbf{e}_\perp. \tag{3.145}$$

For arbitrary eccentricity, the polarizability for perpendicular incidence is still given by (3.142), but $g_\parallel$ and $(\alpha_e)_\parallel$ must now be replaced by $g_\perp$ and $(\alpha_e)_\perp$. When the spheroid is immersed in an *oblique* field $\mathbf{e}$, the field in the dielectric is still uniform, but its direction is no longer parallel to the incident field. The dipole moment is now given by

$$\mathbf{p}_e = \epsilon_0(\alpha_e)_\parallel\mathbf{e}_\parallel + \epsilon_0(\alpha_e)_\perp\mathbf{e}_\perp = \epsilon_0\begin{pmatrix}(\alpha_e)_\parallel & 0\\ 0 & (\alpha_e)_\perp\end{pmatrix}\cdot\begin{pmatrix}\mathbf{e}_\parallel\\ \mathbf{e}_\perp\end{pmatrix} = \epsilon_0\overline{\overline{\alpha}}_e\cdot\mathbf{e} \tag{3.146}$$

where $\overline{\overline{\alpha}}_e$ is the *polarizability dyadic of the spheroid*.

The method of separation of variables can also be applied to *oblate* spheroids of the kind shown in Figure 3.21*b*, for which the coordinates (μ, ν) defined by

$$r = c\mu\nu \qquad z = \pm c[(\mu^2 - 1)(1 - \nu^2)]^{\frac{1}{2}} \tag{3.147}$$

are appropriate (see A2.118). For $\mu_0 = 1$, the ellipsoid of revolution $\mu = \mu_0$ degenerates into a flat disk of radius c; for $\nu_0 = 1$, the hyperboloid of revolution $\nu = \nu_0$ degenerates into a plane with a central hole of radius c. The oblate spheroid in a uniform field can be treated exactly as its prolate counterpart [104, 134]. The weakening of the internal field and the value of the polarizability are still given by the expressions obtained for the prolate spheroid, but $g_\parallel$ and $g_\perp$ must now take the values given in Figure 3.23. In that figure, the eccentricities close to one correspond respectively with a dielectric needle (for the prolate geometry) and a circular dielectric disk (for the oblate geometry).

3.12 NUMERICAL METHODS

When the shape of the dielectric body is arbitrary, separation of variables does not work any longer, and some other method must be found to solve the potential problem. Two of these methods are discussed next.

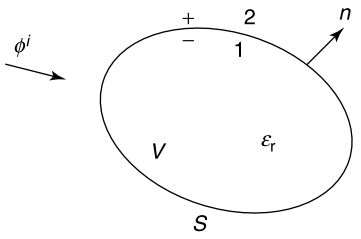

Figure 3.24 Dielectric body in an external field.

3.12.1 Integral Equation for a Homogeneous Dielectric

Let the "obstacle" consist of a homogeneous, isotropic*** dielectric of arbitrary shape, immersed in an incident potential ϕ^i (Fig. 3.24). A solution in terms of an integral equation was given years ago by Phillips.[9] The unknown in that equation is the value of the potential at the boundary surface. The starting point of the derivation is (3.90), which we will first apply to volume 1 and the harmonic function

$$\phi_1 - \frac{1}{\epsilon_r}\phi_i.$$

Thus, for $\mathbf{r}$ inside 1,

$$\phi_1(\mathbf{r}) - \frac{\phi_i(\mathbf{r})}{\epsilon_r} = \frac{1}{4\pi}\int_S \left[\frac{1}{|\mathbf{r}-\mathbf{r}'|}\frac{\partial\phi_1}{\partial n'_-} - \frac{1}{\epsilon_r|\mathbf{r}-\mathbf{r}'|}\frac{\partial\phi_i}{\partial n'_-} - \phi_1\frac{\partial}{\partial n'_-}\left(\frac{1}{|\mathbf{r}-\mathbf{r}'|}\right) + \frac{\phi_i}{\epsilon_r}\frac{\partial}{\partial n'_-}\left(\frac{1}{|\mathbf{r}-\mathbf{r}'|}\right)\right] dS', \tag{3.148}$$

where the subscript $(-)$ refers to a derivative just *inside* S (i.e., on the 1 side of S). We next apply (3.90) to the exterior region. The harmonic function is now $(\phi_2 - \phi_i)$, which is the potential stemming from the induced dipoles. For $\mathbf{r}$ inside 1:

$$0 = \frac{1}{4\pi}\int_S \left[\frac{1}{|\mathbf{r}-\mathbf{r}'|}\frac{\partial\phi_2}{\partial n'_+} - \frac{1}{|\mathbf{r}-\mathbf{r}'|}\frac{\partial\phi_i}{\partial n'_+} - \phi_2\frac{\partial}{\partial n'_+}\left(\frac{1}{|\mathbf{r}-\mathbf{r}'|}\right) + \phi_i\frac{\partial}{\partial n'_+}\left(\frac{1}{|\mathbf{r}-\mathbf{r}'|}\right)\right] dS', \tag{3.149}$$

where the subscript $(+)$ now refers to a derivative just *outside* S. The normal derivatives can be eliminated by multiplying (3.148) by ϵ_r, subtracting (3.149) from the result, and making use of the boundary conditions $\phi_1 = \phi_2$ and $\epsilon_r\dfrac{\partial\phi_1}{\partial n_-} = \dfrac{\partial\phi_2}{\partial n_+}$. This gives the following value for the potential inside the dielectric:

$$\phi(\mathbf{r}) = \frac{\phi_i(\mathbf{r})}{\epsilon_r} - \frac{\epsilon_r - 1}{4\pi\epsilon_r}\int_S \phi(\mathbf{r}')\frac{\partial}{\partial n'_-}\left(\frac{1}{|\mathbf{r}-\mathbf{r}'|}\right) dS'. \tag{3.150}$$

***For an extension to anisotropic media, see Note 8.

The procedure can be repeated for $\mathbf{r}$ outside V, the relevant functions being now $(\epsilon_r\phi_1 - \phi_i)$ and $(\phi_2 - \phi_i)$. This gives

$$\phi(\mathbf{r}) = \phi_i(\mathbf{r}) - \frac{\epsilon_r - 1}{4\pi}\int_S \phi(\mathbf{r}')\frac{\partial}{\partial n'_+}\left(\frac{1}{|\mathbf{r}-\mathbf{r}'|}\right) dS'. \tag{3.151}$$

The third and final step consists in letting the field point $\mathbf{r}$ approach the boundary. The essential difficulty here lies in the behavior of the surface integrals as the limiting process is performed. These integrals have the form of a dipole-layer potential, and their limit value is given by (3.64) and (3.65). Hence, after a few simple manipulations, one arrives at

$$\phi^i(\mathbf{r}) = \frac{\epsilon_r + 1}{2}\phi(\mathbf{r}) + \frac{\epsilon_r - 1}{4\pi}\int_S \phi(\mathbf{r}')\frac{\partial}{\partial n'}\left(\frac{1}{|\mathbf{r}-\mathbf{r}'|}\right) dS' \quad (\mathbf{r} \text{ on } S), \tag{3.152}$$

which is the sought *Phillips integral equation*. It is to be remembered that the surface integral is a convergent improper integral whose value is obtained by excluding a small surface of arbitrary shape containing $\mathbf{r}$ and letting this surface approach zero.

The solution of the integral equation proceeds by methods of the kind discussed in Section 1.11. Typically, in the case of a cube (Fig. 3.25), the boundary surface is subdivided into elementary patches, over which ϕ is assumed constant (a *pulse* type of basis function). The equation is then satisfied by point matching at the center of each subarea.[10] Proper consideration of the symmetries of the structure leads to a reduction of the number of independent values of ϕ. The matrix problem having been solved, physically interesting parameters, such as the induced moment density m_e, are easily derived.[11,12] The data in Figure 3.26 express the dimensionless function $m_e/4\pi\epsilon_0 e^i$ in terms of ϵ_r. For the sphere, from (3.125),

$$\frac{m_e}{4\pi\epsilon_0 e^i} = \frac{3}{4\pi}\frac{\epsilon_r - 1}{\epsilon_r + 2}.$$

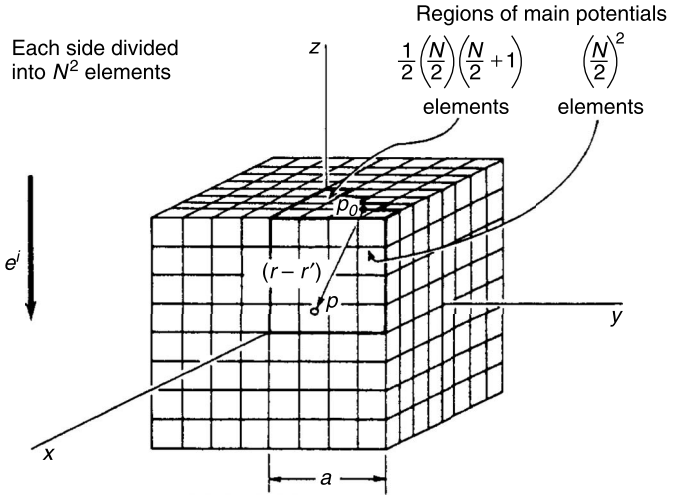

Figure 3.25 A dielectric cube in a uniform field (from T. W. Edwards and J. Van Bladel, Electrostatic dipole moment of a dielectric cube, *Appl. Sci. Res. Sect. B.*, **9**, 151–155, 1961, with permission of Springer Science and Business Media).

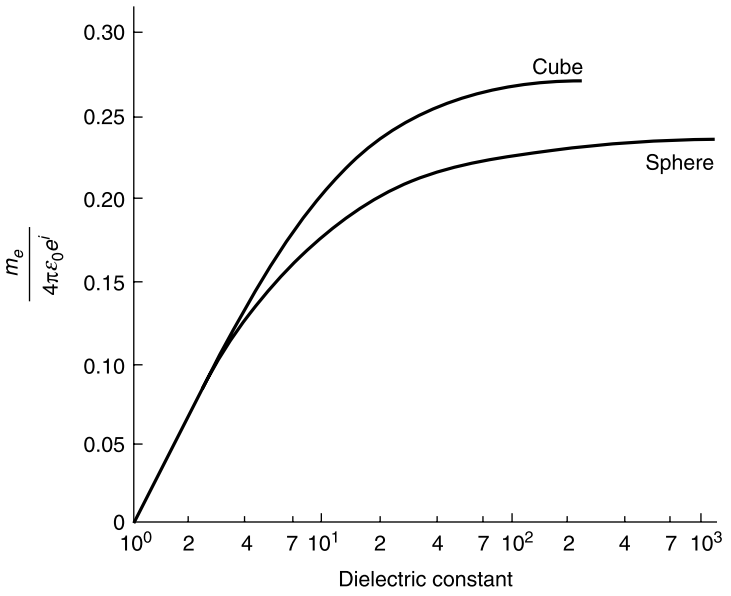

Figure 3.26 Dipole moment per unit volume (from D. F. Herrick and T. B. A. Senior, *IEEE Trans. AP*, **25**, 590–592, 1977, with permission of IEEE).

It is, of course, important to check that the problem embodied in (3.152) is *well-posed*. To that effect, we notice that the integral equation is of the second kind, that is, of the general type discussed under (1.85), with

$$\lambda = -\frac{\epsilon_r - 1}{\epsilon_r + 1}. \tag{3.153}$$

The kernel is

$$K(\mathbf{r}|\mathbf{r}') = \frac{1}{2\pi}\frac{\partial}{\partial n'}\left(\frac{1}{|\mathbf{r} - \mathbf{r}'|}\right). \tag{3.154}$$

Its adjoint has the same form, except that $\partial/\partial n'$ is replaced by $\partial/\partial n$. The $K(\mathbf{r}|\mathbf{r}')$ kernel is of essential importance in potential theory. Some of its principal properties are [158]:

1. $K(\mathbf{r}|\mathbf{r}')$ is weakly singular. In fact, for $\mathbf{r}$ and $\mathbf{r}'$ both on the surface, the discontinuity is not stronger than $1/|\mathbf{r} - \mathbf{r}'|$, so that Fredholm's theory can be applied.
2. If ϕ is continuous on S, the integral appearing in (3.152) satisfies a Hölder condition on S.
3. The eigenvalues are real, and none of them is less than 1 in absolute value.

The value of $|\lambda|$ shown in (3.153) is less than one, hence it does not coincide with an eigenvalue. Under these conditions, Fredholm's theory implies that (3.152) has one and only one solution.

3.12.2 Difference Equations and Finite Element Methods

The basic differential equation (3.109) can be discretized by using finite difference expressions for the operators (see Section 1.14). It is also possible to subdivide the whole

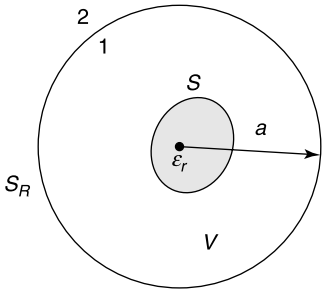

Figure 3.27 Artifical boundary surface S_R.

space into finite-element cells, a method introduced in Section 2.6. Both methods have the advantage of being easily applicable to inhomogeneous (and even anisotropic) dielectrics (Fig. 3.27). They are *three-dimensional* but fortunately give rise to sparsely populated matrices. The Phillips integral equation, on the other hand, is two-dimensional but generates *full* matrices containing a relatively large number of unknown coefficients. The point is further discussed in later chapters, as well as the numerical difficulties arising from the assumption of an infinite three-dimensional domain. This domain can usefully be divided into two regions, one *inside* a mathematical boundary S_R — conveniently chosen to be spherical — and one *outside* that surface. Assume, to simplify matters, that the dielectric is homogeneous. In region 2, the potential due to the "disturbance" is harmonic, hence it may be written as

$$\phi_d(\mathbf{r}) = \sum_{\sigma,m,n} A_{\sigma mn} Y_{\sigma mn}(\theta,\varphi) \left(\frac{a}{R}\right)^{n+1}, \tag{3.155}$$

where the functions $Y_{\delta mn}$ are the normalized surface spherical harmonics

$$Y_{\sigma mn}(\theta,\varphi) = \sqrt{\epsilon_m \frac{2n+1}{4\pi}\frac{(n-m)!}{(n+m)!}} P_n^m(\cos\theta) \begin{Bmatrix} \cos m\varphi \\ \sin m\varphi \end{Bmatrix}. \tag{3.156}$$

The indices must satisfy the condition $0 \le m \le n$ (see Appendix 9). The parity index σ takes the form e (even) for $\cos m\varphi$ and o (odd) for $\sin m\varphi$. The normalization implies that

$$\int_0^{2\pi}\int_0^{\pi} |Y_{\theta mn}|^2 \sin\theta \, d\theta \, d\varphi = 1. \tag{3.157}$$

The incident potential is sourceless in 1, hence it admits the expansion

$$\phi^i(\mathbf{r}) = \sum_{\sigma,m,n} B_{\sigma mn} Y_{\sigma mn}(\theta,\varphi) \left(\frac{R}{a}\right)^n \tag{3.158}$$

in that region. Because phenomena are assumed linear, the *effect* **A** is linearly related to the *cause* **B**. Thus,[13]

$$\mathbf{A} = \overline{\overline{T}} \cdot \mathbf{B}, \tag{3.159}$$

where $\overline{\overline{T}}$ is the *T-matrix*. The determination of its elements requires solution of Laplace's equation inside V, taking continuity of ϕ and $(\partial\phi/\partial R)$ on S_R into account. It is clear that $\overline{\overline{T}}$ is an efficient representation of the effect of the disturbance, as it yields **A** (and therefore ϕ_d) by the simple multiplication shown in (3.159), and this for all possible incident potentials ϕ^i.

PROBLEMS

3.1 Sketch the equipotentials and lines of force of the charge distributions appearing in Figure P3.1.

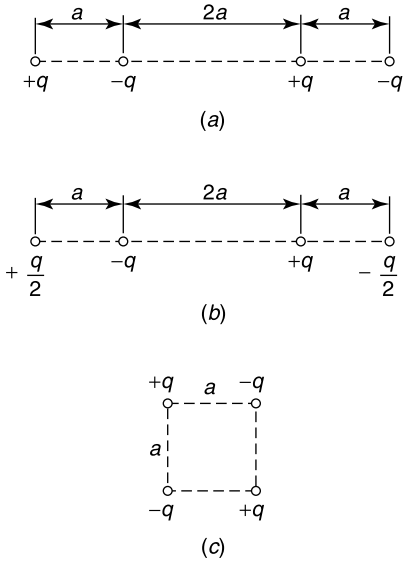

Figure P3.1

3.2 Consider two small bodies, each carrying a charge of $(+1\mu C)$. What is the electric force of interaction when they are placed 1 m apart?

3.3 Find the multipole expansion relative to a circular disk charged with a uniform density ρ_0.

3.4 In a crystal, charges of alternately positive and negative sign form a lattice of the kind shown in Figure P3.2. The periodicity is defined by the three vectors $\mathbf{a}_1, \mathbf{a}_2, \mathbf{a}_3$ or, equivalently, by the vectors $\mathbf{b}_1, \mathbf{b}_2, \mathbf{b}_3$ of the inverse system ($\mathbf{a}_i \cdot \mathbf{b}_j = \delta_{ij}$). If the origin of coordinates is taken at a certain positive charge O, find the potential ϕ' inside a sphere centered at O with radius equal to the distance to the nearest charge. The contribution of the charge in O will be ignored; hence $\phi = \phi - q/(4\pi\epsilon_0 R)$. Use an expansion of the multipole type, and assume that all charges have the same absolute value as in O. (F. W. DeWette et al., *Physica* **24**, 1105, 1958.)

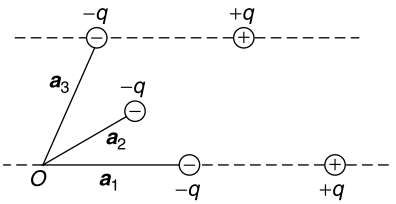

Figure P3.2

3.5 Find the potential generated by two antiparallel dipoles directed along the z-axis and separated by a small distance d. Use a multipole expansion. This axial quadrupole is a good model for molecules such as *p*-dichlorobenzene [37] (Fig. P3.3).

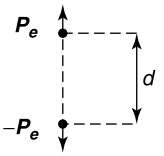

Figure P3.3

3.6 Investigate what happens to the dipole moment $\mathbf{p}_e$ of a cloud of charge when the origin O in Figure 3.3 is shifted by a vectorial distance $\mathbf{a}$.

3.7 In (3.33), the dyadic $(\bar{\bar{I}} - 3\mathbf{u}_R\mathbf{u}_R)$ is called the *dipole-field dyadic*, or dipole-dipole interaction dyadic [37]. On the basis of (A4.86), show that

$$\bar{\bar{I}} - 3\mathbf{u}_R\mathbf{u}_R = -R^3 \operatorname{grad}\operatorname{grad}\left(\frac{1}{R}\right).$$

3.8 Two spherical shells are separated by a radial distance d (Fig. P3.4). They carry respective uniform charge densities $+\rho_S$ and $-\rho_S$. Determine the potential ϕ throughout space, and investigate the limit $d \to 0$ of ϕ under the assumption $\lim \rho_S d = \tau$. Repeat by replacing $+\rho_S$ by the value ρ_{S1} given in (3.59). Compare with the results obtained for an ideal double layer.

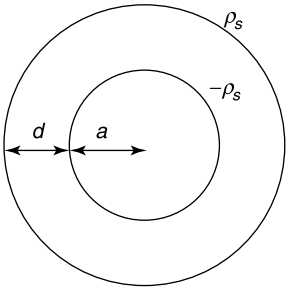

Figure P3.4

3.9 Continuity of $\mathbf{e}_{\tan}$ across a surface S is traditionally proved by applying Stokes' theorem to a small rectangle with sides AD and BC perpendicular to S and letting the separation d approach zero (Fig. P3.5). The proof must obviously break down in the case of a double layer with *variable* τ, as shown by (3.72). Find out why. (J. Van Bladel, *IEEE Ant. Prop. Magazine* **33**, 57–58, 1991; and B. Friedman, Techn. Report 2, Dept. of Math., Univ. of California, Berkeley, 1959.)

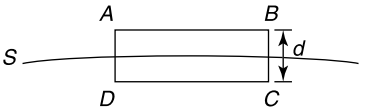

Figure P3.5

3.10 (**a**) Derive equations (3.54) and (3.55) by integrating the potential of an element $\rho_S\, dx$.

(**b**) Derive (3.73), either as the integral of potentials generated by $\tau\, dx$, or as the limit of two surface charges of the type shown in Figure 3.8*a*, letting the separating distance approach zero.

3.11 A straight segment AB is charged with a uniform linear density ρ_l. Show that (Fig. P3.6)

$$e_x = -\frac{\rho_l}{2\pi\epsilon_0 D}\sin\frac{\theta_1+\theta_2}{2}\sin\frac{\theta_2-\theta_1}{2}$$
$$e_y = \frac{\rho_l}{2\pi\epsilon_0 D}\cos\frac{\theta_1+\theta_2}{2}\sin\frac{\theta_2-\theta_1}{2}.$$

(A. R. Panicali, *IEEE Trans.* **EMC-33**, 67–68, 1991.)

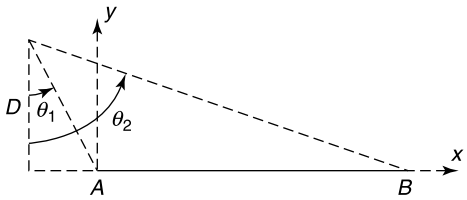

Figure P3.6

3.12 The portion of a spherical surface lying between the polar angles $\theta = \theta_0$ and $\theta = \pi - \theta_0$ is covered with a uniform charge density ρ_S. Find the potential outside the surface.

3.13 In the practical world of particle physics, the dipoles are not ideal, and the charge separation d in Figure 3.4*b*, although small, is not zero. Find the potential created by such a $(+q, -q)$ source, using spherical coordinates and an expansion in Legendre polynomials [37]. Consider, in particular, a few points situated on the **u** axis (e.g., at a distance d above $+q$), for which the solution is trivial, and compare with the results of the expansion when the latter is limited to one or two terms.

3.14 A spherical surface of radius a is covered with a surface charge of density $\sin\varphi$. Find the potential inside and outside the sphere.

3.15 The polarizability α_e is of the order of 10^{-30}m^3 (0.210^{-30} for N_a^+, for example, and 10^{-29} for benzene). Assume a very simplified model in which $\mathbf{p}_e$ is caused by charges q and $-q$ separated by a distance d. If the particles are electrons ($q = -1.6008\ 10^{-19}$ C),
(**a**) Find d in an electric field of $1\ \text{kV m}^{-1}$.
(**b**) Find the resulting dipole moment.

3.16 Show that the value (3.111) of the self-field $\mathbf{e}_s$ can also be obtained by replacing the uniform $\mathbf{m}_e$ by an equivalent charge density ρ'_S. Use this method to show that $\mathbf{e}_s$ is uniform in a sphere, hence that (3.113) holds at every interior point of the latter. Repeat the derivation for the circular cylinder of Figure 3.18*a*. The results can be found in Maxwell's treatise [13, p. 22–25, Vol. 2], where the author investigates the equivalent magnetic problem.

3.17 Find the field due to an elementary dipole situated at the center of a spherical cavity carved out of a homogeneous dielectric of dielectric constant ϵ_r.

3.18 Derive a variational principle for the potential produced by volume charges ρ located in a dielectric of nonuniform dielectric constant ϵ_r.

3.19 The potential at the surface of a dielectric sphere in a uniform field can be found from (3.123). Check that this potential satisfies the Phillips integral equation (3.152).

NOTES

1. H. Weyl, The method of orthogonal projection in potential theory, *Duke Math. J.* **7**, 411–444 (1940).
2. P. Hammond and T. Tsiboukis, Dual finite-element calculations for static electric and magnetic fields, *IEE Proceedings* **130-A**, 105–111 (1983).
3. Coulomb's Law Committee of the AAPT. The teaching of electricity and magnetism at the college level, *Am. J. Phys.* **18**, 1–25, 69–88 (1950).
4. A. D. Yaghjian, Electric dyadic Green's functions in the source region, *Proc. IEEE* **68**, 248–263 (1980).
5. J. Avelin et al., Electric fields in the source region: the depolarization dyadic for a cubic cavity, *Electrical Engineering* **81**, 199–202 (1998).
6. I. V. Lindell, Electrostatic image theory for the dielectric sphere, *Radio Science* **27**, 1–8 (1992).
7. I. V. Lindell, K. I. Nikoskinen and A. Viljanen, Electrostatic image method for the anisotropic half space, *IEE Proc.-Sci. Meas. Technol.* **144**, 156–162 (1997).
8. A. H. Sihvola and I. V. Lindell, Electrostatics of an anisotropic ellipsoid in an anisotropic environment, *AEÜ* **50**, 289–292 (1996).
9. H. B. Phillips, Effect of surface discontinuity on the distribution of potential, *J. Math. and Phys.* **13**, 261–267 (1934).
10. T. W. Edwards and J. Van Bladel, Electrostatic dipole moment of a dielectric cube, *Appl. Sci. Res. Sect. B.* **9**, 151–155 (1961).
11. D. F. Herrick and T. B. A. Senior, The dipole moments of a dielectric cube, *IEEE Trans. AP* **25**, 590–592 (1977).
12. J. Avelin and A. Sihvola, Polarizability of polyhedral dielectric scatterers, *Microwave Opt. Tech. Lett.* **32**, 60–64 (2002).
13. P. C. Waterman, Matrix methods in potential theory and electromagnetic scattering, *J. Appl. Phys.* **50**, 4550–4566 (1979).

Chapter 4

Electrostatic Fields in the Presence of Conductors

Under static conditions, conductors are found either passive or to carry currents. In the *passive* mode, the electric field vanishes inside the conducting volume V, which is therefore at a uniform potential. If the conductor is *charged*, the charges migrate to the surface S of V, where their density ρ_S must be determined. When the conductor is *uncharged*, positive and negative charges will be induced on S under the influence of exterior sources, the net charge remaining zero. In all cases, the electric field is perpendicular to S, and its determination is an *exterior* problem, to which the first part of the current chapter is devoted.

In the *current-carrying* mode, the current is either injected (or extracted) through contact electrodes or generated by applied electric fields (i.e., by factors such as chemical potentials or temperature gradients). In both situations, the fields and currents must be determined *inside* the conductor. This is an *interior* problem, which is discussed in the second part of the chapter.

4.1 CONDUCTIVITY

Conducting bodies contain charges that are free to move under the influence of electrical and nonelectrical forces. The motion of these charges gives rise to electric currents whose strength and direction are measured by the *current density* vector

$$\mathbf{j} = \sum_i \rho_i \mathbf{v}_i = \sum_i n_i q_i \mathbf{v}_i \quad (\mathrm{A\,m^{-2}}), \tag{4.1}$$

where the summation extends over all types of charge carriers. In (4.1), n_i, ρ_i, q_i, and $\mathbf{v}_i$ are, respectively, the number density, charge density, charge, and average velocity of species i. In metallic conductors and alloys, the free charges are electrons moving in a lattice of positive charges. In semiconductors the current can be carried either by electrons with energies in the conduction band or by holes (missing electrons) in the valence band. The carrier density depends strongly on the temperature and the concentration of impurities and can be changed by many orders of magnitude by variations in these parameters. In electrolytic solutions,

Electromagnetic Fields, Second Edition, By Jean G. Van Bladel

the charge carriers are positive and negative ions. In gasses, charges can be produced by processes such as ionizing collisions and X-ray bombardment.

The motion of charge carriers can be ascribed to various influences. One of these is the action of a macroscopic electric field. It is useful to separate the current density into two parts:

$$\mathbf{j} = \mathbf{j}(\mathbf{e}) + \mathbf{j}_a. \tag{4.2}$$

The first part stems from the influence of the electric forces and the second part from the effects of all other forces. We shall first concern ourselves with the electric part. In a large number of media, the relationship between the electric field and the average velocity $\mathbf{v}$ is, for a given species,

$$\mathbf{v} = \overline{\overline{\mu}}_m \cdot \mathbf{e}, \tag{4.3}$$

where $\overline{\overline{\mu}}_m$ is the *mobility tensor*. This tensor has the dimension $\mathrm{m^2\,Vs^{-1}}$, and typical values of μ_m are 0.0032 for Cu and 0.38 for the electrons in intrisic Ge. The linear relationship (4.3) holds for sufficiently low values of the electric field. The corresponding current density is proportional to $\mathbf{v}$ and given by

$$\mathbf{j} = nq\overline{\overline{\mu}}_m \cdot \mathbf{e} = \overline{\overline{\sigma}} \cdot \mathbf{e}, \tag{4.4}$$

where $\overline{\overline{\sigma}}$ is the *conductivity tensor*. To calculate the values of $\overline{\overline{\mu}}_m$ and $\overline{\overline{\sigma}}$, it is necessary to perform statistical averages over all free charges in a small volume. For a body with crystalline structure, the conductivity tensor has three principal directions. In gallium, for example, the conductivities along these directions are in the ratio of 1 to 3.2 to 7. More commonly, two of the principal directions have the same conductivity $\sigma_\perp$, but a different value $\sigma_\parallel$ is associated with the third direction. This is the case for tin, in which $\sigma_\parallel = 11.1 \times 10^6\,\mathrm{S\,m^{-1}}$ and $\sigma_\perp = 7.6 \times 10^6\,\mathrm{S\,m^{-1}}$ at 273 K. In cubic crystals, σ is simply a scalar. In noncubic crystals, a scalar average can be introduced when the individual crystals are oriented at random, so that an isotropic mean conductivity can be used.

Conductivities encountered in practice range from multiples of $10^7\,\mathrm{S\,m^{-1}}$ for metals (which are endowed with large densities of electrons) to about $10^{-17}\,\mathrm{S\,m^{-1}}$ for very good insulators such as quartz. In between we find the semiconductor group, with σ of about $1.6 \times 10^{-3}\,\mathrm{S\,m^{-1}}$ for pure Si and $2.22\,\mathrm{S\,m^{-1}}$ for intrisic, pure Ge. These conductivities can be increased by means of doping with impurities.

We now turn our attention to the current density $\mathbf{j}_a$ in (4.2). Instead of this density, an effective *applied electric field* is frequently introduced, in terms of which $\mathbf{j}$ can be written as

$$\mathbf{j} = \overline{\overline{\sigma}} \cdot (\mathbf{e} + \mathbf{e}_a)$$

with

$$\mathbf{e}_a = \overline{\overline{\sigma}}^{-1} \cdot \mathbf{j}_a. \tag{4.5}$$

The current density $\mathbf{j}_a$ arises by virtue of several factors, one of which is *diffusion* (i.e., a migration of particles from higher to lower concentrations). Thus, if q is the charge of the particles, the current density in an electron gas is

$$\mathbf{j} = nq\mathbf{v}_{\mathrm{ave}} = nq\mu_m\mathbf{e} - qD\ \mathrm{grad}\ n, \tag{4.6}$$

where D is the *diffusion coefficient*. This effect is negligible in metals but is of decisive importance in semiconductors. In electrolytic solutions, we encounter the *battery effect*, which results in a current density

$$\mathbf{j} = \sigma(\mathbf{e} - \alpha \text{ grad } \zeta), \tag{4.7}$$

where ζ is the chemical potential and α a material factor. In a heated metal, the *thermoelectric effect* gives rise to a current density

$$\mathbf{j} = \sigma(\mathbf{e} - \overline{\overline{\beta}} \cdot \text{grad } T), \tag{4.8}$$

where T is the temperature, and $\overline{\overline{\beta}}$ is a tensor if the conductor is anisotropic.

The strong inhomogeneties that exist at the junction between two materials produce large gradients in the transition layer. Throughout this layer, $\mathbf{e}$ must be very large and almost equal to $-\mathbf{e}_a$ to keep the current density finite. Thus, if A and B are two points on opposite sides of the junction,

$$\int_A^B \mathbf{e} \cdot d\mathbf{l} = \phi(A) - \phi(B) = -\int_A^B \mathbf{e}_a \cdot d\mathbf{l}. \tag{4.9}$$

A contact potential consequently appears between the two media.

The conduction process is often influenced by magnetic fields. The conductivity of a plasma, for example, is normally a scalar but becomes a nonsymmetric tensor under the influence of a uniform magnetic flux density $\mathbf{b}_0$. The consequences for wave propagations in such a medium are discussed in Chapter 8. In an isotropic conductor, the $\mathbf{j}(\mathbf{e})$ relationship becomes, for sufficiently small $\mathbf{b}_0$,

$$\mathbf{e} = \frac{1}{\sigma}\mathbf{j} + R(\mathbf{b}_0 \times \mathbf{j}), \tag{4.10}$$

where R is a scalar quantity termed *Hall's constant*. According to this relationship, the Hall effect generates an electric field perpendicular to the current density $\mathbf{j}$. Finally, when gradients of temperature are present, the $\mathbf{e}(\mathbf{j})$ relationship takes the form

$$\mathbf{e} = \frac{1}{\sigma}\mathbf{j} + \beta \text{ grad } T + R(\mathbf{b}_0 \times \mathbf{j}) + N(\mathbf{b}_0 \times \text{ grad } T) \tag{4.11}$$

valid to the first order in $\mathbf{b}_0$. The last term in the right-hand term represents the *Nernst effect*; that is, the effect of the magnetic field on the thermoelectric field [11].

4.2 POTENTIAL OUTSIDE A CHARGED CONDUCTOR

Let a homogeneous isotropic conductor carry a charge q (Fig. 4.1). The volume charge density in V is connected to the current density $\mathbf{j}$ by the *equation of conservation of charge*

$$\text{div } \mathbf{j} = -\frac{\partial \rho}{\partial t} \qquad (\text{A m}^{-3}). \tag{4.12}$$

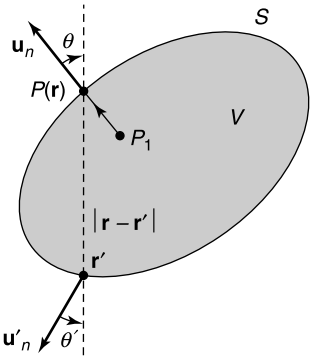

Figure 4.1 Charged conductor.

This is the *point* form of the equation. Its *integral* form is obtained by integrating (4.12) over the fixed volume V. This gives

$$\int_S \mathbf{u}_n \cdot \mathbf{j}\, dS = -\frac{d}{dt}\int_V \rho\, dV \qquad (\mathrm{C\,s^{-1}} = \mathrm{A}).$$

The physical meaning is clear: a flux of charges out of V causes a reduction of the charge accumulated in V.

Under static conditions, (4.12) implies div $\mathbf{j} = 0$. In addition, $\mathbf{u}_n \cdot \mathbf{j}$ must vanish on S, lest charges are accumulated on (or depleted from) the surface, which would create a nonstatic situation. If furthermore there are no applied electric fields in V, we may write $\mathbf{j} = \sigma\mathbf{e} = -\sigma$ grad ϕ. Potential ϕ must therefore satisfy

$$\nabla^2\phi = 0 \qquad (\text{in } V)$$

$$\frac{\partial\phi}{\partial n} = 0 \qquad (\text{on } S).$$

The only solution to this sourceless Neumann problem is $\phi =$ constant. The proof is based on (A1.30), which gives

$$\int_V \left(\phi\nabla^2\phi + \text{grad } \phi \cdot \text{grad } \phi\right) dV = \int_S \phi \frac{\partial\phi}{\partial n}\, dS = 0.$$

This equation implies grad $\phi = 0$ (i.e., ϕ = constant). Under static conditions, therefore, no current flows in the conductor, the potential remains constant and uniform in V, and the charges are concentrated at the surface. The potential varies outside S, however, where it must satisfy

$$\begin{aligned} \text{div}(\epsilon_r \text{ grad } \phi) &= 0 \\ \phi &= \phi_1 \qquad (\text{on } S) \\ -\epsilon_0 \int_S \epsilon_r \frac{\partial\phi}{\partial n} dS &= q \end{aligned} \tag{4.13}$$

ϕ regular at infinity.

The symbol ϵ_r denotes the dielectric constant of the region outside S. The constant potential ϕ_1 is obviously proportional to q. The proportionality ratio $C = q/\phi_1$ is the *capacitance of the conductor*.

In a few cases, the potential problem can be solved by separation of variables. The simplest example is that of a charged metallic sphere of radius a, for which the (exterior) potential at a distance R from the center is

$$\phi = \frac{q}{4\pi\epsilon_0 R} = \phi_1 \frac{a}{R}. \tag{4.14}$$

We recognize the potential generated by a point charge q located at the center of the sphere. From (4.14), the capacitance of the sphere is $C = 4\pi\epsilon_0 a$.

4.2.1 The Prolate Spheroid

A more interesting example is afforded by the charged prolate spheroid. We use the spheroidal coordinates already introduced in Section 3.11. The outer surface of the conductor is defined by $\mu = \mu_0$ (Fig. 3.22). The condition $\phi = \phi_1$ on S can clearly be satisfied by assuming a solution of the form $\phi(\mu)$. Laplace's equation (3.134) becomes, for such a function,

$$\frac{\partial}{\partial \mu}\left[(\mu^2 - 1)\frac{\partial \phi}{\partial \mu}\right] = 0. \tag{4.15}$$

The general solution of (4.15) is

$$\phi(\mu) = A \log_e \frac{\mu + 1}{\mu - 1} + B.$$

A sphere of infinite radius centered at the origin corresponds with $\mu = \infty$. Hence, the condition $\phi(\mu) = 0$ at infinity requires B to vanish. To determine A, we note that the potential at a large distance from the origin is of the form $q/(4\pi\epsilon_0 R)$. From (3.132), the limiting value of R for large μ is $R = (r^2 + z^2)^{\frac{1}{2}} = \mu c$. Accordingly,

$$\lim_{R\to\infty} \phi(\mu) = \frac{q}{4\pi\epsilon_0 \mu c} = A \log_e \frac{1 + \mu^{-1}}{1 - \mu^{-1}} \approx \frac{2A}{\mu}$$

which yields

$$A = \frac{q}{8\pi\epsilon_0 c}$$

and finally

$$\phi(\mu) = \frac{q}{8\pi\epsilon_0 c} \log_e \frac{\mu + 1}{\mu - 1}. \tag{4.16}$$

The capacitance of the spheroid follows immediately by setting $\mu = \mu_0$ in (4.16). Thus,

$$C = \frac{8\pi\epsilon_0 c}{\log_e\left(\dfrac{\mu_0 + 1}{\mu_0 - 1}\right)}. \tag{4.17}$$

To determine the electric field $\mathbf{e} = -\text{grad}\ \phi$, we apply the general formula (A2.114). This gives, at the surface,

$$\mathbf{e} = -\sqrt{\frac{\mu_0^2 - 1}{\mu_0^2 - \nu^2}}\frac{\partial \phi}{\partial \mu}\mathbf{u}_1 \tag{4.18}$$

where $\mathbf{u}_1$ is the unit vector perpendicular to the surface of constant μ. The charge density on the spheroid is $\epsilon_0 e_\mu$, hence

$$\rho_S = \frac{q}{4\pi c^2}\left[(\mu_0^2 - \nu^2)(\mu_0^2 - 1)\right]^{-\frac{1}{2}}. \tag{4.19}$$

At the tip of the conductor, where $\nu = 1$,

$$\rho_S = \frac{q}{4\pi c^2}\frac{1}{\mu_0^2 - 1} = \frac{q}{4\pi b^2}. \tag{4.20}$$

The equivalent linear charge density ρ_l (in C per m along the axis) is defined by $\rho_l\, dz = \rho_S\, dS$, where dS is the area of the annulus formed by moving from ν to $\nu + d\nu$. This move corresponds with a distance $h_\nu\, d\nu$, where the metric coefficient h_ν is given by (A2.113). Thus,

$$h_\nu\, d\nu = c\sqrt{\frac{\mu_0^2 - \nu^2}{1 - \nu^2}}\, d\nu = \frac{1}{\mu_0}\sqrt{\frac{\mu_0^2 - \nu^2}{1 - \nu^2}}\, dz. \tag{4.21}$$

The element of surface dS is therefore

$$dS = \frac{2\pi c}{\mu_0}\sqrt{(\mu_0^2 - 1)(\mu_0^2 - \nu^2)}\, dz, \tag{4.22}$$

which gives a linear charge density

$$\rho_l = \frac{q}{2\mu_0 c} = \frac{q}{2a}. \tag{4.23}$$

This is an interesting result: ρ_l turns out to be uniform, whatever the axial ratio (a/b). The property holds in particular for a sharp needle, which is obtained by letting μ_0 approach unity.[1] The potential and fields around the needle therefore coincide with those around a uniformly charged line segment, a problem already discussed in Section 3.6. The electric field near the tip will consequently exhibit the type of singularity described in (3.84).

The *oblate* spheroid may be discussed in a similar way. In the limit of a flat circular disk of radius a, the charge density takes the value [17]

$$\rho_S = \frac{q}{4\pi a\sqrt{a^2 - r^2}}. \tag{4.24}$$

The capacitance is $C = 8\epsilon_0 a$. The charge density is singular at the edge of the disk, in agreement with the general edge behavior discussed in Section 5.2.

4.2.2 Conductors of Arbitrary Shape

When the shape of the boundary does not lend itself to separation of variables, alternate procedures must be found. The integral equation formulation is a possibility and in fact a very successful one. The *Coulomb equation* is obtained by recognizing that, on an isolated conductor at potential ϕ_1, the surface charge density satisfies

$$\frac{1}{4\pi\epsilon_0}\int_S \frac{\rho_S(\mathbf{r}')dS'}{|\mathbf{r}-\mathbf{r}'|} = \phi_1 \qquad \text{(for all } \mathbf{r} \text{ on } S\text{)}. \tag{4.25}$$

A second type of *equation* was proposed by *Robin*.[2] It is derived from the important relationship (3.45). Because ϕ is constant in the conductor, its normal derivative when P_1 approaches the surface is zero, and we may write (Fig. 4.1)

$$\begin{aligned} 2\epsilon_0 \lim_{P_1\to P}\frac{\partial\phi}{\partial n} &= \rho_S(\mathbf{r}) + \frac{1}{2\pi}\int_S \rho_S(\mathbf{r}')\frac{\partial}{\partial n}\left(\frac{1}{|\mathbf{r}-\mathbf{r}'|}\right)dS' \\ &= \rho_S(\mathbf{r}) - \frac{1}{2\pi}\int_S \rho_S(\mathbf{r}')\frac{\cos\theta}{|\mathbf{r}-\mathbf{r}'|^2}\,dS' = 0. \end{aligned} \tag{4.26}$$

We note that (4.26) determines ρ_S to within a multiplicative constant, which can be determined from a knowledge of the total charge q on the conductor. This property, and the existence and uniqueness of the solution, are discussed in Section 4.3.

As an example of solution of Poisson's equation, consider a hollow circular cylinder raised to potential ϕ_1 (Fig. 4.2). Because the sought charge density ρ_S is independent of the azimuth φ, (4.25) takes the form

$$\frac{1}{4\pi}\int_{-h}^{h}\sigma(z')k(z-z')dz' = 1, \tag{4.27}$$

where σ is the dimensionless quantity $2\pi a\rho_S/\epsilon_0\phi_1$, and

$$k(z-z') = \frac{1}{2\pi}\int_{-\pi}^{\pi}\frac{d\varphi'}{\sqrt{(z-z')^2 + 4a^2\sin^2\dfrac{\varphi'}{2}}}.$$

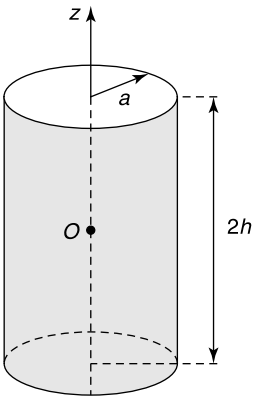

Figure 4.2 Charged hollow cylinder.

With the reduced variable $\beta = |z - z'|/2a$, the — weakly singular — kernel becomes

$$k(\beta) = \frac{1}{\pi a} \int_0^{\frac{\pi}{2}} \frac{d\alpha}{\sqrt{\beta^2 + \sin^2 \alpha}}.$$

The form of the kernel is appropriate for the application of an often used technique: addition and subtraction of singularities.[3] The singular part of $k(\beta)$ can be isolated by writing

$$k(\beta) = \frac{1}{\pi a} \int_0^{\frac{\pi}{2}} \frac{\cos\alpha d\alpha}{\sqrt{\beta^2 + \sin^2 \alpha}} + \frac{1}{\pi a} \int_0^{\frac{\pi}{2}} \frac{(1 - \cos\alpha) d\alpha}{\sqrt{\beta^2 + \sin^2 \alpha}} = k_1(\beta) + k_2(\beta).$$

The second integral does not diverge as $\beta \to 0$ (i.e., as $z \to z'$), but it must be evaluated numerically. The first one can be integrated analytically, however, and yields

$$k_1(\beta) = -\frac{1}{\pi a} \log_e \frac{|\beta|}{1 + \sqrt{1 + \beta^2}}. \tag{4.28}$$

When $a \gg h$ (i.e., for a thin ring), ρ_S is given by

$$\rho_S(z) = \frac{2\epsilon_0 \phi_1}{h} \frac{1}{\log_e \left(\frac{16a}{h}\right)} \frac{1}{\sqrt{1 - \frac{z^2}{h^2}}}. \tag{4.29}$$

The edge singularity is apparent. When the tube is very long (i.e., in the limit $a \ll h$), ρ_S is essentially uniform except for a singularity at the edges. The approximate value of the capacitance for such a tube is

$$C = -4\pi\epsilon_0 \frac{h}{1 + \log_e \frac{a}{4h}}. \tag{4.30}$$

Some values of C are given in Table 4.1.

The charge density on a conductor can also be determined by means of a variational principle. Because the kernel in (4.25) is real and symmetric (in $\mathbf{r}$ and $\mathbf{r}'$), (2.21) implies that the charge density. ρ_S extremizes the functional

$$J_1(\rho_S) = \frac{1}{4\pi\epsilon_0} \int_S \rho_S(\mathbf{r}') dS' \int_S \frac{\rho_S(\mathbf{r}) dS}{|\mathbf{r} - \mathbf{r}'|} \tag{4.31}$$

Table 4.1 Normalized Capacitance $C/\epsilon_0 a$ of a Hollow Tube

a/h	Long tube (4.30)	Short tube (4.29)	Exact (numerical)
0.005	442		446
0.050	74.3		75.8
0.150	36.7		36.8
0.250	28.4	28.5	27.4
1		14.2	14.4
4		9.49	9.44

under the restrictive condition

$$\int_S \rho_S(\mathbf{r})dS = 1.$$

The functional reaches a minimum of $1/C$ for the correct charge density.[4] This property implies that $1/J_1(\phi)$ yields a lower bound for C when an arbitrary function ϕ is used. An upper bound may be found by invoking a complementary variational principle[5] [146]. In the current problem, the functional

$$J_2(\phi) = \frac{\epsilon_0}{\phi_1^2}\int |\text{grad } \phi|^2 dV \qquad (\phi = \phi_1 \text{ on } S), \tag{4.32}$$

where the integral is over the space outside the conductor, yields the sought upper bound. As a result, C may be bracketed by the inequalities

$$\frac{1}{J_1(\rho_S)} \le C \le J_2(\phi). \tag{4.33}$$

The stationary value of $J_2(\phi)$ is proportional to the electrostatic energy outside the conductor, as

$$\mathcal{E} = \frac{1}{2}\epsilon_0 \int |\text{grad } \phi|^2 dV = \frac{1}{2}\phi_1^2 J_2(\phi) = \frac{1}{2}C\phi_1^2. \tag{4.34}$$

4.3 CAPACITANCE MATRIX

Figure 4.3 shows two conductors carrying respective charges q_1 and q_2. Two basic potential problems must be solved to determine the potential in the space surrounding the conductors. With $j = 1, 2$,

$$\begin{aligned} &\nabla^2\phi_j = 0 \\ &\quad \phi_j = 1 \qquad \text{(on conductor } j\text{)} \\ &\quad \phi_j = 0 \qquad \text{(on the other conductor)} \\ &\quad \phi_j \text{ regular at infinity.} \end{aligned} \tag{4.35}$$

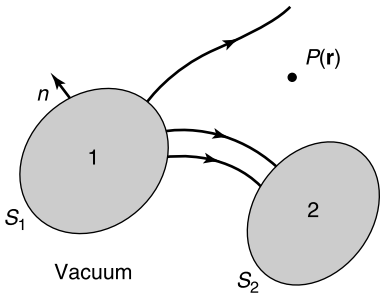

Figure 4.3 Lines of force about two charged bodies.

Solution of these problems allows determination of the potential for an arbitary set of conductor potentials V_j. The linearity of the problem permits writing

$$\phi(\mathbf{r}) = V_1\phi_1(\mathbf{r}) + V_2\phi_2(\mathbf{r}).$$

The charge carried by conductor j is then

$$q_j = -\epsilon_0 \int_{S_j} \frac{\partial \phi}{\partial n} dS = V_1 \left(-\epsilon_0 \int_{S_j} \frac{\partial \phi_1}{\partial n} dS \right) + V_2 \left(-\epsilon_0 \int_{S_j} \frac{\partial \phi_2}{\partial n} dS \right). \tag{4.36}$$

Equations (4.36) show that a linear relationship exists between the q's and the V's. More precisely:

$$\begin{aligned} q_1 &= C_{11}V_1 + C_{12}V_2 \\ q_2 &= C_{21}V_1 + C_{22}V_2. \end{aligned} \tag{4.37}$$

Because a harmonic function cannot have an extremum except at a boundary surface, the magnitude of a potential such as ϕ_1 must lie between 0 and 1 outside S_1. Consequently, with $q_1 > q_2$ the lines of force must emanate from 1, and terminate on 2 or at infinity. We conclude that C_{11} must be positive, whereas C_{12} is negative. In addition, C_{12} is not larger than C_{11} in absolute value.

The detailed solution of (4.35) can be effected by methods similar to those introduced in the solution of the one-conductor problem. For example, separation of variables can be used to determine the capacitance of two coaxial hyperboloids of revolution. As no new elements of importance are involved, the reader is referred to existing textbooks for applications of the method [6, volume 17], [54, volume 2], [140, 165].

The notion of capacitance matrix, introduced for two conductors, can easily be extended to N condutors. The $\overline{\overline{C}}$ matrix is symmetric (i.e., $C_{mn} = C_{nm}$), which implies that the number of independent coefficients is $N(N+1)/2$ rather than N^2 (Problem 4.9). The remark is of importance when the coefficients of the matrix must be determined *experimentally*, in which case it becomes desirable to reduce the number of measurements to a minimum.

4.4 THE DIRICHLET PROBLEM

The potential in a volume V bounded by a conducting screen must satisfy the requirements

$$\begin{aligned} \nabla^2\phi &= -\frac{\rho}{\epsilon_0} \\ \phi &= \phi_0 \qquad (\text{on } S_0). \end{aligned} \tag{4.38}$$

The uniform value ϕ_0 is equal to q/C, where C is the capacitance of the conductor bounded by S_1 (Fig. 4.4*a*) and q is the total charge of the system, equal to the charge on the screen plus that in the interior volume V. We may set $\phi_0 = 0$ without changing the value of the electric field in V. With this homogeneous boundary condition it is elementary to show, on the basis of Green's theorem (A1.30), that the transformation defined by the operator ∇^2

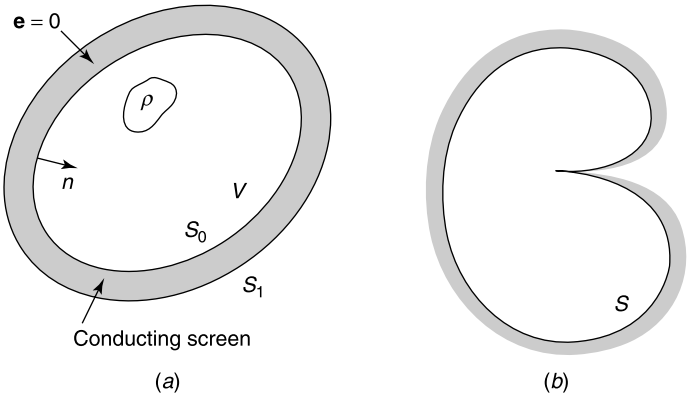

Figure 4.4 (*a*) Volume charges in an enclosure. (*b*) Surface with a spine.

and the boundary condition $\phi = 0$ on S_0 is negative-definite and self-adjoint. Further, the homogeneous problem

$$\begin{aligned} \nabla^2\phi_0 &= 0 \qquad (\text{in } V) \\ \phi_0 &= 0 \qquad (\text{on } S_0) \end{aligned} \tag{4.39}$$

has no nonzero solution. The similarity to the clamped-string problem is evident. In the same vein, one easily verifies that the *eigenfunctions* of the *Dirichlet problem*, given by

$$\begin{aligned} \nabla^2\phi_{mnp} - \lambda_{mnp}\phi_{mnp} &= 0 \qquad (\text{in } V) \\ \phi_{mnp} &= 0 \qquad (\text{on } S_0), \end{aligned} \tag{4.40}$$

form a complete and orthogonal set. All eigenvalues λ_{mnp} are negative, and all eigenfunctions are continuous. When the interior source is a point charge [with charge density $\rho = q\,\delta(\mathbf{r} - \mathbf{r}')$], the potential becomes the Green's function of the enclosure, and its expansion in terms of the ϕ_{mnp} follows from (1.100).

The problem embodied in (4.38) is a particular example of the more *general Dirichlet problem*

$$\begin{aligned} \nabla^2\phi &= g(\mathbf{r}) \qquad (\text{in } V) \\ \phi &= h(\mathbf{r}) \qquad (\text{on } S). \end{aligned} \tag{4.41}$$

If ϕ_c is a particular solution of the first equation, for example (3.16), the difference $\phi - \phi_c = \Omega$ must satisfy

$$\begin{aligned} \nabla^2\Omega &= 0 \qquad (\text{in } V) \\ \Omega &= s(\mathbf{r}) \qquad (\text{on } S), \end{aligned} \tag{4.42}$$

where $s = h - \phi_c$ on S. The existence of a solution to (4.41) is now reduced to that of a solution to (4.42), a problem that is well-suited for an application of the Fredholm theory outlined in Section 1.9. Rigorous analysis shows that (4.42) does not *always* have a solution.

A famous example provided by Lebesgue [158] is that of a surface with a spine (Fig. 4.4*b*). For more regular surfaces, however, (4.42) has a solution of the type (see Fig. 4.1)

$$\Omega(\mathbf{r}) = \frac{1}{4\pi\epsilon_0}\int_S \tau(\mathbf{r}')\frac{\partial}{\partial n'}\left(\frac{1}{|\mathbf{r}-\mathbf{r}'|}\right) dS'. \tag{4.43}$$

This dipole-layer potential satisfies $\nabla^2\Omega = 0$ in V. To satisfy the boundary condition, the limit of Ω as $\mathbf{r}$ approaches the surface from the inside must be $s(\mathbf{r})$. From (3.66), this condition implies that

$$-2\epsilon_0 s(\mathbf{r}) = \tau(\mathbf{r}) - \frac{1}{2\pi}\int_S \tau(\mathbf{r}')\frac{\partial}{\partial n'}\left(\frac{1}{|\mathbf{r}-\mathbf{r}'|}\right) dS'. \tag{4.44}$$

This is an integral equation whose homogeneous version, obtained by setting $s(\mathbf{r}) = 0$, has no nonzero solution [158]. Hence, from Fredholm's theory, (4.43) has a unique solution, which implies that (4.42) has a unique solution too.

The second Dirichlet problem to be investigated concerns the volume *outside* S. The potential problem is now

$$\begin{aligned} \nabla^2\Omega &= 0 \qquad (\text{outside } S) \\ \Omega &= s(\mathbf{r}) \qquad (\text{on } S) \\ \Omega &\text{ regular at infinity.} \end{aligned} \tag{4.45}$$

To solve this problem, it is convenient to express $s(\mathbf{r})$ as the sum of a constant term and a term orthogonal to the solution* $\rho_S(\mathbf{r})$ of (4.25). The desired splitting is then uniquely given by

$$s(\mathbf{r}) = \frac{\displaystyle\int_S s(\mathbf{r}')\rho_S(\mathbf{r}')\,dS'}{\underbrace{\displaystyle\int_S \rho_S(\mathbf{r}')\,dS'}_{\text{constant } A}} + u(\mathbf{r}) \tag{4.46}$$

with

$$\int_S u(\mathbf{r})\rho_S(\mathbf{r})\,dS = 0.$$

We must now solve two partial problems. In the first one, $\Omega = A$ on S. The solution is the surface charge potential associated with the conductor at the uniform potential A; it is of the form (4.25). In the second partial problem, $\Omega = u(\mathbf{r})$ on S. To solve this problem, let us try a dipole-layer potential of the type given in (4.43). From (3.67), satisfaction of the boundary condition on S implies that

$$2\epsilon_0 u(\mathbf{r}) = \tau(\mathbf{r}) + \frac{1}{2\pi}\int_S \tau(\mathbf{r}')\frac{\partial}{\partial n'}\left(\frac{1}{|\mathbf{r}-\mathbf{r}'|}\right) dS'. \tag{4.47}$$

*Function $\rho_S(\mathbf{r})$ is the charge density on a charged conductor bounded by S. It is determined to within a proportionality factor, whose value is determined by requiring the total charge on S to be equal to q.

The associated homogeneous integral equation, obtained by inverting the roles of $\mathbf{r}$ and $\mathbf{r}'$ in the kernel, is given by

$$\eta(\mathbf{r}) + \frac{1}{2\pi}\int_S \eta(\mathbf{r}')\frac{\partial}{\partial n}\left(\frac{1}{|\mathbf{r}-\mathbf{r}'|}\right)dS' = \eta(\mathbf{r}) - \frac{1}{2\pi}\int_S \eta(\mathbf{r}')\frac{\cos\theta}{|\mathbf{r}-\mathbf{r}'|^2}dS' = 0. \quad (4.48)$$

We recognize Robin's integral equation (4.26), the solution of which is $\rho_S(\mathbf{r})$. It follows, from Fredholm's theory, that (4.47) has solutions if, and only if, $u(\mathbf{r})$ is orthogonal to $\rho_S(\mathbf{r})$. But this condition is automatically satisfied because of the way in which $u(\mathbf{r})$ was constructed. We conclude that (4.47) has an infinity of solutions, differing only in an arbitrary additive constant. This constant is trivial, because a constant τ produces zero potential outside S, whence it follows that all solutions of (4.47) give rise to the same potential Ω.

4.5 THE NEUMANN PROBLEM

This companion to Dirichlet's problem consists in finding a function ϕ that satisfies the equation (Fig. 4.1)

$$\nabla^2\phi = g(\mathbf{r}) \qquad (\mathbf{r} \text{ in } V) \quad (4.49)$$

and the boundary condition

$$\frac{\partial\phi}{\partial n} = h(\mathbf{r}) \qquad (\mathbf{r} \text{ on } S).$$

This problem is of considerable importance in mathematical physics, particularly in acoustics and hydrodynamics. It is termed *Neumann's problem*, and the linear transformation whose operator is ∇^2 and whose domain is defined by the condition $\partial\phi/\partial n = 0$ on S is termed *Neumann's transformation*. In accordance with the procedure given in Section 1.3, the first step is to determine the solutions of the homogeneous problem

$$\nabla^2\phi_0 = 0$$
$$\frac{\partial\phi_0}{\partial n} = 0 \qquad (\text{on } S). \quad (4.50)$$

An application of Green's theorem (A1.30) gives

$$\int_V \phi_0\nabla^2\phi_0\,dV + \int_V |\text{grad }\phi_0|^2\,dV = \int_S \phi_0\frac{\partial\phi_0}{\partial n}dS = 0.$$

Clearly, grad ϕ_0 is equal to zero, and the only solution to (4.50) is $\phi_0 =$ constant. The situation is strikingly similar to that which arose in the study of the sliding string (see Section 1.3). Here again, (4.49) does not have a solution unless the *source functions* g and h satisfy the necessary condition (1.30). This condition can be rederived as follows:

$$\int_V \nabla^2\phi\,dV = \int_S \frac{\partial\phi}{\partial n}dS = \int_V g\,dV = \int_S h\,dS. \quad (4.51)$$

The last two members represent the condition on g and h. Clearly, the solution of (4.49), if it exists, is determined to within an additive constant. The core solution is the particular

choice of ϕ for which the average value over V is zero. It can be expressed in terms of a Green's function in the extended sense that, from (1.59), must satisfy the equations

$$\nabla^2 G_e(\mathbf{r}|\mathbf{r}') = \delta(\mathbf{r}-\mathbf{r}') - \frac{1}{V}$$
$$\frac{\partial G_e}{\partial n} = 0 \qquad (\text{on } S). \tag{4.52}$$

It follows, from the nature of the singularity of the δ-function, that the singularity of $G_e(\mathbf{r}|\mathbf{r}')$ is identical with that of the Green's function for unbounded space. Hence,

$$G_e(\mathbf{r}|\mathbf{r}') = -\frac{1}{4\pi|\mathbf{r}-\mathbf{r}'|} + H_e(\mathbf{r}|\mathbf{r}'),$$

where $H_e(\mathbf{r}|\mathbf{r}')$ is a continuous function that satisfies

$$\nabla^2 H_e = -\frac{1}{V}$$
$$\frac{\partial H_e}{\partial n} = \frac{1}{4\pi}\frac{\partial}{\partial n}\left(\frac{1}{|\mathbf{r}-\mathbf{r}'|}\right) \qquad (\text{on } S). \tag{4.53}$$

Function H_e contains an arbitrary additive constant, which can be adjusted to make the average value of G_e equal to zero. The core solution of (4.49) then becomes

$$\phi_c(\mathbf{r}) = \int_V G_e(\mathbf{r}|\mathbf{r}')g(\mathbf{r}')\,dV' - \int_S G_e(\mathbf{r}|\mathbf{r}')h(\mathbf{r}')\,dS'. \tag{4.54}$$

It is a simple matter to verify that Neumann's transformation is self-adjoint. The proof follows from an application of Green's theorem (A1.31). The *eigenfunctions* of the *Neumann transformation*, which are the solutions of

$$\nabla^2\psi_{mnp} - \nu_{mnp}\psi_{mnp} = 0$$
$$\frac{\partial\psi_{mnp}}{\partial n} = 0 \qquad (\text{on } S), \tag{4.55}$$

form a complete orthogonal set. We note that the eigenfunction $\psi_0 =$ constant must be included in the set. The proof of the completeness property depends essentially on the fact that the kernel $G_e(\mathbf{r}|\mathbf{r}')$ is weakly singular. Further, an application of Green's theorem shows that Neumann's transformation is nonpositive. It follows that all nonzero eigenvalues ν_{mnp} are negative.

The conditions embodied in (4.51) are *necessary* for the existence of a solution, but are they *sufficient*? To answer this question, let us transform Neumann's problem by substracting from ϕ one of the infinite number of solutions of $\nabla^2\phi = g$, called ϕ_1 for the purpose of the argument. The difference $(\phi - \phi_1) = \Omega$ must now satisfy

$$\nabla^2\Omega = 0 \qquad (\text{in } V)$$
$$\frac{\partial\Omega}{\partial n} = s \qquad (\text{on } S), \tag{4.56}$$

where s is the given function $h - \partial\phi_1/\partial n$. Because

$$\int_V \nabla^2\phi_1\, dV = \int_V g\, dV = \int_S \frac{\partial\phi_1}{\partial n}\, dS$$

the integral of $s(\mathbf{r})$ over S must vanish. From (4.51), indeed,

$$\int_S s\, dS = \int_S h\, dS - \int_S \frac{\partial\phi_1}{\partial n}\, dS = 0. \tag{4.57}$$

The existence proof for ϕ now reduces to a corresponding proof for the solution of (4.56). The solution will be sought in the form of a surface charge potential

$$\Omega(\mathbf{r}) = \frac{1}{4\pi\epsilon_0}\int_S \frac{\eta(\mathbf{r}')\, dS'}{|\mathbf{r} - \mathbf{r}'|}.$$

It is shown in Section 3.4 that this potential satisfies the equation $\nabla^2\Omega = 0$. The first condition in (4.56) is therefore satisfied. The second condition requires $\partial\Omega/\partial n$ to approach $s(\mathbf{r})$ as $\mathbf{r}$ approaches the surface *from the inside*. The value of the limit of $\partial\Omega/\partial n$ is given by (3.45); hence the boundary condition takes the form

$$\begin{aligned} 2\epsilon_0 s(\mathbf{r}) &= \eta(\mathbf{r}) + \frac{1}{2\pi}\int_S \eta(\mathbf{r}')\frac{\partial}{\partial n}\left(\frac{1}{|\mathbf{r} - \mathbf{r}'|}\right) dS' \qquad (\mathbf{r} \text{ on } S) \\ &= \eta(\mathbf{r}) - \frac{1}{2\pi}\int_S \eta(\mathbf{r}')\frac{\cos\theta}{|\mathbf{r} - \mathbf{r}'|^2}\, dS'. \end{aligned} \tag{4.58}$$

It is mentioned in Section 3.12 that the kernel of this integral equation is weakly singular; Fredholm's theory may therefore be applied. To investigate the existence of a solution to (4.58), the associated homogeneous integral equation

$$\mu(\mathbf{r}) + \frac{1}{2\pi}\int_S \mu(\mathbf{r}')\frac{\partial}{\partial n'}\left(\frac{1}{|\mathbf{r} - \mathbf{r}'|}\right) dS' = \mu(\mathbf{r}) - \frac{1}{2\pi}\int_S \mu(\mathbf{r}')\frac{\cos\theta'}{|\mathbf{r} - \mathbf{r}'|^2} dS' = 0, \tag{4.59}$$

obtained by exchanging $\mathbf{r}$ and $\mathbf{r}'$ in the kernel, must be examined for nonzero solutions. The solutions are given by $\mu(\mathbf{r})$ = constant, a statement that is proved by setting $\mu = 1$ in (4.59) and applying (3.68). The theory given in Section 1.9 now implies that (4.58) has a solution provided $s(\mathbf{r})$ is orthogonal to μ = constant, or, more explicitly, provided

$$\int_S s\, dS = 0.$$

But this is precisely equation (4.57).

4.6 NUMERICAL SOLUTION OF THE CHARGE DENSITY PROBLEM

As a typical example, we shall evaluate the capacitance of a cube, a problem that can be solved by subdividing the surface into subareas, on each of which ρ_S is given a uniform, adjustable value ρ_{Sm}. The basis fuctions are therefore *pulses*.[6] In Figure 4.5, there are

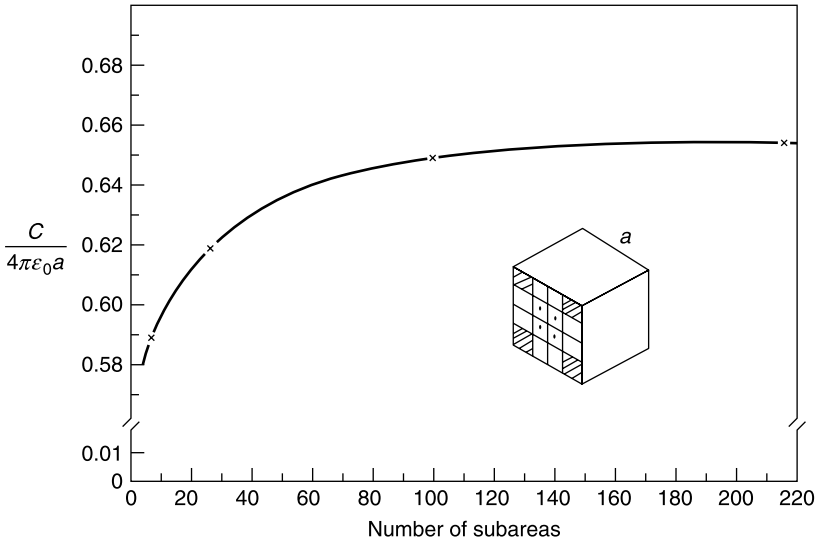

Figure 4.5 Capacitance of a cube evaluated by the method of subareas.

96 subareas but, because of symmetry, only three independent values of ρ_{Sm} should be considered. By using that particular subdivision, it is found that Coulomb's integral equation (4.25) yields three equations with three unknowns that, in the spirit of the collocation method, will be satisfied at the center of three suitably chosen subareas. The main problem is actually the evaluation of the matrix elements. For two coplanar subareas, they are of the form (Fig. 4.6)

$$\Delta L_{mn} = \int_{S_m} \frac{1}{\left[(x-x')^2 + (y-y')^2\right]^{\frac{1}{2}}}\, dS'. \tag{4.60}$$

One of these elements, namely L_{mm}, is proportional to the potential generated at the center of S_m by the charge on that subarea itself. This self-patch value is given in Section 3.4 for rectangular and circular elements. In an approximation that becomes better as the distance between subareas increases, the integration in (4.60) may be avoided and $|\mathbf{r} - \mathbf{r}'|$ replaced

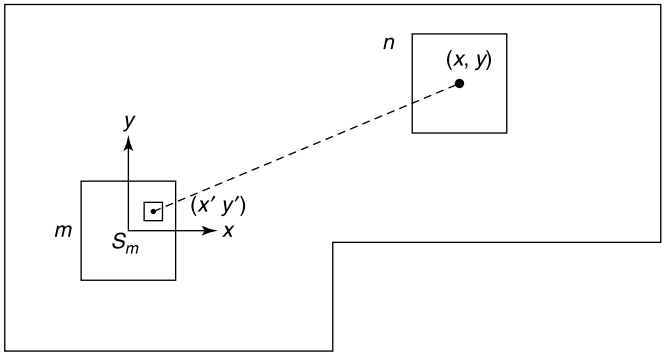

Figure 4.6 Pertinent to the evaluation of a matrix element.

by the distance between centers. Thus, for $x' = y' = 0$,

$$\Delta L_{mn} \approx \frac{S_m}{(x^2 + y^2)^{1/2}}. \tag{4.61}$$

When the subareas are not coplanar, the denominator should be replaced by $(x^2 + y^2 + z^2)^{\frac{1}{2}}$. Results for the capacitance of a cube are given in Table 4.2, which shows $(C/4\pi\epsilon_0 a)$ in terms of the number n of subareas (N is the corresponding number of *independent* equations) [156]. Table 4.2 also gives the results obtained by solving Robin's equation (4.26).

The problem discussed above is a particular case of a more general one, namely

$$\int_S G(\mathbf{r}|\mathbf{r}')\rho_S(\mathbf{r}')\, dS' = V(\mathbf{r}). \tag{4.62}$$

In the spirit of Section 1.11, discretization of (4.62) leads to a matrix equation, with coefficients

$$\begin{aligned} L_{mn} &= \int_S w_m(\mathbf{r})\, dS \int_S G(\mathbf{r}|\mathbf{r}')f_n(\mathbf{r}')\, dS' \\ g_m &= \int_S w_m(\mathbf{r})V(\mathbf{r})\, dS. \end{aligned} \tag{4.63}$$

It is desirable, whenever possible, to choose basis and testing functions that allow the integrations to be performed analytically. Suitable formulas are available for triangular subareas carrying a uniform ρ_S. These triangles are used, in particular, in finite element procedures, because they are well-suited to model surfaces of a general shape.[7] Formulas are also available for polygonal and polyhedral domains.[8]

Various other numerical methods may be used to determine the charge density on a conductor (and the resulting capacitance). A perturbational approach is possible when the shape of the conductor is slightly distorted with respect to another conductor for which the ρ_S problem has been solved.[9] In a more general perspective, variational principle (4.31) can be relied upon to yield a lower bound for the capacitance.[4] In these various methods, the pulse approximation can be improved by introducing the more sophisticated basis functions discussed in Sections 2.6 and 2.7, for example isoparametric elements.[10]

Table 4.2 Normalized Capacitance of a Cube

n	N	Coloumb	Robin
150	6	0.6538	0.6525
294	10	0.6568	0.6558
486	15	0.6582	0.6573
726	21	0.6590	0.6582
1014	28	0.6595	0.6588
1350	36	0.6598	0.6592
1734	45	0.6600	0.6595
2166	55	0.6602	0.6597
2646	66	0.6603	0.6599

4.7 CONDUCTOR IN AN EXTERNAL FIELD

Figure 4.7 shows a conductor immersed in an external (incident) field $\mathbf{e}^i$. This field is generated by a charge density $\rho(\mathbf{r})$. The incident potential satisfies

$$\begin{aligned} \nabla^2\phi^i &= -\frac{\rho}{\epsilon_0} \\ \phi^i &\text{ regular at infinity.} \end{aligned} \tag{4.64}$$

When conductor V is inserted, the equations become

$$\begin{aligned} \nabla^2\phi &= -\frac{\rho}{\epsilon_0} && \text{(outside } V\text{)} \\ \phi &= \text{a constant } \phi_1 && \text{(on } S\text{)} \\ -\epsilon_0 \int_S \frac{\partial\phi}{\partial n} dS &= q \\ \phi &\text{ regular at infinity.} \end{aligned} \tag{4.65}$$

We shall consider two possible situations. Assume first that the conductor is *grounded* (i.e., that $\phi_1 = 0$). The potential can be written as $\phi = \phi^i + \phi^d$, where ϕ^d is the disturbance potential due to the presence of the grounded conductor. This potential satisfies

$$\begin{aligned} \nabla^2\phi^d &= 0 \\ \phi^d &= -\phi^i && \text{(on } S\text{)} \\ \phi^d &\text{ regular at infinity.} \end{aligned} \tag{4.66}$$

Solution of this problem yields the value of the charge density on the grounded conductor, viz.

$$\rho_{S1} = -\epsilon_0 \frac{\partial}{\partial n}(\phi^i + \phi^d) \qquad \text{(on } S\text{)}.$$

Integration of ρ_{S1} over S gives the total charge that the conductor has acquired through its contact with the ground. Function ρ_{S1} can also be obtained by solving the *Coulomb* type of integral equation

$$\phi^i(\mathbf{r}) + \frac{1}{4\pi\epsilon_0} \int_S \frac{\rho_{S1}(\mathbf{r}')\, dS'}{|\mathbf{r} - \mathbf{r}'|} = 0 \qquad (\mathbf{r} \text{ on } S) \tag{4.67}$$

or, alternately, a straightforward extension of Robin's integral equation.

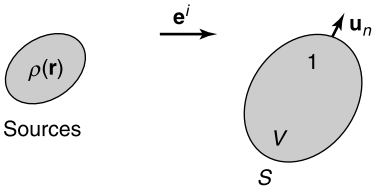

Figure 4.7 Conductor in an external field.

In a second situation, the conductor carries a charge q, and its potential ϕ_1 is unknown. Let ϕ_0 be the potential outside the isolated conductor when the latter is at unit potential. We set $\phi_0 = 1$ on the conductor — thereby making ϕ_0 dimensionless — and denote by

$$\rho_{S0} = -\epsilon_0 \frac{\partial \phi_0}{\partial n} \tag{4.68}$$

the corresponding charge density. Let us assume that ρ_{S0} is known from a previous analysis. The potential and charge are now, by linear superposition,

$$\begin{aligned} \phi &= \phi^i + \phi^d + \phi_1 \phi_0 \\ q &= \int_S \rho_{S1}\, dS + \phi_1 \int_S \rho_{S0}\, dS \;=\; \int_S \rho_{S1}\, dS + C\,\phi_1, \end{aligned} \tag{4.69}$$

where C is the capacitance of the conductor, and ρ_{S1} and ϕ^d have the meaning defined above. Equation (4.69) can serve to evaluate ϕ_1, q being given. It is, in fact, not necessary to know ρ_{S1} in detail to achieve this goal. What we need is $\int_S \rho_{S1}\, dS$, a "global" quantity, which can be evaluated by invoking a reciprocity principle. To that effect, we apply Green's theorem (A1.131) to ϕ_0 and ϕ^d outside the conductor. Both functions satisfy Laplace's equation, hence (Fig. 4.7)

$$\int_{\text{outside } S} \left(\phi_0 \nabla^2 \phi^d - \phi^d \nabla^2 \phi_0 \right) dV = \int_{S+S_\infty} \left(\phi^d \frac{\partial \phi_0}{\partial n} - \phi_0 \frac{\partial \phi^d}{\partial n} \right) dS = 0.$$

Because ϕ_0 and ϕ^d are regular at infinity, the integral over S_∞ vanishes, and we may write

$$\int_S \frac{\partial \phi^d}{\partial n}\, dS = \int_S \frac{\partial \phi^d}{\partial n}\, dS + \underbrace{\int_S \frac{\partial \phi^i}{\partial n}\, dS}_{=0} = \int_S \frac{\partial (\phi^d + \phi^i)}{\partial n}\, dS = \int_S \phi^d \frac{\partial \phi_0}{\partial n}\, dS.$$

If we take into account that $\phi^d = -\phi^i$ on S, we obtain

$$\int_S \rho_{S1}\, dS = \int_S \phi^d \rho_{S0}\, dS = -\int_S \phi^i \rho_{S0}\, dS$$

and, from (4.69),

$$\phi_1 = \frac{q}{C} - \frac{\displaystyle\int_S \phi^i \rho_{S0}\, dS}{\displaystyle\int_S \rho_{S0}\, dS}. \tag{4.70}$$

Only ρ_{S0} is involved in this formula.

4.7.1 Conductor in a Uniform Incident Field

Consider, as an example, an uncharged conducting sphere immersed in a uniform $\mathbf{e}^i$ (Fig. 4.8). The incident potential ϕ^i is defined to within an additive constant, which we choose to be zero at the center of the sphere. Thus,

$$\phi^i = -R \cos\theta e^i. \tag{4.71}$$

Elementary steps, based on separation of variables, give

$$\begin{aligned}\phi^d &= \frac{a^3}{R^2}\cos\theta e^i \\ \rho_{S0} &= \frac{\epsilon_0}{a} \\ \rho_{S1} &= 3\epsilon_0\cos\theta e^i \\ C &= 4\pi\epsilon_0 a \\ \mathbf{p}_e &= 4\pi\epsilon_0 a^3\mathbf{e}^i. \end{aligned} \tag{4.72}$$

Because of symmetry, the potential of the sphere will be zero. From (4.70), this is a general property, which holds whenever an arbitrary conductor is uncharged and $\int_S \phi^i \rho_{S0}\, dS = 0$. Both conditions are clearly satisfied in the current problem.

Separation of variables is applicable to a few additional configurations, such as the ellipsoid in a uniform field parallel to one of the axes [20], or the circular aperture in a conducting plane, on which a uniform field is incident [17], [54, volume 2]. For a prolate conducting spheroid immersed in a field $\mathbf{e}_\parallel$, the techniques discussed in Section 3.11 are pertinent. The potential outside the spheroid is now given by (Fig. 3.21*a*)

$$\phi = -e_\parallel c\mu\nu + e_\parallel c\nu\frac{Q_1(\mu)}{Q_1(\mu_0)} \tag{4.73}$$

where, from (A5.112)

$$Q_1(\mu) = \frac{\mu}{2}\log_e\frac{1+\mu}{1-\mu} - 1.$$

In the particular case of the sphere, the induced dipole moment is parallel to the incident field. For a more general conductor, the moment can be written as

$$\mathbf{p}_e = \epsilon_0\overline{\overline{\alpha}}_e\cdot\mathbf{e}^i. \tag{4.74}$$

Comparison with (4.72) shows that the *polarizability dyadic of the conducting sphere* is

$$\overline{\overline{\alpha}}_e = 4\pi a^3\overline{\overline{I}}. \tag{4.75}$$

For a more general shape, $\mathbf{p}_e$ must be determined by solving the field problem for three orthogonal directions, a process that yields the nine terms of $\overline{\overline{\alpha}}_e$. The $\overline{\overline{\alpha}}_e$ matrix may be shown to be symmetric (Problem 4.13), which means that it can be diagonalized, and that three orthogonal directions exist for which the induced dipole moment $\mathbf{p}_e$ is in the direction of the incident field.

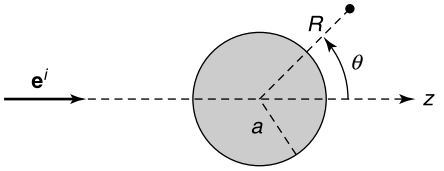

Figure 4.8 Conducting sphere in a uniform field $\mathbf{e}^i$.

4.7.2 Incident Field Produced by a Point Charge

A uniform field may be conceived as produced by a point charge located *far away* from the conductor. When the charge lies *close* to the conductor, the potential $(\phi^i + \phi^d)$ becomes the Green's function corresponding with the boundary condition $G(\mathbf{r}|\mathbf{r}_0) = 0$ on S. Separation of variables can sometimes yield this *unit response*, for example in the case of two unequal (grounded) spheres [22], the interior of a circular cylinder [22], or the interior of a parallelepiped [54, volume 2]. The method of *images* can also yield $G(\mathbf{r}|\mathbf{r}_0)$ in a few cases. The simplest one involves a conducting plane, for which (Fig. 4.9*a*)

$$G(\mathbf{r}|\mathbf{r}_0) = -\frac{1}{4\pi\epsilon_0}\left(\frac{1}{|\mathbf{r}-\mathbf{r}_0|} - \frac{1}{|\mathbf{r}-\mathbf{r}_0'|}\right), \tag{4.76}$$

where $\mathbf{r}_0 = (x_0, y_0, z_0)$ and $\mathbf{r}_0' = (x_0, y_0, -z_0)$.

When the structure consists of two parallel conducting planes, an infinite number of images is generated, and the Green's function turns out to be an infinite sum [54, volume 2]. A problem where a *single* image suffices is illustrated in Figure 4.9*b*. The upper conductor is at potential V, and its image is another conductor, now at potential $(-V)$. Together they form a capacitor across which a potential $2V$ is applied. The surface charge density satisfies

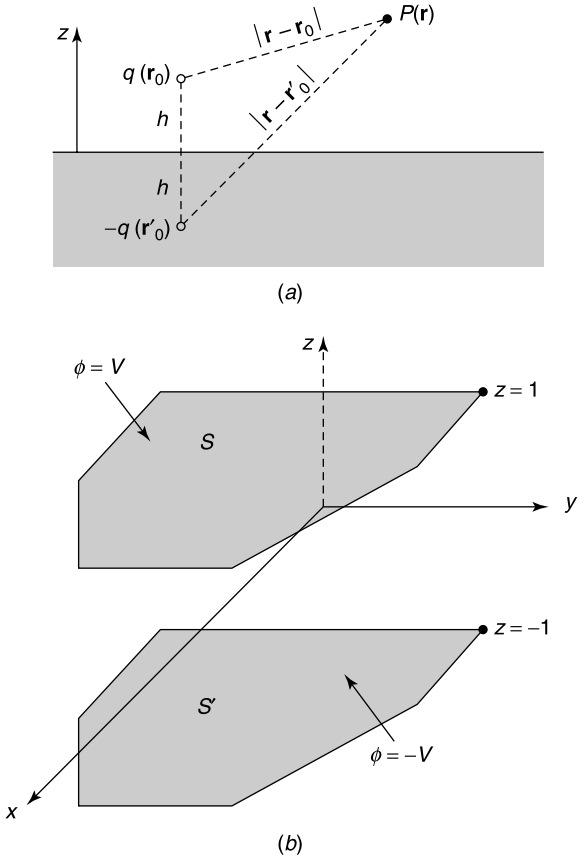

Figure 4.9 (*a*) Point charge above a conducting plane. (*b*) Two flat conductors forming a capacitor.

the integral equation

$$\phi = \frac{1}{4\pi\epsilon_0}\int_{\text{both plates}} \rho_S(\mathbf{r}')\frac{1}{|\mathbf{r}-\mathbf{r}'|}dS' = \phi_c$$

where $\mathbf{r}$ is on S or S', and ϕ_c is V or $(-V)$. Given the symmetry, it suffices to integrate over half the upper plate, in which case the contributions of the remaining parts can be taken into account by a Green's function of the form[10]

$$G(\mathbf{r}|\mathbf{r}') = -\frac{1}{4\pi\epsilon_0}\left(\frac{1}{D_1}+\frac{1}{D_2}-\frac{1}{D_3}-\frac{1}{D_4}\right),$$

where

$$\begin{aligned} D_1 &= \left[(x-x')^2+(y-y')^2+(z-z')^2\right]^{\frac{1}{2}} \\ D_2 &= \left[(x-x')^2+(y+y')^2+(z-z')^2\right]^{\frac{1}{2}} \\ D_3 &= \left[(x-x')^2+(y-y')^2+(z+z')^2\right]^{\frac{1}{2}} \\ D_4 &= \left[(x-x')^2+(y+y')^2+(z+z')^2\right]^{\frac{1}{2}}. \end{aligned} \tag{4.77}$$

4.8 CONDUCTORS IN THE PRESENCE OF DIELECTRICS

In a *first* problem, we consider a dielectric placed in the field of a conductor raised to potential ϕ_c (Fig. 4.10). Bound surface charges ρ'_S appear on the boundary surface of the dielectric. The total potential is the sum of ϕ_1, the contribution from the conductor, and ϕ_2, the contribution from the dielectric. On the conductor (i.e., for $\mathbf{r}$ on S_c),

$$\frac{1}{4\pi\epsilon_0}\int_{S_c}\frac{\rho_S(\mathbf{r}')}{|\mathbf{r}-\mathbf{r}'|}dS' + \frac{1}{4\pi\epsilon_0}\int_{S_d}\frac{\rho'_S(\mathbf{r}')}{|\mathbf{r}-\mathbf{r}'|}dS' = \phi_c. \tag{4.78}$$

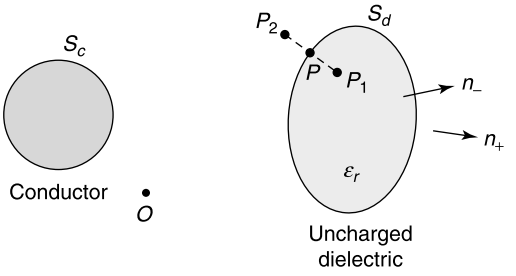

Figure 4.10 Dielectric immersed in an incident potential.

To determine the corresponding equation for $\mathbf{r}$ on S_d, we apply (3.45) and (3.46), and write

$$\lim_{P_1 \to P} \frac{\partial \phi_2}{\partial n_-} = \frac{1}{2\epsilon_0} \rho'_S(\mathbf{r}) + \frac{1}{4\pi\epsilon_0} \fint_{S_d} \rho'_S(\mathbf{r}') \frac{\partial}{\partial n} \left(\frac{1}{|\mathbf{r} - \mathbf{r}'|} \right) dS'$$

$$\lim_{P_2 \to P} \frac{\partial \phi_2}{\partial n_+} = -\frac{1}{2\epsilon_0} \rho'_S(\mathbf{r}) + \frac{1}{4\pi\epsilon_0} \fint_{S_d} \rho'_S(\mathbf{r}') \frac{\partial}{\partial n} \left(\frac{1}{|\mathbf{r} - \mathbf{r}'|} \right) dS'.$$

On S_d:

$$\frac{\partial}{\partial n_+}(\phi_1 + \phi_2) = \epsilon_r \frac{\partial}{\partial n_-}(\phi_1 + \phi_2),$$

from which we deduce that

$$\frac{\partial \phi_2}{\partial n_+} - \epsilon_r \frac{\partial \phi_2}{\partial n_-} = (\epsilon_r - 1) \frac{\partial \phi_1}{\partial n_-}.$$

This leads to the integral equation

$$2\pi(\epsilon_r + 1)\rho'_S(\mathbf{r}) + (\epsilon_r - 1) \fint_{S_d} \rho'_S(\mathbf{r}') \frac{\partial}{\partial n} \left(\frac{1}{|\mathbf{r} - \mathbf{r}'|} \right) dS'$$
$$+ (\epsilon_r - 1) \fint_{S_c} \rho_S(\mathbf{r}') \frac{\partial}{\partial n} \left(\frac{1}{|\mathbf{r} - \mathbf{r}'|} \right) dS' = 0. \tag{4.79}$$

Integral equations (4.78) and (4.79) can be solved by the usual methods, using for example pulse approximations on triangular patches, both as basis and testing functions.[11]

In a *second* problem the conductor is grounded and the source is a unit point charge in 0 (Fig. 4.10). If the potential in the absence of the dielectric (i.e., the Green's function G_c) is known, it suffices to set $\phi_c = 0$ on S_c and replace $(-1/4\pi|\mathbf{r} - \mathbf{r}'|)$ by $G_c(\mathbf{r}|\mathbf{r}')$ in the previous equations to obtain their new form.[12]

In a *third* problem, the conductor is first removed, and the dielectric is kept. The Green's function G_d must now satisfy (Fig. 4.10)

$$\begin{gathered} \nabla^2 G_d = \delta(\mathbf{r} - \mathbf{r}') \\ G_d \text{ continuous across } S_d \\ \frac{\partial G_d}{\partial n_2} = \epsilon_r \frac{\partial G_d}{\partial n_1} \text{ on } S_d \\ G_d \text{ regular at infinity.} \end{gathered} \tag{4.80}$$

Assume now that the conductor is reinserted and raised to a potential ϕ_c. The integral equation of concern is now

$$-\frac{1}{\epsilon_0} \int_{S_c} \rho_S(\mathbf{r}') G_d(\mathbf{r}|\mathbf{r}')\, dS' = \phi_c. \tag{4.81}$$

The pertinent Green's function is known for a few simple dielectric shapes [17, 59]. Given the interest in layered stuctures, solutions involving dielectrics bounded by planes

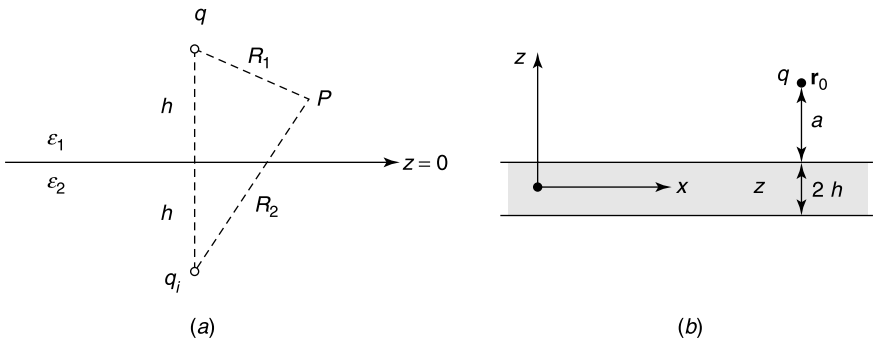

Figure 4.11 (*a*) Green's function by the method of images. (*b*) Green's function for a dielectric slab.

are particularly useful. In the simple configuration of Figure 4.11*a* the method of images solves the problem. In region 1, the potential is given by

$$\phi_1 = \frac{1}{4\pi\epsilon_1}\left(\frac{q}{R_1} + \frac{\epsilon_1 - \epsilon_2}{\epsilon_1 + \epsilon_2}\frac{q}{R_2}\right), \tag{4.82}$$

and in region 2 by

$$\phi_2 = \frac{1}{4\pi\epsilon_2}\frac{2\epsilon_2}{\epsilon_1 + \epsilon_2}\frac{q}{R_2}. \tag{4.83}$$

In the application of the method of images to a dielectric slab, one must add up the contributions of an *infinite* number of sources. With a unit charge located at $(x_0, y_0, a + h)$, the Green's function at a point inside the dielectric becomes[13] (Fig. 4.11*b*)

$$G_d(\mathbf{r}|\mathbf{r}_0) = -\frac{1+\beta}{4\pi}\sum_{n=0}^{\infty}\beta^{2n}\frac{1}{\sqrt{(x-x_0)^2 + (y-y_0)^2 + [z-(4n+1)h-a]^2}}$$
$$-\frac{\beta(1+\beta)}{4\pi}\sum_{n=0}^{\infty}\beta^{2n}\frac{1}{\sqrt{(x-x_0)^2 + (y-y_0)^2 + [z+(4n+3)h+a]^2}}, \tag{4.84}$$

where $\beta = \dfrac{\epsilon_r - 1}{\epsilon_r + 1}$ is the *image coefficient*. If we now place a thin conductor of surface S_c on the plane $z = h$, at potential ϕ_c, the surface charge density on the conductor can be determined by solving

$$-\frac{1}{\epsilon}\int_{S_c} G_d(\mathbf{r}|\mathbf{r}')\rho_S(\mathbf{r}')\,dS' = \phi_c.$$

The method allows determination of, for example, the capacitance of the planar conductor S_c with respect to a ground plane at $z = 0$, a most important quantity for the development of present-day electronic circuits.[14]

4.9 CURRENT INJECTION INTO A CONDUCTING VOLUME

Figure 4.12 shows a resistive conductor V_1 in contact with two perfectly conducting electrodes S_A and S_B. The electric field vanishes in the electrodes, which are therefore at a

constant potential. We assume that there is no applied field in the resistor and write $\mathbf{j} = \sigma \mathbf{e}$. Under static conditions, no charges may accumulate on the sidewalls S_W. It follows that $\mathbf{j}$ must be tangent to S_W. By the same token, the equation of conservation of charge (4.12) requires $\mathbf{j}$ to be solenoidal. The potential must therefore satisfy the system

$$\begin{aligned} \operatorname{div}(\sigma \operatorname{grad} \phi) &= 0 \qquad (\text{in } V_1) \\ \phi &= V \qquad (\text{on } S_A) \\ \phi &= 0 \qquad (\text{on } S_B) \\ \frac{\partial \phi}{\partial n} &= 0 \qquad (\text{on } S_W). \end{aligned} \tag{4.85}$$

This is a *mixed* problem, partly Dirichlet, partly Neumann. The potential is clearly proportional to V, hence it can be written as $V\phi_1$, where ϕ_1 corresponds with the condition $V = 1$. Consider the thin tube of current shown in Figure 4.12. Its cross section dS varies according to a law $k\, dS_A$, where k is a function of the distance l along the line of force. Because the current di in the tube is equal to $\sigma e_l\, dS$ (where e_l is the component of $\mathbf{e}$ in the l-direction), and because $\displaystyle\int_A^B e_l\, dl = V$, we may write

$$di = V \frac{dS_A}{\displaystyle\int_A^B \frac{1}{\sigma k} dl}.$$

Integrating over S_A gives

$$i = V \left[\int_{S_A} \frac{dS}{\displaystyle\int_A^B \frac{dl}{\sigma k}} \right] = gV, \tag{4.86}$$

where g is the conductance of the resistor. From this expression, it is easy to obtain an approximate value of g from an *estimate* of the profile of the tubes of force. An *exact*

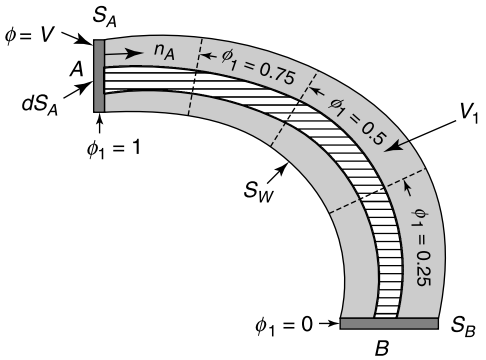

Figure 4.12 Equipotentials in a current-carrying conductor.

determination of the lines of force, however, requires the solution of (4.85). Once this is done, current and conductance follow from

$$i = -\int_{S_A} \sigma \frac{\partial \phi}{\partial n_A}\, dS \tag{4.87}$$

and

$$g = \frac{i}{V} = -\int_{S_A} \sigma \frac{\partial \phi_1}{\partial n_A}\, dS. \tag{4.88}$$

The conductance may also be determined from the stationarity properties of the functional

$$J(\phi) = \int_{V_1} \sigma |\text{grad } \phi|^2\, dV \tag{4.89}$$

with respect to functions that satisfy the same boundary conditions as does ϕ_1. It is left to the reader to check that $J(\phi)$ reaches a minimum for $\phi = \phi_1$ and that this minimum is the conductance (Problem 4.17).

Various methods are available for the solution of (4.85). Separation of variables, for example, is appropriate for determining the potential in a homogeneous sphere into which a current **i** is injected through diametrically opposed point contacts (Fig. 4.13*a*). The configuration is a useful model for the ball-bearing motor,[15,16] a device that, if given an initial push in either azimuthal direction, will continue running in that direction under the influence of volume magnetic forces $\mathbf{j} \times \mathbf{b}$. The determination of **j** under rotation is a problem of the kind discussed in Section 17.10. The solution starts with the evaluation of the currents in the *motionless*, nonrotating sphere. To solve that initial problem, we note that the potential inside the sphere is harmonic and φ-independent. Hence, from (3.95),

$$\phi(R, \theta) = \sum_{\text{odd } n} A_n R^n P_n(\cos\theta),$$

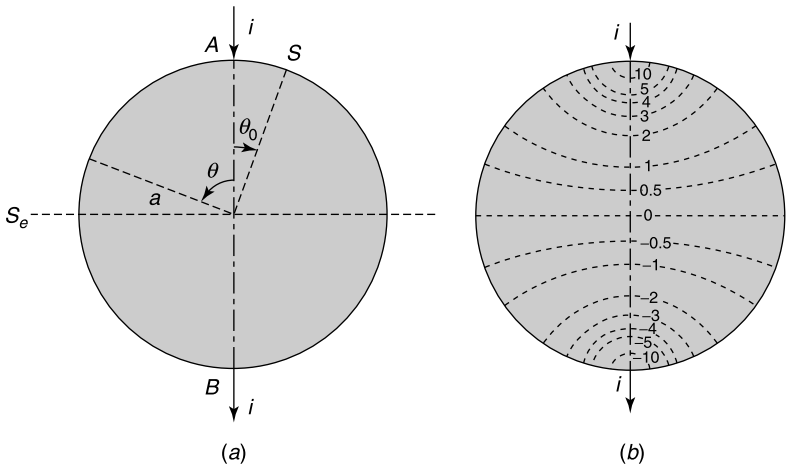

Figure 4.13 (*a*) Conducting sphere with point contacts. (*b*) Potential in the spherical conductor.

where the odd indices alone are needed because the potential is antisymmetric with respect to the equatorial plane S_e, and hence should be an odd function of $\cos\theta$. The same is true of the normal derivative $(\partial\phi/\partial R)$ of at the surface, which we write in the form

$$\left(\frac{\partial\phi}{\partial R}\right)_{R=a} = g(\cos\theta) = \sum_{\text{odd } n} C_n P_n(\cos\theta).$$

This function is zero everywhere, except at the poles where current injection and extraction take place, and where $(\partial\phi/\partial R)$ displays a $\delta(\theta)$ kind of behavior. We shall take that singularity into account by letting the contact electrode occupy a *very small angle* θ_0, with a corresponding value of $\cos\theta_0$ equal to $(1-\theta_0^2/2) = (1-\epsilon)$. In the vicinity of the upper pole:

$$i = \sigma \int_{\text{contact area}} \frac{\partial\phi}{\partial R}\, dS = \sigma \int_0^{\theta_0} g(\cos\theta) 2\pi a^2 \sin\theta\, d\theta.$$

From (A5.133):

$$C_n = \frac{\int_0^1 g(x)P_n(x)\,dx}{\int_0^1 P_n(x)\,dx} = (2n+1)P_n(1)\int_{1-\epsilon}^1 g(x)\,dx = \frac{2n+1}{2\pi a^2\sigma}\, i.$$

This value of C_n can be used to calculate A_n, from which the following expression for the potential is obtained:

$$\phi = \frac{i}{2\pi\sigma a}\sum_{\text{odd } n}\frac{2n+1}{n}\left(\frac{R}{a}\right)^n P_n(\cos\theta). \tag{4.90}$$

The resistance of the sphere and the profile of the lines of current can be determined from this expression. Figure 4.13*b* shows a few values of $(2\pi\sigma a/i)\phi$, a dimensionless quantity proportional to the potential.

A second problem that can be solved by separation of variables is taken from medical technology. It concerns the artificial stimulation of nerves, a technique that can potentially help patients who have lost bladder control or suffered spinal cord injuries (with resulting paralysis of the lower limbs). By proper injection of current in a motor nerve, an action potential is generated, which will eventually activate the muscle. The nerve can be excited by various methods, for example by implanting a cuff that snugly fits the nerve trunk.[17] Discrete dot electrodes are embedded in the cuff, at well-chosen positions. A simplified model of the system is shown in Figure 4.14, where the central region is the nerve, and the exterior region is the cuff. The insulating cuff helps the current flow axially, a direction in which **e** acts optimally. Because of the fiber structure of the nerve, the conductivity is anisotropic and may be written as

$$\overline{\overline{\sigma}} = \sigma_t \overline{\overline{I}}_{xy} + \sigma_z \mathbf{u}_z\mathbf{u}_z. \tag{4.91}$$

Typically $\sigma_z \approx 10\,\text{S m}^{-1}$ and $\sigma_t \approx 1\,\text{S m}^{-1}$. The equation that the potential satisfies, viz.

$$\text{div}\,\mathbf{j} = -\text{div}\,(\overline{\overline{\sigma}}\cdot\text{grad}\,\phi) = 0 \tag{4.92}$$

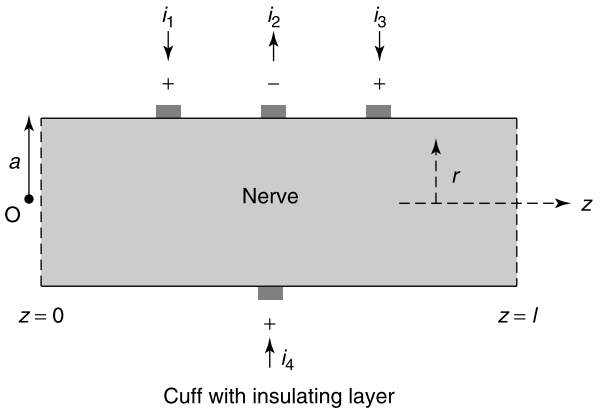

Figure 4.14 Nerve and implanted electrodes.

takes the specific form

$$\frac{1}{r}\frac{\partial}{\partial r}\left(r\frac{\partial \phi}{\partial r}\right) + \frac{1}{r^2}\frac{\partial^2 \phi}{\partial \varphi^2} + \frac{\sigma_z}{\sigma_t}\frac{\partial^2 \phi}{\partial z^2} = 0. \tag{4.93}$$

The boundary conditions are $\phi = 0$ at the end planes $z = 0$ and $z = l$, where the nerve trunk is in contact with a strongly conductive bath. On the lateral walls $\partial\phi/\partial r = 0$, except at the level of the electrodes, where

$$j_{sr} = -\sigma_t \frac{\partial \phi}{\partial r}.$$

In a first approximation, j_{sr} may be assumed constant over the area S of the electrode, and we write $j_{sr} = -(i/S)$ (the validity of such an assumption is discussed in the next section). Solution of (4.93) may now proceed by double Fourier expansion:

$$\phi(\mathbf{r}) = \sum_{m=0}^{\infty}\sum_{n=1}^{\infty}(A_{mn}\cos m\varphi + B_{mn}\sin m\varphi)\sin\frac{n\pi z}{l} f_{mn}(r). \tag{4.94}$$

Separation of variables gives

$$\frac{1}{r}\frac{d}{dr}\left(r\frac{df_{mn}}{dr}\right) - \left[\frac{\sigma_z}{\sigma_t}\left(\frac{n\pi}{l}\right)^2 + \frac{m^2}{r^2}\right] f_{mn} = 0.$$

This is the modified Bessel equation (A5.60), hence

$$f_{mn}(r) = I_m\left(\sqrt{\frac{\sigma_z}{\sigma_t}}\frac{n\pi}{l}r\right).$$

The coefficients A_{mn} and B_{mn} must now be fitted to make the expansion of $\partial\phi/\partial r$ in terms of $\sin(n\pi z/l)$ correspond with the known pulse functions j_{sr}. This should be done for each electrode. Once the coefficients are found, the potential distribution follows from (4.93).

The *double* summation in (4.94) often converges poorly. To remedy this situation, ϕ may be represented by a *single* Fourier expansion, viz.

$$\phi(r,\varphi,z) = \sum_{m=0}^{\infty}[A_m(r,z)\cos m\varphi + B_m(r,z)\sin m\varphi]. \tag{4.95}$$

The problem is now reduced to the solution of a series of differential equations for A_m and B_m, to be solved in the (r,z) plane.[18]

4.10 CONTACT ELECTRODES

In the current section, we investigate the flow of current through *broad* electrodes, thus generalizing the injection by *point contacts* considered in the previous section. The main unknown is now j_n, the normal component of $\mathbf{j}$ on the electrodes, and we will derive an integral equation that must be satisfied by j_n. The technique works when the Green's function with respect to Neumann's boundary condition is known. This function must satisfy (Fig. 4.15*a*)

$$\begin{aligned} &\operatorname{div}[\sigma\ \operatorname{grad} G(\mathbf{r}|\mathbf{r}')] = \delta(\mathbf{r}-\mathbf{r}') \\ &\frac{\partial G}{\partial n} = 0 \qquad (\text{on } S_A + S_B + S_W). \end{aligned} \tag{4.96}$$

When space is anisotropic, which is often the case in geophysical applications, the differential equation that appears in (4.96) must be replaced by

$$\operatorname{div}(\overline{\overline{\sigma}}\cdot\operatorname{grad} G) = \delta(\mathbf{r}-\mathbf{r}') \tag{4.97}$$

with appropriate Dirichlet or Neumann conditions at the boundary surface.[19] We shall assume, for simplicity, that the material is isotropic, and apply (A1.27) and (A1.31) to ϕ

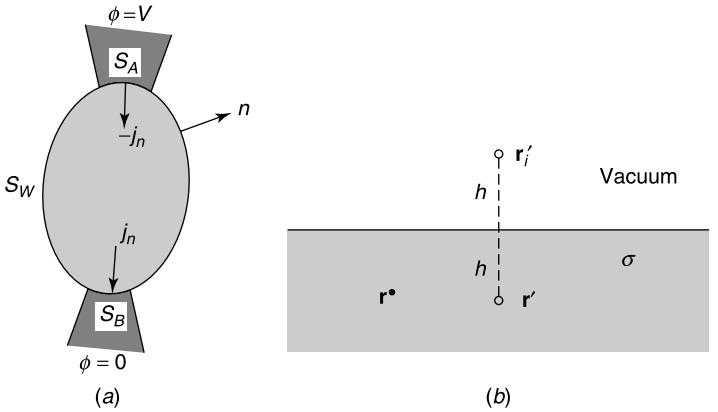

Figure 4.15 (*a*) Conductor with perfectly conducting electrodes. (*b*) Half-infinite homogeneous conductor.

(the solution of 4.85) and $G(\mathbf{r}|\mathbf{r}')$. This gives

$$\phi(\mathbf{r}) = \int_{S_A+S_B} G(\mathbf{r}|\mathbf{r}') j_n(\mathbf{r}')\, dS' \begin{cases} = V & (\text{on } S_A) \\ = 0 & (\text{on } S_B) \end{cases}. \tag{4.98}$$

where n is the outward normal. Once j_n is known, the total current follows from

$$i = \int_{S_A} (-j_n)\, dS = \int_{S_B} j_n\, dS. \tag{4.99}$$

Because j_n is proportonal to V, (4.99), once solved, will yield the value (i/V) of the conductance. To be more specific, let us investigate the current distribution at a contact with a half-infinite conducting space (Fig. 4.16). The relevant Green's function is easily obtained by the method of images. Thus (Fig. 4.15*b*),

$$G(\mathbf{r}|\mathbf{r}') = -\frac{1}{4\pi\sigma}\left(\frac{1}{|\mathbf{r}-\mathbf{r}'|} + \frac{1}{|\mathbf{r}-\mathbf{r}'_i|}\right). \tag{4.100}$$

Integral equation (4.98) now takes the form

$$\frac{1}{2\pi\sigma}\int_{S_A} \frac{1}{|\mathbf{r}-\mathbf{r}'|} j_n(\mathbf{r}')\, dS = V \qquad (\mathbf{r} \text{ on } S_A). \tag{4.101}$$

But the charge density on a conducting disk coinciding with S_A satisfies, in vacuum, the same type of integral equation, viz.

$$\frac{1}{4\pi\epsilon_0}\int_{S_A} \frac{1}{|\mathbf{r}-\mathbf{r}'|} \rho_S(\mathbf{r}')\, dS' = V \qquad (\mathbf{r} \text{ on } S_A).$$

It follows that we may immediately write

$$\begin{aligned} j_n &= \frac{\sigma\rho_S}{2\epsilon_0} \\ i &= \frac{\sigma}{2\epsilon_0} q = \frac{\sigma}{2\epsilon_0} CV \\ g &= \frac{i}{V} = \frac{\sigma}{2\epsilon_0} C. \end{aligned} \tag{4.102}$$

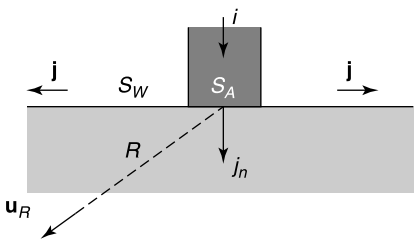

Figure 4.16 Electrode in contact with a conductor bounded by a plane.

The value of ρ_S for a circular disk, for example, is given by (4.24). Hence, for a circular contact area,

$$j_n = \frac{i}{4\pi a^2 \sqrt{1 - \left(\frac{r}{a}\right)^2}}$$

$$g = 4a\sigma. \tag{4.103}$$

These results suggest a few additional comments:

1. The current density is not uniform across the electrode. In fact, it becomes infinite at the rim, as it is proportional to $(1/\sqrt{d})$ where d is the perpendicular distance to the rim. This characteristic behavior is further discussed in Section 5.2.
2. At distances large with respect to the dimensions of S_A, the current density $\mathbf{j}$ becomes insensitive to the details of j_n. The limit form is (Fig. 4.16)

$$\mathbf{j} = \frac{i}{2\pi R^2}\mathbf{u}_R. \tag{4.104}$$

   At these distances it becomes permissible to assume j_n constant, an assumption that was made in the last example discussed in the previous section.
3. For a point contact, (i.e., in the limit $a \to 0$), resistance and potential resulting from an injection of current i become infinite. This behavior is confirmed by the data appearing in Figure 4.13.

For an electrode of arbitrary shape, integral equation (4.101) must be solved numerically (e.g., by finite element techniques). Given the singularity at the contour, special forms should preferably be used in triangles that are in contact with the edge.[20,21] In a triangle of type A, for example (Fig. 4.17) the $(1/\sqrt{d})$ dependence can be enforced by using the basis function

$$\rho(\mathbf{r}) = \rho_1 \sqrt{\frac{h}{d}} = \rho_1 \frac{1}{\sqrt{L_1}}. \tag{4.105}$$

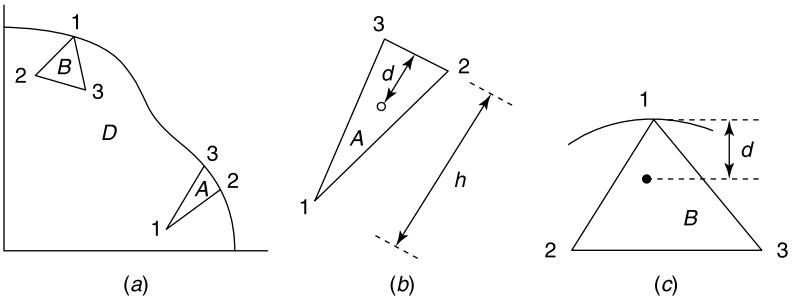

Figure 4.17 (*a*) Subdivision of a domain into triangles. (*b*) A triangle of type *A*. (*c*) A triangle of type *B* (from R. De Smedt and J. Van Bladel, Magnetic polarizability of some small apertures, *IEEE Trans. AP*, **28**, 703–707, 1980, with permission of IEEE).

For a triangle such as B:

$$\rho(\mathbf{r}) = \frac{\rho_2 L_2 + \rho_3 L_3}{(1 - L_1)^{3/2}}. \tag{4.106}$$

where L_1, L_2, L_3 are defined in (2.31).

Current Injection Into a Conducting Shell

In the limit case of a very thin conducting shell, the current density is related to the tangential electric field by the equation (Fig. 4.18)

$$\mathbf{j}_S = \sigma_S \mathbf{e}_S \qquad (\mathrm{A\,m^{-1}}) \tag{4.107}$$

where σ_S is the *surface conductivity* (in units of S). Because the electric field is irrotational, its various components can be derived from a scalar potential, and the tangential component can therefore be represented as

$$\mathbf{e}_S = -\mathrm{grad}_S\, \phi_S(v_1, v_2),$$

where v_1 and v_2 are suitable orthogonal coordinates on the surface (see Appendix 3 for a general discussion of surface operators and coordinate systems). To determine ϕ_S, we make use of the *equation of conservation of charge on a surface*, viz.

$$\mathrm{div}_S\, \mathbf{j}_S = -\frac{\partial \rho_S}{\partial t}. \tag{4.108}$$

Under static conditions the time derivative must vanish, hence $\mathrm{div}_S\, \mathbf{j}_S = 0$. Inserting the values of $\mathbf{j}_S$ and $\mathbf{e}_S$ in the left-hand term of (4.108) yields an equation for the potential. If the sheet has uniform conductivity σ_S, one obtains

$$\nabla_S^2 \phi_S = \frac{1}{h_1 h_2} \frac{\partial}{\partial v_1} \left(\frac{h_2}{h_1} \frac{\partial f}{\partial v_1} \right) + \frac{1}{h_1 h_2} \frac{\partial}{\partial v_2} \left(\frac{h_1}{h_2} \frac{\partial f}{\partial v_2} \right) = 0, \tag{4.109}$$

where h_1 and h_2 are the metric coefficients relative to v_1 and v_2, respectively. When S is an open surface, Neumann and Dirichlet problems on the surface can be introduced as in three dimensions. Of great importance for these problems is Green's theorem (A3.49), repeated here for clarity:

$$\int_S (A \nabla_S^2 B + \mathrm{grad}_S\, A \cdot \mathrm{grad}_S\, B)\, dS = \int_C A \frac{\partial B}{\partial m}\, dc. \tag{4.110}$$

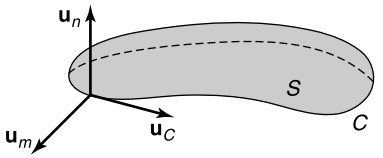

Figure 4.18 Open surface S, with $\mathbf{u}_n$ perpendicular to S, $\mathbf{u}_c$ tangent to C, and $\mathbf{u}_m = \mathbf{u}_c \times \mathbf{u}_n$.

The direction m lies in the tangent plane of S and is perpendicular to C (Fig. 4.18). Equation (4.110) immediately yields the following results:

1. The problem $\nabla_S^2 \phi_S = 0$, with ϕ_S given on C, has a unique solution on S.
2. The problem $\nabla_S^2 \phi_S = 0$, with $\phi_S =$ constant on C, has the unique solution $\phi_S =$ constant.
3. The problem $\nabla_S^2 \phi_S = 0$, with $\partial \phi_S / \partial m$ given on C, has a solution provided $\int_C (\partial \phi_S / \partial m)\, dc = 0$. This solution is determined to within an additive constant.
4. A function that has zero surface Laplacian on a closed surface must reduce to a constant.

To illustrate the solution of (4.109), let us determine the current density on a conducting spherical shell (Fig. 4.13*a*). Current is injected and extracted at two diametrically opposite points. The appropriate coordinates on the spherical surface are $v_1 = \theta$ and $v_2 = \varphi$, with $h_1 = a$ and $h_2 = a \sin\theta$. From (A3.25), Laplace's equation in those coordinates takes the form

$$\operatorname{div}_S \operatorname{grad}_S \phi = \nabla_S^2 \phi_S = \frac{1}{a^2}\left(\frac{\partial^2 \phi}{\partial \theta^2} + \frac{1}{\tan\theta}\frac{\partial \phi}{\partial \theta} + \frac{1}{\sin^2\theta}\frac{\partial^2 \phi}{\partial \varphi^2}\right) = 0. \tag{4.111}$$

The desired potential is φ-independent. Hence

$$\frac{\partial^2 \phi_S}{\partial \theta^2} + \frac{1}{\tan\theta}\frac{\partial \phi_S}{\partial \theta} = 0.$$

Two integrations yield, successively,

$$\frac{\partial \phi_S}{\partial \theta} = \frac{A}{\sin\theta} \tag{4.112}$$

and

$$\phi_S = A \log_e \tan\frac{\theta}{2}, \tag{4.113}$$

where we have taken into account the antisymmetric character of ϕ_S with respect to the plane $\theta = \pi/2$. To determine A, we evaluate the total current through a small circle centered at the injection point. Thus, because $dc = a \sin\theta_0\, d\varphi \approx a\theta_0\, d\varphi$,

$$i = \int_c \mathbf{j}\cdot\mathbf{u}_\theta\, dc = -\frac{\sigma_S}{a}\int_c \frac{\partial \phi_S}{\partial \theta} dc = -\sigma_S 2\pi\theta_0 \frac{\partial \phi_S}{\partial \theta}. \tag{4.114}$$

This relationship implies that $\partial\phi/\partial\theta$ is equal to $-i/2\pi\sigma_S\theta$ for small θ. Comparison with (4.112) yields $A = -i/2\pi\sigma_S$. Consequently, except under the electrodes,

$$\phi_S = -\frac{i}{2\pi\sigma_S}\log_e \tan\frac{\theta}{2}$$

$$\mathbf{j} = \frac{i}{2\pi a \sin\theta}\mathbf{u}_\theta. \tag{4.115}$$

4.11 CHAINS OF CONDUCTORS

Current injection through contact electrodes is not the only way to force current through a conductor; applied electric fields can also perform that task. Let us investigate whether this is possible in a *simply connected* volume (Fig. 4.19*a*). The interior potential must satisfy, from (4.5) and (4.92),

$$\begin{aligned} \operatorname{div}(\sigma \operatorname{grad} \phi) &= \operatorname{div} \mathbf{j}_a \qquad (\text{in } V) \\ \sigma \frac{\partial \phi}{\partial n} &= \mathbf{u}_n \cdot \mathbf{j}_a \qquad (\text{on } S). \end{aligned} \tag{4.116}$$

We illustrate the solution of this system by assuming that the conductor is homogeneous and at a nonuniform temperature. From (4.8), the nonuniformity can produce an *irrotational* applied electric field

$$\mathbf{e}_a = -\beta \operatorname{grad} T.$$

It pays to introduce a new function $\theta = (\phi + \beta T)$, which, from (4.116), satisfies

$$\begin{aligned} \operatorname{div}(\sigma \operatorname{grad} \theta) &= 0 \\ \frac{\partial \theta}{\partial n} &= 0. \end{aligned} \tag{4.117}$$

From the divergence theorem A1.27:

$$\begin{aligned} \int_V \operatorname{div}(\sigma\theta \operatorname{grad} \theta)\, dV &= \int_V \theta \operatorname{div}(\sigma \operatorname{grad} \theta)\, dV + \int_V \sigma |\operatorname{grad} \theta|^2\, dV \\ &= \int_S \sigma\theta \frac{\partial \theta}{\partial n}\, dS = 0. \end{aligned} \tag{4.118}$$

Relationship (4.118) shows that grad θ vanishes throughout the volume or, because $\mathbf{j} = -\sigma \operatorname{grad} \theta$, that *no current exists in the conductor* when $\mathbf{e}_a$ is irrotational. In fact, charges appear at the boundary and create a field that exactly cancels the thermoelectric field. We note that points A and B are not at the same potential, because the constancy of θ implies that

$$\phi_A - \phi_B = \beta(T_B) - \beta(T_A).$$

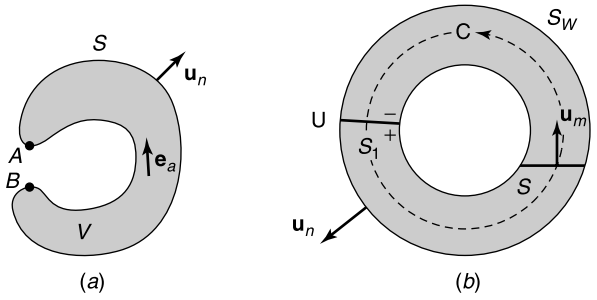

Figure 4.19 (*a*) Homogeneous conductor at a nonuniform temperature. (*b*) A simple ring circuit.

We have actually created a thermal battery, ready to force a current through a circuit connected between A and B. To show how this phenomenon leads to the usual circuit equations, consider now a *doubly connected* volume, more specifically the simple ring circuit shown in Figure 4.19*b*. The material of the ring is homogeneous, hence σ is uniform. Assume now that a uniform potential jump U of the kind appearing in (4.9) is impressed across S_1. To determine the current density $\mathbf{j}$, we integrate (4.5) over contour C and obtain

$$\int_C \frac{1}{\sigma}\mathbf{j}\cdot\mathbf{dc} = \int_C \mathbf{e}\cdot\mathbf{dc} + \int_C \mathbf{e}_a\cdot\mathbf{dc}.$$

But $\displaystyle\int_C \mathbf{e}\cdot\mathbf{dc} = 0$, because curl $\mathbf{e} = 0$ throughout space, and $\displaystyle\int_C \mathbf{e}_a\cdot\mathbf{dc} = U$. It follows that

$$\int_C \mathbf{j}\cdot\mathbf{dc} = \sigma U.$$

In the ring, outside the *slice generator* in S_1, div $\mathbf{j} = 0$ and curl $\mathbf{j} = \text{curl}(\sigma\mathbf{e}) = 0$. We may therefore write $\mathbf{j} = -\sigma$ grad ϕ, where ϕ satisfies

$$\begin{aligned} \nabla^2\phi &= 0 && \\ \frac{\partial\phi}{\partial n} &= 0 && \text{(on } S_W\text{)} \\ \frac{\partial\phi}{\partial c} & && \text{continuous across } S_1 \\ (\phi_+ - \phi_-) &= U && \text{(on } S_1\text{)}. \end{aligned} \tag{4.119}$$

Because U is uniform over S_1, normal and tangential components of $\mathbf{j}$ are continuous across that surface. We may therefore write $\mathbf{j} = \sigma U\mathbf{h}_0$, where $\mathbf{h}_0$ satisfies[†]

$$\begin{aligned} \text{div } \mathbf{h}_0 &= 0 && \\ \text{curl } \mathbf{h}_0 &= 0 && \\ \int_C \mathbf{h}_0\cdot\mathbf{dc} &= 1 && \\ \mathbf{u}_n\cdot\mathbf{h}_0 &= 0 && \text{(on } S_W\text{)}. \end{aligned} \tag{4.120}$$

The solution to that problem is unique (Problem 4.24). Note that $\mathbf{h}_0$ is *harmonic*; that is, it is both solenoidal and irrotational. It can be given an obvious interpretation in terms of fluid flow and plays an important role in electromagnetic theory, for example in the determination of the magnetic flux in a ring-like domain (which is why the $\mathbf{h}_0$ notation was chosen). Given

[†]The existence of a solution to (4.120) has been proved by H. Weyl,[22] who called (4.119) the *magnetostatic problem*. In a torus:

$$\mathbf{h}_0 = \frac{1}{2\pi r}\,\mathbf{u}_\varphi = \text{grad}\left(\frac{\varphi}{2\pi}\right).$$

Potential φ is clearly multivalued.

$\mathbf{h}_0$, the total current through an arbitrary cross section S can be written as

$$\begin{aligned} i &= \int_S \mathbf{j}\cdot\mathbf{u}_m\, dS = \sigma U \int_S \mathbf{u}_m \cdot \mathbf{h}_0\, dS \\ &= U \underbrace{\left[\sigma \int_S \mathbf{u}_m \cdot \mathbf{h}_0\, dS\right]}_{\text{conductance } g} \end{aligned} \tag{4.121}$$

where $\mathbf{u}_n$ is perpendicular to S.

PROBLEMS

4.1 A conducting body consists of two half-spheres in contact along an equatorial plane. The contact potential between the two conductors is given. Assuming that no current exists and that the sphere is uncharged, find the potentials of both half-spheres with respect to infinity. Find an expression for the potential outside the sphere.

4.2 Show that the normal component of the electric field satisfies the equation

$$\frac{\partial e_n}{\partial n} + \left(\frac{1}{R_1} + \frac{1}{R_2}\right) e_n = 0$$

at the surface of a conductor in which no current flows (R_1 and R_2 are the principal radii of curvature of the surface).

4.3 Derive an expression for the capacitance of a short circular cylinder (a thin ring), using the value of ρ_S given in (4.29).

4.4 Show that the potential between a conductor 1 at unit potential and a grounded conductor O surrounding conductor 1 minimizes the functional

$$J(\phi) = \epsilon_0 \int_V |\text{grad } \phi|^2\, dV.$$

What is the physical meaning of the minimum? Apply the variational principle to obtain an approximate value of the potential between two concentric spheres of radius b and $2b$. Compare the approximate value of $J(\phi)$ with the exact one.

4.5 Apply variational principle (4.31) to integral equation (4.27). Take σ = constant as a trial function, and verify that this choice gives a good approximation to C in the case of a long tube (see 4.30).

4.6 With reference to Figure 4.3, show that the quadratic form $\sum_{ij} C_{ij} V_i V_j$ is positive-definite.

4.7 A certain conductor 1 is almost completely surrounded by another conductor 2 (Fig. P4.1). What can be said about the relative values of the coefficients C_{11}, C_{12}, C_{22} in these circumstances?

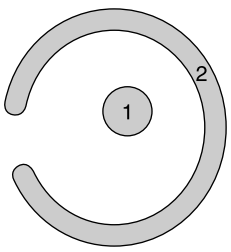

Figure P4.1

When conductor 2 is grounded, V_1 is proportional to q_1. How is the proportionality constant modified when $q_2 = 0$ and the potential of conductor 2 is floating (ungrounded screen)? What is the influence of the charge of conductor 2 on the charge of conductor 1?

4.8 Find an approximate formula for C_{12} when conductors 1 and 2 are separated by a distance much larger than their linear dimensions.

4.9 Show that the capacitance matrix is symmetric. Use a Green's theorem for the purpose. The symmetry property is intimately related to the self-adjoint character of the transformation defined in (4.35).

4.10 A metallic sphere of radius a is placed in the field of a concentric distribution of surface charges of uniform density ρ_S. Make use of the obvious symmetries to determine the potential of the sphere (Fig. P4.2).

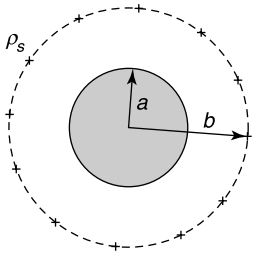

Figure P4.2

4.11 An uncharged metallic sphere is immersed in a uniform field $\mathbf{e}^i$. Find the total potential (a) by separation of variables and (b) by image methods (dipoles). Check that the potential at the center is equal to its incident value.

4.12 As a sequel to Problem 4.11, determine whether there exists, in an arbitrary metallic conductor immersed in a uniform field, a fixed point P such that the potential at that point is equal to the incident potential. Is the location of P a function of the orientation of the body?
(R. Cade *et al.*, *Proc. Phys. Soc. London* **69B**, 175, 1956.)

4.13 Show that the polarizability matrix $\overline{\overline{\alpha}}_e$ given in (4.74) is symmetric. To that effect, immerse the uncharged conductor in incident potentials $\phi_1^i = x$ and $\phi_2^i = y$. Write down expressions for $\mathbf{p}_{e1}$ and $\mathbf{p}_{e2}$, and show that $\mathbf{u}_y \cdot \mathbf{p}_{e1} = \mathbf{u}_x \cdot \mathbf{p}_{e2}$. *Hint*: Apply a suitable Green's theorem, and make use of the property

$$\int_S x \frac{\partial y}{\partial n} dS = \int_S y \frac{\partial x}{\partial n} dS.$$

Remember that the *disturbance* potentials ($\phi - \phi^i$) are $O(1/R^2)$ at large distances.

4.14 Use the results of Section 3.11 to find the polarizability of an oblate conducting spheroid. The conductor corresponds with the limit $\epsilon_r \to \infty$. Investigate, in particular, the limit value for a very small a (Fig. 3.21*b*).

4.15 When the source is a point charge q located at $\mathbf{r}_0$, show that the integral that appears in (4.70) is given by

$$\int \phi^i \rho_{S0}\, dS = q\phi_0(\mathbf{r}_0) \qquad (\phi_0 = 1 \text{ on } S).$$

4.16 Using images, find the potential of the small conducting spheres 1 and 2 with respect to the ground plane (Fig. P4.3). Find the capacitance between 1 and 2 [54, volume 2].

4.17 Show that the functional (4.89) reaches a minimum for ϕ_1 (the solution of 4.85 for V_1), and that this minimum is the conductance.

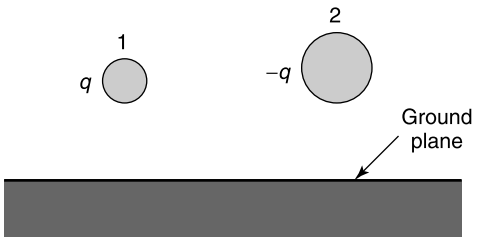

Figure P4.3

4.18 Estimate the conductance of a homogeneous cylindrical conductor of arbitrary cross section by using variational principle (4.89). Use, as a trial function (Fig. P4.4),

(a) A quadratic form in $(z - l)$;

(b) $\phi = \dfrac{1}{e^{-1} - 1} |e^{-1} - e^{-\frac{z}{l}}|$.

Compare the approximative value with the exact one, which is $(\sigma S/l)$.

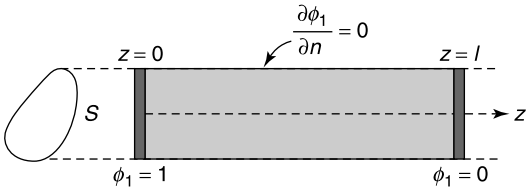

Figure P4.4

4.19 Find the potential within the homogeneous toroidal conductor shown in Figure P4.5. Show that the current density is not uniform in the cross section, and derive a formula for the resistance of the conductor.

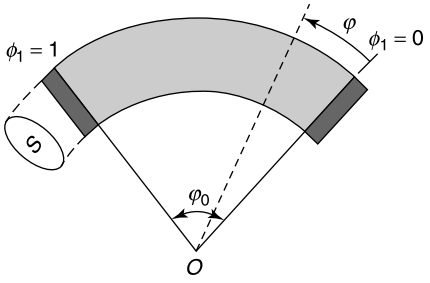

Figure P4.5

4.20 At large distances r from a point contact, the current density in Figure P4.6*a* becomes radial, hence

$$\mathbf{j} = f(r)\mathbf{u}_r$$

$$\phi = g(r)$$

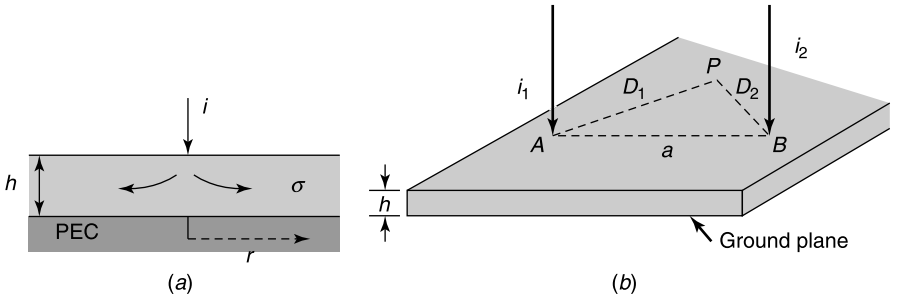

Figure P4.6

(a) Determine $f(r)$ and $g(r)$, given i.

(b) Determine the surface conductance in terms of σ and h, when $h \to 0$.

(c) Determine the potential in P at large distances D_1 and D_2 (Fig. P4.6*b*).

(d) Examine the particular case $i_2 = -i_1$.

(e) Examine the particular case $i_1 = -2i_2$, and show that one of the lines of current is a circle centered in B.

4.21 Find the resistance between two perfectly conducting hemispherical contacts embedded in an Earth of conductivity σ, assuming the distance d to be large compared with the radius a (Fig. P4.7).

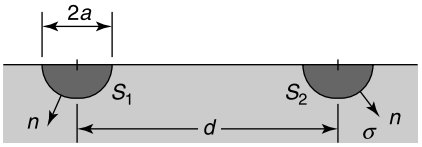

Figure P4.7

4.22 Four metallic wires make point contact with a semi-infinite conducting medium (Fig. P4.8). A current i is injected through contact A and extracted through contact D. Calculate the potential difference that appears between probes B and C, and show that a measurement of $V_B - V_C$ allows determination of the conductivity of the medium, a method that has been used in geophysics. Repeat the problem when the four probes, assumed now to be equally spaced, are placed close to a vertical boundary of the sample. Use the method of images.
(L. B. Valdes, *Proc. IRE* **42**, 420, 1954.)

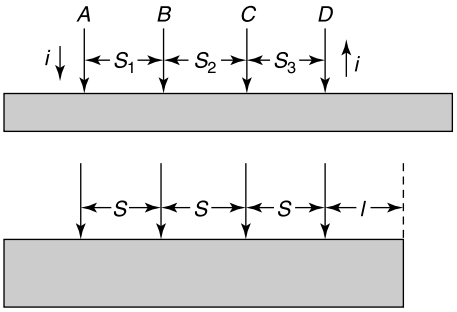

Figure P4.8

4.23 The thermoelectric structure shown in Figure P4.9 is two-dimensional. The two half-circular cylinders, homogeneous with respective conductivities σ_1, σ_2, generate contact potentials U_A and U_B. These potentials are assumed different (e.g., because the cross sections are at different temperatures).

(a) Determine the vector $\mathbf{h}_0$ for this configuration.

(b) Determine the current density $\mathbf{j}$ in 1 and 2, as well as the total current i.

(c) Write down the potential along the outer contour (it varies linearly with φ).

(d) Find the potential *outside* the cylinder by using an expansion in cylindrical harmonics (see Section 5.1).

4.24 Show that the solution of (4.120), if it exists, is unique.

Hint: With $\int \mathbf{h}_0 \cdot d\mathbf{c} = 0$, potential ϕ_0 becomes single-valued.

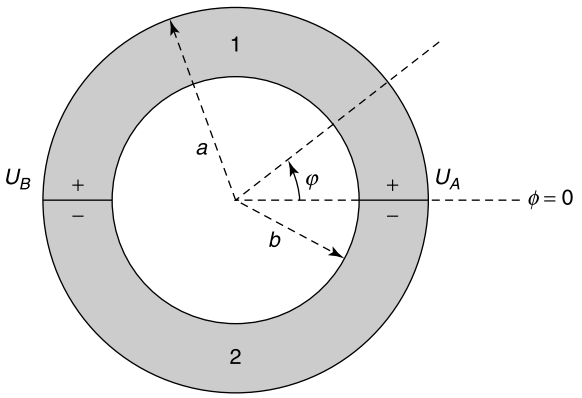

Figure P4.9

NOTES

1. J. Van Bladel, How electromagnetically sharp is a needle?, *IEEE Antennas Prop. Mag.* **45**, 118–122 (2003).
2. G. Robin, Sur la distribution de l'électricité, *Ann. Sci. de l'Ecole Normale Supérieure*, séries 3, **3** (supplément), 1–60 (1886).
3. C. M. Butler, Capacitance of a finite-length conducting cylindrical tube, *J. Appl. Phys.* **51**, 5607–5609 (1980).
4. J. Van Bladel and K. Mei, On the capacitance of a cube, *Appl. Sci. Res. B* **9**, 267–270 (1961).
5. R. Albanese, R. Fresa, and G. Rubinacci, Local error bounds for static and stationary fields, *IEEE Trans. MAG* **36**, 1615–1618 (2000).
6. D. K. Reitan and T. J. Higgins, Calculation of the electrical capacitance of a cube, *J. Appl. Phys.* **22**, 223–226 (1951).
7. S. M. Rao, A. W. Glisson, D. R. Wilton, and B. S. Vidula, A simple numerical solution procedure for statics problems involving arbitrary-shaped surfaces, *IEEE Trans. AP* **27**, 604–608 (1979).
8. D. R. Wilton, S. M. Rao, A. W. Glisson, D. H. Schaubert, O. M. Al-Bundak, and C. M. Butler, Potential integrals for uniform and linear source distributions on polygonal and polyhedral domains, *IEEE Trans. AP* **32**, 276–281 (1984).
9. J. Ureel and D. De Zutter, Shape sensitivities of capacitances of planar conducting surfaces using the method of moments, *IEEE Trans. MTT* **44**, 198–207 (1996).
10. G. Jeng and A. Wexler, Isoparametric, finite element, variational solution of integral equations for three-dimensional fields, *Int. J. Numer. Methods Eng.* **11**, 1455–1471 (1977).
11. S. M. Rao and T. Sarkar, Static analysis of arbitrarily shaped conducting and dielectric structures, *IEEE Trans. MTT* **46**, 1171–1173 (1998).
12. T. G. Bryant and J. A. Weiss, Parameters of microstip transmission lines of coupled pairs of microstrip lines, *IEEE. Trans. MTT* **16**, 1021–1027 (1968).

13. P. Benedek and P. Silvester, Capacitance of parallel rectangular plates separated by a dielectric sheet, *IEEE Trans. MTT* **20**, 504–510 (1972).
14. S. S. Papatheodorou, R. F. Harrington, and J. R. Mautz, The equivalent circuit of a microstrip crossover in a dielectric substrate, *IEEE Trans. MTT* **38**, 135–140 (1990).
15. H. Gruenberg, The ball bearing as a motor, *Am. J. Phys.* **46**, 1213–1219 (1978).
16. D. B. Watson, M. R. Williams, and C. S. Crimp, Ball-bearing motors, *IEE Proc. A.* **140**, 281–286 (1993).
17. J. D. Sweeney, D. A. Ksienski, and J. T. Mortimer, A nerve cuff technique for selective excitation of peripheral nerve trunk regions, *IEEE Trans. Biomed. Eng.* **37**, 706–715 (1990).
18. S. Parrini, J. Delbeke, E. Romero, V. Legat, and C. Veraart, A hybrid finite-elements spectral method for computation of the electric potential generated by a nerve cuff electrode, *Medical Biol. Eng. Computing* **37**, 733–736 (1999).
19. I. V. Lindell, M. E. Ermutlu, K. I. Nikoskinen, and E. H. Eloranta, Static image principle for anisotropic-conducting half-space problems: PEC and PMC boundaries, *Geophysics* **99**, 1861–1864 (1993).
20. R. De Smedt and J. Van Bladel, Magnetic polarizability of some small apertures, *IEEE Trans. AP* **28**, 703–707 (1980).
21. T. F. Eibert and V. Hansen, On the calculation of potential integrals for linear source distributions on triangular domains, *IEEE Trans. AP* **43**, 1499–1502 (1995).
22. H. Weyl, Über die Randwertaufgabe der Strahlungstheorie und Asymptotische Spektralgesetze, *J. Reine Angew. Math.* **143**, 177–202 (1913).

Chapter 5

Special Geometries for the Electrostatic Field

This Chapter is devoted to a number of additional topics in the general area of electrostatics. The "special geometries" mentioned in the title are the two-dimensional Cartesian plane and the axisymmetric and conical volumes. The two-dimensional potential is discussed rigorously in the literature, and we shall only mention the main results of the theory. Proofs of convergence, for example, are similar to those given for the three-dimensional potential in Chapter 3. The list of contents in Chapter 5 includes topics that are of importance not only in electrostatics, but also, in adapted form, for the evaluation of time-dependent fields. For example:

- The analysis of singularities at tips of cones and edges
- The penetration of electric fields through apertures
- The truncation of computational domains
- The use of Fourier transforms in the evaluation of fields in layered media.

5.1 TWO-DIMENSIONAL POTENTIALS IN THE PLANE

The two-dimensional approximation to a three-dimensional problem represents a considerable simplification for the analytical and numerical determination of potential and fields. The approximation is appropriate, for example, for the central part of a slender and cylindrical body, when the independence from the longitudinal coordinate z may reasonably be assumed. The end effects must obviously be investigated separately. A typical application can be found in the determination of the electric field between the wires of a DC transmission line.

In a first step in the analysis of a two-dimensional situation, we determine the potential produced by a linear charge of density ρ_l (in $\mathrm{C\,m^{-1}}$), located at point $\mathbf{r}'(x', y')$. This potential has the nature of a Green's function. The corresponding electric field is purely radial and can be calculated by an application of Gauss' law, according to which the flux of $\epsilon_0\,\mathbf{e}$ through

Electromagnetic Fields, Second Edition, By Jean G. Van Bladel

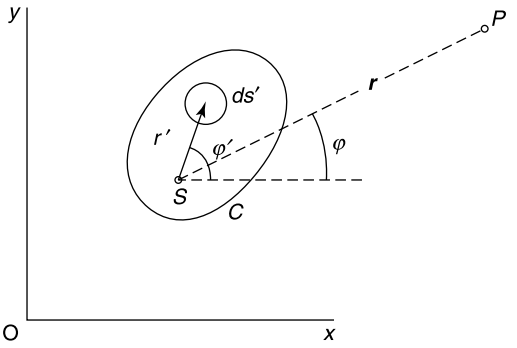

Figure 5.1 Two-dimensional charge distribution.

C is equal to the enclosed charge (i.e., to ρ_l). Thus,

$$\mathbf{e}(\mathbf{r}) = \frac{\rho_l}{2\pi\epsilon_0}\frac{\mathbf{r}-\mathbf{r}'}{|\mathbf{r}-\mathbf{r}'|^2}. \tag{5.1}$$

This field can be derived from a potential

$$\phi(\mathbf{r}) = \frac{\rho_l}{2\pi\epsilon_0}\log_e\frac{L}{|\mathbf{r}-\mathbf{r}'|} + \text{constant}, \tag{5.2}$$

where L is a reference length.* The potential produced by a distributed charge density $\rho(x, y)$ follows by integration. Thus (Fig. 5.1).

$$\phi(\mathbf{r}) = \frac{1}{2\pi\epsilon_0}\int_S \rho(\mathbf{r}')\log_e\frac{L}{|\mathbf{r}-\mathbf{r}'|}\,dS', \tag{5.3}$$

where S is the surface occupied by the charges. Potential (5.3) satisfies Poisson's equation

$$\nabla^2_{xy}\phi = -\frac{\rho}{\epsilon_0}. \tag{5.4}$$

The Green's function for that equation must satisfy

$$\nabla^2_{xy}G(\mathbf{r}|\mathbf{r}') = \delta(\mathbf{r}-\mathbf{r}').$$

From (5.3), the sought function is

$$G(\mathbf{r}|\mathbf{r}') = -\frac{1}{2\pi}\log_e\frac{L}{|\mathbf{r}-\mathbf{r}'|}. \tag{5.5}$$

The potential produced by a dipole line (Fig. 5.2) is the superposition of two *linear charge* potentials. Thus, from (5.2),

$$\phi = \frac{\rho_l}{2\pi\epsilon_0}\log_e\frac{r_2}{r_1}$$

*If we set $L = 1\ m$, $L/|\mathbf{r}-\mathbf{r}'|$ becomes $1/|\mathbf{r}-\mathbf{r}'|$, where $|\mathbf{r}-\mathbf{r}'|$ is expressed in m.

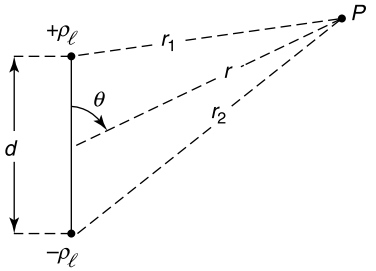

Figure 5.2 A dipole source.

with

$$\lim_{r \gg d} \phi = \frac{1}{2\pi\epsilon_0 r}(\rho_l d)\cos\theta. \tag{5.6}$$

The term $(\rho_l d)$ is the electric dipole moment. It has the dimension C (actually, Cm per m along the axis).

The theory of the two-dimensional potential can be developed along the same lines as in the three-dimensional situation. One can prove, for example, that an integral such as (5.3) is finite and continuous in the entire plane (except at infinity) when ρ_S is bounded and integrable. The same property holds for the first derivatives [158, 172]. A *multipole expansion* can also be derived, following the three-dimensional example, by expanding $\phi(r, \varphi)$ in a Fourier series, valid outside a circle containing all charges:

$$\phi(r, \varphi) = \sum_{n=1}^{\infty} a_n(r)\sin n\varphi + \sum_{n=0}^{\infty} b_n(r)\cos n\varphi.$$

The periodicity of the potential with respect to φ allows termwise differentiation of the series. Introducing the resulting expansion in Laplace's equation gives the differential equation

$$\frac{1}{r}\frac{d}{dr}\left(r\frac{da_n}{dr}\right) - \frac{n^2}{r^2}a_n = 0,$$

to be satisfied by both a_n and b_n. Its general solution is $A\,\log_e(1/r) + B$ for $n = 0$, and $Cr^n + Dr^{-n}$ for $n = 1, 2, \ldots$. The required behavior at large distances leads to the form

$$\phi = A\,\log_e\frac{L}{r} + \sum_{n=1}^{\infty}\frac{1}{r^n}(C_n\sin n\varphi + D_n\cos n\varphi), \tag{5.7}$$

which is valid outside a circle containing all the sources. The coefficients C_n and D_n can be obtained from the expansions

$$\begin{aligned}
\log_e\frac{r'}{|\mathbf{r}-\mathbf{r}'|} &= \sum_{n=1}^{\infty}\frac{1}{n}\left(\frac{r}{r'}\right)^n\cos n(\varphi-\varphi') \quad \text{for } r < r' \\
\log_e\frac{r}{|\mathbf{r}-\mathbf{r}'|} &= \sum_{n=1}^{\infty}\frac{1}{n}\left(\frac{r'}{r}\right)^n\cos n(\varphi-\varphi') \quad \text{for } r > r'.
\end{aligned} \tag{5.8}$$

Insertion of these expansions in (5.3) gives, for $r \gg r'$ (i.e., at large distances)

$$\phi(\mathbf{r}) = \left(\frac{1}{2\pi\epsilon_0}\int_S \rho(\mathbf{r}')\,dS'\right)\log_e\frac{L}{r} + \frac{1}{2\pi\epsilon_0 r}\int_S \rho(\mathbf{r}')r'\cos(\varphi-\varphi')\,dS' + \ldots. \tag{5.9}$$

The first term on the right-hand side corresponds with a linear charge of density $\rho_l = \int \rho(\mathbf{r}')dS'$ (a monopole). The second term represents, according to (5.6), the contribution from a dipole line. The next terms, which are not written out explicitly, are associated with higher-order multipoles.

The properties of single- and double-layer charge distributions depend on the 2D counterparts of (3.68) and (3.69). These are

$$\lim_{P_1\to P}\int_{C_\delta}\frac{\partial}{\partial n}\left(\log_e\frac{L}{|\mathbf{r}-\mathbf{r}'|}\right)dc' = -\lim_{P_1\to P}\int_{C_\delta}\frac{\partial}{\partial n}\left(\log_e\frac{L}{|\mathbf{r}-\mathbf{r}'|}\right)dc' = \pi \tag{5.10}$$

$$\lim_{P_2\to P}\int_{C_\delta}\frac{\partial}{\partial n}\left(\log_e\frac{L}{|\mathbf{r}-\mathbf{r}'|}\right)dc' = -\lim_{P_2\to P}\int_{C_\delta}\frac{\partial}{\partial n}\left(\log_e\frac{L}{|\mathbf{r}-\mathbf{r}'|}\right)dc' = -\pi, \tag{5.11}$$

where C_δ is a small segment of C that contains P (Fig. 5.3*a*). When we apply these formulas to the potential of a *single layer* of charge, viz.

$$\phi(\mathbf{r}) = \frac{1}{2\pi\epsilon_0}\int_C \rho_S(\mathbf{r}')\log_e\frac{L}{|\mathbf{r}-\mathbf{r}'|}\,dc' \tag{5.12}$$

we find that the normal derivatives near C must satisfy

$$\lim_{P_1\to P}\frac{\partial\phi}{\partial n} = \frac{\rho_S(P)}{2\epsilon_0} + \frac{1}{2\pi\epsilon_0}\lim_{\delta\to 0}\int_{C-C_\delta}\rho_S(\mathbf{r}')\frac{\partial}{\partial n}\left(\log_e\frac{L}{|\mathbf{r}-\mathbf{r}'|}\right)dc' \tag{5.13}$$

$$\lim_{P_2\to P}\frac{\partial\phi}{\partial n} = -\frac{\rho_S(P)}{2\epsilon_0} + \frac{1}{2\pi\epsilon_0}\lim_{\delta\to 0}\int_{C-C_\delta}\rho_S(\mathbf{r}')\frac{\partial}{\partial n}\left(\log_e\frac{L}{|\mathbf{r}-\mathbf{r}'|}\right)dc'. \tag{5.14}$$

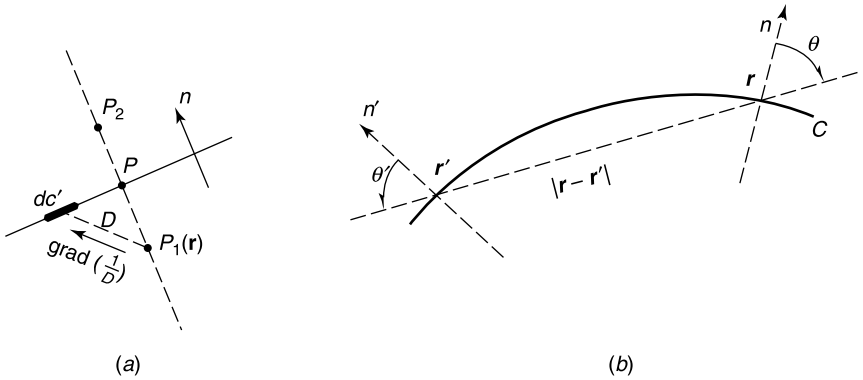

Figure 5.3 (*a*) Evaluation of the self-segment contribution. (*b*) Boundary curve C and relevant angles and distances.

The potential of a *double layer* is given by (Fig. 5.3*b*)

$$\phi(\mathbf{r}) = \frac{1}{2\pi\epsilon_0}\int_C \tau(\mathbf{r}')\frac{\partial}{\partial n'}\log_e\frac{L}{|\mathbf{r}-\mathbf{r}'|}\,dc'. \tag{5.15}$$

This potential is continuous outside C_1, but suffers a step discontinuity across C. More precisely:

$$\lim_{P_1\to P}\phi = -\frac{\tau(P)}{2\epsilon_0} + \frac{1}{2\pi\epsilon_0}\lim_{\delta\to 0}\int_{C-C_\delta}\tau(\mathbf{r}')\frac{\partial}{\partial n'}\left(\log_e\frac{L}{|\mathbf{r}-\mathbf{r}'|}\right)dc' \tag{5.16}$$

$$\lim_{P_2\to P}\phi = \frac{\tau(P)}{2\epsilon_0} + \frac{1}{2\pi\epsilon_0}\lim_{\delta\to 0}\int_{C-C_\delta}\tau(\mathbf{r}')\frac{\partial}{\partial n'}\left(\log_e\frac{L}{|\mathbf{r}-\mathbf{r}'|}\right)dc'. \tag{5.17}$$

The two associated kernels

$$\frac{1}{2\pi}\frac{\partial}{\partial n}\log_e\frac{1}{|\mathbf{r}-\mathbf{r}'|} = -\frac{\cos\theta}{2\pi|\mathbf{r}-\mathbf{r}'|} \tag{5.18}$$

$$\frac{1}{2\pi}\frac{\partial}{\partial n'}\log_e\frac{1}{|\mathbf{r}-\mathbf{r}'|} = -\frac{\cos\theta'}{2\pi|\mathbf{r}-\mathbf{r}'|} \tag{5.19}$$

play a fundamental role in the theory of the logarithmic potential (Fig. 5.3*b*).

5.2 FIELD BEHAVIOR AT A CONDUCTING WEDGE

Structures encountered in practice — airplane frames for example — often exhibit metallic or dielectric wedges, vertices, or corners. Pyramidal corners and vertices, discussed in Section 5.12, are three-dimensional structures. Wedges, on the other hand, may often be considered as two-dimensional (Fig. 5.4). It is important to understand how field and potential behave near the edge, both to incorporate their behavior into a numerical program (if so desired) or to verify the validity of otherwise obtained numerical results.

Metallic wedges are found, for example, at the tips of aircraft wings or at the (sharp) rim of an aperture. When the edge is curved instead of straight, curvature effects may be neglected as long as r remains small with respect to the radius of curvature of the edge. Under these conditions, the potential is, to a good approximation, a function of only r and φ. We write

$$\phi(r,\varphi) = r^{\nu}\Big[a_0(\varphi) + ra_1(\varphi) + r^2a_2(\varphi) + \ldots\Big], \tag{5.20}$$

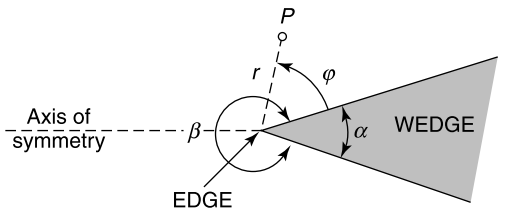

Figure 5.4 Conducting wedge.

where r^ν represents a possible singular factor, the exponent ν remaining temporarily undetermined. The corresponding electric field is

$$\mathbf{e}(r,\varphi) = -r^{\nu-1}(\nu a_0 \mathbf{u}_r + \frac{da_0}{d\varphi}\mathbf{u}_\varphi) - r^\nu[(\nu+1)a_1\mathbf{u}_r + \frac{da_1}{d\varphi}\mathbf{u}_\varphi + \cdots]. \tag{5.21}$$

For physical reasons, the energy density near the edge must remain integrable.[1] Because this density is proportional to $|\mathbf{e}|^2$, a simple integration shows that ν may not be negative; that is, that the singularity of $\mathbf{e}$ may not be stronger than $(1/r)$. To further determine ν, we require (5.20) to satisfy Laplace's equation. This gives

$$\phi(r,\varphi) = r^{\nu-2}\left(\frac{d^2a_0}{d\varphi^2} + \nu^2 a_0\right) + r^{\nu-1}\left[\frac{d^2a_1}{d\varphi^2} + (\nu+1)^2 a_1\right] + \cdots. \tag{5.22}$$

But ϕ must vanish for $\varphi = 0$ and $\varphi = 2\pi - \alpha = \beta$. The coefficient of $r^{\nu-2}$ must consequently vanish, which leads to the form $a_0 = A\sin\nu\varphi$, where ν is a multiple of (π/β). The strongest singularity, which corresponds with the smallest value of ν, is therefore characterized by (Fig. 5.4)

$$\begin{aligned}
\nu &= \frac{\pi}{\beta} = \frac{\pi}{2\pi - \alpha} \\
\phi &= A\, r^{\frac{\pi}{\beta}} \sin\left(\frac{\pi}{\beta}\varphi\right) + \cdots \\
\mathbf{e} &= -A\, r^{\left(\frac{\pi}{\beta}-1\right)}\left[\frac{\pi}{\beta}\sin\left(\frac{\pi}{\beta}\varphi\right)\mathbf{u}_r + \cos\left(\frac{\pi}{\beta}\varphi\right)\mathbf{u}_\varphi\right] + \cdots.
\end{aligned} \tag{5.23}$$

Important particular cases are $\nu = 1/2$ (the half plane) and $\nu = 2/3$ (the 90° corner). The electric field is seen to become infinite at the tip of a sharp edge but to remain finite at a reentrant corner. The charge density on the conductor, equal to $(-\epsilon_0 e_\varphi)$, is

$$\rho_S = -\epsilon_0 e_\varphi = \epsilon_0 A\, r^{\nu-1} = \epsilon_0 A\, r^{\frac{\pi}{\beta}-1}. \tag{5.24}$$

This density becomes infinite at the tip but without charge accumulation because $\int_0^r \rho_S(r')\,dr'$ approaches zero together with r.

The potential in (5.23) is symmetric with respect to the axis of symmetry $\varphi = \beta/2$. It follows that the singularity is not present when the wedge is immersed in an antisymmetric incident potential, in which case the field near the tip remains finite. The infinity also disappears when the edge is rounded off. An estimate of the departure from the idealized sharp edge may be obtained from Figure 5.5, where s is the distance from the tip and R the radius of curvature of the hyperbola that fits the tip. The two curves differ by less than 2% as soon as the distance s is larger than $5R$ [133]. From that distance on, the edge may reasonably be considered as sharp, unless another discontinuity is present in the immediate vicinity. To illustrate this remark, Figure 5.6 shows data concerning a half-infinite conducting slab (e.g., the end of a metallic strip). Near the 90° corners the singularity exponent $\nu = 2/3$ dominates, as expected, but farther away the half-plane value $\nu = 1/2$ progressively takes over. This is confirmed by theoretical results[2] obtained by means of a Schwarz-Christoffel

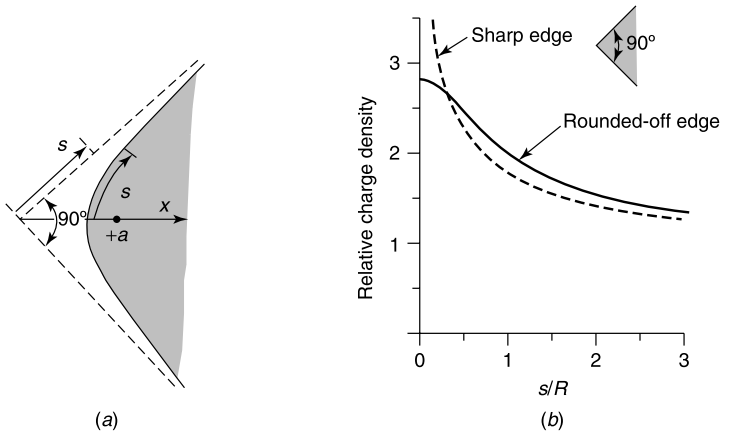

Figure 5.5 (*a*) Hyperbolic conducting wedge. (*b*) Charge density on two types of wedges.

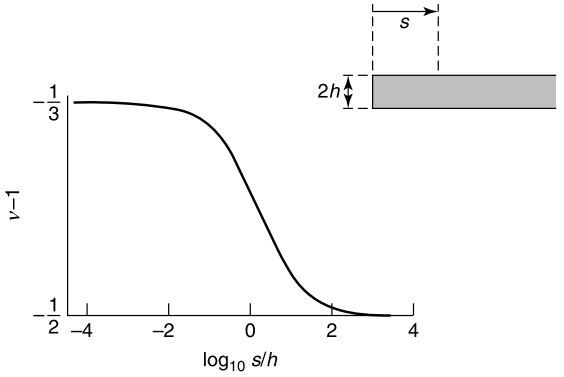

Figure 5.6 Singularity exponent along the faces of a conducting slab (from F. Olyslager and D. De Zutter, Analytical behavior of the surface charge density on a conductor with two consecutive edges with right angles, *Microwave Opt. Tech. Lett.* **6**, 578–581, 1993, with permission of John Wiley & Sons).

transformation [59]. Such a transformation can also be used[3] to derive the variation of ρ_S along the N-corner configuration shown in Figure 5.7.

From a theoretical point of view, satisfaction of the edge behavior guarantees uniqueness of the solution of the potential problem

$$\nabla_{xy}^2 \phi = -\frac{1}{\epsilon_0}\rho$$
$$\phi = 0 \qquad (\text{on } C). \tag{5.25}$$

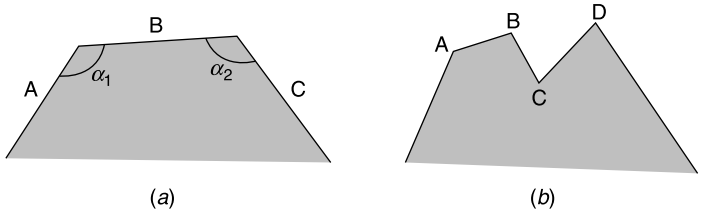

Figure 5.7 Conductors with several edges.

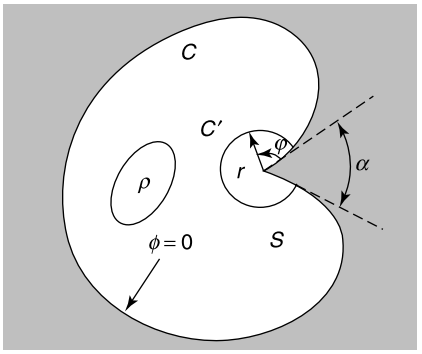

Figure 5.8 Boundary endowed with a sharp edge.

To prove uniqueness, we should prove that the homogeneous problem (with $\rho = 0$) has only the trivial solution $\phi_0 = 0$. The condition $\phi_0 = 0$ on C does not suffice for the purpose. Traditionally, indeed, uniqueness is proved by means of the Green's theorem (Fig. 5.8)

$$\int_S \left[\phi_0 \nabla^2 \phi_0 + |\text{grad } \phi_0|^2\right] dS = \int_C \phi_0 \frac{\partial \phi_0}{\partial n} dc = 0.$$

But this theorem cannot be applied in a region where ϕ_0 is singular. The immediate vicinity of the edge must therefore be excluded. This can be achieved by introducing an additional boundary C', a small circle centered on the edge and of radius r. Uniqueness now requires ϕ_0 to behave in such a fashion that

$$\lim_{r \to 0} \int_{C'} \phi_0 \frac{\partial \phi_0}{\partial r} r \, d\varphi = 0. \tag{5.26}$$

The edge condition requires ϕ to be proportional to $r^\nu \sin \nu\varphi$ (where $\nu \geq \frac{1}{2}$), hence (5.26) is satisfied, and uniqueness is guaranteed.

Numerical Aspects

To take the singular behavior at edges into account, two strategies are possible: either use standard basis functions, and strongly refine the net in the region containing the singularity, or incorporate the singularity into the basis functions themselves.[4] In the one-dimensional problem of a conducting strip of width $2c$, singular quantities near the edges can be efficiently represented by series of the type (Fig. 5.9)

$$f(x) = \frac{1}{\sqrt{[1 - (x/c)^2]}} \left(A_0 + \sum_{n=1}^{\infty} A_n T_n(x/c)\right). \tag{5.27}$$

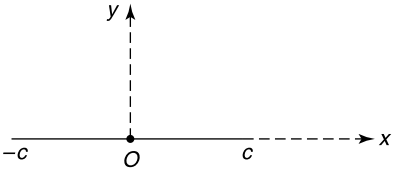

Figure 5.9 Metallic strip.

In this expression, the $T_n(x)$ are the Chebyshev polynomials of the first kind. Their choice is justified by the interesting property (see A5.193)

$$-\frac{1}{\pi}\int_c^c \frac{1}{\sqrt{1-(x'/c)^2}} T_m(x'/c)\log_e|x-x'|\,dx' = \begin{cases} c\log_e\left[\frac{2}{c}\right] T_0(x/c) & \text{for } m=0, \\ (c/m)T_m(x/c) & \text{for } m=1,2,\ldots. \end{cases} \tag{5.28}$$

Such integrals are interesting because the Green's function in the plane is logarithmic (see Section 5.2).

5.3 FIELD BEHAVIOR AT A DIELECTRIC WEDGE

Two examples of structures endowed with dielectric wedges are shown in Figure 5.10*a* and *b*. In a first type of singularity, ϕ is symmetric with respect to the $\varphi = 0$ plane, and the potential close to the edge is of the form[5] [133]

$$\begin{aligned} \phi_1 &= Ar^\nu \cos\nu\varphi && \left(\text{for } -\frac{1}{2}\alpha \le \varphi \le \frac{1}{2}\alpha\right) \\ \phi_2 &= A\frac{\cos\frac{1}{2}\nu\alpha}{\cos\nu\left(\pi-\frac{1}{2}\alpha\right)} r^\nu \cos\nu(\pi-\varphi) && \left(\text{for } \frac{1}{2}\alpha \le \varphi \le 2\pi - \frac{1}{2}\alpha\right). \end{aligned} \tag{5.29}$$

The value of ν follows from enforcing continuity of $\epsilon_r \partial\phi/\partial n$ at the interfaces (Fig. 5.10*c*). The lowest value of ν, which yields the strongest singularity, is given in Table 5.1. Only sharp edges give rise to infinities, because ν is always larger than one for reentrant edges (i.e., for $\alpha > 180°$).

In the second type of singularity ϕ is anti symmetric with respect to the $\varphi = 0$ plane, and we set

$$\begin{aligned} \phi_1 &= Br^\tau \sin\tau\varphi && \left(\text{for } -\frac{1}{2}\alpha \le \varphi \le \frac{1}{2}\alpha\right) \\ \phi_2 &= Br^\tau \frac{\sin\frac{1}{2}\tau\alpha}{\sin\tau\left(\pi-\frac{1}{2}\alpha\right)} \sin\tau(\pi-\varphi) && \left(\text{for } \frac{1}{2}\alpha \le \varphi \le 2\pi - \frac{1}{2}\alpha\right). \end{aligned} \tag{5.30}$$

These potentials have also the correct form for the configuration shown in Figure 5.11, where φ varies between 0 and π. Applying the boundary conditions at the interfaces shows

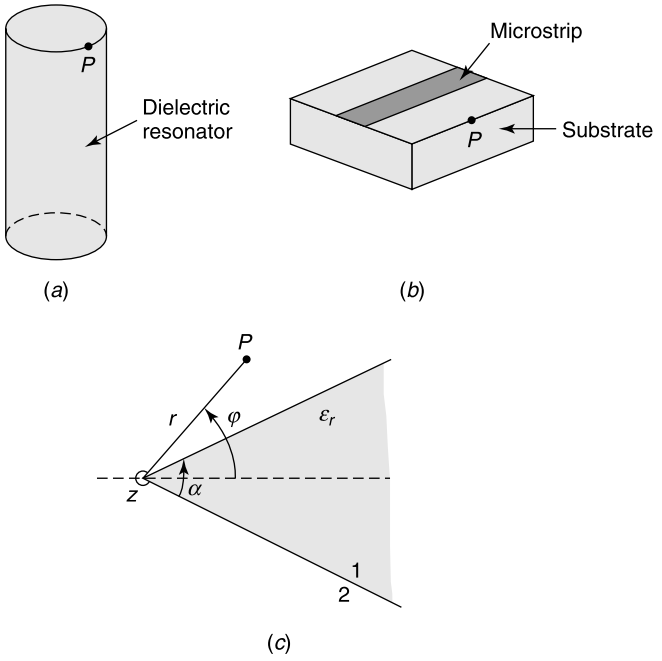

Figure 5.10 (*a*,*b*) Examples of devices exhibiting dielectric wedges. (*c*) Dielectric wedge.

Table 5.1 Lowest Values of ν and τ

α (for ν)	ϵ_r	1	2	5	10	38	50	100	∞	α (for τ)
0°		1.000	1.000	1.000	1.000	1.000	1.000	1.000	.5000	360°
20°		1.000	.9500	.8437	.7486	.6107	.5935	.5635	.5294	340°
40°		1.000	.9156	.7841	.6992	.6062	.5963	.5799	.5625	320°
60°		1.000	.8971	.7679	.6977	.6293	.6226	.6115	.6000	300°
80°		1.000	.8918	.7745	.7169	.6644	.6594	.6512	.6429	280°
100°		1.000	.8974	.7961	.7495	.7086	.7048	.6986	.6923	260°
120°		1.000	.9123	.8300	.7935	.7622	.7594	.7547	.7500	240°
140°		1.000	.9351	.8751	.8489	.8268	.8248	.8215	.8182	220°
160°		1.000	.9649	.9317	.9171	.9048	.9037	.9018	.9000	200°
180°		1.000	1.000	1.000	1.000	1.000	1.000	1.000	1.000	180°

that the singularity exponent τ is related to ν in Table 5.1 by[6]

$$\nu(\alpha) = \tau(2\pi - \alpha) \tag{5.31}$$

Table 5.1 has been adapted to take that remark into account: the extreme left column of α should be used to read off values of ν; the extreme right column to read off those of τ. The table shows that the singularity for the second kind of symmetry (i.e., for ϕ antisymmetric in φ) occurs for reentrant wedges.

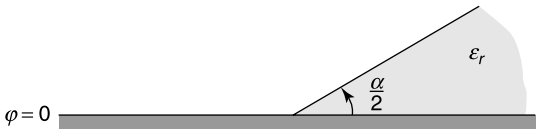

Figure 5.11 Dielectric wedge resting on a conducting plane.

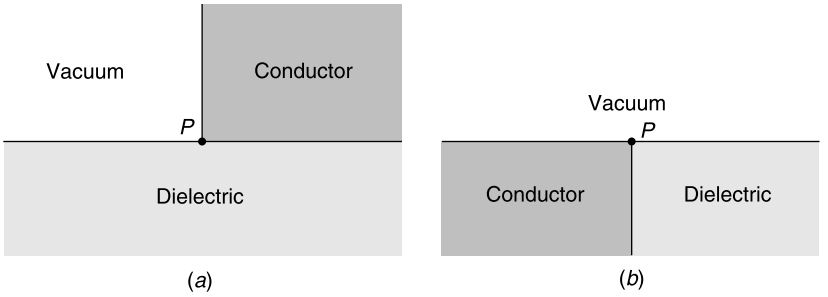

Figure 5.12 Two conductor-dielectric contacts.

Table 5.2 Singularity Exponents for Metal-Dielectric Contacts

ϵ_r	σ	β	ϵ_r	σ	β
1.0	.6667	.6667	10.0	.5290	.8632
1.5	.6310	.7048	15.0	.5199	.8869
2.0	.6082	.7323	20.0	.5152	.9014
2.5	.5922	.7532	25.0	.5122	.9114
3.0	.5804	.7699	38.0	.5082	.9278
4.0	.5641	.7952	50.0	.5062	.9369
5.0	.5533	.8136	100.0	.5032	.9552
7.5	.5375	.8440			

In the previous discussion, a dielectric medium of dielectric constant $\epsilon = \epsilon_r \epsilon_0$ was in contact with vacuum (i.e., a region of dielectric constant ϵ_0). The analysis remains valid when *two* dielectrics are in contact, but now ϵ_r must be interpreted as the ratio $\epsilon_{r1}/\epsilon_{r2}$. The reentrant wedge ($\alpha > \pi$) now becomes a sharp dielectric wedge embedded in a medium of higher dielectric constant.

Structures encountered in practice often contain conductors in contact with dielectrics. Figure 5.12 shows two such examples[7]: a microstrip in contact with a substrate, and a quartz window in contact with a cavity wall. The singularity exponents for the geometries are respectively σ and β. Their value given in Table 5.2. Multiple wedges, involving several conductors and dielectrics, are briefly discussed in [133].

5.4 SEPARATION OF VARIABLES IN TWO DIMENSIONS

Numerous two-dimensional problems have been solved by separation of variables. As an illustration of the method, we shall evaluate the fields in (and around) an elliptic cylinder

immersed in a uniform incident field $\mathbf{e}^i$. Elliptic coordinates are a natural choice for the solution of that problem. Two sets of elliptic coordinates are in use: (μ, ν) and (u, v) (see Appendix 2, equations A2.102 to (A2.106), and Fig. 3.22). The transformation equations from elliptic to Cartesian coordinates are given by

$$\begin{aligned} x &= c \cosh u \cos v = c\mu\nu \\ y &= c \sinh u \sin v = c\sqrt{\mu^2 - 1}\sqrt{1 - \nu^2}. \end{aligned} \tag{5.32}$$

In Section 3.11 the (μ, ν) pair was chosen to solve the problem of a prolate spheroid immersed in an incident field. We shall now switch to the (u, v) pair, and assume that the incident field is x-directed, with corresponding potential (Fig. 5.13*a*)

$$\phi^i = -e^i x = -e^i c \cosh u \cos v. \tag{5.33}$$

The *disturbance* potential must be symmetric with respect to the x-axis, and vanish at infinity [165]. It must also satisfy Laplace's equation, where ∇^2 is given by (A2.109). Separation of variables generates the possible solution

$$\phi_n = \begin{Bmatrix} \sinh nu \\ \cosh nu \end{Bmatrix} \begin{Bmatrix} \sin nv \\ \cos nv \end{Bmatrix} \qquad (n \text{ an integer or zero}).$$

All requirements are satisfied by the choices

$$\frac{\phi^+}{ce^i} = -\cosh u \cos v + Ae^{-u} \cos v \quad \text{(outside the cylinder)} \tag{5.34}$$

$$\frac{\phi^-}{ce^i} = B \cosh u \cos v = Bx \quad \text{(inside the cylinder)}. \tag{5.35}$$

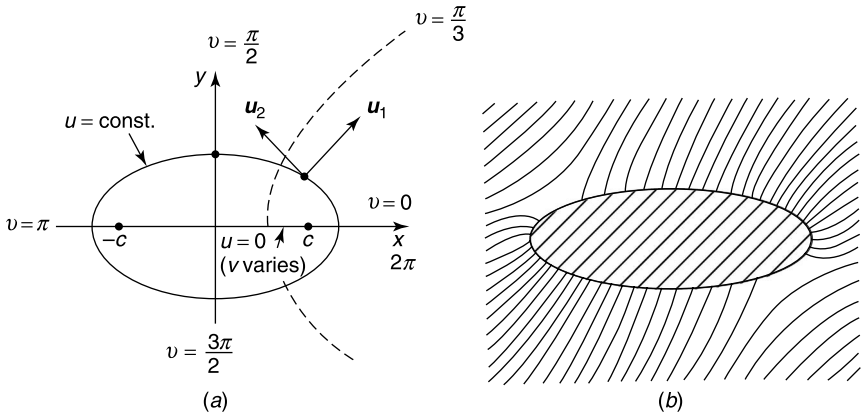

Figure 5.13 (*a*) Elliptic coordinate system. (*b*) Lines of force in an oblique incident field.

The coefficients A and B may be determined from the boundary conditions at $u = u_0$. For a *dielectric* cylinder, from (A2.107), these conditions are

$$\phi^+ = \phi^-$$
$$\left(\frac{\partial \phi}{\partial u}\right)_+ = \epsilon_r \left(\frac{\partial \phi}{\partial u}\right)_- .$$

A few simple steps show that the interior field is equal to

$$\mathbf{e}^- = e^i \frac{\sinh u_0 + \cosh u_0}{\epsilon_r \sinh u_0 + \cosh u_0} \mathbf{u}_x. \tag{5.36}$$

This field is everywhere parallel to the incident field, and the induced dipole moment (per unit length along the z-axis) is given by

$$\mathbf{p}_e = \epsilon_0 \alpha_x \mathbf{e}^i = \epsilon_0 (\epsilon_r - 1)\pi ab \frac{e^{u_0}}{\epsilon_r \sinh u_0 + \cosh u_0} \mathbf{e}^i. \tag{5.37}$$

For a field in the y direction, similarly,

$$\mathbf{e}^- = e^i \frac{\sinh u_0 + \cosh u_0}{\sinh u_0 + \epsilon_r \cosh u_0} \mathbf{u}_y \tag{5.38}$$

$$\mathbf{p}_e = \epsilon_0 \alpha_y \mathbf{e}^i = \epsilon_0 (\epsilon_r - 1)\pi ab \frac{e^{u_0}}{\sinh u_0 + \epsilon_r \cosh u_0} \mathbf{e}^i. \tag{5.39}$$

The interior field is again proportional with the incident field, but with a different proportionality factor than for x-incidence. For arbitrary incidence, therefore, $\mathbf{e}$ is uniform in the dielectric, as shown in Figure 5.13*b*, but not parallel to $\mathbf{e}^i$. The dipole moment is now given by the general formula

$$\mathbf{p}_e = \epsilon_0 \overline{\overline{\alpha}}_e \cdot \mathbf{e}^i = \epsilon_0 \underbrace{\begin{pmatrix} \alpha_x & 0 \\ 0 & \alpha_y \end{pmatrix}}_{\overline{\overline{\alpha}}_e} \cdot \begin{pmatrix} e_x^i \\ e_y^i \end{pmatrix}, \tag{5.40}$$

where $\overline{\overline{\alpha}}_e$ is the *polarizability dyadic* (dimension: m^2).

When the cylinder is *conducting*, expression (5.34) for the exterior potential is still appropriate, but ϕ must now vanish on the surface (i.e., for $u = u_0$). It follows that (Fig. 5.14)

$$\begin{aligned} \frac{\phi}{ce^i} &= \left(-\cosh u + e^{-(u-u_0)} \cosh u_0\right) \cos v \\ \frac{\mathbf{e}}{e^i} &= \frac{1}{\sqrt{\cosh^2 u - \cos^2 v}} \Big[\left(\sinh u + e^{-(u-u_0)} \cosh u_0\right) \cos v \, \mathbf{u}_1 \\ &\quad + \left(-\cosh u + e^{-(u-u_0)} \cosh u_0\right) \sin v \, \mathbf{u}_2 \Big]. \end{aligned} \tag{5.41}$$

Let P be a point on the x-axis, close to the cylinder, and let its u coordinate be $u_0 + \Delta u$. The small distance d can be written as

$$d = c \sinh u_0 (u - u_0) = c \sinh u_0 \Delta u$$

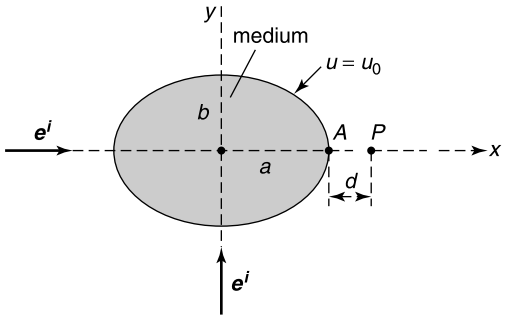

Figure 5.14 Conducting elliptic cylinder in an incident field.

from which it follows, from (5.41), that

$$e_x(P) = e_x(A)\left(1 - \frac{a^2}{b^2}\frac{d}{a}\right), \tag{5.42}$$

where

$$e_x(A) = e^i\left(1 + \frac{a}{b}\right).$$

When b approaches zero, the normal component of the electric field in A becomes

$$e_x(A) \approx \frac{a}{b}e^i = \sqrt{\frac{a}{R_A}}e^i, \tag{5.43}$$

where R_A is the radius of curvature (b^2/a) in A. Expressions (5.42) and (5.43) are useful for estimating the electric field near a conducting rounded-off edge (e.g., near the aileron of an airplane). When u_0 is set equal to zero the ellipse becomes a band, and one obtains, from (A2.107),

$$\frac{\phi}{ce^i} = \sinh u \cos v$$
$$\frac{\mathbf{e}}{e^i} = \frac{1}{(\cosh^2 a - \cos^2 v)^{\frac{1}{2}}}[\cosh u \cos v\, \mathbf{u}_1 + \sinh u \sin v\, \mathbf{u}_2].$$

Near the edge of the band

$$e_x = e_i\sqrt{\frac{c}{2d}}, \tag{5.44}$$

where d is the distance to the edge. This expression confirms the expected $(1/\sqrt{d})$ singularity near a sharp edge (see 5.23).

The previous analysis can easily be extended to an incident field along the y-axis. The details are left to the reader.

5.5 TWO-DIMENSIONAL INTEGRAL EQUATIONS

For a homogeneous dielectric cylinder, the two-dimensional version of the *Phillips integral equation* (3.152) takes the form

$$\phi^i(\mathbf{r}) = \frac{\epsilon_r + 1}{2}\phi(\mathbf{r}) + \frac{\epsilon_r - 1}{2\pi}\int_C \phi(\mathbf{r}')\frac{\partial}{\partial n'}\left(\log_e \frac{1}{|\mathbf{r} - \mathbf{r}'|}\right) dc'. \tag{5.45}$$

Once ϕ is determined, the dipole moment (per unit length along the axis) can be evaluated from the relationship

$$\mathbf{p}_e = (\epsilon_r - 1)\epsilon_0 \int_C \phi(\mathbf{r}')\mathbf{u}'_n dc'. \tag{5.46}$$

Figure 5.15 shows how the two basic polarizabilities of a rectangular cylinder vary in terms of ϵ_r and the cross-sectional dimensions.[8] These results should be compared with the *polarizability of a circular cylinder* of radius a, which is

$$\alpha_e = a^2 2\pi \frac{\epsilon_r - 1}{\epsilon_r + 1}. \tag{5.47}$$

The integral equation solution has several advantages: it is one-dimensional, and its kernel automatically produces the correct behavior at large distances. When the dielectric is inhomogeneous, however, the problem becomes inescapably two-dimensional. Suitable integral equations are available for such cases: they are discussed in Chapter 14.

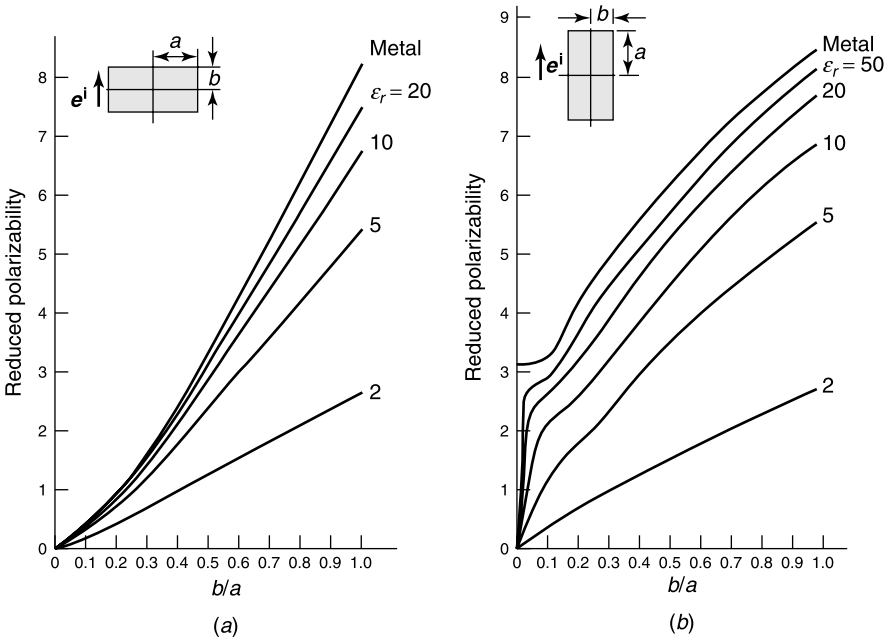

Figure 5.15 Reduced polarizability α/a^2 for (*a*) $\mathbf{e}^i$ perpendicular to the broad side. (*b*) $\mathbf{e}^i$ perpendicular to the narrow side.

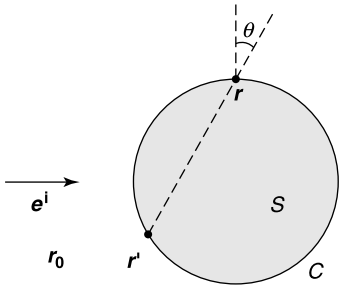

Figure 5.16 Conducting cylinder in an incident field.

When the cylinder is *conducting* we shall assume, as a *first problem*, that the conductor carries a total charge ρ_l, spread over the contour C with a still unknown charge density ρ_S (Fig. 5.16). To determine ρ_S, we write the potential with respect to a reference point $\mathbf{r}_0$ as[8]

$$\phi(\mathbf{r}) - \phi(\mathbf{r}_0) = \frac{1}{2\pi\epsilon_0}\int_C \rho_S(\mathbf{r}')\log_e\frac{|\mathbf{r}_0 - \mathbf{r}'|}{|\mathbf{r} - \mathbf{r}'|}\,dc'. \tag{5.48}$$

When $\mathbf{r}$ approaches C, ϕ must approach the given constant potential of the conductor. Basically, a function $f(\mathbf{r})$ should be found that satisfies the integral equation

$$\frac{1}{2\pi}\int_C f\left(\frac{\mathbf{r}'}{L}\right)\log_e\frac{L}{|\mathbf{r} - \mathbf{r}'|}\frac{dc'}{L} = 1, \tag{5.49}$$

where L is a characteristic length, for example the length of the contour. The sought function depends only on the *shape* of the cross section and not on the *scale* of the latter. The value of f for a rectangle is plotted in Figure 5.17 in terms of its average over the contour. We notice the singularity at the corner, which was not enforced, but automatically came out of the numerical computation. Once $f(\mathbf{r})$ is known, the sought charge density follows from

$$\rho_S = \frac{\rho_l}{L}\left(\frac{f}{f_{\text{ave}}}\right) = (\rho_S)_{\text{ave}}\left(\frac{f}{f_{\text{ave}}}\right). \qquad (\mathbf{r} \text{ on } C) \tag{5.50}$$

In the limit case of a conducting band (Fig. 5.9), ρ_S is given by[†]

$$\rho_S(x) = \frac{\rho_L}{2c}\frac{1}{\pi}\frac{1}{\sqrt{1 - \dfrac{x^2}{c^2}}} \qquad (\text{C m}^{-2}). \tag{5.51}$$

The formula confirms the expected edge behavior of ρ_S at $x = \pm c$.

In a *second problem*, the conducting cylinder is uncharged but lies in the field of an incident potential ϕ^i. The surface charge density satisfies, for $\mathbf{r}$ on C,

$$\frac{1}{2\pi\epsilon_0}\int_C \rho_S(\mathbf{r}')\log_e\frac{L}{|\mathbf{r} - \mathbf{r}'|}\,dc' + \phi^i(\mathbf{r}) = C_1. \tag{5.52}$$

[†]Functions that are orthogonal to ρ_S in (5.51) are useful for certain applications. Examples are all odd functions in x, as well as the even function $\left(x^2 - \frac{1}{2}c^2\right)$, which is orthogonal to ρ_S because $\int_{-c}^{c}\frac{x^2 dx}{\sqrt{c^2 - x^2}} = \frac{\pi}{2}c^2$.

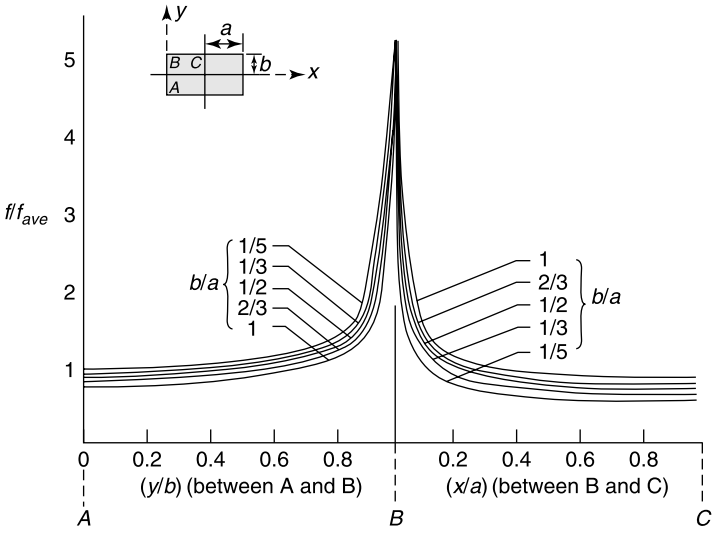

Figure 5.17 Relative variation of the charge density on a rectangular conductor.

The constant C_1 is left undetermined because ϕ^i is known to within an additive constant. In a first step, we solve

$$\frac{1}{2\pi\epsilon_0}\int_C \rho_{S1}(\mathbf{r}')\log_e\frac{L}{|\mathbf{r}-\mathbf{r}'|}\,dc' = -\phi^i(\mathbf{r}). \tag{5.53}$$

To ensure charge neutrality, we add to ρ_{S1} a multiple of the solution f of (5.49). The right combination is

$$\rho_S(\mathbf{r}) = \rho_{S1}(\mathbf{r}) - (\rho_{S1})_{\text{ave}}\frac{f(\mathbf{r})}{f_{\text{ave}}}.$$

Results for a rectangular cylinder[8] are plotted in Figure 5.18. As a corner is approached, ρ_S shows a singularity of the $d^{-\frac{1}{3}}$ type, a behavior predicted by (5.23). The polarizability of the cylinder is given by the curves marked "metal" in Figure 5.15.

In addition to (5.52), the charge density ρ_S also satisfies *Robin's integral equation*

$$\rho_S(\mathbf{r}) - \frac{1}{\pi}\lim_{\sigma\to 0}\int_{C-\sigma}\rho_S(\mathbf{r}')\frac{\cos\theta}{|\mathbf{r}-\mathbf{r}'|}\,dc' = -2\epsilon_0\frac{\partial\phi^i}{\partial n} \qquad (\mathbf{r}\text{ on }C). \tag{5.54}$$

A *third problem* is concerned with the evaluation of the capacitance C between two cylindrical conductors. Consider, for example, the transmission line formed by two parallel bands (Fig. 5.19). The potential above the $y = 0$ plane is the same as when the horizontal plane $y = 0$ is metallized. The relevant Green's functions, taking symmetries into account, is[9]

$$G(x,y|x',c) = -\log_e\left\{\frac{[(x-x')^2+(y-c)^2][(x+x')^2+(y-c)^2]}{[(x-x')^2+(y+c)^2][(x+x')^2+(y+c)^2]}\right\}^{\frac{1}{2}}. \tag{5.55}$$

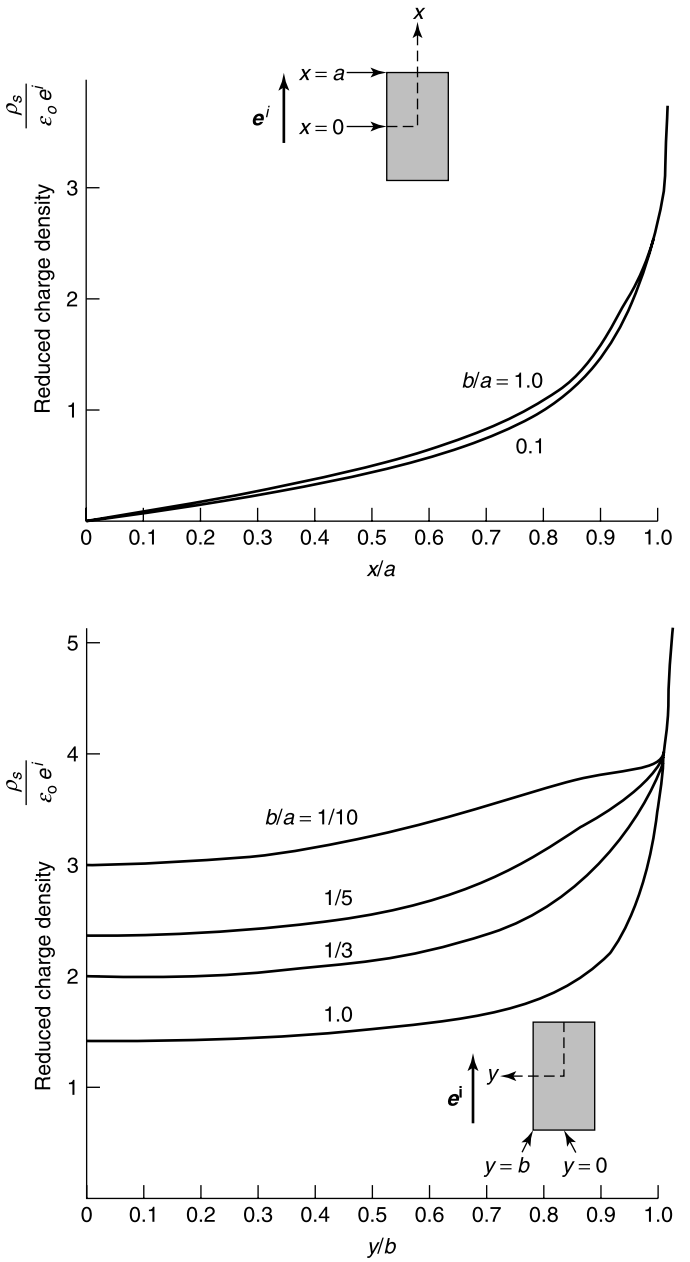

Figure 5.18 Charge density on a rectangular conducting cylinder (*a*) along the side parallel to $\mathbf{e}^i$, (*b*) along the side perpendicular to $\mathbf{e}^i$ (from K. Mei and J. Van Bladel, Low frequency scattering by rectangular cylinders, *IEEE Trans. AP*, **11**, 52–56, 1963, with permission of IEEE).

Using this kernel leads to the integral equation

$$\frac{1}{2\pi\epsilon_0}\int_0^1 \rho_S(x')\, G(x, c|x', c)\, dx' = V.$$

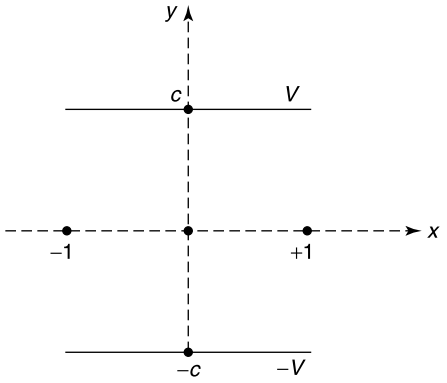

Figure 5.19 Two parallel bands.

From (2.20), this is the Euler equation of the functional

$$J(\rho_S) = \frac{1}{2\pi\epsilon_0}\int_0^1 \rho_S(x)\int_0^1 \rho_S(x')\,G(x,c|x',c)\,dx'dx - 2V\int_0^1 \rho_S(x)\,dx. \tag{5.56}$$

Once $\rho_S(x)$ is known, the capacitance follows from

$$C = \frac{1}{V}\int_0^1 \rho_S(x)\,dx.$$

For a square pattern (i.e., for $c = 1$), C has the known value 18.72 F m^{-1}. This value can serve as a check to verify the accuracy of a numerical solution. To take the edge behavior at $x = \pm 1$ into account, it is useful to use trial functions of the form

$$\rho_S(x) = \frac{a_0}{\sqrt{1-x^2}} + \text{one pulse}$$

or

$$\rho_S(x) = \frac{a_0 + a_1 x}{\sqrt{1-x^2}}.$$

5.6 FINITE METHODS IN TWO DIMENSIONS

In the finite difference solution of Poisson's equation (Fig. 5.20), the basic equation is written in the form (see 1.161)

$$\phi_1 + \phi_2 + \phi_3 + \phi_4 - 4\phi_0 = -h^2\frac{1}{\epsilon_0}\rho(0). \tag{5.57}$$

To illustrate the method, consider a square grounded on three sides. On the fourth side ($y = a$) the potential is given by $\sin\dfrac{\pi x}{a}$. The exact solution is

$$\phi = \frac{\sinh\left(\dfrac{\pi y}{a}\right)}{\sinh\pi}\sin\frac{\pi x}{a}. \tag{5.58}$$

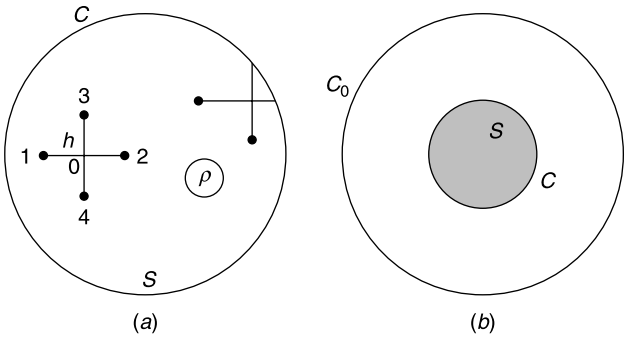

Figure 5.20 (*a*) Two-dimensional interior domain. (*b*) Two-dimensional exterior domain.

We shall use that solution to check the accuracy of the numerical procedure. The net is shown in Figure 5.21. By virtue of the symmetry, only six different values of the potential need be considered. Application of (5.57) at the significant points gives

$$\begin{array}{cccccc|c}
-4\phi_1 & +\phi_2 & +\phi_3 & & & & = -\dfrac{1}{\sqrt{2}} \\
2\phi_1 & -4\phi_2 & & +\phi_4 & & & = -1 \\
\phi_1 & & -4\phi_3 & +\phi_4 & +\phi_5 & & = 0 \\
 & \phi_2 & +2\phi_3 & -4\phi_4 & & +\phi_6 & = 0 \\
 & & \phi_3 & & -4\phi_5 & +\phi_6 & = 0 \\
 & & & \phi_4 & +2\phi_5 & -4\phi_6 & = 0.
\end{array} \tag{5.59}$$

The banded nature of the matrix is already apparent, even with the very rough net used in Figure 5.21. Solution of (5.59) yields approximate values for ϕ_1 to ϕ_6. The values at points 1, 3, and 5, for example, are $\phi_1 = 0.464, \phi_3 = 0.208$, and $\phi_5 = 0.080$. The corresponding exact values, obtained from the solution of the differential equation, are 0.572, 0.225, and 0.085. Better agreement would be obtained with a finer net. Commonly, (5.59) is not solved directly, but the potentials at the net points are determined by iteration. The method consists in choosing initial values, say $\phi_1 = \phi_3 = \phi_5 = 0.70$ and $\phi_2 = \phi_4 = \phi_6 = 1$, for these potentials. Improvement is obtained by replacing these values with new ones by means of the relationship

$$\phi(0) = \frac{\phi_1 + \phi_2 + \phi_3 + \phi_4}{4}, \tag{5.60}$$

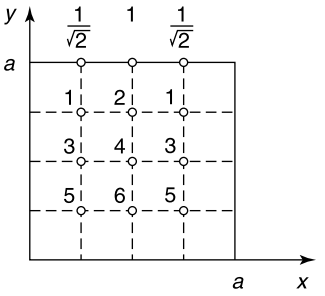

Figure 5.21 Net of points for difference-equation solution.

which holds for a star with equal arms (Fig. 5.20*a*). At point 1, for example, the new value of ϕ is $(0.70 + 1 + 0.70)/4 = 0.6$. The improved value of ϕ_2 is then (1 + 0.6 + 0.6 + 1)/4 = 0.8. The process is repeated until all points of the net have been exhausted. One obtains, successively, $\phi_3 = 0.58, \phi_4 = 0.74, \phi_5 = 0.395, \phi_6 = 0.38$. These results evidence a marked improvement over the initially chosen values. Still better results are obtained by iterating several times around the net. Alternately, updated values can be used immediately, instead of storing them until the scan is completed. It is also possible to overrelax or underrelax according to the prescription

$$\phi_{i,j}^{\text{new}} = \phi_{i,j}^{\text{old}} + \frac{\alpha}{4}\left[\phi_{i-1,j} + \phi_{i+1,j} + \phi_{i,j-1} + \phi_{i,j+1}\right] - \alpha\phi_{i,j}^{\text{old}}. \tag{5.61}$$

Prescription (5.60) corresponds with $\alpha = 1$, while underrelaxation occurs for $0 < \alpha < 1$, and overrelaxation for $\alpha > 1$.

Close to an irregular boundary a full star often steps out of the domain, in which case we may use a discretized Laplacian (Fig. 5.22*a*)

$$\nabla^2\phi = \frac{2}{a^2}\left[\frac{1}{h_1 + h_3}\left(\frac{\phi_1}{h_1} + \frac{\phi_3}{h_3}\right) + \frac{1}{h_2 + h_4}\left(\frac{\phi_2}{h_2} + \frac{\phi_4}{h_4}\right) - \left(\frac{1}{h_1 h_3} + \frac{1}{h_2 h_4}\right)\phi_0\right]. \tag{5.62}$$

In the presence of circular arcs, an expression in polar coordinates is appropriate, viz.

$$\begin{aligned}\nabla^2\phi = {} & \phi_1 \frac{2}{r_0^2\varphi_1(\varphi_1 + \varphi_3)} + \phi_2\left(\frac{2 - h_4(a/r_0)}{a^2 h_2(h_2 + h_4)}\right) + \phi_3\left(\frac{2}{r_0^2\varphi_3(\varphi_1 + \varphi_3)}\right) \\ & + \phi_4 \frac{2 + h_2(a/r_0)}{a^2 h_4(h_2 + h_4)} - \phi_0\left(\frac{2}{a^2 h_2 h_4} + \frac{h_2 - h_4}{a r_0 h_2 h_4} + \frac{2}{r_0^2\varphi_1\varphi_3}\right).\end{aligned} \tag{5.63}$$

When the difference method is applied to an infinite exterior region, as suggested in Figure 5.20*b*, the need arises, for reasons of economy, to truncate the computational domain. This is a major problem, which regularly appears when finite methods, FD or FEM, are resorted to. For our present application, a brute force method consists in setting $\phi = 0$ on a mathematical curve C_0 and applying difference methods between C and C_0. This rough

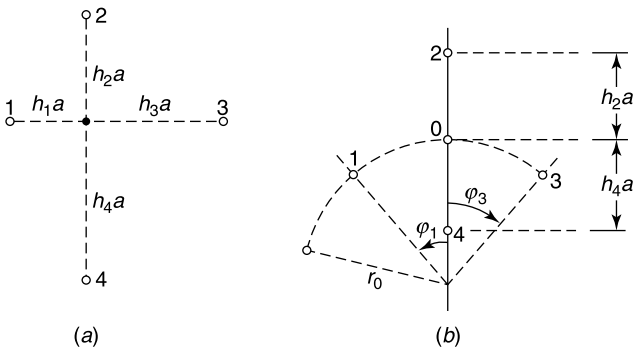

Figure 5.22 (*a*) Four-rayed star with unequal arms. (*b*) Star in cylindrical coordinates.

procedure may be improved by using the already computed values of ϕ at the net points to determine $(\partial\phi/\partial n)$ at the conductor, which leads to an approximate value of ρ_S. New values of ϕ on C can now be computed from those sources. The process is iterated until a stable solution is obtained.[10] It can also be applied to the finite element method.[11] More refined truncation methods are fortunately available, and we shall now discuss three of these.

5.7 INFINITE COMPUTATIONAL DOMAINS

The three methods to be discussed next are quite general. They will be described by means of their application to potential problems, for which the formalism is particularly simple.

5.7.1 The Unimoment Method

Let a two-dimensional obstacle be immersed in an incident potential ϕ^i (Fig. 5.23). The obstacle is assumed uncharged. In Section 3.12, the idea of splitting space into interior and exterior regions with respect to a surface S was discussed in relation with the T-matrix. The same strategy will now be applied to the obstacle problem embodied in Figure 5.23, where we choose the mathematical boundary curve to be a circle, for convenience.[12] The disturbance potential in the region outside C_0 may be written in terms of the multipole expansion (5.7) as

$$\phi^d(\mathbf{r}) = \sum_{m=1}^{N} \frac{1}{r^m}(C_m \sin m\varphi + D_m \cos m\varphi)$$

Term by term differentiation gives

$$\frac{\partial\phi^d}{\partial r}(\mathbf{r}) = -\sum_{m=1}^{N} \frac{m}{r^{m+1}}(C_m \sin m\varphi + D_m \cos m\varphi). \tag{5.64}$$

The term in $\log_e\left(\frac{1}{r}\right)$ is omitted because of the assumed charge neutrality. Corresponding values for ϕ^i and $\frac{\partial\phi^i}{\partial r}$ are similarly written in the form of suitable Fourier expansions. For

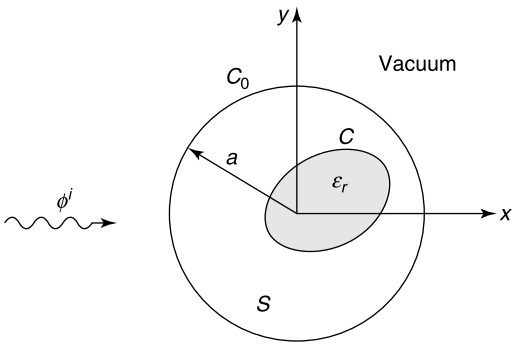

Figure 5.23 Dielectric cylinder in an incident field (from W. R. Smythe, Static and dynamic electricity, 2nd edition. McGraw-Hill, New York).

a uniform incident field $\mathbf{e}^i$ along the x-axis, the expansion boils down to a single term, viz.

$$\begin{aligned} \phi^i(\mathbf{r}) &= -e^i x = -e^i r\cos\varphi \\ \frac{\partial \phi^i}{\partial r}(\mathbf{r}) &= -e^i \cos\varphi. \end{aligned} \tag{5.65}$$

Inside the obstacle, we expand $\phi(\mathbf{r})$ in $2N$ well-chosen functions $\phi_m^-(\mathbf{r})$. Thus,

$$\begin{aligned} \phi^-(\mathbf{r}) &= \sum_{m=1}^{2N} A_m \phi_m^-(\mathbf{r}) \\ \left.\frac{\partial \phi^-(\mathbf{r})}{\partial n}\right|_{r=a} &= \sum_{m=1}^{2N} A_m \left(\frac{\partial \phi_m^-(\mathbf{r})}{\partial n}\right)_{r=a}. \end{aligned} \tag{5.66}$$

The first N functions (with m running from 1 to N) are required to take the value $\cos m\varphi$ on C_0 and the following N functions (with m running from $N+1$ to $2N$) the value $\sin(m-N)\varphi$ on C_0. These $2N$ functions are obtained by solving Dirichlet problems of the kind

$$\begin{aligned} &\operatorname{div}\left[\epsilon_r(\mathbf{r})\operatorname{grad}\phi_m^-\right] = 0 \text{ in } S \\ &\phi_m^- \text{ given} \qquad (\text{on } C_0). \end{aligned} \tag{5.67}$$

The solution can be effected by methods such as finite differences or finite elements. A suitable functional for the latter is

$$J(\phi) = \int_S \epsilon_r(\mathbf{r})|\operatorname{grad}\phi|^2\, dS. \tag{5.68}$$

Once the $2N$ functions ϕ_m^- are determined, the unknown expansion coefficients in (5.64) and (5.66) are found by requiring $(\phi^d + \phi^i)$ and ϕ^- to be continuous on C_0, together with their normal derivatives. We note that the ϕ_m^-'s, once determined, can serve to solve the problem for arbitrary incident potentials ϕ^i.

5.7.2 Asymptotic Boundary Conditions

Setting $\phi = 0$ on C_0 (the brute force approach) is too unsophisticated a way to enforce the large-distance behavior of the disturbance potential. If we switch to three dimensions, the more general case, better accuracy is obtained by remembering that ϕ must approach zero at least as fast as $\left(\frac{1}{R}\right)$. The mathematical boundary becomes a spherical surface S_0 of large radius R. In the absence of sources outside S_0, the following expansion holds in that region:

$$\phi(R,\theta,\varphi) = \frac{1}{R}f_1(\theta,\varphi) + \frac{1}{R^2}f_2(\theta,\varphi) + \frac{1}{R^3}f_3(\theta,\varphi) + \cdots. \tag{5.69}$$

It is useful to form functions that converge faster to zero than ϕ for large R. That goal can be achieved by introducing the operators

$$B_1\phi = \frac{\partial\phi}{\partial R} + \frac{1}{R}\phi = -\frac{1}{R^3}f_2 - \frac{2}{R^4}f_3 + \cdots = O\left(\frac{1}{R^3}\right) \tag{5.70}$$

$$B_2\phi = \frac{\partial}{\partial R}\left(\frac{\partial\phi}{\partial R} + \frac{1}{R}\phi\right) + \frac{3}{R}\left(\frac{\partial\phi}{\partial R} + \frac{1}{R}\phi\right) = \frac{2}{R^5}f_3 + \cdots = O\left(\frac{1}{R^5}\right). \tag{5.71}$$

Further operators, such as $B_3\phi$ or $B_4\phi$, can be similarly generated. To demonstrate the use of a form such as $B_2\phi$, we write Laplace's equation in spherical coordinates by means of (A2.98), extract the value of $\dfrac{\partial^2\phi}{\partial R^2}$ from that relationship, and insert it in (5.71). This simple manipulation yields an interesting value for $\dfrac{\partial\phi}{\partial R}$, viz.

$$\frac{\partial\phi}{\partial R} = -\frac{\phi}{R} + \frac{1}{2R}\left[\frac{\partial^2\phi}{\partial\theta^2} + \frac{1}{\tan\theta}\frac{\partial\phi}{\partial\theta} + \frac{1}{\sin^2\theta}\frac{\partial^2\phi}{\partial\varphi^2}\right] + O\left(\frac{1}{R^4}\right). \tag{5.72}$$

If we start from the value of ϕ on S_0, evaluate the derivatives with respect to θ and φ, and insert these data into (5.72), we obtain a value of $(\partial\phi/\partial R)$, which is correct to $O(1/R^4)$ (i.e., which will become sufficiently accurate at relatively short distances R). Using this value of $(\partial\phi/\partial R)$ as a boundary condition allows S_0 to be brought much closer to sources and obstacles than would be the case with a brute force condition such as $\phi = 0$ on S_0.

The spherical boundary surface is theoretically convenient. In practice, however, the need to limit the number of unknowns requires S_0 to "hug" the domain containing sources and materials more closely, and a box-like surface of the kind shown in Figure 5.24 may be more appropriate. The normal derivatives are now with respect to x, y or z, but they can easily be expressed in terms of their (R, θ, φ) counterparts.[13,14]

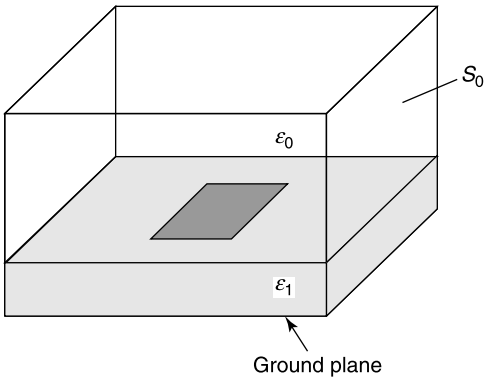

Figure 5.24 A microstrip surrounded by a box (from A. Khebir, A. B. Kouki and R. Mittra, Asymptotic boundaries conditions for finite element analysis of three-dimensional transmission line discontinuities, *IEEE Trans. MTT* **38**, 1427–1432, 1990, with permission of IEEE).

5.7.3 The Generalized Multipole Technique

Consider, as in Section 5.5, an arbitrary conductor in an incident electric field $\mathbf{e}^i$ (Fig. 5.16). The conductor is uncharged, hence the potential generated externally by the induced charges on C is harmonic and bounded at infinity. This potential may therefore be synthesized, approximately at least, by the cumulative contributions of a number of sources located inside the cylinder and so chosen that the boundary conditions on C are satisfied. The sources can be linear charges, dipoles, or higher multipoles. The various contributions have the advantage of not being singular on C. The exterior potential will now be written as a sum of partial (multipole) potentials ϕ_m. Thus,

$$\phi(\mathbf{r}) = \sum_{m=1}^{N} a_m \phi_m(\mathbf{r}). \tag{5.73}$$

For $\mathbf{r}$ on C, the boundary conditions are

$$\sum_{m=1}^{N} a_m \phi_m(\mathbf{r}) + \phi^i(\mathbf{r}) = \text{constant}$$

$$\sum_{m=1}^{N} a_m \frac{\partial \phi_m}{\partial n}(\mathbf{r}) = 0 \qquad \text{(charge neutrality)}. \tag{5.74}$$

These conditions can serve to determine the unknown a_m coefficients. In practice, the choice of matching points on S, or of distances between fictive sources, is not trivial, because the matrix can easily become ill-conditioned [187]. It is therefore often advisable to use more matching points than unknown coefficients, a strategy that generates an overdetermined system of equations (Problem 5.15). In the presence of geometrical singularities at the boundary, such as corners (Fig. 5.25), increased accuracy can be obtained by using elements located *on* the boundary[15] (e.g., pulse functions spread over an interval Δc_k). The potential is now

$$\phi(\mathbf{r}) = \underbrace{\sum_{m} a_m \phi_m(\mathbf{r})}_{\text{multipoles}} + \underbrace{\sum_{k} \rho_{Sk} \psi_k(\mathbf{r})}_{\text{boundary elements}} + \phi^i(\mathbf{r}) \tag{5.75}$$

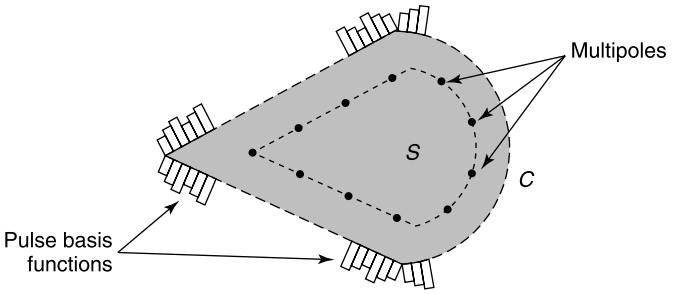

Figure 5.25 Multipoles augmented by boundary elements (from J. L. Rodriguez, F. Obelleiro, and A. G. Pino, A hybrid multipolar-expansion-moment-method approach for electromagnetic scattering problems, *Microwave Opt. Tech. Lett.* **11**, 304–308, 1996, with permission of John Wiley & Sons).

where, for pulse functions,

$$\psi_k(\mathbf{r}) = \frac{1}{2\pi\epsilon_0}\int_{\Delta c_k} \log_e \frac{L}{|\mathbf{r}-\mathbf{r}'|}\, dc'.$$

The variable parameters are a_m and ρ_{Sk}.

5.8 MORE TWO-DIMENSIONAL TECHNIQUES

Expansions in eigenfunctions play an important role in mathematical physics (see Sections 1.8 and 1.10). To illustrate their application to electrostatics, we shall evaluate the fields generated in a metal tube by the action of volume and surface sources.

5.8.1 Eigenfunction Expansions

The two-dimensional eigenfunctions of concern in Figure 5.26 are the *Dirichlet eigenfunctions* defined in (4.40). Because the eigenvalues λ_{mn} are negative, we may rewrite the basic equations in the form

$$\begin{aligned} \nabla_{xy}^2\phi_{mp} + \mu_{mp}^2\phi_{mp} &= 0 \qquad (\text{in } S) \\ \phi_{mp} &= 0 \qquad (\text{on } C) \\ \int_S |\text{grad } \phi_{mp}|^2\, dS &= \mu_{mp}^2 \int_S \phi_{mp}^2\, dS = 1. \end{aligned} \tag{5.76}$$

The last equation is a normalization condition, which makes ϕ_{mp} dimensionless. The area S is the cross section of the hollow cylinder, which itself is connected with the exterior region through an aperture A. The sources are the volume sources $\rho(\mathbf{r})$ and the potential in A. We expand ϕ in the (complete) normalized set ϕ_{mp}. Thus,

$$\phi(x,y,z) = \sum_m \sum_p f_{mp}(z)\phi_{mp}(x,y).$$

Separate expansions are needed for the various terms in Poisson's equation, in harmony with the *derivative of a sum* technique discussed in Section 1.7. We write

$$\rho(x,y,z) = \sum_m \sum_p g_{mp}(z)\phi_{mp}(x,y)$$

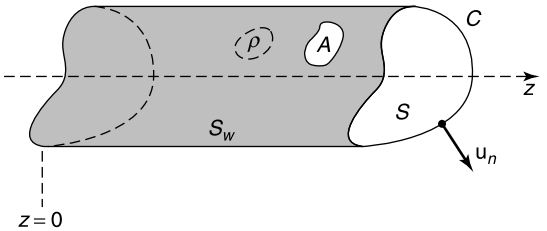

Figure 5.26 Cylindrical volume and its volume and surface sources.

$$\nabla^2\phi(x,y,z) = \sum_m \sum_p h_{mp}(z)\phi_{mp}(x,y),$$

where

$$g_{mp}(z) = \mu_{mp}^2 \int_S \rho(x,y,z)\phi_{mp}(x,y)\, dS.$$

The relationship between f_{mp} and h_{mp} can be established by the following calculation:

$$\begin{aligned} h_{mp}(z) &= \mu_{mp}^2 \int_S \nabla^2\phi(x,y,z)\phi_{mp}(x,y)\, dx\, dy \\ &= \mu_{mp}^2 \int_S \phi_{mp} \frac{\partial^2\phi}{\partial z^2}\, dS + \mu_{mp}^2 \int_S \phi_{mp}\nabla_{xy}^2\phi\, dS. \end{aligned}$$

The first term on the right-hand side is d^2f_{mp}/dz^2. The second term can be transformed by using Green's theorem in the plane. Thus,

$$\begin{aligned} \int_S \phi_{mp}\nabla_{xy}^2\phi\, dS &= \int_S \phi\nabla_{xy}^2\phi_{mp} dS + \int_C \left(\phi_{mp}\frac{\partial\phi}{\partial n} - \phi\frac{\partial\phi_{mp}}{\partial n}\right) dc \\ &= -\mu_{mp}^2 f_{mp}(z) - \int_C \phi(c,z)\frac{\partial\phi_{mp}}{\partial n}\, dc. \end{aligned}$$

where c is a coordinate along contour C. Insertion of the expansion into Poisson's equation gives $h_{mp} = -(1/\epsilon_0)\, g_{mp}$. Hence,

$$\frac{d^2f_{mp}}{dz^2} - \mu_{mp}^2 f_{mp} = \mu_{mp}^2 \int_C \phi(c,z)\frac{\partial\phi_{mp}}{\partial n}\, dc - \frac{\mu_{mp}^2}{\epsilon_0}\int_S \rho(x,y,z)\phi_{mp}\, dS. \tag{5.77}$$

Clearly, the amplitude f_{mp} of the term in ϕ_{mp} depends on the *coupling* of the boundary potential $\phi(c,z)$ to $\partial\phi_{mp}/\partial n$, and of the volume excitation $\rho(\mathbf{r})$ to $\phi_{mp}(\mathbf{r})$.

The final solution of the problem is now reduced to the solution of a doubly infinite set of *ordinary* differential equations of type (5.77). To illustrate the solution, consider the accelerator tube shown in Figure 5.27*a*. The normalized eigenfunctions for the rectangular cross section are

$$\phi_{mp} = A_{mp} \sin\frac{m\pi x}{a} \sin\frac{p\pi y}{b} \tag{5.78}$$

with

$$A_{mp}^2 = \frac{2}{\pi^2}\frac{ab}{m^2b^2 + p^2a^2}$$

and

$$\mu_{mp}^2 = \left(\frac{m\pi}{a}\right)^2 + \left(\frac{p\pi}{b}\right)^2. \tag{5.79}$$

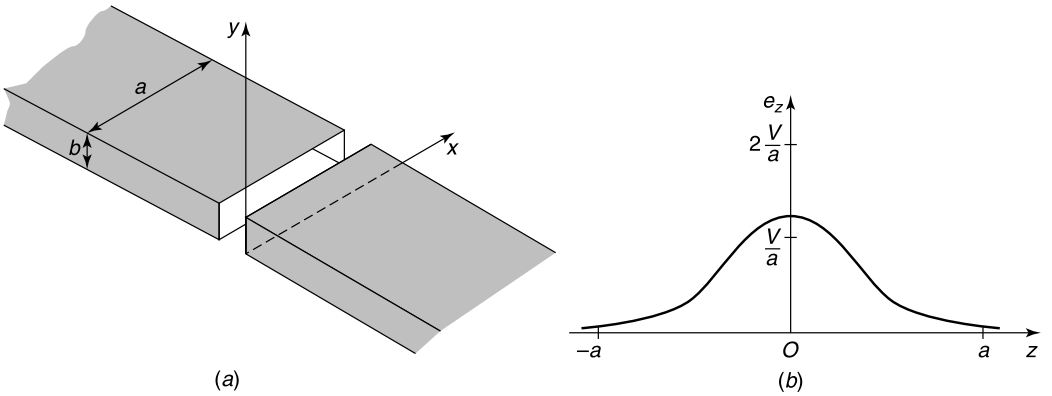

Figure 5.27 (*a*) Rectangular duct with gap. (*b*) Electric field at $x = a/2$, $y = b/2$ (from J. Van Bladel, Fields in gap-excited rectangular ducts, *J. Appl. Phys.* **28**, 1479–1483, with permission of the American Institute of Physics).

A voltage V is applied between the two conducting halves, which are separated by a narrow gap. The boundary values are therefore

$$\phi(c, z) = -\frac{V}{2} + V\,H(z)$$

where $H(z)$ is the *Heaviside unit step function*, equal to zero for $z < 0$ and to one for $z > 0$. Simple calculation shows that the right-hand term of (5.77) vanishes unless both m and p are odd. Repeated solution of (5.77) leads to the final result

$$\phi(x, y, z) = \frac{8}{\pi^2} V \sum_{\text{odd } m} \sum_{\text{odd } p} \frac{1 - \exp\{-z[(m\pi/a)^2 + (p\pi/b)^2]^{\frac{1}{2}}\}}{mp} \times \sin\frac{m\pi x}{a} \sin\frac{p\pi y}{b}. \tag{5.80}$$

The electric field can be obtained by differentiation of ϕ. Illustratively, Figure 5.27*b* shows the variation of e_z along the axis of a square duct. The curve gives an idea of the depth of penetration of the field on both sides of the gap.

5.8.2 Monte Carlo Methods

There are two types of Monte Carlo methods. The first one makes use of random numbers, obtained by pseudo-random generation subroutines. An example is the *fixed random walk method*, which we illustrate by determining a potential ϕ that satisfies Laplace's equation in the rectangle and takes constant values $\phi_1, \phi_2, \phi_3, \phi_4$ on the respective sides 1, 2, 3, 4 (Fig. 5.28). We start from P and proceed to walk from node to node until a boundary is reached. The direction of motion (up, down, left, right) is determined randomly (e.g., by throwing dice). The process is repeated N times. If side 1 has been hit n_1 times, side 2

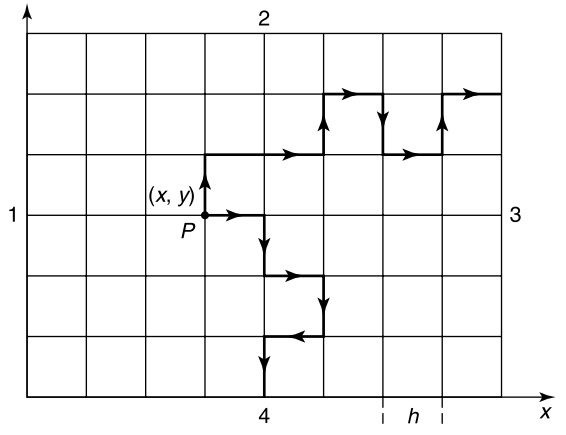

Figure 5.28 Fixed random walk.

correspondingly n_2 times, and so forth, the potential in P is given by the limit

$$\lim_{N\to\infty} \phi(P) = \frac{1}{n_1 + n_2 + n_3 + n_4}(n_1\phi_1 + n_2\phi_2 + n_3\phi_3 + n_4\phi_4), \tag{5.81}$$

where $n_1 + n_2 + n_3 + n_4 = N$. The method is quite simple, because only the current point on the walk must be stored in the computer memory. The rate of convergence is unfortunately proportional to $\sqrt{N}$, hence many random walks are nessessary to obtain reasonable accuracy. The method can also be applied to Poisson's equation and extended to three dimensions.

In the presence of irregular boundaries, or when Neumann boundary conditions are imposed, the *fixed random walk* with fixed h and fixed directions of motion is advantageously replaced by a *floating random walk* procedure. In short, the method consists in moving from a last node i to a circle of radius a_i centered on i, where a_i is the shortest distance between i and the boundary. The radial direction of motion is generated randomly over the interval $(0, 2\pi)$. The process is repeated until the "particle" comes within a prescribed small distance from the boundary. Fewer steps are needed than in the fixed walk version, a feature that reduces computer time.

Random walk procedures give only the value of ϕ at one node and must therefore be repeated many times. This is not so in the *Exodus* method, in which numerous particles (say 10^6) are simultaneously launched in different directions, controlled by probability techniques. No random number generator is needed.[16,17] Potential $\phi(P)$ is still given by (5.81), but n_i is now the number of particles that have reached side i.

5.8.3 Two-Dimensional Images

Assume that a linear charge ρ_l is located in A (Fig. 5.29). The images with respect to a uniform dielectric half-space are as follows:

1. In region 1, an image source in B, of strength

$$\rho_l' = -\rho_L \frac{\epsilon_r - 1}{\epsilon_r + 1}, \tag{5.82}$$

to which should be added the contribution form ρ_l.

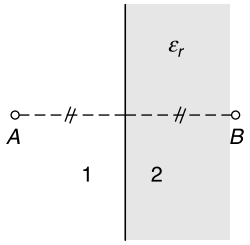

Figure 5.29 Linear charge and its image point.

2. In region 2 (the dielectric), an image source in A, of strength

$$\rho_l'' = \rho_l \frac{2\epsilon_r}{\epsilon_r + 1}. \tag{5.83}$$

This source is assumed immersed in a space totally filled with the dielectric material.

Images can also be found for a line charge located outside a circular cylinder [17], layered (coaxial) structures, and biisotropic cylinders.[18] Also available is the potential generated by a linear source outside a dielectric wedge.[19] The solution is in the form of either a modal series or a series of image sources.[20] An image solution is also available for multilayered bianisotropic media.[21]

5.9 LAYERED MEDIA

Mass production of telecommunication networks has led to the development of structures wherein conductors are sandwiched between layers of dielectric materials. Figure 5.30 shows some examples of such structures, of progressive complexity. They are extensively used as waveguides and are further discussed in Chapters 9 and 15. The density of conductors is such that problems of crosstalk become prominent. At sufficiently low frequencies, the capacities between the conductors play an important role there, and it is to the determination of these static parameters that the current section is devoted.

5.9.1 Transform Methods

In the examples of Figure 5.30, the potentials depend on two coordinates, x and y. Because the boundary lines are parallel to the x-axis, the x-dependence may be erased by means of a spatial Fourier transformation with respect to x. This transform method has found numerous applications in practice,[22] and we shall discuss its main features by analyzing the simple example of the microstrip depicted in Figure 5.30a, where the conducting band is assumed infinitely thin ($t = 0$).

Let the $y = h$ plane be covered with a surface charge density $\rho_S(x)$. The Fourier transform of the latter is[23]

$$P_S(\beta) = \int_{-\infty}^{\infty} \rho_S(x) e^{-j\beta x} dx. \tag{5.84}$$

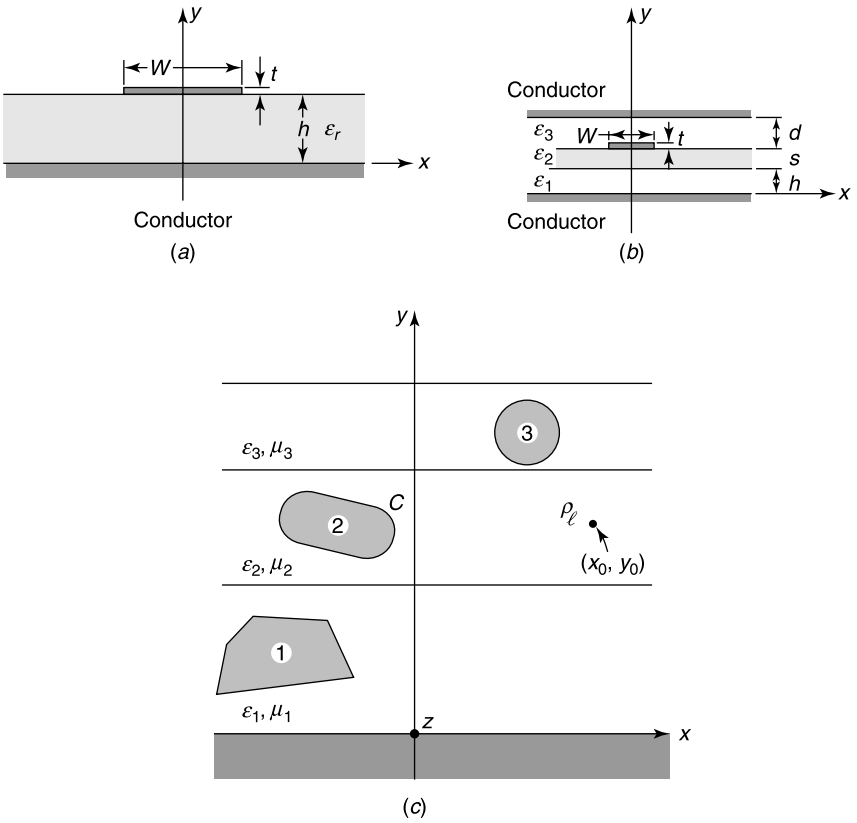

Figure 5.30 Transmission lines and layered media (from E. Yamashita and R. Mittra, Variational methods for the analysis of microstrip lines, *IEEE Trans. MTT* **16**, 251–256, 1968, with permission of IEEE).

The potential $\phi(x, y)$ is likewise transformed into $\Phi(\beta, y)$, where Φ satisfies, after transformation of Laplace's equation,

$$\left(\frac{d^2}{dy^2} - \beta^2\right) \Phi(\beta, y) = 0.$$

Because Φ must vanish for $y = 0$ and remain bounded for $y \to \infty$, the solution must be of the form

$$\begin{aligned} \Phi(\beta, y) &= A\, e^{-|\beta| y} \qquad \text{for } h < y < \infty \\ &= B \sinh \beta y \qquad \text{for } 0 < y < h. \end{aligned} \tag{5.85}$$

The A and B coefficients follow from the boundary conditions at $y = h$, which require Φ to be continuous, and the electric flux density $D(\beta, y)$ to suffer a jump equal to $P_S(\beta)$. The final result is

$$\Phi(\beta, h) = \frac{P_S(\beta)}{\epsilon_0 |\beta| (1 + \epsilon_r \coth |\beta| h)}. \tag{5.86}$$

The actual x-dependence may now be determined by an inverse Fourier transformation. In most applications this is a difficult task, but in the current case it is lightened by noticing

that the correct $\rho_S(x)$ minimizes the electrostatic energy. In consequence, a lower bound for the capacitance may be obtained by relying on the inequality

$$\frac{\rho_l^2}{\displaystyle\int_{-w/2}^{w/2} \rho_S(x)\phi(x,h)\,dx} \leq C \qquad (\mathrm{F\,m^{-1}}), \tag{5.87}$$

where

$$\rho_l = \int_{-w/2}^{w/2} \rho_S\,dx \qquad (\mathrm{C\,m^{-1}})$$

is the linear charge density on the band. The inequality (5.87) can be transferred to "β space" by means of *Parseval's theorem* (A7.33), which takes the following form for $\omega = 0$:

$$\int_{-\infty}^{\infty} f(x)g(x)\,dx = \frac{1}{2\pi}\int_{-\infty}^{\infty} F(-\beta)G(\beta)\,d\beta. \tag{5.88}$$

Because P_S and Φ are symmetric in β, there follows the relationship

$$\frac{1}{\pi\epsilon_0 q^2}\int_0^{\infty} \frac{|P_S(\beta)|^2}{[1+\epsilon_r \coth(\beta h)]\,\beta h}\,d(\beta h) \geq \frac{1}{C}. \tag{5.89}$$

Lower bounds for C, obtained from (5.89) with a trial function $\rho_S(x) = A|x|$ on the conductor and zero elsewhere, are shown in Figure 5.31. The Fourier transform of the chosen trial function is

$$P_S(\beta) = \left\{\frac{\sin 2\nu}{\nu} - \left[\frac{\sin\nu}{\nu}\right]^2\right\}\rho_l, \tag{5.90}$$

where $\nu = \dfrac{\beta w}{4}$.

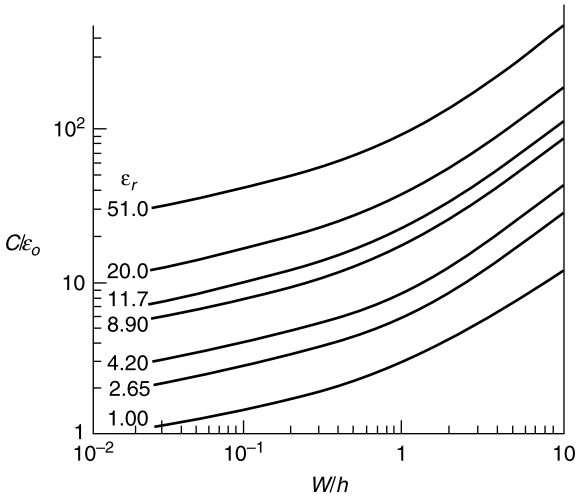

Figure 5.31 Line capacitance versus the ratio strip width/strip height (from E. Yamashita and R. Mittra, Variational methods for the analysis of microstrip lines, *IEEE Trans. MTT* **16**, 251–256, 1968, with permission of IEEE).

5.9.2 Integral Equations

In Figure 5.30*c*, the charge densities on the various conductors satisfy integral equations of the form

$$\int_C \rho_S(\mathbf{r}')G(\mathbf{r}|\mathbf{r}')\,dl' = V. \tag{5.91}$$

The main problem is to determine the Green's function. Spectral methods can give the answer. We outline the steps. Assume that a linear charge of density ρ_l (the unit source) is located at (x_0, y_0). The transform of the corresponding *charge density* ρ_s is

$$P_S(\beta) = \rho_l\, e^{-j\beta x_0}.$$

The transform of the *potential* generated by this charge density may be determined by the method discussed above, suitably extended to several dielectric layers. The potential, written as $\Phi(\beta, y, x_0, y_0)$, is the transform of the sought Green's function. It must be inverted, for example, by approximating $\Phi(\beta, y, x_0, y_0)$ by means of exponential functions.[24] The sought inversion, viz.

$$G(x, y, x_0, y_0) = \frac{1}{2\pi}\int_{-\infty}^{\infty} G(\beta, y, x_0, y_0)e^{j\beta x}d\beta,$$

may also be performed[25] by exploiting the asymptotic form of the transform for high values of $|\beta|$.

The Green's function in (5.91) may sometimes be derived by the method of images. In the presence of a ground plane, as in Figure 5.30*a*, an infinite number of images is needed.[26] In the $x = h$ plane, where the strip is located,

$$G(x, x_0) = \frac{1}{2\pi\epsilon_0(1+\epsilon_r)}\sum_{n=1}^{\infty}\left(\frac{1-\epsilon_r}{1+\epsilon_r}\right)^{n-1}\log_e\frac{4n^2+\left(\dfrac{x+x_0}{h}\right)^2}{4(n-1)^2+\left(\dfrac{x-x_0}{h}\right)^2}. \tag{5.92}$$

Both x and x_0 are *on the strip*.

An alternate integral equation can be formulated on the basis of the free space Green's function G_0. The Green's function is the kernel, and the unknowns are the real charge densities on the conductor-dielectric interfaces, together with the polarization charge densities on the dielectric-dielectric interfaces.[27]

5.10 APERTURES

Apertures are frequently found in metallic structures. Their presence is either planned (a window in a microwave oven) or accidental and undesirable (a crack in a Faraday cage, through which fields may penetrate). In Figure 5.32, the conducting plane S is provided with an aperture A. Sources are located in region 1, and fields penetrate into region 2 through the aperture. The media in regions 1 and 2 are assumed homogeneous. On the S plane the potential ϕ vanishes, except in the aperture A. To evaluate the potential in 2, we shall use

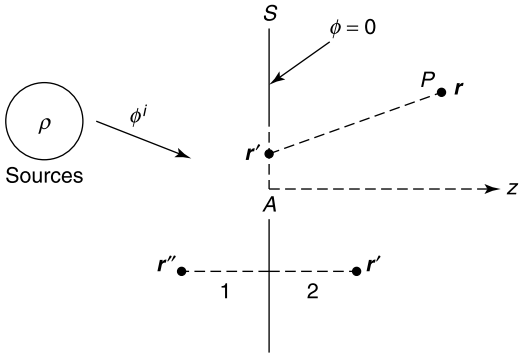

Figure 5.32 Conducting plane with an aperture.

the Dirichlet Green's function relative to the boundary condition $G = 0$ for $\mathbf{r}$ on S. The solution is given by the image method. Thus,

$$G(\mathbf{r}|\mathbf{r}') = -\frac{1}{4\pi|\mathbf{r}-\mathbf{r}'|} + \frac{1}{4\pi|\mathbf{r}-\mathbf{r}''|}, \tag{5.93}$$

where $\mathbf{r}''$ is the image of $\mathbf{r}'$. Applying Green's theorem A1.31 to region 2 gives

$$\int_{z>0} \left[\phi(\mathbf{r}')\nabla^2 G(\mathbf{r}|\mathbf{r}') - G(\mathbf{r}|\mathbf{r}')\nabla^2\phi(\mathbf{r}')\right] dV'$$
$$= \int_{S+S_\infty} \left[\phi(\mathbf{r}')\frac{\partial G(\mathbf{r}|\mathbf{r}')}{\partial n'} - G(\mathbf{r}|\mathbf{r}')\frac{\partial\phi}{\partial n'}\right] dS',$$

where n is the outer normal to S ($-\mathbf{u}_z$ in the current case) and S_∞ is a half-spherical surface of very large radius. The functions G and ϕ must be regular on S_∞. Because

$$\nabla^2\phi = 0 \quad (\text{in } z)$$
$$\frac{\partial}{\partial z'}\left(\frac{1}{|\mathbf{r}-\mathbf{r}'|}\right) = -\frac{\partial}{\partial z'}\left(\frac{1}{|\mathbf{r}-\mathbf{r}''|}\right) \qquad (\mathbf{r}' \text{ on } S)$$

the theorem gives

$$\phi_2(\mathbf{r}) = \frac{1}{2\pi}\int_A \phi(\mathbf{r}')\frac{\partial}{\partial z'}\left(\frac{1}{|\mathbf{r}-\mathbf{r}'|}\right) dS' \qquad (\mathbf{r}' \text{ in } S). \tag{5.94}$$

Similarly, when $\mathbf{r}$ is located in region 1,

$$\phi_1(\mathbf{r}) = \phi^g(\mathbf{r}) - \frac{1}{2\pi}\int_A \phi(\mathbf{r}')\frac{\partial}{\partial z'}\left(\frac{1}{|\mathbf{r}-\mathbf{r}'|}\right) dS', \tag{5.95}$$

where ϕ^g is the *generator* or *short-circuit potential* (i.e., the potential in the absence of an aperture). Comparison with (3.58) shows that ϕ_2 has the nature of a dipole-layer potential. It further follows from (5.94) and (5.95) that the contribution of the aperture to the potential is *symmetric* with respect to S. The z-components of the electric field $\mathbf{e}^a$ stemming from the aperture are therefore *antisymmetric*, as sketched in Figure 5.33*a*. The remark is of

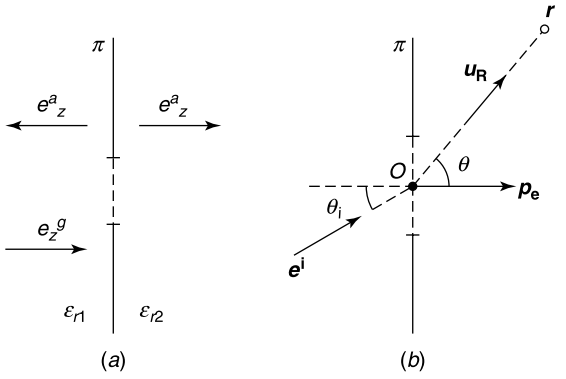

Figure 5.33 (*a*) z-Directed electric fields. (*b*) Uniform incident field and resulting dipole moment.

importance for the derivation of the integro-differential equation satisfied by ϕ in A, which is obtained by requiring the normal component of $\mathbf{d}$ to be continuous on both sides of A. Thus,

$$\epsilon_{r1}\left(e_z^g + e_{z1}^a\right) = \epsilon_{r2}\, e_{z2}^a. \tag{5.96}$$

For $\mathbf{r}$ in the aperture, this condition gives

$$\frac{\partial \phi_2}{\partial z} = \frac{\partial}{\partial z}\left[\frac{1}{2\pi}\int_A \phi(\mathbf{r}')\frac{\partial}{\partial z'}\left(\frac{1}{|\mathbf{r}-\mathbf{r}'|}\right)dS'\right] = \frac{\epsilon_{r1}}{\epsilon_{r1}+\epsilon_{r2}}\left(\frac{\partial \phi^g}{\partial z}\right). \tag{5.97}$$

To solve for ϕ, $\dfrac{\partial}{\partial z}$ may be brought behind the integral sign, but at the cost of introducing a strong singularity, of the order $|\mathbf{r}-\mathbf{r}'|^{-3}$. Such singularities must be handled with care,[28] as shown in Section 3.9. Alternately, the derivative can be pulled outside (5.97) to yield

$$\frac{\partial^2}{\partial z^2}\left[\frac{1}{2\pi}\int_A \frac{\phi(\mathbf{r}')}{|\mathbf{r}-\mathbf{r}'|}\,dS'\right] = \frac{\epsilon_{r1}}{\epsilon_{r1}+\epsilon_{r2}}\, e_z^g(\mathbf{r}). \tag{5.98}$$

The term between brackets is a (continuous) single-layer potential, which satisfies Laplace's equation. Therefore, for $\mathbf{r}$ in S,

$$\nabla_{xy}^2\left[\frac{1}{2\pi}\int_A \frac{\phi(\mathbf{r}')}{|\mathbf{r}-\mathbf{r}'|}dS'\right] = -\frac{\epsilon_{r1}}{\epsilon_{r1}+\epsilon_{r2}}\, e_z^g(\mathbf{r}'). \tag{5.99}$$

This equation may now be solved by the usual discretization methods.

In many applications, the incident field is uniform. For such a case (Fig. 5.33*b*)

$$e_z^g = 2e_z^i = 2\mathbf{u}_z\cdot\mathbf{e}^i = 2e^i\cos\theta_i.$$

Whenever e_z^g may be assumed constant in the aperture, the solution is proportional to a key dimensionless function τ_0 that satisfies

$$\nabla_{xy}^2\left[\frac{1}{2\pi}\int_A \frac{\tau_0(\mathbf{r}')}{|\mathbf{r}-\mathbf{r}'|}\,dS'\right] = -\frac{1}{\sqrt{S_a}}, \tag{5.100}$$

where S_a is the area of the aperture. The potential may now be written as

$$\phi(\mathbf{r}') = \frac{2\epsilon_1}{\epsilon_1 + \epsilon_2}\sqrt{S_a}\,\tau_0(\mathbf{u}_z \cdot \mathbf{e}^i) \qquad (\mathbf{r} \text{ in } A). \tag{5.101}$$

From (5.94), the potential in region 2, at distances large with respect to the dimensions of the aperture, has the asymptotic value

$$\phi_2(\mathbf{r}) = \frac{1}{2\pi}\int_A \phi(\mathbf{r}')\frac{\mathbf{u}_z \cdot \mathbf{u}_R}{|\mathbf{r} - \mathbf{r}'|^2}\,dS' = \frac{1}{2\pi}\frac{1}{R^2}\,\mathbf{u}_R \cdot \int_A \mathbf{u}_z \phi(\mathbf{r}')\,dS'. \tag{5.102}$$

Comparison with (3.29) shows that $\phi_2(\mathbf{r})$ has the form of a dipole potential of moment

$$\mathbf{p}_{e2} = 2\epsilon_2 \int_A \phi\, dS\, \mathbf{u}_z. \tag{5.103}$$

The dipole is assumed located in 0, in an infinite medium of dielectric constant ϵ_{r2}. It could be replaced, on the basis of images, by a dipole of moment $\frac{1}{2}\mathbf{p}_{e2}$, located in front of a *metallized* aperture A (i.e., of a plane S without aperture). Inserting the value (5.101) of $\phi(\mathbf{r})$ into (5.103) gives

$$\mathbf{p}_{e2} = \frac{2\epsilon_2}{\epsilon_1 + \epsilon_2}\, S_a^{3/2}\,(\tau_0)_{\text{ave}}(\epsilon_1 \mathbf{E}_1^g - \epsilon_2 \mathbf{E}_2^g) \qquad (\text{C m}) \tag{5.104}$$

where the subscript *ave* denotes an average over the aperture, and $\mathbf{E}_2^g$ is present when there are sources in region 2 (note that both short-circuit fields $\mathbf{E}_1^g$ and $\mathbf{E}_2^g$ are perpendicular to the screen). It is convenient to rewrite (5.104) as

$$\mathbf{p}_{e2} = \frac{2\epsilon_2}{\epsilon_1 + \epsilon_2}\,\overline{\overline{\alpha}}_e \cdot (\epsilon_1 \mathbf{E}_1^g - \epsilon_2 \mathbf{E}_2^g) \tag{5.105}$$

where $\overline{\overline{\alpha}}_e$ is the *polarizability dyadic of the aperture*, given by

$$\begin{aligned} \overline{\overline{\alpha}}_e &= (\tau_0)_{\text{ave}}\, S_a^{3/2}\, \mathbf{u}_z \mathbf{u}_z \qquad (\text{m}^3) \\ &= S_a^{3/2}\,\overline{\overline{\nu}}_e. \end{aligned} \tag{5.106}$$

The dyadic $\overline{\overline{\nu}}_e$ is a dimensionless shape factor. If we choose the *metallized aperture* convention, the relevant dipole moment becomes

$$\frac{1}{2}\mathbf{p}_{e2} = \frac{\epsilon_2}{\epsilon_1 + \epsilon_2}\,\overline{\overline{\alpha}}_e \cdot (\epsilon_1 \mathbf{E}_1^g - \epsilon_2 \mathbf{E}_2^g). \tag{5.107}$$

For a circular aperture of radius a, the main data are

$$\begin{aligned} \tau_0 &= \frac{2}{\pi\sqrt{\pi}}\sqrt{1 - \frac{r^2}{a^2}} \\ (\tau_0)_{\text{ave}} &= \frac{4}{3\pi\sqrt{\pi}} = 0.24 \\ \alpha_e &= \frac{4a^3}{3}. \end{aligned} \tag{5.108}$$

Results are available for some other shapes: *analytically* for the ellipse, and *numerically*[29] for the rectangle, the diamond, the cross, and the rounded-off rectangle.

5.11 AXISYMMETRIC GEOMETRIES

To exploit the particular symmetry associated with volumes of revolution, it is natural to use Fourier expansions of the kind (Fig. 5.34)

$$\phi(r,z,\varphi) = \sum_{m=0}^{\infty} [a_m(r,z)\cos m\varphi + b_m(r,z)\sin m\varphi]. \tag{5.109}$$

From A2.64,

$$\nabla^2\phi = \sum_{m=0}^{\infty} \left[\left(\nabla_M^2 - \frac{m^2}{r^2} \right) a_m(r,z)\cos m\varphi + \left(\nabla_M^2 - \frac{m^2}{r^2} \right) b_m(r,z)\sin m\varphi \right] \tag{5.110}$$

where, for conciseness, we have written

$$\nabla_M^2 f(r,z) = \frac{1}{r}\frac{\partial}{\partial r}\left(r\frac{\partial f}{\partial r} \right) + \frac{\partial^2 f}{\partial z^2}.$$

The reader will find, in Appendix 3, more details about operators in the (r,z) meridian plane, as well as relationships valid on a surface of revolution. When ϕ is harmonic, separation of variables gives the following double sum as a possible solution of Laplace's equation:

$$\phi(r,z,\varphi) = \sum_{m,n=0}^{\infty} [a_{mn}J_m(\lambda_{mn}\, r) + b_{mn}N_m(\lambda_{mn}\, r)] \tag{5.111}$$
$$[c_{mn}\sinh\lambda_{mn}\, z + d_{mn}\cosh\lambda_{mn}\, z]\cdot[e_{mn}\cos m\varphi + f_{mn}\sin m\varphi].$$

The coefficients a_{mn} to f_{mn}, together with λ_{mn}, are unspecified, and must be so chosen that the various boundary conditions are satisfied. Another useful expansion, also obtained by separation of variables, is

$$\phi(r,z,\varphi) = \sum_{m,n=0}^{\infty} [a_{mn}I_m(\lambda_{mn}\, r) + b_{mn}K_m(\lambda_{mn}\, r)] \tag{5.112}$$
$$[c_{mn}\sin\lambda_{mn}\, z + d_{mn}\cos\lambda_{mn}\, z]\cdot[e_{mn}\cos m\varphi + f_{mn}\sin m\varphi].$$

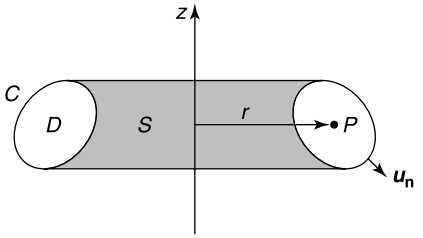

Figure 5.34 Volume of revolution.

The symbols I_m and K_m denote the modified Bessel and Neumann functions, some properties of which can be found in Appendix 5.

When sources and fields are independent of φ, the sums simplify to

$$\phi(r,z) = \sum_{n=0}^{\infty} [a_n J_0(\lambda_n r) + b_n N_0(\lambda_n r)][c_n \sinh(\lambda_n z) + d_n \cosh(\lambda_n z)] \tag{5.113}$$

and

$$\phi(r,z) = \sum_{n=0}^{\infty} [a_n I_0(\lambda_n r) + b_n K_0(\lambda_n r)][c_n \sin \lambda_n z + d_n \cos \lambda_n z]. \tag{5.114}$$

As an application, consider the potential in a grounded metallic tank partially filled with a liquid carrying a uniform electric charge density ρ (Fig. 5.35). In expansion (5.113), the term in N_0 must be dropped because N_0 becomes infinite on the axis. Because ϕ must vanish for $r = a$, we write the term in r as $J_0\left(\lambda_n \frac{r}{a}\right)$, where $J_0(\lambda_n) = 0$. The $J_0\left(\lambda_n \frac{r}{a}\right)$ family forms a complete orthogonal set in the interval $(0, a)$. Because ϕ vanishes for $z = h$, and is harmonic in the gas region, we write

$$\phi_2(r,z) = \sum_n A_n J_0\left(\lambda_n \frac{r}{a}\right) \sinh\left[\frac{\lambda_n}{a}(h-z)\right]. \tag{5.115}$$

In the liquid, in region 1, we expand the potential as

$$\phi_1(r,z) = \sum_n J_0\left(\lambda_n \frac{r}{a}\right) f_n(z), \tag{5.116}$$

where f_n must be determined. On the basis of (A5.32) and (A5.53), the expansion for a uniform ρ equal to ρ_0 is

$$\rho(r,z) = \rho_0 \sum_n \frac{2}{\lambda_n J_1(\lambda_n)} J_0\left(\lambda_n \frac{r}{a}\right). \tag{5.117}$$

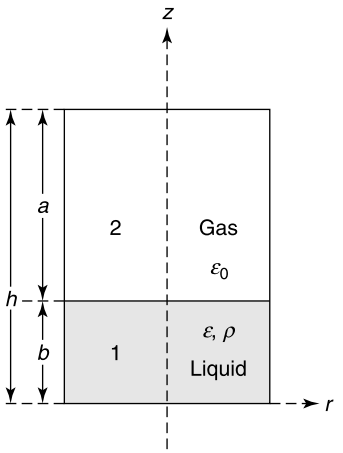

Figure 5.35 A grounded metallic tank.

Inserting into Poisson's equation (3.4) gives

$$\frac{d^2 f_n}{dz^2} - \left(\frac{\lambda_n}{a}\right)^2 f_n = -\frac{\rho_0}{\epsilon}\frac{2}{\lambda_n J_1(\lambda_n)}.$$

It follows, because f_n must vanish for $z = 0$, that

$$f_n = B_n \sinh\left(\lambda_n \frac{z}{a}\right) + \rho_0 \frac{2a^2}{\epsilon \lambda_n^2 J_1(\lambda_n)}\left[1 - \cosh\left(\lambda_n \frac{z}{a}\right)\right]. \tag{5.118}$$

The coefficients A_n and B_n may now be determined by imposing the conditions $\phi_1 = \phi_2$ and $\epsilon_r \dfrac{\partial \phi_1}{\partial z} = \dfrac{\partial \phi_2}{\partial z}$ at the gas-liquid interface [205]. The knowledge of ϕ, and subsequently of **e**, will show whether there is a serious danger of explosion in the tank.

Expansion (5.111) is also pertinent to reformulate the image problem of Figure 5.36 in an interesting way. Because ϕ is φ-independent, $J_0(\lambda r)e^{\pm\lambda z}$ is a possible solution of Laplace's equation. Because the region of interest is unbounded in the r-direction, a summation such as (5.115) must be replaced by an integral. Thus, for $z > 0$,

$$\phi_1(r, z) = \frac{q}{4\pi\epsilon_1}\int_0^\infty \left[e^{-\lambda|z-h|} + K\, e^{-\lambda(z+h)}\right] J_0(\lambda r)\, d\lambda, \tag{5.119}$$

where K is still to be determined. Similarly, for $z < 0$,

$$\phi_2(r, z) = \frac{q}{4\pi\epsilon_2}\int_0^\infty T\, e^{\lambda(z-h)} J_0(\lambda r)\, d\lambda. \tag{5.120}$$

Expressing continuity of ϕ and $\epsilon \dfrac{\partial \phi}{\partial z}$ at $z = 0$ yields

$$K = \frac{\epsilon_1 - \epsilon_2}{\epsilon_1 + \epsilon_2}$$
$$T = \frac{2\epsilon_2}{\epsilon_1 + \epsilon_2}. \tag{5.121}$$

Representations of the kind shown above, while hardly worth deriving for the simple image problem of Figure 5.36, are significant because of their applicability to more general problems involving stratified media [23].

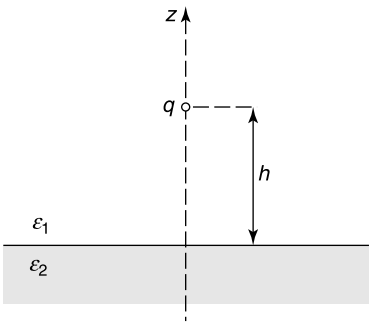

Figure 5.36 Charge q located above a dielectric slab.

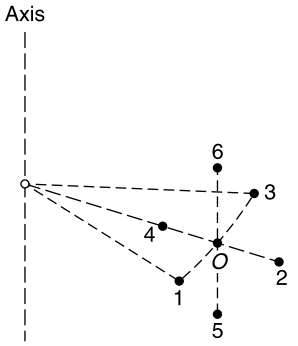

Figure 5.37 Discretization of the Laplacian.

Classic numerical procedures may easily be adapted to axisymmetric problems. In the finite difference method, for example, the pertinent form of the Laplacian becomes (Fig. 5.37)

$$\nabla^2\phi = \frac{\phi_1+\phi_3}{(r_0\Delta\varphi)^2} + \frac{\phi_2+\phi_4}{(\Delta r)^2} + \frac{\phi_5+\phi_6}{(\Delta z)^2} - 2\phi_0\left(\frac{1}{(\Delta r)^2} + \frac{1}{(r_0\Delta\varphi)^2} + \frac{1}{(\Delta z)^2}\right]. \quad (5.122)$$

Here Δr denotes the (common) distance from 0 to 2 and 0 to 4, Δz denotes the distance from 0 to 5 and 0 to 6, and $r_0\Delta\varphi$ denotes the distance from 0 to 1 and 0 to 3.

When the region of interest contains part of the axis, it is important to understand the behavior of ϕ for small values of r. Because the limit of ϕ for $r \to 0$ must be independent of φ, the coefficients in (5.109) must depend on r according to

$$\begin{aligned} a_0(r,z) &= \alpha_{00}(z) + r\alpha_{01}(z) + r^2\alpha_{02}(z) + \cdots \\ a_m(r,z) &= r\alpha_{m1}(z) + r^2\alpha_{m2}(z) + \cdots \qquad (m \neq 0), \end{aligned} \quad (5.123)$$

with similar expressions for the b_m coefficients. The expression for $\nabla^2\phi$ in (5.110) gives additonal information. The φ-independent part, for example, is

$$\begin{aligned} \nabla_M^2 a_0(r,z) &= \frac{\partial^2 a_0}{\partial r^2} + \frac{1}{r}\frac{\partial a_0}{\partial r} + \frac{\partial^2 a_0}{\partial z^2} \\ &= \frac{1}{r}\alpha_{01}(z) + 4\alpha_{02}(z) + \frac{\partial^2 a_0(0,z)}{\partial z^2} + \cdots . \end{aligned} \quad (5.124)$$

For the Laplacian in (5.110) to remain bounded on the axis, $\alpha_{01}(z) = \dfrac{\partial a_0}{\partial r}$ must vanish. The corresponding condition for a_m follows from an expansion of $\nabla^2 a_m$ in powers of r. Thus,

$$\begin{aligned} \nabla^2 a_m(r,z) &= \nabla_M^2 a_m(r,z) - \frac{m^2}{r^2}\, a_m(r,z) \\ &= (1-m^2)\,\frac{\alpha_{m1}(z)}{r} + (4-m^2)\,\alpha_{m2}(z) + \text{terms in } r \text{ and higher.} \end{aligned}$$

Boundedness of $\nabla^2 a_m$ requires $\alpha_{m1}(z)$ to vanish when $m \neq 1$. Similar arguments hold for the $b_m(r,z)$ coefficients.

5.12 CONICAL BOUNDARIES

The singularities at the tip of a conducting circular cone (Fig. 5.38) are characterized by an exponent ν. This exponent appears in the spherical harmonics expansion

$$\phi(R,\theta,\varphi) = \sum_{m=0}^{\infty}\sum_{\nu} R^{\nu} P_{\nu}^{m}(\cos\theta)(A_{m\nu}\sin m\varphi + B_{m\nu}\cos m\varphi), \tag{5.125}$$

where P_{ν}^{m} is an associated Legendre function. The subscript ν actually depends on two indices, and should be written as ν_{mn}. We write ν for the sake of conciseness. The value of ν is determined by requiring ϕ to vanish on the cone, which implies the condition

$$P_{\nu}^{m}(\cos\theta_0) = 0. \tag{5.126}$$

Only values of ν less than 1 are of interest, because they alone give rise to infinite fields. Detailed calculations show that the $m = 0$ mode of revolution is the only one in which infinities can occur. This happens only for sharp cones, and for the first root.[30] The pertinent values are given in Table 5.3, where α is the opening angle (Fig. 5.38*a*). The electric field near the tip is

$$\mathbf{e} = -\nu R^{\nu-1} P_{\nu}(\cos\theta)\mathbf{u}_R - R^{\nu-1}\frac{dP_{\nu}(\cos\theta)}{d\theta}\mathbf{u}_{\theta}. \tag{5.127}$$

Typical lines of force of $\mathbf{e}$, together with values of ϕ, are shown in Figure 5.38*b*. For a sharp needle[31] $\nu = 0$, and the field singularity is of the order of $(1/R)$. The relevant expressions for potential and field are given in (3.84).

Consider next a circular *dielectric* cone of dielectric constant ϵ_r. We now need two expansions, viz.

$$\phi_1(R,\theta,\varphi) = \sum_{m=0}^{\infty}\sum_{\nu} R^{\nu} P_{\nu}^{m}(\cos\theta)(A_{m\nu}\sin m\varphi + B_{m\nu}\cos m\varphi) \tag{5.128}$$

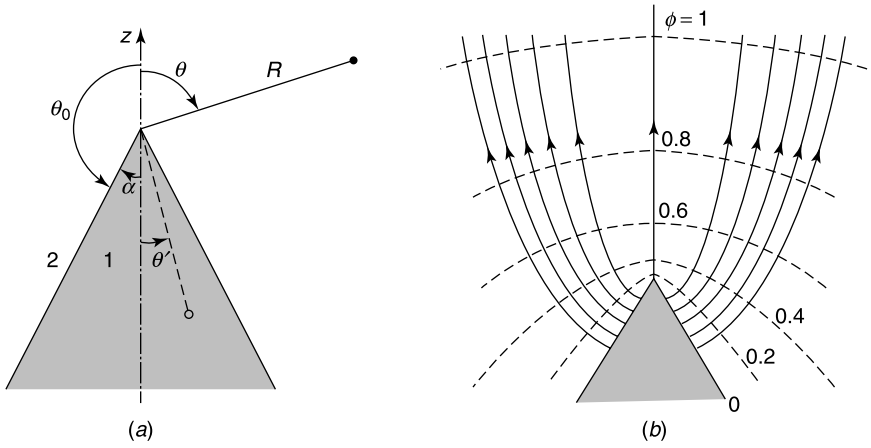

Figure 5.38 (*a*) Angles and coordinates for a circular cone. (*b*) Lines of force and equipotentials (from J. Van Bladel, Field singularities of the tip of a cone, *Proc. IEEE* **71**, 901–902, 1983, with permission of IEEE).

Table 5.3 Singularity Exponent ν for a Conducting Circular Cone

α	ν
90°	1.000
80°	0.8423
70°	0.7118
60°	0.6015
50°	0.5063
40°	0.4223
30°	0.3462
20°	0.2745
15°	0.2387
10°	0.2012
5°	0.1581
4°	0.1479
3°	0.1364
2°	0.1230
1°	0.1052

in the cone, and

$$\phi_2(R,\theta,\varphi) = \sum_{m=0}^{\infty} \sum_{\nu} R^{\nu} P_{\nu}^{m}(\cos\theta)(C_{m\nu}\sin m\varphi + D_{m\nu}\cos m\varphi) \tag{5.129}$$

outside the cone. Applying the classic boundary conditions at the air-dielectric interface quantizes ν. For a sharp cone[32] (i.e., for $0 \le \alpha \le 90°$), singularities arise for the lowest value of ν corresponding with the φ-independent mode (Fig. 5.39*a*). For the reentrant cone ($90° \le \alpha \le 180°$), singularities occur in the $m = 1$ mode (Fig. 5.39*b*). The previous values remain valid when regions 1 and 2 have dielectric constants ϵ_{r1} and ϵ_{r2}. The symbol ϵ_r now stands for $(\epsilon_{r1}/\epsilon_{r2})$.

For arbitrary cross sections, we must rely on a more general method than separation of variables.[‡] The basic ingredients for a general approach are the eigenfunctons ϕ_{mp}, solutions of

$$\nabla^2_{\theta,\varphi}\phi_{mp}(\theta,\varphi) + k^2_{mp}\phi_{mp}(\theta,\varphi) = 0 \qquad \phi_{mp} = 0 \text{ on } C_1, \tag{5.130}$$

where C_1 is the intersection of the conical surface with a sphere of unit radius (Fig. 5.40), S_1 is the enclosed surface, and the Laplacian is the *Beltrami operator*

$$\nabla^2_{\theta,\varphi}\phi = \frac{\partial^2\phi}{\partial\theta^2} + \frac{1}{\tan\theta}\frac{\partial\phi}{\partial\theta} + \frac{1}{\sin^2\theta}\frac{\partial^2\phi}{\partial\varphi^2}.$$

[‡]Separation of variables works, for example, for a cone of elliptic cross section. See J. Boersma and J. K. M. Jansen, Electromagnetic field singularities at the tip of an elliptic cone, EUT Report 90-01. Department of Mathematics and Computing Science, Eindhoven University of Technology (1990).

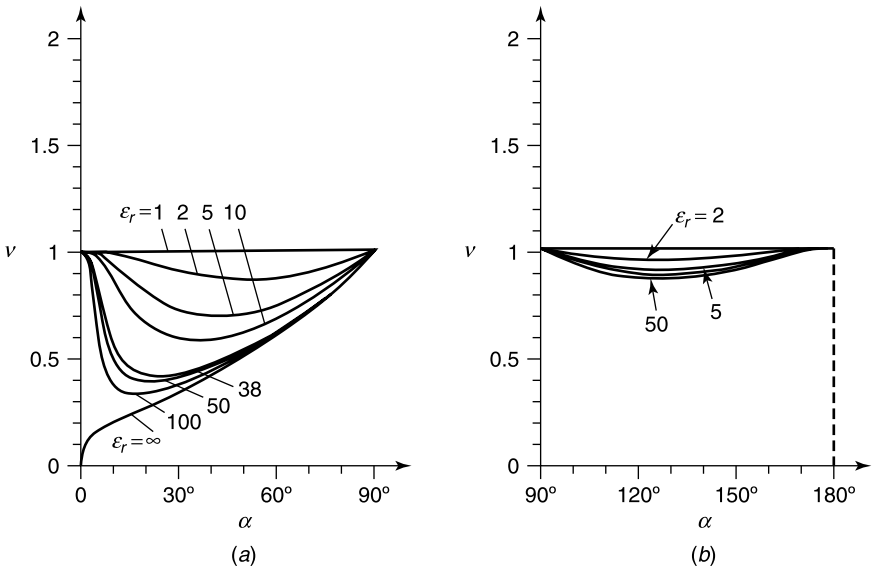

Figure 5.39 Singularity exponent ν for a circular dielectric cone (*a*) for the $m = 0$ mode (salient cone) and (*b*) for the $m = 1$ mode (reentrant cone) (from J. Van Bladel, Field singularities at the tip of a dielectric cone, *IEEE Trans. AP* **33**, 893–895, 1985, with permission of IEEE).

The eigenfunctions are orthogonal and normalized in the sense that

$$\int_{S_1} \phi_{mp}\phi_{m'p'}\, dS = \int_{S_1} \phi_{mp}\phi_{m'p'} \sin\theta\, d\theta\, d\varphi = \delta_{mm'}\delta_{pp'}. \tag{5.131}$$

We use these eigenfunctions to determine the potential when the sources $\rho(R, \theta, \varphi)$ and the values $\phi(R, c)$ of the potential on the outer conical surface are given. To solve that problem, both members of Poisson's equation (3.4) are expanded in terms of the ϕ_{mp}'s. For the potential, in particular, we write

$$\phi = \sum_m \sum_p f_{mp}(R)\phi_{mp}(\theta, \varphi).$$

Following the *derivative of a sum* technique, a differential equation for $f_{mp}(R)$ can be obtained by expressing the expansion coefficients of $\nabla^2\phi$ in terms of those of ϕ. The

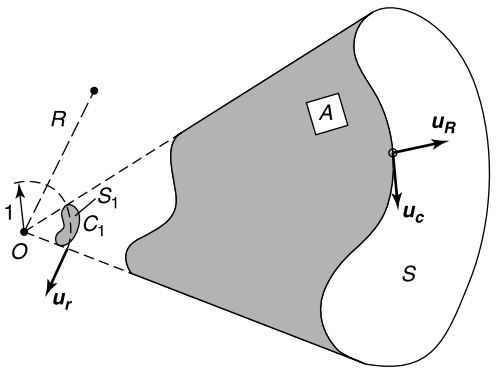

Figure 5.40 Conical waveguide with aperture in the wall.

calculation proceeds as in Section 5.8 and yields

$$\frac{d}{dR}\left(R^2\frac{df_{mp}}{dR}\right) - k_{mp}^2 f_{mp} = \underbrace{\int_c \phi(R,c)\frac{\partial \phi_{mp}}{\partial n}\sin\theta\, d\theta\, d\varphi}_{\text{boundary excitation}} \underbrace{-\frac{R^2}{\epsilon_0}\int_S \rho(R,\theta,\varphi)\phi_{mp}\sin\theta\, d\theta\, d\varphi}_{\text{volume excitation}}. \tag{5.132}$$

The general solution of (5.132) is of the form

$$f_{mp} = \left(A_{mp}R^{\alpha_{mp}} + B_{mp}\frac{1}{R^{\beta_{mp}}}\right) + g_{mp}(R) \qquad (\beta_{mp} = \alpha_{mp} + 1), \tag{5.133}$$

where $g_{mp}(R)$ is a particular solution, and α_{mp} and $-\beta_{mp}$ are the roots of the equation $\nu_{mp}(\nu_{mp}+1) = k_{mp}^2$. To determine the eigenvalues k_{mp}^2, we may start from the functional[33]

$$\begin{aligned} J_1(\phi) &= \int_{S_1}\left[|\text{grad}_{\theta,\varphi}\phi|^2 - k^2\phi^2\right] dS \\ &= \int_0^{\pi}\int_{-\frac{\pi}{2}}^{\frac{\pi}{2}}\left[\left(\frac{\partial\phi}{\partial\theta}\right)^2 + \frac{1}{\sin^2\theta}\left(\frac{\partial\phi}{\partial\varphi}\right)^2 - k^2\phi^2\right]\sin\theta\, d\theta\, d\varphi, \end{aligned} \tag{5.134}$$

which is stationary for the eigenfunctions ϕ_{mp}. To verify that property, let us set $\phi = \phi_0 + \epsilon\eta$, and require the term in ϵ to vanish. This gives

$$\int_{S_1}[\text{grad}_S\,\phi_0 \cdot \text{grad}_S\,\eta - k^2\eta\phi_0]\, dS = 0.$$

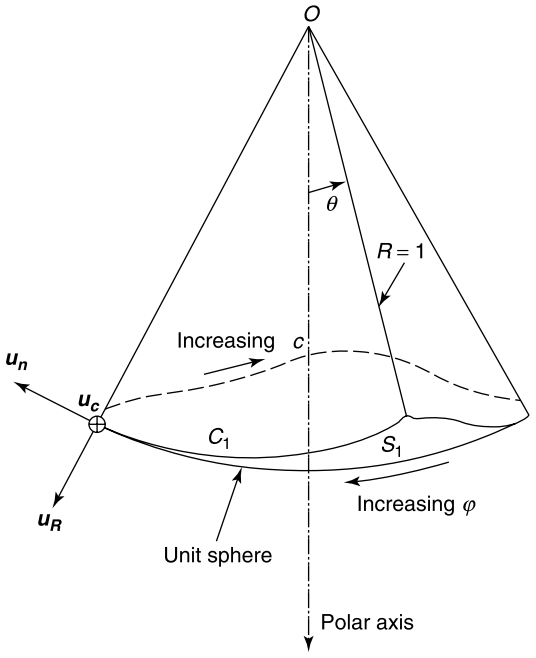

Figure 5.41 A cone of arbitrary cross section.

Applying Green's theorem (A3.49) yields (Fig. 5.41)

$$\int_{S_1} \eta[\nabla^2_{\theta\varphi}\phi_0 + k^2\phi_0]\, dS + \int_{C_1} \eta \mathbf{u}_n \cdot \text{grad}_S\, \phi_0\, dc = 0.$$

The Euler equation is precisely (5.130), and the natural boundary condition, derived from the contour integral, is

$$(\partial\phi_0/\partial n) = 0 \qquad (\text{on } C) \tag{5.135}$$

where n denotes the normal to the conical surface. With the boundary condition $\phi = 0$ on C_1, the line integral vanishes automatically, and an additional boundary condition is not needed.

Another suitable variational principle is based on

$$J_2(\phi) = \frac{\displaystyle\int_{S_1} |\text{grad}_S\, \phi|^2\, dS}{\displaystyle\int_{S_1} \phi^2 dS}. \tag{5.136}$$

The stationary values are the sought k^2_{mp}. The principle has been applied to various cross sections [133]. For a *90° corner* for example, the lowest singularity exponent turns out to be $\nu = 0.4541$ (Fig. 5.42). For a *flat sector* (a degenerate elliptic cone), the lowest value of ν is given in Table 5.4 in terms of the opening angle α of the sector. The transition between salient and reentrant sectors occurs for $\alpha = 180°$ (the half-plane) and the corresponding exponent $\nu = 0.5$ is in agreement with the previously obtained value (5.13). Salient and reentrant corners occur, for example, in certain types of apertures. Details on charge densities and lines of force on the corners can be found elsewhere.[34] The reader is also referred to the literature[35] for data concerning *dielectric* cones, and in particular dielectric pyramids [133].

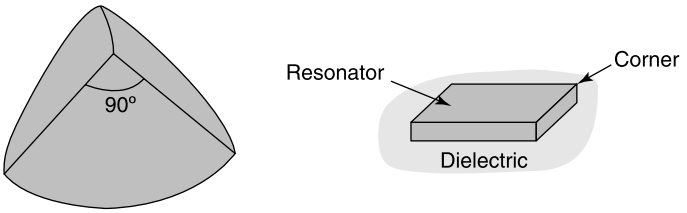

Figure 5.42 (*a*) A 90° corner. (*b*) A resonator showing such a corner (from R. De Smedt and J. Van Bladel, Field singularities at the tip of a metallic cone of arbitrary cross-section, *IEEE Trans. AP* **34**, 865–870, 1986, with permission of IEEE).

Table 5.4 Singularity Exponent for a Conducting (Flat) Sector of Opening Angle α

Salient		Reentrant	
α	ν	α	ν
10°	0.131	180°	0.500
20°	0.159	200°	0.560
40°	0.202	220°	0.625
60°	0.241	240°	0.698
80°	0.279	260°	0.776
90°	0.297	270°	0.816
100°	0.317	280°	0.853
120°	0.357	300°	0.920
140°	0.400	320°	0.966
160°	0.448	340°	0.992
180°	0.500	350°	0.998

PROBLEMS

5.1 An electric field e^i is incident on the wedge structure of Figure P5.1*a*. Show that symmetry implies that the singularities are the same as in the absence of dielectric. The particular case of Figure P5.1*b*, which corresponds with $\alpha = 0$, is clearly relevant for the microstrip line shown in Figure P5.1*c*, because strong singular fields may cause avalanche breakdown in a semiconductor substrate.

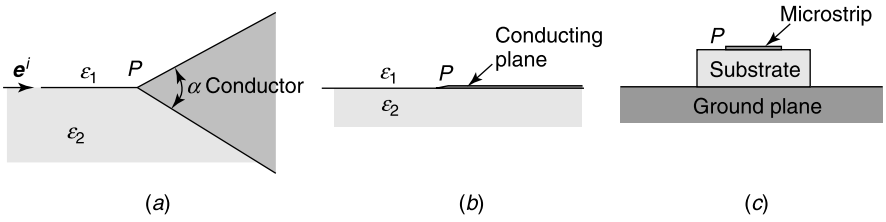

Figure P5.1

5.2 Find the equipotentials in the presence of a source consisting of a linear charge $+\rho_l$ separated by a distance $2d$ from an opposite linear charge $-\rho_l$ (Fig. P5.2). Determine first the image of ρ_l with

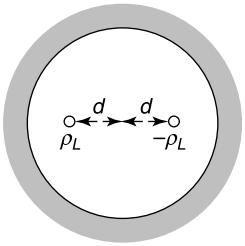

Figure P5.2

respect to a grounded circular cylinder. Repeating for the charge $-\rho_l$, find the potential inside the cylinder and use this result to determine the capacitance of two small cylinders centered on ρ_l and $-\rho_l$ and carrying respective charges q and $-q$. The result, in Fm^{-1}, is the capacitance of the corresponding bifilar line.

5.3 The vacuum tank of a certain particle accelerator can be approximated by a long metallic tube of rectangular cross section (Fig. P5.3). A current of protons of intensity $i = 50$ A and velocity $c_0/2$ is located in the $y = 0$ (equatorial) plane. Find the electric field in that plane, and identify the respective contributions from the protons and the charges induced in the walls.

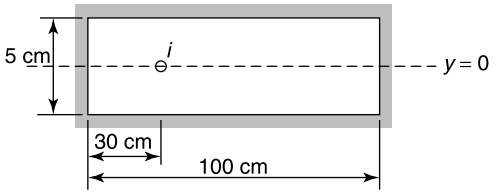

Figure P5.3

5.4 A metallic container bounded by plane surfaces contains a liquid hydrocarbon. The liquid is charged with a density $\rho = 0.1\ \mathrm{Cm}^{-3}$, and its dielectric constant is 2. The tank is only partially filled with liquid (Fig. P5.4). Determine the maximum potential and the maximum field intensity as a function of liquid height. The problem is of importance for the oil industry.

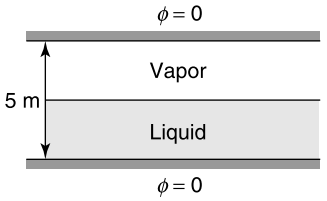

Figure P5.4

5.5 Find the potential outside a circular cylinder, the two halves of which consist of different metals 1 and 2 (Fig. P5.5). The contact potential V_{12} is given. Assume that no current exists in the conductor.

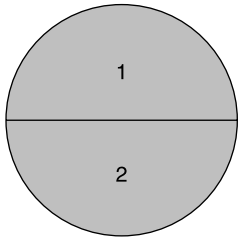

Figure P5.5

5.6 Show, by applying Gauss' law to the square in Figure P5.6, that

$$\phi_0 = \frac{\epsilon_1}{2(\epsilon_1 + \epsilon_2)}\phi_1 + \frac{\epsilon_2}{2(\epsilon_1 + \epsilon_2)}\phi_3 + \frac{1}{4}\phi_2 + \frac{1}{4}\phi_4$$

when ϕ satisfies Laplace's equation. The dielectrics are assumed uncharged [205].

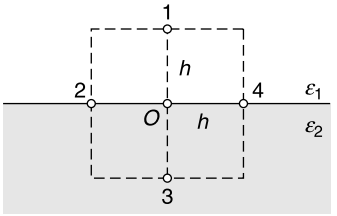

Figure P5.6

5.7 Solve the matrix problem

$$\begin{pmatrix} 2 & 1 \\ 1 & 3 \end{pmatrix} \cdot \begin{pmatrix} x_1 \\ x_2 \end{pmatrix} = \begin{pmatrix} 5 \\ 10 \end{pmatrix}$$

by relaxation techniques, starting with the guess (2, 2.5). Perform only one iteration, using $\alpha = 0.5$, 1, and 1.5. The correct solution is (1, 3).

5.8 Repeat the problem embodied in Figure 5.21 with the same boundary conditions, but with a charge density $\rho \doteq x(y-1)$. Use successive overelaxations.

5.9 The following functional is pertinent for the solution of the interior problem with mixed boundary conditions (Fig. P5.7)

$$J(\phi) = \frac{1}{2}\int_S \epsilon_r |\text{grad}\,\phi|^2\, dS - \int_S g\phi\, dS - \int_{C'} h\phi\, dc'.$$

The admissible functions must satisfy the conditions (a) ϕ given on C'' (b) $\phi = h$ on C'. The dielectric constant is a function of (x, y). Find Euler's equation and the natural boundary conditions.

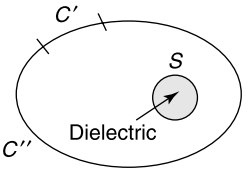

Figure P5.7

5.10 Use image theory to show that the potential in the upper half-space of Figure P5.8 is given by [23].

$$\phi(r,z) = \frac{p_e}{4\pi\epsilon_1}\left(\frac{z-h}{R_1^3} - \frac{\epsilon_1-\epsilon_2}{\epsilon_1+\epsilon_2}\frac{z+h}{R_2^3}\right).$$

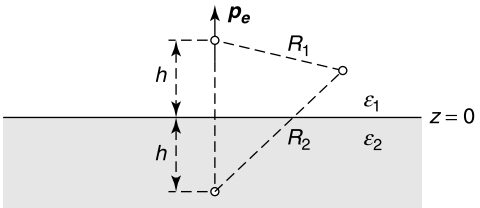

Figure P5.8

5.11 Find the capacitance per unit area of two infinite metallic plates separated by a dielectric of given *tensor* dielectric constant.

5.12 Verify that the charge density $\rho_S(x)$ on a conducting band, given by (5.51), yields the correct total charge density. In other words, check that

$$\int_{-c}^{c} \rho_S(x)\, dx = \rho_l.$$

5.13 The potential on a surface S has a given value $\phi(\mathbf{r})$. Show that the exterior potential minimizes

$$I = \frac{1}{2}\int_V \epsilon_r |\text{grad}\,\phi|^2\, dV$$

where V is the exterior volume (Fig. P5.9). The integral is the electrostatic energy. It is also equal to

$$I = \frac{1}{2}\int_S \epsilon_r \phi \frac{\partial \phi}{\partial n}\, dS.$$

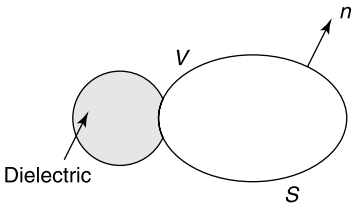

Figure P5.9

5.14 Determine the polarizability dyadic of a conducting elliptic cylinder. Compare with the results in Figure 5.15 obtained for a rectangular cylinder.

5.15 Consider the overdetermined system

$$x + 2y + 1 = 0 \tag{1}$$

$$3x - y - 4 = 0 \tag{2}$$

$$2x + y = 0 \tag{3}$$

Solve (1) and (2), (2) and (3), (1) and (3) separately. Determine the most acceptable "intermediate" solution by the method of least squares.

5.16 Extend the asymptotic boundary condition discussed in Section 5.7 to two-dimensional configurations, such as transmission lines in their TEM mode (A. Khebir et al., *J. Elec. Waves Appl.* **4**, 145–157, 1990).

5.17 The potential on plane $y = h$ has a given value $\phi(x, h) = f(x)$ (Fig. P5.10). Determine the potential everywhere above the ground plane by using a spatial Fourier transform.

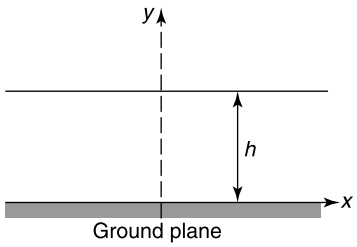

Figure P5.10

5.18 The structure in Figure P5.11 consists of coupled conducting cylindrical rods lying between parallel ground planes. This configuration is found, for example, in microwave filters, where it carries two kinds of modes:

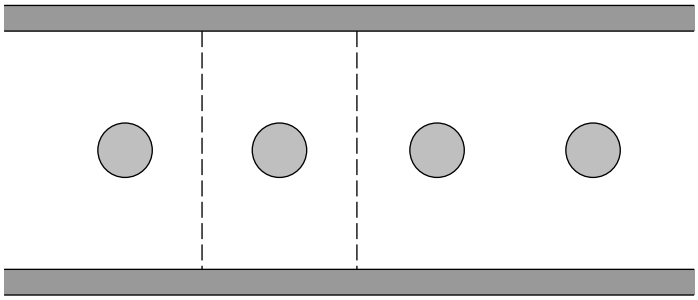

Figure P5.11

(**a**) An even mode, in which all the conductors are at the same potential V;

(**b**) An odd mode, in which the potentials are alternately at $+V$ and $-V$.

Because of the built-in symmetries, the cells are bounded, halfway between rods, by

- Magnetic walls for the even modes;
- Electric walls for the odd modes.

Solve for the various capacities by means of suitable integral equations (E.G. Cristal, *IEEE Trans. MTT* **12**, 428–439, 1964).

5.19 Apply the method of images to determine the (two-dimensional) potential generated by a linear charge located in a right-angle sector bounded by two perpendicular conductors (Fig. P5.12) [23].

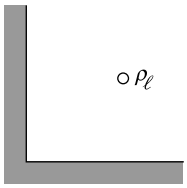

Figure P5.12

5.20 In the configuration of Figure P5.13, assume that the Green's function in the presence of the conductor is known. In the absence of dielectric:

$$\phi(\mathbf{r}) = \phi^i(\mathbf{r}) + \frac{1}{\epsilon_0}\int_1 \rho(\mathbf{r}')G(\mathbf{r}|\mathbf{r}')\,dV'.$$

The dielectric may be replaced by equivalent bound charges ρ'_S on S, equal to $\epsilon_0(e_n^+ - e_n^-)$. Show that ρ'_S may be found by solving the integral equation

$$\mathbf{u}_n \cdot \mathbf{e}^i = \frac{\epsilon_r + 1}{2(\epsilon_r - 1)}\frac{\rho'_S}{\epsilon_0} + \lim_{\delta\to 0}\frac{1}{\epsilon_0}\int_{S-S_\delta} \rho'_S(\mathbf{r}')\frac{\partial G(\mathbf{r}|\mathbf{r}')}{\partial n}\,dS'.$$

(C. Wei et al., *IEEE Trans. MTT* **32**, 439–450, 1984).

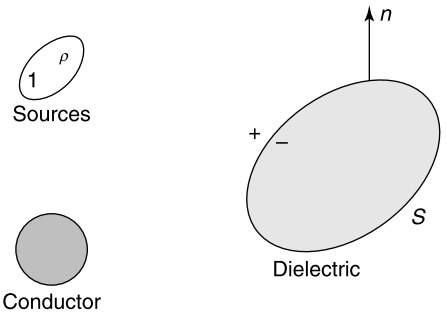

Figure P5.13

5.21 The screen in Figure 5.32 is not infinitely thin in practice. To investigate the influence of thickness, consider the two-dimensional slit in Figure P5.14.
(**a**) Express ϕ in regions 1 and 3 by means of a Fourier transformation in x.

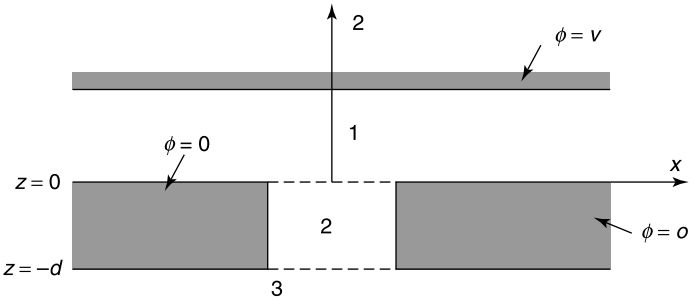

Figure P5.14

(**b**) Use a Fourier sine series in region 2.
(**c**) Match ϕ and $\dfrac{\partial \phi}{\partial z}$ at the interfaces $z = 0$ and $z = -d$.
(**d**) Invert the Fourier transforms.
(Y.S. Kim et al., *IEEE Trans. EMC* **38**, 77–79, 1996.)

5.22 Two conducting cylinders A and B are immersed in an electrolyte C of given conductivity σ (Fig. P5.15). Find the resistance between A and B.

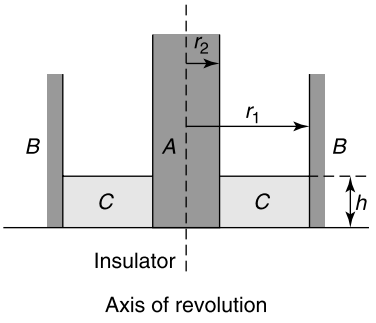

Figure P5.15

5.23 Find the potential in regions 1 and 2 by means of the methods discussed in Section 5.11 (Fig. P5.16).

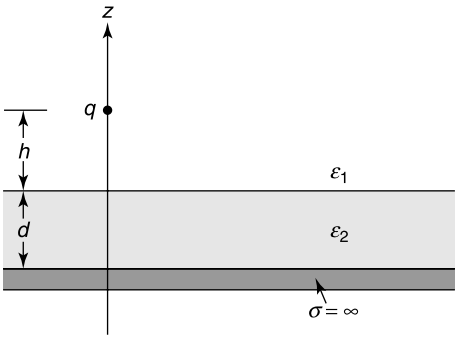

Figure P5.16

5.24 A conical conductor, bounded by a conical surface of vertex O and by two spherical surfaces A and B centered at O, has a uniform conductivity σ. Calculate the resistance between contact surfaces A and B, and determine the profile of the lines of current.

NOTES

1. J. Meixner, Die Kantenbedingung in der Theorie der Beugnung Elektromagnetischer Wellen an Volkommen Leitenden Ebenen Schirmen, *Ann. Phys.* **6**, 2–9 (1949).
2. F. Olyslager and D. De Zutter, Analytical behavior of the surface charge density on a conductor with two consecutive edges with right angles, *Microwave Opt. Tech. Lett.* **6**, 578–581 (1993).
3. F. Olyslager, Behavior of the surface charge density on a conductor with a number of consecutive edges with corners with arbitrary angles, *Electromagn.* **15**, 175–188 (1995).
4. D. R. Wilton and S. Govind, Incorporation of edge conditions in moment method solutions, *IEEE Trans. AP* **25**, 845–850 (1977).
5. J. Meixner, The behavior of electromagnetic fields at edges, *IEEE Trans. AP* **20**, 442–446 (1972).
6. J. Bach Andersen, Field behavior near a dielectric wedge, *IEEE Trans. AP* **26**, 598–602 (1978).
7. J. Van Bladel, Field singularities at metal-dielectric wedges, *IEEE Trans. AP* **33**, 450–455 (1985).
8. K. Mei and J. Van Bladel, Low frequency scattering by rectangular cylinders, *IEEE Trans. AP* **11**, 52–56 (1963).
9. B. H. Mc. Donald, M. Friedman, and A. Wexler, Variational solution of integral equations, *IEEE Trans. MTT* **22**, 237–248 (1974).
10. A. R. Djordevic, T. K. Sarkar, T. Roy, S. M. Rao, and M. Salazar, An exact method for simulatingboundary conditions for mesh termination in finite difference techniques, *Microwave Opt. Tech. Lett.* **8**, 88–90 (1995).
11. T. Roy, T. K. Sarkar, A. R. Djordevic, and M. Salazar, A hybrid method for terminating the finite-element mesh (electrostatic case), *Microwave Opt. Tech. Lett.* **8**, 282–287 (1995).
12. K. K. Mei, Unimoment method of solving antenna and scattering problems, *IEEE Trans. AP* **22**, 760–766 (1974).
13. A. Khebir, A. B. Kouki, and R. Mittra, Aymptotic boundaries conditions for finite element analysis of three-dimensional transmission line discontinuities, *IEEE Trans. MTT* **38**, 1427–1432 (1990).
14. R. K. Gordon and S. H. Fook, A finite difference approach that employs an asymptotic boundary condition on a rectangular outer boundary for modeling two-dimensional transmission line structures, *IEEE Trans. MTT* **41**, 1280–1286 (1993).
15. J. L. Rodriguez, F. Obelleiro and A. G. Pino, A hybrid multipolar-expansion-moment-method approach for electromagnetic scattering problems, *Microwave Opt. Tech. Lett.* **11**, 304–308 (1996).
16. M. N. O. Sadiku and D. T. Hunt, Solution of Dirichlet problems by the Exodus method, *IEEE Trans. MTT* **40**, 89–95 (1992).
17. M. N. O. Sadiku, S. O. Ajose, and Z. Fu, Applying the Exodus method to solve Poisson's equation, *IEEE Trans. MTT* **42**, 661–666 (1994).

18. I. V. Lindell, Static image method for layered isotropic and bi-isotropic cylinders, *Microwave Opt. Tech. Lett.* **6**, 383–387 (1993).
19. R. W. Scharstein, Mellin transform solution for the static line-source excitation of a dielectric wedge, *IEEE Trans. AP* **41**, 1675–1679 (1993).
20. K. I. Nikoskinen and I. V. Lindell, Image solution for Poisson's equation in wedge geometry, *IEEE Trans. AP* **43**, 179–187 (1995).
21. I. V. Lindell, Static image theory for bianisotropic media with plane parallel interfaces, *Microwave Opt. Tech. Lett.* **6**, 228–230 (1993).
22. D. B. Davidson and J. T. Aberle, An introduction to spectral domain method-of-moments formulations, *IEEE Antennas Prop. Mag.* **46**, 11–19 (2004).
23. E. Yamashita and R. Mittra, Variational methods for the analysis of microstrip lines, *IEEE Trans. MTT* **16**, 251–256 (1968).
24. K. S. Oh, D. Kuznetsov, and J. E. Schutt-Aine, Capacitance computations in a multilayered dielectric medium using closed-form spatial Green's functions, *IEEE Trans. MTT* **42**, 1443–1453 (1994).
25. W. Delbare and D. De Zutter, Space-domain Green's function approach to the capacitance calculation of multiconductor lines in multilayered dielectrics with improved surface charge modeling, *IEEE Trans. MTT* **37**, 1562–1568 (1989).
26. P. Silvester and P. Benedek, Equivalent capacitances of microstrip open circuits, *IEEE Trans. MTT* **20**, 511–516 (1972).
27. C. Wei, R. F. Harrington, J. O. Mautz, and T. K. Sarkar, Multiconductor transmission lines in multilayered dielectric media, *IEEE Trans. MTT* **32**, 439–450 (1984).
28. A. Rahhal-Arabi, J. R. Mautz, and R. F. Harrington, On the treatment of the second partial derivative of the integral of the Green's function, *IEEE Trans. MTT* **42**, 1102–1104 (1994).
29. F. De Meulenaere and J. Van Bladel, Polarizability of some small apertures, *IEEE Trans. AP* **25**, 198–205 (1977).
30. J. Van Bladel, Field singularities of the tip of a cone, *Proc. IEEE* **71**, 901–902 (1983).
31. R. De Smedt, Electric singularity near the tip of a sharp cone, *IEEE Trans. AP* **36**, 152–155 (1988).
32. J. Van Bladel, Field singularities at the tip of a dielectric cone, *IEEE Trans. AP* **33**, 893–895 (1985).
33. R. De Smedt and J. Van Bladel, Field singularities at the tip of a metallic cone of arbitrary cross-section, *IEEE Trans. AP* **34**, 865–870 (1986).
34. R. De Smedt and J. Van Bladel, Field singularities near aperture corners, *IEE Proc.* **134-A**, 694–698 (1987).
35. R. De Smedt, Singular field behavior near the tip of a dielectric or dielectric-metallic corner, *Radio Sci.* **22**, 1190–1196 (1987).

Chapter 6

Magnetostatic Fields

The basic equations for the *electrostatic* field in vacuum are curl $\mathbf{e} = 0$ and div $\mathbf{e} = (\rho/\epsilon_0)$. From the first equation, $\mathbf{e}$ can be written as $(-\text{grad}\ \phi)$, where ϕ is the solution of Poisson's equation div grad $\phi = -(\rho/\epsilon_0)$. The *magnetostatic* induction, on the other hand, must satisfy the *dual* equations curl $\mathbf{b} = \mu_0\mathbf{j}$ and div $\mathbf{b} = 0$. The last equation implies that $\mathbf{b}$ can be written as curl $\mathbf{a}$, and the first one that the vector potential $\mathbf{a}$ must be a solution of curl curl $\mathbf{a} = \mu_0\mathbf{j}$. The two operators, div grad and curl curl, are the two fundamental operators of static electromagnetism.[1]

Because curl $\mathbf{b}$ vanishes outside the ringlike current-carrying region V, the magnetic induction can be given the form $\mathbf{b} = -\mu_0\ \text{grad}\ \psi$ *outside* V. Potential ψ is a multivalued function in that case. Various methods have been proposed to restore single-valuedness to ψ, given the advantages of working with a scalar potential. Two of these methods are cuts (or barriers) in space and the replacement of $\mathbf{b}$ as unknown field by $(\mathbf{b}/\mu_0 - \mathbf{t})$, where $\mathbf{t}$ is a particular solution of curl $\mathbf{t} = \mathbf{j}$. The new unknown is irrotational everywhere in space and may therefore be written as grad θ, where θ is *singlevalued*. Such considerations are of great importance for the economy of computing magnetic fields in devices such as large transformers and alternators, which are characterized by a complex geometry and an intricate topology of coils and iron. An additional difficulty arises from the frequent presence of strongly nonlinear ferromagnetic materials and from the irregular time-dependence of transient currents in the coils that generate the fields. This last aspect is briefly discussed in Chapter 13.

6.1 MAGNETIC FIELDS IN FREE SPACE: VECTOR POTENTIAL

In the absence of magnetic materials, the magnetic induction in unbounded space satisfies the equations (Fig. 6.1)

$$\begin{aligned} \text{curl}\ \mathbf{b} &= \mu_0\,\mathbf{j} \\ \text{div}\ \mathbf{b} &= 0 \\ R^2|\mathbf{b}| &\text{bounded at infinity.} \end{aligned} \tag{6.1}$$

Electromagnetic Fields, Second Edition, By Jean G. Van Bladel

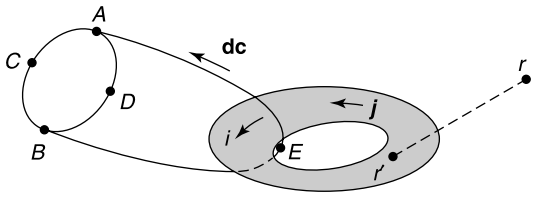

Figure 6.1 Ring current and paths of integration.

It is shown in Section 6.4 that $|\mathbf{b}|$ actually decreases like $(1/R^3)$ at large distances. A few observations emerge:

1. Because curl $\mathbf{b} = 0$ outside the sources, the integral of $\mathbf{b}$ around a contour such as *ACBD* in Figure 6.1 vanishes. It follows that $\mathbf{b}$ can be derived from a scalar potential in that region. The point is further discussed in Section 6.5.
2. Because $\mathbf{b}$ is without divergence throughout space and vanishes strongly at infinity, it can be written as

$$\mathbf{b} = \text{curl } \mathbf{a}, \tag{6.2}$$

where $\mathbf{a}$ is a *vector potential*. This representation is justified by a theorem ascribed to Blumenthal,[2] which states that (6.2) holds when a divergenceless vector, together with its derivatives, vanishes at infinity and is continuous. The property does not necessarily hold for a vector that has zero divergence in a *finite* region only, a point discussed in Appendix 1 (Problem 6.1).

3. Equations (6.1) cannot have a solution unless div $\mathbf{j} = 0$. But the equation of conservation of charge (4.12) shows that this condition is automatically satisfied when the sources are time-independent.

The problem embodied in (6.1) has a unique solution. To prove this assertion, let us apply the usual method, which is to show that there is no nonzero solution $\mathbf{b}_0$ to the homogeneous problem obtained by setting $\mathbf{j} = 0$ in (6.1). Any solution $\mathbf{b}_0$ has zero divergence and curl throughout space, hence it is harmonic. But it is shown in Section 3.7 that a vector that is harmonic throughout space reduces to a constant. The latter, however, must be zero in the current case because $\mathbf{b}_0$ approaches zero for $R \to \infty$.

Combining (6.1) and (6.2) shows that the vector potential satisfies

$$\text{curl curl } \mathbf{a} = \mu_0 \mathbf{j}$$

$$\mathbf{a} \text{ regular at infinity (on a sphere } S_\infty). \tag{6.3}$$

Regularity is defined in Section 3.1. The solution of (6.3) is obviously not unique because $\mathbf{a}$ is determined to within a gradient. Furthermore, the "family" of gradients is the *only* solution of the homogeneous problem

$$\text{curl curl } \mathbf{a}_0 = 0$$

$$\mathbf{a}_0 \text{ regular at infinity.}$$

From (A1.32), indeed,

$$\int_{\text{all space}} \left[-\mathbf{a}_0 \cdot \text{curl curl } \mathbf{a}_0 + |\text{curl } \mathbf{a}_0|^2 \right] dV = \int_{S_\infty} \mathbf{u}_R \cdot (\mathbf{a}_0 \times \text{curl } \mathbf{a}_0) dS.$$

The integral over S_∞ vanishes because of the regularity condition, hence curl $\mathbf{a}_0 = 0$ over all space, which means that $\mathbf{a}_0$ may be written as a gradient. In the parlance of Section 1.3: The null-space of transformation (6.3) consists of irrotational vectors that are regular at infinity. The uncertainty may be lifted by imposing an additional condition on $\mathbf{a}$, for example

$$\operatorname{div} \mathbf{a} = 0. \tag{6.4}$$

The potential now satisfies Poisson's equation

$$\begin{aligned} \nabla^2 \mathbf{a} &= -\mu_0 \mathbf{j} \\ \mathbf{a} &\text{ regular at infinity.} \end{aligned} \tag{6.5}$$

Projection of (6.3) on the x, y, and z axes gives rise to three potential problems of the type discussed in Section 3.1. The solution of these problems is given by (3.16). The value of $\mathbf{a}$ is therefore

$$\mathbf{a}(\mathbf{r}) = \frac{\mu_0}{4\pi} \int_{\text{all space}} \frac{\mathbf{j}(\mathbf{r}')}{|\mathbf{r} - \mathbf{r}'|}\, dV'. \tag{6.6}$$

According to Section 3.2, the three components of $\mathbf{a}$ are continuous, together with their first derivatives, when $\mathbf{j}$ is piecewise continuous.* The expression of $\mathbf{b}$ in terms of $\mathbf{j}$ can now be derived by taking the curl of the right-hand term of (6.6) with respect to the $\mathbf{r}$ coordinates. The result is

$$\begin{aligned} \mathbf{b}(\mathbf{r}) &= \frac{\mu_0}{4\pi} \int_{\text{all space}} \left[\operatorname{grad} \frac{1}{|\mathbf{r} - \mathbf{r}'|} \times \mathbf{j}(\mathbf{r}') \right] dV' \\ &= -\frac{\mu_0}{4\pi} \int_{\text{all space}} \frac{(\mathbf{r} - \mathbf{r}') \times \mathbf{j}(\mathbf{r}')}{|\mathbf{r} - \mathbf{r}'|^3}\, dV'. \end{aligned} \tag{6.7}$$

This equation constitutes a mathematical expression of Ampère's law and at the same time concretizes the *inversion* of the curl operator in (6.1).

Currents and vector potentials satisfy the *reciprocity property*

$$\int_{\text{all space}} \mathbf{j}_1 \cdot \mathbf{a}_2\, dV = \int_{\text{all space}} \mathbf{j}_2 \cdot \mathbf{a}_1\, dV, \tag{6.8}$$

which is sometimes written more concisely as $\langle \mathbf{j}_1, \mathbf{a}_2 \rangle = \langle \mathbf{j}_2, \mathbf{a}_1 \rangle$, or even as $\langle 1, 2 \rangle = \langle 2, 1 \rangle$. The property may be proved by using the specific form of $\mathbf{a}$ given in (6.6) or by a more general procedure consisting of applying Green's theorem (A1.33). Thus,

$$\begin{aligned} \int_{\text{all space}} \mathbf{j}_1 \cdot \mathbf{a}_2\, dV &= \int_{\text{all space}} \operatorname{curl} \operatorname{curl} \mathbf{a}_1 \cdot \mathbf{a}_2\, dV \\ &= \int_{\text{all space}} \operatorname{curl} \operatorname{curl} \mathbf{a}_2 \cdot \mathbf{a}_1\, dV + \int_{S_\infty} [(\mathbf{u}_R \times \mathbf{a}_1) \cdot \operatorname{curl} \mathbf{a}_2 \\ &\quad - (\mathbf{u}_R \times \mathbf{a}_2) \cdot \operatorname{curl} \mathbf{a}_1]\, dS. \end{aligned}$$

The surface integral vanishes because of the regular behavior of $\mathbf{a}$ at infinity.

*The extension of (6.6) to linear and surface currents is discussed in Sections 6.2 and 6.3.

6.2 FIELDS GENERATED BY LINEAR CURRENTS

The vector potential of a linear current is obtained by replacing volume integrals in (6.6) with line integrals. Thus (Fig. 6.2),

$$\mathbf{a}(\mathbf{r}) = \frac{\mu_0}{4\pi} i \int_C \frac{\mathbf{dc}'}{|\mathbf{r} - \mathbf{r}'|}. \tag{6.9}$$

As a simple example, let us evaluate the fields of a circular loop of current. The vector potential of this current distribution is independent of φ (Fig. 6.3). Its value can be obtained from (6.9), which gives

$$\mathbf{a}(r, z) = \frac{\mu_0 i}{4\pi} \int_C \frac{\mathbf{dc}'}{D} = \frac{\mu_0 i}{4\pi} \int_C \frac{a\mathbf{u}_c}{D}\, d\varphi'.$$

The vector potential is φ-directed, and its magnitude is

$$a_\varphi(r, z) = \frac{\mu_0 i}{4\pi} \int_0^\pi \frac{2a \cos \varphi'}{(a^2 + r^2 + z^2 - 2ar \cos \varphi')^{\frac{1}{2}}}\, d\varphi'.$$

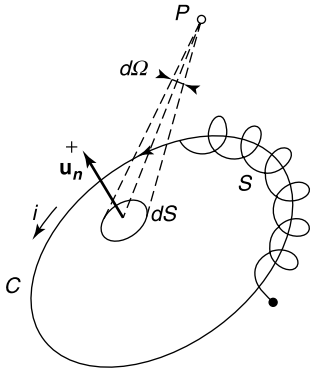

Figure 6.2 Current loop with lines of force.

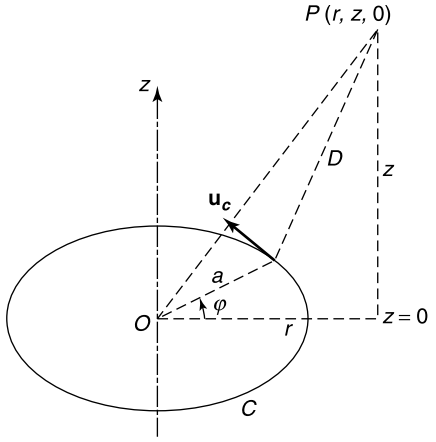

Figure 6.3 Circular loop.

Introduction of the parameter $k = \{4ar/[(a+r)^2 + z^2]\}^{\frac{1}{2}}$ allows rewriting this expression as

$$a_\varphi(r,z) = \frac{\mu_0 i}{k\pi}\left(\frac{a}{r}\right)^{\frac{1}{2}}\left[\left(1-\frac{k^2}{2}\right)K - E\right] = \frac{\mu_0 i}{32}\left(\frac{a}{r}\right)^{\frac{1}{2}} k^3\left(1+\frac{3}{4}k^2+\frac{75}{128}k^4+\cdots\right), \tag{6.10}$$

where K and E are the complete elliptic integrals of the first and second kinds. These are defined by the expressions

$$K = \int_0^{\pi/2} \frac{d\theta}{(1-k^2\sin^2\theta)^{\frac{1}{2}}} \qquad E = \int_0^{\pi/2} (1-k^2\sin^2\theta)^{\frac{1}{2}}\, d\theta. \tag{6.11}$$

E and K are defined for $0 \le k \le 1$ and have the properties [55]

$$K(0) = E(0) = \frac{\pi}{2}$$
$$K(1) = \infty \qquad E(1) = 1.$$

For small values of k:

$$K(k) = \frac{\pi}{2}\left(1+\frac{k^2}{4}+\frac{9}{64}k^4+\cdots\right)$$
$$E(k) = \frac{\pi}{2}\left(1-\frac{k^2}{4}-\frac{3}{64}k^4+\cdots\right). \tag{6.12}$$

The general behavior of these functions is shown in Figure 6.4. In the limit $k \to 1$, K becomes singular according to the law

$$K \approx \log_e \frac{4}{\sqrt{1-k^2}}. \tag{6.13}$$

Some useful comments:

1. On the axis, **b** is z-oriented and equal to

$$b_z = \frac{\mu_0 i a^2}{2(a^2+z^2)^{\frac{3}{2}}}. \tag{6.14}$$

At the center of the loop, $b_z = (\mu_0 i/2a)$.

2. At large distances, in spherical coordinates,

$$a_\varphi = \frac{\mu_0}{4\pi}(\pi a^2 i)\frac{\sin\theta}{R^2}, \tag{6.15}$$

where $\pi a^2 i = iS$ is the *magnetic moment* p_m (further discussed in Section 6.4) and S is the area of the loop. The formula remains valid for a planar loop of arbitrary shape and enclosed area S.

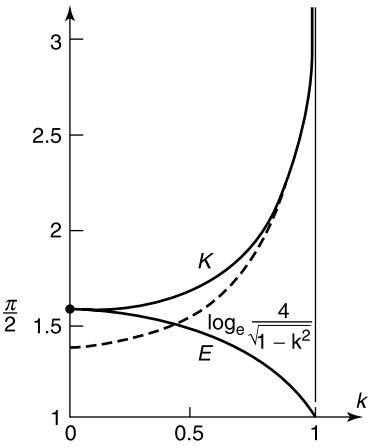

Figure 6.4 Elliptic integrals (from E. Durand. *Magnétostatique*. Masson, Paris, 1968, with permission of Editions Dunod).

3. The lines of force of **b** lie in a meridian plane and form closed loops. Close to the conductor they are circular, and **b** has the value that is obtained for an infinite straight linear current.

Details concerning the fields of other linear sources such as the circular part of a loop[3] or the helix (a model for the windings of an electric machine) can be found in [17, 55]. It should be remarked, in that respect, that the lines of force are *not* closed in general.[4,5,6] For a nonplanar loop, for example, they spiral around the loop, as suggested in Figure 6.2. The precise topology of the lines of force is of great importance for the design of many devices, for example those used to confine high-temperature plasmas. An example of unorthodox topology is offered by the configuration of Figure 6.5, where the current loop consists of two circles connected by two parallel wires. When these wires are very close to one another, the field is reduced to that of two circular loops and can easily be evaluated. A detailed plot of the lines of force in the plane of symmetry shows that these lines are not infinite in length, but emanate from P_1 and terminate on P_2, two points at which the magnetic field is equal to

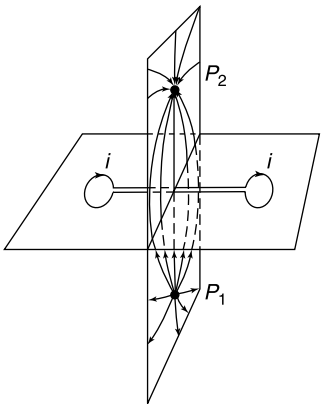

Figure 6.5 Singular lines of force (from K. L. McDonald, Topology of steady current magnetic fields, *Am. J. Phys.* **22**, 586–596, 1954, with permission of the American Institute of Physics).

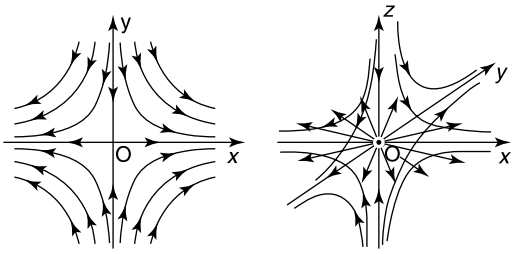

Figure 6.6 Lines of force near a singular point where $\mathbf{b} = 0$ (from E. Durand. *Magnétostatique*. Masson, Paris, 1968, with permission of Editions Dunod).

zero. If several lines of force converge to the same point O, $\mathbf{b}$ must vanish there because the field cannot have different directions in a point. The typical behavior of the lines of force in the vicinity of O is shown in Figure 6.6 [55].

6.3 FIELDS GENERATED BY SURFACE CURRENTS

The vector potential of a current-carrying sheet is given by

$$\mathbf{a}(\mathbf{r}) = \frac{\mu_0}{4\pi} \int_S \frac{\mathbf{j}_S(\mathbf{r}')}{|\mathbf{r} - \mathbf{r}'|}\, dS'. \tag{6.16}$$

When $\mathbf{r}$ is on S, the right-hand term of (6.16) becomes an improper, but convergent, integral. The properties of vector potential (6.16) can be immediately derived from those of the surface-layer potential dicussed in Section 3.4. Thus, $\mathbf{a}(\mathbf{r})$ is continuous throughout space, and its tangential derivatives approach identical limits on both sides of the surface. The behavior of $\mathbf{b}$ across the layer follows from the expression for the curl of a piecewise continuous vector given in A8.91. Applying (6.1) to the surface current yields (Fig. 6.7*a*)

$$\text{curl } \mathbf{b} = \{\text{curl } \mathbf{b}\} + \mathbf{u}_n \times (\mathbf{b}_2 - \mathbf{b}_1)\, \delta_S = \mu_0 \mathbf{j}_S\, \delta_S. \tag{6.17}$$

It follows from (6.17) that b_n is continuous, and that the tangential components experience a jump

$$(\mathbf{b}_2)_{\tan} - (\mathbf{b}_1)_{\tan} = \mu_0 \mathbf{j}_S \times \mathbf{u}_n. \tag{6.18}$$

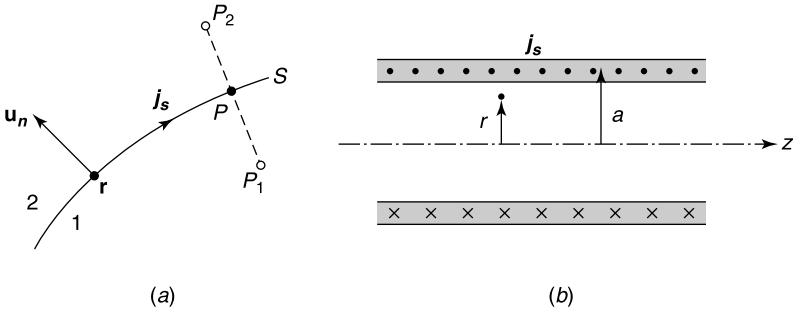

(*a*) (*b*)

Figure 6.7 Layers of surface currents: (*a*) general (*b*) on a circular cylinder.

In terms of the magnetic field $\mathbf{h} = (\mathbf{b}/\mu_0)$, this condition becomes

$$(\mathbf{h}_2)_{\tan} - (\mathbf{h}_1)_{\tan} = \mathbf{j}_S \times \mathbf{u}_n. \tag{6.19}$$

Consider, as an example, a thin layer of uniform azimuthal $\mathbf{j}_S$, wound on a circular cylinder (Fig. 6.7*b*). A few simple steps yield, inside the cylinder,

$$\begin{aligned} b &= b_z = \mu_0 j_S \\ a_\varphi &= \frac{r}{2}\mu_0 j_S, \end{aligned} \tag{6.20}$$

and outside that volume

$$\begin{aligned} b &= b_z = 0 \\ a_\varphi &= \frac{a^2}{2r}\mu_0 j_S. \end{aligned} \tag{6.21}$$

The behavior of $\mathbf{h}$ at points close to the surface can be clarified by the following simple derivation. Assume that $\mathbf{a}_t$ is a tangential vector. At a point $P_1(\mathbf{r})$ just outside S (Figs. 3.6 and 6.7*a*)

$$\begin{aligned} \mathbf{I}(\mathbf{r}) = \operatorname{curl}\left[\int \frac{1}{|\mathbf{r}-\mathbf{r}'|}\,\mathbf{a}_t\,dS'\right] &= \int_S \operatorname{grad}\frac{1}{|\mathbf{r}-\mathbf{r}'|} \times \mathbf{a}_t(\mathbf{r}')\,dS' \\ = \underbrace{\int_{S-S_\delta} \mathbf{a}_t(\mathbf{r}') \times \operatorname{grad}'\left(\frac{1}{|\mathbf{r}-\mathbf{r}'|}\right) dS'}_{\mathbf{I}_1} &+ \underbrace{\int_{S_\delta} \mathbf{a}_t(\mathbf{r}') \times \operatorname{grad}'\left(\frac{1}{|\mathbf{r}-\mathbf{r}'|}\right) dS'}_{\mathbf{I}_2} \end{aligned} \tag{6.22}$$

where S_δ is a small surface of arbitrary shape containing $\mathbf{r}$. To evaluate the self-contribution $\mathbf{I}_2$, we shall assume that S_δ is small enough for $\mathbf{a}_t$ to be uniform over that surface. Cross-multiplying by $\mathbf{u}_n$, and expanding the triple product, gives, from (3.69),

$$\begin{aligned} \lim_{P_1\to P} \mathbf{u}_n(\mathbf{r}) \times \mathbf{I}_2(\mathbf{r}) &= \int_{S_\delta} \mathbf{u}_n(\mathbf{r}) \times \left[\operatorname{grad}\left(\frac{1}{|\mathbf{r}-\mathbf{r}'|}\right) \times \mathbf{a}_t(\mathbf{r}')\right] dS' \\ &= -\mathbf{a}_t(\mathbf{r}) \lim_{P_1\to P} \int_{S_\delta} \frac{\partial}{\partial n}\left(\frac{1}{|\mathbf{r}-\mathbf{r}'|}\right) dS' \;=\; -2\pi\,\mathbf{a}_t(\mathbf{r}). \end{aligned}$$

Inserting this result into (6.22) leads to the important equations [201]

$$\lim_{P_1\to P}(\mathbf{u}_n \times \mathbf{I}) = -2\pi\,\mathbf{a}_t(\mathbf{r}) + \mathbf{u}_n(\mathbf{r}) \times \lim_{\delta\to 0} \int_{S-S_\delta} \mathbf{a}_t(\mathbf{r}') \times \operatorname{grad}'\left(\frac{1}{|\mathbf{r}-\mathbf{r}'|}\right) dS' \tag{6.23}$$

$$\lim_{P_2\to P}(\mathbf{u}_n \times \mathbf{I}) = 2\pi\,\mathbf{a}_t(\mathbf{r}) + \mathbf{u}_n(\mathbf{r}) \times \lim_{\delta\to 0} \int_{S-S_\delta} \mathbf{a}_t(\mathbf{r}') \times \operatorname{grad}'\left(\frac{1}{|\mathbf{r}-\mathbf{r}'|}\right) dS'. \tag{6.24}$$

Applied to $\mathbf{a}_t = (\mathbf{j}_S/4\pi)$, these equations give

$$\lim_{P_1 \to P} (\mathbf{u}_n \times \mathbf{h}) = -\frac{1}{2}\mathbf{j}_S(\mathbf{r}) + \mathbf{u}_n(\mathbf{r}) \times \frac{1}{4\pi} \lim_{\delta \to 0} \int_{S-S_\delta} \mathbf{j}_S(\mathbf{r}') \times \operatorname{grad}' \left(\frac{1}{|\mathbf{r} - \mathbf{r}'|} \right) dS' \tag{6.25}$$

$$\lim_{P_2 \to P} (\mathbf{u}_n \times \mathbf{h}) = \frac{1}{2}\mathbf{j}_S(\mathbf{r}) + \mathbf{u}_n(\mathbf{r}) \times \frac{1}{4\pi} \lim_{\delta \to 0} \int_{S-S_\delta} \mathbf{j}_S(\mathbf{r}') \times \operatorname{grad}' \left(\frac{1}{|\mathbf{r} - \mathbf{r}'|} \right) dS', \tag{6.26}$$

where $\mathbf{u}_n$ is a unit vector along the normal to S, directed from 1 to 2.

Surface currents are often used as a model for tightly wound current layers, as suggested in Figure 6.7*b*. They can also be generated by surface charges of density ρ_S, moving with velocity $\mathbf{v}$. Consider, as an illustration, a uniform ρ_S covering a circular disk of radius a. If the disk rotates with angular velocity Ω, the resulting current density is $\mathbf{j}_S = \Omega r \rho_S \mathbf{u}_\varphi$. From a magnetic point of view, the disk consists of a series of circular currents, and the axial field may be obtained by integrating contributions of the form (6.14). The result, for a point on the axis, is

$$\begin{aligned} b_z(0,z) &= \frac{\mu_0}{2} \int_0^a \frac{j_S r^2}{(r^2+z^2)^{\frac{3}{2}}}\, dr \\ &= \frac{\mu_0 \rho_S \Omega}{2} \int_0^a \left(\frac{r}{\sqrt{r^2+z^2}} \right)^3 dr \\ &= \frac{\mu_0 \rho_S \Omega}{2} \left[\frac{2z^2+a^2}{\sqrt{z^2+a^2}} - 2z \right]. \end{aligned} \tag{6.27}$$

6.4 FIELDS AT LARGE DISTANCES FROM THE SOURCES

From (6.6), the components (a_x, a_y, z_z) of the vector potential have the form of scalar potentials, each of which may be represented by a multipole expansion of type (3.29). It is preferable, however, to treat the problem vectorially from the start and make use of the solenoidal character of $\mathbf{j}$. Starting from (3.24), and remembering that at large distances $|\mathbf{r} - \mathbf{r}'|$ varies little over the source region V, we write (Fig. 6.8*a*)

$$\begin{aligned} \mathbf{a}(\mathbf{r}) &= \lim_{R \to \infty} \frac{\mu_0}{4\pi} \int_V \frac{\mathbf{j}(\mathbf{r}')}{|\mathbf{r} - \mathbf{r}'|}\, dV' \\ &= \frac{\mu_0}{4\pi R} \int_V \mathbf{j}(\mathbf{r})\, dV + \frac{\mu_0}{4\pi} \operatorname{grad}_0 \left(\frac{1}{R} \right) \cdot \int_V \mathbf{r}\mathbf{j}\, dV + \text{ higher terms.} \end{aligned} \tag{6.28}$$

The first term vanishes. To justify this assertion, let us evaluate the x-component of the integral, namely

$$\mathbf{u}_x \cdot \int_V \mathbf{j}(\mathbf{r})\, dV = \int_V \operatorname{grad} x \cdot \mathbf{j}(\mathbf{r})\, dV.$$

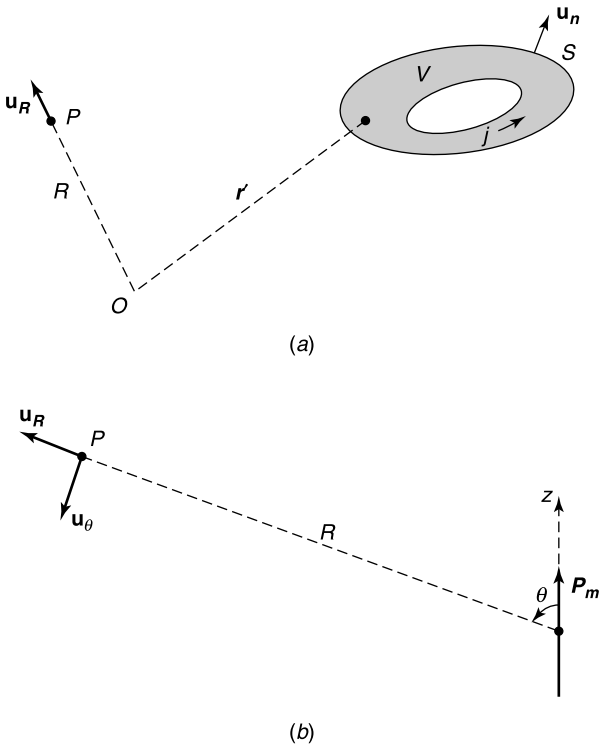

Figure 6.8 (*a*) Typical current source. (*b*) Magnetic dipole.

The right-hand term is a particular example of the more general integral

$$\int_V \mathbf{j}\cdot\text{grad}\,\theta\,dV = \int_V \text{div}\,(\theta\mathbf{j})\,dV - \int_V \theta\,\text{div}\,\mathbf{j}\,dV$$
$$= \int_S \theta\,\mathbf{u_n}\cdot\mathbf{j}\,dS - \int \theta\,\text{div}\,\mathbf{j}\,dV = \mathbf{0}. \tag{6.29}$$

This expression vanishes because $\mathbf{j}$ is solenoidal and tangent to S. Applying this result to θ, successively set equal to x, y, z, shows that the first term in (6.28) must vanish.

To evaluate the second term in (6.28), we scalar multiply the integral (a dyadic) with a constant vector $\mathbf{c}$. We subsequently split the dyadic into its symmetric and antisymmetric parts. Thus,

$$\mathbf{c}\cdot\int_V \mathbf{rj}\,dV = \frac{1}{2}\,\mathbf{c}\cdot\int_V (\mathbf{rj}+\mathbf{jr})\,dV + \frac{1}{2}\,\mathbf{c}\cdot\int_V (\mathbf{rj}-\mathbf{jr})\,dV. \tag{6.30}$$

The first integral vanishes. Consider, indeed, its ik component, which is

$$\int_V \mathbf{u}_i\cdot(\mathbf{rj}+\mathbf{jr})\cdot\mathbf{u}_k\,dV = \int_V [x_i(\mathbf{j}\cdot\mathbf{u}_k) + x_k\,\mathbf{j}\cdot\mathbf{u}_i]\,dV$$
$$= \int_V (x_i\,\text{grad}\,x_k + x_k\,\text{grad}\,x_i)\cdot\mathbf{j}\,dV = \int \text{grad}\,(x_i x_k)\cdot\mathbf{j}\,dV.$$

This expression vanishes because of property (6.29). The second term in (6.30), on the other hand, does *not* vanish and may be transformed as follows:

$$\frac{1}{2}\int_V [(\mathbf{c}\cdot\mathbf{r})\,\mathbf{j} - (\mathbf{c}\cdot\mathbf{j})\,\mathbf{r}]\,dV = \frac{1}{2}\mathbf{c}\times\int_V (\mathbf{j}\times\mathbf{r})\,dV.$$

If we introduce the *magnetic moment*

$$\mathbf{p}_m = \frac{1}{2}\int_V \mathbf{r}\times\mathbf{j}\,dV \qquad (\mathrm{A\,m^2}) \tag{6.31}$$

the vector potential at large distances takes the form

$$\lim_{R\to\infty}\mathbf{a}(\mathbf{r}) = \frac{\mu_0}{4\pi}\mathrm{grad}_p\left(\frac{1}{R}\right)\times\mathbf{p}_m + \text{ higher terms.} \tag{6.32}$$

An evaluation of the higher terms is deferred until radiation fields are discussed in Chapter 7 [133].

It is seen from (6.32) that $|\mathbf{a}|$ is $O(1/R^2)$ at large distances, from which we conclude that $\mathbf{b} = \mathrm{curl}\,\mathbf{a}$ will be $O(1/R^3)$. More specifically, for a z-oriented dipole (Fig. 6.8*b*)

$$\begin{aligned}\mathbf{a} &= \frac{\mu_0}{4\pi}p_m\frac{\sin\theta}{R^2}\,\mathbf{u}_\varphi\\ \mathbf{b} \;=\; \mathrm{curl}\,\mathbf{a} &= \frac{\mu_0}{4\pi}\,\mathrm{curl}\left(\mathrm{grad}\,\frac{1}{R}\times\mathbf{p}_m\right) = \frac{\mu_0}{4\pi}(\mathbf{p}_m\cdot\mathrm{grad})\,\mathrm{grad}\,\frac{1}{R}\\ &= \frac{\mu_0}{2\pi}\frac{p_m\cos\theta}{R^3}\,\mathbf{u}_R + \frac{\mu_0}{4\pi}\frac{p_m\sin\theta}{R^3}\,\mathbf{u}_\theta.\end{aligned} \tag{6.33}$$

An alternate method for the derivation of (6.32) is to represent the *current of a small loop* in $\mathbf{r}_0$ (*a "frill"*) by its distributional expression

$$\mathbf{j} = \mathrm{curl}\,[\delta(\mathbf{r}-\mathbf{r}_0)\,\mathbf{p}_m] = \mathrm{grad}\,\delta(\mathbf{r}-\mathbf{r}_0)\times\mathbf{p}_m. \tag{6.34}$$

If we insert (6.34) into (6.28), and take (A8.76) into account, we obtain

$$\begin{aligned}\mathbf{a}(\mathbf{r}) = \frac{\mu_0}{4\pi}\int_V \mathrm{curl}[\delta(\mathbf{r}-\mathbf{r}_0)\mathbf{p}_m]\frac{dV}{|\mathbf{r}-\mathbf{r}_0|} &= \frac{\mu_0}{4\pi}\int_V \delta(\mathbf{r}-\mathbf{r}_0)\mathbf{p}_m\times\mathrm{grad}\left(\frac{1}{|\mathbf{r}-\mathbf{r}_0|}\right)dV\\ &= \frac{\mu_0}{4\pi}\mathbf{p}_m\times\mathrm{grad}_0\left(\frac{1}{R}\right),\end{aligned}$$

which is exactly (6.32) since $\mathrm{grad}_0 R = -\mathrm{grad}_P R$.

Instead of starting from the integral representation (6.28) of $\mathbf{a}$ to derive the multipole expansion, it is also possible to resort to an expansion in spherical harmonics, in the manner discussed for the scalar potential in Section 3.7. Germane to the procedure is the expansion of $1/|\mathbf{r}-\mathbf{r}'|$ given in (3.99). Details are deferred until radiation fields are discussed in Chapter 7.

6.5 SCALAR POTENTIAL IN VACUUM

The magnetic induction in a region devoid of currents is irrotational and can therefore be written as $-\mu_0$ grad ψ. The point can be clarified by considering the volume outside the ringlike current depicted in Figure 6.1. An application of Stokes' theorem to contours *ACBDA* and *ACBEA* yields

$$\frac{1}{\mu_0}\int_{ACB}\mathbf{b}\cdot d\mathbf{c}=\frac{1}{\mu_0}\int_{ADB}\mathbf{b}\cdot d\mathbf{c}=\frac{1}{\mu_0}\int_{AEB}\mathbf{b}\cdot d\mathbf{c}+i,$$

where i, considered positive in the sense indicated on the figure, is the total current linking the loop *ACBEA*. The scalar potential can be made single-valued (and the line integral independent of the path) by introducing *barriers* or *cuts* of the type shown in Figure 6.9*a*. When this procedure is applied, the scalar potential takes different values on the two sides of the cut. For the linear current in Figure 6.2, for example, the magnetic potential is, to within an additive constant,

$$\psi(\mathbf{r})=\frac{i}{4\pi}\int_S\frac{\partial}{\partial n'}\left(\frac{1}{|\mathbf{r}-\mathbf{r}'|}\right)dS'=\frac{i}{4\pi}\int d\Omega, \tag{6.35}$$

where $d\Omega$, the solid angle subtended by the surface element dS, is positive when P is on the positive side of dS. Note that the positive sides of dS and $\mathbf{u}_n$ are linked to the chosen positive sense of i by the corkscrew rule. For the circular loop shown in Figure 6.3, the scalar potential on the axis is given by

$$\psi=\begin{cases}\dfrac{i}{2}\left(1-\dfrac{z}{a}\right) & \text{for } z>0\\[2ex] -\dfrac{i}{2}\left(1+\dfrac{z}{a}\right) & \text{for } z<0.\end{cases}$$

As expected from (6.35), the value of ψ differs by an amount of i on opposite sides of the $z=0$ plane. The choice of the cuts is rather evident in Figure 6.9*a*, where the region is

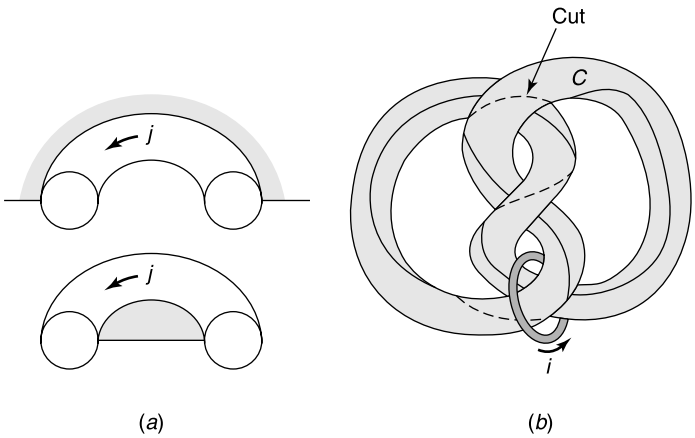

Figure 6.9 (*a*) Cuts for the scalar potential. (*b*) A multiply connected region (from A. Vourdas and K. J. Binns, Magnetostatics with scalar potentials in multiply connected regions, *IEE Proc.* **136A**, 49–54, 1989, with permission of the Institution of Electrical Engineers).

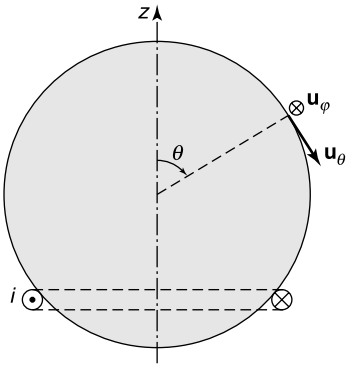

Figure 6.10 Coil wound on a nonmagnetic spherical support.

doubly connected. But in more complicated structures, such as the knotted configuration in Figure 6.9*b*, one must rely on a good feeling for the topology of the coils[7,8,9,10,11,12] [128].

To further illustrate the use of the scalar potential, consider the coil system of Figure 6.10, where the coil is wound in such a fashion that the resulting current density is

$$\mathbf{j}_S = ni \sin\theta \, \mathbf{u}_\varphi. \qquad (\text{n in m}^{-1})$$

Inside the sphere, the scalar potential is single-valued and harmonic. In consequence, from (3.95),

$$\psi_i = \sum_{c_n} R^n P_n(\cos\theta).$$

Similarly, outside the sphere,

$$\psi_e = \sum \frac{d_n}{R^{r+1}} P_n(\cos\theta).$$

The constants c_n and d_n can be determined by making use of the boundary conditions at $R = a$, which require the normal component of $\mathbf{b}$ to be continuous, and the tangential components to experience a jump given by (6.18). A few simple algebraic steps yield

$$\psi_i = -\frac{2ni}{3} R\cos\theta \qquad \psi_e = \frac{ni}{3}\frac{a^3}{R^2}\cos\theta. \tag{6.36}$$

The value of the induction is therefore

$$\begin{aligned} \mathbf{b}_i &= \mu_0 \frac{2ni}{3}(\mathbf{u}_R \cos\theta - \mathbf{u}_\theta \sin\theta) = \mu_0 \frac{2ni}{3}\mathbf{u}_z \\ \mathbf{b}_e &= \mu_0 \frac{ni}{3}\left(\frac{2a^3}{R^3}\cos\theta\,\mathbf{u}_R + \frac{a^3}{R^3}\sin\theta\,\mathbf{u}_\theta\right). \end{aligned} \tag{6.37}$$

The induction inside the sphere is seen to be parallel to the z axis. Outside the sphere, $\mathbf{b}_e$ is the field of a z-oriented dipole of moment $\left(\frac{4\pi a^3}{3}\right) ni$, equal to ni times the volume of

the sphere. The uniformity of the interior field has been exploited in a variety of devices, in particular in the area of magnetic resonance imaging (MRI).

The multivalued nature of the potential can be avoided by introducing a *reduced potential* θ. The method assumes that a field $\mathbf{t}$ can be found that satisfies

$$\begin{aligned} &\text{curl } \mathbf{t} = \mathbf{j} \\ &\mathbf{t} \text{ regular at infinity.} \end{aligned} \tag{6.38}$$

Clearly, $\text{curl}\left(\dfrac{\mathbf{b}}{\mu_0} - \mathbf{t}\right) = 0$ everywhere, hence we may write

$$\frac{1}{\mu_0}\mathbf{b} = \mathbf{t} - \text{grad } \theta, \tag{6.39}$$

where θ is single-valued. As a possible choice for $\mathbf{t}$ we may take the magnetic field in free space given by (6.7). Outside the current-carrying region, we may either use the representation (6.39) or the expression $\mathbf{h} = -\text{grad } \psi$, where ψ is a multivalued *total potential*. Two *approaches* are therefore possible: a first one, the *Ampèrian*, is based on $\mathbf{b}$ and the vector potential $\mathbf{a}$; a second one, named after *Coulomb*, emphasizes $\mathbf{h}$ and the scalar potential ψ.

6.6 MAGNETIC MATERIALS

The magnetic properties of a material result from the magnetic moments of its constituent atoms. The atomic moment finds its origin in three causes:

1. The orbital motion of the electrons around the nucleus
2. The intrinsic magnetic moment of the spinning electron
3. The magnetic moment of the nucleus.

In most materials, the contribution from the third factor is negligible. Immersion of a material in an external magnetic field results in a distortion of the electron orbits and in the production of a magnetic moment. This effect is called *diamagnetism*. In some materials, the atom has a magnetic moment even in the absence of external fields. This effect is termed *paramagnetism*.

The total magnetic moment in a volume dV is obtained by vectorially adding the moments of all atoms contained in dV. Suitable averaging processes introduce the concept of *moment (or dipole) density* $\mathbf{m}_m$, in terms of which the total moment of the volume dV can be written as $\mathbf{m}_m\, dV$. In paramagnetic and diamagnetic materials, $\mathbf{m}_m$ is typically proportional to the macroscopic induction $\mathbf{b}$ within the material. For ferromagnetic substances, however, the $\mathbf{m}_m(\mathbf{b})$ relationship is nonlinear and even multivalued.

From (6.32) and (A1.14), the vector potential produced by the moment distribution outside the magnetic body is given by (Fig. 6.11*a*)

$$\begin{aligned} \mathbf{a}(\mathbf{r}) &= -\frac{\mu_0}{4\pi}\int_V \text{grad}' \frac{1}{|\mathbf{r}-\mathbf{r}'|} \times \mathbf{m}_m(\mathbf{r}')\, dV' \\ &= \frac{\mu_0}{4\pi}\int_V \frac{\text{curl}'\, \mathbf{m}_m(\mathbf{r}')}{|\mathbf{r}-\mathbf{r}'|}\, dV' - \frac{\mu_0}{4\pi}\int_V \text{curl}' \frac{\mathbf{m}_m(\mathbf{r}')}{|\mathbf{r}-\mathbf{r}'|}\, dV'. \end{aligned}$$

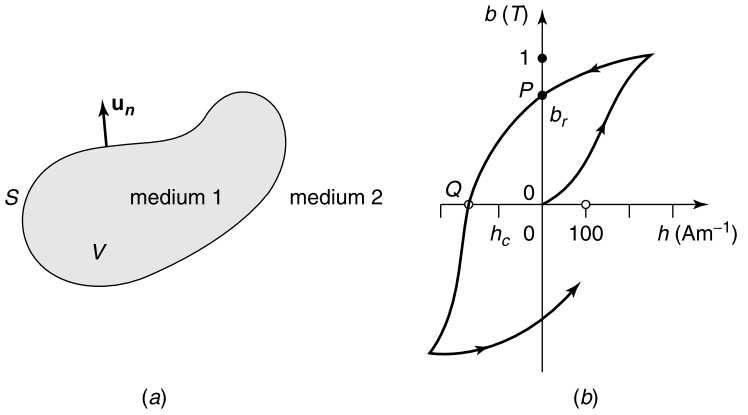

Figure 6.11 (*a*) Magnetic body. (*b*) Typical hysteresis curve.

This relationship can be further transformed by applying (A1.28). Thus,

$$\mathbf{a}(\mathbf{r}) = \frac{\mu_0}{4\pi}\int_V \frac{\text{curl}'\,\mathbf{m}_m(\mathbf{r}')}{|\mathbf{r}-\mathbf{r}'|}\,dV' + \frac{\mu_0}{4\pi}\int_S \frac{\mathbf{m}_m(\mathbf{r}')\times\mathbf{u}_{n'}}{|\mathbf{r}-\mathbf{r}'|}\,dS'. \tag{6.40}$$

In this form, the magnetic body effects the fields by means of equivalent magnetizing currents

$$\begin{aligned}\mathbf{j}' &= \text{curl}\,\mathbf{m}_m\\ \mathbf{j}'_S &= \mathbf{m}_m \times \mathbf{u}_n.\end{aligned} \tag{6.41}$$

These magnetization currents must be inserted into the right-hand term of (6.1), which becomes

$$\text{curl}\,\mathbf{b} = \mu_0\mathbf{j} + \mu_0\mathbf{j}' = \mu_0\mathbf{j} + \mu_0\,\text{curl}\,\mathbf{m}_m \tag{6.42}$$

or, equivalently,

$$\text{curl}\left(\frac{\mathbf{b}}{\mu_0} - \mathbf{m}_m\right) = \mathbf{j}. \tag{6.43}$$

The term between parentheses is the *magnetic field strength* **h** (or more concisely, the magnetic field). The **h** field satisfies the relationships

$$\begin{aligned}\text{curl}\,\mathbf{h} &= \mathbf{j}\\ \mathbf{b} &= \mu_0\mathbf{h} + \mu_0\mathbf{m}_m.\end{aligned} \tag{6.44}$$

The boundary conditions on S are, from (6.18) and (6.41),

$$\begin{aligned}\mathbf{u}_n\cdot(\mathbf{b}_2 - \mathbf{b}_1) &= 0\\ \mathbf{u}_n \times (\mathbf{h}_2 - \mathbf{h}_1) &= \mathbf{j}_S.\end{aligned} \tag{6.45}$$

The equation satisfied by the vector potential now becomes

$$\nabla^2 \mathbf{a} = -\text{curl}\, \mathbf{b} = -\mu_0(\mathbf{j} + \mathbf{j}') = -\mu_0 \mathbf{j} - \mu_0 \{\text{curl}\, \mathbf{m}_m\} - \mu_0(\mathbf{m}_m \times \mathbf{u}_n)\, \delta_S. \quad (6.46)$$

In media for which $\mathbf{m}_m$ is linearly related to $\mathbf{b}$ (and consequently to $\mathbf{h}$):

$$\mathbf{b} = \mu_0(\chi_m + 1)\mathbf{h} = \mu_0 \mu_r \mathbf{h} = \mu \mathbf{h} \quad \text{with} \quad \mathbf{m}_m = \chi_m \mathbf{h}, \quad (6.47)$$

where χ_m is the *magnetic susceptibility* of the material, and μ_r its *magnetic permeability*. For *diamagnetic* materials, χ_m is negative (with absolute value of the order 10^{-5}), and μ_r is less than 1. Examples of diamagnetic substances are He, H_2, and Bi. For *paramagnetic* materials, such as K, O, and rare-earth salts, χ_m is positive and of the order 10^{-3}. In *ferromagnetic* materials, the relationship between $|\mathbf{b}|$ and $|\mathbf{h}|$ is nonlinear and of the type shown schematically in Figure 6.11*b*. The large moment densities in ferromagnetic materials are due to the action of strong quantum-mechanical exchange forces that lock adjacent atomic dipoles into rigid parallelism. The parallel dipoles form regions, termed *domains*, in which there is essentially perfect alignment. The linear dimensions of these regions are of the order 10^{-6} m. The common orientation of the dipoles differs from one domain to the next. An externally applied magnetic field tends to align the various domains, and saturation comes about when this alignment has been completed. Hysteresis occurs because the domain boundaries do not return completely to their original positions when the external field is suppressed. Above a temperature termed the *Curie temperature*, ferromagnetic materials become paramagnetic.

Problems involving materials with nonlinear $b(h)$ characteristic are very difficult to solve. These problems become more tractable when the characteristics are linearized over a small interval. In the vicinity of P (Fig. 6.11*b*), this can be done by writing

$$\mathbf{b} = \mu \mathbf{h} + \mu_0 \mathbf{m}_{m0} = \mu \mathbf{h} + \mathbf{b}_r, \quad (6.48)$$

where $\mathbf{m}_{m0}$ is the *remanent polarization*. More generally, the slope (db/dh) at an arbitrary point of the curve is an important parameter termed the *differential permeability*. Note that the value of μ_r, conceived as the ratio $(b/\mu_0 h)$, varies widely along the curve. For Si-iron, for example, the initial value may be 400, later to reach a maximum of 7000. For 78-Permalloy, the corresponding figures would be 9000 and 100,000.

The magnetic field h needed to bring the induction to zero is the *coercivity* h_c (equal to OQ on Fig. 6.11*b*). Various magnetization models are available to predict the behavior of magnetic materials (e.g., those of Stoner-Wohlfahrt, Jiles-Atherton, Globus and Preisach[13]).

6.7 PERMANENT MAGNETS

Permanent magnets find numerous applications, for example, in small motors and, on a much larger scale, as components of particle accelerators. They are also found in systems where field uniformity is essential, for example in magnetic resonance devices of the kind used in diagnostic medicine, where inductions of up to 1 T must be generated with uniformities of 10 parts per million or better.[14] To a good approximation, the permanent magnet may be characterized by a fixed residual (or remanent) polarization density $\mathbf{m}_{m0}$. The problem therefore consists of determining the fields produced by a rigid, constant $\mathbf{m}_{m0}$ (Fig. 6.12*a*). In the Ampèrian approach, the induction $\mathbf{b}$ satisfies (6.46), in which one should set $\mathbf{j} = 0$

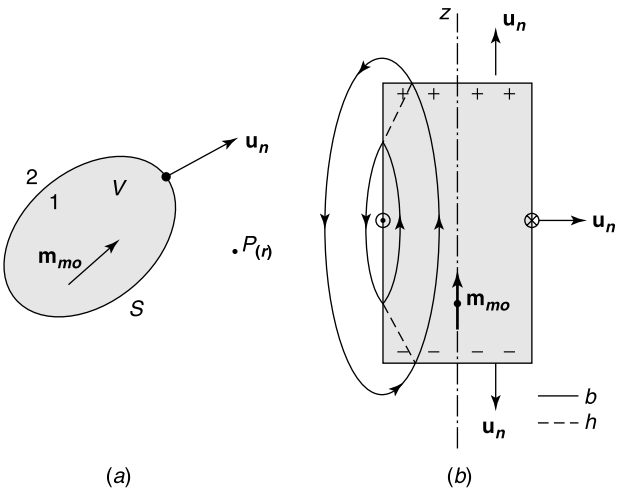

Figure 6.12 (*a*) General permanent magnet. (*b*) Cylindrical permanent magnet.

and $\mathbf{m}_m = \mathbf{m}_{m0}$. Consider, for example, the uniformly polarized cylindrical magnet shown in Figure 6.12*b*. The volume currents vanish because $\mathbf{m}_{m0} = m_{m0}\,\mathbf{u}_z$ is uniform. The surface currents vanish at the top and bottom surfaces but exist on the lateral wall, where they actually follow azimuthal circular paths. The conclusion is immediate: As far as **b** is concerned, the magnet can be replaced by a cylindrical current sheet of axis Oz. In consequence, the lines of **b** are not refracted at the *end* surfaces, but they suffer a discontinuity at the *side* surfaces, where the tangential component of **b** experiences a jump equal to $\mu_0\mathbf{m}_{m0}$. A more detailed plot of **b** may be obtained by determining **a** according to (6.46) and subsequently evaluating curl **a**. Taking (A8.91) into account, we note that the equation satisfied by **a** can be written as

$$\text{curl curl } \mathbf{a} = \{\text{curl } \mathbf{b}_r\} + (\mathbf{b}_r \times \mathbf{u}_n)\,\delta_S. \tag{6.49}$$

In the *Coulomb* approach, based on magnetic charges, one starts from

$$\mathbf{h} = -\text{grad } \psi = \frac{1}{\mu_0}\mathbf{b} - \mathbf{m}_{m0}. \tag{6.50}$$

From (6.44), **h** is irrotational throughout space, hence ψ is single-valued. To derive the equation satisfied by ψ, we take the divergence of both members of (6.50) and obtain, from (A8.90),

$$-\text{div } \mathbf{h} = \nabla^2\psi = \text{div } \mathbf{m}_{m0} = \{\text{div } \mathbf{m}_{m0}\} - (\mathbf{u}_n \cdot \mathbf{m}_{m0})\,\delta_S. \tag{6.51}$$

The two terms on the right-hand side may be interpreted as magnetic volume and surface charges. Further, ψ must be regular at infinity and must satisfy the following boundary conditions on S (Fig. 6.12*a*):

1. $\psi_2 = \psi_1$ (from the continuity of the tangential component of **h**).
2. $(\partial\psi/\partial n)_2 = (\partial\psi/\partial n)_1 - \mathbf{u}_n \cdot \mathbf{m}_{m0}$ (from the continuity of b_n).

These conditions are similar to those satisfied by the electrostatic potential in the presence of volume and surface charges. As in electrostatics, therefore, the solution for ψ is

$$\psi(\mathbf{r}) = -\frac{1}{4\pi}\int_V \frac{\text{div}'\,\mathbf{m}_{m0}(\mathbf{r}')}{|\mathbf{r}-\mathbf{r}'|}\,dV' + \frac{1}{4\pi}\int_S \frac{\mathbf{m}_{m0}(\mathbf{r}')\cdot\mathbf{u}_n}{|\mathbf{r}-\mathbf{r}'|}\,dS'. \tag{6.52}$$

This relationship can be transformed by using (A1.12), which yields

$$\psi(\mathbf{r}) = \frac{1}{4\pi}\int_V \mathbf{m}_{m0}(\mathbf{r}')\cdot\text{grad}'\frac{1}{|\mathbf{r}-\mathbf{r}'|}\,dV' = -\frac{1}{4\pi}\int_V \mathbf{m}_{m0}(\mathbf{r}')\cdot\text{grad}\frac{1}{|\mathbf{r}-\mathbf{r}'|}\,dV'. \tag{6.53}$$

The long-distance fields of the magnet are, not surprisingly, those of a dipole of moment $\mathbf{p}_m = \int_V \mathbf{m}_{m0}\,dV$. Applied to the simple example of Figure 6.12*b*, Equation (6.52), combined with div $\mathbf{m}_{m0} = 0$, shows that the potential must be

$$\psi(\mathbf{r}) = \frac{m_{m0}}{4\pi}\int_S \frac{\mathbf{u}_{n'}\cdot\mathbf{u}_z}{|\mathbf{r}-\mathbf{r}'|}\,dS'. \tag{6.54}$$

This equation shows that ψ is proportional to the electrostatic potential stemming from surface charges $\pm m_{m0}$, located at both ends of the magnet.

The Hertz Potential

The magnetic field stemming from a permanent magnet can be expressed in terms of a *Hertz potential*

$$\boldsymbol{\pi}_m = \frac{1}{4\pi}\int_V \frac{\mathbf{m}_{m0}(\mathbf{r}')}{|\mathbf{r}-\mathbf{r}'|}\,dV' \qquad \text{(A m)}. \tag{6.55}$$

Because

$$\begin{aligned}\text{div}\,\boldsymbol{\pi}_m &= \frac{1}{4\pi}\int_V \text{div}\left[\frac{1}{|\mathbf{r}-\mathbf{r}'|}\mathbf{m}_0(\mathbf{r}')\right]dV' \\ &= \frac{1}{4\pi}\int_V \text{grad}\left(\frac{1}{|\mathbf{r}-\mathbf{r}'|}\right)\cdot\mathbf{m}_0(\mathbf{r}')\,dV',\end{aligned} \tag{6.56}$$

reference to (6.40) and (6.53) shows that

$$\psi = -\text{div}\,\boldsymbol{\pi}_m \qquad \text{(A)} \tag{6.57}$$

and

$$\mathbf{a} = \mu_0\,\text{curl}\,\boldsymbol{\pi}_m \qquad \text{(T m)}. \tag{6.58}$$

The evaluation of $\mathbf{a}$, ψ and $\boldsymbol{\pi}_m$ is a simple matter, in principle at least. Consider, as an illustration, the radially polarized cylinder in Figure 6.13. This type of polarization is

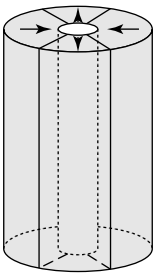

Figure 6.13 Radially polarized cylinder (from E. P. Furlani, S. Reznik, and A. Kroll, A three-dimensional field solution for radially polarized cylinders, *IEEE Trans. MAG* **31**, 844–851, 1995, with permission of IEEE).

used in magnetic encoders or in the controlled movement of small magnetic particles.[15] The magnetization is given by

$$\mathbf{m}_{m0} = \pm m_{m0}\,\mathbf{u}_r \qquad (\mathrm{A\ m^{-1}}),$$

where the + and − signs take into account the alternating polarity of adjacent poles. Because curl $\mathbf{m}_{m0} = 0$, (6.40) implies that the magnet may be replaced by surface currents ($\mathbf{m}_{m0} \times \mathbf{u}_n$). Analyzing each quarter of the cylinder separately leads to currents that are circular (azimuthal) on the top and bottom surfaces and z-directed on the sidewall.

Other magnet shapes can sometimes be approximated by ellipsoids, a geometry for which the fields can be determined by separation of variables.[16] Prolate spheroids, in particular, provide a good model for simulating cylinders, as are oblate spheroids for disks, and oblate ellipsoids for ribbons and films [17, 20].

6.8 THE LIMIT OF INFINITE PERMEABILITY

The permeability μ_r of para- and diamagnetic bodies is very close to one; hence the presence of these bodies may be conceived as a small perturbation. Ferromagnetic bodies, with their nonlinear characteristics and strong equivalent μ_r, warrant more attention. It is meaningful, in a first approximation, to endow them with an infinite μ_r (in which case the material will be called *iron*). The boundary conditions at the interface between two media lead to the relationship (Fig. 6.14*a*)

$$\frac{1}{\mu_1}\tan\theta_1 = \frac{1}{\mu_2}\tan\theta_2. \tag{6.59}$$

When region 1 is filled with iron, two possibilities arise:

1. Either the lines of force in medium 2 are perpendicular to the iron (and $\theta_2 = 0$), or
2. The lines of force in the iron are tangent to S $\left(\text{and } \theta_1 = \dfrac{\pi}{2}\right)$.

The choice depends on the shape of the iron, and more specifically on its connectedness. The influence of connectedness has already been discussed in Section 4.10, and the contents of that section are relevant to the present analysis.

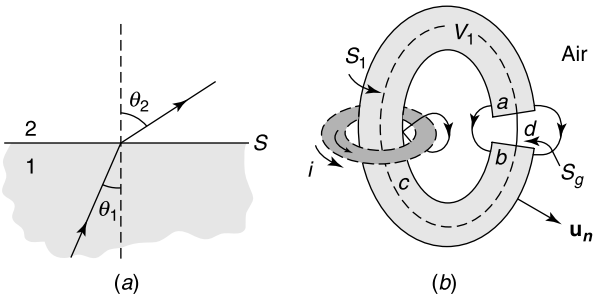

Figure 6.14 (*a*) Refraction of the lines of force of **b**. (*b*) Open magnetic ring.

6.8.1 Simply Connected Region

Assume first that the iron region is simply connected and devoid of current (Fig. 6.14*b*). Inside the iron, **h** is irrotational and can be derived from a single-valued potential satisfying

$$\begin{aligned} \nabla^2 \psi &= 0 \qquad (\text{in } V_1) \\ \frac{\partial \psi}{\partial n} &= 0 \qquad (\text{on } S_1). \end{aligned} \tag{6.60}$$

The discussion of Neumann's problem in Section 4.4 shows that the only solution of (6.60) is ψ = constant, hence that $\mathbf{h} = 0$ in the iron. Because the tangential component of **h** is continuous across S_1, **h** in air must be perpendicular to the iron. Its value may be obtained by solving the exterior problem[17]

$$\begin{aligned} \text{curl } \mathbf{h} &= \mathbf{j} \\ \text{div } \mathbf{h} &= 0 \\ \mathbf{u}_n \times \mathbf{h} &= 0 \qquad (\text{on } S_1) \\ |D^3 \mathbf{h}| &\text{ bounded at infinity.} \end{aligned} \tag{6.61}$$

A few exterior lines of force are sketched in Figure 6.14*b*. As one proceeds along contour C, part of the flux Φ of **b** is lost by leakage through the walls. If a small air gap is present, the **h** field will be strong there, because

$$i = \int_C \mathbf{h} \cdot \mathbf{dc} = \int_a^b \mathbf{h} \cdot \mathbf{dc} \approx hd \approx \frac{b}{\mu_0} d \approx \Phi \left(\frac{d}{\mu_0 S_g} \right).$$

In the limit of small d, most of the flux will be left to flow through the air gap, and its value approaches i divided by the *reluctance* $\left(d/\mu_0 S_g\right)$ of the gap.

The problem remains of finding the (nonzero) field **b** in the iron. This field is irrotational because of the absence of current in V_1. It follows that **b** can be written as grad θ, where θ satisfies

$$\begin{aligned} \nabla^2 \theta &= 0 \qquad (\text{in } V_1) \\ \frac{\partial \theta}{\partial n} &= b_n \qquad (\text{on } S). \end{aligned} \tag{6.62}$$

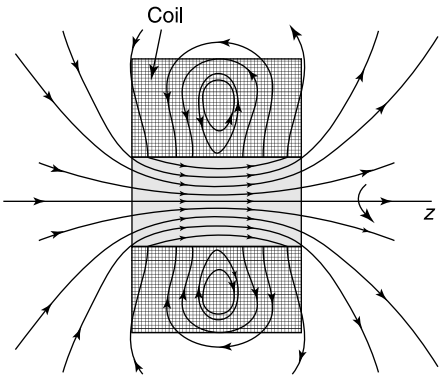

Figure 6.15 A coil wound around a cylinder (from E. Durand. *Magnétostatique*. Masson, Paris, 1968, with permission of Editions Dunod).

The value of b_n results from the solution of (6.6.1). A typical profile for the lines of force of $\mathbf{b}$ is shown in Figure 6.15, in which a thick coil carries a uniform current density J_φ, wound around a circular cylinder of infinite permeability.

6.8.2 Multiply Connected Regions

Assume that the iron region is *doubly-connected* (Fig. 6.16). Two cases must be carefully distinguished. In the *first* one, the total number of ampère-turns linking the iron is equal to zero. The integral $\int_c \mathbf{h}\cdot d\mathbf{c}$ around any closed contour in the iron is therefore equal to zero; hence, $\mathbf{h}$ derives from a *single-valued* scalar potential. It follows that the interior problem can be solved as in the case of a simply connected region, which implies that $\mathbf{h} = 0$ in the iron. This, in turn, means that the lines of force in air are perpendicular to the boundary. Assume now, as a *second* possibility, that a nonzero number of ampère-turns links the iron. The integral of $\mathbf{h}$ around the hole is i. Both curl $\mathbf{h}$ and div $\mathbf{h}$ are zero and, because b_n must remain bounded on S_1, h_n vanishes just inside the iron, which means that $\mathbf{h}$ must be tangent to the boundary. These are precisely the conditions satisfied by the harmonic vector $\mathbf{h}_0$ defined in (4.120), hence we may write[†] $\mathbf{h} = i\mathbf{h}_0$. This relationship shows that the magnetic

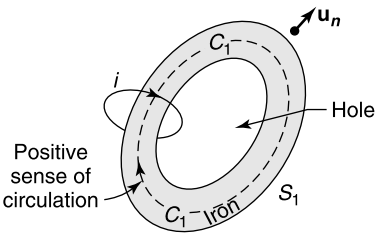

Figure 6.16 Doubly connected iron region (from J. Van Bladel, Magnetostatic fields at an iron-air boundary, *Am. J. Phys.* **29**, 732–736, 1961, with permission of the American Institute of Physics).

[†]A much deeper topological study of fields and their periods appears in A. A. Blank, K. O. Friedricks, and H. Grad, Theory of Maxwell's equations without displacement current, Report NYO-6486, New York University, 1957.

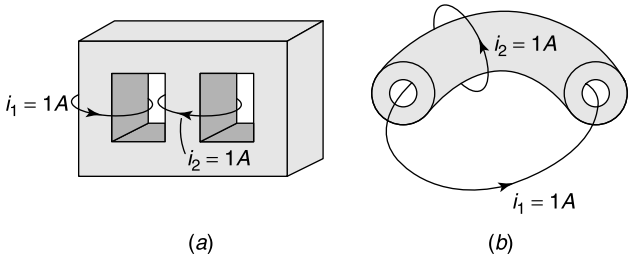

Figure 6.17 Triply connected regions (from J. Van Bladel, Magnetostatic fields at an iron-air boundary, *Am. J. Phys.* **29**, 732–736, 1961, with permission of the American Institute of Physics).

field in the iron is proportional to i and that the shape of its lines of force is independent of the location of the current i. It also implies that the magnetic field at the boundary has a nonzero tangential component $i\mathbf{h}_0$, hence that the lines of force in air are *not* perpendicular to the iron boundary. Further, the induction $\mathbf{b}$ is infinite in the iron. This nonphysical result is a consequence of our nonphysical assumption of infinite μ_r. In actual materials of high (but not infinite) permeability, $\mathbf{b}$ is approximately given by $\mu_r\mu_0 i\mathbf{h}_0$.

The preceding analysis can easily be adapted to more complicated structures such as the three-legged transformer or the hollow torus shown in Figure 6.17. The corresponding iron regions are triply connected, and their analysis requires the introduction of two linearly independent vectors, $\mathbf{h}_{01}$ and $\mathbf{h}_{02}$. Two such vectors are the magnetic fields produced by the unit currents i_1 and i_2 depicted in Figure 6.17.

6.8.3 Edge Condition

The analysis of the behavior of $\mathbf{b}$ and $\mathbf{h}$ near geometrical singularities proceeds as in Sections 5.2, 5.3, and 5.12, where dielectrics and conductors are considered. Extrapolated to iron wedges the results are[18]

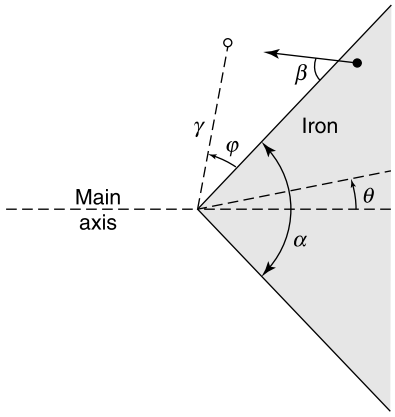

Figure 6.18 Coordinates suitable for the study of fields in air, and in an iron wedge.

1. Outside the wedge (Fig. 6.18), **h** is of the general form

$$\begin{aligned}\mathbf{h} &= A\nu r^{\nu-1}(\sin \nu\varphi \mathbf{u}_r + \cos \nu\varphi \mathbf{u}_\varphi) \\ &= A\mathbf{u}_z \times \text{grad}\,(r^\nu \cos \nu\varphi)\end{aligned} \tag{6.63}$$

where A is some proportionality factor, and $\nu = \pi/(2\pi - \alpha)$. The lines of force correspond with

$$\Gamma = r^\nu \cos \nu\varphi = \text{constant}.$$

The flux between two lines is proportional to the difference between the two corresponding values of Γ. Note that the singularity does not occur when the incident potential is antisymmetric with respect to the main axis.

2. The singularity *within the iron* results from the expression

$$\mathbf{b} = \frac{A\mu_0}{\sin(\nu\alpha/2)} r^{\nu-1}(-\cos \nu\theta \mathbf{u}_r + \sin \nu\theta \mathbf{u}_\theta). \tag{6.64}$$

The lines of force, given by

$$r^\nu \sin(\nu\theta) = \text{constant}$$

form an angle $\beta = \left(\frac{\nu\alpha}{2}\right)$ with the boundary. Outside the iron these lines are perpendicular to the wedge. The profile of the lines of force is illustrated in Figure 6.19 for $\alpha = 90°$ (to which correspond $\nu = \frac{2}{3}$ and $\beta = 30°$). When the wedge is reentrant, (i.e., for $\alpha > 180°$), the field remains finite in air, but **b** in the iron remains singular and of the form

$$\mathbf{b} \doteq r^{\left(\frac{\pi}{\alpha}-1\right)} \left(\sin \frac{\pi}{\alpha}\theta \mathbf{u}_r + \frac{\pi}{\alpha} \cos \frac{\pi}{\alpha}\theta \mathbf{u}_\theta\right). \tag{6.65}$$

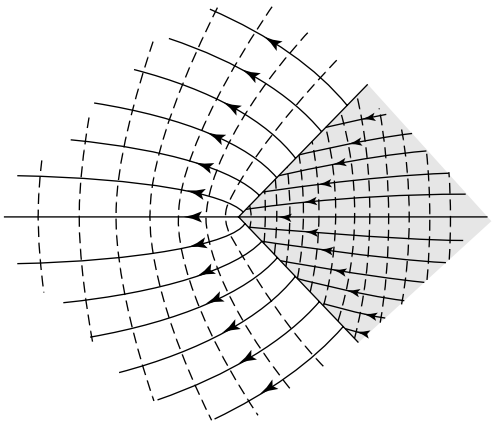

Figure 6.19 Lines of force and equipotentials for a 90° wedge (from J. Van Bladel, Induction at a corner in perfect iron, *IEE Proc.* **128-B**, 219–221, 1981, with permission of the Institution of Electrical Engineers).

In the $\mu_{\mathbf{r}} = \infty$ model, which forms the basis of the current analysis, $\mathbf{b}$ becomes very large near the edge. With actual materials saturation develops in that region and the edge becomes magnetically rounded-off.

6.9 TWO-DIMENSIONAL FIELDS IN THE PLANE

6.9.1 In Vacuum

Let us first assume that the generating current flows *parallel* to the z-axis (Fig. 6.20a). From the general background provided by (6.5) and Section 5.1, the vector potential satisfies

$$\nabla^2 a = -\mu_0 j, \tag{6.66}$$

and its magnitude is

$$a(\mathbf{r}) = \frac{\mu_0}{2\pi} \int_S j(\mathbf{r}') \log_e \frac{L}{|\mathbf{r} - \mathbf{r}'|} dS'. \tag{6.67}$$

At large distances:

$$\lim_{r\to\infty} a = \frac{\mu_0 i}{2\pi} \log_e \frac{L}{r} + \text{ a regular function.} \tag{6.68}$$

The induction generated by the current i $\left(\text{equal to } \int_S j\, dS\right)$ is given by

$$\mathbf{b} = \text{curl } (a\mathbf{u}_z) \;=\; \text{grad } a \times \mathbf{u}_z \;=\; \frac{\partial a}{\partial y}\mathbf{u}_x - \frac{\partial a}{\partial x}\mathbf{u}_y$$

$$\lim_{r\to\infty} \mathbf{b} = \frac{\mu_0 i}{2\pi r}\mathbf{u}_\varphi + \text{ terms in } \frac{1}{r^2}. \tag{6.69}$$

The lines of constant a are the lines of force of $\mathbf{b}$, and a is a flux function because the flux through 1–2 is

$$\int_1^2 (\mathbf{b}\cdot\mathbf{u}_m)\, dl = \int_1^2 (\text{grad } a \times \mathbf{u}_z)\cdot\mathbf{u}_m\, dl = a_2 - a_1. \tag{6.70}$$

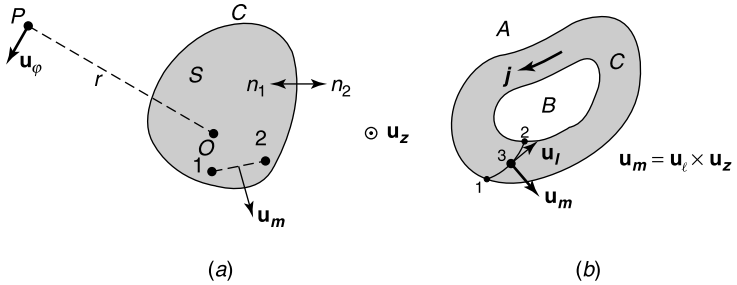

Figure 6.20 (a) Axial currents. (b) Transverse currents.

When the current is *transverse* (Fig. 6.20*b*), both **b** and **h** are z-directed and

$$\text{curl}\,(h\mathbf{u}_z) = \text{grad}\,h \times \mathbf{u}_z = \mathbf{j}. \tag{6.71}$$

In A, outside the current-carrying region, h is uniform, and therefore zero because it must vanish at large distances. In B:

$$\int_1^2 \text{grad}\,h \cdot d\mathbf{l} = h(2) = \int_1^2 (\mathbf{u}_z \times \mathbf{j}) \cdot \mathbf{u}_l\, dl = \int_1^2 (\mathbf{j} \cdot \mathbf{u}_m)\, dl. \tag{6.72}$$

The field in region B is also uniform and equal to the current flowing per unit axial length of the conductor. Further, a corresponding integration between points 1 and 3 shows that the magnetic field at point 3 is numerically equal to the current between points 1 and 3 (both expressed in A m^{-1}). Two examples will illustrate these general considerations. In the first one, the dipole line in Figure 6.21*a* generates a vector potential

$$\begin{aligned} a &= \frac{\mu_0 i}{2\pi} \log_e \frac{r_2}{r_1} \\ \lim_{d \to 0} a &= \frac{\mu_0}{2\pi} \frac{id \sin\theta}{r}. \end{aligned} \tag{6.73}$$

The resulting magnetic field is proportional to $(1/r^2)$. Its lines of force are given by the relationship a = constant or, equivalently, by $(\sin\theta)/r$ = constant. This is the equation of a circle through the dipole (Fig. 6.21*b*). In the second example, the source is an infinite array of equidistant wires, each of which carries a current i (Fig. 6.22*a*). The vector potential is now

$$\begin{aligned} a &= -\frac{\mu_0 i}{4\pi} \log_e \left(r_0^2\, r_1^2\, r_{1'}^2\, r_2^2 r_{2'}^2 \ldots \right) + \text{ constant} \\ &= -\frac{\mu_0 i}{4\pi} \log_e \left(\cosh \frac{2\pi x}{a} - \cos \frac{2\pi y}{a} \right) + \text{ constant}. \end{aligned} \tag{6.74}$$

It generates a magnetic field

$$\mathbf{h} = -\frac{i}{2a} \frac{\sin(2\pi y/a)}{\cosh(2\pi x/a) - \cos(2\pi y/a)} \mathbf{u}_x + \frac{i}{2a} \frac{\sinh(2\pi x/a)}{\cosh(2\pi x/a) - \cos(2\pi y/a)} \mathbf{u}_y. \tag{6.75}$$

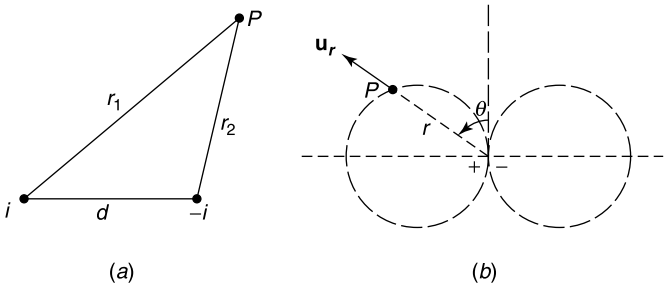

Figure 6.21 (*a*) Parallel lines with opposite currents. (*b*) Lines of force of the dipole line.

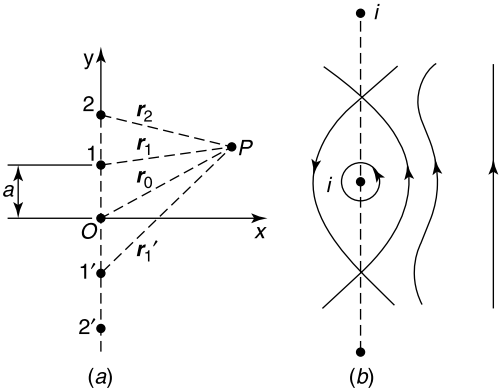

Figure 6.22 (*a*) Infinite array of identical line currents. (*b*) Lines of force.

Some of the lines of force of this field are sketched in Figure 6.22*b*. Far away from the array (i.e., for $|x| \gg a$), the magnetic field becomes parallel to the $x = 0$ plane, and its magnitude approaches the value $i/2a$. This is precisely the field produced by a current sheet of density (i/a) A m^{-1}. We conclude that the discrete nature of the array influences the structure of the field only up to distances of the order of a.

6.9.2 In the Presence of Magnetic Materials

Consider again the geometry of Figure 6.20*a*, but let the z-oriented current flow in a homogeneous magnetic material. The vector potential still satisfies (6.66), but μ_0 must be replaced by μ. Potential a must be continuous across contour C. In the presence of surface currents $j_S\mathbf{u}_z$ on C, the magnetic field suffers a step discontinuity

$$\mathbf{u}_{n1} \times \mathbf{h}_1 + \mathbf{u}_{n2} \times \mathbf{h}_2 = j_S\mathbf{u}_z.$$

From (6.69), therefore, the normal derivatives of a across C are related by

$$\frac{1}{\mu_{r1}}\frac{\partial a}{\partial n_1} + \frac{1}{\mu_{r2}}\frac{\partial a}{\partial n_2} = -\mu_0 j_S. \tag{6.76}$$

A solution by images is available for a linear current i located outside a semi-infinite medium (Fig. 6.23*a*). The field in vacuum is generated by the original current and an image current $i(\mu_r - 1)/(\mu_r + 1)$ located in $\mathbf{r}'$. The field in the material is produced by a current $2i/(\mu_r + 1)$, located in $\mathbf{r}$, assuming space to be homogeneously filled with the magnetic material. The resulting lines of force are shown in Figure 6.23*b*. When a current i is located at $\mathbf{r}'$, inside the material, the field in vacuum is that of a current $2i\,\mu_r/(\mu_r + 1)$ in $\mathbf{r}'$, in an otherwise empty space. The field in the material is that of a current i in $\mathbf{r}'$ and $-i\,(\mu_r - 1)/(\mu_r + 1)$ in $\mathbf{r}$. The lines of force are shown in Figure 6.23*c*.

The method of images is applicable to a few other shapes, such as the elliptic cylinder[19] [22]. As an alternate approach separation of variables has been applied to numerous configurations [17, 55], for example to a circular cylinder immersed in a uniform $\mathbf{b}^i$ (Fig. 6.24). The cylinder carries a uniform axial current density j. The incident potential is

$$a^i = b^i y = b^i r \sin\varphi.$$

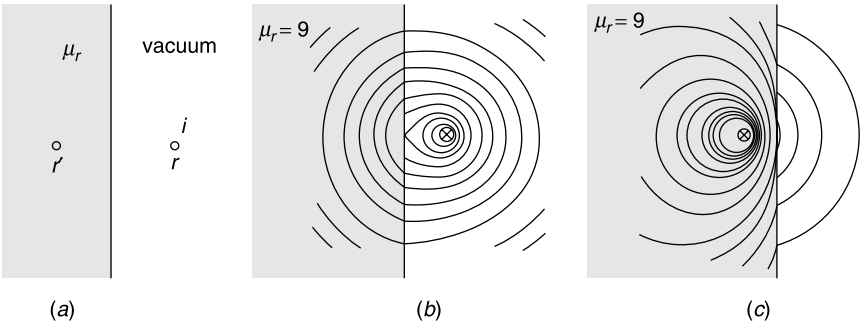

Figure 6.23 (*a*) **r** and its image **r**′. (*b*) Line current in front of the magnetic medium. (*c*) Line current inside the magnetic medium (from B. Hague. *Electromagnetic Problems in Electrical Engineering*. Oxford University Press, 1929, with permission of Oxford University Press).

From (5.7), the *exterior* potential may be written as

$$a_2 = \sum_{n=1}^{\infty} \left(\sin n\varphi \frac{A_n}{r^n} \right) + b^i r \sin \varphi + A_0 \log_e r.$$

The *interior* potential must satisfy Poisson's equation

$$\frac{\partial^2 a_1}{\partial r^2} + \frac{1}{r}\frac{\partial a_1}{\partial r} + \frac{1}{r^2}\frac{\partial^2 a_1}{\partial \varphi^2} = -\mu j.$$

This equation has the particular solution $-(\mu j r^2)/4$. The general solution is therefore

$$a_1 = \sum_{n=1}^{\infty} \sin n\varphi \, B_n r^n + B_0 - \mu j \frac{r^2}{4}.$$

The A and B constants are determined by requiring a to be continuous at $r = b$, and to satisfy (6.76). The final result is

$$a_1 = b^i \sin \varphi \frac{2\mu_r}{\mu_r + 1} r - \frac{1}{4\pi}\mu_r \mu_0 i \left(\frac{r}{b}\right)^2 + \frac{1}{4\pi}\mu_r \mu_0 i$$

$$a_2 = b^i \sin \varphi \left(r + \frac{b^2}{r}\frac{\mu_r - 1}{\mu_r + 1} \right) - \frac{1}{2\pi}\mu_0 \, i \log_e r. \tag{6.77}$$

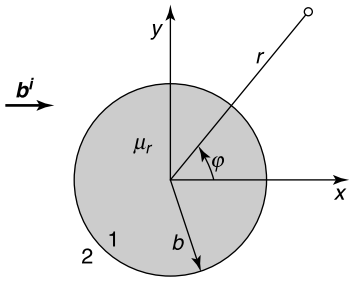

Figure 6.24 Current-carrying magnetic cylinder in a uniform incident field.

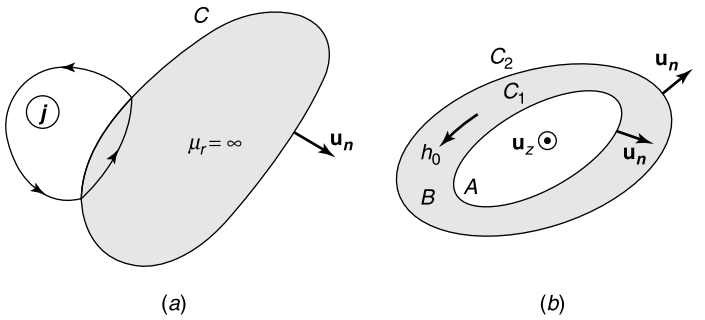

Figure 6.25 Simply and doubly connected regions (from J. Van Bladel, Magnetostatic fields at an iron-air boundary, *Am. J. Phys.* **29**, 732–736, 1961, with permission of the American Institute of Physics).

6.9.3 Infinite Permeability

The results of Section 6.8 can easily be adapted to a two-dimensional situation. If the cross section is simply connected and does not carry any current (Fig. 6.25*a*), **h** vanishes in the iron, and the exterior lines of force are perpendicular to the iron surface. If the region is doubly connected, and does not carry any current (Fig. 6.25*b*), two cases must be distinguished:

1. The total (z-oriented) current in the central vacuum region is zero. For such a case **h** vanishes in the iron, and the lines of force in A and C_2 are perpendicular to the iron. The fields inside and outside the iron are uncoupled and depend only on the currents within their own regions. The iron acts as a perfect screen.
2. The total current i in the central region is different from zero. The magnetic field in the iron does not vanish and can be written as

$$\mathbf{h} = i\mathbf{h}_0 = Ti(\mathbf{u}_z \times \mathbf{e}_0), \tag{6.78}$$

where $\mathbf{e}_0$ is the electric field that results from a unit potential difference impressed between C_1 and C_2 (assumed metallized). Vector $\mathbf{h}_0$ is the two-dimensional equivalent of the three-dimensional harmonic vector $\mathbf{h}_0$ defined in (4.120). It is the unique solution of the system of equations

$$\begin{aligned} \operatorname{div}_{xy} \mathbf{h}_0 &= 0 \\ \operatorname{div}_{xy} (\mathbf{u}_z \times \mathbf{h}_0) &= 0 \\ \mathbf{u}_n \cdot \mathbf{h}_0 &= 0 \quad \text{(on } C_1 \text{ and } C_2\text{)} \\ \int_{C_1} \mathbf{h}_0 \cdot \mathbf{dc} &= \int_{C_2} \mathbf{h}_0 \cdot \mathbf{dc} \; = \; \mathbf{1}. \end{aligned} \tag{6.79}$$

The second equation is the two-dimensional equivalent of curl $\mathbf{h}_0 = 0$. From (A3.44), the line integral of $\mathbf{h}_0$ around C_1 and C_2 (and more generally around any curve C encircling region A) has a constant value. Factor T in (6.78) can therefore be determined by equating the line integrals of $\mathbf{h}_0$ and T $(\mathbf{u}_z \times \mathbf{e}_0)$ around C. Because **h** has a nonzero tangential component on both C_1 and C_2, the lines of force

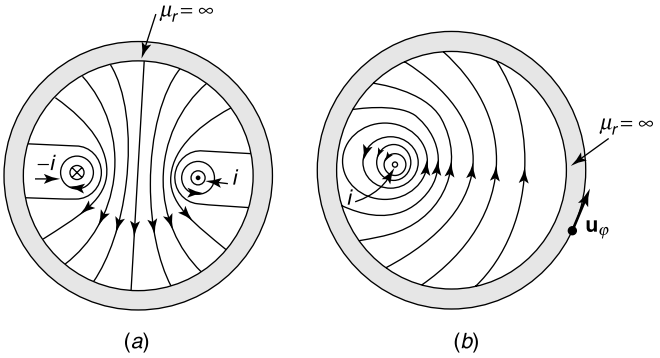

Figure 6.26 Lines of force produced in a "tunnel" (*a*) by a current and its return (*b*) by an eccentric current (from J. Van Bladel, Magnetostatic fields at an iron-air boundary, *Am. J. Phys.* **29**, 732–736, 1961, with permission of the American Institute of Physics).

in vacuum are *not* perpendicular to the iron. These considerations are illustrated by the lines of force shown in Figure 6.26, which have been obtained by the method of images. Figure 6.26*a* relates to aforementioned case 1 and Figure 6.26*b* to case 2.

6.10 AXISYMMETRIC GEOMETRIES

Figure 6.27 shows a ringlike medium and an azimuthal current source $\mathbf{j} = j(r, z)\mathbf{u}_\varphi$. Because $\mathbf{b}$ is solenoidal, it can be written as

$$\mathbf{b} = \text{curl } (a\mathbf{u}_\varphi) = \frac{1}{r} \text{ grad } (ar) \times \mathbf{u}_\varphi = \frac{1}{2\pi r}(\text{grad } \Phi \times \mathbf{u}_\varphi), \tag{6.80}$$

where $\Phi = 2\pi ra$. The use of the function Φ has certain advantages. First, the curves $\Phi =$ constant are the lines of force of the magnetic field. Second, Φ is a flux function. This can be proved by evaluating the flux through an annulus located in a plane perpendicular to the z axis. Thus,

$$\text{Flux} = \int_{r_A}^{r_B} (\mathbf{u}_z \cdot \mathbf{b}) 2\pi r \, dr = \int_{r_A}^{r_B} \mathbf{u}_z \cdot (\text{grad } \Phi \times \mathbf{u}_\varphi) dr = \Phi_B - \Phi_A.$$

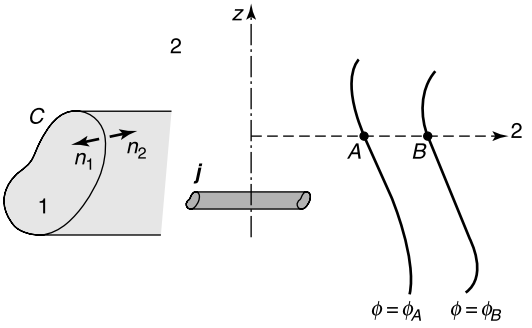

Figure 6.27 Geometry of revolution.

If the media are linear, homogeneous and isotropic, curl $\mathbf{b} = \mu\mathbf{j}$, hence a and Φ must satisfy the respective equations

$$\frac{\partial^2 a}{\partial r^2} + \frac{1}{r}\frac{\partial a}{\partial r} + \frac{\partial^2 a}{\partial z^2} - \frac{a}{r^2} = -\mu j \tag{6.81}$$

$$\frac{\partial^2 \Phi}{\partial r^2} - \frac{1}{r}\frac{\partial \Phi}{\partial r} + \frac{\partial^2 \Phi}{\partial z^2} = -\mu r 2\pi j. \tag{6.82}$$

The boundary conditions to be satisfied by potential a are

$$a_1 = a_2$$

$$\frac{1}{\mu_{r1}}\frac{\partial}{\partial n_1}(ra_1) + \frac{1}{\mu_{r2}}\frac{\partial}{\partial n_2}(ra_2) = 0, \tag{6.83}$$

while Φ must satisfy

$$\Phi_1 = \Phi_2$$

$$\frac{1}{\mu_{r1}}\frac{\partial \Phi_1}{\partial n_1} + \frac{1}{\mu_{r2}}\frac{\partial \Phi_2}{\partial n_2} = 0. \tag{6.84}$$

The solution of the differential problems for a and Φ can be effected by classic methods such as separation of variables, difference equations, etc. Numerous examples of such solutions can be found in the literature [55]. Illustratively, consider a permanent magnet of the type used to close doors magnetically (Fig. 6.28). The magnet carries a uniform polarization $\mathbf{m}_0$ and is embedded in an iron armature that serves to concentrate the flux [55]. Because there are no currents, $\mathbf{h}$ vanishes in the iron, and the lines of force of $\mathbf{b}$ must be perpendicular to the iron (i.e., to the contour *CDEFGH*). Further, in the iron,

$$\text{curl } \mathbf{b} = \mu_0 \text{ curl } \mathbf{m}_0 = 0.$$

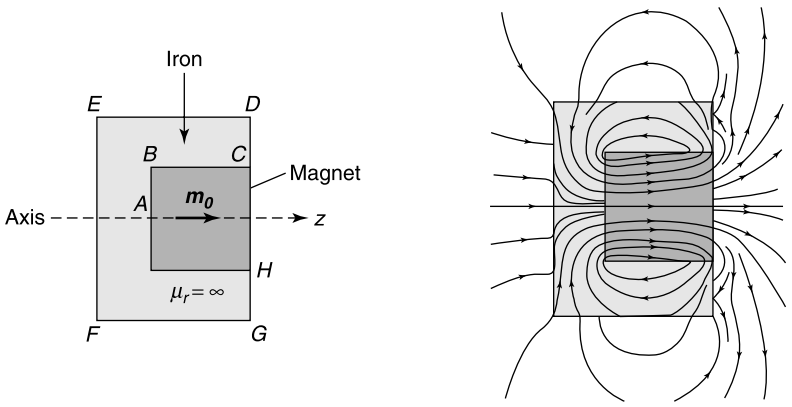

Figure 6.28 Permanent magnet and lines of force of b (from E. Durand. *Magnétostatique*. Masson, Paris, 1968, with kind permission of Editions Dunod).

It follows that the second member in (6.82) must vanish. The boundary conditions are

$$\frac{\partial \Phi}{\partial n} = 0 \text{ on } AB \text{ and } CDEFGH$$
$$\frac{\partial \Phi}{\partial n} = -m_0 \text{ on } BC.$$

The condition on BC stems from the presence of the surface magnetizing current $\mu_0 m_0 \mathbf{u}_\varphi$, which is the source of $\mathbf{b}$.

6.11 NUMERICAL METHODS: INTEGRAL EQUATIONS

When the field problem can be expressed in terms of a scalar potential ψ the various equations discussed in Chapters 3 to 5 can easily be adapted to the magnetic situation. It suffices, to do so, to exploit the duality $(\mathbf{e}^i, \epsilon_r) \rightarrow (\mathbf{h}^i, \mu_r)$. Consider, for example, a dielectric sphere of radius a immersed in a uniform $\mathbf{e}^i$. It acquires a dipole moment $\mathbf{p}_e = \epsilon_0 \overline{\overline{\alpha}}_e \cdot \mathbf{e}^i$ where, from (3.126), $\overline{\overline{\alpha}}_e$ is the electric polarizability dyadic

$$\overline{\overline{\alpha}}_e = 4\pi \frac{\epsilon_r - 1}{\epsilon_r + 2} a^3 \overline{\overline{I}}. \tag{6.85}$$

When the same sphere, now of permeability μ_r, is immersed in a uniform $\mathbf{h}^i$, it acquires a dipole moment $\mathbf{p}_m = \overline{\overline{\alpha}}_m \cdot \mathbf{h}^i$, where

$$\overline{\overline{\alpha}}_m = 4\pi \frac{\mu_r - 1}{\mu_r + 2} a^3 \overline{\overline{I}} \quad (\mathrm{m}^3) \tag{6.86}$$

is the *magnetic polarizability dyadic*. In the Coulomb formulation the material may be replaced, in the evaluation of $\mathbf{h}$, by the volume and surface charges appearing in (6.52). If the material is linear and homogeneous, both $\mathbf{b}$ and $\mathbf{m}_m$ are solenoidal, and we may write, for the disturbance potential generated by the presence of the medium,

$$\psi^d(\mathbf{r}) = \frac{1}{4\pi\mu_0} \int_S \frac{\rho_{ms}(\mathbf{r}')}{|\mathbf{r} - \mathbf{r}'|} \, dS', \tag{6.87}$$

where the surface charge density is

$$\rho_{ms} = \mu_0 (\mathbf{u}_n \cdot \mathbf{m}_m) \quad (\mathrm{T}). \tag{6.88}$$

The normal component of $\mathbf{b}$, equal to $\left(-\mu \dfrac{\partial \psi}{\partial n}\right)$, must be continuous on S. Expressing $\partial\psi/\partial n$ on both sides of S according to (3.43) and (3.44) leads to a Phillips type of integral equation:[20,21,22]

$$\frac{\mu_r + 1}{2(\mu_r - 1)} \frac{\rho_{ms}(\mathbf{r})}{\mu_0} + \frac{1}{4\pi} \lim_{\delta \to 0} \int_{S - S_\delta} \frac{\rho_{ms}(\mathbf{r}')}{\mu_0} \frac{\partial}{\partial n} \left(\frac{1}{|\mathbf{r} - \mathbf{r}'|} \right) dS' = \mathbf{u}_n \cdot \mathbf{h}^i(\mathbf{r}). \tag{6.89}$$

In the formulation of integral equations, the kernel is often a Green's function. In a few cases, this function can be obtained by the method of images. This can be done for the

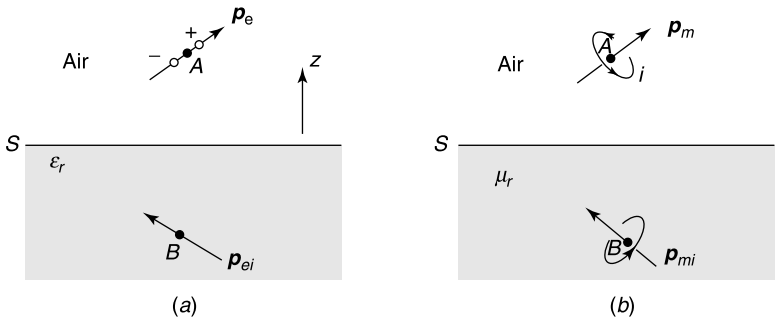

Figure 6.29 Images of dipole sources: (*a*) electric, (*b*) magnetic.

sphere.[23,24] When the sources are dipoles, the images of both $\mathbf{p}_e$ and $\mathbf{p}_m$ with respect to a plane are shown in Figure 6.29. After splitting $\mathbf{p}_e$ into components respectively perpendicular and parallel to S, the field in air is found to be generated by the original dipole $\mathbf{p}_e$ in A and an image dipole

$$\mathbf{p}_{ei} = \left(\mathbf{p}_{e\perp} - \mathbf{p}_{e\parallel}\right) \frac{\epsilon_r - 1}{\epsilon_r + 1} \tag{6.90}$$

in B. The field in the dielectric is generated by a dipole

$$\mathbf{p}_e = \frac{2\epsilon_r}{\epsilon_r + 1} \mathbf{p}_e, \tag{6.91}$$

located in A in a dielectric-filled space. For the magnetic situation of Figure 6.29*b*, (6.90) and (6.91) are still valid, but ϵ_r should be replaced by μ_r. Images of magnetic dipoles and current loops with respect to a sphere are also available.[25,26] When the source consists of a current density $\mathbf{j}(\mathbf{r})$ in A, the sources for the field in air (i.e., for $z > 0$) are the original $\mathbf{j}$ in A, completed by an image current

$$\mathbf{j}_i = \frac{\mu_r - 1}{\mu_r + 1} \left(\mathbf{j}_\parallel - \mathbf{j}_\perp\right) \tag{6.92}$$

in B. The field in the magnetic material is generated by a current density

$$\mathbf{j}_i = \frac{2\mu_r}{\mu_r + 1} \mathbf{j} \tag{6.93}$$

located in B, all space being filled with the magnetic material.

When the material is *para-* or *diamagnetic*,[27] the solution of an integral equation can be avoided by applying a *Born approximation*. In these materials χ_m is a very small number, and the presence of the material represents only a small perturbation. As a first step, therefore, we may set $\mathbf{m}_m \approx \chi_m \mathbf{h}^i$. Each small volume dV may now be replaced by a known dipole moment $d\mathbf{p}_m = \mathbf{m}_m \, dV$. The exterior field results from the cumulative effect of these dipoles, which individually contribute an elementary induction of type (6.33), viz.

$$d\mathbf{b}(r) = \frac{\mu_0}{4\pi} \, d\,\mathbf{p}_m \cdot \text{grad grad} \left(\frac{1}{R}\right).$$

By applying (A4.86), it is found that

$$\text{grad grad}\left(\frac{1}{R}\right) = \frac{1}{R^3}\,(3\mathbf{u}_R\mathbf{u}_R - \bar{\bar{I}}), \tag{6.94}$$

which leads to the following expression for the total field:

$$\mathbf{b}(\mathbf{r}) = \frac{\mu_0}{4\pi}\int_V \chi_m(\mathbf{r}')\mathbf{h}^i(\mathbf{r}')\cdot\bar{\bar{g}}(\mathbf{r}|\mathbf{r}')\,dV'. \tag{6.95}$$

In this equation,

$$\bar{\bar{g}}(\mathbf{r}) = 3\frac{(\mathbf{r}-\mathbf{r}')(\mathbf{r}-\mathbf{r}')}{|\mathbf{r}-\mathbf{r}'|^5} - \frac{1}{|\mathbf{r}-\mathbf{r}'|^3}\,\bar{\bar{I}}. \tag{6.96}$$

Relationship (6.95) can serve to determine an unknown nonuniform $\chi_m(\mathbf{r})$ from a knowledge of $\mathbf{b}$ (a typical *inverse* problem). This method, which allows imaging the interior of an object from measurements made outside, is of potential interest for medical tomography.[28]

Abandoning the assumption $\mu_r \approx 1$, we now consider materials of arbitrary $\mathbf{b}(\mathbf{h})$ characteristic. A very general equation, obtained directly from (6.53), is

$$\mathbf{h}(\mathbf{r}) - \frac{1}{4\pi}\,\text{grad}\int_V \mathbf{m}_m(\mathbf{r}')\cdot\text{grad}\left(\frac{1}{|\mathbf{r}-\mathbf{r}'|}\right)dV' = \mathbf{h}^i(\mathbf{r}). \tag{6.97}$$

This is an integral equation for $\mathbf{h}$ when $\mathbf{r}$ is in V, because $\mathbf{m}_m$ is related to $\mathbf{h}$ by the magnetization curve.[29] The equation is therefore potentially capable of handling nonlinear media. If the material is linear, (6.97) becomes

$$\frac{1}{\chi_m(\mathbf{r})}\mathbf{m}_m(\mathbf{r}) + \frac{1}{4\pi}\,\text{grad}\int_V \mathbf{m}_m(\mathbf{r}')\cdot\text{grad}'\left(\frac{1}{|\mathbf{r}-\mathbf{r}'|}\right)dV' = \mathbf{h}^i(\mathbf{r}). \tag{6.98}$$

As remarked before, the *integral equation formulation* has the advantage of producing solutions that automatically behave correctly at large distances, but the matrices resulting from discretization are dense. The *method of finite elements*, to be discussed in the next section, has the advantage of easily handling nonhomogeneous and nonlinear materials. The features of both approaches can be combined into hybrid procedures, in which finite elements are used in highly nonlinear or anisotropic regions and integral representations in the surrounding air space.[30]

6.12 NUMERICAL METHODS: FINITE ELEMENTS

Let a linear magnetic material (volume V_1) be immersed in the field of a ring-type of current (Fig. 6.30). Assume for a moment that the ring current is replaced by a permanent magnet. In and around V_1, the incident field is irrotational and may therefore be written as $\mathbf{h}^i = -\text{grad}\,\psi^i$. The disturbance field stemming from the material in V_1 may similarly be written as $\mathbf{h}^d = -\text{grad}\,\psi^d$. The total potential ψ must be continuous on S, together with $\left(\mu\dfrac{\partial\psi}{\partial n}\right)$. The problem is therefore identical to that of a linear dielectric body immersed in an incident electric field $\mathbf{e}^i$. Such problems are discussed extensively in Chapter 3. In the

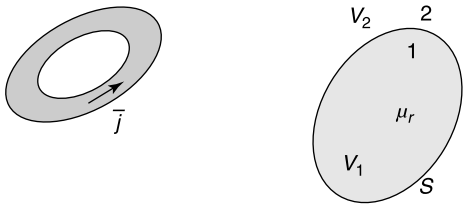

Figure 6.30 Magnetic body and current source.

presence of the ring current, however, the potential becomes multivalued, and the techniques described in Section 6.5, involving cuts and vector fields **t**, should be applied. They are discussed in more detail in Chapter 13. Multivaluedness may also be avoided by using vector potentials. To that effect, we note that the vector potential in a medium of nonuniform permeability μ satisfies.[‡]

$$\text{curl}\left(\frac{1}{\mu}\,\text{curl}\,\mathbf{a}\right) = \text{curl}\,(\nu\,\text{curl}\,\mathbf{a}) = \mathbf{j}$$

$$\mathbf{a} \text{ regular at infinity } (O(R^{-2})). \tag{6.99}$$

From (2.8), Equation (6.99) is the Euler equation of

$$J(\mathbf{a}) = \int_{\text{all space}} \left[\frac{1}{2}\mathbf{a}\cdot\text{curl}\left(\frac{1}{\mu}\,\text{curl}\,\mathbf{a}\right) - \mathbf{j}\cdot\mathbf{a}\right] dV. \tag{6.100}$$

This functional can be replaced by another one, which involves only first derivatives. From (A1.32), this is

$$J(\mathbf{a}) = \int_{\text{all space}} \left[\frac{1}{2\mu}|\text{curl}\,\mathbf{a}|^2 - \mathbf{j}\cdot\mathbf{a}\right] dV. \tag{6.101}$$

This functional reaches a local minimum at the correct value of **a**. It can be rewritten as

$$J = \int_{\text{all space}} \left[\frac{1}{2}\mathbf{h}\cdot\mathbf{b} - \mathbf{j}\cdot\mathbf{a}\right] dV, \tag{6.102}$$

where $\frac{1}{2}\mathbf{h}\cdot\mathbf{b}$ is the magnetic energy density (Problem 6.33).

The numerical solution of (6.99) starts with an expansion of **a** in basis vectors $\mathbf{f}_n$. Thus,

$$\mathbf{a} = \sum_{n=1}^{N} a_n \mathbf{f}_n. \tag{6.103}$$

Discretization leads to N equations of the type

$$\sum_{n=1}^{N} a_n \int_{\text{all space}} \mathbf{f}_m\cdot\text{curl}\left(\frac{1}{\mu}\,\text{curl}\,\mathbf{f}_n\right) dV = \int_{\text{all space}} \mathbf{j}\cdot\mathbf{f}_m\, dV \tag{6.104}$$

[‡]A formulation in terms of **h** directly is also possible; it avoids the errors that arise from differentiating **a**, as well as the difficulties associated with gauging.[31,32]

with $m = 1, \ldots, N$. An integration based on A1.32 yields the form

$$\sum_{n=1}^{N} a_n \int_{\text{all space}} \frac{1}{\mu} \operatorname{curl} \mathbf{f}_m \cdot \operatorname{curl} \mathbf{f}_n \, dV = \int_{\text{all space}} \mathbf{j} \cdot \mathbf{f}_m \, dV. \tag{6.105}$$

It is instructive to work out the details of the variational procedure on the simple example of Figure 6.30, where μ_r is assumed uniform in V_1. Functional (6.101) may now be written in more detail as

$$J(\mathbf{a}) = \frac{1}{\mu_r} \int_{V_1} \frac{1}{2} |\operatorname{curl} \mathbf{a}_1|^2 \, dV + \int_{V_2} \left[\frac{1}{2} |\operatorname{curl} \mathbf{a}_2|^2 - \mathbf{j} \cdot \mathbf{a}_2 \right] dV. \tag{6.106}$$

To seek stationarity, we introduce $\mathbf{a} = \mathbf{a}_0 + \epsilon \boldsymbol{\eta}$ in this expression and set the coefficient of ϵ equal to zero. On the basis of (A1.32), this move yields (6.99) as Euler equation, but also the following condition at the boundary:

$$\frac{1}{\mu_r} \int_S \boldsymbol{\eta}_1 \cdot (\operatorname{curl} \mathbf{a}_{10} \times \mathbf{u}_n) \, dS - \int_S \boldsymbol{\eta}_2 \cdot (\operatorname{curl} \mathbf{a}_{20} \times \mathbf{u}_n) \, dS = 0. \tag{6.107}$$

This condition is satisfied when the tangential components of the $\boldsymbol{\eta}$ vectors are continuous on S, which implies that $\mathbf{u}_n \times \boldsymbol{\eta}_1 = \mathbf{u}_n \times \boldsymbol{\eta}_2$ on S. In addition, the condition introduces the natural boundary condition

$$\frac{1}{\mu_r} \mathbf{u}_n \times \operatorname{curl} \mathbf{a}_1 = \mathbf{u}_n \times \operatorname{curl} \mathbf{a}_2, \tag{6.108}$$

which simply expresses the continuity of the tangential component of $\mathbf{h}$ on S. The remaining condition, continuity of b_n, follows immediately from the continuity condition on $\mathbf{a}$, because

$$\begin{aligned} \mathbf{u}_n \cdot \mathbf{b}_1 &= \mathbf{u}_n \cdot \operatorname{curl} \mathbf{a}_1 = \operatorname{div}_S (\mathbf{a}_1 \times \mathbf{u}_n) \\ \mathbf{u}_n \cdot \mathbf{b}_2 &= \mathbf{u}_n \cdot \operatorname{curl} \mathbf{a}_2 = \operatorname{div}_S (\mathbf{a}_2 \times \mathbf{u}_n) \end{aligned} \qquad (\text{on } S)$$

and $\mathbf{a}_1 \times \mathbf{u}_n = \mathbf{a}_2 \times \mathbf{u}_n$. The conclusion is clear: it is that preferable, in the expansion (6.103), to choose basis vectors $\mathbf{f}_n$ that make $\mathbf{a}_{\tan}$ automatically continuous, both from element to element and at interfaces between media. Note that there is no requirement on the continuity of the normal component a_n, which is left flexible in order to accommodate discontinuities in the properties of the media. An example of such curl-conforming elements, suitable for use in a plane triangle, is (Fig. 6.31)

$$\mathbf{f}_{12} = L_1 \operatorname{grad} L_2 - L_2 \operatorname{grad} L_1, \tag{6.109}$$

where L_1 and L_2 are shape functions of the type defined in (2.31) and (2.32). On the 1–2 side, $L_1 = \left(1 - \dfrac{x}{l_{12}}\right)$ and $L_2 = \dfrac{x}{l_{12}}$, hence $\mathbf{f}_{12} = \dfrac{1}{l_{12}} \mathbf{u}_x$, and the tangential component of the element is seen to be constant along 1–2. If we write

$$\mathbf{a} = a_{12}\mathbf{f}_{12} + a_{23}\mathbf{f}_{23} + a_{31}\mathbf{f}_{31} \tag{6.110}$$

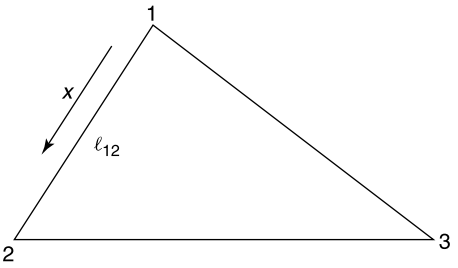

Figure 6.31 Example of an edge element.

the tangential component of $\mathbf{a}$ on 1–2 is $a_{12}\left(\frac{1}{l_{12}}\mathbf{u}_x\right)$, because the corresponding components of $\mathbf{f}_{23}$ and $\mathbf{f}_{31}$ vanish along that side. Continuity of $\mathbf{a}_{\tan}$ therefore requires a_{12} to have the same value in adjacent elements. From (6.110), it follows that

$$\int_C \mathbf{a}\cdot d\mathbf{c} = a_{12} + a_{23} + a_{31} = \sum a_{ij}, \tag{6.111}$$

where C is the contour of the triangle. Applying Stokes theorem to $\mathbf{a}$ shows that (6.111) is also the flux of $\mathbf{b}$ through the triangle. When applied to $\mathbf{h}$, instead of $\mathbf{a}$, $\sum a_{ij}$ is now equal to $\int_C \mathbf{h}\cdot d\mathbf{c}$, and this integral should be equal to the current flowing through the triangle, as required by Ampère's law. Note that the contribution of the element to $\mathbf{b}$ can be obtained from (6.110) in the form

$$\mathbf{b} = \text{curl } \mathbf{a} = \sum a_{ij} \text{ curl } \mathbf{f}_{ij} = \sum a_{ij} 2 \text{ grad } L_i \times \text{grad } L_j. \tag{6.112}$$

These simple principles may be extended to three dimensions, where the elements could be tetrahedra, pyramids with quadrilateral base (useful as a filler in a volume), prisms, bricks, or curvilinear elements [181, 189, 192, 207]. Higher-order bases may advantageously replace the linear variation associated with the simple element $\mathbf{f}_{12}$.[33,34,35,36,37] Additional details are given in Chapter 10.

In the solution of (6.99) $\mathbf{j}$ cannot be specified arbitrarily, because it must be solenoidal to ensure the existence of a solution. To enforce that requirement, one may write $\mathbf{j} = \text{curl } \mathbf{t}$, as in (6.38), and set $\mathbf{h} = \mathbf{t} - \text{grad } \theta$. There is no unique solution for $\mathbf{t}$, because it is defined to within a gradient. A possible choice, already mentioned before, is the field created by $\mathbf{j}$ in free space, which is given by (6.7). Thus,

$$\mathbf{t} = \mathbf{h}^j(\mathbf{r}) = \frac{1}{4\pi}\int_{V_2} \frac{\mathbf{j}(\mathbf{r}')\times(\mathbf{r}-\mathbf{r}')}{|\mathbf{r}-\mathbf{r}'|^3}\, dV'. \tag{6.113}$$

This is the mathematical expression of Biot-Savart's law. The total field is $\mathbf{h}^j$ augmented with the disturbance field generated by the material, which may be written as

$$\mathbf{h}^d(\mathbf{r}) = -\text{grad } \theta^d = \frac{1}{4\pi}\text{ grad}\int_{V_1} \mathbf{m}_m(\mathbf{r}')\cdot\text{grad}\left(\frac{1}{|\mathbf{r}-\mathbf{r}'|}\right) dV'. \tag{6.114}$$

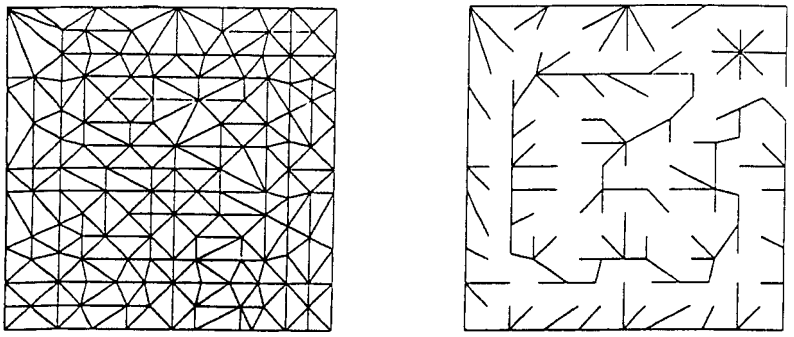

Figure 6.32 A two-dimensional mesh and corresponding tree (from J. B. Manges and Z. J. Cendes, A generalized tree-cotree gauge for magnetic field computation, *IEEE Trans. MAG* **31**, 1342–1347, 1995, with kind permission of IEEE).

The potential θ^d is single-valued and coincides with the total potential ψ^d in V_1, where it satisfies

$$\text{div } (\mu \text{ grad } \theta^d) = \text{div } (\mu \mathbf{t}). \tag{6.115}$$

Other choices for $\mathbf{t}$ are possible besides (6.113). For example, going back to (6.41) and (6.51), $\mathbf{t}$ may be interpreted as a fictive polarization density $\mathbf{m}_m$, which in turn generates equivalent distributions of charge and current[38] (Problem 6.17).

The $(\mathbf{t}, \theta)$ formulation described above has limitations. First, the magnetic medium must not carry any current. In addition, when μ_r is high, $\mathbf{h}$ in V_1 becomes small compared with its value around V_1. This small term is obtained as the difference between two larger ones, namely $\mathbf{h}^j$ and grad θ^d, which in practice are almost equal in magnitude and almost point in the same direction. Small relative inaccuracies in the larger terms lead to much larger uncertainties in their small difference, a fact that may lead to instability in the numerical process.[39] For a variety of reasons, therefore, recent choices for $\mathbf{t}$ have been based on graph theory.[40,41,42,43,44] They involve the *tree* of the finite element mesh (i.e., any set of edges connecting all nodes without forming closed loops). The remaining edges form the *co-tree*. A mesh and a typical tree are shown in Figure 6.32, as a matter of illustration. One can arbitrarily set the values of $\mathbf{t}$ on the tree equal to zero, and subsequently assign values of $\mathbf{t}$ on the co-tree, making sure Ampère's law is satisfied. The advantages of the method are many[§]: the cancellation problem is eliminated, and assigning values of $\mathbf{t}$ to compute the particular solution involves much less work than an evaluation according to (6.113).

Not yet mentioned in this discussion is the ever recurrent problem of the open boundaries (i.e., of an infinite computational space[45,46,47]). The techniques outlined in Section 5.7 for the electric field can be applied, in suitably modified form, to the magnetostatic situation. This is the case for the *asymptotic boundary condition* method, in which the vector potential $\mathbf{a}$ is written in the form $\mathbf{a} = \mathbf{f}(\theta, \varphi)\, R^{-2}$ on a (mathematical) spherical boundary S_O. The *boundary integral method*, to be further discussed in Section 12.6, can also be resorted to.

[§]Private communication from Dr. Z. Cendes.

6.13 NONLINEAR MATERIALS

The permeability μ_r of nonlinear materials must be treated as a variable parameter in equations such as (6.99). In a simplified model, the relationship $\mathbf{b}(\mathbf{h})$ is reduced to a curve relating $|\mathbf{b}|$ to $|\mathbf{h}|$, as shown in Figure 6.33. An analytical expression for this graphical relationship is desirable, for numerical reasons.[48] An example is Fröhlich's formula

$$b = \frac{h}{a + ch} + dh, \tag{6.116}$$

where a, c, and d are suitable constants, chosen to match the curve optimally. More accurate models are needed to accomodate factors such as the major hysteresis loop, the return-point memory, the wiping-out property, or the vectorial character of the relationship (obviously essential in anisotropic materials).

Equations (6.99), when discretized, lead to a classic matrix problem of the form

$$\overline{\overline{S}} \cdot \mathbf{a} = \mathbf{j}. \tag{6.117}$$

The matrix elements contain the variable parameter ν, which means that the problem is nonlinear and must be solved by successive iterations. The *Newton-Raphson method* is very frequently used for the purpose. In its simplest form, it seeks to find the nulls of a function $f(x)$. In a first step, one chooses a trial value x^1, hopefully close to x, and writes

$$f(x) = f(x^1) + (x - x^1) f'(x^1) + \text{ higher terms in } (x - x^1) = 0.$$

This gives, assuming that $f'(x^1)$ is different from zero,

$$x = \underbrace{x^1 - \frac{f(x^1)}{f'(x^1)}}_{x^2} + \cdots. \tag{6.118}$$

In the next step, one goes through the same motions with x^2, and subsequently with x^3, $x^4, \ldots$. The iterations are terminated when the difference between x^n and x^{n-1} is less than a given error criterion (Problem 6.35).

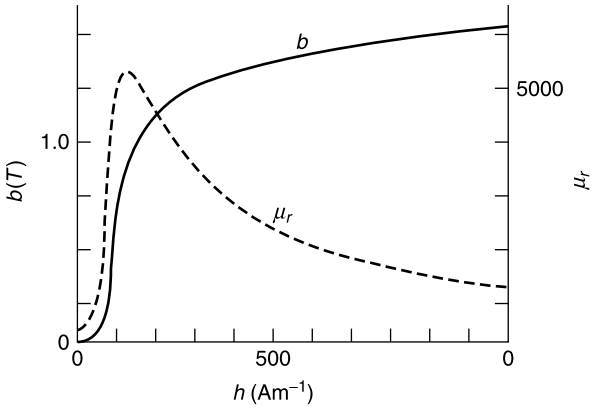

Figure 6.33 Variation of μ_r in a nonlinear material.

Applied to the operator equation $\mathcal{L}f = g$, the method starts with a trial function f^1, in error by $\delta f^1 = f - f^1$. Let $R(f^i) = (\mathcal{L}f^i - g)$ be the residue for a trial function f^i. Expansion (6.118) now takes the form

$$R(f) = R(f^1) + \delta R(f^1) = R(f^1) + \delta f^1 R'(f^1) + \cdots = 0 \tag{6.119}$$

where R' is the *Fréchet derivative* of the R operator.[¶] The correction δf^1 follows as

$$\delta f^1 = -\frac{R(f^1)}{R'(f^1)}. \tag{6.120}$$

To illustrate the application to matrix equation (6.117), consider the simple example

$$\begin{aligned} S_{11}\, a_1 + S_{12}\, a_2 &= j_1 \\ S_{21}\, a_1 + S_{22}\, a_2 &= j_2. \end{aligned}$$

The residual vector is $\mathbf{R}(\mathbf{r}) = \overline{\overline{S}} \cdot \mathbf{a} - \mathbf{j}$. Written out:

$$\begin{aligned} R_1 &= S_{11}\, a_1 + S_{12}\, a_2 - j_1 \\ R_2 &= S_{21}\, a_1 + S_{22}\, a_2 - j_2. \end{aligned}$$

These residues vanish for the exact pair $\mathbf{a} = (a_1, a_2)$, obtained with the correct ν_r. With an approximate solution, one writes $\mathbf{a}^1 = \mathbf{a} - \delta\mathbf{a}^1$, and sets

$$\begin{aligned} R_1(a_1, a_2) &= R_1(a_1^1, a_2^1) + \frac{\partial R_1}{\partial a_1}\delta a_1^1 + \frac{\partial R_1}{\partial a_2}\delta a_2^1 = 0 \\ R_2(a_1, a_2) &= R_2(a_1^1, a_2^1) + \frac{\partial R_2}{\partial a_1}\delta a_1^1 + \frac{\partial R_2}{\partial a_2}\delta a_2^1 = 0. \end{aligned}$$

This gives, in compact form,

$$\overline{\overline{J}} \cdot \delta\mathbf{a}^1 = -\mathbf{R}(\mathbf{a}^1)$$

where $\overline{\overline{J}}$ is the *Jacobian matrix* $J_{ik} = \dfrac{\partial R_i}{\partial a_k}$. The improved solution $\mathbf{a}^2$ follows from

$$\mathbf{a}^2 = \mathbf{a}^1 - (\overline{\overline{J}})^{-1} \cdot \mathbf{R}(\mathbf{a}^1). \tag{6.121}$$

Convergence of the procedure is not ensured [193] but will hopefully occur if the initial trial vector is sufficiently close to the exact solution.[49] Note that, with the new trial vector $\mathbf{a}^2$, a new distribution of ν_r must be introduced throughout the magnetic volume; hence, a new system of equations must be solved at each iteration. In consequence, in each line of (6.117),

[¶]Let x and y be normed linear spaces. If, for a given x there is a bounded linear operator F from x to y such that

$$\lim_{\|h\| \to 0} \frac{\|L(x+h) - L(x) - Fh\|}{\|h\|} = 0,$$

then F is called the Fréchet derivative of L at x and is classically written as $L'(x)$ [193].

a should be replaced by $\mathbf{a} + \delta\mathbf{a}$, and ν by $\nu + \delta\nu$, where $\delta\nu$ is a function of $\delta a_1, \delta a_2, \ldots$. The details of the calculations can be found in [180, 189, 207]. The method has been applied, for example, to the determination of **b** in a 5 kW DC machine, assumed infinitely long in the z-direction.[50] The fields were derived variationally from the functional

$$J = \int_S [\nu b_z \, db_z] \, dS - \int_S j_z \, a_z \, dS.$$

6.14 STRONG MAGNETIC FIELDS AND FORCE-FREE CURRENTS

Values of the induction encountered in practice vary over a wide range, from typically 5×10^{-5} T for the earth's magnetic field, to 1 T in electric machines, and to 22 T (steady state) and even 70 T (pulsed state) in advanced laboratory devices. An induction of 10 T corresponds with $h = 8 \times 10^6 \, \mathrm{A\,m^{-1}}$ in vacuum, and requires a total of 4×10^5 Ampère-turns in the ring circuit of Figure 6.14*b* to generate 10 T across a 5 cm gap. Densities of 10^8 to $10^{10} \, \mathrm{A\,m^{-2}}$ in the conductors are commonly encountered in such applications. The technological problems posed by such densities are considerable, as heavy currents result in large Joule effects, which in turn require efficient cooling systems, and lead to a huge energy consumption. Materials with low (or zero) resistivity are therefore desirable. In that light, superconductors give a potential answer to the problem.

6.14.1 The Superconducting Phase

The main property of superconductors, discovered as early as 1911, is the disappearance of resistivity below a critical temperature T_c. The potential applications of such a property are numerous, for example to the storage of energy by means of currents in superconducting rings (with estimated decay times of the order 10^5 years). On the basis of perfect conductivity, one would expect the magnetic flux created by a conducting ring to be *trapped* as soon as the material becomes superconducting. Experiments conducted by Meissner and Ochsenfeld in 1933 showed that this was not the case, and that the flux is *expelled* from the material as soon as the latter reaches the superconducting phase. It was further observed that, at a temperature $T < T_c$, the material reverted to the normal conduction phase above a critical field h_c, the value of which depends on the temperature according to the law

$$h_c(T) = h_c(0) \left[1 - \left(\frac{T}{T_c} \right)^2 \right]. \tag{6.122}$$

In materials of Type I, such as lead, tin, and mercury, the loss of superconductivity is abrupt (Fig. 6.34). For materials of Type II, such as niobium, vanadium, and various alloys, the loss is progressive, starting at h_{c1} and ending at h_{c2}, the value at which normal conduction resumes [129].

Extensive research has been devoted to a better understanding of the superconductivity phenomenon. Prominent theories are those of Bardeen-Cooper-Schieffer (BCS) and Ginzburg-Landau (GL). Such theories are beyond the pale of the current text. For most engineering purposes, however, a simplified approach based on the two *London equations*

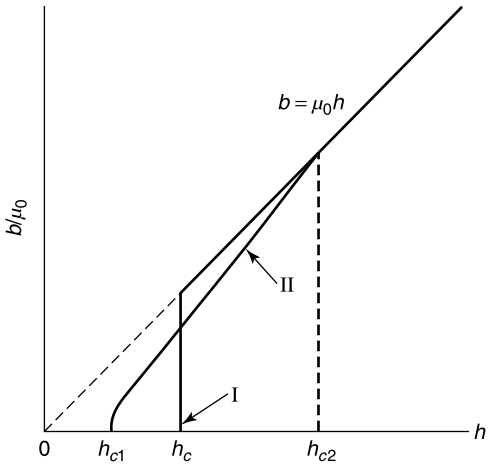

Figure 6.34 The $b(h)$ curve of superconductors (from M. Tinkham. *Introduction to superconductivity*, 2nd edition, with permission of Dover Publications, New York).

is sufficient. These equations, proposed by F. and H. London in 1935, are

$$\mathbf{e} = \Lambda \frac{\partial \mathbf{j}_s}{\partial t} \tag{6.123}$$

$$\mathbf{b} = -\Lambda \text{ curl } \mathbf{j}_s, \tag{6.124}$$

where

$$\Lambda = \frac{m}{n_s q_e^2} \tag{6.125}$$

and m is the mass of the electron. In the superconducting phase, the electrons, with number density n_s, form *Cooper pairs*. These electrons are responsible for the vanishing resistivity, and their density relative to the total electron density n is given by

$$\frac{n_s}{n} = 1 - \left(\frac{T}{T_c}\right)^4. \tag{6.126}$$

The first London equation can be derived from classsic arguments, based on the equation of motion of an electron, which is

$$m\frac{d\mathbf{v}}{dt} = q_e \mathbf{e} - \frac{m\mathbf{v}}{\tau}.$$

Here $\mathbf{v}$ is the average velocity of the electrons, q_e the negative charge of the electron, and τ a phenomenological collision time. Lack of resistivity means $\tau = \infty$, hence

$$\frac{d\mathbf{v}}{dt} = \frac{q_e}{m}\,\mathbf{e}.$$

The current density of the paired electrons is $\mathbf{j}_s = n_s q_e\, \mathbf{v}$. Expressing $\mathbf{v}$ in terms of $\mathbf{j}$ and inserting this value into the previous equation yields

$$\frac{d\mathbf{j}_s}{dt} = \frac{n_s q_e^2}{m}\,\mathbf{e} = \frac{1}{\Lambda}\,\mathbf{e},$$

which is precisely (6.123).

6.14.2 Field Penetration into a Superconductor

Because there are no magnetization currents,

$$\text{curl } \mathbf{b} = \mu_0 \mathbf{j} \approx \mu_0 \mathbf{j}_s.$$

Taking the curl of (6.124) gives

$$-\text{curl curl } \mathbf{j}_s = \frac{\mu_0}{\Lambda} \mathbf{j}_s = \frac{1}{\delta_s^2} \mathbf{j}_s, \tag{6.127}$$

where δ_s is the characteristic length

$$\delta_s = \sqrt{\frac{\Lambda}{\mu_0}} = \sqrt{\frac{m}{\mu_0 n_s q_e^2}}. \tag{6.128}$$

In a similar manner, one finds

$$-\text{curl curl } \mathbf{b} = \frac{1}{\delta_s^2} \mathbf{b}.$$

To interpret the significance of δ_s, consider the penetration of an induction $\mathbf{b}$ into a half-infinite superconductor (Fig. 6.35). Because the fields depend on z alone, b_x satisfies, in the superconductor,

$$\frac{d^2 b_x}{dz^2} - \frac{1}{\delta_s^2} b_x = 0.$$

But b_x must be bounded at $z = \infty$; hence,

$$\begin{aligned} b_x &= b_x(0) e^{-\frac{z}{\delta_s}} \\ j_{sy} &= -\frac{b_x(0)}{\mu_0 \delta_s} e^{-\frac{z}{\delta_s}}. \end{aligned} \tag{6.129}$$

Because δ_s is only a fraction of a micrometer in practice, fields and currents remain concentrated in a narrow transition layer, a property that confirms the Meissner effect. A few values of δ_s:

- For *Pb* (a metal), $T_c = 7.2\,\text{K}$ and $\delta_s(0) = 39\,\text{nm}$
- For $Nb_3\,Ge$ (an alloy), $T_c = 23\,\text{K}$ and $\delta_s(0) = 150\,\text{nm}$.

The symbol $\delta_s(0)$ denotes the *penetration depth* at zero K. At higher temperatures, the variation of δ_s may be adequatly approximated by the law

$$\delta_s(T) = \frac{\delta_s(0)}{\sqrt{1 - \left(\frac{T}{T_c}\right)^4}}. \tag{6.130}$$

The values found experimentally are somewhat larger, essentially because the motion of the electrons is influenced, not only by the *local* $\mathbf{e}$ field in $\mathbf{r}$, but also by the value of $\mathbf{e}$ in the immediate vicinity of $\mathbf{r}$.

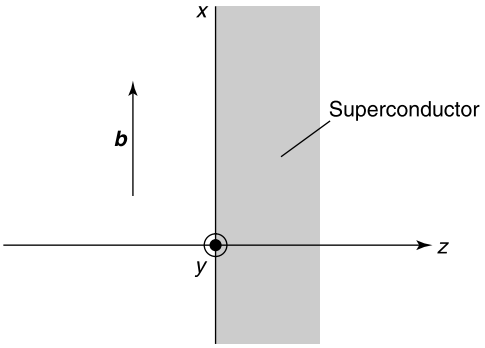

Figure 6.35 Half-infinite superconductor.

6.14.3 Applications

The critical temperature T_c is an important parameter for practical applications, because the classic coolants are liquid *He* (at 4.2 K) and the much cheaper liquid N_2 (at 77 K). Materials with a critical temperature above 77 K are therefore desirable. Recently developed high T_c ceramics have that property, for example:

1. Yttrium barium copper oxide (*YBCO*) ($T_c = 92$ K)
2. Thallium alloys, such as $Hg_{0.8}\ Tl_{0.2}\ Ba_2\ Ca_2\ Cu_3\ O_{8.33}$.

These materials are brittle, but they may be deposited on pliable tapes to produce power cables capable of carrying more than 1000 *A*. The economic implications are considerable, because typically 7% of the energy generated in a power system is lost in the transmission lines.

For many years now, low T_c superconductors have found applications in electric machinery, magnetic levitation of vehicles, and confinement of thermonuclear plasmas. They are routinely used in the coils that generate the magnetic fields of particle accelerators and are also found in magnetic resonance imaging devices.[51] High T_c materials, of more recent vintage, are used in components such as *SQUID* magnetometers and high-frequency filters [74].

6.14.4 Force-Free Currents

Strong currents $\mathbf{j}$ in a material may produce force densities $\mathbf{j} \times \mathbf{b}$ of such magnitude that the conductor literally tears itself apart. These forces also make it hard to design the support structure of the coils. The problem would disappear if current and field were parallel, in which case the force vanishes. The condition is

$$\text{curl}\ \mathbf{b}(\mathbf{r}) = \lambda(\mathbf{r})\mathbf{b}(\mathbf{r}). \tag{6.131}$$

Such fields are *Beltrami fields*, and for constant λ they may be interpreted as eigenvectors of the curl operator.[52] The "λ constant" situation has been the object of extensive research. One can prove, for example, that the most general solution of (6.131) for $\lambda =$ constant is of the form[53]

$$\mathbf{b} = \frac{1}{\lambda}\ \text{curl curl}\ (\psi\mathbf{u}) + \text{curl}\ (\psi\mathbf{u}), \tag{6.132}$$

where $\mathbf{u}$ is a fixed unit vector, and ψ is a solution of the Helmholtz equation

$$\nabla^2\psi + \lambda^2\psi = 0.$$

It has also been shown[54] that the force-free fields with constant λ represent the lowest state of magnetic energy that a closed system may attain.[‖]

Force-free currents are well-known in astrophysics, where they have been proposed to explain the simultaneous existence of magnetic fields and large currents in stellar matter. A simple example will illustrate the concept:

$$\mathbf{b} = z^2\mathbf{u}_x + x^2\mathbf{u}_y + y^2\mathbf{u}_z$$
$$\text{curl } \mathbf{b} = 2y\mathbf{u}_x + 2z\mathbf{u}_y + 2x\mathbf{u}_z.$$

The two vectors are parallel along the line $x = y = z = t$ (where t is a parameter). The field is force-free *locally*. When λ is constant, a solution of (6.131) is also a solution of

$$\nabla^2\mathbf{b} + \lambda^2\mathbf{b} = 0.$$

The property may be used to find force-free fields between spherical boundaries.[54] Force-free currents have also been investigated in toroidal coordinates.[55] The results can be exploited in the design of nuclear fusion reactors such as Tokamaks and more generally in the solution of the difficult problem of hot plasma confinement.

PROBLEMS

6.1 The electric field $\mathbf{e}$ generated by a point charge q is divergenceless outside q, and in particular in the region V bounded by two spherical surfaces centered on q (Fig. P6.1). Show that no vector potential $\mathbf{c}$ can be found such that $\mathbf{e} = \text{curl } \mathbf{c}$ in V.

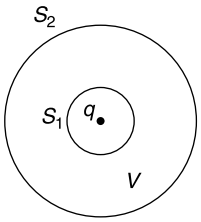

Figure P6.1

6.2 The transformation (6.3) admits a null-element $\mathbf{a}_0$, as discussed in Section 6.1. System (6.3) has no solution, according to (1.30), unless $\mu_0\mathbf{j}$ is orthogonal to $\mathbf{a}_0$. Check whether this requirement is satisfied.

6.3 Evaluate $\mathbf{b}$ at point M in Figure P6.2. The source is a linear current, sharply bent at point O.

[‖]The proof makes use of the property

$$I = \int_V \mathbf{a} \cdot \text{curl } \mathbf{a}\, dV = \text{constant}$$

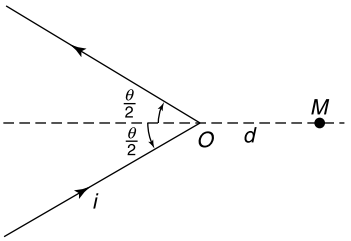

Figure P6.2

6.4 A sphere of radius a carries a uniform surface charge of density ρ_S. The sphere rotates with an angular velocity Ω around the z-axis. Show that the induction has the uniform value $\mathbf{b} = \frac{2}{3}\mu_0\,\Omega\,\rho_S\,a\,\mathbf{u}_z$ inside the sphere. Show that $\mathbf{b}$ outside the sphere is the field of a magnetic dipole located at the center of the sphere.

6.5 Show that the magnetic moment $\mathbf{p}_m$ defined in (6.31) is independent of the choice of the origin O in Figure 6.8*a*.

6.6 A *Helmholtz pair* consists of two loops of radius a, axially separated by the same distance a (Fig. P6.3). Show that b_z in the vicinity of the midpoint C (located halfway between coils, on the z-axis) is given by

$$b_z(z) = b_z(C) + O\left[\left(\frac{z}{a}\right)^4\right].$$

This field varies very slowly in the vicinity of C, a property that has been put to good use in the design of some instruments.

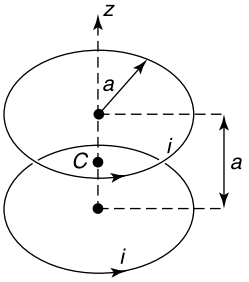

Figure P6.3

6.7 A sphere of radius a is uniformly magnetized in the z-direction. Evaluate $\psi(\mathbf{r})$, and show that $\mathbf{h} = -\frac{1}{3}\mathbf{m}_{m0}$ inside the sphere [22].

6.8 A permanent magnet has the shape of a torus with circular cross section (Fig. P6.4). The magnetization is given by

$$\mathbf{m}_{m0} = m_0\,\frac{a}{a + R\sin\theta}\,\mathbf{u}_\varphi.$$

Determine the magnetic field inside and outside the magnet.

which holds in a closed system if the gauge of $\mathbf{a}$ is suitably chosen. The integral I is the *helicity* of the field, a parameter that is mentioned in Appendix 1. It plays an important role in fluid mechanics, in which case $\mathbf{a}$ is the velocity, curl $\mathbf{a}$ the vorticity, and I the vortex helicity [24].

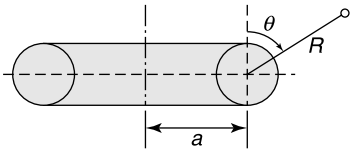

Figure P6.4

6.9 Two permanently magnetized bars, carrying opposite magnetizations, are in contact (Fig. P6.5). Determine the magnetic field by first solving the equivalent electrostatic problem.

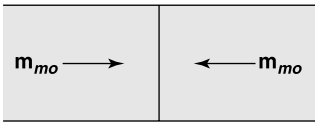

Figure P6.5

6.10 A circular cylinder carries a permanent, uniform magnetic moment density $\mathbf{m}_{m0}$, parallel to the z-axis (Fig. P6.6). Determine the induction on the axis.

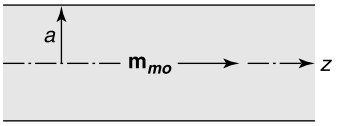

Figure P6.6

6.11 A spherical permanent magnet has a $\mathbf{b}(\mathbf{h})$ relationship of the form given in (6.48), where $\mu \neq \mu_0$. Assume that $\mathbf{m}_{m0}$ is oriented in the z direction. Determine the scalar potential, both inside and outside the sphere.

6.12 A coil with n windings per unit length carries a current i and is wound around a magnetic torus of circular cross section. The windings are so close that the current distribution is essentially a layer of surface current. Determine the induction in the ring.

6.13 A hollow magnetic sphere is immersed in a uniform incident induction $\mathbf{b}^i$ (Fig. P6.7). Determine the magnetic field $\mathbf{h} = -\text{grad } \psi$ in the various regions. Investigate the shielding effect by evaluating $\mathbf{b}$ at the center O as a function of μ_r and the ratio (b/a) [22]. The medium is linear.

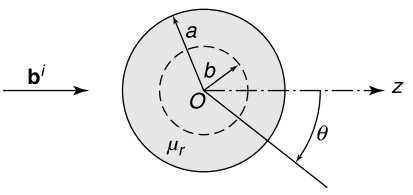

Figure P6.7

6.14 Repeat Problem 6.13, but for a cylindrical shield instead of a spherical one. Show that the induction inside the shell (i.e., for $r \leq b$), is given by

$$\mathbf{b} = \mathbf{b}^i \frac{4\mu_r}{(\mu_r + 1)^2 - (\mu_r - 1)^2 \dfrac{b^2}{a^2}}.$$

The formula shows how well the interior can be shielded from the incident field.

6.15 Repeat Problem 6.13 for a confocal spheroidal shield. Determine the induced dipole moment, a *signature* that may serve to detect the presence of a (hidden) object, often better modeled by a spheroid than by a sphere. Solve for $\mathbf{b}^i$ parallel or perpendicular to the major axis (L. Frumkis *et al.*, *IEEE Trans. MAG* **35**, 4151–4158, 1999).

6.16 Repeat Problem 6.13 for a superconducting spherical shell. The current density is of the form $\mathbf{j} = j_\varphi(R, \theta)\mathbf{u}_\varphi$. Try a solution $j_\varphi = f(R) \sin\theta$.

6.17 A cylindrical volume carries a uniform axial current $\mathbf{j} = j_z\mathbf{u}_z$ (Fig. P6.8). On the basis of Section 6.8, show that this current may be replaced by a moment density $\mathbf{m}_{m0} = xj_z\mathbf{u}_y$, and determine the equivalent surface densities ρ_{ms} and $\mathbf{j}_{ms}$. Particularize the analysis to a cylinder of rectangular cross section, with sides parallel to the coordinate axes (I. R. Ciric, *J. Appl. Phys.* **61**, 2709–2717, 1987).

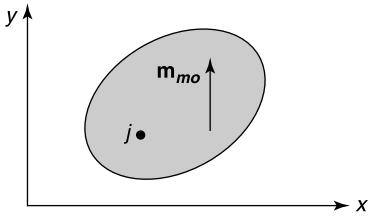

Figure P6.8

6.18 Let the coil in Figure 6.10 be wound on a spherical core of permeability μ_r. Determine the fields in the core, and show that $\mathbf{h}$ approaches zero when $\mu_r \to \infty$, while $\mathbf{b}$ approaches the nonzero limit $2ni\mu_0\mathbf{u}_z$.

6.19 To refine the $\mu_r = \infty$ model, assume that μ_r is large, but finite. Apply a perturbation analysis and expand the fields in a series $\mathbf{b} = \mathbf{b}_0 + \dfrac{1}{\mu_r}\mathbf{b}_1 + \cdots$, where $\mathbf{b}_0$ is the value for infinite μ_r. Solve for the first-order correction (J. Van Bladel, *Proc. IEE* **113**, 1239–1242, 1966).

6.20 In the perturbation theory of Problem 6.19, $\mathbf{h}_0$ vanishes inside the iron (assumed simply connected), but $\mathbf{h}_1 = \dfrac{1}{\mu_0}\mathbf{b}_0$. Check the latter property by determining $\mathbf{b}$ and $\mathbf{h}$ inside a circular cylinder of permeability μ_r immersed in a uniform $\mathbf{b}^i = b^i\mathbf{u}_x$ (Fig. P6.9), and taking the limit $\mu_r \to \infty$.

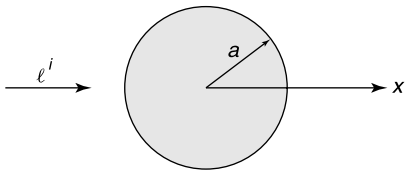

Figure P6.9

6.21 Laminated structures of the type shown in Figure P6.10 are often encountered in practice. Show that the flux density averaged over the magnetic material and air is given by

$$b_{\text{ave}} = [(\mu_r - 1)s + 1]\,\mu_0 h_{\text{ave}}$$

when the incident field is $b_{\parallel}$. In this expression the *stacking factor* s is

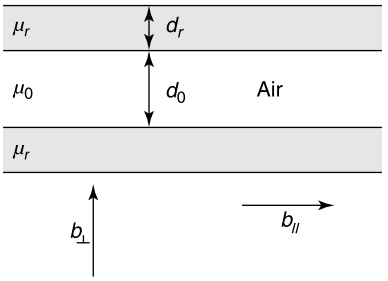

Figure P6.10

$$s = \frac{d_r}{d_r + d_0}.$$

A high value of μ_r has a strong influence in that case. In an incident field $b_{\perp}$, show that

$$b_{\text{ave}} = \frac{\mu_r}{\mu_r - s(\mu_r - 1)}\mu_0 h_{\text{ave}}.$$

The air is now the governing influence. The two results can be combined into a permeability tensor $\overline{\overline{\mu}}_r$ [195]. For the application of the theory to spherical layers, see E. Goto *et al. IEEE Trans. EMC*, **29**, 237-241, 1987.

6.22 Sketch the lines of force in the gap between two concentric iron cylinders (Fig. P6.11) (a) when a current $+i$ is located at A, and (b) when a current $+i$ is located at A and a current $-i$ at B.

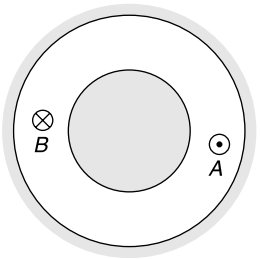

Figure P6.11

6.23 The nonmagnetic rectangular bus bar in Figure P6.12 carries a uniformly distributed z-directed current i. Determine the vector potential as a function of x and y. Check that its value,

for small b, is

$$a = \frac{\mu_0 i}{8\pi c}\left[(x+c)\log_e\frac{(c+x)^2+y^2}{c^2}\right.$$
$$\left.+(c-x)\log_e\frac{(c-x)^2+y^2}{c^2}+2y\left(\tan^{-1}\frac{c+x}{y}+\tan^{-1}\frac{c-x}{y}\right)\right].$$

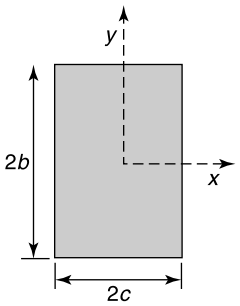

Figure P6.12

6.24 Show that the scalar and vector potentials of the periodic current distribution shown in Figure P6.13 are

$$\psi = \frac{i}{\pi}\sum_n(-1)^{n-1}\left\{\tan^{-1}\frac{\tan(\pi y/2l)}{\tanh(\pi/2l)[x+(2n-1)s]}\right.$$
$$\left.-\tan^{-1}\frac{\tan(\pi y/2l)}{\tanh(\pi/2l)[x-(2n-1)s]}\right\}$$
$$a = -\frac{i}{2\pi}\sum_n(-1)^{n-1}\log_e\frac{\cosh(\pi/l)[x+(2n-1)s]-\cos(\pi y/l)}{\cosh(\pi/l)[x-(2n-1)s]-\cos(\pi y/l)}.$$

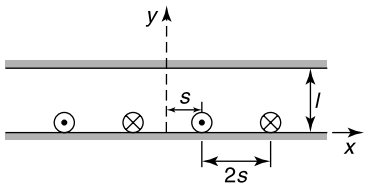

Figure P6.13

6.25 Show that the vector potential of the thin current sheet in Figure P6.14 is

$$a = \frac{i}{4\pi b}\int_{-b}^{+b}\log_e\left[\cosh\frac{\pi}{l}(x-x') - \cos\frac{\pi y}{l}\right]dx'$$

where $i = 2bj_S$ is the z-oriented current carried by the sheet.

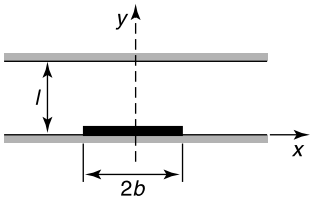

Figure P6.14

6.26 A sleeve of magnetic material surrounds a two-wire transmission line (Fig. P6.15). Find the vector potential in regions 1, 2, and 3, noting that it consists of a contribution $(\mu_0 i/2\pi)\log_e(r_2/r_1)$ from the transmission line, augmented by a harmonic term representing the effect of the screen. Determine, in particular, the field that leaks into region 3, and check that shielding becomes perfect as $\mu_r \to \infty$ [22].

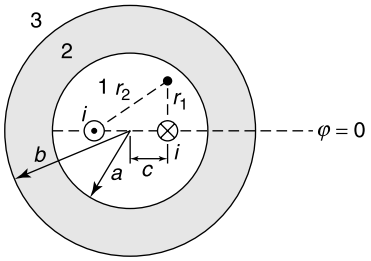

Figure P6.15

6.27 An iron cylinder carries a uniform z-oriented current density **j** (Fig. P6.16). Assume that μ_r is infinite, and verify that the vector potential a is constant on the contour of the rectangle. The differential problem is therefore $\nabla^2 a = -\mu_r \mu_0 j$, with $(\partial a/\partial c) = 0$ on the contour. Solve this problem in a rectangular iron bar

(a) By expanding $a(x, y)$ in a single Fourier series in $\cos mx$, with coefficients proportional to $\cosh my$

(b) By expanding $a(x, y)$ in a double Fourier series in $\dfrac{\pi}{2a}(x + d)$ and $\dfrac{\pi}{2b}(y + b)$.

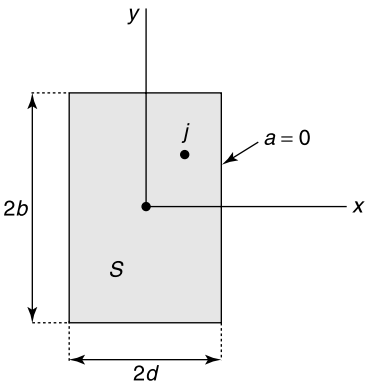

Figure P6.16

(c) By using a trial solution $a = C(x^2 - d^2)(y^2 - b^2) = Cf(x, y)$, and finding C by the Galerkin method, which gives [180]

$$C \int_S f \nabla^2 f dx\, dy = -\mu_0 \mu_r j \int_S f\, dx\, dy.$$

The induction $\mathbf{b}$ is infinite for $\mu_r \to \infty$, but $\mathbf{h}$ remains finite.

6.28 A magnetic sphere of radius a and infinite μ_r is buried in a nonmagnetic soil. An incident field $\mathbf{b}^i$ penetrates into the soil (Fig. P6.17). Show that the induction at the surface $z = 0$ is equal to $\mathbf{b}^i$ augmented with a disturbance field of magnitude

$$|\Delta \mathbf{b}| = b^i \frac{a^3}{d^3} \frac{1}{(1 + X^2 + Y^2)^{\frac{3}{2}}} \left[3 \frac{(X \cos\theta^i - \sin\theta^i)^2}{1 + X^2 + Y^2} - 1 \right],$$

where $X = \dfrac{x}{d}$ and $Y = \dfrac{y}{d}$. In a detection scheme, one may infer the size of the sphere by observing the magnitude of $|\Delta \mathbf{b}|$, and the depth of burial by observing the variation of $|\Delta \mathbf{b}|$ as a function of X and Y. To detect a more general buried dipole $\mathbf{p}_m$ one could register, in addition to $|\Delta \mathbf{b}|$ at the surface, the small local variations, given by [30]

$$\text{grad } \mathbf{b} = \frac{3\mu_0}{4\pi} \left[-5(\mathbf{p}_m \cdot \mathbf{u}_R)\mathbf{u}_R \mathbf{u}_R + \mathbf{p}_m \mathbf{u}_R + \mathbf{u}_R \mathbf{p}_m + (\mathbf{p}_m \cdot \mathbf{u}_R)\bar{\bar{I}} \right].$$

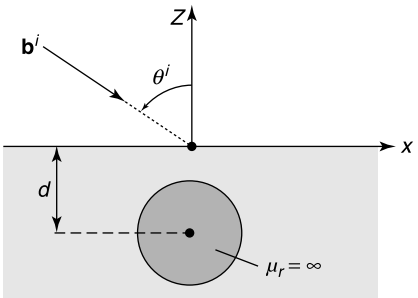

Figure P6.17

6.29 Let a linear magnetic material be immersed in an incident potential ψ^i. Show that the total potential ψ satisfies the integral equation

$$\mu_r \psi(\mathbf{r}) + \frac{1}{4\pi} \int_S \chi(\mathbf{r}') \psi(\mathbf{r}') \frac{\mathbf{r} - \mathbf{r}'}{|\mathbf{r} - \mathbf{r}'|^3}\, dS' - \frac{1}{4\pi} \int_V \psi(\mathbf{r}')\, \text{grad}' \chi \frac{\mathbf{r} - \mathbf{r}'}{|\mathbf{r} - \mathbf{r}'|^3}\, dV' = \psi^i(\mathbf{r})$$

when $\mathbf{r}$ is in V (A. Armstrong *et al.*, *IEEE Trans. MAG* **19**, 2329–2332, 1983, and L. Han *et al.*, *IEEE Trans. MAG* **30**, 2897–2890, 1994).

6.30 In the two-dimensional problem embodied in Figure P6.18, the magnetic cylinder is homogeneous, and $\mathbf{a} = a\mathbf{u}_z = (a^i + a^d)\mathbf{u}_z$. Starting from the Ampèrian approach

$$\nabla^2 \mathbf{a} = -\mu_0(\mathbf{j} + \mathbf{j}') = -\mu_0 \text{ curl } \mathbf{m}_m = -\mu_0(\mathbf{m}_m \times \mathbf{u}_n)\, \delta_S,$$

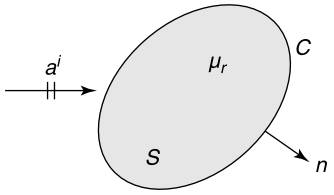

Figure P6.18

show that the polarization surface current satisfies the integral equation

$$\frac{\mu_r + 1}{2(\mu_r - 1)} j'_{sz}(\mathbf{r}) + \frac{1}{2\pi} \int_C j'_{sz}(\mathbf{r}') \frac{\partial}{\partial n} \left[\log_e \frac{L}{|\mathbf{r} - \mathbf{r}'|} \right] dc' = -\frac{\partial a^i}{\partial n}(\mathbf{r}).$$

(M. H. Lean *et al.*, *IEEE Trans. MAG* **18**, 331–335, 1982).

6.31 Show that the functional

$$J(a) = \int_{\text{all space}} \left[\frac{1}{2\mu} |\text{grad } a|^2 - aj \right] dS$$

is stationary for the (two-dimensional) vector potential $a(x, y)$.

6.32 Determine the Euler equation of the functional

$$J(\mathbf{a}) \int_{\text{all space}} \left[|\text{curl } \mathbf{a}|^2 + s|\text{div } \mathbf{a}|^2 - 2\mu_0 \mathbf{j} \cdot \mathbf{a} \right] dV,$$

where $\mathbf{a}$ is regular at infinity, and s is a given number (a penalty factor). For $s = 1$ one obtains Poisson's equation (6.5) in free space. Show that the stationary state $\mathbf{a}_0$ automatically satisfies the Coulomb condition $div\ \mathbf{a} = 0$ (J. L. Coulomb, *IEEE Trans. MAG* **17**, 3241–3246, 1981).

6.33 Find the Euler equation of the functional

$$F(h) = \int_V \left[\int_0^b h\, db - aj \right] dV.$$

The integral between brackets represents the magnetic energy, in a form suitable for the application to nonlinear materials [189, 207].

6.34 The electric field in a coaxial line can be found from an evaluation of the electric potential ϕ (Fig. P6.19). The electric energy is $\frac{1}{2}CV^2$. The magnetic field is obtained by solving the potential problem for ψ, with $\frac{\partial \psi}{\partial n} = 0$ along the metal boundaries. This (multivalued) potential suffers a jump $\psi_+ - \psi_- = i$ along the cut. The magnetic energy is $\frac{1}{2}Li^2$. Because $LC = \epsilon_0 \mu_0$, show that

$$\frac{i^2}{\displaystyle\int_S |\text{grad } \psi|^2\, dS} \leq \frac{C}{\epsilon_0} \leq \frac{\displaystyle\int_S |\text{grad } \phi|^2\, dS}{V^2}.$$

6.35 To illustrate Newton's method described in (6.118), find a zero of

$$f(x) = x^2 - 4x + 3.$$

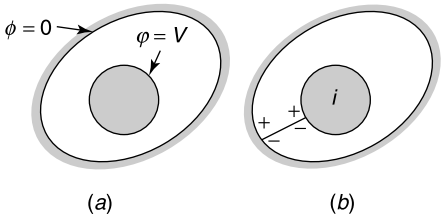

Figure P6.19

Start from $x = 1.2$, and iterate twice.

6.36 A superconducting sphere is immersed in a uniform field $\mathbf{h}^i$ (Fig. P6.20). Neglecting the small transition region of thickness δ_s, assume that $\mathbf{h} = 0$ in the sphere. Solve for the magnetic field at the surface of the sphere, and determine where it reaches a maximum. What is the value of that maximum? Show that when $\dfrac{2h_c}{3} < h^i < h^c$, superconducting and normal regions will coexist in the sphere. Determine the value of the surface currents [129].

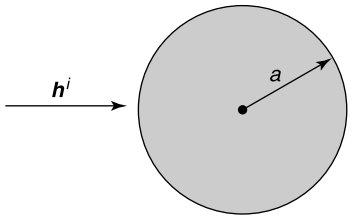

Figure P6.20

6.37 Let a current distribution $\mathbf{j}$ in a cylinder depend only on x and y. The current has both axial and lateral components ($\mathbf{j} = \mathbf{j}_z + \mathbf{j}_t$). Under which conditions are $\mathbf{j}$ and $\mathbf{h}$ parallel? Show that h_z and j_z must be Dirichlet eigenfunctions of S (J. Van Bladel, *Nuclear Instr. Meth.* **16**, 101–112, 1962).

NOTES

1. A. Bossavit, Magnetostatic problems in multiply-connected regions: some properties of the curl operator, *IEE Proc.* **135A**, 179–187 (1988).
2. O. Blumenthal, Über die Zerlegung Unendlicher Vektorfelder, *Math. Ann.* **61**, 235–250 (1905).
3. Y. Chu, Numerical calculation for the magnetic field in current-carrying circular arc filament, *IEEE Trans. MAG* **34**, 502–504 (1998).
4. D. Owen, The lines of force through neutral points in a magnetic field, *Proc. Phys. Soc. London* **59**, 14–18 (1947).
5. J. Slepian, Lines of force in electric and magnetic fields, *Am. J. Phys.* **19**, 87–90 (1951).
6. K. L. McDonald, Topology of steady current magnetic fields, *Am. J. Phys.* **22**, 586–596 (1954).
7. M. L. Brown, Scalar potentials in multiply-connected regions, *Int. J. Numer. Methods Eng.* **20**, 665–680 (1984).
8. C. S. Harrold and J. Simkin, Cutting multiply connected domains, *IEEE Trans. MAG* **21**, 2495-2498 (1985).
9. P. R. Kotiuga, On making cuts for magnetic scalar potentials in multiply-connected regions, *J. Appl. Phys.* **61**, 3916–3918 (1987), with erratum in **64**, 4257 (1988).
10. P. R. Kotiuga, Toward an algorithm to make cuts for magnetic scalar potentials in finite element meshes, *J. Appl. Phys.* **63**, 3357–3359 (1988).
11. A. Vourdas and K. J. Binns, Magnetostatics with scalar potentials in multiply-connected regions, *IEE Proceedings* **136A**, 49–54 (1989), with comments by A. Bossavit on p. 260–261.

12. P. R. Kotiuga, Topological considerations in coupling magnetic scalar potentials to stream functions describing surface currents, *IEEE Trans. MAG* **25**, 2925–2927 (1989).
13. F. Liorzou, B. Phelps, and D. L. Atherton, Macroscopic models of magnetization, *IEEE Trans. MAG* **36**, 418–428, 2000.
14. M. G. Abele, H. Rusinek, and F. Bertora, Field computation in permanent magnets, *IEEE Trans. MAG* **28**, 931–934 (1992).
15. E. P. Furlani, S. Reznik, and A. Kroll, A three-dimensional field solution for radially polarized cylinders, *IEEE Trans. MAG* **31**, 844–851 (1995).
16. M. Tejedor, H. Rubio, L. Elbaile, and R. Iglesias, External fields treated by uniformly magnetized ellipsoids and spheroids, *IEEE Trans. MAG* **31**, 830–836 (1995).
17. J. Van Bladel, Magnetostatic fields at an iron-air boundary, *Am. J. Phys.* **29**, 732–736 (1961).
18. J. Van Bladel, Induction at a corner in perfect iron, *IEE Proc.* **128-B**, 219–221 (1981).
19. J. C.-E. Sten, Magnetostatic image method for the confocally layered elliptic cylinder, *IEEE Trans. MAG* **34**, 199–204 (1998).
20. M. H. Lean and A. Wexler, Accurate field computation with the boundary element method, *IEEE Trans. MAG* **18**, 331–335 (1982).
21. M. Kobayashi and Y. Ishikawa, Surface magnetic charge distributions and demagnetizing factors of circular cylinders, *IEEE Trans. MAG* **28**, 1810–1814 (1992).
22. K. Ozaki, M. Kobayashi, and G. Rowlands, Surface magnetic charge distribution of a long, thin cylinder and its edge singularity, *IEEE Trans. MAG* **34**, 2185–2191 (1998).
23. I. V. Lindell and E. A. Lehtola, Magnetostatic image theory for the permeable sphere, *IEEE Trans. MAG* **28**, 1930–1934 (1992).
24. I. V. Lindell and J. J. Hänninen, Static image principle for the sphere in isotropic or bi-isotropic space, *Radio Science* **35**, 653–660 (2000).
25. I. V. Lindell, Quasi-static image theory for the bi-isotropic sphere, *IEEE Trans. AP* **40**, 228–233 (1992).
26. I. V. Lindell, E. A. Lehtola, and K. I. Nikoskinen, Magnetostatic image theory for an arbitrary current loop in front of a permeable sphere, *IEEE Trans. MAG* **29**, 2202–2206 (1993).
27. K. Ozaki, and M. Kobayashi, Surface magnetic charge densities and demagnetizing factors for rotating astroids, *IEEE Trans. MAG* **36**, 210–215 (2000).
28. N. G. Sepulveda, I. M. Thomas, and J. P. Wikswo, Magnetic susceptibility tomography for three-dimensional imaging of diamagnetic paramagnetic objects, *IEEE Trans. MAG* **30**, 5062–5069 (1994).
29. J. Simkin, and C. W. Trowbridge, On the use of the total scalar potential in the numerical solution of field problems in electromagnetics, *Int. J. Num. Meth. Eng.* **14**, 412–440 (1979).
30. M. V. K. Chari, J. D'Angelo, C. Crowley, J. Roeth, and H. Hurwitz, Solution of open boundary problems by differential and integral methods, *IEEE Trans. MAG* **22**, 1037–1039 (1986).
31. I. E. Lager and G. Mur, Finite element method for stationary and static electromagnetic fields, *J. Appl. Phys.* **81**, 4079–4081 (1997).
32. B. Bandelier and F. Rioux-Damidau, Mixed finite element method for magnetostatics in R^3, *IEEE Trans. MAG* **34**, 2473–2476 (1998).
33. Z. Cendes, Vector finite elements for electromagnetic field computation, *IEEE Trans. MAG* **27**, 3958–3966 (1991).
34. R. D. Graglia, D. R. Wilton, and A. F. Peterson, Higher order interpolatery vector bases for computational electomagnetics, *IEEE Trans. AP* **45**, 329–342 (1997).
35. J. L. Coulomb, F. X. Zgainski, and Y. Maréchal, A pyramidal element to link hexahedral, prismatic and tetrahedral edge finite elements, *IEEE Trans. MAG* **33**, 1362–1365 (1997).
36. R. D. Graglia, D. R. Wilton, and A. F. Peterson, Higher order interpolatory vector bases on prism elements, *IE EE Trans. AP* **46**, 442–450 (1998).
37. R. D. Graglia and I. L. Gheorma, Higher-order interpolatory vector bases on pyramidal elements, *IEEE Trans. AP* **47**, 775–782 (1999).
38. I. R. Ciric, New models for current distributions and scalar potential formulations of magnetic field problems, *J. Appl. Phys.* **61**, 2709–2717 (1987).
39. G. Bedrosian, Magnetostatic cancellation error revisited, *IEEE Trans. MAG* **27**, 4181–4182 (1991).
40. R. Albanese and G. Rubinacci, Magnetostatic field computations in terms of two-component vector potentials, *Int. J. Numer. Methods Eng.* **29**, 515–532 (1990).
41. J. P. Webb and B. Forghani, A single scalar potential method for 3D magnetostatics using edge elements, *IEEE Trans. MAG* **25**, 4126–4128 (1989).
42. J. P. Webb and B. Forghani, The low-frequency performance of H-ϕ and T-Ω methods using edge elements for 3D eddy current problems, *IEEE Trans. MAG* **29**, 2461–2463 (1993).
43. J. B. Manges and Z. J. Cendes, A generalized tree-cotree gauge for magnetic field computation, *IEEE Trans. MAG* **31**, 1342–1347 (1995).
44. O. Biro, K. Preis, and K. R. Richter, On the use of the magnetic vector potential in the nodal and edge finite element analysis of 3D magnetostatic problems, *IEEE Trans. MAG* **32**, 651–654 (1996).
45. Q. Chen and A. Konrad, A review of finite element open boundary techniques for static and quasi-static electromagnetic field problems, *IEEE Trans. MAG* **33**, 663–676 (1997).
46. J. F. Lee and Z. Cendes, Transfinite elements: a highly efficient procedure for modeling open field problems, *J. Appl. Phys.* **61**, 3913–3915 (1987).
47. J. R. Brauer, S. M. Schaefer, J. F. Lee, and R. Mittra, Asymptotic boundary condition for three-dimensional

magnetostatic finite elements, *IEEE Trans. MAG* **27**, 5013–5015, 1991.

48. J. C. Sabonnadière and G. Meunier, Modelling nonlinear magnetic materials for field computation, *J. Electromagnetic Waves Appl.* **4**, 1027–1054, 1990.
49. C. Neagoe and F. Ossart, Analysis of convergence in nonlinear magnetostatic finite elements problems, *IEEE Trans. MAG* **30**, 2865–2868 (1994).
50. M. V. K. Chari and P. Silvester, Finite-element analysis of magnetically saturated D-C machines, Paper 71 TP 3-PWR, *IEEE Winter Power Meeting* 2362–2372 (1970).
51. J. M. Jin, Electromagnetics in magnetic resonance imaging, *IEEE Antennas Prop. Mag.* **40**, 7–22 (1998).
52. A. Lakhtakia and B. Shanker, Beltrami fields within continuous source regions, volume integral equations, scattering algorithms and the extended Maxwell-Garnett model, *Int. J. Applied Electrom. Materials* **4**, 65–82 (1993).
53. S. Chandrasekhar and P. C. Kendall, On force-free magnetic fields, *Astrophys. J.* **126**, 457–460 (1957).
54. L. Woltjer, A theorem on force-free magnetic fields, *Proc. Natl. Acad. Sci.* **44**, 489–491 (1958).
55. G. J. Buck, Force-fee magnetic-field solution in toroidal coordinates, *J. Appl. Phys.* **36**, 2231–2235 (1965).

Chapter 7

Radiation in Free Space

When the sources are time-dependent, the fields **e** and **b**, which satisfied separate equations under static conditions, become coupled through the time derivatives that appear in Maxwell's equations. A time variation of **b**, for example, induces an electric field through the term $\partial \mathbf{b}/\partial t$, and similarly a time variation of $\partial \mathbf{d}/\partial t$ generates a magnetic field. The coupling is weak when the variations are slow, and perturbation methods can be applied in that case, for instance by means of the low-frequency approximations described in Chapter 13.

The coupling of **e** to **b** has a direct consequence for the evaluation of the fields in terms of potentials; *two* potentials, **a** and ϕ (or **c** and ψ), are now needed. An important choice must be made in that respect:

- Either evaluate the fields from **j** and $\mathbf{j}_m$ by means of the potentials (the mixed potential approach), or
- Derive the fields by direct integration of **j** and $\mathbf{j}_m$, multiplied by a suitable Green's dyadic.

Germane to the choice are the singularities of the appropriate Green's functions as $\mathbf{r} \to \mathbf{r}'$. They are weaker in the first method — a clear advantage — but the differentiation of the potentials, which is part of the method, may be a source of inaccuracies when the evaluation of **a** and ϕ has been marred by numerical errors. This type of difficulty does not arise in the second approach, because the integration of a function smoothes out small fluctuations of that function.

Although the developments in the next pages are based on sources radiating in vacuum, they can immediately be extended to sources in a homogeneous, isotropic medium by replacing (ϵ_0, μ_0) by (ϵ, μ), where ϵ and μ can be complex.

7.1 MAXWELL'S EQUATIONS

When the sources are time-dependent, the equations satisfied by the electric and magnetic fields lose their independence, and coupling is introduced by means of the first-order time

Electromagnetic Fields, Second Edition, By Jean G. Van Bladel

derivatives. The basic equations become

$$\text{curl } \mathbf{e} = -\frac{\partial \mathbf{b}}{\partial t} \tag{7.1}$$

$$\text{curl } \mathbf{b} = \mu_0 \mathbf{j} + \epsilon_0 \mu_0 \frac{\partial \mathbf{e}}{\partial t} \tag{7.2}$$

$$\text{div } \mathbf{e} = \frac{\rho}{\epsilon_0} \tag{7.3}$$

$$\text{div } \mathbf{b} = 0. \tag{7.4}$$

Equation (7.2) shows that a magnetic field is produced, not only by a current $\mathbf{j}$, but also by a time-dependent electric field.[1,2] This happens by way of the *displacement current* $\epsilon_0 \dfrac{\partial \mathbf{e}}{\partial t}$, the fundamental term introduced by Maxwell some 140 years ago. This current provides more symmetry between (7.1) and (7.2). Full symmetry is achieved when a magnetic current is added to (7.1), to yield

$$\text{curl } \mathbf{e} + \frac{\partial \mathbf{b}}{\partial t} = -\mathbf{j}_m \tag{7.5}$$

$$\text{curl } \mathbf{b} - \epsilon_0 \mu_0 \frac{\partial \mathbf{e}}{\partial t} = \mu_0 \mathbf{j} \tag{7.6}$$

$$\text{div } \mathbf{e} = \frac{\rho}{\epsilon_0} \tag{7.7}$$

$$\text{div } \mathbf{b} = \rho_m. \tag{7.8}$$

The notation $\mathbf{j}_m$ stands for the *magnetic current density*. At the present time, no experimental evidence exists for such a current, but its introduction has mathematical advantages, which are further discussed in Section 7.12.

The sources that appear in Maxwell's equations are not independent. They are related by the *equations of conservation of charge*

$$\text{div } \mathbf{j} + \frac{\partial \rho}{\partial t} = 0 \tag{7.9}$$

$$\text{div } \mathbf{j}_m + \frac{\partial \rho_m}{\partial t} = 0. \tag{7.10}$$

In integrated form, when the sources are energized at $t = 0$,

$$\rho(\mathbf{r}, t) = -\int_0^t \text{div } \mathbf{j}(\mathbf{r}, t')\, dt' \tag{7.11}$$

$$\rho_m(\mathbf{r}, t) = -\int_0^t \text{div } \mathbf{j}_m(\mathbf{r}, t')\, dt'. \tag{7.12}$$

Such time integrals permit casting Maxwell's equations into a form that does not require the existence of time derivatives of $\mathbf{e}$ and $\mathbf{h}$ [72]. Equation (7.7), for example, becomes

$$\text{div} \int_0^t \mathbf{e}(\mathbf{r}, t')\, dt' = -\frac{1}{\epsilon_0} \text{ div} \int_0^t dt' \int_0^{t'} \mathbf{j}(\mathbf{r}, t'')\, dt''. \tag{7.13}$$

We shall be interested in two classes of phenomena: (1) transient phenomena, in which the fields are zero up to the instant $t = 0$, and (2) steady-state sinusoidal phenomena. The latter are basic because transient fields can be expressed in the form

$$f(t) = \frac{1}{2\pi} \int_{-\infty}^{\infty} F(\omega) e^{j\omega t} d\omega. \tag{7.14}$$

The frequency spectrum $F(\omega)$, which is the unknown in integral equation (7.14), is given by the Fourier transform

$$F(\omega) = \int_{-\infty}^{\infty} f(t) e^{-j\omega t}\, dt. \tag{7.15}$$

Fourier transforms are discussed in Appendix 7.

Transient signals are either man-made or of natural origin. Examples of the latter are radio stars, cosmic noise, Earth currents, and lightning [51, 67]. Transients caused by lightning can damage — and even destroy — sensitive electronic devices.[3,4] A few typical data concerning the discharge current are given in Figure 7.1. The spectrum extends to a few MHz and the amplitude may peak to hundreds of kA (Problem 7.2).

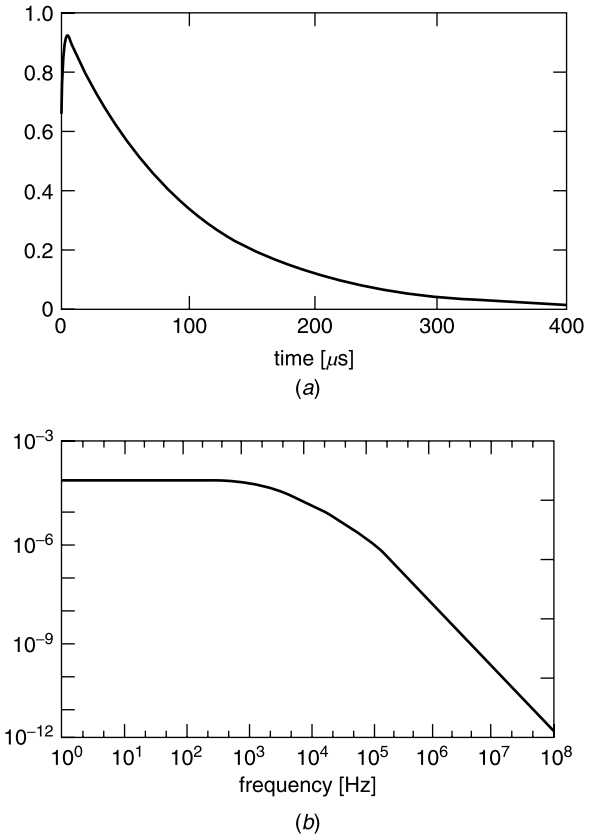

Figure 7.1 Typical curves for the lightning current: (*a*) relative amplitude, (*b*) spectrum (from M. S. Sarto, Innovative absorbing boundary conditions for the efficient FDTD analysis of lightning interaction problems, *IEEE Trans. EMC* **43**, 368–381, 2001, with permission of IEEE).

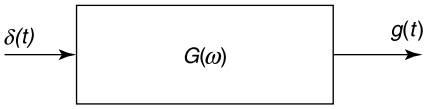

Figure 7.2 Linear system with input and output signals.

Suitably modulated time-harmonic signals play a prominent role in technical applications, but pulsed signals have strongly gained in importance in recent years. A classic example of transient source is the Dirac pulse $f(t) = \delta(t)$, the Fourier spectrum of which is $F(\omega) = 1$. All frequencies are therefore equally present in that signal, which makes it particularly suitable for testing linear systems. Assume that one seeks to determine the frequency response $G(\omega)$ of such a system (which could be a propagation channel, or a cavity resonator). It is clear that $G(\omega)$ is the frequency spectrum of the output $g(t)$ of the system when the latter is excited by a Dirac pulse (Fig. 7.2). A measurement of $g(t)$ therefore suffices to generate $G(\omega)$ by means of (7.15). The broadband properties of the Dirac pulse may be exploited in the detection of targets designed to be "unseen" at frequencies normally contained in the incoming radar pulse but still detectable (and vulnerable) outside that band. Note that a pure $\delta(t)$ signal cannot be generated in practice. An often used substitute — particularly useful in numerical and theoretical studies — is the *Gaussian pulse*

$$f(t) = e^{-\frac{t^2}{t_0^2}}, \tag{7.16}$$

the spectrum of which is

$$F(j\omega) = \sqrt{\pi}\, t_0\, e^{-\frac{\omega^2 t_0^2}{4}}. \tag{7.17}$$

The pulse width, defined as the time the signal rises above $(1/e)$ times its maximum value, is equal to $2t_0$. The analogously defined bandwidth stretches from $f = -\dfrac{1}{\pi t_0}$ to $f = \dfrac{1}{\pi t_0}$.

7.2 THE WAVE EQUATION

The electric field appears in both (7.5) and (7.6). An equation for **e** alone can be obtained by taking the curl of both members of (7.5), and substituting curl **b** from (7.6). This gives

$$-\text{curl curl } \mathbf{e} - \epsilon_0\mu_0 \frac{\partial^2 \mathbf{e}}{\partial t^2} = \mu_0 \frac{\partial \mathbf{j}}{\partial t} + \text{curl } \mathbf{j}_m. \tag{7.18}$$

This equation can be transformed into a wave equation by adding the term grad div **e** to both members; thus,

$$\nabla^2 \mathbf{e} - \epsilon_0\mu_0 \frac{\partial^2 \mathbf{e}}{\partial t^2} = \mu_0 \frac{\partial \mathbf{j}}{\partial t} + \text{curl } \mathbf{j}_m + \frac{1}{\epsilon_0} \text{grad } \rho. \tag{7.19}$$

Similar steps yield the following equations for the magnetic induction:

$$-\text{curl curl } \mathbf{b} - \epsilon_0\mu_0 \frac{\partial^2 \mathbf{b}}{\partial t^2} = \epsilon_0\mu_0 \frac{\partial \mathbf{j}_m}{\partial t} - \mu_0 \text{ curl } \mathbf{j} \tag{7.20}$$

and

$$\nabla^2\mathbf{b} - \epsilon_0\mu_0\frac{\partial^2\mathbf{b}}{\partial t^2} = \epsilon_0\mu_0\frac{\partial\mathbf{j}_m}{\partial t} - \mu_0 \text{ curl } \mathbf{j} + \text{grad } \rho_m. \tag{7.21}$$

Equations (7.19) and (7.21) show that the Cartesian projections of **e** and **b** satisfy the wave equation*

$$\nabla^2\phi - \frac{1}{c_0^2}\frac{\partial^2\phi}{\partial t^2} = f(\mathbf{r}, t). \tag{7.22}$$

In solving this equation, we shall assume that the sources are at a finite distance from the origin, and hence that $f(\mathbf{r}, t)$ vanishes outside a sufficiently large spherical surface S_R. The solution proceeds by first determining the Green's function for (7.22), that is, the solution of

$$\nabla^2 g - \frac{1}{c_0^2}\frac{\partial^2 g}{\partial t^2} = \delta(\mathbf{r})\delta(t). \tag{7.23}$$

Because there is no preferred direction in space, this function can only depend on the distance R to the source. It follows that $g(R, t)$ must satisfy

$$\frac{1}{R^2}\frac{\partial}{\partial R}\left(R^2\frac{\partial g}{\partial R}\right) - \frac{1}{c_0^2}\frac{\partial^2 g}{\partial t^2} = 0 \qquad (\text{for } R > 0).$$

Setting $g = \dfrac{1}{R}f$ gives

$$\frac{\partial^2 f}{\partial R^2} - \frac{1}{c_0^2}\frac{\partial^2 f}{\partial t^2} = 0. \tag{7.24}$$

The general solution of (7.24) is elementary (Problem 7.3). It leads to

$$g(R, t) = \frac{1}{R}h_1\left(t - \frac{R}{c_0}\right) + \frac{1}{R}h_2\left(t + \frac{R}{c_0}\right), \tag{7.25}$$

where h_1 and h_2 are yet to be determined functions. In macroscopic electromagnetism causality prevails (i.e., the effect cannot precede the cause). The $h_2\left(t + \dfrac{R}{c_0}\right)$ term, which represents a wave incident from infinity, must therefore be excluded. To determine h_1, note that the $\delta(\mathbf{r})$ term in (7.23) implies, from (A1.27), that

$$\int_S \frac{\partial g}{\partial R}\, dS = \delta(t),$$

where S is a small spherical surface surrounding the origin. This condition suggests a $\left(-\dfrac{1}{4\pi R}\right)$ dependence, hence a Green's function

$$g(R, t) = -\frac{1}{4\pi R}\,\delta\left(t - \frac{R}{c_0}\right).$$

*The operator in (7.22) is the *Dalembertian*, a name suggested by Lorentz. It is denoted by the symbol

$$\Box = \nabla^2 - \frac{1}{c_0^2}\frac{\partial^2}{\partial t^2}.$$

When the source is a Dirac function centered on source point $(\mathbf{r}', t')$, the *Green's function* becomes

$$g(\mathbf{r}, t|\mathbf{r}', t') = -\frac{1}{4\pi|\mathbf{r}-\mathbf{r}'|}\,\delta\left(t - t' - \frac{|\mathbf{r}-\mathbf{r}'|}{c_0}\right). \tag{7.26}$$

This rather intuitive derivation, which can be given a firmer theoretical basis [165], is further supported by the developments in Section 7.7. Knowledge of g leads to the following solution of (7.22):

$$\phi(\mathbf{r}, t) = -\frac{1}{4\pi}\int_{\text{all space}} \frac{f(\mathbf{r}', t - |\mathbf{r}-\mathbf{r}'|/c_0)}{|\mathbf{r}-\mathbf{r}'|}\,dV'. \tag{7.27}$$

Equation (7.26) implies that an elementary disturbance propagates its effects with a velocity c_0 or, equivalently, that the value of ϕ at point $\mathbf{r}$ at time t is determined solely by the strength of the sources at time $t - |\mathbf{r}-\mathbf{r}'|/c_0$.

Each of the projections of the electromagnetic field satisfies (7.22) and hence is given by a formula similar to (7.27). It follows that the fields radiate progressively into space, and that the domain of space in which they are different from zero is bounded by a wavefront that continuously moves outward.

7.3 POTENTIALS

In the absence of sources at large distances, the induction $\mathbf{b}$ vanishes at infinity and is solenoidal; it can therefore be derived from a vector potential, just as in the static case. Inserting

$$\mathbf{b} = \text{curl}\ \mathbf{a} \tag{7.28}$$

into (7.1) gives

$$\text{curl}\left(\mathbf{e} + \frac{\partial \mathbf{a}}{\partial t}\right) = 0.$$

This relationship implies that the term between brackets can be derived from a scalar potential. We therefore write

$$\mathbf{e} = -\text{grad}\ \phi - \frac{\partial \mathbf{a}}{\partial t}. \tag{7.29}$$

The vector potential is determined to within an additive gradient. If $\mathbf{a}', \phi'$ form a set of vector and scalar potentials, then $\mathbf{a} = \mathbf{a}' - \text{grad}\,\theta$ and $\phi = \phi' + \partial\theta/\partial t$ form another set of potentials that, upon insertion in (7.28) and (7.29), give rise to the same electromagnetic fields. This element of flexibility allows one to choose a set satisfying the auxiliary relationship

$$\text{div}\ \mathbf{a} + \epsilon_0\mu_0\frac{\partial \phi}{\partial t} = 0, \tag{7.30}$$

called the *Lorenz condition*[5,6] after the Danish physicist who first proposed it.[†] The *Lorenz potentials* can be derived from an arbitrary set $\mathbf{a}', \phi'$ by choosing θ to satisfy

$$\nabla^2\theta - \epsilon_0\mu_0\frac{\partial^2\theta}{\partial t^2} = \text{div}\ \mathbf{a}' + \epsilon_0\mu_0\frac{\partial \phi'}{\partial t}.$$

[†]See M. Pihl, The scientific achievements of L. V. Lorenz, in Jordan E. C. (ed.), *Electromagnetic theory and antennas*, Pergamon Press, 1963. Lorenz' contribution was published in the Poggendorff's Annalen in June 1867, and translated into English in *Phil. Mag.* **34**, 287–301 (1867).

Differential equations for $\mathbf{a}$ and ϕ can be obtained by inserting (7.28) and (7.29) into Maxwell's equations. From (7.2),

$$\text{curl curl } \mathbf{a} = \mu_0 \mathbf{j} - \epsilon_0 \mu_0 \frac{\partial^2 \mathbf{a}}{\partial t^2} - \epsilon_0 \mu_0 \text{ grad } \frac{\partial \phi}{\partial t}.$$

Consideration of the Lorenz condition yields

$$\nabla^2 \mathbf{a} - \epsilon_0 \mu_0 \frac{\partial^2 \mathbf{a}}{\partial t^2} = -\mu_0 \mathbf{j}. \tag{7.31}$$

From (7.3) and (7.30) we obtain, by similar steps,

$$\nabla^2 \phi - \epsilon_0 \mu_0 \frac{\partial^2 \phi}{\partial t^2} = -\frac{\rho}{\epsilon_0}. \tag{7.32}$$

The retarded solution of (7.31) and (7.32) must be used to obtain the retarded fields. We therefore take

$$\mathbf{a}(\mathbf{r}, t) = \frac{\mu_0}{4\pi} \int \frac{\mathbf{j}(\mathbf{r}', t - |\mathbf{r} - \mathbf{r}'|/c_0)}{|\mathbf{r} - \mathbf{r}'|} \, dV' \tag{7.33}$$

$$\phi(\mathbf{r}, t) = \frac{1}{4\pi\epsilon_0} \int \frac{\rho(\mathbf{r}', t - |\mathbf{r} - \mathbf{r}'|/c_0)}{|\mathbf{r} - \mathbf{r}'|} \, dV'. \tag{7.34}$$

Another possible gauge is the *Coulomb gauge*

$$\text{div } \mathbf{a} = 0. \tag{7.35}$$

This condition generates a potential that, by taking the divergence of (7.29), is found to satisfy

$$\nabla^2 \phi = -\frac{1}{\epsilon_0} \rho(\mathbf{r}, t).$$

The solution of that *Poisson equation* is

$$\phi(\mathbf{r}, t) = \frac{1}{4\pi\epsilon_0} \int_{\text{all space}} \frac{\rho(\mathbf{r}', t)}{|\mathbf{r} - \mathbf{r}'|} \, dV'. \tag{7.36}$$

The vector potential must now satisfy

$$\nabla^2 \mathbf{a} - \frac{1}{c_0^2} \frac{\partial^2 \mathbf{a}}{\partial t^2} = -\mu_0 \mathbf{j} + \frac{1}{c_0^2} \frac{\partial}{\partial t} (\text{grad } \phi). \tag{7.37}$$

We note that the right-hand term is known once ϕ has been evaluated.

According to Helmholtz' theorem (see Appendix 1), $\mathbf{j}$ may be split into two terms:

- A longitudinal (or irrotational) part

$$\begin{aligned} \mathbf{j}_l(\mathbf{r}) &= -\frac{1}{4\pi} \text{ grad} \int_{\text{all space}} \frac{\text{div}' \, \mathbf{j}}{|\mathbf{r} - \mathbf{r}'|} \, dV' \\ &= \frac{\partial}{\partial t} \text{ grad} \left[\frac{1}{4\pi} \int_{\text{all space}} \frac{\rho(\mathbf{r}')}{|\mathbf{r} - \mathbf{r}'|} \, dV' \right]. \end{aligned} \tag{7.38}$$

- A transverse (or solenoidal) part

$$\mathbf{j}_t(\mathbf{r}) = \frac{1}{4\pi}\,\text{curl}\int_{\text{all space}} \frac{\text{curl}'\,\mathbf{j}(\mathbf{r}')}{|\mathbf{r}-\mathbf{r}'|}\,dV'. \tag{7.39}$$

Inserting (7.38) and (7.39) into (7.37) leaves only $(-\mu_0\mathbf{j}_t)$ in the second member, hence

$$\nabla^2\mathbf{a} - \frac{1}{c_0^2}\frac{\partial^2\mathbf{a}}{\partial t^2} = -\mu_0\mathbf{j}_t. \tag{7.40}$$

In the Coulomb gauge, therefore, the transverse current is the source of the radiated fields, while the longitudinal current, which is related to ρ by the equation of conservation of charge

$$\frac{\partial\rho}{\partial t} = -\text{div}\,\mathbf{j}_l,$$

generates the quasi-static field.

In addition to the Lorenz and Poisson potentials, we may also use *Hertz potentials* $\mathbf{\Pi}_e$. If the sources are activated at $t = 0$, $\mathbf{\Pi}_e$ is given by

$$\mathbf{\Pi}_e(\mathbf{r},t) = \frac{1}{4\pi\epsilon_0}\int_0^t dt'\int_V \frac{\mathbf{j}(\mathbf{r}',t'-|\mathbf{r}-\mathbf{r}'|/c_0)}{|\mathbf{r}-\mathbf{r}'|}\,dV' \quad (\text{V m}). \tag{7.41}$$

The Lorenz potentials and fields are related to $\mathbf{\Pi}_e$ by

$$\mathbf{a} = \epsilon_0\mu_0\frac{\partial\mathbf{\Pi}_e}{\partial t} \tag{7.42}$$

$$\phi = -\text{div}\,\mathbf{\Pi}_e \tag{7.43}$$

$$\mathbf{e} = \text{grad div}\,\mathbf{\Pi}_e - \epsilon_0\mu_0\frac{\partial^2\mathbf{\Pi}_e}{\partial t^2} \tag{7.44}$$

$$\mathbf{b} \;=\; \mu_0\mathbf{h} = \epsilon_0\mu_0\,\text{curl}\,\frac{\partial\mathbf{\Pi}_e}{\partial t}. \tag{7.45}$$

As an illustration, assume that two point charges q and $-q$, initially superimposed, are suddenly pulled apart,[7] thus creating a dipole (Fig. 7.3). The Hertz potential is z-directed, and $\mathbf{j}$ can be written in terms of a linear current i as

$$\mathbf{j}(\mathbf{r},t) = \delta(x)\delta(y)i(t)\,\mathbf{u}_z,$$

where $\displaystyle\int_{-\infty}^{t} i(t')\,dt' = q\,H(t)$. The corresponding Hertz potential takes the value

$$\mathbf{\Pi}_e = \frac{ql}{4\pi\epsilon_0}\frac{H(t-R/c_0)}{R}\,\mathbf{u}_z,$$

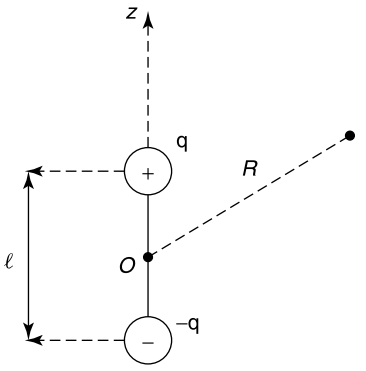

Figure 7.3 Creation of a dipole.

where H is the Heaviside step function. The resulting fields are

$$e_R = \frac{ql\cos\theta}{2\pi\epsilon_0}\left[\frac{H(t-R/c_0)}{R^3} + \frac{\delta(t-R/c_0)}{c_0R^2}\right]$$

$$e_\theta = \frac{ql\sin\theta}{4\pi\epsilon_0}\left[\frac{H(t-R/c_0)}{R^3} + \frac{\delta(t-R/c_0)}{c_0R^2} + \frac{\delta'(t-R/c_0)}{c_0^2R}\right]$$

$$h_\varphi = \frac{ql\sin\theta}{4\pi}\left[\frac{\delta(t-R/c_0)}{R^2} + \frac{\delta'(t-R/c_0)}{c_0R}\right].$$

Magnetic Sources

When the sources are purely magnetic, div **d** vanishes, and it becomes useful to introduce a vector potential **c** (sometimes called *Fitzgerald potential*), in terms of which the fields are expressed by

$$\mathbf{d} = \epsilon_0\mathbf{e} = -\text{curl}\,\mathbf{c}$$

$$\mathbf{h} = -\text{grad}\,\psi - \frac{\partial\mathbf{c}}{\partial t}. \tag{7.46}$$

Given the Lorenz type of condition

$$\text{div}\,\mathbf{c} + \epsilon_0\mu_0\frac{\partial\psi}{\partial t} = 0 \tag{7.47}$$

c must satisfy

$$\nabla^2\mathbf{c} - \frac{1}{c_0^2}\frac{\partial^2\mathbf{c}}{\partial t^2} = \epsilon_0\mathbf{j}_m \tag{7.48}$$

and the potentials follow as

$$\mathbf{c}(\mathbf{r},t) = \frac{\epsilon_0}{4\pi}\int\frac{\mathbf{j}_m(\mathbf{r}',t-|\mathbf{r}-\mathbf{r}'|/c_0)}{|\mathbf{r}-\mathbf{r}'|}\,dV' \qquad (\text{C m}^{-1}) \tag{7.49}$$

$$\psi(\mathbf{r},t) = \frac{1}{4\pi\mu_0}\int\frac{\rho_m(\mathbf{r}',t-|\mathbf{r}-\mathbf{r}'|/c_0)}{|\mathbf{r}-\mathbf{r}'|}\,dV' \qquad (\text{A}). \tag{7.50}$$

The corresponding *magnetic Hertz potential* $\mathbf{\Pi}_m$ can be defined by a relationship similar to (7.41). It gives rise to the equations

$$\mathbf{c} = \epsilon_0 \mu_0 \frac{\partial \mathbf{\Pi}_m}{\partial t} \tag{7.51}$$

$$\psi = -\text{div } \mathbf{\Pi}_m \tag{7.52}$$

$$\mathbf{d} = -\epsilon_0 \mu_0 \text{ curl } \frac{\partial \mathbf{\Pi}_m}{\partial t} \tag{7.53}$$

$$\mathbf{h} = \text{grad div } \mathbf{\Pi}_m - \epsilon_0 \mu_0 \frac{\partial^2 \mathbf{\Pi}_m}{\partial t^2}. \tag{7.54}$$

Note finally that, in a region devoid of sources, the fields can be expressed in terms of *two* scalar functions, both of which must be solutions of the wave equation (7.22) without second member. Thus,

$$\begin{aligned} \mathbf{e} &= \text{grad div } (A\mathbf{u}) - \frac{1}{c_0^2} \frac{\partial^2 A}{\partial t^2} \mathbf{u} - \text{curl } \left(\frac{\partial C}{\partial t} \mathbf{u} \right) \\ \mathbf{b} &= \frac{1}{c_0^2} \text{ curl } \left(\frac{\partial A}{\partial t} \mathbf{u} \right) + \text{grad div } (C\mathbf{u}) - \frac{1}{c_0^2} \frac{\partial^2 C}{\partial t^2} \mathbf{u}, \end{aligned} \tag{7.55}$$

where $\mathbf{u}$ is a constant vector (typically a unit vector).

7.4 SINUSOIDAL TIME DEPENDENCE: POLARIZATION

The three components of a time-harmonic vector of angular frequency ω are of the form

$$\begin{aligned} a_x &= a_{xm}(\mathbf{r}) \cos [\omega t + \phi_x(\mathbf{r})] \\ a_y &= a_{ym}(\mathbf{r}) \cos [\omega t + \phi_y(\mathbf{r})] \\ a_z &= a_{zm}(\mathbf{r}) \cos [\omega t + \phi_z(\mathbf{r})]. \end{aligned}$$

The complex phasor representation of these relationships, which preserves the phase and amplitude information, is

$$\begin{aligned} A_x(\mathbf{r}) &= a_{xm}(\mathbf{r}) e^{j\phi_x(\mathbf{r})} \\ A_y(\mathbf{r}) &= a_{ym}(\mathbf{r}) e^{j\phi_y(\mathbf{r})} \\ A_z(\mathbf{r}) &= a_{zm}(\mathbf{r}) e^{j\phi_z(\mathbf{r})}. \end{aligned}$$

The vector itself can be represented by the vectorial phasor

$$\mathbf{A}(\mathbf{r}) = A_x(\mathbf{r})\mathbf{u}_x + A_y(\mathbf{r})\mathbf{u}_y + A_z(\mathbf{r})\mathbf{u}_z,$$

which is related to the time-dependent form by the simple relationship

$$\mathbf{a}(\mathbf{r}, t) = Re\, [\mathbf{A}(\mathbf{r}) e^{j\omega t}]. \tag{7.56}$$

It is useful to separate $\mathbf{A}$ into its real and imaginary parts. Thus,

$$\begin{aligned}\mathbf{A}(\mathbf{r}) &= \mathbf{a}_r(\mathbf{r}) + j\mathbf{a}_i(\mathbf{r}) \\ &= a_{xm}\cos\phi_x\mathbf{u}_x + a_{ym}\cos\phi_y\mathbf{u}_y + a_{zm}\cos\phi_z\mathbf{u}_z \\ &\quad + j(a_{xm}\sin\phi_x\mathbf{u}_x + a_{ym}\sin\phi_y\mathbf{u}_y + a_{zm}\sin\phi_z\mathbf{u}_z).\end{aligned}$$

Equation (7.56) shows that

$$\mathbf{a}(\mathbf{r}, t) = \mathbf{a}_r\cos\omega t - \mathbf{a}_i\sin\omega t. \tag{7.57}$$

This relationship implies that a time-harmonic vector remains at all times parallel to a fixed plane $(\mathbf{a}_r, \mathbf{a}_i)$ (Fig. 7.4). With respect to an arbitrary set of orthogonal coordinates in that plane, the projections (X, Y) of $\mathbf{a}$ become

$$\begin{aligned}X &= a_{rx}\cos\omega t - a_{ix}\sin\omega t \\ Y &= a_{ry}\cos\omega t - a_{iy}\sin\omega t.\end{aligned}$$

The relationship $\sin^2\omega t + \cos^2\omega t = 1$ yields

$$(Xa_{ry} - Ya_{rx})^2 + (Xa_{iy} - Ya_{ix})^2 = (a_{rx}a_{iy} - a_{ry}a_{ix})^2.$$

This equation shows that the tip of vector $\mathbf{a}$ describes an ellipse. Accordingly, the most general time-harmonic field is said to be *elliptically polarized*. The semi-axes of the ellipse are given by

$$\begin{aligned}\mathbf{a}'_r &= \mathbf{a}_r\cos\delta + \mathbf{a}_i\sin\delta \\ \mathbf{a}'_i &= -\mathbf{a}_r\sin\delta + \mathbf{a}_i\cos\delta,\end{aligned} \tag{7.58}$$

with

$$\tan 2\delta = \frac{2\mathbf{a}_r\cdot\mathbf{a}_i}{a_r^2 - a_i^2}.$$

Comparison with (7.57) shows that δ/ω is the time interval required for the vector to change its value from $\mathbf{a}'_r$ to $\mathbf{a}_r$. We notice that (7.58) can be written more compactly as

$$\mathbf{A} = \mathbf{a}_r + j\mathbf{a}_i = (\mathbf{a}'_r + j\mathbf{a}'_i)\,e^{j\delta}.$$

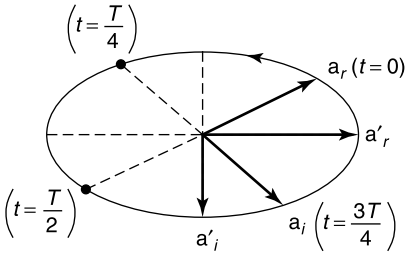

Figure 7.4 Polarization ellipse.

7.4.1 Linear Polarization

When $\mathbf{a}_i$ and $\mathbf{a}_r$ are parallel, $\mathbf{a}$ has a fixed direction in space, and the ellipse degenerates into a line segment. In such a case the vector is said to be *linearly polarized*. It is to be noted that the projections of a linearly polarized vector oscillate in phase. It follows that the phasor of $\mathbf{a}$ can be expressed as

$$\mathbf{A} = \mathbf{a}_m e^{j\phi} = a_m \mathbf{u}_a e^{j\phi},$$

where $\mathbf{a}_m$ is a *real* vector, and $\mathbf{u}_a$ is a unit vector in the direction of $\mathbf{a}_m$.

An arbitrary elliptically polarized vector can be expressed as the sum of two mutually orthogonal linearly polarized vectors. This decomposition, which can be performed in an infinite number of ways, is particularly useful in the study of wave propagation in material media, a topic dealt with in Chapter 8.

7.4.2 Circular Polarization

When $\mathbf{a}_i$ and $\mathbf{a}_r$ are orthogonal and of equal magnitude, the tip of $\mathbf{a}$ describes a circle; the vector is said to be *circularly polarized*. Assume that a positive side has been chosen for the normal to the circle. The polarization is termed as *right* or *left* depending on whether an observer located on the positive side of the circle sees the tip of the vector rotate respectively in the clockwise and the counterclockwise direction. The projections of a circularly polarized vector on two perpendicular axes are of the form

$$a_x = a \cos(\omega t + \phi)$$
$$a_y = a \cos\left(\omega t + \phi \pm \frac{\pi}{2}\right).$$

If the positive side coincides with the positive z-axis, the right and left polarizations correspond respectively with the plus and minus signs in a_y. The complex representation of these two polarizations is shown in Figure 7.5.

An elliptically polarized vector can always be split into two circularly polarized vectors rotating in opposite directions. The proof consists in showing that two complex numbers A' and A'' can be found such that

$$\mathbf{A} = \mathbf{A}_r + j\mathbf{A}_i = A'(\mathbf{u}_x + j\mathbf{u}_y) + A''(\mathbf{u}_x - j\mathbf{u}_y). \tag{7.59}$$

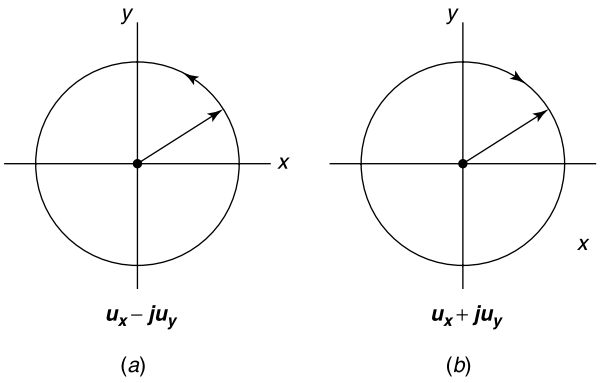

Figure 7.5 Circular polarizations: (*a*) left hand, (*b*) right hand.

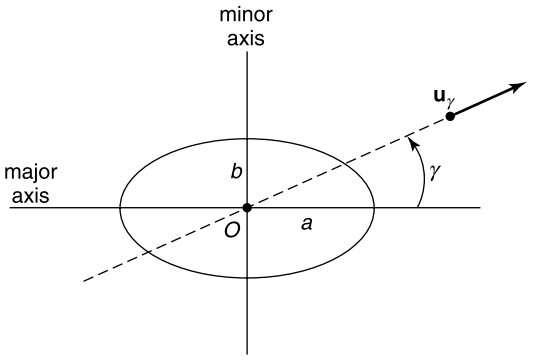

Figure 7.6 Determination of the axes of an ellipse.

This is easy to verify, because the explicit values of A' and A'' can be written by inspection. Thus,

$$A' = \frac{A_{rx} + A_{iy}}{2} + j\frac{A_{ix} - A_{ry}}{2} = \frac{1}{2}(a_{xm}e^{j\phi_x} - ja_{ym}e^{j\phi_y})$$

and

$$A'' = \frac{A_{rx} - A_{iy}}{2} + j\frac{A_{ix} + A_{ry}}{2} = \frac{1}{2}(a_{xm}e^{j\phi_x} + ja_{ym}e^{j\phi_y}).$$

Characteristics of the polarization ellipse, such as the axial ratio (b/a), can be measured by means of a device (e.g., a short dipole-probe) that measures the component of $\mathbf{a}(t)$ in a direction of unit vector $\mathbf{u}_\gamma$ (Fig. 7.6). This projection is

$$\mathbf{a}\cdot\mathbf{u}_\gamma = a\cos\omega t\cos\gamma + b\sin\omega t\sin\gamma.$$

If the detector measures the time-averaged square of $(\mathbf{a}\cdot\mathbf{u}_\gamma)$, its output will be

$$\left\langle a_\gamma^2 \right\rangle = \frac{1}{T}\int_0^T a_\gamma^2(t)\,dt = \frac{a^2}{2}\cos^2\gamma + \frac{b^2}{2}\sin^2\gamma.$$

By rotating the probe over 2π, this output will display successive maxima and minima, obtained when the probe is parallel with respectively the major and the minor axis. The ratio of minimum to maximum is the square of the sought axial ratio.

The state of polarization may be conveniently represented by a point P on the *Poincaré sphere*. The representation is based on two angles (Fig. 7.7*a*):

- An angle $\alpha = \tan^{-1}\left(\frac{b}{a}\right)$, which is a measure of the axial ratio b/a.
- An angle β, which measures the position of the major axis with respect to a reference direction, often chosen to be the horizontal polarization H.

The representation of the state of polarization is shown in Figure 7.7*b*. There the radius of the sphere is unity, and the point P is determined by its latitude 2α and its longitude 2β. The poles correspond with the two circular polarizations, and the equator to linear polarizations. The Poincaré sphere is well-suited to follow the change of polarization that a wave (e.g., a beam of light) suffers when it traverses an inhomogeneous medium. If the ellipse keeps its shape, but not its orientation, α remains constant, and P moves on the small circle shown in Figure 7.7*b*.

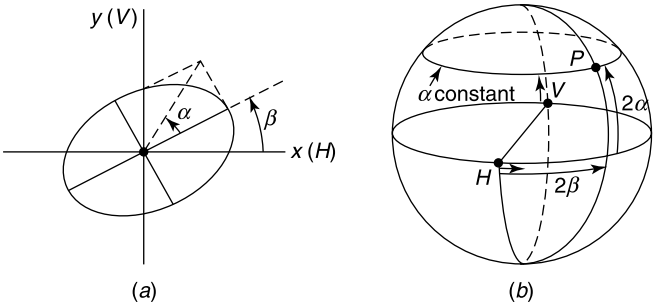

Figure 7.7 (*a*) Angles for the Poincaré sphere. (*b*) Poincaré sphere.

7.5 PARTIALLY POLARIZED FIELDS

The polarization of a *quasi-harmonic field* varies slowly with respect to the main period of the field but rapidly with respect to the time constants of the observed system. For such a field, the "*P*" point wanders around on the Poincaré sphere. In two dimensions (but the extension to three dimensions is immediate), the components of the wave vector may be written as

$$\begin{aligned} e_x(t) &= e_{xm}(t)\cos\left[\omega t + \phi_x(t)\right] \\ e_y(t) &= e_{ym}(t)\cos\left[\omega t + \phi_y(t)\right]. \end{aligned} \tag{7.60}$$

The vector **e** could be the electric field in a plane wave or the vector potential in a radiation zone. As mentioned before, the functions e_{xm}, e_{ym}, ϕ_x, and ϕ_y are assumed to vary slowly with respect to the basic period $T = (2\pi/\omega)$. As in the case of a purely time-harmonic field, it pays to introduce the complex vector

$$\begin{aligned} E_x(t) &= e_{xm}(t)\, e^{j\phi_x(t)} \\ E_y(t) &= e_{ym}(t)\, e^{j\phi_y(t)}. \end{aligned} \tag{7.61}$$

Important parameters for a partially polarized field are time-averages of the kind

$$\begin{aligned} \langle e_x e_y \rangle &= \lim_{T\to\infty} \frac{1}{2T} \int_{-T}^{T} e_x(t) e_y(t)\, dt \\ &= \lim_{T\to\infty} \frac{1}{4T} \left[\int_{-T}^{T} e_{xm}(t) e_{ym}(t) \cos[2\omega t + \phi_x(t) + \phi_y(t)]\, dt \right. \\ &\quad \left. + \int_{-T}^{T} e_{xm}(t) e_{ym}(t) \cos[\phi_x(t) - \phi_y(t)]\, dt \right]. \end{aligned}$$

The integrand in the first integral oscillates rapidly, and the integral averages to zero when it is evaluated over large T. The second integral therefore dominates and may be written as

$$\langle e_x e_y \rangle = \frac{1}{2}\, Re \left\langle E_x E_y^* \right\rangle, \tag{7.62}$$

where

$$\left\langle E_x E_y^* \right\rangle = \lim_{T\to\infty} \int_{-T}^{T} e_{xm}(t)\, e^{j\phi_x(t)}\, e_{ym}(t)\, e^{-j\phi_y(t)}\, dt. \tag{7.63}$$

7.5.1 The Polarization Matrix

The *coherence matrix* is defined by [36]

$$\overline{\overline{\Gamma}} = \begin{pmatrix} \langle E_x E_x^* \rangle & \left\langle E_x E_y^* \right\rangle \\ \langle E_y E_x^* \rangle & \left\langle E_y E_y^* \right\rangle \end{pmatrix} \tag{7.64}$$

From (7.63), this matrix is Hermitian. The diagonal elements are positive; hence, the trace of the matrix is positive as well. Normalization to unit trace yields the *polarization matrix* $\overline{\overline{p}}$. For example:

- In a time-harmonic linearly polarized field making an angle γ with the x-axis, $\overline{\overline{p}}$ is given by

$$\overline{\overline{p}} = \begin{pmatrix} \cos^2\gamma & \sin\gamma\cos\gamma \\ \sin\gamma\cos\gamma & \sin^2\gamma. \end{pmatrix}. \tag{7.65}$$

- In a time-harmonic circularly polarized field,

$$\overline{\overline{p}} = \begin{pmatrix} 0.5 & \pm 0.5j \\ \mp 0.5j & 0.5 \end{pmatrix}. \tag{7.66}$$

- In a totally unpolarized field,

$$\overline{\overline{p}} = \begin{pmatrix} 0.5 & 0 \\ 0 & 0.5 \end{pmatrix}. \tag{7.67}$$

From *Schwartz' inequality* (1.13), viz.

$$|\langle f, g\rangle_H| \leq \| f \| \, \| g \|$$

it follows that

$$\det\ \overline{\overline{p}} = p_{xx}p_{yy} - p_{yx}p_{xy} \geq 0, \tag{7.68}$$

where the equality sign holds only for a purely elliptic polarization. This property leads to the concept of *degree of polarization* ρ, defined by

$$\rho = \sqrt{1 - 4\ \det\ \overline{\overline{p}}}. \tag{7.69}$$

From (7.65) to (7.67), it follows that $\rho = 1$ for time-harmonic linearly or circularly polarized fields, and $\rho = 0$ for totally unpolarized fields. Electromagnetic radiation generated by the sun and radio stars, or encountered in remote sensing radiometry, is partially

polarized. Unwanted noise entering any system tends to be randomly polarized. The *random* component in such fields can be isolated by means of the splitting

$$\overline{\overline{p}} = A \begin{pmatrix} 0.5 & 0 \\ 0 & 0.5 \end{pmatrix} + \begin{pmatrix} B & D \\ D^* & C \end{pmatrix}. \tag{7.70}$$

The first part is the random component. Its weight is given by $A = 4 \det \overline{\overline{p}}$. Note that the determinant $(BC - DD^*)$ of the polarized component is equal to zero.

7.5.2 Stokes Parameters

Both intensity and state of polarization can be efficiently characterized by the — real — *Stokes parameters*[8]

$$\begin{aligned} s_0 &= I = \left\langle E_x E_x^* \right\rangle + \left\langle E_y E_y^* \right\rangle = \Gamma_{xx} + \Gamma_{yy} \\ s_1 &= Q = \left\langle E_x E_x^* \right\rangle - \left\langle E_y E_y^* \right\rangle = \Gamma_{xx} - \Gamma_{yy} \\ s_2 &= U = 2\, Re \left\langle E_x E_y^* \right\rangle = \Gamma_{xy} + \Gamma_{yx} \\ s_3 &= V = -2\, Im \left\langle E_x E_y^* \right\rangle = j(\Gamma_{xy} - \Gamma_{yx}). \end{aligned} \tag{7.71}$$

Both s and I notations are in use. The s_0 parameter is clearly a measure of the intensity of the wave (see also Problem 7.11). Further,

$$\begin{aligned} I^2 &\geq Q^2 + U^2 + V^2 \\ s_0^2 &\geq s_1^2 + s_2^2 + s_3^2, \end{aligned} \tag{7.72}$$

where the equality sign applies only for completely polarized light. The degree of polarization is now

$$\rho = \frac{\sqrt{s_1^2 + s_2^2 + s_3^2}}{s_0}. \tag{7.73}$$

It is common practice to normalize the Stokes vector by setting $s_0 = I = 1$, which amounts to replacing $\overline{\overline{\Gamma}}$ by $\overline{\overline{p}}$ in (7.71). This convention gives, for time-harmonic fields,

$s = (1, 0, 0, \pm 1)$ for circular polarization ($+$ for right circular)

$s = (1, 1, 0, 0)$ for the H-polarization (linear in the x-direction)

$s = (1, -1, 0, 0)$ for the V-polarization (linear in the y-direction).

For unpolarized fields,

$$s = (1, 0, 0, 0). \tag{7.74}$$

The polarization property has been put to good use in numerous technological applications. A transmitter, for example, can be designed to beam two separate signals, one on the vertical polarization, the other one on the horizontal polarization. Both signals are

subsequently separated at the receiving end. Polarization has also been a main element in sensing and imaging applications. It has also been exploited in monitoring the environmental evolution of a region. In a wider perspective, it is interesting to note that humans are almost (but not fully) polarization blind, while some insects and marine creatures are able to distinguish between polarized and unpolarized light, and make use of the fact to navigate and control flight motion [53].

7.6 THE RADIATION CONDITION

The radiation condition, which governs the behavior of the fields at large distances, must be enforced to obtain a unique solution for the exterior problem. The condition, which is based on the causality principle, ensures that outgoing waves are allowed, whereas incoming waves are excluded.

7.6.1 Scalar Fields

Let Φ be a solution of Helmholtz' equation

$$\nabla^2\Phi + k_0^2\Phi = G(\mathbf{r}). \tag{7.75}$$

Outside a sphere S_R containing all the sources Φ satisfies

$$\nabla^2\Phi + k_0^2\Phi = 0. \tag{7.76}$$

The nature of the field at large distances may be clarified by expanding Φ in spherical harmonics, following a method that has successfully been used in Section 3.7 for the electrostatic potential. Thus,

$$\Phi(R,\theta,\varphi) = \sum_{n=0}^{\infty}\left\{A_n(R)P_n(\cos\theta) + \sum_{m=1}^{n}\left[A_{mn}(R)\cos m\varphi + B_{mn}(R)\sin m\varphi\right]P_n^m(\cos\theta)\right\}. \tag{7.77}$$

This expansion holds in a spherical coordinate system whose origin is at the center of S_R. Insertion of the right-hand term of (7.77) into (7.76) leads to the differential equation

$$\frac{d^2A_{mn}}{dR^2} + \frac{2}{R}\frac{dA_{mn}}{dR} + \left[k_0^2 - \frac{n(n+1)}{R^2}\right]A_{mn} = 0. \tag{7.78}$$

where use has been made of (A9.34). The solutions of this equation are the spherical Bessel functions $j_n(k_0R)$ and $n_n(k_0R)$ defined in (A5.84). Of particular interest for the current analysis are the following linear combinations of these functions:

$$h_n^{(1)}(k_0R) = \left(\frac{\pi}{2k_0R}\right)^{\frac{1}{2}}H_{n+\frac{1}{2}}^{(1)}(k_0R)$$

$$h_n^{(2)}(k_0R) = \left(\frac{\pi}{2k_0R}\right)^{\frac{1}{2}}H_{n+\frac{1}{2}}^{(2)}(k_0R). \tag{7.79}$$

For large values of R, the asymptotic values of the functions are given in (A5.100) and (A5.101). Thus,

$$\lim_{R\to\infty} h_n^{(1)}(k_0R) = (-j)^{n+1}\frac{e^{jk_0R}}{k_0R}$$
$$\lim_{R\to\infty} h_n^{(2)}(k_0R) = (j)^{n+1}\frac{e^{-jk_0R}}{k_0R}. \tag{7.80}$$

Because the time factor is $e^{j\omega t}$, the first function gives rise to an incoming wave, the second to an outgoing wave. It is the outgoing-wave solution that is appropriate. The *Sommerfeld radiation condition* [171]

$$\lim_{R\to\infty} R\left(\frac{\partial\Phi}{\partial R} + jk_0\Phi\right) = 0, \tag{7.81}$$

often rewritten as

$$\frac{\partial\Phi}{\partial R} + jk_0\Phi = o\left(\frac{1}{R}\right), \tag{7.82}$$

automatically selects the proper solution. Inserting $h_n^{(2)}(k_0R)$ into the expansion for Φ yields

$$\Phi(R,\theta,\varphi) = \sum_{n,m} A_{mn}h_0^{(2)}(k_0R)Y_{mn}(\theta,\varphi). \tag{7.83}$$

The asymptotic form of $h_n^{(2)}(kR)$ further shows that

$$\lim_{R\to\infty}\Phi(R,\theta,\varphi) = \frac{e^{-jk_0R}}{R}F(\theta,\varphi). \tag{7.84}$$

The function $F(\theta,\varphi)$ is the *radiation characteristic* of the source. A complex function that satisfies both (7.76) and the radiation condition, and that possesses continuous derivatives up to the second order, is termed a *scalar radiation function*.

It is to be noted that Sommerfeld's radiation condition is unnecessarily severe. The milder condition

$$\lim_{R\to\infty}\int_{S_R}\left|\frac{\partial\Phi}{\partial R} + jk_0\Phi\right|^2 dS = 0, \tag{7.85}$$

is sufficient to make the solution unique and generate an outgoing wave at large distances.[9]

7.6.2 Electromagnetic Fields

Outside a sphere that contains all the sources, the **E** and **H** fields satisfy

$$\nabla^2\mathbf{\Phi} + k_0^2\mathbf{\Phi} = 0. \tag{7.86}$$

Applying (7.84) to the three components of Φ yields the large-distance expression

$$\mathbf{\Phi}(R,\theta,\varphi) = \frac{e^{-jk_0R}}{R}\left[\mathbf{F}(\theta,\varphi) + \frac{\mathbf{F}_1(\theta,\varphi)}{R} + \cdots\right]. \tag{7.87}$$

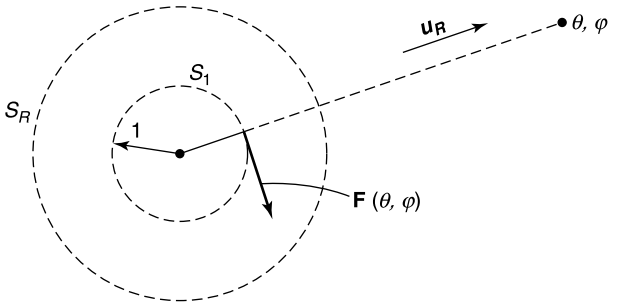

Figure 7.8 Radiation vector and unit sphere.

Additional information is obtained by noting that **E** and **H** have zero divergence. The asymptotic form of div $\mathbf{\Phi}$, for large R, is

$$\text{div } \mathbf{\Phi} = \text{div}\left[\frac{e^{-jk_0R}}{R}\mathbf{F}(\theta,\varphi)\right] = -jk_0\frac{e^{-jk_0R}}{R}(\mathbf{u}_R\cdot\mathbf{F}). \tag{7.88}$$

The condition div $\mathbf{\Phi} = 0$ therefore implies $F_R = 0$. It follows that the radiation vectors of **E** and **H** are *tangent* to the unit sphere S_1 centered at the origin (Fig. 7.8). We note that the radiation vector $\mathbf{F}(\theta, \varphi)$ is a complex vector, whose real and imaginary parts determine the polarization characteristics of the radiation field.

The radiation vectors of **E** and **H** are not independent. The relationship between these vectors can be derived by evaluating the asymptotic form of curl $\mathbf{\Phi}$. Thus, in the limit $R \to \infty$,

$$\text{curl}\left[\frac{e^{-jk_0R}}{R}\mathbf{F}(\theta,\varphi)\right] = -jk_0\frac{e^{-jk_0R}}{R}(\mathbf{u}_R\times\mathbf{F}), \tag{7.89}$$

which implies the *radiation condition*[‡]

$$\mathbf{u}_R\times\text{curl }\mathbf{\Phi} - jk_0\mathbf{\Phi} = o\left(\frac{1}{R}\right). \tag{7.90}$$

Because a divergenceless $\mathbf{\Phi}$ satisfies

$$-\text{curl curl }\mathbf{\Phi} + k_0^2\mathbf{\Phi} = 0 \tag{7.91}$$

outside the sources, it makes sense to call a vector $\mathbf{\Phi}$ satisfying (7.90) and (7.91) a *vector radiation function*. Both **E** and **H** are such functions, and insertion of (7.89) into Maxwell's

[‡]C. H. Wilcox shows that the milder conditions

$$\lim_{R\to\infty}\int_\Sigma\left|\frac{\partial\mathbf{\Phi}}{\partial R} + jk_0\mathbf{\Phi}\right|^2 dS = 0 \quad \text{or} \quad \lim_{R\to\infty}\int_\Sigma|\mathbf{u}_R\times\text{curl }\mathbf{\Phi} - jk_0\mathbf{\Phi}|^2\,dS = 0$$

are sufficient.[9] He also proves that

1. div $\mathbf{\Phi} = 0$ if $\mathbf{\Phi}$ satisfies (7.85) and $\lim_{R\to\infty}\int_\Sigma|\Phi_R|^2dS = 0$
2. curl $\mathbf{\Phi} = 0$ if $\mathbf{\Phi}$ satisfies (7.85) and $\lim_{R\to\infty}\int_\Sigma|\mathbf{u}_R\times\mathbf{\Phi}|^2dS = 0$.

equations shows that, in any direction (θ, φ) of unit vector $\mathbf{u}_R$, the radiation fields must satisfy

$$\mathbf{u}_R \times \mathbf{H} + \frac{1}{R_{co}}\mathbf{E} = o\left(\frac{1}{R}\right)$$
$$\mathbf{u}_R \times \mathbf{E} - R_{co}\mathbf{H} = o\left(\frac{1}{R}\right) \tag{7.92}$$

in the limit $R \to \infty$. These equations imply the following:

1. **E** and **H** are perpendicular, and the ratio of their magnitudes is R_{co}.
2. **E** and **H** oscillate in phase.
3. Both **E** and **H** are transverse (i.e., they are perpendicular to $\mathbf{u}_R$) and their cross product $\mathbf{E} \times \mathbf{H}$ is radial.
4. If $\mathbf{F}_E$ is the radiation vector of **E**, then $\mathbf{u}_R \times \mathbf{F}_E/R_{co}$ is the corresponding radiation vector of **H**.
5. In a small range (in distance and angle) centered on R and (θ, φ), **E** and **H** behave like the fields in a plane wave.

Property 5 justifies the frequent use of plane waves as incident fields in scattering problems of the kind discussed in Chapters 11 and 12.

7.7 TIME-HARMONIC POTENTIALS

The time-harmonic Lorenz potentials satisfy equations, (7.31) and (7.32), which in their complex version take the form

$$\nabla^2\mathbf{A} + k_0^2\mathbf{A} = -\mu_0\mathbf{J}$$
$$\nabla^2\Phi + k_0^2\Phi = -\frac{1}{\epsilon_0}P. \tag{7.93}$$

To solve these Helmholtz equations, it is useful to first determine the relevant Green's function $G_0(\mathbf{r}|\mathbf{r}')$. For a point source at the origin, G_0 satisfies

$$\nabla^2 G_0(\mathbf{r}) + k_0^2 G_0(\mathbf{r}) = \delta(\mathbf{r}). \tag{7.94}$$

Because of the isotropic character of the field, G_0 is a function of R only, hence the general solution of (7.94) is

$$G_0(R) = A\frac{e^{-jk_0R}}{R} + B\frac{e^{jk_0R}}{R}.$$

The term in (e^{jk_0R}/R) must be eliminated because, upon multiplication with $e^{j\omega t}$, it generates an incoming wave. The coefficient A may be determined by requiring $G_0(R)$ to converge to the Green's function (3.13) of potential theory in the limit $k_0 \to 0$. More specifically, for $R \ll \lambda_0$, e^{-jk_0R} may be replaced by unity. It follows that

$$G_0(\mathbf{r}, \mathbf{r}') = -\frac{1}{4\pi}\frac{e^{-jk_0|\mathbf{r}-\mathbf{r}'|}}{|\mathbf{r}-\mathbf{r}'|}. \tag{7.95}$$

Other methods are available to justify the coefficient $-(1/4\pi)$ (see Problem 7.14). Applied to the solution of (7.93), the Green's function leads to

$$\Phi(\mathbf{r}) = \frac{1}{4\pi\epsilon_0} \int \frac{P(\mathbf{r}')e^{-jk_0|\mathbf{r}-\mathbf{r}'|}}{|\mathbf{r}-\mathbf{r}'|}\, dV' \tag{7.96}$$

$$\mathbf{A}(\mathbf{r}) = \frac{\mu_0}{4\pi} \int \frac{\mathbf{J}(\mathbf{r}')e^{-jk_0|\mathbf{r}-\mathbf{r}'|}}{|\mathbf{r}-\mathbf{r}'|}\, dV'. \tag{7.97}$$

These relationships show that the contributions from the various volume elements dV' do not add with their original phase but are affected by an additional phase lag $k_0|\mathbf{r}-\mathbf{r}'| = 2\pi|\mathbf{r}-\mathbf{r}'|/\lambda_0$. If the dimensions of the volume occupied by the sources are larger than λ_0, the additional phase lag covers a range larger than $(0, 2\pi)$. Phase differences of that magnitude create the possibility of constructive interference in certain directions and destructive interference in others. These, in turn, produce corresponding maxima (or lobes) and minima (or zeroes) in the radiation pattern of the sources.

The transition of the general expressions (7.96) and (7.97) to their far-field form can be followed by replacing $|\mathbf{r}-\mathbf{r}'|$ by

$$\begin{aligned} |\mathbf{r}-\mathbf{r}'| &= R\sqrt{1+\left(\frac{R'}{R}\right)^2 - 2\frac{R'}{R}\cos\psi} \\ &\approx R - R'\cos\psi + \frac{1}{2}\left(\frac{R'^2}{R}\right)\sin^2\psi + \cdots . \end{aligned}$$

Inserting this expression into (7.97) yields, in a direction of unit vector $\mathbf{u}$ (Fig. 7.9),

$$\lim_{R\to\infty} \mathbf{A} = \frac{e^{-jk_0R}}{R}\frac{\mu_0}{4\pi}\int_V \mathbf{J}(\mathbf{r}')\, e^{jk_0\mathbf{u}\cdot\mathbf{r}'} e^{-j\frac{k_0}{2}\frac{(R')^2}{R}\sin^2\psi} dV' + \cdots . \tag{7.98}$$

By definition, the *radiation (or Fraunhofer) zone* corresponds with values of R large enough to satisfy the *small exponent* condition[§]

$$\frac{k_0}{2}\frac{(R')^2}{R}\sin^2\psi \ll 1.$$

An often-used general criterion is

$$R_{\text{rad}} \geq \frac{2d_{\max}^2}{\lambda_0}, \tag{7.99}$$

where $d_{\max}$ is the largest dimension of the source in a direction perpendicular to $\mathbf{u}$. A few radiation distances are given in Figure 7.10 for four values of $d_{\max}$. For a parabolic antenna of 9 m diameter, for example, the radiation distance at 10 GHz is 5.4 km. In the radiation zone,

$$\lim_{R\to\infty} \mathbf{A} = \frac{e^{-jk_0R}}{R}\frac{\mu_0}{4\pi}\int_V \mathbf{J}(\mathbf{r}')e^{jk_0\mathbf{u}\cdot\mathbf{r}'}dV' = \frac{e^{-jk_0R}}{R}\mathbf{N}(\mathbf{u}). \tag{7.100}$$

[§]The *Rayleigh* zone corresponds with distances $R \ll \lambda_0$; the *Fresnel* zone follows, from λ_0 to R_{rad}, and the *Fraunhofer* zone extends beyond R_{rad}.

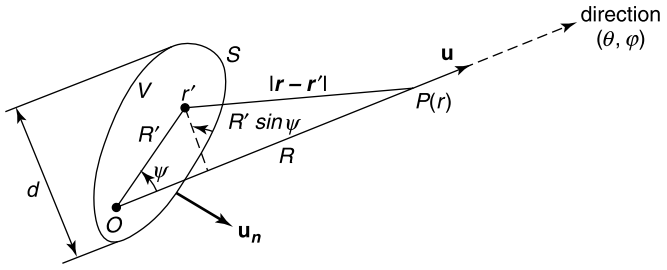

Figure 7.9 Current distribution and field point P.

The complex vector $\mathbf{N}$ represents the (θ, φ) dependence of the radiated potential. As predicted by (7.92), the corresponding fields are asymptotically

$$\begin{aligned} \mathbf{E} &= jk_0 c_0 \frac{e^{-jk_0 R}}{R} \mathbf{u} \times (\mathbf{u} \times \mathbf{N}) = \mathbf{F}(\mathbf{u}) \frac{e^{-jk_0 R}}{R} \\ \mathbf{H} &= \frac{jk_0}{\mu_0} \frac{e^{-jk_0 R}}{R} (\mathbf{N} \times \mathbf{u}) = \frac{1}{R_{c0}} (\mathbf{u} \times \mathbf{F}) \frac{e^{-jk_0 R}}{R}. \end{aligned} \tag{7.101}$$

The transition to the radiation zone can be followed with particular clarity when the source is a z-oriented linear current I located at the origin. If the antenna is small (i.e., if its length ℓ is much less than λ_0), (7.97) becomes

$$\mathbf{A}(\mathbf{r}) = \frac{\mu_0}{4\pi} (I\ell) \frac{e^{-jk_0 R}}{R} \mathbf{u}_z, \tag{7.102}$$

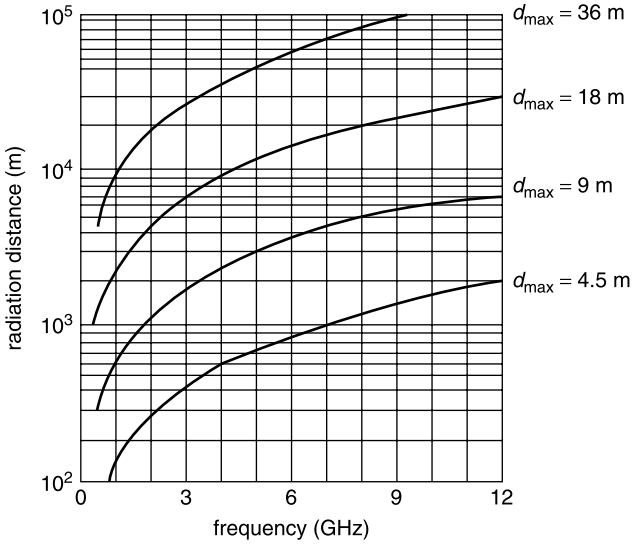

Figure 7.10 Radiation distance for a few source dimensions.

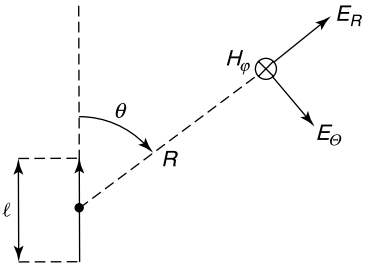

Figure 7.11 Pertinent to the fields from a short antenna.

from which one obtains (Fig. 7.11)

$$\begin{aligned}\mathbf{E} &= R_{c0}\frac{I\ell}{2\pi}\cos\theta k_0^2\left[\frac{1}{k_0^2R^2}-\frac{j}{k_0^3R^3}\right]e^{-jk_0R}\mathbf{u}_R\\ &\quad+R_{c0}\frac{I\ell}{4\pi}\sin\theta k_0^2\left[\frac{j}{k_0R}+\frac{1}{k_0^2R^2}-\frac{j}{k_0^3R^3}\right]e^{-jk_0R}\mathbf{u}_\theta\\ \mathbf{H} &= \frac{I\ell}{4\pi}\sin\theta\left[\frac{e^{-jk_0R}}{R^2}+jk_0\frac{e^{-jk_0R}}{R}\right]\mathbf{u}_\varphi.\end{aligned}\tag{7.103}$$

In the near-field, characterized by

$$|\mathbf{r}-\mathbf{r}'|\ll\frac{1}{k_0}=\frac{\lambda_0}{2\pi}=\text{ƛ}_0,\tag{7.104}$$

the exponentials in (7.96) and (7.97) are very close to one. In that region (the *Rayleigh* zone), the potentials approach their static value. In the current case, the static source is an electric dipole of moment

$$\mathbf{P}_e=\frac{1}{j\omega}I\ell\,\mathbf{u}_z=Q\ell\,\mathbf{u}_z.\tag{7.105}$$

In the radiation zone, the dipole fields become transverse. The electric field, for example, approaches the value

$$\mathbf{E}=jk_0R_{c0}\frac{I\ell}{4\pi}\frac{e^{-jk_0R}}{R}\sin\theta\mathbf{u}_\theta\qquad(R\to\infty).\tag{7.106}$$

The Electric Vector Potential C

In the previous analysis, **E** and **H** were derived from a magnetic vector potential **A**, which itself was generated by electric currents **J**. In the presence of *magnetic* currents $\mathbf{J}_m$, an

electric vector potential **C** must be introduced, and the superimposed effects yield

$$\begin{aligned}\mathbf{E} &= -j\omega\mathbf{A} - j\omega\frac{1}{k_0^2}\,\text{grad div}\,\mathbf{A} - \frac{1}{\epsilon_0}\,\text{curl}\,\mathbf{C}\\ &= -\frac{j\omega}{k_0^2}\,\text{curl curl}\,\mathbf{A} - \frac{1}{j\omega\epsilon_0}\mathbf{J} - \frac{1}{\epsilon_0}\,\text{curl}\,\mathbf{C}\\ \mathbf{H} &= \frac{1}{\mu_0}\,\text{curl}\,\mathbf{A} - j\omega\mathbf{C} - j\omega\frac{1}{k_0^2}\,\text{grad div}\,\mathbf{C}\\ &= \frac{1}{\mu_0}\,\text{curl}\,\mathbf{A} - \frac{j\omega}{k_0^2}\,\text{curl curl}\,\mathbf{C} - \frac{1}{j\omega\mu_0}\mathbf{J}_m \end{aligned} \tag{7.107}$$

where Lorenz gauges have been used for both **A** and **C**. Because

$$\nabla^2\mathbf{C} + k_0^2\mathbf{C} = -\epsilon_0\mathbf{J}_m \tag{7.108}$$

the solution for **C** proceeds as for **A**. Thus,

$$\mathbf{C}(\mathbf{r}) = \frac{\epsilon_0}{4\pi}\int \frac{\mathbf{J}_m(\mathbf{r}')e^{-jk_0|\mathbf{r}-\mathbf{r}'|}}{|\mathbf{r}-\mathbf{r}'|}\,dV' \qquad (\text{C m}^{-1}). \tag{7.109}$$

The analysis of the far-fields generated by **C** follows as in the case of **A**.

7.8 RADIATION PATTERNS

When the sources radiate in a medium of uniform characteristics ϵ, μ, σ Maxwell's equations (7.1) and (7.2) keep their form, but (ϵ_0, μ_0) must be replaced by (ϵ, μ) and **j** by $\sigma\mathbf{e}$. By scalar multiplying (7.1) with **h**, and (7.2) with **e**, we obtain, after subtracting the results,

$$\mathbf{h}\cdot\text{curl}\,\mathbf{e} - \mathbf{e}\cdot\text{curl}\,\mathbf{h} = -\frac{\mu}{2}\frac{\partial}{\partial t}|\mathbf{h}|^2 - \mathbf{j}\cdot\mathbf{e} - \frac{\epsilon}{2}\frac{\partial}{\partial t}|\mathbf{e}|^2. \tag{7.110}$$

The left-hand term is equal to div $(\mathbf{e}\times\mathbf{h})$. Integrating (7.110) over a volume V bounded by S yields

$$-\frac{\partial\mathcal{E}}{\partial t} = \int_V \frac{1}{\sigma}|\mathbf{j}|^2\,dV + \int_S \mathbf{u}_R\cdot(\mathbf{e}\times\mathbf{h})\,dS \qquad (\text{W}), \tag{7.111}$$

where the *energy* $\mathcal{E}$ is the integral over V of the *energy density*

$$\mathcal{W} = \frac{1}{2}\epsilon|\mathbf{e}|^2 + \frac{1}{2}\mu|\mathbf{h}|^2 = \frac{1}{2}(\mathbf{e}\cdot\mathbf{d} + \mathbf{b}\cdot\mathbf{h}) \qquad (\text{W m}^{-3}). \tag{7.112}$$

Equation (7.111) is actually a power budget. The left-hand term represents the power extracted from the electric and magnetic energies stored in V. The right-hand term shows how this power is spent: first in Joule losses (the volume integral) and, second, in delivering power to the region outside S (the surface integral). This radiated power is the flux of the *vector of Poynting*

$$\mathbf{p} = \mathbf{e}\times\mathbf{h}. \tag{7.113}$$

We note that the flux of $\mathbf{p}$ can be negative, in which case power is delivered to V by the exterior sources. Under time-harmonic conditions, the time-averaged power escaping from V is given by

$$P_{\text{ave}} = \frac{1}{2} Re \int_S \mathbf{u}_R \cdot (\mathbf{E} \times \mathbf{H}^*)\, dS. \tag{7.114}$$

7.8.1 Gain and Directivity

The far-field expressions (7.101) show that Poynting's vector is radial in the radiation zone, and that the time-averaged power density on a large sphere S_R of radius R is $(\mathbf{F}\cdot\mathbf{F}^*/2R_{c0}R^2)\,\text{W m}^{-2}$. The power in an elementary solid angle $d\Omega$ is therefore

$$dP = \frac{1}{2R_{c0}}|\mathbf{F}|^2 d\Omega = \frac{1}{2R_{c0}}|\mathbf{F}|^2 \sin\theta\, d\theta\, d\varphi.\ (\text{W}) \tag{7.115}$$

The total power is obtained by integrating dP over all solid angles, and the average power per steradian is that value divided by 4π. The actual power density per steradian is $|\mathbf{F}|^2/2R_{c0}$, and its ratio to the average value over all solid angles is the *directivity*

$$D(\mathbf{u}) = D(\theta,\varphi) = \frac{|\mathbf{F}(\theta,\varphi)|^2}{\dfrac{1}{4\pi}\displaystyle\int_{4\pi} |\mathbf{F}(\theta,\varphi)|^2 d\Omega}. \tag{7.116}$$

The directivity is therefore a measure of the power concentration in the (θ,φ) direction. The radiation pattern is obtained by plotting D as a function of direction (i.e., of θ and φ). The result is a three-dimensional body, of which only a few plane cross sections are typically shown. An often encountered pattern is displayed in Figure 7.12.

An extensive literature has been devoted to the analysis and synthesis of patterns [47, 80, 84, 118, 138]. High values of $D(\mathbf{u})$ in a given direction are desirable when the purpose is to illuminate a tracked target with a high power density. A possible application, still at an experimental stage,[10] is the transmission of power from the earth to a space vehicle or, conversely, from a platform in geostationary orbit, where power is harvested from the sun and subsequently beamed down to the earth.

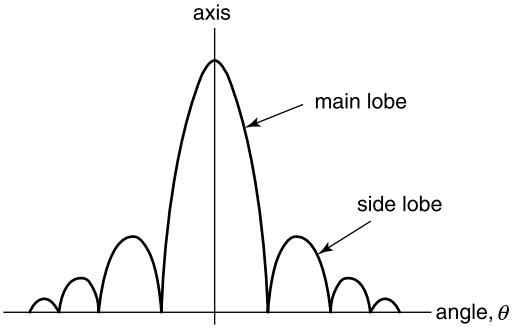

Figure 7.12 Plane cross section of a radiation pattern.

An important factor in the design of antennas is the *efficiency* η, defined by the ratio

$$\eta = \frac{\text{radiated power}}{\text{power into the radiating system}}. \tag{7.117}$$

This parameter is less than unity when losses are present in the system. These may find their origin in Joule dissipation in metal parts, dielectric losses in radomes, or conduction losses in the earth. They give rise to another important concept, the *gain*, defined by

$$G(\mathbf{u}) = \eta D(\mathbf{u}). \tag{7.118}$$

The gain is at most equal to D, and then only in the absence of losses.

7.8.2 The Array Factor

A combination of individual antennas into an array gives great flexibility in the synthesis of desirable radiation patterns. Consider, for example, two identical z-oriented dipole antennas fed by respective currents I and $Ie^{-j\alpha}$ (Fig. 7.13). From (7.106) the electric field in the (x, y) plane is z-polarized and its radiated value is given, to within a constant factor, by

$$E_z \doteq \frac{e^{-jk_0R}}{R}\left[e^{-jk_0\frac{d}{2}\sin\theta} + e^{+jk_0\frac{d}{2}\sin\theta}e^{-j\alpha}\right].$$

The direction of maximum radiation is obtained when the interference between the two patterns is maximally constructive (i.e., when the two exponentials are equal). This happens when

$$\frac{d}{\lambda_0}\sin\theta = \left(\frac{\alpha}{2\pi}\right) + n \qquad (n = 0, \pm 1, \ldots). \tag{7.119}$$

Directions of zero radiation occur when the two fields interfere destructively. The condition is now

$$\frac{d}{\lambda_0}\sin\theta = \frac{\alpha - \pi}{2\pi} + n \qquad (n = 0, \pm 1, \ldots). \tag{7.120}$$

By means of a voltage-controlled phase shifter the lobe structure may be shifted in space. In the *transmitting* mode, a servo-loop can be inserted to keep a lobe of maximum radiation

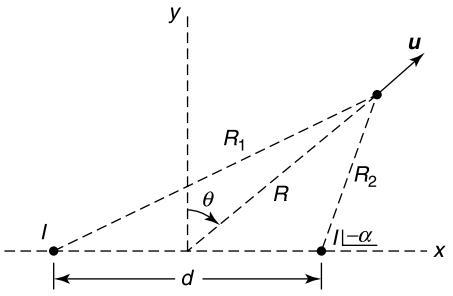

Figure 7.13 Pertinent for the radiation from two vertical dipoles.

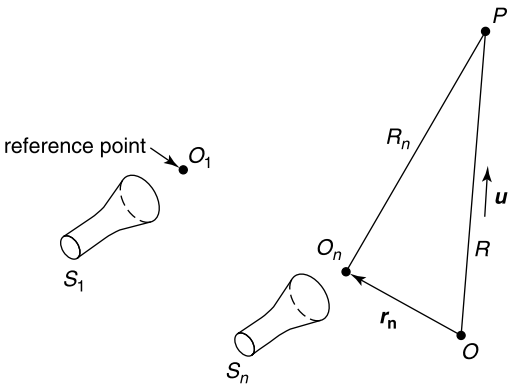

Figure 7.14 General antenna array.

hooked on an evasive target. In the *receiving* mode, an interfering signal may be eliminated by setting a null zone in the direction of the unwanted source.

It is to be noted, from (7.119) and (7.120), that narrow beams ensue when successive maxima and nulls are separated by small angular distances. Such a property requires large values of (d/λ_0). Under these conditions, a small shift in θ is sufficient to destroy a constructive interference and convert it to a totally destructive one.

A more general array is shown in Figure 7.14. It consists of N identical elements, identically oriented. If the antennas are driven by voltages V_n, their radiation vectors will be of the form $V_n\mathbf{F}(\mathbf{u})$, where $\mathbf{F}$ is common to all the elements (provided mutual interferences may be neglected). In the radiation zone, with reference points O_n identically located with respect to their antenna,

$$\begin{aligned}\mathbf{E} &= V_1\mathbf{F}\frac{e^{-jk_0R_1}}{R_1} + \cdots + V_N\mathbf{F}\frac{e^{-jk_0R_N}}{R_N} \\ &= \frac{e^{-jk_0R}}{R}\underbrace{\left[V_1e^{jk_0\mathbf{u}\cdot\mathbf{r}_1} + \cdots + V_Ne^{jk_0\mathbf{u}\cdot\mathbf{r}_N}\right]}_{\text{array factor } \mathcal{R}}\mathbf{F}(\mathbf{u}).\end{aligned} \tag{7.121}$$

The *array factor* $\mathcal{R}$ is independent of the nature of the elements of the array. It only characterizes their geometrical pattern and their respective excitations. In radioastronomical systems, such as the *very long baseline interferometer*, the number of elements (typically parabolic disks) can be very large, as well as the dimensions of the array with respect to λ_0. For such a case, $\mathcal{R}$ is solely responsible for the sharpness of the beam. Assuming that the maximum dimension of the array is 10,000 km and $\lambda_0 = 6$ cm, the resolution may be as high as 1 milli-arc second.

7.9 GREEN'S DYADICS

Evaluation of the fields from potentials implies differentiation with respect to space and time. Such operations generate additional inaccuracies when $\mathbf{J}$ is only approximately known, for instance because of experimental inaccuracies. It is therefore useful to obtain $(\mathbf{E}, \mathbf{H})$ by a direct integration involving $\mathbf{J}(\mathbf{r})$ multiplied by a suitable dyadic $\overline{\overline{G}}(\mathbf{r}|\mathbf{r}')$. By means

of the scalar Green's function in free space (7.95), the *magnetic* field can be written, from (7.97), as[¶]

$$\mathbf{H}(\mathbf{r}) = -\text{curl} \int_V G_0(\mathbf{r}|\mathbf{r}')\mathbf{J}(\mathbf{r}')\, dV'. \tag{7.122}$$

Because

$$\text{grad}\, |\mathbf{r} - \mathbf{r}'| = -\text{grad}'\, |\mathbf{r} - \mathbf{r}'|, \tag{7.123}$$

this expression can be cast into the form

$$\mathbf{H}(\mathbf{r}) = \int_V \text{grad}'\, G_0(\mathbf{r}|\mathbf{r}') \times \mathbf{J}(\mathbf{r}')\, dV'. \tag{7.124}$$

The singularity of the integrand is of the order $|\mathbf{r} - \mathbf{r}'|^{-2}$ hence, as mentioned in Section 3.2, the integral is convergent, even when $\mathbf{r}$ is in the source region V. One may therefore write

$$\mathbf{H}(\mathbf{r}) = \lim_{\delta \to 0} \int_{V - V_\delta} \overline{\overline{G}}_{me}(\mathbf{r}|\mathbf{r}') \cdot \mathbf{J}(\mathbf{r}')\, dV' \tag{7.125}$$

where δ is the maximum chord length, and

$$\overline{\overline{G}}_{me}(\mathbf{r}|\mathbf{r}') = \text{curl}'\, [G_0(\mathbf{r}|\mathbf{r}')\, \overline{\overline{I}}] = -\text{curl}\, [G_0(\mathbf{r}|\mathbf{r}')\, \overline{\overline{I}}]. \tag{7.126}$$

The subscript "*me*" identifies the contribution to the *magnetic* field from the *electric* sources. In Cartesian coordinates, the integrand in (7.124) is explicitly

$$\text{grad}'\, G_0 \times \mathbf{J} = \begin{pmatrix} 0 & -\dfrac{\partial G_0}{\partial z'} & \dfrac{\partial G_0}{\partial y'} \\ \dfrac{\partial G_0}{\partial z'} & 0 & -\dfrac{\partial G_0}{\partial x'} \\ -\dfrac{\partial G_0}{\partial y'} & \dfrac{\partial G_0}{\partial x'} & 0 \end{pmatrix} \cdot \begin{pmatrix} J_x \\ J_y \\ J_z \end{pmatrix}. \tag{7.127}$$

An expression such as (7.125) shows that the contribution of a small volume V_δ containing the field point vanishes as the chord δ approaches zero. From the expression (7.122) for $\mathbf{H}$, we may derive the value of $\mathbf{E}$, viz.

$$\mathbf{E}(\mathbf{r}) = \frac{1}{j\omega\epsilon_0}(\text{curl}\, \mathbf{H} - \mathbf{J}) = -\frac{1}{j\omega\epsilon_0}\, \text{curl curl} \int_V G_0(\mathbf{r}|\mathbf{r}')\, \mathbf{J}(\mathbf{r}')\, dV' - \frac{1}{j\omega\epsilon_0}\, \mathbf{J}(\mathbf{r}). \tag{7.128}$$

It is clear that the determination of a Green's dyadic appropriate for $\mathbf{E}$ involves bringing the operator curl curl behind the integral, thus creating singularities of the order $|\mathbf{r} - \mathbf{r}'|^3$. For such a case, the integrals must be evaluated with the greatest care whenever $\mathbf{r}$ lies inside the current-carrying volume.[11,12] To achieve that goal, we shall excise a small volume V_δ containing $\mathbf{r}$ from V, a strategy already followed in Section 3.9 in a related potential

[¶]When the sources are magnetic currents $\mathbf{J}_m$, the analysis proceeds in an analogous way but starts with the evaluation of $\mathbf{E}$.

problem. The contribution of V_δ, the self-patch, may be obtained by first evaluating the potentials

$$\mathbf{A}(\mathbf{r}) = -\mu_0 \int_{V_\delta} \mathbf{J}(\mathbf{r}')\, G_0(\mathbf{r}|\mathbf{r}')\, dV'$$

$$\phi(\mathbf{r}) = -\frac{1}{j\omega\epsilon_0\mu_0} \operatorname{div} \mathbf{A} = \frac{1}{j\omega\epsilon_0} \int_{V_\delta} \operatorname{div} [G_0(\mathbf{r}|\mathbf{r}')\mathbf{J}(\mathbf{r}')]\, dV'$$

$$= \frac{1}{j\omega\epsilon_0} \int_{V_\delta} \operatorname{grad} G_0(\mathbf{r}|\mathbf{r}') \cdot \mathbf{J}(\mathbf{r}')\, dV. \tag{7.129}$$

The electric field now follows from the formula

$$\mathbf{E}(\mathbf{r}) = j\omega\mu_0 \int_{V\delta} G_0(\mathbf{r}|\mathbf{r}')\mathbf{J}(\mathbf{r}')\, dV'$$

$$- \frac{1}{j\omega\epsilon_0} \operatorname{grad} \int_{V_\delta} \operatorname{grad} G_0(\mathbf{r}|\mathbf{r}') \cdot \mathbf{J}(\mathbf{r}')\, dV'. \tag{7.130}$$

The integrals involved are improper but convergent, a point already stressed in Section 3.2. Assume for the moment that V_δ is small enough for $\mathbf{J}$ to be practically uniform in V_δ. The evaluation of $\mathbf{E}$ should now be performed for three orthogonal directions (i.e., for $\mathbf{J}$ successively equal to $\mathbf{u}_x$, $\mathbf{u}_y$, $\mathbf{u}_z$). Analytical results have been obtained for the sphere and the parallelepiped,[13,14,15] and the theory further shows that the field functions $(\mathbf{E}, \mathbf{H}, \mathbf{A})$ are analytic at all interior points. For a cube of side $2a$, for example, the self-cell electric field at the center is, under J_x excitation,

$$E_x(o) = -\frac{J_x}{3j\omega\epsilon_0}[1 - 1.51520(k_0 a)^2 + j\, 1.27324(k_0 a)^3 + \cdots]. \tag{7.131}$$

The analyticity of the field functions holds for more general density functions than the uniform $\mathbf{J}$, provided conditions such as that of Hölder are satisfied.[16] It is instructive to extend the previous analysis to a volume V_δ of *shrinking dimension* δ. If we assume that $\delta \ll \lambda_0$, the exponential in G_0 may be replaced by unity, and it becomes particularly acceptable to assume $\mathbf{J}$ to be uniform in V_δ. The derivation proceeds by going back to (7.130), and remembering that the grad operator must not be transferred blindly behind the integral sign. As in Section 3.9, we shall split V_δ into a small sphere V_0 containing $\mathbf{r}$ and a remainder $(V_\delta - V_0)$ (Fig. 3.17). The contribution from V_0 can be derived analytically. As in (3.113) and (7.131), it is

$$\mathbf{E}_0(\mathbf{r}) = -\frac{1}{3j\omega\epsilon_0} \mathbf{J}. \tag{7.132}$$

For the remainder volume we must evaluate, as an intermediate step,

$$I(\mathbf{r}) = \int_{V_\delta - V_0} \mathbf{J} \cdot \operatorname{grad} G_0(\mathbf{r}|\mathbf{r}')\, dV' = \frac{1}{4\pi} \mathbf{J} \cdot \int_{V_\delta - V_0} \operatorname{grad} \left(\frac{1}{|\mathbf{r} - \mathbf{r}'|} \right) dV'.$$

The analysis leading to (3.111) in Section 3.9 can be fully duplicated here. It yields, for the field $\mathbf{E}_1(\mathbf{r})$ generated by the currents in $(V_\delta - V_0)$, the value

$$\mathbf{E}_1(\mathbf{r}) = -\frac{1}{j\omega\epsilon_0} \overline{\overline{L}}_{V_\delta} \cdot \mathbf{J} + \frac{1}{j\omega\epsilon_0} \overline{\overline{L}}_0 \cdot \mathbf{J},$$

where the *depolarizing dyadic* $\overline{\overline{L}}$ is defined in (3.112). Adding this value to $\mathbf{E}_0$ gives the self-patch field

$$\mathbf{E}_0(\mathbf{r}) = -\frac{1}{j\omega\epsilon_0}\,\overline{\overline{L}}_{V_\delta}(\mathbf{r})\cdot\mathbf{J}. \tag{7.133}$$

From (7.130) we may now write the total field in the form

$$\begin{aligned}\mathbf{E}(\mathbf{r}) = {} & j\omega\mu_0\int_V G_0(\mathbf{r}|\mathbf{r}')\,\mathbf{J}(\mathbf{r}')\,dV' \\ & -\frac{1}{j\omega\epsilon_0}\lim_{\delta\to 0}\int_{V-V_\delta}\operatorname{grad}'\operatorname{grad}' G_0(\mathbf{r}|\mathbf{r}')\cdot\mathbf{J}(\mathbf{r}')\,dV' \\ & -\frac{1}{j\omega\epsilon_0}\,\overline{\overline{L}}_{V_\delta}(\mathbf{r})\cdot\mathbf{J}(\mathbf{r}).\end{aligned} \tag{7.134}$$

In a more compact version [133, 210]:

$$\mathbf{E}(\mathbf{r}) = j\omega\mu_0\lim_{\delta\to 0}\int_{V-V_\delta}\overline{\overline{\mathbf{G}}}_{ee}(\mathbf{r}|\mathbf{r}')\cdot\mathbf{J}(\mathbf{r}')\,dV' - \frac{1}{j\omega\epsilon_0}\,\overline{\overline{\mathbf{L}}}_{V_\delta}\cdot\mathbf{J}(\mathbf{r}) \tag{7.135}$$

where

$$\begin{aligned}\overline{\overline{\mathbf{G}}}_{ee}(\mathbf{r}|\mathbf{r}') &= \left(\bar{\bar{\mathbf{I}}} + \frac{1}{k_0^2}\operatorname{grad}\operatorname{grad}\right) G_0(\mathbf{r}|\mathbf{r}') \\ &= -\frac{1}{4\pi}\left(\bar{\bar{\mathbf{I}}} + \frac{1}{k_0^2}\operatorname{grad}\operatorname{grad}\right)\frac{e^{-jk_0|\mathbf{r}-\mathbf{r}'|}}{|\mathbf{r}-\mathbf{r}'|}.\end{aligned} \tag{7.136}$$

The limit process in (7.135) must be defined carefully. It requires the linear dimensions of V_δ to approach zero, while the geometry of V_δ (shape, position, orientation with respect to $\mathbf{r}$) is maintained. In other words, V_δ contracts by a similarity transformation with center at $\mathbf{r}$. Under these conditions, $\mathbf{r}$ keeps the same relative position within V_δ (the center of a cube, for example, remains the center), and $\overline{\overline{L}}_{V_\delta}$ remains constant. The integral in (7.135) is a principal value, in which the volume V_δ should be explicitly mentioned. The term in $\overline{\overline{L}}_{V_\delta}$ can be absorbed into $\overline{\overline{G}}_{ee}$ to give the *total Green's dyadic*

$$\overline{\overline{G}}^{tot}_{ee}(\mathbf{r}|\mathbf{r}') = PV\,\overline{\overline{G}}_{ee}(\mathbf{r}|\mathbf{r}') + \frac{1}{k_0^2}\delta(\mathbf{r}-\mathbf{r}')\,\overline{\overline{L}}_{V_\delta}. \tag{7.137}$$

The solution of

$$-\operatorname{curl}\operatorname{curl}\mathbf{E} + k_0^2\mathbf{E} = j\omega\mu_0\,\mathbf{J} \tag{7.138}$$

may now be expressed in terms of the total Green's dyadic as

$$\mathbf{E}(\mathbf{r}) = j\omega\mu_0\int_V \overline{\overline{G}}^{tot}_{ee}(\mathbf{r}|\mathbf{r}')\cdot\mathbf{J}(\mathbf{r}')\,dV'. \tag{7.139}$$

A Green's function is routinely associated with a *point-source*, which in the realm of distribution theory is represented by delta-functions and appropriate derivatives. We shall not dwell upon these aspects, but refer the reader to the nontrivial problems (7.19) to (7.25) for further clarification.

7.10 MULTIPOLE EXPANSION

The integral of concern in this section is of the general form

$$\mathbf{I} = \int_V \phi(\mathbf{r})\mathbf{J}(\mathbf{r})\, dV, \tag{7.140}$$

where $\phi(\mathbf{r})$ varies little over V. As in (3.24), $\phi(\mathbf{r})$, which is assumed continuous with continuous first and second derivatives, is expanded in a power series with respect to an origin in V. Inserting this expansion in (7.140) gives

$$\mathbf{I} = \phi_0 \int_V \mathbf{J}\, dV + \sum_{i=1}^{3} \left(\frac{\partial \phi}{\partial x}\right)_0 \int_V x_i \mathbf{J}\, dV + \frac{1}{2} \sum_{i,j=1}^{3} \left(\frac{\partial^2 \phi}{\partial x_i \partial x_j}\right)_0 \int_V x_i \mathbf{J} x_j\, dV + \cdots . \tag{7.141}$$

We shall evaluate the *first integral* by exploiting (6.29). In magnetostatics, the second member of that equation vanished because $\mathbf{J}$ was solenoidal and tangent to the boundary of the source region. In the time-harmonic situation, however, the current density $\mathbf{J}$ must satisfy the *equations of conservation of charge*, namely (Fig. 7.9)

$$\begin{aligned} \operatorname{div} \mathbf{J} &= -j\omega P = -jk_0 c_0 P \quad (\text{in } V) \\ \mathbf{u}_n \cdot \mathbf{J} &= j\omega P_s = jk_0 c_0 P_s \quad (\text{on } S). \end{aligned}$$

It follows that (6.29) is replaced by

$$\int_V \mathbf{J} \cdot \operatorname{grad} \Theta\, dV = jk_0 c_0 \left(\int_S \Theta P_s\, dS + \int_V \Theta P\, dV \right). \tag{7.142}$$

Applied successively to $\Theta = x, y$, and z, this relationship leads to

$$\int_V \mathbf{J}\, dV = j\omega \mathbf{P}_{e1} = jk_0 c_0 \mathbf{P}_{e1},$$

where $\mathbf{P}_{e1}$ is the *electric dipole moment* defined in (3.27), that is,

$$\mathbf{P}_{e1} = \int_V P\mathbf{r}\, dV + \int_S P_s \mathbf{r}\, dS. \tag{7.143}$$

The *second term* in (7.141) can be written as

$$\sum_{i=1}^{3} \frac{\partial \phi_0}{\partial x_i} \int_V (\mathbf{u}_i \cdot \mathbf{r})\mathbf{J}\, dV = \operatorname{grad}_0 \phi \cdot \int_V \mathbf{r}\mathbf{J}\, dV. \tag{7.144}$$

It is useful to split the dyadic $\mathbf{rJ}$ into its symmetric and antisymmetric parts. Thus,

$$\mathbf{rJ} = \frac{1}{2}(\mathbf{rJ} + \mathbf{Jr}) + \frac{1}{2}(\mathbf{rJ} - \mathbf{Jr}).$$

Consider first the *antisymmetric* part. A vector dotted in such a dyadic gives rise to a cross-product. In the current case,

$$\frac{1}{2}\,\text{grad}_0\,\phi\cdot(\mathbf{rJ}-\mathbf{Jr}) = -\frac{1}{2}\,\text{grad}_0\,\phi\times(\mathbf{r}\times\mathbf{J}).$$

Integration over V now introduces the *magnetic dipole moment* (6.32), viz.

$$\mathbf{P}_m = \frac{1}{2}\int_V \mathbf{r}\times\mathbf{J}\,dV, \tag{7.145}$$

in terms of which the integral can be written as

$$\frac{1}{2}\text{grad}_0\,\phi\cdot\int_V(\mathbf{rJ}-\mathbf{Jr})\,dV = -\text{grad}_0\,\phi\times\mathbf{P}_m.$$

We next evaluate the contribution from the *symmetric* part. Its (i,j) component is

$$\begin{aligned}\frac{1}{2}\mathbf{u}_i\cdot(\mathbf{rJ}+\mathbf{Jr})\cdot\mathbf{u}_j &= \frac{1}{2}[x_i(\mathbf{u}_j\cdot\mathbf{J})+x_j(\mathbf{u}_i\cdot\mathbf{J})]\\ &= \frac{1}{2}(x_i\ \text{grad}\ x_j + x_j\ \text{grad}\ x_i)\cdot\mathbf{J}\\ &= \frac{1}{2}\mathbf{J}\cdot\text{grad}\ (x_ix_j).\end{aligned}$$

When this expression is inserted into the integral in (7.144), a term of type (7.142) is obtained, with $\Theta = x_ix_j$. Simple algebra now shows that

$$\frac{1}{2}\,\text{grad}\,\phi_0\cdot\int_V(\mathbf{rJ}+\mathbf{Jr})\,dV = \frac{1}{2}j\omega\,\text{grad}\,\phi_0\cdot\overline{\overline{\mathbf{Q}}}_e,$$

where $\overline{\overline{\mathbf{Q}}}_e$ is the (symmetric) electric quadrupole dyadic defined in (3.27), viz.

$$\overline{\overline{\mathbf{Q}}}_e = \int_V P\mathbf{rr}\,dV + \int_S P_s\mathbf{rr}\,dS = \frac{1}{j\omega}\int_V(\mathbf{rJ}+\mathbf{Jr})\,dV. \tag{7.146}$$

The term in $\overline{\overline{\mathbf{Q}}}_e$ in the expansion is clearly of the order D/L with respect to the term in $\mathbf{P}_{e1}$, where D is the maximum dimension of the source volume, and L a characteristic length for the variation of ϕ.

The *third term* in (7.141) is the summation

$$\mathbf{I}' = \frac{1}{2}\sum_{i,j=1}^{3}\left(\frac{\partial^2\phi}{\partial x_i\partial x_j}\right)_0\int_V x_i\mathbf{J}x_j\,dV. \tag{7.147}$$

A detailed evaluation of the integral in that expression gives[17]

$$\begin{aligned}\int_V x_i\mathbf{J}x_j\,dV = &-\frac{1}{2}\mathbf{u}_i\times(\mathbf{u}_j\times\overline{\overline{\mathbf{Q}}}_m) - \frac{1}{2}\mathbf{u}_j\times(\mathbf{u}_i\cdot\overline{\overline{\mathbf{Q}}}_m)\\ &-\mathbf{u}_i\times(\mathbf{u}_j\times\mathbf{P}_{e2}) - \mathbf{u}_j\times(\mathbf{u}_i\times\mathbf{P}_{e2}),\end{aligned} \tag{7.148}$$

where

$$\mathbf{P}_{e2} = \frac{1}{6}\int_V \mathbf{r}\times\mathbf{J}\times\mathbf{r}\,dV$$
$$\overline{\overline{\mathbf{Q}}}_m = \frac{1}{3}\int_V [(\mathbf{r}\times\mathbf{J})\mathbf{r} + \mathbf{r}(\mathbf{r}\times\mathbf{J})]\,dV. \tag{7.149}$$

The reason for the notation $\mathbf{P}_{e2}$, which suggests a contribution of the electric dipole type, can be found in the form of the field expansion (7.155). The quantity $\overline{\overline{\mathbf{Q}}}_m$ is the (symmetric) *magnetic quadrupole dyadic*. The terms in $\mathbf{P}_{e2}$ and $\overline{\overline{\mathbf{Q}}}_m$ are clearly of the order D/L with respect to the term in $\mathbf{P}_m$ and must therefore be retained in the expansion. Some elementary algebra involving the term in $\overline{\overline{\mathbf{Q}}}_m$ leads to the final result

$$\mathbf{I} = \int_V \phi\mathbf{J}\,dV = j\omega\phi_0\mathbf{P}_{e1} - \operatorname{grad}_0\phi\times\mathbf{P}_m + \frac{1}{2}j\omega\operatorname{grad}_0\phi\cdot\overline{\overline{\mathbf{Q}}}_e$$
$$+ (\bar{\bar{\mathbf{I}}}\nabla_0^2\phi - \operatorname{grad}\operatorname{grad}_0\phi)\cdot\mathbf{P}_{e2} - \frac{1}{2}\operatorname{curl}(\operatorname{grad}_0\phi\cdot\overline{\overline{\mathbf{Q}}}_m) + \cdots. \tag{7.150}$$

It is interesting to note that this expression can also be derived by inserting the distributional form of $\mathbf{J}$ into (7.140), namely

$$\mathbf{J}(\mathbf{r}) = j\omega\mathbf{P}_e\,\delta(\mathbf{r}-\mathbf{r}_0) + \operatorname{curl}[\delta(\mathbf{r}-\mathbf{r}_0)\mathbf{P}_m] - \frac{1}{2}j\omega\operatorname{grad}\delta(\mathbf{r}-\mathbf{r}_0)\cdot\overline{\overline{\mathbf{Q}}}_e$$
$$-\operatorname{curl}\operatorname{curl}[\delta(\mathbf{r}-\mathbf{r}_0)\mathbf{P}_{e2}] - \frac{1}{2}\operatorname{curl}[\operatorname{grad}\delta(\mathbf{r}-\mathbf{r}_0)\cdot\overline{\overline{\mathbf{Q}}}_m] + \cdots. \tag{7.151}$$

Applied to a slowly varying vector function $\boldsymbol{\phi}$, this formula gives

$$\int_V \boldsymbol{\phi}\cdot\mathbf{J}\,dV = j\omega\mathbf{P}_{e1}\cdot\boldsymbol{\phi}_0 + \mathbf{P}_m\cdot\operatorname{curl}_0\boldsymbol{\phi} + \frac{1}{2}j\omega\operatorname{grad}_0\boldsymbol{\phi} : \mathbf{Q}_e$$
$$-\mathbf{P}_{e2}\cdot\operatorname{curl}\operatorname{curl}_0\boldsymbol{\phi} + \frac{1}{2}\operatorname{grad}\operatorname{curl}_0\boldsymbol{\phi} : \overline{\overline{\mathbf{Q}}}_m + \cdots. \tag{7.152}$$

Integrals of this type are often encountered as excitation coefficients in normal-mode expansions, for example in the expansions of the fields in the interior of a cavity (see Section 10.2).

7.10.1 Radiation by Multipoles

The general moment equation (7.150) may be applied to the integral

$$\mathbf{I} = \int_V \mathbf{J}(r)e^{jk_0\mathbf{u}\cdot\mathbf{r}}\,dV. \tag{7.153}$$

This integral, which already appeared in (7.100) and (7.101), characterizes the radiation properties of a source. The function ϕ in (7.150) is now the exponential factor $e^{jk_0\mathbf{u}\cdot\mathbf{r}}$, which varies slowly when the exponent $k_0(\mathbf{u}\cdot\mathbf{r})$ is small. This happens when L is small with respect to λ_0, for example when an atom of $L \approx 10^{-10}$ m emits in the visible range

($\lambda_0 \approx 0.5\ 10^{-6}$m). One could also expand the exponential directly in a series in $jk_0(\mathbf{u}\cdot\mathbf{r}')$. Both procedures[17] yield the same result, viz.

$$\lim_{R\to\infty} \mathbf{A} = \frac{\mu_0}{4\pi}\frac{e^{-jk_0R}}{R}\left[jk_0c_0\mathbf{P}_{e1} - jk_0\mathbf{u}\times\mathbf{P}_m - \frac{1}{2}k_0^2c_0\mathbf{u}\cdot\overline{\overline{\mathbf{Q}}}_e \right.$$
$$\left. - k_0^2\mathbf{u}\times\mathbf{P}_{e2}\times\mathbf{u} + \frac{1}{2}k_0^2\mathbf{u}\times(\mathbf{u}\cdot\overline{\overline{\mathbf{Q}}}_m) + \cdots\right]. \tag{7.154}$$

The corresponding electric and magnetic fields are

$$\mathbf{E} = \frac{R_{c0}}{4\pi}\frac{e^{-jk_0R}}{R}\left\{-k_0^2c_0\mathbf{u}\times(\mathbf{u}\times\mathbf{P}_{e1}) - k_0^2\mathbf{u}\times\mathbf{P}_m \right.$$
$$\left. -\frac{1}{2}jk_0^3c_0\mathbf{u}\times[\mathbf{u}\times(\mathbf{u}\cdot\overline{\overline{\mathbf{Q}}}_e)] - jk_0^3\mathbf{u}\times(\mathbf{u}\times\mathbf{P}_{e2}) - \frac{1}{2}jk_0^3\mathbf{u}\times(\mathbf{u}\cdot\overline{\overline{\mathbf{Q}}}_m) + \cdots\right\}$$
$$\mathbf{H} = \frac{1}{4\pi}\frac{e^{-jk_0R}}{R}\left\{k_0^2c_0\mathbf{u}\times\mathbf{P}_{e1} - k_0^2\mathbf{u}\times(\mathbf{u}\times\mathbf{P}_m) + \frac{1}{2}jk_0^3c_0\mathbf{u}\times(\mathbf{u}\cdot\overline{\overline{\mathbf{Q}}}_e)\right.$$
$$\left. + jk_0^3\mathbf{u}\times\mathbf{P}_{e2} - \frac{1}{2}jk_0^3\mathbf{u}\times[\mathbf{u}\times(\mathbf{u}\cdot\overline{\overline{\mathbf{Q}}}_m)] + \cdots\right\}. \tag{7.155}$$

We observe that the contributions of $\mathbf{P}_{e1}$ and $\mathbf{P}_{e2}$ are of the same form, which justifies the notation $\mathbf{P}_e$ used for both terms. We also notice the duality between the contributions of $(\mathbf{P}_{e1}, \overline{\overline{\mathbf{Q}}}_e)$ on the one side and $(\mathbf{P}_m, \overline{\overline{\mathbf{Q}}}_m)$ on the other side.

When the various multipole moments in (7.155) are frequency-independent, the terms in k_0^2 clearly become dominant at low frequencies. Those in k_0^3 take over if $\mathbf{P}_{e1}$ and $\mathbf{P}_m$ happen to vanish. These fairly trivial observations lose their validity when the current distribution $\mathbf{J}$ (together with its associated moments) varies with frequency. This can happen when the current-carrying body — a dielectric resonator for example — exhibits resonances[18] [133].

It is clear, from (7.10), that a shift of origin by a fixed amount $\mathbf{a}$ does not affect the value of the electric dipole moment $\mathbf{P}_{e1}$. The magnetic dipole moment $\mathbf{P}_m$, on the other hand, takes the new value

$$\mathbf{P}_m(\mathbf{a}) = \frac{1}{2}\int(\mathbf{r}-\mathbf{a})\times\mathbf{J}\,dV = \mathbf{P}_m(0) - \mathbf{a}\times\frac{1}{2}j\omega\mathbf{P}_{e1}.$$

Shifted values can also be derived for the other terms in the multipole expansion. The parameter $\mathbf{a}$ can be selected to optimize some criterion (e.g., to reinforce the dominance of the dipole moments with respect to the second-order terms). On the basis of a dyadic norm

$$\| \overline{\overline{a}} \|^2 = \overline{\overline{a}} : \overline{\overline{a}}^* \tag{7.156}$$

optimization leads to multipole locations in *complex* space.[19]

7.10.2 Examples of Multipoles

An electric dipole moment is generally elliptically polarized. In the case of a short antenna of length ℓ carrying a current I, the polarization is linear, and the current can be expressed as (Fig. 7.15*a*).

$$\mathbf{J} = I\ell\delta(\mathbf{r}-\mathbf{r}_1)\mathbf{u}_a = j\omega(P_e\mathbf{u}_a)\delta(\mathbf{r}-\mathbf{r}_1). \tag{7.157}$$

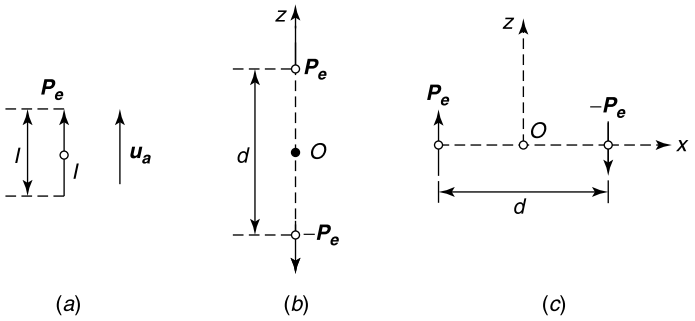

Figure 7.15 Linear current sources.

If the a direction is the z-axis of a system of spherical coordinates, the radiation fields take the form

$$\mathbf{E} = -\frac{1}{4\pi}\,\omega^2\mu_0 P_e\,\frac{e^{-jk_0R}}{R}\,\sin\theta\,\mathbf{u}_\theta$$
$$\mathbf{H} = -\frac{1}{4\pi}\,\omega^2\sqrt{\epsilon_0\mu_0}\,P_e\frac{e^{-jk_0R}}{R}\,\sin\theta\,\mathbf{u}_\varphi. \tag{7.158}$$

The electric dipole $\mathbf{P}_e$ radiates a power

$$\mathrm{P}_e = \frac{1}{12\pi}\,\omega^4\mu_0\sqrt{\epsilon_0\mu_0}\,|\mathbf{P}_e|^2 \qquad \text{(W)}. \tag{7.159}$$

As further examples, we note that the two collinear antennas in Figure 7.15*b* have vanishing $\mathbf{P}_{e1}, \mathbf{P}_{e2}, \mathbf{P}_m, \overline{\overline{\mathbf{Q}}}_m$ when the origin is taken in O. The first nonzero multipole term is

$$\overline{\overline{\mathbf{Q}}}_e = 2P_e d\,\mathbf{u}_z\mathbf{u}_z. \tag{7.160}$$

The current density of the system may be written as

$$\mathbf{J} = -I\ell d\,\frac{\partial}{\partial z_0}[\delta(\mathbf{r}-\mathbf{r}_0)]\,\mathbf{u}_z. \tag{7.161}$$

The two antiparallel short antennas of Figure 7.15*c* form a *doublet*, of current density

$$\mathbf{J} = I\ell d\left(\frac{\partial\delta(x)}{\partial x}\right)_0\delta(y)\delta(z)\,\mathbf{u}_z. \tag{7.162}$$

The nonzero moments are

$$\mathbf{P}_m = -\frac{1}{2}\ell d\,I\mathbf{u}_y$$
$$\overline{\overline{\mathbf{Q}}}_e = -P_e d(\mathbf{u}_x\mathbf{u}_z + \mathbf{u}_z\mathbf{u}_x). \tag{7.163}$$

The magnetic dipole moment is also generally elliptically polarized. An exception is provided by the circular current

$$\mathbf{J} = I\,\delta(r-a)\delta(z)\,\mathbf{u}_\varphi. \tag{7.164}$$

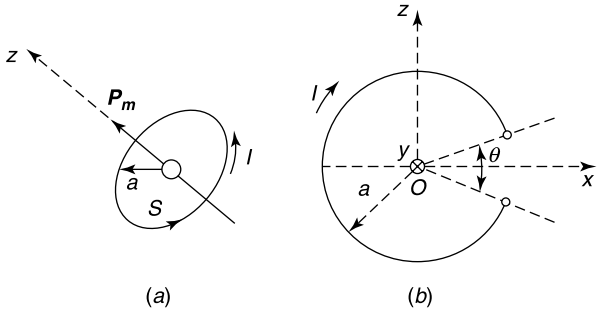

Figure 7.16 Curved current sources.

For this *frill* (Fig. 7.16*a*)

$$\mathbf{P}_m = \pi a^2 I\, \mathbf{u}_z = IS\, \mathbf{u}_z. \tag{7.165}$$

From (7.155), the radiation fields of a z-oriented $\mathbf{P}_m$ are given by

$$\begin{aligned} \mathbf{E} &= \frac{1}{4\pi}\, \omega^2 \mu_0 \sqrt{\epsilon_0 \mu_0}\, P_m\, \frac{e^{-jk_0 R}}{R} \sin\theta\, \mathbf{u}_\varphi \\ \mathbf{H} &= -\frac{1}{4\pi}\, \omega^2 \epsilon_0 \mu_0\, P_m\, \frac{e^{-jk_0 R}}{R} \sin\theta\, \mathbf{u}_\theta. \end{aligned} \tag{7.166}$$

The dipole radiates a power

$$P = \frac{1}{12\pi}\, \omega^4 \mu_0 (\epsilon_0 \mu_0)^{\frac{3}{2}} |\mathbf{P}_m|^2 \quad \text{(W)}. \tag{7.167}$$

The incomplete circular loop of Figure 7.16*b* is a hybrid structure, characterized by the dipole moments

$$\begin{aligned} j\omega \mathbf{P}_{e1} &= 2Ia \sin(\theta/2)\, \mathbf{u}_z \\ \mathbf{P}_m &= Ia^2(\pi - \theta/2)\, \mathbf{u}_y. \end{aligned} \tag{7.168}$$

The electric dipole moment vanishes when the loop is closed (i.e., when $\theta = 0$). The magnetic moment, on the other hand, decreases progressively (and ultimately vanishes) when the loop opens up and becomes, in the limit $\theta \to 2\pi$, a short dipole antenna.

7.10.3 Multipole Expansion for Magnetic Currents

An expression in terms of $\mathbf{J}_m$ can be derived on the basis of the time-harmonic form of (7.49). The integral in that expression is again of the general type (7.153), a property that can be exploited to generate the expansion

$$\begin{aligned} \mathbf{C} = \frac{\epsilon_0}{4\pi} \frac{e^{-jk_0 R}}{R} [&jk_0 c_0 \mathbf{P}'_{m1} + jk_0 \mathbf{u} \times \mathbf{P}'_e - \frac{1}{2} k_0^2 c_0 \mathbf{u} \cdot \overline{\overline{\mathbf{Q}}}'_m \\ &- k_0^2 (\mathbf{u} \times \mathbf{P}'_{m2} \times \mathbf{u}) - \frac{1}{2} k_0^2 \mathbf{u} \times (\mathbf{u} \cdot \overline{\overline{\mathbf{Q}}}'_e) + \cdots], \end{aligned} \tag{7.169}$$

where

$$\begin{aligned}
\mathbf{P}'_{m1} &= \frac{1}{j\omega}\int_V \mathbf{J}_m\, dV \\
\mathbf{P}'_{e} &= \frac{1}{2}\int_V \mathbf{J}_m \times \mathbf{r}\, dV \\
\mathbf{P}'_{m2} &= \frac{1}{6}\int_V \mathbf{r} \times \mathbf{J}_m \times \mathbf{r}\, dV \\
\overline{\overline{\mathbf{Q}}}'_m &= \frac{1}{j\omega}\int_V (\mathbf{r}\mathbf{J}_m + \mathbf{J}_m\mathbf{r})\, dV \\
\overline{\overline{\mathbf{Q}}}'_e &= \frac{1}{3}\int_V [(\mathbf{J}_m \times \mathbf{r})\mathbf{r} + \mathbf{r}(\mathbf{J}_m \times \mathbf{r})]\, dV.
\end{aligned} \tag{7.170}$$

The corresponding far fields are

$$\begin{aligned}
\mathbf{E} = \frac{1}{4\pi}\frac{e^{-jk_0R}}{R}\Big\{ & -k_0^2 c_0 \mathbf{u}\times\mathbf{P}'_{m1} - k_0^2\mathbf{u}\times(\mathbf{u}\times\mathbf{P}'_e) - \frac{1}{2}jk_0^3 c_0\mathbf{u}\times(\mathbf{u}\cdot\overline{\overline{\mathbf{Q}}}'_m) \\
& -jk_0^3\mathbf{u}\times\mathbf{P}'_{m2} - \frac{1}{2}jk_0^3\mathbf{u}\times[\mathbf{u}\times(\mathbf{u}\cdot\overline{\overline{\mathbf{Q}}}'_e)] + \cdots \Big\} \\
\mathbf{H} = \frac{1}{4\pi R_{c0}}\frac{e^{-jk_0R}}{R}\Big\{ & -k_0^2 c_0\mathbf{u}\times(\mathbf{u}\times\mathbf{P}'_{m1}) + k_0^2\mathbf{u}\times\mathbf{P}'_e - \frac{1}{2}jk_0^3 c_0\mathbf{u}\times[\mathbf{u}\times(\mathbf{u}\cdot\overline{\overline{\mathbf{Q}}}'_m)] \\
& -jk_0^3\mathbf{u}\times(\mathbf{u}\times\mathbf{P}'_{m2}) + \frac{1}{2}jk_0^3\mathbf{u}\times(\mathbf{u}\cdot\overline{\overline{\mathbf{Q}}}'_e) + \cdots \Big\}.
\end{aligned} \tag{7.171}$$

7.11 SPHERICAL HARMONICS

In this section the multipole expansion is approached from another point of view than in Section 7.10. The new approach is based on a *vectorial* extension of the analysis in Section 3.7, which was concerned with the *scalar* potential.

7.11.1 Eigenfunctions for a Spherical Surface

The spherical harmonics expansion is based on the functions

$$Y_{mn}(\theta,\varphi) = C_{mn}P_n^m(\cos\theta)\left\{\begin{array}{c}\cos m\varphi\\ \sin m\varphi\end{array}\right\}, \tag{7.172}$$

which were introduced in Section 3.7. These functions are defined on a spherical surface S_1 of unit radius, and their properties are discussed in Appendix 9. The modes associated with $\cos m\varphi$ are termed *even*, and those with $\sin m\varphi$ *odd*. The Y_{mn} eigenfunctions are orthogonal within their parity and also with respect to the other parity. The coefficients C_{mn} are chosen according to (A9.31), which yields the norm

$$\int_{S_1} Y^e_{mn}(\theta,\varphi)Y^e_{m'n'}(\theta,\varphi)\sin\theta\, d\theta\, d\varphi = \delta_{mm'}\delta_{nn'}. \tag{7.173}$$

On a spherical surface S_R of radius R, the orthonormal functions are $Y_{mn}(\theta,\varphi)/R$, and the norm becomes

$$\int_{S_R} \frac{Y^e_{mn}(\theta,\varphi)}{R}\frac{Y^e_{m'n'}(\theta,\varphi)}{R}R^2 d\Omega = \delta_{mm'}\delta_{nn'}, \tag{7.174}$$

where $dS_R = R^2 d\Omega = R^2 \sin\theta\, d\theta\, d\varphi$. A complete set of eigenvectors can be constructed from the Y_{mn} eigenfunctions. On S_1, these are

$$\begin{aligned} \mathbf{f}_{mn} &= \operatorname{grad}_1 Y_{mn} \\ \mathbf{f}_{mn}\times\mathbf{u}_R &= \operatorname{grad}_1 Y_{mn}\times\mathbf{u}_R. \end{aligned} \tag{7.175}$$

Orthogonality and norm follow from the relationship

$$\int_{S_1} \mathbf{f}_{mn}(\theta,\varphi)\cdot\mathbf{f}_{m'n'}(\theta,\varphi)\, d\Omega = n(n+1)\delta_{mn}\delta_{m'n'}. \tag{7.176}$$

This property holds for eigenvectors of the same parity. Eigenvectors of opposite parity are automatically orthogonal. The norm (7.176) is obviously also appropriate for the $\mathbf{f}_{mn}\times\mathbf{u}_R$ eigenvectors. One can also readily demonstrate that the $\mathbf{f}_{mn}$ and $(\mathbf{f}_{mn}\times\mathbf{u}_R)$ families are orthogonal. Note that the $\mathbf{f}_{mn}$ are tangent to the unit sphere.

The Y_{mn} functions satisfy the eigenvalue equation

$$\nabla_1^2 Y_{mn}(\theta,\varphi) = -n(n+1)Y_{mn}(\theta,\varphi). \tag{7.177}$$

One of these eigenfunctions, which corresponds with $m = n = 0$, is $Y =$ constant. Its *unit-norm* version is

$$Y_{00} = \frac{1}{\sqrt{4\pi}}. \tag{7.178}$$

This eigenfunction does not generate any eigenvector, because its gradient vanishes. The detailed form of $\mathbf{f}^{(e)}_{mn}, \mathbf{f}^{(o)}_{mn}, \mathbf{f}^{(e)}_{mn}\times\mathbf{u}_R$ and $\mathbf{f}^{(o)}_{mn}\times\mathbf{u}_R$ can be found in (A9.36) to (A9.39).

7.11.2 Field Expansions

The fields generated by sources $\mathbf{j}(\mathbf{r},t)$ and $\mathbf{j}_m(\mathbf{r},t)$ (Fig. 7.17) can be determined by expanding both fields and sources into elementary blocks, members of two families:

1. *The TE (transverse electric) family.*

   The expansion in the TE family is of the form

$$\begin{aligned} \mathbf{e}(\mathbf{r},t) &= \sum_{m,n} v_{mn}(R,t)\ \operatorname{grad}_1 Y_{mn}\times\mathbf{u}_R \\ \mathbf{h}(\mathbf{r},t) &= \sum_{m,n} i_{mn}(R,t)\ \operatorname{grad}_1 Y_{mn} + \sum_{m,n}\ell_{mn}(R,t)Y_{mn}\mathbf{u}_R + \ell_0(R,t)\frac{1}{\sqrt{4\pi}}\mathbf{u}_R. \end{aligned} \tag{7.179}$$

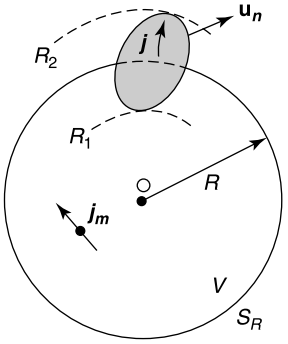

Figure 7.17 Sources in free space.

It is of the type called "unit" expansion in Section 16.5. The expansion includes even and odd modes. The contribution from Y_{00} has been written separately, and the summations therefore exclude the double index $m = n = 0$. The source terms are similarly expanded, and $\mathbf{j}$ in the same eigenvectors as and $\mathbf{e}$, $\mathbf{j}_m$ in the same ones as $\mathbf{h}$. The expansions are inserted into Maxwell's equations, where the *curl of the sum* may be written as *the sum of the curls* (a step that is not allowed in a conical volume, a point discussed in Section 16.5). The following formulas turn out to be most useful for calculation in spherical coordinates:

$$\begin{aligned}
\operatorname{curl}\left[a(R)\ \operatorname{grad}_1 Y_{mn} \times \mathbf{u}_R\right] &= \frac{1}{R}\frac{d(aR)}{dR}\ \operatorname{grad}_1 Y_{mn} + \frac{a}{R}n(n+1)Y_{mn}\mathbf{u}_R \\
\operatorname{curl}\left[a(R)\ \operatorname{grad}_1 Y_{mn}\right] &= \frac{1}{R}\frac{d(aR)}{dR}\mathbf{u}_R \times \operatorname{grad}_1 Y_{mn} \\
\operatorname{curl}\left[a(R) Y_{mn}\mathbf{u}_R\right] &= \frac{a}{R}\operatorname{grad}_1 Y_{mn} \times \mathbf{u}_R. \qquad (7.180)
\end{aligned}$$

Also,

$$\begin{aligned}
\operatorname{curl}\operatorname{curl}\left[a(R)\ \operatorname{grad}_1 Y_{mn} \times \mathbf{u}_R\right] &= \left[\frac{1}{R}\frac{d^2(aR)}{dR^2} - \frac{n(n+1)}{R^2}\,a\right]\mathbf{u}_R \times \operatorname{grad}_1 Y_{mn} \\
\operatorname{curl}\operatorname{curl}\left[a(R)\ \operatorname{grad}_1 Y_{mn}\right] &= -\frac{1}{R}\frac{d^2(aR)}{dR^2}\ \operatorname{grad}_1 Y - \frac{n(n+1)}{R^2}\frac{d(aR)}{dR}Y_{mn}\mathbf{u}_R \\
\operatorname{curl}\operatorname{curl}\left[a(R) Y_{mn}\mathbf{u}_R\right] &= \frac{1}{R}\frac{d(aR)}{dR^2}\ \operatorname{grad}_1 Y + \frac{n(n+1)}{R^2}\,aY_{mn}\mathbf{u}_R. \qquad (7.181)
\end{aligned}$$

On the basis of these expressions, and by equating expansion coefficients on both sides of Maxwell's equations, one obtains

$$\begin{aligned}
\frac{1}{R}\frac{\partial}{\partial R}(Rv_{mn}) + \mu_0\frac{\partial i_{mn}}{\partial t} &= -\frac{1}{n(n+1)}\int_{S_1}\mathbf{j}_m(R,\theta,\varphi,t)\cdot\operatorname{grad}_1 Y_{mn}\,d\Omega \\
&= A_{mn}(R,t) \\
n(n+1)\frac{v_{mn}}{R} + \mu_0\frac{\partial \ell_{mn}}{\partial t} &= -\int_{S_1}\mathbf{u}_R\cdot\mathbf{j}_m(R,\theta,\varphi,t)Y_{mn}\,d\Omega = B_{mn}(R,t)
\end{aligned}$$

$$\epsilon_0 \frac{\partial v_{mn}}{\partial t} + \frac{1}{R}\frac{\partial}{\partial R}(Ri_{mn}) - \frac{1}{R}\ell_{mn} = -\frac{1}{n(n+1)}\int_{S_1} \mathbf{j}(R,\theta,\varphi,t)\cdot(\text{grad}_1 Y_{mn} \times \mathbf{u}_R)\, d\Omega$$
$$= C_{mn}(R,t)$$
$$\mu_0 \frac{\partial \ell_0}{\partial t} = -\frac{1}{\sqrt{4\pi}}\int_{S_1} \mathbf{u}_R \cdot \mathbf{j}_m(R,\theta,t)\, d\Omega. \tag{7.182}$$

Elimination gives a differential equation satisfied by v_{mn} alone, viz.

$$\frac{1}{R}\frac{\partial^2 (Rv_{mn})}{\partial R^2} - \frac{1}{c_0^2}\frac{\partial^2 v_{mn}}{\partial t^2} - n(n+1)\frac{v_{mn}}{R^2}$$
$$= \frac{1}{R}\frac{\partial}{\partial R}(RA_{mn}) - \mu_0 \frac{\partial C_{mn}}{\partial t} - \frac{1}{R}B_{mn}. \tag{7.183}$$

At large distances, away from the sources, this equation reduces to the wave equation in vacuum, and the *outgoing wave* condition must be imposed on v_{mn}. Because the Y_{mn} are mutually orthogonal, all Y_{mn} except Y_{00} (which is a constant) have zero average value over S_1. It follows, from (7.179), that the average value of h_R over S_R is related to ℓ_0 by

$$[h_R(R,t)]_{\text{ave}} = \frac{1}{4\pi R^2}\int_{S_R} h_R R^2 d\Omega = \frac{\ell_0(R,t)}{\sqrt{4\pi}}. \tag{7.184}$$

The magnetic flux ϕ_m of $\mathbf{b}$ through S_R is $\mu_0 4\pi R^2 [h_R]_{\text{ave}}$. Combining this result with (7.182) gives

$$-\frac{\partial \phi_m}{\partial t} = \int_{S_R} (\mathbf{u}_R \cdot \mathbf{j}_m)\, dS. \tag{7.185}$$

2. *The TM (transverse magnetic) family.*

The relevant expansion, again including even and odd modes, is

$$\mathbf{e}(\mathbf{r},t) = \sum_{m,n} v_{mn}(R,t)\ \text{grad}_1 Y_{mn} + \sum_{m,n} w_{mn}(R,t) Y_{mn}\mathbf{u}_R + w_0(R,t)\frac{1}{\sqrt{4\pi}}\mathbf{u}_R$$
$$\mathbf{h}(\mathbf{r},t) = \sum_{m,n} i_{mn}(R,t)\mathbf{u}_R \times \text{grad}_1 Y_{mn}. \tag{7.186}$$

From Maxwell's equations:

$$\frac{1}{R}\frac{\partial}{\partial R}(Rv_{mn}) + \mu_0 \frac{\partial i_{mn}}{\partial t} - \frac{1}{R}w_{mn} = -\frac{1}{n(n+1)}\int_{S_1} \mathbf{j}_m(R,\theta,\varphi,t)$$
$$\cdot(\mathbf{u}_R \times \text{grad}_1 Y_{mn})\, d\Omega = A_{mn}(R,t)$$
$$\frac{1}{R}\frac{\partial}{\partial R}(Ri_{mn}) + \epsilon_0 \frac{\partial v_{mn}}{\partial t} = -\frac{1}{n(n+1)}\int_{S_1} \mathbf{j}(R,\theta,\varphi,t)\cdot \text{grad}_1 Y_{mn}\, d\Omega$$
$$= B_{mn}(R,t)$$
$$n(n+1)\frac{i_{mn}}{R} + \epsilon_0 \frac{\partial w_{mn}}{\partial t} = -\int_{S_1} \mathbf{u}_R \cdot \mathbf{j}(R,\theta,\varphi,t)\, d\Omega = C_{mn}(R,t)$$
$$\epsilon_0 \frac{\partial w_0}{\partial t} = -\frac{1}{\sqrt{4\pi}}\int_{S_1} \mathbf{u}_R \cdot \mathbf{j}(R,\theta,\varphi,t)\, d\Omega. \tag{7.187}$$

Elimination gives

$$\frac{1}{R}\frac{\partial^2(Ri_{mn})}{\partial R^2} - \frac{1}{c_0^2}\frac{\partial^2 i_{mn}}{\partial t^2} - n(n+1)\frac{i_{mn}}{R^2} = \frac{1}{R}\frac{\partial}{\partial R}(RB_{mn}) - \epsilon_0\frac{\partial A_{mn}}{\partial t} - \frac{1}{R}C_{mn}. \tag{7.188}$$

This equation can be solved by Laplace transformation techniques. The average value of e_R is $w_0(R,t)/\sqrt{4\pi}$, and the electric flux ϕ_e of $\mathbf{d} = \epsilon_0\mathbf{e}$ through S_R varies with time according to

$$-\frac{\partial \phi_e}{\partial t} = \int_{S_R} (\mathbf{u}_R \cdot \mathbf{j})\, dS. \tag{7.189}$$

Referring to Figure 7.17, ϕ_e is time-dependent for R between R_1 and R_2, and time-independent outside that interval. Note that (7.189) could have been obtained directly from the equation of conservation of charge. Thus, integrating over a sphere bounded by S_R gives

$$\int_V \operatorname{div} \mathbf{j}\, dV = \int_{S_R} \mathbf{u}_R \cdot \mathbf{j}\, dS = -\frac{\partial}{\partial t}\int_V \rho\, dV = -\frac{\partial}{\partial t}\int_V \operatorname{div} \mathbf{d}\, dV = -\frac{\partial}{\partial t}\int_{S_R} \mathbf{u}_R \cdot \mathbf{d}\, dS.$$

Because $\operatorname{div} \mathbf{d} = \rho$, the flux ϕ_e, in addition to being time-independent between the origin and R_1, must also be zero in that range.

7.11.3 Time-Harmonic Sources

Under time-harmonic conditions, an equation such as (7.183) becomes

$$\frac{1}{R}\frac{d^2(RV_{mn})}{dR^2} + \left(k_0^2 - \frac{n(n+1)}{R^2}\right) V_{mn} = F_{mn}(R), \tag{7.190}$$

where F_{mn} is a given forcing function. Equation (7.190) appears in Appendix 5 under (A5.85). Its solution, for zero second member, is a combination of spherical Bessel functions. In the far field, we must choose the solution $h_n^{(2)}(k_0R)$ to obtain outgoing waves. The basic function in that region is

$$\psi_n^m = h_n^{(2)}(k_0R) \left\{ \begin{array}{c} \cos m\varphi \\ \sin m\varphi \end{array} \right\} P_n^m(\cos\theta). \tag{7.191}$$

A coefficient such as $V_{mn}(R)$ must be a multiple of ψ_n^m. The other coefficients follow from V_{mn} by solving (7.183) or (7.188). The procedure yields multipole fields that, in the case of an *odd* ψ_n^m, are the TM (or *electric*) multipole fields

$$E_R = \frac{n(n+1)}{k_0R} h_n^{(2)}(k_0R) \sin m\varphi\, P_n^m(\cos\theta)$$

$$E_\theta = \frac{1}{k_0R}\frac{d}{dR}\left[Rh_n^{(2)}(k_0R)\right] \sin m\varphi \frac{d}{d\theta}\left[P_n^m(\cos\theta)\right]$$

$$E_\varphi = \frac{m}{k_0R\sin\theta}\frac{d}{dR}\left[Rh_n^{(2)}(k_0R)\right] \cos m\varphi\, P_n^m(\cos\theta)$$

$$H_\theta = \frac{j}{R_{c0}} \frac{m}{\sin\theta} h_n^{(2)}(k_0 R) \cos m\varphi \, P_n^m(\cos\theta)$$
$$H_\varphi = -\frac{j}{R_{c0}} h_n^{(2)}(k_0 R) \sin m\varphi \frac{d}{d\theta} \left[P_n^m(\cos\theta)\right]. \tag{7.192}$$

The *even electric multipoles* are obtained by replacing $\sin m\varphi$ by $\cos m\varphi$ and $\cos m\varphi$ by $-\sin m\varphi$. In similar fashion, the *odd* TE *(or magnetic)* multipole fields are defined by

$$E_\theta = -jR_{c0} \frac{m}{\sin\theta} h_n^{(2)}(k_0 R) \cos m\varphi P_n^m(\cos\theta)$$
$$E_\varphi = jR_{c0} h_n^{(2)}(k_0 R) \sin m\varphi \frac{d}{d\theta} \left[P_n^m(\cos\theta)\right]$$
$$H_R = \frac{n(n+1)}{k_0 R} h_n^{(2)}(k_0 R) \sin m\varphi \, P_n^m(\cos\theta)$$
$$H_\theta = \frac{1}{k_0 R} \frac{d}{dR} \left[R h_n^{(2)}(k_0 R)\right] \sin m\varphi \frac{d}{d\theta} \left[P_n^m(\cos\theta)\right]$$
$$H_\varphi = \frac{m}{k_0 R \sin\theta} \frac{d}{dR} \left[R h_n^{(2)}(k_0 R)\right] \cos m\varphi \, P_n^m(\cos\theta). \tag{7.193}$$

The *even* fields follow by means of the already mentioned substitution. The connection with the multipoles discussed in Section 7.10 may be illustrated by considering the mode $m = 0, n = 1$. Its spatial dependence is governed by a function which, from (A5.93), is of the form

$$h_1^{(2)}(k_0 R) P_1(\cos\theta) = \frac{e^{-jk_0 R}}{k_0 R} \left[-1 + \frac{j}{k_0 R}\right] \cos\theta.$$

At large distances, this function generates electric (or magnetic) dipole fields of the kind described in (7.106).

The various multipole fields can be expressed concisely in terms of the generating function (7.191). Thus, for an electric multipole field,

$$\mathbf{E} = \frac{1}{k_0} \operatorname{curl} \operatorname{curl} (R\psi_n^m \mathbf{u}_R)$$
$$\mathbf{H} = \frac{j}{R_{c0}} \operatorname{curl} (R\psi_n^m \mathbf{u}_R). \tag{7.194}$$

For a magnetic multipole field,

$$\mathbf{E} = -jR_{c0} \operatorname{curl} (R\psi_n^m \mathbf{u}_R)$$
$$\mathbf{H} = \frac{1}{k_0} \operatorname{curl} \operatorname{curl} (R\psi_n^m \mathbf{u}_R). \tag{7.195}$$

The fields outside a sphere containing all the sources can be expanded as a sum of such multipole fields, which form a complete set [22]. The summations, which are actually the

already introduced expansions (7.179) and (7.186), are of the general form

$$\begin{aligned}\mathbf{E} &= \sum_{n,m}\left[\alpha_{nm}\frac{1}{k_0}\,\text{curl curl}\,(\psi_n^m\mathbf{r}) - jR_{c0}\,\beta_{nm}\,\text{curl}\,(\theta_n^m\mathbf{r})\right]\\ \mathbf{H} &= \sum_{n,m}\left[\alpha_{nm}\frac{j}{R_{c0}}\,\text{curl}\,(\psi_n^m\mathbf{r}) + \frac{1}{k_0}\beta_{nm}\,\text{curl curl}\,(\theta_n^m\mathbf{r})\right],\end{aligned} \tag{7.196}$$

where the even and odd terms have been written as one term for the sake of conciseness. These relationships suggest that there exist functions $V(R,\theta,\varphi)$ and $W(R,\theta,\varphi)$ in terms of which the fields can be expressed as

$$\begin{aligned}\mathbf{E} &= \text{curl curl}\,(V\mathbf{r}) - jk_0R_{c0}\,\text{curl}\,(W\mathbf{r})\\ \mathbf{H} &= \frac{jk_0}{R_{c0}}\,\text{curl}\,(V\mathbf{r}) + \text{curl curl}\,(W\mathbf{r}),\end{aligned} \tag{7.197}$$

where V and W are the *Debye potentials*

$$\begin{aligned}V &= \frac{1}{k_0}\sum_{n,m}\alpha_{nm}\psi_n^m \quad \text{(TM)}\\ W &= \frac{1}{k_0}\sum_{n,m}\beta_{nm}\theta_n^m \quad \text{(TE)}.\end{aligned} \tag{7.198}$$

From (7.42), (7.43), (7.51), and (7.52), the fields can also be expressed in terms of *Hertz potentials*. Thus,

$$\begin{aligned}\mathbf{E} &= \text{curl curl}\,\mathbf{\Pi}_e - j\omega\mu_0\,\text{curl}\,\mathbf{\Pi}_m\\ \mathbf{H} &= j\omega\epsilon_0\,\text{curl}\,\mathbf{\Pi}_e + \text{curl curl}\,\mathbf{\Pi}_m.\end{aligned} \tag{7.199}$$

Comparing (7.197) and (7.199) shows that the functions $V\mathbf{r}$ and $W\mathbf{r}$ are Hertz potentials.[‖]

The operators that appear in the previous analysis are sometimes written as

$$\begin{aligned}\mathbf{L}(\psi) &= \text{grad}\,\psi\\ \mathbf{M}(\psi) &= k_0\,\text{curl}\,[\psi R\mathbf{u}_R] = \frac{1}{k_0}\,\text{curl}\,\mathbf{N} \;=\; k_0(\mathbf{L}\times\mathbf{r})\\ \mathbf{N}(\psi) &= \text{curl curl}\,[\psi R\mathbf{u}_R] = \frac{1}{k_0}\,\text{curl}\,\mathbf{M}.\end{aligned} \tag{7.200}$$

In wave mechanics $(\mathbf{r}\times\text{grad})/i$, proportional to $\mathbf{M}$, represents the orbital angular-momentum operator.

[‖]A rigorous proof for the validity of these operations and the existence of Debye potentials is given in Note 20.

7.11.4 Expansion of the Scalar Green's Function

An alternate way to derive the multipole expansion is to start from the vector potential (7.97) and insert the following series into the integrand:

$$\frac{e^{-jk_0|\mathbf{r}-\mathbf{r}'|}}{|\mathbf{r}-\mathbf{r}'|} = \begin{cases} -jk_0 \displaystyle\sum_{n=0}^{\infty} (2n+1) P_n(\cos\psi) j_n(k_0 R') \, h_n^{(2)}(k_0 R) & \text{for } R > R' \\ -jk_0 \displaystyle\sum_{n=0}^{\infty} (2n+1) P_n(\cos\psi) j_n(k_0 R) \, h_n^{(2)}(k_0 R') & \text{for } R < R'. \end{cases} \tag{7.201}$$

In this expression (Fig. 7.9),

$$\cos\psi = \cos\theta\cos\theta' + \sin\theta\sin\theta'\cos(\varphi - \varphi') \tag{7.202}$$

$$P_n(\cos\psi) = P_n(\cos\theta) P_n(\cos\theta') + 2\sum_{m=1}^{n} \frac{(n-m)!}{(n+m)!} \times P_n^m(\cos\theta) P_m^n(\cos\theta') \cos m(\varphi - \varphi'). \tag{7.203}$$

Inserting (7.203) into (7.201) gives, for $R > R'$,

$$\frac{e^{-jk_0|\mathbf{r}-\mathbf{r}'|}}{|\mathbf{r}-\mathbf{r}'|} = -jk_0 \sum_{n=0}^{\infty}\sum_{m=0}^{n} (2n+1) j_n(kR') h_n^{(2)}(kR) \epsilon_m \frac{(n-m)!}{(n+m)!} \times P_n^m(\cos\theta) P_n^m(\cos\theta') \cos m(\varphi - \varphi'). \tag{7.204}$$

The corresponding formula for $R < R'$ follows by exchanging R and R'.

Expression (7.204) generalizes the expansion given in (3.99) for the static Green's function $1/|\mathbf{r}-\mathbf{r}'|$. It is relevant for the evaluation of RE_R and RH_R, two functions from which the full field components can be derived [22] (Problem 7.30).

7.12 EQUIVALENT SOURCES

Equation (7.20) suggests that a time-harmonic current $\mathbf{J}$ may be replaced by a magnetic current

$$\mathbf{J}_m = -\frac{1}{j\omega\epsilon_0} \operatorname{curl} \mathbf{J}. \tag{7.205}$$

This simple statement should be carefully qualified by investigating whether the equivalence holds at points *inside* the (common) source volume V (Fig. 7.18). Also to be checked is the validity of the equivalence for surface currents.

7.12.1 Equivalence Between Electric and Magnetic Currents

The fields generated by $\mathbf{J}$ (the "a" fields) satisfy[21]

$$\operatorname{curl} \mathbf{E}_a = -j\omega\mu_0 \mathbf{H}_a$$

$$\operatorname{curl} \mathbf{H}_a = j\omega\epsilon_0 \mathbf{E}_a + \mathbf{J}.$$

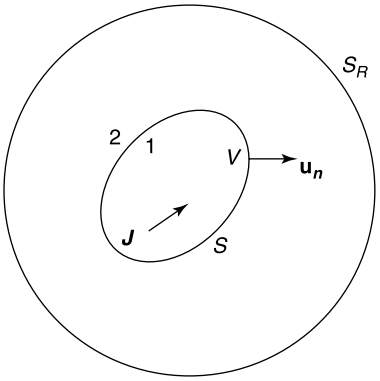

Figure 7.18 A current-carrying volume.

Those generated by $\mathbf{J}_m$ (the "b" fields) satisfy

$$\text{curl } \mathbf{E}_b = -j\omega\mu_0 \mathbf{H}_b - \mathbf{J}_m$$
$$\text{curl } \mathbf{H}_b = j\omega\epsilon_0 \mathbf{E}_b.$$

Subtraction gives

$$\text{curl } (\mathbf{E}_a - \mathbf{E}_b) = -j\omega\mu_0(\mathbf{H}_a - \mathbf{H}_b) + \mathbf{J}_m \tag{7.206}$$
$$\text{curl } (\mathbf{H}_a - \mathbf{H}_b) = j\omega\epsilon_0(\mathbf{E}_a - \mathbf{E}_b) + \mathbf{J}. \tag{7.207}$$

Taking the curl of the first equation and substituting curl $(\mathbf{H}_a - \mathbf{H}_b)$ from the second yields

$$-\text{curl curl } (\mathbf{E}_a - \mathbf{E}_b) + k_0^2(\mathbf{E}_a - \mathbf{E}_b) = -\text{curl } \mathbf{J}_m + j\omega\mu_0 \mathbf{J}. \tag{7.208}$$

Similarly,

$$-\text{curl curl } (\mathbf{H}_a - \mathbf{H}_b) + k_0^2(\mathbf{H}_a - \mathbf{H}_b) = -\text{curl } \mathbf{J} - j\omega\epsilon_0 \mathbf{J}_m. \tag{7.209}$$

If $\mathbf{J}$ and $\mathbf{J}_m$ are to generate the same magnetic field, $(\mathbf{H}_a - \mathbf{H}_b)$ must vanish everywhere, hence the second term in (7.209) must vanish. This condition yields the aforementioned relationship (7.205). The "a" and "b" *electric* fields, however, are not the same. From (7.207), indeed,

$$\mathbf{E}_b = \mathbf{E}_a + \frac{1}{\mathrm{j}\omega\epsilon_0} \mathbf{J}. \tag{7.210}$$

The electric fields therefore coincide, except in the source volume V. In an analogous way, from (7.208), a magnetic current $\mathbf{J}_m$ may be replaced by an electric current

$$\mathbf{J} = \frac{1}{j\omega\mu_0} \text{curl } \mathbf{J}_m. \tag{7.211}$$

In that equivalence the electric fields coincide, but the magnetic fields in V differ because

$$\mathbf{H}_a = \mathbf{H}_b + \frac{1}{j\omega\mu_0}\mathbf{J}_m. \tag{7.212}$$

In the equivalence condition (7.205), the curl must be interpreted in terms of distributions. Thus, in Figure 7.19*a*, (A8.98) gives

$$\mathbf{J}_m = -\frac{1}{j\omega\epsilon_0}\{\text{curl } \mathbf{J}\} + \frac{1}{j\omega\epsilon_0}\mathbf{u}_n \times \mathbf{J}\,\delta_S. \tag{7.213}$$

Because **J** is assumed uniform, (7.213) reduces to a "frill" of magnetic surface current

$$\mathbf{J}_{mS} = \frac{J}{j\omega\epsilon_0}\mathbf{u}_n \times \mathbf{u}_z. \tag{7.214}$$

Such a current gives rise to the electric dipole type of radiation predicted by (7.170).

When **J** is a surface current, the equivalence is governed by the expression (A8.101) for the curl of a surface field. Thus [133],

$$\begin{aligned}\text{curl } (\mathbf{J}_S\delta_S) = &\left[\text{grad}_S J_{Sn} \times \mathbf{u}_n + \overline{\overline{\pi}}\cdot(\mathbf{u}_n \times \mathbf{J}_S) + \mathbf{u}_n \,\text{div}_S(\mathbf{J}_S \times \mathbf{u}_n)\right]\delta_S \\ &+ (\mathbf{u}_n \times \mathbf{J}_S)\frac{\partial\delta_S}{\partial n},\end{aligned} \tag{7.215}$$

where

$$\overline{\overline{\pi}} = \frac{1}{R_1}\mathbf{u}_1\mathbf{u}_1 + \frac{1}{R_2}\mathbf{u}_2\mathbf{u}_2. \tag{7.216}$$

In this expression, the unit vectors $\mathbf{u}_1$ and $\mathbf{u}_2$ are attached to the principal directions, and R_1, R_2 are the principal radii of curvature (see Appendix 3). As an example, consider a uniform planar surface current $J_S\delta(z)\mathbf{u}_x$ (Fig. 7.19*b*). Because $\overline{\overline{\pi}} = 0$ for a plane, the equivalent $\mathbf{J}_m$ is

$$\mathbf{J}_m = -\frac{1}{j\omega\epsilon_0}\mathbf{u}_y\frac{\partial\delta(z)}{\partial z}. \tag{7.217}$$

Such a current density corresponds with a double sheet of magnetic current.[22] The field discontinuities across the various currents in (7.215) are discussed in [133] and, for anisotropic media, in [12].

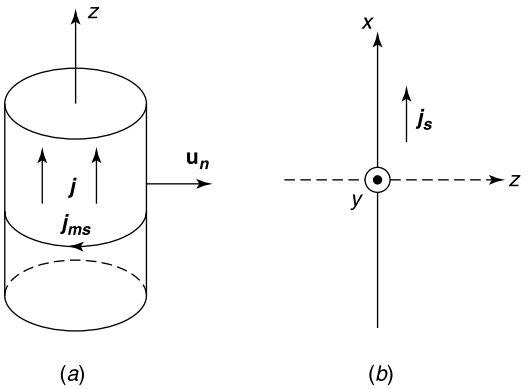

Figure 7.19 (*a*) Uniform current density in a cylinder. (*b*) A sheet of electric surface currents.

7.12.2 Nonradiating Sources

The equivalent sources in (7.205) and (7.210) generate identical fields *outside* V. But this equivalence is not unique, as there exist nonradiating sources $\mathbf{J}^{NR}$ (or $\mathbf{J}_m^{NR}$) that, when added to the equivalent sources, do not modify the exterior fields. The existence of nonradiating sources is germane to the *inverse source* problem. In its simplest form, this problem consists in finding the sources $P(\mathbf{r}')$ in Helmholtz' equation (7.93), given the observed radiated field $\phi(\mathbf{r})$ on S_R (Fig. 7.18). The solution cannot be unique because $P(\mathbf{r}) + P^{NR}(\mathbf{r})$ yields another solution. Uniqueness may be achieved by requiring the solution to have a minimum $\mathcal{L}_2$ norm[23,24]

$$\| P \| = \left[\int_V |P(\mathbf{r})|^2 dV \right]^{\frac{1}{2}}. \tag{7.218}$$

Because of the $\mathcal{L}_2$ nature of this "minimum-energy" solution, single-layer and higher-order singularities at the boundary of V are excluded.

An interesting theorem shows how a nonradiating source can be constructed,[25] starting from a vector field $\mathbf{f}(\mathbf{r})$ that is continuous in V, has continuous partial derivatives up to the third order, and vanishes at all points outside S_R. For such a vector

$$\mathbf{J}(\mathbf{r}) = \frac{1}{j\omega\mu_0} \left[-\text{curl curl } \mathbf{f} + k_0^2 \mathbf{f} \right]. \tag{7.219}$$

is a well-behaved nonradiating current distribution, and $\mathbf{f}$ is precisely the electric field generated by $\mathbf{J}$. This field is therefore confined to V. Conversely, any $\mathbf{J}^{NR}$ can be represented in the form (7.219). A general *radiating* source $\mathbf{J}$, on the other hand, can be split into two components according to

$$\mathbf{J}(\mathbf{r}) = \mathbf{J}^{NR} + \mathbf{J}^{R}. \tag{7.220}$$

The two terms are respectively the nonradiating and the purely radiating components. A *purely radiating* current must satisfy the orthogonality condition[26]

$$\int_V \mathbf{J}^R \cdot \mathbf{f}^* \, dV = 0 \tag{7.221}$$

where V is the support of the source, and $\mathbf{f}$ represents the electric field stemming from any nonradiating source with support in V. Similarly, $\mathbf{J}$ is *nonradiating* if it is orthogonal to all solutions $\mathbf{f}$ of the homogeneous equation[27]

$$-\text{curl curl } \mathbf{f} + k_0^2 \mathbf{f} = 0 \ \text{ in } V.$$

The concept *nonradiating source* can be extended to magnetic currents $\mathbf{J}_m$ and to currents flowing in chiral or bianisotropic materials [12].

7.12.3 Huygens Sources

Let the fields in volume V_1, bounded by a mathematical surface S, be generated by interior sources $\mathbf{J}_1$ and exterior sources $\mathbf{J}_2$ (Fig. 7.20). By means of Huygens sources, we shall express the fields in V_1 as the sum of a contribution from $\mathbf{J}_1$ and a contribution from

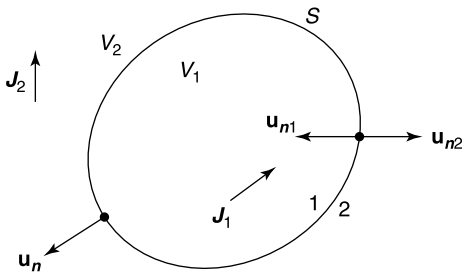

Figure 7.20 Partition of space into regions V_1 and V_2.

appropriate sources on S, which represent the effect of $\mathbf{J}_2$. To demonstrate that equivalence, we start from the differential equations

$$-\text{curl curl}\,\mathbf{E} + k_0^2\,\mathbf{E} = j\omega\mu_0\,\mathbf{J}_1$$
$$\nabla^2 G_0 + k_0^2\,G_0 = \delta(\mathbf{r}-\mathbf{r}').$$

Let us multiply the first equation by $G_0(\mathbf{r}|\mathbf{r}')$, the second one by $\mathbf{E}(\mathbf{r})$, subtract and integrate over V_1 according to (A1.40). This gives, because $j\omega$ div $\epsilon_0\mathbf{E} = -\text{div}\,\mathbf{J}$,

$$\begin{aligned} &j\omega\mu_0\int_{V_1} G_0(\mathbf{r}|\mathbf{r}')\,\mathbf{J}_1(\mathbf{r}')\,dV' + \frac{1}{j\omega\epsilon_0}\int_{V_1}\left[\text{div}'\,\mathbf{J}_1(\mathbf{r}')\ \text{grad}'\,G_0(\mathbf{r}|\mathbf{r}')\right]dV' \\ &+\int_S G_0(\mathbf{r}|\mathbf{r}')\left(\mathbf{u}_n\times\text{curl}'\,\mathbf{E}(\mathbf{r}')\right)dS' + \int_S\left(\mathbf{u}_n\times\mathbf{E}(\mathbf{r}')\right)\times\text{grad}'\,G_0(\mathbf{r}|\mathbf{r}')\,dS' \\ &-\int_S\left(\mathbf{u}_n\cdot\mathbf{E}(\mathbf{r}')\right)\text{grad}'\,G_0(\mathbf{r}|\mathbf{r}')\,dS' = \begin{cases}\mathbf{E}(\mathbf{r}) & \text{for } \mathbf{r} \text{ in } V_1\\ 0 & \text{for } \mathbf{r} \text{ in } V_2.\end{cases} \end{aligned} \tag{7.222}$$

In this equation, the fields on S are the values on the V_1 side of S. We shall now express the surface integrals in terms of only $(\mathbf{u}_n\times\mathbf{E})$ and $(\mathbf{u}_n\times\mathbf{H})$. The *first* surface integral can immediately be cast in the form

$$\mathbf{I}_1(\mathbf{r}) = \int_S G_0(\mathbf{r}|\mathbf{r}')\left[\mathbf{u}_n\times(-j\omega\mu_0\,\mathbf{H}(\mathbf{r}'))\right]dS' = -j\omega\mu_0\int_S \mathbf{u}_n\times\mathbf{H}(\mathbf{r}')\,G_0(\mathbf{r}|\mathbf{r}')\,dS'.$$

The *second* integral can readily be transformed to

$$\mathbf{I}_2(\mathbf{r}) = \int_S \text{grad}\,G_0(\mathbf{r}|\mathbf{r}')\times\left(\mathbf{u}_n\times\mathbf{E}(\mathbf{r}')\right)dS' = \text{curl}\int_S G_0(\mathbf{r}|\mathbf{r}')\,\mathbf{u}_n\times\mathbf{E}(\mathbf{r}')\,dS'.$$

The evaluation of the *third* integral is more subtle. It starts by writing, on the basis of (A3.31),

$$\begin{aligned}\text{div}\int_S G_0(\mathbf{r}|\mathbf{r}')\,\mathbf{u}_n\times\mathbf{H}(\mathbf{r}')\,dS' &= -\int_S \text{grad}_S\,G_0(\mathbf{r}|\mathbf{r}')'\cdot\mathbf{u}_n\times\mathbf{H}(\mathbf{r}')\,dS' \\ &= -\int_S \text{div}'_S\left[G_0(\mathbf{r}|\mathbf{r}')\,\mathbf{u}_n\times\mathbf{H}(\mathbf{r}')\right]dS' \\ &\quad+\int_S G_0(\mathbf{r}|\mathbf{r}')\ \text{div}'_S\left[\mathbf{u}_n\times\mathbf{H}(\mathbf{r}')\right]dS'.\end{aligned}$$

The integral on the second line vanishes, because it represents Gauss' theorem (A3.44) applied to a closed surface. The integral on the third line can be transformed by noting, from (A3.21), that

$$\mathrm{div}_S\,(\mathbf{u}_n \times \mathbf{H}) = -\mathbf{u}_n \cdot \mathrm{curl}\,\mathbf{H} = -j\omega\epsilon_0\,\mathbf{u}_n \cdot \mathbf{E}.$$

This gives

$$\int_S (\mathbf{u}_n \cdot \mathbf{E}(\mathbf{r}))\, G_0(\mathbf{r}|\mathbf{r}')\, dS' = -\frac{1}{j\omega\epsilon_0}\,\mathrm{div} \int_S G_0(\mathbf{r}|\mathbf{r}')\,\mathbf{u}_n \times \mathbf{H}(\mathbf{r}')\, dS'.$$

By taking the gradient of this expression we obtain, for the third surface integral in (7.222),

$$\int_S \mathrm{grad}'\, G_0(\mathbf{r}|\mathbf{r}') \cdot \left[\mathbf{u}_n \cdot \mathbf{E}(\mathbf{r}')\right] dS' = -\frac{1}{j\omega\epsilon_0}\,\mathrm{grad\ div} \int_S G_0(\mathbf{r}|\mathbf{r}')\,\mathbf{u}_n \times \mathbf{H}(\mathbf{r}')\, dS'.$$

For $\mathbf{r}$ in V_1, the integral on the right-hand side is a solution of a sourceless Helmholtz equation, hence we may replace grad div by (curl curl $-k_0^2$). It follows that (7.222) can be given the concise form

$$\begin{aligned}\mathbf{E}(\mathbf{r}) = \mathbf{E}_0(\mathbf{r}) &+ \mathrm{curl} \int_S \mathbf{u}_n \times \mathbf{E}\, G_0(\mathbf{r}|\mathbf{r}')\, dS' \\ &+ \frac{1}{j\omega\epsilon_0}\,\mathrm{curl\ curl} \int_S G_0(\mathbf{r}|\mathbf{r}')\,\mathbf{u}_n \times \mathbf{H}\, dS' \qquad (\mathbf{r} \text{ in } V_1).\end{aligned} \tag{7.223}$$

In this equation $\mathbf{E}_0(\mathbf{r})$, which stands for the sum of the volume integrals in (7.222), is the field created in free space by $\mathbf{J}_1$. When $\mathbf{J}_1 = 0$, the surface integrals represent the contribution to $\mathbf{E}(\mathbf{r})$ from the sources exterior to V_1 (i.e., from $\mathbf{J}_2$). For the magnetic field one finds, analogously,

$$\begin{aligned}\mathbf{H}(\mathbf{r}) = \mathbf{H}_0(\mathbf{r}) &- \frac{1}{j\omega\mu_0}\,\mathrm{curl\ curl} \int_S (\mathbf{u}_n \times \mathbf{E})\, G(\mathbf{r}|\mathbf{r}')\, dS' \\ &+ \mathrm{curl} \int_S G(\mathbf{r}|\mathbf{r}')\mathbf{u}_n \times \mathbf{H}\, dS'.\end{aligned} \tag{7.224}$$

A comparison of (7.223) and (7.224) with (7.107) further reveals that the fields generated by $\mathbf{J}_2$ may be thought of as produced by virtual surface currents

$$\begin{aligned}\mathbf{J}_S &= \mathbf{H} \times \mathbf{u}_n \\ \mathbf{J}_{mS} &= \mathbf{u}_n \times \mathbf{E} \qquad (\text{on } S),\end{aligned} \tag{7.225}$$

radiating in free space. It should be noted that $\mathbf{u}_n$ must be directed along the *outer normal* to V_1. We also remark, from (7.199), that the fields in V_1 are derived from Hertz potentials

$$\begin{aligned}\boldsymbol{\pi}_e(\mathbf{r}) &= \frac{1}{j\omega\epsilon_0} \int_S (\mathbf{u}_n \times \mathbf{H})\, G_0(\mathbf{r}|\mathbf{r}')\, dS' \\ \boldsymbol{\pi}_m(\mathbf{r}) &= \frac{1}{j\omega\mu_0} \int_S (\mathbf{E} \times \mathbf{u}_n)\, G_0(\mathbf{r}|\mathbf{r}')\, dS'.\end{aligned} \tag{7.226}$$

The splitting (7.223), often called the induction theorem[28,29] [15], can be given the more concise form

$$\mathbf{E}_1(\mathbf{r}) = \mathbf{E}_{01} + \mathbf{E}_m(\mathbf{u}_n \times \mathbf{E}_1) + \mathbf{E}_e(\mathbf{H}_1 \times \mathbf{u}_n) \qquad (\mathbf{r} \text{ in } V_1) \tag{7.227}$$

$$0 = \mathbf{E}_{01} + \mathbf{E}_m(\mathbf{u}_n \times \mathbf{E}_1) + \mathbf{E}_e(\mathbf{H}_1 \times \mathbf{u}_n) \qquad (\mathbf{r} \text{ in } V_2). \tag{7.228}$$

The previous results, obtained for region 1, can be extended to region 2 by integrating over V_2 to derive an equation similar to (7.222). The boundary surface now consists of S and S_∞, but the integral over S_∞ vanishes in the limit $R \to \infty$ by virtue of the radiation condition. The outer normal to S is now $(-\mathbf{u}_n)$, but the $\mathbf{E}_m$ and $\mathbf{E}_e$ operators are still appropriate. In short,

$$0 = \mathbf{E}_{02} - \mathbf{E}_m(\mathbf{u}_n \times \mathbf{E}_2) - \mathbf{E}_e(\mathbf{H}_2 \times \mathbf{u}_n) \qquad (\mathbf{r} \text{ in } V_1) \tag{7.229}$$

$$\mathbf{E}_2(\mathbf{r}) = \mathbf{E}_{02} - \mathbf{E}_m(\mathbf{u}_n \times \mathbf{E}_2) - \mathbf{E}_e(\mathbf{H}_2 \times \mathbf{u}_n) \qquad (\mathbf{r} \text{ in } V_2). \tag{7.230}$$

When S is a mathematical boundary, $\mathbf{E}$ and $\mathbf{H}$ are continuous across S, and we may set $\mathbf{u}_n \times \mathbf{E}_1 = \mathbf{u}_n \times \mathbf{E}_2$ and $\mathbf{H}_1 \times \mathbf{u}_n = \mathbf{H}_2 \times \mathbf{u}_n$.

In the previous analysis, the sources were assumed time-harmonic. For an arbitrary time dependence, (7.223) becomes [72]

$$\begin{aligned}\mathbf{e}(\mathbf{r},t) = \mathbf{e}_0(\mathbf{r},t) &+ \frac{1}{4\pi}\,\mathrm{curl}\int_S \mathbf{u}_n' \times \frac{\mathbf{e}\left(\mathbf{r}', t - \dfrac{|\mathbf{r}-\mathbf{r}'|}{c_0}\right)}{|\mathbf{r}-\mathbf{r}'|}\,dS' \\ &- \frac{1}{4\pi\epsilon_0}\,\mathrm{curl}\,\mathrm{curl}\int_S \frac{\mathbf{u}_n' \times \displaystyle\int_{t_0}^{t} \mathbf{h}\left(\mathbf{r}', t' - \dfrac{|\mathbf{r}-\mathbf{r}'|}{c_0}\right)dt'}{|\mathbf{r}-\mathbf{r}'|}\,dS'\end{aligned} \tag{7.231}$$

where t_0 is the time at which the sources are activated. A similar formula can be written for $\mathbf{h}(\mathbf{r},t)$.

7.12.4 Uniqueness

The currents $\mathbf{J}_S$ and $\mathbf{J}_{mS}$ in (7.225) are not known a priori, and their evaluation requires the solution of the full field problem. It is, of course, possible to determine the tangential components of $\mathbf{e}$ and $\mathbf{h}$ *experimentally*.[30] From a *numerical* point of view, approximate values of $\mathbf{J}_S$ and $\mathbf{J}_m$ can sometimes be deduced from the solution of some related canonical problem. In any case, one should investigate whether assigning $\mathbf{u}_n \times \mathbf{e}$ and $\mathbf{h} \times \mathbf{u}_n$ leads to a well-posed problem. We note that, in the absence of sources, an equation such as (7.223) generates the fields in V_1 unambiguously, given $\mathbf{u}_n \times \mathbf{e}$ *and* $\mathbf{h} \times \mathbf{u}_n$. From a fundamental point of view, it is important to remark that *either* $\mathbf{u}_n \times \mathbf{E}$ or $\mathbf{u}_n \times \mathbf{H}$ are sufficient to determine the fields uniquely in V_2 [201]. In Section 10.2, for example, it is shown that the fields generated by an aperture A in a cavity wall can be written as

$$\mathbf{E}(\mathbf{r}) = \int_A \overline{\overline{G}}_{em}(\mathbf{r}|\mathbf{r}') \cdot (\mathbf{u}_n \times \mathbf{E})\, dS'. \tag{7.232}$$

In the absence of volume sources, a knowledge of *only* $\mathbf{u}_n \times \mathbf{E}$ in A therefore suffices to determine $\mathbf{E}$. To prove uniqueness, we should consequently show that setting $\mathbf{u}_n \times \mathbf{E} = 0$

on S implies zero fields in the enclosed volume V. Consider first the exterior region V_2 in Figure 7.20. Because this region is sourceless

$$I = \int_{V_2} \text{div}(\mathbf{E} \times \mathbf{H}^*)\, dV = \int_{V_2} (\mathbf{H}^* \cdot \text{curl}\, \mathbf{E} - \mathbf{E} \cdot \text{curl}\, \mathbf{H}^*)\, dV$$
$$= -j\omega \int_{V_2} \left[\mu_0 |\mathbf{H}|^2 - \epsilon_0 |\mathbf{E}|^2\right] dV. \tag{7.233}$$

This integral is imaginary or zero. A second evaluation of I results from applying the divergence theorem (A1.27) to V_2. Thus,

$$I = \int_{S_\infty} \mathbf{u}_R \cdot (\mathbf{E} \times \mathbf{H}^*)\, dS - \int_S \mathbf{u}_n \cdot (\mathbf{E} \times \mathbf{H}^*)\, dS \tag{7.234}$$

where S_∞ is a spherical surface of very large radius. Because of the radiation condition (7.92), the *first* integral is real, and even positive. It is, in fact, twice the average radiated power emanating from S. The *second* integral vanishes because $\mathbf{u}_n \times \mathbf{E} = 0$ on S. It follows that I is positive or zero. We conclude, by comparing the two values of I, that the only solution is $I = 0$, which implies zero radiated power (i.e., zero exterior fields). Note that a similar analysis for an enclosed cavity only leads to the conclusion $\mu_0 |\mathbf{H}|^2 = \epsilon_0 |\mathbf{E}|^2$. In fact, the cavity admits a triply infinite number of solutions of the sourceless Maxwell equations satisfying the boundary condition $\mathbf{u}_n \times \mathbf{E} = 0$ on S, the electric eigenvectors. Losses in the cavity restore uniqueness (Problem 7.38).

7.13 LINEAR WIRE ANTENNAS

The evaluation of the fields radiated by currents $\mathbf{J}$ and $\mathbf{J}_m$ is a straightforward procedure, in principle at least. The sources, however, are not always known from the onset. In an aperture type of antenna, for example, the tangential electric field in the aperture is the source, and it must be evaluated, a point discussed at length in Chapters 9 and 10. In this section we consider a simple but important example of initially unknown sources, namely the currents on a gap-excited linear antenna (Fig. 7.21*a*). The cross section of the gap is circular, and the material of the antenna is perfectly conducting. Across the gap the electric field is z-directed, and its value $E_g(z)$ is independent of φ. The whole structure is therefore axisymmetric, and the currents on the cylinder are z-directed. Both a and g are further assumed to be small with respect to λ_0. The antenna may be tubular, in which case the current I vanishes at both ends $z = \pm h$, in accordance with the edge conditions (9.242) and (9.243). When the antenna is solid, a capacitive current flows at $z = \pm h$, where it ferries charges to (or from) the two flat ends. In the limit of small a, however, this current becomes negligible.

A practical example of an axisymmetric excitation is shown in Figure 7.21*b*, where the monopole above an infinite ground plane is a good model for some car antennas. The radiated fields are generated by the electric field $E_r(r)$ in the annular gap. The equivalent magnetic current is, from (7.225),

$$\mathbf{J}_{mS} = \mathbf{u}_n \times \mathbf{E} = -(\mathbf{u}_z) \times E_r \mathbf{u}_r = -E_r \mathbf{u}_\varphi \qquad (\text{V m}^{-1}).$$

A voltage $V = \int_a^{a+d} E_r\, dr$ exists across the annular gap, and if d is small with respect to a, it becomes permissible to set $E_r = (V/d)$. From a knowledge of E_r one can readily

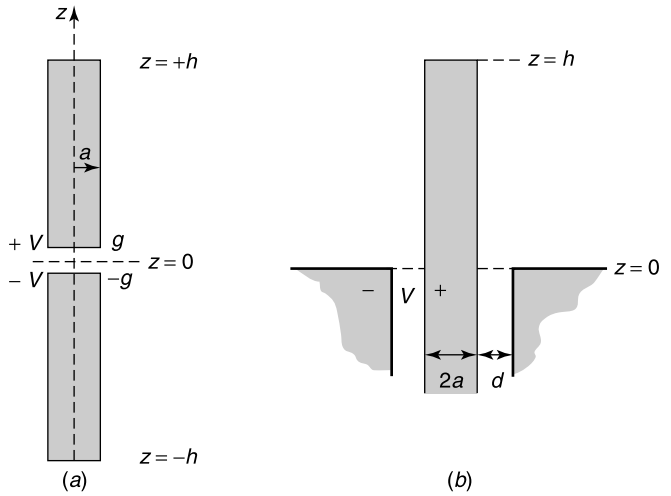

Figure 7.21 (*a*) Gap-excited linear antenna. (*b*) Coaxially excited linear antenna.

determine the fields in the upper half-space and subsequently the current flowing along the monopole. The image sources discussed in Section 9.1 suggest that the ground plane may be suppressed provided the base magnetic currents are doubled. This procedure yields a thin, circular magnetic current of amplitude $I_m = 2V$, located at the center of a monopole of length $2h$.

In the model of Figure 7.21*a*, the exterior fields can be evaluated as soon as E_z is known in the gap. To determine E_z in detail, one should solve a *coupled regions* problem, starting with a derivation of the exterior fields in terms of E_z. This is the only step we will discuss,** because approximate values of E_z, to be mentioned next, can often be used with good results. When the gap is narrow, for example, the details of the variation of E_z are unimportant for the evaluation of the distant fields, and we may choose the convenient law

$$\mathbf{E}_g(z) = -2V\delta(z)\,\mathbf{u}_z. \tag{7.235}$$

7.13.1 Integro-differential Equations

The vector potential generated by the antenna currents is z-directed. From (7.97), its value for a point on the antenna is

$$A(z) = \frac{\mu_0}{8\pi^2}\int_{-h}^{h}\int_{-\pi}^{\pi} I(z')\frac{e^{-jk_0|\mathbf{r}-\mathbf{r}'|}}{|\mathbf{r}-\mathbf{r}'|}\,dz'd\varphi'. \tag{7.236}$$

If we assign $\varphi = 0$ to the observation point, the distance $|\mathbf{r} - \mathbf{r}'|$ takes the form

$$D = |\mathbf{r}-\mathbf{r}'| = \left[(z-z')^2 + 4a^2\sin^2\frac{\varphi}{2}\right]^{\frac{1}{2}}. \tag{7.237}$$

**The second part would consist in determining the fields generated by E_z on the interior side of the gap.

Because

$$\mathbf{E} = -j\omega\,\mathbf{A} - \frac{j\omega}{k_0^2}\,\text{grad div}\,\mathbf{A}$$

$A(z)$ must satisfy

$$\frac{d^2A}{dz^2} + k_0^2 A = j\frac{k_0}{c_0}E_g(z). \tag{7.238}$$

Inserting (7.236) into (7.238) yields *Pocklington's integro-differential equation* for $I(z)$. When $E_g(z)$ is continuous, and if $I(z)$ is required to vanish at $z = \pm h$, this equation has a solution, which furthermore is unique.[31,32,33]

It is useful to rewrite (7.238) more explicitly as

$$\left(\frac{d^2}{dz^2} + k_0^2\right)\int_{-h}^{h} I(z')K(z|z')\,dz' = j\omega\epsilon_0 4\pi E_g(z), \tag{7.239}$$

where

$$K(z|z') = \frac{1}{2\pi}\int_{-\pi}^{\pi} \frac{e^{-jk_0\left[(z-z')^2+4a^2\sin^2\frac{\varphi'}{2}\right]^{\frac{1}{2}}}}{\left[(z-z')^2+4a^2\sin^2\frac{\varphi'}{2}\right]^{\frac{1}{2}}}\,d\varphi'. \tag{7.240}$$

The K kernel and its singularities are essential elements in the analysis of the antenna currents.

The general solution of (7.239), considered as a differential equation in z, is readily found to be

$$\int_{-h}^{h} I(z')K(z|z')\,dz' = A\,\sin k_0 z + B\,\cos k_0 z + j\frac{4\pi}{R_{c0}}\int_{-h}^{z}\sin k_0(z-z')E_g(z')\,dz'. \tag{7.241}$$

The last term on the right-hand side is a particular solution of (7.239) (Problem 7.39). Equation (7.241) is *Hallén's* integral equation.[34] When the gap is very narrow, E_g is given by (7.235). Inserting this value in (7.241), and taking symmetry into account, leads to

$$\int_{-h}^{h} I(z')K(z|z')\,dz' = B\,\cos k_0 z + \frac{4\pi V}{R_{c0}}e^{-jk_0|z|}. \tag{7.242}$$

The constant B is determined by requiring I to vanish at both ends, that is, for $z = \pm h$. For an infinitely long antenna B vanishes, and the vector potential A consists of traveling waves of constant amplitude. For such a situation, Hallén writes the current in the form

$$I(z) = \frac{2\pi V}{R_{c0}}\psi(k_0 z)\,e^{-jk_0|z|}. \tag{7.243}$$

Numerical values of ψ are given in Figure 7.22. The curves show that the current tends to reach a constant amplitude away from the gap. At the gap itself, I becomes proportional to $\log_e|z|$, and therefore infinite at $z = 0$. This singularity is the result of the nonphysical nature of the gap model. The singularity also appears in the admittance of the antenna, which is (Fig. 7.23)

$$Y_a = \frac{I(0)}{V} = \frac{2\pi}{R_{c0}}\psi(0) = G_a + jB_a.$$

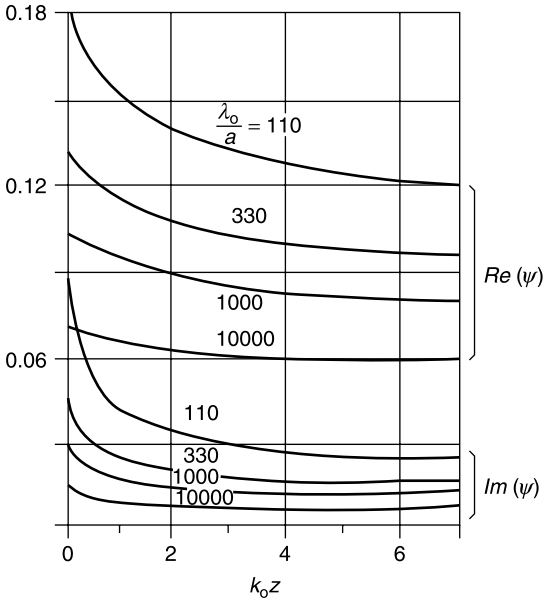

Figure 7.22 Normalized current on an infinite antenna (from E. Hallén, *Electromagnetic theory*, Chapman and Hall, London 1962, with permission of the Taylor & Francis Group).

It is clear, from the figure, that the susceptance B_a becomes infinite at $z = 0$ because it is proportional to Im $\psi(0)$. To avoid this singularity, the figure displays B_a at a distance a from the gap.

The $\delta(z)$ generator is clearly unable to generate the correct *near* fields, although it provides a valid model for the evaluation of the *radiated* fields. An improved model is obtained by assuming[35,36] that $E_g(z)$ has a uniform value $(V/2a)$ in a gap of nonzero

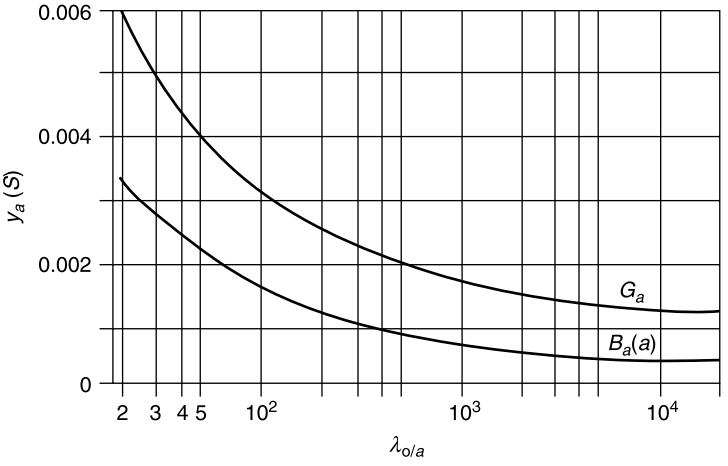

Figure 7.23 Admittance of the infinitely long antenna in the slice generator model (from E. Hallén, *Electromagnetic theory*, Chapman and Hall, London, 1962, with permission of the Taylor & Francis Group).

length $2g$. When the antenna is *tubular*,[††] further improvement results from including the edge behavior by setting

$$E_g(z) = -\frac{V}{\pi}\frac{1}{(g^2 - z^2)^{\frac{1}{2}}}. \tag{7.244}$$

7.13.2 Singularity of the Kernel

It is clear, from (7.240), that K is singular for $D \to 0$ (i.e., for $z \to z'$ and $a \to 0$). The singularity may be extracted by splitting K as follows:

$$\begin{aligned} K(z|z') &= \frac{1}{2\pi}\int_{-\pi}^{\pi} \frac{d\varphi'}{\left[(z-z')^2 + 4a^2 \sin^2 \frac{\varphi'}{2}\right]^{\frac{1}{2}}} + \frac{1}{2\pi}\int_{-\pi}^{\pi} \frac{e^{-jk_0 D} - 1}{D}\, d\varphi' \\ &= K_S(z|z') + K_r(z|z'). \end{aligned} \tag{7.245}$$

The singular part K_S, already discussed under (4.28), is of the form

$$\lim_{z \to z'} K_S = -\frac{1}{\pi a}\log_e \frac{|z - z'|}{8a}. \tag{7.246}$$

This kernel is logarithmically infinite at $z = z'$ for all values of a, and approaches infinity almost proportionally to $(1/a)$ as a approaches zero. More generally [114],

$$K_S(z|z') = \frac{\beta}{\pi a} K(\beta) \tag{7.247}$$

where K is the complete elliptic integral of the first kind defined in (6.11), and

$$\beta = \frac{2a}{\left[(z-z')^2 + 4a^2\right]^{\frac{1}{2}}}.$$

Kernel (7.247) may be expressed as a series in β, with (7.246) as leading singularity. Because of this leading term, the numerical solution of (7.242) typically involves the evaluation of integrals of the type

$$\int_{z-\Delta_1}^{z+\Delta_2} I(z') \log_e |z - z'|\, dz'.$$

Assume, for example, that the numerical solution proceeds by splitting the antenna into N equal segments,[37] each of which is characterized by a given constant value of I (Fig. 7.24*a*). The self-contribution to $k(z/z')$ at z from the segment between $z - (\Delta/2)$ and $z + (\Delta/2)$ can now be written as[38]

$$\frac{1}{2\pi}\int_{-\pi}^{\pi} d\varphi \int_{-\Delta/2}^{\Delta/2} \frac{du}{\left[u^2 + 4a^2 \sin^2 \frac{\varphi}{2}\right]^{\frac{1}{2}}} - jk\Delta + \cdots$$

[††]The tubular antenna of *infinite* length can be investigated by the methods described in Section 15.6 results obtained near the gap remain valid for an antenna of *finite* length.

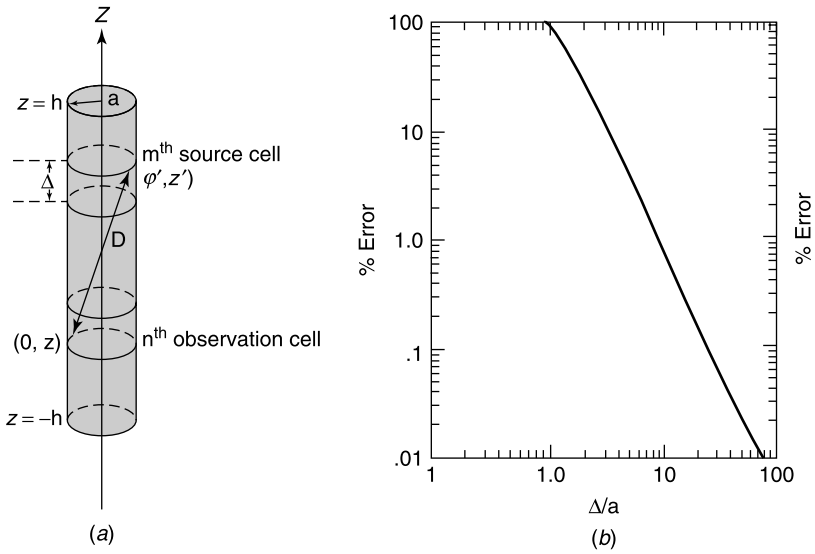

Figure 7.24 (*a*) Antenna subdivided into equal segments Δ. (*b*) Error of the approximate self-patch contribution (from F. M. Tesche, Evaluation of the surface integral equation occurring in the *E*-field integral equations for wire antennas, *IEEE Trans. EMC* **16**, 209–210, with permission of IEEE).

$$= \frac{1}{\pi}\int_{-\pi}^{\pi}\left\{\log_e\left[\frac{\Delta}{4a}+\sqrt{\left(\frac{\Delta}{4a}\right)^2+\sin^2\frac{\varphi}{2}}\right]d\varphi + 2\log_e 2 - jk\Delta + \cdots \right. \tag{7.248}$$

where $u = z - z'$. The integral is nonsingular and can easily be evaluated by machine integration. For separations much larger than the radius (i.e., for $|z - z'| \gg a$), the kernel becomes

$$K(z|z') = \frac{1}{|z-z'|}e^{-jk_0|z-z'|} + \text{terms in } (a/|z-z'|)^2. \tag{7.249}$$

7.13.3 Numerical Solution

The method of moments is particularly suitable[‡‡] for the determination of $I(z)$. If the antenna is subdivided as suggested in Figure 7.24*a*, and if identical basis functions and testing functions are used in the segments, all matrix elements Z_{mn} for which $(m - n)$ is constant have the same value. The matrix is therefore Toeplitz-symmetric and can be inverted by methods that make use of that feature.[40,41] The basis functions may be of the entire-domain type (Chebychev polynomials, Legendre polynomials, Fourier series . . .) or of the subdomain type[42] (pulses, triangles, partial sinusoids . . .) [198].

In an often used approximate solution for $I(z)$, one assumes that the currents are concentrated on the axis of the antenna. Under these conditions, the contributions from elements of current situated at distances $|z - z'|$ of the order a are not properly accounted for, but the relative magnitude of these contributions decreases as a approaches zero. The great

[‡‡]Other methods are also applicable (see, e.g., Note 39).

advantage of the proposed approximation is that the distance D can now be expressed as

$$D = [a^2 + (z - z')^2]^{\frac{1}{2}}.$$

For a $\delta(z)$ type of generator, for example, the resulting *axial* form of *Hallén's equation* is simply[§§]

$$I(z) \int_{-h}^{h} \frac{dz'}{D} + \int_{-h}^{h} \frac{I(z')e^{-jk_0 D} - I(z)}{D}\, dz' = 8\pi^2 \frac{V}{R_{c0}}\, e^{-jk_0 z} + B\, \cos k_0 z. \tag{7.250}$$

The second integral remains finite for $z = z'$ as a approaches zero, while the first one has the explicit value [7]

$$\int_{-h}^{h} \frac{dz^2}{[a^2 + (z - z')^2]^{\frac{1}{2}}} = \log_e \frac{h - z + \left[(h - z)^2 + a^2\right]^{\frac{1}{2}}}{-h - z + \left[(h + z)^2 + a^2\right]^{\frac{1}{2}}}. \tag{7.251}$$

It is, of course, for small D that the difference with the exact kernel becomes more pronounced. A comparison between the exact kernel (7.248) and its axial approximation (7.251) leads to the error curve shown in Figure 7.24*b*. The error is less than 1% when $\Delta \geq 8a$.

7.14 CURVED WIRE ANTENNAS: RADIATION

The current on a thin curved antenna of radius a satisfies a Hallén type of integral equation[45,46]

$$\int_{c_1}^{c_2} I(c')K_c(c|c')\, dc' = A\, \sin k_0|c| + \int_{c_1}^{c_2} I(c')K(0|c')\mathbf{u}_c \cdot \mathbf{u}_{c0} \cos k_0 c\, dc' + F(c) \tag{7.252}$$

where c is the arc length[¶¶] (Fig. 7.25*a*). The term $F(c)$ is the forcing function

$$F(c) = j\frac{4\pi}{R_{c0}} \int_{c_1}^{c} \sin k_0(c - c')E_g(c')\, dc'$$

and the kernel $K_c(c|c')$ is related to the previously defined fundamental kernel

$$K(c|c') = \frac{1}{2\pi} \int_{-\pi}^{\pi} \frac{e^{-jk_0|\mathbf{r}-\mathbf{r}'|}}{|\mathbf{r} - \mathbf{r}'|}\, d\varphi'$$

by the expression

$$K_c(c|c') = K(c|c')(\mathbf{u}_c \cdot \mathbf{u}_{c'}) - \int_0^c \left[\frac{\partial K(s|c')}{\partial s}(\mathbf{u}_s \cdot \mathbf{u}_{c'}) + \frac{\partial K(s|c')}{\partial c'} + K(s|c')\frac{\partial(\mathbf{u}_s \cdot \mathbf{u}_{c'})}{\partial s}\right] \cos k_0(c - s)\, ds. \tag{7.253}$$

[§§]It should be noted that the axial form of Hallén's equation has *no* exact solution[43,44] [47, part 1]. Approximate solutions, however, often yield values of $I(z)$ and Y_a that are in good agreement with experimental data.

[¶¶]The form of (7.252) for a general time-dependence is discussed in [62, 110, 193].

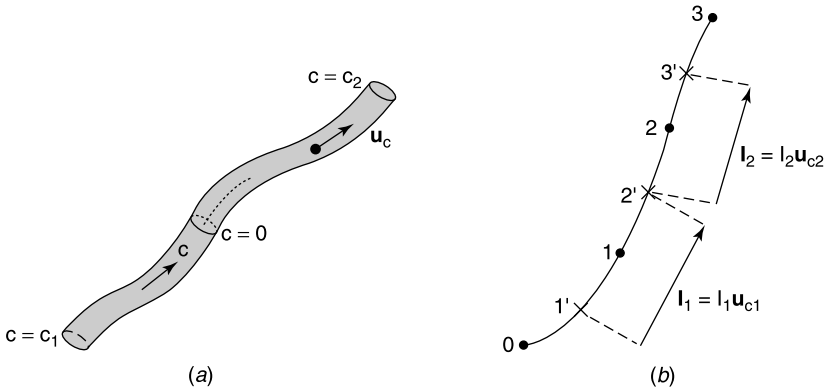

Figure 7.25 (*a*) Curved wire antenna and coordinates. (*b*) Division into equal segments.

A simpler form for K_c can be derived when the antenna can be approximated by a series of linear segments.[47] The problem can also be formulated in terms of vector and scalar potentials, with **E** given by (7.29). Projecting this equation in the c-direction yields

$$\mathbf{u}_c \cdot \mathbf{E}_g = -j\omega \mathbf{u}_c \cdot \mathbf{A} - \frac{\partial \phi}{\partial c}. \tag{7.254}$$

The potentials follow from (7.96) and (7.97). Thus [154]

$$\mathbf{A} = \frac{\mu_0}{4\pi} \int_c I(c') \frac{e^{-jk_0 D}}{D} \mathbf{u}_{c'} \, dc' \tag{7.255}$$

$$\Phi = \frac{1}{4\pi\epsilon_0} \int_c P_c(c') \frac{e^{-jkD}}{D} \, dc' \tag{7.256}$$

where the equation of conservation of charge takes the one-dimensional form

$$j\omega P_c = -\frac{dI}{dc}. \tag{7.257}$$

The problem can be discretized[48] by dividing the antenna into segments of equal length (three in Fig. 7.25*b*). From (7.254):

$$\begin{aligned} E_{gc}(1) &= -j\omega A_c(1) - \frac{\phi(2') - \phi(1')}{\Delta c} \\ E_{gc}(2) &= -j\omega A_c(2) - \frac{\phi(3') - \phi(2')}{\Delta c}. \end{aligned} \tag{7.258}$$

By choosing a uniform current in each segment (Fig. 7.25*b*), the vector potential becomes

$$\mathbf{A}(1) = \frac{\mu_0}{4\pi} \left[I_1 \mathbf{u}_{c1} \int_{1'}^{2'} \frac{e^{-jk_0 D_1}}{D_1} \, dc' + I_2 \mathbf{u}_{c2} \int_{2'}^{3'} \frac{e^{-jk_0 D_1}}{D_1} \, dc' \right] \tag{7.259}$$

where D_1 is the distance from the observation point on the surface to point 1. A similar equation may be written for $\mathbf{A}(2)$. The discretized scalar potential is now[‖‖49]

$$\phi(1') = \frac{1}{4\pi\epsilon_0}\left[\rho_c(1')\int_0^1 \frac{e^{-jk_0 D_{1'}}}{D_{1'}}dc' + \rho_c(2')\int_1^2 \frac{e^{-jk_0 D_{2'}}}{D_{2'}}\,dc' + \rho_c(3')\int_2^3 \frac{e^{-jk_0 D_{3'}}}{D_{3'}}\,dc'\right] \tag{7.260}$$

with similar expressions for $\phi(2')$ and $\phi(3')$. The second member can be written in terms of I_1 and I_2 by taking the equation of conservation of charge (7.257) into account. Thus,

$$\rho_c(1') = -\frac{1}{j\omega}\frac{I_1}{\Delta c}; \qquad \rho_c(2') = -\frac{1}{j\omega}\frac{I_2 - I_1}{\Delta c}; \qquad \rho_c(3') = -\frac{1}{j\omega}\frac{(-I_2)}{\Delta c}.$$

Performing the substitution expresses $\phi(1')$ as a linear function of I_1 and I_2. Combining this result with (7.259) ultimately yields a matrix equation

$$\begin{pmatrix} \Delta c\, E_{gc}(1) \\ \Delta c\, E_{gc}(2) \end{pmatrix} = \begin{pmatrix} Z_{11} & Z_{12} \\ Z_{21} & Z_{22} \end{pmatrix} \cdot \begin{pmatrix} I_1 \\ I_2 \end{pmatrix}. \tag{7.261}$$

The wire antenna is fully characterized by its $\overline{\overline{Z}}$ matrix, which can be used for arbitrary excitations E_g. The main numerical problem resides with the determination of the matrix elements Z_{mn} [154].

Synthesis of Radiation Patterns

The vector potential associated with a linear antenna is given by (Fig. 7.26*a*)

$$\mathbf{A}(\mathbf{r}) = \frac{\mu_0}{4\pi}\mathbf{u}_z \int_{-h}^{h} I(z')\frac{e^{-jk_0|\mathbf{r}-\mathbf{r}'|}}{|\mathbf{r}-\mathbf{r}'|}\,dz'. \tag{7.262}$$

At large distances from the origin O (i.e., for $R \gg \lambda_0$ and $R \gg h$),

$$\begin{aligned} E_\theta = R_0 H_\varphi &= \frac{j\omega\mu_0}{4\pi}\int_{-h}^{h} \sin\gamma \frac{e^{-jk_0 D}}{D} I(z')\,dz' \\ &= \frac{j\omega\mu_0}{4\pi}\sin\theta\frac{e^{-jkR}}{R}\int_{-h}^{h} e^{jk_0 z'\cos\theta} I(z')\,dz' + \text{terms of higher order in } \frac{1}{R}. \end{aligned} \tag{7.263}$$

An often used approximation for the current is the sinusoidal variation

$$I = I_m \sin k_0(h - |z|) \tag{7.264}$$

For a half-wave dipole (i.e., for $h = \lambda_0/4$), this approximation becomes

$$I = I_m \cos k_0 z = I_m \cos\left(\frac{\pi}{2}\frac{z}{h}\right).$$

[‖‖]More refined basis functions, which better take the shape of the antenna into account, are discussed in Note 49.

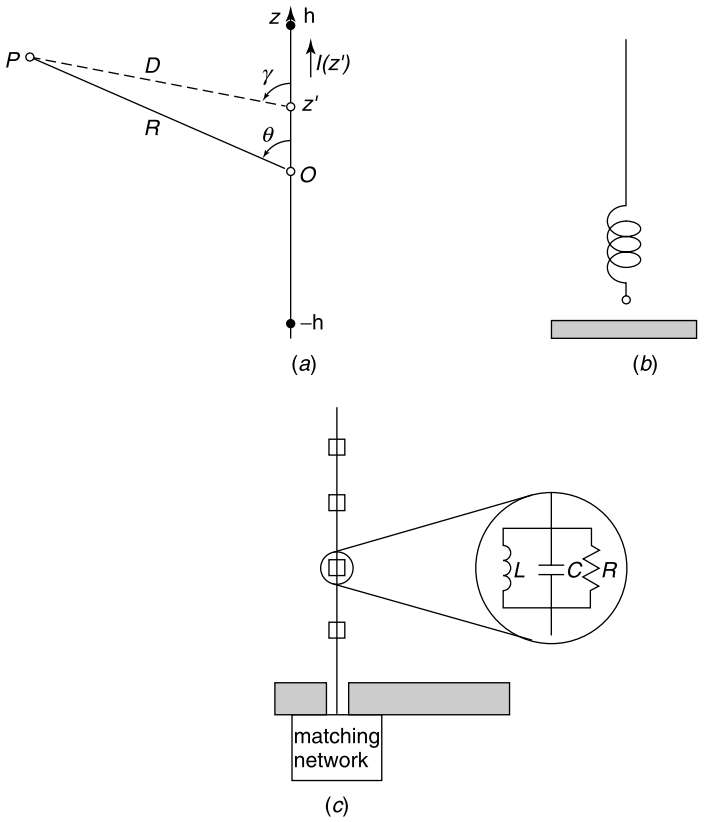

Figure 7.26 (*a*) Linear antenna. (*b*) Short antenna loaded by an inductance (*c*) Loaded linear antenna (from A. Boag, A. Boag, E. Michielssen, and R. Mittra, Design of electrically loaded wire antennas using genetic algorithms, *IEEE Trans. AP* **44**, 687–695, 1996, with permission of IEEE).

It generates a radiated field

$$E_\theta = R_{c0} H_\varphi = jR_{c0} \frac{I_m}{2\pi} \frac{\cos\left(\frac{\pi}{2}\cos\theta\right)}{\sin\theta} \frac{e^{-jk_0 R}}{R}.$$

The sinusoidal approximation breaks down when h is a multiple of $\lambda_0/2$, because (7.264) predicts zero base current for that case (i.e., an infinite base impedance). This result is not acceptable, because radiative losses imply a finite, nonzero input resistance.

A major engineering problem is the determination (and realization) of a current $I(z)$ that satisfies a given criterion, such as the optimization of the directivity in a chosen direction. There are various ways to control $I(z)$. Some of these are

- Top loading with a capacitance. For such a choice, the need to set $I = 0$ at $z = h$ disappears, which gives an additional degree of freedom to the designer.
- Base-loading a short antenna with an inductance (Fig. 7.26*b*). In this system, the capacitive reactance of the gap can be cancelled, which allows larger base currents to flow.
- Loading at various points along the antenna (Fig. 7.26*c*).

Optimization can be achieved by various methods, for example by the use of *genetic algorithms*[50] (GA) [187, 204]. In the case of loading with resonant tank circuits, as in Figure 7.26*c*, the objective might be to enhance the broadband performance by optimizing the parameters of the RLC circuits, the location of these circuits, and the characteristics of the matching network.[51,52,53] The GA method achieves this goal by mimicking natural evolution, that is, by starting from a set of trial solutions, and subsequently evolving toward an optimal solution by means of a criterion-associated fitness function.[54] The parameters (the *genes*) are expressed in coded form. For example, if there are N parameters, the code could be

$$\underbrace{110010}_{P_1} \quad \underbrace{000011}_{P_2} \quad \ldots \quad \underbrace{100010}_{P_N}.$$

The ensemble of these coded values, a bitstring, forms a *chromosome*. The method starts with an initial *population* of chromosomes (say M of them), typically obtained by randomly generating 0's and 1's. The GA method produces series of bitstrings and evaluates these according to a fitness function, which is the actual link with the physical world. In the tank-circuit problem, for example, this function could be the sidelobe level of the radiation pattern, or the system gain G_s, given by

$$G_s = G_a + 10 \log_{10}(1 - |K|^2) \text{ (dB)}$$

where G_a is the antenna gain defined in (7.115), and K is the reflection coefficient of the antenna system. The antenna designer might require the gain to be maximized in certain directions and in a given frequency band. For such a case, programs are needed to determine the current along the antenna for a large number of parameter values. The GA now proceeds by replacing the initial population by a new one by means of a few fundamental operations. In the *decimation* strategy, the genes with poor fitness results are discarded. In the *crossover* strategy, two genes serve as parents. A crossover point in the gene code is chosen, and two new genes, the *children*, are created by swapping all the bits (e.g., those to the right of the crossover point). *Mutation* creates a new gene by selecting a bit from the string and inverting it, so that a "1" becomes a "0," or conversely.

The genetic algorithm method has been applied to problems such as the design of light weight, broadband microwave absorbers, or the extraction of the natural resonances of a target from the target's radar return.[54,55]

7.15 TRANSIENT SOURCES

Pulsed signals are increasingly utilized in technical applications. In tracking-radar systems, for example, highly energetic and directive short pulses are now in frequent use, and the design of suitable beam-shaping antennas has become a topic of active research[56] [29, 31, 42]. Illustratively, Figure 7.27 shows, under (*a*), the relative amplitude of the signal from a pulsed dye laser and, under (*b*), the relative amplitude of the frequency spectrum of that signal. Broad spectra are a source of interference with other systems. To give an extreme example, the typical signal from a possible nuclear explosion is shown under (*c*). This particularly violent source of interference has been investigated extensively[57] [91].

The response to transient currents $\mathbf{j}(\mathbf{r}, t)$ can be derived from the inverse Fourier transformation (7.14), provided the harmonic response $\mathbf{J}(\mathbf{r}, \omega)$ is known. This operation is seldom trivial. In addition, when sources are broadbanded, the harmonic response must be known

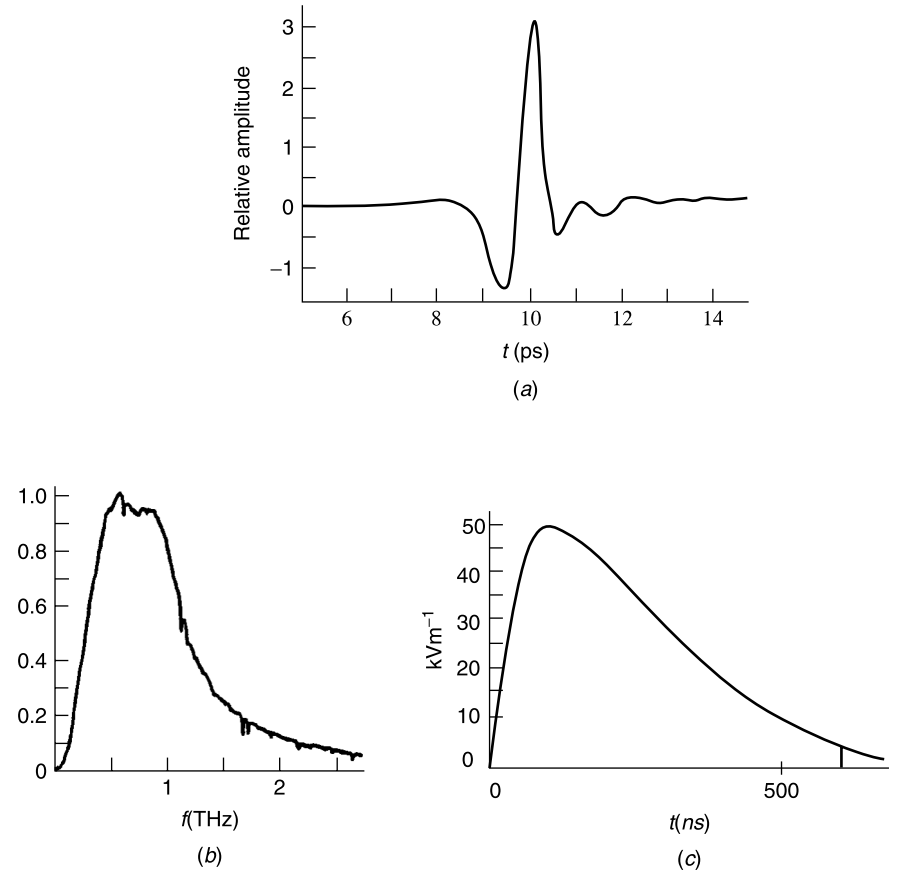

Figure 7.27 (*a*) Very short pulse. (*b*) Spectrum of the pulse. (*c*) Typical field intensity on the ground from a high-altitude nuclear explosion.

(in phase and amplitude) for a large number of discrete frequencies, a time-consuming task. Note that transient sources are often activated over only a short time interval $(-T, T)$, in which case sampling theorem (A7.49) allows one to determine $\mathbf{J}(\mathbf{r}, \omega)$ by sampling values of $\mathbf{J}$ at equidistant frequency points, separated by $\left(\dfrac{1}{2T}\right)$. Further simplification is possible when low- and high-frequency asymptotic forms are available for the frequency spectrum. Given these various factors, *direct time-domain* techniques have become prominent in determining the time-history of a short pulse as to its generation, propagation, and impact on receiving systems. The propagation part is particularly difficult to ascertain in the presence of dispersive media, for which the $\overline{\overline{\epsilon}}_r, \overline{\overline{\mu}}_r, \overline{\overline{\sigma}}$ are frequency dependent, and cannot always be assumed constant over the spectral band covered by the pulsed signal.

7.15.1 Pulsed Linear Antenna

The current on a linear antenna with arbitrary $e_g(z, t)$ can be determined by *Laplace transform* techniques. Thus, *Pocklington's integro-differential equation* (7.239) becomes, in the

s-plane,[58]

$$\left(\frac{d^2}{dz^2} - \frac{1}{c_0^2}s^2\right)\frac{\mu_0}{8\pi^2}\int_{-h}^{h} I(z',s)dz' \int_{-\pi}^{\pi} \frac{e^{-sD/c_0}}{D}\, d\varphi' = \frac{s}{c_0^2}E_g(z,s). \tag{7.265}$$

Once $I(z,s)$ is obtained from this equation, the sought time dependence $i(z,t)$ can be derived by inversion of $I(z,s)$. It is often more efficient to work *directly* in the time domain and to express the field radiated by a current $i(z,t)$ in terms of the mixed $(\mathbf{a},\phi)$ potentials. Thus,

$$\begin{aligned}\mathbf{e}(\mathbf{r},t) &= -\text{grad}\left[\frac{1}{4\pi\epsilon_0}\int_{-h}^{h}\frac{\rho_l\left(z',t-\dfrac{R}{c_0}\right)}{R}\,dz'\right] - \frac{\partial}{\partial t}\left[\frac{\mu_0}{4\pi}\int_{-h}^{h}\frac{i\left(z',t-\dfrac{R}{c_0}\right)}{R}\,dz'\,\mathbf{u}_z\right]\\ &= \frac{\mathbf{u}_R}{4\pi\epsilon_0}\left[\int_{-h}^{h}\frac{\rho_l\left(z',t-\dfrac{R}{c_0}\right)}{R^2}\,dz' + \int_{-h}^{h}\frac{\dfrac{\partial\rho_l}{\partial t}\left(z',t-\dfrac{R}{c_0}\right)}{c_0 R}\,dz'\right]\\ &\quad - \frac{\mu_0}{4\pi}\mathbf{u}_z\int_{-h}^{h}\frac{i\left(z',t-\dfrac{R}{c_0}\right)}{R}\,dz'.\end{aligned} \tag{7.266}$$

To determine $i(z,t)$, and subsequently $\rho_l(z,t)$, we may resort to the solution of time-dependent integral equations, derived directly from the corresponding time-harmonic form. For example, the axial form of Pocklington's equation in the presence of a gap voltage $v_g(t)$ becomes[59]

$$\left(\frac{\partial^2}{\partial z^2} - \frac{1}{c_0^2}\frac{\partial^2}{\partial t^2}\right)\int_{-h}^{h}\frac{i\left(z',t-\dfrac{D}{c_0}\right)}{4\pi D}\,dz' = -\epsilon_0\frac{dv_g(t)}{dt}\,\delta(z) \tag{7.267}$$

with

$$D = \left[(z'-z)^2 + a^2\right]^{\frac{1}{2}}.$$

The *Hallén* type of *equation* follows as[60]

$$\int_{-h}^{h}\frac{i\left(z',t-\dfrac{D}{c_0}\right)}{4\pi D}\,dz' = \frac{1}{2R_{c0}}v_g\left(t-\frac{|z|}{c_0}\right) + i_1\left(t-\frac{z}{c_0}\right) + i_2\left(t+\frac{z}{c_0}\right). \tag{7.268}$$

The first term on the right-hand side is a wave that propagates away from the gap; the last two terms are particular solutions of the homogeneous wave equation. These terms can be determined by requiring i to vanish at both end-points of the antenna. It is clear that i_1 and i_2 respectively represent current waves to positive and negative z, the result of successive reflections at both ends.

Instead of determining $i(z,t)$ — and the resulting fields — from the solution of an integral equation, one may choose to solve Maxwell equations by finite difference methods

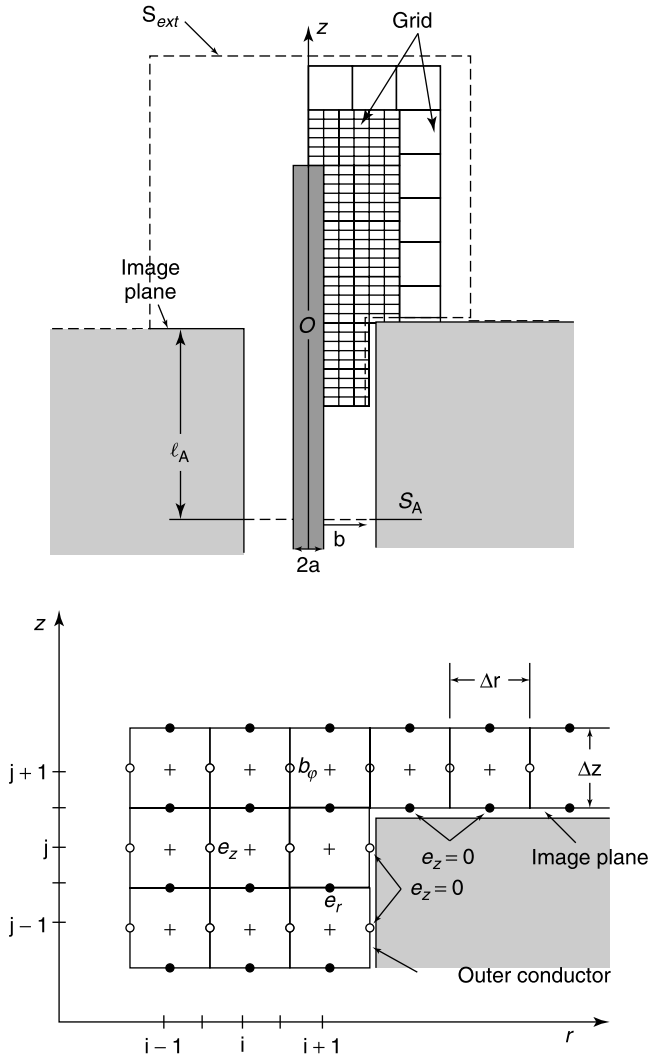

Figure 7.28 Coaxial monopole and associated grid (from J. G. Maloney, G. S. Smith, and W. R. Scott, Accurate computation of the radiation from simple antennas using the finite-difference, time-domain method, *IEEE Trans. AP* **38**, 1059–1068, 1990, with permission of IEEE).

(FDTD). To that effect, derivatives are replaced by their finite difference approximation (see Section 1.14). As an example of application, consider the monopole antenna depicted in Figure 7.28, and assume that the fields are zero until $t = 0$. At $t = 0$, a field appears on S_A. If the TEM mode is the only propagated mode in the coaxial line (see Section 15.1), the electric field on S_A can be written as[61,62]

$$\mathbf{e}(r,t) = \frac{V(t)}{r \log_e(b/a)} \mathbf{u}_r.$$

The wave progresses up the coaxial line and later fans out above the ground plane. The whole field pattern is axisymmetric, and the radial component of (7.2), for example, takes

the form

$$\frac{\partial h_\varphi}{\partial z} = -\epsilon_0 \frac{\partial e_r}{\partial t}. \tag{7.269}$$

Discretization proceeds by evaluating **e** and **h** at interleaved spatial grid points and interleaved time steps. If a typical field component is denoted by

$$e_z(r,z,t) = e_z(i\Delta r, j\Delta z, n\Delta t) = e_z^n(i,j),$$

equation (7.269) becomes, in discretized form,

$$e_r^{n+1}(i,j-0.5) = e_r^n(i,j-0.5) - \frac{\Delta t}{\epsilon_0 \Delta z}\left[h_\varphi^{n+0.5}(i,j) - h_\varphi^{n+0.5}(i,j-1)\right]. \tag{7.270}$$

The spatial and temporal elements (Δr, Δz, Δt) are chosen to satisfy the *Courant-Friedrichs condition*

$$c_0 \Delta t \leq \frac{\Delta r \Delta z}{\left[(\Delta r)^2 + (\Delta z)^2\right]^{\frac{1}{2}}}.$$

If the observation time $0 < t < t_0$ is limited to $t_0 = 2l_A/c_0$, the reflected wave from the ground plane level will not reach S_A before t_0. Hence, the field in S_A won't be disturbed by reflections up to time t_0. If, in addition, $R_{\min} > (c_0 t_0 - l_A)$, the fields on S_{ext} will be zero at least up to t_0. If these conditions are not satisfied, suitable absorbing conditions can be applied on S_{ext}. Figure 7.29 shows numerical results for the base impedance of the monopole antenna, obtained by exciting the coaxial line with a *differentiated Gaussian pulse*[62]

$$V(t) = V_0 \left(\frac{t}{\tau_p}\right) e^{\frac{1}{2}\left[1-\left(\frac{t}{\tau_p}\right)^2\right]}.$$

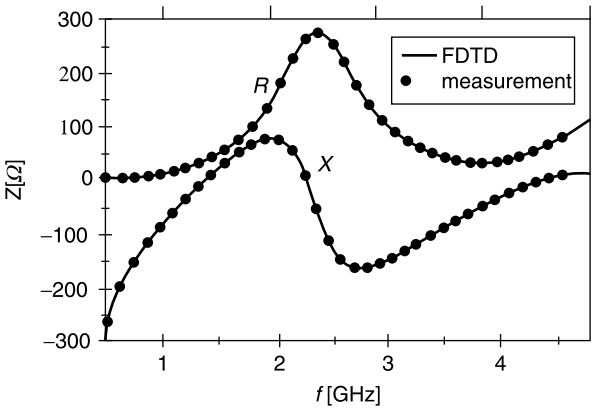

Figure 7.29 Base impedance of a monopole antenna (precision 7 mm line, $h = 32.9a$; $b = 2.3a$) (from T. W. Hertel, and G. S. Smith, The insulated linear antenna-revisited, *IEEE Trans. AP* **48**, 914–920, 2000, with permission of IEEE).

7.15.2 Electromagnetic Missiles

When a transient signal has a broad frequency spectrum, formula (7.99) for the radiation distance shows that, at a given distance R, the observer could be in the far field for the low frequencies but in the near field for the higher ones. In the far field, the power density decreases proportionally to $(1/R^2)$, but in the near field the decrease can be much slower. It follows that a volume of almost constant power density (an electromagnetic bullet) could conceivably be launched in a given direction, provided the signal is sufficiently rich in high frequencies.[63] Possible applications to telecommunications and remote destruction of targets are obvious. To put these considerations on a firmer footing, consider the simple example of a circular disk source carrying a uniform current density [72] (Fig. 7.30)

$$\mathbf{j}_S(\mathbf{r}, t) = j_S(t)\,\mathbf{u}_x. \tag{7.271}$$

To determine the fields on the axis of the antenna (the z-axis), we shall first find the Fourier transforms of these fields and subsequently transform the obtained expressions back to the time domain. The Fourier transform of $\mathbf{j}_S(\mathbf{r}, t)$ is $J_S(\omega)\,\mathbf{u}_x$. From (7.97):

$$\mathbf{A}(\mathbf{r}, \omega) = \mu_0 J_S(\omega) \frac{1}{4\pi} \int_S \frac{e^{-jk_0 D}}{D} dx'\, dy'\, \mathbf{u}_x, \tag{7.272}$$

where

$$D = \sqrt{(x - x')^2 + (y - y')^2 + z^2}. \tag{7.273}$$

By taking the curl of $\mathbf{A}$, one can readily derive the form of the magnetic field at a point on the axis. On the basis of the simple integral

$$\frac{1}{4\pi} \int_S \frac{e^{-jk_0 D}}{D} dS = -\frac{1}{2jk_0} \left(e^{-jk_0\sqrt{z^2+a^2}} - e^{-jk_0 z} \right),$$

which is valid for a point on the axis,

$$\mathbf{H}(0, 0, z, \omega) = -\frac{1}{2} J_S(\omega) \left(e^{-jk_0 z} - \frac{z}{\sqrt{z^2 + a^2}} e^{-jk_0\sqrt{z^2+a^2}} \right) \mathbf{u}_y. \tag{7.274}$$

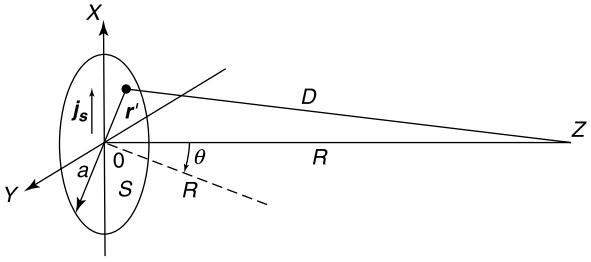

Figure 7.30 A planar current source.

From (7.2), the corresponding electric field on the axis is given by its transform

$$\mathbf{E}(0,0,z,\omega) = -\frac{R_{c0}}{2} J_S(\omega) \left[e^{-jk_0 z} - \left(\frac{z^2 + \frac{a^2}{2}}{z^2 + a^2} + \frac{j}{2k_0} \frac{a^2}{(z^2+a^2)^{3/2}} \right) e^{-jk_0\sqrt{z^2+a^2}} \right] \mathbf{u}_x. \tag{7.275}$$

It is a fairly straightforward matter to derive the value of the time-dependent fields from (7.274) and (7.275). Thus,

$$\mathbf{h}(z,t) = -\frac{1}{2}\left[j_S\left(t - \frac{z}{c_0}\right) - \frac{z}{\sqrt{z^2+a^2}} j_S\left(t - \frac{\sqrt{z^2+a^2}}{c_0}\right)\right] \mathbf{u}_y \tag{7.276}$$

$$\begin{aligned}\mathbf{e}(z,t) = -\frac{R_{c0}}{2}\Bigg[& j_S\left(t - \frac{z}{c_0}\right) - \frac{z^2 + \frac{a^2}{2}}{z^2+a^2} j_S\left(t - \frac{\sqrt{z^2+a^2}}{c_0}\right) \\ & + \frac{1}{2}\frac{c_0 a^2}{(z^2+a^2)^{3/2}} \int_{-\infty}^{t - \frac{\sqrt{z^2+a^2}}{c_0}} j_S(t')dt' \Bigg] \mathbf{u}_x. \end{aligned} \tag{7.277}$$

The first (or leading) pulse in (7.276) emanates from 0, the center of the disk. The second (or trailing) pulse emanates from the rim of the disk. At distances much larger than the radius a:

$$\mathbf{h}(z,t) \approx -\frac{1}{2}\left[j_S\left(t - \frac{z}{c_0}\right) - j_S\left(t - \frac{z}{c_0} - \frac{a^2}{2c_0 z}\right)\right] \mathbf{u}_y \tag{7.278}$$

$$\begin{aligned}\mathbf{e}(z,t) &\approx -\frac{R_{c0}}{2}\left[j_S\left(t - \frac{z}{c_0}\right) - j_S\left(t - \frac{z}{c_0} - \frac{a^2}{2c_0 z}\right)\right] \mathbf{u}_x \\ &\approx R_{c0}\mathbf{h} \times \mathbf{u}_z. \end{aligned} \tag{7.279}$$

The radiated pulse therefore becomes transverse electromagnetic (TEM) at these distances.

These results can be concretized by assuming that $j_S(t)$ is a step function $H(t)\, j_S$, where j_S is a constant. It is clear, from (7.278), that $h(z,t)$ now consists of an outgoing rectangular pulse, traveling with constant amplitude (but decreasing width) down the z-axis (Fig. 7.31).

The more general radiation problem, which is three-dimensional, is much more delicate, and requires a deeper analysis [72]. We shall only quote two important results:

1. The far electric and magnetic fields decay as $\dfrac{1}{R}$ (or faster) as $R \to \infty$, provided the first time-derivative of the source current $\mathbf{j}$ is bounded by an integrable function in the (finite) source volume V.
2. It is only if the first time derivative of $\mathbf{j}$ is infinite at some point in time that the far fields can decay more slowly than $\left(\dfrac{1}{R}\right)$. As a necessary condition, the frequency spectrum of $\mathbf{j}$ must decay *slowly* as $\omega \to \pm\infty$ (in fact, more slowly than ω^{-2}).

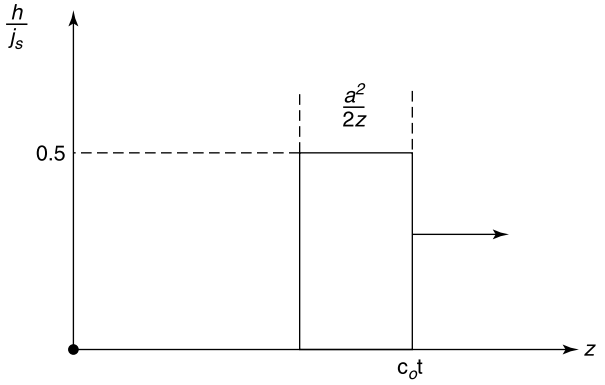

Figure 7.31 Signal traveling down the positive z-axis.

7.15.3 Radiation Evaluated in the Time Domain

Considerable research has been devoted to a better understanding of the propagation of ultra-short pulses [120]. Because of the wide frequency spectrum of the pulses, frequency domain techniques are often less efficient (and less transparent) than a direct analysis in the time domain. We shall briefly describe two important time domain techniques.

In a *first* method,*** one starts from the *multipole expansion* described at length in Section 7.11. The relevant equations are (7.182) and (7.187), and the solution involves the solution of spherical transmission line equations of the type[64,65]

$$\frac{1}{R}\frac{\partial^2(Rf)}{\partial R^2} - \frac{1}{c_0^2}\frac{\partial^2 f}{\partial t^2} - n(n+1)\frac{f}{R^2} = g(R,t).$$

Applied to the disk of Figure 7.30, which carries a current density $\mathbf{j}_S = j_S(t)\mathbf{u}_x$, the analysis shows that the number of spherical modes needed for suitable convergence is of the order $(3a/c_0T)$, where T is the pulse length.

In a *second* method, the starting point is the vector potential of an arbitrary current source. This is

$$\mathbf{a}(\mathbf{r},t) = \frac{\mu_0}{4\pi}\int_V \frac{\mathbf{j}\left(\mathbf{r}', t - \dfrac{|\mathbf{r}-\mathbf{r}'|}{c_0}\right)}{|\mathbf{r}-\mathbf{r}'|}\,dV'. \tag{7.280}$$

From Figure 7.9:

$$|\mathbf{r}-\mathbf{r}'| = R - \mathbf{u}_R\cdot\mathbf{r}' + \frac{1}{2}\frac{(R')^2}{R}\sin^2\psi + \cdots.$$

The term in $(1/R)$ may be dropped if the maximum delay it introduces is much less than the pulse length T. The far field condition is now

$$R \gg \frac{1}{c_0}\frac{d_{\max}^2}{T}. \tag{7.281}$$

***This method can also be applied to radiation in a *conical* volume (see Section 16.6).

This *time-domain Fraunhofer condition* should be compared with its frequency-domain counterpart (7.99). Let ω denote the upper significant angular frequency in the spectrum of a pulse of duration T. This frequency is proportional to T^{-1}, hence we may write $\omega = \alpha T^{-1}$. The ratio of the Fraunhofer distances for pulsed and time-harmonic sources is therefore

$$\frac{R_{\text{pulse}}}{R_{\text{freq}}} = \frac{\pi}{\alpha}.$$

In the far field, the vector potential (7.280) becomes

$$\mathbf{a}(\mathbf{r}, t) = \frac{\mu_0}{4\pi R} \int_V \mathbf{j}\left(\mathbf{r}', t - \frac{R}{c_0} + \frac{1}{c_0}\mathbf{u}_R \cdot \mathbf{r}'\right) dV'. \tag{7.282}$$

The integral, a function of $\tau = t - (R/c_0)$, is the *slant stack transform* of $\mathbf{j}$ (SST). This transform has been put to good use in the solution of radiation problems.[66,67] Consider, for example, an antenna that is energized by the injection of a current i into its terminal. The far-zone electric field of the antenna can be written as

$$\mathbf{e}(\mathbf{r}, t) = -\frac{\mu_0}{4\pi R}\, i(\tau) * \mathbf{h}^t(\mathbf{u}_R, \tau) \tag{7.283}$$

where $\tau = \left(t - \dfrac{R}{c_0}\right)$, and $*$ denotes the convolution operation

$$C(f, g, \tau) = f(t) * g(t) = \int_{-\infty}^{\infty} f(\tau - t)\, g(t)\, dt = g(t) * f(t). \tag{7.284}$$

The vector $\mathbf{h}$ (the effective height) is the far field impulse response of the transmitting antenna. It can be written in the SST form[66]

$$\mathbf{h}^t(\mathbf{u}_R, \tau) = \frac{\partial}{\partial \tau} \int_V (K\mathbf{J}^\delta)_\parallel \left(\mathbf{r}', \tau + \frac{1}{c_0}\mathbf{u}_R \cdot \mathbf{r}'\right) dV' \qquad (\text{m s}^{-2}). \tag{7.285}$$

In (7.285), $K\mathbf{J}^\delta$ denotes the current density in V that results from the injection of a *Dirac* type of current $I\delta(t)$. The subscript $\parallel$ selects the transverse component of $\mathbf{J}^\delta$ with respect to $\mathbf{u}_R$. The basic current $\mathbf{J}^\delta$, which must be known to obtain $\mathbf{h}$ [and subsequently $\mathbf{e}(\mathbf{r}, t)$] must generally be calculated numerically (e.g., by means of FDTD techniques).

The SST can serve to solve a variety of problems. Applied to the planar current (7.271), for example, it leads to the following formula for the vector potential (Fig. 7.30):

$$\mathbf{a}(\mathbf{r}, t) = \frac{\mu_0}{4\pi R}\, \mathbf{u}_x j_S \left(t - \frac{R}{c_0}\right) * D(t, \theta). \tag{7.286}$$

The symbol $D(t, \theta)$ stands for (Problem 7.47)

$$\begin{aligned} D &= \frac{2c_0}{\sin\theta}\left(a^2 - \frac{c_0^2 t^2}{\sin^2\theta}\right)^{\frac{1}{2}} && \text{for } |c_0 t| < a \sin\theta \\ &= 0 && \text{otherwise.} \end{aligned} \tag{7.287}$$

PROBLEMS

7.1 By combining the electric and magnetic fields into a single vector $\mathbf{K} = \mathbf{E} + \lambda\mathbf{H}$, show that there are two values of λ for which Maxwell's equations can be written as

$$\text{curl } \mathbf{K} + m\mathbf{K} = \Phi.$$

(G. Zin, *Ann. Mat. Pura Appl.* **43**, 215, 1957.)

7.2 The standard pulse shape for the current in a lightning discharge is

$$i(t) = i_m(e^{-at} - e^{-bt}),$$

with $0 < a < b$. Show that the Fourier spectrum of $i(t)$ is given by

$$I(\omega) = i_m\left(\frac{1}{a + j\omega} - \frac{1}{b + j\omega}\right),$$

hence that

$$|I(\omega)| = i_m \frac{b - a}{\sqrt{(a^2 + \omega^2)(b^2 + \omega^2)}}.$$

7.3 Derive the general solution (7.25) of the one-dimensional wave equation by introducing the new variables $u = t - \dfrac{R}{c_0}$ and $v = t + \dfrac{R}{c_0}$.

7.4 Show that the solution $\phi(\mathbf{r}, t)$ of the scalar wave equation (7.22) can be written as

$$\phi(\mathbf{r}, t) = -\frac{1}{\pi^2}\int_{-\infty+i\tau}^{\infty+i\tau} d\omega \int_{-\infty}^{\infty} \frac{e^{-j(\mathbf{k}_0 \cdot \mathbf{r} - \omega t)}}{k^2 - k_0^2} f(\mathbf{k}_0, \omega)\, dk_x dk_y dk_z,$$

where $\mathbf{k}_0 = k_x\mathbf{u}_x + k_y\mathbf{u}_y + k_z\mathbf{u}_z$ and

$$f(\mathbf{k}_0, \omega) = -\frac{1}{4\pi}\int dV' \int_0^T dt' f(\mathbf{r}', \mathbf{t}') e^{j(\mathbf{k}_0 \cdot \mathbf{r}' - \omega t')}.$$

(A. J. Devaney *et al.*, *SIAM Review* **15**, 765, 1973.)

7.5 Show by direct differentiation that the potentials (7.33) and (7.34) satisfy Lorenz' condition (7.30).

7.6 Show that the linearly polarized fields

$$\mathbf{e} = E\cos\omega t\left(\mathbf{u}_x \cos\frac{\omega z}{c_0} + \mathbf{u}_y \sin\frac{\omega z}{c_0}\right)$$
$$\mathbf{b} = \frac{E}{c_0}\sin\omega t\left(\mathbf{u}_x \cos\frac{\omega z}{c_0} + \mathbf{u}_y \sin\frac{\omega z}{c_0}\right)$$

are one-dimensional solutions of Maxwell's equations. Verify that these parallel fields consist of the superposition of fields traveling to respectively increasing and decreasing z.
(K. Shimoda *et al.*, *Am. J. Phys.* **58**, 394–396, 1990.)

7.7 Show that:

(**a**) The phasor of an arbitrary elliptically polarized vector can be represented in the form $\mathbf{A} = (a_x\mathbf{u}_x + ja_y\mathbf{u}_y)e^{j\delta}$, where a_x and a_y are real numbers, and $\mathbf{u}_x$ and $\mathbf{u}_y$ are two suitably chosen perpendicular unit vectors.

(**b**) An arbitrary time-harmonic vector can be split uniquely into two linearly polarized components of equal magnitude.

(**c**) The lengths of the main axes of the polarization ellipse are in the ratio $|(|\mathbf{E}_R| - |\mathbf{E}_L|)/(|\mathbf{E}_R| + |\mathbf{E}_L|)|$, where $|\mathbf{E}_R|$ and $|\mathbf{E}_L|$ are the magnitudes of the circularly polarized vectors into which the original vector can be decomposed.

7.8 Starting with (7.58), show that the lengths λ of the semi-axes of the polarization ellipse are the roots of the quadratic equation

$$\begin{vmatrix} \mathbf{a}_r \cdot \mathbf{a}_r - \lambda^2 & -\mathbf{a}_r \cdot \mathbf{a}_i \\ -\mathbf{a}_r \cdot \mathbf{a}_i & \mathbf{a}_i \cdot \mathbf{a}_i - \lambda^2 \end{vmatrix} = 0.$$

Check that the roots are equal when the polarization is circular and that one of the roots is zero when the polarization is linear. Show that the ellipticity is given by the ratio

$$\frac{\mathbf{A} \cdot \mathbf{A}^* - [(\mathbf{A} \cdot \mathbf{A})(\mathbf{A}^* \cdot \mathbf{A}^*)]^{\frac{1}{2}}}{\mathbf{A} \cdot \mathbf{A}^* + [(\mathbf{A} \cdot \mathbf{A})(\mathbf{A}^* \cdot \mathbf{A}^*)]^{\frac{1}{2}}}$$

where $\mathbf{A} = \mathbf{a}_r + j\mathbf{a}_i$.

7.9 Prove that, if a time-harmonic vector is resolved into its x and y components and $E_y/E_x = \tan \gamma e^{j\phi}$,

(**a**) The angle β between the major axis and the x axis is given by $\tan 2\beta = \tan 2\gamma \cos \phi$.

(**b**) The ellipticity r is given by $|r| = \tan \alpha$, where α satisfies $\sin 2\alpha = \sin 2\gamma \sin \phi (-45^\circ < \alpha < 45^\circ)$.

7.10 A field

$$\mathbf{e} = Re(\mathbf{E}\, e^{j\omega t})$$

may be characterized by its *Jones vector* $[E_x, E_y]$. Evaluate this vector for the following polarizations:
(a) horizontal, (b) vertical, (c) 45° linear, (d) −45° linear, (e) circular.

7.11 The physical significance of the normalized Stokes parameters may be illustrated by showing that [124]

(**a**) $s_1^2 + s_2^2 = 1$ for a linear polarization

(**b**) $s_3^2 = 1$ for a circular polarization

(**c**) s_1 measures the portion of the wave which is horizontally polarized

(**d**) s_2 measures the portion of the wave that is polarized at $\pm 45^\circ$

(**e**) s_3 measures the portion of the wave that is circularly polarized.

7.12 It is apparent from the developments leading to (7.83) that a scalar radiation function admits an expansion of the form

$$\Phi = \frac{e^{-jkR}}{R} \sum_{n=0}^{\infty} \frac{f_n(\theta, \varphi)}{R^n}.$$

Prove the following recursion formula:

$$-2jk(n+1) f_{n+1} = \left[n(n+1) + \frac{1}{\sin \theta} \frac{\partial}{\partial \theta} \left(\sin \theta \frac{\partial}{\partial \theta} \right) + \frac{1}{\sin^2 \theta} \frac{\partial^2}{\partial \varphi^2} \right] f_n.$$

7.13 A vector radiation function can be represented as

$$\mathbf{\Phi} = \frac{e^{-jkR}}{R} \sum_{n=0}^{\infty} \frac{\mathbf{F}_n(\theta, \varphi)}{R^n}.$$

Prove the recursion formulas

$$\begin{aligned}
jkF_{1,R} &= \frac{1}{\sin\theta}\left[\frac{\partial}{\partial\theta}(\sin\theta F_{0,\theta}) + \frac{\partial F_{0,\varphi}}{\partial\varphi}\right] = R\ \text{div}\ \mathbf{F}_0 \\
-2jknF_{n+1,R} &= n(n-1)F_{n,R} + DF_{n,R} \qquad (n = 1, 2, \ldots) \\
-2jknF_{n,\theta} &= n(n-1)F_{n-1,\theta} + DF_{n-1,\theta} + D_\theta \mathbf{F}_{n-1} \qquad (n = 1, 2, \ldots) \\
-2jknF_{n,\varphi} &= n(n-1)F_{n-1,\varphi} + DF_{n-1,\varphi} + D_\varphi \mathbf{F}_{n-1} \qquad (n = 1, 2, \ldots)
\end{aligned}$$

where

$$Df = \frac{1}{\sin\theta}\frac{\partial}{\partial\theta}\left(\sin\theta\frac{\partial f}{\partial\theta}\right) + \frac{1}{\sin^2\theta}\frac{\partial^2 f}{\partial\varphi^2}$$

$$D_\theta \mathbf{F} = 2\frac{\partial F_R}{\partial\theta} - \frac{1}{\sin^2\theta}F_\theta - \frac{2\cos\theta}{\sin^2\theta}\frac{\partial F_\varphi}{\partial\varphi}$$

$$D_\varphi \mathbf{F} = \frac{2}{\sin\theta}\frac{\partial F_R}{\partial\varphi} + \frac{2\cos\theta}{\sin^2\theta}\frac{\partial F_\theta}{\partial\varphi} - \frac{1}{\sin^2\theta}F_\varphi.$$

(C. H. Wilcox, *Comm. Pure Appl. Math.* **9**, 115, 1956.)

7.14 Apply the definition of the Laplacian given in A8.61 to a testing function ϕ that is constant in the vicinity of the origin, and show that

$$\int_S \frac{\partial G}{\partial R} dS = 1$$

where S is a small sphere centered on the origin. Use this property to justify the coefficient $(-1/4\pi)$ in (7.95).

7.15 Verify that the transformation defined by the operator $\nabla^2 + k_0^2$ and the radiation condition (7.81) is *not* self-adjoint. Show that the adjoint problem corresponds with the incoming-wave solution. Determine the Green's function of the adjoint problem, and verify that the reciprocity property (1.54) is satisfied. Use a scalar product $\int uv^* dV$.

7.16 Utilizing the relationship

$$\delta(t - t_0) = \frac{1}{2\pi}\int_{-\infty}^{+\infty} e^{j\omega(t-t_0)} d\omega$$

obtain the Green's function (7.26) of the wave equation by performing the integration

$$g(R, t - t_0) = \frac{1}{2\pi}\int_{-\infty}^{+\infty} G_0(R, \omega)\, e^{j\omega(t-t_0)} d\omega.$$

In this expression, G_0 is the Green's function (7.95) of the Helmholtz equation.

7.17 The definition of the array factor $\mathcal{R}$ in (7.121) can be extended to a continuous distribution, conceived as the limit of a dense discrete array. The sum now becomes an integral. Let the voltage density be approximated by

$$V(x) = \sum_1^N C_n V_n(x).$$

Determine the C_n that maximize $|\mathcal{R}|^2$ in a given direction.

7.18 Determine the array factor of the four elements shown in Figure P7.1, where $d = (3\lambda_0/8)$. The elements are identical, but 1 and 3 are in phase, and 2, 4 in opposite phase with respect to (1, 3). Particularize the solution to directions lying in the plane of the elements.

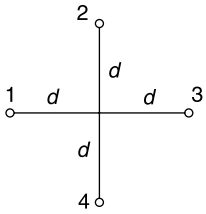

Figure P7.1

7.19 Show that the form of $\overline{\overline{G}}_{ee}(\mathbf{r}|\mathbf{r}')$ in spherical coordinates is [133]

$$\overline{\overline{G}}_{ee}(\mathbf{r}|\mathbf{r}') = G(R)\left[1 - \mathbf{u}_R\mathbf{u}_R - \left(\frac{j}{kR} + \frac{1}{k^2R^2}\right)(\bar{\bar{I}} - 3\mathbf{u}_R\mathbf{u}_R)\right].$$

7.20 The Green's dyadic $\overline{\overline{G}}_{ee}^{tot}$ defined in (7.137) satisfies

$$-\text{curl curl}\,\overline{\overline{G}}_{ee}^{tot}(\mathbf{r}|\mathbf{r}') + k_0^2\,\overline{\overline{G}}_{ee}^{tot}(\mathbf{r}|\mathbf{r}') = \delta(\mathbf{r} - \mathbf{r}')\bar{\bar{I}}.$$

This equation must be interpreted in the sense of distribution theory. Show that it leads to [133]

$$\boldsymbol{\phi}(\mathbf{r}) = \int_V \overline{\overline{G}}_{ee}^{tot}(\mathbf{r}|\mathbf{r}')\cdot(-\text{curl}'\,\text{curl}'\boldsymbol{\phi} + k_0^2\boldsymbol{\phi})\,dV'.$$

When applied to $\mathbf{E}(\mathbf{r})$ — a vector that satisfies (7.138) — this relationship reproduces the representation (7.139).

7.21 Show that the distributional equation satisfied by $\overline{\overline{G}}_{ee}$ is

$$-\text{curl curl}\,PV\,\overline{\overline{G}}_{ee}(\mathbf{r}|\mathbf{r}') + k_0^2\,PV\,\overline{\overline{G}}_{ee}(\mathbf{r}|\mathbf{r}')$$

$$= \delta(\mathbf{r} - \mathbf{r}')\bar{\bar{I}} - \overline{\overline{L}}_{V_\delta}\delta(\mathbf{r} - \mathbf{r}') + \frac{1}{k_0^2}\,\text{curl curl}\left[\delta(\mathbf{r} - \mathbf{r}')\overline{\overline{L}}_{V_\delta}\right].$$

7.22 A Green's function can be interpreted as generated by a unit source. To verify this property in the case of the dyadic $\overline{\overline{G}}_{ee}(\mathbf{r}|\mathbf{r}')$ defined in (7.136), evaluate the fields generated by a short z-directed element of current $\mathbf{J}(\mathbf{r}) = j\omega P_e\delta(\mathbf{r} - \mathbf{r}_0)\mathbf{u}_z$, using (7.135) [133]. Note that $\overline{\overline{G}}_{ee}$ automatically incorporates the effects of both $\mathbf{J}$ (the source of $\mathbf{A}$) and ρ (the source of Φ).

7.23 In the evaluation of the contribution of V_δ to $\mathbf{E}(\mathbf{r})$, use the property

$$-\text{curl curl}\,\overline{\overline{G}}_{ee} + k_0^2\overline{\overline{G}}_{ee} = 0,$$

which holds outside V_δ. Multiplying both members of this equation by $\mathbf{E}$, and integrating outside V_δ, gives an integral over S_δ of the form [210]

$$\int_{S_\delta}\left[(\mathbf{u}_n' \times \mathbf{E})\cdot\text{curl}'\,\overline{\overline{G}}_{ee} + \overline{\overline{G}}_{ee}\cdot(\mathbf{u}_n' \times \text{curl}'\,\mathbf{E})\right]dS'.$$

Show that this integral is equal to $\dfrac{1}{k_0^2}\overline{\overline{L}}_{V_\delta}\cdot(k_0^2\mathbf{E} - \text{curl curl}\,\mathbf{E})$.

(R. E. Collin, *Radio Sci.* **21**, 883–890, 1986.)

7.24 Prove the following properties of the Green's dyadic $\overline{\overline{G}}_{ee}$ defined in (7.136):

(**a**) div $\overline{\overline{G}}_{ee}(\mathbf{r}|\mathbf{r}') = 0$ for $\mathbf{r} \neq \mathbf{r}'$

(**b**) the electric field (7.135) satisfies the radiation condition

(**c**) $-\text{curl curl}\,\overline{\overline{G}}_{ee} + k_0^2\overline{\overline{G}}_{ee} = 0$ for $\mathbf{r} \neq \mathbf{r}'$.

7.25 In relation to the developments in Section 7.9, show that

$$\mathbf{E}(\mathbf{r}) = -\frac{1}{j\omega\epsilon_0}\left[\lim_{\delta\to 0}\int_{V-V_\delta} \text{curl}'\,\overline{\overline{G}}_{me}(\mathbf{r}|\mathbf{r}')\cdot\mathbf{J}(\mathbf{r}')\,dV' + \int_{S_\delta}\left(\overline{\overline{G}}_{me}(\mathbf{r}|\mathbf{r}')\times\mathbf{u}_n(\mathbf{r}')\right)\cdot\mathbf{J}(\mathbf{r}')\,dS'\right] - \frac{\mathbf{J}(\mathbf{r})}{j\omega\epsilon_0}.$$

Particularize the surface integral to the special case of a uniform $\mathbf{J}$.
(A. D. Yaghjian, *Proc. IEEE* **68**, 248–263, 1980 and J. Nachamkin, *IEEE Trans. AP* **38**, 919–921, 1990.)

7.26 Show that

$$\delta(\mathbf{r}-\mathbf{r}')\,\bar{\bar{I}} = \frac{1}{4\pi}\left[-\text{grad div}\left(\frac{1}{|\mathbf{r}-\mathbf{r}'|}\,\bar{\bar{I}}\right) + \text{curl curl}\left(\frac{1}{|\mathbf{r}-\mathbf{r}'|}\,\bar{\bar{I}}\right)\right]$$

and use this relationship to obtain the Helmholtz splitting (7.38), (7.39).

7.27 According to (7.151), the current density associated with a small circular loop parallel to the xy plane and centered at the origin is given by

$$\mathbf{J} = \text{curl}\,[\delta(\mathbf{r})\mathbf{P}_m] = \text{grad}\,\delta\times\mathbf{P}_m.$$

In this expression, $\mathbf{P}_m$ is the magnetic moment $\pi a^2 I\mathbf{u}_z$ of the loop. Show that the corresponding radiated fields can be expressed as

$$\mathbf{E} = j\omega\mu_0(\text{curl}\,\overline{\overline{G}}_{ee}\cdot\mathbf{P}_m) \qquad \mathbf{H} = -k^2\,\overline{\overline{G}}_{ee}\cdot\mathbf{P}_m$$

where $\overline{\overline{G}}_{ee}$ is the dyadic appearing in (7.136).

7.28 A noncircular, but planar current loop lies in the (x, y) plane. Show that the magnetic moment is $IS\mathbf{u}_z$, where S is the area of the loop (Fig. P7.2). Write down the various components of the $(\mathbf{E}, \mathbf{H})$ field, and show in particular that

$$H_\theta = \frac{P_m\cos\theta}{4\pi}\left(\frac{1}{R^3} + \frac{jk_0}{R^2} - \frac{k_0^2}{R}\right)e^{-jk_0R}.$$

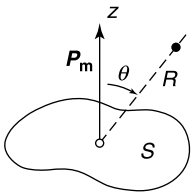

Figure P7.2

7.29 Show that a vector radiation function $\mathbf{A}$ is determined uniquely by the assignment of $\mathbf{r}\cdot\mathbf{A}$ and $\mathbf{r}\cdot\text{curl}\,\mathbf{A}$ [22].
(C. H. Wilcox, *J. Math. Mech.* **6**, 167–202, 1957.)

7.30 Prove that $RH_R = \mathbf{r}\cdot\mathbf{H}$ satisfies the equation

$$(\nabla^2 + k_0^2)(\mathbf{r}\cdot\mathbf{H}) = -\mathbf{r}\cdot\text{curl}\,\mathbf{J}$$

when the sources are electric currents $\mathbf{J}$. The differential equation can be solved by integration to give

$$RH_R = \frac{1}{4\pi}\int_V \mathbf{r}'\cdot\text{curl}'\,\mathbf{J}\,\frac{e^{-jk_0|\mathbf{r}-\mathbf{r}'|}}{|\mathbf{r}-\mathbf{r}'|}\,dV'.$$

Evaluation in terms of (R,θ,φ) follows by inserting the expansion (7.204) into the integral. Show that the equation for RE_R is

$$(\nabla^2 + k_0^2)\cdot R\mathbf{u}_R\left[\mathbf{E} + \frac{\mathbf{J}}{j\omega\epsilon_0}\right] = -\frac{1}{j\omega\epsilon_0}\mathbf{r}\cdot\text{curl curl}\,\mathbf{J}$$

and solve it in the same manner as in the case of RH_R [22].
(C. J. Bouwkamp *et al*., *Physica* **20**, 539–554, 1954.)

7.31 Show that the discontinuity implied by (7.210) is in harmony with the boundary conditions satisfied by $\mathbf{E}$ at an interface [133].

7.32 Consider a spherically symmetric source

$$\begin{aligned}\mathbf{J} &= J(R)\mathbf{u}_R \quad &\text{for } R \le a\\ \mathbf{J} &= 0 \quad &\text{for } R > a.\end{aligned}$$

This (pulsating) radial source radiates isotropically. But it is known that a source radiating equally in all directions cannot exist. Resolve this apparent paradox. The source $\mathbf{J}$ could be a radial stream of charged particles.

7.33 Chiral materials have constitutive equations of the form

$$\mathbf{D} = \epsilon(\mathbf{E} + \beta\,\text{curl}\,\mathbf{E}), \qquad \mathbf{B} = \mu(\mathbf{H} + \beta\,\text{curl}\,\mathbf{H})$$

where β is a chirality parameter. Show that the $(\mathbf{J},\mathbf{J}_m)$ equivalence is now given by the relationships [87]

$$\mathbf{J} + \beta\,\text{curl}\,\mathbf{J} = \frac{1}{j\omega\mu}\,\text{curl}\,\mathbf{J}_m$$

$$\mathbf{J}_m + \beta\,\text{curl}\,\mathbf{J}_m = -\frac{1}{j\omega\epsilon}\,\text{curl}\,\mathbf{J}.$$

7.34 A sphere carries a uniform current $\mathbf{J}$ (Fig. P7.3). Show that it radiates as an electric dipole of moment

$$\mathbf{P}_e = \frac{1}{j\omega}\cdot(\text{volume of the sphere})\cdot\mathbf{J}.$$

Find the equivalent $\mathbf{J}_m$, and verify that $\mathbf{J}$ and $\mathbf{J}_m$ generate the same fields *outside* the sphere.
(J. Van Bladel, *AEÜ* **42**, 314–315, 1988.)

7.35 Applying (7.205) and (7.211) successively seems to imply that $\mathbf{J}$ and $\dfrac{1}{k_0^2}\,\text{curl curl}\,\mathbf{J}$ are equivalent. But this is not likely to happen since $\mathbf{J}$ is arbitrary. Discuss the case of a uniform $\mathbf{J}$ in a given volume V to show that the equivalence actually holds.
(J. Van Bladel, *Microwave Opt. Tech. Lett.* **4**, 423–427, 1991.)

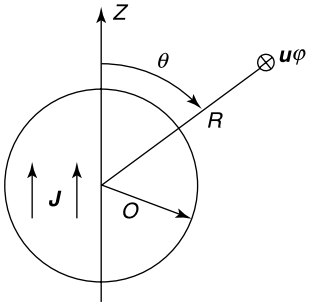

Figure P7.3

7.36 Let V be the support of a vector $\mathbf{F}(\mathbf{r})$. Show that

$$\mathbf{J}_1 = \frac{\partial^2 \mathbf{F}}{\partial z^2} + k_0^2 \mathbf{F}$$

$$\mathbf{J}_2 = -\nabla_{xy}^2 \mathbf{F}$$

are equivalent sources for the evaluation of fields outside V.

7.37 An electric current $\mathbf{J} = J(\mathbf{r})\mathbf{u}$, where $\mathbf{u}$ is a constant unit vector, gives rise to a TM field, that is, a field with $\mathbf{H}$ parallel to $(\mathbf{u} \times \mathbf{u}_R)$. Similarly $\mathbf{J}_m = J_m(\mathbf{r})\mathbf{u}$, which is equivalent to $\mathbf{J} = \dfrac{1}{j\omega\mu_0}$ grad $J_m \times \mathbf{u}$, gives rise to a TE field. Show that any $\mathbf{J}$ can be split as

$$\mathbf{J}(\mathbf{r}) = \mathbf{u} f(\mathbf{r}) + \mathbf{u} \times \text{ grad } g(\mathbf{r}) + \mathbf{J}^{NR}(\mathbf{r})$$

where f and g are zero outside the support of $\mathbf{J}$, and $\mathbf{J}^{NR}$ is nonradiating. Extend the analysis to an arbitrary time dependence [12].
(I. V. Lindell, *IEEE Trans. AP* **36**, 1382–1388, 1988; and *IEEE Trans. AP* **38**, 353–358, 1990.)

7.38 Show that sourceless fields in a bounded volume V are uniquely determined by the value of either $\mathbf{u}_n \times \mathbf{E}$ or $\mathbf{u}_n \times \mathbf{H}$ at the boundary S when V is filled with a homogeneous medium of conductivity σ.

7.39 On the basis of the differentiation rule

$$\frac{d}{dz} \int_{-h}^{z} g(z|z')\, dz' = \int_{-h}^{z} \frac{\partial g(z|z')}{\partial z}\, dz' + g(z|z)$$

show that

$$\frac{d^2 A}{dz^2} + k_0^2 A = f(z)$$

admits the particular solution

$$A = \frac{1}{k_0} \int_{-h}^{z} f(z') \sin k_0(z - z')\, dz'.$$

7.40 Consider two perfectly conducting antennas energized across a narrow gap. Show that

$$V_1 I_{12} = V_2 I_{21}$$

where I_{ik} is the base current flowing in the (shorted) antenna i when a voltage V_k is applied across the gap of antenna k.
(A. F. Stevenson, *Quart. Appl. Math.* **5**, 369, 1948; and E. Roubine, *Onde Elec.* **30**, 259, 1950.)

7.41 Find the right-hand term of Hallén's integral equation (7.241) when $E_g = \dfrac{V}{2g}$ in the gap $-g \le z \le g$, and $E_g = 0$ outside.
(R. E. Collin, *IEEE Trans. AP* **32**, 200–204, 1984.)

7.42 Assuming that the "sinusoidal" approximation $I_m \sin k_0(h - |z|)$ holds for the current on a linear antenna,

(**a**) find a formula for the far-field (with h/λ_0 arbitrary)

(**b**) find the directivity and radiation resistance of a very short antenna ($h \ll \lambda_0$).

7.43 The vector potential for a linear antenna is given by

$$A_z(r,z) = \frac{\mu_0}{4\pi}\int_{-h}^{h} I(z')K(z|z')\,dz'$$

with

$$K(z|z') = \frac{1}{2\pi}\int_0^{2\pi} \frac{e^{-jk_0D}}{D}\,d(\varphi-\varphi')$$

$$D = \left[(z-z')^2 + r^2 + a^2 - 2ar\cos(\varphi-\varphi')\right]^{\frac{1}{2}}.$$

Show that K can be written in the form (valid for arbitrary radius a)

$$K(z|z') = -\frac{e^{-jk_0R}}{R}\sum_{n=0}^{\infty}\sum_{k=0}^{2n} A_{nk}\frac{(k_0^2ar)^{2n}}{(k_0R)^{2n+k}}.$$

(D. H. Werner, *IEEE Trans. AP* **41**, 1009–1018, 1993.)

7.44 Determine the integral equation satisfied by the current on a curved wire antenna when the applied electric field $\mathbf{u}_c \cdot \mathbf{E}_g$ (Figure 7.25) is an arbitrary function of time.
(E. K. Miller *et al.*, *Proc. IEEE* **68**, 1396–1423, 1980.)

7.45 Generalize (7.278) and (7.279) to a current distribution $\mathbf{j}_S = f(t)j_S(\mathbf{r})\,\mathbf{u}_x$, and show that

$$\mathbf{e}(0,0,z,t) = -\frac{\mu_0}{4\pi z}\frac{d\,j_S\left(t-\dfrac{z}{c_0}\right)}{dt}\int_S \mathbf{j}_S(\mathbf{r}')\,dS'$$

$$\mathbf{h}(0,0,z,t) = \frac{1}{R_{c0}}\mathbf{u}_z \times \mathbf{e}(0,0,z,t).$$

Let $\mathbf{j}_S$ be uniform, and equal to $j_S(t)\mathbf{u}_x$. Evaluate $\mathbf{e}$ when

(**a**) j_S is a half-sinusoid $sin\left(\pi\dfrac{t}{T}\right)$ (for $0 < t < T$)

(**b**) j_S is a triangular pulse, with maximum at $T/2$, and base extending from 0 to T.
Evaluate the energy per unit area along the z-axis.
(W. Geyi, *Microwave Opt. Tech. Lett.* **12**, 332–335, 1996.)

7.46 Assume that transient sources are started at $t = 0$. Check the equivalences (in the sense of distributions)

$$\mathbf{j}_m = -\frac{1}{\epsilon_0}\int_0^t \text{curl}\,\mathbf{j}\,dt$$

$$\mathbf{j} = \frac{1}{\mu_0}\int_0^t \text{curl}\,\mathbf{j}_m\,dt.$$

Show that nonradiating currents have the necessary (and sufficient) form

$$\mathbf{j}^{NR}(\mathbf{r},t) = -\text{curl curl}\,\mathbf{f}(\mathbf{r},t) - \frac{1}{c_0^2}\frac{\partial^2 \mathbf{f}(\mathbf{r},t)}{\partial t^2}.$$

(I. V. Lindell, *IEEE Trans. AP* **38**, 353–358, 1990.)

7.47 Show that, for $\theta = 0$, D in (7.287) approaches the value $\pi a^2 \delta(t)$. Show further that the following expressions are valid on the axis:

$$\mathbf{a}(z,t) = \mathbf{u}_x \frac{\mu_0}{4z} a^2 j_S\left(t - \frac{z}{c_0}\right)$$

$$\mathbf{e}(z,t) = -\mathbf{u}_x \frac{\mu_0}{4z} a^2 j_S'\left(t - \frac{z}{c_0}\right).$$

Verify that this value of $\mathbf{e}$ is in agreement with (7.279) as $z \to \infty$ (problem suggested by Prof. E. Heyman).

NOTES

1. R. M. Whitmer, Calculation of magnetic and electric fields from displacement currents, *Am. J. Phys.* **33**, 481–484 (1965).
2. D. F. Bartlett and T.R. Corle, Measuring Maxwell's displacement current inside a capacitor, *Phys. Rev. Letters* **55**, 59–62 (1985).
3. M. Ianoz, Lightning electromagnetic effects: do we know everything?, *IEEE Antennas Prop. Mag.* **304**, 17–33 (2003).
4. M. S. Sarto, Innovative absorbing boundary conditions for the efficient FDTD analysis of lightning interaction problems, *IEEE Trans. EMC* **43**, 368–381 (2001).
5. J. Van Bladel, Lorenz or Lorentz?, *IEEE Antennas Prop. Mag.* **33**, 69 (1991).
6. A. Sihvola, Lorenz-Lorentz or Lorentz-Lorenz?, *IEEE Antennas Prop. Mag.* **33**, 56 (1991).
7. B. van der Pol, On discontinuous electromagnetic waves and the occurrence of a surface wave, *IEEE Trans. AP* **4**, 288–293 (1956).
8. E. Collett, The description of polarization in classical physics, *Am. J. Phys.* **36**, 713–725 (1968).
9. C. H. Wilcox, An expansion theorem for electromagnetic fields, *Comm. Pure Appl. Math.* **9**, 115–134 (1956).
10. W. C. Brown and E. E. Eves, Beamed microwave power transmission and its application to space, *IEEE Trans. MTT* **40**, 1239–1250 (1992).
11. J. Van Bladel, Some remarks on Green's dyadic for infinite space, *IRE Trans. AP* **9**, 563–566 (1961).
12. A.D. Yaghjian, Electric dyadic Green's functions in the source region, *Proc. IEEE*, **68**, 248–263 (1980).
13. J. G. Fikioris, Electromagnetic field inside a current-carrying region, *J. Math. Phys.* **6**, 1617–1620 (1965).
14. J. G. Fikioris, The electromagnetic field of constant-density distributions in finite regions, *J. Electromagn. Waves Applicat.* **2**, 141–153 (1988).
15. J. G. Fikioris, The EM field of constant current density distributions in parallelipiped regions, *IEEE Trans. AP* **46**, 1358–1364 (1998).
16. J. G. Fikioris, Electromagnetic field in the source region of continuously varrying current density, *Quart. Appl. Math.* **44**, 201–209 (1996).
17. J. Van Bladel, The multipole expansion revisited, *AEÜ* **3**, 407–411 (1977).
18. J. Van Bladel, Hierarchy of terms in a multipole expansion, *Electron. Lett.* **24**, 491–492 (1988).
19. I. V. Lindell and K. I. Nikoskinen, Complex space multipole theory for scattering and diffraction problems, *Radio Sci.* **22**, 963–967 (1987).
20. C. H. Wilcox, Debye potentials, *J. Math. Mech.* **6**, 167-202 (1957).
21. P. E. Mayes, The equivalence of electric and magnetic sources, *IRE Trans. AP* **6**, 295–296 (1958).
22. J. Van Bladel, Boundary conditions at a double current sheet, *Electron. Lett.* **25**, 98–99 (1989).
23. E. A. Marengo, A. J. Devaney, and R. W. Ziolkowski, New aspects of the inverse source problem with far-field data, *J. Opt. Soc. Am.* **A16**, 1612–1622 (1999).
24. E. A. Marengo, A. J. Devaney, and R. W. Ziolkowski, Inverse source problem and minimum energy sources, *J. Opt. Soc. Am.* **A17**, 34–45 (2000).
25. A. J. Devaney and E. Wolf, Radiating and nonradiating classical current distributions and the fields they generate, *Phys. Rev.* **D-8**, 1044–1047 (1973).
26. E. A. Marengo and R. W. Ziolkowski, On the radiating and nonradiating components of scalar, electromagnetic

and weak gravitational sources, *Phys. Rev. Lett.* **83**, 3345–3349 (1999).
27. E. A. Marengo and R. W. Ziolkowski, Nonradiating and minimum energy sources and their fields: generalized source inversion theory and applications, *IEEE Trans. AP* **48**, 1553–1562 (2000).
28. S. A. Schelkunoff, Some equivalence theorems of electromagnetics and their application to radiation problems, *Bell Syst. T.J.* **15**, 92–112 (1936).
29. S. A. Schelkunoff, Kirchhoff's formula, its vector analogue and other field equivalence theorems, *Comm. Pure Appl. Math.* **4**, 107–123 (1951).
30. Y. Rahmat-Samii, L. L. Williams, and R. G. Yaccarino, The UCLA bipolar planar-near-field antenna measurement and diagnostics range, *IEEE Antennas Prop. Mag.* **37**, 16–35 (1995).
31. D. S. Jones, Note on the integral equation for a straight wire antenna, *IEE Proc.* **128-H**, 114–116 (1981).
32. B. P. Rynne, The well-posedness of the integral equation for thin wire antennas, *IMA J. Appl. Math.* **49**, 35–44 (1992).
33. B. P. Rynne, On the well-posedness of Pocklington's equation for a straight wire antenna and convergence of numerical solutions, *J. Electromagn. Waves Appl.* **14**: 1489-1503 (2000).
34. E. Hallén, Theoretical investigations into the transmitting and receiving qualities of antennas, *Nova Acta Reg. Soc. Scient. Upsaliensis* **11** (4), 1–44 (1938).
35. R. A. Hurd and J. Jacobsen, Admittance of an infinite cylindrical antenna with realistic gap field, *Electron. Lett.* **4**, 420–421 (1968).
36. J. Jacobsen and R. A. Hurd, Admittance of a thick antenna, *Can. J. Phys.* **48**, 2201–2209 (1970).
37. L. W. Pearson, A separation of the logarithmic singularity in the exact kernel of the cylindrical antenna integral equation, *IEEE Trans. AP* **23**, 256–257 (1975).
38. F. M. Tesche, Evaluation of the surface integral occurring in the *E*-field integral equations for wire antennas, *IEEE Trans. EMC* **16**, 209–210 (1974).
38. T. K. Sarkar, E. Arvas, and S. M. Rao, Application of FFT and the conjugate gradient method for the solution of electromagnetic radiation from electrically large and small conducting bodies, *IEEE Trans. AP* **34**, 635–640 (1986).
40. C. M. Butler and D. R. Wilton, Analysis of various numerical techniques applied to thin-wire scatterers, *IEEE Trans. AP* **23**, 534–551 (1975).
41. D. R. Wilton and C. M. Butler, Effective methods for solving integral and integro-differential equations, *Electromagn.* **1**, 289–308 (1981).
42. J. M. Richmond, Digital computer solutions of the rigorous equations for scattering problems, *Proc. IEEE* **53**, 796–804 (1965).
43. R. E. Collin, Equivalent line current for cylindrical dipole antennas and its asymptotic behavior, *IEEE Trans. AP* **32**, 200–204 (1984).
44. G. Fikioris and T. T. Wu, On the application of numerical methods to Hallén's equation, *IEEE Trans. AP* **49**, 383–392 (2001).
45. K. K. Mei, On the integral equations of thin wire antennas, *IEEE Trans. AP* **13**, 374–378 (1965).
46. G. K. Cambrell and C. T. Carson, On Mei's integral equation of thin wire antennas, *IEEE Trans. AP* **19**, 781–782 (1971).
47. M. Kominami and K. Rokushima, On the integral equation of piecewise linear antennas, *IEEE Trans. AP* **29**, 787–792 (1981).
48. R. F. Harrington, Matrix methods for field problems, *Proc. IEEE* **55**, 136–149 (1967).
49. N. J. Champagne, J. T. Williams, and D.R. Wilton, The use of curved segments for numerically modelling thin wire antennas and scatterers, *IEEE Trans. AP* **40**, 682–689 (1992).
50. D. S. Weile and E. Michielssen, Genetic algorithm optimization applied to electromagnetics: a review, *IEEE Trans. AP* **45**, 343–353 (1997).
51. A. Boag, A. Boag, E. Michielssen, and R. Mittra, Design of electrically loaded wire antennas using genetic algorithms, *IEEE Trans. AP* **44**, 687–695 (1996).
52. J. M. Johnson and Y. Rahmat-Samii, Genetic algorithms in engineering electromagnetics, *IEEE Antennas Prop. Mag.* **39**, 7–21 (1997).
53. S. D. Rogers, C. M. Butler, and A. Q. Martin, Realization of a genetic algorithm – optimized wire antenna with 5:1 bandwith, *Radio Sci.* **36**, 1315–1325 (2001).
54. D. Marcano and F. Duran, Synthesis of antenna arrays using genetic algorithms, *IEEE Antennas Prop. Mag.* **42**, 12–19 (2000).
55. E. E. Altschuler, Design of a vehicular antenna for GPS-Iridium using a genetic algorithm, *IEEE Trans. AP* **48**, 968–972 (2000).
56. C. E. Baum, E. G. Farr, and D. V. Giri, Review of impulse-radiating antennas, in *URSI Review of Radio Science 1996–1999*, Oxford University Press, 1999.
57. C. E. Baum, From the electromagnetic pulse to high-power electromagnetics, *Proc. IEEE.* **80**, 789–817 (1992).
58. L. Marin and T. K. Liu, A simple way of solving transient thin-wire problems, *Radio Sci.* **11**, 149–155 (1976).
59. P. J. Davies, B. P. Rynne, and B. Zubik-Konval, The time domain integral equation for a straight thin-wire antenna with the reduced kernel is not well-posed, *IEEE Trans. AP* **50**, 1165–1166 (2003).
60. J. C. Bogerd, A. G. Tijhuis, and J. J. A. Klaasen, Electromagnetic excitation of a thin wire: a travelling-wave approach, *IEEE Trans. AP* **46**, 1202–1211 (1998).
61. J. G. Maloney, G. S. Smith, and W. R. Scott, Accurate computation of the radiation from simple antennas using the finite-difference, time-domain method, *IEEE Trans. AP* **38**, 1059–1068 (1990).
62. T. W. Hertel and G. S. Smith, The insulated linear antenna-revisited, *IEEE Trans. AP* **48**, 914–920 (2000).

63. T. T. Wu, Electromagnetic missiles, *J. Appl. Phys.* **57**, 2370–2373 (1985).
64. E. Heyman and A. J. Devaney, Time-dependent multipoles and their application for radiation from volume source distributions, *J. Math. Phys.* **37**, 682–692 (1996).
65. A. Shlivinski and E. Heyman, Time-domain near-field analysis of short-pulse antennas, *IEEE Trans. AP* **47**, (1999).
Part I. Spherical wave (multipole) expansion: 271-279.
Part II. Reactive energy and the antenna Q: 280-286.
66. A. Shlivinski, E. Heyman, and R. Kastner, Antenna characterization in the time domain, *IEEE Trans. AP* **45**, 1140–1149 (1997).
67. E. Heyman, Time dependent plane-wave spectrum representations for radiation from volume source distributions, *J. Math. Phys.* **37**, 658–681 (1996).

Chapter 8

Radiation in a Material Medium

The first part of this chapter focuses on the propagation of waves in an *infinite* space filled with a medium of given $\overline{\overline{\epsilon}}$, $\overline{\overline{\mu}}$, $\overline{\overline{\sigma}}$. Propagation in a *limited* space, such as in a waveguide, is discussed in subsequent chapters. The attention is restricted to materials that are linear, time-invariant, and locally reacting. The parameters are assumed to vary smoothly — strong discontinuities, such as the presence of obstacles, are dealt with in chapters on scattering. Two particular types of propagation are emphasized:

- Plane waves in various media
- High-frequency waves. This is a most important topic, which has given birth to an abundant literature, but will only be discussed lightly. More details can be found in Chapter 13.

The second part of the chapter is devoted to the fundamental reciprocity properties of the electromagnetic field. These properties depend on the nature of the $\overline{\overline{\epsilon}}$, $\overline{\overline{\mu}}$, $\overline{\overline{\sigma}}$ parameters and give rise to important applications, for example to the derivation of the equivalent circuit of a receiving antenna. In that particular application, reciprocity provides a connection between the transmitting and receiving properties of the antenna.

8.1 CONSTITUTIVE EQUATIONS

8.1.1 Generalities

In a material medium, the source terms $\mathbf{j}$ and ρ must include contributions from the polarization currents and charges. Maxwell's equations should therefore be written as*

$$\text{curl } \mathbf{e} = -\frac{\partial \mathbf{b}}{\partial t} \tag{8.1}$$

$$\text{curl } \mathbf{b} - \epsilon_0 \mu_0 \frac{\partial \mathbf{e}}{\partial t} = \mu_0 \mathbf{j}_{\text{tot}} \tag{8.2}$$

$$\text{div } \mathbf{e} = \frac{1}{\epsilon_0} \rho_{\text{tot}} \tag{8.3}$$

$$\text{div } \mathbf{b} = 0. \tag{8.4}$$

*A similar analysis can be carried out for $\mathbf{j}_m$ and ρ_m.

Electromagnetic Fields, Second Edition, By Jean G. Van Bladel

The density ρ_{tot} is the sum of the contributions from free and polarization charges. Thus,

$$\rho_{\text{tot}} = \rho_f - \text{div } \mathbf{m}_e. \tag{8.5}$$

The density $\mathbf{j}_{\text{tot}}$ is the sum of four terms, viz.

$$\mathbf{j}_{\text{tot}} = \mathbf{j}_a + \mathbf{j} + \frac{\partial \mathbf{m}_e}{\partial t} + \text{curl } \mathbf{m}_m = \mathbf{j}_f + \frac{\partial \mathbf{m}_e}{\partial t} + \text{curl } \mathbf{m}_m. \tag{8.6}$$

The terms $\mathbf{j}_a$ and $\mathbf{j}$ result from the motion of free charges under the influence of, respectively, nonelectromagnetic and electromagnetic effects. The terms $\partial \mathbf{m}_e/\partial t$ and curl $\mathbf{m}_m$ are the *electric and magnetic polarization current* densities. We will now proceed to analyze some of these current densities from a macroscopic point of view (see, e.g., [37, 50, 58] for a more detailed treatment). Some important categories should be distinguished:

1. **Time-Invariant Media**

   In these media, the relationships between currents and fields are time-independent. Most materials are of that kind, but time-dependent media have found uses in devices such as parametric amplifiers, where the characteristics of the medium are systematically modified by external agencies to achieve some technical purpose.

2. **Instantly Reacting Media**

   In these media, the currents at time t depend only on the value of the fields at that particular time. If, on the contrary, the currents depend on the fields at previous instants, the media are said to have memory and to show relaxation. Note that the principle of causality excludes consideration of *future* instants.

3. **Locally Reacting Media**

   Here the currents in $\mathbf{r}$ depend only on the fields in $\mathbf{r}$ and not on their value at neighboring points. There are materials, such as plasmas, where this property does not hold and in which distant effects must be taken into account.

We shall mainly consider linear, time-invariant, and locally reacting media, for which the constitutive equations are of the general form

$$\begin{aligned} \mathbf{j}(\mathbf{r}, t) &= \overline{\overline{\sigma}}(\mathbf{r}) \cdot \mathbf{e}(\mathbf{r}, t) \\ \mathbf{m}_e(\mathbf{r}, t) &= \epsilon_0 \overline{\overline{\chi}}_e(\mathbf{r}) \cdot \mathbf{e}(\mathbf{r}, t) \\ \mathbf{m}_m(\mathbf{r}, t) &= \overline{\overline{\chi}}_m(\mathbf{r}) \cdot \mathbf{h}(\mathbf{r}, t). \end{aligned} \tag{8.7}$$

For a medium with memory, (8.7) must be replaced by

$$\begin{aligned} \mathbf{j}(\mathbf{r}, t) &= \int_0^\infty \overline{\overline{k}}_c(\mathbf{r}, t') \cdot \mathbf{e}(\mathbf{r}, t - t')\, dt' \\ \mathbf{m}_e(\mathbf{r}, t) &= \epsilon_0 \int_0^\infty \overline{\overline{k}}_e(\mathbf{r}, t') \cdot \mathbf{e}(\mathbf{r}, t - t')\, dt' \\ \mathbf{m}_m(\mathbf{r}, t) &= \int_0^\infty \overline{\overline{k}}_m(\mathbf{r}, t') \cdot \mathbf{h}(\mathbf{r}, t - t')\, dt'. \end{aligned} \tag{8.8}$$

For an instantly reacting medium, the memory function $\overline{\overline{k}}_c$ becomes

$$\overline{\overline{k}}_c(\mathbf{r}, t') = \overline{\overline{\sigma}}(\mathbf{r})\,\delta(t'), \tag{8.9}$$

which leads to

$$\mathbf{j}\,(\mathbf{r}, t) = \overline{\overline{\sigma}}(\mathbf{r})\cdot\mathbf{e}(\mathbf{r}, t). \tag{8.10}$$

Similar relationships hold for $\overline{\overline{k}}_e$ and $\overline{\overline{k}}_m$.

Under time-harmonic conditions, the convolution-type equations (8.8) give rise to relationships between Fourier transforms, such as

$$\begin{aligned}
\mathbf{J}(\mathbf{r}, j\omega) &= \overline{\overline{K}}_c(\mathbf{r}, j\omega)\cdot\mathbf{E}(\mathbf{r}, j\omega) = \overline{\overline{\sigma}}(\mathbf{r}, j\omega)\cdot\mathbf{E}(\mathbf{r}, j\omega)\\
\mathbf{M}_e(\mathbf{r}, j\omega) &= \epsilon_0\overline{\overline{K}}_e(r, j\omega)\cdot\mathbf{E}(\mathbf{r}, j\omega) = \epsilon_0\overline{\overline{\chi}}_e(\mathbf{r}, j\omega)\cdot\mathbf{E}(\mathbf{r}, j\omega)\\
\overline{\overline{M}}_m(\mathbf{r}, j\omega) &= \overline{\overline{K}}_m(\mathbf{r}, j\omega)\cdot\mathbf{H}(\mathbf{r}, j\omega) = \overline{\overline{\chi}}_m(\mathbf{r}, j\omega)\cdot\mathbf{H}(\mathbf{r}, j\omega).
\end{aligned} \tag{8.11}$$

For an *isotropic material*, the constitutive equations (8.8) become

$$\mathbf{m}_e(\mathbf{r}, t) = \epsilon_0 \int_0^\infty k_e(\mathbf{r}, t')\,\mathbf{e}(\mathbf{r}, t - t')\,dt', \tag{8.12}$$

hence

$$\chi_e(\mathbf{r}, j\omega) = \int_{-\infty}^{\infty} k_e(\mathbf{r}, t')\,H(t')\,e^{-j\omega t'}\,dt' = \int_0^\infty k_e(\mathbf{r}, t')\,e^{-j\omega t'}\,dt'. \tag{8.13}$$

The χ_e parameter is complex and may be written as

$$\chi_e(\mathbf{r},j\omega) = \chi_e'(\mathbf{r},j\omega) - j\chi_e''(\mathbf{r},j\omega). \tag{8.14}$$

Similar splittings can be performed for the other parameters. Thus,

$$\begin{aligned}
\epsilon_r(\mathbf{r}, j\omega) &= \epsilon_r'(\mathbf{r}, j\omega) - j\epsilon_r''(\mathbf{r}, j\omega)\\
\sigma\,(\mathbf{r}, j\omega) &= \sigma'(\mathbf{r}, j\omega) - j\sigma''(\mathbf{r}, j\omega)\\
\mu_r(\mathbf{r}, j\omega) &= \mu_r'(\mathbf{r}, j\omega) - j\mu_r''(\mathbf{r}, j\omega).
\end{aligned} \tag{8.15}$$

By invoking the steps that led to (6.44), Maxwell's equation (8.2) can be written as

$$\begin{aligned}
\text{curl}\,\mathbf{H} &= (\sigma' - j\sigma'')\,\mathbf{E} + j\omega\epsilon_0(\epsilon_r' - j\epsilon_r'')\,\mathbf{E}\\
&= \left[(\sigma' + \omega\epsilon_r''\epsilon_0) - j(\sigma'' - \omega\epsilon_r'\epsilon_0)\right]\mathbf{E} \;= \sigma_c\,\mathbf{E}\\
&= \left[j(\omega\epsilon_0\epsilon_r' - \sigma'') + \omega\epsilon_0\epsilon_r'' + \sigma'\right]\mathbf{E} \quad = j\omega\epsilon_c\,\mathbf{E},
\end{aligned} \tag{8.16}$$

where the medium is represented by either a complex σ or a complex ϵ_r. Relationship (8.13), which includes the property of causality, leads to the *Kronig-Kamers relations* between real and imaginary parts of ϵ [37, 50]. These equations are

$$\begin{aligned}
\epsilon'(\omega) &= \epsilon_\infty + \frac{1}{\pi}\,PV\int_{-\infty}^{\infty}\frac{\epsilon''(\omega')}{\omega' - \omega}\,d\omega'\\
\epsilon''(\omega) &= -\frac{1}{\pi}\,PV\int_{-\infty}^{\infty}\frac{\epsilon'(\omega')}{\omega' - \omega}\,d\omega'.
\end{aligned} \tag{8.17}$$

The Cauchy principal value is defined as

$$PV\int_b^a f(x)\,dx = \lim_{\epsilon\to 0}\left[\int_b^{x_0-\epsilon} f(x)\,dx + \int_{x_0+\epsilon}^a f(x)\,dx\right], \tag{8.18}$$

where the singular point x_0 has been isolated from the interval. For example:

$$PV\int_{-\infty}^{\infty}\frac{d\omega'}{\omega'-\omega} = 0.$$

The ϵ' and ϵ'' functions form a Hilbert pair of the kind defined in (A7.41) and (A7.42).

Suitable existence theorems exist for the fields in causal media. Assume, for example, that the (ϵ_r, μ_r) of the medium are complex (with negative imaginary part) and become uniform (in space) for $|\mathbf{r}| > R$. If, in addition, $\mathbf{u}_n \times \mathbf{E}$ is given on a surface S, while the fields satisfy the *radiation conditions*

$$\lim_{R\to\infty}\mathbf{E} = O\left(\frac{1}{R}\right)$$

$$\lim_{R\to\infty}\omega\mu\,\mathbf{u}_R\times\mathbf{H} + \chi\mathbf{E} = o\left(\frac{1}{R}\right) \quad (\text{with } \chi^2 = \omega^2\epsilon\mu \text{ and } 0 \le \arg\chi < \pi)$$

uniformly in all directions, then it may be shown that Maxwell's equations have a solution in the space outside S, and that this solution is unique.[1] It is also possible to show that Maxwell's equations have a unique solution when the normal components $\mathbf{u}_n\cdot\mathbf{E}$ *and* $\mathbf{u}_n\cdot\mathbf{H}$ are prescribed on S.

8.1.2 Dielectrics

There are several mechanisms by which the polarization density $\mathbf{m}_e$ in a dielectric may not immediately follow the variation of $\mathbf{e}$. In polar compounds, for example, the permanent dipoles are not immediately reoriented in the direction of $\mathbf{e}$. If $\mathbf{e}$ suffers a sudden jump at $t = 0$, thermal buffeting may cause $\mathbf{m}_e$ to approach its final value according to a law $\left(1 - e^{-\frac{t}{\tau}}\right)$, where the relaxation time τ measures the extent of the memory of the material. The dielectric constant that corresponds with that time delay is

$$\epsilon = \epsilon_r\epsilon_0 = \epsilon_\infty + \frac{\epsilon_{st}-\epsilon_\infty}{1+j\omega\tau} = \epsilon_0 + \chi\,(j\omega), \tag{8.19}$$

where ϵ_{st} and ϵ_∞ are the limit values for $\omega = 0$ and $\omega = \infty$, respectively. It is useful to split ϵ into a real and an imaginary part. Thus,

$$\begin{aligned}\epsilon &= \epsilon_\infty + \frac{\epsilon_{st}-\epsilon_\infty}{1+\omega^2\tau^2} - j\frac{(\epsilon_{st}-\epsilon_\infty)\omega\tau}{1+\omega^2\tau^2}\\ &= \epsilon' - j\epsilon''.\end{aligned} \tag{8.20}$$

Illustratively, experiments show that the ϵ of pure water is well-described by (8.20), with $(\epsilon_r)_\infty = 1.8, (\epsilon_r)_{st} = 81$ and $\tau = 9.4$ ps. The pole in (8.19) is characteristic of a *Debye*

material, a model that has received much attention in modeling biological and water-based materials, which can often be described by a combination of single pole models. It should be noted that the Debye parameters in (8.20) satisfy the Kramers-Kronig relationships. If the Debye material has conductivity in addition to polarization, it can be described by

$$\epsilon = \frac{\sigma}{j\omega} + \epsilon_\infty + \frac{\epsilon_{st} - \epsilon_\infty}{1 + j\omega\tau}. \tag{8.21}$$

For moist sand, with 1.58% water by weight, typical values between 0.6 and 6 GHz are[2] $(\epsilon_r)_{st} = 2.68, (\epsilon_r)_\infty = 2.14, \tau = 5.5$ ps, $\sigma = 1.38\ 10^{-3}$ S m^{-1}.

The Debye model holds only in a restricted frequency range. At high frequencies, toward the infrared and optical regions, the actual variation of ϵ_r is typically of the type shown in Figure 8.1. A single τ is not sufficient to describe such a variation properly above $\omega\tau \approx 1$. More flexibility in fitting an experimental ϵ_r curve is afforded by the *Lorentz single-resonance model*, for which

$$\epsilon(\omega) = \epsilon_\infty + \frac{(\epsilon_{st} - \epsilon_\infty)\omega_0^2}{\omega_0^2 - \omega^2 + j\chi\omega}. \tag{8.22}$$

Here ω_0 is the resonant angular frequency associated with some restoring force, and the added flexibility is provided by parameter χ.

When one solves a problem directly in the time domain, techniques such as the use of finite differences must be carefully adapted when dispersive media are present [194]. If the frequency spectrum is narrow-banded, ϵ_r may be assumed constant in the field equations. However, such an approximation is not acceptable for ultra-wideband short pulses. The convolution-type of constitutive equations should now be part of the algorithm, including a multiterm Debye relaxation function for biological media.[3,4] Evaluation of the convolution integrals will, in general, require storing a vast number of past-time values of **e** for each cell into which the medium is divided. Various methods have been proposed to accelerate the procedure [203].

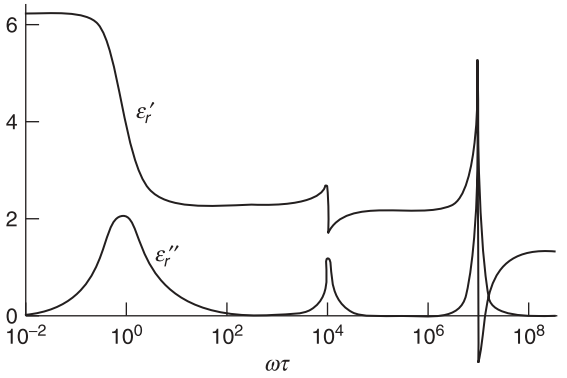

Figure 8.1 Frequency dependence of a dielectric constant (from C. J. F. Böttcher, *Theory of electric polarisation*. Elsevier Publishing Company, Amsterdam, 2nd edition; volume 1: 1973, volume 2: 1978).

8.1.3 Metals

The motion of the free electrons in a metal should be investigated by the methods of statistical mechanics. A simplified theory, however, suffices for most engineering purposes. It is based on the equation of motion of the *average* electron, which, in the absence of a magnetic field, is

$$m\frac{d\mathbf{v}}{dt} = q\mathbf{e} - m\nu\mathbf{v}, \tag{8.23}$$

where m and q denote respectively the mass and the (negative) charge of the electron. The $m\nu\mathbf{v}$ force is the *Langevin force*, a braking force that represents the effect of the collisions with other particles. The parameter ν is the average collision frequency. Under time-harmonic conditions, there results a current density

$$\mathbf{J} = nq\mathbf{V} = \frac{nq^2}{m(j\omega + \nu)}\mathbf{E} = \sigma\mathbf{E}, \tag{8.24}$$

where n is the number density of electrons (in m^{-3}). The formula shows that the conductivity σ is practically real when the frequency is much less than ν. For such a case, the average collision time $\tau = \nu^{-1}$ is much shorter than the period T of the fields, and the motion is collision-dominated. When $\omega \gg \nu$, the metal behaves as a slightly lossy dielectric, in which the fields oscillate so fast that collisions become seldom events. The Langevin approximation leads to the constitutive equation

$$\mathbf{J} = \frac{\sigma_{st}}{1 + j\omega\tau}\mathbf{E} = (\sigma' - j\sigma'')\,\mathbf{E}, \tag{8.25}$$

which is of the *Debye* type. The transition from low to high frequencies takes place around $\omega\tau = 1$, a frequency that lies in the infrared to ultraviolet range for conductors such as Al, Ag, or Ir. Traditional conductors (with $\sigma_{st} \approx 10^7\ \mathrm{S\,m}^{-1}$) are therefore good reflectors in the radio-frequency range, but become much less efficient as mirrors in the ultraviolet range[5] ($\lambda_0 < 0.4\ \mu\mathrm{m}$). The point is illustrated by the typical curve plotted in Figure 8.2 for Al. It is

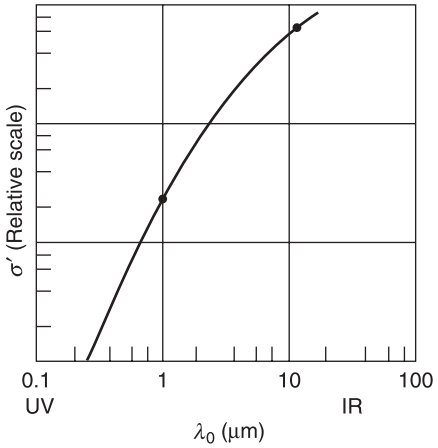

Figure 8.2 Experimental dispersion curve of σ' for Al, on a logarithmic scale.

known that, at the yellow Na spectral line ($\lambda_0 = 0.589\ \mu\text{m}$), the power reflection coefficient is still 0.94 for Ag, but it is already down to 0.83 for Al [36, 76].

Without applied current, the net charge in a conductor diffuses toward the boundary and eventually vanishes in the volume itself. When the medium is homogeneous, the rate at which this happens is given by

$$-\frac{\partial \rho_f}{\partial t} = \text{div}\,\mathbf{j} = \sigma\ \text{div}\,\mathbf{e} = \frac{\sigma}{\epsilon}\rho_f. \tag{8.26}$$

If σ and ϵ are time-independent, this relationship can be integrated to give the free-charge density

$$\rho_f = \rho_f(0)\, e^{-\frac{t}{(\epsilon/\sigma)}}. \tag{8.27}$$

Such a time variation should be looked at critically in the case of metals.[6] By inserting the values $\epsilon = \epsilon_0$ and $\sigma \approx 10^7\ \text{S m}^{-1}$ in (8.27), one arrives at charge relaxation times (ϵ/σ) of the order 10^{-18} s, *much shorter* than the experimentally measured values. The reason is clear: a pulse as short as 10^{-18} s has a spectrum that extends way beyond the frequencies for which σ may be assumed constant. A correct solution[7] for ρ_f must be based on Laplace transforming (8.26), using for $\sigma(s)$ the expression $\sigma(j\omega)$ given in (8.25), in which $j\omega$ must be replaced by s. The solution $\rho_f(s)$ may then be inserted to yield the correct time dependence of ρ_f.

8.1.4 Superconductors

According to the simplified theory of superconduction presented in Section 6.14, all the conduction carriers† form Cooper pairs at OK, and current flows unimpeded. As the temperature increases, some of the carriers are excited out of that state, with a resulting break-up of Cooper pairs. The released normal electrons introduce AC resistance because the electric field, which according to (6.123) must exist in the material, causes these carriers to move and scatter from impurities [129]. Above a critical temperature T_c, the superconducting effect is destroyed, and the material becomes a normal conductor. Superconductivity may also be destroyed by sufficiently high current densities or magnetic fields and by very high operating frequencies. In the latter case, this happens when the photon energy, proportional to f, is sufficiently high to break the Cooper pairs. For a low-temperature semiconductor (LTS) such as Pb, the critical frequency is about 650 GHz; for a high-temperature semiconductor (HTS), it lies in the THz region [74]. These figures show that the usable frequency range for the HTS is at least an order of magnitude higher than that of the LTS. They also indicate that, up to the microwave region (say up to 300 GHz), it is satisfactory to use the two-fluid model, with conductivities governed by the equations of motion

$$j\omega m \mathbf{V}_s = -|q_e|\mathbf{E}$$

for the paired electrons, and

$$j\omega m \langle \mathbf{V}_n \rangle_{\text{ave}} = -|q_e|\mathbf{E} - \frac{m}{\tau_n} \langle \mathbf{V}_n \rangle_{\text{ave}}$$

†The carriers could be electrons or holes. We shall call them electrons, for conciseness.

for the normal electrons. Because

$$\mathbf{J} = -n_s|q_e|\mathbf{V}_s - n_n|q_e|\,\langle \mathbf{V}_n\rangle_{\text{ave}}$$

the medium may be interpreted as endowed with an equivalent dielectric constant[8] [32]

$$\epsilon_r = 1 - \frac{\omega_s^2}{\omega^2} - \frac{\omega_n^2\tau_n^2}{1+\omega^2\tau_n^2} - j\frac{\omega_n^2\tau_n}{\omega(1+\omega^2\tau_n^2)} = \epsilon_r' - j\epsilon_r'', \tag{8.28}$$

where ω_s^2 and ω_n^2 are the *plasma frequencies* of the two fluids, defined by

$$\omega_s^2 = \frac{n_s q_e^2}{m\epsilon_0} \qquad \omega_n^2 = \frac{n_n q_e^2}{m\epsilon_0}. \tag{8.29}$$

In (8.28), τ_n is the collision time of the normal electrons, which is of the order 10^{-12} s. Typically ϵ' is negative, with $|\epsilon'| \gg \epsilon_0 \gg |\epsilon''|$. The conductivities of the fluids follow from

$$\begin{aligned} \mathbf{J}_s &= \frac{n_s q_e^2}{j\omega m}\,\mathbf{E} &&= \sigma_s\mathbf{E} \\ \mathbf{J}_n &= \frac{n_n q_e^2\tau_n}{m(1+j\omega\tau_n)}\,\mathbf{E} &&= \sigma_n\mathbf{E}. \end{aligned} \tag{8.30}$$

The total conductance can be written as

$$\sigma = \sigma_s + \sigma_n = \sigma' - j\sigma''.$$

Well below 10^{12} Hz, σ_n in a typical thin film of high T_c material is about 2×10^5 S m^{-1} at 70 K. Hence, from (6.128),

$$\sigma = \sigma_n - j\frac{1}{\omega\mu_0\delta_s^2}. \tag{8.31}$$

Because δ_s is typically 10^{-7} m, up to 10 GHz one may write

$$\sigma \approx -j\frac{1}{\omega\mu_0\delta_s^2}. \tag{8.32}$$

We note, from (6.128), that δ_s is frequency-independent.

In order to solve field problems in superconductors, due attention must be paid to the surface impedance.[9] This quantity can be expressed in terms of σ by

$$Z_S = \sqrt{\frac{j\omega\mu_0}{\sigma}}. \tag{8.33}$$

With the value (8.32) for σ, Z_S becomes

$$Z_S \approx j\omega\mu_0\delta_s.$$

The parameters used above yield $|Z_S| = 8\,\text{m}\Omega$ at 10 GHz. It is to be noted that the experimentally determined value of δ_s is always larger than the value that appears in (6.128).

Table 8.1 Plasma Frequency for an Electron

$n_e(\mathrm{m}^{-3})$	10^{14}	10^{18}	10^{20}	10^{22}
f_p	90 MHz	9 GHz	90 GHz	0.9 THz

To take this fact into account, the local London equations should be replaced by nonlocal equations, in which **J** in **r** is influenced by the particles located at distances of the order the *coherence distance* ℓ from **r**.

The low resistance that characterizes superconductors — at least an order of magnitude less than that of normal conductors — has been exploited in numerous applications, for example in the design of the high-Q filters often found at the front end of radioastronomical receivers.[10] Such applications became more practical with the advent of HTS materials, whose cooling systems (at 77 K) are significantly cheaper and smaller than those required for the LTS (at 4.2 K).

8.1.5 Ionized Media

Ionization occurs when the kinetic energy of the colliding particles exceeds the ionizing potential of the atoms, which is usually of the order a few eV. The released charged particles move statistically in a complex way because the electrostatic forces between charged particles are *long range* compared with the forces between neutral atoms. It follows that the charge interactions are mostly distant encounters, to which the concept collision can scarcely be applied. When the density of charged particles is sufficiently low, collisions may be ignored and the motion of the particles may adequately be described by the equation

$$m\frac{d\mathbf{v}}{dt} = q(\mathbf{e} + \mathbf{v} \times \mathbf{b}). \tag{8.34}$$

When the induction **b** is associated with an electromagnetic wave, the Lorentz force $q\mathbf{v} \times \mathbf{b}$ is normally negligible with respect to $q\mathbf{e}$, because the ratio (e/h) is of the order R_{c0}. Hence, the ratio vb/e is of the order v/c_0, which is very small at the usual nonrelativistic velocities. Under these circumstances, the medium acts macroscopically as a dielectric of permittivity

$$\epsilon_r = 1 - \frac{\omega_p^2}{\omega^2}, \tag{8.35}$$

with

$$\omega_p^2 = \frac{nq^2}{m\epsilon_0}. \tag{8.36}$$

This dielectric constant is negative below the *plasma frequency* $(\omega_p/2\pi)$ (Table 8.1). In a plasma, where both electrons and positive ions are present, (8.35) should be written for each kind of particle.

The plasma frequencies of the ions are much lower than those of the electrons, because of the higher ionic mass, which results in a more sluggish motion. The influence of collisions may be accounted for by a Langevin force, which leads to a conductivity of the (8.24) type. Typical values of ν for the ionosphere, at a height of 100 km, are $\nu_e = 400$ kHz for the electrons and $\nu_i = 4$ kHz for the ions.

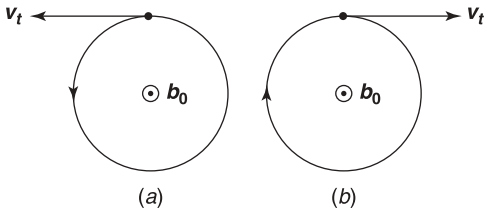

Figure 8.3 Sense of rotation of charged particles: (*a*) electrons ($f_c < 0$), (*b*) ions ($f_c > 0$).

The parameters of the ionized medium change significantly when the induction is given a static value $\mathbf{b}_0$ (in addition to the time-harmonic component). This value could vary from perhaps 70 μT for the earth's magnetic field at the magnetic South Pole, to a few T in devices designed to contain a very hot thermonuclear plasma. In the equations of motion (8.34), the Lorentz term $\mathbf{v} \times \mathbf{b}_0$ must now be carefully kept. Assuming $\mathbf{b}_0$ to be uniform in space, the motion of a charged particle turns out to be helicoidal. In a plane perpendicular to $\mathbf{b}_0$, the particle describes a circle with angular velocity (Problem 8.2).

$$f_c = \frac{\omega_c}{2\pi} = \frac{qb_0}{2\pi m}. \tag{8.37}$$

This frequency is the *cyclotron frequency*, which amounts to 28 GHz per T for an electron, and 15.25 MHz per T for a proton. Averaging over the motion of all particles shows that the medium may be macroscopically described by a tensorial permittivity that, for $\mathbf{b}_0$ along the z-axis, is [92, 123]

$$\overline{\overline{\epsilon}}_r = \begin{pmatrix} \epsilon_r & j\epsilon_r' & 0 \\ -j\epsilon_r' & \epsilon_r & 0 \\ 0 & 0 & \epsilon_r'' \end{pmatrix} = \overline{\overline{\epsilon}}_{rt} + \epsilon_r'' \mathbf{u}_z \mathbf{u}_z, \tag{8.38}$$

where

$$\begin{aligned} \epsilon_r &= 1 - \frac{\omega_{pe}^2(\omega - j\nu_e)}{\omega\left[(\omega - j\nu_e)^2 - \omega_{ce}^2\right]} - \frac{\omega_{pi}^2(\omega - j\nu_i)}{\omega\left[(\omega - j\nu_i)^2 - \omega_{ci}^2\right]} \\ \epsilon_r' &= \frac{\omega_{ce}\omega_{pe}^2}{\omega\left[(\omega - j\nu_e)^2 - \omega_{ce}^2\right]} + \frac{\omega_{ci}\omega_{pi}^2}{\omega\left[(\omega - j\nu_i)^2 - \omega_{ci}^2\right]} \\ \epsilon_r'' &= 1 - \frac{\omega_{pe}^2}{\omega(\omega - j\nu_e)} - \frac{\omega_{pi}^2}{\omega(\omega - j\nu_i)}. \end{aligned} \tag{8.39}$$

It should be noted that ω_c has a sign, in accordance with (8.37), where q can be negative or positive (Fig. 8.3). The description of the medium by the tensorial $\overline{\overline{\epsilon}}_r$ in (8.38) holds only for a uniform $\mathbf{b}_0$ but remains a good approximation as long as $\mathbf{b}_0$ varies little over the cyclotron radius (v_t/ω_c), where $\mathbf{v}_t$ is the component of the velocity perpendicular to $\mathbf{b}_0$.

8.1.6 Anistropic Media

The ionized medium in a uniform $\mathbf{b}_0$ is but a first example of an anisotropic medium. Another example is the ferrite immersed in a magnetic field $\mathbf{b}_0$, whose permeability tensor $\overline{\overline{\mu}}$ can be

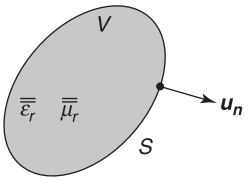

Figure 8.4 Lossless anisotropic medium.

immediately derived from (8.38) by replacing ϵ_r by μ_r. In the absence of collisions (hence in the absence of losses), (8.39) shows that all elements of the tensor become real, that is, that $\overline{\overline{\epsilon}}_r$ becomes Hermitian. This is a very general property of lossless media, which can be proved by evaluating the average power flow into a volume occupied by a linear material of tensorial $\overline{\overline{\epsilon}}$ and $\overline{\overline{\mu}}$ (Fig. 8.4). In V:

$$\begin{aligned}\text{div}\,(\mathbf{E}\times\mathbf{H}^*) &= \mathbf{H}^*\cdot\text{curl}\,\mathbf{E} - \mathbf{E}\cdot\text{curl}\,\mathbf{H}^*\\ &= -j\omega\mathbf{H}^*\cdot\mathbf{B} - \mathbf{E}\cdot(-j\omega\mathbf{D}^*)\\ &= -j\omega\mathbf{H}^*\cdot\overline{\overline{\mu}}\cdot\mathbf{H} + j\omega\mathbf{E}\cdot(\overline{\overline{\epsilon}})^*\cdot\mathbf{E}^*. \end{aligned} \tag{8.40}$$

Integrating over V gives

$$-\text{Re}\,\frac{1}{2}\int_S \mathbf{u}_n\cdot(\mathbf{E}\times\mathbf{H}^*)dS = -\text{Re}\,j\frac{\omega}{2}\int_V(\mathbf{E}\cdot(\overline{\overline{\epsilon}})^*\cdot\mathbf{E}^* - \mathbf{H}^*\cdot\overline{\overline{\mu}}\cdot\mathbf{H})\,dV.$$

The left-hand term is the average power flow into V. It vanishes for a lossless material, in which case the integral in the right-hand term must be real. For this property to hold for any V, both $\mathbf{E}\cdot\overline{\overline{\epsilon}}^*\cdot\mathbf{E}^*$ and $\mathbf{H}^*\cdot\overline{\overline{\mu}}\cdot\mathbf{H}$ must be real. A simple algebraic manipulation shows that this requirement implies $\overline{\overline{\epsilon}} = \overline{\overline{\epsilon}}^+$ and $\overline{\overline{\mu}} = \overline{\overline{\mu}}^+$; that is, the Hermitian character of the parameters.

Materials for which the electric and magnetic polarizations depend on *both* **E** and **H** are termed *magnetoelectric*. An important example is afforded by the *chiral* media, the molecules of which do not coincide with their mirror images, as suggested in Figure 8.5.

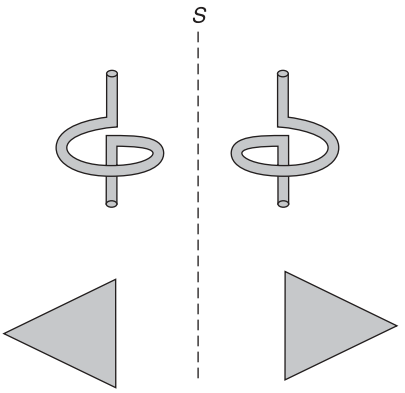

Figure 8.5 Illustrating chirality with respect to a plane of symmetry S.

In an *isotropic chiral medium*, the constitutive equations are [87, 117]

$$\begin{aligned}\mathbf{D} &= \epsilon\mathbf{E} - j\kappa\sqrt{\epsilon_0\mu_0}\,\mathbf{H}\\ \mathbf{B} &= \mu\mathbf{H} + j\kappa\sqrt{\epsilon_0\mu_0}\,\mathbf{E},\end{aligned} \tag{8.41}$$

where κ is the *chirality (or Pasteur) parameter*. It is dimensionless and is real in a lossless medium. A century-old fabrication method for chiral media consists of embedding small metallic spirals in an isotropic medium acting as a host.[11] The current in the helix in Figure 8.5 flows in a small not-completed loop that, according to (7.168), radiates like a combination of electric and magnetic dipoles and therefore generates electric *and* magnetic polarizations.

The most general magnetoelectric medium is called *bianisotropic*, and its constitutive equations can be written as[‡]

$$\begin{aligned}\mathbf{D}(\mathbf{r},\omega) &= \overline{\overline{\epsilon}}(\mathbf{r},\omega)\cdot\mathbf{E}(\mathbf{r},\omega) + \overline{\overline{\alpha}}(\mathbf{r},\omega)\cdot\mathbf{H}(\mathbf{r},\omega)\\ \mathbf{B}(\mathbf{r},\omega) &= \overline{\overline{\mu}}(\mathbf{r},\omega)\cdot\mathbf{H}(\mathbf{r},\omega) + \overline{\overline{\beta}}(\mathbf{r},\omega)\cdot\mathbf{E}(\mathbf{r},\omega).\end{aligned} \tag{8.42}$$

Such materials may be synthesized by inserting properly oriented spherical bianisotropic inclusions into an isotropic matrix. They have been investigated extensively in the optical range. The great flexibility that they afford, thanks to the number of available parameters in (8.42), has been exploited down to the microwave region, for example in the design of frequency filters.[12]

In the electromagnetic study of bianisotropic materials, it is useful to group the fields into two six-vectors, viz.

$$\begin{pmatrix}\mathbf{E}\\ R_{c0}\mathbf{H}\end{pmatrix} \quad \text{and} \quad \begin{pmatrix}c_0R_{c0}\mathbf{D}\\ c_0\mathbf{B}\end{pmatrix},$$

both of which have the dimension $\mathrm{V\,m^{-1}}$. The constitutive equations can be written in terms of these six-vectors and appropriate six-dyadics.[13,14]

8.1.7 Metamaterials

A strong research effort has recently been directed toward materials obtained by embedding prefabricated inhomogeneities into a host material (a matrix). Artificial media obtained in that manner have been known for about a hundred years.[11] The new medium often displays properties that are strongly different from those of the initial components. One of the challenges is to conceive combinations that have desirable properties, even some that may not exist in "natural" materials. Of great potential interest are materials that have negative ϵ_r and μ_r. These doubly negative materials (DNG materials) are often included in the category of *metamaterials*.[§] They can be synthesized, in principle at least, by inserting suitable conducting inhomogeneities in a dielectric matrix. The conductors can be split-ring resonators (SRRs) or Ω particles[16] (Fig. 8.6). These inclusions react by means of the electric and magnetic dipole moments that they acquire under the influence of an incident field. The moments

[‡]This is the **E**, **H** (or Tellegen) representation. In the Boys-Post version, (**D**, **H**) are expressed in terms of **E** and **B**.

[§]For a possible definition of the concept "metamaterial," see A. Sihvola's comments in Note 15.

(*a*) (*b*)

Figure 8.6 Geometry of the insertions: (*a*) split ring resonator, (*b*) omega particle.

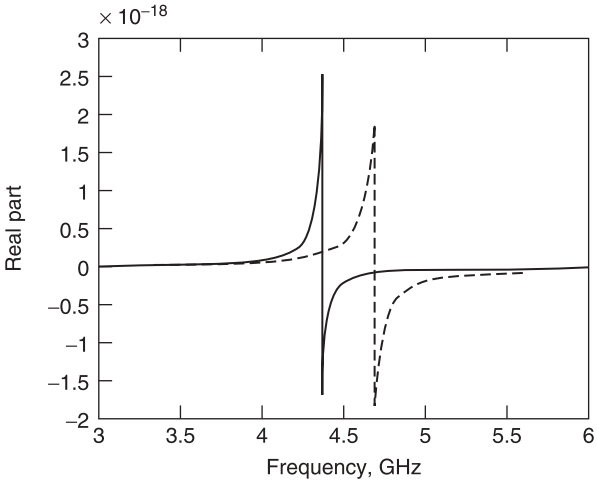

(*a*)

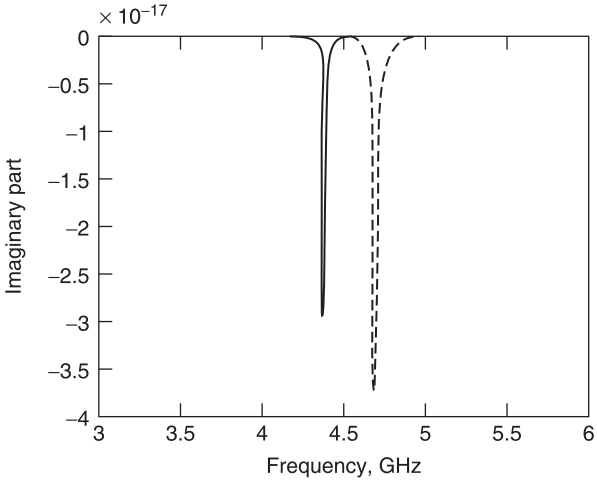

(*b*)

Figure 8.7 Average magnetic polarizability of a split-ring resonator versus frequency. Analytical model (solid) numerical model (dashed) (from C. R. Simovski and B. Sauviac, Toward creating isotropic microwave composites with negative refraction, *Radio Sci.* **39**, RS2014, 1–18, 2004, with permission of the American Geophysical Union).

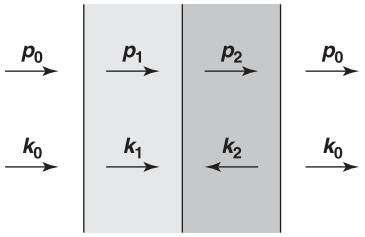

Figure 8.8 A two-layered structure.

of an open circular loop are evaluated in Section 7.10 (see Equation 7.168). The corresponding values for the inclusions shown in Figure 8.6 may be derived on the basis of the inductance and capacitance of these small circuits. Resonances will clearly appear.[17,18] By suitable mixing of inclusions of random orientation[¶] a homogeneous isotropic material can be synthesized. Figure 8.7 shows, as an illustration, a typical frequency dependence of the real and imaginary parts of a SRR with split width 0.1 mm. The analytical results are based on the resonant circuit representation, the numerical ones on a solution by finite elements. The main resonance and the appearance of negative values can easily be recognized.

Materials with negative ϵ_r and μ_r can be expected to have unusual properties. They can support backward waves, a phenomenon further discussed in Section 15.7 (and which is well-known from the operation of some microwave oscillators and amplifiers). In these waves, Poynting's vector $\mathbf{p}$ and the propagation vector $\mathbf{k}$ (see Equation 8.43) point in opposite directions. Figure 8.8 shows a sandwich structure in which 1 refers to a lossless dielectric material and 2 to a DNG medium. As the incident wave progresses to the right, its phase decreases in medium 1 but increases in medium 2 (Problem 8.9). When the two phase shifts compensate each other, entrance and exit waves are in phase. By metallizing the $z = 0$ and $z = l$ planes, a compact, thin cavity resonator can be formed. Numerous other applications can be imagined.[15,19,20] They could be based, for example, on the anomalous refraction of an incident wave impinging on a DNG medium, whose index of refraction is negative (see Section 9.1).

8.2 PLANE WAVES

The fields in a plane wave depend on a single space coordinate, which we will call a. If the fields are time-harmonic, the space dependence will be through a factor $e^{-\gamma a} = e^{-jka}$, where γ (and k) depend on the frequency. The dispersion law $\gamma(\omega)$ is of great importance for the propagation of waves, and we shall derive its form for a number of media.

8.2.1 Isotropic, Homogeneous Medium

A plane wave propagating in a direction a in a medium of scalar characteristics ϵ, μ, σ is of the form

$$\mathbf{E} = \mathbf{A}\, e^{-j\mathbf{k}\cdot\mathbf{r}}$$
$$\mathbf{H} = \frac{1}{Z_c}(\mathbf{u}_a \times \mathbf{A})\, e^{-j\mathbf{k}\cdot\mathbf{r}}, \tag{8.43}$$

[¶]For a medium made up of inclusions in a 3D array, the parameters become tensorial.[18]

Table 8.2 Propagation Parameters for Seawater

f	10 kHz	1 GHz	10 GHz
α (m^{-1})	0.4	80	89
β (m^{-1})	0.4	195	1777
Q	10^{-5}	1	10

where

$$\begin{aligned}
\mathbf{k} &= k\mathbf{u}_a \\
k^2 &= k_0^2 N^2 = \omega^2\epsilon\mu - j\omega\mu\sigma \\
&= -j\omega\mu\sigma(1 + jQ) = \omega^2\epsilon\mu\left(1 - j\frac{1}{Q}\right) \\
Q &= \frac{\omega\epsilon}{\sigma} \\
Z_c &= \sqrt{\frac{\mu}{\epsilon + \dfrac{\sigma}{j\omega}}} = \sqrt{\frac{j\omega\mu}{\sigma + j\omega\epsilon}} = \sqrt{\frac{\mu}{\epsilon}}\frac{1}{\sqrt{1 - \dfrac{j}{Q}}}.
\end{aligned} \tag{8.44}$$

It is useful to introduce the real and imaginary parts of k. Thus,

$$\begin{aligned}
k &= (\beta - j\alpha) \\
e^{-j\mathbf{k}\cdot\mathbf{r}} &= e^{-\alpha(\mathbf{u}_a\cdot\mathbf{r})}e^{-j\beta(\mathbf{u}_a\cdot\mathbf{r})}.
\end{aligned} \tag{8.45}$$

The *propagation coefficients* (α, β) are given by

$$\begin{aligned}
\alpha &= \omega\sqrt{\frac{\mu\epsilon}{2}}\left(\sqrt{1 + \frac{\sigma^2}{\omega^2\epsilon^2}} - 1\right)^{\frac{1}{2}} \\
\beta &= \omega\sqrt{\frac{\mu\epsilon}{2}}\left(\sqrt{1 + \frac{\sigma^2}{\omega^2\epsilon^2}} + 1\right)^{\frac{1}{2}}.
\end{aligned} \tag{8.46}$$

Illustratively, α and β for seawater (with typical values $\sigma = 4\ \mathrm{S\ m}^{-1}$ and $\epsilon_r = 72$) are given in Table 8.2.

In a collisionless cold plasma, with ϵ_r given by (8.35), the electric field of an x-polarized plane wave propagating in the z-direction satisfies

$$\frac{d^2E}{dz^2} + k_0^2\left(1 - \frac{\omega_p^2}{\omega^2}\right)E = 0. \tag{8.47}$$

At sufficiently low frequencies, for $\omega \ll \omega_p$, ϵ_r is negative, and the waves decay (or grow) exponentially as a function of z. Fields that remain bounded at large z must therefore be of

the form

$$E = A\, e^{-k_0 z\sqrt{\frac{\omega_p^2}{\omega^2} - 1}}. \tag{8.48}$$

In the limit $\omega \to 0$, the e-folding distance is

$$d = \frac{1}{2\pi}(\lambda_0)_p. \tag{8.49}$$

where $(\lambda_0)_p$ is the free-space wavelength corresponding with the plasma frequency. If, for example, the wave is generated by a sheet of current $\mathbf{J} = A\,\delta(z)\mathbf{u}_x$ at the origin,

$$\begin{aligned} E(z) &= -\frac{R_{c0}A}{2\sqrt{1 - \dfrac{\omega_p^2}{\omega^2}}}\, e^{-jk_0|z|\sqrt{1-\frac{\omega_p^2}{\omega^2}}} && \text{for } \omega > \omega_p \\ &= -\frac{j}{2}\frac{R_{c0}A}{2\sqrt{\dfrac{\omega_p^2}{\omega^2} - 1}}\, e^{-k_0|z|\sqrt{\frac{\omega_p^2}{\omega^2} - 1}} && \text{for } \omega < \omega_p. \end{aligned} \tag{8.50}$$

The plasma is clearly dispersive.[‖] When it carries a pulsed signal, such as (7.16), the fields may be determined by splitting the signal into its Fourier components, evaluating the propagation of the individual components and subsequently inverse-transforming the sum of the results. For example, if $E(\omega)$ is the Fourier transform of $e(t)$ at $z = 0$, the field at a distance z, in the absence of reflected waves, will be[21]

$$e(z,t) = \frac{1}{2\pi}\int_{-\infty}^{\infty} E(\omega)\, e^{j(\omega t - \sqrt{k_0^2 - k_p^2}z)}\, d\omega \qquad (z > 0). \tag{8.51}$$

Alternately, a direct numerical solution in the time domain is possible by methods such as finite differences. The model describing the medium must be carefully selected in function of the width of the frequency spectrum involved. A dielectric, for example, may require a Debye or Lorentz description in a range for which ϵ_r and σ is may not be assumed constant.[22]

As an example of analytic formulation in the time-domain, consider the two-dimensional fields generated by a z-directed applied current

$$\mathbf{j}_a = i(t)\delta(x)\delta(y)\mathbf{u}_x.$$

The medium in which the fields propagate is a cold, collisionless, homogeneous, and unbounded plasma.[23] From the equation of motion (8.34), the current density associated with the electrons satisfies

$$\frac{d\mathbf{j}_e}{dt} = \epsilon_0\omega_p^2\mathbf{e}.$$

[‖]The dispersive effect decreases as ω increases beyond ω_p and disappears in the limit $\omega \to \infty$.

Differentiating Maxwell's equation

$$\text{curl}\,\mathbf{h} = \epsilon_0 \frac{\partial \mathbf{e}}{\partial t} + \mathbf{j}_e + \mathbf{j}_a$$

with respect to time and inserting the value of $\dfrac{\partial \mathbf{h}}{\partial t}$ from (7.1) gives

$$-\text{curl curl}\,\mathbf{e} - \frac{1}{c_0^2}\frac{\partial^2 \mathbf{e}}{\partial t^2} - \frac{\omega_p^2}{c_0^2}\mathbf{e} = \mu_0 \frac{\partial \mathbf{j}_a}{\partial t}. \tag{8.52}$$

For the two-dimensional problem under discussion, this equation becomes

$$\nabla_{xy}^2 e_z - \frac{1}{c_0^2}\frac{\partial^2 e_z}{\partial t^2} - \frac{\omega_p^2}{c_0^2} e_z = \mu_0 \frac{\partial i}{\partial t}\delta(x)\delta(y). \tag{8.53}$$

It can be solved with the help of an appropriate Green's function. Given the isotropy of space, the relevant $g(\mathbf{r}, \mathbf{r}'|t, t')$ depends only on $r = |\mathbf{r} - \mathbf{r}'|$. If, in addition, the unit source is applied at $t' = 0$, the sought Green's function is obtained by solving

$$\nabla^2 g(r,t) - \frac{1}{c_0^2}\left(\frac{\partial^2}{\partial t^2} + \omega_p^2\right) g(r,t) = -\delta(t)\frac{\delta(r)}{r}. \tag{8.54}$$

Causality requires g to vanish for $t < 0$. This requirement leads to the solution

$$g(r,t) = c_0 \frac{\cos\left[\dfrac{\omega_p}{c_0}\sqrt{(c_0 t)^2 - r^2}\right]}{2\pi\sqrt{(c_0 t)^2 - r^2}} H(c_0 t - r). \tag{8.55}$$

The front of this wave reaches a distance r at time (r/c_0). At long observation times:

$$\lim_{t\to\infty} g(r,t) = \frac{\cos \omega_p t}{2\pi t}. \tag{8.56}$$

This expression represents a field that oscillates at the plasma frequency [62].

8.2.2 Anisotropic Ionized Medium

Let a plane wave propagate in the z-direction in a medium of $\overline{\overline{\epsilon}}_r$ given by (8.38). The time-harmonic Maxwell's equations take the form [10]

$$\begin{aligned}
-\frac{dE_y}{dz} &= -j\omega\mu_0 H_x \\
\frac{dE_x}{dz} &= -j\omega\mu_0 H_y \\
-\frac{dH_y}{dz} &= j\omega\epsilon E_x - \omega\epsilon' E_y \\
\frac{dH_x}{dz} &= \omega\epsilon' E_x + j\omega\epsilon E_y.
\end{aligned} \tag{8.57}$$

To uncouple the last two equations (i.e., to create new equations involving only two functions), we introduce the eigenvectors of $\overline{\overline{\epsilon}}_{rt}$, defined by

$$\overline{\overline{\epsilon}}_{rt} \cdot (\mathbf{u}_x \pm j\mathbf{u}_y) = (\epsilon \mp \epsilon')(\mathbf{u}_x \pm j\mathbf{u}_y). \tag{8.58}$$

It is meaningful to expand the fields in terms of these vectors. Thus,

$$\begin{aligned} \mathbf{E} &= A(\mathbf{u}_x + j\mathbf{u}_y) + B(\mathbf{u}_x - j\mathbf{u}_y) \\ \mathbf{H} &= C(\mathbf{u}_x + j\mathbf{u}_y) + D(\mathbf{u}_x - j\mathbf{u}_y). \end{aligned} \tag{8.59}$$

The two partial waves are circularly polarized, with the sense of rotation shown in Figure 7.5 with respect to the positive z-axis (which is also the direction of the static induction $\mathbf{b}_0$). Inserting expressions (8.59) into (8.57) shows that A and B satisfy the respective equations

$$\frac{d^2A}{dz^2} + \omega^2\mu_0(\epsilon - \epsilon')A = 0 \tag{8.60}$$

and

$$\frac{d^2B}{dz^2} + \omega^2\mu_0(\epsilon + \epsilon')B = 0. \tag{8.61}$$

Once A and B are found, C and D follow from

$$\begin{aligned} C &= \frac{1}{\omega\mu_0}\frac{dA}{dz} \\ D &= -\frac{1}{\omega\mu_0}\frac{dB}{dz}. \end{aligned} \tag{8.62}$$

The (A, C) and (B, D) waves are respectively termed *ionic* and *electronic*, after the corresponding senses of rotation of ions and electrons. The A field satisfies (8.60), which is the propagation equation in a medium of virtual dielectric constant $(\epsilon_r - \epsilon_r')$, while in the case of the B field the medium has a virtual dielectric constant $(\epsilon_r + \epsilon_r')$. The corresponding characteristic impedances are

$$Z_c = R_{c0}\frac{1}{\sqrt{\epsilon_r \mp \epsilon_r'}}. \tag{8.63}$$

In a collisionless medium (if the contributions of the ions are neglected),

$$\begin{aligned} \epsilon_r - \epsilon_r' &= 1 - \frac{\omega_p^2}{\omega(\omega - \omega_c)} = 1 - \frac{\omega_p^2}{\omega(\omega + |\omega_c|)} \\ \epsilon_r + \epsilon_r' &= 1 - \frac{\omega_p^2}{\omega(\omega + \omega_c)} = 1 - \frac{\omega_p^2}{\omega(\omega - |\omega_c|)}. \end{aligned} \tag{8.64}$$

The cyclotron angular frequency for an electron of charge $(-e)$ is

$$\omega_c = -\frac{eb_{0z}}{m_e}, \tag{8.65}$$

where b_{0z} is positive when $\mathbf{b}_0$ is in the direction of propagation, negative otherwise. The equivalent ϵ_r can be positive or negative, depending on the frequency, and the waves are correspondingly propagated or attenuated. The resulting passbands and stopbands do not coincide for the ionic and electronic waves (Problem 8.5). If the frequency is sufficiently high, both partial waves are propagated, but with different wave-numbers, namely

$$\begin{aligned} k_i &= k_0\sqrt{\epsilon_r - \epsilon_r'} \quad \text{(ionic)} \\ k_e &= k_0\sqrt{\epsilon_r + \epsilon_r'} \quad \text{(electronic)}, \end{aligned} \tag{8.66}$$

where $k_i > k_e$, from (8.64). The difference gives rise to the *Faraday effect*. Assume, for example, that $\mathbf{E}$ is x-polarized at $z = 0$. We split this field into its two basic polarizations according to (8.59) and obtain

$$\frac{\mathbf{E}(0)}{E} = \mathbf{u}_x = \frac{1}{2}(\mathbf{u}_x + j\mathbf{u}_y) + \frac{1}{2}(\mathbf{u}_x - j\mathbf{u}_y).$$

Further down the z-axis (Fig. 8.9),

$$\frac{\mathbf{E}(z)}{E} = \frac{1}{2}(\mathbf{u}_x + j\mathbf{u}_y)\, e^{-jk_i z} + \frac{1}{2}(\mathbf{u}_x - j\mathbf{u}_y)e^{-jk_e z}.$$

A simple coordinate transformation shows that $\mathbf{E}(z)$ is again linearly polarized, because it is given by

$$\frac{\mathbf{E}(z)}{E} = \mathbf{u}_{x'} \cdot e^{-j\frac{k_i + k_e}{2}z}. \tag{8.67}$$

The new direction of polarization, defined by $\mathbf{u}_{x'}$, has been shifted by an angle

$$\theta = \frac{1}{2}(k_i - k_e)z \tag{8.68}$$

with respect to the original $\mathbf{u}_x$. A wave traveling toward negative z (i.e., against $\mathbf{b}_0$) suffers a rotation in the opposite sense with respect to the direction of propagation, but in the same sense in space. It follows that a horizontally polarized incident wave at $z = 0$ might be reflected back vertically polarized by the time it reaches $z = 0$. Fundamentally, the non-reciprocal nature of the wave behavior is due to the presence of the off-diagonal terms $j\epsilon_r'$ and $-j\epsilon_r'$ in the $\overline{\overline{\epsilon}}_r$ tensor.

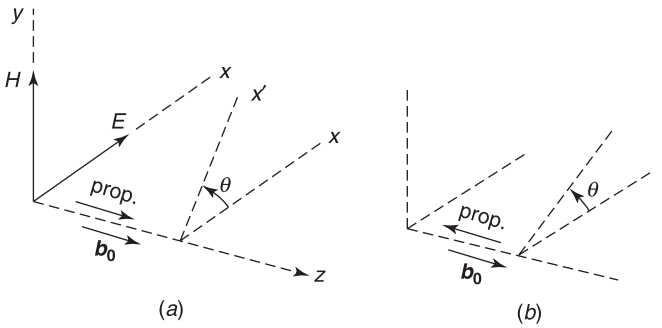

Figure 8.9 Faraday rotation for two directions of propagation: (*a*) to positive z, (*b*) to negative z.

Further aspects of wave propagation in an anisotropic plasma are discussed in texts such as [8, 43, 68, 123]. For example:

- The influence of ionic motion
- Oblique propagation with respect to $\mathbf{b}_0$
- Self-oscillations of the plasma medium
- The temperature of the plasma[23] [61, 62].

8.2.3 Chiral Medium

From (8.41) the fields in a wave propagating in the z-direction satisfy [10]

$$\begin{aligned} -\frac{dE_y}{dz} &= -j\omega\mu\, H_x + k_0\,\kappa\, E_x \\ \frac{dE_x}{dz} &= -j\omega\mu\, H_y + k_0\,\kappa\, E_y \\ -\frac{dH_y}{dz} &= j\omega\epsilon\, E_x + k_0\,\kappa\, H_x \\ \frac{dH_x}{dz} &= j\omega\epsilon\, E_y + k_0\,\kappa\, H_y. \end{aligned} \tag{8.69}$$

If one sets

$$\mathbf{H} = j\sqrt{\frac{\epsilon}{\mu}}\mathbf{E}$$

these equations are satisfied provided

$$\begin{aligned} -\frac{dE_y}{dz} &= k_0(N+\kappa)E_x \\ \frac{dE_x}{dz} &= k_0(N+\kappa)E_y, \end{aligned}$$

where $N = \sqrt{\epsilon_r\mu_r}$. Elimination of E_y yields

$$\frac{d^2E_x}{dz^2} + k_0^2(N+\kappa)^2E_x = 0,$$

from which it follows that the sought solution is

$$\begin{aligned} \mathbf{E} &= A\,(\mathbf{u}_x + j\mathbf{u}_y)\,e^{-jk_0(N+\kappa)z} \\ \mathbf{H} &= j\sqrt{\frac{\epsilon}{\mu}}A\,(\mathbf{u}_x + j\mathbf{u}_y)\,e^{-jk_0(N+\kappa)z}. \end{aligned} \tag{8.70}$$

This partial wave is circularly polarized. Another possible solution, circularly polarized in the opposite sense, is obtained by setting $H = -j\sqrt{\dfrac{\epsilon}{\mu}}\,E$. Thus,

$$\begin{aligned}\mathbf{E} &= B\,(\mathbf{u}_x - j\mathbf{u}_y)\,e^{-jk_0(N-\kappa)z}\\ \mathbf{H} &= -j\sqrt{\frac{\epsilon}{\mu}}B\,(\mathbf{u}_x - j\mathbf{u}_y)\,e^{-jk_0(N-\kappa)z}.\end{aligned} \tag{8.71}$$

The total field is the sum of these partial waves, which propagate with different phase velocities.

The decomposition described above may be extended to *uniaxial chiro-omega media*,[24,25] the constitutive equations of which are

$$\begin{aligned}\mathbf{D} &= \overline{\overline{\epsilon}}\cdot\mathbf{E} + \overline{\overline{\kappa}}_1\cdot\mathbf{H}\\ \mathbf{B} &= \overline{\overline{\mu}}\cdot\mathbf{H} + \overline{\overline{\kappa}}_2\cdot\mathbf{E},\end{aligned} \tag{8.72}$$

where (with $\overline{\overline{I}}_t = \mathbf{u}_x\mathbf{u}_x + \mathbf{u}_y\mathbf{u}_y$)

$$\begin{aligned}\overline{\overline{\epsilon}} &= \epsilon_z\mathbf{u}_z\mathbf{u}_z + \epsilon_t\overline{\overline{I}}_t\\ \overline{\overline{\mu}} &= \mu_z\mathbf{u}_z\mathbf{u}_z + \mu_t\overline{\overline{I}}_t\\ \overline{\overline{\kappa}}_1 &= -j\frac{\kappa}{c_0}\overline{\overline{I}}_t + j\frac{\gamma}{c_0}\mathbf{u}_z\times\overline{\overline{I}}_t\\ \overline{\overline{\kappa}}_2 &= j\frac{\kappa}{c_0}\overline{\overline{I}}_t + j\frac{\gamma}{c_0}\mathbf{u}_z\times\overline{\overline{I}}_t.\end{aligned}$$

The decomposition is also possible for a more general biaxial bianisotropic medium.[26]

8.3 RAY METHODS

Ray methods are concerned with the evaluation of fields at high frequencies, in a region where the parameters of the medium vary little over a wavelength.

8.3.1 The Eikonal Equation

Hemholtz' equation in a sourceless medium of index of refraction N can be written in the form

$$\nabla^2\phi + k_0^2N^2(\mathbf{r})\phi = 0. \tag{8.73}$$

This equation is satisfied by the various components of the $(\mathbf{E},\mathbf{H})$ fields. A fundamental solution when the medium is homogeneous is the plane wave $e^{-jk_0N\mathbf{u}\cdot\mathbf{r}}$. When the medium is *inhomogeneous*, but N varies little over a wavelength, ray theory generalizes the plane wave concept and assumes a solution of (8.73) of the form [122]

$$\phi\,(\mathbf{r}) = A\,(\mathbf{r},k_0)\,e^{-jk_0S(\mathbf{r})}. \tag{8.74}$$

This solution behaves locally as a plane wave. Inserting (8.74) into (8.73) gives, from (A1.22),

$$e^{-jk_0S}\left[\nabla^2 A - jk_0 A\nabla^2 S - 2jk_0 \operatorname{grad} A\cdot\operatorname{grad} S + k_0^2 N^2 A - k_0^2 A(\operatorname{grad} S)^2\right] = 0. \quad (8.75)$$

In the high-frequency limit, for $k_0 \to \infty$, A may be expanded in terms of k_0^{-1} as

$$A(\mathbf{r}, k_0) = A_0(\mathbf{r}) + \frac{1}{jk_0}A_1(\mathbf{r}) + \cdots . \quad (8.76)$$

Setting the coefficients of the various powers of k_0 in (8.75) equal to zero yields first the eikonal equation

$$(\operatorname{grad} S)^2 = N^2 \quad (8.77)$$

and further the transport equations

$$A_0\nabla^2 S + 2\operatorname{grad} A_0\cdot\operatorname{grad} S = 0 \quad (8.78)$$

for $m = 0$, and

$$A_m\nabla^2 S + 2\operatorname{grad} A_m\cdot\operatorname{grad} S = \nabla^2 A_{m-1} \quad (8.79)$$

for $m > 0$. In a *one-dimensional situation*, the Helmholtz equation (8.73) becomes**

$$\frac{d^2\phi}{dx^2} + k_0^2 N^2(x)\phi = 0 \quad (8.80)$$

and the *eikonal equation*

$$\left(\frac{dS}{dx}\right)^2 = N^2(x). \quad (8.81)$$

A simple integration gives

$$S(x) = \pm\int_{x_0}^{x} N(x')\,dx'. \quad (8.82)$$

The first transport equation (8.78) can now be given the form

$$A_0\frac{d^2S}{dx^2} + 2\frac{dA_0}{dx}\cdot\frac{dS}{dx} = A_0\frac{dN}{dx} \pm 2\frac{dA_0}{dx}N = 0.$$

Its solution is

$$A_0(x) = \frac{\text{constant}}{\sqrt{N(x)}}. \quad (8.83)$$

Combining (8.82) and (8.83) gives

$$\phi(x) = \frac{C_1}{\sqrt{N(x)}}\,e^{-jk_0\int_{x_0}^{x} N(x')\,dx'} + \frac{C_2}{\sqrt{N(x)}}\,e^{jk_0\int_{x_0}^{x} N(x')\,dx'}. \quad (8.84)$$

**For an extension to chiral media, see Note 27.

This is the *Wentzel*, *Kramers*, *Brillouin (or WKB) approximation*, which dates from the early days of quantum mechanics.[††] In both terms of the right-hand side, the phase rotates at a rate of $k_0 N$ rad m^{-1}, the value that corresponds with a uniform value of N. Expression (8.84) is a zero-order approximation, which can be refined by means of higher order terms that take into account the variation of wave number and curvature along the ray[28] [61]. The zero-order, however, is often sufficient for propagation studies, because the error on the cumulative phase is frequently comparable with the experimental uncertainties associated with factors such as the fluctuations of the medium. The validity of the approximation deteriorates in regions where $N(x)$ varies strongly, particularly at the *turning points*, where $N = 0$ and *local* methods must be applied to evaluate the fields[29] [9, 61, 165].

8.3.2 Ray Tracing

The rays are the orthogonal trajectories of the wavefronts (which are the surfaces $S =$ constant). The defining equations of the rays are

$$\frac{d\mathbf{r}}{d\sigma} = \text{grad } S = N\mathbf{u}_l, \tag{8.85}$$

where $\mathbf{u}_l$ is the unit vector along the tangent to the ray, and σ is a curve parameter. Differentiating the x-component of (8.85) with respect to σ gives

$$\begin{aligned}\frac{d^2x}{d\sigma^2} = \frac{d}{d\sigma}\left(\frac{\partial S}{\partial x}\right) &= \frac{\partial^2 S}{\partial x^2}\frac{dx}{d\sigma} + \frac{\partial^2 S}{\partial x \partial y}\frac{dy}{d\sigma} + \frac{\partial^2 S}{\partial x \partial z}\frac{dz}{d\sigma} \\ &= \frac{\partial^2 S}{\partial x^2}\frac{\partial S}{dx} + \frac{\partial^2 S}{\partial x \partial y}\frac{\partial S}{\partial y} + \frac{\partial^2 S}{\partial x \partial z}\frac{\partial S}{\partial z} \\ &= \frac{1}{2}\frac{\partial}{\partial x}\left[\left(\frac{\partial S}{\partial x}\right)^2 + \left(\frac{\partial S}{\partial y}\right)^2 + \left(\frac{\partial S}{\partial z}\right)^2\right] = \frac{1}{2}\frac{\partial N^2}{\partial x}.\end{aligned}$$

The ray equations are therefore

$$\frac{d^2\mathbf{r}}{d\sigma^2} = \frac{1}{2}\,\text{grad } N^2.$$

From (8.85), the elementary length along the ray is

$$dl = N d\sigma,$$

which implies that

$$\frac{d}{dl}(N\mathbf{u}_l) = N\frac{d\mathbf{u}_l}{dl} + \mathbf{u}_l\frac{dN}{dl} = \text{grad } N. \tag{8.86}$$

This relationship can be used graphically to trace the rays. Let $\mathbf{u}_l$ be the unit vector at point P, located at coordinate l (Fig. 8.10*a*). At a neighboring point of coordinate $l + dl$, the unit

[††]The approximation is sometimes called WKBJ, to acknowledge the contribution of H. Jeffreys to its conception.

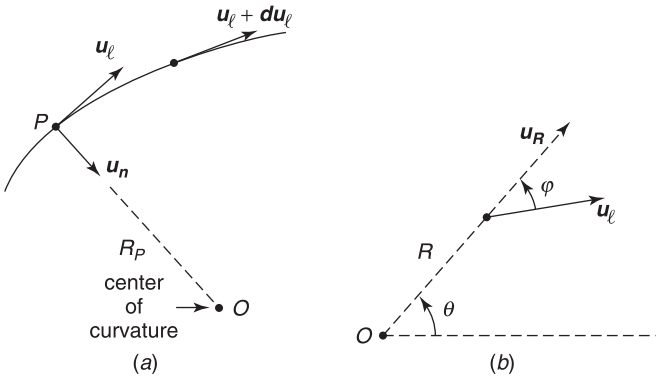

Figure 8.10 (*a*) Geometry of a typical ray. (*b*) Ray in a spherically stratified medium centered on *O*.

vector may be written as $\mathbf{u}_l + d\mathbf{u}_l$. If R_P is the radius of curvature of the ray, and $\mathbf{u}_n$ a unit vector directed toward the center of curvature,

$$d\mathbf{u}_l = \frac{1}{R_P}\mathbf{u}_n\, dl. \tag{8.87}$$

Combining (8.86) and (8.87) gives

$$\frac{1}{R_P} = \mathbf{u}_n \cdot \frac{d\mathbf{u}_l}{dl} = \frac{1}{N}\mathbf{u}_n \cdot \text{grad } N. \tag{8.88}$$

This relationship shows that the ray bends toward the region of higher index N.

As a first illustration, consider ray propagation in a spherically stratified medium, where N is a function of R only (Fig. 8.10*b*). Because both grad N and $\mathbf{r}$ are directed along $\mathbf{u}_R$,

$$\begin{aligned}\frac{d}{dl}(\mathbf{r} \times N\mathbf{u}_l) &= \frac{d\mathbf{r}}{dl} \times N\mathbf{u}_l + \mathbf{r} \times \frac{d}{dl}(N\mathbf{u}_l)\\ &= \mathbf{u}_l \times N\mathbf{u}_l + \mathbf{r} \times \text{grad } N\\ &= 0,\end{aligned} \tag{8.89}$$

and the ray equation becomes

$$\mathbf{r} \times N\mathbf{u}_l = \mathbf{A}, \tag{8.90}$$

where $\mathbf{A}$ is a constant vector. The rays therefore lie in a meridian plane, and we may write

$$NR\sin\varphi = NR\frac{R}{\left[R^2 + \left(\dfrac{dR}{d\theta}\right)^2\right]^{\frac{1}{2}}} = \text{constant},$$

from which it may be deduced that

$$\theta = \theta_0 + A\int_{R_0}^{R} \frac{dR}{R\left[N^2R^2 - A^2\right]^{\frac{1}{2}}}, \tag{8.91}$$

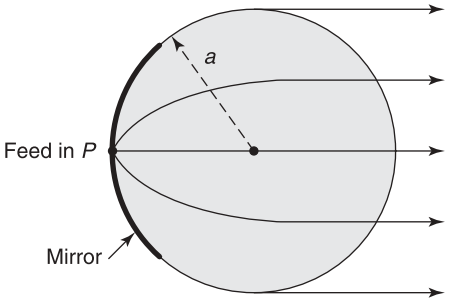

Figure 8.11 Rays in a Luneburg lens.

where A is a constant, different for each ray. By carefully choosing the $N(R)$ dependence, the rays can be given certain desirable properties. An important example is the *Luneburg lens*, for which[30]

$$N = \sqrt{2 - \frac{R^2}{a^2}}. \tag{8.92}$$

The profile of the rays in that medium is shown in Figure 8.11. The rays emanating from a surface point P emerge as a parallel bundle, hence a spherical wave from P is converted into a plane wave. Conversely, an incident plane wave is focused in P and, if reflected by a conducting layer, collimated back in the direction of incidence. This property has led to the use of the Luneburg lens as a radar echo enhancer, installed on a buoy or at the tip of an aircraft wing. The lens could also serve as the main component of a radioastronomical array, for which it would have the following advantages:[31]

- An inherently wide bandwidth
- A very wide field of view
- The potential to form simultaneous beams (for multiple observation) by placing sources at several points P
- The possibility of scanning by simply moving the feed.

The ray analysis of the Luneburg lens is only valid in the limit $\lambda_0 \to 0$. A more refined theory[32,33,34] should therefore be developed, for example by applying the methods discussed in Section 11.3. The improved theory shows that the radiated fields leave the lens as a parallel bundle, but later diverge into a conical beam, which becomes narrower as the frequency increases.

A second important example pertains to the propagation in a stratified atmosphere, where N is assumed to depend only on the altitude z [83, 137]. Symmetry indicates that the rays are in a vertical plane. From (8.77), the phase function is (Fig. 8.12)

$$S = Kx \pm \int_{z_0}^{z} (N^2 - K^2)^{\frac{1}{2}}\, dz, \tag{8.93}$$

where K is an arbitrary constant. The resulting differential equation for the rays has the form

$$\frac{dz}{dx} = \tan\varphi = \pm\frac{(N^2 - K^2)^{\frac{1}{2}}}{K},$$

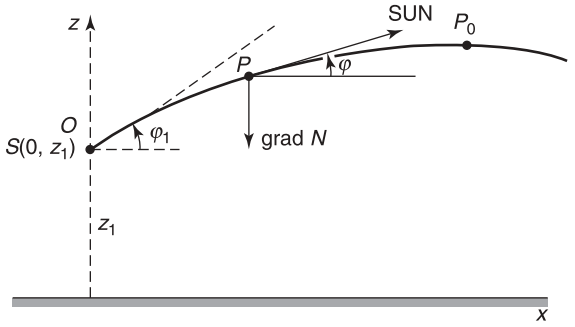

Figure 8.12 Ray in a stratified atmosphere.

which can be integrated to give

$$x = K \int_{z_1}^{z} \frac{dz}{\pm (N^2 - K^2)^{\frac{1}{2}}}. \tag{8.94}$$

The choice between the plus and minus signs depends on whether P is to the left or the right of the turning point P_0. We note that the altitude of P_0 is given by the equation

$$N(z_0) = K$$

and that

$$N(z) \cos \varphi = K = N(z_0) = N(z_1) \cos \varphi_1 \tag{8.95}$$

along a ray. This relationship is useful for a step-by-step determination of the profile of the ray. We notice that a ray that forms an angle φ in P (an incident sun-ray for example) will be seen under a larger angle φ_1 in 0, which implies that a setting sun would appear elevated to the observer.

8.3.3 Transport Equations for the Electromagnetic Field

Vector fields are characterized by polarization. To include this aspect in the analysis, it is appropriate to introduce detailed expansions for the fields in (8.74). We write

$$\begin{aligned} \mathbf{E}(\mathbf{r}) &= \mathbf{e}(\mathbf{r}, k_0)\, e^{-jk_0 S(\mathbf{r})} = \left[\mathbf{e}_0 + \frac{1}{jk_0} \mathbf{e}_1 + \cdots \right] e^{-jk_0 S(\mathbf{r})} \\ \mathbf{H}(\mathbf{r}) &= \mathbf{h}(\mathbf{r}, k_0)\, e^{-jk_0 S(\mathbf{r})} = \left[\mathbf{h}_0 + \frac{1}{jk_0} \mathbf{h}_1 + \cdots \right] e^{-jk_0 S(\mathbf{r})}. \end{aligned} \tag{8.96}$$

Here S is a real function.[‡‡] Expansions (8.96) must now be inserted into Maxwell's equations and terms of equal powers in $(k_0)^{-1}$ equated on both sides of the equations. In an isotropic

[‡‡]The validity of such an expansion is not evident, and examples have been quoted of situations where exponential decay factors and fractional powers of k_0 must be included. See Note 35.

Figure 8.13 (*a*) Orientation of the fields with respect to the rays. (*b*) Bundle of rays.

medium[§§] of scalar characteristics $(\epsilon_r, \mu_r, \sigma)$, the lowest term gives

$$\begin{aligned} \text{grad } S \times \mathbf{e}_0 &= \mu_r R_{c0} \mathbf{h}_0 \\ \mathbf{h}_0 \times \text{grad } S &= \frac{1}{R_{c0}} \epsilon_r \mathbf{e}_0. \end{aligned} \tag{8.97}$$

These equations show that $\mathbf{e}_0, \mathbf{h}_0$, and grad S form a rectangular system of axes (Fig. 8.13). Further,

$$\frac{|\mathbf{e}_0|}{|\mathbf{h}_0|} = R_c = \sqrt{\frac{\mu_r}{\epsilon_r}} R_{c0} \tag{8.98}$$

$$|\text{grad } S|^2 = \epsilon_r \mu_r \; = \; N^2. \tag{8.99}$$

The first equation confirms the quasi-plane wave character of the fields, and the second — the already discussed eikonal equation — confirms the relevance of ray tracing. Because

$$\frac{1}{2}\epsilon |\mathbf{e}_0|^2 = \frac{1}{2}\mu |\mathbf{h}_0|^2 = \frac{1}{2}\mathcal{W} \qquad (\text{J m}^{-3})$$

there is equipartition of energy between $\mathbf{e}_0$ and $\mathbf{h}_0$. One can now write the fields as

$$\begin{aligned} \mathbf{e}_0 &= \sqrt{\frac{\mathcal{W}}{\epsilon}} \mathbf{u}_e \\ \mathbf{h}_0 &= \sqrt{\frac{\mathcal{W}}{\mu}} \mathbf{u}_h, \end{aligned} \tag{8.100}$$

from which it may be deduced that

$$\mathbf{e}_0 \times \mathbf{h}_0^* = \frac{\mathcal{W}}{\sqrt{\epsilon\mu}} \mathbf{u}_l = I \mathbf{u}_l \qquad (\text{W m}^{-2}). \tag{8.101}$$

The vector of Poynting is clearly tangent to the rays, while the energy flux $I\mathbf{u}_l$ is conservative (Fig. 8.13*b*).

[§§] For an extension to chiral media, see Note 27.

Consideration of the next term in the expansion in $(k_0)^{-1}$ leads to the transport equations

$$\begin{aligned} \text{grad } S \times \mathbf{e}_1 - \mu_r R_{c0} \mathbf{h}_1 &= \text{curl } \mathbf{e}_0 \\ \text{grad } S \times \mathbf{h}_1 + \frac{1}{R_{c0}} \epsilon_r \mathbf{e}_1 &= \text{curl } \mathbf{h}_0 - \sigma \mathbf{e}_0. \end{aligned} \tag{8.102}$$

Cross-multiplying the first equation with grad S, and eliminating grad $S \times \mathbf{h}$ by means of the second, yields

$$(\text{grad } S \cdot \mathbf{e}_1) \text{ grad } S = \text{grad } S \times \text{curl } \mathbf{e}_0 + \mu_r R_{c0} (\text{curl } \mathbf{h}_0 - \sigma \mathbf{e}_0).$$

The term in $\mathbf{e}_1$ can be eliminated by cross-multiplying with grad S. Further substitution of $\mathbf{h}_0$ from (8.97) now gives

$$\text{grad } S \times \left\{ \text{grad } S \times \text{curl } \mathbf{e}_0 - \mu_r R_{c0} \sigma \mathbf{e}_0 + \mu_r \text{ curl} \left(\frac{1}{\mu_r} \text{ grad } S \times \mathbf{e}_0 \right) \right\} = 0. \tag{8.103}$$

This is an equation for $\mathbf{e}_0$ alone. The last curl can be transformed by applying (8.85), (A1.11), and (A1.15) to obtain

$$\begin{aligned} \mu_r \text{ curl } \left(\frac{1}{\mu_r} \text{ grad } S \times \mathbf{e}_0 \right) = \text{div } \mathbf{e}_0 \text{ grad } S - \mathbf{e}_0 \mu_r \text{ div} \left(\frac{1}{\mu_r} \text{ grad } S \right) \\ + (\mathbf{e}_0 \cdot \text{ grad}) \text{ grad } S - N \frac{\partial \mathbf{e}_0}{\partial l} \end{aligned}$$

and

$$\begin{aligned} \mu_r \text{ grad} \left(\frac{1}{\mu_r} \text{ grad } S \cdot \mathbf{e}_0 \right) = 0 = \text{grad } S \times \text{curl } \mathbf{e}_0 + \mu_r \mathbf{e}_0 \times \text{curl} \left(\frac{1}{\mu_r} \text{ grad } S \right) \\ + N \frac{\partial \mathbf{e}_0}{\partial l} + (\mathbf{e}_0 \cdot \text{grad}) \text{ grad } S. \end{aligned}$$

As a result, (8.103) becomes

$$\text{grad } S \times \left[\mu_r R_{c0} \sigma \mathbf{e}_0 + 2N \frac{\partial \mathbf{e}_0}{\partial l} + \mathbf{e}_0 \mu_r \text{ div} \left(\frac{1}{\mu_r} \text{ grad } S \right) \right] = 0. \tag{8.104}$$

The term between square brackets must clearly be proportional to grad S. It can therefore be written as α grad S. Dot multiplying that term by grad S gives

$$\alpha N^2 = 2N \text{ grad } S \cdot \frac{\partial \mathbf{e}_0}{\partial l} = -2N \mathbf{e}_0 \cdot \frac{\partial}{\partial l} (\text{grad } S) = -2N \mathbf{e}_0 \cdot \text{grad } N,$$

where use had been made of (8.97). Combining with (8.104) leads to the important result

$$\frac{\partial \mathbf{e}_0}{\partial l} + \frac{\mathbf{e}_0}{2N} \left[\mu_r R_{c0} \sigma + \mu_r \text{ div} \left(\frac{1}{\mu_r} \text{ grad } S \right) \right] + \left(\mathbf{e}_0 \cdot \frac{\text{grad } N}{N} \right) \frac{\text{grad } S}{N} = 0. \tag{8.105}$$

Similarly,

$$\frac{\partial \mathbf{h}_0}{\partial l} + \frac{\mathbf{h}_0}{2N}\left[\frac{\mu_r R_{c0}\sigma}{2} + \epsilon_r \operatorname{div}\left(\frac{1}{\epsilon_r}\operatorname{grad} S\right)\right] + \left(\mathbf{h}_0 \cdot \frac{\operatorname{grad} N}{N}\right)\frac{\operatorname{grad} S}{N} = 0. \tag{8.106}$$

Equation (8.105) gives the rate of variation of $\mathbf{e}_0$ as a function of l. It contains information on the evolution of both the amplitude $|\mathbf{e}_0|$ and the unit polarization vector $\mathbf{u}_e$. Thus, dot multiplying (8.105) with $\mathbf{e}_0^*$ yields

$$\frac{\partial}{\partial l}|\mathbf{e}_0|^2 + \frac{1}{N}|\mathbf{e}_0|^2\left[\mu_r R_{c0}\sigma + \mu_r \operatorname{div}\left(\frac{1}{\mu_r}\operatorname{grad} S\right)\right] = 0. \tag{8.107}$$

Dividing (8.105) by $|\mathbf{e}_0|$ gives, because $\mathbf{e}_0 = |\mathbf{e}_0|\mathbf{u}_e$,

$$\frac{1}{|e_0|}\frac{\partial |e_0|}{\partial l}\mathbf{u}_e + \frac{\partial \mathbf{u}_e}{\partial l} + \frac{\mathbf{u}_e}{2N}\left[\mu_r R_{c0}\sigma + \mu_r \operatorname{div}\left(\frac{1}{\mu_r}\operatorname{grad} S\right)\right] + \left(\mathbf{u}_e \cdot \frac{\operatorname{grad} N}{N}\right)\frac{\operatorname{grad} S}{N} = 0$$

or

$$\frac{\partial \mathbf{u}_e}{\partial l} + \mathbf{u}_e\left\{\frac{1}{2e_0^2}\frac{\partial (e_0^2)}{\partial l} + \frac{1}{2N}\left[\mu_r R_{c0}\sigma + \mu_r \operatorname{div}\left(\frac{1}{\mu_r}\operatorname{grad} S\right)\right]\right\} + \left(\mathbf{u}_e \cdot \frac{\operatorname{grad} N}{N}\right)\frac{\operatorname{grad} S}{N} = 0.$$

From (8.107), the term between square brackets vanishes. Hence,

$$\frac{\partial \mathbf{u}_e}{\partial l} + (\mathbf{u}_e \cdot \operatorname{grad} \log_e N)\frac{\operatorname{grad} S}{N} = 0. \tag{8.108}$$

Analogously,

$$\frac{\partial \mathbf{u}_h}{\partial l} + (\mathbf{u}_h \cdot \operatorname{grad} \log_e N)\frac{\operatorname{grad} S}{N} = 0. \tag{8.109}$$

The complex vectors $\mathbf{u}_e$ and $\mathbf{u}_h$ are unit vectors in the sense that $\mathbf{u} \cdot \mathbf{u}^* = 1$. In a homogeneous medium, $\mathbf{u}_e$ and $\mathbf{u}_h$ remain constant along the ray. From this property, it may be deduced that the polarization ellipses keep their shape and orientation, while their general amplitude varies according to (8.107). In an inhomogeneous medium, the ellipses keep their shape but change their orientation and amplitude. From (8.108), indeed,

$$\begin{aligned} \mathbf{u}_e \cdot \frac{\partial \mathbf{u}_e}{\partial l} &= \frac{1}{2}\frac{\partial}{\partial l}(\mathbf{u}_e \cdot \mathbf{u}_e) = 0 \\ \mathbf{u}_e^* \cdot \frac{\partial \mathbf{u}_e^*}{\partial l} &= \frac{1}{2}\frac{\partial}{\partial l}(\mathbf{u}_e^* \cdot \mathbf{u}_e^*) = 0. \end{aligned} \tag{8.110}$$

Both $(\mathbf{u}_e \cdot \mathbf{u}_e)$ and $\mathbf{u}_e^* \cdot \mathbf{u}_e^*$ remain constant. If we split $\mathbf{u}_e$ along its main axes according to

$$\mathbf{u}_e = \frac{1}{\sqrt{1+\epsilon^2}}(\mathbf{u}_x + j\epsilon \mathbf{u}_y)e^{j\theta},$$

and insert this form into (8.110), the result shows that the ellipticity ϵ remains constant along the ray.[¶¶]

[¶¶] For the corresponding phenomenon in an anisotropic medium, see Note 36.

8.3.4 Two Approximations

In the WKB approximation (8.84), it is assumed that the index of refraction $N(\mathbf{r})$ varies little over a wavelength. In the two approximations to be discussed next, the medium is assumed *weakly scattering*, that is, its $N(\mathbf{r})$ departs little from a reference value $N_r(\mathbf{r})$ for which the solution of (8.73) is known (Fig. 8.14*a*). In the *Born appproximation*, one writes

$$N^2(\mathbf{r}) = N_r^2(\mathbf{r})[1 + \chi(\mathbf{r})], \tag{8.111}$$

where $\chi(\mathbf{r})$ is a (small) contrast function. With $k_r^2 = k_0^2 N_r^2$, the propagation equation may be written as

$$\nabla^2\phi + k_r^2\phi = -(k^2 - k_r^2)\phi = -k_r^2\chi(\mathbf{r})\phi.$$

If the Green's function is known for the reference medium, and if the departure from $N_r(\mathbf{r})$ is localized in a volume V,

$$\phi(\mathbf{r}) = \phi^i(\mathbf{r}) - \int_V \phi(\mathbf{r}')\chi(\mathbf{r}')G(\mathbf{r}|\mathbf{r}')\,dV'. \tag{8.112}$$

This is an integral equation for $\phi(\mathbf{r})$. In the limit of small $\chi(\mathbf{r}), \phi(\mathbf{r})$ departs only slightly from $\phi^i(\mathbf{r})$ and we may write, in a first-order approximation,

$$\phi_1(\mathbf{r}) = \phi^i(\mathbf{r}) - \int_V \phi^i(\mathbf{r}')\chi(\mathbf{r}')G(\mathbf{r}|\mathbf{r}')\,dV'. \tag{8.113}$$

In a one-dimensional situation, for example, the Green's function for a homogeneous reference medium is (Fig. 8.14*b*)

$$G(x|x') = -\frac{1}{2jk_r}e^{-jk_r|x-x'|}.$$

For an incident wave $e^{-jk_r x}$, therefore,

$$\phi_1(x) = e^{-jk_r x} + \frac{1}{2jk_r}\int_A^B e^{-jk_r x'}e^{-jk_r|x-x'|}\chi(x')\,dx'. \tag{8.114}$$

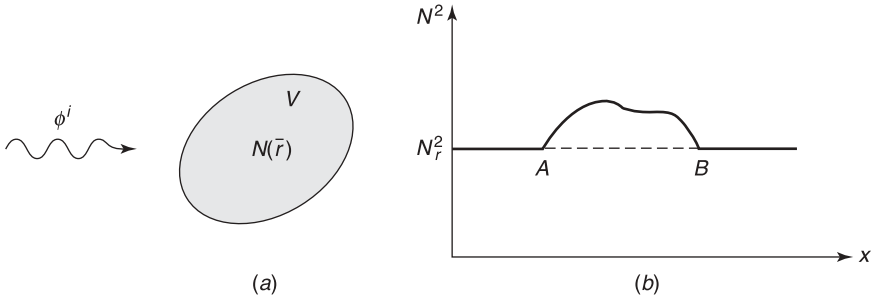

Figure 8.14 Regions of index of refraction slightly different from N_r: (*a*) weakly scattering volume: (*b*) one-dimensional variation of N.

Higher-order corrections are formed iteratively by inserting $\phi_1(\mathbf{r})$ into the integral in (8.112), thereby generating a new approximation $\phi_2(\mathbf{r})$. The procedure may be repeated to yield further approximations, such as ϕ_3 and ϕ_4 [165].

In the *Rytov approach*,[|||] which will only be discussed in its one-dimensional version for the sake of brevity, the function to be approximated is the exponent $\theta(x)$ in the exponential

$$\phi(x) = e^{\theta(x)}.$$

Assume that the wave propagates in free space, and that N^2, almost equal to one, represents a small perturbation [8]. The "incident" exponent θ_i corresponding with $N = 1$ satisfies, from (8.80),

$$\frac{d^2\theta^i}{dx^2} + \left(\frac{d\theta^i}{dx}\right)^2 + k_0^2 = 0.$$

The corresponding equation for the actual θ is

$$\frac{d^2\theta}{dx^2} + \left(\frac{d\theta}{dx}\right)^2 + k_0^2 N^2 = 0.$$

If θ is split as $\theta^i + \theta_1$, the small correction θ_1 is found to satisfy

$$\frac{d^2\theta_1}{dx^2} + 2\frac{d\theta^i}{dx}\frac{d\theta_1}{dx} = -k_0^2(N^2 - 1) - \left(\frac{d\theta_1}{dx}\right)^2,$$

and because

$$2\frac{d\phi^i}{dx}\frac{d\theta_1}{dx} = \frac{d^2}{dx^2}\left(\phi^i\theta_1\right) - \phi^i\frac{d^2\theta_1}{dx^2} + k_0^2\phi^i\theta_1,$$

one finally obtains

$$\frac{d^2}{dx^2}(\phi^i\theta_1) + k_0^2\phi^i\theta_1 = -\phi^i\left[k_0^2(N^2 - 1) + \left(\frac{d\theta_1}{dx}\right)^2\right]. \tag{8.115}$$

The approximation consists in neglecting the contribution of $(d\theta_1/dx)^2$, a term considered to be of quadratic order. Under that assumption, the approximate value of $\phi(x)$ may be written as

$$\phi_1(x) = \phi^i(x)e^{\theta_1(x)}$$

where, from (8.115), the phase correction θ_1 is given by

$$\theta_1(x) = \frac{1}{\phi^i(x)}\int_A^B k_0^2[N^2(x') - 1]\, G(x|x')\phi^i(x')\, dx'. \tag{8.116}$$

[|||] For a comparison of the accuracies of the Born and Rytov approximations, see [8] and Note 37.

8.3.5 Foci and Caustics

The previous discussions have demonstrated that ray theory can generate important information through ray tracing and transport equations. However, the method has important limitations in that it fails in the presence of strong local variations. The derivation of an equation such as (8.75), for example, implicitly assumes that space derivatives in grad A remain bounded. An important example of failure occurs when the rays converge to a focus, where the theory predicts an infinite value for the power density I in (8.101). Difficulties also arise at caustics, which are found when the envelope of the rays degenerates into a line (Fig. 8.15). An early and abundant literature exists on the subject of the actual field variation in the vicinity of these critical points and curves[38] [11, 61, 76, 88, 122]. Difficulties also arise at the transition from light to shadow, where ray theory predicts abrupt discontinuities, while the actual variation is fast, but progressive. The accurate analysis of that particular transition is discussed in Section 9.7. Phenomena that are the consequence of such deviations from geometrical optics are called diffraction phenomena.

It is interesting to note that a related view of geometrical optics was developed by Luneburg, who showed the connection between ray theory and the propagation of discontinuous solutions of Maxwell's equations [61, 86, 89, 93]. If $\phi(\mathbf{r}) = ct$ represents the equation of a wavefront, it can be shown that ϕ is the phase function $S(\mathbf{r})$, which appears in the eikonal equation, and that the $\mathbf{e}$ and $\mathbf{h}$ fields at the wavefront behave precisely like the $\mathbf{e}_0$ and $\mathbf{h}_0$ fields in (8.97), (8.105), and (8.106).

8.4 BEAMLIKE PROPAGATION

To observe the formation of a beam, we start from a Gaussian field amplitude in the $z = 0$ plane, coupled to a slightly curved quadratic front (Fig. 8.16). More precisely, for an axisymmetric beam in a homogeneous medium, we assume an initial field distribution

$$u(x, y, 0) = A_0 \, e^{-\frac{r^2}{w_0^2}} e^{jk\frac{r^2}{2R_0}}. \tag{8.117}$$

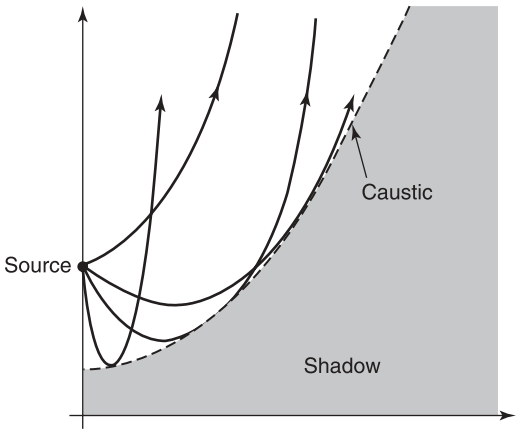

Figure 8.15 An example of caustic (from L. B. Felsen and N. Marcuvitz, *Radiation and scattering of waves*, p. 587, Prentice Hall, 1973, with permission of IEEE Press).

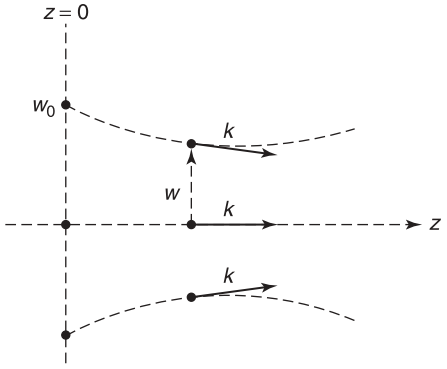

Figure 8.16 Propagation of a Gaussian beam.

Here k is the wave number in the medium, w_0 the width of the beam at $z = 0$, R_0 the radius of curvature of the phase-front, and $r^2 = x^2 + y^2$. The function $u(\mathbf{r})$ is a typical field component, and we shall investigate how $u(\mathbf{r})$ varies as a function of z. If the cross section of the beam decreases to a minimum at $z = z_{\min}$, some power concentration will be achieved there. This feature has been exploited, for example, in the design of applicators used in the hyperthermia treatment of tumors [32].

By setting

$$k\alpha = \frac{2}{w_0^2} - \frac{jk}{R_0}$$

(8.117) takes the form

$$u(r, 0) = A_0\, e^{-\frac{k\alpha r^2}{2}}. \tag{8.118}$$

The field variation in the half-space $z > 0$ can be found by applying Fourier transform techniques to (8.118). From (7.16) and (7.17), the spatial transform of u is

$$\begin{aligned} U(k_x, k_y, 0) &= A_0 \int_{-\infty}^{\infty}\int_{-\infty}^{\infty} e^{-\frac{k\alpha}{2}(x^2+y^2)}\, e^{-j(k_x x + k_y y)}\, dxdy \\ &= \frac{2\pi A_0}{k\alpha}\, e^{-\frac{1}{2k\alpha}(k_x^2+k_y^2)}. \end{aligned} \tag{8.119}$$

The main contribution to the integral comes from the low values of k_x and k_y. To determine $U(k_x, k_y, z)$, we transform Helmholtz' equation to

$$\frac{d^2U}{dz^2} + (k^2 - k_x^2 - k_y^2)\, U = 0,$$

from which it may be deduced that

$$U(k_x, k_y, z) = U(k_x, k_y, 0)\, e^{-j(k^2 - k_x^2 - k_y^2)^{\frac{1}{2}} z}.$$

In the *paraxial approximation* (i.e., for points close to the axis), $\mathbf{k}$ is almost z-oriented, hence k_x and k_y are small with respect to k_z (Problem 8.16). It follows that

$$k_z = (k^2 - k_x^2 - k_y^2)^{\frac{1}{2}} \approx k - \frac{1}{2k}(k_x^2 + k_y^2).$$

Inserting this value in $U(k_x, k_y, z)$ and taking the Fourier transform of U gives the sought variation

$$u(x, y, z) = \frac{A_0}{1 - j\alpha z} e^{-jkz}\, e^{-\frac{k\alpha}{2(1-j\alpha z)} r^2}. \tag{8.120}$$

By analogy with (8.117), the amplitude dependence on r can be written as e^{-r^2/w^2}. At $z = 0$, for example,

$$\left(\frac{1}{w^2}\right)_{z=0} = \frac{k\alpha}{2} = \frac{1}{w_0^2}\left(1 - j\,\frac{\pi l_F}{R_0}\right),$$

where l_F is the *Fresnel length*

$$l_F = \frac{1}{2\pi}\, k w_0^2. \tag{8.121}$$

At a distance z, w^2 is given by

$$\left(\frac{1}{w^2}\right)_z = \left(\frac{1}{w^2}\right)_{z=0} \frac{1}{1 - j\alpha z},$$

from which it follows that

$$(w^2)_z = (w^2)_{z=0}\left(1 - \frac{z}{R_0} - j\,\frac{z}{\pi l_F}\right). \tag{8.122}$$

The waist (or spotsize) $|w|$ is a measure of the radial extension of the beam. When R_0 is positive, w initially decreases, and the beam converges to a minimum waist. When $R_0 = 0$, the initial rays are parallel: the beam is collimated. When $R_0 < 0$, the beam diverges.

There are various ways to represent the fields to the right of the $z = 0$ plane. One possibility is by means of a sum of plane waves of the type $e^{-j\mathbf{k}_i \cdot \mathbf{r}}$, which have an infinite waist, but a compact space spectrum $\delta(\mathbf{k} - \mathbf{k}_i)$. Another possibility is to treat the field as generated by point sources located in the $z = 0$ plane. Such sources are spatially compact and have zero waist. Beam-type elements, on the other hand, have an additional (flexible) parameter w_0. They only evidence a degree of spatial and spectral localization and are less singular than rays. The beam propagators have the advantage of remaining valid at caustics and foci, where ray methods break down [34].

The Gaussian beam (8.117) was assumed axisymmetric. In a more general situation, azimuth-dependent components must be included, for example when the cross section of the beam is elliptical, in which case [143]

$$u \doteq e^{-\frac{x^2}{w_x^2}}\, e^{-\frac{y^2}{w_y^2}}. \tag{8.123}$$

Such beams have been used to study field propagation in biological media[39] [32]. In fact, there exist complete and orthogonal sets of (x, y) dependent functions in terms of which every arbitrary distribution of monochromatic light can be expanded.[40] For a beam of arbitrary cross section, u varies according to[41]

$$u(\mathbf{r}) = \sqrt{\frac{\det\ \overline{\overline{\Gamma}}(z)}{\det\ \overline{\overline{\Gamma}}(0)}}\, e^{-jk(z + \frac{1}{2}\mathbf{r}_t \cdot \overline{\overline{\Gamma}} \cdot \mathbf{r}_t)}, \tag{8.124}$$

where $\overline{\overline{\Gamma}}$ is a symmetric 2×2 complex matrix with positive-definite imaginary part, and $\mathbf{r}_t$ denotes the transverse coordinates (x, y). The real part Re $(\overline{\overline{\Gamma}})$ describes the phase front curvature and Im $(\overline{\overline{\Gamma}})$ the amplitude of the beam. The z-dependence of $\overline{\overline{\Gamma}}$ is expressed by the law

$$\overline{\overline{\Gamma}}(z) = \left[\overline{\overline{\Gamma}}^{-1}(0) + z\bar{\bar{I}}\right]^{-1}. \tag{8.125}$$

Beam techniques can be extended, at greatly added mathematical complexity, to transient sources such as the pulsed beams formed by highly localized space-time wavepackets that propagate along ray trajectories.[41,42]

8.4.1 Point Source at a Complex Location

In a homogeneous medium, the field generated by a point source at $\mathbf{r}_0$ (the Green's function) is given by

$$G(\mathbf{r}|\mathbf{r}_0) = -\frac{1}{4\pi}\frac{e^{-jk|\mathbf{r}-\mathbf{r}_0|}}{|\mathbf{r}-\mathbf{r}_0|}.$$

Let us assume that the source is located at a *complex* point $\mathbf{r}_0 = (0, 0, z_0 = ja)$. For such a location, the Green's function becomes axisymmetric, with a distance $D = |\mathbf{r} - \mathbf{r}_0|$ given by

$$D = \left[r^2 + (z - ja)^2\right]^{\frac{1}{2}}.$$

In the paraxial approximation,*** for $r \ll |z - z_0|$,

$$G(\mathbf{r}|\mathbf{r}_0) \approx -\frac{1}{4\pi(z-ja)} e^{-jk(z-ja)} e^{-j\frac{1}{2}k\frac{r^2}{z-ja}}. \tag{8.126}$$

Comparing this expression with (8.120) shows that the complex point source radiates a paraxial beam, equivalent to a spherical wave centered on a complex location. This concept may be used to solve problems of refraction and scattering when the corresponding solution for G is known.[43] Note that the paraxial approximation is not valid when $|z - z_0|$ is too small, (e.g., in focal regions).

The complex beam approach can be extended to pulsed sources and pulsed beam solutions of the wave equation that are highly directed in space and localized in time. Such beams are of importance for a variety of applications (e.g., for local probing and exploration of the environment[44,45]).

8.4.2 The Beam Propagation Method

In the beam propagation method (BPM), the optical beam is assumed to have a major propagation direction.[46] The method seeks to determine a typical field component $\phi(\mathbf{r})$ in

***Note that k in (8.126) may be complex, which happens when the beam propagates in a lossy medium, for example, in a biological tissue (see [31] and Note 39).

the vicinity of a point $\mathbf{r}_P$ at which $N = N_P$. Let $\phi_0(\mathbf{r})$ denote the solution of Helmholtz' equation in a homogeneous medium of uniform N_P. Function ϕ_0 therefore satisfies

$$\nabla^2\phi_0 + k_0^2 N_P^2 \phi_0 = 0, \tag{8.127}$$

together with the usual radiation conditions. By splitting $N^2(\mathbf{r})$ into a sum, as in

$$N^2(\mathbf{r}) = N_P^2 + \Delta(N^2),$$

Helmholtz' equation can be written as[47] [34]

$$\nabla^2\phi + k_0^2 N_P^2 \phi = -k_0^2 \Delta(N^2)\,\phi, \tag{8.128}$$

where $\Delta(N^2)$ is assumed small if one stays in the vicinity of $\mathbf{r}_P$. By means of the Green's function $G(\mathbf{r}, \mathbf{r}')$ pertinent to (8.128), one can show that an operator $\mathcal{L}$ exists such that

$$\left(\frac{\partial\phi_0}{\partial z}\right)_P = \mathcal{L}(\mathbf{r}_t)\,\phi_0(\mathbf{r}_t, z_P),$$

where $\mathbf{r}_t$ denotes coordinates transverse to the propagation direction. If one further assumes that the reflected fields may be neglected (i.e., that small reflections due to the variation of N) do not add up coherently, a few steps lead to[48]

$$\frac{\partial\phi}{\partial z} = \mathcal{L}\phi - j\frac{k_0}{2N_P}\,\Delta(N^2)\,\phi$$

and, for sufficiently small Δz, to

$$\phi(\mathbf{r}_t, z_0 + \Delta z) = \phi_0(\mathbf{r}_t, z_0 + \Delta z)\, e^{\frac{-jk_0}{2N_P}\Delta(N^2)\,\Delta z}. \tag{8.129}$$

The exponential factor represents the phase correction due to the perturbation of N (a *lens* type of correction). The BPM algorithm now consists in successive applications of (8.129), each step involving first a propagation in a thin slice of uniform medium N_P over a short distance Δz, subsequently followed by a lens correction.

A number of assumptions (some of which are mentioned above) must be made to derive equations (8.128) and (8.129). Many of these restrictions can be weakened, or even eliminated[49,50] [63]. The paraxial approximation, for example, initially included in the theory, can be dropped and the BPM extended to accommodate wide-angle beams, vector fields, and the influence of reflected waves.[51] The ever-increasing complexity of integrated optics circuits, which often contain materials of very different dielectric properties, leads to equally complex field patterns, which are no longer paraxial but propagate in any direction instead of only down a given axis. For such cases, one may have to solve the full Maxwell's equations directly, without the help of simplifying approximations.

8.5 GREEN'S DYADICS

The Green's dyadic concept, discussed in detail in Section 7.9, can be extended to sources embedded in a material medium. We will successively assume that medium to be isotropic, chiral, and bianisotropic.

8.5.1 Isotropic Media

In an *inhomogeneous* medium endowed with (ϵ, μ, σ) parameters, the electric field satisfies the differential equation

$$-\text{curl}\left(\frac{1}{\mu}\,\text{curl}\,\mathbf{e}\right) - \sigma\frac{\partial \mathbf{e}}{\partial t} - \epsilon\frac{\partial^2 \mathbf{e}}{\partial t^2} = \frac{\partial \mathbf{j}}{\partial t} + \frac{1}{\mu}\,\text{curl}\,\mathbf{j}_m. \tag{8.130}$$

When the sources are time-harmonic:

$$-\text{curl}\left(\frac{1}{\mu}\,\text{curl}\,\mathbf{E}\right) + \omega^2\epsilon_c\mathbf{E} = j\omega\mathbf{J} + \text{curl}\left(\frac{1}{\mu}\mathbf{J}_m\right) \tag{8.131}$$

$$-\text{curl}\left(\frac{1}{\epsilon_c}\,\text{curl}\,\mathbf{H}\right) + \omega^2\mu\mathbf{H} = j\omega\mathbf{J}_m - \text{curl}\left(\frac{1}{\epsilon_c}\mathbf{J}\right), \tag{8.132}$$

where the complex dielectric constant ϵ_c stands for $\epsilon + (\sigma/j\omega)$. The response to various dipole excitations — the building blocks of the Green's dyadic — is obtained by replacing $\mathbf{j}$ and $\mathbf{j}_m$ by their appropriate distributional expressions, such as

$$\mathbf{j}(\mathbf{r}, t) = j_a(t)\mathbf{u}_a\delta(\mathbf{r} - \mathbf{r}_0).$$

Solutions for layered media are discussed in Chapter 9 (see also [47]).

In a *homogeneous* medium, the potential representation (7.28), (7.29) remains valid. With a *Lorenz gauge*

$$\text{div}\,\mathbf{a} = -\sigma\mu\phi - \epsilon\mu\frac{\partial \phi}{\partial t} \tag{8.133}$$

the potentials satisfy

$$\nabla^2\mathbf{a} - \sigma\mu\frac{\partial \mathbf{a}}{\partial t} - \epsilon\mu\frac{\partial^2 \mathbf{a}}{\partial t^2} = -\mu\mathbf{j} \tag{8.134}$$

$$\nabla^2\phi - \sigma\mu\frac{\partial \phi}{\partial t} - \epsilon\mu\frac{\partial^2 \phi}{\partial t^2} = -\frac{1}{\epsilon}\rho. \tag{8.135}$$

The corresponding time-harmonic equations are of the form

$$\nabla^2\phi + k^2\phi = \nabla^2\phi + (\omega^2\epsilon\mu - j\omega\sigma\mu)\phi = -\frac{1}{\epsilon}P. \tag{8.136}$$

They may be solved by means of the Green's function

$$G(\mathbf{r}|\mathbf{r}') = -\frac{1}{4\pi}\frac{e^{-jk|\mathbf{r}-\mathbf{r}'|}}{|\mathbf{r} - \mathbf{r}'|}. \tag{8.137}$$

Consider, as an illustration, the dipole fields generated in an (ϵ, μ, σ) medium by a short length l of conductor carrying a current $i(t)$ (Fig. 8.17*a*). By setting $i(t) = I\delta(t)$, one

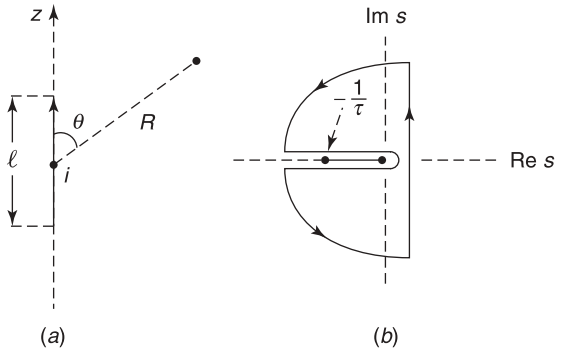

Figure 8.17 (*a*) Time-dependent electric dipole located at the origin. (*b*) Contour for the Bromwhich integral.

obtains the temporal Green's function.[52] For a general current distribution $\mathbf{j}(\mathbf{r}, t)$ the Laplace transform of the vector potential is, from (7.92) and (8.137),

$$\mathbf{a}(\mathbf{r}, s) = \frac{\mu}{4\pi} \int_V \frac{e^{-\sqrt{\epsilon\mu s^2 + \sigma\mu s}|\mathbf{r}-\mathbf{r}'|}}{|\mathbf{r} - \mathbf{r}'|} \mathbf{J}(\mathbf{r}', s)\, dV'. \tag{8.138}$$

Because the Laplace transform of $\delta(t)$ is unity, the transformed potential for the source in Figure 8.17*a* is simply

$$\mathbf{a}(R, s) = \mathbf{u}_z \mu \frac{Il}{4\pi} \frac{e^{-\gamma(s)R}}{R}, \tag{8.139}$$

where

$$\gamma(s) = (\epsilon\mu s^2 + \sigma\mu s)^{\frac{1}{2}} = \frac{1}{c}\left(s^2 + \frac{s}{\tau}\right)^{\frac{1}{2}}.$$

Here c is the velocity $(\epsilon, \mu)^{-\frac{1}{2}}$ and τ is the relaxation time (ϵ/σ). Note that the parameters (ϵ, μ, σ) are assumed time-independent, an assumption whose limitations are discussed in Section 8.1. To obtain the sought $a(R, t)$, one could invert $a(R, s)$ by means of the Bromwhich integral (A7.15), using the contour in Figure 8.17*b*. We note that a branch cut has been drawn between the branch points $s = -(1/\tau)$ and $s = 0$ of $\gamma(s)$ (see Appendix 6). In the current application, the inverse Laplace transform of the exponential in (8.139) happens to be known explicitly. Thus,

$$\begin{aligned} e^{-x\sqrt{as^2+bs+c}} = L_1 \Bigg\{ & e^{-\frac{b}{2\sqrt{a}}x} \delta(t - \sqrt{a}x) \\ & + \frac{1}{2}\sqrt{\frac{d}{a}} x e^{-\frac{b}{2a}t} I_1\left(\frac{\sqrt{d}}{2a}\sqrt{t^2 - ax^2}\right) \frac{H(t - \sqrt{a}x)}{\sqrt{t^2 - ax^2}} \Bigg\}, \end{aligned} \tag{8.140}$$

where $d = (b^2 - 4ac)$, and I_1 is a modified Bessel function. Consequently,

$$a_z(R, t) = \frac{\mu Il}{4\pi R}\left[e^{-\alpha R}\delta\left(t - \frac{R}{c}\right) + \alpha R\, e^{-\frac{t}{2\tau}} I_1\left(\frac{\sqrt{t^2 - \frac{R^2}{c^2}}}{2\tau}\right) \frac{H\left(t - \frac{R}{c}\right)}{2\sqrt{t^2 - \frac{R^2}{c^2}}} \right], \tag{8.141}$$

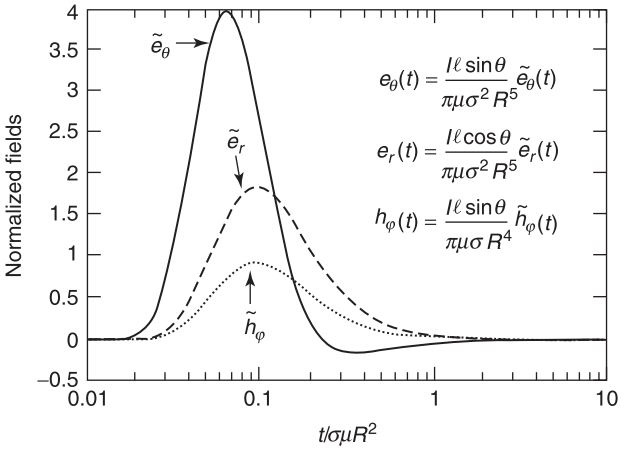

Figure 8.18 Fields from an impulsive current $I\delta(t)$ (from J. Song and K. M. Chen, Propagation of EM pulses excited by an electric dipole in a conducting medium, *IEEE Trans. AP* **41**, 1414–1421, 1993, with permission of IEEE).

where $\alpha = \dfrac{\sigma}{2}\sqrt{\dfrac{\mu}{\epsilon}}$. The $(h_\varphi, e_\theta, e_R)$ components can now be obtained directly from a_z. For example,

$$h_\varphi(R,t) = \frac{Il\sin\theta}{4\pi R^2}\left\{ e^{-\frac{\alpha R}{2}}\left[\left(1+\frac{\alpha R}{2}+\frac{\alpha^2R^2}{8}\right)\delta\left(t-\frac{R}{c}\right)+\frac{R}{c}\delta'\left(t-\frac{R}{c}\right)\right]\right.$$
$$\left. + e^{-\frac{t}{2\tau}} I_2\left(\frac{\sqrt{t^2-\dfrac{R^2}{c^2}}}{2\tau}\right)\frac{\alpha^2R^3 H\left(t-\dfrac{R}{c}\right)}{4c\left(t^2-\dfrac{R^2}{c^2}\right)}\right\}. \tag{8.142}$$

Typical time-variations of the field components are plotted in Figure 8.18 in terms of a normalized time variable.

The discussion of the properties of the Green's dyadic given in Section 7.9 may immediately be transposed to a homogeneous isotropic medium (ϵ, μ, σ). The extension to more general media is more delicate, in particular in the presence of anisotropies, as shown below.

8.5.2 Chiral Media

The constitutive equations for an isotropic chiral medium are given in (8.41). They lead to the following Maxwell equations

$$\begin{aligned} \text{curl}\,\mathbf{E} - k_0\kappa\mathbf{E} &= -j\omega\mu\mathbf{H} - \mathbf{J}_m \\ \text{curl}\,\mathbf{H} - k_0\kappa\mathbf{H} &= j\omega\mathbf{E} + \mathbf{J}. \end{aligned} \tag{8.143}$$

Eliminating **H** gives, for a homogeneous medium,

$$-\text{curl curl } \mathbf{E} + 2k_0\kappa \text{ curl } \mathbf{E} + (\omega^2\epsilon\mu - k_0^2\kappa^2)\mathbf{E} = \text{curl } \mathbf{J}_m - k_0\kappa\mathbf{J}_m + j\omega\mu\mathbf{J}, \quad (8.144)$$

which can usefully be rewritten as

$$\mathcal{L}\mathbf{E} = -(\text{curl} - k_0\kappa)(\text{curl} - k_0\kappa)\mathbf{E} + \omega^2\epsilon\mu\mathbf{E} = j\omega\mu\mathbf{J} + (\text{curl} - k_0\kappa)\mathbf{J}_m. \quad (8.145)$$

The operator $\mathcal{L}$ is the dyadic

$$\overline{\overline{\mathcal{L}}} = -(\text{curl } \overline{\overline{I}} - k_0\kappa\overline{\overline{I}})\cdot(\text{curl } \overline{\overline{I}} - k_0\kappa\overline{\overline{I}}) + \omega^2\epsilon\mu\overline{\overline{I}}. \quad (8.146)$$

By introducing the wavenumbers

$$\begin{aligned} k_+ &= k_0(N + \kappa) \\ k_- &= k_0(N - \kappa), \end{aligned} \quad (8.147)$$

where $N^2 = \epsilon_r\mu_r$, $\mathcal{L}$ becomes

$$\mathcal{L} = -(\text{curl} - k_+)(\text{curl} + k_-). \quad (8.148)$$

According to (8.70) and (8.71), the wavenumbers k_+ and k_- are precisely associated with the two fundamental circularly polarized waves that the medium can carry (the eigenstates). Factorization of the $\mathcal{L}$ operator facilitates the determination of the Green's dyadic $\overline{\overline{G}}_{ee}$, which is the solution of

$$\mathcal{L}\overline{\overline{G}}_{ee}(\mathbf{r} - \mathbf{r}') = \delta(\mathbf{r} - \mathbf{r}')\overline{\overline{I}}. \quad (8.149)$$

One can readily check that[53]

$$\overline{\overline{G}}_{ee} = \frac{1}{k_+ + k_-}(\overline{\overline{G}}^- - \overline{\overline{G}}^+), \quad (8.150)$$

where $\overline{\overline{G}}^+$ and $\overline{\overline{G}}^-$ satisfy respectively

$$\begin{aligned} \mathcal{L}^+\overline{\overline{G}}^+(\mathbf{r} - \mathbf{r}') &= (\text{curl} - k_+)\overline{\overline{G}}^+(\mathbf{r} - \mathbf{r}') = \delta(\mathbf{r} - \mathbf{r}')\overline{\overline{I}} \\ \mathcal{L}^-\overline{\overline{G}}^-(\mathbf{r} - \mathbf{r}') &= (\text{curl} + k_-)\overline{\overline{G}}^-(\mathbf{r} - \mathbf{r}') = \delta(\mathbf{r} - \mathbf{r}')\overline{\overline{I}}. \end{aligned} \quad (8.151)$$

The $\overline{\overline{G}}^+$ dyadic is given by

$$\overline{\overline{G}}^+ = -(\text{curl} + k_+)\overline{\overline{G}}_0^+, \quad (8.152)$$

where $\overline{\overline{G}}_0^+$ is the free-space dyadic (7.95), in which k_0 must be replaced by k_+. A similar expression holds for $\overline{\overline{G}}_0^-$. The singularity of $\overline{\overline{G}}_0^+$ for $\mathbf{r} \to \mathbf{r}'$ is, as in (7.137),

$$\overline{\overline{G}}_0^+ = PV_v\,\overline{\overline{G}}_0^+(\mathbf{r}|\mathbf{r}') + \frac{1}{k_+^2}\delta(\mathbf{r} - \mathbf{r}')\overline{\overline{L}}_v. \quad (8.153)$$

The depolarizing dyadic $\overline{\overline{L}}_v$, extensively discussed in Sections 3.9 and 7.9, represents the contribution $\mathbf{E}_v$ of a small volume v containing $\mathbf{r}$. Note that the method of Fikioris mentioned in Section 7.9, in which v is not assumed vanishingly small, may also be applied to anisotropic media.[54]

8.5.3 Bianisotropic Media

The simplicity of the constitutive equations (8.41) has yielded a closed form for the $\overline{\overline{G}}$ dyadic, from which **E** follows by means of a classic integration. It is clear that this simplicity may not hold when the constitutive equations are of the more general form (8.42) where, from a mathematical point of view, the tensors can have any form. The appropriate $\overline{\overline{\mathcal{L}}}$ operator is now[†††] [87]

$$\overline{\overline{\mathcal{L}}} = -(\text{curl}\,\overline{\overline{I}} - j\omega\overline{\overline{\alpha}})\cdot(\overline{\overline{\mu}})^{-1}\cdot(\text{curl}\,\overline{\overline{I}} + j\omega\overline{\overline{\beta}}) + \omega^2\overline{\overline{\epsilon}}, \tag{8.154}$$

and the Green's dyadic must satisfy

$$\overline{\overline{\mathcal{L}}}\cdot\overline{\overline{G}}_{ee}(\mathbf{r}-\mathbf{r}') = \overline{\overline{I}}\delta(\mathbf{r}-\mathbf{r}'). \tag{8.155}$$

8.6 RECIPROCITY

It is shown in Section 3.1 that the solutions ϕ_a and ϕ_b of Poisson's equation corresponding with sources ρ_a and ρ_b are connected by the "reaction" equation

$$\langle\phi_a, \rho_b\rangle = \langle\phi_b, \rho_a\rangle. \tag{8.156}$$

This is a powerful relationship.[57] Assume, indeed, that ϕ_a is the unknown of the problem. If we know the solution ϕ_b generated by ρ_b (analytically, numerically, or experimentally), Equation (8.156) immediately gives $\langle\phi_a, \rho_b\rangle$, (i.e., the projection of ϕ_a on ρ_b). If ρ_b is the (singular) density $q\delta(\mathbf{r}-\mathbf{r}_0)$ of a point charge in $\mathbf{r}_0$,

$$q\phi_a(\mathbf{r}_0) = \langle\phi_b, \rho_a\rangle. \tag{8.157}$$

The connection with the theory of distributions discussed in Appendix 8 is evident.[58] If we repeat this testing procedure for several b states, a series of projections of ϕ_a is obtained, in a manner reminiscent of the method of moments. Note that the product $\langle\phi_a, \rho_b\rangle$ is often a quantity of physical interest, and that (8.156) shows how it can be evaluated from $\langle\phi_b, \rho_a\rangle$; that is, without explicitly solving for ϕ_a (Problem 8.22).

It is clear that the $\langle a, b\rangle = \langle b, a\rangle$ property in (8.156) is intimately connected with the adjointness of the transformation. This can be shown on the example of the scalar radiation problem

$$\begin{aligned} &\nabla^2\phi + k_0^2\phi = P(\mathbf{r}) \\ &\frac{\partial\phi}{\partial R} + jk_0\phi = o\left(\frac{1}{R}\right) \qquad (R\to\infty). \end{aligned} \tag{8.158}$$

The transformation is self-adjoint with respect to a *symmetric* scalar product, and the Green's function for that type of product is

$$G(\mathbf{r}|\mathbf{r}') = G(\mathbf{r}'|\mathbf{r}) = -\frac{1}{4\pi}\frac{e^{-jk_0|\mathbf{r}-\mathbf{r}'|}}{|\mathbf{r}-\mathbf{r}'|}.$$

[†††] For a survey of the theory, see Notes 55 and 56.

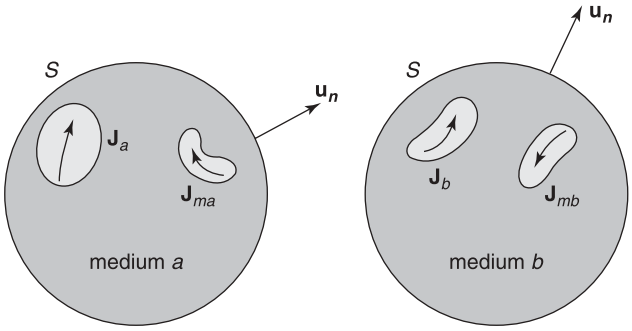

Figure 8.19 Two states and their respective sources.

The adjoint problem with respect to a *Hermitian* scalar product takes the form

$$\nabla^2\phi + k_0^2\phi = P(\mathbf{r})$$
$$\frac{\partial\phi}{\partial R} - jk_0\phi = o\left(\frac{1}{R}\right) \qquad (R \to \infty) \tag{8.159}$$

and the (adjoint) Green's function is now

$$G^a(\mathbf{r}|\mathbf{r}') = -\frac{1}{4\pi}\frac{e^{jk_0|\mathbf{r}-\mathbf{r}'|}}{|\mathbf{r}-\mathbf{r}'|} = G^*(\mathbf{r}'|\mathbf{r}). \tag{8.160}$$

The form of the reciprocity property for a Hermitian scalar product is discussed later in this section.

8.6.1 Time-Harmonic Fields: Symmetric Scalar Product

Let the a state be generated by currents $\mathbf{J}_a$ and $\mathbf{J}_{ma}$ radiating in the presence of a magneto-electric medium of constitutive equations (8.42) (Fig. 8.19). Maxwell's equations take the form

$$\text{curl}\,\mathbf{E}_a = -j\omega\overline{\overline{\mu}}_a\cdot\mathbf{H}_a - j\omega\overline{\overline{\beta}}_a\cdot\mathbf{E}_a - \mathbf{J}_{ma} \tag{8.161}$$
$$\text{curl}\,\mathbf{H}_a = j\omega\overline{\overline{\epsilon}}_a\cdot\mathbf{E}_a + j\omega\overline{\overline{\alpha}}_a\cdot\mathbf{H}_a + \mathbf{J}_a. \tag{8.162}$$

The effect of conduction currents is included in the material parameters. Consider, in the same space domain, a second state b, which may be of a purely mathematical nature. The b sources and media are independent of their a counterparts, but in both cases the media are assumed linear, time-invariant, and locally reacting inside the considered space domain. The b fields satisfy

$$\text{curl}\,\mathbf{E}_b = -j\omega\overline{\overline{\mu}}_b\cdot\mathbf{H}_b - j\omega\overline{\overline{\beta}}_b\cdot\mathbf{E}_b - \mathbf{J}_{mb} \tag{8.163}$$
$$\text{curl}\,\mathbf{H}_b = j\omega\overline{\overline{\epsilon}}_b\cdot\mathbf{E}_b + j\omega\overline{\overline{\alpha}}_b\cdot\mathbf{H}_b + \mathbf{J}_b. \tag{8.164}$$

On the basis of a *symmetric scalar product*, and because

$$(\mathbf{b}\cdot\overline{\overline{a}}\cdot\mathbf{c}) = (\mathbf{c}\cdot\overline{\overline{a}}^{t}\cdot\mathbf{b}), \tag{8.165}$$

we may write

$$\begin{aligned}\operatorname{div}(\mathbf{E}_a\times\mathbf{H}_b-\mathbf{E}_b\times\mathbf{H}_a) &= \mathbf{J}_a\cdot\mathbf{E}_b-\mathbf{J}_b\cdot\mathbf{E}_a-\mathbf{J}_{ma}\cdot\mathbf{H}_b+\mathbf{J}_{mb}\cdot\mathbf{H}_a\\ &\quad+j\omega\mathbf{H}_a\cdot(\overline{\overline{\mu}}_b-\overline{\overline{\mu}}_a^{t})\cdot\mathbf{H}_b-j\omega\mathbf{E}_a\cdot(\overline{\overline{\epsilon}}_b-\overline{\overline{\epsilon}}_a^{t})\cdot\mathbf{E}_b\\ &\quad-j\omega\mathbf{E}_a\cdot(\overline{\overline{\alpha}}_b+\overline{\overline{\beta}}_a^{t})\cdot\mathbf{H}_b+j\omega\mathbf{H}_a\cdot(\overline{\overline{\beta}}_b+\overline{\overline{\alpha}}_a^{t})\cdot\mathbf{E}_b.\end{aligned} \tag{8.166}$$

This expression strongly simplifies when the b state has the characteristics [105]

$$\overline{\overline{\epsilon}}_b=\overline{\overline{\epsilon}}_a^{t}\ ;\ \overline{\overline{\mu}}_b=\overline{\overline{\mu}}_a^{t}\ ;\ \overline{\overline{\alpha}}_b=-\overline{\overline{\beta}}_a^{t}\ ;\ \overline{\overline{\beta}}_b=-\overline{\overline{\alpha}}_a^{t}. \tag{8.167}$$

If we choose this *adjoint medium* for state b, integration of (8.166) yields

$$\begin{aligned}&\int_V(\mathbf{J}_a\cdot\mathbf{E}_b-\mathbf{J}_b\cdot\mathbf{E}_a-\mathbf{J}_{ma}\cdot\mathbf{H}_b+\mathbf{J}_{mb}\cdot\mathbf{H}_a)\,dV\\ &\qquad=\int_S\mathbf{u}_n\cdot(\mathbf{E}_a\times\mathbf{H}_b-\mathbf{E}_b\times\mathbf{H}_a)\,dS.\end{aligned} \tag{8.168}$$

The surface integral vanishes when S is perfectly conducting. It also vanishes when the magnetoelectric medium occupies a bounded region smoothly connected to free space.[‡‡‡] For such a case, S becomes S_∞, a sphere of very large radius, on which the radiation conditions must be satisfied. Thus,

$$\begin{aligned}\mathbf{E}_a&=\frac{1}{R_{c0}}\mathbf{H}_a\times\mathbf{u}_R=\frac{e^{-jk_0R}}{R}\mathbf{F}_a+O_a\left(\frac{1}{R^2}\right)\qquad(R\to\infty)\\ \mathbf{E}_b&=\frac{1}{R_{c0}}\mathbf{H}_b\times\mathbf{u}_R=\frac{e^{-jk_0R}}{R}\mathbf{F}_b+O_b\left(\frac{1}{R^2}\right)\qquad(R\to\infty).\end{aligned} \tag{8.169}$$

It immediately follows that

$$\mathbf{E}_a\times\mathbf{H}_b-\mathbf{E}_b\times\mathbf{H}_a=O\left(\frac{1}{R^3}\right)\qquad(R\to\infty) \tag{8.170}$$

and the surface integral again vanishes. When this condition is satisfied, the following property holds:

$$\int_V(\mathbf{E}_a\cdot\mathbf{J}_b-\mathbf{H}_a\cdot\mathbf{J}_{mb})\,dV=\int_V(\mathbf{E}_b\cdot\mathbf{J}_a-\mathbf{H}_b\cdot\mathbf{J}_{ma})\,dV. \tag{8.171}$$

[‡‡‡]In the presence of abrupt transitions, one would write (8.166) inside and outside the medium, integrate over both regions, and apply continuity of $\mathbf{E}_{\tan}$ and $\mathbf{H}_{\tan}$ to eliminate the contribution of the boundary surface.

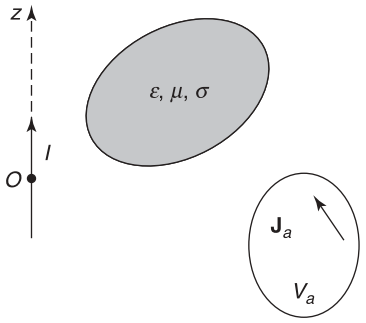

Figure 8.20 Example of use of the reaction principle.

In Rumsey's notation,[58] this equation may be written symbolically as

$$\langle a, b\rangle = \langle b, a\rangle. \tag{8.172}$$

As a simple application of (8.171), consider the evaluation of the electric field in O generated by given currents $\mathbf{J}_a$ (Fig. 8.20). We choose, as a b source a dipole current $\mathbf{J}_b = Il\,\delta(\mathbf{r})\mathbf{u}_z$ located in O. From (8.171):

$$E_{az}(O) = \frac{1}{Il}\int_{V_a} \mathbf{J}_a \cdot \mathbf{E}_b\, dV. \tag{8.173}$$

This component can easily be evaluated if the field generated in V_a by the dipole is known.

The reciprocity idea originated in the middle of the nineteenth century but reached full maturity somewhat later, when H. A. Lorentz[59] showed the fundamental importance of the principle [135]. Note that, while Maxwell's equations are *local*, reciprocity theorems are of a *global* nature, because they describe interactions of two fields in spatial regions and, for arbitrary time-dependence, at all times.[60]

8.6.2 Time-Harmonic Fields: Hilbert Scalar Product

The divergence equation (8.166) is now replaced by

$$\begin{aligned}\operatorname{div}(\mathbf{E}_a \times \mathbf{H}_b^* + \mathbf{E}_b^* \times \mathbf{H}_a) = &-\mathbf{E}_a \cdot \mathbf{J}_b^* - \mathbf{H}_a \cdot \mathbf{J}_{mb}^* - \mathbf{E}_b^* \cdot \mathbf{J}_a - \mathbf{H}_b^* \cdot \mathbf{J}_{ma} \\ &- j\omega \mathbf{E}_a \cdot (\overline{\overline{\epsilon}}_a^t - \overline{\overline{\epsilon}}_b^*) \cdot \mathbf{E}_b^* + j\omega \mathbf{H}_b^* \cdot (\overline{\overline{\mu}}_b^\dagger - \overline{\overline{\mu}}_a) \cdot \mathbf{H}_a \\ &+ j\omega \mathbf{E}_a \cdot (\overline{\overline{\alpha}}_b^* - \overline{\overline{\beta}}_a^t) \cdot \mathbf{H}_b^* + j\omega \mathbf{H}_a \cdot (\overline{\overline{\beta}}_b^* - \overline{\overline{\alpha}}_a^t) \cdot \mathbf{E}_b^*. \end{aligned} \tag{8.174}$$

Only the source terms survive when the *b medium* is the *Hermitian adjoint* of a, that is, when

$$\overline{\overline{\epsilon}}_b = \overline{\overline{\epsilon}}_a^\dagger\ ;\ \overline{\overline{\mu}}_b = \overline{\overline{\mu}}_a^\dagger\ ;\ \overline{\overline{\alpha}}_b = \overline{\overline{\beta}}_a^\dagger\ ;\ \overline{\overline{\beta}} = \overline{\overline{\alpha}}_a^\dagger. \tag{8.175}$$

For such a case (Fig. 8.19):

$$\int_V (\mathbf{E}_a \cdot \mathbf{J}_b^* + \mathbf{E}_b^* \cdot \mathbf{J}_a + \mathbf{H}_a \cdot \mathbf{J}_{mb}^* + \mathbf{H}_b^* \cdot \mathbf{J}_{ma})\, dV$$
$$= -\int_S \mathbf{u}_n \cdot (\mathbf{E}_a \times \mathbf{H}_b^* + \mathbf{E}_b^* \times \mathbf{H}_a)\, dS. \tag{8.176}$$

The surface integral vanishes when S is perfectly conducting. In unbounded space, the same holds if the b field satisfies the far-field condition (8.159) associated with a *convergent* wave. This condition, which implies time reversal and acausality, is

$$\mathbf{E}_b = \frac{e^{jk_0 R}}{R}\mathbf{F}_b + O_b\left(\frac{1}{R^2}\right) = -\frac{1}{R_{c0}}\mathbf{u}_R \times \mathbf{H}_b \qquad (R \to \infty). \tag{8.177}$$

The b state is now of a mathematical, macroscopically nonphysical nature. The reciprocity relationship takes the form

$$\int_V (\mathbf{E}_a \cdot \mathbf{J}_b^* + \mathbf{H}_a \cdot \mathbf{J}_{mb}^*)\, dV = -\int_V (\mathbf{E}_b^* \cdot \mathbf{J}_a + \mathbf{H}_b^* \cdot \mathbf{J}_{ma})\, dV. \tag{8.178}$$

8.6.3 Transient Fields

Let $(\mathbf{e}_a, \mathbf{h}_a)$ denote the retarded fields generated by sources $\mathbf{j}_a, \mathbf{j}_{ma}$ in a lossless, homogeneous medium of parameters ϵ, μ. The sources are activated after a reference time t_a. For state b, we choose the advanced (or acausal) fields $(\mathbf{e}_b, \mathbf{h}_b)$ generated by currents $(\mathbf{j}_b, \mathbf{j}_{mb})$. These fields may be evaluated by means of advanced potentials[§§§]

$$\mathbf{a}_b = \frac{\mu}{4\pi}\int_V \frac{\mathbf{j}_b\left(\mathbf{r}', t + \dfrac{|\mathbf{r} - \mathbf{r}'|}{c}\right)}{|\mathbf{r} - \mathbf{r}'|}\, dV'. \tag{8.179}$$

The sources have been activated from $t = -\infty$, and are turned off when time t_b is reached.[62] The b fields therefore vanish for $t \geq t_b$. From Maxwell's equations, satisfied by both the a and b fields,

$$\operatorname{div}(\mathbf{e}_a \times \mathbf{h}_b + \mathbf{e}_b \times \mathbf{h}_a) = -\mu\frac{\partial}{\partial t}(\mathbf{h}_b \cdot \mathbf{h}_a) - \epsilon\frac{\partial}{\partial t}(\mathbf{e}_b \cdot \mathbf{e}_a)$$
$$- \mathbf{e}_a \cdot \mathbf{j}_b - \mathbf{h}_a \cdot \mathbf{j}_{mb} - \mathbf{h}_b \cdot \mathbf{j}_{ma} - \mathbf{e}_b \cdot \mathbf{j}_a. \tag{8.180}$$

Integration of both members over (t_a, t_b) gives, if $t_b > t_a$,

$$\int_{t_a}^{t_b} dt \int_V (\mathbf{e}_a \cdot \mathbf{j}_{eb} + \mathbf{h}_a \cdot \mathbf{j}_{mb} + \mathbf{h}_b \cdot \mathbf{j}_{ma} + \mathbf{e}_b \cdot \mathbf{j}_{ea})\, dV$$
$$= -\int_{t_a}^{t_b} dt \int_S \mathbf{u}_n \cdot (\mathbf{e}_a \times \mathbf{h}_b + \mathbf{e}_b \times \mathbf{h}_a)\, dS. \tag{8.181}$$

[§§§]The extension to media endowed with conductivity is discussed in Note 61. While the retarded solutions decrease with time because of σ, the advanced solutions grow with time.

Let S be a large spherical surface S_∞. Its radius may be chosen so large that none of the points of S are reached by the (diverging) a wave at time t_b. For such a choice, the surface integral vanishes.

Several reciprocity theorems have been derived in the time domain on the basis of the time-convolution of two signals, a concept that is defined in (7.284) and (A7.5). In a *first* theorem, sources $\mathbf{j}_a(\mathbf{r}, t)$ and $\mathbf{j}_b(\mathbf{r}, t)$ are contained within a volume V, and both vanish before time t_0. Under these conditions, the following result holds[¶¶¶] for all τ:

$$\int_{-\infty}^{\infty} dt \int_V \mathbf{j}_a(\mathbf{r}, \tau - t) \cdot \mathbf{e}_b(\mathbf{r}, t)\, dV = \int_{-\infty}^{\infty} dt \int_V \mathbf{j}_b(\mathbf{r}, t) \cdot \mathbf{e}_a(\mathbf{r}, \tau - t)\, dV. \tag{8.182}$$

This relationship can be derived directly in the time-domain, without introducing intermediate Fourier transforms,[64] an important feature for fields whose time dependence is not Fourier transformable.

In a *second* theorem, the media are assumed to be dispersive, reciprocal, and anisotropic, with constitutive equations of type (8.8). For such media, a relationship combining space and time convolutions can be derived, namely

$$\int_{-\infty}^{\infty} dt' \int_{V_b} \mathbf{e}_a(\mathbf{r} \pm \mathbf{r}', t - t') \cdot \mathbf{j}_b(\mathbf{r}', t')\, dV' = \int_{-\infty}^{\infty} dt' \int_{V_a} \mathbf{e}_b(\mathbf{r} \pm \mathbf{r}', t - t') \cdot \mathbf{j}_a(\mathbf{r}', t')\, dV'. \tag{8.183}$$

Similar equations may be written in terms of magnetic currents and magnetic fields. A *third* theorem, shown in a form valid for time-invariant isotropic media in states a and b, is

$$\int_S \mathbf{u}_n \cdot C(\mathbf{e}_a \times \mathbf{h}_b - \mathbf{e}_b \times \mathbf{h}_a)\, dS = \int_V C\left[-\mathbf{j}_{ma} \cdot \mathbf{h}_b - \mathbf{e}_a \cdot \mathbf{j}_{eb} + \mathbf{j}_{mb} \cdot \mathbf{h}_a + \mathbf{e}_b \cdot \mathbf{j}_{ea}\right] dV$$

$$+ \int_V \left[(\mu_b - \mu_a) \frac{\partial}{\partial \tau} C(\mathbf{h}_a \cdot \mathbf{h}_b) + (\epsilon_a - \epsilon_b) \frac{\partial}{\partial \tau} C(\mathbf{e}_a \cdot \mathbf{e}_b)\right] dV. \tag{8.184}$$

The proof makes use of the property

$$C\left(f_1, \frac{\partial f_2}{\partial t}\right) = C\left(\frac{\partial f_1}{\partial \tau}, f_2\right) = \frac{\partial}{\partial t} C(f_1, f_2). \tag{8.185}$$

Theorem (8.184) may be invoked to solve both the inverse *source* problem and the inverse *profiling* problem (in which the unknowns are the constitutive parameters in some space domain). In the source problem, for example, state a corresponds with the fields generated by the unknown sources, and b is a computational state, often termed *observational*. Medium b is the adjoint of medium a when the latter is anisotropic.[64]

8.7 EQUIVALENT CIRCUIT OF AN ANTENNA

The antenna system of concern is shown in Figure 8.21*a*. It consists of a volume V enclosed by perfectly conducting walls and a transmission line (a waveguide), which connects V to

[¶¶¶]The proof, and the extension to dispersive and anisotropic media, can be found in [50] and in Note 63.

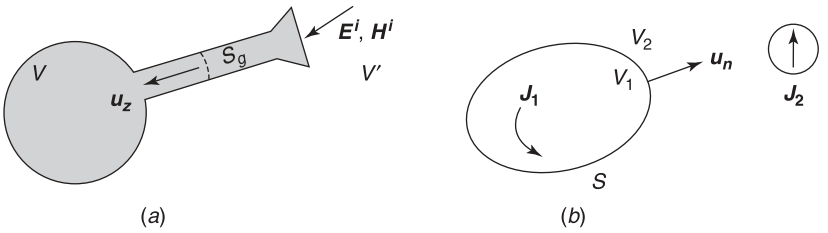

Figure 8.21 (*a*) General antenna system. (*b*) Two regions coupled through boundary S.

a radiating element, for example a horn. The antenna system lies in the field of an incident wave, and the problem is to determine the penetration of the wave into V, where it ultimately dissipates its power in an absorbing load (a receiver). This configuration is a particular case of a more general one, embodied in Figure 8.21*b*, in which volume V_1 is coupled to an exterior volume V_2 by means of a common boundary S. This surface is typically a perfectly conducting wall, provided with an aperture through which the two regions communicate electromagnetically. The wall often serves to shield some electronic system located in V_1, in which case slots and apertures (needed, for example, for heat dissipation or for the in- and out-penetration of cables) tend to jeopardize the shielding effect.

8.7.1 The Coupled Regions Problem

Consider first the fields in region 1 of Figure 8.21*b* (a cavity). Cavity fields are discussed in Chapter 10, where it is shown that they are generated by volume currents $\mathbf{J}_1$ and surface magnetic currents $\mathbf{J}^1_{mS} = \mathbf{u}_n \times \mathbf{E}$. The surface currents represent the contribution from the exterior sources $\mathbf{J}_2$ (see Section 7.12). If the media in V_1 are linear, the two contributions add up, and we may write the magnetic field in the form

$$\mathbf{H}_1(\mathbf{r}) = \mathbf{H}^g_1(\mathbf{r}) + \mathbf{H}(\mathbf{J}^1_{mS}) = \mathbf{H}^g_1(\mathbf{r}) + \mathbf{L}_1(\mathbf{u}_n \times \mathbf{E}). \tag{8.186}$$

The symbol $\mathbf{H}^g_1$ (where g stands for *generator*) denotes the fields generated by $\mathbf{J}_1$ in the presence of a metallized (or short-circuited) surface S. Field $\mathbf{H}^g_1$ is tangent to S and equal to $\mathbf{u}_n \times \mathbf{J}^g_{S1}$, where $\mathbf{J}^g_{S1}$ denotes the current flowing on S on the 1 side. The operator $\mathbf{L}_1$ is further discussed in Section 10.2, and is left unspecified for the moment. In region 2, similarly, the magnetic current is $\mathbf{J}^2_{mS} = (-\mathbf{u}_n) \times \mathbf{E}$ (i.e., minus the already defined $\mathbf{J}^1_{mS}$), and we write,

$$\mathbf{H}_2(\mathbf{r}) = \mathbf{H}^g_2(\mathbf{r}) + \mathbf{H}(\mathbf{J}^2_{mS}) = \mathbf{H}^g_2(\mathbf{r}) + \mathbf{L}_2\,[(-\mathbf{u}_n) \times \mathbf{E}] = \mathbf{H}^g_2(\mathbf{r}) - \mathbf{L}_2(\mathbf{u}_n \times \mathbf{E}). \tag{8.187}$$

The form of operator $\mathbf{L}_2$ is derived in Section 10.7. Expressing continuity of the tangential component $\mathbf{H}_{\tan}$ on S gives, with $\mathbf{J}_{mS} = \mathbf{J}^1_{mS}$,

$$\mathbf{H}_{\tan}(\mathbf{r}) = \mathbf{u}_n \times \mathbf{J}^g_{S1} + \mathbf{L}_{1t}(\mathbf{J}_{mS}) = -\mathbf{u}_n \times \mathbf{J}^g_{S2} - \mathbf{L}_{2t}(\mathbf{J}_{mS}) \qquad (\mathbf{r} \text{ on } S). \tag{8.188}$$

The symbol $\mathbf{L}_t(\mathbf{J}_{mS})$ denotes the tangential component of $\mathbf{L}(\mathbf{J}_{mS})$ on S. Equation (8.188) is fundamental for the solution of $\mathbf{J}_{mS}$, the key unknown in the formulation of the *coupled regions* problem.

The general availability of computer power in the late 1950s made a discretized version of (8.188) desirable. Such a form is obtained, for example,[65] by introducing two sets of real tangential vectors, $\mathbf{a}_m(\mathbf{r})$ and $\mathbf{c}_m(\mathbf{r})$, on boundary surface S. The sets are chosen biorthogonal, in the sense that

$$\int_S \mathbf{a}_m(\mathbf{r}) \cdot \mathbf{c}_n(\mathbf{r})\, dS = \delta_{mn}. \tag{8.189}$$

The tangential fields on the "1" side of S can now be expanded as

$$\mathbf{E}_{\tan}(\mathbf{r}) = \sum_m V_m\, \mathbf{a}_m(\mathbf{r})$$

$$\mathbf{u}_n \times \mathbf{H}(\mathbf{r}) = \sum_n I_n\, \mathbf{c}_n(\mathbf{r}).$$

Invoking (8.189) shows that the "terminal" voltages and currents V_m and I_n are given by

$$V_m = \int_S \mathbf{E}_{\tan} \cdot \mathbf{c}_m\, dS$$

$$I_n = \int_S \mathbf{H}_{\tan} \cdot (\mathbf{a}_n \times \mathbf{u}_n)\, dS.$$

If all media are linear, and if there are no sources in V_1, relationships of the form

$$I_n = \sum_{m=1}^{\infty} Y_{nm} V_m \tag{8.190}$$

must exist. In matrix form:

$$\mathbf{I} = \overline{\overline{Y}} \cdot \mathbf{V}.$$

The power radiated from "1" into "2" is now, averaged over time,

$$P = \frac{1}{2}\, Re \int_S (\mathbf{E}_{\tan} \times \mathbf{H}^*_{\tan}) \cdot \mathbf{u}_n\, dS = \frac{1}{2}\, Re \sum_{m=1}^{\infty} V_m I^*_m. \tag{8.191}$$

With respect to equation (8.188), however, it is $\mathbf{J}_{mS}$, and not $\mathbf{E}_{\tan}$, which should be expanded in an infinite series (truncated in practice). We therefore write[66,67]

$$\mathbf{u}_n \times \mathbf{E} = \mathbf{J}_{mS} = \sum_{n=1}^{N} V_n \mathbf{f}_n(\mathbf{r}) \qquad (\mathbf{r} \text{ on } S). \tag{8.192}$$

Insertion in (8.188) gives

$$\mathbf{H}_{\tan}(\mathbf{r}) = \mathbf{u}_n \times \mathbf{J}^g_{S1} + \sum_{n=1}^{N} V_n \mathbf{L}_{1t}(\mathbf{f}_n) = -\mathbf{u}_n \times \mathbf{J}^g_{S2} - \sum_{n=1}^{N} V_n \mathbf{L}_{2t}(\mathbf{f}_n). \tag{8.193}$$

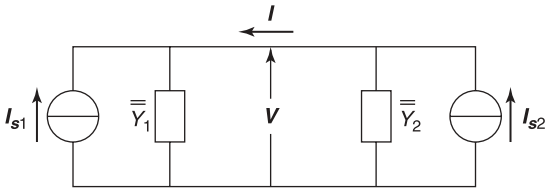

Figure 8.22 Equivalent network for the coupling problem.

This equation will now be tested on S with N testing vectors $\mathbf{w}_i$, and a suitably chosen scalar product. Thus,

$$\begin{aligned}\langle \mathbf{H}_{\tan}, \mathbf{w}_i \rangle &= \left\langle \mathbf{u}_n \times \mathbf{J}^g_{S1}, \mathbf{w}_i \right\rangle + \sum_{n=1}^{N} V_n \langle \mathbf{L}_{1t}(\mathbf{f}_n), \mathbf{w}_i \rangle \\ &= \left\langle \mathbf{u}_n \times \mathbf{J}^g_{S2}, \mathbf{w}_i \right\rangle - \sum_{n=1}^{N} V_n \langle \mathbf{L}_{2t}(\mathbf{f}_n), \mathbf{w}_i \rangle. \end{aligned} \tag{8.194}$$

This system may be written more compactly by means of "N" vectors and "$N \times N$" matrices as

$$\mathbf{I} = -\mathbf{I}_{S1} + \overline{\overline{Y}}_1 \cdot \mathbf{V} = \mathbf{I}_{S2} - \overline{\overline{Y}}_2 \cdot \mathbf{V}. \tag{8.195}$$

Such a relationship may be represented symbolically by the Norton network shown in Figure 8.22. The problem can clearly be split into two mutually exclusive parts, one for each region (typically a waveguide, a resonator, or a half-infinite space). Each region has its specific $\overline{\overline{Y}}$, which can be further used in a variety of configurations. Note that the elements of the admittance depend not only on the region but also on the choice of $\mathbf{f}_n$ (entire domain, subdomain, ...) and of $\mathbf{w}_i$ (equal to $\mathbf{f}_n$ in the Galerkin method).

8.7.2 Application to an Antenna

Anticipating the waveguide theory developed in Chapter 15, we shall assume, for conciseness, that only a single mode propagates in the waveguide shown in Figure 8.21*a*. This mode could be, for example, the TEM mode of a coaxial line. Under these conditions, the fields at a point in S_g can be written in the form

$$\begin{aligned}\mathbf{E}_t &= V\, \boldsymbol{\alpha}(x, y) \\ \mathbf{H} \times \mathbf{u}_z &= I\, \boldsymbol{\alpha}(x, y)\end{aligned} \tag{8.196}$$

where t denotes a component parallel to the transverse (x, y) plane. Vector $\boldsymbol{\alpha}$ is a characteristic eigenvector of the mode, normalized according to the rule

$$\int_{S_g} \boldsymbol{\alpha} \cdot \boldsymbol{\alpha}\, dS = 1.$$

By choosing $\mathbf{u}_z$ to be directed toward the load, the emphasis is on propagation into V, because the average power delivered to V, under time-harmonic conditions, is given by

$$P = \frac{1}{2}\,\mathrm{Re}\int_{S_g} \mathbf{u}_z \cdot (\mathbf{E}\times\mathbf{H}^*)\,dS = \frac{1}{2}\,\mathrm{Re}\,(VI^*). \tag{8.197}$$

If all media are linear in V, there must exist a relationship

$$I = Y_L\,V.$$

The symbol Y_L denotes the admittance of the load for the propagating mode (i.e., the admittance of the volume to the *left* of S_g). The fields in V', to be discussed next, are generated by two sources: first the tangential electric field $V\boldsymbol{\alpha}$ on S_g, second the volume sources $\mathbf{J}$ in V'. At large distances, the first fields can be written as

$$\mathbf{E} = V\,\mathbf{F}(\mathbf{u})\,\frac{e^{-jk_0R}}{R} \qquad (R\to\infty). \tag{8.198}$$

In S_g, the tangential components of $\mathbf{E}_t$ and $\mathbf{H}_t$ are connected by a relationship

$$-I\,\boldsymbol{\alpha} = \mathbf{H}\times(-\mathbf{u}_z) = Y_a\,\mathbf{E}_t = Y_aV\boldsymbol{\alpha} \tag{8.199}$$

where Y_a is the admittance of the antenna (i.e., of the volume to the *right* of S_g). The second fields have the effect of inducing a current $\mathbf{J}_S^g$ in the short-circuited (or "metallized") cross section S_g. This short-circuit current is given by

$$\mathbf{J}_S^g = \mathbf{H}\times\mathbf{u}_z = I^g\,\boldsymbol{\alpha} \qquad (\mathrm{A\,m^{-1}}). \tag{8.200}$$

Expressing continuity of $\mathbf{H}\times\mathbf{u}_z$ on both sides of S_g yields

$$I = Y_LV = I_g - Y_aV \qquad (\mathrm{A}). \tag{8.201}$$

This important relationship corresponds with (8.195), and can be represented graphically by the simple network of Figure 8.23. Such a representation clarifies the ideas, is conceptually satisfactory, but does not solve the main problem, which is to determine Y_a, Y_L, and I^g. Appropriate techniques to solve such problems are described in subsequent chapters. Leaving that point aside, we shall now show that the short-circuit current I^g — a "receiving"

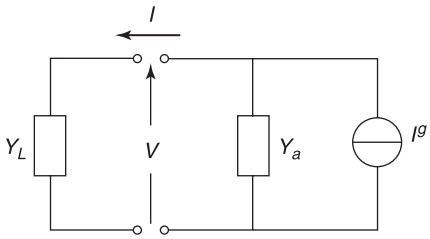

Figure 8.23 Norton equivalent circuit of a receiving antenna.

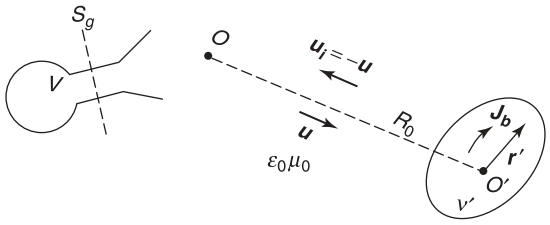

Figure 8.24 An antenna and a distribution of current, partners in a reciprocity theorem.

parameter — can be expressed in terms of the "transmitting" properties of the antenna. The proof consists in applying reciprocity relationship (8.168) to two states:

- A state a in which the antenna radiates in the presence of media $\overline{\overline{\epsilon}}$, $\overline{\overline{\mu}}$ in V'
- A state b in which the sources are a test antenna[68] or an incident plane wave.[69,70]

In the current derivation we choose, for the b state, currents $\mathbf{J}_b$ which radiate in the presence of transpose medium $\overline{\overline{\epsilon}}^t$, $\overline{\overline{\mu}}^t$, cross section S_g being short circuited.[71] Reciprocity theorem (8.168) now gives (Figure 8.21a)

$$-\int_{V'} \mathbf{E}_a \cdot \mathbf{J}_b \, dV = \int_{S_g} \mathbf{u}_t \cdot (\mathbf{E}_a \times \mathbf{H}_b) \, dS = V_a I_b \tag{8.202}$$

from which $I^g = I_b$, the sought short-circuit current, follows immediately. A particularly interesting form is obtained when both antenna and $\mathbf{J}_b$ are in each other's radiation field. We shall assume, for simplicity, that region V' does not contain any materials, hence that the sources radiate in vacuum (Fig. 8.24). For such a case, the far-field of the antenna is (from 8.198)

$$\frac{1}{V_a}\mathbf{E}_a = \mathbf{F}(\mathbf{u})\frac{e^{-jk_0R}}{R} \approx \mathbf{F}(\mathbf{u})\frac{e^{-jk_0R_0}}{R_0}\, e^{-jk_0\mathbf{u}\cdot\mathbf{r}'}$$

where $\mathbf{F}$ is transverse to $\mathbf{u}$, $R_0 = OO'$, and $R \approx R_0 + \mathbf{u}\cdot\mathbf{r}'$. Equation (8.202) now yields

$$I_b = -\frac{e^{-jk_0R_0}}{R_0}\mathbf{F}(\mathbf{u}) \cdot \int_{v'} \mathbf{J}_b(\mathbf{r}')\, e^{jk_0\mathbf{u}_i\cdot\mathbf{r}'}\, dV. \tag{8.203}$$

The integral in (8.203) is directly related to the free-space field radiated by $\mathbf{J}_b$ in the $\mathbf{u}_i = -\mathbf{u}$ direction because, from (7.100)

$$\lim_{R\to\infty} \mathbf{A}^i = \frac{\mu_0}{4\pi}\frac{e^{-jk_0R_0}}{R_0}\int_{v'} \mathbf{J}_b(\mathbf{r}')\, e^{jk_0\mathbf{u}_i\cdot\mathbf{r}'}\, dV' = \mathbf{N}\frac{e^{-jk_0R_0}}{R_0}.$$

The radiated field in O follows as

$$\mathbf{E}^i(O) = j\omega\frac{e^{-jk_0R_0}}{R_0}(\mathbf{N}\times\mathbf{u}_i)\times\mathbf{u}_i. \tag{8.204}$$

Combining (8.203) and (8.204) gives a short-circuit current

$$I^g = I_b = \frac{4\pi}{j\omega\mu_0}\mathbf{F}\cdot\mathbf{E}^i(O) = -2j\lambda_0\left(\mathbf{F}\cdot\frac{\mathbf{E}^i(O)}{R_{c0}}\right) \tag{8.205}$$

for the antenna immersed in a plane wave incident from a direction $\mathbf{u}_i = -\mathbf{u}$ and of electric field $\mathbf{E}^i(O)$ at reference point O. The current density in the short-circuited S_g is therefore, from (8.200),

$$\mathbf{J}_S^g = \frac{4\pi}{j\omega\mu_0}\left[\mathbf{F}(\mathbf{u})\cdot\mathbf{E}^i(O)\right]\boldsymbol{\alpha}. \tag{8.206}$$

Equation (8.205) shows that I^g can be determined by first evaluating $\mathbf{F}$, either analytically, numerically, or experimentally in an anechoic chamber.

A few additional remarks are in order:

1. Equation (8.202), which expresses the intimate relation between the transmitting mode (through $\mathbf{E}_a/V_a$) and the receiving mode (through I^g), is very general, and therefore valid for *near-field* interactions. Given the complexity of near-fields it becomes useful, in that case, to decompose the incident near-fields into partial waves, either plane, or of the spherical harmonic type.[72]

2. When the waveguide in Figure 8.21 carries N propagated modes instead of a single one, (8.196) must be rewitten in the form

$$\begin{aligned}\mathbf{E}_t &= V_1\,\boldsymbol{\alpha}_1 + V_2\,\boldsymbol{\alpha}_2 + \cdots + V_N\,\boldsymbol{\alpha}_N\\ \mathbf{H}\times\mathbf{u}_z &= I_1\,\boldsymbol{\alpha}_1 + I_2\,\boldsymbol{\alpha}_2 + \cdots + I_N\,\boldsymbol{\alpha}_N\end{aligned} \tag{8.207}$$

   with $\displaystyle\int_{S_g}\boldsymbol{\alpha}_i\cdot\boldsymbol{\alpha}_k = \delta_{ik}$. Relationships such as (8.198) to (8.206) are still valid for each mode individually. Equation (8.206), in particular, becomes

$$\mathbf{J}_S^g = \mathbf{H}^g\times\mathbf{u}_z = \frac{4\pi}{j\omega\mu_0}\,\mathbf{E}^i(o)\cdot[\mathbf{F}_1\,\boldsymbol{\alpha}_1 + \cdots + \mathbf{F}_N\boldsymbol{\alpha}_N]. \tag{8.208}$$

3. Further generalization is achieved by considering *two* antennas, with respective waveguide cross sections S_g' and S_g''. Instead of (8.199) we write[68]

$$\begin{aligned}-I_1' &= Y_{11}'V_1' + Y_{12}'V_2' + \cdots + Y_{11}^mV_1'' + Y_{12}^mV_2'' + \cdots\\ -I_2' &= Y_{21}'V_1' + Y_{22}'V_2' + \cdots + Y_{21}^mV_1'' + Y_{22}^mV_2'' + \cdots\end{aligned} \tag{8.209}$$

   and

$$\begin{aligned}-I_1'' &= Y_{11}''V_1'' + Y_{12}''V_2'' + \cdots + Y_{11}^pV_1' + Y_{12}^pV_2' + \cdots\\ -I_2'' &= Y_{21}''V_1'' + Y_{22}''V_2'' + \cdots + Y_{21}^pV_1' + Y_{22}^pV_2' + \cdots.\end{aligned} \tag{8.210}$$

   More concisely:

$$\begin{aligned}\mathbf{I}' &= -\overline{\overline{Y}}'\cdot\mathbf{V}' - \overline{\overline{Y}}^m\cdot\mathbf{V}''\\ \mathbf{I}'' &= -\overline{\overline{Y}}^p\cdot\mathbf{V}' - \overline{\overline{Y}}''\cdot\mathbf{V}''.\end{aligned} \tag{8.211}$$

   If $\overline{\overline{Y}}^m$ is evaluated for a host medium $\overline{\overline{\epsilon}}$, $\overline{\overline{\mu}}$, and if $\overline{\overline{Y}}^p$ is similarly evaluated for the transposed medium $\overline{\overline{\epsilon}}^t$, $\overline{\overline{\mu}}^t$, reciprocity shows that

$$\overline{\overline{Y}}^m_{(\overline{\overline{\epsilon}},\overline{\overline{\mu}})} = \left[\overline{\overline{Y}}^p_{(\overline{\overline{\epsilon}}^t,\overline{\overline{\mu}}^t)}\right]^t. \tag{8.212}$$

If, in particular, the medium is reciprocal,

$$\overline{\overline{Y}}^m = (\overline{\overline{Y}}^p)^t. \tag{8.213}$$

4. The Norton equivalent can be replaced by a Thevenin circuit of open voltage (I^g/Y_a). If we define the *effective length of the antenna* by[73]

$$\mathbf{l}_{\text{eff}} = \frac{4\pi}{j\omega\mu_0}\frac{\mathbf{F}}{Y_a}, \tag{8.214}$$

the open circuit voltage becomes

$$V^g = \frac{I^g}{Y_a} = \mathbf{l}_{\text{eff}} \cdot \mathbf{E}^i(o).$$

8.8 EFFECTIVE ANTENNA AREA

The evaluation of the effective area is based on the equivalent circuit shown in Figure 8.23. We shall assume that the waveguide carries only one mode and that all media are reciprocal.

8.8.1 Power Absorbed by the Load

On the basis of (8.197) and (8.201), the time-averaged power delivered to the receiving antenna (the "load") is given by

$$\begin{aligned} P &= \frac{1}{2}\,\text{Re}\int_{S_g} \mathbf{u}_z \cdot (\mathbf{E}\times\mathbf{H}^*)\,dS = \frac{1}{2}\,\text{Re}\,(VI^*) \\ &= \frac{1}{2}\frac{g_L|I_g|^2}{|Y_a+Y_L|^2} \end{aligned} \tag{8.215}$$

where $g_L = \text{Re}(Y_L)$, and the factor $\frac{1}{2}$ appears because we use peak and not *RMS* values for the fields. It is clear that, as in classic circuit theory, P reaches a maximum P^a for a matched load (i.e., for $Y_L = Y_a^*$). In an unmatched situation,

$$P = \underbrace{\frac{4g_a g_L}{|Y_a+Y_L|^2}}_{\text{mismatch factor } M} P^a \tag{8.216}$$

where $0 \le M \le 1$. The available power P^a is, from the value of I^g in (8.205),

$$P^a = \frac{|I_g|^2}{8g_a} = \frac{\lambda_0^2}{2g_a R_{c0}^2}|\mathbf{F}\cdot\mathbf{E}^i|^2. \tag{8.217}$$

The conductance $g_a(= \mathrm{Re}(Y_a))$ can be eliminated by assuming that the antenna operates in its transmitting mode. Under these conditions, a power[‖‖‖]

$$P = \frac{1}{2} g_a |V|^2$$

flows to the right of S_g. Because of possible losses in the antenna system, only a fraction η of the power is actually radiated. Thus, keeping (8.198) in mind,

$$P^{\mathrm{rad}} = \eta \frac{1}{2} g_a |V|^2 = \frac{|V|^2}{2R_{c0}} \int_{4\pi} |\mathbf{F}(\mathbf{u})|^2 d\Omega \tag{8.218}$$

where $d\Omega$ is an elementary solid angle. Using the definition (7.106) of the directivity gives

$$P^a = \frac{\lambda_0^2}{8\pi R_{c0}} \eta D \frac{|\mathbf{F} \cdot \mathbf{E}^i|^2}{|\mathbf{F}|^2}. \tag{8.219}$$

This power is proportional to the power density $|\mathbf{E}^i|^2/2R_{c0}$ of the incident wave. A crucial property of the antenna, independent of the power level of the incident wave, is the *effective area* (or cross section)

$$S_a = \frac{P^a}{|\mathbf{E}^i|^2/2R_{c0}} = M\eta D \frac{\lambda_0^2}{4\pi} \frac{|\mathbf{F} \cdot \mathbf{E}^i|^2}{|\mathbf{F}|^2 |\mathbf{E}^i|^2}. \tag{8.220}$$

With the definition of the gain given in (7.108), one may write

$$S_a = M P_{\mathrm{rad}} \frac{G(\mathbf{u})\lambda_0^2}{4\pi} \tag{8.221}$$

where P_{rad} is the *polarization factor*, to be discussed next.

8.8.2 The Polarization Factor

Because the mismatch factor may be considered trivial, it is the polarization factor

$$P_{\mathrm{rad}} = \frac{|\mathbf{F} \cdot \mathbf{E}^i|^2}{|\mathbf{F}|^2 \cdot |\mathbf{E}^i|^2} = \frac{|\mathbf{l}_{\mathrm{eff}} \cdot \mathbf{E}^i|^2}{|\mathbf{l}_{\mathrm{eff}}|^2 |\mathbf{E}^i|^2} \tag{8.222}$$

that will require our attention. The value of P_{rad} depends on the properties of the polarization ellipses (Fig. 8.25). The polarization of the radiated field is defined by the complex factor

$$\mathbf{F} \doteq \mathbf{u}_x - j\epsilon \mathbf{u}_y.$$

[‖‖‖]The power dissipated in g_a is not the power backscattered by the antenna operating in its receiving mode. More precisely, the circuit in Figure 8.23 is appropriate for the evaluation of *fields* but not automatically of *powers* (although it gives correct results when applied to the passive load Y_L). The matter has been discussed extensively in the literature[74] [47, 113, 118].

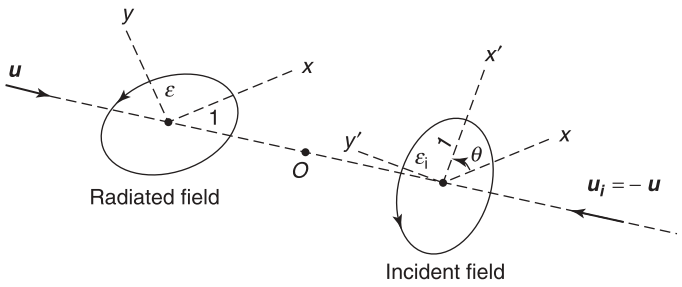

Figure 8.25 Polarization ellipses of radiated and incident fields.

For the incident field:

$$\mathbf{E}^i \doteq \mathbf{u}_{x'} - j\epsilon_i \cdot \mathbf{u}_{y'}. \tag{8.223}$$

When ϵ and ϵ^i have the same sign, the ellipses rotate in the same sense in space but in opposite senses with respect to their respective direction of propagation. A few elementary steps show that

$$P_{\text{rad}} = \frac{|\mathbf{F}\cdot\mathbf{E}^i|^2}{|\mathbf{F}|^2|\mathbf{E}^i|^2} = \frac{(\epsilon_i - \epsilon)^2}{(1+\epsilon_i^2)(1+\epsilon^2)} + \cos^2\theta \frac{(1-\epsilon^2)(1-\epsilon_i^2)}{(1+\epsilon^2)(1+\epsilon_i^2)}. \tag{8.224}$$

According to this important formula:

1. P_{rad} is maximum when $\theta = 0$ (i.e., when the major axes coincide in space). More precisely,

$$0 \le P_{\text{rad}}^{\max} = \frac{(1-\epsilon\epsilon_i)^2}{(1+\epsilon_1^2)(1+\epsilon^2)} \le 1. \tag{8.225}$$

2. P_{rad} is minimum when $\theta = 90^\circ$ (i.e., when the major axes are perpendicular). Thus,

$$0 \le P_{\text{rad}}^{\min} = \frac{(\epsilon_i - \epsilon)^2}{(1+\epsilon_i^2)(1+\epsilon^2)} \le 1. \tag{8.226}$$

3. The maximum maximorum is equal to one and is obtained for $\epsilon_i = -\epsilon$ and $\theta = 0$ (i.e., for ellipses which can be superimposed but rotate in opposite senses in space).
4. The minimum minimorum is zero, and it occurs for $\epsilon_i = \epsilon$ and $\theta = 90^\circ$ (i.e., for ellipses that have the same shape, are described in the same sense in space, and are perpendicular to each other).

Formula (8.224) has found numerous applications in practice. It can serve to evaluate the power transmitted between antennas in a microwave link (Problem 8.30). It can also serve to understand what happens when a circularly polarized wave is incident along the axis of a body of revolution (which could be a sphere or a plane) (Fig. 8.26). The x and y components are reflected with identical phase and amplitude, hence the reflected wave is circularly polarized in the same sense in space as the incident wave. If the same antenna is used to transmit and receive, as in most monostatic radars, P_{rad} vanishes, hence the target will not be "seen." The principle has been applied to weather radar systems to improve the detectability of an obstacle (say a mountain) behind a cloud of interfering raindrops, most of which may be assumed quasi-spherical in shape.

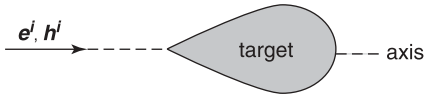

Figure 8.26 Circularly polarized wave, incident on a body of revolution.

8.8.3 Partially Polarized Incident Field

When the time variation of the incident field is arbitrary, the problem of determining the received signal becomes extremely complex, not only because the high-frequency part of the spectrum causes multimode propagation in the waveguide, but also because the time dependence of parameters such as $\mathbf{F}$ or Y_a must be taken into account [47]. The situation is strongly simplified when the receiver is narrow-banded, and G and $\mathbf{F}$ may be considered constant throughout the band. Because the signals are partially polarized, the techniques of Section 7.5 may be applied. For example, assuming that conjugate-matching holds throughout the band,

$$\langle S_a \rangle = \lim_{T\to\infty} \frac{1}{2T} \int_{-T}^{T} S_a(t)\, dt = \frac{G\lambda_0^2}{4\pi} \langle P_{\text{rad}} \rangle. \tag{8.227}$$

The (almost sinusoidal) incident field is of the form (Fig. 8.21*a*)

$$\mathbf{e}^i = e_{ix}(t) \cos[\omega t + \phi_x(t)]\, \mathbf{u}_x + e_{iy}(t) \cos[\omega t + \phi_x(t) + \delta(t)]\, \mathbf{u}_y,$$

where e_{ix}, e_{iy}, and the phase angles vary slowly over a period $(2\pi/\omega)$. It follows that

$$\left\langle |\mathbf{e}^i|^2 \right\rangle = \frac{1}{2} \left\langle e_{ix}^2 \right\rangle + \frac{1}{2} \left\langle e_{iy}^2 \right\rangle.$$

This is $2R_{c0}$ times the time-averaged incident power density. The radiation field is represented by $\mathbf{F} = \mathbf{u}_x - j\epsilon \mathbf{u}_y$, with corresponding time-dependence

$$\mathbf{f}(t) = \cos \omega t\, \mathbf{u}_x + \epsilon \cos\left(\omega t - \frac{\pi}{2}\right) \mathbf{u}_y.$$

Consequently,

$$\left\langle |\mathbf{f}|^2 \right\rangle = \frac{1}{2}(1 + \epsilon^2),$$

and

$$\left\langle |\mathbf{f} \cdot \mathbf{e}^i|^2 \right\rangle = \frac{1}{4} \left[\left\langle e_{ix}^2 \right\rangle + 2\epsilon \left\langle e_{ix} e_{iy} \sin \delta \right\rangle + \epsilon^2 \left\langle e_{iy}^2 \right\rangle \right].$$

This leads to the value

$$\langle P_{\text{rad}} \rangle = \frac{\left\langle e_{ix}^2 \right\rangle + 2\epsilon \left\langle e_{ix} e_{iy} \sin \delta \right\rangle + \epsilon^2 \left\langle e_{iy}^2 \right\rangle}{(1 + \epsilon^2) \left[\left\langle e_{ix}^2 \right\rangle + \left\langle e_{iy}^2 \right\rangle \right]}. \tag{8.228}$$

In terms of the Stokes parameters of the incident wave, defined in (7.71),

$$\langle P_{\text{rad}} \rangle = \frac{1}{2} \frac{(1+\epsilon^2)s_0 + (1-\epsilon^2)s_1 + 2\epsilon s_3}{s_0(1+\epsilon^2)}. \tag{8.229}$$

For a totally unpolarized incident field, characterized by $s_0 = 1, s_1 = s_2 = s_3 = 0$, we obtain the intuitively predictable result[75]

$$\begin{aligned} \langle P_{\text{rad}} \rangle &= \frac{1}{2} \\ \langle S_a \rangle &= \frac{G\lambda_0^2}{8\pi}. \end{aligned} \tag{8.230}$$

Relationship (8.228) can also be written in terms of the polarization matrix introduced in Section 7.5. For the incident field, this matrix is[76,77,78]

$$\overline{\overline{p}}_i = \frac{1}{\langle e_{ix}^2 \rangle + \langle e_{iy}^2 \rangle} \begin{pmatrix} \langle e_{ix}^2 \rangle & \langle e_{ix} e_{iy} e^{-j\delta} \rangle \\ \langle e_{ix} e_{iy} e^{j\delta} \rangle & \langle e_{iy}^2 \rangle \end{pmatrix}. \tag{8.231}$$

For the antenna radiation:

$$\overline{\overline{p}}_a = \frac{1}{1+\epsilon^2} \begin{pmatrix} 1 & j\epsilon \\ -j\epsilon & \epsilon^2 \end{pmatrix}. \tag{8.232}$$

It is easy to verify that

$$\langle P_{\text{rad}} \rangle = tr(\overline{\overline{p}}_i \times \overline{\overline{p}}_a^t). \tag{8.233}$$

PROBLEMS

8.1 Show that the frequency dependence in (8.21) can be simulated by the circuit shown in Figure P8.1. Use the admittance representation.
(E. G. Farr *et al.*, *Measurement Note* **52**, Nov. 1997.)

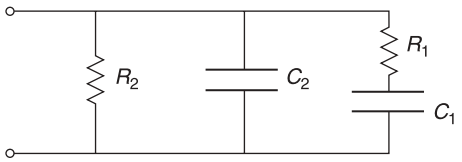

Figure P8.1

8.2 A charged particle moves in crossed static fields $\mathbf{e}_0$ and $\mathbf{b}_0$. In the absence of $\mathbf{e}_0$ the particle is known to describe a circle perpendicular to $\mathbf{b}_0$ (Fig. P8.2). Find the gyration radius and the cyclotron angular frequency of the motion. Show that $\mathbf{e}_0$ produces a general drift velocity $\dfrac{\mathbf{e}_0 \times \mathbf{b}_0}{|\mathbf{b}_0|^2}$ [123].

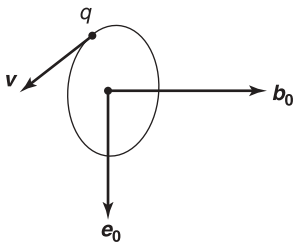

Figure P8.2

8.3 Assume that a material has a diagonal permittivity $\bar{\bar{\epsilon}} = \epsilon_x \mathbf{u}_x\mathbf{u}_x + \epsilon_y \mathbf{u}_y\mathbf{u}_y + \epsilon_z \mathbf{u}_z\mathbf{u}_z$. Identify the axial nature of the medium by writing

$$\bar{\bar{\epsilon}} = \epsilon_x \bar{\bar{I}} + \frac{\epsilon_x - \epsilon_y}{2}(\mathbf{u}_m\mathbf{u}_n + \mathbf{u}_n\mathbf{u}_m).$$

Determine the value of the unit vectors $\mathbf{u}_m, \mathbf{u}_n$.
(W. S. Weiglhofer *et al*., *Electromagn.* **19**, 351–362, 1999.)

8.4 (**a**) Show that the potentials in an inhomogeneous medium can be expressed in the form

$$\phi = -\text{div}(\epsilon \boldsymbol{\pi}_e)$$
$$\mathbf{A} = j\omega\epsilon_0^2\mu_0\boldsymbol{\pi}_e + \epsilon^{-1}\cdot\text{curl}\,\boldsymbol{\pi}_m.$$

(**b**) Find the differential equations satisfied by the electric and magnetic Hertz vectors $\boldsymbol{\pi}_e$ and $\boldsymbol{\pi}_m$.
(A. Nisbet, *Proc. Roy. Soc. London, Ser. A.* **240**, 375, 1957.)

8.5 Sketch the frequency variation of the permittivities $(\epsilon_r - \epsilon_r')$ and $(\epsilon_r + \epsilon_r')$ given in (8.64). Investigate, in particular, the region $\omega < |\omega_c/2|$, and show that the electronic wave can propagate down to the lowest frequencies. This feature explains how low-frequency "whistlers" are able to propagate in the ionosphere in the direction of the earth's magnetic field.

8.6 Show that in a lossless medium with variable ϵ and μ,

$$\nabla^2\mathbf{e} - \frac{N^2}{c^2}\frac{\partial^2\mathbf{e}}{\partial t^2} = -\text{grad}(\mathbf{p}\cdot\mathbf{e}) - \mathbf{q}\times\text{curl}\,\mathbf{e}$$
$$\nabla^2\mathbf{h} - \frac{N^2}{c^2}\frac{\partial^2\mathbf{h}}{\partial t^2} = -\text{grad}(\mathbf{q}\cdot\mathbf{h}) - \mathbf{p}\times\text{curl}\,\mathbf{h},$$

where $\mathbf{p} = (1/\epsilon)\,\text{grad}\,\epsilon, \mathbf{q} = (1/\mu)\,\text{grad}\,\mu$, and $N = (\epsilon_r\mu_r)^{\frac{1}{2}}$.

8.7 *Tellegen* has introduced *media* characterized by the constitutive equations

$$\mathbf{D} = \epsilon\mathbf{E} + \alpha\mathbf{H}$$
$$\mathbf{B} = \beta\mathbf{E} + \mu\mathbf{H}.$$

(**a**) Show that $\mathbf{E}$ and $\mathbf{H}$ satisfy the equation

$$\nabla^2\mathbf{F} + j\omega(\beta - \alpha)\,\text{curl}\,\mathbf{F} + \omega^2(\epsilon\mu - \alpha\beta)\mathbf{F} = 0.$$

(**b**) Show that the same equation is satisfied by the vector potential **A**, provided the gauge is defined by the auxiliary relationship

$$\text{div } \mathbf{A} + j\omega(\epsilon\mu - \alpha\beta)\phi = 0.$$

(**c**) Show that the corresponding scalar potential satisfies

$$\nabla^2\phi + \omega^2(\epsilon\mu - \alpha\beta)\phi = 0.$$

(**d**) Verify that double refraction occurs in the medium.
(L. L. G. Chambers, *Quart. J. Mech. Appl. Math.* **9**, 360, 1956.)

8.8 Consider a uniaxial chiral medium of constitutive equations

$$\mathbf{D} = (\epsilon_t \bar{\bar{I}}_t + \epsilon_z \mathbf{u}_z\mathbf{u}_z)\cdot\mathbf{E} - j\frac{\kappa}{c_0}\mathbf{u}_z\mathbf{u}_z\cdot\mathbf{H}$$

$$\mathbf{B} = (\mu_t \bar{\bar{I}}_t + \mu_z \mathbf{u}_z\mathbf{u}_z)\cdot\mathbf{H} + j\frac{\kappa}{c_0}\mathbf{u}_z\mathbf{u}_z\cdot\mathbf{E}.$$

Show that a slab of that material can transform any polarization to any other polarization. In particular, show that two linearly polarized fields that are perpendicular to each other can be transformed to right-hand and left-hand circularly polarized fields, respectively.
(A. J. Viitanen *et al.*, *Electron. Lett.* **29**, 1074–1075, 1993.)

8.9 A z-dependent plane wave in a medium with positive ϵ_r and μ_r has the components

$$E_x = A\, e^{-j\mathbf{k}\cdot\mathbf{r}} = A\, e^{-jkz}$$

$$H_y = \frac{A}{R_c}\, e^{-jkz}.$$

Pointing's vector $\dfrac{|A|^2}{R_c}\,\mathbf{u}_z$ is directed toward positive z. Consider, on the other hand, a DNG medium, for which $\epsilon_r = -|\epsilon_r|$ and $\mu_r = -|\mu_r|$. Insert these parameters into Maxwell's equations, and show that $k = -k_0\sqrt{|\epsilon_r||\mu_r|}$, which means that **k** is directed toward $(-\mathbf{u}_z)$.

8.10 Consider a horizontally stratified medium in which ϵ and μ depend on z alone. A z-oriented electric dipole produces fields that can be derived from a Hertz potential $\pi\mathbf{u}_z$. Show that π satisfies, for very small values of grad ϵ, the equation $\nabla^2\pi + k_0^2N^2\pi = 0$, where $k_0^2 = \omega^2\epsilon_0\mu_0$, and N is the index of refraction. Show that there exists a solution of the form

$$\pi = \int_0^\infty \lambda J_0(\lambda r)\, v(z,\lambda)\, d\lambda.$$

8.11 Voltage and current on an inhomogeneous lossless transmission line satisfy

$$\frac{dV}{dx} = -j\omega L(x) I$$

$$\frac{dI}{dx} = -j\omega C(x) V.$$

Derive the *WKB* approximation for V and I.

8.12 *Maxwell's fish-eye lens* is a half-sphere of index of refraction

$$N = \frac{2}{1 + \left(\dfrac{R}{a}\right)^2}.$$

Apply (8.91) to show that the rays issued from the pole O (Fig. P8.3) emerge parallel to the z-axis, thereby converting a spherical wave from O into a plane wave [22].

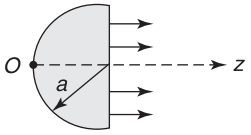

Figure P8.3

8.13 Assume that the index of refraction of the atmosphere varies according to a law $N = N_0\left(1 - \frac{h}{a}\right)$, where h is small with respect to a (Fig. P8.4). Assume also that the ray from A is little inclined with respect to the horizon, a typical situation for a terrestrial radio link. Show that the rays are circles [18].

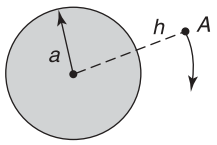

Figure P8.4

8.14 Derive an expression for the reflection and transmission coefficients of the slab in Figure P8.5. Consider, in particular, the value of these coefficients when the interval AB is much less than the wavelength in the slab. Analyze further by evaluating the coefficients for a homogeneous slab. Compare the obtained formulas with the easily derived exact values.

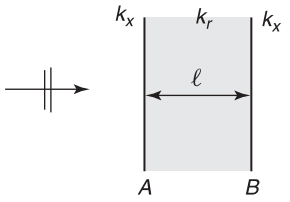

Figure P8.5

8.15 Solve the problem

$$\frac{da(z)}{dz} = \epsilon p(z)\, b(z)$$
$$\frac{db(z)}{dz} = \epsilon q(z)\, a(z),$$

where ϵ is a small parameter. The sought solution proceeds by way of expansions

$$a(z) = a_0(z) + \epsilon a_1(z) + \cdots$$
$$b(z) = b_0(z) + \epsilon b_1(z) + \cdots .$$

If a_0, for example, is a wave propagating to $(+z)$, $\epsilon\, b_1$ will be a reflected wave to $(-z)$. The solution gives a better approximation than the classical *WKB* approach [2, 137].

8.16 A well-known method to investigate paraxial beams consists of writing the field in the form $u(\mathbf{r}) = \psi(x, y, z)e^{-jkz}$, where ψ is a slowly varying function. Such a quasi-plane wave is suitable to represent a laser beam. Neglecting $\partial^2\psi/\partial z^2$, show that ψ satisfies

$$\nabla_{xy}^2\psi - 2jk\frac{\partial\psi}{\partial z} = 0$$

and that the solution is of the form

$$\psi = e^{-jP(z)}e^{-j\frac{kr^2}{2q}}.$$

(H. Kogelnik *et al.*, *Proc. IEEE*, **54**, 1312–1329, 1966.)

8.17 A paraxial ray is characterized by a small radius $r(z)$ and a slope $\dfrac{dr}{dz}$ (Fig. P8.6). Successive values of these parameters are connected by the relationship [143]

$$\begin{pmatrix} r \\ \dfrac{dr}{dz} \end{pmatrix}_2 = \begin{pmatrix} A & B \\ C & D \end{pmatrix} \cdot \begin{pmatrix} r \\ \dfrac{r}{dz} \end{pmatrix}_1.$$

Determine the ray-transfer matrix (*ABCD*)

(**a**) For a homogeneous medium of index N in the space between 1 and 2

(**b**) For a lenslike medium of $N = N_0 - \dfrac{1}{2}N_2r^2$

(**c**) For a thin lens of focal length f (Fig. P8.6*b*).

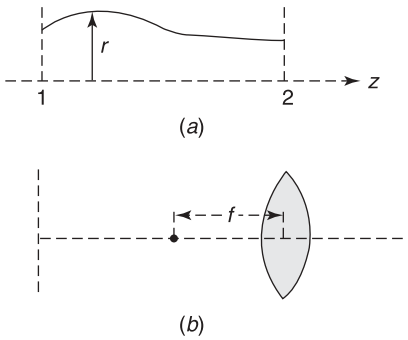

Figure P8.6

8.18 Consider a cylindrical column having an index of refraction (Fig. P8.7)

$$N^2 = N_0^2\left[1 - \frac{r^2}{a^2}\right].$$

Investigate the form of the rays in the paraxial region. Show that the trajectories are sinusoidal [18].

8.19 Particularize the value (8.142) of h_φ to a *lossless* medium. Determine the value of h_φ produced by the step dipole created by suddenly separating charges $+q$ and $-q$ (see Section 7.3).

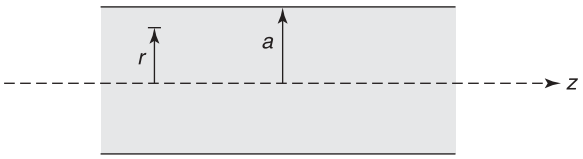

Figure P8.7

8.20 The constitutive equations (8.41) can also be written in the Drude-Born-Fedorov form

$$\mathbf{D} = \epsilon[\mathbf{E} + \beta \text{ curl } \mathbf{E}]$$

$$\mathbf{B} = \mu[\mathbf{H} + \beta \text{ curl } \mathbf{H}].$$

Determine the corresponding form of differential equation (8.144).
(A. Lakhtakia, *AEÜ.* **45**, 57–59, 1991.)

8.21 Extend the reciprocity theorem of Section 8.6 to a medium of finite conductivity.
(W. J. Welch, *IRE Trans. Antennas Propagation* **9**, 114, 1961.)

8.22 A point charge q is located inside a spherical volume bounded by conducting walls. Apply a reciprocity principle to determine the potential at the center of the sphere (Fig. P8.8).

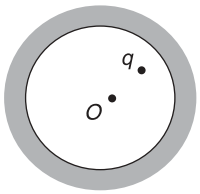

Figure P8.8

8.23 Prove the reciprocity principle (8.171) for the configuration of Figure P8.9, where the medium is a lossless isotropic homogeneous dielectric. To simplify matters, consider only electric currents **J**.

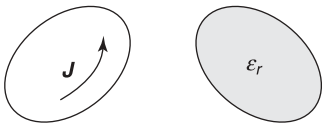

Figure P8.9

8.24 Apply the reciprocity principle (8.171) to determine the magnetic field H_z generated in P by an aperture in a cavity V on which a given ($\mathbf{u}_n \times \mathbf{E}$) is impressed (Fig. P8.10).
Hint: Put a z-oriented magnetic dipole in P, and assume that the induced currents are known on the metallized aperture.

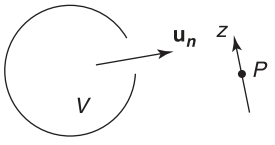

Figure P8.10

8.25 A unit current is injected into the (submerged) loop antenna AB (Fig. P8.11). Determine the voltage that appears between the C and D terminals of a short receiving linear antenna. This voltage is Z_{12}, and it is equal to Z_{21}, by reciprocity. Impedance Z_{21}, on the other hand, follows from evaluating the voltage that appears between A and B when a unit current is injected at CD. At the frequencies typically used for the link, the Q of seawater is very low, and S may be considered as almost perfectly conducting [100].

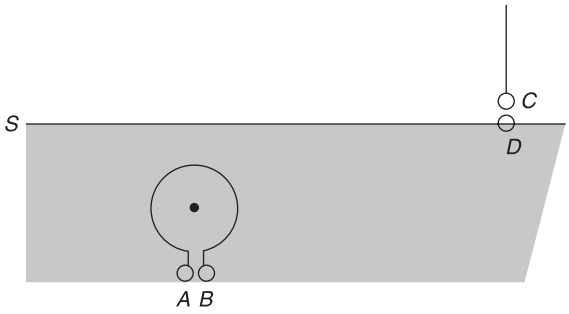

Figure P8.11

8.26 Consider two perfectly conducting antennas energized across a narrow gap. Show that

$$V_1 I_{12} = V_2 I_{21}$$

where I_{ik} is the base current flowing in the (shorted) antenna i when a voltage V_k is applied across the gap of antenna k.
(A. F. Stevenson, *Quart. Appl. Math.* **5**, 371–384, 1948; and E. Roubine, *Onde Elec.* **30**, 259, 1950.)

8.27 In Equation (8.206), $\mathbf{F}_1$ and $\mathbf{E}^i$ are defined with respect to the same reference point O. Show that the product $\mathbf{F}_1 \cdot \mathbf{E}^i$ is invariant with respect to a shift in the position of O.

8.28 Determine the effective length $\mathbf{l}_{\text{eff}}$ of
(**a**) A short center-fed linear antenna
(**b**) A small circular loop antenna [47].

8.29 Determine the effective cross section (8.220) of a short linear antenna. Determine, in particular, the directivity D and the polarization factor P_{rad} of the antenna.

8.30 In a microwave relay, two identical antennas ($\epsilon_1 = -\epsilon_i$) are used, respectively in their transmitting and receiving modes (Fig. P8.12). Evaluate the power picked up by *2* when *1* radiates a power P_1. How does that power vary with θ?

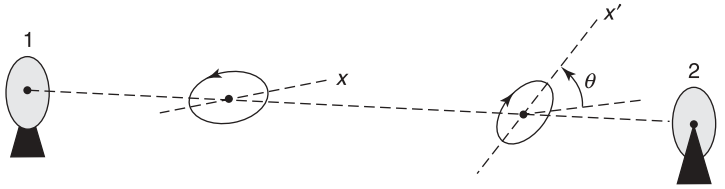

Figure P8.12

8.31 Apply relationship (8.228) to
(**a**) An antenna radiating a linearly polarized wave
(**b**) An antenna radiating a circularly polarized wave
(**c**) An unpolarized incident wave.

NOTES

1. P. Werner, Randwertprobleme für die zeitunabhängigen Maxwellschen Gleichungen mit variablen Koeffizienten, *Arch. Rational Mech. Anal.* **18**, 167–195 (1955).
2. E. G. Farr and C. A. Frost, Impulse propagation measurements of the dielectric properties of water, dry sand, moist sand, and concrete, *Measurement Note* **52** (Nov. 1997).
3. O. P. Gandhi, B. Gao, and J. Chen, A frequency-dependent finite-difference time-domain formulation for general dispersive media, *IEEE Trans. MTT* **41**, 658–665 (1993).
4. C. M. Furse, J. Chen, and O. P. Gandhi, The use of the frequency-dependent finite-difference time-domain method for induced current and SAR calculations for a heterogeneous model of the human body, *IEEE Trans. EMC* **36**, 128–133 (1994).
5. M. P. Givens, Optical properties of metals, *Solid State Physics* **6**, 313–352 (1958).
6. S. Gruber, On charge relaxation in good conductors, *Proc. IEEE* **61**, 237–238 (1973).
7. R. J. Gutmann and J. M. Berrego, Charge density in a conducting medium revisited, *IEEE Trans. AP* **22**, 635–636 (1974).
8. K. K. Mei and G. Liang, Electromagnetics of superconductors, *IEEE Trans. MTT* **39**, 1545–1552 (1991).
9. P. J. Walsh and V. P. Tomaselli, Theory of microwave surface impedance in superconductors and normal metals, *Am. J. Phys.* **58**, 644–650 (1990).
10. R. R. Mansoor, Microwave superconductivity, *IEEE Trans. MTT* **50**, 750–759 (2002).
11. J. C. Bose, On the rotation of the plane of polarization by a twisted structure, *Proc. Roy. Soc. (London)* **63**, 146–152 (1898).
12. H. Cory and I. Rosenhouse, Multi-layered chiral filters, *Electromagn.* **17**, 317–341 (1997).
13. I. V. Lindell, A. H. Sihvola, and K. Suchy, Six-vector formalism in electromagnetics of bianisotropic media, *J. Electromagn. Waves Appl.* **9**, 887–903 (1995).
14. J. Fridén, G. Kristensson, and A. Sihvola, Effect of dissipation on the constitutive relations of bi-anisotropic media — the optical response, *Electromagn.* **17**, 251–267 (1997).
15. S. Zouhdi, A. Sihvola, and M. Arsalane (eds.), *NATO advanced workshop on bianisotropics 2002*, Kluwer Academic Publishers, Dordrecht, The Netherlands.
16. M. M. I. Saadoun and N. Engheta, A reciprocal phase shifter using novel pseudochiral or omega medium, *Microwave Opt. Tech. Lett.* **5**, 184–188 (1992).
17. C. R. Simovski and B. Sauviac, Toward creating isotropic microwave composites with negative refraction, *Radio Sci.* **39**, RS2014, 1–18, 2004.
18. A. Ishimaru, S. W. Lee, Y. Kuga, and V. Jandhyala, Generalized constitutive relations for metamaterials based on the quasi-static Lorentz theory, *IEEE Trans. AP* **51**, 2550–2557 (2003). This paper is part of an issue of the transactions devoted to metamaterials.
19. N. Engheta, An idea for thin subwavelength cavity resonators using metamaterials with negative permittivity and permeability, *IEEE Ant. Wireless Prop. Lett.* **1**, 10–13, 2002.
20. G. F. Eleftheriades, Enabling RFmicrowave devices using negative-refraction index transmission line metamaterials, *URSI Radio Sci. Bull.* **312**, 57–69 (2005).
21. S. L. Dvorak and D. G. Dudley, Propagation of ultra-wideband electromagnetic pulses through dispersive media, *IEEE Trans. EMC* **37**, 192–200 (1995).
22. R. Luebbers, Lossy dielectrics in FDTD, *IEEE Trans. AP* **41**, 1586–1588 (1993).
23. J. L. Young and F. P. Brueckner, A time domain numerical model of a warm plasma, *Radio Sci.* **29**, 451–463 (1994).
24. I. V. Lindell, S. A. Tretyakov, and A. J. Viitanen, Plane wave propagation in a uniaxial chiro-omega medium, *Microwave Opt. Techn. Lett.* **6**, 517–520 (1993).
25. S. He and I. V. Lindell, Propagating eigenmodes for plane waves in a uniaxial bianisotropic medium and reflection from a planar interface, *IEEE Trans. AP* **41**, 1659–1664 (1993).
26. W. S. Weiglhofer and A. Lakhtakia, On electromagnetic waves in biaxial bianisotropic media, *Electromagn.* **19**, 351–362 (1999).
27. I. V. Lindell and A. H. Sihvola, Generalized *WKB* approximation for stratified isotropic chiral media, *J. Electromagn. Waves Appl.* **5**, 857–872 (1991).
28. D. S. Saxon, Modified *WKB* methods for the propagation and scattering of electromagnetic waves, *IRE Trans. AP* **7**, 320–323 (1959).
29. I. Tolstoy, The *WKB* approximation, turning points, and the measurement of phase velocities, *J. Acoust. Soc. Am.* **52**, 356–363 (1972).
30. S. P. Morgan, General solution of the Luneburg lens problem, *J. Appl. Phys.* **29**, 1358–1368 (1958).
31. A. Parfitt, G. James, J. Kot, and P. Hall, A case for the Luneburg lens as the antenna element for the square kilometer array radio telescope, *URSI Radio Sci. Bull.* **293**, 32–38 (2000).

32. J. R. Sanford, Scattering by spherically stratified microwave lens antennas, *IEEE Trans. AP* **42**, 690–698 (1994).
33. H. Sakurai, T. Hashidate, M. Ohki, K. Motoyima and S. Kozaki, Electromagnetic scattering by the Luneburg lens with reflecting cap, *IEEE Trans. EMC* **40**, 94–96 (1998).
34. A. D. Greenwood and J. M. Jin, A field picture of wave propagation in inhomogeneous dielectric lenses, *IEEE Antennas Prop. Mag.* **41**, 9–17 (1999).
35. F. G. Friedlander and J. B. Keller, Asymptotic expansions of solutions of $(\nabla^2 + k^2)u = 0$, Research report EM-67, Division of Electromagnetic Research, New York University, 1954 (10 pages).
36. K. C. Yeh, H. Y. Chao, and K. H. Lin, Polarization transformation of a wave field propagation in an anisotropic medium, *IEEE Antennas Prop. Mag.* **41**, 19–32 (1999).
37. J. B. Keller, Accuracy and validity of the Born and Rytov approximations, *J. Opt. Soc. Am.* **59**, 1003–1004 (1969).
38. P. Debye, Das Verhalten von Lichtwellen in der Nähe eines Brennpunktes oder einer Brennlinie, *Ann. Phys.* **30**, 755–776 (1909).
39. M. L. D. Lumori, J. Bach Andersen, M. K. Gopal, and T. C. Cetas, Gaussian beam representation of aperture fields in layered, lossy media: simulation and experiment, *IEEE Trans. MTT* **38**, 1623–1630 (1990).
40. H. Kogelnik and T. Li, Laser beams and resonators, *Proc. IEEE* **54**, 1312–1329 (1966).
41. E. Heyman, Pulsed beam propagation in inhomogeneous medium, *IEEE Trans. AP* **42**, 311–319 (1994).
42. T. Melamed and L. B. Felsen, Pulsed-beam propagation in dispersive media via pulsed plane wave spectral decomposition, *IEEE Trans. AP* **48**, 901–908 (2000).
43. G. A. Deschamps, Gaussian beam as a bundle of complex rays, *Electron. Lett.* **7**, 684–685 (1971).
44. E. Heyman, Complex source pulsed beams. Properties and applications. *Radio Sci.* **26**, 237–243 (1991).
45. E. Heyman and L. Felsen, Gaussian beam and pulsed-beam dynamics: complex-source and complex-spectrum formulations within and beyond paraxial asymptotics, *J. Opt. Soc. Am.* **18-A**, 1588–1608 (2001).
46. S. M. Saad, Review of numerical methods for the analysis of arbitrarily-shaped microwave and optical waveguides, *IEEE Trans. MTT* **33**, 894–899 (1985).
47. C. Yeh, L. Casperson, and B. Szejn, Propagation of truncated Gaussian beams in multimode fiber guides, *J. Opt. Soc. Am.* **68**, 989–993 (1978).
48. J. Van Roey, J. van der Donk, and P. Lagasse, Beam-propagation method: analysis and assessment, *J. Opt. Soc. Am.* **71**, 803–810 (1981).
49. P. Lagasse and R. Baets, Application of propagating beam methods to electromagnetic and acoustic wave propagation problems: a review, *Radio Sci.* **22**, 1225–1233 (1987).
50. D. Yevick, A guide to electric field propagation techniques for guided-wave optics, *Opt. Quantum Electron.* **26**, 185–197 (1994).
51. R. Scarmozzino, A. Gopinath, R. Pregla, and S. Helfert, Numerical techniques for modeling guided-wave photonic devices, *J. Sel. Topics in Quantum El.* **6**, 150–162 (2000).
52. J. Song and K. M. Chen, Propagation of EM pulses excited by an electric dipole in a conducting medium, *IEEE Trans. AP* **41**, 1414–1421 (1993).
53. I. V. Lindell and A. J. Viitanen, Green dyadic for the general bi-isotropic (non-reciprocal chiral) medium, *Report 72*, Helsinki University of Technology, Electromagnetics laboratory (1990).
54. W. S. Weiglhofer, Electromagnetic field in the source-region: a review, *Electromagn.* **19**, 563–578 (1999).
55. J. A. Kong, Theorems of bianisotropic media, *Proc. IEEE* **60**, 1036–1056 (1972).
56. F. Olyslager and I. V. Lindell, Electromagnetics and exotic media – a quest for the Holy Grail, *IEEE Antennas Prop. Mag.* **44**, 48–58 (2002).
57. V. H. Rumsey, A short way of solving advanced problems in electromagnetic fields and other linear systems, *IEEE Trans. AP* **11**, 73–86 (1963).
58. V. H. Rumsey, Reaction concept in electromagnetic theory, *Phys. Rev.* **94**, 1483–1491 (1954).
59. H. A. Lorentz, Het theorema van Poynting over de energie in het elektromagnetisch veld en een paar algemene stellingen over de voortplanting van het licht (The theorem of Poynting concerning the energy in the electromagnetic field and two general propositions concerning the propagation of light), *Versl. K. Akad. Wet. Amsterdam*, Wis. en nat. afd., **4**, 176–187 (1896).
60. A. T. de Hoop, "Research in Academia — Een Epiloog," 32 pages, Delft University Press, 1997.
61. W. J. Welch, Reciprocity theorems for electromagnetic fields whose time dependence is arbitrary, *IRE Trans. AP* **8**, 68–73 (1960).
62. W. J. Welch, Comment on Ref. 61, *IRE Trans. AP* **9**, 114–115 (1961).
63. A. T. de Hoop, Time-domain reciprocity theorems for electromagnetic fields in dispersive media, *Radio Sci.* **22**, 1171–1178 (1987).
64. R. Ru-shao Cheo, A reciprocity theorem for electromagnetic fields with general time dependence, *IEEE Trans. AP* **13**, 278–284 (1965).
65. A. Tonning, On the network description of electromagnetic problems, AFCRL-62–967, Försvarets Forskningsinsitutet, Kjeller (1962).
66. J. Van Bladel, The matrix formulation of scattering problems, *IEEE Trans. MTT* **14**, 130–135 (1966).
67. R. F. Harrington and J. R. Mautz, A generalized network formulation for aperture problems, *IEEE Trans. AP* **24**, 870–873 (1976).
68. J. Van Bladel, A generalized reciprocity theorem for radiating apertures, *AEÜ* **20**, 447–450 (1966).
69. A. T. de Hoop and G. De Jong, Power reciprocity in antenna theory, *Proc. IEE* **121**, 1051–1056 (1974).
70. A. T. de Hoop, The N-port receiving antenna and its equivalent electrical network, *Philips Research Reports* **30**, 302–315 (1975).

71. J. Van Bladel, On the equivalent circuit of a receiving antenna, *IEEE Antennas Prop. Mag.* **44**, 164–165 (2002).
72. J. C. Bolomey, Réponse d'une antenne de réception à une onde incidente non plane, *Ann. des Telecom.* **34**, 469–476 (1979).
73. G. Sinclair, The transmission and reception of elliptically polarized waves, *Proc. IRE* **38**, 148–151 (1950).
74. R. E. Collin, Limitations of the Thévenin and Norton equivalent circuits for a receiving antenna, *IEEE Antennas Prop. Mag.* **45**, 119–124 (2003).
75. C. T. Tai, On the definition of the effective aperture of an antenna, *IRE Trans. AP* **9**, 224–225 (1961).
76. H. C. Ko, The use of the statistical matrix and the Stokes vector in formulating the effective aperture of antennas, *IRE Trans. AP* **9**, 581–582 (1961).
77. H. C. Ko, On the reception of quasi-monochromatic, partially polarized radio waves, *Proc. IRE* **50**, 1950–1957 (1962).
78. H. C. Ko, Radio-telescope antenna parameters, *IEEE Trans. AP* **12**, 891–898 (1964).

Chapter 9

Plane Boundaries

The way light rays are reflected at the plane boundary of a medium, and possibly further penetrate into the medium, already attracted the attention of physicists in the seventeenth century. The wish to understand better how radio waves propagate along the (plane) surface of the earth, with relatively low attenuation, rekindled the interest of the scientific community in the problem. This was in the early years of "radio," and the names of Sommerfeld, Zenneck, and Weyl are attached to these century-old investigations. More recently, the development of multilayered microwave and optical circuits gave a strong impulse to the need to evaluate fields in these structures with great accuracy. In most theoretical studies, the plane boundaries are assumed infinite. This is a mathematical model, which must be refined in the case of those scatterers that exhibit plane surfaces, such as the rudder of an aircraft or the sides of an armored vehicle. These parts are finite in extent, but the "infinite" theory remains relevant when the dimensions of the planar surface are large with respect to the wavelength. Near the rim of the surface, however, the singularities of fields and currents must be taken into account. The reader will find detailed information on these singularities in Section 9.7.

9.1 PLANE WAVE INCIDENT ON A PLANE BOUNDARY

9.1.1 General Formulas

In Figure 9.1, the homogeneous media 1 and 2 are both characterized by a propagation constant k and a characteristic impedance Z_c, concepts defined in (8.44) and (8.45). Thus,

$$k = (\omega^2 \epsilon\mu - j\omega\mu\sigma)^{\frac{1}{2}} = \omega(\epsilon_c\mu)^{\frac{1}{2}} = \beta - j\alpha$$
$$Z_c = (\mu/\epsilon_c)^{\frac{1}{2}}, \tag{9.1}$$

where ϵ_c is the complex dielectric constant $\epsilon + (\sigma/j\omega)$. Assume that a plane wave propagates in medium 1, with fields

$$\mathbf{E}^i = \mathbf{E}_0^i \, e^{-jk_1 \mathbf{u}_i \cdot \mathbf{r}}$$
$$\mathbf{H}^i = \frac{1}{Z_{c1}} \mathbf{u}_i \times \mathbf{E}_0^i \, e^{-jk_1 \mathbf{u}_i \cdot \mathbf{r}}. \tag{9.2}$$

Electromagnetic Fields, Second Edition, By Jean G. Van Bladel

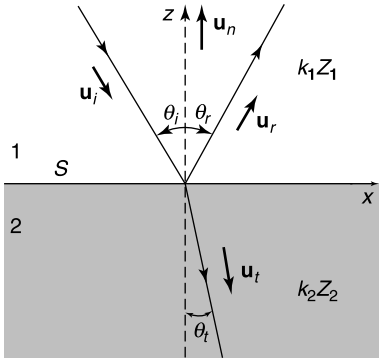

Figure 9.1 Plane wave incident on a plane boundary.

The wave collides with the plane boundary S and generates reflected and transmitted waves. Both are plane waves, and their respective fields are

$$\begin{aligned}\mathbf{E}^r &= \mathbf{E}_0^r\, e^{-jk_1\mathbf{u}_r\cdot\mathbf{r}}\\ \mathbf{H}^r &= \frac{1}{Z_{c1}}(\mathbf{u}_r\times\mathbf{E}_0^r)\, e^{-jk_1\mathbf{u}_r\cdot\mathbf{r}} \;=\; \mathbf{H}_0^r\, e^{-jk_1\mathbf{u}_t\cdot\mathbf{r}}\end{aligned} \tag{9.3}$$

in medium 1, and

$$\begin{aligned}\mathbf{E}^t &= \mathbf{E}_0^t\, e^{-jk_2\mathbf{u}_t\cdot\mathbf{r}}\\ \mathbf{H}^t &= \frac{1}{Z_{c2}}\mathbf{u}_t\times\mathbf{E}_0^t\, e^{-jk_2\mathbf{u}_t\cdot\mathbf{r}} \;=\; \mathbf{H}_0^t\, e^{-jk_2\mathbf{u}_t\cdot\mathbf{r}}\end{aligned} \tag{9.4}$$

in medium 2. The subscript "0" refers to the value at the boundary $z = 0$. The plane wave *ansatz* holds provided the boundary conditions at the interface can be satisfied by a proper choice of the parameters $\mathbf{u}_r, \mathbf{u}_t, \mathbf{E}_0^r$, and $\mathbf{E}_0^t$. Elementary steps lead to the following requirements for $\mathbf{u}_r$ and $\mathbf{u}_t$:

1. $\theta_r = \theta_i$.
2. $\mathbf{u}_i, \mathbf{u}_r$, and $\mathbf{u}_t$ must be in a plane containing the normal n.
3. The direction of $\mathbf{u}_t$ must be such that $k_1\mathbf{u}_i - k_2\mathbf{u}_t$ lies along the normal.

The conditions on $\mathbf{E}_0^r$ and $\mathbf{E}_0^t$ depend on the polarization of the incident wave with respect to the plane of incidence $(\mathbf{u}_i, \mathbf{u}_n)$. Two cases must be carefully distinguished:

1. **Perpendicular (or TE) polarization with respect to** $(\mathbf{u}_i, \mathbf{u}_n)$

   The $\mathbf{E}$ field is y-directed, and

$$(\mathbf{E}_0^r)_\perp = R_\perp\mathbf{E}_0^i = \frac{\mu_2 k_1\cos\theta_i - \mu_1[k_2^2 - k_1^2\sin^2\theta_i]^{\frac{1}{2}}}{\mu_2 k_1\cos\theta_i + \mu_1[k_2^2 - k_1^2\sin^2\theta_i]^{\frac{1}{2}}}\mathbf{E}_0^i \tag{9.5}$$

$$(\mathbf{E}_0^t)_\perp = T_\perp\mathbf{E}_0^i = \frac{2\mu_2 k_1\cos\theta_i}{\mu_2 k_1\cos\theta_i + \mu_1[k_2^2 - k_1^2\sin^2\theta_i]^{\frac{1}{2}}}\mathbf{E}_0^i. \tag{9.6}$$

   The magnetic field follows by applying (9.3) and (9.4). It lies in the plane of incidence.

2. Parallel (or TM) polarization with respect to $(\mathbf{u}_i, \mathbf{u}_n)$

The magnetic field is y-directed, and

$$(\mathbf{H}_0^r)_\parallel = R_\parallel \mathbf{H}_0^i = \frac{\mu_1 k_2^2 \cos\theta_i - \mu_2 k_1 [k_2^2 - k_1^2 \sin^2\theta_i]^{\frac{1}{2}}}{\mu_1 k_2^2 \cos\theta_i + \mu_2 k_1 [k_2^2 - k_1^2 \sin^2\theta_i]^{\frac{1}{2}}} \mathbf{H}_0^i \tag{9.7}$$

$$(\mathbf{H}_0^t)_\parallel = T_\parallel \mathbf{H}_0^i = \frac{2\mu_1 k_2^2 \cos\theta_i}{\mu_1 k_2^2 \cos\theta_i + \mu_2 k_1 [k_2^2 - k_1^2 \sin^2\theta_i]^{\frac{1}{2}}} \mathbf{H}_0^i. \tag{9.8}$$

The electric field follows from (9.3) and (9.4). It lies in the plane of incidence.

In technical applications, medium 1 frequently consists of free space. For such a case,

$$R_\perp = \frac{\mu_r \cos\theta_i - (\mu_r \epsilon_{cr} - \sin^2\theta_i)^{\frac{1}{2}}}{\mu_r \cos\theta_i + (\mu_r \epsilon_{cr} - \sin^2\theta_i)^{\frac{1}{2}}} \tag{9.9}$$

$$T_\perp = \frac{2\mu_r \cos\theta_i}{\mu_r \cos\theta_i + (\mu_r \epsilon_{cr} - \sin^2\theta_i)^{\frac{1}{2}}} \tag{9.10}$$

$$R_\parallel = \frac{\epsilon_{cr} \cos\theta_i - (\mu_r \epsilon_{cr} - \sin^2\theta_i)^{\frac{1}{2}}}{\epsilon_{cr} \cos\theta_i + (\mu_r \epsilon_{cr} - \sin^2\theta_i)^{\frac{1}{2}}} \tag{9.11}$$

$$T_\parallel = \frac{2\epsilon_{cr} \cos\theta_i}{\epsilon_{cr} \cos\theta_i + (\mu_r \epsilon_{cr} - \sin^2\theta_i)^{\frac{1}{2}}}, \tag{9.12}$$

where $\mathbf{u}_n$ and ϵ_{cr} refer to medium 2. The (x, z) dependence of the fields is governed by the exponentials in (9.2) to (9.4). Thus,

$$\begin{aligned} e^{-jk_0 \mathbf{u}_i \cdot \mathbf{r}} &= e^{-jk_0 \sin\theta_i x}\, e^{jk_0 \cos\theta_i z} \\ e^{-jk_0 \mathbf{u}_r \cdot \mathbf{r}} &= e^{-jk_0 \sin\theta_i x}\, e^{-jk_0 \cos\theta_i z} \\ e^{-jk_2 \mathbf{u}_t \cdot \mathbf{r}} &= e^{-jk_2 \sin\theta_t x}\, e^{jk_2 \cos\theta_t z}. \end{aligned} \tag{9.13}$$

Satisfaction of the boundary conditions implies the relationships

$$(k_2 \mathbf{u}_t)_x = k_2 \sin\theta_t = (\beta_2 - j\alpha_2) \sin\theta_t = k_0 \sin\theta_i. \tag{9.14}$$

The angle θ_t is therefore complex. Let N be the (also complex) *index of refraction*

$$N = N_r + jN_i = (\epsilon_{cr}\mu_r)^{\frac{1}{2}} = \left[\left(\epsilon_r + \frac{\sigma}{j\omega}\right)\mu_r\right]^{\frac{1}{2}}, \tag{9.15}$$

where $N_r > 0$ and $N_i < 0$. With that definition of N,

$$\begin{aligned} \sin\theta_t = \frac{k_0}{k_2} \sin\theta_i &= (\mu_r \epsilon_{cr})^{-\frac{1}{2}} \sin\theta_i = \frac{N_r - jN_i}{|N|^2} \sin\theta_i \\ \cos\theta_t = (1 - \sin^2\theta_t)^{\frac{1}{2}} &= \left[1 - \frac{(N_r - jN_i)^2}{|N|^4} \sin^2\theta_i\right]^{\frac{1}{2}}. \end{aligned} \tag{9.16}$$

These values can be used to determine the unit vector $\mathbf{u}_t = \sin\theta_t \mathbf{u}_x - \cos\theta_t \mathbf{u}_z$. The (x, z) dependence of the fields in 2 is now

$$E \doteq e^{-jk_0 \sin\theta_i x}\, e^{jk_2 \cos\theta_t z} = e^{-jk_0 \sin\theta_i x}\, e^{jk_0 z (N^2 - \sin^2\theta_i)^{\frac{1}{2}}}$$

or, if we write $(N^2 - \sin^2\theta_i)^{\frac{1}{2}} = M_r - jM_i$, where M_i is positive,

$$E \doteq e^{-jk_0(\sin\theta_i x - M_r z)}\, e^{k_0 M_i z}. \tag{9.17}$$

The surfaces of constant amplitude in medium 2 are planes parallel to the boundary. Note that the amplitude decreases exponentially as a function of $|z|$, with an e-folding distance given by $\delta = \lambda_0/(2\pi M_i)$. The surfaces of constant phase are oblique planes, defined by $(\sin\theta_i x - M_r z) = \text{constant}$. When $|N| \gg 1$, the term in $\sin^2\theta_i$ is negligible with respect to N^2, $\mathbf{u}_t$ is practically equal to $(-\mathbf{u}_z)$, and the (x, z) dependence becomes

$$f(x, z) = e^{-jk_0(\sin\theta_i x - N_r z)} e^{k_0 |N_i| z}.$$

In Chapter 11, use is made of the *surface impedance* concept Z_S. The surface fields in the TE polarization are, from (9.2) and (9.3),

$$\begin{aligned} \mathbf{E}_{\tan} &= E_0^i (1 + R_\perp)\, e^{-jk_0 \sin\theta_i x} \mathbf{u}_y \\ \mathbf{H}_{\tan} &= \frac{E_0^i}{R_{c0}} (1 - R_\perp) \cos\theta_i\, e^{-jk_0 \sin\theta_i x} \mathbf{u}_x \end{aligned} \tag{9.18}$$

which leads to the relationship

$$\mathbf{E}_{\tan} = R_{c0} \frac{1 + R_\perp}{(1 - R_\perp)\cos\theta_i} \mathbf{u}_n \times \mathbf{H} = Z_S^\perp (\mathbf{u}_n \times \mathbf{H}). \tag{9.19}$$

This equation defines $Z_S^\perp$. In the TM polarization:

$$\begin{aligned} \mathbf{E}_{\tan} &= -\cos\theta_i R_{c0} H_0^i (1 - R_\parallel)\, e^{-jk_0 \sin\theta_i x} \mathbf{u}_x \\ \mathbf{H}_{\tan} &= H_0^i (1 + R_\parallel)\, e^{-jk_0 \sin\theta_i x} \mathbf{u}_y, \end{aligned} \tag{9.20}$$

which leads to the relationship

$$\mathbf{E}_{\tan} = R_{c0} \frac{(1 - R_\parallel)\cos\theta_i}{1 + R_\parallel} \mathbf{u}_n \times \mathbf{H} = Z_S^\parallel (\mathbf{u}_n \times \mathbf{H}). \tag{9.21}$$

The Z_S impedances have the same value at every point of the boundary but obviously depend on factors such as the angle of incidence θ_i and the frequency.

9.1.2 Incidence on a Perfect Conductor

Consider first a *perfect electric conductor* under oblique incidence (Fig. 9.2). The boundary conditions require the tangential component of $\mathbf{E}$ to vanish on the conductor. The figure

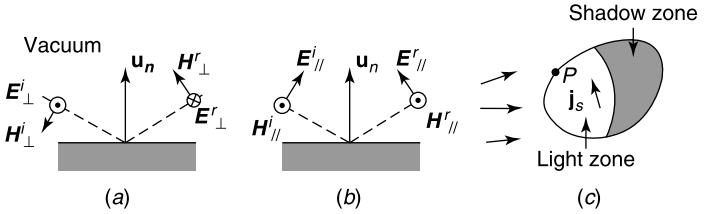

Figure 9.2 (*a*) and (*b*) Reflected fields on a PEC, in the two basic polarizations. (*c*) Relevant for the physical optics approximation.

shows clearly how the incident wave must be reflected to satisfy this condition. In both polarizations, densities of charge and current appear on the interface, viz.

$$\rho_s = \epsilon_0 E_n = 2\epsilon_0 \mathbf{u}_n \cdot \mathbf{E}^i$$
$$\mathbf{J}_s = \mathbf{u}_n \times \mathbf{H} = 2(\mathbf{u}_n \times \mathbf{H}^i). \tag{9.22}$$

When the lower half space is a *perfect magnetic conductor* (boundary condition $\mathbf{H}_{\tan} = 0$), magnetic densities

$$\rho_{ms} = \mu_0 H_n = 2\mu_0(\mathbf{u}_n \cdot \mathbf{H}^i)$$
$$\mathbf{J}_{ms} = \mathbf{E} \times \mathbf{u}_n = 2(\mathbf{E}^i \times \mathbf{u}_n) \tag{9.23}$$

are induced on the interface. It is clear, from Figure 9.2, that the form of the polarization ellipse remains unchanged upon reflection.

The induced densities approximately keep their value (9.22) on a curved body, provided the radii of curvature at the boundary remain very large with respect to λ_0. This remark forms the basis for the (high-frequency) physical optics approximation, in which $\mathbf{J}_s$ is given the value (9.22) on the illuminated part of S and zero in the shadow zone (Fig. 9.2*c*). The point is further discussed in Section 13.1.

When the incident wave is not plane, but generated by arbitrary currents $\mathbf{J}$ and $\mathbf{J}_m$, the fields reflected from a plane boundary may be found by the method of images. The images shown in Figure 9.3 are particularly useful for practical applications. At an *electric wall* (often called perfectly electric), $\mathbf{E}$ is perpendicular to the surface. On a *magnetic wall*, $\mathbf{H}$ is

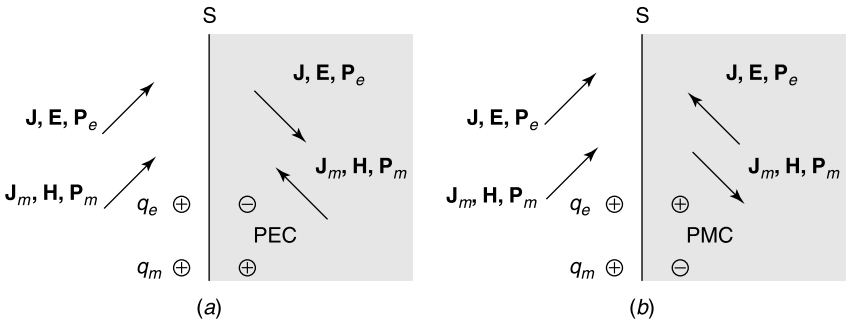

Figure 9.3 (*a*) Images in the presence of an electric wall (PEC). (*b*) Images in the presence of a magnetic wall (PMC).

perpendicular to the surface. In both cases, the vector of Poynting $\frac{1}{2}(\mathbf{E} \times \mathbf{H}^*)$ is tangent to S, hence no power flows into the medium. Both electric and magnetic walls are particular cases of the *ideal* boundary,[1] a boundary on which Poynting's vector is not allowed to have a normal component. Such a boundary neither absorbs nor emits power and is therefore lossless. It is defined mathematically by the boundary conditions

$$\mathbf{u}\cdot\mathbf{E} = 0; \qquad \mathbf{u}^*\cdot\mathbf{H} = 0 \qquad (\mathbf{u}\cdot\mathbf{u}^* = 1), \tag{9.24}$$

where $\mathbf{u}$ is a complex unit vector tangent to S. Other examples of ideal boundaries are the *soft* and *hard interfaces*, which can be realized by covering metallic surfaces with tuned corrugations.[2] The respective appropriate boundary conditions are

$$\mathbf{u}\cdot\mathbf{E} = 0 \qquad \text{and} \qquad \mathbf{u}\cdot\mathbf{H} = 0, \tag{9.25}$$

where $\mathbf{u}$ is a real unit vector tangent to S.

9.1.3 Incidence on a Good Conductor

By definition, a *good conductor* is a medium in which the conduction current $|\sigma\mathbf{E}|$ is much larger than the displacement current $|j\omega\epsilon\mathbf{E}|$. At the frequencies for which this holds, one may write

$$\begin{aligned} \sigma &\gg \omega\epsilon \geq \omega\epsilon_0 \\ \omega\mu\sigma &\gg \omega^2\epsilon_0\mu_0 = k_0^2 \\ \frac{2}{\delta^2} &\gg k_0^2 = \left(\frac{2\pi}{\lambda_0}\right)^2, \end{aligned} \tag{9.26}$$

where δ is the *penetration depth*

$$\delta = \left(\frac{2}{\omega\mu\sigma}\right)^{\frac{1}{2}}. \tag{9.27}$$

It is clear, from (9.26), that $\delta \ll \lambda_0$. In the application of the general formulas (9.5) to (9.12) to good conductors, one must set

$$\begin{aligned} k_2 = (-j\omega\mu\sigma)^{\frac{1}{2}} &= \left(-j\frac{2}{\delta^2}\right)^{\frac{1}{2}} = \pm\left(\frac{1}{\delta} + \frac{j}{\delta}\right) \\ \epsilon_{cr} &= \frac{\sigma}{j\omega\epsilon_0} \\ N^2 = \mu_r\epsilon_{cr} &= -j\frac{2}{(k_0\delta)^2} \\ N &= -\frac{1}{k_0\delta} - \frac{j}{k_0\delta}. \end{aligned} \tag{9.28}$$

From (9.27), therefore, $|\epsilon_{cr}| \gg 1$ and $|N| \gg 1$. The implications for the value of the surface impedance are further discussed in Section 11.6. Whatever the angle of incidence, the angle

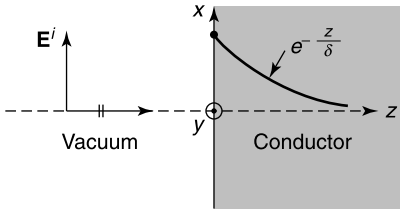

Figure 9.4 Normal incidence on a good conductor.

θ_t in (9.16) turns out to be zero. Hence, $\mathbf{u}_t = (-\mathbf{u}_z)$, and the propagation into the good conductor is governed by a factor

$$f(x,z) = e^{-jk_0 \sin\theta_i x}\, e^{-\frac{|z|}{\delta}}\, e^{-j\frac{|z|}{\delta}}. \tag{9.29}$$

Consider, in particular, the fields at *normal incidence* (Fig. 9.4). In free space, for $z < 0$,

$$\begin{aligned} E_x &= E^i \left(e^{-jk_0 z} + R\, e^{jk_0 z}\right) \\ H_y &= \frac{E^i}{R_{c0}} \left(e^{-jk_0 z} - R\, e^{jk_0 z}\right). \end{aligned} \tag{9.30}$$

In the conductor,

$$\begin{aligned} E_x &= T\, e^{-\frac{z}{\delta}}\, e^{-j\frac{z}{\delta}} \\ H_y &= \frac{T}{Z_c}\, e^{-\frac{z}{\delta}}\, e^{-j\frac{z}{\delta}}, \end{aligned} \tag{9.31}$$

where Z_c is the *characteristic impedance*

$$Z_c = \left(\frac{\mu}{\epsilon_c}\right)^{\frac{1}{2}} = \frac{1+j}{\sigma\delta}. \tag{9.32}$$

Reflection and transmission coefficients are determined by the boundary conditions on E_x and H_y at $z = 0$, which give

$$\begin{aligned} T &= \frac{2Z_c}{R_{c0}} \\ R &= 1 - T. \end{aligned} \tag{9.33}$$

Because

$$|Z_c| = \left|\frac{\mu_r \mu_0}{\epsilon_0 \epsilon_{cr}}\right|^{\frac{1}{2}} = R_{c0} \left|\frac{\mu_r \omega \epsilon_0}{\sigma}\right|^{\frac{1}{2}} = R_{c0} (\mu_r)^{\frac{1}{2}}\, Q^{\frac{1}{2}}, \tag{9.34}$$

it is clear that $|T|$, proportional to $Q^{\frac{1}{2}}$, is very small, and therefore that $|R|$ is almost equal to one as soon as $Q \ll \mu_r^{-1}$.

Table 9.1 Typical Values of $\delta f^{\frac{1}{2}}$ (δ in mm, f in Hz)

Aluminum	85
Copper	66
Silver	64
Seawater	0.23×10^6
Iron	11
Mumetal	2.8

From (9.27) the penetration depth is proportional to $f^{-\frac{1}{2}}$ at constant σ and μ (i.e., decreases with increasing frequency according to a law $f^{-\frac{1}{2}}$). Some indicative values of $\delta f^{\frac{1}{2}}$ are given in Table 9.1.

As ω increases, the penetration depth in metals decreases and eventually becomes of the order of magnitude the mean free path of the conduction electrons. Under these circumstances, the spatial nonuniformity of the fields precludes a macroscopic description of the fields.

In Figure 9.4, the current induced in the good conductor flows in the x-direction. From (9.31),

$$\mathbf{J} = \sigma \mathbf{E} = \sigma T \, e^{-(1+j)\frac{|z|}{\delta}} \, \mathbf{E}^i \qquad (\mathrm{A\,m^{-2}}).$$

Integration over the current-carrying region gives

$$\int_0^\infty \mathbf{J} \, dz = \frac{T\sigma\delta}{1+j}\mathbf{E}^i = \frac{T}{Z_c}\mathbf{E}^i = \frac{2}{R_{c0}}\mathbf{E}^i \qquad (\mathrm{A\,m^{-1}}). \tag{9.35}$$

From (9.23), this is precisely the current density $\mathbf{J}_S$ that flows at the surface of a perfectly conducting plane. We write

$$\mathbf{E}_{\tan} = Z_c \mathbf{J}_S = \left(\frac{Z_c}{R_{c0}}\right)(R_{c0}\mathbf{J}_S). \tag{9.36}$$

Because (Z_c/R_{c0}) is normally very small, (9.36) gives the first-order value of $\mathbf{E}_{\tan}$ for large (but noninfinite) conductivity.

Assume now that the incidence in Figure 9.4 is *oblique*. Because all fields must exhibit an (x, z) dependence of the form $e^{-jk_0 \sin\theta_i x}$ in order to satisfy the boundary conditions, Helmholtz' equation requires the z-variation $f(z)$ to satisfy

$$\frac{d^2 f}{dz^2} + (k_2^2 - k_0^2 \sin^2\theta_i) f = 0. \tag{9.37}$$

In a good conductor, $|k_2^2| = |\omega\mu\sigma|$ is much larger than $k_0^2 \sin^2\theta_i$, hence the typical variation

$$f(z) \doteq e^{-\frac{z}{\sigma}} \, e^{-j\frac{z}{\sigma}}$$

still holds, and

$$\mathbf{E}_{\tan} = Z_c(\mathbf{u}_n \times \mathbf{H}) \tag{9.38}$$

Table 9.2 Relevant Data for Muscle Material

Frequency (MHz)	433	915	2450
λ (cm)	3.57	2.50	1.67
$\lvert T\rvert^2$ at interface	0.36	0.40	0.43

at the interface.

The previous analysis can easily be adapted to *mixed conductors*, in which conduction and displacement currents are both significant. The relevant formula is (9.17), and the penetration depth is now $\delta = \lambda_0/2\pi M_i$, a parameter of decisive importance for heating applications, medical, or industrial. A few typical data for muscle material are given in Table 9.2. At oblique incidence, the transmitted wave becomes a *nonuniform* plane wave, in which the surfaces of constant amplitude and phase are still plane but do not coincide[3] [1, 20].

9.1.4 Two Lossless, Nonmagnetic Dielectrics

When two dielectric media are in contact, the propagation constants, $k_1 = k_0\sqrt{\epsilon_{r1}}$ and $k_2 = k_0\sqrt{\epsilon_{r2}}$, are real and positive in both media. Referring to Figure 9.1, two particular cases should be distinguished:

1. **The Incidence is on a Medium of Higher $\boldsymbol{\epsilon_r}$** (i.e. $\epsilon_{r2} > \epsilon_{r1}$)
   The variation of the reflection coefficients as a function of θ_i is shown in Figure 9.5*a*. The corresponding power transmission coefficients $|T|^2$ are given by $1 - |R|^2$ and can easily be deduced from the figure. The reflected wave is richer in perpendicular polarization than the incident one, because $|R_\perp| > |R_\parallel|$. The parallel polarization even vanishes upon reflection when θ_i is the *Brewster angle*, defined by

   $$\tan\theta_i = \sqrt{\frac{\epsilon_2}{\epsilon_1}} \qquad (\theta_i > \pi/4). \tag{9.39}$$

   This property has been put to good use in the design of windows for laser cavities (Fig. 9.6*a* and Problem 9.2). The transmission angle θ_t, given by

   $$\sin\theta_t = \sqrt{\frac{\epsilon_1}{\epsilon_2}}\sin\theta_i, \tag{9.40}$$

   is clearly less than θ_i.
2. **The Incidence is on a Medium of Lower $\boldsymbol{\epsilon_r}$** (i.e., $\epsilon_{r2} < \epsilon_{r1}$)
   The Brewster angle is now less than $(\pi/4)$ (Fig. 9.5*b*). A new interesting property arises, namely *total reflection*, which occurs for both polarizations when

   $$\sin\theta_i \geq \sqrt{\frac{\epsilon_2}{\epsilon_1}} = \frac{c_1}{c_2}. \tag{9.41}$$

Under these conditions, no *real* unit vector $\mathbf{u}_t$ exists such that $k_1\mathbf{u}_i - k_2\mathbf{u}_t$ is directed along the normal. The transmitted wave is still given by (9.4), but $\mathbf{u}_t$ must be given the *complex*

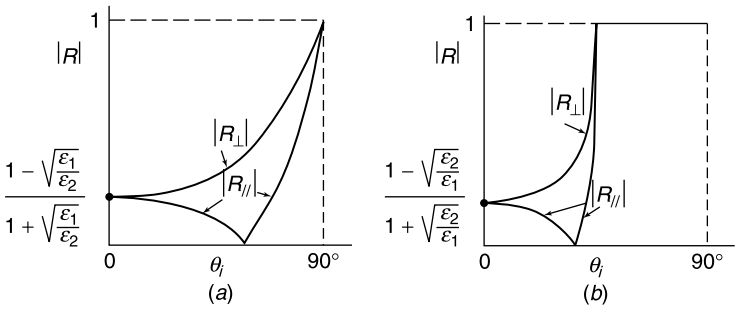

Figure 9.5 Reflection coefficient for (*a*) $\epsilon_2 = 2.25\,\epsilon_1$ and (*b*) $\epsilon_1 = 2.25\,\epsilon_2$.

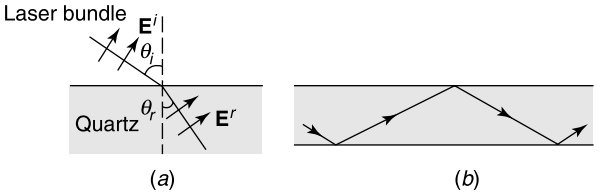

Figure 9.6 (*a*) Full transmission of a laser bundle. (*b*) Wave-guiding by a dielectric slab.

value

$$\mathbf{u}_t = \frac{k_1}{k_2}\sin\theta_i \mathbf{u}_x \pm \frac{j}{k_2}\left[k_1^2\sin^2\theta_i - k_2^2\right]^{\frac{1}{2}}\mathbf{u}_n. \tag{9.42}$$

This choice of $\mathbf{u}_t$ introduces a factor

$$e^{-jk_2\mathbf{u}_t\cdot\mathbf{r}} = e^{-jk_1\sin\theta_i x}\, e^{-|z|[k_1^2\sin^2\theta_i - k_2^2]^{\frac{1}{2}}} \tag{9.43}$$

in the expression for the fields in medium 2. It follows that both **E** and **H** are *attenuated* in a direction perpendicular to the interface, but *propagate* in a direction parallel to the latter. In short, the wave in medium 2 is "glued" to the surface and is guided by the latter. The *wave* is also *slow*, because the propagation velocity $(\omega/k_1\sin\theta_i)$ is less than the corresponding velocity $c_2 = (\omega/k_2)$ in medium 2. From (9.5), the reflection coefficient $R_\perp$ at total reflection is given by

$$R_\perp = \frac{\cos\theta_i - j\sqrt{\dfrac{\epsilon_1}{\epsilon_2}\sin^2\theta_i - 1}}{\cos\theta_i + j\sqrt{\dfrac{\epsilon_1}{\epsilon_2}\sin^2\theta_i - 1}}.$$

Its magnitude is unity — as expected because there is total reflection. Coefficient $R_\perp$ can therefore be written as $e^{-j\theta}$, where θ denotes the *Goos-Hänchen* phase shift [10]. A similar phenomenon occurs with $R_\parallel$.

The property of total reflection may be used to guide a plane wave down the x-axis by means of successive reflections at plane interfaces (Fig. 9.6*b*). From this point of view, the dielectric slab acts as a plane version of the optical fiber, a waveguide discussed in some detail in Section 15.9.

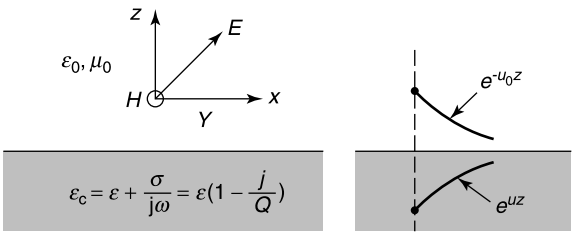

Figure 9.7 Fields in a Zenneck wave.

9.1.5 The Zenneck Wave

This wave, investigated by Zenneck in the early days of radio,[4,5] propagates in a direction parallel to a conductor-vacuum boundary (Fig. 9.7). The wave is of the TM type, with **H** parallel to the *y*-axis. In vacuum, its field components are [21]

$$\begin{aligned} H_y &= H\, e^{-jkx}\, e^{-u_0 z} \\ E_x &= \frac{u_0}{j\omega\epsilon_0} H\, e^{-jkx}\, e^{-u_0 z} \\ E_z &= -\frac{k}{\omega\epsilon_0} H\, e^{-jkx} e^{-u_0 z}, \end{aligned} \tag{9.44}$$

with $u_0 = (k^2 - k_0^2)^{\frac{1}{2}}$. In the conductor:

$$\begin{aligned} H_y &= H\, e^{-jkx}\, e^{uz} \\ E_x &= -\frac{u}{j\omega\epsilon_c} H\, e^{-jkx}\, e^{uz} \\ E_z &= -\frac{k}{\omega\epsilon_c} H\, e^{-jkx}\, e^{uz}, \end{aligned} \tag{9.45}$$

where $u = (k^2 - k_0^2\, \epsilon_{cr})^{\frac{1}{2}}$. Continuity of H_y is automatically satisfied. Expressing continuity of E_x gives

$$\begin{aligned} u_0 &= -jk_0 \frac{1}{(1+\epsilon_{cr})^{\frac{1}{2}}} \\ u &= jk_0 \frac{\epsilon_{cr}}{(1+\epsilon_{cr})^{\frac{1}{2}}} \\ k &= k_0 \left(\frac{\epsilon_{cr}}{1+\epsilon_{cr}} \right)^{\frac{1}{2}}. \end{aligned} \tag{9.46}$$

To obtain a surface wave, the fields should decrease away from the interface, a condition that requires $Re(u_0)$ and $Re(u)$ to be positive. These conditions are not satisfied when the lower medium is a lossless dielectric. For a *poor conductor*, on the other hand, with $Q = \dfrac{\omega\epsilon}{\sigma} \gg 1$,

(9.46) becomes

$$u_0 = -j\frac{k_0}{(1+\epsilon_r)^{\frac{1}{2}}} + \frac{k_0\epsilon_r}{2(1+\epsilon_{cr})^{\frac{3}{2}}Q}$$
$$u = \frac{jk_0\epsilon_r}{(1+\epsilon_{cr})^{\frac{1}{2}}} + \frac{k_0\epsilon_r(\epsilon_r+2)}{2(1+\epsilon_{cr})^{\frac{3}{2}}Q}$$
$$k = k_0\left(\frac{\epsilon_r}{1+\epsilon_r}\right)^{\frac{1}{2}} - jk_0\frac{1}{2Q}\left(\frac{\epsilon_r}{(1+\epsilon_r)^3}\right)^{\frac{1}{2}}. \tag{9.47}$$

The wave is seen to be attenuated in both the x and z directions. The longitudinal attenuation particularly interested Zenneck, who was trying to find a theoretical basis for the then available experimental data on propagation over land. Although land surfaces vary widely in their characteristics, the *poor conductor* model describes their properties realistically. For a rocky surface, for example, Q may be of the order 50 at 500 MHz.

It should be noted that the previous analysis only shows that the Zenneck wave satisfies Maxwell's equations and corresponding boundary conditions. The analysis, however, does not predict "how much" of that wave is excited by a source such as a linear antenna and under which conditions (and in which region) the wave can be the dominant part of the field pattern. This issue is further discussed in Section 9.3.

9.1.6 Reflection on an Ionized Medium

In accordance with (8.35), the ionized medium may be described by a dielectric constant $\epsilon_r = 1 - (\omega_p^2/\omega^2)$ (a very simplified model for a medium such as the ionosphere). The reflection coefficients (9.5) and (9.7) are now (Fig. 9.8*a*)

$$R_\perp = \frac{\cos\theta_i - \sqrt{\epsilon_r - \sin^2\theta_i}}{\cos\theta_i + \sqrt{\epsilon_r - \sin^2\theta_i}} = \frac{\cos\theta_i - \sqrt{\cos^2\theta_i - \dfrac{\omega_p^2}{\omega^2}}}{\cos\theta_i + \sqrt{\cos^2\theta_i - \dfrac{\omega_p^2}{\omega^2}}}$$
$$R_\parallel = \frac{\epsilon_r\cos\theta_i - \sqrt{\epsilon_r - \sin^2\theta_i}}{\epsilon_r\cos\theta_i + \sqrt{\epsilon_r - \sin^2\theta_i}} = \frac{\left(1-\dfrac{\omega_p^2}{\omega^2}\right)\cos\theta_i - \sqrt{\cos^2\theta_i - \dfrac{\omega_p^2}{\omega^2}}}{\left(1-\dfrac{\omega_p^2}{\omega^2}\right)\cos\theta_i + \sqrt{\cos^2\theta_i - \dfrac{\omega_p^2}{\omega^2}}}. \tag{9.48}$$

It is clear that $|R_\perp| = |R_\parallel| = 1$ when

$$\omega < \frac{\omega_p}{\cos\theta_i}. \tag{9.49}$$

At sufficiently low frequencies, therefore, total reflection occurs, and it takes angular frequencies higher than $(\omega_p/\cos\theta_i)$ to penetrate the layer. At normal incidence, when

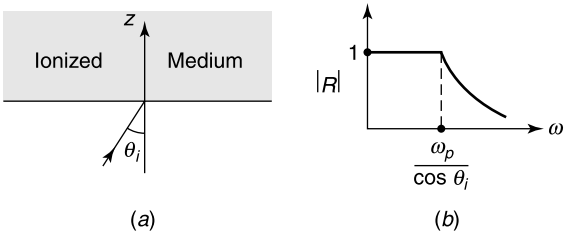

Figure 9.8 (*a*) Wave incident on an ionized layer. (*b*) Reflection coefficient as a function of frequency.

$\omega < \omega_p$, the fields are attenuated in the ionized layer according to a factor

$$e^{-jk_0\sqrt{\epsilon_r}z} = e^{-k_0\sqrt{|\epsilon_r|}z} = e^{-2\pi\frac{z}{\lambda_0}\sqrt{\frac{\omega_p^2}{\omega^2}-1}}. \tag{9.50}$$

The general variation of the reflection coefficient is shown in Figure 9.8*b*. The curve suggests the possibility of long-distance radiocommunication through reflections on the ionosphere, particularly at grazing incidence. It also shows that the medium becomes transparent as $\omega \to \infty$, fundamentally because the amplitude of the electronic motion (the source of the reflected wave) approaches zero in that limit [11].

The model discussed above is too primitive to describe the behavior of the ionosphere in a satisfactory way. Ionospheric layers are poorly modeled by a half-infinite medium, and they are strongly inhomogeneous and time-dependent. Furthermore, they become anisotropic in the presence of the earth's magnetic field [68].

9.1.7 Incidence on an Anisotropic Medium

Anisotropic media are increasingly found in practical devices, in particular through the frequent use of composite materials in structures such as airplane frames. The analysis of reflection and transmission proceeds as for isotropic materials but at a heavier formal cost[6,7] [87]. The constitutive equations of anisotropic materials contain several adjustable parameters, a property that provides added flexibility to the design of components such as polarizers[8] and *wave absorbers*. Earlier solutions to the absorption problem were based on stack-ups of thin screens,[9,10] with as its most rudimentary form the Salisbury screen shown in Figure 9.9 (see Section 11.7). Numerous other structures have been proposed to arrive at a balanced combination of reflection and absorption, often by use of ferrites and magnetic composites.[11] On a purely theoretical basis, a perfect absorber may be synthesized by means of a virtual *uniaxial anisotropic medium*.* The tensorial parameters of the medium are[12]

$$\bar{\bar{\epsilon}}_r = \bar{\bar{\mu}}_r = \begin{pmatrix} a & 0 & 0 \\ 0 & a & 0 \\ 0 & 0 & \dfrac{1}{a} \end{pmatrix}, \tag{9.51}$$

*A more fundamental presentation of the material in this section can be found in [24, Chapter 14], where topics such as causality, reciprocity, and physical realizability of the PML medium are discussed, together with the applicability of the PML-synthesized medium at low frequencies.

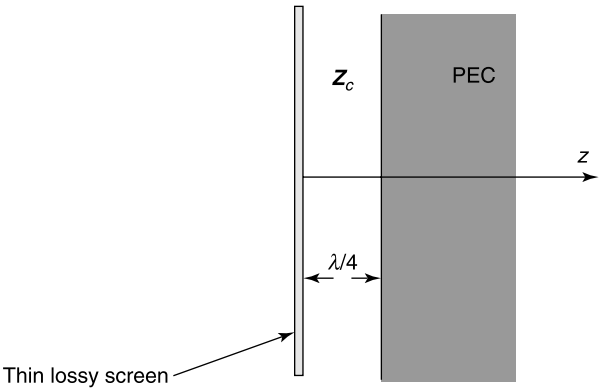

Figure 9.9 The Salisbury screen.

where $a = \alpha - j\beta$ is complex. Let the incident wave be perpendicularly polarized (the parallel polarization can be handled analogously). The incident fields are, from (9.2),

$$\mathbf{E}^i = E^i\, e^{-jk_0(\sin\theta_i x - \cos\theta_i z)}\mathbf{u}_y$$

$$\mathbf{H}^i = \frac{E^i}{R_{c0}} e^{-jk_0(\sin\theta_i x - \cos\theta_i z)}(\cos\theta_i \mathbf{u}_x + \sin\theta_i \mathbf{u}_z). \tag{9.52}$$

The transmitted fields will be of the general form (Fig. 9.1)

$$\mathbf{E}^t = \mathcal{E} e^{-jk_0 \sin\theta_i x} f(z)\mathbf{u}_y$$

$$\mathbf{H}^t = e^{-jk_0 \sin\theta_i x}\left[\mathcal{H}_x(z)\mathbf{u}_x + \mathcal{H}_z(z)\mathbf{u}_z\right], \tag{9.53}$$

where $\mathcal{E}$ is a yet-to-be determined constant factor. Inserting (9.53) into Maxwell's equations yields

$$\mathcal{E}\frac{df}{dz} = j\omega\mu_0\, a\, \mathcal{H}_x \tag{9.54}$$

$$jk_0 \sin\theta_i \mathcal{E} f = j\omega\mu_0 \frac{1}{a}\mathcal{H}_z \tag{9.55}$$

$$\frac{d\mathcal{H}_x}{dz} + jk_0 \sin\theta_i \mathcal{H}_z = j\omega\epsilon_0\, \mathcal{E}\, af. \tag{9.56}$$

Let us assume that $a = \alpha - j\beta$ is independent of z. Differentiating (9.54) with respect to z and substituting from (9.56) leads to

$$\frac{d^2 f}{dz^2} + k_0^2 a^2 \cos^2\theta_i f = 0. \tag{9.57}$$

If β is chosen positive, the wave in the anisotropic medium is attenuated, and

$$\mathbf{E}^t = \mathcal{E}\, e^{-jk_0 \sin\theta_i x}\, e^{jk_0 a \cos\theta_i z}\, \mathbf{u}_y$$

$$\mathbf{H}^t = \frac{\mathcal{E}}{R_{c0}} e^{-jk_0 \sin\theta_i x}\, e^{jk_0 a \cos\theta_i z}(\cos\theta_i \mathbf{u}_x + a \sin\theta_i \mathbf{u}_z). \tag{9.58}$$

The ratio of E_y to H_x at the interface (the surface impedance) is equal to $(R_{c0}/\cos\theta_i)$. This is also the corresponding field ratio in the incident wave, which means that the boundary conditions can be satisfied without having to introduce reflected fields. The interface is therefore a *perfectly matched layer* (a PML), and this property holds irrespective of frequency, angle of incidence and polarization. Within the PML, the z-variation is of the type

$$e^{jk_0 a\cos\theta_i z} = e^{-Im(a)k_0\cos\theta_i|z|}\, e^{-jk_0 Re(a)\cos\theta_i|z|}. \tag{9.59}$$

The penetration depth, proportional to $(1/\cos\theta_i)$, increases as the incidence approaches the grazing limit.

In a pioneering article,[13] Bérenger had initially approached the PML problem from a different point of view. In its simplest form, his method involves a TM plane wave, incident on a medium endowed with electric and magnetic conductivities σ_e and σ_m. These parameters are assumed related by the condition

$$\frac{\sigma_e}{\epsilon_0} = \frac{\sigma_m}{\mu_0}. \tag{9.60}$$

Maxwell's equations are now of the form

$$\begin{aligned} j\omega\epsilon_0 E_x + \sigma_e E_x &= \frac{\partial H_z}{\partial y} \\ j\omega\epsilon_0 E_y + \sigma_e E_y &= -\frac{\partial H_z}{\partial x} \\ j\omega\mu_0 H_z + \sigma_m H_z &= \frac{\partial E_x}{\partial y} - \frac{\partial E_y}{\partial x}. \end{aligned} \tag{9.61}$$

At normal incidence, the fields are y-independent and E_x (and therefore also H_z) vanish (Fig. 9.10*a*). From (9.61), the medium has a characteristic impedance

$$Z_c = \left(\frac{\sigma_m + j\omega\mu_0}{\sigma_e + j\omega\epsilon_0}\right)^{\frac{1}{2}},$$

a value equal to R_{c0} because of (9.60). The impedances are therefore matched, and no reflection takes place. In a general PML, the fields are required to satisfy the non-Maxwellian

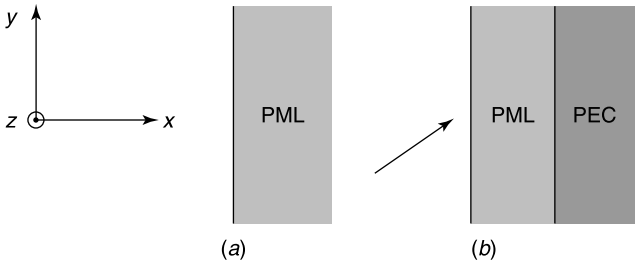

Figure 9.10 (*a*) Normal incidence on a PML. (*b*) Metal-backed PML.

equations

$$\epsilon_0 \frac{\partial e_x}{\partial t} + \sigma_{ey} e_x = \frac{\partial}{\partial y}(h_{zx} + h_{zy})$$
$$\epsilon_0 \frac{\partial e_y}{\partial t} + \sigma_{ex} e_y = -\frac{\partial}{\partial x}(h_{zx} + h_{zy})$$
$$\mu_0 \frac{\partial h_{zx}}{\partial t} + \sigma_{mx} h_{zx} = -\frac{\partial e_y}{\partial x}$$
$$\mu_0 \frac{\partial h_{zy}}{\partial t} + \sigma_{my} h_{zy} = \frac{\partial e_x}{\partial y}, \tag{9.62}$$

where σ_{mx}, σ_{ex} and σ_{my}, σ_{ey} independently satisfy (9.60). We note that the h_z component has been split into two parts, h_{zx} and h_{zy}, and that the sum $(h_{zx} + h_{zy})$ must be equal to the value of h_z on the vacuum side of the interface. Bérenger has shown that, given an adequate set of conductivities, the reflection from a vacuum-PML interface can vanish.[13] The property holds for both the TE and TM waves and for arbitrary incidence and time-dependence. The method can be extended to three dimensions[14] and to waves incident from a linear *dispersive* medium.[15]

The PML is an important tool in the numerical solution of Maxwell's equations in an infinite domain, in particular under arbitrary time variations. In the FDTD method, to be discussed in Section 12.8, sources are energized at $t = 0$ and the fields propagate on a net of points.[15] The net must be truncated at a well-chosen surface, on which free-space conditions should be simulated. This is achieved in Figure 9.11 by means of a series of PML layers, including transition layers in the corners [24, 202]. The finite difference net is extended into the layers, in which the appropriate field equations are discretized. The layer is backed by a perfectly conducting surface in order to limit its extent (Fig. 9.10*b*). This short-circuit generates reflections, which are quite small if the thickness d is sufficiently large. The reflected wave is further attenuated on the return trip. A small residual reflection survives, however, particularly at points where the radiated wave hits the PML at grazing incidence. In the presence of *homogeneous* incident waves, reflections can be minimized by using PMLs of moderate thickness. In the presence of an *evanescent* wave, inhomogeneous

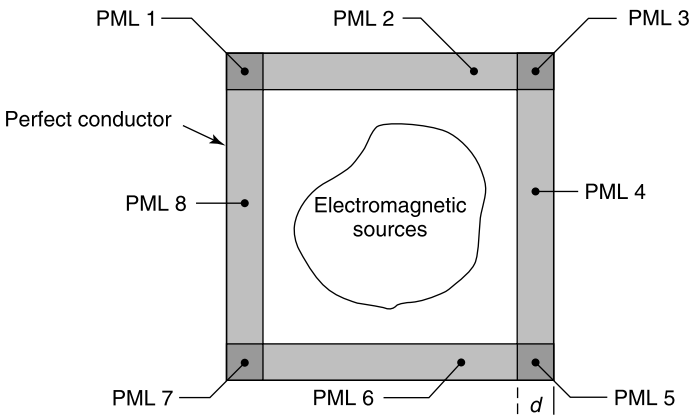

Figure 9.11 PML surrounding a 2D computational domain. (Courtesy of Dr. J. P. Bérenger.)

in a direction perpendicular to the propagation, the numerical reflection may be very large, and total reflection may even occur below a certain frequency.[16,17,18]

The absorbing layer can be looked at from a third point of view. In that third approach, the *z-coordinate* is *stretched* into a new coordinate Z, defined by[19,20]

$$\begin{aligned} dZ &= a(z)\,dz \\ Z &= \int^{z} a(z')\,dz'. \end{aligned} \tag{9.63}$$

The function $a(z)$ is complex, and is typically given the forms:

$$a = \epsilon_r(z) + \frac{\sigma(z)}{j\omega\epsilon_0} \qquad (\epsilon_r \geq 1) \tag{9.64}$$

or

$$a = 1 + (\kappa_0 - 1)g(z) + \frac{\sigma_0}{j\omega\epsilon_0}g(z), \tag{9.65}$$

where κ_0, σ_0, and $g(z)$ describe the properties of the layer. Because a is a function of z, (9.57) must be rewritten as

$$\frac{1}{a}\frac{d}{dz}\left(\frac{1}{a}\frac{df}{dz}\right) + k_0^2 \cos^2\theta_i f = 0.$$

In the stretched coordinates:

$$\frac{d^2 f}{dZ^2} + k_0^2 \cos^2\theta_i f = 0. \tag{9.66}$$

Propagation in these coordinates occurs as in free space, with waves of the type $e^{-jk_0 \cos\theta_i Z}$. In other words, the field at Z, in the PML, has the value that would be obtained in vacuum at a *complex depth* $Z = \int_0^z a(z')\,dz'$. The method is not restricted to planar boundaries but can be extended to three-dimensional orthogonal grids,[21,22] for example to spherical or cylindrical nets [24].

The coordinate-stretching technique has found an interesting application in the study of scattering and reflection of surface waves at the boundaries of a layered substrate. By surrounding this waveguiding structure with a metal-covered PML, the waveguide becomes numerically closed but still behaves as an open waveguide. The point is further discussed in Section 15.10.

9.1.8 Transient Incident Fields

Consider, as an illustrative example, a TE field $e^i(t)\mathbf{u}_y$ incident on a non-magnetic conducting half-space. The field is turned on at $t = 0$. Because every frequency component is reflected along an angle $\theta_r = \theta_i$, the same will be true of the reflected field $e^r(t)\mathbf{u}_y$ (Fig. 9.1). The relation between e^r and e^i is of the convolution type, viz.[23]

$$e^r(t) = \int_{-\infty}^{t} e^i(t-\tau)R_\perp(\tau)\,d\tau \tag{9.67}$$

where $R_\perp(t)$ is the impulse response of the reflection coefficient. From (9.5), the Laplace transform of $R_\perp(t)$ is

$$R_\perp(s) = \frac{\cos\theta_i - \left(\epsilon_r + \dfrac{\sigma}{s\epsilon_0} - \sin^2\theta_i\right)^{\frac{1}{2}}}{\cos\theta_i + \left(\epsilon_r + \dfrac{\sigma}{s\epsilon_0} - \sin^2\theta_i\right)^{\frac{1}{2}}}. \tag{9.68}$$

The convolution theorem A7.5 yields

$$E^r(s) = E^i(s)R_\perp(s). \tag{9.69}$$

The desired response $e^r(t)$ can now be obtained by Laplace inversion of $E^r(s)$. Alternately, the reflected field may also be derived from (9.67), provided $R_\perp(t)$ has been evaluated previously, for example by Laplace inversion of (9.68). This operation, which is not trivial, can be simplified when ϵ_r is sufficiently large (say >10) and the incidence sufficiently close to normal to set $\sin^2\theta_i \approx 0$ and $\cos\theta_i \approx 1$ in (9.68). Thus,

$$R_\perp(s) \approx \frac{\sqrt{s} - \sqrt{\epsilon_r}\sqrt{s+\tau}}{\sqrt{s} + \sqrt{\epsilon_r}\sqrt{s+\tau}} \tag{9.70}$$

where $\tau = \sigma/\epsilon$ is the relaxation time of the conducting material. $R_\perp(s)$ can be expressed as a series $\displaystyle\sum_{n=1} A_n \left(s + \sqrt{s^2 - \tau^2/4}\right)^{-n}$, which can subsequently be inverted term by term.[23]

In the evaluation of the fields *inside* the conducting half-space, the parameter of interest becomes

$$T_\perp(s) = \frac{2\cos\theta_i}{\cos\theta_i + \left(\epsilon_r + \dfrac{\sigma}{s\epsilon_0} - \sin^2\theta_i\right)^{\frac{1}{2}}}. \tag{9.71}$$

The corresponding $T_\perp(t)$ may be obtained (approximately) by assuming ϵ_r large and θ_i small or (exactly) from the evaluation of two canonical integrals.[24,25] Some physical feeling for the nature of the penetration may be gained from Figure 9.12*a*, *b*, which shows the fields for three values of $|z|$, the distance from the interface. The incident wave is the double exponential

$$e^i(t) = A\left(e^{-\alpha_1 t} - e^{-\alpha_2 t}\right)H(t)$$

whose transform is

$$E^i(s) = A\left(\frac{1}{s+\alpha_1} - \frac{1}{s+\alpha_2}\right). \tag{9.72}$$

The parameters in the figure are $\alpha_1 = 5.9 \times 10^7\ \mathrm{s}^{-1}$, $\alpha_2 = 2.1 \times 10^8\ \mathrm{s}^{-1}$, $\epsilon_r = 10$, and $\sigma = 2 \times 10^{-2}\ \mathrm{Sm}^{-1}$.

The previous analysis can serve better to understand the penetration of strong pulses into the earth, often caused by waves induced on power transmission lines. The assumed characteristics of lossy ground are typically $\epsilon_r = 10$ and $\sigma = 0.001$ to $0.1\ \mathrm{Sm}^{-1}$, but in a

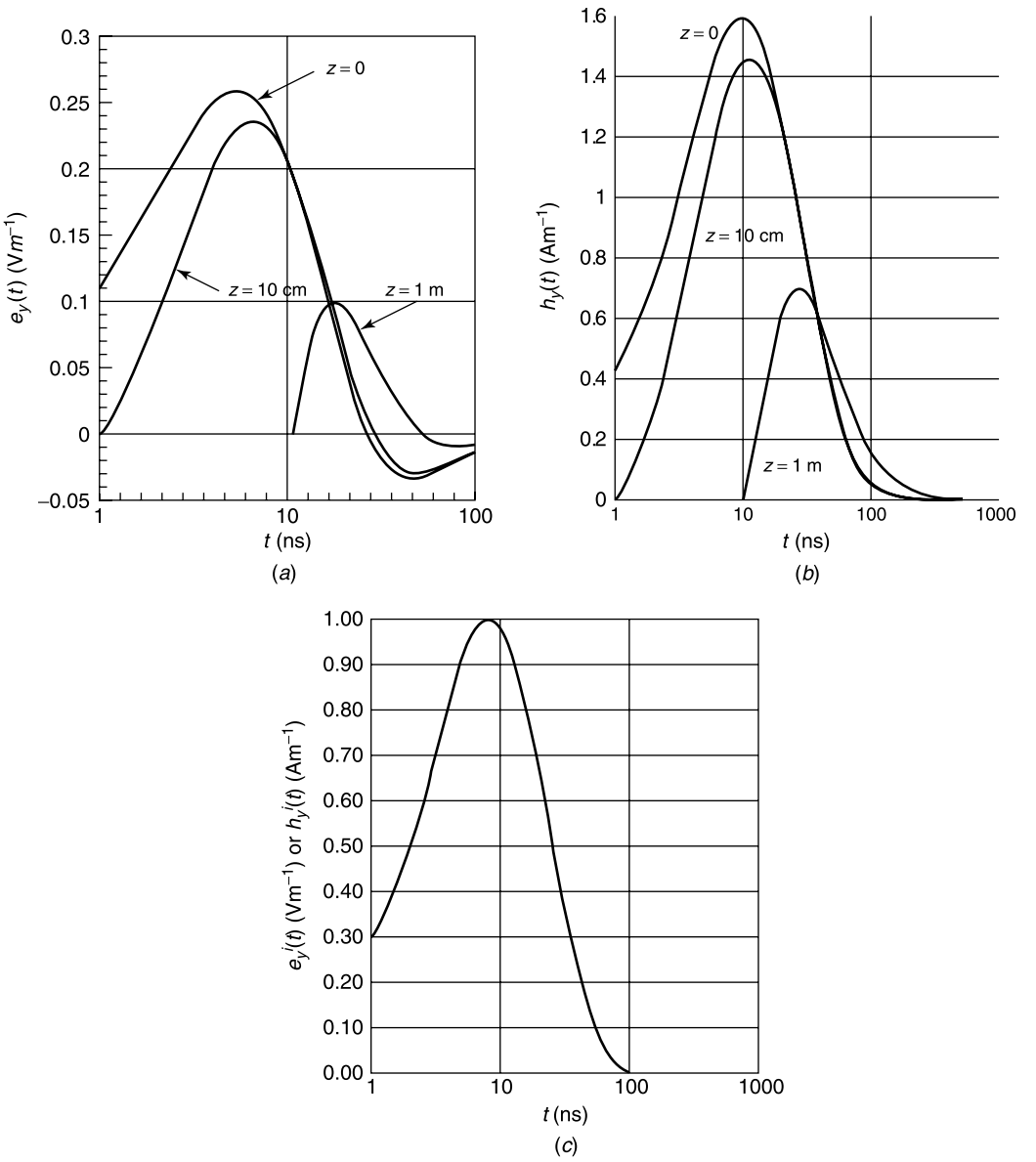

Figure 9.12 (*a*) Penetration in a lossy medium, TE polarization ($\theta_i = 45°$) (**e** parallel to the interface). (*b*) TM polarization ($\theta^i = 45°$) (**h** parallel to the interface). (*c*) Incident double exponential (used for both a and b) (from H. Y. Pao, S. L. Dvorak and D. G. Dudley, An accurate and efficient analysis for transient plane waves obliquely incident on a conductive half space (TE case), *IEEE Trans. AP* **44**, 918–924, (1996), and H. Y. Pao, S. L. Dvorak and D. G. Dudley, An accurate and efficient analysis for transient plane waves obliquely incident on a conductive half space (TM case), *IEEE Trans. AP* **44**, 925–932, (1996), with permission of IEEE).

more exact approach the frequency dependence of these parameters should be taken into account when the frequency spectrum occupies a range in which σ and ϵ_r vary significantly. For such a case a better model is needed, which should fit measured data but also respect the causality requirements embodied in Kramers-Kronig relations (8.17). The Debye and

Lorentz models, defined in (8.21) and (8.22), have been found useful, as well as the *Messier parameters*[26]

$$\epsilon(\omega) = \epsilon_\infty + \left(\frac{2\sigma_0\epsilon_\infty}{\omega}\right)^{\frac{1}{2}}$$
$$\sigma_{\text{eff}}(\omega) = \sigma_0 + (2\sigma_0\epsilon_\infty\omega)^{\frac{1}{2}}. \tag{9.73}$$

9.2 PROPAGATION THROUGH A LAYERED MEDIUM

In Section 9.1, the media were assumed half-infinite. In this section, we shall consider volumes bounded by parallel planes, and in particular slabs and thin films.

9.2.1 Propagation Through a Slab

Figure 9.13 shows a plane wave normally incident on a slab of impedance Z_c and propagation constant $k = \beta - j\alpha$ (see Equations 8.44 and 8.46). In the slab the fields — solutions of Helmholtz' equation — are of the form

$$E(z) = C\,e^{-jkz} + D\,e^{jkz}$$
$$Z_c H(z) = C\,e^{-jkz} - D\,e^{jkz}. \tag{9.74}$$

These relationships, written for $z = 0$ and $z = l$, give, after elimination of C and D,

$$\begin{pmatrix} E \\ H \end{pmatrix}_0 = \begin{pmatrix} \cos kl & jZ_c \sin kl \\ jY_c \sin kl & \cos kl \end{pmatrix} \cdot \begin{pmatrix} E \\ H \end{pmatrix}_l. \tag{9.75}$$

If Z_{c3} is the characteristic impedance of medium 3, the impedance in the $z = 0$ plane is found to be

$$\frac{E(0)}{H(0)} = \frac{Z_{c3}\cos kl + jZ_c \sin kl}{jY_c Z_{c3} \sin kl + \cos kl}. \tag{9.76}$$

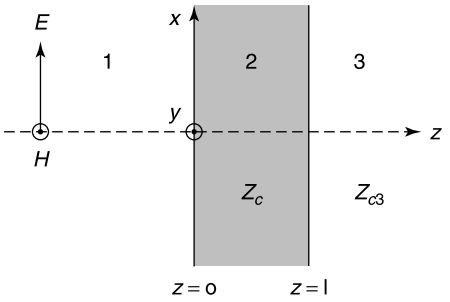

Figure 9.13 Plane wave normally incident on a slab.

If medium 3 is free space, one should set $Z_{c3} = R_{c0}$. If 3 is a perfect conductor [which implies the condition $E(l) = 0$], (9.76) leads to

$$\frac{E(0)}{H(0)} = jZ_c \tan kl. \tag{9.77}$$

This simple analysis allows determination of the fields that leak through the slab. The relevant relationships, obtained from (9.74), are

$$\begin{pmatrix} E \\ H \end{pmatrix}_l = \begin{pmatrix} \cos kl & -jZ_c \sin kl \\ -jY_c \sin kl & \cos kl \end{pmatrix} \cdot \begin{pmatrix} E \\ H \end{pmatrix}_0. \tag{9.78}$$

For a good conductor, for example, $kl = (1-j)\dfrac{l}{\delta}$, and the shielding effect for $|kl| \gg 1$ can easily be evaluated as a function of δ. At low frequencies, materials of high permeability μ_r, such as mumetal, are often used. These materials are highly nonlinear, however, and the determination of the fields in the slab must proceed by iteration. Time-domain techniques of the type discussed in Section 12.8 are particularly suitable for such computations.[27,28,29] When the material is linear, transient penetration becomes easier to analyze. The following simple example — an introduction to some topics discussed in Chapter 13 — shows the importance of a fundamental parameter, the diffusion time [142].

Assume that an induction $\mathbf{b}_0 = b_0 \mathbf{u}_y$ is suddenly applied at both ends of a highly conducting slab (Fig. 9.13). The induction in the slab satisfies the diffusion equation, a direct consequence of Maxwell's equations. Thus, because the displacement current has been assumed negligible,

$$\frac{\partial^2 b(z,t)}{\partial z^2} - \sigma\mu \frac{\partial b(z,t)}{\partial t} = 0. \tag{9.79}$$

Let us Fourier expand $b(z,t)$ in the interval $(0,l)$ as

$$b = \sum_{n=1}^{\infty} a_n(t) \sin \frac{n\pi z}{l} + b_0, \tag{9.80}$$

where only odd n are needed because b is symmetric with respect to the central axis $z = (l/2)$. Inserting (9.80) into (9.79) gives

$$\frac{da_n}{dt} + \frac{1}{\sigma\mu}\left(\frac{n\pi}{l}\right)^2 a_n = 0.$$

The solution of this equation is elementary. It leads to the expansion

$$b = \sum_{n\,odd} b_n \sin \frac{n\pi z}{l}\, e^{-\alpha_n t} + b_0,$$

where

$$\alpha_n = n^2 \frac{\pi^2}{\sigma\mu l^2} = \frac{n^2}{\tau} = \frac{n^2\pi^2}{T_D}$$

and T_D is the *magnetic diffusion time*. Because $b(z,t)$ is zero at $t = 0$, b_n can easily be evaluated. The final result is

$$b = b_0 \left[1 - \sum_{n\,odd} \frac{4}{n\pi} \sin \frac{n\pi z}{l} e^{-n^2 \frac{t}{\tau}} \right]. \tag{9.81}$$

The lowest space harmonic (corresponding with $n = 1$) diffuses more slowly than the higher ones, which have time constants (τ/n^2). The evolution of $b(z,t)$ is shown in Figure 9.14. It is seen that the field has almost completely diffused by the time t exceeds 3τ (Problem 9.11).

The shielding effect of a conducting slab results from two basic mechanisms:

1. Power absorption in the layer

2. A strong impedance mismatch (i.e., strong reflections).

In the application to "stealth" structures, the accent is on minimal reflections, obtained by means of strong absorption and a good match. If this goal is to be achieved over a wide frequency band, a number of adjustable parameters should be available. Multilayered structures can provide some of that flexibility and have been used in the design of filters or in the modeling of the human body as a succession of layers of skin, fat, muscle, and bone.[7,30] Heat will be dissipated in the conducting layers, and the determination of the resulting temperature rise is important for an efficient use of techniques such as hyperthermia,[30] in which tumors are selectively heated and destroyed. In the presence of N layers, (9.75) should be applied N times, yielding an overall matrix equal to the product of the N partial ones [1, 10]. Trade-offs must often be made between reflectivity and total thickness. Genetic algorithms,[31] which act on an initial population of N designs (the chromosomes), have been successful in converging to optimal solutions.

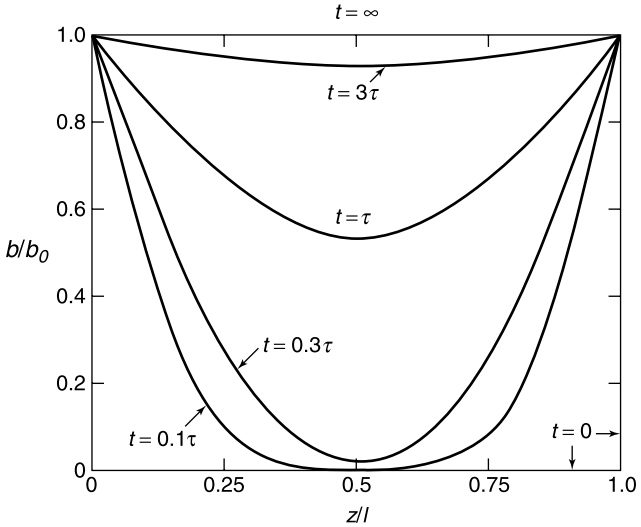

Figure 9.14 Transient diffusion of a magnetic field into a conducting material (from H. H. Woodson and J. R. Melcher, *Electromechanical Dynamics, Part II: Fields, Forces, and Motion*. John Wiley & Sons, New York, 1968, with kind permission of Mrs. J. Melcher).

In the previous analysis, normal incidence of a plane wave on the slab has been assumed. *Oblique* incidence can be investigated by the methods presented in Section 9.1, both for time-harmonic and general transient fields. No new principles are involved, but the formalism becomes heavy.[32]

9.2.2 Thin Films

A thin film is defined by the condition $|kl| \ll 1$. Consider first normal incidence on a good conductor. Because the conductor is highly conducting, a second small parameter, $Q = (\omega\epsilon_0/\sigma)$, becomes relevant, and we write

$$\begin{aligned} kl &= (1-j)\frac{l}{\delta} \\ Z_c &= R_{c0}\sqrt{Q}\,\frac{1+j}{\sqrt{2}} = R_{c0}\sqrt{jQ}. \end{aligned} \tag{9.82}$$

To determine the reflection coefficient R_1 at $z = 0$, let us apply (9.74) there. Assuming unit incident electric field (Fig. 9.13):

$$\begin{aligned} E &= 1 + R_1 = C + D \\ H &= \frac{1}{R_{c0}}(1 - R_1) = \frac{1}{Z_c}(C - D). \end{aligned} \tag{9.83}$$

At $z = l$:

$$\begin{aligned} E &= C(1 - jkl) + D(1 + jkl) = T_3 \\ Z_c H &= C(1 - jkl) - D(1 + jkl) = \frac{Z_c}{R_{c0}}T_3, \end{aligned} \tag{9.84}$$

where T_3 is the transmission coefficient to region 3, assumed to be vacuum.[†] A few elementary steps yield

$$R_1 = \frac{jkl - klQ}{2\sqrt{jQ} - klQ + jkl} \approx -\frac{jkl}{jkl + 2\sqrt{jQ}}. \tag{9.85}$$

This formula shows that the reflection properties, when both kl and Q are small, depend on the *ratio* of these two parameters. By introducing a characteristic length[33]

$$l_0 = \frac{2\sqrt{jQ}}{jk} = \frac{2}{R_{c0}\sigma} = \sqrt{2Q}\delta \tag{9.86}$$

the reflection coefficient takes the form

$$R_1 = -\frac{(l/l_0)}{1 + (l/l_0)}. \tag{9.87}$$

[†]Generalizations to arbitrary media in 3, as well as to oblique incidence, are immediate.

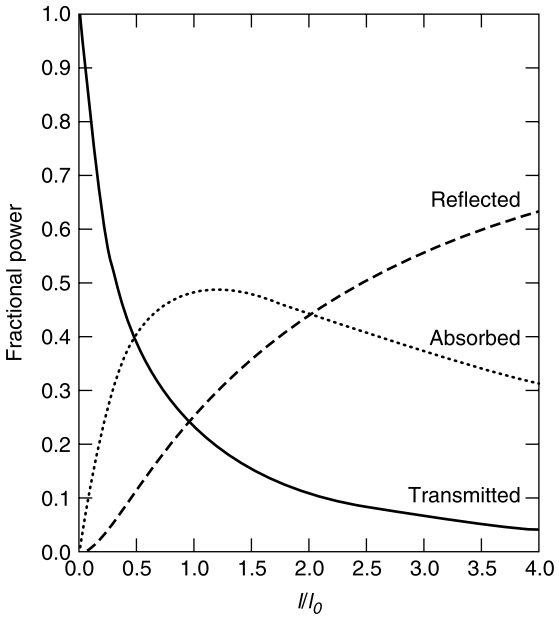

Figure 9.15 Transmission, reflection and absorption of power by a thin film (from S. Fahy, C. Kittel, and S. G. Louie, Electromagnetic screening by metals, *Am. J. Phys.* **54**, 989–992, 1988, with kind permission of Dr. S. G. Louie).

The variation of $|R_1|^2$ is shown in Figure 9.15. The transmission coefficient is given by

$$T_3 = \frac{1}{1 + (l/l_0)}. \tag{9.88}$$

The variation of $|T_3|^2$, the relative power transmission, is displayed on the same figure, as well as that of the absorption coefficient

$$A = 1 - \left[\frac{l/l_0}{1 + (l/l_0)}\right]^2 - \left[\frac{1}{1 + (l/l_0)}\right]^2 = \frac{2(l/l_0)}{\left[1 + (l/l_0)\right]^2}.$$

These curves are particularly interesting from a physical point of view. They show, for example, that increasing l from zero initially increases the power absorbed in the film. Further increases of l increase the reflections, hence reduce the penetration of the fields into the film. The analysis shows that maximum absorption occurs for $l = l_0$. Illustratively, for Cu at 10 GHz, $l_0 = 0.914 \times 10^{-10}$ m and $\delta = 0.66 \times 10^{-6}$ m.

On the basis of (9.78), the fields at the boundary planes of the slab are related by

$$\begin{aligned} E(l) &= E(0) - jklZ_cH(0) \\ Z_cH(l) &= Z_cH(0) - jklE(0). \end{aligned} \tag{9.89}$$

To the first order:

$$\begin{aligned} E(l) &= E(0) = \frac{1}{1+(l/l_0)}E^i \\ H(l) &= H(0) - 2\frac{l}{l_0}\frac{E(0)}{R_{c0}} = H(0) - \frac{2l/l_0}{1+(l/l_0)}H^i \\ &= \frac{H^i}{1+(l/l_0)}. \end{aligned} \tag{9.90}$$

The equations show that a current

$$I_x = \frac{\sigma l}{1+l/l_0}E^i = \frac{2l/l_0}{1+l/l_0}H^i \quad (\mathrm{A\,m^{-1}}) \tag{9.91}$$

flows in the x-direction. This current causes a drop of H across the slab. From Maxwell's equation (7.2), indeed,

$$H(l) = H(0) + l\left(\frac{\partial H}{\partial z}\right)_{z=0} = H(0) - l\sigma E(0) = H(0) - I_x.$$

9.2.3 An Inversion Problem

Let a transient wave

$$\mathbf{e}^i = f\left(t - \frac{z}{c_0}\right)\mathbf{u}_x \tag{9.92}$$

be incident on a nonmagnetic slab of unknown parameters $\epsilon_r(z)$ and $\sigma(z)$ (Fig. 9.13). The function $f(t)$ differs from zero only between 0 and T. The one-sided Laplace transform of e^i is, from A7.4,

$$E^i(s) = e^{-s\frac{z}{c_0}}F(s),$$

where $F(s)$ is the Laplace transform of $f(t)$. Within the slab, $E(z,c)$ satisfies the transform of the wave equation, viz.

$$\frac{\partial^2 E}{\partial z^2} - \frac{s^2}{c_0^2}\left[\epsilon_r(z) + \frac{\sigma(z)}{s\epsilon_0}\right]E = 0. \tag{9.93}$$

By introducing the contrast function

$$C(z,s) = \epsilon_r(z) - 1 + \frac{\sigma(z)}{s\epsilon_0}$$

(9.93) can be recast in the form

$$\frac{\partial^2 E}{\partial z^2} - \frac{s^2 E}{c_0^2} = \frac{s^2}{c_0^2}C(z,s)E. \tag{9.94}$$

The second member may be considered as a forcing function. By means of the one-dimensional Green's function

$$G(z, z', s) = -\frac{c_0}{2s} e^{-\frac{s}{c_0}|z-z'|}$$

the solution $E(z, s)$ of (9.94) is readily shown to be also the solution of

$$E(z, s) + \frac{s^2}{c_0^2} \int_0^l C(z', s)\, G(z,\, z', s)\, E(z', s)\, dz' = E^i(z, s). \tag{9.95}$$

Given $C(z, s)$, (9.95) becomes an integral equation for $E(z, s)$ which, once solved, yields $e(z, t)$ by way of a Laplace inversion. Alternately, $e(z, t)$ may be measured for a given incident wave and $C(z, s)$ determined from the solution of (9.95), where $E(z, s)$ is now the evaluated transform of $e(z, t)$. In an iterative method, one would start with a reasonable estimate of ϵ_r and σ, solve (9.95) for $E(z, s)$, compare the result with the previously computed value of $E(z, s)$, and further iterate on the basis of a suitable error criterion [31, 128].

9.3 THE SOMMERFELD DIPOLE PROBLEM

The Sommerfeld problem of concern consists in evaluating the fields radiated by a dipole in the presence of a half-infinite medium of complex dielectric constant ϵ_c (Fig. 9.16). The dipole can be vertical or horizontal, electric or magnetic. The fields generated by the various dipoles can be combined into appropriate electric or magnetic Green's dyadics. The problem has been discussed extensively in the literature‡ [8, 12, 20, 28, 47, 137, 171]. The first investigators, in the early years of "radio," wished to find out theoretically whether the earth could support a surface wave of low attenuation.[34] Experimental evidence had shown the possibility of long distance propagation, unimpeded by the curvature of the earth. The Zenneck wave, discussed in Section 9.1, was expected to provide a possible theoretical basis for these experimental data. We shall discuss, in very concise form, the solution that Sommerfeld gave to the field problem, and more particularly in the case of a vertical electric dipole source. The primary field (i.e., the field of the dipole in free space) can be derived from a Hertz potential. From (7.41) and (7.105),

$$\boldsymbol{\pi}_e^i(\mathbf{r}) = \frac{P_e}{4\pi\epsilon_0} \frac{e^{-jk_0R}}{R}\, \mathbf{u}_z \qquad \text{(V m)}. \tag{9.96}$$

Given the axial symmetry, $\boldsymbol{\pi}_e^i$ is a function of r and z alone. Because $J_0(\lambda r)\, e^{\pm(\lambda^2-k_0^2)^{\frac{1}{2}}z}$ is a solution of Helmholtz' equation for arbitrary (complex) λ, a superposition of such solutions is also a solution of Helmholtz' equation, hence [171]

$$f(r, z) = \int_0^\infty F(\lambda)\, J_0(\lambda r)\, e^{-(\lambda^2-k_0^2)^{\frac{1}{2}}|z|} d\lambda \qquad (\lambda \text{ in m}^{-1})$$

‡Several papers commemorating Sommerfeld's diffraction problem have been collected into two special issues of *Electromagnetics*, edited by G. Pelosi and J. Volakis (vol. 18, March–April and May–June 1998).

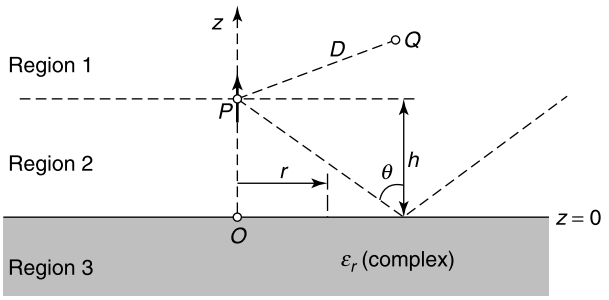

Figure 9.16 Vertical dipole above a dielectric medium.

is a possible form for the primary Hertz potential. We note that satisfaction of the radiation condition requires use of the root with positive real part for $(\lambda^2 - k_0^2)^{\frac{1}{2}}$. To determine the value of $F(\lambda)$, it is convenient to shift the origin of the coordinate system from O to P. The functions $f(r, z)$ and $\pi_e^i(r, z)$ must be equal at the new $z = 0$. In consequence,

$$\int_0^\infty F(\lambda)\, J_0(\lambda r)\, d\lambda = \frac{P_e}{4\pi\epsilon_0} \frac{e^{-jk_0 r}}{r}.$$

The left-hand term is the Hankel transform (A7.58) of $F(\lambda)/\lambda$. Inversion according to (A7.59) gives

$$F(\lambda) = \lambda \int_0^\infty \frac{P_e}{4\pi\epsilon_0}\, e^{-jk_0 z} J_0(\lambda z)\, dz.$$

Using Sommerfeld's integral (A5.49), viz.

$$J_0(\rho) = \frac{1}{2\pi} \int_{-\pi}^{\pi} e^{-j\rho\cos\varphi}\, d\varphi$$

leads to

$$F(\lambda) = \frac{P_e}{4\pi\epsilon_0} \frac{\lambda}{2\pi} \int_{-\pi}^{\pi} d\varphi \int_0^\infty e^{-jz(k_0 + \lambda\cos\varphi)}\, dz.$$

The integral over z can be integrated by parts. If we restrict ourselves to $\lambda's$ that have negative imaginary parts, the contribution from $z = \infty$ vanishes, and

$$F(\lambda) = \frac{P_e}{4\pi\epsilon_0} \frac{\lambda}{2\pi j} \int_{-\pi}^{\pi} \frac{d\varphi}{k_0 + \lambda\cos\varphi} = \frac{P_e}{4\pi\epsilon_0} \frac{\lambda}{(\lambda^2 - k_0^2)^{\frac{1}{2}}}.$$

By reverting to the original system of coordinates centered on O, we obtain the Hertz potential of the primary field in the form

$$\pi_e^i = \frac{P_e}{4\pi\epsilon_0} \int_0^\infty \frac{\lambda}{(\lambda^2 - k_0^2)^{\frac{1}{2}}}\, J_0(\lambda r)\, e^{-(\lambda^2 - k_0^2)^{\frac{1}{2}} |z-h|}\, d\lambda \tag{9.97}$$

where the previously mentioned restriction on λ requires the path of integration to be below the real axis.

The total Hertz potential is the sum of the incident value π_e^i and the secondary contribution from the dielectric region. In region 1, the total potential satisfies Helmholtz equation in vacuum and can therefore be cast in a form similar to (9.97). Thus,

$$\pi_1 = \pi_e^i + \pi_e^d = \frac{P_e}{4\pi\epsilon_0}\left[\int_0^\infty \frac{\lambda}{(\lambda^2 - k_0^2)^{\frac{1}{2}}} J_0(\lambda r)\, e^{-(\lambda^2 - k_0^2)^{\frac{1}{2}}(z-h)}\, d\lambda \right.$$
$$\left. + \int_0^\infty \frac{\lambda}{(\lambda^2 - k_0^2)^{\frac{1}{2}}} R(\lambda)\, J_0(\lambda r)\, e^{-(\lambda^2 - k_0^2)^{\frac{1}{2}}(z+h)}\, d\lambda \right]. \tag{9.98}$$

The function $R(\lambda)$ has the nature of a reflection coefficient. In region 2, the Hertz potential is given by a similar expression, differing only in the sign of the exponent in the first integral. In region 3 we take

$$\pi_3 = \frac{P_e}{4\pi\epsilon_0} \int_0^\infty \frac{\lambda}{(\lambda^2 - k_0^2)^{\frac{1}{2}}} T(\lambda)\, J_0(\lambda r)\, e^{(\lambda^2 - k_0^2\epsilon_{cr})^{\frac{1}{2}} z}\, e^{-(\lambda^2 - k_0^2)h}\, d\lambda \tag{9.99}$$

where $T(\lambda)$ has the nature of a transmission coefficient. We shall set $k^2 = k_0^2\epsilon_{cr}$ in the sequel. To determine the functions R and T, we invoke the boundary conditions at $z = 0$, which require E_r and H_φ to be continuous. In terms of the Hertz potentials, these conditions become

$$\frac{\partial}{\partial r}\left(\frac{\partial \pi_2}{\partial z}\right) = \frac{\partial}{\partial r}\left(\frac{\partial \pi_3}{\partial z}\right) \qquad \text{at } z = 0$$
$$k_0^2 \frac{\partial \pi_2}{\partial r} = k^2 \frac{\partial \pi_3}{\partial r} \qquad \text{at } z = 0.$$

The first condition can be satisfied if $\partial\pi_2/\partial z$ is set equal to $\partial\pi_3/\partial z$. A few simple steps now give

$$R(\lambda) = \frac{\epsilon_{cr}(\lambda^2 - k_0^2)^{\frac{1}{2}} - (\lambda^2 - k^2)^{\frac{1}{2}}}{\epsilon_{cr}(\lambda^2 - k_0^2)^{\frac{1}{2}} + (\lambda^2 - k^2)^{\frac{1}{2}}}$$
$$T(\lambda) = \frac{2(\lambda^2 - k_0^2)^{\frac{1}{2}}}{\epsilon_{cr}(\lambda^2 - k_0^2)^{\frac{1}{2}} + (\lambda^2 - k^2)^{\frac{1}{2}}}, \tag{9.100}$$

which completes the formal solution of the problem.

Theoretical Evaluation of the Potentials

In many applications, interest centers on the secondary wave π_e^d, obtained by inserting the form (9.100) for $R(\lambda)$ into (9.98). The solution can be interpreted as a bundle of plane waves reflected and refracted from the earth's surface at various angles of incidence [20]. The evaluation of the integrals rests on the techniques of complex integration. We note, in that respect, that the form of $R(\lambda)$ evidences branch points at $\pm k_0$ and $\pm k_0(\epsilon_{cr})^{\frac{1}{2}}$. There are also poles at values of λ satisfying

$$\epsilon_{cr}(\lambda^2 - k_0^2)^{\frac{1}{2}} + (\lambda^2 - \epsilon_{cr}k_0^2)^{\frac{1}{2}} = 0. \tag{9.101}$$

The pole

$$\lambda = k_0 \left(\frac{\epsilon_{cr}}{\epsilon_{cr} + 1} \right)^{\frac{1}{2}}$$

is precisely the value (9.46) associated with the Zenneck wave. The integration can be performed by saddle-point techniques, due attention being given to the Zenneck pole and the saddle point k_0 [8]. In the assumption $|\epsilon_{cr}|^{\frac{1}{2}} \gg 1$, normally valid for the earth, the pole is at $\lambda \approx k_0 \left(1 - \dfrac{1}{2\epsilon_{cr}} \right)$.

The results of Sommerfeld's analysis have been a matter of longstanding controversy.[35,36,37,38] As part of his solution, Sommerfeld obtained a radial Zenneck surface wave (i.e., a long distance wave guided along the surface of the earth). This wave could account for some of Marconi's early experimental results. In the solution given by Weyl, the Zenneck wave did *not* appear.[35] The discussion centered on a possible error of sign in Sommerfeld's equations. The reader is referred to two recent articles for a summary of the state of affairs.[5,34] We shall only quote an illustrative result, based on putting the potential of the ground wave in the form

$$\pi_e(r, 0) = \frac{e^{-jk_0 r}}{2\pi r} F(p) \tag{9.102}$$

where both source and observation point are located at the interface. The symbol p is the *numerical distance*

$$p = -j \frac{k_0 r}{2\epsilon_{cr}} = |p| e^{jb}. \tag{9.103}$$

The first factor in (9.102) is the value of π_e on a perfect conductor. The factor F, given by

$$F = 1 - (\pi p)^{\frac{1}{2}} e^{-p} \operatorname{erfc}(j\sqrt{p}), \tag{9.104}$$

is the *attenuation function* [8]. The formula is valid for large $k_0 r$, moderate values of p, and $|\epsilon_r| \gg 1$. The complementary error function is defined by

$$\operatorname{erfc}(jp^{\frac{1}{2}}) = \frac{2}{\sqrt{\pi}} \int_{jp^{\frac{1}{2}}}^{\infty} e^{-z^2} dz,$$

where the contour is from $jp^{\frac{1}{2}}$ via a straight line to the origin and then along the real axis to $+\infty$. Figure 9.17 shows some numerical values for the attenuation function F, with $|p|$ and b as parameters. The data are taken from an article by Norton,[36] who reduced the complex equations of the Sommerfeld theory to a few simple formulas, suitable for use by practicing engineers.

The potentials π_e^d and π_3 can be interpreted as generated by images [12], which in the current case are continuous line sources in complex space.[39,40,41] Such sources are briefly

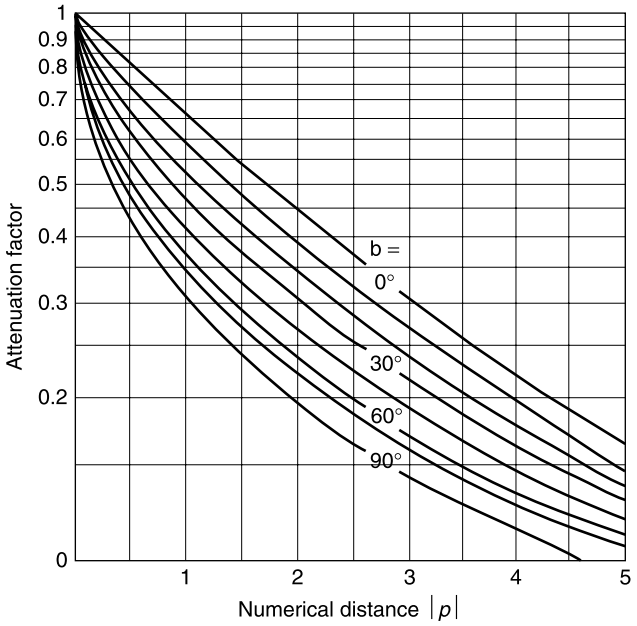

Figure 9.17 Ground-wave attenuation factor as a function of the parameters $|p|$ and b (from K. A. Norton, The propagation of radio waves over the surface of the earth and in the upper atmosphere, Part I: Ground-wave propagation from short antennas, *Proc. IRE* **24**, 1367–1387, 1936, with permission of IEEE).

discussed in Section 8.4. The method provides a rapidly converging alternate representation, which can also be used in the time domain.[42]

9.4 MULTILAYERED STRUCTURES

The extensive use of multilayered geometries in the design of antennas and monolithic integrated circuits has led to considerable interest in a thorough theoretical study of these structures. Typical examples are shown in Figure 9.18. These circuits are tightly packed, and their operation may suffer from electromagnetic coupling, a phenomenon that can't be fully understood without a complete field analysis.

9.4.1 Integral Equations

In the patch configuration of Figure 9.18*a*, the integral equation takes the form[§]

$$\mathbf{E}_t(\mathbf{r}) = \mathbf{E}_t^i(\mathbf{r}) + \left[\int_S \overline{\overline{G}}_{ee}(\mathbf{r}|\mathbf{r}') \cdot \mathbf{J}_S(\mathbf{r}')\, dS'\right]_t = 0 \tag{9.105}$$

where t denotes a tangential component (i.e., a component in the x, y plane), and $\mathbf{r}$ and $\mathbf{r}'$ are points in the interface plane $z = 0$. The patch configuration can serve as a *resonator*,

[§] $\mathbf{E}_t$ has been set equal to zero because the patch is assumed perfectly conducting. When the patch material is characterized by a surface impedance, one should set $\mathbf{E}_t = Z_S \mathbf{J}_S$ [191].

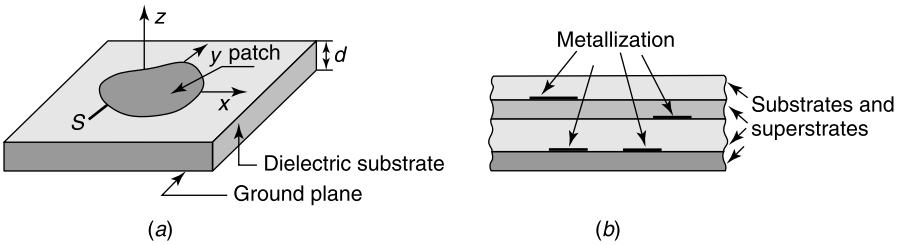

Figure 9.18 (*a*) A patch on a dielectric substrate. (*b*) A multilayer and multistrip structure.

in which case $\mathbf{E}^i = 0$. Integral equation (9.105) now quantizes the complex eigenvalues of the problem and therefore yields the resonant frequency and the damping constant of the resonant modes.[43,44,45] In the *antenna* mode of operation, the patch is excited by an incident field, generated for example by an aperture or a coaxial line [90, 109]. Examples of such couplings are sketched in Figure 9.19. Essential for the theoretical solution is a knowledge of the Green's dyadic, a complex problem made more tractable by exploiting the particular geometry of the problem, which calls for the use of spatial Fourier transforms. The main features of the method will be summarized by considering the simple mathematical problem embodied in Figure 9.20*a*. The geometry is axisymmetric, hence only the r and z coordinates are relevant. On the basis of (A8.18), the Green's function must satisfy the differential equations

$$\begin{aligned} \nabla^2 G_1 + k_1^2 G_1 &= 0 \qquad\qquad\qquad \text{(in region 1)} \\ \nabla^2 G_0 + k_0^2 G_0 &= \frac{1}{2\pi r}\,\delta(r)\delta(z - z_0) \quad \text{(in region 0).} \end{aligned} \tag{9.106}$$

The boundary conditions at $z = 0$ are $G_0 = G_1$ and

$$\frac{\partial G_0}{\partial z} = \gamma \frac{\partial G_1}{\partial z.} \tag{9.107}$$

At the lower boundary (i.e., at $z = -h$), G_1 should vanish. Given the symmetry of the problem, the r-dependence may be erased by means of the Hankel transform (A7.58).

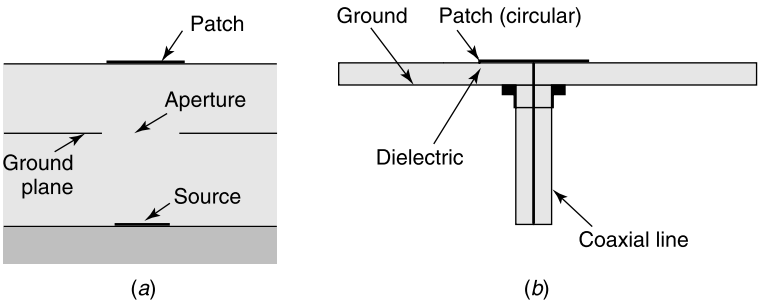

Figure 9.19 (*a*) Excitation by a microstrip, through an aperture. (*b*) Coaxial excitation (from C. Wu, K. L. Wu, Z.-Q. Bi, and J. Litva, Accurate characterization of planar printed antennas using finite-difference time-domain methods, *IEEE Trans. AP* **40**, 526–534, 1992, with permission of IEEE).

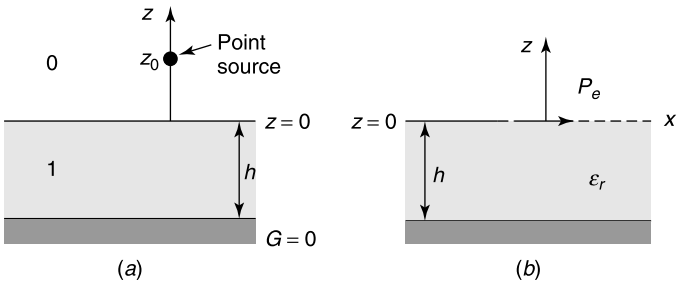

Figure 9.20 (*a*) Layered structure. (*b*) Horizontal electric dipole in the interface $z = 0$.

We write

$$\tilde{G}(\lambda, z, z_0) = \int_0^\infty G(r, z, z_0) J_0(\lambda r) r \, dr \tag{9.108}$$

For $z \neq z_0$, (9.106) implies

$$\frac{d}{dr}\left(r\frac{dG}{dr}\right) + k^2 r G = 0.$$

By combining that equation with

$$\frac{d}{dr}\left(r\frac{dJ_0}{dr}\right) + \lambda^2 r J_0 = 0,$$

one obtains transmission-line equations for the transform of G. Thus[¶]

$$\begin{aligned} &\frac{d^2\tilde{G}_1}{dz^2} + (k_1^2 - \lambda^2)\,\tilde{G}_1 = 0 \\ &\frac{d^2\tilde{G}_0}{dz^2} + (k_0^2 - \lambda^2)\,\tilde{G}_0 = \frac{1}{2\pi}\,\delta(z - z_0). \end{aligned} \tag{9.109}$$

At $z = z_0$, $\tilde{G}$ is continuous, but the presence of the δ-function in (9.109) implies a jump condition

$$\left(\frac{d\tilde{G}_0}{dz}\right)_{z_0^+} - \left(\frac{d\tilde{G}_0}{dz}\right)_{z_0^-} = \frac{1}{2\pi}$$

for the first derivatives. It is useful, for conciseness, to introduce the notation

$$u_i = (\lambda^2 - k_i^2)^{\frac{1}{2}} \tag{9.110}$$

where we select the root with positive real part. In region 1

$$\tilde{G}_1 = A \sinh u_1 (z + h), \tag{9.111}$$

[¶]In a multilayered structure, there would be a cascade of such transmission lines.

because $\tilde{G}_1$ must vanish at $z = -h$. In region 0, below the source,

$$\tilde{G}_0 = B \sinh u_0 z + C \cosh u_0 z. \tag{9.112}$$

In region 0, above the source,

$$\tilde{G}_0 = De^{-u_0 z}. \tag{9.113}$$

Expression (9.113) remains bounded for $z \to \infty$, because the real part of u_0 has been chosen positive. The value of the coefficients A, B, C, D follows from an application of the boundary conditions at $z = 0$ and $z = z_0$. We shall omit the details but note that once a coefficient such as $A(z_0, h, \lambda)$ is obtained, the field at the interface $z = 0$ follows from an inversion of the Hankel transform. Thus, from (A7.59),

$$G_1(r, 0|z_0, h) = \int_0^\infty A(z_0, h, \lambda) \sinh(u_1 h)\, J_0(\lambda r)\lambda \, d\lambda. \tag{9.114}$$

The just outlined steps can be applied, in adapted form, to the patch configuration shown in Figure 9.18*a*, where the x and y coordinates can be erased by performing a Fourier transformation with respect to x and y. We write, for example:

$$\tilde{G}_{xx}(k_x, k_y, z) = \int_{-\infty}^{\infty} \int_{-\infty}^{\infty} G_{xx}(x, y, z)\, e^{-j(k_x x + k_y y)}\, dx\, dy. \tag{9.115}$$

Because the elements of $\overline{\overline{G}}$, given the translation symmetry, depend on x, y, x', y' through the combination $(x - x')$ and $(y - y')$, the convolution theorems A7.5 and A7.30 may be applied, and we obtain, starting from (9.105),

$$\begin{aligned} &\tilde{E}_x^i(k_x, k_y, 0) + \tilde{G}_{xx}(k_x, k_y)\, \tilde{J}_{Sx}(k_x, k_y) + \tilde{G}_{xy}(k_x, k_y)\, \tilde{J}_{Sy}(k_x, k_y) = 0 \\ &\tilde{E}_y^i(k_x, k_y, 0) + \tilde{G}_{yx}(k_x, k_y)\, \tilde{J}_{Sx}(k_x, k_y) + \tilde{G}_{yy}(k_x, k_y)\, \tilde{J}_{Sy}(k_x, k_y) = 0. \end{aligned} \tag{9.116}$$

Let us assume that the spectral Green's functions have been determined. Equation (9.116) may now be solved to yield $\tilde{J}_x$ and $\tilde{J}_y$, from which the space currents J_x and J_y follow by an inverse Fourier transformation. For example:

$$J_{Sx}(x, y) = \frac{1}{(2\pi)^2} \int_{-\infty}^{\infty} \int_{-\infty}^{\infty} \tilde{J}_{Sx}(k_x, k_y)\, e^{j(k_x x + k_y y)}\, dk_x\, dk_y. \tag{9.117}$$

The proposed spectral domain analysis is particularly useful when J_{Sx} can be expressed as a sum of basis functions, each of which is conveniently invertible according to (9.117). In an alternate approach, $\tilde{G}(k_x, k_y)$ is inverted first, and the resulting space-domain dyadic $\overline{\overline{G}}$ is subsequently inserted into (9.105), which can then be solved for $\mathbf{J}_S$.

9.4.2 Solution by Means of Mixed Potentials

In many recent publications,[46,47,48] the fields are expressed in terms of the $\mathbf{A}$ and ϕ potentials, following a method already used in Section 7.14. Thus,

$$\mathbf{E} = -\text{grad}\, \phi - j\omega \mathbf{A}.$$

The solution now centers on the determination of the potentials. Both satisfy Helmholtz' equation, for example,

$$\nabla^2\phi + k^2\phi = \frac{1}{\epsilon_c}P = \frac{1}{j\omega\epsilon_c}\,\text{div}\,\mathbf{J}.$$

As usual $k^2 = \omega^2\epsilon\mu$, where ϵ and μ can be complex. The basic integro-differential equation for $\mathbf{J}_S$ now takes the form

$$\mathbf{E}_t^i(\mathbf{r}) - j\omega\left[\int_S \overline{\overline{G}}^A(\mathbf{r}|\mathbf{r}')\cdot\mathbf{J}_S(\mathbf{r}')\,dS'\right]_t - \text{grad}_t\int_S G^\phi(\mathbf{r}|\mathbf{r}')P_S(\mathbf{r}')\,dS' = 0 \tag{9.118}$$

for $\mathbf{r}$ on S. The advantage of the mixed potential formulation lies in the weak singularity of $\overline{\overline{G}}^A$ and G^ϕ, of the order $\left(\frac{1}{R}\right)$, compared with the stronger singularity of $\overline{\overline{G}}_{ee}$, of the order $\left(\frac{1}{R^3}\right)$. The weaker singularity leads to better convergence in the evaluation of Sommerfeld integrals.[‖]

The elements of $\overline{\overline{G}}^A$ are the fields generated by appropriate elementary dipoles. In Figure 9.20*b*, the dipole is chosen horizontal, a reasonable choice because the currents $\mathbf{J}_S$ lie in the (x, y) plane.[46] With both dipole and observation point in the interface plane $z = 0$,

$$\overline{\overline{G}}^A(\mathbf{r}|\mathbf{r}')\cdot\mathbf{J}_S(\mathbf{r}') = G_{xx}^A(\mathbf{r}|\mathbf{r}')\,\mathbf{J}_{Sx}(\mathbf{r}') + G_{yy}^A(\mathbf{r}|\mathbf{r}')\,\mathbf{J}_{Sy}(\mathbf{r}'). \tag{9.119}$$

The cross-terms in (xy) and (yx) are absent because of symmetry.[49] Also absent are the z indices because neither the z-component of the current nor E_z must be evaluated. By means of the techniques used to solve (9.106), one obtains

$$\begin{aligned}\tilde{G}_{xx}^A = \tilde{G}_{yy}^A &= \frac{\mu_0}{2\pi}e^{-u_0 z}\frac{1}{D_{\text{TE}}} && \text{(in air, } z \geq 0\text{)}\\ &= \frac{\mu_0}{2\pi}\frac{\sinh u(z+h)}{\sinh uh}\frac{1}{D_{\text{TE}}} && \text{(in the dielectric, } -h \leq z \leq 0\text{)}\end{aligned} \tag{9.120}$$

where u and u_o are defined in (9.110), and

$$D_{\text{TE}} = u_0 + u\coth(uh). \tag{9.121}$$

When the observation point is on the interface, as in the integral equation (9.118),

$$\tilde{G}_{xx}^A = \tilde{G}_{yy}^A = \frac{\mu_0}{2\pi}\frac{1}{D_{\text{TE}}}. \tag{9.122}$$

Inversion of the Hankel transform leads to

$$G_{xx}^A(\mathbf{r}|\mathbf{r}') = G_{yy}^A(\mathbf{r}|\mathbf{r}') = \frac{\mu_0}{2\pi}\int_0^\infty \frac{1}{D_{\text{TE}}}J_0(\lambda|\mathbf{r}-\mathbf{r}'|)\lambda\,d\lambda. \tag{9.123}$$

[‖]Basically, the curl curl operator in the equation satisfied by $\overline{\overline{G}}_{ee}$ is replaced by the ∇^2 operator in the equations for $\overline{\overline{G}}_A$ and G^ϕ.

Similarly, again for $\mathbf{r}$ and $\mathbf{r}'$ in the (x, y) plane,

$$\tilde{G}^{\phi}(\mathbf{r}|\mathbf{r}') = \frac{1}{2\pi\epsilon_0} \frac{u_0 + u \tanh(uh)}{D_{\mathrm{TE}} D_{\mathrm{TM}}}, \tag{9.124}$$

where

$$D_{\mathrm{TM}} = \epsilon_{cr} u_0 + u \tanh(uh), \tag{9.125}$$

with corresponding inversion integral.

In the determination of G_{xx}^{A} from (9.123), it pays to write the integral in the form

$$G_{xx}^{A}(r) = \frac{\mu_0}{2\pi} \int_0^{\infty} \frac{1}{2u_0} J_0(\lambda r) \lambda \, d\lambda + \int_0^{\infty} \underbrace{\left[\tilde{G}^{A}(\lambda) - \frac{\mu_0}{4\pi u_0} \right]}_{\tilde{G}_1^{A}(\lambda)} J_0(\lambda r) \lambda \, d\lambda. \tag{9.126}$$

The first integral in the right-hand term can be evaluated by making use of an important result derived by Sommerfeld [171]. For Re $(u) > 0$:

$$\frac{e^{-jk\sqrt{r^2+z^2}}}{\sqrt{r^2+z^2}} = \int_0^{\infty} J_0(\lambda r) \frac{e^{-u|z|}}{u} \lambda \, d\lambda = \frac{1}{2} \int_{-\infty}^{\infty} H_0^{(2)}(\lambda r) \frac{e^{-u|z|}}{u} \lambda \, d\lambda. \tag{9.127}$$

For $z = 0$, in particular,

$$\frac{e^{-jkr}}{r} = \int_0^{\infty} J_0(\lambda r) \frac{1}{u} \lambda \, d\lambda. \tag{9.128}$$

Equation (9.126) can now be put in the form

$$G_{xx}^{A}(r) = \frac{\mu_0}{4\pi} \frac{e^{-jk_0 r}}{r} + \int_0^{\infty} \tilde{G}_1^{A}(\lambda) J_0(\lambda r) \lambda \, d\lambda, \tag{9.129}$$

where the first term** represents the singularity associated with the limit $k_0 r \to 0$.

Typical results for the variation of the Green's functions with distance $|\mathbf{r} - \mathbf{r}'|$ are given in Figure 9.21 for the dipole shown in Figure 9.20*b*.

9.4.3 Numerical Evaluation of the Sommerfeld Integrals

The evaluation of an integral of the type appearing in (9.129) proceeds by applying the techniques of complex integration. The original contour, for example, which lies on the real axis, can be appropriately deformed. The integration remains a very time-consuming process, because the integrands are highly oscillating, and slow convergence occurs whenever

**This static term is sometimes replaced by a quasi-dynamic term[50,51]

$$\frac{\mu_0}{4\pi} \left[\frac{e^{-jk_0 r}}{r} - \frac{e^{-jk_0\sqrt{r^2+4h^2}}}{\sqrt{r^2+4h^2}} \right].$$

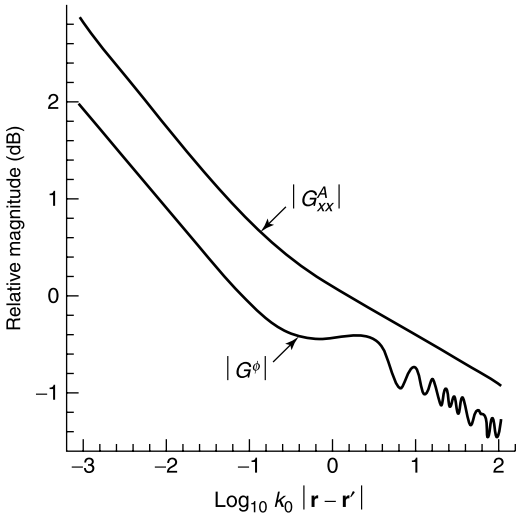

Figure 9.21 Variation of some Green's functions as a function of the distance from the source. The parameters are $\epsilon_r = 12.6$, $h = 1$ mm, and $f = 30$ GHz (from M. J. Tsai, C. Chen, and N. G. Alexopoulos, Sommerfeld integrals in modeling interconnects and microstrip elements in multi-layered media, *Electromagn.* **18**, 267–288, 1998, with permission of the Taylor and Francis Group).

the source and observation points are located on the same interface. The *first term* on the right-hand side of (9.129) extracts the near field, which dominates at distances much less than λ_0. The integrand in the *second* term introduces a number of poles, which give rise to corresponding surface waves. In the example embodied in Figure 9.21, the integrand in (9.123) had two poles:[52]

- One at $\lambda = 1.663\, k_0$, which generates a TE surface wave (transverse with respect to the z-axis)
- One at $\lambda = 2.637\, k_0$, which generates a TM surface wave.

A typical deformed contour C is shown in Figure 9.22 for the Hankel transform with kernel $H_0^{(2)}$ (see 9.127). We notice branch points and branch cuts, together with a few poles. The poles lie on the real axis when the dielectric is lossless but migrate into the second and fourth quadrants when the material is lossy. If we consider the lossless case as the limit of a (vanishingly) lossy situation, the integration path should be deformed as shown on the figure. The contribution of a pole at $\lambda = \lambda_p$ — a surface wave — can be evaluated by the method of residues. These contributions can be extracted from $G_1^A(r)$ and a new function $G_2^A(r)$ introduced according to the splitting

$$G_1^A(r) = \text{sum of residue terms} + G_2^A(r). \tag{9.130}$$

The evaluation of the remainder G_2^A from

$$G_2^A(r) = \int_0^\infty \tilde{G}_2^A(\lambda) J_0(\lambda r) \lambda \, d\lambda, \tag{9.131}$$

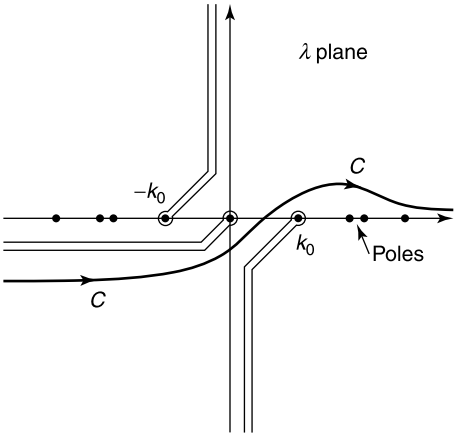

Figure 9.22 Relevant to the evaluation of the Sommerfeld integral (from J. R. Mosig and F. E. Gardiol, Analytical and numerical techniques in the Green's function treatment of microstrip antennas and scatterers, *IEE Proc.* **H130**, 175–182, 1983, with permission of the Institution of Electrical Engineers).

is better adapted to numerical evaluation than the corresponding expression (9.126). The remaining difficulty is the oscillatory behavior of the Bessel function, which is described by

$$\lim_{\lambda r\to\infty} J_0(\lambda r) = \sqrt{\frac{2}{\pi\lambda r}}\cos\left(\lambda r - \frac{\pi}{4}\right). \tag{9.132}$$

The convergence of the tail end of $(0,\infty)$ can be accelerated by splitting this interval into two parts: $(0,a)$ and (a,∞), where a is so chosen that the subinterval (a,∞) is free of singularities. The integral over (a,∞) is then evaluated as the sum of a series of partial integrals over finite subintervals.[53] [160] In another approach, convergence is improved by expanding $\tilde{G}_2^A(\lambda)$ in functions $\tilde{\phi}_n(\lambda)$, typically exponentials.[††] Thus,

$$\tilde{G}_2^A(\lambda) = \sum_{n=1}^{N} a_n \tilde{\phi}_n(\lambda). \tag{9.133}$$

The exponentials can be interpreted as generated by *complex images*.[50,54,55] Introducing (9.133) into (9.131) yields

$$\begin{aligned} G_2^A(r) &= \sum_{n=1}^{N} a_n \int_0^\infty \tilde{\phi}_n(\lambda) J_0(\lambda r)\lambda\, d\lambda \\ &= \sum_{n=1}^{N} a_n \phi_n(r). \end{aligned} \tag{9.134}$$

[††]The procedure requires the preliminary removal of the surface-wave poles from $\tilde{G}_1^A(\lambda)$, because the exponentials are uncapable of producing the slowly decaying far-fields associated with the poles through the factor $H_0^{(2)}(\lambda_p r)$ in (9.130).

If the integrals, which are the inverse Hankel transforms of ϕ_n, could be expressed analytically, the Sommerfeld integrations would be avoided. A suitable choice for ϕ_n is suggested by (9.127). We thus select

$$\tilde{\phi}_n = \frac{e^{-(\lambda^2 - k_0^2)^{\frac{1}{2}} b_n}}{(\lambda^2 - k_0^2)^{\frac{1}{2}}}, \tag{9.135}$$

the inverse of which is

$$\phi_n(r) = \int_0^\infty \tilde{\phi}_n(\lambda) J_0(\lambda r) \lambda \, d\lambda = \frac{e^{-jk_0\sqrt{r^2 + b_n^2}}}{\sqrt{r^2 + b_n^2}}. \tag{9.136}$$

The main problem is to fit $\tilde{G}_2(\lambda)$ accurately by means of an optimal choice of a_n, b_n, and N. Well-known mathematical techniques (Prony, pencil of functions) are available for the purpose.[56,57] Once that task is performed, one arrives at the following expression for a typical Green's function:

$$G_{xx}^A(\mathbf{r}|\mathbf{r}') = \frac{\mu_0}{4\pi} \frac{e^{-jk_0 r}}{r} + \sum_{p=1}^{P} G_p^A(r) + \sum_{n=1}^{N} a_n \phi_n(r).$$

This expression (and similar ones for G_{yy}^A and G^ϕ) can now be inserted in the right-hand term of (9.118). The solution proceeds by the techniques of discretization discussed in Chapters 1 and 2, which imply the expansion of $\mathbf{J}_S(\mathbf{r})$ in suitable basis functions[56,58,59] [90].

The Sommerfeld technique, applied in the preceding pages to a horizontal dipole source, has been extended to include

- Vertical currents,[60] typically carried by probes of the kind shown in Figure 9.19*b*.
- Nonperfect conductors and strips of nonvanishing thickness[61] (a real-life situation) [111]
- Multilayered structures.[62,63,64]

9.5 PERIODIC STRUCTURES

Periodic structures are frequently encountered in electromagnetic devices, particularly so in the area of integrated optics.[65,66] More specifically they are found in filters, beam splitters, antireflection surfaces, polarizers, and distributed feedback (DFB) lasers. A few typical forms are shown in Figure 9.23. The dielectric slab might be a fluid, whose ϵ_r is modulated by a standing wave of acoustic pressure.

9.5.1 Floquet Modes

Consider a one-dimensional structure, periodic along the x-axis, with spatial period a. Figure 9.23*c* is an example of such a structure. Assume, in Floquet's analysis, that the incident field creates a *quasi-periodic* situation, in which the fields in cell $N + 1$ are equal

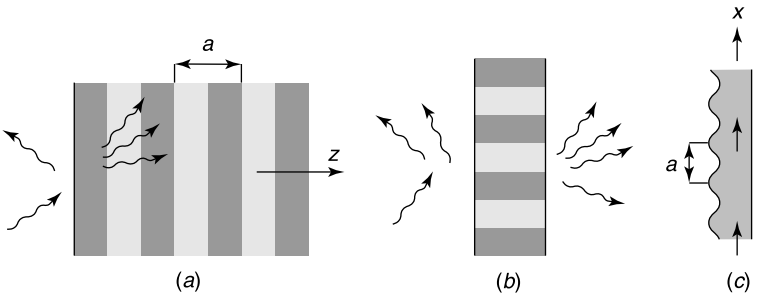

Figure 9.23 Examples of periodic structures: (*a*) Unbounded medium, periodic in the z-direction. (*b*) Dielectric slab, transversely periodic. (*c*) Dielectric waveguide with a periodic boundary.

to those in cell N times a factor $e^{-j\beta_0 a}$, where β_0 may be complex. Quasi-periodicity implies that

$$\frac{\phi(x+a)}{\phi(x)} = \frac{\phi(x+2a)}{\phi(x+a)} = e^{-j\beta_0 a}, \tag{9.137}$$

from which it can be deduced that

$$e^{j\beta_0(x+a)}\phi(x+a) = e^{j\beta_0 x}\phi(x).$$

The right-hand term is clearly periodic, with period a. It may therefore be expanded in a Fourier series. Thus,

$$e^{j\beta_0 x}\phi(x) = \sum_{n=-\infty}^{\infty} A_n\, e^{-jn\frac{2\pi}{a}x}$$

or

$$\phi(x) = \sum_{n=-\infty}^{\infty} A_n\, e^{-j\beta_n x} \tag{9.138}$$

where

$$\beta_n = \beta_0 + n\frac{2\pi}{a} \qquad (n = 0, \pm 1, \ldots). \tag{9.139}$$

The *Floquet modes* in (9.138) represent waves to the *right* (forward waves), but (9.137) also allows waves to the *left* (backward waves). The propagation constant β_0 is a function of frequency. In a *passband*, β_0 is real and the modes propagate without loss. Each mode has its own phase velocity ω/β_n, but the group velocity $(d\beta/d\omega)^{-1}$ is common (Problem 9.17). In a *stopband*, β_0 has an imaginary part and the modes are attenuated. This can occur even when the mode is carried by a lossless structure, in which case the attenuation is due to the destructive interference — the distributive feedback — stemming from the numerous wavelets generated by the nonuniform character of the periodic structure. The passband, on the other hand, is the result of constructive interference.

It is clear, from (9.139), that $\omega(\beta)$ is periodic with period $(2\pi/a)$. A typical plot of ω as a function of β is shown in Figure 9.24. The basic interval $\left(-\frac{\pi}{a}, \frac{\pi}{a}\right)$ is the *Brillouin zone*. As an illustration, consider the propagation of a wave in a material of dielectric constant $\epsilon_r(z)$. If the propagation is along the z-axis, the wave can be split into TE (transverse electric)

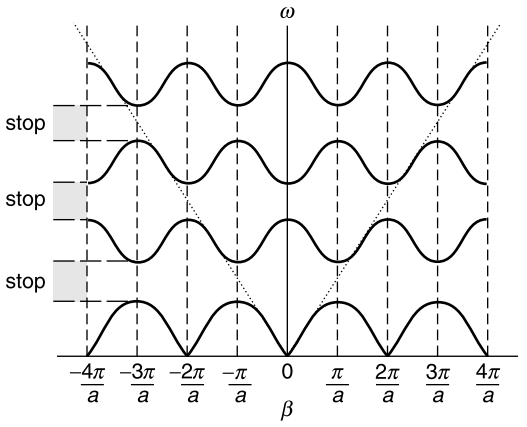

Figure 9.24 Typical $\omega(\beta)$ slot.

and TM (transverse magnetic) modes.[‡‡] In a TE mode, the E_x and E_y fields satisfy the equation[68]

$$\frac{d^2\phi}{dz^2} + k_0^2 \epsilon_r(z)\phi = 0. \tag{9.140}$$

Assume that $\epsilon_r(z)$ is periodically modulated, as suggested in Figure 9.23*a*, and more specifically that the ϵ_r law is a sinusoid superimposed on a constant.[§§] Equation (9.140) now becomes a *Mathieu equation* [40, 46]

$$\frac{d^2\phi}{dz^2} + \omega^2 \left(C_0 + 2C_1 \cos \frac{2\pi z}{a} \right) \phi = 0. \tag{9.141}$$

This equation can be put in the useful form

$$\frac{d^2\phi}{dZ^2} + (D_0 + D_1 \cos 2Z)\phi = 0,$$

with

$$\begin{aligned} Z &= \frac{\pi z}{a} \\ D_0 &= \frac{a^2\omega^2}{\pi^2} C_0 \\ D_1 &= \frac{2a^2\omega^2}{\pi^2} C_1. \end{aligned} \tag{9.142}$$

The basic solutions of Mathieu's equation, discussed in Appendix 5, are the functions Ce_m, even in Z, and Se_m, odd in Z. It is seen, from (9.142), that D_0 and D_1 are proportional to

[‡‡]For the differential equation governing TM mode propagation (Problem 9.18), see Note 67.

[§§]For the analysis of propagation in the presence of an ϵ_r that varies sinusoidally in both the x and y directions, see Note 69.

ω^2, and that their ratio is independent of ω. The straight lines marked ω^2 in Figure 9.25*a* correspond with given ratios $\dfrac{D_1}{D_0} = 2\dfrac{C_1}{C_0}$. As the frequency increases, the operating point moves along the line and goes through shaded areas, which correspond with passbands, and blank areas, which imply stopbands. The band structure of a TM wave with a modulation depth $(D_1/D_0) = 0.4$ is shown in Figure 9.25*b*. The ordinate is $(k_0 a/\pi)^2(\epsilon_r)_{\text{ave}}$, where $(\epsilon_r)_{\text{ave}} = c_0^2 C_0$ is the average value of ϵ_r on the z-axis.

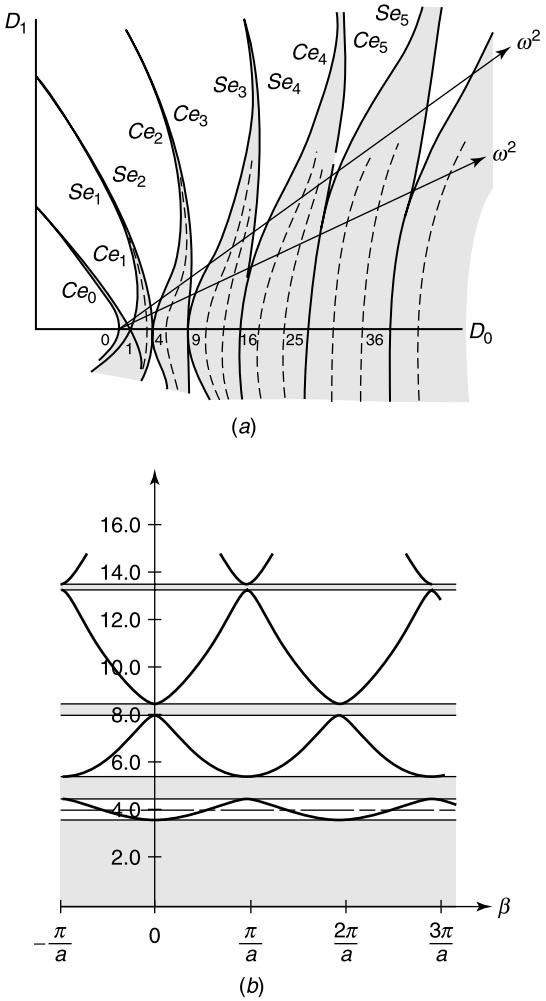

Figure 9.25 (*a*) Relevant to the solution of Mathieu's equation. The stopbands are shaded (from L. Brillouin. *Wave propagation in periodic structures*. Dover Publications, New York, 2nd edition, 1953, with permission of Dover Publications). (*b*) Stop and passbands. The stopbands are shaded. The ordinate is proportional to ω^2 (from C. Yeh, K. F. Casey, and Z. A. Kaprielian, Transverse magnetic wave propagation in sinusoidally stratified dielectric media, *IEEE Trans. MTT* **13**, 297–302, 1965, with permission of IEEE).

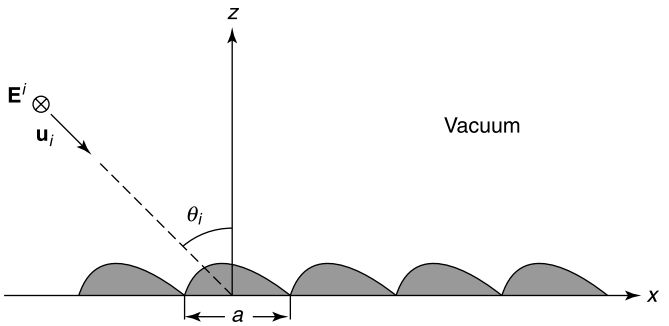

Figure 9.26 A simple grating of period a.

9.5.2 Gratings: Generalities

Figure 9.26 shows a plane wave incident on a periodic grating of spatial period a. Such periodic structures find numerous applications in electromagnetism, particularly in the area of optics, and their theory has been developed extensively [108]. We shall assume, for simplicity, that the grating is perfectly conducting, and that the electric field of the incident wave is parallel to the y-axis, the axis of the grating. The fields depend only on x and z, and they consist of an incident and a scattered part. We write

$$E(x,z) = E^i(x,z) + E^{sc}(x,z).$$

Because of the periodicity in the x direction, an expansion such as (9.138) may be invoked, with an exponential factor

$$e^{-j\beta_0 a} = e^{-jk_0 a \sin\theta_i}.$$

The expansion for the scattered field takes the form

$$E^{sc}(x,z) = \sum_m A_m(z)\, e^{-j\left(k_0 \sin\theta_i + m\frac{2\pi}{a}\right)x} = \sum_m A_m(z)\, e^{-jk_{xm}x},$$

where $m = 0, \pm 1, \pm 2, \ldots$. Coefficient A_m can be determined by remembering that E^{sc} must satisfy Helmholtz' equation, a requirement that leads to the more precise expansion

$$E^{sc}(x,z) = \sum E_m\, e^{-jk_{xm}x}\, e^{-jk_{zm}z}, \tag{9.143}$$

where

$$\begin{aligned} k_{xm} &= k_0\left(\sin\theta_i + m\frac{\lambda_0}{a}\right) \\ k_{zm}^2 &= k_0^2\left[1 - \left(\sin\theta_i + m\frac{\lambda_0}{a}\right)^2\right]. \end{aligned} \tag{9.144}$$

The value of k_{zm}^2 can be positive or negative. When k_{zm}^2 is positive, k_{zm} is real, the partial wave propagates in the z-direction, and the sign of k_{zm} is chosen to ensure that the wave is

outgoing. When k_m^2 is negative, k_{zm} becomes imaginary, and we choose the sign to make sure the wave is attenuated in the z-direction. A partial wave — an *order* — is associated with a given value of m. The *zero order term* ($m = 0$) is characterized by

$$\begin{aligned} k_x &= k_0 \sin\theta_i \\ k_z &= \pm k_0 \cos\theta_i. \end{aligned} \tag{9.145}$$

It consists of two partial waves: one reflected along the direction $(-\mathbf{u}_i)$ and another *specularly* reflected, (i.e., in the same direction as the reflected ray on a "metallized" plane $z = 0$). The zero-order always propagates, while an m order only propagates if

$$\begin{aligned} \frac{\lambda_0}{a} &< \frac{1 - \sin\theta_i}{m} \qquad (\text{for } m > 0) \\ \frac{\lambda_0}{a} &< \frac{1 + \sin\theta_i}{|m|} \qquad (\text{for } m < 0). \end{aligned} \tag{9.146}$$

The various orders are launched in succession as the frequency is raised from $\omega = 0$ to ∞. When the incident field contains a spectrum of frequencies, each λ_0 will launch the propagated orders whose m satisfies (9.146). Each mode has its own direction of propagation, a property that follows from (9.144), and the grating will therefore reflect the incident beam in directions which depend on the frequency (i.e., on the "color"). This feature is exploited in devices such as spectrum analyzers and demultiplexers.

When k_{zm}^2 in (9.144) is negative, the contribution from the mth order is a surface wave, evanescent in the z-direction (i.e., away from the grating) and propagating in the x-direction. Thus,

$$E_m \doteq e^{-jk_0\left(\sin\theta_i + m\frac{\lambda_0}{a}\right)x} e^{-\sqrt{\left(\sin\theta_i + m\frac{\lambda_0}{a}\right)^2 - 1}\, k_0 z}. \tag{9.147}$$

For $m > 0$, for example, a surface wave is generated when

$$\frac{\lambda_0}{a} > \frac{1 - \sin\theta_i}{m}.$$

A phase velocity in the x-direction ensues, given by

$$v_{ph} = \frac{c_0}{\sin\theta_i + m\dfrac{\lambda_0}{a}} < c_0. \tag{9.148}$$

The wave is therefore a *slow wave*, a property that can be exploited in devices where the fields must interact with particles moving with velocities less than c_0.

9.5.3 Gratings: Integral Equation for the Induced Current

The Floquet expansion (9.143) can be written in the slightly different form

$$E^{sc}(x,z) = \sum_m E_m\, e^{-j\alpha_m x}\, e^{-j\beta_m z} = \sum_m E_m \phi_m(x,z), \tag{9.149}$$

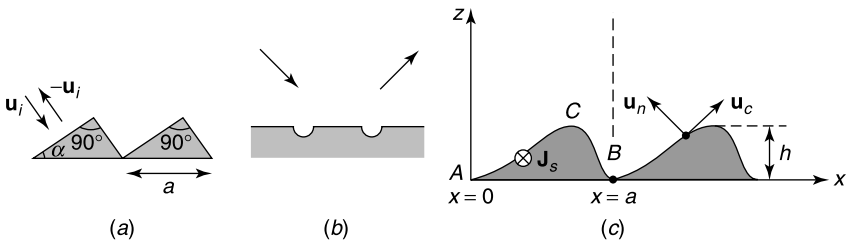

Figure 9.27 (*a*) Echelette type of grating. (*b*) Shallow groove type of grating. (*c*) Unit cells.

where

$$\alpha_m = k_0 \sin\theta_i + m\frac{2\pi}{a}$$
$$\beta_m = (k_0^2 - \alpha_m^2)^{\frac{1}{2}}. \tag{9.150}$$

We note that the $e^{-j\alpha_m x}$ factors form a complete orthogonal set, in the sense that

$$\int_0^a e^{-j\alpha_m x}\left[e^{-j\alpha_n x}\right]^* dx = a\,\delta_{mn}. \tag{9.151}$$

The problem consists in determining the expansion coefficients E_m. In the $m = 0$ order, for example, a strong E_0 in the $(-\mathbf{u}_i)$ direction may be expected when a wave illuminates an echelette grating at normal incidence (Fig. 9.27*a*). At sufficiently low frequencies, for $a \ll \lambda_0$, the $m = 0$ orders are the only propagating ones, and the detailed shape of the grating is not "felt." This characteristic low-frequency behavior is further discussed in Chapter 13. Qualitative arguments can be misleading, however, and should therefore be replaced by a correct theoretical analysis.[¶¶] As an example, we shall derive an integral equation for the problem embodied in Figure 9.27*c*. The incident E-field is y-directed,[‖‖] and the main unknown is the induced surface current density $\mathbf{J}_S = J_S\mathbf{u}_y$ on the perfectly conducting profile [108]. The main step is to express the scattered field in the form of an integral

$$E^{sc}(\mathbf{r}) = j\omega\mu_0 \int_c G(\mathbf{r}|\mathbf{r}'_c)\, J_S(\mathbf{r}'_c)\, dc', \tag{9.152}$$

where c is the boundary of the grating; that is the arc ACB in Figure 9.27*c* (Problem 9.21). An integral equation for J_S is obtained by enforcing the boundary condition $E = E^i + E^{sc} = 0$ on ACB. Central to the solution is the determination of the Green's function $G(\mathbf{r}|\mathbf{r}')$ relative to the unit cell. This (periodic) Green's function must satisfy

$$\nabla_{xz}^2 G(\mathbf{r}|\mathbf{r}') + k_0^2 G(\mathbf{r}|\mathbf{r}') = \delta(\mathbf{r} - \mathbf{r}'), \tag{9.153}$$

[¶¶] This approach is discussed with particular clarity in Note 70.

[‖‖] The analysis can readily be extended to the second basic polarization, in which $\mathbf{H}$ is parallel to the y-axis, and $\mathbf{J}_S$ is tangent to ACB.

where $0 < x < a$, and $\mathbf{r}$ stands for (x, z). On the basis of the orthogonality property (9.151), the δ-function may be expanded as

$$\delta(\mathbf{r} - \mathbf{r}') = \delta(z - z') \sum_{n=-\infty}^{\infty} \frac{1}{a} e^{-j\alpha_n(x-x')}. \tag{9.154}$$

For the Green's function, we write

$$G(\mathbf{r}|\mathbf{r}') = \sum_{n=-\infty}^{\infty} G_n(z)\, e^{-j\alpha_n x}. \tag{9.155}$$

Inserting these expansions in (9.153) yields a differential equation for $G_n(z)$, viz.

$$\frac{d^2G_n(z)}{dz^2} + (k_0^2 - \alpha_n^2)\, G_n(z) = \frac{d^2G_n(z)}{dz^2} + \beta_n^2 G_n(z) = \frac{1}{a} e^{j\alpha_n x'} \delta(z - z'). \tag{9.156}$$

The correct solution should give rise to outgoing waves; that is, to upward propagation for $z > z'$ and downward propagation for $z < z'$. A simple manipulation gives the result

$$G_n(z) = \frac{j}{2a\beta_n} e^{j\alpha_n x'}\, e^{-j\beta_n|z-z'|}. \tag{9.157}$$

At sufficiently low frequencies, for $k_0 < \alpha_n$, β_n becomes imaginary, and should be written as $\beta_n = -j(\alpha_n^2 - k_0^2)^{\frac{1}{2}}$ to ensure an exponential decay for large $|z|$. We finally write $G(\mathbf{r}|\mathbf{r}')$ as

$$G(\mathbf{r}|\mathbf{r}') = \sum_{n=-\infty}^{\infty} \frac{j}{2a\beta_n} e^{-j\alpha_n(x-x')}\, e^{-j\beta_n|z-z'|}. \tag{9.158}$$

On the basis of the equation satisfied by E^{sc}, namely

$$\nabla_{xz}^2 E^{sc} + k_0^2 E^{sc} = j\omega\mu_0 J_y = j\omega\mu_0 J_S \delta_c. \tag{9.159}$$

we may immediately derive the following integral equation for J_S:

$$E_i \beta_n e^{-jk_0 \sin\theta_i x}\, e^{jk_0 \cos\theta_i z} = \frac{\omega\mu_0}{2a\beta_n} \sum_{n=-\infty}^{\infty} e^{-j\alpha_n x}\, e^{-j\beta_n z} \int_{ACB} J_S(c')\, e^{j\alpha_n x'}\, e^{j\beta_n z'}\, dc'. \tag{9.160}$$

Note that (x, z) and (x', z') are the coordinates of a point on profile ACB.

9.5.4 Mode Matching

In a second method, the fields above the grating are evaluated by first dividing the unit cell into two parts: a region 1 above the groove, in which the Rayleigh expansion may definitely be used, and an enclosed region 2, in which a normal-mode representation is appropriate (Fig. 9.28). The two representations are matched along AB, yielding an integral equation for some basic field component [8, 10]. We are clearly confronted with a typical *coupled regions*

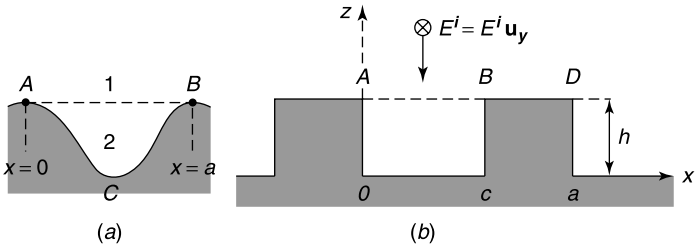

Figure 9.28 Mode matching; (*a*) arbitrary grating, (*b*) corrugated grating.

problem. Illustratively, assume that a plane wave is normally incident on the *lamellar* (or *corrugated*) grating of Figure 9.28*b*. The field above the grating, for $z > h$, has the space period a, and can be written as the sum of an incident and a scattered part. Thus, using a Fourier expansion,

$$\frac{E(x,z)}{E^i} = e^{jk_0 z} + \sum_{n=-\infty}^{\infty} A_n e^{-jn\frac{2\pi x}{a}} e^{-j\sqrt{k_0^2 - \left(\frac{n^2\pi}{a}\right)^2}\, z}. \tag{9.161}$$

The ratio E/E^i is equal to zero between B and D. Its value between A and B is the main unknown of the problem. If we denote this value by $f(x)$ we may write, for $z = h$,

$$\frac{E(x,h)}{E^i} = e^{jk_0 h} + \sum_{n=-\infty}^{\infty} \frac{2}{a} e^{-jn\frac{2\pi x}{a}} \int_0^c f(x')\, e^{jn\frac{2\pi x'}{a}}\, dx'. \tag{9.162}$$

Comparing this expression with (9.161) gives A_n in terms of the integral in (9.162). In the next step, we represent E in the groove by its eigenfunction expansion in the interval, $(0, c)$, viz.

$$\begin{aligned} \frac{E}{E^i} &= \sum_{m=1}^{\infty} B_m \sin\frac{m\pi x}{c} \sin\sqrt{k_0^2 - \left(\frac{m\pi}{c}\right)^2}\, z \quad (\text{for } 0 \le x \le c) \\ &= 0 \qquad\qquad\qquad\qquad\qquad\qquad\quad (\text{for } c \le x \le a). \end{aligned} \tag{9.163}$$

In the aperture AB, for $z = h$,

$$\frac{E}{E^i} = \sum_{m=1}^{\infty} \sin\frac{m\pi x}{c} \frac{2}{c} \int_0^c f(x') \sin\frac{m\pi x'}{c}\, dx'. \tag{9.164}$$

The coefficients B_m can be expressed in terms of the integral in (9.164). The key function $f(x)$ is now the solution of the integral equation obtained by requiring

$$H_x = \frac{1}{j\omega\mu_0} \frac{\partial E}{\partial z}$$

to have the same value just above and just below AB.

9.5.5 Extensions

Besides the integral equation formulation, other numerical approaches of the kind discussed in Chapter 12 can be resorted to, to solve the grating problem. They are based, for example, on the differential equation satisfied by E or H, and/or on the use of finite elements to subdivide the computational domain.[71,72] It should be noted, when choosing a method, that representation (9.152) for the scattered field is valid for any point above the grating. The same does not automatically hold when E^{sc} is determined by forcing the *Rayleigh expansion* (9.149), limited to N terms, to be equal to $(-E^i)$ at N points on ACB (Fig. 9.27*c*). The process yields N equations for the N coefficients B_n. Practice shows that the series often does not converge for points *in the groove* (region 2 in Fig. 9.28*a*), fundamentally because the expansion is based on Helmholtz' equation, i.e., on the existence of $\nabla^2 E$ from $x = 0$ to $x = a$. This existence is not guaranteed when one crosses from vacuum to metal. For a sinusoidal grating with profile $z = f(x) = h\cos(2\pi x/a)$, for example, the series diverges for $h > 0.0713a$, but converges[73,74] for $h < 0.0713a$ [108]. More general criteria are available for profiles that can be described by an analytic function of the arc length.[75]

Perfectly conducting gratings have found numerous uses, for example in frequency scanning or the exploitation of polarization sensitivity. Dielectric gratings (and dielectric-coated gratings) have also been utilized, in particular in certain types of lasers, beam deflectors, and waveguide couplers.[76,77] Note also that metal conductors become increasingly penetrable as the frequency rizes above the visible range, a point of fundamental importance for the design of UV gratings.

9.5.6 Multidimensional Periodic Structures

The two-dimensional configuration in Figure 9.29 depicts a typical rectangular periodic pattern, illuminated by an incident plane wave of phase factor

$$e^{-jk_0\mathbf{u}_i\cdot\mathbf{r}} = e^{-jk_0(\mathbf{u}_x\cdot\mathbf{u}_i)x}\, e^{-jk_0(\mathbf{u}_y\cdot\mathbf{u}_i)y} = e^{-j(k_x^i x + k_y^i y)}. \tag{9.165}$$

The two-dimensional Floquet harmonics are given by (Problem 9.24)

$$\phi_{mn}(x,y) = e^{-j\left(k_x + m\frac{2\pi}{a}\right)x} e^{-j\left(k_y + n\frac{2\pi}{b}\right)y} = e^{-j(\alpha_m x + \beta_n y)}. \tag{9.166}$$

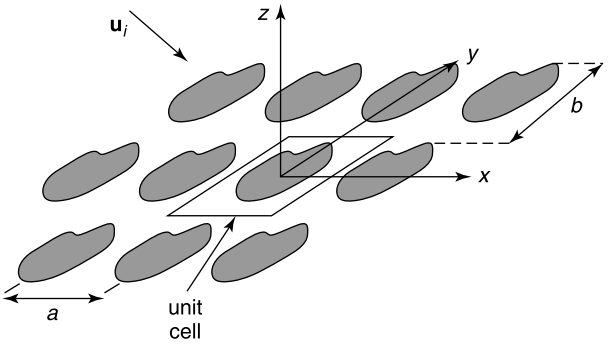

Figure 9.29 A frequency-selective surface (from R. Mittra, C. H. Chan, and T. Cwik, Techniques for analyzing frequency selective surfaces — A review, *Proc. IEEE* **76**, 1593–1615, 1988, with permission of IEEE).

The orthogonality property corresponding with (9.151) is now

$$\int_0^a \int_0^b \phi_{mn}(x'y')\,\phi_{rs}^*(x'y')\,dx'dy' = ab\,\delta_{mr}\delta_{ns}. \tag{9.167}$$

The scattered field will be of the general form

$$\mathbf{E}(x,y,z) = \sum_{m=0}^{\infty}\sum_{n=0}^{\infty} \mathbf{E}_{mn}(\alpha_m,\beta_n)\,e^{-j(\alpha_m x+\beta_n y)}\,e^{-j\sqrt{k_0^2-\alpha_m^2-\beta_n^2}\,z}.$$

It clearly consists of a finite number of propagating waves, which generate radiated beams (the grating lobes) and an infinite number of surface waves. The structure behaves like an antenna array, in which the strength of the radiating modes depends on factors such as the frequency, the angle of incidence, and the polarization of the incident wave. By proper choice of the elements (Fig. 9.30), possibly embedded in a stratified medium, the reflected power (and hence the leaked transmitted power) can be given a desirable frequency variation [103]. If the elements in Figure 9.29 are perfectly conducting, the frequency response is conditioned by the interplay between the magnetic energy around the current-carrying elements and the electric energy associated with the electric field in the gaps between elements. This interplay gives rise to resonances, which may result, for example, in strong reflections in a narrow band, while an infinite, perfectly conducting plane reflects at all frequencies.

The scattered field can be determined by the various methods discussed in Chapter 12. We shall only consider the integral equation formulation, applied to the current density

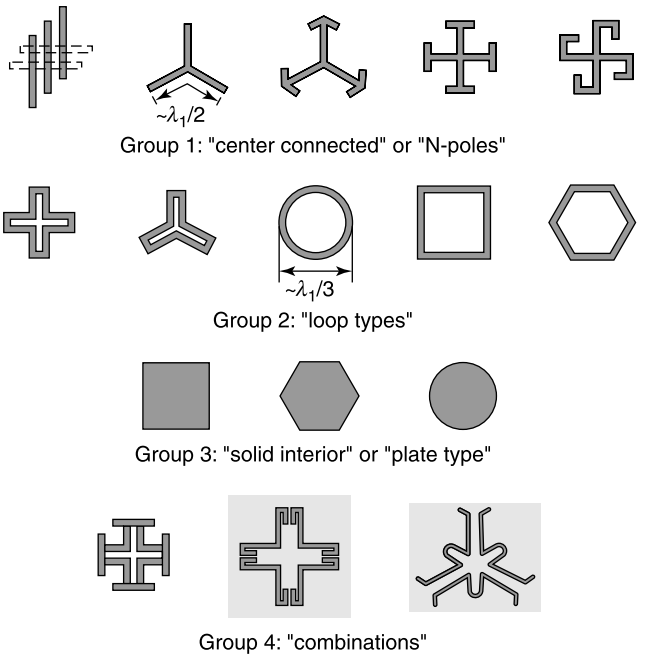

Figure 9.30 Typical elements, arranged in groups (from B. A. Munk. *Frequency Selective Surfaces*, 2000, Copyright 2000, with permission of John Wiley & Sons).

$\mathbf{J}_S = J_{Sx}\mathbf{u}_x + J_{Sy}\mathbf{u}_y$ induced on thin, perfectly conducting patches.*** The currents generate a vector potential

$$\mathbf{A}(\mathbf{r}) = \frac{\mu_0}{4\pi}\int_{\text{patches}} \mathbf{J}_S(\mathbf{r}')\frac{e^{-jk_0|\mathbf{r}-\mathbf{r}'|}}{|\mathbf{r}-\mathbf{r}'|}\,dx'dy', \tag{9.168}$$

which is parallel to the (x, y) plane. From (7.55), the (x, y) component of the resulting electric field is

$$\mathbf{E}^{sc}_{xy} = -j\omega\mathbf{A}(\mathbf{r}) - \frac{j\omega}{k_0^2}\left[\left(\frac{\partial^2 A_x}{\partial x^2} + \frac{\partial^2 A_y}{\partial x\partial y}\right)\mathbf{u}_x + \left(\frac{\partial^2 A_x}{\partial x\partial y} + \frac{\partial^2 A_y}{\partial y^2}\right)\mathbf{u}_y\right]. \tag{9.169}$$

To take periodicity into account, we shall introduce three expansions in Floquet harmonics, viz.[79]

$$\begin{aligned}
\mathbf{J}_S(x, y) &= \sum_{m,n=-\infty}^{\infty} \mathbf{J}_{mn}\, e^{-j(\alpha_m x+\beta_n y)} \\
\mathbf{A}(x, y, 0) &= \sum_{m,n=-\infty}^{\infty} \mathbf{A}_{mn}\, e^{-j(\alpha_m x+\beta_n y)} \\
\mathbf{E}^{sc}_{xy}(x, y, 0) &= \sum_{m,n=-\infty}^{\infty} \mathbf{E}_{mn}\, e^{-j(\alpha_m x+\beta_n y)}.
\end{aligned} \tag{9.170}$$

Inserting the expansions for $\mathbf{E}$ and $\mathbf{A}$ into (9.169) yields

$$\mathbf{E}_{mn}(\alpha_m, \beta_n) = -\frac{j\omega}{k_0^2}\begin{bmatrix} k_0^2 - \alpha_m^2 & -\alpha_m\beta_n \\ -\alpha_m\beta_n & k_0^2 - \beta_n^2 \end{bmatrix} \cdot \mathbf{A}_{mn}(\alpha_m, \beta_n). \tag{9.171}$$

The connection between $\mathbf{A}_{mn}$ and $\mathbf{J}_{mn}$ can be derived from (9.168). Thus,

$$\mathbf{A}_{mn}(\alpha_m, \beta_n) = G_{mn}(\alpha_m, \beta_n)\mathbf{J}_{mn}(\alpha_m, \beta_n), \tag{9.172}$$

where

$$G_{mn}(\alpha_m, \beta_n) = \frac{1}{ab}\int\!\!\int_{-\infty}^{\infty} G(x, y)\, e^{j(\alpha_m x+\beta_n y)}\,dx\,dy. \tag{9.173}$$

In this expression,

$$G(x, y) = \frac{\mu_0}{4\pi}\frac{e^{-jk_o|\mathbf{r}-\mathbf{r}'|}}{|\mathbf{r}-\mathbf{r}'|},$$

where $\mathbf{r}$ and $\mathbf{r}'$ are vectors in the (x, y) plane. On the basis of (A5.50) and (A5.52), the integration in (9.173), performed in polar coordinates, gives

$$\begin{aligned}
G_{mn}(\alpha_m, \beta_n) &= \frac{\mu_0}{2ab\sqrt{\alpha_m^2 + \beta_n^2 - k_0^2}} \qquad (\text{for } k_0^2 < \alpha_m^2 + \beta_n^2) \\
&= -j\frac{\mu_0}{2ab\sqrt{k_0^2 - \alpha_m^2 - \beta_n^2}} \qquad (\text{for } k_0^2 > \alpha_m^2 + \beta_n).
\end{aligned} \tag{9.174}$$

***For an extension to patches characterized by a surface impedance, see Note 78.

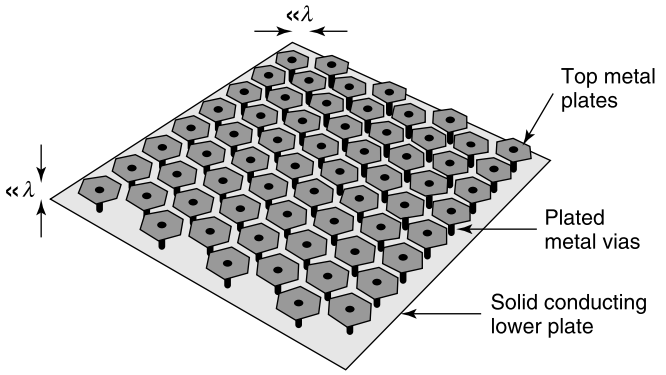

Figure 9.31 Square periodic pattern. (Courtesy of Dr. D. Sievenpiper.)

G_{mn} becomes imaginary when the frequency is high enough for the m, n Floquet mode to propagate. Taking (9.170) to (9.173) into account leads to an expression of the general form

$$\mathbf{E}_{xy}^{sc}(x, y, 0) = \sum_{m,n=-\infty}^{\infty} \overline{\overline{Z}}_{mn}(\alpha_m, \beta_n) \cdot \mathbf{J}_{mn}(\alpha_m, \beta_n)\, e^{-j(\alpha_m x + \beta_n y)}. \tag{9.175}$$

The sought equation for $\mathbf{J}_S$ is obtained by enforcing the condition $\mathbf{E}_{xy}^{sc} = -\mathbf{E}_{xy}^{i}$ on the conducting patch. Because of the periodicity, this condition must only be applied over a single cell of the lattice.

An equation such as (9.175) is of the general linear form (1.18). It can be solved by expanding $\mathbf{J}$ and $\mathbf{E}$ in basis functions, of either the subdomain or the entire-domain type. The form of the entire-domain functions is known for a few shapes such as the circle, the rectangle, the thin dipole, the cross dipole, and the Jerusalem cross.[79]

A periodic texture can serve to alter the electromagnetic properties of metal surfaces, in particular by means of the impedance Z_S of the surface. Quarter-wavelength corrugations have been used for years to provide a high Z_S for a given polarization, and a low Z_S for another polarization. Figure 9.31 displays a lattice consisting of metal plates connected to a ground plane by means of vias.[80] This configuration can provide, in a given frequency band, a high Z_S for the two basic polarizations, thus synthesizing a magnetic conductor surface. In elementary circuit terms, the impedance can be modeled by means of a resonant LC circuit, where C is associated with the capacity between the plates and L with the conducting loops that link the plates to the ground plane. The network of parallel LC resonant circuits develops an infinite impedance to surface currents at resonance. Typical experimental results are shown in Figure 9.32 for the three-layered structure obtained by letting the metal plates in Figure 9.31 overlap. Such a move increases C and decreases $\omega_0 = (LC)^{-\frac{1}{2}}$. Figure 9.32*a* displays the variation of the phase of the reflected waves. At low frequencies, where $\phi = \pi$, the lattice reflects like a perfectly conducting plane. As the frequency increases, ϕ goes through zero at the resonant frequency and later approaches $(-\pi)$ under the influence of the capacitive effect. Figure 9.32*b* illustrates another interesting phenomenon: the much lowered excitation of surface waves in the bandgap.[†††] The resulting almost total reflection

[†††]These waves can significantly degrade the radiation pattern of the antenna.

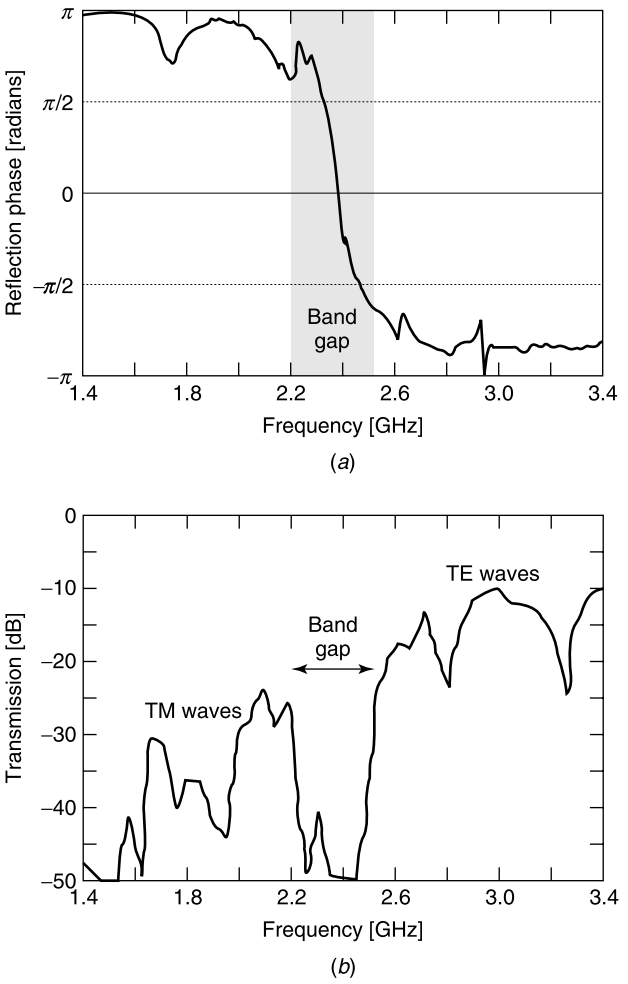

Figure 9.32 (*a*) Phase of the reflected wave as a function of frequency. (*b*) Transmission between two probes parallel to the surface (from D. Sievenpiper, L. Zhang, R. F. Jimenez Broas, N. G. Alexopoulos, and E. Jablonovitch, High-impedance electromagnetic surfaces with a forbidden frequency band, *IEEE Trans. MTT* **47**, 2059–2074, 1999, with permission of IEEE).

can be exploited in the design of handset telephones by incorporating a lattice to serve as a ground plane.[81] Such a solution — now made less practical by the size reduction of handsets — reduces the power radiated into the user's head, and therefore a potential health hazard. In another application, C is modulated in time, for example by means of varactor diodes. This variation modulates the resonant frequency, and therefore the phase of the reflected wave, a property that can be exploited to steer the beam radiated from an antenna.[82]

9.5.7 The Complementary Lattice

In Figure 9.29, a complementary lattice is obtained by replacing patches by holes perforated in a perfectly conducting screen. This substitution creates a typical Babinet situation,[83,84] and the theory of the hole structure can therefore be developed directly from that of the

patches, provided the incident fields are modified as discussed in Section 9.6. The induced electric currents on the patches are now replaced by the excited magnetic currents in the apertures. The perforated screen can be used as a ground plane in a microstrip circuit, given its bandpass-bandstop characteristics[85,86] (Fig. 9.33*a*). The screen can also serve as a filter,[87] a point illustrated by the power transmission coefficient of an array of crosses at broadside incidence (Fig. 9.33*b*).

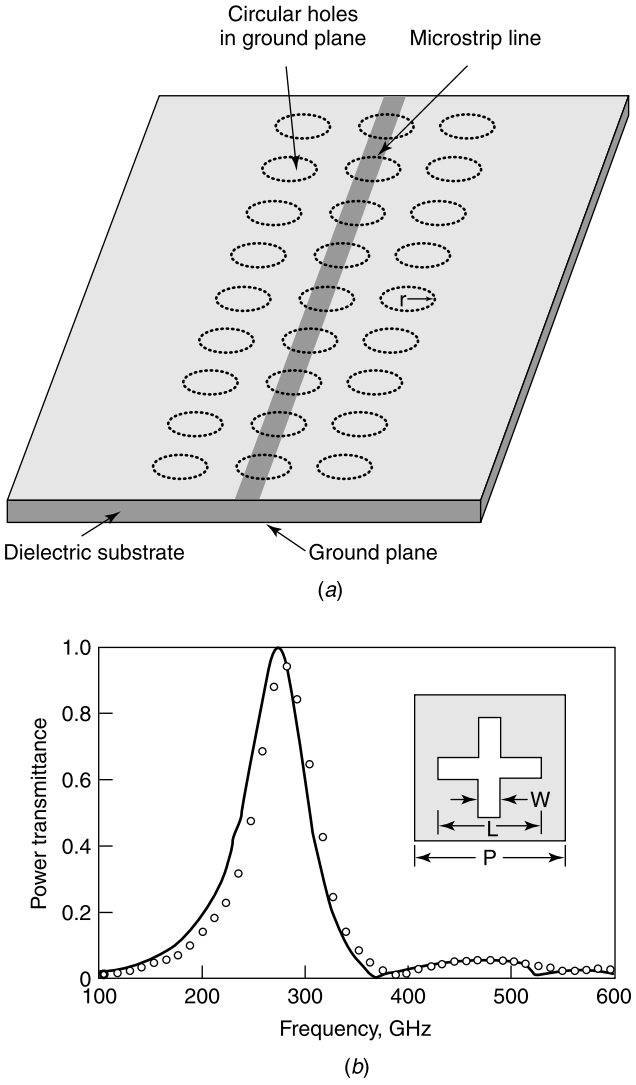

Figure 9.33 (*a*) Microstrip with perforated screen (from V. Radisic, Y. Qian, R. Coccioli, and T. Itoh, Novel 2-D photonic bandgap structure for microstrip lines, *IEEE Microwave Guided Wave Lett.* **8**, 69–71, 1998, with permission of IEEE). (*b*) Power transmission of cross-shaped bandpass filter ($L = 0.57$ mm, $W = 0.16$ mm, periodic $P = 0.81$ mm). *o*: measurements (from M. Bozzi and L. Perregrini, Efficient analysis of thin conductive screens perforated periodically with arbitrarily shaped apertures, *Electron. Lett.* **35**, 1085–1087, 1999, with permission of the Institution of Electrical Engineers).

The remarkable frequency-sensitive properties mentioned above can be extended, at increased complexity, to three dimensional lattices. The lattice can be oblique, in which case it is characterized by three noncoplanar primitive vectors $\mathbf{a}_1, \mathbf{a}_2, \mathbf{a}_3$, in terms of which a cell is identified by its position vector

$$\mathbf{a} = m_1\mathbf{a}_1 + m_2\mathbf{a}_2 + m_3\mathbf{a}_3$$

where m_1, m_2, m_3 are integers. Also needed in the theory is the *reciprocal* lattice, based on vectors $\mathbf{b}_j$ defined by (Problem 9.25).

$$\mathbf{a}_i \cdot \mathbf{b}_j = 2\pi\delta_{ij}. \tag{9.176}$$

For an orthogonal two-dimensional lattice:

$$\begin{aligned} \mathbf{a}_1 &= a\mathbf{u}_x \qquad & \mathbf{a}_2 &= b\mathbf{u}_y \\ \mathbf{b}_1 &= \frac{2\pi}{a}\mathbf{u}_y \qquad & \mathbf{b}_2 &= \frac{2\pi}{b}\mathbf{u}_x. \end{aligned} \tag{9.177}$$

In analogy with electronic bandgaps in semiconductor crystal lattices, a periodic array of electromagnetic scatterers can generate frequency gaps in which waves do not propagate but suffer exponential attenuation. Fundamental parameters are the geometry of the lattice and the nature of the scatterers. In the *optoelectronic* frequency range, the artificial crystals typically take the form of *photonic band-gap materials* (PBG), built around metallic, dielectric, or even active implants. The lattice inhibits propagation in given passbands and in certain directions, eventually forbidding light to exist in the interior of the crystal. As in solid-state devices, the lattice can be manipulated, for example by removing several rows of inclusions, thereby creating a tunnel that can serve as a waveguide.[88]

9.5.8 Periodic Green's Functions

The direct summation of the Green's function (9.158), and of analog expressions in two dimensions, is not computationally efficient. Improving the convergence can be obtained by several methods, such as those of Poisson, Ewald, Shanks, and Kummer [203]. We shall briefly describe some of their main features.[89,90]

9.5.8.1 The Poisson Transformation

The series to be evaluated is

$$S = \sum_{n=-\infty}^{\infty} f(n). \tag{9.178}$$

Let us introduce a function $f_e(x)$ equal to $f(n)$ for $x = 0, \pm 1, \pm 2, \ldots$. The Fourier transform of that function is

$$F_e(\nu) = \int_{-\infty}^{\infty} f_e(x)\, e^{-j\nu x}\, dx.$$

By writing S as $\int_{-\infty}^{\infty} f_e(x)\,\mathrm{comb}(x)\,dx$, where $\mathrm{comb}(x)$ is the comb function

$$\mathrm{comb}(x) = \sum_{n=-\infty}^{\infty} \delta(x-n) \tag{9.179}$$

the summation takes the form

$$S = \sum_{n=-\infty}^{\infty} F_e(n2\pi). \tag{9.180}$$

If $f_e(x)$ is a smooth function, which in addition approaches zero gradually as $x \to \infty$, $F_e(\nu)$ will be highly localized, and (9.180) will converge rapidly. A simple example:

$$\begin{aligned}\sum_{n=-\infty}^{\infty} f(n) &= \sum_{n=-\infty}^{\infty} \frac{1}{2jk}\, e^{-jk|x-nd|} \\ &= \sum_{n=-\infty}^{\infty} \frac{1}{d}\left[\frac{2\pi n}{d} - k^2\right]^{-1} e^{-j\frac{2\pi n x}{d}} \;=\; -\frac{1}{2k}\,\frac{\cos\left[\left(\frac{d}{2}-x\right)k\right]}{\sin\frac{kd}{2}}.\end{aligned} \tag{9.181}$$

Poisson sums are also available in closed form for[91]

$$\sum_{n=-\infty}^{\infty} \frac{1}{4j} H_0^{(2)}(kD_2); \qquad \sum_{n=-\infty}^{\infty} \frac{1}{2\pi}\log_e D_2; \qquad \sum_{n=-\infty}^{\infty} \frac{1}{4\pi D_3}; \qquad \sum_{n=-\infty}^{\infty} \frac{1}{4\pi D_3}\, e^{-jkD_3}$$

where

$$D_2 = \left[(x-x')^2 + (y-nd)^2\right]^{\frac{1}{2}}$$

$$D_3 = \left[(x-x')^2 + (y-y')^2 + (z-nd)^2\right]^{\frac{1}{2}}.$$

9.5.8.2 The Kummer Transformation

The asymptotic part of a series plays an important role in determining the rate of convergence of the series. The Kummer transform makes use of the fact by subtracting the asymptotic part from $S(n)$. Assume that $f(n)$ is asymptotic to a function

$$f_1(n) = \lim_{n\to\infty} f(n).$$

One writes[92]

$$S = \sum_{n=-\infty}^{\infty} [f(n) - f_1(n)] + \sum_{n=-\infty}^{\infty} f_1(n) = S_1(n) + S_2(n). \tag{9.182}$$

The idea is to choose a $f_1(n)$ that makes the second series highly convergent or even expressible in closed form. By taking the *Poisson* transformation of this series, one obtains

$$\sum_{n=-\infty}^{\infty} f_1(n) = \sum_{n=-\infty}^{\infty} F_1(n2\pi) \tag{9.183}$$

where F_1 is the Fourier transform of $f_1(x)$. It is further possible, in certain cases,[93] to split S_2 into an analytical expression S_2' and a fast converging series S_2''.

9.5.8.3 The Shanks Transformation

In this method, the transform is computed from the algorithm

$$e_{s+1}(S_n) = e_{s-1}(S_{n+1}) + \frac{1}{e_s(S_{n+1}) - e_s(S_n)} \qquad (s = 1, 2, \ldots)$$

where

$$e_0(S_n) = S_n; \qquad e_1(S_n) = \frac{1}{e_0(S_{n+1}) - e_0(S_n)} \tag{9.184}$$

and S_n is a sequence of partial sums. Details on the procedure can be found in Notes 89, 94, 95.

9.5.8.4 The Ewald Transformation

The Ewald transformation was born from the solution of a crystallographic problem[96]. The reader is referred to the literature for a full description of the procedure,[97,98,99] which will be summarized by considering the very simple example of the Green's function of a two-dimensional periodic array, of respective periods a and b in the x and y directions [203]. The array lies in the $z = 0$ plane, and the relevant Green's function is[99]

$$G(\mathbf{r}|\mathbf{r}') = \frac{1}{4\pi} \sum_{mn} \frac{e^{-jk_0 R_{mn}}}{R_{mn}},$$

where

$$R_{mn} = \sqrt{(x - x' - ma)^2 + (y - y' - nb)^2 + z^2}.$$

R_{mn} is the distance between the observation point (x, y, z) and the periodic sources in the $z = 0$ plane. The Green's function can be split into two terms, viz.

$$\begin{aligned} G_1 &= \frac{1}{8ab} \sum_{m,n=-\infty}^{\infty} \frac{e^{-j2\pi\left[\frac{m(x-x')}{a} + \frac{n(y-y')}{b}\right]}}{\alpha_{mn}} \\ &\quad \times \left[e^{2\alpha_{mn} z} \operatorname{erfc}\left(\frac{\alpha_{mn}}{E} + zE\right) + e^{-2\alpha_{mn} z} \operatorname{erfc}\left(\frac{\alpha_{mn}}{E} - zE\right)\right] \\ G_2 &= \frac{1}{4\pi} \sum_{m,n=-\infty}^{\infty} \frac{1}{R_{mn}} \operatorname{Re}\left[e^{-jk_0 R_{mn}} \operatorname{erfc}\left(R_{mn} E - \frac{jk_0}{2E}\right)\right], \end{aligned} \tag{9.185}$$

where

$$\alpha_{mn} = \sqrt{\underbrace{\left(\frac{m\pi}{a}\right)^2 + \left(\frac{n\pi}{b}\right)^2 - \frac{k_0^2}{4}}_{A_{mn}}} = \sqrt{A_{mn}} \text{ when } A_{mn} \text{ is positive,}$$

$$= j\sqrt{-A_{mn}} \text{ when } A_{mn} \text{ is negative.}$$

The symbol erfc denotes the complementary error function, defined in Section 9.3 and (A5.175). Parameter E is adjustable, and selected to ensure optimum convergence.[99] Rapid convergence is based on the property [144]

$$\operatorname{erfc} z = O\left(\frac{e^{-z^2}}{\pi z}\right)$$

which holds for $z \to \infty$ and $|\arg\ z| < \dfrac{3\pi}{4}$.

9.6 FIELD PENETRATION THROUGH APERTURES

Apertures in metallic surfaces are frequently encountered, for example in input-output connections, visual access windows, and cracks around doors. The basic theory for the field penetration through these apertures will be developed by considering the important case of a plane screen.

9.6.1 General Theory

The problem in hand consists in evaluating the fields that leak into region 2 through aperture A, given the sources in region 1 (Fig 9.34). Screen S is assumed perfectly conducting.[‡‡‡] In the absence of an aperture, the fields in 1 may be obtained from the image scheme depicted in Figure 9.3*a*. Let $\mathbf{E}^g$, $\mathbf{H}^g$ denote these "generator" (or "short-circuit") fields. On S, from (9.22),

$$\begin{aligned} \mathbf{u}_z \cdot \mathbf{E}^g &= 2\mathbf{u}_z \cdot \mathbf{E}^i \\ \mathbf{u}_z \times \mathbf{H}^g &= 2\mathbf{u}_z \times \mathbf{H}^i. \end{aligned} \tag{9.186}$$

From the equivalence principle discussed in Section 7.12, the fields in region 2 are generated by a fictitious magnetic current $\mathbf{J}_{ms} = \mathbf{E} \times \mathbf{u}_z$, spread over the aperture area. Figure 9.3*a* is again relevant here; it shows that the fields in "2" may be thought of as stemming from a magnetic current 2 ($\mathbf{E} \times \mathbf{u}_z$) radiating in free space.[100] From (7.49) to (7.54),

$$\begin{aligned} \mathbf{E}(\mathbf{r}) &= \operatorname{curl} \frac{1}{2\pi} \int_A \mathbf{u}_z \times \mathbf{E}(\mathbf{r}') \frac{e^{-jk_0|\mathbf{r}-\mathbf{r}'|}}{|\mathbf{r}-\mathbf{r}'|}\, dS' = -\operatorname{curl}(\mathbf{C}/\epsilon_0) \\ \mathbf{H}(\mathbf{r}) &= \frac{1}{j\omega\mu_0\epsilon_0} \operatorname{curl}\operatorname{curl} \mathbf{C} \qquad (\mathbf{r} \text{ in } 2). \end{aligned} \tag{9.187}$$

[‡‡‡]The extension to a magnetic wall proceeds analogously. Possible realizations of such walls are discussed in Section 9.5.

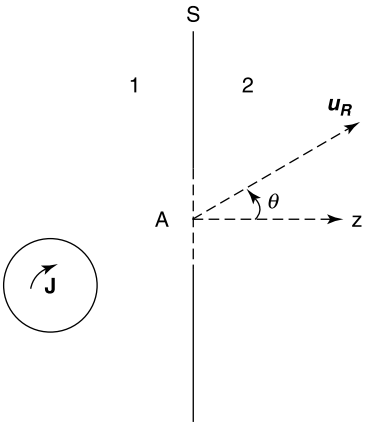

Figure 9.34 Plane screen with aperture.

The fields radiated by the aperture into region 1 are given by analogous formulas, but $\mathbf{u}_z$ must now be replaced by $(-\mathbf{u}_z)$. Keeping the value of $\mathbf{C}$ defined in (9.187), the fields in 1 may be written as

$$\begin{aligned}\mathbf{E}(\mathbf{r}) &= \mathbf{E}^g(\mathbf{r}) + \operatorname{curl} \frac{\mathbf{C}}{\epsilon_0} \\ \mathbf{H}(\mathbf{r}) &= \mathbf{H}^g(\mathbf{r}) - \frac{1}{j\omega\mu_0} \operatorname{curl}\operatorname{curl}\left(\frac{\mathbf{C}}{\epsilon_0}\right).\end{aligned} \tag{9.188}$$

The fundamental unknown of the problem is $\mathbf{u}_z \times \mathbf{E}$. The required continuity of the tangential component of $\mathbf{H}$ in the aperture leads to an integro-differential equation for $\mathbf{u}_z \times \mathbf{E}$, viz.

$$\mathbf{H}_t(\mathbf{r}) = \mathbf{H}^g(\mathbf{r}) - \frac{1}{j\omega\mu_0}\left(\operatorname{curl}\operatorname{curl}\frac{\mathbf{C}}{\epsilon_0}\right)_t = \frac{1}{j\omega\mu_0}\left(\operatorname{curl}\operatorname{curl}\frac{\mathbf{C}}{\epsilon_0}\right)_t (\mathbf{r} \text{ in } A), \tag{9.189}$$

where t denotes a component parallel to S (i.e., in the (x, y) plane). Because $\mathbf{H}^g = 2(\mathbf{H}^i)_t$ in the aperture, (9.189) may be rewritten as

$$\left(\operatorname{curl}\operatorname{curl}\frac{\mathbf{C}}{\epsilon_0}\right)_t = \frac{1}{\epsilon_0}\left(\operatorname{grad}\operatorname{div}\mathbf{C} - \nabla^2\mathbf{C}\right)_t = \operatorname{grad}_t \operatorname{div}_t \frac{\mathbf{C}}{\epsilon_0} + k_0^2\frac{\mathbf{C}}{\epsilon_0} = j\omega\mu_0\mathbf{H}_t^i \quad (\mathbf{r} \text{ in } A). \tag{9.190}$$

Once $\mathbf{u}_z \times \mathbf{E}$ is determined, the fields throughout space can be obtained from (9.187) and (9.188). The far field in region 2, for example, follows from the limit (7.100), which here yields

$$\begin{aligned}\lim_{R\to\infty}\frac{\mathbf{C}}{\epsilon_0} &= -\frac{1}{2\pi}\frac{e^{-jk_0R}}{R}\int_A \mathbf{u}_z \times \mathbf{E}(\mathbf{r}')\, e^{jk_0\mathbf{u}_R\cdot\mathbf{r}'}\, dS' \\ &= \frac{e^{-jk_0R}}{R}\,\mathbf{M}(\theta,\varphi),\end{aligned} \tag{9.191}$$

from which it may be deduced that.

$$\lim_{R\to\infty} \mathbf{E} = jk_0 \frac{e^{-jk_0R}}{R}\, \mathbf{u}_R \times \mathbf{M} \;=\; \mathbf{F}(\theta,\varphi)\frac{e^{-jk_0R}}{R}$$
$$\lim_{R\to\infty} \mathbf{H} = \frac{1}{R_{c0}}(\mathbf{u}_R \times \mathbf{F})\, \frac{e^{-jk_0R}}{R}. \tag{9.192}$$

The radiation pattern depends on the detailed distribution of $\mathbf{u}_z \times \mathbf{E}$ in the aperture, which can be modified, in amplitude and phase, by a variety of methods [47]. Tapering the amplitude of the field to smaller values near the edge, for example, reduces the effective aperture area and therefore broadens the main lobe and lowers the directivity. It has the advantage of potentially reducing the side lobe ratio.

The time-averaged power radiated into half-space 2 follows from (9.192), which gives

$$P^{\text{rad}} = \frac{1}{2}\,\text{Re}\int_{S_\infty/2} \mathbf{u}_R\cdot(\mathbf{E}\times\mathbf{H}^*)\,dS = \frac{1}{2R_{c0}}\int_0^{\pi/2}\int_0^{2\pi} |\mathbf{F}(\theta,\varphi)|^2 \sin\theta\, d\theta\, d\varphi. \tag{9.193}$$

Dividing this power by the average power density in an incident plane wave gives the *transmission cross-section*

$$\sigma^{tr} = \frac{P^{\text{rad}}}{\dfrac{1}{2R_{c0}}|\mathbf{E}^i|^2} = \frac{\displaystyle\int_0^{\Omega=2\pi} |\mathbf{F}(\theta,\varphi)|^2 d\Omega}{|\mathbf{E}^i|^2}, \tag{9.194}$$

where $d\Omega$ denotes the elementary solid angle $\sin\theta\, d\theta\, d\varphi$.

In the previous analysis, screen and sources were embedded in free space. The generalization to half spaces of different parameters (ϵ, μ), both containing sources, is immediate. In region 2:

$$\mathbf{E}(\mathbf{r}) = \mathbf{E}_2^g(\mathbf{r}) + \text{curl}\,\frac{1}{2\pi}\int_A \mathbf{u}_z \times \mathbf{E}(\mathbf{r}')\frac{e^{-jk_2|\mathbf{r}-\mathbf{r}'|}}{|\mathbf{r}-\mathbf{r}'|}\,dS' \;=\; \mathbf{E}_2^g(\mathbf{r}) - \text{curl}\,\frac{\mathbf{C}_2}{\epsilon_2}$$
$$\mathbf{H}(\mathbf{r}) = \mathbf{H}_2^g(\mathbf{r}) + \frac{1}{j\omega\mu_2}\,\text{curl curl}\,\frac{\mathbf{C}_2}{\epsilon_2}. \tag{9.195}$$

In region 1, similarly,

$$\mathbf{E}(\mathbf{r}) = \mathbf{E}_1^g(\mathbf{r}) - \text{curl}\,\frac{1}{2\pi}\int_A \mathbf{u}_z \times \mathbf{E}(\mathbf{r}')\frac{e^{-jk_1|\mathbf{r}-\mathbf{r}'|}}{|\mathbf{r}-\mathbf{r}'|}dS' \;=\; \mathbf{E}_1^g(\mathbf{r}) + \text{curl}\,\frac{\mathbf{C}_1}{\epsilon_1}$$
$$\mathbf{H}(\mathbf{r}) = \mathbf{H}_1^g(\mathbf{r}) - \frac{1}{j\omega\mu_1}\,\text{curl curl}\,\frac{\mathbf{C}_1}{\epsilon_1}. \tag{9.196}$$

Continuity of $\mathbf{H}_t$ in the aperture now leads to the equation

$$\frac{1}{2\pi}\,\text{curl curl}\int_A \mathbf{E}(\mathbf{r}')\times\mathbf{u}_z \frac{\dfrac{1}{\mu_1}e^{-jk_1|\mathbf{r}-\mathbf{r}'|} + \dfrac{1}{\mu_2}e^{-jk_2|\mathbf{r}-\mathbf{r}'|}}{|\mathbf{r}-\mathbf{r}'|}\,dS' = j\omega(\mathbf{H}_1^g - \mathbf{H}_2^g). \tag{9.197}$$

We note that $\mathbf{H}_1^g - \mathbf{H}_2^g = \mathbf{u}_z \times \mathbf{J}_S$, where $\mathbf{J}_S$ is the total surface current induced on the short-circuited aperture A by the sources in both 1 and 2. The sources in 2, for example, could be the currents induced on (or in) a scatterer irradiated by the fields from the aperture.[101,102] In a typical situation, the conductor is a wire belonging to the communication system of an aircraft, the aperture is a window, and the source in region 1 is a jamming signal or the intense transient of a lightning discharge. These unwanted signals can also leak into region 2 by traveling along a wire penetrating from 1 to 2 through a small hole.[103,104] Transient fields radiated from an aperture can be derived from a potential[105]

$$\frac{\mathbf{c}(\mathbf{r},t)}{\epsilon_0} = \frac{1}{2\pi}\int_A \frac{\mathbf{e}\left(\mathbf{r}', t - \dfrac{|\mathbf{r}-\mathbf{r}'|}{c_0}\right) \times \mathbf{u}_z}{|\mathbf{r}-\mathbf{r}'|}\, dS'. \tag{9.198}$$

9.6.2 Babinet's Principle

Consider a perfectly conducting planar disk immersed in an incident wave $\mathbf{E}^i = \mathbf{f}, \mathbf{H}^i = \mathbf{g}$ (Fig. 9.35*a*). The scattered field can be derived from a magnetic potential

$$\mathbf{A}(\mathbf{r}) = \frac{\mu_0}{4\pi}\int_S \mathbf{J}_s(\mathbf{r}')\frac{e^{-jk_0|\mathbf{r}-\mathbf{r}'|}}{|\mathbf{r}-\mathbf{r}'|}\, dS'$$

where $\mathbf{J}_s = 2[\mathbf{u}_z \times \mathbf{H}(z = 0^+)]$. In the $z > 0$ half-space,

$$\mathbf{H}^{sc}(\mathbf{r}) = \operatorname{curl}\frac{1}{2\pi}\int_S \mathbf{u}_z \times \mathbf{H}(\mathbf{r}')\frac{e^{-jk_0|\mathbf{r}-\mathbf{r}'|}}{|\mathbf{r}-\mathbf{r}'|}\, dS' = \operatorname{curl}\left(\frac{\mathbf{A}}{\mu_0}\right). \tag{9.199}$$

The analogy with (9.187) is evident. It implies that the disk problem is equivalent to the complementary problem in which a wave $\mathbf{E}^i = -R_{c0}\mathbf{g}, \mathbf{H}^i = \mathbf{f}/R_{c0}$ impinges on an aperture with the same shape as the disk (Fig. 9.35*b*). The fields are related by $\mathbf{E}' = R_{c0}\mathbf{H}$ and $\mathbf{H}' = -\mathbf{E}/R_{c0}$, relationships in which $\mathbf{E}', \mathbf{H}'$ are the transmitted fields on the shadow side of the aperture and $\mathbf{E}$, $\mathbf{H}$ the scattered fields on the $z > 0$ side of the disk. This duality constitutes Babinet's principle. Illustratively, the principle allows replacement of the circular-hole problem with an equivalent circular-disk problem, for which a solution by separation of variables is available.[106,107] The same principle can be applied to a rectangular aperture.[108]

9.6.3 Numerical Solution

Figure 9.36 shows the amplitude distribution of the electric field in a $1\lambda_0 \times 1\lambda_0$ square aperture, excited by a normally incident plane wave $\mathbf{E}^i = E^i\mathbf{u}_y$. The singularities at the

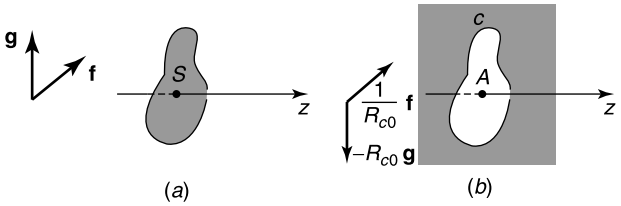

Figure 9.35 (*a*) Perfectly conducting planar disk in a plane wave. (*b*) Complementary problem.

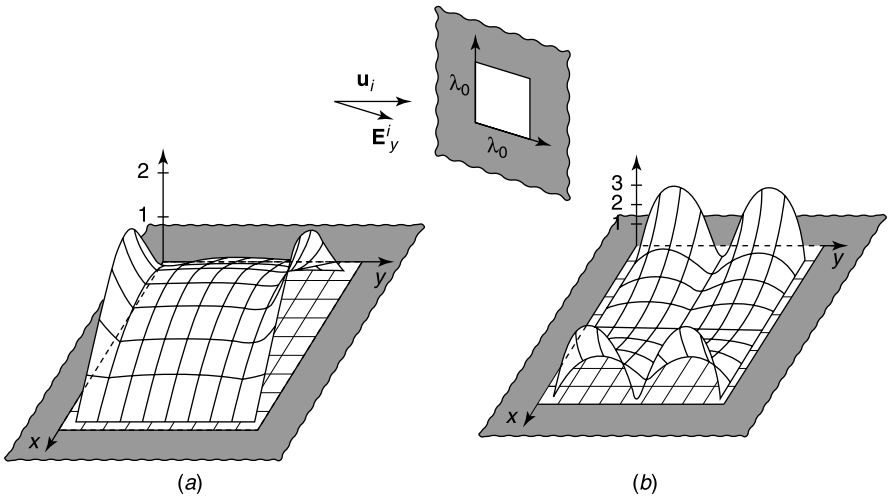

Figure 9.36 Plot of the electric field components in a square aperture. (*a*) Component $|E_y/E^i|$ parallel to the incident field. (*b*) Component $|E_x/E^i_y|$ perpendicular to the incident field (from C. M. Butler, Y. Rahmat-Samii, and R. Mittra, Electromagnetic penetration through apertures in conducting surfaces, *IEEE Trans. AP*, **26**, 82–93, 1978, with permission of IEEE).

edges are apparent.[109] It is often useful, in the numerical solution, to take these singularities into account, for instance on the basis of Helmholtz' theorem in the plane, according to which $\mathbf{E}_t$ can be written as (Fig. 9.37)

$$\mathbf{E}_t(\mathbf{r}) = \text{grad}_t\, \phi(\mathbf{r}) + \mathbf{u}_z \times \text{grad}_t\, \psi(\mathbf{r}) \qquad (\mathbf{r} \text{ in } A). \tag{9.200}$$

The condition $\mathbf{u}_m \times \mathbf{E} = 0$ on contour C (where $\mathbf{u}_m$ is in the aperture plane) requires satisfaction of the conditions $\phi = 0$ and $(\partial\psi/\partial m) = 0$ on C [119]. In addition, from (5.23), $\mathbf{E}\cdot\mathbf{u}_m$ has a singularity of the $d^{-\frac{1}{2}}$ type, which implies that ϕ and $(\partial\psi/\partial m)$ approach zero proportionally to $d^{\frac{1}{2}}$.

Many apertures occurring in practice exhibit corners, sharp or reentrant (Fig. 9.38). The electric field in the aperture plane, close to a corner, is of the form[110]

$$\mathbf{E} = \frac{1}{R^{1-\nu}}\left(\nu Y \mathbf{u}_R + \frac{\partial Y}{\partial \theta}\mathbf{u}_\theta\right) = \text{grad}\,(R^\nu Y). \tag{9.201}$$

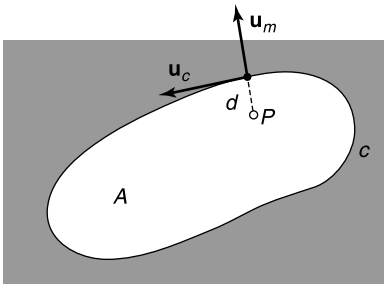

Figure 9.37 Relevant to the singularities at contour C.

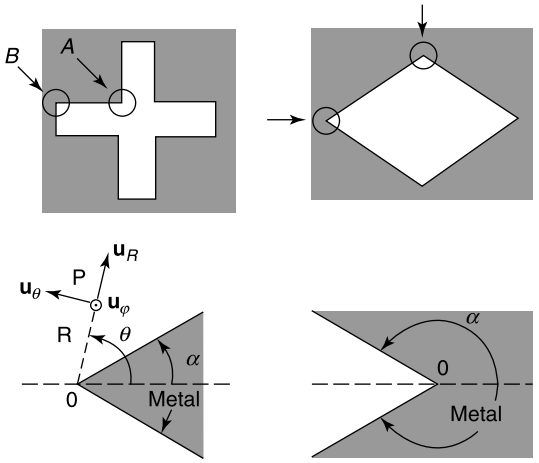

Figure 9.38 Flat sector (corner) singularities (from R. De Smedt and J. Van Bladel, Field singularities near aperture corners, *IEE Proc.* **134-A**, 694–698, 1987, with permission of the Institution of Electrical Engineers).

The function $Y(\theta)$ is discussed in Section 16A, and the value of ν in terms of the opening angle α can be found in Table 5.4. At corner $\boldsymbol{A}$, for example, $\nu = 0.297$, while in B, $\nu = 0.816$. The magnetic field is given by

$$\mathbf{H} = \text{grad}\left[R^{\tau} Z(\theta)\right]. \tag{9.202}$$

The nature of $Z(\theta)$ is also discussed in Section 16.7, and the value of τ can be read from Table 16.1. In $\boldsymbol{A}$, for example, Table 16.1 gives $\tau = 0.816$.

The numerical solution of the aperture problem proceeds typically by discretization. Basic equation (9.197) can be rewritten, for a point in the aperture, as

$$\mathbf{H}_1(\mathbf{J}^1_{ms}) + \mathbf{H}^g_1 = \mathbf{H}_2(\mathbf{J}^2_{ms}) + \mathbf{H}^g_2 \tag{9.203}$$

where $\mathbf{J}^1_{ms} = \mathbf{u}_z \times \mathbf{E}$ and $\mathbf{J}^2_{ms} = \mathbf{E} \times \mathbf{u}_z$. If we set $\mathbf{J}_{ms} = \mathbf{E} \times \mathbf{u}_z$ and use the notation introduced in (8.186), Equation (9.203) becomes

$$\mathbf{L_{1t}} + (\mathbf{J_{ms}}) + \mathbf{L}_{2\text{t}} + (\mathbf{J_{ms}}) = \mathbf{H}^g_1 - \mathbf{H}^g_2. \tag{9.204}$$

Discretization now proceeds by means of an expansion[111]

$$\mathbf{J_{ms}} = \sum_{1}^{N} V_m \mathbf{f}_m. \tag{9.205}$$

The basis functions $\mathbf{f}_m$ may belong to an orthonormal set, for example $\mathbf{f}_m = \mathbf{u}_z \times \text{grad}_t\, \phi_m$, where the ϕ_m are the eigenfunctions satisfying

$$\begin{aligned} \nabla_t^2 \phi_m(\mathbf{r}) + \mu_m^2 \phi_m(\mathbf{r}) &= 0 \qquad (\mathbf{r} \text{ in } A) \\ \phi_m &= 0 \qquad (\text{on } C). \end{aligned} \tag{9.206}$$

The characteristic vectors of the aperture discussed in Section 11.8 may also be considered.[112,113] Great flexibility results from choosing finite elements as basis functions. Whatever the choice, inserting the expansion for $\mathbf{J}_{ms}$ into (9.204) leads to

$$\sum_{1}^{N} V_m \mathbf{L_{1t}}(\mathbf{f_m}) + \sum_{\mathbf{1}}^{\mathbf{N}} \mathbf{V_m L_{2t}} + (\mathbf{f_m}) = \mathbf{H_1^g} - \mathbf{H_2^g}. \tag{9.207}$$

Following the method outlined in Section 8.7, we now multiply both sides of (9.207) with testing functions $\mathbf{W}_n$ to obtain, with a symmetric scalar product $\langle \mathbf{a}, \mathbf{b} \rangle = \int_A \mathbf{a} \cdot \mathbf{b}\, dS$,

$$\sum_{m=1}^{N} V_m \langle \mathbf{W_n}, \mathbf{L_{1t}}(\mathbf{f_m}) \rangle + \sum_{m=1}^{N} V_m \langle \mathbf{W_n}, \mathbf{L_{2t}}(\mathbf{f_m}) \rangle = \langle \mathbf{W_n}, \mathbf{H_1^g} \rangle - \langle \mathbf{W_n}, \mathbf{H_2^g} \rangle$$

$$= \langle \mathbf{W_n}, \mathbf{u_z} \times \mathbf{J_{S1}} \rangle + \langle \mathbf{W_n}, \mathbf{u_z} \times \mathbf{J_{S2}} \rangle \quad (n = 1, 2, \ldots, N)$$

or, in matrix form,

$$\overline{\overline{Y}}_1 \cdot \mathbf{V} + \overline{\overline{\mathbf{Y}}}_{\mathbf{2}} \cdot \mathbf{V} = \mathbf{I_1^g} + \mathbf{I_2^g}. \tag{9.208}$$

This relationship can be represented symbolically by the equivalent circuit of Figure 9.39, where

$$\mathbf{I} = -\mathbf{I_1^g} + \overline{\overline{\mathbf{Y}}}_{\mathbf{1}} \cdot \mathbf{V} = \mathbf{I_2^g} - \overline{\overline{\mathbf{Y}}}_{\mathbf{2}} \cdot \mathbf{V}.$$

As an example of solution, let a rectangular aperture be illuminated by a plane wave at normal incidence, as shown in Figure 9.40*a*. In a rough approximation, suggested by the direction of $\mathbf{E}^i$ and the need for E_y to vanish along the sides $x = 0$ and $x = L$, let expansion (9.205) be reduced to the single term[114]

$$\mathbf{J}_{ms} = (\mathbf{E} \times \mathbf{u}_z) = V\mathbf{f} = \frac{V}{W} \sin \frac{\pi x}{L} \mathbf{u}_x. \tag{9.209}$$

In Figure 9.40*b*, the computed values of V are plotted as a function of $(L/\lambda_0) = (k_0 L/2\pi)$. Resonances are seen to occur around $L = (\lambda_0/2)$. They clearly become sharper when the rectangle gets narrower. In that particular limit, the approximation (9.209) becomes more realistic, a point confirmed by referring to the electric currents induced in a narrow rectangular strip (the equivalent "Babinet" problem).

The half-space admittance matrix for the approximation (9.209) reduces to a single scalar admittance Y, for which representative values of G and B are depicted in Figure 9.41.

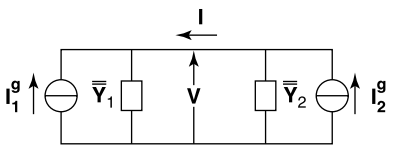

Figure 9.39 Equivalent circuit of aperture-coupled regions.

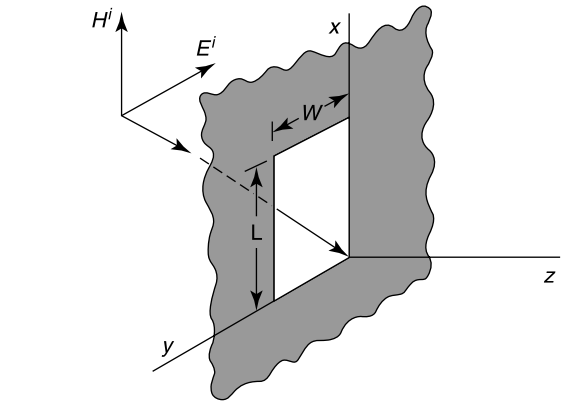

(*a*)

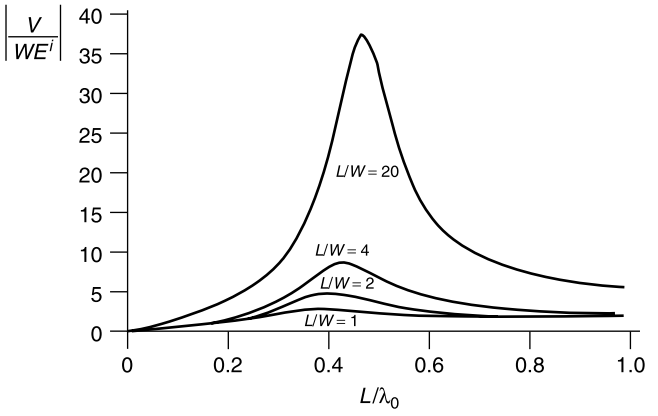

(*b*)

Figure 9.40 (*a*) Rectangular aperture. (*b*) Normalized voltage V across the aperture (from I. C. Jan, R. F. Harrington, and J. R. Mautz, Aperture admittance of a rectangular aperture and its use, *IEEE Trans. AP* **39**, 423–425, 1991, with permission of IEEE).

9.6.4 High-Frequency Limit

Penetration through a circular aperture, a classic canonical problem, can be investigated by separation of variables.[115] The analysis yields, in particular, the *high-frequency transmission cross-section* at normal incidence, which is[116]

$$\lim_{k_0 a \to \infty} \frac{\sigma^{tr}}{\pi a^2} = 1 - \frac{1}{\pi^{1/2}(k_0 a)^{\frac{3}{2}}} \sin\left(2k_0 a - \frac{\pi}{4}\right) + \frac{1}{(k_0 a)^2}\left[\frac{3}{4} + \frac{1}{2\pi}\sin 2\left(2k_0 a - \frac{\pi}{4}\right)\right] + \cdots . \tag{9.210}$$

The actual variation of σ^{tr} is shown in Figure 9.42, where the *exact* curve is taken from Ref. 107. The variational value is obtained from a functional[117,118] whose stationary value is intimately related to σ^{tr}. We notice that the cross-section approaches the optical value πa^2

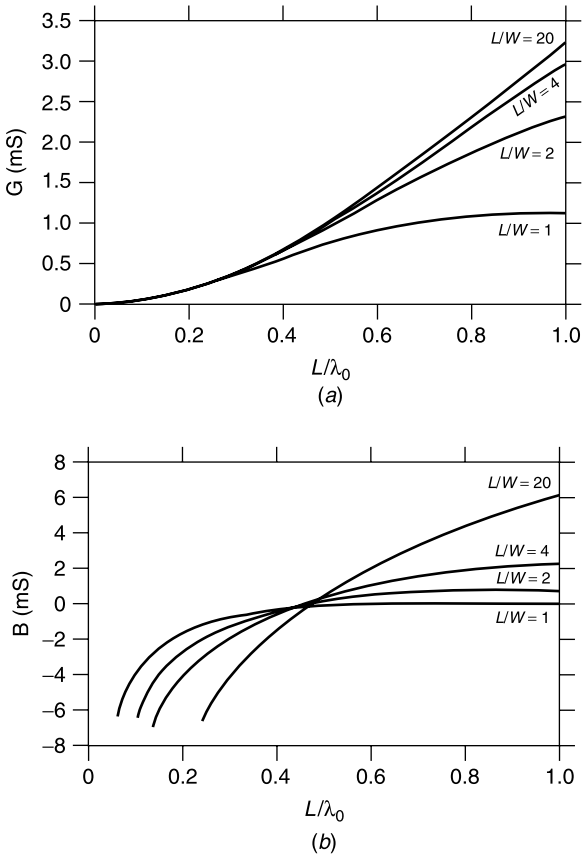

Figure 9.41 Plot of the half-space admittance versus L/λ_0 (from I. C. Jan, R. F. Harrington, and J. R. Mautz, Aperture admittance of a rectangular aperture and its use, *IEEE Trans. AP* **39**, 423–425, 1991, with kind permission of IEEE).

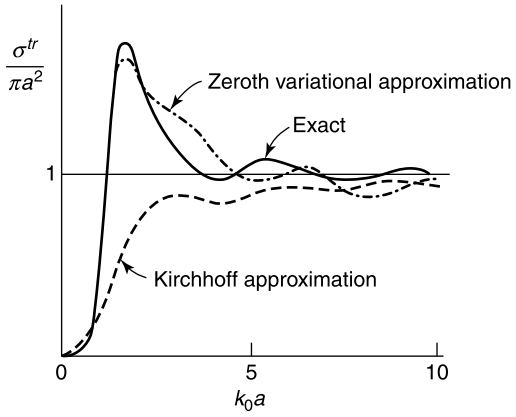

Figure 9.42 Transmission cross section of a circular aperture of radius a (from C. Huang, R. D. Kodis, and H. Levine, Diffraction by apertures, *J. Appl. Phys.* **26**, 151–165, 1955, with permission of the American Institute of Physics).

as the frequency increases. As shown in Section 9.7, at high frequencies the field in the plane aperture is equal to the incident value, except in a narrow band along the rim. An acceptable approximation may therefore be obtained by setting $\mathbf{u}_z \times \mathbf{E} = \mathbf{u}_z \times \mathbf{E}^i$ in the aperture. The influence of the rim can be evaluated by the techniques of the geometrical theory of diffraction,[119,120] which are briefly discussed in Section 13.3. A classic approximation method is that of Kirchhoff [9], in which $\mathbf{E}_t$ *and* $\mathbf{H}_t$ are set equal to their incident values in the aperture, while the fields on the dark side of the metallic screen are set equal to zero. On the basis of these assumptions, the fields *behind* the screen can readily be evaluated. The method is obviously not rigorous. It is also inconsistent, because the calculated fields in the aperture are different from the initially assumed values. These discrepancies are not surprising if one remembers that the fields are uniquely determined by the value of $\mathbf{u}_n \times \mathbf{E}$ in the aperture, so that specification of $\mathbf{u}_n \times \mathbf{E}$ *and* $\mathbf{u}_n \times \mathbf{H}$ overdetermines the problem.

9.6.5 Low-Frequency Limit (Small Holes)

The effect of small apertures, for example the holes drilled in a parabolic reflector to decrease the wind pressure, cannot be ignored in many applications. In the evaluation of the power which leaks through these openings, we should remember that the electric and magnetic fields become unconnected in the $k_0 \to 0$ limit. At distances from the aperture less than λ_0 the magnetic field $\mathbf{H}^a$ generated by the aperture can be written as a field quasi-static[§§§] $\mathbf{H}^a = -\text{grad}\ \psi^a$. The scalar potential ψ^a in region 2 is given by (Problem 9.29)

$$\begin{aligned}\psi^a(\mathbf{r}) &= -\frac{1}{2\pi}\int_A \frac{\partial \psi^a}{\partial z'}\frac{1}{|\mathbf{r}-\mathbf{r}'|}\,dS' \\ &= \frac{1}{\mu_2}\frac{1}{2\pi}\int_A B_z(\mathbf{r}')\frac{1}{|\mathbf{r}-\mathbf{r}'|}\,dS'. \end{aligned} \tag{9.211}$$

An analogous expression may be written in region 1, with the same value of B_z because the normal component of $\mathbf{B}$ is continuous across the aperture. Expressing continuity of the tangential component of $\mathbf{H}$ gives

$$\text{grad}_t\left[\frac{1}{2\pi}\int_A \frac{B_z(\mathbf{r}')}{|\mathbf{r}-\mathbf{r}'|}\,dS'\right] = \frac{\mu_1\mu_2}{\mu_1+\mu_2}(\mathbf{H}_2^g - \mathbf{H}_1^g). \tag{9.212}$$

If the aperture is small enough for $(\mathbf{H}_2^g - \mathbf{H}_1^g)$ to be practically constant in A, the common value of B_z may be written as

$$B_z = \frac{\mu_1\mu_2}{\mu_1+\mu_2}\boldsymbol{\rho}\cdot(\mathbf{H}_2^g - \mathbf{H}_1^g) \tag{9.213}$$

[§§§]Correction terms to this static form can be obtained by suitable expansions of the fields in powers of jk_0. See e.g. [119] and Note 121.

where the dimensionless vector $\boldsymbol{\rho} = \rho_x \mathbf{u}_x + \rho_y \mathbf{u}_y$ can be obtained by solving the integral equations[¶¶¶]

$$\begin{aligned} \operatorname{grad}_t \left[\frac{1}{2\pi} \int_A \rho_x(\mathbf{r}') \frac{1}{|\mathbf{r} - \mathbf{r}'|} \, dS' \right] &= \mathbf{u}_x \\ \operatorname{grad}_t \left[\frac{1}{2\pi} \int_A \rho_y(\mathbf{r}') \frac{1}{|\mathbf{r} - \mathbf{r}'|} \, dS' \right] &= \mathbf{u}_y. \end{aligned} \tag{9.214}$$

The bracketed terms are linear functions of respectively x and y. The interpretation of (9.214) is obvious: ρ_x and ρ_y are proportional to the charge densities that are induced on the scatterer formed by the metallized aperture when the latter is immersed in incident electrostatic fields $\mathbf{u}_x$ or $\mathbf{u}_y$. To make the solution unique, we must add the requirement of charge neutrality[122,123]

$$\int_A \rho_x \, dS = \int_A \rho_y \, dS = 0. \tag{9.215}$$

This requirement is a consequence of the relationship (Problem 9.30)

$$\int_A B_z \, dS = 0. \tag{9.216}$$

We notice that ρ_x and ρ_y are dimensionless. For a circle of radius a, for example,

$$\boldsymbol{\rho} = \frac{4}{\pi} \frac{r}{\sqrt{a^2 - r^2}} \mathbf{u}_r. \tag{9.217}$$

The functions ρ_x and ρ_y, are proportional to charge densities on metallic conductors, hence they should become infinite like $1/\sqrt{d}$ near the edge. The variation of ρ_x and ρ_y in a rectangle, shown in Figure 9.43, confirms this behavior[124].

9.6.6 Dipole Moments and Polarizabilities

From (9.191) and (9.192), the *magnetic* field radiated into region 2 becomes, in the low-frequency limit,

$$\lim_{R \to \infty} \mathbf{H} = \frac{j\omega\epsilon_2}{2\pi} \mathbf{u}_R \times \left[\mathbf{u}_R \times \int_A (\mathbf{E} \times \mathbf{u}_z) \, dS \right] \frac{e^{-jk_2 R}}{R}. \tag{9.218}$$

A comparison with (7.155) shows that this is the field of a magnetic dipole radiating in an infinite homogeneous medium (ϵ_2, μ_2). The equivalent dipole moment of the aperture is[‖‖‖]

$$\mathbf{P}_{m2} = \frac{1}{j\omega\mu_2} \int_A \underbrace{2(\mathbf{E} \times \mathbf{u}_z)}_{\mathbf{J}_{mS}} \, dS = \frac{1}{jk_2 R_{c2}} \int_A \mathbf{J}_{mS} \, dS \qquad (A \text{ m}^2). \tag{9.219}$$

[¶¶¶]The functions ρ_x, ρ_y and τ_0 are also relevant for two related acoustic problems. See Notes 122 and 123.

[‖‖‖]Alternately, one may obtain the far field by assuming that a dipole moment $(\mathbf{P}_m/2)$ is located in front of the short-circuited aperture.

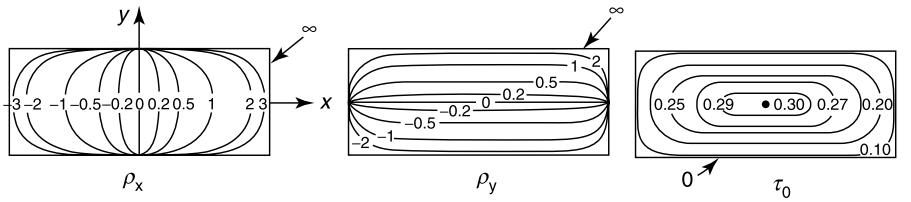

Figure 9.43 Variation of some important parameters in a rectangular aperture (from F. De Meulenaere and J. Van Bladel, Polarizability of some small apertures, *IEEE Trans. AP* **25**, 198–205, 1977, with permission of IEEE).

This moment lies in the plane of the aperture. It can be evaluated starting from

$$\int_A \mathbf{J}_{mS}\, dS = \mathbf{u}_x \int_A \operatorname{grad}_t x \cdot \mathbf{J}_{mS}\, dS + \mathbf{u}_y \int_A \operatorname{grad}_t y \cdot \mathbf{J}_{mS}\, dS.$$

Both integrals can be transformed according to (A3.44). For example:

$$\int_A \operatorname{grad}_t x \cdot \mathbf{J}_{mS}\, dS = \int_A \operatorname{div}_t (x\mathbf{J}_{mS}) - \int_A x \operatorname{div}_t \mathbf{J}_{mS}\, dS.$$

Because $\mathbf{J}_{mS} = 2(\mathbf{E} \times \mathbf{u}_z)$ is tangent to the rim of the aperture, Gauss' theorem (A3.44) shows that the first integral in the right-hand term must vanish. From the formula for the curl, and the value of H_z given in (9.213),

$$\begin{aligned} \operatorname{div}_t (\mathbf{E} \times \mathbf{u}_z) = \mathbf{u}_z \cdot \operatorname{curl} \mathbf{E} \; &= \; -j\omega\mu_2 H_z \\ &= -j\omega \frac{\mu_1\mu_2}{\mu_1 + \mu_2} \boldsymbol{\rho} \cdot (\mathbf{H}_2^g - \mathbf{H}_1^g). \end{aligned}$$

Collecting these results gives

$$\int_A \mathbf{J}_{mS}\, dS = \int_A 2(\mathbf{E} \times \mathbf{u}_z)\, dS = j\omega \frac{2\mu_1\mu_2}{\mu_1 + \mu_2} (\mathbf{H}_1^g - \mathbf{H}_2^g) \cdot \int_A \boldsymbol{\rho}\mathbf{r}\, dS$$

and

$$\mathbf{P}_{m2} = \frac{2\mu_1}{\mu_1 + \mu_2} \bar{\bar{\alpha}}_m \cdot (\mathbf{H}_1^g - \mathbf{H}_2^g) \tag{9.220}$$

where $\bar{\bar{\alpha}}_m$, in units of m^3, is the *magnetic polarizability* of the aperture. Thus, if S_a is the area of the aperture,

$$\bar{\bar{\alpha}}_m = \int_A \boldsymbol{\rho}\mathbf{r}\, dS = S_a^{\frac{3}{2}}\, \bar{\bar{\nu}}_m. \tag{9.221}$$

The polarizability dyadic is symmetric, and can be diagonalized by choosing the x and y axes to coincide with its principal axes. The dimensionless form $\bar{\bar{\nu}}_m$ is a shape factor. For a circle,**** for example,

$$\begin{aligned} \bar{\bar{\alpha}}_m &= \frac{8a^3}{3}\, \bar{\bar{I}}_{xy} \\ \bar{\bar{\nu}}_m &= \frac{8}{3\pi\sqrt{\pi}}\, \bar{\bar{I}}_{xy}. \end{aligned} \tag{9.222}$$

****For data on other shapes, including the electric polarizability, see Notes 124 to 128.

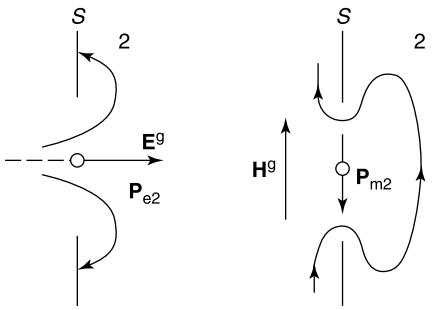

Figure 9.44 Field penetration through a small aperture (from F. De Meulenaere and J. Van Bladel, Polarizability of some small apertures, *IEEE Trans. AP*, **25**, 198–205, 1977, with permission of IEEE).

In the low-frequency limit the *electric* field is independent of the magnetic field. Its electrostatic value is discussed in Section 5.10, where it is shown that the fields radiated in region 2 may be thought of as generated by an electric dipole of moment (5.105). We write

$$\mathbf{P}_{e2} = \frac{2\epsilon_2}{\epsilon_1 + \epsilon_2}\,\overline{\overline{\alpha}}_e \cdot (\epsilon_1 \mathbf{E}_1^g - \epsilon_2 \mathbf{E}_2^g) \qquad \text{(C m)}. \tag{9.223}$$

In this expression

$$\overline{\overline{\alpha}}_e = (\tau_o)_{\text{ave}}\, S_a^{\frac{3}{2}}\, \mathbf{u}_z\mathbf{u}_z = \alpha_e\, \mathbf{u}_z\mathbf{u}_z. \tag{9.224}$$

For a circle,

$$\alpha_e = \frac{4a^3}{3}.$$

The dipole is assumed immersed in an infinite space filled with material 2. A general picture of the lines of force of the total **E** and **H** fields is shown in Figure 9.44. Once $\mathbf{P}_{e2}$, and $\mathbf{P}_{m2}$ are known, the power transmitted into region 2 (devoid of sources) can easily be determined, together with the *transmission cross section* (9.194). *For a circular hole* at normal incidence, for example, the power expansion of σ^{tr} in terms of $(k_0 a)$ is, in vacuum,

$$\lim_{k_0 a \to 0} \frac{\sigma^{tr}}{\pi a^2} = \frac{64}{27\pi^2}(k_0 a)^4 \left[1 + \frac{22}{25}(k_0 a)^2 + \frac{7312}{18375}(k_0 a)^4 + \cdots\right]. \tag{9.225}$$

This formula confirms that little power leaks through small holes (Problem 9.26).

9.7 EDGE DIFFRACTION

9.7.1 The Sommerfeld Diffraction Problem

The problem in hand is to determine the fields scattered by a perfectly conducting half-plane. Various analytical solutions, based on complex integration techniques, are available, including Sommerfeld's use of two-sided Riemann surfaces [45, 77, 122, 196]. The following simple approach was proposed by Bouwkamp.[100] Assume that a plane wave is normally

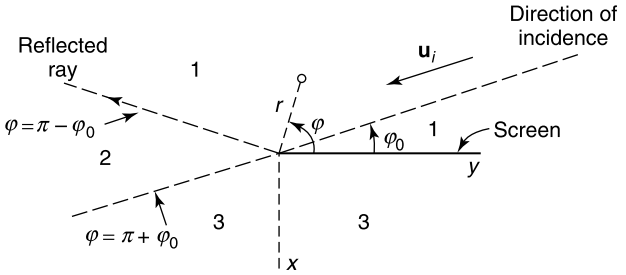

Figure 9.45 Perfectly conducting half-plane and incident plane wave.

incident on the edge of the screen (Fig. 9.45). The wave can be of the E-type, with E_z as the main unknown and the boundary condition $E_z = 0$ at $\varphi = 0$ and $\varphi = 2\pi$. It can also be of the H-type, with H_z as the main unknown, and $\dfrac{\partial H_z}{\partial \varphi} = 0$ at $\varphi = 0$ and $\varphi = 2\pi$. The incident wave is

$$\phi^i = e^{-jk_0 \mathbf{u}_i \cdot \mathbf{r}} = e^{jk_0 r \cos(\varphi - \varphi_0)}.$$

Let us introduce a new set of coordinates, viz.

$$u = 2r\cos^2\frac{\varphi}{2} \qquad v = -r\cos\varphi.$$

The field ϕ, which can be E_z or H_z, satisfies Helmholtz' equation. In the u, v coordinates, this equation takes the form

$$\nabla^2\phi + k_0^2\phi = \left[\frac{\partial^2}{\partial v^2} + \frac{2u}{u+v}\left(\frac{\partial^2}{\partial u^2} - \frac{\partial^2}{\partial u \partial v}\right) + \frac{1}{u+v}\frac{\partial}{\partial u} + k_0^2\right]\phi = 0. \tag{9.226}$$

It is a simple matter to show that a product of the form $\phi = F(v)G(u)$ is a possible solution provided $F(v)$ and $G(u)$ satisfy

$$\frac{d^2F}{dv^2} + k_0^2 F = 0$$
$$F\left(\frac{d^2G}{du^2} + \frac{1}{2u}\frac{dG}{du}\right) - \frac{dF}{dv}\frac{dG}{du} = 0. \tag{9.227}$$

Because the total solution must contain the incident field, the choice for F is

$$F = e^{-jk_0 v} = e^{jk_0 r\cos\varphi}.$$

Introducing this form into (9.227), and setting

$$\frac{dG}{du} = \frac{1}{\sqrt{u}}Z(u) \tag{9.228}$$

leads to

$$\frac{dZ}{du} + jk_0 Z = 0.$$

$Z = e^{-jk_0 u}$ is clearly a possible solution. It follows that a particular solution of Helmholtz' equation is

$$\phi = e^{jk_0 r\cos\varphi} \int_{\text{constant}}^{2r\cos^2(\frac{\varphi}{2})} \frac{e^{-jk_0 u}}{(u)^{\frac{1}{2}}}\, du.$$

Other particular solutions can be obtained by replacing φ with $(\varphi + \varphi_0)$ or $(\varphi - \varphi_0)$. As a result, the linear combination

$$\phi = A\, e^{jk_0 r\cos(\varphi-\varphi_0)} \int_{-\infty}^{2(k_0 r/\pi)^{\frac{1}{2}}\cos[(\varphi-\varphi_0)/2]} e^{-j(\pi/2)\tau^2} d\tau,$$

$$+B\, e^{jk_0 r\cos(\varphi+\varphi_0)} \int_{-\infty}^{2(k_0 r/\pi)^{\frac{1}{2}}\cos[(\varphi+\varphi_0)/2]} e^{-j(\pi/2)\tau^2} d\tau, \tag{9.229}$$

which is obtained by setting $k_0 u = \pi\tau^2/2$, is also a solution of Helmholtz' equation. To determine A and B, we note that the boundary conditions are $A + B = 0$ for the E wave (the *Dirichlet* or *"soft" condition*), and $A - B = 0$ for the H wave (the *Neumann* or *"hard" condition*). The final result for a unit incident field is

$$\left.\begin{matrix} E_z \\ H_z \end{matrix}\right\} = e^{jk_0 r\cos(\varphi-\varphi_0)} \frac{1+j}{2} \int_{-\infty}^{2(k_0 r/\pi)^{\frac{1}{2}}\cos[(\varphi-\varphi_0)/2]} e^{-j\pi\tau^2/2} d\tau$$

$$\mp\ e^{jk_0 r\cos(\varphi+\varphi_0)} \frac{1+j}{2} \int_{-\infty}^{2(k_0 r/\pi)^{\frac{1}{2}}\cos[(\varphi+\varphi_0)/2]} e^{-j\pi\tau^2/2} d\tau. \tag{9.230}$$

Fundamental to the interpretation of this result is a knowledge of the value of the *Fresnel integral*

$$F(W) = \int_0^W e^{-j(\pi\tau^2/2)} d\tau = \int_0^W \cos\left(\frac{\pi}{2}\tau^2\right) d\tau - j\int_0^W \sin\left(\frac{\pi}{2}\tau^2\right) d\tau$$
$$= C(W) - jS(W). \tag{9.231}$$

The Cornu spiral in Figure 9.46 shows the dependence of C and S on W (extensive numerical data are available in [144]). Some particular values of $F(w)$ are worth mentioning [76, 122]:

$$F(0) = 0 \qquad F(\infty) = \frac{1-j}{2} \qquad F(-\infty) = -\frac{1-j}{2}$$
$$\lim_{W\to 0} F(W) = W\left(1 - j\frac{\pi}{2}W^2 + \cdots\right)$$
$$\lim_{W\to\infty} F(W) = \frac{1-j}{2} + \frac{j}{\pi W} e^{-j\frac{\pi W^2}{2}} \left(1 + \frac{j}{\pi W^2} + \cdots\right) \tag{9.232}$$
$$\lim_{W\to\infty} \int_W^\infty e^{-j\pi\tau^2/2}\, d\tau = -\frac{j}{\pi W} e^{-j\frac{\pi W^2}{2}} + \cdots.$$

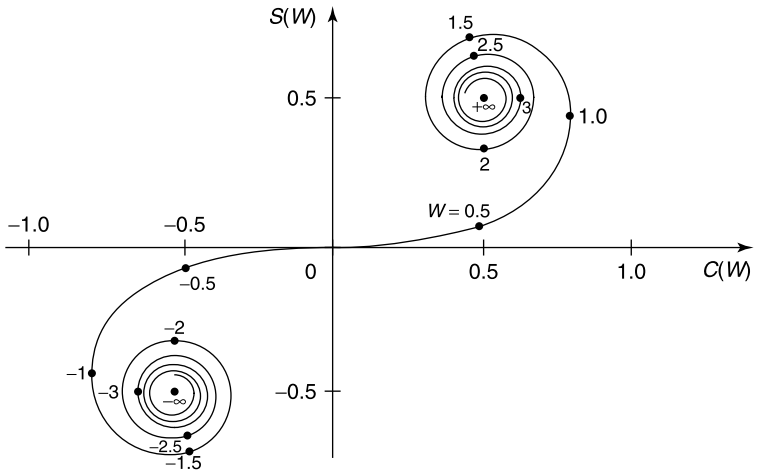

Figure 9.46 Cornu spiral.

9.7.2 The Diffracted Field

Let us first exclude the directions $\varphi = (\pi - \varphi_0)$ and $\varphi = (\pi + \varphi_0)$. With this restriction, both $\cos(\varphi - \varphi_0)/2$ and $\cos(\varphi + \varphi_0)/2$ differ from zero. In consequence, the upper limits of the integrals in (9.230) approach infinity in region 1 when $r \to \infty$ (Fig. 9.45). The fields in 1 then take the form

$$\left.\begin{matrix} E_z \\ H_z \end{matrix}\right\} = e^{jk_0 r\cos(\varphi-\varphi_0)} \mp e^{jk_0 r\cos(\varphi+\varphi_0)}. \tag{9.233}$$

The first and second terms are respectively the incident wave and the specularly reflected wave (which propagates along $\varphi = \pi - \varphi_0$). Region 2 carries only the incident wave, while zone 3 lies in the shadow. These results are in harmony with the ray-approximation of geometrical optics. At large, but not infinite distances, an additional *diffracted* field must be taken into account. From (9.232):

$$\begin{aligned} E_z^d &= -\frac{E_z^i}{\sqrt{8\pi k_0 r}}\left(\frac{1}{\cos\dfrac{\varphi-\varphi_0}{2}} - \frac{1}{\cos\dfrac{\varphi+\varphi_0}{2}}\right) e^{-j(k_0 r+\frac{\pi}{4})} = D^e(\varphi,\varphi_0)\frac{e^{-jk_0 r}}{\sqrt{r}}E_z^i \\ H_z^d &= -\frac{H_z^i}{\sqrt{8\pi k_0 r}}\left(\frac{1}{\cos\dfrac{\varphi-\varphi_0}{2}} + \frac{1}{\cos\dfrac{\varphi+\varphi_0}{2}}\right) e^{-j(k_0 r+\frac{\pi}{4})} = D^h(\varphi,\varphi_0)\frac{e^{-jk_0 r}}{\sqrt{r}}H_z^i. \end{aligned} \tag{9.234}$$

The D's are *diffraction coefficients*, proportional to $k_0^{-\frac{1}{2}}$ (i.e., to $\lambda_0^{\frac{1}{2}}$). As φ approaches the excluded directions $\pi \pm \varphi_0$, the expressions (9.234) become infinite, showing that the analysis must be modified. Along the boundary $\varphi = \pi - \varphi_0$, the general expressions (9.230) give rise to the incident field plus *one-half* the reflected field. Along the light-shadow

boundary, that is, for $\varphi = (\pi + \varphi_0)$, the field is *half* the incident field. It pays to investigate what happens in the immediate vicinity of these two boundaries. For the light-shadow boundary, for example, we shall write $\varphi = (\varphi_0 + \pi + \Delta\varphi)$, where $\Delta\varphi$ is small. The second term on the right-hand side of (9.230) vanishes, but the first term becomes

$$\left.\begin{matrix} E_z \\ H_z \end{matrix}\right\} = e^{-jk_0 r}\frac{1+j}{2}\int_{-\infty}^{-\sqrt{\frac{2r}{\lambda_0}}\Delta\varphi} e^{\frac{-j\pi\tau^2}{2}}\,d\tau. \tag{9.235}$$

The value of this field can be read from the Cornu spiral and associated tables. The result is shown in Figure 9.47. The angular width of the light-shadow transition zone is of the order $\Delta\varphi = \pm 2(\lambda_0/r)^{\frac{1}{2}}$.

9.7.3 Near Field

At short distances r, the approximation (9.232) gives, in the limit $W \to 0$,

$$\begin{aligned} E_z &= 2(1+j)\sqrt{\frac{k_0 r}{\pi}}\sin\frac{\varphi_0}{2}\sin\frac{\varphi}{2} \\ R_{c0}H_r &= -(1-j)\frac{1}{\sqrt{\pi k_0 r}}\sin\frac{\varphi_0}{2}\cos\frac{\varphi}{2} \\ R_{c0}H_\varphi &= (1-j)\frac{1}{\sqrt{\pi k_0 r}}\sin\frac{\varphi_0}{2}\sin\frac{\varphi}{2} \end{aligned} \tag{9.236}$$

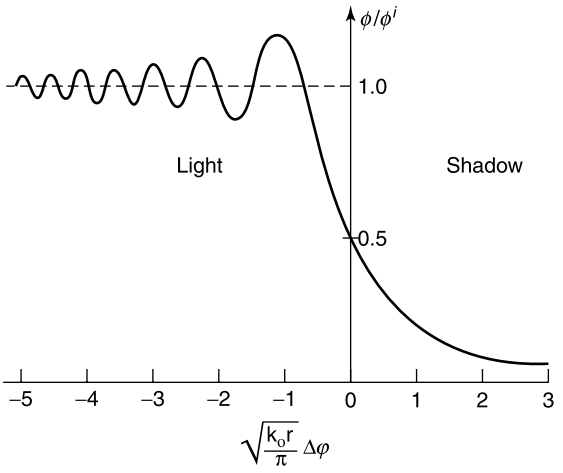

Figure 9.47 Fields in the vicinity of the light-shadow boundary.

for an E wave, and

$$\begin{aligned} H_z &= 1 + 2(1+j)\sqrt{\frac{k_0 r}{\pi}} \cos\frac{\varphi_0}{2} \cos\frac{\varphi}{2} \\ \frac{1}{R_{c0}} E_r &= -(1-j)\frac{1}{\sqrt{\pi k_0 r}} \cos\frac{\varphi_0}{2} \sin\frac{\varphi}{2} \\ \frac{1}{R_{c0}} E_\varphi &= -(1-j)\frac{1}{\sqrt{\pi k_0 r}} \cos\frac{\varphi_0}{2} \cos\frac{\varphi}{2} \end{aligned} \tag{9.237}$$

for an H wave. The edge singularities of the near field are in agreement with more general results mentioned at the end of this section.

The fields in the $\varphi = \pi$ half-plane (i.e., in the continuation of the conducting half-plane) deserve particular attention. They are obtained from (9.230) by inserting an upper limit $2(k_0 r/\pi)^{\frac{1}{2}} \sin\dfrac{\varphi_0}{2}$ in the first integral, and minus this value in the second one. It is clear, from Cornu's spiral, that the second term becomes negligible as soon as

$$r \gg \frac{\lambda_0}{\sin\left(\dfrac{\varphi_0}{2}\right)}. \tag{9.238}$$

Under these conditions the first term, which is equal to the incident field, predominates. Extrapolating this result to an aperture bounded by a sharp perfectly conducting edge, we may conclude that the disturbing effect of the edge is limited to distances of the order of $\lambda_0 \left[\sin\left(\dfrac{\varphi_0}{2}\right)\right]^{-1}$, that is, of the order λ_0, unless φ_0 is small. At larger distances, the incident field penetrates undisturbed below the $\varphi = \pi$ plane.

The near field on the conducting half-plane itself is obtained from (9.236) and (9.237) by setting $\varphi = 0$ for the upper face and $\varphi = 2\pi$ for the lower one. The results show that different values of H_r and H_z appear on both sides of the screen, thus revealing the presence of a surface current

$$\mathbf{J}_S = (1-j)\frac{2}{\sqrt{\pi k_0 r}} \sin\frac{\varphi_0}{2} \frac{E^i}{R_{c0}} \mathbf{u}_z + (1-j)\, 4\sqrt{\frac{k_0 r}{\pi}} \cos\frac{\varphi_0}{2} H^i\, \mathbf{u}_r. \tag{9.239}$$

The only singular component of $\mathbf{J}_S$ is *parallel* to the edge, and it is only present when the incident wave is of the E-type.

The screen in the previous discussions was assumed perfectly conducting. The extension of the theory to an *imperfectly* conducting half-plane is more difficult but worthwhile considering because of its potential application to the reduction of scattering from structural edges.[129,130]

9.7.4 Oblique Incidence

The incident field at oblique incidence is of the general form

$$\mathbf{E} = \mathbf{E}^i e^{-jk_0(x\cos\varphi_0 \sin\theta_0 + y\sin\varphi_0 \sin\varphi_0 \sin\theta_0 + z\cos\theta_0)}. \tag{9.240}$$

Normal incidence corresponds with $\theta_0 = (\pi/2)$ (Fig. 9.48). To satisfy the boundary conditions, all field components must exhibit a phase factor $e^{-jk_0 z\cos\theta_0}$. The equations for normal

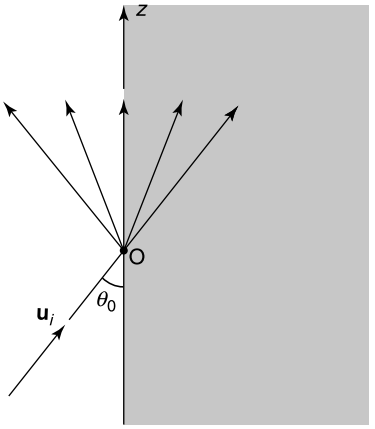

Figure 9.48 Incident and diffracted rays.

incidence can now be adapted to oblique incidence by replacing k_0 by $k_0 \sin\theta_0$. Detailed calculations show [76, 122] that the diffracted field at large distances consists of an ensemble of plane waves, or "rays," which all make an angle θ_0 with the sharp edge. For any given ray, we shall use subscripts $\parallel$ and $\perp$ to denote components respectively in the ray-edge plane or perpendicular to that plane. For such a choice, there exist *diffraction coefficients* $D_\parallel$ and $D_\perp$ in terms of which [76]

$$\begin{pmatrix} E_\perp^d \\ E_\parallel^d \end{pmatrix} = \frac{1}{\sin\theta_0} \begin{pmatrix} D_\perp & 0 \\ 0 & D_\parallel \end{pmatrix} \cdot \begin{pmatrix} E_\perp^i \\ E_\parallel^i \end{pmatrix}_{\text{in } O} \frac{e^{-jk_0 r}}{\sqrt{r}}. \tag{9.241}$$

In the geometrical theory of diffraction (the GTD), a powerful tool further discussed in Section 13.3, one assumes that the same cone of diffracted rays emerges from O even when the edge is *curved*. The solution breaks down at shadow boundaries, where it predicts infinite fields.

9.7.5 Edge Condition

At distances r much less than λ_0, the field singularities near the edge of a wedge are of the type discussed in Sections 5.2 and 5.3 for static fields. For a *perfectly conducting* wedge, and with **E** parallel to the edge (Fig. 9.49),

$$\begin{aligned} E_z &= j\omega\mu_0 A r^\nu \sin\nu\varphi \\ \mathbf{H}_t &= \frac{\nu A}{r^{1-\nu}} (-\mathbf{u}_r \cos\nu\varphi + \mathbf{u}_\varphi \sin\nu\varphi) \\ \rho_S &= 0 \\ \mathbf{J}_S &= \frac{\nu A}{r^{1-\nu}} \mathbf{u}_z \end{aligned} \tag{9.242}$$

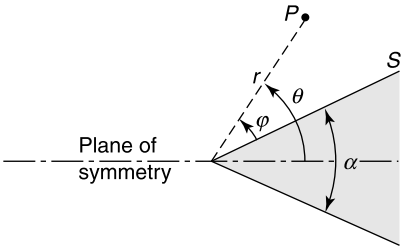

Figure 9.49 Geometry of a wedge.

where the subscript S denotes the sides of the wedge, and t is a component in the xy plane. The singularity exponent is $\nu = \pi/(2\pi - \alpha)$. For **H** parallel to the edge:

$$
\begin{aligned}
H_z &= j\omega\epsilon_0 B r^{\nu} \cos \nu\varphi + \text{constant} \\
\mathbf{E}_t &= -\frac{\nu B}{r^{1-\nu}} (\mathbf{u}_r \sin \nu\varphi + \mathbf{u}_\varphi \cos \nu\varphi) \\
\rho_S &= -\frac{\nu B \epsilon_0}{r^{1-\nu}} \\
\mathbf{J}_S &= j\omega\epsilon_0 B r^{\nu} \mathbf{u}_r.
\end{aligned} \tag{9.243}
$$

The field components parallel to the edge are bounded, but the perpendicular components are singular. The surface charge ρ_S is only singular in an H-wave, and the current density $\mathbf{J}_S$ in an E-wave. The A and B coefficients depend on the nature of the incident fields. In a numerical procedure, it is often advantageous, in order to accelerate convergence, to incorporate the singularity into the basis functions. Near the sharp edge bounding a planar aperture, for example, $(h/d)^{\frac{1}{2}}$ would be a suitable function for a triangular element because it enforces the $1/\sqrt{d}$ dependence (Fig. 9.50). Note that, under special conditions of symmetry, the A and B coefficients may vanish; that is, the singularity may not be excited [133]. This would be the case when the incident E_z field is *antisymmetric* with respect to the plane of symmetry $\varphi = \pi - (\alpha/2)$, or when the H_z field is *symmetric* with respect to that plane. Under these circumstances, enforcing the singularity may lead to numerical problems.[131]

In the presence of a *dielectric* wedge, no singularities occur when the incident wave is of the E-type. Because the incident field satisfies all boundary conditions at the air-dielectric interface, it will propagate undisturbed by the presence of the dielectric. In an H-wave, however, **E** is transverse, and the singularities appear, as shown by the field

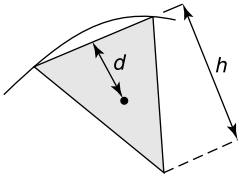

Figure 9.50 Subarea near a sharp edge.

expressions [133]

$$H_z^k = j\omega\epsilon^k A^k r^\nu \sin \nu(\varphi + \alpha_k)$$

$$\mathbf{E}_t^k = \text{grad}\ \phi_k = \frac{A^k \nu}{r^{1-\nu}} \left[\cos \nu(\varphi + \alpha^k)\, \mathbf{u}_r - \sin \nu(\varphi + \alpha^k)\, \mathbf{u}_\varphi\right] \tag{9.244}$$

where $k = 0$ in air, and $k = 1$ in the dielectric. The value of ν is determined by the requirement that E_r and $\epsilon_r E_\varphi$ be continuous at the air-dielectric interface. There are two fundamental symmetries. In the first one, *ϕ is symmetric*. In terms of the angle θ shown in Figure 9.49:

$$\phi_0 = A\, r^\nu \cos \nu\theta$$

in air, and

$$\phi_1 = A\, \frac{\cos\left(\nu \dfrac{\alpha}{2}\right)}{\cos \nu \left(\pi - \dfrac{\alpha}{2}\right)}\, r^\nu \cos \nu(\pi - \theta) \tag{9.245}$$

in the dielectric. The value of the exponent ν can be found in Table 5.1. In the second symmetry, *ϕ is antisymmetric*, and its value is

$$\phi_0 = B\, r^\tau \sin \tau\theta$$

in air, and

$$\phi_1 = B\, \frac{\sin\left(\tau \dfrac{\alpha}{2}\right)}{\sin \tau \left(\pi - \dfrac{\alpha}{2}\right)}\, r^\tau \sin \tau(\pi - \theta) \tag{9.246}$$

in the dielectric. The values of τ can be found in Table 5.1.

When the wedge is *magnetic*, it is now the incident H-wave that is undisturbed by the presence of the wedge. The previous results can be duplicated, provided (9.244) is replaced by

$$E_z^k = -j\omega\mu^k B^k r^\nu \sin \nu(\varphi + \alpha_k)$$

$$\mathbf{H}_t^k = \frac{B^k \nu}{r^{1-\nu}} \left[\cos \nu(\varphi + \alpha^k)\, \mathbf{u}_r - \sin \nu(\varphi + \alpha^k)\, \mathbf{u}_\varphi\right]. \tag{9.247}$$

Further data on singularities are available for

- A few composite wedges, formed by adjacent metal and dielectric bodies [133]
- Imperfectly conducting wedges[132]
- Biisotropic and bianisotropic wedges.[133]

PROBLEMS

9.1 A circularly-polarized wave $\mathbf{E}^i = E(\mathbf{u}_x + j\mathbf{u}_y)$ is incident on a dielectric medium ($\epsilon_r = 4$, Fig. P9.1). Determine the reflected electric field, and in particular its two circularly polarized components. Evaluate $|R|^2$ for the component that rotates in the same sense with respect to the direction of propagation as the incident field (i.e., the component $\mathbf{u}_{x'} + j\mathbf{u}_{y'}$). Plot $|R|^2$ as a function of θ_i, and compare with the $|R_\parallel|^2$ that is obtained for a wave polarized in the y-direction.

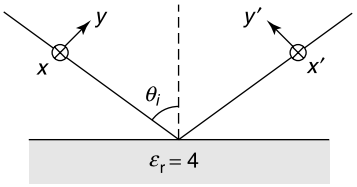

Figure P9.1

9.2 With reference to Figure 9.5, assume that a plane wave is incident, under Brewster's angle (9.39), on the exit interface of a quartz window (Fig. P9.2). Evaluate the reflection coefficient when θ_i is Brewster's angle (9.39), and show that total transmission takes place.

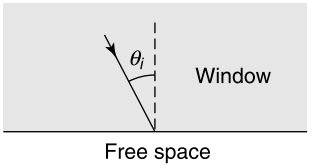

Figure P9.2

9.3 The Zenneck wave is described by Equations (9.44) and (9.45). Show that the tilt of the electric field at the interface is

$$\left(\frac{E_x}{E_z}\right)_{z=0} = \left(\frac{j\omega\epsilon_0}{\sigma + j\omega\epsilon}\right)^{\frac{1}{2}}.$$

9.4 A plane wave illuminates a lossless plasma at normal incidence (Fig. 9.8). For $\omega < \omega_p$ there is total reflection. Show that the reflection coefficient R can be written in the form $R = e^{-j2\varphi}$. Verify that the plasma reflects like a perfect conductor located at a depth $z = l$, and determine l (the *effective altitude*).

9.5 Assume that a plane wave is normally incident on a good conductor, as depicted in Figure 9.4. Let now $\sigma = \infty$ (i.e., let the good conductor become perfect). Find the limit value of both the magnetic field at the interface and the induced current density $\mathbf{J} = \sigma\mathbf{E}$. By integrating $\mathbf{J}$ along the z-axis, find the equivalent $\mathbf{J}_S$, and verify that $\mathbf{J}_S$ and $\mathbf{H}$ are connected by the classic formula given in (9.23).

9.6 With respect to Figure 9.4 evaluate the power dissipated in the good conductor (in $W\ m^{-2}$) as a function of frequency. Generalize to normal incidence on a slab of thickness d.
(G. Bouchitté et al., *Radio Sci.* **24**, 13–26, 1989).

9.7 A perpendicularly polarized plane wave is obliquely incident on a slab in which ϵ_r and μ_r are smooth functions of z (Fig. P9.3).

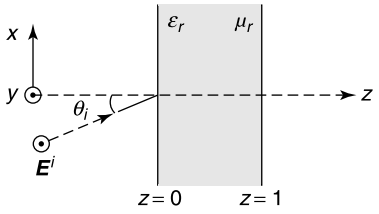

Figure P9.3

(a) Find the differential equation satisfied by $\mathbf{E} = \mathbf{E}\mathbf{u}_y$

(b) Derive the (9.75) matrix for this configuration.

9.8 A slab of dielectric material is illuminated under the Brewster angle $\theta_i = \tan^{-1}\sqrt{\epsilon_r}$ (Fig. P9.4). Determine the field in the dielectric. $\mathbf{E}^i$ is polarized in the plane of incidence.

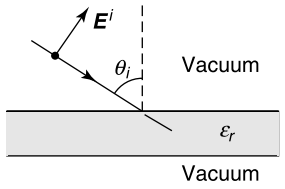

Figure P9.4

9.9 A medium of dielectric constant $\epsilon_r = 16$ is covered with a layer of dielectric constant $\epsilon_r = 4$ and thickness $d = 3.75$ mm (Fig. P9.5). Determine the reflection coefficient for normal incidence in the frequency range 8 to 12 GHz. Is the name "antireflection layer" justified, and at which frequencies?

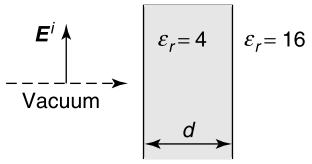

Figure P9.5

9.10 In the configuration of Figure P9.5, formulate the problem as a Sturm-Liouville boundary value problem for either E or H, depending on the polarization. Derive an appropriate variational formulation, in which the functional is an integral extending from $z = 0$ to $z = d$.
(C. H. Chen et al., *IEEE Trans. AP* **28**, 762–769, 1980).

9.11 Evaluate the current $\mathbf{j} = \sigma\mathbf{e}$ that is induced in the conducting slab of Figure 9.13 when the induction is given by (9.80). What is the current distribution right after $\mathbf{b}_0$ is applied (i.e., at $t = 0^+$)? Could that value be expected on the basis of elementary physics?

9.12 A conducting coaxial cylinder is immersed in an AC magnetic field $H^i e^{j\omega t}\mathbf{u}_z$ (Fig. P9.6). Assume that $d \ll \delta \ll a \ll \lambda_0$. Show that good shielding can occur although δ is much larger than d. Plot the ratio of H to H^i in region 1 as a function of (δ^2/a), which turns out to be the main parameter.

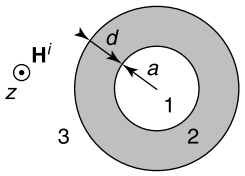

Figure P9.6

(S. Fahy et al., *Am. J. Phys.* **56**, 989–992, 1988).

9.13 Show that the expressions D_{TE} and D_{TM} in (9.121) and (9.125) are related to the reflection coefficients R_{TE} and R_{TM} of the TE or TM waves by

$$R_{\mathrm{TE}} = \frac{2u_0}{D_{\mathrm{TE}}} - 1$$

$$R_{\mathrm{TM}} = 1 - \frac{2u\tan uh}{D_{\mathrm{TM}}}.$$

The waves are assumed normally incident on the layered structure shown in Figure 9.20*b*.
(J. R. Mosig et al., *IEE Proc.* **130-H**, 175–182, 1983.)

9.14 Apply the Sommerfeld techniques to determine the fields generated by a horizontal electric dipole located between two perfectly conducting ground planes.
(J. J. Yang et al., *IEEE Trans. MTT* **40**, 595–600, 1992.)

9.15 Show that, when an x-directed horizontal electric dipole is located at a height $z' > 0$, the Hankel transforms of the Green's functions are

$$\tilde{G}^A_{xx} = \frac{\mu_0}{2\pi}\frac{1}{2u_0}\left[e^{-u_0(z-z')} + R_{\mathrm{TE}}\, e^{-u_0(z+z')}\right]$$

$$\tilde{G}^\phi = \frac{1}{2\pi\epsilon_0}\frac{1}{2u_0}\left[e^{-u_0(z-z')} + (R_{\mathrm{TE}} + R_\phi)\, e^{-u_0(z+z')}\right].$$

(Y. L. Chow et al., *IEEE Trans. MTT* **39**, 588–592, 1991).

9.16 Starting from the form of $\overline{\overline{G}}_A$ (the dyadic appropriate to the vector potential $\mathbf{A}$), determine the elements of the dyadics $\overline{\overline{G}}_{ee}$ and $\overline{\overline{G}}_{mm}$ pertinent to the $\mathbf{E}$ and $\mathbf{H}$ fields.

9.17 Show that each space-harmonic in (9.138) has the same group velocity $\left(\dfrac{d\beta_n}{d\omega}\right)^{-1}$.

9.18 Equation (9.140) describes the variation of the fields in an H mode (characterized by $E_z = 0$). Show that the corresponding equation for an E-mode is

$$\frac{d^2\phi}{dz^2} + k_0^2\epsilon_r(z)\phi - \frac{1}{\epsilon_r(z)}\frac{d\epsilon_r(z)}{dz}\frac{d\phi}{dz} = 0.$$

(T. Tamir et al., *IEEE Trans. MTT* **12**, 323–335, 1964).

9.19 A periodic grating is illuminated under an angle θ_i. The angle of diffraction of the p^{th} order is θ_p (Fig. P9.7*a*). Show that, when the grating is illuminated under θ_p (Fig. P9.7*b*), the p^{th} diffracted wave propagates in the direction θ_1 [108].

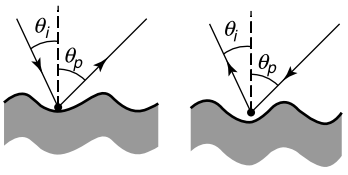

Figure P9.7

9.20 With respect to the grating shown in Figure 9.27*c*, derive the integral equation for J_S in the perpendicular polarization i.e., for an incident field $\mathbf{H}^i = H^i \mathbf{u}_y$. Show that the equation is of the form

$$\int_0^a G[x, f(x), x'] J_S(x')\, dx' + H^i(x) = \frac{1}{2} J_S(x).$$

Section 12.2 should be consulted to understand the form of the second member.

9.21 Prove relationship (9.152) by applying Green's theorem (A1.31), to the unit cell. Make use of both the periodicity of $G(\mathbf{r}|\mathbf{r}')$ and the relationship $\dfrac{\partial E}{\partial n} = j\omega\mu_0 J_S$ (Fig. 9.27*c*).

9.22 Let a periodic medium be characterized by a given $\epsilon_r(x)$. A two-dimensional wave $\phi(x, z)$ satisfies Helmholtz' equation $\nabla^2\phi + k^2(x)\phi = 0$ (see Problem 9.18). Let ϕ be expanded as in (9.138). Thus,

$$\phi(x, z) = \sum q_n(z)\, e^{-j\beta_n x}.$$

Show that the column vector $\mathbf{q}(z)$ satisfies

$$\frac{d\mathbf{q}}{dz} = -\overline{\overline{P}} \cdot \mathbf{q}$$

where $\overline{\overline{P}}$ is independent of z. Setting $\mathbf{q}(z) = \mathbf{c}e^{-j\kappa z}$, where κ is a propagation constant along z, show that κ must satisfy the characteristic equation

$$\det\left[\overline{\overline{P}} - \kappa^2 \overline{\overline{I}}\right] = 0.$$

(S. T. Peng et al., *IEEE Trans. MTT* **23**, 123–133, 1975.)

9.23 In Figure 9.23*a*, assume that the law $\epsilon_r(z)$ in (9.140) is generated by an alternance of slabs of uniform ϵ_{r1} and ϵ_{r2}. The (ABCD) matrix of the unit cell is given as a function of frequency. Thus,

$$\begin{pmatrix} V_1 \\ I_1 \end{pmatrix} = \begin{pmatrix} A & B \\ C & D \end{pmatrix} \cdot \begin{pmatrix} V_2 \\ I_2 \end{pmatrix}$$

According to Floquet, there should be relationships $V_2 = V_1 e^{-jqa}$ and $I_2 = I_1 e^{-jqa}$. Show that [8]

$$qa = \pm \cos^{-1} \frac{A + D}{2}.$$

9.24 With respect to (9.166) show that the periodic Green's function can be written as

$$G(\mathbf{r}|\mathbf{r}') = \frac{1}{2ab} \sum_{m=-\infty}^{\infty} \sum_{n=-\infty}^{\infty} \frac{1}{\gamma_{mn}} e^{-j(\alpha_m(x-x')+\beta_n(y-y'))} e^{-\gamma_{mn}|z-z'|}$$

where $\gamma_{mn}^2 = \alpha_m^2 + \beta_n^2 - k_0^2$.
(N. Marly et al., *IEEE Trans. EMC* **36**, 14–22, 1994.)

9.25 Derive a formula that explicitly gives the reciprocal lattice vectors $\mathbf{b}_i$ in terms of the lattice vectors $\mathbf{a}_k$ [78].

9.26 A perfectly conducting screen is perforated by a periodic array of circular holes of radius a = 5 mm. The pattern is square, with period 5 cm in both x and y directions. A plane wave of power density $10^5 W\ \mathrm{m}^{-2}$ is normally incident on the screen. How much power per m^2 will leak through the holes at 10 GHz? The holes might be useful in decreasing the wind pressure on the screen (a crude model for a radar antenna).

9.27 On the basis of (9.190), show that $\mathbf{C}$ satisfies the equations [22]

$$\nabla^2 \mathbf{C} + k_0^2 \mathbf{C} = -\epsilon_0 \frac{\partial}{\partial z}(\mathbf{u}_z \times \mathbf{E}^i)$$

$$\text{div}\,(\mathbf{u}_z \times \mathbf{C}) = \epsilon_0 \mathbf{u}_z \cdot \mathbf{E}^i.$$

9.28 Let a coaxial aperture carry an electric field $\mathbf{E} = \dfrac{1}{\log_e(a/b)} \dfrac{\mathbf{u}_r}{r}$ (Fig. P9.8). The aperture radiates like a circular loop of magnetic current (a magnetic frill). Evaluate the far field of this source [197].

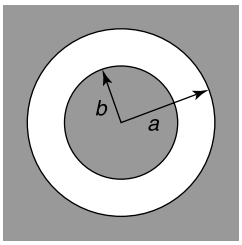

Figure P9.8

9.29 Derive (9.211) by making use of the Green's function relative to a half infinite space that satisfies a Neumann boundary condition on the screen.

9.30 Justify why the average value of $\boldsymbol{\rho}$ in (9.214) must vanish over the cross section. Remember that the low-frequency value of the induction $\mathbf{B}$ behaves like a magnetostatic field, in particular at large distances.

9.31 A small aperture radiates in medium 2 by way of both its magnetic dipole moment (9.220) and its electric dipole moment (9.223).

(a) Derive the total radiated fields $\mathbf{E}$ and $\mathbf{H}$.

(b) Write down the value of $\mathbf{P}_e$ and $\mathbf{P}_m$ for a circular aperture, assuming that the normally incident field is a plane wave with $\mathbf{E}^i$ parallel to the x-direction.

(c) Evaluate the power radiated into half-space 2.

(d) Evaluate the transmission cross section, and compare your result with the exact value (9.225).

9.32 Show that the tangential electric field in a small aperture is given by

$$\mathbf{E}_t(\mathbf{r}) = \frac{\rho_S}{\epsilon_1 + \epsilon_2}\sqrt{S_a}\ \text{grad}_t\ \tau_0(\mathbf{r})$$

where ρ_S is the charge density induced on the short circuited aperture by the presence of sources in 1 and 2.

9.33 A plane wave illuminates a perfectly conducting half-plane from a direction tangent to the conductor (Fig. P9.9). Discuss the nature of the scattered fields for both the E and H polarizations.

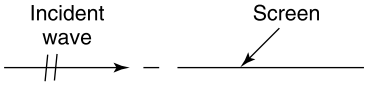

Figure P9.9

NOTES

1. I. V. Lindell, Generalized soft-and-hard surface, *IEEE Trans. AP* **50**, 926–929 (2002).
2. P. S. Kildal, Artificially soft and hard surfaces in electromagnetics, *IEEE Trans. AP* **38**, 1537–1544 (1990).
3. R. De Roo and C. T. Tai, Plane wave reflection and refraction involving a finitely conducting medium, *IEEE Antennas Prop. Mag.* **45**, 54–60 (2003).
4. J. Zenneck, Über die Fortpflanzung ebener elektromagnetischer Wellen längs einer ebenen Leiterfläche und ihre Beziehung zur drahtlosen Telegraphie, *Ann. Phys. (Leipzig)* **23**, 846–866 (1907).
5. J. R. Wait, The ancient and modern history of EM ground-wave propagation, *IEEE Antennas Prop. Mag.* **40**, 7–24 (1998).
6. A. Lakhtakia, V. V. Varadan, and V. K. Varadan, A parametric study of microwave reflection characteristics of a planar achiral-chiral interface, *IEEE Trans. EMC* **28**, 90–95 (1986).
7. S. Bassiri, C. H. Papas, and N. Engheta, Electromagnetic wave propagation through a dielectric-chiral interface and through a chiral slab, *J. Opt. Soc. Am. A* **5**, 1450–1459 (1988).
8. I. V. Lindell and A. Sihvola, Plane-wave reflection from uniaxial chiral interface and its application to polarization transformation, *IEEE Trans. AP* **43**, 1397–1404 (1995).
9. R. L. Fante and M. T. Mc Cormack, Reflection properties of the Salisbury screen, *IEEE Trans. AP* **36**, 1443–1454 (1988).
10. D. L. Jaggard, N. Engheta, and J. Liu, Chiroshield: a Salisbury-Dallenbach shield alternative, *Electron. Lett.* **28 (17)**, 1332–1334 (1990).
11. Y. Lee and R. Mittra, Investigation of an artificially synthesized electromagnetic absorber, *Microwave Opt. Tech. Lett.* **27**, 384–386 (2000).
12. Z. S. Sacks, D. M. Kingsland, R. Lee, and J. F. Lee, A perfectly matched anisotropic absorber for use as an absorbing boundary condition, *IEEE Trans. AP* **43**, 1460–1463 (1995).
13. J. P. Bérenger, A perfectly matched layer for the absorption of electromagnetic waves, *J. Comput. Phys.* **114**, 185–200 (1994).
14. J. P. Bérenger, Three-dimensional perfectly matched layer for the absorption of electromagnetic waves, *J. Comput. Phys.* **127**, 363–379 (1996).
15. S. Gedney, An anisotropic PML absorbing medium for FDTD simulation of fields in lossy and dispersive media, *Electromagn.* **16**, 399–415 (1996).
16. J. P. Bérenger, Evanescent waves in PML's. Origin of the numerical reflection in wave-structure interaction problems, *IEEE Trans. AP* **47**, 1497–1503 (1999).
17. J. P. Bérenger, Numerical reflection of evanescent waves by PMLs: origin and interpretation in the FDTD case. Expected consequences to other finite methods, *Int. J. Numer. Model*. **13**, 103–114 (2000).
18. J. P. Bérenger, Numerical reflection from FDTD-PMLs: A comparison of the split PML with the unsplit and CFS PMLs, *IEEE Trans. AP* **50**, 258–265 (2002).
19. W. C. Chew and W. H. Weedon, A 3D perfectly matched medium from modified Maxwell's equations with stretched coordinates, *Microwave Opt. Tech. Lett.* **7**, 599–604 (1994).
20. W. C. Chew, J. M. Jin and E. Michielssen, Complex coordinate stretching as a generalized absorbing boundary condition, *Micowave Opt. Tech. Lett.* **15**, 363–369 (1997).
21. F. L. Teixeira and W. C. Chew, PML-FDTD in cylindrical and spherical grids, *IEEE Microwave Guided Wave Lett.* **7**, 285–287 (1997).

22. L. Knockaert and D. De Zutter, On the stretching of Maxwell's equations in general orthogonal coordinate systems and the perfectly matched layer, *Microwave Opt. Tech. Lett.* **24**, 31–34 (2000).
23. P. R. Barnes and F. M. Tesche, On the direct calculation of a transient plane wave reflected from a finitely conducting half space, *IEEE Trans. EMC* **33**, 90–96 (1991).
24. H. Y. Pao, S. L. Dvorak, and D. G. Dudley, An accurate and efficient analysis for transient plane waves obliquely incident on a conductive half space (TE case), *IEEE Trans. AP* **44**, 918–924 (1996).
25. H. Y. Pao, S. L. Dvorak, and D. G. Dudley, An accurate and efficient analysis for transient plane waves obliquely incident on a conductive half space (TM case), *IEEE Trans. AP* **44**, 925–932 (1996).
26. F. M. Tesche, On the modeling and representation of a lossy earth for transient electromagnetic field calculations, *Theoretical note 367*, AFRL, Kirtland AFB, July 2002.
27. R. B. Schulz, V. C. Plantz, and D. R. Bush, Shielding theory and practice, *IEEE Trans. EMC* **30**, 187–201 (1988).
28. R. Luebbers, K. Kumagai, S. Adachi and T. Uno, FDTD calculation of transient pulse propagation through a nonlinear magnetic sheet, *IEEE Trans. EMC* **35**, 90–94 (1993).
29. S. Celozzi and M. D'Amore, Magnetic field attenuation of nonlinear shields, *IEEE Trans. EMC* **38**, 318–326 (1996).
30. C. De Wagter, Computer simulation for local temperature control during microwave-induced hyperthermia, *J. Microwave Power* **20**, 31–42 (1985).
31. D. S. Weile, E. Michielssen, and D.E. Goldberg, Genetic algorithm design of Pareto optimal broadband microwave absorbers, *IEEE Trans. EMC* **38**, 518–524 (1996).
32. C. E. Baum, The boundary-connection supermatrix for uniform isotropic walls, *Interaction note 562*, October 22, 2000.
33. S. Fahy, C. Kittel, and S.G. Louie, Electromagnetic screening by metals, *Am. J. Phys.* **54**, 989–992 (1988).
34. R. E. Collin, Hertzian dipole radiating over a lossy earth or sea: some early and late 20^{th} century controversies, *IEEE Antennas Prop. Mag.* **46**, 64–79 (2004).
35. H. Weyl, Ausbreitung elektromagnetischer Wellen über einem ebenen Leiter, *Ann. Phys.* **60**, 481–500 (1919).
36. K. A. Norton, The propagation of radio waves over the surface of the earth and in the upper atmosphere, Part I: Ground-wave propagation from short antennas, *Proc. IRE* **24**, 1367–1387 (1936).
37. K. A. Norton, The propagation of radio waves over the surface of the earth and in the upper atmosphere, Part II: The propagation from vertical, horizontal and loop antennas over a plane earth of finite conductivity, *Proc. IRE* **25**, 1203–1236 (1937).
38. B. van der Pol, On discontinuous electromagnetic waves and the occurrence of a surface wave, *IRE Trans. AP* **4**, 288–293 (1956).
39. I. V. Lindell and E. Alanen, Exact image theory for the Sommerfeld half-space problem. Part I: vertical magnetic dipole. Part II: vertical electric dipole. Part III: general formulation, *IEEE Trans. AP* **32**, 126–137, 811–847, 1027–1032 (1984).
40. I. V. Lindell, E. Alanen, and H. von Bagh, Exact image theory for the calculation of fields transmitted through a planar interface of two media, *IEEE Trans. AP* **34**, 129–137 (1986).
41. J. R. Wait, Complex image theory-revisited, *IEEE Antennas Prop. Mag.* **33**, 27–29, 1991.
42. K. I. Nikoskinen and I. V. Lindell, Time-domain analysis of the Sommerfeld VMD problem based on the exact image theory, *IEEE Trans. AP* **38**, 241–250 (1990).
43. T. Itoh, Analysis of microstrip resonators, *IEEE Trans. MTT* **22**, 946–952 (1974).
44. T. Itoh and W. Menzel, A full-wave analysis method for open microstrip structures, *IEEE Trans. MTT* **29**, 63–68 (1981).
45. K. A. Michalski and D. Zheng, Analysis of microstrip resonators of arbitrary shape, *IEEE Trans. MTT* **40**, 112–119 (1992).
46. J. R. Mosig and F.E. Gardiol, Analytical and numerical techniques in the Green's function treatment of microstrip antennas and scatterers, *IEE Proc.* **130H**, 175–182 (1983).
47. K. A. Michalski, The mixed-potential electric field integral equation for objects in layered media, *A.E.Ü.* **39**, 317–322 (1985).
48. K. A. Michalski and J. R. Mosig, Multilayered media Green's functions in integral equation formulations, *IEEE Trans. AP* **45**, 508–519 (1997).
49. J. R. Mosig, Arbitrarily shaped microstrip structures and their analysis with a mixed potential integral equation, *IEEE Trans. MTT* **36**, 314–1301 (1988).
50. Y. L. Chow, J. J. Yang, D. G. Fang, and G. E. Howard, A closed-form spatial Green's function for the thick microstrip substrate, *IEEE Trans. MTT* **39**, 588–592 (1991).
51. F. Ling and J.M. Jin, Scattering and radiation analysis of microstrip antennas using discrete complex image method and reciprocity theorem, *Microwave Opt. Tech. Lett.* **16**, 212–216 (1997).
52. M. J. Tsai, C. Chen, and N.G. Alexopoulos, Sommerfeld integrals in modeling interconnects and microstrip elements in multi-layered media, *Electromagn.* **18**, 267–288 (1998).
53. K. A. Michalski, Extrapolation methods for Sommerfeld integral tails, *IEEE Trans. AP* **46**, 1405–1418 (1998).
54. D. G. Fang, J.J. Yang, and G.Y. Delisle, Discrete image theory for horizontal electric dipoles in a multilayered medium, *IEE Proc.* **135-H**, 297–303 (1988).
55. R. A. Kipp and C. H. Chan, Complex image method for sources in bounded regions of multilayer structures, *IEEE Trans. MTT* **42**, 860–865 (1994).
56. M. I. Aksun, A robust approach for the derivation of closed-form Green's functions, *IEEE Trans. MTT* **44**, 651–658 (1996).
57. M. I. Aksun and R. Mittra, Choices of expansion and testing functions for the method of moments applied to

a class of electromagnetic problems, *IEEE Trans. MTT* **41**, 503–508 (1993).
58. M. I. Aksun, F. Caliskan, and L. Gürel, An efficient method for electromagnetic characterization of 2-D geometries in stratified media, *IEEE Trans. MTT* **50**, 1264–1274 (2002).
59. D. C. Chang and J.X. Zheng, Electromagnetic modeling of passive circuit elements in MMIC, *IEEE Trans. MTT* **40**, 1741–1747 (1992).
60. K. A. Michalski and J. R. Mosig, Discrete complex image mixed-potential integral equation analysis of microstrip patch antennas with vertical probe feeds, *Electromagn.* **15**, 377–392 (1995).
61. M. Farina and T. Rozzi, A 3-D integral equation-based approach to the analysis of real-life MMICs - Application to microelectromechanical systems, *IEEE Trans. MTT* **49**, 2235–2240 (2001).
62. J. Sercu, N. Faché, F. Libbrecht, and P. Lagasse, Mixed potential integral equation technique for hybrid microstrip-slotline multilayered circuits using a mixed rectangular - triangular mesh, *IEEE Trans. MTT* **43**, 1162–1172 (1995).
63. K. Michalski and D. Zheng, Electromagnetic scattering and radiation by surfaces of arbitrary shape in layered media. Part I: theory, *IEEE Trans. AP* **38**, 335–344 (1990).
64. G. Dural and M.I. Aksun, Closed form Green's functions for general sources and stratified media, *IEEE Trans. MTT* **43**, 1545–1552 (1995).
65. C. Elachi, Waves in active and passive periodic structures, *Proc. IEEE* **64**, 1666–1698 (1976).
66. T. K. Gaylord and M. G. Moharam, Analysis and applications of optical diffraction by gratings, *Proc. IEEE* **73**, 894–937 (1985).
67. C. Yeh, K. F. Casey, and Z. A. Kaprielian, Transverse magnetic wave propagation in sinusoidally stratified dielectric media, *IEEE Trans. MTT* **13**, 297–302 (1965).
68. T. Tamir, H. C. Wang, and A. A. Oliner, Wave propagation in sinusoidally stratified dielectric media, *IEEE Trans. MTT* **12**, 323–335 (1964).
69. C. Caloz, A. K. Skrivervik, and F. E. Gardiol, An efficient method to determine Green's functions of a two-dimensional photonic crystal excited by a line source - the phased array method, *IEEE Trans. MTT* **50**, 1380–1391 (2002).
70. R. Petit and M. Cadilhac, On the roles of physical intuition, computation, and mathematical analysis in electromagnetic diffraction theory, *Radio Sci.* **22**, 1247–1259 (1987).
71. S. Gedney, J. F. Lee, and R. Mittra, A combined FEM/MOM approach to analyze the plane wave diffraction by arbitrary gratings, *IEEE Trans. MTT* **40**, 363–370 (1992).
72. A. F. Peterson, An outward-looking differential equation formulation for scattering from one-dimensional periodic diffraction gratings, *Electromagn.* **14**, 227–238 (1994).
73. R. F. Millar, The Rayleigh hypothesis and a related least-squares solution to scattering problems for periodic surfaces and other scatterers, *Radio Sci.* **8**, 785–796 (1973).
74. S. Christiansen and R. E. Kleinman, On a misconception involving point collocation and the Rayleigh hypothesis, *IEEE Trans. AP* **44**, 1309–1316 (1996).
75. P. M. van den Berg and J. T. Fokkema, The Rayleigh hypothesis in the theory of reflection by a grating, *J. Opt. Soc. Am.* **69**, 27–31 (1979).
76. J. Moore, H. Ling, and C. S. Liang, The scattering and absorption characteristics of material-coated periodic gratings under oblique incidence, *IEEE Trans. AP* **41**, 1281–1288 (1993).
77. W. P. Pinello, R. Lee, and A. C. Cangellaris, Finite element modeling of electromagnetic wave interactions with periodic dielectric structures, *IEEE Trans. MTT* **42**, 2294–2301 (1994).
78. T. A. Cwik and R. Mittra, Scattering from a periodic array of free-standing arbitrarily shaped perfectly conducting or resistive patches, *IEEE Trans. AP* **35**, 1226–1234 (1987).
79. R. Mittra, C. H. Chan, and T. Cwik, Techniques for analyzing frequency selective surfaces—A review, *Proc. IEEE* **76**, 1593–1615 (1988).
80. D. Sievenpiper, L. Zhang, R. F. Jimenez Broas, N. G. Alexopoulos, and E. Jablonovitch, High-impedance electromagnetic surfaces with a forbidden frequency band, *IEEE Trans. MTT* **47**, 2059–2074 (1999).
81. R. F. Jimenez Broas, D. F. Sievenpiper, and E. Jablonovitch, A high-impedance ground plane applied to a cellphone handset geometry, *IEEE Trans. MTT* **49**, 1262–1265 (2001).
82. D. Sievenpiper and J. Schaffner, Beam steering reflector based on electrically tunable impedance surface, *Electron. Lett.* **38**, 1237–1238 (2002).
83. C. C. Chen, Transmission through a conducting screen perforated periodically with apertures, *IEEE Trans. MTT* **18**, 627–632 (1970).
84. C. C. Chen, Diffraction of electromagnetic waves by a conducting screen perforated periodically with circular holes, *IEEE Trans. MTT* **19**, 475–479 (1971).
85. V. Radisic, Y. Qian, R. Coccioli, and T. Itoh, Novel 2-D photonic bandgap structure for microstrip lines, *IEEE Microwave Guided Wave Lett.* **8**, 69–71 (1998).
86. Y. Zhang, M. Youmis, C. Fischer, J. van Hagen, and W. Wiesbeck, Artificial magnetic conductors as reflectors for low sidelobe antenna arrays, *Microwave Opt. Tech. Lett.* **36**, 267–270 (2003).
87. M. Bozzi and L. Perregrini, Efficient analysis of thin conductive screens perforated periodically with arbitrarily shaped apertures, *Electron. Lett.* **35**, 1085–1087 (1999).
88. J. D. Joannopoulos, P. R. Villeneuve, and S. Fan, Photonic crystals: putting a new twist on light, *Nature* **386**, 143–149 (1997).
89. S. Singh, W.F. Richards, J.R. Zinecker, and D.R. Wilton, Accelerating the convergence of series representing the

free space periodic Green's function, *IEEE Trans. AP* **38**, 1958–1962 (1990).
90. Özlem Aydin Civi, P. H. Pathak, and H. T. Chou, On the Poisson formula for the analysis of wave radiation and scattering from large finite arrays, *IEEE Trans. AP* **47**, 958–959 (1999).
91. R. Lampe, P. Klock, and P. Mayes, Integral transforms useful for the accelerated summation of periodic, free-space Green's functions, *IEEE Trans. MTT* **33**, 734–736 (1985).
92. N. Kinayman and M. I. Aksun, Comparative study of acceleration techniques for integrals and series in electromagnetic problems, *Radio Sci.* **30**, 1713–1722 (1995).
93. B. Baekelandt, D. De Zutter, and F. Olyslager, Arbitrary order asymptotic approximation of a Green's function series, *A.E.Ü.* **51**, 224–230 (1997).
94. D. Shanks, Non-linear transformations of divergent and slowly convergent sequences, *J. Math. Phys.* **34**, 1–42 (1955).
95. S. Singh and R. Singh, Application of transforms to accelerate the summation of periodic free-space Green's functions, *IEEE Trans. MTT* **38**, 1746–1748 (1990).
96. P. P. Ewald, Die Berechnung optischer und elektrostatischer Gitterpotentiale, *Ann. der Physik* **64**, 253–287 (1921).
97. K. E. Jordan, G. R. Richter, and P. Sheng, An efficient numerical evalution of the Green's function for the Helmholtz operator on periodic structures, *J. Comp. Phys.* **63**, 222–235 (1986).
98. T. F. Eibert, J. L. Volakis, D. R. Wilton, and D. R. Jackson, Hybrid FE/BI modeling of 3-D doubly periodic structures utilizing triangular prismatic elements and an MPIE formulation accelerated by the Ewald transformation, *IEEE Trans. AP* **47**, 843–850 (1999).
99. A. Kustepeli an A. Q. Martin, On the splitting parameter in the Ewald method, *Microwave Guided Wave Lett.* **10**, 168–170 (2000).
100. C. J. Bouwkamp, Diffraction Theory, Research Report EM-50, New York University, 1953.
101. C. M. Butler and K.R. Umashankar, Electromagnetic excitation of a wire through an aperture-perforated conducting screen, *IEEE Trans. AP* **24**, 456–462 (1976).
102. G. Manara, M. Bandinelli, and A. Monorchio, Electromagnetic penetration and coupling to wires through apertures of arbitrary shape, *IEEE Trans. EMC* **40**, 391–396 (1998).
103. R. Lee and D. G. Dudley, Electromagnetic coupling by a wire through a circular aperture in an infinite planar screen, *J. Electromagn. Waves Appl.* **3**, 281–305 (1989).
104. R. Lee and D. G. Dudley, Transient current propagation along a wire penetrating a circular aperture in an infinite planar conducting screen, *IEEE Trans. EMC* **32**, 137–143 (1990).
105. E. K. Reed and C. M. Butler, Time-domain electromagnetic penetration through arbitrarily shaped narrow slots in conducting screens, *IEEE Trans. EMC* **34**, 161–172 (1992).
106. J. Meixner and W. Andrejewski, Strenge Theorie der Beugung ebener elektromagnetischer Wellen an der volkommen leitenden Kreisscheibe und an der kreisformigen Öffnung in volkommen leitenden ebenen Schirm, *Ann. Phys.* **7**, 157–168 (1950).
107. W. Andrejewski, Die Beugung elektromagnetischer Wellen an der leitenden Kreisscheibe und an der kreisformigen Öffnung in leitenden ebenen Schirm, *Z. Angew. Phys.* **5**, 178–186 (1953).
108. K. Hongo and H. Serizawa, Diffraction of electromagnetic plane wave by a rectangular plate and a rectangular hole in the conducting plate, *IEEE Trans. AP* **47**, 1029–1041 (1999).
109. C. M. Butler, Y. Rahmat-Samii, and R. Mittra, Electromagnetic penetration through apertures in conducting surfaces, *IEEE Trans. AP* **26**, 82–93 (1978).
110. R. De Smedt and J. Van Bladel, Field singularities near aperture corners, *IEE Proc.* **134-A**, 694–698 (1987).
111. R. F. Harrington and J.R. Mautz, Electromagnetic transmission through an aperture in a conducting plane, *A.E.Ü.* **31**, 81–87 (1977).
112. R. F. Harrington and J. R. Mautz, Characteristic modes for aperture problems, *IEEE Trans. MTT* **33**, 500–505 (1985).
113. T. Wang, J.R. Mautz, and R.F. Harrington, Characteristic modes and dipole representations of small apertures, *Radio Sci.* **22**, 1289–1297 (1987).
114. I. C. Jan, R. F. Harrington, and J. R. Mautz, Aperture admittance of a rectangular aperture and its use, *IEEE Trans. AP* **39**, 423–425 (1991).
115. C. J. Bouwkamp, Theoretical and numerical treatment of diffraction through a circular aperture, *IEEE Trans. AP* **18**, 152–176 (1970).
116. S. R. Seshadri and T. T. Wu, High-frequency diffraction of electromagnetic waves by a circular aperture in an infinite plane conducting screen, *IRE Trans. AP* **8**, 27–36 (1960).
117. H. Levine and J. Schwinger, On the theory of electromagnetic wave diffraction by an aperture in an infinite plane conducting screen, *Comm. Pure. Appl. Math.* **3**, 355–391 (1950).
118. C. Huang, R. D. Kodis, and H. Levine, Diffraction by apertures, *J. Appl. Phys.* **26**, 151–165 (1955).
119. J. B. Keller, Diffraction by an aperture I, *J. Appl. Phys.* **28**, 426 (1957).
120. J. B. Keller, R. M. Lewis, and B. D. Seckler, Diffraction by an aperture II, *J. Appl. Phys.* **28**, 570 (1957).
121. J. Van Bladel, Field penetration through small apertures: the first-order correction, *Radio Sci.* **14**, 319–331 (1979).
122. J. Van Bladel, Low frequency scattering through an aperture in a rigid screen, *J. Sound Vib.* **6**, 386–395 (1967).
123. J. Van Bladel, Low frequency scattering through an aperture in a soft screen, *J. Sound Vib.* **8**, 186–195 (1968).

124. F. De Meulenaere and J. Van Bladel, Polarizability of some small apertures, *IEEE Trans. AP* **25**, 198–205 (1977).
125. R. De Smedt and J. Van Bladel, Magnetic polarizability of some small apertures, *IEEE Trans. AP* **28**, 703–707 (1980).
126. N. A. McDonald, Polynomial approximations for the electric polarizabilities of some small apertures, *IEEE Trans. MTT* **33**, 1146–1149 (1985).
127. N. A. McDonald, Polynomial approximations for the transverse magnetic polarizabilities of some small apertures, *IEEE Trans. MTT* **35**, 20–23 (1987).
128. N. A. McDonald, Simple approximations for the longitudinal magnetic polarizabilities of some small apertures, *IEEE Trans. MTT* **36**, 1141–1144 (1988).
129. T. B. A. Senior, Half plane edge diffraction, *Radio Sci.* **10**, 645–650 (1975).
130. T. B. A. Senior, Diffraction by a resistive half plane, *Electromagn.* **11**, 183–192 (1991).
131. P. Ya. Ufimtsev, B. Khayatian and Y. Rahmat-Samii, Singular edge behaviour: to impose or not impose - that is the question, *Microwave Opt. Tech. Lett.* **24**, 218–223 (2000).
132. M. Farina and T. Rozzi, Numerical investigation of the field and current behavior near lossy edges, *IEEE Trans. MTT* **49**, 1355–1358 (2001).
133. F. Olyslager, Overview of the singular behavior of electromagnetic fields at edges and tips in bi-isotropic and special bianisotropic media, *Radio Sci.* **30**, 1349–1354 (1995).

Chapter 10

Resonators

A simple example of a resonator is the lossless transmission line, short circuited at its end points $x = 0$ and $x = l$. A resonant mode is a field pattern (in casu a voltage) that can exist in the absence of sources. For a line of length l that voltage is $v_n = \sin n\pi \dfrac{x}{l}$, with $n = 1, 2, \ldots$. The associated frequency of oscillation is $f_n = \dfrac{\omega_n}{2\pi} = \dfrac{n}{2l}(LC)^{-\frac{1}{2}}$ (see Section 1.8). The time-harmonic function $v_n e^{j\omega_n t}$ is actually a standing pattern, which can be written as

$$V_n = \sin n\pi \frac{x}{l} = -\frac{1}{2j} e^{-jn\pi \frac{x}{l}} + \frac{1}{2j} e^{jn\pi \frac{x}{l}}.$$

The standing pattern is seen to result from the interference between waves propagating respectively to the right and the left. Resonances occur when a wave propagating from $x = 0$ to $x = l$ is reflected at $x = l$, returns to $x = 0$ and, upon reflection there, retrieves its original phase; the cycle can now be perpetuated.

These elementary considerations remain valid for the more complicated three-dimensional situation. The waves are now reflected at the conducting walls of the resonator, and the resonant modes are again in the form of a — now more complex — standing wave pattern. The mathematics lose their one-dimensional transparency, but nevertheless easily reveal the existence of resonances when the fields are excited by current sources. In the absence of sources, the self-oscillations are damped by losses, which in a cavity occur in the imperfectly conducting walls, in the enclosed materials, or by way of the power that escapes through apertures in the wall. The radiative losses become crucially important when the resonator is open, which is the case for the dielectric resonator, a component to which much attention is devoted in Section 10.5.

10.1 EIGENVECTORS FOR AN ENCLOSED VOLUME

Let volume V in Figure 10.1 be bounded by perfectly conducting walls, and let it contain an inhomogeneous linear medium of dyadic characteristics $\overline{\overline{\epsilon}}(\mathbf{r}), \overline{\overline{\mu}}(\mathbf{r})$. Maxwell's equations

Electromagnetic Fields, Second Edition, By Jean G. Van Bladel

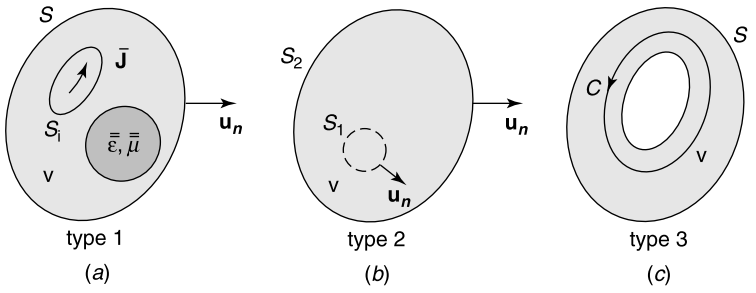

Figure 10.1 Three typical volumes: (*a*) singly bounded and simply connected, (*b*) doubly bounded, (*c*) doubly connected (ringlike).

in the cavity are now of the general form

$$\begin{aligned} \text{curl } \mathbf{E} &= -j\omega\, \overline{\overline{\mu}}(\mathbf{r})\cdot\mathbf{H} - \mathbf{J}_m \\ \text{curl } \mathbf{H} &= j\omega\, \overline{\overline{\epsilon}}(\mathbf{r})\cdot\mathbf{E} + \mathbf{J}. \end{aligned} \tag{10.1}$$

The eigenfields $(\mathbf{e}_m, \mathbf{h}_m)$ are patterns that can exist without sources. From (10.1), they satisfy

$$-\text{curl}\left[(\overline{\overline{\mu}}_r)^{-1}\cdot\text{curl }\mathbf{e}_m\right] + k_m^2\overline{\overline{\epsilon}}_r\cdot\mathbf{e}_m = 0 \tag{10.2}$$

$$-\text{curl}\left[(\overline{\overline{\epsilon}}_r)^{-1}\cdot\text{curl }\mathbf{h}_m\right] + k_m^2\overline{\overline{\mu}}_r\cdot\mathbf{h}_m = 0, \tag{10.3}$$

where m stands for a triple index. The inhomogeneity may be due to a load, for example in an industrial or domestic heating process, or it may possibly consist of a ferroelectric volume of variable ϵ_r, used to tune the cavity of an accelerator to the programmed rotation frequency of the particles. We shall restrict our analysis to isotropic media of parameters $\epsilon = \epsilon' - j\epsilon''$ and $\mu = \mu' - j\mu''$, where ϵ'' and μ'' are positive or zero, depending on whether the media are lossy or lossless. It is a simple matter to show that the solution of (10.1) is unique for lossy media. Uniqueness depends on the nonexistence of a solution to the homogeneous problem

$$\begin{aligned} \text{curl } \mathbf{E}_0 &= -j\omega\mu\, \mathbf{H}_0 \\ \text{curl } \mathbf{H}_0 &= j\omega\epsilon\, \mathbf{E}_0. \end{aligned}$$

Applying the divergence theorem A1.27 to $\mathbf{E}_0 \times \mathbf{H}_0^*$ yields

$$\begin{aligned} \int_S \mathbf{u}_n\cdot(\mathbf{E}_0\times\mathbf{H}_0^*)\,dS = &-\int_V \left[\omega\epsilon''|\mathbf{E}_0|^2 + \omega\mu''|\mathbf{H}_0|^2\right]dV \\ &+ j\omega\int_V \left[\epsilon'|\mathbf{E}_0|^2 - \mu'|\mathbf{H}_0|^2\right]dV. \end{aligned} \tag{10.4}$$

The surface integral vanishes because the walls are perfectly conducting, in which case $\mathbf{E}_0$ is perpendicular to S. Both the real and imaginary parts of the right-hand term must vanish separately, which is only possible if $\mathbf{E}_0 = 0$ and $\mathbf{H}_0 = 0$. This concludes the proof. The proof also holds when the *walls* are lossy (Problem 10.2). If the material is lossless

(i.e., when $\epsilon'' = \mu'' = 0$), (10.4) allows a nonzero solution provided the integral over V of $(\epsilon\,\mathbf{E}_0^2 - \mu\,\mathbf{H}_0^2)$ vanishes. It is shown later in this section that this test is satisfied by the resonant fields $\mathbf{e}_m$ and $\mathbf{h}_m$ of the cavity. To define these eigenvectors, we shall first assume that the media are homogeneous, scalar, and lossless,* with a uniform ϵ and μ. The restriction to lossless media turns out to be adequate, even if the resonator contains lossy media (as shown in Section 10.2).

10.1.1 Electric Eigenvectors

They are the eigenvectors of the *electric transformation*†

$$\begin{aligned} \mathcal{L}_e\mathbf{f} &= \nabla^2\mathbf{f} \\ \operatorname{div}\mathbf{f} &= 0 \qquad (\text{on } S) \\ \mathbf{u}_n \times \mathbf{f} &= 0 \qquad (\text{on } S). \end{aligned} \tag{10.5}$$

The eigenvectors are defined by the relationship $\mathcal{L}_e\mathbf{f} = \lambda\mathbf{f}$. They belong to two classes:

1. Irrotational eigenvectors $\mathbf{f}_m = \operatorname{grad}\phi_m$, where ϕ_m satisfies

$$\begin{aligned} \nabla^2\phi_m + \mu_m^2\phi_m &= 0 \qquad (\text{in } V) \\ \phi_m &= 0 \qquad (\text{on } S). \end{aligned} \tag{10.6}$$

In a doubly-bounded region (Fig. 10.1*b*), one of the eigenvectors has the eigenvalue zero. Its mother-function ϕ_0 satisfies

$$\begin{aligned} \nabla^2\phi_0 &= 0 \qquad (\text{in } V) \\ \phi_0 &= c_1 \qquad (\text{on } S_1) \\ \phi_0 &= c_2 \qquad (\text{on } S_2). \end{aligned} \tag{10.7}$$

The eigenvector $\mathbf{f}_0 = \operatorname{grad}\phi_0$ (discussed in Appendix 1 in relation to Helmholtz' theorem) is proportional to the electrostatic field that exists between the metallized surfaces S_1 and S_2 when they are raised to different potentials, c_1 and c_2.

2. Solenoidal eigenvectors satisfying

$$\begin{aligned} -\operatorname{curl}\operatorname{curl}\mathbf{e}_m + \tau_m^2\mathbf{e}_m &= 0 \qquad (\text{in } V) \\ \mathbf{u}_n \times \mathbf{e}_m &= 0 \qquad (\text{on } S). \end{aligned} \tag{10.8}$$

It is a simple matter to show that the eigenvectors are orthogonal with respect to the scalar product

$$\langle \mathbf{u}, \mathbf{v} \rangle = \int_V \mathbf{u}\cdot\mathbf{v}\, dV. \tag{10.9}$$

*For an extension to anisotropic media, see, for example, Note 1.

†In a first analysis[2] Weyl had chosen the boundary condition $\mathbf{u}_n \cdot \dfrac{\partial \mathbf{f}}{\partial n} = 0$ instead of div $\mathbf{f} = 0$, but Levi-Civita convinced him to switch to the new form.[3]

If several eigenvectors correspond with the same eigenvalue, they can be orthogonalized by the Schmidt process described in Section 1.3.

10.1.2 Magnetic Eigenvectors

They are the eigenvectors of the *magnetic transformation*

$$\begin{aligned} \mathcal{L}_h \mathbf{f} &= \nabla^2 \mathbf{f} \\ \mathbf{u}_n \cdot \mathbf{f} &= 0 \qquad (\text{on } S) \\ \mathbf{u}_n \times \operatorname{curl} \mathbf{f} &= 0 \qquad (\text{on } S). \end{aligned} \tag{10.10}$$

We again distinguish two classes of eigenvectors:

1. Irrotational eigenvectors $\mathbf{g}_m = \operatorname{grad} \psi_m$, where ψ_m satisfies

$$\begin{aligned} \nabla^2 \psi_m + \nu_m^2 \psi &= 0 \qquad (\text{in } V) \\ \mathbf{u}_n \cdot \operatorname{grad} \psi_m &= 0 \qquad (\text{on } S). \end{aligned} \tag{10.11}$$

In a doubly connected region, as in Figure 10.1*c*, one of the eigenvectors has the eigenvalue zero, and is defined by[‡]

$$\begin{aligned} \operatorname{div} \mathbf{g}_0 &= 0 \qquad (\text{in } V) \\ \operatorname{curl} \mathbf{g}_0 &= 0 \\ \mathbf{u}_n \cdot \mathbf{g}_0 &= 0 \qquad (\text{on } S). \end{aligned} \tag{10.12}$$

This eigenvector is the important harmonic vector $\mathbf{h}_0$ defined in Section 4.10.

2. Solenoidal eigenvectors satisfying[§]

$$\begin{aligned} -\operatorname{curl} \operatorname{curl} \mathbf{h}_m + \lambda_m^2 \mathbf{h}_m &= 0 \qquad (\text{in } V) \\ \mathbf{u}_n \times \operatorname{curl} \mathbf{h}_m &= 0 \qquad (\text{on } S). \end{aligned} \tag{10.13}$$

These various eigenvectors are orthogonal with respect to scalar product (10.9).

A few simple steps show that curl $\mathbf{h}_m$ is a possible electric eigenvector, and curl $\mathbf{e}_m$ a possible magnetic eigenvector. In addition, $\lambda_m^2 = \tau_m^2$, and we may write

$$\lambda_m^2 = \tau_m^2 = k_m^2.$$

The proportionality factors in $\mathbf{e}_m$ and $\mathbf{h}_m$ can be so chosen that

$$\begin{aligned} \mathbf{e}_m &= \frac{1}{k_m} \operatorname{curl} \mathbf{h}_m \\ \mathbf{h}_m &= \frac{1}{k_m} \operatorname{curl} \mathbf{e}_m. \end{aligned} \tag{10.14}$$

[‡]In an N-connected region, there would be $(N-1)$ such eigenvectors.

[§]In a first paper,[2] Weyl had chosen the boundary condition $\mathbf{u}_n \times \dfrac{\partial \mathbf{f}}{\partial n} = 0$ instead of $\mathbf{u}_n \times \operatorname{curl} \mathbf{f} = 0$.

For such a choice, the fields can be normalized to unity according to the condition

$$\int_V \mathbf{e}_m \cdot \mathbf{e}_k \, dV = \int_V \mathbf{h}_m \cdot \mathbf{h}_k \, dV = \delta_{mk}. \tag{10.15}$$

The corresponding orthonormalization conditions for the irrotational eigenvectors are

$$\int_V \mathbf{f}_m \cdot \mathbf{f}_k \, dV = \int_V \text{grad } \phi_m \cdot \text{grad } \phi_k \, dV \; = \; \delta_{mk} \tag{10.16}$$

$$\int_V \mathbf{g}_m \cdot \mathbf{g}_k \, dV = \int_V \text{grad } \psi_m \cdot \text{grad } \psi_k \, dV \; = \; \delta_{mk}. \tag{10.17}$$

The scalar eigenfunctions satisfy

$$\int_V \phi_m \phi_k \, dV = \frac{1}{\mu_m^2} \, \delta_{mk} \quad \text{or} \quad \int_V \psi_m \psi_k \, dV = \frac{1}{\nu_m^2} \, \delta_{mk}. \tag{10.18}$$

10.1.3 Inhomogeneous Media

In the next section, it is shown that the solenoidal eigenvectors are the source of the resonance properties of the cavity. It is therefore appropriate to show which equations they satisfy in an inhomogeneous medium of $\epsilon(\mathbf{r})$, $\mu(\mathbf{r})$ characteristics. From (10.2) and (10.3), these equations are

$$\begin{aligned} -\text{curl} \left(\frac{1}{\mu_r} \text{ curl } \mathbf{e}_m \right) + k_m^2 \epsilon_r \mathbf{e}_m = 0 \qquad & (\text{in } V) \\ \mathbf{u}_n \times \mathbf{e}_n = 0 \qquad & (\text{on } S) \end{aligned} \tag{10.19}$$

and

$$\begin{aligned} -\text{curl} \left(\frac{1}{\epsilon_r} \text{curl } \mathbf{h}_m \right) + k_m^2 \mu_r \mathbf{h}_m = 0 \qquad & (\text{in } V) \\ \mathbf{u}_n \times \text{curl } \mathbf{h}_m = 0 \qquad & (\text{on } S). \end{aligned} \tag{10.20}$$

The electric-magnetic connection is now

$$\begin{aligned} \mathbf{e}_m &= \frac{1}{k_m \epsilon_r} \text{ curl } \mathbf{h}_m \\ \mathbf{h}_m &= \frac{1}{k_m \mu_r} \text{ curl } \mathbf{e}_m. \end{aligned} \tag{10.21}$$

A simple manipulation, based on (A1.32) and (A1.33), shows that the normalization relationships become

$$\int_V \epsilon_r \, \mathbf{e}_m \cdot \mathbf{e}_k \, dV = \int_V \mu_r \, \mathbf{h}_m \cdot \mathbf{h}_k \, dV = \delta_{mk}. \tag{10.22}$$

The irrotational eigenvectors are again $\mathbf{f}_m = \text{grad}\ \phi_m$ and $\mathbf{g}_m = \text{grad}\ \psi_m$, where

$$\begin{aligned} \text{div}\ (\epsilon_r\ \text{grad}\ \phi_m) + \mu_m^2 \phi_m &= 0 \qquad (\text{in } V) \\ \phi_m &= 0 \qquad (\text{on } S) \end{aligned} \tag{10.23}$$

and

$$\begin{aligned} \text{div}\ (\mu_r\ \text{grad}\ \psi_m) + \nu_m^2 \psi_m &= 0 \qquad (\text{in } V) \\ \mathbf{u}_n \cdot \text{grad}\ \psi_m &= 0 \qquad (\text{on } S). \end{aligned} \tag{10.24}$$

The orthonormalization integrals are readily shown to be

$$\int_V \epsilon_r\, \mathbf{f}_m \cdot \mathbf{f}_k\, dV = \delta_{mk} = \int_V \mu_r\, \mathbf{g}_m \cdot \mathbf{g}_k\, dV. \tag{10.25}$$

10.2 EXCITATION OF A CAVITY

To simplify matters, let the cavity be filled with a *homogeneous* medium (ϵ, μ, σ), an important particular case.[¶] We shall also assume that the volume is of type 1, but the extension to types 2 and 3 follows easily by adding terms in $\mathbf{f}_0$ and $\mathbf{g}_0$ to the field expansions[4,5] (Fig. 10.1). The expansions are in terms of electric eigenvectors for $\mathbf{e}$ and $\mathbf{j}$, and magnetic eigenvectors for $\mathbf{h}$ and $\mathbf{j}_m$. Thus,

$$\begin{aligned} \mathbf{e}(\mathbf{r}, t) &= \sum_m e_m(t)\, \mathbf{f}_m(\mathbf{r}) + \sum_m d_m(t)\, \mathbf{e}_m(\mathbf{r}) \\ \mathbf{h}(\mathbf{r}, t) &= \sum_m l_m(t)\, \mathbf{g}_m(\mathbf{r}) + \sum_m u_m(t)\, \mathbf{h}_m(\mathbf{r}) \\ \mathbf{j}(\mathbf{r}, t) &= \sum_m p_m(t)\, \mathbf{f}_m(\mathbf{r}) + \sum_m q_m(t)\, \mathbf{e}_m(\mathbf{r}) \\ \mathbf{j}_m(\mathbf{r}, t) &= \sum_m r_m(t)\, \mathbf{g}_m(\mathbf{r}) + \sum_m s_m(t)\, \mathbf{h}_m(\mathbf{r}). \end{aligned} \tag{10.26}$$

The sources $\mathbf{j}$ and $\mathbf{j}_m$ are *impressed* currents. There are also conduction currents, but these are automatically taken into account by terms in $\sigma_{\mathbf{e}}$ in Maxwell's equations. Expansion (10.26) must now be inserted in (7.1) and (7.2). It should be remarked, in that respect, that the curl of an infinite sum is only equal to the sum of the curls when $\mathbf{e}$ and $\mathbf{h}$ satisfy the same boundary conditions as the corresponding eigenvectors. Otherwise the *derivative of a sum* technique must be invoked, which in the current case entails separate expansions for curl $\mathbf{e}$ and curl $\mathbf{h}$. We write

$$\begin{aligned} \text{curl}\ \mathbf{e} &= \sum_m \alpha_m \mathbf{g}_m + \sum_m \beta_m \mathbf{h}_m \\ \text{curl}\ \mathbf{h} &= \sum_m \gamma_m \mathbf{f}_m + \sum_m \delta_m \mathbf{e}_m. \end{aligned}$$

[¶]The extension to inhomogeneous materials is further discussed in Section 10.3. It readily follows from the equations derived in the previous section.

From Maxwell's equations (10.1) it follows that

$$\alpha_m = -\mu \frac{\partial l_m}{\partial t} - r_m$$

$$\beta_m = -\mu \frac{\partial u_m}{\partial t} - s_m$$

$$\gamma_m = \left(\sigma + \epsilon \frac{\partial}{\partial t}\right) c_m + p_m$$

$$\delta_m = \left(\sigma + \epsilon \frac{\partial}{\partial t}\right) d_m + q_m.$$

The $(\alpha, \beta, \gamma, \delta)$ coefficients must now be eliminated. Because the eigenvectors are normalized to unity,

$$\beta_m = \int_V \text{curl } \mathbf{e} \cdot \mathbf{h}_m \, dV = \int_V \mathbf{e} \cdot \text{curl } \mathbf{h}_m \, dV + \int_S \mathbf{u}_n \cdot (\mathbf{e} \times \mathbf{h}_m) \, dS$$
$$= k_m d_m + \int_S (\mathbf{u}_n \times \mathbf{e}) \cdot \mathbf{h}_m \, dS.$$

Analogous steps for the other coefficients lead to

$$\epsilon \frac{dc_m}{dt} + \sigma c_m = -\int_V \mathbf{j} \cdot \mathbf{f}_m \, dV$$

$$\epsilon\mu \frac{d^2 d_m}{dt^2} + \sigma\mu \frac{dd_m}{dt} + k_m^2 d_m = -\mu \int_V \frac{\partial \mathbf{j}}{\partial t} \cdot \mathbf{e}_m \, dV - k_m \int_V \mathbf{j}_m \cdot \mathbf{h}_m \, dV$$
$$- k_m \int_S (\mathbf{u}_n \times \mathbf{e}) \cdot \mathbf{h}_m \, dS$$

$$\mu \frac{dl_m}{dt} = -\int_V \mathbf{j}_m \cdot \mathbf{g}_m \, dV - \int_S (\mathbf{u}_n \times \mathbf{e}) \cdot \mathbf{g}_m \, dS$$

$$\epsilon\mu \frac{d^2 u_m}{dt^2} + \sigma\mu \frac{du_m}{dt} + k_m^2 u_m = k_m \int_V \mathbf{j} \cdot \mathbf{e}_m \, dV - \left(\sigma + \epsilon \frac{d}{dt}\right) \int_V \mathbf{j}_m \cdot \mathbf{h}_m \, dV$$
$$- \left(\sigma + \epsilon \frac{d}{dt}\right) \int_S (\mathbf{u}_n \times \mathbf{e}) \cdot \mathbf{h}_m \, dS. \tag{10.27}$$

It is interesting to observe the behavior of the fields after the sources are cut off. The irrotational coefficient c_m decreases exponentially, with a time constant (ϵ/σ). Its magnetic equivalent l_m remains constant, fundamentally because of the absence of magnetic losses. The solenoidal coefficients u_m and d_m, on the other hand, see their amplitude decrease according to a damped sinusoidal oscillation. It is to be further noted

- That the term in $\mathbf{u}_n \times \mathbf{e}$ acts as an equivalent *surface* magnetic current, in accordance with the equivalence formulas (7.225).
- That the electric currents $\mathbf{j}$ couple only to the electric eigenvectors (through integrals such as $\int_V \mathbf{j} \cdot \mathbf{e}_m \, dV$) and the magnetic currents $\mathbf{j}_m$ to magnetic eigenvectors.

The time-harmonic version of (10.27) consists of the expansions

$$\mathbf{E}(\mathbf{r}) = -\sum_m \frac{\mathbf{f}_m(\mathbf{r})}{\sigma + j\omega\epsilon} \int_V \mathbf{J}\cdot\mathbf{f}_m \, dV + \sum_m \frac{\mathbf{e}_m(\mathbf{r})}{k^2 - j\omega\mu\sigma - k_m^2}$$
$$\left[j\omega\mu \int_V \mathbf{J}\cdot\mathbf{e}_m \, dV + k_m \int_V \mathbf{J}_m\cdot\mathbf{h}_m \, dV + k_m \int_S (\mathbf{u}_n \times \mathbf{E})\cdot\mathbf{h}_m \, dS \right] \tag{10.28}$$

$$\mathbf{H}(\mathbf{r}) = -\frac{1}{j\omega\mu} \sum_m \mathbf{g}_m(\mathbf{r}) \left[\int_V \mathbf{J}_m\cdot\mathbf{g}_m \, dV + \int_S (\mathbf{u}_n \times \mathbf{E})\cdot\mathbf{g}_m \, dS \right]$$
$$+ \sum \frac{\mathbf{h}_m(\mathbf{r})}{k^2 - j\omega\mu\sigma - k_m^2} \left[-k_m \int_V \mathbf{J}\cdot\mathbf{e}_m \, dV + (\sigma + j\omega\epsilon) \right.$$
$$\left. \int_V \mathbf{J}_m\cdot\mathbf{h}_m \, dV + (\sigma + j\omega\epsilon) \int_S (\mathbf{u}_n \times \mathbf{E})\cdot\mathbf{h}_m \, dS \right] \tag{10.29}$$

where $k^2 = \omega^2\epsilon\mu = \epsilon_r\mu_r k_0^2$.

The eigenvectors in (10.28) are perpendicular to the boundary S, yet $\mathbf{E}$ is not necessarily perpendicular to S. The convergence difficulties associated with such a behavior are analyzed in Section 1.7 for the case of a Fourier sine series. In the case of the cavity, the eigenvector expansion converges uniformly with respect to the *normal* component but nonuniformly with respect to the *tangential* component. Correspondingly, the expansion for $\mathbf{H}$ in (10.29) is uniformly convergent with respect to the tangential component, but nonuniformly convergent with respect to the normal component. We also note that the electric and magnetic eigenvectors are real vectors. It follows that the fields associated with a given mode are linearly polarized vectors. By the same token, the directions of $\mathbf{u}_n \times \mathbf{g}_m$ and $\mathbf{u}_n \times \mathbf{h}_m$ at the boundary remain constant during a cycle. This implies that the wall currents of a given mode flow along permanent lines. In consequence, a narrow slot cut along the lines of current remains parallel to $\mathbf{u}_n \times \mathbf{g}_m$ (or $\mathbf{u}_n \times \mathbf{h}_m$) during the entire cycle. A slot of this type does not disturb the lines of current and hence does not contribute to the excitation of the mode. An alternate method of proving this result consists in noting that the tangential electric field in the slot is directed along $\mathbf{u}_a$ (except close to the corners, Fig. 10.2). The corresponding term $\int_{slot} (\mathbf{u}_n \times \mathbf{E})\cdot\mathbf{h}_m \, dS$ becomes practically zero in (10.28) and (10.29), confirming that the narrow slot does not excite the mode of concern. Note also[6] that the irrotational modes play an important role in a lossless medium when the frequency approaches zero, basically because their coefficient is proportional to $(1/\omega)$,

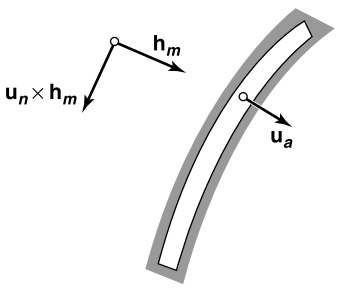

Figure 10.2 Slot in a wall.

while the denominator $k^2 - k_m^2$ of the solenoidal modes approaches a nonzero limit $(-k_m^2)$. Further important properties of the expansions are mentioned in Problems 10.8 to 10.11.

10.3 DETERMINATION OF THE EIGENVECTORS

The triple summations in (10.28) and (10.29) converge poorly, particularly so when the observation point is close to a source point. When the cavity is of a simple shape, however, methods exist to accelerate the modal convergence.[7] Some of these methods are described in Section 9.5. The great merit of the expansion is to reveal the existence of resonances, a point that is further discussed in Section 10.4. It is therefore important to determine the resonant frequency and the field structure of a few well-chosen modes. The desired accuracy may be high, for example in cavities associated with atomic clocks, where the resonant frequency must rigorously coincide with the frequency corresponding with changes in atomic energy levels.[8]

For a few simple shapes, the eigenvectors may be obtained by separation of variables. Data can be found in Appendix 9 on the spherical cavity and a few cavities derived from waveguides by metallizing two end planes perpendicularly to the axis. In most cases, however, numerical methods must be relied upon. They can be based, for example, on a variational principle derived from (10.19). The transformations in (10.5) and (10.10) are self-adjoint and negative-definite (Problem 10.4). As a result, the eigenvalues $(-k_m^2)$ are negative, and the k_m^2's are positive. Under these conditions, variational principle (2.16) may be applied. It shows that the functional

$$F(\mathbf{a}) = \frac{\displaystyle\int_V \mathbf{a}\cdot\text{curl curl }\mathbf{a}\, dV}{\displaystyle\int_V |\mathbf{a}|^2\, dV} = \frac{\displaystyle\int_V |\text{curl }\mathbf{a}|^2\, dV}{\displaystyle\int_V |\mathbf{a}|^2\, dV} \tag{10.30}$$

is minimized by the "lowest" eigenvector, with a minimum equal to the lowest eigenvalue k_1^2. The resonant wavelength of the corresponding mode is $\lambda_1 = 2\pi/k_1$. The method has been applied to the reentrant cavity shown in Figure 10.3*a* (Problem 10.17). This type of cavity is widely used in high-frequency tubes. The modes of interest are those that have a large axial electric field on the axis of the cavity and are capable of efficiently accelerating a beam of particles traveling along the axis. Genetic algorithms have been found useful, for

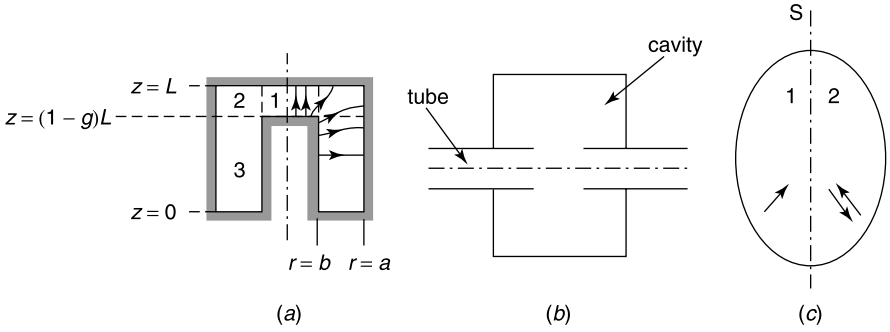

Figure 10.3 (*a*) Reentrant cavity. (*b*) Coaxial cavity wrapped around a circular tube. (*c*) Cavity with plane of symmetry.

example in generating the shape of a cavity required to satisfy some important criterion. For the accelerator cavity of Figure 10.3*b*, this criterion might be the need to maximize the ratio between the energy transferred to the beam and the energy supplied by the RF generator that feeds the coaxial cavity.[9]

In the first two examples of Figure 10.3, rotational symmetry simplifies the problem. The relevant theory is discussed in Chapter 16. Also simplifying is the presence of a plane of symmetry, by which the modes are split into two families, one where S is an *electric* wall, and a second one where S is a *magnetic* wall (Fig. 10.3*c*). From Figure 9.3*a*, an electric wall is associated with an $\mathbf{e}_m$ perpendicular to S and an $\mathbf{h}_m$ tangent to S. These modes are excited by sources that have the symmetries displayed in Figure 9.3*a*. Similar conclusions can be drawn from Figure 9.3*b* for the magnetic wall. In the presence of an *arbitrary* source $\mathbf{J}$, the fields are the sum of two contributions:

1. $\frac{1}{2}\mathbf{J}$ on side 1, and its image on side 2 according to Figure 9.3*a*
2. $\frac{1}{2}\mathbf{J}$ on side 1, and its image on side 2 according to Figure 9.3*b*.

The first pair excites the electric wall modes, the second one the magnetic wall modes.

10.3.1 Spurious Modes

The electric eigenvectors[‖] in a linear, isotropic medium are defined by (10.19). Let volume V be simply connected and singly bounded (the extension to the other two types is immediate). A weak form of the problem is obtained by multiplying (10.19) with testing vectors $\mathbf{w}_j$ and subsequently integrating over V. This gives, for the left-hand term of (10.19),

$$I = -\int_V \mathbf{w}_j \cdot \operatorname{curl}\left(\frac{1}{\mu_r}\operatorname{curl}\mathbf{e}_m\right) dV + k_m^2 \int_V \epsilon_r\, \mathbf{w}_j \cdot \mathbf{e}_m\, dV = 0 \qquad (j = 1, \ldots, N). \tag{10.31}$$

Elimination of the second derivatives is obtained by invoking (A1.13), which transforms the first integral in (10.31) into

$$\int_V \mathbf{w}_j \cdot \operatorname{curl}\left(\frac{1}{\mu_r}\operatorname{curl}\mathbf{e}_m\right) dV = \int_V \frac{1}{\mu_r}\operatorname{curl}\mathbf{w}_j \cdot \operatorname{curl}\mathbf{e}_m\, dV + \int_S \mathbf{w}_j \cdot \left(\mathbf{u}_n \times \frac{1}{\mu_r}\operatorname{curl}\mathbf{e}_m\right) dS. \tag{10.32}$$

It is desirable to eliminate the surface integral in the second term. This goal is achieved by requiring $\mathbf{w}_j$ to be perpendicular to S. Following the customary method, $\mathbf{e}_m$ is expanded in a series of basis vectors. Thus,

$$\mathbf{e}_m(\mathbf{r}) = \sum_{i=1}^{N} a_{mi}\mathbf{v}_i(\mathbf{r}). \tag{10.33}$$

The $\mathbf{v}_i$ may be entire domain functions, but in the great majority of cases V is subdivided into N cells (or subdomains) V_i, and $\mathbf{v}_i$ is defined in V_i only. Series (10.33) is now inserted

[‖] One could equally well discuss the dual problem (10.20), formulated in terms of $\mathbf{h}_m$.

into (10.32) to yield

$$\sum_{i=1}^{N} a_{mi} \underbrace{\left[-\int_V \frac{1}{\mu_r} \text{ curl } \mathbf{w}_j \cdot \text{curl } \mathbf{v}_i \, dV \right]}_{L_{ji}} + k_m^2 \sum_{i=1}^{N} a_{mi} \underbrace{\int_V \epsilon_r \mathbf{w}_j \cdot \mathbf{v}_i \, dV}_{M_{ji}} = 0, \tag{10.34}$$

where i and j range from 1 to N. In matrix form:

$$\overline{\overline{L}} \cdot \mathbf{a}_m + k_m^2 \overline{\overline{M}} \cdot \mathbf{a}_m = 0. \tag{10.35}$$

The solutions of (10.19) that correspond with values of k_m^2 different from zero automatically satisfy the condition** div $(\epsilon_r \mathbf{e}_m) = 0$ (i.e., they produce a solenoidal electric flux density $\epsilon_r \mathbf{e}_m$). There are, however, eigenvectors associated with $k_m^2 = 0$. These vectors must satisfy

$$\begin{aligned} \text{curl} \left(\frac{1}{\mu_r} \text{ curl } \mathbf{e}_0 \right) &= 0 \qquad (\text{in } V) \\ \mathbf{u}_n \times \mathbf{e}_0 &= 0 \qquad (\text{on } S). \end{aligned} \tag{10.36}$$

The first equation implies that there exists a (potential) function ψ such that

$$\frac{1}{\mu_r} \text{ curl } \mathbf{e}_0 = \text{grad } \psi.$$

Because $\mathbf{e}_0$ is perpendicular to S, its curl, from (A3.21), is tangent to S. Hence,

$$\begin{aligned} \text{div } (\mu_r \text{ grad } \psi) &= 0 \qquad (\text{in } V) \\ \frac{\partial \psi}{\partial n} &= 0 \qquad (\text{on } S). \end{aligned} \tag{10.37}$$

But (A1.12) and (A1.27) imply that

$$\begin{aligned} \int_V \text{div } (\psi \, \mu_r \text{ grad } \psi) \, dV &= \int_S \mu_r \, \psi \frac{\partial \psi}{\partial n} \, dS = 0 \\ &= \int_V \mu_r |\text{grad } \psi|^2 \, dV + \int_V \psi \text{ div } (\mu_r \text{ grad } \psi) \, dV. \end{aligned}$$

This equation shows that the only solution of (10.37) is $\psi =$ constant, from which may be deduced that curl $\mathbf{e}_0 = 0$. Clearly, any solution of (10.36) is a gradient, and the *null space* of the curl curl operator in (10.19) consists of all irrotational vectors grad θ perpendicular to S. These vectors do not belong to the resonant family, and may be eliminated by imposing

**The condition also implies, from (A8.90), that $\mathbf{u}_n \cdot \mathbf{d}_m$ is continuous at an interface, the expected behavior in the absence of real charges on the surface.

the additional condition div $(\epsilon_r \mathbf{e}_m) = 0$. This may be shown by applying the divergence condition to grad θ. Thus,

$$\int_V \text{div}\,(\epsilon_r\,\theta\ \text{grad}\,\theta)\,dV = \int_S \epsilon_r\,\theta\frac{\partial\theta}{\partial n}\,dS = 0$$
$$= \int_V \epsilon_r|\text{grad}\,\theta|^2\,dV + \int_V \theta\ \underbrace{\text{div}\,(\epsilon_r\ \text{grad}\,\theta)}_{=0}\,dV.$$

This equation implies that

$$\int_V \epsilon_r|\text{grad}\,\theta|^2 dV = 0,$$

and therefore that grad $\theta = 0$, (provided ϵ_r is not equal to zero, which could happen in a plasma).

The difficulty arising from zero (or very small) eigenvalues is discussed in Section 1.13 in the light of a simple matrix problem. Various methods have been proposed to eliminate the spurious solutions. The *penalty term* approach,[10,11] for instance, is based on the functional[††]

$$J(\mathbf{e}) = \int_V \Big[|\text{curl}\,\mathbf{e}|^2 - k_m^2|\mathbf{e}|^2\Big]\,dV + s\int_V |\text{div}\,\mathbf{e}|^2 dV, \tag{10.38}$$

where the divergence condition is enforced by choosing an appropriate s factor [192].

The most often applied numerical methods rely on the use of curl-conforming edge elements, which enforce the tangential continuity of the fields, a property already discussed in Section 6.12. Other approaches are possible, and *finite difference* methods in the time domain have been successful in revealing resonances by exciting the cavity with suitable broadbanded impulse signals.[14,15] These methods are further discussed in Section 12.8.

10.3.2 An Important Cell

The *tetrahedron* with nodes 1, 2, 3, 4 (Fig. 10.4) is often used as a unit *cell*. Its basis vectors $\mathbf{v}_i$ are defined in terms of the *shape functions* L_i already introduced in (2.31), but now extended to three dimensions [189, 192, 203, 211]. Function L_1, for example, is linear in (x, y, z), equal to one in 1, and zero in 2, 3, 4 (hence also on the face 234). At a point P it is given by

$$L_1(P) = \frac{\text{volume } P_{234}}{\text{volume of the cell}} = \frac{PQ}{h_1}. \tag{10.39}$$

It follows that

$$\text{grad}\,L_1 = \frac{1}{h_1}\mathbf{u}_1. \tag{10.40}$$

We shall use basis vectors of the kind

$$\mathbf{v}_{12} = (L_1\ \text{grad}\,L_2 - L_2\ \text{grad}\,L_1)\,l_{12}. \tag{10.41}$$

[††]Variational principles in the presence of lossy materials (ϵ_r and/or μ_r complex) are derived in Notes 12 and 13.

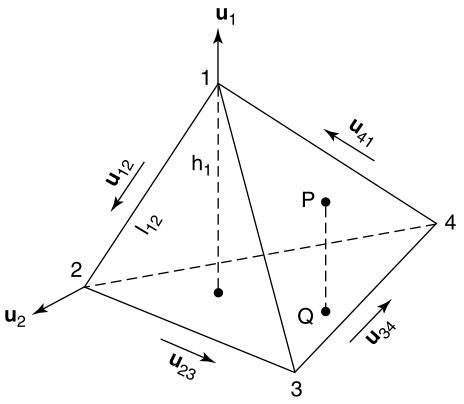

Figure 10.4 Tetrahedron and relevant geometrical parameters.

Simple manipulations show that

$$\text{div } \mathbf{v}_{12} = 0 \tag{10.42}$$

$$\text{curl } \mathbf{v}_{12} = \frac{2l_{12}}{h_1 h_2}\mathbf{u}_1 \times \mathbf{u}_2 = 2l_{12} \text{ grad } L_1 \times \text{grad } L_2 \tag{10.43}$$

$$\mathbf{u}_{12} \cdot \text{grad } L_1 = -\frac{1}{l_{12}} \tag{10.44}$$

$$\mathbf{u}_{12} \cdot \text{grad } L_2 = \frac{1}{l_{12}} \tag{10.45}$$

$$\mathbf{u}_{12} \cdot \mathbf{v}_{12} = (L_1 + L_2) = 1. \tag{10.46}$$

It is seen that $\mathbf{v}_{12}$ is solenoidal within its own tetrahedron. Further, the tangential component of $\mathbf{v}_{12}$ along side 12 is a constant equal to one. Similar relationships hold for the other five sides. Note also

- That the tangential components of the various $\mathbf{v}_{ik}$ ($\mathbf{v}_{12}$ excepted) vanish on side 12.
- That $\mathbf{v}_{12}$ has tangential components on the element faces that contain side 12, but none on the other faces.

The six $\mathbf{v}_{mn}$ are now combined to form the basis vector $\mathbf{v}_i$ for cell "i," viz.

$$\mathbf{v}_i(\mathbf{r}) = A_{12}\mathbf{v}_{12}(\mathbf{r}) + A_{13}\mathbf{v}_{13}(\mathbf{r}) + A_{14}\mathbf{v}_{14}(\mathbf{r}) + A_{23}\mathbf{v}_{23}(\mathbf{r}) + A_{24}\mathbf{v}_{24}(\mathbf{r}) + A_{34}\mathbf{v}_{34}(\mathbf{r}), \tag{10.47}$$

where the A_{ik} coefficients are adjustable. In particular, continuity of the tangential components across edges (and faces) can be obtained by sharing the coefficient A_{ik} with all cells having side ik in common.

The $\mathbf{v}_i$ must now be inserted in (10.34). The matrix elements L_{ki} contain products curl $\mathbf{w}_k \cdot$curl $\mathbf{v}_i$. In a Galerkin solution, the $\mathbf{v}$ and the $\mathbf{w}$ coincide. For such a case, the following relationships are useful [203]:

$$\int_{V_i} \text{curl } \mathbf{v}_{jk} \cdot \text{curl } \mathbf{v}_{mn}\, dV$$

$$= 4V_i\, l_{jk}\, l_{mn}\, (\text{grad } L_j \times \text{grad } L_k) \cdot (\text{grad } L_m \times \text{grad } L_n) \tag{10.48}$$

and

$$\frac{1}{V_i}\int_{V_i} L_j L_k \, dV = \begin{cases} \dfrac{1}{10} & \text{for } j = k \\ \dfrac{1}{20} & \text{for } j \neq k. \end{cases} \tag{10.49}$$

In a practical situation, the cells are so chosen that material parameters such as ϵ_r, μ_r are constant in the cell (or assumed constant there), and jump discontinuities only occur at cell boundaries.[16]

10.3.3 Other Edge Elements

Beside tetrahedra, other volumes such as triangular prisms, bricks, and hexahedra are in frequent use (Fig. 10.5). Details on suitable basis vectors for these cells, and on the evaluation of the corresponding elements, can be found in [192, 203, 211]. Within these cells, basis vectors can be constructed by means of the linear (x, y, z) variation of the L_i shape functions. The $\mathbf{v}_{ik}$ defined in (10.41) are sometimes called (CT, LN) because of the constancy of their tangential component and the linear variation of their normal component. Other choices are possible, such as the (LT, QN) vectors, characterized by a linear tangential variation and a quadratic normal variation [203]. One can further apply a hierarchal strategy, choose a fixed polynomial degree p for the polynomials, and obtain the desired accuracy by refining the net, or keep a fixed net and improve accuracy by increasing p.[17,18]

Nodal elements, discussed in Sections 2.6 and 2.7, are used extensively to solve potential problems. Vector problems, however, focus the attention on edge elements, not only because of the *spurious modes* difficulty, but also because tangential continuity, and the absence of constraints on the normal component, allow the field to change direction abruptly, a desirable feature in the vicinity of an edge.[19] Nodal elements, however, have retained their usefulness in formulations based on potential pairs $(\mathbf{A}, \phi)$ or $(\mathbf{C}, \psi)$ instead of field pairs $(\mathbf{E}, \mathbf{H})$. Edge elements can be used for $\mathbf{A}$ and nodal elements for ϕ. The potential formulation is robust: it yields reliable solutions throughout the frequency spectrum, while field formulations may become unstable at very low frequencies, where the system of equations becomes nearly singular[20,21] [211].

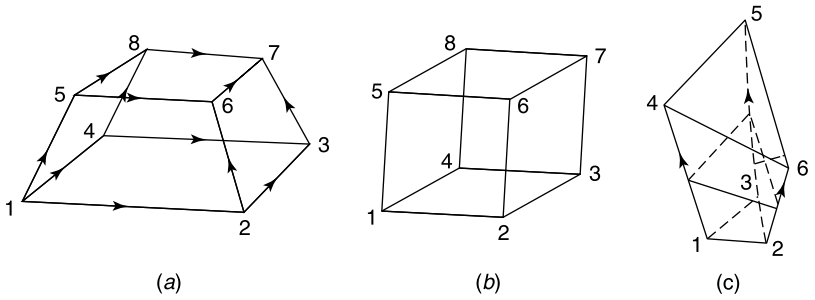

Figure 10.5 Three useful cells: (*a*) hexahedral, (*b*) cubic, (*c*) diagonal prism (from J. L. Volakis, A. Chatterjee, and L. C. Kempel. *Finite element method for electromagnetics*. IEEE Press, New York, and Oxford University Press, Oxford, 1998, with permission of IEEE Press).

10.3.4 Perturbation Methods

Assume that the eigenvectors $\mathbf{e}_m, \mathbf{h}_m$ of an evacuated cavity are known. A medium of characteristics

$$\begin{aligned} \epsilon_r^{-1}(\mathbf{r}) &= 1 + \lambda\, \phi(\mathbf{r}) \\ \mu_r^{-1}(\epsilon_{\boldsymbol{r}}) &= 1 + \lambda\, \theta(\mathbf{r}), \end{aligned} \tag{10.50}$$

where λ is a small parameter, is now introduced in the cavity. The new eigenvectors satisfy, from (10.21),

$$\begin{aligned} \text{curl}\ \mathbf{e}'_m &= k_m\, \mu_r\, \mathbf{h}'_m \\ \text{curl}\ \mathbf{h}'_m &= k_m\, \epsilon_r\, \mathbf{e}'_m. \end{aligned} \tag{10.51}$$

In the spirit of the general method discussed in Section 1.15, we introduce expansions

$$\begin{aligned} k_m &= k_{m0} \left(1 + \lambda\, C_m + \lambda^2 D_m + \cdots\right) \\ \epsilon_r\, \mathbf{e}'_m &= \mathbf{e}_m + \lambda \sum_{i=1}^{\infty} A_{mi}\, \mathbf{e}_i \\ \mu_r\, \mathbf{h}'_m &= \mathbf{h}_m + \lambda \sum_{k=1}^{\infty} B_{mk} \mathbf{h}_k. \end{aligned} \tag{10.52}$$

The eigenvectors are connected by the relationship

$$\begin{aligned} \int_V \text{div}\, (\mathbf{e}'_m \times \mathbf{h}_i)\, dV &= \int_S \mathbf{u}_n \cdot (\mathbf{e}'_m \times \mathbf{h}_i)\, dS \;=\; 0 \\ &= \int_V \left[\mathbf{h}_i \cdot \text{curl}\ \mathbf{e}'_m - \mathbf{e}'_m \cdot \text{curl}\ \mathbf{h}_i\right] dV. \end{aligned}$$

From (10.21), this implies

$$k_m \int_V \mu_r \mathbf{h}_i \cdot \mathbf{h}'_m\, dV = k_i \int_V \mathbf{e}'_m \cdot \mathbf{e}_i\, dV.$$

Inserting the power expansions into this equation, and equating terms of equal order in λ, gives

$$\begin{aligned} C_m + B_{mm} &= A_{mm} + \phi_{mm} && (\text{for } i = m) \\ k_{m0}\, B_{mi} &= k_{i0}\, A_{mi} + k_{i0}\, \phi_{mi} && (\text{for } i \neq m), \end{aligned}$$

where

$$\phi_{mi} = \int_V \phi\, \mathbf{e}_m \cdot \mathbf{e}_i\, dV.$$

Additional relationships can be obtained by equating terms in λ^2, and developing $\int_V \text{div}\,(\mathbf{h}'_m \times \mathbf{e}_i)\,dV$. Omitting the details, we quote the results, which are

$$C_m = \frac{1}{2}(\phi_{mm} + \theta_{mm})$$

$$D_m = -\frac{1}{8}(\phi_{mm} - \theta_{mm})^2 + \frac{1}{2}\sum_{i\neq m}\left[\frac{k_{i0}^2}{k_{m0}^2 - k_{i0}^2}\left(\phi_{mi}^2 + \theta_{mi}^2\right) + 2\,\phi_{mi}\,\theta_{mi}\frac{k_{m0}\,k_{i0}}{k_m^2 - k_i^2}\right], \tag{10.53}$$

where

$$\theta_{mi} = \int_V \theta\,\mathbf{h}_m \cdot \mathbf{h}_i\,dV.$$

Let us apply these results to the cavity of Figure 10.6 and the mode

$$\mathbf{h}_m = J_1\left(2.405\,\frac{r}{a}\right)\cos\frac{\pi z}{L}\mathbf{u}_\varphi.$$

A flat disk of nonmagnetic material, with dielectric constant $\epsilon_r \approx 1$, is introduced along the axis of the cavity. For such a sample, the function $\lambda\,\phi(\mathbf{r})$ is equal to zero outside the disk and to $(1 - \epsilon_r)$ inside the disk. Applied to the mode of concern, (10.53) gives,[22] because $\theta_{mi} = 0$,

$$k_m = k_{m0}\left[1 - 3.28\ 10^{-6}(\epsilon_r - 1) - 0.992\ 10^{-8}(\epsilon_r - 1)^2 + \cdots\right], \tag{10.54}$$

with $a = 6.61$ cm, $L = 8.29$ cm, $b = 0.5$ cm, $t = 0.075$ cm, and $d = 4.145$ cm.

Perturbation methods can be applied to a host of other situations. Assume, for example, that a homogeneous sample of volume V is introduced in the cavity. In this case, the first-order correction to the resonant wave-number is

$$k_m = k_{m0}\left[1 - \frac{1}{2}(\epsilon_r - 1)\int_V |\mathbf{e}_m|^2\,dV - \frac{1}{2}(\mu_r - 1)\int_V |\mathbf{h}_m|^2\,dV\right]. \tag{10.55}$$

This formula shows clearly where to put the sample to obtain maximum frequency shift, namely near a peak of $|\mathbf{e}_m|$ when ϵ_r is perturbed, or near a peak of $\mathbf{h}_m$ when μ_r is perturbed. Results are also available for biisotropic samples,[23] for small deformations of cavity walls [46, 73] (Problem 10.22), and for the insertion of a sample of *arbitrary* ϵ_r, μ_r, but vanishing dimensions, into the cavity (Problem 10.24).

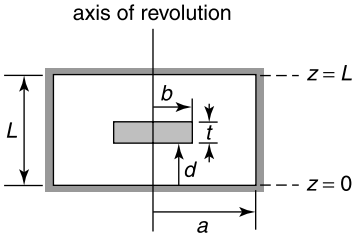

Figure 10.6 Circular cylindrical cavity with flat dielectric disk (from A. Cunliffe, R. N. Gould, and K. D. Hall, On cavity resonators with non-homogeneous media, *Monograph 91*, January 1954, with permission of the Institution of Electrical Engineers).

10.4 RESONANCES

10.4.1 Quality Factor *Q*

It is clear, from (10.28) and (10.29), that the irrotational modes $\mathbf{f}_m$ and $\mathbf{g}_m$ do not evidence any resonances. The solenoidal modes, on the other hand, *do* resonate, in casu in the vicinity of $k = k_m$, and with an amplitude that is ultimately bounded by energy losses. If a given mode has a very high Q, its contribution tends to dominate. If we introduce the notations

$$k = \omega\sqrt{\epsilon\mu}; \quad k_c^2 = k^2\left(1 - \frac{j}{Q}\right); \quad \Delta k = k - k_m; \quad Q = \frac{\omega\epsilon}{\sigma}; \quad R_c = \sqrt{\frac{\mu}{\epsilon}}, \tag{10.56}$$

the fields of a mode near resonance may be given the form

$$\begin{aligned} \mathbf{E} &\approx A\,\frac{1}{\dfrac{\Delta k}{k_m} - \dfrac{j}{2Q}}\,\mathbf{e}_m \\ R_c\mathbf{H} &= jA\,\frac{1}{\dfrac{\Delta k}{k_m} - \dfrac{j}{2Q}}\,\mathbf{h}_m, \end{aligned} \tag{10.57}$$

where

$$A = \frac{1}{2k_m^2}\left[j\omega\mu\int_V \mathbf{J}\cdot\mathbf{e}_m\,dV + k_m\int_V \mathbf{J}_m\cdot\mathbf{h}_m\,dV + k_m\int_S (\mathbf{u}_n\times\mathbf{E})\cdot\mathbf{h}_m\right]dS.$$

In the presence of loss mechanisms, the *quality factor* is given by

$$\frac{1}{Q} = \sum_{i=1}^{N}\frac{1}{Q_i} = \frac{1}{2\pi}\,\frac{\text{energy dissipated per cycle}}{\text{energy in the mode at resonance}}. \tag{10.58}$$

Losses can occur either in the medium filling the cavity (in which case $Q = \omega\epsilon/\sigma$) or in the imperfectly conducting walls. The penetration depth δ in the wall is typically much less than the radii of curvature of S, hence it is permissible to apply the results of Section 9.1, in particular (9.32) and (9.38). We write

$$\begin{aligned} \mathbf{E}_{\tan} &= Z_w\mathbf{J}_S = (1+j)\left(\frac{\omega\mu_w}{2\sigma_w}\right)^{\frac{1}{2}}(\mathbf{H}\times\mathbf{u}_n) \\ &= \frac{1+j}{\sigma_w\delta_w}(\mathbf{H}\times\mathbf{u}_n) = R_w(1+j)\,\mathbf{J}_S, \end{aligned} \tag{10.59}$$

where the subscript w refers to the material of the wall, and $\mathbf{u}_n$ points toward the wall. The magnitude of R_w is generally quite small (e.g., of the order 0.02 Ω for copper at 10 GHz). The time-averaged power loss in the wall is

$$P = \frac{1}{2}R_w\int_S |\mathbf{H}_{\tan}|^2\,dS = \frac{1}{2}R_w\int_S |\mathbf{J}_S|^2\,dS \quad (W). \tag{10.60}$$

To a good approximation, $\mathbf{H}_{\tan}$ can be replaced with the value corresponding to a perfectly conducting wall. This value is often obtained in the form of a series, as in (10.29). It is to be noted, in this respect, that the eigenvectors $\mathbf{g}_m$ and $\mathbf{h}_m$ do *not* have orthogonality properties on S, hence that P is not the sum of the power losses in the individual modes. At a strong resonance, $\mathbf{H}_{\tan}$ may be replaced by the value given in (10.57), while the mode energy, divided equally between electric and magnetic parts, is obtained by integrating $\epsilon\,|\mathbf{E}|^2$ or $\mu\,|\mathbf{H}|^2$ over the cavity volume. When all media are nonmagnetic, Q is roughly equal to

$$Q = 2\frac{\text{volume}}{\delta_{\text{res}} \times \text{area of wall}} = k_m \frac{R_c}{R_w}\left(\frac{V}{S}\right). \tag{10.61}$$

This result only holds when the average values of $|\mathbf{h}_m|^2$, on S and in V, are practically equal.

Layers of superconducting material on the walls can yield very high values of Q and are attractive when the reduced losses more than compensate the inconvenience and cost of a cooling system.[24,25] The characteristic impedance of the superconductor is of the form[26]

$$Z_w = \frac{1}{2}\omega^2 \mu_0\, \delta_s^3 \sigma_n + j\omega\mu_0\, \delta_s,$$

where the real part is contributed by the unpaired charge carriers. When $\omega\tau_n \ll 1$ (typically up to the high microwave region), R_w is proportional to ω^2, while (10.59) shows that the proportionality is to $\sqrt{\omega}$ for a conductor such as copper. There is therefore a diminishing reward in using high-temperature superconductors as the frequency increases. Illustratively: at 5 GHz and 77 K, R_w could be 1 mΩ for YBCO, and as little as 9 mΩ for Au.

10.4.2 The Frequency Curve

Given the losses, the general level of the fields at a point in the resonator varies with frequency in the manner sketched in Figure 10.7*a*. As the losses increase, the resonant modes lose their impact, and the total field, to which many modes contribute, becomes spatially more uniform. Homogeneity is desirable in industrial heating applications, where hot spots must normally be avoided.‡‡ Pronounced resonances are also detrimental to the use of the cavity as a shielded space, in which case Q-lowering material may have to be inserted in the room to obtain a flatter response.[28]

A numerical analysis of the number of modes per Hz can easily be conducted for a rectangular parallelepiped of sides a, b, d (Fig. 10.7*b*). The parallelepiped is derived from a rectangular waveguide, and its eigenvectors can be obtained by the method outlined in Section 15.2. The resonant frequencies of an air-filled parallelepiped are

$$f_{mnq} = c_0 \left[\left(\frac{m}{2a}\right)^2 + \left(\frac{n}{2b}\right)^2 + \left(\frac{q}{2d}\right)^2\right],$$

where the indices are integers or zero. To a good approximation,[2] the number of modes between 0 and f is given, for large f, by the formula

$$\lim_{f\to\infty} N = \frac{8\pi}{3}\frac{f^3}{c_0^3} \times \text{volume } V. \tag{10.62}$$

‡‡The homogeneous field can also be generated in a mode-stirred chamber, where the simultaneously excited modes are stirred by a rotating conductive paddle. See Note 27.

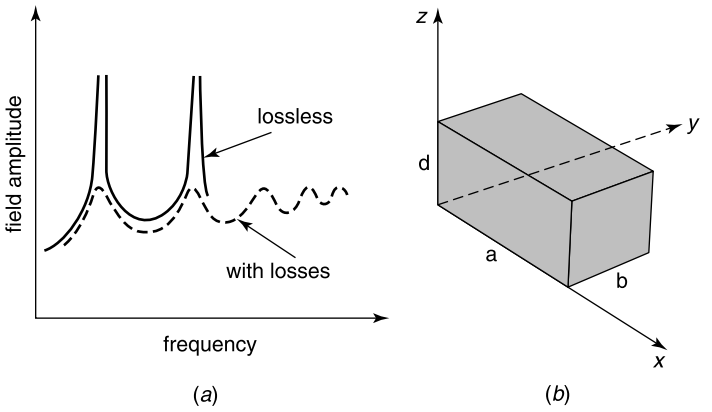

Figure 10.7 (*a*) Damped and undamped resonances. (*b*) Parallelepipedic cavity.

In a $(f, f + \Delta f)$ interval, there are

$$dN = \frac{8\pi}{c_0^3} V f^2 \Delta f \tag{10.63}$$

modes. Note that some of these may resonate at the same frequency, a degeneracy that occurs, in particular, in the presence of symmetries (for example in a cube, or a circular cylinder). It can be shown that, in the limit of large f,

$$\begin{aligned} \sum_m |\mathbf{e}_m(\mathbf{r})|^2 &= \sum |\mathbf{h}_m(\mathbf{r})|^2 = \frac{8\pi}{3} \frac{f^3}{c_0^3} \\ \sum_m \frac{|\mathbf{e}_m(\mathbf{r})|^2}{f_m^2} &= \sum \frac{|\mathbf{h}_m(\mathbf{r})|^2}{f_m^2} = 8\pi \frac{f}{c_0^3}, \end{aligned} \tag{10.64}$$

where the summation is over all modes with resonant frequency less than f. Because this relationship holds for all $\mathbf{r}$, it follows that the energy tends to be distributed evenly throughout the cavity, as assumed in Planck's analysis of black body radiation.[29]

10.4.3 A Simple Example

The currents $\mathbf{J}$ and $\mathbf{J}_m$ in (10.28) and (10.29) are assumed given, but the contribution from $\mathbf{u}_n \times \mathbf{E}$ is normally unknown. When the walls are only slightly lossy, we may write $\mathbf{u}_n \times \mathbf{E} = Z_w \mathbf{u}_n \times \mathbf{J}_S$, where $\mathbf{J}_S$ is the current flowing on a perfectly conducting wall. More generally, however, $\mathbf{u}_n \times \mathbf{E}$ must be determined by solving a coupled regions problem. Consider, for example, the penetration of the fields in the imperfectly conducting wall of a spherical cavity. The primary source is an electric dipole located at the center of the cavity (Fig. 10.8). From (7.103), the primary magnetic field generated by the dipole radiating in free space has the φ-independent value

$$(H_\varphi)_{\text{dipole}} = \frac{Il}{4\pi} \left(jk_0 + \frac{1}{R} \right) \sin\theta \, \frac{e^{-jk_0 R}}{R}. \tag{10.65}$$

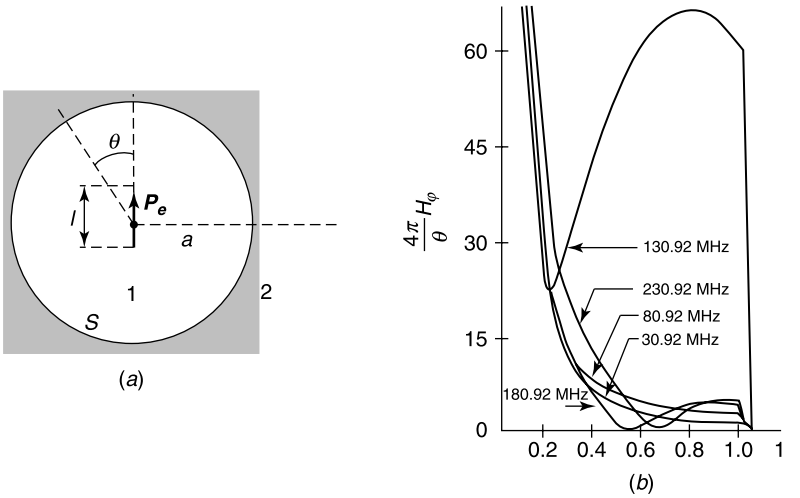

Figure 10.8 (*a*) Electric dipole at the center of a spherical cavity. (*b*) Radial variation of the normalized H_φ at a few frequencies (from C. M. Butler and J. Van Bladel, Electromagnetic fields in a spherical cavity embedded in a dissipative medium, *IEEE Trans. AP* **12**, 110–118, 1964, with permission of IEEE).

The H_φ component in the cavity should exhibit the same $\sin\theta$ dependence. The problem is usefully formulated in terms of the Debye potentials introduced in (7.197). Given the TM character of the fields, only the V potential is needed and we may write $V(R,\theta) = f(R)\cos\theta$. The function $f(R)$ is a combination of spherical Bessel functions. Because the field generated by the reflections on the wall is finite at $R = 0$, the appropriate function is $j_1(k_0R)$. It follows that the total field inside the cavity may be written as

$$H_\varphi^- = \left[\frac{Il}{4\pi}\frac{e^{-jk_0R}}{R}\left(jk_0 + \frac{1}{R}\right) + A_1 j_1(k_0R)\right]\sin\theta \qquad R \le a. \tag{10.66}$$

By similar arguments, the field in the outside medium is found to be

$$H_\varphi^+ = B_1 h_1^{(2)}(k_2R)\sin\theta \qquad R \ge a, \tag{10.67}$$

where $k_2^2 = \omega^2\epsilon_2\mu_2 - j\omega\mu_2\sigma_2$. The unknown constants A_1 and B_1 are determined from the boundary conditions at $R = a$, which require

1. H_φ to be continuous;
2. E_θ, the tangential electric field, to be continuous.

From Maxwell's equations, E_θ can be written in the form

$$E_\theta = -\frac{1}{j\omega\epsilon R}\frac{\partial}{\partial R}(RH_\varphi), \tag{10.68}$$

where ϵ may be complex. A few simple steps lead to the coefficients[30] [22]

$$A_1 = \frac{Il}{4\pi\Delta} e^{-jk_0 a} \frac{\epsilon_0}{\epsilon_{c2}} \left(\frac{jk_0}{a} + \frac{1}{a^2} \right) \left[k_2 R h_1^{(2)}(k_2 R) \right]'_{R=a}$$

$$B_1 = \frac{Il}{4\pi\Delta} e^{-jk_0 a} \left\{ \left(\frac{jk_0}{a} + \frac{1}{a^2} \right) \left[k_0 R j_1(k_0 R) \right]'_{R=a} - j_1(k_0 a) \left[k_0^2 - \frac{1}{a^2} - \frac{jk_0}{a} \right] \right\}, \tag{10.69}$$

where

$$\epsilon_{c2} = \epsilon_2 - \frac{j\sigma_2}{\omega}$$

and

$$\Delta = h_1^{(2)}(k_2 a) \left[k_0 R j_1(k_0 R) \right]'_{R=a} - \frac{\epsilon_0}{\epsilon_{c2}} j_1(k_0 a) \left[k_2 R h_1^{(2)}(k_2 R) \right]'_{R=a}. \tag{10.70}$$

A few typical curves for H_φ are shown in Figure 10.8*b* for $a = 1$ m and seawater as external medium ($\sigma_2 = 4$ S m^{-1}, $\epsilon_2 = 7 \times 10^{-7}$F m^{-1}). The fields are seen to peak around 130.92 MHz, the resonant frequency associated with a perfectly conducting wall.

10.5 OPEN RESONATORS: DIELECTRIC RESONANCES

Microwave integrated circuits, given their *open waveguide* structure, are in need of resonators of another type than the classic enclosed cavity. This section focuses on the properties of *dielectric* resonators, bodies of arbitrary shape but high ϵ_r, which resonate at well-defined frequencies. Enhanced scattering at certain frequencies from conducting or dielectric spheres is discussed in Section 11.3 and confirms the existence of these resonances. Figure 10.9*a*, a useful guide for further discussions, shows the resonant scattering peaks for a circular dielectric cylinder immersed in a plane H-wave. It is seen that higher ϵ_r lead, first, to sharper resonances and, second, to smaller resonator dimensions for a given resonant frequency. The modes are actually oscillations that can be sustained when the sources are cut off. Their time evolution is proportional to $e^{j\omega t}$, where ω must be complex, with a positive imaginary part when losses are present, in particular as a result of radiation. In the case of a *perfectly conducting* sphere, the oscillating modes are the multipoles discussed in Section 7.11. The $m = 0$, $n = 1$ electric multipole, for example, is characterized by a field

$$E_\theta = e^{jk_0 c_0 t} \sin\theta \frac{1}{k_0 R} \frac{d}{dR} \left[R h_1^{(2)}(k_0 R) \right]. \tag{10.71}$$

The wave-number $k_0 = (\omega/c_0)$ is quantized by the condition $E_\theta = 0$ at $R = a$. With the value of $h_1^{(2)}(k_0 R)$ given in (A5.93), this condition yields a factor

$$e^{j\omega t} = e^{-\frac{c_0}{2a} t} e^{+j\frac{\sqrt{3} c_0}{2a} t}. \tag{10.72}$$

Scattering by a *dielectric* sphere, and the determination of the corresponding resonant modes, can be investigated by similar multipole techniques[31] [9].

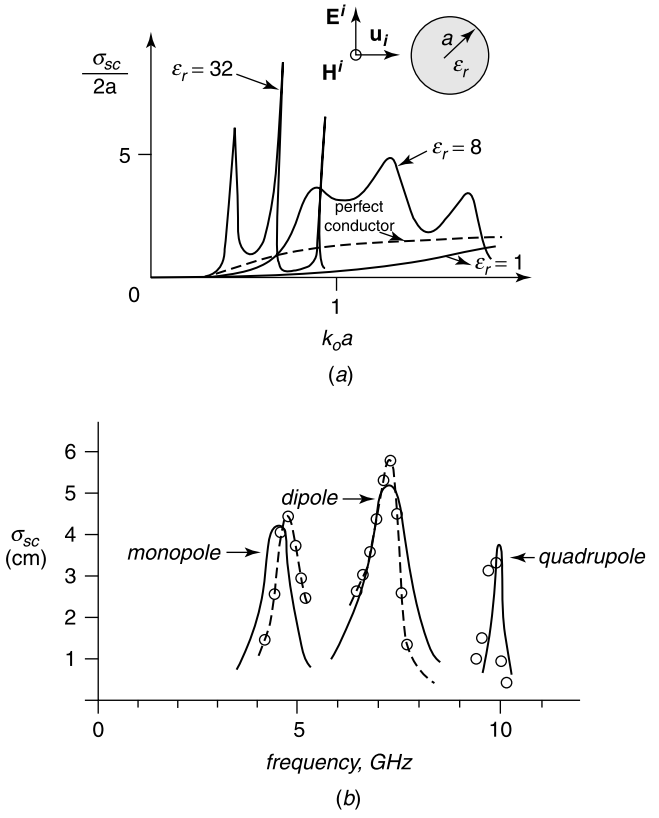

Figure 10.9 (*a*) Scattering cross section of a circular cylinder. (*b*) The first three peaks for the cylinder in an H-wave ($\epsilon_r = 16, a = 6$ mm). Solid lines: asymptotic theory. Small circles: exact numerical values (from J. Van Bladel, Resonant scattering by dielectric cylinders, *IEE Microwaves, Optics and Acoustics* **1**, 41–50, 1977, with permission of the Institution of Electrical Engineers).

10.5.1 The Dielectric Post Resonator

Total shielding of resonators has the advantage of suppressing the radiative losses. In the shielded volume, the resonant fields can be evaluated[32] by the various methods discussed in Section 10.3. *Partial* shielding often occurs, for example when the resonator is inserted between two perfectly conducting ground planes[33] (Fig. 10.10). To obtain high Q's (of the order 10^6 at 90 K) the planes may be covered with a superconducting film. We shall only analyze the simple configuration of Figure 10.10*a* and more particularly the $m = 0$, axisymmetric TE mode. Maxwell's equations yield [82]

$$\mathbf{H} = \frac{1}{j\omega\mu_0}\left[\frac{\partial E}{\partial z}\,\mathbf{u}_r - \frac{1}{r}\frac{\partial}{\partial r}(rE)\,\mathbf{u}_z\right]$$

$$\mathbf{E} = \frac{1}{j\omega\epsilon}\left[\frac{\partial H_r}{\partial z} - \frac{\partial H_z}{\partial r}\right]\mathbf{u}_\varphi.$$

$$= E\mathbf{u}_\varphi \tag{10.73}$$

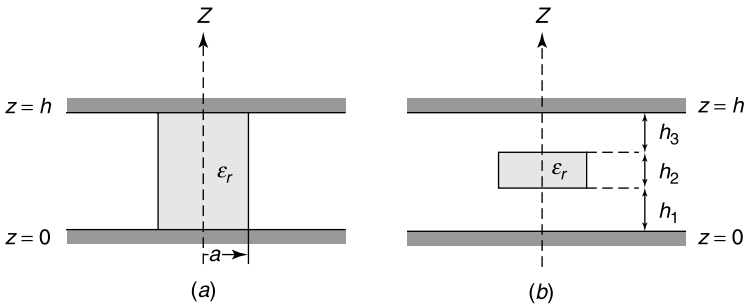

Figure 10.10 (*a*) Circular cylindrical post. (*b*) Pillbox located between ground planes.

Because div $\mathbf{H} = 0$, H_z must satisfy

$$\frac{1}{r}\frac{\partial}{\partial r}\left(r\frac{\partial H_z}{\partial r}\right) + \frac{\partial^2 H_z}{\partial z^2} + k_0^2 \epsilon_r H_z = 0. \tag{10.74}$$

But H_z must vanish on the perfectly conducting planes $z = 0$ and $z = h$. This prompts us to introduce the Fourier expansion

$$H_z(r, z) = \sum_{n=1}^{\infty} \sin k_n z \, f_n(r), \tag{10.75}$$

where $k_n = (n\pi/h)$. Inserting (10.75) into (10.74) shows that $f_n(r)$ satisfies a Bessel type of equation. We therefore write, for the nth mode,

$$\begin{aligned} H_z &= A_n J_0\left[(k_0^2\epsilon_r - k_n^2)^{\frac{1}{2}}\, r\right] \sin k_n z \qquad (\text{for } r < a) \\ H_z &= B_n H_0^{(2)}\left[(k_0^2 - k_n^2)^{\frac{1}{2}}\, r\right] \sin k_n z \qquad (\text{for } r > a). \end{aligned} \tag{10.76}$$

The electric field follows as

$$\begin{aligned} E_\varphi &= \frac{j\omega\mu_0}{\left[k_0^2\epsilon_r - k_n^2\right]^{\frac{1}{2}}} A_n J_0'\left[(k_0^2\epsilon_r - k_n^2)^{\frac{1}{2}}\, r\right] \sin k_n z \qquad (\text{for } r < a) \\ E_\varphi &= \frac{j\omega\mu_0}{\left[k_0^2 - k_n^2\right]^{\frac{1}{2}}} B_n \left\{H_0^{(2)}\left[(k_0^2 - k_n^2)^{\frac{1}{2}}\, r\right]\right\}' \sin k_n z \qquad (\text{for } r > a). \end{aligned} \tag{10.77}$$

Expressing continuity of H_z and E_φ at $r = a$ generates two homogeneous equations in A_n and B_n, which are only compatible for certain values of $k_0 a$, that is, for certain (resonant) frequencies [82]. It should be noted that terms such as $(k_0^2\epsilon_r - k_n^2)$ can be negative, in which case the arguments of the Bessel functions become imaginary, and the functions switch over to their *modified* form (see A5.61). Under these conditions, the resonant fields decrease exponentially in the r direction. There are therefore two kinds of *modes*: *leaky*, and *trapped* (or confined).[34]

In many applications, the resonating pillbox is not in direct contact with the ground planes (Fig. 10.10*b*). For such a case, the fields may be determined by assuming the dielectric

to be sandwiched between the horizontal planes, $z = h_1$ and $z = h_1 + h_2$ and using mode matching (see Section 9.5) to connect the fields in the three regions.[35] Alternately, one may assume the resonator to be part of the cylindrical volume $r = a$ and again use mode matching at $r = a$ to find the modal fields.[36] Numerical procedures such as the FDTD method discussed in Section 12.8 are also convenient. Briefly, the method consists in making the resonator part of an axisymmetric grid, in which all fields are initially assumed to be zero. At one selected point, **e** is suddenly set equal to one. This step impulse excites a large number of modes, and the computed time-response is subsequently Fourier inverted to reveal the frequency spectrum, and in particular the resonant peaks.[37]

10.5.2 The Modes of an Isolated Dielectric Resonator

Finding the modes and resonant frequencies is a first but fundamental step in understanding how the resonator behaves when it is part of an external circuit. Various methods are available for the purpose. To keep the computational volume bounded, one may decide, for example, to locate the dielectric in a shielded enclosure. Because the fields decay rapidly away from the resonator (a point to be expanded upon later on in this section), computed eigenvalues will be very close to those of the unshielded resonator, provided the dimensions of the enclosure are sufficiently large.[38] In general, the chosen numerical technique should exploit the assumed high value of ϵ_r. Such high values are needed to obtain resonances of sufficient sharpness and quality factor. Note that they are realistic because almost lossless materials with ϵ_r of 40 or higher are now available, with good temperature stability. It is clear that high ϵ_r's tend to confine the energy to the resonator volume, a property that may be understood from the following simple argument. Let a plane wave be normally incident from a region of high ϵ_r to the plane interface separating the dielectric from vacuum. From (9.5), the reflection coefficient is

$$R = \frac{\sqrt{\epsilon_r} - 1}{\sqrt{\epsilon_r} + 1}. \tag{10.78}$$

The formula shows that total reflection takes place in the limit $\epsilon_r \to \infty$. We also note that high material contrasts (in casu high ϵ_r) require special care in the application of numerical procedures.[39]

Several *simplified models* have been proposed to evaluate the resonant fields. In one of these, the dielectric volume is assumed bounded by magnetic walls. Such an approach ignores the radiative losses, because Poynting's vector is tangent to a magnetic wall. We must therefore consider exact methods, of the kind presented in Chapter 12 for the related problem of scattering [82]. They include the use of finite elements,[40] finite differences,[41] and integral equation techniques.[42] An example of the latter starts by expressing the fields in terms of electric and magnetic potentials.[43] This classic procedure is based on the Huyghens sources $\mathbf{J}_S = \mathbf{H} \times \mathbf{u}_n$ and $\mathbf{J}_{mS} = \mathbf{u}_n \times \mathbf{E}$ defined in Section 7.12. From (7.29) and (7.107), the fields in the nonmagnetic resonator (region 1 in Fig. 10.11*a*) can be written as

$$\begin{aligned} \mathbf{E} &= -j\omega\mathbf{A}_1 - \text{grad}\ \phi_1 - \frac{1}{\epsilon}\ \text{curl}\ \mathbf{C}_1 \\ \mathbf{H} &= \frac{1}{\mu_0}\ \text{curl}\ \mathbf{A}_1 - j\omega\mathbf{C}_1 - \text{grad}\ \psi_1. \end{aligned} \tag{10.79}$$

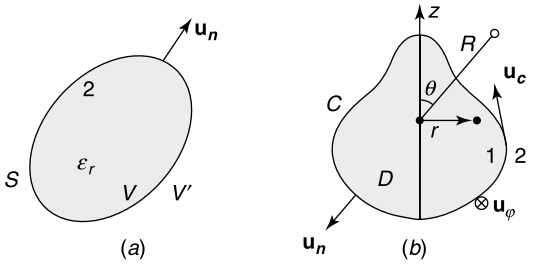

Figure 10.11 (*a*) General resonator volume. (*b*) Axisymmetric resonator.

The potentials have the advantage of being expressible in terms of the free space Green's function. Thus, on the basis of (7.33), (7.34), (7.49), and (7.50),

$$\mathbf{A}_1(\mathbf{r}) = \frac{\mu_0}{4\pi}\int_S \mathbf{J}_S(\mathbf{r}')\,\frac{e^{-jk_0\sqrt{\epsilon_r}D}}{D}\,dS' \tag{10.80}$$

$$\mathbf{C}_1(\mathbf{r}) = \frac{\epsilon_r\epsilon_0}{4\pi}\int_S \mathbf{J}_{mS}(\mathbf{r}')\,\frac{e^{-jk_0\sqrt{\epsilon_r}D}}{D}\,dS' \tag{10.81}$$

$$\phi_1(\mathbf{r}) = \frac{1}{4\pi\epsilon_r\epsilon_0}\int_S \rho_S(\mathbf{r}')\,\frac{e^{-jk_0\sqrt{\epsilon_r}D}}{D}\,dS' \tag{10.82}$$

$$\psi_1(\mathbf{r}) = \frac{1}{4\pi\mu_0}\int_S \rho_{mS}(\mathbf{r}')\,\frac{e^{-jk_0\sqrt{\epsilon_r}D}}{D}\,dS', \tag{10.83}$$

where D is the distance

$$D = \left[r^2 + r'^2 2rr'\cos(\varphi-\varphi') + (z-z')^2\right]^{\frac{1}{2}}. \tag{10.84}$$

From conservation of charge on S:

$$\rho_S = -\frac{1}{j\omega}\,\mathrm{div}_S\,\mathbf{J}_S \tag{10.85}$$

$$\rho_{mS} = -\frac{1}{j\omega}\,\mathrm{div}_S\,\mathbf{J}_{mS}. \tag{10.86}$$

Similar expressions hold in medium 2 ($\epsilon_r = 1$), where the virtual sources are $-\mathbf{J}_S, -\mathbf{J}_{mS}, -\rho_S, -\rho_{mS}$. The sought integral equations are obtained by requiring the tangential components of $\mathbf{E}$ and $\mathbf{H}$ to be continuous across S. The analysis simplifies when the resonator is axisymmetric (Fig. 10.11*b*). Fourier expansions in φ are now useful and we write, anticipating the discussions in Section 16.2,

$$\mathbf{J}_S = \sum_{n=-\infty}^{\infty} J_{nc}(c)\,e^{jn\varphi}\mathbf{u}_c + \sum_{n=-\infty}^{\infty} J_{n\varphi}(c)\,e^{jn\varphi}\mathbf{u}_\varphi. \tag{10.87}$$

Discretization follows by expanding the c-dependent coefficients in basis functions, for example subdomain pulses. There results a $\overline{\overline{Z}}_n \cdot \mathbf{J}_n = 0$ type of matrix equation for the nth

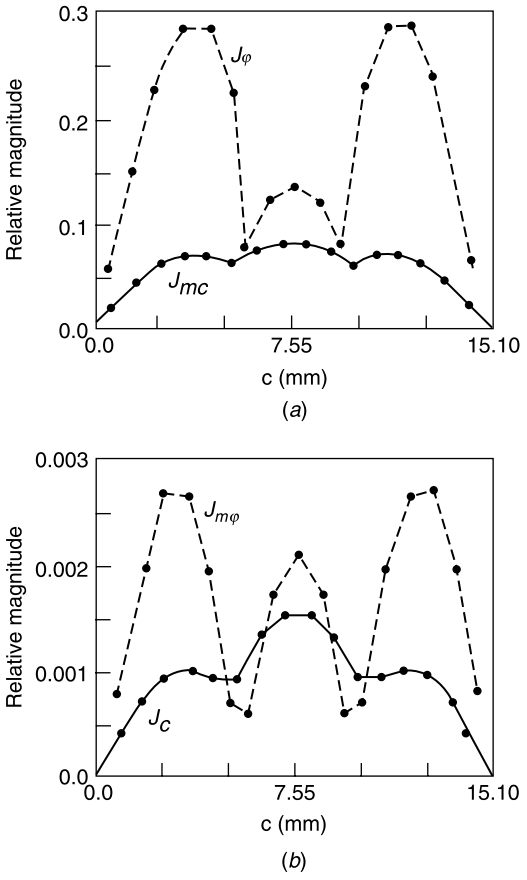

Figure 10.12 Surface currents on a dielectric pillbox. (*a*) Lowest TE mode (f_{res} = 4.83 GHz, Q = 46). (*b*) Lowest TM mode (f_{res} = 7.52 GHz, Q = 77) (from A. W. Glisson, D. Kajfez, and J. James, Evaluation of modes in dielectric resonators using a surface integral equation formulation, *IEEE Trans. MTT* **31**, 1023–1029, 1983, with permission of IEEE).

mode, the complex resonant frequencies of which are found by setting $\det \overline{\overline{Z}}_n = 0$. Typical results for the surface currents are shown in Figure 10.12 for a pillbox of radius 5.25 mm, height 4.6 mm, and ϵ_r = 38. The modes are the two lowest (φ-independent) transverse modes. The c coordinate is measured along the contour, starting with 0 on the axis and ending with 15.10, again on the axis.

When the material of the resonator is inhomogeneous, the surface integral equation is replaced by a volume integral equation, the unknowns of which are the polarization currents $\mathbf{J} = j\omega\epsilon_0[\epsilon_r(\mathbf{r}) - 1]\,\mathbf{E}$ in the dielectric.[44] The method is further discussed in Section 12.5.

10.5.3 Higher Modes

The lowest resonant frequency is associated with the lowest value of k_m, the wavenumber in the dielectric. This lowest k_m is of the order L^{-1}, where L is a typical dimension of the resonator. Because $k = 2\pi/\lambda_d$, the corresponding wavelength λ_d *in the dielectric* is of the order $(L/2\pi)$. The successive modes, for increasing values of k_m, radiate like dipoles,

quadrupoles, and higher-order multipoles. If one decides to increase the desired resonant frequency of the lowest mode, L must decrease accordingly, until at 50 GHz and $\epsilon_r = 100$, L becomes of the order 0.6 mm, too small for many applications. Resonances in higher modes, which at that (desired) frequency require larger L, may therefore be preferred. It should be remarked, however, that λ_d becomes correspondingly smaller with respect to L, hence that a quasi-optical situation progressively develops. The resonant waves now tend to graze the resonator boundary at small angles of incidence, and the total reflection phenomenon discussed in Section 9.1 becomes relevant. For such a limit, the *modes* become of the "*whispering gallery*" type, with fields progressively concentrated near the boundary. According to (9.43), in the air region the fields decrease exponentially in a direction perpendicular to the boundary. High values of Q result from this confinement, a property that has been put to good use in the millimeter and submillimeter ranges, in particular in certain applications to spectroscopy.[45,46,47]

10.5.4 An Asymptotic Theory

The properties of a resonator of given shape, size and ϵ_r can be determined with great accuracy by present day numerical facilities. The method to be discussed next is only approximate, because it is concerned with the limit $\epsilon_r \to \infty$. It can nevertheless be useful in shedding more light on the physical phenomenon of resonance. The method starts with an expansion of the fields in terms of $(1/N)$, where N is the index of refraction, equal to $\sqrt{\epsilon_r}$. Thus, because $\mathbf{E}$ must vanish in the limit $\epsilon_r \to \infty$,

$$\begin{aligned} \mathbf{E} &= \frac{1}{N}\mathbf{E}_1 + \frac{1}{N^3}\mathbf{E}_3 + \cdots \\ \mathbf{H} &= \mathbf{H}_0 + \frac{1}{N^2}\mathbf{H}_2 + \cdots . \end{aligned} \tag{10.88}$$

Let $k = Nk_0$ be the wave number in the dielectric. Inserting the expansions into Maxwell's equations, and equating coefficients of equal powers of $(1/N)$ on both sides, yields

$$\begin{aligned} \text{curl } \mathbf{E}_1 &= -jkR_{c0}\mathbf{H}_0 \\ \text{curl } \mathbf{H}_0 &= \frac{jk}{R_{c0}}\mathbf{E}_1 \end{aligned} \tag{10.89}$$

in the dielectric, and

$$\begin{aligned} \text{curl } \mathbf{E}_1' &= -jkR_{c0}\mathbf{H}_0' \\ \text{curl } \mathbf{H}_0' &= 0 \\ \text{curl } \mathbf{H}_2' &= \frac{jk}{R_{c0}}\mathbf{E}_1' \end{aligned} \tag{10.90}$$

outside the dielectric. At the boundary S between vacuum and dielectric, the tangential components of $\mathbf{E}_1$ and $\mathbf{E}_1'$, $\mathbf{H}_0$ and $\mathbf{H}_0'$ must be equal (Fig. 10.11*a*). The normal component of $\mathbf{D}$ is also continuous, which gives the conditions

$$\begin{aligned} \mathbf{u}_n \cdot \mathbf{E}_1 &= 0 \\ \mathbf{u}_n \cdot \mathbf{E}_3 &= \mathbf{u}_n \cdot \mathbf{E}_1'. \end{aligned} \tag{10.91}$$

The dominant term of $\mathbf{E}$ in the dielectric therefore becomes, in the limit $\epsilon_r \to \infty$, tangent to the boundary.

The only zero-order term in the expansions (10.88) is $\mathbf{H}_0$. Each mode has its own $\mathbf{H}_0$, which, after elimination of $\mathbf{E}_1$ in (10.89), is found to satisfy[48]

$$\begin{aligned} -\text{curl curl } \mathbf{H}_{0m} + k_m^2 \mathbf{H}_{0m} &= 0 \qquad (\text{in } V) \\ \text{curl } \mathbf{H}'_{0m} &= 0 \qquad (\text{in } V') \\ \mathbf{H}_{0m} &= \mathbf{H}'_{0m} \quad (\text{on } S). \end{aligned} \tag{10.92}$$

This system of equations quantizes k_m, and yields a corresponding resonant frequency f_m given by

$$k_{0m} = \frac{2\pi f_m}{c_0} = \frac{1}{N} k_m. \tag{10.93}$$

Because k_m is independent of N, increasing ϵ_r decreases the resonant frequency proportionally to $1/N$. The formula therefore confirms the behavior shown in Figure 10.9*a*. The electric field corresponding to $\mathbf{H}_{0m}$ is

$$\mathbf{E} = \frac{1}{N} \mathbf{E}_{1m} = -\frac{jR_{c0}}{Nk_m} \text{ curl } \mathbf{H}_{0m}. \tag{10.94}$$

In the limit $N \to \infty$, $\mathbf{E}$ approaches zero, but the energy density $\epsilon |\mathbf{E}|^2$ in the dielectric approaches a nonzero (and finite) limit. The fields radiated by the resonator find their origin in the polarization currents

$$\mathbf{J}_{\text{pol}} = j\omega\epsilon_0 (N^2 - 1)\mathbf{E} \approx j\omega\epsilon_0 N^2 \mathbf{E} = \text{curl } \mathbf{H}_{0m}. \tag{10.95}$$

Because the dimension L of the resonator is much less than λ_0, the radiation of the lowest mode may be expected to be of the dipole type. We note, in that respect, that the *electric* dipole moment vanishes. From (A3.56) and (10.92), indeed,

$$\begin{aligned} \mathbf{P}_e = \frac{1}{j\omega} \int_V \text{curl } \mathbf{H}_{0m} \, dV &= \frac{1}{j\omega} \int_S \mathbf{u}_n \times \mathbf{H}_{0m} \, dS = \frac{1}{j\omega} \int_S \mathbf{u}_n \times \mathbf{H}'_{0m} \, dS \\ = \frac{1}{j\omega} \int_S \mathbf{u}_n \times \text{grad}_S \, \psi'_{0m} \, dS &= 0. \end{aligned} \tag{10.96}$$

The *magnetic* dipole moment, on the other hand, survives, with a moment equal to

$$\mathbf{P}_m = \frac{1}{2} \int \mathbf{r} \times \text{curl } \mathbf{H}_{0m} \, dV. \tag{10.97}$$

and a quality factor[48]

$$Q = \frac{6\pi N^3}{k_m^5} \frac{\int_V |\text{curl } \mathbf{H}_{0m}|^2 dV}{|\mathbf{P}_m|^2}. \tag{10.98}$$

Because Q is proportional to N^3, the resonances get significantly sharper as ϵ_r increases. As an example, consider the field pattern of one of the axisymmetric modes of a sphere of radius a:

$$\begin{aligned}\mathbf{H}_{0m} &= 2\cos\theta\left(\frac{\sin kR}{R^3} - k\frac{\cos kR}{R^2}\right)\mathbf{u}_R \\ &\quad + \sin\theta\left(\frac{\sin kR}{R^3} - k^2\frac{\sin kR}{R} - k\frac{\cos kR}{R^2}\right)\mathbf{u}_\theta \\ &\quad (\text{in } V) \end{aligned} \tag{10.99}$$

$$\begin{aligned}\mathbf{H}'_{0m} &= ka\cos ka\ \text{grad}\left(\frac{\cos\theta}{R^2}\right) \\ &= -\frac{2ka\cos ka}{R^3}\cos\theta\,\mathbf{u}_R - \frac{ka\cos ka}{R^3}\sin\theta\,\mathbf{u}_\theta \\ &\quad (\text{in } V'). \end{aligned} \tag{10.100}$$

This particular solution confirms the fast decay of the fields outside the sphere. Continuity of $\mathbf{H}$ gives the (asymptotic) condition $\sin k_m a = 0$; that is, $k_m a = m\pi$ (m an integer). This value of $k_m a$ is only valid in the limit $\epsilon_r \to \infty$. To obtain an idea of its accuracy, we will compare the asymptotic $k_m a = \pi$ of the lowest mode ($m = 1$) with two *exact* values: 3.08 for $\epsilon_r = 40$ and 3.11 for $\epsilon_r = 80$. The asymptotic expression for the Q of the mode is

$$Q = \frac{N^3}{2k_m a} = \frac{N^3}{2\pi}. \tag{10.101}$$

This yields $Q = 40$ and 127.5 for the two ϵ_r quoted above, while the exact values are 50 and 141.

To further illustrate the application of the method, some numerical data are given in Figures 10.13 and 10.14 for an important shape, the ring resonator[49] (which becomes a pillbox for $b = 0$). The solid lines in Figure 10.14 are for the dipole mode (with azimuthal currents), the dashed lines for the quadrupole mode, which has the symmetry that would result from metallizing the $z = 0$ plane. The corresponding curves are therefore relevant for a resonator resting on a ground plane. In both cases, the wavenumbers represent a zero-order approximation. Higher order corrections for k_m and Q have been developed for the magnetic dipole mode of the ring.[50] They include terms in $\dfrac{1}{N^2}$ and $\dfrac{1}{N^4}$ in the formula for k_m^2.

10.5.5 Confined Modes

A *mode* is *confined* when its fields, in the limit $N \to \infty$, *do not* leak outside the resonator. This is a strong requirement indeed. Because $\mathbf{H}_{0m} = \mathbf{H}'_{0m}$ on S, $\mathbf{H}_{0m}$ must satisfy

$$\begin{aligned} -\text{curl curl}\,\mathbf{H}_m + k_m^2\mathbf{H}_m &= 0 \qquad (\text{in } V) \\ \mathbf{H}_m &= 0 \qquad (\text{on } S). \end{aligned} \tag{10.102}$$

The sought modes clearly belong to the family of electric eigenvectors of the enclosed cavity bounded by S. There is, however, an important additional requirement: the normal

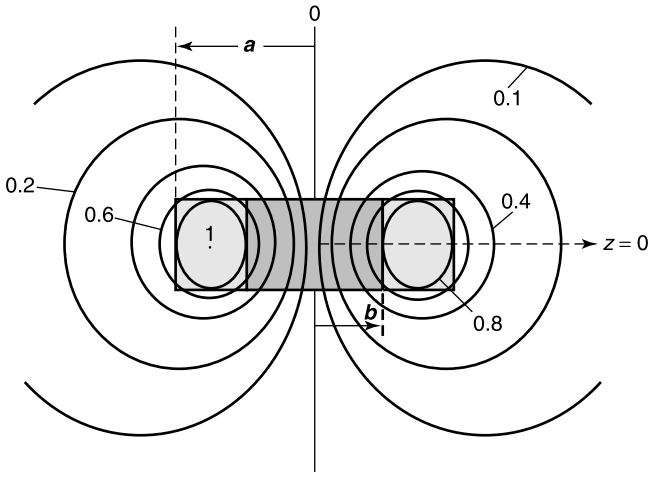

Figure 10.13 Dielectric ring resonator with lines of force of $\mathbf{H}_{0m} = \text{curl}\,(\alpha\,\mathbf{u}_\varphi)$. Curves of contant α (from M. Verplanken and J. Van Bladel, The magnetic-dipole resonances of ring resonators of very high permittivity, *IEEE Trans. MTT* **27**, 328–333, 1979, with permission of IEEE).

component of the eigenvector must also vanish everywhere on S. This condition makes the problem overdetermined for an arbitrary shape of V. The possibility nevertheless exists for bodies of revolution, in which case the sought modes have a magnetic field of the form (Fig. 10.11*b*)

$$\mathbf{H}_{0m} = \beta_m(r, z)\mathbf{u}_\varphi.$$

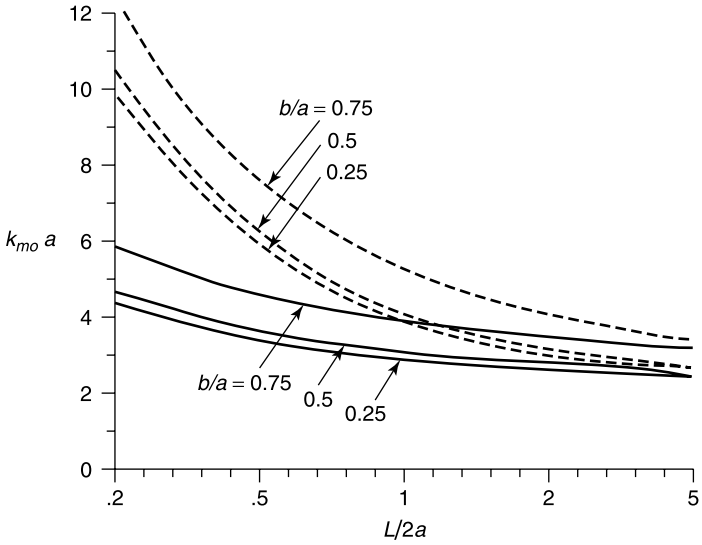

Figure 10.14 Asymptotic value of the resonant wavenumber (from R. De Smedt, Correction due to a finite permittivity for a ring resonator in free space, *IEEE Trans. MTT* **32**, 1288–1292, 1984, with permission of IEEE).

The meridian function β_m satisfies

$$\frac{\partial^2 \beta_m}{\partial r^2} + \frac{1}{r}\frac{\partial \beta_m}{\partial r} - \frac{\beta_m}{r^2} + k_m^2 \beta_m = 0 \qquad \beta_m = 0 \quad \text{(on the axis and on } C\text{)}. \tag{10.103}$$

For a circular cavity of radius a, for example,

$$\beta_{ps} = \sin \frac{p\pi z}{L} J_1\left(x_s \frac{r}{a}\right), \tag{10.104}$$

with $J_1(x_s) = 0$, and

$$k_{ps}^2 = \left(\frac{p\pi}{L}\right)^2 + \left(\frac{x_s}{a}\right)^2.$$

In such a mode, the resonator radiates like an *electric* dipole,[48] with a moment generated by the term in $(\mathbf{H}_2/N^2)$ in expansion (10.88). The resulting Q is proportional to N^5. The sphere, in particular, supports a large number of confined modes, given its special properties of symmetry. For example:

$$\mathbf{H}_{0m} = \sin\theta \left(\frac{\sin kR}{R^2} - k\frac{\cos kR}{R}\right)\mathbf{u}_\varphi. \tag{10.105}$$

Data on $\mathbf{P}_e$ and Q are available for the confined modes of the ring resonator.[51]

10.5.6 The Influence of Conductors

Dielectric resonators are normally located near conductors, which may be ground planes, microstrip lines, or shielding enclosures. The presence of conductors influences the value of both the resonant frequency and the Q of the mode. Several phenomena are involved here: the modification of the radiative losses (they will disappear if the resonator is fully shielded), the losses in the conductor, and the modification of the reactive energy with respect to its free-space value. These factors come more strongly to the fore when the resonator is close to the metal, whose surface is often locally plane (or almost so). It is therefore pertinent to investigate a resonator located above a ground plane, which may be electric or magnetic.[52] Figure 10.15*b* shows some (asymptotic) results for a pillbox in its lowest TE-mode. Clearly, the influence of the wall becomes negligible when $h \gg a$. We note that the theory of weakly coupled resonators, which holds for resonators of arbitrary shape and orientation, may be applied in the present case.[53] The resonances are actually those of the resonator coupled to its image, with symmetries that depend on the nature of the wall, electric or magnetic.

The presence of a ground plane is but a first step in understanding the behavior of the resonator in a realistic environment. Alone, or mounted on top of a ground plane (possibly covered with a substrate),[54] the resonator can function as an antenna with high radiation efficiency,[55] possibly excited by a coaxial conducting probe,[56] by coupling to a microstrip line, or by means of an aperture in a ground plane. There are numerous other applications of dielectric resonators [82], for example to frequency filters.

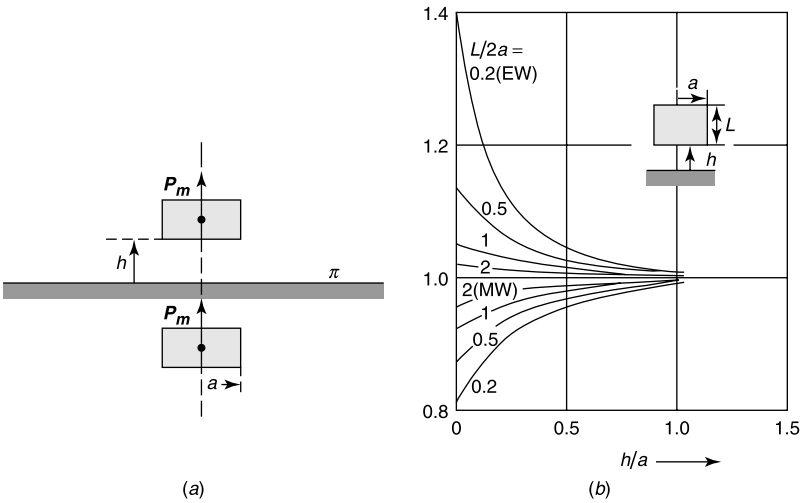

Figure 10.15 (*a*) Circular cylindrical resonator and its image. (*b*) Ratio of the resonant frequency to its value in free space, for both the electric (EW) and magnetic (MW) walls (from R. De Smedt, Dielectric resonator above an electric or magnetic wall, *A.E.Ü.* **37**, 6–14, 1983, with permission of Elsevier Science Publishers).

10.5.7 Dielectric Resonances of Cylinders

The asymptotic method can be extended to the resonances of cylinders.[57,58] The curves in Figure 10.9 display some typical results obtained for the scattering cross section of a circular cylinder. At very low frequencies (i.e., in the *Rayleigh region*), the formulas derived in Section 14.8 may be applied. The asymptotic theory subsequently locates the first few resonant peaks and the shape of the curve in their vicinity. The method has a number of advantages:

1. The curves are derived from formulas that are valid for arbitrary (high) values of N. As a result, no new calculations are required when N is modified to another (large) value.
2. Higher-order corrections are possible to improve the accuracy of the asymptotic predictions.
3. Numerical determination of the peak in an exact method is difficult in the vicinity of a sharp resonance, because the peak may be missed if the density of computed points is too low.
4. The asymptotic formulas can easily determine the effect of a small variation of ϵ_r on parameters such as the resonant frequency and the quality factor Q.

It should finally be remarked that the successive approximate resonances can only be trusted if the corresponding k_m remains much less than $(2\pi N/L)$, a condition that makes sure λ_0 remains much larger than L.

10.6 APERTURE COUPLING

The fields in a cavity can be excited by sources such as coaxial probes or small loops protruding from the wall, or by the action of particle beams shot through the cavity. Aperture

coupling, however, provides the main mechanism. Such coupling is often undesirable, for example when it occurs through small cracks in the wall of a shielded enclosure, or when the strong wave from a lightning discharge penetrates into an aircraft through the plane's windows, and damages the electronic navigation systems. In these examples, the fundamental problem — to be discussed next — is the determination of the fields in regions coupled by a common boundary.

Separation of Variables

The method is applicable to a few simple geometries. Consider, as a first example, a spherical shell provided with a gap across which the tangential field $\mathbf{E}_t$ is prescribed[59] (Fig. 10.16*a*). To simplify matters, assume that the fields are φ-independent, in which case $\mathbf{E}_t$ reduces to its E_θ component. We shall seek to determine the resulting H_φ through a relationship of the form $\mathbf{H}_t = \mathbf{L}(\mathbf{u}_n \times \mathbf{E})$. It is convenient to express the *exterior* fields in terms of a Debye potential. Thus, from Section 7.11,

$$\begin{aligned} \mathbf{E} &= \text{curl curl } (v R \mathbf{u}_R) \\ \mathbf{H} &= j\omega\epsilon_0 \text{ curl } (v R \mathbf{u}_R), \end{aligned} \tag{10.106}$$

with

$$v = \sum_{n=1}^{\infty} A_n h_n^{(2)}(k_0 R) P_n(\cos\theta). \tag{10.107}$$

The summation represents a superposition of TM modes with fields that satisfy equations (7.192). The three mode components are obtained by inserting (10.107) into (10.106), which yields

$$\begin{aligned} E_R &= \sum_{n=1}^{\infty} A_n \frac{n(n+1)}{R} h_n^{(2)}(k_0 R) P_n(\cos\theta) \\ E_\theta &= \sum_{n=1}^{\infty} A_n \frac{1}{R}\frac{d}{dR}\left[R h_n^{(2)}(k_0 r)\right]\frac{d}{d\theta}[P_n(\cos\theta)] \\ H_\varphi &= -\sum_{n=1}^{\infty} j\omega\epsilon_0 A_n h_n^{(2)}(k_0 R)\frac{d}{d\theta}[P_n(\cos\theta)]. \end{aligned} \tag{10.108}$$

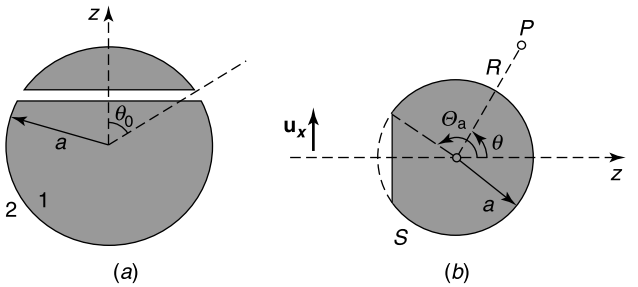

Figure 10.16 (*a*) Perfectly conducting shell with circumferential gap. (*b*) Spherical shell with circular aperture.

At the boundary, E_θ is given by

$$E_\theta(a,\theta) = -\sum_{n=1}^{\infty} A_n \frac{1}{a} \left\{ \frac{d}{dR}\left[Rh_n^{(2)}(k_0R)\right] \right\}_{R=a} P_n^1(\cos\theta).$$

This value must coincide with the given value $E_\theta(\theta)$. Hence, from (A9.34),

$$A_n = -\frac{a(2n+1)}{2n(n+1)} \frac{\displaystyle\int_0^\pi E_\theta(\theta') P_n^1(\cos\theta') \sin\theta' d\theta'}{\left\{ (d/dR)\left[Rh_n^{(2)}(k_0R)\right] \right\}_{R=a}}. \tag{10.109}$$

Inserting this value of A_n into (10.108) gives H_φ in terms of E_θ, where E_θ appears behind an integral sign. This is the sought relationship $H_\varphi = L(E_\theta)$. A similar analysis may be conducted for the *interior* of the sphere, with $h_n^{(2)}(k_0R)$ replaced by $j_n(k_0R)$ and A_n by B_n. In the presence of sources (e.g., an incident plane wave), the unknown E_θ can be determined by requiring the two $L(E_\theta)$ to be equal at the boundary. The solution of that difficult problem is not always necessary. If the aperture is a narrow gap across which a voltage V is applied, the tangential electric field is of the form $\mathbf{E}_{\tan} = (V/a)\delta(\theta - \theta_0)\mathbf{u}_\theta$. It follows that the value of A_n in (10.109) reduces to

$$A_n = -\frac{a(2n+1)}{2n(n+1)} \frac{P_n^1(\cos\theta_0)\sin\theta_0}{\left\{ (d/dR)\left[Rh_n^{(2)}(k_0R)\right] \right\}_{R=a}} \frac{V}{a}. \tag{10.110}$$

From these values of A_n, it is easy to derive expressions for the far field in region 2, in particular when the gap is narrow and the radius a of the sphere is much less than λ_0 [22].

As a second example, we investigate the more difficult problem of a spherical shell with a circular aperture, immersed in an incident plane wave $\mathbf{E}^i = \mathbf{u}_x e^{-jk_0z}$ [91] (Fig. 10.16*b*). Both angles θ and φ are now involved in the analysis.[§§] The incident fields should be expressed in spherical coordinates. We examine these expressions in detail, because they are useful for all scattering problems involving spherical shells or spherical volumes. Thus, for a field of unit amplitude,

$$\begin{aligned} \mathbf{E}^i &= \mathbf{u}_x e^{-jk_0z} = \mathbf{u}_x e^{-jk_0R\cos\theta} \\ &= e^{-jk_0R\cos\theta}(\mathbf{u}_R \sin\theta\cos\varphi + \mathbf{u}_\theta \cos\theta\cos\varphi - \mathbf{u}_\varphi \sin\varphi), \end{aligned} \tag{10.111}$$

$$e^{-jk_0R\cos\theta} = \sum_{n=0}^{\infty} A_n P_n(\cos\theta) = \sum_{n=1}^{\infty} (-j)^n (2n+1) P_n(\cos\theta) j_n(k_0R), \tag{10.112}$$

$$\frac{d}{d\theta}(e^{-jk_0R\cos\theta}) = jk_0R\sin\theta\, e^{-jk_0R\cos\theta} = -\sum_{n=0}^{\infty} (-j)^n j_n(k_0R) P_n^1(\cos\theta). \tag{10.113}$$

[§§]The extension to an incident wave of arbitrary polarization and angle of incidence can be found in Note 60.

These equations, together with the recursion formulas for Legendre polynomials and spherical Bessel functions, yield

$$\mathbf{E}^i = \sum_{n=1}^{\infty}(-j)^n \frac{2n+1}{n(n+1)} \left\{ \frac{jn(n+1)}{k_0 R} j_n(k_0 R) P_n^1(\cos\theta)\cos\varphi\, \mathbf{u}_R \right.$$
$$+ \left[\frac{1}{\sin\theta} j_n(k_0 R) P_n^1(\cos\theta) + \frac{j}{k_0 R}\frac{d}{dR}\left[R j_n(k_0 R)\right] \frac{dP_n^1(\cos\theta)}{d\theta} \right] \cos\varphi\, \mathbf{u}_\theta$$
$$\left. - \left[j_n(k_0 R) \frac{dP_n^1(\cos\theta)}{d\theta} + \frac{j}{k_0 R \sin\theta}\frac{d}{dR}\left[R j_n(k_0 R)\right] P_n^1(\cos\theta) \right] \sin\varphi\, \mathbf{u}_\varphi \right\}. \quad (10.114)$$

We shall merely outline the subsequent steps. The form of $\mathbf{E}^i$ shows that the $\cos\varphi$ dependence must be kept for E_R, E_θ, H_φ, and the $\sin\varphi$ dependence for E_φ, H_R, H_θ. According to (7.197), the incident field can be expressed as follows in terms of Debye potentials:

$$\mathbf{E}^i = \text{curl curl}\,(v_i R\mathbf{u}_R) - j\omega\mu_0\,\text{curl}\,(w_i R\mathbf{u}_R) \quad (10.115)$$

$$v_i = \frac{j}{k}\sum_{n=1}^{\infty}\frac{(-j)^n 2n+1}{n(n+1)} j_n(kR)\cos\varphi P_n^1(\cos\theta) \quad (10.116)$$

$$w_i = \frac{j}{\omega\mu_0}\sum_{n=1}^{\infty}\frac{2n+1}{n(n+1)} j_n(kR)\sin\varphi P_n^1(\cos\theta). \quad (10.117)$$

The fields inside the spherical shell can similarly be written as

$$\mathbf{E} = \text{curl curl}\,(vR\mathbf{u}_R) - j\omega\mu_0\,\text{curl}\,(wR\mathbf{u}_R) \quad (10.118)$$

$$\mathbf{H} = j\omega\epsilon_0\,\text{curl}\,(vR\mathbf{u}_R) + \text{curl curl}\,(wR\mathbf{u}_R). \quad (10.119)$$

The φ dependence of v and w must be the same as for the incident potentials. Accordingly,

$$v = \frac{j}{k_0}\cos\varphi\sum_{n=1}^{\infty}(-j)^n\frac{2n+1}{n(n+1)} c_n j_n(k_0 R) P_n^1(\cos\theta) \quad (10.120)$$

$$w = \frac{j}{\omega\mu_0}\sin\varphi\sum_{n=1}^{\infty}(-j)^n\frac{2n+1}{n(n+1)} d_n j_n(k_0 R) P_n^1(\cos\theta), \quad (10.121)$$

where c_n and d_n must be determined. Outside the shell, the Debye potentials consist of an incident part (10.116), (10.117), and a part contributed by the scattered fields. Thus,

$$v_{\text{out}} = \frac{j}{k_0}\sum_{n=1}^{\infty}(-j)^n\frac{2n+1}{n(n+1)}\cos\varphi P_n^1(\cos\theta)\left[j_n(k_0 R) - a_n h_n^{(2)}(k_0 R)\right] \quad (10.122)$$

$$w_{\text{out}} = \frac{j}{\omega\mu_0}\sum_{n=1}^{\infty}(-j)^n\frac{2n+1}{n(n+1)}\sin\varphi P_n^1(\cos\theta)\left[j_n(k_0 R) - b_n h_n^{(2)}(k_0 R)\right]. \quad (10.123)$$

The unknown coefficients a_n, b_n, c_n, d_n can now be determined by requiring E_θ, E_φ to vanish on the metal (on both sides of the shell) and E_θ, E_φ, H_θ, H_φ to be continuous in the aperture. The procedure yields two infinite sets of equations for a_n and b_n, one holding for $0 < \theta < \theta_a$, and the other for $\theta_a < \theta < \pi$. Convergence of the series expansions is poor and can be remedied by taking into account the singular behavior of the fields close to the edge.[61]

A similar analysis can be applied to the penetration of a plane wave through an elliptic aperture in a spherical shell[62] [24]. The aperture is formed by the intersection of the shell with an elliptic cone with apex at the center of the sphere. The analysis is conducted in *sphero-conal coordinates*, in which the multipole functions involve products of Bessel functions and Lamé products. Details on these techniques are given in Section 16.7.

10.7 GREEN'S DYADICS

A general coupling situation is shown in Figure 10.17. The perfectly conducting boundary S may typically function as a shield for some electronic system located in V_1, while slots and apertures (needed, for example, for heat dissipation or for the in- and out-penetration of cables) tend to jeopardize the shielding effect. Except for a few simple geometries, the determination of important parameters such as the resonant frequencies, or the shielding efficiency, must rely on numerical approaches, typically of a FDTD or FETD nature.[63,64,65] These powerful techniques are applicable to cavities with complex geometries, possibly filled with strongly inhomogeneous media. As a starting point for the discussion, we take the equation satisfied by the electric field in the cavity, viz.

$$-\text{curl curl}\,\mathbf{E} + k^2\mathbf{E} = j\omega\mu\,\mathbf{J}. \tag{10.124}$$

This equation can be solved, in weak form, by multiplying both members with testing vectors $\mathbf{w}_k$. The same procedure can be applied to the exterior region, bounded by a surface on which an absorbing boundary condition (*ABC*) is applied (see Section 12.6). Details of the method can be found in [192], [203], and [211]. In the FDTD approach, the penetration of an electromagnetic wave into the cavity can be followed, in the time domain, by tracking the fields as they propagate toward the cavity, and ultimately "hit" wall and aperture.[63,64] The relevant techniques, based on finite differences, are discussed in Section 12.8, and the combination of FDTD and ray tracing is briefly discussed in Section 13.5. Time-domain techniques can serve to identify resonant frequencies by Fourier transforming the data obtained in the time domain.[65,66] Notwithstanding these vast capabilities, coupled to the flexibility of the TD methods, there is considerable merit in formulating the penetration

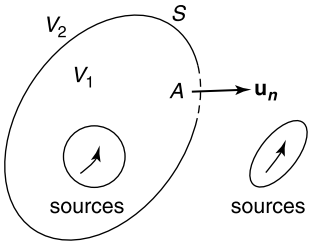

Figure 10.17 Two regions coupled by an aperture.

problem in terms of Green's dyadics, an approach that sheds much clarity on the fundamental coupling mechanism. It is described in the remainder of the section.

10.7.1 Green's Dyadics for the Exterior Region

We shall first derive expressions for the dyadics associated with *electric* current sources [192]. Let $\mathbf{J}^a(\mathbf{r})$ and $\mathbf{J}^b(\mathbf{r})$ denote two current sources located in the exterior region 2 (Fig. 10.18). The generated electric fields satisfy, respectively,

$$\begin{aligned} -\text{curl curl}\,\mathbf{E}^a + k_0^2\mathbf{E}^a &= j\omega\mu_0\,\mathbf{J}^a \\ -\text{curl curl}\,\mathbf{E}^b + k_0^2\mathbf{E}^b &= j\omega\mu_0\,\mathbf{J}^b. \end{aligned} \tag{10.125}$$

Using (A1.33), and taking the radiation condition (7.90) into account, leads to the "reaction" result

$$\begin{aligned} &\int_S \Big[(\mathbf{u}_n \times \mathbf{E}^a)\cdot \text{curl}\,\mathbf{E}^b - (\mathbf{u}_n \times \mathbf{E}^b)\cdot\text{curl}\,\mathbf{E}^a\Big]\,dS \\ &\quad = j\omega\mu_0\left[\int_{V_a}\mathbf{J}^a\cdot\mathbf{E}^b\,dV - \int_{V_b}\mathbf{J}^b\cdot\mathbf{E}^a\,dV\right]. \end{aligned} \tag{10.126}$$

Let us introduce a Green's vector $\mathbf{G}_x$, which satisfies

$$-\text{curl curl}\,\mathbf{G}_x(\mathbf{r}|\mathbf{r}_0) + k_0^2\mathbf{G}_x(\mathbf{r}|\mathbf{r}_0) = \delta(\mathbf{r}-\mathbf{r}_0)\,\mathbf{u}_x. \tag{10.127}$$

and the radiation conditions. Applying (A1.33) to $\mathbf{G}_x$ and an arbitrary current $\mathbf{J}$ gives, when $\mathbf{r}_0$ lies in the exterior region V_2,

$$\begin{aligned} E_x(\mathbf{r}_0) &= j\omega\mu_0\int_{V_2}\mathbf{J}(\mathbf{r})\cdot\mathbf{G}_x(\mathbf{r}|\mathbf{r}_0)\,dV \\ &\quad + \int_S\left[-[\mathbf{u}_n\times\mathbf{G}_x(\mathbf{r}|\mathbf{r}_0)]\cdot\text{curl}\,\mathbf{E}(\mathbf{r}) + (\mathbf{u}_n\times\mathbf{E})\cdot\text{curl}\,\mathbf{G}_x(\mathbf{r}|\mathbf{r}_0)\right]dS. \end{aligned} \tag{10.128}$$

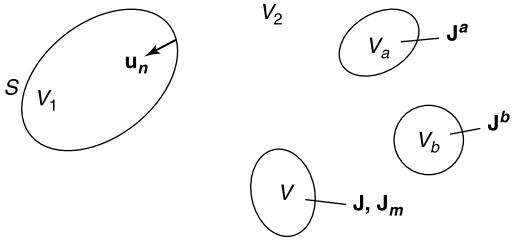

Figure 10.18 Exterior electric current sources.

When $\mathbf{r}_0$ lies in V_1, the left-hand term of the equation vanishes. Repeating the procedure for sources $\delta(\mathbf{r}-\mathbf{r}_0)\mathbf{u}_y$ and $\delta(\mathbf{r}-\mathbf{r}_0)\mathbf{u}_z$ yields, for the total field $\mathbf{E}$, at a point $\mathbf{r}_0$ in V_2

$$\begin{aligned}\mathbf{E}(\mathbf{r}_0) = j\omega\mu_0 \int_{V_2} \mathbf{J}(\mathbf{r})\cdot\left[\mathbf{G}_x(\mathbf{r}|\mathbf{r}_0)\mathbf{u}_x + \mathbf{G}_y(\mathbf{r}|\mathbf{r}_0)\mathbf{u}_y + \mathbf{G}_z(\mathbf{r}|\mathbf{r}_0)\mathbf{u}_z\right] dV \\ + \int_S (\mathbf{u}_n \times \operatorname{curl}\mathbf{E})\cdot\left[\mathbf{G}_x(\mathbf{r}|\mathbf{r}_0)\mathbf{u}_x + \mathbf{G}_y(\mathbf{r}|\mathbf{r}_0)\mathbf{u}_y + \mathbf{G}_z(\mathbf{r}|\mathbf{r}_0)\mathbf{u}_z\right] dS \\ + \int_S (\mathbf{u}_n \times \mathbf{E})\cdot\left[\operatorname{curl}\mathbf{G}_x(\mathbf{r}|\mathbf{r}_0)\mathbf{u}_x + \operatorname{curl}\mathbf{G}_y(\mathbf{r}|\mathbf{r}_0)\mathbf{u}_y + \operatorname{curl}\mathbf{G}_z(\mathbf{r}|\mathbf{r}_0)\mathbf{u}_z\right] dS.\end{aligned} \tag{10.129}$$

This can be written more compactly as

$$\begin{aligned}\mathbf{E}(\mathbf{r}_0) = j\omega\mu_0 \int_{V_2} \mathbf{J}(\mathbf{r})\cdot\overline{\overline{G}}(\mathbf{r}|\mathbf{r}_0)\, dV + j\omega\mu_0 \int_S \mathbf{J}_S\cdot\overline{\overline{G}}(\mathbf{r}|\mathbf{r}_0)\, dS \\ + \int_S \mathbf{J}_{mS}\cdot\operatorname{curl}\overline{\overline{G}}(\mathbf{r}|\mathbf{r}_0)\, dS\end{aligned} \tag{10.130}$$

where $\mathbf{J}_S = \mathbf{H}\times\mathbf{u}_n$ and $\mathbf{J}_{mS} = \mathbf{u}_n \times \mathbf{E}$. In (10.130), the volume integral represents the contribution from the sources in V_2 (radiating in free space), and the sum of the surface integrals represents the contribution from the sources in region 1. We note that the expressions for $\mathbf{J}_S$ and $\mathbf{J}_{mS}$ are in agreement with the Huygens values given in (7.225).

By comparing (10.130) with (7.139), we may conclude that $\overline{\overline{G}}(\mathbf{r}|\mathbf{r}_0)$ is the *total* free-space dyadic defined in (7.137). This dyadic is strongly singular when $\mathbf{r}\to\mathbf{r}_0$, and should be evaluated according to (7.135) when $\mathbf{r}$ is in the source volume V [46]. The singularity problem is even more delicate for the last surface integral in (10.130), which has a factor curl $\overline{\overline{G}}(\mathbf{r}|\mathbf{r}_0)$ in its integrand. Techniques to handle this difficulty are discussed in Chapter 12. For the remainder of this section, we shall assume that $\mathbf{r}_0 \neq \mathbf{r}$ (i.e., *that* $\mathbf{r}_0$ *is neither in* V *nor on* S, but typically denotes a point at large distances), in which case the dyadic can serve to evaluate the radiated fields.

It is useful to write out the nine components of $\overline{\overline{G}}(\mathbf{r}|\mathbf{r}_0)$ in full. Thus,

$$\overline{\overline{G}}(\mathbf{r}|\mathbf{r}_0) = \begin{pmatrix} \mathbf{u}_x\cdot\mathbf{G}_x(\mathbf{r}|\mathbf{r}_0) & \mathbf{u}_x\cdot\mathbf{G}_y(\mathbf{r}|\mathbf{r}_0) & \mathbf{u}_x\cdot\mathbf{G}_z(\mathbf{r}|\mathbf{r}_0) \\ \mathbf{u}_y\cdot\mathbf{G}_x(\mathbf{r}|\mathbf{r}_0) & \mathbf{u}_y\cdot\mathbf{G}_y(\mathbf{r}|\mathbf{r}_0) & \mathbf{u}_y\cdot\mathbf{G}_z(\mathbf{r}|\mathbf{r}_0) \\ \mathbf{u}_z\cdot\mathbf{G}_x(\mathbf{r}|\mathbf{r}_0) & \mathbf{u}_z\cdot\mathbf{G}_y(\mathbf{r}|\mathbf{r}_0) & \mathbf{u}_z\cdot\mathbf{G}_z(\mathbf{r}|\mathbf{r}_0) \end{pmatrix}. \tag{10.131}$$

The detailed form of curl $\overline{\overline{G}}$ is obtained from (10.131) by replacing $\mathbf{G}$ by curl $\mathbf{G}$. We shall now specialize the general $\overline{\overline{G}}$ dyadic to the specific forms $\overline{\overline{G}}_{ee}$ and $\overline{\overline{G}}_{mm}$, where $\overline{\overline{G}}_{ee}$ has been defined for free space in Section 7.9 [210]. Let the vectors $\mathbf{G}_i (i = x, y, z)$ first satisfy the *Dirichlet boundary condition*[¶¶]

$$\mathbf{u}_n(\mathbf{r})\times\mathbf{G}_i(\mathbf{r}|\mathbf{r}_0) = 0 \qquad (\mathbf{r}\text{ on }S). \tag{10.132}$$

[¶¶]From (10.127), div $\overline{\overline{G}}(\mathbf{r}|\mathbf{r}_0) = 0$ for $\mathbf{r}\neq\mathbf{r}_0$, which means that the dyadic satisfies an *electric* boundary condition on S.

Methods to determine vectors such as $\mathbf{G}_i$ are discussed in detail in Chapter 12. Once these vectors are found, they can be combined to construct an *electric dyadic* $\overline{\overline{G}}_{ee}(\mathbf{r}|\mathbf{r}_0)$, which in turn allows writing the electric field in the form

$$\mathbf{E}(\mathbf{r}_0) = j\omega\mu_0 \int_V \mathbf{J}(\mathbf{r}) \cdot \overline{\overline{G}}_{ee}(\mathbf{r}|\mathbf{r}_0)\, dV + \int_S \mathbf{J}_{mS}(\mathbf{r}) \cdot \text{curl}\, \overline{\overline{G}}_{ee}(\mathbf{r}|\mathbf{r}_0)\, dS. \tag{10.133}$$

$\overline{\overline{G}}_{ee}$ is endowed with an important reciprocity property, which can easily be derived by applying (10.126) to the sources $\mathbf{J}^a = \delta(\mathbf{r} - \mathbf{r}_1)\mathbf{u}_i$ and $\mathbf{J}^b = \delta(\mathbf{r} - \mathbf{r}_2)\mathbf{u}_k$. The result is

$$\mathbf{u}_i \cdot \mathbf{G}_k(\mathbf{r}_2|\mathbf{r}_1) = \mathbf{u}_k \cdot \mathbf{G}_i(\mathbf{r}_1|\mathbf{r}_2) \tag{10.134}$$

or, in terms of the full dyadic,

$$\overline{\overline{G}}^t_{ee}(\mathbf{r}|\mathbf{r}_0) = \overline{\overline{G}}_{ee}(\mathbf{r}_0|\mathbf{r}). \tag{10.135}$$

By virtue of this property, the volume integral in (10.133) (i.e., the electric field with short-circuited S) can be written as

$$\mathbf{E}(\mathbf{r}_0) = j\omega\mu_0 \int_{V_z} \overline{\overline{G}}_{ee}(\mathbf{r}_0|\mathbf{r}) \cdot \mathbf{J}(\mathbf{r})\, dV. \tag{10.136}$$

In this more traditional form, the field point $\mathbf{r}_0$ appears *first* in $\overline{\overline{G}}_{ee}(\mathbf{r}_0|\mathbf{r})$, followed by the source point $\mathbf{r}$. The magnetic field generated by $\mathbf{J}(\mathbf{r})$ can be formally derived from (10.136) by taking the curl of both members. The volume integral, for example, gives rise to a contribution

$$\mathbf{H}(\mathbf{r}_0) = -\frac{1}{j\omega\mu_0} \text{curl}_0\, \mathbf{E}(\mathbf{r}_0) = -\int_V \text{curl}_0\, \overline{\overline{G}}_{ee}(\mathbf{r}_0|\mathbf{r}) \cdot \mathbf{J}(\mathbf{r})\, dV. \tag{10.137}$$

As in (7.125), this relationship can be put in the form

$$\mathbf{H}(\mathbf{r}_0) = \int_V \overline{\overline{G}}_{me}(\mathbf{r}_0|\mathbf{r}) \cdot \mathbf{J}(\mathbf{r})\, dV, \tag{10.138}$$

with

$$\overline{\overline{G}}_{me}(\mathbf{r}_0|\mathbf{r}) = -\text{curl}_0\, \overline{\overline{G}}_{ee}(\mathbf{r}_0|\mathbf{r}). \tag{10.139}$$

In the presence of *magnetic* sources $\mathbf{J}_m$, a *magnetic Green's dyadic* $\overline{\overline{G}}_{mm}$ must be introduced. It is constructed from vectors satisfying the *Neumann boundary condition*[‖‖]

$$\mathbf{u}_n(\mathbf{r}) \times \text{curl}\, \mathbf{G}_i(\mathbf{r}|\mathbf{r}_0) = 0 \qquad (\mathbf{r} \text{ on } S). \tag{10.140}$$

[‖‖] For $\mathbf{r}_0$ on S, (10.127) implies that

$$\mathbf{u}_n \cdot \mathbf{G}_i = \frac{1}{k_0^2}\, \mathbf{u}_n \cdot \text{curl}\, (\text{curl}\, \mathbf{G}_i) = -\frac{1}{k_0^2}\, \text{div}_S\, [\mathbf{u}_n \times \text{curl}\, \mathbf{G}_i] = 0.$$

$\mathbf{G}_i$ therefore satisfies the *magnetic* boundary condition (10.10).

The $\mathbf{G}_i$ vectors must still satisfy (10.127). Starting with the differential equation for $\mathbf{H}$, viz.

$$-\text{curl curl}\,\mathbf{H} + k_0^2\mathbf{H} = j\omega\epsilon_0\,\mathbf{J}_m, \tag{10.141}$$

we repeat the steps leading to (10.130), and obtain

$$\begin{aligned}\mathbf{H}(\mathbf{r}_0) &= j\omega\epsilon_0 \int_V \mathbf{J}_m(\mathbf{r})\cdot\left[\mathbf{G}_x(\mathbf{r}|\mathbf{r}_0)\mathbf{u}_x + \mathbf{G}_y(\mathbf{r}|\mathbf{r}_0)\mathbf{u}_y + \mathbf{G}_z(\mathbf{r}|\mathbf{r}_0)\mathbf{u}_z\right] dV \\ &\quad + j\omega\epsilon_0 \int_S (\mathbf{u}_n\times\mathbf{E})\cdot\left[\mathbf{G}_x(\mathbf{r}|\mathbf{r}_0)\mathbf{u}_x + \mathbf{G}_y(\mathbf{r}|\mathbf{r}_0)\mathbf{u}_y + \mathbf{G}_z(\mathbf{r}|\mathbf{r}_0)\mathbf{u}_z\right] dS \\ &= j\omega\epsilon_0 \int_V \overline{\overline{G}}_{mm}(\mathbf{r}_0|\mathbf{r})\cdot\mathbf{J}_m(\mathbf{r})\,dV + j\omega\epsilon_0 \int_S \overline{\overline{G}}_{mm}(\mathbf{r}_0|\mathbf{r})\cdot\mathbf{J}_{mS}(\mathbf{r})\,dS. \end{aligned}\tag{10.142}$$

If we set $\mathbf{r}_0$ on S, the volume integral is seen to represent the $\mathbf{H}$ field with short-circuited S, that is, the *generator* field denoted by $\mathbf{H}_2^g$ in (8.187). The surface integral, on the other hand, represents the $\mathbf{H}(\mathbf{J}_{mS})$ term in the same equation. Further,

$$\begin{aligned}\mathbf{E}(\mathbf{r}_0) &= \frac{1}{j\omega\epsilon_0}\text{curl}_0\,\mathbf{H} = \int_V \text{curl}_0\,\overline{\overline{G}}_{mm}(\mathbf{r}_0|\mathbf{r})\cdot\mathbf{J}_m(\mathbf{r})\,dV \\ &\quad + \int_S \text{curl}_0\,\overline{\overline{G}}_{mm}(\mathbf{r}_0|\mathbf{r})\cdot\mathbf{J}_{mS}(\mathbf{r})\,dS. \end{aligned}\tag{10.143}$$

10.7.2 Green's Dyadics for the Interior Region

The form of the relevant dyadics can be derived, by mere inspection, from (10.28) and (10.29). With the notations $\epsilon_c = \epsilon - j\dfrac{\sigma}{\omega}$ and $k_c^2 = \omega^2\mu\epsilon_c$, we find

$$\begin{aligned}\overline{\overline{G}}_{ee}^{st}(\mathbf{r}|\mathbf{r}') &= \frac{1}{k_c^2}\sum_m \mathbf{f}_m(\mathbf{r})\mathbf{f}_m(\mathbf{r}') & \overline{\overline{G}}_{mm}^{st}(\mathbf{r}|\mathbf{r}') &= \frac{1}{k_c^2}\sum_m \mathbf{g}_m(\mathbf{r})\mathbf{g}_m(\mathbf{r}') \\ \overline{\overline{G}}_{ee}^{r}(\mathbf{r}|\mathbf{r}') &= \sum_m \frac{\mathbf{e}_m(\mathbf{r})\mathbf{e}_m(\mathbf{r}')}{k_c^2 - k_m^2} & \overline{\overline{G}}_{mm}^{r}(\mathbf{r}|\mathbf{r}') &= \sum_m \frac{\mathbf{h}_m(\mathbf{r})\mathbf{h}_m(\mathbf{r}')}{k_c^2 - k_m^2} \\ \overline{\overline{G}}_{em}^{r}(\mathbf{r}|\mathbf{r}') &= \sum_m \frac{k_m\mathbf{e}_m(\mathbf{r})\mathbf{h}_m(\mathbf{r}')}{k_c^2 - k_m^2} & \overline{\overline{G}}_{me}^{r}(\mathbf{r}|\mathbf{r}') &= -\sum_m \frac{k_m\mathbf{h}_m(\mathbf{r})\mathbf{e}_m(\mathbf{r}')}{k_c^2 - k_m^2}, \end{aligned}\tag{10.144}$$

where the superscripts "*st*" and "*r*" stand for *static* and *resonant*, respectively. Equations (10.28) and (10.29) become

$$\begin{aligned}\mathbf{E}(\mathbf{r}) &= j\omega\mu\int_V \overline{\overline{G}}_{ee}(\mathbf{r}|\mathbf{r}')\cdot\mathbf{J}(\mathbf{r}')\,dV' + \int_V \overline{\overline{G}}_{em}(\mathbf{r}|\mathbf{r}')\cdot\mathbf{J}_m(\mathbf{r}')\,dV' \\ &\quad + \int_S \overline{\overline{G}}_{em}(\mathbf{r}|\mathbf{r}')\cdot\mathbf{J}_{mS}(\mathbf{r}')\,dS', \end{aligned}\tag{10.145}$$

$$\begin{aligned}\mathbf{H}(\mathbf{r}) &= \int_V \overline{\overline{G}}_{me}(\mathbf{r}|\mathbf{r}')\cdot\mathbf{J}(\mathbf{r}')\,dV' + j\omega\epsilon_c\int_V \overline{\overline{G}}_{mm}(\mathbf{r}|\mathbf{r}')\cdot\mathbf{J}_m(\mathbf{r}')\,dV' \\ &\quad + j\omega\epsilon_c\int_S \overline{\overline{G}}_{mm}(\mathbf{r}|\mathbf{r}')\cdot\mathbf{J}_{mS}(\mathbf{r}')\,dS', \end{aligned}\tag{10.146}$$

where we have set

$$\begin{aligned}\overline{\overline{G}}_{ee}(\mathbf{r}|\mathbf{r}') &= \overline{\overline{G}}^{st}_{ee}(\mathbf{r}|\mathbf{r}') + \overline{\overline{G}}^{r}_{ee}(\mathbf{r}|\mathbf{r}') \\ \overline{\overline{G}}_{mm}(\mathbf{r}|\mathbf{r}') &= \overline{\overline{G}}^{st}_{mm}(\mathbf{r}|\mathbf{r}') + \overline{\overline{G}}^{r}_{mm}(\mathbf{r}|\mathbf{r}').\end{aligned} \tag{10.147}$$

It is apparent, from (10.144), that $\overline{\overline{G}}_{ee}(\mathbf{r}|\mathbf{r}') = \overline{\overline{G}}^{t}_{ee}(\mathbf{r}'|\mathbf{r})$, precisely the reciprocity property (10.135) that holds for the exterior Green's dyadic. Similarly $\overline{\overline{G}}_{mm}(\mathbf{r}|\mathbf{r}') = \overline{\overline{G}}^{t}_{mm}(\mathbf{r}'|\mathbf{r})$. It is further clear, from (10.144), that the static term in a lossless medium prevails in the limit $k_0 \to 0$. That term can be interpreted by recognizing that (10.28) is actually the electric splitting

$$\mathbf{E} = -\text{grad}\ \phi - j\omega\,\mathbf{A}, \tag{10.148}$$

with $\phi = 0$ on S. In the Coulomb gauge, with div $\mathbf{A} = 0$, (10.148) can be written in the form

$$\mathbf{E} = -\text{grad}\ \phi + \text{curl}\ \mathbf{v}.$$

The first term stems from $\overline{\overline{G}}^{st}_{ee}$, the second one from $\overline{\overline{G}}^{r}_{ee}$. It is shown in Section 7.9 that the fundamental singularity of $\overline{\overline{G}}_{ee}$ resides with the static term, which is the source of the poor convergence of a series such as (10.28) when $\mathbf{r}$ approaches a source point $\mathbf{r}'$. Improved convergence is obtained by isolating that singularity, and writing, from (7.136),

$$\overline{\overline{G}}_{ee}(\mathbf{r}|\mathbf{r}') = -\frac{1}{4\pi k^2}\ \text{grad grad}\left(\frac{1}{|\mathbf{r}-\mathbf{r}'|}\right) + \overline{\overline{G}}^{1}_{ee}(\mathbf{r}|\mathbf{r}'). \tag{10.149}$$

The remainder dyadic $\overline{\overline{G}}^{1}_{ee}$ still contains a $|\mathbf{r}-\mathbf{r}'|^{-1}$ singularity, but this can also be isolated[67] (Problem 10.11).

10.7.3 Aperture Coupling

With reference to Figure 10.17, the fundamental equations are

$$\mathbf{H}_1 = \mathbf{H}^g_1 + \mathbf{H}_1(\mathbf{u}_n \times \mathbf{E}) = \mathbf{H}^g_1 + \mathbf{L}_1(\mathbf{J}_{mS}) \tag{10.150}$$

in region 1, and

$$\mathbf{H}_2 = \mathbf{H}^g_2 + \mathbf{H}_2(-\mathbf{u}_n \times \mathbf{E}) = \mathbf{H}^g_2 - \mathbf{L}_2(\mathbf{J}_{mS}) \tag{10.151}$$

in region 2. The notation is that of Section 8.7. The main unknown is $\mathbf{J}_{mS} = \mathbf{u}_n \times \mathbf{E}$, the surface magnetic current relative to region 1. To determine $\mathbf{J}_{mS}$, we express continuity of the tangential component of $\mathbf{H}$ in the aperture. Thus,

$$\mathbf{H}_{1t}(\mathbf{r}) = \mathbf{H}^g_1(\mathbf{r}) + \mathbf{L}_{1t}\,[\mathbf{J}_{mS}(\mathbf{r})] = \mathbf{H}^g_2(\mathbf{r}) - \mathbf{L}_{2t}\,[\mathbf{J}_{mS}(\mathbf{r})] \qquad (\mathbf{r}\ \text{in}\ A). \tag{10.152}$$

It is shown in Section 8.7 that this equation leads to the (symbolic) equivalent circuit of Figure 8.23. The operator $\mathbf{L}_1$ can be identified by referring to the various dyadics introduced

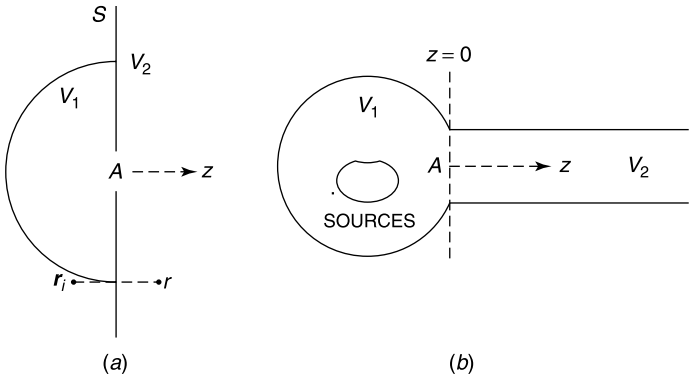

Figure 10.19 (*a*) Cavity coupled to a half-space. (*b*) Cavity coupled to a waveguide.

in (10.144). Assume, for example, that cavity V_1 does not contain any sources. For such a case,

$$\mathbf{H}_1(\mathbf{r}) = j\omega\epsilon_c \left[\int_S \overline{\overline{G}}_{mm}(\mathbf{r}|\mathbf{r}') \cdot \mathbf{J}_{mS}(\mathbf{r}')\, dS' \right]_t = \mathbf{L}_1(\mathbf{J}_{mS}), \tag{10.153}$$

while in the closed cavity containing electric currents $\mathbf{J}$,

$$\mathbf{H}_1(\mathbf{r}) = \mathbf{H}_1^g(\mathbf{r}) = \int_V \overline{\overline{G}}_{me}(\mathbf{r}|\mathbf{r}') \cdot \mathbf{J}(\mathbf{r}')\, dV'. \tag{10.154}$$

The form of these dyadics can sometimes be determined by separation of variables, for example when the boundary surface S is spherical [210]. The solution of the two spherical problems discussed in Section 10.6 actually involves steps that coincide with those resulting from the use of a Green's dyadic. Two types of region are particularly important for applications: the half-infinite space and the cylindrical waveguide.

Consider first a half-infinite space bounded by a perfectly conducting screen (Fig. 10.19*a*). Such an infinite screen is often used as a model to represent a planar surface of limited, but fairly large extent (e.g., the wall of a perfectly conducting parallelepiped). The $\overline{\overline{G}}_{ee}$ and $\overline{\overline{G}}_{mm}$ dyadics of V_2 can be synthesized by the method of images, starting from the free-space dyadic

$$\begin{aligned} \overline{\overline{G}}_f(\mathbf{r}_0|\mathbf{r}) &= -\frac{1}{4\pi}\left(\bar{\bar{I}} + \frac{1}{k_0^2}\,\text{grad grad}\right)\frac{e^{-jk_0|\mathbf{r}-\mathbf{r}_0|}}{|\mathbf{r}-\mathbf{r}_0|} \\ &= -\frac{1}{4\pi k_0^2}\,\text{curl curl}\left(\frac{e^{-jk_0|\mathbf{r}-\mathbf{r}_0|}}{|\mathbf{r}-\mathbf{r}_0|}\,\bar{\bar{I}}\right). \end{aligned} \tag{10.155}$$

Guided by Figure 9.3 we write, for example,

$$\begin{aligned} \overline{\overline{G}}_{ee}(\mathbf{r}_0|\mathbf{r}) &= \big[\mathbf{G}_{fx}(\mathbf{r}_0|\mathbf{r}) - \mathbf{G}_{fx}(\mathbf{r}_0|\mathbf{r}_i)\big]\mathbf{u}_x + \big[\mathbf{G}_{fy}(\mathbf{r}_0|\mathbf{r}) - \mathbf{G}_{fy}(\mathbf{r}_0|\mathbf{r}_i)\big]\mathbf{u}_y \\ &\quad + \big[\mathbf{G}_{fz}(\mathbf{r}_0|\mathbf{r}) + \mathbf{G}_{fz}(\mathbf{r}_0|\mathbf{r})\big]\mathbf{u}_z \\ &= \overline{\overline{G}}_f(\mathbf{r}_0|\mathbf{r}) - \overline{\overline{G}}_f(\mathbf{r}_0|\mathbf{r}_i) + 2\mathbf{G}_{fz}(\mathbf{r}_0|\mathbf{r})\mathbf{u}_z. \end{aligned} \tag{10.156}$$

A second important exterior region is the cylindrical waveguide of arbitrary cross section S (Fig. 10.19*b*). It is shown in Section 15.3 that the transverse fields in the waveguide (assumed semi-infinite for simplicity) may be represented by modal expansions

$$\mathbf{E}_t(x,y,z) = V_1\mathbf{e}_1 e^{-j\gamma_1 z} + \sum_{m=2}^{\infty} V_m\,\mathbf{e}_m e^{-\delta_m z} \tag{10.157}$$

$$\begin{aligned}\mathbf{H}_t(x,y,z) &= \frac{V_1}{R_1}\mathbf{u}_z \times \mathbf{e}_1 e^{-j\gamma_1 z} + \sum_{m=2}^{\infty}\frac{V_m}{jX_m}(\mathbf{u}_n \times \mathbf{e}_m)\, e^{-\delta_m z} \\ &= I_1\mathbf{h}_1 e^{-j\gamma_1 z} + \sum_{m=2}^{\infty} I_m\mathbf{h}_m\, e^{-\delta_m z},\end{aligned} \tag{10.158}$$

where the subscript t denotes a transverse component; that is, a component in the (x, y) plane. In these expressions it is assumed that only the lowest mode (labeled "1") is propagates, and that all other modes are evanescent. The eigenvectors $\mathbf{e}_m$ are orthonormalized according to the condition

$$\int_A \mathbf{e}_m\cdot\mathbf{e}_n\, dS = \int_A \mathbf{h}_m\cdot\mathbf{h}_n\, dS = \delta_{mn}. \tag{10.159}$$

By means of that condition, V_1 can be expressed as

$$\begin{aligned}V_1 &= \int_A \mathbf{E}_t(x,y,0)\cdot\mathbf{e}_1(x,y)\, dS \\ &= \int_A (\mathbf{u}_z \times \mathbf{E}_t)_{z=0}\cdot\mathbf{h}_1(x,y)\, dS \;=\; \int_A \mathbf{J}_{mS}(x,y)\cdot\mathbf{h}_1(x,y)\, dS.\end{aligned}$$

Inserting this value into (10.158) gives, in the waveguide,

$$\mathbf{H}_t(x,y,z) = \int_A \underbrace{\left[\frac{1}{R_1}\, e^{-j\gamma_1 z}\,\mathbf{h}_1(x,y)\,\mathbf{h}_1(x',y') + \frac{1}{jX_2}\, e^{-\delta_2 z}\,\mathbf{h}_2(x,y)\,\mathbf{h}_2(x',y') + \cdots\right]}_{\overline{\overline{G}}_{mm}(x,y,z|x',y',0)}$$

$$\cdot\mathbf{J}_{mS}(x',y')\, dS'. \tag{10.160}$$

This is precisely the $\mathbf{H}_2(\mathbf{J}_{mS})$ term in Equation (10.151), written here in concrete form to illustrate the meaning of the operator $\mathbf{L}_2$. This relationship may now be projected on the $\mathbf{h}_m$ space, in casu by testing it with the $\mathbf{h}_m$ eigenvectors. If we truncate the series to m terms, this gives

$$\underbrace{\begin{pmatrix} I_1 \\ I_2 \\ \vdots \\ I_m \end{pmatrix}}_{\mathbf{I}} = \underbrace{\begin{pmatrix} \frac{1}{R_1} & & & \\ & \frac{1}{jX_2} & & \\ & & \ddots & \\ & & & \frac{1}{jX_m} \end{pmatrix}}_{\overline{\overline{Y}}_2} \cdot \underbrace{\begin{pmatrix} V_1 \\ V_2 \\ \vdots \\ V_m \end{pmatrix}}_{\mathbf{V}}. \tag{10.161}$$

According to the theory in Section 8.7, the matrix is the admittance $\overline{\overline{Y}}_2$ of region 2, which in this case is the semi-infinite waveguide. The matrix is diagonal — a consequence of the orthogonality property (10.159) — and complex. It becomes imaginary below the cut off frequency of the lowest mode, because R_1 becomes jX_1 under these circumstances. Note that the conductance $\left(\frac{1}{R_1}\right)$ represents the radiative losses associated with the power carried by the lowest mode down the axis of the waveguide.

10.7.4 The Use of Potentials

The strong singularity of a dyadic such as $\overline{\overline{G}}_{mm}(\mathbf{r}|\mathbf{r}')$ can be avoided by formulating the aperture problem in terms of potentials, for which the Green's functions are less singular than their field counterparts. It is the same motivation that led to the introduction of mixed potentials to solve the Sommerfeld problem in Section 9.4. The policy has been applied in Section 9.6 to evaluate the magnetic field that leaks through the aperture in region 2 (Fig. 9.34). That field is given by

$$\begin{aligned}\mathbf{H}_2(\mathbf{r}) &= \frac{1}{j\omega\epsilon_0\mu_0}\,\text{curl curl}\,\mathbf{C}(\mathbf{r}) \\ &= \frac{1}{j\omega\epsilon_0\mu_0}\Big(\text{grad div}\,\mathbf{C} + k_0^2\,\mathbf{C}\Big),\end{aligned} \tag{10.162}$$

where the *Fitzgerald potential* $\mathbf{C}$ is equal to

$$\mathbf{C}(\mathbf{r}) = \frac{\epsilon_0}{2\pi}\int_A (\mathbf{E}(\mathbf{r}')\times\mathbf{u}_z)\,\frac{e^{-jk_0|\mathbf{r}-\mathbf{r}'|}}{|\mathbf{r}-\mathbf{r}'|}\,dS'(\text{Cm}^{-1}).$$

The singularity of the integrand is of the $\left(\frac{1}{R}\right)$ type and is therefore mild. We note that Equation (10.162) can be given the form

$$\mathbf{H} = -\text{grad}\,\psi - j\omega\mathbf{C}, \tag{10.163}$$

which is a *Lorenz splitting*;*** that is, a decomposition based on the condition

$$\text{div}\,\mathbf{C} + j\omega\epsilon_0\mu_0\,\psi = 0. \tag{10.164}$$

Splitting (10.163), introduced in Section (9.6) for a plane boundary, can also be exploited to evaluate the fields outside a boundary of arbitrary shape. The use of potentials ψ and $\mathbf{C}$ is also helpful when the magnetic field must be evaluated as $\mathbf{r}$ approaches a point on the boundary surface S (or in the aperture A) (Fig. 10.19). Over distances $|\mathbf{r}-\mathbf{r}'|$ small with respect to both λ_0 and the radii of curvature of S, $\mathbf{C}$ behaves locally as the potential of a surface layer of charge, to which the important results derived in Section 3.4 may be applied. In the same vein, when the aperture is small (in the sense mentioned above), it

***In the *Helmholtz splitting* discussed in Appendix 1, the condition is div $\mathbf{C} = 0$, which leads to the free-space potential equations $\nabla^2\psi = 0$ and $\nabla^2\mathbf{C} = 0$.

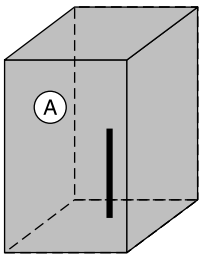

Figure 10.20 Wire in a screened enclosure.

radiates through its electric and magnetic dipoles $\mathbf{P}_e$ and $\mathbf{P}_m$, *located in front of the short-circuited aperture*.[68,69] From (9.220) and (9.223), the moments of these dipoles are, with vacuum in regions 1 and 2,

$$\mathbf{P}_e = \frac{1}{2}\epsilon_0 \overline{\overline{\alpha}}_e \cdot (\mathbf{E}_1^g - \mathbf{E}_2^g)$$
$$\mathbf{P}_m = \frac{1}{2}\overline{\overline{\alpha}}_m \cdot (\mathbf{H}_1^g - \mathbf{H}_2^g). \tag{10.165}$$

The power radiated into region 2 can easily be evaluated when the aperture is located in an infinite screen, as in Figure 9.34. The relevant formulas are (7.159) and (7.167), and they show that the radiative losses are proportional to ω^4. They consequently increase rapidly with frequency. Because $\overline{\overline{\alpha}}_e$ and $\overline{\overline{\alpha}}_m$ are proportional to L^3, where L is a characteristic length of the aperture, the losses will also increase proportionally to L^6, a point confirmed by the value of the transmission cross section of a circular aperture given in (9.225). It follows that increasing L strongly increases the losses and produces a correspondingly strong reduction of the resonant Q's. Illustrative numerical data are available[70] for the geometry of Figure 10.20, where the vertical bar represents an electric dipole, and the side containing the aperture is assumed infinite in extent.[†††] For a cube of edge $a = 50$ cm, for example, a horizontal aperture of dimensions 20 cm $\times$ 5 cm shifts the resonant frequency of one of the modes from 423.97 MHz to 420.0 MHz and introduces a quality factor $Q = 609$. These effects result from the reactive and radiative powers associated with the aperture. When the dimensions of the slot are reduced to 4 cm $\times$ 1 cm, the frequency shift decreases to 20 kHz, and the quality factor associated with the radiative losses rises to a (high) value of $Q = 23.8 \times 10^6$. The moments $\mathbf{P}_e$ and $\mathbf{P}_m$ have another interesting property. Following the steps outlined in Section 9.6, one can easily show that

$$\int_A (\mathbf{u}_n \times \mathbf{E}) \cdot \mathbf{f}\, dS = j\omega\mu_0\, \mathbf{P}_m \cdot \mathbf{f} + \frac{1}{\epsilon_0}\, \mathbf{P}_e \cdot \text{curl}\, \mathbf{f}. \tag{10.166}$$

This formula can be applied to the surface integrals that appear in the (10.28) and (10.29) expansions.

[†††] In Note 70, the fields in the cavity are evaluated by means of an eigenvector expansion, the slow convergence of which is remedied by utilizing an Ewald transform. The same field problem has been solved in Note 71 by means of finite elements in both the frequency and time domains.

PROBLEMS

10.1 Let the $(\overline{\overline{\epsilon}}, \overline{\overline{\mu}})$ sample in Figure 10.1*a* be lossless. For such a case $\overline{\overline{\epsilon}}_r$ and $\overline{\overline{\mu}}_r$ are Hermitian. Reproduce the developments in Sections 10.1 and 10.2, using the scalar products

$$\langle \mathbf{u}, \mathbf{v} \rangle = \int \mathbf{u}^* \cdot \overline{\overline{\epsilon}}_r \cdot \mathbf{v} \, dV$$

or

$$\langle \mathbf{u}, \mathbf{v} \rangle = \int \mathbf{u}^* \cdot \overline{\overline{\mu}}_r \cdot \mathbf{v} \, dV.$$

10.2 Extend the uniqueness proof given in Section 10.1 to lossy walls characterized by a wall impedance $Z_w = (1 + j)R_w$. The resistance R_w is positive, and $\mathbf{E}_{\tan} = Z_w \mathbf{J}_S = Z_w(\mathbf{H} \times \mathbf{u}_n)$.

10.3 Using essentially (A1.32), show that the eigenvectors in (10.6) and (10.8) are orthogonal not only within their own family but also from family to family. Show that the same holds for the magnetic eigenvectors defined in (10.11) and (10.13).

10.4 Prove the self-adjoint and negative-definite characters of the transformations defined in (10.5) and (10.10).

10.5 Show that the solution of $\mathcal{L}_e \mathbf{f} = \mathbf{s}$ can be written in the form

$$\mathbf{f}(\mathbf{r}) = \int_V \underbrace{\left[-\sum_m \frac{\mathbf{f}_m(\mathbf{r}) \mathbf{f}_m(\mathbf{r}')}{\mu_m^2} - \sum_m \frac{\mathbf{e}_m(\mathbf{r}) \mathbf{e}_m(\mathbf{r}')}{k_m^2} \right]}_{\overline{\overline{G}}(\mathbf{r}|\mathbf{r}')} \cdot \mathbf{s}(\mathbf{r}') \, dV'.$$

In region 2, a term in $\mathbf{f}_0$ must be included, in which case the Green's dyadic $\overline{\overline{G}}$ becomes *extended*. Derive a similar relationship for the magnetic problem

$$\nabla^2 \mathbf{f} = s \quad (\text{in } V)$$
$$\mathbf{u}_n \cdot \mathbf{f} = 0 \quad (\text{on } S)$$
$$\mathbf{u}_n \times \operatorname{curl} \mathbf{f} = 0 \quad (\text{on } S).$$

Remember that, in a ring type of region 2, a term in $\mathbf{g}_0$ must be included in the eigenvector expansion [22].

10.6 Show that the eigenvector $\mathbf{f}_0 = \operatorname{grad} \phi_0$ defined in (10.7) is unique when the volume is doubly bounded.

10.7 Assuming (to simplify) that $\epsilon_r = \mu_r = 1$, investigate the null space of the electric and magnetic transformations; that is, the solutions $\mathbf{e}_0$ and $\mathbf{h}_0$ that correspond with the eigenvalue zero (Fig. 10.1). Show (1) that these solutions are harmonic vectors, (2) that $\mathbf{e}_0$ exists only in a doubly bounded region, (3) that $\mathbf{h}_0$ exists only in a doubly connected region.
Hint: Use A1.36, and refer to (10.7) and (10.12).

10.8 Noting that the summation over $\mathbf{f}_m$ in the right-hand term of (10.28) can be written as $(-\operatorname{grad} \phi)$, prove that this summation represents the electrostatic field $\mathbf{E}_0$ produced by the instantaneous electric charges in the cavity. The relevant charge density is (Fig. P10.1).

$$P = -\frac{1}{j\omega} \left[\{\operatorname{div} \mathbf{J}\} - (\mathbf{u}_n \cdot \mathbf{J}) \delta_{S_i} \right] = \epsilon \operatorname{div} \mathbf{E}_0.$$

Show that (10.28) therefore realizes the electric splitting discussed in Appendix 1.

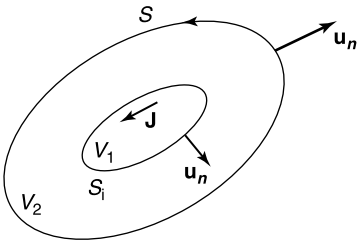

Figure P10.1

10.9 Repeat this analysis for the magnetic field $\mathbf{H}_0$, which is the limit of $\mathbf{H}$ for $k \to 0$ in (10.29). The sources are $\rho_m = -\dfrac{1}{j\omega}\ \text{div}\ \mathbf{J}_m$ and $\rho_{mS} = \dfrac{1}{j\omega}\mathbf{u}_n \cdot \mathbf{J}_m$ on S_i (Fig. 10.1*a*). Show that the terms in $\mathbf{g}_m$ in (10.29) represent $\mathbf{H}_0$.

Hint: Use A1.27 to evaluate $\displaystyle\int \mathbf{H}_0 \cdot \text{grad}\ \psi_n\, dV$, and note that $\mathbf{u}_n \cdot \mathbf{H} = -(\mathbf{u}_n \cdot \text{curl}\ \mathbf{E})/j\omega\mu = \dfrac{1}{j\omega\mu}\ \text{div}_S\ (\mathbf{u}_n \times \mathbf{E})$.

10.10 Show that the expansion of $\left(\mathbf{E} + \dfrac{1}{j\omega\epsilon}\mathbf{J}\right)$ in electric eigenvectors $\mathbf{e}_m$ yields the *resonant* terms in the expansion (10.28) for $\mathbf{E}$, the terms in $\mathbf{f}_m$ being excluded. Compare the convergence properties of the two expansions.
(A. S. Omar et al., *IEEE Trans. MTT* **40**, 1730–1738, 1992.)

10.11 In the Coulomb gauge (div $\mathbf{A} = 0$), the fields are expressed in terms of potentials by

$$\mathbf{E} = -\text{grad}\ \phi - j\omega\mathbf{A} \qquad (\text{div}\ \mathbf{A} = 0)$$

$$\mathbf{H} = \mu^{-1}\ \text{curl}\ \mathbf{A}.$$

Show that, in the presence of interior electric sources [185],

$$\phi(\mathbf{r}) = \epsilon^{-1} \sum_m \phi_m(\mathbf{r}) \left[\int_V \rho(\mathbf{r}')\, \phi_m(\mathbf{r}')\, dV' + \int_S \underbrace{\rho_S(\mathbf{r}')\, \phi_m(\mathbf{r}')\, dS'}_{=0} \right]$$

$$\mathbf{A}(\mathbf{r}) = \mu \sum_m \frac{\mathbf{e}_m(\mathbf{r})}{k_m^2 - k^2} \left[\int_V \mathbf{J}(\mathbf{r}') \cdot \mathbf{e}_m(\mathbf{r}')\, dV' + \int_S \underbrace{\mathbf{J}_S(\mathbf{r}') \cdot \mathbf{e}_m(\mathbf{r}')\, dS'}_{=0} \right].$$

Determine the Green's functions G^ϕ and $\overline{\overline{G}}^A$, by means of which the expansions can be written in compact form. Show that $\overline{\overline{G}}^A$ can be split according to

$$\overline{\overline{G}}^A(\mathbf{r}|\mathbf{r}'|k) = \overline{\overline{G}}^A(\mathbf{r}|\mathbf{r}'|0) + k_c^2 \sum_m \frac{\mathbf{e}_m(\mathbf{r})\, \mathbf{e}_m(\mathbf{r}')}{k_m^2(k_m^2 - k_c^2)}$$

where the low-frequency limit is

$$\overline{\overline{G}}^A(\mathbf{r}|\mathbf{r}'|0) = \frac{1}{8\pi|\mathbf{r} - \mathbf{r}'|} \left(\bar{\bar{I}} + \frac{(\mathbf{r} - \mathbf{r}')(\mathbf{r} - \mathbf{r}')}{|\mathbf{r} - \mathbf{r}'|^2} \right) + \overline{\overline{G}}_1^A.$$

The $\overline{\overline{G}}_1^A$ dyadic is nonsingular [185].

10.12 A circular loop of current of radius b is located in a spherical cavity of radius a, and its center is at a distance d from the center of the cavity. Determine the position of the loop for which maximum excitation of the nth φ-independent TE mode is obtained.
(R. N. Ghose, *IRE Trans. MTT* **5**, 18, 1957.)

10.13 A circular accelerator of rectangular cross section contains a narrow beam of particles of charge density

$$\rho_l = (\rho_l)_{\max}\, g(\varphi - \Omega t) \qquad \text{C m}^{-1}.$$

This cloud of charge rotates with angular velocity Ω. Determine the fields produced by the resulting current.
Hint: Expand $g(\varphi)$ in a Fourier series in φ.

10.14 The circular cavity in Figure P10.2 carries a magnetic field of the form

$$\mathbf{H} = H(r, z)\mathbf{u}_\varphi.$$

Determine the form of $\mathbf{E}$ and $\mathbf{H}$ is regions 1 and 2, knowing that ϵ_r is real and uniform. Determine the lowest resonant frequency ω_r and compare with the value ω_{r0} that holds in the absence of the dielectric. Determine also the resonant frequency in the limit $(b/a) \to 0$ (i.e., for a very thin dielectric post). Show that ω_r is equal to ω_{r0} minus a term proportional to $(b/a)^2$.

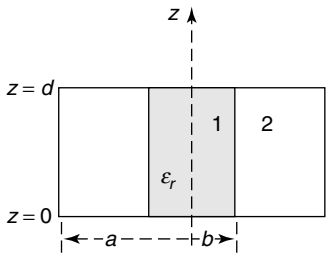

Figure P10.2

10.15 Show that the functionals

$$k^2(\mathbf{E}) = \frac{\displaystyle\int_V \text{curl}\,\mathbf{E}^* \cdot \overline{\overline{\mu}}_r^{-1} \cdot \text{curl}\,\mathbf{E}\, dV}{\displaystyle\int_V \mathbf{E}^* \cdot \overline{\overline{\epsilon}}_r \cdot \mathbf{E}\, dV}; \quad k^2(\mathbf{H}) = \frac{\displaystyle\int_V \text{curl}\,\mathbf{H}^* \cdot \overline{\overline{\epsilon}}_r^{-1} \cdot \text{curl}\,\mathbf{H}\, dV}{\displaystyle\int_V \mathbf{H}^* \cdot \overline{\overline{\mu}}_r \cdot \mathbf{H}\, dV}$$

may be used to determine the eigenvectors in cavities containing anisotropic media. The trial vectors for $k^2(\mathbf{E})$ must be perpendicular to S and must satisfy the equation div $(\overline{\overline{\epsilon}} \cdot \mathbf{E}) = 0$. The trial vectors for $k^2(\mathbf{H})$ must satisfy the conditions div $(\overline{\overline{\mu}} \cdot \mathbf{H}) = 0$ in V and $\mathbf{u}_n \cdot \overline{\overline{\mu}} \cdot \mathbf{H} = 0$ on S.
(A. D. Berk, *IRE Trans. AP* **4**, 104, 1956.)

10.16 Investigate the Euler equations of the functional

$$F(\mathbf{e}, \mathbf{h}) = j\omega \int_V \left[\frac{1}{\epsilon_r} |\mathbf{d} - \epsilon \mathbf{e}|^2 + \frac{1}{\mu_r} |\mathbf{b} - \mu \mathbf{h}|^2 \right] dV$$

where $j\omega\mathbf{d} = \text{curl}\,\mathbf{h}$ and $j\omega\mathbf{b} = -\text{curl}\,\mathbf{e}$. (L. Pichon et al., *IEEE Trans. MAG* **29**, 1595–1600, 1993.)

10.17 Consider the φ-independent modes in the reentrant cavity of Figure 10.3a, and in particular the electric field

$$\mathbf{e} = \frac{R_{co}}{jk_0}\, \text{curl}\,(h\mathbf{u}_\varphi) = \frac{R_{co}}{jk_0^r}\, \text{grad}\,(rh) \times \mathbf{u}_\varphi.$$

The lines of force of $\mathbf{e}$ are given by the equation $rh(r,z) = \text{constant}$. Find an approximate value for the resonant frequency by inserting a suitable trial function in variational principle (10.30). The lines of force in Figure 10.3*a* suggest an appropriate choice for this function in the three regions 1, 2, and 3 [22].

10.18 Show that (10.19) is the Euler equation of the functional

$$J(\mathbf{e}_m) = \int_V \left[\frac{1}{\mu_r}|\text{curl } \mathbf{e}_m|^2 - k_m^2 \epsilon_r |\mathbf{e}_m|^2\right] dV.$$

10.19 The discussion starting with (10.31) is based on the eigenvector $\mathbf{e}_m$. Repeat the argument by focusing on $\mathbf{h}_m$, solution of the dual problem

$$\begin{aligned} -\text{curl curl } \mathbf{h}_m + k_m^2 \mathbf{h}_m &= 0 \qquad (\text{in } V) \\ \mathbf{u}_n \times \text{curl } \mathbf{h}_m &= 0 \qquad (\text{on } S). \end{aligned}$$

10.20 Show that the first-order tetrahedral edge element $\mathbf{f}_{ik} = L_i \text{ grad } L_k - L_k \text{ grad } L_i$ can be put in the general form $\mathbf{f}_{ik} = \boldsymbol{\alpha}_{ik} + (\boldsymbol{\beta}_{ik} \times \mathbf{r})$, where $\boldsymbol{\alpha}_{ik}$ and $\boldsymbol{\beta}_{ik}$ are independent of (x, y, z).
Hint: Express L_i and L_k as linear functions of (x, y, z).

10.21 A spherical cavity is excited in a TM mode whose magnetic eigenvector is $\mathbf{h}_m = j_1(2.743\ R/a)\sin\theta\, \mathbf{u}_\varphi$. Determine the frequency shift resulting from insertion of a small dielectric sphere of radius b at the center of the cavity. Apply the formula to a sphere of radius 13.1 cm in which a polystyrene sphere ($\epsilon_r = 2.5$) of radius 0.5 cm is introduced.

10.22 Assume that the wall of a cavity has been slightly deformed at a point P, so that the volume of the cavity is decreased by an amount Δv. Show that the resulting frequency shift is

$$\frac{k_m - k_{m0}}{k_{m0}} = \frac{\displaystyle\int_{\Delta V} (|\mathbf{h}_m|^2 - |\mathbf{e}_m|^2)\, dV}{\displaystyle 2\int_V |\mathbf{e}_m|^2 dV} \approx \frac{\Delta v[|\mathbf{h}_m(P)|^2 - |\mathbf{e}_m(P)|]^2}{\displaystyle 2\int_V |\mathbf{e}_m|^2 dV}$$

where k_{m0}, $\mathbf{e}_m$, and $\mathbf{h}_m$ refer to the unperturbed mode. Utilize this relationship to analyze the tuning properties of a metallic screw inserted in the wall.

10.23 A resonant cavity with perfectly conducting walls resonates in a mode whose electric and magnetic fields are $\mathbf{E}_0$ and $\mathbf{H}_0$. Assume that the walls are given a (small) impedance Z_w, so that $\mathbf{u}_n \times \mathbf{E} = Z_w \mathbf{H}_{\tan}$. Show that the resulting frequency shift is

$$\Delta f = -j \frac{\displaystyle\int_S Z_w \mathbf{H}\cdot\mathbf{H}_0\, dS}{\displaystyle\int_V (\epsilon \mathbf{E}\cdot\mathbf{E}_0 - \mu \mathbf{H}\cdot\mathbf{H}_0)\, dV}.$$

In this expression, $\mathbf{E}$ and $\mathbf{H}$ are the fields that exist in the presence of the perturbation.

10.24 Show that inserting a vanishingly small sample of given characteristics (ϵ_r, μ_r) shifts the resonant frequency of a cavity by [22]

$$\frac{\Delta f_{\text{res}}}{f_{\text{res}}} = \frac{\mu_0 \mathbf{h}_0\cdot\mathbf{P}_m - \mathbf{e}_0\cdot\mathbf{P}_e}{\displaystyle\int_V [\mathbf{e}_0\cdot\mathbf{d}_0 - \mathbf{h}_0\cdot\mathbf{b}_0]\, dV}.$$

In this expression, $\mathbf{P}_e$ and $\mathbf{P}_m$ are the static electric and magnetic moments induced in the sample by a static field $(\mathbf{e}_0, \mathbf{h}_0)$. These moments are obtained by multiplying $\mathbf{e}_0$ and $\mathbf{h}_0$ with

the polarizability tensors $\overline{\overline{\alpha}}_e$ and $\overline{\overline{\alpha}}_m$, respectively. The fields $(\mathbf{e}_0, \mathbf{h}_0)$ are defined by

$$\mathbf{e}_0 = A\mathbf{e}_m$$
$$\mathbf{h}_0 = j\frac{A}{k_m R_{c0}} \operatorname{curl} \mathbf{e}_m = j\frac{A}{R_{c0}}\mathbf{h}_m.$$

10.25 Design a circular cylinder cavity to resonate in the TM_{010} mode at 10 GHz, with a Q equal to 10.000 (Fig. P10.3). The walls are made of copper (conductivity $\sigma = 0.58\ 10^8$ S m^{-1}). The electric field is of the form

$$\mathbf{e}_m \doteqdot J_0\left(\lambda\frac{r}{a}\right)\mathbf{u}_z$$

where λ is the lowest zero of $J_0(\lambda)$.

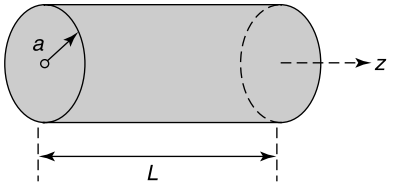

Figure P10.3

10.26 Determine the electric and magnetic eigenvectors of a parallelepiped. Justify formulas (10.62) and (10.63), and discuss their limitations. Determine also the resonant frequencies of a cube (side 50 cm) in the frequency interval 0 to 1 GHz.

10.27 Show that the dielectric resonator fields satisfying (10.92) are orthogonal in the sense that

$$\int_{V+V'} \mathbf{H}_m \cdot \mathbf{H}_n \, dV = 0.$$

Here $\mathbf{H}_m$ and $\mathbf{H}_n$ belong to different eigenvalues, and V and V' are respectively the interior and exterior volumes of the resonator. Show also that

$$\int_V \operatorname{curl} \mathbf{H}_m \cdot \operatorname{curl} \mathbf{H}_n \, dV = 0.$$

This relationship is important because curl $\mathbf{H}_m$ is proportional to the electric field.
(J. Van Bladel, *IEEE Trans. MTT*, **23**, 199–208, 1975).

10.28 Let $\mathbf{r}_0$ lie outside a current-carrying region (Fig. P10.4). The magnetic field is given by (10.142) in terms of $\overline{\overline{G}}_{mm}$ and $\mathbf{J}_m$ and by (10.137) in terms of $\overline{\overline{G}}_{ee}$ and $\mathbf{J}$. Replace $\mathbf{J}_m$ by its electric equivalent $\mathbf{J}$, as given in (7.211), and confirm the reciprocity relationship (10.135).

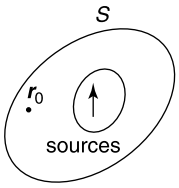

Figure P10.4

10.29 Investigate whether dyadic $\overline{\overline{G}}_{ee}$ defined in (10.144) satisfies the differential equation

$$-\text{curl curl}\,\overline{\overline{G}}_{ee}(\mathbf{r}|\mathbf{r}') + k_c^2\overline{\overline{G}}_{ee}(\mathbf{r}|\mathbf{r}') = \overline{\overline{I}}\delta(\mathbf{r}-\mathbf{r}').$$

Hint: Expand the second member as

$$\overline{\overline{I}}\delta(\mathbf{r}-\mathbf{r}') = \underbrace{\sum_m \mathbf{f}_m(\mathbf{r})\mathbf{f}_m(\mathbf{r}')}_{\overline{\overline{D}}_{\text{irr}}(\mathbf{r}|\mathbf{r}')} + \underbrace{\sum \mathbf{e}_m(\mathbf{r})\mathbf{e}_m(\mathbf{r}')}_{\overline{\overline{D}}_{\text{sol}}(\mathbf{r}|\mathbf{r}')}.$$

(W. A. Johnson et al., *Radio Sci.* **14**, 961–967, 1979.)

NOTES

1. J. Van Bladel, Field expansions in cavities containing gyrotropic media, *IRE Trans. MTT* **10**, 9–13 (1962).
2. H. Weyl, Über das Spektrum der Hohlraumsthralung, *Z. Reine Angew. Math.* **141**, 163–181 (1912).
3. H. Weyl, Über die Randwertaufgabe der Strahlungstheorie und Asymptotische Spektralgesetze, *Z. Reine Angew. Math.* **143**, 177–202 (1913).
4. S. A. Schelkunoff, On representation of electromagnetic fields in cavities in terms of natural modes of oscillation, *J. Appl. Phys.* **26**, 1231–1234 (1955).
5. K. Kurokawa, The expansions of electromagnetic fields in cavities, *IRE Trans. MTT* **4**, 178–187 (1958).
6. H. A. Mendez, On the theory of low-frequency excitation of cavity resonators, *IEEE Trans. MTT* **18**, 444 – 448 (1970).
7. M. J. Park, J. Park, and S. Nam, Efficient calculation of the Green's function for the rectangular cavity, *IEEE Microwave Guided Wave Lett.* **8**, 124–126 (1998).
8. L. Pichon and A. Razek, Electromagnetic field computations in a three-dimensional cavity with a waveguide junction of a frequency standard, *Proc. IEE* **139-H**, 343–346 (1992).
9. A. Chincarini, P. Fabbricatore, G. Genume, K. Musenich, R. Parodi, B. Zhang, Headway in cavity design through genetic algorithms, *IEEE Trans. MAG* **31**, 1566–1569 (1995).
10. J. P. Webb, The finite-element method for finding modes of dielectric-loaded cavities, *IEEE Trans. MTT* **33**, 635–639 (1985).
11. J. P. Webb, Efficient generation of divergence-free fields for the finite element analysis of 3D cavity resonances, *IEEE Trans. MAG* **24**, 162–165 (1988).
12. A. Bossavit, Solving Maxwell equations in a closed cavity, and the question of spurious modes, *IEEE Trans. MAG* **26**, 702–705 (1990).
13. L. Pichon and A. Bossavit, A new variational formulation, free of spurious modes, for the problem of loaded cavities, *IEEE Trans. MAG* **29**, 1595–1600 (1993).
14. P. H. Harms, J. F. Lee, and R. Mittra, A study of the nonorthogonal FDTD method versus the conventional FDTD technique for constant resonant frequencies of cylindrical cavities, *IEEE Trans. MTT* **40**, 741–746 (1992). A correction appeared in **40**, 2115–2116 (1992).
15. L. Zhao, L. S. Tong, and R. G. Carter, The influence of boundary conditions on resonant frequencies in cavities in 3-D FDTD algorithm using non-orthogonal co-ordinates, *IEEE Trans. MAG* **30**, 3570–3573 (1994).
16. J. F. Lee and R. Mittra, A note on the application of edge-elements for modeling three-dimensional inhomogeneously-filled cavities, *IEEE Trans. MTT* **40**, 1767–1773 (1992).
17. Y. Wang, P. Monk, and B. Szabo, Computing cavity modes using the *p*-version of the finite element method, *IEEE Trans. MAG* **32**, 1934–1940 (1996).
18. J. P. Webb, Hierarchal vector basis functions of arbitrary order for triangular and tetrahedral finite elements, *IEEE Trans. AP* **47**, 1244–1253 (1999).
19. J. P. Webb, Edge elements and what they can do for you, *IEEE Trans. MAG* **29**, 1460–1465 (1993).
20. I. Bardi, O. Biro, and K. Preis, Finite element scheme for 3D cavities without spurious modes, *IEEE Trans. MAG* **27**, 4036–4039 (1991).
21. R. Dyczij and O. Biro, A joint vector and scalar potential formulation for driven high frequency problems using hybrid edge and nodal finite elements, *IEEE Trans. MTT* **44**, 15–23 (1996).
22. A. Cunliffe, R. N. Gould, and K. D. Hall, On cavity resonators with non-homogeneous media, *Institution of Electrical Engineers (London) monograph 91*, January 1954.
23. S. A. Tretyakov and A. J. Viitanen, Perturbation theory for a cavity resonator with a bi-isotropic sample: applications to measurement techniques, *Microwave Opt. Tech. Lett.* **5**, 174–177 (1992).
24. L. E. Davis and P. A. Smith, *Q* of a coaxial cavity with a superconducting inner conductor, *IEE Proc. A* **138**, 313–319 (1991).

25. G. L. Matthaei and G. L. Hey-Shipton, Concerning the use of high-temperature superconductivity in planar microwave filters, *IEEE Trans. MTT* **42**, 1287–1294 (1994).
26. H. Piel and G. Müller, The microwave surface impedance of high-T_c superconductors, *IEEE Trans. MAG* **27**, 854–862 (1991).
27. M. Petirsch and A. J. Schwab, Investigation of the field uniformity of a mode-stirred chamber using diffusors based on acoustic theory, *IEEE Trans. EMC* **41**, 446–451 (1999).
28. F. Olyslager, E. Laermans, D. De Zutter, S. Criel, R. De Smedt, N. Lietaert, and A. De Clercq, Numerical and experimental study of the shielding effectiveness of a metallic enclosure, *IEEE Trans. EMC* **41**, 202–213 (1999).
29. C. Müller and H. Niemeyer, Greensche Tensoren und asymptotische Gesetze der elektromagnetischen Hohlraumschwingungen, *Arch. Rational Mech. Anal.* **7**, 305–348 (1961).
30. C. M. Butler and J. Van Bladel, Electromagnetic fields in a spherical cavity embedded in a dissipative medium, *IEEE Trans. AP* **12**, 110–118 (1964).
31. M. Gastine, L. Courtois, and J. L. Dormann, Electromagnetic resonances of free dielectric spheres, *IEEE Trans. MTT* **15**, 694–700 (1967).
32. B. Sauviac, P. Guillot, and H. Baudrand, Rigorous analysis of shielded cylindrical dielectric resonators by dyadic Green's functions, *IEEE Trans. MTT* **42**, 1484–1493 (1994).
33. A. A. Kucharski, Resonances in inhomogeneous dielectric bodies of revolution placed in the multilayered media-TE modes, *Microwave Opt. Tech. Lett.* **21**, 1–4 (1999).
34. Y. Kobayashi and S. Tanaka, Resonant modes of a dielectric rod resonator short-circuited at both ends by parallel conducting planes, *IEEE Trans. MTT* **28**, 1077–1085 (1980).
35. M. W. Pospieszalski, Cylindrical dielectric resonators and their applications in TEM line microwave circuits, *IEEE Trans. MTT* **27**, 233–238 (1979).
36. Y. Kobayashi, T. Aoki, and Y. Kabe, Influence of conductor shields on the Q-factors of a TE_0 dielectric resonator, *IEEE Trans. MTT* **33**, 1361–1366 (1985).
37. Z. Bi, Y. Shen, K. Wu, and J. Litva, Fast finite-difference time-domain analysis of resonators using digital filtering and spectrum estimation techniques, *IEEE Trans. MTT* **40**, 1611–1619 (1992).
38. R. E. Collin and D. A. Ksienski, Boundary element method for dielectric resonators and waveguides, *Radio Sci.* **22**, 1155–1167 (1987).
39. J. M. Jin, J. L. Volakis, and V. V. Lipa, A moment method solution of a volume-surface integral equation using isoparametric elements and point matching, *IEEE Trans. MTT* **37**, 1641–1645 (1989).
40. S. Hyun, J. Hwang, Y. Lee, and S. Kim, Computation of resonant modes of open resonators using the FEM and the anisotropic perfectly matched layer boundary condition, *Microwave Opt. Tech. Lett.* **16**, 352–356 (1997).
41. S. G. O' Keefe, S. P. Kingsley, and S. Saario, FDTD simulation of radiation characteristics of half-volume HEM- and TE-mode dielectric resonator antennas, *IEEE Trans. AP* **50**, 175–179 (2002).
42. J. E. Lebaric and D. Kajfez, Analysis of dielectric resonator cavities using the finite integration technique, *IEEE Trans. MTT* **37**, 1740–1748 (1989).
43. A. W. Glisson, D. Kajfez, and J. James, Evaluation of modes in dielectric resonators using a surface integral equation formulation, *IEEE Trans. MTT* **31**, 1023–1029 (1983).
44. A. A. Kucharski, Resonances in heterogeneous dielectric bodies with rotational symmetry-volume integral equation formulations, *IEEE Trans. MTT* **48**, 766–770 (2000).
45. D. Cros and P. Guillon, Whispering gallery dielectric resonator modes for W-band devices, *IEEE Trans. MTT* **38**, 1667–1674 (1990).
46. J. Krupka, D. Cros, M. Aubourgh, and P. Guillon, Study of whispering gallery modes in anisotropic single-crystal dielectric resonators, *IEEE Trans. MTT* **42**, 56–61 (1994).
47. G. Annino, M. Cassettari, I. Longo, and M. Martinelli, Whispering gallery modes in a dielectric resonator: characterization at millimeter wavelength, *IEEE Trans. MTT* **45**, 2025–2034 (1997).
48. J. Van Bladel, On the resonances of a dielectric resonator of very high permittivity, *IEEE Trans. MTT* **23**, 199–208 (1975).
49. M. Verplanken and J. Van Bladel, The magnetic-dipole resonances of ring resonators of very high permittivity, *IEEE Trans. MTT* **27**, 328–333 (1979).
50. R. De Smedt, Correction due to a finite permittivity for a ring resonator in free space, *IEEE Trans. MTT* **32**, 1288–1292 (1984).
51. M. Verplanken and J. Van Bladel, The electric-dipole resonances of ring resonators of very high permittivity, *IEEE Trans. MTT* **24**, 108–112 (1976).
52. R. De Smedt, Dielectric resonator above an electric or magnetic wall, *A.E.Ü.* **37**, 6–14 (1983).
53. J. Van Bladel, Weakly coupled dielectric resonators, *IEEE Trans. MTT* **30**, 1907–1914 (1982).
54. A. A. Kishk, M. R. Zunoubi, and D. Kajfez, A numerical study of a dielectric disk antenna above grounded dielectric substrate, *IEEE Trans. AP* **41**, 813–821 (1993).
55. S. A. Long, M. W. Mc Allister, and L. C. Shen, The resonant dielectric cavity antenna, *IEEE Trans. AP* **31**, 406–412 (1983).
56. G. F. Yunker, A. P. Kishk, and A. W. Glisson, Input impedance of dielectric resonator antennas excited by a coaxial probe, *IEEE Trans. AP* **42**, 960–966 (1994).
57. J. Van Bladel, Resonant scattering by dielectric cylinders, *IEE Microwaves, Optics and Acoustics* **1**, 41–50 (1977).
58. M. Verplanken and J. Van Bladel, Resonances of rectangular dielectric cylinders, *IEE Microwaves, Optics and Acoustics* **1**, 185–191 (1977).

59. P. R. Karr, Radiation properties of spherical antennas as a function of the location of the driving force, *J. Research Natl. Bur. Standards* **46**, 422–436 (1951).
60. R. W. Ziolkowski and W. A. Johnson, Electromagnetic scattering of an arbitrary plane wave from a spherical shell with a circular aperture, *J. Math. Phys.* **28**, 1293–1314 (1987).
61. T. B. A. Senior and G. A. Desjardins, Electromagnetic field penetration into a spherical cavity, *IEEE Trans. EMC* **16**, 205–208 (1974).
62. S. Blume and L. Klinkenbusch, Scattering of a plane electromagnetic wave by a spherical shell with an elliptical aperture, *IEEE Trans. EMC* **34**, 308–314 (1992).
63. S. V. Georgakopoulos, C. R. Birtcher, and C. A. Balanis, HIRF penetration through apertures: FDTD versus measurements, *IEEE Trans. EMC* **43**, 282–294 (2001).
64. Z. S. Sacks and J. F. Lee, A finite-element time-domain method using prism elements for microwave cavities, *IEEE Trans. EMC* **37**, 519–527 (1995).
65. Y. Shen, Z. Bi, K. Wu, and J. Litva, FD-TD analysis of open cylindrical dielectric resonators, *Microwave Opt. Tech. Lett.* **5**, 261–265 (1992).
66. E. Semouchkina, G. Semouchkin, R. Mittra, and W. Cao, Finite-difference time-domain simulation of resonant modes of rectangular dielectric resonators, *Microwave Opt. Tech. Lett.* **36**, 160–164 (2003).
67. M. Bressan and G. Conciauro, Singularity extraction from the electric Green's function for a spherical resonator, *IEEE Trans. MTT* **33**, 407–414 (1985).
68. J. Van Bladel, Small-hole coupling of resonant cavities and waveguides, *Proc. IEE* **117**, 1098–1104 (1970).
69. R. Gluckstern, Ru Li, and R. Cooper, Electric polarizability and magnetic susceptibility of small holes in a thin screen, *IEEE Trans. MTT* **38**, 186–192 (1990).
70. W. Wallyn, D. De Zutter, and H. Rogier, Predictions of the shielding and resonant behavior of multisection enclosures based on magnetic current modeling, *IEEE Trans. EMC* **44**, 130–138 (2002).
71. W. P. Carpes, L. Pichon, and A. Razek, Analysis of the coupling of an incident wave with a wire inside a cavity using an FEM in frequency and time domains, *IEEE Trans. EMC* **44**, 470–475 (2002).

Chapter 11

Scattering: Generalities

Chapter 11 introduces a number of fundamental concepts of scattering theory, in preparation for Chapter 12, which describes the main numerical methods used for the evaluation of the scattered fields. Some of the topics under discussion in the following pages are the various *cross sections* of a scatterer, the *characteristic modes* of the current induced on the scatterer's surface, and the influence of *thin films* on the scattering properties of targets. Much attention is devoted to the perfectly conducting sphere, a shape for which the scattered fields can be determined by separation of variables. The abundantly available results for that particular geometry reveal the existence of *resonances* at certain frequencies, a phenomenon that also exists for other shapes and plays an important role in the analysis of the transient response from targets. It has been observed experimentally, for example, that the late-time part of the time response, under $\delta(t)$ irradiation, can be interpreted as the ringing of a number of (R, L, C) circuits. The theory confirms this interpretation, which can be exploited to obtain information on the target from the complex exponents of the decaying oscillations of its radar return.

Resonances also occur when the scatterer is penetrable. They are particularly sharp when the material of the scatterer is a dielectric of high ϵ_r, a property that is the basis for the popularity of dielectric resonators as circuit elements at microwave frequencies.

11.1 THE SCATTERING MATRIX

Figure 11.1 shows an obstacle V immersed in the field $\mathbf{E}^i, \mathbf{H}^i$ of a primary source $\mathbf{J}$ (electric or magnetic). The incident fields generate currents in the obstacle, which in turn reradiates and possibly causes a redistribution of the source currents $\mathbf{J}$. This effect is negligible when the obstacle (or *scatterer*) is far away from the sources, a condition often encountered in practice. In fact, the obstacle is frequently in the radiation field of the sources, and the solid angle that it subtends is often so small that the incident wave has all the characteristics of a plane wave. For such a case, the incident fields in a direction of unit vector $\mathbf{u}$ are of the

Electromagnetic Fields, Second Edition, By Jean G. Van Bladel

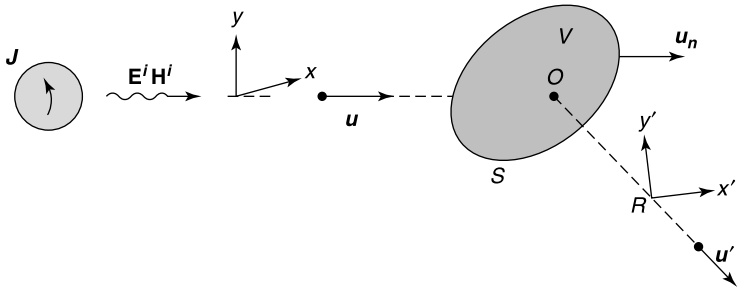

Figure 11.1 Scattering of an incident wave by an obstacle V.

form

$$\mathbf{E}^i(\mathbf{r}) = \mathbf{A}\, e^{-jk_0\mathbf{u}\cdot\mathbf{r}}$$
$$\mathbf{H}^i(\mathbf{r}) = \frac{1}{R_{c0}}(\mathbf{u}\times\mathbf{A})\, e^{-jk_0\mathbf{u}\cdot\mathbf{r}}. \tag{11.1}$$

It is useful to decompose the incident field into a pair of linearly polarized waves. Thus,

$$\mathbf{E}^i = A_x\mathbf{u}_x\, e^{-jk_0\mathbf{u}\cdot\mathbf{r}} + A_y\mathbf{u}_y\, e^{-jk_0\mathbf{u}\cdot\mathbf{r}} = \mathbf{A}\, e^{-jk_0\mathbf{u}\cdot\mathbf{r}}, \tag{11.2}$$

where $\mathbf{u}_x$, $\mathbf{u}_y$, and $\mathbf{u}$ form an orthogonal set of unit vectors. The choice of the directions x and y depends on the application in hand.* On the ground, one often chooses V and H, the vertical and horizontal directions. In *antenna* applications, x and y could be the main axes of the radiated polarization ellipse. In *scattering* problems, two natural directions of the target may be chosen, such as the axes of the rectangular plate in Figure 11.2*a*. For the sphere, on the other hand, all directions are equivalent.

The x-component of $\mathbf{E}^i$ gives rise to scattered fields which, at large R and in a direction of unit vector $\mathbf{u}'$, may be written as (Fig. 11.1)

$$\mathbf{E}^{sc} = \frac{e^{-jk_0R}}{R} A_x\mathbf{F}'_x(\mathbf{u}') = \frac{e^{-jk_0R}}{R}\mathbf{F}_x(\mathbf{u}')$$
$$\mathbf{H}^{sc} = \frac{1}{R_{c0}}\frac{e^{-jk_0R}}{R} A_x\mathbf{u}'\times\mathbf{F}'_x(\mathbf{u}'). \tag{11.3}$$

The origin O is the phase center of the fields, and $\mathbf{F}_x$ is a transverse complex vector, the real and imaginary parts of which determine the polarization characteristics of $\mathbf{E}^{sc}$. The $\mathbf{u}_y$ incident component similarly generates a scattered field of the form (11.3), with its own radiation vector $\mathbf{F}_y$. By superposition, the radiation vector of the general scattered field (11.2) becomes

$$\mathbf{F} = A_x\mathbf{F}'_x + A_y\mathbf{F}'_y = (\mathbf{F}'_x\mathbf{u}_x + \mathbf{F}'_y\mathbf{u}_y)\cdot\mathbf{A}$$
$$= \overline{\overline{S}}(\mathbf{u}'|\mathbf{u})\cdot\mathbf{A} \qquad (V). \tag{11.4}$$

*In Figure 11.1, $\mathbf{u}_x\times\mathbf{u}_y$ is directed toward the target and $\mathbf{u}_{x'}\times\mathbf{u}_{y'}$ away from it. This is the *forward scattering alignment* [130].

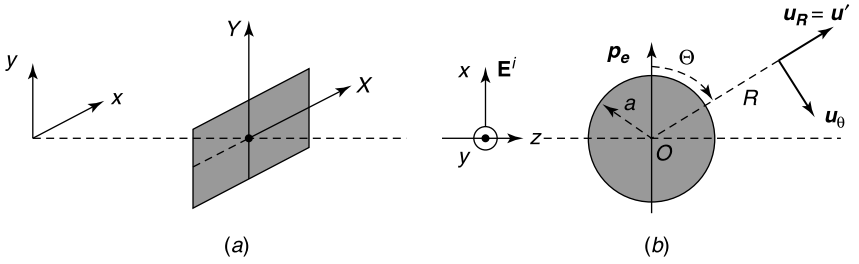

Figure 11.2 Two scatterers: (*a*) rectangular plate, (*b*) perfectly conducting sphere.

In this equation, $\overline{\overline{S}}$ is the *scattering matrix* relative to the scattering direction $\mathbf{u}'$ and the incident direction $\mathbf{u}$. It is a function of frequency. In radar applications, one is mostly interested in the *backscattered* direction $\mathbf{u}' = -\mathbf{u}$ and the corresponding matrix $\overline{\overline{S}}(-\mathbf{u}|\mathbf{u})$.

As an illustration, consider the problem embodied in Figure 11.2*b*, where a perfectly conducting sphere is immersed in an incident field

$$\mathbf{E}^i = A_x\,\mathbf{u}_x\,e^{-jk_0z}.$$

When the radius a of the sphere is very small with respect to λ_0, the *target* reradiates like an electric dipole of moment

$$\mathbf{p}_e = 4\pi\epsilon_0 a^3 A_x \mathbf{u}_x.$$

This is the static moment (4.75), and the justification for this value is discussed in Section 13.8. The scattered field in a direction $\mathbf{u}' = \mathbf{u}_R$ becomes, from (7.158),

$$\begin{aligned}\mathbf{E}^{sc} &= -\frac{\omega^2\mu_0}{4\pi}\frac{e^{-jk_0R}}{R}\,p_e\sin\theta\,\mathbf{u}_\theta \\ &= \underbrace{-k_0^2a^3\sin\theta\,\mathbf{u}_\theta}_{\mathbf{F}'_x}\,A_x\frac{e^{-jk_0R}}{R},\end{aligned} \tag{11.5}$$

where R and θ are spherical coordinates based on $\mathbf{p}_e$ as polar axis. In the backscattered direction, in particular,

$$\mathbf{F}'_x(-\mathbf{u}_z,\mathbf{u}_z) = k_0^2a^3\mathbf{u}_x.$$

For a wave linearly polarized in the $\mathbf{u}_y$ direction, one similarly obtains

$$\mathbf{F}'_y(-\mathbf{u}_z,\mathbf{u}_z) = k_0^2a^3\mathbf{u}_y,$$

from which it follows that

$$\overline{\overline{S}}(-\mathbf{u}_z|\mathbf{u}_z) = k_0^2a^3(\mathbf{u}_x\mathbf{u}_x + \mathbf{u}_y\mathbf{u}_y) = k_0^2a^3\overline{\overline{I}}_{xy} \qquad (m) \tag{11.6}$$

With an incident field $\mathbf{A}\,e^{-jk_0z}$, the backscattered field, far away from the sphere, is therefore

$$\mathbf{E}^{sc} = \frac{k_0^2a^3}{|z|}\,\mathbf{A}\,e^{jk_0z}. \tag{11.7}$$

We note that the polarization ellipse is conserved upon backscattering, in shape, orientation, and sense of rotation in space. This feature is due to the symmetry of the sphere and holds for head-on axial illumination of any axisymmetric target. In fact, a measurement of the four components of $\overline{\overline{S}}$ for various regimes of frequency and time can be exploited to identify targets by comparison with a known library of "signatures." The $\overline{\overline{S}}$ matrix is clearly an extension of the concept *radar cross section*, because it includes information on the polarization sensitivity of the target.

The direct determination of the four elements of $\overline{\overline{S}}$ requires phase and amplitude measurements, typically obtained by alternately radiating orthogonally polarized waves, and measuring the respective scattered wave components. Note that the requirement for *phase* measurements can be dropped by applying methods based on *amplitude* measurements only, performed for several polarizations.[1]

Operating at a single frequency gives only limited information on the target. More information can be extracted by using pulses or multiple frequencies, in which case the elements of $\overline{\overline{S}}$ become Laplace transforms.[2]

Reciprocity

In Figure 11.3, a target of characteristics $(\overline{\overline{\epsilon}}, \overline{\overline{\mu}})$ is immersed in an incident plane wave

$$\begin{aligned} \mathbf{E}_a^i &= \mathbf{A}\, e^{-jk_0 \mathbf{u}_a \cdot \mathbf{r}} \\ \mathbf{H}_a^i &= \frac{1}{R_{c0}} (\mathbf{u}_a \times \mathbf{A})\, e^{-jk_0 \mathbf{u}_a \cdot \mathbf{r}}. \end{aligned} \tag{11.8}$$

This is state a. In state b, the body is endowed with the *transpose* characteristics $(\overline{\overline{\epsilon}}^t, \overline{\overline{\mu}}^t)$ and is immersed in a plane wave[†]

$$\begin{aligned} \mathbf{E}_b^i &= \mathbf{B}\, e^{-jk_0 \mathbf{u}_b \cdot \mathbf{r}} \\ \mathbf{H}_b^i &= \frac{1}{R_{c0}} (\mathbf{u}_b \times \mathbf{B})\, e^{-jk_0 \mathbf{u}_b \cdot \mathbf{r}}. \end{aligned} \tag{11.9}$$

In the absence of sources in V, Maxwell's equations and (A4.35) yield

$$\operatorname{div} (\mathbf{E}_a \times \mathbf{H}_b) = \operatorname{div} (\mathbf{E}_b \times \mathbf{H}_a) \qquad (\text{in } V). \tag{11.10}$$

Integrating over V gives

$$\int_S \mathbf{u}_n \cdot (\mathbf{E}_a \times \mathbf{H}_b)\, dS = \int_S \mathbf{u}_n \cdot (\mathbf{E}_b \times \mathbf{H}_a)\, dS. \tag{11.11}$$

Because both incident and scattered fields are sourceless in V, we may write

$$\int_S \mathbf{u}_n \cdot \left[(\mathbf{E}_a^i + \mathbf{E}_a^{sc}) \times (\mathbf{H}_b^i + \mathbf{H}_b^{sc}) - (\mathbf{E}_b^i + \mathbf{E}_b^{sc}) \times (\mathbf{H}_a^i + \mathbf{H}_a^{sc}) \right] dS = 0$$

[†]This is a slight modification of a paper by A. T. de Hoop (see Note 3).

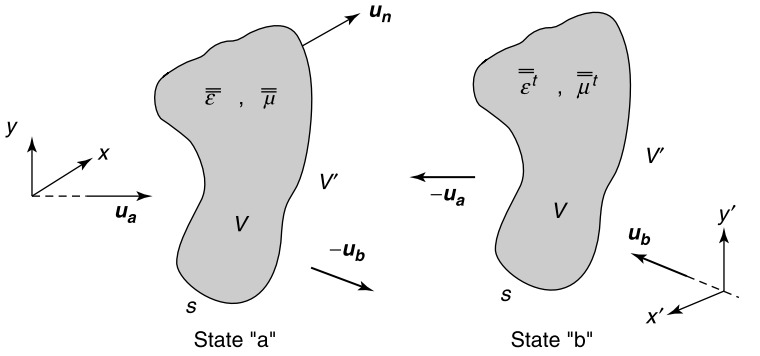

Figure 11.3 Relevant to the reciprocity theorem.

and

$$\int_S \mathbf{u}_n \cdot \left[\mathbf{E}_a^i \times \mathbf{H}_b^i - \mathbf{E}_b^i \times \mathbf{H}_a^i\right] dS = 0.$$

Subtraction of corresponding members of these equations gives

$$\int_S \mathbf{u}_n \cdot \left(\mathbf{E}_a^{sc} \times \mathbf{H}_b^{sc} - \mathbf{E}_b^{sc} \times \mathbf{H}_a^{sc}\right) dS + \int_S \mathbf{u}_n \cdot \left(\mathbf{E}_a^{sc} \times \mathbf{H}_b^i + \mathbf{E}_a^i \times \mathbf{H}_b^{sc}\right) dS$$
$$- \int_S \mathbf{u}_n \cdot \left(\mathbf{E}_b^{sc} \times \mathbf{H}_a^i + \mathbf{E}_b^i \times \mathbf{H}_a^{sc}\right) dS = 0. \tag{11.12}$$

The first integral in the left-hand term is equal to zero. This can be seen by applying (11.11) to the scattered fields in the volume V' *outside* S, where these fields are sourceless. The boundary surface of V' consists of S and a sphere S_∞ at infinity, hence the surface integral over S is equal to

$$\int_{S_\infty} \mathbf{u}_R \cdot \left(\mathbf{E}_a^{sc} \times \mathbf{H}_b^{sc} - \mathbf{E}_b^{sc} \times \mathbf{H}_a^{sc}\right) dS,$$

and this integral vanishes because of the radiation condition (7.92). Inserting the value of the incident fields into (11.12) now gives

$$\mathbf{A} \cdot \int_S \left[\mathbf{H}_b^{sc} \times \mathbf{u}_n + \frac{1}{R_{c0}} \mathbf{u}_a \times (\mathbf{u}_n \times \mathbf{E}_b^{sc})\right] e^{-jk_0 \mathbf{u}_a \cdot \mathbf{r}}\, dS$$
$$= \mathbf{B} \cdot \int_S \left[\mathbf{H}_a^{sc} \times \mathbf{u}_n + \frac{1}{R_{c0}} \mathbf{u}_b \times (\mathbf{u}_n \times \mathbf{E}_a^{sc})\right] e^{-jk_0 \mathbf{u}_b \cdot \mathbf{r}}\, dS. \tag{11.13}$$

It is shown in Section 7.12 that the scattered fields may be thought of as generated by virtual surface currents $\mathbf{J}_S = \mathbf{u}_n \times \mathbf{H}$ and $\mathbf{J}_{mS} = \mathbf{E} \times \mathbf{u}_n$ on S, where $\mathbf{u}_n$ is directed as in Figure 11.3. From (7.101), the fields radiated by $\mathbf{J}_S$ in a direction of unit vector $\mathbf{u}$ have a radiation vector

$$\mathbf{F}_e = j \frac{k_0 R_{c0}}{4\pi} \mathbf{u} \times \left(\mathbf{u} \times \int_S (\mathbf{u}_n \times \mathbf{H})\, e^{jk_0 \mathbf{u} \cdot \mathbf{r}'} dS'\right)$$
$$= -j \frac{k_0 R_{c0}}{4\pi} \left[\int_S (\mathbf{u}_n \times \mathbf{H})\, e^{jk_0 \mathbf{u} \cdot \mathbf{r}'} dS'\right]_t \qquad (V). \tag{11.14}$$

where t means *transverse* (i.e., a component perpendicular to $\mathbf{u}$). Adapting (7.101) to magnetic currents by means of the value of $\mathbf{C}$ given in (7.109) produces similarly a radiation vector

$$\mathbf{F}_m = j\frac{k_0}{4\pi}\mathbf{u} \times \int_S (\mathbf{E} \times \mathbf{u}_n)\, e^{jk_0 \mathbf{u}\cdot\mathbf{r}'} dS' \qquad (V). \tag{11.15}$$

The total radiation vector is $\mathbf{F} = \mathbf{F}_e + \mathbf{F}_m$. Going back to (11.13), it becomes clear, because $\mathbf{A}$ is transverse to $\mathbf{u}_a$ and $\mathbf{B}$ to $\mathbf{u}_b$, that

$$\mathbf{A}\cdot\mathbf{F}_b(-\mathbf{u}_a|\mathbf{u}_b) = \mathbf{B}\cdot\mathbf{F}_a(-\mathbf{u}_b|\mathbf{u}_a). \tag{11.16}$$

In terms of scattering matrices:

$$\mathbf{A}\cdot\overline{\overline{S}}_b(-\mathbf{u}_a|\mathbf{u}_b)\cdot\mathbf{B} = \mathbf{B}\cdot\overline{\overline{S}}_a(-\mathbf{u}_b|\mathbf{u}_a)\cdot\mathbf{A}. \tag{11.17}$$

From (A4.35), it follows that the matrices $\overline{\overline{S}}_a(-\mathbf{u}_b|\mathbf{u}_a)$ and $\overline{\overline{S}}_b(-\mathbf{u}_a|\mathbf{u}_b)$ are each other's transpose. For a *symmetric* medium, the fields in states a and b concern the same scatterer material, hence $\mathbf{F}_a$ and $\mathbf{F}_b$ are the same functions provided the same definitions are used; that is, provided $\mathbf{u}_x \times \mathbf{u}_y$ and $\mathbf{u}_{x'} \times \mathbf{u}_{y'}$ are *both* directed toward the scatterer (or away from it). For such a case

$$F_{xy'}(-\mathbf{u}_b|\mathbf{u}_a) = F_{y'x}(-\mathbf{u}_a|\mathbf{u}_b), \tag{11.18}$$

and the scattering matrix, being the same for the a and b states, is now symmetric. In the backscattered direction, in particular,

$$F_{xy}(-\mathbf{u}_z|\mathbf{u}_z) = F_{yx}(-\mathbf{u}_z|\mathbf{u}_z). \tag{11.19}$$

11.2 CROSS SECTIONS

The time-averaged power scattered by an obstacle is given by (Fig. 11.1)

$$P^{sc} = \frac{1}{2}\,\mathrm{Re}\int_S \mathbf{u}_n\cdot(\mathbf{E}^{sc} \times \mathbf{H}^{sc*})\, dS. \tag{11.20}$$

When the obstacle is irradiated by an incident plane wave of type (11.8), this power is proportional to the power density of the wave, which is

$$\mathcal{P}^i = \frac{1}{2}\,\mathrm{Re}\,(\mathbf{E}^i \times \mathbf{H}^{i*}) = \frac{1}{2R_{c0}}\mathbf{A}\cdot\mathbf{A}^* = \frac{1}{2R_{c0}}|\mathbf{A}|^2 \qquad (\mathrm{Wm}^{-2}). \tag{11.21}$$

The proportionality constant has the dimension m^2 and is independent of the power level. It is therefore meaningful to define a *scattering cross section*

$$\sigma^{sc} = \frac{P^{sc}}{\mathcal{P}^i} = \frac{1}{|A|^2}\int_{4\pi} |\mathbf{F}|^2 d\Omega \qquad (\mathrm{m}^2). \tag{11.22}$$

One can similarly define, for a lossy obstacle, an *absorption cross section*

$$\sigma^{abs} = \frac{P^{abs}}{\mathcal{P}^i} \qquad (\mathrm{m}^2), \tag{11.23}$$

where the absorbed power is given by

$$P^{abs} = -\frac{1}{2}\,\mathrm{Re}\int_S \mathbf{u}_n \cdot (\mathbf{E}\times\mathbf{H}^*)\,dS. \tag{11.24}$$

Also useful is the *extinction cross section*

$$\sigma^{ext} = \sigma^{abs} + \sigma^{sc} \qquad (\mathrm{m}^2). \tag{11.25}$$

To evaluate σ^{ext}, we note that the total power extracted from the incident wave is

$$P^{abs} + P^{sc} = -\frac{1}{2}\,\mathrm{Re}\int_S \mathbf{u}_n \cdot (\mathbf{E}\times\mathbf{H}^* - \mathbf{E}^{sc}\times\mathbf{H}^{sc*})\,dS. \tag{11.26}$$

We also note that the total fields on S are $\mathbf{E} = \mathbf{E}^i + \mathbf{E}^{sc}$ and $\mathbf{H} = \mathbf{H}^i + \mathbf{H}^{sc}$. In the absence of an obstacle, the average power carried across S by the incident wave is zero. In mathematical form:

$$\frac{1}{2}\,\mathrm{Re}\int_S \mathbf{u}_n \cdot (\mathbf{E}^i\times\mathbf{H}^{i*})\,dS = 0. \tag{11.27}$$

It follows, by subtracting (11.27) from (11.26), that

$$P^{ext} = P^{abs} + P^{sc} = -\frac{1}{2}\,\mathrm{Re}\int_S \mathbf{u}_n \cdot (\mathbf{E}^i\times\mathbf{H}^{sc*} + \mathbf{E}^{sc}\times\mathbf{H}^{i*})\,dS. \tag{11.28}$$

Let the incident wave be of the form (11.1). For such a choice, (11.28) becomes[4]

$$P^{ext} = \frac{1}{2}\,\mathrm{Re}\left\{\mathbf{A}^*\cdot\int_S\left[\mathbf{u}_n\times\mathbf{H}^{sc} + \frac{1}{R_{c0}}\mathbf{u}\times(\mathbf{u}_n\times\mathbf{E}^{sc})\right]e^{jk_0\mathbf{u}\cdot\mathbf{r}}dS\right\}.$$

From (11.14) and (11.15):

$$P^{ext} = \frac{1}{2}\,\mathrm{Re}\left\{\mathbf{A}^*\cdot\frac{j4\pi}{k_0R_{c0}}\mathbf{F}(\mathbf{u})\right\} = -\frac{2\pi}{k_0R_{c0}}\,\mathrm{Im}\left\{\mathbf{A}^*\cdot\mathbf{F}(\mathbf{u})\right\}. \tag{11.29}$$

Dividing by $\mathcal{P}_i$ gives, for the extinction cross section,

$$\sigma^{ext} = -\frac{4\pi}{k_0}\,\mathrm{Im}\left(\frac{\mathbf{A}^*\cdot\mathbf{F}(\mathbf{u})}{\mathbf{A}\cdot\mathbf{A}^*}\right). \tag{11.30}$$

This remarkable result shows that the value of σ^{ext} can be derived from a knowledge, in phase and amplitude, of the field scattered in the direction in which the incident wave propagates (the *forward* direction).

11.2.1 Radar Cross Section

The intensity of the scattered wave in a direction $\mathbf{u}'$ is measured by the *bistatic cross section* (Fig. 11.4)

$$\sigma^b(\mathbf{u}'|\mathbf{u}) = \frac{4\pi|\mathbf{F}(\mathbf{u}')|^2}{|\mathbf{A}|^2} \qquad (\mathrm{m}^2), \tag{11.31}$$

in terms of which the power radiated in a solid angle $d\Omega$ centered on $\mathbf{u}'$ can be expressed as

$$dP^{sc} = \frac{1}{2R_{c0}}\sigma^b(\mathbf{u}'|\mathbf{u})|\mathbf{A}|^2\frac{d\Omega}{4\pi} = \sigma^b(\mathbf{u}'|\mathbf{u})\frac{d\Omega}{4\pi}\mathcal{P}^i \qquad (W).$$

Of particular importance for radar applications is the *monostatic or radar cross section*

$$\sigma^{rad}(-\mathbf{u}|\mathbf{u}) = \frac{4\pi|\mathbf{F}(-\mathbf{u})|^2}{|\mathbf{A}|^2}, \tag{11.32}$$

a knowledge of which is necessary for calculation of the backscattered power.

The power density of the scattered wave in the direction $\mathbf{u}'$ is

$$P^{sc} = \mathcal{P}^i\frac{\sigma^b(\mathbf{u}'|\mathbf{u})}{4\pi R^2} \qquad (\mathrm{Wm}^{-2}). \tag{11.33}$$

According to Section 8.8, an antenna B located in a direction $\mathbf{u}'$ collects an available power

$$P^a = \frac{G'(-\mathbf{u}')\lambda_0^2}{4\pi}P_{pol}P^{sc} = \frac{G'(-\mathbf{u}')\lambda_0^2}{4\pi}\mathcal{P}^i\frac{\sigma^b(\mathbf{u}'|\mathbf{u})}{4\pi R^2}P_{pol}, \tag{11.34}$$

where P_{pol} is the polarization factor and G' the gain of the receiving antenna B in the direction $(-\mathbf{u}')$. Note that $\mathcal{P}^i$ is the incident power density *at the target*. If the latter is in the far field of the transmitter, we may write

$$\mathcal{P}^i = \frac{P^{tr}}{4\pi R^2}G(\mathbf{u}), \tag{11.35}$$

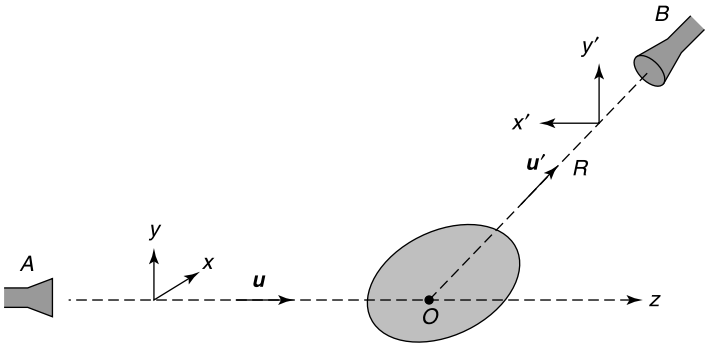

Figure 11.4 Scattered field and receiving antenna.

where P^{tr} is the transmitted power and G the gain of the transmitting antenna A in the direction $\mathbf{u}$. It is seen that the received power is proportional to R^{-4} and to P_{pol}, which, according to (8.222), is given by

$$P_{pol} = \frac{|\mathbf{F}^B_{ant} \cdot \mathbf{E}^i_B|^2}{|\mathbf{F}^B_{ant}|^2 |\mathbf{E}^i_B|^2}. \tag{11.36}$$

Here, $\mathbf{F}^B_{ant}$ is the radiation vector of antenna B and $\mathbf{E}^i_B$ the incident field on that antenna, viz.

$$\begin{aligned} \mathbf{E}^{sc} \;=\; \mathbf{E}^i_B &= \left[A_x \mathbf{F}^B_x(\mathbf{u}'|\mathbf{u}) + A_y \mathbf{F}^B_y(\mathbf{u}'|\mathbf{u})\right] \frac{e^{-jk_0R}}{R} \\ &= \overline{\overline{S}}(\mathbf{u}'|\mathbf{u}) \cdot \mathbf{A} \frac{e^{-jk_0R}}{R}. \end{aligned} \tag{11.37}$$

Vector $\mathbf{F}'$ and scattering matrix $\overline{\overline{S}}$ refer to the target. Let us particularize the analysis to backscattering from the target. For such a choice, antennas A and B coincide (Fig. 11.5). If, in addition, the target has symmetric bulk parameters $(\overline{\overline{\epsilon}}, \overline{\overline{\mu}}, \overline{\overline{\sigma}})$, the backscattering matrix becomes symmetric and can therefore be diagonalized. There are, in other words, directions X and Y for which $S_{XY} = S_{YX} = 0$ and for which the backscattered field becomes

$$\mathbf{E}^{sc} = (A_X F'_{XX} \mathbf{u}_X + A_Y F'_{YY} \mathbf{u}_Y) \frac{e^{-jk_0R}}{R}. \tag{11.38}$$

For these directions, which for the rectangular plate of Figure 11.2*a* are obvious from symmetry considerations, an X-polarized incident wave is reflected polarized in the same direction (i.e., without cross polarization). The same holds for the Y-polarization. The radiation vector of antenna A in the z-direction is proportional to

$$\mathbf{F}^A_{ant} \doteq A_X \mathbf{u}_X + A_Y \mathbf{u}_Y. \tag{11.39}$$

Inserting (11.38) and (11.39) into (11.36) gives a polarization factor

$$P_{pol} = \frac{\left|A_X F'_{XX} A_X + A_Y F'_{YY} A_Y\right|^2}{\left(|A_X F'_{XX}|^2 + |A_Y F'_{YY}|^2\right) \cdot \left(|A_X|^2 + |A_Y|^2\right)}. \tag{11.40}$$

There is *no* received signal when $P_{pol} = 0$; that is, when $\mathbf{A}$ and $\mathbf{F}$ are related by

$$\frac{A_Y}{A_X} = \pm j\sqrt{Q}\, e^{j\frac{\theta}{2}}, \tag{11.41}$$

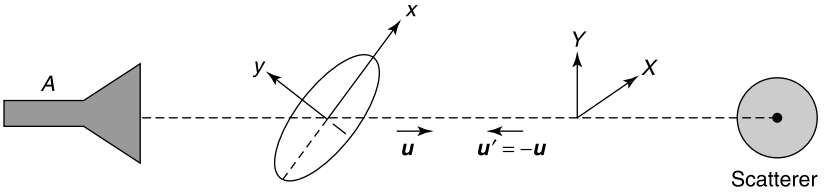

Figure 11.5 Backscattering and polarization factor.

where

$$Qe^{j\theta} = \frac{F'_{XX}(-\mathbf{u}/\mathbf{u})}{F'_{YY}(-\mathbf{u}/\mathbf{u})}.$$

If $F'_{XX} = F'_{YY}$, which is the case for a homogeneous sphere or a square plate, the *null polarizations* correspond with $A_Y = \pm jA_X$ (i.e., with the left and right circular polarizations), a result already obtained in Section 8.8. For the linear X polarization, setting $A_Y = 0$ in (11.40) gives the optimum value $P_{pol} = 1$. An analogous result holds for the Y-polarization.

The diagonalized scattering matrix can be given the form[5]

$$\overline{\overline{S}} = \begin{pmatrix} |F'_{XX}|e^{j\phi_X} & 0 \\ 0 & |F'_{YY}|e^{j\phi_Y} \end{pmatrix} = \underbrace{\begin{pmatrix} e^{j\phi_X} & 0 \\ 0 & e^{j\phi_Y} \end{pmatrix}}_{\overline{\overline{\phi}}} \cdot \underbrace{\begin{pmatrix} |F'_{XX}| & 0 \\ 0 & |F'_{YY}| \end{pmatrix}}_{\overline{\overline{P}}}, \tag{11.42}$$

in which we have written $\overline{\overline{S}}$ as the product of a *phase matrix* $\overline{\overline{\phi}}$ and a nonnegative matrix $\overline{\overline{P}}$. The *power matrix*, defined as

$$\overline{\overline{P}} \cdot \overline{\overline{P}} = \overline{\overline{P}}^2 = \begin{pmatrix} |F'_{XX}|^2 & 0 \\ 0 & |F'_{YY}|^2 \end{pmatrix} = \overline{\overline{S}}^+ \cdot \overline{\overline{S}}, \tag{11.43}$$

is useful in deriving an expression for the backscattered power density. To within a proportionality factor:

$$P^{sc} \doteq |A_X F'_{XX}|^2 + |A_Y F'_{YY}|^2$$

$$= \begin{pmatrix} A_X \\ A_Y \end{pmatrix} \cdot \begin{pmatrix} |F'_{XX}|^2 & 0 \\ 0 & |F'_{YY}|^2 \end{pmatrix} \cdot \begin{pmatrix} A_X^* \\ A_Y^* \end{pmatrix} = \mathbf{A} \cdot \overline{\overline{P}}^2 \cdot \mathbf{A}^*. \tag{11.44}$$

The elements of $\overline{\overline{P}}^2$ can be determined by power measurements only: no phase measurements are necessary.

11.2.2 Partially Polarized Fields

Basic concepts concerning partial polarization are discussed in Sections 7.5 and 8.8. We shall assume that the signals are quasi-harmonic, and represented by their *Stokes' vectors* (7.71). These vectors are of the form

$$\begin{pmatrix} s_0 \\ s_1 \\ s_2 \\ s_3 \end{pmatrix} = s_0(1-\rho) \begin{pmatrix} 1 \\ 0 \\ 0 \\ 0 \end{pmatrix} + \begin{pmatrix} \rho s_0 \\ s_1 \\ s_2 \\ s_3 \end{pmatrix}, \tag{11.45}$$

where ρ is the degree of polarization defined in (7.73). From (7.74), the first term on the right side of (11.45) is a completely unpolarized component and the second one a completely polarized one. One often uses the *modified Stokes vector*, of components $\frac{1}{2}(s_0 + s_1), \frac{1}{2}(s_0 - s_1), s_2, s_3$. These components, written for $\mathbf{A}(t)$ and the backscattered

$\mathbf{F}(t)$, are linearly connected through the 4×4 *Mueller matrix*.[‡] Thus [35, 70, 120] (Problem 11.4)

$$\begin{pmatrix} \langle F_x F_x^* \rangle \\ \langle F_y F_y^* \rangle \\ 2\,\mathrm{Re}\langle F_x F_y^* \rangle \\ -2\,\mathrm{Im}\langle F_x F_y^* \rangle \end{pmatrix} = \overline{\overline{M}} \cdot \begin{bmatrix} \langle A_x A_x^* \rangle \\ \langle A_y A_y^* \rangle \\ 2\,\mathrm{Re}\langle A_x A_y^* \rangle \\ -2\,\mathrm{Im}\langle A_x A_y^* \rangle \end{bmatrix}. \tag{11.46}$$

In accordance with (11.4):

$$\overline{\overline{M}} = \begin{bmatrix} |S_{xx}|^2 & |S_{xy}|^2 & \mathrm{Re}\,(S_{xx}S_{xy}^*) & \mathrm{Im}\,(S_{xx}S_{xy}^*) \\ |S_{yx}|^2 & |S_{yy}|^2 & \mathrm{Re}\,(S_{yx}S_{yy}^*) & \mathrm{Im}\,(S_{yx}S_{yy}^*) \\ 2\,\mathrm{Re}\,(S_{xx}S_{yx}^*) & 2\,\mathrm{Re}\,(S_{xy}S_{yy}^*) & \mathrm{Re}\,(S_{xx}S_{yy}^* + S_{xy}S_{yx}^*) & \mathrm{Im}\,(S_{xx}S_{yy}^* - S_{xy}S_{yx}^*) \\ -2\,\mathrm{Im}\,(S_{xx}S_{yx}^*) & -2\,\mathrm{Im}\,(S_{xy}S_{yy}^*) & -\mathrm{Im}\,(S_{xx}S_{yy}^* + S_{xy}S_{yx}^*) & \mathrm{Re}\,(S_{xx}S_{yy}^* - S_{xy}S_{yx}^*) \end{bmatrix}. \tag{11.47}$$

Because the terms of both the Stokes vectors and the Mueller matrix are real numbers, they can be determined by power measurements only. The Mueller matrix can alternately be expressed in terms of nine *Huynen descriptors*, the values of which are simply related to the elements of $\overline{\overline{S}}$. The new form is[6]

$$\overline{\overline{M}} = \begin{pmatrix} A_0 + B_0 & F & C & H \\ F & -A_0 + B_0 & G & D \\ C & G & A_0 + B_0 & E \\ H & D & E & A_0 - B_0 \end{pmatrix}. \tag{11.48}$$

For time-harmonic targets, the nine elements are not all independent but connected by four auxiliary equations. For a general time dependence, they become independent. It can be shown that the time-averaged Mueller matrix $\left\langle \overline{\overline{M}}(t) \right\rangle$ can be split into a mean non-time-dependent *target* matrix, to which is added a noise *residue* part [56]. Such a splitting can separate motional effects from the target signature.

The $\overline{\overline{M}}$ matrix is available for a variety of shapes [130, 131]. When the target is characterized by $F_{XX} = F_{YY}$, $\overline{\overline{M}}$ becomes proportional to the identity matrix. For a perfectly conducting sphere of radius a, for example, the proportionality factor, in the high-frequency limit, is $(a^2/4)$. For a metallic helix:[7]

$$\overline{\overline{S}} \doteq \frac{1}{2} \begin{pmatrix} 1 & \pm j \\ \pm j & -1 \end{pmatrix} \qquad \overline{\overline{M}} \doteq \frac{1}{4} \begin{pmatrix} 1 & 1 & 0 & \mp 1 \\ 1 & 2 & 0 & \mp 1 \\ 0 & 0 & 0 & 0 \\ \pm 2 & \pm 2 & 0 & -2 \end{pmatrix}, \tag{11.49}$$

where the upper and lower signs correspond with respectively a left and a right screw.

[‡]In addition to the Mueller matrix, one can also introduce the Hermitian 3×3 covariance matrix, formed from the correlations of the field components [120, 130].

The decomposition principle may also be applied to the scattering matrix, which Huynen splits as [35, 131]

$$\overline{\overline{S}}(t) = \underbrace{a_0(t)\overline{\overline{S}}_0}_{\text{signal}} + \underbrace{\overline{\overline{S}}_N(t)}_{\text{noise}}. \tag{11.50}$$

Here $a_0(t)$ is a complex scalar amplitude, and $\overline{\overline{S}}_0$ characterizes a structured target. By means of (11.50), basic information about the target (symmetry, nonsymmetry, convexity …) can be extracted from the fluctuating $\overline{\overline{S}}(t)$. The *noise* term $\overline{\overline{S}}_N(t)$ originates from factors such as sea and ground clutter, weather patterns, or foliage motion. They form the *residue* target. For a sphere, for example, $\overline{\overline{S}}_0$ is proportional to the identity matrix, while for a long straight wire it is

$$\overline{\overline{S}}_0 \doteq \begin{pmatrix} 1 & 0 \\ 0 & 0 \end{pmatrix}. \tag{11.51}$$

For a helix, $\overline{\overline{S}}_0$ is given by (11.49). The $\overline{\overline{S}}_N$ matrix can be put in the general form[§]

$$\overline{\overline{S}}_N = \begin{pmatrix} b & c \\ c & -b \end{pmatrix}. \tag{11.52}$$

By making full use of the vector nature of electromagnetic waves, polarimetric radars can achieve a considerable improvement over standard "amplitude-only" systems. Such radars are often used in conjunction with the interferometric determination of the full $\overline{\overline{S}}$ matrix by means of measurements at both ends of a baseline.[9] The potential applications of polarimetric methods are numerous: detection of buried objects or oil spills, crop assessment, sea-ice monitoring, forest height mapping, and more generally remote sensing of important biological and geophysical parameters of both the earth surface and the atmosphere [130].

11.3 SCATTERING BY A SPHERE

Field determination by separation of variables works in a few cases, notably for prolate and oblate spheroids (of which the straight wire and the disk are particular cases), rings, paraboloids, hyperboloids, and cones. By the early 1970s, most of these problems had been solved and their solution collected in various specialized treatises [38, 49, 113]. The number of papers relying on the method is nevertheless still growing.[10,11,12,13,14] We shall only consider the application of the method to a spherical scatterer, not only because of the intrinsic importance of that particular shape, but also because of the availability of abundant numerical data, which may serve to illustrate the physics of the scattering process, and in particular the phenomenon of resonance.

[§]For details on the electromagnetic characterization of precipitation echoes, land and sea clutter or *chaff* (a deliberately created airborne cloud of reflecting objects), see Ref. 8.

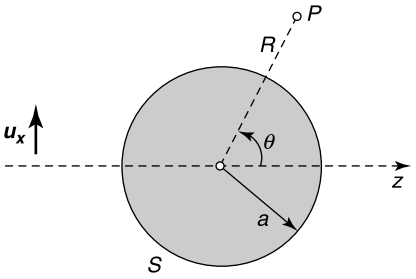

Figure 11.6 Spherical scatterer.

11.3.1 The Homogeneous Penetrable Sphere

Let a sphere of given isotropic[¶] characteristics (ϵ, μ) be immersed in an x-polarized plane wave of electric field (Fig. 11.6)

$$\mathbf{E}^i = \mathbf{u}_x e^{-jk_0 z}.$$

As in Section 10.6, we shall express the fields in terms of Debye potentials and write, for an incident electric field of unit amplitude,

$$\mathbf{E} = \text{curl curl}\,(v R\mathbf{u}_R) - j\omega\mu\ \text{curl}\,(wR\mathbf{u}_R) \tag{11.53}$$

$$\mathbf{H} = \underbrace{j\omega\epsilon\ \text{curl}\,(vR\mathbf{u}_R)}_{\text{TM}} + \underbrace{\text{curl curl}\,(wR\mathbf{u}_R)}_{\text{TE}}. \tag{11.54}$$

Outside the scatterer, $\epsilon = \epsilon_0$ and $\mu = \mu_0$. The Debye potentials for the incident field are given by (10.116) and (10.117) and for the total field outside the sphere by (10.122) and (10.123). We repeat these results for convenience:

$$v^{out} = \frac{j}{k_0}\sum_{n=1}^{\infty}(-j)^n \frac{2n+1}{n(n+1)}\cos\varphi P_n^1(\cos\theta)\left[j_n(k_0R) - a_n h_n^{(2)}(k_0R)\right] \tag{11.55}$$

$$w^{out} = \frac{j}{\omega\mu_0}\sum_{n=1}^{\infty}(-j)^n \frac{2n+1}{n(n+1)}\sin\varphi P_n^1(\cos\theta)\left[j_n(k_0R) - b_n h_n^{(2)}(k_0R)\right]. \tag{11.56}$$

Inside the sphere, we keep the $(\sin\varphi, \cos\varphi)$ dependence and use spherical Bessel functions instead of Hankel functions in order to avoid the singularity at $R = 0$. Thus,

$$v^{in} = \frac{j}{Nk_0}\cos\varphi\sum_{n=1}^{\infty}(-j)^n \frac{2n+1}{n(n+1)}c_n j_n(Nk_0R)P_n^1(\cos\theta) \tag{11.57}$$

$$w^{in} = \frac{j}{k_0 NZ_c}\sin\varphi\sum_{n=1}^{\infty}(-j)^n \frac{2n+1}{n(n+1)}d_n j_n(Nk_0R)P_n^1(\cos\theta). \tag{11.58}$$

[¶]For an extension to anisotropic media, see, for example, [87].

In these equations, $N = (\epsilon_r \mu_r)^{\frac{1}{2}}$ is the index of refraction, and $Z_c = (\mu/\epsilon)^{\frac{1}{2}}$ is the characteristic impedance of the medium filling the sphere. The constants a_n, b_n, c_n, and d_n can be determined by requiring the tangential components of **E** and **H** to be continuous at the surface of the scatterer (i.e., at $R = a$). In terms of Debye potentials, these conditions take the form

$$\begin{aligned}
\frac{\partial}{\partial R}\left(R\frac{\partial v^{in}}{\partial \theta}\right) &= \frac{\partial}{\partial R}\left(R\frac{\partial v^{out}}{\partial \theta}\right) \\
\mu_r \frac{\partial w^{in}}{\partial \theta} &= \frac{\partial w^{out}}{\partial \theta} \\
\frac{\partial}{\partial R}\left(R\frac{\partial w^{in}}{\partial \theta}\right) &= \frac{\partial}{\partial R}\left(R\frac{\partial w^{out}}{\partial \theta}\right) \\
\epsilon_r \frac{\partial v^{in}}{\partial \theta} &= \frac{\partial v^{out}}{\partial \theta}.
\end{aligned} \tag{11.59}$$

We are particularly interested in the coefficients a_n and b_n, which determine the strength of the scattered fields. Solution of the system of equations obtained by inserting the series expansions (11.55) to (11.58) into (11.59) gives

$$a_n = \frac{\epsilon_r j_n(Nk_0a)\left[xj_n(x)\right]'_{k_0a} - j_n(k_0a)\left[xj_n(x)\right]'_{Nk_0a}}{\epsilon_r j_n(Nk_0a)\left[xh_n^{(2)}(x)\right]'_{k_0a} - h_n^{(2)}(k_0a)\left[xj_n(x)\right]'_{Nk_0a}} \tag{11.60}$$

$$b_n = \frac{\mu_r j_n(Nk_0a)\left[xj_n(x)\right]'_{k_0a} - j_n(k_0a)\left[xj_n(x)\right]'_{Nk_0a}}{\mu_r j_n(Nk_0a)\left[xh_n^{(2)}(x)\right]'_{k_0a} - h_n^{(2)}(k_0a)\left[xj_n(x)\right]'_{Nk_0a}}. \tag{11.61}$$

It is particularly interesting to evaluate the scattered fields in the *radiation region*. This can be done by introducing the asymptotic value (A5.101) of $h_n^{(2)}(k_0R)$ into a_n and b_n. Thus, because

$$\lim_{R\to\infty} h_n^{(2)}(k_0R) = j^{n+1}\frac{e^{-jk_0R}}{k_0R}; \qquad \lim_{R\to\infty}\frac{d}{dR}\left[Rh_n^{(2)}(k_0R)\right] = j^n e^{-jk_0R}, \tag{11.62}$$

we obtain the scattered field

$$\begin{aligned}
\mathbf{E}^{sc} = \frac{e^{-jk_0R}}{R}\Bigg\{ &-\frac{j}{k_0}\sum_n \frac{2n+1}{n(n+1)}\, a_n \,\mathrm{grad}_1\left[\cos\varphi P_n^1(\cos\theta)\right] \\
&+ \frac{j}{k_0}\frac{2n+1}{n(n+1)}\, b_n \mathbf{u}_R \times \mathrm{grad}_1\left[\sin\varphi P_n^1(\cos\theta)\right]\Bigg\}.
\end{aligned} \tag{11.63}$$

Based on that expression, detailed calculations give the following formulas for the cross sections:

$$\sigma^{sc} = \frac{2\pi}{k_0^2} \sum_{n=1}^{\infty} (2n+1) \left(|a_n|^2 + |b_n|^2 \right) \tag{11.64}$$

$$\sigma^{ext} = \frac{2\pi}{k_0^2} \operatorname{Re} \left[\sum_n (2n+1)(a_n + b_n) \right] \tag{11.65}$$

$$\sigma^{rad} = \frac{\pi}{k_0^2} \left| \sum_n (-1)^n (2n+1)(a_n - b_n) \right|^2 . \tag{11.66}$$

Extensive numerical data for these quantities can be found in [134], including approximate expressions valid for small or large $k_0 a$, or for N close to unity. Typical results are shown in Figure 11.7. The curve $N = 8.90 - j\,0.69$, drawn for water at 20°C and $\lambda_0 = 10$ cm, displays two resonant peaks. Such peaks are also present in Figure 11.8, which is drawn for a wider range of frequencies.[15] Also of interest are the curves in Figure 11.9, drawn for respectively a perfectly conducting sphere ($N = \infty$) and a spherical drop of water ($N = 3.41 - j\,1.94$ at $\lambda_0 = 3$ mm).

The equations for the scattering coefficients a_n and b_n take a particularly simple form when $k_0 a$ and $N k_0 a$ are small, in which case we may use the small-argument approximations (A5.94) and (A5.96), namely

$$\lim_{\rho \to 0} \left[\rho j_n(\rho) \right]' = 2^n \frac{(n+1)!}{(2n+1)!} \rho^n ; \qquad \lim_{\rho \to 0} \left[\rho h_n^{(2)}(\rho) \right]' = \frac{j}{2^n} \frac{(2n)!}{(n-1)!} \frac{1}{\rho^{n+1}} .$$

Under these circumstances, and with $\rho = k_0 a$,

$$a_n = -j \rho^{2n+1} 2^{2n} \frac{n!(n+1)!(\epsilon_r - 1)}{(2n)!(2n+1)![n(\epsilon_r + 1) + 1]} (1 + \text{terms in } \rho^2) \tag{11.67}$$

$$b_n = -j \rho^{2n+1} 2^{2n} \frac{n!(n+1)!(\mu_r - 1)}{(2n)!(2n+1)![n(\mu_r + 1) + 1]} (1 + \text{terms in } \rho^2). \tag{11.68}$$

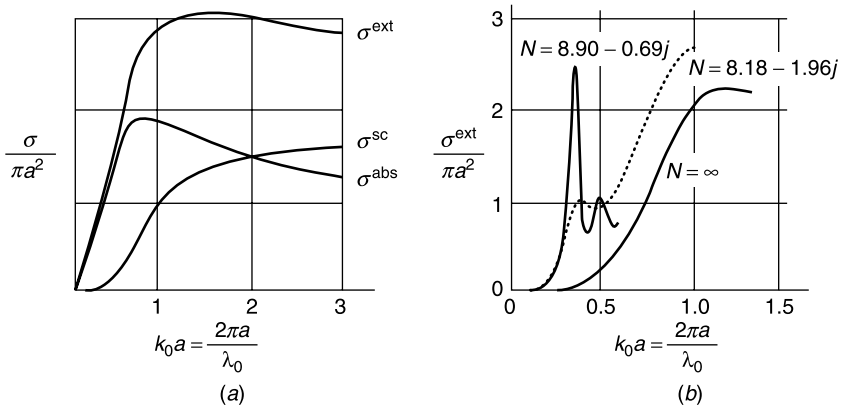

Figure 11.7 (*a*) Cross sections for iron ($\lambda_0 = 0.42$ μm, $N = 1.27 - j1.37$). (*b*) Typical extinction cross sections (from H. C. van de Hulst, *Light scattering by small particles*. John Wiley & Sons, New York, 1957).

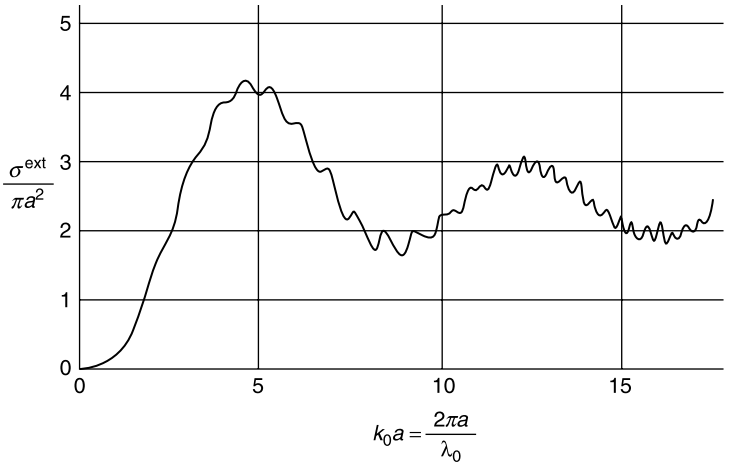

Figure 11.8 The fine structure of the curve for the extinction cross section of a dielectric sphere of index $N = 1.49$ (from J. Mével, Etude de la structure détaillée des courbes de diffusion des ondes electromagnétiques par les sphères diélectriques, *J. Phys. Radium* **19**, 630–636, 1958, with permission of EDP Sciences).

For a nonmagnetic dielectric, the dominant contribution in these multipole expansions stems from the term in a_1, an electric dipole term of moment $\mathbf{P}_e$ equal to the static value obtained for $\mathbf{e}^i = \mathbf{u}_x$ (Problem 11.5). The scattering cross section resulting from this dipole term is

$$\frac{\sigma^{sc}}{\pi a^2} = \frac{8}{3}\left|\frac{\epsilon_r - 1}{\epsilon_r + 2}\right|^2 (k_0 a)^4, \tag{11.69}$$

which shows that the low-frequency scattering cross section is proportional to the fourth power of the frequency. This frequency dependence, which is a characteristic of the *Rayleigh region*, is responsible for the slow start of the curves in Figures 11.7 to 11.9.

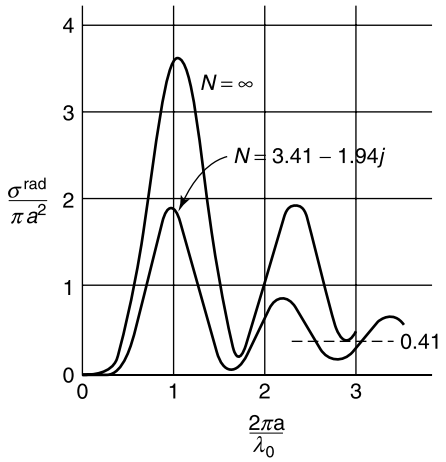

Figure 11.9 Typical radar cross sections (from H. C. van de Hulst, *Light scattering by small particles*. John Wiley & Sons, New York, 1957).

11.3.2 The Perfectly Conducting Sphere

The boundary conditions at $R = a$ now take the form $E_\theta = 0$ and $E_\varphi = 0$. Using (11.53) and (11.54) leads to the expansion coefficients

$$a_n = \frac{\left[xj_n(x)\right]'_{x=k_0a}}{\left[xh_n^{(2)}(x)\right]'_{x=k_0a}} \qquad b_n = \frac{j_n(k_0a)}{h_n^{(2)}(k_0a)}. \tag{11.70}$$

Knowledge of a_n and b_n allows evaluation of the various cross sections. The variation of σ^{ext}, σ^{sc}, and σ^{rad} with frequency is given in Figures 11.7 and 11.9 by the curves marked $N = \infty$. This infinite index of refraction stems from the value of N_σ for a good conductor, which is

$$N_\sigma = \left(\frac{\sigma}{j\omega\epsilon_0}\right)^{\frac{1}{2}} = \left(\frac{\sigma}{2\omega\epsilon_0}\right)^{\frac{1}{2}}(1-j). \tag{11.71}$$

Index N_σ clearly becomes infinite in the limit $\sigma \to \infty$. In the *low-frequency limit*, the coefficients a_n and b_n approach the values

$$a_n = -j2^{2n}\frac{(n-1)!(n+1)!}{(2n)!(2n+1)!}(k_0a)^{2n+1}$$

$$b_n = j2^{2n}\frac{(n!)^2}{(2n)!(2n+1)!}(k_0a)^{2n+1}.$$

According to these expressions, the leading terms in the series for σ^{sc} are the terms in $n = 1$, which correspond with the coefficients $a_1 = -j\frac{2}{3}(k_0a)^3$ and $b_1 = j\frac{1}{3}(k_0a)^3$. In consequence,

$$\lim_{k_0a\to 0}\sigma^{sc} = \frac{10\pi}{3}k_0^4a^6. \tag{11.72}$$

This relationship confirms the fourth-power dependence on frequency that is characteristic of Rayleigh scattering. Similarly, the low-frequency value of the monostatic (radar) cross section is given by

$$\lim_{k_0a\to 0}\sigma^{rad} = \pi k_0^4a^6. \tag{11.73}$$

Data on the *high-frequency limit* [38, 85] show that the cross sections σ^{rad} and σ^{sc} approach the respective values πa^2 and $2\pi a^2$ when $\omega \to \infty$. The limit $2\pi a^2$ implies that a large spherical particle removes from the incident beam exactly twice the amount of light it can intercept. This apparent paradox is due to the intense lobe that develops in a very narrow region about the forward direction[16] [134]. The transition to the *optical* region, obtained as the frequency increases, can be followed on Figure 11.10*a*, which displays the variation of $|J_{S\theta}/H^i|$ along a great circle whose plane is perpendicular to the incident magnetic field. The figure also displays the value predicted by geometrical optics, which is $|\mathbf{J}_S| = 2H^i$ up to 90° and $|\mathbf{J}_S| = 0$ between 90° and 180°. Figure 11.10*b* shows the variation of $|\mathbf{J}_S|$ along a great circle perpendicular to the incident electric field. We notice that $\mathbf{J}_S$ is perpendicular to the great circle. In the geometrical optics limit, $|\mathbf{J}_S|$ is proportional to $\cos\alpha$ when α lies between 0° and 90° and equal to zero for α lying between 90° and 180°.

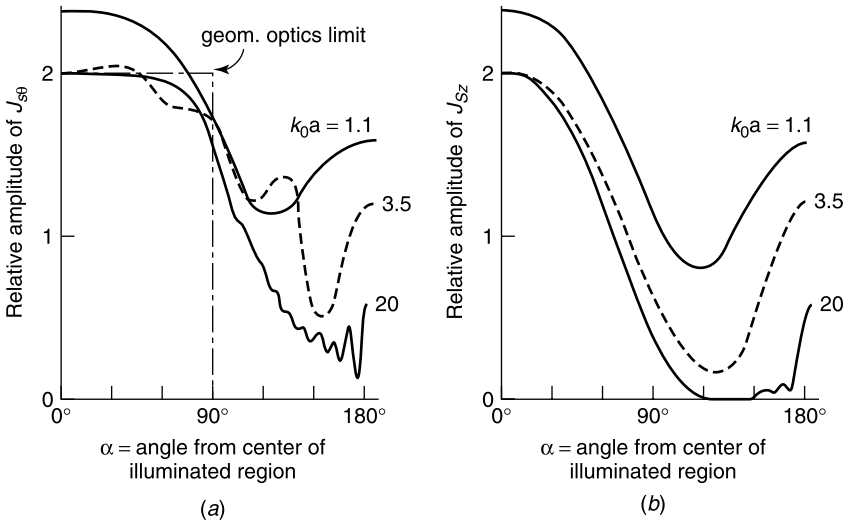

Figure 11.10 Current density at the surface of the sphere (reprinted by permission of the publishers (from *The scattering and diffraction of waves*, by Ronald W. P. King and Tai Tsun Wu, Cambridge, Mass., Harvard University Press, Copyright 1959 by the President and Fellows of Harvard College).

11.3.3 The Radially Inhomogeneous Sphere

Let (ϵ, μ) depend only on R. In solving for the fields we start from the spherical harmonics expansions in Section 7.11 and notice that equations (7.182) and (7.187) remain valid when ϵ_0 and μ_0 are replaced by $\epsilon(R)$ and $\mu(R)$. In the TE family, the main expansion coefficient v_{mn} now satisfies

$$\frac{\mu}{R}\frac{\partial}{\partial R}\left[\frac{1}{\mu}\frac{\partial}{\partial R}(Rv_{mn})\right] - \epsilon\mu\frac{\partial^2 v_{mn}}{\partial t^2} - n(n+1)\frac{v_{mn}}{R^2}$$

$$= \frac{\mu}{R}\frac{\partial}{\partial R}\left(\frac{1}{\mu}RA_{mn}\right) - \mu\frac{\partial C_{mn}}{\partial t} - \frac{1}{R}B_{mn}. \tag{11.74}$$

For the TM family, (7.188) is replaced by

$$\frac{\epsilon}{R}\frac{\partial}{\partial R}\left[\frac{1}{\epsilon}\frac{\partial}{\partial R}(Ri_{mn})\right] - \epsilon\mu\frac{\partial^2 i_{mn}}{\partial t^2} - n(n+1)\frac{i_{mn}}{R^2}$$

$$= \frac{\epsilon}{R}\frac{\partial}{\partial R}\left(\frac{1}{\epsilon}RB_{mn}\right) - \frac{1}{R}C_{mn} - \epsilon\frac{\partial A_{mn}}{\partial t}. \tag{11.75}$$

At large R, the parameters (ϵ, μ) normally taper off to (ϵ_0, μ_0), and the radiation conditions for free space may be applied. In a sinusoidal time regime, these conditions imply a $h_n^{(2)}(k_0R)$ variation for both v_{mn} and i_{mn}.

A configuration of great practical importance is that of a spherical Earth of radius a surrounded by an atmosphere whose parameters depend on altitude only. In this case, the expansion in spherical harmonics converges very poorly. It is found, indeed, that terms

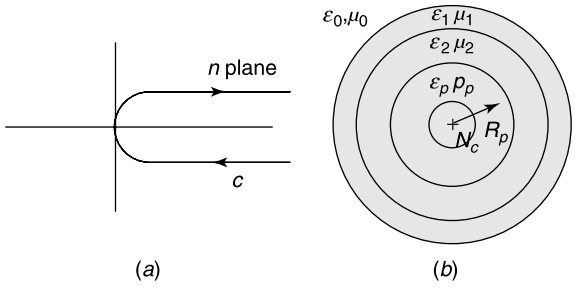

Figure 11.11 (*a*) Contour of integration for Watson's transformation. (*b*) Typical multishell structure.

up to the order $n = 2\pi a/\lambda_0 = k_0 a$ must be included in the expansion to ensure reasonable convergence. This number lies between 10^3 and 10^9 at typical radio frequencies. The convergence difficulties can be avoided by use of the *Watson transformation*[17]

$$\sum_0^\infty (2n+1) f(n) P_n(\cos\theta) = \frac{1}{j}\int_c \frac{n\,dn}{\cos n\pi} f\left(n-\frac{1}{2}\right) P_{n-\frac{1}{2}}[\cos(\pi-\theta)] \qquad (11.76)$$

through which the expansion can be replaced by an integral in the complex plane. The contour for the integral is shown in Figure 11.11*a*. By suitable deformation of the contour, the integral can be expressed as a sum of residues whose convergence properties are much better than those of the original spherical-harmonics expansion [137].

In many applications, in particular those that involve general inhomogeneous materials, direct solution by finite elements or finite differences is the preferred choice. Figure 11.12 displays results obtained by finite elements for a *Luneburg lens* excited by a Hertzian dipole at its surface[18] (see Section 8.3). As expected, the radiation is directive and becomes increasingly so as the frequency increases (or as the size of the lens increases).

11.3.4 Spherical Shells

A succession of concentric shells of homogeneous material is often used as a *numerical model* to approximate a continuous $\epsilon_r(R)$ variation (Fig. 11.11*b*). In each shell, the R-dependent coefficients in the field expansions are combinations of spherical Bessel functions. In the central sphere, one should choose $j_n(N_c k_0 R)$; in a typical shell $j_n(N_p k_0 R) + c_p n_n(N_p k_0 R)$; and in the exterior region $h_n^{(2)}(k_0 R)$. By such methods, each

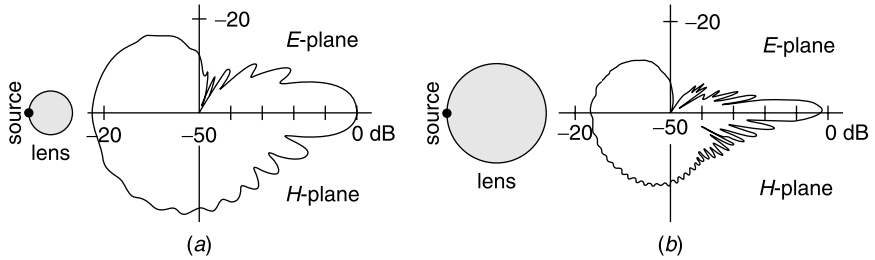

Figure 11.12 Radiation from a Luneburg lens: (*a*) diameter = 4 λ_0, (*b*) diameter = 10 λ_0 (from A. D. Greenwood and J. M. Jin, A field picture of wave propagation in inhomogeneous dielectric lenses, *IEEE Antennas Prop. Mag.* **41**, 9–17, 1999, with permission of IEEE).

shell may be characterized by a transition matrix, and it becomes possible, for example, to derive the form of the appropriate Green's dyadics.[19,20,21] The multishell structure, in addition to being a useful model, is used in the real-life design of Luneburg lenses. The desired $N(R)$ variation is difficult to realize and is typically simulated by a succession of discrete steps. For economic reasons, the number of steps should be as small as possible, and acceptable gain and sidelobe performance must be maintained. The genetic method discussed in Section 7.14 is well-equipped to solve the problem. In the application to the lens, the following fitness function has been used:[22]

$$F(\epsilon_{r1}, t_1, \ldots, \epsilon_{rm}, t_m) = \alpha\, G_{\max} + \beta\, \text{Min}\left[f(\theta) - G(\theta)\right]_{\text{sidelobe region}}. \tag{11.77}$$

In this expression, ϵ_{r_i} and t_i are respectively the dielectric constant and the thickness of the "i" layer, $G(\theta)$ is the gain pattern in the E plane, and $f(\theta)$ is the selected sidelobe envelope function. By a proper choice of $f(\theta)$ and the parameters (α, β), it becomes possible to control the gain and sidelobe levels.

11.3.5 Transient Fields

The solution of the time-dependent equations (11.74) and (11.75) may be effected by Laplace transformation techniques [35, 91, 113]. In a homogeneous sourceless region, for example, one would write

$$\frac{d^2}{dR^2}\left[R\, V_{mn}(s)\right] + \left[-\frac{s^2}{c_0^2} - n(n+1)\right] V_{mn}(s) = 0, \tag{11.78}$$

or, with a slight change of notation,

$$\frac{d^2}{dR^2}\left[R\, V_{mn}(s)\right] + \left[\left(\frac{js}{c_0}\right)^2 - n(n+1)\right] V_{mn}(s) = 0. \tag{11.79}$$

In expression (11.60) for a_n, $(k_0 a)$ should be replaced by $\left(\frac{js}{c_0}\right)a$, which introduces spherical Bessel functions of the complex argument $\left(\frac{js}{c_0}\right)a$ into the analysis.

11.4 RESONANT SCATTERING

A resonant mode is a field pattern that can exist in the absence of sources. For a *perfectly conducting* sphere, the resonances occur when the denominators in (11.70) vanish. For a TE (or magnetic) mode, the condition is

$$h_n^{(2)}(k_0 a) = 0. \tag{11.80}$$

For a TM (or electric) mode it becomes

$$\frac{d}{dR}\left[R h_n^{(2)}(k_0 R)\right]_{R=a} = 0. \tag{11.81}$$

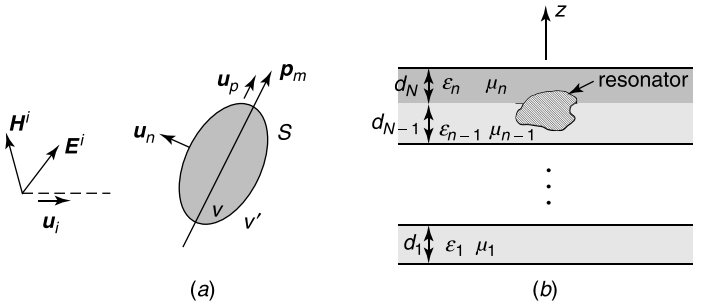

Figure 11.13 (*a*) Dielectric resonator in an incident wave. (*b*) Resonator embedded in a multilayered circuit.

The $n = 1$ mode, for example, has a resonance at $k_0a = \pm 0.86 + j\,0.5$ [134]. A complex value of k_0a leads to a time factor $e^{j\omega t}$ of the form $e^{\alpha t}e^{j\beta t}$, where α must be negative [and therefore $\mathrm{Im}(k_0a)$ positive] in order to take the radiative losses into account. When the incident wave is swept in frequency, the various modes resonate successively, producing peaks in the radar cross section that may serve to identify the nature of the target. The topic is discussed at length in Section 11.5.

Resonances also occur for *dielectric* bodies, a property that is illustrated by Figure 11.8, where the peaks are actually hardly observable because of the low value of N. One expects them to become more pronounced when N increases (i.e., for higher contrasts). A component of great importance for the design of microwave circuits is the dielectric resonator discussed in Section 10.5. Its usefulness is based on these resonances, and the popularity of the device rests on advantages of smallness, low cost, low loss, and potentially wide bandwidth[23] (Fig. 11.13*a*). The resonator is often incorporated in a multilayer structure,[24,25] in which case the field problem may be formulated in terms of a mixed potential integral equation of the type discussed in Section 9.4 (Fig. 11.13*b*). The resonator is often coupled to a waveguide, for example to a microstrip. In Figure 11.14*a*, the coupling results from the linking of the **H**-fields of the microstrip (dashed line) to the fields of the $\mathrm{TE}_{01\delta}$ mode of a circular pillbox[26] (solid line, see also Fig. 10.13). The $\mathrm{TE}_{01\delta}$ mode has a high quality factor and is therefore often chosen for *resonator* applications. Another mode of low resonant frequency, the $\mathrm{HEM}_{11\delta}$, radiates efficiently and is particularly suitable for *antenna* applications [82]. The theoretical microstrip-resonator problem can be solved[27] by methods already described

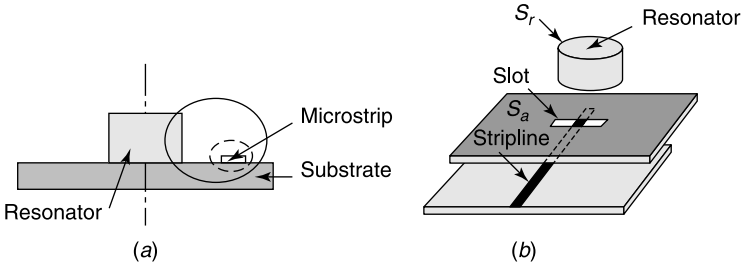

Figure 11.14 (*a*) Coupling between a microstrip and a resonator. (*b*) Aperture-coupling between resonator and microstrip feed (from P. Guillon, B. Byzery, and M. Chaubet, Coupling parameters between a dielectric resonasstor and a microstripline, *IEEE Trans. MTT* **33**, 222–226, 1985, with permission of IEEE, and K. W. Leung, M. L. Poon, W. C. Wong, K. M. Luk, and E. K. N. Jung, Aperture-coupled dielectric resonator antenna using a strip-line feed, *Microwave Opt. Tech. Lett.* **24**, 120–121, 2000, with permission of John Wiley & Sons).

in Section 10.5 (see Equations 10.79 to 10.87). The potentials in these equations must now be expressed in terms of the Green's dyadic of the *microstrip* instead of that of free space.

Another frequently encountered coupling mechanism is shown in Figure 11.14*b*. Here the fields can be determined by integral equation techniques involving several unknowns[28,29]: the equivalent sources $\mathbf{J}_S$ and $\mathbf{J}_{mS}$ on the resonator surface S_r, the surface current $\mathbf{J}_S$ on the feed line, and the equivalent magnetic current $\mathbf{J}_{mS}$ in the coupling aperture S_a.

The Asymptotic Theory

In Figure 11.13*a*, the scattered fields may be conveniently expanded in a series

$$\mathbf{H}(\mathbf{r}) = \sum A_n \mathbf{H}_{0n}(\mathbf{r}), \tag{11.82}$$

where the $\mathbf{H}_{0n}$ are the eigenvectors defined in (10.92). To simplify the notation, we shall drop the subscript 0, and write $\mathbf{H}_n$ instead of $\mathbf{H}_{0n}$. The $\mathbf{H}_n$ form an orthogonal set in the sense that (Problem 10.27)

$$\int_{V+V'} \mathbf{H}_n \cdot \mathbf{H}_p \, dV = 0 \qquad \text{for } k_n \neq k_p. \tag{11.83}$$

It follows that

$$A_n = \frac{\displaystyle\int_{V+V'} \mathbf{H} \cdot \mathbf{H}_n \, dV}{\displaystyle\int_{V+V'} |\mathbf{H}_n|^2 dV}. \tag{11.84}$$

Expansion (11.82) converges well because $\mathbf{H}$ and $\mathbf{H}_n$ behave similarly in the vicinity of V (a vanishingly small volume for large N). Both fieds are irrotational and decrease like $(1/R^3)$ away from the body, a characteristic of the magnetostatic field.[30] From the respective field equations satisfied by $\mathbf{H}^i$ and the total field $\mathbf{H}_{\text{total}} = \mathbf{H} + \mathbf{H}^i$, it is easy to show that

$$-\text{curl curl } \mathbf{H} + k^2 \mathbf{H} = -k^2 \mathbf{H}^i \left(1 - \frac{1}{N^2}\right), \tag{11.85}$$

where $k = k_0 N$ is the wave number in the dielectric. A few manipulations based on (11.85) lead to[30,31]

$$\mathbf{H}(\mathbf{r}) = \sum_n \frac{\displaystyle\int_S \psi_n \mathbf{u}_n \cdot \mathbf{H}^i \, dS - \int_V \mathbf{H}^i \cdot \mathbf{H}_n \, dV}{2k_n^2 \left(\dfrac{\Delta k}{k_n} - \dfrac{j}{2Q_n}\right) \displaystyle\int_V |\text{curl } \mathbf{H}_n|^2 \, dV} \mathbf{H}_n(\mathbf{r}), \tag{11.86}$$

where grad ψ_n is the form of $\mathbf{H}_n$ outside the resonator, k_n is the resonant wavenumber, and $\Delta k = (k - k_n)$. The value of Q_n is given in (10.98). For a given resonant frequency, the resonator becomes very small as N increases, and $\mathbf{H}^i$ may therefore be assumed uniform over V. For such a case, the numerator in (11.86) can be written in terms of the characteristic magnetic dipole moment $(\mathbf{p}_m)_n$ of the nth mode, the value of which is given in (10.97).

This expression contains the integral $\int_V dV\mathbf{r}\times$, an operator that is often encountered in mathematical physics. It can be transformed as follows:

$$(\mathbf{p}_m)_n = \frac{1}{2}\int_V \mathbf{r}\times \text{curl}\,\mathbf{H}_n\,dV = \frac{1}{2}\sum_{i=1}^{3}\mathbf{u}_{x_i}\times\int_V x_i\,\text{curl}\,\mathbf{H}_n\,dV$$

$$= \frac{1}{2}\sum_{i=1}^{3}\mathbf{u}_{x_i}\times\left[\int_V \text{curl}\,(x_i\mathbf{H}_n)\,dV - \int_V \text{grad}\,x_i\times\mathbf{H}_n\,dV\right].$$

By means of (A1.28), and because $\mathbf{H}_n = \text{grad}\,\psi_n$ on S, we may write the first integral of the term between square brackets as

$$\int_S \mathbf{u}_n\times(x_i\,\text{grad}\,\psi_n)\,dS = \int_S \mathbf{u}_n\times\text{grad}\,(x_i\psi_n)\,dS - \int_S \psi_n\mathbf{u}_n\times\mathbf{u}_{x_i}.$$

From (A3.56), the first integral in the right-hand term vanishes, hence

$$\mathbf{p}_{mn} = p_{mn}\mathbf{u}_{pn} = -\int_S \psi_n\mathbf{u}_n\,dS + \int_V \mathbf{H}_n\,dV. \tag{11.87}$$

The numerator in (11.86) is therefore minus $\mathbf{p}_{mn}\cdot\mathbf{H}^i$. The peak magnetic field at the k_n resonance follows as

$$\mathbf{H}_{\text{peak}} = -jQ_n\frac{k_n^2\mathbf{p}_{mn}\cdot\mathbf{H}^i}{\int_V |\text{curl}\,\mathbf{H}_n|^2 dV}. \tag{11.88}$$

The value of Q_n given in (10.98) leads to the following expression for the induced dipole moment in the vicinity of the k_n resonance:

$$(\mathbf{P}_m)_n = -j\frac{3}{4\pi^2}\lambda_0^3(\mathbf{H}^i)_{pn}\frac{1}{1+j2Q_n(\Delta k/k_n)}. \tag{11.89}$$

In this expression, λ_0 is the free-space wavelength at resonance, and $(\mathbf{H}^i)_{pn} = (\mathbf{u}_{pn}\cdot\mathbf{H}^i)\mathbf{u}_{pn}$ is the component of $\mathbf{H}^i$ in the direction of the dipole moment $\mathbf{p}_{mn}$. The peak scattering cross section at resonance is easily found to be

$$\sigma_n^{sc} = \frac{3\lambda_0^2}{2\pi}\frac{|\mathbf{u}_{pn}\cdot\mathbf{H}^i|^2}{|\mathbf{H}^i|^2}. \tag{11.90}$$

We note that only the *direction* of $\mathbf{p}_{mn}$ must be known to evaluate both $(\mathbf{P}_m)_n$ and σ_n^{sc}, while the *magnitude* of $\mathbf{p}_{mn}$ is not involved. We also note that the optimum values of $(\mathbf{P}_m)_n$ and σ_n^{sc} are obtained when $\mathbf{p}_{mn}$ is oriented along $\mathbf{H}^i$, and that these values are independent of the shape and dielectric constant of the resonator. These interesting results hold only for $N\to\infty$, and require, in particular, that λ_0 should remain much larger than the dimensions of the resonator.

A similar analysis can be developed for the resonances of the confined modes. We only quote two results, valid for the lowest *electric dipole* mode. Its moment around resonance varies according to the law

$$\mathbf{P}_e = -j\frac{6\pi N^3 \epsilon_0}{k_n^3}(\mathbf{E}^i)_{pn}\,\frac{1}{1+j2Q_n(\Delta k/k_n)} \tag{11.91}$$

and the peak scattering cross section is

$$\sigma_n^{sc} = \frac{3\lambda_0^2}{2\pi}\frac{|\mathbf{u}_{pn}\cdot\mathbf{E}^i|^2}{|\mathbf{E}^i|^2}. \tag{11.92}$$

Thanks to these formulas, the lowest resonances on a curve σ^{sc} (frequency) can be asymptotically predicted, both in their peak value [from (11.90) and (11.92)] and in the sharpness of their flanks (from the known value of Q). Figure 10.9*b* illustrates the kind of approximation that can be obtained by such methods.

11.5 THE SINGULARITY EXPANSION METHOD

It is clear from the previous section that conducting and dielectric bodies *resonate* at certain frequencies. The resonant peaks of the scattering cross section appear clearly in Figure 11.15, where the data have been obtained by separation of variables[32] (the *Mie method*). The shape of the resonances, and in particular their sharpness, gives information on N and therefore on the nature of the target. It has been observed[33] that the frequency response in the range $\frac{\pi}{2} < k_0 L < 4\pi$ (or $10L > \lambda_0 > 0.5L$, with L a characteristic dimension of the target) can provide much useful information on bulk dimensions, approximate shape, and material composition of the scatterer.[34] The higher frequencies, on the other hand, characterize the fine details. A more sophisticated identification method emerged some 30 years ago, after numerous observations had shown that the late-time scattered fields could be represented by a series of damped sinusoidal oscillations. The (complex) frequencies of these oscillations depended only on the geometry and the material parameters of the scatterer and not on the nature of the incident fields[35] [91, 127]. Figure 11.16*a* shows the experimentally observed current on a wire located in an aircraft exposed to a pulsed electromagnetic field.[36] This response reminds one of the oscillation of an R-L-C circuit. The response of such circuits is of the form $e^{-\alpha t}e^{\pm j\omega t}$, and it is associated with the presence of poles $(-\alpha \pm j\omega)$ in the Laplace transform of the current. Figure 11.16*b* and *c* show the first two resonant currents on a 707 aircraft, modeled by a few conducting sticks. The dashed lines represent the amplitude of the current and the arrows the current's direction. Figure 11.16*d* displays the first-quadrant poles of the lowest modes of the 707 and 747 aircrafts. Resonances in the frequency domain are discussed in Sections 10.4 and 11.4. They will now be investigated in the time domain.

11.5.1 The Ringing of an R, L, C Circuit

The current in the circuit of Figure 11.17*a* satisfies the differential equation

$$\left(L\frac{d^2}{dt^2} + R\frac{d}{dt} + \frac{1}{C}\right) i(t) = \frac{dv(t)}{dt}. \tag{11.93}$$

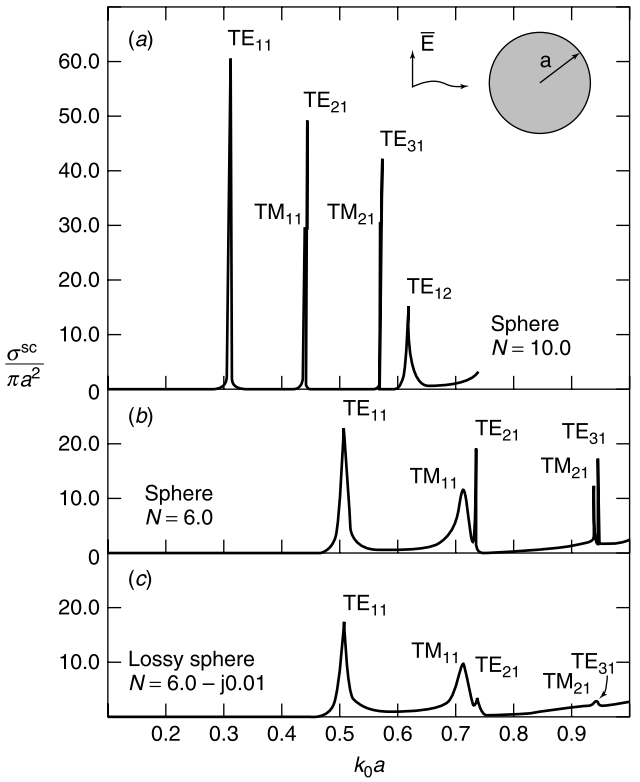

Figure 11.15 Scattering cross section for three spheres (from P. W. Barber, J. F. Owen, and R. K. Chang, Resonant scattering for characterization of axisymmetric dielectric objects, *IEEE Trans. AP* **30**, 168–172, 1982, with permission of IEEE).

By taking the bilateral Laplace transforms of both sides, this equation becomes [91]

$$\mathcal{L}(s)I(s) = \left(s^2L + Rs + \frac{1}{C}\right) I(s) = s\,V(s). \tag{11.94}$$

The unknown $I(s)$ can be determined by inverting (11.94). Thus,

$$I(s) = \mathcal{L}^{-1}(s)V(s) = \frac{s}{s^2L + sR + \dfrac{1}{C}} V(s) = Y(s)V(s). \tag{11.95}$$

The admittance function $Y(s)$ has two simple poles, located at

$$s^{\pm} = -\frac{R}{2L} \pm j\left[\left(\frac{R}{2L}\right)^2 - \frac{1}{LC}\right]^{\frac{1}{2}} = -\alpha \pm j\beta. \tag{11.96}$$

Depending on the sign of $R^2 - 4(L/C)$, the poles, which lie in the left half-plane, are real or complex conjugate. The admittance $Y(s)$ can be written in *singularity expansion* form as

$$Y(s) = \frac{1}{L(s^+ - s^-)}\left(\frac{s^+}{s - s^+} - \frac{s^-}{s - s^-}\right). \tag{11.97}$$

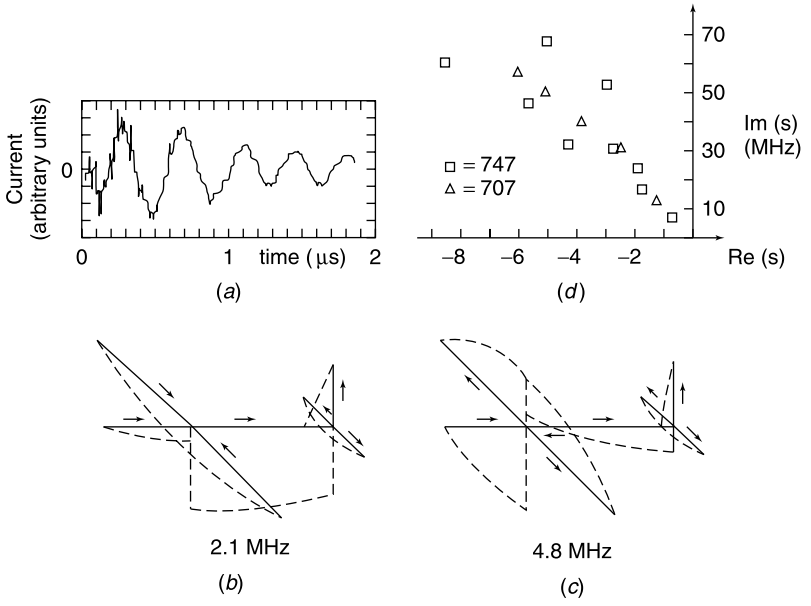

Figure 11.16 (*a*) Typical experimental response curve. (*b*, *c*) The two lowest resonant currents for the 707. (*d*) The lowest resonant poles for the 707 and the 747 (from L. Marin, Major results and unresolved issues in singularity expansion method, *Electromagn.* **1**, 361–373, 1981, with permission of the Taylor & Francis Group).

Let us assume that a step voltage V_0 is suddenly applied at $t = 0$, for example by closing a switch. The voltage $v(t)$ is equal to $V_0 H(t)$, and its transform is found, from Table A7.2, to be (V_0/s). For such a case

$$I(s) = \frac{V_0}{L(s - s^+)(s - s^-)} = \frac{V_0}{L(s^+ - s^-)} \left(\frac{1}{s - s^+} - \frac{1}{s - s^-} \right). \tag{11.98}$$

The value of $i(t)$ can easily be derived from Table A7.2, according to which $(s - a)^{-1}$ is the transform of e^{at}. Alternately, the inverse of $I(s)$ can be determined by means of the Bromwich integral (A7.15). Because $i(t)$ is zero for $t < 0$, the integral will converge for $\mathrm{Re}\,(s) > -(R/2L)$. The vertical path AB in Figure A7.1 may therefore coincide with the imaginary axis and the path closed by a left semicircle at infinity. Application of Cauchy's

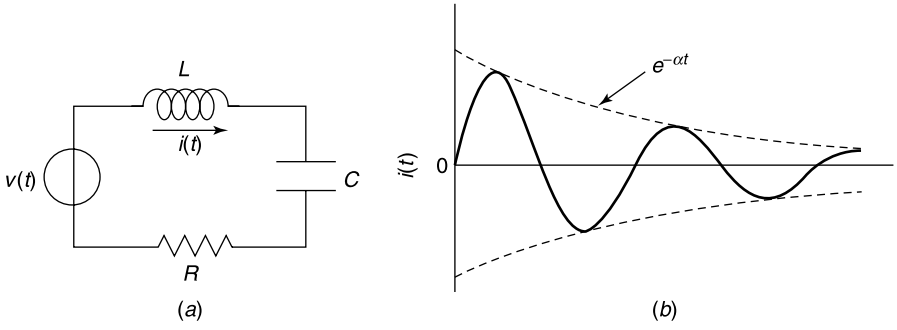

Figure 11.17 (*a*) RLC circuit and transient voltage source. (*b*) Response to a step-input.

theorem gives, after evaluation of the residues at the two poles,

$$\begin{aligned} i(t) &= \frac{V_0}{L(s^+ - s^-)} \left(e^{s^+ t} - e^{s^- t} \right) \\ &= \frac{V_0}{L} e^{-\alpha t} \frac{\sin \beta t}{\beta} \qquad (\text{for } t \geq 0). \end{aligned} \tag{11.99}$$

11.5.2 The Transmission Line

A transmission line open at both ends provides a good example of a system endowed with an infinite number of resonant modes. From (1.2), the bilateral Laplace transform of $i(x,t)$ must satisfy [91]

$$\mathcal{L}(s) I(x,s) = \frac{d^2 I(x,s)}{dx^2} + k^2(s) I(x,s) = -Y(s) V_a'(s), \tag{11.100}$$

where $V_a' = \dfrac{dV_a}{dx}$, $Y(s) = G + sC$, $Z(s) = R + sL$, and $k^2(s) = -Y(s)Z(s)$. To invert the operator $\mathcal{L}$, we shall expand $I(x,s)$ in the orthonormal set

$$\psi_n(x) = \sqrt{\frac{2}{l}} \sin\left(\frac{n\pi}{l} x \right) = \sqrt{\frac{2}{l}} \sin(k_n x). \tag{11.101}$$

Because $I(x,s)$ vanishes at both ends of the line (i.e., for $x = 0$ and $x = l$), the expansion takes the form

$$I(x,s) = \mathcal{L}^{-1} V_a'(s) = \sum_{n=1}^{\infty} \frac{Y(s)}{k_n^2 - k^2(s)} \psi_n(x) V_n(s), \tag{11.102}$$

where $\mathcal{L}^{-1}$ is the resolvent operator, and

$$V_n(s) = \int_0^l V_a'(x,s) \psi_n(x)\, dx.$$

The resonances are associated with poles, which can be identified by the condition $k^2(s) - k_n^2 = 0$. This condition yields

$$s_n^{\pm} = -\frac{1}{2} \left(\frac{R}{L} + \frac{G}{C} \right) \pm \frac{j}{2} \left[\frac{4\pi^2 n^2}{l^2 LC} - \left(\frac{R}{L} - \frac{G}{C} \right)^2 \right]^{\frac{1}{2}} \tag{11.103}$$

and

$$\frac{Y(s)}{k_n^2 - k^2(s)} = \frac{1}{LC(s_n^+ - s_n^-)} \left(\frac{Y(s_n^+)}{s - s_n^+} - \frac{Y(s_n^-)}{s - s_n^-} \right). \tag{11.104}$$

The (simple) poles correspond with the natural frequencies of the open-circuited line. Singularities can also be present in the source term $V_n(s)$. For such a case, one splits $I(x,s)$

into two terms, $I_1(x,s)$ and $I_2(x,s)$, given by

$$I_1(x,s)=\sum_{n=1}^{\infty}\frac{\psi_n(x)}{LC(s_n^+-s_n^-)}\left[\frac{V_n(s_n^+)Y(s_n^+)}{s-s_n^+}-\frac{V_n(s_n^-)Y(s_n^-)}{s-s_n^-}\right] \tag{11.105}$$

$$I_2(x,s)=\sum_{n=1}^{\infty}\frac{\psi_n(x)}{LC(s_n^+-s_n^-)}\left[\frac{[V_n(s)-V_n(s_n^+)]Y(s_n^+)}{s-s_n^+}-\frac{[V_n(s)-V_n(s_n^-)]Y(s_n^-)}{s-s_n^-}\right]. \tag{11.106}$$

The $I_2(x,s)$ term remains analytic at the natural frequencies of the line, and its sole singularities stem from $V_a'(x,s)$. The $I_1(x,s)$ term yields, upon inversion, exponentials of the type (11.99).

When the line is infinite, the summation (11.102) is replaced by an integral [91]

$$I(x,s)=\int_{-\infty}^{\infty}\frac{Y(s)}{\lambda^2-k^2(s)}\frac{1}{\sqrt{2\pi}}e^{-jx\lambda}V_a(s)\,d\lambda,$$

where

$$V_a(s)=\int_{-\infty}^{\infty}V_a'(x,s)\frac{1}{\sqrt{2\pi}}e^{jx\lambda}\,dx. \tag{11.107}$$

Singularities may be contributed by the excitation term $V_a(s)$. The line itself introduces poles, which can be extracted by solving the equation

$$\lambda^2-k^2(s)=LC(s-s_\lambda^+)(s-s_\lambda^-)=0,$$

from which it follows that

$$s_\lambda^{\pm}=-\frac{1}{2}\left(\frac{R}{L}+\frac{G}{C}\right)\pm\frac{j}{2}\sqrt{\frac{4\lambda^2}{LC}-\left(\frac{R}{L}-\frac{G}{C}\right)^2}. \tag{11.108}$$

The poles, infinite in number, form a continuous spectrum and crowd together on the vertical line

$$\mathrm{Re}\,(s)=-\frac{1}{2}\left(\frac{R}{L}+\frac{G}{C}\right).$$

This line traces part of a branch cut for the integral. The other part is formed by the portion of the real axis for which the square root in (11.108) is imaginary. The evaluation of the Bromwich integral must take these branch cuts into account.

11.5.3 The Linear Antenna

Pocklington's equation (7.238) for a short-circuited antenna becomes,[‖] *in s form* (Fig. 7.21),

$$-s\epsilon_0E_z^i(z,s)=\left(\frac{d^2}{dz^2}-\frac{s^2}{c_0^2}\right)\int_{-h}^{h}I(z',s)K(z,z',s)\,dz'. \tag{11.109}$$

[‖]The analysis can be extended to bent wires and to aircrafts modeled by a combination of wires. See for example, Notes 37 and 38.

The kernel is the (transformed) value of (7.240), viz.[39,40]

$$K(z,z',s) = \frac{1}{2\pi}\int_{-\pi}^{\pi} \frac{e^{-\frac{s}{c_0}[(z-z')^2+4a^2\sin^2\frac{\varphi}{2}]^{\frac{1}{2}}}}{\left[(z-z')^2+4a^2\sin^2\dfrac{\varphi}{2}\right]^{\frac{1}{2}}}\,d\varphi. \tag{11.110}$$

The incident wave is often a plane wave propagating in a direction $\mathbf{u}_i$ and polarized in the $(\mathbf{u}_i, \mathbf{u}_z)$ plane. For such a case,

$$E_z^i(z,s) = E_0(s)\sin\theta_i\, e^{-z\frac{\cos\theta_i}{c_0}s}, \tag{11.111}$$

where $\cos\theta_i = (\mathbf{u}_i \cdot \mathbf{u}_z)$, $E_0 = \dfrac{1}{s}$ for a unit step function, and $E_0 = 1$ for a unit delta function input. The integro-differential equation (11.109) is of the general form

$$\mathcal{L}(z,s)[I(z,s)] = V(z,s). \tag{11.112}$$

Expanding $I(z,s)$ in a series $\sum \mathcal{I}_m(s) f_m(z)$, and testing the result with functions $w_n(z)$, leads to the system of equations

$$\sum_{m=1}^{N} \mathcal{I}_m(s)\,\langle w_n, \mathcal{L}(s) f_m\rangle = \langle w_n, V(z,s)\rangle = \mathcal{V}_n(s).$$

In matrix form:

$$\overline{\overline{Z}}(s)\cdot\boldsymbol{\mathcal{I}}(s) = \boldsymbol{\mathcal{V}}(s). \tag{11.113}$$

The various modes are characterized by vectors $\mathbf{M}_k$ satisfying

$$\overline{\overline{Z}}(s_k)\cdot\boldsymbol{\mathcal{I}}(s_k) = \overline{\overline{Z}}(s_k)\cdot\mathbf{M}_k = 0, \tag{11.114}$$

where the *resonant* s_k's are obtained by solving

$$\det\ \overline{\overline{Z}}(s_k) = 0. \tag{11.115}$$

The solution of (11.113) can be formally written in terms of a resolvent matrix as

$$\boldsymbol{\mathcal{I}}(s) = \overline{\overline{Z}}^{-1}(s)\cdot\boldsymbol{\mathcal{V}}(s), \tag{11.116}$$

which leads to the Bromwich integral

$$\boldsymbol{\mathcal{I}}(t) = \frac{1}{2\pi j}\int_{\sigma_0-j\infty}^{\sigma_0+j\infty} \overline{\overline{Z}}^{-1}(s)\cdot\boldsymbol{\mathcal{V}}(s)\, e^{st}\,ds. \tag{11.117}$$

Here $\boldsymbol{\mathcal{I}}(t)$ is the column vector formed by the expansion coefficients of the antenna current $i(t)$ in terms of the $f_m(z)$. The transform of $i(z,t)$, for $\delta(t)$ excitation, turns out to be of the type [127]

$$I(s,z) = \sum_{k=1}^{\infty} \frac{\eta_k A_k(z)}{s-s_k} + F_e(s,z). \tag{11.118}$$

The symbol η_k denotes the coupling coefficient

$$\eta_k = \int_{-h}^{h} \mathbf{C}_k(z') \cdot \mathbf{V}(z', s_k)\, dz', \tag{11.119}$$

where $\mathbf{C}_k$ is defined by

$$\left[\overline{\overline{Z}}(s_k)\right]^t \cdot \mathbf{C}_k = 0$$

and the A_k depend on the components of $\mathbf{M}_k$ [127]. Equation (11.118) reveals the presence of poles at $s = s_k$. Upon inversion, and after evaluation of the residues, these poles give rise to damped resonances, which are dominant at late times. The notation F_e denotes an entire function, which plays an important role in the construction of the early and intermediate

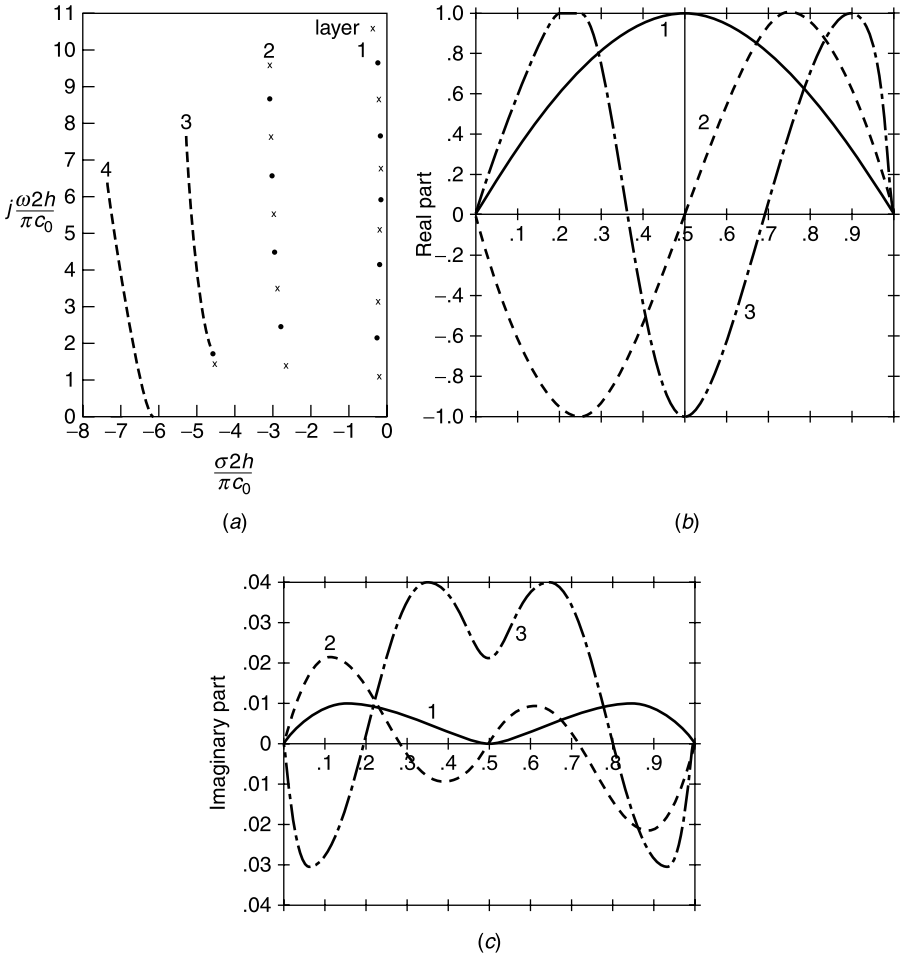

Figure 11.18 (*a*) Poles ($\sigma + j\omega$) of a thin wire. (*b*) Real part of three mode currents. (*c*) Imaginary part of these currents (from F. M. Tesche, On the analysis of scattering and antenna problems using the singularity expansion technique, *IEEE Trans. AP* **21**, 53–62, 1973, with permission of IEEE).

time responses. Figure 11.18*a* shows the distribution of poles for $(a/h) = 0.01$ (Fig. 7.21). The resonances are clearly distributed in *layers*. The real and imaginary parts of the currents, for the three lowest modes of layer 1, are displayed in parts *b* and *c*, where the abscissa runs from $z = -h$ (at 0) to $z = h$ (at 1). The amplitude factor $e^{\sigma t} = e^{-|\sigma| t}$ of the mode shows that a pole far from the imaginary axis gives rise to a strongly damped oscillation. At late times, say for $t > (6h/c_0)$, only a few poles are therefore needed to represent $i(t)$ adequately, because the contributions from the other poles have died away. The SEM is consequently a potentially economical method, the more so because the value of s_k is independent of the nature of the incident wave, which only influences the coupling coefficient η_k.

11.5.4 Transient Scattering

The far fields must satisfy a *radiation condition*, which *in the s-plane* takes the form [62]

$$\begin{aligned}
\lim_{R\to\infty} \left(\frac{\partial}{\partial R} + \frac{s}{c_0} \right) G_0(\mathbf{r}, \mathbf{r}', s) &= o\left(\frac{1}{R}\right) \\
\lim_{R\to\infty} \left(\text{curl} + \frac{s}{c_0} \mathbf{u}_R \times \right) \overline{\overline{G}}_0(\mathbf{r}, \mathbf{r}', s) &= o\left(\frac{1}{R}\right) \\
\lim_{R\to\infty} \left(\text{curl} + \frac{s}{c_0} \mathbf{u}_R \times \right) \mathbf{E}(\mathbf{r}, s) &= o\left(\frac{1}{R}\right).
\end{aligned} \tag{11.120}$$

In free space, the transforms of the Green's functions are

$$\begin{aligned}
G_0(\mathbf{r}, \mathbf{r}', s) &= -\frac{e^{-\frac{s}{c_0}|\mathbf{r}-\mathbf{r}'|}}{4\pi |\mathbf{r} - \mathbf{r}'|} \\
\overline{\overline{G}}_0(\mathbf{r}, \mathbf{r}', s) &= \left(\overline{\overline{I}} - \frac{c_0^2}{s^2} \text{grad grad} \right) G_0(\mathbf{r}, \mathbf{r}', s).
\end{aligned} \tag{11.121}$$

The integral equations satisfied by the current on a perfectly conducting scatterer are derived in Sections 12.1 and 12.2 in time-harmonic form. In *s* form the MFIE, for example, becomes

$$\frac{1}{2} \mathbf{J}_S(\mathbf{r}, s) - \mathbf{u}_n |\mathbf{r}| \times \lim_{\delta\to 0} \int_{S-S_\delta} \text{grad}' \, G_0(\mathbf{r}, \mathbf{r}', s) \times \mathbf{J}_S(\mathbf{r}', s) \, dS' = \mathbf{u}_n(\mathbf{r}) \times \mathbf{H}^i(\mathbf{r}, s) \tag{11.122}$$

or, more concisely,

$$\frac{1}{2} \mathbf{J}_S(\mathbf{r}, s) - \overline{\overline{L}} \cdot \mathbf{J}_S(\mathbf{r}, s) = \mathbf{u}_n(\mathbf{r}) \times \mathbf{H}^i(\mathbf{r}, s). \tag{11.123}$$

The solution depends formally on the existence of a resolvent dyadic $\overline{\overline{R}}(\mathbf{r}, \mathbf{r}', s)$, by means of which the sought $\mathbf{J}_S$ can be obtained from the prescription [193]

$$\mathbf{J}_S(\mathbf{r}, s) = 2\mathbf{u}_n(\mathbf{r}) \times \mathbf{H}^i(\mathbf{r}, s) + \int_S \overline{\overline{R}}(\mathbf{r}, \mathbf{r}', s) \cdot \left[\mathbf{u}_n(\mathbf{r}') \times \mathbf{H}^i(\mathbf{r}', s) \right] dS'. \tag{11.124}$$

Note that integral equation (11.123) can be given the more compact form

$$\left[\frac{1}{2}\bar{\bar{I}} - \bar{\bar{L}}(s)\right] \cdot \mathbf{J}_S = \mathbf{u}_n \times \mathbf{H}^i. \tag{11.125}$$

The formal solution of this equation is

$$\mathbf{J}_S = \left(\frac{1}{2}\bar{\bar{I}} - \bar{\bar{L}}\right)^{-1} \cdot (\mathbf{u}_n \times \mathbf{H}^i). \tag{11.126}$$

At the natural (complex) frequencies, the homogeneous integral equation and its adjoint have nontrivial solutions. Thus[36]

$$\begin{aligned}\left[\frac{1}{2}\bar{\bar{I}} - \bar{\bar{L}}(s_k)\right] \cdot \mathbf{J}_k &= 0\\ \left[\frac{1}{2}\bar{\bar{I}} - \bar{\bar{L}}^a(s_k)\right] \cdot \mathbf{N}_k &= 0.\end{aligned} \tag{11.127}$$

Written in full [193]:

$$\frac{1}{2}\mathbf{J}_k(\mathbf{r}, s_k) + \mathbf{u}_n(\mathbf{r}) \times \oint_S \mathbf{J}_k(\mathbf{r}', s_k) \times \operatorname{grad}' G_0(\mathbf{r}, \mathbf{r}', s_k)\, dS' = 0 \tag{11.128}$$

$$\frac{1}{2}\mathbf{N}_k(\mathbf{r}, s_k) - \oint_S \left[\mathbf{u}_n(\mathbf{r}') \times \mathbf{N}_k(\mathbf{r}', s_k)\right] \times \operatorname{grad}' G_0^*(\mathbf{r}, \mathbf{r}', s_k)\, dS' = 0. \tag{11.129}$$

In writing these equations, we have implicitly made use of the Fredholm alternative discussed in Section 1.10. This is permissible because the operator $\bar{\bar{L}}$ is compact** [193].

Illustratively, Figure 11.19 shows the pole distribution for the magnetic modes of a perfectly conducting sphere. A similar pattern holds for the electric modes[39,40,41] [62].

The analysis given above can be extended to the EFIE, which becomes, in terms of Laplace transforms,

$$\mathbf{E}^i_{\tan}(\mathbf{r}, s) = \frac{s\mu_0}{4\pi}\left[\lim_{\delta\to 0}\int_{S-S_\delta} \mathbf{J}_S(\mathbf{r}', s)\frac{e^{-\frac{s}{c_0}|\mathbf{r}-\mathbf{r}'|}}{|\mathbf{r}-\mathbf{r}'|}\, dS'\right]_{\tan} \tag{11.130}$$

$$+ \frac{1}{4\pi s\epsilon_0}\left[\lim_{\delta\to 0}\int_{S-S_\delta} \operatorname{div}'_S \mathbf{J}_S(\mathbf{r}, s)\operatorname{grad}' \frac{e^{-\frac{s}{c_0}|\mathbf{r}-\mathbf{r}'|}}{|\mathbf{r}-\mathbf{r}'|}\, dS' + \mathbf{T}\operatorname{div}'_S \mathbf{J}_S(\mathbf{r}', s)\right]_{\tan}.$$

A typical example of incident field is

$$\mathbf{e}^i(\mathbf{r}, t) = E_0 f\left(t - \frac{\mathbf{u}_i \cdot \mathbf{r}}{c_0}\right)\mathbf{u}_e.$$

**A *linear operator L is bounded* if there is a real number M such that $\| Lx \| \leq M \| x \|$ for all $x \in E$, where E is a normed linear space. This bounded *operator* becomes *compact* (or completely continuous) if, and only if, for every infinite sequence y_i of bounded elements the sequence Ly_i has a convergent subsequence. Note that the sequence is bounded if $\| y_i \| < c$ for all i.

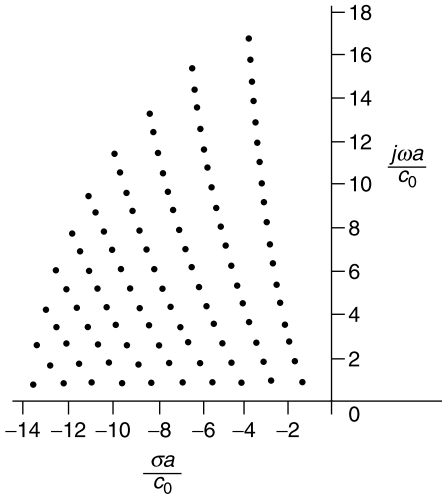

Figure 11.19 Poles of the magnetic modes of a perfectly conducting sphere (from F. M. Tesche, On the analysis of scattering and antenna problems using the singularity expansion technique, *IEEE Trans. AP* **21**, 53–62, 1973, with permission of IEEE).

In the s-plane:

$$\mathbf{E}^i(\mathbf{r}, s) = E_0 F(s)\, e^{-\frac{s}{c_0}\mathbf{u}_i \cdot \mathbf{r}} \mathbf{u}_e,$$

where $F(s)$ is the two-sided Laplace transform of $f(t)$.

11.5.5 The Time Response

The induced current $\mathbf{J}_S(\mathbf{r}, s)$ and the scattered fields $\mathbf{E}^{sc}(\mathbf{r}, s)$, $\mathbf{H}^{sc}(\mathbf{r}, s)$ are meromorphic functions of frequency.[36,42] Under these conditions, the Mittag-Leffler theorem may be applied, and a $\delta(t)$ input irradiating a perfectly conducting scatterer can be shown to give a response[43]

$$\mathbf{H}^{sc}(\mathbf{r}, s) = \sum_{k=1}^{\infty} \frac{R_k(\mathbf{r})}{s - s_k} + \mathbf{F}_e(\mathbf{r}, s). \tag{11.131}$$

This expansion is similar to (11.118). When the poles are single, the resulting time variation is

$$\mathbf{h}^{sc}(\mathbf{r}, t) = \sum_{k=1}^{\infty} \mathbf{R}_k(\mathbf{r}) e^{s_k t} + f_e(\mathbf{r}, t). \tag{11.132}$$

In addition to the poles, branch points occur when the scatterer is embedded in a conducting medium,[44,45] in which case a branch cut must be taken into account in the evaluation of the Bromwich integral. As in (11.118), the numerator $\mathbf{R}_k(\mathbf{r})$ is the product of a coupling coefficient η_k and a function of $\mathbf{M}_k$, which can be defined precisely as in (11.114) [62]. The incident fields intervene through the value of η_k but do not influence the poles.[46]

11.5.6 The Early Time Response

The time evolution of the scattered fields, under $\delta(t)$ irradiation, can be split into two regions: the early times and the late times. Some *qualitative* statements can be made about these

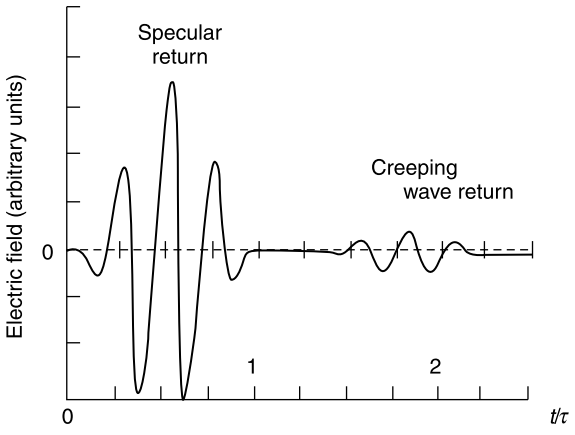

Figure 11.20 Pulse scattered from a PEC sphere (from J. Rheinstein, Scattering of short pulses of electromagnetic waves, *Proc. IEEE* **53**, 1069–1070, 1965, with permission of IEEE).

two zones, which are separated by a transition time t_k, the time it takes the incident wave to traverse the scatterer. Typically $t_k \approx L/c_0$, where L is the largest dimension of the obstacle. According to (A7.1) and (A7.6), the *very early time response* is governed by the limit $s \to \infty$ of the Laplace transforms. A look at expansion (11.131) shows that the contribution of the entire function $\mathbf{F}_e(\mathbf{r}, s)$ must be important in that range.[††] The contribution of the resonant modes may not be neglected, however, because their fields have not decayed significantly at early times. To avoid performing the cumbersome mode summation, it is useful to note that the fields change abruptly near the incident wave front and may therefore be represented by a small number of high-frequency terms of the kind discussed in Chapter 13. Creeping waves associated with rays circumnavigating the scatterer may therefore be expected. Watson's transformation, mentioned in Section 11.3, confirms the theoretical existence of these waves in the case of a spherical reflector.[50] Their importance is also confirmed[51] by the numerical data in Figure 11.20, which show the time variation of the far field scattered from a sphere illuminated by a pulse of length $\tau = (4a/c_0) = 2t_k$. The specular return arrives first, followed by the creeping wave generated by the fields diffracted around the sphere. The SEM resonances have been attributed to these creeping waves, which, after one revolution, return in phase coherence with their initial value. This connection suggests a hybrid approach, efficient at all times, in which wavefronts and resonances are combined self-consistently. In this scheme, wavefronts dominate at early times, and resonances take over later on[52,53] [63].

11.5.7 The Late Time Response

The high-frequency approximation, valid at early times, becomes cumbersome at later times when a growing number of rays had time to reach the observer. The pole series, on the other hand, increases in simplicity as more modes get strongly attenuated, and only a few survive.

[††] It remains important up to times of the order t_k. See Ref. 47. The role of the entire function has been the subject of an extensive literature. See, for example, [63] and Notes 48, 49,

These terms give rise to a representation

$$f(t) = \sum_{n=1}^{N} R_n e^{s_n t}$$

$$F(s) = \sum_{n=1}^{N} \frac{R_n}{s - s_n}. \tag{11.133}$$

The poles can be extracted, in principle at least, from an observation of $f(t)$. The problem is classic in signal analysis, where it is solved by methods such as Prony's [30, 31, 62, 193]. The s_n's characterize the target, in size and shape, independently of the nature of the incident wave. The oscillatory part of $e^{s_n t}$ is more sensitive to *size* because of its dependence on path length. On the other hand, the attenuated part is more sensitive to *shape*, because radiation damping is influenced by curves, bends, and edges [110]. Poles could therefore conceivably give rise to an aspect-independent method of discriminating radar targets.[54,55,56] The late-time resonant response, however, is weak as compared with the earlier values of the echo signal, and this causes low signal-to-noise ratios. It follows that a method such as Prony's might not be able to extract more than a few poles. This ambiguity may be lifted by combining early and late responses into a single identification process.[57]

11.5.8 An Illustrative Example

The previous qualitative statements will now be concretized by considering a lossless dielectric slab, exposed to an incident field $e^i(z,t) = f\left(t - \dfrac{z}{c_0}\right)$. The function $f(t)$ is assumed to vanish everywhere but in the interval 0 to T [128]. An integral equation for $E(z,s)$ has been derived in (9.95), and its solution in the zones 1, 2, and 3 is given by (Fig. 11.21*a*)

$$E_1(z,s) = F(s)\left\{e^{-s\frac{z}{c_0}} + e^{s\frac{z}{c_0}}\left[-\frac{N-1}{N+1} + \frac{4N(N-1)}{N+1}\frac{e^{-2N\frac{s}{c_0}l}}{(N+1)^2 - (N-1)^2\, e^{+2N\frac{s}{c_0}l}}\right]\right\} \tag{11.134}$$

$$E_2(z,s) = F(s)\left[\frac{2(N+1)\, e^{-Ns\frac{z}{c_0}}}{(N+1)^2 - (N-1)^2 e^{-2N\frac{s}{c_0}l}} + \frac{2(N-1)\, e^{-2N\frac{s}{c_0}l}\, e^{N\frac{s}{c_0}z}}{(N+1)^2 - (N-1)^2 e^{-2N\frac{s}{c_0}l}}\right] \tag{11.135}$$

$$E_3(z,s) = F(s)\left[\frac{4N}{(N+1)^2 - (N-1)^2\, e^{-2N\frac{s}{c_0}l}}\, e^{-\frac{s}{c_0}(z-l)}\right], \tag{11.136}$$

where $N = \sqrt{\epsilon_r}$ and $F(s)$ is the transform of $f(t)$. The terms between square brackets result from the presence of the dielectric slab. They introduce poles at the zeros of the

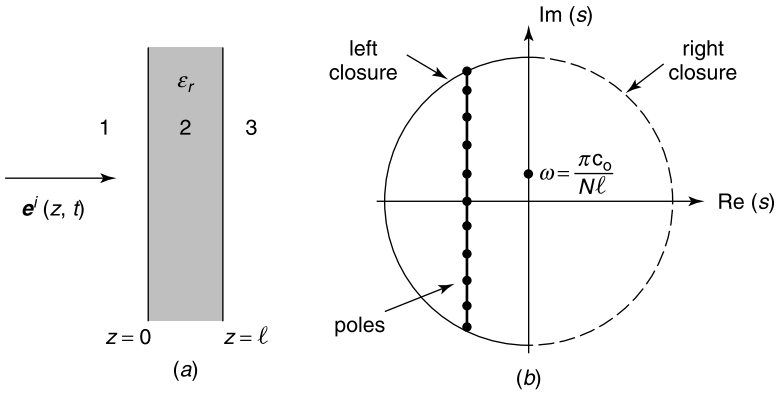

Figure 11.21 (*a*) Normal incidence of a linearly polarized wave. (*b*) Poles at frequency intervals $(c_0/2Nl)$, and half circles at infinity.

denominators, that is, at

$$s_k = (\sigma + j\omega)_k = -\frac{c_0}{Nl}\log_e\frac{N+1}{N-1} + j\frac{k\pi}{N}\frac{c_0}{l} \qquad (k = 0, \pm 1, \pm 2, \ldots). \tag{11.137}$$

As expected from the *real* function $e(z, t)$, the poles are on the real axis or occur in complex conjugate pairs. When the expressions for $E(z, s)$ are inserted in their respective Bromwich integrals, the imaginary axis may be chosen as AB axis (Fig. A7.1). There are no branch points, hence left closure will give rise to the SEM terms $e^{s_k t}$, augmented by the contribution from the large semicircle $|s| \to \infty$. This, in turn, may be interpreted as generated by the entire function $\mathbf{F}_e$ that appears in (11.131). When z is in *region 3*, there is no contribution from the arc of right closure when $t < t_k + \dfrac{z-l}{c_0}$, where t_k is the transit time $\dfrac{l}{c} = \dfrac{Nl}{c_0}$. If we use left closure, the contribution from the arc will vanish for $t > T - t_k + \dfrac{z-l}{c_0}$, leaving only the attenuated modes after that time. In short: in addition to the SEM resonances there are (potential) additions from closure-arcs when t lies in the window

$$t_k + \frac{z-l}{c_0} < t < T - t_k + \frac{z-l}{c_0}. \tag{11.138}$$

These additions, only exist if $T > 2t_k$. In *region 2*, the two terms in (11.135) yield waves that travel back and forth in the slab and can be interpreted as high-frequency rays. The ray-SEM connection has been carefully investigated in a related configuration,[58] in which the slab is short-circuited at the interface $z = l$ (Fig. 11.21*a*).

11.6 IMPEDANCE BOUNDARY CONDITIONS

11.6.1 Surface Impedances

The difficult scattering problem embodied in Figure 11.13*a* involves *two regions* when V is penetrable. The solution would be considerably simplified if the presence of the scatterer could be simulated by a boundary condition on S. For such a case, the problem would only

involve a *single region*. It is clear that many factors stand in the way of such a simplification: curvature, penetration depth, nature of the incident wave. In fact, attaching a *local* parameter at each point of S is bound to be hazardous, because such a move ignores what happens at neighboring points, as well as the complexity of the internal structure beneath the surface. In a search for configurations that could possibly accommodate the *one region* assumption, let us first examine the case of a highly conducting scatterer. An exclusively *local* reaction requires, as a minimum, a form of boundary condition that is independent of the angle of incidence of an incoming plane wave. We shall promptly check this requirement on the plane boundary, for which the relevant equation is (9.19). For the TE polarization, this equation predicts a surface impedance

$$Z_S = R_{c0} \frac{1 + R_\perp}{(1 - R_\perp) \cos \theta_i}.$$

The index of refraction N_σ of a good conductor is given by

$$N_\sigma^2 = \epsilon_r = \frac{\sigma}{j\omega\epsilon_0} = -j \frac{1}{2\pi^2} \left(\frac{\lambda_0}{\delta} \right)^2, \tag{11.139}$$

where δ is the penetration depth (9.27). The magnitude of N is very large because $\sigma \gg \omega\epsilon_0$, hence the reflection coefficient (9.9) may be written as

$$R_\perp \approx -1 + \frac{2 \cos \theta_i}{N}.$$

Inserting $R_\perp$ into (11.139) gives

$$Z_S = \frac{R_{c0}}{N} = \sqrt{\frac{\mu_0}{\epsilon_0 \epsilon_r}}, \tag{11.140}$$

which is precisely the characteristic impedance Z_c of the good conductor. The result is obviously independent of θ_i. A quick check shows that such a property also holds for the TM polarization. We may therefore write that the tangential components of $\mathbf{E}$ and $\mathbf{H}$ just outside V are connected by the relationship

$$\mathbf{E}_{\tan} = Z_S \, (\mathbf{u}_n \times \mathbf{H}) = Z_c (\mathbf{u}_n \times \mathbf{H}), \tag{11.141}$$

where $\mathbf{u}_n$ refers to the outward normal to the scatterer. If the medium is anisotropic, Z_c becomes tensorial.

In the 1940s, Leontovich and Shchukin independently proposed to extend the use of the impedance condition (11.141) to more general materials and surfaces.[59] It is clear that the fields should only vary slowly over distances of the order the skin depth (or of the internal λ) if the *Leontovich* condition is to hold [116]. In the problem of the land-sea contact, for example, it would be erroneous to assume that the surface impedance of the land remains constant down to the coast line.[60]

In order to extend the time-harmonic impedance condition to an arbitrary time-dependence, (11.141) will be rewritten as[61] [194]

$$\mathbf{E}(j\omega) = \underbrace{\left[\frac{Z_c(j\omega)}{j\omega} \right]}_{Z_c'(j\omega)} \mathbf{u}_n \times \left[j\omega \mathbf{H}(j\omega) \right].$$

From (A7.5) and (A7.30), it follows that

$$\mathbf{e}(t) = Z_c'(t) * \frac{\partial \mathbf{h}(t)}{\partial t}, \tag{11.142}$$

where $*$ denotes the convolution operator defined in A7.5. For a good conductor:

$$\begin{aligned} Z_c'(j\omega) &= \sqrt{\frac{\mu_0}{j\omega\sigma}} \qquad \text{and} \qquad Z_c'(s) = \sqrt{\frac{\mu_0}{s\sigma}} \\ Z_c'(t) &= \sqrt{\frac{\mu_0}{\pi\sigma t}} \qquad (\text{for } t > 0) \\ &= 0 \qquad\qquad (\text{for } t < 0). \end{aligned} \tag{11.143}$$

When the medium has both σ and ϵ, (11.143) should be replaced by[62]

$$\begin{aligned} Z_c(s) &= \sqrt{\frac{\mu_0}{\epsilon}} \frac{\sqrt{s}}{\sqrt{s + \frac{1}{\tau}}} \\ Z_c(t) &= \sqrt{\frac{\mu_0}{\epsilon}} \left\{ a e^{at} \left[I_0(at) + I_1(at) \right] H(t) + \delta(t) \right\}, \end{aligned} \tag{11.144}$$

where I_0 and I_1 are the modified Bessel functions defined in (A5.61), τ is the relaxation time (ϵ/σ), and $a = -(\sigma/2\epsilon)$.

11.6.2 The Boundary Condition Along the Normal

Let E_z' be the z-oriented field component in a space $z \geq 0$ filled with a medium of high N. The E_z' field satisfies

$$\frac{\partial^2 E_z'}{\partial x^2} + \frac{\partial^2 E_z'}{\partial y^2} + \frac{\partial^2 E_z'}{\partial z^2} + k_0^2 N^2 E_z' = 0.$$

If the field varies much more rapidly in the z-direction than laterally, the derivative with respect to z predominates, and one may approximately write[63]

$$E_z'(x, y, z) = E_z'(x, y, 0)\, e^{jk_0 N z}, \tag{11.145}$$

provided the root of N^2 with positive imaginary part is chosen. In consequence,

$$\frac{\partial E_z'}{\partial z} = jk_0 N E_z' \tag{11.146}$$

on the medium side of boundary plane $z = 0$. If E_z denotes the component in air, just to the left of that plane, (11.146) yields

$$\begin{aligned} E_z &= \epsilon_r E_z' \\ \frac{\partial E_z}{\partial z} &= \frac{\partial E_z'}{\partial z}, \end{aligned}$$

from which it follows that

$$\frac{\partial E_z}{\partial z} = \frac{jk_0}{N} E_z. \tag{11.147}$$

A similar analysis for H_z, based on the boundary conditions

$$H_z = H_z'$$
$$\frac{\partial H_z}{\partial z} = \frac{\partial H_z'}{\partial z},$$

gives

$$\frac{\partial H_z}{\partial z} = jk_0 N H_z. \tag{11.148}$$

11.6.3 Extension to Curved Surfaces

The validity of the *Leontovich* and *normal* conditions for curved surfaces is not evident. It has been confirmed, however, in a few special cases involving mainly cylinders and spheres.[64] The extension to *dielectric* media, on the other hand, can be justified only under very restricted circumstances. For a *conducting* medium, the field should vary little within a wavelength along the surface, a condition that requires, in addition to $|N| \gg 1$, satisfaction of the inequality

$$|\mathrm{Im}\, N|\, k_0 R_{\min} \gg 1, \tag{11.149}$$

where $R_{\min}$ is the smallest radius of curvature at the field point. In some circumstances (but they are exceptional), (11.149) may be replaced by the weaker restriction

$$|N|\, k_0 R_{\min} \gg 1. \tag{11.150}$$

In the presence of an *inhomogeneous* material (i.e., of an N that varies along the boundary surface S), the *normal* conditions (11.147) and (11.148) are replaced by[65]

$$\frac{\partial E_n}{\partial n} = j\frac{k_0}{N} E_n - \frac{1}{N}\, \mathbf{E}_{\tan} \cdot \mathrm{grad}_S\, N \tag{11.151}$$

$$\frac{\partial H_n}{\partial n} = jk_0 N H_n + \frac{1}{R_{c0} N}\, (\mathbf{u}_n \times \mathbf{E}_{\tan}) \cdot \mathrm{grad}_S\, N. \tag{11.152}$$

These relationships do not contain lateral derivatives of the fields, although these are needed to take curvature effects into account. Suitable expressions have been proposed to accomodate this need[65,66] [32].

11.7 THIN LAYERS

Thin layers are generated either naturally, for example by ice forming on an aircraft frame, or artificially, as in the case of a protective coat of paint on an antenna,[67] or of a microwave-absorbing layer on a radar target. In Figure 11.22, the electromagnetic problem involves *three* regions, and any simplification of this complex configuration would be welcome. This goal can be achieved when the layer is *thin*. The basic theory is given in Section 9.2. We shall only consider three important special cases.

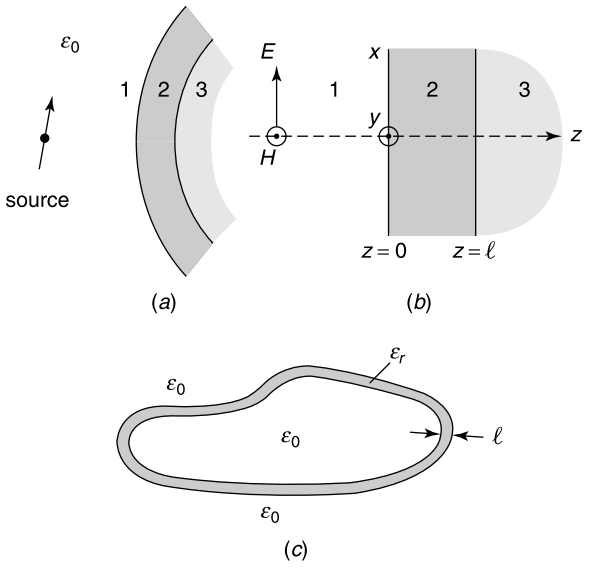

Figure 11.22 (*a*) Layer 2 on main body 3. (*b*) Plane layered structure. (*c*) Thin shell in free space.

11.7.1 A Nonmagnetic Layer of High Dielectric Constant

In the limit of high ϵ_r the electric field at the ends of slab 2 (i.e., for $z = 0$ and $z = l$), must be tangential. We shall assume that the fields propagate along the z-axis, in which case Figure 11.22*b* becomes an acceptable model for the slab, if we further assume that curvature effects are negligible. The assumption "thin layer" implies the condition $kl = \sqrt{\epsilon_r}\, k_0 l \ll 1$ (and a fortiori $k_0 l \ll 1$); in other words, l must be much less than the wavelength in the dielectric. A transition equation such as (9.75) now becomes[‡‡]

$$\begin{pmatrix} E_x \\ H_y \end{pmatrix}_0 = \begin{pmatrix} 1 & jklZ_c \\ jklY_c & 1 \end{pmatrix} \begin{pmatrix} E_x \\ H_y \end{pmatrix}_l, \tag{11.153}$$

which leads to the following surface admittance at $z = 0$:

$$(Y_S)_0 = \frac{1}{R_{c0}} \frac{1 + jZ'_{c3}\epsilon_r k_0 l}{Z'_{c3} + jk_0 l} = \frac{(H_y)_0}{(E_x)_0}, \tag{11.154}$$

where $Z'_{c3} = (Z_{c3}/R_{c0})$. For a thin dielectric shell in free space $Z'_{c3} = 1$, hence

$$(Y_S)_0 \approx \frac{1}{R_{c0}} + j\omega(\epsilon - \epsilon_0)\, l. \tag{11.155}$$

This is the admittance formed by $(R_{c0})^{-1}$ in parallel with a capacitance $C = (\epsilon - \epsilon_0)\, l$. In this case, the thin layer clearly represents a *reactive* load,[69,70] from (9.74), the electric field varies very little in the slab, but the tangential magnetic field suffers a discontinuity given by

$$H_0 - H_l \approx j\omega\epsilon\, El. \tag{11.156}$$

[‡‡]In a more general time-dependence, the matrix in (11.153) contains Laplace-transforms of the terms, as in (11.143). See, for example, Note 68.

A small portion $j\omega\epsilon_0 El$ of that discontinuity is due to propagation in vacuum, the rest may be attributed to the polarization currents $\mathbf{J} = j\omega(\epsilon - \epsilon_0)\mathbf{E}$ induced in the slab. These volume currents may be concentrated in an equivalent surface current

$$\mathbf{J}_S = j\omega(\epsilon - \epsilon_0)\, l\, \mathbf{E} = j\omega C\, \mathbf{E}. \tag{11.157}$$

The electric field actually varies linearly (but slowly) across the slab. From (11.153):

$$E_0 \approx E_l + jZ_c klH_l = E_l + jk_0 l(R_{c0}H_l). \tag{11.158}$$

In the transition condition (11.156), E should therefore be replaced by $(E_0 + E_l)/2$.

11.7.2 A Highly Permeable Magnetic Layer

This shell is the dual of the preceding one. The impedance at $z = 0$ is

$$(Z_S)_0 = R_{c0}\frac{Z'_{c3} + j\mu_r k_0 l}{1 + jZ'_{c3}k_0 l} = \frac{(E_x)_0}{(H_y)_0}. \tag{11.159}$$

When the sheet is in free space:

$$Z_S \approx R_{c0} + j\omega(\mu - \mu_0)\, l = R_{c0} + j\omega L. \tag{11.160}$$

To first order the magnetic field is uniform in the slab, but the electric field suffers a jump

$$E_0 = j\omega\mu\, Hl + E_l, \tag{11.161}$$

which is generated by the magnetic polarization current $\mathbf{J}_m = j\omega(\mu - \mu_0)\mathbf{H} \approx j\omega\mu\, \mathbf{H}$, or the equivalent surface current

$$\mathbf{J}_{mS} = j\omega(\mu - \mu_0)\, l\, \mathbf{H} = j\omega L\, \mathbf{H}. \tag{11.162}$$

The magnetic field actually varies slowly across the slab and obeys the linear law

$$H_0 \approx H_l + jk_0 l\frac{E_l}{R_{c0}}. \tag{11.163}$$

11.7.3 A Thin Highly Conducting Layer

In this case, "thin" implies that l is much smaller than the penetration depth δ. In a very good conductor, propagation occurs perpendicularly to the end faces, and $\mathbf{E}$ is tangent to the latter. With the slab in free space, (9.76) gives

$$(Y_S)_0 = \frac{1}{R_{c0}}\frac{1 + j\dfrac{kl}{Z'_c}}{1 + jklZ'_c}. \tag{11.164}$$

From (9.82), $Z_c' = \sqrt{jQ}$ in a good conductor. This reduced impedance is a very small quantity, of the order 10^{-4} for copper at 10 GHz. Under these conditions, the admittance at $z = 0$ is approximately

$$(Y_S)_0 \approx \frac{1}{R_{c0}} + \frac{jkl}{Z_c} = \frac{1}{R_{c0}} + \sigma l(1 + jQ) \approx \frac{1}{R_{c0}} + \sigma l. \tag{11.165}$$

At $z = 0$, the layer therefore represents a resistance $(1/\sigma l)$ in parallel with R_{c0}. E_x is practically constant in the slab, but H_y suffers a jump, actually produced by the equivalent surface current

$$\mathbf{J}_S = \sigma l\, \mathbf{E}. \tag{11.166}$$

11.7.4 Restrictions

The validity of the three simple models discussed above rests on two assumptions. *First*, the effect of a possible curvature of the boundary surface must be negligible. Correction terms are available to take curvature into account.[71] In addition, guidelines are provided by the solution of a few canonical problems involving coated cylinders and spheres [75, 116]. It should be noted that a *planar* slab endowed with both ϵ_r and μ_r supports electrically resistive *and* magnetically conductive sheets, which scatter independently. Curvature, however, introduces coupling between the two.[72]

It has *secondly* been assumed that propagation takes place in a direction *perpendicular* to the plane boundaries of the slab. This assumption implies that an obliquely incident wave is bent to nearly perpendicularity when it enters the slab. Such an approximation is appropriate for coatings with a high N and/or significant losses. Many practical coatings do not meet these criteria.[73,74] Under these circumstances the influence of the angle of incidence may be taken into account by including higher order terms in the equations.

11.8 CHARACTERISTIC MODES

The concept of characteristic mode is very general and can easily be applied to arbitrary *perfectly conducting* surfaces[75,76] [198]. From (7.29), (7.33) and (7.34), the induced current density $\mathbf{J}_S$ on such a surface satisfies the equation

$$\mathbf{E}^i_{\tan}(\mathbf{r}) = -\mathbf{E}^{sc}_{\tan}(\mathbf{r}) = j\omega\mu_0\, \mathbf{L}_t\, (\mathbf{J}_S) = \mathbf{Z}(\mathbf{J}_S) \qquad (\mathbf{r} \text{ on } S), \tag{11.167}$$

where the symbol $\mathbf{L}_t$ stands for the tangential operator

$$\mathbf{L}_t(\mathbf{f}_S) = \left[\int_S \mathbf{f}_S(\mathbf{r}') \frac{e^{-jk_0|\mathbf{r}-\mathbf{r}'|}}{4\pi|\mathbf{r}-\mathbf{r}'|}\, dS'\right]_{\tan} + \frac{1}{k_0^2}\, \mathrm{grad}_S \int_S \mathrm{div}'_S\, \mathbf{f}_S(\mathbf{r}') \frac{e^{-jk_0|\mathbf{r}-\mathbf{r}'|}}{4\pi|\mathbf{r}-\mathbf{r}'|}\, dS'. \tag{11.168}$$

In that equation $\mathbf{r}$ and $\mathbf{r}'$ are on S, and $\mathbf{f}_S(\mathbf{r})$ is a tangential vector. The term $\mathbf{E}^i_{\tan}(\mathbf{r})$ can be interpreted as a forcing function and the operator $\mathbf{Z}$ as an impedance (of which it has the dimension Ω). On the basis of the reciprocity property (8.171), the $\mathbf{Z}$ operator is symmetric with respect to the symmetric scalar product

$$\langle \mathbf{a}_S, \mathbf{b}_S \rangle_S = \int_S \mathbf{a}_S \cdot \mathbf{b}_S\, dS. \tag{11.169}$$

More precisely,

$$\left\langle \mathbf{J}_S^a, Z\left(\mathbf{J}_S^b\right)\right\rangle = \left\langle \mathbf{Z}\left(\mathbf{J}_S^a\right), \mathbf{J}_S^b\right\rangle. \tag{11.170}$$

It is useful to split $\mathbf{Z}$ into its real and imaginary parts, and write

$$\mathbf{Z} = \mathbf{R} + j\mathbf{X},$$

where $\mathbf{R}$ and $\mathbf{X}$ are real. Clearly,

$$\mathbf{R} = \frac{1}{2}(\mathbf{Z} + \mathbf{Z}^*)$$
$$\mathbf{X} = \frac{1}{2j}(\mathbf{Z} - \mathbf{Z}^*).$$

The *characteristic currents* are defined by the eigenvector equation

$$\mathbf{Z}(\mathbf{J}_n) = (\mathbf{R} + j\mathbf{X})(\mathbf{J}_n) = \nu_n \mathbf{R}(\mathbf{J}_n) = (1 + j\lambda_n)\mathbf{R}(\mathbf{J}_n), \tag{11.171}$$

where the $\mathbf{J}_n$ are surface vectors. One may write, equivalently,

$$\mathbf{X}(\mathbf{J}_n) = \lambda_n \mathbf{R}(\mathbf{J}_n). \tag{11.172}$$

Because $\mathbf{X}$ and $\mathbf{R}$ are real and symmetric, all λ_n are real, and the $\mathbf{J}_n$ can be chosen real. The following orthogonality relationships hold (for $k \neq n$):

$$\begin{aligned} \langle \mathbf{J}_k, \mathbf{R}(\mathbf{J}_n)\rangle_S &= 0 \\ \langle \mathbf{J}_k, \mathbf{X}(\mathbf{J}_n)\rangle_S &= 0 \\ \langle \mathbf{J}_k, \mathbf{Z}(\mathbf{J}_n)\rangle_S &= 0. \end{aligned} \tag{11.173}$$

These relationships remain valid for a Hermitian scalar product because the $\mathbf{J}_n$ are real. Choosing the $\mathbf{J}_n$ as basis functions leads to diagonal matrix representations for $\mathbf{R}$, $\mathbf{X}$, and $\mathbf{Z}$. For $k = n$, normalization can be imposed on the basis of the complex source power needed to keep $\mathbf{J}_n$ on the surface S, viz.

$$P = \frac{1}{2}\int_S \mathbf{u}_n \cdot (\mathbf{E}_n \times \mathbf{H}_n^*)\, dS = \frac{1}{2}\int_S \mathbf{Z}(\mathbf{J}_n)\cdot \mathbf{J}_n^*\, dS. \tag{11.174}$$

In that equation, $\mathbf{E}_n$ and $\mathbf{H}_n$ are the fields generated by $\mathbf{J}_n$ (Fig. 11.23). The real part of P may serve to normalize $\mathbf{J}_n$ according to the law

$$\frac{1}{2}\langle \mathbf{R}(\mathbf{J}_n), \mathbf{J}_n\rangle_H = 1 \quad \text{(W)}. \tag{11.175}$$

This condition gives $\mathbf{J}_n$ the dimension Am^{-1} of a surface current.

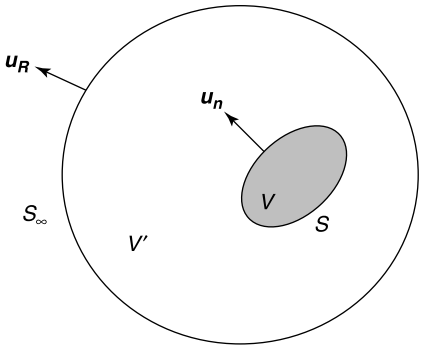

Figure 11.23 Scatterer and sphere at infinity.

11.8.1 Scattering

Orthogonality properties such as (11.173) can also be derived for the radiation vectors $\mathbf{F}_n$ of the eigencurrents $\mathbf{J}_n$. The radiation vectors are defined on a spherical surface S_∞ of infinite radius and are tangent to the latter[§§] The orthogonality proof starts by writing, between S and S_∞,

$$\begin{aligned}\text{div}\,(\mathbf{E}_k \times \mathbf{H}_n^*) &= \mathbf{H}_n^* \cdot \text{curl}\,\mathbf{E}_k - \mathbf{E}_k \cdot \text{curl}\,\mathbf{H}_n^* \\ &= -j\omega\left[\mu_0 \mathbf{H}_n^* \cdot \mathbf{H}_k - \epsilon_0 \mathbf{E}_k \cdot \mathbf{E}_n^*\right].\end{aligned}$$

This expression, integrated over V', gives (Fig. 11.23)

$$\begin{aligned}&-j\omega \int_{V'} \left[\mu_0 \mathbf{H}_n^* \cdot \mathbf{H}_k - \epsilon_0 \mathbf{E}_k \cdot \mathbf{E}_n^*\right] dV \\ &\quad = -\int_S \mathbf{u}_n \cdot (\mathbf{E}_k \times \mathbf{H}_n^*)\, dS + \int_{S_\infty} \mathbf{u}_R \cdot (\mathbf{E}_k \times \mathbf{H}_n^*)\, dS \\ &\quad = -\int_S \mathbf{Z}(\mathbf{J}_k) \cdot \mathbf{J}_n^*\, dS + \frac{1}{R_{c0}} \int_{S_\infty} \mathbf{F}_k \cdot \mathbf{F}_n^*\, dS. \qquad (11.176)\end{aligned}$$

The integral over S vanishes, from (11.173). By exchanging the indices k and n in (11.176), and taking the complex conjugate of the result, one easily shows that

$$\int_{S_\infty} \mathbf{F}_k \cdot \mathbf{F}_n^*\, dS = 0. \qquad (11.177)$$

The radiation vectors therefore form an orthogonal set over S_∞ (Problem 11.12). The modes consequently radiate independently, and power orthogonality holds.

The orthogonality properties (11.173) can be exploited to formulate the scattering problem in a particularly clear way. To that effect, we expand the unknown $\mathbf{J}_S$ in terms of the (assumed known) $\mathbf{J}_n$. Thus,

$$\mathbf{J}_S(\mathbf{r}) = \sum A_n \mathbf{J}_n(\mathbf{r}) \qquad (\mathbf{r} \text{ on } S). \qquad (11.178)$$

[§§]The characteristic modes can be adapted to exhibit orthogonality properties over other regions of space than the sphere at infinity. See Note 77.

Inserting this expansion into (11.167) gives

$$\mathbf{E}^i_{\tan}(\mathbf{r}) = \sum A_n \mathbf{Z}(\mathbf{J}_n) = \sum A_n(1 + j\lambda_n)\mathbf{R}(\mathbf{J}_n(\mathbf{r})).$$

After testing with $\mathbf{J}_n$ we obtain

$$\left\langle \mathbf{E}^i, \mathbf{J}_n \right\rangle = V^i_n = A_n(1 + j\lambda_n)\,\langle \mathbf{J}_n, \mathbf{R}(\mathbf{J}_n)\rangle.$$

Inserting the normalization condition (11.175) into this expression leads to

$$\mathbf{J}_S(\mathbf{r}) = \frac{1}{2}\sum \frac{V^i_n}{1 + j\lambda_n}\mathbf{J}_n(\mathbf{r}), \tag{11.179}$$

where V^i_m is the modal excitation coefficient (Problem 11.14). On the whole, modes with small $|\lambda_n|$ scatter strongly, modes with large $|\lambda_n|$ poorly. Because of the resonant type of response, only a few modes are often sufficient to represent $\mathbf{J}_S$ with sufficient accuracy. Note that, in the presence of *multiple* scatterers of equal size and shape, the characteristic modes of a *single* isolated scatterer can be used to expand the electric current on each scatterer.[78]

The series (11.179) suggests a few interesting applications. It shows, for example, that the efficiency of a small antenna located on a ship or a tank can be improved by placing the antenna at points where the highly radiating modes are optimally excited. To maximize V^i_n, the source should be located near a maximum of $\mathbf{J}_n$ and so oriented that $\mathbf{E}^i$ and $\mathbf{J}_n$ are parallel.[79] The formula can also serve to determine the current $\mathbf{J}_S$, which radiates according to a prescribed radiation vector $\mathbf{F}(\theta, \varphi)$. The solution to this synthesis problem is obtained,[80,81] in principle at least, by expanding $\mathbf{F}$ as [198]

$$\mathbf{F}(\theta, \varphi) = \sum A_n \mathbf{F}_n(\theta, \varphi).$$

The coefficients A_n can now be determined by means of the orthogonality property (11.177), whereupon the desired $\mathbf{J}_S$ follows from (11.178).

11.8.2 Penetrable Bodies

Let volume V in Figure 11.23 be filled with a linear homogeneous dielectric. The electric field generated by the polarization currents $\mathbf{J}$ is given by[¶¶]

$$\mathbf{E}^{sc}(\mathbf{r}) = -j\omega\mu_0\,\mathbf{L}(\mathbf{J}) = -\mathbf{Z}_V(\mathbf{J}),$$

where[‖‖]

$$\mathbf{J} = j\omega(\epsilon - \epsilon_0)(\mathbf{E}^i + \mathbf{E}^{sc}) \qquad (\text{in } V), \tag{11.180}$$

[¶¶] A treatment in terms of equivalent surface currents can be found in Note 82.

[‖‖] The form of operator $\mathbf{L}$ for a surface vector $\mathbf{f_s}$ is given in (11.168).

and

$$\mathbf{L}(\mathbf{f}) = \int_V \mathbf{f}(\mathbf{r}') \frac{e^{-jk_0|\mathbf{r}-\mathbf{r}'|}}{4\pi|\mathbf{r}-\mathbf{r}'|}\, dV' + \frac{1}{k_0^2} \operatorname{grad} \int_V \operatorname{div}' \mathbf{f}(\mathbf{r}') \frac{e^{-jk_0|\mathbf{r}-\mathbf{r}'|}}{4\pi|\mathbf{r}-\mathbf{r}'|}\, dV'. \tag{11.181}$$

An equation for $\mathbf{J}$ follows by combining these equations into

$$\mathbf{E}^i(\mathbf{r}) = \frac{1}{j\omega(\epsilon - \epsilon_0)} \mathbf{J} + \mathbf{Z}_V(\mathbf{J}) = \mathbf{Z}_p(\mathbf{J}). \tag{11.182}$$

The analysis of the properties of the $\mathbf{Z}_p$ operator proceeds as for the perfectly conducting scatterer, but with respect to a volume scalar product[83]

$$\langle \mathbf{a}, \mathbf{b} \rangle = \int_V \mathbf{a} \cdot \mathbf{b}\, dV.$$

Under conditions discussed in Section 11.6, the penetrable body may sometimes be modeled by a surface impedance. The tangential electric field just outside the scatterer is then given by

$$\mathbf{E}_{\tan} = Z_S \mathbf{J}_S = \mathbf{E}^i_{\tan} + \mathbf{E}^{sc}_{\tan} = \mathbf{E}^i_{\tan} - \mathbf{Z}(\mathbf{J}_S), \tag{11.183}$$

or

$$\mathbf{E}^i_{\tan}(\mathbf{r}) = Z_S \mathbf{J}_S + \mathbf{Z}(\mathbf{J}_S), \qquad (\mathbf{r} \text{ on } S), \tag{11.184}$$

which corresponds with (11.167). It is clear that by proper choice of Z_S (i.e., by suitable *impedance loading*[84]), the radar cross section of the body can be significantly modified. Further, any real $\mathbf{J}_S$ can be made into the dominant mode current $\mathbf{J}_n$ of the body [198]. Loading of the scatterer can also be achieved by means of *ports* to which lumped impedances or networks are connected. Characteristic modes may again be defined for such hybrid systems.[85,86]

11.8.3 Apertures

Aperture modes can be introduced on the basis of the theory given in Section 10.7, in which the main unknown is the surface magnetic current $\mathbf{J}_{mS} = \mathbf{u}_n \times \mathbf{E}$ in the aperture (Fig. 10.17). This current must satisfy (10.152), repeated here for convenience:

$$\mathbf{L}_{1t}(\mathbf{J}_{mS}) + \mathbf{L}_{2t}(\mathbf{J}_{mS}) = \mathbf{J}_S \times \mathbf{u}_n. \tag{11.185}$$

The symbol $\mathbf{J}_S$ denotes the total current density induced in the *short-circuited* aperture by the sources in both regions 1 and 2, acting together. We write, in short,***

$$\mathbf{L}_t(\mathbf{J}_{mS}) = \mathbf{J}_S \times \mathbf{u}_n. \tag{11.186}$$

The operator $\mathbf{L}_t$ is symmetric with respect to a scalar product[87]

$$\langle \mathbf{a}, \mathbf{b} \rangle = \int_A \mathbf{a} \cdot \mathbf{b}\, dS, \tag{11.187}$$

***The form of $\mathbf{L}_t$ for a perfectly conducting plane is given in (11.191).

where A is the surface of the aperture. Note that $\mathbf{L}_t$ has the dimension of an *admittance*, and that its discretization leads to the admittance matrices defined in Section 10.7. By means of the splitting

$$\mathbf{L}_t = \mathbf{G}_t + j\mathbf{B}_t \tag{11.188}$$

we may write the eigenvector equation for the characteristic modes in the form

$$\mathbf{L}_t(\mathbf{M}_n) = \mu_n \mathbf{G}_t(\mathbf{M}_n). \tag{11.189}$$

The theory proceeds precisely as in the case of a perfectly conducting surface. Similar steps, in particular, show that the $\mathbf{M}_n$ have orthogonality properties, and that they can be normalized by requiring the power through A to be unity. The particular case of an infinite slot is discussed in detail in Section 14.9.

11.8.4 Numerical Procedure

The eigenvalue problems (11.172) and (11.189) are discretized by writing $\mathbf{J}_n = \sum_j I_j \mathbf{w}_j$, and testing the equation with appropriate vector functions. In the Galerkin method this approach leads to relationships of the form[88]

$$\sum_j I_j \langle \mathbf{w}_i, \mathbf{X}(\mathbf{w}_j) \rangle = \lambda_n \sum_j I_j \langle \mathbf{w}_i, \mathbf{R}(\mathbf{w}_j) \rangle \qquad i = 1, 2, \ldots.$$

In matrix notation:

$$\begin{aligned} \overline{\overline{X}} \cdot \mathbf{I}_n &= \lambda_n \overline{\overline{R}} \cdot \mathbf{I}_n \\ \overline{\overline{Z}} \cdot \mathbf{I}_n &= (1 + j\lambda_n) \overline{\overline{R}} \cdot \mathbf{I}_n. \end{aligned} \tag{11.190}$$

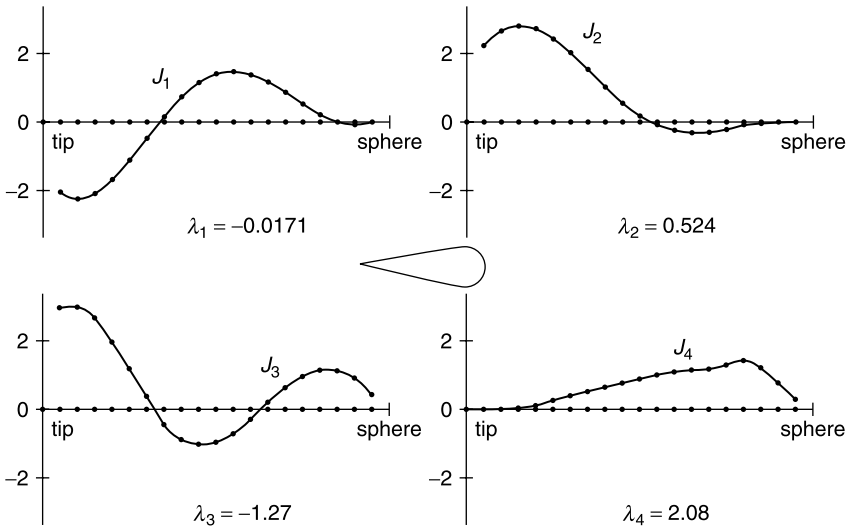

Figure 11.24 Characteristic currents for a cone-sphere structure (from R. F. Harrington and J. R. Mautz, Computation of characteristic modes for conducting bodies, *IEEE Trans. AP* **19**, 629–639, 1971, with permission of IEEE).

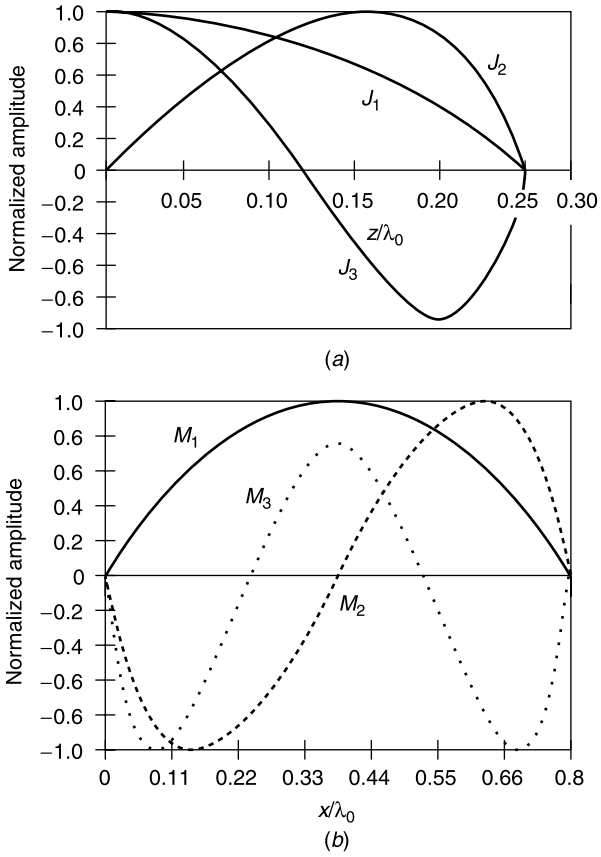

Figure 11.25 First three characteristic modes: (*a*) of a half-wave dipole, (*b*) of a narrow rectangular aperture of length 0.8 λ_0 and width 0.025 λ_0 (from Ali El-Hajj and K. Y. Kabalan, Characteristic modes of a rectangular aperture in a perfectly conducting plane, *IEEE Trans. AP* **42**, 1447–1450, 1994, with permission of IEEE).

Illustratively, Figure 11.24 shows the four lowest-order, axisymmetric eigencurrents $\mathbf{J}_n$ of a *cone-sphere* scatterer of length 1.36 λ_0 and sphere diameter 0.4 λ_0. Corresponding data are given in Figure 11.25*a* for a *straight wire* of length $\lambda_0/2$ (a half-wave dipole). The figure shows the amplitudes of $\mathbf{J}_1, \mathbf{J}_2, \mathbf{J}_3$, normalized to unity, for a wire of radius 0.0025 $|\lambda_0|$. The eigenvalues are $\lambda_1 = 0.5941$, $\lambda_2 = -98.48$, $\lambda_3 = -6264$, and the abscissas 0 and 0.25 correspond with respectively the center and the tip of the antenna. We note the very large increase in the eigenvalue λ_n as one proceeds from λ_1 to λ_2 (and further). The remark is important for the interpretation of (11.179). Finally, Figure 11.25*b* gives data concerning an *aperture* in a perfectly conducting plane.[89,90] The operator $\mathbf{L}_t$ is given, in this case, by (9.187). Thus (Fig. 9.34)

$$\mathbf{L}_t(\mathbf{J}_{mS}) = -\frac{2}{j\omega\mu_0}\frac{1}{2\pi}\left[\text{curl curl}\int_A \mathbf{J}_{mS}(\mathbf{r}')\frac{e^{-jk_0|\mathbf{r}-\mathbf{r}'|}}{|\mathbf{r}-\mathbf{r}'|}\,dS'\right]_{\text{tan}}, \tag{11.191}$$

where $\mathbf{J}_{mS} = \mathbf{E} \times \mathbf{u}_n$.

PROBLEMS

11.1 Equation (11.6) gives the backscattering matrix of a small, perfectly conducting sphere. Extend the analysis to the determination of $\overline{\overline{S}}(\mathbf{u}'|\mathbf{u}_z)$, where $\mathbf{u}'$ is *arbitrary*.

11.2 The fields of an external source are incident on an obstacle of arbitrary constitutive parameters. Investigate whether these parameters can be chosen to maximize the absorbed power. (A. T. de Hoop, *Radio Sci.* **16**, 971–974, 1981.)

11.3 Determine the modified Stokes' vector of an unpolarized field.

11.4 Determine the form of the modified Stokes vector of $\mathbf{F}$ in (11.46) when the input $\mathbf{A}$ is unpolarized. Consider more particularly the backscattered field from a target with symmetric $\overline{\overline{\sigma}}, \overline{\overline{\mu}}, \overline{\overline{\epsilon}}$. Under which conditions is $\mathbf{F}$ still unpolarized? Bring the $\overline{\overline{S}}$ matrix to its F_{XX}, F_{YY} form, and evaluate the $\overline{\overline{M}}$ matrix, which is now diagonal.

11.5 Verify that the multipole coefficients a_n, b_n in (11.67) and (11.68) reduce to a_1 in the low-frequency limit when the sphere is nonmagnetic. Determine the scattered fields and the dipole moment $\mathbf{P}_e$ that produces them.

11.6 Show that the electromagnetic fields in a sourceless, homogeneous region can be written in the form

$$\mathbf{e} = \text{grad}\,\frac{\partial}{\partial R}(RA) - \epsilon\mu\frac{\partial^2 A}{\partial t^2}\mathbf{r} - \text{curl}\left(\frac{\partial B}{\partial t}\mathbf{r}\right)$$

$$\mathbf{h} = \frac{1}{c^2}\,\text{curl}\left(\frac{\partial A}{\partial t}\mathbf{r}\right) + \text{curl curl}\,(B\mathbf{r})$$

where A and B satisfy the wave equation in medium (ϵ, μ) [9].

11.7 Helmholtz's theorem on the sphere allows representation of an arbitrary vector $\mathbf{A}(R, \theta, \varphi)$ as

$$\mathbf{A} = F(R, \theta, \varphi)\mathbf{u}_R + \text{grad}_{\theta\varphi} S(R, \theta, \varphi) + \mathbf{u}_R \times \text{grad}_{\theta\varphi} T(R, \theta, \varphi).$$

(**a**) Calculate the corresponding functions F, S, T for curl $\mathbf{A}$.

(**b**) Show that in a region $a < R < b$ free of sources, and where ϵ and μ depend on R alone, the fields are given by

$$\mathbf{E} = \frac{1}{j\omega\epsilon}\,\text{curl curl}\,(u\mathbf{r}) + \text{curl}\,(v\mathbf{r})$$

$$\mathbf{H} = -\frac{1}{j\omega\mu}\,\text{curl curl}\,(v\mathbf{r}) + \text{curl}\,(u\mathbf{r}),$$

where u and v satisfy

$$\nabla^2 u + \omega^2\epsilon\mu u - \frac{1}{\epsilon R}\frac{d\epsilon}{dR}\frac{\partial}{\partial R}(Ru) = 0$$

$$\nabla^2 v + \omega^2\epsilon\mu v - \frac{1}{\mu R}\frac{d\mu}{dR}\frac{\partial}{\partial R}(Rv) = 0$$

and the auxiliary conditions

$$\int_\Omega u\, d\Omega = \int_\Omega v\, d\Omega = 0.$$

(C. H. Wilcox, *J. Math. Mech.* **6**, 167, 1957.)

11.8 A target of high ϵ_r is illuminated by the far-field of an elliptically polarized antenna (Fig. P11.1). Determine the form of the backscattered field in the vicinity of a $\mathbf{p}_m$ resonance, using (11.89). Determine also the power received by the receiving antenna, using the appropriate form of the polarization factor.

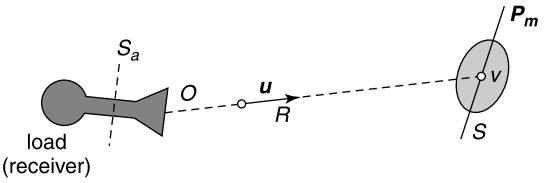

Figure P11.1

11.9 Evaluate $I_2(x, s)$ in (11.106) when the voltage is a step function given by $v_a(x, t) = H(t)\, v_a(x)$. Determine the singularity associated with this term [91].

11.10 Starting from (11.124), derive a formal expression for $\mathbf{j}_S(\mathbf{r}, t)$, given an incident field

$$\mathbf{h}^i = H_0 \mathbf{u}_h\, \delta\left(t - \frac{\mathbf{u}_i \cdot \mathbf{r}}{c_0}\right).$$

(L. Marin, *Electromagn.* **1**, 361–373, 1981.)

11.11 Under oblique incidence, the tangential current in the thin dielectric slab of Figure P11.2 is given by (11.157), viz.

$$(\mathbf{J}_S)_{\tan} = \underbrace{j\omega(\epsilon - \epsilon_0)l}_{j\omega C} \frac{\mathbf{E}^1_{\tan} + \mathbf{E}^2_{\tan}}{2}.$$

Show that there is also a (small) normal component

$$(\mathbf{J}_S)_n = \frac{j\omega C}{\epsilon_r} \frac{E^1_n + E^2_n}{2}.$$

(T. B. A. Senior et al., *Radio Sci.* **22**, 1261–1272, 1987.)

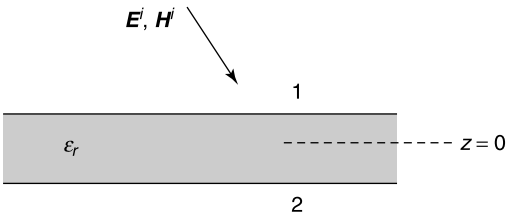

Figure P11.2

11.12 Show that $\mathbf{F}_n$, radiation vector of $\mathbf{J}_n$, is automatically normalized on S_∞ when $\mathbf{J}_n$ is normalized according to (11.175).

Hint: Start from Equation (11.176), and find the explicit value of $\displaystyle\int_{S_\infty} \mathbf{F}_n \cdot \mathbf{F}_n^*\, dS$.

11.13 Show that the time-domain version of (11.184) is

$$\mathbf{u}_n \times \mathbf{e}^i(\mathbf{r},t) = \frac{\mathbf{u}_n}{2\pi} \times \int_S \left[\frac{\mu_0}{|\mathbf{r}-\mathbf{r}'|} \frac{\partial}{\partial \tau} \mathbf{j}_S(\mathbf{r}',\tau) - \frac{\rho_S(\mathbf{r},\tau)}{\epsilon_0} \frac{(\mathbf{r}-\mathbf{r}')}{|\mathbf{r}-\mathbf{r}'|^3} \right.$$
$$\left. - \frac{1}{\epsilon_0} \frac{\partial}{\partial \tau} \rho_S(\mathbf{r}',\tau) \frac{(\mathbf{r}-\mathbf{r}')}{c_0|\mathbf{r}-\mathbf{r}'|^2} \right] dS' + \mathbf{u}_n \times \int_0^t Z_c'(\tau) \frac{\partial}{\partial \tau} \mathbf{j}_S(\mathbf{r}', \tau - t)\, d\tau$$

where $Z_c'(t)$ is defined in (11.143) and $\tau = t - (|\mathbf{r}-\mathbf{r}'|/c_0)$.
(F. M. Tesche, *IEEE Trans. EMC* **32**, 1–4, 1990.)

11.14 Using expansion (11.179) for $\mathbf{J}_S$, find a formula for the bistatic scattering cross section of a perfectly conducting obstacle immersed in a plane wave.
(R. F. Harrington et al., *IEEE Trans. AP* **19**, 622–628, 1971.)

11.15 An iterative solution of

$$\mathbf{x} = \overline{\overline{B}} \cdot \mathbf{x} + \mathbf{C}$$

can be obtained by using the scheme

$$\mathbf{x}_{n+1} = \overline{\overline{B}} \cdot \mathbf{x}_n + \mathbf{C}$$

starting with a well-chosen $\mathbf{x}_0$. The error $\mathbf{e}_n = \mathbf{x}_n - \mathbf{x}$ satisfies $\mathbf{e}_{n+1} = \overline{\overline{B}} \cdot \mathbf{e}_n$. Show that the process converges to the correct solution if, and only if, the spectral radius of $\overline{\overline{B}}$ defined in (1.135) is less than unity.

NOTES

1. J. R. Huynen, Measurement of the target scattering matrix, *Proc. IEEE* **53**, 936–946 (1965).
2. C. E. Baum, Decomposition of the backscattering dyadic, *Interaction Note 533* (1997).
3. A. T. de Hoop, A reciprocity theorem for the electromagnetic field scattered by an obstacle, *Appl. Sci. Res. B* **8**, 135–140 (1959).
4. A. T. de Hoop, On the plane-wave extinction cross section of an obstacle, *Appl. Sci. Res. B* **7**, 463–469 (1958).
5. C. D. Graves, Radar polarization power scattering matrix, *Proc. IRE* **44**, 248–252 (1956).
6. J. J. van Zijl, H. A. Zebker, and C. Elachi, Imaging radar polarization signatures: theory and observation, *Radio Sci.* **22**, 529–543 (1987).
7. W. M. Boerner, M. B. El-Arini, C. Y. Chan, and P. M. Mastoris, Polarization dependence in electromagnetic inverse problems, *IEEE Trans. AP* **29**, 262–271 (1981).
8. D. Giuli, Polarization diversity in radars, *Proc. IEEE* **74**, 245–269 (1986).
9. E. Pottier, S. R. Cloude, and W. M. Boerner, Recent development of data processing in polarimetric and interferometric SAR, *Radio Sci. Bull.* **304**, 48–58 (2003).
10. J. Björkberg, Current distribution on a perfectly conducting elliptic disk, *IEEE Trans. AP* **39**, 318–326 (1991).
11. I. R. Ciric and M. F. R. Cooray, Scattering of a plane wave by a hemispheroidal boss on an infinite plane, *Can. J. Phys.* **70**, 615–622 (1992).
12. S. Hong, Electromagnetic backscattering by spheroids for axial incidence, *Microwave Opt. Tech. Lett.* **13**, 229–233 (1996).
13. I. R. Ciric and F. R. Cooray, Separation of variables for electromagnetic scattering by spheroidal particles, in *Light scattering by nonspherical particles: theory, measurements and applications*, p. 89–130, Academic Press, New York, 2000.
14. L. W. Li, M. S. Leong, P. S. Kooi, and T. S. Yeo, Spheroidal vector wave eigenfunction expansion of dyadic Green's functions for a dielectric spheroid, *IEEE Trans. AP* **49**, 645–659 (2001).
15. J. Mével, Etude de la structure détaillée des courbes de diffusion des ondes electromagnétiques par les sphères diélectriques, *J. Phys. Radium* **19**, 630–636 (1958).
16. L. Brillouin, Scattering cross section of spheres for electromagnetic waves, *J. Appl. Phys.* **20**, 1110–1125 (1949). See also *Letters to the Editor* in *Proc. IRE* **48**, 1781–1782 (1960).
17. G. N. Watson, The diffraction of electric waves by the earth, *Proc. Roy. Soc. London* **95**, 83–99 (1918).
18. A. D. Greenwood and J. M. Jin, A field picture of wave propagation in inhomogeneous dielectric lenses, *IEEE Antennas Prop. Mag.* **41**, 9–17 (1999).

19. J. R. Sanford, Scattering by spherically stratified microwave lens antennas, *IEEE Trans. AP* **42**, 690–698 (1994).
20. L. W. Li, P. S. Kooi, M. S. Leong, and T. S. Yeo, Electromagnetic Green's function in spherically multilayered media, *IEEE Trans. MTT* **42**, 2302–2310 (1994).
21. S. M. S. Reyhani and R. J. Glover, Electromagnetic dyadic Green's function for a multilayered homogeneous lossy dielectric spherical head model for numerical EMC investigation, *Electromagn.* **20**, 141–153 (2000).
22. H. Mosallaei and Y. Rahmat-Samii, Nonuniform Luneburg and two-shell lens antennas: radiation characteristics and design optimization, *IEEE Trans. AP* **49**, 60–69 (2001).
23. A. Petosa, A. Ittipiboon, Y. M. M. Antar, D. Roscoe, and M. Cuhaci, Recent advances in dielectric resonator-antenna technology, *IEEE Antennas Prop. Mag.* **40**, 35–48 (1998).
24. J. Chen, A. A. Kishk, and A. W. Glisson, Applications of a new MPIE formulation to the analysis of a dielectric resonator embedded in a multilayered medium coupled to a microstrip circuit, *IEEE Trans. MTT* **49**, 263–279 (2001).
25. S. Y. Ke and Y.-T. Cheng, Integration equation analysis on resonant frequencies and quality factors of rectangular dielectric resonators, *IEEE Trans. MTT* **49**, 571–574 (2001).
26. P. Guillon, B. Byzery, and M. Chaubet, Coupling parameters between a dielectric resonator and a microstripline, *IEEE Trans. MTT* **33**, 222–226 (1985).
27. J. Chen, A. A. Kishk, and A. W. Glisson, A 3D interpolation model for the calculation of the Sommerfeld integrals to analyze dielectric resonators in a multilayered medium, *Electromagn.* **20**, 1–15 (2000).
28. K. W. Leung, M. L. Poon, W. C. Wong, K. M. Luk, and E. K. N. Jung, Aperture-coupled dielectric resonator antenna using a strip-line feed, *Microwave Opt. Tech. Lett.* **24**, 120–121 (2000).
29. Z. Liu, W. C. Chew, and E. Michielssen, Numerical modeling of dielectric-resonator antennas in a complex environment using the method of moments, *IEEE Trans. AP* **50**, 79–82 (2002).
30. J. Van Bladel, On the resonances of a dielectric resonator of very high permittivity, *IEEE Trans. MTT* **23**, 199–208 (1975)
31. J. Van Bladel, The excitation of dielectric resonators of very high permittivity, *IEEE Trans. MTT* **23**, 208–217 (1975).
32. P. W. Barber, J. F. Owen, and R. K. Chang, Resonant scattering for characterization of axisymmetric dielectric objects, *IEEE Trans. AP* **30**, 168–172 (1982).
33. D. L. Moffatt and R. K. Mains, Detection and discrimination of radar target, *IEEE Trans. AP* **23**, 358–367 (1975).
34. A. A. Ksienski, Y. T. Lin, and L. J. White, Low-frequency approach to target identification, *Proc. IEEE* **63**, 1651–1660 (1975).
35. C. E. Baum, Emerging technology for transient and broad-band analysis and synthesis of antennas and scatterers, *Proc. IEEE* **64**, 1598–1616 (1976).
36. L. Marin, Major results and unresolved issues in singularity expansion method, *Electromagn.* **1**, 361–373 (1981).
37. E. J. Rothwell, J. Baker, K. M. Chen, and D. P. Nyquist, Approximate natural response of an arbitrarily shaped thin wire scatterer, *IEEE Trans. AP* **39**, 1457–1462 (1991).
38. C. A. Lin and J. T. Cordaro, Determination of the SEM parameters for an aircraft model from the transient surface current, *Electromagn.* **3**, 65–75 (1983).
39. F. M. Tesche, On the analysis of scattering and antenna problems using the singularity expansion technique, *IEEE Trans. AP* **21**, 53–62 (1973).
40. M. A. Richards, T. H. Shumpert, and L. S. Riggs, SEM formulation of the fields scattered from arbitrary wire structures, *IEEE Trans. EMC* **35**, 249–254 (1993).
41. S. R. Vechinski and T. H. Shumpert, Natural resonances of conducting bodies of revolution, *IEEE Trans. AP* **38**, 1133–1136 (1990).
42. L. Marin, Natural-mode representation of transient scattered fields, *IEEE Trans. AP* **21**, 809–818 (1973).
43. D. G. Dudley, A state-space formulation of transient electromagnetic scattering, *IEEE Trans. AP* **33**, 1127–1136 (1985)
44. D. V. Giri and F. M. Tesche, On the use of singularity expansion method for analysis of antennas in conducting media, *Electromagn.* **1**, 455–471 (1981).
45. C. E. Baum, The SEM representation of scattering from perfectly conducting targets in simple lossy media, *Interaction Note 492* (1993).
46. L. W. Pearson, D. R. Wilton and R. Mittra, Some implications of the Laplace transform inversion on SEM coupling coefficients in the time domain, *Electromagn.* **2**, 181–200 (1982).
47. C. E. Baum, An observation concerning the entire function in SEM scattering, *Interaction Note 567* (2001).
48. C. E. Baum and L. W. Pearson, On the convergence and numerical sensitivity of the SEM pole-series in early-time scattering response, *Electromagn.* **1**, 209–228 (1981).
49. L. W. Pearson, A note on the representation of scattered fields as a singularity expansion, *IEEE Trans. AP* **32**, 520–524 (1984).
50. H. Überall and G. C. Gaunaurd, Relation between the ringing of resonances and surface waves in radar scattering, *IEEE Trans. AP* **32**, 1071–1079 (1984).
51. J. Rheinstein, Scattering of short pulses of electromagnetic waves, *Proc. IEEE* **53**, 1069–1070 (1965).
52. E. Heyman and L. B. Felsen, Creeping waves and resonances in transient scattering by smooth convex objects, *IEEE Trans. AP* **31**, 426–437 (1983).
53. E. Heyman and L. B. Felsen, A wavefront interpretation of the singularity expansion method, *IEEE Trans. AP* **33**, 706–718 (1985).
54. T. K. Sarkar and O. Pereira, Using the matrix pencil method to estimate the parameters of a sum of complex

exponentials, *IEEE Antennas Prop. Mag.* **37**, 48–54 (1995).
55. C. E. Baum, E. J. Rothwell, K. M. Chen, and D. P. Nyquist, The singularity expansion method and its application to target identification, *Proc. IEEE* **79**, 1481–1492 (1991).
56. C. E. Baum, Signature-based target identification, *Interaction Note 500* (1994).
57. Q. Li, P. Ilavarasan, J. E. Ross, E. J. Rothwell, K. M. Chen, and D. P. Nyquist, Radar target identification using a combined early-time/late-time *E*-pulse technique, *IEEE Trans. AP* **46**, 1272–1278 (1998).
58. K. A. Nabulsi and D. G. Dudley, Hybrid formulations for scattering from the dielectric slab, *IEEE Trans. AP* **40**, 959–965 (1992).
59. G. Pelosi and P. Y. Ufimtsev, The impedance-boundary condition, *IEEE Antennas Prop. Mag.* **38**, 31–34 (1996).
60. J. R. Wait, Use and misuse of impedance boundary conditions in electromagnetics, *PIERS 1989 Proceedings*, 358.
61. J. H. Beggs, R. J. Luebbers, K. S. Yee, and K. S. Kunz, Finite-difference time-domain implementation of surface impedance boundary conditions, *IEEE Trans. AP* **40**, 49–56 (1992).
62. J. G. Maloney and G. S. Smith, The use of surface impedance concepts in the finite-difference time-domain method, *IEEE Trans. AP* **40**, 38–48 (1992).
63. T. B. A. Senior, Impedance boundary conditions for imperfectly conducting surfaces, *Appl. Sci. Res. B* **138**, 418–436 (1960).
64. D. S. Wang, Limits and validity of the impedance boundary condition on penetrable surfaces, *IEEE Trans. AP* **35**, 453–457 (1987).
65. T. B. A. Senior, Generalized boundary and transition conditions and the question of uniqueness, *Radio Sci.* **27**, 929–934 (1992).
66. T. B. A. Senior, J. L. Volakis, and S. R. Legault, Higher order impedance and absorbing boundary conditions, *IEEE Trans. AP* **45**, 107–114 (1997).
67. T. Y. Otoshi, Y. Rahmat-Samii, R. Cirillo, Jr., and J. Sosnowksi, Noise temperature and gain loss due to paints and primers: a case study of DSN antennas, *IEEE Antennas Prop. Mag.* **43**, 11–28 (2001).
68. M. Feliziani and F. Maradei, Finite difference time-domain modeling of thin shields, *IEEE Trans. Mag.* **36**, 848–851 (2000).
69. R. F. Harrington and J. R. Mautz, An impedance sheet approximation for thin dielectric shells, *IEEE Trans. AP* **23**, 531–534 (1975).
70. T. B. A. Senior, Approximate boundary conditions, *IEEE Trans. AP* **29**, 826–829 (1981).
71. K. M. Mitzner, Effective boundary conditions for reflection and transmission by an absorbing shell of arbitrary shape, *IEEE Trans. AP* **16**, 706–712 (1968).
72. T. B. A. Senior, Combined resistive and conductive sheets, *IEEE Trans. AP* **33**, 577–579 (1985).
73. T. B. A. Senior and J. L. Volakis, Generalized impedance boundary conditions in scattering, *Proc. IEEE* **79**, 1413–1420 (1991).
74. D. J. Hoppe and Y. Rahmat-Samii, Higer order impedance boundary conditions applied to scattering by coated bodies of revolution, *IEEE Trans. AP* **42**, 1600–1611 (1994).
75. R. J. Garbacz, Modal expansions for resonance scattering phenomena, *Proc. IEEE* **53**, 856–864 (1965).
76. R. F. Harrington and J. R. Mautz, Theory of characteristic modes for conducting bodies, *IEEE Trans. AP* **19**, 622–628 (1971).
77. D. Liu, R. J. Garbacz and D. M. Pozar, Antenna synthesis and optimization using generalized characteristic modes, *IEEE Trans. AP* **38**, 862–868 (1990).
78. G. Angiulli, G. Amendola, and G. Di Massa, Characteristic modes in multiple scattering by conducting cylinders of arbitrary shape, *Electromagn.* **18**, 593–612 (1998).
79. E. H. Newman, Small antenna location synthesis using characteristic modes, *IEEE Trans. AP* **27**, 530–531 (1979).
80. R. J. Garbacz and R. H. Turpin, A generalized expansion for radiated and scattered fields, *IEEE Trans. AP* **19**, 348–358 (1971).
81. B. A. Austin and K. P. Murray, The application of characteristic-mode techniques to vehicle-mounted NVIS antennas, *IEEE Antennas Prop. Mag.* **40**, 7–21 (1998).
82. Y. Chang and R. F. Harrington, A surface formulation for characteristic modes of material bodies, *IEEE Trans. AP* **25**, 789–795 (1977).
83. R. F. Harrington, J. R. Mautz, and Y. Chang, Characteristic modes for dielectric and magnetic bodies, *IEEE Trans. AP* **20**, 194–198 (1972).
84. R. F. Harrington and J. R. Mautz, Control of radar scattering by reactive loading, *IEEE Trans. AP* **20**, 446–454 (1972).
85. J. R. Mautz and R. F. Harrington, Modal analysis of loaded *N*-port scatterers, *IEEE Trans. AP* **21**, 188–199 (1973).
86. R. F. Harrington and J. R. Mautz, Pattern synthesis for loaded *N*-port scatterers, *IEEE Trans. AP* **22**, 184–190 (1974).
87. R. F. Harrington and J. R. Mautz, Characteristic modes for aperture problems, *IEEE Trans. MTT* **33**, 500–505 (1985).
88. R. F. Harrington and J. R. Mautz, Computation of characteristic modes for conducting bodies, *IEEE Trans. AP* **19**, 629–639 (1971).
89. W. Sun, K. M. Chen, D. P. Nyquist, and E. J. Rothwell, Determination of the natural modes for a rectangular plate, *IEEE Trans. AP* **38**, 643–652 (1990).
90. Ali El-Hajj and K. Y. Kabalan, Characteristic modes of a rectangular aperture in a perfectly conducting plane, *IEEE Trans. AP* **42**, 1447–1450 (1994).

Chapter 12

Scattering: Numerical Methods

The search for ever more performing numerical methods is a constantly recurrent theme in the recent literature. Given that strong interest, this chapter is devoted to the formulation of the scattering problem in ways that can be conveniently exploited by the numerical analyst. The approach is general, and the specialization to high and low frequencies — or to particular geometries — is left to Chapters 13 to 16. The discussion of techniques such as the adaptive integral method does not go further than a light exposé of the principles; matters of stability, convergence, and minimization of the number of steps are left to the numerical analyst.

12.1 THE ELECTRIC FIELD INTEGRAL EQUATION

When a perfectly conducting scatterer is irradiated by an incident wave, the fundamental unknown quantity is the current $\mathbf{J}_S$ induced on the boundary surface S of the scatterer. In a first approach, $\mathbf{J}_S$ is determined by imposing the boundary condition $\mathbf{E}^{sc}_{\tan}(\mathbf{J}_S) = -\mathbf{E}^{i}_{\tan}$ on S. This requirement leads to an *integro-differential* equation for $\mathbf{J}_S$, the *electric field integral equation* (EFIE). In a second approach, the scattered *magnetic* field is expressed in terms of $\mathbf{J}_S$, and the condition $\mathbf{H}_{\tan}(\mathbf{J}_S) = \mathbf{J}_S \times \mathbf{u}_n$ is imposed on S (Fig. 12.1). This strategy leads to an *integral* equation for $\mathbf{J}_S$, the *magnetic field integral equation* (MFIE). Both integral equations were derived by Maue,[1] whose paper remained somewhat forgotten until, in the late 1950s, performant digital computers became widely available and were promptly used to solve the rediscovered (and sometimes rederived) Maue equations [6, 22].

To derive the EFIE, we start from the potential form of the scattered field:

$$\mathbf{E}^{sc}(\mathbf{r}) = -j\omega\mathbf{A} - \operatorname{grad}\phi = -j\omega\mu_0\,\mathbf{L}(\mathbf{J}_S). \tag{12.1}$$

The operator $\mathbf{L}(\mathbf{J}_S)$ is defined in (11.168) and (11.181). Repeated for convenience:

$$\mathbf{L}(\mathbf{J}_S) = \int_S \mathbf{J}_S(\mathbf{r}')\frac{e^{-jk_0|\mathbf{r}-\mathbf{r}'|}}{4\pi|\mathbf{r}-\mathbf{r}'|}\,dS' + \frac{1}{k_0^2}\operatorname{grad}\int_S \operatorname{div}'_S\,\mathbf{J}_S(\mathbf{r}')\frac{e^{-jk_0|\mathbf{r}-\mathbf{r}'|}}{4\pi|\mathbf{r}-\mathbf{r}'|}\,dS'. \tag{12.2}$$

Electromagnetic Fields, Second Edition, By Jean G. Van Bladel

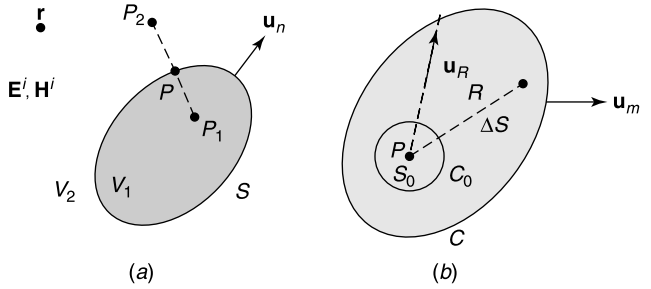

Figure 12.1 (*a*) Perfectly conducting scatterer in an incident field. (*b*) Flat self-patch of arbitrary shape $S_\delta = S_0 + \Delta S$.

It is actually the operator $\mathbf{L}$ of Equation (11.181) but applied to a surface current. Relationship (12.1) is written more explicitly as

$$\mathbf{E}^{sc}(\mathbf{r}) = \underbrace{-\frac{j\omega\mu_0}{4\pi}\int_S \mathbf{J}_S(\mathbf{r}')\frac{e^{-jk_0|\mathbf{r}-\mathbf{r}'|}}{|\mathbf{r}-\mathbf{r}'|}\,dS'}_{\text{“magnetic,” inductive part}} + \underbrace{\operatorname{grad}\frac{1}{4\pi j\omega\epsilon_0}\int_S \operatorname{div}'_S \mathbf{J}_S(\mathbf{r}')\frac{e^{-jk_0|\mathbf{r}-\mathbf{r}'|}}{|\mathbf{r}-\mathbf{r}'|}\,dS'}_{\text{“electric,” capacitive part}}. \tag{12.3}$$

The EFIE is obtained by enforcing the condition $\mathbf{E}^{sc}_{\tan}(\mathbf{r}) = -\mathbf{E}^{i}_{\tan}(\mathbf{r})$ for $\mathbf{r}$ on S; that is, by letting P_2 approach P along the normal (Fig. 12.1). Thus, in a concise notation,

$$\mathbf{E}^{i}_{\tan}(\mathbf{r}) = -\mathbf{E}^{sc}_{\tan}(\mathbf{r}) = j\omega\mu_0\,\mathbf{L}_t(\mathbf{J}_S) = \mathbf{Z}(\mathbf{J}_S) \qquad (\mathbf{r} \text{ on } S) \tag{12.4}$$

where the tangential operator $\mathbf{L}_t$ is defined in (11.168). The *magnetic* part of $\mathbf{E}^{sc}$ is continuous throughout space, as mentioned in Section 3.4, and its value for $\mathbf{r}$ on S is equal to the limit of the integral over $S - S_\delta$ when $\delta \to 0$, and S_δ is a small patch of arbitrary shape and maximum chord δ including $\mathbf{r}$. The potential integral in the *electric* part of $\mathbf{E}^{sc}$ behaves in a similar way. If, however, it is desired to bring the grad operator behind the integral sign, great care should be exercised because a singularity in $|\mathbf{r}-\mathbf{r}'|^{-2}$ is introduced. The difficulty is touched upon in Section 3.4, where it is mentioned that

$$\mathbf{J}_{\tan} = \lim_{\delta\to 0}\int_{S-S_\delta} f(\mathbf{r}')\frac{\mathbf{r}-\mathbf{r}'}{|\mathbf{r}-\mathbf{r}'|^3}\,dS$$

approaches a limit as $\mathbf{r}$ approaches a point P on S and S_δ is a *small circle* centered on P. We shall now investigate how that property is modified when the shape of S_δ is arbitrary.

To that effect, we rewrite the gradient term in (12.3) as

$$\begin{aligned}\mathbf{I}(\mathbf{r}) &= \operatorname{grad}_S \int_S f(\mathbf{r}') \frac{e^{-jk_0|\mathbf{r}-\mathbf{r}'|}}{|\mathbf{r}-\mathbf{r}'|}\, dS' \\ &= \underbrace{\operatorname{grad}_S \int_S f(\mathbf{r}') \left[\frac{e^{-jk_0|\mathbf{r}-\mathbf{r}'|}}{|\mathbf{r}-\mathbf{r}'|} - \frac{1}{|\mathbf{r}-\mathbf{r}'|}\right] dS'}_{\mathbf{I}_1} + \underbrace{\operatorname{grad}_S \int_S f(\mathbf{r}') \frac{1}{|\mathbf{r}-\mathbf{r}'|}\, dS'}_{\mathbf{I}_2}, \quad (12.5)\end{aligned}$$

where we have set

$$f(\mathbf{r}) = \frac{1}{4\pi j\omega\epsilon_0} \operatorname{div}_S \mathbf{J}_S(\mathbf{r}).$$

Bringing the gradient behind the integral gives

$$\mathbf{I}(\mathbf{r}) = \left\{ -\int_S f(\mathbf{r}') \operatorname{grad}' \left[\frac{e^{-jk_0|\mathbf{r}-\mathbf{r}'|}}{|\mathbf{r}-\mathbf{r}'|} - \frac{1}{|\mathbf{r}-\mathbf{r}'|}\right] dS' - \int_S f(\mathbf{r}') \operatorname{grad}' \frac{1}{|\mathbf{r}-\mathbf{r}'|}\, dS' \right\}_{\tan}. \quad (12.6)$$

The first term is not singular because

$$\operatorname{grad}' \left[\frac{e^{-jk_0|\mathbf{r}-\mathbf{r}'|}}{|\mathbf{r}-\mathbf{r}'|} - \frac{1}{|\mathbf{r}-\mathbf{r}'|}\right] \approx \operatorname{grad}' \left[-jk_0 - \frac{1}{2} k_0^2 |\mathbf{r}-\mathbf{r}'| + \cdots\right] = \frac{1}{2} k_0^2 \mathbf{u}_D + \cdots, \quad (12.7)$$

where $\mathbf{u}_D$ is the unit vector in the direction connecting $\mathbf{r}'$ to $\mathbf{r}$. The main problem therefore resides with the second term, which is the tangential electrostatic field $\mathbf{e}_{\tan}$ generated by a charge density proportional to $f(\mathbf{r})$. This component has been carefully investigated in the specialized literature [148, 153, 158]. When P_2 approaches a point P on S (Fig. 12.1*a*), the term $\mathbf{I}_2$ in (12.5) gives rise to a limit

$$\begin{aligned}&\lim_{P_2 \to P} \int_S f(\mathbf{r}') \operatorname{grad}' \left(\frac{1}{|\mathbf{r}-\mathbf{r}'|}\right) dS \\ &\quad = \lim_{\delta \to 0} \int_{S - S_\delta} f(\mathbf{r}') \operatorname{grad}' \left(\frac{1}{|\mathbf{r}-\mathbf{r}'|}\right) dS + \int_{S_\delta} f(\mathbf{r}') \operatorname{grad}' \left(\frac{1}{|\mathbf{r}-\mathbf{r}'|}\right) dS.\end{aligned}$$

The contribution from S_δ may be transformed according to[2] (Fig. 12.1*b*)

$$\int_{S_\delta} f(\mathbf{r}') \operatorname{grad}' \left(\frac{1}{|\mathbf{r}-\mathbf{r}'|}\right) dS' = f(0) \int_{S_\delta} \operatorname{grad}'_S \left(\frac{1}{R}\right) dS',$$

where $f(\mathbf{r}')$ is assumed constant over the (very small) *quasi-planar* area S_δ. Further, if S_0 is a small circle centered on P (Fig. 12.1*b*),

$$\int_{S_\delta} \operatorname{grad}'_S \left(\frac{1}{R}\right) dS' = \int_{S_0} \operatorname{grad}'_S \left(\frac{1}{R}\right) dS' + \int_{\Delta S} \operatorname{grad}'_S \left(\frac{1}{R}\right) dS'.$$

The integral over the circle S_0 vanishes by symmetry, thus confirming the conditional convergence mentioned in Section 3.4. In evaluating the integral over ΔS, we may apply (A3.45), because the integrand remains finite in ΔS, and write

$$\left[\int_{\Delta S} \text{grad}'\left(\frac{1}{R}\right) dS\right]_{\tan} = \left[\int_C \frac{\mathbf{u}_m}{R}\, dc - \int_{C_0} \frac{\mathbf{u}_R}{R}\, dc\right]_{\tan}$$

where $\mathbf{u}_m$ and $\mathbf{u}_R$ are unit vectors respectively perpendicular to C and C_0. The integral over C_0 vanishes, again by symmetry, hence (Problem 12.1)

$$\left[\int_{S_\delta} \text{grad}'_S\left(\frac{1}{R}\right) dS\right]_{\tan} = \left[\int_C \frac{\mathbf{u}_m dc}{R}\right]_{\tan} = \mathbf{T}. \tag{12.8}$$

The tangential vector $\mathbf{T}$ depends on the shape, position, and orientation of S_δ but not on the *scale* of that surface (it vanishes for a circle, for example). Collecting all terms in (12.5) shows that

$$\mathbf{I}(\mathbf{r}) = -\lim_{\delta\to 0}\left[\int_{S-S_\delta} f(\mathbf{r}')\ \text{grad}'\left(\frac{e^{-jk_0|\mathbf{r}-\mathbf{r}'|}}{|\mathbf{r}-\mathbf{r}'|}\right) dS'\right]_{\tan} - f(P_0)\,\mathbf{T}. \tag{12.9}$$

This result can be applied to (12.3) and (12.4) to yield the *sought EFIE*, viz.

$$\begin{aligned}\mathbf{E}^i_{\tan}(\mathbf{r}) = \frac{j\omega\mu_0}{4\pi}\lim_{\delta\to 0}&\left[\int_{S-S_\delta} \mathbf{J}_S(\mathbf{r}')\frac{e^{-jk_0|\mathbf{r}-\mathbf{r}'|}}{|\mathbf{r}-\mathbf{r}'|}\, dS\right]_{\tan}\\ &+ \frac{1}{4\pi j\omega\epsilon_0}\left[\lim_{\delta\to 0}\int_{S-S_\delta} \text{div}'_S\,\mathbf{J}_S(\mathbf{r}')\ \text{grad}'\left(\frac{e^{-jk_0|\mathbf{r}-\mathbf{r}'|}}{|\mathbf{r}-\mathbf{r}'|}\right) dS'\right.\\ &\left.+\ \mathbf{T}\ \text{div}'_S\,\mathbf{J}_S(\mathbf{r})\right]_{\tan} \qquad (\mathbf{r}\text{ on }S).\end{aligned} \tag{12.10}$$

12.1.1 Uniqueness of the Solution

Whether or not (12.10) has a unique solution depends on the existence of a nonzero solution for the homogeneous equation obtained by setting $\mathbf{E}^i(\mathbf{r}) = 0$ in (12.10). We shall now show that such a solution exists when $k_0 = k_m$ (i.e., at the resonant frequencies of the interior volume V_1). The solution is proportional to $(\mathbf{u}_n \times \mathbf{h}_m)$, where $\mathbf{h}_m$ is defined in (10.13). To prove this assertion, let us apply (A1.40) to $\mathbf{e}_m$ and $G_0(\mathbf{r}|\mathbf{r}')$, where G_0 is the Green's function* (7.95). Thus,

$$\begin{aligned}&\int_{V_1}\left[G_0(\mathbf{r}|\mathbf{r}')\ \text{curl}'\,\text{curl}'\,\mathbf{e}_m + \mathbf{e}_m\nabla^2 G_0(\mathbf{r}|\mathbf{r}')\right] dV'\\ &\quad= \int_S\left[G_0(\mathbf{r}|\mathbf{r}')(\mathbf{u}'_n \times \text{curl}'\,\mathbf{e}_m) + (\mathbf{u}_n\cdot\mathbf{e}_m)\ \text{grad}'\,G_0(\mathbf{r}|\mathbf{r}')\right] dS'.\end{aligned}$$

*The eigenvectors $\mathbf{e}_m$ and $\mathbf{h}_m$, and their eigenvalue k_m, are discussed at length in Section 10.1.

Inserting the appropriate values of $\nabla^2 G_0$ and curl curl $\mathbf{e}_m$ yields

$$\int_S \left[k_m G_0(\mathbf{r}|\mathbf{r}')\,\mathbf{u}'_n \times \mathbf{h}_m + (\mathbf{u}_n \cdot \mathbf{e}_m)\,\text{grad}'\, G_0(\mathbf{r}|\mathbf{r}')\right] dS' = 0 \qquad (\mathbf{r} \text{ in } V_2).$$

But $(\mathbf{u}_n \cdot \mathbf{e}_m) = k_m^{-1}\mathbf{u}_n \cdot \text{curl}\, \mathbf{h}_m = -k_m^{-1}\,\text{div}_S\,(\mathbf{u}_n \times \mathbf{h}_m)$. It follows that

$$\int_S \left[G_0(\mathbf{r}|\mathbf{r}')(\mathbf{u}'_n \times \mathbf{h}_m) - k_m^{-2}\,\text{div}'_S\,(\mathbf{u}'_n \times \mathbf{h}_m)\,\text{grad}'\, G_0(\mathbf{r}|\mathbf{r}')\right] dS' = 0 \qquad (\mathbf{r} \text{ on } S). \tag{12.11}$$

To within a trivial factor, this is Equation (12.4), in which the left-hand side should be set equal to zero. This result confirms that $(\mathbf{u}_n \times \mathbf{h}_m)$ satisfies (12.10) with $\mathbf{E}^i = 0$. From the theory in Section 1.4, either the inhomogeneous equation does not have any solution or it has an infinite number of them, all of these differing by an arbitrary multiple[†] of $\mathbf{u}_n \times \mathbf{h}_m$. Because the $\mathbf{Z}$ operator in (12.4) is self-adjoint, as mentioned in Section 11.8, criterion (1.30) takes the form

$$\int_S (\mathbf{u}_n \times \mathbf{h}_m) \cdot \mathbf{E}^i_{\tan}\, dS = 0 \qquad (\text{for } k_0 = k_m). \tag{12.12}$$

It is easy to show that this condition is automatically satisfied (Problem 12.3). Consequently, when k_0 coincides with a resonant value, (12.10) determines $\mathbf{J}_S$ to within a multiple of $(\mathbf{u}_n \times \mathbf{h}_m)$. This indeterminacy has no influence on the scattered field because, from (12.11), the fields associated with $\mathbf{u}_n \times \mathbf{h}_m$ vanish outside V_1. But the consequences for the numerical determination of $\mathbf{J}_S$ are serious and cannot be ignored. Suitable remedies are briefly discussed in Section 12.2. In the *discretized* version of (12.10), the difficulties are also present, compounded with numerical and truncation errors, leading to highly ill-conditioned matrices in the vicinity of resonances. The problem worsens as the frequency increases, because a higher frequency implies a higher density of modes. Another difficulty arises at *low* frequencies, way below the first resonance.[3] As $\omega \to 0$, the inductive part in (12.3) becomes progressively insignificant with respect to its capacitive counterpart. The problem therefore becomes quasi-electrostatic, and its solution tends to produce $\text{div}_S\, \mathbf{J}_S$ instead of $\mathbf{J}_S$. Because the tangential vector $\mathbf{J}_S$ can be split, in Helmholtz fashion, as

$$\mathbf{J}_S = \text{grad}_S\, \phi + \mathbf{u}_n \times \text{grad}_S\, \psi \tag{12.13}$$

a knowledge of $\text{div}_S\, \mathbf{J}_S$ only gives the *longitudinal* term $\text{grad}_S\, \phi$, obtained by solving

$$\nabla_S^2 \phi(\mathbf{r}) = \text{div}_S\, \mathbf{J}_S(\mathbf{r}) \qquad (\mathbf{r} \text{ on } S). \tag{12.14}$$

Note that the Helmholtz splitting can serve to generate efficient iterative solvers, which remain performant down to very low frequencies[4] [183]. The low-frequency region, extensively dealt with in Chapter 13, is of fundamental interest, not only for power applications but also for techniques such as the electromagnetic prospection of underground layers of oil, where the desired large penetration depths require the use of very low frequencies.

[†]Note that the tangent vector $(\mathbf{u}_n \times \mathbf{h}_m)$ is proportional to the surface current associated with the mth resonant mode.

12.1.2 Transient Fields

The potential-based functional equation

$$-\mathbf{e}^{sc}_{\tan}(\mathbf{r}) = \left(\frac{\partial \mathbf{a}}{\partial t} + \text{grad}\,\phi\right)_{\tan} = \mathbf{e}^{i}_{\tan} \qquad (\mathbf{r} \text{ on } S) \tag{12.15}$$

gives rise, in view of (7.33) and (7.34), to the time-dependent EFIE

$$\left[\frac{\mu_0}{4\pi}\frac{\partial}{\partial t}\int_S \frac{\mathbf{j}_S(\mathbf{r}',\tau)}{|\mathbf{r}-\mathbf{r}'|}\,dS' + \text{grad}\,\frac{1}{4\pi\epsilon_0}\int_S \frac{\rho_S(\mathbf{r}',\tau)}{|\mathbf{r}-\mathbf{r}'|}\,dS'\right]_{\tan} = \mathbf{e}^{i}_{\tan}(\mathbf{r},t), \tag{12.16}$$

where τ is the *retarded time*

$$\tau = t - \frac{|\mathbf{r}-\mathbf{r}'|}{c_0}. \tag{12.17}$$

With the notation

$$\frac{\partial f(\tau)}{\partial \tau} = \left[\frac{\partial f(t)}{\partial t}\right]_{t=\tau} \tag{12.18}$$

a few steps lead to [62]

$$\frac{1}{4\pi}\mathbf{u}_n(\mathbf{r}) \times \lim_{\delta\to 0}\int_{S-S_\delta}\left[\frac{\mu_0}{|\mathbf{r}-\mathbf{r}'|}\frac{\partial \mathbf{j}_S(\mathbf{r}',\tau)}{\partial \tau} - \frac{1}{\epsilon_0}\rho_S(\mathbf{r}',\tau)\frac{\mathbf{r}-\mathbf{r}'}{|\mathbf{r}-\mathbf{r}'|^3}\right.$$
$$\left. -R_{c0}\frac{\partial \rho_S(\mathbf{r}',\tau)}{\partial \tau}\frac{\mathbf{r}-\mathbf{r}'}{|\mathbf{r}-\mathbf{r}'|^3}\right] dS' = \mathbf{u}_n(\mathbf{r}) \times \mathbf{e}^{i}(\mathbf{r},t). \tag{12.19}$$

Note that cross-multiplying with $\mathbf{u}_n(\mathbf{r})$ has the sole purpose of extracting the tangential component of both members of the equation. In solving the integral equation, difference approximations are used for the time derivatives. Thus, dividing the time axis in equal intervals Δt, and writing $t_i = i\Delta t$, (12.15) becomes[5]

$$\left[\frac{\mathbf{a}(\mathbf{r},t_i) - \mathbf{a}(\mathbf{r},t_{i-1})}{\Delta t} + \frac{\text{grad}\,\phi(\mathbf{r},t_i) + \text{grad}\,\phi(\mathbf{r},t_{i-1})}{2}\right]_{\tan} = \mathbf{e}^{i}_{\tan}(\mathbf{r},t_{i-\frac{1}{2}}), \tag{12.20}$$

where the central finite difference scheme is used for the time derivative of $\mathbf{a}$, and time averaging for the scalar potential term. The space dependence of $\mathbf{j}_S$ is introduced by inserting a summation

$$\mathbf{j}_S(\mathbf{r},t) = \sum_{n=1}^{N}\sum_{m=1}^{M} A_{nm}\mathbf{f}_n(\mathbf{r})T_m(t)$$

into (12.19), where the $\mathbf{f}_n$ are suitable basis vectors[6,7,8] (see Section 12.4). Illustratively, Figure 12.2 shows the backscattered field from a sphere of diameter 2 m, immersed in the incident field of a Gaussian pulse of width 4 light-meters.‡ The solid line is the Mie

‡The *light-meter* is a time unit, equal to the time it takes light to cover a distance of 1 m in vacuum. Thus, 1 ns = 0.3 LM.

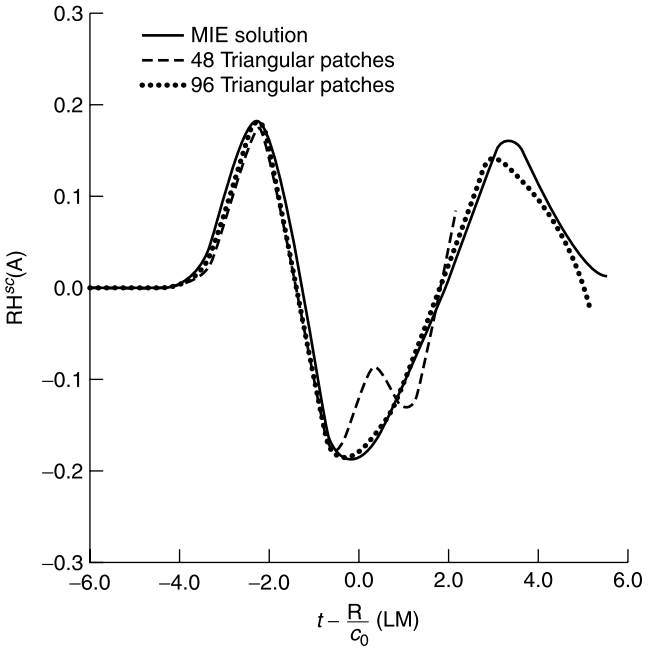

Figure 12.2 Backscattered field from a sphere (from S. M. Rao and D. R. Wilton, Transient scattering by conducting surfaces of arbitrary shape, *IEEE Trans. AP* **39**, 56–61, 1991, with permission of IEEE).

solution, obtained by separation of variables in the frequency domain, and subsequently Fourier transformed to the time domain. The numerical solution by means of the EFIE is characterized by late-time instabilities.[9] These are displayed in Figure 12.3, which shows the field backscattered from a pair of parallel square plates (side a, separation a). The late-time instability results from the growing "beating" interference between two resonances

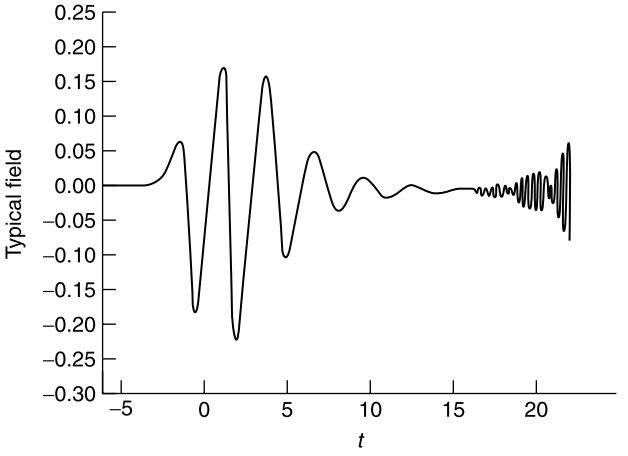

Figure 12.3 Backscattered field from parallel plates (from B. P. Rynne and P. D. Smith, Stability of time marching algorithms for the electric field integral equation, *J. Electromagn. Waves Appl.* **4**, 1181–1205, 1990, with permission of Brill N.V.).

of the plate structure.[10] The unstable tail can be eliminated by taking a weighted average across three time-steps, or by space averaging the value of $\mathbf{J}_S(\mathbf{r})$ over the centroids of the adjacent subareas. A four-step average has been found necessary for closed bodies with internal resonances.[11] Implicit methods offer a way to solve the instability problem. In an *explicit* approach, the time step Δt is at most equal to $(R_{\min}/c_0)$, where $R_{\min}$ is the minimum spatial sampling interval. At each time step, each unknown value can then be written in terms of values determined at previous steps. The size of the time-step, however, becomes unnecessarily small when the spatial mesh is refined over *portions* of the scatterer where fast variations are expected. In an *implicit* scheme, on the other hand, one may take $\Delta t > (R_{\min}/c_0)$, but interactions between adjacent fields and sources will take place. Advancing the solution from time-step i to step $i+1$ now requires the solution of a matrix problem [110].

12.2 THE MAGNETIC FIELD INTEGRAL EQUATION

The magnetic field generated by the induced currents is given by (7.124). If we introduce the operator $\mathbf{M}$, defined by

$$\begin{aligned}\mathbf{M}(\mathbf{f}) &= \operatorname{curl} \int_V \mathbf{f}(\mathbf{r}') \frac{e^{-jk_0|\mathbf{r}-\mathbf{r}'|}}{4\pi|\mathbf{r}-\mathbf{r}'|}\, dV' \\ &= \int_V \operatorname{grad} \frac{e^{-jk_0|\mathbf{r}-\mathbf{r}'|}}{4\pi|\mathbf{r}-\mathbf{r}'|} \times \mathbf{f}(\mathbf{r}')\, dV' \;=\; \int_V \mathbf{f}(\mathbf{r}') \times \operatorname{grad}' \frac{e^{-jk_0|\mathbf{r}-\mathbf{r}'|}}{4\pi|\mathbf{r}-\mathbf{r}'|}\, dV',\end{aligned} \tag{12.21}$$

the scattered field can be written as

$$\mathbf{H}^{sc}(\mathbf{r}) = \mathbf{M}(\mathbf{J}_S) = \frac{1}{4\pi} \int_S \mathbf{J}_S(\mathbf{r}') \times \operatorname{grad}' \left(\frac{e^{-jk_0|\mathbf{r}-\mathbf{r}'|}}{|\mathbf{r}-\mathbf{r}'|} \right) dS'. \tag{12.22}$$

We shall need the limit of the tangential component of this expression when $\mathbf{r}$ approaches S; that is, when P_1 and P_2 approach P (Fig. 12.1*a*). The answer is provided by the important relationship [201]

$$\begin{aligned}&\mathbf{u}_n(\mathbf{r}_0) \times \lim_{\mathbf{r}\to\mathbf{r}_0} \int_S \mathbf{a}_t(\mathbf{r}') \times \operatorname{grad}' \phi\,(\mathbf{r}_0|\mathbf{r}')\, dS' \\ &\quad = \pm 2\pi\, \mathbf{a}_t(\mathbf{r}_0) + \mathbf{u}_n(\mathbf{r}_0) \times \lim_{\delta\to 0} \int_{S-S_\delta} \mathbf{a}_t(\mathbf{r}') \times \operatorname{grad}' \phi\,(\mathbf{r}_0|\mathbf{r}')\, dS\end{aligned} \tag{12.23}$$

where $\mathbf{r}_0$ refers to P, ϕ stands for $e^{-jk_0|\mathbf{r}-\mathbf{r}'|}|\mathbf{r}-\mathbf{r}'|^{-1}$, the $(+)$ sign corresponds with the approach $P_2 \to P$, and the $(-)$ sign to the approach $P_1 \to P$. Equation (12.23), which can readily be derived from (6.23) and (6.24) (Problem 12.5), is valid for a tangential vector $\mathbf{a}_t$.

It leads to[§]

$$\lim_{P_1\to P}\mathbf{H}^{sc}_{\tan}(\mathbf{r}) = -\left[\frac{1}{2}\mathbf{J}_S\times\mathbf{u}_n\right]_P + \lim_{\delta\to 0}\left[\int_{S-S_\delta}\mathbf{J}_S(\mathbf{r}')\times\operatorname{grad}'\left(\frac{e^{-jk_0|\mathbf{r}-\mathbf{r}'|}}{4\pi|\mathbf{r}-\mathbf{r}'|}\right)dS'\right]_{\tan} \tag{12.24}$$

$$\lim_{P_2\to P}\mathbf{H}^{sc}_{\tan}(\mathbf{r}) = \left[\frac{1}{2}\mathbf{J}_S\times\mathbf{u}_n\right]_P + \lim_{\delta\to 0}\left[\int_{S-S_\delta}\mathbf{J}_S(\mathbf{r}')\times\operatorname{grad}'\left(\frac{e^{-jk_0|\mathbf{r}-\mathbf{r}'|}}{4\pi|\mathbf{r}-\mathbf{r}'|}\right)dS'\right]_{\tan} \tag{12.25}$$

where S_δ is a small area of arbitrary shape centered on P. The boundary condition

$$\lim_{P_2\to P}\mathbf{H}(\mathbf{r}) = \mathbf{H}^i_{\tan}(P) + \lim_{P_2\to P}\mathbf{H}^{sc}_{\tan}(\mathbf{r}) = (\mathbf{J}_S\times\mathbf{u}_n)_P$$

leads to the *integral equation*

$$\mathbf{N}(\mathbf{J}_S) = \mathbf{J}_S(\mathbf{r}) - \mathbf{u}_n(\mathbf{r})\times\lim_{\delta\to 0}\int_{S-S_\delta}\mathbf{J}_S(\mathbf{r}')\times\operatorname{grad}'\left(\frac{e^{-jk_0|\mathbf{r}-\mathbf{r}'|}}{2\pi|\mathbf{r}-\mathbf{r}'|}\right)dS' = 2\mathbf{u}_n(\mathbf{r})\times\mathbf{H}^i(\mathbf{r}) \tag{12.26}$$

for $\mathbf{r}$ on S. It is instructive to rewrite this equation as

$$\mathbf{J}_S(\mathbf{r}) = 2\mathbf{u}_n(\mathbf{r}\times\mathbf{H}^i(\mathbf{r})) + \mathbf{u}_n(\mathbf{r})\times\text{the integral.} \tag{12.27}$$

The first term, $2\mathbf{u}_n\times\mathbf{H}^i$, is the current density induced on the illuminated side of a perfectly conducting *plane*, hence the integral may be interpreted as a curvature effect.

12.2.1 Uniqueness of the Solution

Integral equation (12.26) is of the second kind, and its solution should be discussed in the light of Fredholm's alternative. We shall use a Hilbert scalar product [46, 193]

$$\langle\mathbf{a},\mathbf{b}\rangle = \int_S \mathbf{a}\cdot\mathbf{b}^*\,dS.$$

With respect to this product, and according to (1.88), the adjoint operator of $\mathbf{N}(\mathbf{f}_S)$ takes the form

$$\mathbf{N}^a(\mathbf{f}_S) = \mathbf{f}_S(\mathbf{r}) + \mathbf{u}_n(\mathbf{r})\times\lim_{\delta\to 0}\int_{S-S_\delta}\mathbf{f}_S(\mathbf{r}')\times\operatorname{grad}'\left(\frac{e^{+jk_0|\mathbf{r}-\mathbf{r}'|}}{2\pi|\mathbf{r}-\mathbf{r}'|}\right)dS'. \tag{12.28}$$

If the homogeneous equation $\mathbf{N}^a(\mathbf{f}_S) = 0$ has a nonzero solution, the homogeneous equation $\mathbf{N}(\mathbf{J}_S) = 0$ will also have a solution, which may be interpreted as an eigenvector with

[§]The factor $\frac{1}{2}$ holds when S_δ is plane. When it is a part of a strongly curved part of S, in particular when it contains an edge, the factor becomes $(\Omega/4\pi)$, where Ω is the solid angle under which S_δ is "seen" as P approaches the edge. See, for example, Note 12.

eigenvalue zero (the null space of $\mathbf{N}$). We shall now show that $\mathbf{u}_n \times \mathbf{h}_m$ (a real vector) is a solution of $\mathbf{N}^a(\mathbf{u}_n \times \mathbf{h}_m) = 0$, or, equivalently, of $[\mathbf{N}^a(\mathbf{u}_n \times \mathbf{h}_m]^* = 0$. Written in full, this condition is

$$[\mathbf{N}^a(\mathbf{f}_S)]^* = \mathbf{f}_S^*(\mathbf{r}) + \mathbf{u}_n(\mathbf{r}) \times \lim_{\delta \to 0} \int_{S-S_\delta} \mathbf{f}_S^*(\mathbf{r}') \times \text{grad}' \left(\frac{e^{-jk_0|\mathbf{r}-\mathbf{r}'|}}{2\pi|\mathbf{r}-\mathbf{r}'|} \right) dS' = 0. \quad (12.29)$$

Applying A1.40 to $G_0(\mathbf{r}|\mathbf{r}')$ and $\mathbf{h}_m(\mathbf{r})$ shows that, for $\mathbf{r}$ in V_1,

$$\mathbf{h}_m(\mathbf{r}) = \int_S \left[\mathbf{h}_m(\mathbf{r}') \times \mathbf{u}_n(\mathbf{r}') \right] \times \text{grad}' \left(\frac{e^{-jk_m|\mathbf{r}-\mathbf{r}'|}}{4\pi|\mathbf{r}-\mathbf{r}'|} \right) dS'.$$

Letting $\mathbf{r}$ approach the surface from inside gives, from (12.23),

$$\lim_{P_1 \to P} \mathbf{h}_m(\mathbf{r}) = \frac{1}{2}\mathbf{u}_n \times (\mathbf{h}_m \times \mathbf{u}_n) + \lim_{\delta \to 0} \int_{S-S_\delta} \left[\mathbf{h}_m(\mathbf{r}') \times \mathbf{u}_n(\mathbf{r}') \right] \times \text{grad}' \left(\frac{e^{-jk_m|\mathbf{r}-\mathbf{r}'|}}{4\pi|\mathbf{r}-\mathbf{r}'|} \right) dS'. \quad (12.30)$$

This is precisely (12.29) if one sets $\mathbf{f}_S^* = \mathbf{h}_m \times \mathbf{u}_n$. The usual alternative now holds, but because it can be shown that a solution exists [193], we may conclude that (12.26) has an infinite number of solutions for $k_0 = k_m$, all of which differ by a multiple of the solution of the homogeneous equation $\mathbf{N}(\mathbf{J}_S) = 0$. Note that this solution does not coincide with the solution $\mathbf{u}_n \times \mathbf{h}_m$ of the homogeneous EFIE. Furthermore, the associated $\mathbf{J}_S$ *radiates* outside S, which implies that the indeterminacy *must* be lifted if the scattered fields are to be evaluated correctly.

The use of the MFIE is restricted to closed surfaces,[9] a limitation that does not apply to the EFIE. Equation (12.26) shows that the integrand of the MFIE contains the cross-product $\mathbf{J}_S \times \text{grad}' G_0(\mathbf{r}|\mathbf{r}')$, where $\text{grad}' G$ is parallel to the direction connecting $\mathbf{r}'$ to $\mathbf{r}$. It follows that this cross-product is almost zero for a straight wire, because $\mathbf{J}_S$ and the gradient are almost parallel in that case. This situation is a source of numerical instability. The form of (12.10), on the other hand, shows that the EFIE does not suffer from the same limitation and is therefore better suited to elongated scatterers.

12.2.2 Transient Fields

The current density $\mathbf{j}_S(\mathbf{r}, t)$ satisfies the integral equation[13] [62, 193]

$$\mathbf{j}_S(\mathbf{r}, t) - \frac{1}{2\pi}\mathbf{u}_n(\mathbf{r}) \times \lim_{\delta \to 0} \int_{S-S_\delta} \left[\frac{1}{c_0} \frac{\partial}{\partial \tau} \mathbf{j}_S(\mathbf{r}', \tau) + \frac{\mathbf{j}_S(\mathbf{r}', \tau)}{|\mathbf{r}-\mathbf{r}'|} \right] \times \frac{\mathbf{r}-\mathbf{r}'}{|\mathbf{r}-\mathbf{r}'|^2} \, dS' = 2\mathbf{u}_n(\mathbf{r}) \times \mathbf{h}^i(\mathbf{r}, t) \quad (12.31)$$

for $\mathbf{r}$ on S. The kernel has spatial singularities of the order of respectively $|\mathbf{r}-\mathbf{r}'|^{-1}$ and $|\mathbf{r}-\mathbf{r}'|^{-2}$, which require a careful evaluation of the self-patch contribution.[14,15] As in the case of the EFIE, the solution nearly always becomes unstable as time progresses. The origin of the oscillations has been attributed to the interior resonances, whose influence can be eliminated by methods to be discussed next.[16,17,18]

12.2.3 Avoiding the Resonance Problem

Several schemes have been proposed to avoid the difficulties associated with the interior resonances. We enumerate some of these concisely.

1. In a first method, the EFIE and the MFIE are replaced by a *combined field integral equation*

$$\alpha\, j\omega\mu_0\, \mathbf{L}_t(\mathbf{J}_S) + (1-\alpha) R_{c0} \mathbf{N}_t(\mathbf{J}_S) = \alpha \mathbf{E}^i_{\tan} + (1-\alpha) R_{c0} \mathbf{u}_n \times \mathbf{H}^i. \qquad (12.32)$$

   Because the solutions of the homogeneous equations $\mathbf{L}(\mathbf{J}_S) = 0$ and $\mathbf{N}(\mathbf{J}_S) = 0$ are different for $k_0 = k_m$, neither of these will be a solution of the homogeneous CFIE at that frequency. Note that the CFIE has a unique solution provided the real part of α differs from zero [193]. The equation has the drawback of requiring a special treatment when the scatterer is axisymmetric. In addition, the matrix elements resulting from the discretization of the CFIE require more computation time than those of the original EFIE or MFIE.

2. It may be shown[2] that the electric field resulting from the solution of the MFIE does not automatically respect the condition $\mathbf{E}_{\tan} = 0$ on S. The situation may be straightened out by *augmenting* that equation by means of the condition

$$\mathbf{u}_n \cdot \mathbf{H} = -\frac{1}{j\omega\mu_0}\, \mathbf{u}_n \cdot \text{curl}\, \mathbf{E} = -\frac{1}{j\omega\mu_0}\, \text{div}_S\, (\mathbf{E} \times \mathbf{u}_n) = 0 \qquad (\text{on } S). \qquad (12.33)$$

   Similarly, the solution of the EFIE does not automatically respect the condition $\mathbf{H}_{\tan} = \mathbf{J}_S \times \mathbf{u}_n$ on S. There again, the remedy consists in adding a supplementary condition, viz.

$$\mathbf{u}_n \cdot \mathbf{E} = \frac{\rho_S}{\epsilon_0} = -\frac{1}{j\omega\epsilon_0}\, \text{div}_S\, \mathbf{J}_S. \qquad (12.34)$$

   Note that the added condition transforms the EFIE into an integro-differential equation of the second kind, which may be more amenable to a stable numerical solution than the original one.

3. In the *extended boundary condition method*, the total fields, sum of the incident and disturbance parts, are constrained to vanish at all points $\mathbf{r}_i$ of the interior volume V_1 [198]. In mathematical terms, the condition implies, from (12.1) and (12.22), that

$$\begin{aligned} j\omega\mu_0\, \mathbf{L}(\mathbf{J}_S) &= \mathbf{E}^i(\mathbf{r}_i) \\ -\mathbf{M}(\mathbf{J}_S) &= \mathbf{H}^i(\mathbf{r}_i). \end{aligned} \qquad (12.35)$$

   Requirement (12.35) should actually be satisfied for all $\mathbf{r}_i$. It is sufficient, however, to involve only the points of an interior *surface* S^d parallel to the actual surface S and at a small distance d from the latter. Let $\mathbf{r}^d$ denote the point on S^d that corresponds with a point $\mathbf{r}$ on S. If we multiply (12.35) with $\mathbf{u}_n(\mathbf{r})$, and add the result to the

original EFIE and MFIE, we obtain the dual surface equations[19,20,21]

$$\mathbf{u}_n(\mathbf{r}) \times \mathbf{E}^{id}(\mathbf{r}) = \mathbf{u}_n(\mathbf{r}) \times \frac{1}{j\omega\epsilon_0} \int_S \Big[k_0^2 \mathbf{J}_S(\mathbf{r}')\, G_0^d(\mathbf{r}, \mathbf{r}') - \operatorname{div}'_S \mathbf{J}_S(\mathbf{r}') \operatorname{grad}' G_0^d(\mathbf{r}|\mathbf{r}') \Big]\, dS' \tag{12.36}$$

$$\mathbf{u}_n(\mathbf{r}) \times \mathbf{H}^{id}(\mathbf{r}) = \frac{1}{2}\mathbf{J}_S(\mathbf{r}) + \mathbf{u}_n(\mathbf{r}) \times \int_S \mathbf{J}_S(\mathbf{r}') \times \operatorname{grad}' G_0^d(\mathbf{r}, \mathbf{r}')\, dS', \tag{12.37}$$

where $\mathbf{r}$ is on S, and

$$\begin{aligned} \mathbf{E}^{id}(\mathbf{r}) &= \mathbf{E}^i(\mathbf{r}) + \alpha\, \mathbf{E}^i(\mathbf{r}^d) \\ \mathbf{H}^{id}(\mathbf{r}) &= \mathbf{H}^i(\mathbf{r}) + \alpha\, \mathbf{H}^i(\mathbf{r}^d) \\ G_0^d(\mathbf{r}|\mathbf{r}') &= G_0(\mathbf{r}|\mathbf{r}') + \alpha\, G_0(\mathbf{r}^d, \mathbf{r}'). \end{aligned} \tag{12.38}$$

The equations are identical in form with the original EFIE and MFIE and comparable in complexity. They have a unique solution at all frequencies provided α has an imaginary part, and $d < \lambda_0/2$. Note that the higher computation cost attached to the matrix elements may be reduced by imposing the null condition on a smaller interior surface.[22]

4. In an approach reminiscent of the multipole technique discussed in Section 5.7, a fictitious current $\mathbf{J}_S^K$ is assumed on a smooth surface S^K contained within interior volume V_1 (Fig. 12.1*a*). This current generates fields outside S^K, and in particular on S. At points of S, one now imposes the condition $\mathbf{E}(\mathbf{J}_S^K)_{\tan} = -\mathbf{E}^i_{\tan}$, which ensures uniqueness, and sees to it that $\mathbf{E}(\mathbf{J}_S^K)$ creates the correct scattered field outside S. Resonances associated with S^K will not coincide with the original ones and furthermore will not radiate fields outside S^K, leaving the scattered fields undisturbed.[23]

12.2.4 Scatterer with a Surface Impedance

When a target is perfectly conducting, the scattered fields can be found from the value of the induced current $\mathbf{J}_S = \mathbf{u}_n \times \mathbf{H}$ on S (Fig. 12.1*a*). From (12.1), the relevant formula is $\mathbf{E}^{sc} = -j\omega\mu_0\, \mathbf{L}(\mathbf{J}_S)$. If the sources are magnetic surface currents $\mathbf{J}_{mS}$, the radiated fields are the dual of (12.22). More specifically, from (7.107) and (7.109),

$$\mathbf{E}(\mathbf{r}) = -\operatorname{curl} \frac{1}{4\pi} \int_S \mathbf{J}_{mS}(\mathbf{r}') \frac{e^{-jk_0|\mathbf{r}-\mathbf{r}'|}}{|\mathbf{r}-\mathbf{r}'|}\, dS' = -\mathbf{M}(\mathbf{J}_{mS}).$$

The fields generated by the combination of the surface currents may now be written formally as

$$\mathbf{E}^{sc}(\mathbf{r}) = -j\omega\mu_0\, \mathbf{L}(\mathbf{J}_S) - \mathbf{M}(\mathbf{J}_{mS}) \tag{12.39}$$

and

$$\mathbf{H}^{sc}(\mathbf{r}) = \mathbf{M}(\mathbf{J}_S) - j\omega\epsilon_0\, \mathbf{L}(\mathbf{J}_{mS}). \tag{12.40}$$

An important simplification occurs when the scatterer is characterized by an impedance boundary condition. For such a case, from (11.141),

$$\begin{aligned} \mathbf{E}_{\tan} &= Z_S \mathbf{J}_S = \mathbf{u}_n \times \mathbf{J}_{mS} \\ \mathbf{H}_{\tan} &= \frac{1}{Z_S} \mathbf{J}_{mS} = \mathbf{J}_S \times \mathbf{u}_n. \end{aligned} \tag{12.41}$$

The fields can now be expressed in terms of *either* $\mathbf{J}_S$ or $\mathbf{J}_{mS}$. For example:

$$\mathbf{E}^{sc}(\mathbf{r}) = j\omega\mu_0 \mathbf{L}\mathbf{J}_S - \mathbf{M}[Z_S \mathbf{J}_S \times \mathbf{u}_n]. \tag{12.42}$$

By letting $\mathbf{r}$ approach a point on the surface S, and applying the methods leading to the EFIE and the MFIE, one arrives at the integro-differential equation[24,25]

$$\begin{aligned} -\mathbf{E}^i_{\tan} = \mathbf{E}^{sc}_{\tan} = &\left[+j\omega\mu_0 \int_S \mathbf{J}_S(\mathbf{r}')\, G_0(\mathbf{r}|\mathbf{r}')\, dS' \right]_{\tan} \\ &- \frac{1}{j\omega\epsilon_0} \operatorname{grad}_S \int_S \operatorname{div}' \mathbf{J}_S(\mathbf{r}')\, G_0(\mathbf{r}|\mathbf{r}')\, dS' \\ &+ \frac{1}{2} Z_S(\mathbf{r}_S)\, \mathbf{J}_S(\mathbf{r}_S) + \lim_{\delta \to 0} \left[\int_{S-S_\delta} Z_S(\mathbf{r}')\, (\mathbf{J}_S \times \mathbf{u}'_n) \times \operatorname{grad}' G_0(\mathbf{r}|\mathbf{r}')\, dS' \right]_{\tan}, \end{aligned} \tag{12.43}$$

where G_0 is the Green's function of free space. The corresponding equation for a perfect conductor — which is (12.10) — follows by setting $Z_S = 0$. When the scatterer is a good conductor, (Z_S/R_{c0}) is small, and the equation can be solved iteratively, starting from the surface current $\mathbf{J}_S = \mathbf{u}_n \times \mathbf{H}_0$ on the scatterer, assumed perfectly conducting.[26] The initial value of $\mathbf{E}_{\tan}$ is zero, but a first-order correction can be obtained by setting

$$\mathbf{E}_{\tan} = Z_S(\mathbf{u}_n \times \mathbf{H}_0) = Z_S \mathbf{J}_S.$$

The fields associated with this tangential component can be evaluated by the methods discussed in Section 12.1. When a perfectly conducting scatterer is *coated*, the appropriate Z_S can be evaluated according to the formulas derived in Section 11.7. A coating of high ϵ_r and small thickness l, for example, is characterized[¶] by an admittance[28,29] $Y_S = Z_S^{-1} = jk_0 l\, R_{c0}^{-1}(\epsilon_r - 1)$.

12.3 THE T-MATRIX

The application of the *T-matrix method* to potential problems is briefly discussed in Section 3.12. The main idea is to expand an incident potential ϕ^i in terms of spherical harmonics, and to write[30]

$$\phi^i = \sum_{\sigma,m,n} B_{\sigma mn} Y_{\sigma mn}(\theta, \varphi) \left(\frac{R}{a} \right)^n.$$

[¶]For the effect of a multilayered coating, see Note 27.

In the (σ, m, n) index, m goes from 0 to n, n from 0 to ∞ and σ is o or e (odd or even). The additional potential due to the obstacle admits a similar expansion

$$\phi^d = \sum_{\sigma,m,n} A_{\sigma mn} Y_{\sigma mn}(\theta, \varphi) \left(\frac{a}{R}\right)^{n+1},$$

valid outside a sphere of radius a. The A and B coefficients, grouped into vectors, are linearly related by

$$\mathbf{A} = \overline{\overline{\mathbf{T}}} \cdot \mathbf{B}.$$

The *transition matrix* $\overline{\overline{T}}$ is a characteristic of the obstacle alone and is independent of the incident potential; it can therefore be used with any kind of ϕ^i. In this section, we shall discuss the extension of the method to time-harmonic fields, and in particular to perfectly conducting scatterers[30] [197]. The basic unknown $\mathbf{J}_S$ is determined by a null-field principle (i.e., by requiring the total field $\mathbf{E} = \mathbf{E}^i + \mathbf{E}^J$ to vanish inside the scatterer). By expressing $\mathbf{E}^J$ — the field generated by $\mathbf{J}_S$ — in terms of the vector potential $\mathbf{A}$, the condition becomes, from (7.107),

$$\mathbf{E}^J = \frac{1}{j4\pi\omega\epsilon_0} \operatorname{curl}\operatorname{curl} \int_S \mathbf{J}_S(\mathbf{r}') \frac{e^{-jk_0|\mathbf{r}-\mathbf{r}'|}}{|\mathbf{r}-\mathbf{r}'|} dS' = -\mathbf{E}^i(\mathbf{r}), \tag{12.44}$$

where $\mathbf{r}$ is in V_1 (Fig. 12.1). Both $\mathbf{J}_S$ and $\mathbf{E}^i$ should now be expanded in spherical harmonics. The calculations are lengthy, and only the main steps will be outlined. Some relationships, however, are given in extenso, because they are of general use in mathematical physics. In (12.44), for example, $\mathbf{J}_S(\mathbf{r}')$ will be written as $\overline{\overline{I}} \cdot \mathbf{J}_S(\mathbf{r}')$, and the following important expansion will be used [165]:

$$\frac{e^{-jk_0|\mathbf{r}-\mathbf{r}'|}}{|\mathbf{r}-\mathbf{r}'|} \overline{\overline{I}} = -jk_0 \sum_{n=0}^{\infty} \frac{2n+1}{n(n+1)} \sum_{m,\sigma} \epsilon_m \frac{(n-m)!}{(n+m)!} \Big[\mathbf{M}^1_{\sigma mn}(\mathbf{r}') \mathbf{M}^3_{\sigma mn}(\mathbf{r}) + \mathbf{N}^1_{\sigma mn}(\mathbf{r}') \mathbf{N}^3_{\sigma mn}(\mathbf{r}) + n(n+1) \mathbf{L}^1_{\sigma mn}(\mathbf{r}') \mathbf{L}^3_{\sigma mn}(\mathbf{r}) \Big]. \tag{12.45}$$

This expression is valid for $R > R'$. When $R < R'$, $\mathbf{r}$ and $\mathbf{r}'$ should be exchanged in the series. The eigenvectors $\mathbf{L}$, $\mathbf{M}$, $\mathbf{N}$ are defined in (7.200). Thus [165],

$$\begin{aligned}
\mathbf{L}^1_{\sigma mn}(\mathbf{r}) &= \frac{1}{k_0} \operatorname{grad} \left[Y_{\sigma mn}(\theta, \varphi) j_n(k_0 R) \right] \\
&= \frac{1}{k_0 R} j_n(k_0 R) \operatorname{grad}_1 Y^{(\theta,\varphi)}_{\sigma mn} + \frac{1}{k_0} \frac{d}{dR} [j_n(k_0 R)] Y_{\sigma mn}(\theta, \varphi) \mathbf{u}_R \\
\mathbf{M}^1_{\sigma mn}(\mathbf{r}) &= \operatorname{curl} [Y_{\sigma mn}(\theta, \varphi) j_n(k_0 R) \mathbf{r}] = j_n(k_0 R) \operatorname{grad}_1 Y_{\sigma mn}(\theta, \varphi) \times \mathbf{u}_R \\
\mathbf{N}^1_{\sigma mn}(\mathbf{r}) &= \frac{1}{k_0} \operatorname{curl} \mathbf{M}^1_{\sigma mn}(\mathbf{r}) = \frac{1}{k_0^2} \operatorname{curl}\operatorname{curl} \mathbf{N}^1_{\sigma mn}(\mathbf{r}).
\end{aligned} \tag{12.46}$$

In these expressions, $Y_{\sigma mn}$ denotes $P^m_n(\cos\theta)\cos m\varphi$ or $P^m_n(\cos\theta)\sin m\varphi$ (see Appendix 9). The eigenvectors with superscript 3 are obtained by substituting $h^{(2)}_n(k_0 R)$ for $j_n(k_0 R)$.

Also of general use are the vectors

$$\begin{aligned}\mathbf{B}_{\sigma mn}(\theta,\varphi) &= [n(n+1)]^{-\frac{1}{2}}\ \mathrm{grad}_1\, Y_{\sigma mn}(\theta,\varphi)\\ \mathbf{C}_{\sigma mn}(\theta,\varphi) &= [n(n+1)]^{-\frac{1}{2}}\ \mathrm{grad}_1\, Y_{\sigma mn}(\theta,\varphi)\times\mathbf{u}_R\\ \mathbf{P}_{\sigma mn}(\theta,\varphi) &= Y_{\sigma mn}(\theta,\varphi)\mathbf{u}_R.\end{aligned}\tag{12.47}$$

They are needed for the expansion in spherical harmonics of the fields of the incident plane wave

$$\mathbf{E}^i(\mathbf{r}) = \mathbf{e}^i e^{-jk_0\mathbf{u}_i\cdot\mathbf{r}} = \mathbf{e}^i e^{-j\mathbf{k}^i\cdot\mathbf{r}}.\tag{12.48}$$

Here the exponential can be represented by the series [165]

$$\begin{aligned}e^{-jk_0\mathbf{u}_i\cdot\mathbf{r}}\bar{\bar{I}} = \sum_{\sigma mn}\epsilon_m\frac{1}{j^n}\frac{(n-m)!}{(n+m)!}\Bigg\{&j\mathbf{P}_{\sigma mn}(\theta_i,\varphi_i)\mathbf{L}^1_{\sigma mn}(\mathbf{r})\\ &+\frac{1}{\sqrt{n(n+1)}}\Big[\mathbf{C}_{\sigma mn}(\theta_i,\varphi_i)\mathbf{M}^1_{\sigma mn}(\mathbf{r})+j\mathbf{B}^e_{mn}(\theta_i,\varphi_i)\mathbf{N}^1_{\sigma mn}(\mathbf{r})\Big]\Bigg\}\end{aligned}\tag{12.49}$$

where θ_i and φ_i are the angles characterizing the direction of incidence $\mathbf{u}_i$. For a wave incident along the z-axis, in particular,

$$\begin{aligned}e^{-jk_0z}\bar{\bar{I}} = \sum_{n=0}^{\infty}\frac{2n+1}{j^n n(n+1)}\Big\{&\mathbf{u}_x\Big[\mathbf{M}^1_{o1n}(\mathbf{r})+j\mathbf{N}^1_{e1n}(\mathbf{r})\Big]\\ &+\mathbf{u}_y\Big[\mathbf{M}^1_{e1n}-j\mathbf{N}^1_{o1n}(\mathbf{r})\Big]+j\mathbf{u}_z n(n+1)\mathbf{L}^1_{eon}(\mathbf{r})\Big\}.\end{aligned}\tag{12.50}$$

After these preliminaries, we now introduce (12.45) into the left-hand term of the null-field condition (12.44) and (12.49) into the right-hand term. It is sufficient to impose this condition inside a sphere v of center O, located inside the scatterer, and with radius equal to the distance from O to the nearest point of S. For such a case, the left-hand term will, after integration, contain terms in $\mathbf{L}^1_{\sigma mn}(\mathbf{r})$, $\mathbf{M}^1_{\sigma mn}(\mathbf{r})$, and $\mathbf{N}^1_{\sigma mn}(\mathbf{r})$. The same will be true for the right-hand term. Equating coefficients on both sides yields

$$\begin{aligned}\int_S dS\,\mathbf{J}_S(\mathbf{r})\cdot\mathbf{M}^3_{\sigma mn}(\mathbf{r}) &= \frac{4\pi}{j^{n+1}k_0^3}\sqrt{n(n+1)}\ \mathbf{e}^i\cdot\mathbf{C}_{\sigma mn}(\mathbf{k}^i)\\ \int_S dS\,\mathbf{J}_S(\mathbf{r})\cdot\mathbf{N}^3_{\sigma mn}(\mathbf{r}) &= \frac{4\pi}{j^{n+1}k_0^3}\sqrt{n(n+1)}\ \mathbf{e}^i\cdot\mathbf{B}_{\sigma mn}(\mathbf{k}^i)\end{aligned}\tag{12.51}$$

where $\mathbf{k}_i$ stands for (θ_i,φ_i). These relationships suggest[31] expanding $\mathbf{J}_S$ in terms of the tangential vectors $\mathbf{u}_n\times\mathbf{M}^3_{\sigma mn}$ and $\mathbf{u}_n\times\mathbf{N}^3_{\sigma mn}$, which form a complete set on S. Thus,[‖]

$$\mathbf{J}_S(\mathbf{r}) = \frac{4j}{k_0}\sum_{\sigma mn}\Big[a_{\sigma mn}\mathbf{u}_n(\mathbf{r})\times\mathbf{N}^3_{\sigma mn}(\mathbf{r})+b_{\sigma mn}\mathbf{u}_n(\mathbf{r})\times\mathbf{N}^3_{\sigma mn}(\mathbf{r})\Big].\tag{12.52}$$

[‖]The completeness property holds for a star-shaped surface; that is, a surface for which there exists an interior origin O such that the vector $R(\theta,\varphi)\mathbf{u}_R$ connecting O to arbitrary point on S is determined by a single-valued continuous function $R(\theta,\varphi)$.

Skipping the details, we note that the procedure leads to a matrix type of equation for the coefficients a and b, written concisely as [197]

$$\begin{aligned} \overline{\overline{M}} \cdot \mathbf{a} + \overline{\overline{N}} \cdot \mathbf{b} &= \mathbf{e}^i \cdot \overline{\overline{C}} \\ \overline{\overline{P}} \cdot \mathbf{a} + \overline{\overline{Q}} \cdot \mathbf{b} &= j\mathbf{e}^i \cdot \overline{\overline{B}} \end{aligned} \tag{12.53}$$

or even more concisely as

$$\begin{pmatrix} \mathbf{a} \\ \mathbf{b} \end{pmatrix} = \overline{\overline{D}} \cdot \begin{pmatrix} \mathbf{e}^i \cdot \overline{\overline{C}} \\ j\mathbf{e}^i \cdot \overline{\overline{B}} \end{pmatrix}. \tag{12.54}$$

Illustratively, a typical element of $\overline{\overline{M}}$ is

$$M_{pp'} = \frac{k_0^2}{\pi} \int_S \mathbf{u}_n \cdot \left[\mathbf{M}_p^3(\mathbf{r}) \times \mathbf{M}_{p'}^1(\mathbf{r}) \right] dS \tag{12.55}$$

where p stands for a collective index (σ, m, n). Analogous expressions hold for N_{pp}, P_{pp}, and Q_{pp}, involving respectively $\mathbf{M}^3 \times \mathbf{N}^1$, $\mathbf{N}^3 \times \mathbf{M}^1$, and $\mathbf{N}^3 \times \mathbf{N}^1$. The symbols $\overline{\overline{B}}$ and $\overline{\overline{C}}$ denote column matrices having, as elements, $(-j)^n\ [n(n+1)]^{\frac{1}{2}}\ \mathbf{B}_{\sigma mn}(\mathbf{k}^i)$ and $(-j)^n [n(n+1)]^{\frac{1}{2}}\ \mathbf{C}_{\sigma mn}(\mathbf{k}^i)$.

Solution of (12.53) produces the surface currents $\mathbf{J}_S$. The latter in turn generate a scattered field given by the left-hand term of (12.44). The far field, written in terms of the transverse vector $\mathbf{M}^3$ and $\mathbf{N}^3$, is of the general form [197]

$$\mathbf{E}^{sc}(\mathbf{r}) = 4 \sum_{\sigma mn} \left[f_{\sigma mn} \mathbf{M}_{\sigma mn}^3(\mathbf{r}) + g_{\sigma mn} \mathbf{N}_{\sigma mn}^3(\mathbf{r}) \right]. \tag{12.56}$$

The f and g coefficients are linearly related to the a and b. The connection, expressed in block matrix form, may be written concisely as

$$\begin{pmatrix} \mathbf{f} \\ \mathbf{g} \end{pmatrix} = \overline{\overline{K}} \cdot \begin{pmatrix} \mathbf{a} \\ \mathbf{b} \end{pmatrix}. \tag{12.57}$$

Relationships (12.54) and (12.57) may be combined into an expression giving $\mathbf{f}$ and $\mathbf{g}$ in terms of the incident (plane wave) fields directly, thus skipping the preliminary determination of $\mathbf{a}$ and $\mathbf{b}$ (i.e., of $\mathbf{J}_S$). Specifically,

$$\begin{pmatrix} \mathbf{f} \\ \mathbf{g} \end{pmatrix} = \overline{\overline{K}} \cdot \overline{\overline{D}} \cdot \begin{pmatrix} \mathbf{e}^i \cdot \overline{\overline{C}} \\ j\mathbf{e}^i \cdot \overline{\overline{B}} \end{pmatrix}. \tag{12.58}$$

A few additional remarks are of interest:

1. The method can serve to determine the eigenfrequencies of the interior volume of the scatterer. This is achieved by writing $\mathbf{e}^i = 0$ in (12.53) and setting the determinant of the matrix equal to zero.[32]
2. The method can be extended to the N-body problem, each scatterer being characterized by its own transition matrix.[33]

3. The method has also been successfully applied to dielectric scatterers, particularly in the preresonance frequency range, and for shapes that do not deviate too much from the sphere.[31,34,35]
4. A full study of the T-matrix formalism should include the convergence properties of the method,[36] as well as a discussion of the symmetry and unitarity properties of the matrices involved in the algorithm[37] [197].

12.4 NUMERICAL PROCEDURES

Discretization of integral equation (12.4) proceeds by expanding $\mathbf{J}_S$ in a truncated series

$$\mathbf{J}_S = \sum_{n=1}^{N} A_n \mathbf{f}_n(\mathbf{r}) \qquad (\mathbf{r} \text{ on } S). \tag{12.59}$$

Insertion of this series into (12.4) gives

$$\sum_{n=1}^{N} A_n [\mathbf{Z}(\mathbf{f}_n)]_{\tan} = \mathbf{E}^i_{\tan}(\mathbf{r}) \qquad (\mathbf{r} \text{ on } S). \tag{12.60}$$

Testing with vectors $\mathbf{w}_k$ yields, given a suitable scalar product, a linear system of equations

$$\sum_{n=1}^{N} A_n \langle \mathbf{Z}(\mathbf{f}_n), \mathbf{w}_k \rangle = \langle \mathbf{E}^i, \mathbf{w}_k \rangle = B_k \qquad (k = 1, \ldots, N). \tag{12.61}$$

In short:

$$\overline{\overline{Z}} \cdot \mathbf{A} = \mathbf{B}. \tag{12.62}$$

If we choose a symmetric scalar product

$$\langle \mathbf{a}, \mathbf{b} \rangle = \int_S \mathbf{a} \cdot \mathbf{b} \, dS.$$

$\overline{\overline{Z}}$ will be self-adjoint, and the Galerkin choice $\mathbf{w}_k = \mathbf{f}_k$ produces a symmetric matrix (Problem 12.2). Let $\mathbf{f}_k$ be a subdomain function on S_k. The matrix element

$$Z_{nk} = \langle \mathbf{Z}(\mathbf{f}_n), \mathbf{f}_k \rangle = \int_{S_k} \mathbf{Z}(\mathbf{f}_n) \cdot \mathbf{f}_k \, dS \tag{12.63}$$

expresses the mutual coupling of $\mathbf{f}_n$ and $\mathbf{f}_k$. It tends to decrease as the distance between S_n and S_k increases.

It is clear from these preliminary remarks that one should select

- An efficient type of $\mathbf{f}_n$, with an easy to evaluate Z_{nk}
- An efficient (and economical) way of solving the resulting matrix equation.

An extremely extensive bibliography exists on the subject, which is of general interest for many branches of physics, but evidences special aspects in its application to electromagnetism [131, 183, 193, 197, 198, 200, 203, 211, 212].

12.4.1 The Basis Functions

In the early history of the method, a grid model was often used to simulate a continuous surface. Figure 12.4*b* shows the application of this principle to a perfectly conducting circular plate. The elementary scatterer is a short piece of wire carrying a uniform (complex) current I on its surface. In cylindrical coordinates this current radiates an electric field (Fig. 12.4*a*)

$$E_r = rR_{c0}I\left[\frac{1+jk_0R}{4\pi jk_0}\frac{e^{-jkR}}{R^3}\right]_{R_1}^{R_2}$$

$$E_\varphi = 0 \tag{12.64}$$

$$E_z = \frac{R_{c0}I}{4\pi jk_0}\int_{-h}^{h}\left[2R^2(1+jk_0R)-(r^2+a^2)(3+3jk_0R-k_0^2R^2)\right]\frac{e^{-jk_0R}}{R^5}\,dz',$$

where

$$R = [r^2 + a^2 + (z-z')^2]^{\frac{1}{2}}.$$

The values R_1 and R_2 correspond respectively with $z' = -h$ and $z' = h$. A system of linear equations can now be generated by forcing the total tangential electric field to vanish at the center of each segment.[38] Other choices are possible, and the accuracy of the procedure will depend on factors such as the wire radius [193, 198] or the choice of points where the condition $\mathbf{E}_{\tan} = 0$ is enforced. These points are typically chosen[39,40] on the axis or on the outer surface of the wire. It is clear that the net should be sufficiently dense; five wires per λ_0 has been found satisfactory.

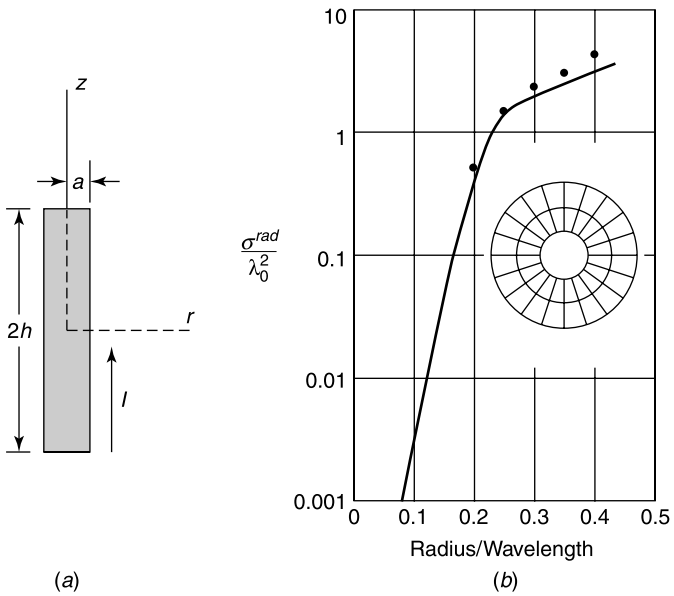

Figure 12.4 (*a*) Elementary wire segment. (*b*) Broadside scattering cross section of a thin circular plate: – measured, • calculated (from J. H. Richmond, A wire-grid model for scattering by conducting bodies, *IEEE Trans. AP* **14**, 782–786, 1966, with permission of IEEE).

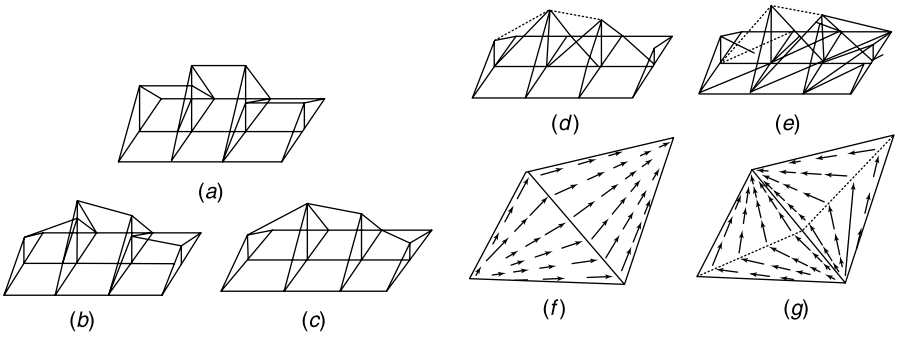

Figure 12.5 A few basis functions: (*a*) the rooftop, (*b*) the higher-order rooftop, (*c*) the transversely continuous higher order rooftop, (*d*) pyramids with rectangular bases, (*e*) pyramids with triangular bases, (*f*) the Rao-Wilton-Glisson rooftop, (*g*) the Jacobus and Landstorfer magnetic type (from L. Gürck, K. Sertel, and I. K. Sendur, On the choice of basis functions to model surface electric current densities in computational electromagnetics, *Radio Sci.* **34**, 1373–1387, 1999, with permission of the American Geophysical Union).

The limitations of the wire-grid model led to a strong interest in patch-modeling. There are numerous types of patches and associated basis functions.[41] Some of these are shown in Figure 12.5. The *RWG* (*Rao, Wilton, Glisson*) triangular rooftop function shown under (f) has many desirable features.[42,43] It has the advantage of using the versatile triangular patch in modeling arbitrarily shaped surfaces. It is also free of the fictitious line and point charges that would appear if the normal component of $\mathbf{J}_S$ were discontinuous across a surface edge. Analytically, the basis function is given by (Fig. 12.6)

$$\mathbf{f}_n = \begin{cases} \dfrac{l_n}{2A_n^+}\,\mathbf{r}_n^+ & (\mathbf{r} \text{ in } S_n^+) \\ \dfrac{l_n}{2A_n^-}\,\mathbf{r}_n^- & (\mathbf{r} \text{ in } S_n^-) \\ 0 & (\text{otherwise}). \end{cases} \tag{12.65}$$

The symbol A denotes the area of the corresponding surface. It is clear that $\mathbf{f}_n$ is tangential to the lateral edges, and that its component perpendicular to C_n is constant along C_n, and

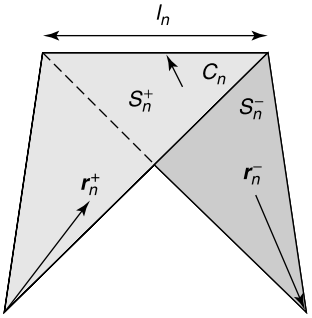

Figure 12.6 Triangle pair and geometrical parameters.

continuous across it. The surface divergence, which is needed for the EFIE, is given by

$$\operatorname{div}_S \mathbf{f}_n = \begin{cases} \dfrac{l_n}{A_n^+} & (\text{on } S_n^+) \\ -\dfrac{l_n}{A_n^-} & (\text{on } S_n^-). \end{cases} \tag{12.66}$$

The corresponding charge density is therefore constant in each triangle, and the total charge is zero, giving a dipole type of distribution.

The number of papers advocating possible new forms of basis functions is still growing. Some authors address the need to develop elements that take the curvature of the surface into account.[44,45,46,47] Other ones propose the use of entire-domain basis functions instead of subdomain functions.[48] Higher-order elements have also been proposed to improve the representation of fields and currents compared with conventional low-order elements. As mentioned in Section 10.3, a net can be adapted to improve the accuracy of the solution according to an error indicator.[49] In the *h*-type scheme, the mesh is refined, but the elements have a fixed order. In the *p*-type scheme, the mesh remains untouched, but convergence is achieved by increasing the polynomial order of the basis functions. A mixed $h - p$ type is also in use[50] [183]. Because in electromagnetism the curl of a vector is often as important as the vector itself, one may choose to represent the field as a polynomial of order p, and its curl by a polynomial of order $(p - 1)$, using separate representations for the irrotational and solenoidal parts of the field.[51]

12.4.2 Solving the Matrix Problem

The matrix $\overline{\overline{Z}}$ in (12.62) is a dense, fully populated matrix. For bodies large with respect to λ_0, the rank of the $N \times N$ matrix, and the number of matrix elements, become very large, because a good "feeling" of the phase and amplitude variation of $\mathbf{J}_S$ requires some 200 to 300 subdomains per λ_0^2. In a Gaussian elimination process, the number of required multiplications grows very fast, because it is $O(N^3)$. It therefore becomes essential to accelerate the solution of such large systems of equations.[52] A prominent method to do so is the conjugate-gradient method briefly discussed in Section 2.9. It has been reported[53,54,55] that this iterative algorithm typically requires $N/4$ to $N/2$ steps to converge to acceptable accuracy (where N is the order of the matrix). Because a large number of products of the type $\overline{\overline{Z}} \cdot \mathbf{f}_n$ must be evaluated, each of which requires $O(N^2)$ operations, considerable energy has been devoted to lighten this task. The *Fast multipole method*, to be discussed in Section 14.6, is an example of such an endeavor, by which the $O(N^2)$ criterion is reduced to $O(N \log N)$ [183].

12.4.3 The Adaptive Integral Method

Several acceleration methods are based on the property that fields at large distances from the sources can be computed by using a reduced amount of information on the source currents. In the *adaptive integral method* (AIM), this goal is achieved by splitting $\overline{\overline{Z}}$ into near-field and far-field components.[56,57] Thus,

$$\overline{\overline{Z}} = \overline{\overline{Z}}_{near} + \overline{\overline{Z}}_{far}. \tag{12.67}$$

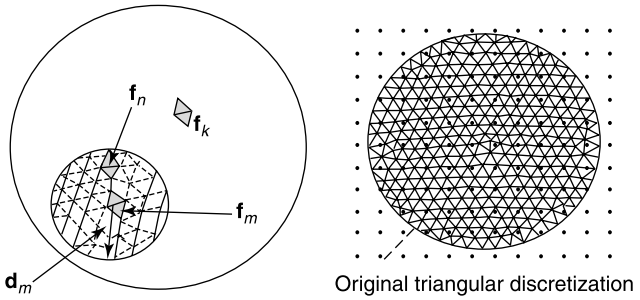

Figure 12.7 (*a*) Far- and near-field regions. (*b*) Mapping of an original grid to a uniform AIM grid (from J. L. Volakis, A. Chatterjee, and L. C. Kempel. *Finite element method for electromagnetics*. IEEE Press, New York and Oxford University Press, Oxford, 1998, with permission of IEEE Press).

In Figure 12.7*a*, a surface is discretized into small triangular patches (for example of the RWG type). With respect to patch $\mathbf{f}_m$, a radius d_m separates elements in the near-field (say $\mathbf{f}_n$) from those in the far-field (say $\mathbf{f}_k$). The value of d_m is chosen according to the desired accuracy. Only near-neighbors contribute to $\overline{\overline{Z}}_{near}$, hence this matrix will be sparse. Its elements are computed by evaluating the integrals shown in (12.63). In the computation of $\overline{\overline{Z}}_{far}$, the original current distribution is replaced by an approximately equivalent set of point currents. If these currents are located at nodes of a regular Cartesian grid, as shown in Figure 12.7*b*, the fields they generate can be computed using the *Fast fourier transform* algorithm (see Appendix 7). Fundamentally, this is because the kernel in the integral equations of concern, such as (12.10), is a function of $\mathbf{r}$ and $\mathbf{r}'$ through the combination $|\mathbf{r} - \mathbf{r}'|$, a property that expresses translational space invariance. Detailed developments show that $\overline{\overline{Z}}_{far}$ can be written in the numerically useful form

$$\overline{\overline{Z}}_{far} = \overline{\overline{A}} \cdot \overline{\overline{T}} \cdot \overline{\overline{A}}^t \tag{12.68}$$

where $\overline{\overline{A}}$ is sparse, and $\overline{\overline{T}}$ is of the Toeplitz type. The decision to treat distant basis functions as a group is an essential ingredient in many other acceleration methods. Several functions, for example, can be collected into a cluster, a technique used in the *Fast multipole* approach. By assigning appropriate weights to the individual basis functions within a cluster, it is possible to reduce the latter's influence at some preselected points of the structure, thereby converting the $\overline{\overline{Z}}$ matrix into a highly dominant diagonal form, with practically ignorable off-diagonal terms.[58]

12.4.4 The Asymptotic Waveform Evaluation

In many applications, the characteristics of a device (the input impedance of an antenna, the radar cross section of a target, . . .) must be evaluated over a wide frequency band, say from 20 to 80 GHz. In a brute force approach, the evaluation is fully repeated at discrete intervals, for instance every GHz. If the variation is expected to be rapid in certain frequency ranges, perhaps because of resonance phenomena, the interval may have to be shortened, which obviously creates problems of computational cost. In such a situation, interpolation

procedures become particularly valuable. The various problems encountered in the current text are often formulated in terms of a matrix equation

$$\overline{\overline{Z}}(k)\cdot\mathbf{I}(k)=\mathbf{V}(k), \tag{12.69}$$

where k is an appropriate wavenumber. The EFIE (12.10) is a case in point, in which the frequency dependence of the terms is apparent — and is carried over to the discretized version. Assume now that (12.69) has been solved for a given central wavenumber k_c. A natural extension on the frequency axis is by means of a Taylor expansion[59,60] [183]

$$\mathbf{I}(k)=\mathbf{i}_0(k_c)+\mathbf{i}_1(k_c)(k-k_c)+\mathbf{i}_2(k_c)(k-k_c)^2+\cdots. \tag{12.70}$$

To determine the expansion coefficients, one must introduce derivatives of the $\overline{\overline{Z}}$ operator with respect to k, evaluated at k_c. The end result is

$$\begin{aligned}\mathbf{i}_0(k_c)&=\overline{\overline{Z}}^{-1}(k_c)\cdot\mathbf{V}(k_c)\\ \mathbf{i}_n(k_c)&=\overline{\overline{Z}}^{-1}(k_c)\cdot\left[\frac{\mathbf{V}^{(n)}(k_c)}{n!}-\sum_{q=1}^{n}\frac{\overline{\overline{Z}}^{(q)}(k_c)\cdot\mathbf{i}_{n-q}}{q!}\right]\qquad(n\geq 1),\end{aligned} \tag{12.71}$$

where the superscript (n) stands for the nth derivative with respect to k. The reader will notice that the method requires only a single matrix inversion. On the other hand, the accuracy of the expansion is limited by its radius of convergence, a difficulty that appears clearly in Figure 12.8, which displays the frequency-dependence of the radar cross section of a perfectly conducting square plate of dimensions 1 cm × 1 cm. The incidence is normal, and 30 GHz is the reference frequency f_c. The small squares correspond with exact solutions of (12.69), repeated at 1 GHz intervals, and the Taylor expansion has been truncated to seventh order. A wider frequency coverage is afforded by the Padé approximation, which consists in expressing the Taylor expansion as a ratio of polynomials. Thus,

$$\mathbf{i}_0(k_c)+(k-k_c)\,\mathbf{i}_1(k_c)+\cdots+(k-k_c)^{L+M}\mathbf{i}_{L+M}(k_c)=\frac{\mathbf{P}_L(k-k_c)}{Q_M(k-k_c)}. \tag{12.72}$$

The polynomials are explicitly

$$\begin{aligned}\mathbf{P}_L(x)&=\mathbf{a}_0+x\mathbf{a}_1+\cdots+x^L\mathbf{a}_L\\ Q_M(x)&=1+xb_1+\cdots+x^Mb_M.\end{aligned}$$

By matching coefficients of equal powers of $(k-k_c)$ on both sides of (12.72), first multiplied by Q_M, matrix equation (12.73) is obtained. It connects the unknown b^k coefficients to the previously evaluated $\mathbf{i}_k$:

$$\begin{bmatrix}\mathbf{i}_{L-M+1} & \mathbf{i}_{L-M+2} & \cdots & \mathbf{i}_L\\ \mathbf{i}_{L-M+2} & \mathbf{i}_{L-M+3} & \cdots & \mathbf{i}_{L+1}\\ \vdots & \vdots & & \vdots\\ \mathbf{i}_L & \mathbf{i}_{L+1} & \cdots & \mathbf{i}_{L+M-1}\end{bmatrix}\cdot\begin{bmatrix}b_M\\ b_{M-1}\\ \vdots\\ b_1\end{bmatrix}=-\begin{bmatrix}\mathbf{i}_{L+1}\\ \mathbf{i}_{L+2}\\ \vdots\\ \mathbf{i}_{L+M}\end{bmatrix}. \tag{12.73}$$

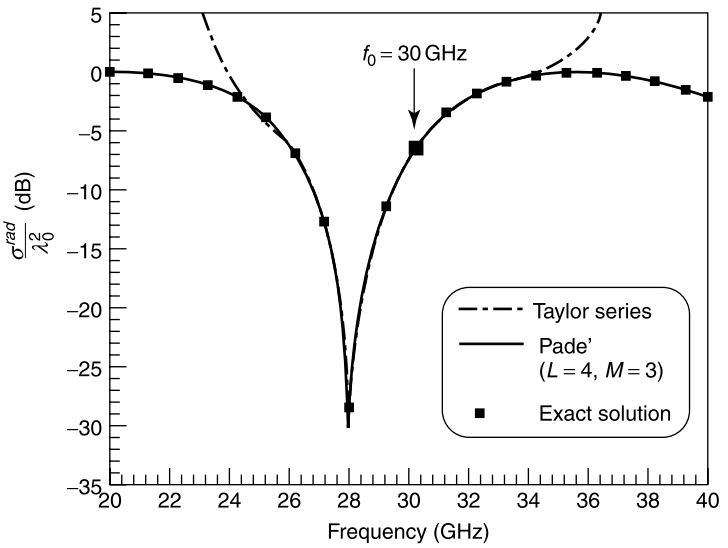

Figure 12.8 Radar cross section of a square plate at normal incidence (from C. J. Reddy, M. D. Deshpande, C. R. Cockrell, and F. B. Beck, Fast RCS computation over a frequency band using method of moments in conjunction with asymptotic waveform evaluation technique, *IEEE Trans. AP* **46**, 1229–1233, 1998, with permission of IEEE).

Once the b_k coefficients are found, the $\mathbf{a}_k$ follow by the simple operation

$$\mathbf{a}_k = \sum_{s=1}^{k} b_s \mathbf{i}_{k-s} \qquad (0 \le k \le L). \tag{12.74}$$

The application of the method to the square plate in Figure 12.8, again with 30 GHz as a reference frequency, yields the solid line in the figure. It is seen that the dip in the curve is remarkably predicted.

The AWE technique can be extended to arbitrary time-dependences,[61] in which case the fields are represented by their Laplace transforms, and the expansions are in terms of "s" instead of "k."

12.5 INTEGRAL EQUATIONS FOR PENETRABLE BODIES

When the (ϵ, μ) parameters of a body vary throughout the volume, a problem formulation in terms of a surface equation on S is not feasible because it would not "feel" the spatial variations of (ϵ, μ). The approach becomes realistic, however, when ϵ and μ are uniform in the scatterer. The analysis for such a case requires the use of the Green's functions

$$G_i(\mathbf{r}|\mathbf{r}') = -\frac{1}{4\pi} \frac{e^{-jk_i|\mathbf{r}-\mathbf{r}'|}}{|\mathbf{r}-\mathbf{r}'|} \qquad (i = 1, 2) \tag{12.75}$$

where $k_i^2 = \omega^2 \epsilon_i \mu_i$, and ϵ_i, μ_i may be complex (Fig. 12.9).

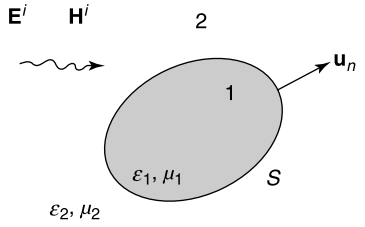

Figure 12.9 Penetrable body in an incident wave.

12.5.1 Homogeneous Scatterer

The unknowns of the problem are the surface currents $\mathbf{J}_S = \mathbf{u}_n \times \mathbf{H}$ and $\mathbf{J}_{mS} = \mathbf{E} \times \mathbf{u}_n$. From (7.222), with $\mathbf{u}_n$ oriented as in Figure 12.9,

$$\mathbf{E}_2(\mathbf{r}) = \mathbf{E}^i(\mathbf{r}) + \int_S [j\omega\mu_2\, G_2(\mathbf{r}|\mathbf{r}')\, \mathbf{J}_S(\mathbf{r}') + \mathbf{J}_{mS}(\mathbf{r}') \times \operatorname{grad}' G_2(\mathbf{r}|\mathbf{r}') + \frac{1}{j\omega\epsilon_2} \operatorname{div}'_S \mathbf{J}_S \operatorname{grad}' G_2(\mathbf{r}|\mathbf{r}')]\, dS' \tag{12.76}$$

$$\mathbf{H}_2(\mathbf{r}) = \mathbf{H}^i(\mathbf{r}) + \int_S [j\omega\epsilon_2\, G_2(\mathbf{r}|\mathbf{r}')\, \mathbf{J}_{mS}(\mathbf{r}') - \mathbf{J}_S(\mathbf{r}') \times \operatorname{grad}' G_2(\mathbf{r}|\mathbf{r}') - \frac{1}{j\omega\mu_2} \operatorname{div}'_S \mathbf{J}_{mS} \operatorname{grad}' G_2(\mathbf{r}|\mathbf{r}')]\, dS'. \tag{12.77}$$

The fields in medium 1 are given by similar expressions but without source terms. Thus, keeping in mind that $\mathbf{u}_n \times \mathbf{H}$ and $\mathbf{E} \times \mathbf{u}_n$ are continuous across S,

$$\mathbf{E}_1(\mathbf{r}) = \int_S [-j\omega\mu_1\, G_1(\mathbf{r}|\mathbf{r}')\, \mathbf{J}_S(\mathbf{r}') - \mathbf{J}_{mS}(\mathbf{r}') \times \operatorname{grad}' G_1(\mathbf{r}|\mathbf{r}') + \frac{1}{j\omega\epsilon_1} \operatorname{div}'_S \mathbf{J}_S \operatorname{grad}' G_1(\mathbf{r}|\mathbf{r}')]\, dS' \tag{12.78}$$

$$\mathbf{H}_1(\mathbf{r}) = \int_S [-j\omega\epsilon_1\, G_1(\mathbf{r}|\mathbf{r}')\, \mathbf{J}_{mS}(\mathbf{r}') + \mathbf{J}_S(\mathbf{r}') \times \operatorname{grad}' G_1(\mathbf{r}|\mathbf{r}') - \frac{1}{j\omega\mu_1} \operatorname{div}'_S \mathbf{J}_{mS} \operatorname{grad}' G_1(\mathbf{r}|\mathbf{r}')]\, dS'. \tag{12.79}$$

The sought coupled integral equations are obtained by expressing continuity of the tangential components of $(\mathbf{E}_1, \mathbf{E}_2)$ and $(\mathbf{H}_1, \mathbf{H}_2)$. Thus [197, 212]

$$-\mathbf{u}_n \times \mathbf{E}^i = \mathbf{u}_n \times \int_S \left[j\omega(\mu_1 G_1 + \mu_2 G_2)\, \mathbf{J}_S + \mathbf{J}_{mS} \times \operatorname{grad}'(G_1 + G_2) + \frac{1}{j\omega} \operatorname{div}'_S \mathbf{J}_S \left(\frac{G_1}{\epsilon_1} + \frac{G_2}{\epsilon_2} \right) \right] dS' \tag{12.80}$$

$$-\mathbf{u}_n \times \mathbf{H}^i = \mathbf{u}_n \times \int_S \left[j\omega(\epsilon_1 G_1 + \epsilon_2 G_2)\, \mathbf{J}_{mS} - \mathbf{J}_S \times \operatorname{grad}'(G_1 + G_2) \right.$$
$$\left. + \frac{1}{j\omega} \operatorname{div}'_S \mathbf{J}_{mS} \left(\frac{G_1}{\mu_1} + \frac{G_2}{\mu_2} \right) \right] dS'. \tag{12.81}$$

The integrals are the limits obtained by letting $\mathbf{r}$ approach S. These limits must be evaluated according to the rules spelled out in Sections 12.1 and 12.2. Solution proceeds by the usual discretization steps (i.e., by expanding $\mathbf{J}_S$ and $\mathbf{J}_{mS}$ in terms of basis vectors[62,63]). The method can be extended to scatterers consisting of several homogeneous parts and to dielectric-coated conductors, both in the frequency and time domains.[64,65,66,67]

In the coupled integral equations (12.80) and (12.81) *two* unknowns, $\mathbf{J}_S$ and $\mathbf{J}_{mS}$, are involved, and the Green's functions G_1 and G_2 have a very simple form. It is possible, however, to formulate the problem in terms of a *single* tangential field satisfying a *single* surface equation, but the price to pay is added complexity.[68,69,70] Note that the original integral equations (12.80) and (12.81) may serve to determine the resonant modes and frequencies of a dielectric resonator [82]. It suffices, for that purpose, to set $\mathbf{E}^i = 0$ and $\mathbf{H}^i = 0$ in the equations and to solve the resulting homogeneous problem.[71] The method has been applied to the axisymmetric resonators discussed in Section 10.5.

12.5.2 Inhomogeneous Scatterers

In many situations encountered in practice, the (ϵ, μ) parameters vary within the scattering volume. The *obstacle* in Figure 12.9 might serve, for example, to modify the radiation pattern of an antenna. The Luneburg lens is a case in point. In the industrial and medical areas, the obstacle could be a conducting volume, to be heated up by the Joule effect of the induced currents. This effect is measured by the value of $\sigma|\mathbf{e}|^2$, a parameter termed *Specific absorption rate* (SAR) when it is expressed in $\mathrm{W\,kg^{-1}}$. Examples of industrial applications are numerous: the drying of wood, the thawing of frozen foods, or the vulcanization of rubber tires. In *medical* applications, the target is often strongly inhomogeneous, because it may consist of fat, muscle, bones, and skin. It could also be markedly anisotropic, particularly in the presence of fiber-rich muscular tissue. The inhomogeneity could also be concentrated in a small part of a volume, as in the case of a tumor, the target of the hyperthermia treatment of cancer.

To solve for the fields in the scatterer, we start from Maxwell's equations, written in the form

$$\operatorname{curl} \mathbf{E} = -j\omega\mu_0 \mathbf{H} - j\omega(\mu - \mu_0)\mathbf{H} = -j\omega\mu_0 \mathbf{H} - \mathbf{J}_m$$
$$\operatorname{curl} \mathbf{H} = j\omega\epsilon_0 \mathbf{E} + [\sigma + j\omega(\epsilon - \epsilon_0)]\mathbf{E} = j\omega\epsilon_0 \mathbf{E} + \mathbf{J}. \tag{12.82}$$

The sources $\mathbf{J}$ and $\mathbf{J}_m$ are the polarization (or contrast) currents

$$\mathbf{J} = [\sigma + j\omega(\epsilon - \epsilon_0)]\mathbf{E}$$
$$\mathbf{J}_m = j\omega(\mu - \mu_0)\mathbf{H}. \tag{12.83}$$

The corresponding charge densities are

$$\begin{aligned} \rho &= -\frac{1}{j\omega}\,\text{div}\,\mathbf{J} \qquad & \rho_m &= -\frac{1}{j\omega}\,\text{div}\,\mathbf{J}_m \\ \rho_S &= \frac{1}{j\omega}\,\mathbf{u}_n\cdot\mathbf{J} \qquad & \rho_{mS} &= \frac{1}{j\omega}\,\mathbf{u}_n\cdot\mathbf{J}_m \end{aligned} \tag{12.84}$$

On the basis of (7.107), the fields may be written as

$$\begin{aligned} \mathbf{E}(\mathbf{r}) &= \frac{\mathbf{J}}{\sigma - j\omega(\epsilon-\epsilon_0)} \\ &= \mathbf{E}^i(\mathbf{r}) + j\omega\mu_0\int_V \mathbf{J}(\mathbf{r}')\,G_0(\mathbf{r}|\mathbf{r}')\,dV' + \frac{1}{\epsilon_0}\,\text{grad}\int_V \rho(\mathbf{r}')\,G_0(\mathbf{r}|\mathbf{r}')\,dV' \\ &\quad + \frac{1}{\epsilon_0}\,\text{grad}\int_S \rho_S(\mathbf{r})\,G_0(\mathbf{r}|\mathbf{r}')\,dS' + \text{curl}\int_V \mathbf{J}_m(\mathbf{r}')\,G_0(\mathbf{r}|\mathbf{r}')\,dV' \end{aligned} \tag{12.85}$$

and

$$\begin{aligned} \mathbf{H}(\mathbf{r}) &= \frac{\mathbf{J}_m}{j\omega(\mu-\mu_0)} \\ &= \mathbf{H}^i(\mathbf{r}) - \text{curl}\int_V \mathbf{J}(\mathbf{r}')\,G_0(\mathbf{r}|\mathbf{r}')\,dV' + j\omega\epsilon_0\int_V \mathbf{J}_m(\mathbf{r}')\,G_0(\mathbf{r}|\mathbf{r}')\,dV' \\ &\quad + \frac{1}{\mu_0}\,\text{grad}\int_V \rho_m(\mathbf{r}')\,G_0(\mathbf{r}|\mathbf{r}')\,dV' + \frac{1}{\mu_0}\,\text{grad}\int_S \rho_{mS}(\mathbf{r}')\,G_0(\mathbf{r}|\mathbf{r}')\,dS'. \end{aligned} \tag{12.86}$$

These are functional equations to be satisfied by $\mathbf{J}$ and $\mathbf{J}_m$. The singularity of $G_0(\mathbf{r}|\mathbf{r}')$ is weak and easy to handle numerically. On the other hand, space derivatives must be evaluated because of the presence of the *grad* and *curl* operators. Both symbols may be brought behind the integral sign to operate on $G_0(\mathbf{r}|\mathbf{r}')$, but at the cost of increasing the singularity of the integrand, and consequently requiring the careful steps outlined in Sections 3.8 and 7.9. The result of such an operation is a set of integral equations

$$\begin{aligned} \frac{\mathbf{J}}{\sigma + j\omega(\epsilon-\epsilon_0)} &= \mathbf{E}^i(\mathbf{r}) + j\omega\mu_0 \lim_{\delta\to 0}\int_{V-V_\delta} \overline{\overline{G}}_{ee}(\mathbf{r}|\mathbf{r}')\cdot\mathbf{J}(\mathbf{r}')\,dV' \\ &\quad - \frac{1}{j\omega\epsilon_0}\overline{\overline{L}}_{V_\delta}(\mathbf{r})\cdot\mathbf{J}(\mathbf{r}) - \lim_{\delta\to 0}\int_{V-V_\delta} \overline{\overline{G}}_{me}(\mathbf{r}|\mathbf{r}')\cdot\mathbf{J}_m(\mathbf{r}')\,dV' \end{aligned} \tag{12.87}$$

$$\begin{aligned} \frac{\mathbf{J}_m}{j\omega(\mu-\mu_0)} &= \mathbf{H}^i(\mathbf{r}) + j\omega\epsilon_0 \lim_{\delta\to 0}\int_{V-V_\delta} \overline{\overline{G}}_{ee}(\mathbf{r}|\mathbf{r}')\cdot\mathbf{J}_m(\mathbf{r}')\,dV' \\ &\quad - \frac{1}{j\omega\mu_0}\overline{\overline{L}}_{V_\delta}(\mathbf{r})\cdot\mathbf{J}_m(\mathbf{r}) + \lim_{\delta\to 0}\int_{V-V_\delta} \overline{\overline{G}}_{me}(\mathbf{r}|\mathbf{r}')\cdot\mathbf{J}(\mathbf{r}')\,dV' \end{aligned} \tag{12.88}$$

where $\overline{\overline{G}}_{ee}$ and $\overline{\overline{G}}_{me}$ are defined in (7.136) and (7.126). These equations reduce to a single one when the body is nonmagnetic, in which case one may set $\mathbf{J}_m = 0$. Note that it is always possible to replace $\mathbf{J}_m$ by an equivalent $\mathbf{J}$ and, conversely, $\mathbf{J}$ by an equivalent $\mathbf{J}_m$.

The relevant formulas are given in (7.205) and (7.211). The two equations now become uncoupled.[72]

In the previous analysis, the unknowns were $\mathbf{J}$ and $\mathbf{J}_m$. The field problem can also be formulated in terms of the *displacement* $\mathbf{D}$. This vector has the advantage of having a continuous normal component at media interfaces. It satisfies, in the scatterer,[73,74,75] the equation

$$\frac{\mathbf{D}}{\epsilon(\mathbf{r})} = \mathbf{E} = \mathbf{E}^i + \mathbf{E}^{sc} = \mathbf{E}^i - j\omega \left[\mathbf{A}^{sc} + \frac{1}{k_0^2} \operatorname{grad} \operatorname{div} \mathbf{A}^{sc} \right] \tag{12.89}$$

where

$$\mathbf{A}^{sc} = -\mu_0 \int_V G_0(\mathbf{r}|\mathbf{r}')\, \mathbf{J}(\mathbf{r}')\, dV' = -j\omega\mu_0 \int_V G_0(\mathbf{r}|\mathbf{r}')\, \chi(\mathbf{r}')\, \mathbf{D}(\mathbf{r}')\, dV' \tag{12.90}$$

and $\chi(\mathbf{r})$ is a contrast function

$$\chi(\mathbf{r}) = \frac{\epsilon(\mathbf{r}) - \epsilon_0}{\epsilon(\mathbf{r})} = 1 - \frac{1}{\epsilon_r(\mathbf{r})}. \tag{12.91}$$

Inserting (12.90) into (12.89) yields an integro-differential equation for $\mathbf{D}$.

12.5.3 Numerical Solution

Figure 12.10 shows two important biomedical applications.[76] The first figure represents a body exposed to the near field of an *applicator* (an antenna). The penetration of the fields is governed by the (ϵ, σ) characteristics of the tissues.[77] Table 12.1 shows, on the first line, some average values of these parameters for skin, muscle, and other tissues of high water content. The second line refers to fat, bone, and tissues of low water content. Penetration is weak at high frequencies because of the important absorption in the outer layers.

The second figure refers to a problem that is of considerable interest to the general public: the coupling of a transceiver handset to the head of an operator.[78] The unknowns are the current $I(z)$ in the antenna and the fields in the head. This coupled problem may be solved by a range of numerical methods: coupled integral equations or finite differences in the time domain. The value of the fields, for realistic parameters, is an important factor in the evaluation of potential dangers to brain or eyes.[79,80] Safety levels for such situations are still under discussion.

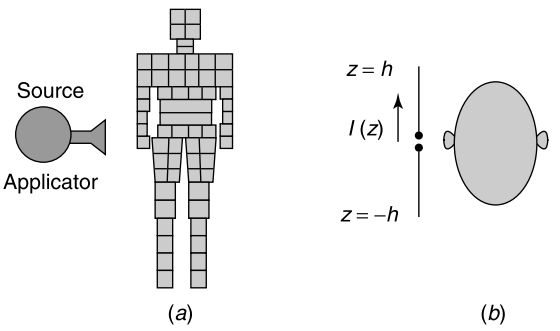

Figure 12.10 (*a*) Man in the field of an applicator. (*b*) Head coupled to an antenna.

Table 12.1 Characteristics of Some Biological Materials

	Frequency	100 MHz	915 MHz	2.45 GHz	10 GHz
Skin	ϵ_r	71.7	51	47	40
	σ (S m^{-1})	0.885	1.28	2.17	10
Fat	ϵ_r	7.45	5.6	5.5	4.5
	σ (S m^{-1})	0.019–0.076	0.056–0.147	0.096–0.213	0.324–0.55

Early numerical solutions to the *whole body* problem were based on the division of the volume into cubic cells of various sizes, with basis functions in the form of pulses[81] (Fig. 12.10*a*). Many other basis functions have been proposed since, for example:

- Entire-domain, higher-order expansion functions, defined on electrically large geometrical volumes[82]
- Curvilinear hexahedra, particularly suited to curvilinear volumes.[83,84]

A particularly popular cell consists of two tetrahedra, T_n^+ and T_n^-, of respective volumes V_n^+ and V_n^-, separated by an nth common face of area a_n (Fig. 12.11*a*). The basis vector function is[73]

$$\mathbf{f}_n(\mathbf{r}) = \begin{cases} \dfrac{a_n}{3V_n^+}\mathbf{r}_n^+ & (\text{in } T_n^+) \\ \dfrac{a_n}{3V_n^-}\mathbf{r}_n^- & (\text{in } T_n^-,) \end{cases} \tag{12.92}$$

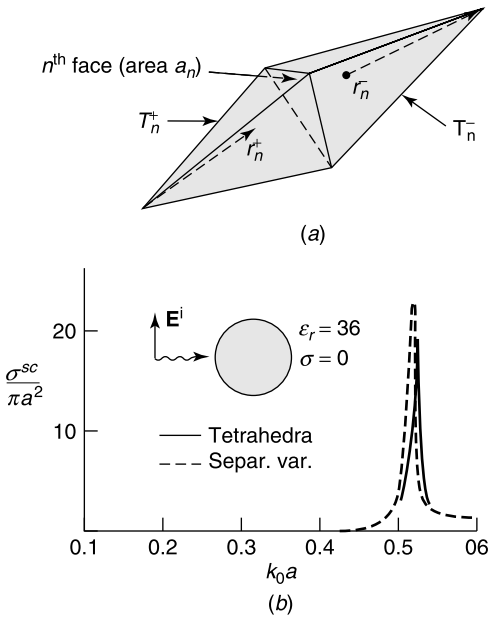

Figure 12.11 (*a*) Pair of tetrahedra. (*b*) Total scattering cross section of a dielectric sphere (from D. H. Schaubert, D. R. Wilton, and A. W. Glisson, A tetrahedral modeling method for electromagnetic scattering by arbitrarily shaped inhomogeneous dielectric bodies, *IEEE Trans. AP* **32**, 77–85, 1984, with permission of IEEE).

and as such is the three-dimensional counterpart of the two-dimensional RWG rooftop function shown in Figure 12.6. Within each tetrahedron, four basis functions should be used, one per face. The various $\mathbf{f}_n$ are tangent to the lateral faces but have a component perpendicular to the common edge, which furthermore has the same value on both sides of the edge. In each tetrahedron div $\mathbf{f}_n$ is constant, equal to (a_n/V_n^+) in T_n^+, and to $-(a_n/V_n^-)$ in T_n^-.

In Figure 12.11*b*, the subdivision of a sphere into 512 tetrahedra has been used to evaluate the scattering cross-section of the body (full curve). The dashed curve is obtained from a Mie type of expansion. It is interesting to check what the asymptotic method would predict. From Section 10.5, the lowest $\mathbf{P}_m$ mode is characterized by $ka = \pi$ (i.e., by $k_0 a = (\pi/\sqrt{\epsilon_r}) \approx 0.52$), and the quality factor $Q = (N^3/2\pi)$ is about 34. Further, (11.90) predicts a scattering cross-section $(\sigma^{sc}/\pi a^2) = 6/(k_0 a)^2 = 22$. These figures are in good agreement with the Mie results.

12.5.4 Transient Fields

The extension to arbitrary time dependences follows essentially the same steps as in the time-harmonic situation.[85] With reference to Figure 12.9, we start with the potential form of the electric field in 1. From (7.107):

$$\mathbf{e}_1(\mathbf{r}, t) = -\frac{\partial \mathbf{a}_1}{\partial t} - \text{grad}\, \phi_1 - \frac{1}{\epsilon_1} \text{curl}\, \mathbf{c}_1. \tag{12.93}$$

Let us assume that the medium is homogeneous and time-invariant.** From the equivalence theorem, the fields may be thought of as generated by surface currents $\mathbf{j}_S = \mathbf{h}_1 \times \mathbf{u}_n$ and $\mathbf{j}_{mS} = \mathbf{u}_n \times \mathbf{e}_1$. The associated potentials are

$$\begin{aligned}
\mathbf{a}_1(\mathbf{r}, t) &= \frac{\mu_1}{4\pi} \int_S \frac{\mathbf{j}_S \left(\mathbf{r}', t - \dfrac{|\mathbf{r} - \mathbf{r}'|}{c_1} \right)}{|\mathbf{r} - \mathbf{r}'|}\, dS' \\
\mathbf{c}_1(\mathbf{r}, t) &= \frac{\epsilon_1}{4\pi} \int_S \frac{\mathbf{j}_{mS} \left(\mathbf{r}', t - \dfrac{|\mathbf{r} - \mathbf{r}'|}{c_1} \right)}{|\mathbf{r} - \mathbf{r}'|}\, dS' \\
\phi_1(\mathbf{r}, t) &= \frac{1}{4\pi\epsilon_1} \int_S \frac{\rho_S \left(\mathbf{r}', t - \dfrac{|\mathbf{r} - \mathbf{r}'|}{c_1} \right)}{|\mathbf{r} - \mathbf{r}'|}\, dS'.
\end{aligned} \tag{12.94}$$

An equation similar to (12.93) can be written for $\mathbf{h}_1(\mathbf{r}, t)$. The same procedure may be further applied to the exterior region 2, provided (c_1, ϵ_1, μ_1) are replaced by (c_2, ϵ_2, μ_2) and fictive sources $\mathbf{h}_2 \times (-\mathbf{u}_n)$ and $(-\mathbf{u}_n) \times \mathbf{e}_2$ are introduced. Expressing continuity of $\mathbf{e}_{\text{tan}}$ and $\mathbf{h}_{\text{tan}}$ on S leads to coupled integral equations [110]. The stability problem associated with explicit solutions is again encountered here,[87] as in Section 12.1, and implicit solutions are therefore often preferred.[88]

**When the scatterer is inhomogeneous, volume integral equations must be considered. See Note 86.

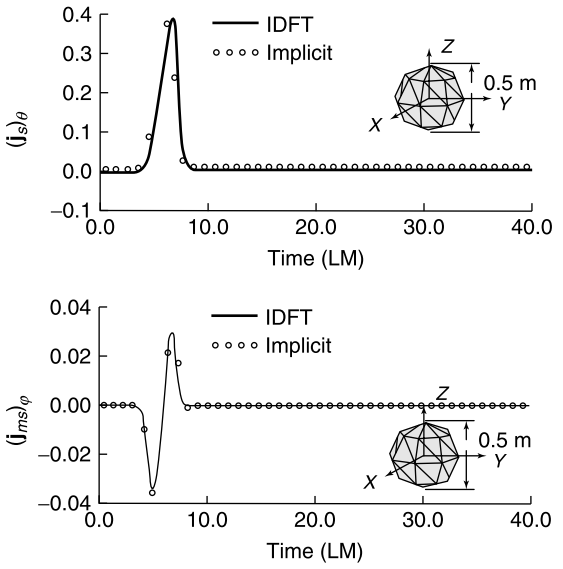

Figure 12.12 Equivalent currents on a dielectric sphere (from S. M. Rao and T. K. Sarkar, Implicit solution of time-domain integral equations for arbitrarily shaped dielectric bodies, *Microwave Opt. Tech. Lett.* **21**, 201–205, 1999, with permission of John Wiley & Sons).

In an illustrative numerical example, consider the scattering of a Gaussian pulse

$$\mathbf{e}^i = 120\pi\, \mathbf{u}_x\, e^{-(t+z/c_0)^2}$$

by a dielectric sphere ($\epsilon_r = 3, a = 0.25$ m). Data are shown in Figure 12.12. The equivalent currents (in A m^{-1} for j_S, and in V m^{-1} for j_{mS}) have been obtained with a time-step of 0.25 LM, much larger than the value allowed in an explicit solution. For comparison, IDFT denotes the solution obtained by Fourier transforming the frequency-domain results.

12.6 ABSORBING BOUNDARY CONDITIONS

Direct numerical solution of the differential equations, by finite differences or finite elements, has great advantages of flexibility in the presence of complicated geometries and inhomogeneous media, isotropic or anisotropic. These methods exploit the local character of the equations, through which only neighboring points appear in the numerical algorithms. The resulting matrices are sparse, a great advantage. There are problems, however. Discretization of the fields often results in grid dispersion. More importantly, the computational space, which in scattering problems extends to infinity, must necessarily be truncated and its boundary S_0 brought closer to the scatterer. Suitable absorbing conditions must be imposed on S_0 to simulate free space there. These conditions can be local or global. *Local ABCs* specify the derivatives of the outgoing waves and make sure the waves leave the solution region without reflections. They are approximate but keep the matrices sparse. *Global*

ABCs, on the other hand, are based on surface integral relationships. They are exact but lead to dense matrices.[††]

12.6.1 Annihilation Operators

The form of the ABCs for potential problems is discussed in Section 5.7. In the extension to time-harmonic fields, let us first consider two-dimensional scattered fields. They satisfy Helmholtz' equation

$$\nabla^2\phi + k_0^2\phi = \frac{1}{r}\frac{\partial}{\partial r}\left(r\frac{\partial\phi}{\partial r}\right) + \frac{1}{r^2}\frac{\partial^2\phi}{\partial\varphi^2} + k_0^2\phi = 0. \tag{12.95}$$

At large distances, the solution of this equation is of the general form (Fig. 12.13*a*)

$$\begin{aligned}\phi = {} & \frac{e^{-jk_0r}}{\sqrt{r}}\left[A_0(\varphi) + \frac{1}{r}A_1(\varphi) + \frac{1}{r^2}A_2(\varphi) + \cdots\right] \\ & + \frac{e^{+jk_0r}}{\sqrt{r}}\left[D_0(\varphi) + \frac{1}{r}D_1(\varphi) + \frac{1}{r^2}D_2(\varphi) + \frac{1}{r^3}D_3(\varphi) + \frac{1}{r^4}D_4(\varphi) + \cdots\right].\end{aligned} \tag{12.96}$$

To enforce the radiation condition, one forms the operator [209]

$$\begin{aligned}B_1(\phi) = {} & \frac{\partial\phi}{\partial r} + jk_0\phi = \frac{e^{-jk_0r}}{\sqrt{r}}\left[-\frac{1}{2r}A_0(\varphi) - \frac{3}{2r^2}A_1(\varphi)\ldots\right] \\ & + \frac{e^{jk_0r}}{\sqrt{r}}\left[2jk_0D_0(\varphi) - \frac{1}{2r}D_0(\varphi) + 2jk_0\frac{1}{r}D_1(\varphi) - \frac{3}{2r^2}D_1(\varphi)\ldots\right].\end{aligned} \tag{12.97}$$

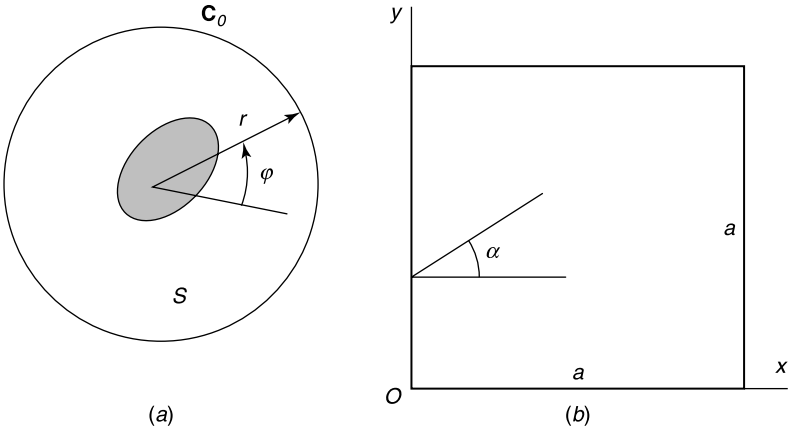

Figure 12.13 (*a*) Scatterer and surrounding circle C_0. (*b*) Relevant for the Engquist-Majda condition.

[††]For a general survey of the absorbing boundary conditions, see the July–August 1996 issue of *Electromagnetics* **16** (4).

The Sommerfeld radiation condition requires $B_1(\phi)$ to be $o(r^{-\frac{1}{2}})$. Enforcing $B_1(\phi) = 0$ on C_0 consequently eliminates the term in $D_0(\varphi)$, which is $O(r^{-\frac{1}{2}})$, and therefore does not approach zero fast enough. The main outgoing wave A_0 is *not* annihilated and, from (12.96), dominates at large distances. To accelerate that desirable dominance and help bring C_0 closer to the scatterer, one may form the higher-order operator

$$\begin{aligned} B_2(\phi) &= \frac{\partial \phi}{\partial r} + jk_0\phi + \frac{1}{2r}\phi \\ &= -\frac{1}{r^2}\frac{e^{-jkr}}{\sqrt{r}}A_1(\varphi) + \cdots + \frac{e^{jk_0 r}}{\sqrt{r}}\left[2jk_0 D_0 + 2jk_0\frac{D_1}{r} - \frac{1}{r^2}D_1 \ldots\right]. \end{aligned} \tag{12.98}$$

The radiation condition requires $B_2(\varphi)$ to be $o(r^{-\frac{3}{2}})$. Imposing $B_2(\phi) = 0$ therefore annihilates D_0 and D_1 but keeps A_0 and A_1 alive. The residual inward-directed wave (the reflection) starts with the term in D_2 and is $O(r^{-\frac{5}{2}})$. One can proceed further [203] and introduce the second-order operator

$$B_3(\phi) = \left(jk_0 + \frac{\partial}{\partial r} + \frac{5}{2r}\right)\left(jk_0 + \frac{\partial}{\partial r} + \frac{1}{2r}\right)\phi. \tag{12.99}$$

Enforcing $B_3(\phi) = o(r^{-\frac{7}{2}})$ eliminates D_0, D_1, D_2, D_3, but keeps A_0, A_1, A_2, A_3 in the expansion. The residual reflection is now $O(r^{-\frac{9}{2}})$. Note that, from (12.95), $\dfrac{\partial^2\phi}{\partial r^2}$ can be expressed in terms of tangential derivatives, which gives $B_3(\phi) = 0$ the equivalent form

$$\frac{\partial \phi}{\partial r} = \underbrace{\frac{k_0^2 r - \frac{3}{2}jk_0 - \frac{3}{8r}}{1 + jk_0 r}}_{\alpha(r)}\phi + \underbrace{\frac{1}{2r(1+jk_0 r)}}_{\beta(r)}\frac{\partial^2\phi}{\partial\varphi^2}. \tag{12.100}$$

This expression is convenient because $(\partial^2\phi/\partial\varphi^2)$ can be discretized by using points on c_0, a move that reduces the number of mesh points.

The same kind of approach can be extended to the *scalar three-dimensional wave equation*, the general solution of which is[89]

$$\phi = \frac{1}{R}\phi^1(c_0 t - R, \theta, \varphi) + \frac{1}{R^2}\phi^2(c_0 t - R, \theta, \varphi) + \cdots. \tag{12.101}$$

The relevant operators are now[90,91]

$$\begin{aligned} B_0\phi \;&=\; \mathcal{L}\phi = \left(\frac{1}{c_0}\frac{\partial}{\partial t} + \frac{\partial}{\partial R}\right)\phi \;=\; O\left(\frac{1}{R^2}\right) \\ B_1\phi &= \left(\frac{1}{c_0}\frac{\partial}{\partial t} + \frac{\partial}{\partial R} + \frac{1}{R}\right)\phi \;=\; O\left(\frac{1}{R^3}\right) \\ B_2\phi &= \left(\mathcal{L} + \frac{3}{R}\right)\left(\mathcal{L} + \frac{1}{R}\right) \;=\; O\left(\frac{1}{R^5}\right). \end{aligned} \tag{12.102}$$

In solving for *three-dimensional time-harmonic* vector fields one may first apply the radiation condition on a large spherical surface S_0, viz. [192, 203]

$$\mathbf{u}_R \times \text{curl}\, \mathbf{E}^{sc} - jk_0\, \mathbf{E}^{sc}_{\tan} = o\left(\frac{1}{R}\right). \tag{12.103}$$

The next order is (Fig. 12.14)

$$\left(\mathbf{u}_R \times \text{curl} - jk_0 - \frac{2}{R}\right)\left(\mathbf{u}_R \times \text{curl}\, \mathbf{E}^{sc} - jk_0\, \mathbf{E}^{sc}_{\tan}\right) = 0. \tag{12.104}$$

Written out:[92]

$$\begin{aligned}\mathbf{u}_R \times \text{curl}\, \mathbf{E}^{sc} = {} & jk_0\, \mathbf{E}^{sc}_{\tan} + \beta(R)\, \text{curl}\left[\mathbf{u}_R(\mathbf{u}_R \cdot \text{curl}\, \mathbf{E}^{sc})\right] \\ & + jk_0\beta(R)\, \text{grad}_S\, (\mathbf{u}_R \cdot \mathbf{E}^{sc}),\end{aligned} \tag{12.105}$$

where

$$\beta(R) = \frac{R}{2(1 + jk_0R)}.$$

The annihilation method can be further extended to nonspherical terminal surfaces S_0, a useful option when the scatterer is elongated[93,94,95,96] [211].

12.6.2 One-Way Wave Equation

The *two-dimensional* wave equation may be written symbolically in the form[97] [209]

$$\begin{aligned} L\phi \;&=\; L^+L^-\phi = 0 \\ &= \left(\frac{\partial}{\partial x} + \frac{1}{c_0}\frac{\partial}{\partial t}\sqrt{1 - S^2}\right)\left(\frac{\partial}{\partial x} - \frac{1}{c_0}\frac{\partial}{\partial t}\sqrt{1 - S^2}\right)\phi \;=\; 0,\end{aligned} \tag{12.106}$$

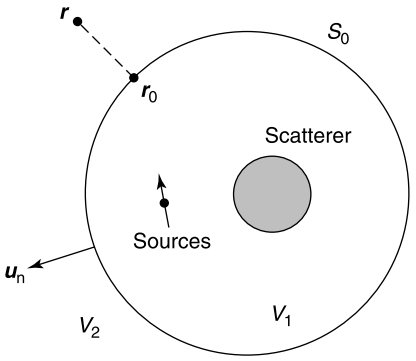

Figure 12.14 Relevant to the boundary integral method.

where

$$S = \frac{\dfrac{\partial}{\partial y}}{\dfrac{1}{c_0}\dfrac{\partial}{\partial t}}.$$

At $x = 0$ (i.e., on the outer side of the mesh), the condition

$$L^{-}\phi = \frac{\partial \phi}{\partial x} - \frac{1}{c_0}\frac{\partial}{\partial t}\sqrt{1 - S^2}\,\phi = 0 \tag{12.107}$$

can be shown to absorb a plane wave propagating toward the boundary, whatever the angle α (Fig. 12.13*b*). The condition $L^{+}\phi = 0$ performs the same function for the boundary $x = a$. These conditions simplify when S^2 is small with respect to unity; that is, when $\dfrac{\partial}{\partial y}$ is small with respect to $\partial/\partial(c_0 t)$. By writing $\sqrt{1 - S^2} \approx 1 - \dfrac{1}{2}S^2$, for example, $L^{-}\phi = 0$ at $x = 0$ becomes approximately [192]

$$\frac{\partial^2 \phi}{\partial x \partial t} - \frac{1}{c_0}\frac{\partial^2 \phi}{\partial t^2} + \frac{c_0}{2}\frac{\partial^2 \phi}{\partial y^2} = 0. \tag{12.108}$$

In *three dimensions*, (12.108) is replaced by[98]

$$\frac{\partial^2 E}{\partial x \partial t} - \frac{1}{c_0}\frac{\partial^2 E}{\partial t^2} + \frac{c_0}{2}\left(\frac{\partial^2 E}{\partial y^2} + \frac{\partial^2 E}{\partial z^2}\right) = 0 \tag{12.109}$$

where E designates the tangential electric field at the $x = 0$ wall. From the wave equations, the previous equation can be given the alternate form[99]

$$\left(\frac{\partial E}{\partial x} - \frac{1}{c_0}\frac{\partial E}{\partial t}\right)\left(\frac{\partial E}{\partial x} - \frac{1}{c_0}\frac{\partial E}{\partial t}\right) = 0. \tag{12.110}$$

This version involves only the normal derivative, whereas (12.109) contains the (tangential) derivatives with respect to y and z.

A number of other absorbing conditions have been proposed [194, 209], in particular those of Trefethen-Halpern, Higdon, Lee, Mei, and Fang.[100,101,102,103,104] In recent years, the *perfectly-matched layer* condition discussed in Section 9.1 has been applied with great success to the closure of the mesh.[105] While most of the methods mentioned above provide effective reflection coefficients of the order 0.5% to 5%, a reduction by a factor of 100 or more can be obtained with the PML technique, bringing the figure to the level achieved in anechoic chambers [209]. The PML has the further advantage of being efficient for arbitrary angles of incidence and of displaying a virtually flat frequency response, an important feature in the presence of ultra-wideband signals.

12.6.3 Global Approaches

In Figure 12.14, a surface S_0 partitions the infinite field domain into interior and exterior regions. In the interior region, the electric field can be represented by a series $\sum a_n \mathbf{f}_n$,

with yet to be determined coefficients. A suitable field representation for **E** and **H** must subsequently be found for the exterior region, also with unknown coefficients. The solution proceeds by "soldering" the two regions smoothly on S_0 (i.e., by expressing continuity of $\mathbf{u}_n \times \mathbf{E}$ and $\mathbf{u}_n \times \mathbf{H}$ across S_0). One such approach is the *unimoment* method, further discussed in Chapter 14. In another method, the influence of the exterior region is represented by a *boundary integral relationship*. The determination of the electric field in the interior region typically involves integrals of the form

$$I = j\omega\mu_0 \int_{S_0} \mathbf{w} \cdot (\mathbf{u}_n \times \mathbf{H})\, dS. \tag{12.111}$$

Our aim is to express $(\mathbf{u}_n \times \mathbf{H})$ in terms of $\mathbf{u}_n \times \mathbf{E}$ (i.e., in terms of the a_n coefficients). The proposed relationship performs this task in an *exact* way. The method is global in the sense that $\mathbf{u}_n \times \mathbf{H}$ at a point $\mathbf{r}$ of S_0 is expressed in terms of the value of $\mathbf{u}_n \times \mathbf{E}$ at *all* points of S_0. Because there are no sources in V_2, basic equation (7.222) may be applied, to yield

$$\begin{aligned}\mathbf{E}(\mathbf{r}) = \int_{S_0} &[j\omega\mu_0 G_0(\mathbf{r}|\mathbf{r}')\mathbf{u}_n' \times \mathbf{H}(\mathbf{r}') + \big(\mathbf{E}(\mathbf{r}') \times \mathbf{u}_n'\big) \times \operatorname{grad}' G_0(\mathbf{r}|\mathbf{r}') \\ &+ \frac{1}{j\omega\epsilon_0} \operatorname{div}_S'[\mathbf{u}_n' \times \mathbf{H}(\mathbf{r}')] \operatorname{grad}' G_0(\mathbf{r}|\mathbf{r}')]\, dS'. \end{aligned} \tag{12.112}$$

This expression gives **E** at a point *outside* S_0. The desired integral relationship is obtained by letting $\mathbf{r}$ approach $\mathbf{r}_0$. Singularities must be taken into account in that approach. For the first and third terms in the integral, they are discussed in Section 12.1, for the second term in Section 12.2. Let us now expand $\mathbf{J}_S = \mathbf{u}_n \times \mathbf{H}$ in a series with coefficients b_m. Because the magnetic current $\mathbf{J}_{mS} = \mathbf{E} \times \mathbf{u}_n$ has already been expanded in a series with coefficients a_n, discretization of the boundary integral law will generate a matrix connecting the b_m to the a_n. This matrix is unfortunately dense and destroys the sparsity that had been obtained by the application of the finite element method in V_1 [190, 192, 203, 211].

The analysis discussed above can, if so desired, be repeated by starting from **H** in V_1 and deriving a law expressing $(\mathbf{E} \times \mathbf{u}_n)$ in terms of $(\mathbf{u}_n \times \mathbf{H})$. These functional dependences, of the type $\mathbf{H}_{\tan} = L(\mathbf{E} \times \mathbf{u}_n)$ on S, have been encountered in Sections 8.7 and 10.7, where they gave rise to the concept of boundary admittance $\overline{\overline{Y}}$, and in Section 11.8, where the scattered field was written as $\mathbf{E}^{sc}_{\tan} = -\mathbf{Z}(\mathbf{J}_S)$ to characterize the *impedance loading* of the interior region by the exterior region.[‡‡]

The steps in the derivation of the boundary integral relationship duplicate those that lead to the EFIE or the MFIE. Interior resonance problems may therefore be expected. They can be avoided[107] by taking the CFIE as a basis for the discussion.

12.7 FINITE ELEMENTS

Let the computational domain V_1 in Figure 12.14 be filled with an inhomogeneous (but isotropic) medium.[108] The differential equations satisfied by the fields are elementary

[‡‡]This methodology can be extended to volumes consisting of several subregions. See Note 106.

extensions of (7.18) and (7.20), viz.

$$-\text{curl}\left(\frac{1}{\mu_r}\,\text{curl}\,\mathbf{E}\right)+k_0^2\epsilon_r\,\mathbf{E}\;=\;jk_0R_{c0}\mathbf{J}+\text{curl}\left(\frac{1}{\mu_r}\mathbf{J}_m\right)=\mathbf{J}_1 \tag{12.113}$$

$$-\text{curl}\left(\frac{1}{\epsilon_r}\,\text{curl}\,\mathbf{H}\right)+k_0^2\mu_r\,\mathbf{H}\;=\;\frac{jk_0}{R_{c0}}\mathbf{J}_m-\text{curl}\left(\frac{1}{\epsilon_r}\mathbf{J}\right)=\mathbf{J}_2. \tag{12.114}$$

When the medium is tensorial, the corresponding equations become

$$-\text{curl}\left((\overline{\overline{\mu}}_r)^{-1}\cdot\text{curl}\,\mathbf{E}\right)+k_0^2\,\overline{\overline{\epsilon}}_r\cdot\mathbf{E}=jk_0R_{c0}\mathbf{J}+\text{curl}\left[(\overline{\overline{\mu}}_r)^{-1}\cdot\mathbf{J}_m\right]=\mathbf{J}_1 \tag{12.115}$$

$$-\text{curl}\left((\overline{\overline{\epsilon}}_r)^{-1}\cdot\text{curl}\,\mathbf{H}\right)+k_0^2\,\overline{\overline{\mu}}_r\cdot\mathbf{H}=\frac{jk_0}{R_{c0}}\mathbf{J}_m-\text{curl}\left[(\overline{\overline{\epsilon}}_r)^{-1}\cdot\mathbf{J}\right]=\mathbf{J}_2. \tag{12.116}$$

The domain will now be paved with small finite elements, as suggested in Figure 12.15, and $\mathbf{E}$ (or $\mathbf{H}$) expanded in basis vectors $\mathbf{f}_n$ of the type mentioned in Sections 10.3 and 12.5, yet to be determined coefficients A_n. Testing (12.113) with vector functions $\mathbf{w}_m$ leads to the weak form

$$\int_{V_1}\left[-\text{curl}\left(\frac{1}{\mu_r}\,\text{curl}\,\mathbf{E}\right)+k_0^2\epsilon_r\,\mathbf{E}\right]\cdot\mathbf{w}_m\,dV=\int_{V_1}\mathbf{J}_1\cdot\mathbf{w}_m\,dV. \tag{12.117}$$

The second derivatives in the double curl term can be eliminated by means of the relationship

$$\text{div}\left[\mathbf{w}_m\times\left(\frac{1}{\mu_r}\,\text{curl}\,\mathbf{E}\right)\right]=\frac{1}{\mu_r}\,\text{curl}\,\mathbf{E}\cdot\text{curl}\,\mathbf{w}_m-\mathbf{w}_m\cdot\text{curl}\left(\frac{1}{\mu_r}\,\text{curl}\,\mathbf{E}\right).$$

The weak form (12.117) can therefore be recast as:[92]

$$\begin{aligned}&-\int_{V_1}\frac{1}{\mu_r}\,\text{curl}\,\mathbf{E}\cdot\text{curl}\,\mathbf{w}_m\,dV+k_0^2\int_{V_1}\epsilon_r\mathbf{w}_m\cdot\mathbf{E}\,dV\\&+\int_{S_0}\mathbf{w}_m\cdot\left(\frac{1}{\mu_r}\,\text{curl}\,\mathbf{E}\times\mathbf{u}_n\right)dS=\int_{V_1}\mathbf{J}_1\cdot\mathbf{w}_m\,dV.\end{aligned} \tag{12.118}$$

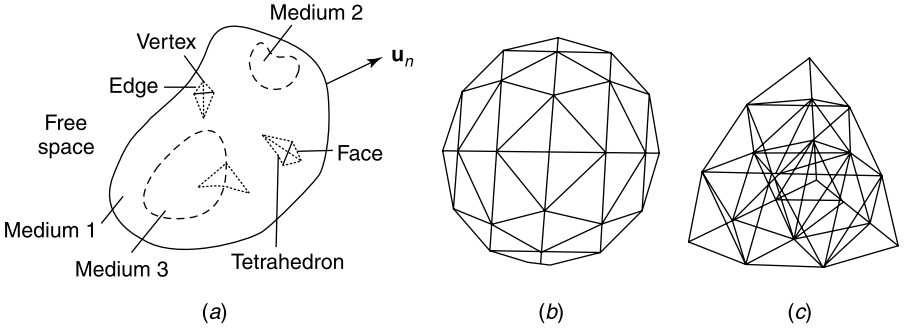

Figure 12.15 (*a*) Piecewise homogeneous dielectric body modeled by tetrahedral volume elements. (*b*) Top view of sphere modeled by three layers of tetrahedra .(*c*) Subdivision of 1/8 of sphere into 27 tetrahedra (from D. H. Schaubert, D. R. Wilton, and A. W. Glisson, A tetrahedral modeling method for electromagnetic scattering by arbitrarily shaped inhomogeneous dielectric bodies, *IEEE Trans. AP* **32**, 77–85, 1984, with permission of IEEE).

The surface integral in that equation is of the general form

$$I = j\omega\mu_0 \int_{S_0} \mathbf{w}_m \cdot (\mathbf{u}_n \times \mathbf{H})\, dS.$$

This is precisely (12.111) and justifies the choice of that equation in the presentation of the *boundary integral* condition. When the computational volume is closed by a perfectly matched layer, the left-hand term of (12.118) must be augmented by a contribution from the layer itself[109] [190, 202, 211]. If the latter is characterized by diagonal tensors $\overline{\overline{\epsilon}}_r = \overline{\overline{\mu}}_r = \overline{\overline{\Lambda}}$, the contribution becomes of the form

$$-\int_{PML} \left[\text{curl } \mathbf{w}_m \cdot \overline{\overline{\Lambda}}^{-1} \cdot \text{curl } \mathbf{E} + k_0^2 \mathbf{w}_m \overline{\overline{\Lambda}} \cdot \mathbf{E}\right] dV + \int_S (\mathbf{w}_m \times \mathbf{u}_n) \cdot \overline{\overline{\Lambda}}^{-1} \cdot \text{curl } \mathbf{E}\, dS, \tag{12.119}$$

where S denotes the two boundary surfaces of the layer. Note that the integral over the metal backing vanishes when one chooses $\mathbf{w}_n$ to be perpendicular to the metal.

On the basis of the previous results, the expansion of $\mathbf{E}$ in $\mathbf{f}_n$ leads to a matrix equation

$$\overline{\overline{L}} \cdot \mathbf{A} = \mathbf{J}, \tag{12.120}$$

where the matrix elements are

$$L_{nm} = \int_{V_n} \left[-\text{curl}\left(\frac{1}{\mu_r} \text{ curl } \mathbf{f}_n\right) + k_0^2 \epsilon_r \mathbf{f}_n\right] \cdot \mathbf{w}_m\, dV. \tag{12.121}$$

The small volume V_n bounded by S_n is the support of $\mathbf{f}_n$.

The $\mathbf{E}$ and $\mathbf{H}$ fields can also be determined by means of *functionals*, selected to have one of the equations (12.113) to (12.116) as Euler equation. For (12.113), for example, the steps outlined in Section 2.2 generate the functional

$$\begin{aligned} J(\mathbf{E}) = &\int_{V_1} \left(-\frac{1}{\mu_r} \text{ curl } \mathbf{E} \cdot \text{curl } \mathbf{E} + k_0^2 \epsilon_r\, \mathbf{E} \cdot \mathbf{E}\right) dV \\ &+ \int_{S_0} \frac{1}{\mu_r} (\mathbf{u}_n \times \mathbf{E}) \cdot \text{curl } \mathbf{E}\, dS - 2 \int_V \mathbf{E} \cdot \mathbf{J}_1\, dV. \end{aligned} \tag{12.122}$$

Note that ϵ_r and μ_r may be complex and/or tensorial[110] (Problem 12.12). A functional suitable for the potentials $\mathbf{A}$ and ϕ is also available, namely [211]

$$\begin{aligned} J(\mathbf{A}, \phi) = &\frac{1}{2} \int_{V_1} \frac{1}{\mu} \text{ curl } \mathbf{A} \cdot \text{curl } \mathbf{A} - \omega^2 \epsilon (\mathbf{A} + \text{grad } \phi) \cdot \mathbf{A}\, dV \\ &- \frac{1}{2} \int_{V_1} \omega^2 \epsilon (\mathbf{A} + \alpha^2 \text{ grad } \phi) \cdot \text{grad } \phi\, dV \\ &+ \frac{1}{2} \int_{S_0} \left[(\mathbf{u}_n \times \mathbf{H}) \cdot \mathbf{A} + (\mathbf{u}_n \times \mathbf{H}) \cdot \text{grad } \phi\right] dS, \end{aligned} \tag{12.123}$$

where α is a scalar used to provide a gauge. The potential formulation gives reliable results down to very low frequencies, a region where the solution in terms of $\mathbf{E}$ or $\mathbf{H}$ often produces

unstable, nearly singular systems of equations.[111] A disadvantage of the potential approach: The discretization of the scalar potential introduces nodal unknowns in addition to the edge elements needed for the vector potential **A**.

Finite Elements in the Time Domain

The basic differential equation is now

$$-\text{curl}\left(\frac{1}{\mu}\,\text{curl}\,\mathbf{e}\right)-\epsilon\frac{\partial^2\mathbf{e}}{\partial t^2}=\frac{\partial\mathbf{j}}{\partial t}.$$

It leads to the weak form[112]

$$\int_V\frac{1}{\mu}\,\text{curl}\,\mathbf{e}\cdot\text{curl}\,\mathbf{w}\,dV+\int_V\epsilon\,\mathbf{w}\cdot\frac{\partial^2\mathbf{e}}{\partial t^2}\,dV$$
$$+\int_{S_0}\mathbf{w}\cdot\left(\frac{1}{\mu}\,\text{curl}\,\mathbf{e}\times\mathbf{u}_n\right)dS+\int_V\mathbf{w}\cdot\frac{\partial\mathbf{j}}{\partial t}\,dV=0 \tag{12.124}$$

Alternately,[113] one can start from the weak form of Maxwell's equations, viz.

$$\int_V\mathbf{w}\cdot\left(\frac{\partial\mathbf{d}}{\partial t}-\text{curl}\,\mathbf{b}+\mathbf{j}\right)dV=0$$
$$\int_V\mathbf{w}\cdot\left(\text{curl}\,\mathbf{e}+\frac{\partial\mathbf{b}}{\partial t}\right)dV=0. \tag{12.125}$$

If **e** is expanded as a sum $\sum_n a_n(t)\mathbf{f}_n(\mathbf{r})$, discretization of (12.124) leads to a matrix equation of the form

$$\overline{\overline{A}}\cdot\frac{d^2\mathbf{a}(t)}{dt^2}+\overline{\overline{B}}\cdot\frac{d\,\mathbf{a}(t)}{dt}+\overline{\overline{C}}\cdot\mathbf{a}(t)=\mathbf{j}(t). \tag{12.126}$$

The numerical implementation of the problem requires an efficient choice of mesh, finite elements, and absorbing boundary conditions.[114,115,116,117,118]

12.8 FINITE DIFFERENCES IN THE TIME DOMAIN

In the FDTD method, a wave is followed as it progresses through a medium. The computational steps are local, because they involve only the closest neighbors and the most recent data in the space-time mesh. The method, which is suited to massive parallel computing,[119] can handle materials with all kinds of characteristics, such as nonlinearity and time-dependence of the ϵ, μ, σ parameters. When the input signal is a delta-function (in practice a very short pulse), the whole frequency response can be generated in a single swing, revealing sharp resonances that a point-by-point approach might miss. The FDTD technique is widely used in a host of applications, for example, in the determination of the resonant fields and frequencies of an aperture-coupled cavity, or in the evaluation of the fields in the head of a telephone operator.[120]

There are several methods to extract the frequency response from the time response. One of these is the *Fast Fourier transform* technique, briefly discussed in Appendix 7. Another approach is the *N equations – N unknowns method*,[121] which requires sampling the response at $2N$ time intervals. Illustratively, if the response is desired at two frequencies (in which case $N = 2$), four unknowns — two per frequency — should be determined, namely the amplitudes a_n and the phases φ_n ($n = 1, 2$). If the response $v(t)$ is sampled at four times, say t_1, t_2, t_3, t_4, the (a_n, φ_n) are found by solving the equations

$$\begin{aligned} a_1 \sin(\omega_1 t_1 + \varphi_1) + a_2 \sin(\omega_2 t_1 + \varphi_2) &= v(t_1) \\ a_1 \sin(\omega_1 t_2 + \varphi_1) + a_2 \sin(\omega_2 t_2 + \varphi_2) &= v(t_2) \\ a_1 \sin(\omega_1 t_3 + \varphi_1) + a_2 \sin(\omega_2 t_3 + \varphi_2) &= v(t_3) \\ a_1 \sin(\omega_1 t_4 + \varphi_1) + a_2 \sin(\omega_2 t_4 + \varphi_2) &= v(t_4). \end{aligned} \tag{12.127}$$

For N frequencies, a $(2N \times 2N)$ matrix equation must be solved (e.g., by Gaussian elimination). The efficiency of the method, as compared with its transform competitors, depends on the number of frequencies, parameters, and locations required by the application in hand.

12.8.1 A Simple One-Dimensional Example

Voltage and current on a lossless transmission line satisfy, on a source-free stretch, the system of equations (Fig. 12.16)

$$\begin{aligned} \frac{\partial v}{\partial x} &= -L \frac{\partial i}{\partial t} \\ \frac{\partial i}{\partial x} &= -C \frac{\partial v}{\partial t}. \end{aligned} \tag{12.128}$$

The difference version of this system is obtained by the techniques outlined in Section 1.14, which yield [125]

$$v^{n+\frac{1}{2}}(k) = v^{n-\frac{1}{2}}(k) - \frac{\Delta t}{C\Delta x}\left[i^n\left(k + \frac{1}{2}\right) - i^n\left(k - \frac{1}{2}\right)\right] \tag{12.129}$$

$$i^{n+1}\left(k + \frac{1}{2}\right) = i^n\left(k + \frac{1}{2}\right) - \frac{\Delta t}{L\Delta x}\left[v^{n+\frac{1}{2}}(k+1) - v^{n+\frac{1}{2}}(k)\right]. \tag{12.130}$$

Here $\phi^n(k)$ stands for the value of ϕ at time $n\Delta t$ and coordinate $k\Delta x$. It is seen that the values of v and i are interleaved in time and space. Equation (12.129) shows how to "march" from

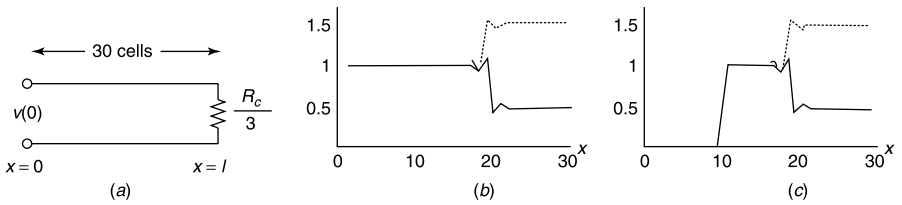

Figure 12.16 (*a*) Terminated transmission line. (*b*) v and i for a step input. (*c*) v and i for a rectangular pulse input.

Table 12.2 Propagation of v and i on a Transmission Line

		Space							
Time		$k=0$ $(x=0)$		$k=1$ $(x=1/3)$		$k=2$ $(x=2/3)$		$k=3$ $(x=1)$	
$n=0$	v	1		0		0		0	
$n=\frac{1}{2}$	$R_c i$		1		0		0		
$n=1$	v	1		1		0		$-\frac{1}{15}$	
$n=\frac{3}{2}$	$R_c i$		1		1		$\frac{1}{15}$		
$n=2$	v	1		1		$\frac{14}{15}$		$\frac{17}{225}$	
$n=\frac{5}{2}$	$R_c i$		1		$\frac{16}{15}$		$\frac{208}{225}$		
$n=3$	v	1		$\frac{14}{15}$		$\frac{242}{225}$		$\frac{1526}{3375}$	

the value of v at $\left(n-\frac{1}{2}\right)\Delta t$ to the value at $\left(n+\frac{1}{2}\right)\Delta t$, using the value of i at neighboring points and at $t=n\Delta t$. The stability of the numerical process requires satisfaction of the *Courant condition*

$$\Delta t \leq \frac{\Delta x}{c}, \tag{12.131}$$

where c is the wave-velocity $(LC)^{-\frac{1}{2}}$. In other words, the sampling interval Δt may not exceed the travel time of the wave through the cell. Figure 12.16 shows the application of the method to a line subdivided into 30 cells and terminated in $\frac{1}{3}R_c = \frac{1}{3}\left(\frac{L}{C}\right)^{\frac{1}{2}}$. The source voltages are[§§]

- A step function $v(0,t) = H(t)$ (Fig. 12.16*b*)
- A rectangular pulse of length $30\Delta t$; that is, of time dependence $v(0,t) = H(t) - H(t-30\Delta t)$ (Fig. 12.16*c*)

The solid lines represent $v(x)$ at time $40\ \Delta t$ and the dashed lines $R_c\ i(x)$ at the same time. The small departures with respect to the (easily derived) theoretical curves are due to numerical dispersion. To further clarify the marching process, Table 12.2 shows the successive results of the progression. For the sake of conciseness, the line has been split into only three cells, and a step input is assumed, with $\Delta t = (\Delta x/c)$. The first line corresponds with the initial condition. The second line is obtained by means of (12.130), and the third one by applying (12.129). The process then continues as shown in the table (Problem 12.13).

[§§]Numerical results courtesy of Dr. F. Olyslager.

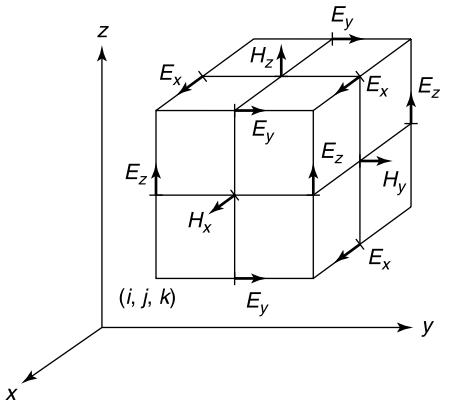

Figure 12.17 Position of various field components (from A. Taflove and K. R. Umashankar, Review of FD-TD numerical modeling of electromagnetic wave scattering and radar cross section, *Proc. IEEE* **77**, 682–699, 1989, with permission of IEEE).

12.8.2 The Marching-on Procedure

The basic *lattice* introduced by K. S. Yee is shown in Figure 12.17. By use of this configuration, a typical Maxwell equation such as

$$\frac{\partial d_x}{\partial t} = \left(\frac{\partial h_z}{\partial y} - \frac{\partial h_y}{\partial z}\right) - j_x$$

is discretized in the form[122]

$$\begin{aligned}
&\frac{d_x^n\left(i+\frac{1}{2},j,k\right) - d_x^{n-1}\left(i+\frac{1}{2},j,k\right)}{\Delta t} \\
&\quad = \frac{h_z^{n-\frac{1}{2}}\left(i+\frac{1}{2},j+\frac{1}{2},k\right) - h_z^{n-\frac{1}{2}}\left(i+\frac{1}{2},j-\frac{1}{2},k\right)}{\Delta y} \\
&\quad\quad - \frac{h_y^{n-\frac{1}{2}}\left(i+\frac{1}{2},j,k+\frac{1}{2}\right) - h_y^{n-\frac{1}{2}}\left(i+\frac{1}{2},j,k-\frac{1}{2}\right)}{\Delta z} - j_x^{n-\frac{1}{2}}\left(i+\frac{1}{2},j,k\right).
\end{aligned} \tag{12.132}$$

The notation $\phi^n(i,j,k)$ refers to a point $(i\Delta x,\ j\Delta y,\ k\Delta z)$. The grid points for the **e** components are in the middle of — and parallel to — the edges. The grid points for the **h** components are in the center of — and perpendicular to — the faces of the parallelepiped. The procedure has the advantage of not requiring the inversion of a matrix. The following points should be kept in mind:

1. The unit cell should be *small* enough to achieve acceptable accuracy at the highest frequency of interest. It should also be *large* enough to limit computational cost.[123]

2. To ensure the stability of the time-stepping algorithm, Δt should satisfy a criterion such as the *Courant condition*

$$\Delta t \leq \frac{1}{c_{\max}\sqrt{\left(\frac{1}{\Delta x}\right)^2 + \left(\frac{1}{\Delta y}\right)^2 + \left(\frac{1}{\Delta z}\right)^2}}, \tag{12.133}$$

where $c_{\max}$ is the maximum phase velocity of the wave within the model. For a cubic lattice:

$$\Delta t \leq \frac{\Delta x_i}{\sqrt{3}\, c_{\max}}. \tag{12.134}$$

The criterion gives only conditional stability and should be strengthened in highly conducting media [194].

3. As time stepping proceeds, it is found that different frequencies propagate at slightly different velocities on the numerical grid. As a result of this *numerical dispersion*, pulses are distorted as they propagate through the mesh. The effect, which depends on the direction of propagation with respect to the grid, introduces a spurious anisotropy[124] [209].

12.8.3 Materials

The parameters of the medium supporting the wave should be inserted into an equation such as (12.132). For a conducting isotropic medium, for example, one should set $\mathbf{d} = \epsilon\mathbf{e}$ and $\mathbf{j} = \sigma\mathbf{e}$ in the equation. Note that the value of $\mathbf{j}$ in (12.132) is selected at time $\left(n - \frac{1}{2}\right)\Delta t$, while $\mathbf{e}$ is evaluated at times $(n-1)\Delta t$ and $n\Delta t$. This discordance can be remedied by writing

$$j_x^{n-\frac{1}{2}} = \frac{\sigma}{2}\left(e_x^n + e_x^{n-1}\right),$$

which leads to

$$e_x^n(i,j,k) = \frac{1 - \dfrac{\Delta t}{2\tau(i,j,k)}}{1 + \dfrac{\Delta t}{2\tau(i,j,k)}}\, e_x^{n-1}(i,j,k) + \frac{\Delta t}{\epsilon(i,j,k)\left(1 + \dfrac{\Delta t}{\tau(i,j,k)}\right)} A, \tag{12.135}$$

where $\tau = (\epsilon/\sigma)$, and

$$A = \frac{h_z^{n-\frac{1}{2}}\left(i, j+\frac{1}{2}, k\right) - h_z^{n-\frac{1}{2}}\left(i, j-\frac{1}{2}, k\right)}{\Delta y} - \frac{h_y^{n-\frac{1}{2}}\left(i, j, k+\frac{1}{2}\right) - h_y^{n-\frac{1}{2}}\left(i, j, k-\frac{1}{2}\right)}{\Delta z}. \tag{12.136}$$

There are other possible time-stepping formulas,[125] in particular those taking into account the exponential decay of the fields in a highly lossy medium or in a perfectly matched layer. There the decay is so rapid that the standard Yee algorithm cannot follow. Suitable schemes are also available for nonlinear and anisotropic media, such as plasmas and magnetized ferrites. When the medium is dispersive, the chosen model (Drude, Lorentz, ...) determines the form of the marching-on formula.[126] It should further be noted that lumped elements can be incorporated in the computational scheme, a possibility that allows the designer of microelectronic circuits to apply FDTD techniques to nonlinear electronic or photonic devices[127] [209]. A resistor block carrying a current I in the x-direction, for example, can be modeled by inserting a current density $\mathbf{j} = (I/\Delta y\,\Delta z)\,\mathbf{u}_x$ into (12.132).

12.8.4 Sources and Initial Conditions

Initial conditions can be imposed by inserting the values $\mathbf{e}^0(i,j,k)$ and $\mathbf{h}^{\frac{1}{2}}(i,j,k)$ at each point of the grid. The sign and magnitude of each component are chosen to yield appropriate propagation direction, phase velocity, and polarization.[128] The method results in excessive lengthening of the grid when the input is of long duration. This difficulty can be avoided by choosing *hard* sources, for example by assigning a desired time dependence to specific $(\mathbf{e}, \mathbf{h})$ components at a restricted number of points on the lattice. The actual choice of the source is important because it influences accuracy, computing time, and stability of the simulation.[129] Several injection schemes have been used frequently. In the case of a linear antenna, the gap and coaxial feeds sketched in Figures 7.21 and 7.28 are obvious choices. In Figure 12.18, the applied electric field has only an e_y component, directed along the wire.[130] In Figure 12.19, the fields are excited through the radial components of $\mathbf{e}$ on the ground plane. More precisely,[131,132]

$$\begin{aligned} e_x^n(i,j,k) = -e_x^n(i-1,j,k) &= \frac{2v(n\Delta t)}{\Delta x \log_e\left(\dfrac{\Delta x}{a}\right)} \\ e_y^n(i,j,k) = -e_y^n(i,j-1,k) &= \frac{2v(n\Delta t)}{\Delta y \log_e\left(\dfrac{\Delta y}{a}\right)}, \end{aligned} \tag{12.137}$$

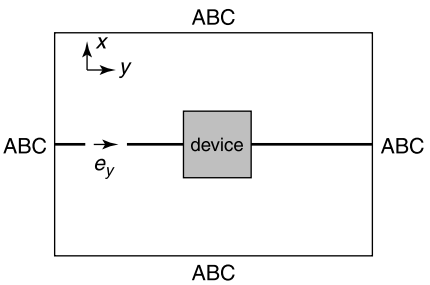

Figure 12.18 *e*-Field excitation by means of a gap (from E. Semouchkina, W. Cao, and R. Mittra, Source excitation methods for the finite-difference time-domain modeling of circuits and devices, *Microwave Opt. Tech. Lett.* **21**, 93–100, 1999, with permission of John Wiley & Sons).

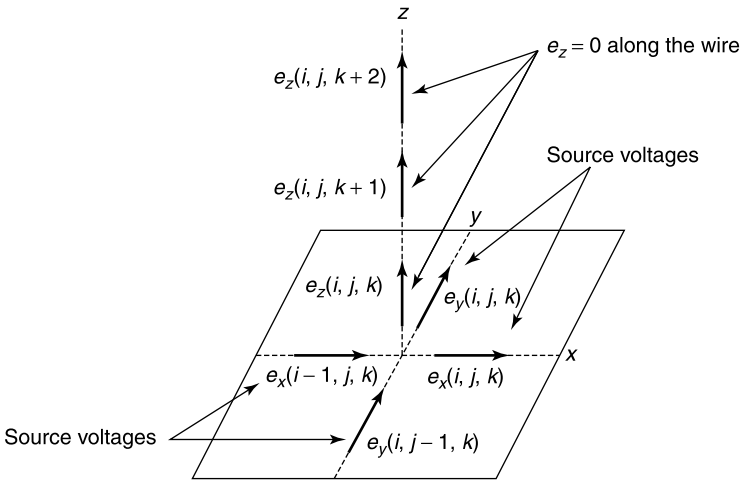

Figure 12.19 Radial electric field model (from W. V. Andrew, C. A. Balanis, P. A. Tirkas, J. Peng, and C. R. Birtcher, Finite-difference time-domain analysis of HF antennas on helicopter airframes, *IEEE Trans. EMC* **39**, 100–113, 1997, with permission of IEEE).

where a is the radius of the wire. It is also possible to impose the tangential component of **e** on a surface that is part of an electric or magnetic wall (Fig. 12.20). The voltage source is simulated by imposing e_z in the rectangular region below the microstrip port and setting it equal to zero on the other parts of the source plane.[133]

12.8.5 Input Waveforms

The excitation signal should be injected sufficiently gently to avoid exciting frequencies higher than those for which the model is valid. A Dirac $\delta(t)$ input is theoretically interesting because, after its output is computed and stored, it can serve to evaluate the response for an arbitrary $v(t)$ by a simple convolution.[134] The Dirac function, however, is a mathematical limit, which is often replaced by an ultra-wideband pulse that contains all the frequencies of interest. The pulse could be "flat top" rectangular, or Gaussian with a time-dependence

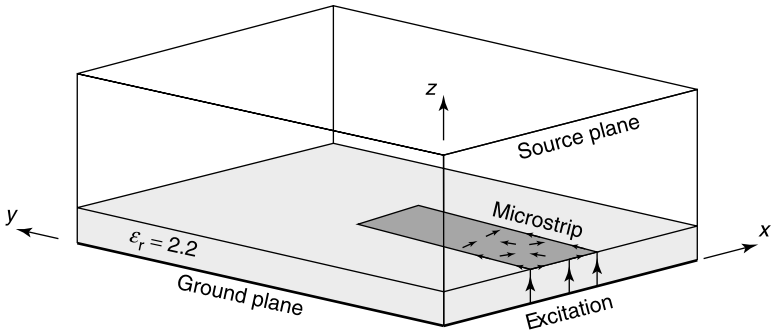

Figure 12.20 Computational domain for a microstrip (from D. M. Sheen, S. M. Ali, M. D. Abouzahra, and J. A. Kong, Application of the three-dimensional finite-difference time-domain method to the analysis of planar microstrip circuits, *IEEE Trans. MTT* **38**, 849–857, 1990, with permission of IEEE).

$e^{-\frac{t^2}{t_0^2}}$. Other inputs of interest are the *Gaussian modulated sinusoid*

$$v(t) = e^{-\frac{t^2}{t_0^2}} \sin \omega t, \tag{12.138}$$

which has no DC component (as opposed to the pure Gaussian) and the *Rayleigh pulse*

$$v(t) = (t - T)\, e^{-\left(\frac{t-T}{t_0}\right)^2}, \tag{12.139}$$

which is proportional to the time-derivative of the Gaussian pulse. Typical characteristics of the Rayleigh pulse are shown in Figure 12.21.

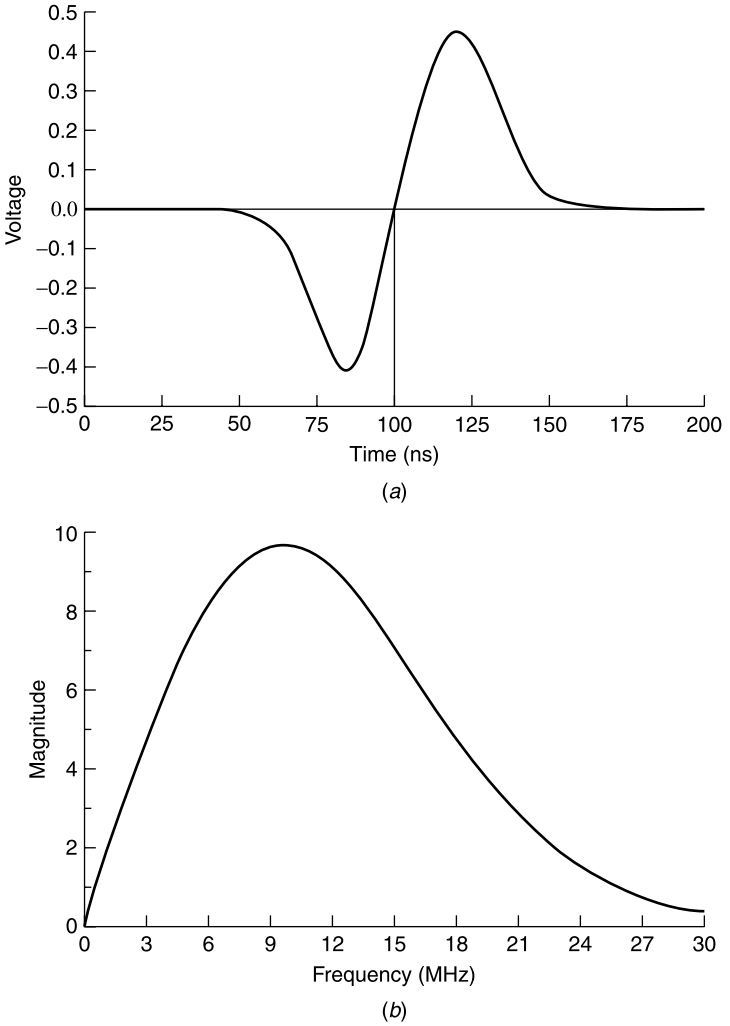

Figure 12.21 (*a*) Amplitude of a wideband Rayleigh pulse. (*b*) Frequency content of the pulse (from W. V. Andrew, C. A. Balanis, P. A. Tirkas, J. Peng, and C. R. Birtcher, Finite-difference time-domain analysis of HF antennas on helicopter airframes, *IEEE Trans. EMC* **39**, 100–113, 1997, with permission of IEEE).

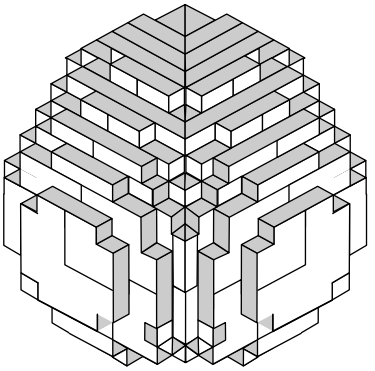

Figure 12.22 Staircased subdivision of a dielectric sphere (from R. Holland, L. Simpson, and K. S. Kunz, Finite-difference analysis of EMP coupling to lossy dielectric structures, *IEEE Trans. EMC* **22**, 203–209, 1980, with permission of IEEE).

12.8.6 Curved Surfaces

The normal Yee grid is a union of parallelepipeds that, when extended to the curved surface of a scatterer, can be modulated to *staircase* the surface[135] (Fig. 12.22). The method clearly introduces errors,[136] but remedies are available,[137] for example [110, 194, 209]:

1. The introduction of a global curvilinear coordinate system that conforms to the boundary surface of the scatterer.[138,139]
2. The use of a regular mesh away from the surface, subsequently modified in the vicinity of the latter by means of a body-fitting mesh.[140,141,142]
3. The implementation of a hybrid scheme, in which the surface and its vicinity are modeled by a finite-element subdivision.[143,144,145]

PROBLEMS

12.1 Determine the value of **T** in (12.8) for a square patch at point O. (Fig. P12.1). The sought value is a function of the ratio (d/a); it should vanish, by symmetry, for $d = 0$.
(A. D. Yaghjian, *Radio Sci.* **16**, 987–1001, 1981.)

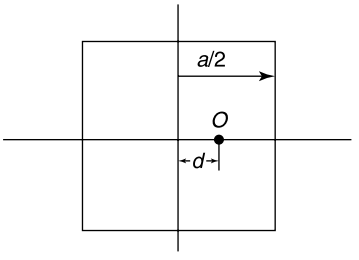

Figure P12.1

12.2 The EFIE (12.10) can be written as

$$\mathbf{u}_n \times \int_S \overline{\overline{Z}}(\mathbf{r}|\mathbf{r}') \cdot \mathbf{J}_S(\mathbf{r}')\, dS' = \mathbf{u}_n \times \mathbf{V}(\mathbf{r}) = \mathbf{u}_n \times \mathbf{E}^i(\mathbf{r}).$$

Consider the backscattered amplitude $f = \int_S \mathbf{V}(\mathbf{r}) \cdot \mathbf{J}_S(\mathbf{r})\, dS$. Show that, if $\mathbf{J}_S$ is off by $\Delta\mathbf{J}_S$ (so that $\mathbf{J}_S = (\mathbf{J}_S)_{\text{exact}} + \Delta\mathbf{J}_S$), the following holds:

$$\Delta f = -j \int_S dS\, \mathbf{J}_S(\mathbf{r}) \cdot \left[\mathbf{V}(\mathbf{r}) - \int_S \overline{\overline{Z}}(\mathbf{r}|\mathbf{r}') \cdot \mathbf{J}_S(\mathbf{r}')\, dS' \right] + \text{terms in } |\Delta\mathbf{J}_S|^2.$$

Investigate whether a Galerkin choice of testing vectors minimizes Δf (i.e., whether it leaves only the term in $|\Delta\mathbf{J}_S|^2$ in Δf).
(S. Wandzura, *Microwave Opt. Tech. Lett.* **4**, 199–200, 1991.)

12.3 Prove condition (12.12) by making use of the relationship

$$\text{div}\left(\mathbf{E}^i \times \mathbf{h}_m - jR_{c0}\, \mathbf{H}^i \times \mathbf{e}_m\right) = 0 \qquad (\text{for } k_0 = k_m).$$

Hint: Check this relationship, and integrate over the volume V_1 of the scatterer.

12.4 Investigate whether (12.26) has a solution at $k = k_m$; that is, whether $(\mathbf{u}_n \times \mathbf{h}_m)$ and $(\mathbf{u}_n \times \mathbf{H}^i)$ are orthogonal.

12.5 Prove (12.23), starting from the analog potential problem

$$\lim_{\delta \to 0} \left[\int_S \mathbf{f}_S(\mathbf{r}') \times \text{grad}' \left(\frac{1}{|\mathbf{r} - \mathbf{r}'|} \right) dS' \right]_{\text{tan}},$$

where $\mathbf{f}_S$ is a vector in the tangent plane.

12.6 Formulate the time-dependent EFIE for a scatterer that is not perfectly conducting but characterized by a surface impedance $Z_S(\omega)$, in terms of which

$$\mathbf{u}_n \times \mathbf{E}(\mathbf{r}, \omega) = \mathbf{u}_n \times [Z_S(\omega)\mathbf{J}_S(\mathbf{r}, \omega)].$$

Hint: Use the convolution

$$\mathbf{u}_n \times \mathbf{e}(\mathbf{r}, t) = \mathbf{u}_n \times \int_{-\infty}^{t} z_s(\tau)\, \mathbf{j}_S(\mathbf{r}, \tau - t)\, d\tau,$$

where $z_s(t)$ is the inverse Fourier transform of $Z_S(\omega)$.
(F. M. Tesche, *IEEE Trans. EMC* **32**, 1–4, 1990.)

12.7 At the surface of a rough body, the tangential components of $\mathbf{E}$ and $\mathbf{H}$ are often approximately related by an impedance condition

$$\mathbf{E}_{\text{tan}} = Z_S \mathbf{u}_n \times \mathbf{H}.$$

This relationship is quite accurate when the surface irregularities are small and distributed at random. Utilize this boundary condition to investigate the field scattered by a rough sphere immersed in an incident plane wave. The radius of the sphere is much larger than λ_0.
(R. E. Hiatt et al., *Proc. IRE* **48**, 2008, 1960.)

12.8 Show that the electric field in an inhomogeneous body satisfies the (uncoupled) equation

$$\mathbf{E}(\mathbf{r}) = \mathbf{E}^i(\mathbf{r}) + \int_V \overline{\overline{G}}(\mathbf{r}|\mathbf{r}') \cdot \left[k^2(\mathbf{r}) - k_0^2(\mathbf{r})\right] \cdot \mathbf{E}(\mathbf{r}')\, dV' - \int_V \overline{\overline{G}}(\mathbf{r}|\mathbf{r}') \cdot \left[\mu \operatorname{grad}\left(\frac{1}{\mu}\right) \times \operatorname{curl} \mathbf{E}(\mathbf{r}')\right] dV'.$$

([44] and H. Wang et al., *Electromagn.* **14**, 153–179, 1994.)

12.9 Show that the weighted residual solution of (12.95) can be written in the form (Fig. 12.13)

$$\int_S (\operatorname{grad} w \cdot \operatorname{grad} \phi^{sc} - k_0^2\, w\, \phi^{sc})\, dS + \int_{C_0} \left[w\, \alpha(r)\, \phi^{sc} - \beta(r) r^2 \frac{\partial w}{\partial c} \frac{\partial \phi^{sc}}{\partial c}\right] dc = -\int_S (\operatorname{grad} w \cdot \operatorname{grad} \phi^i + k_0^2\, w\, \phi^i)\, dS + \int_{C_0} w \frac{\partial \phi^i}{\partial r}\, dc.$$

The boundary conditions on the scatterer are either Dirichlet or Neumann.
(See [202, 203] and O. M. Ramahi et al., *IEEE Trans. MAG* **25**, 3043–3045, 1989.)

12.10 Determine the corresponding form based on the vector radiation condition.
(A. Chatterjee et al., *IEEE Trans. AP* **41**, 221–226, 1993.)

12.11 Show that a perfectly matched layer suitable for electrostatic fields can be constructed by means of a layer of fictitious anisotropic material with given $\epsilon_r < 1$ in a direction z perpendicular to the layer and with permittivity $(\epsilon_r)^{-1}$ in a direction tangent to the layer. The choice $\epsilon_r < 1$ ensures a fast decay in the z-direction.
(I. Ticar et al., *IEEE Trans. MAG* **35**, 1139–1142, 1999.)

12.12 Show that, when ϵ_r and μ_r are real, the following functional may be used to determine $\mathbf{E}$ [192]:

$$J(\mathbf{E}) = \int_V \left(-\frac{1}{\mu_r} \operatorname{curl} \mathbf{E} \cdot \operatorname{curl} \mathbf{E}^* + k_0^2 \epsilon_r\, \mathbf{E} \cdot \mathbf{E}^*\right) dV - \int_V \left(\mathbf{E} \cdot \mathbf{J}_1^* + \mathbf{E}^* \cdot \mathbf{J}_1\right) dV + \int_S \frac{1}{\mu_r} \left[(\mathbf{u}_n \times \mathbf{E}) \cdot \operatorname{curl} \mathbf{E}^* + (\mathbf{u}_n \times \mathbf{E}^*) \cdot \operatorname{curl} \mathbf{E}\right] dS.$$

12.13 In the transmission line problem of Figure 12.16, show that a resistive termination R_L imposes the condition

$$v^n(k) = \frac{3R_L}{4}\left[i^{n+\frac{1}{2}}\left(k - \frac{1}{2}\right) + i^{n-\frac{1}{2}}\left(k - \frac{1}{2}\right)\right] - \frac{R_L}{4}\left[i^{n+\frac{1}{2}}\left(k - \frac{3}{2}\right) + i^{n-\frac{1}{2}}\left(k - \frac{3}{2}\right)\right]$$

$$i^{n+\frac{1}{2}}\left(k-\frac{1}{2}\right)=\frac{1-\dfrac{3R_L\Delta t}{4L\Delta x}}{1+\dfrac{3R_L\Delta t}{4L\Delta x}}\,i^{n-\frac{1}{2}}\left(k-\frac{1}{2}\right)+\frac{\dfrac{\Delta t}{L\Delta x}}{1+\dfrac{3R_L\Delta t}{4L\Delta x}}\left\{\frac{R_L}{4}\left[i^{n+\frac{1}{2}}\left(k-\frac{3}{2}\right)+i^{n-\frac{1}{2}}\left(k-\frac{3}{2}\right)\right]+v^n(k-1)\right\},$$

where $k=(l/\Delta x)$ refers to the end point.

12.14 With respect to Figure 12.19, derive an expression for the input current $I\left[\left(n+\frac{1}{2}\right)\Delta t\right]$ one-half cell above the feed.
Hint: Express the current in terms of the circulating magnetic fields.
(W. V. Andrew et al., *IEEE Trans. EMC* **39**, 100–113, 1997.)

NOTES

1. A. W. Maue, Zur Formuliering eines Allgemeinen Beugungsproblem durch eine Integralgleichung, *Z. Physik* **126**, 601–618 (1949).
2. A. D. Yaghjian, Augmented electric — and magnetic — field integral equations, *Radio Sci.* **16**, 987–1001 (1981).
3. J. R. Mautz and R. F. Harrington, An *E*-field solution for a conducting surface small or comparable to the wavelength, *IEEE Trans. AP* **32**, 330–339 (1984).
4. J. S. Zhao and W. C. Chew, Integral equation solution of Maxwell's equations from zero frequency to microwave frequencies, *IEEE Trans. AP* **48**, 1635–1645 (2000).
5. B. H. Jung and T. K. Sarkar, Time-domain electric-field integral equation with central finite difference, *Microwave Opt. Tech. Lett.* **31**, 429–435 (2001).
6. S. M. Rao and D. R. Wilton, Transient scattering by conducting surfaces of arbitrary shape, *IEEE Trans. AP* **39**, 56–61 (1991).
7. G. Manara, A. Monorchio, and R. Reggiannini, A space-time discretization criterion for a stable time-marching solution of the electric field integral equation, *IEEE Trans. AP* **45**, 527–532 (1997).
8. S. M. Rao and T. K. Sarkar, An efficient method to evaluate the time-domain scattering from arbitrarily shaped conducting bodies, *Microwave Opt. Tech. Lett.* **17**, 321–325 (1998).
9. D. R. Wilton, Review of current status and trends in the use of integral equations in computational electromagnetics, *Electromagn.* **12**, 287–341 (1992).
10. B. P. Rynne and P. D. Smith, Stability of time marching algorithms for the electric field integral equation, *J. Electromagn. Waves Appl.* **4**, 1181–1205 (1990).
11. P. J. Davies, On the stability of time-marching schemes for the general surface electric-field integral equation, *IEEE Trans. AP* **44**, 1467–1473 (1996).
12. J. M. Rino, E. Úbeda, and J. Parrón, On the testing of the magnetic field equation with RWG basis functions in method of moments, *IEEE Trans. AP* **49**, 1550–1553 (2001).
13. C. L. Bennett and G. F. Ross, Time-domain electromagnetics and its applications, *Proc. IEEE* **66**, 299–318 (1978).
14. S. P. Walker, Developments in time-domain integral-equation modeling at Imperial College, *IEEE Antennas Prop. Mag.* **39**, 7–19 (1997).
15. M. J. Bluck, M. D. Pocock, and S. P. Walker, An accurate method for the calculation of singular integrals arising in time-domain integral equation analysis of electromagnetic scattering, *IEEE Trans. AP* **45**, 1793–1798 (1997).
16. P. D. Smith, Instabilities in time marching methods for scattering: cause and rectification, *Electromagn.* **10**, 439–451 (1990).
17. B. Shanker, A. A. Ergin, K. Aygün, and E. Michielssen, Analysis of transient electromagnetic scattering from closed surfaces using a combined field integral equation, *IEEE Trans. AP* **48**, 1064–1074 (2000).
18. B. H. Jung and T. K. Sarkar, Time domain CFIE for the analysis of transient scattering from arbitrarily shaped 3D conducting objects, *Microwave Opt. Tech. Lett.* **34**, 289–296 (2002).
19. M. B. Woodworth and A. D. Yaghjian, Derivation, application, and conjugate gradient solution of dual-surface integral equations for three-dimensional, multi-wavelength perfect conductors, in *PIER 5*,

J. A. Kong and T. K. Sarkar (eds.), Elsevier, New York (1991).

20. M. B. Woodworth and A. D. Yaghjian, Multiwavelength three-dimensional scattering with dual-surface integral equations, *J. Opt. Soc. Am.* **A-11**, 1399–1413 (1994).
21. R. A. Shore and A. D. Yaghjian, Dual surface electric field equation, Air Force Research Laboratory Report AFRL-SN-HS-TR-2001-013 (2001).
22. P. M. van den Berg, E. Korkmaz, and A. Abubakar, A constrained conjugate gradient method for solving the magnetic field boundary integral equation, *IEEE Trans. AP* **51**, 1168–1176 (2003).
23. Y. Leviatan and Z. Baharav, Overcoming the onset of ill conditioning at interior resonances by using generalized formulations, *Microwave Opt. Tech. Lett.* **9**, 49–52 (1995).
24. L. N. Medgyesi-Mitschang and J. M. Putnam, Integral equation formulations for imperfectly conducting scatterers, *IEEE Trans. AP* **33**, 206–214 (1985).
25. A. W. Glisson, Electromagnetic scattering by arbitrarely shaped surfaces with impedance boundary conditions, *Radio Sci.* **27**, 935–943 (1992).
26. K. M. Mitzner, An integral equation approach to scattering from a body of finite conductivity, *Radio Sci.* **2**, 1459–1470 (1967).
27. E. H. Newman, A sheet impedance approximation for electrically thick multilayered shields, *IEEE Trans. AP* **51**, 67–73 (2003).
28. J. G. Maloney and G. S. Smith, The efficient modeling of thin material sheets in the finite-difference time domain method, *IEEE Trans. AP* **40**, 323–330 (1992).
29. E. Bleszynski, M. Bleszynski, and T. Jaroszewickz, Surface-integral equations for electromagnetic scattering from impenetrable and penetrable sheets, *IEEE Antennas Prop. Mag.* **35**, 14–25 (1993).
30. P. C. Waterman, Matrix formulation of electromagnetic scattering, *Proc. IEEE* **53**, 805–812 (1965).
31. S. Ström and W. Zheng, Basic features of the null field method for dielectric scatterers, *Radio Sci.* **22**, 1273–1281 (1987).
32. J. Björkberg, Natural frequencies and eigencurrents of the elliptic disk, *Radio Sci.* **26**, 149–160 (1991).
33. Y. M. Wang and W. C. Chew, An efficient algorithm for solution of a scattering problem, *Microwave Opt. Tech. Lett.* **3**, 102–106 (1990).
34. P. C. Waterman, Matrix methods in potential theory and electromagnetic scattering, *J. Appl. Phys.* **50**, 4550–4566 (1979).
35. S. Ström and W. Zheng, Null-field computations of radar cross sections of composite objects, *Proc. IEEE* **77**, 761–769 (1989).
36. G. Kristensson, A. G. Ramm, and S. Ström, Convergence of the T-matrix approach in scattering theory II, *J. Math. Phys.* **24**, 2619–2631 (1983).
37. P. C. Waterman, Symmetry, unitarity and geometry in electromagnetic scattering, *Phys. Rev. D* **3**, 825–839 (1971).
38. J. H. Richmond, A wire-grid model for scattering by conducting bodies, *IEEE Trans. AP* **14**, 782–786 (1966).
39. K. S. H. Lee, L. Marin, and J. P. Castillo, Limitations of wire-grid modeling of a closed surface, *IEEE Trans. EMC* **18**, 123–129 (1976).
40. A. C. Ludwig, Wire grid modeling of surfaces, *IEEE Trans. AP* **35**, 1045–1048 (1987).
41. L. Gürck, K. Sertel, and I. K. Sendur, On the choice of basis functions to model surface electric current densities in computational electromagnetics, *Radio Sci.* **34**, 1373–1387 (1999).
42. A. W. Glisson, On the development of numerical techniques for treating arbitrarily-shaped surfaces, Ph.D. dissertation, University of Mississippi (1978).
43. S. M. Rao, D. R. Wilton, and A. W. Glisson, Electromagnetic scattering by surfaces of arbitrary shape, *IEEE Trans. AP* **30**, 409–418 (1982).
44. S. Wandzura, Electric current basis functions for curved surfaces, *Electromagn.* **12**, 77–91 (1992).
45. N. Y. Zhu and F. M. Landstorfer, Application of curved parametric triangular and quadrilateral edge elements in the moment method solution of the EFIE, *IEEE Microwave Guided Wave Lett.* **3**, 319–321 (1993).
46. C. J. Huber, W. Rieger, M. Haas, and W. M. Rucker, Application of curvilinear higher order edge elements to scattering problems using the boundary element method, *IEEE Trans. MAG* **35**, 1510–1513 (1999).
47. W. J. Brown and D. R. Wilton, Singular basis functions and curvilinear triangles in the solution of the electric field integral equations, *IEEE Trans. AP* **47**, 347–353 (1999).
48. B. M. Kolundzya and B. D. Popovic, Entire-domain Galerkin method for analysis of metallic antennas and scatterers, *IEE Proc.* **140-H**, 1–10 (1993).
49. G. Kang, J. Song, W. C. Chew, D. Donepudi, and J. M. Jin, A novel grid-robust higher order vector basis function for the method of moments, *IEEE Trans. AP* **49**, 908–915 (2001).
50. J. Wang and J. P. Webb, Hierarchal vector boundary elements and p-adaption for 3-D electromagnetic scattering, *IEEE Trans. AP* **45**, 1869–1879 (1997).
51. J. P. Webb, Hierarchal vector basis functions of arbitrary order for triangular and tetrahedral finite elements, *IEEE Trans. AP* **47**, 1244–1253 (1999).
52. T. K. Sarkar, K. R. Starkiewicz, and R. F. Stratton, Survey of numerical methods for solution of large systems of linear equations for electromagnetic field problems, *IEEE Trans. AP* **29**, 847–856 (1981).
53. A. F. Peterson and R. Mittra, Method of conjugate gradients for the numerical solution of large-body electromagnetic scattering problems, *J. Opt. Soc. Am. A* **2**, 971–977 (1985).
54. A. F. Peterson and R. Mittra, Convergence of the conjugate gradient method when applied to matrix equations representing electromagnetic scattering problems, *IEEE Trans. AP* **34**, 1447–1454 (1986).

55. A. F. Peterson, C. F. Smith, and R. Mittra, Eigenvalues of the moment-method matrix and their effect on the convergence of the conjugate gradient algorithm, *IEEE Trans. AP* **36**, 1177–1179 (1988).
56. E. Bleszynski, M. Bleszynski, and T. Jaroszewicz, AIM: adaptive integral method for solving large-scale electromagnetic scattering and radiation problems, *Radio Sci.* **31**, 1225–1251 (1996).
57. H. T. Anastassiu, M. Smeljansky, S. Bindiganavale, and J. L. Volakis, Scattering from relatively flat surfaces using the adaptive integral method, *Radio Sci.* **33**, 7–16 (1998).
58. M. L. Waller and S. M. Rao, Application of adaptive basis functions for a diagonal moment matrix solution of arbitrarily-shaped three dimensional conducting body problems, *IEEE Trans. AP* **50**, 1445–1452 (2002).
59. C. J. Reddy, M. D. Deshpande, C. R. Cockrell, and F. B. Beck, Fast RCS computation over a frequency band using method of moments in conjunction with asymptotic waveform evaluation technique, *IEEE Trans. AP* **46**, 1229–1233 (1998).
60. D. Jiao, X. Y. Zhu, and J. M. Jin, Fast and accurate frequency-sweep calculations using asymptotic waveform evaluation and the combined-field integral equation, *Radio Sci.* **34**, 1055–1063 (1999).
61. J. E. Bracken, D. K. Sun, and Z. J. Cendes, *S*-domain methods for simultaneous time and frequency characterization of electromagnetic devices, *IEEE Trans. MTT* **46**, 1277–1290 (1998).
62. K. Umashankar, A. Taflove, and S. M. Rao, Electromagnetic scattering by arbitrary shaped three-dimensional homogeneous lossy dielectric objects, *IEEE Trans. AP* **34**, 758–765 (1986).
63. L. N. Medgyesi, J. M. Putnam, and M. B. Gedera, Generalized method of moments for three-dimensional penetrable scatterers, *J. Opt. Soc. Am. A* **11**, 1383–1398 (1994).
64. P. L. Huddleston, L. N. Medgyesi-Mitschang, and J. M. Putnam, Combined field integral equation formulation for scattering by dielectrically coated conducting bodies, *IEEE Trans. AP* **34**, 510–520 (1986).
65. P. M. Goggans, A. A. Kishk, and A. W. Glisson, Electromagnetic scattering from objects composed of multiple homogeneous regions using a region-by-region solution, *IEEE Trans. AP* **42**, 865–871 (1994).
66. A. Herschlein, J. von Hagen, and W. Wiesbeck, A generalized integral equation formulation for mixed dielectric - PEC scatterers, *Radio Sci.* **37**, 11-1 to 11-15 (2002).
67. S. M. Rao and T. K. Sarkar, Numerical solution of time domain integral equations for arbitrarily shaped conductor-dielectric composite bodies, *IEEE Trans. AP* **50**, 1831–1837 (2002).
68. A. W. Glisson, An integral equation for electromagnetic scattering from homogeneous dielectric bodies, *IEEE Trans. AP* **32**, 173–175 (1984).
69. E. Marx, Integral equation for scattering by a dielectric, *IEEE Trans. AP* **32**, 166–172 (1984).
70. M. S. Yeung, Single integral equation for electromagnetic scattering by three-dimensional homogeneous dielectric objects, *IEEE Trans. AP* **47**, 1615–1622 (1999).
71. D. Kajfez, A. W. Glisson, and J. James, Computed modal field distributions for isolated dielectric resonators, *IEEE Trans. MTT* **32**, 1609–1616 (1984).
72. J. L. Volakis, Alternative field representations and integral equations for modeling inhomogeneous dielectrics, *IEEE Trans. MTT* **40**, 604–608 (1992).
73. D. H. Schaubert, D. R. Wilton, and A. W. Glisson, A tetrahedral modeling method for electromagnetic scattering by arbitrarily shaped inhomogeneous dielectric bodies, *IEEE Trans. AP* **32**, 77–85 (1984).
74. P. Zwamborn and P. M. van den Berg, The three-dimensional weak form of the conjugate gradient FFT method for solving scattering problems, *IEEE Trans. MTT* **40**, 1757–1765 (1992).
75. P. Zwamborn and P. M. van den Berg, Computation of electromagnetic fields inside strongly inhomogeneous objects by the weak-conjugate gradient Fast-Fourier-Transform method: *J. Opt. Soc. Am. A* **11**, 1414–1421 (1994).
76. D. E. Livesay and K. M. Chen, Electromagnetic fields induced inside arbitrarily shaped biological bodies, *IEEE Trans. MTT* **22**, 1273–1280 (1974).
77. W. D. Hurt, J. M. Zirias, and P. A. Mason, Variability in EMF permittivity values: implications for SAR calculations, *IEEE Trans. Biomed. Eng.* **47**, 396–401 (2000).
78. M. A. Jensen and Y. Rahmat-Samii, EM interaction of handset antennas and a human in personal communications, *Proc. IEEE* **83**, 7–17 (1995).
79. K. R. Foster, L. S. Erdreich, and J. E. Moulder, Weak electromagnetic fields and cancer in the context of risk assessment, *Proc. IEEE* **85**, 733–746 (1997).
80. J. C. Lin, Lens specification and radio-frequency electromagnetic radiation, *URSI Radio Sci. Bull.* **305**, 51–54 (2003).
81. H. Massoudi, C. H. Durney, and M. F. Iskander, Limitations of the cubical block model of man in calculating SAR distributions, *IEEE Trans. MTT* **32**, 746–752 (1984).
82. B. M. Notaroš, B. D. Popović, J. P. Weem, R. A. Brown, and Z. Popović, Efficient large domain MoM solutions to electrically large practical EM problems, *IEEE Trans. MTT* **49**, 151–159 (2001).
83. K. Sertel and J. L. Volakis, Method of moments solution of volume integral equations using parametric geometry modeling, *Radio Sci.* **37**, 10-1 to 10-7 (2002).
84. B. C. Usner, K. Sertel, and J. L. Volakis, Conformal Galerkin testing for VIE using parametric geometry, *Electron. Lett.* **40**, 926–928 (2004).
85. S. M. Rao and T. K. Sarkar, Implicit solution of time-domain integral equations for arbitrarily shaped dielectric bodies, *Microwave Opt. Tech. Lett.* **21**, 201–205 (1999).

86. N. T. Gres, A. A. Ergin, and E. Michielssen, Volume-integral-equation-based analysis of transient electromagnetic scattering from three-dimensional inhomogeneous dielectric objects, *Radio Sci.* **36**, 379–386 (2001).
87. B. P. Rynne, Time domain scattering from dielectric bodies, *Electromagn.* **14**, 181–193 (1994).
88. M. D. Pocock, M. J. Bluck, and S. P. Walker, Electromagnetic scattering from 3-D curved dielectric bodies using time-domain integral equations, *IEEE Trans. AP* **46**, 1212–1219 (1998).
89. C. H. Wilcox, An expansion theorem for electromagnetic fields, *Comm. Pure Appl. Math.* **9**, 115–134 (1956).
90. A. Bayliss and E. Turkel, Radiation boundary conditions for wave-like equations, *Comm. Pure Appl. Math.* **33**, 707–725 (1980).
91. A. Bayliss, M. Gunzburger, and E. Turkel, Boundary conditions for the numerical solution of elliptic equations in exterior regions, *SIAM J. Appl. Math.* **47**, 430–451 (1982).
92. A. F. Peterson, Accuracy of the 3-D radiation boundary conditions for use with the vector Helmholtz equation, *IEEE Trans. AP* **40**, 351–355 (1992).
93. J. L. Volakis, A. Chatterjee, and L. C. Kempel, Review of the finite-element method for three-dimensional electromagnetic scattering, *J. Opt. Soc. Am. A* **11**, 1422–1433 (1994).
94. A. Chatterjee and J. L. Volakis, Conformal absorbing boundary conditions for the vector wave equation, *Microwave Opt. Tech. Lett.* **6**, 886–889 (1993).
95. D. B. Meade, G. W. Slade, A. F. Peterson, and K. J. Webb, Comparison of local boundary conditions for the scalar Helmholtz equation with general boundary shapes, *IEEE Trans. AP* **43**, 6–10 (1995).
96. O. M. Ramahi, Absorbing boundary conditions for convex object-conformable boundaries, *IEEE Trans. AP* **47**, 1141–1145 (1999).
97. B. Engquist and A. Majda, Absorbing boundary conditions for the numerical solution of waves, *Math. Comp.* **31**, 629–651 (1977).
98. G. Mur, Absorbing boundary conditions for the finite-difference approximation of the time-domain electromagnetic-field equations, *IEEE Trans. EMC* **23**, 377–382 (1981).
99. A. Rahhah-Arabi and R. Mittra, An alternate form of the Mur second-order absorbing boundary condition, *Microwave Opt. Tech. Lett.* **9**, 336–338 (1995).
100. C. J. Railton and E. M. Daniel, A comparison of the properties of radiating boundary conditions in the FDTD method for finite discretisation and non-planar waves, *IEEE Trans. AP* **42**, 276–281 (1994).
101. J. A. Svigelj and R. Mittra, The dispersive boundary condition applied to nonuniform orthogonal meshes, *IEEE Trans. MTT* **47**, 257–264 (1999).
102. N. Sachdeva, N. Bclakrishnan, and S. M. Rao, A new absorbing boundary condition for FDTD, *Microwave Opt. Tech. Lett.* **25**, 86–90 (2000).
103. M. S. Sarto, Innovative absorbing-boundary conditions for the efficient FDTD analysis of lightning-interaction problems, *IEEE Trans. EMC* **43**, 368–381 (2001).
104. K. K. Mei and J. Fang, Superabsorption — a method to improve absorbing boundary conditions, *IEEE Trans. AP* **40**, 1001–1010 (1992).
105. D. S. Katz, E. T. Thiele, and A. Taflove, Validation and extension to three dimensions of the Bérenger PML absorbing boundary condition for FD-TD meshes, *IEEE Microwave Guided Wave Lett.* **4**, 268–270 (1994).
106. H. Rogier, D. De Zutter, and F. Olyslager, A new FDTD-boundary integral equation technique with biconjugate gradient solver for analyzing scattering problems, *A.E.Ü.* **54**, 227–232 (2000).
107. X. Q. Sheng, J. M. Jin, J. Song, C. C. Lu, and W. C. Chew, On the formulation of hybrid finite-element and boundary-integral methods for 3D scattering, *IEEE Trans. AP* **46**, 303–311 (1998).
108. G. Mur, The finite-element modeling of three-dimensional electromagnetic fields using edge and nodal elements, *IEEE Trans. AP* **41**, 948–953 (1993).
109. Y. Y. Botros and J. L. Volakis, Perfectly matched layer termination for finite-element meshes: implementation and application, *Microwave Opt. Tech. Lett.* **23**, 166–172 (1999).
110. J. Jin and W. C. Chew, Variational formulation of the electromagnetic boundary-value problems involving anisotropic media, *Microwave Opt. Tech. Lett.* **7**, 348–351 (1994).
111. R. Dyczij, G. Peng, and J. F. Lee, A fast vector-potential method using tangentially continuous vector finite elements, *IEEE Trans. MTT* **46**, 863–867 (1998).
112. J. F. Lee and Z. Sacks, Whitney elements time domain methods, *IEEE Trans. MAG* **31**, 1325–1329 (1995).
113. J. F. Lee, R. Lee, and A. Cangellaris, Time-domain finite-element methods, *IEEE Trans. AP* **45**, 430–442 (1997).
114. K. Mahadevan and R. Mittra, Radar cross section computation of inhomogeneous scatterers using edge-based finite element methods in frequency and time domains, *Radio Sci.* **28**, 1181–1193 (1993).
115. M. Feliziani and F. Maradei, Hybrid finite element solutions of time dependent Maxwell's curl equations, *IEEE Trans. MAG* **31**, 1330–1335 (1995).
116. D. Jiao, A. A. Ergin, B. Shanker, E. Michielssen, and J. M. Jin, A fast higher-order time-domain finite-element boundary integral method for 3-D electromagnetic scattering analysis, *IEEE Trans. AP* **50**, 1192–1201 (2002).
117. D. Jiao and J. M. Jin, Three-dimensional orthogonal vector basis functions for time-domain finite element solution of vector wave equations, *IEEE Trans. AP* **51**, 59–66 (2003).
118. D. Jiao, J. M. Jin, E. Michielssen, and D. J. Riley, Time-domain finite-element simulation of three-dimensional scattering and radiation problems using perfectly matched layers, *IEEE Trans. AP* **51**, 296–304 (2003).

119. A. Fijany, M. A. Jensen, Y. Rahmat-Samii, and J. Barthen, A massively parallel computation strategy for FDTD: time and space parallelism applied to electromagnetics problems, *IEEE Trans. AP* **43**, 1441–1449 (1995).
120. L. Martens, J. De Moerloose, D. De Zutter, J. De Poorter, and C. De Wagter, Calculation of the electromagnetic fields induced in the head of an operator of a cordless telephone, *Radio Sci.* **30**, 283–290 (1995).
121. C. M. Furse, Faster than Fourier: ultra-efficient time-to-frequency-domain conversions for FDTD simulations, *IEEE Ant. Prop. Mag.* **42**, 24–33 (2000).
122. K. S. Yee, Numerical solution of initial boundary value problems involving Maxwell's equations in isotropic media, *IEEE Trans. AP* **14**, 302–307 (1966).
123. A. Taflove and K. R. Umashankar, Review of FD-TD numerical modeling of electromagnetic wave scattering and radar cross section, *Proc. IEEE* **77**, 682–699 (1989).
124. A. Taflove, Review of the formulation and applications of the finite-difference time-domain method for numerical modeling of electromagnetic wave interactions with arbitrary structures, *Wave Motion* **10**, 547–582 (1988).
125. C. Schuster, A. Christ, and W. Fichtner, Review of FDTD time-stepping schemes for efficient simulation of electric conductive media, *Microwave Opt. Tech. Lett.* **25**, 16–21 (2000).
126. R. Luebbers, F. P. Hunsberger, K. S. Kunz, R. B. Standler, and M. Schneider, A frequency-dependent finite-difference time-domain formulation for dispersive materials, *IEEE Trans. EMC* **32**, 222–227 (1990).
127. M. Piket-May, A. Taflove, and J. Baron, FD-TD modeling of digital signal propagation in 3-D circuits with passive and active loads, *IEEE Trans. MTT* **42**, 1514–1523 (1994).
128. U. Oguz and L. Gürel, Interpolation techniques to improve the accuracy of the plane wave excitations in the finite difference time domain method, *Radio Sci.* **32**, 2189–2199 (1997).
129. W. Yuan, C. Liang, X. Shi, and B. Wang, Effects of current source models on numerical performances in FDTD simulations, *Microwave Opt. Tech. Lett.* **27**, 4–7 (2000).
130. E. Semouchkina, W. Cao, and R. Mittra, Source excitation methods for the finite-difference time-domain modeling of circuits and devices, *Microwave Opt. Tech. Lett.* **21**, 93–100 (1999).
131. W. V. Andrew, C. A. Balanis, P. A. Tirkas, J. Peng, and C. R. Birtcher, Finite-difference time-domain analysis of HF antennas on helicopter airframes, *IEEE Trans. EMC* **39**, 100–113 (1997).
132. R. Luebbers, L. Chen, T. Uno, and S. Adachi, FDTD calculation of radiation patterns, impedance and gain for a monopole antenna on a conducting box, *IEEE Trans. AP* **40**, 1577–1582 (1992).
133. D. M. Sheen, S. M. Ali, M. D. Abouzahra, and J. A. Kong, Application of the three-dimensional finite-difference time-domain method to the analysis of planar microstrip circuits, *IEEE Trans. MTT* **38**, 849–857 (1990).
134. J. Y. Chen, C. M. Furse, and O. P. Gandhi, A simple convolution procedure for calculating currents induced in the human body for exposure to electromagnetic pulses, *IEEE Trans. MTT* **42**, 1172–1175 (1994).
135. R. Holland, L. Simpson, and K. S. Kunz, Finite-difference analysis of EMP coupling to lossy dielectric structures, *IEEE Trans. EMC* **22**, 203–209 (1980).
136. A. C. Cangellaris and D. B. Wright, Analysis of the numerical error caused by the stair-stepped approximation of a conducting boundary in FDTD simulations of electromagnetic phenomena, *IEEE Trans. AP* **39**, 1518–1525 (1991).
137. T. G. Jurgens, A. Taflove, K. Umashankar, and T. G. Moore, Finite-difference time-domain modeling of curved surfaces, *IEEE Trans. AP* **40**, 357–366 (1992).
138. R. Holland, Finite-difference solution of Maxwell's equations in generalized nonorthogonal coordinates, *IEEE Trans. NS* **30**, 4589–4591 (1983).
139. M. A. Fusco, M. V. Smith, and L. W. Gordon, A three-dimensional FDTD algorithm in curvilinear coordinates, *IEEE Trans. AP* **39**, 1463–1471 (1991).
140. K. S. Yee, J. S. Chen, and A. H. Chang, Conformal finite-difference time-domain (FDTD) with overlapping grids, *IEEE Trans. AP* **40**, 1068–1075 (1992).
141. S. Dey and R. Mittra, A modified locally conformal finite-difference, time-domain algorithm for modeling three-dimensional perfectly conducting objects, *Microwave Opt. Tech. Lett.* **17**, 349–352 (1998).
142. S. Dey and R. Mittra, A conformal finite-difference time-domain technique for modeling cylindrical dielectric resonators, *IEEE Trans. MTT* **47**, 1737–1739 (1999).
143. N. K. Madsen and R. W. Ziolkowski, A three-dimensional modified finite volume technique for Maxwell's equations, *Electromagn.* **10**, 147–161 (1990).
144. K. S. Yee and J. S. Chen, Conformal hybrid finite difference time domain and finite volume time domain, *IEEE Trans. AP* **42**, 1450–1455 (1994).
145. R. B. Wu and T. Itoh, Hybrid finite-difference time-domain modeling of curved surfaces using tetrahedral edge elements, *IEEE Trans. AP* **45**, 1302–1309 (1997).

Chapter 13

High- and Low-Frequency Fields

The outer regions of the frequency range — high and low — have received unequal attention in the *radio* literature. Much more emphasis has been laid on high-frequency techniques, which become predominant when the characteristic length L of the scatterer is much larger than the wavelength λ_0 of the incident wave. Such a situation exists, for example, when a large aircraft is illuminated by a 10 GHz radar pulse. Some elementary results of HF theory are derived in Sections 8.3 and 8.4, basically by expanding the **E** and **H** fields in terms of the small parameter $(1/k_0L)$. A few additions to the theory are presented in Sections 13.1 to 13.5. They hardly do justice to the difficulty — and elegance — of the subject; a separate volume would be needed for the purpose. Such books exist, of course, and are frequently referred to in the text.

The situation is different at the low-frequency end of the spectrum. The small parameter is now k_0L, and an expansion of the fields in terms of k_0L — the *Rayleigh method* — is the basic approach. The literature on the LF region is not very abundant, and the theory is relatively simple. A fairly detailed description of the subject can therefore be developed within a reasonable number of pages. The *radio scientist* will find the LF approximation useful in starting a "σ^{sc} vs. frequency" curve on the LF side and even extending it toward the resonance region by including additional terms in the (k_0L) expansion. But it is for the *power engineer* that the quasi-static approximation becomes indispensable, for example for the evaluation of the magnetic field near transformers and alternators. The geometry of these devices can be very complex, and the materials are generally nonlinear and inhomogeneous. The numerical problems, in particular under transient conditions, can therefore become quite formidable. Their solution forms a most active part of the current electromagnetic literature.

13.1 PHYSICAL OPTICS

The solution of field problems at high frequencies can seldom be effected by the methods used so successfully at low and median frequencies. Separation of variables, whenever possible, often converges too slowly to be of practical interest. Integral equations do not fare better: they require at least 10 points per λ_0 to achieve acceptable accuracy; that is, 100 points per λ_0^2, or 1000 points per λ_0^3. Approximate methods, based on *Physical optics* and *Geometrical optics*, avoid these lengthy computations but run into difficulties when the scatterer has singularities such as edges, corners, or vertices or when the contribution

Electromagnetic Fields, Second Edition, By Jean G. Van Bladel

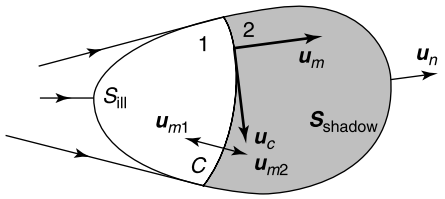

Figure 13.1 Light-shadow boundary C on a scatterer.

from the geometrical shadow region becomes important. Two theories have been proposed to correct this situation: the *geometrical theory of diffraction* (GTD), which introduces additional rays generated by the discontinuities, and the *physical theory of diffraction* (PTD). Both methods rely on the known solution of some *canonical* problems.

13.1.1 Physical Optics

Let a convex perfectly conducting scatterer be immersed in the field of a bundle of rays (Fig. 13.1). The scatterer is of simple shape, with clearly distinguished illuminated and shadow zones. The *physical optics* approximation (P.O.) assumes that the current density vanishes on the shadow side and has the value

$$\mathbf{J}_S = 2(\mathbf{u}_n \times \mathbf{H}^i) \tag{13.1}$$

on the illuminated side of the scatterer. From (9.22), this is precisely the current induced on a perfectly conducting plane. It is clear that the P.O. assumption suffers from two shortcomings:

- The transition from light to shadow is abrupt, while continuity may be expected.
- The curvature of the surface is neglected. The method must therefore fail in the presence of surfaces with strong curvature, in particular at edges and vertices.

With the assumed value of (13.1) $\mathbf{J}_S$, the vector potential becomes

$$\mathbf{A}^{sc} = \frac{\mu_0}{2\pi} \int_{S_{ill}} (\mathbf{u}_n \times \mathbf{H}^i) \frac{e^{-jk_0|\mathbf{r}-\mathbf{r}'|}}{|\mathbf{r}-\mathbf{r}'|}\, dS'. \tag{13.2}$$

In the radiation zone, in a direction of unit vector $\mathbf{u}$,

$$\lim_{R\to\infty} \mathbf{A}^{sc} = \frac{e^{-jk_0R}}{R} \frac{\mu_0}{2\pi} \int_{S_{ill}} (\mathbf{u}_n \times \mathbf{H}^i) \cdot e^{jk_0\mathbf{u}\cdot\mathbf{r}'}\, dS' = \frac{e^{-jk_0R}}{R} \mathbf{N}(\mathbf{u}). \tag{13.3}$$

The resulting electric field is*

$$\mathbf{E}^{sc} = j\omega \frac{e^{-jk_0R}}{R} \mathbf{u} \times [\mathbf{u} \times \mathbf{N}(\mathbf{u})] \qquad (R \to \infty). \tag{13.4}$$

The assumed discontinuity of $\mathbf{J}_S$ on the surface does not create any problem for the evaluation of $\mathbf{A}^{sc}$, and the same holds for $\mathbf{E}^{sc}$ when it is obtained by differentiation of $\mathbf{A}^{sc}$. The situation

*For a typical application, see Note 1.

is different, however, where $\mathbf{E}$ is expressed *directly* in terms of $\mathbf{J}_S$ by means of (7.222). The term $(\mathbf{u}_n \cdot \mathbf{E})$ in this equation is strongly singular because

$$\mathbf{u}_n \cdot \mathbf{E} = \frac{1}{j\omega\epsilon_0}\, \mathbf{u}_n \cdot \operatorname{curl} \mathbf{H} = \frac{1}{j\omega\epsilon_0}\, \operatorname{div}_S (\mathbf{H} \times \mathbf{u}_n) = -\frac{1}{j\omega\epsilon_0}\, \operatorname{div}_S \mathbf{J}_S = \frac{1}{\epsilon_0} P_S. \tag{13.5}$$

Because the assumed $\mathbf{J}_S$ suffers a step discontinuity, P_S becomes infinite at the light-shadow boundary, which implies that a linear charge density P_L appears there. From the equation of continuity, it follows that

$$j\omega P_L = \mathbf{u}_m \cdot \mathbf{J}_S = \mathbf{u}_m \cdot 2(\mathbf{u}_n \times \mathbf{H}^i) = 2(\mathbf{u}_c \cdot \mathbf{H}^i). \tag{13.6}$$

In this equation, $\mathbf{u}_m$ is a unit vector perpendicular to C and situated in the tangent plane (Fig. 13.1). In the language of distributions one could write, as in (A8.90),

$$\operatorname{div}_S \mathbf{J}_S = \{\operatorname{div}_S \mathbf{J}_S\} + (\mathbf{u}_{m1} \cdot \mathbf{J}_{S1} + \mathbf{u}_{m2} \cdot \mathbf{J}_{S2})\, \delta_c. \tag{13.7}$$

To gain a better idea of the accuracy of the P.O. approximation, it may be noted that the exact value of $\mathbf{J}_S$ is not (13.1) but is given more accurately by (12.26), that is, by

$$\mathbf{J}_S(\mathbf{r}) = 2\left(\mathbf{u}_n \times \mathbf{H}^i(\mathbf{r})\right) + 2\mathbf{u}_n(\mathbf{r}) \times \lim_{\delta \to 0} \int_{S - S_\delta} \operatorname{grad}' G_0(\mathbf{r}|\mathbf{r}') \times \mathbf{J}_S(\mathbf{r}')\, dS'. \tag{13.8}$$

The second term in the right-hand side can be shown, by careful evaluation, to approach zero (to first order in k_0^{-1}) when $\mathbf{r}$ is on the *light* side, and $-2(\mathbf{u}_n \times \mathbf{H}^i)$ when $\mathbf{r}$ is in the *shadow*.[2] The departure from these limit values is a correction to the P.O. approximation.

13.1.2 Points of Stationary Phase

The field scattered from an obstacle is given by (13.4). In the simple configuration of Figure 13.2, where the scatterer is a circular cylinder, $\mathbf{u}_n \times \mathbf{H}^i$ is proportional to $\cos\theta\, e^{jk_0 z}\, \mathbf{u}_y$. When this value is inserted into (13.3), the backscattered E field is found to be proportional to the integral

$$I = \int_{\theta=0}^{2\pi} \cos\theta'\, e^{j2k_0 z'}\, dc'. \tag{13.9}$$

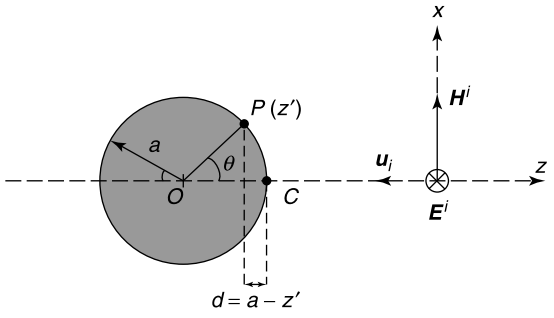

Figure 13.2 Point of stationary phase C.

Let us investigate the contribution to this integral from the vicinity of the point marked C, for which $\theta \approx 0$. Because

$$d = a - z' = a(1 - \cos\theta_P) = 2a \sin^2 \frac{\theta_P}{2} \approx \frac{a}{2}\theta_P^2,$$

the integral can be written in the approximate form

$$I \doteq \int_{\theta}^{\theta_P} e^{-jk_0 a\,\theta^2}\, d\theta \doteq \int_0^{\tau_P} e^{-j\frac{\pi}{2}\tau^2}\, d\tau. \tag{13.10}$$

This is actually the Fresnel integral (9.231), which varies with τ_P in accordance with the data in Figure 9.46. The main contribution stems from the vicinity of C, where the phase $(k_0 a\,\theta^2)$ remains stationary, and fields add up constructively. This remains so up to a distance d of the order $(\lambda_0/4)$, which defines the first *Fresnel zone*. Further away from C, on the contour, the phase loses its stationary character, starts oscillating rapidly, and creates destructive interferences between the contributions of the successive zones.

The conclusions reached for the simple scatterer considered above can be extrapolated to other targets, in particular to the sphere. More generally, the phase in an integral of the form

$$I = \int_S g(\mathbf{r})\, e^{-jk_0\phi(\mathbf{r})}\, dS \tag{13.11}$$

is stationary at points where $\text{grad}_S\, \phi(\mathbf{r}) = 0$. These points have been called *critical points of the first kind*.[3] Critical points of the *second kind* are found when, in an integral similar to (13.11) but taken on a curve C (e.g., along the rim of an aperture), the condition $(\partial\phi/\partial c) = 0$ is satisfied. Discontinuous variations of the tangent along the curve give rise to *critical points of the third kind*.

In many cases, the dominant high-frequency fields scattered from a (large) target originate mainly from a discrete set of critical points located on the target, the *scattering centers* (Fig. 13.3). Various methods are available to determine the location of these centers,[4] for example by first obtaining the target characteristics through numerical simulation or actual measurement.[5] Symbolically, the image pattern can be represented by the sum

$$\text{Image}\,(\mathbf{r}) \approx \sum_{n=1}^{N} A_n\, h(\mathbf{r} - \mathbf{r}_n).$$

Such a finite sum of contributions is computationally economical. If, for example, the target is a large rectangular plate illuminated obliquely by a plane wave, a large number of rays may be needed to generate the scattering pattern, while it might take only four scattering centers at the corners of the plate to accomplish the same purpose.

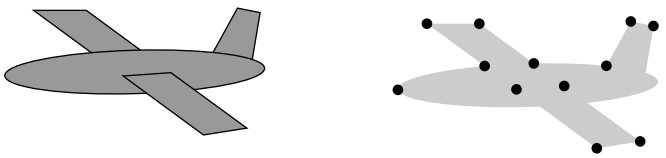

Figure 13.3 Scattering center representation of a target (from R. Bhalla and H. Ling, Three-dimensional scattering center extraction using the shooting and bouncing ray technique, *IEEE Trans. AP* **44**, 1445–1453, 1996, with permission of IEEE).

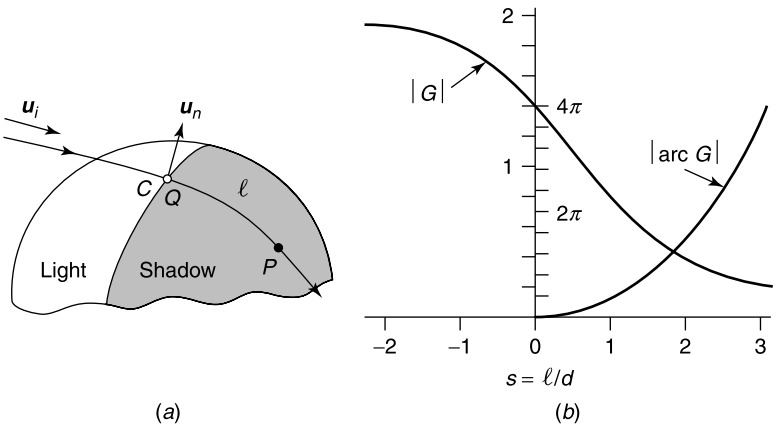

Figure 13.4 (*a*) Point P in the near shadow zone. (*b*) Variation of the complex function $G(s)$.

13.1.3 The Light-Shadow Transition

The current does not suddenly stop at the light-shadow boundary C but penetrates into the shadow zone, albeit with fast decreasing amplitude (Fig. 13.4*a*). The transition takes place in a narrow strip, of width of the order

$$d = \left[\frac{\lambda_0}{\pi} R_0^2\right]^{\frac{1}{3}}, \tag{13.12}$$

where R_0 is the radius of curvature of the surface in the $(\mathbf{u}^i, \mathbf{u}_n)$ plane [63, 113]. The way $\mathbf{J}_S$ varies is obtained by means of *Fock'sprinciple of the local field*, according to which $\mathbf{J}_S$ in P depends only on the geometrical shape of S *near* P (in particular between Q and P) and on the polarization of the fields. Current $\mathbf{J}_S$ is otherwise independent of its value at distant points. The important parameters are therefore the principal radii of curvature of the surface, and a universal law can be obtained by solving for a well-chosen convex body, for example a paraboloid of revolution, which can have a range of values of R_1 and R_2. The result, for a perfectly conducting surface, is

$$\mathbf{J}_S(P) = (\mathbf{u}_n \times \mathbf{H}^i)_Q \, G\left(\frac{l}{d}\right)_P, \tag{13.13}$$

where l is the distance from the C boundary, measured in the $(\mathbf{u}_i, \mathbf{u}_n)$ plane (a principal plane), and in the direction of the geodesic surface ray. The function $G(s)$ results from a complex integration involving Airy functions. We shall only give the end result, more precisely the variation of G as a function of $s = (l/d)$, for $\mathbf{E}$ polarized along $\mathbf{u}_n$ at Q. Data are shown graphically in Figure 13.4*b* and numerically in Table 13.1. The amplitude $|G|$ starts from 2 on the illuminated side and decreases exponentially into the shadow zone.

Table 13.1 Some Values of $|G(s)|$

s	−4	−3	−2	−1	0	1	2	3	4
$\|G\|$	1.9995	1.988	1.982	1.861	1.399	0.738	0.315	0.13	0.0537

The phase of G remains close to zero initially, reaches $(-45°)$ at $s = 1$, and dips further in the shadow, where the current generates a creeping wave.

The theory of Fock can be extended to scatterers characterized by a *Leontovich surface impedance*. It can also yield the value of the fields close to the surface [38]. The case of a flat section smoothly joined to a parabolic section is instructive,[6] because it shows the effect of a step discontinuity in curvature on the propagation of the surface wave. The topic is further discussed in Section 13.3.

13.2 GEOMETRICAL OPTICS

High-frequency propagation and ray tracing are discussed briefly in Sections 8.3 and 8.4. It is shown there that the fields $(\mathbf{E}, \mathbf{H})$ behave locally as in a plane wave, provided the wavelength is much shorter than the scale of variation of the parameters of the medium. The ray approach will now be invoked to determine the scattered fields from a perfectly conducting target, immersed in the far field of a source S radiating in free space (Fig. 13.5*a*). The radiated field can always be represented as the sum of two linearly polarized fields. It is therefore sufficient to investigate the scattering phenomenon for an arbitrary linearly polarized wave. Assume that the incident electric field in the direction 0 is given by the expression

$$\mathbf{E}^i = \mathbf{u}_p(0)\frac{e^{-jk_0R}}{R}F_t(0). \tag{13.14}$$

The basic tenet of *geometrical optics* (G.O.) consists in assuming that an incident ray is reflected by the scatterer as if the latter's surface were plane at the reflection point. Clearly, the quality of the approximation depends on how small λ_0 is with respect to the principal radii of curvature R_1 and R_2. In accordance with the results of Section 9.1, the reflected wave in the direction 1 is also linearly polarized. Its far field, which can be calculated by fairly straightforward methods, is given by [118]

$$\mathbf{E} = \frac{e^{-jk_0s}}{s}RD^{\frac{1}{2}}\mathbf{E}^r(P), \tag{13.15}$$

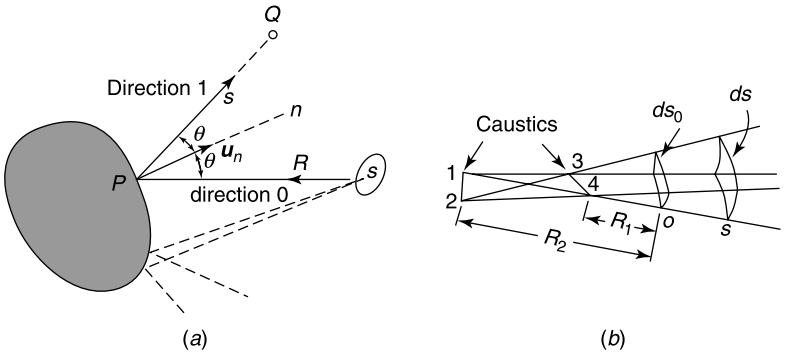

Figure 13.5 (*a*) Scattering according to *geometrical optics*. (*b*) Caustics.

where $\mathbf{E}^r$ is the reflected field at the surface, calculated as if the latter were plane.† More precisely,

$$\mathbf{E}^r(P) = (\mathbf{u}_n \cdot \mathbf{E}^i)\,\mathbf{u}_n + \mathbf{u}_n \times (\mathbf{u}_n \times \mathbf{E}^i) = \mathbf{E}^i(P) \cdot \overline{\overline{R}} \tag{13.16}$$

where $\overline{\overline{R}}$ is the reflection matrix. It is clear, from Figure 13.5, that the reflected rays diverge strongly at points of strong curvature. This "fanning out" causes a progressive decrease of the field amplitudes, a tendency that is expressed quantitatively by the *divergence factor D* (i.e., by the ratio of the power per unit solid angle in the direction 1 to the power per unit solid angle in the direction 0). The D factor is given by [118]

$$D = \frac{R_1 R_2 \cos\theta}{(4R^2 + R_1 R_2)\cos\theta + 2R(R_1 \sin^2\theta_1 + R_2 \sin^2\theta_2)}, \tag{13.17}$$

where θ_1 and θ_2 are the angles between the incident ray and the directions of principal curvature 1 and 2. The field varies along the reflected ray according to the law

$$\mathbf{E}^r = \mathbf{E}^i(P) \cdot \overline{\overline{R}} \underbrace{\left[\frac{R_1^r R_2^r}{(R_1^r + s)(R_2^r + s)}\right]^{\frac{1}{2}}}_{\text{spatial attenuation}} \underbrace{e^{-jk_0 s}}_{\text{phase factor}}, \tag{13.18}$$

where R_1^r and R_2^r are the principal radii of curvature of the reflected wavefront at P. They can be obtained from the corresponding radii of the incident wave[7] [94, 198]. We notice that the field (13.18) becomes infinite when $s = -R_1^r$ or $s = -R_2^r$. This singularity of the divergence factor

$$D = \frac{R_1 R_2}{(R_1 + s)(R_2 + s)} \tag{13.19}$$

occurs at *caustics*, which in Figure 13.5*b* are the lines 1–2 and 3–4. As one passes through a caustic in the direction of propagation, the sign of $(R + s)$ changes, and a phase shift of $(\pi/2)$ is introduced. Caustics appear, in particular, when the reflector is concave. Figure 13.6 shows the reflected-rays pattern from a source of spherical waves illuminating a concave-convex surface of revolution. The rays are seen to form a smooth caustic surface of revolution. On the lit side of the caustic there are two reflected rays that contribute to the field at A. Conventional G.O. fails to predict the existence of the fields at B, on the shadow side of the caustic, where no real reflected ray exists. The method must therefore be supplemented by other approaches, such as the *uniform* theories discussed in Section 13.3. Figure 13.7 suggests how some rays form a zone where the energy is trapped near the surface,[8,9] and where the fields are associated with the whispering-gallery modes briefly mentioned in Section 10.5.

13.2.1 A Simple Application

The problem in hand is to reconstruct the properties of a scatterer, for example its shape and composition, from the characteristics of the radiation scattered in each direction. This *inverse*

†Note that (13.15) is valid only if R is much larger than R_1 and R_2. Note also that R_1 and R_2 are considered positive when the center of curvature is on the interior side of the normal.

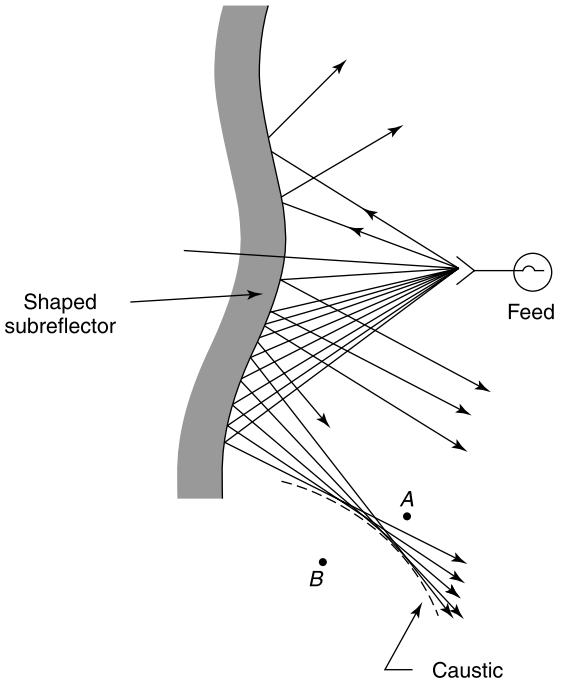

Figure 13.6 Ray caustic generated by a shaped reflector (from P. H. Pathak, High-frequency techniques for antenna analysis, *Proc. IEEE* **80**, 44–65, 1992, with permission of IEEE).

problem is encountered in many branches of physics, notably in quantum mechanics. As an illustration, consider a convex cylinder immersed in the field of a high-frequency plane wave, represented by a bundle of parallel rays (Fig. 13.8*a*). The cylinder is opaque, with

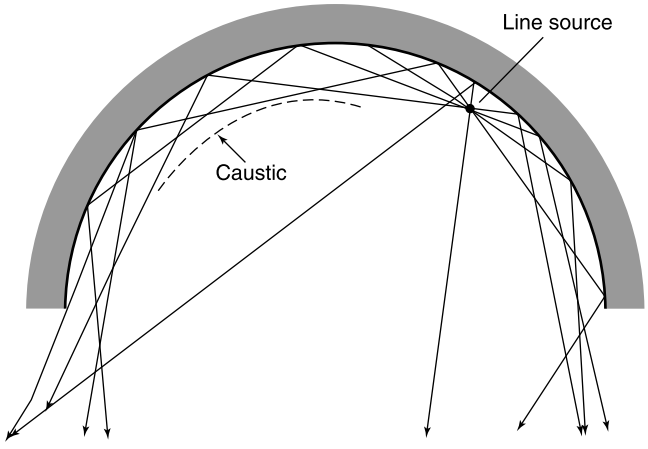

Figure 13.7 Ray-generated whispering-gallery mode (from W. Wasylkiwskyj, Diffraction by a concave perfectly conducting circular cylinder, *IEEE Trans. AP* **23**, 480–492, 1975, with permission of IEEE).

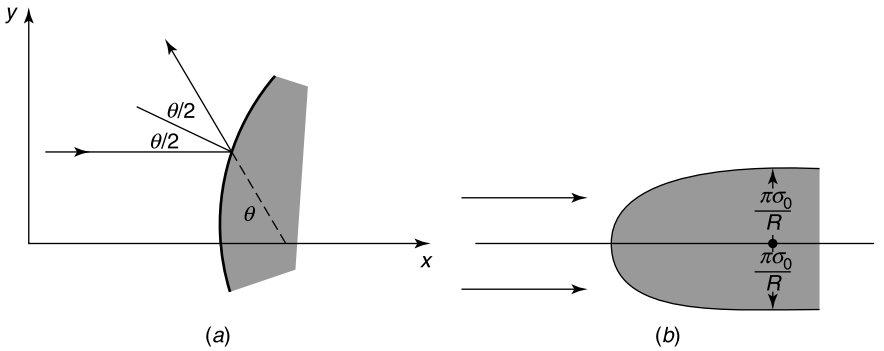

Figure 13.8 (*a*) Incident and reflected rays. (*b*) Shape of an isotropic scatterer (from J. B. Keller, The inverse scattering problem in geometrical optics and the design of reflectors, *IRE Trans. AP* **7**, 146–149, 1959, with permission of IEEE).

a uniform energy reflection coefficient R. In a rather crude approach,[‡] the power incident between rays separated by dy is written as $I\,dy$, where I is the power density, assumed constant and equal to 1 W m^{-1}. A power $R\,dy$ is reflected between the angles θ and $\theta + d\theta$. More precisely,

$$R\,dy = \sigma(\theta)\,d\theta, \tag{13.20}$$

where $\sigma(\theta)$ is the differential cross section. It is the observable of the problem. Integrating (13.20) over θ gives

$$y = y_0 + \frac{1}{R}\int_0^\theta \sigma(\theta')\,d\theta'. \tag{13.21}$$

Because

$$\frac{dy}{dx} = \cot\frac{\theta}{2},$$

one obtains similarly

$$x = x_0 + \frac{1}{R}\int_0^\theta \sigma(\theta')\tan\frac{\theta'}{2}\,d\theta'. \tag{13.22}$$

Equations (13.21) and (13.22) together are the parametric equations of the reflector, and the constants (x_0, y_0) determine the location of the target.[11] An omnidirectional scattering pattern, with $\sigma(\theta)$ equal to a constant σ_0, would reveal the presence of a scatterer of parametric equations

$$\begin{aligned} x &= x_0 - \frac{2\sigma_0}{R}\log_e\cos\frac{\theta}{2} \\ y &= y_0 + \frac{\sigma_0\theta}{R}. \end{aligned} \tag{13.23}$$

[‡]For a much more rigorous approach to this difficult problem, see Note 10.

The profile of this scatterer is shown in Figure 13.8*b*. A similar analysis can be applied to convex bodies of revolution[12] and, more generally, to an arbitrary convex three-dimensional body, for which the differential scattering cross section takes the form

$$\sigma(\theta,\varphi) = \frac{R}{4K\left(\frac{\theta}{2},\varphi\right)}, \tag{13.24}$$

where $K\left(\frac{\theta}{2},\varphi\right)$ is the Gaussian curvature defined in A3.5, evaluated at the point of reflection. Measurements of $\sigma(\theta,\varphi)$ for two opposite directions of incidence, gives the Gaussian curvature for the whole range of values of θ and φ. This spherical image determines the surface uniquely provided

$$\int_{4\pi} \frac{\mathbf{u}_n(\theta,\varphi)}{K(\theta,\varphi)}\, d\Omega = 0, \tag{13.25}$$

where $K(\theta,\varphi)$ is assumed smooth and positive.

13.2.2 Determination of the Reflection Point

Figure 13.5*a* suggests the existence of a ray that, issued from S, hits the scatterer in P and bounces back ultimately to reach Q. The problem is to find P. This can be done by invoking Fermat's principle, which states that the rays between two points P_1 and P_2 are those curves along which the optical path length $\int_{P_1}^{P_2} N\, ds$ is stationary (but not necessarily minimal) with respect to infinitesimal variations of the path (Problem 13.3). When the outside medium is homogeneous the rays are straight, and it is found that incident ray, reflected ray, and normal lie in the same plane [193]. The optical length from S to Q is proportional to

$$L = \left[(x_Q - x_P)^2 + (y_Q - y_P)^2 + (z_Q - z_P)^2\right]^{\frac{1}{2}} + \left[(x_S - x_P)^2 + (y_S - y_P)^2 + (z_S - z_P)^2\right]^{\frac{1}{2}}. \tag{13.26}$$

The unknowns are (x_P, y_P, z_P). If $z = f(x,y)$ denotes the surface of the scatterer,

$$\frac{\partial L}{\partial x} = \frac{x_P - x_Q}{PQ} - \frac{x_S - x_P}{SP} + \left(\frac{z_P - z_Q}{PQ} - \frac{z_S - z_P}{SP}\right)\frac{\partial f}{\partial x}.$$

A similar relationship can be written for $(\partial L/\partial y)$. The coordinates of the points of reflection can now be found by solving the system of equations

$$z = f(x,y); \qquad \frac{\partial L}{\partial x} = 0; \qquad \frac{\partial L}{\partial y} = 0. \tag{13.27}$$

The solution is usually obtained by means of numerical search procedures [94, 119].

The region around the *specular point* (the *flash point*) contributes strongly to the scattered field. It should therefore be possible to decrease the radar return of a target by modifying the shape and surface characteristics of the target to either reduce the number of specular points or neutralize their effect by means of absorbing layers on the metallic surface. Note that specular points do not always exist, in particular when the scatterer is axisymmetric.[13]

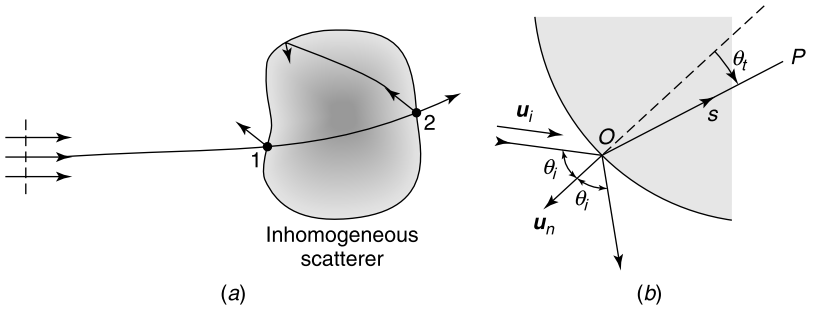

Figure 13.9 (*a*) Scattering investigated by ray tracing. (*b*) A single ray hitting a dielectric (from H. Kim and H. Ling, Electromagnetic scattering from an inhomogeneous object of ray tracing, *IEEE Trans. AP* **40**, 517–525, 1992, with permission of IEEE).

13.2.3 Ray Tracing in Dielectrics

An inhomogeneous dielectric scatterer illuminated by a plane wave is shown in Figure 13.9*a*. The plane wave is represented by a large number of rays, shot toward the target in an approach often called the "*shooting and bouncing*" *procedure*.[14,15] The history of each ray is followed by the methods of *geometrical optics*, which generate a succession of reflected, refracted, and exit rays. The intensities of the rays become weaker after every reflection, hence the process can be terminated after a few bounces. The exiting rays build up the scattered field. More quantitatively,[16] consider the single incident ray in Figure 13.9*b*. The associated fields should be split into parallel and perpendicular components with respect to the plane of incidence $(\mathbf{u}_i, \mathbf{u}_n)$. Reflection and transmission occur as if the surface were plane provided λ_0 is much smaller than the radii of curvature in O. The relevant formulas are (9.9) to (9.12). When $\mathbf{E}^i$ is perpendicular to the plane of incidence, for example,

$$T_\perp = \frac{2\cos\theta^i}{\cos\theta^i + (N^2 - \sin^2\theta^i)^{\frac{1}{2}}}, \tag{13.28}$$

where N is the index of refraction in O, assumed constant over a region of a few λ_0. The field along the refracted ray OP will be of the form

$$\mathbf{E}_\perp(P) = T_\perp\, \mathbf{E}^i_\perp(O)\, D\, e^{-jks}, \tag{13.29}$$

where $k = Nk_0$, and D is the divergence factor (13.19). The radii R_1 and R_2 are the principal radii of curvature of the transmitted wavefront passing through O. The determination of these radii for an arbitrary incident ray (and similarly for the reflected ray) is a difficult task, which requires a knowledge of the curvature matrices of both surface and wavefront.[16] When the dielectric is inhomogeneous, the rays are curved, and the evolution of the field follows the rules discussed in Chapter 8.

13.3 GEOMETRIC THEORY OF DIFFRACTION

The fields scattered by a perfectly conducting obstacle can be expressed as the sum of two parts: a contribution from geometrical optics, and a diffracted field. The G.O. contributes rays of the first kind, which originate from points of stationary phase (shining points or flash

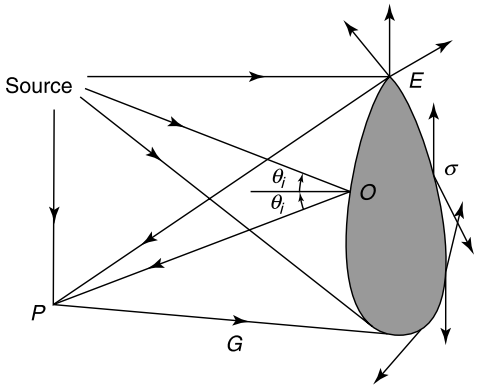

Figure 13.10 Incident rays. P = observation point, O = flash point, G = grazing ray, σ = surface rays, E = sharp edge.

points) located on the smooth parts of the scatterer, away from singularities (Fig. 13.10). Rays of the *second kind* (the diffracted rays) originate from stationary points on edges, corners, vertices, or graze the surface of the scatterer.[§] Diffracted rays clearly play a fundamental role in the absence of specular reflections. Their amplitude and phase are a *local* phenomenon, which depends only on the nature of boundary surface and incident field in the immediate neighborhood of the point of diffraction. The solution of *canonical* problems involving, for example, spheres, cones, paraboloids, or circular cylinders is therefore essential whenever curvature effects, material properties, and incident fields can be matched to those of the original problem. The diffracted wave further propagates along its ray, with an amplitude governed by the principle of power conservation in a tube and a phase delay equal to the product of the wave number of the medium and the distance. Diffraction coefficients must therefore be determined to quantify the process. Figure 13.10 shows the various rays that should be taken into account when a two-dimensional source illuminates a PEC cylinder.

13.3.1 The Edge of a Thin Screen

In a general statement of Fermat's principle, a ray may be defined as any path from P to Q that satisfies the constraints of the problem and whose optical length is stationary with respect to small variations of the path. In Figure 13.11*a*, for example, the *stationary* ray is *SOP*, and O is the stationary point (Problem 13.3). The *plane of incidence* is formed by the ray and the edge (the z-axis), and the components $\perp$ and $\parallel$ are taken with respect to that plane. We shall first assume that the incident ray lies in the plane of the screen. This two-dimensional case is discussed in Section 9.7 for both the E_z and H_z polarizations. From (9.234) and for large values of $k_0 r$ (Fig. 9.45),

$$E_z^d = \underbrace{\frac{1}{\sqrt{8\pi k_0}} \left(-\frac{1}{\cos\dfrac{\varphi - \varphi_0}{2}} + \frac{1}{\cos\dfrac{\varphi + \varphi_0}{2}} \right) \frac{1-j}{\sqrt{2}}}_{D^e(\varphi, \varphi_0)} \frac{e^{-jk_0 r}}{\sqrt{r}} E_z^i(O) \tag{13.30}$$

[§]For a general survey, see Note 17.

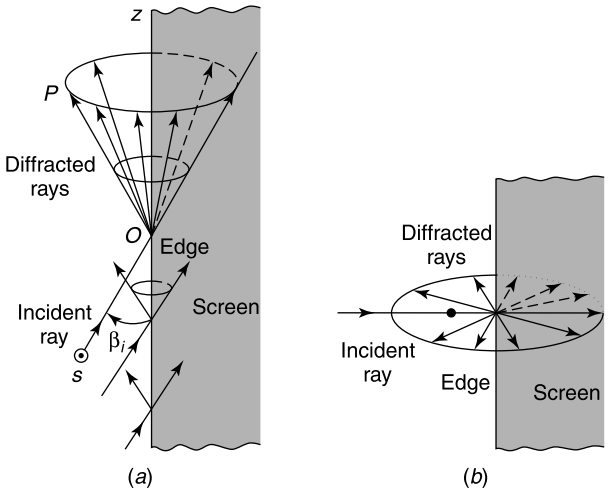

Figure 13.11 (*a*) Cone of diffracted rays for oblique incidence. (*b*) Plane of diffracted rays for normal incidence (from J. B. Keller, Geometrical theory of diffraction, *J. Opt. Soc. Am.* **52**, 116–130, 1962, with permission of the Optical Society of America).

$$H_z^d = \underbrace{\frac{1}{\sqrt{8\pi k_0}}\left(-\frac{1}{\cos\dfrac{\varphi-\varphi_0}{2}}-\frac{1}{\cos\dfrac{\varphi+\varphi_0}{2}}\right)\frac{1-j}{\sqrt{2}}}_{D^h(\varphi,\varphi_0)}\frac{e^{-jk_0r}}{\sqrt{r}}H_z^i(O). \tag{13.31}$$

In a more concise notation:[18]

$$\begin{pmatrix} E_\parallel^{sc} \\ E_\perp^{sc} \end{pmatrix} = \frac{e^{-jk_0r}}{\sqrt{r}}\underbrace{\begin{pmatrix} D^e & 0 \\ 0 & D^h \end{pmatrix}}_{\overline{\overline{D}}}\cdot\begin{pmatrix} E_\parallel^i \\ E_\perp^i \end{pmatrix}, \tag{13.32}$$

where $\parallel$ means parallel to the z-axis. The more difficult case of oblique incidence is discussed in detail in [36], where expressions for the fields are given for various incident plane waves and for sources such as line currents parallel to the edge or electric dipoles perpendicular to the screen. The theory shows that a diagonal form of $\overline{\overline{D}}$ can be found for oblique incidence[19] and further that valuable results can be obtained from a plane wave spectral representation of the incident field.[20,21] The passage from perpendicular to oblique can be realized by a simple manipulations based on the value of the phase factor for an oblique ray, which is

$$e^{-jk_0S} = e^{-jk_0(x\cos\varphi\sin\beta_i + y\sin\varphi\sin\beta_i + z\cos\beta_i)},$$

where β_i is shown on Figure 13.11*a*. This phase variation can be derived from the two-dimensional form by replacing k_0 by $k_0\sin\beta_i$ and multiplying the field expressions by $e^{-jk_0\cos\beta_i z}$.

It is mentioned in Section 9.7 that an oblique ray gives rise to a circular cone of diffracted rays, all of which form an angle β_i with respect to the straight edge. These rays and their cone are not mere analytical tools for the determination of scattered fields; they can be observed experimentally.[22]

13.3.2 Wedge Diffraction

In Figure 13.12*a*, both the incident and diffracted rays form an angle β_i with the edge. The analog acoustic problem is characterized by diffraction coeffients $D^e = D^s$ (relative to a *soft* or Dirichlet boundary condition) and D^h (relative to a *hard* or Neumann boundary condition) [198]. If P is not close to a shadow or reflection boundary, and φ is different from 0 or a multiple of π,

$$D^{s,h} = \frac{e^{-j\frac{\pi}{4}} \sin\frac{\pi}{n}}{n\sqrt{2\pi k_0}\sin\beta_i}\left[\frac{1}{\cos\frac{\pi}{n} - \cos\frac{\varphi-\varphi_i}{n}} \mp \frac{1}{\cos\frac{\pi}{n} - \cos\frac{\varphi+\varphi_i}{n}}\right], \tag{13.33}$$

where $n = \dfrac{2\pi - \alpha}{\pi}$, the upper sign holds for D^s and the lower sign for D^h. It is found that these parameters are also relevant for the electromagnetic situation. More specifically:

$$\mathbf{E}^d(P) = \mathbf{E}^i(0)\cdot\overline{\overline{D}}(\varphi,\varphi',\beta_i)\sqrt{\frac{\rho}{s(\rho+s)}}\,e^{-jk_0 s}, \tag{13.34}$$

where

$$\overline{\overline{D}}(\varphi,\varphi',\beta_i) = -D^s\mathbf{u}_{\beta_i}\mathbf{u}_\beta - D^h\mathbf{u}_{\varphi_i}\mathbf{u}_\varphi, \tag{13.35}$$

and $\mathbf{u}_{\beta_i} = \mathbf{u}_{si} \times \mathbf{u}_{\varphi_i}$, $\mathbf{u}_\beta = \mathbf{u}_s \times \mathbf{u}_\varphi$. In the divergence factor, ρ is the distance between the caustic on the boundary surface (the point of diffraction) and the second caustic of the diffracted ray, located away from this surface. Note that setting $n = 2$ in (13.33) to (13.35) gives the solution for oblique incidence on a thin screen.

The diffraction coefficients D^s and D^h become infinite for $\varphi = (\varphi_i + \pi)$, the light-shadow boundary, and $\varphi = (\pi - \varphi_i)$, the reflection boundary. This difficulty has been

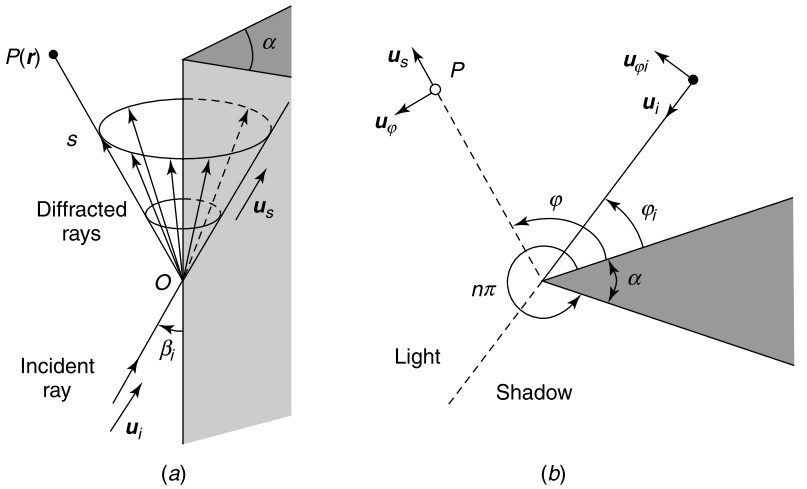

Figure 13.12 (*a*) Reflection and diffraction from a wedge. (*b*) Projection on a plane perpendicular to the wedge.

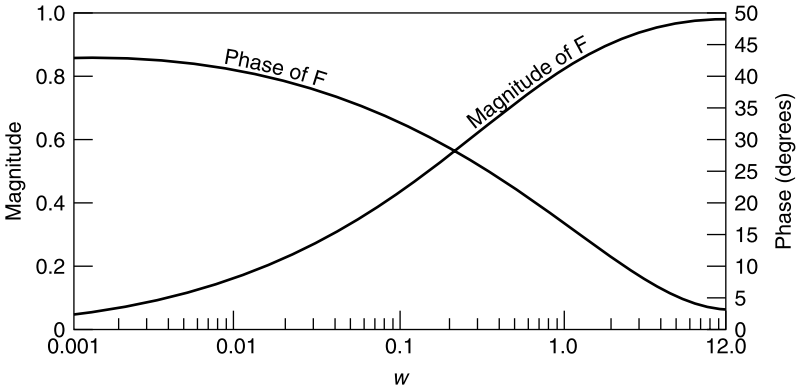

Figure 13.13 The transition function $F(w)$ (from R. G. Kouyoumjian and P. H. Pathak, A uniform geometrical theory of diffraction for an edge in a perfectly conducting surface, *Proc. IEEE* **62**, 1448–1460, 1974, with permission of IEEE).

encountered, and discussed, in Section 9.7. The *Keller* type of D is consequently not *uniformly* valid.[19] To ensure field continuity at the shadow and reflection boundaries,[¶] the *uniform geometrical theory of diffraction* (UTD) introduces modified diffraction coefficients D^s, D^h in (13.33) [198]. The new values involve the important *Fresnel transition function*, given here for general reference (Fig. 13.13):

$$F(w) = 2j\sqrt{w}\, e^{jw} \int_{\sqrt{w}}^{\infty} e^{-j\tau^2} d\tau. \tag{13.36}$$

In the integral, the principal (positive) branch of the square root should be chosen. The F function keeps the fields bounded at the shadow boundary, and becomes unity outside that region, ensuring that the UTD solution automatically reproduces the predictions of the GTD. In the *uniform asymptotic theory of edge diffraction* (UAT), the Keller diffracted field for a thin screen is supplemented by a term $\mathbf{E}_G$, which replaces the *geometrical optics* field.[24,25] This term is given by [131]

$$\mathbf{E}_G(\mathbf{r}) = \left[F(d^i) - \tilde{F}(d^i)\right] \mathbf{E}^i(\mathbf{r}). \tag{13.37}$$

In this expression, F is the Fresnel-type integral

$$F(w) = \frac{e^{j\frac{\pi}{4}}}{\sqrt{\pi}} \int_w^{\infty} e^{-jt^2} dt$$

and $\tilde{F}$ is the dominant asymptotic term of $F(w)$ as $w \to +\infty$. Thus,

$$\tilde{F}(w) = \frac{1}{2\sqrt{\pi}\, w}\, e^{-j\left(w^2 + \frac{\pi}{4}\right)}.$$

The symbol d^i denotes the *detour parameter*. For an incident E_z wave, this parameter is the difference between the phase of the diffracted ray reaching $\mathbf{r}$ via the edge and the phase

[¶]The method can also be applied to dielectric wedges. See, for example, Note 23.

of the incident field that would reach **r** directly (in the absence of the half plane). More generally,

$$d^i(\mathbf{r}) = \epsilon^i(\mathbf{r})\sqrt{k_0 S(\mathbf{r}) - k_0 S^i(\mathbf{r})}, \tag{13.38}$$

where S and S^i are the eikonals of, respectively, the diffracted ray and the incident field. The symbol ϵ^i, the *shadow indicator*, is equal to $(+1)$ in the shadow region of $(\mathbf{E}^i, \mathbf{H}^i)$ and to (-1) in the illuminated region. It has been verified, in the case of a thin screen, that the total field obtained from the UAT under oblique plane wave incidence is equal to the exact solution.[26]

13.3.3 Surface Rays

In Figure 13.14*a*, a ray issued from O reaches a field point P after creeping along the perfectly conducting surface S, from P_1 ro P_2. The surrounding medium is assumed homogeneous, hence the portions OP_1 and P_2P are straight. According to Fermat's principle the ray's trajectory is a path of shortest distance, which means that the portion P_1P_2 must be a geodesic of the surface. In general the geodesics are not easily found, except in the particular cases of cylindrical, spherical, and conical surfaces. Their determination usually requires the numerical solution of a differential equation. The figure shows a second ray — the dashed curve — which can also reach P. Other rays contribute to the field at P after going around the obstacle a certain number of times. Field point P will therefore be hit by a succession of *creeping rays*, which are actually the only relevant ones when P lies in the shadow. When P is in the illuminated zone, there will be, in addition, a direct ray and possibly one or more specular rays.

The ray between P_1 and P_2 is expected to suffer attenuation because it sheds radiated energy on its way, more specifically by means of rays diffracted tangentially from the surface. As a result, the summation of the encircling rays can frequently be limited to a few terms, the other ones being damped out of significance.

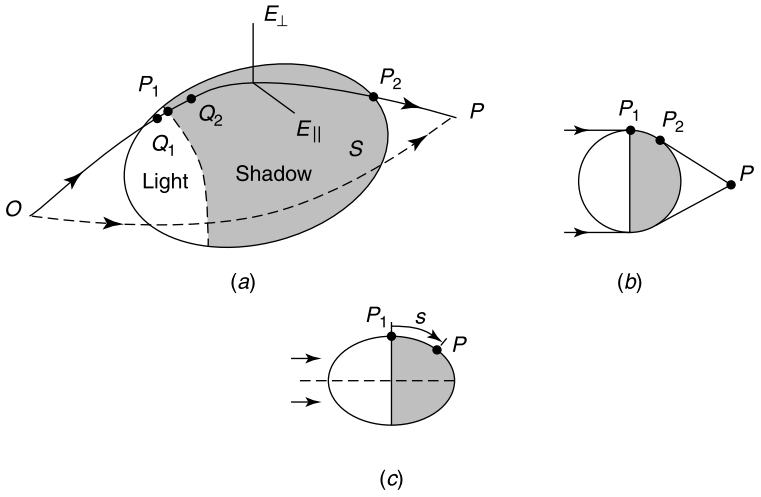

Figure 13.14 (*a*) Surface ray on a perfectly conducting scatterer. (*b*) Circular cylinder in a plane wave. (*c*) Elliptic cylinder.

In Figure 13.14*a*, the source O is located outside the scatterer. The case of a source *on* the scatterer — say an antenna placed conformally on a smooth, convex portion of a spacecraft — is also of considerable interest. The reader is referred to the literature for the solution of this difficult problem [77, 113, 136, 198].

13.3.4 A Few Canonical Problems

Consider first a *circular* cylinder, immersed in the field of a line source parallel to the axis of the cylinder (an incident plane wave is a particular case of such a source). The problem is two-dimensional and of the kind discussed in Chapter 14, where it is shown that the field is the sum of the contributions of an E-wave and an H-wave. In both cases, the solution consists of a summation over an infinite number of modes, where each mode can be associated with a surface diffracted ray, and suffers an attenuation of the form $e^{-\alpha_n P_1 P_2}$ on its path along the cylinder. The diffracted ray in the deep shadow can be written, for the 2D case, as[27,28] [77, 193, 198] (Fig. 13.14*b*)

$$\begin{pmatrix} E_{\parallel}^{d}(P) \\ E_{\perp}^{d}(P) \end{pmatrix} = \sum_{n=1}^{\infty} \begin{pmatrix} D_n^e & 0 \\ 0 & D_n^h \end{pmatrix} \cdot \begin{pmatrix} E_{\parallel}^{i}(P_1) \\ E_{\perp}^{i}(P_1) \end{pmatrix} \frac{e^{-jk_0(l+P_2P)}}{\sqrt{P_2P}}, \tag{13.39}$$

where l denotes the arc length P_1P_2, $E_\perp$ is the component along the normal (as in Figure 13.14*a*), and the D coefficients contain an attenuation factor $e^{-\alpha_n^e l}$ (or $e^{-\alpha_n^h l}$).

When P is deep in the shadow, only the first few terms are required to achieve reasonable accuracy when the radii of curvature of the surface are larger than a wavelength or so. For P_2 close to P_1, the number of terms increases, and it becomes appropriate to replace the series by an integral representation, which turns out to involve Fock-type functions [198]. This is not unexpected, because P_2 moves progressively into the Fock region (behind P_1), represented symbolically by the arc Q_1Q_2 in Figure 13.14*a*.

The analysis can be extended to convex scatterers of variable curvature, such as parabolic or elliptic cylinders.[29] In the case of the elliptic cylinder[30] (Fig. 13.14*c*), the field in P (for both E and H waves) can be expressed as an infinite sum, each term of which contains a factor

$$D_n(P)e^{-jk_0 s}\, e^{-\int_{P_1}^{P} \alpha_n(s')ds'},$$

where $D_n = D^{s,h}(P_1) \cdot D^{s,h}(P_2)$, and $\alpha_n = \alpha^{s,h}$. The D_n and α_n are functions of the local radius of curvature of the ellipse. On the basis of the local character of the high-frequency fields, the formula may be assumed to carry over to arbitrary convex cylinders, in which case one may adopt, for D_n and α_n, the values that are found for the ellipse of identical local curvature.[‖] Alternately, one could also introduce the value of α_n, which holds for the circular cylinder of identical radius of curvature.[29] Curvature must also be taken into account when its variation suffers a *step* discontinuity, while the slope (in the case of a cylinder) remains continuous (Fig. 13.15*a*, point O). The extreme case of a sharp edge, previously discussed in this section, therefore falls outside the pale of the analysis. The mentioned effect is important for an adequate treatment of scattering by bodies such as cone-spheres and hemispherically capped cylinders. The consequences of the discontinuity can be given a quantitative basis by means of the canonical problem of two perfectly

[‖]That assumption has been validated by comparison with results obtained by other methods.

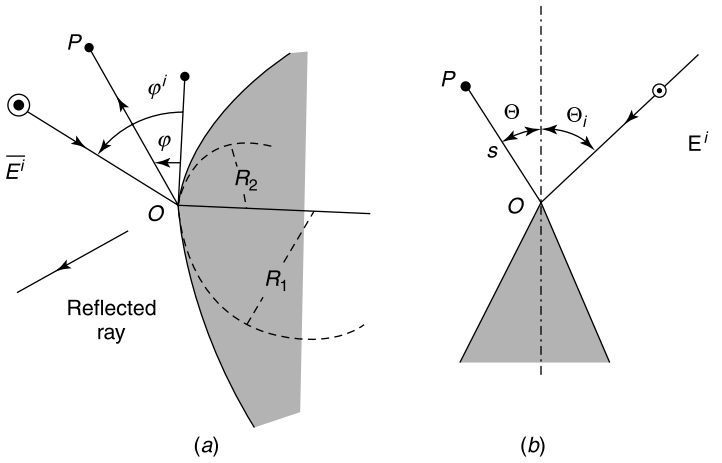

Figure 13.15 (*a*) The junction of two parabolic cylinders. (*b*) Cone in an incident field.

conducting cylinders, circular and parabolic, joined together at a boundary across which the curvature is discontinuous [77, 193]. As a typical example, Figure 13.15*a* shows the junction in O of two parabolic cylinders.[31] The discontinuity in curvature gives rise, for an E-wave for example, to a diffracted field

$$E^d(P) = e^{j\frac{\pi}{4}} \sqrt{\frac{2}{\pi k_0^3}} \frac{\sin\varphi_i \sin\varphi}{(\cos\varphi_i + \cos\varphi)^3} \left(\frac{1}{R_2} - \frac{1}{R_1}\right) \frac{e^{-jk_0 r}}{\sqrt{r}} E^i(0). \tag{13.40}$$

This expression is valid provided the junction is illuminated (i.e., provided $0 < \varphi_i < \pi$). Note that the denominator vanishes in the direction $\varphi = (\pi - \varphi_i)$ of the reflected wave. A uniform solution must therefore be derived for the transition region around the specular direction [77].

13.3.5 Tip Diffraction

Scattering from a cone is discussed more extensively in Chapter 16. In the high-frequency approximation, GTD methods can be applied to yield diffracted rays of the general form (Fig. 13.15*b*)

$$\mathbf{E}(P) = \overline{\overline{D}}(\theta, \varphi, \theta_i, \varphi_i) \cdot \mathbf{E}^i(0) \frac{e^{-jk_0 s}}{s}. \tag{13.41}$$

The diffraction coefficients are proportional to k_0^{-1}, while the corresponding coefficients for a wedge, given in (13.33), are proportional to $k_0^{-\frac{1}{2}}$. Cone diffraction therefore tends to lose relative importance as frequency increases. The literature on the subject is extensive, in particular with respect to circular cones, either semi-infinite,[32,33,34] flat-based, or rounded-based[35,36,37] [113]. A general approach valid for perfectly conducting cones of arbitrary cross section is also available,[38] as well as data on the sector, a limit form of the elliptic cone.[39,40]

13.4 EDGE CURRENTS AND EQUIVALENT CURRENTS

The radar cross sections evaluated by *physical optics* methods are usually quite accurate. For large-angle bistatic scattering or relatively low backscattering, however, errors of several decibels may occur. The major sources for these errors can be traced back to neglected currents near the edges or the light-shadow boundaries of the scatterers. It is useful, in that respect, to write

$$\mathbf{J}_S = (\mathbf{J}_S)_{PO} + (\mathbf{J}_S)_{NU}, \tag{13.42}$$

where *NU* stands for nonuniform. Such a move does not solve the problem, of course, because the nonuniform current must now be determined. This task is facilitated by the *local character of high-frequency fields*, which allows one to replace $(\mathbf{J}_S)_{NU}$ by the value obtained for a canonical problem involving the same (locally plane) incident fields, and a surface that conforms locally to the actual surface of the scatterer. Once this well-approximated value of $(\mathbf{J}_S)_{NU}$ is obtained, the far-field it contributes can easily be deduced by summing the contributions of the various $(\mathbf{J}_S)_{NU}\ dS$ elements on the surface of the original scatterer. Because these currents decay rapidly away from edge or light-shadow boundary, great simplification occurs because surface integrations can be replaced by line integrations, as described later in this section.

13.4.1 The Physical Theory of Diffraction

This theory, in its application to a perfect conductor endowed with a sharp edge, utilizes an infinite wedge as a canonical model. The faces of the wedge in *P* are chosen to coincide with the tangent planes of the original conductor (Fig. 13.16) and the incident wave is replaced by its local (plane) approximation (see Section 8.3). The main problem is now to evaluate $\mathbf{J}_S$ on the wedge and subsequently to obtain $(\mathbf{J}_S)_{NU}$ by simply subtracting $(\mathbf{J}_S)_{PO}$ from $\mathbf{J}_S$. The solution of this canonical problem can be obtained in terms of fast convergent integrals in the complex plane.[41,42] Given the value of $(\mathbf{J}_S)_{NU}$, common to wedge and scatterer, it becomes an easy matter to determine the *edge waves* generated by the nonuniform currents. The corresponding fields are free of singularities away from the edge. When the scatterer is a thin reflector, for example a parabolic antenna, the *NU* currents are the currents near the edge of a perfectly conducting half plane.

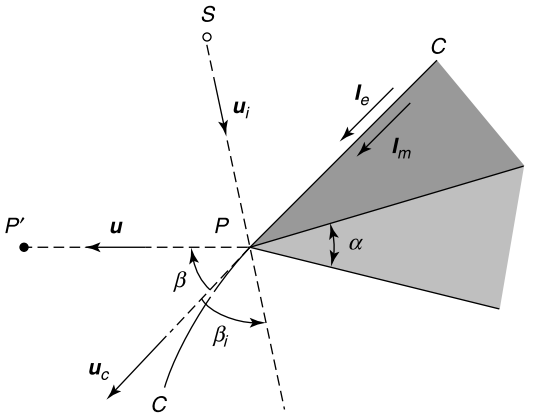

Figure 13.16 Curved edge and rays.

13.4.2 Equivalent Currents

In the method of equivalent currents (MEC), the source of the diffracted field is ascribed to fictitious *line* currents, electric and magnetic, flowing along the edge. The procedure involves only line integrals, as distinct from the surface integrals of the *physical theory of diffraction*. The main idea is suggested by the form of the field diffracted by a half-plane at perpendicular incidence. According to (9.234), (13.30), and (13.31), this field can be written, at large distances, as

$$u(r,\varphi) = D(\varphi,\varphi_i)\,\frac{e^{-jk_0 r}}{\sqrt{r}}\,u^i$$

where D is either D^{e} or D^h. Field u depends on the directions of incidence and observation and can be interpreted as a cylindrical wave radiated from the edge. The *current concentration on the edge* idea, which can be traced back to Thomas Young, was revived in the past century in studies of diffraction by a large aperture in a plane screen.[43] More recently, investigators have sought to find currents $I_e\mathbf{u}_c$ and $I_m\mathbf{u}_c$ which, flowing along the edge (Fig. 13.16), allow expressing the diffracted field in a direction $\mathbf{u}$ as

$$\mathbf{E}^d(\mathbf{r}) = jk_0 \int_C -\left[R_{c0}\,I_e(\mathbf{r}')\,\mathbf{u}\times\left(\mathbf{u}\times\mathbf{u}_c(\mathbf{r}')\right) + I_m(\mathbf{r}')\,\mathbf{u}\times\mathbf{u}_{\mathrm{c}}(\mathbf{r}')\right]\frac{e^{-jk_0|\mathbf{r}-\mathbf{r}'|}}{4\pi|\mathbf{r}-\mathbf{r}'|}\,dc'. \tag{13.43}$$

The currents I_e and I_m can be determined by comparing (13.43) with the results obtained by the PTD method. According to Michaeli, the comparison produces the values

$$\begin{aligned} I_e &= -2j\frac{D_1}{k_0 R_{c0}\sin^2\beta_i}\,(\mathbf{u}_c\cdot\mathbf{E}^i) - 2j\frac{D_2}{k_0\sin\beta_i}\,(\mathbf{u}_c\cdot\mathbf{H}^i) \\ I_m &= 2j\frac{R_{c0}D_3}{k_0\sin\beta\sin\beta_i}\,(\mathbf{u}_c\cdot\mathbf{H}^i), \end{aligned} \tag{13.44}$$

where the D's are suitable diffraction coefficients[44,45,46,47] that depend on β and β_i (Fig. 13.16). The diffracted field can now be formally written as**

$$\mathbf{E}^d(\mathbf{r}) = \int_C \underbrace{\left[\overline{\overline{K}}_e(\mathbf{r},c')\cdot\mathbf{E}^i(c') + \overline{\overline{K}}_m(\mathbf{r},c')\cdot\mathbf{H}^i(c')\right]}_{\text{Incremental contributions}} dc'. \tag{13.45}$$

Note that the currents in (13.44) become infinite for certain combinations of incidence and scattering directions. Appropriate steps can remedy that particular difficulty.[51,52]

13.4.3 Incremental Length Diffraction

In the ILD method, the attention is focused on the *radiation fields* generated by the nonuniform currents, and the details of these currents are left aside.[53] In a symbolic way, one writes

**Applications of the method can be found in Notes. 48, 49, and 50.

the nonuniform fields as

$$E^d_{NU}(\mathbf{r}) = \int_C K(\mathbf{r}, c')\, E^i(c')\, dc', \tag{13.46}$$

where C is a singularity curve (the edge of a wedge-like structure, or a light-shadow boundary). The *incremental length* is the element of arc dc'. In three-dimensional problems E and E^i are vectors, as in (13.45), and polarization becomes important. For such a case, the incremental contribution from dc' should be split into two components with respect to a given reference plane. Thus,

$$d\,\mathbf{E}^d_{NU} = E^i_{\perp}\, d\,\mathbf{E}^d_{\perp} + E^i_{\parallel}\, d\,\mathbf{E}^d_{\parallel}. \tag{13.47}$$

Coefficient $K(\mathbf{r}, c')$, the ILDC, has the nature of a Green's function. The crucial point is the possibility of replacing the $K(\mathbf{r}, c')$ of the scatterer by the value obtained in a companion canonical problem, thus following the spirit of the *local hypothesis* mentioned above. The actual value of the currents must not be known: it is the *far field* of the canonical currents that should be available in closed form. The method has first been applied to scatterers composed of plane surfaces, such as the wedge, the strip, and the polygonal cylinder.[54] In its application to the light-shadow transition on a convex, perfectly conducting scatterer (Fig. 13.17*a*), a suitable, canonical model is provided by the circular cylinder, illuminated by a plane wave at normal or oblique incidence (Fig. 13.17*b*). The diffracted radiation field due to the light-shadow discontinuity is obtained by subtracting the *physical optics* contribution from the total field,[55,56] derived by methods of the kind discussed in Section 14.2. The analysis leads to the following general form of the field diffracted by the circular cylinder:

$$E^d_{NU} \doteq \frac{e^{-jk_0 r}}{\sqrt{r}}\, M(\varphi, z, \theta_i)\, E^i \tag{13.48}$$

where θ_i is the angle between $\mathbf{u}_i$ and $\mathbf{u}_z$. From these results, one can extract the value of $d\,\mathbf{E}^d_{NU}$, which can then be used for the original scatterer. The steps are as follows (Fig. 13.17*a*):

- Determine the oblique angle of incidence that $\mathbf{u}_i$ makes with the light-shadow boundary at P.
- Align both the normal $\mathbf{u}_n$ and the light-shadow boundary of canonical cylinder and scatterer.
- Set the radius R of the circular cylinder equal to the corresponding radius for the curve drawn on S perpendicularly to the LS boundary.

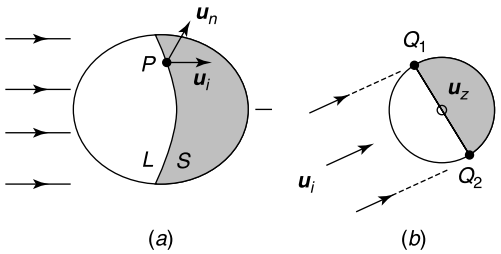

Figure 13.17 (*a*) Scatterer in an incident field. (*b*) Circular cylinder in an incident plane wave, possibly at oblique incidence.

- Use the $d\,\mathbf{E}^d_{NU}$ value of the circular cylinder for the actual cylinder, and integrate according to (13.46).

The validity of the method has been confirmed by comparing its predictions with independent numerical results obtained for a prolate spheroid,[57] a shape that has the advantage over the sphere — the classic test case — of having variable radii of curvature.

The ILD method, as well as its generalized form,[58] has several advantages:[††] it eliminates singularities in caustic and transition regions and yields corrections to *physical optics* that are valid for all angles of observation. Neither ray tracing nor searching for critical points (such as points of stationary phase) are necessary.

13.5 HYBRID METHODS

In many applications, the advantages of the high-frequency techniques can only be exploited in certain regions of space, while other methods might be preferable outside these regions. A few examples will illustrate the point.

13.5.1 Integral Equations and Optical Approximations

Consider a large perfectly conducting scatterer immersed in an incident field (Fig. 13.18*a*). The current density $\mathbf{J}_S$ satisfies an electric field integral equation that, in the notation of (11.168), may be concisely written as

$$j\omega\mu_0\,\mathbf{L}_t(\mathbf{J}_S) = \mathbf{E}^i_{\tan}. \tag{13.49}$$

This equation must be satisfied at points on the surface. When the latter has singularities (a vertex, an edge), these may be included in a (nonoptical) subsurface S_2. Over the remaining

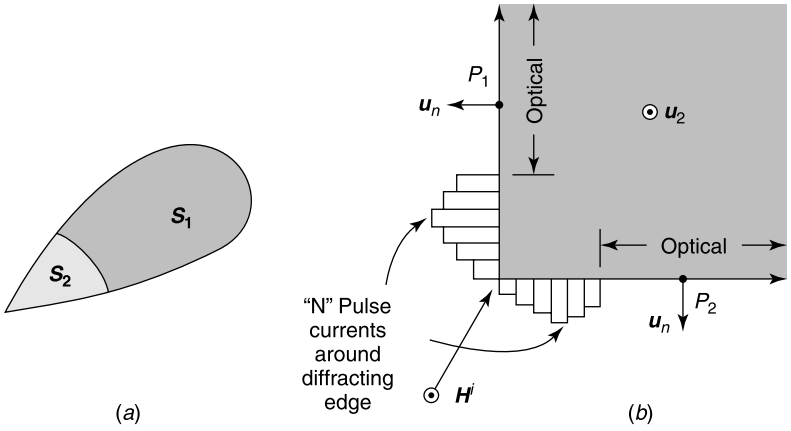

Figure 13.18 (*a*) Division of the scatterer's surface into *optical* and *non-optical* parts. (*b*) Currents on a 90° wedge (from W. D. Burnside, C. L. Yu, and R. J. Marhefka, A technique to combine the geometrical theory of diffraction and the moment method, *IEEE Trans. AP* **23**, 551–558, 1975, with permission of IEEE).

[††]For a comparison with other equivalence methods, see Note 59.

(optical) part (i.e., on S_1), the current in (13.49) can be represented by some optical approximation, possibly containing a few adjustable parameters. On S_2, the representation will be in terms of a sum of appropriate basis functions.[60,61,62,63] Thus,

$$\mathbf{J}_S(\mathbf{r}) = \underbrace{\mathbf{J}_S^{opt}(\mathbf{r}, c_1, c_2, \ldots, c_N)}_{\text{on } S_1} + \underbrace{\sum a_n \mathbf{f}_n(\mathbf{r})}_{\text{on } S_2}. \tag{13.50}$$

As *optical* current, one may choose the P.O. limit $2(\mathbf{u}_n \times \mathbf{H}^i)$, the GTD or, if S_1 is the smooth part of the surface, the sum of a few complex exponential functions of the surface coordinates.[64,65] The basis functions on S_2 are of the usual type, typically pulses or RWG triangle pairs. The unknown coefficients are subsequently determined by testing (13.49) with a set of weighting functions.

To concretize the method, consider the 90° wedge in Figure 13.18*b*, illuminated by a plane H-wave. This is a classic problem, the solution of which is of the form

$$H_z(\mathbf{r}) = H_z^i(\mathbf{r}) + H_z^r(\mathbf{r}) + C\,\frac{e^{-jk_0 r}}{\sqrt{r}}. \tag{13.51}$$

Here H^r is the field associated with the reflected rays, and r is the distance to the edge. The coefficient C in the last term (the diffracted field) is left floating, although in the current case it is known from (13.33). Representation (13.51) is used in the optical regions, at points such as P_1 and P_2, where we write

$$\begin{aligned}\mathbf{J}_S^{opt} &= \mathbf{u}_n \times \mathbf{u}_z(H_z^i + H_z^r + H_z^d)\\ &= \mathbf{J}_S^i + \mathbf{J}_S^r + (\mathbf{u}_n \times \mathbf{u}_z)\,C\,\frac{e^{-jk_0 r}}{\sqrt{r}}.\end{aligned} \tag{13.52}$$

This expression is acceptable down to $r \approx (\lambda_0/4)$. The region 2 of the problem is the vicinity of the edge, where the (tangential) current is expanded in pulse functions of unknown amplitude (Fig. 13.18*b*). The various expressions for the current are now inserted in (13.49), which in the current case is the MFIE discussed in Section 14.6.

13.5.2 Scattering by Large Open Cavities

Much attention has recently been devoted to the evaluation of the radar echo from a large conducting surface provided with an aperture.[66] The fields penetrate into the interior volume, which acts as a cavity. In an important application, the cavity is the jet engine of an aircraft (Fig. 13.19). Assume that the aperture S_A is plane, and that a dense grid of rays is shot toward the target.[67,68] These rays are subsequently traced in the cavity according to the laws of *geometrical optics*. The scattered field consists of two contributions. The first one stems from the currents induced on the exterior surface and the equivalent currents on the rim of the aperture. These currents can be determined by the methods, described in Section 13.4. The second one originates from the tangential fields that appear in the aperture S_A and act as radiating elements [211]. When the aperture is very large with respect to λ_0, the fields there are equal to the incident fields, except for a small zone of depth of the order λ_0 in the vicinity of the edge (see Section 9.7). In the *Kirchhoff approximation*, these edge fields

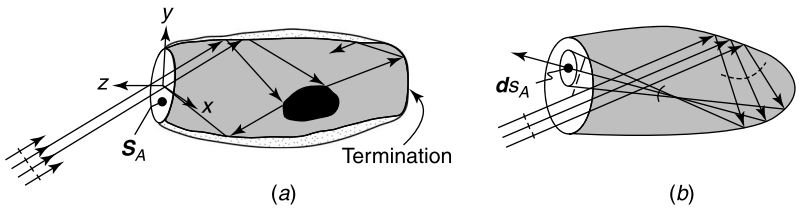

Figure 13.19 (*a*) Ray-bouncing technique. The aperture is in the (x, y) plane. (*b*) More detailed ray pattern, showing the presence of foci (from H. Ling, R. C. Chou, and S. W. Lee, Shooting and bouncing rays: calculating the RCS of an arbitrarily shaped cavity, *IEEE Trans. AP* **37**, 194–205, 1989, with permission of IEEE).

are neglected, and the rays penetrate undisturbed into the cavity, where they bounce from conductors, penetrate through materials, and finally return to the aperture[69] (Fig. 13.19*a*). The ray paths are found by ray tracing, and the reflections on the wall are governed by Snell's laws. The amplitude of the fields along the ray depends on the tube divergence factor [see (13.18) and Fig. 13.5]. The returning rays illuminate S_A, where they induce a magnetic current $\mathbf{J}_{mS} = \mathbf{E} \times \mathbf{u}_z$. If the fields are assumed to vanish on the remaining parts of the aperture plane, the scattered fields can be evaluated by the techniques developed in Section 9.6 for an aperture in a screen. These fields, the result of backscattering from the cavity, are normally much larger than the (neglected) rim diffracted fields.[70]

Various extensions of the method have been proposed, for example:

- Shooting *Gaussian beams* into the cavity instead of rays.[70,71] The method has the advantage of using a small number of beams compared with the number of rays required by the *geometrical optics* approach.
- Applying the *General ray expansion method* (GRE). In this method, the aperture is subdivided into a number of subapertures, each of which is assumed to be the source of an inhomogeneous spherical wave.[72]
- Solving an integral equation of the MFIE type for the currents induced in the cavity walls[73] by the incident magnetic field $\mathbf{H}^i$. This field stems from the aperture fields, which may be given the values $\mathbf{E}^i_{\tan}$ and $\mathbf{H}^i_{\tan}$, in agreement with the Kirchhoff approximation. The MFIE is solved by iteration, using the P.O. current $2(\mathbf{u}_n \times \mathbf{H}^i)$ as initial *seed* current.

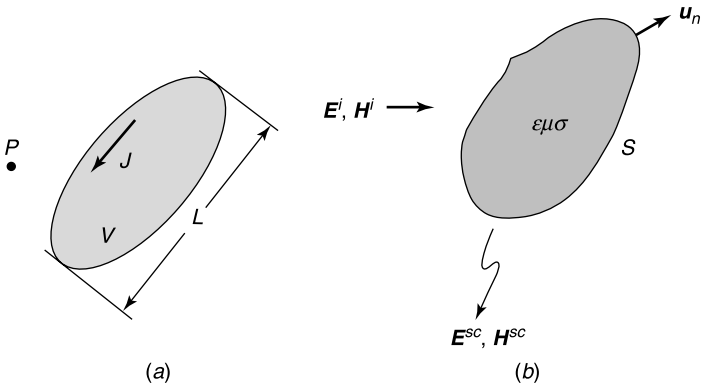

Figure 13.20 (*a*) Current-carrying volume of dimensions much less than λ_0. (*b*) Scatterer in a low-frequency field.

13.6 LOW-FREQUENCY FIELDS: THE RAYLEIGH REGION

With a view toward using low-frequency approximations, we shall assume that volume V in Figure 13.20 has a maximum dimension L much less than the wavelength λ_0. The potentials produced in P by the (electric) currents flowing in V are given by (7.96) and (7.97). If the distance from P to all points of V is also much less than λ_0, the exponent $k_0|\mathbf{r}-\mathbf{r}'|$ is very small, and the potentials are given approximately by[‡‡]

$$\mathbf{A} \approx \frac{\mu_0}{4\pi}\int_V \frac{\mathbf{J}(\mathbf{r}')\,dV'}{|\mathbf{r}-\mathbf{r}'|} \qquad \Phi \approx \frac{1}{4\pi\epsilon_0}\int_V \frac{P(\mathbf{r}')\,dV'}{|\mathbf{r}-\mathbf{r}'|}. \tag{13.53}$$

Under these conditions, the electric and magnetic fields are identical with the static fields generated by the instantaneous values of charges and currents. It is only at distances of the order λ_0 that the finite velocity of the waves and the associated retardation effects produce the $1/R$ variation associated with the radiation fields. In the radiation region, the fields are represented by the multipole expansion (7.155), and the energy densities $\frac{1}{2}\epsilon_0|\mathbf{E}|^2$ and $\frac{1}{2}\mu_0|\mathbf{H}|^2$ are equal. In the near field, however, one of the energies is normally dominant. In the equatorial plane of an electric dipole, for example (Fig. 7.11),

$$E_\theta = \frac{P_e}{4\pi\epsilon_0}\frac{1}{R^3}$$
$$H_\varphi = \frac{j\omega P_e}{4\pi}\frac{1}{R^2}$$

from which it may be deduced that

$$H_\varphi = jk_0R\frac{E_\theta}{R_{c0}}.$$

The electric field clearly dominates. On the other hand, if the current forms a loop, it generates a magnetic dipole, and it is the magnetic energy that now dominates. This situation arises in the vicinity of power devices such as alternators and transformers.

The low-frequency analysis proceeds by expanding the fields in a series in (jk_0). For an x-polarized incident plane wave, for example, one writes[§§]

$$\begin{aligned}\mathbf{E}^i &= e^{-jk_0z}\mathbf{u}_x = \left(1 - jk_0z - \frac{k_0^2}{2}z^2 + \cdots\right)\mathbf{u}_x \\ \mathbf{H}^i &= \frac{1}{R_{c0}}e^{-jk_0z}\mathbf{u}_y = \frac{1}{R_{c0}}\left(1 - jk_0z - \frac{k_0^2}{2}z^2 + \cdots\right)\mathbf{u}_y.\end{aligned} \tag{13.54}$$

[‡‡]The value of $\mathbf{J}$ (or $\mathbf{J}_m$) may be frequency dependent, in which case a separate expansion in jk_0 of these currents should be inserted in (13.53). The actual $\mathbf{J}(k_0)$ law depends on the nature of the sources. In dielectric volumes, for example, the approach $k_0 \to 0$ may cross sudden resonances.

[§§]One could also expand in terms of the dimensionless parameter (k_0L). For such a choice, all coefficients of the expansion have the same dimension.

From (7.155), the leading terms in the expansion of the far fields are

$$\mathbf{E} = k_0^2 \frac{e^{-jk_0R}}{4\pi R}\left[-\frac{1}{\epsilon_0}\mathbf{u}\times(\mathbf{u}\times\mathbf{P}_e) - R_{c0}\mathbf{u}\times\mathbf{P}_m\right]$$
$$\mathbf{H} = k_0^2 \frac{e^{-jk_0R}}{4\pi R}\left[c_0\mathbf{u}\times\mathbf{P}_e - \mathbf{u}\times(\mathbf{u}\times\mathbf{P}_m)\right]. \tag{13.55}$$

The time-averaged radiated power, from (7.159) and (7.167), is equal to

$$P_{\text{ave}} = \frac{k_0^4 c_0}{12\pi}\left[\frac{1}{\epsilon_0}|\mathbf{P}_e|^2 + \mu_0|\mathbf{P}_m|^2\right]. \tag{13.56}$$

The low-frequency (or *Rayleigh*) *region*[74] may be defined — in three dimensions[¶¶] — as the range of frequencies for which the (jk_0) series converges, with a finite radius of convergence.[75] In a more restrictive definition, it is the region for which the series is well-represented, in the far field, by its first nonzero term (or terms), for example those in $\mathbf{P}_e$ and $\mathbf{P}_m$.

13.7 NON-CONDUCTING SCATTERERS AT LOW FREQUENCIES

In *Stevenson's method*[76] the incident, scattered, and interior fields are expanded in a series in jk_0. The series are subsequently inserted into Maxwell's equations and like powers of jk_0 are equated on both sides. This gives, for the scattered field,

$$\begin{cases} \text{curl}\,\mathbf{E}_0^{sc} = 0 \\ \text{curl}\,\mathbf{E}_1^{sc} = -R_{c0}\,\mathbf{H}_0^{sc} \\ \text{curl}\,\mathbf{E}_2^{sc} = -R_{c0}\,\mathbf{H}_1^{sc} \\ \quad\vdots \end{cases} \qquad \begin{cases} \text{curl}\,\mathbf{H}_0^{sc} = 0 \\ \text{curl}\,\mathbf{H}_1^{sc} = \dfrac{1}{R_{c0}}\,\mathbf{E}_0^{sc} \\ \text{curl}\,\mathbf{H}_2^{sc} = \dfrac{1}{R_{c0}}\,\mathbf{E}_1^{sc}. \\ \quad\vdots \end{cases} \tag{13.57}$$

All $\mathbf{E}_n^{sc}$ and $\mathbf{H}_n^{sc}$ are divergenceless. Similar equations may be written for the incident fields. Inside the scatterer, the expansions become

$$\begin{cases} \text{curl}\,\mathbf{E}_0 = 0 \\ \text{curl}\,\mathbf{E}_1 = -\mu_r R_{c0}\,\mathbf{H}_0 \\ \text{curl}\,\mathbf{E}_2 = -\mu_r R_{c0}\,\mathbf{H}_1 \end{cases} \qquad \begin{cases} \text{curl}\,\mathbf{H}_0 = 0 \\ \text{curl}\,\mathbf{H}_1 = \dfrac{\epsilon_r}{R_{c0}}\,\mathbf{E}_0 \\ \text{curl}\,\mathbf{H}_2 = \dfrac{\epsilon_r}{R_{c0}}\,\mathbf{E}_1. \end{cases} \tag{13.58}$$

[¶¶] In two dimensions there is no convergent expansion in terms of jk_0, given the branch point of $H_0^{(2)}(z)$ at $z = 0$. A logarithmic singularity appears. The point is belabored in Section 14.8.

These fields are again divergenceless. Interior and exterior fields are coupled by the boundary conditions on S, viz. (Fig. 13.20*b*)

$$\begin{aligned}
\mathbf{u}_n \times \mathbf{E}_m &= \mathbf{u}_n \times \mathbf{E}_m^i + \mathbf{u}_n \times \mathbf{E}_m^{sc} \\
\epsilon_r \mathbf{u}_n \cdot \mathbf{E}_m &= \mathbf{u}_n \cdot \mathbf{E}_m^i + \mathbf{u}_n \cdot \mathbf{E}_m^{sc} \\
\mathbf{u}_n \times \mathbf{H}_m &= \mathbf{u}_n \times \mathbf{H}_m^i + \mathbf{u}_n \times \mathbf{H}_m^{sc}.
\end{aligned} \tag{13.59}$$

It is clear that, to zero-order, the **E** and **H** fields are *uncoupled static fields*, regular at infinity, and obtainable from (13.53). The sources of the scattered fields are the induced polarization currents and charges. From (13.58), $\mathbf{H}_1$ in the scatterer must be proportional to ϵ_r. If we write $\mathbf{H}_1 = \epsilon_r \mathbf{h}_1$, the expansion takes the form

$$\mathbf{H} = \mathbf{H}_0 + jk_0\epsilon_r\, \mathbf{h}_1 + \cdots .$$

The expansion parameter is now $(k_0\epsilon_r)$, and it should be sufficiently small to ensure convergence. More precisely, because

$$k_0\epsilon_r = \frac{2\pi}{\lambda}\sqrt{\frac{\epsilon_r}{\mu_r}}$$

the wavelength λ in the dielectric should remain large with respect to L. When λ decreases to values of the order L, dielectric resonances of the kind discussed in Section 10.5 will start appearing.

13.7.1 The Scattered Field

The scattered fields are given by equations (7.223) and (7.224), into which the expansions for $\mathbf{E}^{sc}$ and $\mathbf{H}^{sc}$ should be inserted. If $e^{-jk_0|\mathbf{r}-\mathbf{r}'|}$ is similarly expanded in terms of jk_0, the leading terms are found to be

$$\mathbf{E}_0^{sc}(\mathbf{r}) = -\text{grad}\int_S \frac{\mathbf{u}_n \cdot \mathbf{E}_0^{sc}}{4\pi|\mathbf{r}-\mathbf{r}'|}\,dS' + \text{curl}\int_S \frac{\mathbf{u}_n \times \mathbf{E}_0^{sc}}{4\pi|\mathbf{r}-\mathbf{r}'|}\,dS' \quad (\text{V m}^{-1}) \tag{13.60}$$

$$\begin{aligned}
\mathbf{E}_1^{sc}(\mathbf{r}) = &-\text{grad}\int_S \frac{\mathbf{u}_n \cdot \mathbf{E}_1^{sc}}{|\mathbf{r}-\mathbf{r}'|}\,dS' + R_{c0}\int_S \frac{\mathbf{u}_n \times \mathbf{H}_0^{sc}}{|\mathbf{r}-\mathbf{r}'|}\,dS' \\
&+ \text{curl}\int_S \frac{\mathbf{u}_n \times \mathbf{E}_1^{sc}}{4\pi|\mathbf{r}-\mathbf{r}'|}\,dS' \qquad (\text{V}).
\end{aligned} \tag{13.61}$$

The field (13.60) is clearly $O(R^{-2})$ at large distances and therefore satisfies the regularity requirement. The same holds for $\mathbf{E}_1^{sc}$, because, the second term on the right-hand side of (13.61) is also $O(R^{-2})$ because

$$\int_S (\mathbf{u}_n \times \mathbf{H}_0^{sc})\,dS = \int_V \text{curl}\,\mathbf{H}_0\,dV = 0.$$

Similar results can be derived for $\mathbf{H}_0^{sc}$ and $\mathbf{H}_1^{sc}$. These considerations, however, hold only for the near field. As the distance R increases, convergence deteriorates because the expansion

of $e^{-jk_0|\mathbf{r}-\mathbf{r}'|}$ introduces progressively higher powers of $|\mathbf{r}-\mathbf{r}'| = R$ into the integrals. To obtain accurate fields because one could use the expansions for $\mathbf{E}^{sc}$ and $\mathbf{H}^{sc}$ to calculate the fields on some small spherical surface surrounding the scatterer and represent the fields outside the sphere by a multipole expansion. The coefficients of the multipole expansion are determined by matching the fields at the spherical surface. Alternately, one could start from a multipole expansion such as (13.55) and insert the static values of the multipole moments into the equations. If $\mathbf{E}_0^i$ and $\mathbf{H}_0^i$ are uniform in the scatterer, which would be the case when the incident wave is plane, the required dipole moments are[77]

$$\begin{aligned} \mathbf{P}_e &= \epsilon_0 \overline{\overline{\alpha}}_e \cdot \mathbf{E}_0^i \\ \mathbf{P}_m &= \overline{\overline{\alpha}}_m \cdot \mathbf{H}_0^i \end{aligned} \tag{13.62}$$

where $\overline{\overline{\alpha}}_e$ and $\overline{\overline{\alpha}}_m$ (both expressed in m^3) are the polarizabilities defined in (3.125) and (6.86). Equations (13.60) and (13.61) show that the zero-order fields suffice to determine the leading terms in the multipole expansion. More generally, a knowledge of N near-field terms is sufficient to determine the first N terms in the multipole series.[78]

13.7.2 A Dielectric Sphere in an Incident Plane Wave

Assume that a nonmagnetic dielectric sphere is immersed in the field of a linearly polarized incident plane wave (Fig. 13.21). From Section 3.10, the relevant (zero-order) static fields are

$$\begin{aligned} \frac{\mathbf{E}_0}{E_0^i} &= \frac{3}{2+\epsilon_r}\,\mathbf{u}_z \;=\; -\frac{3}{\epsilon_r+2}\,\mathrm{curl}\,(y\,\mathbf{u}_x) \qquad (R \le a) \\ \frac{\mathbf{E}_0^i}{E_0^i} + \frac{\mathbf{E}_0^{sc}}{E_0^i} &= \mathbf{u}_z - \mathrm{grad}\left(\frac{\epsilon_r-1}{\epsilon_r+2}\,a^3\frac{\cos\theta}{R^2}\right) \\ &= \mathbf{u}_z + \frac{\epsilon_r-1}{\epsilon_r+2}\,a^3\,\mathrm{curl}\left(\frac{\sin\theta}{R^2}\,\mathbf{u}_\varphi\right) \qquad (R \ge a) \\ \mathbf{P}_e &= 4\pi\epsilon_0\,a^3\frac{\epsilon_r-1}{\epsilon_r+2}\,\mathbf{E}_0^i. \end{aligned} \tag{13.63}$$

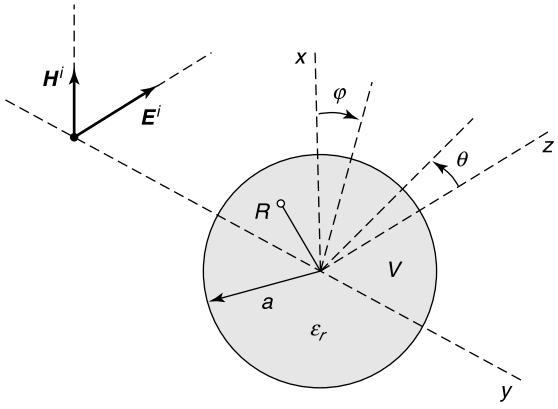

Figure 13.21 Dielectric sphere in an incident low-frequency wave.

There is no static magnetic field because the sphere is nonmagnetic. A first-order field $\mathbf{H}_1$ exists, however, and its source can be traced to the electric polarization currents. The equations for $\mathbf{H}_1$, that is, (13.57) and (13.58), give only the curl of that vector, which therefore is defined to within an additive gradient. We write, from (13.63),

$$\begin{aligned}\mathbf{H}_1 &= -\frac{3\epsilon_r}{R_{c0}(\epsilon_r+2)}\, y\, E_0^i\, \mathbf{u}_x + \text{grad}\ \phi \qquad (R \le a)\\ \mathbf{H}_1^{sc} &= \frac{\epsilon_r - 1}{R_{c0}(\epsilon_r+2)}\, a^3\, E_0^i \frac{\sin\theta}{R^2}\mathbf{u}_\varphi + \text{grad}\ \psi \qquad (R \ge a).\end{aligned} \tag{13.64}$$

Because $\mathbf{H}_1$ is solenoidal, the potentials ϕ and ψ must be harmonic. Their determination — a static problem — can be achieved by separation of variables. It should be remembered, in the process, (1) that grad ϕ must be finite at $R = 0$, (2) that ψ must be regular at large distances, and (3) that $\mathbf{H}_1 = \mathbf{H}_1^{sc} + \mathbf{H}_1^i$ at $R = a$. The final result is

$$\begin{aligned}R_{c0}\,\mathbf{H}_1^{sc} &= \frac{\epsilon_r - 1}{\epsilon_r + 2}\, a^3 \frac{\sin\theta}{R^2}\,\mathbf{u}_\varphi\\ R_{c0}\,\mathbf{H}_1 &= -\frac{R}{2}\sin^2\theta\sin 2\varphi\,\mathbf{u}_R - \frac{R}{4}\sin 2\theta\sin 2\varphi\,\mathbf{u}_\theta\\ &\quad + \left(R\sin\theta\sin^2\varphi + \frac{\epsilon_r - 1}{\epsilon_r + 2}R\sin\theta\right)\mathbf{u}_\varphi.\end{aligned} \tag{13.65}$$

The same approach can be applied to $\mathbf{E}_1$ and $\mathbf{E}_1^{sc}$ [22]. It can also be adapted to spherical scatterers with chiral constitutive equations

$$\begin{aligned}\mathbf{D} &= \epsilon\mathbf{E} - j\kappa\sqrt{\epsilon_0\mu_0}\,\mathbf{H}\\ \mathbf{B} &= \mu\mathbf{H} + j\kappa\sqrt{\epsilon_0\mu_0}\,\mathbf{E}.\end{aligned}$$

The solution proceeds by introducing the field and source combinations[79]

$$\begin{aligned}\mathbf{E}_\pm &= \frac{1}{2}\left(\mathbf{E} \mp j\sqrt{\frac{\mu}{\epsilon}}\,\mathbf{H}\right)\\ \mathbf{J}_\pm &= \frac{1}{2}\left(\mathbf{J} \pm \frac{1}{j\sqrt{\dfrac{\mu}{\epsilon}}}\,\mathbf{J}_m\right).\end{aligned}$$

Electric and magnetic dipoles are again induced in the sphere, but both have cross-polarized components (i.e., $\mathbf{P}_e$ has a component perpendicular to $\mathbf{E}_0^i$).

13.8 PERFECTLY CONDUCTING SCATTERERS AT LOW FREQUENCIES

The scattered field at the surface of the conductor must satisfy the boundary conditions

$$\begin{aligned}\mathbf{u}_n \times \mathbf{E}^{sc} &= -\mathbf{u}_n \times \mathbf{E}^i\\ \mathbf{u}_n \cdot \mathbf{H}^{sc} &= -\mathbf{u}_n \cdot \mathbf{H}^i.\end{aligned} \tag{13.66}$$

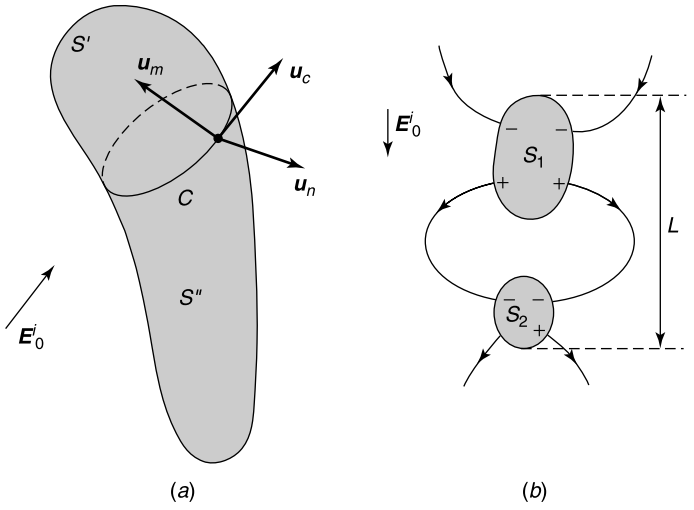

Figure 13.22 (*a*) Simply connected conductor ($S = S' + S''$). (*b*) Two-conductor configuration.

We shall assume that the conductor is simply connected, leaving to Section 13.11 a discussion of ring-type geometries. The low-frequency limit of $\mathbf{E}$ is the static field that exists outside the conductor when the latter is immersed in the incident field $\mathbf{E}_0^i$ (Fig. 13.22*a*). Under these conditions, a charge density

$$P_{S0} = \epsilon_0 \mathbf{u}_n \cdot \mathbf{E}_0 \tag{13.67}$$

appears on S. The zero-order *magnetic* field is also static-like, and its scattered part can be written as $\mathbf{H}_0^{sc} = -\text{grad}\ \psi_0^{sc}$, where

$$\begin{aligned} &\nabla^2 \psi_0^{sc} = 0 && \text{(outside } S\text{)} \\ &\frac{\partial \psi_0^{sc}}{\partial n} = -\frac{\partial \psi_0^{i}}{\partial n} = \mathbf{u}_n \cdot \mathbf{H}_0^i && \text{(on } S\text{)} \\ &\psi_0^{sc} && \text{regular at infinity.} \end{aligned} \tag{13.68}$$

The determination of ψ_0^{sc} is a Neumann type of problem. The induced current density on S can be given the Helmholtz form

$$\mathbf{J}_S = \text{grad}_S A + \mathbf{u}_n \times \text{grad}_S B. \tag{13.69}$$

$\mathbf{J}_S$ is also related to the tangential magnetic field by

$$\mathbf{J}_S = \mathbf{u}_n \times \mathbf{H} = \underbrace{\mathbf{u}_n \times \mathbf{H}_0}_{\mathbf{J}_{S0}} + jk_0 \underbrace{\mathbf{u}_n \times \mathbf{H}_1}_{\mathbf{J}_{S1}} + \cdots, \tag{13.70}$$

where

$$\mathbf{J}_{S0} = -\mathbf{u}_n \times \text{grad}_S\, (\psi_0^i + \psi_0^{sc}).$$

The term $\text{grad}_S A$ in (13.69) is of the first order because, from (13.67),

$$\begin{aligned}\nabla_S^2 A = \text{div}_S \mathbf{J}_S &= -j\omega P_{S0} = -jk_0 c_0 P_{S0} \\ &= jk_0 \,\text{div}\, \mathbf{J}_{S1} + \cdots .\end{aligned} \tag{13.71}$$

This term is therefore associated with $jk_0(\mathbf{u}_n \times \mathbf{H}_1)$ in (13.70). The zero-order current through a curve such as C in Figure 13.22*a* is given by

$$I_0 = \int_C \mathbf{J}_{S0} \cdot \mathbf{u}_m \, dc = \int_C (\mathbf{u}_n \times \mathbf{H}_0) \cdot \mathbf{u}_m \, dc = \int_C \mathbf{H}_0 \cdot \mathbf{u}_c \, dc, \tag{13.72}$$

where $\mathbf{H}_0$ is the value of the magnetic field just outside the scatterer. Applying Stokes' theorem to C and S' transforms $\displaystyle\int_C \mathbf{H}_0 \cdot \mathbf{u}_c \, dc$ into the flux of curl $\mathbf{H}_0$ through S', and this is automatically zero because $\mathbf{H}_0$ is irrotational at all points of S'. Alternately, $\displaystyle\int_C \mathbf{H}_0 \cdot \mathbf{u}_c \, dc$ remains constant as C is shifted along S, and therefore reduces to zero when C shrinks to a point. We conclude that there is no net zero-order current. There is a *first-order* current, however. Flowing from S'' to S', it is

$$\begin{aligned}I = \int_C \mathbf{u}_m \cdot \mathbf{J}_S \, dc &= -\int_{S'} \text{div}_S \, \mathbf{J}_S \, dS \\ &= jk_0 \, c_0 \int_{S'} P_{S0} \, dS = j\omega Q_0,\end{aligned} \tag{13.73}$$

where Q_0 is the total electric charge induced on S' by $\mathbf{E}_0^i$. It is clear that I is the *capacitive current* that ferries charges from S'' to S'. As an illustration, consider the sphere of Figure 13.21, now assumed perfectly conducting. Based on (4.72), the relevant data are

$$\begin{aligned}\mathbf{E}_0 &= \left[\left(1 + 2\frac{a^3}{R^3}\right)\cos\theta \, \mathbf{u}_R + \left(\frac{a^3}{R^3} - 1\right)\sin\theta \, \mathbf{u}_\theta\right] E_0^i \\ P_{S0} &= 3\epsilon_0 \cos\theta E_0^i \\ \psi_0^i &= -H_0^i R \sin\theta \cos\varphi \\ \psi_0^{sc} &= -H_0^i \frac{a^3}{2R^2} \sin\theta \cos\varphi \\ \mathbf{H}_0 &= H_0^i \left[\left(1 - \frac{a^3}{R^3}\right)\sin\theta\cos\varphi \, \mathbf{u}_R + \left(1 + \frac{a^3}{2R^3}\right)\cos\theta\cos\varphi \, \mathbf{u}_\theta \right. \\ &\quad \left. - \left(1 + \frac{a^3}{2R^3}\right)\sin\varphi \, \mathbf{u}_\varphi\right] \\ \mathbf{J}_{S0} &= \frac{3}{2} H_0^i \left[\cos\theta\cos\varphi \, \mathbf{u}_\varphi + \sin\varphi \, \mathbf{u}_\theta\right] = \frac{3}{2} \mathbf{u}_R \times \mathbf{H}_0^i.\end{aligned} \tag{13.74}$$

The zero-order current $\mathbf{J}_{S0}$ flows in circles in a plane perpendicular to $\mathbf{u}_x$. It is a *transformer current*, which does not contribute to the current through C and radiates like a *magnetic dipole* of moment

$$\mathbf{P}_m = \frac{1}{2}\int_S \mathbf{r} \times \mathbf{J}_{S0} \, dS = -2\pi a^3 \, \mathbf{H}_0^i. \tag{13.75}$$

The *capacitive* current density, which must satisfy (13.69), and is θ-oriented by symmetry, is

$$jk_0\mathbf{J}_{S1} = -\frac{3}{2}jk_0 a\, H_0^i \sin\theta\, \mathbf{u}_\theta. \tag{13.76}$$

It radiates like an *electric dipole* of moment

$$\mathbf{P}_e = \int_S P_{S0}\, \mathbf{r}\, dS = 4\pi\epsilon_0 a^3\, \mathbf{E}_0^i. \tag{13.77}$$

The corresponding *polarizability dyadics* are

$$\begin{aligned} \overline{\overline{\alpha}}_e &= 4\pi a^3\, \overline{\overline{I}} \\ \overline{\overline{\alpha}}_m &= -2\pi a^3\, \overline{\overline{I}}. \end{aligned} \tag{13.78}$$

13.8.1 Cross Sections

A perfectly conducting scatterer is characterized, at low frequencies, by its symmetric polarizability dyadics $\overline{\overline{\alpha}}_e$ and $\overline{\overline{\alpha}}_m$. Each dyadic can be constructed from the solution of three potential problems, corresponding with three orthogonal directions of incidence. The case of a simply connected body of revolution $\overline{\overline{\alpha}}_e$ can be given the diagonal form

$$\overline{\overline{\alpha}}_e = \begin{pmatrix} P_{tr} & 0 & 0 \\ 0 & P_{tr} & 0 \\ 0 & 0 & P_{zz} \end{pmatrix} \tag{13.79}$$

where Oz is the axis of revolution, and *tr* means transverse with respect to Oz. One may similarly write

$$\overline{\overline{\alpha}}_m = \begin{pmatrix} M_{tr} & 0 & 0 \\ 0 & M_{tr} & 0 \\ 0 & 0 & M_{zz} \end{pmatrix}. \tag{13.80}$$

The interesting property $M_{zz} = \dfrac{1}{2}P_{zz}$ shows that the two polarizability dyadics contain only three independent terms[80,81] [94]. Values of the three dimensionless coefficients (P_{tr}/V), (P_{zz}/V), and (M_{tr}/V) — where V is the volume of the scatterer — are available for a variety of shapes, for example for the cone-sphere[82] (Problem 13.7). From (11.22), the scattering cross section in an incident plane wave may be written as

$$\sigma^{sc} = \frac{k_0^4 V^2}{6\pi} \underbrace{\left[\left| \frac{\mathbf{u}_e \cdot \overline{\overline{\alpha}}_e}{V} \right|^2 + \left| \frac{\mathbf{u}_h \cdot \overline{\overline{\alpha}}_m}{V} \right|^2 \right]}_{\text{dimensionless factor}} \tag{13.81}$$

where $\mathbf{u}_e$ and $\mathbf{u}_h$ are the — possibly complex — unit vectors in the respective directions of $\mathbf{E}_0^i$ and $\mathbf{H}_0^i$. As a general rule, it may be stated that low-frequency scattering is mainly a bulk effect, and that a phase distribution of the incident field over S is needed to "feel"

the shape of the scatterer. This phase effect does not come to the fore until λ_0 decreases to values of the order the largest dimension L of the scatterer. It is remarked in Section 11.5 that the range $10L > \lambda_0 > L/2$ is capable of providing much initial information on overall dimensions, approximate shape, and material composition of a target.[83]

13.8.2 Two Coupled Conductors

Low-frequency methods can also be applied to scatterers consisting of several conductors (e.g., to the two halves of a receiving *dipole-antenna*). In an incident field $\mathbf{E}_0^i$, a difference of potential $\Delta\phi$ appears between the conductors, with lines of force of the type suggested in Figure 13.22*b*. In a uniform $\mathbf{E}_0^i$, $\Delta\phi$ is given by

$$\Delta\phi = \phi_1 - \phi_2 = \mathbf{E}_0^i \cdot \mathbf{h} \tag{13.82}$$

where $\mathbf{h}$, a real vector, is the *effective length of the antenna*.‖‖ It is easy to show, using reciprocity, that $\mathbf{h}$ is also the distance between the centers of gravity of the positive and negative charges that appear on the armatures of the capacitor formed by S_1 and S_2 (Problem 13.10).

13.8.3 The Mathematical Approach to Zero Frequency

The problem in hand is to prove that the time-harmonic fields $\mathbf{E}(\mathbf{r}, \omega)$ and $\mathbf{H}(\mathbf{r}, \omega)$ *rigorously* approach the zero-order limits $\mathbf{E}_0$ and $\mathbf{H}_0$ introduced in Stevenson's method. Consider first a simply connected, perfectly conducting volume, surrounded by free-space*** (Fig. 13.23*a*). The boundary condition on S may be written as

$$\mathbf{u}_n \times \mathbf{E}^{sc} = -\mathbf{u}_n \times \mathbf{E}^i = \mathbf{C}. \tag{13.83}$$

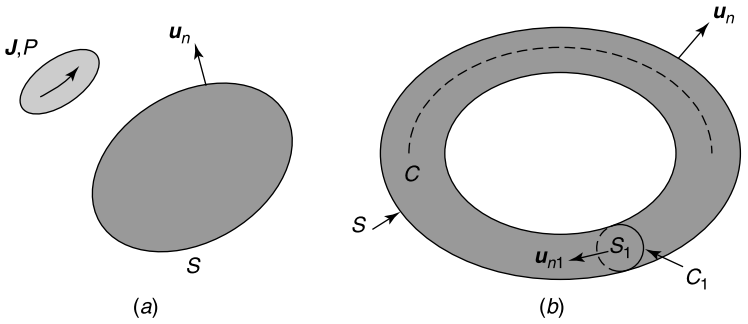

Figure 13.23 (*a*) Simply connected conductor. (*b*) Toroidal volume. S = outer surface, S_1 = cross section.

‖‖For an application to two circular cylinders, see Note 84.

***See Note 85, in which the surrounding medium is allowed to have complex (ϵ, μ) parameters, and the conducting regions may be multiply bounded.

From (7.107) and (7.109), the electric field associated with this *boundary excitation* may be given the tentative form

$$\begin{aligned}\mathbf{E}^{sc}(\mathbf{r}) &= \operatorname{curl} \int_S \mathbf{A}(\mathbf{r}') \frac{e^{-jk_0|\mathbf{r}-\mathbf{r}'|}}{|\mathbf{r}-\mathbf{r}'|}\, dS' \\ &= \int_S \mathbf{A}(\mathbf{r}') \times \operatorname{grad}' \left(\frac{e^{-jk_0|\mathbf{r}-\mathbf{r}'|}}{|\mathbf{r}-\mathbf{r}'|} \right) dS', \end{aligned} \tag{13.84}$$

where $\mathbf{A}$, which has the nature of a magnetic surface current, is assumed tangent to S. If $\mathbf{r}$ is allowed to approach S, the limit form (12.23) of the integral shows that $\mathbf{A}$ must satisfy the integral equation[†††]

$$2\pi\, \mathbf{A}(\mathbf{r}) + \mathbf{u}_n(\mathbf{r}) \times \lim_{\delta \to 0} \int_{S-S_\delta} \mathbf{A}(\mathbf{r}') \times \operatorname{grad}' \left(\frac{e^{-jk_0|\mathbf{r}-\mathbf{r}'|}}{|\mathbf{r}-\mathbf{r}'|} \right) dS' = \mathbf{C}(\mathbf{r}). \tag{13.85}$$

The corresponding homogeneous zero-order version

$$2\pi\, \mathbf{A}_0(\mathbf{r}) + \mathbf{u}_n(\mathbf{r}) \times \lim_{\delta \to 0} \int_{S-S_\delta} \mathbf{A}_0(\mathbf{r}') \times \operatorname{grad}' \left(\frac{1}{|\mathbf{r}-\mathbf{r}'|} \right) dS' = 0 \tag{13.86}$$

can be shown to admit only the solution $\mathbf{A}_0(\mathbf{r}) = 0$ when the volume is simply connected.[‡‡‡] This property can be exploited to prove that a unique solution to (13.85) exists in the limit $\omega \to 0$, and that the limit field $\mathbf{E}_0^{sc}(\mathbf{r})$ derived from $\mathbf{A}_0(\mathbf{r})$ satisfies the properties

$$\begin{aligned} \operatorname{curl} \operatorname{curl} \mathbf{E}_0^{sc} &= 0 && \text{(in } V+S\text{)} \\ \operatorname{div} \mathbf{E}_0^{sc} &= 0 && \text{(in } V+S\text{)} \\ \mathbf{u}_n \times \mathbf{E}_0^{sc} &= \mathbf{C} && \text{(on } S\text{)} \\ \int_S \mathbf{u}_n \cdot \mathbf{E}_0^{sc}\, dS &= 0 && \text{(charge neutrality)} \\ \lim_{R \to \infty} \mathbf{E}_0 &= 0\left(\frac{1}{R}\right) && \text{(for all directions).} \end{aligned} \tag{13.87}$$

The field $\mathbf{E}_0^{sc}$ becomes irrotational if, and only if, $\lim_{\omega \to 0} \operatorname{div}_S \mathbf{C} = 0$ on S. With $\mathbf{C}$ defined by (13.73), the condition is automatically satisfied because

$$\operatorname{div}_S \mathbf{C} = \operatorname{div}_S (\mathbf{E}^i \times \mathbf{u}_n) = \mathbf{u}_n \cdot \operatorname{curl} \mathbf{E}^i = -j\omega\mu_0\, \mathbf{u}_n \cdot \mathbf{H}^i. \tag{13.88}$$

The limit of the *magnetic* field follows on the basis of the expression[86]

$$\mathbf{H} = -(j\omega\mu_0)^{-1} \operatorname{curl} \mathbf{E},$$

[†††]The problems associated with interior resonances resurface here, but they can be taken into account by modifying the *ansatz* (13.84). The point is not relevant at very low frequencies, way below the lowest resonance.

[‡‡‡]In a multiply connected region of genus p, the equation admits p independent solutions.

from which it may be deduced that $\mathbf{H}_0$ is solenoidal and irrotational and satisfies the conditions

$$\begin{aligned} \mathbf{u}_n \cdot \mathbf{H}_0 &= \frac{1}{j\omega\mu_0} \operatorname{div}_S \mathbf{C}_0 \\ \lim \mathbf{H}_0 &= O\left(\frac{1}{R^2}\right) \qquad \text{(at large distances).} \end{aligned} \tag{13.89}$$

Similar results can be obtained for *volume sources*, (Fig. 13.23*a*), in which case the fields converge to values satisfying

$$\begin{aligned} \operatorname{curl} \mathbf{E}_0 &= 0 && \text{(in } V\text{)} \\ \operatorname{div} \mathbf{E}_0 &= \frac{1}{\epsilon_0} P_0 \;=\; -\frac{1}{\epsilon_0} \lim_{\omega \to 0} \frac{1}{j\omega} \operatorname{div} \mathbf{J} && \text{(in } V\text{)} \\ \mathbf{u}_n \times \mathbf{E}_0 &= 0 && \text{(on } S\text{)} \\ \lim_{R \to \infty} \mathbf{E}_0 &= O\left(\frac{1}{R^2}\right) && \text{(for all directions)} \end{aligned} \tag{13.90}$$

and

$$\begin{aligned} \operatorname{curl} \mathbf{H}_0 &= \mathbf{J}_0 && \text{(in } V\text{)} \\ \operatorname{div} \mathbf{H}_0 &= 0 && \text{(in } V\text{)} \\ \mathbf{u}_n \cdot \mathbf{H}_0 &= 0 && \text{(on } S\text{)} \\ \lim_{R \to \infty} \mathbf{H}_0 &= O\left(\frac{1}{R^2}\right) && \text{(at large distances).} \end{aligned} \tag{13.91}$$

The condition $\mathbf{u}_n \cdot \mathbf{H}_0 = 0$ on S, which stems from the mathematical limiting process, deserves some comments. The *perfectly conducting* assumption requires $\mathbf{e}$ to vanish inside the conductor, lest $\mathbf{j}$ becomes infinite there. Maxwell's equation (7.1) therefore implies that $\mathbf{b}(\mathbf{r}, \mathbf{t})$ must be independent of time, hence that the only possible magnetic field inside the conductor is a truly magnetostatic one. It follows, from the continuity of $\mathbf{b}_n$, that $(\mathbf{u}_n \cdot \mathbf{b})$ must be time-independent. If we are only interested in the nonstatic part of $\mathbf{b}$, we may therefore set $\mathbf{u}_n \cdot \mathbf{b} = 0$ on S.

The brief survey of the mathematical argument presented above is far from rigorous. A correct analysis would require, for example, $\mathbf{J}$ and its first derivatives to be continuous functions of ω, and P_0 to be Hölder continuous in space. It would also require S to be a thrice differentiable closed surface. The reader is referred to the quoted papers for a much more sophisticated approach to the problem.

13.8.4 Multiply Connected Conductors

The previous mathematical discussion can be extended to penetrable bodies, of which real-life conductors are an important example. For such bodies, connectedness is irrelevant because the whole of space is involved.[87] If the infinite-conductivity model is kept, the mathematical problem becomes more delicate, and connectedness must be taken into

account. We shall only consider the simplest configuration, a doubly connected ring, for which the interior and exterior problems must be considered separately[88] (Fig. 13.23*b*). The *interior* problem — the only one to be briefly discussed here — is relevant for many applications (e.g., for the evaluation of the fields in the "doughnut" of a particle accelerator). We shall also only consider *boundary excitation* of such a ring, which occurs by way of the condition

$$\mathbf{u}_n \times \mathbf{E} = \mathbf{C} \qquad (\text{on } S). \tag{13.92}$$

The function $\mathbf{C}$ could be, for example, the magnetic current in the aperture of a toroidal cavity. If the limits

$$\begin{aligned} \lim_{\omega \to 0} \mathbf{C} &= \mathbf{C}_0 \\ \lim_{\omega \to 0} \operatorname{div}_S \mathbf{C} &= \operatorname{div}_S \mathbf{C}_0 \end{aligned} \tag{13.93}$$

exist, the electric field converges to the solution $\mathbf{E}_0$ of the *generalized electrostatic problem*

$$\begin{aligned} \operatorname{curl} \operatorname{curl} \mathbf{E}_0 &= 0 \qquad && (\text{in } V) \\ \operatorname{div} \mathbf{E}_0 &= 0 \qquad && (\text{in } V) \\ \mathbf{u}_n \times \mathbf{E}_0 &= \mathbf{C}_0 \qquad && (\text{on } S) \\ \int_S (\mathbf{u}_n \cdot \mathbf{E}_0)\, dS &= 0 \qquad && (\text{charge neutrality}). \end{aligned} \tag{13.94}$$

The proof is based on ansatz (13.84), augmented by the knowledge that integral equation (13.86) has a single nontrivial solution (defined to within a multiplicative constant). If, in addition, there are numbers δ and ν such that

$$\lim_{\omega \to 0} \operatorname{div}_S \mathbf{C} = \omega \delta \tag{13.95}$$

and

$$\lim_{\omega \to 0} \int_{C_1} \mathbf{C} \cdot \mathbf{dc}_1 = \omega \nu, \tag{13.96}$$

then $\mathbf{E}_0$ will satisfy $\operatorname{curl} \mathbf{E}_0 = 0$ in addition to (13.94). Note that (13.95) implies that $\mathbf{C}_0$ is of the form $\mathbf{u}_n \times \operatorname{grad} \phi_0$, which may be expected because $\mathbf{C} = \mathbf{u}_n \times \mathbf{E}_0$, and $\mathbf{E}_0$ is a gradient. Under the same conditions, the magnetic field approaches a limit $\mathbf{H}_0$, which is the solution of the magnetostatic-like problem

$$\begin{aligned} \operatorname{curl} \mathbf{H}_0 &= 0 \\ \operatorname{div} \mathbf{H}_0 &= 0 \\ \mathbf{u}_n \cdot \mathbf{H}_0 = \frac{\delta}{j\mu_0} &= \lim_{\omega \to 0} \left(\frac{1}{j\omega\mu_0} \operatorname{div}_S \mathbf{C} \right) \\ \int_{S_1} \mathbf{u}_{n_1} \cdot \mathbf{H}_0\, dS = \frac{\nu}{j\mu_0} &= \lim_{\omega \to 0} \left(\frac{1}{j\omega\mu_0} \int_{C_1} \mathbf{C} \cdot \mathbf{dc}_1 \right). \end{aligned} \tag{13.97}$$

Similar considerations lead to the equations that are satisfied by $\mathbf{E}_0$ and $\mathbf{H}_0$ under excitation by volume currents.[88]

13.9 GOOD CONDUCTORS

In a sourceless medium endowed with uniform (ϵ, μ, σ), the electric field satisfies the equation

$$-\text{curl curl } \mathbf{e} - \sigma\mu\frac{\partial \mathbf{e}}{\partial t} - \epsilon\mu\frac{\partial^2 \mathbf{e}}{\partial t^2} = 0. \tag{13.98}$$

In time-harmonic form:

$$-\text{curl curl } \mathbf{E} + (\omega^2\epsilon\mu - j\omega\mu\sigma)\,\mathbf{E} = 0. \tag{13.99}$$

The material characteristics are frequency-dependent, a point that is discussed in Section 8.1 in the case of metals. The dependence on frequency also holds for

$$\begin{aligned} &\text{the } \textit{charge}-\textit{relaxation time} \quad T_{rel} = \epsilon/\sigma \\ &\text{the } \textit{wave}-\textit{propagation time} \quad T_w = L/c \;=\; L\sqrt{\epsilon\mu} \\ &\text{the } \textit{magnetic}-\textit{diffusion time} \quad T_D = \sigma\mu L^2. \end{aligned} \tag{13.100}$$

Here L is the largest dimension of the material region. The relationship

$$T_w = \sqrt{T_{rel}T_D} \tag{13.101}$$

shows that T_w lies between T_{rel} and T_D.

By definition, a medium is a *good conductor* when the displacement current $\dfrac{\partial}{\partial t}(\epsilon\mathbf{e})$ is negligible with respect to the conduction current $\sigma\mathbf{e}$. For a time-harmonic field of period T, this requirement is expressed by the condition

$$Q = \frac{\omega\epsilon}{\sigma} = 2\pi\frac{T_{rel}}{T} \ll 1. \tag{13.102}$$

It is satisfied by metals throughout the frequency range for which σ can be regarded as constant. With σ of the order 10^7 S m^{-1}, the Q of metals is of the order 5×10^{-12} at 1 MHz. For materials with a σ ranging from 0.1 to 1 S m^{-1}, and ϵ_r from 10 to 90, Q varies between 0.0056 and 2.5 in the frequency band 10 to 50 MHz. Such material characteristics are often encountered in medical applications.

A most important parameter for good conductors is the *penetration depth* δ, for which a few data are given in Table 9.1. The penetration depth is of the order 1 μm for metals at 10 GHz. At lower frequencies δ increases, because it is inversely proportional to $\sqrt{\omega}$ and becomes as large as 1.1 cm for Al at 60 Hz. Figure 13.24 further illustrates the point. In many applications, in particular for high values of μ_r, δ is so small that a surface impedance representation of the obstacle is in order. At power frequencies, however, the current frequently flows throughout the conducting volume and is not restricted to a thin layer. In a nichrome wire, for example, δ is about 6 cm at 60 Hz. But the occurrence of such a deep penetration is not restricted to power frequencies. At 10 MHz, the penetration depth in muscle material is of the order 20 cm, and in many medical applications (e.g., in hyperthermia), such an important penetration is essential. Even at microwave frequencies, significant occupancy of the conductor by current can occur in microstrip circuits, where the thickness of the metallic

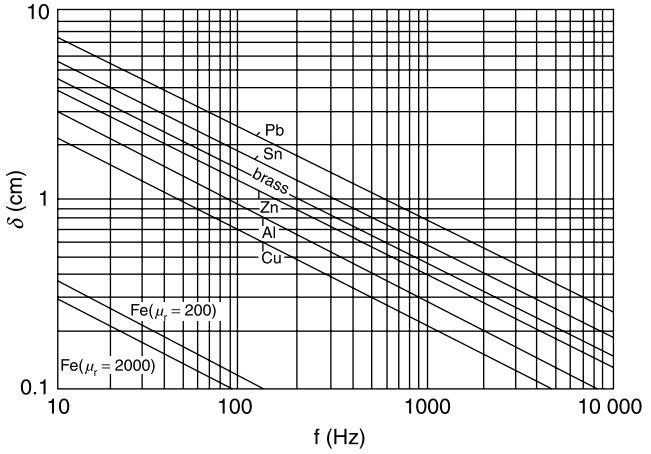

Figure 13.24 Penetration depth as a function of frequency (from H. Kaden, *Wirbelströme und Schirmung in der Nachrichtentechnik.* Springer Verlag, Berlin, 1959, with permission of Springer Verlag).

band may be of the order 1 μm. A case can therefore be made for a systematic study of the progressive invasion of the conducting volume by currents as δ increases (see Section 14.3).

The penetration depth is related to the quality factor Q by the equations

$$k\delta = \sqrt{2Q}$$

$$Q = \frac{1}{2}\left(\frac{\delta}{L}\right)^2 (kL)^2$$

$$kL = 2\pi \frac{T_w}{T} \tag{13.103}$$

where $k = \omega\sqrt{\epsilon_0\mu}$, and $Q = (\omega\epsilon_0/\sigma)$. Some useful data on Q are given in Table 13.2. The short horizontal lines correspond with $Q = 0.1$, and the part of the table above these lines represents the *good conductor* region of the material. It is seen that very small values of Q are associated with low values of kL, that is, with lengths L much less than $(\lambda/2\pi)$, where λ

Table 13.2 Values of Q

	kL					
δ/L	1	0.3	0.1	0.03	0.01	0.003
0	0	0	0	0	0	0
0.2	0.02	0.0018	0.2×10^{-3}	0.018×10^{-3}	2×10^{-6}	0.18×10^{-6}
0.5	0.125	0.01125	1.25×10^{-3}	0.1125×10^{-3}	12.5×10^{-6}	1.125×10^{-6}
1	0.5	0.045	5×10^{-3}	0.45×10^{-3}	50×10^{-6}	4.5×10^{-6}
2	2	0.180	20×10^{-3}	1.8×10^{-3}	200×10^{-6}	18×10^{-6}
5	12.5	1.125	0.125	11.25×10^{-3}	1.25×10^{-3}	112.5×10^{-6}
10	50	4.50	0.5	45×10^{-3}	5×10^{-3}	450×10^{-6}
20	200	18	2	180×10^{-3}	20×10^{-3}	1.8×10^{-3}
∞	∞	∞	∞	∞	∞	∞

is the wavelength $\dfrac{\lambda_0}{\sqrt{\mu_r}}$ in the material. Low-frequency techniques may therefore be applied in that range.

The Diffusion Equation

In the *good conductor* approximation, Maxwell's equations take the form

$$\begin{aligned} \text{curl } \mathbf{e} &= -\frac{\partial \mathbf{b}}{\partial t} = -\mu \frac{\partial \mathbf{h}}{\partial t} \qquad \text{(Faraday's law)} \\ \text{curl } \mathbf{b} &= \mu \mathbf{j} = \mu \sigma \mathbf{e} \qquad\quad \text{(Ampère's law).} \end{aligned} \tag{13.104}$$

This set of pre-Maxwellian equations is mathematically very different from Maxwell's own. It is clear, for example, that equations (13.104) are invariant under Galilean transformations, which make them particularly appropriate for fluid magnetics, where the fluid equations are given in nonrelativistic form. Maxwell's equations, on the other hand, are invariant with respect to the Lorentz transformations discussed in Chapter 17. It cannot automatically be assumed, therefore, that a solution of (13.104) approximates a corresponding Maxwellian solution.[89]

If the displacement current is kept in the curl **h** equation, and the divergence of both sides is taken, one obtains the relationship

$$(\text{div } \mathbf{d}) + \frac{\epsilon}{\sigma} \frac{\partial}{\partial t} (\text{div } \mathbf{d}) = 0, \tag{13.105}$$

from which it may be deduced that, in the limit $t \to \infty$, div **d** vanishes, hence that no volume charges can survive in a good conductor. Because (13.104) implies[§§§] div $\mathbf{e} = 0$ and div $\mathbf{h} = 0$, **e** and **h** are seen to satisfy the diffusion equations

$$\begin{aligned} -\text{curl curl } \mathbf{e} - \sigma \mu \frac{\partial \mathbf{e}}{\partial t} &= \nabla^2 \mathbf{e} - \sigma \mu \frac{\partial \mathbf{e}}{\partial t} = 0 \\ -\text{curl curl } \mathbf{h} - \sigma \mu \frac{\partial \mathbf{h}}{\partial t} &= \nabla^2 \mathbf{h} - \sigma \mu \frac{\partial \mathbf{h}}{\partial t} = 0. \end{aligned} \tag{13.106}$$

The last equation is sometimes written as [48]

$$\frac{\partial \mathbf{h}}{\partial t} = \eta_d \nabla^2 \mathbf{h} \tag{13.107}$$

where $\eta_d = (\sigma \mu)^{-1}$ is the *magnetic diffusivity* (in $\text{m}^2\ \text{s}^{-1}$).

The diffusion equation plays an important role in many branches of physics. The temperature in a homogeneous isotropic body, for example, satisfies the diffusion equation

$$\nabla^2 \theta - \frac{1}{\kappa} \frac{\partial \theta}{\partial t} = -\frac{1}{K} q(\mathbf{r}, t), \tag{13.108}$$

[§§§]The implication is actually div **h** = a constant, but the constant is zero if the fields are initially zero.

where κ is the diffusivity of the substance, K the thermal conductivity, and $q(\mathbf{r}, t)$ the thermal power supplied per unit volume. This power often originates from an electromagnetic Joule effect, in which case (13.108), coupled to Maxwell's equations, forms the basis for a correct analysis of electromagnetic heating.[90]

It is seen that (13.108) implies *directionality* in time, while the wave equation is *symmetric* in t. This directionality is expressed mathematically by the presence of the odd derivative $\dfrac{\partial\theta}{\partial t}$ in the diffusion equation. The form of the diffusive Green's function shows with particular clarity the damping effect of the loss mechanisms associated with $\dfrac{\partial}{\partial t}$. The sought function satisfies the differential equation

$$\nabla^2 G - a^2 \frac{\partial G}{\partial t} = \delta(\mathbf{r} - \mathbf{r}')\,\delta(t - t'), \tag{13.109}$$

where $a^2 = \sigma\mu = \eta_d^{-1}$. In n-dimensional space (with $n = 1, 2, 3$), the solution is[¶¶¶]

$$G(\mathbf{r}, t|\mathbf{r}', t') = -\frac{1}{a^2}\left(\frac{a}{2\sqrt{\pi(t - t')}}\right)^n e^{-a^2\frac{|\mathbf{r}-\mathbf{r}'|^2}{4(t-t')}} H(t - t'). \tag{13.111}$$

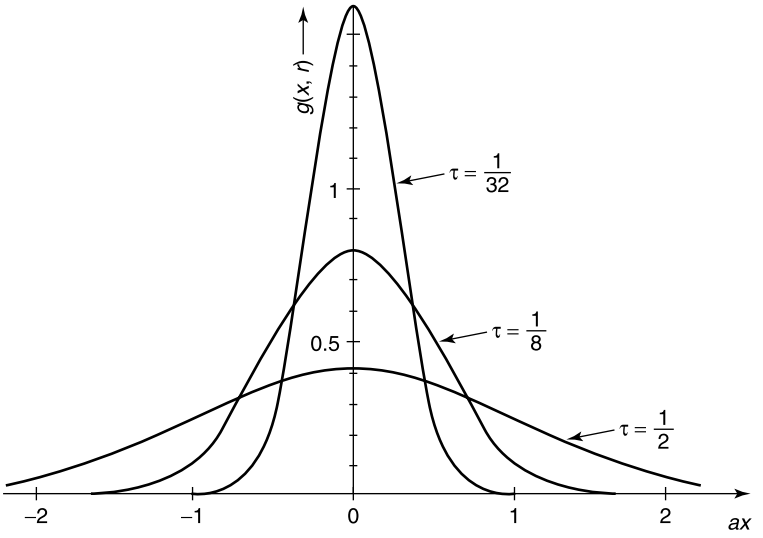

Figure 13.25 One-dimensional Green's function (from P. M. Morse and H. Feshbach. *Methods of theoretical physics.* McGraw-Hill Book Company, Inc., New York, 1953, with permission of Feshbach Publishing, Minneapolis).

[¶¶¶]The time-harmonic two-dimensional form of G is

$$G = \frac{1}{2\pi} K_0(\alpha r), \tag{13.110}$$

where $\alpha^2 = j\omega\mu\sigma = j\omega a^2$ [181]. Note that the adjoint of the diffusion equation is

$$\nabla^2\phi + a^2\frac{\partial\phi}{\partial t} = 0.$$

The Heaviside function $H(t-t')$ sees to it that causality is respected (i.e., that G remains zero until the source is energized). Illustratively, the variation of the one-dimensional Green's function is shown in Figure 13.25, where $\tau = t - t'$. As time progresses, the *point source* effect disappears, the fields spread out, and the amplitude decreases at each point on the axis.

13.10 STEVENSON'S METHOD APPLIED TO GOOD CONDUCTORS

When δ is small with respect to the radii of curvature of S (Fig. 13.26), an impedance boundary condition may be used to determine the exterior fields. We shall leave that particular problem aside and focus our attention on configurations where δ becomes of the order the dimensions L of the conductor, and the induced currents significantly penetrate into the volume. Sometimes the effect is not sought for and is simply the result of miniaturization (e.g., in the case of very thin microstrip lines). Quite frequently, on the other hand, penetration of current throughout the conductor is desired; for example, to reach a device embedded in a conducting medium (a submarine in a conducting sea . . .) or to heat in depth (in industrial and medical applications such as microwave hyperthermia).

In the conductor, the zero- and first-order terms of Stevenson's method satisfy the equations[‖‖‖]

$$\begin{cases} \operatorname{curl} \mathbf{E}_0^- = 0 \\ \operatorname{curl} \mathbf{E}_1^- = -\mu_r R_{c0} \mathbf{H}_0^- \end{cases} \tag{13.112}$$

$$\begin{cases} \operatorname{curl} \mathbf{H}_0^- = \sigma \mathbf{E}_0^- \\ \operatorname{curl} \mathbf{H}_1^- = \sigma \mathbf{E}_1^- + \epsilon_r \dfrac{\mathbf{E}_0^-}{R_{c0}}. \end{cases} \tag{13.113}$$

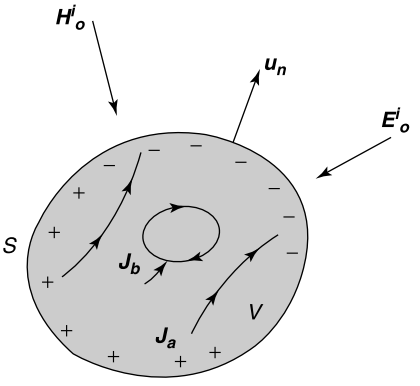

Figure 13.26 Inductive and capacitive currents in a good conductor.

[‖‖‖]For an application of the method to biological tissues, including the evaluation of the dissipated power, see Note 91.

All orders of $\mathbf{E}$ and $\mathbf{H}$ are divergenceless. Outside V, the scattered fields satisfy (Fig. 13.26)

$$\begin{cases} \text{curl } \mathbf{E}_0^{sc} = 0 \\ \text{curl } \mathbf{E}_1^{sc} = -R_{c0}\,\mathbf{H}_0^{sc} \end{cases} \tag{13.114}$$

$$\begin{cases} \text{curl } \mathbf{H}_0^{sc} = 0 \\ \text{curl } \mathbf{H}_1^{sc} = \dfrac{1}{R_{c0}}\mathbf{E}_0^{sc}. \end{cases} \tag{13.115}$$

The boundary conditions require $\mathbf{E}_{\text{tan}}$ and $\mathbf{H}_{\text{tan}}$ to be continuous on S. The same holds for $\mathbf{u}_n \cdot \text{curl } \mathbf{H} = \text{div}_S\,(\mathbf{H} \times \mathbf{u}_n)$. It follows that

$$\begin{aligned} \mathbf{u_n} \cdot \mathbf{E_0^-} &= 0 \\ \sigma\,\mathbf{u}_n \cdot \mathbf{E}_1^- = \frac{1}{R_{c0}}\,\mathbf{u}_n \cdot \mathbf{E}_0^+ &= \frac{1}{R_{c0}}\,\mathbf{u}_n \cdot (\mathbf{E}_0^i + \mathbf{E}_0^{sc}). \end{aligned} \tag{13.116}$$

The $\mathbf{E}_0^-$ field must therefore satisfy

$$\begin{aligned} &\text{curl } \mathbf{E}_0^- = 0; \quad \text{div } \mathbf{E}_0^- = 0 \qquad (\text{in } V) \\ &\mathbf{u_n} \cdot \mathbf{E_0^-} = 0 \qquad\qquad\qquad\quad (\text{on } S). \end{aligned} \tag{13.117}$$

Let us assume that the conductor is simply connected.**** Under these conditions it is shown in Section 4.10 that the only solution to (13.117) is $\mathbf{E}_0^- = 0$. It follows that $\mathbf{E}_0^+$ must be perpendicular to S. In addition, from (13.116), $\mathbf{E}_0^+$ is seen to be independent of σ, which implies that its value is the same as if V were perfectly conducting. Although there is no volume charge in V, a zero-order surface charge density appears on S, viz.

$$P_{S0} = \epsilon_0 \mathbf{u}_n \cdot (\mathbf{E}_0^i + \mathbf{E}_0^{sc}) = -\epsilon_0 \frac{\partial}{\partial n}(\phi_0^i + \phi_0^{sc}). \tag{13.118}$$

It is the first term in an expansion

$$P_S = P_{S0} + jk_0\,P_{S1} - k_0^2\,P_{S2} + \cdots. \tag{13.119}$$

The zero-order *magnetic field* is similarly the static magnetic field that arises when the scatterer is introduced in a magnetic field $\mathbf{H}_0^i$. For a nonmagnetic body $\mathbf{H}_0^{sc} = 0$, and the zero-order magnetic field is equal to $\mathbf{H}_0^i$ everywhere.

Because $\mathbf{E}_0^- = 0$, the leading term in the induced current density is $\mathbf{J} = jk_0\,\sigma\,\mathbf{E}_1^-$. Two separate contributions to $\mathbf{J}$ should be recognized. On the basis of (13.116), the first one is generated by the partial field $\mathbf{E}_{1a}^-$, itself the solution of

$$\begin{aligned} \text{curl } \mathbf{E}_{1a}^- &= 0 \qquad (\text{in } V) \\ \text{div } \mathbf{E}_{1a}^- &= 0 \qquad (\text{in } V) \\ \sigma\,\mathbf{u}_n \cdot \mathbf{E}_{1a}^- &= c_0 P_{S0} \quad (\text{on } S). \end{aligned} \tag{13.120}$$

****Ring-like circuits are discussed in Section 13.11.

The corresponding current density $\mathbf{J}_S$ satisfies the boundary condition

$$\mathbf{u}_n \cdot \mathbf{J}_a = j\omega P_{S0} \qquad (\text{on } S). \tag{13.121}$$

It is the *capacitive current* that ferries charges across the conductor from one point of the boundary to another (Fig. 13.26). This current is a function of $\mathbf{E}_0^i$ alone and is independent of the (finite) conductivity of the body. From (13.112), the second contribution originates from the solution of

$$\begin{aligned} \text{curl } \mathbf{E}_{1b}^- &= -\mu_r R_{c0}\, \mathbf{H}_0^- \\ \text{div } \mathbf{E}_{1b}^- &= 0 \\ \mathbf{u_n} \cdot \mathbf{E_{1b}^-} &= 0 \qquad (\text{on } S). \end{aligned} \tag{13.122}$$

The corresponding *transformer current* $\mathbf{J}_b$ is tangent to the boundary and is generated by the incident magnetic field $\mathbf{H}_0^i$. Its curl is different from zero, which justifies the name *eddy current*, which is often given to that type of current. To solve (13.122), it is useful to write $\mu \mathbf{H}_0^- = \text{curl } \mathbf{A}_0^-$, where $\mathbf{A}_0^-$ is a vector potential, and to express the electric field in the form

$$\mathbf{E}_{1b}^- = -c_0 \mathbf{A}_0^- + \text{grad } \psi_1. \tag{13.123}$$

Insertion of this expression into (13.122) leads to a Neumann type of potential problem for ψ_1.

An order of magnitude for the ratio of the two currents can be obtained by assuming that $|\text{curl } \mathbf{a}| \approx \dfrac{1}{L}|\mathbf{a}|$. If the conductor is nonmagnetic, a few easy steps, based on (13.120) and (13.122), show that

$$\frac{|\mathbf{J}_a|}{|\mathbf{J}_b|} \approx \frac{|\omega \epsilon_0\, \mathbf{E}_0^i|}{k_0 \sigma\, |R_{c0}\, \mathbf{H}_0^i|\, L} \approx \frac{L_c}{L} \left| \frac{\mathbf{E}_0^i}{R_{c0}\, \mathbf{H}_0^i} \right|. \tag{13.124}$$

In this expression, L_c is the characteristic length $(\sigma\, R_{c0})^{-1}$. For metals, L_c is of the order 10^{-9} m, and for $\sigma \approx 1\,\text{S m}^{-1}$ it is of the order a few millimeters. We may conclude — at least in the case of a good conductor – that the capacitive current is normally negligible with respect to its transformer counterpart.

A Simple Example

Consider again the sphere in Figure 13.21, now assumed highly conducting. The zero-order incident fields are $\mathbf{E}_0^i = E\mathbf{u}_z$ and $R_{c0}\, \mathbf{H}_0^i = E\mathbf{u}_x$. A few elementary steps yield

$$\begin{aligned} \frac{1}{E} P_{S0} &= 3\, \epsilon_0 \cos\theta \\ &= \mathbf{u}_z - \text{grad} \left(\frac{a^3 \cos\theta}{R^2} \right) \\ \frac{1}{E}\, \mathbf{E}_0^+ &= \cos\theta \left(1 + \frac{2a^3}{R^3} \right) \mathbf{u}_R - \sin\theta \left(1 - \frac{a^3}{R^3} \right) \mathbf{u}_\theta \end{aligned}$$

$$\frac{1}{E}\mathbf{E}_{1a}^{-} = 3L_c\,\mathbf{u}_z$$
$$\frac{1}{E}\mathbf{E}_{1b}^{-} = \frac{1}{2}(\mathbf{r}\times\mathbf{u}_z). \tag{13.125}$$

The current density follows as

$$\begin{aligned}\mathbf{J} &= jk_0\frac{3E}{R_{c0}}\mathbf{u}_z + jk_0\frac{\sigma E}{2}(\mathbf{r}\times\mathbf{u}_z)\\ &= \underbrace{3j\omega\epsilon_0 E\mathbf{u}_z}_{\text{capacitive current}} \underbrace{-\frac{1}{2}j\omega\epsilon_0 E\frac{R}{L_c}\sin\theta\,\mathbf{u}_\varphi}_{\text{transformer current}}.\end{aligned} \tag{13.126}$$

The lines of current are sketched in Figure 13.27. Because $k_0\sigma R_{c0} = (2/\delta^2)$, the transformer current can be given the alternate form

$$\mathbf{J}_b = -j\frac{R}{\delta^2}\frac{E}{R_{c0}}\sin\theta\,\mathbf{u}_\varphi. \tag{13.127}$$

It is clear that this first-order current can become very large for small δ, a point that suggests Stevenson's series will not converge well unless δ is much larger than a (i.e., unless the field deeply penetrates into the sphere). The point is confirmed by the LF value of the magnetic field in the conductor, which is[92]

$$\begin{aligned}\frac{1}{E}(R_{c0}\,\mathbf{H}) = \mathbf{u}_x - jk_0\left[3y\,\mathbf{u}_z - \frac{1}{2}\operatorname{grad}\left(R^2\sin 2\varphi\sin^2\theta\right)\right]\\ -\frac{j}{\delta^2}\left\{R^2\cos\varphi\sin\theta\,\mathbf{u}_R + 2\operatorname{grad}\left[\cos\varphi\sin\theta\left(\frac{a^2R}{6}-\frac{R^3}{5}\right)\right]\right\}.\end{aligned} \tag{13.128}$$

The transformer part of this expression is of the order (a^2/δ^2). To follow what happens when δ decreases — and ultimately approaches zero — note that the *exact* value, valid for arbitrary δ, is available for a nonmagnetic sphere immersed in an incident field (Fig. 13.27b)

$$\mathbf{H}_0^i = H\,\mathbf{u}_z = H\cos\theta\,\mathbf{u}_R - H\,\sin\theta\,\mathbf{u}_\theta.$$

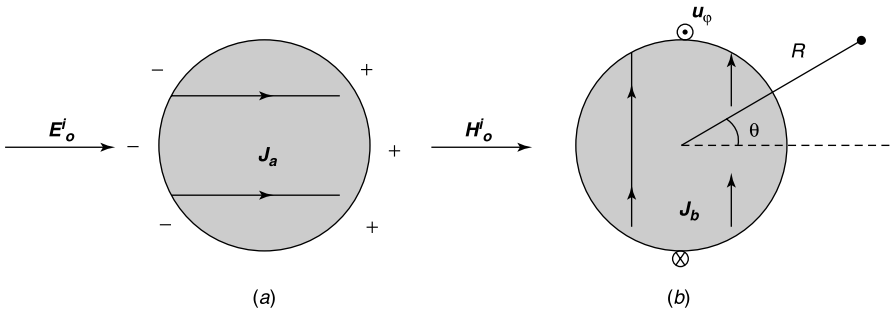

Figure 13.27 (*a*) Capacitive current in a sphere. (*b*) Inductive current in a sphere.

By separation of variables one finds [22], for all δ's,

$$\mathbf{J}_b = -3\sqrt{\frac{j}{2}}\frac{1}{\delta} H \sin\theta \sqrt{\frac{a}{R}} \frac{I_{\frac{3}{2}}\left(\sqrt{2j}\,\frac{R}{\delta}\right)}{I_{\frac{1}{2}}\left(\sqrt{2j}\,\frac{a}{\delta}\right)} \mathbf{u}_\varphi. \tag{13.129}$$

At deep penetrations, the limit forms

$$\lim_{z\to 0} I_{\frac{1}{2}}(z) = \sqrt{\frac{2}{\pi}}\, z^{\frac{1}{2}} \tag{13.130}$$

$$\lim_{z\to 0} I_{\frac{3}{2}}(z) = \frac{1}{3}\sqrt{\frac{2}{\pi}}\, z^{\frac{3}{2}}, \tag{13.131}$$

when they are inserted in (13.129), reproduce the previously obtained *Stevenson* value (13.127). At $R = a$, in particular,

$$J_b(a) \doteq \frac{a^2}{\delta^2}\left(1 - j\frac{2}{15}\frac{a^2}{\delta^2} + \cdots\right). \tag{13.132}$$

The second term, which represents the proportional deviation of the current from Stevenson's result, is less than 3.3% as long as δ is larger than the diameter of the sphere. At small penetrations, for $\delta \ll a$, the asymptotic limits

$$\lim_{z\to\infty} I_{\frac{1}{2}}(z) = \lim_{z\to\infty} I_{\frac{-1}{2}}(z) = \lim_{z\to\infty} I_{\frac{3}{2}}(z) = \frac{e^z}{(2\pi z)^{\frac{1}{2}}} \tag{13.133}$$

lead to

$$J_b \doteq e^{-(1+j)\frac{a-R}{\delta}} \tag{13.134}$$

which is the classic small-δ approximation [81].

13.11 CIRCUIT PARAMETERS

We shall assume, throughout this section, that Stevenson's expansion converges (i.e., that δ is substantially larger than the cross-sectional dimensions of the conductor). Two geometries will be considered: a simply connected region and a doubly connected ring.[93]

13.11.1 The Slice Generator

Consider first the uncharged simply connected conductor in Figure 13.28*a*. An electric field $\mathbf{E}_a$ is applied throughout its volume. In the conductor:

$$\begin{aligned} \text{curl}\,\mathbf{E}^- &= -jk_0\mu_r R_{c0}\,\mathbf{H}^- \\ \text{curl}\,\mathbf{H}^- = \mathbf{J} &= \sigma(\mathbf{E}^- + \mathbf{E}_a). \end{aligned} \tag{13.135}$$

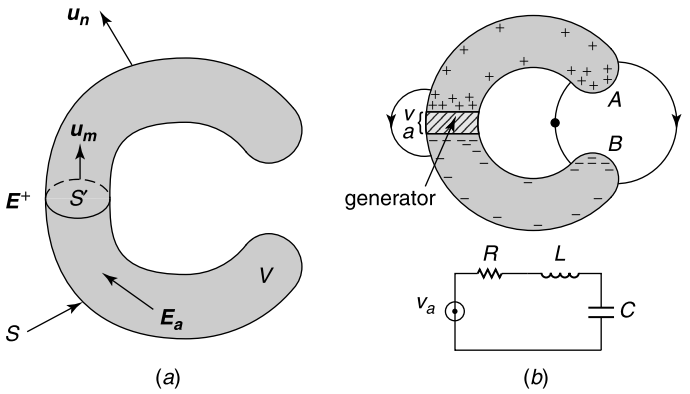

Figure 13.28 (*a*) Simply connected conductor with applied electric field. (*b*) Conductor with slice generator.

On boundary surface S:

$$\sigma \mathbf{u}_n \cdot (\mathbf{E}^- + \mathbf{E}_a) = jk_0 \frac{1}{R_{c0}} \mathbf{u}_n \cdot \mathbf{E}^+. \tag{13.136}$$

To zero-order, (13.135) and (13.136) give rise to the interior problem

$$\begin{aligned} \text{curl } \mathbf{E}_0^- &= 0 \quad (\text{in } V) \\ \text{div } (\mathbf{E}_0^- + \mathbf{E}_a) &= 0 \quad (\text{in } V) \\ \mathbf{u}_n \cdot (\mathbf{E}^- + \mathbf{E}_a) &= 0 \quad (\text{on } S). \end{aligned} \tag{13.137}$$

Equivalently:

$$\begin{aligned} \text{curl } \mathbf{J}_0 &= \sigma \text{ curl } \mathbf{E}_a \quad (\text{in } V) \\ \text{div } \mathbf{J}_0 &= 0 \quad (\text{in } V) \\ \mathbf{u}_n \cdot \mathbf{J}_0 &= 0 \quad (\text{on } S). \end{aligned} \tag{13.138}$$

The last two equations show that there is no net current I_0 through a cross section such as S'. To further simplify the analysis, assume that $\mathbf{E}_a$ is the gradient of a physical quantity, typically concentrated in a thin slice of the conductor (Fig. 13.28*b*). Examples of such "slice" geometries are the short gap-excited linear antenna and the (almost completed) gap-excited circular loop. Note that the capacity C in the loop circuit is mainly determined by the charges accumulated near the end tips A and B. Because curl $\mathbf{E}_a = 0$, $\mathbf{J}_0$ is a harmonic vector, and this must be zero because the volume is simply connected (see Section 4.11). If follows that $\mathbf{E}_0^- = -\mathbf{E}_a$ throughout V and, because $\mathbf{E}_0^- = -\text{grad } \phi_0$, that the potential ϕ_0 suffers a jump $V_a = \int \mathbf{E}_a \cdot \mathbf{dc}$ across the slice generator. The absence of $\mathbf{J}_0$ means that there is no zero-order magnetic field and no first-order *transformer* current either. There will be a first-order *capacitive* current, though, namely the solution of

$$\begin{aligned} \text{curl } \mathbf{J}_a &= 0 \\ \text{div } \mathbf{J}_a &= 0 \\ \mathbf{u}_n \cdot \mathbf{J}_a &= j\omega\epsilon_0 \, \mathbf{u}_n \cdot \mathbf{E}_0^+ \; = \; j\omega P_{S0}, \end{aligned} \tag{13.139}$$

where $\mathbf{E}_0^+$ is the zero-order exterior electrostatic field generated by the boundary condition

$$\mathbf{u}_n \times \mathbf{E}_0^+ = \mathbf{u}_n \times \mathbf{E}_0^- = -\mathbf{u}_n \times \mathbf{E}_a \qquad (\text{on } S).$$

Because $\mathbf{E}_a$ is proportional to V_a, P_{S0} and $\mathbf{J}_a$ are also proportional to V_a, and the same must be true of the net current I at the slice. This current is

$$I = \int_{S'} \mathbf{J}_a \cdot \mathbf{u}_m \, dS = j\omega CV. \tag{13.140}$$

Equation (13.140) allows[††††] evaluation of the capacitance C.

13.11.2 Ring Circuits

The slice generator system was dominated by electric fields and capacitive currents. In the ring-like circuit of Figure 13.29, immersed in an incident field $(\mathbf{E}^i, \mathbf{H}^i)$, the magnetic aspect predominates. We shall only consider the transformer current $\mathbf{J}_b$, known to be much stronger than its capacitive counterpart.

In a classic, somewhat simplistic approach, the current i in a thin ring is assumed conservative, and the current density is written as $\mathbf{j} = i\mathbf{f}$, where $\mathbf{f}$ is a function of c and some transverse coordinates (u, v) (Fig. 13.29*a*). Under the influence of an applied field $\mathbf{e}_a$, $\mathbf{j}$ is given by the vectorial Ohm's law

$$\mathbf{j} = \sigma(\mathbf{e}_a + \mathbf{e}) = \sigma\left(\mathbf{e}_a - \frac{\partial \mathbf{a}}{\partial t} - \text{grad}\,\phi\right). \tag{13.141}$$

Integrating along a close contour C gives

$$\begin{aligned} V_a = \int_C \mathbf{e}_a \cdot d\mathbf{c} &= \int_C \frac{\mathbf{j}}{\sigma} \cdot d\mathbf{c} + \int_C \frac{\partial \mathbf{a}}{\partial t} \cdot d\mathbf{c} \\ &= iR + \frac{d}{dt}\int_C \mathbf{a}^i \cdot d\mathbf{c} + \frac{d}{dt}\int_C \mathbf{a}^j \cdot d\mathbf{c}. \end{aligned} \tag{13.142}$$

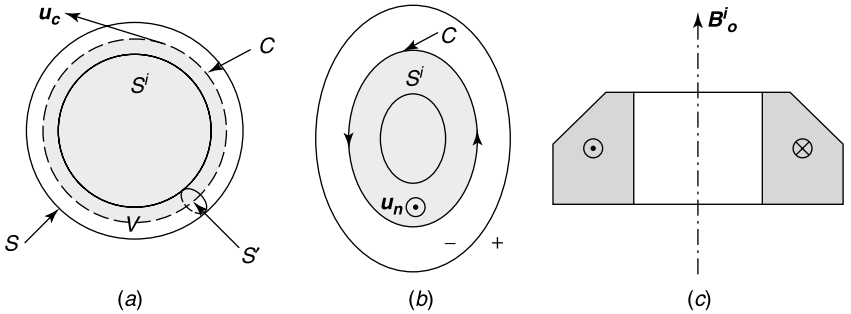

Figure 13.29 (*a*) A thin conducting ring. (*b*) Relevant to the induction law. (*c*) Axisymmetric ring.

[††††]The determination of the other circuit elements requires solving the equations for higher-order terms in the expansions for fields and currents. The matter is not pursued here.

The vector potential $\mathbf{a}^i$ is due to the incident fields. Its contour integral is

$$\int_C \mathbf{a}^i \cdot d\mathbf{c} = \int_{S_i} \text{curl } \mathbf{a}^i \cdot d\mathbf{S} = \int_{S_i} \mathbf{b}^i \cdot d\mathbf{S} = \text{magnetic flux } \Phi^{\mathbf{i}}, \tag{13.143}$$

where S_i is a surface bounded by C. The vector potential $\mathbf{a}^j$, on the other hand, is due to the induced currents and is of the form

$$\mathbf{a}^j = \frac{\mu_0}{4\pi} i \int_V \frac{\mathbf{f}(u', v', c')}{|\mathbf{r} - \mathbf{r}'|}\, dV' = i\mathbf{F}(u, v, c).$$

Its integral is therefore

$$\int_C \mathbf{a}^j \cdot d\mathbf{c} = i \int_C \mathbf{F}(u, v, c) \cdot \mathbf{u}_c\, dV = iL.$$

The circuit equation (13.142) now takes the familiar form

$$iR = V_a - \frac{d\phi^i}{dt} - L\frac{di}{dt}. \tag{13.144}$$

A more satisfactory analysis is provided by Stevenson's method. On the basis of previous arguments, the surface charge effects may be neglected and the transformer current density $\mathbf{J}_b$ assumed tangent to the boundary.[93] We shall also assume, for simplicity, that there is no applied field $\mathbf{E}_a$, and that the conductor is nonmagnetic. The dominant term in $\mathbf{J}_b$ satisfies

$$\begin{aligned} \text{curl } \mathbf{J}_b &= -j\omega\mu_0\, \sigma\, \mathbf{H}_0^i \qquad (\text{in } V) \\ \text{div } \mathbf{J}_b &= 0 \qquad (\text{in } V) \\ \mathbf{u}_n \cdot \mathbf{J}_b &= j\omega\epsilon_0\, \mathbf{u}_n \cdot \mathbf{E}_0^+ \qquad (\text{on } S). \end{aligned} \tag{13.145}$$

Setting $\omega = 0$ in these equations shows that the zero-order term $\mathbf{J}_{b0}$ must be proportional to the harmonic ring-vector $\mathbf{h}_0$ defined in (4.120). The proportionality factor can be determined from (Fig. 13.29*b*)

$$\int_C \mathbf{J}_{b0} \cdot d\mathbf{c} = \sigma \int_C \mathbf{E}_{b0}^- \cdot d\mathbf{c}.$$

To show that the integral over $\mathbf{E}_{b0}^-$ vanishes, let us apply Stokes' theorem to a surface S_i bounded by a curve C lying on the surface of the ring and situated outside the ring itself. For such a choice, because the tangential component of $\mathbf{E}_{b0}$ is continuous on S,

$$\int_C \mathbf{E}_{b0}^- \cdot d\mathbf{c} = \int_C \mathbf{E}_{b0}^+ \cdot d\mathbf{c} = \int_{S_i} \underbrace{\text{curl } \mathbf{E}_{b0}^+}_{=0} \cdot d\mathbf{S} = 0.$$

It may therefore be concluded that there is no zero-order transformer current density.[‡‡‡‡] There is, however, a first-order current, the solution of

$$\text{curl } \mathbf{J}_{b1} = -\sigma\, R_{c0}\, \mathbf{H}_0^i \quad (\text{in } V)$$

[‡‡‡‡]The situation is different with a slice generator, which excites a zero-order current density proportional to $\mathbf{h}_0$ (see Section 4.11).

$$\begin{aligned} \operatorname{div} \mathbf{J}_{b1} &= 0 \quad (\text{in } V) \\ \mathbf{u}_n \cdot \mathbf{J}_{b1} &= 0 \quad (\text{on } S). \end{aligned} \tag{13.146}$$

From these equations, it may be deduced that

$$\int_C \mathbf{J}_b \cdot \mathbf{u}_c \, dc = -j\omega\sigma \int_{S_i} \mathbf{B}_0^i \cdot d\mathbf{S} = -j\omega\sigma \, \Phi_0^i. \tag{13.147}$$

From (13.146), the flux of $\mathbf{J}_b$ through an arbitrary cross section S' (i.e., the net current I) is conservative. It follows that $\mathbf{J}_b$ is proportional to both σ and the uniform value I. We may therefore write, after averaging over the cross section of the ring,

$$\underbrace{I \left[\frac{1}{\sigma} \int_C \frac{\mathbf{J}_b}{I} \cdot d\mathbf{c} \right]_{\text{ave}}}_{R} = -j\omega \left[\Phi_0^i \right]_{\text{ave}}. \tag{13.148}$$

Current I is therefore resistance-controlled. As a matter of illustration, the actual values of $\mathbf{h}_0$ and $\mathbf{J}_b$ in an axisymmetric ring are (Fig. 13.29*c*),

$$\begin{aligned} \mathbf{h}_0 &= \frac{1}{2\pi r} \mathbf{u}_\varphi \\ \mathbf{J}_b &= -\frac{1}{2} j\omega\sigma \, B_0^i r \, \mathbf{u}_\varphi. \end{aligned} \tag{13.149}$$

The determination of L requires consideration of the higher terms in the jk_0 expansion for the current. The analogy with an (R, L) circuit is evident, because

$$I = \frac{V}{R + j\omega L} \approx \frac{V}{R} \left(1 - j\omega \frac{L}{R} + \cdots \right).$$

In the current application, V is proportional to ω (and the inductive current to ω^2), hence it is not surprising that the determination of the self-inductance L requires evaluation of the *second-order* fields $\mathbf{E}_{b2}$ and $\mathbf{J}_{b2}$, the self-induced components generated by the magnetic field produced by $\mathbf{J}_{b1}$. The steps to determine $\mathbf{J}_{b2}$ within the ring volume are based on

$$\operatorname{curl} \mathbf{J}_{b2} = -\sigma R_{c0} \, \mathbf{H}_{b1} - \sigma R_{c0} \, \mathbf{H}_1^i = -\frac{1}{L_c} (\mathbf{H}_{b1} + \mathbf{H}_1^i). \tag{13.150}$$

13.12 TRANSIENT EDDY CURRENTS

This section is concerned with problems of a kind often encountered in power engineering. The typical example of Figure 13.30 shows the main characteristics of the situation:

1. The geometry is often complicated, and the materials can be nonlinear, inhomogeneous, temperature sensitive, and/or frequency-dependent.

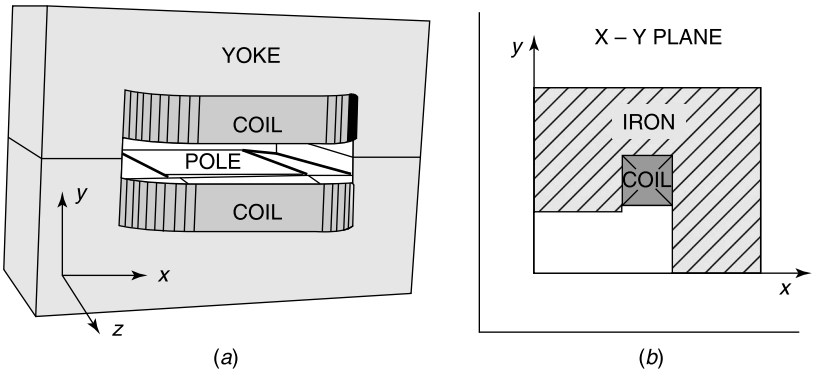

Figure 13.30 (*a*) Particle beam bending magnet. (*b*) One quarter of the $x-y$ plane cross section (from K. J. Binns, P. J. Lawrenson, and C. W. Trowbridge, *The analytical and numerical solution of electric and magnetic fields.* John Wiley & Sons, Chichester, 1992, with permission of John Wiley & Sons).

2. The time-dependence is arbitrary, and strong transients are often the rule, for example in nuclear fusion devices.
3. The time variations are sufficiently slow for the displacement current to remain negligible with respect to the conduction current. In time-harmonic problems, in particular, this means that the period T must be much longer than the relaxation time (ϵ/σ).
4. Great accuracy is sometimes required in the numerical evaluation of the fields. Six significant digits may be needed, for example in the case of nuclear magnetic resonance systems.

The general problem in hand is represented in Figure 13.31*a*, which shows a source $\mathbf{j}^i$ and a body in the field of that source. Distances and dimensions are assumed small with respect to the wavelengths involved, and the *near fields* are of particular concern. The main unknowns in many applications are the current densities in the conductors. They generate Joule effects, on purpose in the case of some industrial and medical applications,[94,95] but detrimental when parts of the conductor are heated above a tolerated maximum temperature. Electrodynamic forces generated by currents, while fundamental for the operation of motors, can also create problems, for example when they endanger the safe anchoring of busbars. This great variety of situations has generated an abundant literature [115, 180, 181, 188, 189].

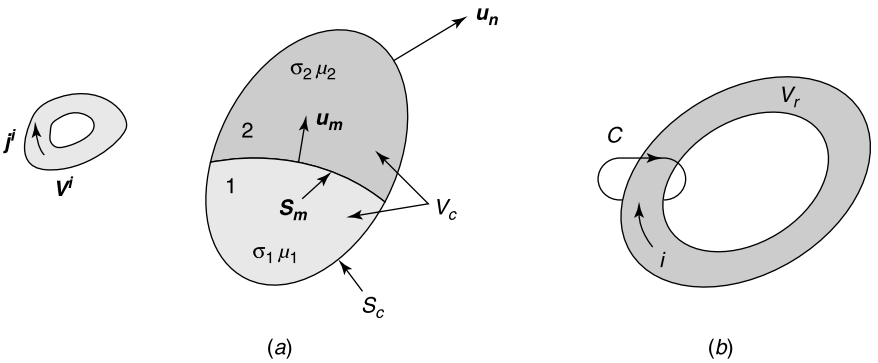

Figure 13.31 General configuration of concern (*a*) Simply connected conductor V_c. (*b*) Ring conductor.

The type of equations of concern is

$$\begin{aligned} \text{curl } \mathbf{e} &= -\frac{\partial \mathbf{b}}{\partial t} && (\textit{Faraday's law}) \\ \text{curl } \mathbf{h} = \mathbf{j} &= \sigma \mathbf{e} + \mathbf{j}_a && (\textit{Ampère's law}) \\ \mathbf{b} &= \mathbf{b}(\mathbf{h}). \end{aligned} \tag{13.151}$$

The various numerical techniques discussed in previous chapters have been exploited to solve these equations, for example finite elements[96] and the method of moments.[97] Either fields or potentials have been chosen as main unknowns. Potentials are less singular than fields and add flexibility in formulating boundary conditions. But direct evaluation of fields avoids the enhancement of errors that the differentiation of potentials may bring about.[98,99] The choice depends on the application in hand.[100,101]

13.12.1 The $(\mathbf{a}, \phi)$ Formulation

As in (7.28) and (7.29), we write

$$\begin{aligned} \mathbf{e} &= -\text{grad } \phi - \frac{\partial \mathbf{a}}{\partial t} \\ \mathbf{b} &= \text{curl } \mathbf{a}. \end{aligned}$$

These are the fields that appear in Faraday's law. Combining these representations with (13.151) shows that, in a linear medium,

$$-\text{curl}\left(\frac{1}{\mu}\ \text{curl } \mathbf{a}\right) - \sigma \frac{\partial \mathbf{a}}{\partial t} = \sigma\ \text{grad } \phi - \mathbf{j}_a, \tag{13.152}$$

and, by taking the divergence of both members,

$$\text{div } (\sigma\ \text{grad } \phi) = -\frac{\partial}{\partial t}(\text{div } \sigma \mathbf{a}) + \text{div } \mathbf{j}_a. \tag{13.153}$$

We shall now assume, for simplicity, that the media are homogeneous, and that $\mathbf{j}_a = 0$. Various gauges have been proposed to solve the resulting potential equations.[102] In the *Coulomb* gauge, one sets div $\mathbf{a} = 0$, which implies that the potentials satisfy

$$\begin{aligned} \nabla^2 \mathbf{a}_c - \sigma \mu \frac{\partial \mathbf{a}_c}{\partial t} - \sigma \mu\ \text{grad } \phi_c = 0 \quad & (\text{in } V_c) \\ \nabla^2 \phi_c = 0 \quad & (\text{in } V_c), \end{aligned} \tag{13.154}$$

where the subscript c refers to V_c. Outside the conductor, that is, in $(R^3 - V_c)$ (Fig. 13.31*a*),

$$\begin{aligned} \nabla^2 \mathbf{a}_e &= -\mu_0 \mathbf{j}^i \\ \nabla^2 \phi_e &= 0. \end{aligned} \tag{13.155}$$

The exterior problem is of a magnetostatic nature, hence $\mathbf{a}_e$ should be $O(R^{-2})$ at large distances. In accordance with the developments in Section 13.10, the effect of the electric

charges will be neglected in V_c, and $\mathbf{j}$ assumed tangent to S_c. On S_c, therefore,

$$\mathbf{u}_n \cdot \mathbf{j} = -\sigma\, \mathbf{u}_n \cdot \left(\frac{\partial \mathbf{a}_c}{\partial t} + \text{grad}\, \phi_c \right) = 0$$

or

$$\frac{\partial a_{cn}}{\partial t} + \frac{\partial \phi_c}{\partial n} = 0. \tag{13.156}$$

At the interface S_m between conductors, a transition condition must be respected, viz.

$$\sigma_1\, \mathbf{u}_m \cdot \left(\frac{\partial \mathbf{a}_{c1}}{\partial t} + \text{grad}\, \phi_{c1} \right) = \sigma_2\, \mathbf{u}_m \cdot \left(\frac{\partial \mathbf{a}_{c2}}{\partial t} + \text{grad}\, \phi_{c2} \right), \tag{13.157}$$

where $\mathbf{u}_m$ is perpendicular to S_m. This condition means that $\sigma \left(\dfrac{\partial a_{cm}}{\partial t} + \dfrac{\partial \phi_c}{\partial m} \right)$ must be continuous. We shall also require $\mathbf{a}_{\text{tan}}$ to be continuous at the various interfaces. Such a choice ensures, from (A3.23), continuity of the normal component of $\mathbf{b}$. If, in addition, a_n is also chosen continuous, ϕ_c can easily be adapted to respect condition (13.156). In short, the boundary conditions satisfied by $\mathbf{a}$ are now

$$\begin{aligned} \mathbf{a_c} &= \mathbf{a}_e && \text{(on } S_c\text{)} \\ \left(\frac{1}{\mu} \text{ curl } \mathbf{a}_c \right)_{\text{tan}} &= \left(\frac{1}{\mu_0} \text{ curl } \mathbf{a}_e \right)_{\text{tan}} && \text{(on } S_c\text{).} \end{aligned} \tag{13.158}$$

The second equation expresses continuity of $\mathbf{h}_{\text{tan}}$. On the basis of (A3.20), div $\mathbf{a} = 0$ implies

$$\frac{\partial a_{cn}}{\partial n} = \frac{\partial a_{en}}{\partial n} \qquad \text{(on } S_c\text{).} \tag{13.159}$$

One can make further use of the flexibility in the choice of potentials by deciding that $\mathbf{a}_c$ should be tangent to S_c. For such a choice, (13.154) and (13.155) have the only solution $\phi_c =$ constant, and the fields may now be expressed in terms of a *modified vector potential* $\mathbf{a}^*$ as

$$\begin{aligned} \mathbf{e} &= -\frac{\partial \mathbf{a}^*}{\partial t} \\ \mathbf{b} &= \text{curl } \mathbf{a}^*, \end{aligned} \tag{13.160}$$

where $\mathbf{a}^*$, tangent to S_c, satisfies

$$-\text{curl} \left(\frac{1}{\mu} \text{ curl } \mathbf{a}^* \right) - \sigma \frac{\partial \mathbf{a}^*}{\partial t} = -\mathbf{j}_a. \tag{13.161}$$

By taking the divergence of both members, one obtains

$$\frac{\partial}{\partial t} (\text{div } \mathbf{a}^*) = \frac{1}{\sigma} \text{ div } \mathbf{j}_a.$$

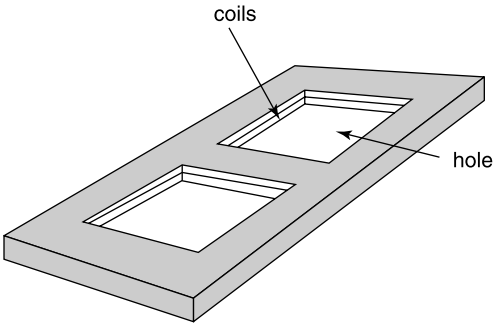

Figure 13.32 The "conductivity ladder" body (from D. Rodger and J. F. Eastham, Multiply connected regions in the $\mathbf{a}-\psi$ three-dimensional eddy-current formulation, *IEE Proc.* **134-A**, 58–66, 1987, with permission of the Institution of Electrical Engineers).

If div $\mathbf{j}_a = 0$, this condition implies the Coulomb gauge in the conductor, provided the fields and sources start from zero at $t = 0$.

The $\mathbf{a}^*$ formulation is economical in the sense that it involves only three unknown functions, the three components of $\mathbf{a}^*$. Keeping ϕ in the analysis adds a fourth unknown but gives more flexibility, because discontinuities in μ and σ can now be taken into account by choosing continuous shape functions in the numerical formulation.[103] The exterior magnetic field may, in any case, be represented in terms of a scalar potential ψ. When the volume is multiply connected, as in Figures 13.31*b* and 13.32, ψ becomes multivalued when a net current flows in the ring circuit. This difficulty can be taken care of by methods discussed in Section 6.5 (e.g., by introducing *barriers* or *cuts* that exclude curves such as C in Fig. 13.31*b* from computational space[104,105]). When a boundary integral condition is used, the cut should be a line on the boundary.[105] Various methods have been proposed to avoid the difficulties that result from the presence of a "hole," for example spanning the hole with either a film of conducting material[104] or a layer of elements.[106]

13.12.2 Other Gauges

In a homogeneous medium, the *Lorenz gauge*

$$\text{div } \mathbf{a} + \sigma\mu\phi = 0 \tag{13.162}$$

gives rise, in the absence of $\mathbf{j}_a$, to uncoupled equations for the potentials, viz.

$$\begin{aligned} \nabla^2\mathbf{a} - \sigma\mu\frac{\partial \mathbf{a}}{\partial t} &= 0 \\ \nabla^2\phi - \sigma\mu\frac{\partial \phi}{\partial t} &= 0. \end{aligned} \tag{13.163}$$

Both $\mathbf{a}$ and ϕ satisfy Laplace's equation outside the conductor. At the boundary:

$$\sigma\mu\phi_c + \frac{\partial a_{cn}}{\partial n} = \frac{\partial a_{en}}{\partial n} \quad (\text{on } S_c). \tag{13.164}$$

Other gauges have been proposed, for example the *continuity gauge*, which is based on the equation of continuity of charge,[107] and has been applied to media endowed with both a σ and an ϵ. In yet another approach, the component of $\mathbf{a}$ is prescribed in the direction of a

vector $\mathbf{w}$ that does not possess closed field lines.[96] The prescribed value could be zero, in which case one sets

$$\mathbf{a}\cdot\mathbf{w} = 0. \tag{13.165}$$

In the case of the electric potential $\mathbf{t}$, to be discussed next, the condition becomes

$$\mathbf{t}\cdot\mathbf{w} = 0. \tag{13.166}$$

A simple example of an admissible $\mathbf{w}$ is the radial field $(\mathbf{r}_0 - \mathbf{r})$, which connects the field point $\mathbf{r}$ to a reference point $\mathbf{r}_0$.

13.12.3 The $(\mathbf{t}, \theta)$ Formalism

This *magnetodynamic* formalism is the dual of its $(\mathbf{a}, \phi)$ electric counterpart. It is now $\mathbf{h}$ that is split, in a manner previously introduced in (6.39), as

$$\mathbf{h} = \mathbf{t} - \text{grad}\,\theta \qquad (\text{in } V_c) \tag{13.167}$$

where the *reduced potential* θ is single-valued. In the presence of an incident field, one writes[108,109,110]

$$\begin{aligned} \mathbf{h} &= \mathbf{h}^i + (\mathbf{t} - \text{grad}\,\theta) \qquad (\text{in } V_c) \\ \mathbf{h} &= \mathbf{h}^i - \text{grad}\,\theta \qquad\quad (\text{in } R^3 - V_c). \end{aligned} \tag{13.168}$$

Any solution of

$$\text{curl}\,\mathbf{t} = \text{curl}\,\mathbf{h} = \mathbf{j}$$

generates a possible $\mathbf{t}$, for example the *Biot-Savart magnetostatic field* (6.7). The potentials satisfy the differential equations

$$\begin{aligned} -\text{curl curl}\,\mathbf{t} - \sigma\mu\frac{\partial \mathbf{t}}{\partial t} &= -\sigma\mu\ \text{grad}\,\frac{\partial \theta}{\partial t} \\ \nabla^2\theta &= \text{div}\,\mathbf{t}. \end{aligned} \tag{13.169}$$

Once $\mathbf{t}$ is found, the electric field follows from

$$\mathbf{e} = \frac{1}{\sigma}\,\text{curl}\,\mathbf{h} = \frac{1}{\sigma}\,\text{curl}\,\mathbf{t}. \tag{13.170}$$

Most developments valid for the $(\mathbf{a}, \phi)$ potentials can be reproduced here. It is possible, in particular, to introduce either a Coulomb gauge, with $\text{div}\,\mathbf{t} = \mathbf{0}$, or a Lorenz gauge

$$\text{div}\,\mathbf{t} = \sigma\mu\frac{\partial \theta}{\partial t}. \tag{13.171}$$

The wish to have $\mathbf{j}$ tangent to S_c leads to the requirement

$$\mathbf{u}_n\cdot\mathbf{j} = \mathbf{u}_n\cdot\text{curl}\,\mathbf{h} = \text{div}_S\,(\mathbf{h}\times\mathbf{u}_n) = \text{div}_S\,(\mathbf{t}\times\mathbf{u}_n) = 0 \qquad (\text{on } S_c). \tag{13.172}$$

This condition can be satisfied by taking $\mathbf{t}$ perpendicular to S_c.

13.12.4 Numerical Solution

A full array of numerical techniques is available to evaluate the eddy currents. The previously mentioned characteristics of the problem make finite element solutions particularly efficient, for example in the presence of nonlinear magnetic materials.[111] The vector fields are typically represented by Whitney edge elements and scalar potentials by nodal elements.[112] When the computational domain extends to infinity, it should be truncated and appropriate conditions enforced at the outer boundary S_0 of the truncated volume. In early investigations, the brute force method of setting all fields equal to zero on S_0 was often used. The absorbing boundary conditions discussed in Section 12.7 are more frequently applied nowadays,[113] for example in the form of boundary integrals,[114,115,116] or by means of perfectly matched layers.[117] Annihilation operators, based on the expansion

$$\mathbf{a}(R,\theta,\varphi) = \sum_{n=1}^{\infty} \frac{\mathbf{a}_n(\theta,\varphi)}{R^n} \tag{13.173}$$

can be used for the quasi-static vector potential.[118]

PROBLEMS

13.1 The scattered electric field given by (7.135) is rewritten here for a surface source $\mathbf{J}_S = 2(\mathbf{u}_n \times \mathbf{H}^i)$ as

$$\mathbf{E}^{sc}(\mathbf{r}) = j\omega\mu_0 \int_{S_{ill}} \overline{\overline{G}}_{ee}(\mathbf{r}|\mathbf{r}') \cdot \mathbf{J}_S(\mathbf{r}')\, dS'.$$

Use the expression for $\overline{\overline{G}}_{ee}$ in spherical coordinates (see Problem 7.19) to rederive expression (13.4) for $\mathbf{E}^{sc}(\mathbf{r})$.

13.2 A parabolic reflector is illuminated by a point source located at the focus S (Fig. P13.1). The incident field is linearly polarized in a direction of unit vector $\mathbf{u}_p$. Show that the reflected field is of the form

$$\mathbf{E}^r = \mathbf{F}\frac{e^{-jk_0R}}{R}\,\mathbf{u}_p \qquad (\text{in } P)$$

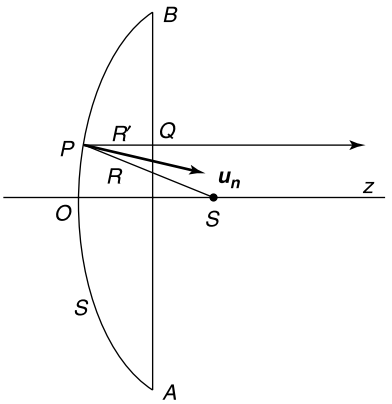

Figure P13.1

and

$$\mathbf{E}^r = \mathbf{F}\frac{e^{-jk_0(R+PQ)}}{R}\,\mathbf{u}_p \qquad (\text{in } Q).$$

13.3 As an illustration of Fermat's principle, show that the shortest optical path $SO + OP$ is obtained for $\beta_1 = \beta_2$ (Fig. P13.2). Find the coordinates of the reflection point. Interpret the result in terms of images.

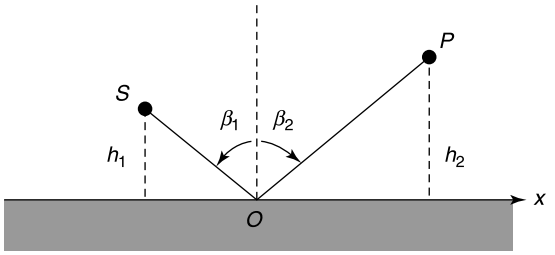

Figure P13.2

13.4 Investigate low-frequency scattering by a perfectly conducting sphere of radius a covered with a coating of thickness d and of characteristics ϵ_2, μ_2. Show that the electric and magnetic dipoles are characterized by the expansion coefficients

$$a_1 = -j\frac{(k_0 b)^3}{3}\,\frac{2+\rho-\mu_{r2}(1-\rho)}{2+\rho+\mu_{r2}(1-\rho)}$$

$$b_1 = -j\frac{(k_0 b)^3}{3}\,\frac{2(1-\rho)-2\epsilon_{r2}(2\rho+1)}{2(1-\rho)+\epsilon_{r2}(2\rho+1)}$$

with $b = a + d$ and $\rho = a^3/b^3$. Show that a nonmagnetic coating tends to increase the radar cross section, but that a magnetic coating is capable of reducing it.
(R. E. Hiatt et al., *Proc. IRE* **48**, 1636–1642, 1960.)

13.5 The zero-order currents on a perfectly conducting scatterer generate an interior field equal to $-\mathbf{H}_0^i$. This simple remark forms the basis of an approximate method of determining $\mathbf{J}_{S0}$ that consists in assuming a parameter-laden form for $\mathbf{J}_{S0}$ and optimizing the parameters by requiring maximum cancellation of the interior fields. Apply the method to a circular cylinder of dimensions much smaller than λ_0 and obtain an approximate value for the magnetic scattering dyadic.
(T. T. Taylor, *J. Research Natl. Bur. Standards* **64B**, 199, 1960.)

13.6 Prove that the dipole moment $\mathbf{P}_e$ in (13.77) can be obtained from the formula

$$\mathbf{P}_e = \frac{1}{j\omega}\int_S jk_0\mathbf{J}_{S1}\,dS$$

where $\mathbf{J}_{S1}$ is given in (13.76).

13.7 Use the results in Section 3.11 to determine the electric dipole moment of a perfectly conducting prolate spheroidal antenna.

13.8 Let a perfectly conducting scatterer be immersed in a linearly polarized plane wave $\mathbf{E}^i = \mathbf{u}_e\, e^{-jk_0\mathbf{u}_i\cdot\mathbf{r}}$. The copolarized component $\mathbf{u}_e\cdot\mathbf{E}^{sc}(-\mathbf{u}_i)$ of the backscattered field is an important radar parameter. Show that it is given by, in the low frequency limit,

$$\mathbf{u}_e\cdot\mathbf{E}^{sc}(-\mathbf{u}_i) = k_0^2\,\frac{e^{jk_0\mathbf{u}_i\cdot\mathbf{r}}}{4\pi R}\left(\mathbf{u}_e\cdot\overline{\overline{\alpha}}_e\cdot\mathbf{u}_e + \mathbf{u}_h\cdot\overline{\overline{\alpha}}_m\cdot\mathbf{u}_h\right).$$

(W. B. Goggins et al., *IEEE Trans. AP* **22**, 774–780, 1974.)

13.9 On the basis of (13.79) and (13.80), show that the scattered field from a perfectly conducting axisymmetric target is given by

$$\lim_{|\mathbf{r}|\to\infty} \mathbf{E}^{sc}(\mathbf{r}) = -\frac{e^{-jkR}}{4\pi R} k_0^2 [P_{tr}\mathbf{u}_R \times (\mathbf{u}_R \times \mathbf{u}_e) + (P_{zz} - P_{tr})\,(\mathbf{u}_z \cdot \mathbf{u}_e)\,\mathbf{u}_R \times (\mathbf{u}_R \times \mathbf{u}_z) - M_{tr}\mathbf{u}_R \times \mathbf{u}_h - (M_{zz} - M_{tr})\,(\mathbf{u}_z \cdot \mathbf{u}_h)\,\mathbf{u}_R \times \mathbf{u}_z],$$

where $\mathbf{u}_e, \mathbf{u}_h$ refer respectively to the incident electric and magnetic polarizations. Show that the backscattering cross section is

$$\sigma^{rad} = \frac{k_0^4}{4\pi}\{P_{tr} + M_{tr} + (P_{zz} - P_{tr})\,(\mathbf{u}_z \cdot \mathbf{u}_e)^2 + (M_{zz} - M_{tr})\,(\mathbf{u}_z \cdot \mathbf{u}_h)^2 + (P_{zz} - P_{tr} + M_{tr} - M_{zz})^2 (\mathbf{u}_z \cdot \mathbf{u}_e)^2 (\mathbf{u}_z \cdot \mathbf{u}_h)^2\}.$$

(R. E. Kleinman et al., *IEEE Trans. AES* **11**, 672–675, 1975.)

13.10 In the two-conductor antenna problem of Figure 13.22*b*, prove that **h** is equal to the distance between the two charges mentioned in the text. Make use of the reciprocity theorem linking the two following states:

- Charges $+q$ and $-q$ on the conductors
- Uncharged conductors in a uniform $\mathbf{E}_0^i$.

13.11 Going back to the nonmagnetic highly conducting sphere in Figure 13.27, show that the fields outside the sphere are given by

$$\frac{\mathbf{E}^{sc}}{E} = -\text{grad}\left(\frac{a^3 \cos\theta}{R^2}\right) + jk_0\left[\frac{a^5}{4}\,\text{grad}\left(\frac{\sin 2\theta \sin\varphi}{R^3}\right) + \frac{3a^3}{\sigma R_{c0}}\,\text{grad}\left(\frac{\cos\theta}{R^2}\right)\right] + \cdots$$

$$\frac{R_{c0}\mathbf{H}^{sc}}{E} = jk_0\left[\frac{a^3}{R^2}\sin\theta\,\mathbf{u}_\varphi + \frac{\sigma R_{c0}}{30}\,\text{grad}\left(\frac{\cos\varphi \sin\theta}{R^2}\right)\right] + \cdots.$$

(J. Van Bladel, *IRE Trans. AP* **10**, 625–633, 1962.)

13.12 Solve for the current density in a highly conducting strip immersed in a low-frequency incident induction

$$\mathbf{b}_i = b_i \cos\omega t\,\mathbf{u}_z.$$

The strip is infinite in the z-direction (Fig. P13.3). In a first approximation, assume that **b** in the strip is equal to $\mathbf{b}^i$, thus neglecting the reaction of the induced currents. Sketch the lines of current, and show that the Joule losses are about $\frac{1}{24}\sigma\omega^2 h^2 b_i^2$ when $h \ll L$ [189].

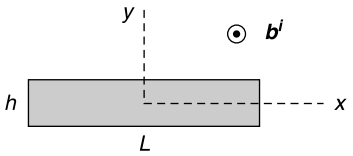

Figure P13.3

13.13 A highly conducting toroidal core of rectangular cross section carries a uniformly wound coil over the entire perimeter of the core (Fig. P13.4). The magnetic field is purely azimuthal. Write down the differential equation satisfied by the induced H_φ, and solve it by expanding the fields in terms of the eigenmodes of the coaxial cavity.
(K. V. Namijoshi et al., *IEEE Trans. MAG* **34**, 636–641, 1998.)

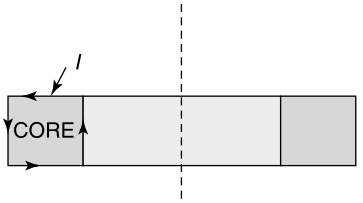

Figure P13.4

13.14 To clarify the penetration of transients in a highly conducting medium, consider a conducting half-space $0 < x < \infty$ on which a magnetic field $H_z(0,t) = H_0\,H(t)$ is suddenly impressed at $x = 0$. The factor H_0 being a constant, show, by taking Laplace transforms, that

$$E_y(x,t) = H_0\sqrt{\frac{\mu}{\pi\sigma t}}\,\exp\left(-\frac{\mu\sigma x^2}{4t}\right)H(t)$$

$$H_z(x,t) = H_0\,\text{erfc}\left(\sqrt{\frac{\mu\sigma x^2}{4t}}\right)H(t),$$

where

$$\text{erfc}\,(x) = \frac{2}{\sqrt{\pi}}\int_x^\infty e^{-t^2}dt$$

is the complementary error function.
(S. R. Seshadri, *IEEE Trans. ED* **14**, 74–76, 1971.)

13.15 Let R be a region devoid of sources, but containing a homogeneous material of characteristics (ϵ, μ, σ). Derive the Euler equations of

$$J_E = \int_R \left[\frac{(\text{curl }\mathbf{E})^2}{j\omega\mu} + (j\omega\epsilon + \sigma)(\mathbf{E})^2\right]dV$$

$$J_H = \int_R \left[j\omega\mu(\mathbf{H})^2 + \frac{(\text{curl }\mathbf{H})^2}{j\omega\epsilon + \sigma}\right]dV.$$

(R. L. Ferrari, *IEE Proc.* **132A**, 157–164, 1985.)

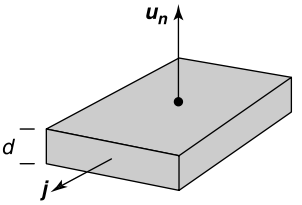

Figure P13.5

13.16 In a thin well-conducting shell, the current density $\mathbf{J}$ flows parallel to the boundary surfaces and can be replaced by a surface current of density $\mathbf{j}_S = \mathbf{j}_d$ (Fig. P13.5). Show that $\mathbf{j}_S$ can be written as $\text{grad}_S\, \phi \times \mathbf{u}_n = \text{curl}_S\, (\phi \mathbf{u}_n)$.

NOTES

1. Y. Rahmat-Samii and V. Galindo-Israel, Shaped reflector antenna analysis using the Jacobi-Bessel series, *IEEE Trans. AP* **28**, 425–435 (1980).
2. J. A. Cullen, Surface currents induced by short-wavelength radiation, *Phys. Rev. (2^d series)* **109**, 1863–1867 (1958).
3. N. Van Kampen, An asymptotic treatment of diffraction problems, *Physica* **XIV**, 575–589 (1949).
4. S. Y. Wang and S. K. Jeng, A deterministic method for generating a scattering-center model to reconstruct the RCS pattern of complex radar targets, *IEEE Trans. EMC* **39**, 315–323 (1997).
5. R. Bhalla and H. Ling, Three-dimensional scattering center extraction using the shooting and bouncing ray technique, *IEEE Trans. AP* **44**, 1445–1453 (1996).
6. V. H. Weston, Extension of Fock theory for currents in the penumbra region, *Radio Sci.* **69D**, 1257–1270 (1965).
7. R. G. Kouyoumjian and P. H. Pathak, A uniform geometrical theory of diffraction for an edge in a perfectly conducting surface, *Proc. IEEE* **62**, 1448–1461 (1974).
8. W. Wasylkiwskyj, Diffraction by a concave perfectly conducting circular cylinder, *IEEE Trans. AP* **23**, 480–492 (1975).
9. H. Idemen and L.B. Felsen, Diffraction of a whispering gallery mode by the edge of a thin concave cylindrically curved surface, *IEEE Trans. AP* **29**, 571–579 (1981).
10. N. J. Bojarski, A survey of the physical optics inverse scattering identity, *IEEE Trans. AP* **30**, 980–989 (1982).
11. J. B. Keller, The inverse scattering problem in geometrical optics and the design of reflectors, *IRE Trans. AP* **7**, 146–149 (1959).
12. M. R. Weiss, Inverse scattering in the geometric-optics limit, *J. Opt. Soc. Am.* **58**, 1524–1528 (1968).
13. W. V. T. Rush and O. Sørenson, On determining if a specular point exists, *IEEE Trans. AP* **27**, 99–101 (1979).
14. H. Kim and H. Ling, Electromagnetic scattering from an inhomogeneous object of ray tracing, *IEEE Trans. AP* **40**, 517–525 (1992).
15. R. Bhalla and H. Ling, Image domain ray tube integration formula for the shooting and bouncing ray technique, *Radio Sci.* **30**, 1435–1446 (1995).
16. S. W. Lee, M. S. Seshadri, V. J Jamnejad, and R. Mittra, Refraction at a curved dielectric interface: geometrical optics solution, *IEEE Trans. MTT* **30**, 12–19 (1982).
17. P. H. Pathak, High-frequency techniques for antenna analysis, *Proc. IEEE* **80**, 44–65 (1992).
18. J. B. Keller, Geometrical theory of diffraction, *J. Opt. Soc. Am.* **52**, 116–130 (1962).
19. R. G. Kouyoumjian and P. H. Pathak, A uniform geometrical theory of diffraction for an edge in a perfectly conducting surface, *Proc. IEEE* **62**, 1448–1460 (1974).
20. Y. Rahmat-Samii and R. Mittra, Spectral analysis of high-frequency diffraction of an arbitrary incident field by a half plane-comparison with four asymptotic techniques, *Radio Sci.* **13**, 31–48 (1978).
21. J. Boersma, and Y. Rahmat-Samii, Comparison of two leading uniform theories of edge diffraction with the exact uniform asymptotic solution, *Radio Sci.* **15**, 1179–1194 (1980).
22. T. B. A. Senior, Experimental detection of the edge-diffraction cone, *Proc. IEEE* **60**, 1448 (1972).
23. J. F. Rouvière, N. Douchin, and P. F. Combes, Diffraction by lossy dielectric wedges using both heuristic UTD formulations and FDTD, *IEEE Trans. AP* **47**, 1702–1708 (1999).
24. R. M. Lewis and J. Boersma, Uniform asymptotic theory of edge diffraction, *J. Math. Phys.* **10**, 2291–2305 (1969)
25. S. W. Lee and G. A. Deschamps, A uniform asymptotic theory of electromagnetic diffraction by a curved wedge, *IEEE Trans. AP* **24**, 25–34 (1976).
26. G. A. Deschamps, J. Boersma, and S. W. Lee, Three-dimensional half-plane diffraction: exact solution and testing of uniform theories, *IEEE Trans. AP* **32**, 264–271 (1984).
27. J. B. Keller, Diffraction by a convex cylinder, *IRE Trans. AP* **4**, 312–321 (1956).
28. P. H. Pathak, An asymptotic analysis of the scattering of plane waves by a smooth convex cylinder, *Radio Sci.* **14**, 419–435 (1979).
29. P. H. Pathak, W. D. Burnside, and R. J. Marhefka, A uniform GTD analysis of the diffraction of electromagnetic waves by a smooth convex surface, *IEEE Trans. AP* **28**, 631–642 (1980).
30. J. B. Keller and B. R. Levy, Decay exponents and diffraction coefficients for surface waves on surfaces on nonconstant curvature, *IRE Trans. AP* **7** (special supplement): 52–61 (1959).
31. T. B. A. Senior, The diffraction matrix for a discontinuity in curvature, *IEEE Trans. AP* **20**, 326–333 (1972).
32. L. B. Felsen, Backscattering from wide-angle and narrow-angle cones, *J. Appl. Phys.* **26**, 138–151 (1955).
33. L. B. Felsen, Plane-wave scattering by small-angle cones, *IRE Trans. AP* **5**, 121–129 (1957).
34. L. B. Felsen, Asymptotic expansion of the diffracted wave for a semi-infinite cone, *IRE Trans. AP* **5**, 402–404 (1957).

35. J. B. Keller, Backscattering from a finite cone, *IRE Trans. AP* **8**, 175–182 (1960).
36. M. E. Bechtel, Application of geometric diffraction theory to scattering from cones and disks, *Proc. IEEE* **53**, 877–882 (1965).
37. T. B. A. Senior and P. L. E. Uslenghi, High-frequency backscattering from a finite cone, *Radio Sci.* **6**, 393–406 (1971).
38. V. M. Babich, V. P. Smyshlyaev, D. B. Dement'v, and B. A. Samokish, Numerical calculation of the diffraction coefficients for an arbitrary shaped perfectly conducting cone, *IEEE Trans. AP* **44**, 740–747 (1996).
39. R. Satterwhite, Diffraction by a quarter plane, the exact solution, and some numerical results, *IEEE Trans. AP* **22**, 500–503 (1974).
40. T. B. Hansen, Corner diffraction coefficients for the quarter plane, *IEEE Trans. AP* **39**, 976–984 (1991).
41. P. Ya. Ufimtsev, Elementary edge waves and the physical theory of diffraction, *Electromagn.* **11**, 125–160 (1991).
42. P. Ya. Ufimtsev, Fast convergent integrals for nonuniform currents on wedge faces, *Electromagn.* **18**, 289–313 (1998).
43. P. C. Clemmow, Edge currents in diffraction theory, *IRE Trans. AP* **4** (special supplement): 282–287 (1956).
44. A. Michaeli, Equivalent edge currents for arbitrary aspects of observation, *IEEE Trans. AP* **32**, 252–258 (1984).
45. E. F. Knott, The relationship between Mitzner's ILDC and Michaeli's equivalent currents, *IEEE Trans. AP* **33**, 112–114 (1985).
46. M. Ando and M. Oodo, Physical optics equivalent edge currents for a half sheet and mechanism extraction of high frequency diffraction analysis, *Electromagn.* **18**, 245–266 (1998).
47. E. F. Knott and T. B. A. Senior, Comparison of three high-frequency diffraction techniques, *Proc. IEEE* **62**, 1468–1474 (1974).
48. A. Michaeli, Equivalent currents for second-order diffraction by the edges of perfectly conducting polygonal surfaces, *IEEE Trans. AP* **35**, 183–190 (1987).
49. O. Breinbjerg, Higher order equivalent edge currents for fringe wave radar scattering by perfectly conducting polygonal plates, *IEEE Trans. AP* **40**, 1543–1554 (1992).
50. P. M. Johansen, Uniform physical theory of diffraction equivalent edge currents for truncated wedge strips, *IEEE Trans. AP* **44**, 989–995 (1996).
51. A. Michaeli, Elimination of infinities in equivalent edge currents, Part I: fringe current components, *IEEE Trans. AP* **34**, 912–918 (1986).
52. A. Michaeli, Elimination of infinities in equivalent edge currents, Part II: physical optics components, *IEEE Trans. AP* **34**, 1034–1037 (1986).
53. K. M. Mitzner, Incremental length diffraction coefficients, AFAL report TR-73–296 (1974).
54. R. A. Shore and A. D. Yaghjian, Incremental diffraction coefficients for planar surfaces, *IEEE Trans. AP* **36**, 55–70 (1988). Correction in *IEEE Trans. AP* **37**, 1342 (1989).
55. A. D.Yaghjian, R. A. Shore, and M. B. Woodworth, Shadow boundary incremental length diffraction coefficients for perfectly conducting smooth, convex surfaces, *Radio Sci.* **31**, 1681–1695 (1996). Correction in *Radio Sci.* **32**, 673 (1997).
56. T. B. Hansen and R. A. Shore, Incremental length of diffraction coefficients for the shadow boundary of a convex cylinder, *IEEE Trans. AP* **46**, 1458–1466 (1998).
57. R. A. Shore and A. D. Yaghjian, Shadow boundary incremental length diffraction coefficients applied to scattering from 3D bodies, *IEEE Trans. AP* **49**, 200–210 (2001).
58. R. Tiberio, A. Toccafondi, A. Polerni, and S. Maci, Incremental theory of diffraction: a new-improved formulation, *IEEE Trans. AP* **52**, 2234–2243 (2004).
59. R. A. Shore and A. D. Yaghjian, A comparison of high-frequency scattering determined from PO fields enhanced with alternative ILDC's, *IEEE Trans. AP* **52**, 336–341 (2004).
60. W. D. Burnside, C. L. Yu, and R. J. Marhefka, A technique to combine the geometrical theory of diffraction and the moment method, *IEEE Trans. AP* **23**, 551–558 (1975).
61. W. D. Burnside and P. H. Pathak, A summary of hybrid solutions involving moment methods and GTD. In *Applications of the method of moments to electromagnetic fields*, IEEE Press (1980).
62. L. N. Medgyesi-Mitschang and D. S. Wang, Hybrid methods for analysis of complex scatterers, *Proc. IEEE* **77**, 770–779 (1989).
63. G. A. Thiele, Overview of selected hybrid methods, *Proc. IEEE* **80**, 66–78 (1992).
64. Z. Altman, R. Mittra, O. Hashimoto, and E. Michielssen, Efficient representation of induced currents on large scatterers using the generalized pencil of functions method, *IEEE Trans. AP* **44**, 51–57 (1996).
65. D.-H. Kwon, R. Burkholder, and P. Pathak, Efficient method of moments formulation for large PEC scattering problems using asymptotic phasefront extraction (APE), *IEEE Trans. AP* **49**, 583–591 (2001).
66. H. Anastassiu, A review of electromagnetic scattering analysis for inlets, cavities, and open duets, *IEEE Antennas Prop. Mag.* **45**, 27–40 (2003).
67. R. Bhalla, J. Moore, and H. Ling, A global scattering center representation of complex targets using the shooting and bouncing ray technique, *IEEE Trans. AP* **45**, 1850–1856 (1997).
68. R. Bhalla, H. Ling, J. Moore, D. J. Andersh, S. W. Lee, and J. Hughes, 3D scattering center representation of complex targets using the shooting and bouncing ray technique: a review, *IEEE Antennas Prop. Mag.* **40**, 30–39 (1998).
69. H. Ling, R. C. Chou, and S. W. Lee, Shooting and bouncing rays: calculating the RCS of an arbitrarily shaped cavity, *IEEE Trans. AP* **37**, 194–205 (1989).
70. P. H. Pathak and R. J. Burkholder, High-frequency electromagnetic scattering by open-ended waveguide cavities, *Radio Sci.* **26**, 211–218 (1991).
71. R. J. Burkholder and P. H. Pathak, Analysis of EM penetration into and scattering by electrically large open

waveguide cavities using Gaussian beam shooting, *Proc. IEEE* **79**, 1401–1412 (1991).

72. A. Garcia-Pino, F. Obelleiro, and J. L. Rodriguez, Scattering from conducting open cavities by generalized ray expansion (GRE), *IEEE Trans. AP* **41**, 989–992 (1993).
73. F. Obelleiro-Basteiro, J. L. Rodriguez, and R. J. Burkholder, An iterative physical optics approach for analyzing the electromagnetic scattering by large open-ended cavities, *IEEE Trans. AP* **43**, 356–361 (1995).
74. Lord Rayleigh, On the incidence of aerial and electric waves upon small obstacles in the form of ellipsoids or elliptic cylinders, and on the passage of electric waves through a circular aperture in a conducting screen, *Philos. Mag.* **XLIV**, 28–52 (1897).
75. R. E. Kleinman, The Rayleigh region, *Proc. IEEE* **53**, 848–856 (1965).
76. A. F. Stevenson, Solution of electromagnetic scattering problems as power series in the ratio (dimension of scatterer)/(wavelength), *J. Appl. Phys.* **24**, 1134–1142 (1953).
77. T. B. A. Senior, Low-frequency scattering by a dielectric body, *Radio Sci.* **11**, 477–482 (1976).
78. R. E. Kleinman, Far field scattering at low frequencies, *Appl. Sci. Res.* **18**, 1–8 (1967).
79. I. V. Lindell and A. H. Sihvola, Quasi-static analysis of scattering from a chiral sphere, *J. Electromagn. Waves Appl.* **4**, 1223–1231 (1990).
80. R. E. Kleinman and T. B. A. Senior, Rayleigh scattering cross sections, *Radio Sci.* **7**, 937–942 (1972).
81. J. B. Keller, R. E. Kleinman, and T. B. A. Senior, Dipole moments in Rayleigh scattering, *J. Inst. Maths Appl.* **9**, 14–22 (1972).
82. R. E. Kleinman and T. B. A. Senior, Low-frequency scattering by space objects, *IEEE Trans. AES* **11**, 672–675 (1975).
83. A. A. Ksienski, Y. T. Lin, and L. J. White, Low-frequency approach to target identification, *Proc. IEEE* **63**, 1651–1660 (1975).
84. L. Marin, Electrostatic properties of two, collinear, solid cylinders, *Int. J. Electronics* **38**, 563–568 (1975).
85. P. Werner, On the exterior boundary value problem of perfect reflection for stationary electromagnetic wave fields, *J. Math. Anal. Appl.* **7**, 348–396 (1963).
86. P. Werner, On the behavior of stationary electromagnetic fields for small frequencies, *J. Math. Anal. Appl.* **15**, 447–496 (1966).
87. K. Steinbrunn, Über das Verhalten stationärer elektromagnetischer Wellenfelder für kleine Frequenzen, *J. Math. Anal. Appl.* **27**, 127–163 (1969).
88. P. Werner, Über das Verhalten elektromagnetischer Felder für kleine Frequenzen in mehrfach zusammenhängenden Gebieten, I. Innenraumprobleme, *J. Reine Angew. Math.* **278–279**, 365–397 (1972). II. Aussenraumprobleme, *J. Reine Angew. Math.* **280**, 98–121 (1976).
89. A. A. Blank, K. O. Friedrichs, and H. Grad, Theory of Maxwell's equations without displacement current, Report N.Y.O.-6486, Institute of Mathematical Sciences, New York University, Nov. 1, 1957.
90. H. Janssen, E. ter Maten, and D. van Houwelingen, Simulation of coupled electromagnetic and heat dissipation problems, *IEEE Trans. MAG* **30**, 3331–3334 (1994).
91. C. C. Johnson, C. H. Durney. and H. Massoudi, Long wavelength electromagnetic power absorption in prolate spheroidal models of man and animals, *IEEE Trans. MTT* **23**, 739–747 (1975).
92. J. Van Bladel, Good conductors in low-frequency fields, *IRE Trans. AP* **10**, 625–633 (1962).
93. J. Van Bladel, Circuit parameters from Maxwell's equations, *Appl. Sci. Res.* **28**, 381–397 (1973).
94. M. Newborough and S.D. Probert, Electromagnetic heating: an interdisciplinary activity, *IEE Proc.* **137A**, 280–286 (1990).
95. J. M. Osepchuk, Microwave power applications, *IEEE Trans. MTT* **50**, 975–985 (2002).
96. R. Albanese and G. Rubinacci, Finite element methods for the solution of the 3D eddy current problem, *Adv. Imaging Electron Phys.* **102**, 1–86 (1998).
97. Y. Zhang, T. J. Cui, W. C. Chew, and J. S. Zhao, Magnetic field integral equation at very low frequencies, *IEEE Trans. AP* **51**, 1864–1871 (2003).
98. A. Bossavit and J. C. Vérité, The "Trifon" code: solving the 3D eddy-current problems in using H as a state variable, *IEEE Trans. MAG* **19**, 2465–2470 (1983).
99. J. S. van Welij, Calculation of eddy currents in terms of **H** on hexahedra, *IEEE Trans. MAG* **21**, 2239–2241 (1985).
100. T. Nakata, N. Takahashi, K. Fujiwara, K. Muramatsu, and Z. G. Cheng, Comparison of various methods for 3D eddy current analysis, *IEEE Trans. MAG* **24**, 3159–3161 (1988).
101. Z. Ren and A. Razek, Comparison of some 3D eddy current formulations in dual systems, *IEEE Trans. MAG* **36**, 751–755 (2000).
102. T. Morisue, A comparison of the Coulomb gauge and Lorenz gauge. Magnetic vector potential formulations for 3D eddy current calculations, *IEEE Trans. MAG* **29**, 1372–1375 (1993).
103. R. Albanese and G. Rubinacci, Formulation of the eddy-current problem, *IEE Proc.* **137-A**, 16–22 (1990).
104. D. Rodger and J. F. Eastham, Multiply connected regions in the $\mathbf{a} - \psi$ three-dimensional eddy-current formulation, *IEE Proc.* **134-A**, 58–66 (1987).
105. J. C. Vérité, Calculation of multivalued potentials in exterior regions, *IEEE Trans. MAG* **23**, 1881–1887 (1987).
106. P. J. Leonard and D. Rodger, A new method for cutting the magnetic scalar potential in multiply connected eddy current problems, *IEEE Trans. MAG* **25**, 4132–4134 (1989).
107. A. Konrad and G. Bedrosian, The continuity gauge — does it work?, *J. Electromagn. Waves Appl.* **4**, 1117–1133 (1990).
108. M. R. Krakowski, On certain properties of the electric vector potential in eddy-current problems, *IEE Proc.*

132-A, 445–449 (1985). Comments by R. Albanese and G. Rubinacci can be found in *IEE Proc.* **134-A**, 814–815 (1987) and **136**, 255–267 (1989).

109. O. Biró and K. Preis, An edge finite element eddy current formulation using a reduced magnetic and a current vector potential, *IEEE Trans. MAG* **36**, 3128–3130 (2000).
110. I. D. Mayergoyz, Some remarks concerning electromagnetic potentials, *IEEE Trans. MAG* **29**, 1301–1305 (1993).
111. J. P. Webb and B. Forghani, $T - \Omega$ method using hierarchal edge elements, *IEE Proc.-Sci. Meas. Technol.* **142**, 133–141 (1995).
112. R. Dyczij-Edlinger and O. Biró, A joint vector and scalar potential formulation for driven high-frequency problems using hybrid edge and nodal finite elements, *IEEE Trans. MTT* **44**, 15–23 (1996).
113. Q. Chen and A. Konrad, A review of finite element open boundary techniques for static and quasi-static electromagnetic field problems, *IEEE Trans. MAG* **33**, 663–676 (1997).
114. A. Bossavit and J. C. Vérité, A mixed FEM-BIEM method to solve 3-D eddy-current problems, *IEEE Trans. MAG* **18**, 431–435 (1982).
115. A. Bossavit and I. Mayergoyz, Edge-elements for scattering problems, *IEEE Trans. MAG* **25**, 2816–2821 (1989).
116. Z. Ren, F. Bouillaut, A. Razek, A. Bossavit, and J.C. Vérité, A new hybrid model using electric field formulation for 3D eddy current problems, *IEEE Trans. MAG* **26**, 470–473 (1990).
117. T. I. Kosmanis, T. V. Yioultsis, and T. D. Tsiboukis, Perfectly matched anisotropic layer for the numerical analysis of unbounded eddy-current problems, *IEEE Trans. MAG* **35**, 4452–4458 (1999).
118. Q. Chen, A. Konrad, and P. P. Biringer, Computation of three-dimensional unbounded eddy current problems using asymptotic boundary conditions, *IEEE Trans. MAG* **31**, 1348–1351 (1995).

Chapter 14

Two-Dimensional Problems

The two-dimensional surface of concern in this chapter is the infinite plane. The relevant coordinates, grouped into the symbol $\mathbf{r}$, are (x, y) or (r, φ), and operations such as div or grad are effected with respect to these coordinates. The sources (and therefore the fields) are assumed independent of z, an assumption that results in considerable mathematical simplification. Maxwell's equations, for example, immediately show that a two-dimensional field can be split into a contribution from an E-wave (with E_z as main component) and a contribution from an H-wave (with H_z as main component). The basic problems become scalar instead of vectorial. Quite a few numerical methods, already discussed in previous chapters in their three-dimensional form, become much more transparent in two dimensions. Similarly, new methods can be described with greater clarity when they are applied to scalar problems first.

Two-dimensional configurations are mathematical models. They can be physically relevant, however, for the evaluation of fields in limited regions of space. Consider, for example, a straight metallic wire of finite length, irradiated by a plane wave propagating perpendicularly to the wire. The current in the wire can be well-approximated by its two-dimensional value, except near the ends, where the three-dimensional aspects must be taken into account.

14.1 *E* AND *H* WAVES

Because the fields are independent of the perpendicular coordinate z, the z-derivatives in Maxwell's equations may be dropped, and the equations become

$$\begin{aligned} &\frac{\partial e_z}{\partial y}\,\mathbf{u}_x - \frac{\partial e_z}{\partial x}\,\mathbf{u}_y + \left(\frac{\partial e_y}{\partial x} - \frac{\partial e_x}{\partial y}\right)\mathbf{u}_z \\ &= -\left(\mu_0 \frac{\partial h_x}{\partial t} + j_{mx}\right)\mathbf{u}_x - \left(\mu_0 \frac{\partial h_y}{\partial t} + j_{my}\right)\mathbf{u}_y - \left(\mu_0 \frac{\partial h_z}{\partial t} + j_{mz}\right)\mathbf{u}_z. \end{aligned} \tag{14.1}$$

$$\begin{aligned} &\frac{\partial h_z}{\partial y}\,\mathbf{u}_x - \frac{\partial h_z}{\partial x}\,\mathbf{u}_y + \left(\frac{\partial h_y}{\partial x} - \frac{\partial h_x}{\partial y}\right)\mathbf{u}_z \\ &= \left(\epsilon_0 \frac{\partial e_x}{\partial t} + j_x\right)\mathbf{u}_x + \left(\epsilon_0 \frac{\partial e_y}{\partial t} + j_y\right)\mathbf{u}_y + \left(\epsilon_0 \frac{\partial e_z}{\partial t} + j_z\right)\mathbf{u}_z. \end{aligned} \tag{14.2}$$

Electromagnetic Fields, Second Edition, By Jean G. Van Bladel

These equations are valid in vacuum, but the extension to a general medium follows easily. It is clear from (14.1) and (14.2) that there is coupling between j_z, e_z and the transverse components h_x, h_y, j_{mx}, j_{my}, and similarly between j_{mz}, h_z and e_x, e_y, j_x, j_y. One may therefore distinguish two kinds of waves, respectively termed E (or TM) and H (or TE). The fundamental equations for an E-wave can be written in the form

$$-\mathbf{u}_z \times \text{grad}\, e_z = -\mu_0 \frac{\partial \mathbf{h}_t}{\partial t} - \mathbf{j}_{mt} \tag{14.3}$$

$$-\text{div}(\mathbf{u}_z \times \mathbf{h}_t) = \mathbf{u}_z \cdot \text{curl}\, \mathbf{h}_t = \epsilon_0 \frac{\partial e_z}{\partial t} + j_z, \tag{14.4}$$

where the subscript t denotes the component of a vector in the xy plane. Elimination of $\mathbf{h}_t$ gives

$$\nabla^2 e_z - \epsilon_0 \mu_0 \frac{\partial^2 e_z}{\partial t^2} = \mu_0 \frac{\partial j_z}{\partial t} - \text{div}\,(\mathbf{u}_z \times \mathbf{j}_{mt}). \tag{14.5}$$

The fundamental equations for an H-wave are, similarly,

$$-\mathbf{u}_z \times \text{grad}\, h_z = \epsilon_0 \frac{\partial \mathbf{e}_t}{\partial t} + \mathbf{j}_t \tag{14.6}$$

$$-\text{div}(\mathbf{u}_z \times \mathbf{e}_t) = -\mu_0 \frac{\partial h_z}{\partial t} - j_{mz} = \mathbf{u}_z \cdot \text{curl}\, \mathbf{e}_t. \tag{14.7}$$

Elimination of $\mathbf{e}_t$ yields

$$\nabla^2 h_z - \epsilon_0 \mu_0 \frac{\partial^2 h_z}{\partial t^2} = \epsilon_0 \frac{\partial j_{mz}}{\partial t} + \text{div}(\mathbf{u}_z \times \mathbf{j}_t). \tag{14.8}$$

When the sources are time-harmonic, both E_z and H_z satisfy the differential equation

$$\nabla^2 \Phi + k_0^2 \Phi = P \tag{14.9}$$

and the radiation condition

$$\frac{\partial \Phi}{\partial r} + jk_0 \Phi = o\left(\frac{1}{r^{\frac{1}{2}}}\right), \tag{14.10}$$

in which r is the distance from the origin. The *Green's function* of the problem is the solution of the equation

$$\nabla_{xy}^2 G_0(\mathbf{r}|\mathbf{r}') + k_0^2 G(\mathbf{r}|\mathbf{r}') = \delta(\mathbf{r} - \mathbf{r}') \tag{14.11}$$

that satisfies the radiation condition at large distances r. By methods similar to those used in Sections 7.2 and 7.7, one finds (Problem 14.1)

$$G_0(\mathbf{r}|\mathbf{r}') = \frac{j}{4} H_0^{(2)}(k_0|\mathbf{r} - \mathbf{r}'|). \tag{14.12}$$

From (A5.10), the asymptotic value for large $|\mathbf{r} - \mathbf{r}'|$ is

$$\lim_{|\mathbf{r}-\mathbf{r}'|\to\infty} G_0(\mathbf{r}|\mathbf{r}') = \frac{j}{4}\left(\frac{2j}{\pi k_0}\right)^{\frac{1}{2}} \frac{e^{-jk_0|\mathbf{r}-\mathbf{r}'|}}{|\mathbf{r} - \mathbf{r}'|^{\frac{1}{2}}}. \tag{14.13}$$

For small values of $|\mathbf{r} - \mathbf{r}'|$:

$$\lim_{|\mathbf{r}-\mathbf{r}'|\to 0} G_0(\mathbf{r}|\mathbf{r}') = \frac{j}{4}\left(1 + j\frac{2}{\pi}\log_e \frac{2}{k_0|\mathbf{r}-\mathbf{r}'|}\right). \tag{14.14}$$

Higher-order correction terms can be deduced from (A5.22).

On the basis of (14.12), the electric field produced by *electric* currents parallel to the z axis is given by

$$E_z(\mathbf{r}) = j\omega\mu_0 \int_S J_z(\mathbf{r}')G_0(\mathbf{r}|\mathbf{r}')\, dS' = -\frac{\omega\mu_0}{4}\int_S J_z(\mathbf{r}')H_0^{(2)}(k_0|\mathbf{r}-\mathbf{r}'|)\, dS'. \tag{14.15}$$

For a line current I, located at the origin, J_z is equal to $\delta(\mathbf{r})I$, hence

$$\begin{aligned} E_z &= -I\frac{k_0 R_{c0}}{4}H_0^{(2)}(k_0 r) \\ \mathbf{H}_t &= -\frac{j}{\omega\mu_0}\frac{\partial E_z}{\partial r}\,\mathbf{u}_\varphi = I\frac{j}{4}\frac{d}{dr}[H_0^{(2)}(k_0 r)]\,\mathbf{u}_\varphi. \end{aligned} \tag{14.16}$$

At large distances:

$$E_z(r) = -I\,R_{c0}\sqrt{\frac{jk_0}{8\pi}}\,\frac{e^{-jk_0 r}}{\sqrt{r}}. \tag{14.17}$$

This expression indicates that the radiation is isotropic, as expected. For two lines separated by a small distance l and carrying opposite currents $+I$ and $-I$ (Fig. 14.1a),

$$E_z = -\frac{k_0^2 R_{c0}}{4}\,Il\,H_1^{(2)}(k_0 r)\cos\varphi. \tag{14.18}$$

For the quadrupole structure of Figure 14.1b:

$$E_z = -\frac{k_0^3 R_{c0}}{8}\,Il_1 l_2 H_2^{(2)}(k_0 r)\sin 2\varphi. \tag{14.19}$$

Similar equations can be written for the magnetic field produced by *magnetic* currents parallel to the z-axis.

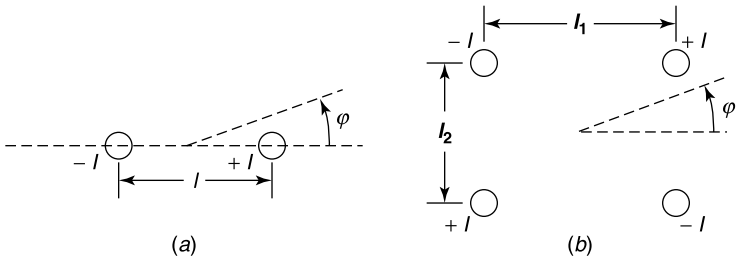

Figure 14.1 Some particular current distributions.

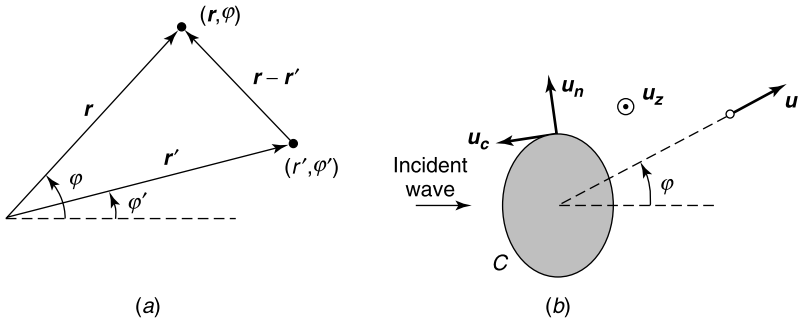

Figure 14.2 (*a*) Relevant for the addition theorem. (*b*) Cylindrical scatterer.

It is often useful, when evaluating the integral in (14.15), to apply the *addition theorem*, according to which (Fig. 14.2*a*)

$$H_0^{(2)}(k_0|\mathbf{r}-\mathbf{r}'|) = \sum_{m=-\infty}^{\infty} J_m(k_0 r') H_m^{(2)}(k_0 r)\, e^{jm(\varphi-\varphi')} \tag{14.20}$$

for $r' < r$, and

$$H_0^{(2)}(k_0|\mathbf{r}-\mathbf{r}'|) = \sum_{m=-\infty}^{\infty} H_m^{(2)}(k_0 r') J_m(k_0 r)\, e^{jm(\varphi-\varphi')} \tag{14.21}$$

for $r' > r$.

The *Green's function* for an infinite homogeneous medium follows from (14.12) by replacing k_0 by the (possibly complex) k of the medium. *For a good conductor*, in particular [144],

$$G(\mathbf{r}|\mathbf{r}') = -\frac{1}{2\pi}\left[ker\left(\sqrt{2}\,\frac{|\mathbf{r}-\mathbf{r}'|}{\delta}\right) + j\,kei\left(\sqrt{2}\,\frac{|\mathbf{r}-\mathbf{r}'|}{\delta}\right)\right], \tag{14.22}$$

where *ker* and *kei* denote the zero-order *Kelvin functions*, defined by

$$ker(x) + j\,kei(x) = -j\frac{\pi}{2} H_0^{(2)}\left(xe^{-j\frac{\pi}{4}}\right). \tag{14.23}$$

Note that, for an inhomogeneous medium of nonuniform ϵ, μ, (14.5) and (14.8) are replaced by

$$\mu\ \mathrm{div}\left(\frac{1}{\mu}\ \mathrm{grad}\ e_z\right) - \epsilon\mu\frac{\partial^2 e_z}{\partial t^2} = \mu\frac{\partial j_z}{\partial t} + \mu\ \mathrm{div}\left(\frac{1}{\mu}\,\mathbf{j}_m \times \mathbf{u}_z\right) \tag{14.24}$$

and

$$\epsilon\ \mathrm{div}\left(\frac{1}{\epsilon}\ \mathrm{grad}\ h_z\right) - \epsilon\mu\frac{\partial^2 h_z}{\partial t^2} = \epsilon\frac{\partial j_{mz}}{\partial t} + \epsilon\ \mathrm{div}\left(\frac{1}{\epsilon}\,\mathbf{u}_z \times \mathbf{j}\right). \tag{14.25}$$

14.1.1 Boundary Conditions

At the junction between two media, the boundary conditions are, for an *E-wave* and in the absence of surface magnetic currents (Fig. 14.2*b*),

1. e_z continuous
2. $(1/\mu)(\partial e_z/\partial n)$ continuous.

At the surface of a perfect conductor, the boundary conditions reduce to $e_z = 0$. The surface then carries a z-oriented electric current, which under time-harmonic conditions is given by

$$\mathbf{J}_S = J_S\,\mathbf{u}_z = \frac{1}{j\omega\mu}\frac{\partial E_z}{\partial n}. \tag{14.26}$$

In (14.26), μ and $\partial E_z/\partial n$ refer to the medium outside the conductor.

The boundary conditions for an *H-wave* produced by transverse electric currents are, again under time-harmonic conditions,

1. $H_{z2} - H_{z1} = \mathbf{J}_S \cdot \mathbf{u}_c$
2. $[1/(\sigma + j\omega\epsilon)](\partial H_z/\partial n)$ continuous.

At the surface of a perfect conductor, the external field satisfies the condition $\partial H_z/\partial n = 0$, and the surface current is given by

$$\mathbf{J}_S = -H_z\,\mathbf{u}_c. \tag{14.27}$$

14.1.2 Scattering Cross Sections

The concept of *scattering cross section*, defined in Section 11.2, can easily be adapted to two-dimensional problems. Consider, for example, a cylindrical scatterer immersed in an incident E-wave whose electric field is $E_z^i\,\mathbf{u}_z$ (Fig. 14.2*b*). The scattered field at large distances is of the form

$$E_z = \frac{e^{-jk_0 r}}{r^{\frac{1}{2}}}F(\varphi) = \left(\frac{2j}{\pi k_0}\right)^{\frac{1}{2}}\frac{e^{-jk_0 r}}{r^{\frac{1}{2}}}f(\varphi). \tag{14.28}$$

The power radiated through a circle C_∞ at infinity is given by

$$\begin{aligned} P^{sc} &= \frac{1}{2}\,\mathrm{Re}\left\{\int_{C_\infty}\left[\mathbf{E}^{sc}\times(\mathbf{H}^{sc})^*\right]\cdot\mathbf{u}_r\,dc\right\} \\ &= \frac{1}{2R_{c0}}\int_0^{2\pi}|F(\varphi)|^2 d\varphi \qquad (\mathrm{W\ m^{-1}}). \end{aligned} \tag{14.29}$$

For an incident plane wave of (complex) amplitude E^i, the *scattering cross section* is defined by the relationship

$$\begin{aligned} \sigma^{sc} &= \frac{\text{time-averaged scattered power per unit length}}{\text{time-averaged incident power per unit area}} \\ &= \frac{1}{|E^i|^2}\int_0^{2\pi}|F(\varphi)|^2\,d\varphi. \end{aligned} \tag{14.30}$$

This cross section has the dimension of a length (more precisely, of m^2 per m along the axis).

The power absorbed in the scatterer is, from (7.114),

$$P^{abs} = -\frac{1}{2}\,\mathrm{Re}\left[\int_C (\mathbf{E}\times\mathbf{H}^*)\cdot\mathbf{u}_n\,dc\right] = -\frac{1}{2}\,\mathrm{Re}\left(\int_C \frac{1}{j\omega\mu_0}E_z\frac{\partial E_z^*}{\partial n}dc\right). \tag{14.31}$$

The total power per unit axial length extracted from the incident wave is the sum of the absorbed and scattered powers. Thus,

$$\begin{aligned} P^{ext} = P^{abs} + P^{sc} &= -\frac{1}{2}\,\mathrm{Re}\left\{\int_C \mathbf{E}\times\mathbf{H}^* - \mathbf{E}^{sc}\times(\mathbf{H}^{sc})^*]\cdot\mathbf{u}_n\,dc\right\} \\ &= -\frac{1}{2}\,\mathrm{Re}\left\{\int_C \frac{1}{j\omega\mu_0}\left[E_z\frac{\partial E_z^*}{\partial n} - E_z^{sc}\frac{\partial (E_z^{sc})^*}{\partial n}\right]dc\right\}. \end{aligned}$$

This expression is basic to the evaluation of the *extinction cross section*, defined by

$$\sigma^{ext} = \frac{P^{abs}+P^{sc}}{\frac{1}{2R_{c_0}}|E^i|^2} \qquad \text{(m)}. \tag{14.32}$$

The formulas derived for an E-wave can easily be extended to an H-wave. The radiation field H_z^{sc} is now

$$H_z^{sc} = \frac{e^{-jk_0r}}{r^{\frac{1}{2}}}\frac{F(\varphi)}{R_{c0}} = \frac{e^{-jk_0r}}{r^{\frac{1}{2}}}\left(\frac{2j}{\pi k_0}\right)^{\frac{1}{2}}\frac{f(\varphi)}{R_{c0}}. \tag{14.33}$$

If the incident field is $H_z^i = A/R_{c0}$, the scattered power and the scattering cross section are given by (14.29) and (14.30). The *absorbed* power takes the form

$$P^{abs} = -\frac{1}{2}\,\mathrm{Re}\left(\int_c \frac{1}{j\omega\epsilon_0}H_z\frac{\partial H_z^*}{\partial n}dc\right). \tag{14.34}$$

The *bistatic cross section*, defined in (11.31), becomes

$$\sigma(\mathbf{u}|\mathbf{u}') = \frac{2\pi\times\text{power scattered per unit angle in direction }\mathbf{u}}{\text{incident power per unit area}} = \frac{2\pi|F(\mathbf{u}')|^2}{|E^i|^2}. \tag{14.35}$$

The monostatic cross section is $\sigma(\mathbf{u}|-\mathbf{u})$.

14.2 SCATTERING BY PERFECTLY CONDUCTING CYLINDERS

The fields scattered by cylinders can be determined by separation of variables in a few cases, for example for the strip, the wedge, and the elliptic, hyperbolic, and parabolic cylinders [38, 113]. In this section, the important canonical case of a *circular* cylinder is discussed in some detail.

Assume first that the cylinder is immersed in an E-wave of incident field* (Fig. 14.3)

$$E_z^i = e^{-jk_0x} = e^{-jk_0r\cos\varphi}. \tag{14.36}$$

*For incident fields generated by a step-current in a parallel line, see Note 1.

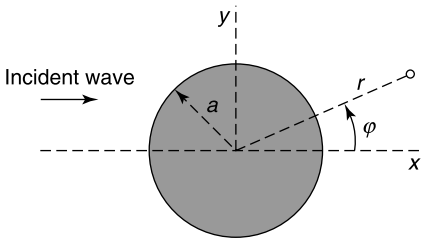

Figure 14.3 Circular cylinder in an incident plane wave.

The formal solution of this problem is quite simple. The incident field is expanded in a Fourier series in φ, whose r-dependent coefficients are found, by insertion into Helmholtz' equation, to satisfy Bessel's equation. Thus, because E_z^i must be finite at $r = 0$,

$$E_z^i = \sum_{n=-\infty}^{\infty} j^{-n} J_n(k_0 r)\, e^{jn\varphi}. \tag{14.37}$$

Because of the radiation condition (14.10), the scattered field must have a Fourier series of the form

$$E_z^{sc} = \sum_{n=-\infty}^{\infty} a_n j^{-n} H_n^{(2)}(k_0 r)\, e^{jn\varphi}. \tag{14.38}$$

When the cylinder is perfectly conducting, the boundary condition

$$E_z = E_z^i + E_z^{sc} = 0$$

at $r = a$ yields

$$a_n = -\frac{J_n(k_0 a)}{H_n^{(2)}(k_0 a)}.$$

It follows that the surface current is given by the expression

$$J_S = H_\varphi\big|_{r=a} = \frac{1}{j\omega\mu}\frac{\partial E_z}{\partial r}\bigg|_{r=a} = -\frac{2}{\omega\mu_0\pi a}\sum_{n=-\infty}^{\infty}\frac{j^{-n}e^{jn\varphi}}{H_n^{(2)}(k_0 a)} \tag{14.39}$$

and the far field by

$$E_z^{sc} = \left(\frac{2j}{\pi k_0 r}\right)^{\frac{1}{2}} e^{-jk_0 r}\sum_{n=-\infty}^{\infty} a_n e^{jn\varphi} = \frac{e^{-jk_0 r}}{r^{\frac{1}{2}}}\left(\frac{2j}{\pi k_0}\right)^{\frac{1}{2}}\sum_{n=-\infty}^{\infty} -\frac{J_n(k_0 a)}{H_n^{(2)}(k_0 a)} e^{jn\varphi}. \tag{14.40}$$

The convergence of these series is quite slow for large values of $k_0 a$. Whereas six terms give satisfactory results for $k_0 a = 3$, more than 100 terms may be needed for $k_0 a = 100$. A few typical results are shown in Figure 14.4. The left part of the figure shows the variation of the electric field $E_z = E_z^i + E_z^{sc}$ along the x axis for $k_0 a = 3.1$, a typical value in the intermediate-frequency range. The standing wave pattern that can be observed on the left part of the x axis results from the interference of the small wavelets scattered from the

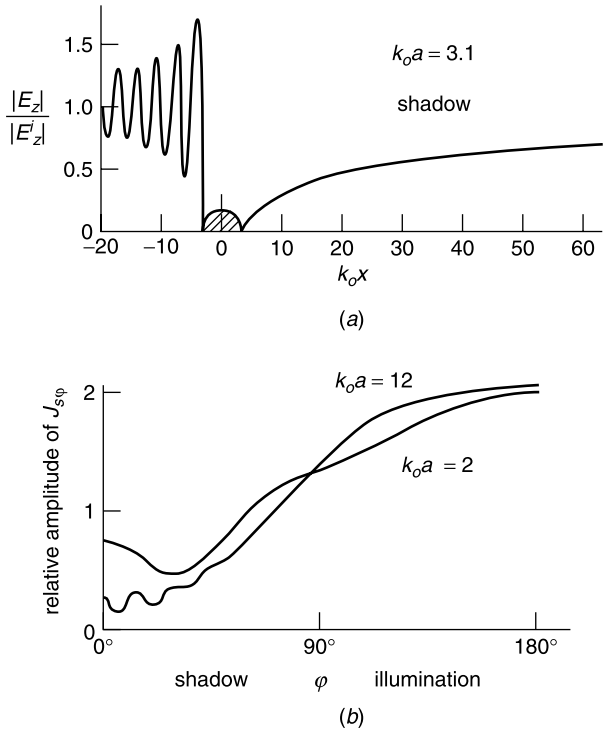

Figure 14.4 (a) E field along an axis parallel to the direction of incidence. (b) Current on a circular cylinder immersed in an H-wave (reprinted by permission of the publishers from *The scattering and diffraction of waves* by Ronald W. P. King and Tai Tsun Wu, Cambridge, Mass.: Harvard University Press, Copyright 1959 by the President and Fellows of Harvard College).

illuminated parts of the cylinder. We also note that the shadow, on the right part of the axis, is not very dark at the chosen frequency.

The analysis for an incident H-wave proceeds much as for an E-wave. For an incident magnetic field e^{-jk_0x}, for example, the boundary condition

$$\frac{\partial}{\partial r}(H_z^i + H_z^{sc}) = 0 \qquad \text{at } r = a$$

leads to the following value for the scattered field:

$$H_z^{sc} = -\sum_{n=-\infty}^{+\infty} j^{-n} H_n^{(2)}(k_0 r) \frac{J_n'(k_0 a)}{[H_n^{(2)}(k_0 a)]'} e^{jn\varphi}. \tag{14.41}$$

The corresponding surface current is

$$J_{S\varphi} = H_z|_{r=a} = \frac{2j}{\pi k_0 a} \sum_{n=-\infty}^{\infty} \frac{j^{-n} e^{jn\varphi}}{[H_n^{(2)}(k_0 a)]'}. \tag{14.42}$$

A typical variation of $J_{S\varphi}$ is displayed in Figure 14.4*b*.

14.2.1 The Low-Frequency Limit

The low-frequency limit of the scattered E field can be obtained by utilizing the small argument values of the Bessel and Neumann functions, given in (A5.16) and (A5.19). The dominant coefficient in expansion (14.38) is

$$a_0 = -\frac{J_0(k_0a)}{H_0^{(2)}(k_0a)} = -\frac{1}{1 - j(2/\pi)\log_e(\gamma k_0a/2)}$$
$$= -j\frac{\pi}{2\log_e k_0a} - \frac{\pi^2}{4(\log_e k_0a)^2} + \cdots .$$

The resulting far field is of the form

$$E_z^{sc} = -\left(\frac{2j}{\pi k_0}\right)^{\frac{1}{2}} \frac{e^{-jk_0r}}{r^{\frac{1}{2}}} \frac{\pi}{2} \frac{j}{\log_e k_0a} \tag{14.43}$$

and the current density has the uniform value

$$J_{Sz} = -\frac{j}{\omega\mu_0 a \log_e k_0a}. \tag{14.44}$$

The scattering pattern is clearly isotropic, with a *scattering cross section* equal to

$$\sigma^{sc} = \frac{\pi^2}{k_0(\log_e k_0a)^2}. \tag{14.45}$$

For an H-wave, the dominant coefficients are

$$a_0 = j\frac{\pi}{4}(k_0a)^2 \qquad a_1 = a_{-1} = -j\frac{\pi}{4}(k_0a)^2.$$

They give rise to a far field

$$H_z^{sc} = \left(\frac{2j}{\pi k_0}\right)^{\frac{1}{2}} \frac{e^{-jk_0r}}{r^{\frac{1}{2}}} j\frac{\pi}{4}(k_0a)^2|1 - 2\cos\varphi|, \tag{14.46}$$

which is the sum of a field stemming from a filamentary magnetic current (associated with the term in a_0) and a field produced by a y-directed electric dipole (associated with the terms in a_1 and a_{-1}). The *scattering cross section* resulting from these currents is

$$\sigma^{sc} = \frac{3\pi^2}{4}a(k_0a)^3. \tag{14.47}$$

14.2.2 The High-Frequency Limit

In this limit, the convergence of the Fourier series for E_z^{sc} or H_z^{sc} becomes very poor. To remedy this situation, the series can be replaced by an integral in the complex plane, based on *Watson's transformation*. The integral is of the form [6, volume 25], [21, 65, 85, 134]

$$E = -\frac{j}{2}\int_{-\infty}^{\infty} \frac{\cos\nu(\varphi - \pi)}{\sin\nu\pi} B_\nu \, d\nu, \tag{14.48}$$

where B_ν is an expression involving $J_\nu(k_0 r)$ and $H_\nu^{(2)}(k_0 r)$. The residue series converges rapidly in the shadow region of the cylinder and reveals the existence of the creeping waves mentioned in Section 11.5. The *scattering cross section in an E-wave* is given asymptotically by[2]

$$\sigma_{sc} = 4a\left[1 + \frac{0.49807659}{(k_0 a)^{\frac{2}{3}}} - \frac{0.01117656}{(k_0 a)^{\frac{4}{3}}} + \cdots\right], \tag{14.49}$$

and in *an H-wave* by

$$\sigma_{sc} = 4a\left[1 + \frac{0.43211998}{(k_0 a)^{\frac{2}{3}}} - \frac{0.21371236}{(k_0 a)^{\frac{4}{3}}} + \cdots\right]. \tag{14.50}$$

14.2.3 A Transient Problem

The problem to be solved next can serve to illustrate the early-time, late-time transition discussed in Section 11.5. It concerns a circular cylinder illuminated from the right by an x-directed E-wave of doubly exponential time variation[3]

$$e^i(x,t) = A\left[e^{-\alpha_1\left(t+\frac{x-a}{c_0}\right)} - e^{-\alpha_2\left(t+\frac{x-a}{c_0}\right)}\right] H\left(t + \frac{x-a}{c_0}\right). \tag{14.51}$$

The incident wavefront hits the cylinder at time $t = 0$ (Fig. 14.3). To evaluate the surface currents $j_s(\varphi, t)$ in the time domain, we start with the time-harmonic solution (14.39). By substituting s for $j\omega$ in that equation, we obtain the Laplace transform

$$J_S(\varphi, s) = \frac{A}{R_{c0}}\frac{a}{c}\sum_{m=0}^{\infty} \epsilon_m \cos m\varphi \left(\frac{1}{s' + \alpha_1'} - \frac{1}{s' + \alpha_2'}\right)\frac{e^{-s'}}{s' K_m(s')}, \tag{14.52}$$

where $s' = \dfrac{a}{c_0}s$ and $\alpha' = \dfrac{a}{c_0}\alpha$ are dimensionless, normalized parameters, and K_m is the modified Bessel function defined in (A5.64). The actual time-dependence $j_S(\varphi, t)$ follows from $J_S(\varphi, s)$ by evaluating the Bromwich integral (A7.15), which gives (Fig. 14.5*a*)

$$j_S(\varphi, t) = \sum_{m=0}^{\infty} \epsilon_m h_m(\tau) \cos m\varphi, \tag{14.53}$$

where $\tau = \dfrac{c_0 t}{a}$ is a normalized time, and

$$h_m(\tau) = \frac{1}{2\pi j}\int_{\sigma - j\infty}^{\sigma + j\infty} H_m(s', \tau)\, ds'.$$

The integrand in the integral is

$$H_m(s', \tau) = A\left(\frac{1}{s' + \alpha_1'} - \frac{1}{s' + \alpha_2'}\right)\frac{e^{s'(\tau - 1)}}{s' K_m(s')}.$$

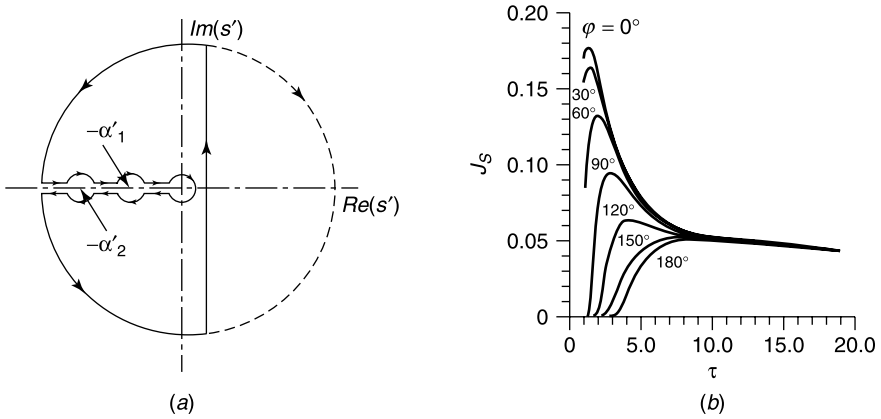

Figure 14.5 (a) Integration contour. (b) Current density response for $\alpha'_1 = 1$, $\alpha'_2 = 1.2$ (from J. Ma and I. R. Ciric, Transient response of a circular cylinder to an electromagnetic pulse, *Radio Sci.* **27**, 561–567, 1992, with permission of the American Geophysical Union).

A typical variation of $j_S(\varphi)$ is shown in Figure 14.5*b*. The series (14.53) is analytically valid for all time ranges. It converges rapidly everywhere, except in the range $0 < \tau < 1$, (i.e., from the impact time $t = 0$ up to the time it takes the incident wave to reach the axis of the cylinder). The value of j_S in that early range can be obtained by various methods, such as a combination of rays and creeping waves, or the application of the Watson transformation to the $J_S(\varphi, s)$ series.[4]

14.3 SCATTERING BY PENETRABLE CIRCULAR CYLINDERS

The method of separation of variables, applied successfully in Section 14.2 to a perfectly conducting circular cylinder, works equally well for a dielectric cylinder. Consider, for example, a layered circular cylinder immersed in the field of an E-wave. In the nth layer, one may write

$$E_n = \sum_{m=0}^{\infty} [A_{nm} J_m(k_n r) + B_{nm} N_m(k_n r)] \cos m\varphi, \tag{14.54}$$

where k_n is the propagation constant in the material of the layer. The corresponding tangential magnetic field is

$$H_{\varphi n} = \frac{k_n}{j\omega\mu_n} \sum_{m=0}^{\infty} \left[A_{nm} J'_m(k_n r) + B_{nm} N'_n(k_n r)\right] \cos m\varphi. \tag{14.55}$$

In the central cylinder, only the A coefficients should be kept. The A and B coefficients are coupled by sets of linear equations, obtained by imposing the boundary conditions at each interface. The resulting chain set of equations can be solved iteratively.[5]

Several other problems involving circular cross sections admit a solution by separation of variables or the method of images.[6,7] We shall only consider the important particular case of the homogeneous, nonmagnetic *highly conducting* cylinder.[8] The fields penetrate into such a cylinder, to a depth determined by the value of the penetration depth δ. To analyze

the phenomenon, assume that the circular cylinder is immersed in an incident E-wave propagating in the x-direction.† From (A5.47):

$$\begin{aligned} E^i &= Ae^{-k_0 x} = A\, e^{-jk_0 r\cos\varphi} \\ &= A\left[J_0(k_0 r) - 2jJ_1(k_0 r)\cos\varphi - 2J_2(k_0 r)\cos 2\varphi + \cdots\right]. \end{aligned} \tag{14.56}$$

At low frequencies, for small $k_0 r$,

$$\begin{aligned} E^i = A\Bigg[1 - \frac{1}{4}k_0^2 r^2 - jk_0 r\left(1 - \frac{1}{8}k_0^2 r^2\right)\cos\varphi \\ -\frac{1}{4}k_0^2 r^2\left(1 - \frac{1}{24}k^2 r^2\right)\cos 2\varphi + \cdots\Bigg]. \end{aligned} \tag{14.57}$$

The dominant contributions come from the φ-independent and $(\cos\varphi, \sin\varphi)$ terms in the expansions. We shall therefore concentrate our attention on these terms — also at higher frequencies — and use, for the various fields, expressions of the form

$$E = E_0(r) + \cos\varphi E_1(r) + \cdots. \tag{14.58}$$

From Maxwell's equation (7.1) the magnetic field is related to E by

$$R_{c0}H_\varphi = \frac{1}{jk_0}\frac{\partial E}{\partial r}$$

$$R_{c0}H_r = -\frac{1}{jk_0 r}\frac{\partial E}{\partial \varphi}.$$

Outside the cylinder the total fields (incident plus scattered) are

$$\begin{aligned} \frac{E^+}{A} &= J_0(k_0 r) + BH_0^{(2)}(k_0 r) - 2jJ_1(k_0 r)\cos\varphi \\ &\quad + MH_1^{(2)}(k_0 r)\cos\varphi + \cdots \end{aligned} \tag{14.59}$$

$$\begin{aligned} \frac{R_{c0}H_\varphi^+}{A} &= jJ_1(k_0 r) + jBH_1^{(2)}(k_0 r) \\ &\quad - 2J_1'(k_0 r)\cos\varphi - jM[H_1^{(2)}(k_0 r)]'\cos\varphi + \cdots. \end{aligned} \tag{14.60}$$

If we set

$$m = (1-j)(a/\delta) = \sqrt{2}\, e^{-j\frac{\pi}{4}}(a/\delta), \tag{14.61}$$

the *interior* fields take the form

$$\frac{E^-}{A} = CJ_0\left[m\frac{r}{a}\right] + NJ_1\left[m\frac{r}{a}\right]\cos\varphi + \cdots \tag{14.62}$$

$$\frac{R_{c0}H_\varphi^-}{A} = -\frac{C}{jka}mJ_1\left[m\frac{r}{a}\right] + \frac{N}{jka}mJ_1'\left[m\frac{r}{a}\right]\cos\varphi + \cdots. \tag{14.63}$$

†The problem of the circular cylinder in an incident H-wave is discussed in Note 9.

Values of the Bessel functions of the complex arguments (mr/a) are given in [144]. The unknown coefficients B, C, M, N can be determined by means of the boundary conditions at $r = a$, which require the total E fields, E^+ and E^-, to be equal, together with their derivatives with respect to r. Because

$$k_0\delta = \sqrt{2Q} \ll 1 \tag{14.64}$$

in a good conductor, the three dimensionless parameters k_0a, Q, and (δ/a) may not be chosen independently because they are connected by the relationship

$$k_0a = \sqrt{2Q}\,\frac{a}{\delta}. \tag{14.65}$$

The condition $Q \ll 1$, to be satisfied by priority, implies $\delta \ll \lambda_0$, but not necessarily $a \ll \lambda_0$, unless δ is of the order a or larger. With this remark in mind, we will discuss two particular cases:

1. In the limit of *very small penetrations depths* (i.e., for $\delta \ll a$), the asymptotic value of $J_0(m)$ for $|m| \to \infty$ may be used. It produces the well-known exponential decay away from the boundary. Thus, to the first order in (δ/a),

$$B = -\frac{J_0(k_0a)}{H_0^{(2)}(k_0a)}\left[1 - \frac{1+j}{\pi}\,\frac{1}{J_0(k_0a)H_0^{(2)}(k_0a)}\,\frac{\delta}{a}\right] \tag{14.66}$$

$$M = 2j\frac{J_0(k_0a)}{H_0^{(2)}(k_0a)}\left[1 - \frac{1+j}{\pi}\,\frac{1}{J_1(k_0a)H_1^{(2)}(k_0a)}\,\frac{\delta}{a}\right]. \tag{14.67}$$

These formulas display the *perfect conductor* values of B and M, obtained by setting $\delta = 0$, as well as the first-order correction terms due to a nonzero δ. They can be used to derive low (δ/a) approximations of various quantities, for example of the electric field at the boundary, which is

$$\frac{E_\varphi}{A} = \frac{1+j}{\pi}\left[\frac{1}{H_0^{(2)}(k_0a)} - 2j\frac{1}{H_1^{(2)}(k_0a)}\cos\varphi\right]\frac{\delta}{a}. \tag{14.68}$$

2. In the limit of *very high penetration depths* (i.e., for $\delta \gg a$), k_0a and $|m|$ become small parameters, and the small-argument expressions of Bessel and Hankel functions may be used in the general formulas for B and M. This gives

$$B = -j\frac{\pi}{4}\,\frac{m^2 - k_0^2a^2}{1 - \dfrac{m^2}{4}(1 - j\pi)} \approx -\frac{\pi}{2}\,\frac{a^2}{\delta^2} \tag{14.69}$$

$$M = -\frac{\pi}{16}k_0^2a^2\,\frac{m^2 - k_0^2a^2}{1 + \dfrac{m^2}{4}} \approx j\frac{\pi}{8}k_0^2a^2\left(\frac{a^2}{\delta^2}\right). \tag{14.70}$$

The corresponding boundary field takes the form

$$\frac{E_\varphi}{A} = 1 - j\log_e\left(\frac{1}{k_0a}\right)\frac{a^2}{\delta^2} - jk_0a\cos\varphi - \frac{1}{4}k_0a\frac{a^2}{\delta^2}\cos\varphi + \cdots. \tag{14.71}$$

The part contributed by the cylinder is proportional to (a^2/δ^2), from which it may be concluded that the cylinder becomes transparent in the limit $(\delta/a) \to \infty$.

One of the important parameters in the scattering problem is the surface impedance $Z_s = (E/H_\varphi)$. For *small* penetration depths

$$Z_s' = \frac{Z_s}{R_{c0}} = \sqrt{Q}\left(1 + \frac{1}{4}\frac{\delta}{a}\right) e^{j((\pi/4)-(1/4)(\delta/a))}. \tag{14.72}$$

This yields the well-known surface impedance

$$Z_s' = \sqrt{\frac{Q}{2}}(1+j) \tag{14.73}$$

of a very good conductor, obtained by setting $\delta \approx 0$. For *deep* penetrations, on the other hand,

$$Z_s' = \sqrt{2Q}\,\frac{\delta}{a} = 2\pi a \frac{r_{dc}}{R_{c0}}, \tag{14.74}$$

where $r_{dc} = (\sigma \pi a^2)^{-1}$ is the *dc* resistance of the wire per *m* along the axis. The current I induced in the cylinder is equal to $2\pi a H_\varphi$, hence

$$I \approx \frac{E^i}{r_{dc}}.$$

14.4 SCATTERING BY ELLIPTIC CYLINDERS

This classic problem was solved in detail a century ago, in the early days of electromagnetic research.[10] It is amenable to a solution by separation of variables, in which Mathieu functions play a major role. Data on these functions can be found in Appendix 5.

Let the elliptic cylinder be immersed in the incident E-wave (Fig. 14.6)

$$E^i = E_0\, e^{-jk_0 \mathbf{u}_i \cdot \mathbf{r}} = E_0\, e^{-jk_0(x\cos\varphi_i + y\sin\varphi_i)}. \tag{14.75}$$

On the basis of (A5.174), this field admits the series representation

$$\frac{E^i}{E_0} = \sum_m \left[A_m^e S_m^e(k_0 c, v)\, J_m^e(kc, u) + A_m^o S_m^o(k_0 c, v)\, J_m^o(k_0 c, u)\right], \tag{14.76}$$

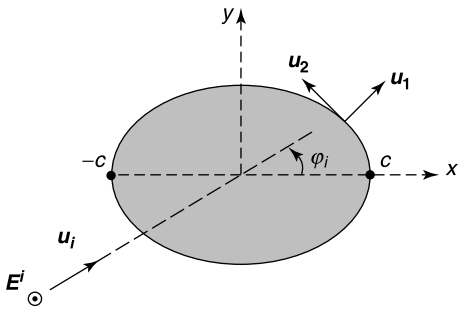

Figure 14.6 Elliptic cylinder in an incident E-wave.

where the A_m coefficients are functions of k_0c and φ_i. The scattered field can similarly be expanded as

$$\frac{E^{sc}}{E_0} = \sum_m \left[B_m^e S_m^e(k_0c, v)\, H_m^e(k_0c, u) + B_m^o S_m^o(k_0c, v)\, H_m^o(k_0c, u)\right]. \tag{14.77}$$

We note that the choice $H_m = J_m - jN_m$ ensures satisfaction of the radiation condition.

14.4.1 Perfectly Conducting Cylinder

The contour C in Figure 14.6 is characterized by a constant value of u, say u_0 (the strip corresponds with $u_0 = 0$) (Fig. 5.13). The boundary conditions at $u = u_0$ are

$$\begin{aligned} E^i + E^{sc} &= 0 \qquad \text{(for an } E\text{-wave, Dirichlet type)} \\ \frac{\partial}{\partial n}(H^i + H^{sc}) &= 0 \qquad \text{(for an } H\text{-wave, Neumann type).} \end{aligned} \tag{14.78}$$

According to (A5.168), the $S_m(k_0c, v)$ functions form a complete orthogonal set in the interval $(0, 2\pi)$. On the basis of that property, the unknown coefficients B_m of the scattered field can be expressed in terms of the known A_m coefficients of the incident field. In an E-wave, for example,[11]

$$\begin{aligned} B_m^e &= -\frac{J_m^e(k_0c, u_0)}{H_m^e(k_0c, u_0)}\, A_m^e(k_0c, \varphi_i) \\ B_m^o &= -\frac{J_m^o(k_0c, u_0)}{H_m^o(k_0c, u_0)}\, A_m^o(k_0c, \varphi_i). \end{aligned} \tag{14.79}$$

Once these coefficients are known, the far field can be determined by inserting the asymptotic form (A5.170) of the radial Mathieu functions into (14.77). The magnetic field follows from E by applying (14.3), which yields

$$\begin{aligned} \mathbf{H} &= \frac{1}{j\omega\mu_0}\, \mathbf{u}_z \times \operatorname{grad} E \\ &= \frac{1}{j\omega\mu_0} \frac{1}{c\sqrt{\cosh^2 u - \cos^2 \varphi}} \left[-\frac{\partial E}{\partial v}\, \mathbf{u}_1 + \frac{\partial E}{\partial u}\, \mathbf{u}_2\right]. \end{aligned} \tag{14.80}$$

On contour C, therefore,

$$\mathbf{J}_S = \mathbf{u}_1 \times \mathbf{H} = \frac{1}{R_{c0}\, jk_0c\, \sqrt{\cosh^2 u_0 - \cos^2 v}} \left[\frac{\partial (E^{sc} + E^i)}{\partial u}\right]_{u=u_0} E_0\, \mathbf{u}_z. \tag{14.81}$$

Similar developments hold for a cylinder immersed in an H-wave. The transverse field is now the electric field $\mathbf{E}$, which can be derived from H by the relationship

$$\begin{aligned} \mathbf{E} &= \frac{1}{j\omega\epsilon_0}\, \operatorname{grad} H \times \mathbf{u}_z \\ &= \frac{1}{j\omega\epsilon_0} \frac{1}{c\sqrt{\cosh^2 u - \cos^2 v}} \left[\frac{\partial H}{\partial v}\, \mathbf{u}_1 - \frac{\partial H}{\partial u}\, \mathbf{u}_2\right]. \end{aligned} \tag{14.82}$$

The surface current is now

$$\mathbf{J}_S = -(H^i + H^{sc})_{u=u_0}\,\mathbf{u}_2. \tag{14.83}$$

14.4.2 Penetrable Cylinder

In a *homogeneous* elliptic cylinder, exposed to an incident E-wave, the interior field admits the expansion

$$\frac{E^{int}}{E_0} = \sum_{m=0}^{\infty} \left[C_m^e(kc, \varphi_i)\, S_m^e(kc, v)\, J_m^e(kc, u) + C_m^o(kc, \varphi_i)\, S_m^o(kc, v)\, J_m^o(kc, u) \right]. \tag{14.84}$$

When the cylinder is *layered*, and consists of several confocal elliptic shells, expansions such as (14.84) can be written in each layer, using for k the propagation constant $k_0(\epsilon_r \mu_r)^{\frac{1}{2}}$ of the layer. The shell structure has been used to model parts of the human body, for example arms and legs. The constant k can be complex,[12,13,14] in which case Mathieu functions of a complex argument appear in (14.84). In the low-frequency limit,[15] one should make use of the small argument form of the Mathieu functions, given in (A5.167) and (A5.169).

The solution of the *homogeneous* cylinder problem proceeds by matching the expansions for $(E^i + E^{sc})$ and E^{int}, given in (14.76), (14.77), and (14.84), at the boundary $u = u_0$. The matching conditions

$$\begin{aligned} E^i + E^{sc} &= E^{int} \\ \frac{1}{jk_0 R_{c0}} \frac{\partial}{\partial u}(E^i + E^{sc}) &= \frac{1}{jkZ_c} \frac{\partial E^{int}}{\partial u} \end{aligned} \tag{14.85}$$

express continuity of the tangential components of $\mathbf{E}$ and $\mathbf{H}$. They allow determination of the B_m and C_m coefficients in terms of the A_m coefficients of the incident wave.[16,17] A major difficulty arises, however: The $S_m(k_0 c, v)$ and $S_m(kc, v)$ functions form *different* orthogonal sets without cross-orthogonality properties.[‡] A possible solution consists in expanding one set in terms of the other, for example as

$$S_m(kc, v) = \sum_{n=0}^{\infty} D_{mn} S_n(k_0 c, v). \tag{14.86}$$

Summation (14.84) now becomes (in shortened form)

$$\frac{E^{int}}{E_0} = \sum_{m=0}^{\infty} S_m(k_0 c, v)\, J_m(kc, u) \sum_{n=0}^{\infty} C_n D_{nm}. \tag{14.87}$$

Equating the coefficients of $S_m(k_0 c, v)$ on both sides of the boundary leads to a matrix relationship between the C coefficients and their A counterparts. The method therefore requires the inversion of a fully populated matrix. It is also possible to replace the functions $S^e(k_0 c, v)$ and $S^h(kc, v)$ [and analogously $S^o(k_0 c, v)$ and $S^o(kc, v)$] by their expansions in terms of $\cos nv$, (or $\sin nv$).

[‡]When $k = k_0$, that is, when $\epsilon\mu = \epsilon_0\mu_0$, the material of the cylinder is termed *isorefractive*, and the two sets *do* coincide. See, for example, Note 18.

14.5 SCATTERING BY WEDGES

The surface of a scatterer often exhibits wedges, which can be perfectly conducting or penetrable. Typical examples are the back edge of an aircraft wing, or the 90° corner of a building. In propagation studies, the wedge often provides a better model for a surface singularity than the half-plane edge[19] (Fig. 14.7). The relevant scattering problem has been investigated extensively [1, 77, 116, 193]. The analytic developments are far from elementary, and only the main steps will be outlined.

14.5.1 The Perfectly Conducting Wedge

Let the wedge lie in the field of an electric line source I (Fig. 14.8). From (14.16), (14.20), and (14.21) the incident field may be written as

$$E^i = -k_0 \frac{R_{c0} I}{4} \begin{cases} \displaystyle\sum_{m=-\infty}^{\infty} J_m(k_0 r_i)\, H_m^{(2)}(k_0 r)\, e^{jm(\varphi-\varphi_i)} & \text{for } r > r_i \\ \displaystyle\sum_{m=-\infty}^{\infty} J_m(k_0 r)\, H_m^{(2)}(k_0 r_i)\, e^{jm(\varphi-\varphi_i)} & \text{for } r < r_i. \end{cases} \tag{14.88}$$

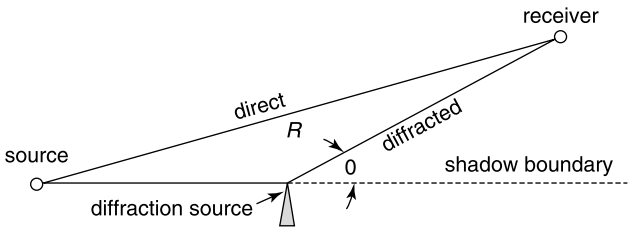

Figure 14.7 Propagation influenced by a wedge (from A. R. Lopez, Cellular telecommunications: estimating shadowing effects using wedge diffraction, *IEEE Antennas Prop. Mag.* **40**, 53–57, 1998, with permission of IEEE).

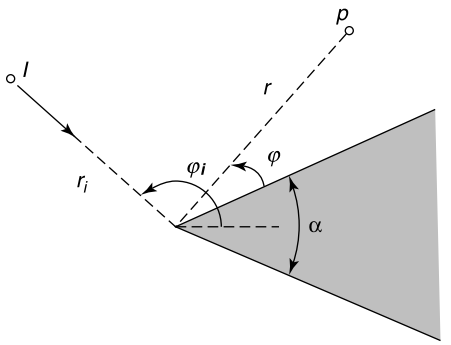

Figure 14.8 Line source and wedge.

The total electric field, sum of the incident and scattered contributions, is found to be

$$E(r,\varphi) = -\frac{1}{2}\nu k_0 R_{c0} I \begin{cases} \displaystyle\sum_{m=0}^{\infty} J_{m\nu}(k_0 r_i)\, H_{m\nu}^{(2)}(k_0 r) \sin(m\nu\varphi_i) \sin(m\nu\varphi) & (\text{for } r > r_i) \\ \displaystyle\sum_{m=0}^{\infty} J_{m\nu}(k_0 r)\, H_{m\nu}^{(2)}(k_0 r_i) \sin(m\nu\varphi) \sin(m\nu\varphi_i) & (\text{for } r < r_i), \end{cases} \tag{14.89}$$

where $\nu = \pi/(2\pi - \alpha)$. In more compact form:

$$E(r,\varphi) = -\frac{k_0 R_{c0} I}{4} G(r, r_i, \varphi, \varphi_i, \nu). \tag{14.90}$$

From the expression for E, one can derive the components H_φ, H_r of the magnetic field and the scattered field at large distances. Note that by taking the limit $k_0 r_i \to \infty$, the incident field becomes a plane wave. The far field derived from (14.89) becomes, in that particular case,

$$\lim_{r\to\infty} E(r,\varphi) = -\nu k_0 R_{c0} \sqrt{\frac{2j}{\pi}} \left[\sum_{m=0}^{\infty} j^m J_{m\nu}(k_0 r_i) \sin(m\nu\varphi_i) \sin(m\nu\varphi) \right] \frac{e^{-jk_0 r}}{\sqrt{k_0 r}}. \tag{14.91}$$

A similar analysis can be conducted for a wedge in the field of a *magnetic* line source I_m. The expansion (14.89) is now replaced by

$$H(r,\varphi) = \frac{1}{2R_{c0}}\, \nu k_0 I_m \begin{cases} \displaystyle\sum_{m=0}^{\infty} \epsilon_m J_{m\nu}(k_0 r_i) H_{m\nu}(k_0 r) \cos(m\nu\varphi_i) \cos(m\nu\varphi) & \text{for } r > r_i \\ \displaystyle\sum_{m=0}^{\infty} \epsilon_m J_{m\nu}(k_0 r) H_{m\nu}(k_0 r_i) \cos(m\nu\varphi) \cos(m\nu\varphi_i) & \text{for } r < r_i, \end{cases} \tag{14.92}$$

where ϵ_m is Neumann's factor.

A series such as (14.91) converges rapidly for small values of $k_0 r_i$ but only slowly for larger values. In the latter case, high-frequency asymptotic methods, involving complex integrals and their evaluation by the method of steepest descent, provide a remedy to the slow convergence [1, 77]. The contour integral solution can be manipulated to yield a transform representation of the scattered field in terms of currents flowing on the two faces of the wedge[20] [131].

14.5.2 Penetrable Wedge

Separation of variables cannot be applied to the general penetrable wedge, fundamentally because of the different wavenumbers in vacuum and wedge. A solution can be found, however, when the material of the wedge is isorefractive (i.e., when the two wavenumbers are equal[21]). A solution is also available when the faces of the wedge carry a surface impedance, say of the Leontovich type[22,23] [116]. Whether the impedance concept remains valid close to the edge or on the face lying in the shadow should clearly be investigated. It has been shown that the actual Z_S of highly conducting and high-contrast wedges can

be assumed constant, on both faces, down to edge distances r of the order λ_0. At shorter distances, waves from one face, although attenuated, can reach the other face with sufficient strength to create interference.[24,25] What happens *very* close to the edge has been the subject of extensive discussions. The assumption that the field components may be represented, as in Section 5.3, by a series of the form

$$\phi(r,\varphi) = r^{\nu}\left[a_0(\varphi) + ra_1(\varphi) + r^2 a_2(\varphi) + \cdots\right] \tag{14.93}$$

remains valid for a perfectly conducting wedge but becomes shaky for a dielectric one. It has been found[26] that the dominant term $a_0(\varphi)$ is equal to the static value, as expected, but that the supplementary (dynamic) term cannot be obtained from the series when the opening angle α is a rational multiple of π. The analysis of the isorefractive wedge confirms that the series is not sufficient to describe the fields correctly.[21] Given these analytical difficulties, attempts have been made to solve the problem numerically in an integral equation formulation and with patches as short as $10^{-10}\lambda_0$ close to the edge. The results have been inconclusive.[27,28]

14.6 INTEGRAL EQUATIONS FOR PERFECTLY CONDUCTING CYLINDERS

The fundamental components, E_z in an E-wave and H_z in an H-wave, satisfy Helmholtz' equation outside contour C (Fig. 14.9*a*). In both cases, the scattered field satisfies the sourcesless version of the equation, viz.

$$\nabla^2\phi^{sc}(\mathbf{r}) + k_0^2\phi^{sc}(\mathbf{r}) = 0. \tag{14.94}$$

Applying Green's theorem (A1.31) to ϕ^{sc} and $G_0(\mathbf{r}|\mathbf{r}')$ in the region outside S gives, for an exterior point $\mathbf{r}$,

$$\phi^{sc}(\mathbf{r}) = \int_C \left[G_0(\mathbf{r}|\mathbf{r}')\frac{\partial\phi^{sc}(\mathbf{r}')}{\partial n'} - \phi^{sc}(\mathbf{r}')\frac{\partial G_0(\mathbf{r}|\mathbf{r}')}{\partial n'}\right] dc'. \tag{14.95}$$

When the same Green's theorem is applied to ϕ^i and G_0, and the integration is performed over S, one obtains

$$o = \int_C \left[G_0(\mathbf{r}|\mathbf{r}')\frac{\partial\phi^{i}(\mathbf{r}')}{\partial n'} - \phi^{i}(\mathbf{r}')\frac{\partial G_0(\mathbf{r}|\mathbf{r}')}{\partial n'}\right] dc' \tag{14.96}$$

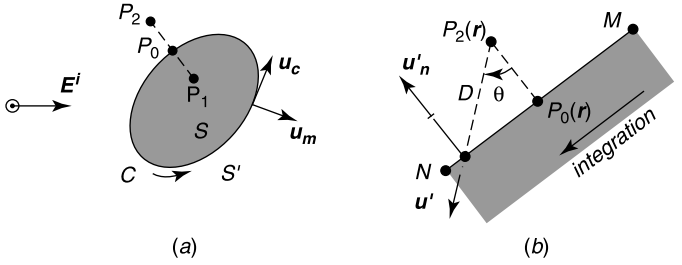

Figure 14.9 (*a*) Perfectly conducting scatterer. (*b*) P_2 approaching P_0.

for an interior point $\mathbf{r}$. Combining (14.95) and (14.96) yields

$$\begin{aligned}\phi(\mathbf{r}) &= \phi^i(\mathbf{r}) + \phi^{sc}(\mathbf{r}) \\ &= \phi^i(\mathbf{r}) + \int_C \left[G_0(\mathbf{r}|\mathbf{r}') \frac{\partial \phi(\mathbf{r}')}{\partial n'} - \phi(\mathbf{r}') \frac{\partial G_0(\mathbf{r}|\mathbf{r}')}{\partial n'} \right] dc'. \end{aligned} \tag{14.97}$$

This basic relationship will now serve to derive the two fundamental integral equations. Note that the scalar problem in hand has been investigated extensively in acoustics.[29]

14.6.1 The EFIE

In an E-wave, ϕ represents the E_z component. Because $E_z = E$ vanishes on C, (14.97) yields

$$E(\mathbf{r}) = E^i(\mathbf{r}) + \int_C G_0(\mathbf{r}|\mathbf{r}') \frac{\partial E}{\partial n'} \, dc'. \tag{14.98}$$

The incident field induces z-directed currents on the boundary C of the cylinder. From (14.3):

$$j\omega\mu_0 J_S = \frac{\partial E}{\partial n}. \tag{14.99}$$

Inserting this expression into (14.98) gives, for $\mathbf{r}$ outside S,

$$E(\mathbf{r}) = E^i(\mathbf{r}) + j\omega\mu_0 \int_C G_0(\mathbf{r}|\mathbf{r}') \, J_S(\mathbf{r}') \, dc'. \tag{14.100}$$

Note that this relationship can be derived directly from (14.15). The sought integral equation is obtained by letting P_2 approach P_0 (Fig. 14.9*b*). The weak (logarithmic) character of the singularity of G_0 ensures convergence of the integral. The approach generates an *integral equation of the first kind, the EFIE*:

$$j\omega\mu_0 \lim_{\delta \to 0} \int_{C - C_\delta} G_0(\mathbf{r}|\mathbf{r}') \, J_S(\mathbf{r}') \, dc' = -E^i(\mathbf{r}) \qquad (\mathbf{r} \text{ on } C). \tag{14.101}$$

Here C_δ is a small segment of length δ that includes P_0. Once J_S is determined, the far field in a direction of unit vector $\mathbf{u}$ follows from (14.13) and (14.15). Thus,

$$\lim_{r \to \infty} E^{sc}(\mathbf{r}) = -\frac{e^{-jk_0 r}}{\sqrt{k_0 r}} \sqrt{\frac{2j}{\pi}} \, k_0 R_{c0} \int_C J_S(\mathbf{r}') \, e^{jk_0 \mathbf{u} \cdot \mathbf{r}'} dc'. \tag{14.102}$$

At low frequencies the pattern becomes omnidirectional.

14.6.2 Uniqueness of the Solution

In an early numerical solution of the EFIE, the curves drawn in Fig. 14.10 were obtained for the axial current on a square cylinder.[30] The numerical procedure was unsophisticated: pulses as basis functions and testing by point matching. Other researchers promptly

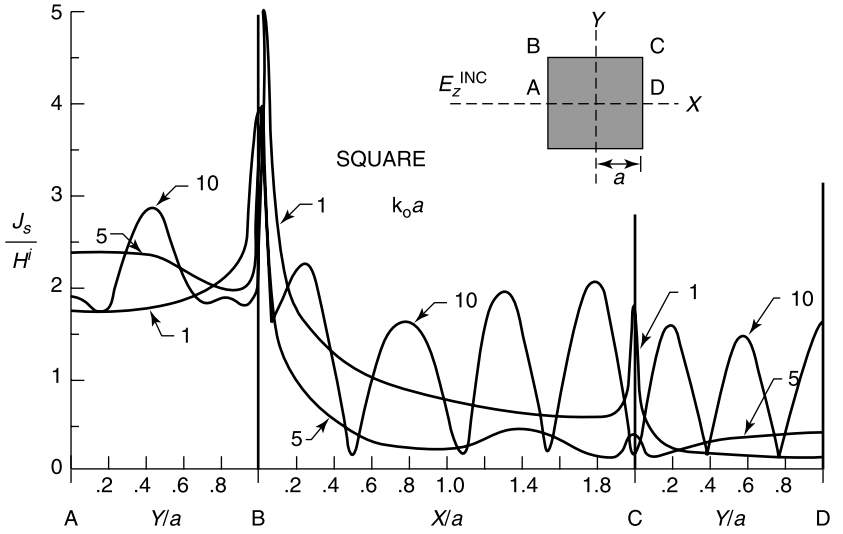

Figure 14.10 Current density on a square cylinder (from K. K. Mei and J. Van Bladel, Scattering by perfectly conducting rectangular cylinders, *IEEE Trans. AP* **11**, 185–192, 1963, with permission of IEEE).

remarked that they had found different values for J_S, but that the scattering patterns were in agreement. The apparent standing wave pattern on the curve $k_0a = 10$ was also found puzzling.[31] The origin of the ambiguity could have been detected from a careful reading of Maue's basic paper, in which the influence of the interior resonances is clearly discussed.[32] These resonances, already encountered in Sections 12.1 and 12.2 in the corresponding three-dimensional problem, are now associated with the Dirichlet eigenfunctions ϕ_m, the solutions of

$$\begin{aligned} \nabla^2\phi_m + k_m^2\phi_m &= 0 \quad \text{(in } S\text{)} \\ \phi_m &= 0 \quad \text{(on } C\text{)}. \end{aligned} \tag{14.103}$$

For a square cross section, the eigenvalues are $k_{mn}a = \dfrac{\pi}{2}\sqrt{m^2+n^2}$, and two of these, $k_0a = 9.935$ and $k_0a = 10.058$, lie in the immediate vicinity of $k_0a = 10$. Ambiguity, or at least instability, could therefore have been expected. To analyze the phenomenon in more detail, we shall again invoke Green's theorem (A1.31), applied to $\phi(\mathbf{r})$, the Green's function $G_0(\mathbf{r}|\mathbf{r}')$, and $k_0 = k_m$. For $\mathbf{r}$ in S, this gives

$$\phi_m(\mathbf{r}) = -\int_C G_0(\mathbf{r},\mathbf{r}',k_m)\frac{\partial\phi_m}{\partial n'}\,dc'. \tag{14.104}$$

By letting $\mathbf{r}$ approach C, it becomes clear that $\dfrac{\partial\phi_m}{\partial n}$ satisfies the homogeneous version of Equation (14.101). The solution of the latter is therefore determined to within a multiple of $\dfrac{\partial\phi_m}{\partial n}$. Applying once more (A1.31), for $\mathbf{r}$ outside C, gives

$$o = \int_C G_0(\mathbf{r}|\mathbf{r}')\,\frac{\partial\phi_m}{\partial n'}\,dc'. \tag{14.105}$$

The integral on the right-hand side is precisely the expression for the scattered field, which therefore vanishes (Problem 14.11). This result confirms the *insensitivity* of the scattering pattern to the addition of multiples of $(\partial\phi_m/\partial n)$ to J_S.

14.6.3 The MFIE

This integral equation concerns an H-wave. From (14.1), because $\mathbf{E}$ must be perpendicular to C, the boundary condition on C is $(\partial H/\partial n) = 0$. The general relationship (14.97) now gives, for an exterior point $\mathbf{r}$,

$$H(\mathbf{r}) = H^i(\mathbf{r}) - \int_C H(\mathbf{r}')\frac{\partial G_0(\mathbf{r}|\mathbf{r}')}{\partial n'}\,dc' = H^i(\mathbf{r}) + \int_C J_S(\mathbf{r}')\frac{\partial G_0(\mathbf{r}|\mathbf{r}')}{\partial n'}\,dc', \quad (14.106)$$

where the tangential surface current is given by

$$\mathbf{J}_S = \mathbf{u}_n \times (H\,\mathbf{u}_z) = -H\,\mathbf{u}_c. \quad (14.107)$$

The sought MFIE is obtained by letting P_2 approach P_0 in Figure 14.9*b*. The contribution of the small segment $MP_0N = C_\delta$ should be investigated carefully, because the singularity resides there. From the small argument approximation (14.14) of the Green's function:

$$\begin{aligned}\frac{\partial G_0(\mathbf{r}|\mathbf{r}')}{\partial n'} &= \mathbf{u}_n' \cdot \operatorname{grad}' G_0(\mathbf{r}|\mathbf{r}') \;=\; \mathbf{u}_n' \cdot \operatorname{grad}' \left(\frac{1}{2\pi}\log_e k_0|\mathbf{r}-\mathbf{r}'|\right)\\ &= \frac{1}{2\pi|\mathbf{r}-\mathbf{r}'|}\operatorname{grad}'(|\mathbf{r}-\mathbf{r}'|)\cdot\mathbf{u}_n'. \end{aligned} \quad (14.108)$$

Reference to Figure 14.9*b* shows that

$$\begin{aligned}\operatorname{grad}'|\mathbf{r}-\mathbf{r}'| &= \operatorname{grad}' D \;=\; \mathbf{u}'\\ \mathbf{u}_n \cdot \operatorname{grad}'|\mathbf{r}-\mathbf{r}'| &= -\cos\theta\\ dc' &= \frac{1}{\cos\theta}\,D\,d\theta. \end{aligned} \quad (14.109)$$

This gives

$$\int_{C_\delta}\frac{\partial G_0(\mathbf{r}|\mathbf{r}')}{\partial n'}\,dc' = -\frac{1}{2\pi}\int_M^N d\theta = -\frac{1}{2\pi}(\theta_N - \theta_M). \quad (14.110)$$

In the limit $P_2 \to P_0$, the angle $(\theta_N - \theta_M)$ approaches π, hence

$$\lim_{\substack{\delta\to 0\\ P_2\to P_0}} \int_{C_\delta}\frac{\partial G_0(\mathbf{r}|\mathbf{r}')}{\partial n'}\,dc' = -\frac{1}{2}, \quad (14.111)$$

where $\mathbf{r}$ is on the positive side of n. Similarly,

$$\lim_{\substack{\delta\to 0\\ P_2\to P_0}} \int_{C_\delta}\frac{\partial G_0(\mathbf{r}|\mathbf{r}')}{\partial n}\,dc' = \frac{1}{2}. \quad (14.112)$$

For the approach $P_1 \to P_0$, with P_1 on the negative side of n, the second members should be changed to respectively $\left(\frac{1}{2}\right)$ and $\left(-\frac{1}{2}\right)$. If J_S may be assumed constant over C_δ, (14.99) and (14.107) give rise to an *integral equation of the second kind (the MFIE)*:

$$\frac{1}{2}J_S(\mathbf{r}) + \lim_{\delta\to 0}\int_{C-C_\delta} J_S(\mathbf{r}')\frac{\partial G_0(\mathbf{r}|\mathbf{r}')}{\partial n'}\,dc' = -H^i(\mathbf{r}). \tag{14.113}$$

We note, for general use, the limits of the normal derivatives of the integral

$$\psi(\mathbf{r}) = \int_C f(\mathbf{r}')\,G_0(\mathbf{r}|\mathbf{r}')\,dc'. \tag{14.114}$$

From (14.112), these are (Fig. 14.9*a*)

$$\lim_{P_2\to P_0}\frac{\partial\psi}{\partial n} = \frac{1}{2}f(P_0) + \lim_{\delta\to 0}\int_{C-C_\delta} f(\mathbf{r}')\frac{\partial G_0(\mathbf{r}|\mathbf{r}')}{\partial n}\,dc' \tag{14.115}$$

$$\lim_{P_1\to P_0}\frac{\partial\psi}{\partial n} = -\frac{1}{2}f(P_0) + \lim_{\delta\to 0}\int_{C-C_\delta} f(\mathbf{r}')\frac{\partial G_0(\mathbf{r}|\mathbf{r}')}{\partial n}\,dc'. \tag{14.116}$$

These limits correspond with the three-dimensional versions given in (3.43) and (3.44).

The uniqueness of the solution of (14.113) is spoiled by interior resonances, just as in the three-dimensional case. The critical frequencies are $k = k_m$, the same as for the EFIE, but the solution of the homogeneous equation (14.113) is not the same as for the EFIE; that is, it is different from $(\partial\phi_m/\partial n)$. The corresponding current J_S *does* radiate, and a correct determination of the scattering pattern requires lifting the indeterminacy. This can be done by methods already mentioned in Section 12.2 (combined or augmented field integral equations, extended boundary conditions[33]).

14.6.4 Discretization

The discretization of both the EFIE and the MFIE leads to a matrix equation of the type

$$\overline{\overline{Z}}\cdot[\mathbf{J}_S] = -[\mathbf{E}^i]. \tag{14.117}$$

The basis functions could be pulse functions, equal to one in the cell and zero outside, and testing could be effected by point matching (i.e., by means of delta functions). In that case, the matrix elements for the EFIE are [203]

$$Z_{mn} = -\frac{\omega\mu_0}{4}\int_{cell\,n} H_0^{(2)}(k_0 R_{mn})\,dc', \tag{14.118}$$

with (Fig. 14.11*a*)

$$R_{mn} = \left\{\left[x_m - x_n(c')\right]^2 + \left[y_m - y_n(c')\right]^2\right\}^{\frac{1}{2}} = |\mathbf{r}_m - \mathbf{r}_n|.$$

The impedance Z_{mn} measures the influence of the point source n on the electric field at the observation point m. For $n \neq m$, the integrand in (14.118) is not singular, and the integral

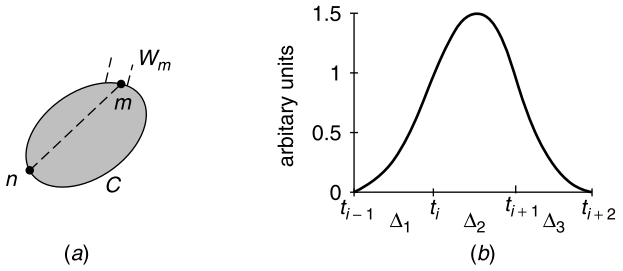

Figure 14.11 (*a*) Relevant for the definition of Z_{mn}. (*b*) The spline function.

can be evaluated accurately by simple numerical integration methods. The evaluation of the self-impedance Z_{mm} requires more care, because the Hankel function is singular in the range of integration. The distance R_{mn} is now the distance s between two points in the cell. To evaluate the integral, we assume that the subcontour of length w_m is approximated by a straight line, and that $k_0 s$ is small enough for the small argument approximation of the Hankel function, given in (A5.20), to be valid. This condition requires s to be sufficiently small with respect to λ_0. Assuming that this restriction is respected, we add the singular part of $H_0^{(2)}(k_0 s)$ to the integrand in (14.118) and subsequently subtract it from $H_0^{(2)}(k_0 s)$. Having thus isolated the basic singularity, its contribution to Z_{mm} can be expressed analytically,[§] leading to the following formula for Z_{mm}:

$$\begin{aligned} Z_{mm} &= -\frac{\omega\mu_0}{4} w_m \left[1 + j\frac{2}{\pi}\left(1 - \log_e \frac{\gamma k_0 w_m}{4}\right)\right] \\ &= -\frac{\omega\mu_0}{2} \int_0^{\frac{w_m}{2}} \left[H_0^{(2)}(k_0 s) - \left(1 - j\frac{2}{\pi}\log_e \frac{\gamma k_0 s}{2}\right)\right] ds, \end{aligned} \tag{14.119}$$

where γ is Euler's constant $0.5772\ldots$, and the distance s is measured from the center of the subcontour. The integrand in (14.119) is small and smooth, and the integration can be performed readily and accurately.

Splines have often been chosen as basis functions (Fig. 14.11*b*). Each spline function spans three segments and varies according to the formulas [75]

$$\begin{aligned} S_i(t) &= \frac{(t - t_{i-1})^2}{\Delta_1^2} && (t_{i-1} < t < t_i) \\ &= 1 + 2\frac{(t - t_i)}{\Delta_1} - \frac{(\Delta_1 + 2\Delta_2 + \Delta_3)(t - t_i)^2}{\Delta_1 \Delta_2 (\Delta_2 + \Delta_3)} && (t_i < t < t_{i+1}) \\ &= \frac{(\Delta_1 + \Delta_2)(t - t_{i+2})^2}{\Delta_1 \Delta_3 (\Delta_2 + \Delta_3)} && (t_{i+1} < t < t_{i+2}). \end{aligned} \tag{14.120}$$

An advantage of the spline is that its first derivative is a piecewise linear function. Note that the second derivative is represented by three pulses.

In the presence of edges, it is often advisable[34] — but not essential[35] — to choose basis functions that take the edge singularities into account.

[§]Result communicated by Prof. C. M. Butler (see Note 8 of Chapter 4).

14.6.5 Fast Methods

Discretization of the integral equations leads to large systems of linear equations and concomitant large, dense matrices. The equations are most often solved by iteration techniques, in which the matrix is repeatedly required to multiply recursively generated vectors (see Section 2.9). The wish to reduce the number of operations was soon recognized as a major challenge by numerical analysts, and several large groups of researchers are known to devote their energy to that important goal. The relevant literature on the topic is extensive, and we shall limit our ambition to an elementary presentation of one of the recent procedures, the *Fast multipole method*, abbreviated as FMM[¶] [192, 203].

The method was first applied to the two-dimensional Helmholtz equation, an equation that happens to be of particular interest for the current chapter.[37,38] Referring to (14.118), it is clear that a Z_{mn} element expresses how a segment m "communicates" with a segment n. The FMM's purpose is to expedite the $\overline{\overline{Z}} \cdot \mathbf{f}$ multiplications by dividing the N subscatterers into groups of M, for a total of N/M groups. Instead of a series of individual reactions of the type m to n, the method seeks to establish reactions from group to group. The procedure has been compared with the replacement of direct flight routes between N cities by a pattern of relaying hubs[39] [183] (Fig. 14.12). As in the *adaptive integral method* discussed in Section 12.4, the interactions between cells will be termed either *near-field* or *far-field*, and the impedance written accordingly as

$$\overline{\overline{Z}} = \overline{\overline{Z}}_{near} + \overline{\overline{Z}}_{far}. \tag{14.121}$$

When the m and n elements are close to each other, the value of Z_{mn} given in (14.118) should be used. It is for the far-distant elements that grouping becomes efficient. In Figure 14.13, two groups of segments are shown, G_m and G_n. Element i of G_m is under the influence of element j of G_n, which contributes a field

$$\Delta E^{sc}(\mathbf{r}_i) = -\frac{\omega\mu_0}{4} J_S(\mathbf{r}_j)\, H_0^{(2)}(k_0|\mathbf{r}_i - \mathbf{r}_j|)\, w_j, \tag{14.122}$$

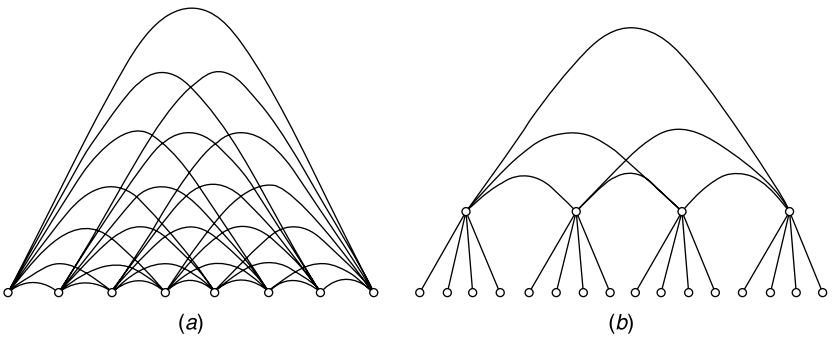

Figure 14.12 (a) Direct flight connections. (b) Two-level hub structure (from W. C. Chew, J. M. Jin, C. C. Lu, E. Michielssen, and J. M. Song, Fast solution methods in electromagnetics, *IEEE Trans. AP* **45**, 533–543, 1997, with permission of IEEE).

[¶]For a general presentation of the method, see Note 36.

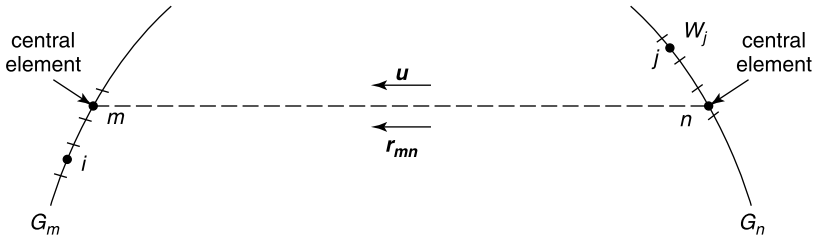

Figure 14.13 Interactions between groups of elements.

where w_j is the length of the segment of which j is the center. Let m and n refer to the central elements of the groups. We write

$$\mathbf{r}_i - \mathbf{r}_j = \underbrace{(\mathbf{r}_i - \mathbf{r}_m)}_{\Delta\mathbf{r}_i} + \underbrace{(\mathbf{r}_m - \mathbf{r}_n)}_{\mathbf{r}_{mn}} + \underbrace{(\mathbf{r}_n - \mathbf{r}_j)}_{-\Delta\mathbf{r}_j}.$$

In the far-away zone, $|\mathbf{r}_m - \mathbf{r}_n|$ is much larger than both $|\Delta\mathbf{r}_i|$ and $|\Delta\mathbf{r}_j|$. We may therefore write

$$|\mathbf{r}_i - \mathbf{r}_j| \approx r_{mn} + \mathbf{u}\cdot\Delta\mathbf{r}_i - \mathbf{u}\cdot\Delta\mathbf{r}_j,$$

where $\mathbf{u}$ is the unit vector in the direction from n to m. Summing over the (N/M) segments in G_n gives the total contribution in $\mathbf{r}_i$, which, using the large argument approximation of $H_0^{(2)}(x)$, becomes [203]

$$E^{sc}_{mn}(\mathbf{r}_i) = \underbrace{-\frac{\omega\mu_0}{4}H_0^{(2)}(k_0 r_{mn})}_{A_{mn}} \underbrace{e^{-jk_0\mathbf{u}\cdot\Delta\mathbf{r}_i}}_{B_m} \underbrace{\sum_{j=1}^{N/M} J_S(\mathbf{r}_j)\, w_j\, e^{jk_0\mathbf{u}\cdot\Delta\mathbf{r}_j}}_{C_n}. \tag{14.123}$$

This equation shows that the field in $\mathbf{r}_i$ is obtained by means of a simple summation and a single Hankel function calculation. The factor C_n *aggregates* the effects of the segments in G_n, the translation factor A_{mn} shifts the field from center to center, and the factor B_m redistributes the field from the center m to the individual subscatterers i (a process called *disaggregation*).

The actual application of the fast method requires the greatest ingenuity from the numerical analyst. Numerous improvements and modifications of the basic pattern discussed above have been introduced, for example by invoking the addition theorem (14.20), which expresses $H_0^{(2)}[k_0|\mathbf{r} - \mathbf{r}'|]$ (i.e., the field generated in $\mathbf{r}$ by a point source in $\mathbf{r}'$) in terms of functions of $\mathbf{r}$, vector distance from a reference origin [211]. In any case, the evaluation of the elements of $\overline{\overline{Z}}_{far}$ requires numerous computations of the Hankel function, which can sometimes be usefully represented by the complex integral[40,41]

$$H_0^{(2)}(k_0|\mathbf{r} - \mathbf{r}'|) = \frac{1}{\pi}\int_\Gamma d\alpha\, e^{-jk_0(\alpha)\cdot(\mathbf{r}-\mathbf{r}')}, \tag{14.124}$$

where $\mathbf{k}_0(\alpha) = k_0(\sin\alpha\mathbf{u}_x + \cos\alpha\mathbf{u}_y)$, and Γ is a suitably chosen steepest descent contour in the complex plane α.

The following additional comments may be useful:

1. $\overline{\overline{Z}}_{far}$ can be sparsified by choosing basis functions that radiate strongly in preferred directions, in the manner of a directive antenna. The interaction of the *emitter* group G_n with distant groups is therefore limited to a few *receiver* cells, whereby only a few Z_{mn} matrix elements should be retained, the remaining ones being negligible.[42]
2. The two-level approach in Figure 14.12*b* can be extended to *multiple* levels.[43,44,45]
3. The $\overline{\overline{Z}}$ matrix can be sparsified by means of a transformation based on multiplication with a matrix $\overline{\overline{A}}$, through which the original matrix equation (14.117) is transformed to[42,46,47]

$$\overline{\overline{T}} \cdot \mathbf{I} = -\mathbf{V}^i, \tag{14.125}$$

where

$$\overline{\overline{T}} = \overline{\overline{A}} \cdot \overline{\overline{Z}} \cdot \overline{\overline{A}}^t; \quad \mathbf{J}_S = \overline{\overline{A}}^t \cdot \mathbf{I}; \quad \mathbf{V}^i = \overline{\overline{A}} \cdot \mathbf{E}^i.$$

By proper choice of $\overline{\overline{A}}$, the important physical interactions within $\overline{\overline{T}}$ can be localized to a small number of groups of large matrix elements.

4. Special measures must be taken to apply the method to low frequencies, for which the argument of the Hankel function in the translation term A_{mn} in (14.123) becomes very small. This tendency, if not corrected, can lead to large numerical errors.[48,49]

14.7 SCATTERING BY PENETRABLE CYLINDERS

When the scatterer is penetrable, two cases should be considered: the homogeneous cylinder, for which contour integral equations can be formulated, and the inhomogeneous cylinder. When the inhomogeneity consists of homogeneous regions in contact with each other, as in a layered cylinder, a formulation in terms of contour integrals is still possible. For a more general inhomogeneity, however, the appropriate integral equations become two-dimensional, and the integrals extend over the whole cross section of the cylinder.[50]

14.7.1 Homogeneous Cylinders

From (14.97), the E field in the exterior region 2 can be given the integral representation (Fig. 14.14)

$$E_2(\mathbf{r}) = E^i(\mathbf{r}) + \int_C \left[G_0(\mathbf{r}|\mathbf{r}') \frac{\partial E_2}{\partial n'} - E_2(\mathbf{r}') \frac{\partial G_0(\mathbf{r}|\mathbf{r}')}{\partial n'} \right] dc'. \tag{14.126}$$

For points in S, analogously,

$$E_1(\mathbf{r}) = \int_C \left[E_1(\mathbf{r}') \frac{\partial G_1(\mathbf{r}|\mathbf{r}')}{\partial n'} - G_1(\mathbf{r}|\mathbf{r}') \frac{\partial E_1}{\partial n'} \right] dc', \tag{14.127}$$

where

$$G_1(\mathbf{r}|\mathbf{r}') = \frac{j}{4} H_0^{(2)}(k_1|\mathbf{r} - \mathbf{r}'|). \tag{14.128}$$

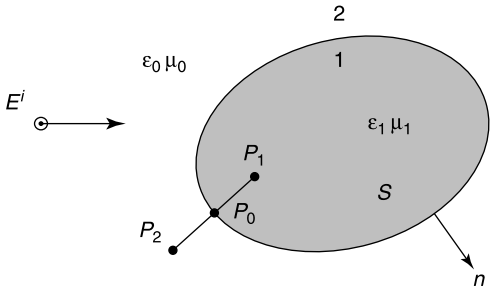

Figure 14.14 Penetrable cylinder in an incident wave.

Let $\mathbf{r}$ approach C from outside (i.e., let $P_2 \to P_0$). On the basis of (14.111), which expresses the contribution of the singularity of $\dfrac{\partial G_0}{\partial n'}$, (14.126) generates the limit form

$$\frac{1}{2}E_2(\mathbf{r}) + \lim_{\delta\to 0}\int_{C-C_\delta}\left[E_2(\mathbf{r}')\frac{\partial G_0(\mathbf{r}|\mathbf{r}')}{\partial n'} - G_0(\mathbf{r}|\mathbf{r}')\frac{\partial E_2}{\partial n'}\right]dc' = E^i(\mathbf{r}). \tag{14.129}$$

For the approach $P_1 \to P$, the singularity contribution becomes

$$\lim_{\delta\to 0}\int_{C_\delta}\frac{\partial G_0(\mathbf{r}|\mathbf{r}')}{\partial n'}dc' = \frac{1}{2}, \tag{14.130}$$

where n' is directed as in Figure 14.14. The limit form is now

$$\frac{1}{2}E_1(\mathbf{r}) - \lim_{\delta\to 0}\int_{C-C_\delta}\left[E_1(\mathbf{r}')\frac{\partial G_1(\mathbf{r}|\mathbf{r}')}{\partial n'} - G_1(\mathbf{r}|\mathbf{r}')\frac{\partial E_1}{\partial n'}\right]dc' = 0. \tag{14.131}$$

If we choose E_2 and $\dfrac{\partial E_2}{\partial n}$ on C as the main unknowns, E_1 and $\dfrac{\partial E_1}{\partial n}$ can be eliminated from (14.129) and (14.131) by means of the boundary conditions

$$\begin{aligned} E_1 &= E_2 \\ \frac{1}{\mu_1}\frac{\partial E_1}{\partial n} = \frac{1}{\mu_0}\frac{\partial E_2}{\partial n} &= j\omega(\mathbf{u}_c\cdot\mathbf{H}), \end{aligned} \tag{14.132}$$

where the second condition expresses continuity of $\mu_r^{-1}\dfrac{\partial E}{\partial n}$. The problem is now reduced to the solution of a pair of integral equations with two unknowns.

In an incident *H-wave*, relationships (14.129) and (14.131) remain valid, provided E and $\dfrac{\partial E}{\partial n}$ are replaced by H and $\dfrac{\partial H}{\partial n}$. The boundary conditions now require continuity of H and $\epsilon_r^{-1}\dfrac{\partial H}{\partial n}$. For a lossy medium:

$$\epsilon_{r1} = \frac{\sigma_1 + j\omega\epsilon_1}{j\omega\epsilon_0}.$$

For a nonmagnectic good conductor, one may write $\epsilon_{r1} = (\sigma_1/j\omega\epsilon_0)$ and $k_1 = (1+j)/\delta_1$.

14.7.2 Inhomogeneous Cylinders

The inhomogeneity may be in the form of a series of homogeneous layers.[51] For such a case, integral equations of types (14.129) and (14.131) can be written at the boundaries of each individual layer, with unknowns E and $\dfrac{\partial E}{\partial n}$ (or H and $\dfrac{\partial H}{\partial n}$) at each boundary surface. These unknowns are common to two layers and must satisfy boundary conditions such as (14.132). The result is a chain of connected integral equations.

For a more general variation of $\epsilon_r(\mathbf{r})$ and $\mu_r(\mathbf{r})$ — both possibly complex — integral equations of the type already discussed in Section 12.5 can readily be formulated. If we assume the scatterer to be nonmagnetic, for simplicity, the currents in an E-wave are polarization currents $J^{pol} = j\omega(\epsilon - \epsilon_0)E$. It follows, from (14.5) and (14.15), that [212]

$$E(\mathbf{r}) = E^i(\mathbf{r}) + j\omega\mu_0 \int_S j\omega\,(\epsilon - \epsilon_0)E(\mathbf{r}')\,G_0(\mathbf{r}|\mathbf{r}')\,dS'. \tag{14.133}$$

By setting $\mathbf{r}$ in the cross section, we obtain a two-dimensional integral equation[52]

$$E(\mathbf{r}) + \frac{jk_0^2}{4}\int_S \chi_e(\mathbf{r}')\,E(\mathbf{r}')\,H_0^{(2)}(k_0|\mathbf{r} - \mathbf{r}'|)\,dS' = E^i(\mathbf{r}), \tag{14.134}$$

where $\chi_e(\mathbf{r})$ is the contrast function $\chi_e(\mathbf{r}) = \epsilon_r(\mathbf{r}) - 1$ (i.e., the susceptibility of the material).

In an H-wave, the polarization current is transverse, and the field $\mathbf{E}^d$ generated by that current is

$$\mathbf{E}^d = \frac{\mathbf{J}^{pol}}{j\omega(\epsilon - \epsilon_0)} - \mathbf{E}^i. \tag{14.135}$$

It can also be expressed in terms of potentials as

$$\begin{aligned}\mathbf{E}^d(\mathbf{r}) &= -\text{grad}\,\phi - j\omega\mathbf{A}\\ &= \frac{j}{4\epsilon_0}\,\text{grad}\int_S P^{pol}(\mathbf{r}')H_0^{(2)}(k_0|\mathbf{r} - \mathbf{r}'|)\,dS'\\ &\quad - \frac{\omega\mu_0}{4}\int_S \mathbf{J}^{pol}(\mathbf{r}')H_0^{(2)}(k_0|\mathbf{r} - \mathbf{r}'|)\,dS',\end{aligned} \tag{14.136}$$

where

$$P^{pol}(\mathbf{r}) = -\frac{1}{j\omega}\,\text{div}\,\mathbf{J}^{pol}(\mathbf{r}). \tag{14.137}$$

Equating the values of $\mathbf{E}^d$ in (14.135) and (14.136) leads to an integro-differential equation for $\mathbf{J}^{pol}$.

When the cylinder has both dielectric *and* magnetic properties, electric and magnetic polarization currents should be taken into account. It is also possible to formulate the problem in terms of a *single* unknown field component, which must then satisfy an equation containing both a surface integral *and* a contour integral.[53] The numerical solution of the integral equations proceeds by the usual discretization techniques. In certain applications, high resolution may be needed, in particular in the medical field, and more specifically in RF dosimetry or in the determination of specific absorption rates. For such cases the cross

section must be subdivided into a large number of cells with, as a result, a large number of equations. Such large systems are typically solved by iteration techniques, or by the use of *fast Fourier transforms*.[54,55] It is often numerically advantageous to abandon integral equations[56] and to switch to the FDTD approach discussed in Section 12.8. For electrically large cylinders, a spatial decomposition technique has been proposed, in which the cylinder is subdivided into a multiplicity of subzones.[57,58]

14.7.3 Transient Scattering

To derive the time-dependent integral equation for an E-wave one may start from the potential representation [110]

$$\mathbf{e}^{sc}(\mathbf{r},t) = -\frac{\partial \mathbf{a}(\mathbf{r},t)}{\partial t} - \text{grad}\ \phi(\mathbf{r},t) \tag{14.138}$$

If the cylinder is perfectly conducting, axial currents are induced on its surface, hence $\mathbf{a}$ will be z-directed. Because ϕ is independent of z, grad ϕ has only transverse components and we may write, for $\mathbf{r}$ on C,

$$e_z^{sc}(\mathbf{r},t) = -\frac{\partial a_z(\mathbf{r},t)}{\partial t} = -e_z^i(\mathbf{r},t). \tag{14.139}$$

If all sources are inactive up to $t = 0$, $a_z(\mathbf{r},t)$ must satisfy

$$a_z(\mathbf{r},t) = \int_0^t e_z^i(\mathbf{r},t')\,dt'. \tag{14.140}$$

When the cylinder is a dielectric, the constitutive equation takes the form

$$j_z(\mathbf{r},t) = \frac{\partial}{\partial t}\left[\epsilon(\mathbf{r},t)\,e_z(\mathbf{r},t)\right] = \epsilon_0\frac{\partial e_z(\mathbf{r},t)}{\partial t} + \epsilon_0\frac{\partial}{\partial t}\left[\chi_e(\mathbf{r},t)\,e_z(\mathbf{r},t)\right]. \tag{14.141}$$

where e_z is the total field $e_z^{sc} + e_z^i$. The term in $\chi_e(\mathbf{r},t)$ may be looked upon as an applied current, to be inserted into the wave equation (14.5). This gives[59]

$$\nabla^2 e_z^{sc} - \frac{1}{c_0^2}\frac{\partial^2 e_z^{sc}}{\partial t^2} = \frac{1}{c_0^2}\frac{\partial^2}{\partial t^2}\left[\chi_e(\mathbf{r},t)\,e_z(\mathbf{r},t)\right] = \mu_0\frac{\partial^2 m_e}{\partial t^2}. \tag{14.142}$$

With the help of the Green's function for the two-dimensional wave equation, namely [165]

$$G(\mathbf{r},t|\mathbf{r}',t') = -\frac{1}{2\pi}\frac{H\left(t-t'-\dfrac{|\mathbf{r}-\mathbf{r}'|}{c_0}\right)}{\left[(t-t')^2 - \dfrac{|\mathbf{r}-\mathbf{r}'|^2}{c_0^2}\right]^{\frac{1}{2}}}, \tag{14.143}$$

the electric field may be written as

$$e_z(\mathbf{r},t) = e^i(\mathbf{r},t) + \mu_0\int_{plane} dS' \int G(|\mathbf{r}-\mathbf{r}'|, t-t')\frac{\partial^2 m_e(\mathbf{r}',t')}{\partial t'^2}\,dt', \tag{14.144}$$

which is an integral equation[‖] for $e_z(\mathbf{r}, t)$, once the constitutive equation $m_e(e)$ is inserted into the integrand.[59]

In the application of finite methods (FDTD or FEM) to a *good conductor*, the net size h must be much less than δ. This requirement may lead to an uneconomically dense mesh when the frequency increases (and δ therefore decreases). In certain portions of the boundary region, it may be permissible to apply a surface impedance condition.[64] This simplification is not acceptable, however, when the rapid decay of the fields near the boundary must be modeled correctly, for example when the power losses must be determined accurately. A possible remedy is to use δ-dependent shape functions in the current-carrying region.[65] The rapid field variations near edges pose similar problems. To solve them, one may turn to singular elements that incorporate the edge behavior.[66]

14.7.4 Fictitious Sources: The Generalized Multipole Technique

The main features of the method are discussed in Section 5.7 [187]. In short,[**] the field scattered by a perfectly conducting cylinder S is approximated by a sum[68] (Fig. 14.15)

$$E^{sc}(\mathbf{r}) = \sum_{n=1}^{N} I_n E_n(\mathbf{r}|\mathbf{r}_n). \tag{14.145}$$

The symbol $E_n(\mathbf{r}|\mathbf{r}_n)$ denotes the field in $\mathbf{r}$ generated by a *fictitious source* located at an interior point $\mathbf{r}_n$. This field automatically satisfies the homogeneous Helmholtz equation outside the cylinder. The source itself could be a linear current, with exterior field given by (14.16), or one of the combinations shown in Figure 14.1. More generally, one often uses higher-order multipoles, which radiate fields of the general form[69]

$$E_n(\mathbf{r}|\mathbf{r}_n) = H_p^{(2)}(k_0|\mathbf{r} - \mathbf{r}_n|)\, e^{\pm jp(\varphi - \varphi_n)}. \tag{14.146}$$

The complex amplitudes I_n must now be adjusted to enforce the boundary condition $E^{sc}(\mathbf{r}) + E^{i}(\mathbf{r}) = 0$ at M points on contour C. If $M = N$, one obtains just enough equations to determine the N amplitudes I_n. The resulting system of equations can be written as $\overline{\overline{Z}} \cdot \mathbf{I} = \mathbf{V}$, where Z_{mn} represents the field created at point m by a fictitious source in $\mathbf{r}_n$. These matrix elements are easy to evaluate because no integrations are involved. The method is beautifully simple, but as in many other attractive numerical techniques, great care should be exercised in its application. It is clear, for example, that while the boundary condition is enforced at M points, the behavior of the field between these points is not tested. Singularities may be missed, typically in the form of edges. To remedy the situation, a better exploration of the singular region by means of subsectional rectangular pulses, as in Figure 5.25, may be appropriate.[70,71] The position of the sources with respect to contour C is also delicate. If sources $\mathbf{r}_n$ and $\mathbf{r}_{n+1}$ are close to each other, and far from C, the resulting incident fields at neighboring test points m and $m + 1$ will be very similar, and the resulting equations will also be similar. This is a source of numerical instability. To enforce stability, it is common practice to choose $M > N$ and to solve the resulting overdetermined system of equations by applying the boundary condition in a *least squares* sense.

[‖]The solution of integral equations by marching-on-in-time methods is discussed in Notes 60, 61, 62, 63.

[**]For a general survey of the method, see Note 67.

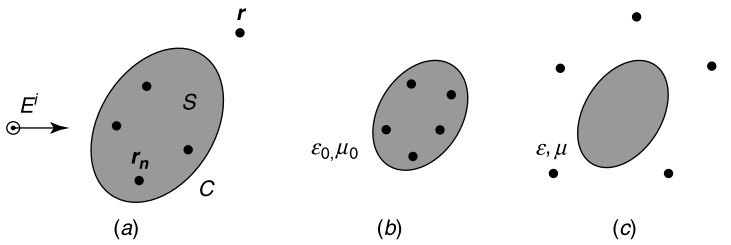

Figure 14.15 (*a*) Fictitious currents for a perfectly conducting scatterer. (*b*) Interior fictitious sources for a penetrable scatterer. (*c*) Exterior fictitious sources for a penetrable scatterer.

The $\overline{\overline{Z}}$ matrix of the method is dense but can be sparsified by choosing directive sources, which irradiate only a few test points. These sources could be arrays, synthesized either by grouping a number of isotropic sources or by shifting a point source (or a multipole) to complex space. As shown in Section 8.4, such sources produce in real space beam-type fields that are nearly Gaussian.[72,73,74] It is also possible to group the (isotropic) point-receptors to form testing arrays with directional receiving patterns, further increasing the sparseness of the matrix. This improvement is equivalent to a mathematical transformation of the original $\overline{\overline{Z}}$ matrix.[75]

The fictitious-sources method can be further applied to three-dimensional problems[67] and to scatterers endowed with a surface impedance.[76] In the case of a penetrable homogeneous cylinder, currents should be inserted both inside and outside the cylinder[77,78] (Fig. 14.15, *b* and *c*). The *interior* sources radiate into the exterior region, the pattern being expressed in terms of Hankel functions containing the wave number k_0, as in (14.146). The *exterior* currents radiate into the cylinder, with patterns relative to an unbounded space filled with the material of the cylinder. The wave number is now k. The two systems are connected by the need to respect continuity of the tangential components of **E** and **H** on C. The method, which has the advantage of using only free-space Green's functions, can be extended to inhomogeneous cylinders consisting of a succession of shells, a suitable model for some biological structures and some types of electric cables.[79]

14.8 LOW-FREQUENCY SCATTERING BY CYLINDERS

In an *E-wave*, both polarization and conduction currents are z-directed. From (14.13) and (14.15), these currents generate a far field

$$\lim_{r\to\infty} E^{sc} = -\frac{\omega\mu_0}{4}\sqrt{\frac{2j}{\pi}}\frac{e^{-jk_0r}}{\sqrt{k_0r}}\int_S J(\mathbf{r}')\, e^{jk_0\mathbf{u}\,\cdot\,\mathbf{r}'}\,dS'. \tag{14.147}$$

If the source is small with respect to λ_0, an expansion of the exponential in terms of powers of jk_0 gives

$$\lim_{r\to\infty} E^{sc} = -\omega\mu_0\sqrt{\frac{j}{8\pi}}\frac{e^{-jk_0r}}{\sqrt{k_0r}}\left[\int_S J(\mathbf{r}')\,dS' + jk_0\mathbf{u}\cdot\int_S J(\mathbf{r}')\mathbf{r}'\,dS' + \cdots\right]. \tag{14.148}$$

This expression can serve as a basis for a *two-dimensional multipole expansion*. The first term, for example, represents the omnidirectional (or monopole) radiation of a line source

of net current $\int_S J\,dS$ (Problem 14.13). The next terms generate various types of multipole fields. Similar considerations hold for an *H-wave*, with J replaced by J_m. The basic equation is now (14.8), and in the absence of J_m the leading term in the multipole expansion stems from $\text{div}_{xy}(\mathbf{u}_z \times \mathbf{J}_t)$. This term radiates like a magnetic monopole of strength

$$\int_S \text{div}_{xy}(\mathbf{u}_z \times \mathbf{J}_t)\,dS = \int_C \mathbf{u}_n \cdot (\mathbf{u}_z \times \mathbf{J}_t)\,dc = \int_C (\mathbf{u}_c \cdot \mathbf{J}_t)\,dc. \tag{14.149}$$

The radiation may therefore be attributed to a loop of electric current. This result is in agreement with the current equivalence principle discussed in Section 7.12. Corresponding with (7.211) and (7.213), the *equivalences* are now

$$J_z = -\frac{1}{j\omega\mu_0}\,\text{div}_{xy}\,(\mathbf{u}_z \times \mathbf{J}_{mt}) \tag{14.150}$$

$$J_{mz} = \frac{1}{j\omega\epsilon_0}\,\text{div}_{xy}\,(\mathbf{u}_z \times \mathbf{J}_t). \tag{14.151}$$

The divergence operator must be interpreted in terms of distributions. Relationship (A8.90), for example, should be applied when the transverse currents have a component perpendicular to contour C.

The previous results were obtained by assuming that the currents are known. A method to determine these currents is discussed next.

14.8.1 E-wave Scattering

When the cylinder is *perfectly conducting*, the low-frequency version of integral equation (14.101) is obtained by inserting the small argument value (14.14) of $G_0(\mathbf{r}|\mathbf{r}')$ into the integrand. This gives

$$\frac{\omega\mu_0}{4}\int_C J_S(\mathbf{r}')\left[1 + j\frac{2}{\pi}\log_e\frac{2}{k_0|\mathbf{r}-\mathbf{r}'|} + \cdots\right]dc' = E^i(\mathbf{r}). \tag{14.152}$$

In the limit $k_0 \to 0$, the term in $\log_e k_0|\mathbf{r}-\mathbf{r}'|$ becomes dominant, and one may write

$$\frac{1}{2\pi}\int_C J_S(\mathbf{r}')\log_e\frac{1}{k_0|\mathbf{r}-\mathbf{r}'|}dc' = -j\frac{E^i}{\omega\mu_0} + BI, \tag{14.153}$$

where I is the total current $\int_C J_S\,dc$ and B an easily derived coefficient, independent of $\mathbf{r}$. In the zero-order approximation, E^i should be replaced by E_0^i in the right-hand term of (14.153), yielding

$$\frac{1}{2\pi}\int_C J_S(\mathbf{r}')\log_e\frac{1}{k_0|\mathbf{r}-\mathbf{r}'|}\,dc' = -j\frac{E_0^i}{\omega\mu_0} + BI. \tag{14.154}$$

If L is a reference length of the cross section (e.g., the longest chord), (14.154) may be rewritten as

$$\frac{1}{2\pi}\int_C J_S(\mathbf{r}')\log_e\frac{L}{|\mathbf{r}-\mathbf{r}'|}\frac{dc'}{L} = -j\frac{E_0^i}{k_0R_{c0}L} - \frac{I}{2\pi L}\log_e\left(\frac{1}{k_0L}\right) + \frac{BI}{L}. \tag{14.155}$$

In many problems — in particular when the incident wave is plane — E_0^i is uniform over S, and in that case we note that (14.155) is precisely of the form (5.49), hence that J_S is proportional to the static charge density ρ_S that appears on the surface of the charged cylinder. Setting $J_S(c) = Af(c)$, and inserting this value into (14.155), gives the value of A and leads to[80]

$$J_S(c) \approx -j \frac{2\pi}{k_0 L \log_e \left(\dfrac{1}{k_0 L}\right)} \frac{f(c)}{f_{\text{ave}}} \frac{E_0^i}{R_{c0}} = \frac{I}{L} \frac{f(c)}{f_{\text{ave}}}. \tag{14.156}$$

To zero-order the scattering pattern is omnidirectional, with a far field given by

$$\lim_{r \to \infty} E^{sc} = \sqrt{\frac{\pi}{2j}} \frac{1}{\log_e (k_0 L)} \frac{e^{-jk_0 r}}{\sqrt{k_0 r}} E_0^i \tag{14.157}$$

and a *cross section*

$$\sigma^{sc} = \frac{\pi^2}{k_0 (\log_e k_0 L)^2}. \tag{14.158}$$

This value is not very sensitive to the choice of L, because $\lim_{k \to 0} \log_e (\alpha\, kL) \approx \log_e kL$ when α is a positive constant. *For a circular cylinder*, (14.45) gives the exact limit

$$\sigma^{sc} = \frac{\pi^2}{k_0 (\log_e k_0 a)^2}.$$

The best value of L for that particular case is clearly the radius. For a strip extending from $(-c)$ to $(+c)$, integral equation (14.154) becomes

$$\int_{-1}^{+1} J_S(X') \log_e k_0 c\, |X - X'|\, dX' = j \frac{2\pi E_0^i}{k_0 c\, R_{c0}}, \tag{14.159}$$

where $X = (x/c)$. On the basis of the value (5.51) for ρ_S, and using formulas (A5.193) and (A5.194), the *current density* is found to be

$$J_S\left(\frac{x}{c}\right) = j \frac{2E_0^i}{R_{c0}\, k_0 c \log_e \dfrac{k_0 c}{2}} \frac{1}{\sqrt{1 - \dfrac{x^2}{c^2}}}, \tag{14.160}$$

from which it may be deduced that

$$\sigma^{sc} = \frac{\pi^2}{k_0 \left(\log_e \dfrac{k_0 c}{2}\right)^2}. \tag{14.161}$$

The best value of L is now $(c/2)$. For some other shapes, this value (sometimes called the *equivalent radius*[81]) is shown graphically in Figure 14.16.

Expressions such as (14.158) evidence the importance of the parameter $\log_e k_0 L$. It should be noted, in that context, that E and J_S do not in general admit a convergent expansion in powers of k_0, as assumed in the three-dimensional Stevenson method.

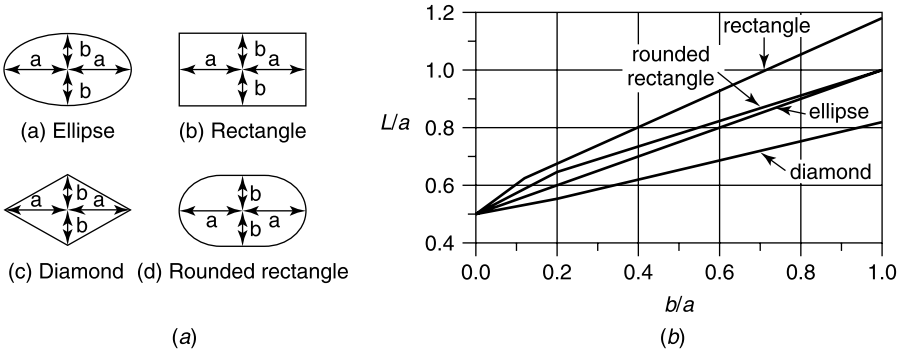

Figure 14.16 (*a*) Cross sections of cylinders. (*b*) Equivalent radius, normalized to half main axis (from R. De Smedt, Low-frequency illumination by an *E*-wave of infinitely long, parallel, perfect conductors, *URSI Radio Sci. Bull.* **305**, 23–31, Sept. 2003, with permission of URSI).

Fundamentally, this is because $H_0^{(2)}(z)$ has a branch point at $z = 0$, while the three-dimensional Green's function is analytic in $(k_0 R)$. To take that remark into account, integral equation (14.152) was derived by inserting the low frequency value of $G_0(\mathbf{r}|\mathbf{r}')$ into the integrand of (14.100), and *not* by expanding J_S in powers of jk_0.

The low-frequency scattering cross section of a homogeneous *dielectric* cylinder immersed in an *E*-wave can be evaluated by replacing the dielectric cylinder with its (equivalent) polarization currents. Inserting these currents into (14.148) yields a dominant term

$$\lim_{r\to\infty} E^{sc} = \frac{k_0^2}{\sqrt{8\pi}}\, e^{-j\frac{\pi}{4}}\, \frac{e^{-jk_0 r}}{\sqrt{k_0 r}} (\epsilon_r - 1) \int_S E(\mathbf{r})\, dS. \tag{14.162}$$

We note that a uniform (static) field $\mathbf{e}_0$ is not disturbed when an infinite dielectric cylinder is introduced parallel to the direction of the field. The reason is simple: $\mathbf{e}_0$ satisfies the boundary conditions on its own, and an additional field is not needed. This property implies that $E_z(\mathbf{r})$ approaches $E_z^i(\mathbf{r})$ as k_0 approaches zero. In consequence,

$$\lim_{r\to\infty} E^{sc} = \frac{k_0^2}{\sqrt{8\pi}}\, e^{-j\frac{\pi}{4}}\, S(\epsilon_r - 1) \frac{e^{-jk_0 r}}{\sqrt{k_0 r}}\, E_0^i \tag{14.163}$$

and

$$\sigma^{sc} = (\epsilon_r - 1)^2 \frac{k_0^3 S^2}{4} \tag{14.164}$$

where S is the cross-sectional area of the cylinder. When higher-order terms in k_0 are taken into account, the omnidirectional scattering pattern is disturbed, and a ripple appears. In the expression (14.148), for the far-field, this effect is associated with the term $\mathbf{u} \cdot \int_S J\mathbf{r}\, dS$, which generates a dipole type of radiation. There results an improved value of σ^{sc}, viz.[82]

$$\sigma^{sc} = (\epsilon_r - 1)^2 \frac{k_0^3 S^2}{4} \left[1 + \frac{k_0^2 S}{\pi} (\epsilon_r - 1) \log_e \frac{1}{k_0 \sqrt{S}} + \cdots \right]. \tag{14.165}$$

The two leading terms are shape-insensitive and depend only on the bulk of the obstacle. This improved approximation can serve to effect a smooth transition from the Rayleigh region to the resonance region.

14.8.2 H-wave Scattering

Consider first a *perfectly conducting* cylinder. The contour current J_S may be determined[83] from the MFIE (14.113), in which $\dfrac{\partial G_0}{\partial n'}$ should be replaced by its small-argument value.[82] If one is particularly interested in the scattered field, the basic equation is (14.95), and the field in a direction $\mathbf{u}$ takes the form

$$\lim_{r\to\infty} H^{sc}(\mathbf{r}) = j\sqrt{\frac{j}{8\pi}}\,\frac{e^{-jk_0 r}}{\sqrt{k_0 r}}\int_C e^{jk_0\mathbf{u}\,\cdot\,\mathbf{r}'}\left(\frac{\partial H^{sc}}{\partial n'} - jk_0\,H^{sc}\,\mathbf{u}\,\cdot\,\mathbf{u}_{n'}\right)dc'.$$

The detailed calculations, which are fairly long, lead to the simple result[80] [22]

$$\lim_{r\to\infty} H^{sc} = j\sqrt{\frac{j}{8\pi}}k_0^2\frac{e^{-jk_0 r}}{\sqrt{k_0 r}}\left[H_0^i S + c_0\mathbf{u}\cdot(\mathbf{u}_z\times\mathbf{P}_e)\right], \tag{14.166}$$

where

$$\mathbf{P}_e = \int_C P_S(\mathbf{r})\,\mathbf{r}\,dc$$

is the dipole moment of the static charges induced on the cylinder by the static field $\mathbf{E}_0^i$. The first term, $H^i S$, represents the omnidirectional pattern of a magnetic line current $I_m = -j\omega\mu_0 H_0^i S$. The second term represents a dipole type of radiation. Because there is power orthogonality in the multipole expansion, the total scattered power is the sum of the two partial powers, hence

$$\sigma^{sc} = \frac{1}{4}k_0^3\left(S^2 + \frac{c_0^2|\mathbf{P}_e|^2}{2|H^i|^2}\right). \tag{14.167}$$

For a circular cylinder:

$$\mathbf{P}_e = 2\pi a^2\epsilon_0\mathbf{E}^i = 2\pi a^2\frac{1}{c_0}H^i(\mathbf{u}_z\times\mathbf{u}_i) \tag{14.168}$$

and

$$\sigma^{sc} = \frac{3}{4}\pi^2 a(k_0 a)^3. \tag{14.169}$$

This cross section is the value already obtained under (14.47).

The *scattering cross section* of a *homogeneous dielectric cylinder* in a plane H-wave is obtained from (14.167) by deleting the term in S^2 (which represents the contribution of the surface currents) and keeping the term in $|\mathbf{P}_e|^2$ (which for the dielectric represents the contribution of the polarization currents). Accordingly,

$$\begin{aligned}\sigma^{sc} &= \frac{1}{4}k_0^3\frac{c_0^2|\mathbf{P}_e|^2}{2|H^i|^2}\\ &= \frac{1}{8}k_0^3\left|\frac{\mathbf{P}_e}{\epsilon_0\mathbf{E}^i}\right|^2 = \frac{1}{8}k_0^3\left|\frac{\bar{\bar{\alpha}}_e\cdot\mathbf{E}^i}{\mathbf{E}^i}\right|^2.\end{aligned} \tag{14.170}$$

For a circular cylinder:

$$\bar{\bar{\alpha}}_e = 2\pi a^2\frac{\epsilon_r - 1}{\epsilon_r + 1}\bar{\bar{I}}_{xy}. \tag{14.171}$$

14.8.3 Deep Field Penetration

Electric currents frequently flow in the full volume of a conductor. This happens routinely at low frequencies, typically in the form of eddy currents in power devices. Full current occupancy can be a desirable feature, and power transmission cables, for example, are stranded to obtain practically uniform current density throughout the cross section, thus ensuring good utilization of the metal. Deep penetration also occurs at much higher frequencies (e.g., in the thin microstrips of a multilayered device). To understand the phenomenon in more detail, we shall develop a "small (L/δ)" approximation, and consider, as an example, a nonmagnetic, highly conducting cylinder immersed in an E field (Fig. 14.17). From (13.103),

$$k_0 L = 2\pi \frac{L}{\lambda_0} = \frac{L}{\delta}\sqrt{2Q} \ll 1. \tag{14.172}$$

Deep penetration therefore implies $L \ll \lambda_0$, which means that low-frequency techniques may be applied.[84] Accordingly, only two terms will be kept in the expansion $E^i = E_0^i + jk_0 E_1^i$. The cylinder creates a disturbance field E^d, which satisfies

$$\begin{aligned} \nabla^2 E^d + k_0^2 E^d &= j\omega\mu_0 J = \frac{2j}{\delta^2}(E^d + E^i) \qquad \text{(in } S\text{)} \\ \nabla^2 E^d + k_0^2 E^d &= 0 \qquad\qquad\qquad\qquad\quad \text{(outside } S\text{)}. \end{aligned} \tag{14.173}$$

Continuity of the tangential components of $\mathbf{E}$ and $\mathbf{H}$ requires, from (14.3), continuity of E and $\dfrac{\partial E}{\partial n}$ across C. Because E^i obviously satisfies these conditions, they must also hold for E^d. It follows that E^d approaches zero as $\delta \to \infty$, because the right-hand term of (14.173) vanishes in that limit. The main disturbance field must therefore satisfy

$$E(\mathbf{r}) = E^i(\mathbf{r}) + E^d(\mathbf{r}) = E^i(\mathbf{r}) - \frac{1}{2\delta^2}\int_S E^i(\mathbf{r}') H_0^{(2)}(k_0|\mathbf{r} - \mathbf{r}'|)\, dS'. \tag{14.174}$$

The cross section area S is of the order L^2 hence the disturbance term is proportional to $(L/\delta)^2$. From (14.174), it becomes easy to evaluate the *scattered* field, which is predominately omnidirectional. The *near* field (i.e., the field at distances much less than λ_0) is obtained by replacing, in (14.174), the Hankel function by its small argument limit (A5.20). Thus,

$$E^d(\mathbf{r}) = \frac{j}{\pi\delta^2}\int_S E^i(\mathbf{r}') \log_e(k_0|\mathbf{r} - \mathbf{r}'|)\, dS'. \tag{14.175}$$

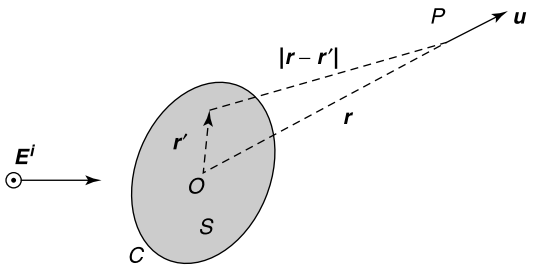

Figure 14.17 General cylinder in an incident field.

The dominant term in the current density is $J_S = \sigma E_0^i$. It follows that a field E_0^i parallel to the axis induces a net axial current $I = (\sigma S)\, E_0^i$ in the conductor.

The actual form of E^d for a circular cylinder can be obtained by separation of variables. The results confirm the previous arguments, because the dominant disturbance is[8]

$$\begin{aligned} \frac{E^d}{E_0^i} &= j\frac{a^2}{\delta^2}\log_e(k_0 a) - j\frac{a^2}{2\delta^2}\left(1 - \frac{r^2}{a^2}\right) \qquad (r < a) \\ \frac{E^d}{E_0^i} &= j\frac{a^2}{\delta^2}\log_e k_0 r \qquad\qquad\qquad\qquad (r > a). \end{aligned} \tag{14.176}$$

In an incident plane wave

$$E^i = E_0^i(1 - jk_0 r\cos\varphi + \cdots),$$

it is the term in $k_0 r$ that introduces the already mentioned ripple in the scattered field. This effect is represented by the first-order correction term

$$\begin{aligned} \frac{E_1^d}{E_0^i} &= \left(\frac{1}{4}\frac{k_0 r^3}{\delta^2} - \frac{1}{2}\frac{k_0 a^2 r}{\delta^2}\right)\cos\varphi \qquad (\mathbf{r} \text{ in } S) \\ \frac{E_1^d}{E_0^i} &= -\frac{1}{4}\frac{k_0 a^4}{r\delta^2}\cos\varphi \qquad\qquad\qquad (\mathbf{r} \text{ outside } S). \end{aligned} \tag{14.177}$$

A similar analysis can be developed for an incident H-wave.[84]

14.9 SLOTS IN A PLANAR SCREEN

The problem of the slot in a perfectly conducting screen is two-dimensional and therefore simpler to solve than its three-dimensional counterpart. There is, indeed, only one unknown, E_z or E_y, depending on whether the incident wave is of the E or the H type. These two polarizations will be considered in succession.

14.9.1 Penetration of an *E*-wave Through a Slot

The unknown is $E_z(y)$ in the slot AB (Fig. 14.18). This component vanishes on the other parts of the metallic screen S. The relevant Green's function $G_e(\mathbf{r}|\mathbf{r}')$ should vanish when $\mathbf{r}$ is on S. By means of images, its value in region 2 is easily found to be

$$G_{e2}(\mathbf{r}|\mathbf{r}') = G_2(\mathbf{r}|\mathbf{r}') - G_2(\mathbf{r}|\mathbf{r}_i') = \frac{j}{4}\left[H_0^{(2)}(k_2|\mathbf{r} - \mathbf{r}'|) - H_0^{(2)}(k_2|\mathbf{r} - \mathbf{r}_i'|)\right]. \tag{14.178}$$

Here G_2 denotes the Green's function for an infinite space filled with a homogeneous material of characteristics (ϵ_2, μ_2). By using Green's theorem (A1.31), combined with the radiation condition (14.10), E_z can be represented by the integral

$$E_z(\mathbf{r}) = -\int_A^B E_z(y')\frac{\partial G_{e2}(\mathbf{r}|\mathbf{r}')}{\partial x'}\, dy' \qquad (\mathbf{r} \text{ in } 2). \tag{14.179}$$

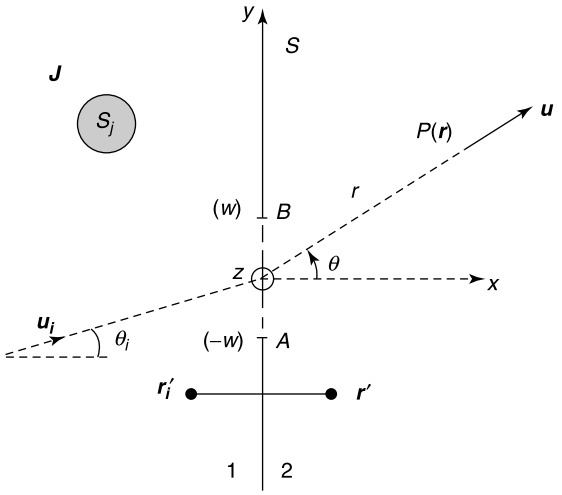

Figure 14.18 Slot in a perfectly conducting plane.

Because $\mathbf{r}'$ and $\mathbf{r}_i'$ coincide when $\mathbf{r}'$ is in the slot,

$$\frac{\partial G_{e2}(\mathbf{r}|\mathbf{r}')}{\partial x'} = 2\frac{\partial G_2(\mathbf{r}|\mathbf{r}')}{\partial x'},$$

which gives, for the field in half-space 2,

$$E_z(\mathbf{r}) = -2\int_A^B E_z(y')\frac{\partial G_2(\mathbf{r}|0,y')}{\partial x'}\,dy'. \tag{14.180}$$

In half-space 1, which contains the sources, one may similarly write

$$E_z(\mathbf{r}) = E_z^g(\mathbf{r}) + 2\int_A^B E_z(y')\frac{\partial G_1(\mathbf{r}|0,y')}{\partial x'}\,dy'. \tag{14.181}$$

In this equation, E_z^g is the *generator* field (i.e., the field that exists between A and B when the slot is short-circuited). It is given by

$$E_z^g(\mathbf{r}) = j\omega\mu_1\int_{S_j} J(\mathbf{r}')\,G_{e1}(\mathbf{r}|\mathbf{r}')\,dS'. \tag{14.182}$$

An integro-differential equation for E_z can now be derived by expressing continuity of the tangential component H_y across the slot. From (14.3), H_y is related to E_z by

$$H_y = \frac{1}{j\omega\mu_i}\frac{\partial E_z}{\partial x} \qquad (i = 1, 2). \tag{14.183}$$

For the sake of conciseness, we will now assume that the screen is located in free-space,[††] which means that $\epsilon_1 = \epsilon_2 = \epsilon_0$ and $\mu_1 = \mu_2 = \mu_0$. Requiring $\dfrac{\partial E_z}{\partial x}$ to be continuous in the

[††]The extension to different media is discussed in [119] and in Note 85.

slot leads to the relationship

$$\frac{\partial E_z^g}{\partial x} = 4\frac{\partial^2}{\partial x^2}\int_A^B E_z(y')\,G(0,y|0,y')\,dy'.$$

Because the integral is a solution of Helmholtz' equation, $\dfrac{\partial^2}{\partial x^2}$ may be replaced by $\left(-k_0^2 - \dfrac{\partial^2}{\partial y^2}\right)$. It follows that, for y in AB,

$$\left(\frac{d^2}{dy^2} + k_0^2\right)\int_A^B E_z(y')\,H_0^{(2)}(k_0|y-y'|)\,dy' = j\frac{\partial E_z^g}{\partial x} = -k_0 R_{c0} H_y^g(y). \tag{14.184}$$

This is the sought integro-differential equation for E. With respect to region 2, the equivalent magnetic current is $\mathbf{J}_{mS} = \mathbf{E} \times \mathbf{u}_n$, where $\mathbf{u}_n$ (here equal to $\mathbf{u}_x$) points toward 2; we may therefore write $\mathbf{J}_{mS} = E_z\,\mathbf{u}_y$. From (9.22), the generator field is equal to

$$H_y^g(y) = 2H_y^i(y). \tag{14.185}$$

A typical variation of the dimensionless ratio $(E_z/R_{c0}\,H_y^i)$ is shown in Figure 14.19, in which it is assumed that a plane wave is incident along the x-axis.

When the slot is narrow, the small argument form of $H_0^{(2)}(x)$ should be inserted into (14.184), which now takes the form

$$\left(\frac{d^2}{dy^2} + k_0^2\right)\int_A^B E_z(y')\log_e\frac{1}{k_0|y-y'|}\,dy' + k_0^2\log_e\frac{2}{\gamma}\int_A^B E_z(y')\,dy' = j\pi k_0\left[R_{c0}H_y^i(y)\right]. \tag{14.186}$$

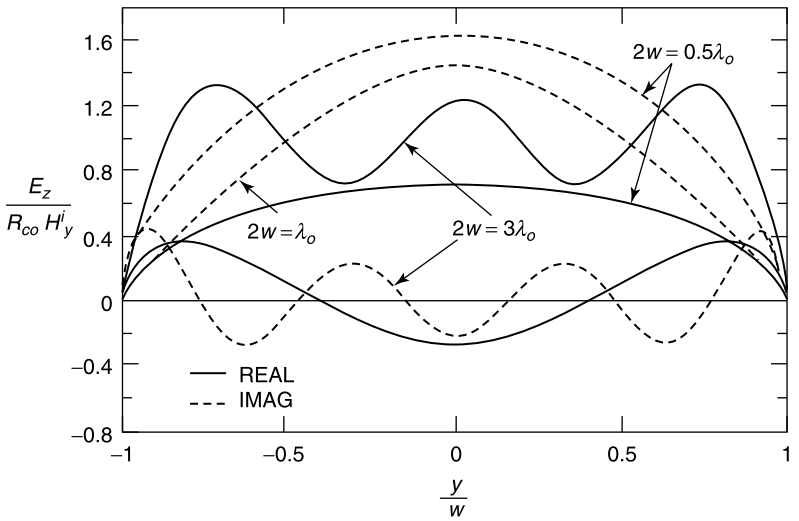

Figure 14.19 E in slots of various widths (from C. M. Butler and K. R. Umashankar, Electromagnetic penetration through an aperture in an infinite, planar screen separating two half spaces of different electromagnetic properties, *Radio Sci.* **11**, 611–619, 1976, with permission of the American Geographical Union).

In the solution of this equation [and of (14.184)] it is useful to remember that the edge condition requires E_z to be proportional to $\sqrt{w^2 - y^2}$ in the vicinity of $y = \pm w$. The condition suggests the use of basis functions of the form $\sqrt{w^2 - y^2} f(y)$, where the Chebyshev polynomials of the second kind $U_n(x)$ are an excellent choice for $f(y)$ given their favorable orthonormality properties (Problem 14.18). Useful integrals for U_0, U_1, and U_2, derived from (A5.197), are

$$\begin{aligned} \int_{-1}^{+1} \sqrt{1 - y^2}\, dy &= \frac{\pi}{2} \\ \int_{-1}^{+1} y^2 \sqrt{1 - y^2}\, dy &= \frac{\pi}{8} \\ \int_{-1}^{+1} y^4 \sqrt{1 - y^2}\, dy &= \frac{\pi}{16}. \end{aligned} \tag{14.187}$$

When the slot is narrow, the relevant reference equation becomes (A5.198).

14.9.2 Penetration of an *H*-wave Through a Slot

In an H-wave, the main unknown is E_y in the slot. Because

$$E_y = -\frac{1}{j\omega\epsilon} \frac{\partial H_z}{\partial x} \tag{14.188}$$

the boundary condition on the (unslotted) screen S is $\dfrac{\partial H_z}{\partial x} = 0$. The appropriate Green's function should satisfy the same boundary condition and is therefore

$$G_{m2}(\mathbf{r}|\mathbf{r}') = G_2(\mathbf{r}|\mathbf{r}') + G_2(\mathbf{r}|\mathbf{r}_i') = \frac{j}{4}\left[H_0^{(2)}(k_2|\mathbf{r} - \mathbf{r}'|) + H_0^{(2)}(k_2|\mathbf{r} - \mathbf{r}'|)\right]. \tag{14.189}$$

The relationship corresponding with (14.180) is now

$$H_z(\mathbf{r}) = \int_A^B G_{m2}(\mathbf{r}|\mathbf{r}') \frac{\partial H_z}{\partial x'}\, dy' = -2j\omega\epsilon_2 \int_A^B G_2(\mathbf{r}|\mathbf{r}')\, E_y(y')\, dy', \tag{14.190}$$

where $\mathbf{r}'$ is in the slot (Problem 14.16). In region 1, similarly,

$$H_z(\mathbf{r}) = H_z^g(\mathbf{r}) + 2j\omega\epsilon_1 \int_A^B G_1(\mathbf{r}|\mathbf{r}')\, E_y(y')\, dy'. \tag{14.191}$$

Enforcing continuity of H_z across the slot yields an integral equation for E_y. When $\epsilon_1 = \epsilon_2 = \epsilon_0$, this equation takes the form

$$\omega\epsilon_0 \int_A^B H_0^{(2)}(k_0|y - y'|)\, E_y(y')\, dy' = H_z^g(y) \tag{14.192}$$

for y in the slot. Note that the current density in the short-circuited aperture is $\mathbf{J}_S = H_z^g(y)\, \mathbf{u}_y = 2H_z^i(y)\, \mathbf{u}_y$, where $H_z^i(y)$ is the incident field in free space.

In the numerical solution of (14.192), it is useful to take the edge behavior of E_y into account and to select basis functions of the form

$$E_n(y) = \frac{f_n(y)}{\sqrt{w^2 - y^2}}, \tag{14.193}$$

where $f_n(y)$ is regular at $y = \pm w$. The function $f_n(y)$ can be usefully expanded in Chebyshev polynomials of the first kind, which are endowed with the orthogonality property (A5.192). The following relationships, derived from (A5.193), are helpful for the detailed computations:[86,87]

$$\begin{aligned}
&\int_{-1}^{1} \frac{1}{\sqrt{1-y'^2}} \log_e |y - y'|\, dy' = -\pi \log_e 2 \\
&\int_{-1}^{1} \frac{y'}{\sqrt{1-y'^2}} \log_e |y - y'|\, dy' = -\pi y \\
&\int_{-1}^{1} \frac{y'^2}{\sqrt{1-y'^2}} \log_e |y - y'|\, dy' = -\frac{\pi}{2}\left[y^2 - \frac{1}{2} + \log_e 2\right] \\
&\int_{-1}^{1} \frac{y'^3}{\sqrt{1-y'^2}} \log_e |y - y'|\, dy' = -\frac{\pi}{6}\left[2y^3 + 3y\right].
\end{aligned} \tag{14.194}$$

They are valid for y in the slot (i.e., for $-1 < y < 1$). It should be noted that, according to Babinet's principle, the solution for the slot automatically generates the solution for the dual problem of a conducting strip of width AB. The same remark holds for several slots and several strips[88] [119].

14.9.3 Characteristic Modes of a Slot

Consider first the slot in an incident wave of the H type. The induced magnetic current is $\mathbf{J}_{mS} = E_y \mathbf{u}_z$. Let integral equation (14.192) be rewritten as[89]

$$\underbrace{\omega\epsilon_0 \int_{-w}^{w} J_{mS}(y')\, J_0(k_0|y - y'|)\, dy'}_{G(J_{mS})} \underbrace{-j\omega\epsilon_0 \int_{-w}^{w} J_{mS}(y')\, N_0(k_0|y - y'|)\, dy'}_{+jB(J_{mS})} = \underbrace{-2e^{-jk_0 \sin\theta_i y} H_0^i}_{I(y)}, \tag{14.195}$$

where θ_i is the angle of incidence shown in Figure 14.18. Note that G and B have the nature of an admittance. The characteristic functions are the solutions of

$$B(J_n) = \lambda_n G(J_n). \tag{14.196}$$

As in Section 11.8, G can be shown to be positive definite and λ_n real. We choose J_n, defined to within an arbitrary factor, to be real. The orthonormalization conditions are

$$\begin{aligned}
&\langle J_m, G(J_n)\rangle = \delta_{mn} \\
&\langle J_m, B(J_n)\rangle = \lambda_n \delta_{mn},
\end{aligned} \tag{14.197}$$

where

$$\langle a, b\rangle = \int_{-w}^{w} a^*(y)b(y)\,dy. \tag{14.198}$$

To solve (14.195), J_{mS} may be expanded in the eigenfunctions $J_n(y)$, which in that case play the role of entire-domain basis functions. We write

$$J_{mS}(y) = \sum_n V_n J_n(y).$$

The coefficients V_n can be determined by means of the normalization conditions. Thus,

$$J_{mS}(y) = \sum_n \frac{\langle J_n, I\rangle}{1 + j\lambda_n} J_n(y). \tag{14.199}$$

In general, $(8w/\lambda_0)$ terms in the series suffice to obtain an acceptable approximation to the sought slot field. Figure 14.20 displays the relative variation of J_n across the slot, the

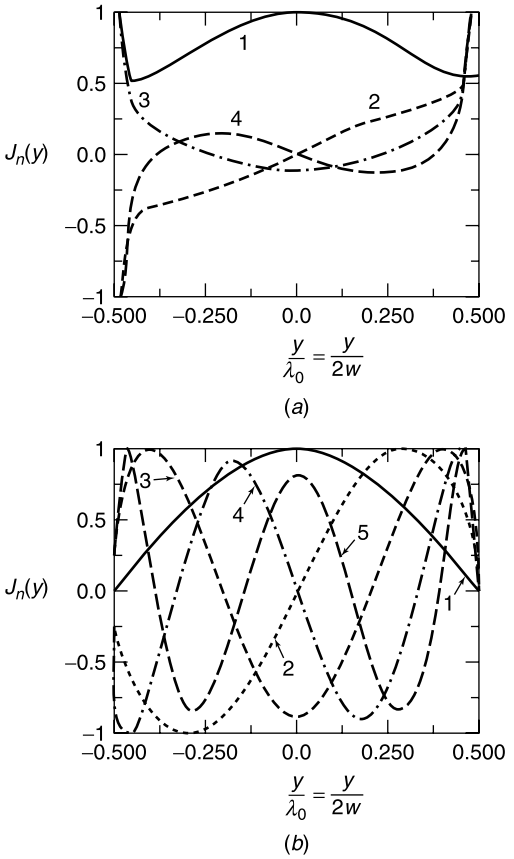

Figure 14.20 (*a*) First four $J_n(y)$ functions in an H-wave, for $2w = \lambda_0$. (*b*) Same for an E-wave (from K. Y. Kabalan, R. F. Harrington, H. A. Auda, and J. R. Mautz, Characteristic modes for slots in a conducting plane, TE case, *IEEE Trans. AP* **35**, 162–168, 1987, with permission of IEEE).

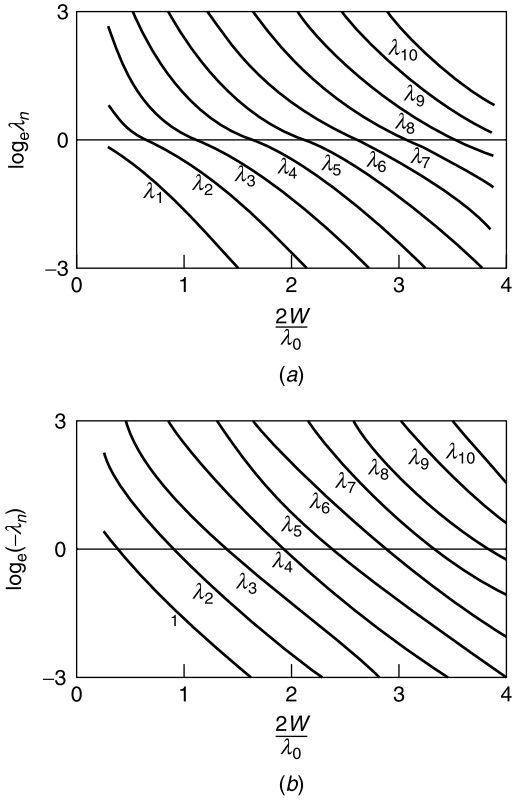

Figure 14.21 (*a*) First ten eigenvalues as a function of $(2w/\lambda_0)$, for an H-wave. (*b*) Same for an E-wave (from O. M. Bucci and G. Di Massa, Use of characteristic modes in multiple-scattering problems, *J. Phys. D. Appl. Phys.* **28**, 2235–2244, 1995, with permission of the Institute of Physics).

maximum amplitude set equal to one. Figure 14.21 shows the variation of λ_n as a function of the relative width $(2w/\lambda_0)$ of the slot.[90] This information can be used to determine how many terms should be kept in expansion (14.199).

When the incident wave is of the E type, the eigenfunction equation becomes,[91] from (14.184),

$$\lambda_n \underbrace{\left(\frac{d^2}{dy^2}+k_0^2\right)\int_{-w}^{w} J_n(y')J_0(k_0|y-y'|)dy}_{G(J_n)} + j\underbrace{\left(\frac{d^2}{dy^2}+k_0^2\right)\int_{-w}^{w} J_n(y')N_0(k_0|y-y'|)dy'}_{-B(J_n)} = 1. \tag{14.200}$$

14.9.4 Radiation from a Slot

From (14.190), the H field radiated into region 2 is given by

$$\lim_{r\to\infty} H(\mathbf{r}) \doteq \frac{e^{-jk_0 r}}{\sqrt{k_0 r}} \underbrace{\int_{-w}^{w} E_y(y')\, e^{jk_0 y' \sin\theta} dy'}_{g(\theta)}, \tag{14.201}$$

where $\doteq$ denotes "proportional to" and $k_2 = k_0$. Relationship (14.201) is a particular case of the more general equation

$$\mathcal{L}f = g. \tag{14.202}$$

In (14.201), f is $E_y(y)$ and g is the radiation pattern $g(k_0 w \sin\theta)$. In a *source-identification* problem g is given, and f should be determined as accurately as possible. In a *synthesis* problem,[92] on the other hand, a function f is sought that generates a desired g. The criterion is now to make $\mathcal{L}f$ as close to g as possible. The meaning of *close* depends on the chosen *norm*, which in turn determines the notion of *distance*. Some often used norms (of the unit, Euclidean, and infinite types) are defined in Section 1.2. Another possible example is

$$\| f \|^2 = \int_{-w}^{w} \left[a|f|^2 + b|f'|^2 \right] dy, \tag{14.203}$$

where a and b are positive. For that choice, closeness of f_1 to f_2 means not only that f_1 and f_2 must be close, but also that the same must hold for their first derivatives.

In the numerical solution of (14.202), g is not known with infinite precision, either because it results from measurements (in the identification problem) or because it is given in sampled form (in the synthesis problem). The solution may therefore suffer from instability, for example when small fluctuations in g strongly affect f in the identification problem. Similarly, if f is not realized exactly in the synthesis problem, the effect on $\mathcal{L}f$ (i.e., on the realized gain) may be drastic. In general, in ill-posed problems, the solution may not exist or be unacceptable. For such a case, a compromise must often be found between conflicting requirements. It might be necessary, for example, to limit the size of $\| f \|$ while keeping

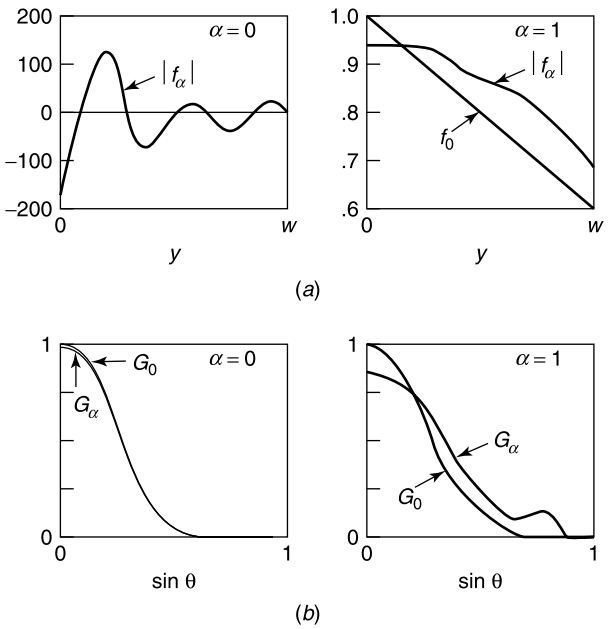

Figure 14.22 (*a*) Aperture field. (*b*) Radiation pattern (from G. A. Deschamps and H. S. Cabayan, Antenna synthesis and solution of inverse problems by regularization methods, *IEEE Trans. AP* **20**, 268–274, 1972, with permission of IEEE).

a sufficiently good approximation for $\| g \|$. This difficult *regularization* problem may be solved by several methods [175], one of which is to minimize

$$J(f) = \| \mathcal{L}f - g \|^2 + \alpha \| f \|^2, \tag{14.204}$$

where α is positive. As α is increased, larger values of $\| f \|$ are more heavily penalized, but concurrently the error $\| \mathcal{L}f - g \|$ becomes larger. The choice of α will therefore be a matter of compromise. The influence of this choice is illustrated in Figure 14.22, which displays data for the synthesis problem relative to a slot of width $2w = \lambda_0$. The desired pattern amplitude $G_0 = |g_0|$ is generated by a current f_0 that varies linearly from a maximum of one at $y = 0$ to zero at $y = \pm w = \pm\lambda_0$. The field distribution f, now for $w = \lambda_0/2$ is obtained by minimizing $J(f)$ in (14.204). The choice $\alpha = 0$ puts the accent on a good approximation for $\mathcal{L}f$ (i.e., for G_α). The aperture fields, however, are highly oscillatory and exhibit a large norm. With the choice $\alpha = 1$, the large values of f have been drastically reduced, but the approximation of G_0 by $\mathcal{L}f$ has deteriorated.

14.10 MORE SLOT COUPLINGS

Slots are frequently encountered as coupling element between regions, for example from cavity to cavity or from shielded microstrip to free space. In the previous section, the coupling effect is investigated between two half-spaces. The theory will now be extended to slots in a thick screen and in the wall of a cylinder.

14.10.1 Slot in a Thick Screen

The slot in Figure 14.23*a* is in the form of an (infinitely broad) tunnel, and the slot region 2 may be considered as a parallel plate waveguide. The field problem is the two-dimensional version of the three-dimensional problem embodied in Figure 10.19*b*.

Assume that the incident wave is of the H type[‡‡] and, for simplicity, that the slot region extends to infinity (Fig. 14.23*b*). To solve for the fields in that region (marked 2 in the figure), it is useful to expand the transverse component E_x in a series of orthogonal functions $\psi_m(x)$. Thus,

$$E_x(x,z) = \frac{1}{\sqrt{a}} f_0(z) + \sum_{m=1}^{\infty} \underbrace{\left(\sqrt{\frac{2}{a}} \cos \frac{m\pi x}{a} \right)}_{\psi_m(x)} f_m(z). \tag{14.205}$$

Because $E_x(x,z)$ satisfies Helmholtz' equation, $f_n(z)$ must be a solution of

$$\frac{d^2 f_n}{dz^2} + \underbrace{\left(k_0^2 - \left(\frac{m\pi}{a} \right)^2 \right)}_{\gamma_m^2 = -\delta_m^2} f_n = 0. \tag{14.206}$$

[‡‡]The solution for an incident E-wave proceeds by similar steps.

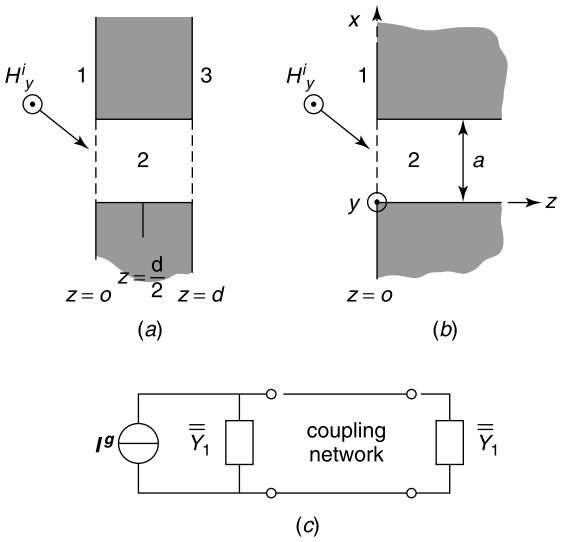

Figure 14.23 (*a*) Thick conducting screen. (*b*) Coupling to a semi-infinite parallel plate waveguide. (*c*) Equivalent circuit for the thick conducting screen.

For $m < (2a/\lambda_0)$ (i.e., for $\gamma_m^2 > 0$), the solution consists of propagating waves, while for $m > (2a/\lambda_0)$ the waves are attenuated. Taking into account the behavior of the fields for $z \to \infty$, the solution for E_x must be of the form

$$E_x(x,z) = \frac{V_a}{\sqrt{a}}\, e^{-jk_0 z} + \sum_{m=1}^{M} V_m\, e^{-j\gamma_m z}\sqrt{\frac{2}{a}}\cos\frac{m\pi x}{a} + \sum_{m=M+1}^{\infty} V_m\, e^{-\delta_m z}\sqrt{\frac{2}{a}}\cos\frac{m\pi x}{a}, \tag{14.207}$$

where we have assumed that M modes propagate. A corresponding expansion can be written for H_y, viz.

$$H_y(x,z) = \frac{I_a}{\sqrt{a}}\, e^{-jk_0 z} + \sum_{m=1}^{M} I_m\, e^{-j\gamma_m z}\sqrt{\frac{2}{a}}\cos\frac{m\pi x}{a} + \sum_{m=M+1}^{\infty} I_m\, e^{-\delta_m z}\sqrt{\frac{2}{a}}\cos\frac{m\pi x}{a}. \tag{14.208}$$

Because $j\omega\epsilon_0 E_x = -\left(\dfrac{\partial H_y}{\partial z}\right)$, it is easy to show that

$$I_0 = \frac{1}{R_{c0}} V_0 = G_{c0} V_0 \tag{14.209}$$

for the $m = 0$ mode. For a general propagating mode:

$$I_m = \frac{\omega\epsilon_0}{\gamma_m} V_m = \frac{k_0}{\gamma_m} G_{c0} V_m = G_m V_m, \tag{14.210}$$

and for an attenuated mode,

$$I_m = \frac{j\omega\epsilon_0}{\delta_m} V_m = j\frac{k_0}{\delta_m} G_{c0} V_m = jB_m V_m. \tag{14.211}$$

The relationship between the I_m and the V_m can be neatly written in matrix form as

$$\begin{pmatrix} I_0 \\ I_1 \\ \vdots \\ I_M \\ I_{M+1} \\ I_{M+2} \\ \vdots \end{pmatrix} = \underbrace{\begin{pmatrix} G_{c0} & & & & & & & \\ & G_1 & & & & & & \\ & & \ddots & & & & & \\ & & & G_M & & & & \\ & & & & jB_{M+1} & & & \\ & & & & & jB_{M+2} & & \\ & & & & & & \ddots & \end{pmatrix}}_{\overline{\overline{Y}}_2 \text{ of the waveguide}} \cdot \begin{pmatrix} V_0 \\ V_1 \\ \vdots \\ V_M \\ V_{M+1} \\ V_{M+2} \\ \vdots \end{pmatrix}. \tag{14.212}$$

The infinite, diagonal[§§] matrix $\overline{\overline{Y}}_2$ is the admittance matrix of region 2, a concept that is discussed theoretically in Sections 8.7 and 10.7 and finds a welcome concretization in the current application.

Remaining is the problem of determining the I_m (or the V_m). For that purpose, we must look at the relationship between H_y and E_x in the aperture. In region 1, this relationship is given by (14.188) and (14.191), which leads to

$$H_y(x) = H_y^g(x) - \frac{\omega\epsilon_0}{2} \int_0^a H_0^{(2)}(k_0|x - x'|)\, E_x(x')\, dx'. \tag{14.213}$$

Inserting the expansion (14.207) for E_x into the integral in the right-hand term gives

$$\begin{aligned} H_y(x) = H_y^g(x) &- \frac{\omega\epsilon_0}{2\sqrt{a}} V_0 \int_0^a H_0^{(2)}(k_0|x - x'|)\, dx' \\ &- \frac{\omega\epsilon_0}{2}\sqrt{\frac{2}{a}} \sum_{m=1}^{\infty} V_m \int_0^a \cos\frac{m\pi x'}{a} H_0^{(2)}(k_0|x - x'|)\, dx'. \end{aligned} \tag{14.214}$$

For x between 0 and a, this must be equal to the field on the region 2 side, viz.

$$H_y(x) = \frac{1}{\sqrt{a}} G_{c0} V_0 + \sum_{m=1}^{M} G_m V_m \sqrt{\frac{2}{a}} \cos\frac{m\pi x}{a} + \sum_{m=M+1}^{\infty} j\, B_m V_m \sqrt{\frac{2}{a}} \cos\frac{m\pi x}{a}. \tag{14.215}$$

Equating the two values of $H_y(x)$ yields an equation that can be efficiently solved by testing with the mode functions; that is, by multiplying with $\psi_n(x)$ and integrating from 0 to a. This leads to an infinite number of equations of the form

$$I_n^g - \sum_{m=0}^{\infty} V_m Y_{nm}^1 = Y_n^2 V_n. \tag{14.216}$$

[§§]It is to be noted that the diagonal character of $\overline{\overline{Y}}_2$ is a consequence of the orthogonality properties of the expansion functions $\psi_m(x)$.

Illustratively, if n is a propagating mode,

$$I_n^g = \sqrt{\frac{2}{a}} \int_0^a H^g(x) \cos \frac{m\pi x}{a}\, dx$$

$$Y_{nm}^1 = \frac{k_0 G_{c0}}{a} \int_0^a \cos \frac{n\pi x}{a} \left[\int_0^a \cos \frac{m\pi x'}{a} H_0^{(2)}(k_0|x - x'|)\, dx' \right] dx$$

$$Y_n^2 = G_n. \tag{14.217}$$

In matrix form, (14.216) gives rise to a *network equation*

$$\mathbf{I}^g = (\overline{\overline{Y}}_1 + \overline{\overline{Y}}_2) \cdot \mathbf{V}, \tag{14.218}$$

which may be usefully represented by the equivalent network shown in Figure 8.22.

Let us go back to the original "crack in the wall" problem of Figure 14.23*a*. The field expansions in region 2 must now include waves in both the $(+z)$ and $(-z)$ directions. In concise form:

$$E_x(x,z) = \sum_{m=0}^{\infty} \left(V_m^+ e^{-j\gamma_m z} + V_m^- e^{j\gamma_m z} \right) \psi_m(x)$$

$$H_y(x,z) = \sum_{m=0}^{\infty} \left(I_m^+ e^{-j\gamma_m z} + I_m^- e^{j\gamma_m z} \right) \psi_m(x), \tag{14.219}$$

where $\gamma_m = -j\delta_m$ for an attenuated mode. Expressing continuity of H_y in both slots (i.e., at $z = 0$ and $z = d$) yields two sets of equations of either type (14.213) or type (14.215). The symbolic network is shown in Figure 14.23*c*, where region 2 is represented by an equivalent transmission line (Problem 14.19). Note that the symmetry of the structure gives rise to two partial problems: one with an electric wall at $z = (d/2)$ and another one with a magnetic wall there. The electric wall situation corresponds with a plane screen provided with a cylindrical depression (a groove).

When the slot is very narrow[93] (i.e., when $a \ll \lambda_0$), only the $m = 0$ mode propagates, and the other modes decay exponentially. The $m = 1$ mode suffers the slowest decay, characterized by an e-folding distance (a/π). When the slot length d is much larger than a, one may therefore assume that one-mode propagation dominates in the connecting space 2. Note that the $m = 0$ mode is a TEM wave, propagating with wave number k_0.

The two-dimensional analysis developed above can be extended to *cylindrical* tunnels of arbitrary cross section, where the slots become apertures, and region 2 turns into a cylindrical waveguide. An interesting example is that of a tunnel of small cross section connecting two cavities.[94] In practical situations, the tunnel region may be filled with inhomogeneous materials, and the coupling apertures may occupy only part of the cross section of the waveguide. For such problems, it pays to use finite elements for the evaluation of the fields in the tunnel.[95] The relationship between $\mathbf{E}_{\tan}$ and $\mathbf{H}_{\tan}$ in the end apertures becomes a boundary integral condition of the type discussed in Section 12.6.

14.10.2 Slotted Cylinder in an *E*-wave

Assume that an E-wave is incident on the slotted cylinder shown in Figure 14.24*a*. The main unknown is $E = E_z$ in the slot. Because E must vanish on a metallic wall, it is natural to

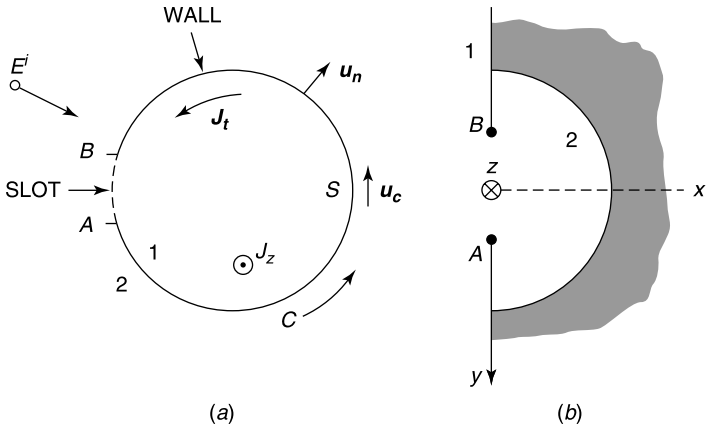

Figure 14.24 (*a*) Slotted cylinder in an incident wave. (*b*) Cavity with slot in an infinite ground plane.

expand the interior field in terms of the Dirichlet eigenfunctions of the cross section. Thus,

$$E(\mathbf{r}) = \sum A_m \phi_m(\mathbf{r}) \qquad (\mathbf{r} \text{ in } S), \tag{14.220}$$

where the dimensionless, normalized ϕ_m's are defined in (5.76). As in Section 10.2, the magnetic field and the sources are given appropriate expansions, viz.

$$\begin{aligned} \mathbf{H}(\mathbf{r}) &= \sum B_m \mathbf{u}_z \times \text{grad } \phi_m(\mathbf{r}) \\ J_z &= \sum C_m \phi_m(\mathbf{r}) \\ \mathbf{J}_{mt} &= \sum D_m \mathbf{u}_z \times \text{grad } \phi_m(\mathbf{r}). \end{aligned} \tag{14.221}$$

These expansions are subsequently inserted into Maxwell's equations. The developments need the form of the operators curl **v** and curl **v** when **v** does not depend on z. These useful formulas are:

$$\text{curl } \mathbf{v} = \text{grad } v_z \times \mathbf{u}_z + \mathbf{u}_z \text{ div } (\mathbf{v}_t \times \mathbf{u}_z) \tag{14.222}$$

$$-\text{curl curl } \mathbf{v} = \mathbf{u}_z \times \text{grad div } (\mathbf{v}_t \times \mathbf{u}_z) + \mathbf{u}_z \nabla^2 v_z. \tag{14.223}$$

If $\mathbf{v}_t$ is given by its Helmholtz representation $\mathbf{v}_t = \text{grad } \phi + \mathbf{u}_z \times \text{grad } \psi$, the potentials satisfy

$$\begin{aligned} \nabla^2 \phi = \text{div } \mathbf{v}_t &= \text{curl } (\mathbf{u}_z \times \mathbf{v}) \cdot \mathbf{u}_z \\ \nabla^2 \psi = \text{div } (\mathbf{v}_t \times \mathbf{u}_z) &= \text{curl } \mathbf{v} \cdot \mathbf{u}_z. \end{aligned} \tag{14.224}$$

Using these various formulas in separate expansions for curl **E** and curl **H** gives, for **r** in the cylinder,

$$E(\mathbf{r}) = \sum_m \frac{\mu_m^2 \phi_m(\mathbf{r})}{k_0^2 - \mu_m^2} \left[j\omega\mu_0 \int_S J_z \phi_m \, dS + \int_B^A E \frac{\partial \phi_m}{\partial n} \, dc \right. \tag{14.225}$$

$$\left. - \int_S \mathbf{J}_{mt} \cdot (\mathbf{u}_z \times \text{grad } \phi_m) \, dS \right]$$

$$\mathbf{H}(\mathbf{r}) = \sum_m \frac{1}{k_0^2 - \mu_m^2} \mathbf{u}_z \times \text{grad } \phi_m(\mathbf{r}) \left[\mu_m^2 \int_S J_z \phi_m \, dS - j\omega\epsilon_0 \int_B^A E \frac{\partial \phi_m}{\partial n} \, dc \right.$$

$$\left. + j\omega\epsilon_0 \int_S \mathbf{J}_{mt} \cdot (\mathbf{u}_z \times \text{grad } \phi_m) \, dS \right]. \tag{14.226}$$

Note that the magnetic current in the slot, as seen from the cavity, is $\mathbf{J}_{mS} = -E\mathbf{u}_c$. In the absence of volume sources in the cavity, (14.226) becomes

$$E(\mathbf{r}) = \sum_m \phi_m(\mathbf{r}) \frac{\mu_m^2}{k_0^2 - \mu_m^2} \int_B^A E \frac{\partial \phi_m}{\partial n} \, dc$$

$$\mathbf{H}(\mathbf{r}) = -j\omega\epsilon_0 \sum_m (\mathbf{u}_z \times \text{grad } \phi_m) \frac{1}{k_0^2 - \mu_m^2} \int_B^A E \frac{\partial \phi_m}{\partial n} \, dc. \tag{14.227}$$

When **r** is in the slot,

$$H_c(\mathbf{r}) = -j\omega\epsilon_0 \sum_m \frac{\partial \phi_m}{\partial n}(c) \frac{1}{k_0^2 - \mu_m^2} \int_B^A E \cos \frac{\partial \phi_m}{\partial n} \, dc$$

$$= \int_B^A J_{mS}(c') \underbrace{\left[jk_0 G_{c0} \sum_m \frac{1}{k_0^2 - \mu_m^2} \frac{\partial \phi_m}{\partial n}(c) \frac{\partial \phi_m}{\partial n'}(c') \right]}_{G_{cav}(c|c')} dc'. \tag{14.228}$$

To determine E, we must find a corresponding relationship $H_c(E)$ on the exterior side of the slot and equate the two values of H_c. The sought relationship can seldom be obtained in analytical form, except in cases when separation of variables is possible. It is available for the left half-infinite space in Figure 14.24*b*, in which case (14.184) gives

$$H_y(y) = H_y^g(y) + \frac{1}{\omega\mu_0} \left(\frac{\partial^2}{\partial y^2} + k_0^2 \right) \int_B^A E(y') H_0^{(2)}(k_0|y - y'|) \, dy'. \tag{14.229}$$

Equating the two tangential components of **H** in the slot yields an integro-differential equation for $E(y)$.

14.10.3 Slotted Cylinder in an *H*-wave

The main unknown is E_c, the tangential component of $\mathbf{E}$ in the slot. The expansions are now in terms of the Neumann eigenfunctions $\psi_n(x, y)$, the (normalized) solutions of

$$\begin{aligned} \nabla_{xy}^2 \psi_n + \nu_n^2 \psi_n &= 0 \qquad \text{(in } S\text{)} \\ \frac{\partial \psi_n}{\partial n} &= 0 \qquad \text{(on } C\text{)} \\ \int_S |\text{grad } \psi_n|^2 \, dS &= \nu_n^2 \int_S \psi_n^2 \, dS = 1. \end{aligned} \tag{14.230}$$

One of these eigenfunctions is $\psi_0 =$ a constant, which we set equal to one for normalization purposes. Fields and sources are given the expansions

$$\begin{aligned} H(\mathbf{r}) &= A_0 + \sum_{n=1}^{\infty} A_n \psi_n(\mathbf{r}) \\ \mathbf{E}(\mathbf{r}) &= \sum_{n=1}^{\infty} B_n \, \text{grad } \psi_n(\mathbf{r}) \times \mathbf{u}_z \\ \mathbf{J}_t &= \sum_{n=1}^{m} C_n \, \text{grad } \psi_n(\mathbf{r}) \times \mathbf{u}_z \\ J_{mz} &= D_0 + \sum_{n=1}^{\infty} D_n \psi_n(\mathbf{r}). \end{aligned} \tag{14.231}$$

Because of the orthogonality properties of the eigenfunctions, A_0 and D_0 are the average values of respectively H and J_{mz} over the cross section S. To evaluate A_0, we start from (14.7) and integrate over S to obtain

$$\int_S \text{div } (\mathbf{E}_t \times \mathbf{u}_z) \, dS = \int_B^A E_z \, dc = -j\omega\mu_0 \underbrace{\int_S H \, dS}_{A_0 S} - \int J_{mz} \, dS,$$

from which one easily deduces that

$$A_0 = -\frac{1}{j\omega\mu_0} \left[\frac{1}{S} \int_B^A E_c \, dc + \frac{1}{S} \int_S J_{mz} \, dS \right]. \tag{14.232}$$

Coefficients A_n and B_n are evaluated by introducing separate expansions for curl $\mathbf{E}$ and curl $\mathbf{H}$. Following the pattern set in Section 10.2, we obtain

$$\begin{aligned} H(\mathbf{r}) = A_0 + \sum_{n=1}^{\infty} \frac{\nu_n^2 \psi_n(\mathbf{r})}{k_0^2 - \nu_n^2} \Bigg[& j\omega\epsilon_0 \int_B^A E \psi_n \, dc + j\omega\epsilon_0 \int_S J_{mz} \psi_n \, dS \\ & - \int_S \mathbf{J}_t \cdot (\text{grad } \psi_n \times \mathbf{u}_z) \, dS \Bigg] \end{aligned}$$

$$\mathbf{E}(\mathbf{r}) = \sum_{n=1}^{\infty} \frac{\text{grad } \psi_n(\mathbf{r}) \times \mathbf{u}_z}{k_0^2 - \nu_n^2} \left[\nu_n^2 \int_B^A E\psi_n \, dc + \nu_n^2 \int_S J_{mz}\psi_n \, dS \right.$$
$$\left. + j\omega\mu_0 \int_S \mathbf{J}_t \cdot (\text{grad } \psi_n \times \mathbf{u}_z) \, dS \right]. \tag{14.233}$$

The equivalent surface magnetic current is $\mathbf{J}_{mS} = E_c \mathbf{u}_z$. In the absence of sources in the cylinder, the tangential magnetic field in the slot becomes

$$H(c) = \int_B^A J_{mS}(c') \left[\frac{j}{k_0 S} G_{c0} + jk_0 \underbrace{G_{c0} \sum_{n=1}^{\infty} \frac{\nu_n^2}{k_0^2 - \nu_n^2} \psi_n(c)\psi_n(c')}_{G_{cav}(c|c')} \right] dc'. \tag{14.234}$$

An equation for the unknown J_{mS} (or E_c) is obtained by evaluating $H(J_{ms})$ on the exterior side and equating the two values of H in the slot. For half-space 1 in Figure 14.24*b*, the appropriate relationship is (14.191).

14.10.4 Numerical Solution for the Slotted Cylinder

The cylindrical cross sections for which ϕ_m and ψ_n are known in closed form are few in number. A particularly simple example is the circle (Fig. 14.25). Assume that the circular cylinder is illuminated by an incident plane wave propagating in the x-direction. For an H-wave, the main unknown is the tangential electric field E_φ in the slot. Equations (14.37) and (14.38) show that E_φ has the following value outside the cylinder:

$$E_\varphi = -\frac{1}{j\omega\epsilon_0} \frac{\partial}{\partial r}(H^i + H^{sc})$$
$$= -\frac{1}{j\omega\epsilon_0} \frac{\partial}{\partial r} \left\{ \sum_{n=-\infty}^{\infty} j^{-n} e^{jn\varphi} \left[J_n(k_0 r) + a_n H_n^{(2)}(k_0 r) \right] \right\}, \tag{14.235}$$

where the a_n are the unknown coefficients in the expansion of H^{sc}. In the interior region, we write similarly[¶¶]

$$E_\varphi = -\frac{1}{j\omega\epsilon_0} \frac{\partial H}{\partial r} = -\frac{1}{j\omega\epsilon_0} \frac{\partial}{\partial r} \left\{ \sum_{n=-\infty}^{\infty} j^{-n} e^{jn\varphi} b_n J_n(k_0 r) \right\}. \tag{14.236}$$

The b_n's are the unknown coefficients of the expansion of H inside the cylinder. To determine a_n and b_n, we shall equate H and E_φ in the slot, (i.e., for $r = a$ and $-\varphi_0 \le \varphi \le \varphi_0$). The

[¶¶] If the penetration is weak (e.g., when the slot is narrow), the interior fields are very small and easily contaminated by round-off errors.

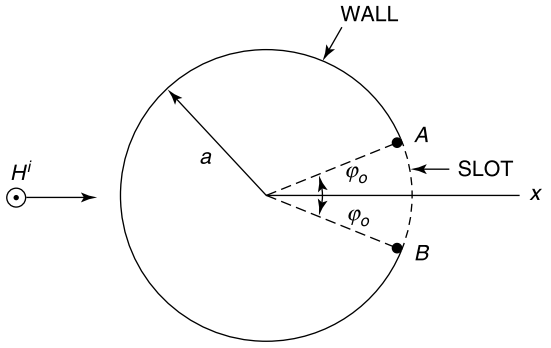

Figure 14.25 Circular cylinder with gap.

slot field E_φ may be usefully represented by the series[|||]

$$E_\varphi(\varphi) = \sum_{n=1}^{N} V_n f_n(\varphi) = \sum_{n=1}^{N} V_n \frac{\left(\dfrac{\varphi}{\varphi_0}\right)^{2n-2}}{\sqrt{1-\left(\dfrac{\varphi}{\varphi_0}\right)^2}}. \tag{14.237}$$

The basis functions f_n clearly take the edge behavior into account. They are set equal to zero outside the gap, and each of them can be expanded in a Fourier series in $e^{jn\varphi}$, which generates a corresponding expansion for E_φ.

The approach described above focuses on the tangential E-field in the slot. Other methods are possible. In the *scatterer method*, for example,[98,99] the metal wall of the slotted cylinder is considered as a scatterer, and the wall current $\mathbf{J}_S$ is determined by one of the many available methods (e.g., by solving an integral equation or, when the cylindrical cavity is filled with an inhomogeneous material, by using finite element methods[100,101,102]). The problem resulting from spurious solutions may be avoided by using the integral form of Maxwell's equations, applied to a discrete conformal grid.[103]

14.11 TERMINATION OF A TRUNCATED DOMAIN

Suitable methods to terminate a computational domain are discussed in Section 12.6. They can be immediately adapted to two-dimensional situations, in most cases in simpler form. In addition to *local* and *global* approaches, we shall discuss *intermediate* methods, in which the field at a point of the boundary is connected to the corresponding fields at *a few* neighboring points.

[|||]The details of the method can be found in Notes 96 and 97.

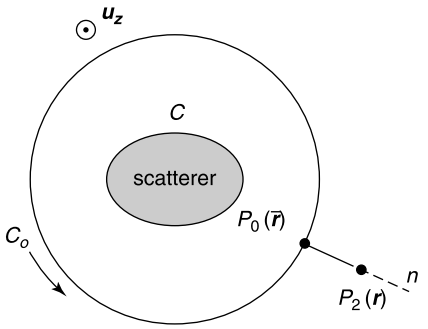

Figure 14.26 Scatterer and mathematical boundary C_0.

14.11.1 Local Conditions

The two-dimensional condition (12.100), valid for a circular boundary, can be extended to a more general boundary. Thus,

$$\frac{\partial \phi^{sc}}{\partial n} = \frac{2k_0^2 - 3\dfrac{jk_0}{R} - \dfrac{3}{4R^2}}{2\left(jk_0 + \dfrac{1}{R}\right)} \phi^{sc} + \frac{1}{2\left(jk_0 + \dfrac{1}{R}\right)} \frac{\partial^2 \phi^{sc}}{\partial c^2}. \tag{14.238}$$

Here c is a tangential coordinate, and $R(c)$ is the local radius of curvature [192] (Fig. 14.26). Details of other local methods (Mur, Engquist-Majda, and so forth) can be found in the references quoted in Section 12.6.

In a recent iterative approach,[104] pairs of points are considered in a finite difference net. A first point $\mathbf{r}_i$ is located on the outer boundary and a neighboring point $\mathbf{r}_j$ on the normal to C (Fig. 14.27). Applied to an E-wave, the method starts by assuming a reasonable trial value for J_S. The fields radiated by that current are evaluated from (14.15), and the resulting ratio

$$A_{ij} = \frac{E(\mathbf{r}_i)}{E(\mathbf{r}_j)} \tag{14.239}$$

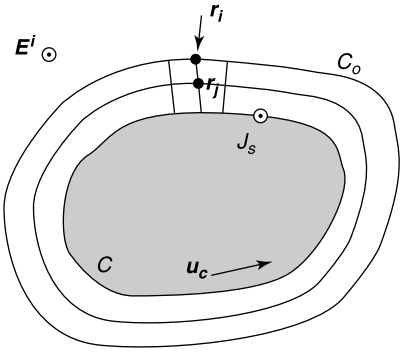

Figure 14.27 Two points on a conformal FD mesh (from Y. L. Luo, K. M. Luk, and S. M. Shum, A novel exact two-point field equation for solving electromagnetic scattering problems, *IEEE Trans. AP* **46**, 1833–1841, 1998, with permission of IEEE).

is noted for each point $\mathbf{r}_i$. The scattered electric field between C and C_0 is subsequently computed by requiring E^{sc} to be equal to $(-E^i)$ on C, and enforcing the ratio (14.239) at each point $\mathbf{r}_i$ to terminate the FD mesh. From this value of E^{sc}, a new surface current J_S is derived according to (14.3). Thus, on C,

$$J_S = \frac{1}{j\omega\mu_0}\frac{\partial E}{\partial n} = \frac{1}{j\omega\mu_0}\frac{\partial}{\partial n}(E^{sc} + E^i). \tag{14.240}$$

The process is repeated iteratively until a steady solution is obtained.

14.11.2 The Measured Equation of Invariance

While a condition such as (14.238) gives $\dfrac{\partial\phi}{\partial n}$ at a point P_0 in terms of the value of ϕ (and tangential derivatives) at the same point, the MEI approach involves P_0 and $(N-1)$ neighboring points.[105] The method assumes the existence of a linear relationship between the values of the scattered field at these N points. Thus,

$$\sum_{n=0}^{N-1} a_n\phi_n = 0. \tag{14.241}$$

Figure 14.28*a* shows the P_0 node (here denoted by 0), connected respectively to one, three, and five neighboring nodes. It may first be remarked that a relationship of the type (14.241) exists when ϕ (in the current case E_z or H_z) is the solution of a Helmholtz' equation. This classic relationship is

$$\phi_1 + \phi_2 + \phi_3 + \phi_4 - (4 - k_0^2h^2)\phi_0 = 0, \tag{14.242}$$

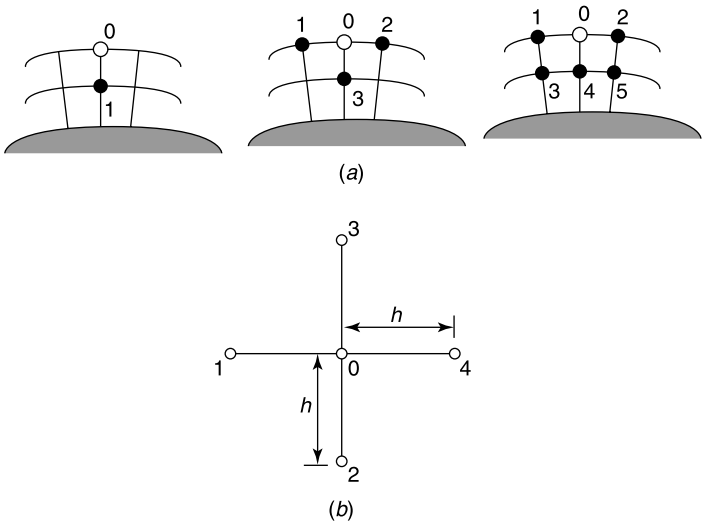

Figure 14.28 (a) Nodes for the MEI method. (b) Finite difference mesh points (from J. Chen, W. Hong, and J. M. Jin, An iterative measured equation technique for electromagnetic problems, *IEEE Trans. MTT* **46**, 25–30, 1998, with permission of IEEE).

and it holds in free space, in particular close to the scatterer (Fig. 14.28*b*). It is independent of the geometry of the scatterer, however, and does not "feel" the shape of the latter. In the MEI method, on the other hand, an equation of type (14.241) is postulated at each node, in such a form that the relationship is

- Location dependent
- Geometry-specific
- Invariant to the incident wave (i.e., to the field of excitation).

One of the coefficients, say a_0, may be arbitrarily set equal to one. To determine the $(N-1)$ remaining a_n's, $(N-1)$ solutions of the Helmholtz equation (the *measuring functions* ϕ_n) are inserted into (14.241), thus generating $(N-1)$ equations for the $(N-1)$ unknowns (a *measure* for the coefficients). A good choice for a measuring function is the field generated by a current J_S flowing on the surface of the scatterer (a *metron*) (Fig. 14.29). From (14.15) this field, in an E-wave, can be written as

$$E(\mathbf{r}) = j\omega\mu_0 \int_C J_S(c')\, G_0(\mathbf{r}, c')\, dc'. \tag{14.243}$$

$E(\mathbf{r})$ is first evaluated at P_0 and $(N-1)$ neighboring nodes by inserting a first metron J_1 into (14.243). Inserting the obtained value of $E(\mathbf{r})$ into (14.241) gives

$$\sum_{i=0}^{N} a_i\, j\omega\mu_0 \int_C J_1(c')\, G_0(\mathbf{r}_i, c')\, dc' = 0. \tag{14.244}$$

The process is repeated with metrons $J_2, J_3, \ldots, J_{N-1}$, yielding $(N-1)$ equations for the $(N-1)$ unknown coefficients. The functional form of the metrons is a matter of choice; it could be quadratic, for example, or sinusoidal, as in

$$J_k(c) = \cos\left[(k-1)2\pi\frac{c}{L}\right]$$

where L is the circumferential length of the contour. Experience shows that the scattered fields obtained from various sets of "reasonable" metrons are normally insensitive to the choice of the set. The accuracy depends mostly on the number of mesh layers, the number

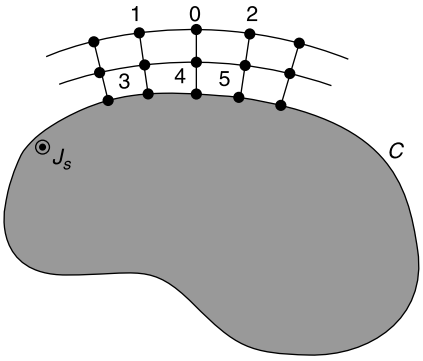

Figure 14.29 PEC scatterer and net.

N of nodes, and the number of metrons. Iterative improvements are obtained by using the fields produced by an initial set of metrons to generate a *new* metron according to (14.240). The fields are thereafter recomputed with the new metron,[106] and a second (new) metron is subsequently generated from (14.240). The process is continued until convergence is achieved.

The most time consuming part of the MEI method is the determination of the a_n coefficients. When their number becomes large, which happens when the frequency is progressively raised, it may be advantageous to compute those coefficients at a restricted number of nodes and to interpolate between these values to derive the a_n of the initially neglected nodes.[107] Difficulties also arise when the scatterer exhibits deep concave parts[108,109] (in which case multiple reflections take place) or when it is penetrable.[110] In both cases these difficulties can be avoided by filling the region of concern with FD or FE meshes.

14.11.3 The Boundary Integral Condition

This global condition takes a particularly simple form in two dimensions.[111] If the wave is of the H type, the sought relationship must connect $H(c)$ to $E_c(c)$. Applying (14.97) to $H(\mathbf{r})$ gives, in the region outside the computational boundary C_0 (Fig. 14.26),

$$H(\mathbf{r}) = H^i(\mathbf{r}) + \int_{C_0} \frac{\partial H(\mathbf{r}')}{\partial n'} G_0(\mathbf{r}|\mathbf{r}')\, dc' - \int_{C_0} H(\mathbf{r}') \frac{\partial G_0(\mathbf{r}|\mathbf{r}')}{\partial n'}\, dc'. \tag{14.245}$$

From (14.6), $\left(\dfrac{\partial H}{\partial n}\right)$ in the first integral can be replaced by

$$\frac{\partial H}{\partial n} = -j\omega\epsilon_0\, E_c. \tag{14.246}$$

This substitution introduces E_c into the equation. Let $\mathbf{r}$ (i.e., P_2) approach a point P_0 on the contour. The convergence of the first integral does not pose any problem because $G_0(\mathbf{r}|\mathbf{r}')$ is weakly singular. The second integral, however, requires application of (14.111), which expresses the connection between E_c and H in the form

$$j\omega\epsilon_0 \lim_{\delta\to 0} \int_{C_0 - C_{0\delta}} E_c(\mathbf{r}')\, G_0(\mathbf{r}|\mathbf{r}')\, dc' + \frac{1}{2} H(\mathbf{r}) + \lim_{\delta\to 0} \int_{C_0 - C_{0\delta}} H(\mathbf{r}') \frac{\partial G_0(\mathbf{r}|\mathbf{r}')}{\partial n'}\, dS' = H^i(\mathbf{r}), \tag{14.247}$$

where $\mathbf{r}$ and $\mathbf{r}'$ are on C_0. We note that the integral operators in (14.247) appear in either the EFIE or the MFIE. In both cases, interior resonances may cause problems. The same difficulties can therefore be expected in the solution of (14.247), where they can be alleviated by introducing small (artificial) losses, that is, by replacing the propagation constant k_0 in the Green's function $G_0(\mathbf{r}|\mathbf{r}')$ by $k_0\left(1 - \dfrac{j}{2Q}\right)$, where Q is a (large) quality factor.[112]

The boundary integral method is a global, nonlocal method. Another nonlocal approach[113] consists in first setting $E = E^i$ on C_0 and $E = 0$ on C (Fig. 14.30). The E-field between C and C_0 is subsequently evaluated by the FEM, using for example a functional of the form

$$J(E) = \frac{1}{2} \int_S \Big[|\text{grad } E|^2 - k_0^2 |E|^2 \Big]\, dS. \tag{14.248}$$

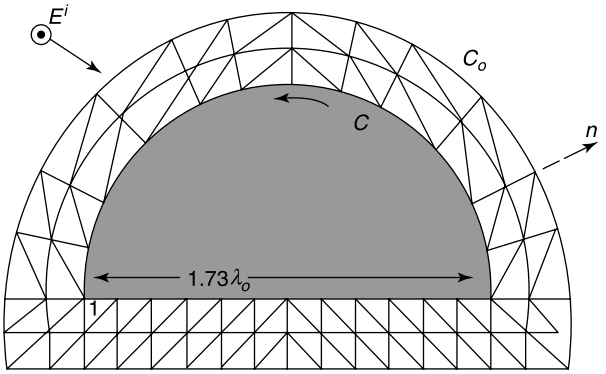

Figure 14.30 Finite element mesh in an E-wave (from T. Roy, T. K. Sarkar, A. R. Djordjević and M. Salazar-Palma, A hybrid method solution of scattering by conducting cylinders (TM case), *IEEE Trans. MTT* **44**, 2145–2151, 1996, with permission of IEEE).

From this solution, an approximate value of J_S on C can be derived from (14.240). This current radiates a scattered field E^{sc} (originally neglected in the first step), which is now added to E^i on C_0 to obtain a new value of E. The process is repeated iteratively until convergence is achieved.

In recent years, the *perfectly matched layer (PML)* has been used extensively to close the computational domain. The layer can be placed as close as two FDTD cells to the scatterer. The advantages of the method are discussed in Section 9.1. There may be difficulties, however, when the PML is thin and placed very close to the scatterer, in which case strong numerical reflections may develop.[114] It should be noted, as a side remark, that the idea of placing a perfectly absorbing material on C_0 has been applied in anechoic chambers for quite a number of years. This experimental realization of the absorption principle can be carried over to the numerical area by covering C_0 with a PEC (or PMC), coated with layers of a fictitious dielectric medium, so proportioned that absorption is obtained over a wide range of angles of incidence.[115]

14.11.4 The Unimoment Method

The method, already discussed in Section 5.7 in its application to potential problems, can be extended to time-harmonic fields. The function ϕ is now either E_z or H_z (Fig. 14.26). The scattered field in the region exterior to the circular boundary C_0 is represented by its Fourier series[116]

$$\phi^{sc}(\mathbf{r}) = \phi^{+}(\mathbf{r}) = \sum_{n=0}^{N-1} (C_n \cos n\varphi + D_n \sin n\varphi)\ H_n^{(2)}(k_0 r). \tag{14.249}$$

The normal component follows as

$$\left.\frac{\partial \phi^{sc}(r,\varphi)}{\partial r}\right|_{r=a} = \sum_{n=0}^{N-1} (C_n \cos n\varphi + D_n \sin n\varphi) \left.\frac{dH_n^{(2)}(k_0 r)}{dr}\right|_{r=a}. \tag{14.250}$$

Inside C_0, the representation takes the form

$$\phi^-(\mathbf{r}) = \sum_{n=0}^{2N-1} a_n \psi_n(\mathbf{r}) \tag{14.251}$$

$$\left.\frac{\partial \phi^-(r,\varphi)}{\partial r}\right|_{r=a} = \left.\sum_{n=0}^{2N-1} a_n \frac{\partial \psi_n}{\partial r}\right|_{r=a}. \tag{14.252}$$

The ψ_n are required to take given values on C_0, for example $\cos n\varphi$ for $n \le N$ and $\sin(n-N)\varphi$ for $n > N$. The values of ψ_n inside C_0 are subsequently determined by numerically solving the differential equations satisfied by ϕ^-. Such an approach — typically based on the FEM — can easily accommodate inhomogeneous or anisotropic materials inside C_0. Once the ψ_n are determined for a given scatterer, they can be used to solve the scattering problem for arbitrary incident fields ϕ^i. When ϕ^i is given, the 4N coefficients in (14.249) and (14.251) are determined by enforcing the boundary conditions on C_0 (i.e., for $r = a$). Thus,

$$\phi^i(a,\varphi) + \phi^{sc}(a,\varphi) = \phi^-(a,\varphi) \tag{14.253}$$

$$\left[\frac{\partial}{\partial r}\phi^i(r,\varphi) + \phi^{sc}(r,\varphi)\right]_{r=a} = \left[\frac{\partial}{\partial r}\phi^-(r,\varphi)\right]_{r=a}. \tag{14.254}$$

With a testing function $w_k(\varphi)$, the first condition yields[117]

$$\begin{aligned}\int_0^{2\pi} \left[\sum_{n=0}^{2N-1} a_n \psi_n(a,\varphi)\right] w_k(\varphi)\, d\varphi \\ = \int_0^{2\pi} \left[\sum_{n=0}^{N-1} (C_n \cos n\varphi + D_n \sin n\varphi)\, H_n^{(2)}(k_0 a)\right] w_k(\varphi)\, d\varphi + \int_0^{2\pi} \phi^i(a,\varphi)\, w_k(\varphi)\, d\varphi.\end{aligned} \tag{14.255}$$

The integrations become particularly simple when the $w_k(\varphi)$ are sinusoidal functions of φ. A similar set of equations can be written for the second condition.

In the application of the unimoment method, the C_0 boundary does not have to be circular, and an elliptic boundary may be preferable for elongated scatterers [192]. The terms of the expansion in (14.249) now involve Mathieu functions. This expansion may more generally be written in terms of known free-space solutions of Helmholtz' equation satisfying the radiation condition. This principle is in fact the basis of the *generalized multipole technique* discussed in Section 14.7.

14.12 LINE METHODS

In this section, two methods are discussed that are related to transmission line theory. In the *transmission line matrix* technique, one recognizes that Maxwell's equations satisfied by fields such as e_x and h_y often take the form of transmission line equations. This remark

opens the possibility of replacing a field problem with a similar one involving currents and voltages on an analog line network. In the *method of lines*, all variables but one (say l) are discretized. The *lines* are the curves along which l only varies, and the fields satisfy ordinary second-order differential equations along these lines.

14.12.1 The Transmission Line Matrix Method

Before the advent of powerful digital computers, problems in many branches of physics and engineering were solved by analog methods. Network analyzers, for example, were extensively used to investigate the stability of electric power systems. These basic techniques gave birth to the TLM method.[118] Consider, for example, the equations satisfied by the fields in a z-directed plane wave propagating in vacuum:

$$\begin{aligned} \frac{\partial e_x}{\partial z} &= -\mu_0 \frac{\partial h_y}{\partial t} \\ \frac{\partial h_y}{\partial z} &= -\epsilon_0 \frac{\partial e_x}{\partial t}. \end{aligned} \tag{14.256}$$

These are precisely the equations (1.2) satisfied by v and i on a lossless transmission line, provided one identifies $(e_x, h_y, \epsilon_0, \mu_0)$ with (v, i, C, L). The variation of v and i over a length Δl of transmission line can therefore simulate the corresponding field propagation. In two dimensions, two perpendicular directions should be considered, and the "analog" circuit consists of short segments of transmission line (stubs and links). These lines, in turn, can be replaced by lumped elements, a classic move. If the structures shown in Figure 14.31*a* and *b* are repeated, one obtains a net, partly shown in Figure 14.32. Assume now that a $\delta(t)$ impulse of unit power is incident on node 0 (Fig. 14.32*a*). The energy is scattered isotropically in all four directions[119] at the rate of $1/4$ per line, or correspondingly $1/2$ V per line (Fig. 14.32*b*). For such a case, 1 sees a resistance $(R_c/3)$, which gives rise to a reflection coefficient $(-1/2)$ and transmission coefficients $(1/2)$ to the other lines. In the more general case of four impulses incident on the four branches of the node, the reflected voltages at time $(n+1)\Delta t$ are related to the (previous) incident voltages at time $n\Delta t$ by a scattering matrix

$$\begin{pmatrix} V_1 \\ V_2 \\ V_3 \\ V_4 \end{pmatrix}_{refl}^{n+1} = \frac{1}{2} \begin{pmatrix} -1 & 1 & 1 & 1 \\ 1 & -1 & 1 & 1 \\ 1 & 1 & -1 & 1 \\ 1 & 1 & 1 & -1 \end{pmatrix} \cdot \begin{pmatrix} V_1 \\ V_2 \\ V_3 \\ V_4 \end{pmatrix}_{inc}^{n}. \tag{14.257}$$

The outgoing waves hit new nodes, and a propagating pattern develops, as sketched in Figure 14.32*c* [184]. If the magnitudes, positions, and directions of all impulses are known at time $n\Delta t$, the corresponding values at times $(n+1)\Delta t$ can now be evaluated. It has been remarked[120] [34] that the process is in full harmony with Huygens' model of light propagation in a medium, according to which light is a mechanical vibration of densely packed spherical particles. The wave propagates by elastic shock from one particle to the next, and each particle becomes the source of a further disturbance.

The detailed application of the method requires a deeper analysis*** [32, 34, 184, 191, 205]. To accommodate dielectric or magnetic materials, for example, nodes should be

***The September–October 1996 issue of *Electromagnetics* (vol. 16, no. 5) is devoted to the TLM method.

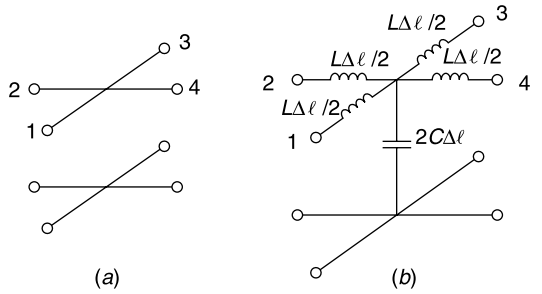

Figure 14.31 (*a*) Shunt node with four sections of transmission line of length ($\Delta l/2$). (*b*) Lumped element model (from W. R. Hoefer, The transmission-line matrix method — theory and applications, *IEEE Trans. MTT* **33**, 882–893, 1985, with permission of IEEE).

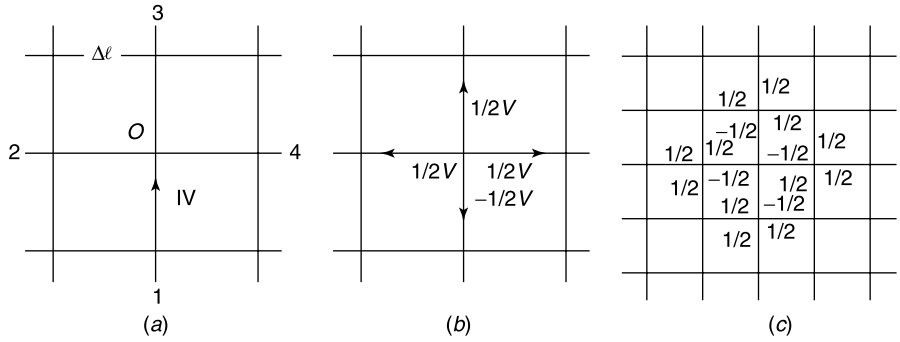

Figure 14.32 Scattering of an initial Dirac impulse (from W. R. Hoefer, The transmission-line matrix method – theory and applications, *IEEE Trans. MTT* **33**, 882–893, 1985, with permission of IEEE).

loaded with reactive stubs of appropriate characteristic impedance and of length ($\Delta l/2$). Losses in the material can be accounted for by inserting lossy transmission lines in the mesh or by loading with lossy stubs [184]. The main step forward, however, is the extension of the method to three dimensions. The shunt node most now be replaced[121,122] by a cell with three shunt nodes (for **H**) and three series nodes (for **E**) (Fig. 14.33) [184]. Other important aspects are a correct representation of boundaries in the presence of highly conducting materials[123] and a proper truncation of the computational domain.[124,125,126]

The TLM method has several advantages:

- It requires only simple arithmetic operations, and no matrix inversions are needed.
- Because the mesh consists of passive circuits, stability problems do not arise.
- Scattering and connection are local processes, which involve at most a node and its immediate neighbors.

The method has its limitations, however, in particular because of the increasing dispersion and computational anisotropy that develop on a mesh as frequency increases, in which case a fixed Δl will eventually become of the order λ_0 or larger.

The TLM has been applied extensively to electromagnetic problems, in particular in the areas of scattering[127] and waveguide propagation[128,129,130] [184]. Although it is fundamentally a time-domain technique, it can also be used in the frequency domain[131] [184].

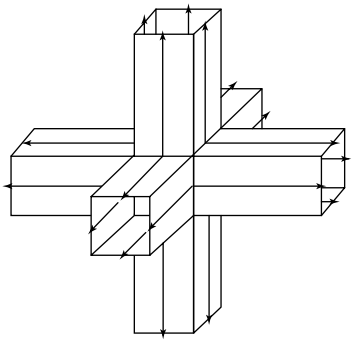

Figure 14.33 Three-dimensional symmetrical condensed node (from C. Christopoulos and J. L. Herring, The application of transmission-line modeling (TLM) to electromagnetic compatibility problems, *IEEE Trans. EMC* **35**, 185–191, 1993, with permission of IEEE).

It has further been found useful in the study of electric circuits, both linear and nonlinear,[132] and in the evaluation of static fields and eddy currents.[133,134]

14.12.2 The Method of Lines

In this very general numerical method, the derivatives with respect to a given variable (say l) are left untouched, and all other derivatives are discretized [205]. A partial differential equation is now replaced by a set of ordinary *differential* equations in l, and *difference* equations in the other variables. The selected variable may be the time or a space coordinate. In a layered medium, the natural choice is to select lines perpendicular to the layers (i.e., parallel to the z-axis). Each line corresponds with a discretization point in the (x, y) plane.

In order to illustrate the principle of the method,[135,136] consider Helmholtz' equation in polar coordinates, viz.

$$\frac{\partial^2 \phi}{\partial r^2} + \frac{1}{r}\frac{\partial \phi}{\partial r} + \frac{1}{r^2}\frac{\partial^2 \phi}{\partial \varphi^2} + k_0^2 \phi = 0. \tag{14.258}$$

Discretization in the φ-direction is obtained by choosing N points on a circle of constant r and expressing the second derivative with respect to φ by its discretized version

$$\frac{1}{r^2}\frac{\partial^2 \phi}{\partial \varphi^2} = \frac{1}{(r\Delta\varphi)^2}\left(\phi_{n+1} + \phi_{n-1} - 2\phi_n\right), \tag{14.259}$$

where $\Delta\phi = (2\pi/N)$ (Fig. 14.34*a*). If we denote the ensemble of values $(\phi_1, \phi_2, \ldots, \phi_N)$ by the vector $\boldsymbol{\phi}(r)$, the differential equation in r, to be solved along radial lines, may be written as

$$\frac{d^2 \boldsymbol{\phi}}{dr^2} + \frac{1}{r}\frac{d\boldsymbol{\phi}}{\partial r} + k_0^2 \boldsymbol{\phi} - \frac{1}{(r\Delta\varphi)^2}\,\overline{\overline{D}}\cdot\boldsymbol{\phi} = 0, \tag{14.260}$$

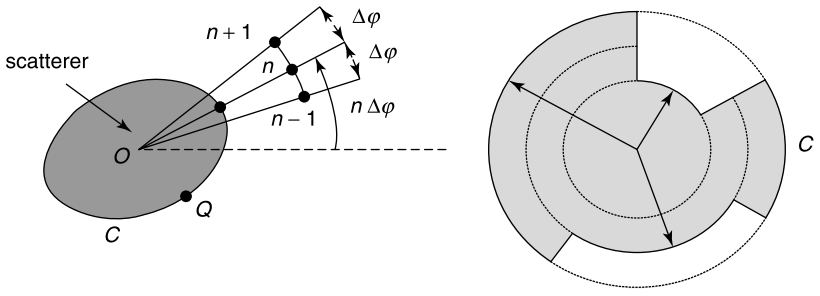

Figure 14.34 (*a*) Radial lines and lateral discretization. (*b*) Circular ridge waveguide (from S. Xiao, R. Vahldieck, and J. Hesselbarth, Analysis of cylindrical transmission lines with the method of lines, *IEEE Trans. MTT* **44**, 993–999, 1996, with permission of IEEE).

where $\overline{\overline{D}}$ is the square N × N matrix

$$\overline{\overline{D}} = \begin{bmatrix} 2 & -1 & 0 & 0 & \dots & 0 & 0 & -1 \\ -1 & 2 & -1 & 0 & \dots & 0 & 0 & 0 \\ 0 & -1 & 2 & -1 & \dots & 0 & 0 & 0 \\ \vdots & \vdots & \vdots & \vdots & \dots & \vdots & \vdots & \vdots \\ 0 & 0 & 0 & 0 & \dots & -1 & 2 & -1 \\ -1 & 0 & 0 & 0 & \dots & 0 & -1 & 2 \end{bmatrix}. \tag{14.261}$$

This matrix is real and symmetric and is independent of the geometry of the scatterer. Equation (14.260) actually represents a set of coupled differential equations, each one involving several ϕ. This remark is confirmed by the nondiagonal character of $\overline{\overline{D}}$. Uncoupling the equations can be achieved by the eigenvector method, which amounts to diagonalizing $\overline{\overline{D}}$ by means of a transformation matrix $\overline{\overline{T}}$. The method requires the preliminary determination of the eigenvectors $\mathbf{w}_m$ of $\overline{\overline{D}}$, which are the solutions of

$$\overline{\overline{D}} \cdot \mathbf{w}_m = \lambda_m \mathbf{w}_m, \tag{14.262}$$

where λ_m is real. Given the $\mathbf{w}_m$, $\boldsymbol{\phi}(\mathbf{r})$ may be expanded as

$$\boldsymbol{\phi}(r) = \sum_{m=1}^{N} C_m(r)\, \mathbf{w}_m = \overline{\overline{C}} \cdot \mathbf{w}. \tag{14.263}$$

Substitution into (14.260) shows that C_m must satisfy the (uncoupled) differential equation

$$\frac{d^2 C_m}{dr^2} + \frac{1}{r}\frac{dC_m}{dr} + \left(k_0^2 - \frac{\lambda_m}{r^2(\Delta\varphi)^2}\right) C_m = 0. \tag{14.264}$$

From (A5.1), the outgoing solution, which represents the scattered field, is given by

$$C_m(r) = A_m H_{\nu_m}^{(2)}(k_0 r), \tag{14.265}$$

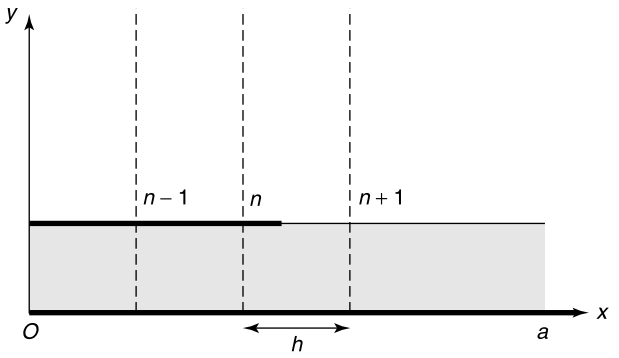

Figure 14.35 Microstrip structure with line.

where $\nu_m = (\sqrt{\lambda_m}/\Delta\varphi)$. Coefficients A_m can be determined by enforcing the boundary condition at the contour (i.e., at points such as Q in Fig. 14.34*a*). For an E-wave, for example, one would impose $E^{sc} = -E^i$ in Q.

The method of lines can easily be applied to scatterers bounded by radial lines and circular arcs, or to multilayered structures consisting of a succession of concentric layers.[137] When contour C is metallized, as in Figure 14.34*b*, a waveguide bounded by C is formed, and the technique described above may serve to determine the normal modes of the guide.[138] The method of lines can be further adapted to transient fields,[139] and it easily handles materials of very general characteristics.[140,141] It has also been successful in its application to waveguide networks and cavities[142,143,144,145] and in particular to planar waveguides.[146] An interesting example is the microstrip shown in Figure 14.35. It is proved in Section 15.10 that the modes of the microstrip may be expressed in terms of scalar potentials ϕ and ψ. These potentials contain a propagation factor $e^{-j\beta z}$, and their (x, y) variation satisfies

$$\frac{\partial^2 \phi}{\partial x^2} + \frac{\partial^2 \phi}{\partial y^2} + (k_i^2 - \beta^2)\,\phi = 0, \tag{14.266}$$

where k_i takes a different value in each layer. The preferred direction is clearly y, and a differential equation in y is obtained by discretizing in the x direction. The lines are the verticals at $x = nh$, along which

$$\left(\frac{d^2\phi}{dy^2}\right)_n + \frac{1}{h^2}\left[\phi_{n+1}(y) + \phi_{n-1}(y) - 2\phi_n(y)\right] + (k_i^2 - \beta^2)\,\phi_n(y) = 0. \tag{14.267}$$

Introducing again the vector $\boldsymbol{\phi}$ gives

$$\frac{d^2\boldsymbol{\phi}}{dy^2} + \left[(k_i^2 - \beta^2)\,\bar{\bar{I}} - \frac{1}{h^2}\,\bar{\bar{D}}\right] \cdot \boldsymbol{\phi} = 0, \tag{14.268}$$

where

$$\bar{\bar{D}} = \begin{pmatrix} p_1 & -1 & & & \\ -1 & 2 & -1 & & \bigcirc \\ & \ddots & \ddots & \ddots & \\ \bigcirc & & -1 & 2 & -1 \\ & & & -1 & p_2 \end{pmatrix}. \tag{14.269}$$

The values of p_1 and p_2 depend on the lateral boundary conditions at $x = a$ and $x = -a$. For a Dirichlet condition one takes $p = 2$, and for a Neumann condition $p = 1$. The method of eigenvectors can again be applied, this time to the solution of (14.268). It yields differential equations in y, one per region, which are solved with the help of boundary conditions at interfaces and on the strip. The metallic strip is often assumed infinitely thin, to simplify matters, but its thickness must be taken into account when a knowledge of the power losses is required.[147,148]

14.12.3 Coupled Transmission Lines

Miniaturized circuits at microwave and optical frequencies are densely packed. As a result, transmission lines lie close to each other, and problems of interference and crosstalk arise. The theory of the coupling mechanism, to be presented next, is very general and can be applied to the many areas of theoretical physics in which coupled differential equations play a role. Of specific interest for this chapter is the system formed by lines *1* and *2* in Figure 14.36. The lines are coupled, and their voltages and currents satisfy the equations

$$\begin{aligned} \frac{dV_1}{dz} &= -Z_{11}I_1 - Z_{12}I_2 \\ \frac{dV_2}{dz} &= -Z_{21}I_1 - Z_{22}I_2 \end{aligned} \tag{14.270}$$

and

$$\begin{aligned} \frac{dI_1}{dz} &= -Y_{11}V_1 - Y_{12}V_2 \\ \frac{dI_2}{dz} &= -Y_{21}V_1 - Y_{22}V_2. \end{aligned} \tag{14.271}$$

Note that the voltages are measured with respect to a reference conductor 3 (typically a ground plane). The lines may be embedded in materials, which we shall assume linear, isotropic, and of z-independent characteristics. We shall also assume that the Z_{ik} (or Y_{ik}) coefficients are known, either by experiment or by means of previous computations.

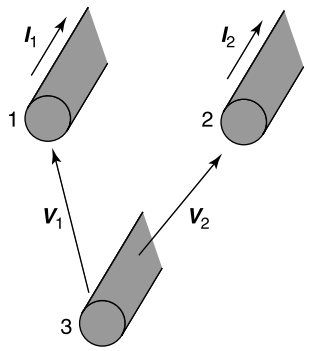

Figure 14.36 Coupled lines and reference conductor 3.

Equations (14.270) and (14.271) admit the more compact forms

$$\frac{d\mathbf{V}}{dz} = -\overline{\overline{Z}} \cdot \mathbf{I} \tag{14.272}$$

$$\frac{d\mathbf{I}}{dz} = -\overline{\overline{Y}} \cdot \mathbf{V}. \tag{14.273}$$

The currents can be eliminated from (14.270) and (14.271) by differentiating $\dfrac{d\mathbf{V}}{dz}$ with respect to z. Thus,

$$\begin{aligned}\frac{d^2V_1}{dz^2} &= (Z_{11}Y_{11} + Z_{12}Y_{21})\,V_1 + (Z_{11}Y_{12} + Z_{12}Y_{22})\,V_2\\ \frac{d^2V_2}{dz^2} &= (Z_{21}Y_{11} + Z_{22}Y_{21})\,V_1 + (Z_{21}Y_{12} + Z_{22}Y_{22})\,V_2.\end{aligned} \tag{14.274}$$

In matrix notation:

$$\frac{d^2\mathbf{V}}{dz^2} = (\overline{\overline{Z}} \cdot \overline{\overline{Y}}) \cdot \mathbf{V}. \tag{14.275}$$

Elimination of the voltages gives analogously

$$\begin{aligned}\frac{d^2I_1}{dz^2} &= (Y_{11}Z_{11} + Y_{12}Z_{21})\,I_1 + (Y_{11}Z_{12} + Y_{12}Z_{22})\,I_2\\ \frac{d^2I_2}{dz^2} &= (Y_{21}Z_{11} + Y_{22}Z_{21})\,I_1 + (Y_{21}Z_{12} + Y_{22}Z_{22})\,I_2.\end{aligned} \tag{14.276}$$

In matrix notation:

$$\frac{d^2\mathbf{I}}{dz^2} = (\overline{\overline{Y}} \cdot \overline{\overline{Z}}) \cdot \mathbf{I}. \tag{14.277}$$

When the system is reciprocal, that is, when $Z_{12} = Z_{21} = Z_M$ and $Y_{12} = Y_{21} = Y_M$, it is easy to check that

$$\left(\overline{\overline{Y}} \cdot \overline{\overline{Z}}\right) = (\overline{\overline{Z}} \cdot \overline{\overline{Y}})^t. \tag{14.278}$$

The equations in (14.274) are coupled because both V_1 and V_2 appear in the respective right-hand terms. Decoupling can be achieved by means of the eigenvectors of $(\overline{\overline{Z}} \cdot \overline{\overline{Y}})$, which are the solutions of[149] [106]

$$\begin{aligned}(\overline{\overline{Z}} \cdot \overline{\overline{Y}}) \cdot \mathbf{x}^a &= \gamma_a^2 \mathbf{x}^a\\ (\overline{\overline{Z}} \cdot \overline{\overline{Y}}) \cdot \mathbf{x}^b &= \gamma_b^2 \mathbf{x}^b,\end{aligned} \tag{14.279}$$

where we have chosen superscripts a and b instead of 1 and 2 in order to avoid confusion with the numbering of the lines. The voltage vector $\mathbf{V}$ can now be expressed as a linear

combination of $\mathbf{x}^a$ and $\mathbf{x}^b$. Thus,

$$\mathbf{V}(z) = \begin{pmatrix} V_1 \\ V_2 \end{pmatrix} = a(z) \begin{pmatrix} x_1^a \\ x_2^a \end{pmatrix} + b(z) \begin{pmatrix} x_1^b \\ x_2^b \end{pmatrix} = a(z)\,\mathbf{x}^a + b(z)\,\mathbf{x}^b. \tag{14.280}$$

Inserting this (two-term) expansion into (14.275) gives

$$\mathbf{V}(z) = \left(C_a\, e^{-\gamma_a z} + D_a\, e^{\gamma_a z}\right)\mathbf{x}^a + \left(C_b\, e^{-\gamma_b z} + D_b\, e^{\gamma_b z}\right)\mathbf{x}^b. \tag{14.281}$$

More explicitly:

$$\begin{aligned} \begin{pmatrix} V_1 \\ V_2 \end{pmatrix} = &\begin{pmatrix} x_1^a & x_1^b \\ x_2^a & x_2^b \end{pmatrix} \cdot \begin{pmatrix} e^{-\gamma_a z} & 0 \\ 0 & e^{-\gamma_b z} \end{pmatrix} \cdot \begin{pmatrix} C_a \\ C_b \end{pmatrix} \\ &+ \begin{pmatrix} x_1^a & x_1^b \\ x_2^a & x_2^b \end{pmatrix} \cdot \begin{pmatrix} e^{\gamma_a z} & 0 \\ 0 & e^{\gamma_b z} \end{pmatrix} \cdot \begin{pmatrix} D_a \\ D_b \end{pmatrix}. \end{aligned} \tag{14.282}$$

This expression contains the *circuit voltage matrix*

$$\overline{\overline{V}}_c = \begin{pmatrix} x_1^a & x_1^b \\ x_2^a & x_2^b \end{pmatrix} = \mathbf{x}^a \mathbf{u}_1 + \mathbf{x}^b \mathbf{u}_2, \tag{14.283}$$

where $\mathbf{u}_1$ and $\mathbf{u}_2$ are formal unit vectors satisfying the condition $\mathbf{u}_i \cdot \mathbf{u}_k = \delta_{ik}$. An analogous (dual) approach for $\mathbf{I}$ is based on the eigenvectors of $\left(\overline{\overline{Y}} \cdot \overline{\overline{Z}}\right)$, which are the solutions of

$$\begin{aligned} \left(\overline{\overline{Y}} \cdot \overline{\overline{Z}}\right) \cdot \mathbf{y}^a &= \lambda_a^2 \mathbf{y}^a \\ \left(\overline{\overline{Y}} \cdot \overline{\overline{Z}}\right) \cdot \mathbf{y}^b &= \lambda_b^2 \mathbf{y}^b. \end{aligned} \tag{14.284}$$

A solution of the first equation is $\mathbf{y}^a = \overline{\overline{Z}}^{-1} \cdot \mathbf{x}^a$. To prove this assertion, note first that

$$\left(\overline{\overline{Y}} \cdot \overline{\overline{Z}}\right) \cdot \left(\overline{\overline{Z}}^{-1} \cdot \mathbf{x}^a\right) = \overline{\overline{Y}} \cdot \mathbf{x}^a,$$

where use has been made of the property

$$(\overline{\overline{a}} \cdot \overline{\overline{b}}) \cdot \overline{\overline{c}} = \overline{\overline{a}} \cdot (\overline{\overline{b}} \cdot \overline{\overline{c}}). \tag{14.285}$$

But (14.279), premultiplied by $\overline{\overline{Z}}^{-1}$, gives

$$\overline{\overline{Y}} \cdot \mathbf{x}^a = \gamma_a^2 \left(\overline{\overline{Z}}^{-1}\right) \cdot \mathbf{x}^a$$

and, equivalently,

$$\left(\overline{\overline{Y}} \cdot \overline{\overline{Z}}\right) \cdot \left(\overline{\overline{Z}}^{-1} \cdot \mathbf{x}^a\right) = \gamma_a^2 \left(\overline{\overline{Z}}^{-1} \cdot \mathbf{x}^a\right).$$

We may therefore set

$$\begin{aligned} \mathbf{y}^a &= A\left(\overline{\overline{Z}}^{-1}\right)\cdot\mathbf{x}^a \qquad (\text{with } \lambda_a^2=\gamma_a^2)\\ \mathbf{y}^b &= B\left(\overline{\overline{Z}}^{-1}\right)\cdot\mathbf{x}^b \qquad (\text{with } \lambda_b^2=\gamma_b^2), \end{aligned} \tag{14.286}$$

where A and B are undetermined coefficients. We could first choose solution $A=\gamma_a$, viz.

$$\begin{aligned} \mathbf{x}^a &= \gamma_a\,\overline{\overline{Y}}^{-1}\cdot\mathbf{y}^a\\ \mathbf{y}^a &= \gamma_a\,\overline{\overline{Z}}^{-1}\cdot\mathbf{x}^a, \end{aligned} \tag{14.287}$$

where the second equation is an immediate consequence of the first. Similar choices are made for $\mathbf{x}^b$ and $\mathbf{y}^b$. Under these conditions, the ratio (x_a/y_a) has the dimension Ω. We could therefore give $\mathbf{x}^a$, used to expand $\mathbf{V}$, the dimension Volt, and to $\mathbf{y}^a$, used for $\mathbf{I}$, the dimension Ampère. *Alternately*, we could require $\mathbf{x}^a$ and $\mathbf{y}^a$ to have the same dimension, which can be achieved by replacing $\overline{\overline{Z}}$ and $\overline{\overline{Y}}$ by values normalized with respect to a reference, say 50 Ω or R_{c0}. We choose

$$\begin{aligned} \overline{\overline{Z}}' &= \frac{1}{R_{c0}}\,\overline{\overline{Z}} \qquad (\mathrm{m}^{-1})\\ \overline{\overline{Y}}' &= R_{c0}\,\overline{\overline{Y}} \qquad (\mathrm{m}^{-1}) \end{aligned}$$

and replace (14.287) by

$$\begin{aligned} \mathbf{x}^a &= \gamma_a\left(\overline{\overline{Y}}'\right)^{-1}\cdot\mathbf{y}^a\\ \mathbf{y}_a &= \gamma_a\left(\overline{\overline{Z}}'\right)^{-1}\cdot\mathbf{x}^a. \end{aligned} \tag{14.288}$$

The second equation is again a consequence of the first. We shall choose both $\mathbf{x}^a$ and $\mathbf{y}^a$ to be dimensionless. In the expansion (14.282), the coefficients C and D are now voltages. The same kind of analysis can now be made for the currents. The dual of (14.281), for example, is

$$\mathbf{I}(z)=\left(F_a\,e^{-\gamma_a z}+G_a\,e^{\gamma_a z}\right)\mathbf{y}^a+\left(F_b\,e^{-\gamma_b z}+G_b\,e^{\gamma_b z}\right)\mathbf{y}^b. \tag{14.289}$$

In full:

$$\begin{aligned} \begin{pmatrix} I_1\\ I_2 \end{pmatrix} &= \begin{pmatrix} y_1^a & y_1^b\\ y_2^a & y_2^b \end{pmatrix}\cdot\begin{pmatrix} e^{-\gamma_a z} & 0\\ 0 & e^{-\gamma_b z} \end{pmatrix}\cdot\begin{pmatrix} F_a\\ F_b \end{pmatrix}\\ &\quad+\begin{pmatrix} y_1^a & y_1^b\\ y_2^a & y_2^b \end{pmatrix}\cdot\begin{pmatrix} e^{\gamma_a z} & 0\\ 0 & e^{\gamma_b z} \end{pmatrix}\cdot\begin{pmatrix} G_a\\ G_b \end{pmatrix}. \end{aligned} \tag{14.290}$$

This expression contains the *circuit current matrix*

$$\overline{\overline{I}}_c=\begin{pmatrix} y_1^a & y_1^b\\ y_2^a & y_2^b \end{pmatrix}=\mathbf{y}^a\,\mathbf{u}_1+\mathbf{y}^b\,\mathbf{u}_2. \tag{14.291}$$

With the choice (14.288), the expansions for $\mathbf{V}$ and $\mathbf{I}$ are related by

$$\begin{aligned}\mathbf{I}(z) &= -\left(\overline{\overline{Z}}\right)^{-1}\cdot\frac{d\mathbf{V}}{dz} \;=\; -R_{c0}^{-1}\left(\overline{\overline{Z}}'\right)^{-1}\cdot\frac{d\mathbf{V}}{dz}\\ &= \frac{1}{R_{c0}}\left(C_a\,e^{-\gamma_a z}-D_a\,e^{\gamma_a z}\right)\underbrace{\gamma^a\left(\overline{\overline{Z}}'\right)^{-1}\cdot\mathbf{x}^a}_{\mathbf{y}^a}\\ &\quad+\left(C_b\,e^{-\gamma_b z}-D_b\,e^{\gamma_b z}\right)\underbrace{\gamma_b\left(\overline{\overline{Z}}'\right)^{-1}\cdot\mathbf{x}^b}_{\mathbf{y}^b}.\end{aligned}\tag{14.292}$$

Comparison with (14.290) shows that $F_a = C_a R_{c0}^{-1}$ and $G_a = -D_a R_{c0}^{-1}$, with similar relationships for F_b and G_b.

14.12.4 Orthogonality and Normalization

We shall assume that the $\overline{\overline{Z}}$ and $\overline{\overline{Y}}$ matrices are symmetric, which is always the case when the transmission line is reciprocal [105]. Reciprocity for a line holds when, given two arbitrary pairs of line voltages and currents $(\mathbf{v}_m, \mathbf{i}_m)$ and $(\mathbf{v}_n, \mathbf{i}_n)$, the following condition is satisfied:

$$\frac{d}{dz}\left[\mathbf{v}_m(z)\cdot\mathbf{i}_n(z)-\mathbf{i}_m(z)\cdot\mathbf{v}_n(z)\right]=0.$$

Propagation in a reciprocal line is governed by the same constant γ for both directions, hence waves $e^{-\gamma z}$ and $e^{\gamma z}$ may exist on the line. If the latter is lossless,[†††] $\overline{\overline{L}}$ and $\overline{\overline{C}}$ are symmetric, and $\overline{\overline{R}} = \overline{\overline{G}} = 0$. If $j\overline{\overline{Z}}$ and $j\overline{\overline{Y}}$ are both positive-definite (or both negative-definite), γ will be imaginary. If one of the two is positive-definite and the other negative-definite, γ will be real. If nothing can be concluded regarding the definiteness of $j\overline{\overline{Z}}$ and $j\overline{\overline{Y}}$, then some of the γ's are real and some imaginary [105].

After this incursion into the properties of more general transmission lines, we revert to the orthogonality properties associated with *symmetric* $\overline{\overline{Z}}$ and $\overline{\overline{Y}}$. For such matrices, (14.278) shows that $\overline{\overline{Y}}\cdot\overline{\overline{Z}}$ is the adjoint (or transpose) of $\overline{\overline{Z}}\cdot\overline{\overline{Y}}$. We may therefore write, applying (A4.22),

$$\mathbf{b}\cdot\left[\left(\overline{\overline{Z}}\cdot\overline{\overline{Y}}\right)\cdot\mathbf{c}\right]=\mathbf{b}\cdot\left[\mathbf{c}\cdot\left(\overline{\overline{Y}}\cdot\overline{\overline{Z}}\right)\right]=\mathbf{c}\cdot\left[\left(\overline{\overline{Y}}\cdot\overline{\overline{Z}}\right)\cdot\mathbf{b}\right].\tag{14.293}$$

Premultiplication of (14.279) with $\mathbf{y}^n$, and of (14.284) with $\mathbf{x}^m$, (where m, n stand for a or b) gives

$$\begin{aligned}\mathbf{y}^n\cdot\left(\overline{\overline{Z}}\cdot\overline{\overline{Y}}\right)\cdot\mathbf{x}^m &= \gamma_m^2\mathbf{y}^n\cdot\mathbf{x}^m\\ \mathbf{x}^m\cdot\left(\overline{\overline{Y}}\cdot\overline{\overline{Z}}\right)\cdot\mathbf{y}^n &= \gamma_n^2\mathbf{x}^m\cdot\mathbf{y}^n.\end{aligned}$$

[†††] When the lossless line is *nonreciprocal*, $\overline{\overline{L}}$ and $\overline{\overline{C}}$ remain symmetric, but $\overline{\overline{R}}$ and $\overline{\overline{G}}$ are anti symmetric [105].

It follows from (14.293) that $\mathbf{x}^m \cdot \mathbf{y}^n = 0$ for $\gamma_m^2 \neq \gamma_n^2$. The eigenvectors therefore satisfy the *biorthogonality* properties

$$\begin{aligned} \mathbf{x}^a \cdot \mathbf{y}^b &= 0 \\ \mathbf{x}^b \cdot \mathbf{y}^a &= 0. \end{aligned} \tag{14.294}$$

Normalization is effected by means of the conditions (Problem 14.23)

$$\begin{aligned} \mathbf{x}^a \cdot \mathbf{y}^a &= 1 \\ \mathbf{x}^b \cdot \mathbf{y}^b &= 1, \end{aligned} \tag{14.295}$$

which imply that the eigenvectors are dimensionless. From (14.283) and (14.291), such a choice leads to the property

$$\overline{\overline{V}}_c^t \cdot \overline{\overline{I}}_c = \overline{\overline{I}} \tag{14.296}$$

or, equivalently,

$$\overline{\overline{V}}_c^t = \left(\overline{\overline{I}}_c\right)^{-1}. \tag{14.297}$$

The concept of *characteristic impedance* (and *admittance*), familiar from elementary transmission line theory, can be introduced by means of the definitions

$$\begin{aligned} \overline{\overline{Z}}'_c &= \overline{\overline{V}}_c \cdot \left(\overline{\overline{I}}_c\right)^{-1} = \overline{\overline{V}}_c \cdot \overline{\overline{V}}_c^t = \mathbf{x}^a\mathbf{x}^a + \mathbf{x}^b\mathbf{x}^b \\ \overline{\overline{Y}}'_c &= \overline{\overline{I}}_c \cdot \left(\overline{\overline{V}}_c\right)^{-1} = \overline{\overline{I}}_c \cdot \overline{\overline{I}}_c^t = \mathbf{y}^a\mathbf{y}^a + \mathbf{y}^b\mathbf{y}^b. \end{aligned} \tag{14.298}$$

If we consider the wave to the right,

$$\mathbf{V}(z) = C_a\, e^{-\gamma_a z}\mathbf{x}^a + C_b\, e^{-\gamma_b z}\,\mathbf{x}^b,$$

we may expect $\mathbf{I}(z)$ to be given by $\overline{\overline{Y}}_c \cdot \mathbf{V}(z)$. The verification is immediate, because

$$\overline{\overline{Y}}'_c \cdot \mathbf{x}^a = \mathbf{y}^a \underbrace{\mathbf{y}^a \cdot \mathbf{x}^a}_{1} + \mathbf{y}^b \underbrace{\mathbf{y}^b \cdot \mathbf{x}^a}_{0} = \mathbf{y}^a.$$

As a result,

$$\mathbf{I}(z) = \frac{1}{R_{c0}}\left[C_a\, e^{-\gamma_a z}\,\mathbf{y}^a + C_b\, e^{-\gamma_b z}\,\mathbf{y}^b\right],$$

which is precisely the form obtained in (14.292). The line impedance and admittance can also be expressed in terms of the eigenvectors. Thus (Problem 14.25),

$$\begin{aligned} \overline{\overline{Z}}' &= \gamma_a\,\mathbf{x}^a\mathbf{x}^a + \gamma_b\,\mathbf{x}^b\mathbf{x}^b \\ \overline{\overline{Y}}' &= \gamma_a\,\mathbf{y}^a\mathbf{y}^a + \gamma_b\,\mathbf{y}^b\mathbf{y}^b. \end{aligned} \tag{14.299}$$

The complex power that flows down the lines, that is, $P(z) = 1/2VI^*$, can easily be derived from (14.281) and (14.292). The resulting expression contains terms in $\mathbf{x}^a \cdot (\mathbf{y}^a)^*$ or $\mathbf{x}^b \cdot (\mathbf{y}^b)^*$ that do not, in general, obey orthonormal conditions such as (14.294) or (14.295). The form of $P(z)$ becomes much simpler, however, when the line is reciprocal and lossless, in which case $\mathbf{x}$ and $\mathbf{y}$ can be chosen real and γ imaginary. If we set $\gamma = j\beta$:

$$P(z) = \frac{1}{2}\mathbf{V}\cdot\mathbf{I}^* = \frac{1}{2}\left[|C_a|^2 - |D_a|^2 + C_a^* D_a\, e^{2j\beta_a z} - C_a D_a^*\, e^{-2j\beta_a z}\right] + \frac{1}{2}\left[|C_b|^2 - |D_b|^2 + C_b^* D_b\, e^{2j\beta_b z} - C_b D_b^*\, e^{-2j\beta_b z}\right]. \tag{14.300}$$

It is also useful to introduce the *field expression* $s(z) = \dfrac{1}{2}\mathbf{V}\cdot\mathbf{I}$. In the evaluation of $s(z)$, terms such as $\mathbf{x}^a \cdot \mathbf{y}^a$ or $\mathbf{x}^b \cdot \mathbf{y}^b$ appear, and the orthonormal conditions may immediately be applied. Thus, even if the line is lossy,

$$s(z) = \frac{1}{2}\mathbf{V}\cdot\mathbf{I} = \frac{1}{2}\left(C_a^2 e^{-2\gamma_a z} - D_a^2\, e^{2\gamma_a z} + C_b^2\, e^{-2\gamma_b z} - D_b^2\, e^{2\gamma_b z}\right). \tag{14.301}$$

Note that, by introducing the factors $\dfrac{1}{2}$ in both $p(z)$ and $s(z)$, we have assumed that $|\mathbf{V}|$ and $|\mathbf{I}|$ represent the *peak* values of voltage or current.

PROBLEMS

14.1 Verify that the Green's function (14.12) is the solution of (14.11).

14.2 Let an electric current be distributed on a circular cylindrical surface with a density $\mathbf{J}_S = \cos\varphi\,\mathbf{u}_z$. Use the ansatz $E_z = \cos\varphi f(r)$ to show that the exterior field, for $r > a$, is [22]

$$E_z = R_{c0}\frac{\pi}{2}k_0 a\, J_1(k_0 a) H_1^{(2)}(k_0 r)\cos\varphi.$$

14.3 Show that the extinction cross section (14.32) is given by

$$\sigma^{ext} = \frac{P^{abs} + P^{sc}}{\dfrac{1}{2}R_{c0}} = -\frac{4}{k_0}\,\mathrm{Re} f(\mathbf{u}|\mathbf{u})$$

for a plane wave of unit electric field propagating in the $\mathbf{u}$ direction. This is the two-dimensional form of (11.30). Extend the analysis to an H-wave [22].

14.4 Show that, on a circular contour C_0 of radius a,

$$\frac{\partial\phi^{sc}}{\partial r} = \frac{k_0}{2\pi}\sum_{n=-\infty}^{\infty}\frac{1}{H_n^{(2)}(k_0 a)}\left[\frac{dH_n^{(2)}(x)}{dx}\right]_{x=k_0 a}\int_0^{2\pi}\phi^{sc}(a,\varphi')\, e^{jn(\varphi-\varphi')}\, d\varphi'.$$

This is an (integral) boundary relationship of the type

$$\frac{\partial\phi^{sc}}{\partial r} + \gamma(\phi^{sc}) = 0 \qquad \text{for } r = a.$$

Show also that the incident field — a plane wave — satisfies

$$\frac{\partial \phi^i}{\partial r} = \frac{k_0}{2\pi} \sum_{n=-\infty}^{\infty} \frac{J_n'(k_0 a)}{J_n(k_0 a)} \int_0^{2\pi} \phi^i(a, \varphi')\, e^{jn(\varphi - \varphi')}\, d\varphi'.$$

Combine the two expansions to find a relationship between the total ϕ and $\dfrac{\partial \phi}{\partial r}$ [192, 203].

14.5 Set up the scattering problem for a circular cylinder filled with a homogeneous superconducting medium. Model the medium by the dielectric constant ϵ_r given in (8.28), in terms of which the characteristic impedance is ($Z_c = R_{c0}/\sqrt{\epsilon_r}$). Consider both E and H incident waves [32].

14.6 Determine the scattered fields for a plane wave of either E or H type, incident on a circular cylinder of given uniform ϵ_r. Use separation of variables [8].

14.7 Determine the characteristic modes of the boundary of an elliptic cylinder. (G. Amendola et al., *Microwave Opt. Tech. Lett.* **16**, 243–249, 1997.)

14.8 A thin circular shell of (small) thickness d is immersed in an E-wave. In the limit $d \to 0$, J_z in the shell may be assumed uniform across the shell and replaced by a surface current $J_{Sz} = J_z d$. Show that the fictitious surface current satisfies the integral equation

$$Z J_{Sz}(\mathbf{r}) + \frac{k_0 R_{c0}}{4} \int_C J_{Sz}(c') H_0^{(2)}(k_0 |\mathbf{r} - \mathbf{r}'|)\, dc' = E^i(\mathbf{r}).$$

If the shell material is a good conductor, with negligible displacement current, Z becomes $Z = 1/\sigma d$. (T. K. Wu et al., *IEEE Trans. EMC* **20**, 349–351, 1978.)

14.9 The scattered field in an E-wave is of the general form

$$E^{sc} = \frac{e^{-jk_0 r}}{\sqrt{r}} f(\varphi).$$

Let $f(\mathbf{u}|\mathbf{u}')$ refer to scattering in a direction $\mathbf{u}'$ for a plane wave incident in a direction $\mathbf{u}$. Prove the reciprocity relationship

$$f(\mathbf{u}'|\mathbf{u}) = f(-\mathbf{u}| - \mathbf{u}').$$

14.10 A perfectly conducting sheet (often termed *lamina*) is immersed in an incident plane wave. Show that the problem can be formulated in terms of an integral equation. (A. W. Maue, *Z. Phys.* **126**, 601, 1949.)

14.11 When k_0 coincides with an eigenvalue of the cross section, the homogeneous version of (14.101) has a nontrivial solution. For such a case, (14.101) has either an infinite number of solutions or none, depending on the value of E^i. Show that solutions *do* exist. *Hint*: Apply Green's theorem A1.31 to ϕ_m and E^i.

14.12 Show analogously that (14.110) has an infinite number of solutions for $k_0 = k_m$ by checking that Fredholm's alternative is satisfied. In the current case, the condition is

$$\int_C H^i \frac{\partial \phi_m}{\partial n}\, dc = 0.$$

Hint: Apply Green's theorem A1.31 to H^i and ϕ^m.

14.13 Consider the multipole expansion (14.148), and let J consist of two sources of zero total value (i.e., such that $\int J\, dS = 0$). Show that the radiation pattern is that of a dipole source, and find the equivalent line configuration. *Hint*: Try two lines carrying opposite currents.

14.14 Equation (14.164) gives the low-frequency limit of the scattering cross section of a dielectric cylinder. Verify the validity of this expression by considering the particular case of a circular cylinder, for which σ^{sc} can be determined by separation of variables.

Figure P14.1

14.15 Taking electric-wall symmetries into account, investigate low-frequency scattering by a perfectly conducting cylindrical bump (Fig. P14.1). (T. B. Hansen et al., *IEEE Trans. AP* **40**, 1389–1402, 1992.)

14.16 Starting from (14.190), derive an expression for the far field in half-space 2. Show that the directional properties in a direction of unit vector $\mathbf{u}$ are governed by the value of the integral

$$\int_A^B E_y(y')\, e^{jk_0(\mathbf{u}\,\cdot\,\mathbf{u}_y)}\, dy'.$$

Specialize to a narrow slot, and evaluate the transmission cross section. *Hint*: Use asymptotic form (14.13).

14.17 Solve the H-field equation (14.192) by replacing $E_n(y)$ by the approximation

$$E_n(y) = \frac{C_{n0}T_0\left(\frac{y}{w}\right) + C_{n1}T_1\left(\frac{y}{w}\right) + C_{n2}T_2\left(\frac{y}{w}\right)}{\sqrt{w^2 - y^2}}.$$

From (A5.191):

$$E_1(y) \doteq \frac{1}{\sqrt{w^2 - y^2}}; \qquad E_2(y) \doteq \frac{y}{w\sqrt{w^2 - y^2}}$$

$$E_3(y) \doteq \frac{2y^2 - w^2}{w^2\sqrt{w^2 - y^2}}.$$

Show that the solution for a narrow slot is

$$J_{mS}(y) \approx \frac{1}{2k_0\sqrt{w^2 - y^2}}\left[\frac{jR_{c0}H^g(0)}{\log_e\left(\frac{\gamma k_0 w}{4}\right) + j\frac{\pi}{2}} + k_0 y\, E_x^g(0)\right].$$

(K. Y. Kabalan et al., *IEEE Trans. AP* **35**, 162–168, 1987.)

14.18 Repeat this analysis for an incident E-wave, but express the basis functions J_n in terms of Chebyshev polynomials of the second kind, U_0, U_1, and U_2. From (A5.197),

$$J_1(y) \doteq \sqrt{w^2 - y^2}; \qquad J_2(y) \doteq \frac{y}{w}\sqrt{w^2 - y^2}; \qquad J_3(y) \doteq \frac{4y^2 - w^2}{w^2}\sqrt{w^2 - y^2}.$$

Show that the solution of (14.184) for a narrow slot is

$$J_{mS}(y) = \frac{jk_0R_{c0}}{2}\sqrt{w^2 - y^2}\left[H_y^g(0) + \frac{y}{2}\left(\frac{d}{dy}H_y^g\right)_0 + \cdots\right].$$

(H. Y. Kabalan et al., *IEEE Trans. AP* **35**, 331–335, 1987.)

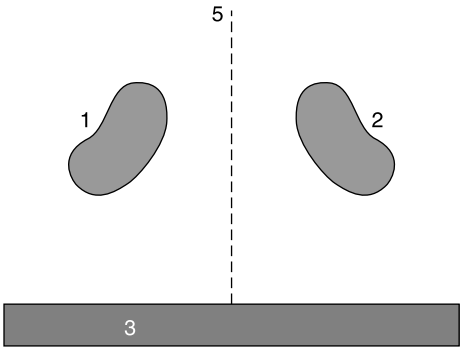

Figure P14.2

14.19 Determine the value of the elements of the equivalent circuit in Figure 14.23*c* when the slot in the thick screen is filled with a material of given (ϵ_r, μ_r). (D. T. Auckland et al., *IEEE Trans. MTT* **26**, 499–505, 1978.)

14.20 The fields of an H-wave that penetrates into a circular cylinder through a slot can be determined by separation of variables. Express $\mathbf{E}_t$ and H_z as a Fourier series in $e^{jm\varphi}$, both outside and inside the cylinder, and determine the unknown coefficients by requiring H_z to be continuous in the slot. (W. A. Johnson et al., *Radio Sci.* **19**, 275–291, 1984.)

14.21 Repeat for a slotted elliptic cylinder, possibly covered with a dielectric layer. Use expansions in Mathieu functions.
(J. H. Richmond, *IEEE Trans. AP* **37**, 1235–1241, 1989, and M. Hussein et al., *IEEE Trans. EMC* **36**, 76–81, 1994.)

14.22 Check that the dyadic relationship (14.285) is valid.

14.23 Starting with given $\mathbf{x}^a$ and $\mathbf{x}^b$, show that corresponding $\mathbf{y}^a$ and $\mathbf{y}^b$ can be found that satisfy the normalization conditions (14.295). *Hint*: Use (14.287).

14.24 Let lines 1 and 2 display the symmetry shown in Figure P14.2, so that $Z_{11} = Z_{22} = Z$. Show that the a and b eigenvectors are respectively symmetric or anti symmetric with respect to S. Determine the characteristic impedances of these modes. Write down the explicit expansions (14.282) and (14.289) that hold when the lines are lossless. *Hint*: $\mathbf{x}^a \doteq (1, 1)$; $\mathbf{x}^b \doteq (1, -1)$.

14.25 On the basis of (14.299), evaluate $\overline{\overline{Z}} \cdot \overline{\overline{Y}}$ and $\overline{\overline{Y}} \cdot \overline{\overline{Z}}$. Use these forms to verify the eigenvector equations (14.279) and (14.284).

NOTES

1. I. R. Ciric and J. Ma, Transient currents on a cylinder excited by a parallel line-current, *Can. J. Phys.* **69**, 1242–1248 (1991).
2. T. T. Wu, High-frequency scattering, *Phys. Rev.* **104**, 1201–1212 (1956).
3. J. Ma and I. R. Ciric, Transient response of a circular cylinder to an electromagnetic pulse, *Radio Sci.* **27**, 561–567 (1992).
4. J. Ma and I. R. Ciric, Early-time currents induced on a cylinder by a cylindrical electromagnetic wave, *IEEE Trans. AP* **39**, 455–463 (1991).
5. H. E. Bussey and J. H. Richmond, Scattering by a lossy dielectric circular cylindrical multilayer, numerical values, *IEEE Trans. AP* **23**, 723–725 (1975). Correction in **43**, 751 (1995).
6. I. V. Lindell and K. I. Nikoskinen, Two-dimensional image method for time-harmonic line current in front of a material cylinder, *Electrical Eng.* **81**, 357–362 (1999).
7. I. V. Lindell and K. I. Nikoskinen, Two-dimensional image method for time-harmonic line current in front of a PEC cylinder, *Microwave Opt. Tech. Lett.* **21**, 217–222 (1999).
8. J. Van Bladel, Penetration of a low-frequency E-wave into a conducting circular cylinder, *IEEE Trans. EMC* **37**, 536–542 (1995).

9. J. Van Bladel, Penetration of a low-frequency H-wave into a conducting circular cylinder, *IEEE Trans. EMC* **38**, 441–449 (1996).
10. B. Sieger, Die Beugung einer ebenen elektrischen Welle an einen Schirm von elliptischen Querschnitt, *Ann. Physik* **27**, 626–664 (1908).
11. R. Barakat, Diffraction of plane waves by an elliptic cylinder, *J. Acoust. Soc. Am.* **35**, 1990–1996 (1963).
12. S. Caorsi, M. Pastorino, and M. Raffetto, Electromagnetic scattering by a multilayer elliptic cylinder under transverse-magnetic illumination: Series solution in terms of Mathieu functions, *IEEE Trans. AP* **45**, 926–935 (1997).
13. S. Caorsi, M. Pastorino, and M. Raffetto, Electromagnetic scattering by weakly lossy multilayer elliptic cylinders, *IEEE Trans. AP* **46**, 1750–1751 (1998).
14. S. Caorsi, M. Pastorino, and M. Raffetto, EM field prediction inside lossy multilayer elliptic cylinders for biological-body modeling and numerical-procedure testing, *IEEE Trans. Biomed. Eng.* **46**, 1304–1309 (1999).
15. J. E. Burke, Low-frequency approximations for scattering by penetrable elliptic cylinders, *J. Acoust. Soc. Am.* **36**, 2059–2070 (1964).
16. C. Yeh, Backscattering cross section of a dielectric elliptical cylinder, *J. Opt. Soc. Am.* **55**, 309–314 (1965).
17. R. Holland and V. P. Cable, Mathieu functions and their applications to scattering by a coated strip, *IEEE Trans. EMC* **34**, 9–16 (1992).
18. P. L. E. Uslenghi, Exact scattering by isorefractive bodies, *IEEE Trans. AP* **45**, 1382–1385 (1997).
19. A. R. Lopez, Cellular telecommunications: estimating shadowing effects using wedge diffraction, *IEEE Antennas Prop. Mag.* **40**, 53–57 (1998).
20. A. Ciarkowski, J. Boersma, and R. Mittra, Plane-wave diffraction by a wedge — a spectral domain approach, *IEEE Trans. AP* **32**, 20–29 (1984).
21. L. Knockaert, F. Olyslager, and D. De Zutter, The diaphanous wedge, *IEEE Trans. AP* **45**, 1374–1381 (1997).
22. T. B. A. Senior, Solution of a class of imperfect wedge problems for skew incidence, *Radio Sci.* **21**, 185–191 (1986).
23. T. B. A. Senior and S. R. Legault, Second-order difference equations in diffraction theory, *Radio Sci.* **35**, 683–690 (2000).
24. D. S. Jones, Impedance of an absorbing wedge, *Quart. J. Mech. Appl. Math.* **54**, 257–271 (2000).
25. D. S. Jones, Impedance of a lossy wedge, *IMA Journ. Appl. Math.* **66**, 411–422 (2001).
26. J. Bach Andersen and V. V. Solodukhov, Field behavior near a dielectric wedge, *IEEE Trans. AP* **26**, 598–602 (1978).
27. E. Marx, Computed fields near the edge of a dielectric wedge, *IEEE Trans. AP* **38**, 1438–1442 (1990).
28. E. Marx, Electromagnetic scattering from a dielectric wedge and the single hypersingular integral equation, *IEEE Trans. AP* **41**, 1001–1008 (1993).
29. H. A. Schenk, Improved integral formulation for acoustic radiation problems, *J. Acoust. Soc. Am.* **44**, 41–58 (1968).
30. K. K. Mei and J. Van Bladel, Scattering by perfectly conducting rectangular cylinders, *IEEE Trans. AP* **11**, 185–192 (1963).
31. M. G. Andreasen, Comments on "Scattering by conducting rectangular cylinders", *IEEE Trans. AP* **12**, 235–236 (1964).
32. A. W. Maue, Zur Formulierung eines Allgemeinen Beugeugsproblem durch eine Integralgleichung, *Z. physik* **126**, 601–618 (1949).
33. A. F. Peterson, The "interior resonance" problem associated with surface integral equations of electromagnetics: numerical consequences and a survey of remedies, *Electromagn.* **10**, 293–312 (1990).
34. D. R. Wilton and S. Govind, Incorporation of edge conditions in moment method solution, *IEEE Trans. AP* **25**, 845–850 (1977).
35. A. W. Glisson and D. R. Wilton, Simple and efficient numerical methods for problems of electromagnetic radiation and scattering from surfaces, *IEEE Trans. AP* **28**, 593–603 (1980).
36. R. Coifman, V. Rokhlin, and S. Wandzura, The fast multipole method for the wave equation: a pedestrian description, *IEEE Antennas Prop. Mag.* **35**, 7–12 (1993).
37. V. Rokhlin, Rapid solution of integral equations of scattering theory in two dimensions, *J. Comput. Phys.* **86**, 414–439 (1990).
38. N. Engheta, W. O. Murphy, V. Rokhlin, and M. S. Vassiliou, The fast multipole method (FMM) for electromagnetic scattering problems, *IEEE Trans. AP* **40**, 634–641 (1992).
39. W. C. Chew, J. M. Jin, C. C. Lu, E. Michielssen, and J. M. Song, Fast solution methods in electromagnetics, *IEEE Trans. AP* **45**, 533–543 (1997).
40. E. Michielssen and W. C. Chew, Fast steepest descent path algorithm for analyzing scattering from two-dimensional objects, *Radio Sci.* **31**, 1215–1224 (1996).
41. B. Hu, W. C. Chew, E. Michielssen, and J. Zhao, Fast inhomogeneous plane wave algorithm for the fast analysis of two-dimensional scattering problems, *Radio Sci.* **34**, 759–772 (1999).
42. S. K. Han, E. Michielssen, B. Shankar, and W. C. Chew, Impedance matrix localization based fast multipole acceleration, *Radio Sci.* **33**, 1475–1488 (1998).
43. C. C. Lu and W. C. Chew, A multilevel algorithm for solving a boundary integral equation of wave scattering, *Microwave Opt. Tech. Lett.* **7**, 466–470 (1994).
44. E. Michielssen and A. Boag, A multilevel matrix decomposition algorithm for analyzing scattering from large structures, *IEEE Trans. AP* **44**, 1086–1093 (1996).
45. J. M. Song, C. C. Lu, and W. C. Chew, Multilevel fast multipole algorithm for electromagnetic scattering by large complex objects, *IEEE Trans. AP* **45**, 1488–1493 (1997).
46. F. X. Canning, The impedance matrix localization method for moment-method calculations, *IEEE Antennas Prop. Mag.* **32**, 18–30 (1990).

47. F. X. Canning, Improved impedance matrix localization method, *IEEE Trans. AP* **41**, 659–667 (1993).
48. J. S. Zhao and W. C. Chew, MLFMA for solving integral equations of 2-D electromagnetic problems from static to electrodynamic, *Microwave Opt. Tech. Lett.* **20**, 306–311 (1999).
49. J. S. Zhao and W. C. Chew, Three-dimensional multilevel fast multipole algorithm from static to electrodynamic, *Microwave Opt. Tech. Lett.* **26**, 43–48 (2000).
50. T. K. Wu and L. L. Tsai, Electromagnetic fields induced inside arbitrary cylinders of biological tissue, *IEEE Trans. MTT* **25**, 61–65 (1977).
51. T. K. Wu and L. Tsai, Scattering by arbitrarily cross-sectioned layered lossy dielectric cylinders, *IEEE Trans. AP* **25**, 518–524 (1977).
52. J. H. Richmond, Scattering by a dielectric cylinder of arbitrary cross section shape, *IEEE Trans. AP* **13**, 334–341 (1965).
53. J. M. Jin, V. V. Liepa, and C. T. Tai, A volume-surface integral equation for electromagnetic scattering by inhomogeneous cylinders, *J. Electromagn. Waves Appl.* **2**, 573–588 (1988).
54. M. F. Sultan and R. Mittra, An iterative moment method for analyzing the electromagnetic field distribution inside inhomogeneous lossy dielectric objects, *IEEE Trans. MTT* **33**, 163–168 (1985).
55. D. T. Borup and O. P. Gandhi, Calculation of high-resolution SAR distributions in biological bodies using the FFT algorithm and conjugate gradient method, *IEEE Trans. MTT* **33**, 417–419 (1985).
56. D. T. Borup, D. M. Sullivan, and O. P. Gandhi, Comparison of the FFT conjugate gradient method and the finite difference time-domain method for the 2-D absorption problem, *IEEE Trans. MTT* **35**, 383–395 (1987).
57. K. R. Umashankar, S. Nimmagadda, and A. Taflove, Numerical analysis of electromagnetic scattering by electrically large objects using spatial decomposition technique, *IEEE Trans. AP* **40**, 867–877 (1992).
58. D. R. Swatek and I. R. Ciric, A recursive single-source surface integral equation analysis for wave scattering by heterogeneous dielectric bodies, *IEEE Trans. AP* **48**, 1175–1785 (2000).
59. J. Wang, M. Lu, and E. Michielssen, A time-domain volume-integral equation approach for analyzing scattering from 2D nonlinear objects under TM illumination, *Microwave Opt. Tech. Lett.* **26**, 419–423 (2000).
60. D. A. Vechinski and S. M. Rao, Transient scattering by conducting cylinders — TE case, *IEEE Trans. AP* **40**, 1103–1106 (1992).
61. D. A. Vechinski and S. M. Rao, Transient scattering from dielectric cylinders: *E*-field, *H*-field, and combined field equations, *Radio Sci.* **27**, 611–622 (1992).
62. D. A. Vechinski and S. M. Rao, Transient scattering from two-dimensional dielectric cylinders of arbitrary shape, *IEEE Trans. AP* **40**, 1054–1060 (1992).
63. S. M. Rao, D. A. Vechinksi, and T. K. Sarkar, Transient scattering by conducting cylinders—implicit solution for the transverse electric case, *Microwave Opt. Techn. Lett.* **21**, 129–134 (1999).
64. S. Celozzi and M. Feliziani, Analysis of fast transient electromagnetic fields: a frequency dependent 2D procedure, *IEEE Trans. MAG* **28**, 1146–1149 (1992).
65. S. Gratkowski and M. Ziolkowski, Special finite element shape functions for 2D eddy current problems, *Arch. Elektrotechnik* **73**, 239–244 (1990).
66. Z. Pantic-Tanner, J. S. Savage, D. R. Tanner, and A.F. Peterson, Two-dimensional singular vector elements for finite-element analysis, *IEEE Trans. MTT* **46**, 178–184 (1998).
67. D. I. Kaklamani and H. T. Anastassiu, Aspects of the method of auxiliary sources (MAS) in computational electromagnetics, *IEEE Antennas Prop. Mag.* **44**, 48–64 (2002).
68. C. Hafner and N. Kuster, Computation of electromagnetic fields by the multiple multipole method (generalized multipole technique), *Radio Sci.* **26**, 291–297 (1991).
69. N. Kuster, Multiple multipole method for simulating EM problems involving biological bodies, *IEEE Trans. Biomed. Eng.* **40**, 611–620 (1993).
70. F. Obelleiro, J. L. Rodriguez, and A. G. Pino, Hybrid GMT-MoM method for solving electromagnetic scattering problems, *IEEE Trans. MAG* **33**, 1424–1427 (1997).
71. U. Jakobus, H. O. Ruoss, and F. M. Landstorfer, Analysis of electromagnetic scattering problems by an iterative combination of MoM with GMT using MPI for the communication, *Microwave Opt. Tech. Lett.* **19**, 1–4 (1998).
72. A. Boag and R. Mittra, Complex multipole beam approach to electromagnetic scattering problems, *IEEE Trans. AP* **42**, 366–372 (1994).
73. E. Erez and Y. Leviatan, Electromagnetic scattering analysis using a model of dipoles located in complex space, *IEEE Trans. AP* **42**, 1620–1624 (1994).
74. F. Obeilleiro, L. Landesa, J. L. Rodriguez, M.R. Pino, R.V. Sabariego, and Y. Leviatan, Localized iterative generalized multipole technique for large two-dimensional scattering problems, *IEEE Trans. AP* **49**, 961–970 (2001).
75. Y. Leviatan, Z. Baharav, and E. Heyman, Analysis of electromagnetic scattering using arrays of fictitious sources, *IEEE Trans. AP* **43**, 1091–1098 (1995).
76. M. Onda and A. Sebak, Scattering from lossy dielectric cylinders using a multifilament current model with impedance boundary conditions, *IEE Proc.* **139-H**, 429–434 (1992).
77. Y. Leviatan and A. Boag, Analysis of electromagnetic scattering from dielectric cylinders using a multifilament current model, *IEEE Trans. AP* **35**, 1119–1127 (1987).
78. Y. Leviatan and A. Boag, Analysis of TE scattering from dielectric cylinders using a multifilament magnetic current model, *IEEE Trans. AP* **36**, 1026–1031 (1988).
79. P. R. Renaud and J. J. Laurin, Shielding and scattering analysis of lossy cylindrical shells using an extended multifilament current approach, *IEEE Trans. EMC* **41**, 320–334 (1999).

80. J. Van Bladel, Low-frequency scattering by cylindrical bodies, *Appl. Sci. Res. B* **10**, 195–202 (1963).
81. R. De Smedt, Low-frequency illumination by an E-wave of infinitely long, parallel, perfect conductors, *URSI Radio Sci. Bull.* **305**, 23–31 (2003).
82. J. Van Bladel, Scattering of low-frequency E-waves by dielectric cylinders, *IEEE Trans. AP* **24**, 255–258 (1976).
83. T. B. Hansen and A. D. Yaghjian, Low-frequency scattering from two-dimensional perfect conductors, *IEEE Trans. AP* **40**, 1389–1402 (1992).
84. J. Van Bladel, Deep field penetration into a conducting cylinder, *IEEE Trans. EMC* **38**, 549–556 (1996).
85. C. M. Butler and K. R. Umashankar, Electromagnetic penetration through an aperture in an infinit e, planar screen separating two half spaces of different electromagnetic properties, *Radio Sci.* **11**, 611–619 (1976).
86. C. M. Butler and D. R. Wilton, General analysis of narrow strips and slots, *IEEE Trans. AP* **28**, 42–48 (1980).
87. C. M. Butler, General analysis of a narrow slot in a conducting screen between half-spaces of different electromagnetic properties, *Radio Sci.* **22**, 1149–1154 (1987).
88. A. Q. Martin and C. M. Butler, Current on an array of narrow strips at a planar interface for transverse magnetic excitation, *Radio Sci.* **33**, 231–237 (1998).
89. K. Y. Kabalan, R. F. Harrington, H. A. Auda, and J. R. Mautz, Characteristic modes for slots in a conducting plane, TE case, *IEEE Trans. AP* **35**, 162–168 (1987).
90. O. M. Bucci and G. Di Massa, Use of characteristic modes in multiple-scattering problems, *J. Phys. D. Appl. Phys.* **28**, 2235–2244 (1995).
91. K. Y. Kabalan, R. F. Harrington, J. R. Mautz, and H. A. Auda, Characteristic modes for a slot in a conducting plane, TM case, *IEEE Trans. AP* **35**, 331–335 (1987).
92. G. A. Deschamps and H. S. Cabayan, Antenna synthesis and solution of inverse problems by regularization methods, *IEEE Trans. AP* **20**, 268–274 (1972).
93. R. F. Harrington and D. T. Auckland, Electromagnetic transmission through narrow slots in thick conductings screens, *IEEE Trans. AP* **28**, 612–622 (1980).
94. N. A. Mc Donald, Electric and magnetic coupling through small apertures in shield walls of any thickness, *IEEE Trans. MTT* **20**, 689–695 (1972).
95. J. M. Jin and J. L. Volakis, Electromagnetic scattering by and transmission through a three-dimensional slot in a thick conducting plane, *IEEE Trans. AP* **39**, 543–550 (1991).
96. J. R. Mautz and R. F. Harrington, Electromagnetic penetration into a conducting circular cylinder through a narrow slot, TM case, *J. Electromagn. Waves Appl.* **2**, 269–293 (1988).
97. J. R. Mautz and R. F. Harrington, Electromagnetic penetration into a conducting circular cylinder through a narrow slot, TE case, *J. Electromagn. Waves Appl.* **3**, 307–336 (1989).
98. J. D. Schumpert and C. M. Butler, Penetration through slots in conducting cylinders—Part I: TE case, *IEEE Trans. AP* **46**, 1612–1621 (1998).
99. J. D. Schumpert and C. M. Butler, Penetration through slots in conducting cylinders—Part 2: TM case, *IEEE Trans. AP* **46**, 1622–1628 (1998).
100. S. K. Jeng, Scattering from a cavity-backed slit in a ground plane—TE case, *IEEE Trans. AP* **38**, 1523–1529 (1990).
101. S. K. Jeng and S. T. Tzeng, Scattering from a cavity-backed slit in a ground plane—TM case, *IEEE Trans. AP* **39**, 661–663 (1991).
102. G. Pelosi, R. Coccioli, G. Manara, and A. Monorchio, Scattering from axially slotted cylinders: a finite-element approach, *Microwave Opt. Tech. Lett.* **9**, 122–124 (1995).
103. S. M. Rao, G. K. Gothard, and D. R. Wilton, Application of finite-integral technique to electromagnetic scattering by two-dimensional cavity-backed aperture in ground plane, *IEEE Trans. AP* **46**, 679–685 (1998).
104. Y. L. Luo, K. M. Luk, and S. M. Shum, A novel exact two-point field equation for solving electromagnetic scattering problems, *IEEE Trans. AP* **46**, 1833–1841 (1998).
105. K. K. Mei, R. Pous, Z. Chen, Y. W. Liu, and M. Prouty, Measured equation of invariance, *IEEE Trans. AP* **42**, 320–328 (1994).
106. J. Chen, W. Hong, and J. M. Jin, An iterative measured equation technique for electromagnetic problems, *IEEE Trans. MTT* **46**, 25–30 (1998).
107. Y. W. Liu, E. K. N. Yung, and K. K. Mei, Interpolation, extrapolation and application of the measured equation of invariance to scattering by very large cylinders, *IEEE Trans. AP* **45**, 1325–1331 (1997).
108. Y. W. Liu, K. K. Mei, and K. N. Yung, The MEI-MoM method for solving conducting concave scattering, *Microwave Opt. Tech. Lett.* **18**, 375–377 (1998).
109. Y. W. Liu, Y. Song, Y. Zhao, and K. K. Mei, Scattering of 2-D conducting concave object by MoM matrix decomposition technique, *Microwave Opt. Tech. Lett.* **25**, 149–152 (2000).
110. W. Hong, Y. W. Liu, and K. K. Mei, Application of the measured equation of invariance to solve scattering problems involving a penetrable medium, *Radio Sci.* **29**, 897–906 (1994).
111. L. W. Pearson, A. F. Peterson, L. J. Bahrmasel, and R. A. Whitaker, Inward-looking and outward-looking formulations for scattering from penetrable objects, *IEEE Trans. AP* **40**, 714–720 (1992).
112. J. D. Collins, J. M. Jin, and J. L. Volakis, Eliminating interior resonances in finite element-boundary integral methods, *IEEE Trans. AP* **40**, 1583–1585 (1992).
113. T. Roy, T. K. Sarkar, A. R. Djordjević, and M. Salazar-Palma, A hybrid method solution of scattering by conducting cylinders (TM case), *IEEE Trans. MTT* **44**, 2145–2151 (1996).
114. J. P. Bérenger, Making use of the PML absorbing boundary condition in coupling and scattering FDTD computer codes, *IEEE Trans. EMC* **45**, 189–197 (2003).

115. J. M. Jin, J. L. Volakis, and V. V. Liepa, Fictitious absorber for truncating finite element meshes in scattering, *IEE Proc.* **139-H**, 472–476 (1992).
116. S. K. Chang and K. K. Mei, Application of the unimoment method to electromagnetic scattering of dielectric cylinders, *IEEE Trans. AP* **24**, 35–42 (1976).
117. K. K. Mei, Unimoment method for electromagnetic scattering, *J. Electromagn. Waves Appli.* **1**, 201–222 (1987).
118. P. B. Johns and R. L. Beurle, Numerical solution of 2-dimensional scattering problems using a transmission-line matrix, *Proc. IEE* **118**, 1203–1208 (1971).
119. W. R. Hoefer, The transmission-line matrix method—theory and applications, *IEEE Trans. MTT* **33**, 882–893 (1985).
120. W. J. R. Hoefer, Huygens and the computer—A powerful alliance in numerical electromagnetics, *Proc. IEEE* **79**, 1459–1471 (1991).
121. P. B. Johns, A symmetrical condensed node for the TLM method, *IEEE Trans. MTT* **35**, 370–376 (1987).
122. C. Christopoulos and J. L. Herring, The application of transmission-line modeling (TLM) to electromagnetic compatibility problems, *IEEE Trans. EMC* **35**, 185–191 (1993).
123. M. M. Ney, Modeling of highly conducting boundaries with TLM, *Electromagn.* **16**, 521–535 (1996).
124. C. Eswarappa and W. R. Hoefer, Absorbing boundary conditions for time-domain TLM and FDTD analysis of electromagnetic structures, *Electromagn.* **16**, 489–519 (1996).
125. J. L. Dubard and D. Pompei, Optimization of the PML efficiency in 3-D TLM method, *IEEE Trans. MTT* **48**, 1081–1087 (2000).
126. D. Pasalic, J. Bornemann, and R. Vahldieck, Absorbing boundary conditions in the frequency-domain TLM method and their application to planar circuits, *IEEE Trans. MTT* **49**, 1469–1476 (2001).
127. P. Sewell, Y. K. Choong, and C. Christopoulos, An accurate thin-wire model for 3D TLM simulations, *IEEE Trans. EMC* **45**, 207–217 (2003).
128. P. B. Johns, The solution of inhomogeneous waveguide problems using a transmission-line matrix, *IEEE Trans. MTT* **22**, 209–215 (1974).
129. M. Walter, P. Waldow, and A. Beyer, Simulation of waveguide structures using the TLM method in time domain, *Electromagn.* **22**, 639–658 (2002).
130. L. Pierantoni, C. Tomassoni, and T. Rozzi, A new termination condition for the application of the TLM method to discontinuity problems in closed homogeneous waveguide, *IEEE Trans. MTT* **50**, 2513–2518 (2002).
131. R. Vahldieck, S. Chen, J. Huang, and H. Jin, The frequency-domain TLM method — theory and application, *Electromagn.* **16**, 591–609 (1996).
132. P. B. Johns and M. O'Brien, Use of the transmission-line modelling (t.l.m.) method to solve non-linear lumped networks, *Radio Electron. Eng.* **50**, 59–70 (1980).
133. J. Lobry, J. Trécat, and C. Broche, The transmission line modeling (TLM) method as a new iterative technique in nonlinear 2D magnetostatics, *IEEE Trans. MAG* **32**, 559-566 (1996).
134. O. Deblecker, J. Lobry, and C. Broche, Novel algorithm based on transmission-line modeling in the finite-element method for nonlinear quasi-static field analysis, *IEEE Trans. MAG* **39**, 524–538 (2003).
135. J. G. Ma and Z. Chen, Application of the method of lines to the Laplace equation, *Microwave Opt. Tech. Lett.* **14**, 330–333 (1997).
136. J. G. Ma, T. K. Chia, T. W. Tan, and K. Y. See, Electromagnetic wave scattering from 2-D cylinder by using the method of lines, *Microwave Opt. Tech. Lett.* **24**, 275–277 (2000).
137. R. Pregla, General formulas for the method of lines in cylindrical coordinates, *IEEE Trans. MTT* **43**, 1617–1620 (1995).
138. S. Xiao, R. Vahldieck, and J. Hesselbarth, Analysis of cylindrical transmission lines with the method of lines, *IEEE Trans. MTT* **44**, 993–999 (1996).
139. S. Nam, H. Ling, and T. Itoh, Characterization of uniform microstrip lines and its discontinuities using the time-domain method of lines, *IEEE Trans. MTT* **37**, 2052–2057 (1989).
140. A. Kornatz and R. Pregla, Analysis of electromagnetic boundary-value problems in inhomogeneous media with the method of lines, *IEEE Trans. MTT* **44**, 2296–2299 (1996).
141. R. Pregla, Efficient and accurate modeling of planar anisotropic microwave structures by the method of lines, *IEEE Trans. MTT* **50**, 1469–1479 (2002).
142. W. Pascher and R. Pregla, Analysis of rectangular waveguide junctions by the method of lines, *IEEE Trans. MTT* **43**, 2649–2653 (1995).
143. H. Zhao, I. Turner, and F. W. Liu, Numerical simulation of the power density distribution generated in a multimode cavity by using the method of lines technique to solve directly for the electric field, *IEEE Trans. MTT* **40**, 2185–2194 (1996).
144. S. Helfert and R. Pregla, The method of lines: a versatile tool for the analysis of waveguide structures, *Electromagn.* **22**, 615–637 (2002).
145. R. Pregla, The method of lines for the unified analysis of microstrip and dielectric waveguides, *Electromagn.* **15**, 441–456 (1995).
146. U. Schulz and R. Pregla, A new technique for the analysis of the dispersion characteristics of planar waveguides, *AEÜ* **34**, 169–173 (1980).
147. F. J. Schmückle and R. Pregla, The method of lines for the analysis of lossy planar waveguides, *IEEE Trans. MTT* **38**, 1473–1479 (1990).
148. L. Vietzorreck and R. Pregla, Hybrid analysis of three-dimensional MMIC elements by the method of lines, *IEEE Trans. MTT* **44**, 2580–2586 (1996).
149. C. R. Paul, Decoupling the multiconductor transmission line equations, *IEEE Trans. MTT* **44**, 1429–1440 (1996).

Chapter 15

Cylindrical Waveguides

The waveguides of concern in this chapter aim at guiding power — or signals — from a source to an end point while maintaining low attenuation and, in the case of a signal, low distortion. The two-wire line, the traditional solution at low frequencies, becomes progressively inefficient as the operating frequency increases. This is predicted by (14.18), which shows that the far field is proportional to $(k_0 l)$, a clear sign that radiation losses become important when l, the separation l between wires, becomes comparable with or larger than λ_0. To suppress the radiative losses while providing mechanical and chemical protection from the environment, the coaxial line was introduced as early as 1850, notably in the form of submarine cables. Joule losses in the line, however, soon limited its usefulness as operating frequencies progressively increased. The closed waveguide, strongly developed from the mid-1930s on, provided a suitable solution for wavelengths down to the millimeter range. It is to these closed "pipes" — familiar from their use in microwave radar sets — that the *first part* of this chapter is devoted. Closed waveguides have kept their importance in carrying power from a source to a load, for example from a 9.4 GHz radar transmitter to an antenna on top of a mast. The tremendous pressure, in the past decades, to increase the information content carried by electronic circuits, and the need densely to package and miniaturize these systems, led to the explosive development of integrated microwave and optical circuits. In those circuits the connecting lines are *open* and therefore exposed to interference and radiative losses. It is on these open lines, and their difficult electromagnetic analysis, that the *second part* of the chapter focuses.

The waveguides of concern in the following pages are, in very general terms, structures that are invariant with respect to a given, preferred direction, in casu the z-axis. These waveguides are therefore *cylindrical*, with as well-known examples the coaxial cable and the circular optical fiber. *Conical* waveguides, for which the preferred direction is radial, are discussed in Chapter 16.

Electromagnetic Fields, Second Edition, By Jean G. Van Bladel

15.1 FIELD EXPANSIONS IN A CLOSED WAVEGUIDE

Figure 15.1 shows a cylindrical volume containing sources $\mathbf{j}(\mathbf{r},t)$ and $\mathbf{j}_m(\mathbf{r},t)$. Given the translation invariance of the structure, it is natural to expand the fields in the form

$$\mathbf{e}(\mathbf{r},t) = \sum_{m=1}^{\infty} v_m(z,t)\underbrace{\operatorname{grad}\phi_m}_{\mathbf{e}_m} + \sum_{n=1}^{\infty} v_n(z,t)\underbrace{\operatorname{grad}\psi_n \times \mathbf{u}_z}_{\mathbf{e}_n} + \sum_{m=1}^{\infty} w_m(z,t)\,\phi_m\mathbf{u}_z + \left[v_0(z,t)\underbrace{\operatorname{grad}\phi_0}_{\mathbf{e}_0} \right]. \tag{15.1}$$

Similarly,

$$\mathbf{h}(\mathbf{r},t) = \sum_{m=1}^{\infty} i_m(z,t)\underbrace{\mathbf{u}_z \times \operatorname{grad}\phi_m}_{\mathbf{h}_m} + \sum_{n=1}^{\infty} i_n(z,t)\underbrace{\operatorname{grad}\psi_n}_{\mathbf{h}_n} + \sum_{n=0}^{\infty} l_n(z,t)\,\psi_n\mathbf{u}_z + \left[i_0(z,t)\underbrace{\mathbf{u}_z \times \operatorname{grad}\phi_0}_{\mathbf{h}_0} \right]. \tag{15.2}$$

The functions $\phi_m(x,y)$ and $\psi_n(x,y)$ are the Dirichlet and Neumann eigenfunctions of the cross section, defined in (5.76) and (14.230). The m and n indices are actually double indices, and the $(\mathbf{e}_m, \mathbf{e}_n)$ and $(\mathbf{h}_m, \mathbf{h}_n)$ eigenvectors form two separate orthogonal sets, the first one consisting of vectors perpendicular to the wall and the second one of vectors tangent to the wall.

The terms between square brackets in the expansions are present when the cross section is of the coaxial type (Fig. 15.1*c*). Such cross sections are both doubly bounded and doubly

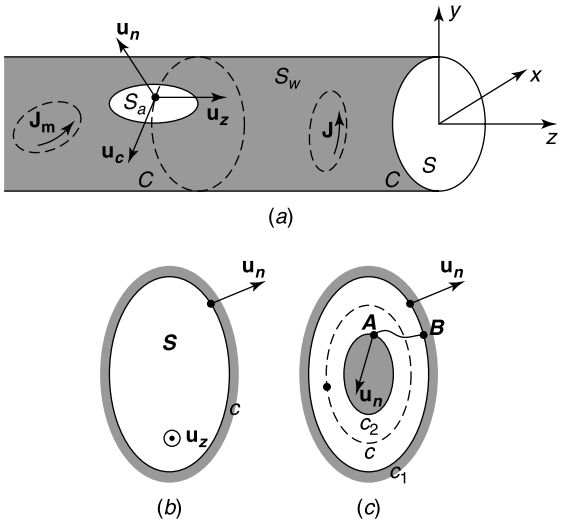

Figure 15.1 (*a*) Waveguide with electric and magnetic sources. (*b*, *c*) Waveguide cross sections.

connected.* The *doubly bounded* property results in the presence of the term in $\mathbf{e}_0$ in (15.1), where $\mathbf{e}_0$ is the electric field that appears between C_1 and C_2 when these cylinders are raised to different potentials. The function ϕ_0, which satisfies $\nabla_t^2 \phi_0 = 0$ in S, is constant on both C_1 and C_2. Eigenvector $\mathbf{e}_0$ will be normalized according to the condition†

$$\int_S |\text{grad}_t\, \phi_0|^2\, dS = 1. \tag{15.3}$$

For a circular coaxial cable of radii a (central conductor) and b (shield), the eigenvector is

$$\text{grad}\, \phi_0 = \mathbf{e}_0 = \left(2\pi\, \log_e \frac{b}{a}\right)^{-\frac{1}{2}} \frac{\mathbf{u}_r}{r}. \tag{15.4}$$

The *double-connectedness*, on the other hand, generates an eigenvector $\mathbf{h}_0(x, y)$ tangent to the boundaries and satisfying the equations $\text{div}_t\, \mathbf{h}_0 = 0$ and $\text{div}_t\, (\mathbf{h}_0 \times \mathbf{u}_z) = 0$ in S. From (A3.23), the second condition means that $\mathbf{h}_0$ is irrotational in the (x, y) plane, whence it follows that $\mathbf{h}_0$ is the two-dimensional version of the important vector $\mathbf{h}_0$ defined in (4.120) for a ringlike volume. For a circular coaxial cable:

$$\mathbf{u}_z \times \text{grad}\, \phi_0 = \mathbf{h}_0 = \left(2\pi\, \log_e \frac{b}{a}\right)^{-\frac{1}{2}} \frac{\mathbf{u}_\varphi}{r}. \tag{15.5}$$

The "0" mode under discussion is a *TEM mode*, and its fields are those of the classic low-frequency mode of the coaxial cable.

An important remark concerns the $\psi_0 = \textit{constant mode}$, which belongs to the Neumann set. Its coefficient is $l_0(z, t)$ in (15.2), and the mode has only one field component, namely h_z. We shall use the normalization condition

$$\int_S \psi_0^2\, dS = 1, \tag{15.6}$$

from which it follows that $\psi_0 = S^{-\frac{1}{2}}$. The field associated with the mode is therefore

$$\mathbf{h} = l_0(z, t)\, S^{-\frac{1}{2}}\, \mathbf{u}_z. \tag{15.7}$$

15.1.1 The Coefficients in the Field Expansions

To determine these coefficients, expansions (15.1) and (15.2) are inserted into Maxwell's equations, together with corresponding expansions for $\mathbf{j}$ (in terms of $\mathbf{e}_m$, $\mathbf{e}_n$) and $\mathbf{j}_m$ (in terms of $\mathbf{h}_m$, $\mathbf{h}_n$). Following the *derivative of a sum* principle, separate equations are used for curl $\mathbf{e}$ and curl $\mathbf{h}$. The coefficients of these expansions are subsequently expressed in terms of the

*The extension to N central conductors is immediate.

†In this chapter, the subscript t, when used to define an operator, implies differentiation with respect to only x and y. When qualifying a vector such as $\mathbf{e}_t$, it means *transverse* and denotes a vector in the (x, y) plane.

expansion coefficients for **e** and **h**. The steps, which are quite elementary, make use of the useful relationships

$$\begin{aligned}
\text{curl}\,[f(z)\,A(x,y)\,\mathbf{u}_z] &= f(z)\,\text{grad}_t\,A \times \mathbf{u}_z,\\
\text{curl}\,[f(z)\,\text{grad}_t\,A(x,y)] &= \frac{df}{dz}\,\mathbf{u}_z \times \text{grad}_t\,A,\\
\text{curl}\,[f(z)\,\text{grad}_t\,A \times \mathbf{u}_z] &= \text{curl curl}\,[f(z)\,A(x,y)\,\mathbf{u}_z],\\
&= \frac{df}{dz}\,\text{grad}_t\,A - f(z)\nabla_t^2 A\,\mathbf{u}_z. \qquad (15.8)
\end{aligned}$$

We only quote the end results, valid for a waveguide filled with a homogeneous medium of characteristics (σ, ϵ, μ):

1. *Coefficients of a TEM (or "0") mode*

$$\begin{aligned}
\frac{\partial v_0}{\partial z} + \mu\frac{\partial i_0}{\partial t} &= -\int_S \mathbf{j}_m \cdot (\mathbf{u}_z \times \text{grad}\,\phi_0)\,dS\\
&\quad - \int_C (\mathbf{u}_n \times \mathbf{e}) \cdot (\mathbf{u}_z \times \text{grad}\,\phi_0)\,dc. \qquad (15.9)
\end{aligned}$$

$$\frac{\partial i_0}{\partial z} + \left(\sigma + \epsilon\,\frac{\partial}{\partial t}\right) v_0 = -\int_S \mathbf{j} \cdot \text{grad}\,\phi_0\,dS. \qquad (15.10)$$

2. *Coefficients of a TM (or E) mode*

$$\begin{aligned}
\frac{\partial v_m}{\partial z} + \mu\frac{\partial i_m}{\partial t} - w_m &= -\int_S \mathbf{j}_m \cdot (\mathbf{u}_z \times \text{grad}\,\phi_m)\,dS\\
&\quad - \int_C (\mathbf{u}_n \times \mathbf{e}) \cdot (\mathbf{u}_z \times \text{grad}\,\phi_m)\,dc. \qquad (15.11)
\end{aligned}$$

$$i_m + \left(\sigma + \epsilon\,\frac{\partial}{\partial t}\right)\frac{w_m}{\mu_m^2} = -\int_S \mathbf{j} \cdot (\phi_m\,\mathbf{u}_z)\,dS. \qquad (15.12)$$

$$\frac{\partial i_m}{\partial z} + \left(\sigma + \epsilon\,\frac{\partial}{\partial t}\right) v_m = -\int_S \mathbf{j} \cdot \text{grad}\,\phi_m\,dS. \qquad (15.13)$$

3. *Coefficients of a TE (or H) mode*

$$\begin{aligned}
\frac{\partial v_n}{\partial z} + \mu\frac{\partial i_n}{\partial t} &= -\int_S \mathbf{j}_m \cdot \text{grad}\,\psi_n\,dS\\
&\quad - \int_C (\mathbf{u}_n \times \mathbf{e}) \cdot \text{grad}\,\psi_n\,dc. \qquad (15.14)
\end{aligned}$$

$$\begin{aligned}
v_n + \frac{\mu}{\nu_n^2}\frac{\partial l_n}{\partial t} &= -\int_S \mathbf{j}_m \cdot (\psi_n\,\mathbf{u}_z)\,dS\\
&\quad - \int_C (\mathbf{u}_n \times \mathbf{e}) \cdot (\psi_n\,\mathbf{u}_z)\,dc. \qquad (15.15)
\end{aligned}$$

$$\frac{\partial i_n}{\partial z} + \left(\sigma + \epsilon \frac{\partial}{\partial t}\right) v_n - l_n = -\int_S \mathbf{j}\cdot(\text{grad } \psi_n \times \mathbf{u}_z)\, dS. \tag{15.16}$$

It should be noted that the neat division into TE, TM, and TEM modes holds for homogeneously filled waveguides but disappears when the interior medium is inhomogeneous, in which case modes are generally hybrid, with both E_z and H_z components. The point is further discussed in the second part of the chapter.

The $l_0(z,t)$ mode, already defined in (15.7), deserves some special attention.[1,2,3] Because of the orthogonality properties of the Neumann set, all ψ_n, except ψ_0, have zero average values over S. It follows that

$$(h_z)_{\text{ave}} = \frac{1}{S}\int_S h_z\, dS = \frac{1}{\sqrt{S}}\, l_0. \tag{15.17}$$

To determine the time dependence of l_0, we project Maxwell's equation (7.1) on the z-axis. This gives

$$\mathbf{u}_z\cdot\text{curl } \mathbf{e} = \text{div}_t(\mathbf{e}\times\mathbf{u}_z) = -\mu\frac{\partial h_z}{\partial t} - \mathbf{u}_z\cdot\mathbf{j}_m. \tag{15.18}$$

Integration over the cross section yields

$$\mu\sqrt{S}\,\frac{\partial l_0}{\partial t} = -\int_S \mathbf{j}_m\cdot\mathbf{u}_z\, dS - \int_C (\mathbf{u}_n\times\mathbf{e})\cdot\mathbf{u}_z\, dc. \tag{15.19}$$

This equation can be rewritten in terms of the flux ϕ of $\mathbf{b}$ through a cross section as

$$\frac{\partial \Phi}{\partial t} = -\int_S \mathbf{j}_m\cdot\mathbf{u}_z\, dS - \int_C (\mathbf{u}_n\times\mathbf{e})\cdot\mathbf{u}_z\, dc. \tag{15.20}$$

This flux is a function of z and t. In a portion of the waveguide containing neither magnetic sources nor apertures, Φ is constant in time and independent of z. Φ will vary, however, in a $\mathbf{j}_m$-carrying part of the guide, or under an aperture, through which flux can penetrate or escape. Note that the classic flux conservation property of $\mathbf{b}$ does not hold in the presence of magnetic sources, because div $\mathbf{b}$ does not vanish, but satisfies from (7.5)

$$\frac{\partial}{\partial t}\,\text{div } \mathbf{b} = -\text{div } \mathbf{j}_m. \tag{15.21}$$

It is clear, from (15.19), that the l_0 mode does not propagate; its contribution remains local and only influences the *reactive* power in the guide. Notwithstanding that restriction, the contribution of the l_0 mode must not be ignored in many applications. Its incorporation is essential, for example, for a correct evaluation of the equivalent *reactance* of a slot in a waveguide wall[‡] [133].

[‡]Ignoring l_0 does not affect the equivalent *resistance* of the slot, because the mode does not radiate into the waveguide.

15.2 DETERMINATION OF THE EIGENVECTORS

The eigenvalue problem has been discussed extensively in the literature. Separation of variables provides an answer in a few well-documented cases [1, 46, 97], in particular for the rectangular, circular, and coaxial cross sections. A few data on these important examples are included in Appendix 9. The elliptical waveguide has also been the object of much attention.[4,5,6,7] From (A2.109), Helmholtz' equation in elliptic coordinates takes the form

$$\frac{\partial^2 f}{\partial u^2} + \frac{\partial^2 f}{\partial v^2} + k_m^2 c^2 (\cosh^2 u - \cos^2 v) f = 0. \tag{15.22}$$

Setting $f(u, v) = A(u)B(v)$ in that equation shows that $A(u)$ must satisfy Mathieu's equation (A5.163) and $B(v)$ the modified equation (A5.165). One therefore writes (Fig. 5.13)

$$f = \begin{Bmatrix} S_m^e(k_m c, v) & J_m^e(k_m c, u) \\ S_m^o(k_m c, v) & J_m^o(k_m c, u) \end{Bmatrix}. \tag{15.23}$$

The $N_m(u)$ functions are excluded because they are singular in the interior of the cross section. Let the elliptic contour of the cross section be defined by $u = u_0$. The Dirichlet and Neumann eigenvalues are now determined from the respective conditions

$$J_m(k_m c, u_0) = 0 \tag{15.24}$$

$$\left(\frac{\partial J_n(k_n c, u)}{\partial u} \right)_{u=u_0} = 0. \tag{15.25}$$

The corresponding eigenvectors follow from (A2.107), which expresses the gradient in elliptic coordinates.

When the cross section is arbitrary, several numerical methods can be relied upon to determine the eigenfunctions.[8] In the process, the following inequalities can be useful in obtaining estimates of eigenvalues and checking numerical results.[9] Let the eigenvalues of the E modes and the H modes be written, in ordered sequence, according to the scheme

$$\begin{aligned} 0 < \mu_0 < \mu_1 \leq \mu_2 \leq \mu_3 \leq \cdots \\ 0 = \nu_0 < \nu_1 \leq \nu_2 \leq \nu_3 \leq \cdots . \end{aligned} \tag{15.26}$$

The following properties then hold:

1. $\nu_k \leq \mu_k$.
2. $\nu_1 < \mu_0$; this implies that the lowest mode is always an H mode.
3. For a given cross-sectional area S, the circle has the largest ν_1 and the smallest μ_0.
4. $\nu_1 \leq A/I$, where I is the greater principal moment of inertia of the cross section with respect to the center of gravity.

Following a classic pattern, one proceeds by expanding the sought eigenfunctions in a series of the form $\phi = \sum a_n f_n$, where the f_n's are chosen to satisfy the boundary conditions on C. The series is inserted into (5.76), upon which testing with w_m casts the equation into the weak form

$$\sum a_n \underbrace{\int_S w_m \nabla^2 f_n \, dS}_{L_{mn}} + \mu^2 \sum a_n \underbrace{\int_S w_m f_n \, dS}_{C_{mn}} = 0. \tag{15.27}$$

Additional properties may be imposed on the f_n's; for example, with a view toward "feeling" the curvature of the boundary more accurately[10] or incorporating the edge behavior in the basis functions.[11,12] Variational formulations have also been proposed. We note, for example, that the two-dimensional *Dirichlet* eigenfunctions are the eigenfunctions of a self-adjoint negative-definite transformation. Variational principle (2.16) may therefore be applied. The appropriate functional

$$J_1(\phi) = -\frac{\int_S \phi \nabla^2 \phi \, dS}{\int_S \phi^2 \, dS} = \frac{\int_S |\text{grad } \phi|^2 \, dS}{\int_S \phi^2 \, dS} \tag{15.28}$$

is minimized by the *lowest* eigenfunction, and the minimum is equal to μ_1^2, the negative of the lowest eigenvalue. The admissible functions are required to vanish at the boundary. Higher-order eigenfunctions can be obtained by the procedure outlined in Sections 2.3 and 2.4 (Problem 15.1).

The set of two-dimensional *Neumann* eigenfunctions includes the function $\psi = \text{const}$. This lowest eigenfunction has the eigenvalue zero. Interest therefore centers on the evaluation of the lowest *nonzero* eigenvalue. This can be obtained by the variational principle given in (15.28), but the admissible functions are now required to be orthogonal to $\psi = \text{const}$ (i.e., to have zero average value over the cross section) and to have zero normal derivative at the contour. Other functionals, this time derived from (2.8), are

$$J_2(\phi) = \int_S \left[\phi \nabla^2 \phi + \mu^2 \phi^2\right] dS \tag{15.29}$$

or, after elimination of the second derivatives,

$$J_3(\phi) = \int_S \left[|\text{grad } \phi|^2 - \mu^2 \phi^2\right] dS. \tag{15.30}$$

From (A1.30), the Euler equations of these functionals are of the form (14.230), with $(\partial\psi/\partial n) = 0$ as a natural boundary condition. If the trial functions are assigned the value zero on contour C, the functional becomes stationary with respect to the Dirichlet eigenfunctions ϕ_m.

A few less traditional methods have been developed recently to determine the eigenvectors. In the examples shown in Figure 15.2, the cross section is subdivided into partial, slot-coupled domains. The unknowns are the tangential components of $\mathbf{E}$ in the slots c_1 to c_4. The fields are expanded in appropriate eigenmodes in each sub-waveguide, with coefficients that depend on the still unknown $\mathbf{E}_{\text{tan}}$'s. An equation for $\mathbf{E}_{\text{tan}}$ is found by requiring $\mathbf{H}_{\text{tan}}$ to be continuous across each slot.[13] Another method, of an integral equation nature, concentrates on the boundary sources $\mathbf{J}_s$ and ρ_S that are induced on the walls of the waveguide. In an H-type of mode[14,15] (7.96), (7.97) and (14.12) show that the potentials resulting from these sources are

$$\begin{aligned} \mathbf{A} &= -j\frac{\mu}{4} \int_C \mathbf{J}_S(\mathbf{r}') H_0^{(2)}(k|\mathbf{r} - \mathbf{r}'|) \, dc' \\ \phi &= -j\frac{1}{4\epsilon} \int_C \rho_S(\mathbf{r}') H_0^{(2)}(k|\mathbf{r} - \mathbf{r}'|) \, dc', \end{aligned} \tag{15.31}$$

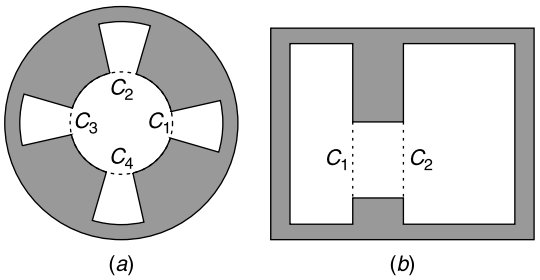

Figure 15.2 (*a*) Slotted circular waveguide. (*b*) Ridge waveguide (from A. S. Omar, A. Jöstingmeier, C. Rieckmann, and S. Lütgert, Application of the generalized spectral domain technique (GSD) to the analysis of slot coupled waveguides, *IEEE Trans. MTT* **42**, 2139–2148, 1994, with permission of IEEE).

with

$$\rho_S(\mathbf{r}') = -\frac{1}{j\omega}\,\mathrm{div}'_S\,\mathbf{J}_S(\mathbf{r}').$$

A functional equation for $\mathbf{J}_S$ follows by enforcing the boundary condition

$$\mathbf{u}_n(\mathbf{r}) \times \left[-j\omega\,\mathbf{A}(\mathbf{r}) - \mathrm{grad}\;\phi(\mathbf{r})\right] = 0 \qquad (\mathbf{r}\text{ on } C). \tag{15.32}$$

In an *E-type* of mode, $\mathbf{J}_S$ is parallel to the waveguide axis, and so is $\mathbf{A}$. No charge density appears on C, and (15.31) is replaced by the single equation

$$A(\mathbf{r}) = -j\frac{\mu}{4}\int_C J_S(\mathbf{r}')H_0^{(2)}(k|\mathbf{r}-\mathbf{r}'|)\,dc'. \tag{15.33}$$

The functional equation for $\mathbf{J}_S$ is now $A(\mathbf{r}) = 0$, for $\mathbf{r}$ on C.

A third recent approach is based on the *boundary integral resonant mode* method. First developed to determine the eigenvalues of waveguides strongly perturbed by axial inserts,[16] the method has been usefully applied to the determination of both the eigenvalues of a cavity[17] and the characteristics of waveguide components[18,19] [185]. Two examples of inserts are shown in Figure 15.3: in part (a), the perturbation is a conducting sheet C (a fin for example); in part (b), a closed shell C. The shell defines two partial waveguides, of respective cross sections S_1 and S_2. Consider, for example, a φ-independent E-mode in the circular waveguide shown in (a). The current density J_S on C is z-directed. The current generates an electric field

$$E_z(\mathbf{r}) = j\omega\mu_0\int_C J_S(c')\,G(\mathbf{r},c')\,dc', \tag{15.34}$$

where $G(\mathbf{r},\mathbf{r}',k)$ is the Dirichlet Green's function of cross section S. This function is the solution of

$$\begin{aligned}\nabla_t^2 G(\mathbf{r},\mathbf{r}',k) + k^2\,G(\mathbf{r},\mathbf{r}',k) &= \delta(\mathbf{r}-\mathbf{r}') \quad (\mathbf{r}\text{ and }\mathbf{r}'\text{ in } S)\\ G(\mathbf{r},\mathbf{r}',k) &= 0 \qquad\qquad (\mathbf{r}\text{ on } C_w).\end{aligned} \tag{15.35}$$

Imposing the boundary condition $E_z(\mathbf{r}) = 0$ for $\mathbf{r}$ on C quantizes k and yields the sought eigenvalues. The usual precautions should be taken in the approach of $\mathbf{r}$ to C, given the

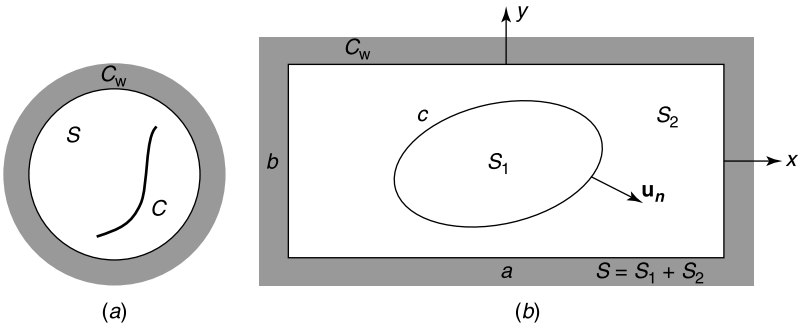

Figure 15.3 (*a*) Circular waveguide with a metallic inset. (*b*) Rectangular waveguide enclosing another waveguide.

singularities of $G(\mathbf{r}, \mathbf{r}', k)$. The method has the advantage of limiting the unknown J_S to the (small) support formed by C, with a corresponding limitation of the size of the matrix. Its application clearly depends on the availability of a suitable form for G. In terms of the normalized Dirichlet eigenfunctions we may write, from (5.76),

$$\delta(\mathbf{r} - \mathbf{r}') = \sum_m \mu_m^2 \phi_m(\mathbf{r}) \phi_m(\mathbf{r}') \tag{15.36}$$

$$\begin{aligned} G(\mathbf{r}, \mathbf{r}', k) &= \sum_m \frac{\mu_m^2}{k^2 - \mu_m^2} \phi_m(\mathbf{r}) \phi_m(\mathbf{r}') \\ &= \underbrace{-\sum_m \phi_m(\mathbf{r}) \phi_m(\mathbf{r}')}_{G_0(\mathbf{r}, \mathbf{r}')} + k^2 \underbrace{\sum_m \frac{\phi_m(\mathbf{r}) \phi_m(\mathbf{r}')}{k^2 - \mu_m^2}}_{G_1(\mathbf{r}, \mathbf{r}', k)}. \end{aligned} \tag{15.37}$$

The function G_0, which is independent of k, is the quasi-static potential part of G, while G_1 is a rapidly converging resonant-like expansion. This expansion can be approximated, in the prescribed range $(0, k_{\max})$, by retaining a reasonable number of terms. For the rectangle in Figure 15.3*b*, for example,

$$G_0 = -\frac{1}{4\pi} \sum_{m=-\infty}^{\infty} (-1)^m \log_e \frac{\cosh X_m - \cos Y_m^+}{\cosh X_m - \cos Y_m^-}, \tag{15.38}$$

where[17]

$$\begin{aligned} X_m &= \frac{\pi}{b} \left\{ x - ma - \frac{a}{2} \left(1 - (-1)^m\right) - (-1)^m x' \right\} \\ Y^{\pm} &= \frac{\pi}{b} (y \pm y'). \end{aligned}$$

The application of the method to the waveguide shown in Figure 15.3*b* yields the modes of *both* partial waveguides, S_1 and S_2.

15.3 PROPAGATION IN A CLOSED WAVEGUIDE

The possibility of propagating signals down a hollow metallic duct has been predicted theoretically — and checked experimentally — as early as the end of the nineteenth century.[20] The topic remained dormant because of the absence of suitable high-frequency sources, long restricted to the popular spark gap and its relatively broad spectral output. In the mid-1930s, however, research resumed, in particular at the hands of Southworth and Barrow.[21] The theory shows that wave propagation in the duct is only possible if the frequency is sufficiently high or, more precisely, if the wavelength is less than some cross-sectional dimension of the waveguide. At wavelengths of 1 m or so, the "pipe" would therefore have dimensions of the order 1 m, which explains why its use did not become practical until sources in the decimeter range became available. This evolution culminated, in World War II, with the development of magnetrons, which could generate sufficient power in the centimeter range to make airborne radar a practical proposition.

15.3.1 *Cut-off Frequency*

The two-wire line, and its enclosed version the coaxial line, can carry electromagnetic waves down to zero frequency. This everyday experimental evidence is confirmed by the solution of (15.9) and (15.10) in a portion of coaxial line devoid of sources. Under time-harmonic conditions, for example, one easily finds that

$$\begin{aligned} V_0(z) &= A\, e^{-jkz} + B\, e^{jkz} \\ I_0(z) &= \frac{1}{Z_c}\left(A\, e^{-jkz} - B\, e^{jkz}\right), \end{aligned} \tag{15.39}$$

where $k^2 = \omega^2\epsilon\mu - j\omega\mu\sigma$ and $Z_c = [j\omega\mu/(\sigma + j\omega\epsilon)]^{\frac{1}{2}}$. Propagation is clearly possible at all frequencies, although the fields are attenuated when the medium in the guide is lossy. In the absence of losses, the basic TEM wave propagates with a velocity $c = (\epsilon\mu)^{-\frac{1}{2}}$ (i.e., with the velocity of light in the medium filling the guide). It is useful to note that the V_0 and I_0 expansion coefficients are related to the classic voltage and current of the line by (Fig. 15.1*c*)

$$\begin{aligned} \int_A^B \mathbf{E}\cdot d\mathbf{l} = V_A - V_B \;&=\; V_0 \int_A^B \text{grad}\,\phi_0 \cdot d\mathbf{l} \;=\; V_0[\phi_0(B) - \phi_0(A)] \\ \int_C \mathbf{H}\cdot d\mathbf{c} = I \;&=\; I_0 \int_C \frac{\partial \phi_0}{\partial n}\, dc. \end{aligned} \tag{15.40}$$

The *one-conductor* waveguide, on the other hand, does *not* support a TEM mode, and its TE and TM modes do *not* propagate until the frequency exceeds a threshold value termed cut-off. In verifying this statement, we shall assume that the waveguide is lossless, leaving to Section 15.4 an analysis of the influence of losses. From (15.11) to (15.16), the expansion coefficients in a sourceless region satisfy equations of the general type

$$\frac{d^2 V_p}{dz^2} + (k^2 - k_p^2)\, V_p = 0. \tag{15.41}$$

When $(k^2 - k_p^2) = \gamma_p^2$ is positive, the variation of V_p will be of the form

$$V_p(z) = C_p\, e^{-j\gamma_p z} + D_p\, e^{j\gamma_p z}. \tag{15.42}$$

Under these conditions, the mode contributes progressive waves. This can only happen when the frequency rises above the threshold value $(ck_p/2\pi)$. Applying this argument to a *TM mode* shows that the coefficients of a propagating wave are

$$\begin{aligned} V_m &= A_m\, e^{\mp j\beta_m z} \\ I_m &= \pm\frac{\omega\epsilon}{\beta_m} A_m\, e^{\mp j\beta_m z} \;=\; \pm G_m V_m \\ W_m &= \pm j\frac{\mu_m^2}{\beta_m} A_m\, e^{\mp j\beta_m z}, \end{aligned} \tag{15.43}$$

where $\beta_m^2 = k^2 - \mu_m^2$. For a propagating *TE mode*, with $\beta_n^2 = k^2 - \nu_n^2$,

$$\begin{aligned} V_n &= \pm\frac{\omega\mu}{\beta_n} C_n\, e^{\mp j\beta_n z} \;=\; \pm R_n I_n \\ I_n &= C_n\, e^{\mp j\beta_n z} \\ W_n &= \pm j\frac{\nu_n^2}{\beta_n} C_n\, e^{\mp j\beta_n z}. \end{aligned} \tag{15.44}$$

Propagating waves give rise to interferences (and standing wave patterns) of the kind encountered in transmission-line problems. It follows that most of the techniques used in transmission-line technology (matching procedures for example) can be applied to waveguide systems.

When $(k^2 - k_p^2) = -\delta_p^2$ is negative, which is the case below cut-off, the propagating waves in (15.42) are replaced by evanescent waves. Thus,

$$V_p(z) = C_p\, e^{-\delta_p z} + D_p\, e^{\delta_p z}. \tag{15.45}$$

The mode contribution now consists of the superposition of two exponentially attenuated terms. Only one of these terms is acceptable at large axial distances $|z|$. To the right of the sources, for example, the term $\exp\left[(k_p^2 - k^2)^{\frac{1}{2}} z\right]$ must be excluded because its magnitude becomes infinite at large positive z. The attenuated waves are therefore, in a *TM mode*,

$$\begin{aligned} V_m &= A_m\, e^{\mp\delta_m z} \\ I_m &= \pm A_m \frac{j\omega\epsilon}{\delta_m}\, e^{\mp\delta_m z} \;=\; \pm jB_m V_m, \end{aligned} \tag{15.46}$$

where $\delta_m^2 = \mu_m^2 - k^2$, and B_m is the susceptance of the mode. In a *TE mode*:

$$\begin{aligned} V_n &= \pm\frac{j\omega\mu}{\delta_n} C_n\, e^{\mp\delta_n z} = \pm jX_n I_n \\ I_n &= C_n\, e^{\mp\delta_n z}, \end{aligned} \tag{15.47}$$

where $\delta_n^2 = \nu_n^2 - k^2$, and X_n is the reactance of the mode. Both in (15.46) and (15.47), the upper signs are associated with attenuation toward positive z and the lower signs with attenuation toward negative z.

The modal forms discussed above hold in sourceless regions. To evaluate coefficients such as A_m and C_n, the sources $\mathbf{j}$, $\mathbf{j}_m$ and $\mathbf{u}_n \times \mathbf{e}$ must be brought into play. We shall illustrate the point by solving a few examples.

15.3.2 Fields Generated by a Magnetic Dipole

Let the source be a time-harmonic magnetic dipole of moment $\mathbf{P}_m$ located at $(x_0, y_0, 0)$ (Fig. 15.4*a*). From (7.151), the equivalent electric current is

$$\begin{aligned}\mathbf{J} \;&=\; \operatorname{curl}\left[\delta(\mathbf{r}-\mathbf{r}_0)\mathbf{P}_m\right] = \operatorname{grad}\delta(\mathbf{r}-\mathbf{r}_0)\times\mathbf{P}_m \\ &= \frac{d\delta(z)}{dz}\,\mathbf{u}_z\times\mathbf{P}_m + \operatorname{grad}_{xy}\delta(\mathbf{r}-\mathbf{r}_0)\times\mathbf{P}_m. \qquad (15.48)\end{aligned}$$

We shall assume that the waveguide carries only its lowest mode, which, from (15.26), is always a TE mode. To evaluate the contribution of $\mathbf{P}_m$ to this mode, (15.14) to (15.16) should be solved. It is immediately clear that the only nonzero second member in these equations is the *forcing function* in (15.16). This function can be evaluated by means of the sifting properties (A8.74) and (A8.76). Thus,

$$\int_S \mathbf{J}(\mathbf{r})\cdot\boldsymbol{\phi}(\mathbf{r})\,dS = \mathbf{P}_m\cdot(\operatorname{curl}_t\boldsymbol{\phi})_0\,\delta(z) + \mathbf{P}_m\cdot\left[\boldsymbol{\phi}(\mathbf{r}_0)\times\mathbf{u}_z\right]\delta'(z), \qquad (15.49)$$

where the subscript 0 means the value at $\mathbf{r}_0$, and

$$\operatorname{curl}_t\boldsymbol{\phi} = \mathbf{u}_x\times\frac{\partial\boldsymbol{\phi}}{\partial x} + \mathbf{u}_y\times\frac{\partial\boldsymbol{\phi}}{\partial y} = \operatorname{curl}\boldsymbol{\phi} - \mathbf{u}_z\times\frac{\partial\boldsymbol{\phi}}{\partial z}. \qquad (15.50)$$

With the $(\mathbf{e}_n, \mathbf{h}_n)$ notation introduced in (15.1) and (15.2):

$$\int_S \mathbf{J}\cdot\mathbf{e}_1\,dS = j\beta_1(\mathbf{P}_m\cdot\mathbf{h}_{1z})_0\,\delta(z) - (\mathbf{P}_m\cdot\mathbf{h}_{1t})_0\,\delta'(z), \qquad (15.51)$$

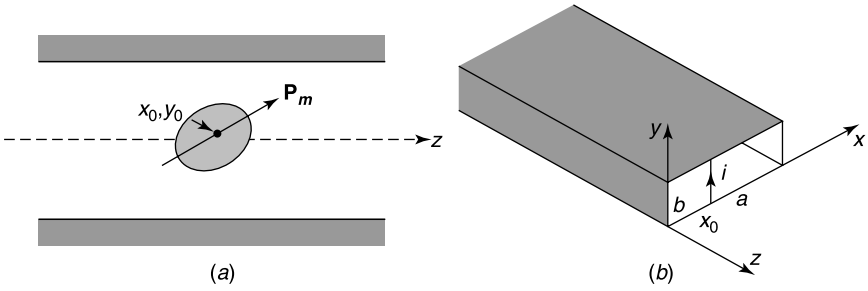

Figure 15.4 Two sources in a waveguide. (*a*) Concentrated dipole moment. (*b*) Line current in a rectangular waveguide.

where we have set

$$\mathbf{h}_{1z} = \frac{\nu_1^2 \psi_1}{\beta_1}\,\mathbf{u}_z. \tag{15.52}$$

Elimination of I_1 and W_1 from the coefficient equations (15.14) to (15.16) gives an equation for V_1 alone, viz.

$$\frac{d^2 V_1}{dz^2} + (k^2 - \nu_1^2)\, V_1 = j\omega\mu_0 \left[j\beta_1 (\mathbf{P}_m \cdot \mathbf{h}_{1z})_0\, \delta(z) - (\mathbf{P}_m \cdot \mathbf{h}_{1t})_0\, \delta'(z) \right]. \tag{15.53}$$

Solving this equation for V_1, and taking the outgoing-waves requirement into account, gives the following electric field for $z > 0$:

$$\mathbf{E}_t = -\frac{1}{2}\, j\omega\mu_0 \left[\mathbf{P}_m \cdot \mathbf{h}_{1t} - j\mathbf{P}_m \cdot \mathbf{h}_{1z} \right]_0 \mathbf{e}_1\, e^{-j\beta_1 z}. \tag{15.54}$$

For $z < 0$:

$$\mathbf{E}_t = -\frac{1}{2}\, j\omega\mu_0 \left[\mathbf{P}_m \cdot \mathbf{h}_{1t} + j\mathbf{P}_m \cdot \mathbf{h}_{1z} \right]_0 \mathbf{e}_1\, e^{j\beta_1 z}. \tag{15.55}$$

The dipole radiates a power

$$P = \frac{1}{8}\, \beta_1 \omega\mu_0 \left[|\mathbf{P}_m \cdot \mathbf{h}_{1t}|^2 + |\mathbf{P}_m \cdot \mathbf{h}_{1z}|^2 \right] \tag{15.56}$$

in both the $(+z)$ and $(-z)$ directions (Problem 15.3).

In the previous analysis, $\mathbf{P}_m$ was treated as a *given* primary source. In many applications, this moment is *induced* in an *obstacle* and is not known from the start. When the obstacle is small enough, $\mathbf{H}^i$ at $(x_0, y_0, 0)$ may be considered uniform, and $\mathbf{P}_m$ can be obtained from the relationship

$$\mathbf{P}_m = \overline{\overline{\alpha}}_m \cdot (\mathbf{H}^i)_0, \tag{15.57}$$

where $\overline{\overline{\alpha}}_m$ is a polarizability dyadic. When the latter takes the form

$$\overline{\overline{\alpha}}_m = \alpha_m \mathbf{u}_p \mathbf{u}_p, \tag{15.58}$$

the induced moment is parallel to the p direction. More precisely, $\mathbf{P}_m$ is given by

$$\mathbf{P}_m = \alpha_m (\mathbf{H}^i \cdot \mathbf{u}_p)_0\, \mathbf{u}_p. \tag{15.59}$$

For such a case, it is clear that the strength of the scattered fields can be adjusted by modifying the location and orientation of the scatterer. If the incident mode is the lowest propagating TE mode, that is, if

$$\begin{aligned} \mathbf{E}^i &= V_1\, \mathbf{e}_1\, e^{-j\beta_1 z} \\ \mathbf{H}^i &= \frac{V_1}{R_1}\, e^{-j\beta_1 z} \left[\mathbf{h}_{1t} + j\mathbf{h}_{1z} \right], \end{aligned} \tag{15.60}$$

the induced moment becomes

$$\mathbf{P}_m = \frac{V_1}{R_1}\,\alpha_m \left(\mathbf{u}_p \cdot \mathbf{h}_{t1} + j\mathbf{u}_p \cdot \mathbf{h}_{z1}\right)_0 \mathbf{u}_p. \tag{15.61}$$

An obstacle for which the (15.59) type of polarizability dyadic is valid is the dielectric resonator discussed in Section 11.4. In the magnetic dipole resonance of the dielectric, the α_m factor is of the general form

$$\alpha_m = \frac{(\alpha_m)_{peak}}{1 + 2jQ\left(\dfrac{\Delta f}{f_{res}}\right)}, \tag{15.62}$$

where Q is determined by the various losses. These comprise the Joule losses in the scatterer and the radiative losses resulting from the power carried down the guide by the scattered fields. For a more general small scatterer, say a small metallic obstacle, the appropriate form of $\overline{\overline{\alpha}}_m$ should be inserted into (15.57) to obtain the scattered fields and subsequently the elements of the scattering matrix (a concept defined in Section 15.5).

15.3.3 A Transient Source

The propagation of transient fields in a waveguide can be clarified by means of the following simple example. Let the (transient) source consist of a unit current, suddenly applied parallel to the narrow side of a rectangular waveguide (Fig. 15.4*b*). The pertinent current density, for $i = \mathrm{A}$, is

$$\mathbf{j} = \delta(x - x_0)\,\delta(z)H(t)\,\mathbf{u}_y. \tag{15.63}$$

Its Laplace transform is

$$\mathbf{J}(s) = \frac{1}{s}\,\delta(x - x_0)\,\delta(z)\,\mathbf{u}_y. \tag{15.64}$$

A few trivial steps, based on the form of ϕ_m given in (A9.1), show that all right-hand terms in (15.11) to (15.13) vanish. The source therefore does not excite the TM modes and only couples to the TE modes. In the second set of equations, (15.14) to (15.16), the only nonzero source term is

$$I_{nq} = \int_S \mathbf{J}(s) \cdot (\text{grad}\ \psi_{nq} \times \mathbf{u}_z) dS.$$

From (A9.3):

$$\text{grad}\ \psi_{nq} \times \mathbf{u}_z = \frac{1}{N_{nq}}\left[-\frac{q\pi}{b}\cos\frac{n\pi x}{a}\sin\frac{q\pi y}{b}\,\mathbf{u}_x + \frac{n\pi}{a}\sin\frac{n\pi x}{a}\cos\frac{q\pi y}{b}\,\mathbf{u}_y\right]. \tag{15.65}$$

Combining (15.64) and (15.65) shows that

$$I_{nq} = \frac{1}{N_{nq}}\frac{n\pi}{a}\sin\frac{n\pi x_0}{a}\,\delta(z)\frac{1}{s}\int_0^b \cos\frac{q\pi y}{b}\,dy.$$

The value of the last integral is zero unless $q = 0$. We conclude that the y-independent modes are the only ones to be excited. Consider, for example, the mode with eigenfunction $\psi_m = \cos n\pi x/a$. Elimination of I_n and L_n from (15.14) to (15.16) shows that V_n must satisfy

$$\frac{d^2V_n(z,s)}{dz^2} - \underbrace{\left(s^2\epsilon\mu + \frac{n^2\pi^2}{a^2}\right)}_{\gamma_n^2(s)} V_n(z,s) = \mu \sin\frac{n\pi x_0}{a}\,\delta(z)\left(\frac{2b}{a}\right)^{\frac{1}{2}}. \tag{15.66}$$

The symmetry of the configuration implies that V_n must be an even function of z. Moreover, the modes must consist of outgoing waves radiating *from* the sources. In consequence,

$$V_n(z,s) = -\mu \sin\frac{n\pi x_0}{a}\left(\frac{b}{2a}\right)^{\frac{1}{2}} \frac{1}{\gamma_n(s)}\, e^{-\gamma_n(s)|z|}. \tag{15.67}$$

The transform of the electric field follows as

$$E_y(x,z,s) = -\frac{\mu}{a}\sum_{n=1}^{\infty} \sin\frac{n\pi x}{a}\sin\frac{n\pi x_0}{a}\frac{e^{-\gamma_n(s)|z|}}{\gamma_n(s)}. \tag{15.68}$$

The time-dependent form of e_y may now be obtained by means of the known transform (see Note 5 of A7)

$$\frac{1}{\sqrt{s^2+1}}\, e^{-a\sqrt{s^2+1}} = L_2\left[J_0\left(\sqrt{t^2-a^2}\right)H(t-a)\right]. \tag{15.69}$$

This gives

$$e_y(\mathbf{r},t) = \begin{cases} -\dfrac{R_c}{a}\displaystyle\sum_{n=1}^{\infty} \sin\frac{n\pi x}{a}\sin\frac{n\pi x_0}{a} J_0\left[\frac{n\pi}{a}(c^2t^2 - z^2)^{\frac{1}{2}}\right] & \text{for } t > \dfrac{|z|}{c} \\ 0 & \text{for } t < \dfrac{|z|}{c}. \end{cases} \tag{15.70}$$

This interesting result shows that the signal propagates with a velocity c. It also shows that the shape of the signal is distorted during propagation. The distortion results from the different propagation constants that characterize the various frequencies present in the Fourier spectrum of the source. It follows that a signal with a fairly wide frequency spectrum (say a pulsed sinusoidal signal lasting for a few periods) can be expected to experience considerable distortion. Another source of distortion resides with the losses in the walls, which are also frequency-dependent.

The source in the current example is a mathematical model. More realistic sources are coaxial probes and small loops protruding from the waveguide wall. The current in these antennas is not known from the start and should be determined by solving an appropriate integral equation [46]. Given the smallness of the antennas, however, low-frequency approximations to the currents are often acceptable (Problem 15.4). The source could also be an aperture in the waveguide wall, a case to be discussed in Section 15.6, or an assigned value of the transverse electric field in a given cross section, for example $\mathbf{e}(x,y,t) = \mathbf{e}_t(x,y)\, e^{-(t^2/t_0^2)}$. The propagation of the resulting wave can subsequently be followed by FDTD techniques.[22]

15.3.4 The General Excitation Problem

As a basis for the discussion, consider the excitation of a TE mode by the boundary source $(\mathbf{u}_n \times \mathbf{E})$. From (15.14) to (15.16):

$$\frac{d^2 I_n}{dz^2} + (k^2 - \nu_n^2)\, I_n = -\frac{k^2 - \nu_n^2}{j\omega\mu}\, I_a - \frac{\nu_n^2}{j\omega\mu}\frac{dI_b}{dz}$$

$$\frac{d^2 W_n}{dz^2} + (k^2 - \nu_n^2)\, W_n = -\frac{\nu_n^2}{j\omega\mu}\left[\frac{d^2 I_b}{dz^2} + k^2 I_b - \frac{dI_a}{dz}\right], \tag{15.71}$$

where

$$I_a(z) = \int_c (\mathbf{u}_n \times \mathbf{E}) \cdot \text{grad}\ \psi_n\, dc$$

$$I_b(z) = \int_c (\mathbf{u}_n \times \mathbf{E}) \cdot (\psi_n \mathbf{u}_z)\, dc.$$

These equations are examples of the often encountered equations

$$\frac{d^2 f}{dz^2} - \gamma^2 f = g(z) \tag{15.72}$$

or

$$\frac{d^2 f}{dz^2} - \gamma^2 f = \frac{dq(z)}{dz}. \tag{15.73}$$

When γ^2 is negative (and γ imaginary), the mode propagates; when γ^2 is positive (and γ real), the mode is attenuated. The solution of (15.72) is most conveniently effected by means of a Green's function. In an infinite guide (i.e., in the interval $-\infty < z < \infty$), application of the radiation condition (or the damping condition) requires the Green's function to be of the type

$$G_1(z, z', \gamma) = -\left(\frac{1}{2}\gamma\right) e^{-\gamma|z - z'|} = G_1(z', z, \gamma). \tag{15.74}$$

The sought function $f(z)$ is therefore

$$\begin{aligned} f(z) &= \int_{-\infty}^{\infty} G_1(z, z', \gamma)\, g(z')\, dz' \\ &= -\frac{1}{2\gamma} e^{-\gamma z} \int_{-\infty}^{z} e^{\gamma z'} g(z')\, dz' - \frac{1}{2\gamma} e^{\gamma z} \int_{z}^{\infty} e^{-\gamma z'} g(z')\, dz'. \end{aligned} \tag{15.75}$$

The solution of (15.73) in an infinite guide is similarly obtained by means of an appropriate Green's function, in this case

$$G_2(z, z', \gamma) = \frac{1}{2}\,\text{sgn}(z - z')\, e^{-\gamma|z - z'|}. \tag{15.76}$$

Explicitly:

$$f(z) = \int_{-\infty}^{\infty} G_2(z, z', \gamma)\, q(z')\, dz' \;=\; \int_{-\infty}^{\infty} \frac{dG_1(z, z', \gamma)}{dz}\, q(z')\, dz',$$
$$= \frac{1}{2}\, e^{-\gamma z} \int_{-\infty}^{z} e^{\gamma z'} q(z')\, dz' - \frac{1}{2}\, e^{\gamma z} \int_{z}^{\infty} e^{-\gamma z'} q(z')\, dz'. \tag{15.77}$$

Outside the source regions, the components of a propagating mode contain an *outgoing wave factor* that, for positive z, depends on z according to the law

$$\phi \doteq \text{Re}\left[e^{j\omega t}\, e^{-j\sqrt{\omega^2 \epsilon \mu - \mu_m^2}\, z}\right]. \tag{15.78}$$

This factor is a particular case of the more general form[§]

$$\phi = \text{Re}\, e^{j[\omega t - k(\omega) z]}. \tag{15.79}$$

For such a frequency dependence, it is meaningful to define two basic velocities. The first one is the *phase velocity*

$$v_{ph} = \frac{\omega}{k(\omega)}. \tag{15.80}$$

An observer following the (15.79) wave with that particular velocity would detect a constant phase. When several modes propagate, each one has its own phase velocity, hence distorsion of the field pattern occurs as the signal moves down the z-axis. Added distorsion takes place when a wide spectrum of frequencies is present, such as in a fast transient. A careful analysis[23] shows that, even when the signal evidences many different phase velocities in its modal components, the front of the wave (the precursor) propagates down the waveguide with the velocity of light in the medium filling the waveguide (Problem 15.5).

The second basic velocity is the *group velocity* [40, 46]

$$v_g = \frac{\partial \omega}{\partial k}. \tag{15.81}$$

It is the speed at which energy propagates.[24,25] Relativity requires this speed not to exceed c_0. For a waveguide mode, for example, the $\omega(k)$ relationship is of the form (Fig. 15.5*a*)

$$\omega^2 = k^2 c^2 + \omega_c^2 \tag{15.82}$$

[§]Dispersive propagation is encountered, for example, in a cold collisionless plasma. When $\omega > \omega_p$, a plane wave in that medium is characterized by a factor (see 8.64)

$$e^{j\left[\omega t - k_0 \sqrt{1 - \frac{\omega_p^2}{\omega^2}}\, z\right]}.$$

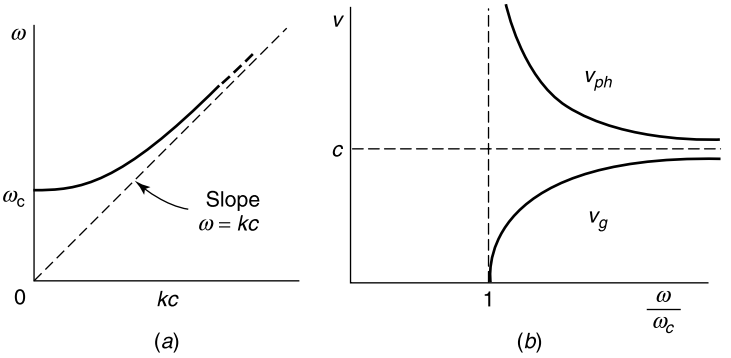

Figure 15.5 (*a*) The $\omega(k)$ relationship for a waveguide mode. (*b*) The frequency dependence of v_{ph} and v_g for a given mode.

where ω_c is the cut-off angular frequency. For such a law, the two velocities are (Problems 15.6 and 15.7)

$$v_{ph} = \frac{c}{\sqrt{1 - \left(\frac{\omega_c}{\omega}\right)^2}} \tag{15.83}$$

$$v_g = c\sqrt{1 - \left(\frac{\omega_c}{\omega}\right)^2}. \tag{15.84}$$

Their variation is depicted on Figure 15.5*b*.

In a *nondispersive* medium, the phase and group velocities are equal. In a *dispersive* medium, the definition of energy velocity requires consideration of a group of waves (a wave packet). Note that, when the medium is lossy, v_g ceases to have a clear physical meaning [40].

15.3.5 Waveguide Resonators

A *waveguide resonator* is formed by closing a sourceless waveguide with two transverse electric walls. The eigenvectors of the cavity can be expressed in terms of the eigenfunctions of the waveguide. For the *TM eigenvectors*, for example,

$$\mathbf{e}_{mpn} = \frac{n\pi}{L} \sin \frac{n\pi z}{L} \operatorname{grad} \phi_{mp} - \mu_{mp}^2 \cos \frac{n\pi z}{L} \phi_{mp} \mathbf{u}_z, \tag{15.85}$$

$$\mathbf{h}_{mpn} = \frac{1}{k_{mpn}} \operatorname{curl} \mathbf{e}_{mpn} = \left[\mu_{mp}^2 + \left(\frac{n\pi}{L}\right)^2\right]^{\frac{1}{2}} \cos \frac{n\pi z}{L} \mathbf{u}_z \times \operatorname{grad} \phi_{mp}, \tag{15.86}$$

with eigenvalues

$$k_{mpn}^2 = \left(\frac{n\pi}{L}\right)^2 + \mu_{mp}^2. \tag{15.87}$$

For the *TE eigenvectors*:

$$\mathbf{e}_{nsp} = \sin\frac{p\pi z}{L}\,\mathbf{u}_z \times \text{grad}\,\psi_{ns}, \tag{15.88}$$

$$\mathbf{h}_{nsp} = \frac{1}{k_{nsp}}\,\text{curl}\,\mathbf{e}_{nsp} = -\frac{1}{[\nu_{ns}^2 + (p\pi/L)^2]^{\frac{1}{2}}} \times \left(\nu_{ns}^2 \sin\frac{p\pi z}{L}\,\psi_{ns}\,\mathbf{u}_z + \frac{p\pi}{L}\cos\frac{p\pi z}{L}\,\text{grad}\,\psi_{ns}\right), \tag{15.89}$$

with eigenvalues

$$k_{nsp}^2 = \left(\frac{p\pi}{L}\right)^2 + \nu_{ns}^2. \tag{15.90}$$

We note that the electric field of the z-independent transverse magnetic modes is parallel to the z-axis. More specifically, for such modes,

$$\mathbf{e}_{0mp} = \phi_{mp}\,\mathbf{u}_z \tag{15.91}$$

$$\mathbf{h}_{0mp} = \frac{1}{k_{0mp}}\,\text{curl}\,\mathbf{e}_{0mp} = \frac{1}{\mu_{mp}}\,\text{grad}\,\phi_{mp} \times \mathbf{u}_z. \tag{15.92}$$

The corresponding eigenvalues are

$$k_{0mp}^2 = \mu_{mp}^2. \tag{15.93}$$

We also note that a set of TEM modes exists in a cylindrical cavity when the cross section is doubly connected. The pertinent eigenvectors are

$$\mathbf{e}_0 = \sin\frac{p\pi z}{L}\,\text{grad}\,\phi_0 \tag{15.94}$$

$$\frac{1}{k_0}\,\text{curl}\,\mathbf{e}_0 = \frac{L}{p\pi}\frac{p\pi}{L}\cos\frac{p\pi z}{L}\,\mathbf{u}_z \times \text{grad}\,\phi_0 = \cos\frac{p\pi z}{L}\,\mathbf{u}_z \times \text{grad}\,\phi_0, \tag{15.95}$$

and their eigenvalues are simply

$$k_0^2 = \left(\frac{p\pi}{L}\right)^2. \tag{15.96}$$

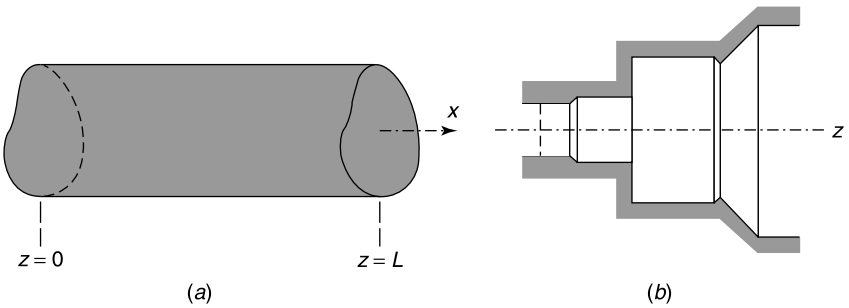

Figure 15.6 (*a*) General cylindrical cavity. (*b*) Composite cavity (from A. Jöstingmeier, C. Rieckmann, and A. S. Omar, Computation of the irrotational magnetic eigenfunctions belonging to complex cavities, *IEEE Trans. MTT* **42**, 2285–2293, 1994, with permission of IEEE).

Complex cavities can be formed by cascading resonant cells, coupled together by apertures in the end sections (Fig. 15.6*b*). The determination of the modal fields reduces to a series of *coupled regions* problems, to be solved by modal expansions in the various cells. The main unknowns are the fields in the apertures. Note that the contribution from the $\psi_0 = constant$ mode may not be ignored.[26]

15.4 WAVEGUIDE LOSSES

Losses may occur either in the medium filling the waveguide or in the walls. In the first case, they are accounted for by the presence of terms in σ in the equations satisfied by the expansion coefficients and can be included in the analysis by writing $k^2 = \omega^2\epsilon\mu - j\omega\mu\sigma$ in the various propagation equations. In the second case, they occur because the wall is not perfectly conducting but penetrable. The waveguide structure then becomes one of the *open-waveguide* type, because the fields are no longer confined to the cylindrical volume. It is possible, however, to avoid a full-fledged analysis if the conductivity of the walls is very high, in which case an impedance boundary condition may serve to represent coupling to the exterior region. It is then permissible to write

$$\mathbf{u}_n \times \mathbf{E} = Z_S \mathbf{H}_{\tan} = \mathbf{J}_{mS}, \tag{15.97}$$

where Z_S will be assumed uniform, for simplicity (a variation of Z_S along boundary C can easily be included in the analysis).

15.4.1 Equations for the Mode Coefficients

In an *E (or TM) mode*, (15.11) and (15.12) can be combined to give[27]

$$\frac{dV_m}{dz} + j\omega\mu\left(1 - \frac{\mu_m^2}{k^2}\right) I_m = -\int_C \mathbf{J}_{mS} \cdot (\mathbf{u}_z \times \operatorname{grad} \phi_m)\, dc. \tag{15.98}$$

The second member can be rewritten as

$$\begin{aligned} -\int_C \frac{\partial \phi_m}{\partial n}\, \mathbf{u}_c \cdot \mathbf{J}_{mS}\, dc &= -Z_S \int_C \frac{\partial \phi_m}{\partial n}\, \mathbf{u}_c \cdot \mathbf{H}\, dc \\ &= -Z_S \int_C \frac{\partial \phi_m}{\partial n} \left[+ \sum_{k=0}^{\infty} I_k \frac{\partial \phi_k}{\partial n} + \sum_{s=0}^{\infty} I_s \frac{\partial \psi_s}{\partial c} \right] dc \\ &= -Z_S \sum_{k=0}^{\infty} I_k(z) \underbrace{\int_C \frac{\partial \phi_m}{\partial n} \frac{\partial \phi_k}{\partial n}\, dc}_{A_{mk}} - Z_S \sum_{s=0}^{\infty} I_s(z) \underbrace{\int_C \frac{\partial \phi_m}{\partial n} \frac{\partial \psi_s}{\partial c}\, dc}_{B_{ms}}. \end{aligned} \tag{15.99}$$

Equation (15.98) now becomes

$$\begin{aligned} \frac{dV_m(z)}{dz} = &-\left(j\omega\mu - j\frac{\mu_m^2}{\omega\epsilon} + Z_S A_{mm}\right) I_m(z) \\ &- Z_S \sum_{k \neq m}^{\infty} A_{mk} I_k(z) - Z_S \sum_{s=0}^{\infty} B_{nS} I_s(z), \end{aligned} \tag{15.100}$$

with

$$\frac{dI_m}{dz} = -j\omega\epsilon\, V_m.$$

Equations (15.100) are of the type encountered in the theory of coupled transmission lines developed in Section 14.12. The solution is simplified when the waveguide carries only a *single* TM mode in the undisturbed state (i.e., when the walls are perfectly conducting). For such a case, all I_k and I_s, with the exception of I_m, are perturbations proportional to Z_S when the walls become penetrable. Keeping only first-order terms in Z_S leads to

$$\frac{d^2V_m}{dz^2} + \underbrace{(k^2 - \mu_m^2 - j\omega\epsilon\, Z_S A_{mm})}_{\gamma_m^2}\, V_m = 0. \tag{15.101}$$

The wall impedance Z_S clearly influences the propagation constant. If we set $\gamma_m = \beta_m - j\alpha_m$, the propagation factor becomes

$$e^{-j\gamma_m z} = e^{-\alpha_m z}\, e^{-j\beta_m z}. \tag{15.102}$$

Splitting $Z_S(\omega)$ into its real and imaginary parts, R_S and jX_S, gives

$$\alpha_m = \frac{1}{2}\frac{R_S}{R_c}\frac{k}{\sqrt{k^2 - \mu_m^2}}\, A_{mm} \tag{15.103}$$

$$\beta_m = \sqrt{k^2 - \mu_m^2} + \frac{1}{2}\frac{X_S}{R_c}\frac{k}{\sqrt{k^2 - \mu_m^2}}\, A_{mm}, \tag{15.104}$$

where $R_c = \sqrt{\dfrac{\mu}{\epsilon}}$ is the characteristic resistance of the medium in the guide, and A_{mm}, of dimension m^{-1}, is a characteristic parameter of the mode. For a good conductor

$$Z_S = \sqrt{\frac{\omega\mu_w}{2\sigma_w}}(1 + j), \tag{15.105}$$

where σ_w and μ_w refer to the material of the wall. With that particular value of Z_S, the *attenuation factor* α_m and the *shift in* β_m are equal. More precisely,

$$\alpha_m = \Delta\beta_m = \sqrt{\frac{\mu_w\epsilon}{8\sigma_w\mu}}\sqrt{\frac{\omega^3}{\omega^2 - \omega_c^2}}\int_C \left(\frac{\partial\phi_m}{\partial n}\right)^2 dc, \tag{15.106}$$

where ω_c denotes the cut-off angular frequency of the mode. A similar analysis can be performed for the *TE modes* (Problems 15.8 and 15.9). In the limit of small Z_S, and when only a single mode propagates, one obtains

$$\alpha_n = \frac{\nu_n^4}{2k\sqrt{k^2 - \nu_n^2}}\frac{R_S}{R_c}C_{nn} + \frac{\sqrt{k^2 - \nu_n^2}}{2k}\frac{R_S}{R_c}\, D_{nn}, \tag{15.107}$$

$$\beta_n = \sqrt{k^2 - \nu_n^2} + \frac{\nu_n^4}{2k\sqrt{k^2 - \nu_n^2}}\frac{X_S}{R_c}\, C_{nn} + \frac{\sqrt{k^2 - \nu_n^2}}{2k}\frac{X_S}{R_c}\, D_{nn}, \tag{15.108}$$

where

$$C_{nn} = \int_C \psi_n^2 \, dc; \qquad D_{nn} = \int_C \left(\frac{\partial \psi_n}{\partial c} \right)^2 dc. \tag{15.109}$$

For a good conductor:

$$\alpha_n = \Delta\beta_n = \sqrt{\frac{\mu_w \epsilon}{8\sigma_w \mu}} \sqrt{\frac{\omega^2 - \omega_c^2}{\omega}} \left[\frac{\omega_c^2}{\omega^2 - \omega_c^2} \, \nu_n^2 \int_C \psi_n^2 \, dc + \int_C \left(\frac{\partial \psi_n}{\partial c} \right)^2 dc \right]. \tag{15.110}$$

The formulas for α_m and α_n are based on the validity of the surface impedance concept and in particular on the assumption that the penetration depth δ is small with respect to the cross-sectional dimensions of the guide.[28] The method could therefore fail in the microwave region when applied to conducting strips, which often have dimensions of the order 1 μm, comparable with the microwave values of δ.

15.4.2 Frequency Dependence of the Attenuation

From (15.103), the attenuation coefficient α_m of a *TM mode* varies proportionally to $\frac{\omega}{\omega_c} \left(\frac{\omega^2}{\omega_c^2} - 1 \right)^{-\frac{1}{2}}$. This universal variation is plotted in Figure 15.7*a*, which shows that a minimum is reached for $\omega = \sqrt{3}\,\omega_c$. The variation of α_n for a *TE mode*, given in (15.107), depends again on (ω/ω_c) but also on the ratio of the two terms on the right-hand side of the equation.[29] The term in C_{nn} is generated by H_z (i.e., by currents flowing along the contour C of the cross section). The term in D_{nn}, on the other hand, is generated by H_c (i.e., by currents flowing in the z-direction). The dimensionless ratio of the two terms is

$$F_{nn} = \frac{\displaystyle\int_C \left(\frac{\partial \psi_n}{\partial c} \right)^2 dc}{\nu_n^2 \displaystyle\int_C \psi_n^2 \, dc}. \tag{15.111}$$

The corresponding set of curves is shown in Figure 15.7*b*. The variations of α in Figure 15.7 are *relative*. Actual values of the attenuation are given in Figure 15.8 for three modes of a circular waveguide with copper walls and a diameter of 5 cm. The minimum attenuation is of the order tens of dB km^{-1}, an unacceptable value for long-distance communications. One exception immediately catches the eye: the H_{01} mode, whose attenuation decreases monotonically for increasing frequencies. This behavior corresponds with $F_{nn} = 0$ in Figure 15.7*b* and implies, from (15.110), a mode with uniform ψ_n along the cross-sectional contour. Such a property requires rotational symmetry and holds only for the H_{0n} modes of the circle. The potentially low attenuation of these modes led to attempts, from the 1930s on, to use the H_{01} mode for long-distance links. There were obstacles: The capital investment was high, in particular because H_{01} is not the lowest mode, and unwanted excitation of the lower modes had to be suppressed. This required the use of devices such as mode filters. The explosive development of the optical fibers, from the 1960s on, led to the de facto abandonment of the H_{01} *technology*.

It is clear, from Figure 15.7, that standard waveguides suffer increasing losses as the frequency progressively increases beyond a certain limit. These losses can reach 10 dB m^{-1}

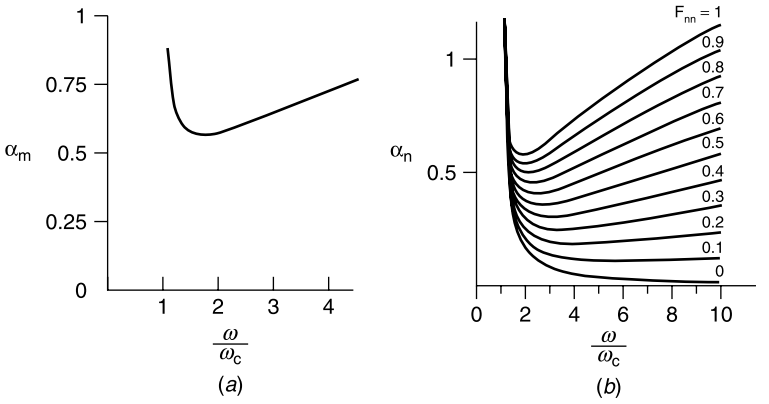

Figure 15.7 (*a*) Relative variation of α_m (TM modes). (*b*) Relative variation of α_n (TE modes) (from P. Lagasse and J. Van Bladel, Square and rectangular waveguides with rounded corners, *IEEE Trans. MTT* **20**, 331–337, 1972, with permission of IEEE).

at 200 GHz. Covering the wall with a superconducting layer could reduce the attenuation to acceptable levels.[30] Other wall coatings have been proposed, for example photonic surfaces (PBG), which create a magnetic wall condition in the stopband of the surface[31] (see Section 9.5 and Fig. 15.9). In Figure 15.10, a series of dielectric-filled corrugations create a wall impedance that, if $s \ll a$ and d is much less than the wavelength λ_g in the guide, becomes a reactive, dyadic impedance $\overline{\overline{Z}}_S$. The anisotropic character of $\overline{\overline{Z}}_S$ is expressed by the equations[32]

$$\frac{E_z}{H_\varphi} = -j\frac{R_{c0}}{\sqrt{\epsilon_r}}\tan(k_0\sqrt{\epsilon_r}s) \qquad \text{and} \qquad \frac{E_\varphi}{H_z} = 0. \tag{15.112}$$

It is interesting to note that the closed metallic guide was once considered as a potential waveguide for the optical range.[33] This was just before the breakthrough of the optical fiber and was based on the fact that metals have a comparatively large dielectric constant at optical frequencies[34] (see Section 8.1).

15.4.3 Degeneracies

The analysis of losses presented above is not directly applicable when two (or more) modes have the same eigenvalue. Such *degenerate modes* are unavoidably coupled together by the

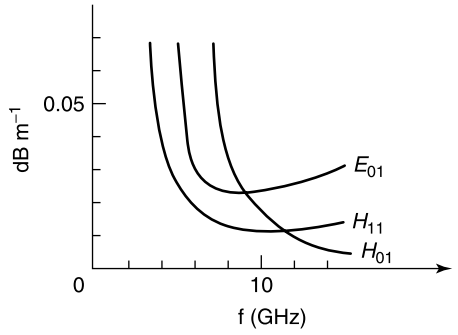

Figure 15.8 Attenuation coefficient of three modes in a circular waveguide.

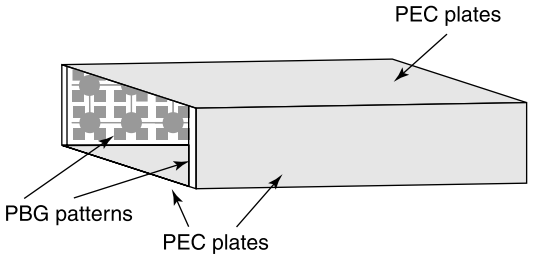

Figure 15.9 Photonic wall waveguide (from F.-R. Yang, K.-P. Ma, Y. Qian, and T. Itoh, A novel TEM waveguide using uniplanar compact photonic-bandgap (UC-PBG) structure, *IEEE Trans. MTT* **47**, 2092–2098, 1999, with permission of IEEE).

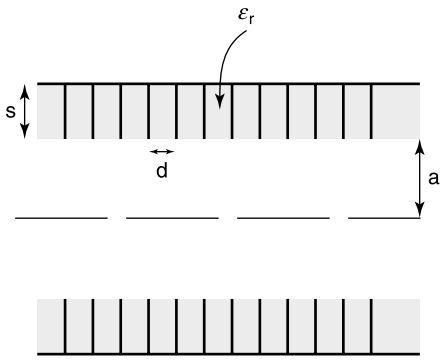

Figure 15.10 Corrugations in a circular waveguide (from I. V. Lindell, Variational methods for nonstandard eigenvalue problems in waveguide and resonator analysis, *IEEE Trans. MTT* **30**, 1194–1204, 1982, with permission of IEEE).

wall impedance. They occur frequently, for example in the presence of special symmetries, as in the circular or square waveguides[35] [18, 46]. Assume that two TM modes, here called 1 and 2, propagate, and that all other modes are not excited. In the spirit of the previous discussion, (15.101) is now replaced by the coupled equations,[27]

$$\begin{aligned}\frac{d^2V_1}{dz^2} &= \left(\mu^2 - k^2 + jk\frac{Z_S}{R_c}A_{11}\right)V_1 + jk\frac{Z_S}{R_c}A_{12}V_2 \\ \frac{d^2V_2}{dz^2} &= jk\frac{Z_S}{R_c}A_{21}V_1 + \left(\mu^2 - k^2 + jk\frac{Z_S}{R_c}A_{22}\right)V_2,\end{aligned} \tag{15.113}$$

where μ^2 is the common value $\mu_1^2 = \mu_2^2$, and A_{mk} is defined in (15.99). System (15.113) is of the general form

$$\frac{d^2\mathbf{V}}{dz^2} = \overline{\overline{M}}\cdot\mathbf{V}. \tag{15.114}$$

This equation is similar to (14.272), which is satisfied by the voltages on two coupled transmission lines. As in Section 14.12, the solution proceeds by determining the eigenvectors and eigenvalues of the matrix. The analysis shows that two *uncoupled* modes are

found, which propagate with *separate* attenuation and propagation constants.[¶] The situation reminds one of the magnetic coupling between two identical (LC) circuits, which splits the common resonant frequency.

15.5 WAVEGUIDE NETWORKS

A general waveguide network is shown in Figure 15.11*a*. We shall assume that the materials in the enclosed volume are linear and that the walls are perfectly conducting.

15.5.1 One Port Junction

The *load* in the junction could be an antenna or a cavity containing lossy materials (Fig. 15.11*b*). From (5.76), (14.230), (15.1), and (15.2), the time averaged power delivered to the load is given by

$$P = \frac{1}{2}\,\mathrm{Re}\int_S (\mathbf{E}_t \times \mathbf{H}_t^*)\cdot \mathbf{u}_z\, dS = \frac{1}{2}\,\mathrm{Re}\left[\sum_m V_m I_m^* + \sum_n V_n I_n^*\right]. \tag{15.115}$$

This relationship shows that the modes are power-orthogonal (i.e., that the power is the sum of the individual powers in the modes). Consider, for example, a propagating *TM mode*. It normally contributes a wave to the left and one to the right. From (15.43), we write

$$\begin{aligned}\mathbf{E}_{mt} &= \left(A_m\, e^{-j\beta_m z} + D_m\, e^{j\beta_m z}\right)\,\mathrm{grad}\,\phi_m\\ \mathbf{H}_{mt} &= G_m\left(A_m\, e^{-j\beta_m z} - D_m\, e^{j\beta_m z}\right)\mathbf{u}_z \times \mathrm{grad}\,\phi_m,\end{aligned} \tag{15.116}$$

where G_m is the *characteristic conductance of the mode*, defined in (15.43). The power flowing to positive z is given by

$$P = \frac{1}{2}\,\mathrm{Re}\,(V_m I_m^*) = \frac{1}{2}\,G_m(|A_m|^2 - |D_m|^2). \tag{15.117}$$

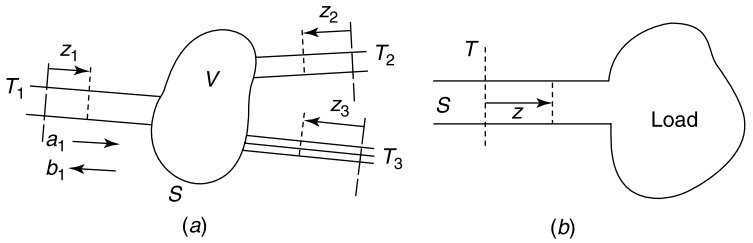

Figure 15.11 (*a*) General waveguide junction. (*b*) One-port junction (terminated guide).

The wave to the left may be interpreted as reflected from the load, which in that case can be characterized by a reflection coefficient

$$K(z) = \frac{D_m}{A_m}\, e^{2j\beta_m z}, \tag{15.118}$$

[¶]As in many similar situations in physics, coupling has removed the degeneracy.

which corresponds with an equivalent load impedance

$$Z_m(z) = \frac{\beta_m}{\omega\epsilon}\frac{1+K}{1-K}. \tag{15.119}$$

These formulas are identical with those obtained in classic transmission line theory. It is not surprising, therefore, that the methods of analysis used in transmission line work (in particular the graphical methods based on the use of the Smith chart) can be applied to waveguide problems [101].

It is useful to introduce the concept of *unit power wave*, a progressive wave for which P in (15.115) is equal to 1 W. The transverse fields for such a wave are, in a *TM mode*,

$$\begin{aligned}\sqrt{\frac{2}{G_m}}\, e^{-j\beta_m z}\,\text{grad}\,\phi_m &= \mathbf{e}'_m\, e^{-j\beta_m z}\\ \sqrt{2G_m}\, e^{-j\beta_m z}\,\mathbf{u}_z \times \text{grad}\,\phi_m &= \mathbf{h}'_m\, e^{-j\beta_m z}.\end{aligned} \tag{15.120}$$

If the waveguide fields are written in the form

$$\begin{aligned}\mathbf{E}_t &= \left(a_m\, e^{-j\beta_m z} + d_m\, e^{j\beta_m z}\right)\mathbf{e}'_m\\ \mathbf{H}_t &= \left(a_m\, e^{-j\beta_m z} - d_m\, e^{j\beta_m z}\right)\mathbf{h}'_m,\end{aligned} \tag{15.121}$$

the power to the load becomes

$$P = |a_m|^2 - |d_m|^2, \tag{15.122}$$

where a_m and d_m have the dimension $W^{\frac{1}{2}}$. Similar steps can be retraced for the *TE modes*, for which the wave carrying unit power has the tranverse fields

$$\begin{aligned}\sqrt{2R_n}\, e^{-j\beta_n z}\,\text{grad}\,\psi_n \times \mathbf{u}_z &= \mathbf{e}'_n\, e^{-j\beta_n z}\\ \sqrt{\frac{2}{R_n}}\, e^{-j\beta_n z}\,\text{grad}\,\psi_n &= \mathbf{h}'_n\, e^{-j\beta_n z},\end{aligned} \tag{15.123}$$

where R_n is the *characteristic resistance of the mode*, defined in (15.44).

15.5.2 Multiport Junctions: The Scattering Matrix

In general, the N waveguide arms of the junction shown in Figure 15.11*a* have different cross sections (hence different cut-off frequencies), but we shall assume, for simplicity, that the operating frequency allows propagation of only a single mode in each waveguide arm. The extension to several propagating modes is immediate. In the absence of sources, a linear relationship must exist between the (complex) amplitudes of the reflected and incident waves. We shall choose the amplitudes on the basis of the unit power representation (15.121) and write (Fig. 15.12)

$$\begin{aligned}b_1 &= S_{11}\, a_1 + S_{12}\, a_2\\ b_2 &= S_{21}\, a_1 + S_{22}\, a_2.\end{aligned} \tag{15.124}$$

In matrix form:

$$\mathbf{b} = \overline{\overline{S}} \cdot \mathbf{a}. \tag{15.125}$$

The dimensionless matrix $\overline{\overline{S}}$ is the *scattering matrix of the junction* [46, 97]. Its various elements can be given useful physical interpretations. S_{11}, for example, is the reflection coefficient at T_1 when arm 2 is matched (i.e., when $a_2 = 0$). The interpretation of S_{21} is equally interesting. With arm 2 matched, $S_{21}a_1$ is the transmitted wave b_2 at T_2 resulting from an incident wave a_1 at T_1. Clearly, $|S_{12}|^2$ has the nature of a power transmission coefficient, and its inverse that of an attenuation coefficient (Problem 15.10). The junction may also be described in terms of impedances. Thus, assuming that fields $\mathbf{E} = V\,\mathbf{e}_m$ and $\mathbf{H} = I\,\mathbf{h}_n$ exist at the end planes T_1, T_2, we write (Problems 15.11 and 15.12)

$$\begin{aligned} V_1 &= Z_{11}\,I_1 + Z_{12}\,I_2 \\ V_2 &= Z_{21}\,I_1 + Z_{22}\,I_2 \end{aligned} \tag{15.126}$$

and

$$\begin{aligned} I_1 &= Y_{11}\,V_1 + Y_{12}\,V_2 \\ I_2 &= Y_{21}\,V_1 + Y_{22}\,V_2. \end{aligned} \tag{15.127}$$

The $\overline{\overline{S}}$, $\overline{\overline{Y}}$, and $\overline{\overline{Z}}$ matrices have important symmetry properties, which can be proved by the following argument. Consider a volume V bounded by a surface S through which no energy can escape. The volume contains an inhomogeneous anisotropic material of characteristics $\overline{\overline{\epsilon}}$ and $\overline{\overline{\mu}}$. Assume, first, that T_2 is short-circuited by a perfectly conducting plane (state a, Fig. 15.12a). The fields at T_1 are given by expressions of the form

$$\mathbf{E}_{ta} = V_{1a}\,\mathbf{e}_1; \qquad \mathbf{H}_{ta} = I_{1a}\,\mathbf{h}_1.$$

At T_2:

$$\mathbf{E}_{ta} = 0; \qquad \mathbf{H}_{ta} = I_{2a}\,\mathbf{h}_2 = Y_{21}^a V_{1a}\,\mathbf{h}_2.$$

In state b (Fig. 15.12b), the junction is filled with a material of *transpose* characteristics $\overline{\overline{\epsilon}}^t$, $\overline{\overline{\mu}}^t$. With T_1 short-circuited, the fields at T_1 are

$$\mathbf{E}_{tb} = 0; \qquad \mathbf{H}_{tb} = I_{1b}\,\mathbf{h}_1 = Y_{12}^b V_{2b}\,\mathbf{h}_1.$$

At T_2:

$$\mathbf{E}_{tb} = V_{2b}\,\mathbf{e}_2; \qquad \mathbf{H}_{tb} = I_{2b}\,\mathbf{h}_2.$$

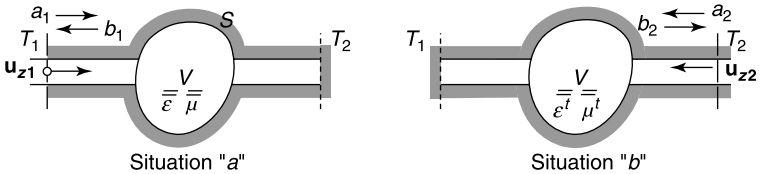

Figure 15.12 Relevant to the reciprocity theorem.

The next steps are very similar to those followed in Section 8.6. From Maxwell's equations we may write

$$\operatorname{div}(\mathbf{E}_a \times \mathbf{H}_b - \mathbf{E}_b \times \mathbf{H}_a) = -j\omega\,(\mathbf{H}_b \cdot \overline{\overline{\mu}} \cdot \mathbf{H}_a - \mathbf{H}_a \cdot \overline{\overline{\mu}}^t \cdot \mathbf{H}_b + \mathbf{E}_a \cdot \overline{\overline{\epsilon}}^t \cdot \mathbf{E}_b - \mathbf{E}_b \cdot \overline{\overline{\epsilon}} \cdot \mathbf{E}_a). \tag{15.128}$$

On the basis of (A4.35) the right-hand term of this equation vanishes. Let now the divergence term in (15.128) be integrated over the volume bounded by T_1, T_2, and S. Use of the divergence theorem transforms the integral to a surface integral. The impenetrability of the walls implies that the surface integral vanishes everywhere except on T_1 and T_2. The contributions from these two surfaces can be further evaluated by remembering that $\mathbf{E}_a$ is perpendicular to T_1 and $\mathbf{E}_b$ to T_2. The integrated left-hand term of (15.128) then becomes

$$\begin{aligned} &-\int_{T_1} \mathbf{u}_{z1} \cdot (\mathbf{E}_a \times \mathbf{H}_b)\, dS_1 + \int_{T_2} \mathbf{u}_{z2} \cdot (\mathbf{E}_b \times \mathbf{H}_a)\, dS_2 \\ &= -\int_{T_1} \mathbf{u}_{z1} \cdot (V_{za}\, \mathbf{e}_1 \times I_{1b}\, \mathbf{h}_1)\, dS_1 + \int_{T_2} \mathbf{u}_{z2} \cdot (V_{2b}\, \mathbf{e}_2 \times I_{2a}\, \mathbf{h}_2)\, dS_2 = 0. \end{aligned}$$

Taking the normalization conditions (5.76) or (14.230) into account, and replacing I_{1b} and I_{2a} by their values in terms of V_{2b} or V_{1b}, gives

$$-V_{1a}\, I_{1b} + V_{2b}\, I_{2a} = -V_{1a}\, Y_{12}^b\, V_{2b} + V_{2b}\, Y_{21}^a\, V_{1b} = 0.$$

It follows that $Y_{21}^a = Y_{12}^b$ or, more generally, that

$$\overline{\overline{Y}}^a = \left(\overline{\overline{Y}}^b\right)^t. \tag{15.129}$$

If, in particular, $\overline{\overline{\epsilon}}$ and $\overline{\overline{\mu}}$ are symmetric, $\overline{\overline{Y}}$ will be symmetric, too. Similar properties hold for the $\overline{\overline{Z}}$ and $\overline{\overline{S}}$ matrices (Problem 15.13).

15.5.3 Further Data on the Scattering Matrix

Additional relationships between the coefficients of $\overline{\overline{S}}$ can be derived from energy considerations. Equations (15.122) and (15.124) show that if a unit wave is incident from arm 1, and if arm 2 is matched, the power entering the junction is $1 - |S_{11}|^2$, and the power leaving the junction is $|S_{21}|^2$. It follows, from the principle of conservation of energy, that

$$1 - |S_{11}|^2 \geq |S_{21}|^2, \tag{15.130}$$

where the *equality* holds for a lossless junction. If the junction is lossless, we may write analogously

$$1 - |S_{22}|^2 = |S_{12}|^2, \tag{15.131}$$

from which the following can be deduced:

$$|S_{11}|^2 + |S_{21}|^2 = |S_{12}|^2 + |S_{22}|^2 = 1. \tag{15.132}$$

In consequence, when the media are reciprocal (and $\overline{\overline{S}}$ consequently symmetric),

$$|S_{11}| = |S_{22}|. \tag{15.133}$$

More generally, the $\overline{\overline{S}}$ *matrix* of a lossless N-armed junction can be shown to be *unitary*, that is, to satisfy the equation

$$\overline{\overline{S}}^{-1} = \overline{\overline{S}}^{\dagger}. \tag{15.134}$$

As an application, consider the two-port junction in Figure 15.13, and assume that arm 2 is loaded at T_2 by a device of reflection coefficient K. It is desired to determine the reflection coefficient K' at T_1. Because K is the reflection coefficient at T_2, incident and reflected waves there are related by the equation

$$\frac{a_2}{b_2} = K.$$

It follows, from (15.124), that

$$b_1 = S_{11}\, a_1 + S_{12}\, a_2 = S_{11}\, a_1 + S_{12}\, K b_2$$
$$b_2 = S_{21}\, a_1 + S_{22}\, a_2 = S_{21}\, a_1 + S_{22}\, K b_2.$$

Elimination of b_2 gives

$$K' = \frac{b_1}{a_1} = S_{11} + \frac{S_{21} S_{21} K}{1 - K S_{22}}, \tag{15.135}$$

which is the desired relationship.

Equation (15.126) implies that a two-armed junction containing a reciprocal medium can be represented by the equivalent circuit shown in Figure 15.13*b*. If the junction is lossless, the various impedances are purely imaginary, and *three* real numbers are sufficient to describe the circuit properties of the junction. We note that these numbers depend on both the operating frequency and the location of the terminal planes.

The $\overline{\overline{S}}$ description of a network reveals the main properties of the structure and in particular how the latter reacts under the impact of various incident waves (Problems 15.14 and 15.15). Much effort has therefore been invested in the determination of the elements of $\overline{\overline{S}}$. This may be done experimentally or theoretically. Theoretical solutions have often focused on waveguides coupled by an aperture in a plane perpendicular to a common axis [46, 97, 101, 191] (Fig. 15.14*a* and *b*). The solution often proceeds by *mode matching*, a method that is particularly suitable for the iris "network" shown in Figure 15.14*a* (Problem 15.16).

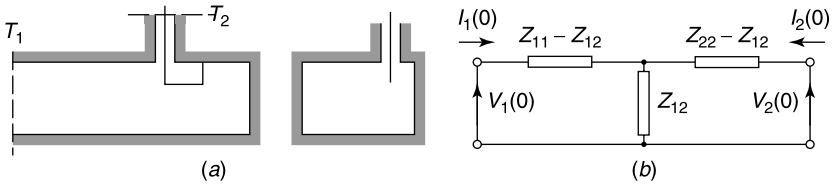

Figure 15.13 (*a*) Waveguide-to-coaxial transition. (*b*) Equivalent circuit for a propagating mode.

We shall assume, for simplicity, that the guide carries only its lowest mode (a TE mode). The transverse fields in part 1 may be written as

$$\mathbf{E}_t = R_1 A_1 \left(e^{-j\beta_1 z} + K\, e^{j\beta_1 z}\right) \mathbf{e}_1 + \sum_{n=2}^{\infty} jX_n A_n\, e^{\delta_n z} \mathbf{e}_n \tag{15.136}$$

$$\mathbf{H}_t = A_1 \left(e^{-j\beta_1 z} - K\, e^{j\beta_1 z}\right) \mathbf{h}_1 + \sum_{n=2}^{\infty} A_n\, e^{\delta_n z} \mathbf{h}_n. \tag{15.137}$$

We shall further simplify by assuming that there are two incident waves, one from each side, with the type of symmetry shown in Figure 15.14*a*. For such a case, $\mathbf{E}_t$ and $\mathbf{H}_t$ are respectively even and odd with respect to the $z = 0$ plane, hence $\mathbf{H}_t$ must vanish in the aperture S_a. This condition — which in fact expresses mode matching between sections 1 and 2 — gives, because $\mathbf{h}_n = \mathbf{u}_z \times \mathbf{e}_n$,

$$A_1(1 - K)\, \mathbf{e}_1(\mathbf{r}) + \sum_{n=2}^{\infty} A_n\, \mathbf{e}_n(\mathbf{r}) = 0 \tag{15.138}$$

for $\mathbf{r}$ in S_a. Because (15.138) is only valid over part of cross section S_1, the coefficients in the eigenvector expansion are not necessarily equal to zero. On the other hand, (15.136), written for $z = 0$, gives

$$\mathbf{E}_t(0) = R_1 A_1(1 + K)\, \mathbf{e}_1 + \sum_{n \neq 1}^{\infty} jX_n A_n\, \mathbf{e}_n(\mathbf{r}), \tag{15.139}$$

and this expression remains valid over the whole cross section S_1. We may therefore write

$$\begin{aligned} R_1 A_1(1 + K) &= \int_{S_1} \mathbf{E}_t(0) \cdot \mathbf{e}_1\, dS \\ jX_n A_n &= \int_{S_1} \mathbf{E}_t(0) \cdot \mathbf{e}_n\, dS. \end{aligned} \tag{15.140}$$

Inserting these values of A_1 and A_n into (15.138) yields an integral equation for $\mathbf{E}_t(0)$. The usual methods can now be applied to the solution of that equation, for example variational procedures [22]. The unknown $\mathbf{E}_t(0)$ can usefully be expanded in basis functions in the

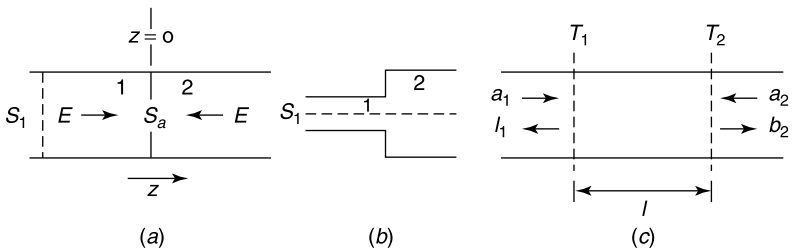

Figure 15.14 (*a*) Perfectly conducting diaphragm. (*b*) Transition between waveguides. (*c*) A section of waveguide.

aperture S_a. When the latter occupies the whole cross section of one of the guides, say S_1 in Figure 15.14*b*, one often chooses the eigenvectors of guide 1 or, to accelerate convergence, functions that incorporate the edge condition.[36] Genetic algorithms have also been used successfully, for example in the design of performant microwave filters.[37]

15.5.4 Evanescent Modes

Modes under cut-off decrease exponentially along the axis (i.e., according to a law $e^{-\delta|z|}$). This decrease can be very accurately predicted from a knowledge of the dimensions of the guide, and a valuable primary attenuation standard has been designed on that basis.[38] In general, evanescent modes may not be neglected in the mode expansions whenever distances from sources and scatterers are less than a few times $(1/\delta)$. It is useful, therefore, to absorb the contribution from the evanescent modes into the $\overline{\overline{S}}$ matrix formalism.[39] To that effect, consider a portion of waveguide located between T_1 and T_2 (Fig. 15.14*c*). If we assume that a_1 is the only incident wave (i.e., if we set $a_2 = 0$), we obtain $b_2 = e^{-\delta l} a_1 = S_{12}\, a_1$ and $b_1 = S_{11}\, a_1 = 0$. This yields the scattering matrix

$$\overline{\overline{S}} = \begin{pmatrix} 0 & e^{-\delta l} \\ e^{-\delta l} & 0 \end{pmatrix}. \tag{15.141}$$

This matrix is *not* unitary because

$$\overline{\overline{S}} \cdot \overline{\overline{S}}^{\dagger} = \begin{pmatrix} e^{-2\delta l} & 0 \\ 0 & e^{-2\delta l} \end{pmatrix} \neq \overline{\overline{I}}. \tag{15.142}$$

On the other hand, for a section carrying a propagating mode, $\overline{\overline{S}}$ would be

$$\overline{\overline{S}} = \begin{pmatrix} 0 & e^{-j\beta l} \\ e^{-j\beta l} & 0 \end{pmatrix}. \tag{15.143}$$

This matrix *is* unitary. It should be noted that the matrix relative to an evanescent mode can be made unitary by a suitable mode normalization.[40]

The $\overline{\overline{S}}$ concept, which has been defined for a single mode, propagating or evanescent, can be extended to include all modes.[41] Such a generalized matrix is infinite but can be limited in size by considering only N (important) modes in the analysis. The submatrices formed by the propagating modes remain unitary [191].

15.6 APERTURE EXCITATION AND COUPLING

Apertures in the wall of a waveguide allow power and signals to leak out of the waveguide and conversely allow fields to penetrate into the guide under the impact of external sources. The field problem is of a *coupled regions* nature, and it can be solved by evaluating the tangential magnetic field in terms of $\mathbf{u}_n \times \mathbf{E}$ on both sides of the aperture, and subsequently equating the two values of $\mathbf{H}_{\tan}$. The procedure yields an equation for $\mathbf{u}_n \times \mathbf{E}$. We shall first discuss two examples of evaluation of $\mathbf{H}_{\tan}$ inside the guide, given $\mathbf{u}_n \times \mathbf{E}$ in the aperture. This will be followed by a third example, in which the full integral equation satisfied by $\mathbf{u}_n \times \mathbf{E}$ is derived. Various types of apertures, continuous or periodic, are discussed thereafter.

In the first example, a circular duct is provided with a narrow circumferential gap, across which a uniform voltage $V \cos \omega t$ is applied (Fig. 15.15*a*). Such a configuration may be found in particle accelerators, in which case the duct is operated below cut-off, and the fields remain located in the gap region, where they interact with the passing particle beams. We seek an expression for the fields in the duct.

Because the gap is narrow, the tangential electric field may be written as

$$\mathbf{E}_{\tan} = V\,\delta(z)\,\mathbf{u}_z. \tag{15.144}$$

It follows that

$$\mathbf{J}_{mS} = \mathbf{u}_n \times \mathbf{E} = -V\,\delta(z)\,\mathbf{u}_c. \tag{15.145}$$

If we introduce that particular value of $\mathbf{u}_n \times \mathbf{E}$ into the right-hand terms of (15.11) to (15.16), we immediately notice that the only excited modes are those whose components are φ-independent. This implies that the H modes are *not* excited, because $\partial \psi_n / \partial c = 0$ for a φ-independent eigenfunction. In consequence, the field expansions contain E modes only. The expansion coefficients for the magnetic field can be determined from (15.11) to (15.13). We shall omit the index 0, for conciseness, in the expression for the mode functions given in (A9.6), and write

$$\operatorname{grad} \phi_p = -\frac{1}{\sqrt{\pi}\,a} \frac{J_1\left(x_p \dfrac{r}{a}\right)}{J_1(x_p)}\,\mathbf{u}_r, \tag{15.146}$$

where

$$J_0(x_p) = 0 \quad \text{and} \quad \mu_p^2 = \left(\frac{x_p}{a}\right)^2.$$

The index p now refers to the order of the zero of $J_0(x)$. The magnetic field must be symmetric with respect to the plane of the gap, hence its coefficients must be even in z. A few elementary steps give [22]

$$\mathbf{h}(r,z,t) = -\omega\epsilon_0 \frac{V}{a} \left\{ \sum_p \frac{J_1(x_p\, r/a)\, \exp\left\{ -\left[(x_p/a)^2 - k_0^2\right]^{\frac{1}{2}} |z| \right\}}{J_1(x_p)\left[(x_p/a)^2 - k_0^2\right]^{\frac{1}{2}}} \right\} \sin \omega t\, \mathbf{u}_\varphi. \tag{15.147}$$

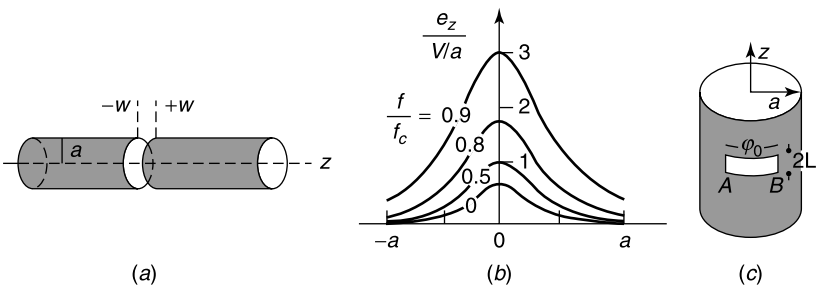

Figure 15.15 (*a*) Circular duct with circumferential gap. (*b*) Electric field on the axis of a circular duct (from J. A. Dattillo and J. Van Bladel, Fields in gap-excited circular ducts, *Nucl. Instr. Methods* **6**, 283–285, 1960, with permission of Elsevier Science Publishers). (*c*) Transverse slot.

Similar steps lead to

$$\mathbf{e}(r,z,t) = \left(\pm \sum_p \frac{J_1(x_p\, r/a)\ \exp\left\{ -\left[(x_p/a)^2 - k_0^2 \right]^{\frac{1}{2}} |z| \right\}}{J_1(x_p)} \mathbf{u}_r \right. \tag{15.148}$$

$$\left. + \sum_p \frac{x_p J_0(x_p\, r/a)\ \exp\left\{ -\left[(x_p/a)^2 - k_0^2 \right]^{\frac{1}{2}} |z| \right\}}{a J_1(x_p) \left[(x_p/a)^2 - k_0^2 \right]^{\frac{1}{2}}} \mathbf{u}_z \right) \frac{V}{a} \cos \omega t.$$

The plus and minus signs in front of the first right-hand term correspond with positive and negative z's, respectively. A few curves for the z component of the electric field are given in Figure 15.15*b*, where the parameter (f/f_c) is the ratio of the frequency to the cut-off frequency. The curves show that the fields penetrate deeper and deeper into the waveguide as the frequency increases. When the cut-off frequency $f_c = 0.383 c_0/a$ is reached, the lowest mode is launched, and the fields propagate down the whole length of the tube.

In a second example, the slot is transverse (Fig. 15.15*c*), and the interior fields are evaluated by assuming a reasonable form for the electric field in the aperture. When the latter is narrow, the field will be essentially z-oriented (except locally at the end points A and B), and we may set[42]

$$E_z = \frac{V}{2L} \cos\left(\pi \frac{\varphi}{\varphi_0} \right), \tag{15.149}$$

where $-L < z < L$. This type of approximation (where V is the voltage across the slot) is acceptable when the length $(\varphi_0 a)$ of the slot is in the neighborhood of $(\lambda_0/2)$.

Assume now that the aperture is of arbitrary shape, and *small* with respect to all characteristic lengths such as the wavelengths and the lateral guide dimensions.[43,44,45] For such an aperture, the integrals over $(\mathbf{u}_n \times \mathbf{E})$ that appear in the right-hand terms of (15.9) to (15.15) can be transformed according to (10.166). The electric and magnetic dipole moments, $\mathbf{P}_m$ and $\mathbf{P}_e$, are given by (10.165). The evaluation of these moments requires a knowledge of the generator fields $\mathbf{E}^g$, $\mathbf{H}^g$ that exist in the aperture when the latter is short-circuited. If the waveguide carries only its lowest mode, these fields are, from (15.1) and (15.44),

$$\mathbf{E}^g = \frac{\omega \mu_0}{\beta_1} (\text{grad}\ \psi_1 \times \mathbf{u}_z) I_1 \ = \ R_1 \frac{\partial \psi_1}{\partial c} \mathbf{u}_n I_1$$

$$\mathbf{H}^g = I_1\, \text{grad}\ \psi_1 + j I_1 \frac{V_1^2}{\beta_1} \psi_1\, \mathbf{u}_z, \tag{15.150}$$

where I_1 represents the amplitude of the incident magnetic field (see 15.2), and the aperture is assumed located at $z = 0$. For a circular hole of radius a, the dipole moments are

$$\mathbf{P}_e = \frac{2}{3} \frac{\omega a^3}{\beta_1 c_0^2} \left(\frac{\partial \psi_1}{\partial c} \right)_A I_1\, \mathbf{u}_n$$

$$\mathbf{P}_m = \frac{4}{3} \mu_0 a^3 \left[\frac{\partial \psi_1}{\partial c} \mathbf{u}_c + j \frac{V_1^2}{\beta_1} \psi_1\, \mathbf{u}_z \right]_A I_1, \tag{15.151}$$

where the subscript A denotes the value at the aperture. These dipoles, placed in front of the short-circuited aperture, radiate fields back into the waveguide according to the equations derived in Section 15.3 [46] (Problem 15.20).

15.6.1 A solved Coupled Regions Problem

The exterior region is sometimes a *closed volume*, possibly wrapped around the waveguide in the form of a coaxial cavity (Fig. 15.16*a*). When the waveguide is circular, the fields in its interior are expanded in the known modes of the circular cross section, the fields in the cavity in the modes of the coaxial volume, and an integral equation for $(\mathbf{u}_n \times \mathbf{E})$ in the gap is subsequently obtained by enforcing continuity of $\mathbf{H}_{\tan}$ across the gap. The guide could, for example, be part of a particle accelerator, in which case the exterior region is an accelerating cavity whose fields penetrate into the tube to deliver momentum kicks to the passing (charged) particles.[46,47]

Coupling to an *open exterior region* poses a greater challenger. We shall only discuss this problem by considering a circular guide coupled to free space by an aperture A (Fig. 15.16*b*). The determination of the interior fields follows steps similar to those outlined in (15.48) and (15.49). The exterior problem (i.e., the determination of the exterior fields in terms of $\mathbf{u}_n \times \mathbf{E}$) has been solved — in principle at least — for an arbitrary aperture.[48] The solution consists in expanding the fields in a series of cylindrical waves, each of which has a z-dependence of the form e^{-jhz} [22]. For simplicity, we shall only discuss the example of a *circumferential gap* (Fig. 15.15*a*). The gap fields are excited by the lowest φ-independent TE mode, assumed to be the only propagating one.[49] This incident mode has components

$$E^i_\varphi(r,z) = V^i(z)\, J_1\left(y_1 \frac{r}{a}\right)$$
$$H^i_z(r,z) = -\frac{1}{j\omega\mu_0} V^i(z) \frac{1}{r}\frac{d}{dr}\left[rJ_1\left(y_1 \frac{r}{a}\right)\right], \tag{15.152}$$

where $y_1 = 3.832$ is the first zero of $J_1(x)$. The tangential electric field in the gap is φ-independent, and its only nonzero component is E_φ, which we denote by $f(z)$. Thus,

$$E_\varphi(a,z) = f(z). \tag{15.153}$$

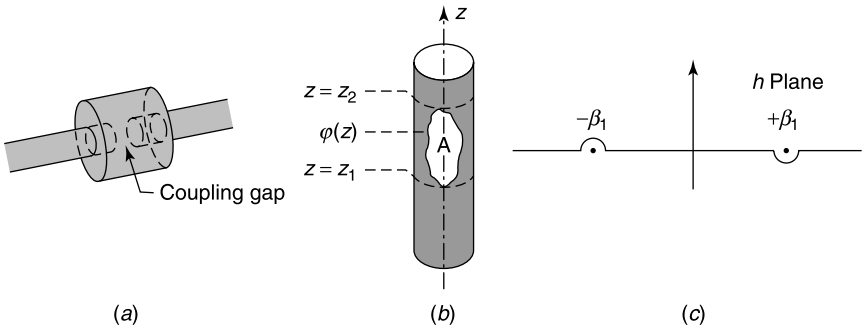

Figure 15.16 (*a*) Coupling to a cavity. (*b*) General aperture in a circular waveguide. (*c*) Contour of integration.

We shall represent a z-dependent function $g(z)$, such as E_φ, by its spatial Fourier transformation (A7.53). Thus,

$$g(z) = \frac{1}{2\pi}\int_{-\infty}^{\infty} e^{jhz} dh \underbrace{\int_{-\infty}^{\infty} g(z')\, e^{-jhz'} dz'}_{\mathcal{G}(h)}. \tag{15.154}$$

Because E_φ satisfies Helmholtz' equation, its transform $\mathcal{E}_\varphi(r,h)$ must satisfy the ordinary differential equation

$$\frac{d^2\mathcal{E}_\varphi}{dr^2} + \frac{1}{r}\frac{d\mathcal{E}_\varphi}{dr} + \underbrace{(k_0^2 - h^2)}_{\Lambda^2}\,\mathcal{E}_\varphi = 0. \tag{15.155}$$

In the exterior region, the solution that respects the radial radiation condition is of the general form

$$\mathcal{E}_\varphi(r,h) = C\,\frac{dH_0^{(2)}(\Lambda r)}{dr}. \tag{15.156}$$

To determine C we require $\mathcal{E}_\varphi(a,h)$ to coincide with the Fourier transform of $f(z)$. This step leads to the value

$$C = \frac{\displaystyle\int_{-w}^{w} f(z)\, e^{-jhz}\, dz}{\Lambda\left[H_0^{(2)}(x)\right]'_{x=\Lambda a}}.$$

Because

$$\mathcal{H}_z(r,h) = -\frac{1}{j\omega\mu_0}\frac{1}{r}\frac{\partial}{\partial r}\left[r\,\mathcal{E}_\varphi(r,h)\right],$$

H_z *outside* the duct may be represented by the integral

$$\begin{aligned} H_z(r,z) &= \frac{1}{2\pi}\frac{1}{j\omega\mu_0}\int_{-w}^{w} f(z')\,dz' \int_{-\infty}^{\infty} \frac{e^{jh(z-z')}\Lambda^{1/2}H_0^{(2)}(\Lambda r)}{\left[H_0^{(2)}(\Lambda r)\right]'}\,dh \\ &= \int_{-w}^{w} f(z')K^+(z-z',r)\,dz'. \end{aligned} \tag{15.157}$$

The magnetic field *inside* the duct is given by an analog expression, provided the Hankel functions are replaced by Bessel functions to ensure finiteness of the fields on the axis. Thus,

$$\begin{aligned} H_z(r,z) &= H^i(r,z) - \frac{1}{2\pi j\omega\mu_0}\int_{-w}^{w} f(z')\,dz' \int_{-\infty}^{\infty} \frac{e^{jh(z-z')}\Lambda^{1/2}J_0(\Lambda r)}{J_1(\Lambda a)}\,dh \\ &= H_z^i(r,z) + \int_{-w}^{w} f(z')\,K^-(z-z',r)\,dz'. \end{aligned} \tag{15.158}$$

If the TE_{01} mode is the only propagating one the wave number k_0 is bracketed by the inequalities

$$y_1^2 < k_0^2 a^2 < y_2^2.$$

It follows that the denominator in the integrand of (15.158) has real zeros at those values of h for which

$$\Lambda^2 a^2 = y_1^2 = (k_0^2 - h^2)\, a^2$$

that is, for

$$h = \pm \left(k_0^2 - \frac{y_1^2}{a^2} \right)^{\frac{1}{2}} = \pm \beta_1,$$

where β_1 is the propagation constant of the TE_{01} mode. The other zeros are on the imaginary axis. The integration contour must therefore encircle the zeros in the manner indicated in Figure 15.16*c*. This requirement ensures that the waves behave properly at large distances and, in particular, that they radiate *away* from the slot.

Once the integrations are performed, the values of $H_z(r, z)$ in (15.157) and (15.158) are equated in the gap (i.e., for $r = a$ and $-w \leq z \leq w$), a move that generates an integral equation for $f(z)$, the tangential electric field E_φ in the gap. The incident voltage $V^i(z)$, which is $e^{-j\beta_1 z}$ or $e^{j\beta_1 z}$, appears in the right-hand term as a forcing function. Once $f(z)$ is determined, for example by variational methods, the scattering matrix of the gap, considered as a (symmetric) obstacle, can easily be determined[49] [22].

15.6.2 Infinite Axial Slot

Apertures in the wall can serve to establish electromagnetic contact between a wave propagating down the waveguide and the outside world. Two well-known applications of that principle are the slotted waveguide antenna and the slotted coaxial cable used in coal mines and road tunnels. Conversely, signals can be picked up from outside sources, as in an obstacle-detecting system. The aperture is often in the form of a continuous longitudinal slot, a shape that has the advantage of being easy to fabricate. It is to that particular aperture that we shall first direct our attention.

Consider, for example, the slotted rectangular waveguide shown in Figure 15.17*a*. An incident wave in the duct radiates fields through the slot. We shall not endeavor to determine these fields in detail but will only mention their general characteristics. Because of the presence of the slot, a mode that originally propagated in the closed waveguide now leaks out and suffers an additional attenuation because of the ensuing radiative losses. Early investigations[50] proved that the new (complex) propagation constant γ is the stationary value of the functional

$$\int_{-w}^{+w} \left[E_y (H_z^- - H_z^+) + E_z (H_y^- - H_y^+) \right] dy = 0. \tag{15.159}$$

Results show that the radiated fields generally decay in the direction of propagation and build up laterally, away from the structure [47, 139]. The detailed form of the fields can be obtained from the complex integration of an appropriate Green's function.[51] Typical

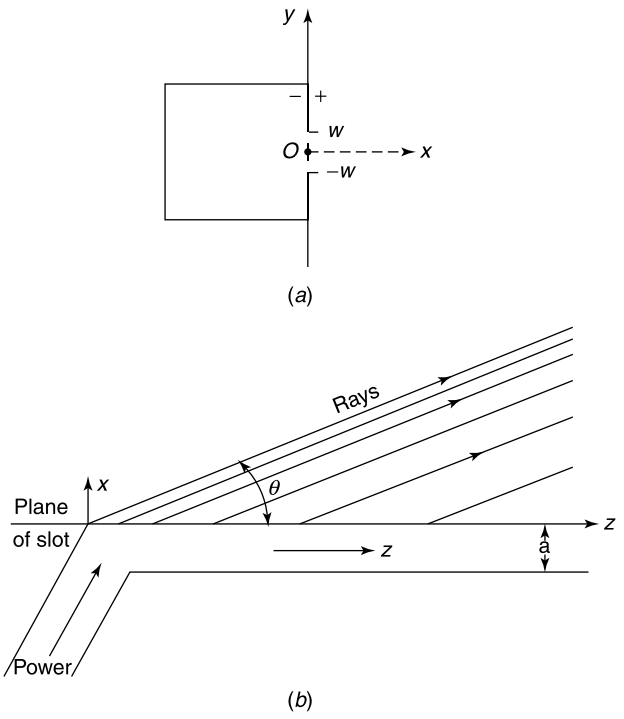

Figure 15.17 (*a*) Waveguide with longitudinal slot. (*b*) Radiation from a semi-infinite slotted waveguide (from L. O. Goldstone and A. A. Oliner, Leaky-wave antennas I: rectangular waveguides, *IRE Trans. AP* **7**, 307–313, 1959, with permission of IEEE).

results for the semi-infinite waveguide in Figure 15.17*a* are shown in Figure 15.18, where the curves display the variation of the propagation constant

$$\gamma = \alpha + j\beta = \alpha + j\frac{2\pi}{\lambda_g} = \alpha + j2\pi\frac{c_0}{v_{ph}\lambda_0}.$$

It is seen that the phase velocity is larger than c_0. The launching angle θ (see Fig. 15.17) is given by

$$\cos\theta = \frac{\lambda_0}{\lambda_g}.$$

This angle can be modified by modulating the frequency, a property that can be exploited in the design of *sweeping beam* antennas.

Another example of slotted waveguide is the *coaxial line* shown in Figure 15.19*a*. The cable is filled with a dielectric of given ϵ_1 (region 1) and is coupled to free space (region 2) by a slot of opening angle $2\varphi_0$. Except in a few special cases, all the modes are hybrid, and it is convenient to derive the fields from the z-oriented Hertz vectors $\pi_e = \pi_e \mathbf{u}_z$ and $\boldsymbol{\pi}_m = \pi_m \mathbf{u}_z$. From (7.199), the components of the E and H fields can be expressed in terms

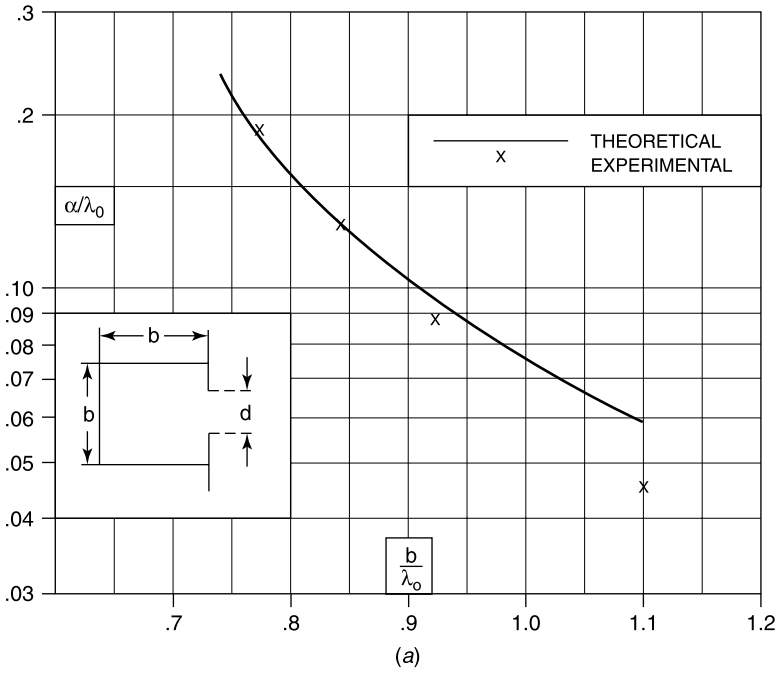

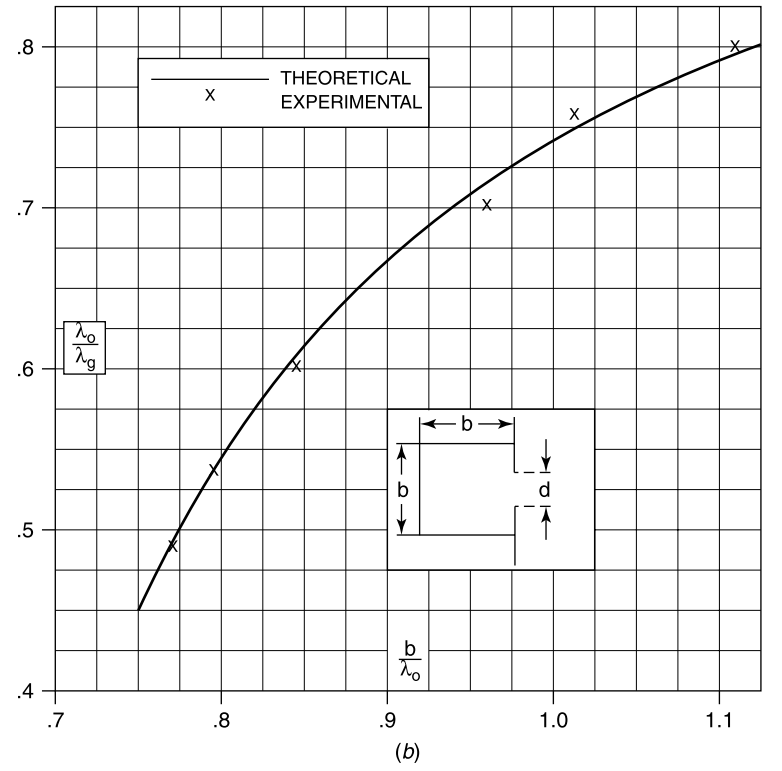

Figure 15.18 (*a*) Attenuation constant α for a slotted square waveguide. (*b*) Guide wavelength for the same waveguide (from L. O. Goldstone and A. A. Oliner, Leaky-wave antennas I: rectangular waveguides, *IRE Trans. AP* **7**, 307–313, 1959, with permission of IEEE).

of π_e and π_m by means of the relationships

$$\begin{cases} E_r = \dfrac{\partial^2 \pi_e}{\partial r \partial z} - \dfrac{j\omega\mu_0}{r}\dfrac{\partial \pi_m}{\partial \varphi} \\ E_\varphi = \dfrac{1}{r}\dfrac{\partial^2 \pi_e}{\partial \varphi \partial z} + j\omega\mu_0 \dfrac{\partial \pi_m}{\partial r} \\ E_z = \left(\dfrac{\partial^2}{\partial z^2} + k^2\right)\pi_e \end{cases} \tag{15.160}$$

$$\begin{cases} H_r = \dfrac{j\omega\epsilon}{r}\dfrac{\partial \pi_e}{\partial \varphi} + \dfrac{\partial^2 \pi_m}{\partial r \partial z} \\ H_\varphi = -j\omega\epsilon \dfrac{\partial \pi_e}{\partial r} + \dfrac{1}{r}\dfrac{\partial^2 \pi_m}{\partial \varphi \partial z} \\ H_z = \left(\dfrac{\partial^2}{\partial z^2} + k^2\right)\pi_e. \end{cases} \tag{15.161}$$

Both potentials satisfy

$$\left(\frac{\partial^2}{\partial r^2} + \frac{1}{r}\frac{\partial}{\partial r} + \frac{1}{r^2}\frac{\partial^2}{\partial \varphi^2} + \frac{\partial^2}{\partial z^2} + k^2\right)\pi = 0. \tag{15.162}$$

The z-dependence will be assumed of the form e^{-jhz} — a previously made assumption — while the rotational symmetry is taken into account by including an $e^{jm\varphi}$ factor in the field components. On the basis of (A9.11), the potentials in region 1 can be written as

$$\begin{aligned} \pi_e &= \sum_{n=0}^{\infty} A_n R_n(\Lambda_1 r)\cos n\varphi \\ \pi_m &= \sum_{n=1}^{\infty} B_n S_n(\Lambda_1 r)\sin n\varphi, \end{aligned} \tag{15.163}$$

where we have dropped the e^{-jhz} factor. In these expressions

$$\begin{aligned} R_n(\Lambda_1 r) &= J_n(\Lambda_1 r) - \frac{J_n(\Lambda_1 a)}{N_n(\Lambda_1 a)} N_n(\Lambda_1 r) \\ S_n(\Lambda_1 r) &= J_n(\Lambda_1 r) - \frac{J_n'(\Lambda_1 a)}{N_n'(\Lambda_1 a)} N_n(\Lambda_1 r), \end{aligned}$$

and

$$\Lambda_1 = \sqrt{k_1^2 - h^2}.$$

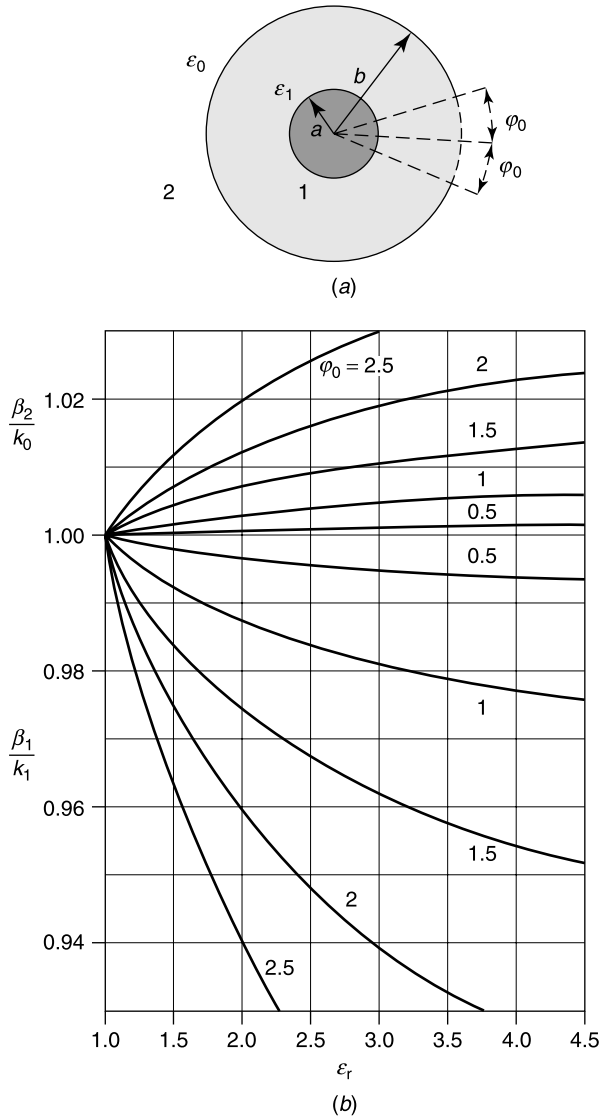

Figure 15.19 (*a*) Slotted coaxial cable. (*b*) Propagation constants in regions 1 and 2 (from R. A. Hurd, The modes of an axially slotted coaxial waveguide, *Radio Sci.* **14**, 741–751, 1979, with permission of the American Geophysical Union).

In region 2, similarly,

$$\pi_e = \sum_{n=0}^{\infty} C_n H_n^{(2)}(\Lambda_2 r) \cos n\varphi$$

$$\pi_m = \sum_{n=1}^{\infty} D_n H_n^{(2)}(\Lambda_2 r) \sin n\varphi, \tag{15.164}$$

with

$$\Lambda_2 = \sqrt{k_0^2 - h^2}.$$

The coefficients A_n, B_n, C_n, and D_n may now be expressed in terms of the values of E_φ and E_z in the slot. The continuity of H_φ and H_z across the slot must subsequently be enforced.[44,52,53] Alternately, variational principle (15.159) can be exploited[54] to find h. The following trial fields have been found useful for the purpose (Fig. 15.19):

$$\mathcal{E}_\varphi = \frac{a_0 \sin\varphi}{\sqrt{1-(\varphi/\varphi_0)^2}} + \sum_{n=1}^{N} a_n \sin\frac{n\pi\varphi}{\varphi_0}$$

$$\mathcal{E}_z = \sum_{n=1}^{N} b_n \cos\frac{n\pi\varphi}{\varphi_0}, \tag{15.165}$$

where the script notation is defined in (15.174). We note that the $\mathcal{E}_\varphi$ component takes the edge condition into account. The solution yields the spectrum of values of h, which consists of a continuous part and a discrete one.[52] Two discrete modes, termed respectively monofilar and bifilar, deserve special attention. They both propagate at all frequencies (i.e., without experiencing any cut-off). In the *bifilar* (or coaxial) mode, most of the energy is concentrated *inside* the cable, with some leakage to the surrounding medium. This mode is related to the TEM mode of the unslotted coaxial line. In the *monofilar* mode, the fields exist mostly *outside* the cable, while some of the energy penetrates inside the coaxial line. The leakage field from the coaxial cable serves to communicate with mobile transceivers located in the exterior region, typically a tunnel. The dielectric constant of the cable plays an important function here: it slows down the coaxial mode, it influences the effective radius of the leakage fields, and it slows down the monofilar mode to phase velocities slightly less than c_0. The presence of the slot, on the other hand, increases the phase velocity of the coaxial mode above that of the closed cable.[52] Some values of the propagation constants β_1 and β_2 are shown in Figure 15.19*b* for $k_0 b = 0.02$ and $a = 0.25b$. The dielectric is nonmagnetic and φ_0 is expressed in radians.

15.6.3 Periodic Slots

Consider a waveguide radiating through a periodic distribution of slots. In determining the radiation pattern of that particular antenna, the tangential electric field in the typical slot is the main unknown, and one of the steps consists in determining the $\mathbf{H}_{\tan}$ ($\mathbf{E}_{\tan}$) relationship on the exterior side of the slot. This is a difficult problem that can be simplified when the waveguide is rectangular and the slots are milled in one of the broad faces of the guide. For such a geometry, a useful approximation consists in assuming that the broad face is part of an infinite ground plane. The Green's dyadic for the half-infinite space above the plane is known for homogeneous media (see Section 9.6), and can be invoked to derive the exterior $\mathbf{H}_{\tan}(\mathbf{E}_{\tan})$ relationship. The form of the dyadic, when the plane is covered with a dielectric layer,[55] is less evident, and its determination requires the use of the techniques described in Section 9.4. The choice of slots in shape, orientation, and dimensions gives great flexibility in synthesizing radiation patterns. There is a wealth of information on that topic in the literature, and we shall restrict ourselves to a discussion of the periodically slotted

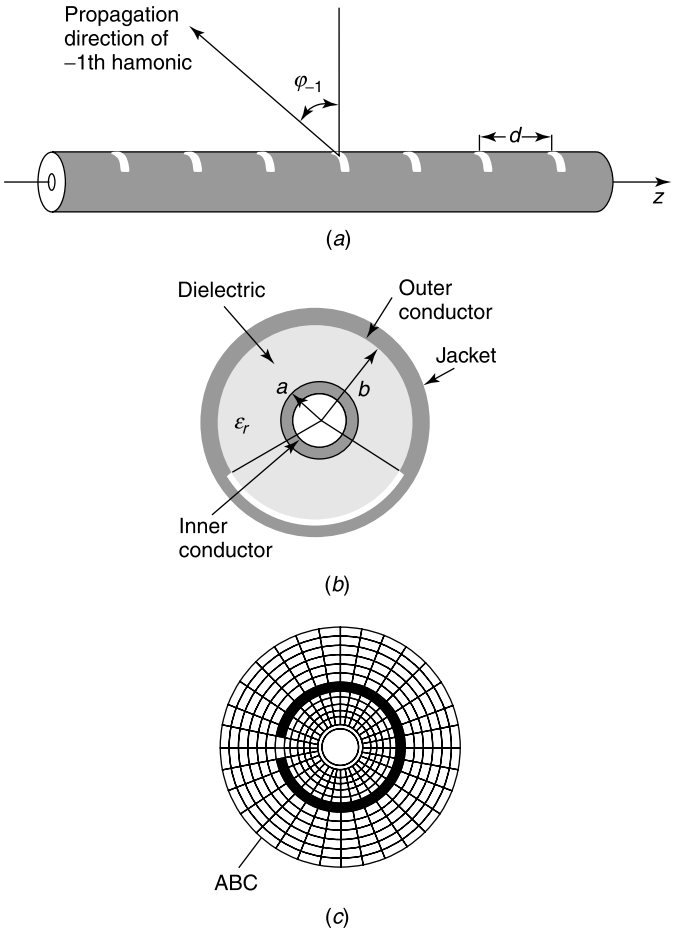

Figure 15.20 (*a*) Leaky coaxial cable. (*b*) Cross section of the coaxial cable. (*c*) Discretized net (from J. H. Wang and K. K. Mei, Theory and analysis of leaky coaxial cables with periodic slots, *IEEE Trans. AP* **49**, 1723–1732, 2001, with permission of IEEE).

array shown in Figure 15.20*a*. On the basis of the general theory presented in Section 9.5, periodic fields that propagate down the axis of the cable may be represented by a sum of partial waves. Thus,[56]

$$\mathbf{E}(r,\varphi,z) = e^{-\alpha z} \sum_{n=-\infty}^{\infty} \mathbf{E}_n(r,\varphi)\, e^{-j\left(\beta_0 + n\frac{2\pi}{d}\right)z}. \tag{15.166}$$

The propagation constant in the *radial* direction is given by the formula

$$k_{rn}^2 = k_0^2 - \left(\beta_0 + n\frac{2\pi}{d}\right)^2. \tag{15.167}$$

When the guide is filled with a dielectric of low ϵ_r, β_0 is approximately equal to $k_0\sqrt{\epsilon_r}$, and we may write

$$k_{rn}^2 = -\left[k_0(\sqrt{\epsilon_r}+1) + n\frac{2\pi}{d}\right]\left[n\frac{2\pi}{d} + k_0(\sqrt{\epsilon_r}-1)\right]. \tag{15.168}$$

When $k_{rn}^2 \leq 0$, the nth harmonic does not radiate radically, and propagates as a surface wave. It is only when k_{rn}^2 is positive that radiation occurs. It is clear, from (15.168), that this can only happen for negative values of n. More precisely, the nth harmonic radiates if the frequency satisfies the inequalities

$$|n|\,\frac{c_0}{a(\sqrt{\epsilon_r}+1)} < f < |n|\,\frac{c_0}{a(\sqrt{\epsilon_r}-1)}. \tag{15.169}$$

As the frequency is progressively raised, the $n = -1$ harmonic radiates first, initially in a backfire direction. The $n = -2$ harmonic radiates next, again initially in the backfire direction, while the $n = -1$ harmonic turns to a forward endfire direction. Usually, the cable is designed to only radiate in the $n = -1$ harmonic to avoid the fluctuations caused by the radiation from higher harmonics. Note that methods are available to control the frequency band in which single harmonic radiation occurs.[57]

Once the frequency is chosen, the main problem is to determine the fields radiated from an incident wave propagating down the coaxial cable. The traditional coupled regions approach is of considerable complexity and may elegantly be replaced by an FDTD technique, in which one impresses a time-harmonic voltage across the cable to launch the wave. The net, shown in Figure 15.20*c*, extends through the slots and terminates at an exterior cylinder, over which absorbing boundary conditions (ABCs) are enforced. The computation generates the value of $\mathbf{E}_{\tan}$ (or its equivalent $\mathbf{J}_{mS}$) in the slot, the main goal of the computation. The radiated fields can now be obtained from the integral representation (10.143), viz.

$$\mathbf{E}(\mathbf{r}_0) = \int_S \operatorname{curl}_0 \overline{\overline{G}}_{mm}(\mathbf{r}_0|\mathbf{r})\cdot\mathbf{J}_{mS}(\mathbf{r})\,dS. \tag{15.170}$$

In this equation, S is the exterior surface of the cable, $\mathbf{J}_{mS}$ is only different from zero in the slots, and $\overline{\overline{G}}_{mm}$ is the Green's dyadic for the exterior of the circular cylinder [210].

15.6.4 Propagation in Tunnels

Experience shows that waves do not propagate well in tunnels, a limitation that constitutes a major problem for underground communications in dangerous environments such as coal mines. A tunnel with *uniform* cross section may be considered as a waveguide. Propagation along this guide, and the nature of the modes, depend on the characteristics of the wall material. In most cases, the bulk properties are isotropic and the materials are nonmagnetic, with ϵ_r's ranging from perhaps 2 to 70, and conductivities ranging from 10^{-6} S m^{-1} to 1 S m^{-1} [52]. Assuming the walls to be perfectly conducting is clearly unrealistic in practice. Representing the wall by a surface impedance, as in Section 15.4, does not hold either, because the penetration depth may not be negligible with respect to the transverse dimensions of the guide. Instead, the tunnel should be modeled as a low-loss open waveguide of the type discussed extensively in Sections 15.7 and 15.8. For cellular radiotelephone applications, with frequencies around 1 GHz and $\lambda_0 \approx 30$ cm, the typical tunnel can

propagate a large number of modes. For such a case, ray tracing is an efficient alternative to the mode expansion.[58] Computations and experiments show that, at sufficiently large axial distances from the sources, the field magnitudes decrease nearly exponentially with z. The validity of that observation is confirmed by the theoretical analysis of the fields in a circular tunnel, excited by a loop of current, electric or magnetic[59] (Fig. 15.21*a*). In the figure an *electric* current excites the φ-independent H modes and a *magnetic* current the φ-independent E modes. Assume that the walls are lossy and have a complex dielectric constant $\epsilon_r + (\sigma/j\omega\epsilon_0)$, with corresponding propagation constant $k_2 = k_0\left(\epsilon_r + \dfrac{\sigma}{j\omega\epsilon_0}\right)^{\frac{1}{2}}$. By means of previously discussed Fourier transform methods [see (15.163) and (15.164)] it is found that an *electric* loop current I_e excites an E_φ, H_r, H_z field given by, for $b < r < a$,

$$E_\varphi(r,z) = -\frac{\omega\mu_0 I_e b}{4}\int_{-\infty}^{\infty} J_1(\Lambda_1 b)\, H_1^{(2)}(\Lambda_1 r)\, e^{-jhz}\, dh + \frac{\omega\mu_0 I_e b}{4}\int_{-\infty}^{\infty} \Gamma J_1(\Lambda_1 r)\, e^{-jhz} dh, \tag{15.171}$$

where $\Lambda_1 = (k_0^2 - h^2)^{\frac{1}{2}}$, $\Lambda_2 = (k_2^2 - h^2)^{\frac{1}{2}}$, and

$$\Gamma = \frac{\Lambda_1 H_0^{(2)}(\Lambda_1 a)\, H_1^{(2)}(\Lambda_2 a) - \Lambda_2 H_0^{(2)}(\Lambda_2 a)\, H_1^{(2)}(\Lambda_1 a)}{\Lambda_1 J_0(\Lambda_1 a)\, H_1^{(2)}(\Lambda_2 a) - \Lambda_2 H_0^{(2)}(\Lambda_2 a)\, J_1(\Lambda_1 a)}.$$

The first term on the right-hand side of (15.171) represents the field radiated by the loop in free space and the second term the field scattered by the walls. The integrals must now be evaluated by contour integration methods. There is a branch point in Λ_2, and poles at a series of complex values of (ha). Some of the poles are shown in Figure 15.21*b* where the parameters are $a = 2\,\text{m}$, $\epsilon_r = 12$, $\sigma = 0.02\,\text{S m}^{-1}$, and $f = 1\,\text{GHz}$. Far from the loop, the contribution from the branch cut turns out to be negligible. A typical result for the propagated E field is displayed in Figure 15.21*c*, where E_φ is obtained from the sum of the residues of the first sixteen poles. The plot reveals the existence of two-zones.[58] For $z < 400\,\text{m}$, a rapid variation of E_φ occurs over small distances, caused by interference between many modes traveling with different phase velocities. For $z > 400\,\text{m}$, the variations becomes smoother, most modes are strongly attenuated, and only the modes $n = 1$ and $n = 2$ actually contribute to the curve. The general exponential decay for increasing z is therefore confirmed.

Propagation predictions based on the *modes* of a cylindrical tunnel suffer from serious drawbacks. The mode picture becomes blurred because the cross section does not remain constant, except over short distances; bends occur, and all kinds of obstacles scatter the propagating mode.[60] In a first practical improvement to the empty tunnel method, a *single axial wire* conductor was strung along the length of the tunnel. The so-created coaxial structure (formed by wire plus wall) can support a quasi-TEM mode and avoids the cut-off limitations.[‖] The current flows down the wire and returns through the earth, where its distribution, and the resulting losses, depend on the proximity of the wire to the wall. To

[‖]The cut-off frequency in road tunnels ranges typically from 30 to 70 MHz. These values explain why AM broadcasting signals are strongly attenuated in tunnels, while FM signals have a much greater range.

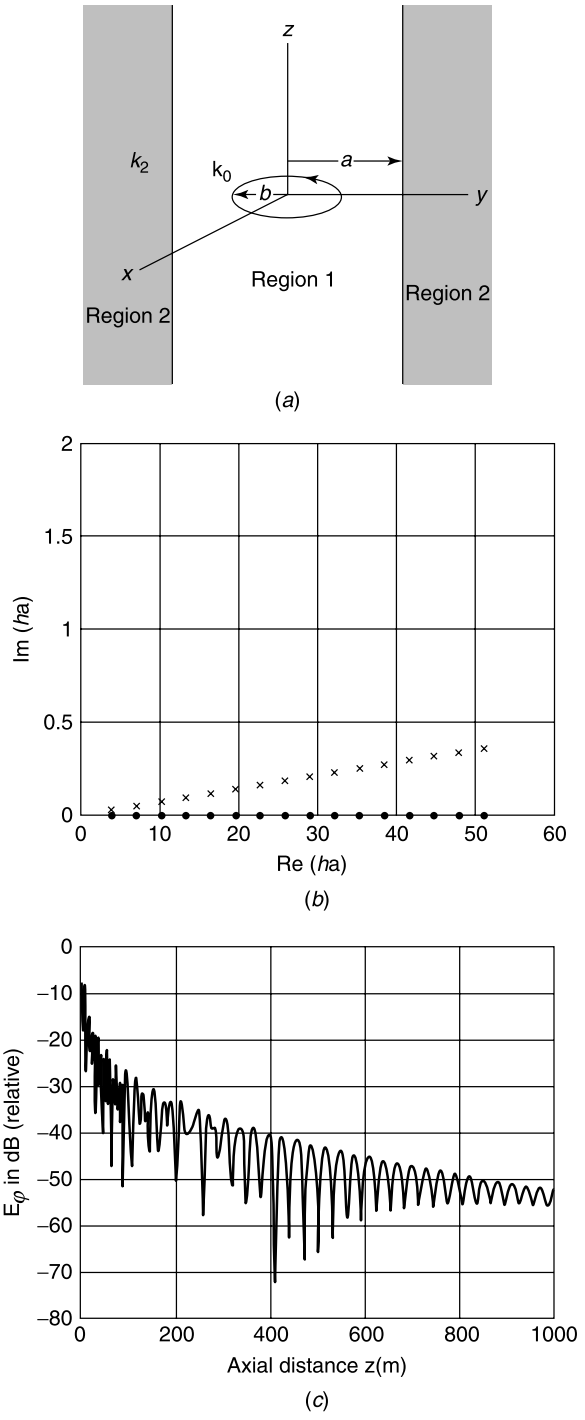

Figure 15.21 (*a*) Circular tunnel with loop current. (*b*) Poles in the *h* plane. The poles marked • are those for a perfectly conducting wall. (*c*) E_φ as a function of *z* (from D. G. Dudley, Wireless propagation in circular tunnels, *IEEE Trans. AP* **53**, 435–441, 2005, with permission of IEEE).

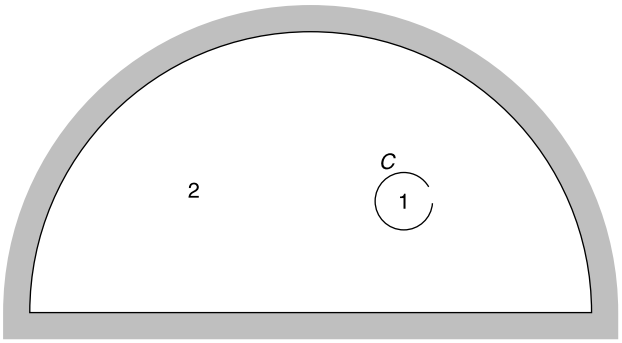

Figure 15.22 Slotted coaxial cable in a tunnel.

reduce the losses, one often relies on a *coaxial* leaky feeder, with either a continuous aperture or a succession of small apertures, as in Figures 15.19*a* and 15.20*a*. The field variations in the two basic modes, monofilar and bifilar, are governed by Equations (15.163) and (15.164). The relative distribution of energy in the two modes depends on various factors, one of which is the effective radius within which most of the exterior fields are contained [52].

The two-mode problem is actually of a *coupled transmission lines* nature, and it can be solved by the methods discussed in Section 14.12 (Fig. 15.22). The subscripts c (for coaxial) and m (for monofilar) will be used instead of the 1 and 2 that appear in (14.270) and (14.271). Practical data show that the network equations may be written as[61]

$$\begin{cases} \dfrac{dV_c}{dz} = -Z_{cc}I_c - Z_{cm}I_m \\ \dfrac{dV_m}{dz} = -Z_{cm}I_c - Z_{mm}I_m \end{cases}$$
$$\begin{cases} \dfrac{dI_c}{dz} = -Y_{cc}I_c \\ \dfrac{dI_m}{dz} = -Y_{mm}I_m. \end{cases} \tag{15.172}$$

The Z_{cc}, Z_{mm}, Y_{cc}, Y_{mm} characterize the configuration in the absence of coupling aperture. Coupling takes place through the mutual impedance Z_{cm} (the mutual admittance Y_{cm} has a negligible effect in practice and is omitted from the equations). The coupling associated with the resistance of screen is also negligible. The dominant influence is therefore the magnetic coupling caused by the leakage of $\mathbf{H}$ through the slot, as expressed by the impedance $Z_{cm} = j\omega M$. When M is small, its effect can be treated as a small perturbation, and two coupling coefficients can usefully be defined:

$$C_1 = \frac{M}{2\sqrt{L_m L_c}} \frac{1}{e^{\frac{1}{4}} - e^{-\frac{1}{4}}}$$
$$C_2 = \frac{M}{2\sqrt{L_m L_c}} \frac{1}{e^{\frac{1}{4}} + e^{-\frac{1}{4}}},$$

where L_c and L_m are the linear inductances of the respective lines, c and m. Detailed calculations show that, to the first order, the propagation constants (β_c, β_m) and the attenuation

constant α_m are unaffected by M. On the other hand, α_c becomes

$$\alpha_c = \alpha_{c0} + (C_1 - C_2)^2 \, \alpha_m$$

where α_{c0} is the attenuation of the unslotted coaxial cable.

15.7 GUIDED WAVES IN GENERAL MEDIA

Let us assume that the materials contained in the waveguide are linear and locally reacting (see Section 8.1). Their most general constitutive equations are those of a bianisotropic medium, viz.

$$\begin{aligned} \mathbf{D}(\mathbf{r}) &= \overline{\overline{\epsilon}}(\mathbf{r}) \cdot \mathbf{E}(\mathbf{r}) + \overline{\overline{\alpha}}(\mathbf{r}) \cdot \mathbf{H}(\mathbf{r}) \\ \mathbf{B}(\mathbf{r}) &= \overline{\overline{\beta}}(\mathbf{r}) \cdot \mathbf{E}(\mathbf{r}) + \overline{\overline{\mu}}(\mathbf{r}) \cdot \mathbf{H}(\mathbf{r}). \end{aligned} \tag{15.173}$$

The fields of the guided waves will be factored as follows:

$$\mathbf{E}(\mathbf{r}) = \boldsymbol{\mathcal{E}}(\mathbf{r}_t) \, e^{-\gamma z} = \boldsymbol{\mathcal{E}}(\mathbf{r}_t) \, e^{-(\alpha + j\beta) z}. \tag{15.174}$$

$\boldsymbol{\mathcal{E}}$ is a *wave field*, and $\mathbf{r}_t$ stands for coordinates in the transverse plane. In accordance with the assumed cylindrical symmetry, $\overline{\overline{\epsilon}}$, $\overline{\overline{\mu}}$, $\overline{\overline{\alpha}}$, and $\overline{\overline{\beta}}$ in (15.173) are independent of z.

15.7.1 Maxwell's Equations in General Media

In the important case of *isotropic media*, the time-harmonic Maxwell's equations, projected transversely and longitudinally, give

$$\begin{cases} \operatorname{grad}_t E_z \times \mathbf{u}_z + \dfrac{\partial}{\partial z}(\mathbf{u}_z \times \mathbf{E}_t) = -j\omega\mu \, \mathbf{H}_t - \mathbf{J}_{mt} \\ \operatorname{div}_t (\mathbf{E}_t \times \mathbf{u}_z) = -j\omega\mu \, H_z - J_{mz} \end{cases} \tag{15.175}$$

$$\begin{cases} \operatorname{grad}_t H_z \times \mathbf{u}_z + \dfrac{\partial}{\partial z}(\mathbf{u}_z \times \mathbf{H}_t) = j\omega\epsilon \, \mathbf{E}_t + \mathbf{J}_t \\ \operatorname{div}_t (\mathbf{H}_t \times \mathbf{u}_z) = j\omega\epsilon \, E_z + J_z, \end{cases} \tag{15.176}$$

where ϵ and μ depend only on $\mathbf{r}_t$. Elimination of E_z and H_z leads to

$$\begin{aligned} \frac{\partial \mathbf{E}_t(\mathbf{r})}{\partial z} + \overline{\overline{L}}_e(\mathbf{r}_t) \cdot \mathbf{H}_t(\mathbf{r}) &= \mathbf{F}_t(\mathbf{r}) \\ \frac{\partial \mathbf{H}_t(\mathbf{r})}{\partial z} + \overline{\overline{L}}_h(\mathbf{r}_t) \cdot \mathbf{E}_t(\mathbf{r}) &= \mathbf{G}_t(\mathbf{r}), \end{aligned} \tag{15.177}$$

with

$$\begin{aligned} \overline{\overline{L}}_e \cdot \mathbf{H}_t &= -j\omega\mu \, \mathbf{u}_z \times \mathbf{H}_t + \operatorname{grad}_t \left[\frac{1}{j\omega\epsilon} \operatorname{div}_t (\mathbf{u}_z \times \mathbf{H}_t) \right] \\ \overline{\overline{L}}_h \cdot \mathbf{E}_t &= j\omega\epsilon \, \mathbf{u}_z \times \mathbf{E}_t - \operatorname{grad}_t \left[\frac{1}{j\omega\mu} \operatorname{div}_t (\mathbf{u}_z \times \mathbf{E}_t) \right]. \end{aligned} \tag{15.178}$$

The dimension of $\overline{\overline{L}}_e$ is $\Omega\,\mathrm{m}^{-1}$ and that of $\overline{\overline{L}}_h$ is $\mathrm{S\,m}^{-1}$. The forcing functions are

$$\begin{aligned}\mathbf{F}_t &= \mathbf{u}_z \times \mathbf{J}_m(\mathbf{r}) - \mathrm{grad}_t\left[\frac{1}{j\omega\epsilon} J_z(\mathbf{r})\right] \quad (\mathrm{V\,m}^{-2})\\ \mathbf{G}_t &= -\mathbf{u}_z \times \mathbf{J}(\mathbf{r}) - \mathrm{grad}_t\left[\frac{1}{j\omega\mu} J_{mz}(\mathbf{r})\right] \quad (\mathrm{A\,m}^{-2}).\end{aligned} \tag{15.179}$$

Equations for $\mathbf{E}_t$ or $\mathbf{H}_t$ alone can be derived by eliminating E_z and H_z from (15.174) and (15.175). Thus,

$$\begin{aligned}\frac{\partial^2 \mathbf{E}_t(\mathbf{r})}{\partial z^2} - \left(\overline{\overline{L}}_e \cdot \overline{\overline{L}}_h\right)\cdot \mathbf{E}_t(\mathbf{r}) &= \frac{\partial \mathbf{F}_t(\mathbf{r})}{\partial z} - \overline{\overline{L}}_e(\mathbf{r}_t)\cdot \mathbf{G}_t(\mathbf{r})\\ \frac{\partial^2 \mathbf{H}_t(\mathbf{r})}{\partial z^2} - \left(\overline{\overline{L}}_h \cdot \overline{\overline{L}}_e\right)\cdot \mathbf{H}_t(\mathbf{r}) &= \frac{\partial \mathbf{G}_t(\mathbf{r})}{\partial z} - \overline{\overline{L}}_h(\mathbf{r}_t)\cdot \mathbf{F}_t(\mathbf{r}).\end{aligned} \tag{15.180}$$

When the material in the guide is *bianisotropic*, (15.175) and (15.176) become

$$\begin{cases} \mathrm{grad}_t\, E_z \times \mathbf{u}_z + \dfrac{\partial}{\partial z}(\mathbf{u}_z \times \mathbf{E}_t) \\ \quad = -j\omega\overline{\overline{\mu}}_{tt}\cdot \mathbf{H}_t - j\omega \boldsymbol{\mu}_{tz} H_z - j\omega\overline{\overline{\beta}}_{tt}\cdot \mathbf{E}_t - j\omega\boldsymbol{\beta}_{tz}E_z - \mathbf{J}_{mt} \\ \mathrm{div}_t\,(\mathbf{E}_t \times \mathbf{u}_z) = -j\omega\mu_{zz}H_z - j\omega\boldsymbol{\mu}_{zt}\cdot\mathbf{H}_t - j\omega\beta_{zz}E_z - j\omega\boldsymbol{\beta}_{zt}\cdot\mathbf{E}_t - J_{mz} \end{cases} \tag{15.181}$$

$$\begin{cases} \mathrm{grad}_t\, H_z \times \mathbf{u}_z + \dfrac{\partial}{\partial z}(\mathbf{u}_z \times \mathbf{H}_t) \\ \quad = j\omega\overline{\overline{\epsilon}}_{tt}\cdot \mathbf{E}_t + j\omega\boldsymbol{\epsilon}_{tz}E_z + j\omega\overline{\overline{\alpha}}_{tt}\cdot\mathbf{H}_t + j\omega\boldsymbol{\alpha}_{tz}H_z + \mathbf{J}_t \\ \mathrm{div}_t\,(\mathbf{H}_t \times \mathbf{u}_z) = j\omega\epsilon_{zz}E_z + j\omega\boldsymbol{\epsilon}_{zt}\cdot\mathbf{E}_t + j\omega\alpha_{zz}H_z + j\omega\boldsymbol{\alpha}_{zt}\cdot\mathbf{H}_t + J_z, \end{cases} \tag{15.182}$$

where, for example,

$$\overline{\overline{\mu}}\cdot\mathbf{a} = \overline{\overline{\mu}}_{tt}\cdot\mathbf{a}_t + \underbrace{(\mathbf{u}_z\boldsymbol{\mu}_{zz})}_{\overline{\overline{\mu}}_{zt}}\cdot\mathbf{a}_t + \underbrace{(\boldsymbol{\mu}_{tz}\mathbf{u}_z)}_{\overline{\overline{\mu}}_{tz}}\cdot\mathbf{a}_z + \underbrace{(\mu_{zz}\mathbf{u}_z\mathbf{u}_z)}_{\overline{\overline{\mu}}_{zz}}\cdot\mathbf{a}_z$$

and

$$\begin{aligned}\boldsymbol{\mu}_{zt} &= \mu_{zx}\mathbf{u}_x + \mu_{zy}\mathbf{u}_y\\ \boldsymbol{\mu}_{tz} &= \mu_{xz}\mathbf{u}_x + \mu_{yz}\mathbf{u}_y.\end{aligned}$$

It is useful to mention a few special forms of the constitutive tensors:

1. In a *reciprocal medium*

$$\overline{\overline{\epsilon}}(\mathbf{r}_t) = \overline{\overline{\epsilon}}^t(\mathbf{r}_t); \quad \overline{\overline{\mu}}(\mathbf{r}_t) = \overline{\overline{\mu}}^t(\mathbf{r}_t); \quad \overline{\overline{\beta}}(\mathbf{r}_t) = -\overline{\overline{\alpha}}^t(\mathbf{r}_t). \tag{15.183}$$

2. In a symmetric *uniaxial medium*, the tensors are diagonal.

3. In a *biisotropic* material, $\overline{\overline{\alpha}}$ and $\overline{\overline{\beta}}$ are scalars, often written as

$$\alpha = \frac{1}{c_0}(\chi - j\kappa); \quad \beta = \frac{1}{c_0}(\chi + j\kappa), \tag{15.184}$$

where κ is the *chirality parameter* and χ the *Tellegen parameter*. The material becomes *chiral* when $\chi = 0$.

4. In a *lossless material*

$$\overline{\overline{\epsilon}}(\mathbf{r}_t) = \overline{\overline{\epsilon}}^{\dagger}(\mathbf{r}_t); \quad \overline{\overline{\mu}}(\mathbf{r}_t) = \overline{\overline{\mu}}^{\dagger}(\mathbf{r}_t); \quad \overline{\overline{\beta}}(\mathbf{r}_t) = \overline{\overline{\alpha}}^{\dagger}(\mathbf{r}_t). \tag{15.185}$$

When the lossless material is biisotropic, ϵ_r, μ_r, κ, and χ must therefore be real.

5. In a *non-lossless* waveguide, the important parameter is the 6×6 matrix

$$-j\omega \begin{pmatrix} \overline{\overline{\epsilon}}^{*} - \overline{\overline{\epsilon}}^{t} & \overline{\overline{\alpha}}^{*} - \overline{\overline{\alpha}}^{t} \\ \overline{\overline{\beta}}^{*} - \overline{\overline{\beta}}^{t} & \overline{\overline{\mu}}^{*} - \overline{\overline{\mu}}^{t} \end{pmatrix}.$$

If this matrix is everywhere positive-definite, the waveguide is lossy. If it is everywhere negative-definite, the waveguide has gain. In other cases, no strict classification between losses and gain can be made [105].

15.7.2 Wave Fields

Equations for the wave fields are obtained by replacing $\partial/\partial z$ by $(-\gamma)$ in (15.175) to (15.180) and setting $\mathbf{J} = 0$ and $\mathbf{J}_m = 0$ in the right-hand terms of these equations. The fields in a sourceless part of an *isotropic* guide satisfy

$$\begin{aligned} \operatorname{grad}_t \mathcal{E}_z \times \mathbf{u}_z + \gamma(\boldsymbol{\mathcal{E}}_t \times \mathbf{u}_z) &= -j\omega\mu\, \boldsymbol{\mathcal{H}}_t \\ \operatorname{div}_t (\boldsymbol{\mathcal{E}}_t \times \mathbf{u}_z) &= -j\omega\mu\, \mathcal{H}_z \end{aligned} \tag{15.186}$$

$$\begin{aligned} \operatorname{grad}_t \mathcal{H}_z \times \mathbf{u}_z + \gamma(\boldsymbol{\mathcal{H}}_t \times \mathbf{u}_z) &= j\omega\epsilon\, \boldsymbol{\mathcal{E}}_t \\ \operatorname{div}_t (\boldsymbol{\mathcal{H}}_t \times \mathbf{u}_z) &= j\omega\epsilon\, \mathcal{E}_z. \end{aligned} \tag{15.187}$$

The $(-\gamma, \boldsymbol{\mathcal{E}}_t, -\mathcal{E}_z, -\boldsymbol{\mathcal{H}}_t, \mathcal{H}_z)$ mode — the *mirror* mode — is also a solution of Maxwell's equations, hence the guide is *bidirectional*. Elimination of $\mathcal{E}_z$ and $\mathcal{H}_z$ from (15.186) and (15.187) yields the following equations for the transverse components:

$$\operatorname{grad}_t \left[\frac{1}{j\omega\epsilon} \operatorname{div}_t(\boldsymbol{\mathcal{H}}_t \times \mathbf{u}_z) \right] - j\omega\mu\, (\boldsymbol{\mathcal{H}}_t \times \mathbf{u}_z) + \gamma \boldsymbol{\mathcal{E}}_t = 0 \tag{15.188}$$

$$\operatorname{grad}_t \left[\frac{1}{-j\omega\mu} \operatorname{div}_t(\boldsymbol{\mathcal{E}}_t \times \mathbf{u}_z) \right] + j\omega\epsilon\, (\boldsymbol{\mathcal{E}}_t \times \mathbf{u}_z) + \gamma \boldsymbol{\mathcal{H}}_t = 0. \tag{15.189}$$

These components can be expressed in terms of $\mathcal{E}_z$ and $\mathcal{H}_z$ by means of the relationships

$$(k^2 + \gamma^2)\, \boldsymbol{\mathcal{E}}_t = -\gamma \operatorname{grad}_t \mathcal{E}_z - j\omega\mu\, (\operatorname{grad}_t \mathcal{H}_z \times \mathbf{u}_z) \tag{15.190}$$

$$(k^2 + \gamma^2)\, \boldsymbol{\mathcal{H}}_t = -\gamma \operatorname{grad}_t \mathcal{H}_z + j\omega\epsilon\, (\operatorname{grad}_t \mathcal{E}_z \times \mathbf{u}_z). \tag{15.191}$$

One can eliminate further and derive an equation for $\boldsymbol{\mathcal{H}}_t$ (or $\boldsymbol{\mathcal{E}}_t$) alone. Assuming that the guide is filled with an isotropic, nonmagnetic dielectric, the equation for $\boldsymbol{\mathcal{H}}_t$ is obtained by cross-multiplying (15.188) with $\mathbf{u}_z$ from the left, to yield

$$\mathbf{u}_z \times \text{grad}_t \left[\frac{1}{j\omega\epsilon} \text{div}_t(\boldsymbol{\mathcal{H}}_t \times \mathbf{u}_z) \right] + \gamma(\mathbf{u}_z \times \boldsymbol{\mathcal{E}}_t) = j\omega\mu_0 \boldsymbol{\mathcal{H}}_t.$$

To eliminate $\mathbf{u}_z \times \boldsymbol{\mathcal{E}}_t$, we combine (15.187), written as

$$\mathbf{u}_z \times \boldsymbol{\mathcal{E}}_t = \frac{1}{j\omega\epsilon} \left[\text{grad}_t \mathcal{H}_z + \gamma \boldsymbol{\mathcal{H}}_t \right], \tag{15.192}$$

with the zero-divergence condition for $\mathbf{B} = \mu_0 \mathbf{H}$, viz.

$$\gamma \mathcal{H}_z = \text{div}_t \boldsymbol{\mathcal{H}}_t. \tag{15.193}$$

A few simple steps now give the desired equation

$$\mathbf{u}_z \times \text{grad}_t \left[\frac{1}{\epsilon_r} \text{div}_t (\boldsymbol{\mathcal{H}}_t \times \mathbf{u}_z) \right] + \frac{1}{\epsilon_r} \text{grad}_t \, \text{div}_t \boldsymbol{\mathcal{H}}_t + k_0^2 \boldsymbol{\mathcal{H}}_t + \frac{1}{\epsilon_r} \gamma^2 \boldsymbol{\mathcal{H}}_t = 0. \tag{15.194}$$

15.7.3 The Propagation Constant

Equations (15.186) to (15.194), combined with appropriate boundary conditions, can be exploited to evaluate the eigenvalue $\gamma = \alpha + j\beta$. In the discrete part of the spectrum, modes are found that can propagate without loss when the media are lossless. For such modes $\gamma = j\beta$, where β is real. Consider first an inhomogeneous waveguide composed of several homogeneous regions (Fig. 15.23). Each region has its own uniform (ϵ_i, μ_i). Combining Equations (15.186) to (15.191) shows that $\mathcal{E}_z$ and $\mathcal{H}_z$ must satisfy the Helmholtz equations

$$\begin{aligned} \nabla^2 \mathcal{E}_z + (k_i^2 + \gamma^2) \mathcal{E}_z &= 0 \\ \nabla^2 \mathcal{H}_z + (k_i^2 + \gamma^2) \mathcal{H}_z &= 0, \end{aligned} \tag{15.195}$$

where $k_i^2 = \omega^2 \epsilon_i \mu_i$. These fields must also satisfy the boundary conditions at the perfectly conducting surfaces, as well as the interface conditions at the junction of two media. These conditions, based on (15.190) and (15.191), show that $\mathcal{E}_z$ and $\mathcal{H}_z$ are coupled components, hence that pure E and H waves cannot be sustained on inhomogeneous guides (except under special conditions of symmetry and coordinate dependence [22]). At a perfectly conducting boundary, the conditions are $\mathbf{u}_n \times \boldsymbol{\mathcal{E}} = 0$ and $\mathbf{u}_n \times \boldsymbol{\mathcal{H}} = 0$, which implies, from (15.187) and (15.189), that

$$\begin{aligned} \mathcal{E}_z &= \frac{1}{j\omega\epsilon} \text{div}_t(\boldsymbol{\mathcal{H}}_t \times \mathbf{u}_z) = 0 \\ \frac{\partial \mathcal{H}_z}{\partial n} &= -\frac{1}{j\omega\mu} \frac{\partial}{\partial n} \left[\text{div}_t(\boldsymbol{\mathcal{E}}_t \times \mathbf{u}_z) \right] = 0. \end{aligned} \tag{15.196}$$

The particular configuration of a slab-loaded rectangular waveguide is discussed in Section 15.10.

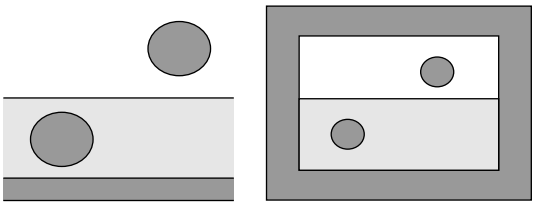

Figure 15.23 (*a*) Open hybrid waveguide. (*b*) Closed hybrid waveguide (from N. Faché and D. De Zutter, New high-frequency circuit model for coupled lossless and lossy waveguide structures, *IEEE Trans. MTT* **38**, 252–259, 1998, with permission of IEEE).

When the inhomogeneity is arbitrary, various numerical methods are available to determine γ. If $\boldsymbol{\mathcal{H}}_t$ is chosen as the main unknown, a weak form of (15.194) can be derived by multiplying both sides of the equation with a testing vector $\mathbf{w}$ and integrating over the whole cross sectional plane.[62] The second derivatives involving $\boldsymbol{\mathcal{H}}_t$ can be eliminated by invoking the divergence theorem (A1.27). Thus,

$$\int_S \left[-\frac{1}{\epsilon_r} \operatorname{div}_t(\mathbf{w} \times \mathbf{u}_z) \operatorname{div}_t(\boldsymbol{\mathcal{H}}_t \times \mathbf{u}_z) - \operatorname{div}_t \left(\frac{\mathbf{w}}{\epsilon_r} \right) \operatorname{div}_t \boldsymbol{\mathcal{H}}_t + \left(k_0^2 + \frac{\gamma^2}{\epsilon_r} \right) \mathbf{w} \cdot \boldsymbol{\mathcal{H}}_t \right] dV$$
$$+ \int_C \left[(\mathbf{u}_n \times \mathbf{w}) \cdot \mathbf{u}_z \operatorname{div}_t(\boldsymbol{\mathcal{H}}_t \times \mathbf{u}_z) + (\mathbf{u}_n \cdot \mathbf{w}) \frac{1}{\epsilon_r} \operatorname{div}_t \boldsymbol{\mathcal{H}}_t \right] dc = 0. \tag{15.197}$$

In this equation, the curve C is the boundary of the computational domain. When C is a *perfectly conducting wall*, as in a closed waveguide, the contour integral vanishes, from (15.187), provided $\mathbf{w}$ is chosen tangent to the boundary. When the waveguide is *open*, absorbing conditions should be applied. Various choices are possible for that purpose: a boundary integral condition[63] or the closure of the domain with a *perfectly matched layer*, a method that is discussed at some length in Section 15.10.

Several variational formulations are available for the determination of γ. They involve either $(\mathcal{E}_z, \mathcal{H}_z)$, or a combination of *two* components such as $\boldsymbol{\mathcal{E}}_t$ or $\boldsymbol{\mathcal{H}}_t$, or a larger number of components, for example $\boldsymbol{\mathcal{E}}_t$ *and* $\boldsymbol{\mathcal{H}}_t$, or even the full $\boldsymbol{\mathcal{E}}$ and $\boldsymbol{\mathcal{H}}$ (Problem 15.23). One of the basic functionals for lossless media is[64]

$$F(\mathbf{H}) = \frac{\displaystyle\int_V (\operatorname{curl} \mathbf{H})^* \cdot \overline{\overline{\epsilon}}^{-1} \cdot \operatorname{curl} \mathbf{H}\, dV}{\displaystyle\int_V \mathbf{H}^* \cdot \overline{\overline{\mu}} \cdot \mathbf{H}\, dV} \tag{15.198}$$

where $\overline{\overline{\epsilon}}$ and $\overline{\overline{\mu}}$ are Hermitian. *Specialized* variational principles have been proposed for biisotropic waveguides, as well as for waveguides filled with a material of dielectric constant $\overline{\overline{\epsilon}} = \overline{\overline{\epsilon}}_{tt} + \epsilon_{zz} \mathbf{u}_z \mathbf{u}_z$, where $\overline{\overline{\epsilon}}_{tt}$ is symmetric.[65,66,67,68] Finite elements are routinely used in the numerical solution of the chosen equations. Spurious solutions may appear, for a variety of causes,[69,70] but edge elements can remedy the difficulty. Other possible improvements are the incorporation of edge singularities into the elements themselves[71] or an appropriate modulation of the density of the mesh in lossy regions having dimensions of the order of the skin depth.[72]

15.7.4 Complex Waves

Early numerical results obtained for γ in *closed inhomogeneous* waveguides revealed a phenomenon that does not exist in homogeneous waveguides: the possible appearance, at certain frequencies, of complex values $\gamma = \alpha + j\beta$. This behavior was observed although the media in the guides were isotropic and lossless. The complex waves could even be of the *backward* type, in which case energy flows in a direction opposite to that of the wavefronts. Such waves are known to exist in periodic structures and are basic to the

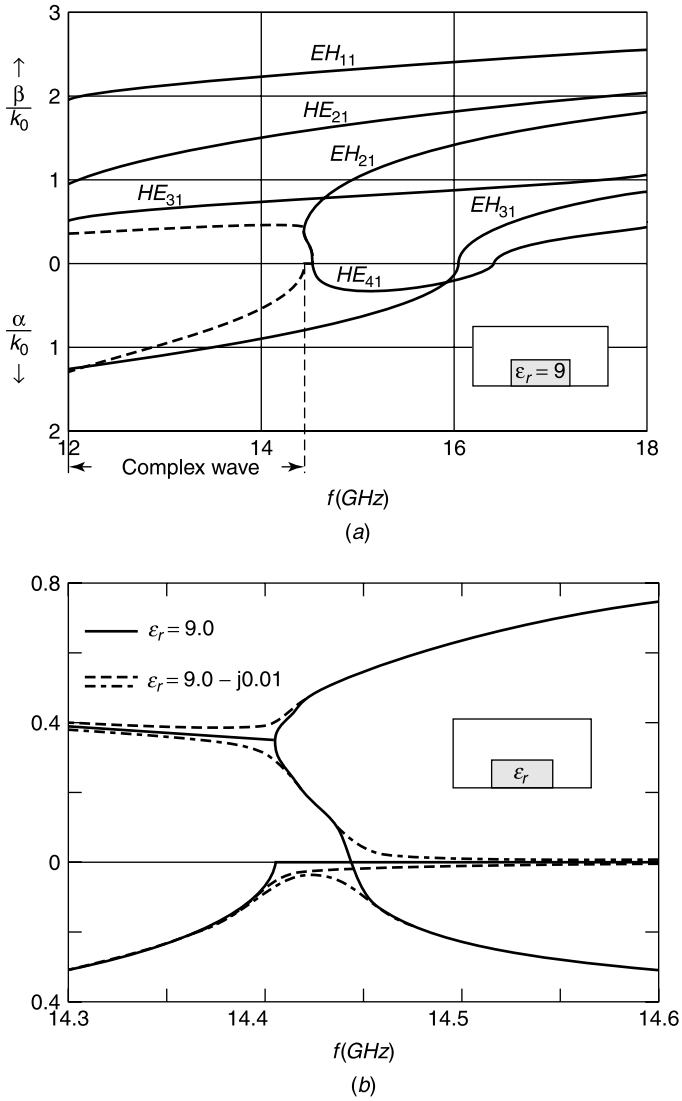

Figure 15.24 (*a*) Propagation constant of the first six modes, including a complex mode (dotted lines). (*b*) Detailed behavior of the complex mode, with and without losses (from F. Fernandez, Y. Lu, J. B. Davies and S. Zhu, Finite element analysis of complex modes in inhomogeneous waveguides, *IEEE Trans. MAG* **29**, 1601–1604, 1993, with permission of IEEE).

operation of backward-wave oscillators. Complex waves, some of them backward, have first been observed in circular waveguides containing an axial dielectric rod.[73,74] They have also been found in dielectric image guides[75,76] and in waveguides containing a microstrip.[77] The data in Figure 15.24*a*, which concern an image dielectric guide of width 15.8 mm, illustrate the complexity of the mode evolution as frequency increases. The dotted line shows a complex mode, which suddenly disappears at 14.4 GHz and gives birth to both the EH_{21} and HE_{41} modes. The bifurcation is shown in more detail in Figure 15.24*b*. When the material becomes slightly lossy, with $\epsilon_r = 9 - j\,0.01$, the sudden bifurcation disappears, as shown by the dashed lines.

Complex modes always appear in pairs, with conjugate (complex) propagation constants. They can not propagate separately, and a correct modal expansion should therefore include *both* of them. The conjugate pair does not transport any active power down the guide but only contributes to the local storage of reactive power. A theoretical understanding of the onset of complex waves, and of their further mutations, remains a challenging problem[78,79] [102, 111, 112]. The identification of these waves is not of purely theoretical interest, because they are indispensible for a correct application of mode matching techniques at discontinuities.[80]

15.8 ORTHOGONALITY AND NORMALIZATION

The orthogonality properties of the modes can be readily derived by invoking the Lorentz reciprocity theorem (8.171) [105]. Applied to the portion of sourceless waveguide shown in Figure 15.25, the theorem gives

$$\int_{S_1+S_2+S_w} \mathbf{u}_n \cdot (\mathbf{E}_a \times \mathbf{H}_b - \mathbf{E}_b \times \mathbf{H}_a)\, dS = 0. \tag{15.199}$$

The subscripts a and b refer to fields in *adjoint waveguides*; that is, in waveguides filled with media of characteristics $\overline{\overline{\epsilon}}_b = \overline{\overline{\epsilon}}_a^t$; $\overline{\overline{\mu}}_b = \overline{\overline{\mu}}_a^t$; $\overline{\overline{\alpha}}_b = -\overline{\overline{\beta}}_a^t$ and $\overline{\overline{\beta}}_b = -\overline{\overline{\alpha}}_a^t$ in (15.173). We shall first consider *isotropic* media, which are inherently self-adjoint, and for the a and b fields we choose two *discrete* modes, m in the original guide, and n in the adjoint guide. Their respective propagation coefficients are γ_m and γ_n. The integral over S_w vanishes when the waveguide is closed by perfectly conducting walls. It also vanishes when the waveguide is open, and the modes are *guided*, in which case the modal fields decrease exponentially

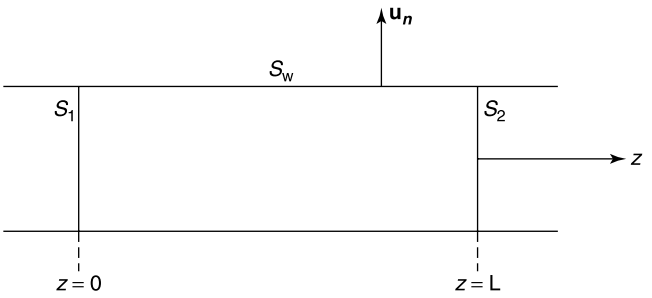

Figure 15.25 A portion of waveguide between two cross sections.

in the transverse directions. The integral over S_1 in (15.199) may be written as

$$I_1 = \int_S (-\mathbf{u}_z) \cdot [\boldsymbol{\mathcal{E}}_{tm} \times \boldsymbol{\mathcal{H}}_{tn} - \boldsymbol{\mathcal{E}}_{tn} \times \boldsymbol{\mathcal{H}}_{tm}]\, dS,$$

where S is the cross section of the waveguide. Over S_2, similarly,

$$I_2 = \int_S \mathbf{u}_z \cdot \left[\boldsymbol{\mathcal{E}}_{tm}\, e^{-\gamma_m L} \times \boldsymbol{\mathcal{H}}_{tn}\, e^{-\gamma_n L} - \boldsymbol{\mathcal{E}}_{tn}\, e^{-\gamma_n L} \times \boldsymbol{\mathcal{H}}_{tm}\, e^{-\gamma_m L}\right] dS.$$

The sum of the two must vanish, from (15.199), hence

$$I_1 + I_2 = \left(e^{-(\gamma_m+\gamma_n)L} - 1\right) \mathbf{u}_z \cdot \int_S (\boldsymbol{\mathcal{E}}_{tm} \times \boldsymbol{\mathcal{H}}_{tn} - \boldsymbol{\mathcal{E}}_{tn} \times \boldsymbol{\mathcal{H}}_{tm})\, dS = 0.$$

If we choose the mirror mode of n as b field, the integrals become

$$I_1' = \int_S (-\mathbf{u}_z) \cdot [\boldsymbol{\mathcal{E}}_{tm} \times (-\boldsymbol{\mathcal{H}}_{tn}) - \boldsymbol{\mathcal{E}}_{tn} \times \boldsymbol{\mathcal{H}}_{tm}]\, dS$$

and

$$I_2' = \int_S \mathbf{u}_z \cdot \left[\boldsymbol{\mathcal{E}}_{tm}\, e^{-\gamma_m z} \times (-\boldsymbol{\mathcal{H}}_{tn})\, e^{\gamma_n z} - \boldsymbol{\mathcal{E}}_{tn}\, e^{\gamma_n z} \times \boldsymbol{\mathcal{H}}_{tm}\, e^{-\gamma_m z}\right] dS.$$

The sum of the two is now

$$I_1' + I_2' = -\left[e^{-(\gamma_m-\gamma_n)L} - 1\right] \mathbf{u}_z \cdot \int_S [\boldsymbol{\mathcal{E}}_{tm} \times \boldsymbol{\mathcal{H}}_{tn} + \boldsymbol{\mathcal{E}}_{tn} \times \boldsymbol{\mathcal{H}}_{tm}]\, dS = 0.$$

When γ_m is different from both γ_n and $(-\gamma_n)$, the orthogonality condition

$$\mathbf{u}_z \cdot \int_S (\boldsymbol{\mathcal{E}}_{tm} \times \boldsymbol{\mathcal{H}}_{tn})\, dS = 0 \tag{15.200}$$

must therefore hold. If m and n coincide, the complex amplitudes of the modes may be chosen to satisfy the normalization condition

$$\mathbf{u}_z \cdot \int_S (\boldsymbol{\mathcal{E}}_{tm} \times \boldsymbol{\mathcal{H}}_{tn})\, dS = \delta_{mn}. \tag{15.201}$$

This condition corresponds with (14.295) in the theory of coupled transmission lines. It is not a *power normalization condition*, a concept that becomes only meaningful when the materials are *lossless* (i.e., when ϵ and μ are real and positive). For such a case $\gamma = j\beta$, with β real, and (15.186), (15.187) show that $\boldsymbol{\mathcal{E}}_t$ and $\boldsymbol{\mathcal{H}}_t$ may be chosen real, and $\mathcal{E}_z$ and $\mathcal{H}_z$ imaginary. From (15.200) and (15.201), it follows that (Problem 15.24)

$$\mathbf{u}_z \cdot \int_S \left(\boldsymbol{\mathcal{E}}_{tm} \times \boldsymbol{\mathcal{H}}_{tn}^*\right) dS = \delta_{mn}. \tag{15.202}$$

If the mode fields are written as

$$\mathbf{E}_t = V_m \boldsymbol{\mathcal{E}}_{tm} e^{-j\beta_m z}$$
$$\mathbf{H}_t = I_m \boldsymbol{\mathcal{H}}_{tm} e^{-j\beta_m z},$$

the time-averaged power flowing to positive z is

$$P = \frac{1}{2} \operatorname{Re} \int_S \mathbf{u}_z \cdot (\mathbf{E}_t \times \mathbf{H}_t^*)\, dS = \frac{1}{2} \operatorname{Re} \sum_m V_m I_m^*. \tag{15.203}$$

The power is therefore the sum of the individual powers carried by the modes, a property that does not hold in a waveguide containing either *lossy* or *active* materials.

Before generalizing the orthogonality property to anisotropic materials, it is useful to discuss the nature of the propagation constant γ in an arbitrary waveguide. In general, each mode includes two branches, corresponding respectively with propagation in the $(+z)$ and the $(-z)$ directions, with respective propagation constants γ_m^+ and γ_m^-. A waveguide is *bidirectional* when there are pairs of modes such that $\gamma_n^- = -\gamma_m^+$. As mentioned in Section 15.7, a *waveguide* is *mirroring* when a mode $(\gamma_m, \boldsymbol{\mathcal{E}}_{tm}, \mathcal{E}_{zm}, \boldsymbol{\mathcal{H}}_{tm}, \mathcal{H}_{zm})$ is accompanied by a companion mode $(-\gamma_m, \boldsymbol{\mathcal{E}}_{tm}, -\mathcal{E}_{zm}, -\boldsymbol{\mathcal{H}}_{tm}, \mathcal{H}_{zm})$. Isotropic waveguides are both bidirectional and mirroring. Bianisotropic waveguides, on the other hand, are generally neither bidirectional nor mirroring, although they will have both properties if [105]

$$\boldsymbol{\epsilon}_{zt} = \boldsymbol{\epsilon}_{tz} = \boldsymbol{\mu}_{zt} = \boldsymbol{\mu}_{tz} = 0; \quad \alpha_{zz} = \beta_{zz} = 0; \quad \overline{\overline{\alpha}}_{tt} = \overline{\overline{\beta}}_{tt} = 0. \tag{15.204}$$

A *reciprocal waveguide*, whose characteristics are defined in (15.183), is also bidirectional. A waveguide, reciprocal or not, and its adjoint waveguide are *mutually bidirectional*, which means that if γ_m characterizes a mode in one of the waveguides, then $(-\gamma_m)$ will be the propagation coefficient of an eigenmode in the other waveguide.

It is interesting to note[81] that a sufficient — though not necessary — condition for a waveguide to be bidirectional is to possess at least one of three basic symmetries, namely:

- Reflection symmetry with respect to a plane perpendicular to the z-axis
- 180° rotation symmetry about an axis perpendicular to the z-axis
- Rotary reflection symmetry, a geometry in which the structure is invariant to a rotation of (π/n) radians about the z-axis, followed by a reflection in a plane perpendicular to the z-axis.

When a reciprocal waveguide does not satisfy one of the three basic symmetry conditions, it remains bidirectional, but there is no special relation between the fields of mode m and those of mode n for which $\gamma_n^- = -\gamma_m^+$.

Going back to our goal of generalizing the orthogonality property (15.200) to bianisotropic media, let us again apply reciprocity theorem (15.199) and choose, as a field, an eigenmode of the original waveguide, propagating with propagation constant γ_m. For the b field we take an eigenmode propagating in the adjoint waveguide with propagating constant $\gamma_n^{(a)}$. Steps similar to those leading to (15.200) now give

$$\left[e^{-(\gamma_m + \gamma_n^{(a)})L} - 1\right] \int_S \mathbf{u}_z \cdot \left[\boldsymbol{\mathcal{H}}_{tm} \times \boldsymbol{\mathcal{E}}_{tn}^{(a)} - \boldsymbol{\mathcal{H}}_{tn}^{(a)} \times \boldsymbol{\mathcal{E}}_{tm}\right] dS = 0.$$

This relationship holds for reciprocal or nonreciprocal bianisotropic waveguides. It implies that the integral is zero when $\gamma_m \neq -\gamma_n^{(a)}$. Thus,

$$\int_S \mathbf{u}_z \cdot \left[\boldsymbol{\mathcal{H}}_{tm} \times \boldsymbol{\mathcal{E}}_{tn}^{(a)} - \boldsymbol{\mathcal{H}}_{tn}^{(a)} \times \boldsymbol{\mathcal{E}}_{tm} \right] dS = 0. \tag{15.205}$$

This biorthogonality property is reminiscent of the similar condition (14.294), derived for a system of coupled transmission lines [105]. When $\gamma_n^{(a)} = -\gamma_m$, there follows the normalization condition

$$\frac{1}{2} \int_S \mathbf{u}_z \cdot \left[\boldsymbol{\mathcal{E}}_{tm}^{+} \times (\boldsymbol{\mathcal{H}}_{tn}^{(a)})^{-} + (\boldsymbol{\mathcal{E}}_{tn}^{(a)})^{-} \times \boldsymbol{\mathcal{H}}_{tm}^{+} \right] dS = 1, \tag{15.206}$$

where $+$ and $-$ refer to the direction of propagation on the z-axis.

15.8.1 Modal Expansion of the Fields

Consider first a closed waveguide containing an inhomogeneous, isotropic medium. Following the steps outlined in Section 15.1, we expand the fields in the form

$$\begin{aligned} \mathbf{E}_t(\mathbf{r}) &= \sum_{m=1}^{N} V_m(z)\, \boldsymbol{\mathcal{E}}_{tm}(\mathbf{r}_t) \\ \mathbf{H}_t(\mathbf{r}) &= \sum_{m=1}^{N} I_m(z)\, \boldsymbol{\mathcal{H}}_{tm}(\mathbf{r}_t). \end{aligned} \tag{15.207}$$

The sum has been limited to the N propagating modes, the remaining modes assumed either fully attenuated or not excited. The equations satisfied by the fields in the presence of volume sources are given in (15.177). To exploit these equations properly, we expand $\mathbf{F}_t$ in terms of the $\boldsymbol{\mathcal{E}}_{tm}$ set and $\mathbf{G}_t$ in terms of the $\boldsymbol{\mathcal{H}}_{tm}$ set. On the basis of the normalization condition (15.201), the expansions are

$$\begin{aligned} \mathbf{F}_t(\mathbf{r}) &= \sum_{m=1}^{N} \boldsymbol{\mathcal{E}}_{tm}(\mathbf{r}_t) \int_S \mathbf{F}_t(\mathbf{r}) \cdot (\boldsymbol{\mathcal{H}}_{tm} \times \mathbf{u}_z)\, dS \qquad = \sum_{m=1}^{N} \boldsymbol{\mathcal{E}}_{tm}(\mathbf{r}_t)\, F_m(z) \\ \mathbf{G}_t(\mathbf{r}) &= \sum_{m=1}^{N} \boldsymbol{\mathcal{H}}_{tm}(\mathbf{r}_t) \int_S \mathbf{G}_t(\mathbf{r}) \cdot (\mathbf{u}_z \times \boldsymbol{\mathcal{E}}_{tm})\, dS \qquad = \sum_{m=1}^{N} \boldsymbol{\mathcal{H}}_{tm}(\mathbf{r}_t)\, G_m(z). \end{aligned} \tag{15.208}$$

The eigenvectors $\boldsymbol{\mathcal{E}}_{tm}$ and $\boldsymbol{\mathcal{H}}_{tm}$ are determined to within a multiplicative constant, which we adjust to give the dimension m^{-1} to both $\boldsymbol{\mathcal{E}}_{tm}$ and $\boldsymbol{\mathcal{H}}_{tm}$. Such a choice, which is in agreement with the normalization condition (15.201), implies that the respective dimensions of V_m and I_m are V and A. In accordance with (15.177) and (15.178), we shall require the eigenvectors to satisfy

$$\begin{aligned} \frac{1}{R_{c0}} \overline{\overline{L}}_e \cdot \boldsymbol{\mathcal{H}}_{tm} &= \gamma_m \boldsymbol{\mathcal{E}}_{tm} \\ R_{c0}\, \overline{\overline{L}}_h \cdot \boldsymbol{\mathcal{E}}_{tm} &= \gamma_m \boldsymbol{\mathcal{H}}_{tm}. \end{aligned} \tag{15.209}$$

As mentioned before, the dimension of $\overline{\overline{L}}_e$ is $\Omega\,\mathrm{m}^{-1}$ (a linear impedance) and the dimension of $\overline{\overline{L}}_h$ is $\mathrm{S\,m}^{-1}$ (a linear admittance). Introducing the expansions (15.207) and (15.208) into (15.177) leads to

$$\begin{aligned} \frac{dV_m}{dz} &= -\gamma_m R_{c0} I_m + F_m(z) \qquad (\mathrm{V\,m}^{-1}) \\ \frac{dI_m}{dz} &= -\gamma_m \frac{V_m}{R_{c0}} + G_m(z) \qquad (\mathrm{A\,m}^{-1}). \end{aligned} \tag{15.210}$$

These are the transmission line equations for the mode under consideration. In a portion of waveguide devoid of sources, the solution of (15.210) is of the general form

$$\begin{aligned} \mathbf{E}_t(\mathbf{r}) &= \sum_{m=1}^{N} \left[A_m \boldsymbol{\mathcal{E}}_{tm}(\mathbf{r}_t)\, e^{-\gamma_m z} + B_m \boldsymbol{\mathcal{E}}_{tm}(\mathbf{r}_t)\, e^{\gamma_m z} \right] \\ \mathbf{H}_t(\mathbf{r}) &= \sum_{m=1}^{N} \left[\frac{A_m}{R_{c0}} \boldsymbol{\mathcal{H}}_{tm}(\mathbf{r}_t)\, e^{-\gamma_m z} - \frac{B_m}{R_{c0}} \boldsymbol{\mathcal{H}}_{tm}(\mathbf{r}_t)\, e^{\gamma_m z} \right]. \end{aligned} \tag{15.211}$$

The important *field integral* $s(z)$, already introduced in (14.301), follows as

$$s(z) = \frac{1}{2} \int_S \mathbf{u}_z \cdot (\mathbf{E}_t \times \mathbf{H}_t)\, dS = \frac{1}{2} \sum_{m=1}^{N} \left[(A_m)^2\, e^{-2\gamma_m z} - (B_m)^2\, e^{2\gamma_m z} \right]. \tag{15.212}$$

Because there are no cross terms, the modes are seen to contribute *individually* to $s(z)$. The situation is different for the complex *power integral*, which is

$$\begin{aligned} P(z) &= \frac{1}{2} \int_S \mathbf{u}_z \cdot \left(\mathbf{E}_t \times \mathbf{H}_t^* \right) dS \\ &= \frac{1}{2} \sum_{m=1}^{N} \sum_{n=1}^{N} \Big[A_m A_n^*\, e^{-(\gamma_m + \gamma_n^*) z} + B_m A_n^*\, e^{(\gamma_m - \gamma_n^*) z} \\ &\quad - A_m B_n^*\, e^{-(\gamma_m - \gamma_n^*) z} - B_m B_n^*\, e^{(\gamma_m + \gamma_n^*) z} \Big] P_{mn}, \end{aligned} \tag{15.213}$$

where the element P_{mn} of the cross power matrix $\overline{\overline{P}}$ is given by

$$P_{mn} = \int_S \mathbf{u}_z \cdot \left(\boldsymbol{\mathcal{E}}_{tn} \times \boldsymbol{\mathcal{H}}_{tn}^* \right) dS. \tag{15.214}$$

In a lossless medium, $P_{mn} = \delta_{mn}$.

Modal expansions have also been used to evaluate the fields in *bianisotropic* and *open* waveguides [105]. In the open case, part of the expansion is contributed by the radiation modes, a point discussed in more detail in Sections 15.9 and 15.10. A summation such as (15.207) now includes both discrete and integral sums. Thus [126],

$$\mathbf{E}_t(\mathbf{r}) = \sum_{mn} \sum V_{mn}(z)\, \boldsymbol{\mathcal{E}}_{tmn}(\mathbf{r}_t) + \int_0^\infty \int_0^\infty V(\mu, \nu, z)\, \boldsymbol{\mathcal{E}}_t(\mu, \nu, \mathbf{r}_t)\, d\mu\, d\nu. \tag{15.215}$$

The double indices have been written in full, for the sake of clarity.

15.8.2 Transmission Line Model for Waveguide Modes

Equations (15.207) and (15.210) strongly suggest that each waveguide mode can be potentially represented by an equivalent transmission line. If N modes propagate in the guide, the representation would involve N coupled transmission lines. Such a model could be particularly valuable for circuit designers, because transmission lines are known circuit elements and are easily incorporated in existing *computer-aided design* programs (CAD). The representation is immediate for the fundamental TEM mode of a coaxial cable. It is also readily derived for the quasi-TEM mode that can propagate, at sufficiently low frequencies, on a microstrip line (see Fig. 15.37). The situation is less clear at higher frequencies or for higher-order modes. An obvious difficulty is the identification of the currents and voltages on the lines with corresponding elements in the waveguide. In the example of Figure 15.27*a*, where the current I_g is concentrated in one point, the evident solution consists in setting I_{line} equal to I_g. When the current is distributed over the contour of perfect conductors, as in Figure 15.26, the *current model* suggests choosing

$$I_1 = \int_{C_1} \mathbf{H}\cdot\mathbf{u}_c \, dc \quad ; \quad I_2 = \int_{C_2} \mathbf{H}\cdot\mathbf{u}_c \, dc. \tag{15.216}$$

The identification of the voltages is more difficult, because the value of $\int_A^B \mathbf{E}\cdot d\mathbf{l}$ depends on the chosen path AB. In the *voltage model*, one identifies V_{line} by performing the integration over a suitable, but freely chosen path. The development of the various models requires predetermination of both the propagation constant γ and fields of the waveguide modes. A first step in the identification, termed *conservation of dispersion*, consists in choosing $\gamma_{line} = \gamma_{mode}$ (i.e., in requiring the $\overline{\overline{Z}}\cdot\overline{\overline{Y}}$ matrix of the lines to have γ^2_{mode} as eigenvalues). This condition is not sufficient to solve for $\overline{\overline{Z}}$ and $\overline{\overline{Y}}$, however. A possible second reasonable step consists in invoking the principle of *conservation of complex power*. This implies requiring the time-averaged propagated complex power (in both its real and reactive parts) to have the same value in waveguide and lines [60]. In simpler terms: $\frac{1}{2}VI^*$ should be conserved. A difficulty arises, however, when the waveguide contains lossy materials, in which case the method may produce nonreciprocal transmission lines, although the original waveguide was reciprocal[82] [60]. Such models cannot be realized with classic transmission lines. Fundamentally, the reason lies in the lack of orthogonality of the modes, as evidenced by (15.213) [105]. Several authors have therefore proposed[83] to replace conservation of

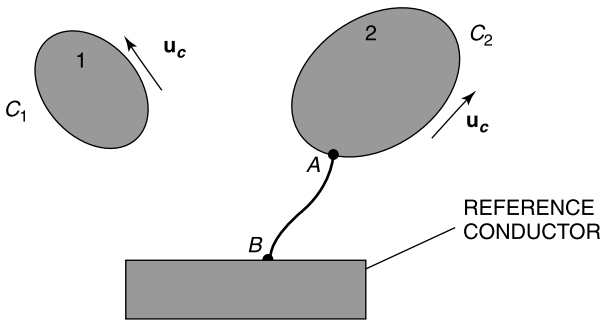

Figure 15.26 Multiconductor waveguide.

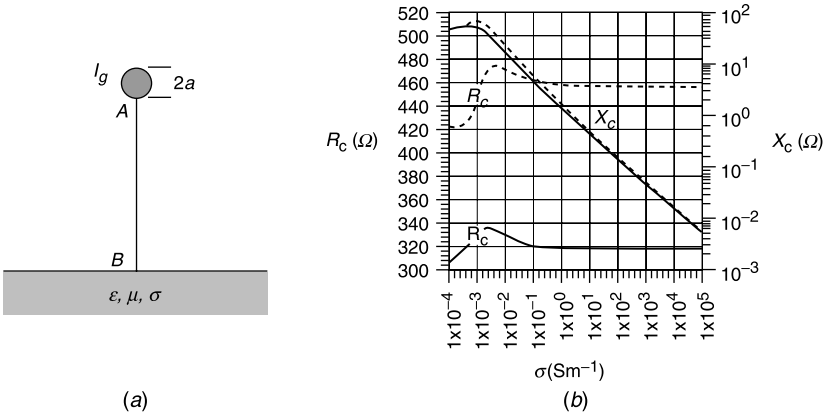

Figure 15.27 (*a*) Thin wire above conducting ground. (*b*) Z_c for the current model as a function of σ, for two radii (— $a = 0.1$ m; - - - $a = 0.01$ m) (from F. Olyslager and D. De Zutter, High-frequency transmission line models for a thin wire above a conducting ground, *IEEE Trans. EMC* **37**, 234–240, 1995, with permission of IEEE).

power by *conservation of reciprocity* (i.e., of $\frac{1}{2}VI$). We note that, when the waveguide is lossless, both $P(z)$ and $s(z)$ give equal results, and both orthogonality properties (15.201) and (15.202) hold.

To concretize these general comments, consider the simple example of a perfectly conducting circular wire, of radius a, located above a lossy half space (Fig. 15.27*a*). We assume from the start that propagation constant and fields of the lowest mode have been determined, for example by means of spectral domain methods[84] (see Section 15.10). Our problem is to determine the Z and Y of the equivalent two-wire line. From (15.211), the fields propagating in the waveguide are of the form

$$\begin{aligned} \mathbf{E}_t(\mathbf{r}) &= C\, e^{-\gamma z}\, \boldsymbol{\mathcal{E}}_t(\mathbf{r}_t) = V_1(z)\, \boldsymbol{\mathcal{E}}_t(\mathbf{r}_t) \\ \mathbf{H}_t(\mathbf{r}) &= \frac{1}{R_{c0}}\, C\, e^{-\gamma z}\, \boldsymbol{\mathcal{H}}_t(\mathbf{r}_t) = I_1(z)\, \boldsymbol{\mathcal{H}}_t(\mathbf{r}_t). \end{aligned} \tag{15.217}$$

where C is a trivial proportionality factor. In the yet-to-be determined equivalent line, the corresponding equations are

$$\begin{aligned} V_2(z) &= A\, e^{-\gamma z} \\ I_2(z) &= \frac{1}{Z_c}\, A\, e^{-\gamma z}. \end{aligned} \tag{15.218}$$

Conservation of dispersion gives a first condition, viz.

$$ZY = \gamma^2. \tag{15.219}$$

To exploit conservation of reciprocity, we use the normalization condition (15.200) to obtain, in the waveguide,

$$s(z) = \frac{1}{2}\int_S \mathbf{u}_z \cdot (\mathbf{E}_t \times \mathbf{H}_t)\, dS = \frac{C^2}{2R_{c0}}\, e^{-2\gamma z}$$
$$= \frac{1}{2} V_1(z)\, I_1(z). \tag{15.220}$$

This quantity is proportional to C^2. The mode current I_g in the wire is proportional to C, hence it can be written as $I_g = \alpha \dfrac{C}{R_{c0}}\, e^{-\gamma z}$, where α depends on the geometry and the chosen materials in Figure 15.27*a*. We may therefore write, from (15.220),

$$s = \frac{1}{2} V_1\, I_1 = \frac{R_{c0}}{2\alpha^2}\, I_g^2 = \frac{1}{2}\, Z_g\, I_g^2.$$

In the *current* model, we set $I_{line} = I_g$, which implies that, on the equivalent line,

$$\frac{V_2}{I_2} = Z_c = \frac{V_2 I_2}{I_2^2} = \frac{V_1 I_1}{I_g^2} = Z_g$$

or

$$Z_c^2 = Z\, Y^{-1} = Z_g^2. \tag{15.221}$$

Combining (15.219) and (15.221) gives the sought values

$$Z = \gamma\, Z_g$$
$$Y = \gamma\, Z_g^{-1}. \tag{15.222}$$

Illustratively, Figure 15.27*b* shows data concerning Z_c for $\epsilon_r = 15$, $h = 10\,\text{m}$, and $f = 1\,\text{MHz}$.

In the *voltage* model, we choose V_{line} to be a given integral of $\mathbf{E}$, say (Fig. 15.27*a*)

$$V_{line} = \int_A^B \mathbf{E} \cdot d\mathbf{l} = V_g.$$

For such a choice, we write

$$V_1 I_1 = Y_V\, V_g^2,$$

where Y_V follows from the characteristics of the waveguide, and obtain the condition

$$\frac{I}{V} = Y_c = \frac{VI}{V^2} = \frac{V_1 I_1}{V_g^2} = Y_V,$$

which gives

$$Z = \gamma\, Y_V^{-1}$$
$$Y = \gamma\, Y_V. \tag{15.223}$$

15.9 DIELECTRIC WAVEGUIDES

At optical frequencies, from the low infrared to the high ultraviolet, metals act as lossy dielectrics and lose their capacity strongly to confine energy in a finite volume. In the dielectric waveguides, now used extensively in the optical range in the form of fibers and planar structures, the desired guiding effect is mostly based on the phenomenon of total reflection discussed in Section 9.1. Total reflection occurs when the angle of incidence θ_i satisfies the condition $\sin\theta_i \geq (\epsilon_r)^{-\frac{1}{2}}$ (i.e., when the *ray* is sufficiently grazing). The fields propagate in the z-direction according to a law (Fig. 15.28*a*)

$$e^{-jk\sin\theta_i z} = e^{-jk_0\sqrt{\epsilon_r}\sin\theta_i z}. \tag{15.224}$$

Such a variation represents a *slow wave*, in the sense that the phase velocity $v_{ph} = c_0/(\sqrt{\epsilon_r}\sin\theta_i)$ is less than the phase velocity c_0 in the exterior medium. Inserting (15.224) into Helmholtz' equation shows that the x-dependence must be of the general form

$$e^{-k_0 x\sqrt{\left(\frac{c_0}{v_{ph}}\right)^2 - 1}}.$$

Except for the trivial case $\sqrt{\epsilon_r}\sin\theta_i = 1$, for which $v_{ph} = c_0$, the fields decrease exponentially in the x-direction, and the wave behaves like a trapped, nonradiating surface wave. If the incidence is too sharp (i.e., for $\sin\theta_i < (\epsilon_r)^{-\frac{1}{2}}$), the ray escapes, and the wave propagates in both the x and z directions.

Total reflection thus clarifies how a trapped wave can progress by means of successive bounces, as suggested in Figure 9.6*b*. This simplistic, intuitive picture of the guidance mechanism is given a more quantitative basis in the following pages.

15.9.1 The Dielectric Slab

The dielectric slab, the simplest planar structure, is discussed extensively in the literature [3, 46, 95, 96, 112, 121]. The slab can sustain both TE and TM modes. In a *TE mode*, the field components are $\mathcal{E}_y$, $\mathcal{H}_x$, and $\mathcal{H}_z$ (using the notation of (15.174)), and these components

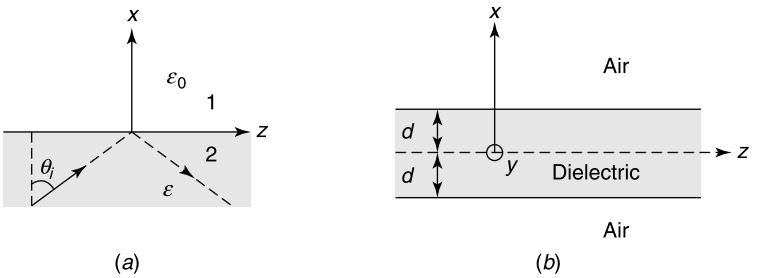

Figure 15.28 (*a*) Totally reflected field. (*b*) A dielectric slab.

depend only on x (Fig. 15.28b). Component $\mathcal{H}_z$, for example, satisfies

$$\frac{d^2\mathcal{H}_z}{dx^2} + \underbrace{(k^2+\gamma^2)}_{k_x^2}\mathcal{H}_z = 0, \tag{15.225}$$

where $k = k_0$ in air and $k = k_d = k_0\sqrt{\epsilon_r}$ in the dielectric. From Maxwell's equations:

$$\begin{aligned}\mathcal{E}_y &= -\frac{j\omega\mu_0}{\gamma}\mathcal{H}_x \;=\; \frac{j\omega\mu_0}{k_x^2}\frac{d\mathcal{H}_z}{dx}\\ \mathcal{H}_z &= -\frac{1}{j\omega\mu_0}\frac{d\mathcal{E}_y}{dx}.\end{aligned} \tag{15.226}$$

Assume first that $\mathcal{E}_y$ is *even* in x, and that the mode propagates (which prompts us to set $\gamma = j\beta$). Because $\mathcal{E}_y$ must be continuous at the interfaces $x = \pm d$, it must be of the form

$$\begin{aligned}&\mathcal{E}_y(x) = \cos\sqrt{k_d^2-\beta^2}\,x && \text{(in the slab)}\\ &\mathcal{E}_y(x) = \cos\left(\sqrt{k_d^2-\beta^2}\,d\right)e^{-\sqrt{\beta^2-k_0^2}(x-d)} && \text{(above the slab).}\end{aligned} \tag{15.227}$$

The magnetic field $\mathcal{H}_z$ must also be continuous at the interfaces, and (15.226) shows that the same must hold for $(d\mathcal{E}_y/dx)$. This requirement results in the dispersion equation

$$\sqrt{k_0^2\epsilon_r-\beta^2}\,\tan\left(\sqrt{k_0^2\epsilon_r-\beta^2}\,d\right) = \sqrt{(\beta^2-k_0^2}, \tag{15.228}$$

from which the law $\beta(\omega)$ may be deduced. The two square roots are real in the range $k_0^2 < \beta^2 < k_0^2\epsilon_r$, in which case (15.227) implies that the fields decrease exponentially away from the slab. The mode is therefore *trapped*, and its velocity of propagation in the z-direction is less than c_0 (making it into a slow wave), while it is higher than the velocity $(c_0/\sqrt{\epsilon_r})$ in the dielectric.

Similar dispersion laws can be derived for $\mathcal{E}_y$ *odd*, as well as for the *TM modes*, where the parity is now determined by $\mathcal{H}_y$. If we set $q = \sqrt{k_d^2-\beta^2}$ and $\gamma_x = \sqrt{\beta^2-k_0^2}$, the various dispersion laws can be written concisely as

$$(qd)\tan(qd) = \gamma_x d \qquad \text{for TE even} \tag{15.229}$$

$$(qd)\cot(qd) = -\gamma_x d \qquad \text{for TE odd} \tag{15.230}$$

$$\frac{1}{\epsilon_r}(qd)\tan(qd) = (\gamma_x d) \qquad \text{for TM even} \tag{15.231}$$

$$\frac{1}{\epsilon_r}(qd)\cot(qd) = -(\gamma_x d) \qquad \text{for TM odd.} \tag{15.232}$$

A trapped mode corresponds with real q and real γ_x. Under these circumstances, a graphical method can be used to solve an equation such as (15.231). In Figure 15.29, the coordinates are $X = qd$ and $Y = \gamma_x d$ [46]. Two sets of curves should be considered:

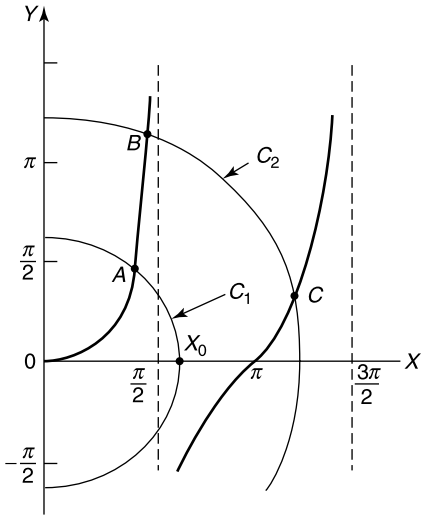

Figure 15.29 Identification of the trapped modes (from R. E. Collin. *Field theory of guided waves*. IEEE Press, New York, 2nd edition, 1991, with permission of IEEE Press).

- The curve $Y = \dfrac{1}{\epsilon_r} X \tan X$, which consists of many branches
- The curves $Y = \gamma_x d = \left[(k^2 - k_0^2)\, d^2 - X^2\right]^{\frac{1}{2}} = [X_0^2 - X^2]^{\frac{1}{2}}$, which are circles of radius X_0.

Any intersection of these curves corresponds with a trapped mode. In Figure 15.29, circle C_1 generates only one intersection (point A), hence only the lowest mode propagates. Because $X_0 = k_0 d(\sqrt{\epsilon_r - 1})$, the radius X_0 of the circle increases with frequency (circle C_2), and eventually two intersections are found, in B and C. Two modes are now trapped.

In addition to imaginary γ's, which are associated with propagating modes, there are also real γ's (evanescent modes) and modes with a general complex γ. Figure 15.30*b* shows how the eigenvalues are distributed in the complex γ plane, more specifically in the case of an enclosed dielectric slab[85] (Fig. 15.30*a*). The *air* modes are represented by points on the β axis (propagating form) or on the α axis (evanescent form). They behave like modes in conventional waveguides, and when the thickness of the dielectric layer decreases to zero, they approach the modes in the empty parallel plate waveguide. The *dielectric* modes, infinite in number, generally have complex eigenvalues (i.e., both an α and a β). A finite

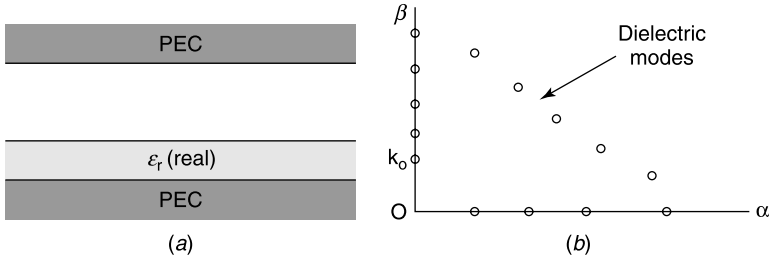

Figure 15.30 (*a*) Parallel plate waveguide with dielectric layer. (*b*) Distribution of eigenvalues $\gamma = \alpha + j\beta$.

number of modes may propagate, with a γ located on the β axis. These correspond with *surface* waves, while the off-axis values correspond with *leaky* waves. If the upper metallic boundary is removed, the waveguide becomes open, and the air modes crowd together into a continuous spectrum, extending down from $\beta = k_0$ to zero, and from there to the whole α axis.

15.9.2 Optical Fibers

The light-guiding properties of a dielectric rod were predicted almost a century ago by Hondros and Debye.[86,87] Guiding resulted fundamentally from either total reflection or ray bending in a radially inhomogeneous medium. These phenomena form the basis for an intuitive understanding of propagation in the three types of fiber shown in Figure 15.31 (where typical dimensions are expressed in μm). In (*a*) and (*b*), the rod has been replaced by a central core (index of reflection N_1) embedded in a cladding layer of index N_2. In (*c*), the index of the central core varies progressively from a maximum of N_1 on the axis to a lower value N_2 at the cladding. For such a variation, the ray is bent toward higher N (i.e., toward the axis of the fiber). Although the propagation theory had been known since the time of Debye, the industrial use of the fiber, motivated by advantages of weight, compactness, and low losses, had to await the development of low-cost materials of sufficient optical purity to become competitive. Such materials became progressively available in the 1960s.

The fibers in Figure 15.31 can be of the monomode type, in which case a single mode propagates, or they may sustain a large number of propagating modes. In the latter case, the different phase velocities of the modes spread out a traveling pulse in time, a phenomenon that limits the frequency of occurrence of distinguishable periodic pulses. Given the large number of modes, a description of wave propagation in terms of rays, instead of modes, was promptly proposed once the interest in the fiber developed in strength.[88] The three types of fibers will be briefly discussed but only under the assumptions of circular symmetry and isotropy of the materials. The more specialized literature may be consulted for the theory of anisotropic and elliptic fibers.[89,90,91,92,93]

15.9.3 The Step-Index Fiber

This type of waveguide has been discussed extensively in a number of textbooks [8, 46, 95, 126, 143, 193]. We shall focus our attention on the modes that *propagate* down the fiber and write therefore $\gamma = j\beta$. Because the media are homogeneous and isotropic, $\mathcal{E}_z$ and $\mathcal{H}_z$

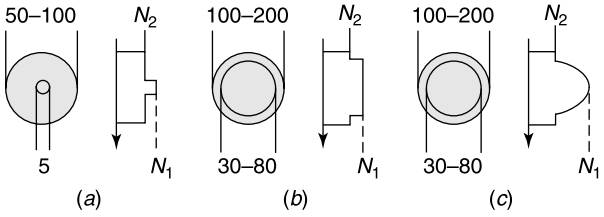

Figure 15.31 (*a*) Single-mode fiber (step index). (*b*) Multimode fiber (step index). (*c*) Multimode fiber (graded index).

satisfy (15.195), now written as

$$\nabla^2 \mathcal{E}_z + (k_0^2 N_i^2 - \beta^2)\, \mathcal{E}_z = 0$$
$$\nabla_t^2 \mathcal{H}_z + (k_0^2 N_i^2 - \beta^2)\, \mathcal{H}_z = 0 \qquad (i = 1, 2). \tag{15.233}$$

The azimuthal variation of the fields is expressed through a factor $e^{\pm jm\varphi}$, and each mode will be characterized by a double index m, n. The radial dependence is governed by a Bessel type of equation, which gives, in the *inner core*,

$$(\mathcal{E}_z)_{mn} = A\, J_m \left(u_{mn} \frac{r}{a}\right) \begin{Bmatrix} \cos m\varphi \\ \sin m\varphi \end{Bmatrix}$$
$$(\mathcal{H}_z)_{mn} = B\, J_m \left(u_{mn} \frac{r}{a}\right) \begin{Bmatrix} \sin m\varphi \\ -\cos m\varphi \end{Bmatrix}, \tag{15.234}$$

where a is the radius of the core, u_{mn} is given by

$$u_{mn}(\omega) = a\sqrt{k_0^2 N_1^2 - \beta_{mn}^2}, \tag{15.235}$$

and $\beta_{mn}(\omega)$ is the propagation constant of the mode. We shall assume that region 2, the cladding, is radially infinite, a justifiable assumption because in most fibers the guided mode is strongly attenuated radially and does not reach the outer boundary of the cladding. Anticipating that the mode is trapped, we introduce the parameter

$$w_{mn}(\omega) = ja\sqrt{k_0^2 N_2^2 - \beta_{mn}^2} = a\sqrt{\beta_{mn}^2 - k_0^2 N_2^2}. \tag{15.236}$$

With that notation, the fields in the *cladding* take the form

$$(\mathcal{E}_z)_{mn} = C\, K_m \left(w_{mn} \frac{r}{a}\right) \begin{Bmatrix} \cos m\varphi \\ \sin m\varphi \end{Bmatrix}$$
$$(\mathcal{H}_z)_{mn} = D\, K_m \left(w_{mn} \frac{r}{a}\right) \begin{Bmatrix} \sin m\varphi \\ -\cos m\varphi \end{Bmatrix}. \tag{15.237}$$

Here K_m is the modified Bessel function defined in (A5.64). When w is real, (A5.82) shows that

$$\lim_{r\to\infty} K_m \left(\frac{w}{a} r\right) = \sqrt{\frac{\pi a}{2wr}}\, e^{-\frac{w}{a} r}. \tag{15.238}$$

This form confirms the radial attenuation of the mode, which propagates (and is trapped) when both u_{mn} and w_{mn} are real. The condition is

$$k_0 N_2 \le \beta_{mn} \le k_0 N_1. \tag{15.239}$$

The lower limit corresponds with $w_{mn} = 0$ and marks the end of the trapped condition; w_{mn} subsequently becomes imaginary, upon which the fields start propagating in the radial direction [95].

To determine a relationship between the A, B, C, D coefficients in (15.234) and (15.237), we must enforce continuity of $\mathcal{E}_z$, $\mathcal{H}_z$, $\mathcal{E}_\varphi$, and $\mathcal{H}_\varphi$ at $r = a$. The azimuthal components may be expressed in terms of $\mathcal{E}_z$ and $\mathcal{H}_z$ by means of (15.190) and (15.191). Thus,

$$\mathcal{E}_\varphi = \frac{1}{k_i^2 - \beta^2}\left[-j\beta\frac{1}{r}\frac{\partial \mathcal{E}_z}{\partial \varphi} + j\omega\mu_0\frac{\partial \mathcal{H}_z}{\partial r}\right]$$
$$\mathcal{H}_\varphi = \frac{1}{k_i^2 - \beta^2}\left[-j\beta\frac{1}{r}\frac{\partial \mathcal{H}_z}{\partial \varphi} - j\omega\epsilon\frac{\partial \mathcal{E}_z}{\partial r}\right]. \tag{15.240}$$

The continuity conditions generate four homogeneous equations for the coefficients. These equations have nontrivial solutions provided the determinant of the system vanishes. Detailed calculations lead to the condition [143]

$$\left[\frac{J_m'(u)}{uJ_m(u)} + \frac{K_m'(w)}{wK_m(w)}\right]\cdot\left[\frac{N_1^2 J_m'(u)}{uJ_m(u)} + \frac{N_2^2 K_m'(w)}{w_n K_m(w)}\right] = \left(\frac{m\beta}{k_0}\right)^2\left(\frac{1}{u^2} + \frac{1}{w^2}\right)^2. \tag{15.241}$$

There is such an equation for each trapped mode, and the solution yields the dispersion law $\beta(\omega)$ of the mode. Instead of ω one often uses the dimensionless parameter

$$v = k_0 a\sqrt{N_1^2 - N_2^2}. \tag{15.242}$$

Further analysis shows that the φ-independent modes are of either the TE or the TM type, but that $m \neq 0$ requires the presence of both $\mathcal{E}_z$ and $\mathcal{H}_z$ in the modal fields. Such *hybrid* modes are denoted by the symbols EH_{mn} or HE_{mn}, where n refers to the order of the mode in its "m" family. The first letter, E or H, indicates whether the fields can be related, by a progressive evolution, to those of an E (or H) mode in a closed circular waveguide completely filled with the rod material.** Ranked according to increasing cut-off frequencies, the modes form the sequence

$$\begin{aligned} &HE_{11} && (v_c = 0)\\ &HE_{21};\quad E_{01}\ (\text{or TM}_{01});\quad H_{01}\ (\text{or TE}_{01}) && (v_c = 2.4048)\\ &EH_{11};\quad HE_{31};\quad HE_{12} && (v_c = 3.8317). \end{aligned} \tag{15.243}$$

The importance of the HE_{11} mode is obvious; it has no cut-off and is the only propagating mode up to $v_c = 2.4048$. The difference $N_1 - N_2 = \Delta N$ is small in practice, because typical values are $N_1 = 1.58$ and $N_2 = 1.52$. Monomode operation will therefore be achieved up to frequencies satisfying

$$v \approx \frac{\omega a}{c_0} N_{\text{ave}}\sqrt{\frac{2\Delta N}{N_{\text{ave}}}} \leq 2.4048, \tag{15.244}$$

where $N_{\text{ave}} = \dfrac{1}{2}(N_1 + N_2)$. In the near infrared, the quoted values of N lead to core diameters of the order of a few micrometers.

**The criterion can also be based on the detailed contributions of $\mathcal{E}_z$ (or $\mathcal{H}_z$) to the transverse components of the fields at some reference point.[94]

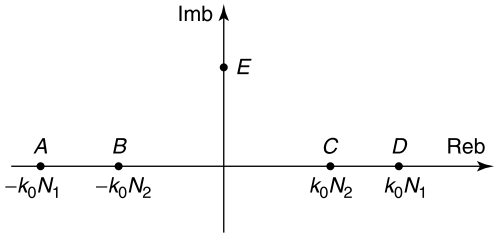

Figure 15.32 Complex β plane.

The *trapped* modes of the fiber are finite in number. They must be augmented by the radiation modes to form a complete orthogonal set, capable of correctly representing the fields excited by either outside sources or discontinuities (such as bends or imperfections in the material). With reference to Figure 15.32*b*, the intervals (*AB*) and (*CD*) correspond with guided (trapped) modes, finite in number. Between *B* and *C*, u_{mn} is real and w_{mn} imaginary, and the mode propagates in the z-direction but also radially. For β imaginary (point *E*), the mode is evanescent in the z-direction but propagates radially [95]. A knowledge of the Green's dyadic for the rod-cladding structure allows one to generate the whole modal spectrum by means of a complex integration. The guided modes are found from pole singularities and the radiating ones from branch cuts.[94,95]

15.9.4 Graded-Index Fibers

Graded-index fibers are typically circular, with a dielectric constant that depends only on the radial distance r. A range of variations is possible within these limitations, and biaxial anisotropic fibers, for example, have been given some attention.[96] We shall only consider isotropic materials, with an index of refraction that varies as in Figure 15.33. The variation between N_1 and N_1' is often parabolic, with $N_1' = N_2$ at the junction $r = a$. Wave propagation in such a medium may be understood in terms of modes or rays [94]. We shall first examine the nature of the propagating *modes*. Given the circular symmetry, a component such as E_z may be written as[97]

$$E_z(\mathbf{r}) = e_z(r)\, e^{jm\varphi}\, e^{-j\beta z}, \tag{15.245}$$

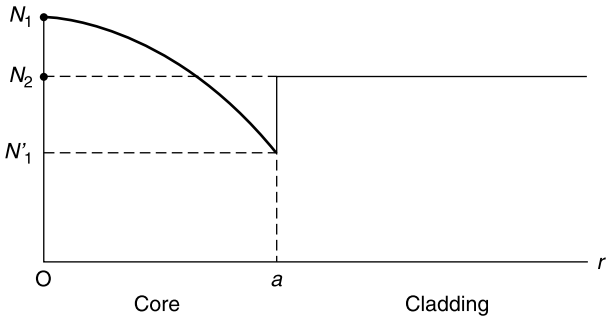

Figure 15.33 A graded-index variation.

where the factors e or h represent the radial dependence. Maxwell's equations yield

$$\begin{cases} \dfrac{1}{r} jme_z + j\beta e_\varphi & = -j\omega\mu_0 h_r \\ -j\beta e_r - \dfrac{\partial e_z}{\partial r} & = -j\omega\mu_0 h_\varphi \\ \dfrac{1}{r}\dfrac{\partial}{\partial r}(re_\varphi) - \dfrac{jm}{r} e_r & = -j\omega\mu_0 h_z \end{cases} \qquad \begin{cases} \dfrac{1}{r} jmh_z + j\beta h_\varphi & = j\omega\epsilon(r)\, e_r \\ -j\beta h_r - \dfrac{\partial h_z}{\partial r} & = j\omega\epsilon(r)\, e_\varphi \\ \dfrac{1}{r}\dfrac{\partial}{\partial r}(rh_\varphi) - \dfrac{jm}{r} h_r & = j\omega\epsilon(r)\, e_z. \end{cases} \tag{15.246}$$

Because the φ and z components remain continuous throughout the fiber volume, it pays to emphasize their role and eliminate the discontinuous e_r and h_r. The result is a system of four equations in four unknowns, which can be written concisely as

$$\frac{d\mathbf{f}}{dr} = \overline{\overline{M}} \cdot \mathbf{f}. \tag{15.247}$$

The four-dimensional quantities are[98]

$$\mathbf{f} = (e_z, re_\varphi, R_{c0}\, h_z, R_{c0}\, rh_\varphi)$$

$$\overline{\overline{M}} = \left[\begin{array}{cc|cc} 0 & 0 & -\dfrac{j\beta m}{\epsilon_r k_0 r} & \dfrac{1}{\epsilon_r}\dfrac{j(k^2-\beta^2)}{k_0 r} \\ 0 & 0 & -\dfrac{1}{\epsilon_r}\dfrac{jr}{k_0}\left(k^2 - m^2\, r^2\right) & \dfrac{j\beta_m}{\epsilon_r k_0 r} \\ \hline \dfrac{j\beta m}{k_0 r} & -j\dfrac{(k^2-\beta^2)}{k_0 r} & 0 & 0 \\ \dfrac{jr}{k_0}\left(k^2 - \dfrac{m^2}{r^2}\right) & -\dfrac{j\beta_m}{k_0 r} & 0 & 0 \end{array}\right] \tag{15.248}$$

with $k^2(r) = k_0^2 \epsilon_r(r)$. The solution of (15.247) may be effected by classic methods of matrix analysis, noting that

$$\overline{\overline{M}} \cdot \overline{\overline{M}} = -\left(k^2 - \beta^2 - \frac{m^2}{r^2}\right)\bar{\bar{I}}. \tag{15.249}$$

The 4-vector $\mathbf{f}$ can be evaluated from (15.247) by direct numerical integration[99,100] or by replacing the continuous variation of $\epsilon(r)$ by a staircase approximation.[101,102]

Considerable simplification in the analysis is possible when ϵ_r varies slowly as a function of r. By *slowly* is meant that the scale L of the radial inhomogeneities is much larger than the wavelengths of interest. For such a gentle profile,

$$\text{grad}\,(\log_e N) = \frac{\text{grad}\, N}{N} \approx \frac{1}{L} \ll \frac{1}{\lambda}. \tag{15.250}$$

Because

$$\text{div}\,(\text{curl}\,\mathbf{H}) = \text{div}\,(\epsilon\mathbf{E}) = 0,$$

we may write

$$\text{grad}\,\epsilon \cdot \mathbf{E} + \epsilon\ \text{div}\,\mathbf{E} = 0$$

or

$$\text{div } \mathbf{E} = -\frac{1}{N}(\text{grad } N \cdot \mathbf{E}).$$

As a result:

$$\text{grad div } \mathbf{E} - \text{curl curl } \mathbf{E} + k_0^2 \epsilon_r \mathbf{E} = -\text{grad}\left(\frac{1}{N}\ \text{grad } N \cdot \mathbf{E}\right). \tag{15.251}$$

The simplification consists in neglecting the second term, which is of the order $(1/L^2)\,E$, while in the first term $k_0^2 \epsilon_r E$ is of the order $(1/\lambda^2)\,E$. With such an approximation, both $\mathbf{E}$ and $\mathbf{H}$ satisfy the vector wave equation

$$\nabla^2 \mathbf{E} + k_0^2 N^2(r)\,\mathbf{E} = 0. \tag{15.252}$$

The x, y, and z components are seen to satisfy separate *scalar* wave equations. Written in terms of the notation in (15.245) this means that e_z, for example, satisfies the separate equation[††] [143]

$$\frac{1}{r}\frac{d}{dr}\left(r\frac{de_z}{dr}\right) + \underbrace{(k_0^2 \epsilon_r - \frac{m^2}{r^2} - \beta^2)}_{p^2(r)}\ e_z = 0. \tag{15.253}$$

The factor $p^2(r)$, which already appears in (15.249), reveals the presence of a *turning point* at $p^2 = 0$. In a region where p^2 is positive the solution will be oscillatory, while a negative p^2 generates an exponential behavior. A trapped mode is therefore only possible if $p^2(r)$ is negative at large radial distances. In the WKB approximation, already discussed in Section 8.3, a solution to (15.253) is sought in the form [165]

$$e_z(r) = e^{jS(r)}. \tag{15.254}$$

Inserting this value into (15.253) gives

$$j\frac{d^2S}{dr^2} + j\,\frac{1}{r}\frac{dS}{dr} - \left(\frac{dS}{dr}\right)^2 = -p^2(r). \tag{15.255}$$

This is a nonlinear, first-order equation for $S'(r)$, the logarithmic derivative of e_z. In a first-order approximation, one assumes that the term in $\left(\dfrac{dS}{dr}\right)^2$ dominates in the left-hand term of (15.255). For such a case, the general solution is a linear combination of the two partial solutions

$$S - S_0 = \pm \int_{r_0}^{r} p(r)\,dr. \tag{15.256}$$

A better approximation, similar to (8.84), is given by (Problem 15.25)

$$e_z(r) = \frac{1}{\sqrt{r\,p(r)}}\left[c_1\, e^{j\int p(r)\,dr} + c_2\, e^{-j\int p(r)\,dr}\right], \tag{15.257}$$

[††]The equation for e_z contains neither e_x nor e_y, which implies that polarization effects are ignored.

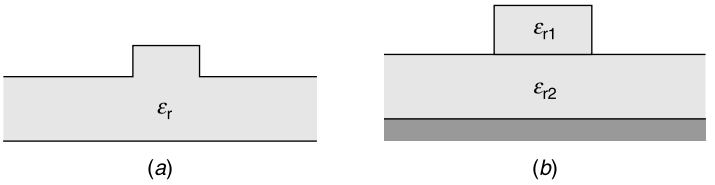

Figure 15.34 (*a*) Rib waveguide. (*b*) Strip dielectric waveguide.

where c_1 and c_2 are arbitrary constants. Special precautions must be taken near the points r_t at which $p^2(r_t) = 0$. At such turning points, the assumed dominance of $\left(\frac{dS}{dr}\right)^2$, which led to (15.257), cannot hold because $S'(r)$ vanishes. The solution must now proceed by expanding $p^2(r)$ in a Taylor series about r_t [143].

15.9.5 Dielectric Waveguides of Arbitrary Cross Section

Planar waveguides, of which two examples are shown in Figure 15.34, are of frequent use in *integrated optics*. The basic equations satisfied by the *modal fields* are derived in Section 15.7. A possible formulation of the problem is in terms of $\mathcal{E}_z$ and $\mathcal{H}_z$. Thus, in an *isotropic* material, (15.190) gives

$$\boldsymbol{\mathcal{E}}_t \times \mathbf{u}_z = -\frac{\gamma}{k^2+\gamma^2} \operatorname{grad} \mathcal{E}_z \times \mathbf{u}_z + \frac{j\omega\mu}{k^2+\gamma^2} \operatorname{grad} \mathcal{H}_z.$$

Taking the divergence of both members yields, from (15.186),

$$\operatorname{grad}_t \left(\frac{\gamma}{k^2+\gamma^2}\right) \cdot (\operatorname{grad} \mathcal{E}_z \times \mathbf{u}_z) + \operatorname{div}_t \left(\frac{j\omega\mu}{k^2+\gamma^2} \operatorname{grad} \mathcal{H}_z\right) + j\omega\mu\, \mathcal{H}_z = 0. \quad (15.258)$$

Similarly, from (15.191),

$$-\operatorname{grad}_t \left(\frac{\gamma}{k^2+\gamma^2}\right) \cdot (\operatorname{grad} \mathcal{H}_z \times \mathbf{u}_z) + \operatorname{div}_t \left(\frac{j\omega\epsilon}{k^2+\gamma^2} \operatorname{grad} \mathcal{E}_z\right) + j\omega\epsilon\, \mathcal{E}_z = 0. \quad (15.259)$$

The numerical solution of these equations can be effected by means of a variational principle[103] (Problem 15.27). More generally, the array of methods described in previous sections is available,[104,105] in particular integral equations,[106,107] finite differences, and finite elements.[108,109,110]

The modal approach is frequently inefficient in its application to *integrated optics* components, which are often complicated three-dimensional structures of dimensions much larger than the relevant wavelengths. The alternative is to resort to approaches such as the *beam propagation method* (BPM), a technique briefly discussed in Section 8.4.

15.10 OTHER EXAMPLES OF WAVEGUIDES

The chosen examples are a closed dielectric-loaded waveguide (in which the dielectric can serve to lower the cut-off frequency), the microstrip and its use as a feed line for networks,

and finally the application of PML techniques to the evaluation of the modes of an open waveguide. Before discussing these various problems, we first mention two transmission lines of historical interest. The first one was investigated by A. Sommerfeld a century or so ago, the second one by G. Goubau one-half century later. The *Sommerfeld* line is simply a circular conductor of *finite* conductivity σ. Of all the modes it can carry, only the symmetric, φ-independent modes are not strongly attenuated [20]. The principal mode is transverse magnetic, and it can only exist when the conductivity is *finite*. Various problems have impeded the practical use of this line, mainly because of the large radial extent of the fields. This difficulty could be reduced by lowering σ, but only at the cost of higher losses. To remedy the situation, the surface of the wire can be modified by covering it with a dielectric coating. This idea gave birth to the *Goubau line*, which enjoyed some popularity in the 1950s, just before the advent of the optical fiber.[111,112] The central core of the line, for $r < a$, is perfectly conducting. With a propagation factor $e^{-j\beta z}$, a field component in the dielectric (i.e., for $a < r < b$) will be of the form

$$\mathcal{E}_z = A\, J_0\left[r(k^2 - \beta^2)^{\frac{1}{2}}\right] + B\, N_0\left[r(k^2 - \beta^2)^{\frac{1}{2}}\right],$$

with similar relationships for $\mathcal{E}_r$ and $\mathcal{H}_\varphi$. In air we select a solution that decreases in the radial direction. On the basis of (A5.82), this should be

$$\mathcal{E}_z = C\, K_0\left[r(\beta^2 - k_0^2)^{\frac{1}{2}}\right].$$

Imposing the boundary conditions ar $r = a$ and $r = b$ gives the eigenvalue equation

$$\frac{K_1(ub)}{uK_0(ub)} = \frac{\epsilon_r}{v}\,\frac{J_0(va)\,N_1(vb) - J_1(vb)\,N_0(va)}{J_0(vb)\,N_0(va) - J_0(va)\,N_0(vb)}, \tag{15.260}$$

where $u^2 = \beta^2 - k_0^2$ and $v^2 = k^2 - \beta^2$ [46]. Solution of (15.260) yields the $\beta(\omega)$ dispersion law of the mode.

15.10.1 The Slab-Loaded Rectangular Waveguide

The inhomogeneous waveguide depicted in Figure 15.35 has been investigated extensively[113] [46]. Let us assume that the dielectric slab is nonmagnetic and homogeneous. A first set of modes is derived from an x-oriented magnetic Hertz potential

$$\boldsymbol{\pi}^m = \pi^m(x, y)\, e^{-\gamma z}\, \mathbf{u}_x. \tag{15.261}$$

From (15.160), this potential generates an electric field

$$\mathbf{E} = -j\omega\mu_0\left[\text{grad}\,(\pi^m\, e^{-\gamma z}) \times \mathbf{u}_x\right] = j\omega\mu_0\left[\gamma\pi^m\,\mathbf{u}_y + \frac{\partial \pi^m}{\partial y}\,\mathbf{u}_z\right]. \tag{15.262}$$

In our search for the normal modes, we shall use a double index (n, p) to identify π^m and related fields. Following the example of the homogeneously filled waveguide, the y-variation of π^m is given the value $\cos(n\pi y/b)$. Thus,

$$\pi^m_{n,p} = \cos\frac{n\pi y}{b}\, f_{np}(x)\, e^{-\gamma_{np} z} \tag{15.263}$$

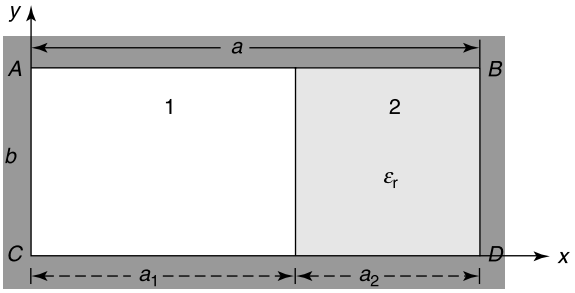

Figure 15.35 Rectangular waveguide with dielectric slab.

and

$$\mathbf{E}_{n,p} = j\omega\mu_0 \left[\gamma_{np} \cos \frac{n\pi y}{b} f_{np}(x)\, \mathbf{u}_y - \frac{n\pi}{b} \sin \frac{n\pi y}{b} f_{np}(x)\, \mathbf{u}_z \right] e^{-\gamma_{np} z}. \tag{15.264}$$

This field is perpendicular to the broad sides AB and CD, as required. Because π^m must satisfy the three-dimensional Helmholtz equation in each layer, $f_{np}(z)$ must be a solution of

$$\frac{d^2 f_{np}}{dx^2} + \underbrace{\left[k_i^2 + \gamma_{np}^2 - \left(\frac{n\pi}{b} \right)^2 \right]}_{h_{npi}^2} f_{np} = 0 \qquad (i = 1, 2). \tag{15.265}$$

We choose

$$\begin{aligned} f_{np1} &= A_1 \sin h_{np1}\, x \qquad &&\text{(in medium 1)} \\ f_{np2} &= A_2 \sin h_{np2}\, (a - x) \qquad &&\text{(in medium 2),} \end{aligned} \tag{15.266}$$

a choice that ensures $\mathbf{E}_{np}$ is perpendicular to the small sides AC and BD. Requiring E_y to be continuous at the interface $x = a_1$ yields the condition

$$A_1 \sin(h_{np1}\, a_1) = A_2 \sin(h_{np2}\, a_2). \tag{15.267}$$

Because

$$\begin{aligned} H_y &= -\frac{1}{j\omega\mu_0} (\text{curl}\, \mathbf{E})_y = \frac{1}{j\omega\mu_0} \frac{\partial E_z}{\partial x} \\ H_z &= -\frac{1}{j\omega\mu_0} (\text{curl}\, \mathbf{E})_z = -\frac{1}{j\omega\mu_0} \frac{\partial E_y}{\partial x}, \end{aligned}$$

continuity of H_y and H_z at the interface gives the additional condition

$$A_1\, h_{np1} \cos(h_{np1}\, a_1) = -A_2\, h_{np2} \cos(h_{np2}\, a_2). \tag{15.268}$$

Combining (15.267) and (15.268) leads to

$$\frac{1}{h_{np1}} \tan(h_{np1}\, a_1) = -\frac{1}{h_{np2}} \tan(h_{np2}\, a_2). \tag{15.269}$$

The quantities h_{np1} and h_{np2} must further satisfy

$$h_{np1}^2 - k_1^2 = h_{np2}^2 - k_2^2 = \gamma_{np}^2 - \left(\frac{n\pi}{b}\right)^2. \tag{15.270}$$

The two conditions, (15.269) and (15.270), generate an infinite number of solutions for h_1 and h_2, with corresponding propagation constants γ. It is interesting to note that the field variation in the x-direction may be interpreted in terms of propagation along two transmission lines, one per region. The first line, in region 1, has a zero impedance $\dfrac{E_y}{H_z} = -\dfrac{E_z}{H_y}$ at the short-circuited end $x = 0$, because E_y and E_z vanish there. At the interface $x = a_1$, conventional transmission line theory gives an impedance Z that, transformed to line 2, should become zero at $x = a$, given the short-circuit at that end. The so-obtained condition reproduces the condition already derived in (15.269). The steps described above form the *transverse resonance* method, here applied to a *longitudinal section electric mode* (an LSE). The method can be extended to *LSM modes*, derived from an electric Hertz potential. It has also been applied to a variety of layered structures and in particular to guides loaded with several dielectric slabs [46, 191].

15.10.2 The Microstrip

The fields in the lowest mode of the microstrip can be evaluated once the surface currents J_{Sx} and J_{Sz} on the strip are known (Fig. 15.36*a*). The equations which form the basis for that evaluation are

$$\begin{aligned}
\mathcal{E}_x(x,y) &= \int_{-\frac{w}{2}}^{\frac{w}{2}} \left[G_{xx}(x-x',y)\, J_{Sx}(x') + G_{xz}(x-x',y)\, J_{Sz}(x')\right] dx' \\
\mathcal{E}_z(x,y) &= \int_{-\frac{w}{2}}^{\frac{w}{2}} \left[G_{zx}(x-x',y)\, J_{Sx}(x') + G_{zz}(x-x',y)\, J_{Sz}(x')\right] dx',
\end{aligned} \tag{15.271}$$

where a common factor $e^{-j\beta z}$ in fields and currents has been dropped. Whenever the Green's functions are known, integral equations for J_{Sx} and J_{Sz} can be derived by setting (x, y) on the strip and requiring both $\mathcal{E}_x$ and $\mathcal{E}_z$ to vanish at these points. The search for the Green's functions is therefore central to the solution. The waveguide geometry, with its boundaries parallel to the x-axis, immediately suggests erasing the x-dependence by means of a spatial Fourier transformation in x. The method has been applied to other layered structures in Sections 5.9 and 9.4. Thus, in accordance with (A7.53) and (A7.54), we introduce the Fourier transform pairs

$$\begin{aligned}
\tilde{f}(\alpha) &= \int_{-\infty}^{\infty} f(x)\, e^{-j\alpha x}\, dx \\
f(x) &= \frac{1}{2\pi} \int_{-\infty}^{\infty} \tilde{f}(\alpha)\, e^{j\alpha x}\, d\alpha.
\end{aligned} \tag{15.272}$$

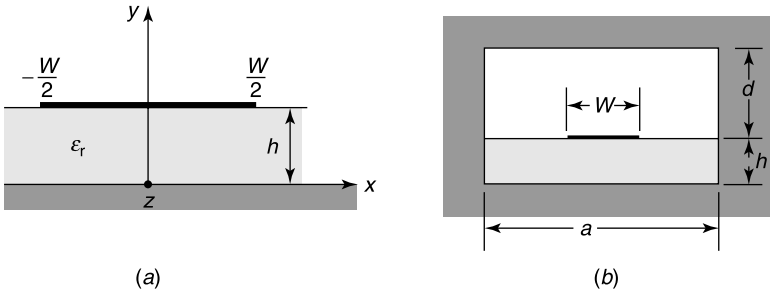

Figure 15.36 (*a*) Microstrip configuration. (*b*) Shielded (boxed in) microstrip.

The fields $\boldsymbol{\mathcal{E}}$ and $\boldsymbol{\mathcal{H}}$ can be expressed in terms of scalar potentials ϕ and ψ. In the spectral domain we write, for example,

$$\tilde{\mathcal{E}}_z(\alpha, y) = -\frac{j\beta}{j\omega\epsilon_i}\frac{\partial\tilde{\phi}}{\partial y} + j\alpha\,\tilde{\psi},$$

where ϵ_i has the value appropriate to each region [191]. The potentials satisfy Helmholtz equations. In transformed form:

$$\left(\frac{d^2}{dy^2} - \alpha^2 - \beta^2\right)\tilde{\phi} + k^2\tilde{\phi} = 0. \tag{15.273}$$

This ordinary differential equation can easily be solved in each region to give

$$\tilde{\phi} = A\sinh\lambda_i\, y + B\cosh\lambda_i\, y,$$

where $\lambda_i^2 = \alpha^2 + \beta^2 - k_i^2$. The coefficients A and B can be determined by enforcing the boundary conditions on the ground plane and at the $y = h$ interface. The magnetic field suffers a jump at $y = h$, because of the presence of a surface current in that plane. Thus,

$$\left(\tilde{H}_x\right)_{h^-} - \left(\tilde{H}_x\right)_{h^+} = \tilde{J}_{Sz}.$$

A similar relationship can be written for $\tilde{H}_z$ and $\tilde{J}_{Sx}$. Fairly lengthy calculations[114] ultimately lead to equations of the form

$$\begin{aligned}\tilde{\mathcal{E}}_x(\alpha) &= \tilde{Z}_{xx}(\alpha)\,\tilde{J}_{Sx}(\alpha) + \tilde{Z}_{xz}\,\tilde{J}_{Sz}(\alpha)\\ \tilde{\mathcal{E}}_z(\alpha) &= \tilde{Z}_{zx}(\alpha)\,\tilde{J}_{Sx}(\alpha) + \tilde{Z}_{zz}\,\tilde{J}_{Sz}(\alpha).\end{aligned} \tag{15.274}$$

The symbol $\tilde{Z}$ has been chosen because the $\tilde{Z}$ coefficients have the nature of an impedance. An application of the convolution theorem (A7.30) further shows that the Z's are actually the transforms of the corresponding Green's functions in (15.271) [191]. In a *first approach*, the Green's functions are kept in their spectral form and are not inverted. The transforms of

the strip currents are subsequently expanded in suitable basis functions. Thus,

$$\tilde{J}_{sx} = \sum_{n=1}^{N} c_n \tilde{\phi}_n(\alpha)$$
$$\tilde{J}_{sz} = \sum_{n=1}^{N} d_n \tilde{\psi}_n(\alpha). \tag{15.275}$$

These expansions are inserted into (15.274), and a weak form of the equations is obtained by weighing with the basis functions themselves. The contributions from the left-hand terms $\tilde{\mathcal{E}}_x$ and $\tilde{\mathcal{E}}_z$ can be evaluated by invoking relationship (A7.33), which gives

$$\frac{1}{2\pi} \int_{-\infty}^{\infty} \tilde{\phi}^*(\alpha)\, \tilde{\mathcal{E}}^*(\alpha)\, d\alpha = \int_{-\infty}^{\infty} \phi(x)\, \mathcal{E}(-x)\, dx. \tag{15.276}$$

If the basis functions $\phi_n(x)$ and $\psi_n(x)$ are chosen to vanish *outside* the strip interval (i.e., for $|x| > w/2$), the right-hand term of (15.276) automatically vanishes because, in addition, $\mathcal{E}(x)$ is zero *on* the strip. Given these basis functions, the weak form of the equations becomes

$$\begin{aligned} \int_{\alpha} \tilde{\phi}_k \left[\tilde{Z}_{xx} \sum_{n=1}^{N} c_n\, \tilde{\phi}_n + \tilde{Z}_{xz} \sum_{n=1}^{N} d_n\, \tilde{\psi}_n \right] d\alpha = 0 \qquad (k = 1, 2, \ldots N) \\ \int_{\alpha} \tilde{\psi}_m \left[\tilde{Z}_{zx} \sum_{n=1}^{N} c_n\, \tilde{\phi}_n + \tilde{Z}_{zz} \sum_{n=1}^{N} d_n\, \tilde{\psi}_n \right] d\alpha = 0 \qquad (m = 1, 2, \ldots N). \end{aligned} \tag{15.277}$$

These are $2N$ homogeneous equations for the $2N$ unknown coefficients C_n, D_n. Setting the determinant of the equations equal to zero yields the dispersion equation for the propagation constant $j\beta$.

A *second approach* consists in inverting the transform of the Green's dyadic,[115,116] thus yielding the space domain form needed for (15.271). A few interesting results obtained by that method are shown in Figure 15.37, which displays the variation of the surface current along the x-axis, for the lowest mode of the microstrip. The same relative scale is used for both J_{Sz} and J_{Sx}, and the parameters are $\epsilon_r = 11.7$, $w = 3.04$ mm, and $h = 3.17$ mm. Note that the J_{Sx} component is 90° out of phase with J_{Sz}. Up to 1 GHz the current is almost entirely longitudinal, as expected from the TEM type of behavior of the lowest mode at low frequencies. Above 1 GHz the transverse components gain progressively in importance, and the hybrid *E-H* character of the mode comes to the fore.

15.10.3 Finite Transforms

It is interesting to note that the spectral method can also be applied to the shielded line depicted in Figure 15.36*b*. The infinite Fourier transform in x is now replaced by its finite version.[117] In the solution of

$$\frac{\partial^2 \phi}{\partial x^2} + \frac{\partial^2 \phi}{\partial y^2} + (k^2 - \beta^2)\, \phi = 0, \tag{15.278}$$

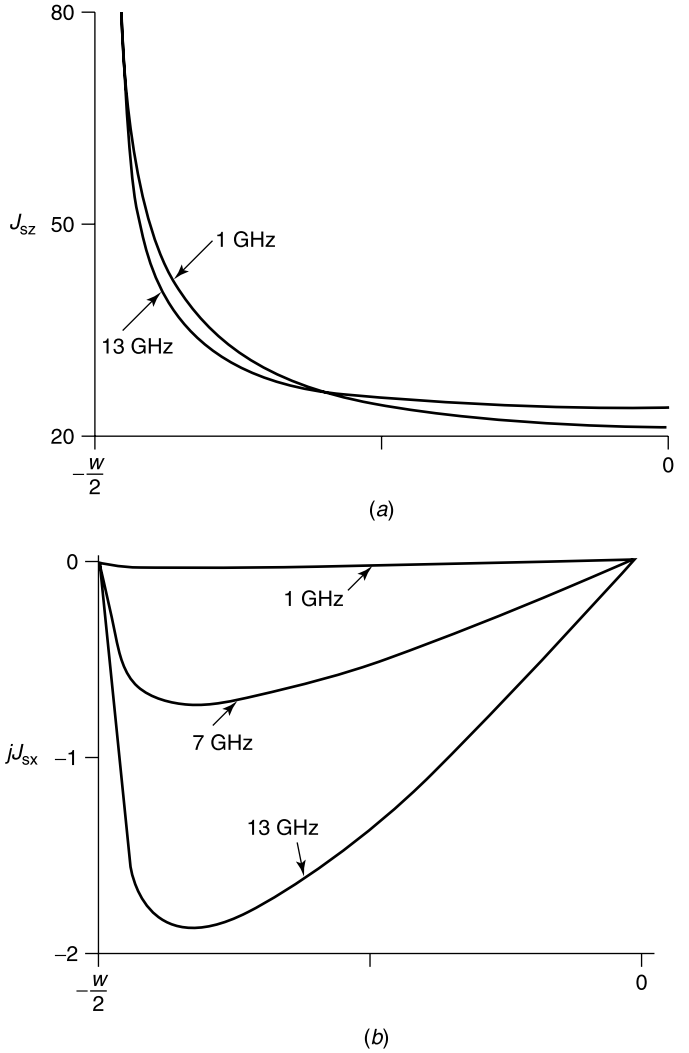

Figure 15.37 (*a*) Variation of J_{Sz} along the strip. (*b*) Variation of J_{Sx} along the strip (from N. Faché and D. De Zutter, Rigorous full-wave space-domain solution for dispersive microstrip lines, *IEEE Trans. MTT* **36**, 731–737, 1988, with permission of IEEE).

the x-variation can be erased by writing

$$\phi(x,y) = \sum_{n=0}^{\infty} \left[A_n(y) \sin\left(n\frac{2\pi x}{a}\right) + B_n(y) \cos\left(n\frac{2\pi x}{a}\right) \right],$$

where $A_n(y)$ is the *finite sine Fourier transform* of ϕ, viz.

$$A_n(y) = \frac{2}{a} \int_0^a \phi(x,y) \sin\left(\frac{n2\pi x}{a}\right) dx, \tag{15.279}$$

and $B_n(y)$ is the corresponding *cosine transform*. Multiplying (15.278) by $\sin\left(\frac{n2\pi x}{a}\right)$, and integrating from $x = 0$ to $x = a$, shows that A_n must satisfy

$$\frac{d^2A_n}{dy^2} + \left[k^2 - \beta^2 - \left(\frac{n2\pi}{a}\right)^2\right] A_n = 0, \tag{15.280}$$

which is the finite counterpart of (15.273).

15.10.4 Microstrip Networks

The scattering parameters of a microstrip network can be evaluated in a number of ways, for example by FDTD methods.[118] In the network of Figure 15.38, the problem can be usefully formulated in terms of an *integral equation* for the surface currents $\mathbf{J}_S$ flowing on the metal.[119] By requiring $\mathbf{E}_{\tan}$ to vanish on the surface S of the upper conductors, one obtains

$$\begin{aligned}
\lim_{z\to h} \int_S \left[G_{xx}(\mathbf{r},\mathbf{r}')\, J_{Sx}(\mathbf{r}') + G_{xy}(\mathbf{r},\mathbf{r}')\, J_{Sy}(\mathbf{r}')\right] dS' &= -E_x^i(\mathbf{r}) \\
\lim_{z\to h} \int_S \left[G_{yx}(\mathbf{r},\mathbf{r}')\, J_{Sx}(\mathbf{r}') + G_{yy}(\mathbf{r},\mathbf{r}')\, J_{Sy}(\mathbf{r}')\right] dS' &= -E_y^i(\mathbf{r}).
\end{aligned} \tag{15.281}$$

The method requires a knowledge of the four Green's functions of the layered medium. These can be determined by the spatial transform method previously discussed in the modal analysis of the microstrip. Once the G_{ik} coefficients are known, they may serve for arbitrary geometries of the metallic planar structure. The incident fields are typically those of the lowest mode of the microstrip, fed into one of the ports. The figure shows the grid of subsections used in the discretization process.

15.10.5 Thick Conductors in a Layered Medium

In many applications, the strip may be assumed infinitely thin. When losses must be taken into account, however, the full cross section of the conductor should be involved in the

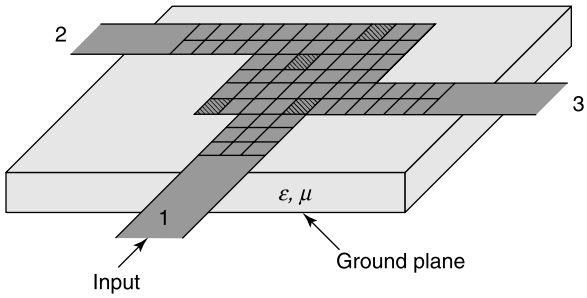

Figure 15.38 Three port microstrip network (from J. Sercu, N. Faché, F. Libbrecht, and D. De Zutter, Full-wave space-domain analysis of open microstrip discontinuities, including the singular current-edge behavior, *IEEE Trans. MTT* **41**, 1581–1588, 1993, with permission of IEEE).

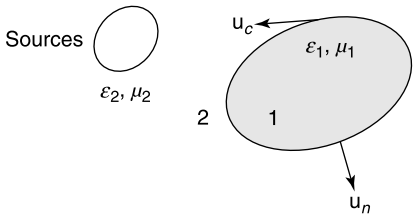

Figure 15.39 A conductor 1 embedded in a region 2.

analysis, as well as the finite conductivity σ of the material. In many cases, the skin depth approximation does not hold, and a more general method must be resorted to.[120] Consider, for example, the simple waveguide shown in Figure 15.39. Both media, 1 and 2, are assumed homogeneous and isotropic, and conductivity is represented by complex values of ϵ. The fields have a common z-dependence $e^{-j\beta z}$, with β complex. From Green's theorem (A1.31), applied to region 1, the fields inside the conductor can be written as

$$\mathcal{E}_z^1(\mathbf{r}_t) = \int_C \left[\mathcal{E}_z^1(\mathbf{r}_t') \frac{\partial G^1(\mathbf{r}_t|\mathbf{r}_t')}{\partial n'} - G^1(\mathbf{r}_t|\mathbf{r}_t') \frac{\partial \mathcal{E}_z'(\mathbf{r}_t')}{\partial n'} \right] dc'$$

$$\mathcal{H}_z^1(\mathbf{r}_t) = \int_C \left[\mathcal{H}_z^1(\mathbf{r}_t') \frac{\partial G^2(\mathbf{r}_t|\mathbf{r}_t')}{\partial n'} - G^1(\mathbf{r}_t|\mathbf{r}_t') \frac{\partial \mathcal{H}_z'(\mathbf{r}_t')}{\partial n'} \right] dc', \tag{15.282}$$

where $\mathbf{r}_t$ is in 1. The notation G^1 denotes the Green's function for a medium of infinite extent endowed with the parameters ϵ_1 and μ_1. This function is the solution of[120]

$$\nabla^2 G^1(\mathbf{r}_t|\mathbf{r}_t') + (k_1^2 - \beta^2)\, G^1(\mathbf{r}_t, \mathbf{r}_t') = \delta(\mathbf{r}_t - \mathbf{r}_t'). \tag{15.283}$$

From (14.12):

$$G^1(\mathbf{r}_t, \mathbf{r}_t') = \frac{j}{4} H_0^{(2)} \left[(k_1^2 - \beta^2)^{1/2} |\mathbf{r}_t - \mathbf{r}_t'| \right]. \tag{15.284}$$

In region 2, the fields consist of an incident part and a scattered part. The scattered fields can be written as

$$\mathcal{E}_z^2(\mathbf{r}_t) = -\int_C \left[\mathcal{E}_z^2(\mathbf{r}_t') \frac{\partial G^2(\mathbf{r}_t|\mathbf{r}_t')}{\partial n'} - G^2(\mathbf{r}_t|\mathbf{r}_t') \frac{\partial \mathcal{E}_z^2(\mathbf{r}_t')}{\partial n'} \right] dc'$$

$$\mathcal{H}_z^2(\mathbf{r}_t) = -\int_C \left[\mathcal{H}_z^2(\mathbf{r}_t') \frac{\partial G^2(\mathbf{r}_t|\mathbf{r}_t')}{\partial n'} - G^2(\mathbf{r}_t|\mathbf{r}_t') \frac{\partial \mathcal{H}_z^2(\mathbf{r}_t')}{\partial n'} \right] dc', \tag{15.285}$$

where G^2 is given by (15.284), provided k_1^2 is replaced by k_2^2. Setting $\mathcal{E}^1 = \mathcal{E}^2$ and $\mathcal{H}^1 = \mathcal{H}^2$ on C yields integral equations, with as unknowns $\mathcal{E}_z$, $\mathcal{H}_z$ and the normal derivatives of these components. Whereas $\mathcal{E}_z$ and $\mathcal{H}_z$ are continuous across C, the same is not true of the normal derivatives. The $\mathcal{E}_c$ and $\mathcal{H}_c$ components, however, *are* continuous and can usefully be used to eliminate the normal derivatives. From (15.190) and (15.191):

$$\mathcal{E}_c = \frac{1}{k^2 - \beta^2} \left[-j\beta \frac{\partial \mathcal{E}_z}{\partial c} + j\omega\mu \frac{\partial \mathcal{H}_z}{\partial n} \right]$$

$$\mathcal{H}_c = \frac{1}{k^2 - \beta^2} \left[-j\beta \frac{\partial \mathcal{H}_z}{\partial c} - j\omega\epsilon \frac{\partial \mathcal{E}_z}{\partial n} \right]. \tag{15.286}$$

The normal derivatives can now be expressed in terms of $\mathcal{E}_c$, $\mathcal{H}_c$, $\dfrac{\partial \mathcal{E}_z}{\partial c}$, and $\dfrac{\partial \mathcal{H}_z}{\partial c}$. These functions are the new unknowns of the integral equations.

The method can be extended to conductors embedded in multilayered structures — the actual application for which it was conceived. The incident fields must now include the effect of the reflections at the planar inter-layer boundaries. Anisotropic materials can also be accommodated, which makes the method suitable for the analysis of a class of *integrated optics* components.[121]

15.10.6 Closing an Open Waveguide with a PML

The modes of the open waveguide shown in Figure 15.40*a* belong to either the discrete or the radiation types. By closing the waveguide with a *perfectly matched layer*, as in Figure 15.40*b*, the radiation modes are eliminated, and the spectrum of the guide becomes fully discrete. This theoretical move has computational advantages because it greatly simplifies the evaluation of the Green's functions of the guide by side-stepping the integrals associated with the continuous spectrum. The litmus test, of course, is whether the new form of the Green's function is a sufficiently accurate substitute for the original one. In the case of Figure 15.40*b*, the original (infinite) air layer is replaced by a finite layer of complex thickness

$$\tilde{h}_a = h_a + h_{PML} = h_a + \int_B^C \alpha(z)\, dz, \tag{15.287}$$

where suitable forms for $\alpha(z)$ are given in (9.64) and (9.65). Finding the form of the modes may now proceed by the methods used for a closed waveguide.[122,123] For a TE mode, with components E_z, H_y, H_z, the dispersion equation $\beta(\omega)$ for a propagation factor $e^{-j\beta y}$ is found to be[122]

$$\gamma_{sub} \cot(\gamma_{sub}\, h) + \gamma_{air} \cot(\gamma_{air}\, \tilde{h}_a) = 0 \tag{15.288}$$

where $\gamma_{sub}^2 = \epsilon_r k_0^2 - \beta^2$ and $\gamma_{air}^2 = k_0^2 - \beta^2$. A typical distribution of discrete (complex) values of β is shown in Figure 15.41, plotted for $h_a = 5\,\text{mm}$, $h = 9\,\text{mm}$, $\epsilon_r = 3$, and $f = 12\,\text{GHz}$. The chosen parameters of the PML are $(\sigma_0/\omega\epsilon_0) = 8$ and $\kappa_0 = 10$. The *Bérenger* modes depend mainly on the characteristics of the PML. For the other modes, most of the field is concentrated in the substrate. Some of these modes, which also exist in the original waveguide, propagate; the other ones belong to the leaky category.

The PML closure has been applied to a variety of waveguides, for example to the optical fiber[124] (Fig. 15.42). Because the PML modes form a complete set, they can be used to

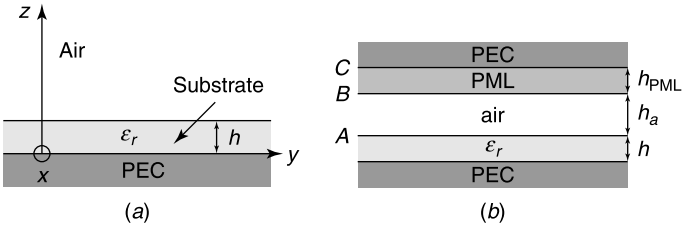

Figure 15.40 (*a*) One-layered structure. (*b*) Substitute waveguide.

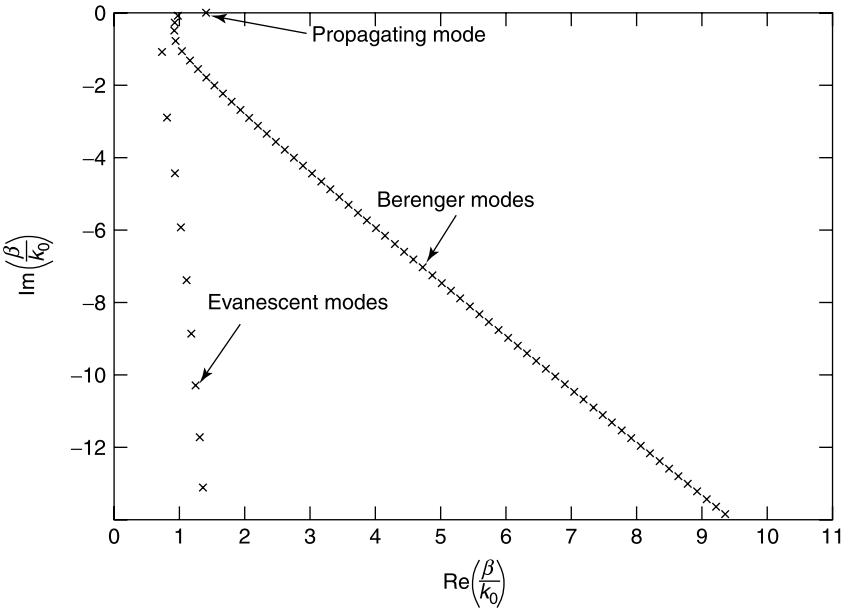

Figure 15.41 The discrete spectrum of the PML-closed microstrip (from H. Derudder, F. Olyslager, and D. De Zutter, An efficient series expansion for the 2D Green's functions of a microstrip substrate using perfectly matched layers, *IEEE Microwave Guided Wave Lett.* **9**, 505–507, 1999, with permission of IEEE).

great advantage in the solution of mode matching problems, because they avoid the need to include radiating modes.[125] The technique has been chosen, for example, for the analysis of the discontinuities between the layers of a vertical-cavity surface-emitting laser (VCSEL) (Fig. 15.43). This axisymmetric structure can be considered as a sequence of cylindrical waveguides.[126] A series expansion of *Green's functions* in terms of the PML modes has also proved to be most useful, in particular when transform methods are applied to accelerate the convergence of the series.[127,128] The PML approach avoids a transformation to the spectral

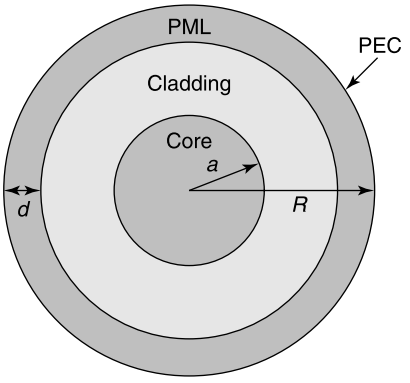

Figure 15.42 PML-closed optical fiber (from H. Rogier and D. De Zutter, Bérenger and leaky modes in optical fibers terminated with a perfectly matched layer, *J. Lightwave Techn.* **20**, 1141–1148, 2002, with permission of IEEE).

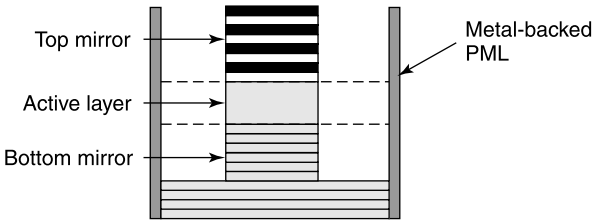

Figure 15.43 Typical VCSEL structure (from P. Bienstman, H. Derudder, R. Baets, F. Olyslager, and D. De Zutter, Analysis of cylindrical waveguide discontinuities using vectorial eigenmodes and perfectly matched layers, *IEEE Trans. MTT* **49**, 349–354, 2001, with permission of IEEE).

domain, which leads to complex and time-consuming inversion schemes. The theoretical challenge resides, as mentioned before, in proving that the PML series converges, and more precisely that it converges to the original Green's function. A careful analysis confirms that the series can be made as accurate as required by adjusting the position in complex space at which the boundary condition is enforced.[129] The main thrust of the argument can be followed by considering the one-dimensional Green's function, which satisfies the differential equation

$$\frac{d^2G(x)}{dx^2} + k^2G(x) = \delta(x). \tag{15.289}$$

The solution that takes the radiation condition into account is

$$G(x) = -\frac{1}{2j}\, e^{-jk|x|}.$$

Let us now introduce a new function G_r that satisfies (15.289) but vanishes at $x = \pm d$. Clearly,

$$G_r(x) = \frac{1}{2}\frac{\sin(|x| - d)}{\cos d}.$$

The PML version is obtained by assigning to d the complex value $\gamma\, e^{-j\alpha}$, with $0 < \alpha < \dfrac{\pi}{2}$. For such a choice,

$$|G_r(x) - G(x)] \leq e^{-2\gamma \sin\alpha},$$

and this limit can be made arbitrarily small by taking γ sufficiently large.

PROBLEMS

15.1 Use the variational principle (15.28) to determine the general cut-off frequency of an elliptic waveguide.
(T. Kihara, *J. Phys. Soc. Japan* **2**, 65, 1947.)

15.2 Show that the magnetic field at a point on the waveguide wall can be written as (Fig. 15.1)

$$\mathbf{u}_n \times \mathbf{J}_S(\mathbf{r}) = \mathbf{H}(\mathbf{r}) = \frac{1}{2j}\int_C \mathbf{J}_S(\mathbf{r}') \times \left[\left(\mathrm{grad}'_t + j\gamma \mathbf{u}_z\right) G(\mathbf{r}, \mathbf{r}')\right] dc',$$

where γ is the phase constant in the z-direction, and

$$G(\mathbf{r}, \mathbf{r}') = H_0^{(2)}\left(\sqrt{k^2 - \gamma^2}\,|\mathbf{r} - \mathbf{r}'|\right).$$

Cut-off corresponds with $\gamma = 0$, in which case k becomes an eigenvalue.
(W. Su et al., *IEEE Trans. MTT* **41**, 1965–1971, 1993.)

15.3 Give an alternate derivation for the fields (15.54) and (15.55) by inserting the value of $\mathbf{P}_m$ in terms of *magnetic* currents $\mathbf{J}_m$ into the second members of (15.14) and (15.15).
Hint: $\mathbf{J}_m = j\omega\mu_0\,\delta(\mathbf{r} - \mathbf{r}_0)\,\mathbf{P}_m$.

15.4 Determine the fields excited in a circular waveguide by a small rectangular loop located in the meridian plane and carrying a uniform alternating current (Fig. P15.1).

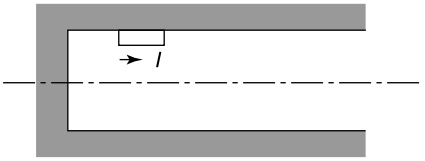

Figure P15.1

15.5 The factor $e^{-j\sqrt{k_0^2 - k_c^2}\,z}$ in (15.78) can be considered as the Fourier transform of the fields produced by a $\delta(t)$ excitation. The corresponding Laplace transform, obtained by replacing $j\omega$ by s, is

$$H(s) = e^{-\frac{\sqrt{s^2 + \omega_c^2}}{c_0}\,z}.$$

Show that the response on the positive z-axis is zero for $t < (z/c_0)$ and that

$$h(z,t) = \delta\left(t - \frac{z}{c_0}\right) - \frac{\omega_c z}{c_0}\,\frac{J_1\left(\omega_c\sqrt{t^2 - \dfrac{z^2}{c_0^2}}\right)}{\sqrt{t - \dfrac{z^2}{c_0^2}}}$$

for $t > (z/c_0)$. The spike $\delta\left(t - \dfrac{z}{c_0}\right)$ is seen to propagate with a velocity c_0.
(E. O. Schulz-Du Bois, *IEEE Trans. MTT* **18**, 455–460, 1970.)

15.6 A given signal propagating down a lossless waveguide is known to have a frequency spectrum centered on ω_0. Each frequency in the spectrum propagates with its own propagation constant $\gamma = (1/c_0)(\omega^2 - \omega_c^2)^{\frac{1}{2}}$. Assume that ω_0 is above cut-off and that the spectrum is sufficiently narrow for γ to be well represented by the first three terms of a Taylor series about $\omega = \omega_0$. Investigate the distortion suffered by the signal as it propagates down the guide. Particularize your results to a pulsed sinusoidal signal (angular frequency ω_0, pulse duration T), and sketch the distorted pulse shape at a distance L from the source.
(R. S. Elliott, *IRE Trans. MTT* **5**, 254, 1957.)

15.7 Determine the phase and group velocities of a plane wave in a plasma, for which $k = k_0\left(1 - \dfrac{\omega_p^2}{\omega^2}\right)^{\frac{1}{2}}$. Plot the ratio of these two velocities to c_0 as a function of (ω/ω_p).

15.8 Let a waveguide carry its lowest TE mode, and let the walls have a small surface impedance Z_S (small in the sense that Z_S is small with respect to the characteristic resistance of the medium filling the waveguide). Show that I_n in (15.2) satisfies

$$\frac{d^2 I_n}{dz^2} + \left[k^2 - k_c^2 - j\frac{\nu_n^4}{k}\frac{Z_S}{R_c}C_{nn} - \frac{j}{k}(k^2 - k_c^2)\frac{Z_S}{R_c}D_{nn}\right]I_n = 0.$$

When the wall is a good conductor, $Z_S = R_S(1 + j)$. Show that the equation for I_n leads to the attenuation factors given in (15.107) and (15.110).

15.9 Prove that the presence of a wall reactance leads to a shift in the cut-off frequency. Use (15.104) and (15.108) to evaluate that shift.
Hint: The condition is $\beta = 0$.

15.10 An N-armed waveguide junction has a known scattering matrix with respect to a set of terminal planes $T_1, \ldots, T_N$. Determine the new form of the matrix when the planes T_i are shifted by a distance L_i toward the junction.

15.11 Show that the scattering matrix is related to the $\overline{\overline{Z}}$ and $\overline{\overline{Y}}$ matrices by the relationships

$$\begin{aligned}\overline{\overline{S}} &= \left(\overline{\overline{Z}} - \overline{\overline{I}}\right)\cdot\left(\overline{\overline{Z}} + \overline{\overline{I}}\right)^{-1}\\ &= \left(\overline{\overline{I}} - \overline{\overline{Y}}\right)\cdot\left(\overline{\overline{I}} + \overline{\overline{Y}}\right)^{-1}.\end{aligned}$$

15.12 A two-armed junction is sometimes characterized by the equations

$$\begin{aligned}V_2 &= T_{vi}I_1 + T_{vv}V_1\\ I_2 &= T_{ii}I_1 + T_{iv}V_1.\end{aligned}$$

These equations are particularly useful in the study of cascaded junctions. Determine the relationships that connect the $\overline{\overline{T}}$ and $\overline{\overline{S}}$ matrices.

15.13 Show that property (15.129), that is, $\overline{\overline{Y}}^a = (\overline{\overline{Y}}^b)^t$, is replaced by $\overline{\overline{Y}}^a = (\overline{\overline{Y}}^b)^\dagger$ when $\overline{\overline{\epsilon}} = \overline{\overline{\epsilon}}^\dagger$ and $\overline{\overline{\mu}} = \overline{\overline{\mu}}^\dagger$ (i.e., when the material is loss less).
Hint: Modify (15.128) to introduce products of the kind $\mathbf{E} \times \mathbf{H}^*$.

15.14 The 4-port junction in Figure P15.2*a* (a directional coupler) has two planes of symmetry, π_1 and π_2. By means of appropriate methods, the junction has been matched in its four arms, so that $S_{ii} = 0$. Show that the resulting scattering matrix is of the form

$$\overline{\overline{S}} = \begin{pmatrix} 0 & \alpha & \beta & \gamma \\ \alpha & 0 & \gamma & \beta \\ \beta & \gamma & 0 & \alpha \\ \gamma & \beta & \alpha & 0 \end{pmatrix}.$$

When the structure is lossless, $\overline{\overline{S}}$ is unitary. Show that β vanishes under these circumstances, that is, that channels 1 and 3 are completely uncoupled, which implies that a signal coming in through port 1 leaks through the aperture to port 4, but not to port 3.

15.15 The four waveguide arms of the *magic-T* in Figure P15.2*b* are assumed to carry only the lowest mode of the guide. The structure is lossless, has one plane of symmetry, and a signal from 3 does

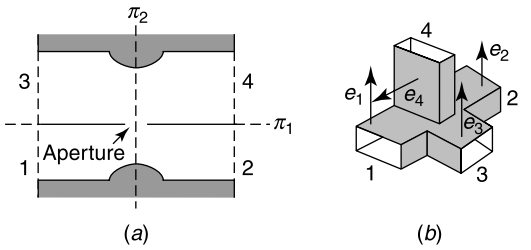

Figure P15.2

not penetrate into 4, given the directions of the electric fields. We conclude that $S_{34} = 0$. By means of tuning elements, the T has been matched as seen from both 3 and 4 ($S_{33} = S_{44} = 0$). Write down the 4×4 $\overline{\overline{S}}$ matrix of the T, and show that the "magic" T can be used to create sum and difference signals.

15.16 A "unit" wave in the TEM mode propagates down a coaxial line terminated in an infinite metallic baffle (Fig. P15.3). Set up an integral equation for the radial electric field in the $z = 0$ plane, and determine the equivalent admittance at $z = 0$.
Hint: The admittance is expected to be very low at low frequencies, but should acquire a significant real (radiative) part when λ_0 decreases to become of the order of the outer radius.

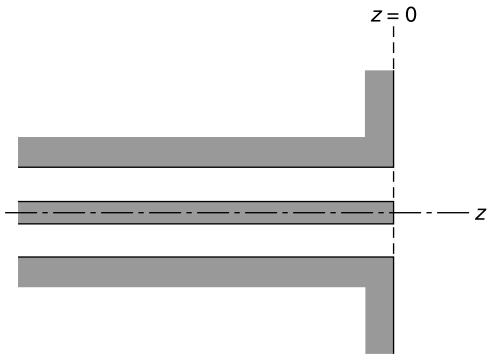

Figure P15.3

15.17 Figure P15.4 shows a cylindrical shield protecting an antenna and its tuned circuits from exterior interfering sources, here symbolized by a frill of magnetic current. Formulate the penetration problem

(a) In terms of longitudinal currents on the two cylinders. Derive the integral equations satisfied by the currents.

(b) As an aperture problem involving E_z and H_φ in the gap (i.e., at $r = b$).
(F. Pisano et al., *IEEE Trans. AP* **50**, 457–468, 2002.)

15.18 Let the voltage along the slot antenna in Figure P15.5 vary according to the law

$$V(z) = V_0 \cos \frac{\pi}{L} (z - z_0).$$

The corresponding electric field is

$$\mathbf{E}_{\tan} = V(z)\, \delta(c - c_0)\, \mathbf{u}_c.$$

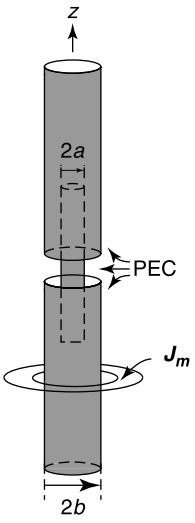

Figure P15.4

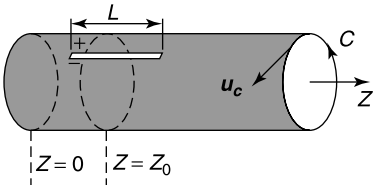

Figure P15.5

Determine the fields radiated into the waveguide, and focus on the contribution from the lowest mode.
(J. Van Bladel, *IEEE Trans. MTT* **14**, 130–135, 1966.)

15.19 Radiating slots are often covered with a dielectric layer, in particular in aerospace applications. This could be either for protection or for aerodynamical reasons. Formulate the corresponding two-region problem, taking the thickness of the screen into account (Fig. P15.6).
(From G. Mazzarello et al., *Electromagn.* **19**, 407–418, 1999, with permission of the Taylor & Francis Group).

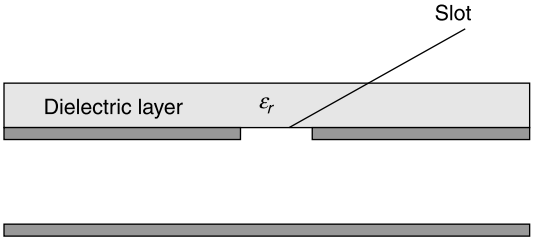

Figure P15.6

15.20 Determine the fields radiated into a waveguide by an electric dipole of moment $\mathbf{P}_e$.
Hint: Set $\mathbf{J} = j\omega\delta\,(\mathbf{r} - \mathbf{r}_0)\,\mathbf{P}_e$.

15.21 Assume that the material of a waveguide has a dielectric constant $\overline{\overline{\epsilon}} = \overline{\overline{\epsilon}}_{tt} + \epsilon_{zz}\mathbf{u}_z\,\mathbf{u}_z$, where ϵ_{tt} is symmetric. Show that $\boldsymbol{\mathcal{H}}_t$ satisfies

$$\mathbf{u}_z \times \operatorname{grad}_t\left[\frac{1}{\epsilon_{zz}}\operatorname{div}_t(\boldsymbol{\mathcal{H}}_t \times \mathbf{u}_z)\right] + \left(\overline{\overline{\epsilon}}_{tt}\right)^{-1}\cdot\operatorname{grad}_t \operatorname{div}_t \boldsymbol{\mathcal{H}}_t$$

$$+ k_0^2\boldsymbol{\mathcal{H}}_t + \gamma^2\left(\overline{\overline{\epsilon}}_{tt}\right)^{-1}\cdot\boldsymbol{\mathcal{H}}_t = 0.$$

(F. A. Fernandez et al., *IEEE Trans. MAG* **27**, 3864–3867, 1991.)

15.22 Show that the eigenvalue problem for an isotropic inhomogeneous waveguide can be given the weak form

$$\int_S\left[-\operatorname{div}_t \mathbf{w}\cdot\operatorname{div}_t(\boldsymbol{\mathcal{E}}_t \times \mathbf{u}_z) + \gamma\mathcal{E}_z \operatorname{div}_t(\mathbf{w}\times\mathbf{u}_z) + (\omega^2\epsilon\mu + \gamma^2)\,\mathbf{w}\cdot(\boldsymbol{\mathcal{E}}_t\times\mathbf{u}_z)\right]dS$$

$$+\int_C \mathbf{w}\cdot\left[\mathbf{u}_n \operatorname{div}_t(\boldsymbol{\mathcal{E}}_t\times\mathbf{u}_z) - \gamma\mathcal{E}_z\,\mathbf{u}_c\right]dc = 0.$$

This is an example of solution in which *three* components are involved.

15.23 A waveguide contains a lossless medium of (tensorial) characteristics $\overline{\overline{\epsilon}}$ and $\overline{\overline{\mu}}$. Show that the functional

$$-\frac{\omega\displaystyle\int_S \boldsymbol{\mathcal{E}}^*\cdot\overline{\overline{\epsilon}}\cdot\boldsymbol{\mathcal{E}}\,dS + \omega\int_S \boldsymbol{\mathcal{H}}^*\cdot\overline{\overline{\mu}}\cdot\boldsymbol{\mathcal{H}}\,dS + j\int_S \boldsymbol{\mathcal{E}}^*\cdot\operatorname{curl}\boldsymbol{\mathcal{H}}\,dS - j\int_S \boldsymbol{\mathcal{H}}^*\cdot\operatorname{curl}\boldsymbol{\mathcal{E}}\,dS}{\displaystyle\int_S \boldsymbol{\mathcal{H}}^*\cdot\mathbf{u}_z\times\boldsymbol{\mathcal{E}}\,dS - \int_S \boldsymbol{\mathcal{E}}^*\cdot\mathbf{u}_z\times\boldsymbol{\mathcal{H}}\,dS}$$

is stationary about the eigenvectors $\boldsymbol{\mathcal{E}}_m$ and $\boldsymbol{\mathcal{H}}_m$ and that the stationary value is equal to γ_m. The admissible vectors must be continuous and differentiable. Furthermore, $\boldsymbol{\mathcal{E}}$ must be perpendicular to the boundary. Apply the principle to a rectangular waveguide containing a centrally located dielectric slab. The waveguide is excited in its lowest mode.
Hint: Use a trial vector $\boldsymbol{\mathcal{E}} = \mathbf{u}_y \sin \pi x/a$.
(A. D. Berk, *IRE Trans. AP* **4**, 104, 1956.)

15.24 Prove (15.202) by methods similar to those leading to the orthogonality relationship (15.200) (i.e., by evaluating corresponding integrals I_1 and I_2).
Hint: Start from $\operatorname{div}(\mathbf{E}_m \times \mathbf{H}_n^* + \mathbf{E}_n^* \times \mathbf{H}_m) = 0$, as in (8.174), and remember that $\epsilon = \epsilon^*$ in a lossless medium.

15.25 Show that the next-order value of $S(r)$, in the WKB approximation to (15.252), is [143]

$$e(r) = \frac{1}{\sqrt{r\,p(r)}}\left\{c_1\, e^{j\int p(r)\,dr} + c_2\, e^{-j\int p(r)dr}\right\}.$$

If r_1 and r_2 are turning points, prove the relationship

$$\int_{r_1}^{r_2}\sqrt{k^2(r) - \beta^2 - \frac{m^2}{r^2}}\,dr = \left(n + \frac{1}{2}\right)\pi \qquad (n = 0, 1, 2, \ldots).$$

15.26 In the scalar approximation to the fields in a graded-index fiber, a field component satisfies

$$\nabla^2\phi + k_0^2 N^2(\mathbf{r}_t, z)\,\phi = 0.$$

To account for the rapid variation of phase in the z-direction, one may write $\phi(\mathbf{r}_t, z) = e^{-jk_0 N_0 z} A(\mathbf{r}_t, z)$, where N_0 is a reference value. Determine the differential equation satisfied by $A(\mathbf{r}_t, z)$, and discuss its form by assuming that $\dfrac{\partial^2 A}{\partial z^2}$ is negligible.
(C. Yeh et al., *J. Opt. Soc. Am.* **68**, 989–993, 1978.)

15.27 Show that the functional

$$J(\mathcal{E}_z, \mathcal{H}_z) = \int_S \frac{\omega\epsilon}{k^2 - \beta^2} (\text{grad } \mathcal{E}_z)^2 \, dS - \int_S \omega\epsilon \, \mathcal{E}_z^2 \, dS + \int_S \frac{\omega\mu}{k^2 - \beta^2} |\text{grad } \mathcal{H}_z|^2 \, dS$$
$$- \int_S \omega\mu \, \mathcal{H}_z^2 \, dS + 2 \int_S \frac{\beta}{k^2 - \beta^2} \mathbf{u}_z \cdot (\text{grad } \mathcal{E}_z \times \text{grad } \mathcal{H}_z) \, dS$$

is stationary for the solutions of (15.258) and (15.259).
(K. Oyamada et al., *Radio Sci.* **17**, 109–116, 1981.)

15.28 Consider an optical waveguide consisting of a material with diagonal tensor $\overline{\overline{\epsilon}} = \mathcal{E}_x \mathbf{u}_x \mathbf{u}_x + \mathcal{E}_y \mathbf{u}_y \mathbf{u}_y$. The differential equations for $\mathcal{E}_z$, $\mathcal{H}_z$ are

$$-\frac{\partial}{\partial x}\left(A_x \mathcal{E}_x \frac{\partial \mathcal{E}_z}{\partial x}\right) + \frac{\partial}{\partial y}\left(A_y \mathcal{E}_y \frac{\partial \mathcal{E}_z}{\partial y}\right) + \frac{\beta}{\omega}\left[\frac{\partial}{\partial y}\left(A_y \frac{\partial \mathcal{H}_z}{\partial x}\right) - \frac{\partial}{\partial x}\left(A_x \frac{\partial \mathcal{H}_z}{\partial y}\right)\right] = \mathcal{E}_z$$
$$\frac{\partial}{\partial x}\left(A_y \frac{\partial \mathcal{H}_z}{\partial x}\right) + \frac{\partial}{\partial y}\left(A_x \frac{\partial \mathcal{H}_z}{\partial y}\right) + \frac{\beta}{\omega\mu_0}\left[\frac{\partial}{\partial y}\left(A_x \frac{\partial \mathcal{E}_z}{\partial x}\right) - \frac{\partial}{\partial x}\left(A_y \frac{\partial \mathcal{E}_z}{\partial y}\right)\right] = -\mathcal{H}_z$$

where $A_x = (k_x^2 - \beta^2)^{-1}$, $A_y = (k_y^2 - \beta^2)^{-1}$, $k_x^2 = k_0^2 \mathcal{E}_{rx}$, $k_y^2 = k_0^2 \mathcal{E}_{ry}$. Find a pertinent functional for these equations.
(N. Mabaya et al., *IEEE Trans. MTT* **29**, 600–605, 1981.)

15.29 The field in an optical beam may be written as $\phi = e^{-jk_r z} u(\mathbf{r})$, where k_r is a fixed reference wave number that takes the rapid variation of the phase into account, and $u(\mathbf{r})$ is a slowly varying factor. Show that u satisfies

$$\frac{\partial^2 u}{\partial z^2} - 2jk_r \frac{\partial u}{\partial z} + \nabla_t^2 u + (k^2 - k_r^2) \, u = 0.$$

In the paraxial approximation $\dfrac{\partial^2 u}{\partial z^2}$ is neglected compared with $\dfrac{\partial u}{\partial z}$, a strategy that allows expressing $\dfrac{\partial u}{\partial z}$ in terms of u and the lateral derivatives of u.

NOTES

1. T. Vu Khai and C. T. Carson, $m = 0$, $n = 0$ mode and rectangular waveguide slot discontinuity, *Electron. Lett.* **9**, 431–432 (1973).
2. R. E. Collin, On the incompleteness of E and H modes in waveguides, *Can. J. Phys.* **51**, 1135–1140 (1973).
3. J. Van Bladel, Contribution of the $\psi =$ constant mode to the modal expansion in a waveguide, *IEE Proc.* **128-H**, 247–251 (1981).
4. J. G. Kretzschmar, Wave propagation in hollow conducting elliptical waveguides, *IEEE Trans. MTT* **18**, 547–554 (1974).
5. F. A. Alhargan and S. R. Judah, Tables of normalized cutoff wavenumbers of elliptic cross section resonators, *IEEE Trans. MTT* **42**, 333–338 (1994).
6. M. Schneider and J. Marquardt, Fast computation of modified Mathieu functions applied to elliptical waveguide problems, *IEEE Trans. MTT* **47**, 573–576 (1999).
7. S. Li and B. S. Wang, Field expressions and patterns in elliptical waveguide, *IEEE Trans. MTT* **48**, 864–867 (2000).
8. F. L. Ng, Tabulation of methods for the numerical solution of the hollow waveguide problem, *IEEE Trans. MTT*

22, 322–329 (1974). This article provides a survey of the methods available in the mid-1970s.

9. E. T. Kornhauser and I. Stakgold, A variational theorem for $\nabla^2 u + \lambda u = 0$ and its application, *J. Math. Phys.* **31**, 45–54 (1952). See also remarks by G. Polya in the same issue, pp. 55-57.
10. K. R. Richter, K. Preis, and W. Rucker, Ein Beitrag zur Berechnung elektromagnetischer Felden mittels numerischer Methoden, *A.E.Ü.* **37**, 174–182 (1983).
11. J. M. Gil and J. Zapata, Efficient singular element for finite element analysis of quasi-TEM transmission lines and waveguides with sharp metal edges, *IEEE Trans. MTT* **42**, 92–98 (1994).
12. J. S. Juntunen and T. D. Tsiboukis, On the FEM treatment of wedge singularities in waveguide problems, *IEEE Trans. MTT* **48**, 1030–1037 (2000).
13. A. S. Omar, A. Jöstingmeier, C. Rieckmann, and S. Lütgert, Application of the generalized spectral domain technique (GSD) to the analysis of slot coupled waveguides, *IEEE Trans. MTT* **42**, 2139–2148 (1994).
14. M. Swaminathan, E. Arvas, T. Sarkar, and A. Djordjevic, Computation of cutoff wavenumbers of TE and TM modes in waveguides of arbitrary cross-sections using a surface integral formulation, *IEEE Trans. MTT* **38**, 154–159 (1990).
15. C. Kim, S. Yu, R. Harrington, J. Ra, and S. Lee, Computation of waveguide modes for waveguides of arbitrary cross section, *IEE Proc.* **137-H**, 145–149 (1990).
16. G. Conciauro, M. Bressan, and C. Zuffada, Waveguide modes via an integral equation leading to a linear matrix eigenvalue problem, *IEEE Trans. MTT* **32**, 1495–1504 (1984).
17. P. Arcioni, M. Bressan, and L. Perregrini, A new boundary integral approach to the determination of the resonant modes of arbitrarily shaped cavities, *IEEE Trans. MTT* **43**, 1848–1855 (1995).
18. P. Arcioni, M. Bressan, G. Conciauro, and L. Perregrini, Wideband modeling of arbitrarily shaped H-plane waveguide components by the boundary integral-resonant mode expansion method, *IEEE Trans. MTT* **44**, 1057–1066 (1996).
19. P. Arcioni, M. Bressan, G. Conciauro, and L. Perregrini, Wideband modeling of arbitrarily shaped E-plane waveguide components by the "Boundary integral-resonant mode expansion method," *IEEE Trans. MTT* **44**, 2083–2092 (1996).
20. R. E. Collin, Introduction to "Some fundamental experiments with wave guides," *Proc. IEEE* **87**, 508–514 (1999).
21. G. C. Southworth, Some fundamental experiments with wave guides, *Proc. IRE* **25**, 807–822 (1937), reprinted in *Proc. IEEE* **87**, 515–521 (1999).
22. W. Dou and E. Yeong, An interesting phenomenon in the finite difference time domain simulation of a Gaussian pulse propagation in a waveguide, *Radio Sci.* **36**, 1307–1314 (2001).
23. E. O. Schulz-Du Bois, Sommerfeld pre- and postcursors in the context of waveguide transients, *IEEE Trans. MTT* **18**, 455–460 (1970).
24. M. J. Lighthill, Group velocity, *J. Inst. Maths. Applics.* **1**, 21–28 (1965).
25. P. Stenius and B. York, On the propagation of transients in waveguides, *IEEE Antennas Prop. Mag.* **37**, 39–44 (April 1995).
26. A. Jöstingmeier, C. Rieckmann, and A. S. Omar, Computation of the irrotational magnetic eigenfunctions belonging to complex cavities, *IEEE Trans. MTT* **42**, 2285–2293 (1994).
27. J. Van Bladel, Mode coupling through wall losses in a waveguide, *Electron. Lett.* **7**, 178–180 (1971).
28. G. L. Matthaei, K. Kiziloglu, N. Dagli, and S. I. Long, The nature of the charges, currents, and fields in and about conductors having cross-sectional dimensions of the order of a skin depth, *IEEE Trans. MTT* **38**, 1031–1036 (1990).
29. P. Lagasse and J. Van Bladel, Square and rectangular waveguides with rounded corners, *IEEE Trans. MTT* **20**, 331–337 (1972).
30. J. H. Winters and C. Rose, High-T_c superconductor waveguides: theory and applications, *IEEE Trans. MTT* **39**, 617–623 (1991).
31. F.-R. Yang, K.-P. Ma, Y. Qian and T. Itoh, A novel TEM waveguide using uniplanar compact photonic-bandgap (UC-PBG) structure, *IEEE Trans. MTT* **47**, 2092–2098 (1999).
32. I. V. Lindell, Variational methods for nonstandard eigenvalue problems in waveguide and resonator analysis, *IEEE Trans. MTT* **30**, 1194–1204 (1982).
33. E. Marcatili and P. Schmeltzer, Hollow metallic and dielectric waveguides for long distance optical transmission and lasers, *B.S.T.J.* **43**, 1783–1808 (1964).
34. Y. Kato and M. Miyagi, Numerical analysis of mode structures and attenuations in dielectric-coated circular hollow waveguides for the infrared, *IEEE Trans. MTT* **42**, 2336–2342 (1994).
35. J. J. Gustincic, A general power loss method for attenuation of cavities and waveguides, *IEEE Trans. MTT* **11**, 83–87 (1963).
36. M. Mongiardo and T. Rozzi, Singular integral equation analysis of flange-mounted rectangular waveguide radiators, *IEEE Trans. AP* **41**, 556–565 (1993).
37. D. S. Weile and E. Michielssen, Community genetic algorithm design of symmetric E-plane microwave filters, *Microwave Opt. Tech. Lett.* **21**, 28–34 (1999).
38. D. H. Russell, The waveguide below-cutoff attenuation standard, *IEEE Trans. MTT* **45**, 2408–2413 (1997).
39. H. Haskal, Matrix description of waveguide discontinuities in the presence of evanescent modes, *IEEE Trans. MTT* **12**, 184–188 (1964).
40. A. Morini and T. Rozzi, On the definition of the generalized scattering matrix of a lossless multiport, *IEEE Trans. MTT* **49**, 160–165 (2001).

41. G. Eleftheriades, A. Omar, L. Katehi, and G. Rebeiz, Some important properties of waveguide junction generalized scattering matrices in the context of the mode matching technique, *IEEE Trans. MTT* **42**, 1896–1903 (1994).
42. S. Papatheodorou, J. R. Mautz, and R. F. Harrington, The aperture admittance of a circumferential slot in a circular cylinder, *IEEE Trans. AP* **40**, 240–244 (1992).
43. J. Van Bladel, Small holes in a waveguide wall, *Proc. IEE* **118**, 43–50 (1971).
44. P. Delogne, Small holes and leaky feeders, *Radio Sci.* **22**, 1179–1189 (1987).
45. R. E. Collin, Small aperture coupling between dissimilar regions, *Electromagn.* **2**, 1–24 (1982).
46. E. G. Cristal and J. Van Bladel, Fields in cavity-excited accelerators, *J. Appl. Phys.* **32**, 1715–1724 (1961).
47. F. Kriegler, F. Mills, and J. Van Bladel, Fields excited by periodic beam currents in a cavity loaded tube, *J. Appl. Phys.* **35**, 1721–1726 (1964).
48. S. Silver and W. K. Saunders, The external field produced by a slot in an infinite circular cylinder, *J. Appl. Phys.* **21**, 153–158 (1950).
49. L. S. Sheingold and J. E. Storer, Circumferential gap in a circular waveguide excited by a dominant circular-electric wave, *J. Appl. Phys.* **25**, 545–552 (1954).
50. V. H. Rumsey, Traveling wave slot antennas, *J. Appl. Phys.* **24**, 1358–1371 (1953).
51. L. O. Goldstone and A. A. Oliner, Leaky-wave antennas I: rectangular waveguides, *IRE Trans. AP* **7**, 307–313 (1959).
52. R. A. Hurd, The modes of an axially slotted coaxial waveguide, *Radio Sci.* **14**, 741–751 (1979).
53. P. Delogne and A. Laloux, Theory of the slotted coaxial cable, *IEEE Trans. MTT* **28**, 1102–1107 (1980).
54. E. Hassan, Field solution and propagation characteristics of monofilar - bifilar modes of axially slotted coaxial cable, *IEEE Trans. MTT* **37**, 553–557 (1989).
55. F. L. Whetten and C. A. Balanis, Effects of a dielectric coating on leaky-wave long-slot waveguide antennas, *IEEE Trans. AP* **44**, 1166–1171 (1996).
56. J. H. Wang and K. K. Mei, Theory and analysis of leaky coaxial cables with periodic slots, *IEEE Trans. AP* **49**, 1723–1732 (2001).
57. J. H. Wang and K. K. Mei, Design of leaky coaxial cables with periodic slots, *Radio Sci.* **37**, 2-1 to 2–10 (2002).
58. P. Mariage, M. Liénard, and P. Degauque, Theoretical and experimental approach of the propagation of high frequency waves in road tunnels, *IEEE Trans. AP* **42**, 75–81 (1994).
59. D. G. Dudley, Wireless propagation in circular tunnels, *IEEE Trans. AP* **53**, 435–441 (2005).
60. P. Delogne, EM propagation in tunnels, *IEEE Trans. AP* **39**, 401–406 (1991).
61. P. Delogne and L. Deryck, Underground use of a coaxial cable with leaky sections, *IEEE Trans. AP* **28**, 875–883 (1980).
62. F. A. Fernandez and Y. Lu, Variational finite element analysis of dielectric waveguides with no spurious solutions, *Electronic Lett.* **26**, 2125–2126 (1990).
63. H. Rogier, F. Olyslager, and D. De Zutter, A hybrid finite element integral equation approach for the eigenmode analysis of complex anisotropic dielectric waveguides, *Radio Sci.* **31**, 999–1010 (1996).
64. A. D. Berk, Variational principles for electromagnetic resonators and waveguides, *IRE Trans. AP* **4**, 104–111 (1956).
65. I. V. Lindell, Variational method for the analysis of lossless bi-isotropic (nonreciprocal chiral) waveguides, *IEEE Trans. MTT* **40**, 402–405 (1992).
66. F. A. Fernandez and Y. Lu, A variational finite element formulation for dielectric waveguides in terms of transverse magnetic fields, *IEEE Trans. MAG* **27**, 3864–3867 (1991).
67. Y. Lu and F. Fernandez, An efficient finite element solution of inhomogeneous anisotropic and lossy dielectric waveguides, *IEEE Trans. MTT* **41**, 1215–1223 (1993).
68. T. Angkaew, M. Matsuhara, and N. Kumagai, Finite-element analysis of waveguide modes: a novel approach that eliminates spurious modes, *IEEE Trans. MTT* **35**, 117–123 (1987).
    Comments on this article, by M. Mrozowksi, can be found in *IEEE Trans. MTT* **39**, 611 (1991).
69. J. B. Davies, Finite element analysis of waveguides and cavities — a review, *IEEE Trans. MAG* **29**, 1578–1583 (1993).
70. B. Dillon and J. Webb, A comparison of formulations for the vector finite element analysis of waveguides, *IEEE Trans. MTT* **42**, 308–316 (1994).
71. J. Gil and J. Webb, A new edge element for the modeling of field singularities in transmission lines and waveguides, *IEEE Trans. MTT* **45**, 2125–2130 (1997).
72. P. Savi, I.-L. Gheorma, and R. D. Graglia, Full-wave high-order FEM modes for lossy anisotropic waveguides, *IEEE Trans. MTT* **50**, 495–500 (2002).
73. P. Clarricoats and K. Slinn, Complex modes of propagation in dielectric-loaded circular waveguides, *Electron. Lett.* **1**, 145–146 (1965).
74. H. Katzier and F. Lange, Grundlegende Eigenschaften komplexer Wellen am Beispiel der geschirmten kreiszylindrischen dielektrischen Leitung, *A.E.Ü.* **37**, 1–5 (1983).
75. U. Crombach, Complex waves on shielded lossless rectangular dielectric image guide, *Electron. Lett.* **19**, 557–558 (1983).
76. F. Fernandez, Y. Lu, J. B. Davies and S. Zhu, Finite element analysis of complex modes in inhomogeneous waveguides, *IEEE Trans. MAG* **29**, 1601–1604 (1993).
77. C. J. Railton and T. Rozzi, Complex modes in boxed microstrip, *IEEE Trans. MTT* **36**, 865–873 (1988).
78. M. Mrozowski and J. Mazur, Matrix theory approach to complex waves, *IEEE Trans. MTT* **40**, 781–785 (1992).
79. T. Rozzi, L. Pierantoni, and M. Farina, General constraints on the propagation of complex waves in closed

lossless isotropic waveguides, *IEEE Trans. MTT* **46**, 512–516 (1998).
80. J. Strube and F. Arndt, Rigorous hybrid-mode analysis of the transition from rectangular waveguide to shielded dielectric image guide, *IEEE Trans. MTT* **33**, 391–401 (1985).
81. P. R. Mc. Isaac, Mode orthogonality in reciprocal and nonreciprocal waveguides, *IEEE Trans. MTT* **39**, 1808–1816 (1991).
82. F. Olyslager, Properties of and generalized full-wave transmission line models for hybrid (bi)(an)isotropic waveguides, *IEEE Trans. MTT* **44**, 2064–2075 (1996).
83. F. Olyslager, D. De Zutter, and A. T. de Hoop, New reciprocal circuit model for lossy waveguide structures based on the orthogonality of the eigenmodes, *IEEE Trans. MTT* **42**, 2261–2269 (1994).
84. F. Olyslager and D. De Zutter, High-frequency transmission line models for a thin wire above a conducting ground, *IEEE Trans. EMC* **37**, 234–240 (1995).
85. T. Tamir, Guided wave methods for optical configurations, *Appl. Phys.* **25**, 201–210 (1981).
86. D. Hondros and P. Debye, Elektromagnetische Wellen an dielektrischen Drähten, *Ann. Phys.* **32**, 465–476 (1910).
87. C. W. Yeh, Optical waveguide theory, *IEEE Trans. CAS.* **26**, 1011–1019 (1979).
88. H. Y. Yee and L. B. Felsen, Ray optics — a novel approach to scattering by discontinuities in a waveguide, *IEEE Trans. MTT* **17**, 73–85 (1969).
89. A. Tonning, Circularly symmetric optical waveguide with strong anisotropy, *IEEE Trans. MTT* **30**, 790–794 (1982).
90. C. Yeh, Modes in weakly guiding elliptical optical fibers, *Opt. Quantum El.* **8**, 43–47 (1976).
91. J. R. Cozens and R. B. Dyott, Higher-mode cutoff in elliptical dielectric waveguides, *Electron. Lett.* **15**, 558–559 (1979).
92. S. M. Saad, On the higher order modes of elliptical optical fibers, *IEEE Trans. MTT* **13**, 1110–1113 (1985).
93. Tom Do-Nhat and F. A. Alhargan, Exact eigenvalue equations of modes in elliptical fibers of step-index profile, *Radio Sci.* **32**, 1337–1345 (1997).
94. E. Snitzer, Cylindrical dielectric waveguide modes, *J. Opt. Soc. Am.* **51**, 491–498 (1961).
95. A. W. Snyder, Continuous mode spectrum of a circular dielectric rod, *IEEE Trans. MTT* **19**, 720–727 (1971).
96. S. F. Kawalko and P. L. E. Uslenghi, A method for the analysis of biaxial graded-index optical fibers, *IEEE Trans. MTT* **39**, 961–968 (1991).
97. A. Vigants and S. P. Schlezinger, Surface waves on radially inhomogeneous cylinders, *IRE Trans. MTT* **10**, 375–382 (1962).
98. A. Tonning, An alternative theory of optical waveguides with radial inhomogeneities, *IEEE Trans. MTT* **30**, 781–789 (1982).
99. J. G. Dil and H. Blok, Propagation of electromagnetic surface waves in a radially inhomogeneous optical waveguide, *Opto-electronics* **5**, 415–428 (1973).
100. M. O. Vassell, Calculation of propagating modes in a graded-index optical fibre, *Opto-electronics* **6**, 271–286 (1974).
101. P. J. B. Clarricoats and K. B. Chan, Electromagnetic-wave propagation along radially inhomogeneous dielectric cylinders, *Electron. Lett.* **6**, 694–695 (1970).
102. C. Yeh and G. Lindgren, Computing the propagation characteristics of radially stratified fibers: an efficient method, *Appl. Optics* **16**, 483–493 (1977).
103. K. Oyamada and T. Okoshi, Two-dimensional finite-element method calculation of propagation characteristics of axially non symmetrical optical fibers, *Radio Sci.* **17**, 109–116 (1982).
104. S. M. Saad, Review of numerical methods for the analysis of arbitrarily-shaped microwave and optical waveguides, *IEEE Trans. MTT* **33**, 894–899 (1985).
105. K. S. Chiang, Review of numerical and approximate methods for the modal analysis of general optical dielectric waveguides, *Opt. Quantum Electron.* **26**, S113–134 (1994).
106. J. F. Kiang, S. M. Ali, and J. A. Kong, Integral equation solution to the guidance and leakage properties of coupled dielectric strip waveguides, *IEEE Trans. MTT* **38**, 193–203 (1990).
107. S. J. Polychronopoulos and N.K. Uzunoglu, Propagation and coupling properties of integrated optical waveguides — an integral equation formulation, *IEEE Trans. MTT* **44**, 641–650 (1996).
108. C. Yeh, K. Ha, S. B. Dong, and W. P. Brown, Single-mode optical waveguides, *Appl. Opt.* **18**, 1490–1504 (1979).
109. N. Mabaya, P. E. Lagasse, and P. Vandenbulcke, Finite element analysis of optical waveguides, *IEEE Trans. MTT* **29**, 600–605 (1981).
110. S. Selleri and M. Zoboli, An improved finite element method formulation for the analysis of nonlinear anisotropic dielectric waveguides, *IEEE Trans. MTT* **43**, 887–892 (1995).
111. G. Goubau, Surface waves and their application to transmission lines, *J. Appl. Phys.* **21**, 1119–1128 (1950).
112. G. Goubau, Single-conductor surface-wave transmission lines, *Proc. IRE* **39**, 619–624 (1951).
113. Z. Czendes and P. Silvester, Numerical solution of dielectric loaded waveguides, I — Finite element analysis, *IEEE Trans. MTT* **13**, 1124–1131 (1970), II — Modal approximation technique, *IEEE Trans. MTT* **19**, 504–509 (1971).
114. T. Itoh and R. Mittra, Spectral-domain approach for calculating the dispersion characteristics of microstrip lines, *IEEE Trans. MTT* **21**, 496–499 (1973).
115. N. Faché and D. De Zutter, Rigorous full-wave space-domain solution for dispersive microstrip lines, *IEEE Trans. MTT* **36**, 731–737 (1988).
116. G. Coen, N. Faché, and D. De Zutter, Comparison between two sets of basis functions for the current modeling in the Galerkin spectral domain solution for microstrips, *IEEE Trans. MTT* **42**, 505–513 (1994).

117. T. Itoh and R. Mittra, A technique for computing dispersion characteristics of shielded microstrip lines, *IEEE Trans. MTT* **22**, 896–898 (1974).
118. P. C. Cherry and M. F. Iskander, FDTD analysis of high-frequency electronic interconnection effects, *IEEE Trans. MTT* **43**, 2445–2451 (1995).
119. J. Sercu, N. Faché, F. Libbrecht, and D. De Zutter, Full-wave space-domain analysis of open microstrip discontinuities, including the singular current-edge behavior, *IEEE Trans. MTT* **41**, 1581–1588 (1993).
120. F. Olyslager, D. De Zutter, and K. Blomme, Rigorous analysis of the propagation characteristics of general lossless and lossy multiconductor transmission lines in multilayered media, *IEEE Trans. MTT* **41**, 79–85 (1993).
121. F. Olyslager and D. De Zutter, Rigorous boundary integral equation solution for general isotropic and unaxial anisotropic dielectric waveguides in multilayered media including losses, gain and leakage, *IEEE Trans. MTT* **41**, 1385–1392 (1993).
122. H. Derudder, F. Olyslager, and D. De Zutter, An efficient series expansion for the 2D Green's functions of a microstrip substrate using perfectly matched layers, *IEEE Microwave Guided Wave Lett.* **9**, 505–507 (1999).
123. H. Rogier and D. De Zutter, Bérenger and leaky modes in microstrips substrates terminated by a perfectly matched layer, *IEEE Trans. MTT* **49**, 712–719 (2001).
124. H. Rogier and D. De Zutter, Bérenger and leaky modes in optical fibers terminated with a perfectly matched layer, *J. Lightwave Techn.* **20**, 1141–1148 (2002).
125. H. Derudder, D. De Zutter, and F. Olyslager, Analysis of waveguide discontinuities using perfectly matched layers, *Electron. Lett.* **34**, 2138–2140 (1998).
126. P. Bienstman, H. Derudder, R. Baets, F. Olyslager, and D. De Zutter, Analysis of cylindrical waveguide discontinuities using vectorial eigenmodes and perfectly matched layers, *IEEE Trans. MTT* **49**, 349–354 (2001).
127. H. Rogier and D. De Zutter, A fast technique based on perfectly matched layers to model electromagnetic scattering from wires embedded in substrates, *Radio Sci.* **37**, 10-1 to 10-6 (2002).
128. H. Rogier and D. De Zutter, Convergence behavior and acceleration of the Bérenger and leaky mode series composing the 2D Green's function for the microstrip substrate, *IEEE Trans. MTT* **50**, 1696–1704 (2002).
129. F. Olyslager, Discretization of continuous spectra based on perfectly matched layers, *SIAM J. Appl. Math.* **64**, 1408–1433 (2004).

Chapter 16

Axisymmetric and Conical Boundaries

The two particular geometries discussed in this chapter play an important role in the electromagnetic literature not only because they provide suitable models for a range of structures, but also because the equations governing their fields have advantages of simplicity. A body of revolution (BOR) can serve as a model for an aircraft fuselage or a rocket — at least in a meaningful approximation. By expanding the fields around a BOR in a Fourier series, with the azimuth φ as a variable, Maxwell's equations are replaced by an (infinite) number of two-dimensional equations in r, z, the meridian coordinates. The reduction to two dimensions is a definite advantage in most problems. When the volume of interest is *conical*, the mathematical simplification resides in the expandability of the fields in modes similar to those that were found so useful in the theory of cylindrical waveguides. Conical structures have been used to model the tip of a rocket or to simulate a chain of mountains in studies of overland radiopropagation. The modeling cone may be circular, elliptic, or of a more extreme shape such as a flat angular sector or a 90° corner.

16.1 FIELD EXPANSIONS FOR AXISYMMETRIC GEOMETRIES

The Fourier expansion of a *vector* field in terms of the azimuth φ is of the general form (Fig. 16.1)

$$\mathbf{a}(r,z,\varphi) = \mathbf{p}_0(r,z) + v_0(r,z)\,\mathbf{u}_\varphi + \sum_{m=0}^{\infty}[\sin m\varphi\,\mathbf{p}_m(r,z) + \cos m\varphi\,\mathbf{q}_m(r,z)]$$
$$+ \sum_{m=0}^{\infty}[-w_m(r,z)\sin m\varphi + v_m(r,z)\cos m\varphi]\,\mathbf{u}_\varphi. \tag{16.1}$$

Here the **p**'s and **q**'s are vectors in the meridian plane. As in the expansion of a *scalar* field, discussed in Section 5.11, it is important to investigate the behavior of the expansion coefficients on the axis of symmetry. When **a** is continuous on that axis, a unique limit must

Electromagnetic Fields, Second Edition, By Jean G. Van Bladel

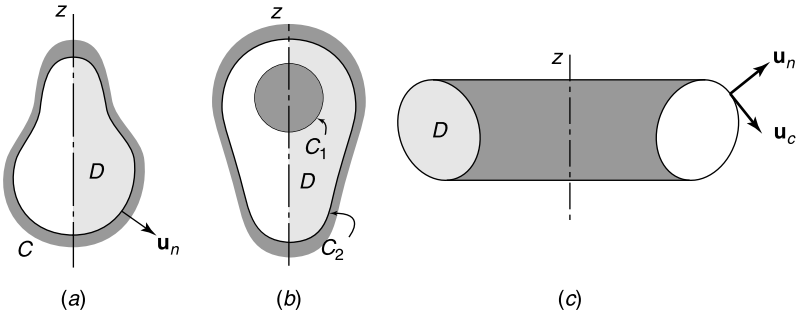

Figure 16.1 Volumes of revolution. (*a*) Simply bounded and simply connected. (*b*) Doubly bounded. (*c*) Toroidal.

be approached for all φ as r approaches zero. This requirement results in the following properties at points on the axis:

1. $\mathbf{p}_0$ is directed along the axis.
2. v_0 vanishes.
3. $\mathbf{p}_1$ and $\mathbf{q}_1$ are purely radial, and the equalities $p_{1r} = v_1$, $q_{1r} = w_1$ hold.
4. $\mathbf{p}_m$, $\mathbf{q}_m$, v_m, and w_m vanish for $m > 1$.

Equations Satisfied by an Azimuthal Harmonic

In expansion (16.1), a typical field harmonic will be written as

$$\mathbf{E}_m(\mathbf{r}) = e^{jm\varphi}\,\boldsymbol{\mathcal{E}}_m(r,z) \qquad (m = 0, \pm 1, \pm 2\ \ldots). \tag{16.2}$$

Similar expressions are used for $\mathbf{H}$ and the currents $\mathbf{J}$ and $\mathbf{J}_m$. If the media are isotropic and homogeneous, the sourceless Maxwell's equations yield, for each Fourier term,

$$\frac{jm}{r}\,\mathcal{E}_z - \frac{\partial \mathcal{E}_\varphi}{\partial z} = -j\omega\mu\,\mathcal{H}_r \tag{16.3}$$

$$\frac{\partial \mathcal{E}_r}{\partial z} - \frac{\partial \mathcal{E}_z}{\partial r} = -j\omega\mu\,\mathcal{H}_\varphi \tag{16.4}$$

$$\frac{1}{r}\frac{\partial}{\partial r}(r\,\mathcal{E}_\varphi) - \frac{jm}{r}\,\mathcal{E}_r = -j\omega\mu\,\mathcal{H}_z \tag{16.5}$$

$$\frac{jm}{r}\,\mathcal{H}_z - \frac{\partial \mathcal{H}_\varphi}{\partial z} = j\omega\epsilon\,\mathcal{E}_r \tag{16.6}$$

$$\frac{\partial \mathcal{H}_r}{\partial z} - \frac{\partial \mathcal{H}_z}{\partial r} = j\omega\epsilon\,\mathcal{E}_\varphi \tag{16.7}$$

$$\frac{1}{r}\frac{\partial}{\partial r}(r\,\mathcal{H}_\varphi) - \frac{jm}{r}\,\mathcal{H}_r = j\omega\epsilon\,\mathcal{E}_z. \tag{16.8}$$

A component such as $\mathcal{H}_z$ should actually be written as $\mathcal{H}_{mz}$, but the subscript m has been temporarily dropped for the sake of compactness. The r and z components of the fields can

be expressed in terms of the φ components, which may then be chosen as main unknowns. Thus,

$$\mathcal{E}_z = \frac{1}{k^2r^2 - m^2}\left[jm\frac{\partial}{\partial z}(r\mathcal{E}_\varphi) - j\omega\mu\, r\frac{\partial}{\partial r}(r\mathcal{H}_\varphi)\right] \tag{16.9}$$

$$\mathcal{E}_r = \frac{1}{k^2r^2 - m^2}\left[jm\frac{\partial}{\partial r}(r\mathcal{E}_\varphi) + j\omega\mu\, r\frac{\partial}{\partial z}(r\mathcal{H}_\varphi)\right] \tag{16.10}$$

$$\mathcal{H}_z = \frac{1}{k^2r^2 - m^2}\left[j\omega\epsilon\, r\frac{\partial}{\partial r}(r\mathcal{E}_\varphi) + jm\frac{\partial(r\mathcal{H}_\varphi)}{\partial z}\right] \tag{16.11}$$

$$\mathcal{H}_r = \frac{1}{k^2r^2 - m^2}\left[-j\omega\epsilon\, r\frac{\partial(r\mathcal{E}_\varphi)}{\partial z} + jm\frac{\partial}{\partial r}(r\mathcal{H}_\varphi)\right]. \tag{16.12}$$

These relationships remain valid when ϵ and μ are not uniform but depend only on r and z. They can be written in more compact form by means of the grad_M operator defined in (A3.60). Thus,

$$\boldsymbol{\mathcal{E}}_M = \frac{1}{k^2r^2 - m^2}\left[jm\ \text{grad}_M(r\mathcal{E}_\varphi) + j\omega\mu\, r\,\mathbf{u}_\varphi \times \text{grad}_M\,(r\mathcal{H}_\varphi)\right] \tag{16.13}$$

$$\boldsymbol{\mathcal{H}}_M = \frac{1}{k^2r^2 - m^2}\left[-j\omega\epsilon\, r\,\mathbf{u}_\varphi \times \text{grad}_M(r\mathcal{E}_\varphi) + jm\ \text{grad}_M\,(r\mathcal{H}_\varphi)\right], \tag{16.14}$$

where the M subscript denotes the component in the meridian plane. If we replace ($\mathcal{E}_r$, $\mathcal{E}_z$, $\mathcal{H}_r$, $\mathcal{H}_z$) in (16.3) to (16.8) by their value in terms of $\mathcal{E}_\varphi$ and $\mathcal{H}_\varphi$, coupled second-order linear partial differential equations are obtained for $\mathcal{E}_\varphi$ and $\mathcal{H}_\varphi$.

The eigenvectors of an axisymmetric cavity[1] are of the general form (16.2) [22]. The solenoidal electric eigenvectors, for example, can be written as

$$\mathbf{e}_{mnp} = \left\{\begin{array}{c}\sin m\varphi\\ \cos m\varphi\end{array}\right\}\mathbf{c}_{mnp} + \left\{\begin{array}{c}\cos m\varphi\\ -\sin m\varphi\end{array}\right\}\beta_{mnp}\,\mathbf{u}_\varphi, \tag{16.15}$$

where $\mathbf{c}_{mnp}$ is a meridian vector. Introduction of this expression into Maxwell's equations leads to the differential equation

$$\nabla_M^2\,\mathbf{c}_{mnp} - \frac{m^2}{r^2}\,\mathbf{c}_{mnp} + \mathbf{u}_r\frac{2}{r}\,\text{div}_M\,\mathbf{c}_{mnp} + k_{mnp}^2\,\mathbf{c}_{mnp} = 0. \tag{16.16}$$

In addition, $\mathbf{c}_{mnp}$ must satisfy the boundary conditions

$$\mathbf{u}_n \times \mathbf{c}_{mnp} = 0 \quad \text{and} \quad \text{div}_M\,\mathbf{c}_{mnp} = 0 \quad (\text{on } C).$$

Once $\mathbf{c}_{mnp}$ is known, the value of β_{mnp} can be obtained from the relationship

$$\beta_{mnp} = \frac{r}{m}\,\text{div}_M\,\mathbf{c}_{mnp} \qquad (m \neq 0). \tag{16.17}$$

For $m = 0$ the eigenvectors are either meridian or azimuthal [22]. If we write the azimuthal eigenvector as $\beta_{onp}\,\mathbf{u}_\varphi$, β_{onp} must be the solution of the system

$$\nabla_M^2\,\beta_{onp} + \mu_{onp}^2\,\beta_{onp} = 0$$

$$\beta_{onp} = 0 \quad (\text{on } C). \tag{16.18}$$

16.2 SCATTERING BY BODIES OF REVOLUTION: INTEGRAL EQUATIONS

The few scatterers whose properties can be determined by separation of variables are often axisymmetric [38, 113]. Oblate and prolate spheroids are obvious examples, together with the sphere, whose scattering characteristics are discussed in Section 11.3. For more general shapes, one must rely on direct numerical methods, in which case semiquantitative results may serve to provide a quick check on already obtained results, and sometimes clarify the physics of the scattering process. Such a semiquantitative guideline exists for low-frequency scattering by a perfectly conducting body of revolution. At low frequencies, scattering depends more on the *volume* of the body than on its *shape*, because a rapid variation of the phase along the scatterer is needed to "feel" the latter's geometry. This volume (or bulk) effect has been evaluated for the nose-on incidence of a plane wave on a BOR. Electric and magnetic dipoles are induced in the conductor, and a simplified theory shows that the backscattering cross section of an elongated body is well approximated by[2]

$$\sigma^{\text{rad}} = \frac{4}{\pi} k_0^4 V^2, \tag{16.19}$$

where V is the volume of the scatterer. As the body gets flatter, however, the approximation deteriorates. A flat disk, for example, has zero volume, but a nonzero radar cross section. A better approximation, based on results obtained for the prolate spheroid, is given by

$$\sigma^{\text{rad}} = \frac{4}{\pi} k_0^4 V^2 \left(1 + \frac{1}{\pi\alpha} e^{-\alpha}\right)^2, \tag{16.20}$$

where α, the ratio of the axial to transverse dimensions, is a measure of the elongation of the body.

16.2.1 Integral Equations for Perfect Conductors

The current density $\mathbf{J}_S$ on a perfectly conducting scatterer satisfies the integro-differential equation (Fig. 16.2)

$$\begin{aligned}\mathbf{E}_t^i(\mathbf{r}) &= j\omega \mathbf{A}_t(\mathbf{r}) + \text{grad}_t\, \phi(\mathbf{r}) \\ &= \frac{j\omega\mu_0}{4\pi} \left\{ \left[\int_S \mathbf{J}_S(\mathbf{r}') \frac{e^{-jk_0|\mathbf{r}-\mathbf{r}'|}}{|\mathbf{r}-\mathbf{r}'|}\, dS' \right]_t \right. \\ &\quad \left. + \frac{1}{k_0^2} \text{grad}_t \int_S \frac{e^{-jk_0|\mathbf{r}-\mathbf{r}'|}}{|\mathbf{r}-\mathbf{r}'|} \text{div}'_S\, \mathbf{J}_S(\mathbf{r}')\, dS' \right\},\end{aligned} \tag{16.21}$$

where $\mathbf{r}$ is on the boundary of the BOR, and t denotes a component in the tangent plane. We shall Fourier-expand $\mathbf{J}_S$ as in (10.87), and write*

$$\mathbf{J}_S = \sum_{m=-\infty}^{\infty} J_{mc}(c)\, e^{jm\varphi}\, \mathbf{u}_c + \sum_{m=-\infty}^{\infty} J_{m\varphi}(c)\, e^{jm\varphi}\, \mathbf{u}_\varphi. \tag{16.22}$$

*The current densities J_c and J_φ can also be evaluated *directly* (i.e., without the intervention of Fourier expansions) by solving a pair of combined integral equations.[3]

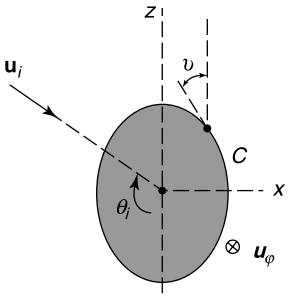

Figure 16.2 Scatterer and incident plane wave.

For points on S:

$$G_0(c,c',\varphi,\varphi') = -\frac{1}{4\pi}\frac{e^{-jk_0|\mathbf{r}-\mathbf{r}'|}}{|\mathbf{r}-\mathbf{r}'|} = \sum_{m=-\infty}^{\infty} G_m(c,c')\, e^{\,jm(\varphi-\varphi')}, \tag{16.23}$$

with

$$G_m(c,c') = \frac{1}{2\pi}\int_{-\pi}^{\pi} G_0(c,c',\alpha)\, e^{-jm\alpha}\, d\alpha. \tag{16.24}$$

The integral in (16.24) must be evaluated numerically.[4] The expansions for $\mathbf{J}_S$ and G_0 are inserted into the right-hand term of (16.21) and the result subsequently compared with the Fourier expansion for $\mathbf{E}_t^i$, upon which coefficients of terms in $e^{\,jm\varphi}$ are equated. This move produces pairs of integral equations for $J_{mc}(c)$ and $J_{m\varphi}(c)$. The plane wave is an important incident wave, and it is useful to give the Fourier expansion of its tangential electric field. This is

$$\mathbf{E}_t^i = \sum_{m=0}^{\infty}\left[E_{cm}^i(c)\left\{\begin{array}{c}\cos m\varphi\\ \sin m\varphi\end{array}\right\}\mathbf{u}_c + E_{\varphi m}^i(c)\left\{\begin{array}{c}\sin m\varphi\\ -\cos m\varphi\end{array}\right\}\mathbf{u}_\varphi\right]. \tag{16.25}$$

Let $\mathbf{E}^i$ be of unit amplitude. In the determination of E_{cm}^i and $E_{\varphi m}^i$, use is made of the following expansion, based on (A5.47):

$$e^{\,jk_0 x\sin\theta_i} = e^{\,jk_0 r\sin\theta_i\cos\varphi} = \sum_{m=0}^{\infty}\epsilon_m j^m J_m(k_0 r\sin\theta_i)\,\cos m\varphi. \tag{16.26}$$

The value of the coefficients E_{cm}^i and $E_{\varphi m}^i$ depends on the polarization of the wave. If $\mathbf{E}^i$ is polarized *parallel* to the plane of incidence (the $\mathbf{u}_i$, $\mathbf{u}_z$ plane), detailed calculations show that[4]

$$\begin{aligned} E_{cm}^i &= -\cos\theta_p\, e^{-jk_0 z\cos\theta_i}\epsilon_m j^{m+1}\left[j\sin\theta_i\cos\upsilon\, J_m(k_0 r\sin\theta_i)\right.\\ &\qquad \left. +\ \cos\theta_i\sin\upsilon\, J_m'(k_0 r\sin\theta_i)\right]\\ E_{\varphi m}^i &= \cos\theta_p\cos\theta_i\, e^{-jk_0 z\cos\theta_i}\,\epsilon_m j^{m+1}\, m\frac{J_m(k_0 r\sin\theta_i)}{k_0 r\sin\theta_i}. \end{aligned} \tag{16.27}$$

The symbol v denotes the angle between $\mathbf{u}_c$ and $\mathbf{u}_z$, and θ_p is the angle between $\mathbf{u}_E$ and $(-\mathbf{u}_\theta)$. For the *perpendicular* polarization:

$$E^i_{cm} = -\sin\theta_p \sin v\, e^{-jk_0 z\cos\theta_i}\, \epsilon_m j^{m+1}\, m\, \frac{J_m(k_0 r\sin\theta_i)}{k_0 r\sin\theta_i}$$
$$E^i_{\varphi m} = \sin\theta_p\, e^{-jk_0 z\cos\theta_i}\, \epsilon_m j^{m+1}\, J'_m(k_0 r\sin\theta_i). \tag{16.28}$$

The numerical solution of the pair of integral equations derived from (16.21) proceeds by expanding $J_{mc}(c)$ and $J_{m\varphi}(c)$ in suitable basis functions, rectangular or triangular.[5] Because the current must be differentiated to obtain $\mathrm{div}_S\, \mathbf{J}_S$, it is often preferable to use triangle functions, which yield a piecewise-linear approximation for the currents, a form that converges well. Discretization leads to a series of matrix problems, each matrix a partition of the total matrix. The total matrix can also be obtained by solving (16.21) directly, without exploiting the axisymmetric character of the scatterer. The Fourier expansion approach, however, has the advantage of requiring the inversion of several *small* matrices, a process often faster than the inversion of a single large one.

Equation (16.21) is the EFIE of the problem on hand. A formulation in terms of the MFIE (the H-field equation) is also possible. In both cases, the usual difficulties with interior resonances are encountered, and it may be preferable to formulate the problem in terms of a *combined* field integral equation.[6]

16.2.2 Integral Equations for Penetrable Scatterers

The basic equations for *homogeneous* penetrable scatterers are (12.80) and (12.81). In the application to axisymmetric bodies, the unknown current densities $\mathbf{J}_S = \mathbf{u}_n \times \mathbf{H}$ and $\mathbf{J}_{mS} = \mathbf{E} \times \mathbf{u}_n$ are expanded as in (16.22), upon which the problem can be solved one partial mode at a time.[7,8] The analysis can be extended to bodies that consist of (or can be modeled by) several parts, each of which is homogeneous and axisymmetric[9,10] (Fig. 16.3).

When the scatterer is *inhomogeneous*, with ϵ and μ functions of r and z — but not of φ — the basic volume integro-differential equations for $\mathbf{J}$ and $\mathbf{J}_m$ are (12.87) and (12.88).

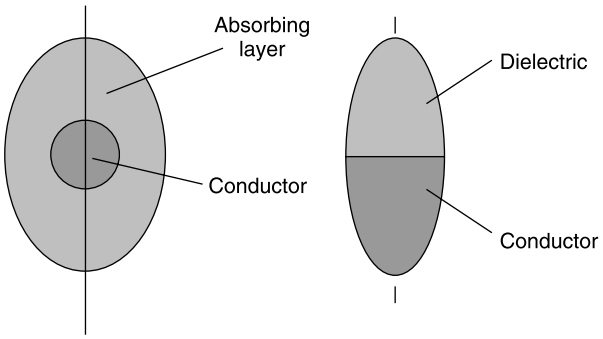

Figure 16.3 Two piecewise homogeneous BORs.

Assuming for simplicity that the scatterer is nonmagnetic we may write, for $\mathbf{r}$ in the scatterer,

$$\mathbf{E}(\mathbf{r}) = \frac{\mathbf{J}(\mathbf{r})}{j\omega\epsilon_0\,\chi(\mathbf{r})} = \mathbf{E}^i(\mathbf{r}) - j\omega\,\mathbf{A}(\mathbf{r}) - \text{grad}\,\phi(\mathbf{r})$$
$$= \mathbf{E}^i(\mathbf{r}) - j\omega\,\mathbf{A}(\mathbf{r}) - \frac{j\omega}{k_0^2}\,\text{grad div}\,\mathbf{A}(\mathbf{r}), \tag{16.29}$$

where $\chi(\mathbf{r}) = \epsilon_r(\mathbf{r}) - 1$ is the susceptibility (a contrast function). The vector potential is given by

$$\mathbf{A}(\mathbf{r}) = \frac{\mu_0}{4\pi}\int_V \mathbf{J}(\mathbf{r})\frac{e^{-jk_0|\mathbf{r}-\mathbf{r}'|}}{|\mathbf{r}-\mathbf{r}'|}\,dV'. \tag{16.30}$$

In the application to a BOR, one writes

$$\mathbf{E}^i = \sum_{n=-\infty}^{\infty} \mathbf{E}_n^i(r,z)\,e^{jn\varphi}$$
$$\mathbf{J} = \sum_{n=-\infty}^{\infty} \mathbf{J}_n(r,z)\,e^{jn\varphi}$$
$$\mathbf{A} = \sum_{n=-\infty}^{\infty} \mathbf{A}_n(r,z)\,e^{jn\varphi}. \tag{16.31}$$

The main unknowns are the $\mathbf{J}_n$ coefficients, and it is therefore necessary, in order to solve (16.29), to find a connection between the $\mathbf{A}_n$'s and the $\mathbf{J}_n$'s. This is found from (16.30), combined with (16.23). With G_n given by (16.24), detailed calculations give[11] (Fig. 16.1*a*)

$$\mathbf{A}_n(r,z) = \frac{\mu_0}{4\pi}\int_D \overline{\overline{\Gamma}}_n(r,z;r',z')\cdot\mathbf{J}_n(r',z')\,r'\,dr'\,dz', \tag{16.32}$$

where

$$\overline{\overline{\Gamma}}_n = \begin{pmatrix} \Gamma_{rr} & \Gamma_{rz} & \Gamma_{r\varphi} \\ \Gamma_{zr} & \Gamma_{zz} & \Gamma_{z\varphi} \\ \Gamma_{\varphi r} & \Gamma_{\varphi z} & \Gamma_{\varphi\varphi} \end{pmatrix}$$
$$= -4\pi^2 \begin{pmatrix} G_{n-1}+G_{n+1} & 0 & \frac{1}{j}(G_{n-1}-G_{n+1}) \\ 0 & 2G_m & 0 \\ \frac{1}{j}(G_{n+1}-G_{n-1}) & 0 & G_{n-1}+G_{n+1} \end{pmatrix}. \tag{16.33}$$

The same type of analysis can be called upon to determine the resonant frequencies of inhomogeneous dielectric resonators[12] or to investigate scattering by BORs endowed with a surface impedance Z_S. The impedance must be independent of φ but may vary along the contour of the scatterer[13] (i.e., along C in Fig. 16.1*a*). Z_S becomes a dyadic when the body is anisotropic.[14]

16.3 SCATTERING BY BODIES OF REVOLUTION: FINITE METHODS

16.3.1 Finite Element Method

In the finite element method, it is often advisable to select $\mathcal{E}_\varphi$ and $\mathcal{H}_\varphi$ as principal unknowns. These components have the advantage of remaining continuous throughout space because they are automatically tangent to an axisymmetric boundary surface. Once $\mathcal{E}_\varphi$ and $\mathcal{H}_\varphi$ are known, the meridian components follow from (16.13) and (16.14). Going one step further,[15] it is helpful to replace $\mathcal{E}_\varphi$ and $\mathcal{H}_\varphi$ by the *coupled azimuthal potentials* $\psi_1 = r\mathcal{E}_\varphi$ and $\psi_2 = R_{c0}\, r\mathcal{H}_\varphi$ (the CAPs). Having made that choice, we may write the electric displacement current in terms of ψ_1 and ψ_2 as

$$\mathcal{D}_M = \epsilon\, \mathcal{E}_M = \frac{\epsilon}{k^2 r^2 - m^2} \left[jm \operatorname{grad}_M \psi_1 + jk_0 r\, \mu_r\, \mathbf{u}_\varphi \times \operatorname{grad}_M \psi_2 \right]. \tag{16.34}$$

Because $\mathcal{D}$ is solenoidal in the absence of sources,

$$\operatorname{div} \mathbf{D} = \operatorname{div} \left[e^{jm\varphi} \mathcal{D}(r, z) \right] = e^{jm\varphi} \left[\operatorname{div}_M (\epsilon\, \mathcal{E}_M) + \frac{jm}{r}\, \epsilon\, \mathcal{E}_\varphi(r, z) \right] = 0. \tag{16.35}$$

After taking the divergence of (16.34), an equation is obtained that must be satisfied by ψ_1 and ψ_2. A second, similar equation follows by rewriting (16.14) in terms of ψ_1 and ψ_2 and exploiting the condition $\operatorname{div} \left[e^{jm\varphi} \mathcal{B}(r, z) \right] = 0$. The resulting system of coupled partial differential equations can be solved by variational methods.[16,17] In the numerical implementation nodal (scalar) basis functions can be used for the two potentials. If the media

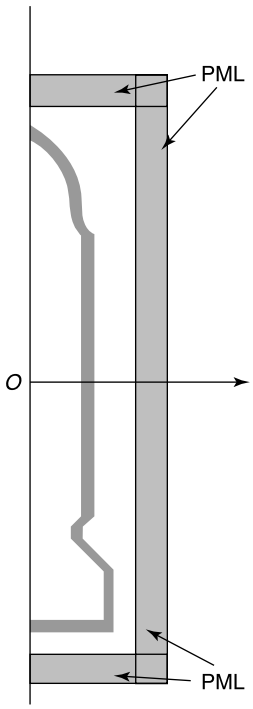

Figure 16.4 Target with PML enclosure (from A. D. Greenwood and J. M. Jin, Computation of the RCS of a complex BOR using FEM with coupled azimuth potentials and PLM, *Electromagn.* **19**, 147–170, 1999, with permission of the Taylor & Francis Group).

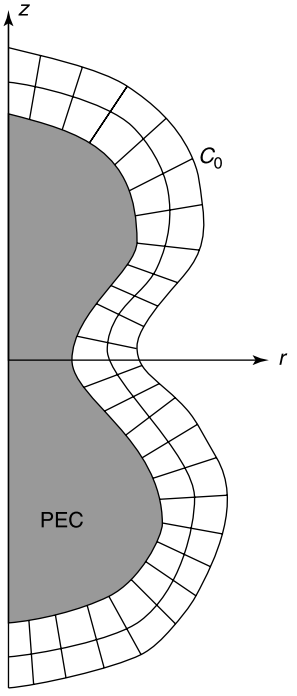

Figure 16.5 Mesh for the MEI method (from T. L. Barkdoll and R. Lee, Finite element analysis of bodies of revolution using the measured equation of invariance, *Radio Sci.* **30**, 803–815, 1995, with permission of the American Geophysical Union).

are lossless, a singularity in (16.34) appears at radii for which $k^2r^2 - m^2 = 0$. This mathematical singularity should be taken into account in order to avoid numerical instabilities. A formulation in terms of the *three* components of the electric field, instead of the two potentials, can avoid the difficulty.[17,18,19] For such a choice, edge-based vector elements are selected for the meridian components of $\boldsymbol{\mathcal{E}}$ and nodal-based scalar basis functions for $\mathcal{E}_\varphi$.

The various ways to truncate the computational domain have been applied — in adapted form — to axisymmetric scatterers. For instance:

- The *boundary integral method*[20,21]
- The *PML closure*, in which the scatterer is enclosed in a capped PML cylinder[17] [192] (Fig. 16.4)
- The *measured equation of invariance*[22,23] (Fig. 16.5).

16.3.2 Finite Differences in the Time Domain

In the application of the FDTD, the axisymmetry of the scatterer is again exploited by expanding the time-dependent fields in Fourier series in φ. Thus [209],

$$\mathbf{e}(\mathbf{r},t) = \sum_{m=0}^{\infty} \left(\boldsymbol{\mathcal{E}}_m^e(r,z,t)\cos m\varphi + \boldsymbol{\mathcal{E}}_m^o(r,z,t)\sin m\varphi\right)$$

$$\mathbf{h}(\mathbf{r},t) = \sum_{m=0}^{\infty} \left(\boldsymbol{\mathcal{H}}_m^e(r,z,t)\cos m\varphi + \boldsymbol{\mathcal{H}}_m^o(r,z,t)\sin m\varphi\right), \tag{16.36}$$

where the e and o superscripts refer to terms respectively *even* and *odd* in φ. The series is subsequently inserted into Maxwell's equations. In an isotropic lossless medium, (7.2) gives, after equating terms in $\cos m\varphi$,

$$\begin{cases} -\dfrac{\partial \mathcal{H}^e_{m\varphi}}{\partial z} + \dfrac{m}{r}\,\mathcal{H}^o_{mz} = \epsilon\,\dfrac{\partial \mathcal{E}^e_{mr}}{\partial t} \\ \dfrac{\partial \mathcal{H}^e_{mr}}{\partial z} - \dfrac{\partial \mathcal{H}^e_{mz}}{\partial r} = \epsilon\,\dfrac{\partial \mathcal{E}^e_{m\varphi}}{\partial t} \\ \dfrac{1}{r}\dfrac{\partial}{\partial r}(r\,\mathcal{H}^e_{m\varphi}) - \dfrac{m}{r}\,\mathcal{H}^o_{m\varphi} = \epsilon\,\dfrac{\partial \mathcal{E}^e_{mz}}{\partial t}. \end{cases} \tag{16.37}$$

From equating the terms in $\sin m\varphi$, one obtains:

$$\begin{cases} -\dfrac{\partial \mathcal{H}^o_{m\varphi}}{\partial z} - \dfrac{m}{r}\,\mathcal{H}^e_{mz} = \epsilon\,\dfrac{\partial \mathcal{E}^o_{mr}}{\partial t} \\ \dfrac{\partial \mathcal{H}^o_{mr}}{\partial z} - \dfrac{\partial \mathcal{H}^o_{mz}}{\partial r} = \epsilon\,\dfrac{\partial \mathcal{E}^o_{m\varphi}}{\partial t} \\ \dfrac{1}{r}\dfrac{\partial}{\partial r}(r\,\mathcal{H}^o_{m\varphi}) + \dfrac{m}{r}\,\mathcal{H}^e_{m\varphi} = \epsilon\,\dfrac{\partial \mathcal{E}^o_{mz}}{\partial t}. \end{cases} \tag{16.38}$$

Equation (7.1) leads to analogous results, with $\mathcal{H}$ replaced by $\mathcal{E}$, and ϵ by $(-\mu)$.

In the discretization process, the traditional Yee-cell shown in Figure 16.6*a* is projected onto the meridian plane[24] [192] (Fig. 16.6*b*). Illustratively, the first equation in (16.37) becomes, in difference form,

$$\mathcal{E}_r^{n+1}(i,j) = \mathcal{E}_r^n(i,j) - \frac{\Delta t}{\epsilon \Delta z}\left[\mathcal{H}_\varphi^{n+\frac{1}{2}}(i,j) - \mathcal{H}_\varphi^{n+\frac{1}{2}}(i,j-1)\right] - \frac{m\Delta t}{\epsilon r}\,\mathcal{H}_z^{n+\frac{1}{2}}(i,j), \tag{16.39}$$

where the m and parity superscripts have been left out for the sake of conciseness. In a typical application, the BOR form of the FDTD can serve to identify the resonances of an axisymmetric resonator, which are revealed by Fourier transforming the computed time response — a classic approach. The method requires a large number of time samples, and

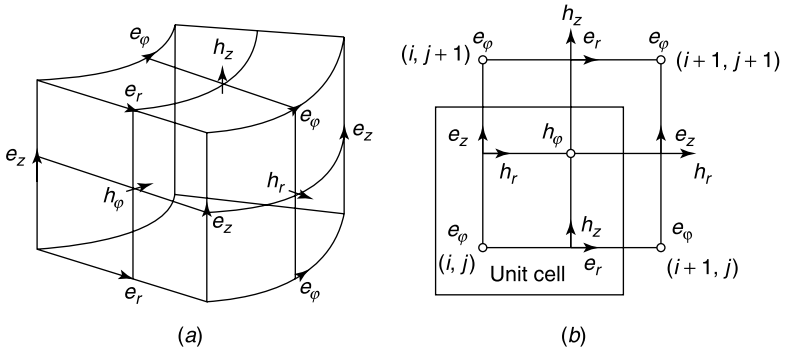

Figure 16.6 (*a*) General 3D lattice in cylindrical coordinates. (*b*) Projection on the meridian plane (from Y. Chen, R. Mittra, and P. Harms, Finite-difference time-domain algorithm for solving Maxwell's equations in rotationally symmetric geometries, *IEEE Trans. MTT* **44**, 832–838, 1996, with permission of IEEE).

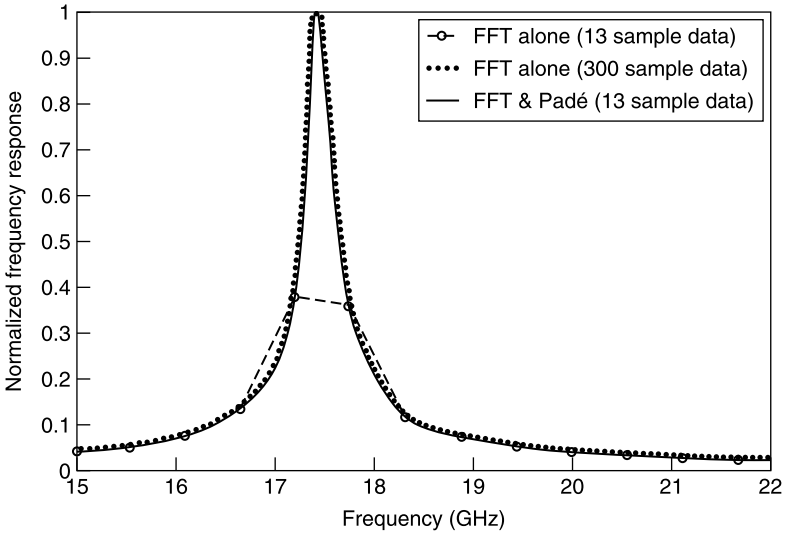

Figure 16.7 Normalized frequency response of a disk (from S. Shi, L. Yang, and D. W. Prather, Numerical study of axisymmetric dielectric resonators, *IEEE Trans. MTT* **9**, 1614–1619, 2001, with permission of IEEE).

its long execution time can be shortened by obtaining first a coarse frequency response and subsequently using the *Padé approximation* to interpolate between frequencies.[25] Some results from this approach are shown in Figure 16.7, which displays part of the frequency response of a dielectric disk of dielectric constant 12, radius 8 mm, and height 8 mm.

16.4 APERTURES IN AXISYMMETRIC SURFACES

To maintain the axisymmetric character of the geometry, we shall assume that the aperture is in the form of a circumferential gap (Fig. 16.8*a*). The problem of determining the fields radiated from such a gap, across which an electric field is impressed, is discussed in Section 10.6 for a sphere. We shall extend the analysis to a circumferential gap in a *prolate spheroid*. The solution proceeds by separation of variables in prolate spheroidal coordinates (see Appendix 2, and in particular A2.112). The determination of $\mathbf{E}_{\tan}$ in the gap is a coupled regions problem, of which only one aspect will be discussed, the evaluation of the exterior fields in the presence of a φ-independent gap excitation. The assumed symmetry implies that the only components of concern are E_r, E_z, and H_φ. It is useful to write

$$H_\varphi = \frac{A(\mu, \nu)}{c\sqrt{(\mu^2 - 1)(1 - \nu^2)}}, \tag{16.40}$$

where $2c$ is the interfocal distance. The electric field can be expressed in terms of $A(\mu, \nu)$ by applying (A2.116), the formula for the curl. Thus,

$$E_\mu = -\frac{jR_{c0}}{k_0 c^2} \frac{1}{\sqrt{(\mu^2 - 1)(\mu^2 - \nu^2)}} \frac{\partial A}{\partial \nu} \tag{16.41}$$

$$E_\nu = \frac{jR_{c0}}{k_0 c^2} \frac{1}{\sqrt{(1 - \nu^2)(\mu^2 - \nu^2)}} \frac{\partial A}{\partial \mu}. \tag{16.42}$$

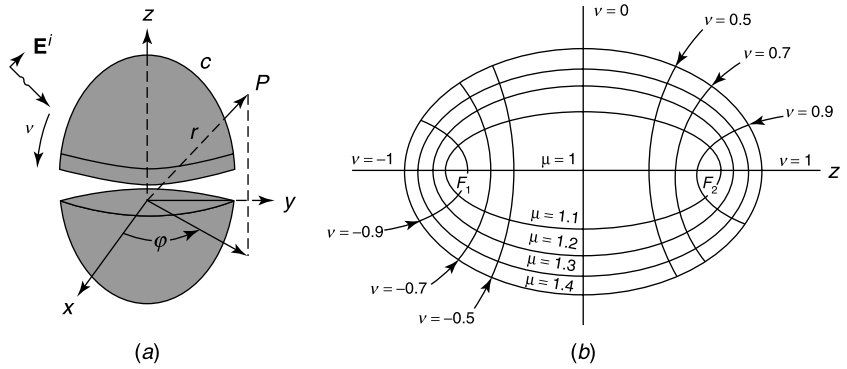

Figure 16.8 (*a*) BOR with circumferential gap. (*b*) Prolate spheroidal coordinates (from H. K. Schuman and D. E. Warren, Aperture coupling in bodies of revolution, *IEEE Trans. AP* **26**, 778–783, 1978, with permission of IEEE).

The function $A(\mu, \nu)$ is $(1/2\pi)$ times the line integral of $\mathbf{H}$ along a circumferential contour. It satisfies the differential equation

$$(\mu^2 - 1)\frac{\partial^2 A}{\partial \mu^2} + (1 - \nu^2)\frac{\partial^2 A}{\partial \nu^2} + k_0^2 c^2 (\mu^2 - \nu^2)\, A = 0. \tag{16.43}$$

This equation may be solved by separation of variables, starting with an assumed solution $A = U(\mu)\, V(\nu)$. Inserting this trial product into (16.43) leads to the separated equations

$$(\mu^2 - 1)\frac{d^2 U}{d\mu^2} + (k_0^2 c^2 \mu^2 - K)\, U = 0 \tag{16.44}$$

$$(1 - \nu^2)\frac{d^2 V}{d\nu} + (K - k_0^2 c^2 \nu^2)\, V = 0, \tag{16.45}$$

where K is the separation constant. The behavior of the fields on the axis requires $V(\nu)$ to be equal to zero for $\nu = \pm 1$. This condition quantizes the possible values of K and defines a set of possible functions $V_K(\nu)$. To determine $U(\mu)$, we note that (16.44) takes the form

$$\frac{d^2 U}{d\mu^2} + k_0^2 c^2\, U = 0 \tag{16.46}$$

for large values of μ. Such values correspond with large distances, because $R = (r^2 + z^2)^{\frac{1}{2}}$ approaches $c\mu$ for large μ. The radiation condition requires U to be proportional to $e^{-jk_0 R}$ for large R. More precisely,

$$\lim_{\mu \to \infty} U \doteq e^{-jk_0 \mu c}. \tag{16.47}$$

Once U and V are determined for a given separation constant K, a solution for (16.43) can be tried in the form[26]

$$A(\mu, \nu) = \sum_K a_K U_K(\mu)\, V_K(\nu). \tag{16.48}$$

From (16.42), the corresponding ν component of the electric field is

$$E_\nu = \frac{jR_{c0}}{k_0 c^2} \frac{1}{\sqrt{(1-\nu^2)(\mu^2-\nu^2)}} \sum_K a_K U'_K(\mu)\, V_K(\nu). \tag{16.49}$$

This component must take the prescribed value $E_\nu(\nu)$ in the gap (i.e., at the value μ_S that defines the shape of the spheroidal boundary). Thus,

$$\frac{jR_{c0}}{k_0 c^2} \frac{1}{\sqrt{(1-\nu^2)(\mu_S^2-\nu^2)}} \sum_K a_K U'_K(\mu_S)\, V_K(\nu) = E_\nu(\nu). \tag{16.50}$$

The coefficients a_K can be derived from the orthogonality property[27]

$$\int_{-1}^{+1} \frac{V_K(\nu) V_{K'}(\nu)}{1-\nu^2}\, d\nu = \delta_{KK'} N_K, \tag{16.51}$$

where N_K, the normalization factor, is given by

$$N_K = \int_{-1}^{1} \frac{V_K^2(\nu)}{1-\nu^2}\, d\nu. \tag{16.52}$$

The desired value of a_K follows as

$$a_K = \frac{jk_0 c^2}{R_{c0} N_K U'_K(\mu_0)} \int_{-1}^{1} E_\nu(\nu) \sqrt{\frac{\mu_S^2-\nu^2}{1-\nu^2}}\, V_K(\nu)\, d\nu. \tag{16.53}$$

For a very narrow gap located at $\nu = \nu_g$, across which a voltage V_g is applied, the formula simplifies to

$$a_K = \frac{jk_0 c}{R_{c0} N_K} \frac{V_K(\nu_g)}{U'_K(\mu_S)}\, V_g. \tag{16.54}$$

The corresponding current crossing a parallel circle $\nu =$ constant is

$$I(\nu) = jV_g \frac{2\pi k_0 c}{R_{c0}} \sum_K \frac{U_K(\mu_S)\, V_K(\nu_g)}{N_K U'_K(\mu_S)}\, V_K(\nu). \tag{16.55}$$

Some radiation patterns[28] obtained from the expansion (16.48) are shown in Figure 16.9 for $k_0 c = 3$, $\mu_S = 1.02$, and $(b/a) = 0.2$.

For an *arbitrary* contour C, separation of variables does not work any longer. In the presence of a wide circumferential gap, across which a given φ-independent E_c is applied, the radiated fields can be evaluated by first solving for $I(z)$, the current through a parallel circle. The determination of $I(z)$ can be formulated in terms of an integral equation[29] (Problem 16.5). A more general situation involves the gap field induced by an incident plane wave.[30,31] This is a coupled regions problem, which can be reduced to the solution of an integro-differential equation for $\mathbf{u}_n \times \mathbf{E}$. One of the steps there is the evaluation of the exterior fields in terms of $\mathbf{u}_n \times \mathbf{E}$. One immediately recognizes that this task is actually performed in Section 16.3 in relation with scattering by a perfectly conducting BOR.

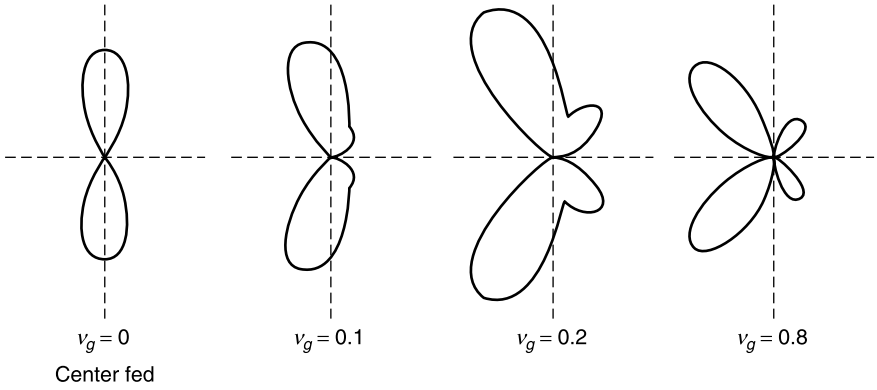

Figure 16.9 Radiation patterns for a prolate spheroidal antenna (from H. A. Myers, Radiation patterns of unsymmetrically fed prolate spheroidal antennas, *IRE Trans. AP* **4**, 58–64, 1956, with permission of IEEE).

16.5 THE CONICAL WAVEGUIDE

To evaluate the fields in a conical volume, we shall rely on mode expansions of the type used in Chapter 15 for cylindrical volumes. The main difference lies in the cross section S of the conical guide, which does not remain constant. The *shape* of S, however, is invariant, with overall dimensions proportional to R, the radial distance from the apex of the cone (Fig. 16.10*a*). The cross section S is, in fact, a blown-up version of S_1, the corresponding cross section on the unit sphere, and it is therefore natural to define eigenvalues and eigenvectors with respect to S_1. This strategy has already been applied in Section 5.12 to the solution of potential problems, and the relevant differential operators are defined in Appendix 9. In the investigation of the fields in the cone, we need the *Dirichlet and Neumann eigenfunctions of* S_1. The Dirichlet functions are defined by the equations

$$\begin{aligned} \nabla_1^2 \phi_m + k_m^2 \phi_m &= 0 \quad (\text{in } S_1) \\ \phi_m &= 0 \quad (\text{on } C_1), \end{aligned} \tag{16.56}$$

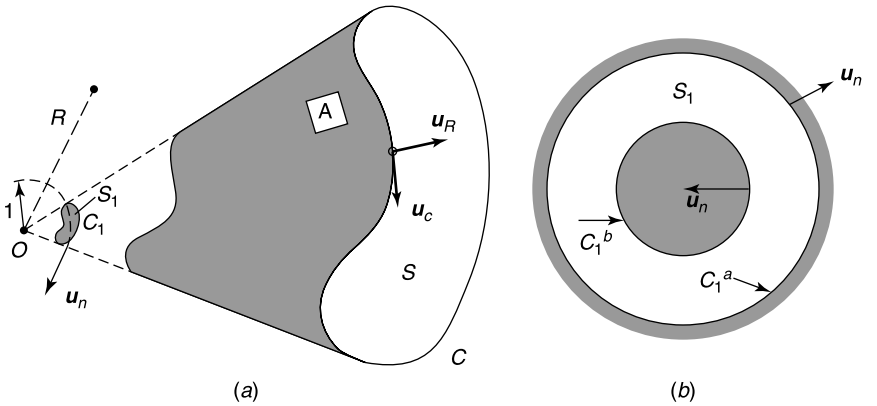

Figure 16.10 (*a*) Conical waveguide with aperture in the wall. (*b*) Doubly bounded contour on S_1.

where ϕ_m is a function of θ and φ, and ∇_1^2 is the Laplacian on the unit surface S_1 (the *Beltrami operator*), viz.

$$\nabla_1^2 \phi_m = \nabla_{\theta,\varphi}^2 \phi_m = \frac{1}{\sin\theta}\frac{\partial}{\partial\theta}\left(\sin\theta \frac{\partial \phi_m}{\partial\theta}\right) + \frac{1}{\sin^2\theta}\frac{\partial^2 \phi_m}{\partial\varphi^2}. \tag{16.57}$$

We note that k_m is dimensionless. For the Neumann eigenfunctions, the defining system is

$$\begin{aligned} \nabla_1^2 \psi_n + k_n^2 \psi_n &= 0 \quad (\text{in } S_1) \\ \frac{\partial \psi_n}{\partial n} &= 0 \quad (\text{on } C_1). \end{aligned} \tag{16.58}$$

The direction n is perpendicular to the outer wall (i.e., to the tangent plane formed by $\mathbf{u}_R$ and $\mathbf{u}_C$). More specifically, $\mathbf{u}_n = \mathbf{u}_C \times \mathbf{u}_R$. From (A3.50), it is easy to show that the ϕ_m form an orthogonal set with respect to the symmetric scalar product

$$\langle a, b \rangle = \int_{S_1} ab \, d\Omega,$$

where $d\Omega = \sin\theta \, d\theta \, d\varphi$ is an elementary solid angle. The orthogonality property also holds for ψ_n. The eigenfunctions are normalized by the conditions

$$\begin{aligned} \int_{S_1} |\text{grad}_1 \, \phi_m|^2 \, d\Omega &= k_m^2 \int_{S_1} (\phi_m)^2 \, d\Omega = 1 \\ \int_{S_1} |\text{grad}_1 \, \psi_n|^2 \, d\Omega &= k_n^2 \int_{S_1} (\psi_n)^2 \, d\Omega = 1. \end{aligned} \tag{16.59}$$

We note that the ϕ_m's and ψ_m's are dimensionless, as well as the grad_1 vectors. We also note that $\psi_0 =$ constant is a member of the Neumann family.[32] The normalized form of that function is $(1/\sqrt{S_1}) = (1/\sqrt{\Omega_1})$, where Ω_1 is the solid angle filled by the conical volume.

In a doubly bounded coaxial structure, of the type shown in Figure 16.10*b*, an eigenfunction ϕ_0 must be added, namely the solution of

$$\begin{aligned} \nabla_1^2 \phi_0 &= 0 \\ \phi_0 &= \text{a constant on } C_1^a \\ \phi_0 &= \text{another constant on } C_1^b. \end{aligned} \tag{16.60}$$

Note that doubly bounded geometries are not exceptional, as evidenced by the examples displayed in Figure 16.11.

16.5.1 The Eigenvectors

Germane to the field expansions are the eigenvectors derived from ϕ_m and ψ_n. These are $\text{grad}_1 \, \phi_m$ and $\text{grad}_1 \, \psi_n$, where

$$\text{grad}_1 \, a(\theta, \varphi) = \frac{\partial a}{\partial\theta}\mathbf{u}_\theta + \frac{1}{\sin\theta}\frac{\partial a}{\partial\varphi}\mathbf{u}_\varphi. \tag{16.61}$$

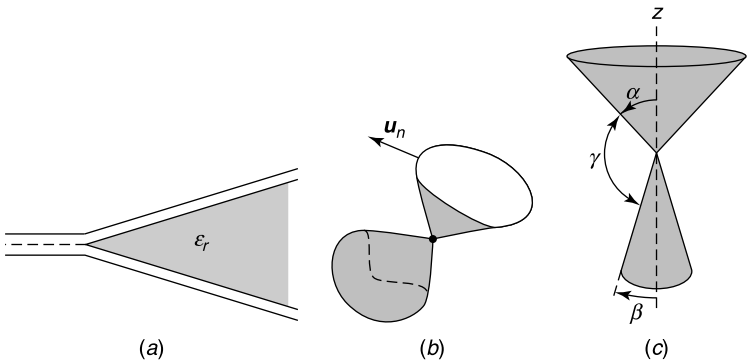

Figure 16.11 (*a*) Dielectric cone in a horn antenna. (*b*) Two concentric cones. (*c*) Biconical circular antenna.

If we introduce a scalar product

$$\langle \mathbf{a}, \mathbf{b} \rangle = \int_{S_1} \mathbf{a} \cdot \mathbf{b} \, d\Omega \tag{16.62}$$

and take Green's theorem (A3.49) into account, it is easy to show that the $\text{grad}_1 \phi_m$ family forms an orthogonal set. The norm of these vectors is related to the norm of ϕ_m by (16.59). The $\text{grad}_1 \phi_m$ vectors are perpendicular to C_1. The vectors $\mathbf{u}_R \times \text{grad}_1 \phi_m$ also form an orthogonal set, with the same norm. The two sets are mutually orthogonal because, from (A3.40) and (A3.44), and because $\phi_m = 0$ on C_1,

$$\int_{S_1} \text{grad}\, \phi_m \cdot (\mathbf{u}_R \times \text{grad}_1 \phi_k) \, d\Omega = \int_{C_1} \mathbf{u}_n \cdot (\phi_m \mathbf{u}_R \times \text{grad}_1 \phi_k) \, d\Omega = 0.$$

A similar analysis shows that $\text{grad}_1 \psi_n$ and $(\mathbf{u}_R \times \text{grad}_1 \psi_n)$ form orthogonal sets, and that the sets $\text{grad}_1 \phi_m$ and $\mathbf{u}_R \times \text{grad}_1 \psi_n$ are cross-orthogonal. Eigenvectors can also be defined with respect to a cross section S at a radial distance R from the origin. The gradient now takes the form

$$\text{grad}_S \, \phi_m(\theta, \varphi) = \frac{1}{R} \frac{\partial \phi_m}{\partial \theta} \mathbf{u}_\theta + \frac{1}{R \sin\theta} \frac{\partial \phi_m}{\partial \varphi} \mathbf{u}_\varphi = \frac{1}{R} \text{grad}_1 \, \phi_m. \tag{16.63}$$

Orthogonality is now with respect to the scalar product

$$\langle \mathbf{a}, \mathbf{b} \rangle = \int_S (\mathbf{a} \cdot \mathbf{b}) \, dS, \tag{16.64}$$

where $dS = R^2 \, d\Omega$. The normalized eigenfunctions are ϕ_m/R and ψ_n/R, including $(\psi_0/R) = (1/\sqrt{S}) = (1/R\sqrt{\Omega})$. Thus,

$$\int_S |\text{grad}_S \, \phi_m|^2 R^2 \, d\Omega = \int_{S_1} |\text{grad}_1 \, \phi_m|^2 \, d\Omega = 1$$

$$\int_S \left(\frac{\phi_m}{R} \right)^2 dS = \int_S \left(\frac{\phi_m}{R} \right)^2 R^2 \, d\Omega = \int_{S_1} \phi_m^2 \, d\Omega \; = \; \frac{1}{k_m^2}. \tag{16.65}$$

16.5.2 The Field Expansions

We shall first assume that the cross section of the cone is simply connected, as in Figure 16.10*a*. Because the electric field is perpendicular to the boundary wall (except in the aperture, if there is one), it is natural to expand **e** in eigenvectors that partake of the same property. Such a move improves convergence. We write[†]

$$\mathbf{e}(\mathbf{r},t) = \sum_m v_m(R,t)\ \mathrm{grad}_S\,\phi_m + \sum_n v_n(R,t)\ \mathrm{grad}_S\,\psi_n \times \mathbf{u}_R + \sum_m w_m(R,t)\frac{1}{R}\,\phi_m\,\mathbf{u}_R. \tag{16.66}$$

The magnetic field, which is tangent to the metal, is similarly expanded as

$$\mathbf{h}(\mathbf{r},t) = \sum_m i_m(R,t)\,\mathbf{u}_R \times \mathrm{grad}_S\,\phi_m + \sum_n i_n(R,t)\ \mathrm{grad}_S\,\psi_n + \sum_{n\neq 0} l_n(R,t)\frac{1}{R}\psi_n\,\mathbf{u}_R + l_0(R,t)\frac{1}{R\sqrt{\Omega}}\,\mathbf{u}_R. \tag{16.67}$$

Because $\mathrm{grad}_S\,\phi_m$ brings in another R dependence through a $\left(\frac{1}{R}\right)$ factor, one may prefer to expand the fields in terms of $\mathrm{grad}_1\,\phi_m$ (and similarly $\mathrm{grad}_1\,\psi_n$) and to rely on a *unit expansion*,

$$\mathbf{e}(\mathbf{r},t) = \sum_n \underbrace{\frac{v_m}{R}}_{V_m}\ \mathrm{grad}_1\,\phi_m + \sum_p \underbrace{\left(\frac{v_n}{R}\right)}_{V_p}\mathrm{grad}_1\,\psi_p \times \mathbf{u}_R + \sum_m \frac{w_m}{R}\,\phi_m\,\mathbf{u}_R \tag{16.68}$$

$$\mathbf{h}(\mathbf{r},t) = \sum_m \underbrace{\frac{i_m}{R}}_{I_m}\ \mathbf{u}_R \times \mathrm{grad}_1\,\phi_m + \sum_n \underbrace{\frac{i_n}{R}}_{I_n}\ \mathrm{grad}_S\,\psi_n + \sum_{n\neq 0} l_n\frac{1}{R}\,\psi_n\,\mathbf{u}_R + l_0\frac{1}{R\sqrt{\Omega}}\,\mathbf{u}_R. \tag{16.69}$$

Both expansions, "*S*" and "*unit*," can be used to evaluate the fields in the cone. The method consists in inserting the expansions into Maxwell's equations, remembering that great care should be exercised in the differentiation of a series. The necessary steps are described in previous chapters, and we shall only quote the results, except for the TEM mode, in which case the details are worked out as a useful exercise and an opportunity to illustrate the mechanics of the method. The calculations make use of the following relationships, written out explicitly because of their general usefulness in spherical coordinates. Assuming that ϕ

[†]The notation for the expansion coefficients is slightly modified compared with the convention used in Section 7.11.

depends only on θ and φ:

$$\operatorname{curl}\left[f(R)\,\operatorname{grad}_S\phi\right] = \frac{df}{dR}\,\mathbf{u}_R \times \operatorname{grad}_S\phi \tag{16.70}$$

$$\operatorname{curl}\left[f(R)\,\operatorname{grad}_1\phi\right] = \frac{1}{R}\frac{d}{dR}(Rf)\,\mathbf{u}_R \times \operatorname{grad}_1\phi \tag{16.71}$$

$$\operatorname{curl}\left[f(R)\,\mathbf{u}_R \times \operatorname{grad}_S\phi\right] = f\nabla_S^2\phi\,\mathbf{u}_R - \frac{df}{dR}\operatorname{grad}_S\phi \tag{16.72}$$

$$\operatorname{curl}\left[f(R)\,\mathbf{u}_R \times \operatorname{grad}_1\phi\right] = \frac{f}{R}\nabla_1^2\phi\,\mathbf{u}_R - \frac{1}{R}\frac{d}{dR}(Rf)\operatorname{grad}_1\phi \tag{16.73}$$

$$\operatorname{curl}\left[f(R)\,\phi\,\mathbf{u}_R\right] = f\operatorname{grad}_S\phi \times \mathbf{u}_R = \frac{f}{R}\operatorname{grad}_1\phi \times \mathbf{u}_R \tag{16.74}$$

$$\operatorname{curl}\left[\frac{1}{R}f(R)\,\phi\,\mathbf{u}_R\right] = \frac{f}{R}\operatorname{grad}_S\phi \times \mathbf{u}_R = \frac{f}{R^2}\operatorname{grad}_1\phi \times \mathbf{u}_R. \tag{16.75}$$

The two Laplacians are connected by the relationship $\nabla_S^2\phi = \dfrac{1}{R^2}\nabla_1^2\phi$. The source terms must also be expanded, $\mathbf{j}$ in terms of the eigenfunctions and eigenvectors appropriate for $\mathbf{e}$, $\mathbf{j}_m$ in terms of those appropriate for $\mathbf{h}$. The expansion coefficients are obtained by means of orthogonality relationships such as (16.65). The results of the derivation are reminiscent of those obtained in Section 15.1 for cylindrical waveguides. They are given here for the expansion coefficients defined in (16.66) and (16.67) (i.e., for the S expansion).

16.5.3 TM Modes

$$\begin{aligned}\frac{\partial v_m}{\partial R} + \mu_0\frac{\partial i_m}{\partial t} - \frac{w_m}{R} &= -\int_S \mathbf{j}_m\cdot(\mathbf{u}_R \times \operatorname{grad}_S\phi_m)\,dS \\ &\quad -\int_C (\mathbf{u}_n \times \mathbf{e})\cdot(\mathbf{u}_R \times \operatorname{grad}_S\phi_m)\,dc \end{aligned}\tag{16.76}$$

$$\frac{\partial i_m}{\partial R} + \epsilon_0\frac{\partial v_m}{\partial t} = -\int_S \mathbf{j}\cdot\operatorname{grad}_S\phi_m\,dS \tag{16.77}$$

$$i_m + \frac{R}{k_m^2}\epsilon_0\frac{\partial w_m}{\partial t} = -\int_S \mathbf{j}\cdot\mathbf{u}_R\,\phi_m\,dS. \tag{16.78}$$

The coefficients in the unit expansion can be found either directly by means of (16.71), (16.73), and (16.75), or more automatically by replacing v_m by RV_m and i_m by RI_m in (16.76) to (16.78). For (16.77), for example, one obtains

$$\frac{1}{R}\frac{\partial}{\partial R}[RI_m] + \epsilon_0\frac{\partial V_m}{\partial t} = -\int_\Omega \mathbf{j}\cdot\operatorname{grad}_1\phi_m\,d\Omega. \tag{16.79}$$

Elimination of v_m and w_m leads to equations for i_m (or I_m) alone. Thus, in a region devoid of sources,

$$\frac{\partial^2 i_m}{\partial R^2} - \frac{1}{c_0^2}\frac{\partial^2 i_m}{\partial t^2} - \frac{k_m^2}{R^2}\,i_m = 0 \tag{16.80}$$

$$\frac{1}{R}\frac{\partial^2(RI_m)}{\partial R^2} - \frac{1}{c_0^2}\frac{\partial^2 I_m}{\partial t^2} - \frac{k_m^2}{R^2} I_m = 0. \tag{16.81}$$

These equations are of the *spherical transmission line* type. For time-harmonic fields, the last equation takes the interesting form

$$\frac{d^2 I_m}{dR^2} + \frac{2}{R}\frac{dI_m}{dR} + \left(k_0^2 - \frac{k_m^2}{R^2}\right) I_m = 0. \tag{16.82}$$

From (A5.85), this is recognized as the equation satisfied by the spherical Bessel functions $j_\nu(k_0R)$, $n_\nu(k_0R)$, and $h_\nu(k_0R)$, provided ν is selected to satisfy $\nu(\nu+1) = k_m^2$.

16.5.4 TE Modes

$$\frac{\partial v_n}{dR} + \mu_0 \frac{\partial i_n}{\partial t} = -\int_S \mathbf{j}_m \cdot \text{grad}_S\, \psi_n\, dS - \int_C (\mathbf{u}_n \times \mathbf{e}) \cdot \text{grad}_S\, \psi_n\, dc \tag{16.83}$$

$$v_n + \frac{R}{k_n^2}\mu_0 \frac{\partial l_n}{\partial t} = -\int_S (\mathbf{j}_m \cdot \mathbf{u}_R)\, \psi_n\, dS - \int_C (\mathbf{u}_n \times \mathbf{e}) \cdot \mathbf{u}_R\, \psi_n\, dc \tag{16.84}$$

$$\frac{\partial i_n}{\partial R} + \epsilon_0 \frac{\partial v_n}{\partial t} - \frac{l_n}{R} = -\int_S \mathbf{j} \cdot (\text{grad}_S\, \psi_n \times \mathbf{u}_R)\, dS \tag{16.85}$$

$$\mu_0 \frac{\partial l_0}{\partial t} = -\frac{1}{R\sqrt{\Omega}} \int_S (\mathbf{j}_m \cdot \mathbf{u}_R)\, dS - \frac{1}{R\sqrt{\Omega}} \int_C (\mathbf{u}_n \times \mathbf{e}) \cdot \mathbf{u}_R\, dc. \tag{16.86}$$

Elimination of i_n and l_n from (16.83) to (16.85) shows that v_n and V_n respectively satisfy (16.80) and (16.81). From (16.67), and because orthogonality of the ψ_n's to ψ_0 implies $\int_S \psi_n\, dS = 0$, it is clear that the term in l_0 yields the average radial component of $\mathbf{h}$ over the cross section. Thus,

$$\frac{l_0(R,t)}{R\sqrt{\Omega}} = [h_R(R,t)]_{\text{ave}}\,. \tag{16.87}$$

The radial magnetic flux is therefore

$$-\frac{\partial \Phi(R,t)}{\partial t} = \int_S (\mathbf{j}_m \cdot \mathbf{u}_R)\, dS + \int_C (\mathbf{u}_n \times \mathbf{e}) \cdot \mathbf{u}_R\, dc. \tag{16.88}$$

This expression corresponds with Equation (7.185), derived in Chapter 7 for the flux variation in free space. We note, from (16.86), that the l_0 mode does not radiate. It represents reactive energy and is therefore important for the evaluation of the near field and the Q of the sources. Radiation, therefore, finds its origin in the remaining modes of the expansion.[32]

The source integrals over $(\mathbf{u}_n \times \mathbf{E})$ in the right-hand terms of (16.76), (16.83), (16.84), and (16.86) can serve to solve coupled regions problems. Such problems are encountered when there are apertures in the wall, through which radiation can leave (or enter) the conical volume. It should be noted, in that respect, that the exterior region in Figure 16.10*a* is also a cone, now of opening solid angle $(4\pi - \Omega_1)$, and endowed with its own eigenvectors. The boundary between the two complementary cross sections is a curve in the (θ, φ) plane. For

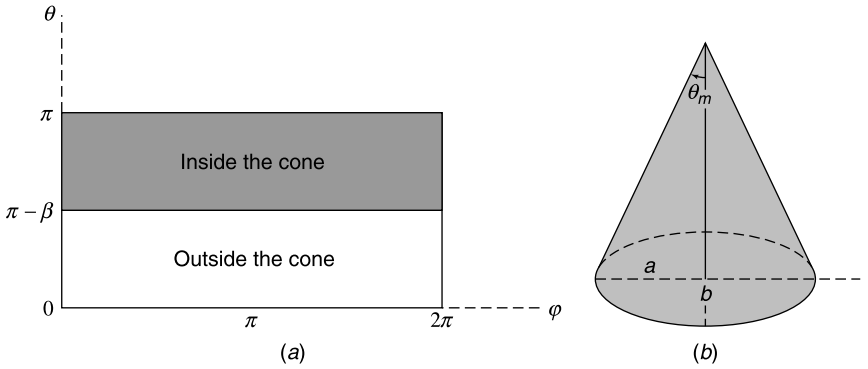

Figure 16.12 (*a*) The (θ, φ) plane. (*b*) Elliptic cone (from R. De Smedt and J. Van Bladel, Field singularities at the tip of a metallic cone of arbitrary cross section, *IEEE Trans. AP* **34**, 865–870, 1986, with permission of IEEE).

a circular cone of opening angle β (Fig. 16.11*c*, lower cone), the curve is the horizontal line in Figure 16.12*a*. For the elliptic cone in Figure 16.12*b*, the curve is defined by[33]

$$\theta(\varphi) = \text{arc tan}\, \frac{\epsilon \tan \theta_m}{\sqrt{\sin^2 \varphi + \epsilon^2 \cos^2 \varphi}}. \tag{16.89}$$

where $\epsilon = (b/a)$.

16.5.5 The TEM Mode

When the cross section of the cone is doubly bounded (and at the same time doubly connected), the field expansions should include a *TEM mode*, whose fields are

$$\mathbf{e}_0(R,t) = v_0(R,t)\, \text{grad}_S\, \phi_0 \;=\; V_0(R,t)\, \text{grad}_1\, \phi_0 \tag{16.90}$$

$$\mathbf{h}_0(R,t) = i_0(R,t)\, \mathbf{u}_R \times \text{grad}_S\, \phi_0 \;=\; I_0(R,t)\, \mathbf{u}_R \times \text{grad}_1\, \phi_0. \tag{16.91}$$

From (16.60), ϕ_0 is proportional to the potential difference between c_1^a and c_1^b, which we choose to satisfy the normalization condition

$$\int_{\Omega_1} |\text{grad}_1\, \phi_0|^2\, d\Omega = \int_S |\text{grad}_S\, \phi_0|^2\, dS = 1. \tag{16.92}$$

To derive equations satisfied by v_0 and i_0, we expand curl $\mathbf{e}$ separately as

$$\text{curl}\, \mathbf{e} = a_0(R,t)\, \mathbf{u}_R \times \text{grad}_S\, \phi_0 + \text{terms in } \phi_m \text{ and } \psi_n. \tag{16.93}$$

It is the $a_0(R,t)$ coefficient that interests us, and our next task is to relate it to v_0 and i_0. Given the normalization condition (16.92), we may write

$$a_0(R,t) = \int_S \text{curl}\, \mathbf{e} \cdot (\mathbf{u}_R \times \text{grad}_S\, \phi_0)\, dS.$$

By invoking (16.72) (and because $\nabla_S^2 \phi_0 = 0$), the integrand can be rewritten as

$$\text{curl } \mathbf{e} \cdot (\mathbf{u}_R \times \text{grad}_S\, \phi_0) = \text{div}\,[\mathbf{e} \times (\mathbf{u}_R \times \text{grad}_S\, \phi_0)].$$

From (A2.90), the divergence in spherical coordinates can be split according to

$$\text{div } \mathbf{a} = \frac{1}{R^2} \frac{\partial}{\partial R}(R^2 a_R) + \text{div}_S\, \mathbf{a}_t.$$

It follows that

$$\begin{aligned} a_0(R,t) &= \int_S \text{div}\,[\mathbf{e} \times (\mathbf{u}_R \times \text{grad}_S\, \phi_0)]\, dS \\ &= \int_S \text{div}_S[\mathbf{e} \times (\mathbf{u}_R \times \text{grad}_S\, \phi_0)]_t\, dS \\ &\quad + \frac{1}{R^2} \frac{\partial}{\partial R} \int_S R^2\, \mathbf{u}_R \cdot [\mathbf{e} \times (\mathbf{u}_R \times \text{grad}_S\, \phi_0)]\, dS \\ &= I(R,t) + \frac{1}{R^2} \frac{\partial}{\partial R}(R^2 v_0). \end{aligned} \tag{16.94}$$

The surface integral $I(R,t)$ can be transformed by applying the surface divergence theorem (A3.44), in which we set J equal to $\dfrac{2}{R}$, the value of the first curvature on a sphere. The unit vectors $\mathbf{u}_m$ and $\mathbf{u}_n$ are respectively $\mathbf{u}_n$ and $\mathbf{u}_R$ in the current case (Fig. 16.10*a*). Thus,

$$I(R,t) = \int_C (\mathbf{u}_n \times \mathbf{e}).(\mathbf{u}_R \times \text{grad}_S\, \phi_0)\, dc - \frac{2}{R} \underbrace{\int_S \mathbf{u}_R \cdot [\mathbf{e} \times (\mathbf{u}_R \times \text{grad}_S\, \phi_0)]\, dS}_{v_0(R,t)}.$$

By inserting $I(R,t)$ into (16.94), we obtain

$$a_0(R,t) = \frac{\partial v_0}{\partial R} + \int_C (\mathbf{u}_n \times \mathbf{e}) \cdot (\mathbf{u}_R \times \text{grad}_S\, \phi_0)\, dS.$$

This is our main result. Combined with Maxwell equation (7.1), it leads to the transmission line equation[‡]

$$\begin{aligned} \frac{\partial v_0}{\partial R} + \mu_0 \frac{\partial i_0}{\partial t} &= -\int_S \mathbf{j}_m \cdot (\mathbf{u}_R \times \text{grad}_S\, \phi_0)\, dS \\ &\quad - \int_C (\mathbf{u}_n \times \mathbf{e}) \cdot (\mathbf{u}_R \times \text{grad}_S\, \phi_0)\, dc \;=\; -A_0(R,t). \end{aligned} \tag{16.95}$$

By similar methods, based on (7.2), one obtains

$$\frac{\partial i_0}{\partial R} + \epsilon_0 \frac{\partial v_0}{\partial t} = -\int_S \mathbf{j} \cdot \text{grad}_S\, \phi_0\, dS \;=\; -B_0(R,t). \tag{16.96}$$

[‡]The contribution of $\mathbf{u}_n \times \mathbf{e}$ to the source term could have been derived directly by remembering that $\mathbf{u}_n \times \mathbf{e}$ is a Huygens equivalent magnetic current [see (7.225)].

By elimination:

$$\frac{\partial^2 v_0}{\partial R^2} - \epsilon_0\mu_0\frac{\partial^2 v_0}{\partial t^2} = -\frac{\partial A_0}{\partial R} + \mu_0\frac{\partial B_0}{\partial t} \tag{16.97}$$

$$\frac{\partial^2 i_0}{\partial R^2} - \epsilon_0\mu_0\frac{\partial^2 i_0}{\partial t^2} = \epsilon_0\frac{\partial A_0}{\partial t} - \frac{\partial B_0}{\partial R}. \tag{16.98}$$

In the absence of source terms, the time-harmonic solutions for v_0 and i_0 are $e^{\pm jk_0R}$ and correspondingly $\dfrac{1}{R}e^{\pm jk_0R}$ for V_0 and I_0.

16.6 SINGULARITIES AT THE TIP OF A CONE

Protuberances on scatterers such as rockets, aircrafts, and ships can often be modeled by cones (which could be circular, elliptic, pyramidal, or in the form of a sector). In the numerical solution of the scattering problem, the convergence of the algorithm can be accelerated by taking the singularities at the tip into account. A knowledge of these singularities also provides an a posteriori check on the validity of some numerical or analytical results.

16.6.1 Simply Bounded Cones

We first assume that the cone is perfectly conducting. In the *electric* singularity, the singularity exponent ν is the smallest root of

$$\nu_m(\nu_m + 1) = k_m^2,$$

where k_m^2 is defined by (16.56). The potential near the apex of the cone can be expanded in harmonics $R^{\nu_m}Y_m(\theta,\varphi)$, where $Y_m(\theta,\varphi)$ satisfies (Fig. 16.10*a*)

$$\begin{aligned} \nabla_1^2 Y_m + \nu_m(\nu_m+1)\,Y_m &= 0 \quad (\text{in } S_1) \\ Y_m &= 0 \quad (\text{on } C_1). \end{aligned} \tag{16.99}$$

The corresponding fields are

$$\begin{aligned} \mathbf{E} &= R^{\nu_m-1}[\nu_m\,Y_m(\theta,\varphi)\,\mathbf{u}_R + \operatorname{grad}_1 Y_m(\theta,\varphi)] \\ \mathbf{H} &= -j\omega\epsilon_0\,\frac{R^{\nu_m}}{\nu_m+1}\,\mathbf{u}_R \times \operatorname{grad}_1 Y_m(\theta,\varphi). \end{aligned} \tag{16.100}$$

For a general conical cross section, the problem narrows down to a search for the values of ν_m less than one. This search can be based on variational principles, as in (5.134) and (5.136) [133]. The *circular cone* is an important particular case, for which data are given in Table 5.3. As mentioned in Section 5.12, the $m = 0$ mode of a *sharp* cone is the only

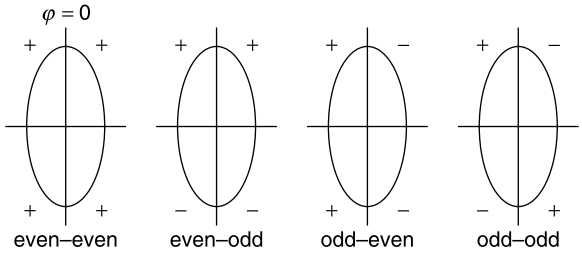

Figure 16.13 Basic symmetries for an elliptic cone.

singular one. For a thin circular needle, in particular (Fig. 5.38),

$$\nu \approx \frac{1}{2\log_e \dfrac{2}{\alpha}}$$

$$P_\nu \approx 1 + 2\nu \log_e \cos\frac{\theta}{2}$$

$$\mathbf{E} = \frac{1}{R}\cos\frac{\theta}{2}\,\mathbf{u}_R - \frac{1}{R}\sin\frac{\theta}{2}\,\mathbf{u}_\theta. \tag{16.101}$$

When the cross section is *elliptic*, *four* basic symmetries of the electric potential should be considered (Fig. 16.13). Detailed calculations show that the strongest singularity appears in the even-even symmetry[33] [133]. When a cone is very sharp, the singular value of ν for a general cross section is

$$\nu = \frac{1}{2\log_e\left(\dfrac{2F}{\alpha_{\max}}\right)}, \tag{16.102}$$

where $\alpha_{\max}$ is the maximum half-opening angle of the cone (so chosen that the circle $\theta = \pi - \alpha_m$ on the unit sphere just encloses C_1) and F is a shape factor, equal to one for the circle. For an elliptic needle:

$$F = 2\,\frac{\alpha_{\max}}{\alpha_{\max} + \alpha_{\min}}. \tag{16.103}$$

The *sector* is a degenerate form of the elliptic cone.[34] Table 16.1 gives its singularity exponent ν in terms of the full opening angle α of the sector.

More details on ν can be found in Table 5.4. The limit values in Table 16.1 are $\nu = 0$ and $\tau = 1$ for $\alpha \to 0$, and $\nu = 1$ and $\tau = 0$ for $\alpha \to 360°$.

The exponent τ of the *magnetic singularity* is related to the eigenvalue k_n^2 in (16.58) by the equation $\tau_n(\tau_n + 1) = k_n^2$. The magnetic potential is proportional to $R^{\tau_n} Z_n(\theta, \varphi)$, where

Table 16.1 Singularity Exponent for a Sector

α	20°	60°	100°	140°	180°	220°	260°	300°	340°
ν	0.159	0.241	0.317	0.400	0.500	0.625	0.776	0.920	0.992
τ	0.992	0.920	0.776	0.625	0.500	0.400	0.317	0.241	0.159
			Salient				Reentrant		

Z_n satisfies (Fig. 5.41)

$$\begin{aligned} \nabla_1^2 Z_n(\theta,\varphi) + \tau_n(\tau_n+1)\, Z_n(\theta,\varphi) = 0 \qquad & (\text{in } S_1) \\ \mathbf{u}_n \cdot \text{grad}_1\, Z_n = 0 \qquad & (\text{on } C_1). \end{aligned} \tag{16.104}$$

The boundary condition on Z_n is precisely of the type that must be satisfied by the magnetic field. The fields corresponding with τ_n are

$$\begin{aligned} \mathbf{E} &= j\omega\mu_0 \frac{R^{\tau_n}}{\tau_n+1}\, \mathbf{u}_R \times \text{grad}_1\, Z_n(\theta,\varphi) \\ \mathbf{H} &= R^{\tau_n-1}\left[\tau_n Z_n(\theta,\varphi)\, \mathbf{u}_R + \text{grad}_1\, Z_n(\theta,\varphi)\right]. \end{aligned} \tag{16.105}$$

It is now the *magnetic* field that evidences the most singular behavior. For the *circular cone*, the strongest singularity is associated with the $m = 1$ harmonic, with field components proportional to $\cos\varphi$ or $\sin\varphi$. Some values of τ_n are given in Table 16.2.

When the cone is *elliptic*, the singularities are found in the odd-even and even-odd symmetries of the magnetic potential [133]. The values of τ for a sector are given in Table 16.1, where it is seen that $\tau(\alpha) = \nu(2\pi - \alpha)$. The field singularities can also be derived from an analytic determination of the fields near the tip of an elliptic cone. The solution of that particular problem is based on separation of variables in sphero-conal coordinates, in which the cone is one of the coordinate surfaces[35,36] (see Section 16.7).

Results for the electric and magnetic singularities of a pyramid are only partially available and concern mainly the 90° corner [133]. Whatever the shape of the cross section, the singularities of the fields cause corresponding singularities of the surface sources. When the singularity is electric, it is the *charge density* that is singular. More precisely,

$$\rho_S = \epsilon_0\, \mathbf{u}_n \cdot \mathbf{E} = \epsilon_0\, R^{\nu_m - 1}\, \mathbf{u}_n \cdot \text{grad}_1\, Y_m(\theta,\varphi). \tag{16.106}$$

When the singularity is magnetic, it is the *current density* that is singular. Thus,

$$\mathbf{J}_S = \mathbf{u}_n \times \mathbf{H} = R^{\tau_n - 1}\left[\tau_n Z_n(\theta,\varphi)\, \mathbf{u}_c - \frac{\partial Z_n(\theta,\varphi)}{\partial c}\, \mathbf{u}_R\right]. \tag{16.107}$$

If the *cone* is filled with a *dielectric material* of dielectric constant $\epsilon_r(\theta,\varphi)$, the search for ν proceeds by assuming potentials of the form $\phi^i = R^\nu Y^i(\theta,\varphi)$ in each region i ($i = 1, 2$). The eigenvalue problem is now

$$\text{div}_1\, [\epsilon_r^i\, \text{grad}_1\, Y^i(\theta,\varphi)] + \nu(\nu+1)\, \epsilon_r^i\, Y_i(\theta,\varphi) = 0 \qquad (\text{in } S^i), \tag{16.108}$$

and the boundary condition requires Y^i and $\epsilon_r^i\, \mathbf{u}_n \cdot \text{grad}_1\, Y^i$ to be continuous on C_1. The electric field is the only one to be potentially singular, and values of the relevant exponent are displayed in Figure 5.39 for a homogeneous circular cone. A few data are also available for the homogeneous pyramid [133].

Table 16.2 Magnetic Singularity Exponent for a Circular Cone

α	90°	80°	70°	60°	50°	40°	30°	20°	10°	5°
τ	1.000	0.928	0.881	0.856	0.852	0.867	0.901	0.945	0.985	0.996

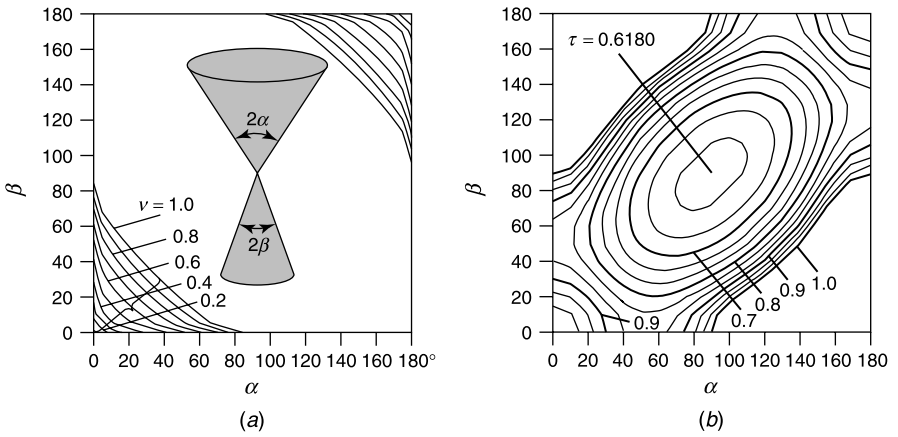

Figure 16.14 Concentric-coaxial perfectly conducting circular cones. (*a*) Electric singularity exponent ν. (*b*) Magnetic singularity exponent (from F. Olyslager, Field singularities at the common tip of a number of concentric biisotropic cones, *Microwave Opt. Tech. Lett.* **6**, 862–867, 1993, with permission of John Wiley & Sons).

16.6.2 Doubly Bounded Cones

The singularity exponent of a biconical scatterer (concentric as in Fig. 16.11*b*, or coaxial as in Fig. 16.11*c*) is only available in a few cases. Data for perfectly conducting concentric-coaxial circular cones can be found in Figure 16.14. The electric singularity is associated with the φ-independent fields ($m = 0$) and the magnetic singularity with $m = 1$ (i.e., with a $\sin\varphi$, $\cos\varphi$ field dependence[37]). Only the zone $\alpha + \beta \leq \pi$ is of physical significance. Some numerical results[§] for the $\alpha = \beta$ *bicone* are given in Tables 16.3 and 16.4.

Singularity exponents have also been evaluated for concentric and coaxial cones consisting of biisotropic materials, and concentric and coaxial circular cones (perfectly

Table 16.3 Electric Singularity Exponent ν

α	2.5°	5°	10°	15°	20°	25°	30°	35°
ν	0.272	0.337	0.445	0.547	0.653	0.768	0.897	1.040

Table 16.4 Magnetic Singularity Exponent τ

α	5°	10°	20°	30°	40°	50°	70°	90°
τ	0.992	0.970	0.898	0.817	0.749	0.698	0.637	0.617

conducting or bianisotropic) embedded in a bianisotropic material.[38,39] Such materials have gained in importance recently because of the added degrees of freedom they provide for the design of components. Also useful are values of ν for two coaxial, coplanar perfectly conducting sectors, in contact through a common apex[40] (a "bowtie" reflector).

[§]Numerical data courtesy of Prof. F. Olyslager.

16.7 RADIATION AND SCATTERING FROM CONES

The radiation problem consists in finding the exterior fields generated by the presence of a magnetic current at the surface of the cone. This current, equal to $\mathbf{u}_n \times \mathbf{E}$, can be concentrated in an aperture or, when the cone is perfectly conducting and immersed in an incident wave, occupy the whole surface of the cone, where it is equal to $-(\mathbf{u}_n \times \mathbf{E}^i)$. The radiation and scattering problems can be solved by separation of variables in only a few cases [113]. We shall currently discuss two of these.

16.7.1 Radiation from a Slot in a Circular Conical Surface

The aperture is a narrow circumferential slot, across which a uniform voltage V is applied (Fig. 16.15*a*). The aperture field has the components

$$E_c = 0; \qquad E_R = V\,\delta(R-a).$$

In more compact form:

$$\mathbf{u}_n \times \mathbf{E} = V\,\delta(R-a)\,\mathbf{u}_c.$$

With this value of $(\mathbf{u}_n \times \mathbf{E})$ the second members in Equations (16.76), (16.83), (16.84), and (16.86) can be evaluated. The analysis requires a knowledge of the eigenfunctions of S_1 when the cone is circular. These are[41] (to within an arbitrary factor)

$$\phi_{mp} = \left\{ \begin{array}{c} \cos m\varphi \\ \sin m\varphi \end{array} \right\} P^m_{\nu_{mp}}(\cos\theta) \tag{16.109}$$

and

$$\psi_{ns} = \left\{ \begin{array}{c} \cos n\varphi \\ \sin n\varphi \end{array} \right\} P^n_{\tau_{ns}}(\cos\theta). \tag{16.110}$$

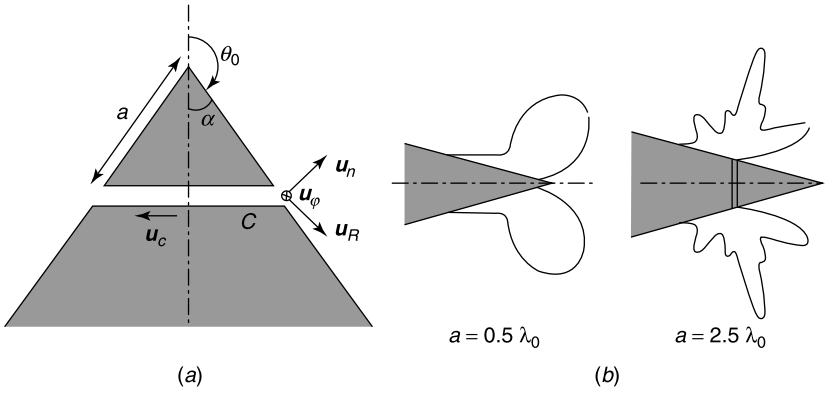

Figure 16.15 (*a*) Circular cone with slot. (*b*) Field patterns (from L. L. Bailin and S. Silver, Exterior electromagnetic boundary value problems for spheres and cones, *IRE Trans. AP* **4**, 5–16, 1956, with permission of IEEE).

The functions P_β^α are associated Legendre functions. The eigenvalues are actually the subscripts ν_{mp} and τ_{ns}, and they are determined from the boundary conditions

$$P^m_{\nu_{mp}}(\cos\theta_0) = 0 \tag{16.111}$$

$$\frac{\partial}{\partial\theta} P^n_{\tau_{ns}}(\cos\theta)\bigg|_{\theta=\theta_0} = 0. \tag{16.112}$$

The normalization integral for the TM eigenfunctions can be written as

$$\begin{aligned}\int_{S_1} |\text{grad}_1\,\phi_{mp}|^2\,dS_1 \;&=\; \nu_{mp}(\nu_{mp}+1)\int_{S_1}|\phi_{mp}|^2\,dS_1\\ &= \nu_{mp}(\nu_{mp}+1)\frac{2\pi}{\epsilon_m}\int_0^{\theta_0}[P^m_{\nu_{mp}}(\cos\theta)]^2\sin\theta\,d\theta\\ &= \frac{2\pi}{\epsilon_m}\frac{\nu_{mp}(\nu_{mp}+1)}{2\nu_{mp}+1}\,\sin\theta_0\,\frac{\partial P^m_{\nu_{mp}}(\cos\theta)}{\partial\theta}\bigg|_{\theta=\theta_0}\frac{\partial P_\nu(\cos\theta)}{\partial\nu}\bigg|_{\substack{\theta=\theta_0\\ \nu=\nu_{mp}}}.\end{aligned} \tag{16.113}$$

For the TE eigenfunctions, similarly,

$$\begin{aligned}\int_{S_1} |\text{grad}_1\,\psi_{ns}|^2\,dS_1 &= \tau_{ns}(\tau_{ns}+1)\int_{S_1}|\psi_{ns}|^2\,dS_1\\ &= -\frac{2\pi}{\epsilon_n}\frac{\tau_{ns}(\tau_{ns}+1)}{2\tau_{ns}+1}\,\sin\theta_0\,P^n_{\tau_{ns}}(\cos\theta_0)\,\frac{\partial^2 P^n_\tau}{\partial\theta\,\partial\tau}\bigg|_{\substack{\theta=\theta_0\\ \tau=\tau_{ns}}}.\end{aligned} \tag{16.114}$$

The particular symmetry of the configuration implies that the φ-independent modes are the only ones to be excited. Under those circumstances, the right-hand terms of (16.83) to (16.86) vanish, from which it may be concluded that the TE modes are not excited. The TM modes, on the other hand, *are* excited through the second term of (16.76), which can be written as

$$B_{0p}(R) = -V\,2\pi\left(\frac{\partial\phi_{0p}}{\partial n}\right)_1\delta(R-a).$$

We shall drop the subscript 0 in the sequel, for conciseness. The main expansion coefficient $i_p(R)$ is found, from (16.76) to (16.78), to satisfy the differential equation

$$\begin{aligned}\frac{d^2 i_p}{dR^2} + \left(k_0^2 - \frac{\nu_p(\nu_p+1)}{R^2}\right) i_p &= j\omega\epsilon_0\,V 2\pi a\left(\frac{\partial\phi_p}{\partial n}\right)_1\delta(R-a)\\ &= a\,P_p\,\delta(R-a).\end{aligned} \tag{16.115}$$

From (16.67), the magnetic field is $i_p\,\mathbf{u}_R\times\text{grad}_S\,\phi_p$. In the *unit* expansion, the main coefficient is $I_p = (i_p/R)$, and it must satisfy

$$\frac{1}{R}\frac{d^2(RI_p)}{dR^2} + \left(k_0^2 - \frac{\nu_p(\nu_p+1)}{R^2}\right) I_p = P_p\,\delta(R-a). \tag{16.116}$$

The linearly independent solutions of the equation without second term are the spherical Bessel functions $j_{\nu_p}(k_0R)$ and $n_{\nu_p}(k_0R)$, defined in (A5.84). From (A5.101), the appropriate linear combination for $R > a$ is $h^{(2)}_{\nu_p}(k_0R)$. For $R < a$, closer to the apex, the need to keep the energy finite in the vicinity of the apex leads to the solution $j_{\nu_p}(k_0R)$ [see (A5.94) and (A5.95)]. To solve (16.116), one further requires $I_p(R)$ to be continuous at $R = a$, and (dI_p/dR) to suffer a jump equal to P_ν. A few simple steps, based on the value of the Wronskian in (A5.106), lead to

$$I_p(R) = jk_0\, a^2 P_p \begin{cases} h^{(2)}_{\nu_p}(k_0R)\, j_{\nu_p}(k_0a) & (\text{for } R > a) \\ h^{(2)}_{\nu_p}(k_0a)\, j_{\nu_p}(k_0R) & (\text{for } R < a). \end{cases} \tag{16.117}$$

The other expansion coefficients can now be determined from (16.77) and (16.78). A few typical radiation patterns are given in Figure 16.15*b* for $\theta_0 = 165^\circ$ (or $\alpha = 15^\circ$) and two different values of (a/λ_0).

It is important to note that the *modal* expansions given above have satisfactory convergence properties as long as the distances from apex to sources, and from apex to field point, are not large compared with the wavelength. These requirements are not satisfied when the field point is in the radiation zone, in which case it is preferable to replace the modal representation with a contour-integral representation, which has better convergence properties.[42]

The solution of the scattering problem for *arbitrary* incident fields implies the excitation of a number of φ-dependent harmonics. Sources for which results are available are the electric and magnetic dipoles [38]. By solving the problem for dipoles oriented along three orthogonal directions, it becomes possible to construct the Green's dyadic for the circular cone [210]. In the solution of the scattering problem for an infinite perfectly conducting cone of *arbitrary* cross section, the following conditions must be satisfied by the fields:

- They should exhibit the previously discussed singularities at the tip of the cone.
- They should satisfy the boundary conditions at a perfectly conducting surface.
- They should satisfy the radiation condition in the form

$$\lim_{R\to\infty} R(\mathbf{E} + \mathbf{u}_R \times \mathbf{H}) \to 0; \qquad \lim_{R\to\infty} R(\mathbf{H} - \mathbf{u}_R \times \mathbf{E}) \to 0$$

  along any radius.

Under these conditions, it can be shown that the solution of the problem is unique, also when the obstacle is only conical outside some finite sphere.[43,44]

16.7.2 Scattering by an Elliptic Cone

The truncated elliptic cone provides a useful model for an obstacle such as a mountain. In its important limit form, the sector, it can simulate parts of a scatterer, for example the wing of an aircraft. The scattering problem for the elliptic cone can be solved in *sphero-conal coordinates* (r, θ, φ) (Fig. 16.16). These coordinates are related to the Cartesian coordinate

system by the transformation[45]

$$\begin{aligned} x &= r\sin\theta\cos\varphi & 0 \le r < \infty \\ y &= r\sqrt{1-k^2\cos^2\theta}\,\sin\varphi & 0 \le \theta \le \pi \\ z &= r\cos\theta\sqrt{1-k'^2\sin^2\varphi} & 0 \le \varphi \le 2\pi, \end{aligned} \tag{16.118}$$

where k and k' are ellipticity parameters, which must satisfy the conditions

$$0 \le k, k' \le 1; \qquad k^2 + k'^2 = 1. \tag{16.119}$$

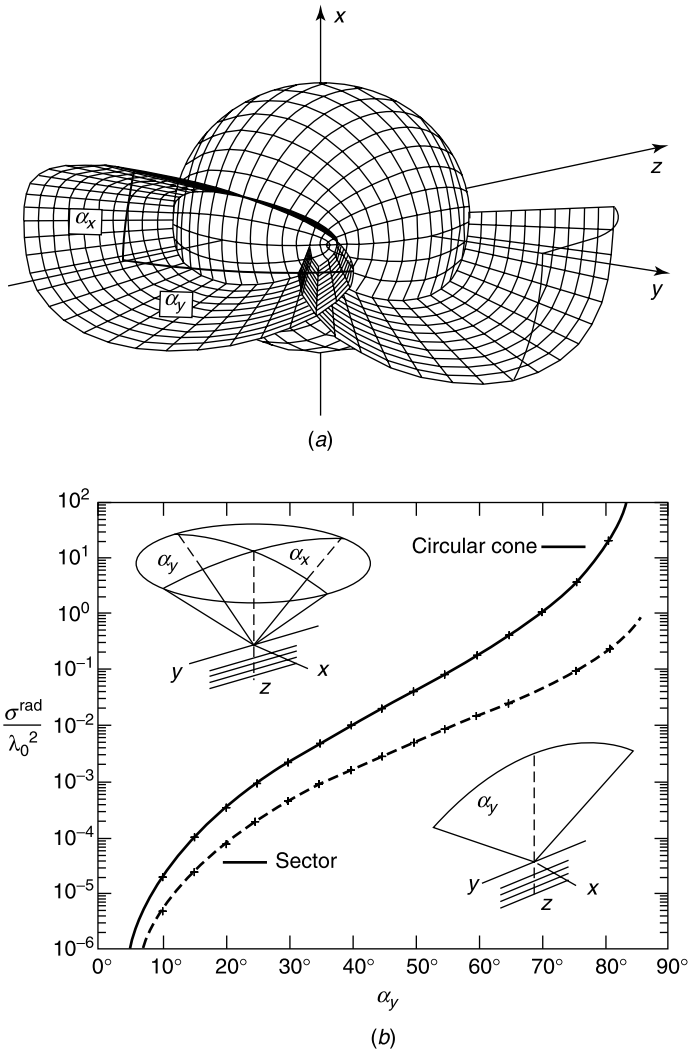

Figure 16.16 (*a*) Sphero-conal coordinate surfaces. (*b*) Nose-on backscattering cross section (from S. Blume, Spherical-multipole analysis of electromagnetic and acoustical scattering by a semi-infinite elliptic cone, *IEEE Antennas Prop. Mag.* **38**, 33–44, 1996, with permission of IEEE).

In the special case $k = 1 (k' = 0)$, the sphero-conal coordinate system (r, θ, φ) reduces to the ordinary spherical coordinate system. The characteristic half-opening angles α_x and α_y (Fig. 16.16*b*) are connected by

$$\cos \alpha_y = k \cos \alpha_x. \tag{16.120}$$

This relationship determines the value of k. Setting $\theta = 0$ (or π) and $\varphi = \dfrac{\pi}{2} \left(\text{or } \dfrac{3\pi}{2} \right)$ produces angular sectors in the (y, z) plane $(\alpha_x = 0)$. A circular cone corresponds with $\alpha_x = \alpha_y$, and a half plane is obtained for $\alpha_x = 0$ and $\alpha_y = \dfrac{\pi}{2}$. The metric coefficients in sphero-conal coordinates are [24]

$$\begin{aligned} h_r &= 1 \\ h_\theta &= r \sqrt{\frac{k^2 \sin^2 \theta + k'^2 \cos^2 \varphi}{1 - k^2 \cos^2 \theta}} = r\, s_\theta \\ h_\varphi &= r \sqrt{\frac{k^2 \sin^2 \theta + k'^2 \cos^2 \varphi}{1 - k'^2 \sin^2 \varphi}} = r\, s_\varphi. \end{aligned} \tag{16.121}$$

The Helmholtz equation now takes the form

$$\frac{1}{r^2} \frac{\partial}{\partial r} \left(r^2 \frac{\partial \phi}{\partial r} \right) + \frac{1}{r^2} \frac{1}{s_\theta s_\varphi} \left\{ \frac{\partial}{\partial \theta} \left(\frac{s_\varphi}{s_\theta} \frac{\partial \phi}{\partial \theta} \right) + \frac{\partial}{\partial \varphi} \left(\frac{s_\theta}{s_\varphi} \frac{\partial \phi}{\partial \varphi} \right) \right\} + k_0^2 \phi = 0. \tag{16.122}$$

Separation of variables applied to that equation gives products $c(r)\, Y_\nu(\theta, \varphi)$, where $c(r)$ is a spherical Bessel function and $Y_\nu(\theta, \varphi)$ a *Lamé product*. Such a product can be written as $f_\nu(\theta)\, g_\nu(\varphi)$, where f and g satisfy the *Lamé differential equations*[45,46] [144]

$$\sqrt{1 - k^2 \cos^2 \theta} \frac{d}{d\theta} \left(\sqrt{1 - k^2 \cos^2 \theta} \frac{df_\nu}{d\theta} \right) + \left[\nu(\nu + 1)(1 - k^2 \cos^2 \theta) - \lambda \right] f_\nu = 0 \tag{16.123}$$

$$\sqrt{1 - k'^2 \sin^2 \varphi} \frac{d}{d\varphi} \left(\sqrt{1 - k'^2 \sin^2 \varphi} \frac{dg_\nu}{d\varphi} \right) + \left[\lambda - \nu(\nu + 1)(k'^2) \sin^2 \varphi \right] g_\nu = 0. \tag{16.124}$$

The constants ν and λ are determined by enforcing the usual boundary conditions at the surface of the cone. Figure 16.16*b* gives, as an illustration, numerical results for the nose-on backscattering cross section of two perfectly conducting semi-infinite scatterers: the circular cone and a metallic sector of half opening angle α_y. The incident plane wave is polarized in the y-direction. The expansion may also serve to determine the electric dyadic of a perfectly conducting elliptic cone;[47] it can also provide an exact solution for the field scattered by a perfectly conducting angular sector.[44,47,48,49] Detailed information is further available for the current density near the tip of a metallic sector[50] and for the currents near the contact between two concentric angular sectors.[51]

16.7.3 The Biconical Antenna

The theory of the *biconical antenna* has received much attention in the past [15, 97, 114]. The two cones, 1 and 2, can be thought of as the two conductors of a coaxial line, with end point in O (Fig. 16.17). The cross section S (i.e., the intersection with a spherical surface of radius $R = a$) is the bracelet-shaped surface S shown in the figure. We shall investigate the TEM mode, whose fields, given the axisymmetric geometry of the waveguide, must be φ-independent. We first note that the φ-independent eigenfunctions of the coaxial structure are linear combinations of $P_\nu(\cos\theta)$ and a second solution,[¶] which can be chosen as either $P_{\nu_m}(-\cos\theta)$ or $Q_{\nu_m}(\cos\theta)$. The two functions are connected by the relationship [161]

$$Q_\nu(\cos\theta) = \frac{\pi}{2\sin(\nu\pi)}\left[\cos(\nu\pi)\,P_\nu(\cos\theta) - P_\nu(-\cos\theta)\right]. \tag{16.125}$$

Conversely,

$$\begin{aligned} P_\nu(\cos\theta) &= \frac{1}{\pi}\tan(\nu\pi)\left[Q_\nu(\cos\theta) - Q_{-\nu-1}(\cos\theta)\right] \\ P_\nu(-\cos\theta) &= -\frac{1}{\pi}\sin(\nu\pi)\left[Q_\nu(\cos\theta) + Q_{-\nu-1}(\cos\theta)\right]. \end{aligned} \tag{16.126}$$

The typical eigenfunction is therefore

$$F_{\nu_m}(\cos\theta) = P_{\nu_m}(\cos\theta) + A_m\,Q_{\nu_m}(\cos\theta). \tag{16.127}$$

The index ν_m and the factor A_m are determined by requiring $F_{\nu_m}(\cos\theta)$ to vanish at $\theta = \alpha$ and $\theta = \pi - \alpha$. It is to be noted that $P_\nu(x)$ has singular points at $x = -1$ and $x = \infty$ (except when ν is an integer) and $Q_\nu(x)$ at $x = \pm 1$ and $x = \infty$. It follows that $P_\nu(\cos\theta)$ is singular at $\theta = \pi$ and $P_\nu(-\cos\theta)$, together with $Q_\nu(\cos\theta)$, at $\theta = 0$. We conclude that $F_{\nu_m}(\cos\theta)$ is appropriate for the region outside the metallic bicone (i.e., for $\alpha < \theta < \pi - \alpha$).

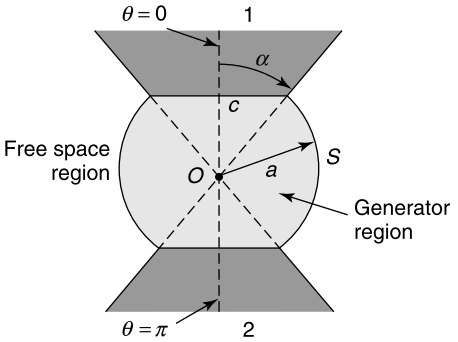

Figure 16.17 Biconical antenna.

[¶]When ν is an integer n, the independent solutions are the Legendre polynomial $P_n(\cos\theta)$ and the function $Q_n(\cos\theta)$ defined in (A5.115).

The "mother" function ϕ_0 of the TEM mode satisfies $\nabla_1^2 \phi_0 = 0$, which in the current case takes the form

$$\frac{1}{\sin\theta}\frac{\partial}{\partial\theta}\left(\sin\theta\,\frac{\partial\phi_0}{\partial\theta}\right) = 0. \tag{16.128}$$

To within an arbitrary factor, therefore,

$$\frac{\partial\phi_0}{\partial\theta} = \frac{1}{\sin\theta}.$$

Because

$$\frac{1}{\sin\theta} = \frac{d}{d\theta}\left(\log_e \tan\frac{\theta}{2}\right),$$

integration over the interval $(\alpha, \pi - \alpha)$ leads to the normalization integral

$$N_0^2 = 2\pi\int_\alpha^{\pi-\alpha}\frac{d\theta}{\sin\theta} = 4\pi\log_e\frac{1}{\tan\dfrac{\alpha}{2}}. \tag{16.129}$$

To satisfy (16.92), we must set

$$\begin{aligned}\phi_0 &= \frac{1}{N_0}\log_e\tan\frac{\theta}{2} + \text{constant}\\ \operatorname{grad}_1\phi_0 &= \frac{\partial\phi_0}{\partial\theta}\mathbf{u}_\theta = \frac{1}{N_0}\frac{1}{\sin\theta}\mathbf{u}_\theta.\end{aligned} \tag{16.130}$$

We shall assume that $E_\theta(\theta)$ is given on S (Fig. 16.17). From (16.90), the TEM components of the fields are

$$\begin{aligned}\mathbf{E}_{0\theta}(R) &= V_0(R)\operatorname{grad}_1\phi_0 = v_0(R)\operatorname{grad}_S\phi_0\\ \mathbf{H}_{0\varphi}(R) &= I_0(R)\,\mathbf{u}_R\times\operatorname{grad}_1\phi_0 = i_0(R)\,\mathbf{u}_R\times\operatorname{grad}_S\phi_0.\end{aligned} \tag{16.131}$$

In detail:

$$\begin{aligned}E_{0\theta}(R) &= V_0(R)\frac{1}{N_0\sin\theta} = v_0(R)\frac{1}{R}\frac{1}{N_0\sin\theta}\\ H_{0\varphi}(R) &= I_0(R)\frac{1}{N_0\sin\theta} = i_0(R)\frac{1}{R}\frac{1}{N_0\sin\theta}.\end{aligned} \tag{16.132}$$

On S (i.e., for $R = a$) $E_\theta(\theta)$ is assumed given, hence $v_0(a)$ can be determined for

$$v_0(a) = \frac{aN_0}{\pi - 2\alpha}\int_\alpha^{\pi-\alpha} E_\theta\,\sin\theta d\theta. \tag{16.133}$$

On the basis of (16.95) and (16.96),

$$\begin{aligned}E_{0\theta}(R) &= \frac{1}{N_0\sin\theta}\left(A\frac{e^{-jk_0R}}{R} + B\frac{e^{jk_0R}}{R}\right) = \frac{1}{RN_0\sin\theta}v_0(R)\\ H_{0\varphi}(R) &= \frac{1}{R_{c0}N_0\sin\theta}\left(A\frac{e^{-jk_0R}}{R} - B\frac{e^{jk_0R}}{R}\right) = \frac{1}{RN_0\sin\theta}i_0(R),\end{aligned} \tag{16.134}$$

where A and B are yet to be determined constants. The current density on the 1 and 2 cones is radial, hence we write, on cone 1 for example, $\mathbf{J}_S = H_\varphi \mathbf{u}_R$. The *current* through a parallel circle such as C in Figure 16.17, where $\theta = \alpha$, is therefore

$$\Im_0(R) = 2\pi R \sin\alpha \, H_\varphi(R, \alpha) = \frac{2\pi}{R_{c0} N_0} \left(A \, e^{-jk_0 R} - B \, e^{jk_0 R} \right). \tag{16.135}$$

A first relationship to be satisfied by A and B follows from (16.133) and (16.134). Thus,

$$v_0(a) = A \, e^{-jk_0 a} + B \, e^{jk_0 a}. \tag{16.136}$$

A second relationship is obtained by considering the fields near the contact point of the cones (i.e., for very small R). If a small insulated bead is inserted between the cones, the current must vanish at $R = 0$, which implies that $A = B$. For small R's,

$$\begin{aligned} E_{0\theta}(R) &\approx \frac{v_0(a)}{N_0 \sin\theta \, \cos k_0 a} \frac{1}{R} \\ H_{0\varphi}(R) &\approx -j \frac{k_0}{R_{c0} N_0 \sin\theta} \frac{v_0(a)}{\cos k_0 a} \\ \Im_0(R) &\approx -j \frac{2\pi}{R_{c0} N_0} \frac{v_0(a)}{\cos k_0 a} k_0 R. \end{aligned} \tag{16.137}$$

When the two tips are in direct contact, the electric field at $R = 0$ must vanish, which now implies that $A = -B$. This condition leads to

$$\begin{aligned} E_{0\theta}(R) &\approx \frac{k_0 \, v_0(a)}{N_0 \sin k_0 a \sin\theta} \\ H_{0\varphi}(R) &\approx \frac{j v_0(a)}{R_{c0} N_0 \sin\theta \sin k_0 a} \frac{1}{R} \\ \Im_0(R) &\approx j \frac{2\pi v_0(a)}{R_{c0} N_0 \sin k_0 a}. \end{aligned} \tag{16.138}$$

These formulas confirm that $v_0(R)$ and $i_0(R)$ vary like the voltage and the current on a transmission line, in harmony with (16.95) and (16.96). At large R, the radial dependence becomes $(e^{-jk_0 R}/R)$ for the TEM fields and $e^{-jk_0 R}$ for both v_0 and i_0.

Actual biconical antennas are truncated by terminal surfaces, which could be planes perpendicular to the axis or spherical surfaces of radius b centered on the contact point of the cones. In the latter case, the geometry of the three regions — generator, spherical, free space — permits use of separation of variables to determine the fields, also when the opening angles of the two cones are different[52] [47]. The use of different angles α and β (Fig. 16.11*c*) gives flexibility and allows the designer to optimize the radiation pattern of the antenna. When the spherically capped region contains inhomogeneous media, a numerical solution such as the unimoment method can be resorted to[53] [47].

PROBLEMS

16.1 Assume that the sources in Figure 16.1*a* are the azimuthal currents $\mathbf{J} = J_\varphi \, \mathbf{u}_\varphi$. Show that the ($\varphi$-oriented) vector potential $\mathbf{A} = A_\varphi \, \mathbf{u}_\varphi$ makes the following functional stationary:

$$J(A_\varphi) = \frac{1}{2} \int_D \left[\nu (\text{curl } \mathbf{A})^2 - 2A_\varphi J_\varphi + j\omega\sigma A_\varphi^2 \right] dS + \int_C A_\varphi \left(\frac{\partial A_\varphi}{\partial n} + \frac{A_\varphi}{r} + \frac{\partial r}{\partial n} \right) dc.$$

Write down the form of $J(A_\varphi)$ in cylindrical coordinates. When the material in the volume is a good conductor, the currents have the nature of eddy currents [211].

16.2 In a cavity bounded by perfectly electric or magnetic surfaces, a useful bilinear functional is

$$J(\mathbf{W}, \mathbf{E}) = \int_V \left[\frac{1}{\mu_r} \text{ curl } \mathbf{W} \cdot \text{curl } \mathbf{E} - k_0^2 \epsilon_r \, \mathbf{W} \cdot \mathbf{E} \right] dV.$$

Express the fields in cylindrical coordinates, the appropriate choice for cavities of revolution. (J. F. Lee et al., *IEEE Trans. MTT* **41**, 1981–1986, 1993.)

16.3 To solve the integro-differential equation (16.21), expand the scalar potential ϕ in a series $\sum_{m=-\infty}^{\infty} \phi_m(r, z) \, e^{jm\varphi}$. Express ϕ_m by means of the integral $\int_D q_m(r', z') \, G_m(r, z | r', z') \, r' \, dr' \, dz'$, where q_n is the Fourier expansion coefficient of $\rho(\mathbf{r})$, and G_m is defined in (16.24).

Hint: $q_m = -\dfrac{1}{j\omega} \left[\dfrac{1}{r} \dfrac{\partial (r J_{mr})}{\partial r} + \dfrac{jm}{r} J_{m\varphi} + \dfrac{\partial J_{mz}}{\partial z} \right]$.

(A. A. Kucharski, *IEEE Trans. AP* **48**, 1202–1210, 2000.)

16.4 In the integro-differential equation (16.29) satisfied by $\mathbf{E}$ in an inhomogeneous scatterer, the term in div $\mathbf{A}$ may be written as

$$\text{div } \mathbf{A} = \frac{\mu_0}{4\pi} \int_V \text{div} \left[\mathbf{J}(\mathbf{r}') \, \frac{e^{-jk_0 |\mathbf{r} - \mathbf{r}'|}}{|\mathbf{r} - \mathbf{r}'|} \right] dV' \; = \; -\frac{\mu_0}{4\pi} \int_V \mathbf{J}(\mathbf{r}') \, \text{grad}' \, \frac{e^{-jk_0 |\mathbf{r} - \mathbf{r}'|}}{|\mathbf{r} - \mathbf{r}'|} \, dV'$$

$$= \frac{\mu_0}{4\pi} \int_V \text{div}' \, \mathbf{J} \, \frac{e^{-jk_0 |\mathbf{r} - \mathbf{r}'|}}{|\mathbf{r} - \mathbf{r}'|} \, dV' - \int_S (\mathbf{u}_n \cdot \mathbf{J}) \, \frac{e^{-jk_0 |\mathbf{r} - \mathbf{r}'|}}{|\mathbf{r} - \mathbf{r}'|} \, dS'.$$

Show that the term in div$'$ $\mathbf{J}$ can be expressed in terms of $\mathbf{J}$, a property that avoids including derivatives of $\mathbf{J}$ in the numerical procedure.
(M. S. Viola, *IEEE Trans. MTT* **43**, 230–233, 1995.)

16.5 Let the shape of an antenna of revolution be defined by a function $a(z)$ (Fig. P16.1). Show that, for a φ-independent excitation, the current $I(z)$ through a parallel circle is the solution of the integral equation

$$\int_{-l_1}^{l_2} \left(k_0^2 \phi + \frac{\partial^2 \phi}{\partial z^2} - \frac{da}{dz} \frac{\partial^2 \phi}{\partial r \partial z} \right) I(z) \, dz = -\frac{2\pi}{j\omega\mu_0} \int_{z-}^{z+} E_c(z) \frac{a^2}{D} \sqrt{1 + \left(\frac{da}{dz} \right)^2} \, dz,$$

where $D^2 = r^2 + (z - z_0)^2$ and $\phi = (e^{-jk_0 D}/D)$. The gap field $E_c(z)$ is assumed given [9, 22].

16.6 With respect to Figure 16.17, in which $E_\theta(\theta)$ is given on S, determine the fields in the region between S and the apex. More specifically:

(**a**) Find the value of the expansion coefficients V_m at $R = a$, using the orthogonality properties of the ϕ_m's and the value of the normalization integral.

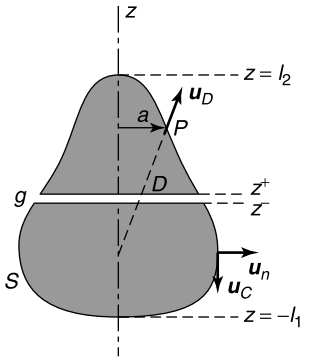

Figure P16.1

(**b**) Write down the equation satisfied by I_m.

Hint: Use (16.117).

(**c**) Match the two steps, (**a**) and (**b**).

Hint: Use (16.77).

Make use of these results to deduce the behavior of the fields near the apex, and verify the existence of singularities.

Hint: $j_{\nu_m}(k_0 R)$ is proportional to $(k_0 R)\nu_m$ for small R.

16.7 Evaluate the fields generated by the linear ring of magnetic current shown in Figure P16.2, where $\mathbf{J}_m$ has the value

$$\mathbf{J}_m = \delta(R - R_0)\,\delta(\theta - \theta_0)\frac{1}{R_0^2 \sin\theta_0}\,\mathbf{u}_\varphi.$$

Show that H_φ is given by

$$H_\varphi = k_0^2 \frac{\partial^2}{\partial\theta\,\partial\theta_0} \sum_n \frac{j_{\nu_n}(k_0 R)\, h_{\nu_n}(k_0 R_0)\, P_{\nu_n}(\cos\theta)\, P_{\nu_n}(\cos\theta_0)}{\nu_n(\nu_n+1)\displaystyle\int_0^\beta |P_{\nu_n}(\cos\theta)|^2 \sin\theta\, d\theta}.$$

(D. S. Jones, *IMA J. Appl. Math.* **60**, 33–53, 1998.)

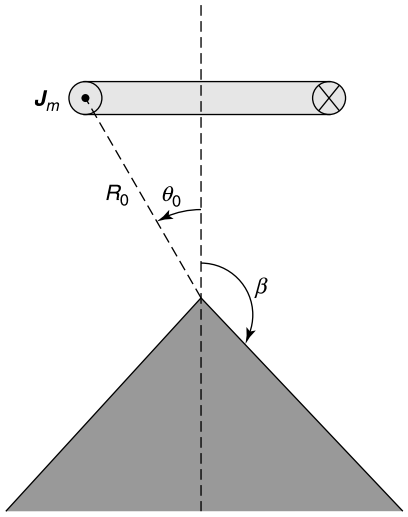

Figure P16.2

16.8 For a given E_θ field between the cones at radius $R = a$, determine the E_θ and H_φ fields in the TEM mode when an impedance Z_L (of very small dimensions) is inserted between the apices of the cones (Fig. 16.17).

NOTES

1. J. E. Lebaric and D. Kajfez, Analysis of dielectric resonator cavities using the finite integration technique, *IEEE Trans. MTT* **37**, 1740–1748 (1989).
2. K. M. Siegel, Far field scattering from bodies of revolution, *Appl. Sci. Res. B* **7**, 293–328 (1959).
3. J. G. Fikioris and A. N. Magoulas, Scattering from axisymmetric scatterers: a hybrid method of solving Maue's equation, *Prog. Electromagn. Res.* **25**, 131–165 (2000).
4. M. G. Andreasen, Scattering from bodies of revolution, *IEEE Trans. AP* **13**, 303–310 (1965).
5. J. R. Mautz and R. F. Harrington, Radiation and scattering from bodies of revolution, *Appl. Sci. Res.* **20**, 405–435 (1969).
6. J. R. Mautz and R. F. Harrington, *H*-field, *E*-field and combined-field solutions for conducting bodies of revolution, *A.E.Ü.* **32**, 157–164 (1978).
7. T. K. Wu and L. I. Tsai, Scattering from arbitrarily-shaped lossy dielectric bodies of revolution, *Radio Sci.* **12**, 709–718 (1977).
8. J. R. Mautz and R. F. Harrington, Electromagnetic scattering from a homogeneous material body of revolution, *A.E.Ü.* **33**, 71–80 (1979).
9. L. N. Medgyesi and J. M. Putnam, Electromagnetic scattering from axially inhomogeneous bodies of revolution, *IEEE Trans. AP* **32**, 797–806 (1984).
10. S. Govind, D. R. Wilton, and A. W. Glisson, Scattering from inhomogeneous penetrable bodies of revolution, *IEEE Trans. AP* **32**, 1163–1173 (1984).
11. A. A. Kucharski, A method of moments solution for electromagnetic scattering by inhomogeneous dielectric bodies of revolution, *IEEE Trans. AP* **48**, 1202–1210 (2000).
12. A. A. Kucharski, Resonances in heterogeneous dielectric bodies with rotational symmetry — volume intregral equation formulation, *IEEE Trans. MTT* **48**, 766–770 (2000).
13. R. D. Graglia, P. L. E. Uslenghi, R. Vitiello, and U. D'Elia, Electromagnetic scattering for oblique incidence on impedance bodies of revolution, *IEEE Trans. AP* **43**, 11–25 (1995).
14. A. H. Chang, K. S. Yee, and J. Prodan, Comparison of different integral equation formulations for bodies of revolution with anisotropic surface impedance boundary conditions, *IEEE Trans. AP* **40**, 989–991 (1992).
15. M. A. Morgan, S. K. Chang, and K. K. Mei, Coupled azimuthal potentials for electromagnetic field problems in inhomogeneous axially symmetric media, *IEEE Trans. AP* **25**, 413–417 (1977).
16. M. A. Morgan and K. Mei, Finite element computation of scattering by inhomogeneous penetrable bodies of revolution, *IEEE Trans. AP* **27**, 202–214 (1979).
17. A. D. Greenwood and J. M. Jin, Computation of the RCS of a complex BOR using FEM with coupled azimuth potentials and PLM, *Electromagn.* **19**, 147–170 (1999).
18. A. D. Greenwood and J. M. Jin, Finite-element analysis of complex axisymmetric radiating structures, *IEEE Trans. AP* **47**, 1260–1266 (1999).
19. J. F. Lee, G. M. Wilkins, and R. Mittra, Finite-element analysis of axisymmetric cavity resonator using a hybrid edge element technique, *IEEE Trans. MTT* **41**, 1981–1986 (1993).
20. M. A. Morgan, C. H. Chen, S. C. Hill, and P. W. Barber, Finite element-boundary integral formulation for electromagnetic scattering, *Wave Motion* **6**, 91–103 (1984).
21. D. J. Hoppe, L. W. Epp, and J. F. Lee, A hybrid symmetric FEM/MOM formulation applied to scattering by inhomogeneous bodies of revolution, *IEEE Trans. AP* **42**, 798–805 (1994).
22. T. L. Barkdoll and R. Lee, Finite element analysis of bodies of revolution using the measured equation of invariance, *Radio Sci.* **30**, 803–815 (1995).
23. Y.-L. Luo, K.-M. Luk, K. K. Mei, and E. K.-N. Yung, Finite difference analysis of electrically large parabolic reflector antennas, *IEEE Trans. AP* **50**, 266–276 (2002).
24. Y. Chen, R. Mittra, and P. Harms, Finite-difference time-domain algorithm for solving Maxwell's equations in rotationally symmetric geometries, *IEEE Trans. MTT* **44**, 832–838 (1996).
25. S. Shi, L. Yang, and D. W. Prather, Numerical study of axisymmetric dielectric resonators, *IEEE Trans. MTT* **9**, 1614–1619 (2001).
26. L. J. Chu and J. A. Stratton, Elliptic and spheroidal wave functions, *J. Math. Phys.* **20**, 259–309 (1941).
27. L. J. Chu and J. A. Stratton, Steady-state solutions of electromagnetic field problems III: forced oscillations of a prolate spheroid, *J. Appl. Phys.* **12**, 241–248 (1941).
28. H. A. Myers, Radiation patterns of unsymmetrically fed prolate spheroidal antennas, *IRE Trans. AP* **4**, 58–64 (1956).
29. G. E. Albert and J. L. Synge, The general problem of antenna radiation and the fundamental integral equation with application to an antenna of revolution, *Quart. Appl. Math.* **6**, 117–156 (1948).
30. H. K. Schuman and D. E. Warren, Aperture coupling in bodies of revolution, *IEEE Trans. AP* **26**, 778–783 (1978).

31. J. R. Mautz and R. F. Harrington, Electromagnetic coupling to a conducting body of revolution with a homogeneous material region, *Electromagn.* **2**, 257–308 (1982).
32. J. Van Bladel, The $\psi_0 =$ constant mode in free space and conical waveguides, *IEEE Trans. MTT* **50**, 1233–1237 (2002).
33. R. De Smedt and J. Van Bladel, Field singularities at the tip of a metallic cone of arbitrary cross section, *IEEE Trans. AP* **34**, 865–870 (1986).
34. R. De Smedt and J. Van Bladel, Field singularities near aperture corners, *IEE Proc.* **134-A**, 694–698 (1987).
35. E. Vafiadis and J. N. Sahalos, Fields at the tip of an elliptic cone, *Proc. IEEE* **72**, 1089–1091 (1984).
36. S. Blume and G. Kahl, Comments on "Fields at the tip of an elliptic cone," *Proc. IEEE* **73**, 1857–1858 (1985).
37. F. Olyslager, Field singularities at the common tip of a number of concentric biisotropic cones, *Microwave Opt. Tech. Lett.* **6**, 862–867 (1993).
38. F. Olyslager, Boundary integral equation technique for the singular behavior of electromagnetic fields at the common tips of metallic and bi-isotropic cones with arbitrary cross section, *IEEE Trans. AP* **42**, 1301–1308 (1994).
39. F. Olyslager, Overview of the singular behavior of electromagnetic fields at edges and tips in bi-isotropic and special bianisotropic media, *Radio Sci.* **30**, 1349–1354 (1995).
40. S. Marchetti and T. Rozzi, Electric field behavior near metallic wedges, *IEEE Trans. AP* **38**, 1333–1340 (1990).
41. L. L. Bailin and S. Silver, Exterior electromagnetic boundary value problems for spheres and cones, *IRE Trans. AP* **4**, 5–16 (1956).
42. L. B. Felsen, Backscattering from wide-angle and narrow-angle cones, *J. Appl. Phys.* **26**, 138–151 (1955).
43. D. S. Jones, Scattering by a cone, *Q. J. Mech. Appl. Math.* **50**, 499–523 (1997).
44. D. S. Jones, Irradiation of a cone by a magnetic dipole, *IMA J. Appl. Math.* **60**, 33–53 (1998).
45. S. Blume, Spherical-multipole analysis of electromagnetic and acoustical scattering by a semi-infinite elliptic cone, *IEEE Antennas Prop. Mag.* **38**, 33–44 (1996).
46. J. K. M. Jansen, Simple-periodic and non-periodic Lamé functions and their application in the theory of conical waveguides (doctoral dissertation), *Mathematisch Centrum*, Amsterdam (1976).
47. S. Blume and V. Krebs, Numerical evaluation of dyadic diffraction coefficients and bistatic radar cross sections for a perfectly conducting semi-infinite elliptic cone, *IEEE Trans. AP* **46**, 414–424 (1998).
48. R. S. Satterwhite and R. G. Kouyoumjian, Electromagnetic diffraction by a perfectly-conducting plane angular section, Electroscience Laboratory, Ohio State University (1970).
49. R. S. Satterwhite, Diffraction by a quarter plane, the exact solution, and some numerical results, *IEEE Trans. AP* **22**, 500–503 (1974).
50. S. Marchetti and T. Rozzi, H-field and J-current singularities at sharp edges in printed circuits, *IEEE Trans. AP* **39**, 1321–1331 (1991).
51. H. Jeuland, B. Uguen, G. Chassay, and E. Grorud, A numerical model for the analysis of a generalized point connection between two surfaces, *Microwave Opt. Tech. Lett.* **16**, 260–265 (1997).
52. S. N. Samaddar and E. L. Mokole, Biconical antennas with unequal cone angles, *IEEE Trans. AP* **46**, 181–193 (1998).
53. R. E. Stovall and K. K. Mei, Application of a unimoment technique to a biconical antenna with inhomogeneous dielectric loading, *IEEE Trans. AP* **23**, 335–342 (1975).

Chapter 17

Electrodynamics of Moving Bodies

Electrical engineers are often confronted with the need to evaluate fields in and around moving bodies. This is certainly the case for *power engineers*, who may be involved with the design of rotating machines, electromagnetic launching pads, or magnetically levitated transportation systems. *Radio scientists*, too, are concerned with the problem, in particular in their wish to interpret (and exploit) the amplitude modulation and frequency shift that result from the motion of a source. The Doppler effect, for example, is the basis of operation of many motion detectors, such as MTI radars (moving target indicators) and burglar alarms.

A fundamental understanding of the electrodynamics of moving bodies deeply preoccupied — and puzzled — the physicists of the second half of the nineteenth century. In this post-Maxwellian period, broad discussions centered on the concepts of ether and absolute time. Ether as a medium was deemed necessary to support the propagation of waves. Various experiments, however, failed to confirm its existence. In this blocked situation, Einstein untied the knot in an epoch-making 1905 article, some ideas of which are summarized in the following pages. Einstein himself considered his theory as the continuation of Maxwell's work,[1] and one may assert that a text on electromagnetic theory is not really complete without some reference to his views. In the current chapter, the structural beauty of the theory and its philosophical implications are hardly touched upon. Numerous specialized texts discuss these aspects authoritatively [25, 26, 27, 99, 107, 122]. Our approach is more humble, almost utilitarian, and focuses on the use of relativistic principles to formulate (and solve) practical problems in a systematic way.*

17.1 FIELDS GENERATED BY A MOVING CHARGE

In this section, we evaluate the fields generated by a charge q moving with variable velocity $\mathbf{v}$ on a trajectory $\mathbf{r}_q(t)$. The problem is of very old vintage. It has been solved by a variety of methods, often based on complex integration in four dimensions, with the time coordinate $x_4 = ict$ as a fourth dimension [20, 120]. Our chosen approach is to start from the expressions (7.33) and (7.34) for the retarded potentials and evaluate these potentials

*Chapter 17 is an extended summary of *Relativity and Engineering*, a book published in 1984 by Springer-Verlag, and now out of print [132]. The author warmly thanks Springer-Verlag for permission to reproduce numerous figures from that text.

Electromagnetic Fields, Second Edition, By Jean G. Van Bladel

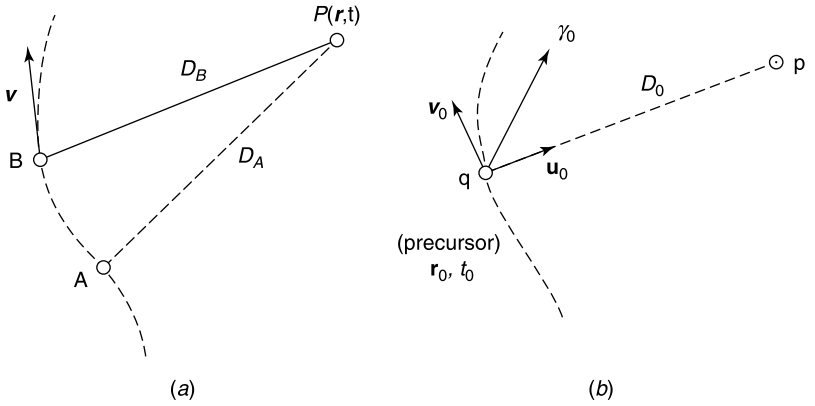

Figure 17.1 (*a*) Possible precursor positions. (*b*) Velocity and acceleration at the precursor.

for the sources [72]

$$\rho(\mathbf{r},t) = q\delta[\mathbf{r} - \mathbf{r}_q(t)]$$
$$\mathbf{j}(\mathbf{r},t) = q\delta[\mathbf{r} - \mathbf{r}_q(t)]\,\mathbf{v}. \tag{17.1}$$

The scalar potential

$$\phi(\mathbf{r},t) = \frac{1}{4\pi\epsilon_0}\int_{sources} \frac{\rho\left(\mathbf{r}', t - \dfrac{|\mathbf{r}-\mathbf{r}'|}{c_0}\right)}{|\mathbf{r}-\mathbf{r}'|}\,dV' \tag{17.2}$$

will be discussed first. Given the form of $\rho(\mathbf{r},t)$, the integral over the sources reduces to the contribution of q at the location the charge occupied at time $t_A = t - (D_A/c_0)$, where t_A can be determined by solving the equation (Fig. 17.1)

$$t = t_A + \frac{|\mathbf{r} - \mathbf{r}_q(t_A)|}{c_0} = t_A + \frac{1}{c}\left\{\left[x - x_q(t_A)\right]^2 + \left[y - y_q(t_A)\right]^2 + \left[z - z_q(t_A)\right]^2\right\}^{\frac{1}{2}}. \tag{17.3}$$

We shall first prove that P lies in the field of only *one* such location, which will be termed the *precursor position*. Assume, indeed, that *two* such positions, A and B, exist. For such a case

$$t_A + \frac{D_A}{c_0} = t_B + \frac{D_B}{c_0} = t$$

or

$$c_0(t_B - t_A) = D_A - D_B.$$

Because the velocity of the charged particle* is less than c_0,

$$t_B - t_A > \frac{|\mathbf{AB}|}{c_0}.$$

*The case of photons is excluded from the current analysis.

Combining the two conditions satisfied by $(t_B - t_A)$ leads to

$$D_A > D_B + |\mathbf{AB}|.$$

A look at the triangle ABP shows that this requirement cannot be met.

Having settled the precursor question, we rewrite (17.2) in the form

$$\phi(\mathbf{r},t) = \frac{1}{4\pi\epsilon_0}\int_{\text{space}}\int_{\text{time}} \frac{\rho(\mathbf{r}',t')}{|\mathbf{r}-\mathbf{r}'|}\,\delta\left(t - t' - \frac{|\mathbf{r}-\mathbf{r}'|}{c_0}\right) dV'\,dt'. \tag{17.4}$$

For the point charge q,

$$\phi(\mathbf{r},t) = \frac{q}{4\pi\epsilon_0}\int_{\text{space}}\int_{\text{time}} \frac{\delta[\mathbf{r}' - \mathbf{r}_q(t')]}{|\mathbf{r}-\mathbf{r}'|}\,\delta\left[t - t' - \frac{|\mathbf{r}-\mathbf{r}'|}{c_0}\right] dV'\,dt'.$$

Integrating over space gives

$$\phi(\mathbf{r},t) = \frac{q}{4\pi\epsilon_0}\int_{-\infty}^{\infty} \frac{1}{|\mathbf{r}-\mathbf{r}_q(t')|}\,\delta\left[t' + \frac{|\mathbf{r}-\mathbf{r}_q(t')|}{c_0} - t\right] dt'. \tag{17.5}$$

The integral is of the general form

$$I = \int_{-\infty}^{\infty} g(t')\,\delta[f(t') - t]\,dt',$$

with

$$g(t') = \frac{q}{4\pi\epsilon_0\,|\mathbf{r}-\mathbf{r}_q(t')|}$$

$$f(t') = t' + \frac{1}{c_0}|\mathbf{r}-\mathbf{r}_q(t')|.$$

The only contribution to I comes from $t = f(t')$. To exploit this property, we introduce the transformation $f(t') = x$ and its inverse $t' = h(x)$. Because $(df/dt') = (dx/dt')$,

$$I = \int_{-\infty}^{\infty} g[h(x)]\,\delta(x-t)\frac{dx}{\left(\dfrac{df}{dt'}\right)} = \left[\frac{g[h(x)]}{\dfrac{df}{dt'}}\right].$$

This result will now be used to evaluate $\phi(\mathbf{r},t)$ in (17.5). We notice, from (17.3), that $t = f(t')$ selects $t' = t_0$, where t_0 is the time corresponding with the precursor location. As a result,

$$\phi(\mathbf{r},t) = \frac{q}{4\pi\epsilon_0|\mathbf{r}-\mathbf{r}_q(t_0)|}\frac{1}{\left.\dfrac{df}{dt'}\right|_{t=t_0}}.$$

From Figure 17.1*b*:

$$\frac{df}{dt'} = 1 + \frac{1}{c_0}\frac{d|\mathbf{r} - \mathbf{r}_q(t')|}{dt'} = 1 - \frac{\mathbf{u}_0 \cdot \mathbf{v}_0}{c_0}.$$

It follows that

$$\phi(\mathbf{r}, t) = \frac{1}{4\pi\epsilon_0}\frac{q}{|\mathbf{r} - \mathbf{r}_0|\left(1 - \dfrac{\mathbf{u}_0 \cdot \mathbf{v}_0}{c_0}\right)}, \tag{17.6}$$

and similarly

$$\mathbf{a}(\mathbf{r}, t) = \frac{\mu_0}{4\pi}\frac{q\,\mathbf{v}_0}{|\mathbf{r} - \mathbf{r}_0|\left(1 - \dfrac{\mathbf{u}_0 \cdot \mathbf{v}_0}{c_0}\right)}. \tag{17.7}$$

These are the *Liénart-Wiechert potentials*,[2,3] from which the fields can be evaluated by means of (7.28) and (7.29). The differentiations are not trivial, however, because t_0 is a complicated function of x, y, z, and t [11, 112]. We shall only quote the results, which are

$$\begin{aligned}
\mathbf{e} &= \frac{q\left(1 - \dfrac{v_0^2}{c_0^2}\right)}{4\pi\epsilon_0 D_0^2\left(1 - \dfrac{\mathbf{u}_0 \cdot \mathbf{v}_0}{c_0}\right)^3}\left(\mathbf{u}_0 - \frac{\mathbf{v}_0}{c_0}\right) + \frac{\mu_0 q}{4\pi D_0\left(1 - \dfrac{\mathbf{u}_0 \cdot \mathbf{v}_0}{c_0}\right)^3}\mathbf{u}_0 \\
&\quad \times \left\{\left(\mathbf{u}_0 - \frac{\mathbf{v}_0}{c_0}\right) \times \gamma_0\right\} \\
\mathbf{b} &= \frac{1}{c_0}(\mathbf{u}_0 \times \mathbf{e}).
\end{aligned} \tag{17.8}$$

The symbol γ_0 denotes the acceleration of q at the precursor location. The first term in $\mathbf{e}$ is the *velocity field*, the second one the *acceleration field*.† The expression for $\mathbf{e}$ shows

- That the magnetic field and the acceleration field are perpendicular to the line connecting precursor to observer
- That the acceleration field, given its $(1/D_0)$ dependence, becomes dominant at sufficiently large distances D_0 (Problem 17.1)

17.2 THE LORENTZ TRANSFORMATION

Interest in the concept *time* — and in particular in the synchronization of clocks — was particularly vivid in the second half of the nineteenth century [66]. The public at large, confronted with a variety of local times, especially in large countries, wanted some kind of rationalization. Some professions were particularly concerned:

- Navigators, often dissatisfied with the available maps and their unreliable longitudinal grids

†It is interesting to note that the theory of the electromagnetic field can be developed from (17.8), taken as a basic postulate. With such a choice, Maxwell's equations can be *derived* by suitable manipulations [104].

- Railroaders responsible for the scheduling of trains, and in particular military planners in charge of the efficient transportation of troops
- Colonial administrators and cartographers

Methods to synchronize clocks started modestly with the injection of modulated air pressure in pipes, followed, from the 1850s on, by the use of electric signals, often carried in transoceanic cables. Physicists were also deeply involved, not only with the true nature of time and the philosophical implications thereof, but also with the concepts of *synchronization* and *simultaneity*. In Newton's physics there existed an *absolute space*; that is, a set of axes K with respect to which all "true" motions should be measured. In this space, a particle left to itself moves in a straight line with constant velocity. Further, this uniform motion (the *law of inertia*) also holds in all other rigid systems K' that move with uniform velocity with respect to K (the *systems of inertia*). Time was also absolute, and should be measured with respect to clocks at rest in K. Such a time was also the time in K'. Events that were simultaneous in K were therefore also simultaneous in K'. Newton's concepts ran into difficulties in the late nineteenth century. It was commonly believed, at the time, that a medium (the *ether*) served as a substratum for the propagation of light, and penetrated into bodies like water in a sponge. Some physicists assumed that moving bodies dragged the ether locally (and partially) in their motion. Others believed that the ether was at absolute rest, and that the earth, for example, was swept by an ether "wind" in its motion through interstellar space. According to these views, fundamental electromagnetic laws should be formulated in the rest axes of the luminiferous ether. In consequence, light should move with velocity c_0 with respect to the ether, but with a different velocity at the surface of the earth. By 1900, however, an impressive series of experiments (in particular those of Michelson and Morley) had shown the fallacy of that point of view [132]. The most prominent physicists of the time, Poincaré and Lorentz, tried to resolve these inconsistencies, which were due to the asymmetry introduced by the special role of K. It was assumed that Maxwell's equations were only valid in K, and the form they subsequently took in K' became consequently quite complex. To reduce this complexity, H.A. Lorentz attached a "local time" to frame K' (in practice the frame of a moving electron). He also assumed that any object moving through the ether suffered a contraction in its direction of travel.[4] These considerations led *Lorentz* to formulate *ad hoc transformation laws* for the space and time coordinates. These laws, written for the axes[‡] used in Figure 17.2*a* (which coincide at times $t = t' = 0$), are

$$\begin{aligned} x' &= x \\ y' &= y \\ z' &= \frac{z - wt}{\sqrt{1-\beta^2}} \\ t' &= \frac{1}{\sqrt{1-\beta^2}} \left(t - \beta \frac{z}{c_0} \right). \end{aligned} \tag{17.9}$$

A simple *mathematical* manipulation shows that, conversely,

$$\begin{aligned} x &= x' \\ y &= y' \end{aligned}$$

[‡]More general forms are available, for example for the axes shown in Figure 17.2*b* [132] (Problem 17.3).

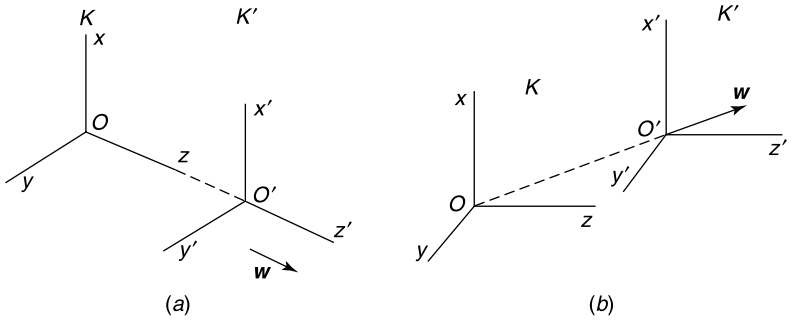

Figure 17.2 (*a*) Axes for the simple Lorentz transformation. (*b*) Two inertial frames in relative motion.

$$z = \frac{z' + wt'}{\sqrt{1-\beta^2}}$$

$$t = \frac{1}{\sqrt{1-\beta^2}}\left(t' + \beta\,\frac{z'}{c_0}\right), \tag{17.10}$$

where $\beta = (w/c_0)$. Lorentz considered his formulas as a convenient mathematical tool. Poincaré reinterpreted them and gave a physical meaning to Lorentz' local time, which he considered to be the time shown by clocks synchronized in K' by means of electromagnetic signals[5] [66]. In his 1905 paper,[6] Einstein did away with absolute time and absolute space and postulated that events that are simultaneous[§] in a frame K are not necessarily simultaneous in a frame K'. In his theory, this relativity of simultaneity found a basis in an extension of (17.9) to arbitrary inertial frames K and K' in uniform motion with respect to each other. It is clear that Einstein's views require a complete reevaluation of the usual concepts of space and time. Time, in particular, cannot remain *universal* and must be interwoven with the spatial coordinates.[¶] It is therefore natural to express (17.9) in terms of four coordinates: the spatial coordinates x^1, x^2, x^3, and the time coordinate $x^0 = c_0 t$. This can be done by means of the following matrix multiplication:

$$\begin{pmatrix} (x')^0 \\ (x')^1 \\ (x')^2 \\ (x')^3 \end{pmatrix} = \underbrace{\begin{pmatrix} \dfrac{1}{\sqrt{1-\beta^2}} & 0 & 0 & -\dfrac{\beta}{\sqrt{1-\beta^2}} \\ 0 & 1 & 0 & 0 \\ 0 & 0 & 1 & 0 \\ -\dfrac{\beta}{\sqrt{1-\beta^2}} & 0 & 0 & \dfrac{1}{\sqrt{1-\beta^2}} \end{pmatrix}}_{\text{coordinate transformation matrix}} \cdot \begin{pmatrix} x^0 \\ x^1 \\ x^2 \\ x^3 \end{pmatrix}. \tag{17.11}$$

In Einstein's theory, the ether is done away with, and no mechanistic justification for the propagation of waves is needed. To use his own words: "the *equations* are essential, and the field intensities that appeared in them are elementary, not derivable from other

[§]Einstein, in a famous *Gedanken experiment*, defines events in A and B to be simultaneous when light signals emitted in A and B at the time of the events arrive at the same time at the center of segment AB (where the common arrival could be monitored by photon detectors and coincidence circuits).

[¶]In 1912, Einstein was asked to write a comprehensive overview of his *special relativity* theory. The original handwritten text has now been reprinted [57].

entities." Einstein paid homage to Maxwell in a 1929 commemoration volume,[1] in which he admired Maxwell's decision to abandon complicated models for the ether (based on rotating cylinders, idle wheels, and such) in favor of a *fundamental* description of reality by differential equations.

A Few Simple Applications of Lorentz' Transformations Laws

1. Let two points A, B be at rest on the z' axis of K', with $l_0 = z'_B - z'_A$. From (17.9):

$$z'_B = \frac{z_B - \omega t}{\sqrt{1-\beta^2}}; \qquad z'_A = \frac{z_A - \omega t}{\sqrt{1-\beta^2}}.$$

If the positions of A and B are noted at the same time t in K, the length measured in K evidences a Lorentz contraction, because

$$z_B - z_A = \sqrt{1-\beta^2}\,(z'_B - z'_A) = \sqrt{1-\beta^2}\,l_0. \tag{17.12}$$

Similarly, if a rigid body of volume V' is at rest in K', and if the points of that body are observed at the same time in K, the observed volume in K will be

$$V = \sqrt{1-\beta^2}\,V'. \tag{17.13}$$

2. Let two events happen simultaneously in A and B in K' (i.e., at a common time t'). The time separation of these events in K is readily found to be a first-order effect in β, namely (Problem 17.4)

$$t_B - t_A = \frac{l_0}{c_0}\,\frac{\beta}{\sqrt{1-\beta^2}}. \tag{17.14}$$

3. Let a body move with velocity v' along the z' axis. Inserting $z' = z'_0 + v't'$ into (17.9) gives, after a few trivial steps,

$$v = \frac{w + v'}{1 + \beta\,\dfrac{v'}{c_0}}. \tag{17.15}$$

At low velocities, v is equal to $(w + v')$, the value predicted by Newtonian mechanics. At the other end of the velocity scale, a photon moving with velocity c_0 in K' is found to move with the *same* velocity in K. This result expresses Einstein's postulate of constancy of c_0, valid irrespectively of the motion of the source.

Transformation formula (17.15) can be extended to a more general $\mathbf{v}'$ to yield

$$v_\parallel = \frac{w + v'_\parallel}{1 + \beta\,\dfrac{v'_\parallel}{c_0}}$$

$$\mathbf{v}_\perp = \frac{\sqrt{1-\beta^2}}{1 + \beta\,\dfrac{v'_\parallel}{c_0}}\,\mathbf{v}'_\perp, \tag{17.16}$$

where the subscripts $\parallel$ and $\perp$ refer to components parallel and perpendicular to $\mathbf{w}$, respectively.

From a relativistic point of view, a derivative operator of the form $\partial/\partial t'$ implies the rate of change experienced by an observer in the moving axes K'. In hydrodynamics, one often uses the *substantial derivative* D/Dt, which is the rate of change of a variable with respect to an oberver moving with velocity $w\mathbf{u}_z$ with respect to the rest axes. This operator is given by

$$\frac{D}{Dt} = \frac{\partial}{\partial t} + w\,\frac{\partial}{\partial z}. \tag{17.17}$$

In the realm of Lorentz' transformations, this should be replaced by $\partial/\partial t'$. It is immediately apparent, from (17.9), that

$$\frac{\partial}{\partial t'} = \frac{1}{\sqrt{1-\beta^2}}\,\frac{D}{Dt}. \tag{17.18}$$

The two operators well approximate each other at low velocities. For $w = 0.05\,c_0$, for example, $\sqrt{1-\beta^2} = 0.99875$. A general remark is in order here. In most engineering problems, β^2 may be completely neglected with respect to 1, and we may set $\sqrt{1-\beta^2} \approx 1$. *Factors* of β, however, may not be ignored, because they may reveal an important physical effect. Numerous examples of such effects are discussed in the sequel.

17.3 TRANSFORMATION OF FIELDS AND CURRENTS

Time and space are the subject of the first part, *Kinematics*, of Einstein's fundamental 1905 paper.[6] In a second part, *Electrodynamics*, the author turns to Maxwell's equations, the Doppler effect, and the radiation pressure exerted by the fields. Because the frames K and K' are completely equivalent, Einstein postulates:

1. That the laws of electrodynamics and optics have the same form in all inertial frames;
2. That light always propagates in empty space with a definite speed c_0, independently of the state of motion of the emitting body.

The requirement that Maxwell's equations *for empty space* should be of the same form in all inertial frames leads automatically to transformation equations for fields and sources from one inertial frame to another. Such equations are of decisive interest for the electrical engineer, because they allow him to solve the field problem in a frame K' in which the solution is particularly simple and to transform the results back to the frame K in which they are actually needed.

17.3.1 Transformation Laws for the Sources

The starting point is the equation of conservation of charge in vacuum. In K:

$$\operatorname{div}\mathbf{j} + \frac{\partial\rho}{\partial t} = \frac{\partial j_x}{\partial x} + \frac{\partial j_y}{\partial y} + \frac{\partial j_z}{\partial z} + \frac{\partial\rho}{\partial t} = 0.$$

On the basis of (17.9), the derivatives in K can be expressed in terms of the primed coordinates in K' by the formulas

$$\begin{aligned}
\frac{\partial}{\partial t} &= \frac{1}{\sqrt{1-\beta^2}}\frac{\partial}{\partial t'} - \frac{\beta c_0}{\sqrt{1-\beta^2}}\frac{\partial}{\partial z'} \\
\frac{\partial}{\partial x} &= \frac{\partial}{\partial x'} \\
\frac{\partial}{\partial y} &= \frac{\partial}{\partial y'} \\
\frac{\partial}{\partial z} &= -\frac{\beta}{c_0\sqrt{1-\beta^2}}\frac{\partial}{\partial t'} + \frac{1}{\sqrt{1-\beta^2}}\frac{\partial}{\partial z'}.
\end{aligned} \tag{17.19}$$

As a result, (17.18) becomes

$$\frac{\partial j_x}{\partial x'} + \frac{\partial j_y}{\partial y'} + \frac{\partial}{\partial z'}\left(\frac{j_z}{\sqrt{1-\beta^2}} - \frac{w\rho}{c_0^2\sqrt{1-\beta^2}}\right) + \frac{\partial}{\partial t'}\left(\frac{\rho}{\sqrt{1-\beta^2}} - \frac{w}{c_0^2\sqrt{1-\beta^2}}j_z\right) = 0.$$

In the K' frame, this should go over to

$$\frac{\partial j'_x}{\partial x'} + \frac{\partial j'_y}{\partial y'} + \frac{\partial j'_z}{\partial z'} + \frac{\partial \rho'}{\partial t'} = 0. \tag{17.20}$$

Identification leads immediately to the desired relationships, namely

$$\begin{aligned}
\rho' &= \frac{\rho}{\sqrt{1-\beta^2}} - \frac{\mathbf{w}\cdot\mathbf{j}}{c_0^2\sqrt{1-\beta^2}} \\
\mathbf{j}'_\perp &= \mathbf{j}_\perp \\
j'_\parallel &= \frac{j_\parallel}{\sqrt{1-\beta^2}} - w\frac{\rho}{\sqrt{1-\beta^2}}.
\end{aligned} \tag{17.21}$$

An analogous transformation, from K' to K, yields

$$\begin{aligned}
\rho &= \frac{\rho'}{\sqrt{1-\beta^2}} + \frac{\mathbf{w}\cdot\mathbf{j}'}{c_0^2\sqrt{1-\beta^2}} \\
\mathbf{j}_\perp &= \mathbf{j}'_\perp \\
j_\parallel &= \frac{j'_\parallel}{\sqrt{1-\beta^2}} + w\frac{\rho'}{\sqrt{1-\beta^2}},
\end{aligned} \tag{17.22}$$

where $\mathbf{w}$ is still the velocity of K' with respect to K. One can easily check that (17.21) and (17.22) are compatible; that is, that solving (17.21) for ρ and $\mathbf{j}$ reproduces (17.22).

At low velocities (17.22) gives, to the first order,

$$\mathbf{j} = \mathbf{j}' + \rho'\mathbf{w}, \tag{17.23}$$

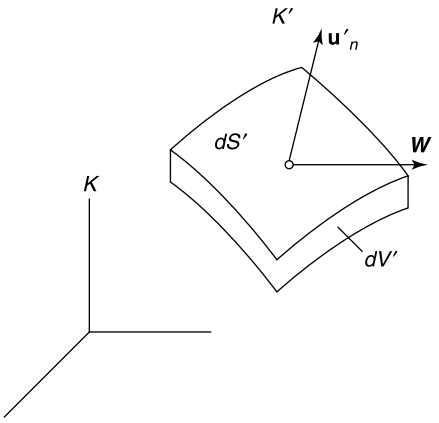

Figure 17.3 Element of surface moving in an arbitrary direction.

a familiar relationship that shows that the current density in K is the current density in K' augmented by a convection current density $\rho'\mathbf{w}$. Similar methods can be applied to derive the transformation laws for the surface sources [132]. If ρ'_S and $\mathbf{j}'_S$ denote the sources in K', then (Fig. 17.3)

$$\rho_S = \frac{1}{\sqrt{1-(w^2/c_0^2)+(\mathbf{w}\cdot\mathbf{u}'_n/c_0)^2}}\left(\rho'_S + \frac{\mathbf{w}\cdot\mathbf{j}'_S}{c_0^2}\right) \tag{17.24}$$

$$\mathbf{j}_S = \frac{1}{\sqrt{1-(w^2/c_0^2)+(\mathbf{w}\cdot\mathbf{u}'_n/c_0)^2}}\left[\sqrt{1-\frac{w^2}{c_0^2}}(\mathbf{j}'_S)_\perp + (\mathbf{j}'_S)_\parallel + \rho'_S\mathbf{w}\right] \tag{17.25}$$

are the corresponding values in K. We also note that dS and $\mathbf{u}_n$, measured synchronously by an observer in K [132], are given by

$$dS = dS'\sqrt{1-(w^2/c_0^2)+(\mathbf{u}'_n\cdot\mathbf{w}/c_0)^2} \tag{17.26}$$

$$\mathbf{u}_n = \frac{\sqrt{1-w^2/c_0^2}\,\mathbf{u}'_{n\perp} + \mathbf{u}'_{n\parallel}}{\sqrt{1-(w^2/c_0^2)+(\mathbf{u}'_n\cdot\mathbf{w}/c_0)^2}}, \tag{17.27}$$

where dS' is at rest in K'.

17.3.2 Transformation Laws for the Fields

The method used for the transformation of the sources can be similarly applied to the fields. The calculations are long but straightforward. They lead to the equations

$$\mathbf{e}' = \mathbf{e}_\parallel + \frac{1}{\sqrt{1-\beta^2}}(\mathbf{e}_\perp + \mathbf{w}\times\mathbf{b})$$

$$\mathbf{b}' = \mathbf{b}_\parallel + \frac{1}{\sqrt{1-\beta^2}}\left(\mathbf{b}_\perp - \frac{\mathbf{w}\times\mathbf{e}}{c_0^2}\right)$$
$$\mathbf{d}' = \mathbf{d}_\parallel + \frac{1}{\sqrt{1-\beta^2}}\left(\mathbf{d}_\perp + \frac{\mathbf{w}\times\mathbf{h}}{c_0^2}\right)$$
$$\mathbf{h}' = \mathbf{h}_\parallel + \frac{1}{\sqrt{1-\beta^2}}(\mathbf{h}_\perp - \mathbf{w}\times\mathbf{d}). \tag{17.28}$$

The components parallel with **w** are seen to be invariant. The remarkable consistency of the relativistic formalism is confirmed by noting that the passage from fields in K' to fields in K, obtained mathematically from (17.28), reproduces (17.28), provided **w** is replaced by $-\mathbf{w}$.

In applications in practice, one often uses the simple Lorentz transformation and the axes shown in Figure 17.2*a*. It is therefore useful to write down (17.28) explicitly for these axes. Thus,

$$e_x' = \frac{1}{\sqrt{1-\beta^2}}(e_x - w\,b_y) \qquad b_x' = \frac{1}{\sqrt{1-\beta^2}}\left(b_x + \frac{w}{c_0^2}\,e_y\right)$$
$$e_y' = \frac{1}{\sqrt{1-\beta^2}}(e_y + w\,b_x) \qquad b_y' = \frac{1}{\sqrt{1-\beta^2}}\left(b_y - \frac{w}{c_0^2}\,e_x\right)$$
$$e_z' = e_z \qquad b_z' = b_z$$
$$d_x' = \frac{1}{\sqrt{1-\beta^2}}\left(d_x - \frac{w}{c_0^2}\,h_y\right) \qquad h_x' = \frac{1}{\sqrt{1-\beta^2}}(h_x + w\,d_y)$$
$$d_y' = \frac{1}{\sqrt{1-\beta^2}}\left(d_y + \frac{w}{c_0^2}\,h_x\right) \qquad h_y' = \frac{1}{\sqrt{1-\beta^2}}(h_y - w\,d_x)$$
$$d_z' = d_z \qquad h_z' = h_z. \tag{17.29}$$

The transformation equations for the potentials can be derived by similar methods. They yield

$$\mathbf{a}_\perp' = \mathbf{a}_\perp$$
$$a_\parallel' = \frac{1}{\sqrt{1-\beta^2}}\left(a_\parallel - \frac{\beta\phi}{c_0}\right)$$
$$\phi' = \frac{1}{\sqrt{1-\beta^2}}\left(\phi - \beta c_0 a_\parallel\right). \tag{17.30}$$

17.3.3 Four-Dimensional Formalism

The three-dimensional formulas (17.19) to (17.30) are in a form appropriate to the solution of practical problems. It is formally interesting, however, to note that the equations for the

fields can be deduced from the transformation of the tensors

$$M^{\alpha\beta} = \begin{bmatrix} 0 & c_0\, d_x & c_0\, d_y & c_0\, d_z \\ -c_0\, d_x & 0 & h_z & -h_y \\ -c_0\, d_y & -h_z & 0 & h_x \\ -c_0\, d_z & h_y & -h_x & 0 \end{bmatrix} \tag{17.31}$$

and

$$N_{\alpha\beta} = \begin{bmatrix} 0 & -\dfrac{e_x}{c_0} & -\dfrac{e_y}{c_0} & -\dfrac{e_z}{c_0} \\ \dfrac{e_x}{c_0} & 0 & b_z & -b_y \\ \dfrac{e_y}{c_0} & -b_z & 0 & b_x \\ \dfrac{e_z}{c_0} & b_y & -b_x & 0 \end{bmatrix}. \tag{17.32}$$

Here, and in the rest of the chapter, greek indices are used for four-dimensional quantities. A *contravariant tensor* such as $M^{\alpha\beta}$ transforms according to the rule

$$(M')^{\alpha\beta} = \sum_{\mu,\nu=0}^{3} \frac{\partial x'^{\alpha}}{\partial x^{\mu}} \frac{\partial x'^{\beta}}{\partial x^{\nu}} M^{\mu\nu}, \tag{17.33}$$

where $x_0 = \mathrm{ct}$. The corresponding formula for a *covariant tensor* is

$$(N')_{\alpha\beta} = \sum_{\mu,\nu=0} \frac{\partial x^{\mu}}{\partial x'^{\alpha}} \frac{\partial x^{\nu}}{\partial x'^{\beta}} N_{\alpha\beta}. \tag{17.34}$$

Maxwell's equations can now be given the concise four-dimensional form

$$\frac{\partial N_{\alpha\beta}}{\partial x^{\gamma}} + \frac{\partial N_{\beta\gamma}}{\partial x^{\alpha}} + \frac{\partial N_{\gamma\alpha}}{\partial x^{\beta}} = 0$$

$$\sum_{\mu=0}^{3} \frac{\partial M^{\alpha\mu}}{\partial x^{\mu}} = J^{\alpha}, \tag{17.35}$$

where J^{α} is the four-vector $(\rho c_0, j^x, j^y, j^z)$ representing the sources. The equation of conservation of charge becomes, four-dimensionally,

$$\sum_{\alpha=0}^{3} \frac{\partial J^{\alpha}}{\partial x^{\alpha}} = 0. \tag{17.36}$$

The form of the tensors $M^{\alpha\beta}$ and $N_{\alpha\beta}$ shows that, from a relativistic point of view, $(\mathbf{e}, \mathbf{b})$ and $(\mathbf{d}, \mathbf{h})$ are natural pairs. The physically important quantities are the *tensors*, and their splitting in $\mathbf{e}, \mathbf{b}, \mathbf{d}, \mathbf{h}$ components, which varies from system to system, may be considered as a mere four-dimensional *perspective effect* [19].

17.4 RADIATION FROM SOURCES: THE DOPPLER EFFECT

When a charge moves uniformly the Liénard-Wiechert procedure can be replaced by an elementary relativistic calculation (Problem 17.9). In the rest frame K' of the particle the magnetic field vanishes, and the electric field is given by its Coulomb value. With the axes shown in Figure 17.4*a* the fields in P are

$$e'_x = \frac{q}{4\pi\epsilon_0}\frac{x'}{(x'^2+z'^2)^{\frac{3}{2}}}$$

$$e'_z = \frac{q}{4\pi\epsilon_0}\frac{z'}{(x'^2+z'^2)^{\frac{3}{2}}}$$

$$\mathbf{h}' = 0.$$

Transformed to K, they become

$$e_x = \frac{e'_x}{\sqrt{1-\beta^2}}$$

$$e_z = e'_z$$

$$h_y = \frac{v\epsilon_0}{\sqrt{1-\beta^2}}\,e'_x. \tag{17.37}$$

Expressing x' and z' in terms of x, z, and t yields, from (17.9),

$$e_x = \frac{q}{4\pi\epsilon_0\sqrt{1-\beta^2}}\frac{x}{\left[x^2+\dfrac{(z-vt)^2}{1-\beta^2}\right]^{\frac{3}{2}}}$$

$$e_z = \frac{q}{4\pi\epsilon_0\sqrt{1-\beta^2}}\frac{z-vt}{\left[x^2+\dfrac{(z-vt)^2}{1-\beta^2}\right]^{\frac{3}{2}}}$$

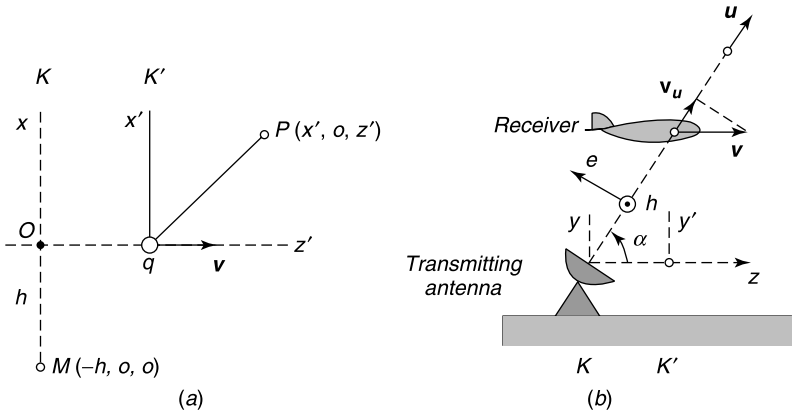

Figure 17.4 (*a*) Charge q in uniform motion. (*b*) Moving receiver in an incident plane wave.

$$h_y = \frac{qv}{4\pi\sqrt{1-\beta^2}} \frac{x}{\left[x^2 + \dfrac{(z-vt)^2}{1-\beta^2}\right]^{\frac{3}{2}}}. \tag{17.38}$$

These are the fields that an observer at rest in K would measure. We notice that the electric field in P, as measured in K, is still radial (i.e., directed along qP) but that the field pattern has become anisotropic. As the charge whizzes by, observer M will receive a pulsed signal, of 3 dB width,

$$\Delta t \approx \frac{h}{c_0} \frac{\sqrt{1-\beta^2}}{\beta}. \tag{17.39}$$

In the limit $v \to c_0$, the signal becomes a Dirac pulse.

Consider now a transmitter radiating a wave of angular frequency ω toward an airplane moving with uniform velocity $\mathbf{v}$ (Fig. 17.4*b*). We wish to determine the characteristics of the signal picked up by a receiver on the airplane.[‖] If the plane is located sufficiently far from the antenna, the incident wave may be assumed plane (at least locally). If $\mathbf{h}$ is polarized horizontally, the incident fields are

$$\begin{aligned} e_z &= -e_1 \sin\alpha \cos\phi \\ e_y &= e_1 \cos\alpha \cos\phi \\ h_x &= -\frac{e_1}{R_{c0}} \cos\phi, \end{aligned} \tag{17.40}$$

where ϕ is the common phase angle

$$\phi = \omega t - k_0 z \cos\alpha - k_0 y \sin\alpha + \phi_1.$$

Applying the field transformation formulas (17.29) gives

$$\begin{aligned} e'_z &= -e_1 \sin\alpha \cos\phi \\ e'_y &= \frac{e_1}{\sqrt{1-\beta^2}} (\cos\alpha - \beta) \cos\phi \\ h'_x &= -\frac{e_1}{R_{c0}\sqrt{1-\beta^2}} (1 - \beta\cos\alpha) \cos\phi. \end{aligned} \tag{17.41}$$

The phase angle is transformed according to

$$\begin{aligned} \phi &= \frac{\omega - k_0 v\cos\alpha}{\sqrt{1-\beta^2}} t' - \frac{k_0\cos\alpha - (\omega v/c_0^2)}{\sqrt{1-\beta^2}} z' - k_0 y' \sin\alpha + \phi_1 \\ &= \omega' t' - k'_z z' - k'_y y' + \phi_1. \end{aligned} \tag{17.42}$$

This relationship shows that the radio operator on the airplane must tune his receiver to a frequency $(\omega'/2\pi)$, where

$$\omega' = \frac{\omega - k\mathbf{u}\cdot\mathbf{v}}{\sqrt{1-\beta^2}} = \frac{\omega}{\sqrt{1-\beta^2}} \left(1 - \frac{v_u}{c_0}\right) = \frac{\omega}{\sqrt{1-\beta^2}} (1 - \beta\cos\alpha). \tag{17.43}$$

[‖]Einstein actually discusses a similar problem in his basic 1905 paper.

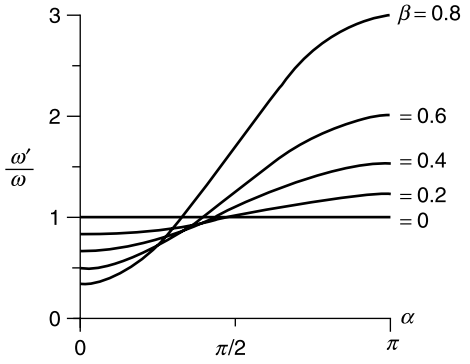

Figure 17.5 Doppler frequency shift.

The velocity v_u in this equation is the projection of $\mathbf{v}$ in the direction of propagation of the incident wave. At low velocities, the *Doppler shift* (ω'/ω) is given by the prerelativistic value

$$\frac{\omega'}{\omega} \approx 1 - \frac{v_\mu}{c_0} = 1 - \cos\alpha \frac{v}{c_0}. \tag{17.44}$$

The ratio (ω'/ω) is plotted in Figure 17.5.

Equation (17.43) shows that all frequencies in the spectrum of an incident wave suffer the same relative shift. Further, the time-harmonic plane wave (17.40) is seen by the radio operator in K' as an incident plane wave of propagation vector

$$\begin{aligned} k'_z &= \frac{1}{\sqrt{1-\beta^2}} \left(k\cos\alpha - \frac{\omega v}{c_0^2} \right) = k' \cos\alpha' \\ k'_y &= k \sin\alpha \qquad\qquad\qquad\quad = k' \sin\alpha'. \end{aligned} \tag{17.45}$$

Completely analogous calculations can be performed for the second basic linear polarization. It is to be noted, in particular, that the transformation of the phase angle ϕ, and the associated results (17.43) to (17.45), are independent of the state of polarization. A more detailed analysis shows that the signals in both polarizations are magnified (or contracted) by the same factor, and that their relative phase differences are maintained. It follows that the state of polarization in both plane waves is invariant, hence that linear remains linear, circular remains circular, and an elliptic polarization conserves its degree of ellipticity.

The dual problem of a transmitter in K' and a receiver in K — on the ground — can be solved by similar methods. If the large distance assumption is dropped, a time-harmonic signal from K' will suffer both amplitude and phase modulation when observed in K. Under these conditions, the fields at a point $\mathbf{r}$ of K can be evaluated by means of a suitable Green's dyadic, more specifically as[7,8]

$$\begin{aligned} \mathbf{E}(\mathbf{r},\omega) &= \frac{\mu_0}{4\pi} \int_{V'} \overline{\overline{G}}_e(\mathbf{r},\mathbf{r}',\omega) \cdot \mathbf{J}'(\mathbf{r}')\, dV' \\ \mathbf{B}(\mathbf{r},\omega) &= \frac{\mu_0}{4\pi} \int_{V'} \overline{\overline{G}}_h(\mathbf{r},\mathbf{r}',\omega) \cdot \mathbf{J}'(\mathbf{r}')\, dV'. \end{aligned} \tag{17.46}$$

The integration is over the volume V' occupied by the sources in K'.

17.5 CONSTITUTIVE EQUATIONS AND BOUNDARY CONDITIONS

When a material medium is in uniform translation with respect to the laboratory K, an inertial frame K' can be found in which all points of the medium are at rest. In that frame, according to *Minkowski*,[9] the traditional constitutive equations for a material at rest hold. For a linear isotropic material, for example,

$$\mathbf{d}' = \epsilon\,\mathbf{e}', \qquad \mathbf{b}' = \mu\,\mathbf{h}', \qquad \mathbf{j}' = \sigma\,\mathbf{e}'.$$

Expressing the primed fields in terms of the unprimed ones according to (17.28) gives

$$\begin{aligned}
\mathbf{d} + \frac{\mathbf{v}\times\mathbf{h}}{c_0^2} &= \epsilon\,(\mathbf{e} + \mathbf{v}\times\mathbf{b}) \\
\mathbf{b} - \frac{\mathbf{v}\times\mathbf{e}}{c_0^2} &= \mu\,(\mathbf{h} - \mathbf{v}\times\mathbf{d}) \\
\mathbf{j} &= \rho\,\mathbf{v} + \sigma\sqrt{1-\beta^2}\,\mathbf{e}_{\parallel} + \frac{\sigma}{\sqrt{1-\beta^2}}\,(\mathbf{e}_{\perp} + \mathbf{v}\times\mathbf{b}).
\end{aligned} \tag{17.47}$$

For practical applications, it is important to write the components explicitly. Thus, from (17.29),

$$\begin{aligned}
d_x - \frac{v}{c_0^2}\,h_y &= \epsilon\,e_x - \epsilon\,v b_y, \qquad d_y + \frac{v}{c_0^2}\,h_x = \epsilon\,e_y + \epsilon\,v b_x, \qquad d_z = \epsilon\,e_z \\
b_x + \frac{v}{c_0^2}\,e_y &= \mu\,h_x + \mu\,v d_y, \qquad b_y - \frac{v}{c_0^2}\,e_x = \mu\,h_y - \mu\,v d_x, \qquad b_z = \mu\,h_z \\
j_x &= \frac{\sigma}{\sqrt{1 - v^2/c_0^2}}\,(e_x - v b_y), \qquad j_y = \frac{\sigma}{\sqrt{1 - v^2/c_0^2}}\,(e_y + v b_x), \\
j_z &= \rho v + \sigma\sqrt{1 - v^2/c_0^2}\,e_z.
\end{aligned} \tag{17.48}$$

In most problems β is exceedingly small, and we write, to the first order,

$$\begin{aligned}
\mathbf{d} &= \epsilon\,\mathbf{e} + \frac{\epsilon_r\,\mu_r - 1}{c_0^2}\,(\mathbf{v}\times\mathbf{h}) \\
\mathbf{b} &= \mu\,\mathbf{h} - \frac{\epsilon_r\,\mu_r - 1}{c_0^2}\,(\mathbf{v}\times\mathbf{e}) \\
\mathbf{j} &= \rho\,\mathbf{v} + \sigma\,(\mathbf{e} + \mathbf{v}\times\mathbf{b}).
\end{aligned} \tag{17.49}$$

Because of the motion, the originally isotropic medium has become bianisotropic with respect to the laboratory. This particularly simple way to derive the *constitutive equations* is in sharp contrast with Lorentz' approach, which rested on appropriate hypotheses concerning the motion of the electrons in the medium.[10]

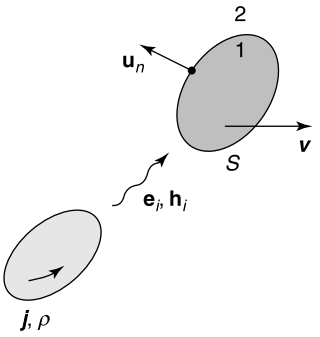

Figure 17.6 A ponderable body moving with uniform velocity in an incident field.

Boundary Conditions

The boundary conditions in the rest frame of the body have their traditional form (Fig. 17.6)

$$\begin{aligned}
\mathbf{u}'_n \times (\mathbf{h}'_2 - \mathbf{h}'_1) &= \mathbf{j}'_S \\
\mathbf{u}'_n \times (\mathbf{e}'_2 - \mathbf{e}'_1) &= 0 \\
\mathbf{u}'_n \cdot (\mathbf{d}'_2 - \mathbf{d}'_1) &= \rho'_S \\
\mathbf{u}'_n \cdot (\mathbf{b}'_2 - \mathbf{b}'_1) &= 0 \qquad (\text{on } S).
\end{aligned}$$

Transformed to K by means of (17.21) and (17.28) they become, after lengthy but trivial calculations,

$$\begin{aligned}
\mathbf{u}_n \times (\mathbf{h}_2 - \mathbf{h}_1) + (\mathbf{u}_n \cdot \mathbf{v})(\mathbf{d}_2 - \mathbf{d}_1) &= \mathbf{j}_S \\
\mathbf{u}_n \times (\mathbf{e}_2 - \mathbf{e}_1) - (\mathbf{u}_n \cdot \mathbf{v})(\mathbf{b}_2 - \mathbf{b}_1) &= 0 \\
\mathbf{u}_n \cdot (\mathbf{d}_2 - \mathbf{d}_1) &= \rho_S \\
\mathbf{u}_n \cdot (\mathbf{b}_2 - \mathbf{b}_1) &= 0. \qquad (17.50)
\end{aligned}$$

When $\mathbf{v}$ is tangent to the boundary, as in Figure 17.7*a*, the boundary conditions are the same as in the absence of motion. The tangential components e_y, e_z, in particular, are continuous

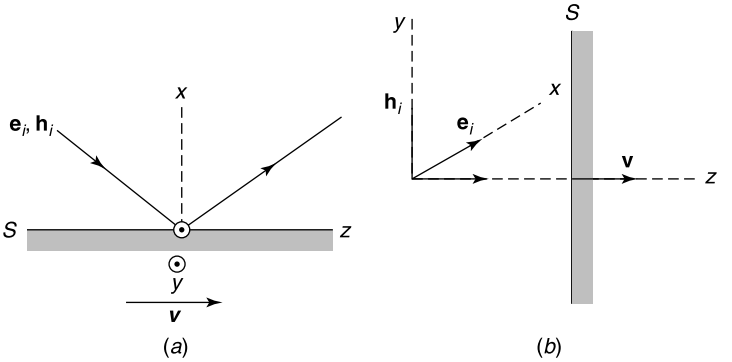

Figure 17.7 (*a*) Motion parallel to a boundary plane. (*b*) Motion perpendicular to a boundary plane.

across S. In Figure 17.7*b*, the motion is perpendicular to S, and the tangential components of $\mathbf{e}$ are *not* continuous. The actual value of these components when the medium is perfectly conducting is derived in Section 17.8.

17.6 MATERIAL BODIES MOVING UNIFORMLY IN STATIC FIELDS

In this section, we discuss two simple applications of the formulas derived in Section 17.5. They involve a method that is used extensively in the sequel: *frame hopping*.

17.6.1 The Moving Dielectric Slab

In Figure 17.8, a slab of material moves with velocity $\mathbf{v}$ in preexisting uniform static fields $\mathbf{e}_i = e_i\,\mathbf{u}_x$ and $\mathbf{b}_i = b_i\,\mathbf{u}_y$. These are the fields that exist when the slab is removed. We transform these fields to the moving axes, where they become

$$\mathbf{e}_i' = \frac{1}{\sqrt{1-\beta^2}}\,(e_i - vb_i)\,\mathbf{u}_x'$$

$$\mathbf{b}_i' = \frac{1}{\sqrt{1-\beta^2}}\left(b_i - \frac{ve_i}{c^2}\right)\mathbf{u}_y'.$$

In the presence of the slab, the total fields in air are

$$\mathbf{e}' = \mathbf{e}_i', \qquad \mathbf{d}' = \epsilon_0\,\mathbf{e}_i'$$

$$\mathbf{b}' = \mathbf{b}_i', \qquad \mathbf{h}' = \frac{1}{\mu_0}\,\mathbf{b}_i'.$$

In the slab, which has macroscopic parameters ϵ_r and μ_r,

$$\mathbf{e}' = \frac{1}{\epsilon_r}\,\mathbf{e}_i', \qquad \mathbf{d}' = \epsilon_0\,\mathbf{e}_i'$$

$$\mathbf{b}' = \mu_r\,\mathbf{b}_i', \qquad \mathbf{h}' = \frac{1}{\mu_0}\,\mathbf{b}_i'.$$

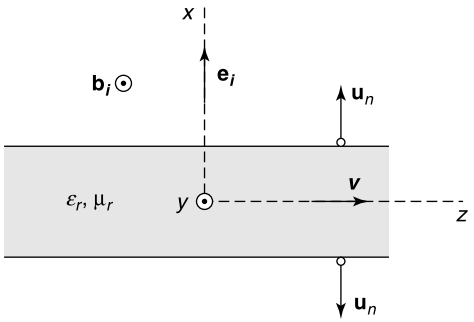

Figure 17.8 Dielectric slab moving in crossed static fields.

The next step is to transform the fields back to the laboratory. In air, one obtains the same values as if the slab was motionless. The same is not true for the fields *in the slab*, which are

$$\begin{aligned}
\mathbf{e} &= \frac{1}{1-\beta^2}\left[e_i\left(\frac{1}{\epsilon_r}-\beta^2\mu_r\right)-vb_i\left(\frac{1}{\epsilon_r}-\mu_r\right)\right]\mathbf{u}_x\\
\mathbf{d} &= \epsilon_0\,\mathbf{e}_i\\
\mathbf{b} &= \frac{1}{1-\beta^2}\left[\frac{v}{c_0^2}\,e_i\left(\frac{1}{\epsilon_r}-\mu_r\right)+b_i\left(\mu_r-\frac{\beta^2}{\epsilon_r}\right)\right]\mathbf{u}_y\\
\mathbf{h} &= \frac{1}{\mu_0}\,\mathbf{b}_i.
\end{aligned} \tag{17.51}$$

When v is very small with respect to c_0,

$$\begin{aligned}
e_x &= \frac{1}{\epsilon_r}\,e_i + vb_i\left(\mu_r-\frac{1}{\epsilon_r}\right)\\
b_y &= \underbrace{\mu_r\,b_i}_{\text{static fields}} \quad \underbrace{-\frac{v}{c_0^2}\,e_i\left(\mu_r-\frac{1}{\epsilon_r}\right)}_{\text{motional fields}}.
\end{aligned} \tag{17.52}$$

The formulas evidence the existence of a flux density b_y, even when the slab is nonmagnetic and the external flux density b_i is removed.** Under those circumstances, the magnetic effect is due to the motion of the electric *polarization* charges, which are of opposite sign on the two sides of the slab, and therefore create two opposite sheets of current in K (Problem 17.14).

17.6.2 Conductors Moving in a Static Magnetic Field

The conductor in Figure 17.9*a* moves with low velocity $\mathbf{v}$ in a preexisting static induction $\mathbf{b}_i(x, y, z)$. Transformed to K', the incident fields become

$$\begin{aligned}
\mathbf{b}_i' &= \mathbf{b}_i\,(x', y', z' + vt')\\
\mathbf{e}_i' &= \mathbf{v}\times\mathbf{b}_i'.
\end{aligned} \tag{17.53}$$

In K', the conductor is therefore immersed in a *transient* field of yet undetermined time complexity. From (17.53), the time rate of change at a fixed point in K' is

$$\frac{\partial\mathbf{b}_i'}{\partial t'} = v\left(\frac{\partial\mathbf{b}_i}{\partial z}\right)_{z=z'+vt'}. \tag{17.54}$$

It is seen that the time derivatives approach zero with v. The incident field may therefore be considered as "low-frequency" when v is small. Assume that the solution has been found. It is of the general form

$$\begin{aligned}
\mathbf{e}' &= \mathbf{e}_i' + \mathbf{e}_s' = \mathbf{v}\times\mathbf{b}_i\,(x', y', z' + vt') + \mathbf{e}_s'\,(x', y', z', t')\\
\mathbf{b}' &= \mathbf{b}_i' + \mathbf{b}_s' = \mathbf{b}_i\,(x', y', z' + vt') + \mathbf{b}_s'\,(x', y', z', t').
\end{aligned} \tag{17.55}$$

**The effects predicted by (17.52) were observed by Röntgen in a well-known experiment performed in 1880.

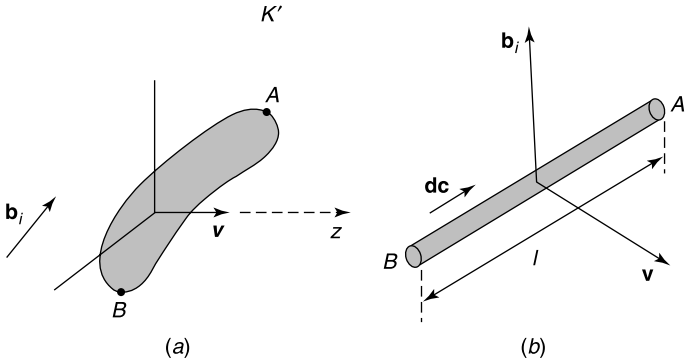

Figure 17.9 (*a*) Conductor moving in a static magnetic field. (*b*) Straight bar moving in a uniform field.

The subscript "*s*" refers to the scattered field (i.e., the field produced by the presence of the conductor). Transferring back to K gives

$$\mathbf{e} = (\mathbf{e}'_s - \mathbf{v} \times \mathbf{b}'_s)$$

$$\mathbf{b} = \mathbf{b}_i(x, y, z) + \left(\mathbf{b}'_s + \frac{1}{c_0^2}\,\mathbf{v} \times \mathbf{e}'_s\right). \tag{17.56}$$

In $\mathbf{e}'_s$ and $\mathbf{b}'_s$, the coordinates $[x', y', z', t']$ must now be replaced by $[x, y, z - vt, t - (vz/c_0^2)]$ to obtain the fields in K. The procedure becomes much simpler when the static fields are uniform. Let for example a nonmagnetic conducting bar move in a uniform $\mathbf{b}_i$, with such velocity that the low-β approximation holds (Fig. 17.9*b*). In K', the incident magnetic induction is $\mathbf{b}'_i = \mathbf{b}_i$. As the body is nonmagnetic, $\mathbf{b}'_i$ is also the total $\mathbf{b}'$. The incident electric field is the homogeneous, static electric field $\mathbf{v} \times \mathbf{b}_i$. As the total $\mathbf{e}'$ in the conductor must be zero, a transformation back to K yields

$$\mathbf{e} = -\mathbf{v} \times \mathbf{b} = -\mathbf{v} \times \mathbf{b}_i \tag{17.57}$$

in the conductor. Integrating from A to B gives an e.m.f.

$$\int_A^B \mathbf{e} \cdot d\mathbf{c} = -\int_A^B (\mathbf{v} \times \mathbf{b}_i) \cdot d\mathbf{c} = \mathbf{v} \cdot \int_A^B d\mathbf{c} \times \mathbf{b}_i = b_i \ell v. \tag{17.58}$$

This is the well-known flux cutting "$B\ell v$" law, familiar from introductory courses in electric machinery.

17.7 MAGNETIC LEVITATION

Advanced ground transportation systems require speeds of the order 400 km h^{-1}. At these speeds, electromagnetic forces are relied upon to eliminate frictional contact with the tracks. The principle of the system, in oversimplified form, is shown in Figure 17.10*a*. Fundamentally, the levitation force f_L arises because of the repulsive action between the primary currents and the secondary currents induced by the motion in either the track coils (not

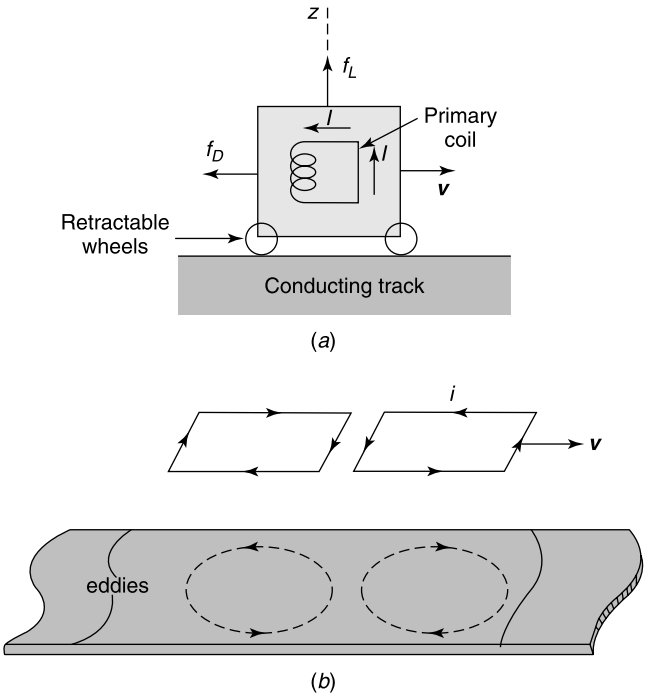

Figure 17.10 Simplified models of the levitation system.

shown in the figure) or in a continuous conducting band[11] (Fig. 17.10*b*). When the vehicle is at rest, no force is developed. Under the influence of a propulsion unit (e.g., ground coils forming a linear motor), the vehicle starts moving. When this happens, the metallic track is swept by a time-dependent magnetic induction **b**. As a result, Foucault currents are induced in the track, and the (secondary) magnetic field of these currents exerts a force on the primary currents i. This force consists of

1. A lift force f_L, and
2. A drag force f_D.

As the vehicle accelerates, the rate of change $\partial \mathbf{b}/\partial t$ in the metal increases, and the width of the Fourier spectrum at each point of the track follows suit. At high v, therefore, high frequencies are present, and the induced currents tend, because of the skin effect, to crowd near the surface of the track. In the limit of infinite v, the track behaves as a perfect conductor, and its effect can be replaced by that of image currents.

The technological complexity of an actual system is considerable. Because heavy primary currents are needed, superconducting coils and associated cryogenic systems must be mounted on the vehicle. Stability against lateral displacements must be ensured. Our purpose is definitely not to discuss these factors, but only to investigate how the f_L and f_D forces develop in the much simplified two-dimensional model[††] sketched in Figure 17.11. A solution in the *rest axes* of the primary current **j** is advantageous, because it ensures time-independence of the fields. A complication arises, however: The slab moves with velocity $(-\mathbf{v})$, hence constitutive equations such as (17.47) must be enforced. In a track of

[††]This model is also relevant for the study of flowmeters and magnetohydrodynamic generators, where the slab becomes a conducting fluid or gas.

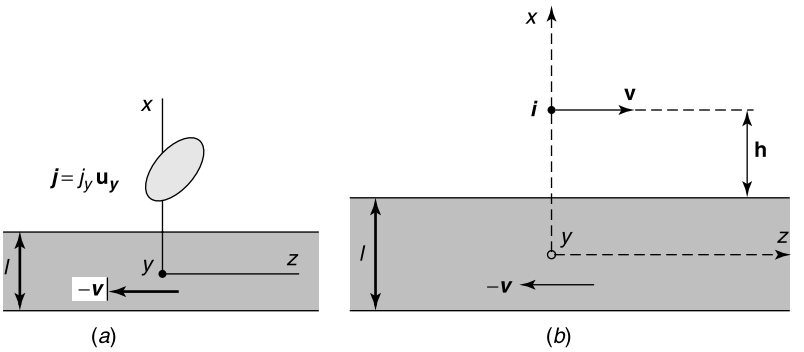

Figure 17.11 (*a*) Two-dimensional track and currents. (*b*) Levitation system with a line current.

characteristics σ, ϵ_r, μ_r these equations are, to the first order in v/c_0,

$$\mathbf{d} = \epsilon\,\mathbf{e} - \frac{\epsilon_r\mu_r - 1}{c_0^2}\,(\mathbf{v}\times\mathbf{h}) \tag{17.59}$$

$$\mathbf{b} = \mu\,\mathbf{h} + \frac{\epsilon_r\mu_r - 1}{c_0^2}\,(\mathbf{v}\times\mathbf{e}) \tag{17.60}$$

$$\mathbf{j} = -\rho\,\mathbf{v} + \sigma(\mathbf{e} - \mathbf{v}\times\mathbf{b}). \tag{17.61}$$

Given the nature of the problem, derivatives with respect to t and y should be set equal to zero in Maxwell's equations. The div $\mathbf{b} = 0$ equation yields, from (17.60),

$$\text{div}\,\mathbf{b} = \mu\,\text{div}\,\mathbf{h} + \frac{\epsilon_r\mu_r - 1}{c_0^2}\,\text{div}\,(\mathbf{v}\times\mathbf{e}) = 0.$$

But, as curl $\mathbf{e} = 0$ for time-independent phenomena,

$$\text{div}\,(\mathbf{v}\times\mathbf{e}) = \mathbf{e}\cdot\text{curl}\,\mathbf{v} - \mathbf{v}\cdot\text{curl}\,\mathbf{e} = 0.$$

We may conclude that div $\mathbf{h} = 0$ everywhere, hence that a flux function A exists such that

$$\mathbf{h}_t = h_x\,\mathbf{u}_x + h_z\,\mathbf{u}_z = \text{grad}\,A\times\mathbf{u}_y = -\frac{\partial A}{\partial z}\,\mathbf{u}_x + \frac{\partial A}{\partial x}\,\mathbf{u}_z. \tag{17.62}$$

From curl $\mathbf{e} = 0$, and because all derivatives with respect to y vanish,

$$\frac{\partial e_y}{\partial x} = \frac{\partial e_y}{\partial z} = 0.$$

A possible e_y component is therefore independent of x and z, which means that it must be zero as the fields must vanish at large distances. We conclude that $e_y = 0$ and, from (17.60) and (17.61), that

$$j_y = -\sigma\,v\,b_x = -\sigma\,v\mu\,h_x = \sigma\,v\mu\,\frac{\partial A}{\partial z}.$$

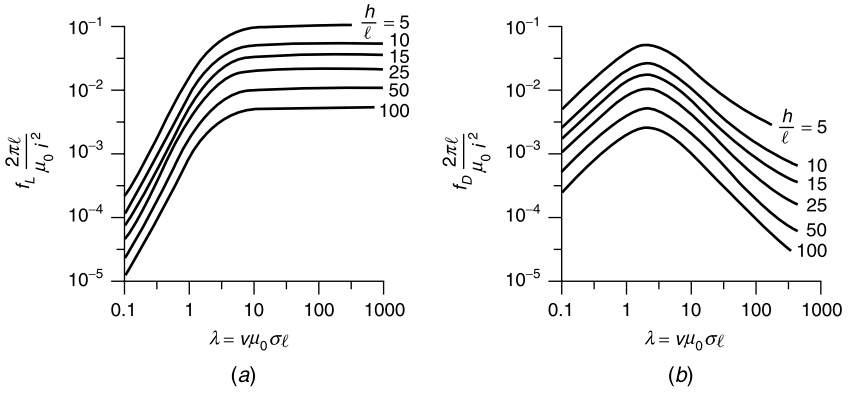

Figure 17.12 (*a*) Vertical (lift) force. (*b*) Horizontal (drag) force (from J. Van Bladel and D. De Zutter, Magnetic levitation: the track currents, *Appl. Phys. B*, **34**, 193–201, 1984, with permission of Springer-Verlag).

Inserting this value into curl $\mathbf{h} = \mathbf{j}$ gives

$$\nabla_{xz}^2 A + \underbrace{\sigma v \mu \frac{\partial A}{\partial z}}_{j_y} = 0 \qquad \text{in the slab.} \tag{17.63}$$

Outside the slab,

$$\nabla_{xz}^2 A = -j_y(x, z). \tag{17.64}$$

where j_y denotes the primary currents shown in Figure 17.11*a*.

To complete the solution, we need to express boundary conditions at the interfaces $x = \pm\ell/2$. Because the motion is parallel to the boundary, these conditions are the same as for a motionless slab. Continuity of b_y, in particular, combined with $e_y = 0$, leads to

$$(\mu_r h_x)_{slab} = -\mu_r \left(\frac{\partial A}{\partial z}\right)_{slab} = (h_x)_{air} = -\left(\frac{\partial A}{\partial z}\right)_{air}. \tag{17.65}$$

We also note that there are no *free* surface currents in the y-direction, hence that h_z is continuous at the boundary. From (17.62) this implies continuity of $\partial A/\partial x$ or, as A must vanish at large distances,

$$(A)_{slab} = (A)_{air}. \tag{17.66}$$

The outlined analysis has been applied to a line current i located above a slab,[12] as in Figure 17.11*b* [132]. Some data[‡‡] on the forces exerted on such a current are given in Figure 17.12. The important parameter there is the dimensionless quantity

$$\lambda = v\mu_0\sigma\ell = \frac{v}{v_r}, \tag{17.67}$$

[‡‡]Results have also been obtained for sources moving above a stratified medium.[13]

which is a *Peclet* or *magnetic Reynolds number*. For copper and $\ell = 10$ cm, $\lambda = 280$ for a velocity of 400 km h^{-1}. In that high velocity range, f_L has reached a constant (asymptotic) value, and f_D decreases monotically for increasing velocities. This behavior is not unexpected, because the drag force f_D finds its origin in the Joule losses in the track, and these disappear in the limit $v \to \infty$ as the (volume) eddy currents progressively migrate to the surface.

17.8 SCATTERERS IN UNIFORM MOTION

The problem in hand is to determine the fields scattered by a material body moving through the field of a radiating source (Fig. 17.13*a*). Currents are induced in the body, and the characteristics of the scattered fields — in both amplitude and time dependence — can be exploited to extract information on the motion of the target. These ideas will be clarified by first discussing the fields reflected by a *perfectly conducting mirror in uniform translation*[§§] (Fig. 17.13*b*).

17.8.1 Reflection from a Mirror Moving Perpendicularly to Its Surface

Let the incident wave be plane, with fields

$$\mathbf{e}_i = E \cos\left(\omega t - \frac{\omega}{c_0} z\right) \mathbf{u}_x$$
$$\mathbf{h}_i = \frac{E}{R_{c0}} \cos\left(\omega t - \frac{\omega}{c_0} z\right) \mathbf{u}_y.$$

Transformed to the rest axes K' of the mirror, the fields become

$$\mathbf{e}'_i = E\sqrt{\frac{1-\beta}{1+\beta}} \cos\left[\omega\sqrt{\frac{1-\beta}{1+\beta}}\left(t' - \frac{z'}{c_0}\right)\right] \mathbf{u}_x$$
$$\mathbf{h}'_i = \frac{1}{R_{c0}} e'_i \mathbf{u}_y. \tag{17.68}$$

In the rest axes, the reflected fields are given by

$$\mathbf{e}'_r = -E\sqrt{\frac{1-\beta}{1+\beta}} \cos\left[\omega\sqrt{\frac{1-\beta}{1+\beta}}\left(t' + \frac{z'}{c_0}\right)\right] \mathbf{u}_x$$
$$\mathbf{h}'_r = \frac{E}{R_{c0}}\sqrt{\frac{1-\beta}{1+\beta}} \cos\left[\omega\sqrt{\frac{1-\beta}{1+\beta}}\left(t' + \frac{z'}{c_0}\right)\right] \mathbf{u}_y. \tag{17.69}$$

[§§]This particular problem is discussed by Einstein in his 1905 paper.

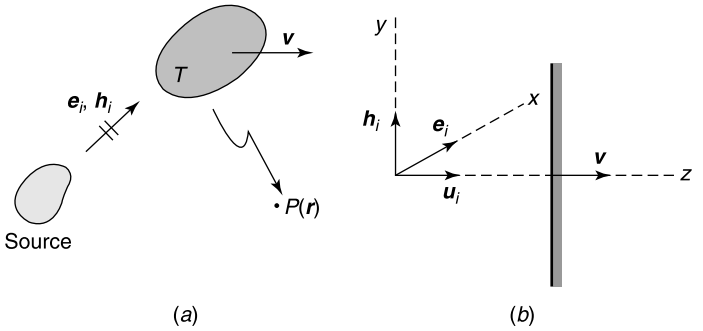

Figure 17.13 (*a*) A target moving past a source. (*b*) Wave incident on a moving mirror.

Transformed back to the laboratory axes, they become

$$\mathbf{e}_r = -E\,\frac{1-\beta}{1+\beta}\,\cos\left[\omega\,\frac{1-\beta}{1+\beta}\left(t+\frac{z}{c_0}\right)\right]\mathbf{u}_x$$
$$\mathbf{h}_r = \frac{1}{R_{c0}}\,E\,\frac{1-\beta}{1+\beta}\,\cos\left[\omega\,\frac{1-\beta}{1+\beta}\left(t+\frac{z}{c_0}\right)\right]\mathbf{u}_y. \tag{17.70}$$

The frequency has clearly suffered a double Doppler shift, which results in a "reflected" frequency

$$\omega_r = \omega\,\frac{1-\beta}{1+\beta}. \tag{17.71}$$

For small v:

$$\omega_r \approx \omega\,(1-2\beta) = \omega\left(1-\frac{2v}{c}\right). \tag{17.72}$$

The total fields at the mirror, at $z = vt$, are given by

$$e_x = \frac{2\beta}{1+\beta}\,\cos\left[\omega\,(1-\beta)\,t\right]$$
$$c_0 b_y = \frac{2}{1+\beta}\,\cos\left[\omega\,(1-\beta)\,t\right]. \tag{17.73}$$

We note that the tangential component e_x does *not* vanish on the perfectly conducting mirror (except for $\beta = 0$, i.e., in the absence of motion). It is clear, from (17.70), that the amplitude of the reflected wave, and hence the latter's power density, are modified by the motion. When the motion is to the left, for example, β is negative, and the power density upon reflection is $\left(\dfrac{1+|\beta|}{1-|\beta|}\right)^2$ times its value for a stationary mirror. Power amplification takes place, the additional power being provided by the force acting on the mirror to overcome the radiation pressure.

The analysis can easily be extended to incident pulses of arbitrary shape and duration. More precisely, let the incident fields in K have the time dependence (Fig. 17.14*a* and *b*)

$$e_{ix} = R_{c0}\,h_{iy} = f\left(t-\frac{z+L}{c_0}\right).$$

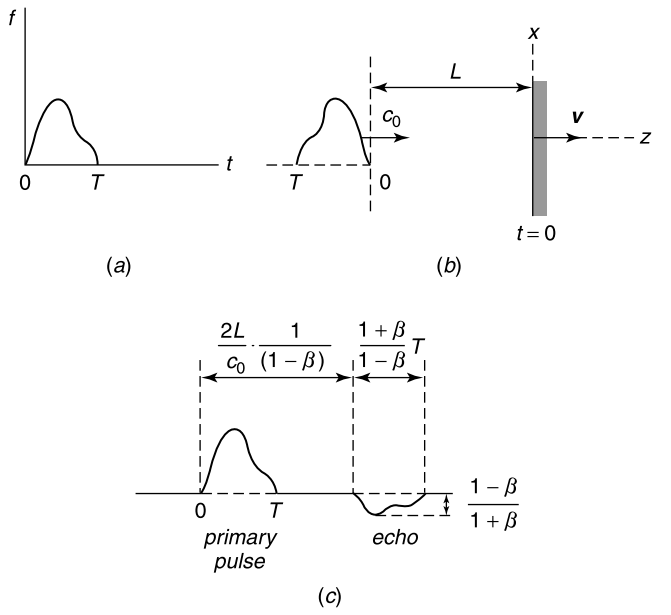

Figure 17.14 Reflection of a pulse on a moving mirror.

In the axes of the mirror, these fields become

$$e'_{ix} = R_{c0}\, h'_{iy} = \sqrt{\frac{1-\beta}{1+\beta}} f\left[\sqrt{\frac{1-\beta}{1+\beta}}\left(t' - \frac{z'}{c}\right) - \frac{L}{c}\right].$$

The corresponding reflected wave is

$$e'_{rx} = -R_{c0}\, h'_{ry} = -\sqrt{\frac{1-\beta}{1+\beta}} f\left[\sqrt{\frac{1-\beta}{1+\beta}}\left(t' + \frac{z'}{c}\right) - \frac{L}{c}\right].$$

Transformed to the laboratory axes, the reflected fields are given by

$$e_{rx} = -R_{c0}\, h_{ry} = -\frac{1-\beta}{1+\beta} f\left[\frac{1-\beta}{1+\beta}\left(t + \frac{z}{c}\right) - \frac{L}{c}\right]. \tag{17.74}$$

In the plane $z = -L$, in particular,

$$\begin{aligned} e_{rx} = -R_{c0}\, h_{ry} &= -\frac{1-\beta}{1+\beta} f\left(\frac{1-\beta}{1+\beta}\, t - \frac{2L}{c_0}\frac{1}{1+\beta}\right) \\ &= -\frac{1-\beta}{1+\beta} f\left[\frac{1-\beta}{1+\beta}\left(t - \frac{2L}{c_0}\frac{1}{1-\beta}\right)\right]. \end{aligned} \tag{17.75}$$

The graphical representation of the echo signal is given in Figure 17.14*c*. We note

1. That the motion of the reflector lengthens the echo time by a factor $1/(1-\beta)$
2. That the motion stretches the received signal along the time axis by a factor $(1+\beta)/(1-\beta)$, and

3. That the motion multiplies the signal in amplitude by a factor $(1-\beta)/(1+\beta)$.

When the incident field is a very short burst, such as the *ns*-long pulse from a laser, the incident field can be modeled by a Dirac pulse $e_{ix} = A\,\delta(t)$. The reflected field is now

$$e_{rx} = -\delta\left[t - \frac{2L}{c_0(1-\beta)}\right], \tag{17.76}$$

a waveform without trailing edge. This conclusion holds only when the mirror may be assumed perfectly conducting.

17.8.2 Two-Dimensional Scatterers

The next step in complexity is to consider a moving material *cylinder* (shown as circular in Fig. 17.15). Let the incident wave be a plane wave of angular frequency ω_i, with fields

$$\begin{aligned}\mathbf{E}_i &= e^{-jk_i\,(x\sin\theta_i + z\cos\theta_i)}\; e^{j\omega_i t}\,\mathbf{u}_y \\ \mathbf{H}_i &= \frac{1}{R_{c0}}\,(\mathbf{u}_i \times \mathbf{E}_i).\end{aligned} \tag{17.77}$$

In the rest frame of the cylinder, these fields become

$$\begin{aligned}\mathbf{E}'_i &= \gamma\,(1-\beta\cos\theta_i)\; e^{-jk'_i(x'\sin\theta'_i + z'\cos\theta'_i)}\; e^{j\omega'_i t'}\,\mathbf{u}'_y \\ \mathbf{H}'_i &= \frac{1}{R_{c0}}\,(\mathbf{u}'_i \times \mathbf{E}'_i),\end{aligned} \tag{17.78}$$

where the often used symbol γ stands for

$$\gamma = \frac{1}{\sqrt{1-\beta^2}}. \tag{17.79}$$

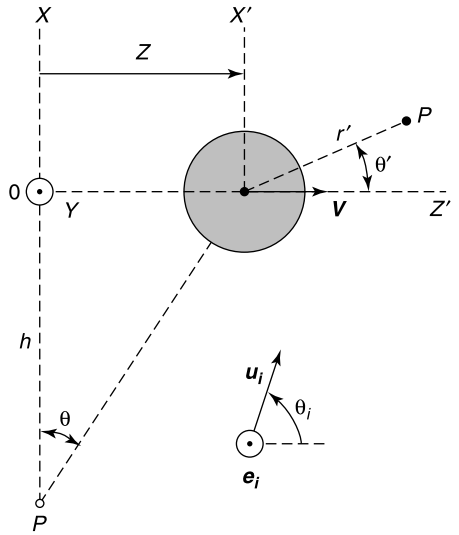

Figure 17.15 Cylinder moving transversally in an incident wave.

The fields are still time-harmonic, but with a new frequency, and a new angle of incidence θ_i'. These are given by

$$\begin{aligned} \omega_i' &= k_i' c = \gamma \omega_i (1 - \beta \cos\theta_i) \\ \sin\theta_i' &= \frac{\sin\theta_i}{\gamma\,(1 - \beta\cos\theta_i)} \\ \cos\theta_i' &= \frac{\cos\theta_i - \beta}{(1 - \beta\cos\theta_i)}. \end{aligned} \tag{17.80}$$

It is seen that θ_i and θ_i' together lie between 0 and π, or between π and 2π. The problem is now reduced to the determination of the fields scattered by a *stationary* cylinder immersed in a plane wave of frequency ω_i'. This is a classic problem, which is discussed extensively in Chapter 14. At distances large with respect to the wavelength λ_i' (i.e., for $k_i' r' \gg 1$), $\mathbf{E}_{sc}'$ is of the general form

$$\mathbf{E}_{sc}' = F'(\theta') \frac{e^{-jk_i' r'}}{\sqrt{r'}} e^{j\omega_i' t'} \mathbf{u}_y'. \tag{17.81}$$

If the cylinder is circular and perfectly conducting, for example, the techniques of Section 14.2 give a radiation pattern

$$F'(\theta') = -\gamma(1 - \beta\cos\theta_i)(1 + j)\frac{1}{\sqrt{\pi k_i'}} \sum_{n=0}^{\infty} \epsilon_n \frac{J_n(k_i' a)}{H_n^{(2)}(k_i' a)} \cos n(\theta' - \theta_i'). \tag{17.82}$$

We will leave $F(\theta')$ unspecified and transform $\mathbf{E}_{sc}'$ back to the laboratory, where the scattered fields are[14] [132]

$$\mathbf{E}_{sc} = \frac{\gamma}{(h^2 + \gamma^2 v^2 t^2)^{\frac{1}{4}}} \left(1 - \frac{\gamma\beta v t}{(h^2 + \gamma^2 v^2 t^2)^{\frac{1}{2}}}\right) e^{j\phi} F'(\theta')\, \mathbf{u}_y \tag{17.83}$$

$$\mathbf{H}_{sc} = \frac{1}{R_{c0}(h^2 + \gamma^2 v^2 t^2)^{\frac{3}{4}}} \left[-h\mathbf{u}_z + \beta\gamma^2 \left(ct - \frac{1}{\gamma}\sqrt{h^2 + \gamma^2 v^2 t^2}\right)\mathbf{u}_x\right] e^{j\phi} F'(\theta').$$

In these formulas, θ' is the value corresponding to P in Figure 17.15; that is,

$$\theta' = \tan^{-1}\left(\frac{h}{\gamma v t}\right) \qquad (\pi \le \theta' \le 2\pi). \tag{17.84}$$

The (fast varying) phase angle is

$$\phi = \gamma^2 \omega_i (1 - \beta\cos\theta_i)\left[t - \frac{1}{c_0}\sqrt{v^2 t^2 + h^2(1 - \beta^2)}\right]. \tag{17.85}$$

An instantaneous frequency may be introduced in the form

$$\omega = \frac{d\phi}{dt} = \frac{\omega_i}{1 - \beta^2}(1 - \beta\cos\theta_i)\left(1 - \beta\frac{t}{\sqrt{t^2 + \dfrac{h^2}{v^2}(1 - \beta^2)}}\right). \tag{17.86}$$

Setting $z_{target} = z_t = vt$ yields, in the low-velocity limit,

$$\omega \approx \omega_i \left(1 - \beta \cos\theta_i - \beta \frac{z_t}{\sqrt{z_t^2 + h^2}} \right). \tag{17.87}$$

This relationship gives an idea of the Doppler shift introduced by the motion of the cylinder.

17.8.3 The General Scattering Problem

In a more accurate analysis, the concept of instantaneous frequency should be replaced by the true frequency spectrum of $\mathbf{E}_{sc}(t)$. The computations are by no means elementary.[14,15,16] They are even more so in three dimensions, even if the source is time-independent and the spectrum is generated by amplitude modulation only.[17] The scattered field is now of the general form

$$\begin{aligned} \mathbf{E}'_{sc} &= \mathbf{F}'(\mathbf{u}') \frac{\exp(-jk'_i R')}{R'} e^{j\omega'_i t'} \\ \mathbf{H}'_{sc} &= \frac{1}{R_{c0}} \mathbf{u}' \times \mathbf{E}'_{sc}. \end{aligned} \tag{17.88}$$

The complexity brought about by this general radiation pattern is evident.

Although the relativistic approach is conceptually correct, it is not surprising that the practicing radio scientist will seek relief in some kind of approximation. The most obvious one is the *quasistationary approach*, which consists in evaluating the scattered fields at ground station P, at time t, as if the scatterer were stationary at the position it occupies at time t (Fig. 17.13*a*). The motion produces both amplitude and phase modulation. The latter in turn results in an instantaneous frequency that, if the motion is very slow, is given by

$$f_{rec} = f_{tr} \left(1 - 2\frac{v_r}{c_0} \right), \tag{17.89}$$

wherein v_r is the radial velocity of the target, and f_{rec} and f_{tr} are respectively the received and transmitted frequencies in P. The approximate character of formula (17.89) is evident, because it implies, for example, that v_r is uniform in the target volume T. The method leads to further difficulties when the target is so large that it no longer looks like a point scatterer with a constant phase center, or when it is illuminated by a wide antenna beam. The quasistationary method also neglects the motion of the target during the travel time of the wave from source to scatterer and back to observation point P. It nevertheless gives acceptable results at low velocities and accelerations. The meaning of "acceptable" and "low" should be examined carefully in each case. For the moving mirror in Figure 17.13, for example, the quasistationary reflected field is

$$e_r = -E \cos[\omega t + k_0(z - z_0) - k_0 z_0], \tag{17.90}$$

where z_0 is the position of the mirror, *frozen in its tracks* at time t. Introducing $z_0 = vt$ in (17.90) leads to the following value for the reflected wave at z:

$$e_r = -E \cos\left[\omega \left(1 - \frac{2v}{c_0} \right) t + k_0 z \right]. \tag{17.91}$$

This quasistationary field should be compared with the exact expression (17.70). The comparison shows that

1. The first-order Doppler effect is correctly predicted
2. The first-order correction in the amplitude is ignored, and
3. The reflected field (17.91) does not satisfy the wave equation in vacuum. In particular, its velocity of propagation is $c_0/(1-2\beta)$ instead of c_0.

We may conclude that the quasistationary (or adiabatic) method should be used with suitable caution.

17.9 MATERIAL BODIES IN NONUNIFORM MOTION

In an accelerated body the internal structure of the material is not in local equilibrium, and the conditions for the derivation of linear laws such as $\mathbf{d} = \epsilon\,\mathbf{e}$ may not be respected. Further, the accelerations generate stresses and deformations, which produce additional changes in the electrical characteristics of the body. For sufficiently low accelerations, however, one often assumes, as a working hypothesis,[¶¶] that the electrical properties in the *instantaneous rest-frame* K' of P are unaffected by the accelerations (Fig. 17.16a). Thus, in a linear medium,

$$\begin{aligned} \mathbf{d}' &= \epsilon\,\mathbf{e}' \\ \mathbf{b}' &= \mu\,\mathbf{h}' \\ \mathbf{j}' &= \sigma\,\mathbf{e}' \qquad (\text{in } P). \end{aligned} \tag{17.92}$$

The effect of the stresses can be included in the values of ϵ, μ, σ. In the laboratory system (i.e., in the inertial frame K), the constitutive equations become, from (17.47),

$$\begin{aligned} \mathbf{d} + \frac{\mathbf{v}\times\mathbf{h}}{c_0^2} &= \epsilon\,(\mathbf{e} + \mathbf{v}\times\mathbf{b}) \\ \mathbf{b} - \frac{\mathbf{v}\times\mathbf{e}}{c_0^2} &= \mu\,(\mathbf{h} - \mathbf{v}\times\mathbf{d}) \\ \mathbf{j} &= \rho\mathbf{v} + \sigma\sqrt{1-\frac{v^2}{c_0^2}}\,\mathbf{e}_\parallel + \frac{\sigma}{\sqrt{1-v^2/c_0^2}}\,(\mathbf{e}_\perp + \mathbf{v}\times\mathbf{b}). \end{aligned} \tag{17.93}$$

The difference with respect to (17.47) is that $\mathbf{v}$ is now a function of position and time. It is to be noted that the *rates* of variation of $\mathbf{v}$ with respect to space and time do not appear in the equations, in agreement with the previous remarks.

A test for the validity of the *instantaneous rest-frame* hypothesis should be based on the internal physics of the accelerated body. This verification has been performed for a uniformly rotating dielectric body.[18] The dielectric is modeled by fixed positive nuclei and free negative electrons, elastically bound to the nuclei (Fig. 17.17). At rest, the number

[¶¶] Private communcation by Professor C. Møller.

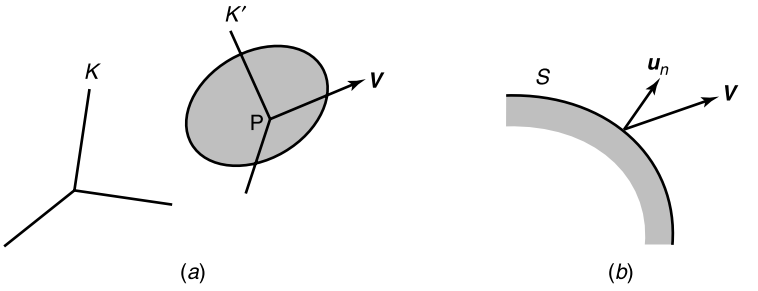

Figure 17.16 (*a*) Accelerated body, together with the instantaneous rest frame in *P*. (*b*) Point *P* at the surface of an accelerated body.

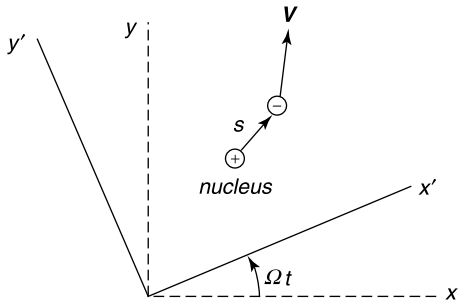

Figure 17.17 Model for a rotating dielectric.

density of both charges is n_0. Under rotation, the electrons shift their position by an amount $\mathbf{s}$ and acquire a new number density $n_0 + n_1(\mathbf{r}')$. The motion of the electrons is governed by

- Elastic forces proportional to $\mathbf{s}$
- Electromagnetic forces $q(\mathbf{e} + \mathbf{v} \times \mathbf{b})$
- Coriolis and centrifugal forces

The solution of the equations of motion shows that acceleration effects can be ignored as long as $\Omega \ll \omega_0$, where ω_0 denotes the angular frequency of the oscillations associated with the mass m_e and the *electron-nucleus* spring. In practice, ω_0 lies in the infrared or ultraviolet parts of the spectrum. The analysis therefore confirms the validity of the instantaneous rest-frame hypothesis for "engineering" values of the rotation frequency $(\Omega/2\pi)$.

A few interesting results can be derived from (17.93) at low velocities:

1. When the moving medium is a perfect conductor, the condition $\mathbf{e}' = 0$ (necessary to keep $\mathbf{j}'$ bounded) leads to

$$\mathbf{e} + \mathbf{v} \times \mathbf{b} = 0 \tag{17.94}$$

everywhere in the body.

2. If the medium is an insulator, the conditions $\rho' = 0$ and $\mathbf{j}' = 0$ in K' yield, in the laboratory,

$$\begin{aligned} \rho &= 0 \\ \mathbf{j} &= 0. \end{aligned} \tag{17.95}$$

In the laboratory frame, the constitutive equations for a general rotating body follow from setting $\mathbf{v} = \Omega r \mathbf{u}_\varphi$ in (17.93).

The instantaneous rest-frame hypothesis can also be invoked to derive the boundary conditions in an *accelerated* frame of reference (Fig. 17.16*b*). The guiding principle is simple: the boundary conditions in the instantaneous rest frame K' of P must be the same as if the body were stationary in K'. This means that (17.50) may be applied. The b'_n and $\mathbf{e}'_{\tan}$ components, in particular, should be continuous across S. It also means that the boundary conditions of a moving body in the laboratory are the same as in the absence of motion at points where $\mathbf{v}$ lies in the tangent plane of the body (in which case $\mathbf{u}_n \cdot \mathbf{v} = 0$).

17.10 ROTATING BODIES OF REVOLUTION

In Figure 17.18, a homogeneous body of revolution, of parameters $(\epsilon_r, \mu_r, \sigma)$, is rotating with uniform angular velocity Ω about the z-axis. This BOR is immersed in an externally applied field, of which two kinds will be considered: static and time-harmonic.

17.10.1 Static Fields

We first assume that the body rotates in an axisymmetric induction $\mathbf{b}_0$, the value that exists in the absence of rotation (but in the presence of the body). The fields and sources in the laboratory axes can be written as

$$\begin{aligned} \mathbf{e} &= \mathbf{e}_1; & \mathbf{d} &= \mathbf{d}_1 \\ \mathbf{b} &= \mathbf{b}_0 + \mathbf{b}_1; & \mathbf{h} &= \mathbf{h}_0 + \mathbf{h}_1 \\ \mathbf{j} &= \mathbf{j}_1; & \rho &= \rho_1, \end{aligned} \tag{17.96}$$

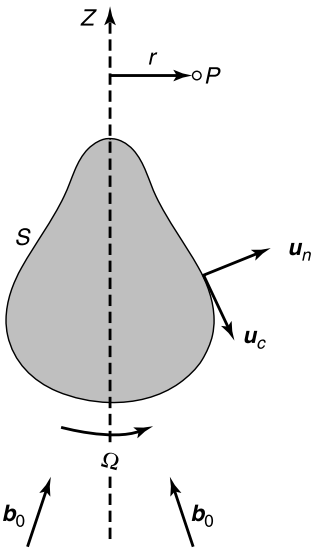

Figure 17.18 Body of revolution rotating in a static field.

wherein the subscript 0 refers to the stationary body and the subscript 1 to the motional contribution. The fields are time-independent, hence Maxwell's equations in the conductor are

$$\text{curl } \mathbf{e} = \text{curl } \mathbf{e}_1 = 0 \tag{17.97}$$

$$\text{curl } \mathbf{h}_0 = 0 \tag{17.98}$$

$$\text{curl } \mathbf{h}_1 = \mathbf{j}_1 \tag{17.99}$$

$$\text{div } \mathbf{d} = \text{div } \mathbf{d}_1 = \rho_1 \tag{17.100}$$

$$\text{div } \mathbf{b}_0 = 0 \tag{17.101}$$

$$\text{div } \mathbf{b}_1 = 0. \tag{17.102}$$

These equations must be complemented by the constitutive equations (17.47), in which (v^2/c_0^2) will be assumed very small with respect to unity. Under these conditions,

$$\mathbf{d}_1 = \epsilon\, \mathbf{e}_1 + \frac{\epsilon_r\, \mu_r - 1}{c_0^2}\, (\mathbf{v} \times \mathbf{h}_0) \tag{17.103}$$

$$\mathbf{b}_0 = \mu\, \mathbf{h}_0 \tag{17.104}$$

$$\mathbf{b}_1 = \mu\, \mathbf{h}_1 - \frac{\epsilon_r\, \mu_r - 1}{c_0^2}\, (\mathbf{v} \times \mathbf{e}_1) \tag{17.105}$$

$$\mathbf{j}_1 = \rho_1\, \mathbf{v} + \sigma\, (\mathbf{e}_1 + \mathbf{v} \times \mathbf{b}_0). \tag{17.106}$$

Because $\mathbf{v}$ lies in the tangent plane, the boundary conditions in K are the same as in the absence of rotation. In solving the field equations, we are particularly interested in the induced Foucault current $\mathbf{j}_1$. This current can be divided into a convective component $\rho_1\, \mathbf{v}$ and a conductive component $\mathbf{j}_{1c}$. More precisely:

$$\mathbf{j}_{1c} = \mathbf{j}_1 - \rho_1\, \mathbf{v} = \sigma\, (\mathbf{e}_1 + \mathbf{v} \times \mathbf{b}). \tag{17.107}$$

The convection current $\rho_1\, \mathbf{v}$ is a second-order effect. To the first order, therefore, we may write

$$\mathbf{j}_{1c} = \mathbf{j}_1 = \sigma\, (\mathbf{e}_1 + \mathbf{v} \times \mathbf{b}_0). \tag{17.108}$$

From (17.99), $\mathbf{j}_1$ is solenoidal. It is also irrotational, because curl $\mathbf{e}_1 = 0$, from (17.97), and

$$\text{curl } (r\, \mathbf{u}_\varphi \times \mathbf{b}_0) = \text{curl } \left[(r\, b_{0z})\, \mathbf{u}_r - (r\, b_{0r})\, \mathbf{u}_z \right]$$

$$= \mathbf{u}_\varphi \left[r \left(\frac{\partial b_{0z}}{sz} + \frac{1}{r} \frac{\partial}{\partial r} (r\, b_{0r}) \right) \right] = \mathbf{u}_\varphi\, r\, \text{div } \mathbf{b}_0 = 0. \tag{17.109}$$

The boundary condition on $\mathbf{j}_1$ results from the equation of conservation of charge (4.108), which takes the form

$$\frac{\partial \rho_{S1}}{\partial t} = \mathbf{u}_n \cdot \mathbf{j}_1 - \text{div}_S\, (\mathbf{j}_{S1}) \qquad (\text{on } S). \tag{17.110}$$

The time derivative vanishes because fields and sources do not depend on time. The surface currents, if they exist, are convection currents and therefore second-order effects. We conclude that $\mathbf{u}_n \cdot \mathbf{j}_1 = 0$. Current $\mathbf{j}_1$ is therefore a harmonic vector tangent to S. Developments similar to those in Section 4.10 prove that such a vector must vanish.[‖‖] To the first order in Ω, therefore,

$$\mathbf{e} = \mathbf{e}_1 = -(\mathbf{v} \times \mathbf{b}) \approx -(\mathbf{v} \times \mathbf{b}_0). \tag{17.111}$$

This relationship is of great importance for practical applications.

The rotation of the conductor generates, in addition to the electric field (17.111), a volume charge density ρ_1. Inserting (17.111) into (17.103) gives, indeed,

$$\operatorname{div} \mathbf{d}_1 = -\frac{\epsilon_0}{\mu_r} \operatorname{div} (\mathbf{v} \times \mathbf{b}_0) = -2\Omega \frac{\epsilon_0}{\mu_r} b_{0z} = -2\Omega \epsilon_0 \mu_0 h_{0z}. \tag{17.112}$$

We conclude that the rotation produces a volume charge density

$$\rho_1 = -\frac{2\Omega}{c_0^2} h_{0z} \qquad (C\,\mathrm{m}^{-3}). \tag{17.113}$$

This density can be either positive or negative, depending on the signs of Ω and h_z. As the body is electrically neutral, charges of a sign opposite to that of ρ_1 appear on the outer surface S.

On the basis of (17.111), it is clear that the rotating conductor can function as a voltage generator. The open circuit voltage that appears between two points M and N located in the same meridian plane is given by

$$\phi_M - \phi_N = \int_M^N \mathbf{e}_1 \cdot d\mathbf{c} = -\int_M^N (\mathbf{v} \times \mathbf{b}_0) \times d\mathbf{c} = \Omega \int_M^N (r b_{0r}\, \mathbf{u}_z - r b_{0z}\, \mathbf{u}_r) \cdot d\mathbf{c}. \tag{17.114}$$

For the drum generator of Figure 17.19*a*, the potential difference is

$$\phi_A - \phi_B = -\Omega a \int_B^A b_{0r}\, dz. \tag{17.115}$$

It is generated by the *radial* component of $\mathbf{b}_0$ and can be positive or negative depending on the sense of rotation. In the device of Figure 17.19*b*, the e.m.f. is generated by the *axial* component b_{0z}.

The results of the previous analysis show that the Foucault currents in the rotating conductor are of an order higher than the first in Ω. The same property does not hold when $\mathbf{b}_0$ loses its axisymmetric character, which is the case for the Faraday disk shown in

[‖‖] The conclusion holds even when the volume is a ring-like term, because $\mathbf{e}$ (and therefore $\mathbf{j}$) is irrotational everywhere in space.

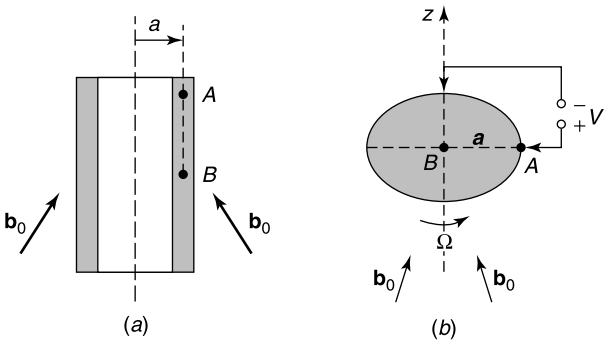

Figure 17.19 Two possible generators of direct voltage.

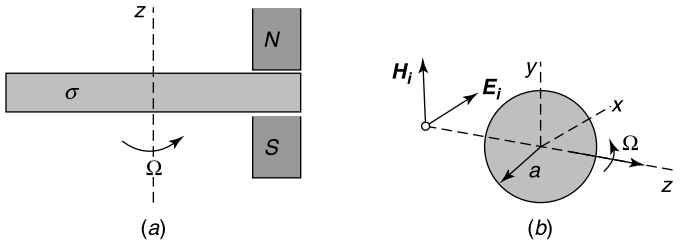

Figure 17.20 (*a*) Rotating conducting circular cylinder (Faraday disk). (*b*) Rotating sphere in an incident wave.

Figure 17.20*a*. In this device, which has been investigated extensively,*** the induced eddy currents act as a brake (Problem 17.21).

17.10.2 Rotating Sphere in an Incident Time-Harmonic Wave

In the simple example shown in Figure 17.20*b*, it is clear that the quasistationary method would not reveal the existence of a rotation, because the successive positions of the (homogeneous) sphere are completely equivalent. The same conclusion would hold for a rotating BOR, provided the body is axisymmetric in shape *and* composition. The instantaneous rest frame assumption, on the other hand, predicts that the rotation influences the fields, specifically by way of the velocity-dependent constitutive equations (17.93). Because the effect disappears as Ω approaches zero, we shall again split the fields and currents into a zero-motion term (say $\mathbf{E}_0$) and a motional term (say $\mathbf{E}_1$). At low velocities, that is, for $\Omega r \ll c_0$, (17.93) gives, to the first order in $(\Omega r/c_0)$,

$$\mathbf{D} \approx \epsilon\,\mathbf{E} + \frac{1}{c_0^2}\,(\epsilon_r\,\mu_r - 1)(\mathbf{v} \times \mathbf{H}) \tag{17.116}$$

$$\mathbf{B} \approx \mu\,\mathbf{H} - \frac{1}{c_0^2}\,(\epsilon_r\,\mu_r - 1)(\mathbf{v} \times \mathbf{E}) \tag{17.117}$$

***The braking effect has been analyzed relativistically for a half infinite slab moving with constant velocity in a static field.[19] A solution in *rotating axes* can be found in B. Hommez, M.S. thesis, Dept. of Information Technology, Ghent University, 1998.

$$\mathbf{J} \approx \sigma\,\mathbf{E} + \sigma\,\mu\,(\mathbf{v} \times \mathbf{H}). \tag{17.118}$$

If the (σ, ϵ, μ) parameters do not vary with time, these equations are time-invariant. It follows that a time-harmonic incident wave is scattered with unchanged frequency by the spherical target; no Doppler shift occurs. The same conclusion could obviously not be drawn for a rotating helicopter blade, whose motion produces amplitude and phase modulation. Inserting the constitutive equations into Maxwell's equations gives (with $\mathbf{\Omega} = \Omega\,\mathbf{u}_z$)

$$\operatorname{curl} \mathbf{H} = -j\omega\,\mathbf{B} = -j\omega\mu\,\mathbf{H} - \underbrace{j\omega\frac{\epsilon_r\,\mu_r - 1}{c_0^2}\,\mathbf{E}_0 \times (\mathbf{\Omega} \times \mathbf{r})}_{\mathbf{J}_{ma}} \tag{17.119}$$

and

$$\operatorname{curl} \mathbf{E} = \sigma\,\mathbf{E} + j\omega\,\mathbf{D} = \sigma\,\mathbf{E} + j\omega\epsilon\,\mathbf{E} + \underbrace{j\omega\frac{\epsilon_r\,\mu_r - 1}{c_0^2}\,(\mathbf{\Omega} \times \mathbf{r}) \times \mathbf{H}_0}_{\mathbf{J}_a}. \tag{17.120}$$

The problem is now to determine[20] the fields generated by the embedded applied currents $\mathbf{J}_a$ and $\mathbf{J}_{ma}$. When the sphere is *perfectly conducting*, the motional part of the scattered fields is found to vanish to the first order in $(\Omega a/c_0)$, which implies that the motion could only be detected through the very small second-order terms.[21] In the case of a *dielectric* sphere, let us assume that low-frequency techniques may be applied[22] (i.e., that $k_0 a \ll 1$). Two small parameters are relevant under these conditions: $k_0 a$ and $(\Omega a/c_0)$. The dominant term in the scattered field, in the absence of rotation, is contributed by an induced electric dipole (see Section 11.3), of value given in (3.125). For a unit incident electric field:

$$\mathbf{P}_{e0} = \frac{4\pi\epsilon_0 a^3(\epsilon_r - 1)}{\epsilon_r + 2}\,\mathbf{u}_x. \tag{17.121}$$

According to (7.155), the corresponding scattered fields are proportional to $(k_0 a)^2$. The rotation generates new moments, viz.

$$(\mathbf{P}_e)_\Omega = jk_0 a\left(\frac{\Omega a}{c_0}\right)\frac{2\pi\epsilon_0 a^3}{5}\,\frac{(\epsilon_r - 1)(5\epsilon_r - 2)}{(\epsilon_r + 2)^2}\,\mathbf{u}_y \tag{17.122}$$

$$(\mathbf{P}_m)_\Omega = -jk_0 a\left(\frac{\Omega a}{c_0}\right)\frac{2\pi a^3}{15R_{c0}}\,\frac{(\epsilon_r - 1)(4\epsilon_r + 1)}{2\epsilon_r + 3}\,\mathbf{u}_x. \tag{17.123}$$

The new scattered fields are proportional to $(k_0 a)^3\left(\frac{\Omega a}{c_0}\right)$. The rotation is seen to add a y-component to $\mathbf{P}_e$, and therefore to convert the polarization of $\mathbf{P}_e$ from linear to elliptic. This effect is *very small* in practice, because it is proportional to $(\Omega a/c_0)$. It should be noted, however, that a term in $(k_0 a)^2$ is often added to (17.122) to improve the low-frequency approximation. The ratio of $(\mathbf{P}_e)_\Omega$ to that correction term is of the order (Ω/ω), a ratio that is not necessarily small,[23] for example at the very low frequencies used for undersea communications.

17.11 MOTIONAL EDDY CURRENTS

In many devices that incorporate moving conductors, the motion of the latter is not uniform; electric motors run with variable speed, conducting fluids flow irregularly. In this section, we seek to evaluate the induced currents under these irregular conditions. The derivative of interest is $\left(\frac{\partial}{\partial t'}\right)$, evaluated in the local rest frame of a point P of the conductor. Because practical velocities are nonrelativistic, (17.18) allows us to replace $\left(\frac{\partial}{\partial t'}\right)$ by the substantial (or total) derivative $\left(\frac{D}{Dt}\right)$. Thus,

$$\frac{\partial f}{\partial t'} \approx \frac{Df}{Dt} = \frac{\partial f}{\partial t} + \mathbf{v} \cdot \text{grad}\, f. \tag{17.124}$$

The $\left(\frac{D}{Dt}\right)$ derivative, sometimes called *mobile operator*, is used extensively in hydrodynamics. It expresses the rate of change experienced in the laboratory by an observer attached to a point P of a moving body. The derivative consists of two terms:

- A term $\left(\frac{\partial f}{\partial t}\right)$, which is due to the time evolution of f at the point of the laboratory through which P passes. This term vanishes for a static f.
- A term $\mathbf{v} \cdot \text{grad}\, f$, which results from the (possibly) nonuniform character of the field in space, an inhomogeneity that is sampled by the observer in his motion.

For a vector field, (17.124) is replaced by

$$\frac{\partial \mathbf{f}}{\partial t'} \approx \frac{D\mathbf{f}}{Dt} = \frac{\partial \mathbf{f}}{\partial t} + (\mathbf{v} \cdot \text{grad})\, \mathbf{f}. \tag{17.125}$$

An important integral theorem involving $\dfrac{D}{Dt}$ will now be reviewed.

17.11.1 Helmholtz' Integral Theorem

Consider an open surface S bounded by a curve C (Fig. 17.21*a*). A flux

$$\phi = \int_S \mathbf{f} \cdot \mathbf{u}_n \, dS = \int_S \mathbf{f} \cdot d\mathbf{S} \tag{17.126}$$

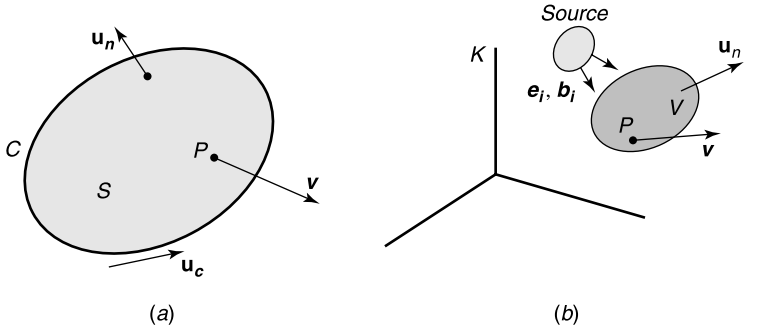

Figure 17.21 (*a*) Relevant for Helmholtz' theorem. (*b*) Good conductor in an external field.

flows through S. The theorem states that the time rate of change of ϕ is given by[24] [173]

$$\frac{D\phi}{Dt} = \int_S \left(\frac{\partial \mathbf{f}}{\partial t} - \text{curl}\,(\mathbf{v} \times \mathbf{f}) + \mathbf{v}\,\text{div}\,\mathbf{f} \right) \cdot d\mathbf{S}. \tag{17.127}$$

In this important relationship, which dates from 1867, the shape of S is allowed to vary with time.[†††] When $\mathbf{f}$ is the magnetic induction $\mathbf{b}$, (17.127) leads to

$$\begin{aligned} \frac{D\phi}{Dt} &= \int_S \frac{\partial \mathbf{b}}{\partial t} \cdot d\mathbf{S} - \int_{\mathbf{C}} (\mathbf{v} \times \mathbf{b}) \cdot \mathbf{dc} \\ &= \int_C \left[\frac{\partial \mathbf{a}}{\partial t} - (\mathbf{v} \times \mathbf{b}) \right] \cdot \mathbf{u}_c \, dc, \end{aligned} \tag{17.128}$$

where $\mathbf{a}$ is the vector potential.

The corresponding *volume-type* of relationship is *Reynolds' transport theorem* [173]

$$\frac{D}{Dt} \int_V \rho \, dV = \int_V \left(\frac{D\rho}{Dt} + \rho \,\text{div}\,\mathbf{v} \right) dV. \tag{17.129}$$

17.11.2 Fields and Sources in a Moving Good Conductor

When the volume V in Figure 17.21*b* is highly conducting the displacement current in the local rest frame of P may be ignored, which justifies writing $\text{curl}'\,\mathbf{h}' = \mathbf{j}' = \sigma \mathbf{e}'$. It follows that $\text{div}'\,\mathbf{j}' = 0$, and therefore that $(\partial \rho'/\partial t') = 0$. We set $\rho' = 0$ because time-independent components are of little interest in our analysis. The transformation equations (17.22) for the sources give, in the laboratory K,

$$\begin{aligned} \rho &= \frac{\mathbf{v} \cdot \mathbf{j}'}{c_0^2} \\ \mathbf{j} &= \mathbf{j}'. \end{aligned} \tag{17.130}$$

The fields transform according to (17.28). Thus, in the rest frame K' of P,

$$\begin{aligned} \mathbf{e}' &= \mathbf{e} + \mathbf{v} \times \mathbf{b} \\ \mathbf{b}' &= \mathbf{b} - \frac{\mathbf{v} \times \mathbf{e}}{c_0^2} \\ \mathbf{d}' &= \mathbf{d} + \frac{\mathbf{v} \times \mathbf{h}}{c_0^2} = 0 \\ \mathbf{h}' &= \mathbf{h} - \mathbf{v} \times \mathbf{d}. \end{aligned} \tag{17.131}$$

To the first order in $\beta = (|\mathbf{v}|/c_0)$, the constitutive equations in K are

$$\mathbf{j} = \mathbf{j} = \sigma\,(\mathbf{e} + \mathbf{v} \times \mathbf{b}) \tag{17.132}$$

$$\mathbf{b} = \mu\,\mathbf{h} + \frac{\mathbf{v} \times \mathbf{e}}{c_0^2}. \tag{17.133}$$

[†††] Because the velocities are nonrelativistic, (17.26) and (17.27) imply that $dS = dS'$ and $\mathbf{u}_n = \mathbf{u}'_n$.

The fields equations are now [11]

$$\begin{aligned} \text{curl } \mathbf{e} &= -\frac{\partial \mathbf{b}}{\partial t} \\ \text{curl } \mathbf{h} &= \sigma\,(\mathbf{e} + \mathbf{v} \times \mathbf{b}) \\ \text{div } \mathbf{b} &= 0. \end{aligned} \tag{17.134}$$

Elimination of **e** gives an equation for **h** and **b**, viz.

$$\frac{\partial \mathbf{b}}{\partial t} - \text{curl}\,(\mathbf{v} \times \mathbf{b}) = -\text{curl}\left(\frac{1}{\sigma}\,\text{curl}\,\mathbf{h}\right). \tag{17.135}$$

In a homogeneous medium:

$$\frac{\partial \mathbf{h}}{\partial t} = \frac{1}{\sigma\mu}\,\nabla^2\mathbf{h} + \text{curl}\,(\mathbf{v} \times \mathbf{h}). \tag{17.136}$$

These equations, important as they are for power applications, become essential in *magnetohydrodynamics* (MHD), a discipline that is concerned with the motion of an electrically conducting fluid in the presence of a magnetic field [48]. This motion can take place *in the laboratory* (where the medium could be mercury or liquid sodium), or on a *cosmic* scale, in vast regions such as the interior of a star. The quantity $(1/\sigma\mu)$ in (17.136) is the *magnetic diffusivity* (see Section 13.9). It determines the speed with which, in the absence of motion, the field leaks through the material to even out possible inhomogeneities in its spatial distribution. The time of decay is of the order $\sigma\mu L^2$, where L is a typical dimension of the region in which the current flows. This time may be of the order seconds for laboratory experiments but could reach 10^{10} years for the magnetic field of the sun.

To gain an idea of the motional effect, let us assume that the material has negligible resistivity. For such a case, (17.136) becomes

$$\frac{\partial \mathbf{h}}{\partial t} = \text{curl}\,(\mathbf{v} \times \mathbf{h}). \tag{17.137}$$

This equation is identical with that satisfied by the velocity in the theory of nonviscous flow. It implies that the field changes are the same as if the magnetic lines of force were constrained to move with the material [48].

The motional term in (17.135) takes an interesting form when the conductor is incompressible (i.e., when div $\mathbf{v} = 0$). Applying (A1.15) allows rewriting (17.135) as [11]

$$\underbrace{\frac{\partial \mathbf{b}}{\partial t} + (\mathbf{v} \cdot \text{grad})\,\mathbf{b}}_{\frac{D\mathbf{b}}{Dt}} - (\mathbf{b} \cdot \text{grad})\,\mathbf{v} = -\text{curl}\left(\frac{1}{\sigma}\,\text{curl}\,\mathbf{h}\right). \tag{17.138}$$

17.11.3 Moving Electric Circuit

Consider the thin tubular circuit of Figure 17.22*a*, moving with nonuniform velocity **v** (i.e., with a shape that may vary with time). Application of (17.127) to the magnetic induction **b**

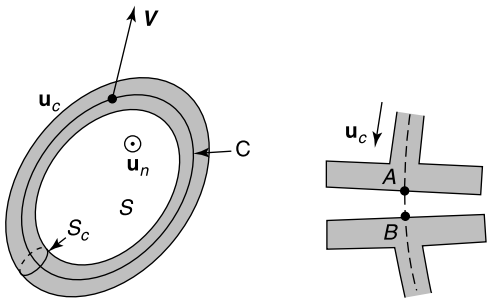

Figure 17.22 (*a*) Typical moving circuit. (*b*) A capacitive region.

gives, in combination with (17.132),

$$\frac{D\phi}{Dt} = \int_S \left[\frac{\partial \mathbf{b}}{\partial t} - \text{curl}\,(\mathbf{v}\times\mathbf{b})\right]\cdot d\mathbf{S} = -\int_S \text{curl}\,(\mathbf{e}+\mathbf{v}\times\mathbf{b})\cdot d\mathbf{S}$$
$$= -\int_C \frac{\mathbf{j}}{\sigma}\cdot d\mathbf{c}. \tag{17.139}$$

For a very thin conductor, and under low-frequency conditions, results obtained in Section 13.11 allow us to write

$$\mathbf{j} = i\,\frac{\mathbf{u}_c}{S_c\,(c)}, \tag{17.140}$$

where S_c is the (variable) cross section of the circuit and i the total current. Inserting this value of $\mathbf{j}$ into (17.139) gives

$$i\int_C \frac{dc}{\sigma S_c} = iR = -\frac{D\phi}{Dt} = -\frac{D\phi_S}{Dt} - \frac{D\phi^i}{Dt}. \tag{17.141}$$

In this equation, ϕ_S is the self-induction flux which, if the media are linear, is proportional to i. We set $\phi_S = \mathcal{L}i$, where $\mathcal{L}$ is a function of time. The incident flux ϕ^i is due to external sources. From (17.128):

$$-\frac{D\phi^i}{Dt} = \underbrace{-\int_S \frac{\partial \mathbf{b}^i}{\partial t}\cdot d\mathbf{S}}_{\text{transformer voltage}} + \underbrace{\int_C (\mathbf{v}\times\mathbf{b}^i)\cdot\mathbf{u}_c\,dc}_{\text{motional voltage}}. \tag{17.142}$$

The first term on the right-hand side is the *transformer e.m.f.*; the second term the *motional* (*or flux-cutting*) *e.m.f.*

In deriving (17.141), it has been assumed that $\mathbf{j}$ is given by (17.132) at all points of the contour. If the circuit contains a capacitor, as in Figure 17.22*b*, $\mathbf{j}$ vanishes in the interval AB, and we must now write

$$\int_C (\mathbf{e}+\mathbf{v}\times\mathbf{b})\cdot d\mathbf{c} = \int_{C-AB}\frac{\mathbf{j}}{\sigma}\cdot d\mathbf{c} + \int_A^B (\mathbf{e}+\mathbf{v}\times\mathbf{b})\cdot d\mathbf{c}$$
$$= iR + (\phi_A - \phi_B). \tag{17.143}$$

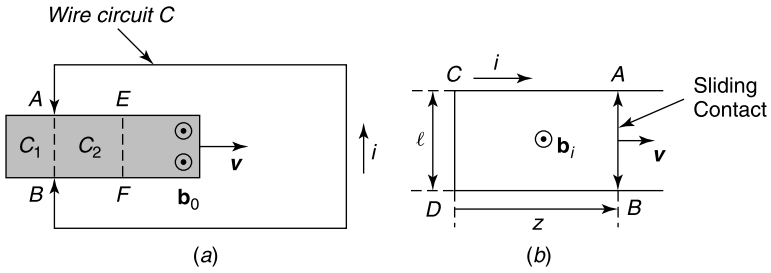

Figure 17.23 (*a*) Moving permanent magnet with sliding contacts. (*b*) Sliding bar and supporting rails.

The difference of potential across the capacitor is

$$\phi_A - \phi_B = \frac{q}{C} = \frac{1}{C}\int i\,dt.$$

Putting these results together leads to the circuit equation

$$iR + \frac{d}{dt}(\mathcal{L}i) + \frac{1}{C}\int i\,dt = \text{transformer e.m.f.} + \text{motional e.m.f.} \tag{17.144}$$

To illustrate the use of this important equation, we briefly discuss two *sliding contact* problems (Fig. 17.23). In the first one, under (a), a uniformly magnetized bar moves with uniform velocity to the right. Let the circuit be closed by a conducting segment AB (circuit C_1). Because of the motion of the magnet, the flux ϕ^i through a surface bounded by C_1 increases linearly with time, hence $-D\phi^i/Dt$ is different from zero. It is known, however, that no current flows through the circuit[25] [33]. The reason for the discrepancy is clear: the derivation of (17.144) is based on constitutive equation (17.132), and that equation holds only if every point of C moves with the material. The situation is different for the curve C_2 formed by the exterior cicuit and the segment $AEFB$, in which E and F are assumed fixed with respect to the material, hence to move to the right with velocity $\mathbf{v}$. In this case, we have a curve that changes shape with time, but in such a fashion that *each point of the curve is at rest with respect to the material*. Under those circumstances, the generalized circuit equation may be applied.

Another sliding contact configuration, shown in Figure 17.23*b*, consists of a bar AB sliding along parallel tracks in a uniform static magnetic field. In the rectangular loop formed by the tracks, the fixed CD and AB, every point is at rest with respect to the conductor, hence[‡‡‡]

$$Ri + \frac{d(\mathcal{L}i)}{dt} = -\frac{D\phi^i}{Dt} = -\frac{D}{Dt}(-b^i lz) = b^i lv. \tag{17.145}$$

This result is in agreement with (17.58).

[‡‡‡]More problems of the same kind are solved in the chapter "Applications and Paradoxes" of a delightful little book published in 1952 by L. Bewley [33]. It has been conjectured that Einstein must have been confronted with many "motional" puzzles during his Patent Office years in Bern (1902–1909).

17.12 ACCELERATED FRAMES OF REFERENCE

In many applications, moving bodies follow arbitrary trajectories, with nonuniform velocities, and possibly instantaneous rotations. Simple solutions in the laboratory, of the type described in Section 17.10, are no longer possible. Two accelerated bodies are shown in Figure 17.24. In part (a), the cross section of the rotating cylinder is arbitrary and does not evidence any kind of symmetry. In part (b), the scatterer is formed by the blades of a helicopter, a most irregular target indeed. In both cases, the rotation angular frequency Ω is low and the distances are short. Under these circumstances, the quasistationary method gives satisfactory results.[26,27,28] The method predicts that, at constant Ω, the return signal from the successive positions of the scatterer has a line spectrum, in which the lines are separated by multiples of $(\Omega/2\pi)$. A theoretically more satisfying solution consists in solving Maxwell's equations in a frame of reference attached to the rigid scatterer — the comoving frame — and transforming the fields back to the laboratory. Suitable coordinates must be defined in the comoving frame. The necessary formalism is described next.

17.12.1 The Metric Tensor

The *world distance ds* between two neighboring events is given, in an inertial frame, by the formula

$$ds^2 = c^2(dT)^2 - (dX)^2 - (dY)^2 - (dZ)^2. \tag{17.146}$$

This incremental distance is equal to zero for two successive positions of a photon. The value of ds^2 is independent of the choice of inertial frame (i.e., it is invariant with respect to Lorentz transformations). Expressed in terms of the chosen x^α coordinates of the comoving frame, ds^2 becomes

$$ds^2 = \sum_{\alpha,\beta=0}^{3} g_{\alpha\beta}\, dx^\alpha\, dx^\beta, \tag{17.147}$$

where the (covariant) component $g_{\alpha\beta}$ of the *metric tensor* is given by

$$g_{\alpha\beta} = c_0^2 \frac{\partial T}{\partial x^\alpha}\frac{\partial T}{\partial x^\beta} - \sum_{i=1}^{3} \frac{\partial X^i}{\partial x^\alpha}\frac{\partial X^i}{\partial x^\beta}. \tag{17.148}$$

The $g_{\alpha\beta}$ tensor is clearly symmetric. We introduce the notations

$$|g| = -\det\,(g_{\alpha\beta}) \tag{17.149}$$

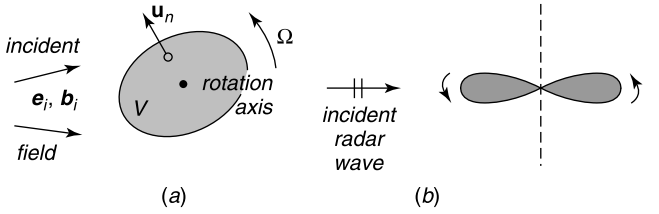

Figure 17.24 Typical configurations involving rotating bodies.

for the negative of the determinant of the $g_{\alpha\beta}$ matrix, and

$$g_i = \frac{g_{0i}}{\sqrt{g_{00}}} \qquad (i = 1, 2, 3) \tag{17.150}$$

for three important coefficients. As an example, consider the use of polar coordinates $(c_0 t, r, \varphi, z)$ in the laboratory. The corresponding ds^2 is

$$ds^2 = c_0^2 (dT)^2 - (dX^1)^2 - (dX^2)^2 - (dX^3)^2. \tag{17.151}$$

If a body rotates uniformly in the laboratory, the appropriate comoving coordinates are

$$x_0 = X_0 = c_0 t = c_0 T; \quad x_1 = X_1 = r; \quad x_2 = r\theta = r\varphi - \Omega\, rt; \quad x_3 = X_3 = z. \tag{17.152}$$

With respect to these coordinates, ds^2 becomes (Fig. 17.25*a*)

$$\begin{aligned} ds^2 &= c_0^2 (dt)^2 - (dx)^2 - (r\, d\varphi)^2 - (dz)^2 \\ &= c_0^2 \left(1 - \frac{\Omega^2 r^2}{c_0^2}\right) dt^2 - (dr)^2 - r^2 (d\theta)^2 - 2r^2 \Omega\, d\theta\, dt - (dz)^2. \end{aligned} \tag{17.153}$$

This gives

$$\begin{aligned} g_{\alpha\beta} &= \begin{pmatrix} 1 - \dfrac{\Omega^2 r^2}{c_0^2} & 0 & -\dfrac{\Omega r^2}{c_0} & 0 \\ 0 & -1 & 0 & 0 \\ -\dfrac{\Omega r^2}{c_0} & 0 & -r^2 & 0 \\ 0 & 0 & 0 & -1 \end{pmatrix} \\ |g| &= r^2 \\ g_1 &= g_3 = 0 \\ g_2 &= -\frac{\Omega r^2}{\sqrt{c_0^2 - \Omega^2 r^2}}. \end{aligned} \tag{17.154}$$

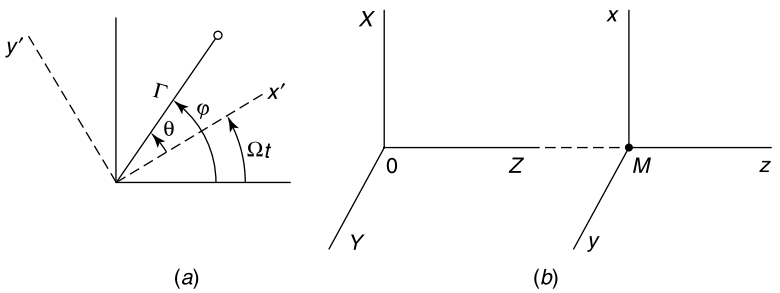

Figure 17.25 Relevant to (*a*) The rotation transformation; (*b*) The translation transformation.

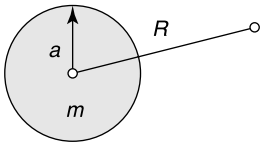

Figure 17.26 Mass distribution with spherical symmetry.

A point at rest on the "merry go round" (i.e., with fixed r, z, θ) describes a circle with velocity Ω in the laboratory. These coordinates are consequently appropriate for problems involving rotating bodies.

Another transformation of interest for practical applications is defined by (Fig. 17.25*b*)

$$x^3 = z = Z - Z_M(T) = X^3 - Z_M(T). \tag{17.155}$$

This transformation is appropriate for problems involving bodies in non-uniform translation[29] (Problems 17.28 and 17.29).

The concept of metric tensor plays a fundamental role in the relativistic theory of gravitation, where the $g_{\alpha\beta}$ components are produced by the presence of masses. Einstein derived in 1916 the (nonlinear) equations satisfied by $g_{\alpha\beta}$ [132]. A simple solution was soon thereafter obtained by Schwarzschild for a mass distribution with spherical symmetry (Fig. 17.26). Outside the mass distribution:

$$ds^2 = \left(1 - \frac{R_S}{R} - \frac{\Lambda R^2}{3}\right) c^2 dt^2 - \frac{dR^2}{1 - (R_S/R) - \Lambda R^2/3} - R^2 d\theta^2 - R^2 \sin^2\theta \, d\varphi^2. \tag{17.156}$$

In this formula, R_S is a critical radius, equal to

$$R_S = \frac{2Gm}{c_0^2}, \tag{17.157}$$

where m is the total mass of the body, and G is the gravitational constant $6.664 \times 10^{-11}\,\mathrm{m^3\,kg^{-1}\,s^{-2}}$. The parameter Λ is a *cosmological* factor, which only plays a role when the system under consideration is of cosmological dimensions. Whether or not Λ is needed to describe the evolution of the universe has been a matter of considerable controversy. If we set $\Lambda = 0$, a singularity occurs when the mass is so concentrated that R_S lies outside the sphere. For such a case, g_{00} vanishes at $R = R_S$, and g_{11} becomes infinite there. Typical values of R_S are

$$\text{For the earth:} \quad R_S = 0.0088\ \mathrm{m} \quad \text{and} \quad \left(\frac{R_S}{a}\right) = 1.4 \times 10^{-9}$$
$$\text{For the sun:} \quad R_S = 2900\ \mathrm{m} \quad \text{and} \quad \left(\frac{R_S}{a}\right) = 4 \times 10^{-6}.$$

The study of the mechanisms that lead dying stars to collapse to a radius a, so small that $R_S > a$, is the province of astrophysics.[§§§] For such a mass concentration, R_S exerts some sort of cosmic censorship and forbids any light to escape from the region inside R_S: the region has become a black hole.

[§§§]The reader is referred to the numerous texts on *general relativity* for a more professional approach to the subject [99, 107].

17.12.2 Maxwell's Equations in a General Metric

From a relativistic point of view, the proper formulation of Maxwell's equations must be valid for any $g_{\alpha\beta}$, whether generated by acceleration or by the presence of masses (Problem 17.31). The sought form is

$$\frac{1}{\sqrt{|g|}} \sum_{\beta=0}^{3} \frac{\partial}{\partial x^\beta} \left(\sqrt{|g|}\, M^{\alpha\beta} \right) = J^\alpha$$

$$\frac{\partial N_{\alpha\beta}}{\partial x^\gamma} + \frac{\partial N_{\beta\gamma}}{\partial x^\alpha} + \frac{\partial N_{\gamma\alpha}}{\partial x^\beta} = 0. \tag{17.158}$$

The antisymmetric tensors $M^{\alpha\beta}$ and $N_{\alpha\beta}$ are given in (17.31) and (17.32) for an inertial frame. In full generality, they become

$$M^{\alpha\beta} = \begin{bmatrix} 0 & c_0 \dfrac{d^1}{\sqrt{g_{00}}} & c_0 \dfrac{d^2}{\sqrt{g_{00}}} & c_0 \dfrac{d^3}{\sqrt{g_{00}}} \\ -c_0 \dfrac{d^1}{\sqrt{g_{00}}} & 0 & \dfrac{h_3}{\sqrt{|g|}} & -\dfrac{h_2}{\sqrt{|g|}} \\ -c_0 \dfrac{d^2}{\sqrt{g_{00}}} & -\dfrac{h_3}{\sqrt{|g|}} & 0 & \dfrac{h_1}{\sqrt{|g|}} \\ -c_0 \dfrac{d^3}{\sqrt{g_{00}}} & \dfrac{h_2}{\sqrt{|g|}} & -\dfrac{h_1}{\sqrt{|g|}} & 0 \end{bmatrix} \tag{17.159}$$

$$N_{\alpha\beta} = \begin{bmatrix} 0 & -\dfrac{e_1}{c_0} & -\dfrac{e_2}{c_0} & -\dfrac{e_3}{c_0} \\ \dfrac{e_1}{c_0} & 0 & \sqrt{|\gamma|}\, b^3 & -\sqrt{|\gamma|}\, b^2 \\ \dfrac{e_2}{c_0} & -\sqrt{|\gamma|}\, b^3 & 0 & -\sqrt{|\gamma|}\, b^1 \\ \dfrac{e_3}{c_0} & \sqrt{|\gamma|}\, b^2 & -\sqrt{|\gamma|}\, b^1 & 0 \end{bmatrix}. \tag{17.160}$$

The symbol $|\gamma|$ denotes the determinant of the three-dimensional tensor

$$\gamma_{ik} = g_i\, g_k - g_{ik}. \tag{17.161}$$

For the rotating coordinate transformation, for example,

$$\gamma_{ik} = \begin{bmatrix} 1 & 0 & 0 \\ 0 & \dfrac{r^2}{1 - \left(\dfrac{\Omega r}{c_0} \right)^2} & 0 \\ 0 & 0 & 1 \end{bmatrix}. \tag{17.162}$$

The fields appearing in the tensors are represented by either their *covariant components* f_α or their *contravariant components* f^α. The two are connected by

$$f_\alpha = \sum_{\beta=0}^{3} g_{\alpha\beta} f^\beta$$

$$f^\alpha = \sum_{\beta=0}^{3} g^{\alpha\beta} f_\beta. \tag{17.163}$$

The transformation equations for vectors are

$$f'_\alpha = \sum_{\beta=0}^{3} \frac{\partial x^\beta}{\partial x'^\alpha} f_\beta. \tag{17.164}$$

For the tensors (Problem 17.30):

$$b^{\alpha\beta} = \sum_{\mu,\nu=0}^{3} g^{\alpha\mu}\, g^{\nu\beta}\, b_{\mu\nu}$$

$$b_{\alpha\beta} = \sum_{\mu,\nu=0}^{3} g_{\alpha\mu}\, g_{\nu\beta}\, b^{\mu\nu}$$

$$b'^{\alpha\beta} = \sum_{\mu,\nu=0}^{3} \frac{\partial x'^\alpha}{\partial x^\mu} \frac{\partial x'^\beta}{\partial x^\nu}\, b^{\mu\nu}$$

$$b'_{\alpha\beta} = \sum_{\mu,\nu=0}^{3} \frac{\partial x^\mu}{\partial x'^\alpha} \frac{\partial x^\nu}{\partial x'^\beta}\, b_{\mu\nu}. \tag{17.165}$$

The source vector J_α in (17.158) has the components

$$J^\alpha = \left(\frac{\rho_c}{\sqrt{g_{00}}}, \frac{j^i}{\sqrt{g_{00}}} \right). \tag{17.166}$$

17.13 ROTATING COMOVING FRAMES

We shall illustrate the solution of Maxwell's equations (17.158) by evaluating the fields scattered by a rotating cylinder (Fig. 17.24*a*). Assume that the incident wave is a z-polarized plane wave of E_z component

$$E_z^i = \mathrm{Re}\left[E_0\, e^{-jk_0 r\cos\varphi}\, e^{j\omega t} \right]. \tag{17.167}$$

The problem is two-dimensional, and the only components of interest are E_z, H_r, H_φ (in the laboratory), e_z, h_r, h_θ (in the *comoving frame*). The field transformation formulas can be

derived by transforming the $M^{\alpha\beta}$ and $N_{\alpha\beta}$ tensors. We only quote the needed result, which is [132]

$$\begin{aligned} e_z^i &= E_z^i - \Omega r\, B_r^i = E_z^i - \frac{\Omega r}{c_0} E_z^i \sin\varphi \\ &= \mathrm{Re}\left\{ E_0 \left[1 + \frac{\Omega r}{c_0} \sin(\theta + \Omega t) \right] e^{-jk_0 r \cos(\theta+\Omega t)}\, e^{j\omega t} \right\}. \end{aligned} \tag{17.168}$$

A rotating observer clearly samples a periodic phase variation, of period $T = (2\pi/\Omega)$ equal to the rotation period. Such a variation is of the classic *phase modulation* type. On the basis of

$$e^{-jkx\cos\alpha} = \sum_{m=-\infty}^{\infty} e^{jm(\alpha-(\frac{\pi}{2}))} J_m(x)$$

and

$$J_{m-1}(x) + J_{m+1}(x) = \frac{2m}{x} J_m(x)$$

we rewrite the incident field as

$$e_z^i = \mathrm{Re}\left\{ E_0 \sum_{m=-\infty}^{\infty} \frac{\omega_m}{\omega} J_m(kr)\, e^{j[\omega_m t + m\theta - m(\pi/2)]} \right\}, \tag{17.169}$$

where $\omega_m = \omega + m\Omega$. This expansion reveals the presence of an infinite but discrete spectrum of frequencies in the incident wave. The expressions for the other field components contain the same frequencies. Because Maxwell's equations are linear in a linear medium, these frequencies (and they alone) will be present in the scattered field. To solve for e_z^{sc}, we must invoke Maxwell's equations (17.158) in the form they take in rotating coordinates [132]. We shall specifically need the equations involving e_z, h_r, h_θ. Given without derivation, these are

$$\begin{aligned} \frac{1}{r}\frac{\partial e_z}{\partial \theta} &= -\frac{1}{\sqrt{1-\beta^2(r)}} \frac{\partial b^r}{\partial t} \\ \frac{\partial e_z}{\partial r} &= \frac{1}{\sqrt{1-\beta^2(r)}} \frac{\partial}{\partial t}(r b^\theta) \\ \frac{1}{r}\frac{\partial h_\theta}{\partial r} - \frac{1}{r}\frac{\partial h_r}{\partial \theta} &= \frac{1}{\sqrt{1-\beta^2(r)}} \frac{\partial d^z}{\partial t}, \end{aligned} \tag{17.170}$$

where we have set $\beta(r) = (\Omega r/c_0)$, for conciseness.[¶¶¶] The constitutive equations outside the cylinder, in vacuum, are derived by transforming $\mathbf{B} = \mu_0 \mathbf{H}$ to rotating coordinates.

[¶¶¶] We note that the co- and contravariant θ-components, h_θ and h^θ, have the respective dimensions A and A m^{-2}. One sometimes introduces the *ordinary (or physical) components*

$$h_{(\theta)} = \frac{r}{\sqrt{1-\beta^2(r)}}\, h^\theta = \frac{1}{r}\sqrt{1-\beta^2(r)}\, h_\theta,$$

and formulates Maxwell's equations in terms of $h_{(\theta)}$, which has the dimension A m^{-1}. Note that $e_{(z)} = e^z = e_z$ and $h_{(r)} = h^r = h_r$.

This gives [132]

$$b^r = \frac{\mu_0}{\sqrt{1-\beta^2(r)}}\left(h_r + \frac{\beta(r)}{R_{c0}}\, e_z\right)$$
$$b^\theta = \frac{\mu_0}{r^2}\sqrt{1-\beta^2(r)}\, h_\theta$$
$$d^z = \epsilon_0\sqrt{1-\beta^2(r)}\, e_z + \frac{1}{R_{c0}}\,\beta(r)\, b^r. \tag{17.171}$$

The scattered field must contain the frequencies ω_m present in the incident field. We therefore write

$$e_z(r,\theta,t) = \mathrm{Re}\sum_{m=-\infty}^{\infty} e_m(r,\theta)\, e^{j\omega_m t}.$$

A few simple manipulations show that e_m must satisfy

$$\frac{1}{r}\frac{\partial}{\partial r}\left(r\,\frac{\partial e_m}{\partial r}\right) + j\,\frac{2\Omega\,\omega_m}{c_0^2}\frac{\partial e_m}{\partial\theta} + \left[1-\left(\frac{\Omega r}{c}\right)^2\right]\frac{1}{r^2}\frac{\partial^2 e_m}{\partial\theta^2} + \frac{\omega_m^2}{c_0^2}\, e_m = 0. \tag{17.172}$$

To solve the resulting set of equations, one for each ω_m, the boundary conditions at the cylinder and at infinity must be taken into account.[30] Classic numerical methods have been used to solve the field problem for cylindrical scatterers, either metallic or dielectric.[31,32] If the cylinder is circular, it pays to express e_z as a Fourier series in θ and write[33]

$$e_m(r,\theta) = \sum_{n=-\infty}^{\infty} e_{mn}(r)\, e^{jn\theta}. \tag{17.173}$$

It is easy to verify that $e_{mn}(r)$ satisfies a Bessel type of differential equation, whose solution leads to the following series for e_z:

$$e_z(r,\theta,t) = \mathrm{Re}\left\{\sum_{m=-\infty}^{\infty} e^{j\omega_m t}\sum_{n=-\infty}^{\infty} C_{mn}H_n^{(2)}(k_{mn}r)\, e^{jn\theta}\right\}, \tag{17.174}$$

where

$$k_{mn} = \frac{\omega}{c_0} + (m-n)\frac{\Omega}{c_0}.$$

The Hankel function is chosen because the fields at large distances must behave, in the limit $\Omega \to 0$, like those obtained for a nonrotating cylinder. To solve for the coefficients C_{mn}, we must derive expressions for the fields inside the cylinder and subsequently enforce appropriate boundary conditions at $r = a$. We shall only consider the particular configuration of a circular cylinder of radius a, carrying a frequency-independent surface reactance $X_S(\theta)$. The resulting boundary condition is

$$\frac{e_\theta}{h_z} = jX_S\frac{a}{\sqrt{1-\left(\dfrac{\Omega a}{c_0}\right)^2}}.$$

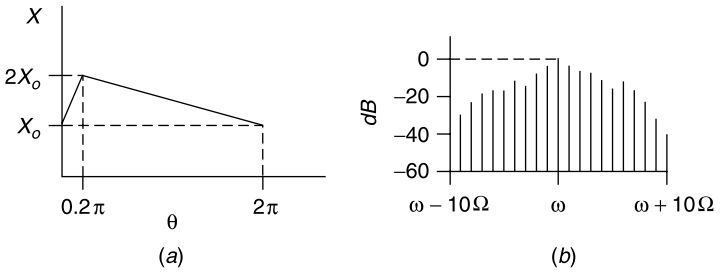

Figure 17.27 (*a*) Sawtooth distribution of reactance. (*b*) Part of the resulting Doppler spectrum for an incident H wave.

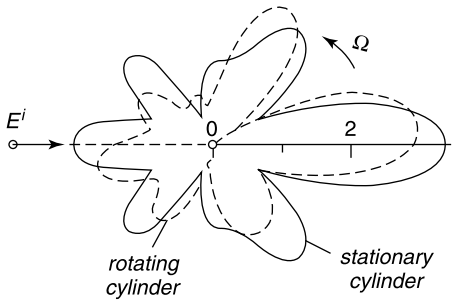

Figure 17.28 Scattering patterns for a dielectric cylinder [$\epsilon_r = 4$, $(\Omega a/c) = 0.03$, $(\Omega/\omega) = 0.01$].

The X_S assumption is appropriate for celestial bodies, the outer crust of which may often be electromagnetically modeled by a surface impedance.[33] For the sawtooth variation shown in Figure 17.27*a*, the spectrum of the scattered field consists of lines centered at the discrete frequencies $\omega_m = \omega + \omega\Omega$ (Fig. 17.27*b*).

The discrete spectrum can serve to reveal the existence of a rotation. When the circular cylinder is *homogeneous*, however, the spectrum reduces to the incident frequency.[34] The relativistic effect now resides with the distortion of the scattering pattern, which is shown in Figure 17.28 for $\epsilon_r = 4$, $(\Omega/\omega) = 0.01$, and $(\Omega a/c_0) = 0.03$. The shift in the pattern is a first-order effect in $(\Omega a/c_0)$, quite negligible unless the peripheral velocity Ωa becomes relativistic.

PROBLEMS

17.1 Derive the form of the acceleration field in (17.8) when $v_0 \ll c_0$. Using Poynting's vector, evaluate the power radiated by the moving charge. Specialize to a circular path, and evaluate the energy lost per revolution. Apply the result to an electron moving with velocity $0.1\ c_0$ on a circular path of radius 1 m.

17.2 The presence of a charged particle, moving uniformly with velocity **v**, can be detected by observing the e.m.f. induced by the particle in a small loop located in the (x, z) plane (i.e., the plane containing q, **v**, and the observer M) (Fig. P17.1). Evaluate both the e.m.f. $(-\partial\phi/\partial t)$ and the flux variation $\Delta\phi$ that result from the passage of the particle.

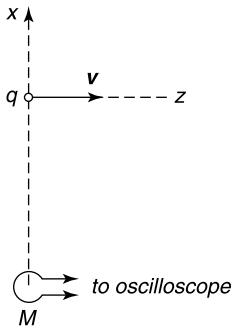

Figure P17.1

17.3 Verify that the transformation equations for the axes shown in Figure 17.2*b* can be written as [132]

$$\mathbf{r}' = \mathbf{r} + \mathbf{w}\left[\frac{\mathbf{r}\cdot\mathbf{w}}{w^2}(\gamma - 1) - \gamma t\right]$$

$$t' = \gamma\left(t - \frac{\mathbf{w}\cdot\mathbf{r}}{c^2}\right),$$

where $\gamma = (1 - \beta^2)^{-\frac{1}{2}}$.

17.4 Assume that two events occur at the same point of K, but not simultaneously. Show that the temporal sequence of these events remains the same in all other initial frames.

17.5 The lifetime of certain pions has been measured to be 2.55×10^{-8} s in their rest frame. Evaluate the average distance that these pions cover in the laboratory when their velocities are 0.75 c_0, 0.9 c_0, 0.99 c_0, 0.995 c_0, 0.9995 c_0, respectively.

17.6 Let $c_0^2 t^2 - x^2 - y^2 - z^2 = 0$ describe the motion of a wavefront in K (Fig. 17.2*a*). The postulates of relativity require c_0, the velocity of light in vacuum, to have the same value in K'. This requirement implies $c_0^2 (t')^2 - (x')^2 - (y')^2 - (z')^2 = 0$. Verify that important property by means of the transformation laws (17.9).

17.7 Two spaceships, A and B, are observed from 0, origin of the inertial frame K (Fig. P17.2). Their positions are separated by ℓ at time $t = 0$, as measured in K. The spaceships have equal (but opposite) velocities $\mathbf{v}$ with respect to K. Find the time at which they collide

(**a**) On the clocks of K

(**b**) on a clock carried by spaceship A

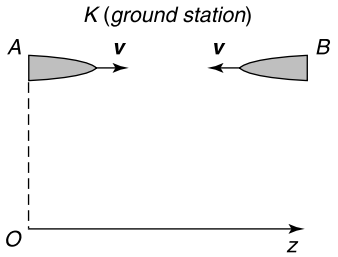

Figure P17.2

17.8 Derive the transformation formulas for the polarization densities $\mathbf{m}_e$ and $\mathbf{m}_m$, remembering that $\mathbf{d} = \epsilon_0\,\mathbf{e} + \mathbf{m}_e$ and $\mathbf{b} = \mu_0\,\mathbf{h} + \mu_0\mathbf{m}_m$ [132].

17.9 To show that the fields (17.38) agree with the predictions of the Liénard-Wiechert formulas, determine first the precursor location P of the uniformly moving charge q (Fig. P17.3). Show that the corresponding time is [132]

$$t_0 = \frac{1}{1-\beta^2}\left[t - \sqrt{\beta^2 t^2 + (1-\beta^2)\,\frac{h^2}{c_0^2}}\right].$$

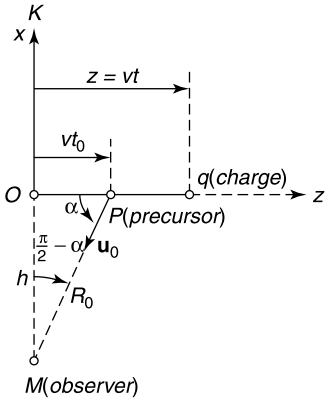

Figure P17.3

17.10 A static dipole is in uniform translational motion with velocity $\mathbf{v}$. The dipole moment is $\mathbf{p}'_\mathbf{e}$ in the rest axes K'. Determine the electric and magnetic fields in the laboratory axes K (Fig. P17.4). Repeat for a magnetic dipole moment $\mathbf{p}'_\mathbf{m}$.

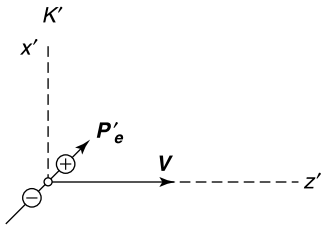

Figure P17.4

17.11 A spaceship recedes radially, with velocity $\mathbf{v}$, from a ground station G (Fig. P17.5). The ground station transmits short pulses toward the spaceship. The interval between pulses is 1 s. What kind of a signal does the radio operator receive on the spaceship?

17.12 A transmitting antenna moves with constant velocity $\mathbf{v}$ with respect to a ground station. The radiation pattern $\mathbf{F}(\mathbf{u})$ of the antenna is given in the rest frame of the antenna. Discuss the frequency spectrum of the received signal on the ground, and determine the Poynting vector at the receiver. Does it lie in the direction precursor-receiver?
(D. De Zutter, *Microwaves Opt. Acoust.*, **3**, 85–92, 1979.)

17.13 A time-harmonic current source $\mathbf{J}(\mathbf{r})$ is stationary in the laboratory. The source is immersed in an (infinite) uniform dielectric medium moving with uniform velocity $\mathbf{v}$. Show that the radiated

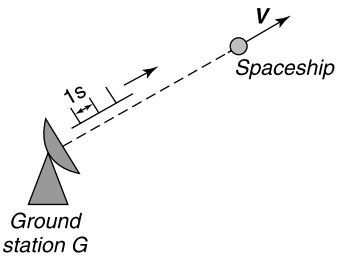

Figure P17.5

field is given by

$$\mathbf{E}(\mathbf{r}) = j\omega\mu \int_V \mathbf{J}(\mathbf{r}') \cdot \underbrace{\overline{\overline{G}}_{ee}(\mathbf{r}|\mathbf{r}')\, e^{j\omega \boldsymbol{\Lambda} \cdot (\mathbf{r}-\mathbf{r}')}}_{\text{motional Green's dyadic}} dV',$$

where $\boldsymbol{\Lambda} = (\epsilon_r \mu_r - 1)\, \frac{\mathbf{v}}{c_0^2}$, and $\overline{\overline{G}}_{ee}$ is the Green's dyadic in the motionless medium.

(R. T. Compton et al., *IEEE Trans. AP*, **13**, 574–577, 1965.)

17.14 In the dielectric slab experiment of Figure 17.8, assume that $b_i = 0$ and $\mu_r = 1$:

(**a**) Evaluate the polarization charges ρ'_p and ρ'_{pS} in the rest axes of the slab (see Problem 17.8).

(**b**) Transform the polarization charges and currents to the laboratory frame, according to (17.22).

(**c**) Verify that ρ_{pS} and $\mathbf{j}_{pS}$ account for the discontinuities of **e** and **b** at the boundaries of the slab [132].

17.15 In an experiment suggested to Wilson by Einstein and Laub in 1908, a magnetic dielectric slab moves parallel to its boundary planes (Fig. P17.6). The boundaries are metallized. An external, preexisting induction $\mathbf{b}_i$ is applied to the dielectric. Show that a difference of potential

$$\phi_A - \phi_B = \left(1 - \frac{1}{\epsilon_r \mu_r}\right) v \mu_r b_i \ell$$

appears between the boundary planes.

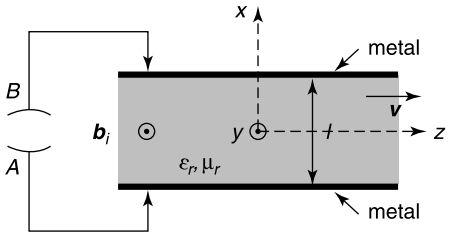

Figure P17.6

17.16 A magnetic conducting circular cylinder, infinite in the y-direction and of given ϵ_r, μ_r, σ, moves with velocity $\mathbf{v} = v\,\mathbf{u}_z$ with respect to K, across a uniform static transverse electric field $\mathbf{e} = e\,\mathbf{u}_x$. Determine the fields in K, inside and outside the cylinder.

17.17 Generalize the levitation problem by adding a dielectric layer to the conducting track shown in Figure 17.11*a*.

(D. De Zutter, *J. Appl. Phys.*, **58**, 2751–2758, 1985.)

17.18 A wave with the polarization shown in Figure P17.7 is totally transmitted, without reflection, provided θ_i is given the *Brewster* value $\theta_B = \tan^{-1}\sqrt{\epsilon_r}$. This value holds for a motionless dielectric. Show that a motion perpendicular to the boundary leads to a new Brewster angle

$$\theta_B = \tan^{-1}\frac{\sqrt{\epsilon_r}\sqrt{1-\beta^2}}{1+\beta\sqrt{\epsilon_r+1}}.$$

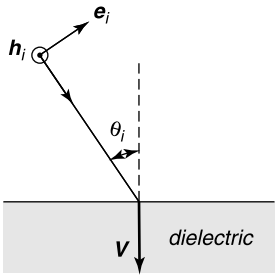

Figure P17.7

17.19 A plane wave is obliquely incident on a perfectly conducting mirror moving perpendicularly to its surface (Fig. P17.8). Determine the angle of reflection θ_r and the frequency of the reflected wave [132].

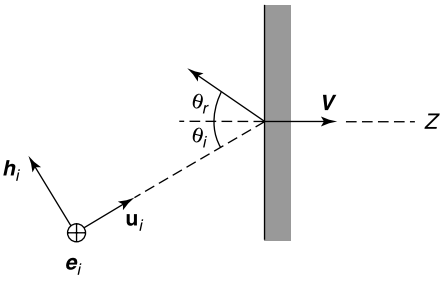

Figure P17.8

17.20 The uniformly rotating sphere in Figure P17.9 carries a rigid magnetization density $\mathbf{m}_m$, whose value is assumed independent of external influences and time. Show that, at low Ω, an electric field $\mathbf{e}_i = -\mathbf{v} \times \mathbf{b}_0$ is generated in the sphere, hence that the motional e.m.f. is given by (17.115). The polarization density $\mathbf{m}_m$ is given by $\mathbf{b}_0 = \mu_0 \mathbf{h}_0 + \mu_0 \mathbf{m}_m$, where $(\mathbf{b}_0, \mathbf{h}_0)$ are the fields that exist when the sphere does not rotate. For a uniformly magnetized sphere, for example,

$$\mathbf{b}_0 = \frac{2}{3}\mu_0 \mathbf{m}_m.$$

17.21 Formulate the problem of the Faraday disk in its translational form (Fig. P17.10), in which a thin nonmagnetic conducting *sheet* moves across a given induction $\mathbf{b}_0$.
(F. Ollendorff, *Arch. Elektrotechnik*, **59**, 305–310, 1977.)

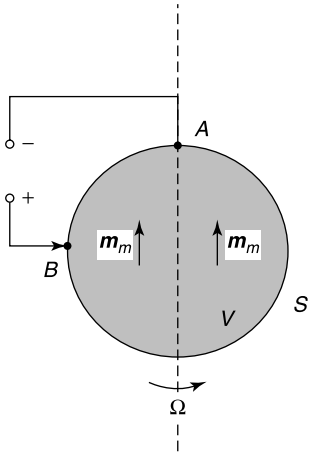

Figure P17.9

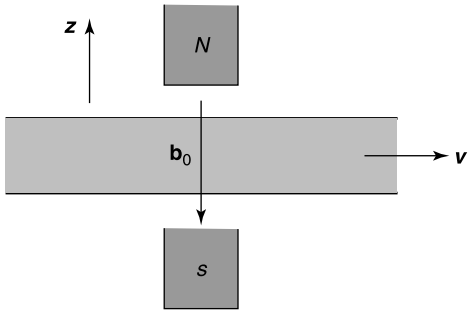

Figure P17.10

17.22 In the Röntgen-Eichenwald experiment, a dielectric disk rotates between the plates of a charged capacitor. The charges apply an electric field $\mathbf{e}_i$ to the disk (Fig. P17.11). The rotation of the polarization charges creates a current, which in turn generates a magnetic field $\mathbf{h}_1 = -\text{grad}\,\psi_1$. Determine the equation and boundary conditions satisfied by ψ_1.
(J. Van Bladel, *Proc. IEEE*, **61**, 260–268, 1973.)

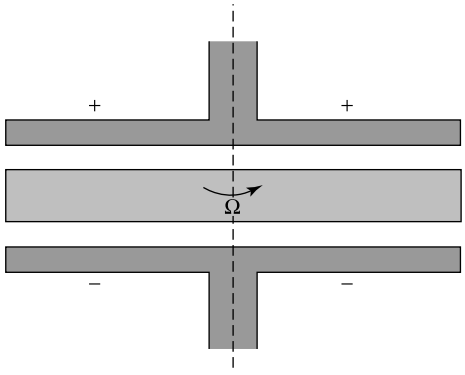

Figure P17.11

17.23 A conducting sphere rotates in an incident induction $\mathbf{b}_0$ (Fig. P17.12). Determine the electric potential inside and outside the sphere (it is proportional to Ω). Determine also the induced volume and surface charge densities [132].

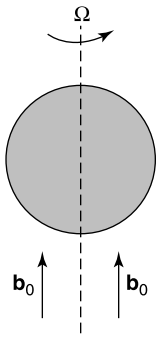

Figure P17.12

17.24 In one of Wilson's experiments, a hollow dielectric cylinder rotates in a uniform magnetic field $\mathbf{h}_0$ (Fig. P17.13). The inner and outer surfaces are metallized. Show that, in the limit of small velocities, a difference of potential

$$\phi_A - \phi_B = \left(\mu_r - \frac{1}{\epsilon_r}\right) \mu_0 \, h_0 \, \Omega \left(\frac{a^2 - b^2}{2}\right)$$

appears across the dielectric cylinder, assumed infinite in length.
(J. Van Bladel, *Proc. IEEE*, **61**, 260–268, 1973.)

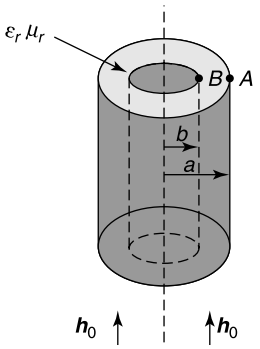

Figure P17.13

17.25 Show that the circuit equation in Figure P17.14 may be written in the form

$$\int_B^A \frac{\mathbf{j}}{\sigma} \cdot d\mathbf{c} = -\frac{D}{Dt} \int_B^A \mathbf{a} \cdot d\mathbf{c} + (\phi - \mathbf{v} \cdot \mathbf{a})_A^B.$$

The term $(\phi - \mathbf{v} \cdot \mathbf{a})$ is a generalized potential.

17.26 Particularize the derivation of the circuit equation given in Section 17.11 to the simpler situation of a *uniform* velocity $\mathbf{v}$, for which a solution in the (common) rest frame is possible.

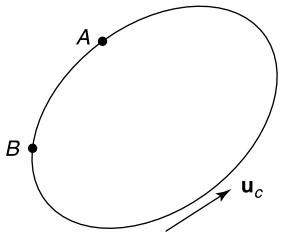

Figure P17.14

Apply this analysis to a rectangular loop moving in a nonuniform static magnetic induction $\mathbf{b}^i$ (Fig. P17.15). Pinpoint the origin of the induced e.m.f.

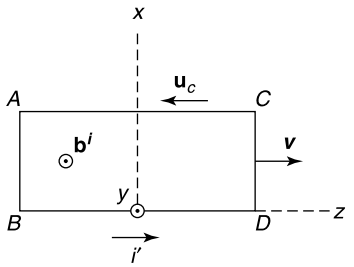

Figure P17.15

17.27 A rigid conducting rectangular loop *ABDC* swings about its side *AC* (Fig. P17.16). The rotation angle varies according to the law $\theta = \theta_M \sin \Omega t$. The swinging circuit moves in a uniform magnetic induction $\mathbf{b}^i = B \cos \omega t \, \mathbf{u}_z$. Write down the circuit equation for this *swinging bar generator*, in particular for small oscillating amplitudes θ. Consider also the resonant situation that arises when $\omega = \Omega$ [33].

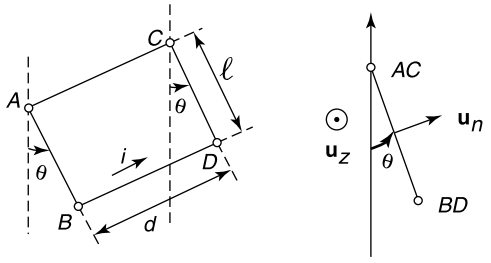

Figure P17.16

17.28 A plane wave impinges perpendicularly on a mirror moving according to a given $z_0(t)$ law (Fig. P17.17).

(**a**) Determine the boundary conditions at the mirror, expressed in the laboratory.

(**b**) Introduce the auxiliary variable u, defined by

$$u + \frac{1}{c_0} z_0(u) = t + \frac{z}{c}.$$

(**c**) Determine the reflected wave in terms of u [132].

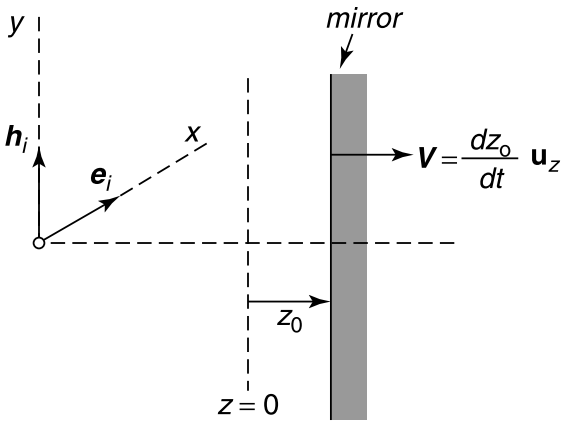

Figure P17.17

17.29 As a particular case of motion in the previous problem, assume that the mirror oscillates sinusoidally, and set $z_0 = \alpha \sin \Omega t$ in Figure P17.17. Write down Maxwell's equations in the "fluttering" axes (i.e., the axes in which the mirror is at rest). Determine the nature of the reflected wave.
(J. Van Bladel et al., *IEEE Trans. AP*, **29**, 629–637, 1981.)
Extend the solution to a plane wave at oblique incidence.
(D. De Zutter, *IEEE Trans. AP*, **30**, 898–903, 1982.)

17.30 Show that the contravariant components of the metric tensor $g_{\alpha\beta}$ are the covariant components of the inverse of this tensor.

17.31 Assume that a high-frequency wave

$$\mathbf{E} = \boldsymbol{\mathcal{E}}\,(\mathbf{r}, k_0)\, e^{-jk_0 S(\mathbf{r})}$$

$$\mathbf{H} = \boldsymbol{\mathcal{H}}\,(\mathbf{r}, k_0)\, e^{-jk_0 S(\mathbf{r})}$$

is incident on the solar mass. Applying the ideas of Section 8.3, show that

$$|\text{grad } S|^2 = \frac{1}{g_{00}} = \frac{1}{1 - \dfrac{R_S}{R}}.$$

This equation replaces the traditional eikonal equation and implies that the gravitational field introduces an equivalent dielectric constant $\epsilon_r = (1 - \frac{R_S}{R})^{-1}$ in the vicinity of the sun. Because a ray is bent toward higher ϵ_r, these simple considerations predict that a grazing ray (the light of a distant star) should be deflected toward the solar mass (for which R_S is about 2900 m, and $a = 7 \times 10^8$ m). According to *general relativity*, therefore, the sun must act as a *gravitational lens*. That revolutionary behavior was confirmed by a well-known experiment performed in 1919.

NOTES

1. Einstein's contribution to *J.C. Maxwell: A Commemoration Volume*, Cambridge University Press, Cambridge, 1931.
2. A. Liénard, Champ électrique et magnétique produit par une charge électrique concentrée en un point et animée d'un mouvement quelconque, *L'Eclairage Electrique* **XVI**, 5–14, 53–59, 106–112 (1898).
3. E. Wiechert, Elektrodynamische Elementargesetze, *Arch. Néerl.* 549–573 (1900).
4. H. A. Lorentz, Elektromagnetische verschijnselen in een stelsel dat zich met willekeurige snelheid, kleiner dan die van het licht, beweegt, Verslagen van de gewone vergaderingen der wis- en natuurkundige afdeling, K. Acad. van Wetenschappen te Amsterdam, deel XII (Juni 1904). An English translation can be found in *The Principle of Relativity, a Collection of Original Memoirs*, Dover Publications, New York.
5. H. M. Schwartz, Poincaré's Rendiconti paper on relativity, Part I, *Am. J. Phys.* **39**, 1287–1294 (1971).
6. A. Einstein, Zur Elektrodynamic Bewegter Körper, *Ann. Phys. (Leipzig)* **17**, 891–921 (1905). An English translation of this fundamental paper can be found in H.M. Schwartz, Einstein's first paper on relativity, *Am. J. Phys.* **45**, 18–25 (1977). It can also be found in the Dover publication mentioned in Ref. 4.
7. D. De Zutter, Doppler effect from a transmitter in translational motion, *Microwave Opt. Tech. Lett.* **3**, 85–92 (1979).
8. D. De Zutter, The dyadic Green's function for the Fourier spectra of the fields from harmonic sources in uniform motion, *Electromagn.* **2**, 221–237 (1982).
9. H. Minkowski, Die Grundgleichungen für die elektromagnetischen Vorgänge in bewegten Körper, *Göttinger Nachrichten* 53–116 (1908), reprinted in *Math. Annalen* **68**, 472–525 (1910).
10. H. Minkowski (bearbeitet von Max Born), Eine Ableitung der Grundgleichungen für die elektromagnetischen Vorgänge in bewegten Körpern vom Standpunkte der Elektronentheorie, *Math. Annalen* **68**, 526–551 (1910).
11. K. Sawada, Development of magnetically levitated high speed transport systems in Japan, *IEEE Trans. MAG* **32**, 2230–2235 (1996).
12. J. Van Bladel and D. De Zutter, Magnetic levitation: the track currents, *Appl. Phys. B* **34**, 193–201 (1984).
13. D. De Zutter, Levitation force acting on a three-dimensional static current source moving over a stratified medium, *J. Appl. Phys.* **58**, 2751–2758 (1985).
14. D. De Zutter and J. Van Bladel, Scattering by cylinders in translational motion, *IEE Microwaves, Optics and Acoustics* **1**, 192–196 (1977).
15. D. De Zutter, Fourier analysis of the signal scattered by three-dimensional objects in translational motion, *Appl. Sci. Res.* **36**, 241–256 and 257–269 (1980).
16. B. L. Michielsen, G. C. Herman, A. T. de Hoop, and D. De Zutter, Three-dimensional relativistic scattering of electromagnetic waves by an object in uniform translational motion, *J. Math. Phys.* **22**, 2716–2722 (1981).
17. J. Van Bladel, Foucault currents in a conducting sphere moving with constant velocity, *IEE Proc. A* **135**, 463–469 (1988).
18. T. Shiozawa, Phenomenological and electron-theoretical study of the electrodynamics of rotating systems, *Proc. IEEE* **61**, 1694–1702 (1973).
19. F. Ollendorff, Relativistische Elektrodynamik der Zählerscheibe, *Archiv. Elektrotechnik* **59**, 305–310 (1977).
20. D. De Zutter, Scattering by a rotating dielectric sphere, *IEEE Trans. AP* **28**, 643–651 (1980).
21. D. De Zutter and D. Goethals, Scattering by a rotating conducting sphere, *IEEE Trans. AP* **32**, 95–98 (1984).
22. J. Van Bladel, Rotating dielectric sphere in a low-frequency field, *Proc. IEEE* **67**, 1654–1655 (1979).
23. D. De Zutter, Scattering by a rotating circular cylinder with finite conductivity, *IEEE Trans. AP* **31**, 166–169 (1983).
24. C. T. Tai, On the presentation of Maxwell's theory, *Proc. IEEE* **60**, 936–945 (1972).
25. P. J. Scanlon, R. N. Henriksen, and J. R. Allen, Approaches to electromagnetic induction, *Am. J. Phys.* **37**, 698–708 (1969).
26. I. J. Lahaie and D. L. Sengupta, Scattering of electromagnetic waves by a slowly rotating rectangular metal plate, *IEEE Trans. AP* **27**, 40–46 (1979).
27. C. R. Birtcher, C. A. Balanis, and D. De Carlo, Rotor-blade modulation on antenna amplitude pattern and polarizations: predictions and measurements, *IEEE Trans. EMC* **41**, 384–393 (1999).
28. A. C. Polycarpou, C. A. Balanis, and A. Stefanov, Helicopter rotor-blade modulation of antenna radiation characteristics, *IEEE Trans. AP* **49**, 688–696 (2001).
29. D. De Zutter, Reflections from linearly vibrating objects: plane mirror at oblique incidence, *IEEE Trans. AP* **30**, 898–903 (1982).
30. J. Van Bladel, Electromagnetic fields in the presence of rotating bodies, *Proc. IEEE* **64**, 301–318 (1976).
31. K. Tanaka, Scattering of electromagnetic waves by a rotating perfectly conducting cylinder with arbitrary cross section: point matching method, *IEEE Trans. AP* **28**, 796–803 (1980).
32. R. Graglia, A. Freni, and G. Pelosi, A finite element approach to the electromagnetic interaction with rotating penetrable cylinders of arbitrary cross-section, *IEEE Trans. AP* **41**, 635–650 (1993).
33. B. M. Petrov, Spectral characteristics of the scatter field from a rotating impedance cylinder in uniform motion, *Radio Eng. Electron. Phys. (USSR) (English transl.)* **17**, 1431–1437 (1972).
34. D. Censor and D. M. Le Vini, The Doppler effect: now you see it, now you don't, *J. Math. Phys.* **25**, 309–316 (1984).

Appendix 1

Vector Analysis in Three Dimensions

MULTIPLICATIVE RELATIONSHIPS

$$\mathbf{a}\cdot(\mathbf{b}\times\mathbf{c}) = \mathbf{c}\cdot(\mathbf{a}\times\mathbf{b}) = \mathbf{b}\cdot(\mathbf{c}\times\mathbf{a}) \tag{A1.1}$$

$$\mathbf{a}\times(\mathbf{b}\times\mathbf{c}) = \mathbf{b}(\mathbf{a}\cdot\mathbf{c}) - \mathbf{c}(\mathbf{a}\cdot\mathbf{b}) \tag{A1.2}$$

$$\mathbf{a}\times(\mathbf{b}\times\mathbf{c}) - \mathbf{c}\times(\mathbf{b}\times\mathbf{a}) = \mathbf{b}\times(\mathbf{a}\times\mathbf{c}) \tag{A1.3}$$

$$(\mathbf{a}\times\mathbf{b})\cdot(\mathbf{c}\times\mathbf{d}) = (\mathbf{a}\cdot\mathbf{c})(\mathbf{b}\cdot\mathbf{d}) - (\mathbf{a}\cdot\mathbf{d})(\mathbf{b}\cdot\mathbf{c}) \tag{A1.4}$$

$$\mathbf{a}\times[\mathbf{b}\times(\mathbf{c}\times\mathbf{d})] = (\mathbf{b}\cdot\mathbf{d})(\mathbf{a}\times\mathbf{c}) - (\mathbf{b}\cdot\mathbf{c})(\mathbf{a}\times\mathbf{d}) \tag{A1.5}$$

$$(\mathbf{a}\times\mathbf{b})\cdot[(\mathbf{b}\times\mathbf{c})\times(\mathbf{c}\times\mathbf{a})] = [\mathbf{a}\cdot(\mathbf{b}\times\mathbf{c})]^2. \tag{A1.6}$$

DIFFERENTIAL RELATIONSHIPS

a and **b** are vector point functions; A and B are scalar point functions; all are provided with the necessary derivatives.

$$\text{grad}(A+B) = \text{grad}\,A + \text{grad}\,B \tag{A1.7}$$

$$\text{div}(\mathbf{a}+\mathbf{b}) = \text{div}\,\mathbf{a} + \text{div}\,\mathbf{b} \tag{A1.8}$$

$$\text{curl}(\mathbf{a}+\mathbf{b}) = \text{curl}\,\mathbf{a} + \text{curl}\,\mathbf{b} \tag{A1.9}$$

$$\text{grad}\,AB = A\,\text{grad}\,B + B\,\text{grad}\,A \tag{A1.10}$$

$$\text{grad}(\mathbf{a}\cdot\mathbf{b}) = \mathbf{a}\times\text{curl}\,\mathbf{b} + \mathbf{b}\times\text{curl}\,\mathbf{a} + (\mathbf{b}\cdot\text{grad})\mathbf{a} + (\mathbf{a}\cdot\text{grad})\mathbf{b} \tag{A1.11}$$

$$\text{div}(A\mathbf{a}) = A\,\text{div}\,\mathbf{a} + \text{grad}\,A\cdot\mathbf{a} \tag{A1.12}$$

$$\text{div}(\mathbf{a}\times\mathbf{b}) = \mathbf{b}\cdot\text{curl}\,\mathbf{a} - \mathbf{a}\cdot\text{curl}\,\mathbf{b} \tag{A1.13}$$

$$\text{curl}(A\mathbf{a}) = (\text{grad}\,A\times\mathbf{a}) + A\,\text{curl}\,\mathbf{a} \tag{A1.14}$$

$$\text{curl}(\mathbf{a}\times\mathbf{b}) = \mathbf{a}\,\text{div}\,\mathbf{b} - \mathbf{b}\,\text{div}\,\mathbf{a} + (\mathbf{b}\cdot\text{grad})\mathbf{a} - (\mathbf{a}\cdot\text{grad})\mathbf{b} \tag{A1.15}$$

$$\text{curl}\,\text{grad}\,A = 0 \tag{A1.16}$$

Electromagnetic Fields, Second Edition, By Jean G. Van Bladel

$$\text{div curl } \mathbf{a} = 0 \tag{A1.17}$$

$$\text{curl curl } \mathbf{a} = \text{grad div } \mathbf{a} - \nabla^2 \mathbf{a} \tag{A1.18}$$

$$\text{div grad } A = \nabla^2 A \tag{A1.19}$$

$$\text{grad } f(A) = f'(A) \cdot \text{grad } A \tag{A1.20}$$

$$\frac{d\mathbf{a}}{dt} = \frac{\partial \mathbf{a}}{\partial t} + \mathbf{a} \text{ div } \mathbf{v} - \text{curl}(\mathbf{a} \times \mathbf{v}) (\mathbf{v} = \text{velocity}) \tag{A1.21}$$

$$\nabla^2 (AB) = A\nabla^2 B + 2 \text{ grad } A \cdot \text{grad } B + B\nabla^2 A \tag{A1.22}$$

$$\nabla^2 (A\mathbf{a}) = A\nabla^2 \mathbf{a} + \mathbf{a}\nabla^2 A + 2(\text{grad } A \cdot \text{grad})\mathbf{a} \tag{A1.23}$$

$$\begin{aligned} \text{grad div } (A\mathbf{a}) = {} & (\text{grad } A) \text{ div } \mathbf{a} + A \text{ grad div } \mathbf{a} + \text{grad } A \times \text{curl } \mathbf{a} \\ & + (\mathbf{a} \cdot \text{grad}) \text{ grad } A + (\text{grad } A \cdot \text{grad})\mathbf{a} \end{aligned} \tag{A1.24}$$

$$\begin{aligned} \text{curl curl } (A\mathbf{a}) = {} & \text{grad } A \times \text{curl } \mathbf{a} - \mathbf{a}\nabla^2 A + (\mathbf{a} \cdot \text{grad}) \text{ grad } A \\ & + A \text{ curl curl } \mathbf{a} + \text{grad } A \text{ div } \mathbf{a} - (\text{grad } A \cdot \text{grad})\mathbf{a}. \end{aligned} \tag{A1.25}$$

INTEGRAL RELATIONSHIPS

These integral relationships are valid for volumes bounded by regular surfaces, a precise definition of which can be found in [158]. It is sufficient, for our purposes, to state that usually encountered surfaces with finite numbers of vertices are regular. The basis for the various relations is the following theorem:

$$\int_V \frac{\partial \phi}{\partial x_i} dV = \int_S \phi (\mathbf{u}_n \cdot \mathbf{u}_i) \, dS \tag{A1.26}$$

where $\mathbf{u}_n$ is the unit vector along the outward-pointing normal. The theorem is valid when ϕ is a single-valued function in V and on its boundary, and has a derivative $\partial\phi/\partial x_i$ that is continuous in the interiors of a finite number of regular regions of which V is the sum. Discontinuities in the derivatives are allowed at the boundaries between the regions. Coordinate x_i is taken along an arbitrary axis with unit vector $\mathbf{u}_i$. Application to three orthogonal directions yields the following *Gauss' theorems*:

$$\int_V \text{div } \mathbf{v} \, dV = \int_S (\mathbf{v} \cdot \mathbf{u}_n) \, dS \tag{A1.27}$$

$$\int_V \text{curl } \mathbf{v} \, dV = \int_S (\mathbf{u}_n \times \mathbf{v}) \, dS = \int_S \mathbf{r} (\mathbf{u}_n \cdot \text{curl } \mathbf{v}) \, dS \tag{A1.28}$$

$$\int_V \text{grad } f \, dV = \int_S f \mathbf{u}_n \, dS. \tag{A1.29}$$

The partial derivatives that appear in the formulas must have the continuity properties stated above for $\partial\phi/\partial x_i$. They can eventually become infinite at the boundary, but the integrals must then be understood to be improper integrals $\lim_{V' \to V} \int_{V'} dV'$. By choosing special vectors, such as A grad B, for insertion in Gauss' theorem, a whole series of *Green's theorems* can

be obtained. The second partial derivatives that appear in the formulas must now satisfy the conditions formerly required of $\partial\phi/\partial x_i$.

$$\int_V [A\nabla^2 B + (\text{grad } A \cdot \text{grad } B)]\, dV = \int_S A \frac{\partial B}{\partial n}\, dS \tag{A1.30}$$

$$\int_V (A\nabla^2 B - B\nabla^2 A)\, dV = \int_S \left(A\frac{\partial B}{\partial n} - B\frac{\partial A}{\partial n} \right) dS \tag{A1.31}$$

$$\int_V (\text{curl } \mathbf{a} \cdot \text{curl } \mathbf{b} - \mathbf{a} \cdot \text{curl curl } \mathbf{b})\, dV = \int_S (\mathbf{a} \times \text{curl } \mathbf{b}) \cdot \mathbf{u}_n\, dS \tag{A1.32}$$

$$\int_V (\mathbf{b} \cdot \text{curl curl } \mathbf{a} - \mathbf{a} \cdot \text{curl curl } \mathbf{b})\, dV$$

$$= \int_S [(\mathbf{u}_n \times \mathbf{a}) \cdot \text{curl } \mathbf{b} - (\mathbf{u}_n \times \mathbf{b}) \cdot \text{curl } \mathbf{a}]\, dS \tag{A1.33}$$

$$\int_V (\text{div } \mathbf{a} \cdot \text{div } \mathbf{b} + \mathbf{b} \cdot \text{grad div } \mathbf{a})\, dV = \int_S \text{div } \mathbf{a} (\mathbf{b} \cdot \mathbf{u}_n)\, dS \tag{A1.34}$$

$$\int_V (\mathbf{a} \cdot \text{grad div } \mathbf{b} - \mathbf{b} \cdot \text{grad div } \mathbf{a})\, dV = \int_S [(\mathbf{a} \cdot \mathbf{u}_n) \text{ div } \mathbf{b} - (\mathbf{b} \cdot \mathbf{u}_n) \text{div } \mathbf{a}]\, dS \tag{A1.35}$$

$$\int_V [\mathbf{a} \cdot \nabla^2 \mathbf{b} + \text{curl } \mathbf{a} \cdot \text{curl } \mathbf{b} + \text{div } \mathbf{a} \cdot \text{div } \mathbf{b})\, dV = \int_S [(\mathbf{u}_n \times \mathbf{a}) \cdot \text{curl } \mathbf{b} + (\mathbf{u}_n \cdot \mathbf{a}) \cdot \text{div } \mathbf{b}]\, dS \tag{A1.36}$$

$$\int_V (\mathbf{a} \cdot \nabla^2 \mathbf{b} - \mathbf{b} \cdot \nabla^2 \mathbf{a})\, dV = \int_S [(\mathbf{u}_n \cdot \mathbf{a}) \text{ div } \mathbf{b} - (\mathbf{b} \cdot \mathbf{u}_n) \text{ div } \mathbf{a} + (\mathbf{u}_n \times \mathbf{a}) \cdot \text{curl } \mathbf{b} - (\mathbf{u}_n \times \mathbf{b}) \cdot \text{curl } \mathbf{a}]\, dS \tag{A1.37}$$

$$\int_V [\mathbf{a} \text{ div } \mathbf{b} + \mathbf{b} \text{ div } \mathbf{a} - (\mathbf{a} \times \text{curl } \mathbf{b}) - (\mathbf{b} \times \text{curl } \mathbf{a})]\, dV$$

$$\int_S [\mathbf{a}(\mathbf{u}_n \cdot \mathbf{b}) + \mathbf{b}(\mathbf{u}_n \cdot \mathbf{a}) - \mathbf{u}_n (\mathbf{a} \cdot \mathbf{b})]\, dS \tag{A1.38}$$

$$\int_V [\mathbf{b} \text{ div } \mathbf{a} + (\mathbf{a} \cdot \text{grad})\mathbf{b}]\, dV = \int_S (\mathbf{u}_n \cdot \mathbf{a})\mathbf{b}\, dS \tag{A1.39}$$

$$\int_V [A \text{ curl curl } \mathbf{v} + \mathbf{v}\nabla^2 A + (\text{div } \mathbf{v}) \text{ grad } A]\, dV$$

$$= \int_S [A\mathbf{u}_n \times \text{curl } \mathbf{v} + (\mathbf{u}_n \times \mathbf{v}) \times \text{grad } A + (\mathbf{u}_n \cdot \mathbf{v}) \text{ grad } A]\, dS \tag{A1.40}$$

$$\int_V \text{grad } A \cdot \text{curl } \mathbf{v}\, dV = \int_S A \text{ curl } \mathbf{v} \cdot \mathbf{u}_n\, dS = \int_S (\mathbf{v} \times \text{grad } A) \cdot \mathbf{u}_n\, dS. \tag{A1.41}$$

When S is a regular two-sided surface, and when the various partial derivatives that appear in the formulas are continuous in a region containing the surface in its interior, the following *Stokes' theorems* hold:

$$\int_S (\mathbf{u}_n \cdot \text{curl } \mathbf{v})\, dS = \int_c \mathbf{v} \cdot d\mathbf{c} \tag{A1.42}$$

$$\int_S (\mathbf{u}_n \times \text{grad } f)\, dS = \int_c f\, d\mathbf{c} \tag{A1.43}$$

$$\int_S (\mathbf{u}_n \times \text{grad}) \times \mathbf{v}\, dS = \int_c d\mathbf{c} \times \mathbf{v} \tag{A1.44}$$

$$\int_S (\text{grad}\, A \times \text{grad}\, B) \cdot \mathbf{u}_n\, dS = \int_c A\, \text{grad}\, B \cdot d\mathbf{c} = -\int_c B\, \text{grad}\, A \cdot d\mathbf{c} \tag{A1.45}$$

where c is a contour on surface S. This contour must be described in the positive sense with respect to $\mathbf{u}_n$.

DEFINITION OF THE MAIN OPERATORS

The usual definition of curl in terms of first derivatives is not valid at points at which some of these derivatives do not exist, for example, at a surface of discontinuity. A more general definition of the curl is obtained by considering the expression

$$\text{curl}^*\mathbf{a} = \lim_{V \to 0} \int_S \mathbf{u}_n \times \mathbf{a}\, dS, \tag{A1.46}$$

where V is a volume surrounding P and bounded by S. If this expression approaches a unique limit when V approaches zero, the limit is termed the *curl of* $\mathbf{a}$ *at* P and is denoted, in Weyl's notation,[1] by $\text{curl}^*\mathbf{a}$. The two definitions of the curl are equivalent when $\mathbf{a}$ is continuously differentiable. Further, many of the properties of the usual curl (Stokes' theorem, for example) can be extended to the curl* operator when the latter is continuous [201]. In a similar manner, a definition of the divergence is obtained by considering

$$\text{div}\, \mathbf{a}^* = \lim_{V \to 0} \frac{1}{V} \int_S \mathbf{u}_n \cdot \mathbf{a}\, dS. \tag{A1.47}$$

If this expression has a unique limit, the limit is termed *divergence* and is denoted by $\text{div}^*\mathbf{a}$. Examples of vectors having a div* but no div are given in [201]. Here, again, the two operators are identical when $\mathbf{a}$ is continuously differentiable. Finally, the gradient is defined by

$$\text{grad}^* f = \lim_{V \to 0} \int_S f \mathbf{u}_n\, dS. \tag{A1.48}$$

The starred definitions have the advantage of being independent of the coordinate system.

The basic operators can also be given a "weak" definition,[2] in particular the distributional forms (A8.72), (A8.75), (A8.78), (A8.79), which can be applied to symbolic functions such as $\delta(\mathbf{r})$. One can also introduce a curl^a operator, based on the notion of fractional derivative of order a, where a can be real or complex.[3] The *linguistic* notations div, grad, curl used in this book are frequently replaced by the Gibbs version, based on the *nabla operator*

$$\nabla = \sum_{n=1}^{3} \mathbf{u}_n \frac{1}{h_n} \frac{\partial}{\partial v_n}, \tag{A1.49}$$

here expressed in the general orthogonal system v_1, v_2, v_3 discussed in Appendix 2. Using that operator, the basic operators are written as ∇f, $\nabla \cdot \mathbf{a}$ and $\nabla \times \mathbf{a}$. The implication is that ∇ is a *constituent* of these operators, and this through scalar and vector products.

A scholarly monograph disputes the desirability of this approach [173] and shows that $\boldsymbol{\nabla}\cdot\mathbf{a}$ as a scalar product can lead to incorrect results in the derivation of formulas valid in a general coordinate system.[4] It is therefore more appropriate to write $(\boldsymbol{\nabla}\cdot)\mathbf{a}$ and $(\boldsymbol{\nabla}\times)\mathbf{a}$, where the object between parentheses is an operator. Following that idea, Tai proposes the notations ∇f, $\nabla\mathbf{a}$ and $\nabla\mathbf{a}$, where ∇ is the expression (A1.49) and

$$\nabla = \sum_{n=1}^{3} \frac{\mathbf{u}_n}{h_n}\cdot\frac{\partial}{\partial v_n} \tag{A1.50}$$

$$\nabla = \sum_{n=1}^{3} \frac{\mathbf{u}_n}{h_n}\times\frac{\partial}{\partial v_n}. \tag{A1.51}$$

This form, valid for orthogonal coordinate systems, emphasizes the independence of the three operators. The Laplacian is now written as $\nabla\nabla f$ or $\nabla\nabla\mathbf{a}$, grad div $\mathbf{a}$ as $\nabla\nabla\mathbf{a}$, and curl curl $\mathbf{a}$ as $\nabla\nabla\mathbf{a}$. The forms (A1.50), (A1.51) are actually derived from definitions of the kind shown in (A1.46) to (A1.48). Tai also proves the invariance of the operators by showing that, in any two curvilinear orthogonal systems,

$$\sum_{n=1}^{3} \frac{\mathbf{u}_n}{h_n} * \frac{\partial}{\partial v_n} = \sum_{n=1}^{3} \frac{\mathbf{u}'_n}{h'_n} * \frac{\partial}{\partial v'_n}$$

where $*$ represents a null, a dot, or a cross. The proof can be extended to nonorthogonal curvilinear systems. Whatever the notation, a formula such as (A2.102), which gives grad div $\mathbf{v}$ in spherical coordinates, has been obtained by first expressing div $\mathbf{v}$ from (A2.92) and subsequently applying the gradient operation (A2.91) to the result. This safe approach has been used consistently in the current text.

HELMHOLTZ' THEOREM IN INFINITE SPACE

Helmholtz' theorem consists in splitting a vector field in the form

$$\mathbf{f}(\mathbf{r}) = \text{grad}\ \phi + \text{curl}\ \mathbf{v}. \tag{A1.52}$$

The term grad ϕ is the irrotational *(lamellar or longitudinal) part*, the term curl $\mathbf{v}$ the *solenoidal (or transverse) part*. The first operator may be thought of as a diagonal matrix, the second one as a skew matrix. The splitting appears on p. 38 of Helmholtz' original paper,[5] in which the author, although mostly concerned with hydrodynamics, mentions the relevance of his theory to electromagnetic problems. Only potential flows in incompressible fluids had been studied at the time, with velocity $\mathbf{w}$ equal to grad ϕ. This explains Helmholtz' interest in vortex motion, which he measures by the *vorticity vector* $\frac{1}{2}\text{curl}\ \mathbf{w}$. Also relevant is the *helicity*

$$h = \int_V \mathbf{f}\cdot\text{curl}\ \mathbf{f}\, dV, \tag{A1.53}$$

which is a topological measure of how much the field rotates about itself in a given volume.[6,7] The concept finds application in magneto-hydrodynamics, where $\mathbf{f}$ is the vector potential. The helicity is gauge invariant in simply connected domains and provides a measure of the linkage of the field lines [24].

Going back to (A1.52), let $\mathbf{f}$ be a field that is bounded, approaches zero at large distances, and has sources, div $\mathbf{f}$ and curl $\mathbf{f}$, which are of finite support V in space. In (A1.52), the two parts keep the same value when a constant is added to ϕ and a gradient to $\mathbf{v}$. With the additional constraint div $\mathbf{v} = 0$, ϕ and $\mathbf{v}$ satisfy

$$\nabla^2\phi = \text{div}\,\mathbf{f}$$
$$\nabla^2\mathbf{v} = -\text{curl}\,\mathbf{f}. \tag{A1.54}$$

The solution becomes unique if we require ϕ and $\mathbf{v}$ (and the two terms of the splitting) to satisfy the classical conditions of regularity at infinity defined in Sections 3.1 and 6.1. Thus,

$$\phi(\mathbf{r}) = -\frac{1}{4\pi}\int_V \text{div}'\mathbf{f}\,\frac{1}{|\mathbf{r}-\mathbf{r}'|}\,dV'$$
$$\mathbf{v}(\mathbf{r}) = \frac{1}{4\pi}\int_V \text{curl}'\mathbf{f}\,\frac{1}{|\mathbf{r}-\mathbf{r}'|}\,dV'. \tag{A1.55}$$

The operators div and curl must be understood in the sense of distributions, that is, according to (A8.90) and (A8.91) if $\mathbf{f}$ is piecewise continuous. To show that the decomposition is unique, let us assume that two sets of functions, $(\phi, \mathbf{v})$ and $(\phi', \mathbf{v}')$, are appropriate for (A1.52). The vector

$$\boldsymbol{\alpha} = \text{grad}(\phi - \phi') = -\text{curl}(\mathbf{v} - \mathbf{v}')$$

is *harmonic*, with div $\boldsymbol{\alpha} = 0$ and curl $\boldsymbol{\alpha} = 0$. It is shown in Section 3.6 that such a vector, if bounded, must have a constant value in space. It follows that $\boldsymbol{\alpha}$ must vanish because the two parts of the splitting are required to approach zero at infinity. This shows that grad ϕ = grad ϕ' and curl $\mathbf{v}$ = curl $\mathbf{v}'$.

The splitting into longitudinal and transverse components can be written formally as [133]

$$\mathbf{f}(\mathbf{r}) = \int \left[\overline{\overline{\delta}}_l(\mathbf{r}|\mathbf{r}') + \overline{\overline{\delta}}_t(\mathbf{r}|\mathbf{r}')\right]\cdot\mathbf{f}(\mathbf{r}')\,dV, \tag{A1.56}$$

where

$$\overline{\overline{\delta}}_l(\mathbf{r}|\mathbf{r}') + \overline{\overline{\delta}}_t(\mathbf{r}|\mathbf{r}') = \overline{\overline{I}}\delta(\mathbf{r}-\mathbf{r}').$$

According to (A4.48),

$$\overline{\overline{\delta}}_l(\mathbf{r}|\mathbf{r}') = -\frac{1}{4\pi}\,\text{grad grad}\,\frac{1}{|\mathbf{r}-\mathbf{r}'|}. \tag{A1.57}$$

It is obvious that $\overline{\overline{\delta}}_l$ and $\overline{\overline{\delta}}_t$ are not concentrated on $\mathbf{r} = \mathbf{r}'$. For example:

$$\text{grad grad}\frac{1}{R} = \frac{1}{R^3}(3\mathbf{u}_R\mathbf{u}_R - \overline{\overline{I}}) \qquad (R \neq 0). \tag{A1.58}$$

The appropriateness of the terms *longitudinal* and *transverse* is confirmed by considering the space transform $\tilde{\mathbf{f}}(\mathbf{k})$ of $\mathbf{f}(\mathbf{r})$, given in (A7.53). From (A7.56) and (A7.57), the transforms of div $\mathbf{f}$ and curl $\mathbf{f}$ are, respectively,

$$\mathcal{F}[\text{div}\,\tilde{\mathbf{f}}] = j\mathbf{k}\cdot\tilde{\mathbf{f}}(\mathbf{k})$$
$$\mathcal{F}\,[\text{curl}\,\tilde{\mathbf{f}}] = j\mathbf{k}\times\tilde{\mathbf{f}}(\mathbf{k}).$$

The div **f** source is associated with the component of **f** in the direction of the propagation vector **k**, and the curl **f** source with the transverse components with respect to **k** [46].

HELMHOLTZ THEOREM IN A FINITE SPACE

A representation such as (A1.52) can be generated from any solution of the equation

$$\mathbf{f} = \text{grad div } \mathbf{a} - \text{curl curl } \mathbf{a} = \nabla^2 \mathbf{a}. \tag{A1.59}$$

Potential theory immediately yields the possible solution (Fig. A1.1*a*)

$$\begin{aligned} \phi = \text{div } \mathbf{a} \quad &= -\frac{1}{4\pi} \int_V \frac{\text{div } \mathbf{f}(\mathbf{r}')}{|\mathbf{r} - \mathbf{r}'|}\, dV' + \frac{1}{4\pi} \int_S \frac{\mathbf{u}'_n \cdot \mathbf{f}(\mathbf{r}')}{|\mathbf{r} - \mathbf{r}'|}\, dS' \\ \mathbf{v} = -\text{curl } \mathbf{a} &= \frac{1}{4\pi} \int_V \frac{\text{curl } \mathbf{f}(\mathbf{r}')}{|\mathbf{r} - \mathbf{r}'|}\, dV' - \frac{1}{4\pi} \int_S \frac{\mathbf{u}_{n'} \times \mathbf{f}(\mathbf{r}')}{|\mathbf{r} - \mathbf{r}'|}\, dS'. \end{aligned} \tag{A1.60}$$

Particular splittings result from boundary conditions imposed on ϕ or **a**. In the *electric splitting*, ϕ is required to vanish on S. The solution is unique, and grad ϕ is easily interpreted as the electrostatic field generated by a volume charge $\rho = \epsilon_0$ div **f** enclosed in a metallized S. In a multiply bounded volume, however, (A1.52) should include harmonic (source-free) terms.[8,9] In the doubly bounded region II of Figure A1.1*b*, one should write

$$\mathbf{f} = \mathbf{f}_0 + \text{grad } \phi + \text{curl } \mathbf{v}. \tag{A1.61}$$

Vector $\mathbf{f}_0$ is proportional to the electric field $\mathbf{e}_0$ resulting from a unit difference of potential applied between the metallized electrodes S_1 and S_2. Although $\mathbf{f}_0$ is solenoidal, it cannot generally be represented as a curl. In a doubly bounded volume, indeed, such a representation requires the flux of the vector through *both* S_1 and S_2 to vanish.[8,10] Because $\mathbf{f}_0$, grad ϕ, and curl **v** are functionally orthogonal [a property easily proven by means of the divergence theorem (A1.27)], $\mathbf{f}_0$ can be determined from the relationship

$$\mathbf{f}_0 = \frac{\int_V \mathbf{f} \cdot \mathbf{e}_0\, dV}{\int_V |\mathbf{e}_0|^2\, dV} \mathbf{e}_0 \tag{A1.62}$$

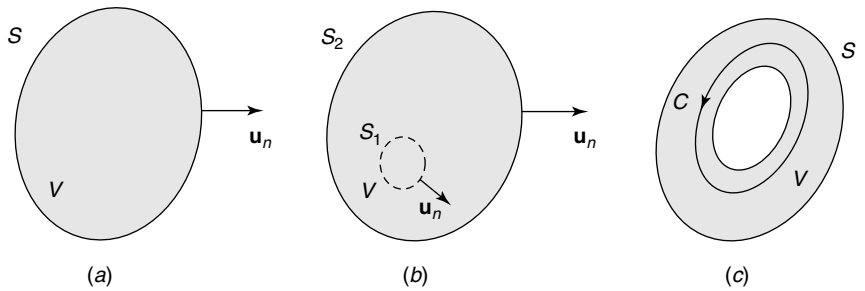

Figure A1.1 Finite volumes: (*a*) simply bounded and connected region I; (*b*) doubly bounded region II; (*c*) doubly connected region III.

where $\mathbf{e}_0 = \text{grad}\,\phi_0$. Potential ϕ_0 satisfies

$$\begin{aligned} \nabla^2\phi_0 &= 0 \\ \phi_0 &= 1 \text{ on } S_2 \\ \phi_0 &= 0 \text{ on } S_1. \end{aligned} \tag{A1.63}$$

When $\mathbf{f}$ is solenoidal, it can only be written as a curl when the term in $\mathbf{f}_0$ is absent (i.e., when the flux of $\mathbf{f}$ vanishes through S_1 and S_2 *individually*).

In the *magnetic splitting*, the potential must satisfy the boundary condition $\partial\phi/\partial n = \mathbf{u}_n \cdot \mathbf{f}$ on S. The solution for ϕ is defined to within an additive constant, which has no influence on the value of grad ϕ. The curl $\mathbf{v}$ term is tangent to S, hence $\mathbf{v}$ may be chosen perpendicular to S. In a ring-like region (Fig. A1.1*c*) splitting (A1.52) takes the form[11]

$$\mathbf{f} = \mathbf{h}_0 \int_V \mathbf{f}\cdot\mathbf{h}_0\, dV + \text{grad}\,\phi + \text{curl}\,\mathbf{v}. \tag{A1.64}$$

Field $\mathbf{h}_0$, introduced in Section 4.10, is sourceless. It can be expressed as a curl or a gradient, but the relevant scalar potential is multivalued. In fluid dynamics, $\mathbf{h}_0$ is the velocity of an incompressible fluid flowing irrotationally in the ring-like volume III.

A Helmholtz theorem can also be written on a surface S. Let $\mathbf{f}_S$ be a tangential vector function. The splitting is now[2]

$$\mathbf{f}_S = \text{grad}_S\,\phi + \mathbf{u}_n \times \text{grad}_S\,\theta. \tag{A1.65}$$

From (A3.40),

$$\begin{aligned} \nabla_S^2\,\phi &= \text{div}_S\,\mathbf{f}_S \\ \nabla_S^2\,\theta &= \text{div}_S(\mathbf{f}_S \times \mathbf{u}_n). \end{aligned} \tag{A1.66}$$

The solution of (A1.66) can be effected, in principle at least, by means of either a Green's function or an expansion in the eigenfunctions of ∇_S^2.

OTHER SPLITTINGS

The representation of fields by means of scalar functions facilitates satisfaction of boundary conditions. The mother functions are typically less singular than the original fields, for example in the vicinity of sharp metallic edges. For a general vector function $\mathbf{f}$, one may write

$$\mathbf{f} = \text{grad}\,\phi + \text{curl}(S\mathbf{u}) + \text{curl curl}(T\mathbf{u}) \tag{A1.67}$$

where $\mathbf{u}$ is a constant unit vector. Another expansion is

$$\begin{aligned} \mathbf{f} &= \text{grad}\,\phi + \text{curl}(S\mathbf{r}) + \text{curl curl}(T\mathbf{r}) \\ &= \text{grad}\,\phi + \text{grad}\,S \times \mathbf{r} + \text{curl}(\text{grad}\,T \times \mathbf{r}) \end{aligned} \tag{A1.68}$$

where S and T are *Debye potentials*. Representation (A1.68) is useful for a multipole analysis in spherical coordinates. Solutions of Maxwell's equations in a sourceless region are afforded by the expressions

$$\begin{aligned} \mathbf{E} &= \operatorname{curl}\operatorname{curl}(T\mathbf{r}) - jk_0 \operatorname{curl}(S\mathbf{r}) \\ R_{c0}\mathbf{H} &= \operatorname{curl}\operatorname{curl}(S\mathbf{r}) + jk_0 \operatorname{curl}(T\mathbf{r}). \end{aligned} \tag{A1.69}$$

By setting $\mathbf{L} = \mathbf{r} \times \operatorname{grad}$, a vector $\mathbf{f}$ can be written as

$$\mathbf{f} = \mathbf{L}\phi + \mathbf{L} \times \mathbf{v} + \mathbf{v}. \tag{A1.70}$$

To within an imaginary factor, the operator $\mathbf{L}$ is the orbital angular momentum encountered in quantum mechanics.[12] Finally, a *solenoidal* vector $\mathbf{f}$ can be expressed in terms of Clebsch potentials S and T. Thus,[13,14]

$$\mathbf{f} = \operatorname{curl}(S \operatorname{grad} T) = \operatorname{grad} S \times \operatorname{grad} T. \tag{A1.71}$$

NOTES

1. H. Weyl, The method of orthogonal projection in potential theory, *Duke Math. J.* **7**, 411–444, 1940.
2. J. Van Bladel, A discussion of Helmholtz' theorem on a surface, *AEÜ* **47**, 131–135, 1993.
3. N. Engheta, Fractional curl operator in electromagnetics, *Microwave Opt. Tech. Lett.* **17**, 86–91, 1998.
4. P. Moon and D. E. Spencer. *Vectors*. D. Van Nostrand Co., Princeton, N.J., 1965.
5. H. Helmholtz, Uber Integrale der hydrodynamischen Gleichungen welche den Wirbelbewegungen entsprechen. *J. Reine Angew. Math.* **55**, 25–55, 1858.
6. N. Anderson and A. M. Arthurs, The helicity of the electromagnetic field, *Int. J. Electronics* **56**, 571–573, 1984.
7. A. Lakhtakia and B. Shanker, Beltrami fields within continuous source regions, volume integral equations, scattering algorithms and the extended Maxwell-Garnett model, *Int. J. Applied Electrom. Materials* **4**, 65–82, 1993.
8. J. Van Bladel, On Helmholtz' theorem in multiply-bounded and multiply-connected regions, *J. Franklin Inst.* **269**, 445–462, 1960.
9. J. Van Bladel, A discussion of Helmholtz' theorem, *Electromagn.* **13**, 95–110, 1993.
10. A. F. Stevenson, Note on the existence and determination of a vector potential, *Quart. Appl. Math.* **12**, 194–198, 1954.
11. A. Bossavit, Magnetostatic problems in multiply connected regions: some properties of the curl operator. *IEE Proc.* **135-A**, 179–187, 1988.
12. J. S. Lemont and H. E. Moses, An angular momentum Helmholtz theorem, *Comm. Pure Appl. Math.* **14**, 69–76, 1961.
13. P. R. Kotiuga, Clebsch potentials and the visualisation of three-dimensional vector fields, *IEEE Trans. MAG* **27**, 3986–3989, 1991.
14. H. Rund, Clebsch potentials in the theory of electromagnetic fields admitting electric and magnetic charge distributions, *J. Math. Phys.* **18**, 84–95, 1977.

Appendix 2

Vector Operators in Several Coordinate Systems

CARTESIAN COORDINATES

$$(\mathbf{a}\cdot\mathbf{b}) = a_x b_x + a_y b_y + a_z b_z \tag{A2.1}$$

$$(\mathbf{a}\times\mathbf{b}) = (a_y b_z - a_z b_y)\mathbf{u}_x + (a_z b_x - a_x b_z)\mathbf{u}_y + (a_x b_y - a_y b_x)\mathbf{u}_z \tag{A2.2}$$

$$\mathbf{u}_z \times (\mathbf{v}\times\mathbf{u}_z) = \mathbf{v}_t (\mathbf{v}_t = \text{component perpendicular to } \mathbf{u}_z) \tag{A2.3}$$

$$\mathbf{u}_z \times \mathbf{a} = -a_y\mathbf{u}_x + a_x\mathbf{u}_y \tag{A2.4}$$

$$\mathbf{u}_x\times\mathbf{u}_y = \mathbf{u}_z \quad \mathbf{u}_y\times\mathbf{u}_z = \mathbf{u}_x \quad \mathbf{u}_z\times\mathbf{u}_x = \mathbf{u}_y \tag{A2.5}$$

$$\text{grad}\, f = \frac{\partial f}{\partial x}\mathbf{u}_x + \frac{\partial f}{\partial y}\mathbf{u}_y + \frac{\partial f}{\partial z}\mathbf{u}_z \tag{A2.6}$$

$$\text{div}\,\mathbf{v} = \frac{\partial v_x}{\partial x} + \frac{\partial v_y}{\partial y} + \frac{\partial v_z}{\partial z} \tag{A2.7}$$

$$\text{curl}\,\mathbf{v} = \left(\frac{\partial v_z}{\partial y} - \frac{\partial v_y}{\partial z}\right)\mathbf{u}_x + \left(\frac{\partial v_x}{\partial z} - \frac{\partial v_z}{\partial x}\right)\mathbf{u}_y + \left(\frac{\partial v_y}{\partial x} - \frac{\partial v_x}{\partial y}\right)\mathbf{u}_z \tag{A2.8}$$

$$\text{div}(\mathbf{u}_z\times\mathbf{v}) = -\mathbf{u}_z\cdot\text{curl}\,\mathbf{v} \tag{A2.9}$$

$$\text{grad}(\mathbf{u}_z\cdot\mathbf{v}) = \mathbf{u}_z\times\text{curl}\,\mathbf{v} + \frac{\partial\mathbf{v}}{\partial z} \tag{A2.10}$$

$$\text{curl}(\mathbf{u}_z\times\mathbf{v}) = \mathbf{u}_z\,\text{div}\,\mathbf{v} - \frac{\partial\mathbf{v}}{\partial z} \tag{A2.11}$$

$$\text{curl}(f\mathbf{u}_z) = \text{grad}\, f\times\mathbf{u}_z \tag{A2.12}$$

$$\text{curl}\big[f(z)A(x,y)\mathbf{u}_z\big] = f(z)\,\text{grad}\,A\times\mathbf{u}_z \tag{A2.13}$$

$$\text{curl}\big[f(z)\,\text{grad}\,A(x,y)\big] = \frac{df}{dz}\mathbf{u}_z\times\text{grad}\,A \tag{A2.14}$$

$$\begin{aligned}\text{curl}\big[f(z)\,\text{grad}\,A\times\mathbf{u}_z\big] &= \text{curl}\,\text{curl}\,\big[f(z)A(x,y)\mathbf{u}_z\big]\\ &= \frac{df}{dz}\,\text{grad}\,A - f(z)\nabla^2 a\mathbf{u}_z\end{aligned} \tag{A2.15}$$

Electromagnetic Fields, Second Edition, By Jean G. Van Bladel

$$\nabla^2 f = \frac{\partial^2 f}{\partial x^2} + \frac{\partial^2 f}{\partial y^2} + \frac{\partial^2 f}{\partial z^2} \tag{A2.16}$$

$$\nabla^2 \mathbf{v} = \nabla^2 v_x \mathbf{u}_x + \nabla^2 v_y \mathbf{u}_y + \nabla^2 v_z \mathbf{u}_z \tag{A2.17}$$

$$\begin{aligned}\text{grad div } \mathbf{v} = &\left(\frac{\partial^2 v_x}{\partial x^2} + \frac{\partial^2 v_y}{\partial x \partial y} + \frac{\partial^2 v_z}{\partial x \partial z}\right)\mathbf{u}_x + \left(\frac{\partial^2 v_x}{\partial x \partial y} + \frac{\partial^2 v_y}{\partial y^2} + \frac{\partial^2 v_z}{\partial y \partial z}\right)\mathbf{u}_y \\ &+ \left(\frac{\partial^2 v_x}{\partial x \partial z} + \frac{\partial^2 v_y}{\partial y \partial z} + \frac{\partial^2 v_z}{\partial z^2}\right)\mathbf{u}_z\end{aligned} \tag{A2.18}$$

$$\begin{aligned}\text{curl curl } \mathbf{v} = &\left(-\frac{\partial^2 v_x}{\partial y^2} - \frac{\partial^2 v_x}{\partial z^2} + \frac{\partial^2 v_y}{\partial x \partial y} + \frac{\partial^2 v_z}{\partial x \partial z}\right)\mathbf{u}_x \\ &+ \left(-\frac{\partial^2 v_y}{\partial x^2} - \frac{\partial^2 v_y}{\partial z^2} + \frac{\partial^2 v_x}{\partial x \partial y} + \frac{\partial^2 v_z}{\partial y \partial z}\right)\mathbf{u}_y \\ &+ \left(-\frac{\partial^2 v_z}{\partial x^2} - \frac{\partial^2 v_z}{\partial y^2} + \frac{\partial^2 v_x}{\partial x \partial z} + \frac{\partial^2 v_y}{\partial y \partial z}\right)\mathbf{u}_z\end{aligned} \tag{A2.19}$$

$$\nabla^2(\mathbf{u}_x \times \mathbf{v}) = \mathbf{u}_z \times \nabla^2 \mathbf{v} \tag{A2.20}$$

$$\text{grad div } (\mathbf{u}_z \times \mathbf{v}) = -\mathbf{u}_z \times \text{curl curl } \mathbf{v} - \text{curl}\frac{\partial \mathbf{v}}{\partial z} \tag{A2.21}$$

$$\text{curl curl } (\mathbf{u}_z \times \mathbf{v}) = -\mathbf{u}_z \times \text{grad div } \mathbf{v} - \text{curl}\frac{\partial \mathbf{v}}{\partial z} \tag{A2.22}$$

$$\nabla^2(f\mathbf{u}_z) = \mathbf{u}_z \nabla^2 f \tag{A2.23}$$

$$\text{grad div } (f\mathbf{u}_z) = \frac{\partial}{\partial z}(\text{grad } f) = \text{grad}\frac{\partial f}{\partial z} \tag{A2.24}$$

$$\text{curl curl } (f\mathbf{u}_z) = -\mathbf{u}_z \nabla^2 f + \text{grad}\frac{\partial f}{\partial z} \tag{A2.25}$$

$$\nabla^2(\sin kz\, \mathbf{v}) = \sin kz(\nabla^2 \mathbf{v} - k^2 \mathbf{v}) + 2k \cos kz \frac{\partial \mathbf{v}}{\partial z} \tag{A2.26}$$

$$\text{grad div } (\sin kz\, \mathbf{v}) = \sin kz(\text{grad div } \mathbf{v} - k^2 \mathbf{v}_z) + k \cos kz(\mathbf{u}_z \text{ div } \mathbf{v} + \text{grad } v_z) \tag{A2.27}$$

$$\begin{aligned}\text{curl curl } (\sin kz\, \mathbf{v}) = &\sin kz(\text{curl curl } \mathbf{v} + k^2 \mathbf{v}_t) \\ &+ k \cos kz \left(\mathbf{u}_z \text{ div } \mathbf{v} - \frac{\partial \mathbf{v}}{\partial z} + \mathbf{u}_z \times \text{curl } \mathbf{v}\right).\end{aligned} \tag{A2.28}$$

CYLINDRICAL COORDINATES

$$x = r\cos\varphi \quad y = r\sin\varphi \quad r = (x^2 + y^2)^{\frac{1}{2}} \quad \tan\varphi = \frac{y}{x} \tag{A2.29}$$

$$\int_0^{2\pi} \sin^4\varphi\, d\varphi = 2\int_0^{2\pi} \cos^4\varphi\, d\varphi = \frac{3\pi}{4}; \quad \int_0^{2\pi} \sin^2\varphi \cos^2\varphi\, d\varphi = \frac{\pi}{4} \tag{A2.30}$$

$$\int_0^{2\pi} \sin^2\varphi\cos 2\varphi\, d\varphi = -\int_0^{2\pi} \cos^2\varphi\cos 2\varphi\, d\varphi = -\frac{\pi}{2} \tag{A2.31}$$

$$\text{Element of length } dl = (dr^2 + r^2 d\varphi^2 + dz^2)^{\frac{1}{2}}$$

$$\text{Element of volume } dV = r\, dr\, d\varphi\, dz \tag{A2.32}$$

$$\mathbf{u}_x \times \mathbf{u}_\varphi = \mathbf{u}_z \cos\varphi; \quad \mathbf{u}_y \times \mathbf{u}_\varphi = \mathbf{u}_z \sin\varphi$$

$$\mathbf{u}_x \times \mathbf{u}_r = \mathbf{u}_z \sin\varphi; \quad \mathbf{u}_y \times \mathbf{u}_r = -\mathbf{u}_z \cos\varphi \tag{A2.33}$$

$$\mathbf{u}_r = \mathbf{u}_x \cos\varphi + \mathbf{u}_y \sin\varphi; \quad \mathbf{u}_\varphi = -\mathbf{u}_x \sin\varphi + \mathbf{u}_y \cos\varphi \tag{A2.34}$$

$$\mathbf{u}_x = \mathbf{u}_r \cos\varphi - \mathbf{u}_\varphi \sin\varphi; \quad \mathbf{u}_y = \mathbf{u}_r \sin\varphi + \mathbf{u}_\varphi \cos\varphi \tag{A2.35}$$

$$\mathbf{a}\cdot\mathbf{b} = a_r b_r + a_\varphi b_\varphi + a_z b_z \tag{A2.36}$$

$$\mathbf{a}\times\mathbf{b} = (a_\varphi b_z - a_z b_\varphi)\mathbf{u}_r + (a_z b_r - a_r b_z)\mathbf{u}_\varphi + (a_r b_\varphi - a_\varphi b_r)\mathbf{u}_z \tag{A2.37}$$

$$\mathbf{u}_r \times \mathbf{u}_\varphi = \mathbf{u}_z; \quad \mathbf{u}_\varphi \times \mathbf{u}_z = \mathbf{u}_r; \quad \mathbf{u}_z \times \mathbf{u}_r = \mathbf{u}_\varphi \tag{A2.38}$$

$$v_r = v_x \cos\varphi + v_y \sin\varphi; \quad v_\varphi = -v_x \sin\varphi + v_y \cos\varphi \tag{A2.39}$$

$$v_x = v_r \cos\varphi - v_\varphi \sin\varphi; \quad v_y = v_r \sin\varphi + v_\varphi \cos\varphi \tag{A2.40}$$

$$\frac{\partial}{\partial x} = \cos\varphi \frac{\partial}{\partial r} - \frac{\sin\varphi}{r}\frac{\partial}{\partial\varphi}; \quad \frac{\partial}{\partial y} = \sin\varphi\frac{\partial}{\partial r} + \frac{\cos\varphi}{r}\frac{\partial}{\partial\varphi} \tag{A2.41}$$

$$\frac{\partial}{\partial r} = \frac{x}{(x^2+y^2)^{\frac{1}{2}}}\frac{\partial}{\partial x} + \frac{y}{(x^2+y^2)^{\frac{1}{2}}}\frac{\partial}{\partial y}; \quad \frac{\partial}{\partial\varphi} = x\frac{\partial}{\partial y} - y\frac{\partial}{\partial x} \tag{A2.42}$$

$$\frac{\partial \mathbf{v}}{\partial r} = \frac{\partial v_r}{\partial r}\mathbf{u}_r + \frac{\partial v_\varphi}{\partial r}\mathbf{u}_\varphi + \frac{\partial v_z}{\partial r}\mathbf{u}_z \tag{A2.43}$$

$$\frac{\partial \mathbf{v}}{\partial \varphi} = (\mathbf{u}_z \times \mathbf{v}) + \frac{\partial v_r}{\partial \varphi}\mathbf{u}_r + \frac{\partial v_\varphi}{\partial \varphi}\mathbf{u}_\varphi + \frac{\partial v_z}{\partial \varphi}\mathbf{u}_z \tag{A2.44}$$

$$\frac{\partial \mathbf{v}}{\partial z} = \frac{\partial v_r}{\partial z}\mathbf{u}_r + \frac{\partial v_\varphi}{\partial z}\mathbf{u}_\varphi + \frac{\partial v_z}{\partial z}\mathbf{u}_z \tag{A2.45}$$

$$\frac{\partial \mathbf{u}_r}{\partial \varphi} = \mathbf{u}_\varphi; \quad \frac{\partial \mathbf{u}_\varphi}{\partial \varphi} = -\mathbf{u}_r;$$

$$\frac{\partial \mathbf{u}_r}{\partial r} = \frac{\partial \mathbf{u}_r}{\partial z} = \frac{\partial \mathbf{u}_\varphi}{\partial r} = \frac{\partial \mathbf{u}_\varphi}{\partial z} = \frac{\partial \mathbf{u}_z}{\partial r} = \frac{\partial \mathbf{u}_z}{\partial \varphi} = \frac{\partial \mathbf{u}_z}{\partial z} = 0 \tag{A2.46}$$

$$\text{grad}\, f = \frac{\partial f}{\partial r}\mathbf{u}_r + \frac{1}{r}\frac{\partial f}{\partial \varphi}\mathbf{u}_\varphi + \frac{\partial f}{\partial z}\mathbf{u}_z \tag{A2.47}$$

$$\text{div}\, \mathbf{v} = \frac{1}{r}\frac{\partial}{\partial r}(r v_r) + \frac{1}{r}\frac{\partial v_\varphi}{\partial \varphi} + \frac{\partial v_z}{\partial z} = \frac{\partial v_r}{\partial r} + \frac{v_r}{r} + \frac{1}{r}\frac{\partial v_\varphi}{\partial \varphi} + \frac{\partial v_z}{\partial z} \tag{A2.48}$$

$$\text{curl}\, \mathbf{v} = \left(\frac{1}{r}\frac{\partial v_z}{\partial \varphi} - \frac{\partial v_\varphi}{\partial z}\right)\mathbf{u}_r + \left(\frac{\partial v_r}{\partial z} - \frac{\partial v_z}{\partial r}\right)\mathbf{u}_\varphi + \left(\frac{1}{r}\frac{\partial}{\partial r}(r v_\varphi) - \frac{1}{r}\frac{\partial v_r}{\partial \varphi}\right)\mathbf{u}_z \tag{A2.49}$$

$$\text{div}\, \mathbf{u}_r = \frac{1}{r}; \quad \text{div}\, \mathbf{u}_\varphi = \text{div}\, \mathbf{u}_z = 0 \tag{A2.50}$$

$$\text{curl}\, \mathbf{u}_\varphi = \frac{\mathbf{u}_z}{r}; \quad \text{curl}\, \mathbf{u}_r = \text{curl}\, \mathbf{u}_z = 0; \quad \text{curl}\, (\mathbf{u}_z \times \mathbf{r}) = 2\mathbf{u}_z \tag{A2.51}$$

$$\text{div}\, (\mathbf{u}_r \times \mathbf{v}) = -\mathbf{u}_r \cdot \text{curl}\, \mathbf{v};$$

$$\operatorname{div}(\mathbf{u}_\varphi \times \mathbf{v}) = \frac{v_z}{r} - \mathbf{u}_\varphi \cdot \operatorname{curl} \mathbf{v}; \quad \operatorname{div}(\mathbf{u}_z \times \mathbf{v}) = -\mathbf{u}_z \cdot \operatorname{curl} \mathbf{v} \tag{A2.52}$$

$$\operatorname{curl}(\mathbf{u}_r \times \mathbf{v}) = \mathbf{u}_r \operatorname{div} \mathbf{v} - \frac{\partial \mathbf{v}}{\partial r} - \frac{\mathbf{v}_m}{r} \text{ (where } \mathbf{v}_m = v_r \mathbf{u}_r + v_z \mathbf{u}_z) \tag{A2.53}$$

$$\operatorname{curl}(\mathbf{u}_\varphi \times \mathbf{v}) = -\mathbf{u}_r \frac{v_\varphi}{r} + \mathbf{u}_\varphi \operatorname{div} \mathbf{v} - \frac{1}{r}\frac{\partial \mathbf{v}}{\partial \varphi} \tag{A2.54}$$

$$\operatorname{curl}(\mathbf{u}_z \times \mathbf{v}) = \mathbf{u}_z \operatorname{div} \mathbf{v} - \frac{\partial \mathbf{v}}{\partial z} \tag{A2.55}$$

$$\operatorname{grad}[\sin m\varphi f(r,z)] = \sin m\varphi \operatorname{grad} f + \cos m\varphi \frac{mf}{r}\mathbf{u}_\varphi \tag{A2.56}$$

$$\operatorname{div}[\sin m\varphi \mathbf{v}(r,z)] = \sin m\varphi \operatorname{div} \mathbf{v} + \cos m\varphi \frac{m v_\varphi}{r}$$

$$\operatorname{div}[\sin m\varphi g(r,z)\mathbf{u}_\varphi] = m \cos m\varphi \frac{g}{r} \tag{A2.57}$$

$$\operatorname{curl}[\sin m\varphi \mathbf{v}(r,z)] = \sin m\varphi \operatorname{curl} \mathbf{v} + \cos m\varphi \frac{m(\mathbf{u}_\varphi \times \mathbf{v})}{r} \tag{A2.58}$$

$$\operatorname{curl}[\sin m\varphi g(r,z)\mathbf{u}_\varphi] = \sin m\varphi \left(\operatorname{grad} g \times \mathbf{u}_\varphi + \frac{g}{r}\mathbf{u}_z\right)$$

$$= \sin m\varphi \frac{\operatorname{grad}(gr) \times \mathbf{u}_\varphi}{r} \tag{A2.59}$$

$$\nabla^2 f = \frac{1}{r}\frac{\partial}{\partial r}\left(r\frac{\partial f}{\partial r}\right) + \frac{1}{r^2}\frac{\partial^2 f}{\partial \varphi^2} + \frac{\partial^2 f}{\partial z^2} = \frac{\partial^2 f}{\partial r^2} + \frac{1}{r}\frac{\partial f}{\partial r} + \frac{1}{r^2}\frac{\partial^2 f}{\partial \varphi^2} + \frac{\partial^2 f}{\partial z^2} \tag{A2.60}$$

$$\nabla^2 \mathbf{v} = \left(\nabla^2 v_r - \frac{v_r}{r^2} - \frac{2}{r^2}\frac{\partial v_\varphi}{\partial \varphi}\right)\mathbf{u}_r$$

$$+ \left(\nabla^2 v_\varphi - \frac{v_\varphi}{r^2} + \frac{2}{r^2}\frac{\partial v_r}{\partial \varphi}\right)\mathbf{u}_\varphi + (\nabla^2 v_z)\mathbf{u}_z \tag{A2.61}$$

$$\operatorname{grad}\operatorname{div} \mathbf{v} = \left(\frac{\partial^2 v_r}{\partial r^2} + \frac{\partial^2 v_z}{\partial r \partial z} + \frac{1}{r}\frac{\partial^2 v_\varphi}{\partial r \partial \varphi} + \frac{1}{r}\frac{\partial v_r}{\partial r} - \frac{1}{r^2}\frac{\partial v_\varphi}{\partial \varphi} - \frac{v_r}{r^2}\right)\mathbf{u}_r$$

$$+ \left(\frac{1}{r}\frac{\partial^2 v_z}{\partial \varphi \partial z} + \frac{1}{r^2}\frac{\partial^2 v_\varphi}{\partial \varphi^2} + \frac{1}{r}\frac{\partial^2 v_r}{\partial r \partial \varphi} + \frac{1}{r^2}\frac{\partial v_r}{\partial \varphi}\right)\mathbf{u}_\varphi$$

$$+ \left(\frac{\partial^2 v_z}{\partial z^2} + \frac{1}{r}\frac{\partial^2 v_\varphi}{\partial \varphi \partial z} + \frac{\partial^2 v_r}{\partial r \partial z} + \frac{1}{r}\frac{\partial v_r}{\partial z}\right)\mathbf{u}_z \tag{A2.62}$$

$$\operatorname{curl}\operatorname{curl} \mathbf{v} = \left(-\frac{1}{r^2}\frac{\partial^2 v_r}{\partial \varphi^2} - \frac{\partial^2 v_r}{\partial z^2} + \frac{\partial^2 v_z}{\partial r \partial z} + \frac{1}{r}\frac{\partial^2 v_\varphi}{\partial r \partial \varphi} + \frac{1}{r^2}\frac{\partial v_\varphi}{\partial \varphi}\right)\mathbf{u}_r$$

$$+ \left(-\frac{\partial^2 v_\varphi}{\partial z^2} + \frac{1}{r}\frac{\partial^2 v_z}{\partial \varphi \partial z} - \frac{\partial^2 v_\varphi}{\partial r^2} - \frac{1}{r}\frac{\partial v_\varphi}{\partial r} + \frac{v_\varphi}{r^2} - \frac{1}{r^2}\frac{\partial v_r}{\partial \varphi} + \frac{1}{r}\frac{\partial^2 v_r}{\partial \varphi \partial r}\right)\mathbf{u}_\varphi$$

$$+ \left(-\frac{\partial^2 v_z}{\partial r^2} - \frac{1}{r^2}\frac{\partial^2 v_z}{\partial \varphi^2} + \frac{\partial^2 v_r}{\partial r \partial z} + \frac{1}{r}\frac{\partial^2 v_\varphi}{\partial \varphi \partial z} + \frac{1}{r}\frac{\partial v_r}{\partial z} - \frac{1}{r}\frac{\partial v_z}{\partial r}\right)\mathbf{u}_z \tag{A2.63}$$

$$\nabla^2[\sin m\varphi\, f(r,z)] = \sin m\varphi \left(\frac{\partial^2 f}{\partial r^2} + \frac{1}{r}\frac{\partial f}{\partial r} + \frac{\partial^2 f}{\partial z^2} - \frac{m^2}{r^2} f\right)$$
$$= \sin m\varphi \left[\nabla^2 f - \frac{m^2}{r^2} f\right] \tag{A2.64}$$

$$\nabla^2[\sin m\varphi\, \mathbf{v}(r,z)] = \sin m\varphi \left[\nabla^2 \mathbf{v} - \frac{m^2}{r^2}\mathbf{v} + \frac{2m}{r^2}\cos m\varphi(\mathbf{u}_z \times \mathbf{v})\right] \tag{A2.65}$$

$$\text{grad div}\,[\sin m\varphi\, \mathbf{v}(r,z)] = \sin m\varphi \left[\text{grad div}\,\mathbf{v} - \frac{m^2}{r^2}\mathbf{v}_\varphi\right]$$
$$+ \frac{m\cos m\varphi}{r}\left[\mathbf{u}_\varphi \text{div}\,\mathbf{v} + (\mathbf{u}_\varphi \times \text{curl}\,\mathbf{v}) - \frac{2v_\varphi}{r}\mathbf{u}_r\right] \tag{A2.66}$$

$$\text{curl curl}\,[\sin m\varphi\, \mathbf{v}(r,z)] = \sin m\varphi \left(\text{curl curl}\,\mathbf{v} + \frac{m^2}{r^2}\mathbf{v}_m\right)$$
$$+ \frac{m\cos m\varphi}{r}\left[\mathbf{u}_\varphi\ \text{div}\,\mathbf{v} + (\mathbf{u}_\varphi \times \text{curl}\,\mathbf{v}) - \frac{2v_r}{r}\mathbf{u}_\varphi\right] \tag{A2.67}$$

where $\mathbf{v}_\varphi = v_\varphi \mathbf{u}_\varphi$ and $\mathbf{v}_m = \mathbf{v} - \mathbf{v}_\varphi$ = projection on the meridian plane.

$$\nabla^2\left[\sin m\varphi\, g(r,z)\mathbf{u}_\varphi\right] = -\frac{2mg}{r^2}\cos m\varphi\, \mathbf{u}_r + \sin m\varphi \left(\nabla^2 g - \frac{m^2+1}{r^2} g\right)\mathbf{u}_\varphi \tag{A2.68}$$

$$\text{grad div}\left[\sin m\varphi\, g(r,z)\mathbf{u}_\varphi\right] = \frac{m\cos m\varphi}{r}\left[\left(\frac{\partial g}{\partial r} - \frac{g}{r}\right)\mathbf{u}_r + \frac{\partial g}{\partial z}\mathbf{u}_z\right] - \frac{m^2 g}{r^2}\sin m\varphi\, \mathbf{u}_\varphi \tag{A2.69}$$

$$\text{curl curl}\,[\sin m\varphi\, g(r,z)\mathbf{u}_\varphi] = \frac{m\cos m\varphi}{r}\left[\left(\frac{\partial g}{\partial r} + \frac{g}{r}\right)\mathbf{u}_r + \frac{\partial g}{\partial z}\mathbf{u}_z\right]$$
$$-\left(\frac{\partial^2 g}{\partial r^2} + \frac{1}{r}\frac{\partial g}{\partial r} + \frac{\partial^2 g}{\partial z^2} - \frac{g}{r^2}\right)\sin m\varphi\, \mathbf{u}_\varphi. \tag{A2.70}$$

Equations (A2.56) to (A2.59) and (A2.64) to (A2.70) are still valid when $\sin m\varphi$ is replaced with $\cos m\varphi$, and $\cos m\varphi$ with $-\sin m\varphi$.

SPHERICAL COORDINATES

$$x = R\sin\theta\cos\varphi; \quad y = R\sin\theta\sin\varphi; \quad z = R\cos\theta; \quad r = R\sin\theta \tag{A2.71}$$

$$R = (x^2 + y^2 + z^2)^{\frac{1}{2}}; \quad \tan\theta = (x^2 + y^2)^{\frac{1}{2}}/z; \quad \tan\varphi = \frac{y}{x} \tag{A2.72}$$

$$\int_0^\pi \sin\theta\cos^2\theta\, d\theta = \frac{2}{3} \qquad \int_0^\pi \sin^2\theta\cos^2\theta\, d\theta = \frac{\pi}{8}$$
$$\int_0^\pi \sin^3\theta\, d\theta = \frac{4}{3} \qquad \int_0^\pi \sin^3\theta\cos^2\theta\, d\theta = \frac{4}{15} \tag{A2.73}$$

$$\text{Element of length } dl = (dR^2 + R^2 d\theta^2 + R^2 \sin^2\theta d\varphi^2)^{\frac{1}{2}}$$

$$\text{Element of solid angle } d\Omega = \sin\theta\, d\theta\, d\varphi$$

$$\text{Area of spherical annulus } dS = 2\pi R^2 \sin\theta\, d\theta$$

$$\text{Element of volume } dV = R^2 dR \sin\theta\, d\theta\, d\varphi \tag{A2.74}$$

$$\mathbf{u}_R \times \mathbf{u}_\theta = \mathbf{u}_\varphi; \quad \mathbf{u}_\varphi \times \mathbf{u}_R = \mathbf{u}_\theta; \quad \mathbf{u}_\theta \times \mathbf{u}_\varphi = \mathbf{u}_R \tag{A2.75}$$

$$\mathbf{u}_R \times \mathbf{u}_x = \cos\theta\cos\varphi\,\mathbf{u}_\varphi + \sin\varphi\,\mathbf{u}_\theta; \quad \mathbf{u}_R \times \mathbf{u}_z = -\sin\theta\,\mathbf{u}_\varphi$$

$$\mathbf{u}_R \times \mathbf{u}_y = \cos\theta\sin\varphi\,\mathbf{u}_\varphi - \cos\varphi\,\mathbf{u}_\theta; \quad \mathbf{u}_\theta \times \mathbf{u}_x = -\sin\varphi\,\mathbf{u}_R - \sin\theta\cos\varphi\,\mathbf{u}_\varphi$$

$$\mathbf{u}_\theta \times \mathbf{u}_y = \cos\varphi\,\mathbf{u}_R - \sin\theta\sin\varphi\,\mathbf{u}_\varphi; \quad \mathbf{u}_\theta \times \mathbf{u}_z = -\cos\theta\,\mathbf{u}_\varphi$$

$$\mathbf{u}_\varphi \times \mathbf{u}_x = -\cos\theta\cos\varphi\,\mathbf{u}_R + \sin\theta\cos\varphi\,\mathbf{u}_\theta; \quad \mathbf{u}_\varphi \times \mathbf{u}_z = \cos\theta\,\mathbf{u}_\theta$$

$$\mathbf{u}_\varphi \times \mathbf{u}_y = \sin\theta\sin\varphi\,\mathbf{u}_\theta - \cos\theta\sin\varphi\,\mathbf{u}_R \tag{A2.76}$$

$$\mathbf{u}_R = \mathbf{u}_x\sin\theta\cos\varphi + \mathbf{u}_y\sin\theta\sin\varphi + \mathbf{u}_z\cos\theta; \quad \mathbf{u}_\varphi = -\mathbf{u}_x\sin\varphi + \mathbf{u}_y\cos\varphi$$

$$\mathbf{u}_\theta = \mathbf{u}_x\cos\theta\cos\varphi + \mathbf{u}_y\cos\theta\sin\varphi - \mathbf{u}_z\sin\theta \tag{A2.77}$$

$$\mathbf{u}_x = \mathbf{u}_R\sin\theta\cos\varphi + \mathbf{u}_\theta\cos\theta\cos\varphi - \mathbf{u}_\varphi\sin\varphi; \quad \mathbf{u}_z = \mathbf{u}_R\cos\theta - \mathbf{u}_\theta\sin\theta$$

$$\mathbf{u}_y = \mathbf{u}_R\sin\theta\sin\varphi + \mathbf{u}_\theta\cos\theta\sin\varphi + \mathbf{u}_\varphi\cos\varphi \tag{A2.78}$$

$$\mathbf{u}_R = \mathbf{u}_r\sin\theta + \mathbf{u}_z\cos\theta; \quad \mathbf{u}_\theta = \mathbf{u}_r\cos\theta - \mathbf{u}_z\sin\theta \tag{A2.79}$$

$$\mathbf{u}_r = \mathbf{u}_R\sin\theta + \mathbf{u}_\theta\cos\theta; \quad \mathbf{u}_z = \mathbf{u}_R\cos\theta - \mathbf{u}_\theta\sin\theta \tag{A2.80}$$

$$\mathbf{a}\cdot\mathbf{b} = a_R b_R + a_\varphi b_\varphi + a_\theta b_\theta \tag{A2.81}$$

$$\mathbf{a}\times\mathbf{b} = (a_\theta b_\varphi - a_\varphi b_\theta)\mathbf{u}_R + (a_\varphi b_R - a_R b_\varphi)\mathbf{u}_\theta + (a_R b_\theta - a_\theta b_R)\mathbf{u}_\varphi \tag{A2.82}$$

$$v_R = \sin\theta\cos\varphi\, v_x + \sin\varphi\sin\theta\, v_y + \cos\theta\, v_z; \quad v_\varphi = -\sin\varphi\, v_x + \cos\varphi\, v_y$$

$$v_\theta = \cos\theta\cos\varphi\, v_x + \cos\theta\sin\varphi\, v_y - \sin\theta\, v_z \tag{A2.83}$$

$$v_x = \sin\theta\cos\varphi\, v_R - \sin\varphi\, v_\varphi + \cos\theta\cos\varphi\, v_\theta; \quad v_z = \cos\theta\, v_R - \sin\theta\, v_\theta$$

$$v_y = \sin\theta\sin\varphi\, v_R + \cos\varphi\, v_\varphi + \cos\theta\sin\varphi\, v_\theta \tag{A2.84}$$

$$\frac{\partial}{\partial x} = \sin\theta\cos\varphi\frac{\partial}{\partial R} + \frac{\cos\theta\cos\varphi}{R}\frac{\partial}{\partial\theta} - \frac{\sin\varphi}{R\sin\theta}\frac{\partial}{\partial\varphi}$$

$$\frac{\partial}{\partial y} = \sin\theta\sin\varphi\frac{\partial}{\partial R} + \frac{\cos\theta\sin\varphi}{R}\frac{\partial}{\partial\theta} + \frac{\cos\varphi}{R\sin\theta}\frac{\partial}{\partial\varphi}$$

$$\frac{\partial}{\partial z} = \cos\theta\frac{\partial}{\partial R} - \frac{\sin\theta}{R}\frac{\partial}{\partial\theta} \tag{A2.85}$$

$$\frac{\partial}{\partial R} = \frac{x}{(x^2+y^2+z^2)^{\frac{1}{2}}}\frac{\partial}{\partial x} + \frac{y}{(x^2+y^2+z^2)^{\frac{1}{2}}}\frac{\partial}{\partial y} + \frac{z}{(x^2+y^2+z^2)^{\frac{1}{2}}}\frac{\partial}{\partial z}$$

$$\frac{\partial}{\partial\theta} = \frac{xz}{(x^2+y^2)^{\frac{1}{2}}}\frac{\partial}{\partial x} + \frac{yz}{(x^2+y^2)^{\frac{1}{2}}}\frac{\partial}{\partial y} - (x^2+y^2)^{\frac{1}{2}}\frac{\partial}{\partial z}$$

$$\frac{\partial}{\partial\varphi} = x\frac{\partial}{\partial y} - y\frac{\partial}{\partial x} \tag{A2.86}$$

$$\frac{\partial \mathbf{v}}{\partial R} = \frac{\partial v_R}{\partial R}\mathbf{u}_R + \frac{\partial v_\theta}{\partial R}\mathbf{u}_\theta + \frac{\partial v_\varphi}{\partial R}\mathbf{u}_\varphi$$

$$\frac{\partial \mathbf{v}}{\partial \theta} = (\mathbf{u}_\varphi \times \mathbf{v}) + \frac{\partial v_R}{\partial \theta}\mathbf{u}_R + \frac{\partial v_\theta}{\partial \theta}\mathbf{u}_\theta + \frac{\partial v_\varphi}{\partial \theta}\mathbf{u}_\varphi$$

$$\frac{\partial \mathbf{v}}{\partial \varphi} = \frac{\partial v_R}{\partial \varphi}\mathbf{u}_R + \frac{\partial v_\theta}{\partial \varphi}\mathbf{u}_\theta + \frac{\partial v_\varphi}{\partial \varphi}\mathbf{u}_\varphi + (\mathbf{u}_z \times \mathbf{v}) \tag{A2.87}$$

$$\frac{\partial \mathbf{u}_R}{\partial \varphi} = \sin\theta\,\mathbf{u}_\varphi; \quad \frac{\partial \mathbf{u}_R}{\partial \theta} = \mathbf{u}_\theta; \quad \frac{\partial \mathbf{u}_\theta}{\partial \theta} = -\mathbf{u}_R; \quad \frac{\partial \mathbf{u}_\theta}{\partial \varphi} = \cos\theta\,\mathbf{u}_\varphi$$

$$\frac{\partial \mathbf{u}_\varphi}{\partial \varphi} = -\mathbf{u}_R\sin\theta - \mathbf{u}_\theta\cos\theta; \quad \frac{\partial \mathbf{u}_R}{\partial R} = \frac{\partial \mathbf{u}_\theta}{\partial R} = \frac{\partial \mathbf{u}_\varphi}{\partial R} = \frac{\partial \mathbf{u}_\varphi}{\partial \theta} = 0 \tag{A2.88}$$

$$\operatorname{grad} f = \frac{\partial f}{\partial R}\mathbf{u}_R + \frac{1}{R}\frac{\partial f}{\partial \theta}\mathbf{u}_\theta + \frac{1}{R\sin\theta}\frac{\partial f}{\partial \varphi}\mathbf{u}_\varphi \tag{A2.89}$$

$$\begin{aligned}\operatorname{div}\mathbf{v} &= \frac{1}{R^2}\frac{\partial}{\partial R}(R^2 v_R) + \frac{1}{R\sin\theta}\frac{\partial}{\partial \theta}(\sin\theta\, v_\theta) + \frac{1}{R\sin\theta}\frac{\partial v_\varphi}{\partial \varphi} \\ &= \frac{\partial v_R}{\partial r} + \frac{2v_R}{R} + \frac{1}{R}\frac{\partial v_\theta}{\partial \theta} + \frac{v_\theta}{R\tan\theta} + \frac{1}{R\sin\theta}\frac{\partial v_\varphi}{\partial \varphi}\end{aligned} \tag{A2.90}$$

$$\begin{aligned}\operatorname{curl}\mathbf{v} &= \frac{1}{R\sin\theta}\left[\frac{\partial}{\partial \theta}(\sin\theta\, v_\varphi) - \frac{\partial v_\theta}{\partial \varphi}\right]\mathbf{u}_R + \frac{1}{R}\left[\frac{1}{\sin\theta}\frac{\partial v_R}{\partial \varphi} - \frac{\partial}{\partial R}(R v_\varphi)\right]\mathbf{u}_\theta \\ &+ \frac{1}{R}\left[\frac{\partial}{\partial R}(R v_\theta) - \frac{\partial v_R}{\partial \theta}\right]\mathbf{u}_\varphi = \left(\frac{1}{R}\frac{\partial v_\varphi}{\partial \theta} + \frac{v_\varphi}{R\tan\theta} - \frac{1}{R\sin\theta}\frac{\partial v_\theta}{\partial \varphi}\right)\mathbf{u}_R \\ &+ \left(\frac{1}{R\sin\theta}\frac{\partial v_R}{\partial \varphi} - \frac{\partial v_\varphi}{\partial R} - \frac{v_\varphi}{R}\right)\mathbf{u}_\theta + \left(\frac{\partial v_\theta}{\partial R} + \frac{v_\theta}{R} - \frac{1}{R}\frac{\partial v_R}{\partial \theta}\right)\mathbf{u}_\varphi\end{aligned} \tag{A2.91}$$

$$\operatorname{div}\mathbf{u}_R = \frac{2}{R}; \quad \operatorname{div}\mathbf{u}_\varphi = 0; \quad \operatorname{div}\mathbf{u}_\theta = \frac{1}{R\tan\theta} \tag{A2.92}$$

$$\operatorname{curl}\mathbf{u}_R = 0; \quad \operatorname{curl}\mathbf{u}_\varphi = \frac{\mathbf{u}_R}{R\tan\theta} - \frac{\mathbf{u}_\theta}{R}; \quad \operatorname{curl}\mathbf{u}_\theta = \frac{\mathbf{u}_\varphi}{R} \tag{A2.93}$$

$$\operatorname{div}(\mathbf{u}_R \times \mathbf{v}) = -\mathbf{u}_R \cdot \operatorname{curl}\mathbf{v}; \quad \operatorname{div}(\mathbf{u}_\varphi \times \mathbf{v}) = \frac{v_R}{R\tan\theta} - \frac{v_\theta}{R} - \mathbf{u}_\varphi \cdot \operatorname{curl}\mathbf{v}$$

$$\operatorname{div}(\mathbf{u}_\theta \times \mathbf{v}) = \frac{v_\varphi}{R} - \mathbf{u}_\theta \cdot \operatorname{curl}\mathbf{v} \tag{A2.94}$$

$$\operatorname{curl}(\mathbf{u}_R \times \mathbf{v}) = \mathbf{u}_R \operatorname{div}\mathbf{v} - \frac{\mathbf{v}}{R} - \frac{\mathbf{v}_R}{R} - \frac{\partial \mathbf{v}}{\partial R} \tag{A2.95}$$

$$\operatorname{curl}(\mathbf{u}_\theta \times \mathbf{v}) = \mathbf{u}_\theta \operatorname{div}\mathbf{v} - \frac{\mathbf{v}_m}{R\tan\theta} - \frac{v_\theta}{R}\mathbf{u}_R - \frac{1}{R}\frac{\partial \mathbf{v}}{\partial \theta}(\mathbf{v}_m = v_R\mathbf{u}_R + v_\theta\mathbf{u}_\theta) \tag{A2.96}$$

$$\begin{aligned}\operatorname{curl}(\mathbf{u}_\varphi \times \mathbf{v}) &= \mathbf{u}_\varphi \operatorname{div}\mathbf{v} - \frac{v_\varphi}{R}\mathbf{u}_R - \frac{v_\varphi}{R\tan\theta}\mathbf{u}_\theta - \frac{1}{R\sin\theta}\frac{\partial \mathbf{v}}{\partial \varphi} \\ &= -\frac{1}{R\sin\theta}\frac{\partial v_R}{\partial \varphi}\mathbf{u}_R - \frac{1}{R\sin\theta}\frac{\partial v_\theta}{\partial \varphi}\mathbf{u}_\theta \\ &+ \left(\frac{\partial v_R}{\partial R} + \frac{v_R}{R} + \frac{1}{R}\frac{\partial v_\theta}{\partial \theta}\right)\mathbf{u}_\varphi\end{aligned} \tag{A2.97}$$

$$\nabla^2 f = \frac{1}{R^2}\frac{\partial}{\partial R}\left(R^2\frac{\partial f}{\partial R}\right) + \frac{1}{R^2\sin\theta}\frac{\partial}{\partial\theta}\left(\sin\theta\frac{\partial f}{\partial\theta}\right) + \frac{1}{R^2\sin^2\theta}\frac{\partial^2 f}{\partial\varphi^2}$$
$$= \frac{\partial^2 f}{\partial R^2} + \frac{2}{R}\frac{\partial f}{\partial R} + \frac{1}{R^2}\frac{\partial^2 f}{\partial\theta^2} + \frac{1}{R^2\tan\theta}\frac{\partial f}{\partial\theta} + \frac{1}{R^2\sin^2\theta}\frac{\partial^2 f}{\partial\varphi^2} \tag{A2.98}$$

$$\nabla^2\mathbf{v} = \left(\nabla^2 v_R - \frac{2v_R}{R^2} - \frac{2\cot\theta}{R^2}v_\theta - \frac{2}{R^2}\frac{\partial v_\theta}{\partial\theta} - \frac{2}{R^2\sin\theta}\frac{\partial v_\varphi}{\partial\varphi}\right)\mathbf{u}_R$$
$$+ \left(\nabla^2 v_\theta + \frac{2}{R^2}\frac{\partial v_R}{\partial\theta} - \frac{v_\theta}{R^2\sin^2\theta} - \frac{2\cos\theta}{R^2\sin^2\theta}\frac{\partial v_\varphi}{\partial\varphi}\right)\mathbf{u}_\theta$$
$$+ \left(\nabla^2 v_\varphi + \frac{2}{R^2\sin\theta}\frac{\partial v_R}{\partial\varphi} - \frac{1}{R^2\sin^2\theta}v_\varphi + \frac{2\cos\theta}{R^2\sin^2\theta}\frac{\partial v_\theta}{\partial\varphi}\right)\mathbf{u}_\varphi \tag{A2.99}$$

$$\text{grad div }\mathbf{v} = \left(\frac{\partial^2 v_R}{\partial R^2} + \frac{2}{R}\frac{\partial v_R}{\partial R} - \frac{2v_R}{R^2} - \frac{v_\theta}{R^2\tan\theta} + \frac{1}{R\tan\theta}\frac{\partial v_\theta}{\partial R} + \frac{1}{R}\frac{\partial^2 v_\theta}{\partial\theta\partial R}\right.$$
$$\left. - \frac{1}{R^2}\frac{\partial v_\theta}{\partial\theta} + \frac{1}{R\sin\theta}\frac{\partial^2 v_\varphi}{\partial\varphi\partial R} - \frac{1}{R^2\sin\theta}\frac{\partial v_\varphi}{\partial\varphi}\right)\mathbf{u}_R$$
$$+ \left(\frac{1}{R}\frac{\partial^2 v_R}{\partial R\partial\theta} + \frac{2}{R^2}\frac{\partial v_R}{\partial\theta} - \frac{v_\theta}{R^2\sin^2\theta} + \frac{1}{R^2\tan\theta}\frac{\partial v_\theta}{\partial\theta} + \frac{1}{R^2}\frac{\partial^2 v_\theta}{\partial\theta^2}\right.$$
$$\left. + \frac{1}{R^2\sin\theta}\frac{\partial^2 v_\varphi}{\partial\varphi\partial\theta} - \frac{\cos\theta}{R^2\sin^2\theta}\frac{\partial v_\varphi}{\partial\varphi}\right)\mathbf{u}_\theta$$
$$+ \left(\frac{1}{R\sin\theta}\frac{\partial^2 v_R}{\partial R\partial\varphi} + \frac{2}{R^2\sin\theta}\frac{\partial v_R}{\partial\varphi} + \frac{\cos\theta}{R^2\sin^2\theta}\frac{\partial v_\theta}{\partial\varphi}\right.$$
$$\left. + \frac{1}{R^2\sin\theta}\frac{\partial^2 v_\varphi}{\partial\varphi\partial\theta} + \frac{1}{R^2\sin^2\theta}\frac{\partial^2 v_\varphi}{\partial\varphi^2}\right)\mathbf{u}_\varphi \tag{A2.100}$$

$$\text{curl curl }\mathbf{v} = \left(\frac{1}{R}\frac{\partial^2 v_\theta}{\partial R\partial\theta} + \frac{1}{R^2}\frac{\partial v_\theta}{\partial\theta} - \frac{1}{R^2}\frac{\partial^2 v_R}{\partial\theta^2} + \frac{1}{R\tan\theta}\frac{\partial v_\theta}{\partial R} + \frac{1}{R\tan\theta}\frac{v_\theta}{R}\right.$$
$$\left. - \frac{1}{R^2\tan\theta}\frac{\partial v_R}{\partial\theta} - \frac{1}{R^2\sin^2\theta}\frac{\partial^2 v_R}{\partial\varphi^2} + \frac{1}{R\sin\theta}\frac{\partial^2 v_\varphi}{\partial R\partial\varphi} + \frac{1}{R^2\sin\theta}\frac{\partial v_\varphi}{\partial\varphi}\right)\mathbf{u}_R$$
$$+ \left(\frac{1}{R^2\sin^2\theta}\frac{\partial^2 v_\varphi}{\partial\varphi\partial\theta} + \frac{\cos\theta}{R^2\sin^2\theta}\frac{\partial v_\varphi}{\partial\varphi} - \frac{1}{R^2\sin^2\theta}\frac{\partial^2 v_\theta}{\partial\varphi^2} - \frac{2}{R}\frac{\partial v_\theta}{\partial R}\right.$$
$$\left. + \frac{1}{R}\frac{\partial^2 v_R}{\partial R\partial\theta} - \frac{\partial^2 v_\theta}{\partial R^2}\right)\mathbf{u}_\theta + \left(\frac{1}{R\sin\theta}\frac{\partial^2 v_R}{\partial\varphi\partial R} - \frac{2}{R}\frac{\partial v_\varphi}{\partial R} - \frac{1}{R^2}\frac{\partial^2 v_\varphi}{\partial\theta^2}\right.$$
$$\left. - \frac{\partial^2 v_\varphi}{\partial R^2} - \frac{1}{R^2\tan\theta}\frac{\partial v_\varphi}{\partial\theta} + \frac{v_\varphi}{R^2\sin^2\theta} + \frac{1}{R^2\sin^2\theta}\frac{\partial^2 v_\theta}{\partial\theta\partial\varphi}\right.$$
$$\left. - \frac{\cos\theta}{R^2\sin^2\theta}\frac{\partial v_\theta}{\partial\varphi}\right)\mathbf{u}_\varphi. \tag{A2.101}$$

ELLIPTIC COORDINATES

$$x = c\cosh u\cos v = c\mu\nu; \quad y = c\sinh u\sin v = c\sqrt{\mu^2-1}\sqrt{1-\nu^2} \tag{A2.102}$$

$$h_u = h_v = c\sqrt{\cosh^2 u - \cos^2 v} = c\sqrt{\frac{\text{ch2u} - \cos 2\text{v}}{2}}$$

$$h_\mu = c\sqrt{\frac{\mu^2-\nu^2}{\mu^2-1}}; \quad h_\nu = c\sqrt{\frac{\mu^2-\nu^2}{1-\nu^2}}. \tag{A2.103}$$

The curves $\mu = \text{const.}$ ($u = \text{const.}$) are ellipses.

At large distances ($\mu \to \infty$), they degenerate into circles of radius $c\mu = ce^u$.

The $(-c, +c)$ segment corresponds with $\mu = 1$ ($u = 0$) (Fig. 5.21).

Half-major axis of the ellipse: $a = c\mu = c\cosh u_0$

Half-minor axis of the ellipse: $b = c\sqrt{\mu^2-1} = c\sinh u_0$ (A2.104)

$$\text{Eccentricity} = \frac{c}{a} = \frac{1}{\cosh u_0} \tag{A2.105}$$

Radius of curvature: (b^2/a) at $x = a$; $\quad (a^2/b)$ at $y = b$ (A2.106)

$$\begin{aligned}\text{grad}\, f &= \frac{1}{c\sqrt{\cosh^2 u - \cos^2 v}}\frac{\partial f}{\partial u}\mathbf{u}_u + \frac{1}{c\sqrt{\cosh^2 u - \cos^2 v}}\frac{\partial f}{\partial v}\mathbf{u}_v \\ &= \frac{1}{c}\sqrt{\frac{\mu^2-1}{\mu^2-\nu^2}}\frac{\partial f}{\partial \mu}\mathbf{u}_\mu + \frac{1}{c}\sqrt{\frac{1-\nu^2}{\mu^2-\nu^2}}\frac{\partial f}{\partial \nu}\mathbf{u}_\nu\end{aligned} \tag{A2.107}$$

$$\begin{aligned}\text{div}\,\mathbf{v} &= \frac{1}{c(\cosh^2 u - \cos^2 v)}\frac{\partial}{\partial u}\left(\sqrt{\cosh^2 u - \cos^2 v}\, v_u\right) \\ &\quad + \frac{1}{c(\cosh^2 u - \cos^2 v)}\frac{\partial}{\partial v}\left(\sqrt{\cosh^2 u - \cos^2 v}\, v_v\right) \\ &= \frac{\sqrt{(\mu^2-1)(1-\nu^2)}}{c(\mu^2-\nu^2)}\left[\frac{\partial}{\partial \mu}\left(\sqrt{\frac{\mu^2-\nu^2}{1-\nu^2}}v_\mu\right) + \frac{\partial}{\partial \nu}\left(\sqrt{\frac{\mu^2-\nu^2}{\mu^2-1}}v_\nu\right)\right]\end{aligned} \tag{A2.108}$$

$$\begin{aligned}\nabla^2 f &= \frac{1}{c^2(\cosh^2 u - \cos^2 v)}\left[\frac{\partial^2 f}{\partial u^2} + \frac{\partial^2 f}{\partial v^2}\right] \\ &= \frac{\sqrt{(\mu^2-1)(1-\nu^2)}}{c^2(\mu^2-\nu^2)}\left[\frac{\partial}{\partial \mu}\left(\sqrt{\frac{\mu^2-1}{1-\nu^2}}\frac{\partial f}{\partial \mu}\right) + \frac{\partial}{\partial \nu}\left(\sqrt{\frac{1-\nu^2}{\mu^2-1}}\frac{\partial f}{\partial \nu}\right)\right]\end{aligned} \tag{A2.109}$$

$$\text{curl}\,(f\mathbf{u}_z) = \frac{1}{c\sqrt{\cosh^2 u - \cos^2 v}}\left(\frac{\partial f}{\partial v}\mathbf{u}_u - \frac{\partial f}{\partial u}\mathbf{u}_v\right)$$

$$\text{with } \mathbf{u}_z = \mathbf{u}_u \times \mathbf{u}_v$$

$$\text{curl}\,(f\mathbf{u}_z) = \frac{1}{c\sqrt{\mu^2-\nu^2}}\left(\sqrt{1-\nu^2}\frac{\partial f}{\partial \nu}\mathbf{u}_\mu - \sqrt{\mu^2-1}\frac{\partial f}{\partial \mu}\mathbf{u}_\nu\right)\mathbf{u}_z$$

$$\text{with } \mathbf{u}_z = \mathbf{u}_\mu \times \mathbf{u}_\nu \tag{A2.110}$$

$$\text{curl}\,(f_u\mathbf{u}_u + f_v\mathbf{u}_v) = \frac{1}{c(\cosh^2 u - \cos^2 v)}$$

$$\left[\frac{\partial}{\partial u}\left(\sqrt{\cosh^2 u - \cos^2 v}f_v\right) - \frac{\partial}{\partial v}\left(\sqrt{\cosh^2 u - \cos^2 v}f_\mu\right)\right]\mathbf{u}_z$$

$$\text{curl}\,(f_\mu\mathbf{u}_\mu + f_\nu\mathbf{u}_\nu) = \frac{1}{c(\mu^2-\nu^2)}$$

$$\left[\sqrt{\mu^2-1}\frac{\partial}{\partial \mu}\left(\sqrt{\mu^2-\nu^2}v_\nu\right) - \sqrt{1-\nu^2}\frac{\partial}{\partial \nu}\left(\sqrt{\mu^2-\nu^2}v_\mu\right)\right]\mathbf{u}_z. \tag{A2.111}$$

The unit vector $\mathbf{u}_a$ is directed to increasing a, hence $\mathbf{u}_u$ and $\mathbf{u}_\mu$ are perpendicular to the ellipse and $(\mathbf{u}_v, \mathbf{u}_\nu)$ tangent to the latter.

SPHEROIDAL COORDINATES

Prolate Coordinates

$$x = c\sqrt{\mu^2-1}\sqrt{1-\nu^2}\cos\varphi; \quad y = c\sqrt{\mu^2-1}\sqrt{1-\nu^2}\sin\varphi; \quad z = c\mu\nu$$

$$r = c\sqrt{\mu^2-1}\sqrt{1-\nu^2}. \tag{A2.112}$$

The z-axis is the rotation axis of the spheroid (also in oblate coordinates)

$$h_\mu = c\frac{\sqrt{\mu^2-\nu^2}}{\mu^2-1}; \quad h_\nu = c\sqrt{\frac{\mu^2-\nu^2}{1-\nu^2}}; \quad h_\varphi = c\sqrt{(\mu^2-1)(1-\nu^2)} \tag{A2.113}$$

$$\text{grad}\, f = \frac{1}{c}\sqrt{\frac{\mu^2-1}{\mu^2-\nu^2}}\frac{\partial f}{\partial \mu}\mathbf{u}_\mu + \frac{1}{c}\sqrt{\frac{1-\nu^2}{\mu^2-\nu^2}}\frac{\partial f}{\partial \nu}\mathbf{u}_\nu + \frac{1}{c\sqrt{(\mu^2-1)(1-\nu^2)}}\frac{\partial f}{\partial \varphi}\mathbf{u}_\varphi \tag{A2.114}$$

$$\text{div}\,\mathbf{v} = \frac{1}{c(\mu^2-\nu^2)}\left[\frac{\partial}{\partial \mu}\sqrt{(\mu^2-\nu^2)(\mu^2-1)}v_\mu\right.$$

$$\left. + \frac{\partial}{\partial \nu}\sqrt{(\mu^2-\nu^2)(1-\nu^2)})v_\nu + \frac{1}{\sqrt{(\mu^2-1)(1-\nu^2)}}\frac{\partial v_\varphi}{\partial \varphi}\right] \tag{A2.115}$$

$$\operatorname{curl}\mathbf{v} = \frac{1}{c}\left[\frac{1}{\sqrt{\mu^2-\nu^2}}\frac{\partial}{\partial\nu}(\sqrt{1-\nu^2}v_\varphi) - \frac{1}{\sqrt{(\mu^2-1)(1-\nu^2)}}\frac{\partial v_\nu}{\partial\varphi}\right]\mathbf{u}_\mu$$
$$+\ \frac{1}{c}\left[\frac{1}{\sqrt{(\mu^2-1)(1-\nu^2)}}\frac{\partial v_\mu}{\partial\varphi} - \frac{1}{\sqrt{\mu^2-\nu^2}}\frac{\partial}{\partial\mu}\left(\sqrt{\mu^2-1}v_\varphi\right)\right]\mathbf{u}_\nu$$
$$+\ \frac{1}{c(\mu^2-\nu^2)}\left[\sqrt{\mu^2-1}\frac{\partial}{\partial\mu}(\sqrt{\mu^2-\nu^2}v_\nu) - \sqrt{1-\nu^2}\frac{\partial}{\partial\nu}\left(\sqrt{\mu^2-\nu^2}v_\mu\right)\right]\mathbf{u}_\varphi \tag{A2.116}$$

$$\nabla^2 f = \frac{1}{c^2(\mu^2-\nu^2)}\left\{\frac{\partial}{\partial\mu}\left[(\mu^2-1)\frac{\partial f}{\partial\mu}\right]\right.$$
$$\left.+\ \frac{\partial}{\partial\nu}\left[(1-\nu^2)\frac{\partial f}{\partial\nu}\right] + \frac{1}{(\mu^2-1)(1-\nu^2)}\frac{\partial^2 f}{\partial\varphi^2}\right\}. \tag{A2.117}$$

Oblate Coordinates

$$x = c\mu\nu\cos\varphi; \quad y = c\mu\nu\sin\varphi; \quad z = c\sqrt{(\mu^2-1)(1-\nu^2)}$$
$$r = c\mu\nu \tag{A2.118}$$

$$h_\mu = c\sqrt{\frac{\mu^2-\nu^2}{\mu^2-1}}; \quad h_\nu = c\sqrt{\frac{\mu^2-\nu^2}{1-\nu^2}}; \quad h_\varphi = c\mu\nu \tag{A2.119}$$

$$\operatorname{grad} f = \frac{1}{c}\sqrt{\frac{\mu^2-1}{\mu^2-\nu^2}}\frac{\partial f}{\partial\mu}\mathbf{u}_\mu + \frac{1}{c}\sqrt{\frac{1-\nu^2}{\mu^2-\nu^2}}\frac{\partial f}{\partial\nu}\mathbf{u}_\nu + \frac{1}{c\mu\nu}\frac{\partial f}{\partial\varphi}\mathbf{u}_\varphi \tag{A2.120}$$

$$\operatorname{div}\mathbf{v} = \frac{1}{c}\frac{\sqrt{\mu^2-1}}{\mu(\mu^2-\nu^2)}\frac{\partial}{\partial\mu}\left(\mu\sqrt{\mu^2-\nu^2}f_\mu\right)$$
$$+\ \frac{\sqrt{1-\nu^2}}{c\nu(\mu^2-\nu^2)}\frac{\partial}{\partial\nu}\left(\nu\sqrt{\mu^2-\nu^2}f_\nu\right) + \frac{1}{c\mu\nu}\frac{\partial f_\varphi}{\partial\varphi} \tag{A2.121}$$

$$\operatorname{curl}\mathbf{v} = \frac{1}{c}\left[\frac{\sqrt{1-\nu^2}}{\nu\sqrt{\mu^2-\nu^2}}\frac{\partial}{\partial\nu}(\nu v_\varphi) - \frac{1}{\mu\nu}\frac{\partial v_\nu}{\partial\varphi}\right]\mathbf{u}_\mu$$
$$+\ \frac{1}{c}\left[\frac{1}{\mu\nu}\frac{\partial v_\mu}{\partial\varphi} - \frac{\sqrt{\mu^2-1}}{\mu\sqrt{\mu^2-\nu^2}}\frac{\partial}{\partial\mu}(\mu v_\varphi)\right]\mathbf{u}_\nu$$
$$+\ \frac{1}{c(\mu^2-\nu^2)}\left[\sqrt{\mu^2-1}\frac{\partial}{\partial\mu}\left(\sqrt{\mu^2-1}v_\nu\right) - \sqrt{1-\nu^2}\frac{\partial}{\partial\nu}(\sqrt{1-\nu^2}v_\mu)\right]\mathbf{u}_\varphi \tag{A2.122}$$

$$\nabla^2 f = \frac{\sqrt{\mu^2-1}}{c^2\mu(\mu^2-\nu^2)}\frac{\partial}{\partial\mu}\left(\mu\sqrt{\mu^2-1}\frac{\partial f}{\partial\mu}\right)$$
$$+\ \frac{\sqrt{1-\nu^2}}{c^2\nu(\mu^2-\nu^2)}\frac{\partial}{\partial\nu}\left(\nu\sqrt{1-\nu^2}\frac{\partial f}{\partial\nu}\right) + \frac{1}{c^2\mu^2\nu^2}\frac{\partial^2 f}{\partial\varphi^2}. \tag{A2.123}$$

RELATIONSHIPS IN GENERAL COORDINATE SYSTEMS

Let $v_1(x, y, z)$, $v_2(x, y, z)$, $v_3(x, y, z)$ be a system of orthogonal curvilinear coordinates and dv_1, dv_2, dv_3 small increments of these coordinates. As coordinate v_i is increased to $v_i + dv_i$, we proceed to a new point of space situated at a distance $h_i dv_i$ from the initial one. The *metrical coefficient*s h_i is given by

$$h_i^2 = \left(\frac{\partial x}{\partial v_i}\right)^2 + \left(\frac{\partial y}{\partial v_i}\right)^2 + \left(\frac{\partial z}{\partial v_i}\right)^2. \tag{A2.124}$$

The elementary volume bounded by coordinate surfaces has the value $dV = h_1 h_2 h_3\, dv_1 dv_2 dv_3$. The magnitude of the displacement resulting from increases dv_1, dv_2, dv_3 is

$$dl = (h_1^2 dv_1^2 + h_2^2 dv_2^2 + h_3^2 dv_3^2)^{\frac{1}{2}}. \tag{A2.125}$$

If $\mathbf{u}_i$ is the unit vector along a coordinate line v_i (along which the other two coordinates are constant), and if $\mathbf{u}_i$ is directed toward increasing v_i, then:

$$\text{grad}\, f = \frac{1}{h_1}\frac{\partial f}{\partial v_1}\mathbf{u}_1 + \frac{1}{h_2}\frac{\partial f}{\partial v_2}\mathbf{u}_2 + \frac{1}{h_3}\frac{\partial f}{\partial v_3}\mathbf{u}_3 \tag{A2.126}$$

$$\text{div}\, \mathbf{v} = \frac{1}{h_1 h_2 h_3}\left[\frac{\partial}{\partial v_1}(h_2 h_3 v_1) + \frac{\partial}{\partial v_2}(h_3 h_1 v_2) + \frac{\partial}{\partial v_3}(h_1 h_2 v_3)\right] \tag{A2.127}$$

$$\begin{aligned}\text{curl}\, \mathbf{v} = {} & \frac{1}{h_2 h_3}\left[\frac{\partial}{\partial v_2}(h_3 v_3) - \frac{\partial}{\partial v_3}(h_2 v_2)\right]\mathbf{u}_1 + \frac{1}{h_3 h_1}\left[\frac{\partial}{\partial v_3}(h_1 v_1) - \frac{\partial}{\partial v_1}(h_3 v_3)\right]\mathbf{u}_2 \\ & + \frac{1}{h_1 h_2}\left[\frac{\partial}{\partial v_1}(h_2 v_2) - \frac{\partial}{\partial v_2}(h_1 v_1)\right]\mathbf{u}_3\end{aligned} \tag{A2.128}$$

$$\nabla^2 f = \frac{1}{h_1 h_2 h_3}\left[\frac{\partial}{\partial v_1}\left(\frac{h_2 h_3}{h_1}\frac{\partial f}{\partial v_1}\right) + \frac{\partial}{\partial v_2}\left(\frac{h_3 h_1}{h_2}\frac{\partial f}{\partial v_2}\right) + \frac{\partial}{\partial v_3}\left(\frac{h_1 h_2}{h_3}\frac{\partial f}{\partial v_3}\right)\right]. \tag{A2.129}$$

Additional formulas for a large number of coordinate systems can be found in P. Moon and D.E. Spencer, '*Field Theory Handbook*', Springer-Verlag, Berlin, 1961.

RELATIONSHIPS INVOLVING THE DISTANCE BETWEEN TWO POINTS

In the formulas given below, D denotes the distance

$$D = |\mathbf{r} - \mathbf{r}_0| = [(x - x_0)^2 + (y - y_0)^2 + (z - z_0)^2]^{\frac{1}{2}}$$

and $\mathbf{u}_D$ the unit vector

$$(x - x_0/D)\mathbf{u}_x + (y - y_0/D)\mathbf{u}_y + (z - z_0)/D)\mathbf{u}_z$$

in the direction joining $\mathbf{r}_0$ to $\mathbf{r}$.

$$\frac{\partial D}{\partial x} = \frac{x - x_0}{D} = -\frac{\partial D}{\partial x_0}; \quad \frac{\partial D}{\partial y} = \frac{y - y_0}{D} = -\frac{\partial D}{\partial y_0}$$

$$\frac{\partial D}{\partial z} = \frac{z - z_0}{D} = -\frac{\partial D}{\partial z_0} \tag{A2.130}$$

$$\text{grad}\, f(D) = f'(D)\mathbf{u}_D = -\text{grad}_0 f(D) \tag{A2.131}$$

where the prime denotes differentiation with respect to the argument

$$\text{grad}\, D^n = nD^{n-1}\mathbf{u}_D; \quad \text{grad}\, D = \mathbf{u}_D \tag{A2.132}$$

$$\text{div}\, [f(D)\mathbf{u}_D] = \frac{2f(D)}{D} + f'(D) = -\text{div}_0 f(D)\mathbf{u}_D \tag{A2.133}$$

$$\text{div}\, (D^n\mathbf{u}_D) = (n+2)D^{n-1}; \quad \text{div}\, \mathbf{u}_D = \frac{2}{D} \tag{A2.134}$$

$$\text{curl}\, [f(D)\mathbf{u}_D] = 0 \tag{A2.135}$$

$$\nabla^2 f(D) = \frac{2f'(D)}{D} + f''(D) = \nabla_0^2 f(D); \quad \nabla^2 D^n = n(n+1)D^{n-2} \tag{A2.136}$$

$$\nabla^2 \frac{1}{D} = -4\pi\delta(\mathbf{r} - \mathbf{r}_0) \tag{A2.137}$$

$$\text{grad}\, f\left(t - \frac{D}{c}\right) = -\frac{f'(t - D/c)}{cD}\mathbf{u}_D = -\text{grad}_0 f\left(t - \frac{D}{c}\right) \tag{A2.138}$$

$$\text{grad}\, \frac{f(t - D/c)}{D} = \left[-\frac{f'(t - D/c)}{cD} + \frac{f(t - D/c)}{D^2}\right]\mathbf{u}_D$$

$$= -\text{grad}_0 \frac{f(t - D/c)}{D} \tag{A2.139}$$

$$\text{div}\, \mathbf{J}\left(t - \frac{D}{c}\right) = -\frac{1}{c}\mathbf{u}_D \cdot \mathbf{J}'\left(t - \frac{D}{c}\right) \tag{A2.140}$$

where $\mathbf{J}' = J_x'\mathbf{u}_x + J_y'\mathbf{u}_y + J_z'\mathbf{u}_z$, and primes denote differentiation with respect to the argument

$$\text{div}\, \frac{\mathbf{J}(t - D/c)}{D} = -\left[\frac{\mathbf{J}(t - D/c)}{D^2} + \frac{\mathbf{J}'(t - D/c)}{cD}\right] \cdot \mathbf{u}_D \tag{A2.141}$$

$$\text{curl}\, \mathbf{J}\left(t - \frac{D}{c}\right) = -\frac{1}{c}\mathbf{u}_D \times \mathbf{J}'\left(t - \frac{D}{c}\right) \tag{A2.142}$$

$$\text{curl}\, \frac{\mathbf{J}(t - D/c)}{D} = -\frac{1}{D^2}\mathbf{u}_D \times \mathbf{J}\left(t - \frac{D}{c}\right) - \frac{1}{cD}\mathbf{u}_D \times \mathbf{J}'\left(t - \frac{D}{c}\right) \tag{A2.143}$$

$$\nabla^2 f\left(t - \frac{D}{c}\right) = -\frac{2}{cD} f'\left(t - \frac{D}{c}\right) + \frac{f''(t - D/c)}{c^2} \tag{A2.144}$$

$$\nabla^2 \mathbf{J}\left(t - \frac{D}{c}\right) = -\frac{2}{cD}\mathbf{J}'\left(t - \frac{D}{c}\right) + \frac{\mathbf{J}''(t - D/c)}{c^2} \tag{A2.145}$$

$$\nabla^2 \frac{\mathbf{J}(t - D/c)}{D} = \frac{\mathbf{J}''(t - D/c)}{c^2 D} \tag{A2.146}$$

$$\text{grad}\ \frac{e^{-jkD}}{D} = -\left(\frac{1}{D} + jk\right)\frac{e^{-jkD}}{D}\mathbf{u}_D \tag{A2.147}$$

$$\text{div}\left(\frac{e^{-jkD}}{D}\mathbf{u}\right) = \left(\frac{1}{D} - jk\right)\frac{e^{-jkD}}{D} \tag{A2.148}$$

$$(\nabla^2 + k^2)\frac{e^{-jkD}}{D} = -4\pi\delta(\mathbf{r} - \mathbf{r}_0). \tag{A2.149}$$

When $\mathbf{a}$ is a constant vector:

$$\text{div}\ (D\mathbf{a}) = \mathbf{u}_D \cdot \mathbf{a}; \quad \text{curl}(D\mathbf{a}) = \mathbf{u}_D \times \mathbf{a}; \quad \text{grad}\ (D\mathbf{u}_D \cdot \mathbf{a}) = \mathbf{a}$$
$$(\mathbf{a} \cdot \text{grad})D = \mathbf{a} \cdot \mathbf{u}_D; \quad \text{curl}\ (\mathbf{a} \times D\mathbf{u}_D) = 2\mathbf{a}. \tag{A2.150}$$

When $\mathbf{a}$ and $\mathbf{b}$ are constant:

$$\mathbf{a} \cdot \text{grad}\left(\mathbf{b} \cdot \text{grad}\ \frac{1}{D}\right) = \frac{3(\mathbf{a} \cdot \mathbf{u}_D) \cdot (\mathbf{b} \cdot \mathbf{u}_D) - (\mathbf{a} \cdot \mathbf{b})}{D^3}. \tag{A2.151}$$

Appendix 3

Vector Analysis on a Surface

CURVILINEAR COORDINATES ON A SURFACE

Let v_1 and v_2 be two parameters that fix the position of a point on a surface. The surface is open or closed, but is assumed to have no singularities. Curves along which one of the parameters remains constant are called *parametric curves*. An increase dv_1, dv_2 in the value of the coordinates results in a displacement of magnitude

$$dl^2 = E_{11}dv_1^2 + 2E_{12}dv_1dv_2 + E_{22}dv_2^2. \tag{A3.1}$$

The quantities E_{11}, E_{12}, E_{22} are the *fundamental magnitudes of the first order*. The parametric curves form an orthogonal system if and only if E_{12} is equal to zero. The expression $E_{11}E_{22} - E_{12}^2$ will be denoted by H^2. Explicit values for E_{11}, E_{12}, E_{22} are

$$E_{11} = \frac{\partial \mathbf{r}}{\partial v_1}\cdot\frac{\partial \mathbf{r}}{\partial v_1}; \quad E_{12} = \frac{\partial \mathbf{r}}{\partial v_1}\cdot\frac{\partial \mathbf{r}}{\partial v_2}; \quad E_{22} = \frac{\partial \mathbf{r}}{\partial v_2}\cdot\frac{\partial \mathbf{r}}{\partial v_2}, \tag{A3.2}$$

where $\mathbf{r}$ is the position vector of a point on the surface. For an orthogonal system (Fig. A3.1*a*)

$$E_{11} = h_1^2; \quad E_{22} = h_2^2; \quad H = h_1h_2; \quad \frac{\partial \mathbf{r}}{\partial v_1} = h_1\mathbf{u}_1; \quad \frac{\partial \mathbf{r}}{\partial v_2} = h_2\mathbf{u}_2, \tag{A3.3}$$

where $\mathbf{u}_i$ is directed toward increasing v_i. The two *fundamental magnitudes of the second order* are

$$l_{11} = \mathbf{u}_n\cdot\frac{\partial^2 \mathbf{r}}{\partial v_1^2}; \quad l_{12} = \mathbf{u}_n\cdot\frac{\partial^2 \mathbf{r}}{\partial v_1\partial v_2}; \quad l_{22} = \mathbf{u}_n\cdot\frac{\partial^2 \mathbf{r}}{\partial v_2^2}, \tag{A3.4}$$

where $\mathbf{u}_n$, the unit vector along the normal, is defined by $(1/H)(\partial \mathbf{r}/\partial v_1) \times (\partial \mathbf{r}/\partial v_2)$. The normals at consecutive points of a surface do not, in general, intersect. At any point P, however, there are two *principal directions*, orthogonal to each other, for which the normals at consecutive points intersect the normal at P. A curve drawn on the surface, and possessing the property that the normals to the surface at consecutive points on the curve intersect, is termed a *line of curvature*. The points of intersection of consecutive normals are the centers of curvature. There are two centers of curvature at each point P. The distances from P to the centers, counted positive in the direction of $\mathbf{u}_n$, are the two *principal radii of curvature*,

Electromagnetic Fields, Second Edition, By Jean G. Van Bladel

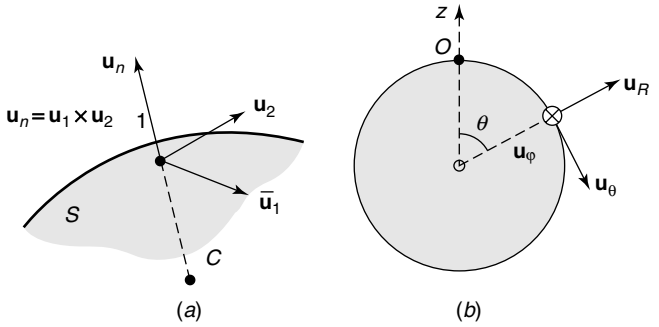

Figure A3.1 (*a*) Coordinates on a surface. (*b*) Coordinates on a spherical surface $h_1 = h_\theta = R$; $h_2 = h_\varphi = R\sin\theta$.

and their reciprocals are the *principal curvatures*. The sum of the principal curvatures is the *first curvature* J, and their product the *second (or Gauss) curvature* K. The radii are positive when n is directed to the center of curvature. On a spherical surface of radius a, $R_1 = R_2 = -a$ (Fig. A3.1*b*), $l_{11} = R$, and $l_{22} = R\sin^2\theta$.

$$J = \frac{1}{R_1} + \frac{1}{R_2} = \frac{1}{H^2}(E_{11}l_{22} - 2E_{12}l_{12} + E_{22}l_{11})$$
$$K = \frac{1}{R_1R_2} = \frac{1}{H^2}(l_{11}l_{22} - l_{12}^2). \tag{A3.5}$$

The path of shortest distance between two points P and Q is a *geodesic line*. Through each point on the surface, there passes a single geodesic line in each direction. It is often useful to choose a simple infinite family of geodesics as parametric curves $v_2 = \text{const}$. One can choose, for instance, the family of geodesics through a fixed point O called a *pole*. The orthogonal trajectories to the geodesics are the *geodesic parallels*, which can be taken as parametric curves $v_1 = \text{const}$. One can always choose v_1 so that $dl^2 = dv_1^2 + E_{22}dv_2^2$. A vector function $\mathbf{P}(v_1v_2)$ is defined by its projections:

$$\mathbf{P} = P_1\mathbf{u}_1 + P_2\mathbf{u}_2 + P_n\mathbf{u}_n = p_1h_1\mathbf{u}_1 + p_2h_2\mathbf{u}_2 + P_n\mathbf{u}_n. \tag{A3.6}$$

From now on, only orthogonal systems will be considered. Scalar and cross products are then

$$\mathbf{P}\cdot\mathbf{Q} = P_1Q_1 + P_2Q_2 + P_nQ_n \tag{A3.7}$$
$$\mathbf{P}\times\mathbf{Q} = (P_2Q_n - P_nQ_2)\mathbf{u}_1 + (P_nQ_1 - P_1Q_n)\mathbf{u}_2 + (P_1Q_2 - P_2Q_1)\mathbf{u}_n. \tag{A3.8}$$

It is often advantageous to choose orthogonal coordinates v_1, v_2 that are constant along the lines of curvature. Then

$$\frac{\partial\mathbf{u}_1}{\partial v_1} = \frac{h_1}{R_1}\mathbf{u}_n - \frac{1}{h_2}\frac{\partial h_1}{\partial v_2}\mathbf{u}_2, \quad \text{with a similar formula for } \frac{\partial\mathbf{u}_2}{\partial v_2} \tag{A3.9}$$
$$\frac{\partial^2\mathbf{r}}{\partial v_1^2} = \frac{\partial}{\partial v_1}\left(\frac{\partial\mathbf{r}}{\partial v_1}\right) = \frac{\partial}{\partial v_1}(h_1\mathbf{u}_1) = \frac{\partial h_1}{\partial v_1}\mathbf{u}_1 - \frac{h_1}{h_2}\frac{\partial h_1}{\partial v_2}\mathbf{u}_2 + \frac{h_1^2}{R_1}\mathbf{u}_n, \tag{A3.10}$$

with a similar relationship for $\partial^2\mathbf{r}/\partial v_2^2$.

$$\frac{\partial \mathbf{u}_2}{\partial v_1} = \frac{1}{h_2}\frac{\partial h_1}{\partial v_2}\mathbf{u}_1, \quad \text{with a similar formula for } \frac{\partial \mathbf{u}_1}{\partial v_2} \tag{A3.11}$$

$$\frac{\partial^2 \mathbf{r}}{\partial v_1 \partial v_2} = \frac{\partial}{\partial v_1}\left(\frac{\partial \mathbf{r}}{\partial v_2}\right) = \frac{\partial}{\partial v_1}(h_2\mathbf{u}_2) = \frac{\partial h_1}{\partial v_2}\mathbf{u}_1 + \frac{\partial h_2}{\partial v_1}\mathbf{u}_2. \tag{A3.12}$$

Relationships (A3.10) and (A3.12) imply that

$$l_{11} = \frac{h_1^2}{R_1}; \quad l_{12} = 0; \quad l_{22} = \frac{h_2^2}{R_2}. \tag{A3.13}$$

The connection between three-dimensional operators and surface operators rests on a fundamental *theorem*, due to *Dupin*, which can be enunciated as follows: An arbitrary surface S belongs to an infinity of triply orthogonal systems. One of these is formed by the surfaces parallel to S and by the two families of developable surfaces generated by the normals to S along its lines of curvature. In other words, v_1, v_2 (along the lines of curvature), and $v_3 = n$ (the distance along the normal with scale factor $h_3 = 1$) form an orthogonal system. For that system (n positive to center of curvature)

$$\frac{\partial \mathbf{u}_1}{\partial n} = \frac{\partial \mathbf{u}_2}{\partial n} = \frac{\partial \mathbf{u}_n}{\partial n} = 0 \tag{A3.14}$$

$$\frac{\partial \mathbf{r}}{\partial n} = \mathbf{u}_n; \quad \frac{\partial^2 \mathbf{r}}{\partial n^2} = 0 \tag{A3.15}$$

$$\frac{\partial h_1}{\partial n} = -\frac{h_1}{R_1}; \quad \frac{\partial h_2}{\partial n} = -\frac{h_2}{R_2}. \tag{A3.16}$$

DIFFERENTIAL OPERATORS

Let $f(v_1, v_2)$ be a scalar function of position. The gradient of f is a vector located in the tangent plane and oriented in the direction of maximum increase of f. Its magnitude is the rate of change of f per unit length. In an orthogonal system

$$\text{grad}_S f = \frac{1}{h_1}\frac{\partial f}{\partial v_1}\mathbf{u}_1 + \frac{1}{h_2}\frac{\partial f}{\partial v_2}\mathbf{u}_2. \tag{A3.17}$$

The gradient of a function is an invariant; that is, its value is independent of the choice of the (v_1, v_2) coordinates. It has the familiar properties of the three-dimensional gradient. Its projection along any direction of the tangent plane, for instance, is the rate of change of the function in that direction. Consider now a vector function of position $\mathbf{P}(v_1, v_2)$ with projection $\mathbf{P}_t$ on the tangent plane to the surface. The *surface divergence* of $\mathbf{P}$ is

$$\text{div}_S \mathbf{P} = \frac{1}{h_1 h_2}\left[\frac{\partial}{\partial v_1}(h_2 P_1) + \frac{\partial}{\partial v_2}(h_1 P_2)\right] - JP_n = \text{div}_S \mathbf{P}_t - JP_n, \tag{A3.18}$$

with

$$\text{div}_S \mathbf{P}_t = \frac{1}{h_1}\mathbf{u}_1 \cdot \frac{\partial \mathbf{P}_t}{\partial v_1} + \frac{1}{h_2}\mathbf{u}_2 \cdot \frac{\partial \mathbf{P}_t}{\partial v_2}. \tag{A3.19}$$

With the coordinates of Dupin's theorem,

$$\operatorname{div}\mathbf{P} = \operatorname{div}_S\mathbf{P} + \frac{\partial P_n}{\partial n} = \operatorname{div}_S\mathbf{P} + \mathbf{u}_n\cdot\frac{\partial \mathbf{P}}{\partial n}. \tag{A3.20}$$

The *surface curl* is defined as

$$\begin{aligned}\operatorname{curl}_S\mathbf{P} = \operatorname{grad}_S P_n \times \mathbf{u}_n + \frac{1}{h_2}\left(l_{12}\frac{P_1}{h_1} + l_{22}\frac{P_2}{h_2}\right)\mathbf{u}_1 \\ - \frac{1}{h_1}\left(l_{11}\frac{P_1}{h_1} + l_{12}\frac{P_2}{h_2}\right)\mathbf{u}_2 + \frac{1}{h_1h_2}\left[\frac{\partial}{\partial v_1}(h_2P_2) - \frac{\partial}{\partial v_2}(h_1P_1)\right]\mathbf{u}_n,\end{aligned} \tag{A3.21}$$

with

$$\operatorname{curl}_S\mathbf{P}_t = \frac{1}{h_1}\mathbf{u}_1 \times \frac{\partial \mathbf{P}_t}{\partial v_1} + \frac{1}{h_2}\mathbf{u}_2 \times \frac{\partial \mathbf{P}_t}{\partial v_2}. \tag{A3.22}$$

If the coordinates are taken along the lines of curvature,

$$\operatorname{curl}_S\mathbf{P} = \operatorname{grad}_S P_n \times \mathbf{u}_n + \frac{P_2}{R_2}\mathbf{u}_1 - \frac{P_1}{R_1}\mathbf{u}_2 + \mathbf{u}_n \operatorname{div}_S(\mathbf{P}\times\mathbf{u}_n) \tag{A3.23}$$

$$\operatorname{curl}\mathbf{P} = \operatorname{curl}_S\mathbf{P} + \mathbf{u}_n \times \frac{\partial \mathbf{P}}{\partial n}$$

$$\mathbf{u}_n \times \operatorname{curl}\mathbf{P} = \operatorname{grad}_S P_n - \frac{P_1}{R_1}\mathbf{u}_1 - \frac{P_2}{R_2}\mathbf{u}_2 - \frac{\partial P_1}{\partial n}\mathbf{u}_1 - \frac{\partial P_2}{\partial n}\mathbf{u}_2. \tag{A3.24}$$

The *surface Laplacian* of a scalar function f is defined by

$$\begin{aligned}\nabla_S^2 f &= \frac{1}{h_1h_2}\frac{\partial}{\partial v_1}\left(\frac{h_2}{h_1}\frac{\partial f}{\partial v_1}\right) + \frac{1}{h_1h_2}\frac{\partial}{\partial v_2}\left(\frac{h_1}{h_2}\frac{\partial f}{\partial v_2}\right) \\ &= \operatorname{div}_S\operatorname{grad}_S f = \nabla^2 f - \frac{\partial^2 f}{\partial n^2} + J\frac{\partial f}{\partial n}.\end{aligned} \tag{A3.25}$$

For a vector,

$$\nabla_S^2\mathbf{P} = \frac{1}{h_1h_2}\frac{\partial}{\partial v_1}\left(\frac{h_2}{h_1}\frac{\partial \mathbf{P}}{\partial v_1}\right) + \frac{1}{h_1h_2}\frac{\partial}{\partial v_2}\left(\frac{h_1}{h_2}\frac{\partial \mathbf{P}}{\partial v_2}\right). \tag{A3.26}$$

If f is a solution of Laplace's equation $\nabla_S^2 f = 0$, there is a conjugate solution g such that $\operatorname{grad}_S g = \mathbf{u}_n \times \operatorname{grad}_S f$. In geodesic polar coordinates, the equation $\nabla_S^2 f = 0$ reduces to (E_{11} being equal to 1)

$$\frac{\partial}{\partial v_1}\left(H\frac{\partial f}{\partial v_1}\right) + \frac{\partial}{\partial v_2}\left(\frac{1}{H}\frac{\partial f}{\partial v_2}\right) = 0.$$

When the pole is one of symmetry, H depends on v_1 only, and $\int (dv_1/H)$ is a solution. The following properties result from the definitions of the various operators:

$$\operatorname{grad}_S v_1 = \frac{\mathbf{u}_1}{h_1}; \quad \operatorname{grad}_S v_2 = \frac{\mathbf{u}_2}{h_2}; \quad \operatorname{grad}_S v_1 \times \operatorname{grad}_S v_2 = \frac{\mathbf{u}_n}{H} \tag{A3.27}$$

$$\operatorname{grad}_S AB = A \operatorname{grad}_S B + B \operatorname{grad}_S A \tag{A3.28}$$

$$\operatorname{grad}_S f(A) = f'(A) \operatorname{grad}_S A \tag{A3.29}$$

$$\operatorname{div}_S (A\mathbf{u}_n) = -AJ; \text{ in particular, } \operatorname{div}_S \mathbf{u}_n = -J \tag{A3.30}$$

$$\operatorname{div}_S (A\mathbf{P}) = \operatorname{grad}_S A \cdot \mathbf{P} + A \operatorname{div}_S \mathbf{P} \tag{A3.31}$$

$$\operatorname{div}_S (\mathbf{P} \times \mathbf{Q}) = \mathbf{Q} \cdot \operatorname{curl}_S \mathbf{P} - \mathbf{P} \cdot \operatorname{curl}_S \mathbf{Q} \tag{A3.32}$$

$$\operatorname{curl}_S A\mathbf{u}_n = \operatorname{grad}_S A \times \mathbf{u}_n \tag{A3.33}$$

$$\operatorname{curl}_S \mathbf{u}_n = \operatorname{curl}_S \mathbf{r} = 0 \tag{A3.34}$$

$$\operatorname{curl}_S (A\mathbf{P}) = \operatorname{grad}_S A \times \mathbf{P} + A \operatorname{curl}_S \mathbf{P} \tag{A3.35}$$

$$\operatorname{div}_S \operatorname{curl}_S A\mathbf{P} = \mathbf{P} \cdot \operatorname{curl}_S \operatorname{grad}_S A + A \operatorname{div}_S \operatorname{curl}_S \mathbf{P} \tag{A3.36}$$

$$\nabla_S^2 \mathbf{r} = J\mathbf{u}_n \tag{A3.37}$$

$$\nabla_S^2 \mathbf{u}_n = -(J^2 - 2K)\mathbf{u}_n - \operatorname{grad}_S J \tag{A3.38}$$

$$\mathbf{u}_n \cdot \operatorname{curl}_S (\mathbf{u}_n \times \operatorname{grad}_S f) = \nabla_S^2 f \tag{A3.39}$$

$$\operatorname{div}_S (\mathbf{u}_n \times \operatorname{grad}_S f) = 0 \tag{A3.40}$$

$$\mathbf{u}_n \cdot \operatorname{curl}_S \operatorname{curl}_S (f\mathbf{u}_n) = -\nabla_S^2 f \tag{A3.41}$$

$$\operatorname{curl}_S \operatorname{grad}_S f = \frac{1}{R_2 h_2} \frac{\partial f}{\partial v_2} \mathbf{u}_1 - \frac{1}{R_1 h_1} \frac{\partial f}{\partial v_1} \mathbf{u}_2 \tag{A3.42}$$

$$\operatorname{div}_S \operatorname{curl}_S \mathbf{P} = \operatorname{div}_S \left(\frac{P_2}{R_2} \mathbf{u}_1 - \frac{P_1}{R_1} \mathbf{u}_2 \right) - J \operatorname{div}_S (\mathbf{P} \times \mathbf{u}_n). \tag{A3.43}$$

In particular, $\operatorname{div}_S \operatorname{curl}_S \mathbf{P} = 0$ for a vector normal to the surface.

INTEGRAL RELATIONSHIPS

Unit vector $\mathbf{u}_m$ is in the tangent plane and perpendicular to curve c. It is drawn outward from the region enclosed by c. Unit vector $\mathbf{u}_t$ is tangent to c and equal to $\mathbf{u}_n \times \mathbf{u}_m$ (Fig. A3.2).

Gauss' Theorems

$$\int_S \operatorname{div}_S \mathbf{P} \, dS = \int_c \mathbf{P} \cdot \mathbf{u}_m \, dc - \int_S J(\mathbf{P} \cdot \mathbf{u}_n) \, dS \tag{A3.44}$$

(vanishes for a closed surface if $\mathbf{P}$ is tangential)

$$\int_S \operatorname{grad}_S f \, dS = \int_c f\mathbf{u}_m \, dc - \int_S Jf\mathbf{u}_n \, dS \tag{A3.45}$$

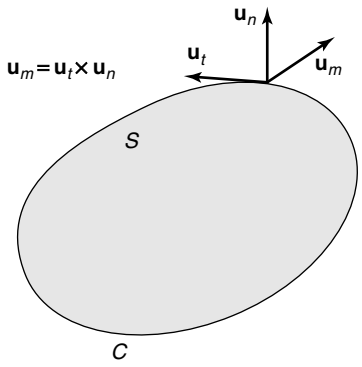

Figure A3.2 Open surface with unit vectors.

$$\int_S \text{curl}_S \, \mathbf{P} \, dS = \int_c \mathbf{u}_m \times \mathbf{P} \, dc - \int_S J(\mathbf{u}_n \times \mathbf{P}) \, dS \tag{A3.46}$$

$$\int_S \mathbf{P} \cdot \text{grad}_S f \, dS = \int_c f \mathbf{P} \cdot \mathbf{u}_m \, dc - \int_S (f \, \text{div}_S \, \mathbf{P} + Jf \mathbf{u}_n \cdot \mathbf{P}) \, dS \tag{A3.47}$$

$$\int_S \mathbf{P} \cdot \text{curl}_S \, \mathbf{Q} \, dS = \int_c \mathbf{Q} \cdot (\mathbf{P} \times \mathbf{u}_m) \, dc + \int_S (\mathbf{Q} \cdot \text{curl}_S \, \mathbf{P} - J\mathbf{Q} \times \mathbf{P} \cdot \mathbf{u}_n) \, dS. \tag{A3.48}$$

Green's Theorems

$$\int_S (A \nabla_S^2 B + \text{grad}_S \, A \cdot \text{grad}_S \, B) \, dS = \int_C A(\mathbf{u}_m \cdot \text{grad} \, B) \, dc \tag{A3.49}$$

$$\int_S (A \nabla_S^2 B - B \nabla_S^2 A) \, dS = \int_c (A \, \text{grad}_S \, B - B \, \text{grad}_S \, A) \cdot \mathbf{u}_m \, dc. \tag{A3.50}$$

In full generality, when e', f', and g' are the coefficients of an invariant quadratic differential form $e' dv_1^2 + 2f' dv_1 dv_2 + g' dv_2^2$,

$$\int_S A \frac{1}{H} \left[\frac{\partial}{\partial v_1} \left(\frac{g'}{H} \frac{\partial B}{\partial v_1} - \frac{f'}{H} \frac{\partial B}{\partial v_2} \right) + \frac{\partial}{\partial v_2} \left(\frac{e'}{H} \frac{\partial B}{\partial v_2} - \frac{f'}{H} \frac{\partial B}{\partial v_2} \right) \right] dS$$
$$+ \int_S \frac{1}{H^2} \left[\left(g' \frac{\partial A}{\partial v_1} - f' \frac{\partial A}{\partial v_2} \right) \frac{\partial B}{\partial v_1} + \left(e' \frac{\partial A}{\partial v_2} - f' \frac{\partial A}{\partial v_1} \right) \frac{\partial B}{\partial v_2} \right] dS = 0, \tag{A3.51}$$

where the integration is performed over a closed surface. The first integral can be written as $\int_S A \mathcal{L} B \, dS$, where $\mathcal{L}$ is an obvious generalization of the Laplacian operator. When the differential form is positive-definite, the relationship $\int_S A \mathcal{L} A \, dS = 0$ implies that A is constant all over the closed surface. In geodesic polar coordinates ($E_{11} = 1, E_{12} = 0$), where v_1 is the geodesic distance from the pole P, the following relationship holds:

$$f(P) = \frac{1}{2\pi} \int_c (f \, \text{grad} \log v_1 - \log v_1 \, \text{grad} \, f) \cdot \mathbf{u}_m \, dc$$
$$+ \frac{1}{2\pi} \int_S \left[(\log v_1) \nabla^2 f - f \nabla^2 (\log v_1) \right] dS, \tag{A3.52}$$

where surface S includes pole P. By use of Green's theorem (A3.50), it is possible[1] to solve the equation $\nabla^2 f = g$ by means of a Green's function, solution of

$$\nabla^2 G = \frac{1}{h_1 h_2}\delta(v_1 - v_1')\delta(v_2 - v_2') - \frac{1}{S}. \tag{A3.53}$$

The singularity of G is given by

$$\lim_{\mathbf{r}_S \to \mathbf{r}_S'} G(\mathbf{r}_S|\mathbf{r}_S') = \frac{1}{2\pi}\log_e \frac{|\mathbf{r}_S - \mathbf{r}_S'|}{L} = \frac{1}{2\pi}\log_e \frac{\rho}{L} \tag{A3.54}$$

where L is a reference length. On a unit sphere with pole in O (Fig. A3.1*b*), (ρ/L) reduces to $(a\theta/a) = \theta$.

Stokes' Theorems

$$\int_S \mathbf{u}_n \cdot \mathrm{curl}_S\, \mathbf{P}\, dS = \int_c \mathbf{P}\cdot\mathbf{u}_t\, dc = \int_c \mathbf{P}\cdot d\mathbf{c}\ (= 0 \text{ for a closed } S) \tag{A3.55}$$

$$\int_S \mathbf{u}_n \times \mathrm{grad}_S f\, dS = \int_c f\mathbf{u}_t\, dc\ (= 0 \text{ for a closed } S) \tag{A3.56}$$

$$\int_S A\mathbf{u}_n \cdot \mathrm{curl}_S\, \mathbf{P}\, dS = \int_c A\mathbf{P}\cdot\mathbf{u}_t\, dc - \int_S (\mathrm{grad}_S A \times \mathbf{P})\cdot\mathbf{u}_n\, dS \tag{A3.57}$$

$$\int_S (\mathrm{grad}_S A \times \mathrm{grad}_S B)\cdot\mathbf{u}_n\, dS = \int_c A(\mathrm{grad}_S B\cdot\mathbf{u}_t)\, dc = -\int_c B(\mathrm{grad}_S A\cdot\mathbf{u}_t)\, dc \tag{A3.58}$$

$$\int_c \mathrm{grad}_S f\cdot\mathbf{u}_t\, dc = \int_c \mathrm{grad}_S f\cdot d\mathbf{c} = 0. \tag{A3.59}$$

Conversely, if a vector point function $\mathbf{P}$ is everywhere tangent to the surface, and if $\int_c \mathbf{P}\cdot\mathbf{u}_t\, dc$ vanishes for every closed curve drawn on the surface, then $\mathbf{P}$ is the gradient of some scalar point function.

RELATIONSHIPS IN A MERIDIAN PLANE

Cylindrical coordinates (r, φ, z) are particularly suitable for configurations with boundaries of revolution. All scalar and vector functions in the following equations depend on r and z only.

$$\mathrm{grad}_M\, g = \frac{\partial g}{\partial r}\mathbf{u}_r + \frac{\partial g}{\partial z}\mathbf{u}_z \tag{A3.60}$$

$$\mathrm{div}_M\, \mathbf{P} = \frac{\partial P_r}{\partial r} + \frac{P_r}{r} + \frac{\partial P_z}{\partial z} = \frac{1}{r}\frac{\partial}{\partial r}(rP_r) + \frac{\partial P_z}{\partial z} \tag{A3.61}$$

$$\text{curl}_M \mathbf{P} = -\frac{\partial P_\varphi}{\partial z}\mathbf{u}_r + \left(\frac{\partial P_r}{\partial z} - \frac{\partial P_z}{\partial r}\right)\mathbf{u}_\varphi + \left(\frac{P_\varphi}{r} + \frac{\partial P_\varphi}{\partial r}\right)\mathbf{u}_z \tag{A3.62}$$

$$\text{curl}_M\,(g\mathbf{u}_\varphi) = \text{grad}\; g \times \mathbf{u}_\varphi + \frac{g}{r}\mathbf{u}_z = \frac{1}{r}\,\text{grad}\,(rg) \times \mathbf{u}_\varphi \tag{A3.63}$$

$$\nabla_M^2 g = \frac{\partial^2 g}{\partial r^2} + \frac{1}{r}\frac{\partial g}{\partial r} + \frac{\partial^2 g}{\partial z^2} = \text{div}_M\,\text{grad}_M\, g \tag{A3.64}$$

$$\text{curl}_M\,\text{grad}_M\, g = 0; \quad \text{div}_M\,\text{curl}_M\,\mathbf{P} = 0 \tag{A3.65}$$

$$\text{div}_M\,(\nabla_M^2 \mathbf{P}) = \nabla_M^2\,(\text{div}_M\,\mathbf{P}) \tag{A3.66}$$

$$\nabla_M^2 g = r\nabla_M^2 \frac{g}{r} + \frac{2}{r}\frac{\partial g}{\partial r} + \frac{g}{r^2} = \frac{1}{r}\nabla^2(rg) - \frac{2}{r}\frac{\partial g}{\partial r} - \frac{g}{r^2} \tag{A3.67}$$

$$\int_S \text{div}_M\,\mathbf{P} r\,dr\,dz = \int_c (\mathbf{u}_m \cdot \mathbf{P}) r\,dc \tag{A3.68}$$

$$\int_S (g\;\text{div}_M \mathbf{P} + \text{grad}_M\, g \cdot \mathbf{P}) r\,dr\,dz = \int_c g(\mathbf{u}_m \cdot \mathbf{P}) r\,dc \tag{A3.69}$$

$$\int_S (h\nabla_M^2 g + \text{grad}_M\, g \cdot \text{grad}_M\, h) r\,dr\,dz = \int_c h\frac{\partial g}{\partial m} r\,dc. \tag{A3.70}$$

(A3.71)

RELATIONSHIPS ON A SURFACE OF REVOLUTION

If the position of a point P is determined by its distance c from some origin O (taken on the generating curve C) and by its azimuth φ (Fig. A3.3),

$$\frac{\partial \mathbf{r}}{\partial c} = \mathbf{u}_c \tag{A3.72}$$

$$\frac{\partial \mathbf{r}}{\partial \varphi} = -r\mathbf{u}_\varphi \tag{A3.73}$$

$$E_{11} = 1; \quad E_{12} = 0; \quad E_{22} = r^2; \quad H = r \tag{A3.74}$$

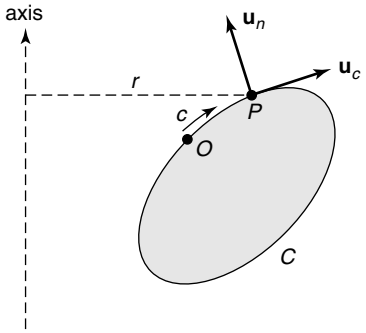

Figure A3.3 Cross section of a surface of revolution.

$$dl^2 = r^2 d\varphi^2 + dc^2 \tag{A3.75}$$

$$dS = -r\, dc\, d\varphi \tag{A3.76}$$

$$l_{11} = -\frac{1}{\rho}; \quad l_{12} = 0; \quad l_{22} = -r(\mathbf{u}_r \cdot \mathbf{u}_n); \quad J = -\frac{1}{\rho} - \frac{\mathbf{u}_r \cdot \mathbf{u}_n}{r} \tag{A3.77}$$

where ρ is the radius of curvature of the generating curve at P, counted positive if the center of curvature is on the inside normal, and negative otherwise. The projections of a vector are denoted by

$$\mathbf{P} = P_c \mathbf{u}_c + rP_\varphi \mathbf{u}_\varphi + P_n \mathbf{u}_n = p_c \mathbf{u}_c + p_\varphi \mathbf{u}_\varphi + p_n \mathbf{u}_n.$$

Formulas for differential operators are as follows:

$$\operatorname{grad}_S f = \frac{\partial f}{\partial c}\mathbf{u}_c + \frac{1}{r}\frac{\partial f}{\partial \varphi}\mathbf{u}_\varphi \tag{A3.78}$$

$$\operatorname{div}_S \mathbf{P} = \frac{1}{r}\left[\frac{\partial}{\partial c}(rP_c) + \frac{\partial}{\partial \varphi}(rP_\varphi)\right] - JP_n = \frac{\partial p_c}{\partial c} + \frac{\mathbf{p}_c \cdot \mathbf{u}_r}{r} + \frac{1}{r}\frac{\partial p_\varphi}{\partial \varphi} - Jp_n \tag{A3.79}$$

$$\begin{aligned}\operatorname{curl}_S \mathbf{P} = {} & \frac{1}{r}\left[\frac{\partial}{\partial c}(r^2 P_\varphi) - \frac{\partial P_c}{\partial \varphi}\right]\mathbf{u}_n + \left[\frac{1}{r}\frac{\partial P_n}{\partial \varphi} - P_\varphi(\mathbf{u}_r \cdot \mathbf{u}_n)\right]\mathbf{u}_c \\ & - \left(\frac{\partial P_n}{\partial c} - \frac{P_c}{\rho}\right)\mathbf{u}_\varphi\end{aligned} \tag{A3.80}$$

$$\nabla_S^2 f = \frac{\partial^2 f}{\partial c^2} + \frac{1}{r^2}\frac{\partial^2 f}{\partial \varphi^2} + \frac{1}{r}\frac{\partial f}{\partial c}(\mathbf{u}_r \cdot \mathbf{u}_c). \tag{A3.81}$$

NOTES

1. J. Van Bladel. A discussion of Helmholtz' theorem. *Electromagn.* **13**, 95–110, 1993.

The following books provide a wider background in differential geometry:

W. Blaschke and H. Reichardt, *Einführung in die Differentialgeometrie*. Springer-Verlag, Berlin, 2nd edition, 1960.

G. Darboux, *Leçons sur la théorie générale des surfaces*. Gauthiers-Villars, Paris, 1941.

L. P. Eisenhart, *A Treatise on the Differential Geometry of Curves and Surfaces*. Reprinted by Dover Publications, New York, 1960.

W. C. Graustein, *Differential Geometry*. Reprinted by Dover Publications, New York, 1966.

H. W. Guggenheimer, *Differential Geometry*. Reprinted by Dover Publications, New York, 1977.

E. Kreyszig, *Differential Geometry*. Reprinted by Dover Publications, New York, 1991.

D. J. Struik, *Lectures on Classical Differential Geometry*. Reprinted by Dover Publications, New York, 2nd edition, 1988.

C. E. Weatherburn, *Differential Geometry of Three Dimensions*. Cambridge University Press, New York, 1927.

Appendix 4

Dyadic Analysis*

DEFINITIONS

Vector $\mathbf{d}'$ is a linear vector function of vector $\mathbf{d}$ when the following relationships hold:

$$\begin{aligned} d'_x &= a_{xx}d_x + a_{xy}d_y + a_{xz}d_z \\ d'_y &= a_{yx}d_x + a_{yy}d_y + a_{yz}d_z \\ d'_z &= a_{zx}d_x + a_{zy}d_y + a_{zz}d_z. \end{aligned} \tag{A4.1}$$

These relationships can be represented in more compact form by means of the matrix notation

$$\mathbf{d}' = \overline{\overline{a}}\cdot\mathbf{d}. \tag{A4.2}$$

The matrix operator itself can be expressed in terms of dyads as

$$\begin{aligned} \overline{\overline{a}} = {} & a_{xx}\mathbf{u}_x\mathbf{u}_x + a_{xy}\mathbf{u}_x\mathbf{u}_y + a_{xz}\mathbf{u}_x\mathbf{u}_z + a_{yx}\mathbf{u}_y\mathbf{u}_x + a_{yy}\mathbf{u}_y\mathbf{u}_y \\ & + a_{yz}\mathbf{u}_y\mathbf{u}_z + a_{zx}\mathbf{u}_z\mathbf{u}_x + a_{zy}\mathbf{u}_z\mathbf{u}_y + a_{zz}\mathbf{u}_z\mathbf{u}_z \end{aligned} \tag{A4.3}$$

provided, by convention, $\mathbf{ab}\cdot\mathbf{c}$ stands for $\mathbf{a}(\mathbf{b}\cdot\mathbf{c})$. The symbol $\mathbf{ab}$ is called a *dyad*, and a sum of dyads such as $\overline{\overline{a}}$ is a *dyadic*. Also by convention, $\mathbf{c}\cdot\mathbf{ab}$ stands for $(\mathbf{c}\cdot\mathbf{a})\mathbf{b}$, so that the dot product of a dyad and a vector is now defined for $\mathbf{ab}$ acting as both a prefactor and a postfactor. The writing of $\overline{\overline{a}}$ in "nonion" form, as shown above, is rather cumbersome, and one often prefers to use the form

$$\begin{aligned} \overline{\overline{a}} = {} & (a_{xx}\mathbf{u}_x + a_{yx}\mathbf{u}_y + a_{zx}\mathbf{u}_z)\mathbf{u}_x + (a_{xy}\mathbf{u}_x + a_{yy}\mathbf{u}_y + a_{zy}\mathbf{u}_z)\mathbf{u}_y \\ & + (a_{xz}\mathbf{u}_x + a_{yz}\mathbf{u}_y + a_{zz}\mathbf{u}_z)\mathbf{u}_z = \mathbf{a}'_x\mathbf{u}_x + \mathbf{a}'_y\mathbf{u}_y + \mathbf{a}'_z\mathbf{u}_z \end{aligned} \tag{A4.4}$$

where the $\mathbf{a}'$ are the column vectors of the matrix of $\overline{\overline{a}}$. Alternatively,

$$\begin{aligned} \overline{\overline{a}} = {} & \mathbf{u}_x(a_{xx}\mathbf{u}_x + a_{xy}\mathbf{u}_y + a_{xz}\mathbf{u}_z) + \mathbf{u}_y(a_{yx}\mathbf{u}_x + a_{yy}\mathbf{u}_y + a_{yz}\mathbf{u}_z) \\ & + \mathbf{u}_z(a_{zx}\mathbf{u}_x + a_{zy}\mathbf{u}_y + a_{zz}\mathbf{u}_z) = \mathbf{u}_x\mathbf{a}_x + \mathbf{u}_y\mathbf{a}_y + \mathbf{u}_z\mathbf{a}_z, \end{aligned} \tag{A4.5}$$

*Professor Lindell has been kind enough to check this appendix, make corrections, and suggest additional formulas.

Electromagnetic Fields, Second Edition, By Jean G. Van Bladel

where the **a** are the row vectors of the matrix of $\overline{\overline{a}}$. It is obvious that $\overline{\overline{a}}\cdot\mathbf{d}$ is, in general, different from $\mathbf{d}\cdot\overline{\overline{a}}$. In other words, the order in which $\overline{\overline{a}}$ and **d** appear should be carefully respected. $\overline{\overline{a}}\cdot\mathbf{d}$ is equal to $\mathbf{d}\cdot\overline{\overline{a}}$ only when the dyadic is symmetric (i.e., when $a_{ik} = a_{ki}$). The *transpose* of $\overline{\overline{a}}$ is *a dyadic* $\overline{\overline{a}}^t$ such that $\overline{\overline{a}}\cdot\mathbf{d}$ is equal to $\mathbf{d}\cdot\overline{\overline{a}}^t$. One may easily check that the transpose is obtained by an interchange of rows and columns. More precisely,

$$\overline{\overline{a}}^t = \mathbf{a}_x\mathbf{u}_x + \mathbf{a}_y\mathbf{u}_y + \mathbf{a}_z\mathbf{u}_z = \mathbf{u}_x\mathbf{a}'_x + \mathbf{u}_y\mathbf{a}'_y + \mathbf{u}_z\mathbf{a}'_z. \tag{A4.6}$$

The *trace of the dyadic* is the sum of its diagonal terms. Thus,

$$tr\ \overline{\overline{a}} = a_{xx} + a_{yy} + a_{zz}. \tag{A4.7}$$

The trace is a scalar (i.e., it is invariant with respect to orthogonal transformations of the base vectors). The trace of **ab** is $\mathbf{a}\cdot\mathbf{b}$. Among dyadics endowed with special properties we note

1. The *unitary dyadic*, which represents a pure rotation. The determinant of its elements is equal to 1.
2. The *identity dyadic*

$$\overline{\overline{I}} = \mathbf{u}_x\mathbf{u}_x + \mathbf{u}_y\mathbf{u}_y + \mathbf{u}_z\mathbf{u}_z. \tag{A4.8}$$

Clearly,

$$\overline{\overline{I}}\cdot\mathbf{d} = \mathbf{d}\cdot\overline{\overline{I}} = \mathbf{d}. \tag{A4.9}$$

3. The *symmetric dyadic*, characterized by $a_{ik} = a_{ki}$, for which $\overline{\overline{a}}^t = \overline{\overline{a}}$. The dyadic **ab** is symmetric when $\mathbf{a}\times\mathbf{b} = 0$. Further,

$$\overline{\overline{a}}\cdot\mathbf{d} = \mathbf{d}\cdot\overline{\overline{a}}. \tag{A4.10}$$

4. The *antisymmetric dyadic*, characterized by $a_{ik} = -a_{ki}$. For such a dyadic $\overline{\overline{a}}^t = -\overline{\overline{a}}$, and

$$\overline{\overline{a}}\cdot\mathbf{d} = -\mathbf{d}\cdot\overline{\overline{a}}. \tag{A4.11}$$

The diagonal elements are zero, and there are only three distinct components. The dyadic can always be written in terms of $\overline{\overline{I}}$ and a suitable vector **b** as

$$\begin{aligned}\overline{\overline{a}} &= -b_z\mathbf{u}_x\mathbf{u}_y + b_y\mathbf{u}_x\mathbf{u}_z + b_z\mathbf{u}_y\mathbf{u}_x \\ &\quad - b_x\mathbf{u}_y\mathbf{u}_z - b_y\mathbf{u}_z\mathbf{u}_x + b_x\mathbf{u}_z\mathbf{u}_y, \\ &= \overline{\overline{I}}\times\mathbf{b},\end{aligned} \tag{A4.12}$$

where the *skew product* is the dyad

$$(\mathbf{bc})\times\mathbf{d} = \mathbf{b}(\mathbf{c}\times\mathbf{d}). \tag{A4.13}$$

The antisymmetric $\overline{\overline{a}}$ can also be expressed as

$$\overline{\overline{a}} = \mathbf{cb} - \mathbf{bc}. \tag{A4.14}$$

5. The *reflection dyadic*

$$\bar{\bar{r}}_f(\mathbf{u}) = \bar{\bar{I}} - 2\mathbf{uu}, \tag{A4.15}$$

where $\mathbf{u}$ is a (real) unit vector. Applied to the position vector $\mathbf{r}$, it performs a reflection with respect to a plane perpendicular to $\mathbf{u}$.

6. The *rotation dyadic*

$$\bar{\bar{r}}_r(\mathbf{u}) = \mathbf{uu} + \sin\theta(\mathbf{u} \times \bar{\bar{I}}) + \cos\theta(\bar{\bar{I}} - \mathbf{uu}). \tag{A4.16}$$

Applied to a vector, it performs a rotation by an angle θ in the right-hand direction around the direction of $\mathbf{u}$.

The elements of a dyadic may be complex (a case in point is the free-space dyadic discussed in Chapter 7). It then becomes useful to introduce concepts such as the *Hermitian dyadic* ($a_{ik} = a_{ki}^*$), or the *anti-Hermitian dyadic* ($a_{ik} = -a_{ki}^*$). Useful *products of dyads* are defined as follows:

$$(\mathbf{ab})\cdot(\mathbf{cd}) = \mathbf{a}(\mathbf{b}\cdot\mathbf{c})\mathbf{d} \quad \text{(the direct product, a dyad).} \tag{A4.17}$$

$$(\mathbf{ab}) : (\mathbf{cd}) = (\mathbf{a}\cdot\mathbf{c})(\mathbf{b}\cdot\mathbf{d}) \quad \text{(the double product, a scalar).} \tag{A4.18}$$

$$(\mathbf{ab}) \overset{\times}{\times} (\mathbf{cd}) = (\mathbf{a} \times \mathbf{c})(\mathbf{b} \times \mathbf{d}) \quad \text{(the double cross-product, a dyad).} \tag{A4.19}$$

$$(\mathbf{ab}) \overset{\times}{\cdot} (\mathbf{cd}) = (\mathbf{a} \times \mathbf{c})(\mathbf{b}\cdot\mathbf{d}) \quad \text{(a vector).} \tag{A4.20}$$

$$(\mathbf{ab}) \overset{\cdot}{\times} (\mathbf{cd}) = (\mathbf{a}\cdot\mathbf{c})(\mathbf{b} \times \mathbf{d}) \quad \text{(a vector).} \tag{A4.21}$$

General Multiplicative Relationships

$$(\mathbf{b}\cdot\bar{\bar{a}})\cdot\mathbf{c} = \mathbf{b}\cdot(\bar{\bar{a}}\cdot\mathbf{c}) = \mathbf{b}\cdot\bar{\bar{a}}\cdot\mathbf{c} \tag{A4.22}$$

$$(\mathbf{b} \times \mathbf{c})\cdot\bar{\bar{a}} = \mathbf{b}\cdot(\mathbf{c} \times \bar{\bar{a}}) = -\mathbf{c}\cdot(\mathbf{b} \times \bar{\bar{a}}) \tag{A4.23}$$

$$(\bar{\bar{a}} \times \mathbf{b})\cdot\mathbf{c} = \bar{\bar{a}}\cdot(\mathbf{b} \times \mathbf{c}) = -(\bar{\bar{a}} \times \mathbf{c})\cdot\mathbf{b} \quad \text{(but not } (\bar{\bar{a}}\cdot\mathbf{b}) \times \mathbf{c}) \tag{A4.24}$$

$$(\mathbf{b} \times \bar{\bar{a}})\cdot\mathbf{c} = \mathbf{b} \times (\bar{\bar{a}}\cdot\mathbf{b}) \tag{A4.25}$$

$$(\mathbf{b}\cdot\bar{\bar{a}}) \times \mathbf{c} = \mathbf{b}\cdot(\bar{\bar{a}} \times \mathbf{c}) \tag{A4.26}$$

$$(\mathbf{b} \times \bar{\bar{a}}) \times \mathbf{c} = \mathbf{b} \times (\bar{\bar{a}} \times \mathbf{c}) = \mathbf{b} \times \bar{\bar{a}} \times \mathbf{c} \tag{A4.27}$$

$$\mathbf{b} \times (\mathbf{c} \times \bar{\bar{a}}) = \mathbf{c}(\mathbf{b}\cdot\bar{\bar{a}}) - \bar{\bar{a}}(\mathbf{b}\cdot\mathbf{c}) \tag{A4.28}$$

$$(\mathbf{bc} - \mathbf{cb})\cdot\mathbf{d} = (\mathbf{c} \times \mathbf{b}) \times \mathbf{d} \tag{A4.29}$$

$$(\mathbf{c}\cdot\bar{\bar{a}})\cdot\bar{\bar{b}} = \mathbf{c}\cdot(\bar{\bar{a}}\cdot\bar{\bar{b}}) = \mathbf{c}\cdot\bar{\bar{a}}\cdot\bar{\bar{b}} \tag{A4.30}$$

$$(\bar{\bar{a}}\cdot\bar{\bar{b}})\cdot\mathbf{c} = \bar{\bar{a}}\cdot(\bar{\bar{b}}\cdot\mathbf{c}) = \bar{\bar{a}}\cdot\bar{\bar{b}}\cdot\mathbf{c} \tag{A4.31}$$

$$(\mathbf{c} \times \bar{\bar{a}})\cdot\bar{\bar{b}} = \mathbf{c} \times (\bar{\bar{a}}\cdot\bar{\bar{b}}) = \mathbf{c} \times \bar{\bar{a}}\cdot\mathbf{b} \tag{A4.32}$$

$$(\bar{\bar{a}}\cdot\bar{\bar{b}}) \times \mathbf{c} = \bar{\bar{a}}\cdot(\bar{\bar{b}} \times \mathbf{c}) = \bar{\bar{a}}\cdot\bar{\bar{b}} \times \mathbf{c} \tag{A4.33}$$

$$(\bar{\bar{a}} \times \mathbf{c})\cdot\bar{\bar{b}} = \bar{\bar{a}}\cdot(\mathbf{c} \times \bar{\bar{b}}) \tag{A4.34}$$

$$\mathbf{b}\cdot\overline{\overline{a}}\cdot\mathbf{c} = \mathbf{c}\cdot\overline{\overline{a}}^{t}\cdot\mathbf{b} \tag{A4.35}$$

$$\overline{\overline{a}}\cdot(\overline{\overline{b}}\cdot\overline{\overline{c}}) = (\overline{\overline{a}}\cdot\overline{\overline{b}})\cdot\overline{\overline{c}}. \tag{A4.36}$$

The identity dyadic satisfies the following relationships:

$$(\overline{\overline{I}}\times\mathbf{b})\cdot\mathbf{c} = \mathbf{b}\cdot(\overline{\overline{I}}\times\mathbf{c}) = \mathbf{b}\times\mathbf{c} \tag{A4.37}$$

$$(\overline{\overline{I}}\times\mathbf{b})\cdot\overline{\overline{a}} = \mathbf{b}\times\overline{\overline{a}} = (\mathbf{b}\times\overline{\overline{I}})\cdot\overline{\overline{a}} \tag{A4.38}$$

$$\overline{\overline{I}}\times(\mathbf{b}\times\mathbf{c}) = \mathbf{cb} - \mathbf{bc}. \tag{A4.39}$$

DIFFERENTIAL RELATIONSHIPS

Differentiation with Respect to a Parameter

$$\frac{d}{dt}(f\overline{\overline{a}}) = \frac{df}{dt}\overline{\overline{a}} + f\frac{d\overline{\overline{a}}}{dt} \tag{A4.40}$$

$$\frac{d}{dt}(\overline{\overline{a}}\cdot\mathbf{b}) = \frac{d\overline{\overline{a}}}{dt}\cdot\mathbf{b} + \overline{\overline{a}}\cdot\frac{d\mathbf{b}}{dt} \tag{A4.41}$$

$$\frac{d}{dt}(\overline{\overline{a}}\times\mathbf{b}) = \frac{d\overline{\overline{a}}}{dt}\times\mathbf{b} + \overline{\overline{a}}\times\frac{d\mathbf{b}}{dt} \tag{A4.42}$$

$$\frac{d}{dt}(\overline{\overline{a}}\cdot\overline{\overline{b}}) = \frac{d\overline{\overline{a}}}{dt}\cdot\overline{\overline{b}} + \overline{\overline{a}}\cdot\frac{d\overline{\overline{b}}}{dt}. \tag{A4.43}$$

Basic Differential Operators

The action of a linear operator $\mathcal{L}$ on a dyadic is defined by the formula

$$\mathcal{L}\overline{\overline{a}} = (\mathcal{L}\mathbf{a}'_x)\mathbf{u}_x + (\mathcal{L}\mathbf{a}'_y)\mathbf{u}_y + (\mathcal{L}\mathbf{a}'_z)\mathbf{u}_z. \tag{A4.44}$$

In particular,

$$\begin{aligned}\operatorname{div}\overline{\overline{a}} = \nabla\cdot\overline{\overline{a}} &= (\operatorname{div}\mathbf{a}'_x)\mathbf{u}_x + (\operatorname{div}\mathbf{a}'_y)\mathbf{u}_y + (\operatorname{div}\mathbf{a}'_z)\mathbf{u}_z \\ &= \frac{\partial\mathbf{a}_x}{\partial x} + \frac{\partial\mathbf{a}_y}{\partial y} + \frac{\partial\mathbf{a}_z}{\partial z}\end{aligned} \tag{A4.45}$$

$$\begin{aligned}\operatorname{curl}\overline{\overline{a}} = \nabla\times\overline{\overline{a}} &= (\operatorname{curl}\mathbf{a}'_x)\mathbf{u}_x + (\operatorname{curl}\mathbf{a}'_y)\mathbf{u}_y + (\operatorname{curl}\mathbf{a}'_z)\mathbf{u}_z \\ &= \mathbf{u}_x\left(\frac{\partial\mathbf{a}_z}{\partial y} - \frac{\partial\mathbf{a}_y}{\partial z}\right) + \mathbf{u}_y\left(\frac{\partial\mathbf{a}_x}{\partial z} - \frac{\partial\mathbf{a}_z}{\partial x}\right) + \mathbf{u}_z\left(\frac{\partial\mathbf{a}_y}{\partial x} - \frac{\partial\mathbf{a}_x}{\partial y}\right)\end{aligned} \tag{A4.46}$$

$$\nabla^2\overline{\overline{a}} = \frac{\partial^2\overline{\overline{a}}}{\partial x^2} + \frac{\partial^2\overline{\overline{a}}}{\partial y^2} + \frac{\partial^2\overline{\overline{a}}}{\partial z^2} = \operatorname{grad}\operatorname{div}\overline{\overline{a}} - \operatorname{curl}\operatorname{curl}\overline{\overline{a}}. \tag{A4.47}$$

Also

$$\text{grad } \mathbf{a} = \nabla \mathbf{a} = \mathbf{u}_x \frac{\partial \mathbf{a}}{\partial x} + \mathbf{u}_y \frac{\partial \mathbf{a}}{\partial y} + \mathbf{u}_z \frac{\partial \mathbf{a}}{\partial z}$$

$$= \text{grad } a_x \mathbf{u}_x + \text{grad } a_y \mathbf{u}_y + \text{grad } a_z \mathbf{u}_z \tag{A4.48}$$

$$\mathbf{a} \text{ grad} = \mathbf{a}\nabla = \mathbf{a}\mathbf{u}_x \frac{\partial}{\partial x} + \mathbf{a}\mathbf{u}_y \frac{\partial}{\partial y} + \mathbf{a}\mathbf{u}_z \frac{\partial}{\partial z}. \tag{A4.49}$$

Derived Relationships

$$\text{grad}(\mathbf{b} \times \mathbf{c}) = (\text{grad } \mathbf{b}) \times \mathbf{c} - (\text{grad } \mathbf{c}) \times \mathbf{b} \tag{A4.50}$$

$$\text{grad}(f\mathbf{b}) = (\text{grad } f)\mathbf{b} + f \text{ grad } \mathbf{b} \quad (f \text{ is any scalar function}) \tag{A4.51}$$

$$(\mathbf{b} \cdot \text{grad})\overline{\overline{a}} = b_x \frac{\partial \overline{\overline{a}}}{\partial x} + b_y \frac{\partial \overline{\overline{a}}}{\partial y} + b_z \frac{\partial \overline{\overline{a}}}{\partial z} \tag{A4.52}$$

$$d\mathbf{r} \cdot \text{grad } \mathbf{a} = d\mathbf{a} \tag{A4.53}$$

$$\text{div}(\mathbf{bc}) = (\text{div } \mathbf{b})\mathbf{c} + \mathbf{b} \cdot \text{grad } \mathbf{c} \tag{A4.54}$$

$$\text{div curl } \overline{\overline{a}} = 0 \tag{A4.55}$$

$$\text{div}(f\overline{\overline{a}}) = \text{grad } f \cdot \overline{\overline{a}} + f \text{ div } \overline{\overline{a}} \tag{A4.56}$$

$$\text{div}(\overline{\overline{a}} \cdot \mathbf{b}) = (\text{div } \overline{\overline{a}}) \cdot \mathbf{b} + tr(\overline{\overline{a}}^t \cdot \text{grad } \mathbf{b}) \tag{A4.57}$$

$$\text{div}(\mathbf{b} \times \overline{\overline{a}}) = (\text{curl } \mathbf{b}) \cdot \overline{\overline{a}} - \mathbf{b} \cdot \text{curl } \overline{\overline{a}} \tag{A4.58}$$

$$\text{div}(\mathbf{bc} - \mathbf{cb}) = \text{curl } (\mathbf{c} \times \mathbf{b}) \tag{A4.59}$$

$$\text{div}(f\overline{\overline{I}}) = \text{grad } f \tag{A4.60}$$

$$\text{div}(\overline{\overline{I}} \times \mathbf{a}) = \text{curl } \mathbf{a} \tag{A4.61}$$

$$\text{curl}(\mathbf{bc}) = (\text{curl } \mathbf{b})\mathbf{c} - \mathbf{b} \times \text{grad } \mathbf{c} \tag{A4.62}$$

$$\text{curl grad } \mathbf{a} = 0 \tag{A4.63}$$

$$\text{curl}(f\overline{\overline{a}}) = \text{grad } f \times \overline{\overline{a}} + f \text{ curl } \overline{\overline{a}} \tag{A4.64}$$

$$\text{curl}(f\overline{\overline{I}}) = \text{grad } f \times \overline{\overline{I}} \tag{A4.65}$$

$$\text{curl}(\overline{\overline{a}} \times \mathbf{b}) = \text{curl } \overline{\overline{a}} \times \mathbf{b} - \text{grad } \mathbf{b} \overset{\times}{\times} \overline{\overline{a}} \tag{A4.66}$$

$$\text{curl curl}(f\overline{\overline{I}}) = \text{curl}(\text{grad } f \times \overline{\overline{I}}) = \text{grad grad } f - \overline{\overline{I}} \nabla^2 f. \tag{A4.67}$$

INTEGRAL RELATIONSHIPS

The integral relationships of vector analysis have their equivalent in dyadic analysis. The most important examples are

$$\int_M^N \mathbf{dc} \cdot \text{grad } \mathbf{a} = \mathbf{a}(N) - \mathbf{a}(M) \tag{A4.68}$$

$$\int_c \mathbf{dc}\,\mathbf{a} = \int_S \mathbf{u}_n \times \text{grad}\,\mathbf{a}\,dS, \tag{A4.69}$$

where the contour is described in the positive sense with respect to $\mathbf{u}_n$.

$$\int_c d\mathbf{c}\cdot\overline{\overline{a}} = \int_S \mathbf{u}_n\cdot\text{curl}\,\overline{\overline{a}}\,dS \tag{A4.70}$$

$$\int_V \text{grad}\,\mathbf{a}\,dV = \int_S \mathbf{u}_n\mathbf{a}\,dS \tag{A4.71}$$

$$\int_V \text{div}\,\overline{\overline{a}}\,dV = \int_S \mathbf{u}_n\cdot\overline{\overline{a}}\,dS \tag{A4.72}$$

$$\int_V \text{curl}\,\overline{\overline{a}}\,dV = \int_S \mathbf{u}_n\times\overline{\overline{a}}\,dS \tag{A4.73}$$

$$\int_V \left[\mathbf{b}\cdot\text{grad div}\,\overline{\overline{a}} - (\text{grad div}\,\mathbf{b})\cdot\overline{\overline{a}}\right]dV = \int_S \left[(\mathbf{u}_n\cdot\mathbf{b})\,\text{div}\,\overline{\overline{a}} - \text{div}\,\mathbf{b}(\mathbf{u}_n\cdot\overline{\overline{a}})\right]dS \tag{A4.74}$$

$$\begin{aligned}\int_V \left[(\text{curl curl}\,\mathbf{b})\cdot\overline{\overline{a}} - \mathbf{b}\cdot\text{curl curl}\,\overline{\overline{a}}\right]dV &= \int_S \left[(\mathbf{u}_n\times\mathbf{b})\cdot\text{curl}\,\overline{\overline{a}} + (\mathbf{u}_n\times\text{curl}\,\mathbf{b})\cdot\overline{\overline{a}}\right]dS \\ &= \int_S \left[\mathbf{u}_n\cdot(\mathbf{b}\times\text{curl}\,\overline{\overline{a}}) + \mathbf{u}_n\cdot(\text{curl}\,\mathbf{b}\times\overline{\overline{a}})\right]dS\end{aligned} \tag{A4.75}$$

$$\begin{aligned}\int_V \left[\mathbf{b}\cdot\nabla^2\overline{\overline{a}} - (\nabla^2\mathbf{b})\cdot\overline{\overline{a}}\right]dV = \int_S \big[&(\mathbf{u}_n\cdot\mathbf{b})\,\text{div}\,\overline{\overline{a}} - \text{div}\,\mathbf{b}(\mathbf{u}_n\cdot\overline{\overline{a}}) \\ &+ \mathbf{u}_n\cdot(\mathbf{b}\times\text{curl}\,\overline{\overline{a}}) + \mathbf{u}_n\cdot(\text{curl}\,\mathbf{b}\times\overline{\overline{a}})\big]\,dS\end{aligned} \tag{A4.76}$$

$$\int_V (\mathbf{a}\nabla^2 f - f\nabla^2\mathbf{a})\,dV = \int_S \mathbf{u}_n\cdot(\text{grad}\,f\,\mathbf{a} - f\,\text{grad}\,\mathbf{a})\,dS. \tag{A4.77}$$

RELATIONSHIPS IN CYLINDRICAL COORDINATES

Dyadic $\overline{\overline{a}}$ can be written as

$$\overline{\overline{a}} = \mathbf{a}'_r\mathbf{u}_r + \mathbf{a}'_\varphi\mathbf{u}_\varphi + \mathbf{a}'_z\mathbf{u}_z = \mathbf{u}_r\mathbf{a}_r + \mathbf{u}_\varphi\mathbf{a}_\varphi + \mathbf{u}_z\mathbf{a}_z.$$

The basic differential operators are then:

$$\begin{aligned}\text{grad}\,\mathbf{a} &= \left(\text{grad}\,a_r - \frac{a_\varphi\mathbf{u}_\varphi}{r}\right)\mathbf{u}_r + \left(\text{grad}\,a_\varphi + \frac{a_r\mathbf{u}_\varphi}{r}\right)\mathbf{u}_\varphi + \text{grad}\,a_z\mathbf{u}_z \\ &= \mathbf{u}_r\frac{\partial\mathbf{a}}{\partial r} + \mathbf{u}_\varphi\frac{1}{r}\frac{\partial\mathbf{a}}{\partial\varphi} + \mathbf{u}_z\frac{\partial\mathbf{a}}{\partial z}\end{aligned} \tag{A4.78}$$

$$\begin{aligned}\text{div}\,\overline{\overline{a}} &= \left(\text{div}\,\mathbf{a}'_r - \frac{a_{\varphi\varphi}}{r}\right)\mathbf{u}_r + \left(\text{div}\,\mathbf{a}'_\varphi + \frac{a_{\varphi r}}{r}\right)\mathbf{u}_\varphi + (\text{div}\,\mathbf{a}'_z)\mathbf{u}_z \\ &= \frac{1}{r}\mathbf{a}_r + \frac{\partial\mathbf{a}}{\partial r} + \frac{1}{r}\frac{\partial\mathbf{a}_\varphi}{\partial\varphi} + \frac{\partial\mathbf{a}_z}{\partial z}\end{aligned} \tag{A4.79}$$

$$\operatorname{curl} \bar{\bar{a}} = \left(\operatorname{curl} \mathbf{a}'_r + \frac{\mathbf{a}'_\varphi \times \mathbf{u}_\varphi}{r}\right)\mathbf{u}_r + \left(\operatorname{curl} \mathbf{a}'_\varphi - \frac{\mathbf{a}'_r \times \mathbf{u}_\varphi}{r}\right)\mathbf{u}_\varphi + \operatorname{curl} \mathbf{a}'_z \mathbf{u}_z$$
$$= \mathbf{u}_r\left(\frac{1}{r}\frac{\partial \mathbf{a}_z}{\partial \varphi} - \frac{\partial \mathbf{a}_\varphi}{\partial z}\right) + \mathbf{u}_\varphi\left(\frac{\partial \mathbf{a}_r}{\partial z} - \frac{\partial \mathbf{a}_z}{\partial r}\right) + \mathbf{u}_z\left(\frac{\mathbf{a}_\varphi}{r} + \frac{\partial \mathbf{a}_\varphi}{\partial r} - \frac{1}{r}\frac{\partial \mathbf{a}_r}{\partial \varphi}\right). \quad \text{(A4.80)}$$

In particular:

$$\operatorname{grad} \mathbf{u}_r = \frac{\mathbf{u}_\varphi \mathbf{u}_\varphi}{r} \quad \text{(A4.81)}$$

$$\operatorname{grad} \mathbf{u}_\varphi = -\frac{\mathbf{u}_\varphi \mathbf{u}_r}{r} \quad \text{(A4.82)}$$

$$\operatorname{grad} \mathbf{u}_z = 0 \quad \text{(A4.83)}$$

$$\operatorname{grad}(r\mathbf{u}_r) = \mathbf{u}_r\mathbf{u}_r + \mathbf{u}_\varphi\mathbf{u}_\varphi = \bar{\bar{I}} - \mathbf{u}_z\mathbf{u}_z. \quad \text{(A4.84)}$$

Note that the dyadic operators expressed in terms of the row vectors **a** are identical with their vector counterparts provided bars are put above scalar projections to transform them into row vectors, and provided the unit vectors are used as *prefactors*. This simple rule, which is also valid in spherical coordinates, allows one to write composite operators such as grad div simply by referring to the vector formula. For example:

$$\nabla^2 \bar{\bar{a}} = \mathbf{u}_r\left(\nabla^2 \mathbf{a}_r - \frac{\mathbf{a}_r}{r^2} - \frac{2}{r^2}\frac{\partial \mathbf{a}_\varphi}{\partial \varphi}\right) + \mathbf{u}_\varphi\left(\nabla^2 \mathbf{a}_\varphi - \frac{\mathbf{a}_\varphi}{r^2} + \frac{2}{r^2}\frac{\partial \mathbf{a}_r}{\partial \varphi}\right) + \mathbf{u}_z \nabla^2 \mathbf{a}_z. \quad \text{(A4.85)}$$

RELATIONSHIPS IN SPHERICAL COORDINATES

Dyadic $\bar{\bar{a}}$ can be written as

$$\bar{\bar{a}} = \mathbf{a}'_R\mathbf{u}_R + \mathbf{a}'_\theta\mathbf{u}_\theta + \mathbf{a}'_\varphi\mathbf{u}_\varphi = \mathbf{u}_R\mathbf{a}_R + \mathbf{u}_\theta\mathbf{a}_\theta + \mathbf{u}_\varphi\mathbf{a}_\varphi.$$

The basic differential operators are

$$\operatorname{grad} \mathbf{a} = \left(\operatorname{grad} a_R - \frac{a_\varphi \mathbf{u}_\varphi}{R} - \frac{a_\theta \mathbf{u}_\theta}{R}\right)\mathbf{u}_R + \left(\operatorname{grad} a_\theta + \frac{a_R \mathbf{u}_\theta}{R} - \frac{a_\varphi \mathbf{u}_\varphi}{R\tan\theta}\right)\mathbf{u}_\theta$$
$$+ \left[\operatorname{grad} a_\varphi + \left(\frac{a_R}{R} + \frac{a_\theta}{R\tan\theta}\right)\mathbf{u}_\varphi\right]\mathbf{u}_\varphi$$
$$= \mathbf{u}_R\frac{\partial \mathbf{a}}{\partial R} + \mathbf{u}_\theta\frac{1}{R}\frac{\partial \mathbf{a}}{\partial \theta} + \mathbf{u}_\varphi\frac{1}{R\sin\theta}\frac{\partial \mathbf{a}}{\partial \varphi} \quad \text{(A4.86)}$$

$$\operatorname{div} \bar{\bar{a}} = \left(\operatorname{div} \mathbf{a}'_R - \frac{a_{\theta\theta} + a_{\varphi\varphi}}{R}\right)\mathbf{u}_R + \left(\operatorname{div} \mathbf{a}'_\theta + \frac{a_{\theta R}}{R} - \frac{a_{\varphi\varphi}}{R\tan\theta}\right)\mathbf{u}_\theta$$
$$+ \left(\operatorname{div} \mathbf{a}'_\varphi + \frac{a_{\varphi R}}{R} + \frac{a_{\varphi\theta}}{R\tan\theta}\right)\mathbf{u}_\varphi$$
$$= \frac{\partial \mathbf{a}_R}{\partial R} + \frac{2\mathbf{a}_R}{R} + \frac{1}{R}\frac{\partial \mathbf{a}_\theta}{\partial \theta} + \frac{\mathbf{a}_\theta}{R\tan\theta} + \frac{1}{R\sin\theta}\frac{\partial \mathbf{a}_\varphi}{\partial \varphi} \quad \text{(A4.87)}$$

$$\begin{aligned}\operatorname{curl}\bar{\bar{a}} &= \left(\operatorname{curl}\mathbf{a}'_R + \frac{\mathbf{a}'_\theta \times \mathbf{u}_\theta}{R} + \frac{\mathbf{a}'_\varphi \times \mathbf{u}_\varphi}{R}\right)\mathbf{u}_R + \left(\operatorname{curl}\mathbf{a}'_\theta - \frac{\mathbf{a}'_R \times \mathbf{u}_\theta}{R} + \frac{\mathbf{a}'_\varphi \times \mathbf{u}_\theta}{R\tan\theta}\right)\mathbf{u}_\theta \\ &\quad + \left(\operatorname{curl}\mathbf{a}'_\varphi - \frac{\mathbf{a}'_R \times \mathbf{u}_\varphi}{R} - \frac{\mathbf{a}'_\theta \times \mathbf{u}_\varphi}{R\tan\theta}\right)\mathbf{u}_\varphi \\ &= \mathbf{u}_R\left(\frac{1}{R}\frac{\partial \mathbf{a}_\varphi}{\partial\theta} + \frac{\mathbf{a}_\varphi}{R\tan\theta} - \frac{1}{R\sin\theta}\frac{\partial \mathbf{a}_\theta}{\partial\varphi}\right) \\ &\quad + \mathbf{u}_\theta\left(\frac{1}{R\sin\theta}\frac{\partial \mathbf{a}_R}{\partial\varphi} - \frac{\partial \mathbf{a}_\varphi}{\partial R} - \frac{\mathbf{a}_\varphi}{R}\right) + \mathbf{u}_\varphi\left(\frac{\partial \mathbf{a}_\theta}{\partial R} + \frac{\mathbf{a}_\theta}{R} - \frac{1}{R}\frac{\partial \mathbf{a}_R}{\partial\theta}\right). \qquad \text{(A4.88)}\end{aligned}$$

In particular:

$$\operatorname{grad}\mathbf{u}_R = \frac{\mathbf{u}_\theta\mathbf{u}_\theta}{R} + \frac{\mathbf{u}_\varphi\mathbf{u}_\varphi}{R} \qquad \text{(A4.89)}$$

$$\operatorname{grad}\mathbf{u}_\theta = -\frac{\mathbf{u}_\theta\mathbf{u}_R}{R} + \frac{\mathbf{u}_\varphi\mathbf{u}_\varphi}{R\tan\theta} \qquad \text{(A4.90)}$$

$$\operatorname{grad}\mathbf{u}_\varphi = -\frac{\mathbf{u}_\varphi\mathbf{u}_R}{R} - \frac{\mathbf{u}_\varphi\mathbf{u}_\theta}{R\tan\theta} \qquad \text{(A4.91)}$$

$$\operatorname{grad}(R\mathbf{u}_R) = \bar{\bar{I}}. \qquad \text{(A4.92)}$$

NOTES

In addition to [12, 165, 173] of the general bibliography:

I. V. Lindell, *Elements of Dyadic Algebra and Its Application in Electromagnetics*. Report S126, Radio Laboratory, Helsinki University of Technology, 1981.

I. V. Lindell, *Complex Vectors and Dyadics for Electromagnetics*. Report 36, Electromagnetics Laboratory, Helsinki University of Technology, 1988.

C. T. Tai, Some essential formulas in dyadic analysis and their applications. *Radio Sci.* **22**, 1283–1288, 1987.

Appendix 5

Special Functions*

BESSEL FUNCTIONS

Bessel's equation is

$$\frac{d^2f}{dz^2} + \frac{1}{z}\frac{df}{dz} + \left(\lambda^2 - \frac{\nu^2}{z^2}\right)f = \frac{1}{z}\frac{d}{dz}\left(z\frac{df}{dz}\right) + \left(\lambda^2 - \frac{\nu^2}{z^2}\right)f = 0 \tag{A5.1}$$

where ν can be complex. When ν is not an integer or zero, $J_\nu(\lambda z)$ and $J_{-\nu}(\lambda z)$, as given by the series

$$J_m = \sum_{n=0}^{\infty} \frac{(-1)^n(\lambda z)^{\nu+2n}}{2^{\nu+2n}\, n!\, \Gamma(\nu + n + 1)} \qquad (m = \pm\nu) \tag{A5.2}$$

form two linearly independent solutions of Bessel's equation. When ν is an integer n or zero, $J_{-n} = (-1)^n J_n$, and the two solutions are no longer independent. Various second solutions have been proposed, notably by Hankel, Neumann, Weber, and Schäfli. The formulas in this appendix are based on the Weber version

$$N_\nu(\lambda z) = \frac{\cos(\nu\pi)J_\nu(\lambda z) - J_{-\nu}(\lambda z)}{\sin \nu\pi}. \tag{A5.3}$$

When ν is an integer n,

$$N_n(\lambda z) = \lim_{\nu \to n} N_\nu(\lambda z). \tag{A5.4}$$

For large values of the argument,

$$\lim_{|\lambda z| \gg |\nu|} J_\nu(\lambda z) = \left(\frac{2}{\pi\lambda z}\right)^{\frac{1}{2}} \cos\left(\lambda z - \frac{2\nu + 1}{4}\pi\right); \quad |\arg \lambda z| < \pi \tag{A5.5}$$

$$\lim_{|\lambda z| \gg |\nu|} N_\nu(\lambda z) = \left(\frac{2}{\pi\lambda z}\right)^{\frac{1}{2}} \sin\left(\lambda z - \frac{2\nu + 1}{4}\pi\right); \quad |\arg \lambda z| < \pi. \tag{A5.6}$$

*The author wishes to thank Professor C. M. Butler — a colleague and friend of almost 50 years — who took the time to check most of the formulas in Appendix 5. He also suggested many improvements to the preliminary version of Appendix 6.

Electromagnetic Fields, Second Edition, By Jean G. Van Bladel

Important linear combinations are the Hankel functions

$$H_\nu^{(1)}(\lambda z) = J_\nu(\lambda z) + jN_\nu(\lambda z) \tag{A5.7}$$

$$H_\nu^{(2)}(\lambda z) = J_\nu(\lambda z) - jN_\nu(\lambda z). \tag{A5.8}$$

Their respective limits are

$$\lim_{|\lambda z|\gg|\nu|} H_\nu^{(1)}(\lambda z) = \left(\frac{2}{\pi\lambda z}\right)^{\frac{1}{2}} e^{j\lambda z - j(\pi/4)(2\nu+1)}; \quad -\pi < \arg\lambda z < 2\pi \tag{A5.9}$$

$$\lim_{|\lambda z|\gg|\nu|} H_\nu^{(2)}(\lambda z) = \left(\frac{2}{\pi\lambda z}\right)^{\frac{1}{2}} e^{-j\lambda z + j(\pi/4)(2\nu+1)}; \quad -2\pi < \arg\lambda z < \pi. \tag{A5.10}$$

Note that

$$H_{-\nu}^{(1)}(\lambda z) = e^{j\nu\pi}\, H_\nu^{(1)}(\lambda z); \quad H_{-\nu}^{(2)}(\lambda z) = e^{-j\nu\pi} H_\nu^{(2)}(\lambda z) \tag{A5.11}$$

$$J_{\frac{1}{2}}(z) = \left(\frac{2}{\pi z}\right)^{\frac{1}{2}} \sin z; \quad J_{\frac{3}{2}}(z) = \left(\frac{2}{\pi z}\right)^{\frac{1}{2}} \left(\frac{\sin z}{z} - \cos z\right) \tag{A5.12}$$

$$J_{-\frac{1}{2}}(z) = \left(\frac{2}{\pi z}\right)^{\frac{1}{2}} \cos z; \quad J_{-\frac{3}{2}}(z) = \left(\frac{2}{\pi z}\right)^{\frac{1}{2}} \left(-\frac{\cos z}{z} - \sin z\right). \tag{A5.13}$$

Approximations for small values of the argument:

$$J_0(z) = 1 - \frac{z^2}{4}; \quad J_1(z) = \frac{z}{2} - \frac{z^3}{16} + \cdots \tag{A5.14}$$

$$J_2(z) = \frac{z^2}{8} - \frac{z^4}{96}; \quad J_n(z) = \frac{z^n}{2^n n!} \tag{A5.15}$$

$$J_\nu(z) = \left(\frac{z}{2}\right)^\nu \frac{1}{\Gamma(\nu+1)}; \quad J_{-\nu}(z) = \left(\frac{2}{z}\right)^\nu \frac{1}{\Gamma(1-\nu)} \tag{A5.16}$$

(ν neither zero nor an integer)

$$N_0(z) = \frac{2}{\pi}\left[\left(1 - \frac{z^2}{4}\right)\log_e z - 0.11593\right] \tag{A5.17}$$

$$N_n(z) = -\frac{2^n(n-1)!}{\pi z^n} \tag{A5.18}$$

$$N_\nu(z) = -\frac{1}{\pi}\Gamma(\nu)\left(\frac{2}{z}\right)^\nu \quad \text{Re}\ \nu > 0 \tag{A5.19}$$

$$H_0^{(2)}(z) = \left(1 - \left(\frac{z}{2}\right)^2\right)\left\{1 - j\frac{2}{\pi}\left[\gamma + \log_e\frac{z}{2}\right]\right\} - j\frac{z^2}{2\pi} \tag{A5.20}$$

$$H_1^{(2)}(z) = j\frac{2}{\pi z} + \frac{z}{2}\left[1 - j\frac{2}{\pi}\left(\gamma - \frac{1}{2} + \log_e\frac{z}{2}\right)\right] \tag{A5.21}$$

where γ is *Euler's constant*, equal to 0.5772153 ...

$$H_n^{(2)}(z) = \frac{z^n}{2^n n!} + j\frac{2^n(n-1)!}{\pi z^n} \tag{A5.22}$$

$$\frac{dH_n^{(2)}(z)}{dz} = \frac{z^{n-1}}{2^n(n-1)!} - j\frac{2^n n!}{\pi z^{n+1}} + \cdots . \tag{A5.23}$$

When $R_\nu = aJ_\nu(z) + bN_\nu(z)$ and $S_\nu = cJ_\nu(z) + dN_\nu(z)$, where a, b, c, and d are independent of ν and z:

$$\frac{2\nu}{\lambda z}R_\nu(\lambda z) = R_{\nu-1}(\lambda z) + R_{\nu+1}(\lambda z) \tag{A5.24}$$

$$\frac{2}{\lambda}\frac{d}{dz}R_\nu(\lambda z) = R_{\nu-1}(\lambda z) - R_{\nu+1}(\lambda z) \tag{A5.25}$$

$$z\frac{d}{dz}R_\nu(\lambda z) = \nu R_\nu(\lambda z) - \lambda z R_{\nu+1}(\lambda z) = -\nu R_\nu(\lambda z) + \lambda z R_{\nu-1}(\lambda z); \tag{A5.26}$$

$$\frac{d}{dz}[z^\nu R_\nu(\lambda z)] = \lambda z^\nu R_{\nu-1}(\lambda z) \tag{A5.27}$$

$$\frac{d}{dz}[z^{-\nu} R_\nu(\lambda z)] = -\lambda z^{-\nu} R_{\nu+1}(\lambda z) \tag{A5.28}$$

$$\text{in particular, } \frac{dR_0(\lambda z)}{dz} = -\lambda R_1(\lambda z). \tag{A5.29}$$

Some useful integrals:

$$(\lambda^2 - \mu^2)\int R_n(\lambda z)S_n(\mu z)z\,dz = \mu z R_n(\lambda z)S_{n-1}(\mu z) - \lambda z R_{n-1}(\lambda z)S_n(\mu z). \tag{A5.30}$$

The normalization integrals are

$$\int [R_n(\lambda z)]^2 z\,dz = \frac{z^2}{2}[R_n^2(\lambda z) - R_{n-1}(\lambda z)R_{n+1}(\lambda z)]. \tag{A5.31}$$

In particular,

$$\int_0^c x[J_n(\lambda_k x)]^2 dx = \frac{c^2}{2}[J_{n+1}(\lambda_k c)]^2 \text{ when } \lambda_k \text{ is a root of } J_n(\lambda_k c) = 0 \tag{A5.32}$$

$$\int_0^c x[J_n(\lambda_k x)]^2 dx = \frac{\lambda_k^2 c^2 + h^2 - n^2}{2\lambda_k^2}[J_n(\lambda_k c)]^2 \tag{A5.33}$$

when λ_k is a root of $\lambda_k c J_n'(\lambda_k c) + hJ_n(\lambda_k c) = 0$.

$$\int_b^a x[R_n(\lambda x)]^2 dx = \frac{a^2}{2}[R_{n+1}(\lambda a)]^2 - \frac{b^2}{2}[R_{n+1}(\lambda b)]^2 \tag{A5.34}$$

when R_n vanishes at $x = a, x = b$.

$$\int_b^a x[R_n(\lambda x)]^2 dx = \left(a^2 - \frac{n^2}{\lambda^2}\right)\frac{R_n^2(\lambda a)}{2} - \left(b^2 - \frac{n^2}{\lambda^2}\right)\frac{R_n^2(\lambda b)}{2} \tag{A5.35}$$

when R_n' vanishes at $x = a, x = b$. Other useful relationships:

$$W[J_\nu, J_{-\nu}] = J_\nu(z)J'_{-\nu}(z) - J'_\nu(z)J_{-\nu}(z) = -\frac{2\sin\nu\pi}{\pi z} \tag{A5.36}$$

$$W[J_\nu, N_\nu] = \frac{2}{\pi z} \tag{A5.37}$$

$$W[H_\nu^{(1)}, H_\nu^{(2)}] = \frac{4}{j\pi z}; \quad W[J_\nu, H_\nu^{(2)}] = \frac{2}{j\pi z} \tag{A5.38}$$

$$J_2(z) = J_0(z) + 2J_0''(z) = J_0''(z) - z^{-1}J_0'(z) \tag{A5.39}$$

$$\cos z = J_0(z) - 2J_2(z) + 2J_4(z) + \cdots \tag{A5.40}$$

$$\sin z = 2J_1(z) - 2J_3(z) + 2J_5(z) + \cdots \tag{A5.41}$$

$$\cos(z\sin\theta) = J_0(z) + 2J_2(z)\cos 2\theta + 2J_4(z)\cos 4\theta + \cdots \tag{A5.42}$$

$$\sin(z\sin\theta) = 2J_1(z)\sin\theta + 2J_3(z)\sin 3\theta + 2J_5(z)\sin 5\theta + \cdots \tag{A5.43}$$

$$[J_0(z)]^2 + 2[J_1(z)]^2 + 2[J_2(z)]^2 + \cdots = 1 \tag{A5.44}$$

$$\left(\frac{\partial^2}{\partial r^2} + \frac{1}{r}\frac{\partial}{\partial r} + \frac{1}{r^2}\frac{\partial^2}{\partial\varphi^2}\right)e^{\pm jn\varphi}R_n(\lambda r) = -\lambda^2 e^{\pm jn\varphi}R_n(\lambda r) \tag{A5.45}$$

$$e^{z(t/2-1/2t)} = \sum_{n=-\infty}^{+\infty} t^n J_n(z) \quad (t \neq 0) \tag{A5.46}$$

$$e^{jz\sin\theta} = \sum_{n=-\infty}^{+\infty} e^{jn\theta}J_n(z); \quad e^{jz\cos\theta} = \sum_{n=-\infty}^{+\infty} e^{jn(\theta+\pi/2)}J_n(z) \tag{A5.47}$$

$$J_0(x) = \frac{2}{\pi}\int_0^\infty \sin(x\cosh t)dt; \quad N_0(x) = -\frac{2}{\pi}\int_0^\infty \cos(x\cosh t)dt \quad (x > 0) \tag{A5.48}$$

$$J_0(x) = \frac{1}{\pi}\int_0^\pi \cos(x\cos t)dt = \frac{1}{\pi}\int_0^\pi \cos(x\sin t)dt$$

$$= \frac{1}{2\pi}\int_0^{2\pi} e^{\pm jx\cos t}dt \tag{A5.49}$$

$$J_0(z) = \frac{2}{\pi}\int_0^1 \cos zu(1-u^2)^{-\frac{1}{2}}du; \quad N_0(z) = -\frac{2}{\pi}\int_0^\infty \cos(z\cosh u)du \tag{A5.50}$$

$$J_n(x) = \frac{1}{\pi}\int_0^\pi \cos(nt - x\sin t)dt \tag{A5.51}$$

$$\int_0^\infty e^{-jkx}J_0(k\rho)dk = (\rho^2 - x^2)^{-\frac{1}{2}} (\rho \text{ and } x \text{ real}) \tag{A5.52}$$

$$\int_0^x x'J_0(x')dx' = xJ_1(x) \tag{A5.53}$$

Table A5.1 Zeros of Bessel functions

m	$s=1$	$s=2$	$s=3$	$s=4$	$s=5$
0	2.405	5.520	8.654	11.792	14.931
1	3.832	7.016	10.173	13.324	16.471
2	5.136	8.417	11.620	14.796	17.960
3	6.380	9.761	13.015	16.223	19.409
4	7.588	11.065	14.373	17.616	20.827

Table A5.2 Zeros of the first derivatives of Bessel functions

m	$s=1$	$s=2$	$s=3$	$s=4$	$s=5$
0	0	3.832	7.016	10.173	13.324
1	1.841	5.331	8.536	11.706	14.864
2	3.054	6.706	9.969	13.170	16.348
3	4.201	8.015	11.346	14.586	17.789
4	5.318	9.282	12.682	15.964	19.196

$$\int_0^\infty J_n(x)dx = 1 \text{ and } \int_0^\infty \frac{J_n(kx)}{x}dx = \frac{1}{n}(n = 1, 2, 3, \ldots) \tag{A5.54}$$

$$\int_0^\infty e^{-at}J_m(bt)\frac{dt}{t} = \frac{1}{mb^m}[(a^2+b^2)^{\frac{1}{2}} - a]^m (a \text{ and } b \text{ real and positive}) \tag{A5.55}$$

$$\int_0^{\frac{\pi}{2}} [J_1(x\sin\theta)]^2 \frac{d\theta}{\sin\theta} = \int_0^1 \frac{[J_1(xu)]^2}{u(1-u^2)^{\frac{1}{2}}}du = \frac{1}{2} - \frac{J_1(2x)}{2x} \tag{A5.56}$$

$$\int_0^\infty e^{-at}N_0(bt)dt = -\frac{2/\pi}{(a^2+b^2)^{\frac{1}{2}}}\log_e\frac{a+(a^2+b^2)^{\frac{1}{2}}}{a} \tag{A5.57}$$

(a and b real and positive)

$$\int_0^\infty J_m(tz)t\,dt \int_0^\infty J_m(tu)F(u)u\,du = F(z) \text{ (Fourier-Bessel integral)} \tag{A5.58}$$

$$\int_0^{\frac{\pi}{2}} \cos(a\cos\theta)\cos(b\sin\theta)d\theta = \frac{\pi}{2}J_0[(a^2+b^2)^{\frac{1}{2}}]. \tag{A5.59}$$

A few zeros of $J_m(x_{ms})$ and related functions are given in Tables A5.1 to A5.3.

Table A5.3 Zeros of $J_0(x)N_0(kx) - N_0(x)J_0(kx)$

k	x_1	x_2	x_3	x_4	x_5
1.2	15.70	31.41	47.12	62.83	78.54
1.5	6.27	12.56	18.85	25.13	31.41
2.0	3.12	6.27	9.42	12.56	15.70
2.5	2.07	4.18	6.28	8.37	10.47
3.0	1.55	3.12	4.70	6.28	7.85
3.5	1.23	2.50	3.76	5.02	6.28
4.0	1.02	2.08	3.13	4.18	5.23

MODIFIED BESSEL FUNCTIONS

The modified Bessel's equation

$$\frac{d^2g}{dz^2} + \frac{1}{z}\frac{dg}{dz} - \left(\lambda^2 + \frac{\nu^2}{z^2}\right) g = 0 \tag{A5.60}$$

has solutions $I_\nu(\lambda z)$ and $K_\nu(\lambda z)$, where

$$I_\nu(\lambda z) = e^{-j\frac{\nu\pi}{2}} J_\nu\left(e^{j\frac{\pi}{2}}\lambda z\right) \qquad \left(-\pi < \arg\lambda z \le \frac{\pi}{2}\right) \tag{A5.61}$$

$$I_\nu(\lambda z) = e^{j\frac{3\nu\pi}{2}} J_\nu\left(e^{-j\frac{3\pi}{2}}\lambda z\right) \quad \left(\frac{\pi}{2} < \arg\lambda z \le \pi\right) \tag{A5.62}$$

$$I_{-\nu}(\lambda z) = j^\nu J_{-\nu}(j\lambda z) \tag{A5.63}$$

$$K_\nu(\lambda z) = \frac{\pi}{2}\frac{I_\nu(\lambda z) - I_{-\nu}(\lambda z)}{\sin\nu\pi}. \tag{A5.64}$$

A few useful values:

$$I_{\frac{1}{2}}(z) = \left(\frac{2}{\pi z}\right)^{\frac{1}{2}} \sinh z = \left(\frac{2}{\pi z}\right)^{\frac{1}{2}} \left(z + \frac{z^3}{6} + \frac{z^5}{120} + \cdots\right) \tag{A5.65}$$

$$I_{\frac{3}{2}}(z) = \left(\frac{2}{\pi z}\right)^{\frac{1}{2}} \left(\cosh z - \frac{\sinh z}{z}\right) \tag{A5.66}$$

$$I_{-\frac{1}{2}}(z) = \left(\frac{2}{\pi z}\right)^{\frac{1}{2}} \cosh z = \left(\frac{2}{\pi z}\right)^{\frac{1}{2}} \left(1 + \frac{z^2}{2} + \frac{z^4}{24} + \cdots\right) \tag{A5.67}$$

$$I_{-\frac{3}{2}}(z) = \left(\frac{2}{\pi z}\right)^{\frac{1}{2}} \left(\sinh z - \frac{\cosh z}{z}\right) \tag{A5.68}$$

$$K_{\frac{1}{2}}(z) = \left(\frac{\pi}{2z}\right)^{\frac{1}{2}} e^{-z}. \tag{A5.69}$$

Some general relationships:

$$\frac{2\nu}{z} I_\nu(z) = I_{\nu-1}(z) - I_{\nu+1}(z) \tag{A5.70}$$

$$2\frac{d}{dz} I_\nu(z) = I_{\nu-1}(z) + I_{\nu+1}(z) \tag{A5.71}$$

$$-\frac{2\nu}{z} K_\nu(z) = K_{\nu-1}(z) - K_{\nu+1}(z) \tag{A5.72}$$

$$-2\frac{dK_\nu(z)}{dz} = K_{\nu-1}(z) + K_{\nu+1}(z) \tag{A5.73}$$

$$\frac{d}{dz}[z^\nu I_\nu(z)] = z^\nu I_{\nu-1}(z) \tag{A5.74}$$

$$\frac{d}{dz}[z^{-\nu}I_\nu(z)] = z^{-\nu}I_{\nu+1}(z) \tag{A5.75}$$

$$W[I_\nu, I_{-\nu}] = -2\frac{\sin \nu\pi}{\pi z} \tag{A5.76}$$

$$\begin{aligned} W[K_\nu, I_\nu] &= K_\nu(z)I'_\nu(z) - K'_\nu(z)I_\nu(z) \\ &= I_\nu(z)K_{\nu-1}(z) + I_{\nu-1}(z)K_\nu(z) = \frac{1}{z}. \end{aligned} \tag{A5.77}$$

When ν is an integer:

$$I_{-n}(z) = I_n(z) \quad (\text{while } J_{-n}(z) = (-1)^n J_n(z)) \tag{A5.78}$$

$$K_n(z) = \lim_{\nu\to n} K_\nu(z) = K_{-n}(z) \tag{A5.79}$$

$$I'_0(z) = I_1(z); \quad K'_0(z) = -K_1(z) \tag{A5.80}$$

$$\lim_{|z|\to\infty} I_n(z) = (2\pi z)^{-\frac{1}{2}} e^z \left(1 - \frac{4n^2-1}{8z} + \cdots\right) \tag{A5.81}$$

$$\lim_{|z|\to\infty} K_n(z) = \left(\frac{\pi}{2z}\right)^{\frac{1}{2}} e^{-z} \left(1 + \frac{4n^2-1}{8z} + \cdots\right). \tag{A5.82}$$

The functions I_n and K_n are real when z is real. If $S_n(\lambda r)$ is any solution of the modified Bessel function (i.e., any linear combination of the I_n, I_{-n}, and K_n), then

$$\nabla^2 e^{\pm jn\varphi} S_n(\lambda r) = \lambda^2 e^{\pm jn\varphi} S_n(\lambda r) = \left(\frac{\partial^2}{\partial r^2} + \frac{1}{r}\frac{\partial}{\partial r} + \frac{1}{r^2}\frac{\partial^2}{\partial \varphi^2}\right) e^{\pm jn\varphi} S_n(\lambda r). \tag{A5.83}$$

SPHERICAL BESSEL FUNCTIONS

These functions are defined by

$$j_\nu(\lambda z) = \left(\frac{\pi}{2\lambda z}\right)^{\frac{1}{2}} J_{\nu+\frac{1}{2}}(\lambda z) \text{ and } n_\nu(\lambda z) = \left(\frac{\pi}{2\lambda z}\right)^{\frac{1}{2}} N_{\nu+\frac{1}{2}}(\lambda z). \tag{A5.84}$$

Any linear combination T_ν of these functions is a solution of

$$\frac{d^2T_\nu}{dz^2} + \frac{2}{z}\frac{dT_\nu}{dz} + \left[\lambda^2 - \frac{\nu(\nu+1)}{z^2}\right] T_n = 0. \tag{A5.85}$$

One may also write the differential operator in the form

$$\frac{d^2T_\nu}{dz^2} + \frac{2}{z}\frac{dT_\nu}{dz} = \frac{1}{z^2}\frac{d}{dz}\left(z^2\frac{dT_\nu}{dz}\right) = \frac{1}{z}\frac{d^2}{dz^2}(zT_\nu). \tag{A5.86}$$

The normalization can be found from the relation

$$\int T_n^2(\lambda z) z^2 dz = \frac{z^3}{2}\left[T_n^2(\lambda z) - T_{n-1}(\lambda z)T_{n+1}(\lambda z)\right]. \tag{A5.87}$$

The function $P_\nu = zT_\nu(\lambda z)$ satisfies

$$\frac{d^2P_\nu(\lambda z)}{dz^2} + \left[\lambda^2 - \frac{\nu(\nu+1)}{z^2}\right]P_\nu(\lambda z) = 0 \tag{A5.88}$$

$$h_\nu^{(1)}(\lambda z) = j_\nu(\lambda z) + jn_\nu(\lambda z); \quad h_\nu^{(2)}(\lambda z) = j_\nu(\lambda z) - jn_\nu(\lambda z). \tag{A5.89}$$

Specific functions:

$$j_0(\lambda z) = \frac{\sin\lambda z}{\lambda z}; \quad n_0(\lambda z) = -\frac{1}{\lambda z}\cos\lambda z \tag{A5.90}$$

$$j_1(\lambda z) = \frac{\sin\lambda z}{\lambda^2 z^2} - \frac{\cos\lambda z}{\lambda z}; \quad n_1(\lambda z) = -\frac{\cos\lambda z}{\lambda^2 z^2} - \frac{\sin\lambda z}{\lambda z} \tag{A5.91}$$

$$h_0^{(1)}(\lambda z) = \frac{e^{j\lambda z}}{j\lambda z}; \quad h_0^{(2)}(\lambda z) = -\frac{e^{-j\lambda z}}{j\lambda z}; \tag{A5.92}$$

$$h_1^{(2)}(\lambda z) = -\frac{e^{-j\lambda z}}{\lambda z} + \frac{j}{(\lambda z)^2}e^{-j\lambda z}. \tag{A5.93}$$

Approximation for small values of the argument, and $n = 0, 1, 2, \ldots$:

$$j_n(\lambda z) = \frac{(\lambda z)^n}{1\cdot 3\cdot 5\cdots(2n+1)} = \frac{2^n n!(\lambda z)^n}{(2n+1)!} \tag{A5.94}$$

$$n_n(\lambda z) = -\frac{1\cdot 3\cdot 5\cdots(2n-1)}{(\lambda z)^{n+1}} \tag{A5.95}$$

$$h_n^{(2)}(\lambda z) = j\frac{(2n)!}{2^n n!(\lambda z)^{n+1}} \tag{A5.96}$$

$$\lambda z\left[h_n^{(2)}(\lambda z)\right]' = -(n+1)h_n^{(2)}(\lambda z). \tag{A5.97}$$

For large values of the argument,

$$\lim_{\lambda z\to\infty} j_n(\lambda z) = \frac{1}{\lambda z}\cos\left[\lambda z - \frac{\pi}{2}(n+1)\right] \tag{A5.98}$$

$$\lim_{\lambda z\to\infty} n_n(\lambda z) = \frac{1}{\lambda z}\sin\left[\lambda z - \frac{\pi}{2}(n+1)\right] \tag{A5.99}$$

$$\lim_{\lambda z\to\infty} h_n^{(1)}(\lambda z) = \frac{(-j)^{n+1}}{\lambda z}e^{j\lambda z} \tag{A5.100}$$

$$\lim_{\lambda z\to\infty} h_n^{(2)}(\lambda z) = \frac{(j)^{n+1}}{\lambda z}e^{-j\lambda z}. \tag{A5.101}$$

General relationships:

$$\frac{(2n+1)}{\lambda z}T_n(\lambda z) = T_{n-1}(\lambda z) + T_{n+1}(\lambda z) \tag{A5.102}$$

$$\frac{(2n+1)}{\lambda}\frac{d}{dz}[T_n(\lambda z)] = nT_{n-1}(\lambda z) - (n+1)T_{n+1}(\lambda z) \tag{A5.103}$$

$$\frac{d}{dz}[z^{n+1}T_n(\lambda z)] = \lambda z^{n+1}T_{n-1}(\lambda z) \tag{A5.104}$$

Table A5.4 Zeros of $j_n(x)$

n	$s=1$	$s=2$	$s=3$	$s=4$	$s=5$
0	π	2π	3π	4π	5π
1	4.493	7.725	10.904	14.066	17.221
2	5.763	9.095	12.323	15.515	18.689
3	6.988	10.417	13.698	16.924	20.122
4	8.183	11.705	15.040	18.301	21.525

Table A5.5 Zeros of the first derivative of $j_n(x)$

n	$s=1$	$s=2$	$s=3$	$s=4$	$s=5$
0	0	4.493	7.725	10.904	14.066
1	2.0816	5.940	9.205	12.404	15.579
2	3.342	7.290	10.613	13.846	17.043
3	4.514	8.583	11.972	15.244	18.468
4	5.646	9.840	13.295	16.609	19.862

Table A5.6 Zeros of the first derivative of $xj_n(x)$

n	$s=1$	$s=2$	$s=3$	$s=4$	$s=5$
0	$\frac{\pi}{2}$	$\frac{3\pi}{2}$	$\frac{5\pi}{2}$	$\frac{7\pi}{2}$	$\frac{9\pi}{2}$
1	2.744	6.117	9.317	12.486	15.644
2	3.870	7.443	10.713	13.921	17.103
3	4.973	8.722	12.064	15.314	18.524
4	6.062	9.968	13.380	16.674	19.915

$$\frac{d}{dz}[z^{-n}T_n(\lambda z)] = -\lambda z^{-n}T_{n+1}(\lambda z) \tag{A5.105}$$

$$\frac{d}{dz}[n_n(\lambda z)]j_n(\lambda z) - n_n(\lambda z)\frac{d}{dz}[j_n(\lambda z)] = \frac{1}{\lambda z^2} \tag{A5.106}$$

$$W[h_n^{(1)}(\lambda z), h_n^{(2)}(\lambda z)] = \frac{2}{j(\lambda z)^2}. \tag{A5.107}$$

A few zeros of $j_n(x)$ and related functions are given in Tables A5.4 to A5.6.

LEGENDRE FUNCTIONS

Legendre's equation is

$$(1-z^2)\frac{d^2f}{dz^2} - 2z\frac{df}{dz} + \nu(\nu+1)f = 0. \tag{A5.108}$$

Note that

$$(1-z^2)\frac{d^2f}{dz^2} - 2z\frac{df}{dz} = \frac{d}{dz}\left[(1-z^2)\frac{df}{dz}\right]. \tag{A5.109}$$

Legendre's equation has two linearly independent solutions called *Legendre functions of the first and the second kinds*. When, in addition, ν is an integer, the function of the first kind is a polynomial of order n, denoted by $P_n(z)$; the first few have the explicit form

$$P_0(z) = 1 \qquad P_1(z) = z \qquad P_2(z) = \frac{3z^2-1}{2} \qquad P_3(z) = \frac{5z^3-3z}{2}. \tag{A5.110}$$

The second solution is a polynomial of order $n-1$ to which is added a logarithmic singularity. For example,

$$Q_0(z) = \frac{1}{2}\log_e\frac{z+1}{z-1} \tag{A5.111}$$

$$Q_1(z) = \frac{z}{2}\log_e\frac{z+1}{z-1} - 1 \tag{A5.112}$$

$$Q_2(z) = \frac{3z^2-1}{4}\log_e\frac{z+1}{z-1} - \frac{3z}{2} \tag{A5.113}$$

$$Q_3(z) = \frac{5z^2-3z}{4}\log_e\frac{z+1}{z-1} - \frac{5}{2}z^2 + \frac{2}{3} \tag{A5.114}$$

$$Q_n(z) = \frac{1}{2}P_n(z)\log_e\frac{z+1}{z-1} + \text{ polynomial of degree } (n-1). \tag{A5.115}$$

The singularity occurs at points $z = \pm 1$. Some important properties:

$$P_{-\nu-1}(z) = P_\nu(z); \quad Q_\nu(-z) = -e^{\pm\nu\pi i}Q_\nu(z) \tag{A5.116}$$

$$\sin(\nu\pi)[Q_\nu(z) - Q_{-\nu-1}(z)] = \pi\cos\nu\pi P_\nu(z). \tag{A5.117}$$

For $\nu \neq -1, -2, \ldots,$

$$Q_\nu(-z) = -e^{\pm j\nu\pi}Q_\nu(z) \tag{A5.118}$$

$$\frac{2\sin\nu\pi}{\pi}Q_\nu(z) = P_\nu(z)e^{\mp j\nu\pi} - P_\nu(-z). \tag{A5.119}$$

The upper sign is chosen if $\text{Im}\, z > 0$, the lower sign if $\text{Im}\, z < 0$, and the exponentials should be replaced by $\cos\nu\pi$ when z is real. When the indices are integers, the following hold:

$$P_n(1) = 1; \quad P_n(-1) = (-1)^n \tag{A5.120}$$

$$P_n(0) = 0 \text{ for } n \text{ odd}; \quad P_n(0) = (-1)^{\frac{n}{2}}\frac{1\cdot3\cdot5\cdots(n-1)}{2\cdot4\cdot6\cdots n} \text{ for } n \text{ even} \tag{A5.121}$$

$$P_n'(1) = \frac{n(n+1)}{2}; \quad P_n(1-x) = 1 - \frac{n(n+1)}{2}x + \cdots \tag{A5.122}$$

$$P_n(\cos\theta) = 1 - \frac{n(n+1)}{4}\theta^2 + \cdots; \quad P_n'(0) = -(n+1)P_{n+1}(0) \tag{A5.123}$$

$$P_n(z) = \frac{1}{2^n n!}\frac{d^n}{dz^n}(z^2-1)^n \tag{A5.124}$$

$$Q_n(0) = 0 \text{ for } n \text{ even} \tag{A5.125}$$

$$Q_n(0) = (-1)^{(n+1)/2}\frac{2\cdot 4\cdot 6\cdots(n-1)}{1\cdot 3\cdot 5\cdots n} \text{ for } n \text{ odd} \tag{A5.126}$$

$$Q_n(1) = \infty; \quad Q_n(\infty) = 0. \tag{A5.127}$$

Useful formulas for ν arbitrary are the following:

$$zP_\nu'(z) - P_{\nu-1}'(z) = \nu P_\nu(z) \tag{A5.128}$$

$$(z^2-1)P_\nu'(z) = \nu z P_\nu(z) - \nu P_{\nu-1}(z) \tag{A5.129}$$

$$P_{\nu+1}'(z) - zP_\nu'(z) = (\nu+1)P_\nu(z) \tag{A5.130}$$

$$(\nu+1)P_{\nu+1}(z) - (2\nu+1)zP_\nu(z) + \nu P_{\nu-1}(z) = 0 \tag{A5.131}$$

$$P_{\nu+1}'(z) - P_{\nu-1}'(z) = (2\nu+1)P_\nu(z). \tag{A5.132}$$

Formulas (A5.128) to (A5.132) are also valid for Q_ν (provided $\nu \neq -1, -2, \ldots$) and any linear combination of P_ν and Q_ν. For m and n integers:

$$\int_{-1}^{1} P_m(x)P_n(x)dx = \frac{2}{2n+1}\delta_{mn} \tag{A5.133}$$

$$\int_0^\pi P_{2n}(\cos\theta)\,d\theta = \pi\left[\frac{(2n)!}{(2^n n!)^2}\right]^2 \tag{A5.134}$$

$$\int_0^\pi P_{2n+1}(\cos\theta)\cos\theta\,d\theta = \pi\frac{(2n)!\,(2n+2)!}{[2^n n!\,2^{n+1}(n+1)!]^2} \tag{A5.135}$$

$$\int_0^\pi P_n(\cos\theta)\sin m\theta\,d\theta$$

$$= \begin{cases} 2\,\dfrac{(m+n-1)(m+n-3)\cdots(m-n+1)}{(m+n)(m+n-2)\cdots(m-n)} & (n < m \text{ and } n+m \text{ odd}) \\ 0 \text{ otherwise} \end{cases} \tag{A5.136}$$

$$\frac{1}{\sqrt{1-2xz+z^2}} = \sum_{n=0}^{\infty} P_n(x)z^n. \tag{A5.137}$$

THE ASSOCIATED LEGENDRE EQUATION

$$(1-z^2)\frac{d^2f}{dz^2} - 2z\frac{df}{dz} + \left[\nu(\nu+1) - \frac{m^2}{1-z^2}\right]f = 0. \tag{A5.138}$$

One often substitutes the variable $\cos\theta$ for z; $f(\cos\theta)$ then satisfies

$$\frac{1}{\sin\theta}\frac{d}{d\theta}\left(\sin\theta\frac{df}{d\theta}\right)+\left[\nu(\nu+1)-\frac{m^2}{\sin^2\theta}\right]f=0. \tag{A5.139}$$

When m is different from zero, the linearly independent solutions are the associated Legendre functions of the first and the second kind. When m is an integer or zero, and $-1<z<1$,

$$P_\nu^m(z)=(1-z^2)^{\frac{m}{2}}\frac{d^m}{dz^m}P_\nu(z) \tag{A5.140}$$

$$Q_\nu^m(z)=(1-z^2)^{\frac{m}{2}}\frac{d^m}{dz^m}Q_\nu(z) \tag{A5.141}$$

$$P_n^m(z)=\frac{(1-z^2)^{\frac{m}{2}}}{2^n n!}\frac{d^{m+n}}{dz^{m+n}}(z^2-1)^n \quad (n \text{ an integer}). \tag{A5.142}$$

In particular,

$$\begin{aligned} P_1^1(z)&=(1-z^2)^{\frac{1}{2}} & P_2^1(z)&=3z(1-z^2)^{\frac{1}{2}}\\ P_2^2(z)&=3(1-z^2) & P_3^1(z)&=\frac{3}{2}(5z^2-1)(1-z^2)^{\frac{1}{2}}\\ P_3^2(z)&=15z(1-z^2) & P_3^3(z)&=15(1-z^2)^{\frac{3}{2}} \end{aligned} \tag{A5.143}$$

$$Q_1^1=(z^2-1)^{\frac{1}{2}}\left(\frac{z}{z^2-1}-\frac{1}{2}\log_e\frac{z+1}{z-1}\right) \tag{A5.144}$$

$$Q_2^1=(z^2-1)^{\frac{1}{2}}\left(\frac{3z^2-2}{z^2-1}-\frac{3}{2}z\log_e\frac{z+1}{z-1}\right) \tag{A5.145}$$

$$Q_2^2=\frac{3}{2}(z^2-1)\log_e\frac{z+1}{z-1}-\frac{3z^3-5z}{z^2-1}. \tag{A5.146}$$

Recurrence formulas satisfied by both P_n^m and Q_n^m are

$$P_{\nu-1}^{m+1}(z)=zP_\nu^{m+1}(z)-(\nu-m)(1-z^2)^{\frac{1}{2}}P_\nu^m(z) \tag{A5.147}$$

$$P_{\nu+1}^{m+1}(z)=zP_\nu^{m+1}(z)+(\nu+m+1)(1-z^2)^{\frac{1}{2}}P_\nu^m(z) \tag{A5.148}$$

$$(1-z^2)^{\frac{1}{2}}P_\nu^m(z)=(\nu+m)zP_\nu^{m-1}(z)-(\nu-m+2)P_{\nu+1}^{m-1} \tag{A5.149}$$

$$\begin{aligned}(1-z^2)^{\frac{1}{2}}P_\nu^m(z)&=2(m-1)zP_\nu^{m-1}(z)\\ &-(\nu+m-1)(\nu-m+2)(1-z^2)^{\frac{1}{2}}P_\nu^{m-2}(z)\end{aligned} \tag{A5.150}$$

$$\begin{aligned}m(1-z^2)^{-\frac{1}{2}}P_\nu^m(z)&=\frac{z}{2}[(\nu-m+1)(\nu+m)P_\nu^{m-1}(z)+P_\nu^{m+1}(z)]\\ &+m(1-z^2)^{\frac{1}{2}}P_\nu^m(z)\end{aligned} \tag{A5.151}$$

$$(2\nu+1)zP_\nu^m(z)=(\nu-m+1)P_{\nu+1}^m(z)+(\nu+m)P_{\nu-1}^m(z) \tag{A5.152}$$

$$(2\nu+1)(1-z^2)^{\frac{1}{2}}P_\nu^m(z) = P_{\nu+1}^{m+1}(z) - P_{\nu-1}^{m+1}(z)$$
$$= (\nu+m)(\nu+m-1)P_{\nu-1}^{m-1}(z) - (\nu-m+1)(\nu-m+2)P_{\nu+1}^{m-1}(z) \tag{A5.153}$$

$$(1-z^2)\frac{d}{dz}P_\nu^m(z) = (\nu+1)zP_\nu^m(z) - (\nu-m+1)P_{\nu+1}^m(z)$$
$$= (\nu+m)P_{\nu-1}^m(z) - \nu zP_\nu^m(z). \tag{A5.154}$$

For integral indices,

$$P_{m+2l+1}^m(0) = 0; \quad P_{m+2l}^m(0) = \frac{(-1)^l(2m+2l)!}{2^{m+2l}l!\,(m+1)!}. \tag{A5.155}$$

For imaginary arguments,

$$P_n(jx)Q_n'(jx) - P_n'(jx)Q_n(jx) = (1+x^2)^{-1} \tag{A5.156}$$

$$P_1^0(jx) = jx; \quad P_1^1(jx) = (1+x^2)^{\frac{1}{2}}; \quad P_2^0(jx) = -\frac{1}{2}(3x^2+1); \tag{A5.157}$$

$$P_2^1(jx) = 3jx(1+x^2)^{\frac{1}{2}} \tag{A5.158}$$

$$Q_0^0(jx) = -j\tan^{-1}\frac{1}{x}; \quad Q_1^0(jx) = x\tan^{-1}\frac{1}{x} - 1. \tag{A5.159}$$

The following integral relationships are important for normalization purposes. For integral indices:

$$\int_{-1}^{+1}\frac{P_n^m(z)P_n^k(z)}{1-z^2}dz = \frac{1}{m}\frac{(n+m)!}{(n-m)!}\delta_{mk} \tag{A5.160}$$

$$\int_{-1}^{+1}P_k^m(x)P_n^m(x)\,dx = \frac{2}{2k+1}\frac{(k+m)!}{(k-m)!}\delta_{nk} \text{ with } k \geq m. \tag{A5.161}$$

When the functions P_n^m have the argument $\cos\theta$:

$$\int_0^\pi\left(\frac{dP_n^m}{d\theta}\frac{dP_k^m}{d\theta} + \frac{m^2}{\sin^2\theta}P_n^mP_k^m\right)\sin\theta\,d\theta = \frac{2}{2n+1}\frac{(n+m)!}{(n-m)!}n(n+1)\delta_{nk}. \tag{A5.162}$$

The associated functions of the first kind P_n^m form a complete orthogonal set in the interval $-1 \leq x \leq +1$. More details about integral representations, Wronskian and functions of half-integral degree are available in the literature.[1,2]

MATHIEU FUNCTIONS

Separation of variables, applied to the Helmholtz equation in elliptic coordinates, yields a Mathieu (angular) equation for the v coordinate, viz.

$$\frac{d^2f}{dv^2} + (b - k^2c^2\cos^2 v)f = 0. \tag{A5.163}$$

This is often written in the form

$$\frac{d^2f}{dv^2} + \left(b - \frac{1}{2}k^2c^2 - \frac{1}{2}k^2c^2\cos 2v\right)f = \frac{d^2f}{dv^2} + (a - 2q\cos 2v)f = 0. \tag{A5.164}$$

It also generates a *modified* (or radial) Mathieu equation for the u coordinate, viz.

$$\frac{d^2g}{du^2} + (k^2c^2\cosh^2 u - b)g = 0 \tag{A5.165}$$

also written as

$$\frac{d^2g}{du^2} - (a - 2q\cosh 2u)g = 0. \tag{A5.166}$$

The angular equation (A5.163) only admits periodic solutions for certain characteristic values of parameter b. These values are real when kc is real. The solutions are either even or odd in v. Several notations unfortunately exist for these functions [144]. The current text uses

$$S_m^e(kc, v) \text{ for the } \textit{cosine-like} \text{ functions, with eigenvalues } b_m^e$$
$$S_m^o(kc, v) \text{ for the } \textit{sine-like} \text{ functions, with eigenvalues } b_m^o$$

Extensive data on these functions and their eigenvalues can be found in [144, 165]. In the limit of small kc, for example,

$$\begin{aligned} &b_0^e \approx \frac{1}{2}k^2c^2; \quad b_1^e \approx 1 + \frac{3}{4}k^2c^2; \quad b_2^e \approx 4 + \frac{1}{2}k^2c^2 \\ &b_1^o \approx 1 + \frac{1}{4}k^2c^2; \quad b_2^o \approx 4 + \frac{1}{2}k^2c^2; \quad b_3^o \approx 9 + \frac{1}{2}k^2c^2. \end{aligned} \tag{A5.167}$$

The S_m^e functions are orthogonal according to the scalar product

$$\left\langle S_m^e, S_n^e \right\rangle = \int_0^{2\pi} S_m^e(v)S_n^e(v)dv = M_m^e\delta_{mn}. \tag{A5.168}$$

The symbol M_m^e denotes the norm. Analogous relationships hold for the S_m^o. Any S_m^e is orthogonal to any S_m^o. Together, they form a complete set in $(0, 2\pi)$. The scale of the functions is determined, either by setting M equal to a given constant (π for example) or by enforcing the conditions $S_m^e = 1$ for $v = 0$ and $\dfrac{d}{dv}[S_m^o] = 1$ for $v = 0$. With the latter choice, a few approximate values for small kc are

$$\begin{aligned} S_o^e &\approx 1 + \frac{1}{8}k^2c^2 - \frac{1}{8}k^2c^2\cos 2v & M_o^e &\approx 2\pi\left(1 + \frac{1}{4}k^2c^2\right) \\ S_1^e &\approx \left(1 + \frac{1}{32}k^2c^2\right)\cos v - \frac{1}{32}k^2c^2\cos 3v & M_1^e &\approx \pi\left(1 + \frac{1}{16}k^2c^2\right) \\ S_1^o &\approx \left(1 + \frac{3}{32}k^2c^2\right)\sin v - \frac{1}{32}k^2c^2\sin 3v & M_1^o &\approx \pi\left(1 + \frac{3}{16}k^2c^2\right) \\ S_2^o &\approx \left(\frac{1}{2} + \frac{1}{48}k^2c^2\right)\sin 2v - \frac{1}{96}k^2c^2\sin 4v & M_2^o &\approx \frac{\pi}{4}\left(1 + \frac{1}{12}k^2c^2\right). \end{aligned} \tag{A5.169}$$

To each even angular function (and its eigenvalue b_m^e) corresponds a radial function, solution of (A5.165) with the same value of b. These functions are of two kinds: $J_m^e(kc, u)$ and $N_m^e(kc, u)$. They are respectively Bessel-like and Neumann-like. The first type does not have any singularities for finite values of its argument, but the second type is singular for $kc \cosh u = 0$. The limits for large u are respectively

$$\lim_{u\to\infty} J_m^e = \frac{1}{\sqrt{kc \cosh u}} \cos\left[kc \cosh u - \frac{\pi}{2}\left(m + \frac{1}{2}\right)\right]$$
$$\lim_{u\to\infty} N_m^e = \frac{1}{\sqrt{kc \cosh u}} \sin\left[kc \cosh u - \frac{\pi}{2}\left(m + \frac{1}{2}\right)\right]. \tag{A5.170}$$

The odd angular functions similarly generate J_m^o and N_m^o, which also behave asymptotically according to (A5.170). For small kc, at $u = 0$,

$$\begin{aligned} J_o^e &\approx \sqrt{\frac{\pi}{2}}\left(1 - \frac{1}{8}k^2c^2\right); & J_1^e &\approx \frac{1}{2}\sqrt{\frac{\pi}{2}}kc \\ N_o^e &\approx \sqrt{\frac{2}{\pi}}\left(1 - \frac{1}{8}k^2c^2\right)\log_e \frac{\gamma kc}{4}; & N_1^e &\approx -\frac{2}{kc}\sqrt{\frac{2}{\pi}}\left(1 + \frac{3}{32}k^2c^2\right) \end{aligned} \tag{A5.171}$$

where $\gamma = 1.781$. At $u = 0$, J_1^o and J_2^o vanish, but

$$N_1^o = -\frac{2}{kc}\sqrt{\frac{2}{\pi}}\left(1 + \frac{1}{32}k^2c^2\right); \quad N_2^o = -\frac{8}{k^2c^2}\sqrt{\frac{2}{\pi}}\left(1 + \frac{1}{24}k^2c^2\right). \tag{A5.172}$$

The Wronskian of the radial function has the simple form

$$J_m^e \frac{dN_m^e}{du} - N_m^e \frac{dJ_m^e}{du} = 1 \tag{A5.173}$$

with an analogous relationship for the "o" functions.

Incoming and outgoing waves can be formed by means of the Hankel-like functions

$$H_m^{e\,(1)} = J_m^e + jN_m^e; \quad H_m^{e\,(2)} = J_m^e - jN_e^m.$$

For large u, both $c \cosh u$ and $c \sinh u$ approach r. From (A5.170), therefore, $H_m^{e\,(1)}$ and $H_m^{e\,(2)}$ become respectively proportional to $\dfrac{e^{jkr}}{\sqrt{r}}$ and $\dfrac{e^{-jkr}}{\sqrt{r}}$. Elementary wave functions can be formed according to the recipes

$$\begin{aligned} &S_m(kc, v)J_m^e(kc, u) \qquad \text{(in a region containing } u = 0) \\ &S_m(kc, v)H_m^e(kc, u) \qquad \text{(in the far field).} \end{aligned}$$

An incident plane wave can usefully be represented by the expansion (Fig. 14.8)

$$e^{-jk(x\cos\varphi_i + y\sin\varphi_i)} = \sqrt{8\pi}\sum_m \frac{1}{jm}\left[\frac{S_m^e(kc, \varphi_i)}{M_m^e(kc)} S_m^e(kc, v)J_m^e(kc, u) + \frac{S_m^o(kc, \varphi_i)}{M_m^o(kc)} S_m^o(kc, v)J_m^o(kc, u)\right]. \tag{A5.174}$$

MISCELLANEOUS FUNCTIONS

The Error Functions

$$\text{erf } x = \frac{2}{\sqrt{\pi}} \int_0^x e^{-t^2} dt$$

$$\text{erfc } x = 1 - \text{erf } x = \frac{2}{\sqrt{\pi}} \int_x^\infty e^{-t^2} dt \tag{A5.175}$$

with erf $\infty = 1$, erf $(-x) = -\text{erf } x$.

$$\frac{d}{dx}(\text{erf } x) = \frac{2}{\sqrt{\pi}} e^{-x^2}$$

$$\frac{d^2}{dx^2}(\text{erf } x) = -\frac{4}{\sqrt{\pi}} x e^{-x^2}. \tag{A5.176}$$

The Gamma Function

$$\Gamma(z) = \int_0^\infty e^{-x} x^{z-1} dx \qquad \text{Re}(z) > 0 \tag{A5.177}$$

$$\Gamma(z+1) = z\,\Gamma(z). \tag{A5.178}$$

When n is an integer or zero,

$$\Gamma(n+1) = n!. \tag{A5.179}$$

The gamma function can be seen as the generalization of the factorial for noninteger values. The complex function $\Gamma(z)$, with z a complex variable, is analytic except at points $z = 0, -1, -2, \ldots$, where it has simple poles.

Airy Functions

The Airy functions are solutions of the differential equation [38]

$$\frac{d^2 f}{dz^2} - zf = 0. \tag{A5.180}$$

They can be expressed as linear combinations of Bessel functions of order $\pm 1/3$. For example,

$$Ai(z) = \frac{1}{3}\sqrt{z}\left[I_{-\frac{1}{3}}\left(\frac{2}{3}z^{\frac{3}{2}}\right) - I_{\frac{1}{3}}\left(\frac{2}{3}z^{\frac{3}{2}}\right)\right]$$

$$Bi(z) = \sqrt{\frac{z}{3}}\left[I_{-\frac{1}{3}}\left(\frac{2}{3}z^{\frac{3}{2}}\right) + I_{\frac{1}{3}}\left(\frac{2}{3}z^{\frac{3}{2}}\right)\right]. \tag{A5.181}$$

Often used are the derived functions

$$\begin{aligned} u(z) &= \sqrt{\pi}\, Bi(z); & v(z) &= \sqrt{\pi}\, Ai(z) \\ w_1(z) &= \sqrt{\pi}[Bi(z) + jAi(z)]; & w_2(z) &= \sqrt{\pi}[Bi(z) - jAi(z)]. \end{aligned} \tag{A5.182}$$

A useful property:

$$Ai\left(ze^{\pm j\frac{2\pi}{3}}\right) = \frac{1}{2}e^{\pm j\frac{\pi}{3}}[Ai(z) \mp jBi(z)]. \tag{A5.183}$$

Laguerre Polynomials

$$x\frac{d^2L_n}{dx^2} + (1-x)\frac{dL_n}{dx} + nL_n = 0 \tag{A5.184}$$

$$L_{n+1}(x) = \frac{1}{n+1}\left[(2n+1-x)L_n(x) - nL_{n-1}(x)\right] \tag{A5.185}$$

$$L_0 = 1; \quad L_1 = 1 - x; \quad L_2 = \frac{1}{2}(x^2 - 4x + 2)$$

$$\int_0^\infty e^{-x}L_n(x)L_m(x)\,dx = \delta_{mn}. \tag{A5.186}$$

Associated polynomials:

$$x\frac{d^2L_n^m}{dx^2} + (m+1-x)\frac{dL_n^m}{dx} + nL_n^m = 0 \tag{A5.187}$$

$$L_{n+1}^m(x) = \frac{1}{n+1}\left[(2n+m+1-x)L_n^m(x) - (n+m)L_{n-1}^m(x)\right] \tag{A5.188}$$

$$L_n^m = 0 \text{ for } m > n$$

$$\int_0^\infty e^{-x}x^m L_n^m(x)L_s^m(x)dx = \frac{(n+m)!}{n!}\delta_{ns}. \tag{A5.189}$$

Chebyshev Polynomials

$$(1-x^2)\frac{d^2T_n}{dx^2} - x\frac{dT_n}{dx} + n^2T_n = 0 \tag{A5.190}$$

$$T_{n+1}(x) = 2xT_n(x) - T_{n-1}(x) \qquad (n \geq 1) \tag{A5.191}$$

$$T_0(x) = 1; \quad T_1(x) = x; \quad T_2(x) = 2x^2 - 1; \quad T_n(1) = 1$$

$$\int_{-1}^{1} \frac{1}{\sqrt{1-x^2}}T_m(x)T_n(x)\,dx = \delta_{mn}\left\{\begin{array}{ll} \pi & \text{for } m = 0 \\ \dfrac{\pi}{2} & \text{for } m = 1, 2, \ldots \end{array}\right\} \tag{A5.192}$$

$$\int_{-1}^{1} \frac{1}{\sqrt{1-x^2}}T_m(x')\log_e|x-x'|\,dx' = \begin{cases} -\pi\,\log_e 2\;T_0(x) & \text{for } m = 0 \\ -\dfrac{\pi}{m}T_m(x) & \text{for } m = 1, 2, \ldots. \end{cases} \tag{A5.193}$$

The following integrals are zero for m odd, while

$$\int_{-1}^{1} \frac{x^m dx}{\sqrt{1-x^2}} = \begin{cases} \pi & \text{for } m = 0 \\ \dfrac{\pi}{m} & \text{for } m = 2, 4, 6, \ldots . \end{cases} \tag{A5.194}$$

Polynomials of the second kind:

$$(1-x^2)\frac{d^2U_n}{dx^2} - 3x\frac{dU_n}{dx} + n(n+1)U_n = 0 \tag{A5.195}$$

$$U_{n+1}(x) = 2xU_n(x) - U_{n-1}(x) \tag{A5.196}$$

$$U_0(x) = 1; \quad U_1(x) = 2x; \quad U_2(x) = 4x^2 - 1$$

$$\int_{-1}^{1} \sqrt{1-x^2}\, U_n(x) U_m(x)\, dx = \frac{\pi}{2}\delta_{mn} \tag{A5.197}$$

$$\frac{d^2}{dx^2}\int_{-1}^{1} \sqrt{1-(x')^2}\, U_m(x') \log_e |x - x'|\, dx' = \pi(m+1)\, U_m(x) \quad \text{for } m = 0, 1, 2, \ldots . \tag{A5.198}$$

The following integrals are zero for m odd, while

$$\int_{-a}^{a} x^m \sqrt{a^2 - x^2} dx = \begin{cases} \dfrac{\pi a^2}{2} & \text{for } m = 0 \\ \dfrac{\pi a^4}{8} & \text{for } m = 2 \cdot \\ \dfrac{\pi a^6}{16} & \text{for } m = 4 \end{cases} \tag{A5.199}$$

Hermite Polynomials

$$\frac{d^2H_n}{dx^2} - 2x\frac{dH_n}{dx} + 2nH_n = 0 \tag{A5.200}$$

$$H_{n+1}(x) = 2xH_n(x) - 2nH_{n-1}(x) \tag{A5.201}$$

$$H_0(x) = 1; \quad H_1(x) = 2x; \quad H_2(x) = 4x^2 - 2$$

$$\int_{-\infty}^{\infty} e^{-x^2} H_m(x) H_n(x) dx = \sqrt{\pi}\, 2^n\, n!\, \delta_{mn}. \tag{A5.202}$$

Polynomials of the second kind:

$$\frac{d^2He_n}{dx^2} - x\frac{dHe_n}{dx} + nHe_n = 0 \tag{A5.203}$$

$$He_{n+1}(x) = xHe_n(x) - nHe_{n-1}(x) \tag{A5.204}$$

$$\int_{-\infty}^{\infty} e^{\frac{-x^2}{2}} He_m(x) He_n(x) dx = \sqrt{2\pi}\, n!\, \delta_{mn}. \tag{A5.205}$$

NOTES

1. N. N. Lebedev, *Special Functions and Their Applications.* Dover Publications, New York, 1972.
2. E. T. Whittaker and G. N. Watson. *A Course of Modern Analysis.* Cambridge University Press, New York, 4th edition, 1927.

A more extended treatment of special functions, including many that are not used in the text, can be found in [144, 165] of the general bibliography and in the following references:

C. F. du Toit, Evaluation of some algorithms and programs for the computation of integer-order Bessel functions of the first and second kind with complex arguments. *IEEE Antennas Prop. Mag.* **35**, 19–25, 1993.

I. S. Gradshteyn and I. M. Ryzhik, *Table of Integrals, Series and Products.* Academic Press, Orlando, 1980.

J. Havil, *Gamma, Exploring Euler's Constant.* Princeton University Press, Princeton and Oxford, 2003.

E. W. Hobson, *The Theory of Spherical and Ellipsoidal Harmonics.* Cambridge University Press, Cambridge, 1955.

E. Jahnke and F. Emde, *Tables of Functions, with Formulae and Curves.* Dover Publications, New York, 1945.

W. Magnus and F. Oberhettinger, *Formeln und Sätze für die speziellen Funktionen der mathematischen Physik.* Springer-Verlag, Berlin, 1943. An English version was published by Chelsea Publishing Company, New York, in 1954.

E. B. Mauring and J. Asmussen, Useful Bessel functions and integrals. *IEEE Trans. Microwave Theory Tech.* **41**, 1468–1471, 1983.

N. W. Mc. Lachlan, *Theory and Application of Mathieu Functions.* Dover Publications, New York, 1964.

J. Meixner and F. W. Schäfke, *Mathieusche Funktionen und Sphäroidfunktionen.* Springer-Verlag, Berlin, 1954.

P. Moon and D. E. Spencer, *Field Theory Handbook.* Springer-Verlag, Berlin, 1961.

R. Paknys, Evaluation of Hankel functions with complex argument and complex order. *IEEE Trans.* **AP40**, 569–578, 1992.

L. Robin, *Fonctions sphériques de Legendre et fonctions sphéroïdales.* Gauthier-Villars, Paris, 1957.

G. N. Watson, *A Treatise on the Theory of Bessel Functions.* Cambridge University Press, Cambridge, 2nd edition, 1958.

Appendix 6

Complex Integration

ANALYTIC FUNCTIONS

A function $f(z) = u(x, y) + jv(x, y)$ has a derivative at a point z if the ratio

$$\frac{f(z + \Delta z) - f(z)}{z} = \frac{u(x + \Delta x, y + \Delta y) + jv(x + \Delta x, y + \Delta y) - u(x, y) - jv(x, y)}{\Delta x + j\Delta y}$$

approaches a well-defined, unique limit when Δx and Δy approach zero independently. This limit is termed the *derivative* of $f(z)$. The function $f(z) = z^2$, for example, has a derivative at $z = 1$, but $f(z) = 1/(z - 1)$ does not have one at that point. *Function* $f(z)$ is *analytic* at a point z if it possesses a derivative at all points in some neighborhood of z. If this holds at every point z of an open connected set, the function is said to be analytic in the set. Analyticity implies that the mapping is conformal; that is, that a given rotation of Δz produces an equal rotation of Δf, both in magnitude and in sense. Analytic functions have remarkable properties; for example:

1. The real and imaginary parts satisfy the Cauchy-Riemann conditions

$$\frac{\partial u}{\partial x} = \frac{\partial v}{\partial y} \qquad \frac{\partial u}{\partial y} = -\frac{\partial v}{\partial x}. \tag{A6.1}$$

These conditions are necessary; they become sufficient when the partial derivatives are continuous.[1,2,3] As mentioned by Goursat,[1] a complex quantity z is essentially a system of two real quantities, ranked in a given order. Analogously, analytic functions of z are fundamentally systems of two functions $u(x, y), v(x, y)$ that satisfy (A6.1). The theory could be developed without reference to the symbol j.

2. A function that is analytic at z has derivatives of all orders at that point. The point is often called a *regular point* of the function. Points at which the function is not analytic are termed *singular*. Let a be a regular point, and let z' be the nearest singularity. Within a circle of radius $|z' - a|$ centered at a, the Taylor expansion

$$f(z) = f(a) + f'(a)(z - a) + \frac{1}{2}f''(a)(z - a)^2 + \cdots \tag{A6.2}$$

is valid (Fig. A6.1). This remarkable relationship can be differentiated term by term, and therefore it allows determination of $f(z)$ and all its derivatives at an

Electromagnetic Fields, Second Edition, By Jean G. Van Bladel

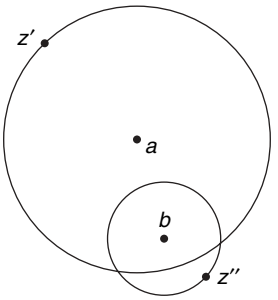

Figure A6.1 Analytic continuation.

arbitrary point $z = b$ located within the circle of convergence. Once these values are obtained, a Taylor expansion can be written about the point $z = b$. The process may be repeated, and an *analytic continuation* of the function can be obtained by fitting the various circles together.

Functions whose power series expansions converge in the entire z-plane are termed *entire functions*. They are necessarily single-valued. It is important to know whether the point at infinity is a regular point or a singular point of $f(z)$. By definition, $f(z)$ behaves at infinity as $f(1/z)$ does at $z = 0$. If the function $f(1/z)$ is regular at the origin, there exists a Taylor-series representation

$$f\left(\frac{1}{z}\right) = a_0 + a_1 z + a_2 z^2 + \cdots, \tag{A6.3}$$

valid within a certain circle of convergence of radius R. Under these conditions, $f(z)$ is regular at infinity and can be represented by the series

$$a_0 + \frac{a_1}{z} + \frac{a_2}{z^2} + \cdots \tag{A6.4}$$

outside a circle of radius $1/R$. For example, the function $(z-1)^{-1}$ is regular at infinity and can be represented by the series $\sum_{n=0}^{\infty} z^{-n}$ outside the unit circle.

MULTIPLE-VALUED FUNCTIONS: BRANCH POINTS

A function is *uniform* in a region D when every path C that connects point z_0 to another point z in D leads to the same final value for $f(z)$. This does not always happen. The criterion is the absence (or presence) of *branch points* within D. Starting from a regular point a, it is possible, by analytic continuation, to compute values of $f(z)$ all along a curvilinear arc C. If the end point b of the arc is allowed to approach a, two cases are possible:

1. The value of $f(z)$ at b approaches $f(a)$.
2. The value of $f(z)$ at b does not approach $f(a)$.

Which case prevails depends on whether or not branch points are contained within the area enclosed by the curve. By definition, $f(z)$ has a branch point at $z = c$ if an arbitrary contour encircling that point (and no other branch point) leads to final values that are different from

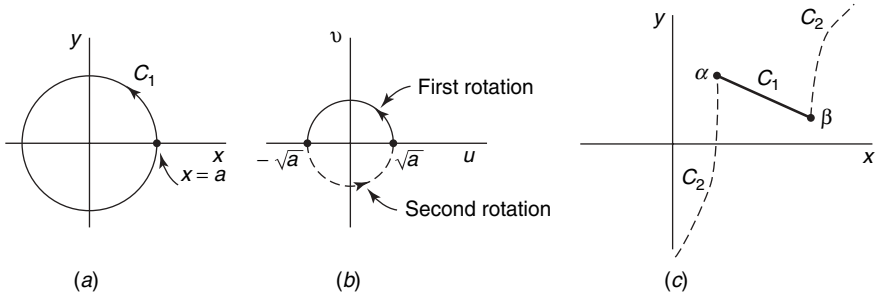

Figure A6.2 (a, b) Branch point of the function $z^{\frac{1}{2}}$. (c) Branch cuts.

the initial ones. For example, the function $z^{\frac{1}{2}}$ has a branch point at the origin $z = 0$. This can be shown by the following argument: let $z^{\frac{1}{2}}$ be equal to the positive root $a^{\frac{1}{2}}e^{j0}$ at a point $x = a$ on the positive real axis (Fig. A6.2a and b). Analytic continuation along a closed contour that does *not* encircle the origin brings one back to the initial value $a^{\frac{1}{2}}e^{j0}$, but the same process along a contour (such as C_1) that encircles the origin yields the value $a^{\frac{1}{2}}e^{j\pi}$. Another rotation around C_1 brings one back to $a^{\frac{1}{2}}e^{j2\pi} = a^{\frac{1}{2}}e^{j0}$. The branch point is then said to be of order 1. More generally, a branch point is of order m if $m + 1$ rotations around $z = c$ reproduce the initial value of $f(z)$. If no finite number of rotations will achieve this result, the function has an infinite number of values, and the branch point is of infinite order. Illustratively,* $\log z$ has a branch point of infinite order at $z = 0$, because each successive counterclockwise rotation increases the value of the function by $2\pi j$.

The usual test for the existence of a branch point at $z = b$ consists in forming $f(b + \rho e^{j\phi})$ (where ρ is a small radius), allowing ϕ to vary from zero to 2π, and determining whether initial and final values are identical. Branch points never occur singly; $z^{\frac{1}{2}}$, for example, has a branch point at the origin, but it has also one at infinity. Some additional criteria for the detection of branch points are

1. If the functions $f_1(z), f_2(z), \ldots$ have individual branch points $a_1, a_2, \ldots$, the product of these functions has the same branch points, provided all the a_i's are different. If some values are common to several factors, these may or may not be branch points of the product. Further analysis is necessary.
2. Let $f(z)$ be analytic at the origin, and let (A6.3) represent its Taylor expansion there. The form of the expansion shows that $f[(z - a)^{\frac{1}{2}}]$ has a branch point at $z = a$ unless $f(z)$ is an even function of z.
3. Let $f(z)$ be analytic at $z = a$, and let (A6.2) represent its Taylor expansion at that point. If $f(a)$ is different from zero, $[f(z)]^{\frac{1}{2}}$ does not have a branch point at $z = a$. The roots of $f(z) = 0$, however, should be investigated. If the first nonzero term in

*Let z be written in polar form as $|z|e^{j\varphi}$. Then

$$\log z = log\,|z| + j(\varphi + 2k\pi) \qquad (k = 0, \pm 1, \ldots).$$

Goursat[1] uses the notation Log z for that function.

the expansion is an odd power of $z - a$, there is a branch point at $z = a$; if it is an even power, there is none.

4. At points at which $f(a)$ is different from zero, $\log f(z)$ has no branch point.

A few examples:

$$\log e^z \text{ has no branch point at } z = 0.$$

Have branch points:

$$\log z \text{ at } z = 0 \text{ and } z = \infty$$

$$\log \sin z \text{ at } k\pi \ (k \text{ an integer})$$

$$\log (z-a)(z-b) \text{ at } a, b, \infty; \quad \log (z-a)(z-b)^{-1} \text{ at } a, b$$

$$(\sin z)^{\frac{1}{2}} \text{ at } k\pi; \quad (\cos z)^{\frac{1}{2}} \text{ at } \frac{\pi}{2} \pm k\pi.$$

If $f(z)$ can be put in the form $e^{g(z)}$, where g is single-valued, $\log f(z)$ has no branch point, and it represents an infinity of single-valued functions $g(z) + k2\pi j$ (k an integer).

BRANCH CUTS

Let us connect two branch points by an arbitrary line—the negative real axis, for example. Any contour that does not cross this line (the *branch cut*) leads back to the initial value of $z^{\frac{1}{2}}$. If we decide not to cross the branch cut, the function becomes single-valued over the entire z plane. This process generates two different branches of $z^{\frac{1}{2}}$, depending on whether $a^{\frac{1}{2}}e^{j0}$ or $a^{\frac{1}{2}}e^{j\pi}$ is taken as the value of $z^{\frac{1}{2}}$ at a point a on the positive real axis. Each of these branches is a single-valued function and partakes of all the properties of these functions. Figure A6.2*c* shows two possible branch cuts, C_1 and C_2, for the function $[(z-\alpha)(z-\beta)]^{\frac{1}{2}}$, whose branch points are α and β. Branch cut C_2 goes through the point at infinity.

POLES AND ESSENTIAL SINGULARITIES

A function $f(z)$ that is analytic inside an annulus and on the latter's boundary can be represented by the Laurent expansion

$$f(z) = \sum_{n=0}^{\infty} a_n (z-a)^n + \sum_{n=1}^{\infty} \frac{b_n}{(z-a)^n} \tag{A6.5}$$

inside the annulus. The coefficients of this expansion are given by the formulas

$$a_n = \frac{1}{2\pi j} \int_{C_1} \frac{f(z)}{(z-a)^{n+1}}\, dz$$

$$b_n = \frac{1}{2\pi j} \int_{C_1} f(z)(z-a)^{n-1}\, dz, \tag{A6.6}$$

where the contour C_1 must be described in the sense that leaves the enclosed area to the left of the contour, and where $z = a$ is the center of the annulus. If the function is analytic in the inner circle, no inverse powers of $(z - a)$ appear in the Laurent expansion. If this is not the case, two possibilities must be considered.

1. The singularities are isolated. A new annulus and a new Laurent expansion can then be introduced around each singularity z_0. If the negative powers of $(z - z_0)$ are finite in number, z_0 is a *pole*. If b_m is the last coefficient which is not zero, z_0 is a *pole of order m*. The modulus of the function is infinite at the pole, but multiplication by $(z - z_0)^m$ gives rise to a function that is analytic at z_0 and in its neighborhood. No smaller power can achieve this result. Examples of functions and their poles are

$$[(z-a)(z-b)]^{\frac{1}{2}} \text{ at } z = \infty; \quad (1 - e^z)^{-1} \text{ at } z = 0, jk2\pi$$

$$\tan z \text{ at } z = \frac{\pi}{2} \pm k\pi; \quad \cot z \text{ at } z = k\pi.$$

   If the negative powers are infinite in number, the *singularity* is said to be *essential*. The function $e^{1/z}$, for example, admits the expansion $\sum_{n=0}^{\infty}(1/n!)(1/z^n)$ about the origin, whence it follows that the origin is an essential singularity. Other examples are

$$e^z \text{ at } z = \infty; \quad \sin z \text{ and } \cos z \text{ at } z = \infty.$$

   Any singularity of a single-valued function other than a pole is essential.

2. The singularities are not isolated. The point at infinity, for example, is a limit point of simple poles for $1/\cos z$. So also is the origin for the function $1/\sin(1/z)$, which has singularities for $z = \pm 1/k\pi$, where k is an integer. A small circle centered at the origin contains an infinite number of these singularities. Other examples of functions having limit points of simple poles are

$$(1 - e^z)^{-1} \text{ at } z = \infty; \quad (\cos z)^{-1} \text{ and } \cot z \text{ at } z = \infty.$$

A uniform function that has no other singular points in a region D than (at most) poles is said to be *meromorphic* in D.

CAUCHY'S THEOREM

Cauchy's theorem states that if $f(z)$ is single-valued and analytic in a simply connected domain, and if C is a closed, piecewise smooth curve in the domain, then $\int_C f(z)\,dz = 0$ for all C. If the region is multiply connected (as in Fig. A6.3*a*) and does not contain any singularities, then

$$\int_{C_0} f(z)\,dz = \int_{C_1} f(z)\,dz + \int_{C_2} f(z)\,dz + \cdots + \int_{C_m} f(z)\,dz, \tag{A6.7}$$

provided all paths are oriented in the same sense. The importance of Cauchy's theorem can be demonstrated by a simple example. Assume that a (difficult) integral must be calculated along the path ABC and that the same integral can easily be evaluated along C'. If the region

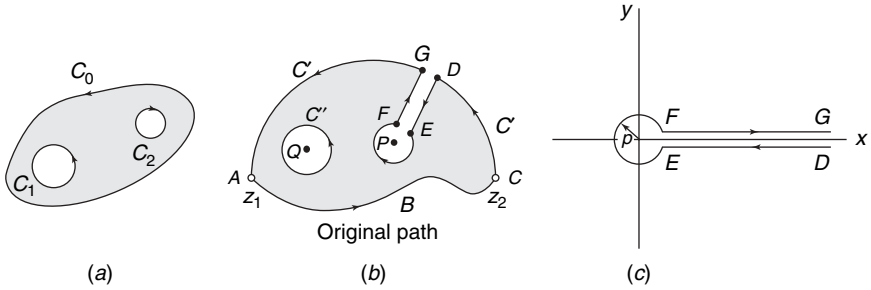

Figure A6.3 (*a*) Relevant to Cauchy's theorem. (*b*) Application of Cauchy's theorem. (*c*) Contribution from a branch cut.

between C' and the original path does not contain any singularities, the desired integral is simply the integral along C'. If, however, singularities are present, they must be excluded from the region. Figure A6.3*b* shows how a branch point P and an isolated singularity Q have been excluded, making the function analytic and single-valued in the dashed region. It is now possible to write

$$\int_{ABC} f(z)\,dz + \int_{CD} f(z)\,dz + \int_{DEFG} f(z)\,dz + \int_{GA} f(z)\,dz = \int_{C''} f(z)\,dz,$$

from which the desired integral can be evaluated if the other integrals are tractable. For CD and GA, the usual method is to choose a path C' that can be expressed in parametric form (i.e., along which z can be expressed as a function of a real parameter t varying from α to β). For such a case,

$$\int_{C'} f(z)\,dz = \int_{\alpha}^{\beta} f[z(t)]z'(t)\,dt.$$

A path often used is an arc of circle of radius ρ centered at a, on which $z = \alpha + \rho e^{jt}$. Consider, for example, $\displaystyle\int_{+1}^{-1} |z|\,dz$, where the integral is along the upper half of the unit circle. It can be evaluated by setting $z = e^{jt}$. In that case, $|z| = 1, dz = je^{jt}dt$, and the integral becomes $\displaystyle j\int_0^{\pi} e^{jt}dt = -2$.

Another typical path is a line segment joining z_1 to z_2, along which $z = z_1 + (z_2 - z_1)t$ (with $0 \le t \le 1$). In the evaluation of $\displaystyle\int_{-\infty}^{+\infty} f(x)\,dx$, where $f(z)$ is analytic in the upper half-plane (except for poles which do not lie on the real axis), it is usual to close the contour with a semicircle of infinite radius centered at the origin. The integral along this semicircle vanishes if $f(z)$ goes to zero at infinity at least as fast as $1/|z|$. An integrand of the form $e^{jkz}/z = e^{-ky}e^{jkx}/z$, for example, gives rise to an integral that vanishes along the upper or lower half-circle at infinity, depending on whether k is positive or negative (see also Jordan's lemma for a more general function).

The branch-cut integral $\displaystyle\int_{DEFG} f\,dz$ can also be evaluated by use of a parametric representation. Assume, for instance, that $f(z) = z^{\frac{1}{2}}g(z)$, where $g(z)$ is an analytic function. Assume also that the branch cut avoiding the origin has been chosen as in Figure A6.3*c*.

The value of F is either $g(\rho)\rho^{\frac{1}{2}}$ or $g(\rho)\rho^{\frac{1}{2}}e^{j\pi}$, depending on which branch is chosen. For the branch $g(\rho)\rho^{\frac{1}{2}}$, for example,

$$\int_F^G f(z)\,dz = \int_0^{x_G} x^{\frac{1}{2}} g(x)\,dx.$$

Along the circle FE of radius ρ, the value of $f(z)$ varies continuously from $g(\rho)\rho^{\frac{1}{2}}$ (at F) to $g(\rho)\rho^{\frac{1}{2}}e^{j\pi}$ (at E). The integral along the circle is therefore

$$\int_E^F f(z)\,dz = -\int_F^E f(z)\,dz = -\int_{\rho=0}^{\rho=2\pi} g(\rho\, e^{j\varphi})\rho^{\frac{1}{2}} j\rho\, e^{j\varphi}\,d\varphi.$$

This integral approaches zero with ρ. The integral along DE is

$$\int_D^E f(z)\,dz = -\int_E^D f(z)\,dz = -\int_0^{x_D} g(x)x^{\frac{1}{2}}e^{j\pi}\,dx = \int_0^{x_D} g(x)x^{\frac{1}{2}}\,dx.$$

RESIDUES

To evaluate the integral around a circle centered at an isolated singularity $z = a$ (the integral along C'' in Fig. A6.3*b*, for example), we make use of the relationship

$$\int_{C''} f(z)\,dz = 2\pi j b_1, \tag{A6.8}$$

which is one of the formulas giving the coefficients of the Laurent expansion. This relationship shows that the integral we seek is proportional to the coefficient b_1 [also termed the *residue of* $f(z)$ at a]. Several methods are available for the evaluation of b_1:

1. In some cases, the coefficient of the Laurent expansion can be calculated directly. The function $e^{1/z}$, for example, admits the expansion $e^{1/z} = 1 + (1/z) + (1/2!)(1/z^2) + \cdots$. This expansion shows that $z = 0$ is an essential singularity with residue 1.
2. The residue of a simple pole is given by $\lim_{z\to a} f(z)(z-a)$. For example, $1/\sin z$ has poles at $z = k\pi$, with residue $\lim_{z\to k\pi}(z - k\pi)/\sin z = (-1)^k$. For a pole of order m, the formula becomes

$$[1/(m-1)!]\lim_{z\to a}\left\{(d^{m-1}/dz^{m-1})[f(z)(z-a)^m]\right\}.$$

3. If $f(z)$ has a pole at a, $1/f(z)$ is analytic at that point. Assume that the Taylor expansion $C_0 + C_1(z-a) + \cdots$ of $1/f(z)$ is known. The Laurent expansion of $f(z)$ can now be obtained by inverting the series. Unless C_0 of the Taylor series of $1/f(z)$ is zero, the function $f(z)$ does not have a pole at $z = a$. If $C_0 = 0$, there is a first-order pole at $z = a$, with residue $1/C_1$. If C_0 and C_1 are zero (and $C_2 \neq 0$), there is a second-order pole, with residue $-C_3/C_2^2$.

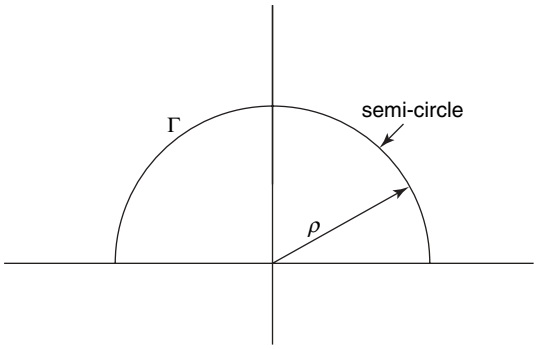

Figure A6.4 Relevant to Jordan's lemma.

4. Let $f(z)$ be the quotient of $g(z)$ divided by $h(z)$, and let z_0 be a zero of the denominator (but not of the numerator). If this zero is simple, the following formula holds in the vicinity of z_0:

$$f(z) = \frac{g(z)}{h(z)} = \frac{a_0 + a_1(z - z_0) + a_2(z - z_0)^2 + \cdots}{b_1(z - z_0) + b_2(z - z_0)^2 + \cdots}. \tag{A6.9}$$

The formula shows that the residue at z_0 is $a_0/b_1 = g(z_0)/h'(z_0)$. If $b_1 = 0$, the zero is of order 2, and z_0 is a pole of order 2 with residue

$$(a_1 b_2 - a_0 b_3)/b_2^2.$$

If $b_1 = 0$ and $b_2 = 0$, the zero is triple, the pole is of order 3, and the residue is

$$(a_0 b^4 - a_0 b_3 b_5 - a_1 b_3 b_4 + a_2 b_3^2)/b_3^3.$$

JORDAN'S LEMMA

Let $z = |z|e^{j\phi}$, and $0 \leq \phi \leq \pi$. If $f(z)$ approaches zero uniformly (for $0 \leq \phi \leq \pi$) with respect to ϕ as $|z| \to \infty$, and if $f(z)$ is analytic when both $|z| > c$ (a constant) and $0 \leq \phi \leq \pi$, then, for λ positive (Fig. A6.4),

$$\lim_{\rho \to \infty} \int_{\Gamma} e^{j\lambda z} f(z)\, dz = 0, \tag{A6.10}$$

where Γ is a semicircle of radius ρ above the real axis, with center at the origin.

MITTAG-LEFFLER'S THEOREM

Assume that $f(z)$ has only a finite number N of singular points a_i in any portion of the plane at a finite distance, and let $G_1\left(\dfrac{1}{z - a_i}\right)$ be a polynomial, or an entire function of $\left(\dfrac{1}{z - a_i}\right)$.

Then there exists a uniform analytic function that is regular for every finite value of $z \neq a_i$, and the principal part of which is G_i in the domain of a_i. This function is[1,3,4,5]

$$f(z) = \sum_{i=1}^{N} \left[G_i \left(\frac{1}{z - a_i} \right) + P_i(z) \right], \tag{A6.11}$$

where $P_i(z)$ is a polynomial. By adding to $f(z)$ a polynomial or an entire function, one keeps the same singular points with the same principal parts. There results the most general expression for all uniform functions that have given singular points with corresponding principal parts. If all the G_i are polynomials, the function is meromorphic in every region of the plane at a finite distance, and conversely.

SADDLE-POINT INTEGRATION

Let $f(z)$ be analytic at a. If the first m derivatives of $f(z)$ vanish at $z = a$, this point is termed a *saddle point* (or point of *stagnation*), and the Taylor expansion takes the form

$$f(z) = f(a) + (z - a)^{m+1} \frac{f^{(m+1)}(a)}{(m+1)!} + \cdots \tag{A6.12}$$

at that point. Under these circumstances, the inverse function $z = \phi(f)$ is multiple-valued and has a branch point of order m at $f = f(a)$. The principle can be immediately verified for the functions z^2 and $z^{\frac{1}{2}}$, which have, respectively, a saddle point and a branch point at the origin. Consider now the integral

$$I_C(\lambda) = \int_C g(z) e^{\lambda f(z)} dz, \tag{A6.13}$$

where λ is real and positive, and C some contour in the complex plane, typically extending to infinity, but possibly ending at finite end-points. The function $f(z)$ is assumed analytic. Our interest centers on the limit of $I_C(\lambda)$ for large λ. In the saddle-point method, C is deformed into a contour C_s, running through a saddle-point z_s, a point at which we assume that $(df/dz) = 0$ (Fig. A6.5*a*). From (A6.1), and because u and v are harmonic, the following

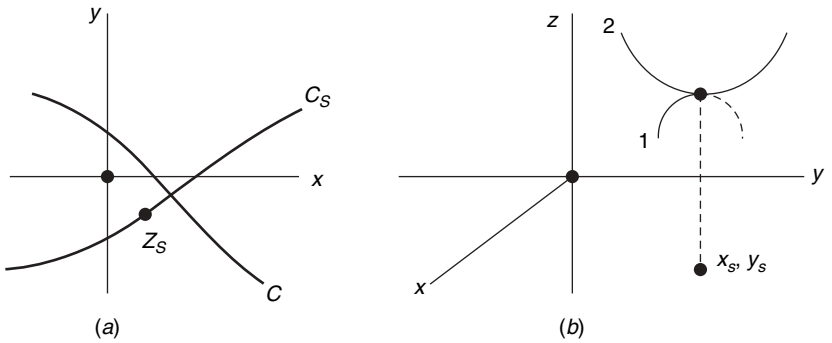

Figure A6.5 (*a*) A contour C and its deformation through z_s. (*b*) Variation of $u(x, y)$ at a saddle point.

relationships hold at z_s:

$$\frac{\partial u}{\partial x} = \frac{\partial u}{\partial y} = \frac{\partial v}{\partial x} = \frac{\partial v}{\partial y} = 0; \quad \frac{\partial^2 u}{\partial x^2} = -\frac{\partial^2 u}{\partial y^2}; \quad \frac{\partial^2 v}{\partial x^2} = -\frac{\partial^2 v}{\partial y^2}.$$

The function u has zero first derivatives at (x_s, y_s), but that point is neither a maximum nor a minimum. If the $u(x, y)$ curve in Figure A6.5*b* has a positive slope in one direction, it must have a negative one at right angles to it. Depending on the choice of path through z_s, the magnitude of $u(x, y)$ may increase, decrease, or remain constant in the vicinity of z_s. The appropriate choice in the current application is the path of steepest descent, marked as 1 in Figure A6.5*b*. From (A6.1), grad u and grad v are perpendicular to each other. It follows that the path of steepest descent for u is at the same time a path of constant value of $v(x, y)$; that is, a path along which the phase of $e^{\lambda f(z)}$ is *stationary*. In the integral

$$I_{C_s}(\lambda) = \int_{C_s} g(z) e^{\lambda u(x,y)} e^{j\lambda v(x,y)} dz \tag{A6.14}$$

the factor $e^{\lambda u}$ reaches a maximum at (x_s, y_s), and, in the limit $\lambda \to \infty$, decreases rapidly on both sides of (x_s, y_s). The main contribution to the integral now comes from the vicinity of z_s or, if there are N saddle-points on C_s, from the vicinities of these N points. In the neighborhood of z_s we may write

$$f(z) \approx f(z_s) + \frac{1}{2}(z - z_s)^2 f''(z) + \cdots .$$

If $g(z)$ varies little around z_s:

$$I_{C_s}(\lambda) \approx g(z_s) e^{\lambda f(z_s)} \int_{C_s} e^{\frac{1}{2}\lambda (z - z_s)^2 f''(z_s)} dz.$$

The exponential factor in the integrand can be written as

$$e^{\frac{1}{2}\lambda |z - z_s|^2 f''(z_s)|(\cos 2\psi + j \sin 2\psi)},$$

where

$$\psi = \arg (z - z_s) + \frac{1}{2} \arg f''(z_s).$$

The *path of steepest descent* corresponds with $\psi = \pm\frac{\pi}{2}$, for which the factor is of the form e^{-s^2}, with

$$s^2 = -\frac{1}{2}(z - z_s)^2 f''(z_s).$$

The typical topography around the saddle point is shown in Figure A6.6, where 1 is the path of steepest ascent, 2 that of steepest descent, and 3, 4 directions of constant value. The integral becomes

$$I_s(\lambda) \approx g(z_s) e^{\lambda f(x_s)} \left[-\frac{1}{2} f''(z_s) \right]^{-\frac{1}{2}} \int e^{-\lambda s^2} ds.$$

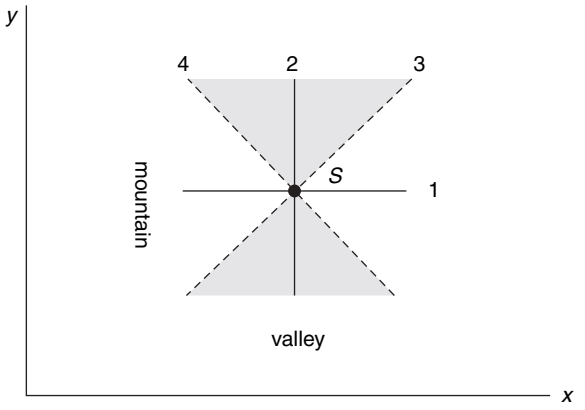

Figure A6.6 Topography around a saddle-point S.

Integration is now along the real axis. Because

$$\int_{-\infty}^{\infty} e^{-\lambda s^2} ds = \sqrt{\frac{\pi}{\lambda}},$$

the end result takes the form

$$I_s(\lambda) \approx g(z_s) e^{\lambda f(z_s)} \sqrt{-\frac{2\pi}{\lambda f''(z_s)}} \qquad (\lambda \to \infty). \tag{A6.15}$$

This simple procedure must be refined in many practical cases. One typically encounters, indeed,

1. Isolated first-order saddle points (the case discussed above)
2. Isolated saddle points of higher order, for which the first nonzero derivative is the mth one, with $m > 2$
3. First-order saddle point near a pole or a branch point[6]
4. Saddle point near an end point.

These items are discussed at great length in specialized texts.[7,8] Note that integral (A6.13) often occurs in the form

$$I_C(\lambda, \phi) = \int_C g(z, \phi) e^{\lambda f(z,\phi)} dz,$$

where ϕ is variable. A varying ϕ may draw the singularities to the vicinity of the saddle point.[9]

The purpose of the saddle-point integration is to replace the original integration path C by C_s. The two corresponding integrals are equal when C can be deformed into C_s without crossing any singularities. If this is not possible, Cauchy's theorem should be applied, together with the requirement that the functions remain single-valued. If a pole is crossed, its residue must be added. If a branch point is encountered, the integral over an appropriate cut should be added.

NOTES

1. E. Goursat, *Cours d'analyse mathématique.* Tome II, 6e édition, Gauthiers-Villars, Paris, 1942. An English translation is available from Dover Publications, New York.
2. B. Friedman, *Lectures on Applications-Oriented Mathematics*. Holden-Day, Inc., San Francisco, 1969.
3. H. and B. Jeffreys, *Methods of Mathematical Physics.* Cambridge University Press, Cambridge, 3rd edition, 1972.
4. E. T. Whittaker and G. N. Watson. *A Course of Modern Analysis*. Cambridge University Press, New York, 4th edition, 1952.
5. K. Knopp. *Funktionentheorie.* Goschen Verlag, Berlin, 1913. An English translation has been published by Dover Publications, New York.
6. R. G. Rojas, Comparison between two asymptotic methods, *IEEE Trans. AP* **35**, 1489–1492 (1987).
7. N. Bleistein and R. A. Handelsman, *Asymptotic Expansions of Integrals.* Holt, Rinehart and Winston, New York, 1975.
8. L. B. Felsen and N. Marcuvitz, *Radiation and Scattering of Waves.* Chapter 4, Prentice-Hall, Englewood Cliffs, N.J., 1973.
9. E. L. Yip and R. J. Chiavetta, Comparison of uniform asymmetric expansions of diffraction integrals, *IEEE Trans. AP* **35**, 1179–1180 (1987).

Appendix 7

Transforms

THE ONE-SIDED LAPLACE TRANSFORM

The one-sided Laplace transform of a function of the real variable t is defined by[1,2,3,4]

$$L_1(f) = F(s) = \int_0^\infty e^{-st} f(t)\, dt. \tag{A7.1}$$

This integral exists, in particular, when the original function $f(t)$ is of exponential order σ_m, that is, when $e^{-\sigma t} f(t)$ is integrable up to $t = \infty$ for all $\sigma > \sigma_m$, and not for $\sigma \leq \sigma_m$. The function $f(t)$ may have finite jumps, and even become infinite at t_0, provided $|(t - t_0)^k f(t)|$ remains bounded at t_0, with $k < 1$. Near the origin, $\lim_{\epsilon \to 0} \int_\epsilon^a f(t)\, dt$ must be absolutely convergent.

The transform is an analytical function in the half-plane to the right of the *abscissa of convergence*, that is, for $\mathrm{Re}(s) > \sigma_m$. On the vertical $\mathrm{Re}(s) = \sigma_m$ there must be at least one singularity, which can be the point at infinity. The whole region to the right of that vertical is devoid of singularities. A few examples:

$$\sigma_m = a \quad \text{for} \quad f(t) = e^{at} (a \text{ real}); \quad \sigma_m = 0 \quad \text{for} \quad t^k.$$

The function e^{-t^2}, on the other hand, is analytical in the whole complex s-plane. Methods to determine σ_m can be found in the literature.[1,2]

A Few Properties of the Laplace Transform

- $$F(s^*) = [F(s)]^* \quad \text{when } f \text{ is real-valued.} \tag{A7.2}$$
- Functions f_1 and f_2, which have the same transform, differ by a null function, that is, they satisfy $\int_0^t |f_1(\tau) - f_2(\tau)| d\tau = 0$ for all t.
- $$F(s + s_0) = L_1(f e^{-s_0 t}) \quad \text{for } \mathrm{Re}\,(s) > \sigma_m - \mathrm{Re}(s_0). \tag{A7.3}$$
- $$L_1[f(t - t_0)] = e^{-st_0}[F(s) - A(s)], \text{where } A(s) = \int_0^{-t_0} f(t) e^{-st} dt. \tag{A7.4}$$
- Assume that the integrals producing the transformations $F_1(s)$ and $F_2(s)$ are absolutely convergent. For such a case, the product $F_1(s)F_2(s)$ is the transform of the

Electromagnetic Fields, Second Edition, By Jean G. Van Bladel

convolution

$$f_1 * f_2 = \int_{-\infty}^{\infty} f_1(t-\tau) f_2(\tau)\, d\tau \tag{A7.5}$$

Some Limit Values

- $F(s)$ always approaches zero when $|s| \to \infty$, but the order of approach depends on the behavior of $f(t)$ and derivatives at the origin. If $f(t)$ and derivatives up to the $(n-1)^{\text{th}}$ order vanish as $t \to 0$, and if $\lim_{t\to 0} f^{(n)}(t)$ is well-defined and nonzero, then

$$\lim_{s\to\infty} F(s) = \frac{f^{(n)}(0)}{s^{n+1}}. \tag{A7.6}$$

- If $\lim_{t\to\infty} f(t) = At^k$, with $k > -1$, then

$$\lim_{s\to 0} F(s) = A\frac{\Gamma(k+1)}{s^{k+1}}. \tag{A7.7}$$

- In particular, if $\lim_{t\to\infty} f(t) = A \neq 0$, then

$$\lim_{s\to 0} F(s) = \frac{A}{s} = \frac{f(\infty)}{s}. \tag{A7.8}$$

Derivative and Integral

- Because differentiation emphasizes the singularities, it is not evident that $f'(t)$ will have a transform. However, if $f(t)$ is differentiable for every $t > 0$ and has a limit $f(+0)$ for $t \to 0$, and if $f'(t)$ has a transform with abscissa σ'_m, then

$$L_1\left(\frac{df}{dt}\right) = sF(s) - f(+0) \qquad (\text{with } \sigma'_m \geq \sigma_m). \tag{A7.9}$$

- In the s-plane, the derivative

$$\frac{d^n F(s)}{ds^n} \tag{A7.10}$$

  is the transform of $(-t)^n f(t)$.

- Integration attenuates the singularities, but because an integral increases faster at $t \to \infty$ than the function itself, the abscissa of convergence of the integral may be larger than that of $f(t)$. Example: $\sigma_m = -1$ for e^{-t}, but $\sigma'_m = 0$ for the integral, equal to $(1 - e^{-t})$. The two transforms are connected by

$$L_1 \int_0^t f(t')\, dt' = \frac{1}{s} F(s). \tag{A7.11}$$

Distributions

The notion "Laplace transform" may be extended to generalized functions T of the type discussed in Appendix 8. The definition is[5,6]

$$T(s) = \langle T, e^{-st} \rangle. \tag{A7.12}$$

Note that e^{-st} is not a test function; it is infinitely differentiable, but not of bounded support, hence the second member of (A7.12) does not necessarily have a meaning. For the *Dirac distribution* at the origin:

$$D(s) = \langle \delta_0, e^{-st} \rangle = 1. \tag{A7.13}$$

The usual rules of differentiation, time shift, etc. . . . can be applied to these transforms when they exist. For example:

$$\left\langle \frac{d^m \delta_0}{ds^m}, e^{-st} \right\rangle = s^m \qquad (m = 0, 1, 2, \ldots). \tag{A7.14}$$

Inversion

Given $F(s)$, the original $f(t)$ can be determined by means of the *Bromwich integral*

$$f(t) = \frac{1}{2\pi j} \lim_{\omega \to \infty} \int_{\sigma - j\omega}^{\sigma + j\omega} e^{st} F(s)\, ds. \tag{A7.15}$$

The integral is defined as a Cauchy principal value, and the vertical is located to the right of all singularities of $F(s)$. When it is taken at the abscissa of convergence itself (i.e., at $\sigma = \sigma_m$), the contour must be slightly deformed to keep all singularities to its left (Fig. A7.1). At points where $f(t)$ has a jump singularity, the right-hand member of (A7.15) converges to $\frac{1}{2}[f(t+0) + f(t-0)]$. In particular, it converges to $\frac{1}{2}f(0)$ at $t = 0$.

To evaluate the integral in (A7.15), the vertical path is closed by a semicircle, a parabolic arc, or a rectangular contour. The choice is governed by the ease with which the integral along C' can be calculated. The usual cuts should be made in the presence of branch points. Cauchy's theorem is subsequently applied to the full contour, and the contributions of poles is taken into account.[7] Part of C' is typically an arc of a circle centered at the origin, and of very large radius. The arcs located left of the imaginary axis contribute a factor e^{st}, which decreases exponentially because $t \geq 0$, and therefore give zero contribution. The difficult parts are AA' and BB', which introduce an exponential increase because $\mathrm{Re}(s) > 0$. When $\sigma_m = 0$, it is a simple matter to eliminate the difficulty by choosing AB on the imaginary axis itself. One can complete, in the absence of branch cuts, AB by a semicircle of large radius. If $F(s)$ approaches zero as $R \to \infty$, and if there are no singularities on Γ, Jordan's lemma (A6.10) shows that the contribution from Γ vanishes. This would hold, for example, when the only singularities are a finite number of poles at a finite distance.

In many problems, the evaluation of the Bromwich integral by complex analysis techniques is too complicated, and one must rely on direct numerical methods (e.g., by

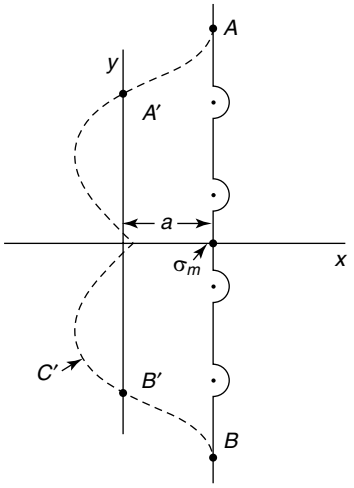

Figure A7.1 Contour for the Bromwich integral.

approximating $F(s)$ by orthogonal polynomials).[8] *Heaviside's expansion theorem* may be used when $F(s)$ is a rational function written as

$$F(s) = \frac{N(s)}{D(s)} = \sum_{n=1}^{N} \sum_{k=1}^{m} \frac{a_{nk}}{(s - s_n)^k} \qquad (\mathrm{Re}(s) > \mathrm{Re}\,(s_n)), \tag{A7.16}$$

where $N(s)$ and $D(s)$ are polynomials, and the degree of N is less than that of D. The denominator D has N poles s_n, of multiplicity m. The original function of $F(s)$ is

$$f(t) = \sum_{n=1}^{N} e^{s_n t} \sum_{k=1}^{m} a_{nk} \frac{t^{k-1}}{(k-1)!}. \tag{A7.17}$$

THE BILATERAL LAPLACE TRANSFORM

This transform is defined by

$$L_2(f) = F(s) = \int_{-\infty}^{\infty} e^{-st} f(t)\, dt. \tag{A7.18}$$

The one-sided (or unilateral) transform $L_1(f)$ is a particular case of L_2, obtained by inserting $f(t)H(t)$ into (A7.18). We note that $L_2(f)$ can be written as the sum of two unilateral transforms. Thus,

$$\begin{aligned} F(s) &= \int_{-\infty}^{0} e^{-st} f(t)\, dt + \int_{0}^{\infty} e^{-st} f(t)\, dt \\ &= \int_{0}^{\infty} e^{st} f(-t)\, dt + \int_{0}^{\infty} e^{-st} f(t)\, dt = F_1(s) + F_2(s). \end{aligned}$$

Assume that $F_2(s)$ converges for $\mathrm{Re}(s) > \sigma_m^+$. The function $F_1(s)$ is seen to be a Laplace integral with respect to $(-s)$. If its abscissa of convergence is $-\sigma_m^-$, then F_1 converges for $\mathrm{Re}(s) < \sigma_m^-$. It follows that $F(s)$ can only converge in the strip defined by (Fig. A7.2)

$$\sigma_m^+ < \mathrm{Re}(s) = \sigma < \sigma_m^-. \tag{A7.19}$$

This strip reduces to a line when $\sigma_m^+ = \sigma_m^-$, while L_2 does not exist if $\sigma_m^- < \sigma_m^+$ (i.e., when the two one-sided integrals do not have a common region of convergence).

The inversion of $L_2(f)$ by the Bromwich integral (A7.15) is still valid, but σ must satisfy (A7.19). Note that different original functions may lead to the same transform, although with different *strips of convergence*. Note also that the transform of a sum is the sum of the transforms, but convergence of the sum is limited to the region where the two original strips overlap. In some cases, however, the addition may cancel a common singularity, which would result in a larger strip.

Most rules valid for $L_1(f)$ also hold for $L_2(f)$, with slight modifications involving mostly the strip of convergence. For example[5]:

- In (A7.3) the strip becomes $\sigma_m^+ - \mathrm{Re}(s_0) < \sigma < \sigma_m^- - \mathrm{Re}(s_0)$.
- In (A7.5) if the strips for 1 and 2 are respectively (α_1, β_1) and (α_2, β_2), then the strip of the convolution is $\max(\alpha_1, \alpha_2) < \mathrm{Re}(s) < \min(\beta_1, \beta_2)$.
- The differentiation rule (A7.9) becomes

$$L_2\left(\frac{df}{dt}\right) = sF(s), \text{ inside the strip of convergence of } f'(t) \tag{A7.20}$$

(if this strip exists).

- The integration rule takes the form:

$$\frac{1}{s}F(s) \text{ is the transform of } \int_{-\infty}^{t} f(t')\,dt' \text{ for } \max(\sigma_m^+, 0) < \mathrm{Re}(s) < \sigma_m^-$$

$$\frac{1}{s}F(s) \text{ is the transform of } \int_{\infty}^{t} f(t')\,dt' \text{ for } \sigma_m^+ < \mathrm{Re}(s) < \min(\sigma_m^-, 0). \tag{A7.21}$$

The behavior of $F(s)$ on the two vertical boundaries of the strip varies from case to case. At points where the integral converges, the latter is the analytic continuation of $F(s)$ inside the

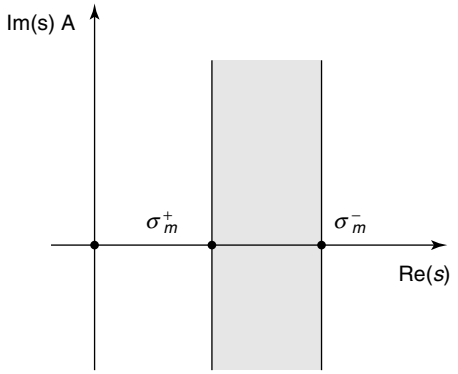

Figure A7.2 Strip of convergence.

strip. On each vertical, there is at least one singularity, for example, a pole, a branch point, or a logarithmic singularity.

THE FOURIER TRANSFORM

This transform is defined by

$$\mathcal{F}[f(t)] = F(\omega) = \int_{-\infty}^{\infty} f(t)e^{-j\omega t}dt. \tag{A7.22}$$

The variable t is typically time, but it could also be a space coordinate such as x, in which case ω is replaced by the more classical notation k_x (dimension m^{-1}), a wave number.

The existence of the Fourier integral is discussed at length in specialized texts. It depends, for example, on the nature of the integral (Riemann, Lebesgue).[9] Two sufficient conditions of existence hold when $f(t)$ is of *bounded variation*, that is, when the curve representing $f(t)$ has a finite length in any interval of time. These conditions are

1. $f(t)$ is absolutely integrable, in the sense that $\displaystyle\int_{-\infty}^{\infty} |f(t)|\,dt < \infty$.
2. $f(t)$ is square integrable, and the Lebesgue integral is taken in the Cauchy sense.

Basic Rules

Some basic rules duplicate those that hold for the Laplace transform. Thus,

- $$F(-\omega) = F^*(\omega) \qquad \text{when } f(t) \text{ is real.} \tag{A7.23}$$
- $$F(\omega - \omega_0) = \Im\left[f(t)e^{j\omega_0 t}\right]. \tag{A7.24}$$
- $$\mathcal{F}\left[f(t - t_0)\right] = e^{-j\omega t_0}F(\omega). \tag{A7.25}$$
- $$\mathcal{F}\left(\frac{df^n}{dt^n}\right) = (j\omega)^n F(\omega) \tag{A7.26}$$

  provided the new Fourier transform exists. It follows that the more a function $f(t)$ is differentiable, with derivatives that have a Fourier transform, the faster $F(\omega)$ will approach zero for $\omega \to \infty$.
- Let $g(t) = \displaystyle\int_{-\infty}^{t} f(t')\,dt'$. If $\lim_{t\to\infty} g(t) = \int_{-\infty}^{\infty} f(t')\,dt' = F(0) = 0$, then

$$\mathcal{F}[g(t)] = \frac{1}{j\omega}F(\omega). \tag{A7.27}$$

Otherwise,

$$\mathcal{F}[g(t)] = \pi F(0)\delta(\omega) + \frac{1}{j\omega}F(\omega). \tag{A7.28}$$

In particular,

$$\mathcal{F}[H(t)] = \pi\delta(\omega) + \frac{1}{j\omega}. \tag{A7.29}$$

- The transform of the convolution (A7.5) is

$$\mathcal{F}(f_1 * f_2) = F_1(\omega)F_2(\omega). \tag{A7.30}$$

As an interesting application, consider the average of $f(t)$ in the interval $(-T, +T)$. This function can be written as

$$f_{\text{ave}}(t) = \frac{1}{2T}\int_{t-T}^{t+T} f(t')\,dt' = \frac{1}{2T}\int_{-\infty}^{\infty} f(t')W_T(t-t')\,dt'$$

where W_T is the window function shown in Figure A7.3. The Fourier transform of W_T is

$$\mathcal{F}[W_T(t)] = 2T\left(\frac{\sin \omega T}{\omega T}\right). \tag{A7.31}$$

Hence

$$\mathcal{F}[f_{\text{ave}}(t)] = F(\omega)\frac{\sin \omega T}{\omega T}. \tag{A7.32}$$

- The transform of a product is given by

$$\mathcal{F}(f_1\, f_2) = \frac{1}{2\pi}\int_{-\infty}^{\infty} F_1(\omega')F_2(\omega - \omega')\,d\omega'. \tag{A7.33}$$

An immediate consequence of (A7.33) is *Parseval's theorem*.

$$\int_{-\infty}^{\infty} |f(t)|^2 dt = \frac{1}{2\pi}\int_{-\infty}^{\infty} |F(\omega)|^2 d\omega \tag{A7.34}$$

where $|F|^2$ is termed the energy spectrum.

- The concept of Fourier transform can be extended to a distribution U in the form

$$\langle U, \varphi\rangle = \int_{-\infty}^{\infty} F_U(\omega)\varphi(\omega)\,d\omega = \int_{-\infty}^{\infty} u(t)\,dt \int_{-\infty}^{\infty} e^{-j\omega t}\varphi(\omega)\,d\omega. \tag{A7.35}$$

The interpretation of these operations depends on the nature of the distribution, which could be tempered, of bounded support or of point support.[6,10]

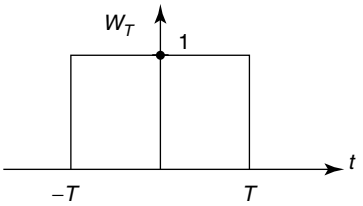

Figure A7.3 Window function.

Inversion

The inversion integral is

$$f(t) = \frac{1}{2\pi} \int_{-\infty}^{\infty} F(\omega) e^{j\omega t} d\omega. \tag{A7.36}$$

At points where $f(t)$ suffers a jump, the formula gives the average value $\frac{1}{2}[f(t+0) + f(t-0)]$. It is useful to look at (A7.36) in the light of the Bromwich integral (A7.15), where the vertical $\mathrm{Re}(s) = \tau$ has now been placed on the imaginary axis. If this axis falls within the strip of convergence, the Fourier transform exists. For example, the Gaussian pulse $f(t) = e^{-t^2}$ has the bilateral Laplace transform

$$L_2(e^{-t^2}) = \sqrt{\pi} e^{\frac{s^2}{4}} \quad (-\infty < \mathrm{Re}(s) < \infty). \tag{A7.37}$$

and also a Fourier transform, namely $\sqrt{\pi}\, e^{-\omega^2/4}$. When the imaginary axis lies outside the strip, there is no Fourier transform. The more difficult cases arise when the imaginary axis *coincides* with one of the limits of the strip. Assume, for example, that $\sigma_m^+ = 0$. Let now the path of integration be shifted to the right by a small amount τ (Fig. A7.4). The Bromwich integral yields, after evaluation, a function $g(t, \tau)$, different from $f(t)$, but such that $f(t) = \lim_{\tau \to 0} g(t, \tau)$. If, in a more usual presentation, one goes over to the *complex* ω *plane*, with $\omega = \omega_r + j\omega_i = \omega - j\tau$, the path lies just under the horizontal axis. In an alternate move, one could shift σ_m^+ slightly to the left and safely perform the integration along the imaginary axis (or along the real axis in the complex ω plane). As an illustrative example, consider the equation satisfied by the voltage on a lossy transmission line, viz.

$$\frac{\partial^2 v}{\partial x^2} - RC\frac{\partial v}{\partial t} - LC\frac{\partial^2 v}{\partial t^2} = f(x, t). \tag{A7.38}$$

The line is short-circuited at both ends $x = 0$ and $x = l$ and is excited by a concentrated pulse $f(x, t) = \delta(x - x_0)\delta(t)$. Taking the Fourier transform of both members of (A7.38) yields

$$\frac{d^2 V}{dx^2} - j\omega RCV + \omega^2 LCV = \delta(x - x_0).$$

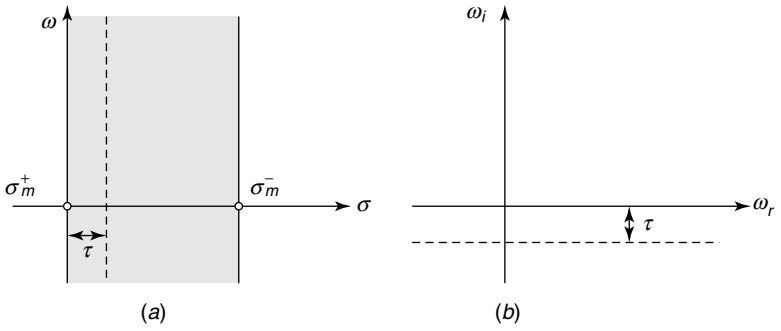

Figure A7.4 (*a*) Shifted axis of integration. (*b*) Complex ω plane.

With $\gamma^2 = \omega^2 LC - j\omega RC$, the Fourier transform takes the form

$$V(x,\omega) = \begin{cases} \dfrac{1}{\gamma}\dfrac{\sin\gamma x \sin\gamma(x_0 - l)}{\sin\gamma l} & \text{for } x < x_0 \\ \dfrac{1}{\gamma}\dfrac{\sin\lambda x_0 \sin\gamma(x - l)}{\sin\gamma l} & \text{for } x > x_0. \end{cases}$$

The original of the transform is obtained by means of (A7.36). Thus,

$$v(x,t) = \frac{1}{2\pi}\int_{-\infty}^{\infty} \frac{\sin\gamma x \sin\gamma(x_0 - l)}{\gamma \sin\gamma l} e^{j\omega t} d\omega \quad \text{for } x < x_0.$$

with a similar formula for $x > x_0$. We note that the values of ω for which γ vanishes are not singular points of the integrand. They are not poles, because the integrand remains finite. They are not branch points, because the integrand is even in γ. The only singularities are poles located at the roots of $\sin\gamma l = 0$, that is, at

$$\omega = j\frac{R}{2L} \pm \left(\frac{n^2\pi^2}{l^2 LC} - \frac{R^2}{4L^2}\right)^{\frac{1}{2}} \qquad (n = 1, 2, 3, \ldots).$$

When R is small, all the poles are located above the real axis. To evaluate the inversion integral for $t < 0$, we close the real axis with a large semicircle Γ in the lower half-plane. The integral along the semicircle is zero. Furthermore, no poles are enclosed between Γ and the real axis. An application of Cauchy's theorem then yields a result that is expected on physical grounds: the voltage is zero before $t = 0$, the time at which the forcing function is applied. For $t > 0$, we use the semicircle in the upper half-plane, where the integral again vanishes, and we find that $v(x,t)$ is equal to the sum of the residues around the poles. We shall not calculate these explicitly; they represent decaying oscillatory terms. It is interesting, however, to note that the poles tend to move closer to the real axis as the resistance decreases. Simultaneously, the decay of the oscillatory terms become slower, and the behavior of the *lossless* transmission line is approached. For such a line, the poles are found on the real ω axis, at the angular frequencies

$$\omega_n = \pm\frac{n\pi}{l\sqrt{LC}} \qquad (n = 1, 2, 3, \ldots).$$

It follows that the inversion integral does not exist at these frequencies. It can be reinstated, however, by introducing a small resistance R, and letting $R \to 0$. Equally efficiently, with $R = 0$, the contour could be shifted slightly below the real axis so as to preserve the contributions from the poles, which are in the form of undamped oscillations.

Causality

A *function* that is zero for negative t is termed *causal*. It is connected to its transform $F(\omega) = R(\omega) + jX(\omega)$ by

$$f(t) = 2\pi\int_0^{\infty} R(\omega)\cos\omega t\, d\omega = -\frac{2}{\pi}\int_0^{\infty} X(\omega)\sin\omega t\, d\omega \qquad (t > 0). \tag{A7.39}$$

At $t = 0$, in particular,

$$f(0) = \frac{1}{\pi}\int_0^\infty R(\omega)\,d\omega = \frac{1}{2}f(0^+). \tag{A7.40}$$

A relationship such as (A7.39) shows that $R(\omega)$ and $X(\omega)$ cannot be chosen independently. In fact, they are each other's Hilbert transform. Thus,[7]

$$R(\omega) = \frac{1}{\pi}\int_{-\infty}^\infty \frac{X(\omega')}{\omega - \omega'}\,d\omega' \tag{A7.41}$$

$$X(\omega) = -\frac{1}{\pi}\int_{-\infty}^\infty \frac{R(\omega')}{\omega - \omega'}\,d\omega', \tag{A7.42}$$

which holds when there is no singularity at the origin, that is, provided $\lim_{\omega\to\infty} F(\omega) = 0$. If, on the other hand, this limit is different from zero, (A7.42) still holds, but (A7.41) is replaced by

$$R(\omega) = R(\infty) + \frac{1}{\pi}\int_{-\infty}^\infty \frac{X(\omega')}{\omega - \omega'}\,d\omega'. \tag{A7.43}$$

Analytic Signal

The *analytic signal* $f^+(t)$ associated with $f(t)$ is defined by its Fourier spectrum, which is twice that of $f(t)$ for $\omega > 0$, and zero for $\omega < 0$. Thus,

$$f^+(t) = \frac{1}{\pi}\int_0^\infty F(\omega)e^{j\omega t}d\omega \qquad (\mathrm{Im}\, t \geq 0). \tag{A7.44}$$

The following property holds for t real:

$$f^+(t) = f(t) + H[f(t)] \tag{A7.45}$$

where H is the Hilbert transform of $f(t)$, viz.

$$H[f(t)] = -\frac{1}{\pi}\lim_{T\to\infty}\int_{-T}^T \frac{f(t')}{t - t'}dt'. \tag{A7.46}$$

If the analytic signal is put in the form

$$f^+(t) = a(t)e^{j\phi(t)} = b(t) + jc(t), \tag{A7.47}$$

the functions $a(t)$ and $\phi(t)$ represent the instantaneous amplitude and phase of the original signal $f(t)$. The functions $b(t)$ and $c(t)$ are Hilbert transforms of each other.

The Sampling Theorem

When $F(\omega)$ vanishes above a certain limit $\omega = \omega_c$ (the Nyquist frequency), the function $f(t)$ is uniquely determined by its value f_n at a sequence of points separated by uniform intervals $T = (\pi/\omega_c) = (1/2f_c)$. More precisely,[11]

$$f(t) = \sum_{n=-\infty}^{\infty} f_n \frac{\sin(\omega_c t - n\pi)}{\omega_c t - n\pi} = \sum f(nT) \sin c \left(\frac{t}{T} - n\right), \tag{A7.48}$$

where $\sin c\, x = \dfrac{\sin \pi x}{\pi x}$. If $f(t)$ is limited, that is, if $f(t) = 0$ for $|t| > T$, then

$$F(\omega) = \sum_{n=-\infty}^{\infty} F\left(n\frac{\pi}{T}\right) \frac{\sin(\omega T - n\pi)}{\omega T - n\pi}. \tag{A7.49}$$

By these theorems, an analog signal is converted into a sequence of numbers, a form that is suitable for handling by digital means.

Discretization

The function $f(t)$ in (A7.22) is often obtained experimentally. For such a case, it is only available over a finite interval (O, T), and not continuously, but at N discrete times. The measurements thus produce values (Fig. A7.5)

$$f_k = f\left(k\frac{T}{N}\right) \qquad (k = 0, 1, \ldots, N-1).$$

The *Fourier transform* is analogously replaced by a *discrete* version, the (DFT), given by

$$F_m = \frac{T}{N} \sum_{k=0}^{N-1} f_k\, e^{-j2\pi \frac{km}{N}}. \tag{A7.50}$$

The inverse is similarly

$$f_k = \frac{1}{T} \sum_{m=0}^{N-1} F_m\, e^{j2\pi \frac{km}{N}}. \tag{A7.51}$$

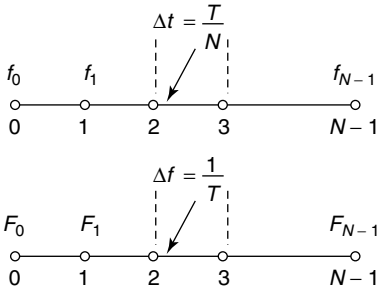

Figure A7.5 Discretized time and frequency functions.

Setting $W_N = e^{j\,2\pi/N}$ gives the perhaps clearer forms

$$F_m = \frac{T}{N}\sum_{k=0}^{N-1} f_k (W_N)^{-km} = \sum f_k B_{km} \tag{A7.52}$$

$$f_k = \frac{1}{T}\sum_{m=0}^{N-1} F_m (W_N)^{km}.$$

To obtain the N values of F_m from the N values of f_k, some N^2 multiplications of complex quantities must be performed. This number may be drastically reduced when N can be expressed as a product of prime numbers. The technique, termed fast Fourier transform (FFT), reduces the number of operations to $N \log_2 N$ when N is a power of 2. This is an important reduction when N is large.[12,13]

Spatial Fourier Transform

The Fourier transform represents a time-dependent function $f(t)$ as an (integral) sum of elementary blocks, the time-harmonic signals $e^{j\omega t}$. In the spatial domain, the Fourier transform represents $f(\mathbf{r})$ as a sum of blocks that are now plane waves. Thus,

$$F(\mathbf{k}) = \int_{\text{all space}} f(\mathbf{r}) e^{-j\mathbf{k}\cdot\mathbf{r}} dV \tag{A7.53}$$

$$f(\mathbf{r}) = \frac{1}{(2\pi)^3}\int F(\mathbf{k}) e^{j\mathbf{k}\cdot\mathbf{r}} dk_x dk_y dk_z = \frac{1}{(2\pi)^3}\int F(\mathbf{k}) e^{j\mathbf{k}\cdot\mathbf{r}} d^3k. \tag{A7.54}$$

The transform of the space derivatives gives

$$\mathcal{F}[\text{grad} f] = j\mathbf{k}F(\mathbf{k}) \tag{A7.55}$$

$$\mathcal{F}[\text{div} f] = j\mathbf{k}\cdot F(\mathbf{k}) \tag{A7.56}$$

$$\mathcal{F}[\text{curl} f] = j\mathbf{k}\times F(\mathbf{k}). \tag{A7.57}$$

OTHER INTEGRAL TRANSFORMS

The *Hankel transform* pair[8,9,17,18]

$$F(s) = \int_0^\infty f(x) x J_n(xs)\, dx \tag{A7.58}$$

$$f(x) = \int_0^\infty F(s) s J_n(xs)\, ds. \tag{A7.59}$$

The *Mellin transform* pair[8,9,15]

$$F(s) = \int_0^\infty f(x) x^{s-1} dx \tag{A7.60}$$

$$f(x) = \frac{1}{2\pi j}\lim_{\omega\to\infty}\int_{\tau-j\omega}^{\tau+j\omega} F(s) x^{-s} ds. \tag{A7.61}$$

The *Hilbert transform*[7,9]

$$F(s) = -\frac{1}{\pi} PV \int_{-\infty}^{\infty} \frac{f(x)}{s-x}\, dx \tag{A7.62}$$

$$f(x) = -\frac{1}{\pi} PV \int_{-\infty}^{\infty} \frac{F(s)}{x-s}\, ds. \tag{A7.63}$$

Table A7.1 Some Bilateral Laplace Transforms[5]

Original function	Transform	Original function	Transform
1	$2\pi\delta(\,js)$	$\sum_{n=0}^{\infty}(-1)^n\delta(t-na)$	$\frac{1}{1+e^{-as}}$
$\delta(t)$	1	$\sum_{n=0}^{\infty}(-1)^n H(t-na)$	$\frac{1}{s(1+e^{-as})}$
$\frac{1}{t}$	$\pi\frac{\lvert s\rvert}{s}$	$\sin t$	$\frac{2\pi}{s}\delta(s^2+1)$
sgn t	$\frac{2}{s}$	$\cos t$	$2\pi\delta(s^2+1)$
erfc(−t)	$\frac{2}{s}e^{s^2/4}$	e^{-t^2}	$\sqrt{\pi}e^{s^2/4}$
$\sum_{n=0}^{\infty}\delta(t-na)$	$\frac{1}{1-e^{-as}}$	$e^{-\alpha\lvert t\rvert}$	$\frac{2\alpha}{\alpha^2-s^2}$

Table A7.1 gives the bilateral Laplace transform of a few important functions. When the function is multiplied by the Heaviside step function $H(t)$, its transform becomes the one-sided Laplace transform. More extensive tables can be found elsewhere.[5,14,15,16]

Table A7.2 Some One-Sided Laplace Transforms[5]

Original function	Transform	Original function	Transform
$H(t)$	$\frac{1}{s}$	$H(t)e^{-at}$	$\frac{1}{s+a}$
$H(t)t^{\upsilon}$	$\frac{\Gamma(\upsilon+1)}{s^{\upsilon+1}}$	$H(t)t^n e^{-at}$	$\frac{n!}{(s+a)^{n+1}}$
$H(t)\frac{1}{a}\sin at$	$\frac{1}{s^2+a^2}$	$H(t)e^{-at}\sin bt$	$\frac{s+a}{(s+a)^2+b^2}$
$H(t)\frac{1}{a}\cos at$	$\frac{s}{s^2+a^2}$	$H(t)e^{-at}\cos bt$	$\frac{b}{(s+a)^2+b^2}$
$H(t)\frac{1}{a^2}(1-\cos at)$	$\frac{1}{s(s^2+a^2)}$	$H(t)\log_e t$	$-\frac{1}{s}(\log_e s+c)\quad(c=0,5772...)$
$H(t)\frac{1}{a^3}(at-\sin at)$	$\frac{1}{s^2(s^2+a^2)}$	$H(t)\frac{1}{a}\sinh(at)$	$\frac{1}{s^2-a^2}$
$H(t)t\sin at$	$\frac{2as}{a(s^2+a^2)^2}$	$H(t)\cosh(at)$	$\frac{s}{s^2-a^2}$

NOTES

1. R. V. Churchill, *Operational Mathematics.* McGraw-Hill Book Company, New York, 2nd edition, 1958.
2. E. Labin, *Calcul opérationnel.* Masson, Paris, 1949.
3. M. R. Spiegel, *Laplace Transforms.* Schaum Publ. Co., New York, 1965.
4. C. J. Tranter, *Integral Transforms in Mathematical Physics.* Methuen Co., Ltd., London, 1951.
5. B. van der Pol and H. Bremmer, *Operational Calculus Based on the Two-Sided Laplace Integral.* Cambridge University Press, Cambridge, 1950.
6. L. Schwartz, *Méthodes mathématiques pour les sciences physiques.* Hermann et Cie., Paris, 1965. An English translation was published by Addison-Wesley in 1966.
7. A. Papoulis, *The Fourier Integral and Its Applications.* McGraw-Hill Book Company, New York, 1962.
8. B. Davies, *Integral Transforms and Their Applications.* Springer-Verlag, New York, 1978.
9. P. M. Morse and H. Feshbach, *Methods of Theoretical Physics.* Chapter 4. McGraw-Hill Book Company, New York, 1953.
10. M. J. Lighthill, *Fourier Analysis and Generalised Functions.* Cambridge University Press, 1959.
11. M. Unser, Sampling — 50 years after Shannon. *Proc. IEEE* **88**, 569–587 (2000).
12. G. D. Bergland, A guided tour of the Fast Fourier Transform. *IEEE Spectrum* **6**, 41–52 (1969).
13. J. W. Cooley, P. A. W. Lewis, and P. D. Welch, *The Fast Fourier Transform.* IBM Research Publications, Yorktown Heights, New York, 1967.
14. M. Abramowitz and I. A. Stegun (eds.), *Handbook of Mathematical Functions.* Dover Publications, New York, 1965.
15. G. Doetsch, *Handbuch der Laplace-transformationen.* Birkhäuser Verlag, Basel, 1950.
16. A. Erdélyi (ed.), *Tables of Integral Transforms,* volumes 1 & 2. McGraw-Hill Book Company, New York, 1953.
17. I. N. Sneddon, *Fourier Transforms.* McGraw-Hill Book Company, New York, 1951.
18. A. H. Zemanian, *Generalized Integral Transformations.* Dover Publications, New York, 1987.

Appendix 8

Distributions

DEFINITIONS

The delta function was conceived as a tool for deriving useful results in a concise way. Its use is now backed by solid mathematical arguments, developed over the years by authors such as Sobolev, Bochner, Mikusinski, and Schwartz. In the following pages, we give the essentials of the Schwartz approach. The level of treatment is purely utilitarian. Rigorous exposés, together with descriptions of the historical evolution of the theory, may be found in the numerous texts quoted in the bibliography.

The idea of the δ-function is quite old and dates back at least to the times of Kirchhoff and Heaviside.[1] In the early days of quantum mechanics, Dirac[2,3] put the emphasis on the following properties of the function:

$$\int_{-\infty}^{\infty} \delta(x)\, dx = 1, \quad \delta(x) = 0 \quad (\text{for } x \neq 0). \tag{A8.1}$$

The notation $\delta(x)$ was inspired by δ_{ik}, the Kronecker delta, equal to 0 for $i \neq k$ and to 1 for $i = k$. Clearly, $\delta(x)$ must be "infinite" at $x = 0$ if the integral in (A8.1) is to be unity. Dirac recognized from the start that $\delta(x)$ was not a function of x in the usual mathematical sense but something more general, which he called an "improper" function. Its use, therefore, had to be confined to certain simple expressions and subjected to careful codification. One of the expressions put forward by Dirac was the *sifting property*

$$\int_{-\infty}^{\infty} f(x)\delta(x)\, dx = f(0). \tag{A8.2}$$

This relationship can serve to define the delta function, not by its value at each point of the x axis, but by the set of its scalar products with suitably chosen "test" functions $f(x)$. The notion of distribution is obtained by generalizing the idea embodied in (A8.2), namely that a function is defined by the totality of its scalar products with reference functions termed *test functions*. The *test functions* used in the Schwartz theory are complex continuous functions $\phi(\mathbf{r})$ endowed with continuous derivatives of all orders. Such functions are often termed *infinitely smooth*. They must vanish outside some *finite* domain, which may be different for each ϕ. They form a space D. The smallest closed set, which contains the set of points for which $\phi(\mathbf{r}) \neq 0$, is the *support of* ϕ. The functions $\phi(x) = x^2$ and $\phi = \sin|x|$ are not

Electromagnetic Fields, Second Edition, By Jean G. Van Bladel

suitable test functions because their support is not bounded. In addition, the derivative of the second function is not continuous at the origin.

In the next step, we define a *linear functional* on D. This is an operation that associates a complex number $t(\phi)$ with every ϕ belonging to D, in such a way that

$$t(\phi_1 + \phi_2) = t(\phi_1) + t(\phi_2); \quad t(\lambda\phi) = \lambda t(\phi), \tag{A8.3}$$

where λ is a complex constant. The complex number $t(\phi)$ is often written in the form

$$t(\phi) = \langle t, \phi \rangle. \tag{A8.4}$$

The functional is *continuous* if, when ϕ_m converges to ϕ for $m \to \infty$, the complex numbers $t(\phi_m)$ converge to $t(\phi)$. *Distributions are continuous linear functionals* on D. They form a vector space D'. To clarify these concepts, assume that $t(x)$ is a locally integrable function (i.e., a function, which is integrable over any compact set). Such a function generates a distribution by the operation[4]

$$t(\phi) = \langle t, \phi \rangle \stackrel{\text{def}}{=} \int_{-\infty}^{\infty} t(x)\phi(x)\, dx. \tag{A8.5}$$

Many distributions cannot be written as an integral of that form, except in a formal way. For such cases, the "generating function" $t(x)$ becomes a symbolic function, and (A8.5) only means that the integral, whenever it is encountered in an analytical development, may be replaced by the value $t(\phi)$. It should be noted, in this respect, that experiments do not yield instantaneous, punctual values of quantities such as a force or an electric field. Instead, they generate *integrated* outputs (i.e., averages over some nonvanishing intervals of time and space). The description of a quantity by scalar products of the form (A8.5) is therefore quite acceptable from a physical point of view.[4]

An obvious example of distribution is the *Dirac distribution* defined by (A8.2), with generating function $\delta(x)$. Because $x^m\phi(x)$ is a test function when $\phi(x)$ is itself a test function and when m is a positive integer, we may write

$$\int_{-\infty}^{\infty} x^m \delta(x)\phi(x)\, dx = \int_{-\infty}^{\infty} \delta(x)[x^m\phi(x)]\, dx = 0.$$

In symbolic form:

$$x^m\delta(x) = 0. \tag{A8.6}$$

As mentioned above, $\delta(x)$ has no "values" on the x axis, but the statement that the delta function $\delta(x)$ is zero in the vicinity of a point such as $x_0 = 1$ can be given a well-defined meaning by introducing the concept *support of a distribution*. A distribution $\langle t, \phi \rangle$ is said to vanish in an interval Δ if, for every $\phi(x)$ that has its support in that interval, $\langle t, \phi \rangle = 0$. This clearly holds, in the case of $\delta(x)$, for intervals Δ that do not contain the origin. The support of t is what remains of the x axis when all the Δ intervals have been excluded.[4] The support of δ_0 is therefore the point $x = 0$. It should be mentioned that each distribution can be extended to a set that is broader than D. The latter space is, in fact, the set that is common to all these functionals. The Dirac distribution, for example, can be extended to all functions that are continuous at the origin.

As a second example of a distribution, we take the integral of ϕ from 0 to ∞. This integral is a distribution, which may be written as

$$\langle H, \phi \rangle \stackrel{\text{def}}{=} \int_0^\infty \phi(x)\, dx = \int_{-\infty}^\infty H(x)\phi(x)\, dx. \tag{A8.7}$$

The generating function is the *Heaviside unit function* $H(x)$, defined by the values

$$H(x) = \begin{cases} 0 & \text{for } x < 0 \\ 1 & \text{for } x \geq 0. \end{cases} \tag{A8.8}$$

Consider next a function $f(x)$ that is possibly undefined at c and unbounded near c, but integrable in the intervals $(a, c-\epsilon)$ and $(c+\eta, b)$, where ϵ and η are positive. If

$$I = \lim_{\substack{\epsilon \to 0 \\ \eta \to 0}} \left(\int_a^{c-\epsilon} f(x)\, dx + \int_{c+\eta}^b f(x)\, dx \right) \tag{A8.9}$$

exists for ϵ and η approaching zero independently of each other, this limit is termed the integral of $f(x)$ from a to b. Sometimes the limit exists only for $\epsilon = \eta$. In such case, its value is the *principal value of Cauchy*, and one writes

$$PV \int_a^b f(x)\, dx = \lim_{\epsilon \to 0} \left(\int_a^{c-\epsilon} f(x)\, dx + \int_{c+\epsilon}^b f(x)\, dx \right). \tag{A8.10}$$

An example of such an integral is

$$\begin{aligned} PV \int_{-a}^a \frac{dx}{x} &= \lim_{\epsilon \to 0} \left(\int_{-a}^{-\epsilon} \frac{dx}{x} + \int_\epsilon^a \frac{dx}{x} \right) \\ &= \lim_{\epsilon \to 0} (\log\epsilon - \log_e a + \log_e a - \log\epsilon) = 0. \end{aligned} \tag{A8.11}$$

The function $1/x$ does not define a distribution because it is not integrable in the vicinity of $x = 0$. But a well-defined meaning may be attached to $PV(1/x)$ by introducing the functional:

$$\langle PV(1/x), \phi \rangle \stackrel{\text{def}}{=} PV \int_{-\infty}^\infty \frac{\phi(x)}{x}\, dx = \int_{-\infty}^\infty PV(1/x)\phi(x)\, dx. \tag{A8.12}$$

THREE-DIMENSIONAL DIRAC DISTRIBUTIONS

The three-dimensional δ-function is defined by the sifting property

$$\langle \delta_0, \phi \rangle \stackrel{\text{def}}{=} \phi(0) = \int \delta(\mathbf{r})\phi(\mathbf{r})\, dV. \tag{A8.13}$$

Here, and in the future, the omission of the integration limits means that the integral is extended over all space.

In Cartesian coordinates, the volume element is $dxdydz$, and $\delta(\mathbf{r})$ can be written explicitly as

$$\delta(\mathbf{r}) = \delta(x)\delta(y)\delta(z). \tag{A8.14}$$

In a more general coordinate system, the form of dV determines that of $\delta(\mathbf{r})$. Let (u, v, w) be a set of curvilinear coordinates. The volume element at a regular point is $J\,du\,dv\,dw$, where J denotes the *Jacobian of the transformation* from the (x, y, z) coordinates to the (u, v, w) coordinates. More explicitly:

$$J = \begin{vmatrix} \dfrac{\partial x}{\partial u} & \dfrac{\partial x}{\partial v} & \dfrac{\partial x}{\partial w} \\ \dfrac{\partial y}{\partial u} & \dfrac{\partial y}{\partial v} & \dfrac{\partial y}{\partial w} \\ \dfrac{\partial z}{\partial u} & \dfrac{\partial z}{\partial v} & \dfrac{\partial z}{\partial w} \end{vmatrix}. \tag{A8.15}$$

The three-dimensional delta function can now be expressed in terms of one-dimensional functions by the relationship

$$\delta(u - u_0, v - v_0, w - w_0) = \frac{\delta(u - u_0)\delta(v - v_0)\delta(w - w_0)}{J(x_0, y_0, z_0)}. \tag{A8.16}$$

The singular points of the coordinate system are these at which the Jacobian vanishes. At such points, the transformation from (x, y, z) into (u, v, w) is no longer of the one-to-one type, and some of the (u, v, w) *coordinates* become *ignorable*; that is, they need not be known to find the corresponding (x, y, z). Let J_k be the integral of J over the ignorable coordinates. Then δ is the product of the δ's relative to the nonignorable coordinates, divided by J_k. In cylindrical coordinates, for example, J is equal to r, and

$$\delta(\mathbf{r} - \mathbf{r}_0) = \delta(r - r_0, \varphi - \varphi_0, z - z_0) = \frac{\delta(r - r_0)\delta(\varphi - \varphi_0)\delta(z - z_0)}{r_0}. \tag{A8.17}$$

Points on the z-axis are singular, and φ is ignorable there. We therefore write

$$\delta(\mathbf{r} - \mathbf{r}_0) = \frac{\delta(r)\delta(z - z_0)}{\int_0^{2\pi} r\,d\varphi} = \frac{1}{2\pi r}\delta(r)\delta(z - z_0). \tag{A8.18}$$

This representation is valid with the convention

$$\int_0^\infty \delta(r)\,dr = 1. \tag{A8.19}$$

If one chooses

$$\int_0^\infty \delta(r)\,dr = \frac{1}{2}, \tag{A8.20}$$

then the $1/2\pi$ factor in (A8.18) should be replaced by $1/\pi$. In spherical coordinates, J is equal to $R^2 \sin\theta$, and

$$\delta(\mathbf{r} - \mathbf{r}_0) = \frac{\delta(R - R_0)\delta(\varphi - \varphi_0)\delta(\theta - \theta_0)}{R^2 \sin\theta}. \tag{A8.21}$$

On the polar axis (where θ_0 is zero or π), the azimuth φ is ignorable, and

$$\delta(\mathbf{r}-\mathbf{r}_0)=\frac{\delta(R-R_0)\delta(\theta-\theta_0)}{2\pi R^2\sin\theta}. \tag{A8.22}$$

At the origin, both φ and θ are ignorable, hence

$$\delta(\mathbf{r}-\mathbf{r}_0)=\frac{\delta(R)}{4\pi R^2}. \tag{A8.23}$$

This formula holds when $\delta(R)$ satisfies (A8.19), with r replaced by R. If $\delta(R)$ is assumed to satisfy (A8.20), then the factor $1/4\pi$ in (A8.23) must be replaced by $1/2\pi$.

SURFACE AND LINE DISTRIBUTIONS

The (generalized) function δ_S is defined by the functional

$$\langle\delta_S,\phi\rangle\overset{\text{def}}{=}\int_S\phi(\mathbf{r})\,dS=\int\delta_S\phi(\mathbf{r})\,dV. \tag{A8.24}$$

The meaning of this relationship is the usual one; that is, whenever the volume integral is encountered in an analytical development, it may be replaced by the surface integral. The support of δ_S is the surface S. Relationship (A8.24) is a sifting operation, suitable to express a surface charge density ρ_S as a volume density. Thus,

$$\rho=\rho_S(v_1,v_2)\,\delta_S. \tag{A8.25}$$

The corresponding functional is[5]

$$\langle\rho_S\delta_S,\phi\rangle\overset{\text{def}}{=}\int_S\rho_S\phi\,dS=\int\rho_S\delta_S\phi\,dV. \tag{A8.26}$$

Similarly, a surface electric current may be written in the form (Fig. A8.1*a*)

$$\mathbf{j}=\mathbf{j}_S(v_1,v_2)\,\delta_S=\mathbf{j}_{St}(v_1,v_2)\,\delta_S+\mathbf{j}_{Sn}(v_1,v_2)\,\delta_S. \tag{A8.27}$$

The normal component of this current represents a surface distribution of elementary currents, oriented along the normal.

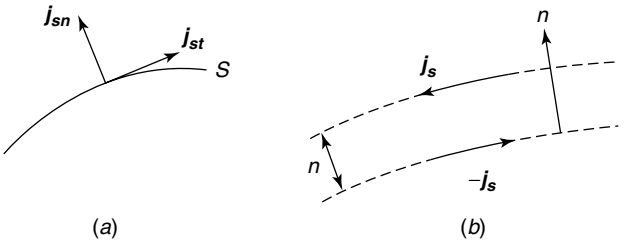

Figure A8.1 (*a*) Current on a surface (*b*) Double layer of current.

Finally, a distribution of linear charge density ρ_c on a curve C may be represented by the volume density

$$\rho = \rho_c \delta_c, \tag{A8.28}$$

where

$$\langle \rho_c \delta_c, \phi \rangle \stackrel{\text{def}}{=} \int_C \rho_c \phi \, dc = \int \rho_c \delta_c \phi \, dV. \tag{A8.29}$$

MULTIPLICATION OF DISTRIBUTIONS

There is no natural way to define the product of two distributions. The product $[\delta(x)]^2$, for example, has no meaning in the theory. The function $1/\sqrt{|x|}$ is locally integrable and can therefore generate a distribution, but its square $1/|x|$ cannot. In general, the more f is irregular, the more g must be regular if the product fg is to have a meaning. Multiplication by an infinitely differentiable function $\alpha(x)$, however, is always meaningful, because $\alpha(x)\phi(x)$ is a test function. For example:

$$\alpha(x)\delta(x - x_0) = \alpha(x_0)\delta(x - x_0). \tag{A8.30}$$

The restriction to infinitely differentiable $\alpha(x)$ is not always necessary. The function $\alpha(x)\delta(x)$, for example, has a meaning, namely $\alpha(0)\delta(x)$, once $\alpha(x)$ is *continuous* at the origin.

It should be noted that multiplication of distributions, even when defined, is not necessarily associative. For example:

$$\left(\frac{1}{x}x\right)\delta(x) = \delta(x); \quad \frac{1}{x}[x\delta(x)] = \frac{1}{x}0 = 0. \tag{A8.31}$$

CHANGE OF VARIABLES

The operation "change of variables" starts from a generating function $t(x)$ and introduces $t[f(x)]$ by means of the formula[6]

$$\int_{-\infty}^{\infty} t[f(x)]\phi(x)\,dx = \int_{-\infty}^{\infty} t(y)\left[\frac{d}{dy}\int_{f(u)<y} \phi(u)\,du\right]dy. \tag{A8.32}$$

The right-hand side has a meaning, provided that the term between brackets is a test function. A few examples:

$$\delta(x) = \delta(-x) \tag{A8.33}$$

$$\delta(\alpha x - \beta) = (1/|\alpha|)\delta(x - \beta/x) \tag{A8.34}$$

$$\delta[(x - a)(x - b)] = [1/(b - a)][\delta(x - a) + \delta(x - b)] \quad (a \neq b) \tag{A8.35}$$

$$\delta(x^2 - a^2) = (1/2|a|)[\delta(x - a) + \delta(x + a)] \tag{A8.36}$$

$$|x|\delta(x^2) = \delta(x). \tag{A8.37}$$

If $f(x)$ varies monotonically, vanishes at $x = x_0$, and satisfies $f'(x_0) \neq 0$:

$$\delta[f(x)] = (1/|f'(x_0)|)\delta(x - x_0) \tag{A8.38}$$

$$\delta[p(x)] = \sum_{\nu} p'(a_\nu)\delta(x - a_\nu), \tag{A8.39}$$

where the a_ν's are the zeros of polynomial $p(x)$, and $p'(a_\nu) \neq 0$.

THE DERIVATIVE OF A DISTRIBUTION

The derivative of a distribution t is a new distribution t', defined by the functional

$$\langle t', \phi \rangle \stackrel{\text{def}}{=} -\int_{-\infty}^{\infty} t\frac{d\phi}{dx}\,dx = \int_{-\infty}^{\infty} \frac{dt}{dx}\phi\,dx. \tag{A8.40}$$

Every distribution, therefore, has a derivative: a property that obviously has no analogue in the classic theory of functions. One expects the generating function $t'(x)$ to coincide with the usual derivative when both t and dt/dx are continuous. That this is so may be shown by the following elementary integration:

$$-\int_{-\infty}^{\infty} t\frac{d\phi}{dx}\,dx = -[t(x)\phi(x)]_{-\infty}^{\infty} + \int_{-\infty}^{\infty} \frac{dt}{dx}\phi\,dx = \int_{-\infty}^{\infty} \frac{dt}{dx}\phi\,dx.$$

To obtain this result, we took into account that $t(x)$ is bounded, and that $\phi(x)$ vanishes at $x = \infty$ and $x = -\infty$. Some important properties of the derivative:

1. A distribution has derivatives of all orders. Further, the ordering of differentiation in a partial derivative may always be permuted.
2. A series of distributions that converges may be differentiated term by term. This holds, for example, for the Fourier series[3]

$$\sum_{k=-\infty}^{\infty} e^{j2kx} = \sum_{k=-\infty}^{\infty} \delta(x - k). \tag{A8.41}$$

   This is the *comb function* defined in Section 9.5. The left-hand member is divergent in the classic sense, but in the sense of distributions it yields periodic sharp spectral lines at $x = 0, \pm 1, \pm 2, \ldots$ Differentiation yields

$$j2\pi \sum_{k=-\infty}^{\infty} k e^{j2\pi kx} = \sum_{k=-\infty}^{\infty} \delta'(x - k). \tag{A8.42}$$

3. The usual differentiation formulas are valid, for instance:

$$\frac{d}{dx}(\alpha t) = \frac{d\alpha}{dx}t + \alpha\frac{dt}{dx}. \tag{A8.43}$$

   Also $dt/dx = ds/dx$ implies that t and s differ by a constant.

4. The operations of differentiation and passing to the limit may always be interchanged. Specifically, if f_m converges to f as $m \to \infty$, then

$$\lim_{m\to\infty} \left\langle \frac{df_m}{dx}, \phi \right\rangle = \left\langle \frac{df}{dx}, \phi \right\rangle. \tag{A8.44}$$

5. The chain rule for differentiation remains valid. Thus,

$$\frac{d}{dx} t[f(x)] = t'[f(x)]\, f'(x). \tag{A8.45}$$

A few important derivatives:

$$\langle \delta', \phi \rangle = -\int_{-\infty}^{\infty} \delta(x) \frac{d\phi}{dx}\, dx = -\phi'(0) \tag{A8.46}$$

$$\left\langle \delta^{(m)}, \phi \right\rangle \stackrel{\text{def}}{=} (-1)^m \phi^{(m)}(0). \tag{A8.47}$$

When $\alpha(x)$ is infinitely differentiable:

$$\alpha(x)\delta'(x) = \alpha(0)\delta'(x) - \alpha'(0)\delta(x). \tag{A8.48}$$

Hence,

$$x\delta'(x) = -\delta(x) \tag{A8.49}$$

$$x^2\delta'(x) = 0. \tag{A8.50}$$

Further,

$$x\delta^{(m)}(x) = -m\delta^{(m-1)}(x) \tag{A8.51}$$

$$x^n\delta^{(m)}(x) = 0 \quad \text{when } n > m \tag{A8.52}$$

$$\frac{d}{dx}\delta[g(x)] = \delta'[g(x)]g'(x) \tag{A8.53}$$

$$\begin{aligned} \frac{d}{dx}\delta(x^2 - a^2) = \delta(x^2 - a^2)2x &= \frac{x}{|a|}[\delta(x-a) + \delta(x+a)] \\ &= \delta(x-a) - \delta(x+a) \end{aligned} \tag{A8.54}$$

$$\frac{d^2}{dx^2}|x| = 2\delta(x) \tag{A8.55}$$

$$\frac{d}{dx}\log_e x = \frac{1}{x} - j\pi\delta(x) \quad \text{(on one branch)}. \tag{A8.56}$$

PARTIAL DERIVATIVES

In three dimensions, the partial derivative $\partial t/\partial x_i$ is defined by the functional

$$\left\langle \frac{\partial t}{\partial x_i}, \phi \right\rangle \stackrel{\text{def}}{=} -\int t \frac{\partial \phi}{\partial x_i}\, dV = \int \frac{\partial t}{\partial x_i}\phi\, dV. \tag{A8.57}$$

A linear differential operator in n dimensions is typically a summation of the form

$$L = \sum_p A_p \left(\frac{\partial}{\partial x_1}\right)^{p_1} \left(\frac{\partial}{\partial x_2}\right)^{p_2} \cdots \left(\frac{\partial}{\partial x_n}\right)^{p_n}, \tag{A8.58}$$

where $p = p_1 + \cdots + p_n$. The *adjoint of* L is

$$L^a = \sum_p A_p (-1)^{p_1+\cdots+p_n} \left(\frac{\partial}{\partial x_1}\right)^{p_1} \left(\frac{\partial}{\partial x_2}\right)^{p_2} \cdots \left(\frac{\partial}{\partial x_n}\right)^{p_n}, \tag{A8.59}$$

and the meaning of Lt follows from

$$\langle Lt, \phi \rangle \stackrel{\text{def}}{=} \langle t, L^a \phi \rangle. \tag{A8.60}$$

Applied to the Laplacian, this gives

$$\langle \nabla^2 t, \phi \rangle = \langle t, \nabla^2 \phi \rangle. \tag{A8.61}$$

In particular:

$$\nabla^2 \log_e \frac{1}{|\mathbf{r} - \mathbf{r}'|} = -2\pi\delta(\mathbf{r} - \mathbf{r}') \quad \text{(in two dimensions)} \tag{A8.62}$$

$$\nabla^2 \frac{1}{|\mathbf{r} - \mathbf{r}'|} = -4\pi\delta(\mathbf{r} - \mathbf{r}') \quad \text{(in three dimensions)}. \tag{A8.63}$$

The "weak" definition of the derivative given above allows recasting a differential equation such as $\nabla^2 f = g$ in the form

$$\langle \nabla^2 f, \phi \rangle = \langle g, \phi \rangle = \langle f, \nabla^2 \phi \rangle. \tag{A8.64}$$

This formulation transfers the operator ∇^2 from the unknown f to the test function ϕ. For the Dirac distribution, the partial derivative is

$$\left\langle \frac{\partial \delta}{\partial x_i}, \phi \right\rangle \stackrel{\text{def}}{=} -\int \delta(\mathbf{r} - \mathbf{r}') \frac{\partial \phi}{\partial x_i} dV = -\left(\frac{\partial \phi}{\partial x_i}\right)_{\mathbf{r}_0}. \tag{A8.65}$$

For Dirac's distribution on a surface, in a direction a,

$$\left\langle \frac{\partial \delta_S}{\partial a}, \phi \right\rangle \stackrel{\text{def}}{=} -\int_S \frac{\partial \phi}{\partial a}\, dS. \tag{A8.66}$$

When a coincides with the normal to S, and f is a function of only the surface coordinates v_1 and v_2,

$$\left\langle f \frac{\partial \delta_S}{\partial n}, \phi \right\rangle \stackrel{\text{def}}{=} -\int_S f \frac{\partial \phi}{\partial n}\, dS. \tag{A8.67}$$

The *volume* density of a double layer of surface density τ can be represented as

$$\rho = -\tau(v_1, v_2)\frac{\partial \delta_S}{\partial n}. \tag{A8.68}$$

In this formula, n is counted positive in the direction of the dipoles. For a double layer of surface currents, we write (Fig. A8.1*b*)

$$\mathbf{j} = -\mathbf{c}_S(v_1, v_2)\frac{\partial \delta_S}{\partial n}. \tag{A8.69}$$

In this equation, we have assumed that $\mathbf{c}_S = \mathbf{j}_S h$ approaches a well-defined (nonzero) limit when the distance h between the two layers approaches zero.

VECTOR OPERATORS

Let $\mathbf{t}$ be a vector distribution (i.e., a triple of scalar distributions t_x, t_y, t_z). The operator div $\mathbf{t}$ is defined, in classic vector analysis, by the expression

$$\text{div } \mathbf{t} = \frac{\partial t_x}{\partial x} + \frac{\partial t_y}{\partial y} + \frac{\partial t_z}{\partial z}.$$

The distributional definition of div t follows by applying (A8.57) to the three derivatives shown above. More specifically:

$$\langle \text{div } \mathbf{t}, \phi \rangle \stackrel{\text{def}}{=} -\int \mathbf{t} \cdot \text{grad } \phi \, dV = \int \phi \text{ div } \mathbf{t} \, dV. \tag{A8.70}$$

Such a definition gives a well-defined meaning to the equation div $\mathbf{d} = \rho$. According to (A8.70), it is

$$-\int \mathbf{d} \cdot \text{grad } \phi \, dV = \int \rho\phi \, dV. \tag{A8.71}$$

This relationship, which must hold for all test functions ϕ, remains valid when $\mathbf{d}$ does not possess everywhere the usual derivatives. In consequence, Maxwell's equation div $\mathbf{b} = 0$ is now interpreted as requiring that, for all ϕ's,

$$\int \mathbf{b} \cdot \text{grad } \phi \, dV = 0. \tag{A8.72}$$

The gradient can be defined similarly as

$$\langle \text{grad } t, \phi \rangle \stackrel{\text{def}}{=} -\int t \text{ grad } \phi \, dV = \int \phi \text{ grad } t \, dV. \tag{A8.73}$$

For the Dirac distribution $\delta(\mathbf{r} - \mathbf{r}_0)$:

$$\langle \text{grad } \delta, \phi \rangle \stackrel{\text{def}}{=} -(\text{grad } \phi)_{\mathbf{r}_0}. \tag{A8.74}$$

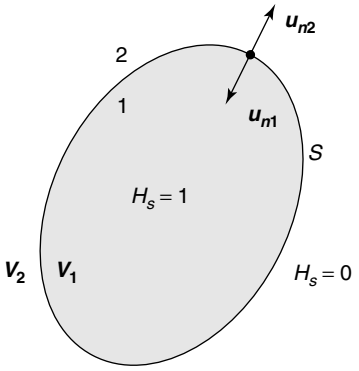

Figure A8.2 A surface of discontinuity.

Applied to the three-dimensional Heaviside unit function H_S, equal to one in V_1, and zero in V_2 (Fig. A8.2), we obtain

$$\langle \text{grad } H_S, \phi \rangle = \int_S \phi \mathbf{u}_{n1}\, dS. \tag{A8.75}$$

The proof follows from the following transformation in V_1:

$$\begin{aligned} -\int_{V_1} H_S \,\text{grad}\,\phi\, dV &= -\int_{V_1} \text{grad}\,(\phi H_S)\, dV + \int_{V_1} \phi\ \text{grad}\, H_S\, dV \\ &= \int_S \phi H_S \mathbf{u}_{n1}\, dS \ = \ \int_S \phi \mathbf{u}_{n1}\, dS, \end{aligned}$$

because $H_S = 1$ just inside S and grad $H_S = 0$ in V_1. The distributional definition of the curl follows from the classic value

$$\text{curl}\,\mathbf{t} = \left(\frac{\partial t_z}{\partial y} - \frac{\partial t_y}{\partial z}, \frac{\partial t_x}{\partial z} - \frac{\partial t_z}{\partial x}, \frac{\partial t_y}{\partial x} - \frac{\partial t_x}{\partial y} \right).$$

The corresponding functionals are

$$\langle \text{curl}\,\mathbf{t}, \phi \rangle \stackrel{\text{def}}{=} \int \mathbf{t} \times \text{grad}\,\phi\, dV = \int \phi\ \text{curl}\,\mathbf{t}\, dV \tag{A8.76}$$

$$\langle \text{curl}\,\mathbf{t}, \boldsymbol{\phi} \rangle \stackrel{\text{def}}{=} \int \mathbf{t} \cdot \text{curl}\,\boldsymbol{\phi}\, dV = \int \boldsymbol{\phi} \cdot \text{curl}\,\mathbf{t}\, dV, \tag{A8.77}$$

where $\boldsymbol{\phi}$ is a triple of testing functions. A relationship such as curl $\mathbf{h} = \mathbf{j}$ now means, in a distributional sense, that

$$\int \phi \mathbf{j}\, dV = \int \mathbf{h} \times \text{grad}\,\phi\, dV \tag{A8.78}$$

$$\int \boldsymbol{\phi} \cdot \mathbf{j}\, dV = \int \mathbf{h} \cdot \text{curl}\,\boldsymbol{\phi}\, dV. \tag{A8.79}$$

An irrotational vector $\mathbf{t}$ is therefore characterized by the properties

$$\int \mathbf{t} \times \operatorname{grad} \phi \, dV = 0 \tag{A8.80}$$

$$\int \mathbf{t} \cdot \operatorname{curl} \boldsymbol{\phi} \, dV = 0. \tag{A8.81}$$

Extension to vector operators involving higher derivatives than the first proceeds in an analogous fashion. For example:

$$\begin{aligned} \langle \operatorname{curl} \operatorname{curl} \mathbf{t}, \phi \rangle &\stackrel{\text{def}}{=} -\int \mathbf{t} \nabla^2 \phi \, dV + \int \mathbf{t} \cdot \operatorname{grad} \operatorname{grad} \phi \, dV \\ &= \int \phi \operatorname{curl} \operatorname{curl} \mathbf{t} \, dV. \end{aligned} \tag{A8.82}$$

$$\langle \operatorname{curl} \operatorname{curl} \mathbf{t}, \boldsymbol{\phi} \rangle \stackrel{\text{def}}{=} \int \mathbf{t} \cdot \operatorname{curl} \operatorname{curl} \boldsymbol{\phi} \, dV = \int \boldsymbol{\phi} \cdot \operatorname{curl} \operatorname{curl} \mathbf{t} \, dV. \tag{A8.83}$$

The symbol grad grad ϕ is defined in (A4.47). Similarly,

$$\langle \operatorname{grad} \operatorname{div} \mathbf{t}, \phi \rangle \stackrel{\text{def}}{=} \int \mathbf{t} \cdot \operatorname{grad} \operatorname{grad} \phi \, dV = \int \phi \operatorname{grad} \operatorname{div} \mathbf{t} \, dV \tag{A8.84}$$

$$\langle \operatorname{grad} \operatorname{div} \mathbf{t}, \boldsymbol{\phi} \rangle \stackrel{\text{def}}{=} \int \mathbf{t} \cdot \operatorname{grad} \operatorname{div} \boldsymbol{\phi} \, dV = \int \boldsymbol{\phi} \cdot \operatorname{grad} \operatorname{div} \mathbf{t} \, dV \tag{A8.85}$$

$$\langle \nabla^2 \mathbf{t}, \phi \rangle \stackrel{\text{def}}{=} \int \mathbf{t} \nabla^2 \phi \, dV = \int \phi \nabla^2 \mathbf{t} \, dV. \tag{A8.86}$$

$$\langle \nabla^2 \mathbf{t}, \boldsymbol{\phi} \rangle \stackrel{\text{def}}{=} \int \mathbf{t} \cdot \nabla^2 \boldsymbol{\phi} \, dV = \int \boldsymbol{\phi} \cdot \nabla^2 \mathbf{t} \, dV. \tag{A8.87}$$

PIECEWISE CONTINUOUS DISTRIBUTIONS

As a first example, consider the distribution $t(x)$ shown in Figure A8.3. By definition, because t remains bounded in x_0,

$$\left\langle \frac{dt}{dx}, \phi \right\rangle = -\int_{-\infty}^{\infty} t \frac{d\phi}{dx} \, dx = -\int_{-\infty}^{x_0^-} t \frac{d\phi}{dx} \, dx - \int_{x_0^+}^{\infty} t \frac{d\phi}{dx} \, dx.$$

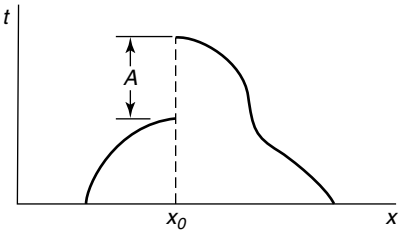

Figure A8.3 Step discontinuity of a function.

Let us transform this expression in such a way that ϕ itself appears in the integral. An integration by parts yields

$$\begin{aligned}\langle t', \phi \rangle &= A\phi(x_0) + \int_{-\infty}^{x_0^-} \frac{dt}{dx}\phi \, dx + \int_{x_0^+}^{\infty} \frac{dt}{dx}\phi \, dx \\ &= \int_{-\infty}^{\infty} \left(A\delta(x - x_0) + \left\{ \frac{dt}{dx} \right\} \right) \phi \, dx.\end{aligned}$$

The factor in front of ϕ is the generating function. Therefore,

$$\frac{dt}{dx} = A\delta(x - x_0) + \left\{ \frac{dt}{dx} \right\}. \tag{A8.88}$$

The notation $\left\{ \dfrac{dt}{dx} \right\}$, used frequently in the text, represents a function that is equal to the usual derivative everywhere but at x_0, where it remains undefined. In a more general way, if g is infinitely differentiable for $x < x_0$ and $x > x_0$, and if g and all its derivatives have left-hand and right-hand limits, then

$$\begin{aligned} g' &= \{g'\} + \sigma_0 \delta(x - x_0) \\ g'' &= \{g''\} + \sigma_0 \delta'(x - x_0) + \sigma_1 \delta(x - x_0) \\ g^{(m)} &= \{g^{(m)}\} + \sigma_0 \delta^{(m-1)}(x - x_0) + \ldots + \sigma_{m-1} \delta(x - x_0), \end{aligned} \tag{A8.89}$$

where σ_i denotes the difference between the right-hand limit and the left-hand limit of the derivative of order i.

In an extension to vector operators, let $\mathbf{t}$ be a continuous vector function that suffers jumps across a surface S but remains bounded throughout space (Fig. A8.2). For such a function,

$$\operatorname{div} \mathbf{t} = \{\operatorname{div} \mathbf{t}\} + (\mathbf{u}_{n1} \cdot \mathbf{t}_1 + \mathbf{u}_{n2} \cdot \mathbf{t}_2) \, \delta_S \tag{A8.90}$$

$$\operatorname{curl} \mathbf{t} = \{\operatorname{curl} \mathbf{t}\} + (\mathbf{u}_{n1} \times \mathbf{t}_1 + \mathbf{u}_{n2} \times \mathbf{t}_2) \, \delta_S. \tag{A8.91}$$

For a discontinuous scalar function:

$$\begin{aligned} \operatorname{grad} t &= \{\operatorname{grad} t\} + (t_1 \mathbf{u}_{n1} + t_2 \mathbf{u}_{n2}) \, \delta_S \\ &= \{\operatorname{grad} t\} + \mathbf{u}_n (t_2 - t_1) \end{aligned} \tag{A8.92}$$

$$\operatorname{grad} H_S = \mathbf{u}_{n1} \delta_S. \tag{A8.93}$$

For a function $\mathbf{t}$ that is discontinuous across S, but remains bounded:

$$\begin{aligned} \operatorname{curl} \operatorname{curl} \mathbf{t} = {} & \{\operatorname{curl} \operatorname{curl} \mathbf{t}\} + \{\mathbf{u}_{n1} \times \operatorname{curl} \mathbf{t}_1 + \mathbf{u}_{n2} \times \operatorname{curl} \mathbf{t}_2\} \delta_S \\ & + \operatorname{curl}[(\mathbf{u}_{n1} \times \mathbf{t}_1 + \mathbf{u}_{n2} \times \mathbf{t}_2) \, \delta_S] \end{aligned} \tag{A8.94}$$

$$\text{grad div } \mathbf{t} = \{\text{grad div } \mathbf{t}\} + (\mathbf{u}_{n1} \text{ div } \mathbf{t}_1 + \mathbf{u}_{n2} \text{ div } \mathbf{t}_2)\delta_S + \text{grad}[(\mathbf{u}_{n1} \cdot \mathbf{t}_1 + \mathbf{u}_{n2} \cdot \mathbf{t}_2)\,\delta_S]. \tag{A8.95}$$

Let a scalar function t suffer jumps in both t and $\dfrac{\partial t}{\partial n}$. Then

$$\nabla^2 t = \{\nabla^2 t\} + \left[\left(\frac{\partial t}{\partial n}\right)_2 - \left(\frac{\partial t}{\partial n}\right)_1\right] + (t_2 - t_1)\frac{\partial \delta_S}{\partial n}. \tag{A8.96}$$

Let a vector distribution $\mathbf{t}$ suffer a discontinuity in its tangential components, while its normal component is infinite in the surface layer,[7] but in such a manner that $\int_1^2 t_n\, dn = v$. Then,

$$\text{div } \mathbf{t} = \{\text{div } \mathbf{t}\} + \mathbf{u}_n \cdot (\mathbf{t}_2 - \mathbf{t}_1)\delta_S + \frac{\partial}{\partial n}(v\delta_S) \tag{A8.97}$$

$$\text{curl } \mathbf{t} = \{\text{curl } \mathbf{t}\} + [\mathbf{u}_n \times (\mathbf{t}_2 - \mathbf{t}_1) + \text{grad}_S\, v \times \mathbf{u}_n]\delta_S. \tag{A8.98}$$

These relationships generalize (A8.87) and (A8.91).

OPERATORS ACTING ON SURFACE SOURCES

The magnetic field in vacuum satisfies (7.20), rewritten here as

$$\text{curl curl } \mathbf{h} + \frac{1}{c_0^2}\frac{\partial^2 \mathbf{h}}{\partial t^2} = \text{curl } \mathbf{j}.$$

When $\mathbf{j}$ is a surface current, it becomes necessary properly to express its curl. More generally, it is desirable to investigate the action of the classic three-dimensional operators on surface sources. The main results are[8,9] [133]:

1. If $\theta\delta_S$ is a scalar function concentrated on S:

$$\text{grad } [\theta\delta_S] = (\text{grad}_S\, \theta + J\theta \mathbf{u}_n)\,\delta_S + \theta u_n \frac{\partial \delta_S}{\partial n}, \tag{A8.99}$$

where J is the first curvature defined in (A3.5).

2. If $\mathbf{a}\delta_S$ is a vector source concentrated on S:

$$\text{div } [\mathbf{a}\delta_S] = \text{div}_S\, \mathbf{a}_t \delta_S + a_n \frac{\partial \delta_S}{\partial n} \tag{A8.100}$$

$$\text{curl } [\mathbf{a}\delta_S] = [\text{grad}_S\, a_n \times \mathbf{u}_n + \overline{\overline{\boldsymbol{\pi}}} \cdot (\mathbf{u}_n \times \mathbf{a}_t) + \mathbf{u}_n \text{ div}_S(\mathbf{a}_t \times \mathbf{u}_n)]\delta_S + (\mathbf{u}_n \times \mathbf{a}_t)\frac{\partial \delta_S}{\partial n}, \tag{A8.101}$$

where $\mathbf{a}_t$ is the tangential component on S, and

$$\overline{\overline{\boldsymbol{\pi}}} = \frac{1}{R_1}\mathbf{u}_1\mathbf{u}_1 + \frac{1}{R_2}\mathbf{u}_2\mathbf{u}_2. \tag{A8.102}$$

NOTES

1. B. van der Pol and H. Bremmer, *Operational Calculus Based on the Two-Sided Laplace Integral.* Cambridge University Press, Cambridge, 1950.
2. P. A. M. Dirac, The physical interpretation of the quantum dynamics, *Proc. Roy. Soc. A.* **CXIII**, 621–641 (1926).
3. P. A. M. Dirac. *The Principles of Quantum Mechanics.* Oxford University Press, Oxford, 4th edition, 1958.
4. L. Schwartz, *Méthodes mathématiques pour les sciences physiques.* Hermann et Cie., Paris, 1965. An English translation was published by Addison-Wesley in 1966.
5. E. M. De Jager, *Applications of Distributions in Mathematical Physics.* Math. Centrum, Amsterdam, 1969.
6. B. Friedman, *Lectures on Applications-Oriented Mathematics.* Holden Day, San Francisco, 1969.
7. J. Van Bladel, On the distributional form of the curl, *Microwave Opt. Tech. Lett.* **23**, 97–100 (1999).
8. J. Van Bladel, Differential operators acting on surface fields, *AEÜ* **45**, 389–391 (1991).
9. J. Van Bladel, Three dimensional operators acting on surface sources, *Radio Sci.* **28**, 841–845 (1993).

For further reading:

J. Arsac, *Transformation de Fourier de théorie des distributions.* Dunod, Paris, 1961.

F. Constantinescu, *Distributionen und ihre Anwendung in der Physik.* Teubner, Stuttgart, 1974.

R. Critescu and G. Marinescu, *Applications of the Theory of Distributions.* John Wiley & Sons, London, 1973 (trans. S. Taleman).

A. Erdélyi (ed.), *Operational Calculus and Generalized Functions.* Holt, Rinehart and Winston, New York, 1962.

F. G. Friedlander, *Introduction to the Theory of Distributions.* Cambridge University Press, Cambridge, 1982.

I. M. Gel'fand and G. E. Shilov, *Generalized Functions.* Academic Press, Inc., New York, 1964.

I. Halperin, *Introduction to the Theory of Distributions.* University of Toronto Press, Toronto, 1952.

R. H. Hoskins, *Generalized Functions.* Ellis Horwood, Chichester, 1979.

D. S. Jones. *The Theory of Generalised Functions*, 2nd edition, Cambridge University Press, Cambridge, 1982.

W. Kecs and P. P. Teodorescu, *Applications of the Theory of Distributions in Mechanics.* Abacus Press, Tunbridge Wells, 1974.

M. J. Lighthill, *An Introduction to Fourier Analysis and Generalised Functions.* Cambridge University Press, Cambridge, 1959.

J. Lützen, *The Prehistory of the Theory of Distributions.* Springer, New York, 1982.

J. P. Marchand, *Distributions: An Outline.* North Holland Publ. Co., Amsterdam, 1962.

R. Petit, *L'outil mathématique*, 2nd edition, Masson, Paris, 1987.

W. Preuss, A. Bleyer, and H. Preuss, *Distributionen und Operatoren: ihre Anwendung in Naturwissenschaft und Technik.* Springer-Verlag, Wien, 1985.

R. D. Richtmyer, *Principles of Advanced Mathematical Physics*, volume 2. Springer, New York, 1978.

L. Schwartz, *Théorie des distributions.* Hermann et Cie, Paris, 1950.

J. Van Bladel, *Singular Electromagnetic Fields and Sources.* Clarendon Press, Oxford, 1991, and IEEE Press, New York, 1995.

V. Vladimirov, *Distributions en physique mathématique.* Editions Mir, Moscou, 1979.

A. H. Zemanian, *Distribution Theory and Transform Analysis.* Dover Publications, New York, 1987. First published in 1965 by McGraw-Hill, New York.

Appendix 9

Some Eigenfunctions and Eigenvectors

IN WAVEGUIDES

The Rectangular Cross Section (Fig. A9.1*a*)

For the E modes,

$$\phi_{mp} = \sin\frac{m\pi x}{a}\sin\frac{p\pi y}{b} \quad m,p = 1,2,3,\ldots \tag{A9.1}$$

$$\mu_{mp}^2 = \left(\frac{m\pi}{a}\right)^2 + \left(\frac{p\pi}{b}\right)^2; \quad N_{mp}^2 = \left(\frac{m^2\pi^2}{a^2} + \frac{p^2\pi^2}{b^2}\right)\frac{ab}{4}, \tag{A9.2}$$

where N^2 is the norm integral of the square of the eigenvector, in the current case of $|\text{grad}\,\phi|^2$.

For the H modes,

$$\psi_{ns} = \cos\frac{n\pi x}{a}\cos\frac{s\pi y}{b} \quad n,s = 0,1,2,\ldots. \tag{A9.3}$$

Except for $n = s = 0$, for which $N_{00}^2 = ab$,

$$\nu_{ns}^2 = \left(\frac{n\pi}{a}\right)^2 + \left(\frac{s\pi}{b}\right)^2$$

$$N_{ns}^2 = \left[(\epsilon_n - 1)\left(\frac{n\pi}{a}\right)^2 + (\epsilon_s - 1)\left(\frac{s\pi}{b}\right)^2\right]\frac{ab}{\epsilon_n\epsilon_s}. \tag{A9.4}$$

The mode with the lowest cutoff frequency is the H_{10} mode ($f_c = c/2a, \lambda_c = 2a$). Its eigenfunctions and eigenvectors are

$$\psi_{10} = \cos\frac{\pi x}{a}; \quad \text{grad}\,\psi_{10} = -\frac{\pi}{a}\sin\frac{\pi x}{a}\mathbf{u}_x. \tag{A9.5}$$

Electromagnetic Fields, Second Edition, By Jean G. Van Bladel

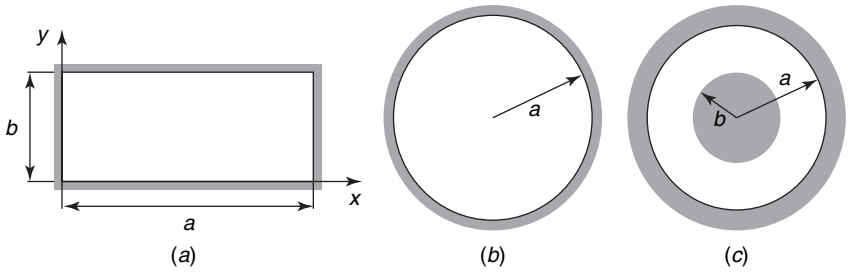

Figure A9.1 Waveguide cross sections: (*a*) rectangular, (*b*) circular, (*c*) coaxial.

The Circular Cross Section (Fig. A9.1*b*)

For the E modes,

$$\phi_{mp} = J_m\left(x_{mp}\frac{r}{a}\right)\begin{Bmatrix}\sin m\varphi\\ \cos m\varphi\end{Bmatrix} \tag{A9.6}$$

$$\mu_{mp}^2 = \left(\frac{x_{mp}}{a}\right)^2; \quad N_{mp}^2 = \frac{2\pi}{\epsilon_m}\frac{x_{mp}^2}{2}J_{m+1}^2(x_{mp}), \tag{A9.7}$$

where the x_{mp}'s are the zeros of $J_m(x)$ (see Table A5.1).

For the H modes,

$$\psi_{ns} = J_n\left(y_{ns}\frac{r}{a}\right)\begin{Bmatrix}\sin n\varphi\\ \cos n\varphi\end{Bmatrix} \tag{A9.8}$$

$$\nu_{ns}^2 = \frac{y_{ns}}{a^2}; \quad N_{ns}^2 = \frac{\pi}{\epsilon_n}J_n^2(y_{ns})(y_{ns}^2 - n^2), \tag{A9.9}$$

where the y_{ns} are the zeros of $dJ_n(x)/dx$ (see Table A5.2). The mode with the lowest cutoff frequency ($\lambda_c = 1.64a$) corresponds with $\psi_{01} = J_0\left(3.832\,\frac{r}{a}\right)$.

The Coaxial Line (Fig. A9.1*c*)

The TEM mode of the coaxial line is defined by the relationships

$$\begin{aligned}\phi_0 &= \log_e r; \qquad \operatorname{grad}\phi_0 = \frac{\mathbf{u}_r}{r}\\ N_0^2 &= 2\pi\,\log_e\frac{a}{b}; \quad \mathbf{u}_z \times \operatorname{grad}\phi_0 = \frac{\mathbf{u}_\varphi}{r}.\end{aligned} \tag{A9.10}$$

The following functions are needed for the other modes:

$$\begin{aligned}R_m\left(\rho_{ms}\frac{r}{a}\right) &= J_m\left(\rho_{ms}\frac{r}{a}\right) + P_{ms}N_m\left(\rho_{ms}\frac{r}{a}\right)\\ S_m\left(\sigma_{ms}\frac{r}{a}\right) &= J_m\left(\sigma_{ms}\frac{r}{a}\right) + Q_{ms}N_m\left(\sigma_{ms}\frac{r}{a}\right).\end{aligned} \tag{A9.11}$$

The functions R_m are defined by the condition $R_m = 0$ at $r = a$ and $r = b$. The condition implies that ρ_{ms} and P_{ms} satisfy the relationship

$$\frac{J_m(\rho_{ms})}{N_m(\rho_{ms})} = \frac{J_m(\rho_{ms}\, b/a)}{N_m(\rho_{ms}\, b/a)} = -P_{ms}. \tag{A9.12}$$

The functions S_m are defined by the condition $dS_m/dr = 0$ at $r = a$ and $r = b$. This condition implies that

$$\frac{J'_m(\sigma_{ms})}{N'_m(\sigma_{ms})} = \frac{J'_m(\sigma_{ms}\, b/a)}{N'_m(\sigma_{ms}\, b/a)} = -Q_{ms}. \tag{A9.13}$$

The E modes are derived from the eigenfunctions

$$\phi_{mp} = R_m\left(\rho_{mp}\frac{r}{a}\right)\begin{Bmatrix}\sin m\varphi\\ \cos m\varphi\end{Bmatrix}. \tag{A9.14}$$

The pertinent eigenvalues can be obtained from the corresponding expressions for the circular waveguide by substituting R_m and ρ_{mp} for J_m and x_{mp}. The normalization integral is now

$$N^2_{mp} = \frac{\pi}{\epsilon_m}\left\{a^2[R'_m(\rho_{mp})]^2 - b^2\left[R'_m\left(\rho_{mp}\frac{b}{a}\right)\right]^2\right\}. \tag{A9.15}$$

For the H modes,

$$\psi_{ns} = S_n\left(\sigma_{ns}\frac{r}{a}\right)\begin{Bmatrix}\sin n\varphi\\ \cos n\varphi\end{Bmatrix} \tag{A9.16}$$

$$N^2_{ns} = \frac{\pi}{\epsilon_n}\left[a^2 S^2_n(\sigma_{ns})\left(1 - \frac{n^2}{\sigma^2_{ns}}\right) - b^2 S^2_n\left(\sigma_{ns}\frac{b}{a}\right)\left(1 - \frac{n^2a^2}{\sigma^2_{ns}b^2}\right)\right]. \tag{A9.17}$$

The transverse components and eigenvalues can be obtained from the corresponding expressions for the circular waveguide by substituting S_n and σ_{ns} for J_n and y_{ns}.

IN CAVITIES

The circular cylindrical and coaxial cavities, as well as the parallelepiped, may be considered as sections of waveguide terminated by metallized end plates. The form of the eigenvectors for these cavities is discussed in Section 15.3. The spherical cavity (of radius a) does not belong to that category. Its Dirichlet eigenfunctions are given by

$$\phi_{mns} = \begin{Bmatrix}\cos m\varphi\\ \sin m\varphi\end{Bmatrix} P^m_n(\cos\theta) j_n(k_{ns}R), \tag{A9.18}$$

where k_{ns} satisfies the equation $j_n(k_{ns}a) = 0$. Some of the roots of this equation are given in Table A5.4. To each ϕ_{mns} there corresponds an *irrotational* eigenvector

$$\begin{aligned}\mathbf{f}_{mns} = {} & \begin{Bmatrix}\cos m\varphi\\ \sin m\varphi\end{Bmatrix} P^m_n(\cos\theta)\frac{dj_n(k_{ns}R)}{dR}\mathbf{u}_R + \frac{1}{R}\begin{Bmatrix}\cos m\varphi\\ \sin m\varphi\end{Bmatrix}\frac{dP^m_n(\cos\theta)}{d\theta} j_n(k_{ns}R)\mathbf{u}_\theta\\ & + \frac{m}{R\sin\theta}\begin{Bmatrix}-\sin m\varphi\\ \cos m\varphi\end{Bmatrix} P^m_n(\cos\theta) j_n(k_{ns}R)\mathbf{u}_\varphi.\end{aligned} \tag{A9.19}$$

The normalization integral for ϕ_{mns} is, from (A5.87),

$$\int_V \phi_{mns}^2 \, dV = -\frac{2\pi(m+n)!a^3}{\epsilon_m(2n+1)(n-m)!}|j_{n+1}(k_{ns}a)|^2. \tag{A9.20}$$

The *divergenceless* electric eigenvectors belong to two different classes. One is associated with the transverse magnetic modes and the other with the transverse electric modes. For the transverse magnetic modes:

$$\begin{aligned} e_{mns} &= \frac{1}{k_{ns}} \operatorname{curl}\operatorname{curl}\left[R\begin{Bmatrix}\sin m\varphi\\ \cos m\varphi\end{Bmatrix} j_n(k_{ns}R)P_n^m(\cos\theta)\mathbf{u}_R\right] \\ &= \frac{n(n+1)}{k_{ns}R} j_n(k_{ns}R)\begin{Bmatrix}\sin m\varphi\\ \cos m\varphi\end{Bmatrix} P_n^m(\cos\theta)\mathbf{u}_R \\ &\quad + \frac{1}{k_{ns}R}\frac{d}{dR}[Rj_n(k_{ns}R)]\begin{Bmatrix}\sin m\varphi\\ \cos m\varphi\end{Bmatrix}\frac{d}{d\theta}[P_n^m(\cos\theta)]\mathbf{u}_\theta \\ &\quad + \frac{m}{k_{ns}R\sin\theta}\frac{d}{dR}[Rj_n(k_{ns}R)]\begin{Bmatrix}\cos m\varphi\\ -\sin m\varphi\end{Bmatrix} P_n^m(\cos\theta)\mathbf{u}_\varphi. \end{aligned} \tag{A9.21}$$

The corresponding eigenvalues are $-k_{ns}^2 = -x_{ns}^2/a^2$, where x_{ns} is a root of $[xj_n(x)]' = 0$. Some of these roots are given in Table A5.6. The resonant wavelengths and frequencies of the cavity are $\lambda = 2\pi a/x$ and $f = cx/2\pi a$. The normalization integral for $\mathbf{e}_{mns}$ can be evaluated by making use of (A5.87). Thus,

$$\begin{aligned} \int_V |\mathbf{e}|^2 \, dV &= \int_V (e_R^2 + b_\theta^2 + e_\varphi^2)\, dV \\ &= \frac{2\pi n(n+1)(n+m)!}{\epsilon_m(2n+1)(n-m)!}a^3\left[1 - \frac{n(n+1)}{x_{ns}^2}\right]j_n^2(x_{ns}). \end{aligned} \tag{A9.22}$$

The transverse electric modes are characterized by the eigenvectors

$$\begin{aligned} \mathbf{e}_{mns} &= \operatorname{curl}\left[Rj_n(k_{ns}R)\begin{Bmatrix}\sin m\varphi\\ \cos m\varphi\end{Bmatrix} P_n^m(\cos\theta)\mathbf{u}_R\right] \\ &= \frac{m}{\sin\theta} j_n(k_{ns}R)\begin{Bmatrix}\cos m\varphi\\ \sin m\varphi\end{Bmatrix} P_n^m(\cos\theta)\mathbf{u}_\theta \\ &\quad - j_n(k_{ns}R)\begin{Bmatrix}\sin m\varphi\\ \cos m\varphi\end{Bmatrix}\frac{d}{d\theta}[P_n^m(\cos\theta)]\mathbf{u}_\varphi, \end{aligned} \tag{A9.23}$$

where $k_{ns} = y_{ns}/a$. The eigenvalues are $k_{ns}^2 = -y_{ns}^2/a^2$, and the resonant wavelengths and frequencies are given by $\lambda = 2\pi a/y$ and $f = cy/2\pi a$. The normalization integral is now

$$\int_V |\mathbf{e}|^2 \, dV = \int_V (e_\theta^2 + e_\varphi^2)\, dV = \frac{2\pi n(n+1)(n+m)!}{\epsilon_m(2n+1)(n-m)!}a^3 j_{n+1}^2(k_{ns}a). \tag{A9.24}$$

The *Neumann* eigenfunctions and corresponding irrotational magnetic eigenvectors are given by the same equations as their electric counterparts (A9.18) and (A9.19). The only

difference lies in the value of k_{ns}, which is now z_{ns}/a, where z_{ns} is a root of $[\,j_n(x)]' = 0$. Some of these roots are given in Table A5.5. The normalization integral is

$$\int_V \psi_{mns}^2\, dV = \frac{2\pi(n+m)!}{\epsilon_m(2n+1)(n-m)!}a^3\left[1 - \frac{n(n+1)}{z_{ns}^2}\right]j_n^2(x_{ns}). \tag{A9.25}$$

It is shown in Section 10.1 that the divergenceless magnetic eigenvectors are given by the equation $\mathbf{h}_m = (1/k_m)$ curl $\mathbf{e}_m$. Application of this equation to the sphere shows that the eigenvectors relative to the TM modes are given by (A9.23) with $k_{ns} = x_{ns}/a$. Similarly, the eigenvectors relative to the TE modes are given by (A9.21), with $k_{ns} = y_{ns}/a$.

ON A SPHERICAL SURFACE

Operators on a spherical surface S_1 of unit radius:

$$\operatorname{div}_1 \mathbf{a} = \operatorname{div}_{\theta\varphi} \mathbf{a}(\theta,\varphi) \;=\; \frac{1}{\sin\theta}\frac{\partial}{\partial\theta}(\sin\theta a_\theta) + \frac{1}{\sin\theta}\frac{\partial a_\varphi}{\partial\varphi} \tag{A9.26}$$

$$\operatorname{grad}_1 a = \operatorname{grad}_{\theta\varphi} a(\theta,\varphi) \;=\; \frac{\partial a}{\partial\theta}\mathbf{u}_\theta + \frac{1}{\sin\theta}\frac{\partial a}{\partial\varphi}\mathbf{u}_\varphi \tag{A9.27}$$

$$\nabla_1^2 a = \nabla_{\theta\varphi}^2 a \;=\; \frac{1}{\sin\theta}\frac{\partial}{\partial\theta}\left(\sin\theta\frac{\partial a}{\partial\theta}\right) + \frac{1}{\sin^2\theta}\frac{\partial^2 a}{\partial\varphi^2}. \tag{A9.28}$$

The basic eigenfunctions, which satisfy

$$\nabla_1^2 Y_{mn} = -n(n+1)Y_{mn} \quad (n = 0, 1, 2, \ldots), \tag{A9.29}$$

are

$$Y_{mn}(\theta,\varphi) = C_{mn}P_n^m(\cos\theta)\begin{Bmatrix}\cos m\varphi\\ \sin m\varphi\end{Bmatrix}. \tag{A9.30}$$

The functions in $\cos m\varphi$ will be termed *even*, those in $\sin m\varphi$ *odd*. The eigenfunction corresponding with $n = 0$, $m = 0$ is a constant. With the choice

$$C_{mn} = \sqrt{\epsilon_m\frac{(2n+1)(n-m)!}{4\pi(n+m)!}}, \tag{A9.31}$$

we obtain an orthonormal set, in the sense that within a given parity (even or odd),

$$\int_{S_1} Y_{mn}(\theta,\varphi)Y_{m',n'}(\theta,\varphi)\sin\theta\, d\theta\, d\theta = \delta_{mm'}\delta_{nn'}. \tag{A9.32}$$

Integration over S_1 implies that φ ranges from 0 to 2π and θ from $(-\pi/2)$ to $(\pi/2)$. Eigenfunctions of different parity are orthogonal. The ensemble of the Y_{mn}^e and Y_{mn}^o forms a complete set, in terms of which a function $f(\theta,\varphi)$ may be expanded as

$$f(\theta,\varphi) = f_{\text{ave}} + \sum_{n=1}^{\infty}\left[A_nP_n(\cos\theta) + \sum_{m=1}^{m=n}(A_{mn}\cos m\varphi + B_{mn}\sin m\varphi)P_n^m(\cos\theta)\right], \tag{A9.33}$$

where f_{ave} is the average value on S_1, (i.e., the average over all solid angles) and

$$A_n = \frac{2n+1}{4\pi} \int_{-\frac{\pi}{2}}^{\frac{\pi}{2}} P_n^m(\cos\theta) \sin\theta \, d\theta \int_0^{2\pi} f(\theta,\varphi) d\varphi$$

$$\begin{Bmatrix} A_{mn} \\ B_{mn} \end{Bmatrix} = \frac{2n+1}{2\pi} \frac{(n-m)!}{(n+m)!} \int_{-\frac{\pi}{2}}^{\frac{\pi}{2}} P_n^m(\cos\theta) \sin\theta \, d\theta \int_0^{2\pi} f(\theta,\varphi) \begin{Bmatrix} \cos m\varphi \\ \sin m\varphi \end{Bmatrix} d\varphi. \quad \text{(A9.34)}$$

The eigenvectors $\text{grad}_1 Y_{nm}^e$; $\text{grad}_1 Y_{nm}^o$; $\text{grad}_1 Y_{nm}^e \times \mathbf{u}_R$; $\text{grad}_1 Y_{nm}^o \times \mathbf{u}_R$ also form a complete orthogonal set. They are not normalized, however. Using (A3.44) and (A3.49), one can show that their N^2 norm is $n(n+1)$, hence that the normalized version is obtained by dividing the above vectors by $\sqrt{n(n+1)}$. With the choice

$$C_{mn} = \sqrt{\epsilon_m \frac{(2n+1)(n-m)!}{4\pi n(n+1)(n+m)!}}, \quad \text{(A9.35)}$$

instead of (A9.31), the gradients are normalized, but the N^2 norm of the Y_{nm} is $[n(n+1)]^{-1}$. Written explicitly, the orthonormal eigenvectors are

$$\mathbf{f}_{m,n}^e = C_{mn} \left\{ -\sin\theta \left[P_n^m(\cos\theta)\right]' \cos m\varphi \, \mathbf{u}_\theta - \frac{m}{\sin\theta} P_n^m(\cos\theta) \sin m\varphi \, \mathbf{u}_\varphi \right\} \quad \text{(A9.36)}$$

$$\mathbf{f}_{m,n}^e \times \mathbf{u}_R = C_{mn} \left\{ -\frac{m}{\sin\theta} P_n^m(\cos\theta) \sin m\varphi \, \mathbf{u}_\theta + \sin\theta \left[P_n^m(\cos\theta)\right]' \cos m\varphi \, \mathbf{u}_\varphi \right\} \quad \text{(A9.37)}$$

$$\mathbf{f}_{m,n}^o = C_{mn} \left\{ -\sin\theta \left[P_n^m(\cos\theta)\right]' \sin m\varphi \, \mathbf{u}_\theta + \frac{m}{\sin\theta} P_n^m(\cos\theta) \cos m\varphi \, \mathbf{u}_\varphi \right\} \quad \text{(A9.38)}$$

$$\mathbf{f}_{m,n}^o \times \mathbf{u}_R = C_{mn} \left\{ \frac{m}{\sin\theta} P_n^m(\cos\theta) \cos m\varphi \, \mathbf{u}_\theta + sin\theta \left[P_n^m(\cos\theta)\right]' \sin m\varphi \, \mathbf{u}_\varphi \right\}, \quad \text{(A9.39)}$$

where

$$\left[P_n^m(x)\right]' = \frac{d}{dx} P_n^m(x), \quad \text{(A9.40)}$$

hence

$$\frac{d}{d\theta} \left[P_n^m(\cos\theta)\right] = -\sin\theta \left[P_n^m(\cos\theta)\right]'. \quad \text{(A9.41)}$$

Appendix 10

Miscellaneous Data

UNITS

Table A10.1 Prefixes

Multiplying factor	Prefix	Symbol
10^{12}	tera	T
10^{9}	giga	G
10^{6}	mega	M
10^{3}	kilo	k
10^{2}	hecto	h
10	deka	da
10^{-1}	deci	d
10^{-2}	centi	c
10^{-3}	milli	m
10^{-6}	micro	μ
10^{-9}	nano	n
10^{-12}	pico	p
10^{-15}	femto	f
10^{-18}	atto	a

SOME PHYSICAL CONSTANTS

Ångström Å (length)	10^{-10} m
Boltzmann constant k	1.3805×10^{-23} J K^{-1}
Charge on an electron e	1.6008×10^{-19} C
Intrinsic impedance of free space $\sqrt{\mu_0/\epsilon_0}$	$120\,\pi = 376.7\,\Omega$
Mass of an electron e	9.1066×10^{-31} kg
Mass of a proton	1.6725×10^{-27} kg
Permittivity of free space ϵ_0	8.854×10^{-12} F m^{-1}

Electromagnetic Fields, Second Edition, By Jean G. Van Bladel

Permeability of free space μ_0	$4\pi \times 10^{-7}\,\mathrm{H\,m^{-1}}$
Planck constant h	$6.624 \times 10^{-34}\,\mathrm{Js}$
Radius of an electron	$2.818\ 10^{-15}\,\mathrm{m}$
Velocity of light c_0 in vacuum	$2.998 \times 10^{8}\,\mathrm{m\,s^{-1}}$

FREQUENCY BANDS

Table A10.2 ITU Frequency Band Nomenclature

ITU band	Designation	Frequency	Wavelength
1	ELF	3–30 Hz	100,000 km to 10,000 km
2	SLF	30–300 Hz	10,000 km to 1000 km
3	ULF	300–3000 Hz	1000 km to 100 km
4	VLF	3–30 kHz	100 km to 10 km
5	LF	30–300 kHz	10 km to 1 km
6	MF	300–3000 kHz	1 km to 100 m
7	HF	3–30 MHz	100 m to 10 m
8	VHF	30–300 MHz	10 m to 1 m
9	UHF	300–3000 MHz	1 m to 10 cm
10	SHF	3–30 GHz	10 cm to 1 cm
11	EHF	30–300 GHz	1 cm to 1 mm

SOME USEFUL EXPANSIONS

These expansions are collected from the main body of the text for easy reference. They are given for $R > R'$ and $r > r'$. The corresponding expansions for $R < R'$ and $r < r'$ follow by exchanging R and R', r and r'. In three dimensions:

$$\frac{1}{|\mathbf{r}-\mathbf{r}'|} = \sum_{n=0}^{\infty}\sum_{m=0}^{n} \epsilon_m \frac{(n-m)!}{(n+m)!} P_n^m(\cos\theta')P_n^m(\cos\theta)\cos m(\varphi-\varphi')\frac{(R')^n}{R^{n+1}} \tag{A10.1}$$

$$\frac{e^{-jk_0|\mathbf{r}-\mathbf{r}'|}}{|\mathbf{r}-\mathbf{r}'|} = -jk_0 \sum_{n=0}^{\infty}\sum_{m=0}^{n} (2n+1) j_n(kR')h_n^{(2)}(kR)\epsilon_m \frac{(n-m)!}{(n+m)!} \times P_n^m(\cos\theta)P_n^m(\cos\theta')\cos m(\varphi-\varphi'). \tag{A10.2}$$

In two dimensions:

$$\log_e \frac{r}{|\mathbf{r}-\mathbf{r}'|} = \sum_{n=1}^{\infty} \frac{1}{n}\left(\frac{r'}{r}\right)^n \cos n(\varphi-\varphi') \tag{A10.3}$$

$$H_0^{(2)}(k_0|\mathbf{r}-\mathbf{r}'|) = \sum_{m=-\infty}^{\infty} J_m(k_0 r')H_m^{(2)}(k_0 r)\, e^{\,jm(\varphi-\varphi')}. \tag{A10.4}$$

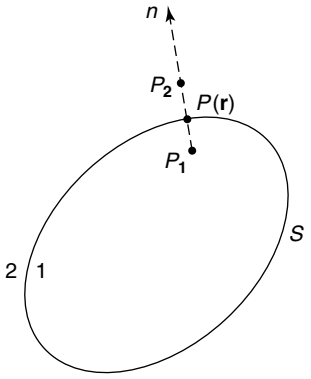

Figure A10.1 Points P_1 and P_2, which approach P along the normal.

SOME FUNDAMENTAL SINGULARITIES

When S_δ is a very small planar area containing P (Fig. A10.1)

$$\lim_{P_1\to P}\int_{S_\delta}\frac{\partial}{\partial n}\left(\frac{1}{|\mathbf{r}-\mathbf{r}'|}\right)dS' = -\lim_{P_1\to P}\int_{S_\delta}\frac{\partial}{\partial n'}\left(\frac{1}{|\mathbf{r}-\mathbf{r}'|}\right)dS' = 2\pi \tag{A10.5}$$

$$\lim_{P_2\to P}\int_{S_\delta}\frac{\partial}{\partial n}\left(\frac{1}{|\mathbf{r}-\mathbf{r}'|}\right)dS' = -\lim_{P_2\to P}\int_{S_\delta}\frac{\partial}{\partial n'}\left(\frac{1}{|\mathbf{r}-\mathbf{r}'|}\right)dS' = -2\pi. \tag{A10.6}$$

Because the dimensions of S_δ are very small with respect to λ_0, the equations remain valid when $|\mathbf{r}-\mathbf{r}'|^{-1}$ is replaced by $|\mathbf{r}-\mathbf{r}'|^{-1}\exp(-k_0|\mathbf{r}-\mathbf{r}'|)$.

Single-Layer Potential

$$I(\mathbf{r}) = \int_S \frac{f(\mathbf{r}')}{|\mathbf{r}-\mathbf{r}'|}\,dS' \quad (\mathbf{r}' \text{ on } S). \tag{A10.7}$$

$$\lim_{P_1\to P}\frac{\partial I}{\partial n} = 2\pi f(\mathbf{r}_P) + \lim_{\delta\to 0}\int_{S-S_\delta} f(\mathbf{r}')\frac{\partial}{\partial n}\left(\frac{1}{|\mathbf{r}-\mathbf{r}_P|}\right)dS' \tag{A10.8}$$

$$\lim_{P_2\to P}\frac{\partial I}{\partial n} = -2\pi f(\mathbf{r}_P) + \lim_{\delta\to 0}\int_{S-S_\delta} f(\mathbf{r}')\frac{\partial}{\partial n}\left(\frac{1}{|\mathbf{r}-\mathbf{r}_P|}\right)dS'. \tag{A10.9}$$

In electrostatics, $f(\mathbf{r})$ is $(\rho_S(\mathbf{r})/4\pi\epsilon_0)$.

Double-Layer Potential

$$I(\mathbf{r}) = \int_S f(\mathbf{r}')\frac{\partial}{\partial n'}\left(\frac{1}{|\mathbf{r}-\mathbf{r}'|}\right)dS'. \tag{A10.10}$$

On the basis of (3.68) and (3.69),

$$\lim_{P_1 \to P} I = -2\pi f(\mathbf{r}_P) + \lim_{\delta \to 0} \int_{S-S_\delta} f(\mathbf{r}') \frac{\partial}{\partial n'} \left(\frac{1}{|\mathbf{r} - \mathbf{r}'|} \right) dS' \tag{A10.11}$$

$$\lim_{P_2 \to P} I = 2\pi f(\mathbf{r}_P) + \lim_{\delta \to 0} \int_{S-S_\delta} f(\mathbf{r}') \frac{\partial}{\partial n'} \left(\frac{1}{|\mathbf{r} - \mathbf{r}'|} \right) dS'. \tag{A10.12}$$

In electrostatics, $f(\mathbf{r})$ is $\tau(\mathbf{r})/4\pi\epsilon_0$.

Vector Potential

Let $\mathbf{a}_t$ be a vector tangent to S. For such a vector,

$$\mathbf{I}(\mathbf{r}) = \operatorname{curl} \left[\int \frac{1}{|\mathbf{r} - \mathbf{r}'|} \mathbf{a}_t \, dS' \right] = \int_S \operatorname{grad} \frac{1}{|\mathbf{r} - \mathbf{r}'|} \times \mathbf{a}_t(\mathbf{r}') \, dS'. \tag{A10.13}$$

For that integral

$$\lim_{P_1 \to P} (\mathbf{u}_n \times \mathbf{I}) = -2\pi \, \mathbf{a}_t(\mathbf{r}) + \mathbf{u}_n(\mathbf{r}) \times \lim_{\delta \to 0} \int_{S-S_\delta} \mathbf{a}_t(\mathbf{r}') \times \operatorname{grad}' \left(\frac{1}{|\mathbf{r} - \mathbf{r}'|} \right) dS' \tag{A10.14}$$

$$\lim_{P_2 \to P} (\mathbf{u}_n \times \mathbf{I}) = 2\pi \, \mathbf{a}_t(\mathbf{r}) + \mathbf{u}_n(\mathbf{r}) \times \lim_{\delta \to 0} \int_{S-S_\delta} \mathbf{a}_t(\mathbf{r}') \times \operatorname{grad}' \left(\frac{1}{|\mathbf{r} - \mathbf{r}'|} \right) dS'. \tag{A10.15}$$

In magnetostatics, $\mathbf{a}_t$ is $(\mathbf{j}_S/4\pi)$, and $\mathbf{I}$ is $\mathbf{h}$.

Two-Dimensional Potentials

$$\lim_{P_1 \to P} \int_{C_\delta} \frac{\partial}{\partial n} \left(\log_e \frac{L}{|\mathbf{r} - \mathbf{r}'|} \right) dc' = -\lim_{P_1 \to P} \int_{C_\delta} \frac{\partial}{\partial n'} \left(\log_e \frac{L}{|\mathbf{r} - \mathbf{r}'|} \right) dc' = \pi \tag{A10.16}$$

$$\lim_{P_2 \to P} \int_{C_\delta} \frac{\partial}{\partial n} \left(\log_e \frac{L}{|\mathbf{r} - \mathbf{r}'|} \right) dc' = -\lim_{P_2 \to P} \int_{C_\delta} \frac{\partial}{\partial n'} \left(\log_e \frac{L}{|\mathbf{r} - \mathbf{r}'|} \right) dc' = -\pi, \tag{A10.17}$$

where C_δ is a small segment of C that contains P. The single-layer potential is of the form

$$I(\mathbf{r}) = \int_C f(\mathbf{r}') \log_e \frac{L}{|\mathbf{r} - \mathbf{r}'|} \, dc'. \tag{A10.18}$$

Its normal derivatives satisfy

$$\lim_{P_1 \to P} \frac{\partial I}{\partial n} = \pi f(\mathbf{r}_P) + \lim_{\delta \to 0} \int_{C-C_\delta} \rho_S(\mathbf{r}') \frac{\partial}{\partial n} \left(\log_e \frac{L}{|\mathbf{r} - \mathbf{r}'|} \right) dc' \tag{A10.19}$$

$$\lim_{P_2 \to P} \frac{\partial I}{\partial n} = -\pi f(\mathbf{r}_P) + \lim_{\delta \to 0} \int_{C-C_\delta} \rho_S(\mathbf{r}') \frac{\partial}{\partial n} \left(\log_e \frac{L}{|\mathbf{r} - \mathbf{r}'|} \right) dc'. \tag{A10.20}$$

In electrostatics, $f(\mathbf{r}) = \rho_S(\mathbf{r})/2\pi\epsilon_0$. The double-layer potential

$$I(\mathbf{r}) = \int_C f(\mathbf{r}') \frac{\partial}{\partial n'} \log_e \frac{L}{|\mathbf{r} - \mathbf{r}'|} \, dc' \tag{A10.21}$$

approaches the following limit values at the surface:

$$\lim_{P_1 \to P} \phi = -\pi f(\mathbf{r}_P) + \lim_{\delta \to 0} \int_{C - C_\delta} \tau(\mathbf{r}') \frac{\partial}{\partial n'} \left(\log_e \frac{L}{|\mathbf{r} - \mathbf{r}'|} \right) dc' \tag{A10.22}$$

$$\lim_{P_2 \to P} \phi = \pi f(\mathbf{r}_P) + \lim_{\delta \to 0} \int_{C - C_\delta} \tau(\mathbf{r}') \frac{\partial}{\partial n'} \left(\log_e \frac{L}{|\mathbf{r} - \mathbf{r}'|} \right) dc'. \tag{A10.23}$$

In electrostatics, $f(\mathbf{r}) = \tau(\mathbf{r})/2\pi\epsilon_0$.

Bibliography

The following books are referenced in the text:

GENERAL TEXTS ON ELECTROMAGNETIC THEORY

[1] C. A. Balanis. *Advanced engineering electromagnetics*. John Wiley & Sons, New York, 1989.

[2] P. R. Clement and W. C. Johnson. *Electrical engineering science*. McGraw-Hill Book Company, New York, 1960.

[3] P. C. Clemmow. *An introduction to electromagnetic theory*. Cambridge University Press, Cambridge, 1973.

[4] E. W. Cowan. *Basic electromagnetism*. Academic Press, New York, 1968.

[5] T. De Donder. *Théorie mathématique de l'électricité*. Gauthier-Villars, Paris, 1925.

[6] S. Flügge (ed.). *Encylopedia of physics*, volume 16: Electric fields and waves, volume 17: Dielectrics, volume 27: Crystal optics—Diffraction. Springer-Verlag, Berlin, 1956, 1958, 1961.

[7] E. Hallén. *Electromagnetic theory*. Chapman and Hall, London, 1962. English translation of the original "Elektricitetslära," Stockholm, 1953.

[8] A. Ishimaru. *Electromagnetic wave propagation, radiation and scattering*. Prentice-Hall, Englewood Cliffs, NJ, 1991.

[9] D. S. Jones. *Acoustic and electromagnetic waves*. Clarendon Press, Oxford, 1986.

[10] J. A. Kong. *Electromagnetic wave theory*. John Wiley & Sons, New York, 1986.

[11] L. D. Landau and E. M. Lifshitz. *Electrodynamics of continous media*. Pergamon Press, New York, 1960.

[12] I. V. Lindell. *Methods for electromagnetic field analysis*. Oxford University Press, Oxford, 1992. 2nd edition published together with IEEE Press, 1995.

[13] J. C. Maxwell. *A treatise on electricity and magnetism*. Oxford University Press, London, 3rd edition, 1891. Reprinted by Dover Publications, New York, in 1954.

[14] R. Petit. *Ondes électromagnétiques en radioélectricité et en optique*. Masson, Paris, 1989.

[15] S. A. Schelkunoff. *Electromagnetic waves*. D. Van Nostrand Co., Princeton, NJ, 1943.

[16] M. Schwartz. *Principles of electrodynamics*. McGraw-Hill Book Company, New York, 1972.

[17] W. R. Smythe. *Static and dynamic electricity*. McGraw-Hill Book Company, New York, 2nd edition, 1950.

[18] C. G. Someda. *Electromagnetic waves*. Chapman and Hall, London, 1998.

[19] A. Sommerfeld. *Elektrodynamik*. Dieterich'sche Verlagsbuchhandlung, Wiesbaden, 1948.

[20] J. A. Stratton. *Electromagnetic theory*. McGraw-Hill Book Company, New York, 1941.

[21] G. Tyras. *Radiation and propagation of electromagnetic waves*. Academic Press, New York, 1969.

[22] J. Van Bladel. *Electromagnetic fields*. McGraw-Hill Book Company, New York, 1st edition, 1964. Revised printing by the Hemisphere Publ. Co., Washington, in 1985.

Electromagnetic Fields, Second Edition, By Jean G. Van Bladel

[23] J. R. Wait. *Electromagnetic wave theory*. Harper and Row, New York, 1985.

[24] D. H. Werner and R. Mittra. *Frontiers in electromagnetics*. IEEE Press, Piscataway, NJ, 2000.

TEXTS THAT DISCUSS PARTICULAR AREAS OF ELECTROMAGNETIC THEORY

[25] H. Arzeliès. *La dynamique relativiste et ses applications*. Gauthier-Villars, Paris, 1957, 1958.

[26] H. Arzeliès. *Milieux conducteurs ou polarisables en mouvement*. Gauthier-Villars, Paris, 1959.

[27] H. Arzeliès. *Relativistic kinematics*. Pergamon Press, Oxford, 1966.

[28] A. Baños. *Dipole radiation in the presence of a conducting half-space*. Pergamon Press, Oxford, 1966.

[29] C. E. Baum, L. Carin, and A. P. Stone (eds.). *Ultra-wideband, short-pulse electromagnetics*, volume 3. Plenum Press, New York, 1997.

[30] C. E. Baum (ed.). *Detection and identification of visually obscured targets*. Taylor & Francis, Philadelphia, 1998.

[31] H. L. Bertoni, L. Carin, and L. B. Felsen (eds.). *Ultra-wideband, short-pulse electromagnetics*, volume 1. Plenum Press, New York, 1993.

[32] H. L. Bertoni and L. B. Felsen (eds.). *Directions in electromagnetic wave modeling*. Plenum Press, New York, 1991.

[33] L. V. Bewley. *Flux linkages and electromagnetic induction*. Macmillan, New York, 1952.

[34] H. Blok, H. A. Ferweda, and H. K. Kuiken (eds.). *Huyghens' principle 1960-1990, theory and applications*. North Holland Publ. Co., Amsterdam, 1992.

[35] W. M. Boerner (ed.). *Inverse methods in electromagnetic imaging*. Reidel Publ. Co., Dordrecht, 1985 (2 vol.).

[36] M. Born and E. Wolf. *Principles of optics*. Cambridge University Press, Cambridge, 7th edition, 1999.

[37] C. J. F. Böttcher. *Theory of electric polarisation*. Elsevier Publishing Company, Amsterdam, 2nd edition, volume 1: 1973, volume 2: 1978.

[38] J. J. Bowman, T. B. A. Senior, and P. L. E. Uslenghi (ed.). *Electromagnetic and acoustic scattering by simple shapes*. North-Holland Publishing Co., Amsterdam, 1969.

[39] H. Bremmer. *Terrestrial radio waves*. Elsevier Publishing Company, Amsterdam, 1949.

[40] L. Brillouin. *Wave propagation in periodic structures*. Dover Publications, New York, 2nd edition, 1953.

[41] H. Buchholz. *Electrische und Magnetische Potentialfelder*. Springer-Verlag, Berlin, 1957.

[42] L. Carin and L. B. Felsen (eds.). *Ultra-wideband short-pulse electromagnetics*, volume 2. Plenum Press, New York, 1995.

[43] F. F. Chen. *Introduction to plasma physics*. Plenum Press, New York, 1974.

[44] W. C. Chew. *Waves and fields in inhomogeneous media*. Van Nostrand, New York, 1990.

[45] P. C. Clemmow. *The plane wave spectrum representation of electromagnetic fields*. IEEE Press, New York, and Oxford University Press, Oxford, 1996.

[46] R. E. Collin. *Field theory of guided waves*. IEEE Press, New York, 2nd edition, 1991.

[47] R. E. Collin and F. J. Zucker (eds.). *Antenna theory*. McGraw-Hill Book Company, New York, 1969. Parts 1 and 2.

[48] T. G. Cowling. *Magnetohydrodynamics*. Interscience Publishers, New York, 1957.

[49] J. W. Crispin and K. M. Siegel (eds.). *Methods of radar cross-section analysis*. Academic Press, Inc., New York, 1968.

[50] A. T. de Hoop. *Handbook of radiation and scattering of waves*. Academic Press, London, 1995.

[51] P. Degauque and J. Hamelin. *Compatibilité électromagnétique*. Dunod, Paris, 1990.

[52] P. Delogne. *Leaky feeders and subsurface radiocommunications*. Peter Peregrinus (on behalf of the IEE), London and Stevenage, 1982.

[53] P. P. Delsanto and A. W. Skenz (eds.). *New perspectives on problems in classical and quantum physics*. Gordon and Breach, Science Publishers, Amsterdam, 1998.

[54] E. Durand. *Electrostatique*. Tome 1: Les distributions, Tome 2: Problèmes généraux. Conducteurs, Tome 3: Méthodes de Calcul. Diélectriques. Masson, Paris, 1964, 1966, 1966.

[55] E. Durand. *Magnétostatique*. Masson, Paris, 1968.

[56] J. L. Eaves and E. K. Reedy. *Principles of modern radar*. Van Nostrand Reinhold Co., New York, 1987.

[57] A. Einstein. *1912 manuscript on the special theory of relativity*. G. Braziller Publ., New York, 1996.

[58] R. S. Elliott. *Electromagnetics. History, theory and applications*. IEEE Press, New York, 1993.

[59] R. S. Elliott. *An introduction to guided waves and microwave circuits*. Prentice-Hall, Englewood Cliffs, NJ, 1993.

[60] N. Faché, F. Olyslager, and D. De Zutter. *Electromagnetic and circuit modelling of multiconductor transmission lines*. Clarendon Press, Oxford, 1993.

[61] L. B. Felsen and N. Marcuvitz. *Radiation and scattering of waves*. Prentice-Hall, Englewood Cliffs, NJ, 1973.

[62] L. B. Felsen (ed.). *Transient electromagnetic fields*. Springer-Verlag, Berlin, 1976.

[63] L. B. Felsen (ed.). *Hybrid formulation of wave propagation and scattering*. Martinus Nijhoff Publishers, Dordrecht, 1984.

[64] V. A. Fock. *Electromagnetic diffraction and propagation problems*. Pergamon Press, Oxford, 1965.

[65] W. Franz. *Theorie der Beugung Elektromagnetischer Wellen*. Springer-Verlag OHG, Berlin, 1957.

[66] P. Galison. *Einstein's clocks, Poincaré's maps*. W. W. Norton and Co., New York, 2003.

[67] R. L. Gardner. *Lightning electromagnetics*. Hemisphere Publ. Corp., New York, 1990.

[68] V. L. Ginzburg. *Propagation of electromagnetic waves in plasma*. Gordon and Breach, New York, 1961.

[69] C. G. Gray and K. Gubbins. *Theory of molecular fluids*, volume 1: Fundamentals. Oxford University Press, Oxford, 1984.

[70] A. Guran, R. Mittra, and P. J. Moser. *Electromagnetic wave interactions*. World Scientific Publ. Co., Singapore, 1996.

[71] B. Hague. *Electromagnetic problems in electrical engineering*. Oxford University Press, Fair Lawn, NJ, 1929.

[72] T. B. Hansen and A. D. Yaghjian. *Plane-wave theory of time-domain fields*. IEEE Press, New York, 1999.

[73] R. F. Harrington. *Time-harmonic electromagnetic fields*. McGraw-Hill Book Company, New York, 1961.

[74] J. H. Hinken. *Superconductor electronics*. Springer-Verlag, Berlin, 1989.

[75] D. J. Hoppe and Y. Rahmat-Samii. *Impedance boundary conditions in electromagnetics*. Taylor & Francis, Philadelphia, 1995.

[76] T. Itoh (ed.). *Planar transmission line structures*. IEEE Press, New York, 1987.

[77] G. L. James. *Geometrical theory of diffraction for electromagnetic waves*. Peter Peregrinus, London, 1976.

[78] J. D. Joannopoulos, R. D. Meade, and J. N. Winn. *Photonic crystals*. Princeton University Press, Princeton, NJ, 1995.

[79] M. Jouguet. *Traité d'électricité théorique,* volumes 1 & 2. Gauthier-Villars, Paris, 1955.

[80] E. V. Jull. *Aperture antennas and diffraction theory*. Peter Peregrinus, London, 1981.

[81] H. Kaden. *Wirbelströme und Schirmung in der Nachrichtentechnik*. Springer-Verlag, Berlin, 1959.

[82] D. Kajfez and P. Guillon (eds.). *Dielectric resonators*. Noble Publ. Co., Atlanta, 1998.

[83] D. E. Kerr (ed.). *Propagation of short radio waves*. McGraw-Hill Book Company, New York, 1951.

[84] R. W. P. King. *The theory of linear antennas*. Harvard University Press, Cambridge, MA, 1956.

[85] R. W. P. King and T. T. Wu. *The scattering and diffraction of waves*. Harvard University Press, Cambridge, MA, 1959.

[86] M. Kline and I. W. Kay. *Electromagnetic theory and geometrical optics*. Interscience Publishers, New York, 1965.

[87] A. Lakhtakia, V. K. Varadan, and V. V. Varadan. *Time-harmonic electromagnetic fields in chiral media*. Springer-Verlag, Berlin, 1989.

[88] L. Landau and E. Lifshitz. *The classical theory of fields*. Addison-Wesley, Cambridge, MA, 1951.

[89] R. E. Langer (ed.). *Electromagnetic waves*. The University of Wisconsin Press, Madison, 1962.

[90] K. F. Lee and W. Chen (eds.). *Advances in microstrip and printed antennas*. John Wiley & Sons, New York, 1997.

[91] K. S. H. Lee (ed.). *EMP interaction: principles, techniques, and reference data*. Hemisphere Publ. Corp., Washington, 1986.

[92] J. G. Linhart. *Plasma physics*. North Holland Publ. Co., Amsterdam, 1960.

[93] R. K. Luneburg. *Mathematical theory of optics*. University of California Press, Berkeley and Los Angeles, 1964.

[94] E. J. Maanders and R. Mittra (eds.). *Modern topics in electromagnetics and antennas*. Peter Peregrinus, Stevenage, 1977.

[95] D. Marcuse. *Light transmission optics*. Van Nostrand Reinhold Co., New York, 1972.

[96] D. Marcuse. *Theory of dielectric optical waveguides*. Academic Press, New York, 1974.

[97] N. Marcuvitz (ed.). *Waveguide handbook*. McGraw-Hill Book Company, New York, 1951.

[98] A. I. Miller. *Albert Einstein's special theory of relativity, emergence (1905) and early interpretation (1905-1911)*. Addison-Wesley, Reading, MA, 1981.

[99] C. Møller. *The theory of relativity*. Clarendon Press, Oxford, 2nd edition, 1972.

[100] G. D. Monteath. *Applications of the electromagnetic reciprocity principle*. Pergamon Press, Oxford, 1973.

[101] C. G. Montgomery, R. H. Dicke, and E. M. Purcell (eds.). *Principles of microwave circuits*. McGraw-Hill Book Company, New York, 1948.

[102] M. Mrozowski. *Guided electromagnetic waves, properties and analysis*. Research Studies Press Ltd., Taunton, UK, and John Wiley & Sons, New York, 1997.

[103] B. A. Munk. *Frequency selective surfaces*. John Wiley & Sons, New York, 2000.

[104] F. Ollendorff. *Potentialfelder der Elektrotechnik*. Springer-Verlag, Berlin, 1932.

[105] F. Olyslager. *Electromagnetic waveguide and transmission lines*. Oxford University Press, Oxford, 1999.

[106] C. R. Paul. *Analysis of multiconductor transmission lines*. John Wiley & Sons, New York, 1994.

[107] W. Pauli. *Theory of relativity*. Pergamon Press, London, 1958.

[108] R. Petit (ed.). *Electromagnetic theory of gratings*. Springer-Verlag, Berlin, 1980.

[109] D. M. Pozar and D. H. Schaubert. *Microstrip antennas*. IEEE Press, New York, 1995.

[110] S. M. Rao (ed.). *Time domain electromagnetics*. Academic Press, San Diego, 1999.

[111] T. Rozzi and M. Farina. *Advanced electromagnetic analysis of passive and active planar structures*. Institution of Electrical Engineers, Stevenage, UK, 1999.

[112] T. Rozzi and M. Mongiardo. *Open electromagnetic waveguides*. Institution of Electrical Engineers, London, 1997.

[113] G. T. Ruck, D. E. Barrick, W. D. Stuart, and C. K. Krichbaum. *Radar cross-section handbook*. Plenum Press, New York, 1970.

[114] S. A. Schelkunoff. *Advanced antenna theory*. John Wiley & Sons, New York, 1952.

[115] D. Schieber. *Electromagnetic induction phenomena*. Springer-Verlag, Berlin, 1986.

[116] T. B. A. Senior and J. L. Volakis. *Approximate boundary conditions in electromagnetics*. The Institution of Electrical Engineers, London, 1995.

[117] A. Serdyukov, I. Semchenko, S. Tretyakov, and A. Sihvola. *Electromagnetics of bi-anisotropic materials*. Gordon and Breach, Science Publishers, Amsterdam, 2001.

[118] S. Silver (ed.). *Microwave antenna theory and design*. McGraw-Hill Book Company, New York, 1949.

[119] J. K. Skwirzynski (ed.). *Theoretical methods for determining the interaction of electromagnetic waves with structures*. NATO advanced study institutes series, Series E: Applied sciences 40, Sijthoff and Noordhoff, Alphen aan den Rijn, 1981.

[120] P. D. Smith and S. R. Cloude (eds.). *Ultra-wideband, short-pulse electromagnetics*, volume 5. Kluwer Academic/Plenum Publishers, New York, Dordrecht, 2002.

[121] A. W. Snyder and J. D. Love. *Optical waveguide theory*. Chapman and Hall, London, 1983.

[122] A. Sommerfeld. *Optik*. Dieterich'sche Verlagsbuchhandlung, Wiesbaden, 1950. An English translation has been published by Academic Press, New York, in 1964.

[123] L. Spitzer. *Physics of fully ionized gases*. Interscience Publishers, New York, 2nd edition, 1962.

[124] W. L. Stutzman. *Polarizations in electromagnetic systems*. Artech House, Norwood, MA, 1993.

[125] D. M. Sullivan. *Electromagnetic simulation using the FDTD method*. IEEE Press, New York, 2000.

[126] T. Tamir (ed.). *Integrated optics*. Springer-Verlag, Berlin, 2nd edition, 1979.

[127] F. M. Tesche, M. V. Ianoz, and T. Karlsson. *EMC analysis methods and computational models*. John Wiley & Sons, New York, 1997.

[128] A. G. Tijhuis. *Electromagnetic inverse profiling*. VNU Science Press, Utrecht, 1987.

[129] M. Tinkham. *Introduction to superconductivity*. McGraw-Hill Book Company, New York, 2nd edition, 1996.

[130] F. T. Ulaby and C. Elachi (eds.). *Radar polarimetry for geoscience applications*. Artech House, Norwood, MA, 1990.

[131] P. L. E. Uslenghi (ed.). *Electromagnetic scattering*. Academic Press, New York, 1978.

[132] J. Van Bladel. *Relativity and engineering*. Springer-Verlag, Berlin, 1984.

[133] J. Van Bladel. *Singular electromagnetic fields and sources*. Oxford University Press, Oxford, 1991, and IEEE Press, New York, 1995.

[134] H. C. van de Hulst. *Light scattering by small particles*. John Wiley & Sons, New York, 1957.

[135] P. M. van den Berg, H. Blok, and J. T. Fokkema. *Wavefields and reciprocity*. Delft University Press, 1996.

[136] V. K. Varadan and V. V. Varadan (eds.). *Acoustic, electromagnetic and elastic wave scattering —Focus on the T-matrix approach*. Pergamon Press, New York, 1979.

[137] J. R. Wait. *Electromagnetic waves in stratified media*. Pergamon Press, Oxford, 2nd edition, 1970.

[138] J. R. Wait. *Introduction to antennas and propagation*. Peter Peregrinus, London, 1986.

[139] C. H. Walter. *Traveling wave antennas*. McGraw-Hill Book Company, New York, 1965.

[140] E. Weber. *Electromagnetic fields*, volume 1: Mapping of fields. John Wiley & Sons, New York, 1950.

[141] E. Whittaker. *A history of the theories of aether and electricity*, volume 1: The classical theories. Thomas Nelson and Sons, London, 1951.

[142] H. H. Woodson and J. R. Melcher. *Electromechanical dynamics, Part II: Fields, forces and motion*. John Wiley & Sons, New York, 1968.

[143] A. Yariv. *Optical electronics*. Holt, Rinehart and Winston, New York, 3rd edition, 1985.

GENERAL MATHEMATICAL BACKGROUND

[144] M. Abramowitz and I. A. Stegun. *Handbook of mathematical functions*. National Bureau of Standards, Applied Mathematics Series 55, 1964. Reprinted by Dover Publications, New York, 1965.

[145] J. H. Ahlberg, E. N. Nilson, and J. L. Walsch. *The theory of splines and their applications*. Academic Press, New York, 1967.

[146] A. M. Arthurs. *Complementary variational principles*. Clarendon Press, Oxford, 1970.

[147] S. Bergman and M. Schiffer. *Kernel functions and elliptic differential equations in mathematical physics*. Academic Press, New York, 1953.

[148] Ll. G. Chambers. *Integral equations: A short course*. International Textbook Co., London, 1976.

[149] J. D. Cole. *Perturbation methods in applied mathematics*. Blaisdell Publishing Company, Waltham, MA, 1968.

[150] B. Friedman. *Principles and techniques of applied mathematics*. John Wiley & Sons, New York, 1956.

[151] H. G. Garnir. *Les problèmes aux limites de la physique mathématique*. Birkhäuser Verlag, Basel, 1958.

[152] G. H. Golub and C. F. Van Loan. *Matrix computations*. John Hopkins University Press, Baltimore, 1983.

[153] N. M. Günter. *Potential theory and its applications to basic problems of mathematical physics*. Frederick Ungar Pub. Co., New York, 1967.

[154] R. F. Harrington. *Field computation by moment methods*. Macmillan, New York, 1968.

[155] M. R. Hestenes. *Conjugate direction methods in optimization*. Springer-Verlag, New York, 1980.

[156] M. A. Jaswon and G. T. Symm. *Integral equation methods in potential theory and elastostatics*. Academic Press, London, 1977.

[157] A. Jennings. *Matrix computation for engineers and scientists*. John Wiley & Sons, Chichester, 1977.

[158] O. D. Kellogg. *Foundations of potential theory*. Springer-Verlag, Berlin, 1929.

[159] M. Krasnov, A. Kissélev, and G. Makarenko. *Equations intégrales*. Editions Mir, Moscow, 1977.

[160] L. A. Ljusternik and W. I. Sobolew. *Elemente der Funktional Analysis*. Akademie-Verlag GmbH, Berlin, 1955.

[161] W. Magnus, F. Oberhettinger, and R. P. Soni. *Formulas and theorems for the special functions of mathematical physics*. Springer-Verlag, Berlin, Third enlarged edition, 1966.

[162] W. D. Mac Millan. *The theory of the potential*. McGraw-Hill Book Company, New York, 1930. Reprinted by Dover Publications, New York, in 1958.

[163] A. R. Mitchell and R. Wait. *The finite element method in partial differential equations*. John Wiley & Sons, Chichester, 1977.

[164] B. L. Moiseiwitsch. *Integral equations*. Longman, London, 1977.

[165] P. M. Morse and H. Feshbach. *Methods of theoretical physics*. McGraw-Hill Book Company, New York, 1953.

[166] R. E. O'Malley. *Introduction to singular perturbations*. Academic Press, New York, 1974.

[167] W. Pogorzelski. *Integral equations and their applications*, volume 1. Pergamon Press, Oxford, 1966.

[168] F. Riesz and B. S. Nagy. *Lecons d'analyse fonctionnelle*. Gauthier-Villars, Paris, 3rd edition, 1955. An English translation has been published by Frederick Ungar Publishing Co., New York.

[169] G. D. Smith. *Numerical solution of partial differential equations: Finite difference methods*. Clarendon Press, Oxford, 3rd edition, 1985.

[170] F. Smithies. *Integral equations*. Cambridge University Press, Cambridge, 1958.

[171] A. Sommerfeld. *Partielle Differentialgleichungen der Physik*. Dieterich'sche Verlagsbuchhandlung, Wiesbaden, 1947. An English translation has been published in 1964 by Academic Press, New York.

[172] W. J. Sternberg and T. L. Smith. *The theory of potential and spherical harmonics*. University of Toronto Press, Toronto, 1952.

[173] C. T. Tai. *Generalized vector and dyadic analysis*. Oxford University Press, Oxford, and IEEE Press, New York, 2nd edition, 1997.

[174] A. E. Taylor. *Introduction to functional analysis*. John Wiley & Sons, New York, 1958.

[175] A. N. Tikhonov and V. Arsenin. *Solution of ill-posed problems*. Winston-Wiley, New York, 1977.

[176] J. R. Westlake. *A handbook of numerical matrix inversion and solution of linear equations*. John Wiley & Sons, New York, 1968.

[177] J. H. Wilkinson. *The algebraic eigenvalue problems*. Clarendon Press, Oxford, 1965.

[178] D. C. Zienkiewicz and R. L. Taylor. *The finite element method*. McGraw-Hill Book Company, London, 4th edition, 1994.

[179] O. C. Zienkiewicz and Y. K. Cheung. *The finite element method in structural and continuous mechanics*. McGraw-Hill Book Company, London, 1967.

MATHEMATICAL TECHNIQUES SPECIFICALLY APPLIED TO ELECTROMAGNETIC THEORY

[180] K. J. Binns, P. J. Lawrenson, and C. W. Trowbridge. *The analytical and numerical solution of electric and magnetic fields*. John Wiley & Sons, Chichester, 1992.

[181] M. V. K. Chari and S. J. Salon. *Numerical methods in electromagnetism*. Academic Press, San Diego, 2000.

[182] M. V. K. Chari and P. P. Silvester. *Finite elements in electrical and magnetic field problems*. John Wiley & Sons, Chichester, 1980.

[183] W. C. Chew, J. M. Jin, E. Michielssen, and J. Song (eds.). *Fast and efficient algorithms in computational electromagnetics*. Artech House, Norwood, MA, 2001.

[184] C. Christopoulos. *The transmission-line modeling method TLM*. IEEE Press and Oxford University Press, New York, 1995.

[185] G. Conciauro, M. Guglielmi, and R. Sorrentino. *Advanced modal analysis*. John Wiley & Sons, Chichester, 2000.

[186] D. G. Dudley. *Mathematical foundations for electromagnetic theory*. IEEE Press, New York, 1994.

[187] C. Hafner. *Post-modern electromagnetics*. John Wiley & Sons, Chichester, 1999.

[188] R. S. H. Hoole. *Computer-aided analysis and design of electromagnetic devices*. Elsevier, New York, 1989.

[189] N. Ida and J. P. A. Bastos. *Electromagnetics and calculation of fields*. Springer-Verlag, New York, 2nd edition, 1997.

[190] T. Itoh, G. Pelosi, and P. P. Silvester (eds.). *Finite element software for microwave engineering*. John Wiley & Sons, New York, 1996.

[191] T. Itoh (ed.). *Numerical techniques for microwave and millimeter-wave passive structures*. John Wiley & Sons, New York, 1989.

[192] J. Jin. *The finite element method in electromagnetics*. John Wiley & Sons, New York, 2nd edition, 2002.

[193] D. S. Jones. *Methods in electromagnetic wave propagation*. Clarendon Press, Oxford, 2nd edition, 1994.

[194] K. S. Kunz and R. J. Luebbers. *The finite difference time-domain method for electromagnetics*. CRC Press, Boca Raton, 1993.

[195] D. A. Lowther and P. P. Silvester. *Computer-aided design in magnetics*. Springer-Verlag, Berlin, 1985.

[196] R. Mittra and S. W. Lee. *Analytical techniques in the theory of guided waves*. Macmillan, New York, 1971.

[197] R. Mittra (ed.). *Computer techniques for electromagnetics*. Pergamon Press, Oxford, 1973.

[198] R. Mittra (ed.). *Numerical and asymptotic techniques in electromagnetics*. Springer-Verlag, Berlin, 1975.

[199] M. A. Morgan (ed.). *Finite element and finite difference methods in electromagnetic scattering*. Elsevier, New York, 1990.

[200] N. Morita, N. Kumagai, and J. R. Mautz. *Integral equation methods for electromagnetics*. Artech House, Boston, 1990.

[201] C. Müller. *Grundprobleme der Mathematischen Theorie Elektromagnetischer Schwingungen*. Springer-Verlag, Berlin, 1957. Translated as "Foundations of the mathematical theory of electromagnetic waves," Springer-Verlag, Berlin, 1969.

[202] G. Pelosi, R. Coccioli, and S. Selleri. *Quick finite elements for electromagnetic waves*. Artech House, Boston, 1998.

[203] A. F. Peterson, S. L. Ray, and R. Mittra. *Computational methods for electromagnetics*. IEEE Press, Oxford University Press, 1998.

[204] Y. Rahmat-Samii and E. Michielssen. *Electromagnetic optimization by genetic algorithms*. John Wiley & Sons, New York, 1999.

[205] M. N. O. Sadiku. *Numerical techniques in electromagnetics*. CRC Press, Boca Raton, 1992.

[206] T. K. Sarkar (ed.). *Application of conjugate gradient method to electromagnetics and signal analysis*. Elsevier, New York, 1991.

[207] P. P. Silvester and R. L. Ferrari. *Finite elements for electrical engineers*. Cambridge University Press, Cambridge, 3rd edition, 1996.

[208] B. J. Strait (ed.). *Applications of the method of moments in electromagnetic fields*. S.C.E.E.E., St. Cloud, FL, 1980.

[209] A. Taflove. *Computational electrodynamics: the finite-difference time-domain method*. Artech House, Boston, 1995.

[210] C. T. Tai. *Dyadic Green functions in electromagnetic theory*. IEEE Press, Piscataway, NJ, 2nd edition, 1994.

[211] J. L. Volakis, A. Chatterjee, and L. C. Kempel. *Finite element method for electromagnetics*. IEEE Press, New York, and Oxford University Press, Oxford, 1998.

[212] J. J. H. Wang. *Generalized moment methods in electromagnetics*. John Wiley & Sons, New York, 1991.

Acronyms and Symbols

Acronyms

ABC	Absorbing boundary condition
AIM	Adaptive integral method
AWE	Asymptotic waveform evaluation
BPM	Beam propagation method
BOR	Body of revolution
CFIE	Combined field integral equation
DNG	Doubly negative materials
EFIE	Electric field integral equation
EW	Electric wall
FD	Finite difference
FDTD	Finite differences in the time domain
FEM	Finite element method
FETD	Finite elements in the time domain
FMM	Fast multipole method
GO	Geometrical optics
GTD	Geometrical theory of diffraction
HTS	High temperature semiconductor
ILD	Incremental length diffraction
LSE	Longitudinal section electric mode
LSM	Longitudinal section magnetic mode
LTS	Low temperature semiconductor
MEC	Method of equivalent currents
MEI	Measured equation of invariance
MFIE	Magnetic field integral equation
MRI	Magnetic resonance imaging
MW	Magnetic wall
PBG	Photonic bandgap material
PEC	Perfect electric conductor
PMC	Perfect magnetic conductor
PML	Perfectly matched layer
PO	Physical optics
PTD	Physical theory of diffraction
PV	Principal value
RWG	Rao-Wilton-Glisson basis function
SAR	Specific absorption rate
SEM	Singularity expansion method

Electromagnetic Fields, Second Edition, By Jean G. Van Bladel

SST	Slant stack transform
TE	Transverse electric
TEM	Transverse electric magnetic
TLM	Transmission line matrix method
TM	Transverse magnetic
UAT	Uniform asymptotic theory of diffraction
UTD	Uniform geometrical theory of diffraction
WKB	Wentzel, Kramers, Brillouin (Jeffreys) approximation

The symbols are essentially the same as in the first edition, including the use of **u** for a unit vector, and the *linguistic* notation for the operators div, grad, curl.

Mathematical symbols

$\doteq$	proportional to
$\approx$	approximately equal to
z^*	complex conjugate of z
Re (z)	real part of z
Im (z)	imaginary part of z
$\|z\|$	amplitude (magnitude) of z
$\overline{\overline{a}}$	a typical dyadic
$\overline{\overline{a}}^t$	transpose of $\overline{\overline{a}}$
$\overline{\overline{a}}^\dagger$	Hermitian transpose of $\overline{\overline{a}}$
$\sup f(x)$	upper bound of $f(x)$
$o\left(\frac{1}{x}\right)$ and $O\left(\frac{1}{x}\right)$	a function $f(x)$ is o or O depending on whether $\lim_{x\to\infty} x f(x)$ is zero or different from zero (but finite)
$\| f \|$	norm of a scalar element
$\| \overline{\overline{\mathbf{a}}} \|$	norm of a dyadic element
$\langle a, b\rangle_S$	symmetric scalar product
$\langle a, b\rangle_H$	Hermitian scalar product
$\text{grad}_S f$	surface gradient of a scalar function
$\text{div}_S \mathbf{f}$	surface divergence of a vector function
$\text{curl}_S \mathbf{f}$	surface curl of a vector function
grad $\mathbf{f}$	gradient of a vector function
div $\overline{\overline{a}}$	divergence of a dyadic function
curl $\overline{\overline{a}}$	curl of a dyadic function
$\text{grad}_1 f$	gradient on a spherical surface of unit radius
$\boldsymbol{\nabla}$	nabla operator
$\nabla_1^2 f$	Laplacian on a spherical surface of unit radius (Beltrami operator)
$\nabla_S^2 f$	surface Laplacian of a scalar function
$\nabla_S^2 \mathbf{f}$	surface Laplacian of a vector function
$\nabla^2 \overline{\overline{a}}$	Laplacian of a dyadic function
$\Box f$	Dalembertian of a scalar function
$\frac{D}{Dt}$	substantial derivative

δ_{mn}	Kronecker delta (=0 for $m \neq n$; =1 for $m = n$)
ϵ_m	Neumann factor (=1 for $m = 0$; =2 for $m = 1, 2, 3, \ldots$)

Symbols for Physical and Mathematical Quantities

Symbols for electrical quantities, static or of arbitrary time dependence, are *lowercase*. Time-harmonic quantities, with time factor $e^{j\omega t}$, are represented by their phasor (*capitals*). Since the supply of symbols is limited, and the number of relevant parameters very large, many symbols are given several meanings. β, for example, denotes either a propagation constant or a velocity expressed in terms of c_0. The various meanings are mostly used locally, hence confusion is negligible in most cases. Most symbols with multiple meanings are not included in the list.

$\mathbf{a}$	magnetic vector potential (Tm)
$\mathbf{b}$	magnetic flux density (or induction) (T)
c_0	velocity of light in vacuum (m s^{-1})
c	velocity of light in a medium (m s^{-1})
$\mathbf{c}$	electric (Fitzgerald) potential (C m^{-1})
comb (x)	comb function
C	capacitance of a conductor (F)
$C(f, g, \tau)$	convolution of the functions f and g
$\mathbf{d}$	electric flux density (or displacement) (C m^{-2})
$D(\mathbf{u})$	directivity of an antenna in a direction of unit vector $\mathbf{u}$
D^e	electric (soft) diffraction coefficient ($m^{\frac{1}{2}}$)
D^h	magnetic (hard) diffraction coefficient ($m^{\frac{1}{2}}$)
$D_\perp$	diffraction coefficient for perpendicular polarization ($m^{\frac{1}{2}}$)
$D_\parallel$	diffraction coefficient for parallel polarization ($m^{\frac{1}{2}}$)
$\mathbf{e}$	electric field strength (intensity) (V m^{-1})
$\mathbf{e}_a$	applied (or impressed) electric field (V m^{-1})
$\mathbf{e}^g$	electric generator field (V m^{-1})
$E(k)$	elliptic integral of the second kind
$\mathcal{E}$	energy (J)
f_p	plasma frequency (Hz)
$\mathbf{F}$	radiation vector (V)
$g_{\alpha\beta}$	metric tensor
$G(\mathbf{u})$	gain of an antenna in a direction of unit vector $\mathbf{u}$
$G(\mathbf{r}\|\mathbf{r}')$	Green's function (effect on $\mathbf{r}$ of an elementary source in $\mathbf{r}'$)
$G^a(\mathbf{r}\|\mathbf{r}')$	Green's function for the adjoint problem
$G_e(\mathbf{r}\|\mathbf{r}')$	Green's function in the extended sense
$G_0(\mathbf{r}\|\mathbf{r}')$	Green's function for Helmholtz equation in vacuum
$\overline{\overline{G}}_{ab}(\mathbf{r}\|\mathbf{r}')$	Green's dyadic, expressing the effect on field a (electric or magnetic) of an elementary source of type b (electric or magnetic) (more specifically: $\overline{\overline{G}}_{ee}$, $\overline{\overline{G}}_{em}$, $\overline{\overline{G}}_{me}$, $\overline{\overline{G}}_{mm}$)
$\overline{\overline{G}}^a(\mathbf{r}\|\mathbf{r}')$	Green's dyadic for the adjoint problem
$\mathbf{h}$	magnetic field strength (or intensity) (A m^{-1})
$\mathbf{h}^g$	generator magnetic field (A m^{-1})
$\mathbf{h}_o$	harmonic vector in a ring, or in an annulus (m^{-1})

h_i	metric coefficient
$H(x)$, $H_S(\mathbf{r})$	Heaviside unit step functions
$\overline{\overline{I}}$	identity (or unit) dyadic
$\mathbf{j}$	electric current density in a volume (A m^{-2})
$\mathbf{j}_S$	electric current density on a surface (A m^{-1})
$\mathbf{j}_a$	applied (or empressed) current density (A m^{-2})
$\mathbf{j}_m$	magnetic current density in a volume (V m^{-2})
$\mathbf{j}_{mS}$	magnetic current density on a surface (V m^{-1})
J	first curvature (m^{-1})
$\overline{\overline{J}}$	Jacobian matrix
$k = \beta - j\alpha$	propagation constant (m^{-1})
k_i	propagation constant of an ionic wave (m^{-1})
k_e	propagation constant of an electronic wave (m^{-1})
K	second curvature (m^{-2})
$K(k)$	elliptic integral of the first kind
$\mathbf{l}_{eff}$	effective length of an antenna (m)
l_F	Fresnel length (m)
$\mathbf{L}(\mathbf{J})$, $\mathbf{L}(\mathbf{J}_S)$	operators producing an electric field from $\mathbf{J}$ or $\mathbf{J}_S$
L_c	characteristic length of a good conductor
L_i	shape function
$\overline{\overline{L}}_v$	depolarization dyadic of a small volume v
$\mathcal{L}_2$	space of Lebesgue square-integrable functions
$\mathbf{m}_e$	electric dipole density (polarization) (C m^{-2})
$\mathbf{m}_m$	magnetic dipole density (polarization) (A m^{-1})
M	mismatch factor
$\mathbf{M}(\mathbf{J})$, $\mathbf{M}(\mathbf{J}_S)$	operators producing a magnetic field from $\mathbf{J}$ or $\mathbf{J}_S$
$M^{\alpha\beta}$	contravariant electromagnetic tensor (for $\mathbf{d}$ and $\mathbf{h}$)
n	number density (m^{-3})
N	index of refraction
$N_{\alpha\beta}$	covariant electromagnetic tensor (for $\mathbf{e}$ and $\mathbf{b}$)
$\mathbf{p}$	Poynting's vector (W m^{-2})
$\mathbf{p}_e$	electric dipole moment (C m)
$\mathbf{p}_m$	magnetic dipole moment (A m^2)
$\overline{\overline{p}}$	polarization matrix
P_{pol}	polarization factor
P^{abs}	absorbed power (W)
P^{sc}	scattered power (W)
P^a	available power (W)
$\mathcal{P}$	power density (W m^{-2})
q	electric charge (C)
$\overline{\overline{q}}_e$	electric quadrupole dyadic (C m^2)
$\overline{\overline{q}}_m$	magnetic quadrupole dyadic (A m^3)
Q	quality factor of a resonance
$\mathbf{r}$	radius vector from the origin (m)
R_1, R_2	radii of curvature of a surface (m)
$R_\perp$	reflection coefficient for perpendicular polarization
$R_\parallel$	reflection coefficient for parallel polarization

R_{c0}	characteristic resistance of free space (Ω)
$s_i (i = 0, 1, 2, 3)$	Stokes' parameters
$s(z)$	field expression (W)
$S(\mathbf{r})$	phase function (m)
S_1	spherical surface of unit radius
S_R	spherical surface of radius R
S_∞	spherical surface of infinite radius
S_a	effective area of an antenna (m^2)
$\overline{\overline{S}}$	scattering matrix
tr	trace of a dyadic
$T_\perp$	transmission coefficient for perpendicular polarization
$T_\parallel$	transmission coefficient for parallel polarization
T_c	critical temperature of a superconductor (K)
T_D	magnetic diffusion time (s)
T_{rel}	charge relaxation time (s)
T_w	wave propagation time (s)
$\overline{\overline{T}}$	transition matrix
$\overline{\overline{\alpha}}_e$	electric polarizability dyadic (m^3)
$\overline{\overline{\alpha}}_m$	magnetic polarizability dyadic (m^3)
$\overline{\overline{\Gamma}}$	coherence matrix
δ	penetration depth in a good conductor (m)
δ_s	penetration depth in a superconductor (m)
$\delta(x)$, $\delta(\mathbf{r})$	Dirac functions
δ_S	Dirac function on a surface (m^{-1})
δ_c	Dirac function on a curve C (m^{-2})
ϵ_r, $\overline{\overline{\epsilon}}_r$	dielectric constant
ϵ_{cr}	complex dielectric constant
η	efficiency of an antenna
η_d	magnetic diffusivity ($m^2\ s^{-1}$)
θ	reduced magnetic potential (A)
κ	chirality (or Pasteur) parameter
κ_{er}, κ_{ei}	Kelvin functions
λ_0	wavelength in vacuum (m)
λ	wavelength in a medium (m)
$\lambda\!\!\!^{-}_0 = (\lambda_0/2\pi)$	(m)
Λ	characteristic parameter of a semiconductor (Ω ms)
μ_r	magnetic permeability
$\mathbf{\Pi}_e$	electric Hertz potential (V m)
$\mathbf{\Pi}_m$	magnetic Hertz potential (A m)
ρ	electric volume charge density (C m^{-3})
ρ_S	electric surface charge density (C m^{-2})
ρ_C	electric linear charge density (C m^{-1})
ρ_m	magnetic volume charge density (T m^{-3})
ρ_{mS}	magnetic surface charge density (T)
$\boldsymbol{\rho}$	characteristic vector of a small aperture
σ_S	surface conductance of a shell (S)
σ^{sc}	scattering cross section (m^2)

σ^{abs}	absorption cross section (m^2)
σ^{ext}	extinction cross section (m^2)
σ^{tr}	transmission cross section of an aperture (m^2)
σ^{rad}	monostatic (radar) cross section (m^2)
σ^{b}	bistatic cross section (m^2)
τ_0	a dimensionless parameter of a small aperture
ϕ	scalar electric potential (V)
ϕ^g	generator electric potential (V)
χ_e, $\overline{\overline{\chi}}_e$	electric susceptibility
χ_m, $\overline{\overline{\chi}}_m$	magnetic susceptibility
χ	Tellegen parameter
ψ	scalar magnetic potential (A)

Author Index

Electromagnetic Fields, Second Edition, By Jean G. Van Bladel

Subject Index

Electromagnetic Fields, Second Edition, By Jean G. Van Bladel